

ASTES

Advances in Science, Technology & Engineering Systems Journal

VOLUME 5-ISSUE 5|SEPT-OCT 2020

www.astesj.com
ISSN: 2415-6698

EDITORIAL BOARD
Editor-in-Chief

Prof. Passerini Kazmerski
University of Chicago, USA

Editorial Board Members

Prof. Rehan Ullah Khan
Qassim University, Saudi Arabia

Prof. María Jesús Espinosa
Universidad Tecnológica Metropolitana, Mexico

Dr. Hongbo Du
Prairie View A&M University, USA

Dr. Nguyen Tung Linh
Electric Power University, Vietnam

Tariq Kamal
University of Nottingham, UK

Sakarya University, Turkey

Dr. Mohmaed Abdel Fattah Ashabrawy
Prince Sattam bin Abdulaziz University, Saudi Arabia

Mohamed Mohamed Abdel-Daim
Suez Canal University, Egypt

Dr. Omeje Maxwell
Covenant University, Nigeria

Prof. Majida Ali Abed Meshari
Tikrit University Campus, Iraq

Dr. Heba Afify
MTI university, Cairo, Egypt

Regional Editors

Dr. Hung-Wei Wu
Kun Shan University, Taiwan

Dr. Maryam Asghari
Shahid Ashrafi Esfahani, Iran

Dr. Shakir Ali
Aligarh Muslim University, India

Dr. Ahmet Kayabasi
Karamanoglu Mehmetbey University, Turkey

Dr. Ebubekir Altuntas
Gaziosmanpasa University, Turkey

Dr. Sabry Ali Abdallah El-Naggar
Tanta University, Egypt

Aamir Nawaz
Gomal University, Pakistan

Dr. Gomathi Periasamy
Mekelle University, Ethiopia

Dr. Walid Wafik Mohamed Badawy
National Organization for Drug Control and Research, Egypt

Dr. Abhishek Shukla
R.D. Engineering College, India

Abdullah El-Bayoumi
Cairo University, Egypt

Ayham Hassan Abazid
Jordan university of science and technology, Jordan

Editorial

Advances in Science, Technology and Engineering Systems Journal (ASTESJ) is an online-only journal dedicated to publishing significant advances covering all aspects of technology relevant to the physical science and engineering communities. The journal regularly publishes articles covering specific topics of interest.

Current Issue features key papers related to multidisciplinary domains involving complex system stemming from numerous disciplines; this is exactly how this journal differs from other interdisciplinary and multidisciplinary engineering journals. This issue contains 158 accepted papers in Computer Science and Electrical Engineering domain.

Editor-in-chief
Prof. Passerini Kazmersk

ADVANCES IN SCIENCE, TECHNOLOGY AND ENGINEERING SYSTEMS JOURNAL

Volume 5 Issue 5 **September-October 2020**

CONTENTS

Mitigating Congestion in Restructured Power System using FACTS Allocation by Sensitivity Factors and Parameter Optimized by GWO 01
Anubha Gautam, Parshram Sharma, Yogendra Kumar

Case Study to Determine the Causes of Fire in Agriculture 11
Marianna Tomašková, Darina Matisková, Michaela Balážiková

Learning the Influence between Partially Observable Processes using Scorebased Structure Learning 16
Ritesh Ajoodha, Benjamin Rosman

Facial Expression Recognition using Facial Landmarks: A Novel Approach 24
Rohith Raj S, Pratiba D, Ramakanth Kumar P

Criteria to Implement a Supervision System in the Petroleum Industry: A Case Study in a Terminal Storage Facility 29
Khalid Chkara, Hamid Seghiouer

The Relation of Compression Strength with Modulus of Rupture and UPV of Concrete Containing M-sand as Fine Aggregate 39
Altamashuddinkhan Nadimalla, Siti Aliyyah Masjuki, Siti Asmahani Saad, Maisarah Ali, Shuhairy Norhisham

A Smart Updater IT Governance Platform Based on Artificial Intelligence 47
Aziza Chakir, Meriyem Chergui, Johanes Fernandes Andry

Analysis of Security-Reliability Trade-off for Multi-hop Cognitive Relaying Protocol with TAS/SC Technique 54
Pham Minh Nam, Phu Tran Tin

Fast Stream Cipher based Chaos Neural Network for Data Security in CAN Bus 63
Zhongda Liu, Takeshi Murakami, Satoshi Kawamura, Hitoaki Yoshida

Low Power Bulk Driven Series Parallel OTA for Low Frequency Applications 69
Sushma Padubidri Shivaprasad, Sreemannarayanay Kulkarni

Power Loss Minimization Using The Integration of DGs And Reconfiguration of Distribution System: Applied on Real Distribution Feeder of Urbain Areas of Kenitra City in Morroco 74
Ismail Moufid, Soukaina Naciri, Hassan EL Moussaoui, Tijani Lamhamdi, Hassane El Markhi

Method of Modelling Prices for R&D Products in the Case of their Transfer from Engineering Universities to the Business 80
Oleksandra Mrykhina, Lidiya Lisovska, Ihor Novakivskyj, Terebukh, Valentyna Zhukovska

Transient Analysis of a Line-Start Synchronous Reluctance Motor with Symmetrical Distributed Brass Rotor Bars 94
Mbika Muteba

Spatial Multi-Layer Perceptron Model for Predicting Dengue Fever Outbreaks in Surabaya 103
Siana Halim, Andreas Handojo, Ivan Enrico Widodo, Felecia, Tanti Octavia

Quantitative Approach in Enhancing Decision Making Through Big Data as An Advanced Technology 109
Hana Yousuf, Asma Yousuf Zainal

A User-Item Collaborative Filtering System to Predict Online Learning Outcome 117
Dina Fitria Murad, Rosilah Hassan, Wahiza Wahi, Bambang Dwi Wijanarko

Search for New Potential Breast Cancer Inhibitors (MCF7) Based on Molecular Docking and Biological Assay of Pyrazoline Analogue Compounds 122
Jasril, Hilwan Yuda Teruna, Ihsan, Neni Frimayanti

The Ludocreative Expression for the Production of Texts in Children of Early Education 127
Giuliana Gaona-Gamarra, Brian Meneses-Claudio, Avid Roman-Gonzalez

Towards Directing Convolutional Neural Networks Using Computational Geometry Algorithms: Application to Handwritten Arabic Character Recognition 137
Mohsine Elkhayati, Youssfi Elkettani

Design of Purebred Dog Recommendation System Using MCDM Approach 148
Phie Chyan

Four-Dimensional Sparse Data Structures for Representing Text Data 154
Martin Marinov, Alexander Efremov

Convolutional Neural Network Based Classification of Patients with Pneumonia using X-ray Lung Images 167
Hicham Moujahid, Bouchaib Cherradi, Oussama El Gannour, Lhoussain Bahatti, Oumaima Terrada & Soufiane Hamida

Detailed Security Evaluation of ARANz, ARAN and AODV Protocols 176
Liana Khamis Qabajeh, Mohammad Moustafa Qabajeh

Evaluation of Disadvantaged Regions in East Java Based-on the 33 Indicators of the Ministry of Villages, Development of Disadvantaged Regions, and Transmigration Using the Ensemble ROCK (Robust Clustering Using Link) Method 193
Luluk Wulandari, Yuniar Farida, Aris Fanani, Nurissaidah Ulinnuha, Putroue Keumala Intan

A Review of RPL Objective Function based Enhancement Approaches 201
Ines Kechiche, Ines Bousnina, Abdelaziz Samet

Learning Tool for Kids on Android Platform 212
Gulam, Afan Galih Salman, Bayu Kanigoro

Thermal Performance Analysis of Parabolic Trough Solar Collector System in Climatic Conditions of Errachidia City, Morocco 217
Mohamed Hajjaj, Amine Tilioua, Abdellah Mellaikhafi, Abella Bouaaddi

Applicability of Generalized Metropolis-Hastings Algorithm to Estimating Aggregate Functions in Wireless Sensor Networks 224
Martin Kenyeres, Jozef Kenyeres

FPGA Acceleration of Tree-based Learning Algorithms 237
Haytham Azmi

Assessing Heutagogical Elements in Learning of Engineering Education: Instrument Validation 245
Mimi Mohaffyza Mohamad, Alias Masek, Jailani Md Yunos, Maizam Alias, Nor Hidayah Hamdan, Andika Bagus Nur Rahma Putra

Differential Evolution based Hyperparameters Tuned Deep Learning Models for Disease Diagnosis and Classification 253
Sathyabama Kaliyapillai, Saruladha Krishnamurthy

A Novel Demand Side Management by Minimizing Cost Deviation 262
Vikas Anand Vatul, Arputha Aravinth, Narayanan K, Gulshan Sharma, Tomonobu Senjyu

A Novel Demand Side Management by Minimizing Cost Deviation 262
Vikas Anand Vatul, Arputha Aravinth, Narayanan K, Gulshan Sharma, Tomonobu Senjyu

Supervised Machine Learning Based Medical Diagnosis Support System for Prediction of Patients with Heart Disease 269
Oumaima Terrada, Soufiane Hamida, Bouchaib Cherradi, Abdelhadi Raihani, Omar Bouattane

Proposal for a Control System to Optimize Water use in Households in Peru 278
Witman Alvarado-Diaz, Brian Meneses-Claudio, Avid Roman-Gonzalez

BISINDO (Bahasa Isyarat Indonesia) Sign Language Recognition Using CNN and LSTM 282
Andi Aljabar, Suharjito

A Didactic Balance to Solve Equations 288
Lhachimi Mohamed Younes, Mamouni My Ismail, Achtaich Naceur

Arduino-Compatible Modular Kit Design and Implementation for Programming Education 295
Gyeongyong Heo

Implementation of a Levitation System for the Visualization of the Magnetic Phenomenon 302
Zeila Torres Santos, Brian Meneses-Claudio

Economic and Environmental Analysis of Life Expectancy in China and India: A Data Driven Approach 308
Nittaya Kerdprasop, Kittisak Kerdprasop, Paradee Chuaybamroong

ISR Data Processing in Military Operations 314
Ladislav Burita, Ales Novak

Design and Implementation of Reconfigurable Neuro-Inspired Computing Model on a FPGA 332
Basutkar Umamaheshwar Venkata Prashanth, Mohammed Riyaz Ahmed

Factors Influencing the Intention to Use Technology Services to Implement Self-Service Technology Case Study: Situation Pandemic Covid-19 342
Erick Fernando, Surjandy Surjandy, Meyliana Meyliana, Henry Antonius Wijadja, Desman Hidayat, Ary W Kusumaningtyas, Roni Heryatno

Water Availability for a Self-Sufficient Water Supply: A Case Study of the Pesanggrahan River, DKI Jakarta, Indonesia 348
Ramadhani Yanidar, Djoko Mulyo Hartono, Setyo Sarwanto Moersidik

Component of Trust for Developing Crowdwork System: A Systematic Literature Review 356
Sugiarto Hartono, Meyliana, Ahmad Nizar Hidayanto, Harjanto Prabowo

Modelling and Simulation of Reduce Harmonic Distortion in Non-linear Loads 364
Agus Junaidi, Rahmaniar, Rudi Salman, Joni Safrin Rambey, Baharuddin

Using Envelope Analysis and Compressive Sensing Method for Intelligent Fault Diagnosis of Ball Bearing 370
Khaldoon Fadhel Brethee, Ghalib Rzayyig Ibrahim, Rashaq Abdullah Mohammed

Semiclassical Theory for Bacteria Motility Under External Electric Fields and Interactions with Nanodevices 376
Huber Nieto-Chaupis

Creating a Website Scoring for High-Order Thinking Skills Game 382
Yogi Udjaja, Sasmoko, Jurike V.Moniaga, Millionsen Christ Lo

Sentiment Analysis on Utilizing Online Transportation of Indonesian Customers Using Tweets in the Normal Era and the Pandemic Covid-19 Era with Support Vector Machine 389
Jajam Haerul Jaman, Rasdi Abdulrohman, Aries Suharso , Nina Sulistiowati, Indah Purnama Dewi

Multi-Objective Optimization when Surface Grinding the 3X13 Steel by Combining the General Reduced Gradient Algorithm and Harmonic Mean Method 395
Nhu-Tung Nguyen, Dung Hoang Tien, Do Duc Trung

Strain–Displacement Expressions and their Effect on the Deflection and Strength of Plate 401
Onyeka, Festus, Edozie Thompson Okeke, Wasiu, John

A hybrid model for Coronary Heart Disease Prediction in Thai Population 414
Chalinee Partanapat, Chuleerat Jaruskulchai, Chanankorn Jandaeng

Shape Optimization of Planar Inductors for RF Circuits using a Metaheuristic Technique based on Evolutionary Approach 426
Imad El Hajjami, Bachir Benhala, Hamid Bouyghf

New Algorithm for the Development of a Musical Words Descriptor for the Artificial Composition of Oriental Music 434
Mehdi Zhar, Omar Bouattane, Lhoussain Bahatti

Newton-Raphson Algorithm as a Power Utility Tool for Network Stability 444
Lambe Mutalub Adesina, Ademola Abdulkareem, James Katende, Olaosebikan Fakolujo

Comparative Study of Cryptocurrency Algorithms: Coronavirus Towards Bitcoin's Expansion 452
Fatma Mallouli, Aya Hellal, Fatimah Abdulraheem Alzahrani, Abdulsalam Ali Almadani, Nahla Sharief Saeed

Bayes Classification and Entropy Discretization of Large Datasets using Multi-Resolution Data Aggregation 460
Safaa Alwajidi, Li Yang

Interpretation of Machine Learning Models for Medical Diagnosis 469
Nghia Duong-Trung, Nga Quynh Thi Tang, Xuan Son Ha

Contextual Word Representation and Deep Neural Networks-based Method for Arabic Question Classification 478
Alami Hamza, Noureddine En-Nahnahi, Said El Alaoui Ouatik

Review of Orange Juice Extractor Machines 485
Ugwu Benedict Nnamdi, Chime Thompson Onyejiuwa, Chime Rufus Ogbuke

Knowledge Mapping of Virtual Academic Communities: A Bibliometric Study Using Visual Analysis 493
Chunlai Yan, Hongxia Li

Simulated Annealing for Traveling Salesman Problem with Hotel Selection for a Distribution Company Based in Mexico 500
Raúl Jiménez-Gutiérrez, Diana Sánchez-Partida, José-Luis Martínez-Flores, Eduardo-Arturo Garzón-Garnica

Growth Models And Age Estimation Of Rice Using Multitemporal Vegetation Index On Landsat 8 Imagery 506
Abdi Sukmono, Arief Laila Nugraha, Arsyad Nur Ariwahid, Nida Shabrina

Genetic Organization and Evolution of Electromechanical Objects with Adaptive Geometry of Active Zone 512
Vasyl Shynkarenko, Ali Makki, Viktoriia Kotliarova, Anna Shymanska, Pavlo Krasovskyi

Multi Closed-loop Adaptive Neuro-Fuzzy Inference System for Quadrotor Position Control 526
Halima Housny, El Ayachi Chater, Hassan El Fadil

Malware classification using XGboost-Gradient Boosted Decision Tree 536
Rajesh Kumar, Geetha S

The Newtonian Model of the Smolensk Catastrophe 550
Józef Pawelec

Butterfly Life Cycle Algorithm for Measuring Company's Growth Performance based on BSC and SWOT Perspectives 554
Kerin Augustin, Natasia, Ditdit Nugeraha Utama

Wideband and High-Gain Aperture Coupled Feed Patch Array Antenna for Millimeter-Wave Application 559
Dat Vuong, Nam Ha-Van, Tran The Son

Advances in Optimisation Algorithms and Techniques for Deep Learning 563
Chigozie Enyinna Nwankpa

Numerical Study of Gas Microflow within a Triangular Lid-driven Cavity 578
Youssef Elguennouni, Mohamed Hssikou, Jamal Baliti, Mohammed Alaoui

Review of Pedagogical Principles of Cyber Security Exercises 592
Mika Karjalainen, Tero Kokkonen

CNN-LSTM Based Model for ECG Arrhythmias and Myocardial Infarction Classification 601
Lana Abdulrazaq Abdullah, Muzhir Shaban Al-Ani

Experimental and Numerical Study of the Mechanical Behavior of Bio-Loaded PVC Subjected to Aging 607
Abdelghani Lakhdar, Aziz Moumen, Laidi Zahiri, Mustapha Jammoukh, Khalifa Mansouri

A Typological Study of Portuguese Mortality from Non-communicable Diseases 613
Ana Paula Nascimento, Cristina Prudêncio, Mónica Vieira, Rui Pimenta, Helena Bacelar-Nicolau

The Design Process in the Improvement of The Experience Between a Brand and its Target Audience Through a Digital Product: The Lexus Portugal's used Car Website Case Study 620
Nuno Martins, Juan-Ramon Martin-Sanroman, Fernando Suárez-Carballo

Sustainable Development Practices in the Moroccan Small and Medium Enterprise: by What means and for What Purpose? 630
Keltoum Rahali, Abdelaziz Chaouch, Elmahjoub Aouane, Sami Chbika, Abderrazzak Khohmimidi, Mustapha Kouzer, Abdellatif Elouali

Overcome Discrimination: A Logistic Regression with 10-year Longitudinal Investigation of Emo Kids' Facebook Posts 637
Proud Arunrangsiwed, Yothin Sawangdee

Finding Association Patterns of Disease Co-occurrence by using Closed Association Rule Generation 645
Panida Songram, Phattanaphong Chompowiset, Chatklaw Jareanpon

Investment of Classic Deep CNNs and SVM for Classifying Remote Sensing Images 652
Khalid A. AlAfandy, Hicham, Mohamed Lazaar, Mohammed Al Achhab

Issues in File Caching and Virtual Memory Paging with Fast SCM Storage 660
Yunjoo Park, Hyokyung Bahn

Investigation of Dielectric Properties of Indigenous Blended Ester oil for Electric System Applications 669
D.M. Srinivasa, Usha Surendra, V.V. Pattanshetti

Multi-layered Security Design and Evaluation for Cloud-based Web Application: Case Study of Human Resource Management System 674
Gautama Wijaya, Nico Surantha

Enterprise Architecture Institutionalization for Health Information Exchange (HIE) Cloud Migration 680
Kofi Osei-Tutu, Yeong-Tae Song

Smartphone Influence Factor of University Student's Academic Achievement 692
Surjandy, Meylian, Kristianus Oktriono, Mika Milenia Catherine, Chutiporn Anutariya, Erick Fernando

Prototype for the Management of Engineering Companies and the ICT to Improve the Quality of Services 698
Segundo Moisés Toapanta Toapanta, Emmanuel Alejandro Narváez Picon, Luis Enrique Mafla Gallegos

Newton-Euler Based Dynamic Modeling and Control Simulation for Dual-Axis Parallel Mechanism Solar Tracker 709
Sarot Srang, Sopagna Ath, Masaki Yamakita

An Empirical Comparison of Different Two-Factor Models in the Context of Portfolio Optimisation 717
Jamal Agouram, Mouncif Harabida, Bouchra Radi, Ghizlane Lakhnati

Modeling and Implementation of Quadcopter Autonomous Flight Based on Alternative Methods to Determine Propeller Parameters 727
Gene Patrick Rible, Nicolette Ann Arriola, Manuel Ramos Jr.

Student's Belief Detection and Segmentation for Real-Time: A Case Study of Indian University 742
Chaman Verma, Zoltan Illes, Veronika Stoffova

Johnson Noise and Optical Characteristics of Polymer Nanocomposites based on Colloidal Quantum Dots and in-situ Nanoparticles Formation 750
Fatin Hana Naning, S. Malik, Lee Feng Koo1, Tze Jin Wong, Pang Hung Yiu

Transient Response & Electromagnetic Behaviour of Flexible Bow-Tie Shaped Chip-less RFID Tag for General IoT Applications 757
Muhammad Usman Ali Khan, Raad Raad, Javad Foroughi

Brain Tumor Classification Using Deep Neural Network 765
Gökalp Çınarer, Bülent Gürsel Emiroğlu, Recep Sinan Arslan, Ahmet Haşim Yurttakal

Using Classic Networks for Classifying Remote Sensing Images: Comparative Study 770
Khalid A. AlAfandy, Hicham Omara, Mohamed Lazaar, Mohammed Al Achhab

Development of a Wireless Displacement Estimation System Using IMU-based Device 781
Tri Nhut Do, Quang Minh Pham, Hoa Binh Le-Nguyen, Cao Tri Nguyen, Hai Minh Nguyen-Tran

Design and Implementation of Quad-Site Testing on FPGA Platform 789
Basavaraj Rabakavi, Saroja V Siddamal

A Study on Methodology of Improvement the Hydraulic System for Cometto Self-Propelled Trailer System 799
Hai Minh Nguyen-Tran, Quang Minh Pham, Hoa Binh Le-Nguyen, Cao Tri Nguyen, Tri Nhut Do

Innovative Solution for Parking-Sharing of Private Institutions Using Various Occupancy Tracking Methods 808
Adrian Florea, Valentin Fleaca, Simona Daniela Marcu

Innovative Course Delivery using Analyze – Group – Design – Optimize (AGDO) Methodology: Case Study of Entity-Relationship Model 820
Aparna Sharma, Rishabh Singh, Prathamesh Churi, Mahesh Mali

Deaf Chat: A Speech-to-Text Communication Aid for Hearing Deficiency 826
Mandlenkosi Shezi, Abejide Ade-Ibijola

The Curriculum Developer Team Assignment Analysis Using Ones Assignment Method 840
Elis Ratna Wulan, Dindin Jamaluddin, Iwan Setiawan, Chaerul Saleh, Dudy Imanuddin Effendi

The Effect of User Experience from Teksologi 847
Yanfi Yanfi, Yogi Udjaja, Adrian Victor Juandi

Design of High Output Impedance, Large Voltage Compliance Output Stage of Implantable Hypoglossal Nerve Stimulator (HGNS) for OSA Treatment 852
Ghada Ben Salah, Karim Abbes, Chokri Abdelmoula, Mohamed Masmoudi

Primary Healthcare Response to COVID 19 in a District of Callao, Peru 864
Juan Morales, Marlene Raquel Basilio-Rojas, Maria Rosa Gonzales-Gonzales, Ana Paula Goyzueta

Path Loss Estimation for Some Korek-Telecom Sites Operating at (1.8) GHz and (2.1) GHz for Urban and Suburban Area in Erbil City 869
Sattar Othman Hasan, Sevan Siyyah Abdullah

User's Demographic Characteristic on the Evaluation of Gamification Interactive Typing for Primary School Visually Impaired with System Usability Scale 876
Yanfi Yanfi, Yogi Udjaja, Azani Cempaka Sari

Using the Neural Network to Diagnose the Severity of Heart Disease in Patients Using General Specifications and ECG Signals Received from the Patients 882
Zahra Jafari, Saman Rajebi, Siyamak Haghipour

English as a Foreign Language Learning Students' Perceptions of Blended Learning in University Institutions: A Case Study of a University in UAE 893
Ghadah Al Murshidi

Need of E-Recruitment System for Universities: Case of Pulchowk Campus, Nepal 902
Vijay Yadav, Ujjwal Gewali, Suman Khatri, Shree Ram Rauniyar, Aman Shakya

Effect of Cover Number on Distilled Water Production of Distillers with a Novel Water Feeding 913
Mirmanto Mirmanto, Made Wirawan, I Made Adi Sayoga, Abdullah Abdullah, Muhamad Faisal

Using Big Data Analytics to Predict Learner Attrition based on First Year Marks at a South African University 920
Gcobisile Matafeni, Ritesh Ajoodha

Performance Analysis of Selective Repeat ARQ Protocol Used in Digital Data Transmission Over Unreliable Channels 927
Fayza A. Nada

Classification of Handwritten Names of Cities and Handwritten Text Recognition using Various Deep Learning Models 934
Daniyar Nurseitov, Kairat Bostanbekov, Maksat Kanatov, Anel Alimova, Abdelrahman Abdallah, Galymzhan Abdimanap

Dense SIFT–Flow based Architecture for Recognizing Hand Gestures 944
Suni S S, K Gopakumar

Scattering of H-Wave by a Moving Dispersive Conducting Complex Object 955
Esmail Mohamed Abuhdima, Gurcan Comert, Ahmed El Qaouaq, Ashleigh Nicole Reeves

Total Family Risk in Families who go to Popular Dining Rooms in a Vulnerable Area of Collique, Comas 960
Hernan Matta-Solis, Rosa Perez-Siguas, Eduardo Matta-Solis, Melissa Yauri-Machaca

Health-Related Quality of life in Students of an Education Institution of Ventanilla 966
Lucia Silva-Bueno, Brian Meneses-Claudio, Hernan Matta-Solis, Lourdes Matta-Zamudio

Covid-19 Pandemic Lockdown: The Consequences Towards Project Success in Malaysian Construction Industry 973
Muneera Binti Esa, Farah Salwati Binti Ibrahim, Ernawati Binti Mustafa Kamal

The Impact of Innovation on the Performance of Manufacturing Enterprises in Vietnam 984
Thi Anh Van Nguyen, Khac Hieu Nguyen

Matrix-based Minimal Cut Method and Applications to System Reliability 991
Emad Kareem Mutar

Renewable Electric Power from the Equine Treadmill: An Evaluation of the Potential 997
Faizan Dastgeer, Hasan Erteza Gelani

Control of Soft Robotic Artificial Muscle with Hand Gesture Using Leap Motion Sensor 1007
Victoria Oguntosin, Akindele Ayoola E

Fabrication and Properties of Hybrid Membranes Based on Poly (Vinyl Alcohol), Sulfosuccinic Acid and Salts of Heteropolyacid with or without Silica for Fuel Cells Applications 1013
Said Maarouf, Zouhair Alouane, Bouchra Tazi, Farhate Guenoun, Khalil Fouad

Dissection of Quantitative Trait Loci (QTL), annotation of Single Nucleotide Polymorphism (SNP), and Identification of Candidate Genes for Grain Yield in Triticum turgidum L. var durum 1020
Issame Farouk, Ahmad Alsaleh, Jihan, Fatima Gaboun, Bouchra Belkadi, Abdelkarim Filali Maltouf, Zakaria Kehel, Ismahane Elouafi, Nasserelhaq Nsarellah, Dimah Habash, M. Miloudi Nachit

Understanding Risk Assessment in the Context of Fractional Ownership using Ethereum Smart Contract 1028
Mohamed Laarabi, Abdelilah Maach

Social skills and Resilience in Adolescent of Secondary Level of a public Educational Institution in Puente Piedra Lima – 2020 1036
Niurka Jacome-Olacua, Joselyne Rodríguez-Paucar, Prhitty Marin-Garcia, Brian Meneses-Claudio, Hernan Solis-Matta, Eduardo Matta-Solis

A Cavity Structure based Flexible Piezoelectric for Low-Frequency Vibration Energy Harvesting 1042
Khairul Azman Ahmad, Siti Noraini Sulaiman, Noramalina Abdullah, Muhammad Khusairi Osman

VLSI Architecture for OMP to Reconstruct Compressive Sensing Image 1050
Santosh Bujari, Saroja V Siddamal

Essential Features/Issues of a Multi-Phase Switching Synchronous Buck Regulator 1056
Hani Ahmad-Assi, Nour Sultan Gammoh, Mariana Awni Al Bader

Comparison by Correlation Metric the TOPSIS and ELECTRE II Multi-Criteria Decision Aid Methods: Application to the Environmental Preservation in the European Union Countries 1064
Mohammed Chaouki Abounaima, Loubna Lamrini, Noureddine EL Makhfi, Mohamed Ouzarf

Nature Inspired and Transform Based Image Encryption Techniques: A Comparative Study 1075
Bhagyashri Pandurangi R, Chaitra Bhat, Meenakshi R. Patil

Posture Recognition Method for Caregivers during Postural Change of a Patient on a Bed using Wearable Sensors 1093
Kodai Kitagawa, Koji Matsumoto, Kensuke Iwanaga, Siti Anom Ahmad, Takayuki Nagasaki, Sota Nakano, Mitsumasa Hida, Shogo Okamatsu, Chikamune Wada

Load Evaluation with Fast Decoupled-Newton Raphson Algorithms: Evidence from Port Harcourt Electricity 1099
Ogbuefi Uche Chinweoke, Ibeni Christopher

Design and Implementation of Aerial Vehicle Remote Sensing and Surveillance System, Dehazing Technique Using Modified Dark Channel Prior 1111
Hasn Mahmood Khudair, Taif Alawsi, Anwaar A. Aldergazly, A. H. Majeed

Design and Implementation a Novel System for Estimation Precise Transfer Function of DC Motor 1118
Falih Salih Alkhafaji, Wan Zuha Wan Hasan, Nasri Sulaiman, Maryam bt. Mohd. Isa

Tolerance of Characteristics and Attributes in Developing Student's Academic Achievements 1126
Wongpanya Nuankaew, Pratya Nuankaew

Feature Extractors Evaluation Based V-SLAM for Autonomous Vehicles 1137
Mounir Amraoui, Rachid Latif, Abdelhafid El Ouardi, Abdelouahed Tajer

Effects of Resting Actions Using Smart Toys During Break Times on Concentration in E-learning 1147
Takashi Ito, Kenichi Takahashi, Tomoko Kajiyama

A Proactive Mobile Edge Cache Policy Based on the Prediction by Partial Matching 1154
Lincan Li, Chiew Foong Kwong, Qianyu Liu

Improvised E-Rickshaws for Indian Roads by Effective Battery-Ultracapacitor Hybridization 1162
Shimin Vayal Veetil, Varsha Shah, Makarand Lokhande

Advanced Control Strategies on Nonlinear Testbench Dynamometer System for Simulating the Fuel Consumption 1172
Marika Fanesi, David Scaradozzi

Development of the Surface Roughness Model in the Grinding Processes 1184
Nhu-Tung Nguyen, Dung Hoang Tien, Do Duc Trung

Synthesis of SQL Queries from South African Local Language Narrations 1189
George Obaido, Abejide Ade-Ibijola, Hima Vadapalli

A Proposal of Exercise and Performance Learning Assistant System for Self-Practice at Home 1196
Irin Tri Anggraini, Achmad Basuki, Nobuo Funabiki, Xiqin Lu, Chih-Peng Fan, Yu-Chung Hsu, Cheng-Hsien Lin

Examination of a Skill Sampling Method of an Athlete Using the Athlete's Movement and Eye Movement for the Development of an AI Coach 1204
Takuya Sarugaku, Jun Lee, Yasuaki Matsumoto, Mitsuho Yamada

Strategic Model to Assess the Sustainability and Competitiveness of Focal Agri-Food Smes and their Supply Chains: A Vision Beyond COVID 19 1214
Yonatan López Santos, Diana Sánchez-Partida, Patricia Cano-Olivos

Interactive Virtual Rehabilitation for Aphasic Arabic-Speaking Patients 1225
Sherif H. ElGohary, Aya Lithy, Shefaa Khamis, Aya Ali, Aya Alaa el-din, Hager Abd El-Azim

Design and Development of Electronic Sensor and Monitoring System of Smart Low-cost Phototherapy Light System for Non-Invasive Monitoring and Treatment of Neonatal Jaundice 1233
Paul Cabacungan, Carlos Oppus, Gregory Tangonan, Nerissa Cabacungan, John Paul Mamaradlo, Neil Angelo Mercado

Resilience Assessment of System Process Through Fuzzy Logic: Case of COVID-19 Context 1247
Saloua Said, Hafida Bouloiz, Maryam Gallab

An Empirical Study on Factors Influencing the Intention to use Mobile Learning 1261
Malik Khlaif Gharaibeh, Natheer Khlaif Gharaibeh

Agricultural Data Fusion for SmartAgro Telemetry System 1266
Ioana Marcu, Ana-Maria Drăgulinescu, Carmen Florea, Cristina Bălăceanu, Marius Alexandru Dobrea, George Suciu

Laser Deprocessing Technique and its Application to Physical Failure Analysis 1273
Yanlin Pan, Jia Rui Thong, Pik Kee Tan, Siong Luong Ting, and Chang Qing Chen

An Overview on CryptDb and Word2vec Approaches 1282
Hana Yousuf, Asma Qassem Al-Hamad, Said Salloum

A Circular Invariant Convolution Model-Based Mapping for Multimodal Change Detection 1288
Redha Touati, Max Mignotte, Mohamed Dahmane

C-Band FMCW Radar Design and Implementation for Breathing Rate Estimation 1299
Mohammad Mohammad Abdul-Atty, Ahmed Sayed Ismail Amar, Mohamed Mabrouk

Approach to a Logistic Model to Reduce Costs for Delivery at Home of a Seller of Supplies in Times of Coronavirus 1308
Hernán Washington Samaniego Guevara

Evaluating the Impact of Semantic Gaps on Estimating the Similarity using Arabic Wordnet 1315
Mamoun Abu Helou

ASTES

Advances in Science, Technology and Engineering Systems Journal Vol. 5, No. 5, 01-10 (2020)

www.astesj.com

Special Issue on Multidisciplinary Innovation in Engineering Science & Technology

ASTESJ

ISSN: 2415-6698

Mitigating Congestion in Restructured Power System using FACTS Allocation by Sensitivity Factors and Parameter Optimized by GWO

Anubha Gautam[1,*], Parshram Sharma[1], Yogendra Kumar[2]

[1]*Department of Electrical Engineering, J C Bose UST, YMCA, Faridabad, 121006, India*

[2]*Department of Electrical Engineering, MANIT, Bhopal, 462003, India*

ARTICLE INFO

Article history:
Received: 07 June, 2020
Accepted: 11 August, 2020
Online: 08 September, 2020

Keywords:
Deregulation
Congestion
ATC
ACPTDF
FACTS
GWO

ABSTRACT

In modern deregulated power industry, private sector has invested a lot to supply for extended power demand using the preexisting power system framework. This resulted into increased loading of transmission lines which has to work now to hit their thermal limits. The overloading of transmission line resulted in congestion and hence increase in loss of power in the system. One of the efficient ways to reduce congestion is by enhancing the available transfer capacity (ATC) of the power system. ATC enhancement can be achieved by application of FACTS devices. This paper presents an innovative method to mitigate congestion by locating TCSC in the IEEE 30 bus system. The allocation of TCSC is done by using ACPTDF sensitivity factors while the parameter setting is done by applying Grey Wolf Optimization (GWO) method. The effective application of GWO is demonstrated in this paper to reduce active power loss, enhancement of ATC value with reduction of reactive power loss and to optimize TCSC size through a multi objective function. The suitability of algorithm is established through concerned figures and tables.

1. Introduction

This paper is an extension of work originally presented in 3rd International Conference on Recent Developments in Control, Automation & Power Engineering (RDCAPE) [1].

With deregulation act in 2003, the reliability of the power system is enhanced in terms of availability and economics. The private sector intervened in the power generation and used the preexisting transmission system for distribution through pools. This resulted in overloading of lines to work under congestion, reaching their thermal and voltage limits [2]. The congestion resulted in huge amount of power losses thus effecting the economy of power transmission. There are two ways to relive the congested system. The cost-free method and the non-cost-free method. The cost-free method is one with no enhancement of operational cost. This is effectively achieved by incorporating Facts devices [3]. Power system is unevenly loaded. This results in inefficient output of the circuits. With uneven sharing of load through the lines, some lines become overloaded while others turn out to be under loaded. This distorts the voltage profile of the interconnected system [4]. FACTS being optimized for their respective parameters such as voltage angles, circuit reactance and voltage magnitudes, can be successfully incorporated in power system to modify the line parameters. This results in establishing a preferred bus and generator voltage profiles [5]. The system efficiency in terms of enhance loadability can be improved by suitably designing the controller of FACTS devices [6]. Maximum load on power system is industrial and domestic inductive load. Thus, there is significant voltage drop at these loads resulting in uneven voltage profile of system. Hence to reduce system inductive voltage drop, the inductive reactance has to be reduced in order to increase the power transfer capacity (PTC) of the system. The series FACTS device such as TCSC plays a vital role in achieving the reactance regulation [7]. To utilize the system at its maximum capacity together with power transmission economics, the transfer capacity of system must be enhanced to maximum value. System loadability improvement by increasing ATC value was achieved by an optimal power-flow-based model, for maximum power transfer by incorporating optimized FACTS control in the system [8]. Properly tuning

*Corresponding Author: Anubha Gautam., gautamanubha.12@gmail.com

FACT controller and its optimal location can reduce the system transmission losses and in return increases the power trans mitting capacity [9]. Different approaches were applied to optimize the location of fact devices. A number of heuristic methods like GA & BA were applied for optimal tuning of FACTS controller to enhance system ATC [10].

Further sensitivity index-based method for optimal allocation of FACTS devices such as SVC and TCSC was applied to enhance system power transfer capacity and hence ATC improvement [11]. The above-mentioned techniques resulted in ATC enhancement but this does not suffice the same improvements in other system parameters such as active power loss, reactive power loss and voltage profile regulation. The main objective of this paper is to develop a method with the incorporation of sensitivity index, ACPTDF together with an heuristic algorithm, Grey Wolf Optimization, (GWO) for minimizing the multi-objective function considered. This paper extends the area of implementation from a single objective of congestion management by ATC enhancement to a multi-objective of reducing active and reactive power losses as well as regulating the voltage profile of the system.

ATC of a power system is the power transfer capacity available above the maximum demand of the system, to be utilized for commercial activities between power suppliers and consumers. ATC is the back bone of any power system as it is directly influencing the power markets technically as well as economically [12]. The ATC of a power system can be enhanced by different methods and FACTS are very efficient in the same. The calculation of ATC can be done by different methods. A method was proposed to first calculate the reactive power flow and then by using PTDF as sensitivity factor ATC was calculated [13]. For enhancing the ATC value, generator terminal voltage and the output power can be worked within the defined security limits. ATC calculation and its values in power system database are therefore very crucial for the power market participants so as it can be used economically for industrial back up [14].

2. Related works

ATC for any system is the basis of restructuring of power system. Power system capability and its strength depends upon it ATC value [15].

The power system is interconnected, hence for enhancing the ATC of a particular system it is required that the power flow during the process must be technically very controlled. In other words, due to interconnection between different areas the ATC enhancement may result in change in power flow levels, resulting in unstable system. FACTS devices are quite a handful solution for this problem. Different types of FACTS devices use their specific properties to dynamically control the voltage magnitude, voltage angles and impedance of the lines while ATC enhancement is worked out. [16], [17].The FACTS devices are operated with the help of controllers. These controllers are either thyristor-controlled switch based or voltage source converter (VCS) based. These controllers helps to enhance the ATC while compensating for reactive power flow and reducing the active power losses [18]. A number of heuristic methods such as GA and PSO have been applied to program the controllers so as the FACTS device can compensate for reactive power and reduce active power loss while regulating the voltage profile of the system [19], [20].

Out of different FACTS devices TCSC is one of the most widely used device. ATC enhancement was done by applying continuation power flow (CPF) method taking thermal limits and voltage profile into account [21] .Other FACTS devices such as SSSC, STATCOM and UPFC have been modeled using heuristic methods like PSO and sensitivity index PTDF for ATC enhancement [22]. The controller of SSSC, UPFC and STATCOM have also been modeled by novel current based modeling for enhancing ATC instead of laying down new transmission line or rescheduling of generator [23]. ATC enhancement have also been done and compared by some more heuristic methods such as GA, PSO & FA under different contingency conditions [24].

3. Calculation of ATC

ATC in a power system can be calculated in numerous ways. Some methods are CPFM (continuous power flow method), linear approximation method etc. In this paper power sensitivity indices method is applied to calculate the ATC for standard IEEE 30 Bus system. The sensitivity factor applied here is Power Transfer Distribution Factor (PTDF). The PTDF can be of two types, DCPTDF and ACPTDF. Here we are applying ACPTDF for the calculation of ATC. ACPTDF determines the change in system power flow with the change in power transaction in some other line at steady state as well as under contingency conditions [25]. For a bilateral transaction between bus m and bus n. Here bus m is considered to sell power to bus n . The PTDF measures the change in real power flow of line i-j due to bilateral transaction between m & n [26].

Mathematically,

$$ACPTDF_{ij,mn} = \frac{\Delta P_{ij}}{P_{mn}} \quad (1)$$

where

P_{mn} is the power transaction between the bus m and n. Here bus m is considered to sell power to bus n. Bus n is considered to buy power in energy pooling system.

ΔP_{ij} is the change in power flow between bus i and j due to the bilateral transaction between bus m and n. This can be calculated as:

$$\Delta P_{ij} = \left[\frac{\partial P_{ij}}{\partial V_i}\right]\Delta V_i + \left[\frac{\partial P_{ij}}{\partial V_i}\right]\Delta V_j + \left[\frac{\partial P_{ij}}{\partial \delta_i}\right]\Delta \delta_i + \left[\frac{\partial P_{ij}}{\partial \delta_i}\right]\Delta \delta_j \quad (2)$$

$$\text{or, } \Delta P_{ij} = \left[\frac{\partial P_{ij}}{\partial \delta_2} \ldots \frac{\partial P_{ij}}{\partial \delta_n} \frac{\partial P_{ij}}{\partial V_2} \ldots \frac{\partial P_{ij}}{\partial V_n}\right] * \begin{bmatrix} \partial\delta_2 \\ . \\ . \\ \partial\delta_n \\ \partial V_2 \\ . \\ . \\ \partial V_n \end{bmatrix} \quad (3)$$

$$\text{or, } \Delta P_{ij} = \left[\frac{\partial P_{ij}}{\partial \delta_2} \ldots \frac{\partial P_{ij}}{\partial \delta_n} \frac{\partial P_{ij}}{\partial V_2} \ldots \frac{\partial P_{ij}}{\partial V_n}\right] * \begin{bmatrix} J1 J2 \\ J3 J4 \end{bmatrix}^{-1} \begin{bmatrix} 0 \\ . \\ . \\ +Pt \\ 0 \\ . \\ . \\ -Pt \\ 0 \end{bmatrix} \quad (4)$$

Now the power transfer in the line between buses i and j can be calculated for different values of PTDF as in equation (5)

$$T_{ij,mn} = \begin{Bmatrix} \dfrac{(P_{ij}^{\max} - P_{ij}^{0})}{PTDF_{ij,mn}}; & PTDF_{ij,mn} > 0 \\ \alpha(\inf inite)\ ; & PTDF_{ij,mn} = 0 \\ \dfrac{(-P_{ij}^{\max} - P_{ij}^{0})}{PTDF_{ij,mn}}; & PTDF_{ij,mn} < 0 \end{Bmatrix} \quad (5)$$

In equation (5)

P_{ij}^{max} is active power flow limit of line *i-j*.

P_{ij}^{0} is base case power flow in line *i-j*.

$PTDF_{ij,\,mn}$ is the Power Transfer Distribution Factor for line i-j due to the exchange of active power between bus m and n.
Then ATC can be calculated as:

$$ATC_{mn} = \min\left\{T_{ij,mn}\right\}, ij \in N_L \quad (6)$$

N_L is the total number of lines.

4. Reactive power flow

A fundamental aspect of the compensation and control of reactive power is its balance. The shunt capacitance of the transmission line yields reactive power proportional to the square of the voltage. Since the voltage must be kept within ± 5% of the rated voltage, the output or consumption of reactive power is relatively constant. The series inductance of the transmission line consumes reactive power proportional to the square of the current. Since the current varies from the duration of maximum demand to the duration of minimum demand, the reactive power consumption is also modified by the transmission line.

Figure number (1) shows the reactive power flow in the transmission system.

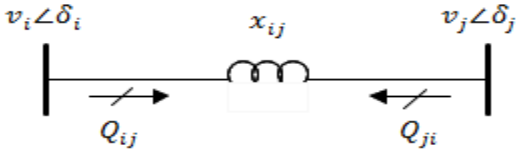


Figure 1: Reactive power flow in the Power system

The reactive power losses in the transmission line can be mathematically expressed as:

$$Q_p = Q_{ij} + Q_{ji} \quad (7)$$

where , Q_{ij} can be written as:

$$Q_{ij} = \frac{v_i}{x_{ij}}\left(v_i - v_j \cos\delta\right) \quad (8)$$

from equation (7) and equation (8) the expression for reactive power loss can be calculated as:

$$Q_p = \frac{v_i^2}{x_{ij}} + \frac{v_j^2}{x_{ij}} - \frac{2v_i v_j}{x_{ij}}\cos\delta \quad (9)$$

On simplification

$$Q_L = min\ \{\textstyle\sum_{k=1}^{nl} g_k(V_i^2 + V_j^2 - 2V_i V_j\, sin(\delta_i - \delta_j))\} \quad (10)$$

5. Modeling of TCSC

During the steady state, the compensator can freely change between reactance values according to its control. To avoid over-compensation of the line, limits are recommended for the TCSC reactance, given by the equation (7).

$$-0{,}8\ X_L \le X_{TCSC} \le 0{,}2\ X_L\ p.u. \quad (11)$$

The proposed limit vary among different research works, but a tendency of capacitive factor greater than 50% of reactance of the line and inductive factor less than 25% of the inductance of the line is maintained.

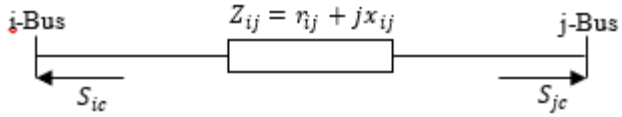


Figure 2: TCSC Power Injection Model [27]

In order to be used in power flow, the TCSC is modelled in form of line impedance with the built-in transformer reactance, in order to obtain the compensation scheme as shown in Figure (2)
The change in admittance is governed by the equation:

$$\Delta y_{ij} = y'_j - y_{ij} = \left(G'_{ij} + jB'_{ij}\right) - \left(G_{ij} + jB_{ij}\right) \quad (12)$$

$$G_{i,j} + jB_{i,j} = \frac{1}{Z_{i,j}} \tag{13}$$

$$\left.\begin{aligned} G_{i,j} &= \frac{r_{i,j}}{r_{i,j}^2 + x_{i,j}^2} \\ B_{i,j} &= \frac{-x_{i,j}}{r_{i,j}^2 + x_{i,j}^2} \end{aligned}\right\} \tag{14}$$

$$G'_{i,j} = \frac{r_{ij}}{r_{i,j}^2 + (x_{i,j} + x_{TCSC})^2} \tag{15}$$

$$B'_{i,j} = \frac{-(x_{i,j} + x_{TCSC})}{r_{ij}^2 + (x_{i,j} + x_{TCSC})^2} \tag{16}$$

where,

G_{ij} is the conductance of line ij before applying TCSC

G'_{ij} is the conductance of line ij after applying TCSC

B_{ij} is the suceptance of line ij before applying TCSC

B'_{ij} is the suceptance of line ij after applying TCSC

Equation (8) depicts that there is a variation of admittances by the application of the TCSC, so the admittances matrix of the system will be modified as indicated (13).

$$Y'_{BUS} = Y_{BUS} + \begin{bmatrix} 0 & 0 & 0 & \cdots & 0 & 0 & 0 \\ 0 & \Delta y_{i,j} & 0 & \cdots & 0 & -\Delta y_{i,j} & 0 \\ 0 & 0 & 0 & \cdots & 0 & 0 & 0 \\ \cdots & \cdots & \cdots & \cdots & \cdots & \cdots & \cdots \\ 0 & 0 & 0 & \cdots & 0 & 0 & 0 \\ 0 & -\Delta y_{i,j} & 0 & \cdots & 0 & \Delta y_{i,j} & 0 \\ 0 & 0 & 0 & \cdots & 0 & 0 & 0 \\ & Col-i & & \ldots & Col-j & & \end{bmatrix} \begin{matrix} \\ \\ \\ \\ \\ Line-i \\ Line-j \end{matrix} \tag{17}$$

The active and reactive power flow, including the admittance variation implemented by the TCSC can be explained by equation (14) & (15):

$$P_{ijrCSC} = V_i^2 G'_{ij} - V_i V_j \left[G'_{ij} Cos(\delta_{ij}) - B'_{ij} Sin(\delta_{ij})\right] \tag{18}$$

6. Objective Function

The objective function includes:

a) ATC maximization:
$ATC_{mn} = \min\{T_{ij,mn}\}$

b) Reactive power loss minimization:
$Q_L = min\{\sum_{k=1}^{nl} g_k(V_i^2 + V_j^2 - 2V_iV_j\, s\, in(\delta_i - \delta_j))\}$

Thus, the multi-objective function can be written as:

$$f(x) = w_1 \times (\max ATC) + w_2 \times \min P_L) \tag{19}$$

7. Constraints and limits

While performing optimal power flow (OPF) on a system, there are certain parameters which are to be implemented with constraints and pre-defined limits as stated in the standard IEEE bus system appendix. Basically, there are two types of parameters. One parameter which involves expenses such as generation of power at generating end, P_i^G. The other parameter which does not involve expenses are magnitude of voltages at generators, V_i^G and the transformer taps, t_{ij}.

The constraints in the system can be represented as summarized in Table number (1) below:

Table 1: Constraints incorporated in the system

Constraints	Equations
Power Balance (MW)	$P_{gn} - P_{dn} - P_n(V_n - \delta_n) = 0$
Power Balance (MVAr)	$Q_{gn} - Q_{dn} - Q_n(V_n - \delta_n) = 0$
Generated Power (MW)	$P_n^{min} \le P_n \le P_n^{max}$
Generated Power (MVAr)	$Q_n^{min} \le Q_n \le Q_n^{max}$
Bus Voltage Limits	$0.95pu \le Vi \le 1.05pu$
Generator Voltage Limits	$0.95pu \le Vg \le 1.50pu$
TCSC Reactance Limits	$-0.8X_L \le X_{tcsc} \le 0.2X_L$

Where,

P_{gn} & Q_{gn} represents real and reactive power generations at *nth* bus

P_{dn} & Q_{dn} represents real and reactive power demand at *nth* bus

P_n & Q_n represents real and reactive power injected at *nth* bus

V_n & δ_n are voltage and resultant angle at *nth* bus

8. Grey Wolf Optimization

The heuristic technique implemented here to optimize the TCSC parameter is Grey Wolf Optimization (GWO). This technique is based on the well-organized social hierarchies of a pack of grey wolf. Grey wolf have a very typical and well defined hunting action. The hunting of prey is led by the most powerful alpha (a) wolf. The next hierarchy is taken by beta (b) wolf and the next one is taken by gamma(g) wolf. Rest of the wolfs in the pack are omega wolf. All the wolfs are guided by the alpha wolf. Hence the alpha wolf position in solution space is considered as the best solution, beta wolf, the next best and gamma wolf position the third best solution. The omega wolfs always follow the three best wolves throughout searching. GWO is divided into three processes, encircling, hunting and attacking the prey. Mathematically, the circling of prey can be symbolized as below [28].

$$\bar{D} = \left| \bar{C} * \bar{X}_{(prey)(t)} - \bar{X}_{GW(t)} \right| \tag{20}$$

$$\bar{X}_{(GW)(t+1)} = \left| \bar{X}_{(prey)(t)} - D \right| \tag{21}$$

where t is the current time, $\bar{X}$ is the vector representing location of the prey, $\bar{X}$ _GW is a vector representing location of grey wolf, C & A are coefficient vectors and mathematically presented as:.

$$\vec{A} = 2\vec{a} * \vec{r}_1 - \vec{a} \tag{22}$$

$$\vec{C} = 2 * \vec{r}_2 \quad (23)$$

where "a", is the error that is introduced in the system so as to avoid premature convergence of the algorithm. Its value is decreased from 2 to 0 through a series of iteration.

$\vec{r}_1$ & $\vec{r}_2$ represents arbitrary values between 0 and 1.

As the power system equations are highly non-linear and the solution can't be realized by traditional methods so Grey wolf algorithm is simulated mathematically to locate the position of prey (solution). First three positions Alpha, Beta & gamma of wolf are best fitness values and position of omega wolves are updated with respect to the position of alpha, beta & gamma wolves and are mathematically be represented as:

$$\vec{X}_1 = \vec{X}_{-a}(t) - \vec{A}_1 * \vec{D}_{-}a$$
$$\vec{X}_2 = \vec{X}_{-b}(t) - \vec{A}_1 * \vec{D}_{-}b$$
$$\vec{X}_3 = \vec{X}_{-g}(t) - \vec{A}_1 * \vec{D}_{-}g$$

where $\vec{D}_{-}a, \vec{D}_{-}b, \vec{D}_{-}g$ are defined as

$$\vec{D}_{-}a = |C * \vec{X}_{-a}(t) - \vec{X}_{GW}(t)| \quad (24)$$
$$\vec{D}_{-}b = |C * \vec{X}_{-b}(t) - \vec{X}_{GW}(t)| \quad (25)$$
$$\vec{D}_{-}g = |C * \vec{X}_{g}(t) - \vec{X}_{GW}(t)| \quad (26)$$

The algebraic sum of three locations of wolves is averaged which gives the best location of grey wolf

$$X_{GW}(t+1) = \frac{\vec{X}_1 + \vec{X}_2 + \vec{X}_3}{3} \quad (27)$$

This algorithm is applied in following steps:

1. The population of grey wolf is initialized with the initialization of initial parameters as:
   - Size of the search space (defined by problem constraints)
   - Number of search agents (here taken as 100)
   - Vectors a, A & C
   - Maximum number of iterations (100)
2. The wolves are randomly distributed in the pre-defined search space
3. The fitness value of each search agent is calculated and then indexed to get the best three fitness values. [from equation (24), (25) and (26)]
4. The three best positions are considered as best fitness values.
5. With respect to these three positions the fitness value of other wolfs are calculated.
6. Again the fitness values are sorted to get the updated positions of the wolfs [using equation (27)]
7. The fitness values are indexed and again first three values are considered as best fitness values.
8. The iterations are carried out till maximum iterations have reached or the fitness value become constant for defined number of iterations (in this paper equals to 50)

8.1 Pseudo code for GWO

Result: Bset value of fitness function

generate (X) / / Initialize the population of grey wolves

initialize Parameter (a, A, C);

evaluate X (0);

select new (Alpha, Beta, Delta, X (0));

for *e = 1 to EVALMAX* to do

  for *every Wolf l in Omega* do

    for *i = 0 to DIM* do

update Position (l, i); // Update current position

. **end for**

adjust parameters (a, A, c); // adjust the algorithm parameters

evaluate X (e + 1);

. select new (Alpha, Beta, Delta, X (e + 1));

. e = e + 1;

  end for

end for

9. Methodology adopted

9.1 For ATC maximization (Without TCSC)

Figure (3) presents the sequence to calculate the ATC value without the application of TCSC. Here GWO is used only in NR with OPF only. While section 9.2 shows the steps followed to calculate ATC value using GWO optimized TCSC size and ACPTDF sorted location of TCSC. In the second case all the calculations are done once TCSC is located at a suitable position.

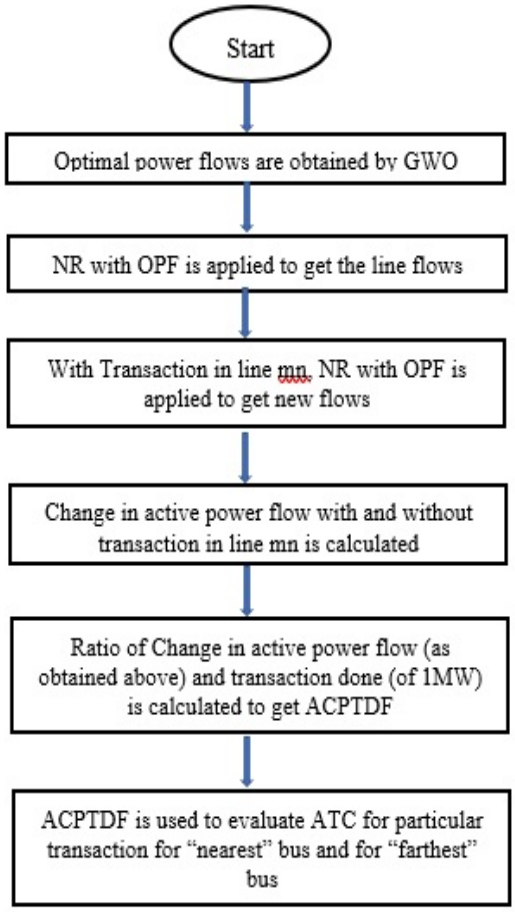


Figure 3: Process to calculate ATC without TCSC

9.2 For Minimization of Reactive power loss (TQL)

For mminimization of power loss same two methods i.e. with and without TCSC are applied but with an objective to minimize reactive power loss only. With decreased value of reactive power loss, it can be observed that the ATC value is also decreased.

Here IEEE 30 bus system with six generators at bus number 1, 2, 5, 8, 11 and 13 is utilized for the application of the selected methodology. ACPTDF values are calculated for the transaction at a particular bus and its effect on power flow at all the other buses. Figure (4) gives the presentation of ACPTDF values when transactions are done between bus number 2 to 5 ad bus 2 to 26.

A number of evolutionary programming methods have been applied enhancement of ATC for a system but GWO turned to be one of the most suitable method to give optimized result for the chosen objective. Firefly algorithm have been used for calculation of ATC with different FACTS devices [29] .GWO when used under similar circumstances with TCSC gave better results. Figure (5) gives a detailed presentation of the values of ATC and active power losses with both the methods are applied.

From fig (5) it can be depicted that while no FACTS device is connected in the system, the ATC value with GWO comes to be 12.18 MW significantly higher with that obtained for FA which comes to be 7.47 MW.

Similarly, when the methods are applied for Total reactive power loss (TQL) reduction the power loss in case of GWO is 4.89 MW which is lesser then 5.01 MW obtained by applying FA. Moreover, the ATC value in case of TPL minimization is 10.54MW which is higher than 6.235 MW obtained by FA.

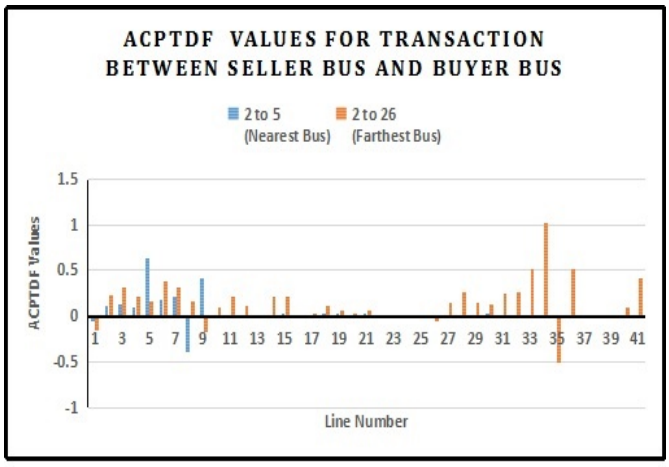


Figure 4: The ACPTDF values calculated for transaction between bus 2-5 and 2-26

10. Results and Analysis

The proposed optimization method is verified on 41 line, six generators, standard IEEE 30 BUS system [30] as shown in figure (6). Here except bus number 2, 5, 8, 11 and 13 where generators are connected, all the buses are considered as load bus. Also, all the generator buses are considered as seller buses while all other buses are the buyer buses.

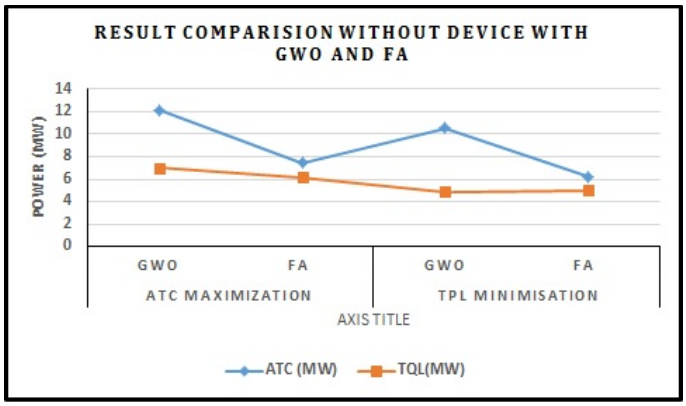


Figure 5: Result comparison between GWO and FA without device

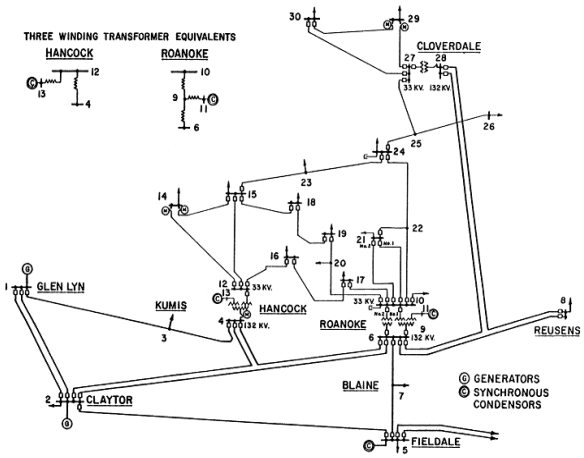


Figure.6: Standard IEEE 30 bus system [30]

10.1 ATC Maximization

The algorithm firstly applied for the objective of enhancement of ATC to reduce the congestion in the given system. The first step in this process is to calculate ATC with the help of ACPTDF. Figure (7) represents the effect of Generator at bus number 2 on ATC values of different parts of the system considered.

It can be seen that bus number 5 is nearest to generator and hence it has maximum value of ATC which equals 116.65 MW. On the other hand, bus number 26 is farthest from bus 2 so have a minimum value of ATC equal to 12.18 MW.

Figure number (8) represents the ATC distribution in the system due to generator at bus number 5 for all transactions. It can be well depicted that ATC value is largest, 184.56 MW for transaction between 5 to 2 and minimum, 12.16 MW for transaction between 5 to 26. The effect of generator at bus number 8 can be seen from figure number (9). This figure shows the distribution of ATC throughout the system for all transactions. Here it can be seen that maximum value of ATC, 70.41 MW is obtained at the line between bus 8-12 as bus 12 is nearest to bus 8. While the minimum value of ATC, 12.86 MW is obtained at line between 8-26.

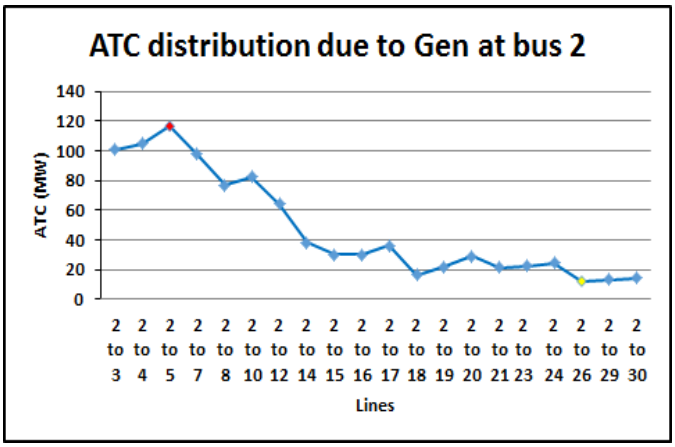


Figure 7: ATC distribution in the system due to generator connected at bus number 2

The effect of generator at bus number 11 on the distribution of ATC in the system for all transactions is shown in figure (10). It is clear from the figure that maximum value of ATC, 7.77 MW,

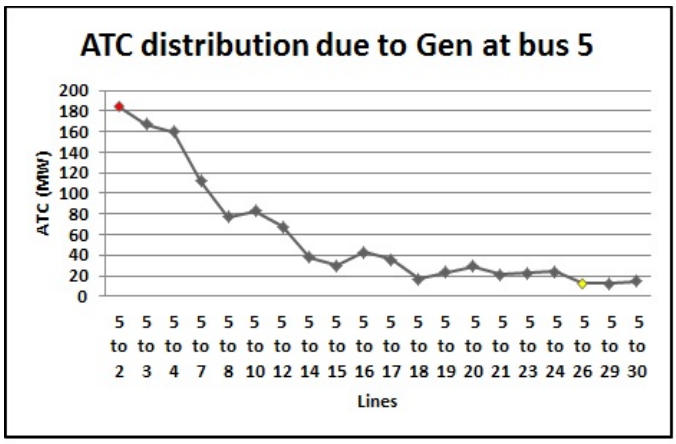


Figure 8: ATC distribution in the system due to generator connected at bus number 5

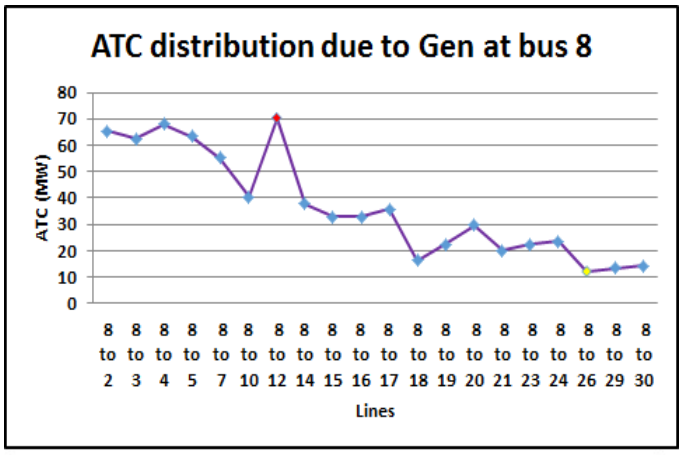


Figure 9: ATC distribution in the system due to generator connected at bus number 8

during all transactions is obtained at the line between seller bus 11 and the buyer bus 16. On the other hand, the minimum ATC value is obtained at the line between bus 11 and 26.

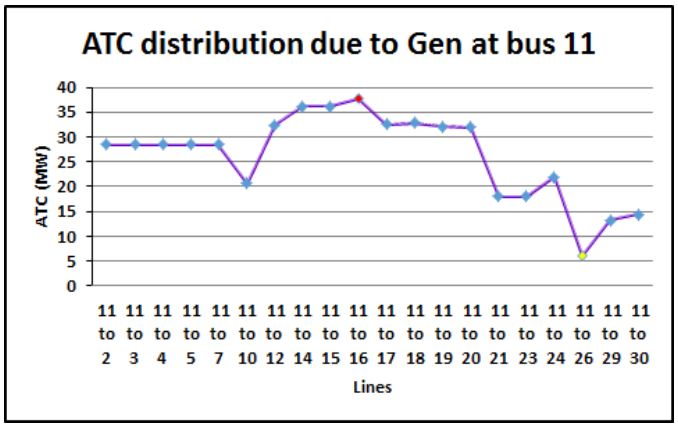


Figure 10: ATC distribution in the system due to generator connected at bus number 11

Effect of generator at bus number 13 is detailed in figure number (11). It is clear from the figure that maximum value of ATC, is obtained at line 13-7 and the minimum value of ATC, 8.89 MW is between bus 13 and 26 which is the farthest bus.

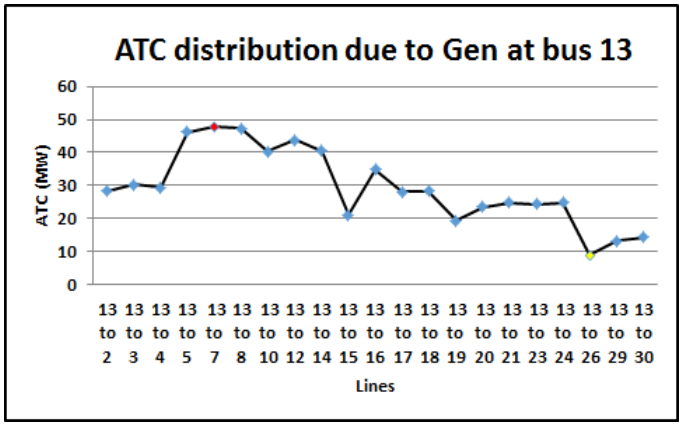


Figure 11: ATC distribution in the system due to generator connected at bus number 13

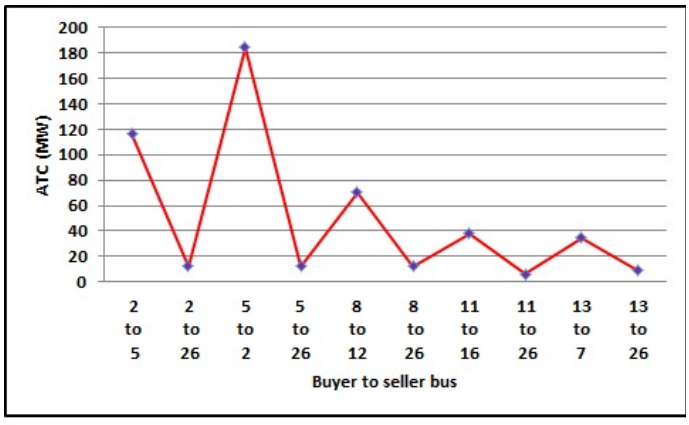


Figure 12: Variation of ATC values for all transactions due to generator at different buses

The maximum and the minimum ATC values can be represented in figure (12) for all generators.

It can be seen that the bus nearer to the generator bus are having higher ATC values. The lines 2-5, 5-2, 8-12, 11-16 and 13-7 are having higher ATC values as compared to their corresponding

farther buses.After ATC being calculated for all generators and all buses, now the ATC value is to be calculated by incorporating TCSC. The position of TCSC is searched by ACPTDF where the value of ATC is maximum after being sorted by GWO for its optimized parameter. NR with OPF is performed to get the enhanced values of ATC after incorporating TCSC the result are being summarized in table number 2. From table no 2 the results for change in ATC and reactive power loss (TPL) can be predicted. The calculations were done by giving weightage to ATC maximization in equation number (19).. Together with the increase of ATC the power loss is also increased.

Table 2: ATC maximization consolidated results

Bus		ATC (MW)		TQL (MVAr)	
SB	BB	Without TCSC	With TCSC	Without TCSC	With TCSC
2	5	116.65	120.75	82.33	30.5
	26	12.18	13.18	28.15	30.3
5	2	184.56	215.13	29.78	30.1
	26	12.26	13.45	28.48	30.7
8	12	70.41	74.056	28.26	30.4
	26	12.18	16.57	28.52	30.8
11	16	37.77	38.08	28.39	30.6
	26	6.09	8.01	29.24	31.3
13	7	34.67	36.89	27.56	29.6
	26	8.89	11.46	28.95	30.5

This increment in ATC value is higher when, percentage increase is compared from ATC enhancement by other optimization methods. In this case the percentage increase in ATP and TQL is shown in figure (13).

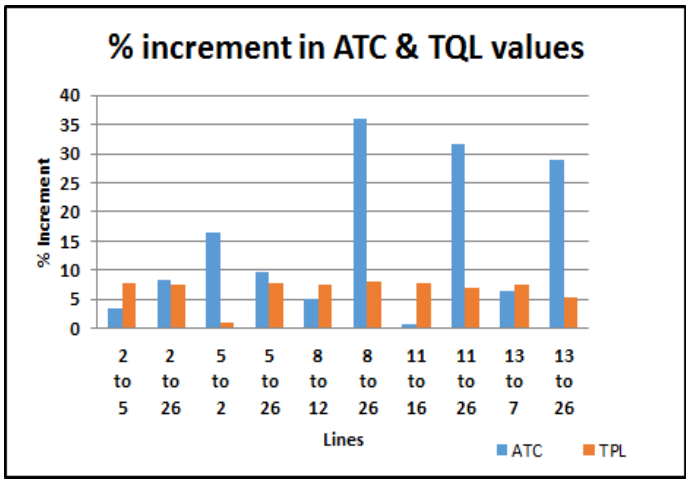


Figure 13: Percentage increment in ATC & TQL values with the incorporation of

TCSC

10.2 Reactive Power loss minimization (TQL)

The second objective to minimize reactive power loss in the system is obtained by giving weightage to the TQL term in the objective function in equation (19).

Reactive power loss minimization results are depicted in table no.3. The table bears consolidated results when to reduce the reactive power losses is the objective. The table shows that reactive power losses are significantly reduced.

Table 3: TQL minimization consolidated results

Bus		ATC (MW)		TQL (MVAr)	
SB	BB	Without TCSC	With TCSC	Without TCSC	With TCSC
2	5	116.65	90.67	28.33	25.36
	26	12.18	8.34	28.15	25.36
5	2	184.56	165.67	29.78	25.36
	26	12.26	9.45	28.48	25.36
8	12	70.41	45.89	28.26	25.36
	26	12.18	7.54	28.52	25.36
11	16	37.77	32.78	28.39	25.36
	26	6.09	6.03	29.24	25.36
13	7	34.67	32.43	27.56	25.36
	26	8.89	9.54	28.95	25.36

Together with reduction in reactive power losses, ATC value is also reduced. Again, in this case, because of the optimized TCSC location, reactive power loss is minimized. The percentage reduction in reactive power loss is higher as compared to other evolutionary programming such as FA. Moreover, the reduction in ATC value with TCSC in line is less as compared to when other FACTS devices are used. Figure (14) shows the percentage reduction in TQL and ATC with GWO optimized TCSC.

Table no 4: OPF result validation for ATC values in IEEE 30 bus system for far end bus

Bilateral Transactions Between Buses		ATC Values (MW)	
From	To	FA [29]	GWO
2	26	7.6697	13.18
5	26	7.67154	13.45
8	26	7.81371	16.57
11	26	7.70317	8.01
13	26	7.66233	11.46

The OPF results for ATC maximization are validated with those obtained by Firefly Algorithm [29] and are presented in Table 4. The ATC value at the bus connected at the far end is low due to the transmission losses. The ATC value obtained by applying GWO is significantly higher as compared to that

obtained by FA when far end values are compared. This validates GWO algorithm.

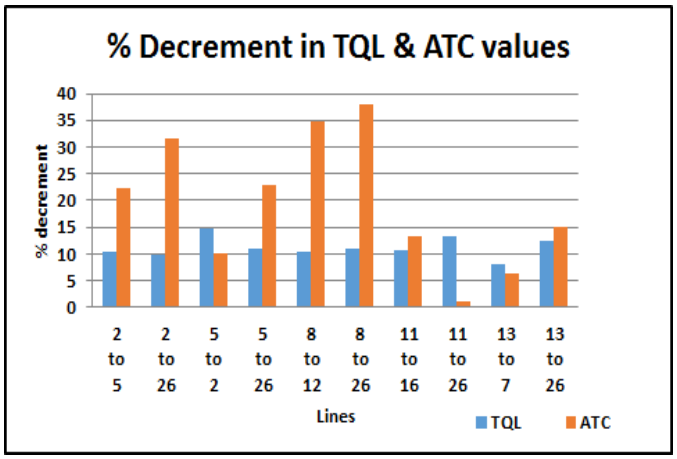


Fig no 14: Percentage decrement in TQL & ATC values with the incorporation of TCSC

11. Conclusion

In the current deregulated version of power system, where the expansion of the power system framework, due to economical and geographical constraints, can't be expanded. Thus, the private market participants supplying their generation through the exiting lines, forcing the lines to work at their voltage and thermal limits hence creating congestion. To overcome this congestion, keeping the operational cost same, a versatile FACTS device, TCSC is tested here in the standard IEEE 30 bus system. TCSC parameters are optimised with the help of very versatile Grey Wolf Optimizer and the location of TCSC is optimized with the help of power system sensitivity factors, ACPTDF. The objectives of enhancing ATC value to reduce congestion in the system and to minimise reactive power loss are achieved. The objectives are achieved here within the prescribed voltage and thermal limit constraints. GWO being guided by the best fitness value (alpha wolf) as well as two more near to best fitness values i.e. beta and gamma wolves. This ensures the speed of convergence. This optimiser uses three more variables a, A and C which ensures that GWO must not get stuck in the local minima and premature convergence. The ATC values for farther buses are quit low but this method optimised the TCSC parameter and its location such that the ATC value at far end should have higher values for greater utilization of lines and hence reduced the congestion. This paper utilised the pre-existing transmission lines for applying GWO and placing TCSC in the system to achieve the objectives of maximising ATC and reduction of reactive power loss to manage congestion in the system.

References

[1] A. Gautam, P.R. Sharma, Y. Kumar, "Placement of TCSC applying Grey Wolf Optimization," 313–318, 2019, doi:10.1109/RDCAPE47089.2019.8979016.

[2] K.S. Verma, "Enhancement of Available Transfer Capability by the use of UPFC in Open Power Market," 463–467, 2002.

[3] M.B. K. Selvi, N. Ramaraj, "Total Transfer Capability Evaluation using Genetic Algorithms," IE(I) Journal, **88**, 60–64, 2007.

[4] Y.H.S. and T.J. L. Gyugyi, Flexible AC Transmission Systems (FACTS), The Institutions of Electrical Engineers, Padstow, 1999.

[5] N.G. Hingorani. and L. Gyugyi, Understanding FACTS, concepts and technology of flexible ac transmission systems, Wiley-IEEE Press, 2000.

[6] S. Gerbex, R. Cherkaoui, A.J. Germond, "Optimal location of multi-type FACTS devices in a power system by means of genetic algorithms," IEEE Transactions on Power Systems, **16**(3), 537–544, 2001, doi:10.1109/59.932292.

[7] A. Arzani, M. Jazaeri, Y. Alinejad-Beromi, "Available transfer capability enhancement using series FACTS devices in a designed multi-machine power system," Proceedings of the Universities Power Engineering Conference, 4–9, 2008, doi:10.1109/UPEC.2008.4651434.

[8] Y. Xiao, Y.H. Song, C. Liu, Y.Z. Sun, "Using FACTS Devices," IEEE Transactions on Power Systems, **18**(1), 305–312, 2003.

[9] W. Ongsakul, P. Jirapong, "Optimal allocation of facts devices to enhance total transfer capability using evolutionary programming," Proceedings - IEEE International Symposium on Circuits and Systems, 4175–4178, 2005, doi:10.1109/ISCAS.2005.1465551.

[10] R. Mohamad Idris, A. Khairuddin, M.W. Mustafa, "A multi-objective bees algorithm for optimum allocation of FACTS devices for restructured power system," IEEE Region 10 Annual International Conference, Proceedings/TENCON, 1–6, 2009, doi:10.1109/TENCON.2009.5395826.

[11] J. Kumar, A. Kumar, W.Z. Gao, S. Yan, J. Wang, S. Gu, "ATC enhancement with SVC and TCSC using PTDF based approach in deregulated electricity markets," Advanced Materials Research, **516**–**517**, 1337–1341, 2012, doi: 10.4028/www.scientific.net/AMR.516-517.1337.

[12] K. Mushfiq-Ur-Rahman, M. Saiduzzaman, M.N. Mahmood, M.R. Khan, "Calculation of available transfer capability (ATC) of Bangladesh power system network," 2013 IEEE Innovative Smart Grid Technologies - Asia, ISGT Asia 2013, 1–5, 2013, doi:10.1109/ISGT-Asia.2013.6698716.

[13] Ibraheem, N.K. Yadav, "Implementation of FACTS Device for Enhancement of ATC Using PTDF," International Journal of Computer and Electrical Engineering, **3**(3), 343–348, 2011, doi:10.7763/ijcee. 2011.v3.338.

[14] P.W. Sauer, "Technical challenges of computing available transfer capability (ATC) in electric power systems," Proceedings of the Hawaii International Conference on System Sciences, **5**(2), 589–593, 1997, doi:10.1109/HICSS.1997.663220.

[15] M.A. Khaburi, M.R. Haghifam, "A probabilistic modeling-based approach for Total Transfer Capability enhancement using FACTS devices," International Journal of Electrical Power and Energy Systems, **32**(1), 12–16, 2010, doi:10.1016/j.ijepes.2009.06.015.

[16] S. Ahmad, F.M. Albatsh, S. Mekhilef, H. Mokhlis, "An approach to improve active power flow capability by using dynamic unified power flow controller," 2014 IEEE Innovative Smart Grid Technologies - Asia, ISGT ASIA 2014, 249–254, 2014, doi:10.1109/ISGT-Asia.2014.6873798.

[17] G. Hamoud, "Assessment of Available Transfer Capability of transmission systems," IEEE Transactions on Power Systems, **15**(1), 27–32, 2000, doi:10.1109/59.852097.

[18] X. Jiang, X. Fang, J.H. Chow, A.A. Edris, E. Uzunovic, M. Parisi, L. Hopkins, "A novel approach for modeling voltage-sourced converter-based FACTS controllers," IEEE Transactions on Power Delivery, **23**(4), 2591–2598, 2008, doi:10.1109/TPWRD.2008.923535.

[19] S. Panda, N.P. Padhy, "Comparison of particle swarm optimization and genetic algorithm for FACTS-based controller design," Applied Soft Computing Journal, **8**(4), 1418–1427, 2008, doi:10.1016/j.asoc.2007.10.009.

[20] R. Eberhart, J. Kennedy, "New optimizer using particle swarm theory," Proceedings of the International Symposium on Micro Machine and Human Science, 39–43, 1995, doi:10.1109/mhs.1995.494215.

[21] T. Nireekshana, G. Kesava Rao, S. Siva Naga Raju, "Enhancement of ATC with FACTS devices using Real-code Genetic Algorithm," International Journal of Electrical Power and Energy Systems, **43**(1), 1276–1284, 2012, doi:10.1016/j.ijepes.2012.06.041.

[22] K. Bavithra, S.C. Raja, P. Venkatesh, "Optimal setting of FACTS devices using particle swarm optimization for ATC enhancement in deregulated power system," IFAC-Papers On Line, **49**(1), 450–455, 2016, doi:10.1016/j.ifacol.2016.03.095.

[23] S. Rahimzadeh, M.T. Bina, "Looking for optimal number and placement of FACTS devices to manage the transmission congestion," Energy Conversion and Management, **52**(1), 437–446, 2011, doi:10.1016/j.enconman.2010.07.019.

[24] A. Gupta, A. Kumar, "ATC Determination with Heuristic techniques and Comparison with Sensitivity based Methods and GAMS," Procedia Computer Science, **125**(2017), 389–397, 2018, doi:10.1016/j.procs.2017.12.051.

[25] A. Kumar, J. Kumar, "ATC determination with FACTS devices using PTDFs approach for multi-transactions in competitive electricity markets," International Journal of Electrical Power and Energy Systems, **44**(1), 308–

317, 2013, doi:10.1016/j.ijepes.2012.07.050.
[26] Shweta, V.K. Nair, V.A. Prakash, S. Kuruseelan, C. Vaithilingam, "ATC Evaluation in A Deregulated Power System," Energy Procedia, **117**, 216–223, 2017, doi:10.1016/j.egypro.2017.05.125.
[27] G.A.N.S.B.S.S. N.M. Tabatabaei, "Optimal Location Of Facts Devices Using Adaptive Particle Swarm Optimization Mixed With Simulated Annealing," International Journal on "Technical and Physical Problems of Engineering, **3**(7), 60–70, 2011.
[28] S. Mirjalili, S.M. Mirjalili, A. Lewis, "Grey Wolf Optimizer," Advances in Engineering Software, **69**, 46–61, 2014, doi:10.1016/j.advengsoft.2013.12.007.
[29] M. Venkateswara Rao, S. Sivanagaraju, C. V. Suresh, "Available transfer capability evaluation and enhancement using various FACTS controllers: Special focus on system security," Ain Shams Engineering Journal, **7**(1), 191–207, 2016, doi:10.1016/j.asej.2015.11.006.
[30] IEEE 30 Bus System. http://www.ee.washington.edu/research/pstca/pf30/pg_tca30bus.htm

ASTES

Advances in Science, Technology and Engineering Systems Journal Vol. 5, No. 5, 11-15 (2020)

www.astesj.com

Special Issue on Multidisciplinary Innovation in Engineering Science & Technology

ASTESJ

ISSN: 2415-6698

Case Study to Determine the Causes of Fire in Agriculture

Marianna Tomašková[*,1], Darina Matisková[2], Michaela Balážiková[1]

[1]*Department of Production Safety and Quality, Technical University of Kosice, Košice, 040 01, Slovakia*

[2]*Department of Industrial Engineering and Informatics, Faculty of Production Technologies in Prešov, Košice, 040 01 Slovakia*

ARTICLE INFO

Article history:
Received: 18 June, 2020
Accepted: 11 August, 2020
Online: 08 September, 2020

Keywords:
Fire analysis in Agriculture
Machine risks
Man - machine - environment system

ABSTRACT

The aim of this paper is to identify a critical link in the man - machine - environment system in the case of an adverse event, such as a hay baling fire, based on a comprehensive risk assessment method. The rate of spread of fires in agriculture depends on meteorological conditions, with large areas affected and potentially endangering the surrounding buildings, facilities. Access to fires is difficult and can extend to forests. Water is often lacking at the scene of a fire, which should be extinguished, and water sources are usually located over long distances. The paper addressed a specific example using a comprehensive method. The process of risk assessment in the work process was determined by the following steps: assessment of the overall risk of the work equipment, assessment of environmental impact, assessment of the person's ability to manage risk, calculation of the resulting risk value, comparison of calculated risk value and acceptability of risk value, proposal of measures. The result of the analysis was the finding that the primary cause of the fire is the environment, i.e. high ambient temperature. The critical element in hay baling work system is the work environment. The risk ratio was estimated at 5.78. The level of risk was low due to the rapid intervention of the human factor. Based on the results, the technical measures mentioned in the paper were proposed to the operator. The paper found that maintenance of the machine is important for protection against agricultural fires, where the human factor plays an important role in the man - machine - environment system.

1. Introduction

Agriculture is one of the most dangerous sectors in terms of accidents at work. There is an accident rate for employees in agriculture without fatalities 1.7 times higher than the average and accident rate with fatalities is three times higher than the average [1].

Fires pose a risk of destroying the environment and human lives [2]. The causes of fire in agricultural machinery are various. The literature [3] lists several possibilities in which a fire may occur: e.g. in the engine, in the bearings, brakes. Maintenance of these machines is an important fire protection.

Maintenance activities in agriculture are very diverse, including the following activities:

- maintenance and repair of machinery, equipment and vehicles,
- maintenance of farmyards and buildings,
- maintenance of silos, tanks, manure tanks and grain tanks,
- maintenance of electrical installations,
- maintenance of drainage and irrigation systems,
- maintenance of paved and unpaved roads.

The following hazards can be identified during these maintenance activities:

- mechanical hazards when working with maintenance machinery, for example crushing, connecting and high-pressure injection means,
- electrical risks,
- thermal risks,
- chemical risks associated with the use of hazardous substances during maintenance or maintenance of equipment containing hazardous substances,
- risk of explosion or fire or during maintenance,
- biological risks in the maintenance of contaminated equipment,
- ergonomic risks, e.g. incorrect construction of tools,
- work activities in enclosed spaces.

[*]Corresponding Author: Marianna Tomašková, marianna.tomaskova@tuke.sk

Wheeled machines, mostly agricultural, are responsible for up to 50% of fatal accidents worldwide. Work safety, work activities and these machines are very important.

For the detection of fires in agriculture, there are almost no studies aimed at identifying the causes in harvesters, respectively. tractors with accessories. Studies to date [4] in which the authors investigated more than 4,000 fires in combines and tractors. They gained access to machines to conduct a detailed study for 265 cases. The authors concluded that 74% of fires occurred in the engine area (e.g. surface heating, flue gas outlet and electrical components). They found that the material that began to burn was crop residues, followed by fuel and oil residues [5].

The tractor is used as a means of accessing hard-to-reach areas, driving and towing connected equipment. For carrying out various agricultural activities, such as harvesting, plowing, fertilizing. Although there are innovative machines and processing methods, there are still risks, such as machine fires, due to low investment in maintenance or machine replacement [6].

To reduce the occurrence of fire, it is possible to apply various systems, e.g. FOGMAKER TM system, which is highly innovative but not available for small businesses. The contribution of the presented paper is to evaluate the risk of hay baling by a complex method in which the bearing was damaged. The press is one of the most risky machines in agriculture. Fires and malfunctions are caused by bearing failure or overheated machine parts.

2. Material and Methods

2.1. Fire safety measures for machines from the Baler company

During harvesting season, fires on agricultural machinery or buildings occur more frequently than in the off-season.

The task of the balers is to continuously pick up the wilted or more often dry material (hay, straw) from the summarized rows, press it and tie it into bales [1,6].

In most cases, presses with variable chambers pose the greatest risk of fire. The fault is most often caused by tensioning and control rollers, which are responsible for the operation of packaging belts [2-7].

Bearings called seasonal bearings used in such machines must be replaced each year before the start of the summer season. Overheated bearings can come into contact with straw, hay and the right hot surface can initiate a negative phenomenon. Before starting work with the press in the field, it is recommended to switch on the press for 5-10 minutes and then check the bearings [7].

Due to the presence of dry straw or hay in the baling chamber, which has a flash point of approximately 300°C depending on the moisture content, as well as rubber bands on the rollers, which are constantly in contact with the hot surface and can heat up during normal operation, they create all the conditions for a fire. The operator of the machine is often able to watch the process only from a mirror.

With such an amount of dry material (straw, hay) it is difficult to extinguish the fire in 1-2 minutes so that the fire does not spread further. In such fires, the greatest chance of rescuing the tractor in the event of a quick uncoupling of the baler [8].

Another important parameter is the parallel guidance of the forming strips at the same distance. If these belts are not lowered in parallel, sooner or later their friction will lead to a fire. Gear bearings also deserve attention even if they are less exposed to direct contact with straw, but accidental dust and other contaminants can also cause a flammable substance to ignite when the bearings are overheated due to wear [9]. There is illustrated in Fig. 1 the baler machine KRONE Big Pack and the same kind of machine damaged after a fire accident is in Fig. 2.



Figure 1: KRONE Big Pack 1290XCHDP



Figure 2: Damaged Big Pack 750 after the fire accident [10]

2.2. Risk analysis of the selected equipment

A comprehensive workplace risk assessment method was used to assess the risks of the selected press [8-10].

The risk assessment at work was performed using a comprehensive method of risk assessment at the workplace [11]. Common practice in small and medium-sized enterprises requires time-saving methods, which, however, presuppose knowledge of the actual state of the monitored technology. The method developed by the international team of the Security Section (represented by France, Germany, Italy and the Czech Republic) can be satisfactory in this respect. The method is based on the knowledge that an injury occurs in most cases for several reasons. The work is performed in the system man (P) - machine (M) - environment (U) and the level of safety depends on all three elements - parameters. These elements are assessed individually by this method, by appropriately assigning a point method and defining an acceptable risk. The method is mainly suitable for immediate risk assessment in order to apply immediate, non-complex measures. The record is kept in the form of a questionnaire [12]. The values in the risk assessment were determined by direct consultation with the tractor driver.

Profession: tractor driver
Equipment under assessment: baler

Description of job: The damaged bearing got stuck and the action of frictional force led to the accumulation of heat, which passes into the chamber of the press and subsequently a machine fire occurred.

Description of the work procedure: After observing the fire, the tractor driver stopped the tractor and the press brake, switched off the drives and exits the tractor, then extinguishes the fire with the help of fire extinguishers**.** Table 1 shows the risk assessment of machinery, namely the baler.

Table 1: Risk assessment of the equipment

Risk element - M Equipment (baler) risk assessment		**Rating**	**Label**	**Range**
Identification of possible damages	Severe consequences (Burns)	S	7	1 - 10
Danger exposure	Frequently repeated exposure	Ex	**1.5**	1 - 2
Probability of a dangerous situation	Central	Wa	**1.5**	0.5-1.5
Possibility of prevention	United	Ve	**0.5**	0.5-1

$$M = S \times Ex \times Wa \times Ve \quad (1)$$
$$\boldsymbol{M = 5.25}$$

The resulting risk level of machinery from the range (0.25-30) is 5.25.
Table 2 shows the risk assessment of the working environment.

Table 2: Environmental impact

Environmental impact - U		**Result**	**Label**	**Range**
Work organization area	On one level	Ua	**0.6**	0.5-1
Work environment	Dust, heat	Ub	**0.6**	0.3-0.6
Other loads	A narrow space	Uc	**0.4**	0.2-0.4

$$U = Ua + Ub + Uc \quad (2)$$
$$\boldsymbol{U = 1.6}$$

The resulting risk level of the working environment from the range (1-2) is 1.6. Here it can be seen that the risk of the working environment is higher. Table 3 shows the risk assessment of the human factor.

The resulting risk factor for human factor from the range (15 - 0) is 15. Here it can be seen that the risk of human factor failure is low.

Table 3: Operator competence manage the risk

Ability of the operator to handle the risk-P		**Rating**	**Label**	**Range**
Person classification	An educated person with experience	Q	**10**	10 - 0
Psychological factors	Appropriate mental ability	φ	**3**	3 - 0
Work organization	The prescribed workflow is not always used	O	**2**	5 - 0

$$P = Q + \varphi + O \quad (3)$$
$$\boldsymbol{P = 15}$$

The resulting degree of risk of the human-machine-environment work system is determined by the following relation (4).

$$R = M \times U - P \times (M/30) \quad (4)$$
$$R = 5.25 \times 1.6 - 15 \times (5.25/30)$$
$$\boldsymbol{\underline{R = 5.78}}$$

The resulting level of risk when baling straw using a tractor with an attachment is low, but the method found that the cause of the fire was the working environment, i.e. high ambient temperature.

Based on the risk assessment, the following measures have been proposed to the operator. The first place of protection against agricultural fires is the maintenance of the machine.

2.3. Proposal of risk minimization measures

This phenomenon can be prevented by inserting a bearing temperature measuring device into a combine or press, thus reducing the risk of fire. Bearing-mounted temperature sensors transmit data to the device, where they are displayed. On the screen it is possible to monitor the bearing temperatures during operation can avoid the risk. It is possible to set the temperature limit, if a bearing with a red circle is signalled, then the temperature has exceeded the value that is set [13].

These bearing thermometers are also designed to detect the temperature of the bearing housing. The tip of the sensor is designed to make the best contact with the measured surface. The sensor should be placed directly in the hole. The clamping ring together with the spring ensures clamping on the surface so that information about the condition of the bearing is available. In the

event of overheating by the sensor signal, the machine can be stopped to prevent damage.

Parameters of the given sensor are:

- maximum ring diameter: 8 mm,
- measuring range: from -25°C to + 250°C,
- wire length: 2 m.

The innovative baler process already has this system built in, but older types are only cleaned mechanically. The hydraulically driven turbo fan, Fig. 3 and Fig. 4, system protects the knotters from pollution and reduces the risk of dust explosion [14].



Figure 3: The hydraulically driven turbo fan system protects the knotters from pollution, a strong air flow with speed 140 km/h. [14]



Figure 4: Two oil pumps supply the input gearbox and the TURBO FAN knot cleaning system with hydraulic oil. [14]

Fires arising from agricultural machinery occur mainly in the engine compartment. The consequence, especially on the damaged construction of the machine, often exceeds the value of the machine. Increased requirements to reduce noise and exhaust emissions are the main reasons for greater insulation and enclosure of the engine compartment, increased fuel pressure and thus an increase in engine compartment temperature.

The fire in the engine compartment spreads often and very quickly and intensively, so it cannot be extinguished with a fire extinguisher. Vehicles and equipment in agriculture, such as harvesters, tractors, loaders, etc. are high power machines that work at a constant load. An increasing number of more powerful electrical and hydraulic equipment pose an increased risk, and it is therefore possible to speak of these machines as potentially dangerous sources. [15-16]

If the engine fire start, the whole machine will burn during 20 minutes. Due to the nature of the work area, it can quickly fall victim to a fire, completely isolating the burning vehicle and its operator.

The FOGMAKER system ™ is an automated closed system that can be operated by direct human intervention and without power supply. On the principle of water mist, the fire in the engine compartment of the machine is extinguished. FOGMAKER ™ may consist of one, two or three fire extinguishing bottles. The construction allows full use of the content of the extinguishing mixture and thus emptying of the entire extinguishing cylinder. This is a positive advantage because the extinguishing roller can be placed vertically or horizontally in confined spaces. [17-18]

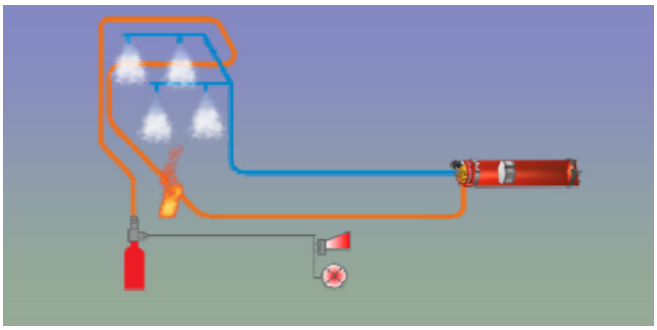


Figure 5: Hydro-pneumatic detection and activation [18]

Detection and activation of the system is performed hydro-pneumatically.

When a fire occurs, the detection hoses expand / burst with pressure and pressure drop, activating the valve on the extinguishing pressure cylinder. The pressure gauge, which is located on the detection cylinder, then alerts you with light and sound signals.

This power-independent system has an extraordinary cooling effect of - 500 ° C in less than 3 seconds. Water high-pressure mist with a pressure of 100 bar and special nozzles turn water into microdroplets with a diameter of 50 μm. The volume of 1 drop with a diameter of 1 mm is sufficient to create 8,000 drops of water mist. Water with a volume of 1 liter absorbs 540,000 calories during evaporation, which gives the extinguishing a completely unique effect. Cooling contributes to rapid extinguishing and thus reduces the risk of re-ignition [19-20].

3. Discussion

The result of the analysis was a finding that the cause of the fire is the environment, i.e. the high ambient temperature. The critical element in hay baling processing system is the working environment. Although the primary cause of the fire was a damaged bearing, the high ambient temperature and the presence of hay in the working environment caused an adverse event, i.e. fire. The risk level of the working environment was estimated at the value 1.6 from the interval < 1; 2 >. The resulting risk level 5.78 was low due to rapid human intervention. The acceptance limit in this method is set at the value 15. Based on the results, the technical measures were proposed to the operator. There was determined in this article that the maintenance of the machine is important for protection against the agricultural fires, where the human factor plays an important role in the man - machine - environment system. As a damaged bearing or electrical installation contributes significantly to a fire in agriculture, maintenance is absolutely necessary in preventing of fires.

4. Conclusion

It can be stated that a damaged bearing, as stated for presses, plays a major role in the fires of agricultural machinery. For tractors, trucks, the main initiator is an electrical short or faults in the electrical installation. In the case of machines intended for harvesting such as a combine harvester or forage harvester, a damaged bearing or electrical installation contributes significantly to a fire. After the risk analysis with a comprehensive method, satisfactory results were obtained, but this does not mean that there is no danger. The proposed measures to improve the situation are feasible, but nowadays smaller companies cannot afford it. Companies with better financial possibilities hire a special service for machines [21-22].

After the service period, maintenance is performed in-house. Today's companies try to have as little as possible, there are 1 maintenance person on about 10 machines [23-24]. Under the pressure of time, maintenance workers carry out repairs to such an extent that the machine is functional-mobile, but safety is significantly neglected. Today's generation of tractor drivers and engineers also neglects the basic maintenance of machines such as bearing lubrication or engine oil change. Some companies motivate their employees by being paid for maintenance. Machines and systems can be improved from a safety point of view, but the human factor plays the biggest role. Fighting fires in agriculture are liquidated according to the methodological sheets of the Fire and Rescue Service.

Conflict of Interest

The authors declare no conflict of interest.

Acknowledgment

APVV 15-0351 Development and application of risk management models in the conditions of technological systems in accordance with the strategy Industry 4.0 and VEGA1/0121/18 Development of methods for implementation and verification of a comprehensive security solution in Smart Factory as part of the Industry 4.0 Strategy.

References

[1] C. Y. Chen, Y.C. Ling, J. T. Wang, H.Y. Chen, "SIMS depth profiling analysis of electrical arc residues in fire investigation", Applied Surface Science, New York, 2003, https://doi.org/10.1016/S0169-4332(02)00817-6

[2] M. P. Filippakou, C.G. Karagiannopoulos, D.P. Agoris, P.D. Bourkas, "Electrical contact overheating under short-circuit currents" 2001 Electric power systems research. https://doi.org/10.1016/S0378- 7796(01)00081-5

[3] M. Balara, D. Dupláková, D. Matisková, "Application of a signal averaging device in robotics" In: Measurement., 115, 125-132, 2018, https://apps.webofknowledge.com/full_record.do?product=WOS&search_mode=GeneralSearch&qid=1&SID=C2GBN... https://doi.org/10.1016/j.measurement.2017.10.037

[4] D. Matisková, Ľ. Ambiško, "Optimization of cutting conditions and improvement of production in economic terms", TEM Journal., **6** (3), 584-590. 2017. ISSN 2217-8309

[5] V. Shah, D. Twidwell, C.L. Wonkka, M.T. Sindelar, J.R. Weir. "First Approximations of Prescribed Fire Risks Relative to Other Management Techniques Used on Private Lands". PLoS ONE 2015

[6] P. J. Val-Aguasca, M. Videgain-Marco, P. Martín-Ramos, M. Vidal-Cortés, A. Boné-Garasa, F. Javier García-Ramos. "Fire Risks Associated with Combine Harvesters: Analysis of Machinery Critical Points", Agronomy 2019, **9**, 877, https://doi.org/10.3390/agronomy9120877

[7] I. Hadade, T. M. Jones, F. Wang, L. di Mare, "Software Prefetching for Unstructured Mesh Applications" in 2018 IEEE/ACM 8th Workshop on Irregular Applications: Architectures and Algorithms (IA3), Dallas, TX, USA, 2018. https://doi.org/10.1109/IA3.2018.00009

[8] J. Shutske, W.E. Field. "An Integrated Loss Control Strategy for Grain Combine Fires". In 1988 International Winter Meeting of the American Society of Agricultural Engineers; American Society of Agricultural Engineers: Chicago, IL, USA, 2014; p. 17.

[9] H. Lihua, "Analysis of Fuel Cell Generation System Application," Ph.D Thesis, Chongqing University, 2005.

[10] Agroinform.hu, Erre vigyázzon bálázáskor, hogy ne gyulladjon ki a gépe, [cit.2018-4-1], https://www.agroinform.hu/gepeszet/erre-vigyazzunk-balazaskor-23427

[11] Agroforum.hu, Ezért gyulladnak ki a bálázók és a kombájnok – Tűzvédelmi tanácsok az aratás kezdetére, [cit. 2018-4-1], https://agroforum.hu/agrarhirek/gepinfo/ezert-gyulladnak-ki-a-balazok-es-a-kombajnok-tuzvedelmi-tanacsok-az-aratas-kezdetere/

[12] Magro.hu, Sok bálázó ég ki munka közben – erre figyeljen Ön is!, [cit. 2018-4-1],https://www.magro.hu/agrarhirek/szines/sok-balazo-eg-ki-munka-kozben-erre-figyeljen/

[13] Agrofarmelectro.com, Csapágy hőfok figyelő, [cit. 2018-4-1], https://www.agroinform.hu/gepeszet/automata-tuzvedelem-a-mezogazdasagban-12305,

[14] Tiszacsege.hu, Aratás előtti gépszemle, [cit.2018-4-1], http://tiszacsege.hu/wp-ontent/uploads/2014/07/betakaritas_tuzvedelem.pdf

[15] Agroinform.hu, Automata tűzvédelem a mezőgazdaságban, [cit. 2018-4-2],:https://www.agroinform.hu/gepeszet/elozzuk-meg-a-kombajntuzet-33150-001

[16] Fogmaker.com, R107, [cit. 2018-4-2], http://fogmaker.com/r107/

[17] Jandjpsv.eu, Meghódította a világot 6 kontinensen több mint 30 országban,[cit.2018-4-2],http://jandjpsv.eu/wp-content/uploads/sajto/Florian-exPress-2013-oktober.pdf

[18] Enatruck.cz, Fogmaker - unikátní hasicí systém, [cit. 2018-4-2], https://www.enatruck.cz/enatruck-cz/eshop/14-1-Signalizacni-a-hasici-systemy/-4-/5/147-Fogmaker-unikatni-hasici-system

[19] Internal documents of the company, consultation with the security technician and mechanizer of the company, 2015.

[20] Maintenance in Agriculture - A Safety and Health Guide, European Agency for Safety and Health at Work, ISBN 978-92-9191-667-2 https://osha.europa.eu/en/publications/reports/maintenance-in-agriculture-a-safety-and-health-guide, 2011.

[21] G.R. Quick. "An Investigation into Combine Harvester Fires"; Grains Research and Development Corporation: Canberra, Australia, 2010.

[22] K. Neubauer, Stroje pro rostlinnou výrobu, (Machines for Agricultural Production), Státní zemědělské nakladatelství, Praha, ISBN 80-209-0075-6, 1989.

[23] J. Sinay, M. Oravec, H. Pačaiová. "Risk assessment methods". Košice: TU, 2001.

[24] T. Henschel, Erfolgreiches Risikomanagement im Mittelstand. Strategien zur Unternehmenssicherung, Erich Schmidt Verlag, Berlin, ISBN 978 3 503 11648 5, 2010.

ASTES

Advances in Science, Technology and Engineering Systems Journal
Vol. 5, No. 5, 16-23 (2020)
www.astesj.com
Special Issue on Multidisciplinary Sciences and Engineering

ASTES Journal
ISSN: 2415-6698

Learning the Influence between Partially Observable Processes using Score-based Structure Learning

Ritesh Ajoodha*, Benjamin Rosman

School of Computer Science and Applied Mathematics. The University of the Witwatersrand, Johannesburg. 2050. South Africa.

ARTICLE INFO

Article history:
Received: 03 July, 2020
Accepted: 11 August, 2020
Online: 08 September, 2020

Keywords:
Stochastic Processes
Dynamic Bayesian Networks
Structure Learning

ABSTRACT

The difficulty of learning the underlying structure between processes is a common task found throughout the sciences, however not much work is dedicated towards this problem. In this paper, we attempt to use the language of structure learning to address learning the dynamic influence network between partially observable processes represented as dynamic Bayesian networks. The significance of learning an influence network is to promote knowledge discovery and improve on density estimation in the temporal space. We learn the influence network, defined by this paper, by learning the optimal structure for each process first, and thereafter apply redefined structure learning algorithms for temporal models. Our procedure builds on the language of probabilistic graphical model representation and learning. This paper provides the following contributions: we (a) provide a definition of influence between stochastic processes represented by dynamic Bayesian networks; (b) expand on the conventional structure learning literature by providing a structure score and learning procedure for temporal models; and (c) introduce the notion of a structural assemble which is used to associate two stochastic processes represented by dynamic Bayesian networks.

1 Introduction

The problem of describing the interaction or influence between stochastic processes has received little scrutiny in the current literature, despite its growing importance. Solving this complex problem has large implications for density estimation and knowledge discovery. In particular, for making predictions about later aspects of the process, or even for learning how processes influence each other.

Usually, the individual structure of each stochastic process is ignored and all are merged into one big process which is modelled by some probabilistic temporal model. This approach undermines the explanatory importance of the relations between these processes. [1] has explored the problems with this approach. The core of the issue mentioned by [1], is that we lose the underlying structure of the relationships between the processes which is essential to learn how one process influences another.

In this paper, we provide a complete method for learning the dynamic influence network between processes. This paper also explores the case when we are learning the influence relationship between partially observable processes. This is a significantly harder problem since the likelihood of the temporal model to the data has multiple optima which is induced from the missing samples [1]. Unfortunately, given that learning parameters from missing data is also a NP-hard problem, heuristic approaches are then needed to solve for a suitable local optimum of the likelihood function of the parameters to the data [1].

We assess this problem by providing an algorithm to learn the influence relations between partially observable stochastic processes by building on the language of probabilistic graphical modelling. In particular, we consider structure learning which searches for an appropriate structure by using scoring metrics and provide evidence for the effectiveness of our approach over the standard benchmarks selected. We notice that our derived penalty-based score paired with a greedy structure search outperforms using a random structure or a tree structure built using the maximum weighted spanning tree algorithm.

The application of this research is broad. Influence networks for stochastic processes can capture the complex relationships of how processes impact others. For example, we can learn the influence of traffic in a network of roads to determine how the traffic condition of a road congestion will impact on another road. In educational data-mining we may want to determine the influence of participants in a lecture environment to encourage student success. We may wish to learn the influence between an IoT network [1, 2]; influence in music [3]; or influence between the skills of learners or their attrition [4, 5].

*Corresponding Author: Ritesh Ajoodha, The University of the Witwatersrand, Johannesburg, +27 74 418 3978 & ritesh.ajoodha@wits.ac.za

An overview of the proposed algorithm in this paper is given by the below instructions. This algorithm is expanded on later in the paper.

(i) The stochastic processes are given as input.

(ii) The parameters for a dynamic Bayesian network is learned for each of the stochastic processes (temporal structure remains static - time invariant and Markov).

(iii) A structure is imposed between the dynamic Bayesian networks (using a relation function called an assemble). This gives us a dynamic influence network (DIN). The parameters for the DIN are relearned.

(iv) The structure score for the DIN is computed.

(v) A structure search algorithm is initiated to find a DIN structure which is has an optimal likelihood to the observable data;

(vi) The optimal DIN is output.

The following contributions is made by this paper:

- The concept of dynamic influence networks (DINs) representing the influence (relationships) between partially observable stochastic processes.
- The derivation of a dynamic Bayesian information criterion (d-BIC score) for DINs.
- The concept of a structural assemble which is able to relate dynamic Bayesian networks.
- The greedy structure learning procedure for learning DINs.

The following structure is used by this paper: Section 2 provides the background and related work on DINs; Section 3 defined the representation of DINs between partially observable stochastic processes; Section 3.3 derives the notion of a dynamic structure score using the notion of an assemble; Section 3.5 provides a greedy structure learning learning algorithm for learning DINs; the results and discussion is illustrated by Section 4; and lastly, Section 5 provides the conclusion of the research and suggestions on future work.

2 Related Work

Many statistical procedures have been used to identify influence between variables [6]–[9]. These statistical procedures have been extended to the temporal environment to learn relationships the between processes (variables over time). A significant contribution is the use of dynamic Bayesian networks which is defined as a set of parameters and conditional independence assumptions which together make up an acyclic structure between variables defined using factors [10, 11]. The values in these factors are referred to as the parameters, and the list of conditional independence assumptions between variables are referred to as the structure of the dynamic Bayesian network.

Learning the independence assertions of a dynamic Bayesian network can be used to make conditional independence inferences over time (density estimation) or to simply learn the relationships between variables (knowledge discovery) [12]–[15]. On the one hand, a sparse graph structure may have more generalisability for density estimation, and on the other hand having a more dense graph can reveal unknown relationships for knowledge discovery. Care must be taken when considering for what purpose is the network required (more on this in the discussion) [11].

A successful approach to structure learning is using score-based structure learning [11, 16]. In score-based structure learning we develop a set of hypothesis structures which are evaluated using a score-based function that computes the likelihood of the data to the hypothesised structure. The likelihood is usually expressed as the information gain (mutual information) of the structure and parameters of the distribution to the data.

A search algorithm is then performed to identify the highest (possible) structure based on the structure score [17]–[20]. Viewing this problem as an optimisation problem allows us to adopt the already established literature on search methods in this super-exponential space to find the optimal structure given the data [21]–[24].

The structure of this section is as follows. In subsection 2.1 we introduce the well established BIC score which offers a way to trade-off the fit to data vs model complexity (the amount of independence assumptions between variables in the data). Finally, in subsection 2.2 we introduce a greedy search method to find the an optimal graph structure.

2.1 The BIC score

The BIC score models the structural fit to data verses the complexity of the conditional independence assumptions between variables, that is, the amount of independence assumptions made on the structure [25]. This makes it a popular choice for structure learning methods since the model complexity has a direct impact on the performance of inference tasks. This is because the amount of conditional independence assumptions on a particular variable increases the factor size of that variable exponentially. The mathematical expression of the BIC score comprises of two terms: the first term models the fit to data; and the second term penalises the fit to data based on the complexity of the structure considered. The complete BIC score is as follows:

$$score_{BIC} = \ell(\hat{\theta}_{\mathcal{G}} : \mathcal{D}) - \frac{\log M}{2} DIM[\mathcal{G}],$$

where the count of instances is denoted by M and the count of independent parameters is denoted by $DIM[\mathcal{G}]$ in the Bayesian network.

The intuition of the Bayesian score is that as the amount of samples increase (ie. M) the score is willing to consider more complicated structures if enough evidence (samples, ie. M) is considered [26, 27]. The BIC core is particularly effective since the likelihood score (one without a penalty to complexity) will always prefer the most complicated network. However, the most complex networks also impose the risk of fragmentation, which is the exponential increase to the size of the factors caused by the increase of the in-degree of a variable. Penalty-based structure scores allows us

to explore the opportunity to adopt more complicated structures if there is enough justification that the likelihood of the structure and parameters to the data is high-enough to compromise on the models speed to perform inference tasks caused by fragmentation.

There has been much contributions in the literature on the properties of the BIC score [25, 28, 29]. Key constitutions include a proof the it is consistent and is score equivalent which are necessary for efficient search procedures [30]–[32].

2.2 Learning General Graph-structured Networks

Since the search space for the optimal Bayesian structure is super-exponential, the difficulty of learning a graph structure for a Bayesian network is NP-hard. More specifically, for any $d \geq 2$, the problem of finding a structure with a maximum score with d parents is NP-hard [21]–[24]. See [33, 34] for a detailed proof.

Despite this, there have been many contributions to learning an optimal structure. A key contribution is using heuristic search procedure to find an optimal acyclic graph structure [35]. These heuristic search procedures make use of search operators (changes to the graph structure) and a search algorithm (e.g. greedy search, best first search or simulated annealing) [36]. The intuition of this approach is find an optimal acyclic structure by gradually improving the choice of the structure using the search operators [37]–[41].

3 Dynamic Influence Networks

We present the following algorithm to learn dynamic influence networks between a set of partially observable processes:

(i) Our stochastic processes are given as a set of partially observed data. This is the input.

(ii) From this data, we learn a dynamic Bayesian network for each partially observable stochastic processes. Expectation maximisation is used to learn the latent variables.

(iii) Build a network with the set of independence assumptions and relearn the parameters for that model.

(iv) Perform expectation maximisation once again to relearn the latent parameters of the resulting network.

(v) Evaluate the resulting dynamic influence network using a scoring function and structural assemble.

(vi) Determine if convergence has occurred or if we exceed the threshold for convergence.

(vii) Apply the structural operator to the model and reevaluate the dynamic influence network using a structure score. Repeat steps (iii - vii) until the structure score can not be improved or a threshold is reached.

(viii) Output the resulting network.

Figure 1 provides a flowchart of our method to learn dynamic influence networks between partially observable processes.

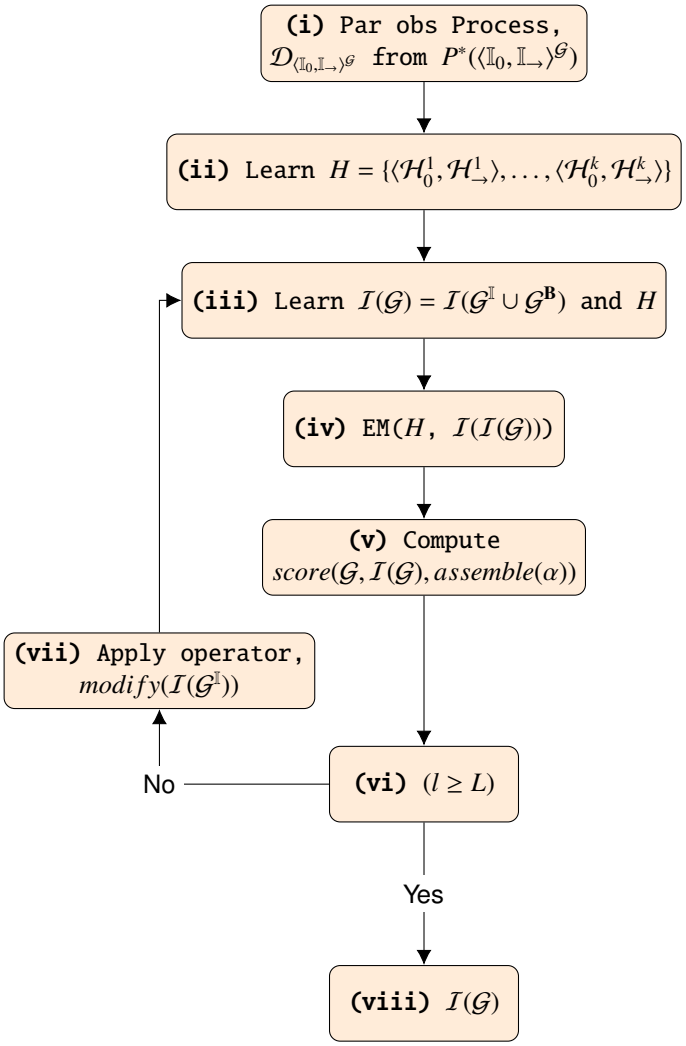


Figure 1: A flowchart of our method to learn dynamic influence networks between partially observable processes.

3.1 Assumptions

There are various assumptions we need to make about our dynamic influence network (DIN). For the below definitions, we denote $\mathcal{B}_i^{(t)}$ to be a shorthand for a Bayesian network $\mathcal{B}_i$ at time-point t.

Time Granularity Assumption We select a time-granularity, denoted $\triangle$, to split observable data into temporal time-slices at different intervals. We use the notation $t\triangle$ to represent the influence state with t time-slices.

The Markov Assumption We also adopted the Markov assumptions between consecutive states.

Definition 1 *The Markov assumption is satisfied for a DIN over the template Bayesian networks,* $\mathbf{B} = \{\mathcal{B}_1, \ldots, \mathcal{B}_R\}$*, if for all* $t \geq 0$*,* $(\mathbf{B}^{(t+1)} \perp\!\!\!\perp \mathbf{B}^{(0:(t-1))} \mid \mathbf{B}^{(t)})$.

The Time-Invariance Finally, we assume that the unrolled template structure of the DIN (which persists through time) does not change.

3.2 Dynamic Influence Networks

Given the assumptions above we define the dynamic influence network as follows:

Definition 2 *A dynamic influence network, denoted as DIN, is a couple* $\langle \mathbb{I}_0, \mathbb{I}_{\rightarrow} \rangle$*, where* $\mathbb{I}_0$ *is an influence network over the set of Bayesian networks,* $\mathbf{B}^{(0)} = \{\mathcal{B}_1, \ldots, \mathcal{B}_R\}$*, representing the starting distribution and* $\mathbb{I}_{\rightarrow}$ *is a 2-time-slice influence network for the rest of the influence distribution (*$P(\mathbf{B}' \mid \mathbf{B}_I) = \prod_{i=1}^{R} P(\mathcal{B}_i^{'} \mid Pa_{\mathcal{B}_i^{'}})$*). For any specified time-span* $T \geq 0$*, the joint distribution over* $\mathbf{B}^{(0:T)}$ *is defined as an unrolled influence network, where, for any* $i = 1, \ldots, n$*: the structure and conditional probability assumptions between variables of* $\mathcal{B}_i^{(0)}$ *are the same as those for* $\mathcal{B}_i$ *in* $\mathbb{I}_0$*; and the structure and conditional probability assumptions between variables of* $\mathcal{B}_i^{(t)}$ *for* $t > 0$ *are the same as those for* $\mathcal{B}_i^{'}$ *in* $\mathbb{I}_{\rightarrow}$*.*

3.3 The Structure Score

In this paper we adapt the celebrated Bayesian information criterion (BIC) to a dynamic Bayesian information criterion (d-BIC) for our dynamic influence networks. The d-BIC score make the same trade-off between model complexity and fit to the data, only the d-BIC can be applied to dynamic networks.

The d-BIC score is as follows:

$$\text{score}_{BIC}(\mathcal{H}_0 : \mathcal{D}) = M \sum_{k=1}^{K} \Big(\sum_{t=1}^{T} \Big(\sum_{i=1}^{N} \big(\mathbf{I}_{\hat{P}} \big(X_i^{\langle \mathcal{H}_0^k, \mathcal{H}_{\rightarrow}^k \rangle^{(t)}} ; \mathbf{Pa}^{\mathcal{G}}_{X_i^{\langle \mathcal{H}_0^k, \mathcal{H}_{\rightarrow}^k \rangle^{(t)}}} \big) \big) \Big) \Big)$$

$$- \frac{\log M}{c} DIM[\mathcal{G}],$$

where the amount of samples is given by M; the amount of dependency models is given by K; the amount of time-slices is given by T for any dependency model; the amount of variables in each time-slice is given by N; $\mathbf{I}_{\hat{P}}$ denotes the information gain in terms of the empirical distribution; and $DIM[\mathcal{G}]$ is the amount of independent parameters in the entire DIN.

The d-BIC score is designed to exchange the complexity of the dynamic influence network, $\frac{\log M}{c} DIM[\mathcal{G}]$, for the fit to the data, $\mathcal{D}$. As the amount of samples increases, the information gain term grows linearly, and the model complexity part logarithmically grows. The intuition of the d-BIC score is that we will be willing to consider more complicated structures, if we have more data that justifies the need for a more complex model (i.e. more conditional independence assumptions).

3.4 Structure Assembles

Choosing the set of parent variables in a DIN establishes the notion of a structural assemble. A structural assemble is a template which relates temporal models. The structural assemble defines the parent sets for variables to construct an dynamic influence network. More sepcifically, the assemble relation is defined as follows:

Definition 3 *Consider a family of dynamic Bayesian networks (D), where* $\langle D_0^0, D_{\rightarrow}^0 \rangle$ *represents the child with the parent set* $\mathbf{Pa}^{\mathcal{G}}_{\langle D_0^0, D_{\rightarrow}^0 \rangle} = \{\langle D_0^1, D_{\rightarrow}^1 \rangle, \ldots, \langle D_0^k, D_{\rightarrow}^k \rangle\}$*. Further assume that* $\mathcal{I}(\langle D_0^j, D_{\rightarrow}^j \rangle)$ *is the same for all* $j = 0, \ldots, k$*. Then the delayed dynamic influence network, denoted by* $\langle \mathcal{A}_0, \mathcal{A}_{\rightarrow} \rangle$*, will satisfy all the independence assumptions in* $\mathcal{I}(\langle D_0^j, D_{\rightarrow}^j \rangle)$ $\forall\, i = 0, \ldots, k$*. In addition,* $\forall\, j$ *and* $\forall\, t$*,* $\langle \mathcal{A}_0, \mathcal{A}_{\rightarrow} \rangle^{(t)}$ *also satisfies the following independence assumptions for each hidden or latent variable denoted* L_i *and some* $t > \alpha \in \mathbb{Z}^+$*:*

$$\forall\, L_i^{\langle D_0^0, D_{\rightarrow}^0 \rangle^{(t)}} : \big(L_i^{\langle D_0^0, D_{\rightarrow}^0 \rangle^{(t)}} \perp\!\!\!\perp NonDescendants_{L_i^{\langle D_0^0, D_{\rightarrow}^0 \rangle^{(t)}}} \mid L_i^{\langle D_0^k, D_{\rightarrow}^k \rangle^{(t)}}, L_i^{\langle D_0^k, D_{\rightarrow}^k \rangle^{(t)-1}}, \ldots, L_i^{\langle D_0^k, D_{\rightarrow}^k \rangle^{(t)-\alpha}}, Pa_{L_i}^{\langle D_0^0, D_{\rightarrow}^0 \rangle^{(t)}} \big).$$

The assemble above an expressive representation to capture influence relationships that persist through time between temporal models. However, the choice of α is important since choosing a large α will render many dependencies on variables cause a fragmentation bottleneck, and therefore a larger computational burden for learning and inference tasks.

3.5 Structure Search

At this point we have the following well-defined optimisation problem:

1. A training set $\mathcal{D}_{\langle \mathbb{I}_0, \mathbb{I}_{\rightarrow} \rangle^{\mathcal{G}}} = \{\mathcal{D}_{\langle D_0^1, D_{\rightarrow}^1 \rangle}, \ldots, \mathcal{D}_{\langle D_0^k, D_{\rightarrow}^k \rangle}\}$, where $\mathcal{D}_{\langle D_0^i, D_{\rightarrow}^i \rangle} = \{\xi_1, \ldots, \xi_M\}$ is a set of M instances from underlying ground-truth DBN $\langle D_0^i, D_{\rightarrow}^i \rangle$;
2. a structure score: $\text{score}(\langle \mathbb{I}_0, \mathbb{I}_{\rightarrow} \rangle : \mathcal{D}_{\langle \mathbb{I}_0, \mathbb{I}_{\rightarrow} \rangle^{\mathcal{G}}})$;
3. and, finally, we have an array of L distinct candidate structures, $\mathcal{G} = \{\mathcal{G}^1, \ldots, \mathcal{G}^L\}$, where each structure $\mathcal{G}^l$ represents a unique list of condition independence assertions $\mathcal{I}(\mathcal{G}) = \mathcal{I}(\mathcal{G}^{\mathbb{I}} \cup \mathcal{G}^{\mathbf{B}})$.

Our objective of this optimisation problem is output the DIN which produces the maximum score. We present the following influence structure search algorithm in Algorithm 1, where $\mathcal{S} = \{\mathcal{S}_{\rightarrow}^1, \ldots, \mathcal{S}_{\rightarrow}^P\}$ represents the set of stochastic processes; *assemble*, is the option of the parameters for an assemble relation; and *score*, the selected scoring function used for the search procedure.

Algorithm 1: Influence structure search

Input: $\mathcal{S} = \{\mathcal{S}_{\rightarrow}^1, \ldots, \mathcal{S}_{\rightarrow}^P\}$, *assemble*, *score*
Output: $\mathcal{G}_i$
For each process we learn a temporal model ($H = \{\langle D_0^1, D_{\rightarrow}^1 \rangle, \ldots, \langle D_0^P, D_{\rightarrow}^P \rangle\}$);
Using the models in H we generate a search space (ie. $\mathbf{G} = \{\mathcal{G}_1, \ldots, \mathcal{G}_n\}$);
Find the structure $\mathcal{G}_i$ which produces the highest *score* (w.r.t. *assemble*) in $\mathbf{G}$;
return $\mathcal{G}_i$

The dynamic influence network, $\langle \mathbb{I}_0, \mathbb{I}_{\rightarrow} \rangle^{\mathcal{G}}$, holds a distribution between a set of DBNs, denoted $\langle D_0^1, D_{\rightarrow}^1 \rangle$, ... , $\langle D_0^k, D_{\rightarrow}^k \rangle$, with the conditional independence assumptions listed by $\mathcal{I}(\langle \mathbb{I}_0, \mathbb{I}_{\rightarrow} \rangle^{\mathcal{G}})$. We further assume that $P^*(\langle \mathbb{I}_0, \mathbb{I}_{\rightarrow} \rangle^{\mathcal{G}})$ is induced by another model, $\mathcal{G}^*(\langle \mathbb{I}_0, \mathbb{I}_{\rightarrow} \rangle^{\mathcal{G}})$, we will refer to this model as the underlying ground-truth model. The model is evaluated by recovering the set of local

independence assertions in $\mathcal{G}^*(\langle \mathbb{I}_0, \mathbb{I}_\rightarrow \rangle^{\mathcal{G}})$, denoted $\mathcal{I}(\mathcal{G}^*(\langle \mathbb{I}_0, \mathbb{I}_\rightarrow \rangle^{\mathcal{G}}))$, by only observing $\mathcal{D}_{\langle \mathbb{I}_0, \mathbb{I}_\rightarrow \rangle^{\mathcal{G}}}$. This structure learning procedure is referred to in this paper as greedy structure search (GESS).

3.6 Computational Complexity and Savings

The overall computational complexity of the above structure search algorithm is given by [42]. In order to allow for notable computational savings we suggest using a cache to store sufficient statistics and the of max priority queues (implemented using heaps) to arrange contending structure using their scores as keys. Random restarts and Tabu lists are also used.

4 Experimental Results

This sections presents the performance of modelling influence between partially observable stochastic processes using dynamic influence networks (DINs). We evaluate the performance of model aside several benchmarks.

The experimental setup is as follows. We constructed a ground-truth DIN which was used to sample sequential data. To simulate a partially observed process, several variables were removed from the sequential data sample. The Algorithm provided in section 3 was used to learn candidate networks. Several variations of the algorithm was also used, such as using the d-AIC score instead of the d-BIC; using prior knowledge of the ground-truth structure such as the maximum in-degree used in the generative distribution; using tree structure for sparse generalisability; a even using no structure.

More specifically, the empirical evaluation of our method was set against the following benchmarks:

1. a random DIN structure;
2. a DIN with no structure (i.e. all DBNs are mutually independent);
3. a DIN with a tree like structure (each DBN has one and only one parent DBN);
4. a structure that incorporates prior knowledge of the true structure;
5. a learned structure with the d-AIC score instead of the d-BIC score, which is the dynamic extension of the AIC score;
6. using the full knowledge of the DIN ground-truth structure.

The parameters for the ground-truth DIN distribution is summarised by Table 1.

Figure 2 illustrates a logarithmic scale plot indicating the relative entropy (also known as KL-divergence) to the ground-truth DIN over the amount of samples alongside the aforementioned benchmarks. The vertical axis represents the logarithmic scale of the relative entropy to the ground-truth generative model (Table 1) and the horizontal axis represents the amount of samples. 10 trials were run for each experiment and the mean of the result was plotted with the standard deviation as error bars (shaded regions). All of the model parameters for each experiment is provided in Table 2 for reproducibility.

In Figure 2 we record that providing no structure, a random structure, tree structures, and finally, learning with knowledge of the maximum order in-degree executes in a same way with reference to their relative entropy to the ground-truth DIN. However, knowledge about the maximum order in-degree executes better on average than the other procedures for a large amount of instances (greater than one thousand). The d-AIC and d-BIC scores execute on average better than the other learning procedures (not counting learning using the true structure). However, the d-BIC and d-AIC penalty scores execute similarly.

Figure 3 illustrates a logarithmic scale plot indicating the execution times (in milliseconds) over the amount of samples alongside the aforementioned benchmarks. The vertical axis represents the logarithmic scale of the execution time of each experiment in milliseconds and the horizontal axis represents the amount of samples. 10 trials were run for each experiment and the mean of the result was plotted with the standard deviation as error bars (shaded regions).

In Figure 3 we provide the results of the execution times for the learning procedures considered. With respect to their execution times, the d-AIC, d-BIC scores, and learning with knowledge of the ground-truth maximum in-degree yield the best run-time. Learning tree-structures, generating a random structures, using no structure, or being given the true structure can be achieved in constant time. It is also noticed that learning with the maximum in-degree from the ground truth can be done faster than using penalty score procedures, which have roughly the same execution time.

In the experimental learning scenario the three penalty-based learning procedures outperformed the benchmarks. Notably these penalty-based learning procedures provide significant improved performance than using no or a random structure for the DIN.

The results also indicate that learning a tree structure for the DIN still significantly outperformed the use of a random structure. This result is particularly useful from a computational saving perspective as tree structures are sparse since they capture less complex dependence relations between variables. Tree structure summarise effective independence assertions and thus offer better generalisability. Another notable result from Figure 2 is that when we have fewer samples (> 250) we may be better suited to use no structure since imposing a structure with little training data weakens the inferences we can draw from the model.

5 Conclusion

In this paper we empirically demonstrated the a score-based structure learning procedure to learn a DIN to represent the influence relationships between partially observable stochastic processes. Why we would want to learn a DIN depends on what the structure will be used for.

On the one hand, if we are trying to identify the original DIN structure for knowledge discovery, then we will need to identify each of the original conditional independence assumptions of the ground-truth network. This means we will need to find the set $\mathcal{I}(\mathcal{G}^*(\langle \mathbb{I}_0, \mathbb{I}_\rightarrow \rangle^{\mathcal{G}}))$. This is not a promising task since there are many perfect maps for $P^*(\langle \mathbb{I}_0, \mathbb{I}_\rightarrow \rangle^{\mathcal{G}})$ that can be derived from $\mathcal{D}_{\langle \mathbb{I}_0, \mathbb{I}_\rightarrow \rangle^{\mathcal{G}}}$.

Recognising $\mathcal{I}(\mathcal{G}^*(\langle \mathbb{I}_0, \mathbb{I}_\rightarrow \rangle^{\mathcal{G}}))$ from the set of structures from $\mathcal{G}^*(\langle \mathbb{I}_0, \mathbb{I}_\rightarrow \rangle^{\mathcal{G}})$ will yield the same fit to the data. Therefore iden-

Table 1: A table summarising the parameters for the ground-truth DIN distribution.

Ground-truth DIN Distribution	
No. DBNs	10
Random variable values	3
No. time-slices	5
No. layers	2
No. CPDs between DBNs	15
max in-degree	2
No. Obs	5 p.t.
No. Latent	3 p.t.

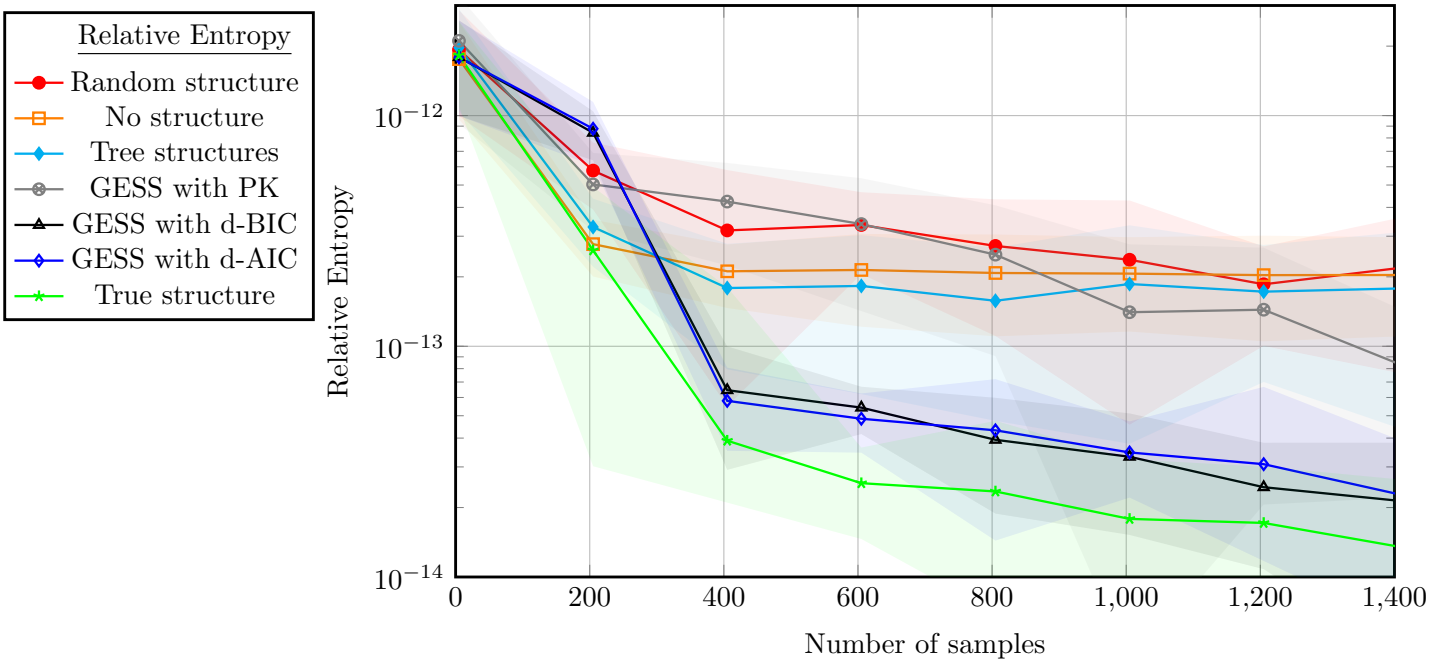


Figure 2: The relative entropy (also known as KL-divergence), to a ground truth DIN, for seven learning tasks to construct a dynamic influence network between dynamic Bayesian networks with respect to the amount of training samples.

Table 2: A table showing all of the parameters used in the structure learning methods in this paper.

	Rand	**No struc**	**Tree**	**GESS with PK**	**GESS with BIC**	**GESS with AIC**	**True**
α	2	2	2	2	2	2	2
No. edges	-	-	-	15	-	-	15
Max in-degree	3	-	-	3	-	-	-
No. observable var	5	5	5	5	5	5	5
Dirichlet prior	5	5	5	5	5	5	5
Parameter threshold	-	-	-	-	5000	5000	-
EM iterations	20	20	20	20	20	20	20
EM accuracy $(\mu\%, \sigma)$					$(76\%, 10)$		
Likelihood score	-	-	Yes	Yes	Yes	Yes	-
Penalty score	-	-	-	-	BIC	AIC	-
Search iterations	-	-	-	50	50	50	-
No. random restarts	-	-	-	5	5	5	-
Tabu-list length	-	-	-	10	10	10	-
α	2	2	2	2	2	2	2

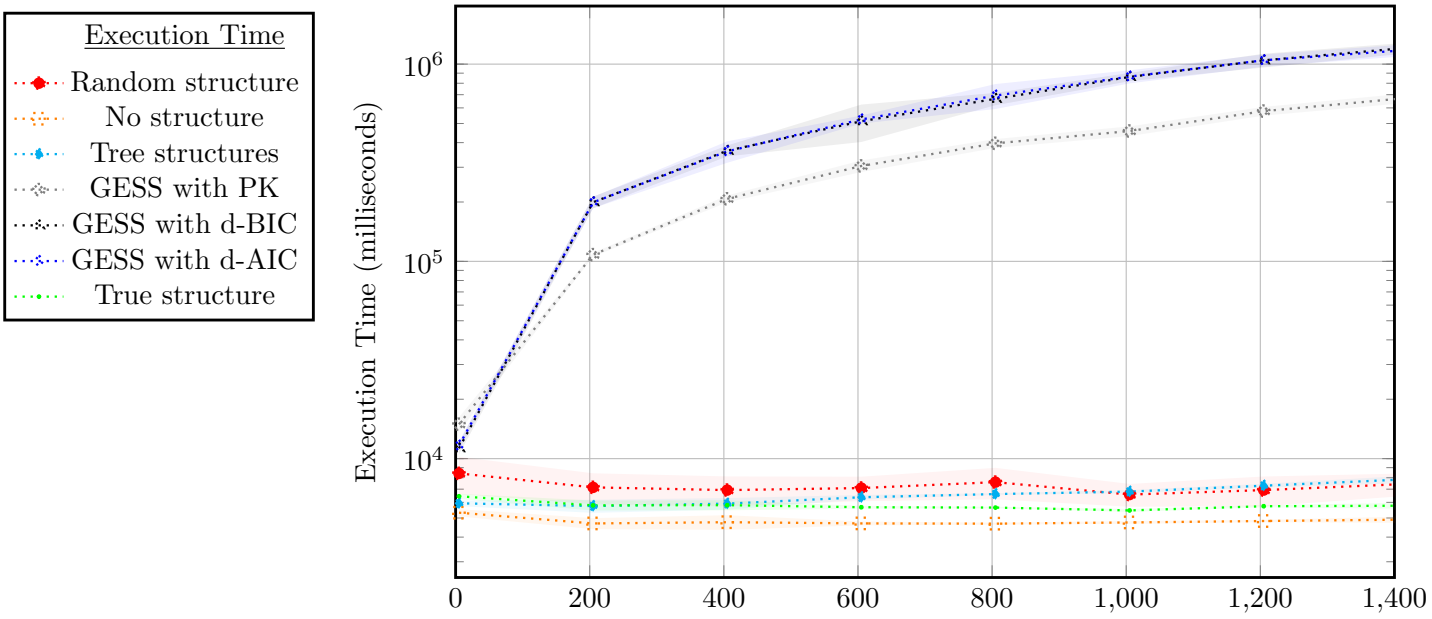


Figure 3: The execution time in milliseconds for seven learning tasks to construct a dynamic influence network between dynamic Bayesian networks with respect to the amount of training samples.

tifying the original ground-truth structure is not identifiable from $\mathcal{D}_{\langle \mathbb{I}_0, \mathbb{I}_{\rightarrow} \rangle^{\mathcal{G}}}$. This is because the structures in the I-equivalent structure set all produces the same numeric likelihood (mutual information) for $\mathcal{D}_{\langle \mathbb{I}_0, \mathbb{I}_{\rightarrow} \rangle^{\mathcal{G}}}$. Therefore, we should rather try to learn a set of structures that are I-equivalent to $\mathcal{G}^*$.

On the other hand, if instead we are trying to learn a DIN structure for density estimation (i.e. to draw probabilistic inferences), then we are interested in capturing the distribution $P^*(\langle \mathbb{I}_0, \mathbb{I}_{\rightarrow} \rangle^{\mathcal{G}})$. If we can successfully constructure such a distribution then we can reason about new data instances and also sample new one.

There are two implications when learning a structure or density estimation: Firstly, Although capturing more independence assertions than specified in $\mathcal{I}(\mathcal{G}^*(\langle \mathbb{I}_0, \mathbb{I}_{\rightarrow} \rangle^{\mathcal{G}}))$ may still allow us to capture $P^*(\langle \mathbb{I}_0, \mathbb{I}_{\rightarrow} \rangle^{\mathcal{G}}$, our selection of more independence assumptions could result in *data fragmentation*. Secondly, selecting too sparse structures can restrict us to never being able to learn the true distribution $P^*(\langle \mathbb{I}_0, \mathbb{I}_{\rightarrow} \rangle^{\mathcal{G}}$ no matter how we change the parameters. However, often sparse DIN structures can be used to promote computational complexity savings [11].

Conflict of Interest The authors declare no conflict of interest.

Acknowledgement This work is based on the research supported in part by the National Research Foundation of South Africa (Grant number: 121835).

References

[1] R. Ajoodha, B. Rosman, "Learning the influence structure between partially observed stochastic processes using IoT sensor data," in Workshops at the Thirty-Second AAAI Conference on Artificial Intelligence, 2018.

[2] R. Ajoodha, B. Rosman, "Tracking influence between naïve Bayes models using score-based structure learning," in 2017 Pattern Recognition Association of South Africa and Robotics and Mechatronics International Conference (PRASA-RobMech), 122–127, IEEE, 2017.

[3] A. Anshel, D. A. Kipper, "The influence of group singing on trust and cooperation," Journal of Music Therapy, **25**(3), 145–155, 1988.

[4] R. Ajoodha, A. Jadhav, S. Dukhan, "Forecasting Learner Attrition for Student Success at a South African University," in In Conference of the South African Institute of Computer Scientists and Information Technologists 2020 (SAICSIT '20), September 14-16, 2020, Cape Town, South Africa. ACM, New York, NY, USA, 10 pages., ACM, 2020, doi:https://doi.org/10.1145/3410886.3410973.

[5] T. Abed, R. Ajoodha, A. Jadhav, "A Prediction Model to Improve Student Placement at a South African Higher Education Institution," in 2020 International SAUPEC/RobMech/PRASA Conference, 1–6, IEEE, 2020.

[6] J. Hatfield, G. J. Faunce, R. Job, "Avoiding confusion surrounding the phrase "correlation does not imply causation"," Teaching of Psychology, **33**(1), 49–51, 2006.

[7] R. Opgen-Rhein, K. Strimmer, "From correlation to causation networks: a simple approximate learning algorithm and its application to high-dimensional plant gene expression data," BMC systems biology, **1**(1), 37, 2007.

[8] T. Grinthal, N. Berkeley Heights, "Correlation vs. Causation," AMERICAN SCIENTIST, **103**(2), 84–84, 2015.

[9] D. Commenges, A. Gégout-Petit, "A general dynamical statistical model with causal interpretation," Journal of the Royal Statistical Society: Series B (Statistical Methodology), **71**(3), 719–736, 2009.

[10] M. Bunge, Causality and modern science, Routledge, 2017.

[11] D. Koller, N. Friedman, Probabilistic graphical models: principles and techniques. (Chapter 16; 17; 18; and 19), MIT press, 2009.

[12] D. Heckerman, D. Geiger, D. M. Chickering, "Learning Bayesian networks: The combination of knowledge and statistical data," Machine learning, **20**(3), 197–243, 1995.

[13] A. Mohammadi, E. C. Wit, "Bayesian structure learning in sparse Gaussian graphical models," Bayesian Analysis, **10**(1), 109–138, 2015.

[14] A. L. Madsen, F. Jensen, A. Salmerón, H. Langseth, T. D. Nielsen, "A parallel algorithm for Bayesian network structure learning from large data sets," Knowledge-Based Systems, **117**, 46–55, 2017.

[15] X. Fan, C. Yuan, B. M. Malone, "Tightening Bounds for Bayesian Network Structure Learning." in AAAI, 2439–2445, 2014.

[16] C. P. d. Campos, Q. Ji, "Efficient structure learning of Bayesian networks using constraints," Journal of Machine Learning Research, **12**(Mar), 663–689, 2011.

[17] S. Kok, P. Domingos, "Learning the structure of Markov logic networks," in Proceedings of the 22nd international conference on Machine learning, 441–448, ACM, 2005.

[18] J. B. Tenenbaum, C. Kemp, T. L. Griffiths, N. D. Goodman, "How to grow a mind: Statistics, structure, and abstraction," science, **331**(6022), 1279–1285, 2011.

[19] I. Tsamardinos, L. E. Brown, C. F. Aliferis, "The max-min hill-climbing Bayesian network structure learning algorithm," Machine learning, **65**(1), 31–78, 2006.

[20] S.-I. Lee, V. Ganapathi, D. Koller, "Efficient structure learning of markov networks using *l*_1-regularization," in Advances in neural Information processing systems, 817–824, 2007.

[21] D. M. Chickering, D. Geiger, D. Heckerman, "Learning Bayesian networks is NP-hard," Technical report, Technical Report MSR-TR-94-17, Microsoft Research, 1994.

[22] D. M. Chickering, "Learning Bayesian networks is NP-complete," Learning from data: Artificial intelligence and statistics V, **112**, 121–130, 1996.

[23] D. M. Chickering, D. Heckerman, C. Meek, "Large-sample learning of Bayesian networks is NP-hard," Journal of Machine Learning Research, **5**(Oct), 1287–1330, 2004.

[24] J. Suzuki, "An Efficient Bayesian Network Structure Learning Strategy," New Generation Computing, **35**(1), 105–124, 2017.

[25] G. Schwarz, et al., "Estimating the dimension of a model," The annals of statistics, **6**(2), 461–464, 1978.

[26] S. Chen, P. Gopalakrishnan, "Speaker, environment and channel change detection and clustering via the bayesian information criterion," in Proc. darpa broadcast news transcription and understanding workshop, volume 8, 127–132, Virginia, USA, 1998.

[27] Y. Tamura, T. Sato, M. Ooe, M. Ishiguro, "A procedure for tidal analysis with a Bayesian information criterion," Geophysical Journal International, **104**(3), 507–516, 1991.

[28] J. Rissanen, "Stochastic complexity," Journal of the Royal Statistical Society. Series B (Methodological), 223–239, 1987.

[29] A. Barron, J. Rissanen, B. Yu, "The minimum description length principle in coding and modeling," IEEE Transactions on Information Theory, **44**(6), 2743–2760, 1998.

[30] D. Geiger, D. Heckerman, H. King, C. Meek, "Stratified exponential families: graphical models and model selection," Annals of statistics, 505–529, 2001.

[31] D. Rusakov, D. Geiger, "Asymptotic model selection for naive Bayesian networks," Journal of Machine Learning Research, **6**(Jan), 1–35, 2005.

[32] R. Settimi, J. Q. Smith, "On the geometry of Bayesian graphical models with hidden variables," in Proceedings of the Fourteenth conference on Uncertainty in artificial intelligence, 472–479, Morgan Kaufmann Publishers Inc., 1998.

[33] M. Koivisto, K. Sood, "Exact Bayesian structure discovery in Bayesian networks," Journal of Machine Learning Research, **5**(May), 549–573, 2004.

[34] T. Silander, P. Myllymaki, "A simple approach for finding the globally optimal Bayesian network structure," arXiv preprint arXiv:1206.6875, 2012.

[35] D. Chickering, D. Geiger, D. Heckerman, "Learning Bayesian networks: Search methods and experimental results," in proceedings of fifth conference on artificial intelligence and statistics, 112–128, 1995.

[36] W. Buntine, "Theory refinement on Bayesian networks," in Proceedings of the Seventh conference on Uncertainty in Artificial Intelligence, 52–60, Morgan Kaufmann Publishers Inc., 1991.

[37] A. Moore, M. S. Lee, "Cached sufficient statistics for efficient machine learning with large datasets," Journal of Artificial Intelligence Research, **8**(3), 67–91, 1998.

[38] K. Deng, A. W. Moore, "Multiresolution instance-based learning," in IJCAI, volume 95, 1233–1239, 1995.

[39] A. W. Moore, "The anchors hierarchy: Using the triangle inequality to survive high dimensional data," in Proceedings of the Sixteenth conference on Uncertainty in artificial intelligence, 397–405, Morgan Kaufmann Publishers Inc., 2000.

[40] P. Komarek, A. W. Moore, "A Dynamic Adaptation of AD-trees for Efficient Machine Learning on Large Data Sets." in ICML, 495–502, 2000.

[41] P. Indyk, "Nearest neighbors in high-dimensional spaces," Citeseer, 2004.

[42] R. Ajoodha, Influence modelling and learning between dynamic Bayesian networks using score-based structure learning, Wirespace, 2019.

ASTES

Advances in Science, Technology and Engineering Systems Journal
Vol. 5, No. 5, 24-28 (2020)
www.astesj.com

ASTES Journal
ISSN: 2415-6698

Facial Expression Recognition using Facial Landmarks: A novel approach

Rohith Raj S*, Pratiba D, Ramakanth Kumar P

Department of Computer Science and Engineering, RV College of Engineering, Bengaluru, 560059, India

ARTICLE INFO

Article history:
Received: 18 July, 2020
Accepted: 11 August, 2020
Online: 08 September, 2020

Keywords:
CLAHE
Facial expression recognition
Facial landmarks
SVM

ABSTRACT

The universally common mode of interaction is the human emotions. Thus, there are several advantages of automated recognition of human facial expressions. The primary objective of the proposed framework in this paper, is to classify a person's facial expression into anger, contempt, disgust, fear, happiness, sadness and surprise. Firstly, CLAHE is performed on the image and the faces are identified using a histogram of oriented gradients. Then, using a model trained with the iBUG 300-W dataset the facial landmarks are predicted. Using the proposed method with the normalized landmarks, a feature vector is calculated. With this calculated feature vector, the emotions can be recognized using a Support Vector Classifier. The Support Vector Classifier was trained and tested for system accuracy using the famous Extended Cohn-Kanade database.

1 Introduction

The primary task of Facial Expression Recognition(FER) is to classify the expressions on human face images into various categories viz., happiness, fear, anger, sadness, surprise and so on. It's a crucial component of psychology as the facial expression of a individual accounts for 55% of a spoken message's impact [1].

Psychologists have historically trained human observers to recognise changes in facial muscles and use a Facial Action Coding System (FACS) to map muscle movements to an emotion [2]. While this method helped to maintain objectivity and had the power of definition, it had many disadvantages such as: ineffective preparation of human observers, mandatory for observers with a strong background in psychology and an average person spent more than 100 hours reading the FACS manual to prepare for certification, the certification itself took about twelve hours, and once certified, FACS professionals could detect emotion with an accuracy of approximately 80%.

Automatic facial expression recognition has become an interesting and challenging area for the fields of computer vision and artificial intelligence with the advent of faster computers and the use of pixels/megapixels for image elements. As we know, the traditional application of FER is in the field of psychology, where facial expressions are used to understand behaviour, detect mental disorders, and detect lies. However, applications of computer-based FER can be broadly classified into three groups, and these are, human computer interaction (HCI), consumer products, and medical research. Human-centered systems need to be built in the field of HCI in such a way that system responds not only according to user input but also according to user behaviour, particularly in ubiquitous computing environments [3]. Automotive fatigue detection systems, entertainment systems such as gaming, human-robot interaction, and protection are a few examples of commercial applications [4]. Identification of clinical depression, pain assessment, and conduct of psychology studies, medicine, are several applications related to medical research [5].

The remainder of the paper is structured as follows. Section II focuses on related research carried out on this area. Section III deals with the proposed methodology. Section IV throws light on the experimental results and analysis. And finally, Section V concludes the paper.

2 Related Work

A lot of research work in the field of human facial expression recognition has been carried out in the recent past, mainly due to the numerous use cases present in this area.

One of the earliest attempt was made by [2] in the year 1978. They had proposed FACS for FER. It was shown that each emotion is a combination of several Action Units (AU) present in FACS. And thus, concluded that facial muscular movement maps to an emotion.

In [6], they trained a Conventional Neural Network (CNN) to perform FER. A 64*64 image is supplied as input to the CNN. The network includes one input layer, five convolution layers, three pooled layers, one fully connected layer, and one output layer. The fully connected layer is combined as the input of the softmax layer to obtain the output class after the convolutional pooling operation. They have used JAFFE and CK+ database for validation.

*Corresponding Author: Rohith Raj S, RV College of Engineering, +91-8095969630 & rohith.june6@gmail.com

In [7], they trained a CNN to perform FER by using CMU MultiPie database for validation. Their proposed method also took advantage of GPU-based parallelism to boost performance.

In [8], they put forward the fact of any FER technique contains 3 steps: feature extraction, dimensionality reduction, and classification. According to them dimensionality and feature selection are major issues concerning FER. They also said that huge amount of memory and processing is required to process the image as a whole. So, they proposed an alternative which is geometric features and have used facial landmark detection for feature extraction and CNN Classifier. They used JAFEE, MUG, CK and MMI database to test effectiveness of their system.

The maximum peak frame chosen is used for the recognition of facial expression in the system designed by [9]. Their approach was relying on the calculation of the distance between the neutral and expressive face. They used eNTERFACE database to test the effectiveness of their system and attained a prediction accuracy of 78.26%.

Using 63 facial landmark points of the active appearance model, a FER system was proposed by [10]. They used those 63 points to calculate the remaining 4 landmark points. Ratio of height to width was used to measure the degree of openness. Facial expression was obtained by multiplying the respective weights with their sum of ratios. Thus, they attained a prediction accuracy of 88%.

3 Proposed Methodology

This section describes the complete proposed methodology. We know from our literature survey, that almost any system designed for Facial Expression Recognition has these three important steps:

- Image pre-processing
- Feature Extraction
- Expression Classification

On similar lines, a system has been proposed using these steps as shown in Figure 1.

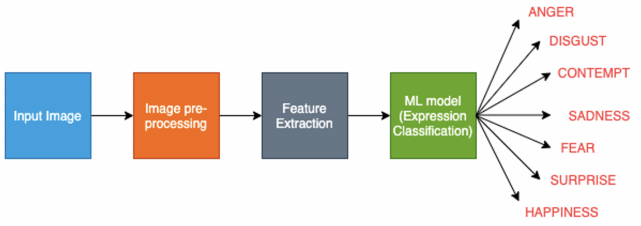


Figure 1: Block diagram of the proposed FER methodology

The way in which image is pre-processed and how the features are extracted makes it a novel technique. Human facial expressions are represented using facial landmark based feature vector. And, Support Vector Classification technique is used to recognise the facial emotions. Python programming language has been used in order to develop the entire system with extensive usage of OpenCV for performing image manipulation tasks. Predominant Scikit-learn python library and Dlib [11], an open source general purpose machine learning library have been used for performing the machine learning tasks. The primary usage of Scikit-learn library is to implement the Support Vector Classifier. Whereas, face detection and facial landmark points prediction is achieved using Dlib library.

3.1 Facial Expression Image Database

Support Vector Classifier (SVC) needs to be trained with a well-known facial expression database, thus, the CK+ dataset is selected. It consists of 7 emotions expressed by 210 adults viz., happiness, surprise, fear, sadness, contempt, disgust and anger. Each image is of size 48*48 pixels. Figure 2 shows a sample of images depicting all seven emotions. Participants are aged 18 to 50 years, 69% are female, 81% are Euro-American, 13% are Afro-American and 6% are other groups [12].



Figure 2: Seven expressions of CK+ database

3.2 Image pre-processing

We know that the dataset consists of images captured in wide range of lighting conditions. Thus, to ensure that all images are equalized to similar lighting conditions, Contrast Limited Adaptive Histogram Equalization (CLAHE) is performed [13] on all the images in the dataset using OpenCV built-in function. The advantage of using CLAHE compared to a general Histogram Equalization is that it doesn't consider the global contrast of the image. In case if the image is in RGB, which is not the case for this dataset, it should be first converted to grayscale and later CLAHE should be applied on it. For visualizing the methodology, input image shown in Figure 3 is considered which is in grayscale. And, Figure 4 shows the image obtained after applying CLAHE on the input image.

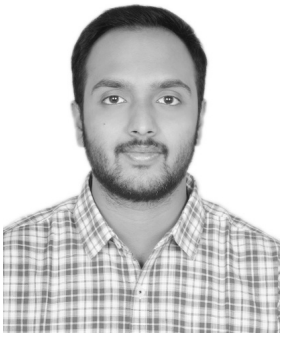


Figure 3: Input image in grayscale



Figure 4: CLAHE applied on grayscale image

3.3 Facial Landmark Prediction

Firstly, to predict the facial landmarks, the face detection algorithm must be run on the image. This was done with built-in Dlib function, which returns an object detector that is capable of identifying faces in the image. Using a classic HOG, the afore-mentioned object detector is developed. Figure 5 shows the detected face with blue bounding box.

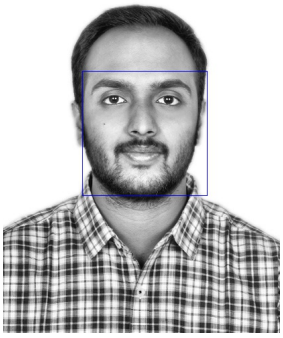


Figure 5: Detected face

Having done with the face detection, again Dlib built-in function is used to predict the facial landmark points. The 68 landmark points prediction is achieved by using the popular pretrained model available for download on the dlib website. This function internally uses the method proposed by [14] for achieving better predictions. The famous iBUG 300-W face landmark dataset is used to train this estimator as it's very robust. Figure 6 shows the predicted facial landmark points marked with red dots.

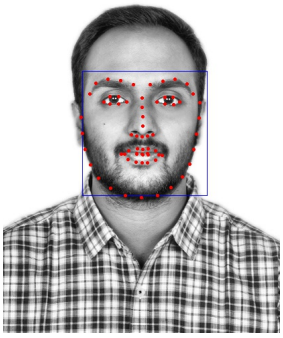


Figure 6: Predicted facial landmarks

3.4 Feature Extraction

Calculation of the feature vector that describes a person's emotion would be the most important step of facial expression identification. It's necessary to know the positions of the facial landmark points relative to each other. This is achieved by calculating mean of both the axes which results in a central point (x_{mean}, y_{mean}) as shown in Figure 7 with a large blue dot near the nose region. We can then get the position of all points relative to this central point. Now a line is drawn between the center point and each other facial landmark location as shown in Figure 7 with green lines. So, each line obtained has magnitude and direction (i.e., it's a vector) and constitutes the feature vector for both training and classification phase. The magnitude is the Euclidean distance between the points under consideration and direction is the angle made by the line with the horizontal reference axis. Therefore the feature vector can be generalized as:

feature_vector = *<point1.x , point1.y , magnitude1 , direction1 , . . . , point68.x , point68.y , magnitude68 , direction68 >*

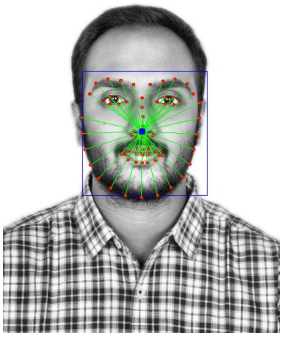


Figure 7: Feature vectors shown alongwith central point (x_{mean}, y_{mean})

3.5 Training and Classification using SVC

It is important to identify the facial expressions after constructing a feature vector. This was achieved by using Support Vector Machine (SVM) as the classification method for evaluation. SVMs are strong but versatile supervised machine learning algorithms used for classification and regression. However, they are commonly used in classification problems. Thus, SVM and SVC can be used interchangeably. SVM classifiers provide excellent accuracy and function well with high dimensional space. Basically, SVM classifiers use a subset of training points and thus use far less memory in the end. However, they have high training time which is not suitable for large data sets in practice. In our case, as we don't have a really large dataset, the training and classification can be achieved with a very good accurcay by just using a SVC. Thus, the use of Decision Trees or Random Forest is not really needed.

The SVC was implemented by using a class called "SVC" present in the "svm" module of Scikit-learn library. To provide versatility, the dataitems in each emotion of the dataset was randomly shuffled and split in the ratio of 80:20 for training data:testing data. In training phase, first each image in the training set of a particular emotion is considered and CLAHE is applied on it. Now face detection is applied to it following which the facial landmarks

can be predicted. From the obtained landmark points, the feature vector is calculated as given in the previous sub-section. Finally, SVC is trained using all the feature vectors that are calculated for the entire dataset, along with the corresponding class labels.

Each image in the testing set is taken through the same steps as that of the training phase for the calculation of the feature vector during the testing/classification phase. One important point to be noted is that training and testing set dataitems are mutually exclusive i.e., testing set consists of images which haven't been used for training. Finally, the determined feature vector for a test image is given as input to the trained SVC which predicts the emotion expressed by the test image under consideration.

4 Experimental Results Analysis

In our experiment, we had considered 80% of the images in the CK+ database for training and used the rest for testing purpose. All the seven emotions available in CK+ database was considered and the number of dataitems in each emotion is given in Figure 8. In order to keep overfitting at bay, training data was ensured to be mutually exclusive with that of the testing data.

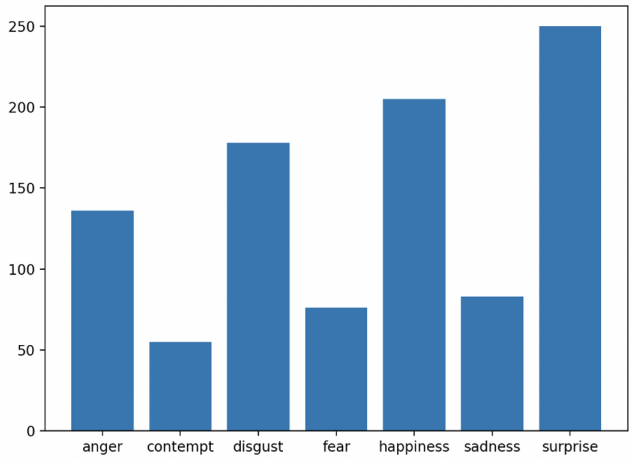


Figure 8: Distribution of the Input database

The developed model was able to classify the images in the test data into one of the 7 emotions (i.e., anger, contempt, disgust, fear, happiness, sadness, surprise) with an average success rate of 89%. This attained accuracy is much better than some of the CNN methods which generally have high training time with an extensive usage of the underlying hardware resources like CPU/GPU.

With the test samples of CK+ dataset, the proposed method was able to achieve 100% accuracy for happiness emotion as shown in the confusion matrix given in Figure 9. And the accuracy obtained for contempt, disgust, sadness and surprise emotions were also reasonably good. However, it can be observed that it's relatively hard to recognize anger and fear.

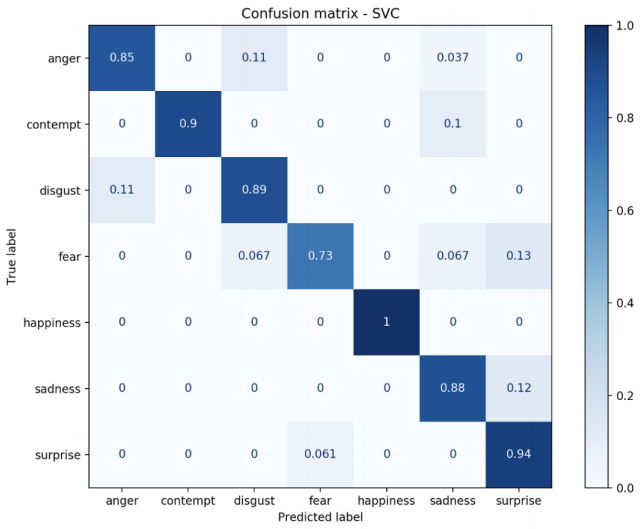


Figure 9: Confusion Matrix on CK+ dataset

To further understand why it's fairly challenging to recognize fear emotion, we need to draw some conclusions from the confusion matrix. It's observed that 13% of the images in test set of fear emotion have been misclassified as surprise. With Figure 10, we can see how challenging it is for certain images to be correctly classified even by humans. This is primarily because, the expression on the face is mixed with fear and surprise, which makes it difficult to give an accurate prediction and results in misclassification.



Figure 10: Images with true label fear incorrectly classified as surprise

5 Conclusion

The potential ability for recognizing facial expression based on facial landmarks is explored in this paper. It shows that facial expressions can be recognized by human brain using just 68 points instead of all face image pixels. Recognition of facial expressions was achieved using a Support Vector Classifier. The famous widely accepted CK+ dataset was used for both the model training and testing phase. The result on our test samples shows that the landmark based approach also has comparable performance with methods based on CNN. However, the precision of the landmark detection algorithm used, is the quintessential factor which decides the performance of the proposed method. The future work would be to explore the model for different facial poses and add support for real-time recognition.

Conflict of Interest The authors declare no conflict of interest.

Acknowledgment The authors would like to thank RV College of Engineering, Bangalore for their constant support and guidance in carrying out this project work.

References

[1] Mehrabian A., Russell J.A., An Approach to Environmental Psychology, The MIT Press: Cambridge, MA, USA, 1974.

[2] P. Ekman and W. Friesen, "Facial action coding system: A technique for the measurement of facial movement", Palo Alto, CA: Consulting Psychologists Press, 1978.

[3] Z. Zeng, M. Pantic, G. I. Roisman and T. S. Huang, "A Survey of Affect Recognition Methods: Audio, Visual, and Spontaneous Expressions," IEEE Transactions on Pattern Analysis and Machine Intelligence, **31**(1), 39–58, 2009, doi:10.1109/TPAMI.2008.52.

[4] Q. Yang, C. Li and Z. Li, "Application of FTGSVM Algorithm in Expression Recognition of Fatigue Driving," Journal of Multimedia , **9**(4), 527–533, 2014, doi:10.4304/jmm.9.4.527-533.

[5] A. R. Daros, K. K. Zakzanis and A. C. Ruocco, "Facial emotion recognition in borderline personality disorder," Psychological Medicine, **43**(9), 1953–1963, 2013, doi:10.1017/S0033291712002607.

[6] M. Wang, Z. Wang, S. Zhang, J. Luan and Z. Jiao, "Face Expression Recognition Based on Deep Convolution Network," in 2018 11th International Congress on Image and Signal Processing, BioMedical Engineering and Informatics (CISP-BMEI), 1–9, 2018, doi:10.1109/CISP-BMEI.2018.8633014.

[7] L. Ivanovsky, V. Khryashchev, A. Lebedev and I. Kosterin, "Facial expression recognition algorithm based on deep convolution neural network," in 2017 21st Conference of Open Innovations Association (FRUCT), 141–147, 2017, doi:10.23919/FRUCT.2017.8250176.

[8] N. P. Gopalan, S. Bellamkonda and V. Saran Chaitanya, "Facial Expression Recognition Using Geometric Landmark Points and Convolutional Neural Networks," in 2018 International Conference on Inventive Research in Computing Applications (ICIRCA), 1149–1153, 2018, doi:10.1109/ICIRCA.2018.8597226.

[9] Sara Zhalehpour, Zahid Akhtar and Cigdem Eroglu Erdem, "Multimodal emotion recognition based on peak frame selection from video", SIViP, **10**, 827–834, 2016, doi:10.1007/s11760-015-0822-0.

[10] Hao Tang and Thomas S. Huang, "3D Facial Expression Recognition Based on Properties of Line Segments Connecting Facial Feature Points", in 2008 8th IEEE International Conference on Automatic Face & Gesture Recognition, 1–6, 2008, doi:10.1109/AFGR.2008.4813304.

[11] D. E. King, "Dlib-ml: A Machine Learning Toolkit," Journal of Machine Learning Research , **10**, 1755–1758, 2009.

[12] P. Lucey, J. F. Cohn, T. Kanade, J. Saragih, Z. Ambadar and I. Matthews, "The Extended Cohn-Kanade Dataset (CK+): A complete dataset for action unit and emotion-specified expression," in 2010 IEEE Computer Society Conference on Computer Vision and Pattern Recognition - Workshops, 94–101, 2010, doi:10.1109/CVPRW.2010.5543262.

[13] G. Yadav, S. Maheshwari and A. Agarwal, "Contrast limited adaptive histogram equalization based enhancement for real time video system," in 2014 International Conference on Advances in Computing, Communications and Informatics (ICACCI), 2392–2397, 2014, doi:10.1109/ICACCI.2014.6968381.

[14] V. Kazemi and J. Sullivan, "One millisecond face alignment with an ensemble of regression trees," in 2014 IEEE Conference on Computer Vision and Pattern Recognition, 1867–1874, 2014, doi:10.1109/CVPR.2014.241.

ASTES

Advances in Science, Technology and Engineering Systems Journal Vol. 5, No. 5, 29-38 (2020)

www.astesj.com

ASTESJ

ISSN: 2415-6698

Criteria to Implement a Supervision System in the Petroleum Industry: A Case Study in a Terminal Storage Facility

Khalid Chkara*, Hamid Seghiouer

Laboratory MOSIL, National School of Applied Sciences, University Abdelmalek Essaâdi, Tétouan, 93000, Morocco

ARTICLE INFO

Article history:
Received: 16 June, 2020
Accepted: 11 August, 2020
Online: 08 September, 2020

Keywords:
Petroleum storage terminal
Supervision system
DCS
SCADA
Project management
Oil & Gas

ABSTRACT

A liquid petroleum storage facility (Terminal), is a platform used to store petroleum products. Terminals plays a strategic role on the oil and gas supply chain. There are three types of terminals: a fully automated terminal, a partially automated terminal and a fully manual terminal. To increase their efficiency and safety in a very competitive market, terminal companies might take the decision to invest in a supervisory control system DCS or SCADA. The advantages of DCS/SCADA systems are: improving the productivity and the proactivity, reducing cost, identifying quickly abnormal operating conditions and finally enhancing the efficiency and the safety. Due to the high cost of this project type, it is deemed vital to take the right decision when comparing the different options. The automation market offers multiple choices and opportunities, and taking the correct decision is a very challenging process. The key criteria for the technical evaluation are: 1) service offered, 2) interface capabilities,3) tender process efficiency and project execution, 4) after sales and product life cycle,5) references and finally 6) additional services. In this paper, the importance of each key criterion is identified and measured, leading to the development of a tool to be used for the assessment of different offers in order to successfully implement a supervision system. It consists of a framework based on a past experience of subject matter expert for a real case related to a successful implementation of a DCS system on a liquid petroleum storage facility. The paper provides as well a valuable feedback for vendors and can be used as a reference when preparing their commercial and technical strategy for future projects.

1. Introduction

The downstream petroleum supply chain (PSC) represents a major economic sector that ensure production, storage and handling of petroleum products in a cost-efficient and safely manner [1].

Liquid petroleum storage facilities play a key role on this supply chain. They are an essential player to import or to export crude or refined products in a given country.

Over the past few years, the global logistics and oil market is transforming rapidly and its complexity compounded by the volatility of petroleum product pricing due to the effect of crude oil price globally (Figure 1) [2,3].

Such volatile and contango crude oil market have driven the traders and even oil majors/producers to use strategic storage facilities for futures trading and consolidation of crude oil and refined petroleum products [4].

Terminal storage facilities are also part of the trading business where petroleum product is stored and transshipped depending on the market evolution. There are two types of terminal operators:

- Terminal operators who own the asset as well as the product which is stored in. Typically, major oil compagnies fall under this category;

* Corresponding Author: Khalid Chkara, Email : k.chkara@gmail.com

- Terminal operators who do not own the product and they are considered as independent storage companies. Their business model is based on providing storage space and handling services for their customers.

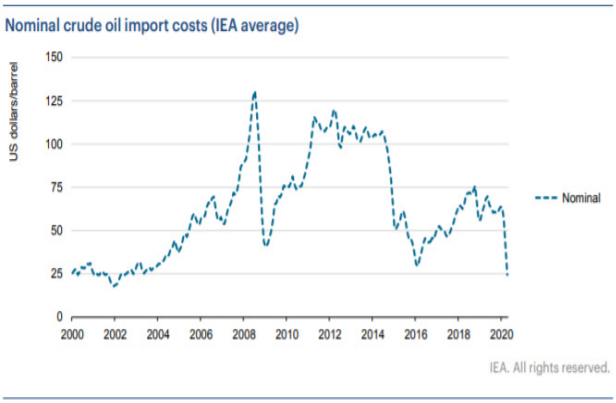


Figure 1: Average crude oil import costs [3]

Petroleum storage facility may store different types of bulk liquid: chemical, refined/semi-refined products, crude oil and LNG. The design of the terminal varies depending on the substances to be stored.

Terminal operations are present worldwide; however, storage hubs have become established in the United States, Europe, Middle East and Asia to provide the necessary storage and handling services required for the international trade of petroleum products.

The tank storage sector is not a static industry but a dynamic one which grows every year.

Estimates are that global tank storage capacity will grow 8% to 1.03 billion cbm in 2020 and even 11.5% to 1.06 billion cbm in 2021 [5].

In Figure 2 can be seen where the largest concentrations of tank terminals are [6].



Figure 2: The world's hottest storage hotspots

Europe provides approximately 30% of the world capacity for bulk liquid storage through a network of hundreds of terminals providing logistical support for industry, authorities and the armed forces. In principle any liquid product that is transported in bulk can be stored in a bulk liquid terminal [7].

Until recent times, refineries as well as terminal storage facilities structures have been fairly static and scarcely investigated due to the lack of detailed information and low market competition. However, nowadays competition has significantly increased and is currently driving the global petroleum supply chain including storage facilities to review the design with a strong focus on automated processes and decision-making effectiveness [8], this can be achieved by implementing a robust supervision system.

The key issue is to clearly define the criteria to compare the exiting solutions. Although some of the works focused on the technical specification of implementing a DCS/SCADA system as well as operation and control techniques [9], only a limited number of works have addressed the qualitative approach to solve the issue, which constitutes a research field with high potential from the project management perspective. In this paper we extend and refine the work of [10] who provide new technological developments and selection criteria of industrial Scada applications. Our work updates the earlier work by considering a qualitative and quantitative methodology to define key criteria and to introduce a decision-making tool to support help Project Managers during the technical evaluation and assessment process.

2. The liquid petroleum storage facility description

A liquid petroleum storage facility provides a vital interface between sea, road, rail and piping systems. A typical terminal is usually located nearby a port area and equipped with different asset to allow efficient and safe handling and storage services (see Fig.3).

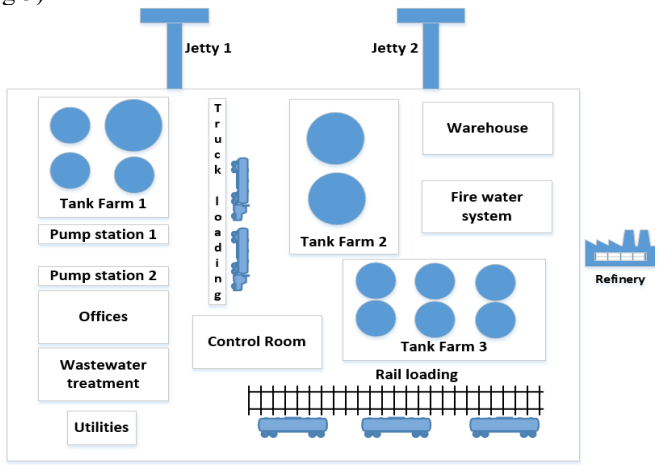


Figure 3: Various parts of a terminal

Those assets are but not limited to:

Marine Berth or deck: usually located in a port, it is used for mooring ship alongside. It provides a safe area where ships can be safely moored to proceed with loading or unloading operations. There are two types of berths: solid structure births or open structure births.

Tank farm: a group of tanks where products are stored, the design of the tank varies in function of the specification of the product to be stored [11], tanks might be fixed roof, floating roof, heated tanks, or insulated tanks.

Piping system: it's the network where the liquid product moves from the terminal into or from the ship. Pipes are made from different qualities of steel: carbon steel, galvanized or inox. For more flexibility it's frequent to use hoses mainly for the ship shore connection.

Pumping system: it's the equipment used to pump the product from the tanks into ships, rail cars or trucks. Pumps come in variety of sizes for a wide range of applications. The most frequent type of pumps used in terminals are: positive displacement and centrifugal.

Truck/rail loading: an asset used to load petroleum products into trucks or rail cars, custody transfer measurement is usually ensured through flowmeters using different technologies such as Coriolis, turbine or positive displacement meters [12]. Also, it's common to use weighbridge for product where weight is considered for the commercial transactions. Figure 3 shows a flow diagram for typical storage facility

Firefighting system: due the high flammability of the products stored, it's essential for any terminal to have a robust firefighting system. The task of fire safety ensuring of such assets becomes very important [13]. Firefighting equipment are divided into two categories: fixed and mobile. The terminal should have also access to a reserve of water and a foam to be used in case of emergency or a fire. Design of the fire system is subject to international standard and regulations [14].

Utilities: in a typical terminal, there are different types of utilities to help providing the handling and the storage services, such utilities are: boilers, compressors, drumming equipment, vapor recovery systems, blending system, nitrogen facilities and water/slop treatment plant.

Supervision system: it consists usually on a DCS or SCADA. It is a purely software package that is positioned on top of hardware to which it is interfaced. The main function is to monitor and control different types of field devices through a unique interface. Field devices could be: level gauges, pressures and temperature transmitters, local alarms, flowmeters, energy consumption and metering, equipment running conditions, pumping start and stop command [15].

Table 1: Acronyms in SCADA/DCS systems

Acronym	Definition
DCS	Digital Control System
HMI	Human Machine Interface
IED	Intelligence Electronic Device
MSU	Master Station Unit
RTU	Remote Terminal Unit
SCADA	Supervisory Control and Data Acquisition
SSU	Slave Station Unit

Supervision system may also provide business solution for some activity like truck/rail loading, shipping loading, material balance and stock reconciliation. Fig.4 represents the general functionality existing on a DCS/SCADA solution [16].

A typical workflow for a petroleum storage facility is from cargo receipt until final delivery is represented on the below flow diagram (See Fig 5).

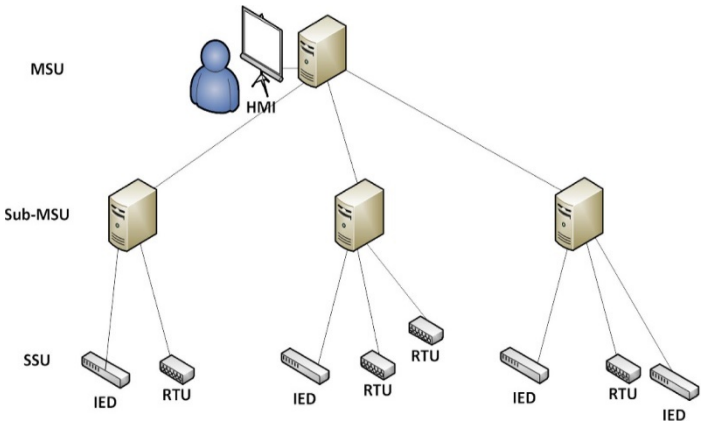


Figure 4: General configuration of DCS solution

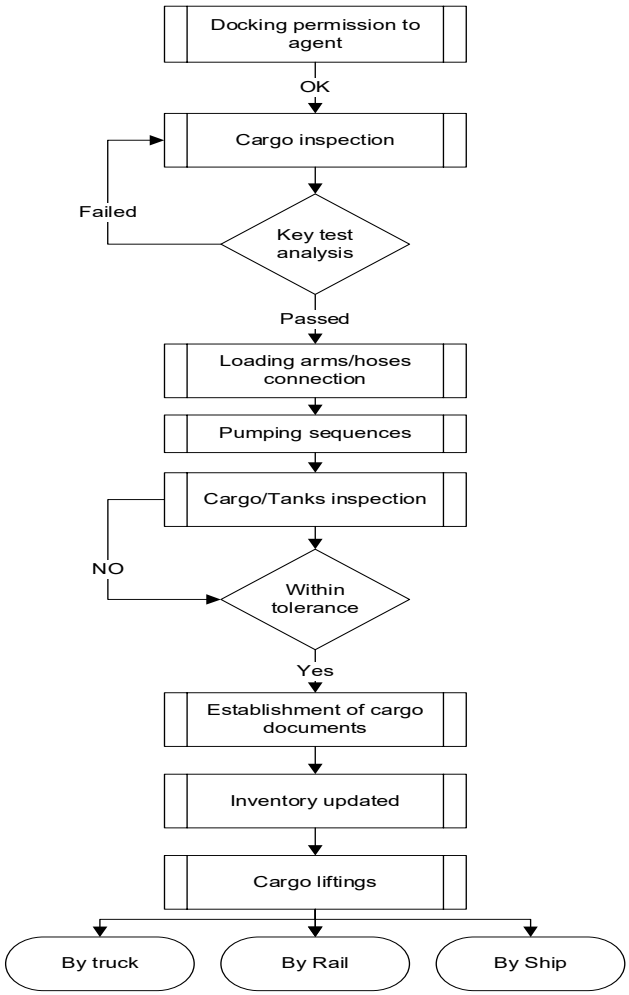


Figure 5: Terminal flow diagram

3. Advantages of implementing a DCS system in a liquid petroleum storage facility

DCSs are used to control industrial processes such as electric power generation, water and wastewater treatment, and chemical, food, and automotive production. DCSs are integrated as a control architecture containing a supervisory level of control overseeing multiple, integrated subsystems that are responsible for controlling the details of a localized process [17].

On the oil and gas, it's very common to find DCS systems implemented in process plants such as refineries. The DCS system plays a key role to automate an oil refinery and to minimize human intervention and consequently reduce failures. While the Scada monitors the system, the PLC is used for the internal storage of instruction for implementing functions such as logic, sequencing, timing and arithmetic to control different type of process devices using digital and analog input/output module [18].

Although the Petroleum storage facility are typically not considered as process plant, market evolution, customers requirement and best practice in the industry push many terminal operators to invest on supervision system. Analysis of the Distributed Control Systems (DCS) Market in India, finds that the market earned approximately $707.9 million in 2012 and estimates this to reach $1,078.9 million in 2016 [19].

Accurate and real time data acquisition is required for decision making to optimize the efficiency and the safety aspect of any liquid petroleum storage facility. Information and communication technologies are of vital importance to almost all aspects of oil and gas operations, from upstream to downstream business [20]. Combined with advanced process controls, terminal's operators may use the DCS not only to achieve regulatory and process controls, but to fully utilize its potential as a direct revenue generator contributing to maintain the company's competitive edge [21].

Another important aspect is safety; because of the dangerous and the valuable nature of the product handled within any terminal, many petroleum storage facilities invest on supervision systems that prevent tragic events from happening by showing exactly where the problem is and by presenting the right information in the right context to the right user. Despite highly equipped process plants' and storage sites' considerable efforts towards effective safety measures, it is still possible that an improbable event, or more likely an unforeseen series of events, may lead to a serious incident. In fact, the task of fire safety becomes very important, major incidents on such facilities can have catastrophic consequences both for neighbouring activities and environment [22]. One of the options that supervision systems might offer is the automation of emergency response plan for petroleum oil storage terminals which is an integral and essential part of a loss prevention strategy [23]. A quick review of the ten largest tank accidents between 1963 and 2002 shows that operational error was the third most frequent cause followed by equipment failure [24].

4. Criteria assessment to choose a DCS provider for a liquid petroleum storage facility

4.1. The study's methodology

In our approach we have adopted a methodology which consists on the definition and the determination of key factors for the right choice and consequently for a successful implementation of a supervision system on a petroleum storage facility. The definition of the criteria list is a key step on the process, this is the primary input that will be used during the development of the final assessment framework. Our aim is to produce an efficient, tested and reliable tool that can be used in other facilities for similar projects.

Figures 6 shows the flow diagram of the process adopted.

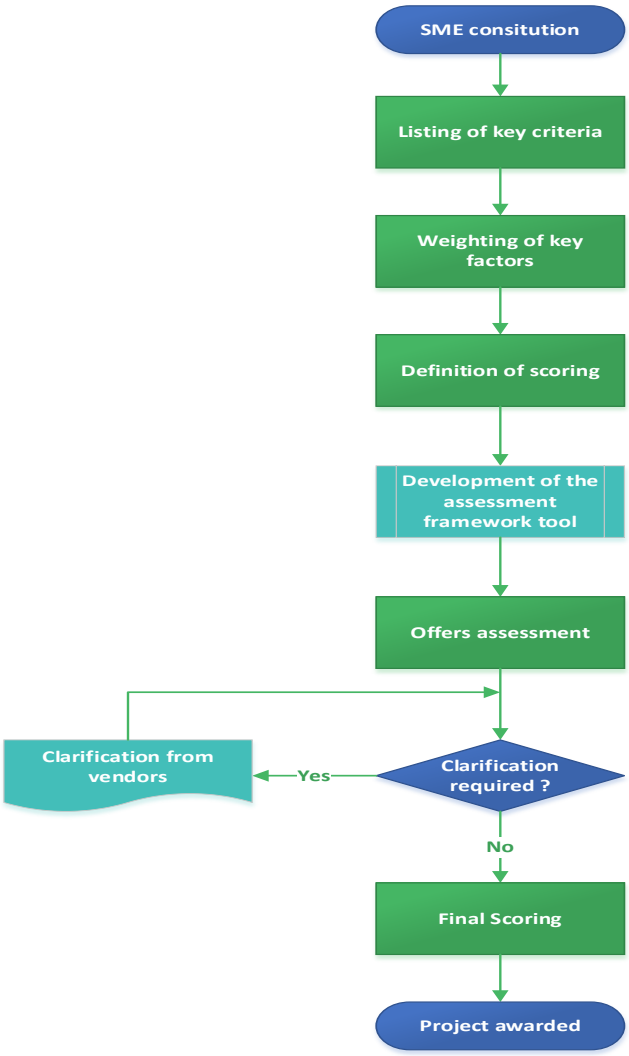


Figure 6: Methodology flowchart

Although this frame work has been tested on a real case study, there is some limitation to be considered:

- Scope of work (SOW): its development might vary from an organization to another; and this could alter the relevance of the proposed framework. As explained below in section b (*The assessment process definition*), the exiting key criterion should match with the requirement of the scope of work, otherwise there will be non-consistency on the assessment process. Vendors should be aware of the relevance of each criteria and this must be clearly stated on the SOW.
- Weightage of the key criteria: definition of the weightage relies basically on the experience of the subject matter expert (SME) committee members of this specific location, to ensure the consistency of the tool, it's will be very useful to review the results of the workshop by other SME.

At this stage, the main purpose of our work is to present a framework that might be the ground for a more complex database. This database could be developed in a way to become a rating platform for the vendors to present the advantages of their solutions and their compliance to a specific checklist, a sort of a Label recognized within the Oil & Gas industry.

4.2. The assessment process definition

Investing on a supervision system is a strategic decision of liquid petroleum storage facility. Due to the high cost of the existing solution on the market, it is vital to have a robust assessment system in place to choose the right vendor. Cost is always a key decision factor but not the only one, determining the key aspect on any solution may help to make the right decision. we have followed the process of a successful implementation of a supervision system in a petroleum storage facility. We have built a tool that might be used by other managers to assess the different offers existing at the right cost but without compromising the quality of the product.

It is important to highlight that a clearly defined scope of work will help the later assessment of the offers in a way that vendors will provide similar offers; therefore, comparison between the advantages and disadvantages of each offer will become straight forward.

- The first step consists of listing the key important factor that will be the basis of the assessment. A brainstorming has been conducted with a multidisciplinary team to determine the most important criteria to retain. The scope of work has been used as a reference to identify such criteria;
- The second step includes providing a weighting to each criterion. The weighting varies from 1 to 4 and it defines the relevance of each criterion. It is a sort of hierarchy of the criteria which allows a more accurate assessment of each item. (See table 2);
- The third step entails providing a score to each item depending on the received offers. The score varies from 0 to 3. (See table 2)

Table 2: Definition of scores

Scoring	Weighting
0 = not available	4 = critical
1 = minimal offering	3 = must have
2 = average offering	2 = nice to have
3 = excellent offering	1 = minimal

4.3. List of the defined criteria

After the workshop with the subject matter experts (SME), a list of the key criteria has been defined and organized by group.

Group 1: Services offered

It covers the different option that the supervision system will provide to meet the needs of the liquid petroleum storage facility such as:

- Holistic Terminal Automation System (TAS);
- General DCS/SCADA functionalities;
- Marine TAS, truck loading TAS;
- Rail loading TAS;
- External pipeline TAS;
- Drumming TAS;
- Utilities & energy management and monitoring TAS.

Group 2: Interfaces capabilities

One of the major challenges that might compromise the success of the supervision system implementation is the capabilities of the solution to communicate with third party software, existing field devices, PLCs and ERPs. List of criteria which fall under this group are:

- Use of common international standards;
- Interfaces with most common L4 ERP systems;
- Interfaces withs most L1 equipment/sensors;
- Interfaces with existing packages.

Group 3: Tender process efficiency and project execution

This group is related to the tender process and project management efficiency. The tender process is a very good opportunity to assess the quality of the provider: response time, site visit, or the respect of the tender deadline date are signs to be considered. Also, the project execution phases and methodology contribute significantly to the success of the implementation. List of criteria which fall under this group are:

- Speed and quality of response;
- Understating of the requirement;
- Factory acceptance test (FAT) testing convenience and facilities;
- FAT testing with integrated with existing equipment;
- Training of operational and maintenance staff;
- Availability of resources during the design phase (in region).

Group 4: After sales and product life cycle

As for any operation technology (OT) Lifecyle and after sales support is considered as important as the implementation itself. One of the disadvantages of a DCS/SCDA solution is the risk of the non-availability of the system due to a breakdown. Shifting from manual operations to automated ones depends highly on the reliability of the solution. Any dysfunction of the system might have major consequences on the business continuity or on the safety of the facility. List of criteria which fall under this group are:

- Availability of remote support 24/7 and its cybersecurity protection;
- Availability of regional or in country support 24/7;
- Size of the support organization;
- Production life cycle duration and software update/upgrade strategy;
- Availability of spare part;
- Provision of support in different languages.

Group 5: Reputation and references

During the amendment of the offers, it is very useful to check the past experience of the providers with similar project, and specially

Table 3: offers comparison using the technical assessment tool

		Supplier 1		Supplier 2		Supplier 3	
	Weighting	Score	max score	Score	max score	Score	max score
1.Services offered							
Holistic Terminal Automation System (TAS)	4	3	12	3	12	3	12
General DCS/SCADA functionalities	4	3	12	3	12	3	12
Marine TAS, truck loading TAS,	4	3	12	3	12	3	12
Rail loading TAS,	4	3	12	3	12	3	12
External pipeline TAS,	1	2	2	2	2	0	0
Drumming TAS	1	2	2	2	2	0	0
Utilities & energy management and monitoring TAS	4	3	12	3	12	3	12
Sub-score 1			**64**		**64**		**60**
%			**97%**		**97%**		**91%**
2.Interfaces capabilities							
Use of common international standards	4	3	12	3	12	3	12
Interfaces with most common L4 ERP systems	3	3	9	3	9	3	9
Interfaces withs most L1 equipment/sensors	3	3	9	3	9	3	9
Interfaces with existing packages	4	2	8	2	8	2	8
Sub-score 2			**38**		**38**		**38**
%			**90%**		**90%**		**90%**
3.Tender process efficiency and project execution							
Speed and quality of response	2	1	2	1	2	2	4
Understating of the requirement	3	3	9	2	6	3	9
Factory acceptance test (FAT) testing convenience and facilities	3	3	9	2	6	3	9
FAT testing with integrated with existing equipment	2	0	0	2	4	0	0
Training of operational and maintenance staff	3	3	9	3	9	3	9
Availability of resources during the design phase (in region)	2	0	0	0	0	2	4
Sub-score 3			**29**		**27**		**35**
%			**64%**		**60%**		**78%**
4.After sales and product life cycle							
Availability of remote support 24/7 and its cybersecurity protection	4	2	8	3	12	3	12
Availability of regional or in country support 24/7	3	0	0	1	3	2	6
Size of the support organization	3	3	9	2	6	2	6
Production life cycle duration and software update/upgrade strategy	3	3	9	2	6	3	9
Availability of spare part	3	2	6	2	6	2	6
Provision of support in different languages.	2	0	0	1	2	3	6
Sub-score 4			**32**		**35**		**45**
%			**59%**		**65%**		**83%**
5.Reputation and references							
Certification to international standards: building SIL (Safety integrity level) rated systems	3	3	9	3	9	3	9
Certification to international standards: integrated management system	2	3	6	3	6	2	4
Proffered vendor with O&G majors or large tank storage companies	2	1	2	2	4	3	6
Sub-score 5			**17**		**19**		**19**
%			**81%**		**90%**		**90%**
6.Additional services							
Alarm management consultancy/support	2	3	6	3	6	3	6
Control room design consultancy	1	2	2	3	3	0	0
Provide services in addition to automation system	1	0	0	0	0	0	0
Sub-score 6			**8**		**9**		**6**
%			**67%**		**75%**		**50%**

TOTAL SCORE	188	192	203
%	**78%**	**80%**	**85%**

with major oil and gas company or with a sister company if the terminal storage facility is part of a group. List of criteria which fall under this group are:

- Certification to international standards: building SIL (Safety integrity level) rated systems;
- Certification to international standards: integrated management system;
- Proffered vendor with O&G majors or large tank storage companies.

Group 6: Additional services

This group covers some additional features and options that usually are not part of the scope of work, however this can be considered as a positive point in favour of the provider in case the offers received from different providers are similar. Availability of an additional option could be a competitive advantage. List of criteria which fall under this group are:

- Alarm management consultancy/support;
- Control room design consultancy;
- Provide services in addition to automation system.

4.4. Assessment of the offers

After listing the defined criteria, the second phase of the workshop was to attribute a weight to each criterion, this process depends highly on the experience of the SME, and the impact on the business. This work can be done prior to the availability of the offers. Final step of the assessment is to assign a score for each supplier against each criterion. Table 3 shows the framework used and the results of the assessment of 3 offers for the implementation of a supervision system within a liquid petroleum storage facility.

4.5. Analysis of the assessment results

Based on the results of table 3, we can assume that Supplier 3's offer should be retained as the best technical offer. However, going deep in our analysis, there is some significant insights to be highlighted. Firstly, we can observe that supplier 1 who has provided the most complete set of offering (97%) compared to Supplier 3 (91%), has the lowest global score. This is due basically to the low sub-score on the tendering process efficiency (64%) and the after sales services (59%). The reason behind this is the non-availability of regional representation of the supplier, this factor is highly important in terms of maintenance contract and also during the engineering/design phase. Being close to your customers is well appreciated by Managers who are in charge of plants working 24/7 such as a petroleum terminal. For business and safety consideration, petroleum storage facilities require high availability of the supervision system.

Regarding the tendering efficiency, Supplier 1 has recorded some delay in providing quick answers during the technical clarification process, this has impacted negatively its image and position. We also notice that Supplier 1 has the lowest sub-score on references (81%) compared to Supplier 2 (90%) and Supplier 3 (90%). This is due to the fact that Supplier 1 is not considered as a preferred vendor with O&G majors who are based worldwide and requiring from any strategic supplier to be present nearby its facilities.

Comparing the overall score for Suppliers 2 and 3 (80% and 85% respectively), we can consider that both suppliers are technically accepted. Suppliers 3 has a competitive advantage related to: support in different languages and a much stronger regional presence compared to Supplier 2.

In the light of this results, the technical choice of Supplier 3 could be made straight forward. On the other hand, Supplier 2 remains a good option, it is present in the region and it offers some additional services related to control room design consultancy. However, before making the final decision, there are other considerations to be taken into account such as the financial offer, the commercial terms and conditions as well as the duration of the project execution. All these factors are part of the decision-making process.

4.6. Gap analysis

On the following paragraph we have produced a Gap analysis (see table 4) to have a wider view and a better understanding of what is required from the supplier and what have been offered by them. Finally, we have suggested some actions to be taken by the supplier to meet the customer's requirement.

Table 4: GAP analysis

	Supplier 1			
	Current	Ideal	Gap	Recommendations
Services offered	The supplier provides a wide range of services covering most of activities carried currently on the terminal storage activity	The offered services should cover the existing services as well as future ones in case of any change on the business model	3%	Supplier should enhance its offer to provide a more robust service related to external pipelines and drumming monitoring
Interfaces capabilities	The supervision system is developed to interface with most common L4/ERP systems and L1 equipment's using common international standards.	The supervision system must interface with all L1 equipment's and sensors without exceptions	10%	It's recommended that during the site survey, provider to collect all relevant data and make sure that all L1 devices will interface with the DCS/SCADA
Tender efficiency and project execution	Suppliers shows low reactivity during the clarification phase. Factory acceptance test is available as well a training material. There is no availably of the project team in the region	The customer's need should be clearly understood. Availability of resources (in region) during the design phase. Factory acceptance testing should be integrated with the existing systems	36%	Supplier to invest on a testing workbench where simulation of the facility conditions and parameters might be tested and verified. Also, it's vital to have resources available (in region) during the design phase, at least temporarily.

After sales and product life cycle	Remote support is cyber-secured and available 24/7 without regional presence and only in English and French. Product lifecycle/updates strategy is well defined	The remote support should be available in region/in country, provided in different languages, available 24/7 and access to be cyber-secured. Software future upgrades and lifecycle strategy should be clearly defined	41%	Supplier to develop regional presence to support customers for troubleshooting. Also, it's important to introduce other languages to break the language barriers
Reputation and references	Supplier and DCS/SCADA systems are certified to international standards. The system has been installed in a limited number of facilities considered as O&G major	The supplier internal organization as well as the DCS/SCADA should be certified to international standard. The proposed system should have been implemented in other similar facilities	11%	Supplier to review the commercial strategy in order to be part of the preferred vendors with O&G majors
Additional services	Supplier provides consultancy services related to alarm management support and control room design	Provide additional services such as alarm management support, control room design consultancy as per ISO 11064 and other services in addition to automation	33%	Supplier to diversify its business model to introduce additional services

	Supplier 2			
	Current	Ideal	Gap	Recommendations
Services offered	The supplier provides a wide range of services covering most of activities carried currently on the terminal storage activity	The offered services should cover the existing services as well as future ones in case of any change on the business model	3%	Supplier should enhance its offer to provide a more robust service related to external pipelines and drumming monitoring
Interfaces capabilities	The supervision system is developed to interface with most common L4/ERP systems and L1 equipment's using common international standards.	The supervision system must interface with ALL L1 equipment's and sensors without exceptions	10%	It's recommended that during the site survey, provider to collect all relevant data and make sure that all L1 devices will interface with the DCS/SCADA
Tender efficiency and project execution	Suppliers shows low reactivity during the clarification phase. factory acceptance test is available as well a training material. The workbench allows an integrated testing with most of the existing equipment. There is no availably of the project team in the region	The customer's need should be clearly understood. Availability of resources (in region) during the design phase. Factory acceptance testing should be integrated with the existing systems	40%	Supplier to review internal process to make sur that tenders are properly followed mainly in term of response time. it's vital to have resources available (in region) during the design phase, at least temporarily
After sales and product life cycle	Remote support is cyber-secured and available 24/7 without regional presence and only in English and French. Product lifecycle/updates strategy is defined	The remote support should be available in region/in country, provided in different languages, available 24/7 and access to be cyber-secured. Software future upgrades and lifecycle strategy should be clearly defined	35%	Supplier to develop regional presence to support customers for troubleshooting. Also, it's important to introduce other languages to break the language barriers
Reputation and references	Supplier and DCS/SCADA systems are certified to international standards. The system has been installed in some facilities considered as O&G major	The supplier internal organization as well as the DCS/SCADA should be certified to international standard. The proposed system should have been implemented in other similar facilities	10%	Supplier to review the commercial strategy in order to be part of the preferred vendors with all O&G majors
Additional services	Supplier provides consultancy services related to alarm management support and control room design as per the required standard	Provide additional services such as alarm management support, control room design consultancy as per ISO 11064 and other services in addition to automation	25%	Supplier to diversify its business model to introduce additional services

	Supplier 3			
	Current	Ideal	Gap	Recommendations

Services offered	The supplier provides a wide range of services covering most of activities carried currently on the terminal storage activity	The offered services should cover the existing services as well as future ones in case of any change on the business model	3%	Supplier should enhance its offer to provide a more robust service related to external pipelines and drumming monitoring
Interfaces capabilities	The supervision system is developed to interface with most common L4/ERP systems and L1 equipment's using common international standards.	The supervision system must interface with ALL L1 equipment's and sensors without exceptions	10%	It's recommended that during the site survey, the supplier has to collect all relevant data and make sure that all L1 devices will interface with the DCS/SCADA
Tender efficiency and project execution	Supplier has clearly understood the customer's requirement. There is a possibility to conduct a factory acceptance test (FAT) and the project team is available in the region	The customer's need should be clearly understood. Availability of resources (in region) during the design phase. Factory acceptance testing should be integrated with the existing systems	22%	Supplier to invest on a testing workbench where simulation of the facility conditions and parameters might be tested and verified.
After sales and product life cycle	Remote support in different languages is cyber-secured and available 24/7 with regional presence. however, the size of the support organization is relatively small. Product lifecycle/updates strategy is defined	The remote support should be available in region/in country, provided in different languages, available 24/7 and access to be cyber-secured. Software future upgrades and lifecycle strategy should be clearly defined	17%	Supplier to invest on developing the local support organization
Reputation and references additional services	Supplier and DCS/SCADA systems are certified to most of international standards. The system has been installed in many facilities considered as O&G major	The supplier internal organization as well as the DCS/SCADA should be certified to international standard. The proposed system should have been implemented in other similar facilities	10%	Supplier to review its process in order to comply with all required international standards
Additional services	Supplier provides consultancy services related to alarm management only	Provide additional services such as alarm management support, control room design consultancy as per ISO 11064 and other services in addition to automation	25%	Supplier to diversify its business model to introduce additional services

5. Recommendations

The decision-making framework presented in this paper is a result of a work of a group of experts for a specific location. It is recommended that this tool is tested, reviewed and used by other terminals with different configurations and constraints in order to verify the consistency of the results and the relevance of the key criteria. It is also recommended to follow up the implementation of the supervision system project in order to confirm the adequacy of the retained supplier to do the required job and to meet the terminal expectations and needs. Moreover, during the project execution, there might be new challenges and new inputs not captured on the early stages of the project and have to be considered as a key criterion on the next iteration.

6. Conclusion

A liquid petroleum storage facility plays a strategic role in the value chain of the petroleum industry. The market is becoming very competitive and terminals are seeking ways to improve their efficiency and productivity in order to meet customers' expectations. Storage facility operators need to streamline their business processes in order to stay competitive and profitable. To answer these challenges, terminal operators need to introduce some automation by investing in a supervision system instead of managing the facility manually. Many supervision solutions provide monitoring, control and management of the entire product handling process, starting from reception to storage to distribution. Due to the high cost of the introducing automation into a facility, it is vital to have a robust system in place to clearly identify the best offer to retain. There is a balance between the cost and the provided options that should be maintained, hence the importance of clearly defining what are the most important options to keep and the less important ones to reject. In this paper, we have introduced a tool that can be gradually introduced and tested in different terminals and similar projects. The methodology can also be adopted for a non-automation project. From the vendor perspective, this work represents a valuable feedback from a real case study where professionals from the oil&gas sector have highlighted what they expect from a supervision system, this might be an inspiration for them to build strong commercial and technical approach to address their current gaps.

Conflict of Interest

The authors declare no conflict of interest.

References

[1] L. J. Fernandes, S. Relvas, and A. P. Barbosa-Póvoa, "Strategic network design of downstream petroleum supply chains: Single versus multi-entity participation" Chem. Eng. Res. Des., **91**(8), 1557–1587, 2013, https://doi: 10.1016/j.cherd.2013.05.028.

[2] M. Z. Ming, N.S. Shah, "Petroleum terminal's operation processes on vessel turnaround," EASTS-International Symposium on Sustainable Transportation incorporating Malaysian Universities Transport Research Forum Conference, Malaysia, 2008.

[3] International Energy Agency (IEA), "Oil information: Overview" France, 2020. [Online]. Available: www.iea.org.

[4] S. Traver, "Current Refining Capacity and Future Storage Requirements in Singapore" Asia Bulk Liq. Storage Transp. Termin. Conf. Singapore, 2007.
[5] J. van den Berge, "The hottest terminal locations of 2020," Insights Global, 2020. https://www.insights-global.com/the-hottest-terminal-locations-of-2020/ (accessed Jul. 10, 2020).
[6] T. Plessas, D. Chroni, A. Papanikolaou, and N. Adamopoulos, "Simulation and optimisation of cargo handling operations of AFRAMAX tankers" Proc IMechE Part M J. Eng. Marit. Environ., 2015, https://doi: 10.1177/1475090215589643.
[7] P. Davidson, "The importance of Bulk Liquid Storage" Chemical Industry Journal., 2020.
[8] K. Al-Qahtani and A. Elkamel, "Multisite facility network integration design and coordination: An application to the refining industry" Comput. Chem. Eng., **32**(10), 2189-2202, 2008, https://doi:10.1016/j.compchemeng.2007.10.017.
[9] A. Nooraii and J. A. Romagnoli, "Implementation of advanced operational and control techniques for a pilot distillation column within a des environment" Comput. Chem. Eng., **22** (4), 695–708, 1998, https://doi: 10.1016/s0098-1354(97)00228-7.
[10] M. Karacor and E. Ozdemir, "New technological developments and selection criteria of industrial SCADA applications" IFAC Proc. Vol., **36**(7), 181–185, 2003, https://doi: 10.1016/S1474-6670(17)35828-7.
[11] American Petroleum Institute (API), "Welded Tanks for oil Storage. API Stand. 650" American Petroleum Institute, 2013.
[12] A. García-Berrocal, C. Montalvo, P. Carmona, and J. Blázquez, "The Coriolis mass flow meter as a volume meter for the custody transfer in liquid hydrocarbons logistics" ISA Trans., **90**, 311–318, 2019, https://doi: 10.1016/j.isatra.2019.01.007.
[13] A. L. Henry Persson, "Tank Fires-Review of fire incidents 1951-2003" BRANDFORSK Project 513-021 report, Swedish National Testing and Research Institute, 2004.
[14] National Fire Protection Association (NFPA), "NFPA 24: Standard for the Installation of Private Fire Service Mains and their Appurtenances" National Fire Protection Association, 2012.
[15] A. A. Bakar, H. Hashim, and M. Z. Ahmad, "Implementation of SCADA System for DC Motor Control" 2010 Int. Conf. Comput. Commun. Eng. (ICCCE 2010), Malaysi, 2010, https://doi: 978-1-4244-6235-3/10/.
[16] A. Rezai, P. Keshavarzi, and Z. Moravej, "Key management issue in SCADA networks: A review" Eng. Sci. Technol. an Int. J., **20**(1), 354–363, 2017, https:/doi: 10.1016/j.jestch.2016.08.011.
[17] K. Stouffer, J. Falco, and K. Scarfone, "Guide to Industrial Control Systems (ICS) Security Recommendations of the National Institute of Standards and Technology" NIST Spec. Publ., **800**(82), 16–16, 2007, https://doi: http://dx.doi.org/10.6028/NIST.SP.800-82r1.
[18] I. Morsi and L. M. El-Din, "SCADA system for oil refinery control" Meas. J. Int. Meas. Confe., **47**(1), 5–13, 2014, https::/doi: 10.1016/j.measurement.2013.08.032.
[19] Frost & Sullivan, "Analysis of the Distributed Control Systems (DCS) Market in India," Frost & Sullivan, 2013.
[20] A. Dike, I. U., Adoghe, A. U., Abdulkareem, "Impact of ICT in Oil and Gas Exploration: A Case Study" Int. J. Comput. Technol., **10**(7), 1831–1835, 2013.
[21] R. S. Bhullar, "Strategies for implementing advanced process controls in a distributed control system (DCS)" ISA Trans., **32**(2), 147–156, 1993, https://doi: 10.1016/0019-0578(93)90037-W.
[22] Y. N. Shebeko et al., "Fire and explosion risk assessment for large-scale oil export terminal" J. Loss Prev. Process Ind., **20**(4–6), 651–658, 2007, https://doi: 10.1016/j.jlp.2007.04.008.
[23] R. K. Sharma, B. R. Gurjar, A. V. Singhal, S. R. Wate, S. P. Ghuge, and R. Agrawal, "Automation of emergency response for petroleum oil storage terminals" Saf. Sci., **72**, 262–273, 2015, https://doi: 10.1016/j.ssci.2014.09.019.
[24] J. I. Chang and C. C. Lin, "A study of storage tank accidents" J. Loss Prev. Process Ind., **19**(1), 51–59, 2006, https://doi: 10.1016/j.jlp.2005.05.015.

ASTES

Advances in Science, Technology and Engineering Systems Journal Vol. 5, No. 5, 39-46 (2020)

www.astesj.com

ASTESJ

ISSN: 2415-6698

The Relation of Compression Strength with Modulus of Rupture and UPV of Concrete Containing M-sand as Fine Aggregate

Altamashuddinkhan Nadimalla[1,*], Siti Aliyyah Masjuki[1], Siti Asmahani Saad[1], Maisarah Ali[1], Shuhairy Norhisham[2]

[1]*Department of Civil Engineering, Kulliyyah of Engineering, International Islamic University Malaysia, Gombak, 53100, Malaysia*

[2]*Department of Civil Engineering, College of Engineering, Universiti Tenaga Nasional, Kajang, 43000, Malaysia*

ARTICLE INFO

Article history:
Received: 23 June, 2020
Accepted: 11 August, 2020
Online: 08 September, 2020

Keywords:
Compression strength
Manufactured Sand (M-sand)
Modulus of rupture
Ultrasonic Pulse Velocity (UPV)

ABSTRACT

The impact of Manufacture sand on UPV, compression strength and modulus of rupture has been experimentally investigated and discussed in this paper. Concrete grade 30 (30Mpa) were produced with different percentage of M sand substitution ranging from 25%, 50%, 75% and 100% by volume were selected as concrete mix design in this project. The strength for different percentage of M-sand incorporation was measured by the destructive test which are compression strength test and modulus of rupture test and non-destructive test which is UPV test for curing ages of 90, 28 and 7 days. Furthermore, the highest compression strength of concrete and modulus of rupture was found on the 90th day containing a proportion of 75% of M-sand as a substitution for natural fine aggregate. A novel empirical equations 1 & 4 are proposed for the relation of compression strength with the modulus of rupture and UPV.

1. Introduction

The construction industry is currently facing a serious problem regarding the shortage of construction material due to the rapid depletion of the sources. The excessive mining activities of natural sand has tremendously dropped the production rate of fine aggregate for concrete production and led to severe depletion of the river beds. The scarcity of the natural sand is already at an alarming rate. Besides, the shortage has resulted in a non-tolerable increase in its price ultimately effecting the construction cost. Since natural sand is non-renewable aggregate resources, a countermeasure needs to be executed. In order to safeguard the enduring availability of construction raw material supplies, the industry needs to start shifting towards sustainable construction materials throughout the concept of recycling. Therefore, the use of recycled aggregates is seen to be the safest choice to replace the consumption of natural aggregate in concrete manufacture [1].

The natural sand that is usually used as fine aggregates in concrete is excavated from river beds. It contains a lot of organic materials such as sulphate, chlorides and silt which can affect the concrete strength and its durability. To protect our river due to high demand of natural sand, there is an alternative of natural sand as fine aggregates in concrete which is Manufactured Sand. M Sand is made from the powder of hard granite rocks. Basically, M Sand are finely graded, have greater durability and their particles are in cubical shape. By using M Sand as fine aggregates in a concrete mixture, the concrete is eco-friendly, have high workability and high durability which lead to the reduction of bleeding, voids and segregation in concrete. Thus, we can use M Sand as partial substitute of fine aggregates in concrete and at the same time protect our river resources from destruction [2].

The article [3] studies the effect of long term concrete compression strength incorporated with M-sand. Nine mix proportion of manufactured sand concrete is developed and tested by using different proportion of manufactured sand combined with 5, 9, and 13 percentage of stone powder. Based on the result obtained, the strength grew tremendously within 3-28 days and grew moderately after 28 days. It is due to the rapid hydration process in the early curing age. After 28 days, the progress rate of compression strength was the same along with different grades of concrete. The studies also showed that the compression strength of manufactured sand concrete obtained is almost similar to the conventional concrete.

The article [4] asserts the particle shape, powder content and gradation of manufactured sand tend to influence the performance of the concrete. The concrete was manufactured with different particle shape (MSA-Diorite, MSC-Altered diorite, MSB-

*Corresponding Author: Altamashuddinkhan Nadimalla, Email: altamashk1987@gmail.com

Metasandstone, MSH-Limestone) and different amount of powder content (0%, 5%, 7.5%, 10% and 12.5%). The specimen is tested to study the difference in performance between reference sand and manufactured sand concrete. It was found that the compression strength of manufactured sand concrete without powder content is lower than the compression strength of concrete with reference sand. However, as the amount of stone powder increase, the compression strength of M-sand concrete also increases. The increment is slightly higher than the concrete with reference sand.

According to the different studies the effects on the compression strength of concrete by substituting the river sand by weight in the concrete with 0 to 100 per cent of manufactured sand. Overall, their results revealed that with the raise of M-sand as a substitution in place of river sand, the compression strength of concrete rises. It has been explained that tremendous bonding between fine and coarse aggregates is the main reason for the compression strength increment of concrete with M-sand [5,6],[7].

Concrete mix with replacement level of 0%, 25% and 100% manufacture sand and tested at the age of 28-days and the maximum modulus of rupture obtained is when the sand is 100% replaced by the M-sand. It was found that the modulus of rupture increase as the compression strength of the concrete increase [7].

The article [8] claimed that the optimal percentage of M sand replacement is only 50%. Based on the experiment, concrete is manufactured with different percentage of M sand (0%, 25%, 50% and 75%). The obtained results reveal that the modulus of rupture of concrete incorporate with M sand is more than the modulus of rupture of conventional concrete. However, the highest increment of modulus of rupture is obtained only up to 50% of replacement. When it goes beyond 50%, the strength is considerably reduced.

The article [9] studies the effect of five different percentage of fine aggregate replacement (0%, 20%, 40%, 60%, 80% and 100%) on the hard properties of the concrete. Type of manufactured sand used is Granite Quarry Dust (GQD). Based on the result obtained, it was found that the UPV of concrete with GQD for all level of replacement is relatively lower in comparison with the reference mix at the initial period of (1 day and 7 days). However, at the period of 28 days, the UPV for all level of replacement shows better performance than the reference mix. This significant increment is due to the slower rate of hydration reaction producing less compact microstructure. Besides, the concrete with GQD within 60%, 80% and 100% shows a better result than those with 0%, 20% and 40%. Thus, as the percentage of fine aggregate replacement with GQD increase, the UPV also increase. It is determined that the presence of GQD improves the performance of the concrete.

The article [7] studies the relation between modulus of rupture and compression strength for concrete with 100%, 25% and 0% fine aggregate replaced by M sand tested at 28 days. The empirical equations were obtained by using power regression analysis in the form of ($y= ax^b$, where a and b are constants, y is modulus of rupture and x is compression strength) for concrete with 100%, 25%, and 0% of fine aggregate replaced by M sand. The equations were evaluated with the equations suggested by IS, ACI, and BS codes of practice for determining the modulus of rupture with the help of the compression strength of concrete. It is found that the equations suggested by the IS, ACI, and BS codes of practice are not reliable to estimate the modulus of rupture of concrete made with manufactured sand.

The article [10] proposed the equation using exponential power regression analysis ($Fc=1.526e^{0.761Vp}$, $R^2=0.8569$) to predict the compression strength of roller-compacted concrete for different curing periods (3,7,28 and 90 days). The UPV and compression strength tests conducted on three types of concrete mixtures (type-1 100% natural sand), (type- 2 100% M sand) and (type-3 50% M sand and 50% natural sand) used in place of natural sand in roller compacted concrete. In each series 0 to 60% of fly ash used as a admixture. Based on the result, it is found that type 3 mixtures yield higher compression strength and UPV. it is also found that UPV increases with the increase in curing ages for all type of concrete mixtures. The UPV of type 2 mixtures is slightly lower compared to UPV of type 1 mixtures. It is due to the harsh mixes which demand more w/c ratio than reference concrete with natural sand as fine aggregate.

Based on studies from the past researchers, it can be presumed that the proper blend of river sand and M sand incorporation in concrete plays an important role in achieving desired concrete strength.

The purpose of this experiment to ascertain the strength of M-Sand incorporated concrete through destructive test analysis namely compression strength and modulus of rupture and non-destructive test analysis UPV. And also, to analyse the relation of compression strength with a modulus of rupture and UPV.

2. Materials Selection and Preparation

In this research, materials are selected in accordance to the specifications to meet the objectives of the project and comply with the appropriate standard. Furthermore, it is to be noted that the grade of all concrete samples designed is G30 (30MPa) according to the Department of Environment (DOE) method.

2.1. Cement

The Ordinary Portland Cement (OPC) 42.5N is used in this project for the production of the concrete samples is which conforms to the Malaysian Standard MS EN 197-1 CEM I.

2.2. Water

Water is an important component that helps to bind the aggregates together. The water must clean and free from harmful chemical, foreign materials and wastages. According to BS EN 1008:2002, the water used is potable water where the water is clean enough without the need to be tested and considered suitable for concrete use.

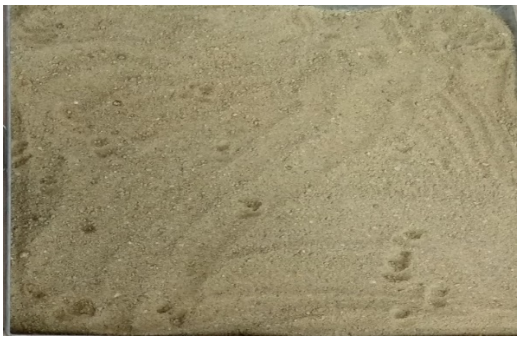


Figure 1: River Sand

2.3. Fine aggregates

Fine aggregates M sand and river sand were used is less than 5mm as specified in BS EN 933-1:2012. Fine aggregates are shown in figure 1 and 2. M Sand is collected from Kajang Rocks Quarry Sdn. Bhd.

2.4. Coarse aggregate

The type of course aggregate that is used to design the concrete mix in this study is crushed aggregate which mainly retained at 5mm sieve and with a maximum size of 20mm as specified in accordance to BS EN 933-1:2012 shown in figure 3.



Figure 2: Manufactured Sand



Figure 3: Gravels

2.5. Mix Design Proportion

Before conducting the concrete mixing, the calculation of the mix is done to obtain the exact weight of the concrete materials in accordance to Department of Environmental Method (DOE) as shown in table 1.

The mixes are designed with 0% replacement which is the conventional concrete production with 100% use of natural sand, increased gradually to 25%, 50%, 75% and 100% of M-sand substitute for fine aggregates in concrete production as tabulated in table 2.

2.6. Concrete mixing

In this research, a concrete mixer machine (figure 4) is used to attain the uniformity in a concrete mix. For the preparation of the concrete, the concrete mixers were cleaned before mixing the concrete. Coarse aggregates, fine aggregates, and cement were placed in the mixers for dry mix. Materials were mixed in a dry state for 3 mins. After dry materials mixed properly required volume of water added to the mixture and it is mixed for 2 mins. After unloading the mixture, it is mixed manually to obtained uniformity in the concrete mix.

The freshly mixed concrete poured into the moulds with the size of 150x150x150 (cubes) and 100mm x 100mm x 500mm (beams) size. The poker vibrator was used to eliminate all the air void in the specimens.

2.7. Curing Method

Curing is one of the important process during concrete hardening. The specimens are kept for 24 hours before the specimens undergo curing process. This curing method is according to BS 1881-113:2011. Type of curing used in this research is water curing method. The concrete samples were deposited in a water tank for 7, 28 and 90 days as demonstrated in figure 7.



Figure 4: Concrete mixing by using concrete mixture machine



Figure 5: Concrete mixing by hand mix

Table 1: Concrete Mix Design

Materials	Weight (kg/m^3)
Water	180
Cement	367
Coarse aggregates	1302
Fine aggregates	531

Table 2: Mix design fine aggregates percentage replacement with manufactured sand

Materials	Conventional Concrete	Manufactured Sand Concrete			
		1	2	3	4
Manufactured Sand	0%	25%	50%	75%	100%
River Sand	100%	75%	50%	25%	0%



Figure 6: Concrete cubes and beams kept for 24 hours before curing

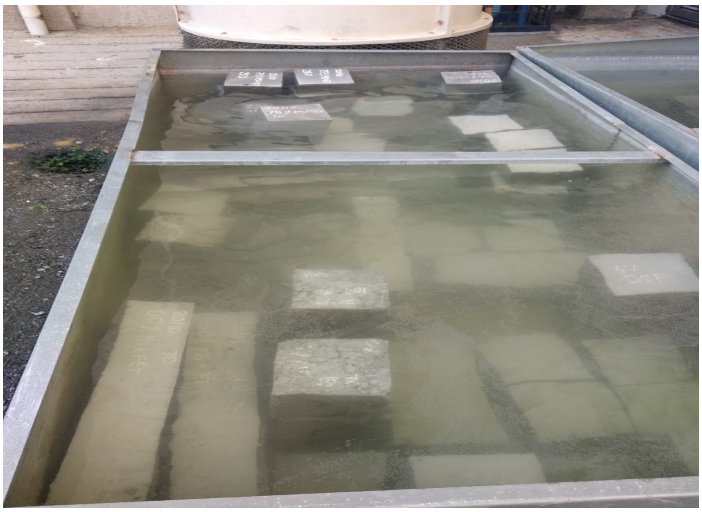


Figure 7: Water curing tank

3. Tests on Hardened Concrete

3.1. Compression strength Test

The test for the compression strength of the hardened concrete that was carried out on all the cube samples of size 150mm x 150mm x150mm in order to measure the development of the strength of each sample of the concrete. The test is conducted as per BS EN 12390-3. For each curing days mentioned, three concrete cubes were tested for all mixtures to obtain the average of compression strength. The readings are taken at 7,28, and 90 days by using a Digital Compression Testing Machine (figure 8). The result of the test shows the maximum load of the concrete can sustain before it fails and the concrete strength after curing days.

3.2. Modulus of rupture Test

This test is performed to investigate the capability of the unreinforced concrete beam to survive the failure in bending. The test is conducted as per BS EN 12390-5. For each curing days mentioned, three beams of size 100mm x 100mm x 500 mm were tested to obtain the average of Modulus of rupture. The readings are taken at 7,28, and 90 days by using a Digital modulus of rupture Testing Machine (figure 9).



Figure 8: Compression test machine



Figure 9: Flexural Testing Machine (Modulus of rupture Test)

3.3. UPV test

In order to investigate the structure and the quality of the concrete containing M-sand as fine aggregate, UPV test was performed on specimen size 150 x 150 x150 mm as per the BS EN 12504-4. 10 Hz pulse is applied to the cube specimen, the wave passed from one side to the other side are recorded as the time taken for the pulse to get through the structure and the result attained are recorded as shown in table 11.



Figure 10: UPV test

Table 3: Quality of concrete as per the UPV test [9] [11].

Velocity (Km/s)	≥4.5	3.5-4.5	3.0-3.5	2.0-2.3	≤2
Concrete quality	Excellent	Generally good	questionable	Generally poor	Very poor

4. Results and Discussion

4.1. Compression strength Test

The test for the compression strength of all the samples has been conducted at 7, 28 and 90 days after curing in a water tank. The proportions of different types of fine aggregate and results obtained are tabulated in tables 4,5, and 6 Furthermore, the bar graph figure 12 represents the results of the compression strength obtained on the 90th, 28th, and 7th day for all the concrete mixes. From the tables (4, 5 & 6) and bar graph, it is observer that the highest compression strength obtained is for concrete containing 75% replacement of M sand as fine aggregates, where the compression strength are 51.35 MPa, 44.63MPa and 36.27 for 90,28, and 7 days respectively. And it is also, observes that up to 75% replacement of M-sand in place of river sand compression strength increases gradually with curing ages. It decreases drastically for 100% replacement of M-sand in place of river sand. The lowest concrete strength produce is for 100% replacement of fine aggregates with M-sand where the strength are 17.38 MPa, 33.03Mpa, and 23,68 Mpa for 90, 28 and 7 curing days. 100% replacement of M-sand sand in place of river sand is not applicable for the concrete production since it produces low concrete strength due to its physical properties. Excessive use of M-sand produces poorly graded of aggregates distribution in the concrete mix and increase the surface area of the particles. It leads to decrease in compression strength of concrete. This can be concluded that the optimum value for the natural sand replacement in concrete production is by using 75% of manufactured sand of natural sand. This result is proven for 7,28, and 90 curing days. It is due to the tremendous bonding between fine and coarse aggregates is the main reason for the compression strength increment of concrete with M-sand [7].

Table 4: Compressive test results for 7 days curing

% of M-Sand	7days			Average cube strength in MPa
	Cube strength in MPa			
	specimen 1	specimen 2	specimen 3	
0	31.23	29.39	29.56	30.06
25	32.92	31.42	29.33	31.22
50	23.56	33.42	38.5	31.83
75	38.08	35.77	34.97	36.27
100	30.39	15.8	24.85	23.68

Table 5: Compressive test results for 28 days curing

% of M-Sand	28 days			Average cube strength in MPa
	Cube strength in MPa			
	specimen 1	specimen 2	specimen 3	
0	32.74	32.86	35.53	33.71
25	40.49	40.22	40.99	40.57
50	42.24	41.09	42.2	41.84
75	43.14	46.71	44.03	44.63
100	32.48	37.99	28.62	33.03

Table 6: Compressive test results for 90 days curing

% of M-Sand	90 days			Average cube strength in MPa
	Cube strength in MPa			
	specimen 1	specimen 2	specimen 3	
0	36.07	34.44	35.31	35.27
25	44.49	42.79	42.91	43.40
50	46.87	45.39	47.87	46.71
75	49.80	52.33	51.92	51.35
100	17.63	17.53	16.97	17.38

4.2. Modulus of rupture Test

The test for the modulus of rupture of all the samples has been conducted at 7, 28 and 90 days after curing in a water tank. The proportions of different types of fine aggregate and results obtained are tabulated in tables 7,8 and 9. Furthermore, the bar graph figure 14 represents the results of the modulus of rupture obtained on the 90th, 28th, and 7th day day for all the concrete mixes.

From the bar graph and tables (7,8 & 9) it is observed that the higher modulus of rupture obtained is for concrete 75% replacement of M sand as fine aggregates where the modulus of rupture are 2.83 Mpa, 2.79 MPa and 2.31 Mpa for 90,28, and 7 days respectively. However, for 90 and 28 days of curing modulus of rupture of conventional concrete is higher i.e 2.76 MPa and 2.49 MPa as compared to concrete with 25% and 50% M sand as fine aggregate replacement. The concrete with 100% of manufactured sand as fine aggregate, enhance the modulus of rupture of the concrete with reference to conventional concrete after 90 days of curing. It can be presumed that up to 100% replacement of M sand in place of river sand enhance the modulus of rupture of concrete [7] .

Modulus of rupture is about 10 to 15 per cent of compression strength depending on the size, volume, and types of aggregate used in concrete. Modulus of rupture can be improved by adding mineral admixtures, fibers and superplasticizer using M sand as fine aggregate [8].



Figure 11: Compression strength test

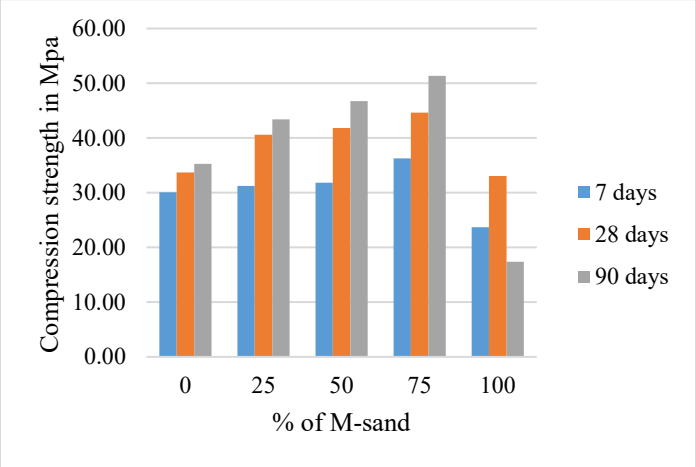


Figure 12: Variation of compression strength at 7,28 and 90 days

4.3. Correlation between modulus of rupture and compression strength

The empirical equation 1 is attained by using MS excel with help the experimental data of compression strength and modulus of rupture of concrete for 28 days of curing. A polynomial relation is attained with a correlation coefficient of 0.7431 between compressive and modulus of rupture.

- $yf = 0.0097x_c^{\,2} - 0.7183x_c + 15.544$

$$R^2 = 0.7431 \quad (1)$$

. The predicted modulus of rupture of concrete is determined using equation 1,2 and 3 with the help of compression strength results obtained from the 28 days of curing. Yusuf, Jimoh, & Salami [12] reported that the equation 2 and 3 equation suggested by the Indian Standard code and Eurocode Code to determine the modulus of rupture of concrete for 28 days of curing.

- $yf = 0.7x_c^{0.5}$ (2)
- $yf = 0.3\ x_c^{\,0.67}$ (3)

where yf is modulus of rupture in MPa and x_c is compression strength in MPa

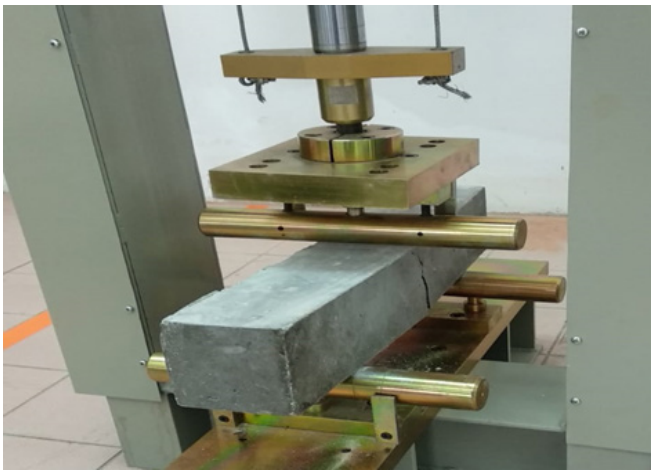


Figure 13: Modulus of rupture test

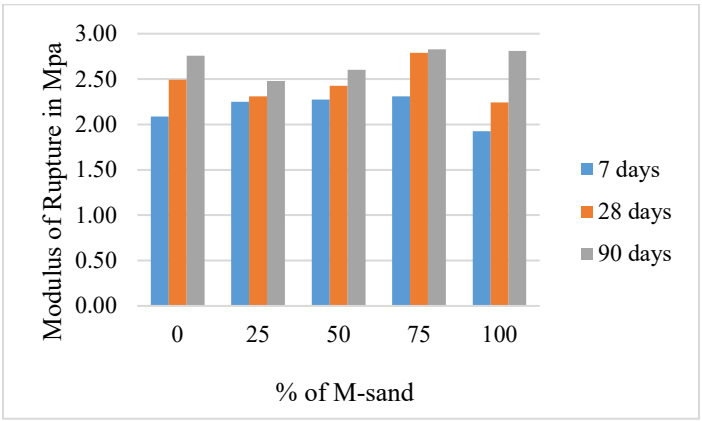


Figure 14: Variation of modulus of rupture at 7,28 and 90 days

From table 10 and figure 15 it is noticed that, the predicted values of modulus of rupture determined using equation 1 is very close to the experimental values of modulus of rupture. The predicated modulus of rupture determined using equation 2 & 3 is very high as compared to equation 1 values. It can be concluded that equation 2 and 3 suggested by IS and EC code is not suitable to evaluate the modulus of rupture of concrete made with M sand.

4.4. UPV test

The UPV test was performed on specimen size 150 x 150 x150 mm according to the BS EN 12504-4 as shown in figure 10. For curing days mentioned, three concrete cubes were tested for all the mixtures to obtain the average of UPV as shown in table 11. From table 11, it is found that UPV is ranging from 3.65 to 4.19 km/s. As per table 3, M-sand and conventional concrete come under good quality concrete.

Table 7: Modulus of rupture test results for 7 days curing

% of M-Sand	7days			Average Modulus of rupture in MPa
	Beam strength in MPa			
	specimen 1	specimen 2	specimen 3	
0	2.34	1.89	2.03	2.09

25	2.39	2.28	2.08	2.25
50	2.31	2.09	2.42	2.27
75	2.23	2.36	2.34	2.31
100	1.96	1.91	1.9	1.92

Table 8: Modulus of rupture test results for 28 days curing

% of M-Sand	28 days			Average Modulus of rupture in MPa
	Beam strength in MPa			
	specimen 1	specimen 2	specimen 3	
0	2.61	2.43	2.44	2.49
25	2.3	2.32	2.31	2.31
50	2.47	2.46	2.35	2.43
75	2.81	2.76	2.8	2.79
100	2.63	2.36	1.74	2.24

Table 9: Modulus of rupture test results for 90 days curing

% of M-Sand	90 days			Average Modulus of rupture in MPa
	Beam strength in MPa			
	specimen 1	specimen 2	specimen 3	
0	2.93	2.432	2.91	2.76
25	2.42	2.47	2.55	2.48
50	2.53	2.66	2.62	2.60
75	2.87	2.79	2.82	2.83
100	2.85	2.76	2.82	2.81

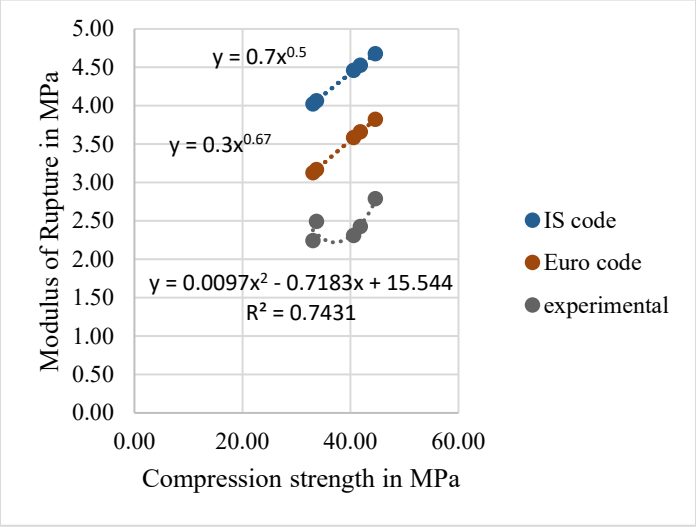


Figure 15: Correlation between modulus of rupture and compression strength for 28 days of curing

4.5. Correlation between compression strength and UPV

The correlation between the UPV and compression strength of the concrete shown in figure 16. It is observed that as the compression strength of concrete increases UPV values also increases as shown in figure 16. Equation 4 is obtained by using MS excel with the help of experimental data of compression strength and UPV of concrete for 28 days of curing. A polynomial relation is attained with a correlation coefficient of 0.8081between compressive and UPV.

- $y_c = 99.001x_v^2 - 686.44x_v + 1219.8$

$$R^2 = 0.8081 \quad (4)$$

where y_c is compression strength in MPa and x_v is UPV in km/s.

Table 10: Evaluation of Modulus of rupture (Experimental and Theoretical)

% M-sand 28 days	Experimental		Predicted Modulus of rupture Mpa		
	Compression strength x Mpa	Modulus of rupture y Mpa	eq 1	eq 2	eq 3
0	33.71	2.49	2.35	4.06	3.17
25	40.57	2.31	2.37	4.46	3.59
50	41.84	2.43	2.47	4.53	3.66
75	44.63	2.79	2.81	4.68	3.82
100	33.03	2.24	2.40	4.02	3.12

Table 11: UPV test results

% of M-Sand	UPV km/s		
	7days	28days	90 days
0	3.65	3.73	3.76
25	3.75	3.74	3.88
50	3.99	3.82	4.16
75	4.1	3.85	4.19
100	3.65	3.64	3.78

5. Conclusion

The replacement of the M-sand in place of river sand in concrete production is a good approach to improve the strength of concrete. From this research, it is determined that the percentage replacement of 75% M Sand as fine aggregates contribute to the best mix design to obtain high durable concrete.

75% replacement of the M-sand in place of river sand exhibit the best compression strength, UPV, and modulus of rupture as compared to other percentages. It is due to the attribute of its physical properties which is rough in surface and angular in shaped exhibit internal friction to produce a good interlocking bond between the particles within the concrete. Even though M Sand can act as fine aggregates in concrete mixtures but fine aggregates cannot be fully replaced with M-sand. Fully replacement of M sand in place of river sand in concrete drastically reduce the compression strength of concrete. However, 100% incorporation of M sand improves the modulus of rupture in concrete.

A novel empirical equations 1 & 4 proposed. Which shows the relationship of compression strength with a modulus of rupture and compression strength with UPV for the concrete containing M-sand as fine aggregate.

According to research conducted and literature review, it is possible to replace the fine aggregate in concrete production by using M-sand. However, a different percentage of the natural sand replacement shows the increasing and decreasing of the concrete strength. Full replacement of the M Sand as fine aggregates in concrete mixing causing the lower performance of the concrete. This concludes that the river sand is still in need of concrete to maintain the eminence of the concrete. Thus, the substitution of M sand in concrete can only as partial substitute of fine aggregates. The natural sand cannot be fully replaced by other material such as M Sand.

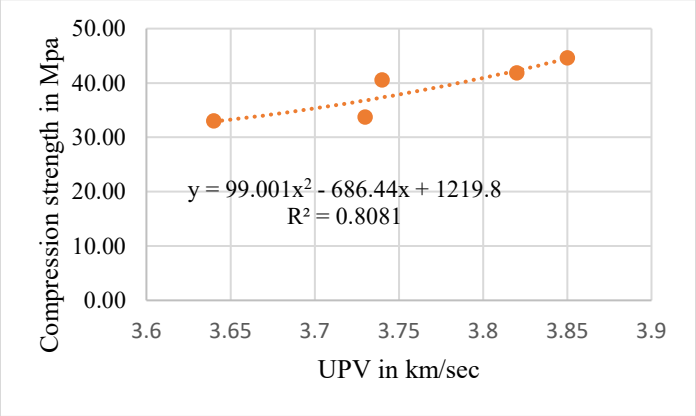


Figure 16: Correlation between UPV and compression strength of concrete for 28 days of curing

Acknowledgment

This research received the financial support from the Ministry of Education, Malaysia (Ref: RACER/1/2019/TK06/UIAM//1).

References

[1] S. Ismail, K.W. Hoe, M. Ramli, "Sustainable Aggregates: The potential and challenge for natural resources conservation," Procedia - Social and Behavioral Sciences, **101**, 100–109, 2013, doi:10.1016/j.sbspro.2013.07.183.

[2] K. V. Sabarish, P. Paul, M. Mohammed Aslam Khan, S. Gowtham, R. Hariharan, "Utilization of M-sand as a partial replacement for fine aggregate in concrete elements," International Journal of Civil Engineering and Technology, **9**(10), 422–426, 2018.

[3] X. Ding, C. Li, Y. Xu, F. Li, S. Zhao, "Experimental study on long-term compressive strength of concrete with manufactured sand," Construction and Building Materials, **108**, 67–73, 2016, doi:10.1016/j.conbuildmat.2016.01.028.

[4] W. Shen, Y. Liu, Z. Wang, L. Cao, D. Wu, Y. Wang, X. Ji, "Influence of manufactured sand's characteristics on its concrete performance," Construction and Building Materials, **172**(May), 574–583, 2018, doi:10.1016/j.conbuildmat.2018.03.139.

[5] P.A. Jadhav, D.K. Kulkarni, "Effect of replacement of natural sand by manufactured sand on the properties of cement mortar," International Journal of Civil and Structural Engineering Volume, **3**(3), 621–628, 2013, doi:10.6088/ijcser.2.

[6] S.L. Chauhan, R.A. Bondre, "Partial replacement of sand by quarry dust in Concrete," International Journal of Scientific and Research Publications, 5(7), 2250–3153, 2014, doi:10.13140/2.1.2742.0804.

[7] B.K. Meisuh, C.K. Kankam, T.K. Buabin, "Effect of quarry rock dust on the flexural strength of concrete," Case Studies in Construction Materials, **8**(July 2017), 16–22, 2018, doi:10.1016/j.cscm.2017.12.002.

[8] T.F. Kala, P. Asha, S. Elavenil, "Properties of concrete using manufactured sand as fine aggregate," International Journal of ChemTech Research, **11**(03), 94–100, 2018, doi:10.20902/ijctr.2018.110337.

[9] C.B. Cheah, J.S. Lim, M.B. Ramli, "The mechanical strength and durability properties of ternary blended cementitious composites containing granite quarry dust (GQD) as natural sand replacement," Construction and Building Materials, **197**, 291–306, 2019, doi:10.1016/j.conbuildmat.2018.11.194.

[10] S.K. Rao, P. Sravana, T.C. Rao, "Experimental studies in ultrasonic pulse velocity of roller compacted concrete pavement containing fly ash and M-sand," International Journal of Pavement Research and Technology, **9**(4), 289–301, 2016, doi:10.1016/j.ijprt.2016.08.003.

[11] S. Akçaözoğlu, K. Akçaözoğlu, C.D. Atiş, "Thermal conductivity, compressive strength and ultrasonic wave velocity of cementitious composite containing waste PET lightweight aggregate (WPLA)," Composites Part B: Engineering, **45**(1), 721–726, 2013, doi:10.1016/j.compositesb.2012.09.012.

[12] I.T. Yusuf, Y.A. Jimoh, W.A. Salami, "An appropriate relationship between flexural strength and compressive strength of palm kernel shell concrete," Alexandria Engineering Journal, **55**(2), 1553–1562, 2016, doi:10.1016/j.aej.2016.04.008.

ASTES

Advances in Science, Technology and Engineering Systems Journal Vol. 5, No. 5, 47-53 (2020)

www.astesj.com

ASTESJ

ISSN: 2415-6698

A Smart Updater IT Governance Platform Based on Artificial Intelligence

Aziza Chakir[1,*], Meriyem Chergui[2], Johanes Fernandes Andry[3]

[1]*Faculty of Law Economics and Social Sciences, Economic Department, Hassan II University, Casablanca, 8110, Morocco*

[2]*Higher National School of Electricity and Mechanics, IT Department, Hassan II University, Casablanca, 8110, Morocco*

[3]*Faculty of Technology and Design, IT Department, Bunda Mulia University, Jakarta, 15143, Indonesia*

ARTICLE INFO

Article history:
Received: 16 June, 2020
Accepted: 19 August, 2020
Online: 08 September, 2020

Keywords:
IT best practices
Information system governance
IT-GRC
Artificial knowledge
ITIL
COBIT
Governance

ABSTRACT

This Information technology (IT) has a crucial role to improve business processes in companies. Getting the best technologies rapidly becomes as significant as understanding and developing the business plan of organizations. Thus, different IT best practices and norms are used by companies to help their services and IT business.

These standards are set of best practices based on the experience and knowledge of numerous organizations; each of them focuses on specific governance issues such as ISO 27001 and ISO 27002 for IT security management, PMBOK and PRINCE2 for project management, ITIL for IT service management and COBIT for overall governance of an organization.

As part of a collective research project that focuses on the IT governance axis, we have developed a smart global IT-GRC platform that allows to IT manager to design his own repository, considering the powers of each best practice, the organization's context and the IT strategic needs expressed by their stakeholders.

To ensure the durability and the continuity of this project, we must consider the evolution of the IT GRC market, the problem posed is how to integrate recent versions of IT GRC frameworks, and how to ensure a periodic update of the knowledge base of the global IT-GRC solution. It is the subject of this paper and the second part of an IT-GRC research project.

1. Introduction

The improving of the strategic sight of an organization is a major requirement of the Information Systems Department, that contributes to the organization's performance. The good functioning of an organization's information system, its evolution, and its effective improvement in its services' quality; is contemplated by the assortment and decent variety of IT best practice. Since the fundamental actors of an organization use set of IT directives which can be COBIT for the General Management [1], ITIL for the Information Systems bearing [2] and the arrangement of ISO 27000 norms for the IT Security [3].

Producing better and cheaper is a necessity common to all companies, whatever their field of activity. Companies working in the domain of information systems are not spared of events. To enhance the quality degree of their products and their services and the control of their processes should be possible by applying several best practices.

The market for the IT Governance Risk Compliance (IT GRC) has extended from a strategic basis on regulatory compliance to a strategic key on company risk management [4]. Numerous organizations are hoping to treat stakeholders' need by incorporating and implementing a repository, and by about management's strategic constraints.

IT-GRC solution gives an elevated level model to IT GRC which empowers the handling of strategic needs in a smart means based on the all the best practices available in the IT GRC market.

In view of the above, the following problem arises "How to integrate updates into the knowledge base of the IT-GRC platform, in order to consider the recent versions of methods, standards,

*Corresponding Author: Aziza CHAKIR, BP 8110 Oasis, Casablanca, aziza1chakir@gmail.com

frameworks and best practices of the IT GRC; that are available on the market".

To answer to this problem, we propose an intelligent architecture of IT governance, in its second version, which allows to process the IT requests remaining lined up with the motivations and goals of the organization's business processes through its facilitators (data, IT processes, services, infrastructure and applications ...). The updated layer is the most important layer in our IT-GRC project, it is the layer which guarantees the continuous improvement of the processing of the stakeholders' strategic needs considering all the IT-GRC solutions.

In section 2, we provide an overview of IT governance risks and compliance. In section 3, we define Artificial Intelligence for IT governance as advanced technical axes.

In section 4, we present the results and analysis of an empirical study showing the motivations of this approach. In section 5, an outline of the principal variant of our smart IT-GRC platform.

In section 6, we present the proposed architecture of the update layer and in the last section; we present a simulation of the global solution.

2. IT Governance, Risk and Compliance (IT-GRC)

2.1. IT governance

The governance of information system or IT governance consists to set the information system objectives related to the company's strategy.

This approach helps to define the way in which the information system contributes to create the value by the company and it specifies the role of the various actors by considering their power stakes; for example determinate the answer of "Is the Information System Department responsible for the implementation of the information system" [5].

The IT governance is a collection of best practices that add to productive management and cooperative energy of all components of its IS so as to get most extreme profit by it. So as to [6]:

- Hold up its value creation goals.
- Improve the IS processes's performance and their client attitude.
- Manager the financial axis related to IS.
- Enhance IS solutions and abilities that the organization will require later on.
- Ensure that IS's risks are overseen.

There are different frameworks developed to define, to assess, to document and to improve internal control, information technology in organizations such as ITIL, COBIT, ISO9000, and CMMI. These methods make it possible to define indicators for monitoring and steering the IS [7].

2.2. IT Risk management

IT risk management is a collection of directives to handle and mastery the company toward risk. we recognize three targets in IT risk the management [8,9]:

- Improvement of information system's security.
- Justification of the budget allocated to secure the information system.
- Provability the information system's credibility using the analyzes carried out.

IT risk management directives and techniques permit an organization to put in practice programs to augment their chances, likewise it gouvern the effect of expected threats [10].

2.3. IT Compliance

IT compliance is a secret piece of a corporate risk management and a critical part of good corporate governance. This concept helps to ensure the corporate governance by identifying, understanding and complying with the large number of laws, regulations and standards that affect the way of functioning an organization [11].

Becoming compliant requires a company to adopt best practices, including internal control procedures for systems' protection, processes' conforming and assets' creating value. A number of risk management regulations have been introduced. These include Sarbanes-Oxley, corporate governance codes, data protection acts, and telecommunications laws [12].

3. Artificial Intelligence for IT Governance

Artificial intelligence (AI) has made techniques and devices for computer-based knowledge handling, and approaches for knowledge based reasoning and critical thinking. These incorporate knowledges obtaining and designing, knowledge modeling, critical thinking, machine learning, analogue reasoning, automatic language handling, neural network, multi-agent systems, and others [13].

In contrast to traditional computing, man-made reasoning is additionally intrigued by humans, since they are the ones who clutch knowledge: how to transmit knowledge, how to model it to make it understandable to the computer, what type of reasoning is the most effective for a given problem, how to program the computer so that it can learn all alone and helps us in our work [14].

IT Governance defines frameworks that orient organizations to manage risk and compliance and to guarantee a moral methodology. The AI can possibly improve administration and decrease costs, however it additionally makes challenges that should be overseen.

IA combined with an IT GRC environment can increase organization's capacity, help to consolidate frameworks', standards' and best practices' necessities into a global framework used to order complex guidelines and help the company's stakeholders to process all the services and the information. Also, it can be useful to ensure the alignment of requirements' regulatory with internal taxonomies and organization's structures and IT GRC data [15].

IT GRC should likewise address the ethical difficulties related with the utilization of AI technologies. These incorporate the need to clarify and to secure privacy, just as vulnerabilities that could be used to assault the system [15][16].

In conclusion, AI technologies offer the potential to govern organization easier by reducing the costs related to integration of new regulations, managing controls, processing compliance data,

discovering hidden knowledge in databases, and searching for relevant information in a large amount of information.

4. Motivation of smart global IT-GRC platform

Many organizations have deployed and integrated IT technologies to manage their business and meet their strategic needs. the use of computer technologies has become essential to rationalize and dematerialize processes and thus optimize work and increase the profitability of the services provided regardless of the organization's sector of activity. Having a quality IT environment is a prerequisite for success because it is the strategic issue that affects the whole organization.

To measure organizational progress towards establishment of the strategic objectives and to make decision organizational, the organization require the foundation of a reliable information system. This IS giving possibility to provide decision help for leaders, to less the degree of uncertainty, and to contribute to the performance of decision-making.

The IS is not a basic instrument to enable the organization to run productively, yet a genuine switch of power.

In this perspective we got on an empirical study on the perception of the impact of the use of information systems on the profitability of Moroccan organizations. The study concerns 262 Moroccan enterprises which have an IS and represent different sectors of activity [17].

Each company in front of the market is looking for profitability: the pure and perfect competition of the company to act on the market. It is therefore only possible to accept the conditions and adapt to them as best as possible. Hence the need to propose an approach to measure the adequacy between the needs of companies in IS and the proposed solutions and to evolve the trends of use in IS, this is the objective of our project. This project concerns good governance of organizations based on IT GRC best practices to add value to the strategy, manage resources, and manage risk while minimizing costs in a cost-effective way [18].

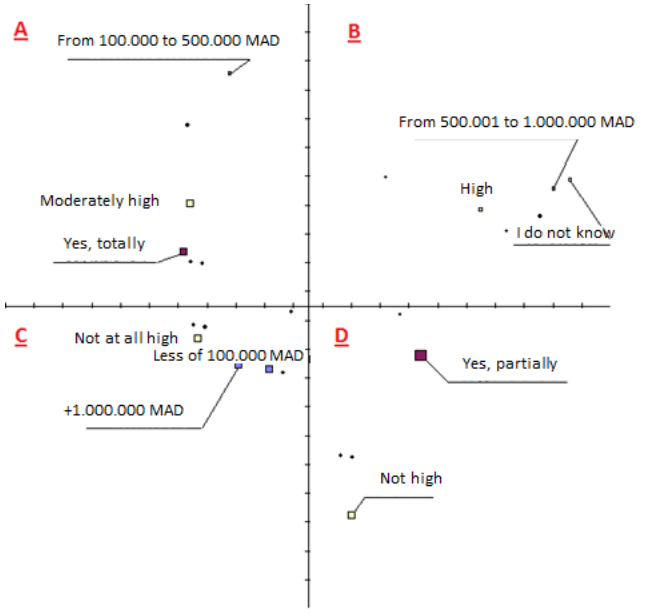


Figure 1: Multiple correspondence analysis "Variables: IS budget department, IS management, IS cost"

Through this empirical study we concluded that the Moroccan organization lacks an IT governance approach that considers its behavior in their choice of an IT framework and which improves their performance by minimizing IT investments [18].

Based on the responses collected; the map below (Figure 1) analyzes the three factors DSI budgets, IS management and IS cost by presenting the perception and interaction between them.

We note that companies which invest a budget of more than 1,000,000 MAD, remain with a moderately high cost and an IS management which partially cover all the IT needs (Zone C).

For the other areas, we can clearly see that there is no equivalence between the three factors that influence the good governance of an IS.

Managers must react to improve the efficiency of investments and govern there IS in a way that performs well to reduce IS costs.

5. Smart global IT-GRC platform: version 1

GSI solutions available on the market have limitations, in particular:

- Specialization in a specific trade of the organization,
- Necessity of coordinated IS management,
- Rigid usage of one of the IT GRC frameworks
- Need for GSI prerequisites from users to be able to use them.

The implementation of an information system that reacts viably to business desires while controlling its effect on performance and profitability; it is one of the significant challenges for organizations.

However, the development of the current IT market, the protection of the environment by be in compliance with regulations and laws, force an iterative questioning of the IS. Consequently, the requirement for an omnipresent governance of IS.

It is in this area fits our project, smart global IT-GRC platform, which aims to design a smart autonomous distributed repository capable of understanding continuously changing business needs, adapting to any type of IS, including heterogeneous parts of the IS and stakeholders, and advancing to collect the expertise of the organization in issues of GSI.

The smart global IT-GRC platform exploits the synergy effects between the organization and the multiple standards adopted. From one viewpoint, organizations can address various areas in an organized and regular manner. Then again, the shortcomings of a solitary reference model can be overwhelmed by the qualities of others. Information systems directors will use the best parts of existing standards to design their own IT framework [19].

Five layers to design the architecture of the smart global IT-GRC platform, namely (Figure 2):

Strategic layer (STR)

The strategic layer is based on COBIT to translate the company's strategy into IT objectives and processes. This layer guarantees an IT strategic alignment with the requirements defined by the stakeholders in an astute way [20].

It depends on inter-organizational workflows (WIO) and multi-agent systems and it is furnished with a semantic motor which makes an interpretation of genuine business goals into a request that can be deciphered by all the frameworks of governance [21].

To implement this solution, we handled as follows:

Design of an inter-organizational workflow explicit to the GSI,

- Integrated mediation expert system in the IOW,
- Setting of a process of IS governance ontology that considers all the best practices.
- Making of "IT Governance Ontology" as the fundamental component for the semantic engine of the global IT GRC solution.

Communication layer (COM)

All interchanges between the various layers are bolstered by this layer. It gives exchange in two distinct modes: synchronous and asynchronous. Every mode is set off as per the particulars of the organization and the strategy being referred to. It incorporates a communication block for each layer and this for ensuring the flows' specificity of each layer and the particularity of the handling to be set upstream before diverting the progression of flow of information to the following layer [22].

Decision-making layer (DM)

This layer implements a savvy smart model fit for picking the best IT framework for an IT request originating from the strategic layer. To do this, it is based on the configuration of the company and criteria for evaluating IT processes by reference [23].

This decision-making model is process-oriented; it generates the best benchmarks based on several stages [24]:

- The first step is to diminish the size of the IT issue by partitioning it into sub-issues, while basing on the mapping between all the best practices and standards of IT GRC. This step guarantees the scheduling of these sub-issues as per environmental variables (organization's type, IT need's priority …).
- In the second step, each sub-issue is formalized as per the measures explicit to the organization and the performance indicators stocked in the data warehouse, and this, so as to generate the most ideal decision of good practice to fulfill IT needs defined as input.
- The third step is to assess IT satisfaction and help make decisions for each chosen benchmark.

A notification of better repositories is immediately sent to the communication layer.

Processing Layer (PROC)

This layer implements all the IT GRC repositories, by attaching for each IT GRC repository a smart system, which deploys the recommendations and the actions of the selected repository in an intelligent manner. Indeed, the interaction is finished by sending a request to the first layer, to demand static data recently configured, or open a questionnaire with an expected user, whose reactions are diverted to the knowledge base of the framework being referred to. From a technical perspective, it has a lot of expert sub-systems connected to knowledge bases explicit to the repository implemented. Its subsystems have a set of intelligent, communicating agents, allowing to dissect the request, to question the concerned user and to analyze the existing one to give an effective and documented answer. Each subsystem of the processing layer is required to send a specification request as a message to the strategic layer, passing through the communication layer [21][25].

Updater Layer (UP)

This layer must guarantee the integration of new versions of the IT GRC frameworks that have showed up on the market. At this level, regulations must be outlined to include new knowledge into the knowledge bases of the various layers of the smart global IT-GRC platform.

This problem produces the second version of our project and this is the subject of this research.

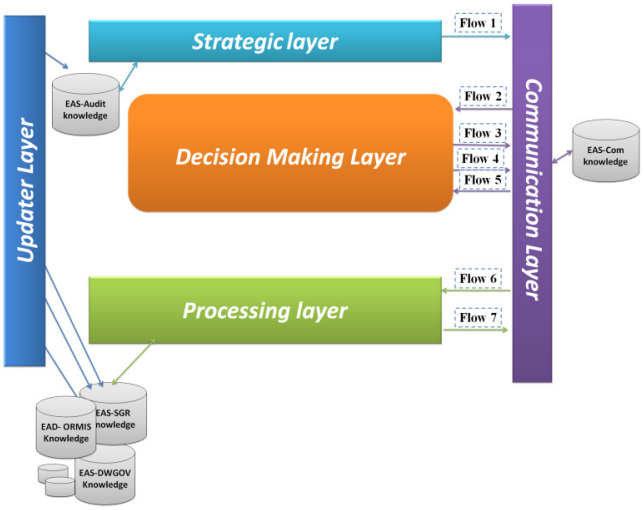


Figure 2: Smart global IT-GRC platform's architecture

6. Discussion

Large companies have changed considerably in recent years. Thousands of new employees have been hired. These newcomers need to know their company's culture, how to apply its procedures, how to govern its information systems, manage risks and remain in compliance with regulations. In addition, the projects they carry out are increasingly complex, and time has accelerated, forcing them to be more reactive.

Adapting and sharing new versions of good practice is a real challenge: the reflex to invent a solution must be substituted for that of finding the solution where it exists. Aware that this challenge, more cultural than technological, was at the heart of productivity, competitiveness and innovation, many companies have developed an organization and roadmap aimed at creating and developing this culture of sharing.

In this perspective, this research focuses on adapting the latest versions of best practices in the smart global IT-GRC platform in order to guarantee the following points:

- Ensure and assess that the organization's business goals be aligned with the IS goals and strategy.
- Govern information streams to address business needs, from its expression to the usage of the action plans of the related processes.
- Manage IT processes according to the recommendations of the repository.

7. Proposed architecture - Updater Layer

The proposed approach Smart-Updater is based on the overall process of integrating the recent versions of the IT frameworks, which is based on four activities carried out by all actors: continuous searching of new versions, collecting, integrating, and innovating knowledge.

The proposed approach requires AI to build aggregate decisions in complex circumstances, to deal with the intricacy of incoming streams (e.g. documents and web), to find knowledge in texts and in databases (for example level documents). AI can enhance the proficiency of aggregate work, the aggregate design of complex hardware, and it can likewise add to global development of the IT-GRC knowledge.

The proposed approach (Figure 3) receives the strategic request with a list of repositories that can implement it; and it process to check if the knowledge base requires an update or no, by using the following entities:

7.1. Knowledge search layer

This layer is able of organizing the sources of knowledge of the governance of information systems: humans, documents, and computers. It receives an IT request from the communication layer (COM-IT request) that present the list of IT objectives with the adequate best framework. In a smart way, this layer searches the recent versions of the adequate best practices.

It is not limited to searching only for the new versions of the proposed frameworks; it also searches for the new IT-GRC framework which appeared recently on the IT market and which is capable to process the IT objective.

7.2. Knowledge seeker

It is the entity responsible for searching for a knowledge of any kinds in the knowledge base of the Smart global IT-GRC platform, in the memory of the organization through its facilitators (data, files, processes, services, infrastructure, applications and web…) if the answer is favorable, it sends an information alert to the layer "Strategic integration of knowledge layer", and if the answer is unfavorable, an information alert will be send it to "Request layer" that ensure the sending of the same IT request to the communication layer.

7.3. Strategic integration of knowledge layer

In a smart mean, this layer manages the knowledge of the IT governance on two stages, the initial step «Knowledge creation» comprises to create new knowledge as indicated by the framework model of the smart global IT-GRC platform's layer (DML-IT Framework Model, PROCL-IT Framework Model,…) and the second step «Knowledge optimization» permits to enhance and to gain by information sources.

7.4. Knowledge update layer

This layer intermittently updates the versions of IT GRC repositories used in the global project. This update is guaranteed from a correspondence between the procedures of the old and the new version if there is just an enhancement of the functionalities, we return to the ongoing adaptation of the knowledge recognized in the knowledge bases of the various layers of the platform, else we include the knowledge on the new processes identified in the knowledge bases of the various layers of the global IT GRC solution.

7.5. Request layer

The request layer prepares the new request (COM-IT request) to be sent to the communication layer, respecting the format required by this layer. It changes the repository and its recent version in the request to send to the communication layer. If there is no appearance of new versions on the IT market, it returns the request received with a notification of the nonexistence of update.

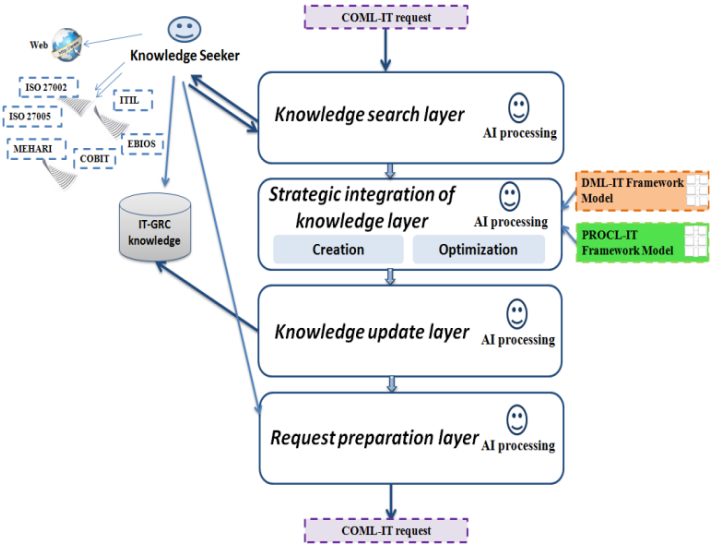


Figure 3: IT-GRC Updater Layer-approach

8. Simulation

Suppose that the smart global IT-GRC platform receives as input the strategic need of the stakeholder [Define a strategic IT plan].

To meet this need, the strategic layer sends the request via the communication layer to the update layer in the format [Define a strategic IT plan, ITIL 3]. At the level of "Knowledge search layer", we seek if there is new knowledge in governance of information systems appeared on the market capable of processing this request.

For the implementation of this request, we have as a proposal framework the ITIL version 3, the "Knowledge seeker" entity will check if there are new versions of ITIL appeared on the market or indeed if there are new frameworks capable of handling this request. This entity will identify the existence of version 4 of ITIL. There after this knowledge will be transmitted to "Strategic integration of knowledge layer", which will be responsible for the

creation of new knowledge according to the knowledge models of each layer of the global platform, for example for the decision-making layer, it must comply with the DML-IT Framework Model. After knowledge creation, knowledge optimization is necessary to optimize and capitalize the knowledge of version 4 of ITIL.

New knowledge is created, at the "Knowledge update layer" level, an upgrade is necessary to make the link between the old and the new processes, subsequently an injection of the new knowledge into all of the knowledge bases of the global platform.

The table (Table 1) below provides the mapping between practices of the recent version of ITIL (version 4) and processes of the old one (Version 3) for the "Service management practices". For the processes which do not present a subject of change, we keep them like for example the process "Availability management". For the others which present an improvement like for example the process "Change enablement" an upgrade is necessary. And for newly developed processes such as "Business analysis" we update the knowledge bases of the global project by injecting the new knowledge [26].

And finally, at the “Request layer” level, the preparation of the new request to be sent to the communication layer with the new version detected.

The objective is to make the ITIL version 4 usable and interpretable by all layers of the smart global IT-GRC platform.

The figure below (Figure 4) represents the global architecture of version 2 of the smart global IT-GRC platform.

Table 1 : ITIL 4 practices vs. ITIL V3 processes - Service management practices

ITIL 4 management practices	Related ITIL V3 processes
Availability management	Availability management
Business analysis	--
Capacity and performance management	Capacity management
	Demand management
Change enablement	Change management
	Change evaluation
Incident management	Incident management
IT asset management	--
Monitoring and event management	Event management
Problem management	Problem management
Release management	Release and deployment management
Service catalogue management	Service catalogue management
Service configuration management	Service asset and configuration management
Service continuity management	IT service continuity management (ITSCM)
Service design	Design coordination
	Service level management
Service desk	Incident management
	Request fulfillment
Service level management	Service level management
Service request management	Request fulfillment
Service validation and testing	Service validation and testing

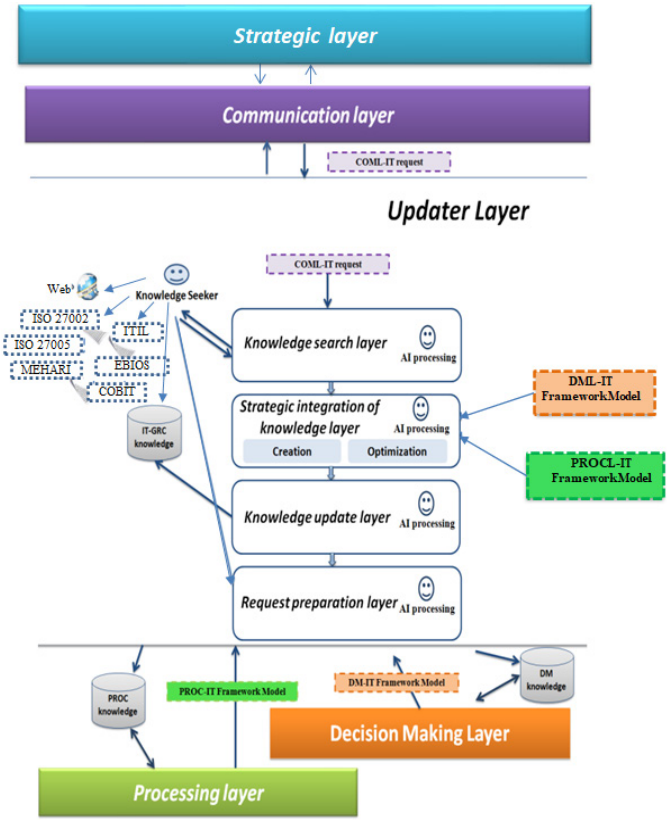


Figure 4: The smart global IT-GRC platform version 2

9. Conclusion

The aim of this paper is to keep up the operability of the generic information systems governance solution which is skilled to guarantee and to assess the alignment of the organization's business targets with the IS's strategy and goals, likewise to manage data streams by answering to business needs from its expression to the execution of actions for related processes.

The generic solution has an updated layer to follow the development of the IT market, based on a new method to

knowledge management based on the powers of artificial intelligence, in order to integrate and share recent versions of IT GRC frameworks in all the knowledge base blocks of the smart global IT-GRC platform.

As perspectives, we plan to integrate ecological governance, Green IT into our smart global IT-GRC solution to achieve more benefits for organizations and more cost savings.

Conflict of Interest

The authors declare no conflict of interest.

Acknowledgment

No funder for this work.

References

[1] S. De Haes, W. Van Grembergen, A. Joshi, T. Huygh, COBIT as a Framework for Enterprise Governance of IT, Springer: 125–162, 2020.
[2] J.L. Rubio, M. Arcilla, "How to Optimize the Implementation of ITIL through a Process Ordering Algorithm," Applied Sciences, **10**(1), 34, 2020.
[3] Z. Hamdi, A.A. Norman, N.N.A. Molok, F. Hassandoust, "A Comparative Review of ISMS Implementation Based on ISO 27000 Series in Organizations of Different Business Sectors," in Journal of Physics: Conference Series, IOP Publishing: 12103, 2019.
[4] J.G. Moreira Campos da Amarante, A. Lange Salvia, M.C. Mifsud, "Governance, risk and compliance: concerns in sustainability research agendas," 2019.
[5] S. De Haes, W. Van Grembergen, A. Joshi, T. Huygh, Enterprise Governance of IT, Alignment, and Value, Springer: 1–13, 2020.
[6] S. De Haes, L. Caluwe, T. Huygh, A. Joshi, Governance Objectives to Lead Digital Transformation, Springer: 47–61, 2020.
[7] N.T.R. Batyashe, Deployment of Information Technology Governance Using Architectural Framework, IGI Global: 199–215.
[8] R.S. Coles, R. Moulton, "Operationalizing IT risk management," Computers & Security, **22**(6), 487–493, 2003.
[9] I. Alsmadi, IT Risk and Security Management, Springer: 55–78, 2020.
[10] N.E. Vincent, R. Pinsker, "IT risk management: interrelationships based on strategy implementation," International Journal of Accounting & Information Management, 2020.
[11] N. Deistler, C. Rentrop, "IT Compliance in SME—State of the art," HMD Praxis Der Wirtschaftsinformatik, 1–11.
[12] S.S. Kim, "The continuance usage of compliance support system: does surveillance concern matter?," Journal of Enterprise Information Management, 2020.
[13] S.S. Ali, B.J. Choi, "State-of-the-Art Artificial Intelligence Techniques for Distributed Smart Grids: A Review," Electronics, **9**(6), 1030, 2020.
[14] C. Webster, S. Ivanov, Robotics, artificial intelligence, and the evolving nature of work, Springer: 127–143, 2020.
[15] G.D. Sharma, A. Yadav, R. Chopra, "Artificial Intelligence and Effective Governance: A Review, Critique and Research Agenda," 2019.
[16] N. Locke, H.L. Bird, "Perspectives on the Current and Imagined Role of Artificial Intelligence and Technology in Corporate Governance Practice and Regulation," Perspectives on the Current and Imagined Role of Artificial Intelligence and Technology in Corporate Governance Practice and Regulation (February 9, 2020). Australian Journal of Corporate Law, 2020.
[17] H. Nahla, A. Chakir, Y. Sekha, M. Chergui, S. Elhasnaoui, S. Lamrani, H. Medromi, "Analysis Of Physionomy Of Is Function In Organizations By Size And Sector Of Activity," International Journal of Computer Engineering & Technology (IJCET), **7**(4), 25–40, 2016.
[18] A. Chakir, H. Nahla, M. Chergui, S. Elhasnaoui, Y. Sekhara, H. Medromi, "An Empirical Study on the information systems in the Moroccan organizations: An explanatory model to decide differently and to optimize the IT governance," International Journal of Advanced Engineering, Management and Science, **2**(5), 239453.
[19] A. Chakir, M. Chergui, S. Elhasnaoui, H. Medromi, A. Sayouti, "Intelligent plateform to select the best IT-GRC framework for treatment the needs of stakeholders," International Journal of Applied Engineering Research, **11**(12), 2016.
[20] M. Chergui, A. Chakir, A. Sayouti, H. Medromi, "Intelligent IT Governance Platform: Strategic level," International Journal of Advanced Engineering Research and Science, **3**(12), 141–147, 2016, doi:10.22161/ijaers/3.12.28.
[21] M. Chergui, Conception et Réalisation d'une Plateforme de Gouvernance des Systèmes d'Information à base des Workflows inter-organisations, du Web sémantique et des Systèmes Multi Agents., Ph. D Thesis, ENSEM-Hassan II University, Casablanca, 2017.
[22] S. Elhasnaoui, H. Iguer, S. Faris, H. Medromi, "Multi-agent architecture for distributed IT GRC platform," International Journal of Computer Science and Information Security (IJCSIS), **16**(2), 2018.
[23] A. Chakir, M. Chergui, S. Elhasnaou, H. Medromi, A. Sayouti, "A decision approach to select the best framework to treat an IT problem by using multi-agent system and expert systems," in Lecture Notes in Electrical Engineering, 2016, doi:10.1007/978-981-287-990-5_40.
[24] C. Aziza, C. Meriyem, Using Multi-Agent System to Govern the IT Needs of Stakeholders, IntechOpen, 2020, doi:10.5772/intechopen.91440.
[25] A. Chakir, Conception et réalisation d'une architecture ITGRC de gouvernance des systèmes d'information décisionnelle à base de l'approche orientée agent, Ph. D Thesis, ENSEM- Hassan II University, 2017.
[26] C. Agutter, ITIL foundation essentials: ITIL 4 edition: the ultimate revision guide, IT Governance Publishing, 2019.

ASTES

Advances in Science, Technology and Engineering Systems Journal Vol. 5, No. 5, 54-62 (2020)

www.astesj.com

ASTESJ

ISSN: 2415-6698

Analysis of Security-Reliability Trade-off for Multi-hop Cognitive Relaying Protocol with TAS/SC Technique

Pham Minh Nam*, Phu Tran Tin

Faculty of Electronics Technology, Industrial University of Ho Chi Minh City, Ho Chi Minh City 700000, Vietnam

ARTICLE INFO

Article history:
Received: 29 June, 2020
Accepted: 11 August, 2020
Online: 08 September, 2020

Keywords:
Intercept Probability
Multi-hop Relaying Network
Outage Probability
Physical-layer Security
Selection combining (SC)
Transmit antenna selection (TAS)
Underlay Cognitive Radio

ABSTRACT

This paper studies a trade-off between security (intercept probability (IP)) and reliability (outage probability (OP)) for a multi-hop decode-and-forward (DF) relaying protocol in an underlay cognitive radio network, in presence of a multi-antenna eavesdropper. In the considered protocol, all primary and secondary terminals are equipped with multiple antennas, and they employ transmit antenna selection (TAS) (at transmitter sides) and selection combining (SC) (at receiver sides) techniques to enhance the system performance. Relying on channel state information (CSI) of the primary-to-secondary interference links known or unknown, two efficient TAS/SC techniques are proposed for the secondary networks. Moreover, operating on the underlay spectrum sharing mode, the secondary transmitters including source and relays must adapt their transmit power so that OP of the primary network is not higher than a pre-determined threshold. Under impact of Rayleigh fading and co-channel interference, the end-to-end (e2e) OP and IP are expressed by exact closed-form expressions that are verified by Monte-Carlo simulations. Then, both simulation and theoretical results are presented to show the OP-IP trade-off.

1. Introduction

MIMO (Multiple Input Multiple Output) [1, 2] and diversity relaying [3-4] are efficient techniques used for wireless communication systems operating on interference, path-loss, fading, noise environment. In MIMO, transmitters and receivers are equipped with multiple antennas, and use transmit and receive diversity techniques to enhance data rate, channel capacity, diversity order as well as to reduce outage probability (OP), error rates. Efficient combiners such as SC (Selection Combining) [5, 6], EGC (Equal-Gain Combining) [7], MRC (Maximal Ratio Combining) [8] are commonly used by the receivers to enhance reliability of the data decoding. The best combiner is MRC, but its implementation is too difficult, while the SC combiner is simplest. Indeed, using SC, the receivers only use the receive antenna which provides the highest signal-to-interference plus noise ratio (SINR) to decode the received signals. In transmit diversity techniques, transmit antenna selection (TAS) [9, 10] and maximal ratio transmission (MRT) [11] are often used. In TAS, the transmitters select one of their antennas to send data to the receivers. To obtain the highest SINR, TAS requires feedback channel state information (CSI) from the receivers for selecting the best transmit antenna. Unlike TAS, the receivers employing MRT use all the antennas to transmit data. The implementation of MRT is hence more difficult than that of TAS, but it obtains higher performance. To further enhance the system performances for wireless communication systems, combination between the transmit diversity and receiver diversity techniques, such as TAS/SC [12], TAS/MRC [12], MRT/SC [13], MRT/MRC [14], were proposed.

Relaying techniques can be efficiently used when the distance between a source and a destination is enough far or a source node cannot directly communicate with a destination node. In these techniques, intermediate nodes or relay nodes are employed to help the source-destination data transmission [3-4, 15-16]. Depends on the signal processing methods, the relays are categorized into two main groups: DF (decode and forward) [15-16] and AF (amplify and forward) [17-18]. The DF relays first decode the received data, encode it again, before sending the encoded signal to the destination. On the contrary, the AF relays only forward the amplified signals to the destination without performing the decoding. Hence, the AF technique is simpler than the DF one, but DF outperforms AF because the noises can be removed at the DF relays. Until now, published works concerned with performance evaluation of the relaying scenarios have mainly focused on dual-hop networks, e.g. [3-4, 15-18]. In [19-20], the authors considered multi-hop relaying models, where the source data are relayed to

*Corresponding Author: Pham Minh Nam, phamminhnam@iuh.edu.vn

the destination over multi-hop or multi-relay. Reference [19] evaluated end-to-end (e2e) symbol error rate of the multi-hop AF relaying protocol. In [20], the multi-hop DF relaying protocol was proposed and analyzed. To enhance the e2e system performances for the multi-hop relaying networks over fading environments, various diversity relaying methods were proposed. References [20, 21] introduced path-selection strategies to exploit spatial diversity. The authors in [22, 23] studied the e2e OP of multi-hop MIMO relaying protocols where the TAS/MRC technique was used to obtain diversity gain at each hop.

In wireless communication systems, security is a critical issue because the transmitted data can be easily overheard by eavesdroppers. Recently, physical-layer security (PLS) [24, 25] has gained much attention as a promising solution to guarantee secure communication. PLS can be simply implemented in practice because the security can be attained, relying on physical channel information such as link distances and channel quality. Indeed, the data transmission can be considered to be secure if the data channel is better than the eavesdropping one. The secrecy performances of the PLS systems can be evaluated via secrecy capacity defined as difference of channel capacity obtained on the data and eavesdropping links. References [26-29] proposed the transmit and receive diversity techniques to enhance secrecy performances for the MIMO systems. In [30-31], secure communication relaying protocols operating over fading channels were proposed and analyzed. Conventionally, the source and relays cooperate together to confuse the eavesdropper, i.e., they randomly generate code-books as transmitting the data [31]. Reference [32] analyzed the e2e secrecy performance of the multi-hop DF relaying protocol over Nakagami-*m* fading channels with imperfect transceiver hardware. Unlike [26-32], performance metrics of the PLS systems considered in [33, 34] are OP of the data transmission and intercept probability (IP) of the eavesdroppers. As shown in [33, 34], trade-off between IP and OP was investigated.

Due to rapid increasing of wireless devices, J. Mitola proposed cognitive radio (CR) [35] to solve spectrum scarcity issue. In CR, primary users can share their licensed bands to secondary users provided that the primary QoS is guaranteed. To realize this, the secondary users have to adjust their transmit power appropriately so that co-channel interference at the primary receivers must be below a given threshold [36, 37]. Recently, PLS in CR [38, 39] has been much attention of researchers. Reference [40] investigated trade-off between IP and OP of the secure communication in the secondary network operating over Rician fading channels. Moreover, in [40], the TAS/SC technique is used for the primary data transmission. The authors in [41] proposed a cooperative routing approach to enhance the e2e secrecy performances for the underlay CR networks, as compared with a conventional multi-hop relaying method. In [42], the TAS/SC technique is used at each hop in the secondary network to obtain better secrecy performance in presence of hardware imperfection. In [43], a best-path selection strategy was proposed for secrecy performance enhancement of cluster-based CR networks using cooperative jamming technique.

This paper investigates the e2e IP and OP performance of the multi-hop MIMO relaying protocol in the underlay CR network with presence of a secondary multi-antenna eavesdropper. In the proposed scheme, the TAS/SC technique is used by both the primary and secondary networks. More particularly, the secondary source and relays must reduce their transmit power to guarantee that OP at the primary receiver is always below a required threshold. Under the joint impact of the limited transmit power and co-channel interference, the secondary transmitters use TAS/SC at each hop to improve the reliability of the data transmission. Also in the secondary network, the eavesdropper with the SC combiner attempts to illegally decode the transmitted data over multiple hops. Moreover, we consider two cases where the interference from the primary transmitter on the secondary nodes is known or not. From two these cases, we propose different TAS/SC techniques for the secondary network. Different with [40, 43] in which the wireless devices only have single antenna; all the nodes in our proposed protocol have multiple antennas, and employ TAS/SC to attain higher diversity order. While references [41-44] derived the secrecy performance by using secrecy capacity, this paper investigates the trade-off between IP and OP. Moreover, references [42, 43] do not consider the presence of the primary transmitter, as well as ignore the impact of the co-channel interference from the primary network.

In the following, we summarize the main contribution of this paper as

- We propose TAS/SC-based multi-hop MIMO relaying protocols in PLS underlay CR networks. Moreover, under impact of the co-channel interference, we consider two efficient TAS/SC techniques applied for the secondary network, depending on channel state information (CSI) between the secondary nodes and the primary transmitter is known or not.
- From an exact closed-form formula of the outage performance of the primary network, we derive expressions of the transmit power for the secondary transmitters including source and relays.
- Exact closed-form expressions of the e2e OP and IP over Rayleigh fading channel are derived, and are validated by Monte-Carlo simulations.

This paper is organized into sections as follows. Section 2 describes system model and operation principle of the proposed model. Section 3 measures the system performances in terms of IP and OP. Both simulation results and analytical results are presented in Section 4. Finally, conclusions are provided in Section 5.

2. System Model

In Fig. 1, the primary transmitter (T) and the primary receiver (R) are equipped N_{T} N_{R} antennas, respectively, and they use TAS/SC to communicate with each other. Considering the secondary network; the source node S_0 wants to sends its data to the destination S_K via $(K-1)$ intermediate relays named S_1, S_2, …, S_{K-1}. Assume that all of the nodes $\mathrm{S}_k\,(k=0,1,...,K)$ have N_{S} antennas, and the $\mathrm{S}_0 \to \mathrm{S}_K$ data transmission is accomplished via K orthogonal time slots. In addition, at the $k-$th hop, S_{k-1} sends the data to S_k by performing TAS/SC. Also in the secondary

network, an N_{E}-antenna eavesdropper (E) attempts to overhear the data transmitted at each hop.

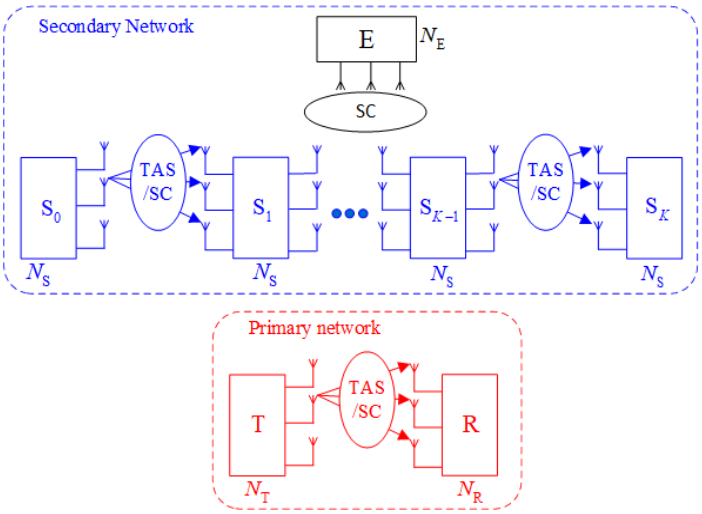


Figure 1: System model of the proposed TAS/SC-based multi-hop relaying protocol in the underlay CR networks.

We denote γ_{XY} as channel gain of the $\mathrm{X}-\mathrm{Y}$ Rayleigh fading channel, and hence the channel gain is an exponential random variable (RV). Similar to [3], parameter of γ_{XY} is $\lambda_{\mathrm{XY}} = d_{\mathrm{XY}}^{\beta}$, where d_{XY} is X-Y distance, and β is path-loss exponent. More particularly, distribution functions of γ_{XY} are given as follows:

$$F_{\gamma_{\mathrm{XY}}}(x) = 1 - \exp(-\lambda_{\mathrm{XY}} x), f_{\gamma_{\mathrm{XY}}}(x) = \lambda_{\mathrm{XY}} \exp(-\lambda_{\mathrm{XY}} x), \quad (1)$$

where $F_U(.)$ and $f_U(.)$ are CDF (cumulative distribution function) and PDF (probability density function) of RV U, respectively.

Next, we consider the primary and secondary data transmission at the $k-$th time slot, in which S_{k-1} and T at the same time send their data to S_k and R, respectively. Assume that S_{k-1} uses the $m-$th transmit antenna, T uses the $p-$th the antenna, S_k uses the $n-$th receive antenna and R uses the $q-$th receive antenna, where $m \in \{1,2,...,N_{\mathrm{S}}\}$, $n \in \{1,2,...,N_{\mathrm{S}}\}$, $p \in \{1,2,...,N_{\mathrm{T}}\}$, $q \in \{1,2,...,N_{\mathrm{R}}\}$. Due to the cross co-channel interference between two networks, the instantaneous SINR obtained at S_k and R can be formulated by (2) and (3), respectively as

$$\varphi_{\mathrm{T}^p\mathrm{R}^q} = \frac{P_{\mathrm{T}}\gamma_{\mathrm{T}^p\mathrm{R}^q}}{P_{\mathrm{S}_{k-1}}\gamma_{\mathrm{S}_{k-1}^m\mathrm{R}^q} + \sigma_0^2}, \quad (2)$$

$$\varphi_{\mathrm{S}_{k-1}^m\mathrm{S}_k^n} = \frac{P_{\mathrm{S}_{k-1}}\gamma_{\mathrm{S}_{k-1}^m\mathrm{S}_k^n}}{P_{\mathrm{T}}\gamma_{\mathrm{T}^p\mathrm{S}_k^n} + \sigma_0^2}. \quad (3)$$

Now, we introduce notations used in (2)-(3). P_{T} is transmit power of each antenna of T. σ_0^2 is variance of Gaussian noises at R, and it is also variance at all the receivers. $P_{\mathrm{S}_{k-1}}$ is transmit power of S_{k-1}. $\gamma_{\mathrm{X}^a\mathrm{Y}^b}$ is channel gain between the $a-$th antenna of X and the $b-$th antenna of Y, where $(\mathrm{X},\mathrm{Y}) \in \{\mathrm{S}_{k-1}, \mathrm{S}_k, \mathrm{T}, \mathrm{R}\}$ and $(a,b) \in \{m,n,p,q\}$.

Considering the $\mathrm{T} \to \mathrm{R}$ transmission; the TAS/SC technique is used to obtain the maximum SINR between T and R, as

$$\varphi_{\mathrm{T}^u\mathrm{R}^v} = \max_{p=1,2,...,N_{\mathrm{T}}} \left(\max_{q=1,2,...,N_{\mathrm{R}}} \left(\varphi_{\mathrm{T}^p\mathrm{R}^q} \right) \right), \quad (4)$$

where u and v are the optimal transmit-receive pair, $u \in \{1,2,...,N_{\mathrm{T}}\}$, $v \in \{1,2,...,N_{\mathrm{R}}\}$.

Comment 1: To realize the strategy given in (4), the T and R nodes have to know the interference component $P_{\mathrm{S}_{k-1}}\gamma_{\mathrm{S}_{k-1}^m\mathrm{R}^q}$ which can be obtained by requesting the cooperation from S_{k-1}.

2.1. OP of Primary Network

From (4), the instantaneous channel capacity of the T-R link is given as

$$C_{\mathrm{P},k} = \frac{1}{K}\log_2\left(1 + \varphi_{\mathrm{T}^u\mathrm{R}^v}\right), \quad (5)$$

where the fraction $1/K$ implies that the data transmission in the secondary network is realized in K orthogonal time slots.

Next, OP of the primary network is defined as the probability that $C_{\mathrm{P},k}$ is below a positive value denoted by C_{Pth}. Then, combining (2), (4) and (5), we can formulate OP at R as

$$\begin{aligned} \mathrm{OP}_{\mathrm{P},k} &= \Pr\left(C_{\mathrm{P},k} < C_{\mathrm{Pth}}\right) = \Pr\left(\varphi_{\mathrm{T}^u\mathrm{R}^v} < \rho_{\mathrm{Pth}}\right) \\ &= \prod_{p=1}^{N_{\mathrm{T}}}\prod_{q=1}^{N_{\mathrm{R}}} \underbrace{\Pr\left(\frac{P_{\mathrm{T}}\gamma_{\mathrm{T}^p\mathrm{R}^q}}{P_{\mathrm{S}_{k-1}}\gamma_{\mathrm{S}_{k-1}^m\mathrm{R}^q} + \sigma_0^2} < \rho_{\mathrm{Pth}}\right)}_{I_1}, \end{aligned} \quad (6)$$

where

$$\rho_{\mathrm{Pth}} = 2^{KC_{\mathrm{Pth}}} - 1. \quad (7)$$

Next, we rewrite the probability I_1 marked in (6) as

$$\begin{aligned} I_1 &= \Pr\left(P_{\mathrm{T}}\gamma_{\mathrm{T}^p\mathrm{R}^q} < P_{\mathrm{S}_{k-1}}\rho_{\mathrm{Pth}}\gamma_{\mathrm{S}_{k-1}^m\mathrm{R}^q} + \sigma_0^2\rho_{\mathrm{Pth}}\right) \\ &= \int_0^{+\infty} F_{\gamma_{\mathrm{T}^p\mathrm{R}^q}}\left(\mu_1 P_{\mathrm{S}_{k-1}}x + \mu_2\right) f_{\gamma_{\mathrm{S}_{k-1}^m\mathrm{R}^q}}(x)\,dx, \end{aligned} \quad (8)$$

where

$$\mu_1 = \frac{\rho_{\mathrm{Pth}}}{P_{\mathrm{T}}}, \mu_2 = \frac{\sigma_0^2\rho_{\mathrm{Pth}}}{P_{\mathrm{T}}}. \quad (9)$$

Substituting CDF $F_{\gamma_{\mathrm{T}P_{\mathrm{R}}q}}\left(\mu_1 P_{\mathrm{S}_{k-1}} x+\mu_2\right)$ and PDF $f_{\gamma_{\mathrm{S}_{k-1}^m \mathrm{R}^q}}(x)$ obtained in (1) into (8); which yields

$$\begin{aligned} I_1 &= 1-\lambda_{\mathrm{S}_{k-1}\mathrm{R}} \exp\left(-\lambda_{\mathrm{TR}}\mu_2\right) \\ &\quad \times \int_0^{+\infty} \exp\left(-\lambda_{\mathrm{TR}} P_{\mathrm{S}_{k-1}}\mu_1 x\right)\exp\left(-\lambda_{\mathrm{S}_{k-1}\mathrm{R}} x\right) dx \\ &= 1-\frac{\lambda_{\mathrm{S}_{k-1}\mathrm{R}}}{\lambda_{\mathrm{S}_{k-1}\mathrm{R}}+\lambda_{\mathrm{TR}} P_{\mathrm{S}_{k-1}}\mu_1}\exp\left(-\lambda_{\mathrm{TR}}\mu_2\right). \end{aligned} \quad (10)$$

Then, substituting (10) into (6), we obtain

$$\mathrm{OP}_{\mathrm{P},k} = \left[1-\frac{\lambda_{\mathrm{S}_{k-1}\mathrm{R}}}{\lambda_{\mathrm{S}_{k-1}\mathrm{R}}+\lambda_{\mathrm{TR}} P_{\mathrm{S}_{k-1}}\mu_1}\exp\left(-\lambda_{\mathrm{TR}}\mu_2\right)\right]^{N_{\mathrm{T}}N_{\mathrm{R}}}. \quad (11)$$

2.2. Transmit Power of Secondary Transmitters

At first, the primary QoS is defined as $\mathrm{OP}_{\mathrm{P},k} \le \varepsilon_{\mathrm{Pth}}\left(\forall k\right)$, where $\varepsilon_{\mathrm{Pth}}$ is a predefined threshold. By solving $\mathrm{OP}_{\mathrm{P},k} = \varepsilon_{\mathrm{Pth}}$, an exact closed-form expression of $P_{\mathrm{S}_{k-1}}$ can be given as

$$P_{\mathrm{S}_{k-1}} = \left[\left(\frac{\exp\left(-\lambda_{\mathrm{TR}}\mu_2\right)}{1-\left(\varepsilon_{\mathrm{Pth}}\right)^{\frac{1}{N_{\mathrm{T}}N_{\mathrm{R}}}}}-1\right)\frac{\lambda_{\mathrm{S}_{k-1}\mathrm{R}}}{\lambda_{\mathrm{TR}}\mu_1}\right]^{+}, \quad (12)$$

where $\left[x\right]^{+} = \max\left(0,x\right)$.

At high transmit power values of P_{T}, i.e., $P_{\mathrm{T}} \to +\infty$, we can approximate $P_{\mathrm{S}_{k-1}}$ as in (13):

$$P_{\mathrm{S}_{k-1}} \overset{P_{\mathrm{T}}\to+\infty}{\approx} \left(\frac{1}{1-\left(\varepsilon_{\mathrm{Pth}}\right)^{\frac{1}{N_{\mathrm{T}}N_{\mathrm{R}}}}}-1\right)\frac{\lambda_{\mathrm{S}_{k-1}\mathrm{R}}P_{\mathrm{T}}}{\lambda_{\mathrm{TR}}\rho_{\mathrm{Pth}}} = \xi P_{\mathrm{T}}, \quad (13)$$

where

$$\xi = \left(\frac{1}{1-\left(\varepsilon_{\mathrm{Pth}}\right)^{\frac{1}{N_{\mathrm{T}}N_{\mathrm{R}}}}}-1\right)\frac{\lambda_{\mathrm{S}_{k-1}\mathrm{R}}}{\lambda_{\mathrm{TR}}\rho_{\mathrm{Pth}}}. \quad (14)$$

Comment 2: The transmit power of the secondary transmitters is calculated by the primary network as in (12), and then sent to the S_{k-1} node. Next, it is worth noting that $P_{\mathrm{S}_{k-1}} = 0$ means the primary network does not obtain the required QoS, i.e., $\mathrm{OP}_{\mathrm{P},k} > \varepsilon_{\mathrm{Pth}}$. Finally, equation (13) shows that as P_{T} is high enough, the primary QoS is always satisfied, and the transmit power $P_{\mathrm{S}_{k-1}}$ becomes a linear function of P_{T}.

2.3. TAS/SC methods

In this section, two practical TAS/SC techniques are considered. The TAS/SC technique is proposed in [12], in which the transmitter and receiver select an optimal transmit-receive antennas to maximize the instantaneous SINR of the data link. However, with presence of the co-channel interference, the TAS/SC technique in [12] may not be optimal any more. This motivates us to reconsider the TAS/SC technique in the interference environment.

Case 1: Co-channel interference from P_{T} is known

In this case, we assume that the co-channel interference can be perfectly estimated by the secondary nodes. Hence, similar to (4), the TAS/SC technique can be set up by S_{k-1} and S_k as

$$\varphi_{\mathrm{S}_{k-1}^z\mathrm{S}_k^t} = \max_{m=1,2,...,N_{\mathrm{S}}}\left(\max_{n=1,2,...,N_{\mathrm{S}}}\left(\frac{P_{\mathrm{S}_{k-1}}\gamma_{\mathrm{S}_{k-1}^m\mathrm{S}_k^n}}{P_{\mathrm{T}}\gamma_{\mathrm{T}^u\mathrm{S}_k^n}+\sigma_0^2}\right)\right), \quad (15)$$

where z and t are the selected transmit-receive antenna pair at S_{k-1} and S_k, respectively, $\left(z,t\right) \in \left\{1,2,...,N_{\mathrm{S}}\right\}$.

For a fair comparison, assume that the interference from the primary network is also known by E. With the SC combiner, the SINR obtained at E can be given as

$$\varphi_{\mathrm{S}_{k-1}^z\mathrm{E}^e} = \max_{r=1,2,...,N_{\mathrm{E}}}\left(\frac{P_{\mathrm{S}_{k-1}}\gamma_{\mathrm{S}_{k-1}^z\mathrm{E}^r}}{P_{\mathrm{T}}\gamma_{\mathrm{T}^u\mathrm{E}^r}+\sigma_0^2}\right), \quad (16)$$

where e is the selected antennas at E for decoding the source data, and $e \in \left\{1,2,...,N_{\mathrm{E}}\right\}$.

Case 2: Co-channel interference from P_{T} is unknown

It is worth noting that in practice the primary network does not need to cooperate with the secondary network (but the secondary network must cooperate with the primary network). Hence, the secondary nodes may not obtain perfectly the information about the co-channel interference caused by PT. In this case, the TAS/SC technique should be performed, only relying on CSIs of the data links, i.e.

$$\gamma_{\mathrm{S}_{k-1}^a\mathrm{S}_k^b} = \max_{m=1,2,...,N_{\mathrm{S}}}\left(\max_{n=1,2,...,N_{\mathrm{S}}}\left(\gamma_{\mathrm{S}_{k-1}^m\mathrm{S}_k^n}\right)\right), \quad (17)$$

where a and b are the chosen antennas at S_{k-1} and S_k, respectively, $\left(a,b\right) \in \left\{1,2,...,N_{\mathrm{S}}\right\}$.

We can observe that the TAS/SC technique in (17) is only sub-optimal because the S_{k-1} and S_k nodes have not perfect information of the channel gain $\gamma_{\mathrm{T}^u\mathrm{S}_k^n}$.

Hence, the SINR obtained at S_k in this case can be given as

$$\varphi_{\mathrm{S}_{k-1}^a\mathrm{S}_k^b} = \frac{P_{\mathrm{S}_{k-1}}\gamma_{\mathrm{S}_{k-1}^a\mathrm{S}_k^b}}{P_{\mathrm{T}}\gamma_{\mathrm{T}^u\mathrm{S}_k^b}+\sigma_0^2}. \quad (18)$$

Also, it is assumed that E has no information of the co-channel interference links, and hence the best antenna selected by E is given as

$$\gamma_{\mathrm{S}_{k-1}^{a}\mathrm{E}^{l}}=\max_{r=1,2,...,N_{\mathrm{E}}}\left(\gamma_{\mathrm{S}_{k-1}^{z}\mathrm{E}^{r}}\right), \tag{19}$$

where $l\left(l\in\{1,2,...,N_{\mathrm{E}}\}\right)$ is the selected antennas at E for decoding the source data. Then, we can formulate the SINR obtained at E as

$$\varphi_{\mathrm{S}_{k-1}^{a}\mathrm{E}^{l}}=\frac{P_{\mathrm{S}_{k-1}}\gamma_{\mathrm{S}_{k-1}^{a}\mathrm{E}^{l}}}{P_{\mathrm{T}}\gamma_{\mathrm{T}^{u}\mathrm{E}^{e}}+\sigma_{0}^{2}}. \tag{20}$$

At high transmit power P_{T}, i.e. $P_{\mathrm{T}}\to+\infty$, $P_{\mathrm{T}}\gg\sigma_{0}^{2}$, from (13), equations (15), (16), (18) and (20) can be approximated respectively as

$$\varphi_{\mathrm{S}_{k-1}^{z}\mathrm{S}_{k}^{t}}\overset{P_{\mathrm{T}}\to+\infty}{\approx}\max_{m=1,2,...,N_{\mathrm{S}}}\left(\max_{n=1,2,...,N_{\mathrm{S}}}\left(\frac{\xi\gamma_{\mathrm{S}_{k-1}^{m}\mathrm{S}_{k}^{n}}}{\gamma_{\mathrm{T}^{u}\mathrm{S}_{k}^{n}}}\right)\right), \tag{21}$$

$$\varphi_{\mathrm{S}_{k-1}^{z}\mathrm{E}^{e}}\overset{P_{\mathrm{T}}\to+\infty}{\approx}\max_{r=1,2,...,N_{\mathrm{E}}}\left(\frac{\xi\gamma_{\mathrm{S}_{k-1}^{z}\mathrm{E}^{r}}}{\gamma_{\mathrm{T}^{u}\mathrm{E}^{r}}}\right), \tag{22}$$

$$\varphi_{\mathrm{S}_{k-1}^{a}\mathrm{S}_{k}^{b}}\overset{P_{\mathrm{T}}\to+\infty}{\approx}\frac{\xi\gamma_{\mathrm{S}_{k-1}^{a}\mathrm{S}_{k}^{b}}}{\gamma_{\mathrm{T}^{u}\mathrm{S}_{k}^{b}}}, \tag{23}$$

$$\varphi_{\mathrm{S}_{k-1}^{a}\mathrm{E}^{l}}\overset{P_{\mathrm{T}}\to+\infty}{\approx}\frac{\xi\gamma_{\mathrm{S}_{k-1}^{z}\mathrm{E}^{l}}}{\gamma_{\mathrm{T}^{u}\mathrm{E}^{e}}}. \tag{24}$$

Comment 3: As observed from (21)-(24), at high P_{T} values, the obtained SINRs do not depend on P_{T}.

2.4. E2e Channel Capacity of Data and Eavesdropping Links

Due to usage of the DF relaying technique, the e2e channel capacity of the $\mathrm{S}_0\to\mathrm{S}_K$ link in the first and second cases can be respectively given as (see [19, 29])

$$C_{\mathrm{D,e2e}}^{\text{Case 1}}=\frac{1}{K}\log_{2}\left(1+\min_{k=1,2,...,K}\left(\varphi_{\mathrm{S}_{k-1}^{z}\mathrm{S}_{k}^{t}}\right)\right), \tag{25}$$

$$C_{\mathrm{D,e2e}}^{\text{Case 2}}=\frac{1}{K}\log_{2}\left(1+\min_{k=1,2,...,K}\left(\varphi_{\mathrm{S}_{k-1}^{a}\mathrm{S}_{k}^{b}}\right)\right). \tag{26}$$

Considering the channel capacity obtained at the eavesdropper. Because of the random code-book generation at each hop, the channel capacity at E in Case 1 and Case 2 can be formulated, respectively as

$$C_{\mathrm{E,e2e}}^{\text{Case 1}}=\frac{1}{K}\log_{2}\left(1+\max_{k=1,2,...,K}\left(\varphi_{\mathrm{S}_{k-1}^{z}\mathrm{E}^{e}}\right)\right), \tag{27}$$

$$C_{\mathrm{E,e2e}}^{\text{Case 2}}=\frac{1}{K}\log_{2}\left(1+\max_{k=1,2,...,K}\left(\varphi_{\mathrm{S}_{k-1}^{a}\mathrm{E}^{l}}\right)\right). \tag{28}$$

3. Evaluation of E2e OP and IP

At first, the e2e OP and IP are respectively defined as in [36]:

$$\mathrm{OP}_{\mathrm{e2e}}^{\text{Case }i}=\Pr\left(C_{\mathrm{D,e2e}}^{\text{Case }i}<C_{\mathrm{Sth}}\right), \tag{29}$$

$$\mathrm{IP}_{\mathrm{e2e}}^{\text{Case }i}=\Pr\left(C_{\mathrm{E,e2e}}^{\text{Case }i}\geq C_{\mathrm{Sth}}\right), \tag{30}$$

where C_{Sth} is a pre-determined threshold, $i\in\{1,2\}$.

3.1. E2e OP

In this sub-section, we exactly and asymptotically evaluate the e2e OP in two cases considered in Sub-section 2.3. At first, combining (25), (26) and (29), we can obtain (31) as

$$\begin{aligned}\mathrm{OP}_{\mathrm{e2e}}^{\text{Case }i}&=\Pr\left(\min_{k=1,2,...,K}\left(\varphi_{\mathrm{S}_{k-1}^{x}\mathrm{S}_{k}^{y}}\right)<\rho_{\mathrm{Sth}}\right)\\&=1-\prod_{k=1}^{K}\left(1-\Pr\left(\varphi_{\mathrm{S}_{k-1}^{x}\mathrm{S}_{k}^{y}}<\rho_{\mathrm{Sth}}\right)\right)\\&=1-\prod_{k=1}^{K}\left(1-\mathrm{OP}_{k}^{\text{Case }i}\right),\end{aligned} \tag{31}$$

where

$$\begin{aligned}&\rho_{\mathrm{Sth}}=2^{KC_{\mathrm{Sth}}}-1,\mathrm{OP}_{k}^{\text{Case }i}=\Pr\left(\varphi_{\mathrm{S}_{k-1}^{x}\mathrm{S}_{k}^{y}}<\rho_{\mathrm{Sth}}\right),\\&(x,y)=\begin{cases}(z,t),\text{ if }i=1\\(a,b),\text{ if }i=2\end{cases}\end{aligned} \tag{32}$$

Case 1: Co-channel interference from P_{T} is known

Substituting (15) into $\mathrm{OP}_{k}^{\text{Case 1}}$, which yields

$$\begin{aligned}\mathrm{OP}_{k}^{\text{Case 1}}&=\prod_{m=1}^{N_{\mathrm{S}}}\prod_{n=1}^{N_{\mathrm{S}}}\Pr\left(\frac{P_{\mathrm{S}_{k-1}}\gamma_{\mathrm{S}_{k-1}^{m}\mathrm{S}_{k}^{n}}}{P_{\mathrm{T}}\gamma_{\mathrm{T}^{u}\mathrm{S}_{k}^{n}}+\sigma_{0}^{2}}<\rho_{\mathrm{Sth}}\right)\\&=\prod_{m=1}^{N_{\mathrm{S}}}\prod_{n=1}^{N_{\mathrm{S}}}\Pr\left(\gamma_{\mathrm{S}_{k-1}^{m}\mathrm{S}_{k}^{n}}<\mu_{3}\gamma_{\mathrm{T}^{u}\mathrm{S}_{k}^{n}}+\mu_{4}\right)\\&=\left[\int_{0}^{+\infty}F_{\gamma_{\mathrm{S}_{k-1}^{m}\mathrm{S}_{k}^{n}}}\left(\mu_{3}x+\mu_{4}\right)f_{\gamma_{\mathrm{T}^{u}\mathrm{S}_{k}^{n}}}\left(x\right)dx\right]^{N_{\mathrm{S}}^{2}},\end{aligned} \tag{33}$$

where

$$\mu_{3}=\frac{\rho_{\mathrm{Sth}}P_{\mathrm{T}}}{P_{\mathrm{S}_{k-1}}},\mu_{4}=\frac{\rho_{\mathrm{Sth}}\sigma_{0}^{2}}{P_{\mathrm{S}_{k-1}}}. \tag{34}$$

Similar to the derivation steps in (8)-(10); substituting CDF $F_{\gamma_{\mathrm{S}_{k-1}^{m}\mathrm{S}_{k}^{n}}}\left(\mu_{3}x+\mu_{4}\right)$ and PDF $f_{\gamma_{\mathrm{T}^{u}\mathrm{S}_{k}^{n}}}\left(x\right)$ obtained in (1) into (33), after some manipulation, we can obtain (35) as follows:

$$\mathrm{OP}_{k}^{\text{Case 1}}=\left[1-\frac{\lambda_{\mathrm{TS}_{k}}}{\lambda_{\mathrm{TS}_{k}}+\lambda_{\mathrm{S}_{k-1}\mathrm{S}_{k}}\mu_{3}}\exp\left(-\lambda_{\mathrm{S}_{k-1}\mathrm{S}_{k}}\mu_{4}\right)\right]^{N_{\mathrm{S}}^{2}}. \tag{35}$$

Substituting (35) into (31), an exact closed-form formula of the e2e OP in the first case can be written as

$$\mathrm{OP}_{\mathrm{e2e}}^{\mathrm{Case\ 1}} = 1-\prod_{k=1}^{K}\left\{1-\left[1-\frac{\lambda_{\mathrm{TS}_k}}{\lambda_{\mathrm{TS}_k}+\lambda_{\mathrm{S}_{k-1}\mathrm{S}_k}\mu_3}\exp\left(-\lambda_{\mathrm{S}_{k-1}\mathrm{S}_k}\mu_4\right)\right]^{N_{\mathrm{S}}^2}\right\}, \quad (36)$$

At high P_{T} values, by using the approximate expression of $\varphi_{\mathrm{S}_{k-1}^z\mathrm{S}_k^t}$ in (21), with the same derivation method, $\mathrm{OP}_{\mathrm{e2e}}^{\mathrm{Case\ 1}}$ can be approximated as follows:

$$\mathrm{OP}_{\mathrm{e2e}}^{\mathrm{Case\ 1}} \overset{P_{\mathrm{T}}\to+\infty}{\approx} 1-\prod_{k=1}^{K}\left[1-\left(\frac{\lambda_{\mathrm{S}_{k-1}\mathrm{S}_k}\mu_3}{\lambda_{\mathrm{TS}_k}+\lambda_{\mathrm{S}_{k-1}\mathrm{S}_k}\mu_3}\right)^{N_{\mathrm{S}}^2}\right]. \quad (37)$$

Case 2: Co-channel interference from P_{T} is unknown

Substituting (18) into $\mathrm{OP}_k^{\mathrm{Case\ 2}}$, we can obtain (38) as

$$\mathrm{OP}_k^{\mathrm{Case\ 2}} = \int_0^{+\infty} F_{\gamma_{\mathrm{S}_{k-1}^a\mathrm{S}_k^b}}\left(\mu_3 x+\mu_4\right) f_{\gamma_{\mathrm{T}^u\mathrm{S}_k^b}}(x)\,dx. \quad (38)$$

From (17), we can write $F_{\gamma_{\mathrm{S}_{k-1}^a\mathrm{S}_k^b}}\left(\mu_3 x+\mu_4\right)$ as

$$\begin{aligned} F_{\gamma_{\mathrm{S}_{k-1}^a\mathrm{S}_k^b}}\left(\mu_3 x+\mu_4\right) &= \prod_{m=1}^{N_{\mathrm{S}}}\prod_{n=1}^{N_{\mathrm{S}}} F_{\gamma_{\mathrm{S}_{k-1}^m\mathrm{S}_k^n}}\left(\mu_3 x+\mu_4\right) \\ &= \left(1-\exp\left(-\lambda_{\mathrm{S}_{k-1}\mathrm{S}_k}\left(\mu_3 x+\mu_4\right)\right)\right)^{N_{\mathrm{S}}^2} \\ &= 1+\sum_{m=1}^{N_{\mathrm{S}}^2}(-1)^m C_{N_{\mathrm{S}}^2}^m \exp\left(-m\lambda_{\mathrm{S}_{k-1}\mathrm{S}_k}\mu_4\right)\exp\left(-m\lambda_{\mathrm{S}_{k-1}\mathrm{S}_k}\mu_3 x\right), \end{aligned} \quad (39)$$

where $C_{N_{\mathrm{S}}^2}^m$ is binomial coefficient which is expressed as

$$C_{N_{\mathrm{S}}^2}^m = \frac{\left(N_S^2\right)!}{m!\left(N_S^2-m\right)!}. \quad (40)$$

Substituting (39) and PDF $f_{\gamma_{\mathrm{T}^u\mathrm{S}_k^b}}(x)$ into (38), after some manipulation, we obtain

$$\mathrm{OP}_k^{\mathrm{Case\ 2}} = 1+\sum_{m=1}^{N_{\mathrm{S}}^2}(-1)^m \frac{C_{N_{\mathrm{S}}^2}^m \lambda_{\mathrm{TS}_k}\exp\left(-m\lambda_{\mathrm{S}_{k-1}\mathrm{S}_k}\mu_4\right)}{\lambda_{\mathrm{TS}_k}+m\lambda_{\mathrm{S}_{k-1}\mathrm{S}_k}\mu_3}. \quad (41)$$

Hence, the e2e OP in this case can be expressed as

$$\mathrm{OP}_{\mathrm{e2e}}^{\mathrm{Case\ 2}} = 1-\prod_{k=1}^{K}\left[\sum_{m=1}^{N_{\mathrm{S}}^2}\frac{(-1)^{m+1} C_{N_{\mathrm{S}}^2}^m \lambda_{\mathrm{TS}_k}\exp\left(-m\lambda_{\mathrm{S}_{k-1}\mathrm{S}_k}\mu_4\right)}{\lambda_{\mathrm{TS}_k}+m\lambda_{\mathrm{S}_{k-1}\mathrm{S}_k}\mu_3}\right]. \quad (42)$$

As P_{T} is high enough, $\mathrm{OP}_{\mathrm{e2e}}^{\mathrm{Case\ 2}}$ can be approximated as

$$\mathrm{OP}_{\mathrm{e2e}}^{\mathrm{Case\ 2}} \overset{P_{\mathrm{T}}\to+\infty}{\approx} 1-\prod_{k=1}^{K}\left[\sum_{m=1}^{N_{\mathrm{S}}^2}(-1)^{m+1}\frac{C_{N_{\mathrm{S}}^2}^m \lambda_{\mathrm{TS}_k}}{\lambda_{\mathrm{TS}_k}+\lambda_{\mathrm{S}_{k-1}\mathrm{S}_k}\mu_3}\right]. \quad (43)$$

3.2. E2e IP

Combining (27), (28) and (30), which yields

$$\begin{aligned} \mathrm{IP}_{\mathrm{e2e}}^{\mathrm{Case}\ i} &= \Pr\left(\max_{k=1,2,..,K}\left(\varphi_{\mathrm{S}_{k-1}^x\mathrm{E}^y}\right)\geq\rho_{\mathrm{Sth}}\right) \\ &= 1-\prod_{k=1}^{K}\left(\Pr\left(\varphi_{\mathrm{S}_{k-1}^x\mathrm{E}^y}<\rho_{\mathrm{Sth}}\right)\right), \end{aligned} \quad (44)$$

where

$$(x,y) = \begin{cases}(z,e), \text{ if } i=1\\(a,l), \text{ if } i=2\end{cases} \quad (45)$$

With the same derivation methods of $\mathrm{OP}_{\mathrm{e2e}}^{\mathrm{Case\ 1}}$ and $\mathrm{OP}_{\mathrm{e2e}}^{\mathrm{Case\ 2}}$, we can calculate $\Pr\left(\varphi_{\mathrm{S}_{k-1}^x\mathrm{E}^y}<\rho_{\mathrm{Sth}}\right)$, and then $\mathrm{IP}_{\mathrm{e2e}}^{\mathrm{Case\ 1}}$ and $\mathrm{IP}_{\mathrm{e2e}}^{\mathrm{Case\ 2}}$ can be respectively written as in (46) and (47):

$$\mathrm{IP}_{\mathrm{e2e}}^{\mathrm{Case\ 1}} = 1-\prod_{k=1}^{K}\left\{\left[1-\frac{\lambda_{\mathrm{TE}}\exp\left(-\lambda_{\mathrm{S}_{k-1}\mathrm{E}}\mu_4\right)}{\lambda_{\mathrm{TE}}+\lambda_{\mathrm{S}_{k-1}\mathrm{E}}\mu_3}\right]^{N_{\mathrm{E}}}\right\}, \quad (46)$$

$$\mathrm{IP}_{\mathrm{e2e}}^{\mathrm{Case\ 2}} = 1-\prod_{k=1}^{K}\left[1+\sum_{n=1}^{N_{\mathrm{E}}}(-1)^n\frac{C_{N_{\mathrm{E}}}^n\lambda_{\mathrm{TE}}\exp\left(-n\lambda_{\mathrm{S}_{k-1}\mathrm{E}}\mu_4\right)}{\lambda_{\mathrm{TE}}+n\lambda_{\mathrm{S}_{k-1}\mathrm{E}}\mu_3}\right]. \quad (47)$$

At high P_{T} regions, (46) and (47) can be approximated by

$$\mathrm{IP}_{\mathrm{e2e}}^{\mathrm{Case\ 1}} \overset{P_{\mathrm{T}}\to+\infty}{\approx} 1-\prod_{k=1}^{K}\left(\frac{\lambda_{\mathrm{S}_{k-1}\mathrm{E}}\mu_3}{\lambda_{\mathrm{TE}}+\lambda_{\mathrm{S}_{k-1}\mathrm{E}}\mu_3}\right)^{N_{\mathrm{E}}}, \quad (48)$$

$$\mathrm{IP}_{\mathrm{e2e}}^{\mathrm{Case\ 2}} \overset{P_{\mathrm{T}}\to+\infty}{\approx} 1-\prod_{k=1}^{K}\left[1+\sum_{n=1}^{N_{\mathrm{E}}}(-1)^n\frac{C_{N_{\mathrm{E}}}^n\lambda_{\mathrm{TE}}}{\lambda_{\mathrm{TE}}+n\lambda_{\mathrm{S}_{k-1}\mathrm{E}}\mu_3}\right]. \quad (49)$$

4. Simulation Results

Section 4 verifies the formulas obtained in Section 3 by Monte-Carlo simulations realized by MATLAB. Assume that the nodes T, R, S_k, and E are located at $(x_{\mathrm{T}}, y_{\mathrm{T}})$, $(x_{\mathrm{R}}, y_{\mathrm{R}})$, $(k/K, 0)$, and $(x_{\mathrm{E}}, y_{\mathrm{E}})$, respectively. In all the simulations, the system parameters are set as follows: $x_{\mathrm{E}}=0.5$, $y_{\mathrm{E}}=0.3$, and the by $\beta=3$, $\sigma_0^2=1$, $C_{\mathrm{Pth}}=1.5$, $C_{\mathrm{Sth}}=0.2$, $N_{\mathrm{S}}=N_{\mathrm{E}}=2$, $\varepsilon_{\mathrm{P}}=0.01$.

4.1. OP of Primary Network and Transmit Power of Secondary Transmitters

Figure 2 presents OP of the primary network as a function of P_{T}

$0.5, 0.6)$ and $(0.35, 0.3$

$N_T = N_R = 1$, OP at T is higher than ε_P when $P_T < 15$dB, and when $N_T = N_R = 2$, OP at T is higher than ε_P when $P_T < 0$dB. This means that the primary network can obtain the required QoS with lower transmit power P_T by equipping more antennas at T and R. It is shown in this figure that the OP value converges to ε_P at high P_T value due to the data transmission of the secondary networks. Finally, we can observe from Fig. 2 that the simulation results verify the theoretical ones.

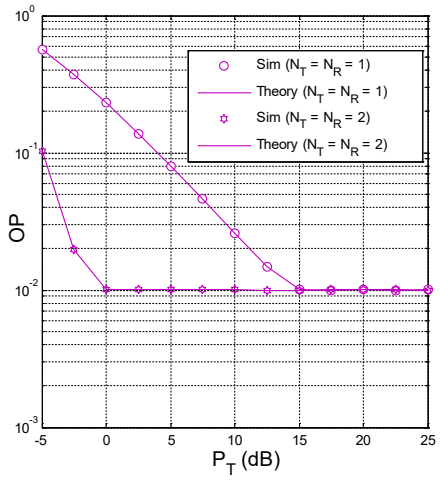


Figure 2: OP of the primary network as a function of P_T (dB) when $x_T = 0.5$, $y_T = 0.6$, $x_R = 0.35$, $y_R = 0.3$, $K = 2$.

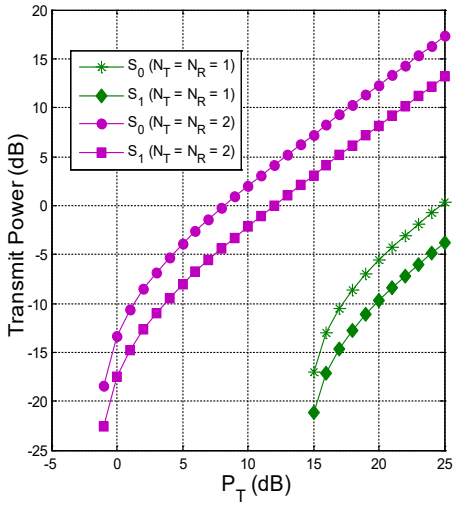


Figure 3: Transmit power of the secondary transmitters as a function of P_T (dB) when $x_T = 0.5$, $y_T = 0.6$, $x_R = 0.35$, $y_R = 0.3$, $K = 2$.

Figure 3 illustrates the transmit power of S_0 and S_1 as a function of P_T in dB. We note that the system parameters in Fig. 3 are same with those in Fig. 2. As shown in Fig. 3, the secondary transmitters S_0 and S_1 can use the licensed bands when P_T is high enough, i.e., when $N_T = N_R = 1$ then $P_T \geq 15$dB, and when $N_T = N_R = 2$ then $P_T \geq -1$dB. Because the OP performance of the primary network is better when the T and R nodes are equipped with more antennas, the secondary network has more opportunity to access the licensed bands. Finally, we can see that the transmit power of S_0 is higher than that of S_1 because the $S_0 - R$ distance is higher than the $S_1 - R$ one.

4.2. OP and IP of Secondary Network

In this sub-section, we present the e2e OP and IP of the proposed protocol in two cases considered in Section 3. In all of the presented figures, we fix the number of antennas at T and R by 2 ($N_T = N_R = 2$), and the positions of T and R at $(0.5, 0.6)$ and $(0.5, 0.4)$, respectively.

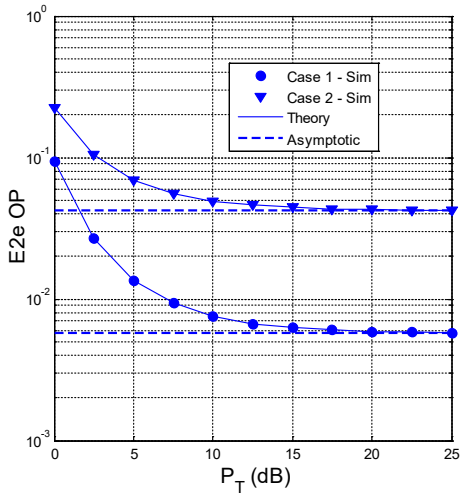


Figure 4: E2e OP as a function of P_T (dB) when $x_T = 0.5$, $y_T = 0.6$, $x_R = 0.5$, $y_R = 0.4$, $N_T = N_R = 2$, $K = 3$.

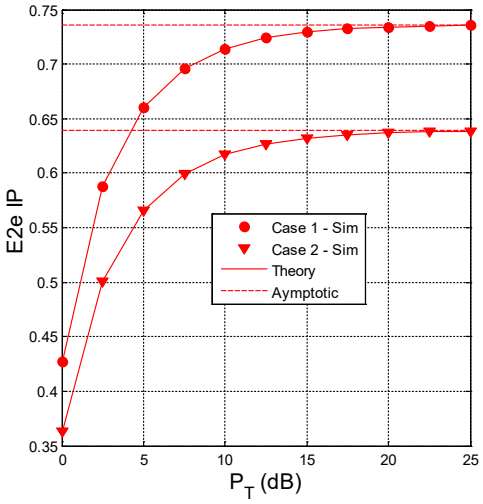


Figure 5: E2e IP as a function of P_T (dB) when $x_T = 0.5$, $y_T = 0.6$, $x_R = 0.5$, $y_R = 0.4$, $N_T = N_R = 2$, $K = 3$.

Figures 4 and 5 present OP and IP as a function of P_T in dB when the number of hops (K) equals to 3. As we can see, the OP and IP values at high P_T region do not depend on P_T, as proved in Section 3. This also means that with the impact of the co-channel interference from the primary network, the secondary network cannot obtain diversity order, i.e., there exists the error floor in the OP performance. As shown in Fig. 4, the e2e OP in Case 1 is much lower than that in Case 2. However, Figure 5 presents that the e2e IP in Case 1 is higher than that in Case 2. From Figs. 4 and 5, it is clearly presented the trade-off between OP and IP. Particularly, if the transmit power P_T is higher, the e2e OP is lower but the e2e IP is higher. Also, if the TAS/SC technique in Case 1 is used, the OP performance is better, but the IP performance is worse. Finally, it is also illustrated that the simulation results verify the derived formulas of the e2e OP and IP in Section 3.

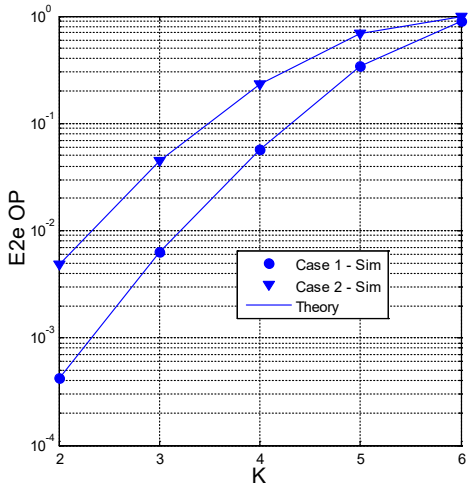


Figure 6: E2e OP as a function of K when $x_T = 0.5$, $y_T = 0.6$, $x_R = 0.5$, $y_R = 0.4$, $N_T = N_R = 2$, $P_T = 15$ (dB).

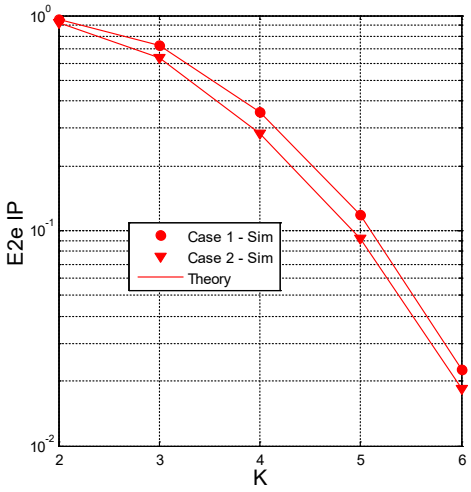


Figure 7: E2e IP as a function of K when $x_T = 0.5$, $y_T = 0.6$, $x_R = 0.5$, $y_R = 0.4$, $N_T = N_R = 2$, $P_T = 15$ (dB).

In Figs. 6-7, the e2e OP and IP is presented as a function of the number of hops (K) with $P_T = 15$ (dB). As presented, the OP values increase with the increasing of the number of hops, but the IP values decrease. Similar to Figs. 4-5, the OP and IP values in Case 1 are lower and higher than those in Case 2. Again, it is shown that there exists the trade-off between the e2e OP and IP performance, and the value of K should be carefully designed. For example, if the required OP of the secondary network is 0.1, then the optimal number of hops used in Case 1 and 2 (to obtain minimum value of IP) is 4 and 3, respectively.

5. Conclusion

This paper proposed the TAS/SC based multi-hop relaying protocol in the PLS underlay CR networks. The practical applications of the proposed protocol are listed as: i) enhancing the spectrum usage efficiency with underlay CR approach; ii) enhancing the performance of the primary and secondary networks with the TAS/SC techniques; iii) two practical TAS/SC techniques are applied for the secondary network; iv) all the derived expressions are in closed-form, which can be easily used for evaluating and optimizing the systems. Moreover, the results showed the trade-off between the IP and OP at the secondary network, and the bad effect of the co-channel interference from the primary network. Finally, the important parameters such as the number of hops and the transmit power of the primary transmitter should be carefully designed.

Conflict of Interest

The authors declare no conflict of interest.

Acknowledgment

This research is funded by Vietnam National Foundation for Science and Technology Development (NAFOSTED) under grant number 102.04-2017.317.

References

[1] L. Liu, R. Chen, S. Geirhofer, K. Sayana, Z. Shi, Y. Zhou, "Downlink MIMO in LTE-advanced: SU-MIMO vs. MU-MIMO" IEEE Commun. Mag., **50**(2), 140–147, 2012. https://doi.org/10.1109/MCOM.2012.6146493

[2] Y. Kim, H. Ji, J. Lee, Y.-H. Nam, B. Loong Ng, I. Tzanidis, Y. Li, "Full Dimension MIMO (FD-MIMO): The Next Evolution of MIMO in LTE Systems" IEEE Wireless Commun., **21**(3), 92-100, 2014. https://doi.org/10.1109/MWC.2014.6845053

[3] J. N. Laneman, D. N. Tse, G. W. Wornell, "Cooperative Diversity in Wireless Networks: Efficient Protocols and Outage Behavior" IEEE Trans. Inform. Theory, **50**(12), 3062–3080, 2004. https://doi.org/10.1109/TIT.2004.838089

[4] M. A. Beserra de Melo, D. Benevides da Costa, "An Efficient Relay–Destination Selection Scheme for Multiuser Multirelay Downlink Cooperative Networks" IEEE Trans. Veh. Techn., **61**(5), 2354 – 2360, 2012. https://doi.org/ 10.1109/TVT.2012.2192488

[5] M. D. Selvaraj, Ranjan K. Mallik , "Performance of Full CSI Selection Combining for Cooperative Diversity Systems" IEEE Trans. Commun., **60**(9), 2482 – 2488, 2012. https://doi.org/10.1109/TCOMM.2012.071212.110101

[6] O. S. Badarneh, D. B. da Costa, M. Benjillali and M. Alouini, "Selection Combining Over Double α-μ Fading Channels," IEEE Trans. Veh. Techn., **69**(3), 3444-3448, 2020. https://doi.org/10.1109/TVT.2020.2969224

[7] Y. Song, S.D. Blostein, J. Cheng, "Exact Outage Probability for Equal Gain Combining with Cochannel Interference in Rayleigh Fading" IEEE Trans. Wireless Commun., **2**(5), 865-870, 2003. https://doi.org/10.1109/TWC.2003.816796

[8] X.W. Cui, Q.T. Zhang, Z.M. Feng, "Outage Probability for Maximal Ratio Combining of Arbitrarily Correlated Faded Signals Corrupted by Multiple Rayleigh Interferers" IEEE Trans. Veh. Techn., **55**(1), 383- 386, 2006. https://doi.org/10.1109/TVT.2005.861186

[9] S. Kim, M. Shin, C. Lee, "Transmit Antenna Selection Scheme for Iterative Receivers in MIMO Systems" IEEE Sig. Proces. Lett., **14**(12), 916 – 919, 2007. https://doi.org/10.1109/LSP.2007.906230

[10] S. Kim, "Transmit Antenna Selection for Precoding-Aided Spatial Modulation," IEEE Access, **8**, 40723-40731, 2020. https://doi.org/10.1109/ACCESS.2020.2976732

[11] M. K. Arti, M. R. Bhatnagar, "Maximal Ratio Transmission in AF MIMO Relay Systems Over Nakagami-*m* Fading Channels," IEEE Trans. Veh. Techn., **64**(5), 1895-1903, 2015. https://doi.org/10.1109/TVT.2014.2334631

[12] D. T. Hung, T. T. Duy, T. T. Phuong, D. Q. Trinh, T. Hanh, "Performance Comparison between Fountain Codes-Based Secure MIMO Protocols With and Without using Non-Orthogonal Multiple Access" Entropy, **21**(10), 928, 2019. https://doi.org/10.3390/e21100982

[13] A. F. Coskun, O. Kucur, "Performance Analysis of Maximal-Ratio Transmission/Receive Antenna Selection in Nakagami-*m* Fading Channels With Channel Estimation Errors and Feedback Delay" IEEE Trans. Veh. Techn., **61**(3), 1099-1108, 2012. https://doi.org/10.1109/TVT.2012.2183650

[14] V. C. Papamichael, P. Karadimas, "Performance Evaluation of Actual Multielement Antenna Systems Under Transmit Antenna Selection/Maximal Ratio Combining," IEEE Antennas Wireless Propag. Lett., **10**, 690 – 692, 2011. https://doi.org/10.1109/LAWP.2011.2161662

[15] T. T. Duy, Trung Q. Duong, D.B. da Costa, V.N.Q. Bao, M. Elkashlan, "Proactive Relay Selection with Joint Impact of Hardware Impairment and Co-channel Interference" IEEE Trans. Commun., **63**(5), 1594-1606, 2015. https://doi.org/10.1109/TCOMM.2015.2396517

[16] P. N. Son, T. T. Duy, "A New Approach for Two-Way Relaying Networks: Improving Performance by Successive Interference Cancellation, Digital Network Coding and Opportunistic Relay Selection" Wireless Netw., **26**(2), 1315-1329, 2020. https://doi.org/10.1007/s11276-019-02186-1

[17] E. Bjornson, M. Matthaiou, M. Debbah, "A New Look at Dual-Hop Relaying: Performance Limits with Hardware Impairments," IEEE Trans. Commun., **61**(11), 4512-4525, 2013. https://doi.org/10.1109/TCOMM.2013.100913.130282

[18] J. Ma, C. Huang, S. Cui, Q. Li, "Energy Efficiency of Amplify-and-Forward Full-Duplex Relay Channels," IEEE Wireless Commun. Lett., **8**(5), 1365 - 1368, 2019. https://doi.org/10.1109/LWC.2019.2918290

[19] G. Farhadi, N. C. Beaulieu, "A General Framework for Symbol Error Probability Analysis of Wireless Systems and Its Application in Amplify-and-Forward Multihop Relaying" IEEE Trans. Veh. Techn., 59(3), 1505 - 1511, 2010. https://doi.org/10.1109/TVT.2009.2037642

[20] M. R. Bhatnagar, "Performance Analysis of a Path Selection Scheme in Multi-Hop Decode-and-Forward Protocol" IEEE Commun. Lett., **16**(12), 1980 - 1983, 2012. https://doi.org/10.1109/TVT.2009.2037642

[21] T. D. Hieu, T. T. Duy, B.-S. Kim, "Performance Enhancement for Multi-hop Harvest-to-Transmit WSNs With Path-Selection Methods in Presence of Eavesdroppers and Hardware Noises" IEEE Sensors Journal, **18**(12), 5173 - 5186, 2018. https://doi.org/10.1109/JSEN.2018.2829145

[22] I. H. Lee, D. Kim, "Outage Probability of Multi-Hop MIMO Relaying With Transmit Antenna Selection and Ideal Relay Gain Over Rayleigh Fading Channels" IEEE Trans. Commun., **57**(2), 357 - 360, 2009. https://doi.org/10.1109/TCOMM.2009.02.070058

[23] A. A. AbdelNabi, F. S. Al-Qahtani, M. Shaqfeh, S. S. Ikki, H. M. Alnuweiri, "Performance Analysis of MIMO Multi-Hop System With TAS/MRC in Poisson Field of Interferers," IEEE Trans. Commun., **64**(2), 525-540, 2016. https://doi.org/10.1109/TCOMM.2015.2496291

[24] A. D. Wyner, "The Wire-tap Channel" Bell System Technical Journal, **54**(8), 1355 – 1387, 1975. https://doi.org/10.1002/j.1538-7305.1975.tb02040.x

[25] I. Csiszar, J. Korner, "Broadcast Channels with Confidential Messages" IEEE Trans. Inform. Theory, **24**(3), 339 – 348, 1978. https://doi.org/10.1109/TIT.1978.1055892

[26] N. S. Ferdinand, D. B. da Costa, A. L. F. de Almeida, M. Latva-aho, "Physical Layer Secrecy Performance of TAS Wiretap Channels with Correlated Main and Eavesdropper Channels" IEEE Wireless Commun. Lett., **3**(1), 86-89, 2014. https://doi.org/10.1109/WCL.2013.112313.130733

[27] J. Xiong, Y. Tang, D. Ma, P. Xiao, K. Wong, "Secrecy Performance Analysis for TAS-MRC System With Imperfect Feedback" IEEE Trans. Inf. Forensics Security, **10**(8), 1617-1629, 2015. https://doi.org/10.1109/TIFS.2015.2421358

[28] J. Si, Z. Li, J. Cheng, C. Zhong, "Asymptotic Secrecy Outage Performance for TAS/MRC Over Correlated Nakagami-*m* Fading Channels," IEEE Trans. Commun., **67**(11), 7700-7714, 2019. https://doi.org/10.1109/TCOMM.2019.2935444

[29] D. Tran, H. Tran, D. Ha, G. Kaddoum, "Secure Transmit Antenna Selection Protocol for MIMO NOMA Networks Over Nakagami-m Channels," IEEE Systems Journal, 14(1), 253-264, 2020. https://doi.org/10.1109/JSYST.2019.2900090

[30] I. Krikidis, "Opportunistic Relay Selection For Cooperative Networks With Secrecy Constraints" IET Commun., **4**(15), 1787 – 1791, 2010. https://doi.org/ 10.1049/iet-com.2009.0634

[31] J. Mo, M. Tao, Y. Liu, "Relay Placement for Physical Layer Security: A Secure Connection Perspective," IEEE Commun. Lett., **16**(6), 878–881, 2012. https://doi.org/10.1109/LCOMM.2012.042312.120582

[32] P. T. Tin, D. T. Hung, T. T. Duy, M. Voznak, "Analysis of Probability of Non-zero Secrecy Capacity for Multi-hop Networks in Presence of Hardware Impairments over Nakagami-*m* Fading Channels" RadioEngineering, **25**(4), 774-782, 2016. http://dx.doi.org/10.13164/re.2016.0774

[33] Y. Zou, B. Champagne, W. P. Zhu, L. Hanzo, "Relay-Selection Improves the Security-Reliability Trade-off in Cognitive Radio Systems," IEEE Trans. Commun., **63**(1), 215 – 228, 2015. http://dx.doi.org/10.1109/TCOMM.2014.2377239

[34] G. Zhang, Y. Gao, H. Luo, S. Wang, M. Guo and N. Sha, "Security Performance Analysis for Best Relay Selection in Energy-Harvesting Cooperative Communication Networks," IEEE Access, vol. 8, pp. 26-2020, http://dx.doi.org/10.1109/ACCESS.2019.2960819

[35] J. Mitola, G. Q. Maguire, "Cognitive Radio: Making Software Radios More Personal" IEEE Pers. Commun., **6**(4), 13-18, 1999. http://dx.doi.org/10.1109/98.788210

[36] Y. Guo, G. Kang, N. Zhang, W. Zhou, P. Zhang, "Outage Performance of Relay-Assisted Cognitive-Radio System Under Spectrum-Sharing Constraints" Electronics Lett., **46**(2), 1-2, 2010. http://dx.doi.org/10.1049/el.2010.2159

[37] K. Tourki, K. A. Qaraqe, M.-S. Alouini, "Outage Analysis for Underlay Cognitive Networks Using Incremental Regenerative Relaying" IEEE Trans. Veh. Techn., **62**(2), 721-734, 2013. http://dx.doi.org/ 10.1109/TVT.2012.2222947

[38] Y. Liu, L. Wang, T. D. Tran, M. Elkashlan, T. Q. Duong, "Relay Selection for Security Enhancement in Cognitive Relay Networks" IEEE Wireless Commun. Lett., **4**(1): 46-49, 2015. http://dx.doi.org/10.1109/LWC.2014.2365808

[39] M. Elkashlan, L. Wang, T. Q Duong, G. K. Karagiannidis, A. Nallanathan, "On the Security of Cognitive Radio Networks" IEEE Trans. Veh. Techn., **64**(8), 3790 – 3795, 2015. http://dx.doi.org/10.1109/TVT.2014.2358624

[40] P. M. Nam, T. T. Duy, P. V. Ca, "End-to-end Security-Reliability Analysis of Multi-hop Cognitive Relaying Protocol with TAS/SC-based Primary Communication, Total Interference Constraint and Asymmetric Fading Channels" International Journal of Communication Systems, **32**(2), 1-16, 2019. http://dx.doi.org/10.1002/DAC.3854

[41] H. D. Hung, T. T. Duy, M. Voznak, ""Secrecy Outage Performance of Multi-hop LEACH Networks Using Power Beacon Aided Cooperative Jamming With Jammer Selection Methods," AEU International Journal of Electronics and Communications, **124**, 1-24, 2020. https://doi.org/10.1016/j.aeue.2020.153357

[42] P. T. Tin, D. T. Hung, N. N. Tan, T. T. Duy, M. Voznak, "Secrecy Performance Enhancement for Underlay Cognitive Radio Networks Employing Cooperative Multi-hop Transmission With and Without Presence of Hardware Impairments" Entropy, **21**(2), 217, 2019. https://doi.org/10.3390/e21020217

[43] P. T. Tin, P. M. Nam, T. T. Duy, T. T. Phuong, M. Voznak, "Secrecy Performance of TAS/SC-based Multi-hop Harvest-to-Transmit Cognitive WSNs under Joint Constraint of Interference and Hardware Imperfection" Sensors, **19**(5), 1160, 2019. https://doi.org/10.3390/s19051160

[44] P. M. Nam, P. V. Ca, T. T. Duy, Khoa N. Le, "Secrecy Performance Enhancement Using Path Selection Over Cluster-Based Cognitive Radio Networks" in 5th EAI International Conference on Industrial Networks and Intelligent Systems, HoChiMinh city, Vietnam, 2019. https://doi.org/10.1007/978-3-030-30149-1_6

ASTES

Advances in Science, Technology and Engineering Systems Journal
Vol. 5, No. 5, 63-68 (2020)
www.astesj.com
Special Issue on Multidisciplinary Innovation in Engineering Science & Technology

ASTES Journal
ISSN: 2415-6698

Fast Stream Cipher based Chaos Neural Network for Data Security in CAN Bus

Zhongda Liu[*,1], Takeshi Murakami[2], Satoshi Kawamura[3], Hitoaki Yoshida[4]

[1]*Faculty of Science and Engineering, Ishinomaki Senshu University, Ishinomaki, 986-8580, Japan*

[2]*Technical Division, Iwate University, Morioka, 020-8550, Japan*

[3]*Faculty of Humanities, Morioka University, Takizawa,020-8550, Japan*

[4]*Faculty of Education, Iwate University, Morioka, 020-8550, Japan*

ARTICLE INFO

Article history:
Received: 02 July, 2020
Accepted: 24 August, 2020
Online: 09 September, 2020

Keywords:
Stream cipher
CAN
Chaos
Encryption and decryption

ABSTRACT

Vehicle systems are controlled by embedded electronic devices called electronic control units (ECUs). These ECUs are connected together with network protocols. The Controller Area Network (CAN) protocol is widely implemented due to its high fault tolerance. However, the CAN is a serial broadcast bus, and it has no protection against security threats. In this paper, we propose a fast stream cipher based on a chaos neural network (CNN) that is able to generate pseudo-random numbers at a high speed, faster than that of the Advanced Encryption Standard, to protect ECUs on the CAN bus by encrypting CAN messages. We discuss the chaotic orbit of the CNN and statistical properties of pseudo-random numbers from the CNN. For a stream cipher, it is very important to share the symmetric key. We designed a symmetric key that is shared with ID-based encryption without the need to use digital certificates. We evaluated our method's performance with embedded boards and showed that the stream cipher is efficient for the embedded software of the ECU. Further, it does not need a hardware security module to accelerate the encryption.

1 Introduction

This paper is an extension of work originally presented at the IEEE 10th International Conference on Awareness Science and Technology [1]. In that work, we found that a chaos neural network (CNN) is able to generate pseudo-random numbers (PRNs) at high speed, 49% faster than that produced with the Advanced Encryption Standard (AES) [2], [3], and it can be easily implemented even for embedded devices.

Generally, electronic devices embedded in vehicles to control vehicle systems are called electronic control units (ECUs). A modern vehicle is usually equipped with more than 70 ECUs [4]. To share information and control the subsystems, those ECUs are connected together with network protocols, such as a Controller Area Network (CAN), Local Interconnect Network (LIN), Media Oriented Systems Transport (MOST), or FlexRay.

The CAN is a broadcast serial communications bus that is widely introduced because of its fault tolerance. The CAN identifier (ID) (see Sec. 2 and Fig. 1) is used for prioritizing messages on the bus and avoids collisions by design. However, security issues were ignored during designing since people took it for granted that a vehicle would be a closed system [5], [6]. Unfortunately, messages are broadcast on the CAN bus, and external devices, such as on-board diagnostics readers, are able to access the CAN bus in modern vehicles.

A pseudo-random number generation (PRNG) is crucial to a stream cipher in information security field. We have reported various PRNG methods [7]–[11] and the property of PRNs from a CNN [9] has been confirmed [10] by National Institute of Standards and Technology (NIST) Special Publication 800-22 [12]. An ultra-long period PRNs that has reached 10^{22432} [11] can be generated with the chaotic time series from the CNNs. The chaotic time series is hard to predict because it is sensitive to tiny change of the initial status.

In this paper, we propose a fast stream cipher based on a CNN to

[*]Corresponding Author: Zhongda Liu, Faculty of Science and Engineering, Ishinomaki Senshu University, Ishinomaki, 986-8580, Japan
Email: liuzd@isenshu-u.ac.jp

protect CAN messages by encrypting them. The remainder of this paper is organized as follows: Section 2 introduces CAN and security issues and surveys some related work. Section 3 describes our CNN and discusses some of its characteristics. Section 4 presents the CNN stream cipher, including sharing of the symmetric key and the procedure for encryption and decryption of the stream cipher. A performance evaluation of the proposed CNN stream cipher is given in Section 5. Finally, Section 6 concludes this paper.

2 Related Work

A CAN is a serial communications bus defined by the International Organization for Standardization (ISO) and originally developed for the automotive industry to replace the complex wiring harness with a two-wire bus [13]. Balanced differential signaling reduces noise coupling and enables high noise immunity in the CAN bus.

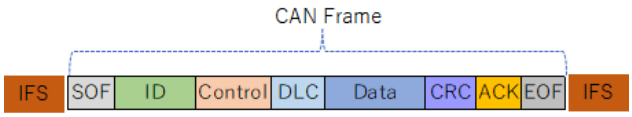


Figure 1: Structure of the CAN data frame

The CAN communication protocol is a carrier-sense multiple access protocol with collision detection and arbitration on message priority. A CAN message contains a unique ID field that represents the priority and function of the message. The CAN protocol supports four different message types: overload, error, remote, and data frame. The CAN data frame begins with a start-of-frame (SOF) bit and is followed by the ID, a control field (6 bits), 4-bit data length code (DLC), 0-64 bits of data, a cyclic redundancy check (CRC) sequence (15 bits), a 2-bit acknowledgment (ACK), and a 7-bit end of frame (EOF) sequence that marks the end of the frame. Between CAN frames, a 7-bit inter-frame space (IFS) is required by the CAN controller to provide time for moving a received frame to a message buffer area (see Fig. 1).

The CAN was subsequently adopted as ISO standards. ISO 11519 (low-speed CAN) is for applications up to 125 kbps with a standard 11-bit ID, while ISO 11898 (high-speed CAN) provides for signaling rates from 125 kbps to 1 Mbps. Furthermore, high-speed CAN supports two data frame formats, where the standard frame consists of an 11-bit ID, while the extended format contains a 29-bit ID.

Unfortunately, security issues were ignored during designing because people took it for granted that CANs would be a closed system in automobiles [5], [6]. Security issues with CANs relate mainly to authentication and encryption at the present time.

Authentication: To identify whether an ECU is authorized, several authentication proposals based on message authentication codes (MACs) have been released. Key sharing is a matter of grave concern. CANAuth [14] implements a backward-compatible message authentication protocol on the CAN bus. One or more pre-shared 128-bit MAC keys are to be available on each CANAuth node. CANAuth assumes that the keys are intended to be stored in tamper-proof storage that cannot be queried by anything but the node itself. LiBrA-CAN [15] splits authentication keys between groups of multiple nodes, rather than achieving authentication independently for each node.

Encryption: A CAN frame is broadcast over the bus. In modern vehicles, external devices, such as on-board diagnostics readers, are able to access the CAN bus, making it is easy to intercept a CAN message. Cryptographic approaches based on the AES have been proposed to guard against such interception. The problem is the computation load of the AES, which might have an undue influence on the response of the ECU. Wolf and Gendrullis [16] and the EVITA Project [17], [18] implemented a hardware security module (HSM) to accelerate the AES measures. However, even if a HSM is used, the cryptographic measure requires 60 clock cycles (at 100 MHz) for the encryption of one AES block [18]. This is insufficient for dealing with the real-time response required of an ECU. Also, the additional hardware increases the cost of the ECU.

In this study, we focused on the encryption issues in CANs. We propose a fast stream cipher based on a CNN that does not need the additional HSM hardware.

3 Chaos Neural Network

As a chaos generator the CNN consisted of 4 neurons in a discrete time system (see Fig. 2).

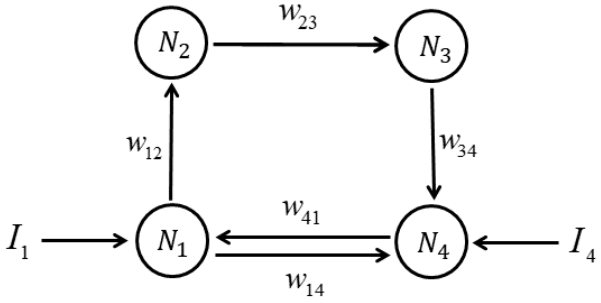


Figure 2: CNN consisting of four artificial neurons

An output from the jth neuron at time $t+1$ is defined as:

$$x_j(t+1) = f[u_j(t)] \tag{1}$$

Here, An activation-function f (see Fig. 3) is an asymmetric piecewise-linear function (APLF).

For the jth neuron, the total value of inputs at time t is defined as :

$$u_j(t) = \sum_{i=1}^{n} w_{ij} x_i(t) + I_j \tag{2}$$

I_j is an external input of the jth neuron. $x_i(t)$ is an input from the ith neuron at time t, and w_{ij} is a synaptic. Generally, the start value of x_i is set as 0, and the synaptic weights are set as follows: $w_{12} = -12.60001$, $w_{14} = 4.511$, $w_{23} = 5.951$, $w_{34} = -4.7004$ and $w_{41} = -7.345007$. The synaptic weights adjust the input values

from other neurons. If extreme synaptic weights were set, the output range of neurons would be limited [19]. The external inputs I_1 and I_4 share a common value ($I_1 = I_4$), and I_2 and I_3 are set as 0 ($I_2 = I_3 = 0$). Thus, a different CNN would be obtained if a different value for I_1 and I_4 were set.

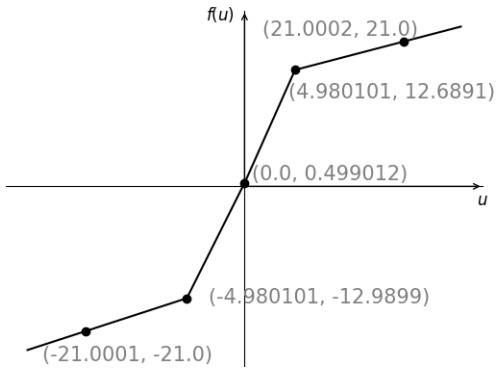


Figure 3: An activation-function f (APLF)

An activation-function APLF can avoid a periodic window corresponding to a non-chaotic periodic orbit. The activation-function APLF composed of linear functions by connecting five points. Those points can be changed as independent parameters. In a cipher system, the points of APLF can be selected as secret keys [9], [10], [20].

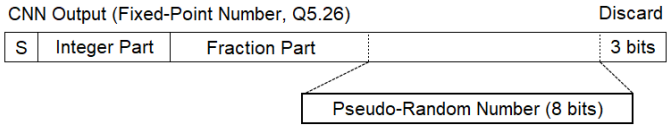


Figure 4: The extraction method of a PRN from a CNN output

Generally, discrete time system of the CNN is implemented with floating-point arithmetic [9]. But many embedded devices do not support 64-bit floating-point arithmetic. In this paper, the CNN is computed by 32-bit fixed-point arithmetic (Q5.26) and it allows overflow and underflow of variables. Comparing to 32-bit floating-point arithmetic, the fractional part of Q5.26 has enough long bit length. PRNs are extracted by the method presented in Figure 4. With regard to the CNN output, the lowest 3 bits of the fraction are discarded [8] and the lower 8 bits of the fraction are extracted as a PRN. Those PRNs from the CNN are applied to the proposed stream cipher .

3.1 Chaotic Orbit

A chaotic orbit is hard to predict because it is sensitive to tiny changes of the initial status. Here, Figure 5 shows time series from a CNN (Q5.26). Corresponding to all external inputs, output time series in the diagram present no bifurcation pattern but chaotic characteristics. It suggests that all external inputs can be used for chaos generation. In fact, the CNN generates the same time series on the ARM CPU and X86 CPU when the same parameters are set. Therefore the CNN is portable between different machines. Moreover, the Lyapunov exponents λ are computed per time series. The maximum Lyapunov exponents is about 2.5 and all of value is $\lambda > 0$. The Kolmogorov-Sinai entropy [21] is also computed by use of Lyapunov exponents, it is about 4.2. Those results demonstrate that the time series from the CNN has chaotic orbit and a high degree of randomness.

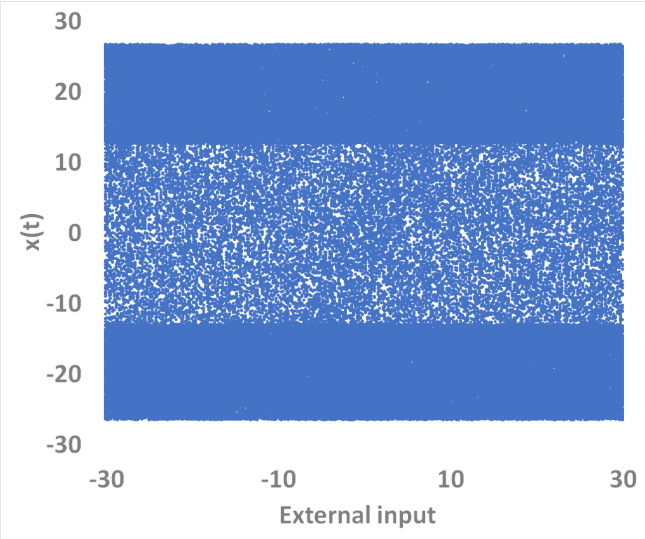


Figure 5: The input-output characteristics of time series from a CNN

3.2 Randomness

Randomness of the PRNs that were extracted from the CNN was confirmed by NIST Special Publication 800-22 statistical test suite [12]. Since NIST test has a couple of trouble (asymptotic approximation, etc.) even the test suite is updated [22], [23], NIST test method presented in the literature [24] was adopted.

We performed the NIST test for 1,000 times. And $10^6 \times 1,000$ bits of PRNs were generated by the method shown in Fig. 4 for per test. NIST test results are presented in Table 1. The failure ratio for the proportion is under 1%, and the failure ratio for the P-values that check for uniformity of distribution is less than 0.1%. All of those results suggest that all of tests passed these criteria, and the tested PRNs from the CNN have good statistical properties.

4 CNN Stream Cipher

The proposed stream cipher has two phases: an ID-based encryption (IBE) phase and a stream phase (see Fig. 6). Each phase uses different CAN IDs; that is, the CAN ID associates a CAN frame with a specific phase. In the advance IBE phase, the symmetric key is shared with IBE [25], [26] among authorized ECUs. Subsequently, an authorized ECU sends encrypted data frames to other authorized ECUs and those ECUs can decrypt data using the symmetric key in the stream phase.

Table 1: NIST SP800-22 statistical test results

	FR[a]	BF[a]	CS[a]	RU[a]	LR[a]	RK[a]	FF[a]	NT[a]
Proportion	0.3	0.2	0.3	0.5	0.4	0.4	0.9	0.2
P-value	0.0	0.0	0.0	0.0	0.1	0.0	0.1	0.0
	OT[a]	UN[a]	AE[a]	RE[a]	RV[a]	SE[a]	LC[a]	
Proportion	0.3	0.7	0.2	0.4	0.2	0.2	0.1	
P-value	0.0	0.0	0.0	0.0	0.0	0.0	0.1	

FR: Frequency, BF: Block Frequency, CS: Cumulative Sums, RU: Runs, LR: Longest Run, RK: Rank, FF: FFT, NT: Non-overlapping Template, OT: Overlapping Template, UN: Universal, AE: Approximate Entropy, RE: Random Excursions, RV: Random Excursions Variant, SE: Serial, LC: Linear Complexity

[a] Numbers are average ratio of failed tests (%).

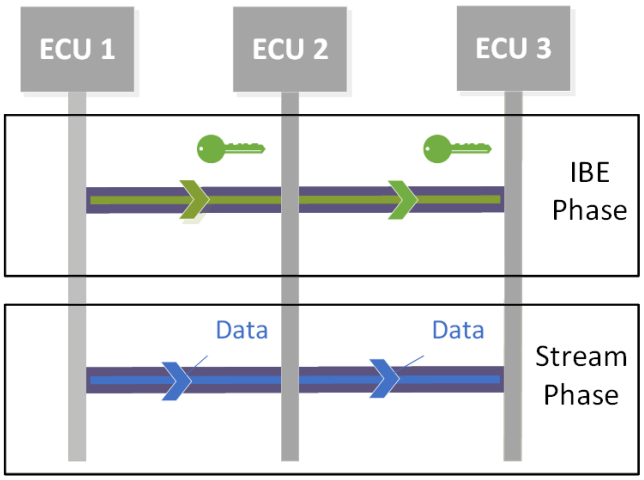


Figure 6: Overview of CNN stream cipher

4.1 IBE phase

It is an important step for the stream cipher to create, manage, and share the symmetric key. A public key infrastructure is used in the Internet to ensure secure communication generally. With this infrastructure, an on-line certificate authority (CA) is necessary, and the cost for issuing digital certificates may become prohibitive [27].

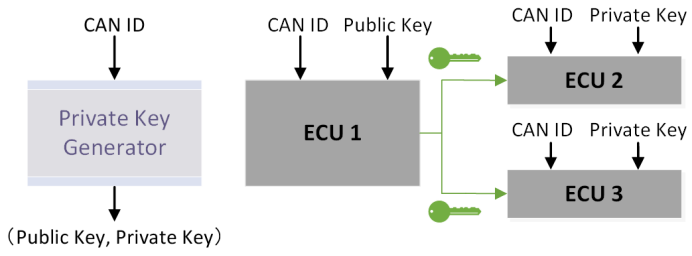


Figure 7: IBE phase

In the proposed stream cipher, we use IBE [26] to create, manage, and share the symmetric key. Fig. 7 shows how the symmetric key is shared among authorized ECUs. The private key generator (PKG) can be offline and does not need to use digital certificates instead of a CA. The PKG initially defines which CAN IDs are used in the IBE phase. For each valid CAN ID, the PKG outputs a public and private key pair that is issued to authorized ECUs. Thus, an ECU can use the public key to encrypt the symmetric key that is used in the stream phase and send it over the CAN bus. When an ECU receives a CAN frame, it checks the CAN ID to confirm the phase and decrypts the data in the CAN frame to obtain the symmetric key in the IBE phase.

4.2 Stream phase

In the stream phase, authorized ECUs use the symmetric key that was obtained during the IBE phase to encrypt and decrypt CAN frames (see Fig. 8). The CNN implemented in authorized ECUs generates a stream of pseudo-random bits: R_1, R_2, R_3, ..., R_i with the symmetric key. This stream is XORed with a stream of bits, D_1, D_2, D_3, ..., D_i, which are from the data in a CAN frame, to produce the stream of cipher text bits. Then each cipher text character is given by $C_i = D_i \oplus R_i$, which is loaded into a CAN frame and translated with the CAN bus. The procedure of decryption is almost the same: when an authorized ECU has received a CAN data frame, the CNN in the ECU generates the same stream of pseudo-random bits R_i and the original data is obtained by $D_i = C_i \oplus R_i$.

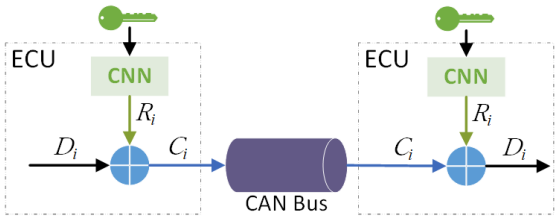


Figure 8: Stream phase

5 Evaluation

It is most important to ensure the safety of the vehicle and its passengers. Therefore, the embedded software of the ECU must run quickly to deal with the constraints of a real-time response. This section describes the performance evaluation of the CNN stream cipher with two embedded CAN boards (listed as Board A and B in Table 2) that were provided by P&A Technologies Inc. These CPUs have a different architecture, where Board A was implemented with a SH2A CPU, while Board B used an ARM CPU. Those boards are connected by a length of about 80*cm* twisted pair cable with D-sub connector.

Table 2: Specifications of experimental CAN boards

Component	Board A	Board B
CPU	R5S72630P200FP SH2A-FPU core (196 MHz)	SAMA5D27C-D1G ARM Cortex-A5 (492 MHz)
RAM	SDR SDRAM (64 MHz)	DDR2-SDRAM (120 MHz)
CAN Controller	Built-in CPU	FPGA IP

5.1 Experimental setup

In our experiments, we tested only the high-speed CAN whose bit rate is typically 500 Kbps, up to 1 Mbps. In fact, another CAN standard specifies low-speed CAN (see Sec. 2) at transmission rates above 40 Kbps up to 125 Kbps. It is more difficult to deal with real-time constraints at the high-speed CAN bit rate. Thus, we assumed that our stream cipher would work well at the low-speed CAN bit rate if it successfully ran with the high-speed CAN.

The PKG can be performed offline. Thus, we assume that Boards A and B are two authorized ECUs and they have already gained the symmetric key. Then we implemented the CNN on Boards A and B. According to the symmetric key, the same stream of pseudo-random numbers was generated in both boards and used to encrypt the data part of a CAN frame in one board and decrypt it in the other board.

5.2 Experimental Results

One thousand CAN message frames were sent between Boards A and B to confirm the validity of the CNN stream cipher and measure the encryption and decryption time. We tested with 500-Kbps and 1-Mbps bit rates. The CAN bus was loaded with over 60% higher-priority traffic.

Table 3: Results of performance testing with CAN boards

	average time
Board A	44 μs
Board B	4 μs

We confirmed the CAN log data of Boards A and B, which showed that each board encrypted and decrypted CAN data frames successfully. With Board A, the procedure for encryption or decryption was performed within 44 μs on average. With Board B, the procedure only took 4 μs on average (see Table 3). The results suggest that the performance of the CNN stream cipher is adequate for real-time requirements of an ECU without additional HSM hardware.

6 Conclusions

In this paper, we have proposed and evaluated a fast stream cipher based on a CNN to provide security for the ECUs on a CAN bus. We have shown that the CNN is chaotic and have strong randomness, and that PRNs with a high degree of randomness can be generated from a CNN. In the proposed stream cipher, IBE is used to create, manage, and share the symmetric key. The PKG can be performed offline and does not need to use digital certificates. The stream cipher was evaluated with embedded CAN boards. The performance test results suggested that our method is efficient for software embedded in an ECU and has no need for a HSM to accelerate the encryption process.

As future work, we will design a new activation-function APLF to extend randomness of the CNN and improve the performance of the stream cipher based on the CNN.

References

[1] Z. Liu, T. Murakami, S. Kawamura, H. Yoshida, "Parallel Implementation of Chaos Neural Networks for an Embedded GPU," in 2019 IEEE 10th International Conference on Awareness Science and Technology (iCAST), 1–6, IEEE, 2019, doi:10.1109/ICAwST.2019.8923383.

[2] NIST FIPS PUB, "197, Advanced Encryption Standard (AES)," Federal information processing standards publication, **197**(441), 0311, 2001, doi:10.6028/NIST.FIPS.197.

[3] J. Daemen, V. Rijmen, Rijndael/AES, 520–524, Springer US, 2005, doi:10.1007/0-387-23483-7_358.

[4] A. Albert, et al., "Comparison of event-triggered and time-triggered concepts with regard to distributed control systems," Embedded world, **2004**, 235–252, 2004.

[5] P. Carsten, T. R. Andel, M. Yampolskiy, J. T. McDonald, S. Russ, "A system to recognize intruders in controller area network (CAN)," in 3rd International Symposium for ICS & SCADA Cyber Security Research 2015 (ICS-CSR 2015) 3, 111–114, 2015, doi:10.14236/ewic/ICS2015.15.

[6] R. Buttigieg, M. Farrugia, C. Meli, "Security issues in controller area networks in automobiles," in 2017 18th International Conference on Sciences and Techniques of Automatic Control and Computer Engineering (STA), 93–98, IEEE, 2017, doi:10.1109/STA.2017.8314877.

[7] H. Yoshida, Y. Nihei, T. Nakanishi, "Comparative study on structurally different chaos neural network," in Proceedings of Papers, International Symposium on Information Theory and its Applications, ISITA 2004, 1046–1050, 2004.

[8] S. Kawamura, H. Yoshida, M. Miura, M. Abe, "Implementation of Uniform Pseudo Random Number Generator and Application to Stream Cipher based on Chaos Neural Network," in The International Conference on Fundamentals of Electronics, Communications and Computer Sciences, 2002, 4–9, 2002.

[9] H. Yoshida, T. Murakami, Z. Liu, "High-speed and highly secure pseudo-random number generator based on chaos neural network," New Trends on System Science and Engineering: Proceedings of ICSSE, **276**, 224–237, 2015, doi:10.3233/978-1-61499-522-7-224.

[10] H. Yoshida, T. Murakami, T. Inao, S. Kawamura, "Origin of Randomness on Chaos Neural Network," Trends in Applied Knowledge-Based Systems and Data Science, **9799**, 587–598, 2016, doi:10.1007/978-3-319-42007-3_51.

[11] H. Yoshida, Y. Akatsuka, T. Murakami, "Implementation of High-Performance Pseudo-Random Number Generator by Choas Neural Networks using Fix-Point Arithmetic with Perturbation," in Proceedings of Papers, The 2018 International Symposium on Nonlinear Theory and Its Applications, NOLTA2018, 46–49, 2018.

[12] A. Rukhin, J. Soto, J. Nechvatal, M. Smid, E. Barker, editors, A statistical test suite for random and pseudorandom number generators for cryptographic applications, NIST Special Publication 800-22, 2001.

[13] S. C. HPL, "Introduction to the controller area network (CAN)," Appl. Rep. SLOA101, 1–17, 2002.

[14] A. Van Herrewege, D. Singelee, I. Verbauwhede, "CANAuth - a simple, backward compatible broadcast authentication protocol for CAN bus," in ECRYPT Workshop on Lightweight Cryptography, volume 2011, 2011.

[15] B. Groza, S. Murvay, A. Van Herrewege, I. Verbauwhede, "LiBrA-CAN: a lightweight broadcast authentication protocol for controller area networks," in International Conference on Cryptology and Network Security, 185–200, Springer, 2012, doi:10.1007/978-3-642-35404-5_15.

[16] M. Wolf, T. Gendrullis, "Design, implementation, and evaluation of a vehicular hardware security module," in International Conference on Information Security and Cryptology, 302–318, Springer, 2011, doi:10.1007/978-3-642-31912-9_20.

[17] O. Henniger, A. Ruddle, H. Seudié, B. Weyl, M. Wolf, T. Wollinger, "Securing vehicular on-board IT systems: The evita project," in VDI/VW Automotive Security Conference, 41, 2009.

[18] H. Schweppe, Y. Roudier, B. Weyl, L. Apvrille, D. Scheuermann, "Car2x communication: securing the last meter-a cost-effective approach for ensuring trust in car2x applications using in-vehicle symmetric cryptography," in 2011 IEEE Vehicular Technology Conference (VTC Fall), 1–5, IEEE, 2011, doi:10.1109/VETECF.2011.6093081.

[19] H. Yoshida, H. Fukuchi, T. Murakami, "Implementation of High-Speed Pseudo-Random-Number Generator with Chaotic and Random Neural Networks," in Proceedings of the 53rd Hawaii International Conference on System Sciences, 2020, doi:10.24251/HICSS.2020.786.

[20] H. Yoshida, T. Murakami, Japan patent JP5504501B, 2014.

[21] T. S. Parker, L. O. Chua, "Chaos: A tutorial for engineers," Proceedings of the IEEE, **75**(8), 982–1008, 1987, doi:10.1109/PROC.1987.13845.

[22] K. Hamano, T. Kaneko, "Correction of overlapping template matching test included in NIST randomness test suite," IEICE transactions on fundamentals of electronics, communications and computer sciences, **90**(9), 1788–1792, 2007, doi:10.1093/ietfec/e90-a.9.1788.

[23] H. Okutomi, K. Nakamura, "A study on rational judgement method of randomness property using NIST randomness test (NIST SP. 800-22)," IEICE Trans. A, **93**(1), 11–22, 2010.

[24] H. Yoshida, T. Murakami, S. Kawamura, "Study on testing for randomness of pseudo-random number sequence with NIST SP800-22 rev. 1a," Technical report, IEICE Technical Report, 2012.

[25] A. Shamir, "Identity-based cryptosystems and signature schemes," in Workshop on the theory and application of cryptographic techniques, 47–53, Springer, 1984, doi:10.1007/3-540-39568-7_5.

[26] D. Boneh, M. Franklin, "Identity-based encryption from the Weil pairing," in Annual international cryptology conference, 213–229, Springer, 2001, doi:10.1007/3-540-44647-8_13.

[27] A. Nash, W. Duane, C. Joseph, PKI: Implementing and Managing E-security, McGraw-Hill, Inc., 2001.

ASTES

Advances in Science, Technology and Engineering Systems Journal Vol. 5, No. 5, 69-73 (2020)

www.astesj.com

Special Issue on Multidisciplinary Innovation in Engineering Science & Technology

ASTESJ

ISSN: 2415-6698

Low Power Bulk Driven Series Parallel OTA for Low Frequency Applications

Sushma Padubidri Shivaprasad[1,*], Sreemannarayanay Kulkarni[2]

[1]*Department of Electronics and Communication Engineering, NMAM Institute of Technology, Nitte, 574110, India*

[2]*School of Electronics and Communication Engineering, Reva University, Bangalore, 560064, India*

ARTICLE INFO

Article history:
Received: 14 June, 2020
Accepted: 16 August, 2020
Online: 09 September, 2020

Keywords:
Low power OTA
Low cutoff frequency
Multifunction filter
Bulk driven
Series parallel current mirror
Biquad

ABSTRACT

Low power OTAs are the most preferred circuits in the realization of continuous time filters of analog front end of wearable healthcare devices. A low transconductance OTA with series parallel current mirror to realize large time constant of the filter is designed. The differential pair of the OTA uses bulk driven PMOSFETs and the subthreshold operation of the circuit achieves 44 nW power with supply voltage of ±0.4 V. The designed OTA has DC gain of 29.59 dB and UGBW of 34.28 KHz. Using the proposed OTA, a multifunction filter which can operate as low pass and high pass filter, having cut-off frequency in the range 25 Hz - 225 Hz is designed in gpdk 180 nm CMOS technology. The simulation is performed using Cadence virtuoso design environment.

1. Introduction

Energy efficient wearable biomedical devices are most widely used in modern healthcare services. In such systems, the design of analog front end (AFE) circuits using existing CMOS technology has multiple design constraints having tradeoffs. As the AFE circuits need to remain on all the time to sense the bioelectric signals continuously, they consume largest share of the overall power budget. So, the energy efficiency of these circuits is major concern along with other performance parameters.

As shown in Figure 1, the analog front end (AFE) consists of low noise amplifier followed by continuous time active filters. Using the sensors or electrodes, biomedical signals such as ECG, EEG, EMG etc. are captured. These signals are having amplitude in the range of μV to few mV and frequencies in the range of dc to few Hz. Therefore, these circuits have to be designed with good low frequency performance. As the signal from the electrodes has dc component, large off chip capacitors are used. However, use of subhertz cutoff frequency high pass filter eliminates these large capacitors. The low pass and band pass filters are used to select the required signal.

The analog filters were designed using opamps. The bandwidth of opamp-RC filters is limited by the excessive gain-bandwidth product requirement for the opamp, to obtain ideal filter response. The high gain-bandwidth product of opamp based topologies consume more power. Therefore, in recent designs, Operational Transconductance Amplifier (OTA) are used in place of opamps. OTAs are also used as the low noise amplifier (LNA), where they need to have high gain and less noise. Therefore, OTA is an important circuit in the analog front end (AFE) of low power systems. OTA is a voltage controlled current source and it converts differential input voltage to output current. The circuit symbol for OTA is shown in Figure 2.

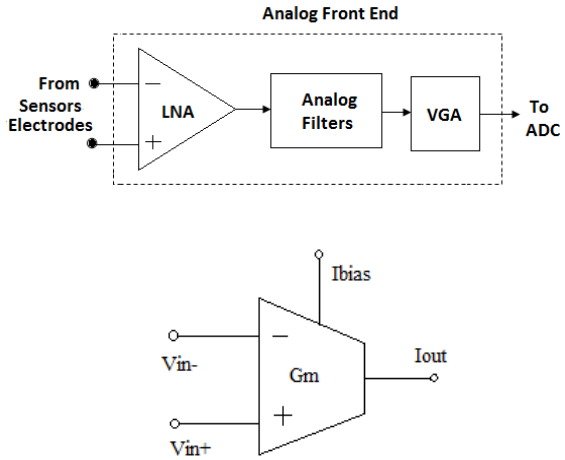


Figure 2: Circuit symbol for OTA

*Corresponding Author: Sushma Padubidri Shivaprasad, pssushma@nitte.edu.in

Figure 3 shows the circuit diagram of single ended current mirror OTA with bulk driven PMOS differential pair, where all nodes have either drain-gate connected or source connected MOSFETs except for input devices. The diffential input (V_{in+} - V_{in-}) is applied to the bulk terminal of PMOSFET pair M1 and M2 that results in output current given by (1). The transconductance of the OTA is constant for the specifies range of differential input and is controlled by bias current I_{bias}.

$$I_{out} = G_m \, (V_{in+} - V_{in-}) \tag{1}$$

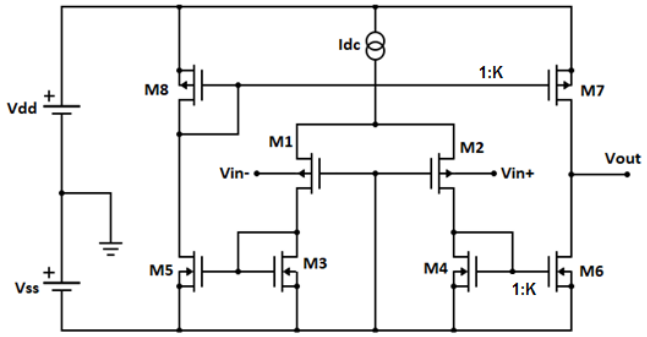


Figure 3: Schematic of current mirror OTA with bulk driven PMOS differential pair

The low voltage operation of OTA is necessary for low power operation. In strong inversion region operating voltage cannot be lowered below the threshold voltage of the MOSFETs. The state of the art digital circuits are operating at 0.3 V to 0.5 V range. To make analog circuits work with same supply voltage range in a chip, they are operated in subthreshold or weak inversion region by choosing appropriate inversion level i_f[1][2]. To lower the operating current level bulk driven MOSFETs are used, resulting in low transconductane and increased linearity. The bulk driven MOSFETs have low cutoff frequency leading to poor frequency response characteristics. The low frequency operation requires large time constants which can be achieved by designing OTAs with small transconductance. In weak inversion gm/Id is high. In order to reduce gm series parallel current mirror [2] is used wherein small bias current and large division factor is used to reduce the output current. Choice of small bias current leads to poor input linear range. Compared to low transconductor design techniques like current division [3], bulk driven [4], attenuator based modular reduction of transconductance [5], current steering [6], source degeneration [7], current cancellation and series parallel current division technique gives lowest transconductance, low offset and better linearity. However, there is trade off with low power.

The proposed series parallel bulk driven OTA (SPOTA) is explained in section 2. The simulation results of the OTA is discussed in section 3. In Section 4, second order multifunction Gm-C filter with tunable cut-off frequency as an application of the proposed SPOTA is explained followed by conclusion in Section 5.

2. Proposed Bulk Driven Series Parallel OTA

In low power analog designs, choice of circuit topology significantly matters for power reduction. In the design of analog filters, OTAs are suitable alternative for opamps. The transconductance of the OTA is an important parameter in the design of active filters. In analog filter applications, the transconductance value is chosen depending on the cutoff frequency range. For low cut off frequency analog filters, large capacitors and resistors are required. As integration of the large resistor is not area efficient, small transconductance cells are designed. In series parallel current division technique, output current is divided by high ratio to achieve very small transconductance [2]. The bulk driven PMOSFET differential pair further reduces overall transconductance.

The OTA shown in Figure 3 is modified to obtain bulk driven series parallel (SP) OTA as shown in Figure 4. The differential input voltage is connected to the substrate of PMOSFETs M1 and M2 and the gates are connected to V_{ss} . Therefore, the transconductance of the OTA depends on g_{mb} , the body conductance which is 0.2 to 0.4 times g_m, the transconductance of the MOSFET. The bulk driven PMOS differential pair at the input with series-parallel current mirror load reduces the transconductance and increases the linearity of the OTA. All devices in the circuit are biased to operate in weak inversion region, by maintaining gate voltage $V_{GS} < V_{th}$, the threshold voltage and drain to source voltages $V_{DS} \geq 4V_T$. The weak inversion drain current I_D under these condition is as given in (2),

$$I_D = 2 \, n \, K \, V_T^2 \, (W / L) \, exp((V_{GS} - V_{th}) / n \, V_T) \tag{2}$$

where $K = \mu_n C_{ox}$, the process dependent parameter which is the product of mobility of charge carrier and the unit gate capacitance, V_T is the volt equivalent of temperature approximately equal to 26 mV at room temperature and n is given by (3),

$$n = (g_m + g_{mb}) / g_m \tag{3}$$

The transconductance g_m in subthreshold region is as given in (4),

$$g_m = I_D / n \, V_T \tag{4}$$

Also, the drain conductance g_o is expressed as in (5),

$$g_o \approx \lambda \, I_D \tag{5}$$

The current mirror load of the differential pair has series and parallel placed MOSFETs so that output current is small. The overall transconductance of the OTA is calculated using (6),

$$G_m = g_{mb1} / N^2 \tag{6}$$

where g_{mb1} is the body transconductance of PMOS M1 and N is the number of series-parallel connected transistors of current mirror load of the differential pair. The current source I_{dc} is realized using PMOS current mirror to provide bias current.

The voltage gain of the circuit is given by (7), with K=1.

$$A_v = g_{mb1} / (g_{o7} + g_{on}) \tag{7}$$

where g_{on} is the overall output conductance of series connected NMOSFETs at the output node. The unity gain cutoff frequency is given by (8),

$$f_T = g_{mb1} / 2 \, \pi \, C_L \tag{8}$$

The transconductance in pS to few nS can be realized when current is divided at the load instead of at the input side. The advantages of series parallel current mirror OTA are low input noise, wide linear input range, small transconductance and nano

watt power. This OTA is used as Gm-cells of a second order Gm-C filter.

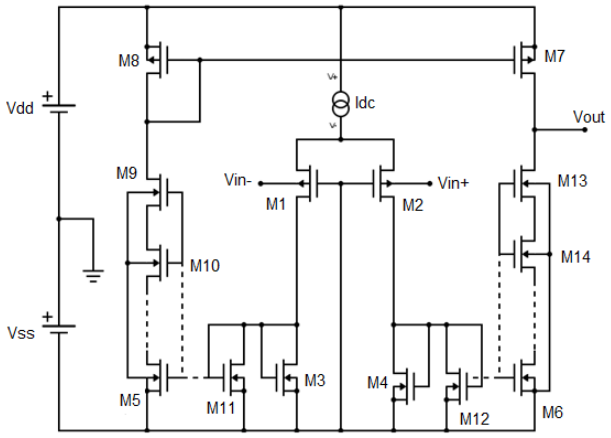


Figure 4: Schematic of proposed bulk driven series-parallel OTA

3. Discussion on Simulation Results of SPOTA

The series parallel current division technique is applied to the current mirror OTA for gate driven and bulk driven input PMOS differential pair. Using the spectre simulation in Cadence Virtuoso tool power dissipation, DC gain, unity gain bandwidth, transconductance, gain and phase margin of circuit are determined and compared. The CMOS technology used is gpdk 180nm. The gate driven SPOTA has power supply of 1.6 V while bulk driven circuit is operated at supply voltage of ± 0.4 V. The input and output waveforms of the bulk driven SPOTA is shown in Figure 5. For ± 1mV input, output voltage of 128 mVpp is obtained. The DC gain is 29.59 dB and 44 nW of power is consumed as can be seen in Figure 6 and in Figure 7 respectively. The SPOTA is stable with 53o of phase margin and has gain margin of 28.2 dB. The OTA has unity gain cutoff frequency of 34. 28 kHz and CMRR of 74.68 dB. The output is linear for ± 50 mV differential input voltage, which is a good range for biomedical applications.

Table 1 gives the comparison of bulk driven SPOTA with gate driven circuit. It is observed that the bulk driven MOSFETs can be operated with supply voltage near the threshold voltage, while for gate driven MOSFETs overdrive voltage requirement has to be met. Therefore, gate driven SPOTA with 1.6 V supply voltage has higher power consumption of 194.336 nW whereas bulk SPOTA power is reduced to 44 nW. The transconductance of the OTA is function of bias current. For bulk driven circuits,

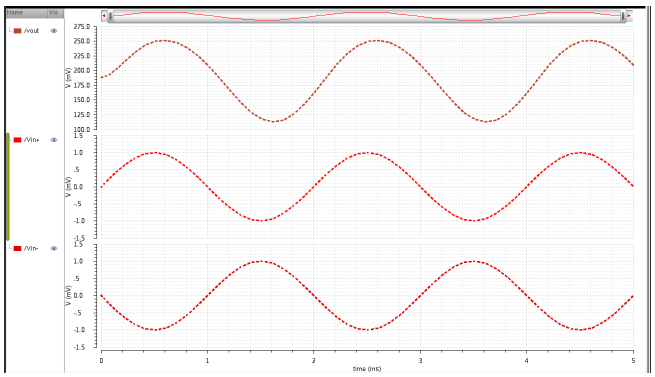


Figure 5: Input and output waveforms of bulk driven SPOTA

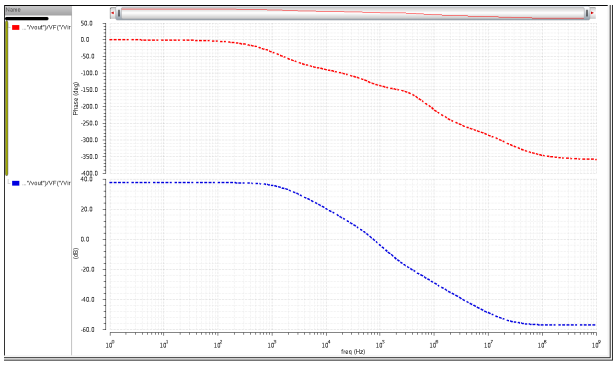


Figure 6: Plot of DC gain and phase of bulk driven SPOTA

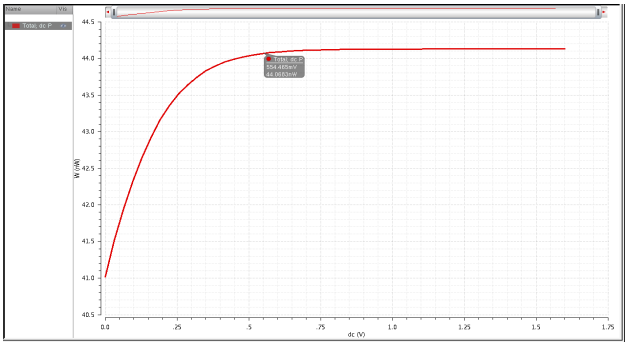


Figure 7: Power dissipation curve of SPOTA

the operating current can be very small. A transconductance of 6.03 nS for bulk driven and 24.63 nS for gate driven is achieved using series parallel technique for N=7 and can be reduced to pS by choosing large value for N. Hence the transconductance of the bulk driven SPOTA is small compared to that of gate driven at the cost of reduced bandwidth, gain margin and phase margin. The CMRR is improved in bulk SPOTA.

4. Gm-C Filter Design

The SPOTA proposed has small transconductance, hence its use in analog filter design for low frequency applications is demonstrated. The circuit structures in CMOS for active filters include Gm-C, OTA-C, switched capacitor integrator and Opamp-RC structures. The Gm-C filter is preferred because of its simplicity, ease of cascading, less area and minimum power consumption.

Table 1: Comparison of Bulk Driven SPOTA with Gate Driven SPOTA

Design Parameter	Gate SPOTA	Bulk SPOTA
Technology (nm)	180 nm	180 nm
V_{DD}(V)	1.6	0.4
Bandwidth (kHz)	74.93	3.504
DC gain (dB)	21.15	29.59
Phase Margin	62.6º	53º
Gain Margin (dB)	38.1	28.2
CMRR (dB)	62.96	74.68
Transconductance	24.63 nS	6.03 nS
Power (nW)	194.336	44

Gm-C filters rely on OTAs and capacitors to realise the transfer function of the filter. Since the transconductance of proposed SPOTA is less than 10 nS and can be even pS if N is chosen large, the integrated capacitor value can be limited in the order of fF to few pF. A second order Gm-C filter realized using biquad structure [8] [9] is shown in Figure 8. It can be set as low pass or high pass filter using the inputs $V_{in\,LP}$ and $V_{in\,HP}$. The two OTAs are used in unity gain mode. For low pass filter, the input is connected to $V_{in\,LP}$ with $V_{in\,HP}$ grounded, whereas it is connected to V_{inHP} with V_{inLP} grounded for high pass filter. The filter is synthesized by neglecting the nonidealities. In Figure 8, voltage $V1$ is as given by (9),

$$V1 = G_{m1}(V_{out} - V_{in\,LP}) / sC_1 \quad (9)$$

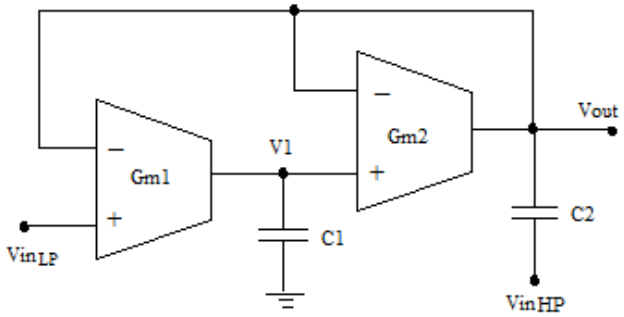


Figure 8: Block schematic of biquad Gm-C filter

Also, the output voltage is as given by (10),

$$V_{out} = (G_{m2}V1 + sC_2V_{in\,HP}) / (sC_2 + G_{m2}) \quad (10)$$

Substituting (9) in (10) we obtain the output voltage V_{out} as in (11),

$$V_{out}(s) = ((G_{m1}\,G_{m2} / C_1\,C_2)\,V_{in\,LP} + S_2\,V_{in\,HP}) / (s^2 + s\,(G_{m2} / C_2) + G_{m1}\,G_{m2} / C_1\,C_2) \quad (11)$$

Choosing $G_{m1} = G_{m2}$ the transfer function of biquad Gm-C low pass filter is obtained by setting $V_{in\,HP} = 0$ and is given by (12),

$$H_{LP}(s) = (G_m^2 / C_1\,C_2) / (s^2 + s\,(G_m / C_2) + G_m^2 / C_1\,C_2) \quad (12)$$

Similarly, the transfer function of high pass filter is obtained by setting $V_{in\,LP} = 0$ and is given by (13),

$$H_{HP}(s) = s^2 / (s^2 + s\,(G_{m2} / C_2) + G_{m1}\,G_{m2} / C_1\,C_2) \quad (13)$$

The 3 dB cutoff frequency and the quality factor of the filter is as given in (14),

$$f_c = (1/2\pi)\,sqrt\,(G_m^2 / C_1\,C_2) \text{ and } Q = sqrt\,(C_2 / C_1) \quad (14)$$

5. Simulation Results of Biquad Gm-C Filter

The simulation of biquad Gm-C filter is carried out using Cadence Virtuoso Tool with gpdk180nm CMOS technology. The magnitude response of the low pass and high pass filter are shown in Figure 9 and Figure 10. The proposed OTA connected as voltage follower is used as Gm cell. The filters have butterworth magnitude response with cutoff frequency in the range 25 Hz to 225 Hz for C_1 = 10 pF. Gain and power consumption are around -7.4 dB to -7.8 dB and 91.7 nW respectively.

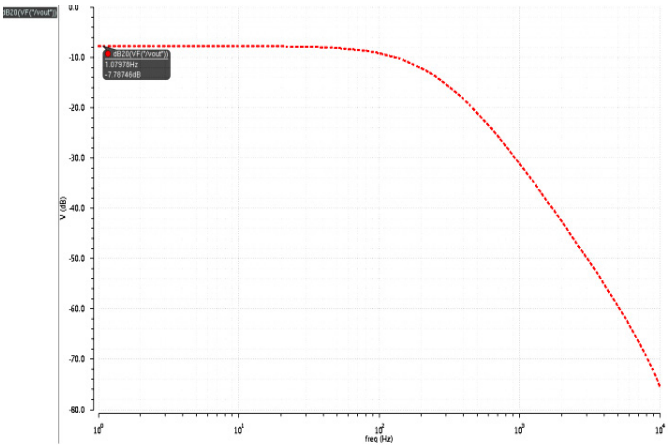


Figure 9: Magnitude response of low pass filter using bulk driven SPOTA

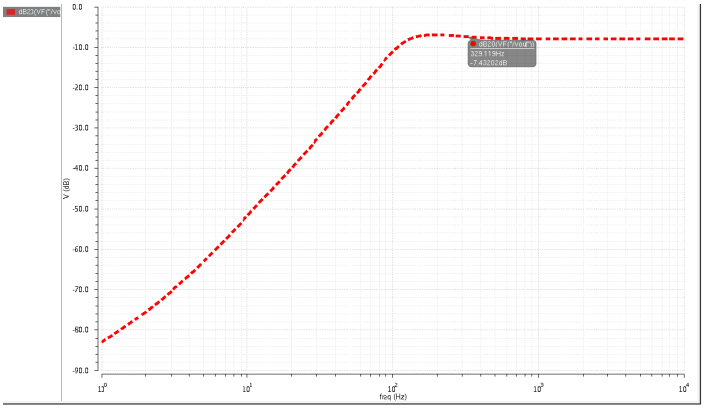


Figure10: Magnitude response of high pass filter using bulk driven SPOTA

By varying capacitor values or by varying the bias current to SPOTA, required cutoff frequency for the filter can be set. When the input signal is applied to $V_{in\,LP}$ with $V_{in\,HP}$ connected to ground, biquad filter is configured as low pass filter, whose cutoff frequency can be tuned by varying C_2 from 25 Hz to 225 Hz. Therefore it can be used to select biomedical signals such as ECG. When the signal is applied to $V_{in\,HP}$ with $V_{in\,LP}$ connected to ground, it is configured as high pass filter, which can be used to allow signals starting from DC to 225 Hz. The series parallel technique reduces the transconductance of the filter to very minimum value. Implementation of low cut off frequency filters using bulk driven SPOTA, results in small capacitors for the filter because of low transconductance. Also the bulk driven SPOTA consumes low power, hence it is useful in active filter section of the low power biomedical AFE.

Table 2 gives comparison of Gm-C filter implementations with different types of OTA. It can be seen from the table that the series parallel current division technique gives smallest transconductance value. The series and parallel connected unit transistors are used to realize the circuit. The designed Gm-C filter is a multifunction filter as low pass and high pass operations can be realized in the same circuit. Also filter can be electronically tunable if the dc current to the OTA is varied. The range of 3 dB frequency of the filter is suitable for selection of biomedical signals. The circuit operating voltage is less than 0.5V hence can be used in the analog section of low voltage, low power system on chip (SoC).

Table 2: Comparison of Gm-C filter Implementations

Parameters	Ref [3] 2002	Ref [1] 2006	Ref [5] 2014	Ref [6] 2018	This work
Technology	1.2 µm	0.8 µm	0.35 µm	180 nm	180 nm
V_{DD} (V)	±1.35	2	1	1	±0.4
Transconuctance	10 nS	33pS-2.35nS	33ps	50pF/pole	6.03 nS
Power	8.2µ (OTA+bias circuit)	100 nW	82 n	1.75µW	91.7 nW
Type of OTA used in the filter	Current division, bulk driven current mirror OTA	Series parallel current mirror OTA	Preattenuated input, current mirror OTA with bump transistor	Current steering current mirror OTA	Series parallel current mirror Bulk driven OTA
Cut-off frequency	0.17Hz	10 Hz-1.2 kHz	0.69 -72 Hz	0.225- 16 kHz	25-225 Hz

6. Conclusion

An OTA operating at ±0.4 V supply, consuming around 44 nW power with transconductance as low as 6.03 pS is designed. Very small transconductance is obtained by series parallel current division technique. Further reduction is transconductance is obtained using bulk driven input PMOS differential pair. The bias current and the number of series-parallel connected NMOS current mirror determine the transconductance of the OTA.

A low cutoff frequency Gm-C biquad filter is then realized using the SPOTA proposed, which can be configured as low pass or high pass filter. The second order filter thus designed consumes 91.7 nW of power. The small value of transconductance of the SPOTA has led to small capacitors in the design. So this multifunction filter can have on-chip capacitors. The filter has Butterworth response with low power consumption, low cutoff frequency and hence suitable for AFE of biomedical devices.

Conflict of Interest

The authors declare no conflict of interest.

References

[1] A. Arnaud et al., "Nanowatt Sub-nS OTAs With Sub-10 mV Input Offset Using Series-Parallel Current Mirrors," IEEE Journal of Solid-State Circuits, **41**(9), 2009–2018, 2006, doi:10.1109/JSSC.2006.880606.

[2] A. Arnaud, C. Galup-Montoro, "Pico-A/V range CMOS transconductors using series-parallel current division," Electronics Letters, **39**(18), 1295–1296, 2003, doi: 10.1049/el:20030840.

[3] A. Veeravalli et al., "A CMOS transconductance amplifier architecture with wide tuning range for very low frequency applications," IEEE Journal of Solid-State Circuits, **37**(6), 776–781, 2002, doi:10.1109/JSSC.2002.1004583.

[4] D. Arbet, M. Rak, V. Stopjakov,"Comparison of Gate-Driven and Bulk-Driven Current Mirror Topologies," in 2016 IEEE 19th International Symposium on Design and Diagnostics of Electronic Circuits & Systems (DDECS), 1–4, 2016, doi::10.1109/DDECS.2016.7482457.

[5] S. Thanapitak, "An 1-V, 74-dB, sub-Hz Gm-C filter based on a modular transconductance reduction technique," in 2014 IEEE 11th International Conference on Electrical Engineering/Electronics, Computer, Telecommunications and Information Technology (ECTI-CON), 1–5, 2014, doi.org/10.1109/ECTICon. 2014.6839763.

[6] J. Perez-Bailon, Marquez, A., Calvo, B., Medrano, N., Sanz-Pascual, M.T., "A 1V–1.75µW Gm-C low pass filter for bio-sensing applications," in 2018 IEEE 9th Latin American Symposium on Circuits & Systems (LASCAS), 1–4, 2018, doi10.1109/LASCAS.2018.8399960.

[7] K. Garradhi, "Low-voltage and low-power OTA using source-degeneration technique and its application in Gm-C filter," in 2016 IEEE 11th International Conference on Integration, Design & Test Symposium (IDT), 221-226, 2016, doi: 10.1109/IDT.2016.7843044.

[8] M. Kumngern, Dejhan K., "Voltage-mode low-pass, high-pass, band-pass biquad filter using simple CMOS OTAs," in 2009 IEEE International Conference on Instrumentation and Measurement Technology (I2MTC'09), 924-927, 2009, doi: 10.1109/IMTC.2009.5168583.

[9] C. Chanapromma et al., "High even-order fully-differential biquadratic continuous-time low-pass Gm-C filter," in 2014 IEEE International Electrical Engineering Congress (IEECON), 1–4, 2014, doi:10.1109/iEECON.2014.6925853.

ASTES

Advances in Science, Technology and Engineering Systems Journal Vol. 5, No. 5, 74-79 (2020)

www.astesj.com

Special Issue on Multidisciplinary Innovation in Engineering Science & Technology

ASTESJ

ISSN: 2415-6698

Power Loss Minimization using the Integration of DGs and Reconfiguration of Distribution System: Applied on Real Distribution Feeder of Urbain Areas of Kenitra City in Morroco

Ismail Moufid*, Soukaina Naciri, Hassan EL Moussaoui, Tijani Lamhamdi, Hassane El Markhi

Intelligent Systems, Georessources and Renewable Energies laboratory (ISGREL), Sidi Mohamed Ben Abdelah University; FST,Fez, 2202, Morocco

ARTICLE INFO

Article history:
Received: 29 June, 2020
Accepted: 21 August, 2020
Online: 09 September, 2020

Keywords:
NOP
Distributed generation
Power loss
Distribution network

ABSTRACT

Optimal integration of distributed generation (DG) into the distribution system results in reduced power losses and improved bus voltages. In this article, a combination of two techniques has been analyzed:
The integration of DG and reconfiguration of the distribution system by removing the Normally Open Point NOP in different places of the system.
These two techniques are applied to a real distribution network " distribution network of Kenitra city in Morroco", considering as key objectives the reduction of power loss and improvement of voltage profile.
To investigate the effectiveness and robustness of our system a model was performed using ETAP. The simulation results improve that we can minimize greatly the power losses in the distribution network by the implementation of DGs and reconfiguring our distribution network.

1. Introduction

The role of the distribution network transfers the electrical energy directly from the substations to consumers. The distribution network administrator currently faces several challenges resulting from increased penetration of renewable energy resources and the demand of customers. The Distribution Network Operators (DNO) has noted that the traditional solution of the network may not be sufficient. The increasing load demand in the distribution network creates an important challenge for research in phases of studying the management of the distribution network to satisfy the need with the actual infrastructure.

The determination of the grid concept of the distribution system depends on special specifications and side conditions [1]. distribution of electrical energy in a grid network is done in two ways: closed-ring networks and radial networks as presented in Fig.1.

Radial grid: The open ring is generally the structure of the distribution network as presented in Figure 1, the advantage of this structure is that during a fault, the currents propagate in one unidirectional direction, so the detection and the position of faults became more flexible than in closed rings arrangement. Moreover, the inconvenience of this architecture is that when a fault befalls, the part of the network after the fault is detached from the substation, this situation makes the management of the distribution system more complicated.

Closed-ring grid: The closed ring grid has the same structure as the radial structure, just that a part of the rings is performed as closed rings as we can see in Figure 1 b. the problem of this kind of structure that the protection of the grid became more complicated than in the radial case because when a fault happens the currents propagate in different ways. The disadvantage of a radial configuration can be skipped by adopting the closed-ring structure [1].

The benefit of the closed-ring structure is that more than one charger feeds the system, so if a feeder is inoperative or in maintenance, the grid is stay powered by the other feeders. In this way, customers are not concerned, even if one of the feeders is down or becomes inoperative. Moreover, the ring dispensing of the network is provided with many isolated parts. Furthermore, in the case of a fault in a section, this section is isolated by opening the corresponding breakers.

Usually, the structure of distribution networks is carried out according to the network shown in Figure 1.the closed-ring distribution network is created with a NOP, dividing the circle into two outlets from an open electrical point [2].

*Corresponding Author: Ismail Moufid, ismail.moufid@usmba.ac.ma

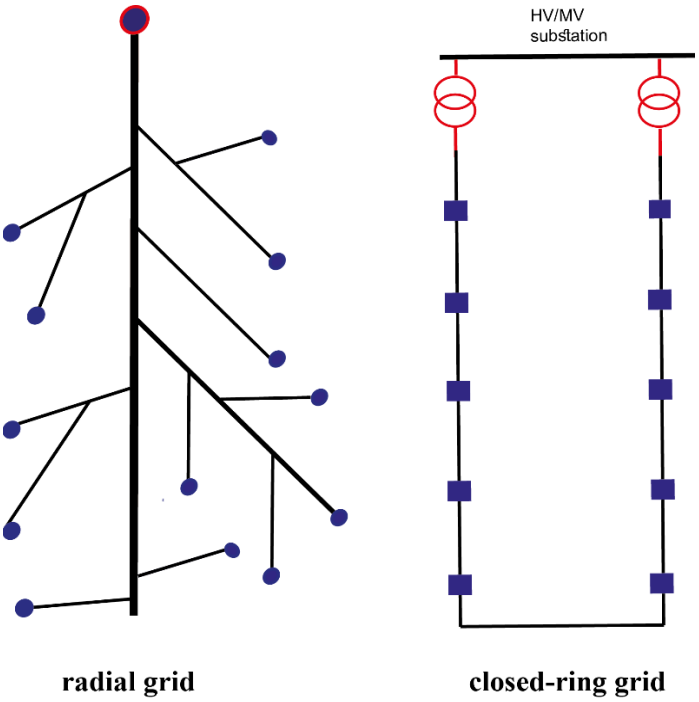


Figure 1: The structure of the closed-ring grid and radial grid.

By using NOP in the distribution network we assure the selectivity of the protection systems and minimize the consequence of faults; so the number of customers affected in the event of failure can be reduced in this case.

The power flow can be affected by the position of NOP. Throughout the day, the number of customers changes, so the power flow also changes.

Consequently, the optimal position of the NOP would change, so the current in each power line became nearly equal. we can reduce power losses and improve the voltage profile of the distribution network by adjusting the loads between the adjacents feeders.

Authors in [3] have proposed a strategy to determine the suitable best location for DG "Distributed Generations" to reduce distribution power losses. The approach is based on a specific loss equation. The strategy has been examined with different size of DG. The authors in [4] have defined an objective function of cost to place solar, wind, and fuel cell. An analytic hierarchy method has been utilized to decide on finding the optimal positions for various sorts of DGs.

The improvement of voltages profile placing DGs in different positions has been discussed in [5]. They have suggested voltage sensitivity to install DGs. Authors in [6] have defined the position of DG to minimize the power losses, the algorithm of Kalma is used to determine the optimal size of DG.

Authors in [7], proposes an approach to determine the Hosting Capacity of distributed generation (DG). The approach proposes a model of the lines utilizing the π type. The capacitance of different lines is not neglected, and we obtained a higher value of HC. we are concentrate on this study on line overloading.

An optimal power flow method and hybrid PSO for optimal position and sizing of DG considering the power loss reduction and DG cost minimization was proposed in [8]. The optimization problem satisfies some constraints like the thermal limit of the transformer and lines and the limit of the voltage profile. Authors in [9] proposed a method for the optimal position of DGs. They have also discussed the sensibility factor to choose the best place of DG. In [10] a GA methodology respecting indices of power loss and voltage profile was discussed. Authors in [11]have suggested a strategy to choose the position and the size of the DG regarding the constraints of minimizing power losses and harmonic distortion. They adopted a multi-objective PSO approach based on conventional weighted aggregation which may lead to a suboptimal solution in some cases. The optimal DG placement is determined based on voltage stability study as a security estimate by authors in [12].A method to evaluate the Sizing and sitting of various DGs based on the reduction of power loss was proposed by authors in [13].

In [14], authors have presented a technique to choose the optimal DG placement Based on Power Stability Index (PSI) based DG placement. In this method, the value of PSI is calculated for each row and sorted from the most important value to the most inferior value. DG was placed at the bus terminal of the most important PSI branch. The PSI value has been recalculated and by the same method location for the next DG. Authors in [15] have discussed a loss sensitivity based DG placement strategy. They used the bus ranking approach based on loss sensitivity and for the placement of DG they are placed in the buses who have the highest loss-sensitive. A simple strategy for the optimal position and sizing of generators in different buses was presented in [16]. The most important aim of this strategy is to minimize the power loss and cost of the distribution network. The authors also discuss the optimization of the weighting factor, which equilibrate loss factors and cost in order to achieve the desired aims with the highest advantage possible. In [17] an optimal placement and sizing of CBs and DGs in distribution systems the based on Spring Search Algorithm (SSA) are proposed. The authors in [18] have studied the impact of using SOP in the distribution system to reduce power losses and improving the voltage profile. Authors in [19] have proposed a new strategy for distribution systems including DG. The principal objects were the reduction of the risk factor and the cost reduction of total installation and operational. The optimal size and position of the DG are fixed in the planning step. The optimization of real power loss and the DG injection index are the two objective functions studied in this DG planning. Authors in [20] have analyzed the optimal placement of DG in order to assure voltage stability and power loss minimization of the distribution network. They have also adopted the PSO technique to find the optimal size and the position of DG. The optimal size and location of a single DG unit in different distribution systems are studied in the paper.

This paper proposes a comparison between two approaches in order to minimize power loss and improving the voltage profile of the distribution network. The paper is organized as follows.

In the first section, the formulation of the problem of power loss minimization and voltage improvement is discussed. In the second part, a description of our test network was discussed.

The third section is divided into two parts. In the first part, the efficiency of the suggested approach is tested to choose the best point of the open point in our distribution systems.

In the second part, DG is placed in a different place to choose the best point of the minimum of power loss, and the achieved results are presented. Lastly, some important conclusions are drawn.

2. Problem formulation

2.1. Power and current in the branches

we consider a distribution network with a radial configuration formed of a set of branches as presented in fig.2. Each branch of this network is modeled as a resistance in series with a pure inductance. The impedance of any branch "i" of this network is written as follows:

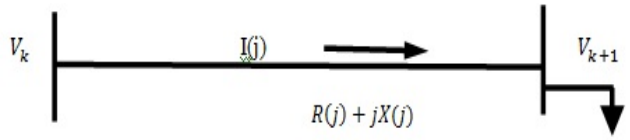


Figure 2: Distribution network with a radial configuration formed of two buses.

The load flow in this type of network is done using a BIBC matrix (**b**us **i**njection to **b**ranch **c**urrent) to calculate the currents flowing through all branches of the network.

For a busbar to which a load is connected, the apparent power S is represented by:

$$S_i = P_i + jQ_i \tag{1}$$

where $i = 1,2,3, \dots, n$

The equivalent current charge corresponding to the k^{th} iteration is represented by:

$$I_i^k = I_i^r + jI_i^l = \left(\frac{P_i + jQ_i}{V_i^k}\right)^* \tag{2}$$

where:

V_i^k and I_i^k : are the voltage load and current of the busbar for the k^{th} iteration.

$I_i^l and\ I_i^r$: are the imaginary and real parts of the busbar load.

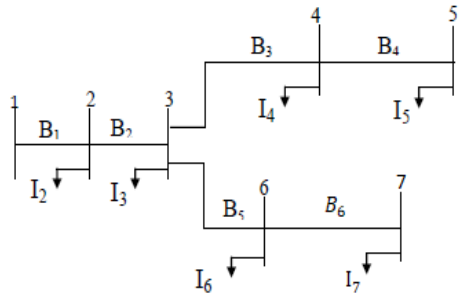


Figure 3: A simple distribution network of 7 busbars and 6 branches.

2.2. The BIBC Matrix

The load currents at the busbar are obtained using equation (2), as well as the currents circulating through the branches are determined by utilizing Kirchhoff's law to the studied distribution network. A simple distribution network constituted of 7 busbars and 6 branches presented in Figure 3 is used as an example to facilitate the description of the method for determining the BIBC matrix.

The branches currents can be represented as a function of load currents as results:

$$\begin{aligned} B_1 &= I_2 + I_3 + I_4 + I_5 + I_6 + I_7 \\ B_2 &= I_3 + I_4 + I_5 + I_6 + I_7 \\ B_3 &= I_4 + I_5 \\ B_4 &= I_5 \\ B_5 &= I_6 + I_7 \\ B_6 &= I_7 \end{aligned} \tag{3}$$

This means that the relation between the load currents of the busbars and the branch currents can be written as follows:

$$\begin{pmatrix} B_1 \\ B_2 \\ B_3 \\ B_4 \\ B_5 \\ B_6 \end{pmatrix} = \begin{pmatrix} 1 & 1 & 1 & 1 & 1 & 1 \\ 0 & 1 & 1 & 1 & 1 & 1 \\ 0 & 0 & 1 & 1 & 0 & 0 \\ 0 & 0 & 0 & 1 & 0 & 0 \\ 0 & 0 & 0 & 0 & 1 & 1 \\ 0 & 0 & 0 & 0 & 0 & 1 \end{pmatrix} \begin{pmatrix} I_2 \\ I_3 \\ I_4 \\ I_5 \\ I_6 \\ I_7 \end{pmatrix}$$

In general, equation (3) can be written as follows:

[B] = [BIBC] [I].

where BIBC represent the matrix of currents injected into the busbars which are a matrix containing only the values 0 and 1.

2.3. Active and reactive power losses:

The determination of the power flow is essential to locate the overloaded electric lines and to calculate the value of the power losses.

The active power losses at a branch (i) are written as follows:

$$P_{loss,i} = R_i \frac{(P_i^2 + Q_i^2)}{|V|_i^2} \tag{4}$$

We can determine the total power losses of the network by summing the losses of all branches of the equation (4).

$$P_{T,loss} = \sum_{i=1}^{Nbr} P_{loss,i} \tag{5}$$

The reactive power losses at a branch (i) may be written as follows:

$$Q_{loss,i} = X_i \frac{(P_i^2 + Q_i^2)}{|V|_i^2} \tag{6}$$

We can also determine the total reactive power losses of the network by summing the losses of all branches of the equation (6)

$$Q_{T,loss} = \sum_{i=1}^{Nbr} Q_{loss,i} \tag{7}$$

2.4. Objective function:

The objective function is the measure of the system considered. The primary aim is improving the voltage profile and keep it between regulatory limits. But, this goal is transcribed mathematically as a constraint, because the voltage limits are strict

limits that the system cannot exceed and therefore they cannot be expressed as an objective function.

There are several possible objectives for solving the problem of choosing the optimal location of DGs in the distribution system. Among the most common goals are:

- Improvement of voltage profile: we seek to balance voltage profile while trying to minimize the sum of the relative deviations of the voltage in each node compared to the nominal tension.
- Minimization of online losses: Reducing Joules losses is becoming a priority for distribution network operators. This allows an increase in transit margins on power lines in addition to improving the voltage profile.

$$F_{objectif} = \min \sum_{i=1}^{Nbr} P_{loss,i} \quad (8)$$

So the objective function is associated with the nature of decision variables, constraints, and depends on the type of optimization adopted.

2.5. Technical constraints related to the problem

Voltage constraint: The value of the voltage profile of each busbar must be limited as follows:

$$V_{min} \leqslant V_i \leqslant V_{max}$$

Where Vmin = 0.95 p.u. and Vmax = 1.05 p.u. are the minimum and maximum of voltage amplitude values at each busbar, respectively. Active and reactive power balance constraints :

$$P_G = P_{loss} + P_D \quad \text{and} \quad Q_G = Q_{loss} + Q_D$$

where

Q_G and P_G are the reactive and active powers injected by the D_G while Q_D and P_D are the reactive and active load powers at the k^{th} node.

Q_{loss} and P_{Loss} are reactive and active power losses in the system.

3. Test Network

The network studied is the MV network of the Kenitra city in Morroco it consists of a source substation with an installed power of 36MVA and a short-circuit power of 397.15 MVA, which supplies two distribution lines L1 and L2, its lengths are 9.4 km and 12 km respectively. This line has various characteristics (Blue, green and orange) which are shown in Table 1. This feeder aliments a load of more than 4.5 MW and 2.76 MVAR.

Table 1: Cables Parameters

Cables	Parameters		
	Impedance Ω/km	Capacitance nF/km	Maximum current A
Green	0.239+j0.11	300	300
orange	0.372+j0.13	220	225
blue	0.145+j0.1	370	400

The characteristics of this distribution network in Figure 4 are given as follows:

- Number of busbars = 40;
- Number of branches = 39;
- Slack bus N ° = 1;
- Nominal voltage 20 kV

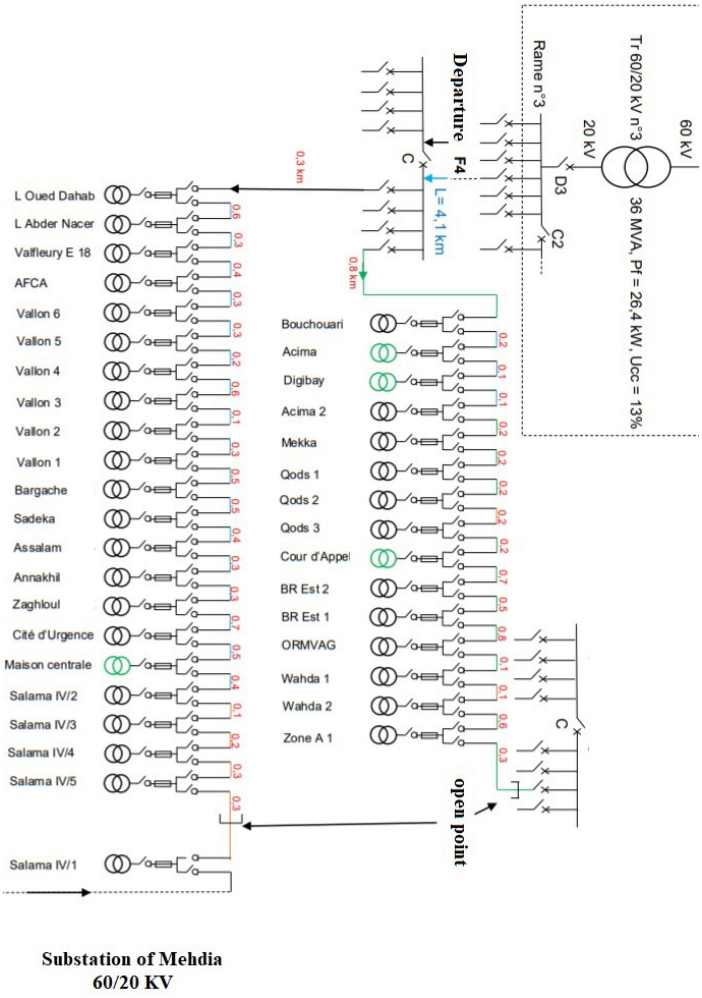


Figure 4: Studied distribution network

4. Simulation and discussion

For simulation purposes, the network studied was implemented in ETAP environment. The objective of this part is to choose the best position of DG for our distribution networks, so here we are interested in two constraints, the power losses and the voltage profile.

In this paper, we considered two cases:
Case 1 we fixed the position of the NOP and we remove the DG to have the minimum of power losses and we ameliorate the voltage profile.
Case 2 we fixed the DG in the optimal position and we change the position of NOP to minimize the power losses.

4.1. Simulation of case 1

We study the network for the first time by removing the DG place. The attitude of the distribution network after changing the position of DG is illustrated in Figures 5 & 6.

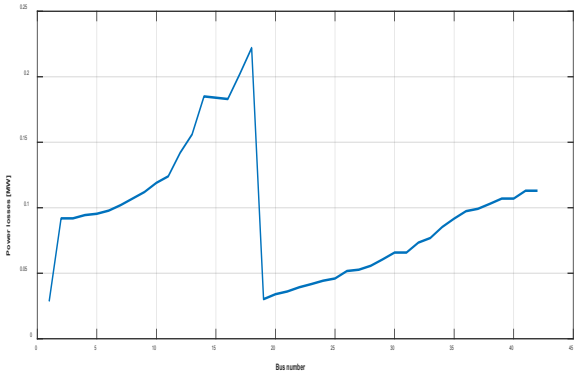


Figure 5: Power losses after the integration of DG in different buses

As presented in Fig. 5 we can see that the power losses change after removing DGs for different positions in our distribution system. However, we can remarque also that the power losses are minimum after the integration of DG in busbar number 18.

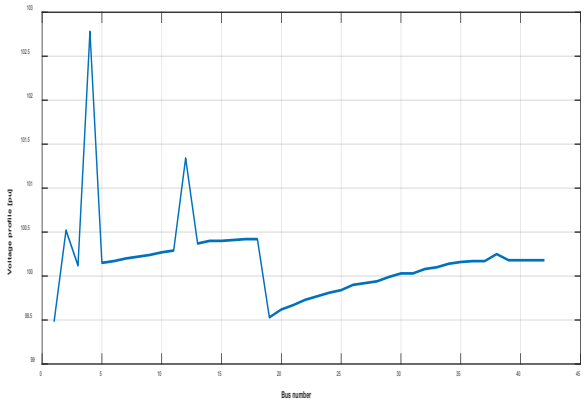


Figure 6: The voltage profile after the integration of DG in different buses

For the voltage profile, we took the average voltage value for the buses because for each DG location we have 41 voltage values.

As we can see in fig.6 the voltage profile for all buses of our distribution system is improved after the integration of DG in different positions, so with the integration of DGs, we can avoid the voltage drop. for the best place of DGs, we can remarque that for bus 18 the voltage profile is near to 1 pu.

4.2. Discussion of case 1

We can note in Fig. 5 that the integration of DG in our system can greatly reduce the total power losses of 0.15 MW, this reduction of power losses are important in bus bar 18; so the best place to integrate our DG is in this busbar, however, we can also observe in fig.6 the improvement of the voltage profile after using dg in our distribution network, we can remarque that for bus 18 the voltage profile is near to 1 pu, we can express this by the integration of DG in this place.

4.3. Simulation of case 2

We study now the performance of our network with DG fix in busbar 20 and we will move the position of NOP. The results are given in Fig.7

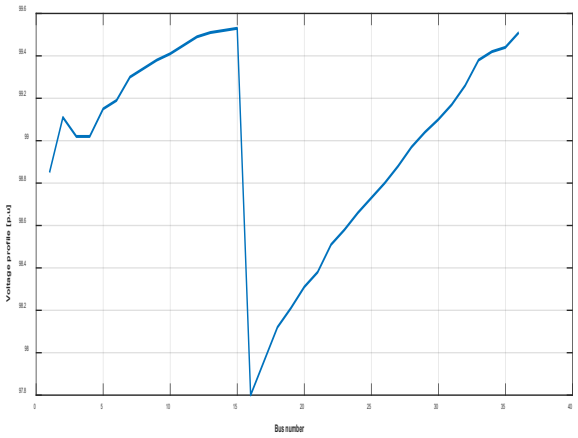


Figure 7: Voltage profile after removing the position of NOP

As presented in Fig. 7 the voltage profile of our distribution network changes proportionally after removing NOP in the different positions, however, we show that the voltage profile is great when the position of the NOP is between bus 16-17 and 36-37.

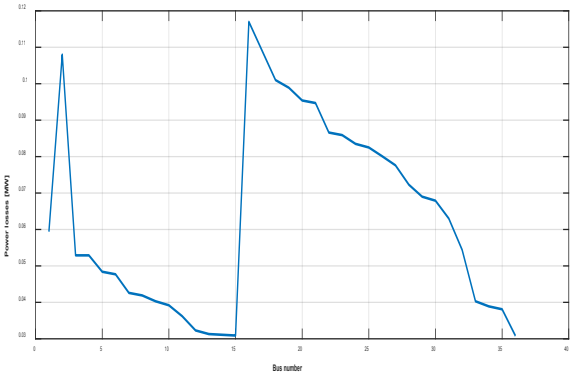


Figure 8: Power losses after removing the position of NOP

For Fig. 8 we can observe that removing NOP between buses influence also the power losses, but we can remarque that the power losses are minimum when the NOP position is is between bus 16-17 and 36-37.

4.4. Discussion of case 2

We can remarque in Fig.7 that the removing NOP greatly reduces the power losses of 0.03 MW, this reduction of power losses are important when it's between bus 16-17 and 36-37, so the best for NOP is between this busbar.

We can also remarque in fig. 8 that the voltage profile is maximum when NOP is between the same buses.

We can explain that by balancing the loads between the feeders of our system.

4.5. Synthesis

To compare the two cases, we will draw the power losses of the two cases in the same graph.

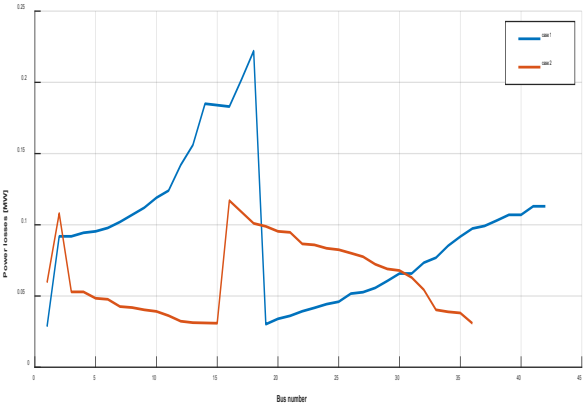


Figure 9: Power losses in case 1 & 2

As presented in Fig.9 the power losses are lower in case 2 compared to case 1.

We can recapitulate that by integrating NOP to balance the loads between feeder we can minimize power losses in the distribution network more than integrating DG in a different position.

5. Conclusion & Perspective

This paper has proposed two approaches to reduce power losses in the distribution network, so we considered two constraints, reduce power losses and improving the voltage profile. To evaluate the effectiveness of this approach we worked on two cases:

Case 1 we fixed the position of the NOP and we remove the DG to have the minimum of power losses.

Case 2 we fixed the DG in the optimal position from the first case and we change the position of NOP. The principal objective was to decrease the power losses in the distribution network. To study the influence on grid losses we considered a Medium Voltage distribution network which is the MV network of the Kenitra city in Morroco it consists of a source substation with an installed power of 36MVA and a short-circuit power of 397.15 MVA was implemented using Etap and Matlab/Simulink. The results presented illustrate that we can decrease power losses in distribution systems by displacing the position of NOP more than integrating DGs in our system.

For Future work, it will be interesting to integrate metaheuristics algorithms like Butterfly optimization algorithm BOA [21] and particle swarm optimization algorithm PSO [22] to reduce power losses and choosing the best place for DGs and NOP.

Conflict of Interest

The authors declare no conflict of interest.

References

[1] L. Thurner, A. Scheidler, A. Probst, M. Braun, "Analysing the Degree of Meshing in Medium Voltage Target Grids-An Automated Technical and Economical Impact Assessment," ArXiv Preprint ArXiv:1802.01492, 2018, doi:arXiv:1802.01492.

[2] T. Schnelle, M. Schmidt, P. Schegner, "Power converters in distribution grids-new alternatives for grid planning and operation," IEEE: 1–6, 2015, doi:arXiv:1802.01492.

[3] N. Acharya, P. Mahat, N. Mithulananthan, "An analytical approach for DG allocation in primary distribution network," International Journal of Electrical Power & Energy Systems, **28**(10), 669–678, 2006, doi:10.1016/j.ijepes.2006.02.013.

[4] A. Singh, S. Parida, "Combined optimal placement of solar; wind and fuel cell based DGs using AHP," Linköping University Electronic Press: 3113–3120, 2011, doi:10.3384/ecp110573113.

[5] M. Kashem, G. Ledwich, "Multiple distributed generators for distribution feeder voltage support," IEEE Transactions on Energy Conversion, **20**(3), 676–684, 2005, doi: 10.1109/TEC.2004.832090.

[6] S.-H. Lee, J.-W. Park, "Selection of optimal location and size of multiple distributed generations by using Kalman filter algorithm," IEEE Transactions on Power Systems, **24**(3), 1393–1400, 2009 doi: 10.1109/TPWRS.2009.2016540.

[7] N. Soukaina, E. Hassane, L. Tijani, "Hosting capacity estimation of underground distribution feeder in Urbain Areas," IEEE: 1–5, 2019, doi:10.1109/WITS.2019.8723822.

[8] M. Gomez-Gonzalez, A. López, F. Jurado, "Optimization of distributed generation systems using a new discrete PSO and OPF," Electric Power Systems Research, **84**(1), 174–180, 2012doi:org/10.1016/j.epsr.2011.11.016.

[9] D.K. Khatod, V. Pant, J. Sharma, "Evolutionary programming based optimal placement of renewable distributed generators," IEEE Transactions on Power Systems, **28**(2), 683–695, 2012 doi: 10.1109/TPWRS.2012.2211044.

[10] D. Singh, D. Singh, K. Verma, "Multiobjective optimization for DG planning with load models," IEEE Transactions on Power Systems, **24**(1), 427–436, 2009, doi: 10.1109/TPWRS.2008.2009483.

[11] M. Sedighi, A. Igderi, A. Parastar, "Sitting and sizing of distributed generation in distribution network to improve of several parameters by PSO algorithm," IEEE: 1083–1087, 2010, doi: 10.1109/IPECON.2010.5696977.

[12] M. Ettehadi, H. Ghasemi, S. Vaez-Zadeh, "Voltage stability-based DG placement in distribution networks," Ieee Transactions on Power Delivery, **28**(1), 171–178, 2012,doi:10.1109/TPWRD.2012.2214241.

[13] F. Ugranlı, E. Karatepe, "Multiple-distributed generation planning under load uncertainty and different penetration levels," International Journal of Electrical Power & Energy Systems, **46**, 132–144, 2013, doi:org/10.1016/j.ijepes.2012.10.043.

[14] M. Aman, G. Jasmon, H. Mokhlis, A. Bakar, "Optimal placement and sizing of a DG based on a new power stability index and line losses," International Journal of Electrical Power & Energy Systems, **43**(1), 1296–1304, 2012, doi:org/10.1016/j.ijepes.2012.05.053.

[15] S.K. Injeti, N.P. Kumar, "A novel approach to identify optimal access point and capacity of multiple DGs in a small, medium and large scale radial distribution systems," International Journal of Electrical Power & Energy Systems, **45**(1), 142–151, 2013, doi:org/10.1016/j.ijepes.2012.08.043.

[16] S. Ghosh, S.P. Ghoshal, S. Ghosh, "Optimal sizing and placement of distributed generation in a network system," International Journal of Electrical Power & Energy Systems, **32**(8), 849–856, 2010, doi:org/10.1016/j.ijepes.2010.01.029.

[17] M. Dehghani, Z. Montazeri, O. Malik, "Optimal sizing and placement of capacitor banks and distributed generation in distribution systems using spring search algorithm," International Journal of Emerging Electric Power Systems, 21(1), 2020, doi:https://doi.org/10.1515/ijeeps-2019-0217.

[18] M. Ismail, E. Hassane, E.M. Hassan, L. Tijani, "Power Losses Minimization in Distribution System Using Soft Open Point," IEEE: 1–5, 2020, doi: 10.1109/IRASET48871.2020.9092002.

[19] S. Ganguly, N. Sahoo, D. Das, "Multi-objective particle swarm optimization based on fuzzy-Pareto-dominance for possibilistic planning of electrical distribution systems incorporating distributed generation," Fuzzy Sets and Systems, **213**, 47–73, 2013, doi:org/10.1016/j.fss.2012.07.005.

[20] M. Aman, G. Jasmon, A. Bakar, H. Mokhlis, "A new approach for optimum DG placement and sizing based on voltage stability maximization and minimization of power losses," Energy Conversion and Management, 70, 202–210, 2013, doi:org/10.1016/j.enconman.2013.02.015.

[21] S. Arora, S. Singh, "Butterfly optimization algorithm: a novel approach for global optimization," Soft Computing, **23**(3), 715–734, 2019, doi:10.1007/s00500-018-3102-4.

[22] R. Pegado, Z. Ñaupari, Y. Molina, C. Castillo, "Radial distribution network reconfiguration for power losses reduction based on improved selective BPSO," Electric Power Systems Research, **169**, 206–213, 2019, doi:org/10.1016/j.epsr.2018.12.030.

ASTES

Advances in Science, Technology and Engineering Systems Journal Vol. 5, No. 5, 80-93 (2020)

www.astesj.com

Special Issue on Multidisciplinary Innovation in Engineering Science & Technology

ASTESJ

ISSN: 2415-6698

Method of Modelling Prices for R&D Products in the Case of their Transfer from Engineering Universities to the Business

Oleksandra Mrykhina[1], Lidiya Lisovska[2,*], Ihor Novakivskyj[2], Terebukh Andrii[3], Valentyna Zhukovska[4]

[1]*Lviv Polytechnic National University, Department of Business Economics and Investment, 12, Banderu, Lviv, 79013, Ukraine*

[2]*Lviv Polytechnic National University, Management of Organizations Department, 12, Banderu, Lviv, 79013, Ukraine*

[3]*Lviv Polytechnic National University, Tourism Department, 12, Banderu, Lviv, 79013, Ukraine*

[4]*Kyiv National University of Trade & Economics, Department of Management, 54/1, Prospect Peremogy, Kyiv, 03057, Ukraine*

ARTICLE INFO

Article history:
Received: 02 July, 2020
Accepted: 21 August, 2020
Online: 09 September, 2020

Keywords:
Pricing
R&D product
Transfer
Commercialization

ABSTRACT

Global changes caused by the IV Industrial revolution and globalization processes resulted in a redistribution of roles of participants in innovative infrastructures of countries. Universities are leading both in terms of generating R&D products and in terms of developing business activities. Now there is a problem of insufficient methodological support of technological universities for pricing R&D products developed and prepared for transfer to the business environment. Existing methods and models do not meet the needs of the market, which is growing rapidly. At the same time, the market is characterized by a high degree of volatility. The purpose of the article is to develop a method for modelling prices for R&D products from universities to the business environment, which takes into account: the specifics of the R&D product, modern market features for this R&D product; the nature of the transfer and commercialization of this R&D product. The article identifies the factors that determine the processes of transfer, commercialization and market launch of R&D products, which affect the pricing of R&D products. Groups of characteristics that characterize systematize these factors: 1) consumer value of R&D product; 2) market susceptibility of R&D product; 3) transfer and commercialization processes of R&D product. Justified a number of factor attributes within the formed groups and assigned them the values of linguistic terms for adjusting the price of R&D product using fuzzy set theory algorithms. The method takes into account elements of cost, revenue and comparative estimation approaches. The method makes it possible to adjust prices for R&D products, taking into account heterogeneous features in the composition of R&D products and compare them with market analogues of R&D products. This contributes to achieving a higher level of pricing accuracy for R&D products when they are transferred from the university to the business environment. The resulting prices are compared with market prices for competitive analogues, which makes it possible to determine the scenario of transfer and commercialization of R&D product; justify the strategy of market development of R&D product; increase the level of manoeuvrability of pricing management for R&D product. The model was tested on a number of R&D products developed at Lviv Polytechnic National University (Ukraine). Application of the proposed method is advisable in the short-and medium-term forecasting period.

1. Introduction

1.1. Framework of theme relevance

This work is a continuation of the development of issues raised by the team of authors at the 14th International Scientific and

* Lidiya Lisovska, Address: Apt. 3, 136, Gen.Chuprunku str., Lviv, 79057, Ukraine, Contact No: +380679260337, Email: lida_lissovcka@ukr.net

Technical Conference on Computer Sciences and Information Technologies [1].

Global changes caused by the IV Industrial revolution, the popularization of the open innovation paradigm and the concept of Society 5.0, the virtualization of many areas of human activity, as well as other events and phenomena, caused the redistribution of roles of almost all participants in the innovation infrastructure of regions of countries. Leading positions are increasingly held by technological universities, both in terms of technology development opportunities and in terms of entrepreneurial development. Universities have become hotbeds for generating, transferring, commercializing, and even providing market support for technologies. Now they are the main providers of interaction between business, government and society.

This requires universities to constantly study the market needs for R&D products in the context of prospective requests due to scientific and technological progress and timely and reasonable response to such requests. Thus, today the processes of transferring R&D products from universities to the business environment are taking place against the background of market uncertainty. In contrast to business structures that are more mobile in the market competition, universities should act on the basis of careful strategic planning of R&D products transfer opportunities, evaluating the level of efficiency of technology transfer in general, being still at the beginning of the "R&D – market" chain.

The commercialization processes of University R&D products are both goals and tools. Goals, since commercialization means the relevance and expediency of further scientific research, and tools – since commercialization makes it possible to make a profit for their implementation. This requires providing universities with the necessary resources and methodological tools. In particular, pricing for R&D products prepared for transfer from universities to the business environment requires priority attention in this process.

As a result of unsubstantiated management decisions in pricing their R&D products, universities can have significant negative results both in the long term (loss of competitive positions, loss of business reputation in research schools) and in current activities (loss of revenue, revaluation of their own positions, loss of qualified personnel), which can lead to a weakening of interaction in the system of participants in the innovation infrastructure.

Until now, the world economic science has not paid much attention to the specifics of pricing for university R&D products as part of their transfer processes. However, the growing integration role of universities in the interaction of participants in the innovation infrastructure and the rapid development of technological universities in the world have led to the need to review this issue.

1.2. Statistical Background

The importance and relevance of research on pricing issues for R&D products prepared for transfer from universities to the business environment, confirm the pace of dynamic growth in the world of R&D products that are transferred by universities to the market.

According to statistics, the overall effect of transferring R&D products from universities to businesses to the global economy is estimated at Supporting regional economic growth and new job creation — up to $1.7 trillion in gross industrial output and 5.9 million jobs since 1996 [2].

According to this year's study, the global trend in R&D spending continues to grow worldwide, reflecting a surge to $240 billion in the Information & Technology sector. As in previous years, the growth in global R&D investments is being driven by spending in Asian countries, in particular China, which exceeds $500 billion in spending accounting for a 22 percent global share in investments [3].

Association of University Technology Managers (AUTM) in their research note that the contribution of universities to GDP as a whole appears to be growing faster than U.S. GDP as a whole, and faster than the manufacturing industries used in prior reports [4]. However, when considering the research-intensive industries, the modelled AUTM contribution to GDP appears to be growing, in relative terms, about as quickly as these research-intensive industries. In numbers it is the $723 billion contribution to gross output, $374 billion contribution to GDP, and providing support for 2.676 million jobs over the 22-year period, is based on an assumption of a 5% earned royalty rate on licensees' product sales.

The World University Rankings in their methodology for evaluating knowledge-intensive universities, they use achievement levels in all their main tasks: teaching, research, knowledge transfer, and worldview [5]. In the research task (takes 30%) on the rating scale, the profit from commercialization of R&D products is estimated at 9%. Despite the different size of universities and the scope of scientific activities, this indicator is adjusted to take into account the number of teachers.

Solving pricing problems when commercializing R&D products is particularly relevant for universities that have technology transfer centres or other similar divisions. A study of the world's leading university technology transfer centres (Oxford, MIT, Stanford, Cambridge, Ruprecht-Karl University of Heidelberg, the National University of Singapore, the University of Toronto, etc.) has shown that even if there is methodological support for their activities, they cannot always effectively apply it. The pace of development and market needs for R&D products is growing significantly faster than the corresponding methodological support is being developed for them, in particular in the field of pricing.

The world's leading science-intensive universities publish annual reports on commercialization to improve their reputation in business circles R&D products. Universities create specialized technology transfer units that implement programs to promote their own R&D products. In particular, start up companies based on discoveries and inventions by University researchers. The most popular form of knowledge transfer in the world, which is developing, is Creative works (no patented technologies). They may be trademarked or copyrighted and are often ready to be licensed when the inventor discloses the invention. In FY2019 [6], creative works earned $6.3 million in revenue from 109 licenses across 55 technologies and leveraged online automated licensing for over 1,000 additional transactions. There were 27 technologies made available via online app platforms with more than 47,000 app downloads. Creative works come from colleges and centres across all UMN campuses.

Paying attention to pricing for R&D products is important when universities enter into contract research based on its contractual obligations. Such transactions, providing business advice is an important source for the development of universities.

According to the annual reports of universities, sometimes such an item of income can reach 10% of the total cost of maintaining the university [7].

1.3. Formulation of the problem

Each engineering university is unique in terms of access to resources, the scale and focus of their research efforts, and the level of expertise in technology licensing, patenting, and sharing. However, most of them have similar problems related to taking into account these and other features in pricing for university-generated R&D products, in particular in a changing market and globalizing processes.

Existing approaches to pricing for R&D products cannot be applied in modern market conditions due to a number of factors, namely:

- accelerated pace and unpredictability of changes in environmental factors;
- increasing the number of participants in the innovation infrastructure, which is increasingly attracted to the region's communities;
- acceleration of changes in market conditions due to digitalization;
- spreading the use of open models of the innovation process;
- diversification of forms and methods of transmission R&D products (Express licenses available online, Fast-track opportunity licenses for early-stage technologies, Negotiated, exclusive, and nonexclusive license agreements, Sponsored research agreements (MN-IP), University start up companies (Venture Centre and Discovery Launchpad));
- limited financial and time resources for full development of R&D products by the developer (often before commercialization, R&D products can be offered at different levels of readiness);
- increasing the level of technology intellectualization;
- maturation of scientific technologies at early stages outside of scientific organizations, using the resources of commercial partners willing and able to continue the applied research and experimental development necessary for the market launch of the product;
- the emergence of unpredictable effects from the commercialization and implementation of R&D products in various sectors of the economy (convergence, spillover, crowd effect, diffusion, multiplicative effect, etc.);
- increasing dependence of the developed functional characteristics of R&D products, taking into account the specifics of the conditions for their future implementation, and so on.

The decrease in the level of predictability and objectivity of results from the use of existing pricing methods for R&D products, their low adaptability to the dynamics of the innovation environment, the growth of the impact of economic consequences from this, and other factors led to the search for new methodological tools for effective pricing of R&D products prepared for commercialization and transfer from universities to the business environment.

2. Theoretical Background

The processes of transfer and commercialization of R&D products is a complex multi-attribute mechanism, the effectiveness of which is largely determined by a reasonable choice of approaches, methods and pricing models for R&D products.

R&D product can result in different products (products, technology, organizational and management decision, etc.) and be at different Technology Readiness Levels (TRL's). Since R&D product is a commodity in the innovation market, General methodological approaches of the market economy are used for basic pricing [8].

Pricing refers to the field of strategic management decisions [9], so specialists in the system of strategic management mainly consider the approaches to its implementation. There are study three types of technology transfer strategies: income-generation strategy, service-to-faculty strategy, and local development strategy [10]. The highlighted strategies differ in the priorities for implementing the transfer strategy.

R&D product transfer, as a process of technology transfer, has its own pricing features in terms of technology transfer transactions between countries [11, 12] .

It is necessary to highlight the influence of such a factor on pricing as a form of calculation the main payment types in use by University Technology Transfer Units (TTUs) [13]. The more frequent types of payment are the running royalties, but other payment types are frequently included in the technology transfer agreements, such as the minimums, the milestone payments, and the patent costs reimbursement and maintenance.

Pricing strategy based on the subscription model could be an effective strategy for any organization to increase its revenue and maintain customer satisfaction at the same time [14]. The strategy enables the organizations to get more revenue from their subscribers over a longer period. It also reduces the upfront cost paid by users, making it more affordable, which would help increase, the number of subscribers.

The complexity of managing the transfer process and, consequently, technology pricing is complicated by the growing importance of the support package, which is «diversified and performance of three key business-community services – provision of consultancy, provision of continuous professional development courses (CPD), and leasing of facilities and equipment» [15].

The complexity of pricing for technology transfers also lies in the fact that the transaction process must be based on balance the needs of the university, researchers, licensing firms and financiers with government entities and the public that support – and ultimately benefit from – the products and services created, along with the economic vitality and job creation derived from the commercialization process.

Pricing is influenced by many factors, including [16]: (1) the characteristics of the property or service, (2) functional analysis, (3) contractual terms, (4) economic circumstances, and (5) business strategies.

In general, all the traditional approaches to R&D product pricing known in the world can be divided into three areas: cost-based, profitable and comparative, represented by many methods and methods of their application.

2.1. Cost approach

For situations with the pricing of R&D products developed in universities, with the purpose of their further transfer and

commercialisation are mostly used methods are the cost approach (for purposes of the base assessment, the definition of "bottom border" prices R&D product, development of cost estimates for studies, preparation of applications for grants and the like).

Scientists studies in modern research the valuation methods used by universities, the concerns of usage, and the difficulties in implementing the valuation methods. The author concluded that the universities typically use cost approach, market approach, income approach and auction to value the academic technologies [17]. Among which, cost approach is the most widely used one. The difficulties suffered by Taiwanese universities include lacking staffs specialized in valuation, expensive valuation service by external consultants, and the restrictions by government regulations. Based on the interview findings and previous studies, this study further designs a technology valuation framework for Taiwan universities and applies the framework to valuing the vaccines of duck viral hepatitis owned by a Taiwan university. At last, this study offers suggestion for valuing academic technologies by integrating the results from interviews and the experiences in empirical applications.

Scientists [18] use a cost-based approach in their research. When forming the price, they recommend operating the Setting standard cost. To reduce the cost of R&D product is offered the optimization method of standard cost setting.

Cost-based pricing methods for R&D product technology developed within the University have their drawbacks and limitations. Focusing on the amount of expenses incurred can completely separate the developer from the real economic situation on the market. Accordingly, the formation of estimates for development will be carried out according to the priorities of the University's development. Since research and development can take many years, often with significant interruptions, it is difficult to justify discount rates to bring costs to today's conditions, especially for countries with unstable economies.

2.2. Income approach

The revenue-based approach to pricing is widely used in the modern business environment. Scientists explore revenue approaches through econometric multifactor asset pricing models, which identifying the best factor-pricing model(s) is conspicuously lacking in investment research applications [19, 20].

In scientific works the authors use a generic reduced-form model economy with moderate risk premium nonlinearity to examine the size of the resulting misspecification-induced pricing errors [21].

Also some authors generalized model, what is presented to jointly characterize the optimal pricing and inventory policies to maximize the retailer's total expected profit [22].

The revenue approach was considered on the example of pricing for Massive Open Online Courses (MOOCs) [23]. Authors adopt a game-theoretic framework to model the interaction and strategic choices of a MOOC platform, learners, and universities. Based on the certificate prices and revenue sharing ratios chosen by the platform for courses with various certificate-purchasing rates, universities consider the competition intensity and decide their course quality levels, to attract learners.

The complexity of applying the revenue approach methods for university developments is related to the subjectivity of the justification of cash flows, which are often determined by the place of application of the development. Paying attention to the revenue approach is important in connection with the development of value-based pricing in recent years.

Some scientists pay special attention to conceptualize key stakeholders' perceptions of their experiences, opportunities, and barriers to implementing value-based pricing [24, 25].

2.3. Comparative approach

Among the methods of this direction, the most common are competitive methods, the essence of which is in comparison with its analogue to determine the competitive advantages and bottlenecks of R&D product. In particular, this method is used as a price formation tool Bert Rand price game Based on game theory, this paper studies the strategy of purchasing technology and upgrading from a technology supplier in a duopoly market, and analyses the pricing of products under different technology procurement strategies [26]. The research shows that, under the competition of product price, the game results of the enterprise's purchase of technology will be divided into symmetrical Nash equilibrium or asymmetric Nash equilibrium. Group of authors developed the complex of methodical support of the implementation and commercialization of domestic innovative devices [27].

The competitive pricing model has been developed for vintage capital model that combines a competitive market structure with an exogenous rapid rate of innovation [28].

There are many methods of estimating cost but as it is clear that we cannot consider any single technique to be the best one as each of the techniques have their own advantages and disadvantages. Efforts should be made to use a combination of the estimation techniques to arrive at a better cost and quality estimate [29]. This will allow you to justify the best pricing option for R&D products for the purpose of transferring it.

The developed approaches to determining the cost and price of R&D products by NASA and the Software Engineering Institute (federally funded research and development centre sponsored by the U.S. Department of Defense). Both teams of authors use the concept of technological readiness in their methods and promote the idea of combining different approaches.

NASA's pricing methodology is aimed at using yet-to-be-completed developments, for estimating the cost and schedule of low TRL technology research and development projects. The method involves using a system of 20 unique technology parameters that are subsequently reduced in number and suitable for use in characterizing these technologies. Further, a discussion of data acquisition effort and criteria established for data quality are provided. The authors offer recommendations on the gaps identified, description of a spreadsheet-based estimating tool initiated. The main cost analysis tool was parametric analysis.

TCASE generates anticipated ranges of cost and schedule duration for a technology development project by drawing analogies to historical and current project. Data for historical and current projects is stored in an accompanying database.

The Software Engineering Institute uses TRL Calculator (one for hardware and one for software) developed by Mr. Nolte at AFRL, it is the negotiation of the answers that is labour intensive. Thus, a good consensus building and conflict-resolution process is also needed. Therefore, the accuracy of calculating the cost

(price) of R&D products is determined by the quantity and quality of negotiations between participants in the technology transfer process. Therefore, an important issue is the choice of a rational range of interviewees. The use of this technique is limited to system components.

2.4. Theoretical generalization

Consequently, most existing methods and pricing models for R&D products are inflexible. They are difficult to adapt to the dynamic characteristics of R&D products. At the same time, appraisers often do not take into account a significant number of changing factors of the internal and external environment.

For a long time, the development of R&D products within universities leads to an increase in the duration of the chain of innovation "generation – commercialization – market diffusion", so the use of exclusively expensive methods is impossible.

Since the sources of generating R&D products are not the parameters of market demand, but the scientific achievements of the university, the use of comparative approaches can also be used in a limited format.

In turn, profitable approaches are also difficult to use in their pure form due to the growing level of convergence of markets and technologies, the emergence of new forms of business, the emergence of unexpected effects of use, and so on.

Taking into account the above, the use of quantitative methods alone will not give an adequate result of pricing, since there is a risk of not taking into account many important situational factors of a volatile market environment. The use of qualitative methods carries the risk of obtaining such an indicator of the price of R&D product that is not subject to adequate adjustment (the price, although competitive in the market, but it is difficult to adjust it under the conditions of market changes).

Currently, there are no methodological developments that would provide a flexible pricing mechanism for R&D products for their transfer from universities to the business environment in a changing market. The lack of such developments causes problems for universities:

- failure to provide an adequate contract price for R&D products during their transfer from universities to the business environment;
- it is impossible to take into account a number of important indicators of an investment project for R&D product (discount parameters, profitability indicators, cash flows, etc.);
- inefficiency of pricing strategies for R&D product (overestimating the price of R&D product in some cases, in others – underestimation, which leads to loss of profit);
- lying of R&D products projects "on the shelves", etc.

It is important to develop a method that would make it possible to adjust the price of an R&D product, depending on changes in market conditions, and overcome the disadvantages of existing methods. At the same time, this method should create the ground for changing the target setting of pricing tasks for R&D products, which will contribute to the formation of effective pricing strategies.

3. Research design

3.1. Methodology approach

The aim of this work is to develop a method for modelling prices for R&D products for their transfer from universities to the business environment, taking into account the conditions of market variability.

The development of a method for modelling the price of R&D products, taking into account the conditions of market variability, is based on a combination of cost, comparative and profitable approaches to pricing. The market is characterized by a variety of features that affect the pricing of R&D products. In practice, appraisers often neglect individual parameters of R&D products; artificially simplify the interdisciplinarity of indicators and their relationship, which reduces the effectiveness of pricing for R&D products. This complicates the processes of transfer and commercialization of R&D products, reduces the competitive stability of the product in the market.

A scientific search has shown that prices for R&D products that are being prepared for transfer from universities to the business environment can be adjusted to take into account the variability of market conditions, in particular by applying the appropriate correction factor. This coefficient is essentially an aggregate indicator that includes a number of relevant factors that influence the pricing of R&D products.

Therefore, for further research and implementation of the goal, the following hypotheses were formed.

Hypothesis 1. The methodological approach to modelling prices for R&D products when they are transferred from universities to the business environment, which takes into account changing market conditions, should be based on: 1) based on the amount of expenses incurred by developers, since the sources of their formation can be justified; 2) taking into account the correction coefficient developed to clarify the price of R&D product.

This coefficient shows the influence of a combination of factors (external and internal relative to the R&D product environment) on pricing for this R&D product.

To do this, you should develop a correction factor that takes into account expert assessments of the set of factors that affect this R&D product. These are the factors that can indicate a possible change (increase or decrease) in the value of the analysed R&D product, and which can be transferred to the pricing plane.

This hypothesis will be tested by a comparative analysis of the average market prices for a number of R&D products and prices obtained by applying a correction coefficient for the proposed author's method.

Hypothesis 2. The list of features used to model the price of an R&D product prepared for transfer from a university to a business environment is universal and exhaustive.

The signs that determine the change in the price adjustment coefficient must be analysed in the process of practical research of R&D products. This hypothesis will be tested by comparing the features used for price modelling between different R&D products.

Hypothesis 3. The methodological approach to calculating the correction factor for improving the pricing of R&D products when they are transferred from universities to the business environment is universal and effective for strategic pricing purposes.

When forming a correction coefficient, the problem arises not so much in the economic as in the mathematical context: indicators that reflect the specific features of R&D product and its transfer processes, market uncertainty, and so on are quite heterogeneous. These indicators are characterized by a complex level of mutual correlation, and their influence on the integral indicator (correction coefficient) is not always obvious.

In order to justify the method of adjusting prices for R&D products when they are transferred from universities to the business environment, which takes into account different types of indicators and their dependencies of different levels of complexity, it is advisable to use approaches within the theory of fuzzy sets.

It is proposed to develop an R&D product price adjustment coefficient based on the algorithms of fuzzy set theory, which will effectively respond to changes in market conditions (in particular, by adding or subtracting the corresponding scenarios in the knowledge base, adjusting features, etc.). One of the promising approaches of this theory for modelling and forecasting economic processes is the fuzzy logic approach, which gained popularity in economic applications in the second half of the last century.

The application of the fuzzy logic approach to develop a method for adjusting prices for R&D products during their transfer from universities to the business environment is justified by the following arguments.

- *The ability to take into account the interaction of factors of influence on the R&D product that are interrelated with different levels of complexity*. Factors that influence the price change for an R&D product can be both the specific characteristics of the R&D product itself, and the characteristics of the market to which this R&D product is displayed (in particular, the market susceptibility of this R&D product), as well as the processes of its transfer. These factors are not in a linear relationship, but are closely related, so considering them in the system using fuzzy set theory algorithms will help refine the price of an R&D product.
- *Adaptive capacity of expert assessments.* Methods based on the theory of fuzzy sets have a high adaptive capacity according to expert estimates and are quite adequate in practical use.
- *Combination of qualitative and quantitative assessments.* The development of the R&D product price correction coefficient within the framework of fuzzy set theory operates with both qualitative and quantitative forms of its implementation, which makes it possible to evaluate the features, external and internal features, properties of the R&D product market, and so on. The method also allows you to take into account estimates that pass from one state to another.
- *Feedback.* The R&D product price adjustment method is based on a number of indicators that can change during the calculation of the adjustment coefficient. For example, if some indicators are outdated or other indicators need to be introduced, they can be replaced, along with appropriate modification of scenarios in the knowledge base. This is based on the principles of feedback-from the market entity (consumer, enterprise, etc.) to the university.

By adjusting the price of R&D products based on fuzzy set theory, we understand the process by which, based on available data, you can set significant parameters that are not directly measured, but determine the nature of pricing for R&D products and make it possible to analyse changes in its state.

The criterion for the effectiveness of price adjustment for R&D products in the framework of fuzzy set theory is expressed by maximizing the degree of suitability of the obtained estimates for a specific market situation.

In economics, the most common models used for this type of problem are Mamdani, Sugeno, Tzukamoto, Larsen, and others. To adjust the price of R&D products based on fuzzy sets, we selected the Mamdani model, which differs from other models in that its rules in sequences contain fuzzy values (membership functions).

The methodology of estimation processes based on the theory of fuzzy sets is based on a number of theoretical assumptions, in particular, stated by Zadeh L. (1976).

First, it is assumed that the object of research can enter a state that belongs to a finite set of states S (the action of external and internal processes changes, but the lack of its measurement leads to a restriction of the set S). On the set S, there are two disjoint subsets $S_1 \cup S_2$, where S_1 is a subset of states that are consistent with the characteristics of the desired state by the level of development of features; S_2 is a subset of states that are not consistent with the characteristics of the desired (normative or reference) state by the level of development of features. The subset $S_1 = \{s_i\}, i = \overline{1,n}$ contains state types that allow for functioning and development. The subset $S_2 = \{s_j\}, i = \overline{1,m}$ contains state types that respond to changes in parameters or structural relationships that contribute to deviations from the desired result.

Second, the solution to the issue of inventory and evaluation of the real state of the object is based on the analysis of the set S or a subset of S_1 and S_2.

Third, the assessment is based on the appraisers' positions and methods of conducting it.

Fourth, detecting deviations from the characteristics of the desired state means that the object is in the process of transitioning from the S_k state to the S_l state, but the operating conditions may not be violated if S_k and S_l belong to a subset of S_1 states.

3.2. Data analysis

Based on the research, the factors that determine the processes of transfer, commercialization and market launch of R&D products, which affect the pricing of R&D products, are identified and systematized by groups of features:

Group A ($f(x_1)$) – characteristics that characterize the consumer value of an R&D product;

Group B ($f(x_2)$) – features that characterize the market susceptibility of the R&D product;

Group C ($f(x_3)$) – features that characterize the processes of transfer and commercialization of R&D product.

Group A combines comparative indicators that allow us to assess the value of R&D products for consumers. Consumer value characterizes the utility of an R&D product to meet the consumer's needs. The value that the developer creates in the form of an R&D product determines the consumer value of the R&D product in the form of a finished product and the consumer value of the product that is obtained using the R&D product. This group of attributes is not personalized and is directly related to the

characteristics of the R&D product. The level of this group of attributes allows us to assess the potential consumer value of R&D product in meeting the consumer's needs.

In particular, the indicators include three levels of R&D product readiness for commercialization (technological, patent, and analytical). These three levels of readiness are related to the assessment of the completeness (feasibility) of the R&D product and determine the level of consumer value of the R&D product as a commodity.

NASA development can be used to determine the level of technological readiness [30]. This organization has developed and successfully uses a methodology for assessing the levels of technological readiness (TRL).

The level of patent readiness includes an assessment of the availability (absence) of documents for intellectual property objects or the process of obtaining them. The level of patent readiness is evaluated as the level of protection of the R&D product and directly affects the consumer value of the R&D product.

The level of analytical readiness (ARL) can be assessed by the degree of development of analytical documents by R&D product developers. The lowest level of analytical readiness is associated with the justification of the R&D product concept. The highest level of ARL is considered a business plan for introducing innovations to the market. The development of analytical documents is based on marketing information and allows you to simplify the process of using R&D product.

Signs of the level of novelty and level of improvement of R&D product characterize the competitive advantages of R&D product as an object of innovation. The level of novelty of R&D product is related to the number of technological parameters that are introduced by the developer for the first time and distinguish R&D product from analogues. If R&D is product improving or modifying an innovation to address customer needs, R&D product has a certain level of improvement, such as increasing the level of existing technological options, R&D product.

The level of quality and competitiveness of a product that is obtained on the basis of R&D product, related to the evaluation of indicators of competitive advantages of the product (products, work, service), which is expected to be obtained as a result of the application of R&D product.

The level of possible unauthorized reproduction of an R&D product is related to the level of complexity of the R&D product. A low level of complexity may expose the consumer to the risk of losing the value of the R&D product.

The level of environmental friendliness of R&D product provides an assessment of the impact of R&D product on the environment when using R&D product or a product made on the basis of R&D product (environmental cleanliness of the development application, reducing environmental pollution, energy saving, reducing raw material costs, etc.) development.

R&D product may not affect the ecology of society, or reduce (increase) its influence on the analogue, both positive and negative. Accordingly, the level of environmental friendliness of the R&D product can increase or decrease the consumer value of the R&D product.

Group B includes features that are correlated with the assessment of the conditions for the introduction of R&D product in a particular market (segment). These indicators allow us to assess the level of attractiveness of market conditions for R & D products (direct action marketing environment).

In particular, the market susceptibility of an R&D product is directly determined by the state and intensity of competition in the target market. A high level of competition, i. e. a large number of similar R&D products and R&D product substitutes, impairs market sensitivity and reduces the level of consumer value of the R&D product [31, 32].

The size of the sales market and the rate of change in its value directly affect the market signs of the introduction of R&D product. These attributes are related to the quantitative parameters of the sales market. Their high level allows us to assess the market sensitivity of the technology as high.

The update level of the market for R&D product provides an opportunity to assess the level of intensity of innovation in a particular economic activity and is associated with the estimation of time expected use R&D to product replacement or improvement.

The level of readiness of consumers to use the product that is obtained based on R&D product is associated with the stage of the life cycle of the need and technology and affects the marketing costs for the consumer.

Group C allows you to evaluate the features of transferring R&D product to a specific consumer and the specifics of implementing R&D product in its activities.

Therefore, the second and third groups of attributes and their estimates are adaptive to the conditions of a specific R&D product transfer transaction.

The third group of features involves comparing and determining the level of attractiveness of the conditions for transferring rights to R&D product to the consumer and the conditions for introducing R&D product to the consumer.

The transfer terms are evaluated by the components of the transaction (the level of attractiveness of the financial terms of the R&D product transfer-providing discounts, instalment payments, rentals, etc.), as well as by the competitive advantages that the developer provides when implementing the R&D product (the level of completeness of technological support by technology developers).

Becoming increasingly important the signs associated with the direct introduction of R&D product from the consumer to evaluate the need for and scope of additional time, financial and other resources to conduct additional tests (the level of difficulty implementation R&D product, the level of necessary material resource support integration of R&D product, the level of initial investment costs that should be involved to implement the R&D product).

This group includes indicators of commercial (investment) attractiveness of R&D product (the level of payback, the level of indicators of economic efficiency of investment costs (commercialization)).

The hierarchical order of factors of influence (f (x)) and their features (p) on the price of R&D products is shown in Fig. 1.

The elements of the hierarchy of factors of influence and attributes in Fig. 1 are interpreted as follows: *S* – relative indicator of price change of R&D product (top of the hierarchy*), %; x1, x2, x3* – generalizing factors influencing the price of R&D product (thermal peaks); $p_{11} \dots p_{1n}$, $p_{21} \dots p_{2n}$, $p_{31} \dots p_{3n}$ –signs of factors influencing the price of the R&D product.

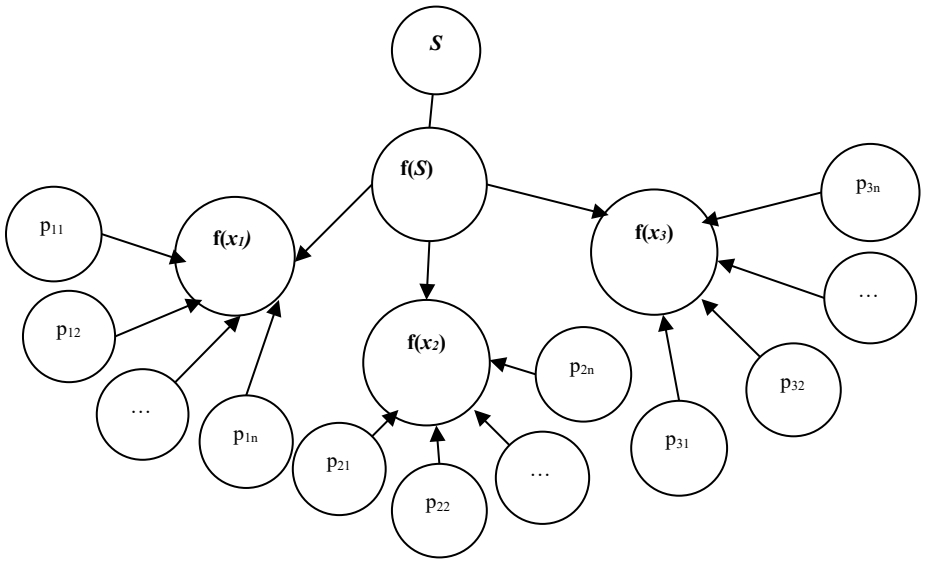


Figure 1: Hierarchical order of the influence of factors and attributes they contain on the price of R&D products

Reductions of f_S, f_{x1}, f_{x2}, f_{x3} are performed based on a logical output with fuzzy knowledge bases. A fuzzy subset of a set S is defined as a set of ordered pairs $A = \{x, \mu_A(x); x \in S\}$, where $\mu_A(x)$ is the characteristic function that takes values from some ordered set M = [0, 1] – many accessories $\mu_x\ (x) > 0, \forall x \in S, \mu_x\ (x) > 0, \forall x \nexists S, sup_{x \in S}[\mu_x\ (x)] = 1$.

In this case, the function $\mu_x\ (x)$ indicates the degree of belonging of element x to a subset of A and is a tool for converting linguistic variables to a mathematical language for further application of the fuzzy logic method.

The description of the R&D product price adjustment process based on the application of fuzzy set theory can be divided into stages: 1) fuzzification; 2) development of fuzzy rules (generalization of antecedents and consequents; inference using logical connections); 3) defazzification.

4. Empirical results

The analysis made it possible to identify the most popular features of factors within groups A, B, and C at this time and assign them the value of linguistic terms for adjusting the price of R&D product using the Mamdani model (table 1).

Table 1: Signs and values of linguistic terms of factors influencing the price of R&D product

Factors	Signs	Meaning and explanation of linguistic terms of the factor
1	2	3
Group A ($f(x_1)$) – features of the consumer value of an R&D product	The technological readiness level of R&D product	L – low indicator level [0; 1.25; 2.5]; T – tolerable indicator level [2.5; 3.75; 5]; A – applicable indicator level [5; 6.25; 7.5]; H – high indicator level [7.5; 8.75; 10].
	The patent readiness level of R&D product	
	The analytical readiness level of R&D product	
	The level of innovation of R&D product	
	The improvement of R&D product	
	The level of possible unauthorized reproduction of R&D product	
	The level of probability of unexpected effects from the introduction and use of R&D product	
	The level of quality and competitiveness of the product that is obtained on the basis of R&D product	
	The environmental level of R&D product	
Group B ($f(x_2)$) – features of the market susceptibility of the R&D product	The level of direct competition	L – low indicator level [0; 1.25; 2.5]; T – tolerable indicator level [2.5; 3.75; 5]; A – applicable indicator level [5; 6.25; 7.5]; H – high indicator level [7.5; 8.75; 10].
	The level of competition among substitutes	
	The size of the market for R&D product	
	The growth rate of the R&D product sales market	
	The update level of the market for R&D product	
	The level of readiness of consumers to use the product that is obtained on the basis of R&D product	
	The level of time expected to use an R&D product before replacement or improvement	
Group C ($f(x_3)$) – features of the	The level of initial investment costs that need to be raised for the implementation of R&D product	L – low indicator level [0; 1.25; 2.5];

processes of transfer and commercialization of R&D product	The cost level for ongoing R&D product maintenance	T – tolerable indicator level [2.5; 3.75; 5]; A – applicable indicator level [5; 6.25; 7.5]; H – high indicator level [7.5; 8.75; 10].
	The difficulty level of the integration of R&D product	
	The level of time spent on implementation and revision	
	The level of required regulatory support for R&D product implementation (obtaining permits, etc.)	
	The level of indicators of economic efficiency of investment costs (commercialization)	
	The level of attractiveness of financial terms of R&D product transfer	
	The level of recoupment	
	The level of expenses for marketing support of commercialization	
	The level of necessary material resource support for R&D product implementation	
	The level of access to the necessary resources to use R&D product	
	The level of need to establish various forms of interaction to use (or the level of sufficient capacity for self-implementation) R&D product	
	The level of completeness of technological support by technology developers	

The model for adjusting product R&D prices when they are transferred from universities to the business environment can be expressed as a function:

$S = f$ (the value of consumption of R&D products, and the market susceptibility of R&D products, production and transfer processes and commercialization of scientific and technical products), which is a system of functions in the following order:

$f(x_1) = f$ (*the technological readiness level of R&D product; the patent readiness level of R&D product; the analytical readiness level of R&D product; the level of innovation of R&D product; the improvement of R&D product; the level of possible unauthorized reproduction of R&D product; the level of probability of unexpected effects from the introduction and use of R&D product; the level of quality and competitiveness of the product that is obtained on the basis of R&D product; the environmental level of R&D product);*

$f(x_2) = f$ (*the level of direct competition; the level of competition among substitutes; the size of the market for R&D product; the growth rate of the R&D product sales market; the update level of the market for R&D product; the level of readiness of consumers to use the product that is obtained on the basis of R&D product; the level of time expected to use an R&D product before replacement or improvement);*

$f(x_3) = f$ (*the level of initial investment costs that need to be raised for the implementation of R&D product; the cost level for ongoing R&D product maintenance; the difficulty level of the integration of R&D product; the level of time spent on implementation and revision; the level of required regulatory support for R&D product implementation (obtaining permits, etc.); the level of indicators of economic efficiency of investment costs (commercialization); the level of attractiveness of financial terms of R&D product transfer; the level of recoupment; the level of expenses for marketing support of commercialization; the level of necessary material resource support for R&D product implementation; the level of access to the necessary resources to use R&D product; the level of need to establish various forms of interaction to use (or the level of sufficient capacity for self-implementation) R&D product; the level of completeness of technological support by technology developers).*

Using the *Mamdani* model in the Fuzzy Logic Toolbox component of the MATLAB software package, a model was developed for adjusting prices for R&D products when they are transferred from universities to the business environment.

Based on the generated set of factor terms (table 1), a knowledge base has been developed – possible scenarios for the ratio of R&D product consumer value factors (Group A), market susceptibility R&D product (Group B), R&D product transfer and commercialization processes (Group C). 33 rules have been established and justified. Note that in some scenarios, the weight of the rule is applied, which is measured in the range [0 ... 1] and indicates the level of significance of a particular scenario when adjusting R&D product prices. A fragment of this rule base is shown in figure 2.

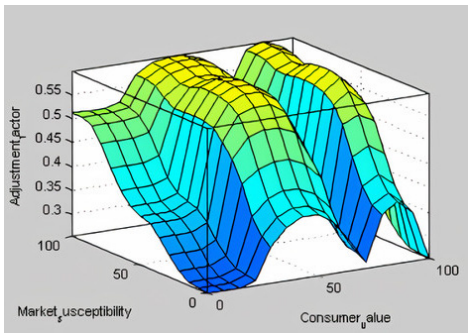
Developed model of R&D product price adjustment from universities in the business environment based on the theory of fuzzy sets enables:

- to enter grades for groups of signs, A, B, C (previously prepared by experts) and to obtain the correction factor prices R&D product;
- the resulting coefficient takes into account the current market volatility conditions and can serve as a basis for developing a strategy for R&D product market development.

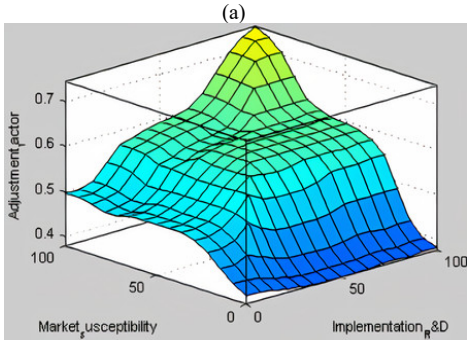
A fuzzy model for adjusting the price of R&D product when transferring from universities to the business environment is shown in figure 3.

1. If (Consumer_value is Low) or (Market_susceptibility is Low) or (Implementation_R&D is Low) then (Adjustment_factor is Low) (1)
2. If (Consumer_value is Low) and (Market_susceptibility is Average) and (Implementation_R&D is Low) then (Adjustment_factor is Average) (1)
3. If (Consumer_value is Low) and (Market_susceptibility is High) and (Implementation_R&D is Low) then (Adjustment_factor is Average) (1)
4. If (Consumer_value is Low) and (Market_susceptibility is Average) and (Implementation_R&D is Average) then (Adjustment_factor is Average) (1)
5. If (Consumer_value is Low) and (Market_susceptibility is Average) and (Implementation_R&D is High) then (Adjustment_factor is Tolerable) (1)
6. If (Consumer_value is Low) and (Market_susceptibility is High) and (Implementation_R&D is High) then (Adjustment_factor is Tolerable) (1)
7. If (Consumer_value is Low) and (Market_susceptibility is High) and (Implementation_R&D is Average) then (Adjustment_factor is Tolerable) (1)
8. If (Consumer_value is Average) or (Market_susceptibility is Average) or (Implementation_R&D is Average) then (Adjustment_factor is Average) (1)
9. If (Consumer_value is Average) and (Market_susceptibility is Average) and (Implementation_R&D is Low) then (Adjustment_factor is Average) (1)
10. If (Consumer_value is Average) and (Market_susceptibility is Average) and (Implementation_R&D is High) then (Adjustment_factor is Average) (1)
11. If (Consumer_value is Average) and (Market_susceptibility is High) and (Implementation_R&D is Average) then (Adjustment_factor is Average) (1)
12. If (Consumer_value is Average) and (Market_susceptibility is High) and (Implementation_R&D is Low) then (Adjustment_factor is Average) (1)
13. If (Consumer_value is Average) and (Market_susceptibility is Low) and (Implementation_R&D is Average) then (Adjustment_factor is Average) (1)
14. If (Consumer_value is Tolerable) and (Market_susceptibility is Low) and (Implementation_R&D is Low) then (Adjustment_factor is Low) (1)
15. If (Consumer_value is Tolerable) and (Market_susceptibility is Average) and (Implementation_R&D is Average) then (Adjustment_factor is Average) (1)
16. If (Consumer_value is Tolerable) and (Market_susceptibility is High) and (Implementation_R&D is High) then (Adjustment_factor is Tolerable) (1)
17. If (Consumer_value is Tolerable) and (Market_susceptibility is Low) and (Implementation_R&D is High) then (Adjustment_factor is Average) (1)
18. If (Consumer_value is Tolerable) and (Market_susceptibility is Average) and (Implementation_R&D is Average) then (Adjustment_factor is Average) (1)
19. If (Consumer_value is Tolerable) or (Market_susceptibility is High) or (Implementation_R&D is High) then (Adjustment_factor is High) (1)
20. If (Consumer_value is Tolerable) and (Market_susceptibility is Average) and (Implementation_R&D is Low) then (Adjustment_factor is Average) (1)
21. If (Consumer_value is Tolerable) and (Market_susceptibility is High) and (Implementation_R&D is Low) then (Adjustment_factor is Average) (1)
22. If (Consumer_value is High) or (Market_susceptibility is High) or (Implementation_R&D is High) then (Adjustment_factor is High) (1)
23. If (Consumer_value is High) and (Market_susceptibility is Average) and (Implementation_R&D is Low) then (Adjustment_factor is Average) (1)
24. If (Consumer_value is High) and (Market_susceptibility is Average) and (Implementation_R&D is High) then (Adjustment_factor is Tolerable) (1)
25. If (Consumer_value is High) and (Market_susceptibility is High) and (Implementation_R&D is Low) then (Adjustment_factor is Average) (1)
26. If (Consumer_value is High) and (Market_susceptibility is High) and (Implementation_R&D is Average) then (Adjustment_factor is Tolerable) (1)

Figure 2: Fragment of the database of rules for adjusting prices for R&D products when they are transferred from universities to the business environment



(a)



(b)

Fig. 3. Fuzzy model of R&D product price adjustment transfer from universities to the business environment: (a) influence customer value R&D product and market receptivity to corrective cost ratio R&D product; (b) influence of market receptivity, R&D product and the nature of its transfer and commercialization at the correct price ratio of R&D product

Using the described methodology, we will adjust the prices of a number of R&D products in the sequence (table 2):

1) *Expert assessment.* Each feature of R&D product is characterized by the level of its manifestation, which is proposed to be assessed by experts, in points, in the range 1...3 where 1 is little or no effect symptom, 2 – moderate effect of the symptom, 3 – severe impact signs (col. *3*), and then summarize the points and assign them a percentage (for example, on the first group: 9 points – the probability of a minimum 27 – maximum probable). Based on this, a generalized estimate is formed for a group of factor attributes, in %. Indicators for the corresponding R&D product are evaluated by experts based on questionnaires. The reliability of the evaluation results is confirmed by a sample of at least 15 experts;

2) *identification of the obtained factor value*, % (col. *4*);

3) *entering the obtained values into the developed model for determining the correction coefficient*. The obtained factor value with the average values of this indicator in the Fuzzy Logic Toolbox component of the MATLAB software package (based on a pre-formed knowledge base) are compared.

Therefore, the proposed method takes into account the ratio of elements of income, cost and comparative estimation approaches.

The method makes it possible to conduct economic forecasting in conditions of uncertainty; in particular, it is especially important at the stage of conceptual decision-making, planning the transfer and commercialization of R&D products from the university to the business environment, and so on. The proposed method has been tested on a number of R&D products developed at Lviv Polytechnic National University (Ukraine) and prepared for transfer to the business environment.

Table 2: Factors, signs of R&D product and their estimates

Factors	Signs	The level of feature manifestation, points	Meaning and explanation of linguistic terms of the factor
1	2	3	4
Group A ($f(x_1)$)	The technological readiness level of R&D product	1…3	L – low level of sign – 0 …25%; T – tolerable level of sign – 26 …50%; A – applicable level of sign – 51 … 75%; H – high level of sign – 76 …100%
	The patent readiness level of R&D product	1…3	
	The analytical readiness level of R&D product	1…3	
	The level of innovation of R&D product	1…3	
	The improvement of R&D product	1…3	
	The level of possible unauthorized reproduction of R&D product	1…3	
	The level of probability of unexpected effects from the introduction and use of R&D product	1…3	
	The level of quality and competitiveness of the product that is obtained on the basis of R&D product	1…3	
	The environmental level of R&D product	1…3	
	Factor estimate, %	0…100%	
Group B ($f(x_2)$)	The level of direct competition	1…3	L – low level of sign – 0 …25%; T – tolerable level of sign – 26 …50%; A – applicable level of sign – 51 … 75%; H – high level of sign – 76 …100%
	The level of competition among substitutes	1…3	
	The size of the market for R&D product	1…3	
	The growth rate of the R&D product sales market	1…3	
	The update level of the market for R&D product	1…3	
	The level of readiness of consumers to use the product that is obtained on the basis of R&D product	1…3	
	The level of time expected to use an R&D product before replacement or improvement	1…3	

	Factor estimate, %	0…100%	
Group C ($f(x_3)$)	The level of initial investment costs that need to be raised for the implementation of R&D product	1…3	L – low level of sign – 0 …25%; T – tolerable level of sign – 26 …50%; A – applicable level of sign – 51 … 75%; H – high level of sign – 76 …100%
	The cost level for ongoing R&D product maintenance	1…3	
	The difficulty level of the integration of R&D product	1…3	
	The level of time spent on implementation and revision	1…3	
	The level of required regulatory support for R&D product implementation (obtaining permits, etc.)	1…3	
	The level of indicators of economic efficiency of investment costs (commercialization)	1…3	
	The level of attractiveness of financial terms of R&D product transfer	1…3	
	The level of recoupment	1…3	
	The level of expenses for marketing support of commercialization	1…3	
	The level of necessary material resource support for R&D product implementation	1…3	
	The level of access to the necessary resources to use R&D product	1…3	
	The level of need to establish various forms of interaction to use (or the level of sufficient capacity for self-implementation) R&D product	1…3	
	The level of completeness of technological support by technology developers	1…3	
	Factor estimate, %	0…100%	

5. Discussion

Taking into account peculiarities of market situation, groups of attributes can be supplemented and / or modified.

The proposed method is tested on a number of scientific and technological complexes, developed at Lviv Polytechnic National University and prepared for transfer to business environment. The obtained results are shown in Table 3.

Table 3: Results of testing the R&D product price adjustment method prepared for transfer from the university to the business environment

№	R&D products	Factor / factor estimate, %			Correction factor, %	Current price, ths. USD	Adjusted price, ths. USD	Price change, + / -; ths.USD	Market price, analogue price, ths. USD
		Group A	Group B	Group C					
1	2	3	4	5	6	7	8	9	10
1	Technology of optically-stimulated luminescent dosimetry	13% (L)	44% (T)	87% (H)	-0,0876	23 020,80	22 999,63	-21,16	25 600
2	Ensuring Technological Strength of Welded Joints with Armored Steel of ARMSTAL 500-Type	11% (L)	34% (T)	61% (A)	0,0698	120,890	129,328	+8,438	142,300
3	Technology of surface friction strengthening of working surfaces of machine parts	27% (T)	44% (T)	71% (A)	0,0321	156,90	161,936	+5,036	165,89
4	Mobile robotic platforms: MRP-05 "Borsuk" and MRP-07 "Kubik"	47% (T)	73% (H)	82% (H)	-0,023	345,90	334,94	-10,96	340,90
5	Continuation of the	41% (T)	44%	73%	0,067	110,78	118,202	+7,42	129,97

	life of machine parts by the method of surfacing under a layer of flux		(T)	(H)					
6	Autonomous system for detection of smoke and carbon leakage monoxide	51% (A)	78% (A)	77% (H)	-0,036	0,084	0,081	-0,003	0,205
7	Predicting and providing a set value of the initial resistance of heterogeneous and homogeneous materials of small thicknesses and cross sections with a point capacitor contact micro-welding	39% (T)	42% (T)	72% (A)	0,0912	0,370	0,403	+0,033	0,518
8	Equipment for contact point capacitor micro-welding	34% (T)	67% (A)	45% (T)	-0,027	0,074	0,072	+0,002	0,096
9	Technology of surface friction displacement of working surfaces of machine parts	43% (T)	32% (H)	68% (A)	0,33	2,10	2,73	+0,63	22,00
10	Pocket City	90% (H)	45% (T)	81% (A)	0,002	3,20	3,2064	+0,0064	28,00
11	Bulk food mixer	50% (T)	48% (T)	63% (A)	0, 0731	3,10	3,32	+0,22	17,80

From the obtained results it can be seen, for example, in the cases of R&D products from the positions 2,3, 5, 7, 9, 10 and 7 (according to table. 3) it is quite possible to set the price at a higher level (in particular, at the level of corrected estimates).

It is predicted that sales of such products will not decrease, but will remain at the same level. After all, the adjusted estimate is based on a number of indicators that reflect the market perception of the product, the level of which in these cases significantly exceeds the level previously included in the cost of R&D product.

In cases 1, 4, 6 and 8, the price of the R&D product should be slightly reduced, which will help to increase its price competitiveness in the market, and, consequently, increase sales volumes.

The values obtained as a result of applying the model are characterized by an indistinct number with a certain range of values, which makes it possible to operate not with probabilistic estimates, but with project data. This helps to achieve a higher level of price accuracy for R&D product when it is transferred from the university to the business environment.

6. Conclusions

Hypothesis 1 comes true. A methodological approach to pricing for R&D products during their transfer from universities to the business environment is developed based on taking into account changing market conditions, which in particular were given in table 2 and on the basis of certain expenses for the R&D products. The result can become the initial price of R&D products in the process of discussing the transaction for its transfer.

A practical study of R&D products for signs that determine the impact on their prices has shown that *hypothesis 2* does not come true. Since each specific situation with R&D product has its own pricing features, due to many factors. For example, those features from factor groups A, B, and C that are relevant for their consideration when modelling prices for R&D products in the field of industrial electronics will not be relevant for R&D products in the field of it. In addition, the same evaluation criteria for R&D products in different industries may have different approaches to the interpretation of their essence. Therefore, the proposed list of features is not exhaustive, and may vary depending on the types of R&D products, their branches of application, features of transfer from the university to the business environment, and so on.

Hypothesis 3 is confirmed, since the methodological approach to calculating the correction factor for improving the pricing of R&D products when they are transferred from universities to the business environment is universal. This approach can be applied regardless of the stage of readiness of R&D products, and depending on the possibility of its transfer (in particular, in situations where the buyer is ready to purchase these R&D products at the initial stage of readiness). The methodological approach is effective for strategic pricing purposes.

The criterion for the effectiveness of modelling prices for

R&D products in the framework of fuzzy set theory is expressed by maximizing the degree of suitability of the obtained estimates for a specific market situation.

The advantages of the proposed methodological approach to pricing for R&D products are as follows:

- justification of the price based on the principles of the author's method gives a more reliable result (takes into account changing market conditions, implementation conditions for a specific buyer, is characterized by flexibility in accounting indicators, etc., the level of novelty);
- the method is aimed at accounting not only for static expenses (which sometimes even become irrelevant because they are spread over a long period of time), but also for dynamic market conditions of R&D products, conditions of the consumer's operating environment, and so on;
- the developer (university) has a lot of flexibility in terms of profit management (in particular, according to the results of the study, in most cases, the margin profit increases);
- the level of trust of business partners is growing at the university, as the procedures for modelling prices for R&D products prepared for transfer from universities to the business environment become significantly more transparent;
- the author's approach can be used not only for the price, but also for other pricing parameters for R&D products;
- the metrics used in the method can be modified depending on the type of R&D product (technological, product, etc.) and market conditions;
- Disadvantages:
- the use of the proposed method is advisable only in the short- and medium-term forecasting period;
- the method is essentially based on the competence of experts. Experts should have a proper level of knowledge, rely on the results of marketing research, and have operational data on the given characteristics.

The approach developed by the authors develops the principles of marketing pricing, providing opportunities to clarify the mechanism of influence of factors on the formation of the value of R&D products, and therefore their prices.

Conflict of Interest

The authors declare no conflict of interest.

Acknowledgment

We thank the developers of R&D products and scientists of Lviv Polytechnic National University (Ukraine), who shared the pearls of their knowledge and experience, which made it possible to conduct research and justify the results.

References

[1] N. Chukhray, N. Shakhovska, O. Mrykhina, M. Bublyk, L. Lisovska, "Consumer aspects in assessing the suitability of technologies for the transfer", in 2019 Proceedings IEEE /14th International Scientific and Technical Conference on Computer Sciences and Information Technologies, 142-147, 2019, doi:10.1109/STC-CSIT.2019.8929879.

[2] About Tech Transfer [online] Available at: https://autm.net/about-tech-transfer / Pages/ https://www.autm.net/AUTMMain/media/Advocacy/Documents/Points_to_Consider.pdf [Accessed 21.03.2020]

[3] Global Funding Forecast Predicts Growth of R&D Spending Worldwide [online] Available at: https://www.rdworldonline.com/global-funding-forecast-predicts-growth-of-rd-spending-worldwide/ [Accessed 11.02.2020]

[4] The Economic Contribution of University/Nonprofit Inventions in the United States: 1996 – 2017. [online] Available at: https://autm.net/AUTM/media/About-Tech-Transfer/Documents/Economic_Contribution_Report_BIO_AUTM_JUN2019_web.pdf/ [Accessed 12.02.2020].

[5] Young University Rankings 2019 [online] Available at: https://www.timeshighereducation.com/world-university-rankings/2019/young-university-rankings#!/page/0/length/25/sort_by/rank/sort_order/asc/cols/stats/ [Accessed 12.04.2020].

[6] Technology Commercialization [online] Available at: https://research.umn.edu/units/techcomm/about-us/overview/ [Accessed 19.04.2020].

[7] Deakin University Annual Report 2018 [online] Available at: https://www.deakin.edu.au/__data/assets/pdf_file/0007/1906819/300519-Deakin_AR_2018_pages_web.pdf/ [Accessed 17.04.2020].

[8] D. Hague, Pricing in business (Vol. 23), Routledge, 2018.

[9] F. Brescia, G. Colombo, P. Landoni, "Organizational structures of Knowledge Transfer Offices: an analysis of the world's top-ranked universities", J. Technol. Transf,. **41**(1),132–151, 2016, doi:10.1007/s10961-014-9384-5.

[10] P. Giuri, F. Munari, A. Scandura, L. Toschi, "The strategic orientation of universities in knowledge transfer activities", Technological Forecasting and Social Change, **138**, 261-278, 2019, doi:10.1016/j.techfore.2018.09.030.

[11] A. M. Rugman, L.Eden, (Eds.), Multinationals and transfer pricing. Routledge, 2017.

[12] D. Mescall, K. J. Klassen, "How Does Transfer Pricing Risk Affect Premiums in Cross-Border Mergers and Acquisitions? ", Contemporary Accounting Research, **35**(2), 830-865, 2018, doi:10.1111/1911-3846.12397.

[13] A. Rocha, R. Lima, M. Amorim, F. Romero, "Payment types included on technology licensing agreements and earnings distribution among Portuguese universities", Tékhne, **15**(2), 100-107, 2017, doi:10.1016/j.tekhne.2017.11.001

[14] A. Singh, Technology software pricing in cloud computing era, Ph. D Thesis, Massachusetts Institute of Technology, 2017.

[15] R. Zhou, P. Tang, "The role of university Knowledge Transfer Offices: Not just commercialize research outputs!", Technovation, 102100, 2019, doi:10.1016/j.technovation.2019.102100.

[16] C. P. Rossing, M.Cools, C. Rohde, "International transfer pricing in multinational enterprises", Journal of Accounting Education, **39**, 55-67, 2017, doi:10.1016/j.jaccedu.2017.02.002.

[17] M. Y. Wang, "The valuation methods and applications for academic technologies in Taiwan", in 2016 Portland International Conference on Management of Engineering and Technology (PICMET), IEEE, 1320-1327, 2016. doi:10.1109/PICMET.2016.7806739.

[18] Q. Meng, J. Lou, J. Zhu, X. Bai, "Standard cost setting and application of improved ant colony optimization algorithm", Systems Engineering-Theory & Practice, (**7**), 9, 2016.

[19] F. Barillas, J. Shanken, "Comparing asset pricing models", The Journal of Finance, **73**(2), 715-754, 2018, doi:10.1111/jofi.12607.

[20] Y. Jin, P. Lu, Q. Qi, Z. G. Tang, T. Xiao, "Tight approximation ratio of anonymous pricing", in 2019 Proceedings of the 51st Annual ACM SIGACT Symposium on Theory of Computing, 674-685, 2019, doi:10.1145/3313276.3316331.

[21] M. W. Brandt, D. A. Chapman, "Linear approximations and tests of conditional pricing models", Review of Finance, **22**(2), 455-489, 2018, doi:10.1093/rof/rfy003.

[22] Q.Wang, N.Zhao, J.Wu, Q.Zhu, "Optimal Pricing and Inventory Policies with Reference Price Effect and Loss-Averse Customers", Omega,102174,2019, doi:10.1016/j.omega.2019.102174.

[23] L. C. Kung, W. C. Lee, "Pricing and Diversification of Massive Online Open Course Platforms", in 2017 PACIS , Twenty First Pacific Asia Conference on Information Systems Langkawi, 2017, 202. [online] Available at: https://aisel.aisnet.org/cgi/viewcontent.cgi?article=1077&context=pacis2017 [Accessed 23.11.2019].

[24] A. Mejía, R. Gilardino, F. B.Kristensen, L. P. Garrison, I. H. T. A. L. America, "Value-Based Pricing in Latin America: How Far Away Are We?", Value in health regional issues, **17**, 219-223, 2018, doi:10.1016/j.vhri.2018.09.007.

[25] P. M. Danzon, "Affordability challenges to value-based pricing: mass diseases, orphan diseases, and cures", Value in Health, **21**(3), 252-257. 2018, doi:10.1016/j.jval.2017.12.018.

[26] X. Qian, W. Liu, J. Yang, "Game theory analysis of technology adoption timing and pricing decision in supply chain system under asymmetric nash

equilibrium", Journal of Intelligent & Fuzzy Systems, **35**(3), 3101-3111, 2018, doi:10.3233/JIFS-169664.

[27] T. J. Kudryavtseva, E. A. Ivanova, E. A. Kozlova, A. E. Skhvediani, "Pricing and assessment of competitiveness of innovative medical devices in the context of commercialization strategy", Academy of Strategic Management Journal, **16**, 110, 2017.

[28] A. Copeland, A. H. Shapiro, "Price setting and rapid technology adoption: The case of the PC industry", Review of Economics and Statistics, **98**(3), 601-616, 2016, doi:10.1162/REST_a_00539.

[29] S. Shekhar, U. Kumar, "Review of various software cost estimation techniques", International Journal of Computer Applications, **141**(11), 31-34, 2016, doi:10.5120/ijca2016909867.

[30] S. Hirshorn, S. Jefferies, "Final Report of the NASA Technology Readiness Assessment (TRA)", Study Team, 2016. [online] Available at: https://ntrs.nasa.gov/archive/nasa/casi.ntrs.nasa.gov/20170005794.pdf[Accessed 27.12.2019]

[31] O. I. Karyy, H. V. Podvalna, "Relationship marketing of automobile transportation companies: The need of establishing mutual understanding with a client", Actual problems of economics, **10**(184), 149-158, 2016.

[32] G. T. Piatnytska, V. M. Zhukovska, "Domestic trade development: Current transformation and priopities in socialization", Actual problems of economics, **11**(173), 106-119, 2016.

ASTES

Advances in Science, Technology and Engineering Systems Journal Vol. 5, No. 5, 94-102 (2020)

www.astesj.com

Special Issue on Multidisciplinary Innovation in Engineering Science & Technology

ASTESJ

ISSN: 2415-6698

Transient Analysis of a Line-Start Synchronous Reluctance Motor with Symmetrical Distributed Brass Rotor Bars

Mbika Muteba*

Department of Electrical and Electronic Engineering Technology, University of Johannesburg, Johannesburg, 2193, Republic of South Africa

ARTICLE INFO

Article history:
Received: 14 July, 2020
Accepted: 31 August, 2020
Online: 09 September, 2020

Keywords:
Brass Rotor Bars
Dynamic Response
Line-Start AC Motor
Starting Transients
Synchronous Reluctance Motor

ABSTRACT

In this paper, the performance evaluation of a line-start three-phase Synchronous Reluctance Motor (SynRM) with symmetrical distributed brass rotor bars is presented. The machine, which has been designed from a conventional three-phase induction motor (IM) NEMA frame stator is proposed as an alternative to a squirrel cage induction motor (SCIM). The 2D Finite Element Analysis (FEA) under ac magnetic transient solution was used to study some performance parameters of interest during starting transients. The experimental measurements were carried out in order to validate the numerical computation, to analyze the starting transients, and to explore the dynamic responses due to load variations. The FEA and experimental results of the synchronous reluctance motor with brass rotor bars (SynRM-BRBs) are compared to the results of a conventional three-phase SCIM of the same NEMA frame stator. The results evidenced that the reluctance torque developed by the SynRM-BRBs has a compounding effect on the accelerating torque, reaching its steady-state operational condition faster than the SCIM. The dynamic response of the SynRM-BRBs is faster in contrast to the SCIM during load variations. Furthermore, it was noted through measured results that the proposed line-start three-phase SynRM had a reduced dynamic no-load, and load current as opposed to the SCIM, thus positioning itself as a good candidate to replace the SCIM in applications that require a line-start ac motor with good starting transients and fast dynamic responses.

1. Introduction

In recent years, the increase in consciousness towards future sustainable growth, as required by international energy regulations, electric motor technologies for households, irrigation systems and industrial applications are endlessly under exploration for additional enhancements as far as the performance and prime costs are concerned [1]. Thus, the need to broaden ac machines' technologies with good starting and dynamic abilities has surfaced [2]. The SCIMs are the most used singly fed line-start ac motors in households, irrigations systems and industrial applications. Despite their robustness and ease of usability, they suffer low efficiency, low power factor and longer time dynamic responses. The possibility to replace squirrel cage IMs with synchronous machines has emerged with several work focusing on the line-start permanent magnet synchronous motors (PMSynMs) that sought to bring solution to problems associated with the squirrel cage IMs low efficiency and low power factor. Therefore, the line-start PMSynMs are high-class alternatives to SCIMs, as they are well within the proposed IE4 efficiency levels, despite having excessive cost per kW [3]. Aside from the high cost of PM materials and high risk of demagnetization, the manufacturing process turns to be expensive, especially when permanent magnets with high hardness are necessitated [4], [5]. Consequently, line-start PMSynMs cannot easily substitute the very entrenched SCIMs [4].

During the last few decades, various scholars have extended their interests beyond the line-start PMSynMs by investigating the line-start SynRM that incorporates the constructional attributes of three-phase SCIM and SynRM. The line-start SynRM can develop an induction torque at starting and a reluctance torque during acceleration, and at synchronous speed. The rotor copper loss is zero during synchronous operation because there is no current induced in rotor bars. To solidify the possibility to replace the SCIMs with line-start SynRMs, several good work have

*Mbika Muteba, 5151 John Orr, Doornfontein, +27115996089, mmuteba@uj.ac.za

sought to compare the performance between the three-phase SCIM and three-phase SynRM with cage bars on the rotor, for various applications [3-4, 6-7]. The Rotor design and dynamic equations that govern the performance of line-start SynRM with round copper bars are investigated in [8]. The dynamic model and transient analysis of line-start SynRM with copper bars in flux barriers are reported in [9] and [10]. Although the copper cage bars have lower rotor resistance and offer a finer synchronization ability than the aluminium, they contribute to the increase in rotor moment of inertia due to their high net weight.

However, modern line-start SynRMs possess a die-casted aluminium cage inside the rotor air barriers [4], [6], [7]. In principle, manufacturing costs of a squirrel cage IM are the same compared to SynRM with die-casted aluminium cage, but at full-load synchronous speed, the efficiency of the line-start SynRM with die-casted aluminium is higher, for the same frame size [7]. The weight of an aluminium conductor is less than the weight of a copper conductor, subjecting the rotor to less stress from centrifugal forces and reduced starting inertia, slighter vibration while running, and it is easily movable than an analogous copper rotor. Moreover, the low yield strength, low Young's Modulus of elasticity and low melting point of the aluminium conductor serve as a good motivation to investigate other conducting materials to be used on the rotors of line-start SynRMs.

Therefore, this paper proposes a line-start SynRM with brass rotor bars. The line-start capabilities are acquired through round brass bars placed inside the air barriers on *direct*-axis and in the rotor core on the *quadrature*-axis as shown in Figure 1 (a). The characteristics of brass used in the proposed machine are well presented in [11]. Despite having a high electric resistivity compared to aluminium and copper, the brass presents a high yield strength, high Young's Modulus of elasticity and high melting point. In the proposed motor, the brass bars are surrounded by cast epoxy resin. The latter permits to keep the bars steady and provide good electric insulation between the brass bars and the steel laminations. The bars are bolted, soldered and brazed to a brass end-ring at both end-points of stack lamination to form a cage.

The organization of this paper is in this manner: section 2 elaborates on ratings and specifications of the proposed SynRM-BRBs, and section 3 presents the model of the SynRM-BRBs. Section 4 deals with the ramifications of the number of rotor brass bars on synchronous parasitic torques during starting, while section 5 focuses on the performance evaluation of the proposed SynRM-BRBs by means of FEA. Section 6 provides details related to experimental validation, while section 7 summarizes the key findings of this paper and further elaborations regarding possible future work.

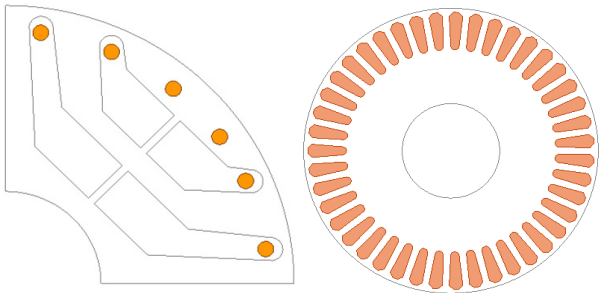
2. Motor Specifications and Ratings

In this paper, the starting transients and dynamic responses of the SynRM-BRBs is compared to a squirrel cage IM that has identical stator frame. Table 1 shows the ratings and specifications of the SynRM-BRBs and SCIM, while Figure1 depicts the rotor cross sections of both machines. The proposed SynRM has 24 symmetrical distributed brass rotor bars, thus only a pole is illustrated in Figure 1 (a). At the same time, the three-phase SCIM has 43 rotor copper bars as depicted in Figure 1 (b). From a design point of view, the number of stator slots and rotor brass bars should not equate [12]. The selection of the number of brass rotor bars depends on the number of air barriers per pole, and on the adequate combination between the number of stator slots and rotor bars for an un-skewed rotor.

Figure 2 depicts the brass bars and end rings for the SynRM, while Figures 3 (a) and (b) picture the prototype rotors for the SynRM with brass bars and squirrel cage induction motor respectively.

Table 1: Ratings and Specifications

Description	Values
Stator slots	36
Poles pairs	2
Full-load line voltage, V	380
Base frequency, Hz	50
Full-load current, A	12
Full-load power, kW	5.5
Series conductors per phase	144
Stator external radius, mm	105
Stator inner radius, mm	73.33
Rotor inner radius, mm	72.8
Shaft radius, mm	24
Airgap Length, mm	0.35
Stack length , mm	160



(a) (b)

Figure 1: Rotors 'cross section, (a) SynRM with brass bars, (b) squirrel cage induction motor

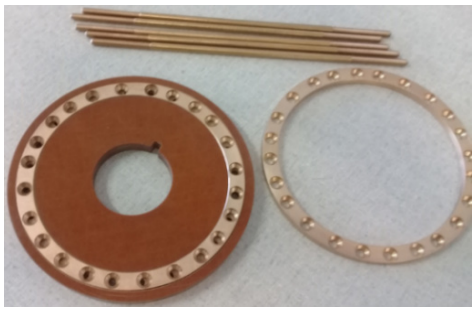


Figure 2: Photograph of brass bars and end rings

The adequate number of stator slots and rotor bars combinations for a 4-pole, 36-slot machine with a skewed rotor should be 36/25, 36/27, 36/28, 36/29, 36/30 and 36/43 [12]. In this paper, the combination of stator slots and rotor bars is 36/24 for the SynRM and 36/43 for SCIM. The rotor of the SCIM is skewed by a slot pitch. Alternatively, a non-skewed rotor design was

opted for the SynRM-BRBs, thus making the combination of 36/24 to be adequate.



(a)



(b)

Figure 3: Photographs of prototype rotors (a) SynRM-BRBs (b) SCIM

3. Model of the SynRM with Brass Rotor Bars

The brass rotor winding is modelled as two identical windings, one on the *direct*-axis and the other on the *quadrature*-axis. Figure.4 illustrates the *d*-and *q*-axis equivalent circuital models of the SynRM-BRBs. The voltage equations that describe the electrical characteristic of the SynRM-BRBs, in rotating arbitrary reference frame are in (1)-(4).

$$V_{sd}^{r} = R_s\, i_{sd}^{r} - \omega\lambda_{sq}^{r} + \rho\lambda_{sd}^{r} \tag{1}$$

$$V_{sq}^{r} = R_s\, i_{sq}^{r} + \omega\lambda_{sd}^{r} + \rho\lambda_{sq}^{r} \tag{2}$$

$$0 = R_{rd}\, i_{rd} + \rho\lambda_{rd} - \left(\omega - \omega_r\right)\lambda_q \tag{3}$$

$$0 = R_{rq}\, i_{rq} + \rho\lambda_{rq} + \left(\omega - \omega_r\right)\lambda_d \tag{4}$$

where $\rho = (d/dt)$, the subscripts *s* and *r* indicate the variables associated with the stator and rotor respectively, while the superscript *r* refers to the rotating reference frame, λ_{sd} and λ_{sq} are the *d*-and *q*-axis stator flux-linkages, λ_{rd} and λ_{rq} are the *d*- and *q*-axis rotor flux-linkages, ω and ω_r are the synchronous and rotor speeds, in electric radians respectively. The two values of rotor resistance for *d*-and *q*-axis in (3) and (4) contemplate the non-isotropic character of the SynRM rotor. The flux-linkages equations are given in (5)-(10).

$$\lambda_{sd}^{r} = L_{\sigma s}\, i_{sd}^{r} + L_{md}\, i_{md}^{r} \tag{5}$$

$$\lambda_{sq}^{r} = L_{\sigma s}\, i_{sq}^{r} + L_{mq}\, i_{mq}^{r} \tag{6}$$

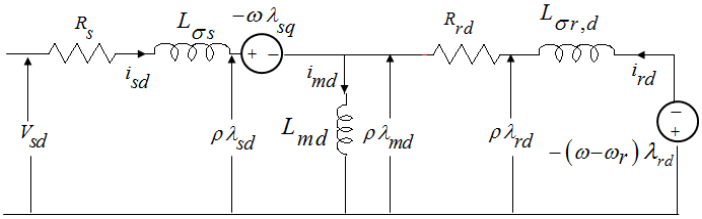
$$\lambda_{md}^{r} = L_{md}\ \ i_{md}^{r} \tag{7}$$

$$\lambda_{mq}^{r} = L_{mq}\ \ i_{mq}^{r} \tag{8}$$

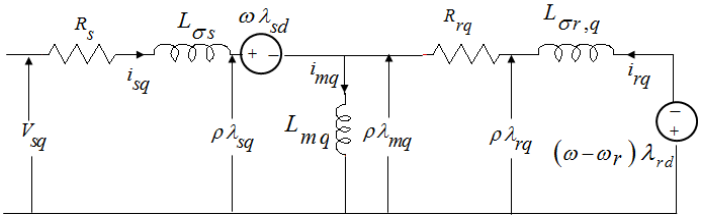
$$\lambda_{rd} = L_{\sigma r,d}\ \ i_{rd} \tag{9}$$

$$\lambda_{rq} = L_{\sigma r,q}\ \ i_{rq} \tag{10}$$

here $L_{\sigma s}$ and $L_{\sigma s}$ are the stator and rotor leakage inductances, L_{md} and L_{mq} are *direct*-and *quadrature*-axis magnetizing inductances.



(a)



(b)

Figure 4: Equivalent circuit of the SynRM-BRBs, (a) *direct*-axis circuital model, (b) *quadrature*-axis circuital model

The torque developed by the three-phase SynRM with brass rotor bars is expressed in (11).

$$T_{em} = \frac{3}{4}\, p\left[\left(L_{ds} - L_{qs}\right) i_{ds}^{r} i_{qs}^{r} + \left(L_{mds}\, i_{dr} i_{qs}^{r} - L_{mqs}\, i_{qr} i_{ds}^{r}\right)\right] \tag{11}$$

Ignoring the friction coefficient, the dynamic equation of the SynRM with cage bars that governs the torque balance at the shaft is generally expressed as

$$T_{em} = \frac{2J}{p}\frac{d\omega_r}{dt} + T_L \tag{12}$$

here *p* is the number of poles, *J* is the total rotor moment of inertia and T_L is the load torque. The electromagnetic torque in (11) has two integrant expressions. The first expression is the reluctance torque, which is the torque at rated synchronous speed, and this torque pulsates at two times the slip frequency during holding phase of the motor [4]. The second expression is the asynchronous torque, which is the torque developed at standstill, also known as

pullout torque. This torque exists only when the SynRM is out of synchronism. A detailed derivation of the asynchronous and reluctance torques is delineated in [7].

4. Space harmonics and Parasitic Torques

The field harmonic caused by the rotor bar current, stator slotting and stator winding phase-spread can be obtained using (13), (14) and (15) respectively [11-12].

$$n_r = x\frac{R_b}{p_1} + 1 \tag{13}$$

$$v_s = x\left(\frac{Q_s}{p_1}\right) + 1 \tag{14}$$

$$u_s = 2x\left(\frac{\pi}{\sigma}\right) + 1 \tag{15}$$

where x is any positive or negative number, R_b is the number of rotor bars, p_1 is the number of fundamental pairs of poles, Q_s is the total number of stator slots and σ is the phase-belt angle. The analysis pertaining to the existence of field harmonics owing to stator slotting, stator winding phase-belt and number of rotor bars in the SynRM-BRBs and SCIM is well documented in [11]. Furthermore, the field harmonic components emanated from the rotor gave rise to synchronous parasitic torques when linking with the field harmonics arisen from the stator with the same order [12-13]. From [11], it was noted that the synchronous parasitic torques occur in both the SynRM-BRBs and the squirrel cage IM. The effect of parasitic torques is more pronounced in the SynRM-BRBs than the squirrel cage IM [11]. To circumvent the synchronous parasitic torque caused by the interactivity between the stator field harmonics and rotor slot harmonics, (13) should not correlate (14) [11-12]. The effects of synchronous parasitic torques on starting transients of both machines are discussed in the succeeding section through FEA.

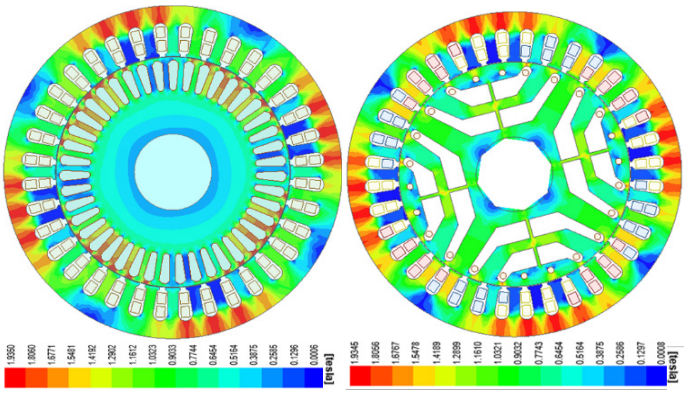
5. Finite Element Analysis

5.1. Machines' flux density

The FEA has been carried out at nameplate voltage. The distributed three-phase double layer stator windings are supplied by three-phase sinusoidal voltage. The skin effect and core loss are not disregarded in the FEA. The skew of the SCIM rotor is accounted for in the FEA.

Figure 5 shows the flux density distribution plots; Figure 6 depicts the airgap flux density profiles, and their FFTs are given in Figure 7. It is clear from the FEA results in Figure 5 that there are localized saturations of stator back iron in both the conventional squirrel cage IM and SynRM with brass rotor bars. Localized saturations are also observed between some rotor teeth, and on some magnetic wedges of conventional squirrel cage IM. High flux density of about ± 1.2 tesla is noticed on the magnetic radial ribs of the SynRM-BRBs. In the latter, some magnetic tangential bridges of the upper air barriers exhibit a flux density of about ± 1.4 tesla, while the flux density in other magnetic tangential bridges levels between 1.2 tesla and 1.3 tesla.

The effects of stator slot openings are noticeable in the airgap flux density waveforms illustrated in Figure 6. The FFT results in Figure 7 (a) evidenced that the SynRM-BRBs has achieved a fundamental airgap flux density of 0.61 tesla. Elseways, the achieved fundamental airgap flux density of SCIM is 0.57 tesla. The 17th space harmonic are dominant in both machines. These harmonics are mainly due to stator slotting, and are reliant on the stator slots and pole pairs' numbers. The 17th airgap space harmonics do not contribute to any asynchronous parasitic torque that may occur during starting because they do not produce rotor bar currents in both machines, whose magneto-motive force (MMF) harmonic has the same order. The 3rd airgap space harmonic is high in the SynRM-BRBs compared to the SCIM. The net airgap flux density is the result of the MMF harmonics and the airgap conductance harmonics. The latter is due to slot opening, leakage, skew, and saturation harmonics. The 3rd space harmonics are mainly caused by main flux path saturation in the stator back iron as noticed in Figure 5, and they are also due to airgap conductance harmonics caused by leakage slot magnetic saturation.



(a) (b)

Figure 5: Flux density distribution, (a) Squirrel cage induction motor, (b) SynRM with brass bars

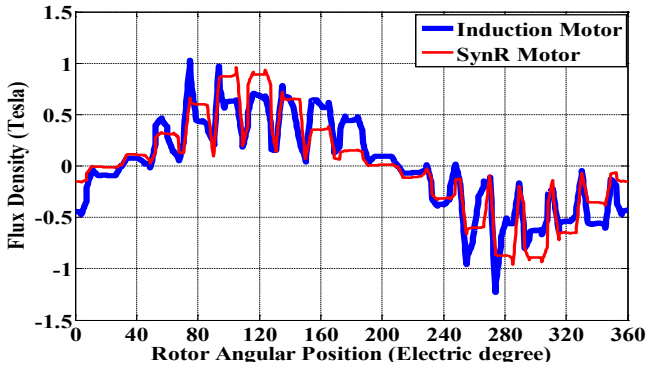
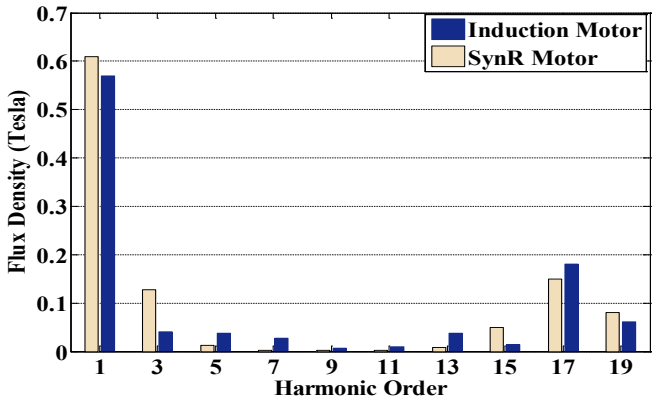


Figure 6: Airgap flux density profile

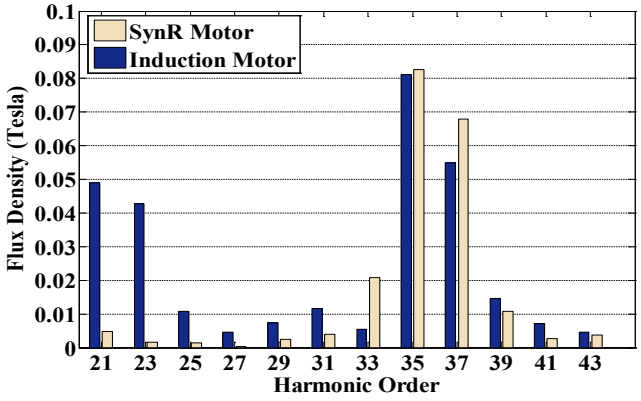
Although both conventional SCIM and SynRM with brass rotor bars show almost the same level of localized flux saturation in the stator back iron, the rotor of SynRM with brass bars shows a well-distributed main flux path saturation between air barriers, thus increasing the airgap 3rd flux density harmonic components.

These airgap 3rd flux density harmonics have the advantage to positively contribute to the average airgap flux density and the machine torque density [14-16].

From figure 7 (b), it is clear that the 35th and 37th airgap flux density harmonics are dominant as far as high order number is concerned. They are mainly due to stator slot and phase-belt magneto-motive force harmonics. In the SynRM-BRBs the 35th and 37th airgap flux density harmonics produced in the brass bars currents with the 35th and 37th MMF harmonics, thus producing synchronous parasitic torques. On the other hand, the 21st and 23rd airgap flux density harmonics in the squirrel cage IM produced rotor currents with the 21st and 23rd MMF harmonics. The same can be stated for the 41st and 43rd airgap flux density harmonics. The latter produced rotor currents with 41st and 43rd MMF harmonics in the SCIM. The interaction of these space harmonics which are originated from different sources (stator and rotor), and having the same order number would contribute to the occurrence of asynchronous or synchronous parasitic torques [12-13].



(a)



(b)

Figure 7: Airgap flux density harmonic components, (a) low order harmonics (b) high order harmonics

5.2. Motors' performance parameters

The rated performance parameters in Table 2 were directly obtained from FEA at the nameplate values. The magnetizing reactance, which depends on the fundamental stator winding number of turns, winding factor, effective stack length, effective inverse airgap and saturation factor, is higher for the SynRM-BRBs compared to the SCIM. This justifies the SynRM with brass bars high value of the airgap fundamental flux density as observed in the previous subsection. The effective inverse airgap is proportional to the carter factor. It should be noted that the carter factor of the SynRM with brass bars does not account for rotor slot opening, which is not the case for the SCIM.

Table 2: Performance Parameters

Description	Value	
	IM	SynRM
Stator resistance , Ω	0.559	0.559
Stator leakage reactance, Ω	0.976	1.030
Stator slot leakage reactance	0.602	0.599
Stator end leakage reactance	0.212	0.212
Stator differential leakage reactance, Ω	0.162	0.217
Magnetizing reactance, Ω	31.21	41.95
Rotor resistance, Ω	1.002	2.377
Rotor leakage reactance, Ω	4.605	5.832
Rotor end leakage reactance, Ω	0.071	0.062
Rotor slot leakage reactance, Ω	4.069	6.659
Rotor differential leakage reactance, Ω	0.250	1.077
Rotor skewing leakage reactance, Ω	0.111	0

From Table 2, it is noticed that the value of the SynRM-BRBs rotor resistance is more than twice the rotor resistance of the SCIM. In addition to a high value of the brass resistivity compared to copper resistivity, the brass bars have a low section area compared to the squirrel cage bars. The skin effects, which are associated with the flux and current density distribution in brass bars or copper cage bars, influence both the rotor resistances and rotor slot leakage reactances. The skin effects are more significant in the SynRM with brass bars because 16 of the 24 brass rotor bars are surrounded by great amount of cast epoxy resin having small air bubbles. The skewing of the SCIM rotor has introduced the skewing magneto-motive force responsible for additional leakage component known as rotor skewing leakage reactance, thus slightly reducing the magnetizing reactance, while increasing the rotor leakage inductance. Though the SynRM with brass bars rotor differential leakage reactance is high, there is a huge difference as far as the stator differential leakage reactances are concerned. It should be noted that the stator differential leakage reactances are attenuated by the reaction of the rotor bars [12]. The two machines use the same stator NEMA frame and they have the same series conductors per phase, therefore given rise to almost the same values of stator resistance, slot leakage reactance and end connection leakage reactance.

5.3. Transient currents and mass rotor torques

Excluding the shaft, the inertia of the rotor is 0.08087 kg.m^2 for the SynRM with brass bars and 0.122 kg.m^2 for the squirrel cage IM. In the latter, the total weight of bars and end rings is found to be 6.418 kg, while it is found to be 3.279 kg for the SynRM-BRBs. The low rotor inertia in the SynRM with brass bars contributes to a fast response as far as the dynamic associated with the mass rotor torque is concerned, as evidenced in Figure 9. Furthermore, the transient currents shown in Figure 8 evidence that the SynRM with brass bars draws low starting currents compared to the SCIM.

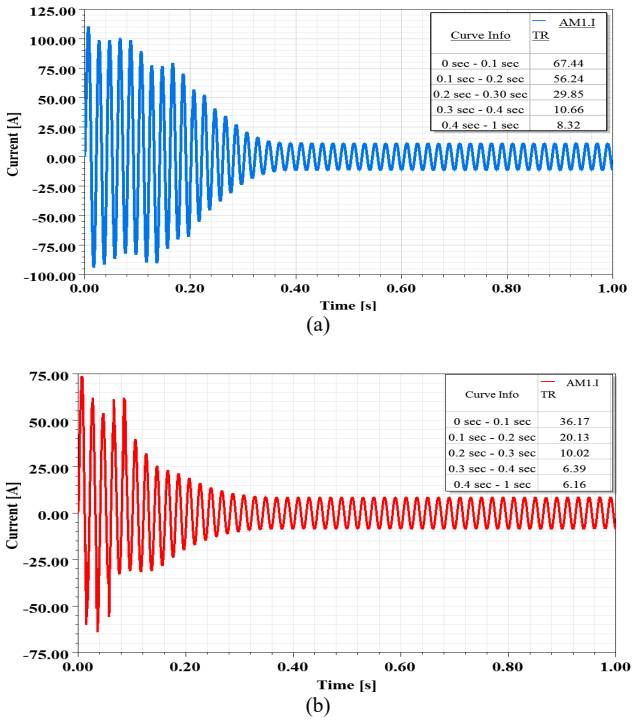


Figure 8: Transient current, (a) Squirrel cage IM, (b) SynRM with brass bars

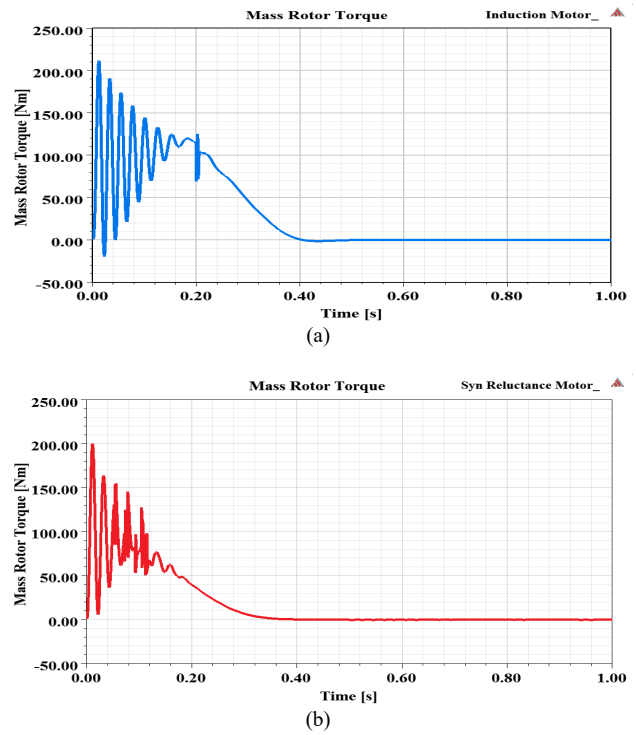


Figure 9: Transient mass rotor torque, (a) Squirrel cage IM, (b) SynRM with brass bars

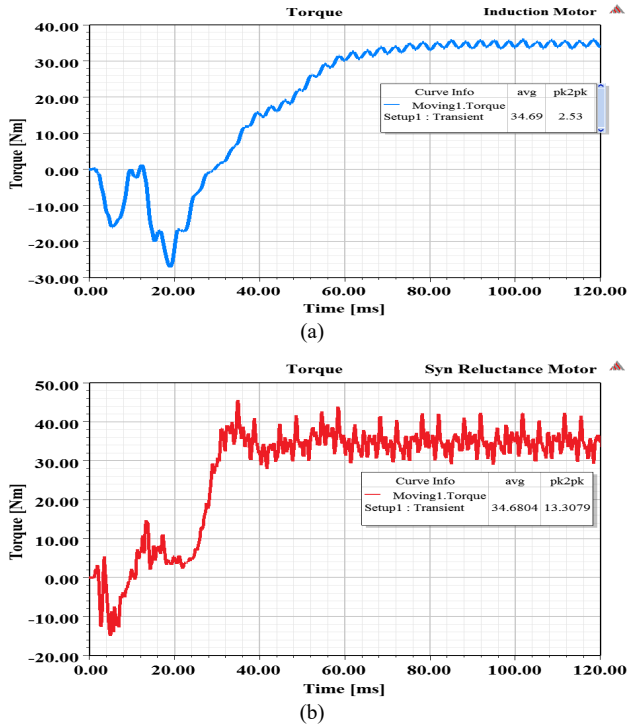


Figure 10: Starting torque, (a) Squirrel cage IM, (b) SynRM with brass bars

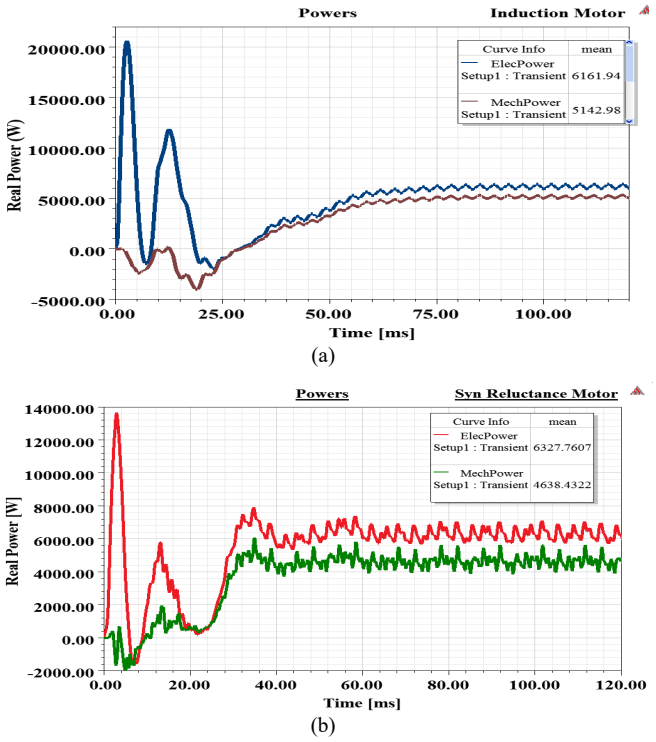


Figure 11. Transient input and output powers, (a) Squirrel cage IM, (b) SynRM with brass bars

5.4. Transient torques and Powers

The total winding energy losses during motor starting and acceleration depend on the stator current, rotor current, starting stator resistance and starting rotor resistance. The starting torque characteristics in Figure 10 indicate that the SynRM-BRBs has a shorter transient response time compared to the squirrel cage IM.

The SynRM with brass bars acceleration begins as early as 6 mSec, crawls for about ± 8 mSec before accelerating up to synchronous operation. The interactivity of the 1st rotor slot field harmonic (11th order) and the 2nd stator winding phase-spread (11th order) field harmonic has given rise to synchronous parasitic torque which are partly responsible for the crawling effect in SynRM with brass bars as discussed earlier on. However, the

squirrel cage IM has shown to have good acceleration without the crawling effect. Both motors have almost the same steady-state average torque, but the SynRM with brass bars exhibits high torque ripple contents compared to the squirrel cage IM. The interactivity of field harmonics of the electrical loading and the rotor anisotropy is responsible for the high ripple contents in the SynRM with brass bars. In addition to skewing the rotor, the optimization of rotor flux barriers microscopic design variables may assist with the mitigation of some torque harmonics that contribute to excessive torque ripple in the SynRM with brass rotor bars [17-23].

Operating at 80% of full-load, the input electric and output mechanical powers transient behaviors of the squirrel cage IM and the SynRM with brass bars are given in Figure 11 (a) and (b) respectively. The FEA results evidenced that the squirrel cage IM absorbs a high real power during starting as opposed to the SynRM-BRBs. This is because the squirrel cage IM locked rotor current is also high.

However, the steady-state squirrel cage IM absorbed real power is less as opposed to the power absorbed by the SynRM with brass bars. The mechanical out powers follow the torque pattern as observed in Figure 10. For the same torque density, the squirrel cage IM delivers more output power in comparison to the SynRM-BRBs. The low output mechanical power of the SynRM-BRBs is caused by high transient rotor winding losses and high critical slip. The latter is reached faster in the SynRM-BRBs, and it is mainly dependent on the rotor resistance and total rotor leakage reactance. Operating at 80 % of full-load, the efficiency of the SynRM-BRBs is found to be 73.3 %, while that of the squirrel cage IM is 79.58 % for the same operational condition.

6. Experimental Results

6.1. Motors' starting transients

The SynRM with brass rotor bars analysed in this paper starts directly online with applied rated line voltage of 380 V. Neglecting the stator resistance, the maximum pullout torque that the motor is proficient to develop at a designated voltage V is [4]

$$\frac{\partial T_s}{\partial \theta} = 0 \rightarrow T_s = \frac{3}{4} p \frac{V_s^2}{2} \frac{\left(L_d - L_q\right)}{\left(X_d X_q\right)} \tag{16}$$

where $L_d = (L_{\sigma s} + L_{md})$, $L_q = (L_{\sigma s} + L_{mq})$, θ is the load angle, X_d and X_q are the d-and q-axis synchronous reactances respectively. The d-and q-axis magnetizing inductances measured values are 34.3 mH and 10.77 mH respectively. Furthermore, the mesured value of stator leakage inductance is 4.2 mH. Figure 12 shows a photo of the experimental setup.

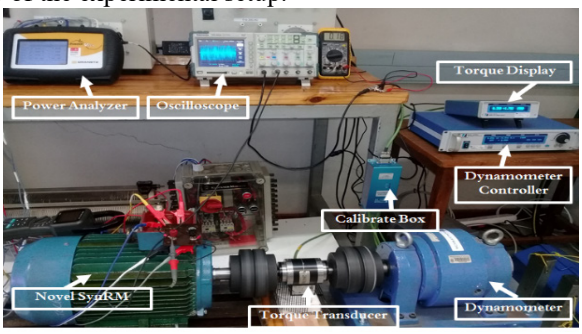
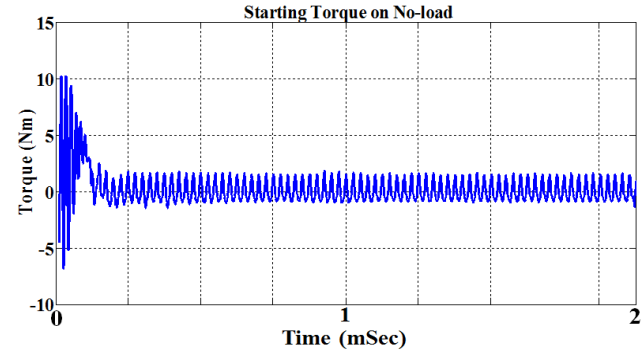
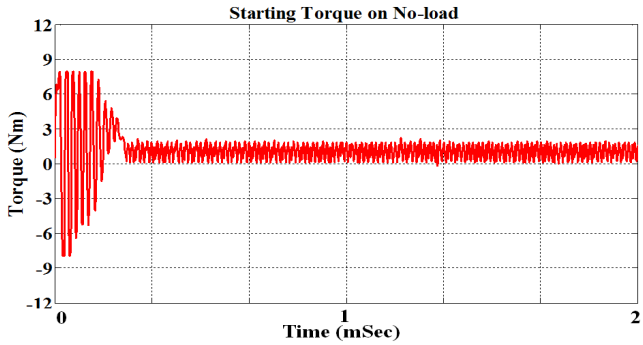


Figure 12: Experimental setup rig photo

Figures 13 (a) and (b) express the no-load starting transient torques of the squirrel cage IM and SynRM with brass bars respectively, while Figures 14 (a) and (b) depict the no-load starting transient currents. At starting, the SynRM developed an asynchronous torque owing to great value of induced current in the brass rotor bars.



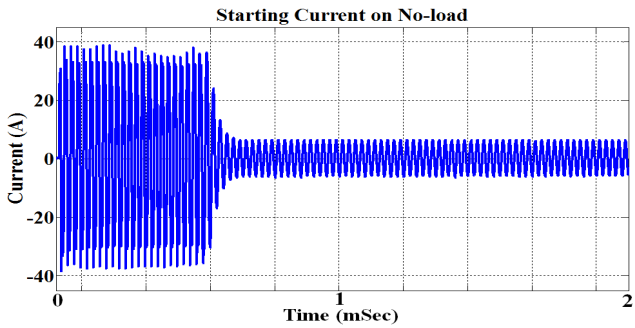
(a)



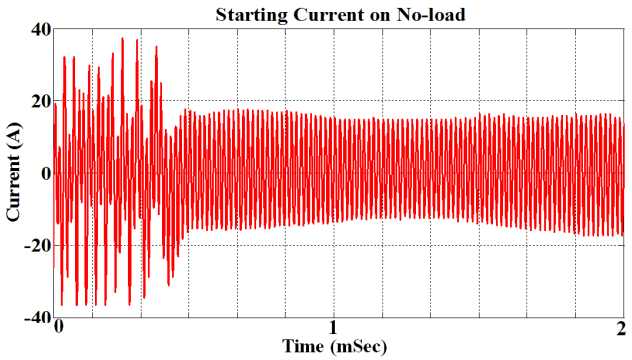
(b)

Figure 13: Starting transient torque at no-load (a) squirrel cage IM (b) SynRM with brass bars

Furthermore, the starting currents on no-load of both motors are more than three times the rated currents. The squirrel cage IM motor starting current dropped fast once it begins to accelerate. The crawling effects during acceleration mode are significant in SynRM with brass bars as it was the case in the FEA results illustrated in the previous section. The crawling effects are caused by synchronous parasitic torques, and they may be mitigated by exploring new designs of the SynRM with brass rotor bars, with adequate combination between the number of brass rotor bars, flux-barriers per pole and that of stator slots for an un-skewed rotor [12-13].



(a)



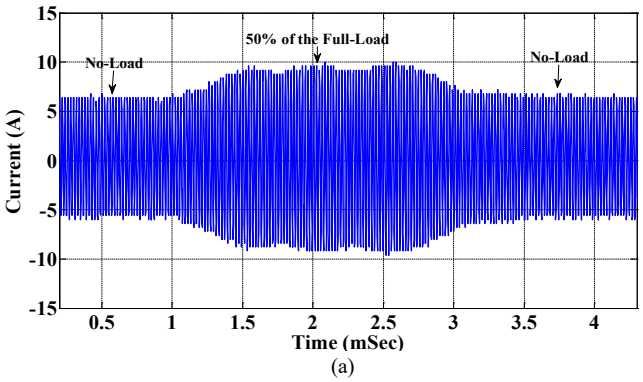
(b)

Figure 14: Starting transient current at no-load (a) squirrel cage IM, (b) starting current of SynRM

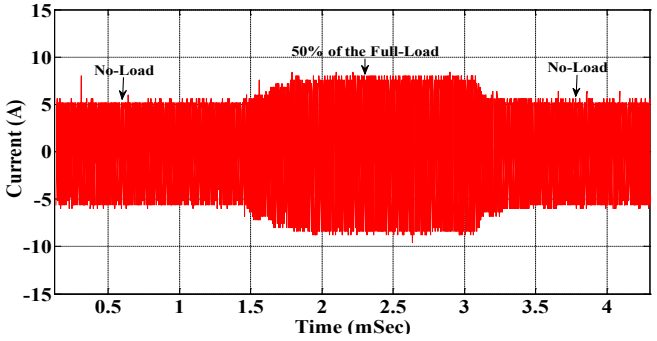
6.2. Motors' dynamic responses

This subsection deals with transients associated with the dynamic responses when the motor mechanical load is abruptly varied. The dynamic responses for currents of the SCIM and SynRM with brass rotor bars are shown in Figures 15 and 16 respectively. The results in Figure 15 denote that the no-load peak-to-peak current is low in the SynRM-BRBs compared to the squirrel cage IM. In the latter, there is a steady increase of currents for about 0.5 mSec and 1 mSec to peak-to-peak values of ± 9 A and ± 12 A, when the load is varied from no-load to 50% and 60% of the full-load respectively. There is a fast decrease of peak-to-peak current for about 0.35 mSec and 0.6 mSec, when the load is varied to no-load from 50% and 60% of the full-load respectively.

However, the results in Figure 16 indicate that the SynRM-BRBs exhibits a fast dynamic response compared to the squirrel cage IM, with a steady increase in currents for about 0.27 mSec and 0.35 mSec, to a peak-to-peak values of ± 8 A and ± 10 A, when the loads of 50% and 60% of the full-load are respectively applied. The decrease of peak-to-peak current lasts for about 0.1 mSec and 0.2 mSec when the loads of 50% and 60% of the full-load are respectively removed. Simply put, the SynRM-BRBs' dynamic response is 0.23 mSec and 0.65 mSec faster than the squirrel cage IM when there is a load variation from no-load to 50% and 60% of the full-load respectively. Furthermore, the SynRM-BRBs' dynamic response is 0.25 mSec and 0.4 mSec faster than the squirrel cage IM when the loads of 50% and 60% of full-load are respectively removed.

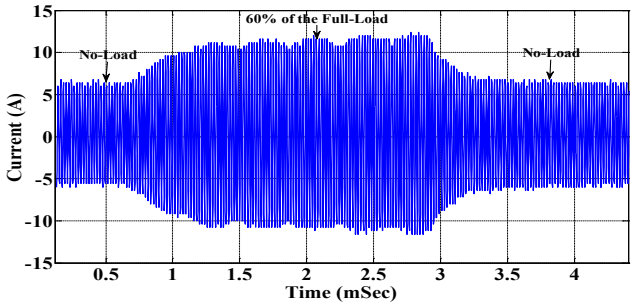


(a)

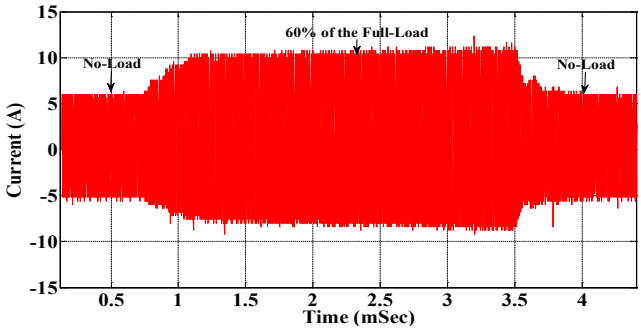


(b)

Figure 15: Dynamic responses, no-load to 50% of the full-load current (a) squirrel cage IM, (b) SynRM with brass bars



(a)



(b)

Figure 16: Dynamic responses, no-load to 60% of the full-load (a) squirrel cage IM, (b) SynRM with brass bars

7. Conclusion

This paper presented the analysis of a SynRM-BRBs as a strong candidate to replace the squirrel cage IM in applications that require a line-start ac motor with good starting transients and fast dynamic responses. The FEA results evidenced that the low rotor inertia of the SynRM-BRBs contributed to fast transient responses. Furthermore, the reluctance torque has been observed to have a compounding effect in both FEA and experimental results, on the accelerating torque of the proposed SynRM-BRBs.

The proposed line-start motor has proved to have fast dynamic responses, reduced steady state no-load, and load current compared to the squirrel cage IM. The main contribution of the proposed design is in the use of brass bars and end-rings on the rotor, having a high yield strength, high Young's Modulus of elasticity and high melting point in contrast to copper and aluminium cages used in modern line-start SynRMs.

For future work, new designs of the SynRM with brass rotor bars, with adequate combination between the number of brass rotor bars, air barriers per pole and that of stator slots for a skewed and an un-skewed rotor may intensively be explored in order to alleviate the crawling effect due to synchronous parasitic torques. The optimization of rotor flux barriers microscopic design variables may also assist with the mitigation of some torque harmonics that contribute to high torque ripple contents in SynRM with brass rotor bars during synchronous operation.

References

[1] A.T. de Almeida, F.J.T.E. Ferreira and G. Baoming, Beyond Induction Motors Technology Trends to Move up Efficiency, IEEE Tran. Ind. Appl. **50** (3), 2103-2114, 2014, https://doi.org/10.1109/TIA.2013.2288425

[2] A. Castagnini, T. Känsäkangas, J. Kolehmainen, and P. Savio Termini, Analysis of the starting transient of a synchronous reluctance motor for direct-on-line applications, Coeur d'Alene, ID, USA, May 10-13, 2015, https://doi.org/10.1109/IEMDC.2015.7409047

[3] A.H. Isfahani and S. Vaez-Zadeh, Line start permanent magnet synchronous motors: Challenges and opportunities, Energy, **34**(11), 1755-1763, 2009, https/doi.org/10.1016/j.energy.2009.04.022

[4] M. Gamba, E. Armando, G. Pellegrino, A. Vagati, B. Janjic and J. Schaab, Line-start synchronous reluctance motors: Design guidelines and testing via active inertia emulation, in IEEE Energy Conversion Congress and Exposition, Montreal, QC, Canada, Sept 20-24, 2015, ,https://doi.org/10.1109/ECCE.2015.7310340

[5] D. Mingardi and N. Bianchi, Line-start PM-assisted synchronous motor design, optimization, and tests, IEEE Tran. Ind. Elec, **64** (12), 9739-9747, 2017, https://doi.org/10.1109/TIE.2017.2711557

[6] A. Kersten, Y. Liu and D. Pehrman, Rotor Design of a Line-Start Synchronous Reluctance Machine with Respect to Induction Machine for Industrial Applications, in 13th IEEE International Conference on Electrical Machines, Alexandroupoli, Greece, Sept 3-6, 2018, https://doi.org/10.1109/ICELMACH.2018.8507053

[7] M. Gamba, G. Pellegrino, A. Vagati, and F. Villata, Design of a line-start synchronous reluctance motor," in IEEE International Electric Machines Drives Conference, Chicago, IL, USA, May 12-15, 2013, https://doi.org/10.1109/IEMDC.2013.6556163

[8] A. Kersten, Y. Liu, D. Pehrman, and T. Thiringer, Rotor design of line-start synchronous reluctance machine with round bars, IEEE Tran. Ind. Appl, **55** (4), 3685-3696, 2019, https://doi.org/ 10.1109/TIA.2019.2914010

[9] V. Aguba, M. Muteba, D.V. Nicolae, Dynamic modelling and transient analysis of synchronous reluctance motor with cage bars in the rotor structure, in International Symposium on Power Electronics, Electrical Drives, Automation and Motion, Amalfi, Italy, June 20-22, 2018, https://doi.org/10.1109/SPEEDAM.2018.8445292

[10] V. Aguba., M. Muteba, D.V. Nicolae, Transient analysis of a start-up synchronous reluctance motor with symmetrical distributed rotor cage bars, in 2017 IEEE AFRICON, Cape Town, South Africa, Sept 28-20, 2017, https://doi.org/10.1109/AFRCON.2017.8095668

[11] M. Muteba, Comparison of dynamic behaviors between a synchronous reluctance motor with brass rotor bars and a squirrel cage induction motor, in IEEE PES/IAS PowerAfrica, Abuja, Nigeria, Aug 20-23, 2019, https://doi.org/10.1109/PowerAfrica.2019.8928746

[12] I. Boldea, S. A. Nasar, The induction machine handbook , CRC Press, New York, 2002.

[13] L. Wang, X. Bao, C. Di, Y. Zhou and Q. Lu, Analysis of synchronous parasitic torque in dual skew cage rotor induction motors with equivalent slot number, IET Elect. Power Appl., 2017, Vol. **11**(8), 1357-1365, 2017, https://doi.org/10.1049/iet-epa.2016.0565

[14] K. Wang, Z. Q. Zhu, G. Ombach and W. Chlebosz, Average torque improvement of interior permanent magnet machine using Third Harmonic in Rotor Shape, IEEE Tran. Ind. Elec, **61** (9), 5047-5057, 2014, https://doi.org/10.1109/TIE.2013.2286085

[15] R. O. C. Lyra and T.A. Lipo, Torque Density Improvement in a Six-Phase Induction Motor With Third Harmonic Current Injection, IEEE Tran. Ind. Appl, **48** (5), 1351-1360, 2002, https://doi.org/10.1109/IAS.2001.955773

[16] H. A. Toliyat, S. P. Waikar, and T.A. Lipo, Analysis and Simulation of Five-Phase Synchronous Reluctance Machines Including Third Harmonic of Airgap MMF, IEEE Tran. Ind. Appl, **34** (2), 332-339, 1998, https://doi.org/10.1109/28.663476

[17] X. L. Bomela and J. Kamper, Effect of stator chording and rotor skewing on performance of reluctance synchronous machines. IEEE Tran. Ind. Appl., **38**(1), 91-100, 2002, https://doi.org/10.1109/28.980362

[18] N. Bianchi, S. Bolognami, D. Bond, D and M. D. Pre, Rotor flux-barrier design for torque ripple reduction in Synchronous Reluctance and PM-assisted Synchronous Reluctance Motors. IEEE Trans. Ind. Appl, **45**(3), pp. 921-928, 2009, https://doi.org/10.1109/TIA.2009.2018960

[19] V. Bilyi, D. Gerling and D. Bilyi, Flux barrier design method for torque ripple reduction in synchronous reluctance machines. in IEEE Transportation Electrification Conference and Expo, Asia- Pacific, Busan, Korea, June 1-4, 2016, https://doi.org/10.1109/ITEC-AP.2016.7512918

[20] M. N. F. Ibrahim, P. Sergeant and E. E. M. Rashad, Simple Design Approach for Low Torque Ripple and High Output Torque Synchronous Reluctance Motors, Energies, **9** (11), 1-14, 2016, https://doi.org/10.3390/en9110942

[21] N. Bianchi, M. Degano and E. Fornasiero, Sensitivity Analysis of Torque Ripple Reduction of Synchronous Reluctance and Interior PM Motors, IEEE Trans. Ind. Appl, **51**(1), 2014, 187-195, https://doi.org/10.1109/TIA.2014.2327143

[22] N. Bianchi, S. Bolognani, D. Bon, and M. Dai Pre, ''Torque harmonic compensation in a synchronous reluctance motor,'' IEEE Trans. Energy. Con., **23**(2), 466–473, 2008, https://doi.org/ 10.1109/TEC.2007.914357

[23] M. Muteba, B. Twala and D.V. Nicolae, Torque ripple minimization in synchronous reluctance motor using a sinusoidal rotor lamination shape, in the IEEE 22nd International Conference on Electrical Machines, Lausanne, Switzerland, Sept 4-7, 2016, https://doi.org/ 10.1109/ICELMACH.2016.7732588

ASTES

Advances in Science, Technology and Engineering Systems Journal Vol. 5, No. 5, 103-108 (2020)

www.astesj.com

Special Issue on Multidisciplinary Sciences and Engineering

ASTESJ

ISSN: 2415-6698

Spatial Multi-Layer Perceptron Model for Predicting Dengue Fever Outbreaks in Surabaya

Siana Halim[1,*], Andreas Handojo[2], Ivan Enrico Widodo[2], Felecia[1], Tanti Octavia[1]

[1]*Petra Christian University, Industrial Engineering Department, Surabaya 60238, Indonesia*

[2]*Petra Christian University, Informatics Engineering Department, Surabaya 60238, Indonesia*

ARTICLE INFO

Article history:
Received: 21 July, 2020
Accepted: 04 August, 2020
Online: 09 September, 2020

Keywords:
Multilayer Perceptron
Spatial
Dengue Fever Outbreak

ABSTRACT

Dengue fever (DF) is a tropical disease spread by mosquitoes of the Aedes type. Therefore, a DF outbreak needs to be predicted to minimize the spread and death caused by it. The spread of dengue fever is a spatial problem. In this paper, we adopted the Multi Linear Perceptron (MLP) to solve the spatial problem, and we called it a spatial multi-layer perceptron model (Spatial MLP). In this proposed model, we consider two types of input neurons in the Spatial MLP, a region and the neighbourhood of that region. The spatial inputs dynamically change to the region. Additionally, the neighbourhood numbers of a region are also varied. So, the spatial inputs are changed in terms of the number of inputs and the neighbourhoods. As a result, the proposed model is outperformed the traditional MLP since it can adapt to the neighbourhoods. We can conclude the spatial MLP model can manage the information and predict the dengue fever outbreak in Surabaya

1. Introduction

Dengue Fever (DF) outbreak happened annually, but every year the number of victims is very high. In the present decade, Ketharpal mentioned that dengue is endemic to 128 countries, mostly developing nations, posing a risk of death to approximately 3.97 billion people annually [1]. Cartographic approaches estimated that 390 million dengue infections annually, out of which 96 million cases evident apparently [2,3]. World health organization (WHO) stated that more than 70% of the population at risk for dengue worldwide live in member states of the WHO South-East Asia Region and Western Pacific Region [4]. WHO categorized the variable endemicity of dengue fever into four categories. Indonesia is included in category A which means the endemic occurs due significant public health problem, a leading cause of hospitalization and death among children, hyperendemicity with all four serotypes circulating in urban areas, and spreading to rural areas [5].

More than thirty-nine thousand (39,876) DF cases and 254 deaths were reported by Indonesian Health Ministry from January to March 2020 [6,7,8]. For significant reduction of dengue mortality, the strategies for the prevention of dengue include prompt diagnosis of fever cases, providing appro-priate clinical management, and controlling vector, and personal protection methods. Therefore, severe cases can be managed with appropriate treatment, and health personnel at all level can be trained. Improved outbreak prediction and detection through coordinated surveillance will be able to reduce DF spread and effected area [9, 10].

Many types of research have been done in predicting the spread and DF affected area. A five years dataset from Sleman, a district in Central Java Indonesia are used for predicting the spread of the DF [11]. Mahdiana's model is based on vector autoregressive spatial autocorrelation (varsa). A four years dataset from Bandung stated that the incidence rate of dengue fever was not related to annual rainfall, population density, larva free index, and prevention Program [12]. The spreading of DF in Surabaya, Indonesia, is modelled using statistical learning [13,14]. Besides of statistical learning approach, many researchers also developed the model in the machine learning approach. Various machine learning algorithms are compared, such as naive Bayes, random forests, minimal sequential optimization [15]. They collected data from the health department, Karuna medical hospital, Kerala, and online sources. The authors stated random forests gives better accuracy for the early detection of dengue disease.

On the other hand, the use of neural networks as an algorithm for predicting disease has been widely used. An artificial neural network is used to predict the DF outbreak in Srilanka [16], using similar approach [17,18] the DF outbreak in Thailand modelled and in the Northwest Coast of Yucatan, Mexico and San Juan,

*Corresponding Author: Siana Halim, Email: halim@petra.ac.id

Puerto Rico, respectively. Most of the artificial neural network that has been used to develop the model is multi-layer perceptron, with the input as the population characteristics in each region and number of DF infected in the previous years for predicting the number of DF infected in the current or next year.

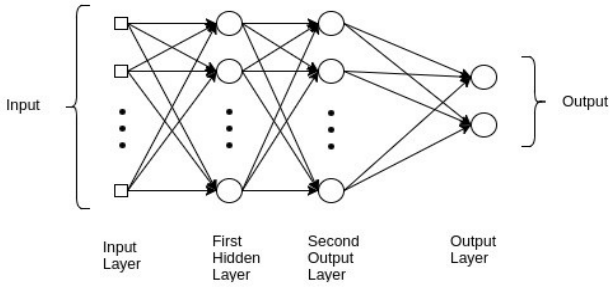


Figure 1. Multi-Layer Perceptron Neural Network

In this research, we proposed a spatial multi-layer perceptron model for predicting the DF outbreak. As a case study, we used DF data in Surabaya. The proposed model adopts the spatial approach in statistical learning as well as the multi-layer perceptron in the machine learning approach. This proposed model tries to accommodate the nature of DF disease spreading. Because DF is a type of disease that spreads through dengue mosquitoes, if DF infects a particular area, the surrounding areas will be vulnerable to the spread of the disease (spatially correlated). Therefore, disease prediction in a particular area is greatly influenced by the DF disease in the surrounding area. So, to predict the possibility of the spread of dengue fever in a particular area, we need to calculate the spread DF data from the surrounding areas. This data will be calculated separately for each region (spatial dependent). This proposed model will implement in Multi-Layer Perceptron Model (MLP) Neural Network. The MLP NN model does not accommodate the spatial dependency in the neural-network construction. This proposed model tries to build a spatial MLP model to accommodate the nature of DF decease spreading.

Additionally, we also present the model for predicting the DF web basely. Since currently, the data for DF victims is manually collected at community health centers, and it will be reported to the regional health department. Based on this DF data, the city and province will take a curative and preventive action to prevent DF outbreak in next year. Urgent measures also being taken by community health centers during outbreaks such as fogging or spreading abate powder in water collecting area. Without a sound information system on DF outbreak location and spreading, the government cannot control and minimize dengue mortality.

2. Research Methods

2.1. Multilayer Perceptron

Multilayer perceptron (MLP), also often called as feedforward neural networks consists of neurons that are ordered into layers (Figure 1). The first layer is called the input layer, and the last one is called as the output layer, the layers between are hidden layers [19].

The main goal of MLP is to approximate some function f; e.g. in a regression, $Y = \theta_0 + \theta_1 X_1 + \cdots + \theta_n X_n$; the function $Y = f(X)$ maps the input vector X into the a value Y. The feedforward network defines a mapping $Y = f(X;\theta)$ and learns the value of the parameters θ that result in the best function approximation.

In the general MLP (Figure 1), we know that each layer can be modelled as a function of

$$Y = f(\theta X + b) \tag{1}$$

where f is the activation function, θ are weights in the layer, X is the input vector, which can also be the output of the previous layer, and b is the bias vector. The hidden layers, which are located in between the input and the output of a neural network, will perform nonlinear transformations of the input in the network. The number of the hidden layers are varied. It depends of the function of the neural network. Similarly, the number of the layers may vary. It depends on their associate weights [20].

The function f is called the transfer function. The transfer function used in this research is ReLu (Rectified Linear Unit) [21]. This function is defined as $y = \max(0, X)$. Visually it can be seen in Figure 2.

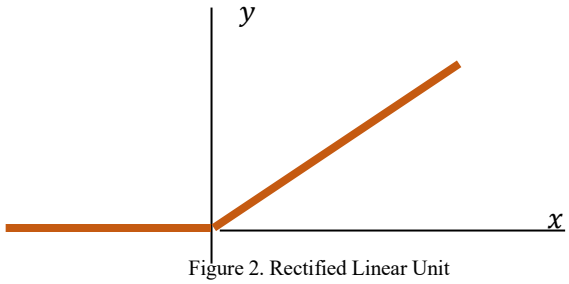


Figure 2. Rectified Linear Unit

2.2 Spatial Multilayer Perceptron

It is well known that the dengue fever happening most in tropical countries and considered as the fastest spreading mosquito-borne disease. It is transmitted by Aedes mosquito which infected with a dengue virus. The spreading of this diseases is spatially correlated [13]. The MLP model does not accommodate the spatial dependent in the neural-network construction. Therefore, in this paper we modified the Multilayer Perceptron Model (MLP), to accommodate the spatial nature of the disease.

In this model, we assumed that the spread of the diseases is in the first-order contiguity level. That is, the number of cases in location s is contagious to its north, east, south, and west neighborhoods. Some additional explanatory variables are also included in the model. They are sex ratio, poverty percentage, population density. In this proposed model, the first layer equation can be written as follows:

$$Y(s) = f\left(\sum_{j=1}^{N}\left(\sum_{i=1}^{M} w_{ij}^{1} X_i(s) + \sum_{k\in(nr,es,st,wt)} w_j^2(s_k) Y(s_k)\right) + \varepsilon\right) \tag{2}$$

where:

$Y(s)$: Number of cases in the location s
w_{ij}^{1} : The jth neuron weight w.r.t explanatory variable i

$X_i(s)$	:	The explanatory variable i in the location s
$w_j^2(s_k)$	:	The j-th neuron weight w.r.t response variable Y in the location s_k
$Y(s_k)$	:	Number of dengue fever cases in the location s_k
s_k	:	The k (north, east, south, west) location of the location s
ε	:	Bias
M	:	Number of explanatory variables ($M = 3$)
N	:	Number of neurons
i, j, k	:	index

In this model the input of the MLP is changed depend on the location s. To give an illustration, let predicts the number of cases in sub-district Balongsari (Figure 3). This region shares borders to sub-district Asemrowo (north), sub-district Tanjungsari (east), sub-district Lontar (south) and sub-district Manukan Kulon (west).

	(A) Asemrowo	
(M) Manukan Kulon	(B) Balongsari	(T) Tanjungsari
	(L) Lontar	

Figure 3: Sub-district Balongsari surrounding area

So, the model can be written as

$$Y(B) = f\left(\sum_{j=1}^{N} w_{1j}^1 X_1(B) + w_{2j}^1 X_2(B) + w_{3j}^1 X_3(B) + w_1^2(A)Y(A) + w_2^2(T)Y(T) + w_3^2(L)Y(L) + w_4^2(M)Y(M)\right)$$

here $X_1(B)$ is the sex ratio in Balongsari, $X_2(B)$ is the poverty percentage in Balongsari, $X_3(B)$ is the population density in Balongsari. $Y(A), Y(T), Y(L)$ and $Y(M)$ are the number of DF case in Asemrowo, Tanjungsari, Lontar and Manukan Kulon respectively. The input neurons of the model adaptively changes with respect to the region s.

2.3 Design Spatial Multi-Layer Perceptron Neural Network

The design uses seven neurons; three neurons represent sex ratio, percentage of poverty and population density of each region under health community center *s* recorded in 2018. The other four neurons are dynamic neurons. They represent the number of cases in the north, east, south, and west. These neurons depend on the location *s* (See Figure 4).

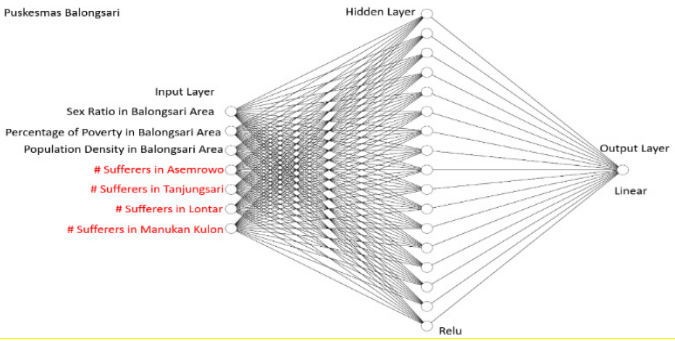


Figure 4: Ilustration for sub-district Balongsari

We used 252 data training (data from 2012-2015) and 126 (data from 2017-2018) data testing. The training process used 3500 epochs (Table 1), and mean squared error is used to measure the loss/error function and we used the stochastic gradient descent as the optimizer.

After some modeling the best design for this case used 1 hidden layer with 17 neurons and 1 output layer (Table 2). The activation function is rectified linear unit (Relu) on the hidden layer and linear on the output layer (Figure 5). This model is implemented as Python functions. It can be used to the other regions as far as the dataset is provided.

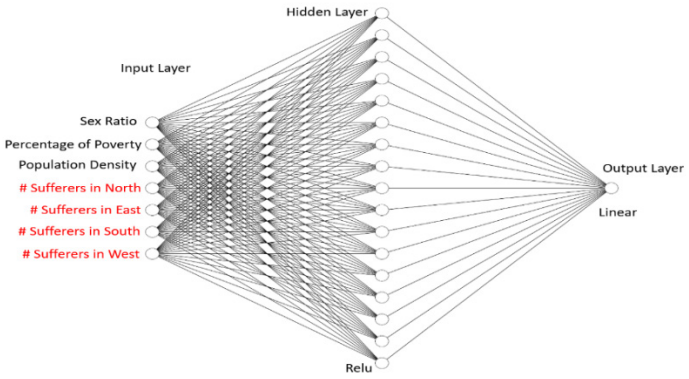


Figure 5: The design of spatial MLP model

Table 1: Setting the Number of Epochs and Neuron

Model	Epochs	Neuron	Loss on Data Training	Loss on Data Validation
1	1500	15	0.0198	0.0403
2		17	0.0187	0.0407
3		20	0.0196	0.039
4		22	0.0182	0.039
5	**3500**	15	0.0189	0.0304
6		**17**	**0.0176**	**0.0294**
7		20	0.0184	0.0383
8		22	0.0171	0.0399
9	4000	15	0.0184	0.0309
10		17	0.0171	0.0304
11		20	0.0181	0.0381
12		22	0.0169	0.0302

Table 2: Setting the Hidden Layer

Model	Layer	#Neuron Hidden Layer 1	# Neuron Hidden Layer 2	Loss on Data Training	Loss on Data Validation
1 hidden	1	17	-	0.0176	0.0294
2 hidden	2	17	7	0.0181	0.0297

3. Result and Discussion

3.1. Data Collection

Data we collected from Surabaya city consist of weather and population characteristic data. Weather data records the number of rainy days in a year, precipitation, maximum and minimum temperature, maximum and minimum humidity. The result shows that Surabaya weather is not significantly different, so it will not be used as the model's explanatory factor. Population characteristic

data will be used in the model, and they are sex ratio, population density, and poverty percentage.

3.2. Data Training and Testing

We use the recorded data from 2012-2015 as the training dataset and the data from 2016 to validate the model. The training dataset consists of 63x4 = 252 data. As usual, we normalized the data set in advanced. The loss of the training data is 0.0176. Figure 5 shows the fitting of the real data to the prediction one. The horizontal axe represents the community health center, the vertical axe represents the number of cases in each community health center, recorded from 2012-2015. Figure 6 shows that the prediction can follow the pattern of the real dataset. During 2012-2013 the number of cases was high, and it started to drop in 2014-2015. The box plot of the data training (Figure 7) shows that there are several outliers in the real dataset and those outliers cannot be captured by the proposed model. The median of the prediction is not significantly different from the real one, but the interquartile range of the prediction is smaller than the real dataset. The two-samples t-test for the training data set is summarized in Table 4 The one-sided p-value is 0.335, we can conclude that there is no mean difference between the real dataset and the predicted one. The mean difference is -0.53 and the 95% confidence interval of the mean difference is (-2.96, 1.91).

Table 3: Surabaya Statistics in 2018

	Min	Mean	Max
Population (thousand)	12541	45802	87561
Area (Km2)	0.915	2.001	14.400
Density (thousand/Km2)	2733	46992	541022
Sex Ratio (Men/Women)	91.5	99.27	110.93
Poverty percentage (%)	4.03	18.02	55.46
Rainy day (days/month)	9.83	13.99	16.00
Precipitation (mm/month)	129.9	164.6	194.9
Max Humidity per month	70	88.72	94.75
Min Humidity per month	46.08	53.14	57.83
Max Temperature	28.21	33.30	34.43
Min Temperature	23.11	26.29	28.73

Table 4: Two-samples t-test for Data Training

	Real	*Predicted*
Mean	18.86508	19.39285714
Variance	262.0455	125.4745304
Observations	252	252
Hypothesized Mean Difference	0	
df	447	
t Stat	-0.425602637	
P(T<=t) one-tail	0.335301126	
t Critical one-tail	1.648269625	
P(T<=t) two-tail	0.670602253	
t Critical two-tail	1.965285234	



Figure 6: The real and prediction line chart of data training from 2012-2015.

We use the recorded data from 2017-2018. There are 126 data. Applying the modelled, the loss value of the testing dataset is 0.052. Some of the prediction are lower/higher than the reality (see Figure 8). Some community health centers reported that there were no dengue fever cases in their area (the number of cases equal to zero), but in their surrounded areas reported highly dengue fever cases. As the result, the real zero number cannot be captured as zero in the model. The model will predict the number of infected in that area as the mean value of the neighborhood. This situation is acceptable, since the predicted number will give early warning to that region to prevent the outbreak in that area.

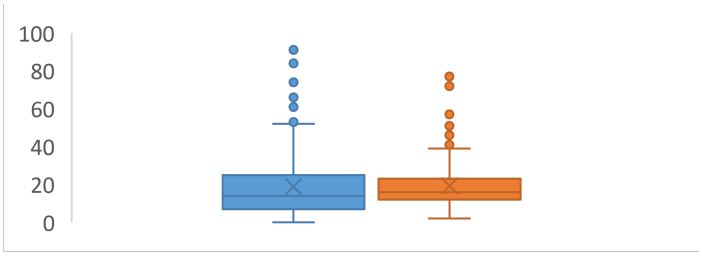


Figure 7: Box plot of the training dataset

3.3. Discussion

In this study, we prosed a spatial-MLP model, which accommodate the spatial property of the dataset. Comparing the other NN models which are used by [16,17,18,19,20] this model uses dynamic variables, which depend on the neighborhood of a region as well as the external variables. The model by [16,17,18,19,20] used only external variables, which do not depend on the neighborhood of a region.

The same dataset has been modelled using the Geostatistical Weighted Regression (GWR) [13]. In [13], the predicted model can follow the pattern of the actual dataset. However, the MSE of the prediction for the years 2017-2018 is 8.59. Compare to this model, the mean square error of the testing data set in the same years is lower, that is 8.07. The t-test shows that there is no significant difference between the mean of the real and the mean of predicted of the testing dataset (Table 5). This model is better than the GWR. However, the computation time of GWR is faster than the spatial-MLP. Since in the spatial-MLP, we have to do the hyperparameter tuning for finding the best model. This model has limitation. It cannot capture the zero in the dataset. The zeros will be predicted as the mean values of the surrounding areas. In this study we prosed a spatial-MLP model, which accommodate the spatial property of the dataset. Comparing the other NN models which are used by [16,17,18] this model uses dynamic variables, which depend on the neighborhood of a region as well as the external variables. The model by [16,17,18] used only external variables, which are not depend on the neighborhood of a region.

The same dataset has been modelled using the Geostatistical Weighted Regression (GWR) [13]. In [13], the predicted model can follow the pattern of the true dataset. However, the MSE of the prediction for the years 2017-2018 is 8.59. Compare to this model, the mean square error of the testing data set in the same

years is lower, that is 8.07. The t-test shows that there is no significant difference between the mean of the real and the mean of predicted of the testing dataset (Table 5). This model is better than the GWR. However, the computation time of GWR is faster than the spatial-MLP. Since in the spatial-MLP, we have to do the hyperparameter tuning for finding the best model. This model has limitation. It cannot capture the zero in the dataset. The zeros will be predicted as the mean values of the surrounding areas.

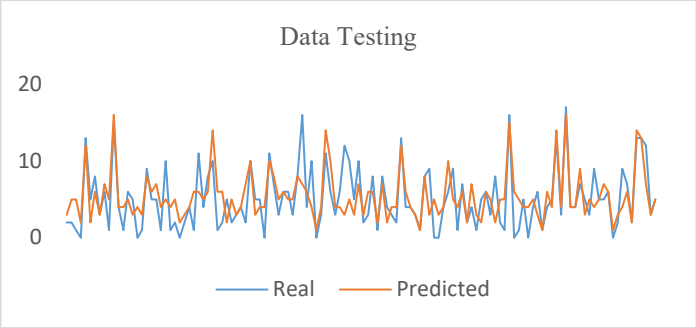


Figure 8: The real and prediction line chart of data training from 2017-2018.

Table 5: Two-samples t-test for Data Testing

	Real	*Predicted*
Mean	5.126984	5.428571
Variance	16.01575	10.10286
Observations	126	126
Hypothesized Mean Difference	0	
df	238	
t Stat	-0.6624	
P(T<=t) one-tail	0.254176	
t Critical one-tail	1.651281	
P(T<=t) two-tail	0.508353	
t Critical two-tail	1.969982	

3.4 Web implementation

This modeled is implemented in a website base to help the "Dinas Kesehatan Surabaya" (The Surabaya Public Health Department) monitoring the dengue fever outbreak. From this website, users can see DF spreading data for each district in Surabaya in the selected year (Figure 9). Data on the number of victims in each sub-district will be displayed in red, yellow and green, with red representing the largest number of victims and green representing the smallest number of victims. Users can specify the upper limit of each color representative. The application will then automatically determine the color gradation based on the input, so that the user can see number of victims in each sub-district that representing in color information. The legend from this gradation color information will display next to the map. User also could choose and see detail information from each sub-district and number of DF victims.

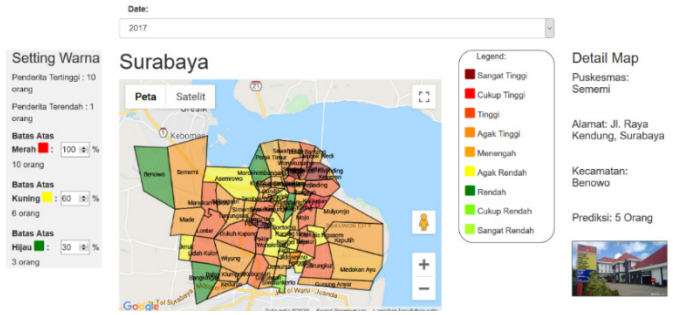


Figure 9: The web design for implemented model

Users can also see details of the number of patients in each sub-district and compare the movement of the number of patients in 3 years presented in tabular form (Figure 10). This data also can be viewed in graphical form (Figure 11).

This visual information will provide more informative information to help The Surabaya Public Health Department monitoring and prevent the dengue fever outbreak for each sub-district.

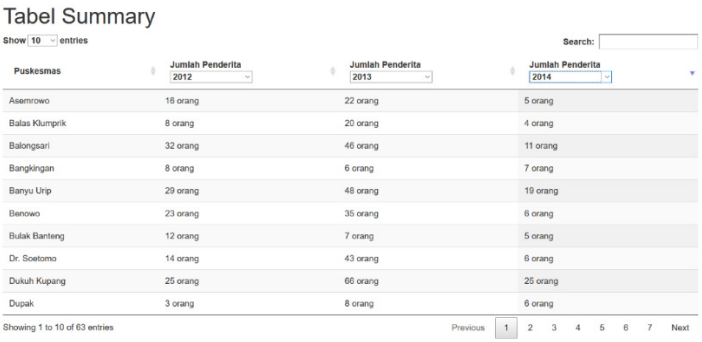


Figure 10: Summarize comparizon spreading DF disease data for each sub-district in Surabaya

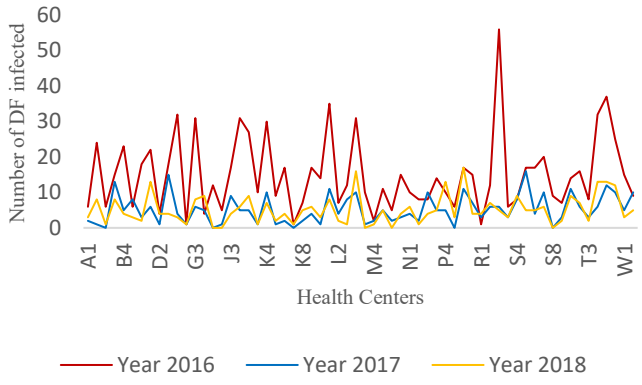


Figure 11: Summarize comparizon spreading DF disease data for each sub-district in Surabaya

4. Conclusion

In this paper we proposed spatial multi-layer perceptron (spatial MLP) model for predicting dengue fever in Surabaya. The model can capture the data pattern. Additionally, the model is implemented in the web-based database. The Surabaya Public

Health Department (Dinas Kesehatan Surabaya) can input the data and predict the outbreak online. However, right now in some regions the predictions are not performed well, especially when that region has zero value. The zeros will be predicted as the mean values it's neighborhood. In the next research, we will expand the model into spatial-temporal multi-layer perceptron (spatial-temporal MLP) model, which can capture data dependencies not only spatially, but also temporally.

Acknowledgement

The authors would like to express their gratitude to the reviewers' feedbacks which certainly improve the clarity of this paper. We also would like to thank to Surabaya Public Health Office (Dinas Kesehatan Surabaya), for the fruitfull discussions. Thanks to Holiyed Hadi for the fruitful discussion on the data base web-design construction. This research is funded by the Ministry of Research, Technology, and Higher Education Republic of Indonesia and the Petra Christian University Institute of Research and Community Outreach.

References

[1] N. Khetarpal N, I. Khanna, "Dengue fever: causes, complications, and vaccine strategies", Journal of Immunology Research, **2016**, 1-14, 2016, doi.org/10.1155/2016/6803098

[2] S. Bhatt, P.W. Gething, O.J. Brady, J.P. Messina, A.W. Farlow, Moyes CL, J.M. Drake, J.S. Brownstein, A.G. Hoen, O. Sankoh, M.F. Myers, D.B. George, T. Jaenisch , G.R.W. Wint, C.P. Simmons, T.W. Scott, J.J. Farrar, S.I. Hay, "The global distribution and burden of dengue", Nature, **496** (7446), 504–507, 2013, doi: 10.1038/nature12060

[3] O.J. Brady, P.W. Gething, S. Bhatt, J.P Messina, J.S. Brownstein, A.G. Hoen, C.L. Moyes, A.W. Farlow, T.W. Scott, S.I., Hay SI, "Refining the global spatial limits of dengue virus transmission by evidence-based consensus", PLoS Neglected Tropical Diseases, **6** (8), 1-15, 2012, doi.org/10.1371/journal.pntd.0001760

[4] WHO, "Dengue guidelines or diagnosis, treatment, prevention and control", World Health Organization, 2009

[5] WHO, "Comprehensive Guidelines for prevention and control of dengue and dengue haemorrhagic fever", World Health Organization- Regional Office for South-East Asia, World Health Organization, 2011.

[6] Tempo, "Dengue fever claims 254 Indonesian lives amid COVID-19 Outbreak", 7 April 2020. Retreived from https://en.tempo.co/read/1328820/dengue-fever-claims-254-indonesian-lives-amid-covid-19-outbreak, accessed on 5 May 2020

[7] Kompas, "Higher than corona, dengue cases reach 17,820 Indonesia". 11 Maret 2020. Retreived from https://nasional.kompas.com/read/2020/03/11/17091361/lebih-tinggi-dari-corona-kasus-dbd-tembus-17820-se-indonesia, accessed on 5 April 2020

[8] Kompas, "Increase rapidly, 2016 cases of dengue fever in East Java, 20 died" 13 Maret 2020. Retrieved from https://surabaya.kompas.com/read/2020/03/13/22200881/bertambah-2016-kasus-dbd-di-jatim-20-meninggal, access on 10 April 2020.

[9] WHO, "Global strategy for dengue prevention and control 2012-2020", World Health Organization, 2012.

[10] W. Wen-Hung, N.U. Aspiro, R.C. Max, A. Wanchai, L. Po-Liang, C. Yen-Hsu, Sheng-Fan, "Dengue hemorrhagic fever a systemic literature review of current perspectives on pathogenesis, prevention and control", Journal of Microbiology, Immunology and Infection, Article in Press. 2020

[11] D. Mahdiana, E. Winarko, A. Ashari, H. Kusnanto, "A model for forecasting the number of cases and distribution pattern of dengue hemorrhagic fever in Indonesia" International Journal of Advanced Computer Science and Applications, **8**(11): 143-150, 2017, DOI:10.14569/IJACSA.2017.081118

[12] K. Anggia, S.Y.I. Sari, H.U. Sumardi, E.P. Setiawati, "Incidence of dengue hemorrhagic fever related to annual rainfall, population density, larval free index and prevention program in Bandung 2008 to 2011", Althea Medical Journal, **2**(2), 262-267, 2015.

[13] S. Halim, T. Octavia, Felecia, A. Handojo, "Dengue fever outbreak prediction in Surabaya using a geographically weighted Regression". Times-Icon Proceeding, 2019, DOI: 10.1109/TIMES-iCON47539.2019.9024438

[14] S. Halim, Felecia, T. Octavia, "Statistical learning for predicting dengue fever rate in Surabaya", Jurnal Teknik Industri, **22**(1), 37-45, 2020, doi.org/10.9744/jti.22.1.37-46

[15] N. Rajathi, S. Kanagaraj, R. Brahmanambika, K. Manjubarkavi, "Early detection of dengue using machine learning algorithms" International Journal of Pure and Applied Mathematics, **118**(18), 3881-3887, 2018.

[16] P.H.M.N. Herath, A.A.I. Perera, H.P. Wijekoon, "Prediction of dengue outbreaks in Srilanka using artificial neural network", International Journal of Computer Applications, **101**, 1-5, 2014, doi:10.1.1.735.9487

[17] B. Jongmuenwai, S. Lowanichchai, S. Jabjone, "Prediction model of dengue hemorrhagic fever outbreak using artificial neural networks in Northeast of Thailand", International Journal of Pure and Applied Mathematics, **118**(8), 3407-3417, 2018.

[18] A.E. Laureano-Rosario, A.P. Duncan, P.A. Mendez-Lazaro, J.E. Garcia-Rejon, S. Gomez-Carro, J. Farfan-Ale, D.A. Savic, F.E. Muller-Karger, "Application of artificial neural networks for dengue fever outbreak predictions in the Northwest Coast of Yucatan, Mexico and San Juan, Puerto Rico", Tropical Medicine Infectious Disease, **3**(5), 1-16, 2018, doi:10.3390/tropicalmed3010005

[19] D. Svozil, V. Kvasnicka, J. Pospichal, "Introduction to multi-layer feed-forward neural networks", Chemometrics and Intelligent Laboratory Systems,**39**,43-62, 1997, doi.org/10.1016/S0169-7439(97)00061-0

[20] R. Collobert, S. Bengio, "Links between perceptrons, MLPs and SVMs", Proceeding of International Conference on Machine Learning (ICML), 2004, doi.org/10.1145/1015330.1015415

[21] L. Yann, Y. Bengio, H. Geoffrey, "Deep learning", Nature, **521**(7553), 436-444, 2015.

ASTES

Advances in Science, Technology and Engineering Systems Journal Vol. 5, No. 5, 109-116 (2020)

www.astesj.com

Special Issue on Innovative Research in Applied Science, Engineering and Technology

ASTESJ

ISSN: 2415-6698

Quantitative Approach in Enhancing Decision Making Through Big Data as An Advanced Technology

Hana Yousuf[1,*], Asma Yousuf Zainal[2]

[1]*Faculty of Engineering & IT, The British University in Dubai, 345015, United Arab Emirates*

[2]*Faculty of Business Management, The British University in Dubai, 345015, United Arab Emirates*

ARTICLE INFO

Article history:
Received: 23 July, 2020
Accepted: 23 August, 2020
Online: 09 September, 2020

Keywords:
Big Data
Discussion Making
Quantitative Method
Percentage Analysis
Chi-Square
Correlation Analysis
Regression Analysis

ABSTRACT

The technology of Big Data got the capability to process large amounts of data, manage them effectively and make retrieval whenever it is required. Decision making in any organisation is a challenging task since decisions need to be made based on the accessibility of data and its status, this becomes more challenging especially in large organisations that generate massive amount of information and data every single day.
Implementation of latest advanced technologies like Big Data is imperative for any organization to make decisions which reduces time and pave the fourth industrial revolution. Even though this is vital in today's business world, there are still few organizations that are hesitant to adopt it.
This paper illustrates the relation between Big Data and effective decision making by implementing a quantitative analysis through questionnaire. The conducted analysis is implemented using SPSS through correlational perspective, where percentage analysis, Chi-Square, correlation, and regression analyses are performed to obtain results.
It is clearly depicted that large organizations transition to adopt Big Data to aid their decision making, where medium and smaller organizations were slowly transitioning the adoption. In spite of this, most of employees, irrespective of the type of organization agree that Big Data is indeed a powerful advanced technology as they were satisfied by the organizational direction they have taken.

1. Introduction

1.1. Background

Digital technologies are transforming the way organizations function sparking the necessity for creative approaches and a wide range of highly functional presentations [1]. Facilities of storing have grown drastically in the past years along with data collection approaches where large amounts of data are also becoming readily accessible. In every moment, new set of data are being generated by various sources, these data need to be processed and evaluated in new forms to derive value. In addition, organizations should get as much value as possible from enormous sources & amounts of data stored [2]. Further technologies and devices are available now to corporations and people to generate and collect more data from various groups. These days, an individual entity can own multiple devices, where each device carries extremely large amount of vital information. These types of information are described as Big Data, or data with a volume, velocity, variety and depth that standard techniques make it difficult to handle [3].

Big Data can contain various combinations of data including texts with social emotions, news feeds, site logfiles for audio / video, as well as geographical and location data, Multimedia, xml data, etc [4]. Due to the size, wide range, dramatic changes, different types of storage and analytical techniques, such these information needs fresh type of Big Data analytics. The rising of these kinds of information need to utilize a Big Data and take advantage of its capability in the organizations who have already a clear, simple roadmap and guidelines for managing Big Data in their departments.

Organizations today are enabled to achieve their target and exceed it if they were able to adopt new technologies which consequently leads to generating profit from Big Data analysis. In other sectors, the capability to create transition would distinguish those who are going to lead and those who are going to left behind. Nevertheless, conducting data analysis only is not enough, it must

*Corresponding Author: Hana Yousuf, The British University in Dubai, Tel: +971501010008, Email: hana.yousuf@gmail.com.

be circulated effectively to the employees within the organization in attempt to influence decisions and therefore obtain specific role at the heart of decision-making processes instead of intuition [5]. In order to make smart choices, organizations should be sharing right information to the right individuals at the right time [6]. As such, Big Data attains great expectations, and the effect on enhancing the decision has been explored by various researchers, with McAfee & Brynjolfsson as the strategic front-runners. However, since it is a relatively new area of concept and research, it is essential to have more empirical studies in specific sectors to the research of what impacts Big Data analytics will have on decision-making.

Organizations need contract terms and interpersonal governance, Big Data analytics competences, information sharing, coordination, process integration, flexible infrastructure, quality data sources and decision making qualities to effectively manage a large data chain and make quality decisions [7,8]. Contract compliance relates to the formalization of arrangements with Big Data vendors to increase the consistency of the results. Relational governance that involves collaboration and information sharing for data interpretation and processing maintains trust between organizational entities. To design a Big Data network and overcome the smaller data groups, various participants of the organisation who are part of the Big Data based decision-making environment require collaboration. It is also necessary to connect operations and procedures to cut the price of Big Data and its related analytics. Big Data networks and its operations must be part of the organizational routine, since this will enhance information speed. The flexibility of the network often allows data collection and retrieval. Information accuracy, with respect to the data provider's interest, is also necessary to avoid making mistake decisions that may prove to be quite expensive. In fact, decision-makers will have the capacity to analyse the findings of Big Data analyses and consider their consequences in order to strengthen evidence-driven decision-making capabilities and increase consistency [7].

1.2. Problem Statement

Existing literature on the use of Big Data for decision making system focuses primarily on the issues and advantages of business intelligence and Big Data[8], whereas the practical effects of Big Data analysis to improve business intelligence are still relatively under-researched[9][10][11]. Some research is usually focused on methods, technical issues and their possible solutions in using Big Data analytics for business intelligence, but there is a shortage of literature on the practical implications of using Big Data analytics in general for decision making.

1.3. Research Questions

This research aims to understand employee's perception of Big Data among in enhancing decision making systems. Therefore, the research questions are:

- How relevant is Big Data for decision making in an organization?
- What percentage of the organizations are currently using Big Data?
- Do the employees feel that Big Data is relevant in the current scenarios?

1.4. Literature Review

Big Data is increasingly transforming the way businesses make choices, because new decision-making skills are required in the Big Data era in order to make better judgments [7]. In the available research the dynamic capabilities are often used to address the strengths of Big Data analytics [12].

This research explores the antecedents of large data decision taking capability. Even though its potential effect has been described with respect to the dynamic capabilities [13,14], many elements of the organizations that affect the Big Data sustaining value of a firm remain unexplored.

The capacity of Big Data has defined by [7] as the capacity of a business to start making high-quality Big Data based decisions by handling a Big Data network effectively. [15] have also presented crucial and in-depth insights into diverse Big Data functionalities; however, the study is much more applicable to Big Data value creation. Conversely, the factors that affect the quality of Big Data decision making has discussed by [7]. Effective management of a Big Data networks requires organizations to build up their capacity and capabilities for Big Data management and analytics. The related literature also demonstrates the ability of a organization to interpret data can affect its efficiency and that the ability of the Big Data processing and analytics organizations to make strategic decision is likely to impact.

Leadership plays a vital role in the development and reconfiguration of dynamic capabilities as an effective way of providing direction to organizational members [6]. The leadership contingency principle often implies members will produce the required results by choosing their leadership style appropriately [16]. The existing literature also recognizes the effect of leadership style on various organizational and the behavioural outcomes for example, a leadership focus on knowledge management influences it positively within an organization [17], [18]. Leaders can also influence the information analysis trend by adopting appropriate leadership behaviours [19].

Leadership is an essential impactor of Big Data development, which is generally done through procedure, social and systemic interactions and complementarities [20]. It is further agreed by [21] that leadership is essential to a firm's development of using technology. Specifically, it is correlated with leadership propensity to adapt, understanding of incentives to improve current practices and services in a constructive way, and desire and capacity to incorporate these improvements. Managerial leadership cognition is critical to the improvement of Diagnostic Control Systems (DCS) that are used to manage the environment change [22].

In a wide spectrum of firms, talent management, which is emerging as a key organizational challenge, is considered very important [23]. Researchers have concluded that, despite the limited consequences of current talent management for implementing Big Data, its role in various situations and environments needs to be analysed [24]. Considering the essential function of the talent harnessing, indicated that the application of Big Data may be improved by effective talent management. As information is now more cost effective for organizations, the data analysis components have become more valuable, which means it is easier to hire data scientists.

The growing worth of Big Data specialists makes retaining them valuable to the organizations. While the expertise of statistics is essential, the use of Big Data demands more than conventional statistical abilities. Big Data management requires specific techniques and abilities that might not be easily available at certain locations [25], but are commonly held by the current generation of informatics scientists. Big Data use also requires skills involved in data cleaning and visualization, which suggests that organizations need to nurture key talents The acknowledgment by [26] that HR experts and expertise play in a Big Data setting, who are able to speak the market language and therefore make it easy for leaders to devise strategies to tackle Big Data.

According to the existing literature, efficient talent management practices improve organizational decision-making capabilities [27]. The resource-based perspective suggests organizations should use their strategic resources to achieve sustained competitive advantages [28]. The knowledge-based view argues that knowledge which is connected to its staff is the most essential strategic asset of a firm [18]. Using employee knowledge and skills to reap the maximum benefit., for instance, as long as success is concerned, organizations will incorporate acceptable talent acquisition practices, as indicated in the literature on the usage of Big Data [15].

The decision-making on data analytics requires quality decision-makers and Big Data analysts experts, asserted done by [7] . In addition to performing data analysis, the latter will also deal with contract terms and interpersonal leadership to improve information cooperation and information sharing across organization boundaries, which can affect the quality of Big Data decision. A lack of dedicated talent has been perceived as the major barrier to capturing value from Big Data [25]. Even though there are currently lots of professionals working with Big Data, there is a great amount of talent shortage for the next three to five years [28].

Many developing countries are in the race to utilize AI capabilities linked to Big Data; therefore, effective talent management is essential for businesses to reap the benefits of Big Data and digital technology[29]. As data gets cheaper, the domain's scientists become much more valuable, that further rises the need for integrated talent management procedures to hire, retain and recruit employees required at all levels to fulfil the standards of data analytics aimed at quality decision making. As such, effective talent management plays a significant role in building capacity for organizations [30]-[31].

2. Methodology

2.1. Research Design

Quantitative methodology is used in this work to gather data and conduct the necessary analysis. It is a type of research method that performs mathematical, computational, and statistical approaches using quantifiable data. To carry out the study, the data must be gathered entirely first. Until obtaining the results, the appropriate sample population must be defined depending upon the necessity. Here the target group is the employees of corporate organizations, about the use of Big Data for decision making. The research design will be as correlational research, where percentage analysis, Chi-Square analysis, correlation analysis and regression analysis will be applied.

It is necessary to identify the respondent population to compile the data and to build the questionnaire. Since the work deals with usage of Big Data in different organisations, employees of these organisations must be considered as community sample. Other related technologies like working of Big Data and its advantages which are related to the principles of Big Data and decision making have been extensively discussed in the literature review section.

The data are gathered in the form of questionnaires from specified respondents. The questions are posed to the respondents in the questionnaire, esponses are compiled. The questionnaire are posted directly in the form of (google forms) and sent via email. The answers must be translated into the graphical format for quantitative methods, so that they are appropriate for study. Any variables are established during the study for grouping the questions and answers into categories. There are numerous factors that rely heavily on this to be considered. In this work, it is identified whether the organisations are willing to use Big Data for decision making, and whether they have trust in them. The employees of certain organisations are taken into account for collecting the data for this study.

2.2. Scaling

Scaling is done to simplify data analysis and enable the researchers to better understand the data. Likert scaling is used in this work. Likert scale suggests that an ability / magnitude of attitude is linear, i.e. on a scale from strongly agreeing to disagreeing, and appears to conclude that attitudes will be calculated. There are various types of Likert scale depending on the number of opinions that are captured for each question [32]. A 4-point Likert scale is used in this research which contains 4 options, which are: Strongly Agree, Agree, Disagree and Strongly Disagree.

2.3. Questionnaire Development

The survey questions are deemed more accurate for gathering answers, they are used to gather answers in this research. The biggest drawback in utilizing questionnaires is that the queries tend to be determined at the outset and the subsequent questions cannot be changed on the basis of the first query. In this work, though, only a few questions will be asked, questionnaires are enough. A questionnaire that contains various questions related to the use of bigdata for decision making, and its effectiveness in enhancing the decision-making process is used. The questionnaire consists of a total of ten questions and it is attached in the appendix. Questions 2 and 3 can be considered as independent responses, while the other questions are dependent on these two questions.

2.4. Sampling Technique

When survey is conducted, there are different ways the population sample must be identified. This is because, it won't be feasible to conduct analysis with the entire population. In this case, we must conduct the study on the employees working small, medium and large organizations, where there would be millions of employees around the world. Hence, certain mixture of small- and large-scale organizations are identified randomly. The research paper will adopt Random Sampling technique.

2.5. Field Work

The respondents are randomly chosen and the questionnaires built using Google forms. The employees working in the same research field of different organisations are identified and the form sent to them by emails. Even though the forms are shared with many employees, only some of them had responded, out of which we round the number of respondents to 50 response. The answers are collected in a single dataset, and then SPSS tools used to perform different statistical approaches for quantitative research.

3. Data Analysis

3.1. Methodology

The responses are obtained from the respondents and then analysed through SPSS tool. The methodology used here are the percentage analysis, Chi-square test, correlation analysis, and regression analysis. The collected data analysed in form of statistical analysis as part of quantitative methodology.

Percentage analysis is among the simple mathematical methods that is commonly utilized in primary data processing and understanding. This deals with the number of respondents to a specific query is the proportion arrived from the overall chosen population for the analysis. A Chi-square test is a mathematical hypothesis check that is true while the Chi-square function is applied under the null hypothesis, called the Chi-square test of Pearson and its variants. Correlation coefficient is a statistical calculation of any form of correlation which implies a statistical association between two variables. The variables may be two columns of a specified series of results, also referred to as a survey, or major aspects of a random multivariate vector with a defined distribution. Regression analysis is an effective mathematical tool that analyses the association between two or more relevant variables. While there are several forms of regression analysis, they all analyse at the heart the effect of one or more independent variables on a dependent variable

4. Result

4.1. Percentage Analysis

Out of the four techniques, percentage analysis first analysed as given below. Out of the 50 respondents, 25 respondents, which considered as 50% of the respondents worked in a medium scale organization that had between 100 and 500 as shown in Table 1. The rest of the respondents were range between small and large organizations where 24% employed in small organizations less than 100 employees, and 26% employed in organizations more than 500 employees.

Table 1: Employees contribution based on the organization size

Organization Size	Frequency	Percent
1-100 employees	12	24.0
100-500 employees	25	50.0
More than 500 employees	13	26.0
Total	50	100

The number of respondents whose organization work with Big Data is shown in table 2. Most of the respondents are using Big Data in their organisation systems which is around 72% in, whereas 20% of the respondents' organizations did not use Big Data and 8% said that their organization is studying the implementation of Big Data in near future as shown in Table 2.

Table 2: Organization working with Big Data

Response	Frequency	Percentage
Yes	36	72.0
No	10	20.0
In future	4	8.0
Total	50	100.0

Out of the smaller organizations below 100 employees, around 67% of them are using Big Data in decision making, while 25% of them are not using it and 8% will implement it soon. Among the medium scale organization with employees between 100 and 500, 60% of them are using Big Data in making decision, while 28% of them are not using it and 12% will implement it soon. Among the large organizations with more than 500 employees, all of them use Big Data for decision making systems. The result is shown in Table 3

Table 3: employees' implantation and preference in using Big Data

Employee Size	Frequency	Implementation	Working with Big Data	Percentage
1 – 100 Employees	12	Implemented	8	66.67 %
		Not implemented	3	25.00 %
		Soon will be implemented	1	8.33 %
100-500 employees	25	Implemented	15	60%
		Not implemented	7	28%
		Soon will be implemented	3	12%
> 500 Employees	13	Implemented	13	100%
		Not implemented	0	0%
		Soon will be implemented	0	0%

The importance of the Big Data as recorded from the employee working in different organization size is shown in Table 4. 68% of the respondents said that it is very necessary for making decisions in the organization, while 24% slightly agreed and thought it is might be necessary to be implemented in some

departments and only 8 % of the respondents felt that it is not necessary at all.

Table 4: Importance of Big Data in decision making

Response	Frequency	Percentage
Not Necessary	4	8.0
Slightly necessary	12	24.0
Very necessary	34	68.0
Total	50	100.0

The availability of some form of strategy for Big Data is shown in Table 5. While 32% of the respondents confirmed that there is some form of strategy being used by the company for decision making analysis, 34% of them said that there is no strategy for this, while another 34% of them were not sure of this.

Table 1: Availability of Big Data strategies

Response	Frequency	Percentage
There is a strategy for Big Data	16	32.0
There isn't a strategy for Big Data	17	34.0
Not sure of the availability of a strategy for Big Data	17	34.0
Total	50	100.0

4.2. Chi- Square Test

Chi-square test is used which checks the null hypothesis between different questions. Since the second question influences the other questions, its relationship and hypothesis with other questions are tabulated in tables 6 to 8. The Chi-square value for having a strategy for Big Data, and those working with Big Data is shown in table 6. There are 16 respondents that use Big Data in the organization besides a strategy for usage and implementation, which accounts to 32% of the overall respondents. 20% of the respondents neither use Big Data nor have any strategy for Big Data in the organization. Around 26% of the respondents use Big Data but are not sure whether the organization have any kind of strategy adopts the Big Data implementation or not. A Chi-square of 31.2 is obtained for the relation, and p-value is 0, which shows that this is significant.

Table 2: Association between organisation work with Big Data and organization has any strategy for Big Data

Organization work with Big Data	Organization have any strategy for Big Data			Total	*P*-value
	Yes	No	Not sure		
	n(%)				
Yes	16 (100.0)	7 (41.2)	13 (76.5)	36 (72.0)	0.000**
No	0 (0.0)	10 (58.8)	0 (0.0)	10 (20.0)	
In future	0 (0.0)	0 (0.0)	4 (23.5)	4 (8.0)	
Total	16 (100.0)	17 (100.0)	17 (100.0)	50 (100.0)	

Chi-Square: 31.209, **P<0.001

Similar analysis is done for those working with Big Data and for those organisations that have qualified experts in Big Data. Most of the experts, 72% agree that they have a qualified expert, since their organization works with Big Data. 20% of the respondents do not work with Big Data and claim that they do not have any qualified Big Data experts. It has a very high Chi-square value of 50, and p-value of 0, showing that the result is significant as shown in table 7.

Table 7: Association between organization work with Big Data and organization with qualified Big Data experts

Importance of using Big Data for decision making	Organization with qualified Big Data experts				Total	*P* value
	Strongly Disagree	Disagree	Agree	Strongly agree		
	n(%)		n(%)			
Not Necessary	4 (100.0)	0 (0.0)	0 (0.0)	0 (0.0)	4 (8.0)	0.00**
Slightly necessary	0 (0.0)	0 (0.0)	3 (20.0)	9 (31.0)	12 (24.0)	
Very necessary	0 (0.0)	2 (100.0)	12 (80.0)	20 (69.0)	34 (68.0)	
Total	4 (100.0)	2 (100.0)	15 (100.0)	29 (100.0)	50 (100.0)	

Chi-Square: 50.000, **P<0.001

Similar Chi-square analysis is done for the opinion of importance of working with Big Data and whether the organization has qualified experts. 64% of the respondents feel that using Big Data is necessary and have qualified experts. Out of this 40% strongly agree, and 24% generally agree. Among those who feel Big Data is necessary, only 4% think that they do not have a qualified expert. With correlation too, a high Chi-square value of 51.48 is obtained along with significant results as shown in Table 8.

4.3. Correlation Analysis

Correlation analysis is performed to identify the correlation between two questions. The correlation coefficient implies the statistical association between two variables. Here, the variables are the two columns of the results. The correlation between the questions 2, 6, 7 and 10 are given in table 14. The questions 6,7, and 10 depend on question 2, they have high amount of correlation

with one another. All the coefficients have a value about 0.6, with some even exceeding 0.87 as shown in Table 9.

Table 3: Association between qualified experts and importance of working with Big Data

Importance of using Big Data for decision making	Organization with qualified Big Data experts				Total	*P* value
	Strongly Disagree	Disagree	Agree	Strongly agree		
	n(%)		n(%)			
Not Necessary	4 (100.0)	0 (0.0)	0 (0.0)	0 (0.0)	4 (8.0)	
Slightly necessary	0 (0.0)	0 (0.0)	3 (20.0)	9 (31.0)	12 (24.0)	0.00
Very necessary	0 (0.0)	2 (100.0)	12 (80.0)	20 (69.0)	34 (68.0)	**
Total	4 (100.0)	2 (100.0)	15 (100.0)	29 (100.0)	50 (100.0)	

Chi-Square: 51.481, **P<0.001

Table 9: Correlations analysis organization with Big Data

Questions	Organization working with Big Data	Organization with qualified Big Data experts	Satisfied with the organization in the integration of Big Data tools in the	Organization uses other tools in besides Big Data for decision making.
Organization work with Big Data	1			
Organization contains qualified Big Data experts.	.874**	1		
Satisfied with the organization in the integration of Big Data tools in the	.659**	.661**	1	
Organization uses other tools in besides Big Data for decision making	.659**	.661**	.870**	1

**p<0.001

The correlation between the questions 3, 5, 8 and 9 are given in table 10. The questions 5,8, and 9 depend on question 2, they have high amount of correlation with one another. While compared to the previous table, the correlation coefficient is slightly lesser. All the coefficients have a value about 0.35, with some even exceeding 0.5 as shown.

4.4. Regression Analysis

Regression analysis analyses the association between two or more relevant variables. Here, the correlation between the dependent and the independent variables are assigned. The regression between the 3impact of decision making and the importance of Big Data for decision making is shown in table 11. The Beta represents the slope of the line which shows that the line is very much dependent on the former variable. The standard error is low at 0.185. Hence, the points are not very much spread out from the main line. From the test value of 3.993, the probability variable is calculated, which comes at 0, showing that result is significant.

Table 4: Correlations analysis

Question	Important of Big Data in decision making	Organizations impact of the decision it makes.	Reduces uncertainty in making decisions	Improve decision making process in an organization
Important of Big Data in decision making	1			
Organizations impact of the decision it makes.	.499**	1		
Reduces uncertainty in making decisions	.518**	.389**	1	
Improve decision making process in an organization	.518**	.389**	.560**	1

**p<0.001

H11: There is a significant impact of the importance of Big Data in decision making on the organisations impact for decision making, which is the dependent variable. Hence, there is no null hypothesis here, and there is an alternate hypothesis. The probabilistic values must be less than 0.001, hence ours shows significant results.

Table 5: Association between important Big Data for decision making and organizations' impact for decision making

	Unstandardized Coefficients		R-Square	t value	*P* value
	Beta	SE			
(Constant)	1.116	0.496	0.249	2.251	0.029
Importance of Big Data for decision making	0.740	0.185		3.993	**0.000****

Dependent Variable: Organizations' impact for decision making, **p<0.001
SE: Standard Error

The regression for the association between the organisations working with Big Data and the availability of strategies of Big Data for decision making is shown in table 12. The Beta represents the slope of the line at 0.391which shows that the line is very much dependent on the former variable. The standard error is low at 0.179. Hence, the points are not very much spread out from the main line. From the test value of 2.1888, the probability

variable is calculated, which comes at 0, showing that result is significant.

H11: There is a significant impact of the organisations working with bigdata on the strategies used for Big Data in the organization, which is the dependent variable. Hence, there is no null hypothesis here, and there is an alternate hypothesis. The probabilistic values must be less than 0.001, hence ours shows significant results.

Table 6: Association between Organization work with Big Data and Strategies for Big Data for analytics

	Unstandardized Coefficients		R-Square	t value	*P* value
	Beta	SE			
(Constant)	1.488	0.268	0.191	5.556	0.000
Organization work with Big Data	0.391	0.179		2.188	0.000**

Dependent Variable: Strategies for Big Data for analytics, **p<0.001
SE: Standard Error

The regression for the association between the organisations working with Big Data and the satisfaction of using Big Data is shown in table 13. The Beta represents the slope of the line at 1.193. The standard error is low at 0.179. Hence, the points are not very much spread out from the main line. From the test value of 6.071, the probability variable is calculated, which comes at 0, showing that result is significant.

H11: There is a significant impact of the organisations working with bigdata on the satisfaction of using Big Data in the organization, which is the dependent variable. Hence, there is no null hypothesis here, and there is an alternate hypothesis. The probabilistic values must be less than 0.001, hence ours shows significant results.

Table 7: Association between Organization work with Big Data and Satisfaction

	Unstandardized Coefficients		R-Square	t value	*P* value
	Beta	SE			
(Constant)	4.582	0.294	0.434	15.585	0.000
Organization work with Big Data	1.193	0.196		6.071	**0.000****

Dependent Variable: Satisfaction, **p<0.001
SE: Standard Error

5. Conclusions and Recommendations

From the above analysis, it is depicted that most of the large organizations have already transitioned to using Big Data for decision making in their companies, where medium scale and smaller scale organizations are slowly transitioning. In spite of that, most employees regardless of the type of their organizations agree that Big Data technology is useful, and they are also satisfied by the organization on the direction they have taken. This work has presented a quantitative methodology for understanding the perception of Big Data used in their company. Initially, a brief introduction on decision making and Big Data systems were studied, followed by relevant literature were illustrated in the literature review section. A questionnaire was initiated to perform interview on the public to understand their perception Big Data. Data is collected in through online forms and then analysed through SPSS. The results illustrate that Big Data is very much relevant in the current scenario in corporate organizations. Most of the organizations seem to have already implemented Big Data for decision making purposes and others are rapidly following their footsteps. The same perception was accepted by employees too, where they showcased that using Big Data is indeed useful and most of the employees are satisfied with the way their company is using Big Data.

6. Limitation and Caveats

The Big Data technology can be used to improve effectiveness of decision-making systems. This work used SPSS as a tool to perform percentage analysis, Chi-square, correlation analysis, and regression analysis. The main limitations that hinders the adoption of Big Data is its awareness and knowledge. Many managers are still struggling with older technologies and are not ready to adopt them soon due to fear of change and its related challenges. Upgrading and seeking expert advice can be a good approach to convince them to adopt Big Data. In the future, the same analysis can be performed with more in-depth questions based on different organizational sectors. This work has only used quantitative methodology. In the future, both quantitative and qualitative methodology can be implemented to explore further. There are no caveats to consider in this work.

Acknowledgment

This work is a part of a project undertaken at the British University in Dubai.

References

[1] S. Brunswicker, E. Bertino, S. Matei, "Big Data for Open Digital Innovation - A Research Roadmap," Big Data Research, **2**(2), 53–58, 2015, doi:10.1016/j.bdr.2015.01.008.

[2] M.C.M. Oo, T. Thein, An efficient predictive analytics system for high dimensional big data, Journal of King Saud University - Computer and Information Sciences, 2019, doi:10.1016/j.jksuci.2019.09.001.

[3] S. Fan, R.Y.K. Lau, J.L. Zhao, Demystifying Big Data Analytics for Business Intelligence Through the Lens of Marketing Mix, Big Data Research, **2**(1), 28–32, 2015, doi:10.1016/j.bdr.2015.02.006.

[4] P. Törnberg, A. Törnberg, "The limits of computation: A philosophical critique of contemporary Big Data research," Big Data and Society, **5**(2), 2018, doi:10.1177/2053951718811843.

[5] M. Muniswamaiah, T. Agerwala, C. Tappert, "Big Data in Cloud Computing Review and Opportunities," International Journal of Computer Science and Information Technology, **11**(4), 43–57, 2019, doi:10.5121/ijcsit.2019.11404.

[6] P.J.H. Schoemaker, S. Heaton, D. Teece, "Innovation, Dynamic Capabilities, and Leadership," California Management Review, **61**(1), 15–42, 2018, doi:10.1177/0008125618790246.

[7] M. Janssen, H. van der Voort, A. Wahyudi, "Factors influencing big data decision-making quality," Journal of Business Research, **70**, 338–345, 2017, doi:10.1016/j.jbusres.2016.08.007.

[8] A.Y. Zainal, H. Yousuf, S.A. Salloum, "Dimensions of Agility Capabilities Organizational Competitiveness in Sustaining," in Joint European-US

Workshop on Applications of Invariance in Computer Vision, Springer: 762–772, 2020.
[9] H. Yousuf, M. Lahzi, S.A. Salloum, K. Shaalan, Systematic Review on Fully Homomorphic Encryption Scheme and Its Application, Springer: 537–551, 2021, doi:10.1007/978-3-030-47411-9_29.
[10] S.A. Salloum, M. Al-Emran, K. Shaalan, "Mining Social Media Text: Extracting Knowledge from Facebook," International Journal of Computing and Digital Systems, **6**(2), 2210–142, 2017, doi:10.12785/ijcds/060203.
[11] S.A. Salloum, M. Al-Emran, K. Shaalan, A. Tarhini, "Factors affecting the E-learning acceptance: A case study from UAE," Education and Information Technologies, **24**(1), 509–530, 2019, doi:10.1007/s10639-018-9786-3.
[12] S.F. Wamba, A. Gunasekaran, S. Akter, S.J. fan Ren, R. Dubey, S.J. Childe, "Big data analytics and firm performance: Effects of dynamic capabilities," Journal of Business Research, **70**, 356–365, 2017, doi:10.1016/j.jbusres.2016.08.009.
[13] S. Erevelles, N. Fukawa, L. Swayne, "Big Data consumer analytics and the transformation of marketing," Journal of Business Research, **69**(2), 897–904, 2016, doi:10.1016/j.jbusres.2015.07.001.
[14] R. Dubey, A. Gunasekaran, S.J. Childe, Z. Luo, S.F. Wamba, D. Roubaud, C. Foropon, "Examining the role of big data and predictive analytics on collaborative performance in context to sustainable consumption and production behaviour," Journal of Cleaner Production, **196**, 1508–1521, 2018, doi:10.1016/j.jclepro.2018.06.097.
[15] J. Zeng, K.W. Glaister, "Value creation from big data: Looking inside the black box," Strategic Organization, **16**(2), 105–140, 2018, doi:10.1177/1476127017697510.
[16] Organisational Behaviour - Stephen Robbins, Timothy A. Judge, Bruce Millett, Maree Boyle - Google Books.
[17] M.J. Donate, J.D. Sánchez de Pablo, "The role of knowledge-oriented leadership in knowledge management practices and innovation," Journal of Business Research, **68**(2), 360–370, 2015, doi:10.1016/j.jbusres.2014.06.022.
[18] S. Shamim, S. Cang, H. Yu, "Impact of knowledge oriented leadership on knowledge management behaviour through employee work attitudes," International Journal of Human Resource Management, **30**(16), 2387–2417, 2019, doi:10.1080/09585192.2017.1323772.
[19] S. Shamim, S. Gang, H. Yu, "Influencers of information system usage among employees for knowledge creation. A future research agenda," in SKIMA 2016 - 2016 10th International Conference on Software, Knowledge, Information Management and Applications, Institute of Electrical and Electronics Engineers Inc.: 134–141, 2017, doi:10.1109/SKIMA.2016.7916210.
[20] T. Felin, N.J. Foss, K.H. Heimeriks, T.L. Madsen, "Microfoundations of Routines and Capabilities: Individuals, Processes, and Structure," Journal of Management Studies, **49**(8), 1351–1374, 2012, doi:10.1111/j.1467-6486.2012.01052.x.
[21] O. Koryak, K.F. Mole, A. Lockett, J.C. Hayton, D. Ucbasaran, G.P. Hodgkinson, "Entrepreneurial leadership, capabilities and firm growth," International Small Business Journal: Researching Entrepreneurship, **33**(1), 89–105, 2015, doi:10.1177/0266242614558315.
[22] M. Waleed Fakhr, M. Lahzi Gaid, G. Ibrahim Selim, Secure Translation Using Fully Homomorphic Encryption and Sequence-to-Sequence Neural Networks, 2018.
[23] D.G. Collings, K. Mellahi, W.F. Cascio, "Global Talent Management and Performance in Multinational Enterprises: A Multilevel Perspective," Journal of Management, **45**(2), 540–566, 2019, doi:10.1177/0149206318757018.
[24] T.N. Krishnan, H. Scullion, "Talent management and dynamic view of talent in small and medium enterprises," Human Resource Management Review, **27**(3), 431–441, 2017, doi:10.1016/j.hrmr.2016.10.003.
[25] P. Tambe, "Big data investment, skills, and firm value," Management Science, **60**(6), 1452–1469, 2014, doi:10.1287/mnsc.2014.1899.
[26] D. Angrave, A. Charlwood, I. Kirkpatrick, M. Lawrence, M. Stuart, "HR and analytics: why HR is set to fail the big data challenge," Human Resource Management Journal, **26**(1), 1–11, 2016, doi:10.1111/1748-8583.12090.
[27] L.J. Gutierrez-Gutierrez, V. Barrales-Molina, H. Kaynak, "The role of human resource-related quality management practices in new product development: A dynamic capability perspective," International Journal of Operations and Production Management, **38**(1), 43–66, 2018, doi:10.1108/IJOPM-07-2016-0387.
[28] J.B. Barney, D.J. Ketchen, M. Wright, "The Future of Resource-Based Theory," Journal of Management, **37**(5), 1299–1315, 2011, doi:10.1177/0149206310391805.
[29] H. Yousuf, A.Y. Zainal, M. Alshurideh, S.A. Salloum, Artificial Intelligence Models in Power System Analysis, Springer: 231–242.
[30] W.F. Joyce, J.W. Slocum, "Top management talent, strategic capabilities, and firm performance," Organizational Dynamics, **41**(3), 183–193, 2012, doi:10.1016/j.orgdyn.2012.03.001.
[31] A. Almansoori, M. AlShamsi, S.A. Salloum, K. Shaalan, Critical Review of Knowledge Management in Healthcare, Springer: 99–119, 2021, doi:10.1007/978-3-030-47411-9_6.
[32] D. Kriksciuniene, V. Sakalauskas, R. Lewandowski, "Evaluating the Interdependent Effect for Likert Scale Items," in Lecture Notes in Business Information Processing, Springer: 26–38, 2019, doi:10.1007/978-3-030-36691-9_3.

ASTES

Advances in Science, Technology and Engineering Systems Journal Vol. 5, No. 5, 117-121 (2020)

www.astesj.com

ASTESJ

ISSN: 2415-6698

A User-Item Collaborative Filtering System to Predict Online Learning Outcome

Dina Fitria Murad[*,1], Rosilah Hassan[2], Wahiza Wahi[3], Bambang Dwi Wijanarko[4]

[1]*Information Systems Department, BINUS Online Learning, Bina Nusantara University, Jakarta, 11480, Indonesia*

[2]*Center for Cyber Security, Faculty of Information Science and Technology, University Kebangsaan Malaysia. Selangor, 45500, Malaysia*

[3]*Pusat Citra Universiti (Centre for Liberal Studiess), Universiti Kebangsaan Malaysia. Selangor, 45500, Malaysia*

[4]*Computer Science Department, BINUS Online Learning, Bina Nusantara University, Jakarta, 11480, Indonesia*

ARTICLE INFO

Article history:
Received: 27 June, 2020
Accepted: 31 August, 2020
Online: 09 September, 2020

Keywords:
Grade prediction
Recommendation system
User-item base collaborative filtering
Online Learning
Learning Materials

ABSTRACT

Education has seen the rapid development of online learning. Many researchers have conducted studies on the use of recommendation systems in online learning. However, until now, several similar studies still focus on the accuracy of the prediction results. Various obstacles were encountered related to changes in the face to face learning process into online learning. This study uses the User-Item Collaborative Filtering method to predict student learning outcomes as a basis for providing recommendations to students. Data on student online learning outcomes were extracted using several methods as a basis for determining and assessing their learning outcomes. The dataset we use is dummy to match the original data. The findings of this study reveal that one of the reinforcing factors that affect student achievement in online learning is the quiz score. The students' high achievement in the quizzes was also balanced by their active involvement during the learning process. Based on the evaluation of the recommendation system, it is known that the gradient boosted tree model is the best model for predicting the final score of student online learning with an accuracy calculated using the highest correlation of 0.7 and the smallest absolute error of 13.0 and root mean square error of 17.9. Based on the results of the evaluation, this study provides recommendations in the form of material links and learning archives that are useful for students to be able to carry out independent learning.

1. Introduction

The Fourth Industrial revolution (4IR) has brought about significant impact to the global public and private sectors. One sector that has been immensely affected by the 4IR is education. This is especially true given the evolving technological approaches to teaching and learning applied by many educators across different levels of education. For example, the 4IR has seen a crucial role of learners when carrying out their learning activities and a flexibility of the approach and ambiance of learning offered to the learners as seen in many online classes conducted by higher learning institutions. This is illustrated in Graphic 1 below. Along the same line, many researches have reported on effective interactions amongst learners who are largely involve in the use of simulation, advanced technologies, and online learning as compared to the conventional methods of learning through book references [1].

In addition, the Internet of Things (IoT) is deemed essential in the educational settings nowadays as it is the fundamental tools required for any online learning to take place. The IoT devices are particularly useful in the process of interchanging information through wireless or wired network connections [2].

Online learning is a learning model that has become increasingly in demand among various groups of learners. On the same note, most researchers are currently focusing on finding the best means and approaches of online learning that fit in the continuous developments of the 4IR such as the strategies utilized by students when conducting online discussion [3] the use of

*Corresponding Author: Dina Fitria Murad, Email: dmurad@binus.edu

various interface to enhance and encourage online learning [4], [5], or the production of expressive web designs [6].

	First Industrial Revolution	Fourth Industrial Revolution
Learning Objectives	Mastery of basic skills and knowledge (e.g., reading, math)	Development of whole person across multiple intelligences (e.g., emotional, intellectual, social)
Role of Educator	Expert	Facilitator
Learner Experience	'Factory model' - Passive, structured, directed, en masse	'Custom model' - Active, self-directed, exploratory
Target Age	K-12	Lifelong learning
Expertise	"Teacher knows best"	"Anyone can teach"
Access	Physical classroom	Anytime, anywhere, any device

Figure 1: Development of learning in education from first to fourth industrial revolution

The escalating popularity of e-learning has instigated various challenges for higher learning institutions to provide massive educational resources and the dire need to search for relevant learning references. Generally, in a university environment that runs the e-learning process, students are equipped with some necessary materials for learning and some additional references. These large amount of learning resources sometimes leads to excessive information received by the students. Hence, this has sparked researchers' interest to utilize a recommendation system that focuses on how students obtain their learning references either by using their profile [7], [8], or behavior [9], [10], and style or preferences which came to be known as personalization.

Starting with a basic theory, related to social studies [11], the recommendation system in the field of Education continues to develop and adapt several methods that successfully used in the field of e-commerce. Some of these studies state that the recommendation system in the area of Education needs personalized [12][13]. In general, the recommendation system can be grouped into four groups, namely (1) collaborative filtering, (2) content-base, (3) hybrid and (4) context-sensitive [14].

In the Education field, the collaborative filtering method is observed to be used effectively in the recommendation system [15], [16] in line with the success of the content-based approach [17], [18] and recently the most widely used method is hybrid [19], [20] and context- aware/context-sensitive [21], [22]. However, some researchers also found that rating determination in the recommendation system in the field of Education stated as a cold start [24] In this regard, this study adopts a cognitive theory that describes learning as a business process which involves mental activities occurring in humans as a result of an active interaction with their environment to obtain a change in the form of knowledge, understanding, behavior, skills, values and attitude that are related and important. This study uses data on students online learning outcomes as a basis to determine and rate their learning materials. Subsequently, this study provides recommendations on the links to learning materials and archives that are useful for the students to be able to conduct their self-directed learning. Specifically for this study, a User-Item Collaborative Filtering method of the recommendation system is employed to predict the outcomes of students online learning. The set of data deployed for the purpose of this study consists of (1) student profiles, (2) learning process results and (3) contextual information regarding students' perceptions and confidence in online learning.

Collaborative filtering techniques are used in recommendation systems as one technique for personalization [23], [24]. User base collaborative filtering (UBCF) works by collecting feedback from users in the form of ratings for items in a given domain. In our previous study [25] it was found that user collaborative filtering was the most dominant method for producing predictive accuracy. In this research we use User-Item collaborative filtering to predict the final grades of students by taking into account the personal values of students assessed based on learning activity (on student grades in other subjects). meanwhile, item base collaborative filtering is used to predict the student's final grade based on the proximity of the course that students have taken with other courses which are then averaged against other students in the same course.

Therefore, the collaborative filtering user-item technique is used by comparing the two techniques, UBCF with IBCF to maximize the predicted results of the student's final grade.

This study is guided by this research question, "Which machine learning model has the highest accuracy to predict the value of online learning students"?.

2. Research Method

Using the preliminary data set that was gathered at the initial stage of the study which comprises of the completeness of the attributes, the filter of the outlier values, and the standardization of the data used, a combination of python and sklearn was further deployed to process the data. The stages of the research process are shown in Figure 2.

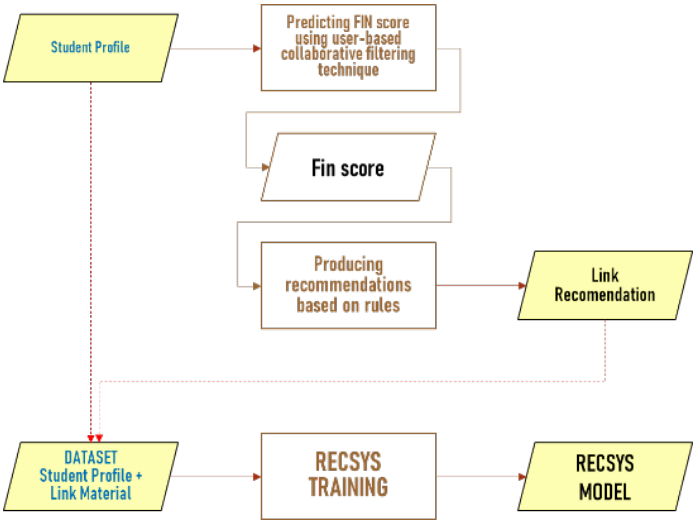


Figure 2: Research Framework

This study uses User-Item Collaborative Filtering method as preliminary data to find out the pattern of online learning process applied by students from previous session to be recommended to targeted students in this study. The structure of the data set used based on the results of the 2007-2018 student learning process at

BINUS Online Learning is shown in Table 1. We have dummy this data set so that it maintains the confidentiality of the original student data. Although officially we have received permission from the institution.

The data set incorporates several attributes that are grouped together into 3 main parts which are:

- Student profile (id and name)
- The output of the learning process (att, fod, pas1, pas2, qiz1, qiz2)
- Contextual information (student perception and student confidence)

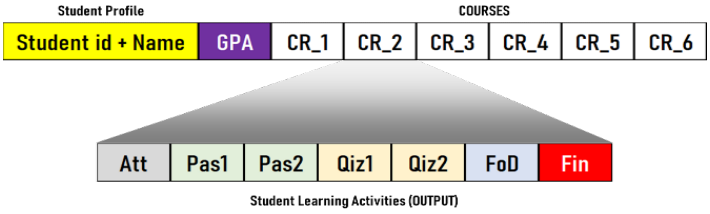


Figure 3: Data set the attribute for UBCF

Points (2) and (3) represent student learning activities using the user-item base collaboratife filtering method (figure 3) with various contextual information as student learning styles (figure 4).

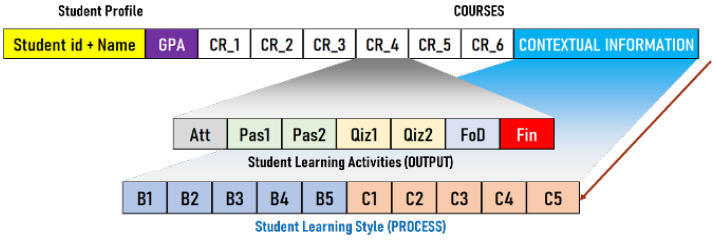


Figure 4: Attribute Dataset for user-item base collaboratife filtering + Multi Context Information

Table 1: Data Set Used

NAMA_MAHASISWA	ATT	FIN	FOD	PAS1	PAS2	QIZ1	QIZ2	TAS1	TAS2	TAS3	B1	B2	B3	B4	B5	C1	C2	C3	C4	C5	MATAKULIAH
1801437451_DONI	0	55	80	75	85	0	0	90	80	90	2	4	2	3	2	6	3	3	5	5	I0192_RESEAF
1801437451_DONI	0	49	60	100	100	0	0	82	50	100	2	4	2	3	2	6	3	3	5	5	K0442_QUAN
1801437451_DONI	0	82	0	0	0	0	0	0	0	0	2	4	2	3	2	6	3	3	5	5	M0244_INFOF
1801437451_DONI	0	94	60	97	95	0	0	100	90	90	2	4	2	3	2	6	3	3	5	5	M0304_CORP
1801437464_DANIE	0	82	100	100	100	0	0	100	100	100	2	4	3	4	5	5	4	5	4	4	CB432_CB: IN
1801437464_DANIE	0	55	100	85	80	0	0	80	80	90	2	4	3	4	5	5	4	5	4	4	I0192_RESEAF
1801437464_DANIE	0	25	100	100	60	0	0	80	65	100	2	4	3	4	5	5	4	5	4	4	K0442_QUAN
1801437464_DANIE	0	70	0	0	0	0	0	0	0	0	2	4	3	4	5	5	4	5	4	4	M0244_INFOF
1801437464_DANIE	0	94	100	80	97	0	0	99	100	90	2	4	3	4	5	5	4	5	4	4	M0304_CORP
1801437533_EKO R	0	86	100	100	100	0	0	100	100	100	2	5	3	3	4	5	5	5	4	5	CB432_CB: IN
1801437533_EKO R	0	60	95	75	80	0	0	90	80	60	2	5	3	3	4	5	5	5	4	5	I0192_RESEAF
1801437533_EKO R	0	39	100	40	100	0	0	95	65	100	2	5	3	3	4	5	5	5	4	5	K0442_QUAN
1801437533_EKO R	0	76	0	0	0	0	0	0	0	0	2	5	3	3	4	5	5	5	4	5	M0244_INFOF
1801437533_EKO R	0	100	90	97	95	0	0	100	90	90	2	5	3	3	4	5	5	5	4	5	M0304_CORP
1801437546_IMAM	0	76	100	100	100	0	0	100	100	100	2	2	4	4	4	4	4	4	4	3	CB432_CB: IN
1801437546_IMAM	0	90	100	80	80	0	0	75	70	70	2	2	4	4	4	4	4	4	4	3	I0192_RESEAF
1801437546_IMAM	0	72	100	40	100	0	0	80	65	100	2	2	4	4	4	4	4	4	4	3	K0442_QUAN
1801437546_IMAM	0	83	0	0	0	0	0	0	0	0	2	2	4	4	4	4	4	4	4	3	M0244_INFOF
1801437546_IMAM	0	94	90	0	95	0	0	99	100	90	2	2	4	4	4	4	4	4	4	3	M0304_CORP
1801437552_RAHM	0	78	90	100	100	0	0	100	100	100	2	6	4	4	3	3	3	6	5	3	CB432_CB: IN
1801437552_RAHM	0	55	70	75	80	0	0	70	80	80	2	6	4	4	3	3	3	6	5	3	I0192_RESEAF
1801437552_RAHM	0	70	75	40	100	0	0	50	60	100	2	6	4	4	3	3	3	6	5	3	K0442_QUAN
1801437552_RAHM	0	95	0	0	0	0	0	0	0	0	2	6	4	4	3	3	3	6	5	3	M0244_INFOF
1801437552_RAHM	0	89	65	100	95	0	0	90	100	90	2	6	4	4	3	3	3	6	5	3	M0304_CORP
1801437565_AGUN	0	76	50	85	88	0	0	97	90	97	2	3	4	4	4	4	4	4	4	3	CB432_CB: IN
1801437565_AGUN	0	55	55	84	94	0	0	76	83	70	2	3	4	4	4	4	4	4	4	3	I0192_RESEAF

with,

ATT = attendance
FOD = forum discussion
PAS1 = personal assignment1
PAS2 = personal assignment2
Qiz1 = quiz1
Qiz2 = quiz2
FIN = predictive target
B1-B5 = measure student perception toward courses
C1-C5 =measure student confidence toward courses
B1-B5, C1-C5 are multi-context information

In addition, a table that contains the list of materials (Refer to Table 2) is utilized to identify similar items related to student learning process and student context to be recommended to the targeted students. The list of materials provides a basis for the recommendations of students online learning outcomes on each learning material per topic per week. Learning outcomes are adjusted to the assessment of each learning material listed in the course outline with close reference to the Bloom taxonomy in line with the guidelines for course provisions as required by the higher learning institution in which the students are studying.

Table 2: List of Materials

M0124_ADVANCED INFORMATION S	10.001	LO1-The Systems Analyst and Information	https://www.or
ISYS6299_INFORMATION SYSTEMS (	10.001	LO1-Introduction to Information Systems	https://learning
M0124_ADVANCED INFORMATION S	10.002	LO1-Requirements Determination	https://www.or
ISYS6299_INFORMATION SYSTEMS (	10.002	LO1-Ethics;Privacy and Information Securit	https://learning
M0124_ADVANCED INFORMATION S	10.003	LO1-Use Case Analysis	https://learning
ISYS6299_INFORMATION SYSTEMS (	10.003	LO1-Telecommunications; Networking;Wir	https://learning
M0124_ADVANCED INFORMATION S	10.004	LO2-Process Modeling	https://learning
ISYS6299_INFORMATION SYSTEMS (	10.004	LO2-Hardware and Software	https://learning
M0124_ADVANCED INFORMATION S	10.005	LO2-Data Modeling	https://learning
ISYS6299_INFORMATION SYSTEMS (	10.005	LO2-E-Business And E-Commerce	https://learning
M0124_ADVANCED INFORMATION S	10.006	LO2-The Design Phase;Design Strategy;and	https://learning
ISYS6299_INFORMATION SYSTEMS (	10.006	LO2-Social Computing	https://learning
M0124_ADVANCED INFORMATION S	10.007	LO2-User Interface Design	https://learning
ISYS6299_INFORMATION SYSTEMS (	10.007	LO2-Cloud Computing	https://learning
M0124_ADVANCED INFORMATION S	10.008	LO3-Program Design	https://learning
ISYS6299_INFORMATION SYSTEMS (	10.008	LO3-Customer Relationship Management a	https://learning
M0124_ADVANCED INFORMATION S	10.009	LO3-Data Storage Design	https://learning
ISYS6299_INFORMATION SYSTEMS (	10.009	LO3-Business Analytics	https://learning
M0124_ADVANCED INFORMATION S	10.01	LO3-Moving Into Implementation	https://learning
ISYS6299_INFORMATION SYSTEMS (	10.01	LO3-Acquiring Information Systems and Ap	https://learning
M0124_ADVANCED INFORMATION S	20.001	LO1-Requirements Determination	https://www.or

3. Result and Discussion

In reference to the data set used, the student profile was the first input collated from this study to predict students' grades. The student profile was complemented by the results of the learning process and students' contextual information. Using the UBCF method, the value prediction is performed. The predictive value used to provide recommendations using a rule base and produce recommendations in the form of learning material links.

Prediction of student grades was made using several techniques including:

- Generalized linier model
- Deep learning
- Decision tree
- Random forest
- Gradient boosted trees
- Support vector machine

In reference to the six models above, the predicted value of student scores was compared with real student values. The results are presented in a scatter diagram in Figure 5.

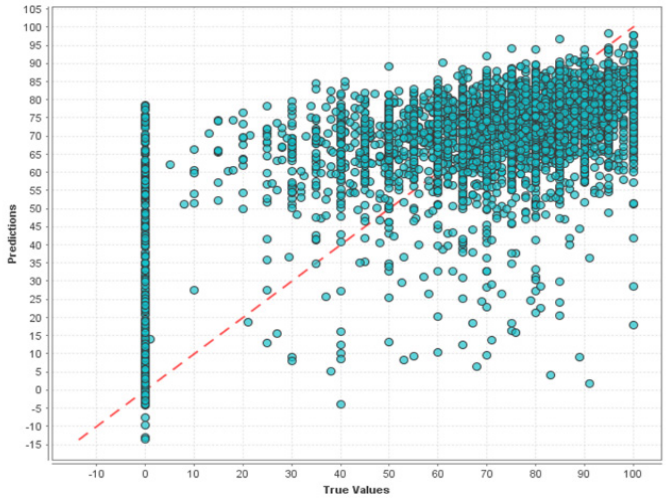


Figure 5: Scatter Diagram – Gradient Boosted Trees Model

Based on the results of the comparison, an evaluation was conducted using root mean square error, and the results are shown in Figure 6.

Model	Correlation	Standard Deviation	Squared Error	Standard Deviation	Relative Error	Standard Deviation	Absolute Error	Standard Deviation	Root Mean Squared Error	Standard Deviation
Generalized Linear Model	0.62	0.01	393.22	8.61	0.23	0.00	14.93	0.11	19.83	0.22
Deep Learning	0.67	0.02	355.41	15.02	0.23	0.00	13.95	0.24	18.85	0.40
Decision Tree	0.62	0.02	390.26	16.75	0.23	0.00	14.53	0.23	19.75	0.43
Random Forest	0.65	0.01	374.63	3.27	0.23	0.00	14.56	0.07	19.36	0.08
Gradient Boosted Trees	0.71	0.01	314.84	6.19	0.22	0.00	12.89	0.06	17.74	0.17
Support Vector Machine	0.47	0.01	550.42	30.97	0.22	0.01	15.99	0.53	23.45	0.67

Figure 6: Comparation: Error of Model

The results of the evaluation on the six learning models indicated that the gradient boosted trees model scored the most significant correlation with the smallest error compared to other models. Gradient boosted trees have the smallest root means square error of 17.74 (generalized linier model 19.83, deep learning 18.85, decision tree 19.75, random forest 19.36, and support vector machine 23.45). The results were then broken down into parts as seen in Figure 7.

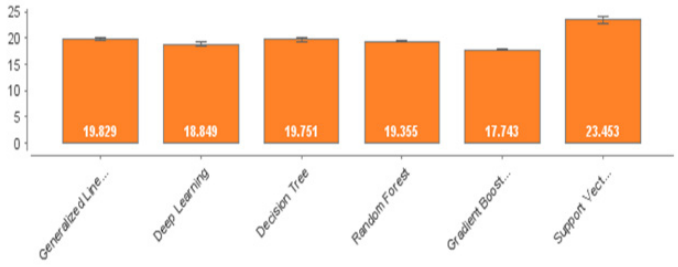


Figure 7: Comparation: Root Mean Square Error

To complement the results of previous study [26] on the dominant factors that affect student attendance, we continue this research by processing data to look for correlations between each attribute (see Figure 8).

Based on the results of our previous research [25], it is known that the dominant factor affecting student achievement or failure of certain learning materials is the active involvement of students in discussion forums, followed by student achievement in quizzes. The results of this study are a little similar to previous studies except that the quiz score is placed as a dominant factor while the active involvement of students in discussion forums is a supporting factor.

	ATT	B1	B2	B3	B4	B5	C1	C2	C3	C4	C5	FIN	FOD	IPK	PAS1	PAS2	QIZ1	QIZ2	TAS1	TAS2	TAS3
ATT	1.00	0.03	0.01	0.01	0.02	0.01	0.01	0.01	0.01	0.01	0.00	0.19	0.22	0.20	0.20	0.21	0.68	0.68	0.04	0.07	0.02
B1	0.03	1.00	0.54	0.45	0.34	0.27	0.23	0.27	0.27	0.26	0.21	0.01	0.00	0.03	0.02	0.02	0.03	0.03	0.00	-0.01	-0.01
B2	0.01	0.54	1.00	0.48	0.46	0.42	0.28	0.30	0.23	0.24	0.16	0.01	0.01	0.02	0.01	0.02	0.00	0.01	0.00	0.00	0.00
B3	0.01	0.45	0.48	1.00	0.46	0.43	0.29	0.29	0.26	0.30	0.17	-0.02	0.00	-0.03	-0.01	-0.01	0.00	0.00	0.00	0.00	-0.01
B4	0.02	0.34	0.46	0.46	1.00	0.72	0.27	0.38	0.21	0.30	0.28	-0.01	0.01	-0.01	-0.01	0.00	0.00	0.00	-0.01	-0.01	-0.01
B5	0.01	0.27	0.42	0.43	0.72	1.00	0.23	0.36	0.20	0.25	0.32	-0.03	0.00	-0.03	-0.02	-0.02	-0.01	-0.01	-0.01	-0.01	-0.02
C1	0.01	0.23	0.28	0.29	0.27	0.23	1.00	0.52	0.36	0.46	0.38	-0.01	-0.01	0.00	-0.01	-0.01	0.00	0.00	0.00	-0.01	0.00
C2	0.01	0.27	0.30	0.29	0.38	0.36	0.52	1.00	0.44	0.42	0.56	0.00	0.00	0.02	0.00	0.00	0.00	0.01	0.00	0.00	-0.01
C3	0.01	0.27	0.23	0.26	0.21	0.20	0.36	0.44	1.00	0.44	0.43	0.00	0.00	0.00	0.00	0.00	0.00	0.01	0.00	0.00	0.00
C4	0.01	0.26	0.24	0.30	0.30	0.25	0.46	0.42	0.44	1.00	0.52	0.00	-0.01	0.00	-0.01	-0.02	0.01	0.01	-0.01	0.00	-0.01
C5	0.00	0.21	0.16	0.17	0.28	0.32	0.38	0.56	0.43	0.52	1.00	-0.01	-0.02	-0.01	-0.01	-0.01	-0.01	0.00	-0.01	-0.01	-0.01
FIN	0.19	0.01	0.01	-0.02	-0.01	-0.03	-0.01	0.00	0.00	0.00	-0.01	1.00	0.51	0.52	0.46	0.50	0.27	0.31	0.20	0.22	0.15
FOD	0.22	0.00	0.01	0.00	0.01	0.00	-0.01	0.00	0.00	-0.01	-0.02	0.51	1.00	0.63	0.56	0.59	0.29	0.32	0.20	0.22	0.16
IPK	0.20	0.03	0.02	-0.03	-0.01	-0.03	0.00	0.02	0.00	0.00	-0.01	0.52	0.63	1.00	0.49	0.52	0.31	0.34	0.10	0.13	0.09
PAS1	0.20	0.02	0.01	-0.01	-0.01	-0.02	-0.01	0.00	0.00	-0.01	-0.01	0.46	0.56	0.49	1.00	0.56	0.29	0.30	0.27	0.28	0.23
PAS2	0.21	0.02	0.02	-0.01	0.00	-0.02	-0.01	0.00	0.00	-0.02	-0.01	0.50	0.59	0.52	0.56	1.00	0.30	0.33	0.26	0.29	0.24
QIZ1	0.68	0.03	0.00	0.00	0.00	-0.01	0.00	0.00	0.00	0.01	-0.01	0.27	0.29	0.31	0.29	0.30	1.00	0.75	0.12	0.14	0.05
QIZ2	0.68	0.03	0.01	0.00	0.00	-0.01	0.00	0.01	0.01	0.01	0.00	0.31	0.32	0.34	0.30	0.33	0.75	1.00	0.11	0.14	0.07
TAS1	0.04	0.00	0.00	0.00	-0.01	-0.01	0.00	0.00	0.00	-0.01	-0.01	0.20	0.20	0.10	0.27	0.26	0.12	0.11	1.00	0.70	0.54
TAS2	0.07	-0.01	0.00	0.00	-0.01	-0.01	-0.01	0.00	0.00	0.00	-0.01	0.22	0.22	0.13	0.28	0.29	0.14	0.14	0.70	1.00	0.55
TAS3	0.02	-0.01	0.00	-0.01	-0.01	-0.02	0.00	-0.01	0.00	-0.01	-0.01	0.15	0.16	0.09	0.23	0.24	0.05	0.07	0.54	0.55	1.00

Figure 8: Correlation between Attribute

4. Conclusion and Next Future

The results of this study complement our previous research regarding the attributes that most dominantly influence student achievement or failure, namely active participation in discussions / forums and quiz scores. These findings confirm that the active involvement of students in discussions / forums and quiz factors are important factors that contribute to meaningful and effective learning. In line with the fundamental social theory [11] and the cognitive learning theory which states that a person can learn from the success of others and tends to influence that person's results, this study also proves that the success of the user collaborative method in e-commerce has also been successfully applied in the field of education. This method was also successful in influencing student learning outcomes. In this study, Gradient boosted trees model is the most accurate machine learning model that can predict student grades.

In the forthcoming research, we will conduct trainings on the use of the recommendation system. The results of the trainings will be become our foundation to build machine learning models for the recommendation system in the field of Education, more specifically for online learning.

Conflict of Interest

This paper is the result of joint research. We declare that there is no conflict of interest regarding the publication of this paper.

Acknowledgment

This work is supported by Bina Nusantara University through the Office of Research and Technology Transfer, as part of the Bina Nusantara University (BINUS) International Research Grant with Universiti Kebangsaan Malaysia (UKM) entitled "New Technology in Education Towards Fourth Industrial Revolution: Case Study Indonesia & Malaysia "contract number: No.026 / VR.RTT / IV / 2020 and contract date: April 6, 2020.

References

[1] Z. Mohd Tawil, N., Hassan, R., Ramlee, S., & K-Batcha, "Enhancing entrepreneurship skill among university's students by online business simulation," Journal of Engineering Science and Technology, 10 (Spec. Issue, (on 4th International Technical Conference (ITC)), 71–80, 2015.

[2] H. Mojib, G., Aman, A.H.M., Khalaf, M. y Hassan, "Simulation analysis for QoS in Internet of Things wireless network," 3C Tecnología. Glosas de Innovación Aplicadas a La Pyme, (Edición Especial), 77-83.

[3] A. Omar, Z. Amir, M. Mohamad, "Facilitating online learning: Students' online discussion strategies for a project work at a technical university in Malaysia," 3L: Language, Linguistics, Literature, **24**(4), 102–114, 2018, doi:10.17576/3L-2018-2404-08.

[4] A. Ramakrisnan, P., & Jaafar, "Usable, aesthetic, sociable and motivating interface for students' online knowledge sharing," In Learning and Collaboration Technologies : 3rd International Conference, LCT 2016 and Held as Part of HCI International (Lecture Notes in Computer Science (Including Subseries Lecture Notes in Artificial Intelligence and Lecture Notes in Bioinformatics), **9753**, 550–561, 2016.

[5] A. Ramakrisnan, P., & Jaafar, "Motivation design methodology for online knowledge sharing interface," In Advances in Visual Informatics - 5th International Visual Informatics Conference, IVIC 2017 (Lecture Notes in Computer Science (Including Subseries Lecture Notes in Artificial Intelligence and Lecture Notes in Bioinformatics), **10645 LNCS**, 224–232, 2017.

[6] Z. Daud, N. A., Redzuan, F., Nasruddin, Z. A., Sahari @ Ashaari, N., & Muda, "Persuasive web design for online islamic education," in In Proceedings of the 2017 6th International Conference on Electrical Engineering and Informatics: Sustainable Society Through Digital Institute of Electrical and Electronics Engineers Inc. Innovation, ICEEI 2017, 1–6, 2018.

[7] O. Bourkoukou, E. El Bachari, M. El Adnani, "A Personalized E-Learning Based on Recommender System," **2**(2), 99–103, 2016, doi:10.18178/ijlt.2.2.99-103.

[8] O. Khribi, M. K., Jemni, M., & Nasraoui, "Toward a hybrid recommender system for e-learning personalization based on web usage mining techniques and information retrieval," In E-Learn: World Conference on E-Learning in Corporate, Government, Healthcare, and Higher Education, (pp. 6136-6145), 2007.

[9] N. Taghipour, A. Kardan, S. Ghidary, "Usage-based web recommendations: a reinforcement learning approach," … of the 2007 ACM Conference on …, 113–120, 2007, doi:10.1145/1297231.1297250.

[10] T. Mahmood, F. Ricci, "Improving recommender systems with adaptive conversational strategies," Proceedings of the 20th ACM Conference on Hypertext and Hypermedia - HT '09, (January), 73, 2009, doi:10.1145/1557914.1557930.

[11] A.J. Chournazidis, "Functionality and Feasibility of Knowledge Management in Enterprises," Procedia - Social and Behavioral Sciences, **73**, 327–336, 2013, doi:10.1016/j.sbspro.2013.02.059.

[12] N. Thai-Nghe, L. Drumond, T. Horváth, A. Nanopoulos, L. Schmidt-Thieme, "Matrix and Tensor Factorization for Predicting Student Performance," Undefined, 2011.

[13] A. Klašnja-Milićević, B. Vesin, M. Ivanović, Z. Budimac, "E-Learning personalization based on hybrid recommendation strategy and learning style identification," Computers and Education, **56**(3), 885–899, 2011, doi:10.1016/j.compedu.2010.11.001.

[14] B. Ricci, F., Rokach, L., & Shapira, Recommender systems: introduction and challenges, 2015.

[15] M. Dhanda, V. Verma, "Recommender System for Academic Literature with Incremental Dataset," Procedia Computer Science, **89**, 483–491, 2016, doi:10.1016/j.procs.2016.06.109.

[16] M.F. Caro Piñeres, J. Hernández, J.A. Jiménez Builes, "Diseño De Un Sistema De Recomendación En Repositorios De Objetos De Aprendizaje Basado En La Percepción Del Usuario: Caso Rodas," Ciencia e Ingeniería Neogranadina, **21**(1), 51–72, 2011.

[17] F. Matematika, P. Alam, U.G. Mada, "Sistem Rekomendasi Pada E-Commerce Menggunakan K-Nearest," **4**(3), 194–200, 2017.

[18] F.O. Isinkaye, "Recommendation systems : Principles , methods and evaluation," Egyptian Informatics Journal, 2015, doi:10.1016/j.eij.2015.06.005.

[19] C. Wang, Z. Zheng, Z. Yang, "The research of recommendation system based on Hadoop cloud platform," in Proceedings of the 9th International Conference on Computer Science and Education, ICCCSE 2014, 193–196, 2014, doi:10.1109/ICCSE.2014.6926453.

[20] G. Article, "Recommender Systems - Comparison of Content-based Filtering and Collaborative Filtering," International Journal of Current Engineering and Technology, **4**(5), 3131–3133, 2014.

[21] T. Morrow, A.R. Hurson, S.S. Sarvestani, "A Multi-Stage Approach to Personalized Course Selection and Scheduling," 2017, doi:10.1109/IRI.2017.58.

[22] Y. Li, L. Mei, J. Wang, "A personalized recommendation system in E-Learning environment based on semantic analysis," in 2012 6th International Conference on New Trends in Information Science, Service Science and Data Mining (ISSDM2012), 2012.

[23] G. Adomavicius, A. Tuzhilin, "Context-aware recommender systems," Recommender Systems Handbook, Second Edition, 191–226, 2015, doi:10.1007/978-1-4899-7637-6_6.

[24] J.L. Herlocker, J.A. Konstan, L.G. Terveen, J.T. Riedl, "Evaluating collaborative filtering recommender systems," ACM Transactions on Information Systems, **22**(1), 5–53, 2004, doi:10.1145/963770.963772.

[25] D.F. Murad, Y. Heryadi, S.M. Isa, W. Budiharto, "Personalization of Study Material based on Predicted Final Grades using Multi-criteria User-collaborative Filtering Recommender System," Education and Information Technologies, **May**(III), 2020, doi:10.1007/s10639-020-10238-9.

[26] D.F. Murad, S.M. Isa, "Text Mining Analysis in the Log Discussion Forum for Online Learning Recommendation Systems," International Seminar on Research of Information Technology and Intelligent Systems (ISRITI) 2018.

ASTES

Advances in Science, Technology and Engineering Systems Journal Vol. 5, No. 5, 121-126 (2020)

www.astesj.com

ASTESJ

ISSN: 2415-6698

Search for New Potential Breast Cancer Inhibitors (MCF7) Based on Molecular Docking and Biological Assay of Pyrazoline Analogue Compounds

Jasril[1], Hilwan Yuda Teruna[1], Ihsan Ikhtiarudin[2], Neni Frimayanti[2,*]

[1]*Department of Chemistry, Faculty of Mathematics and Natural Sciences, Universitas Riau. Kampus Bina Widya, Jl. HR Subantas Km 12.5, Pekanbaru 28293, Indonesia*

[2]*Sekolah Tinggi Ilmu Farmasi (STIFAR) Riau, Jalan Kamboja, Pekanbaru, 28293, Indonesia*

ARTICLE INFO

Article history:
Received: 10 July, 2020
Accepted: 02 September, 2020
Online: 09 September, 2020

Keywords:
pyrazoline
breast cancer
MTT assay
Molecular docking

ABSTRACT

Cancer is the leading cause of death in world. Currently, there are no approved vaccines to avoid the spreading of this disease. Drug discovery have played important role for discover of new potent drugs that could efficiently and cost-effectively. Pyrazoline analogue compounds known to have good potency as anti-cancer. The aim of this study is to observe the potency of these pyrazoline analogue as anticancer using molecular docking. In this study, ten pyrazoline analogue compounds were docked and tested on MCF7 cell line using MTT assay. Based on docking results, compound PH CN1-4F explored three interations with amino acid residues. These interactions are hydrogen bonding with Arg791, hydrophobic interaction with His790 and van der Waals interaction with Asp810. Biological assay was shown that this compound is also have big potency as breast cancer inhibitor with IC_{50} value of 61.22 µg/mL. Thus, this strategy can be used to identify new potent drugs as new inhibitor for breast cancer.

1. Introduction

Breast cancer is begun with development of an abnormal breast cells in men and women. There are some types of cancers such as lung cancer, breast cancer, blood cancer, etc. Currently, breast cancer is one type of cancer that caused of death after lung cancer [1]. Cancer is a very serious problem for human health and this disease grow from the body's cells, which are characterized by uncontrolled, uncoordinated and unwanted cell division [2].

There are some treatment for breast cancer such as using chemotherapy. Chemotherapy is characterized by targeting the functions of receptor such as ERα (alpha estrogen receptor), PR (progesterone receptor), EGFR (epidermal growth factor receptor) etc. Epidermal growth factor receptor (EGFR) is a receptor of tyrosine kinase that plays an important role in normal physiological and cancer conditions [3]. EGFR can be defined as the first receptor that provided evidence for a relationship between cancer and receptor overexpression.

Wala and co-workers [4] has been tested for biological assay of pyrazoline as inhibitor for microbial, anti-inflammatory, antidepressant, and anticancer effects. Sorrounded the reported of biological assay, it is an urgent to say that pyrazolines are not only acceptable for therapy of some type of cancer but it is also can be used for treat another disease. Some of pyrazoline are also can act as an agents for cancer chemopreventive [5]. Surgery, chemotherapy and radiation therapy are some kind of traditional way for cancer treatment. Exspecially for chemotherapy, the crucial goal of this treatment is to discover the specific target of cancer cells without affecting to the normal cells and also to avoid the side effect. Searching for new agents with highly potential and selective anticancer activities is highly demanded [6].

Drug discovery is very complicated and it is always needed a laborious process. Generally, it will begun with screening of compounds from a large database for then will find out the lead of compounds. It is needed high cost and will spend longer time [7, 8]. Thus, computational approach have created a major impact into drug design process. Calculation will reduce the the cost and also the time for research, in addition, it would also help the rapid development of theraupetic methods [9].

One application of computational approach is using molecular docking is very potent way to discover new potential agent like breast cancer inhibitor [10]. Molecular docking can be applied to determine the binding interaction between the protein and ligand, thus it can estimate the ability of thus compounds (i.e. ligand). The

*Corresponding Author: Neni Frimayanti, Email: nenifrimayanti@gmail.com

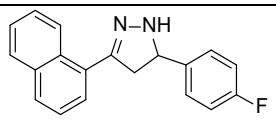
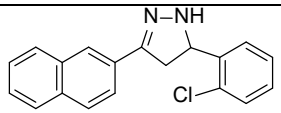
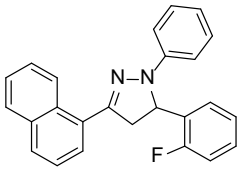
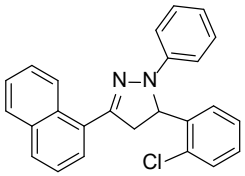
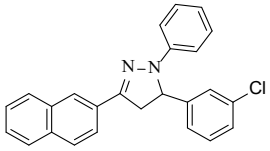
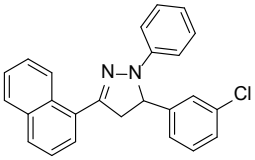
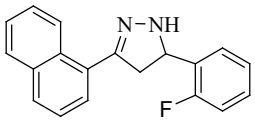
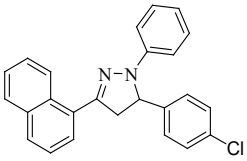
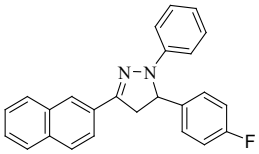
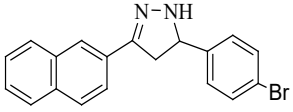
aim of this research is to discover new pyrazoline analogue compounds with good activity for treat breast cancer using molecular docking and approved using biological assay test.

2. Research Methodology

2.1. Receptor 3D Structure

Autodock 1.5.4 software packages was used to perform the molecular docking. Protein data bank (http://www.rscb.org/pdb) was then used to download the protein molecular structure. In this research, the protein tyrosine kinase with PDB ID 1t46 was applied as receptor. It was obtained with resolution of 1.6 Å and also must kept in rigid position. Next step are process to add atoms, merging, checking and repairing missing atoms. This step is begun with added hydrogen atoms, following with merging non-polar hydrogen atoms, checking and repairing missing atoms. For atoms charge, it was started with added Gasteiger charges, following with checking charges and fixing charges on the residue amino acids. Finally, it is assigning atom types to the protein. Autogrid 4 sofware packages with the protein grid box with dimension of 122 x 116 x 120 point along x, y and z axes and centered on the protein for docking. The grid box was settled with grid spacing of 0.35 Å, it also have to default with some atoms such as carbon, hydrogen an nitrogen.

Table 1 Molecular structure of Ligand

Structure	Struture
 PH-CN_1-4F	 PH-CN_2-2Cl
 PF-CN_1-2F	 PF-CN_1-2Cl
 PF-CN_2-3Cl	 PF-CN_1-3Cl
 PH-CN_1-2F	 PF-CN_1-4Cl
 PH-CN_2-4F	 PH-CN_2-4Br

2.2. Preparation of Ligand

Ligands consisted of ten compounds were depicted in Table 1. ChemBioDraw 13.0 ultra software package was used to draw each molecular structure of these ligands. These ligands must be kept in flexible. Energy minimization was required for each ligand for then the minimized structure were subsequently prepared with detected root of torsion. Flexible ligand with number of torsions were detected using Autodocktools 1.5.4 softwarre packages.

2.3. Docking of Pyrazoline

Autodock 1.5.4. software package was used to contruct the molecular docking. Lamarckian genetic algorithm (LGA) with the local minimization energy was used to search the best poses with the lowest binding energy. This is used to enable modification of the gene population. Docking was then performed with output clustered, it was selected based on the value of the root –mean-square-deviation (RMSD) tolerance pf 2.0 Å. The rank of docking poses were rank used the docking scores. The scoring function in Autodock software was used to predict the binding free energy between a ligand and the molecule receptor. Furthermore, the complex of protein-ligand with the lowest binding free energy is needed for analysis for each docking poses. The molecular visualization for 2D and 3D dimension of those complexes were performed using the Biovia Discovery Studio Visualizer.

2.4. Biological Assay

Biological activity was determined using MTT assay. It was begun with the MCF-7 cells preparation. 96-well plates are provided for seed the cellst with the size of cell density is approximately of 3 x 104 cells cm-3. Incubation was performed for 24 h for cell attachment and growth by adding samples with variation concentration. The next step is dissolving compounds with DMSO based on the required concentration. Subsequently, six desirable concentrations were prepared using PBS (phosphoric buffer solution at pH of 7.30 - 7.65). Different treatment was done for control, it dissolved only with DMSO. The incubation period of 48 h was terminated for the biological assay, it is then added with MTT reagent [3- (4,5-dimethyltiazol-2-yl) -2,5-diphenyl tetrazolium bromide; can also be referred to as thiazole blue] and can incubate continuously for 4 hours. The addition of the MTT reagent should be stopped when a solution containing SDS (sodium dodecyl sulfate) is added, while the required incubation period of 24 hours is also carried out. Microplate reader at 550 nm was used to read the opticacal density. A plot graph that explains the percentage of living cells are compared with the standard (%), it can be used to take the IC_{50} value and the biological activity value were taken when only PBS and DMSO are accepted, versus the concentration of the tested compound (µM). The IC_{50} value is the concentration required to inhibit the growth of 50% of infected cells. Each test and analysis was carried out three times and then the values were averaged.The cytotoxic activity of the isolated compounds 1-4 was evaluated against the MCF-7 breast cancer

cells according to a method described [11] and Cisplatin (IC_{50} 27.0 µM) was used as a positive control [12].

3. Results and Discussion

3.1. Docking of Pyrazoline

Generally, the main purpose of molecular docking are to identify the binding interaction between a ligand and specific receptor. In addition, it is also to identify the binding pose and the binding free energy. Binding pose is the best pose with the best and selective interaction and orientation between ligand and specific receptor. The scoring fucntion was used to predict and to estimate the binding affinities for then to generate the ligand poses in order to determine the best binding mode. The docking results for these ten pyrazoles are depicted in Table 2.

Table 2: Docking results

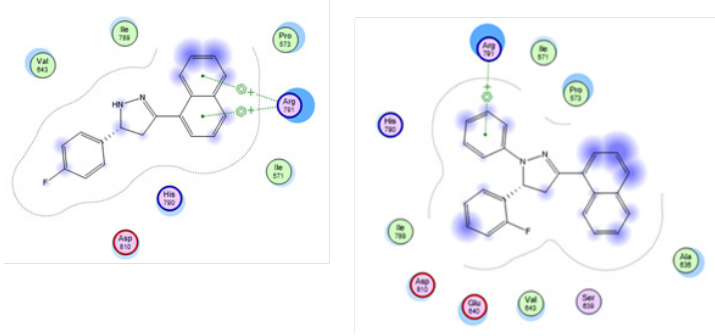
Cpd No	Binding free energy (kcal/mol)	Interaction		
		Hydrogen bond	Van der Waals	Hydrophobic
1	-10.98	Arg791	Asp810	His790, Arg791
2	-2.01	Arg791		His790
3	-5.13	Arg791	Glu640, Asp810	His790
4	-9.21	Arg791		His790
5	-8.97	His790	Asp810	Arg791
6	-8.64	His790	Asp810	Arg791
7	-5.47	Arg791	Glu640, Asp810	Arg791
8	-3.09	Arg791	Glu640	His790
9	-6.79	Arg791	His790, Asp810	
10	-4.58	Arg791	Glu640	His790

The best docking results are selected with some chriteria, they are lowest binding free energy and RMSD (root mean square deviation) less than two. Binding free energy is minimum energy is needed for the ligand to bind with the receptor. RMSD should less than two, it is indicated that the complex of ligand and protein is more stable compare than complex with RMSD is higher than two [13, 14]

According to the docking results, **PH CN1-4F** was explored some interactions such as hydrogen bonding interaction with Arg791. Van der Waals interaction is also observed with the important amino acid. The hydrogen bonding is constructed between nitrogen of ligand with residue Arg791. Van der Waals interaction was observed with the important residue Asp810. In addition, hydrophobic interaction were also observed with amino acid His790 and Arg791. The computed binding free energy from docking results of -17.65 kcal/mol, it is indicated that the existence of amino acid residue like Arg791, His790 presumably made this compound become active. In addition, the availability of hydrogen bonding, van der Waals and hydrophobic interaction are seem to play an important role in its antagonistic activity [15, 16].

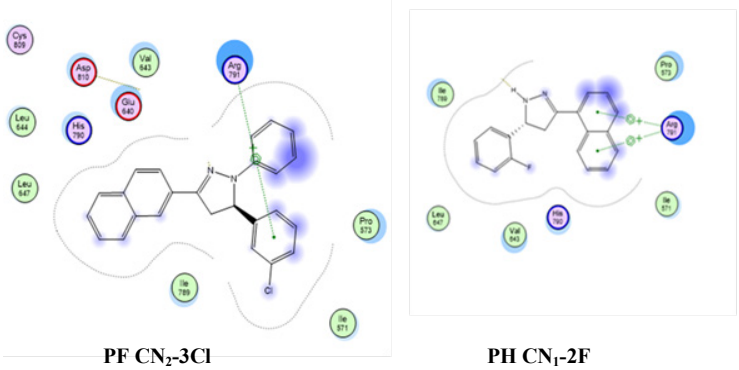
PH CN1-2F, this compound was also observed with one hydrogen bonding. Ligand was bind with Arg791 through hydrogen bonding, hydrophobic interaction was also conducted with amino acid residue His790. Unfortunately, there is no van der Waals interaction between this compound and amino acid. The computed binding free energy value of -10.98 kcal/mol. The absence of van der Waals interaction caused the binding free energy higher than PH-CN1-4F [17]. The spatial arrangement of PH-CN1-4F and PH CN1-2F are depicted in Figure 1.

PF CN2-3Cl and **PF CN1-2F** were also docked into MCF7 cell line. For **PF CN2-3Cl**, docking results shown that this compound was able to conduct the hydrogen bonding with Arg791, van der Waals interaction with Glu640 and Asp810. This compound was also able to conduct the hydrophobic interaction with His790, unfortunately this compound has high computed binding energy value of -9.21 kcal/mol. **PF CN1-2F** was observed hydrogen bonding and hydrophobic interaction with amino acid Arg791 and His790, respectively. The best docking pose for these compounds are depicted in Figure 2.



PF CN_1-4F **PF CN_1-2F**

Figure 1: the spatial arrangement for PH CN1-4F and PF CN1-2F



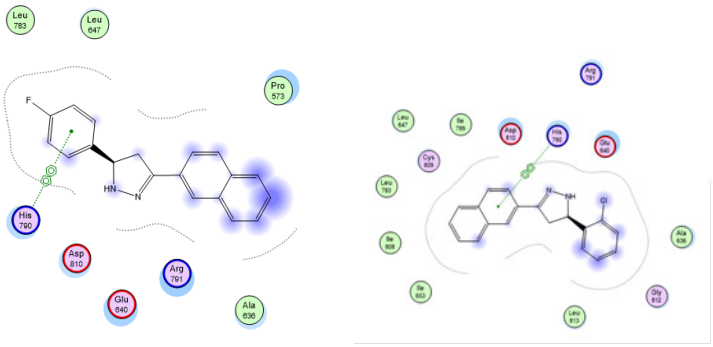
PF CN_2-3Cl **PH CN_1-2F**

Figure 2: The best docking pose for PF CN2-3Cl and PH CN1-2F

The docking results **PH CN2-4F** and **PH CN2-2Cl** were observed with another spatial arrangement like four previous compounds. Hydrogen bonding was exhibited with His790, van der Waals interaction with Asp810 and hydrophobic interaction with Ar791. This seem that those compounds are less active for inhibiting the MCF7 cell line. The spatial arrangement of **PH CN2-4F** and **PH CN2-2Cl** are presented in Figure 3.

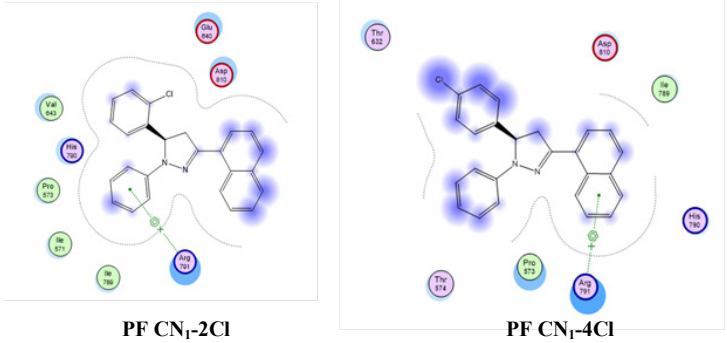
PF CN1-2Cl showed to have one hydrogen bonds (blue dashed line) with residue Arg791. In addition, van der Waals interaction was also found between ligand and residue Glu640 and

Asp810. Residue His790 showed interaction with the ligand through hydrophobic interaction suggesting the importance of this residue in the formation of hydrophobic binding pocket. Likewise, in the case of PF CN1-4Cl, one hydrogen bond was observed between the ligand and residues Arg791. This ligand also displayed van der Waals interaction and hydrophobic interaction via Asp810 and His790, respectively. Best pose for those compounds are presented in Figure 4.



PH CN_2-4F **PH CN_2-2Cl**

Figure 3. Spatial arrangement of PH CN2-4F dan PH CN2-2Cl



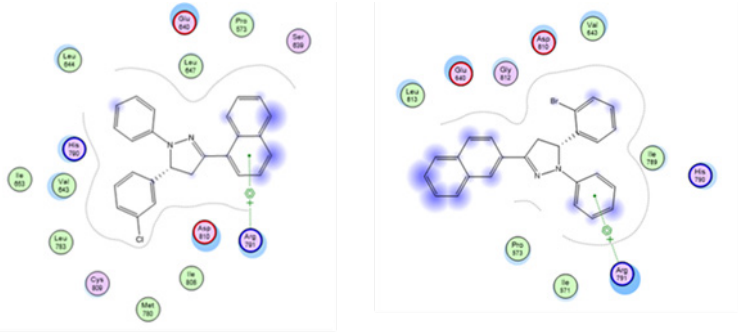
PF CN_1-2Cl **PF CN_1-4Cl**

Figure 4. Best pose for PF CN1-2Cl and PF CN1-4Cl

Our results showed **PF CN1-3Cl** and **PF CN2-4Br** exhibited Van der Waals interactions with Glu640 and His790. In addition, hydrogen bonding interaction was also observed between these two ligands and the residues Arg791, indicating another possible mode of interaction between these ligands and MCF7 cell line. Existance of van der Waals interaction with Glu640 and His790 indicated that this compound has anoter mode of interaction and it may caused this compund become not active compound. The spatial arrangement of those compounds are depicted in Figure 5.

3.2. Bioasssay of Pyrazoline

Invitro toxicity of pyrazole analogue compounds was determined using MTT assay method against MCF7 cell line. The biological assay for ten pyrazoles are presented in Table 3. Based on Inhibition concentration (IC_{50}), it was observed that there is only one active compounds i.e. **PH CN1-4F** with IC_{50} value of 61.22 µg/mL. This data was validated by data from computational calculations (i.e. docking) which is indicated with low value of the binding free energy of this compound. PH CN1-2F, PF CN1-2F, PF CN2-3Cl, PH CN2-4F, PH CN2-2Cl, PF CN1-2Cl, PF CN1-3Cl, PF CN1-4Cl and PH CN2-4Br were shown to have low inhibition activity against MCF7.



PF CN1-3Cl PF CN2-4Br

Figure 5. Best pose for PF CN1-3Cl and PF CN2-4Br

Table 3: Biological assay of pyrazoline anologue compounds

No	Compound	IC_{50} (µg/mL)
1	PH CN_1-4F	61.22
2	PF CN_1-2F	12739.17
3	PF CN_2-3Cl	6575.00
4	PH CN_1-2F	99.78
5	PH CN_2-4F	123.88
6	PH CN_2-2Cl	181.45
7	PF CN_1-2Cl	3665.75
8	PF CN_1-3Cl	32115.00
9	PF CN_1-4Cl	1507.88
10	PH CN_2-4Br	3374.75

4. Conclusion

Ten pyrazoline analogue compounds were docked and tested on MCF7 cell line using MTT assay. Based on docking results, compound PH CN1-4F explored three interactions with amino acid residues. These interactions are hydrogen bonding with Arg791, hydrophobic interaction with His790 and van der Waals interaction with Asp810. Biological assay was shown that this compound is also have big potency as breast cancer inhibitor with IC50 value of 61.22 µg/mL. Thus, this strategy can be used to identify new potent drugs as new inhibitor for breast cancer.

Conflict of Interest

The authors declare no conflict of interest.

Acknowledgment

This research was supported by the ministry of Research, Technology and Higher Education of the Republic of Indonesia, i.e. DRPM KEMENRISTEK for research scheme PDUPT

References

[1] M.S. Charpentier, R. A. Whipple, M. J. Vitolo, Boggs, J. Slovic, K. N. Tompson, L. Bhandary, S. S Martin. " Curcumin targets breast cancer steam-like cells with microtentacles that persist in mamospheres and promote reattachment " Cancer Res, **74**(4),1250-1260, 2014. https://doi.org/10.1158/0008-5472.CAN-13-1778.

[2] C. A. Lipinski, F. Lombardo, B. W. Dominy, and P. J. Feeney. "Experimental and computational approaches to estimate solubility and permeablility in

drug:discovery and development setting." Advanced Drug Delivery Reviews, **46** (1-3), 3-26, 2001. https://doi.org/10.1016/S0169-409X(96)00423-1

[3] T. Mitsudomi, Y. Yatabe, Y. "Epidermal growth factor receptor in relation to tumor development: EGFR gene and cancer". FEBS, **277**, 301- 308, 2010. https://doi.org/ 10.1111/j.1742-4658.2009.07448.x.

[4] X. Y. Meng, H. X. Zhang, M. Mezei, M. Cui. 2011. "Molecular Docking: A Powerful Approach for Structure-Based Drug Discovery". Curr Comput Aided Drug Des. **7**, 146-157, 2011. https://doi.org/10.2174/157340911795677602.

[5] S. E. Wala, A. M. Neama, M. K. Emad, K.. Mahmoud, M. M. Mounier. "Synthesis, Biological Evaluation and Docking Analysis of Some Novel Quinazolin Derivatives as Antitumor Agents" Iranian J Pharm Res, **15**, 179-196, 2016

[6] A. Baldi. "Computational Approaches for Drug Design and Discovery: An Overview" Sys Rev Pharm, **1**(1), 99-105, 2010. https://doi.org/10.4103/0975-8453.59519

[7] Z. Shu-Feng, and Z.Wei-Zhu. "Drug Design and Discovery: Principles and Applications." Molecules, **22**, 279-284, 2017. https://doi.org/ :10.3390/molecules22020279

[8] S. H. Reich, S. E, Webber. Structure-based drug design (SBDD): Every structure tells a story. Perspectives in Drug Discovery and Design **1**, 371–390, 1993. https://doi.org/10.1007/BF02174536

[9] C. A. Anderson. The Process of Structure-Based Drug Design. Chemistry and Biology, **10**(9), 787-797. https://doi.org/10.1016/j.chembiol.2003.09.002

[10] P. Skehan, R. Storeng, D. Scudiero, A. Monks, J. McMahon, D. Vistica, D. J. T. Warren, H. Bokesch, S. Kenney, R. M. Boyd. "New Colorimetric Cytotoxicity Assay for Anticancer-Drug Screening" J. Natl. Cancer Inst, **82**, 1107-1112, 1990. https://doi. Org/10.1093/jnci/82.13.1107

[11] Y. E. Hadisaputri, D. Pharm. T. Miyazaki, S. Suzuki, T. Yokobori, T. Kobayashi, N. Tanaka, T. Inose, M. Sohda, H. Kuwano. " TNFAIP8 Overexpression: Clinical Relevance to Esophageal Squamous Cell Carcinoma". Ann. Surg. Oncol, **19**, S589-S596, 2012. https://doi.org/10.1245/s10434-011-2097-1

[12] O. Unsal-Tan, T.Tüylü Küçükkılınç,b B. Ayazgök, A. Balkan and K. Ozadali-Saria. "Synthesis, molecular docking, and biological evaluation of novel 2-pyrazoline derivatives as multifunctional agents for the treatment of Alzheimer's disease". Medchemcomm., **10**(6), 1018–1026, 2019. https://doi: 10.1039/c9md00030e

[13] F. Turkan, A. Cetin, P.Taslimi, S. Halide S. K. İ. Gulçin, Synthesis, characterization, molecular docking and biological activities of novel pyrazoline derivatives. Archiv der Pharmazie. **352**, 6, 2019. https://doi.org/10.1002/ardp.201800359

[14] N. Frimayanti, V. S. Lee, S. M. Zain, H. A. Wahab, N. A. Rahman. " 2D, 3D QSAR and pharmacophore studies on thiazoline-4-carboxylic acid derivatives as neuraminidase inhibitors in H3N2 influenza virus" Med. Chem. Res. **23**, 1447-1453, 2014. https://doi.org/10.1007/s00044-013-0750-x

[15] N. Frimayanti, B. Iskandar, M. Yaeghoobi, C. H. Han, S. M. Zain, R. Yusof, N. Arahman. " Docking, synthesis and bioassay studies of imine derivatives as potential inhibitors for dengue Den2 NS2B/NS3 serine protease". Asian Pac J Trop. Dis. **7**(12), 762-766, 2017. https://doi.org/10.12980/apjtd.7.2017D7-177

[16] M. Kumari, S. Chandra, N. Tiwari, Subbarao. "3D QSAR, pharmacophore and molecular docking studies of known inhibtors and designing of novel inhibitors for M18 aspartyl aminopeptidase of Plasmodium falciparum". BMC Struc. Biol. **16**(12), 1-11, 2016. https://doi.org/ 10.1186/s12900-016-0063-7.

ASTES

Advances in Science, Technology and Engineering Systems Journal Vol. 5, No. 5, 127-136 (2020)

www.astesj.com

ASTESJ

ISSN: 2415-6698

The Ludocreative Expression for the Production of Texts in Children of Early Education

Giuliana Gaona-Gamarra[1], Brian Meneses-Claudio[2,*], Avid Roman-Gonzalez[2]

[1]*Faculty of Humanities Education and Social Sciences, Universidad de Ciencias y Humanidades, Lima, 15314, Perú*

[2]*Image Processing Research Laboratory (INTI-Lab), Universidad de Ciencias y Humanidades, Lima, 15314, Perú*

ARTICLE INFO

Article history:
Received: 13 July, 2020
Accepted: 14 August, 2020
Online: 09 September, 2020

Keywords:
Texts' Production
Ludocreative Expression
5-year-old Children
Improving Scores
Evaluation to Children

ABSTRACT

The text's production carried out in this research aimed to 5-year-old children from the IE 555 Inmaculada Concepción, under the modality dictated to adult, had a design and application of 22 sessions during three months with the experimental group. On their methodological approach was based on the expression ludocreative, articulating the written experience jointly with the art expression in the pedagogical fields of plastic, musical, scenography and corporal expression, propitiating the children´s prominence through a playful tone with deductive situations in the learning processes. For this, a quasi-experimental design was considered, with a control group of 15 children and an experimental group of 20 children. After selecting the groups in an intentional non-probabilistic manner, the questionnaire was applied to assess the production of texts to the respective groups. The results indicate the effect of the application of the proposal. This could be evidenced in the establishment of differences in the pre-test and post-test of both groups, and differences in the scores between both groups. In particular, it was found that the difference between pre and post-test was greater in the experimental group, obtaining a fundamental achievement to continue deepening in this playful and creative within the framework of pedagogical innovation.

1. Introduction

The ludocreative expression has as a main purpose to develop a subject from its own cultural environment, affirming its identity, without the induction of predetermined models with the aim of highlighting the role of doing and feeling in order to learn and think.

The research presented in [1], it mentions that " To learn to think, it is necessary to exercise our limbs, our senses, our organs, which are the instruments of our intelligence". The creativity links with various experiences that invite to the symbolic imaginary from the interactions of the subject-objects-subjects through the dimensions of plastic, musical, corporal, scenography and cultural expression, which give new transformative perspectives since they articulate aesthetic and cognitive values for the systematization of new concepts [2].

The research presented in [3], this research consists of a playful strategies action plan that aims to develop oral expression skills and abilities in 4-year-old children at the early education level. Due to the problem that was found in them, the low level of oral expression evidencing in practice, the little participation and initiative to express themselves, pronounce words, sounds and ability to express themselves. To validate this research work, the hypothesis to defend is the action plan "Dilo Jugando" is developed and applied, based on the development of playful strategies, then they will significantly increase oral expression in 4-year-old boys and girls. from the early education level of the kindergarten 1861 –October 9– Huamachuco Sánchez Carrión in 2015, based on the theories as in [4] by Piaget and Vygotsky and the playful strategies of Raimundo Dinello. The results obtained in the application of the action plan based on the development of recreational strategies, significantly demonstrate the solution to the problem, achieving a significant increase in the level of oral expression. These skills helped children to achieve better oral expression in the abilities and skills to express themselves, pronounce words, develop phonology, syntax, semantics, speaking, listening, and self-expression and learning.

*Corresponding Author: Brian Meneses-Claudio, Sr., +51 1 950159924
bmeneses@uch.edu.pe

The research presented in [5], this research responds to a qualitative-quantitative approach, since, for the analysis of the information and its subsequent organization, techniques were applied that allowed detailing the strategies used by the teacher in the classroom for the development of the oral language. The research work modality is socio-educational and due to the depth level, it is correlational descriptive in order to determine the relationship between both variables, for which the Pearson Correlation Coefficient was applied, which is 0.63. The Cronbach's alpha reliability coefficient allowed a reliability of 0.84 to be obtained in the observation sheet and in the questionnaire with a reliability of 0.85. As conclusions, it was found that most teachers do not apply ludocreative strategies for oral development. And finally, a proposal of activities framed in the dimensions is made: linguistic games, dramatic games and the traveling story, carried out through play and playful as an integrating element of learning. Among its results, it can be affirmed that ludocreative strategies could help in the development of oral language in children of the Early Education Sub level.

The research presented in [6], this research developed a research work entitled: "Producing texts at the beginning of schooling: the production of oral texts, dictated to an adult and written, in the 5th and 1st grade room. Comparison between different pedagogical approached". This comparative study refers to the knowledge of the written language that children of these ages. They relate the knowledge made by them with the type of teaching proposals. Among the results, the children's narrative capacity was evidenced from their different levels of construction of the conventional writing system, the ability to produce oral, dictated and written texts, and knowledge of the narrative genre. Likewise, differences in textual production were observed in two teaching contexts (formal and constructivist); demonstrating greater achievements in children's learning in the constructivist approach.

The research presented in [1], it mentioned in his book "Emilio o la Educación", that in order to learn to think it is necessary to exercise our limbs, our senses, our organs, which are the instruments of our intelligence. That is why the game that etymologically means free movement, is the essence that leads to this immediate pleasure and joy that engages children in the development of all their abilities.

Dinello and Huizinga cited by [7] states that playful is not limited to the game or vice versa since playful is a much more complex concept that encompasses the man in its entirety. The playful activity dynamizes the educational processes of childhood, since it allows creating significant scenarios for the development of competence in a comprehensive and harmonious way. Those gratifying experiences for human development are linked in turn with creativity through various experiences that invite to the symbolic imaginary with the interactions of the subject-objects-subjects. In the ludocreative expression, the following pedagogical fields are considered through areas of expression related to the arts: plastic expression, musical expression, body expression, scenography expression and the area of cultural initiation, which allow new transformative perspectives since they articulate aesthetic and cognitive values for the systematization of new concepts. As [8] affirms, articulation is a possibility of transforming cognitive acquisitions and emotional states into different domains of thought and application possibilities, since an evolution of the imaginary and understanding of the symbolism of expression is evident.

In Chapter II, the materials and methodology used to carry out the study, the hypotheses and variables, as well as the distribution of the population and sample, based on certain criteria; data collection and processing techniques are also pointed out. In chapter III, the results and analysis are presented (it is consolidated with the psychometric analysis of the instrument used and the processing and analysis of the results through inferential statistics, in such a way that it evidences the aspects of measurement and impact of the object program of this research). In chapter IV, the discussions of the research are shown, also the revalidation of the results shown in the research work. Finally, in chapter V, conclusions and some recommendations on the results obtained through the application of the sessions developed with the children in the applied program are presented, which can be a reference for the development of future research in this area.

2. Methodology

This research has been carried out to improve the production of texts in 5-year-old children from IEI 555 Inmaculada Concepción, based on the teaching-learning methodology of the ludocreative expression.

This practice promoted the development of text production, with respect to planning, textualization, and revision in messages, stories, riddles, poetry.

In this way, the children during the planning organized their ideas about the type of text and its purpose, in the textualization, they created the information, through the modality dictated to an adult, and in the revision a rereading was made to make the improvements, through the opinion and the exchange of ideas.

Subsequently, once the proposal was completed, the publication of their creations in craft books was made, taking into account his drawings and a spontaneous writing of lines and graphics, being located in the library sector.

Regarding the context, it should be noted that I.E.I. N° 555 Inmaculada Concepción is located in the Santiago de Surco district, province and department of Lima. The geographical scope corresponds to the urban area. The I.E.I. has a morning and afternoon shift. The afternoon shift was considered for the present research, with a sample of 22 children, whose age ranges are from 5 to 6 years old.

For the evaluation of the children's progress, a questionnaire was made that was completed by the teacher in charge of the group, in addition to determining an evaluation range for them.

2.1. Population and Sample

The population consisted of 210 students from the institutions distributed in 4 classrooms on morning and afternoon shifts, respectively. It should be noted that educational institutions are state, of medium socioeconomic level from the Santiago de Surco district, UGEL 07.

The sample was consisted of 20 children of both sexes in the experimental group of IEI 555 Inmaculada Concepción and the control group was made up of 15 children of both sexes of IEI

Nuestra Señora del Carmen, all with an early level of education between 5 and 6 years old.

For this, inclusion criteria were taken into account considering the evolutionary development of children according to their age, considered in the respective checklist, as well as the permanence of attendance at the learning sessions, in terms of the exclusion criteria, it should be noted that the sample did not take into account children under 5 years old and with special educational needs.

2.2. Evaluation Criteria

For the application of the text production assessment questionnaire, some basic conditions regarding the arrangement of the environment were envisaged, ensuring that it is comfortable, illuminated and without major distractions for the child. In addition, the necessary material for the completion of the questionnaire was previously organized, such as: sheets, notebook, pencil, pen, six images in sequence to be organized freely by the children for the story creation, an apple for the assessment of the riddle creation area and a flower puppet for the creation of poetry.

Before starting with the questionnaire, an atmosphere of relaxation and trust was provided to the children, in order to facilitate interaction with each one, making a motivating activity.

In addition, some evaluation criteria were defined to provide a preliminary result for each of the variables of the text production. These were the criteria:

- Clarity (C): It is written in appropriate and precise language.
- Performance (P): It is adequate, useful, consistent, appropriate or relevant according to its purpose and function.
- Sufficiency (S): The items are sufficient per analysis factor.
- Objectivity (O): It is in accordance with the proposed objectives.

To generate the statistics and verify the development of the control and experimental population, a scoring system was created following certain criteria, these are the following with their corresponding scores:

- Excellent (4): Evaluation criteria are met.
- Good (3): Meets the criteria, needs minimal modifications.
- Regular (2): Meets the criteria, needs major modifications.
- Poor (1): The evaluation criteria are not met.

The evaluation was carried out independently for each child based on his/her progress and development of the different activities proposed.

2.3. Text Production Questionnaires

The assessment questionnaire is made up of 4 subtests, whose total score is 24 points and whose 16 items are distributed as follows:

Text Production Steps with a total of 8 items, as shown in Table 1: Planning (PL) 3 items, textualization (T) 1 item, revision (R) 1 item, publication (P) 1 item; whose general value obtained is 8 points.

Types of literary texts with a total score of 6 points, having 4 items, as shown in Table 2: Story creation: planning (PL) and textualization (T) 2 items, revision (R) 2 items.

Table 1: Text Production Steps Evaluation Chart (English Version)

I. STEPS IN THE PRODUCTION OF TEXTS	**CRITERIA**			
	C	P	S	O
PLANNING (PL) **The teacher writes verbatim what the child says**				
1 a. Who would you like to write to?				
1 b. What would you like to write to him or her?				
1 c. What would you write to him or her for?				
TEXTUALIZATION (T) **The teacher writes verbatim what the child says**				
2 a. What is the message you want to communicate? (Thank him or her, make an order, or another.)				
REVISION (R) **The teacher reads the text produced for the child to decide whether or not he or she wants to modify it.**				
3 a. Do we leave the message like that or would you change it?				
PUBLICATION (P) **The teacher writes verbatim what the child says. If the child has the initiative to produce another presentation of the text, they are provided with consumable materials (colors, sheets, stickers.)**				
4 a. How will you get this message to "x"? (friend, parents or another person)				

Table 2: Story Creation Evaluation Chart (English Version)

II. TYPE OF TEXTS: LITERARY	**CRITERIA**			
	C	P	S	O
A. STORY CREATION **The teacher presents six images; the child organizes them and creates a story.** **The teacher copies verbatim what the child says.**				
PLANNING (PL) AND TEXTUALIZATION (T)				
1. How would you create a story from these images?				
2. What title would you give it?				
REVISION (R)				
3. Would you change any part of the story?				
If the answer is yes: 4. Which one?				

Creation of a riddle with a total score of 5 points, having 3 items, as shown in Table 3: Planning (PL) and textualization (T) 1 item, revision (R) 2 items.

Table 3: Riddle Creation Evaluation Chart (English Version)

B. CREATION OF RIDDLE	**CRITERIA**			
	C	P	S	O
PLANNING (PL) AND TEXTUALIZATION (T)				
1. How would you create a riddle from this object?				
REVISION (R)				
2. Would you change any part of the riddle?				
If the answer is yes: 3. Which one?				

Poetry Creation with the total score of 5 points, having 3 items, as shown in Table 4: Planning (PL) and textualization (T) 1 item, revision (R) 2 items.

Table 4: Poetry Creation Evaluation Chart (English Version)

C. POETRY CREATION	**CRITERIA**			
	C	P	S	O
PLANNING (PL) AND TEXTUALIZATION (T)				
1. How would you create poetry for this puppet?				
REVISION (R)				
2. Would you change any part of the poetry?				
If the answer is yes: 3. Which one?				

The 16 items correctly resolved in the four corresponding sections, were organized with the total results.

2.4. Data Collection

The text production test mentioned above was applied to the experimental group, before and after the experiment carried out (Teaching module – Create and Have Fun based on the ludocreative expression). Likewise, the same test was carried out on the control group, to measure if the level of text production in both groups was similar or if there were differences.

It is worth mentioning that the application of the interview was semi structured, since it was adapted to the children through the questionnaire, which, although there were pre-established questions, were interspersed with some of the open type during the dialogue with the children. The interview was conducted in a quiet and neutral place in the I.E.I. (the office and / or library of the Inmaculada Concepción educational center were organized to be a relax place for children). In the case of the control group, it was carried out in a neutral place in the classroom, which the other children did not have access to, and on some other occasions in the management office.

The "Create and Have Fun" module has 22 learning sessions and are designed to achieve a text production competition. They were carried out between 2 to 3 times per week in an approximate time of 50 minutes, between the months of June to September of the year 2017, taking into account the proposal of the ludocreative expression. [9]

For the development of the learning sessions, the suggested materials and spaces in the classroom, a psychomotor environment, a library environment and a playground were organized.

Both group and individual activities were carried out with the support of the classroom tutor and an assistant to carry out each of the sessions.

It worked through processes, the first being the Playful Introduction, as shown in Figure 1, beginning with an initial game where children are required to move around the classroom, thus recognizing their environment and their classmates.



Figure 1: Beginning Movement Game

It is about the children trying to produce texts through their memories and imagination of the situations that they have gone through. In session 9, it was called "Our best vacation times" where they dramatized an imaginary trip, as well as shown in Figure 2.



Figure 2: Dramatic Representation Expression simulating an Imaginary Trip

The next step is to do the experimentation, being the group textualization with children's drawings, as seen in Figure 3; this step requires a bit more time because it is a real-time capture of children's ideas. As can be seen in Figure 3, children are required to work as a group in order to speed up and also create complementary stories and ideas.



Figure 3: Group Textualization with Children's Drawings

At the end of the session, a plenary was held to observe the different productions, as shown in Figure 4.



Figure 4: Revision: Plenary of the Creations made

On the other hand, at the end of the pedagogical proposal, the children in the environment of the library of the Educational Institution listened to the oral narration of some of their productions and later, these were located in the library sector of the classroom, this helps the children look their text productions and the progress of their works, some examples of these works were books, drawing and compositions as shown in Figure 5.



Figure 5: Group and Individual Book and Composition of Rhymes

3. Results

The purpose of this research was to determine how the design and application of the methodological proposal based on the ludocreative expression influences the production of texts and each of its planning, textualization and revision aspects, by 5-year-old children. For this, various experiences were carried out in which the studied group participated in playful situations in different learning fields.

The results of the statistical analysis revealed that before developing the intervention, the performance of children in both the control group (Nuestra Señora del Carmen) and the ex-experimental group (Inmaculada Concepción) in the evaluated steps of text production, such as: planning, textualization and revision in its different types: message, story, riddle and poetry, it was equivalent and therefore its performance was similar with which these could be subjected to subsequent comparisons. In this sense, it was found that the groups had a different performance related to the type of intervention they received (intervention of the ludocreative expression methodology and non-intervention), as can be seen in Table 5 and Table 6 (Shapiro Wilk Test) the results obtained from the Entrance and Exit tests.

Table 5: Shapiro Wilk Test for Entrance Test Scores

Description	Group	Statistic	Gl	p value
Text Production	Control	0.965	15	0.776*
	Experimental	0.892	20	0.03**
Planning	Control	0.949	15	0.505*
	Experimental	0.903	20	0.047**
Textualization	Control	0.905	15	0.114*
	Experimental	0.955	20	0.457**
Revision	Control	0.499	15	0.000**
	Experimental	0.672	20	0.000**

*P > 0.05; **P < 0.05

The results of the Shapiro Wilk normality test allow to establish that in the control group the scores for text production, planning and textualization fit a normal distribution ($p>0.05$) and the revision score does not fit a distribution normal ($p<0.05$), while in the experimental group the text production, planning and revision scores do not fit a normal distribution ($p<0.05$) and the textualization score fits a normal distribution ($p>0.05$).

Table 6: Shapiro Wilk Test for Exit Test Scores

Description	Group	Statistic	Gl	p value
Text Production	Control	0.848	15	0.016**
	Experimental	0.929	20	0.148*
Planning	Control	0.864	15	0.028**
	Experimental	0.887	20	0.024**
Textualization	Control	0.906	15	0.116*
	Experimental	0.857	20	0.007**
Revision	Control	0.499	15	0.000**
	Experimental	0.803	20	0.001**

*P > 0.05; **P < 0.05

The results of the Shapiro Wilk normality test allow to establish that in the control group the scores for text production, planning and revision do not fit a normal distribution ($p<0.05$) and the textualization score fits a distribution normal ($p>0.05$), while in the experimental group the planning, textualization and revision scores do not fit a normal distribution ($p<0.05$) and the text production score fits a normal distribution ($p>0.05$).

Through of the preliminary data obtained, the mean and standard deviation of the Entrance Test and the Exit Test were evaluated in both Control and Experimental cases, these results are shown in Table 7 and Table 8.

Table 7: Mean and Standard Deviation of the Entrance Test

Description	Group	Mean	Standard Deviation
Text Production	Control	8.80	2.76
	Experimental	9.60	2.56
Planning	Control	6.67	1.72
	Experimental	6.60	1.19
Textualization	Control	6.07	1.91
	Experimental	6.75	1.45
Revision	Control	0.20	0.41
	Experimental	0.65	1.04

Note: Control = 15, Experimental = 20

Table 8: Mean and Standard Deviation of the Exit Test

Description	Group	Mean	Standard Deviation
Text Production	Control	11.07	2.63
	Experimental	16.35	2.30
Planning	Control	8.40	1.77
	Experimental	11.55	1.00
Textualization	Control	7.53	2.13
	Experimental	11.40	1.14
Revision	Control	0.20	0.41
	Experimental	1.30	1.59

Note: Control = 15, Experimental = 20

In the exit test of the text production, the results demonstrate the effect of the methodological proposal based on ludocreative expression in the 5-year-old children of IEI Inmaculada Concepción, who have gradually become familiar with it, where their productions were accompanied by images (drawings, collage, paintings of different types) of shorts dramatizations (role plays, puppet play, symbolic representations, motor games, body expression) and musical games. It is observed that these experiences allowed them to learn to discover, recognize and in some cases, to use the signs of written language, the need arose to decipher the medium, to appropriate its signs [10]. Which is a good indicator since it sees that this process has opened up the possibility of free expression, exchange and contrast of ideas with their classmates, presenting an investigative attitude, curiosity about their surroundings, respect for their own achievements and those of others.

It should be noted that at first, there were no greater notions about some types of productions such as the use of poetry, riddles and tongue twisters, compared to the stories or messages which they were more used. Therefore, it deserves that these fields can be deepened and developed specifically and/or with a longer application time for better effects.

It can be verified that the scores presented by the experimental group demonstrate a considerable improvement in their performance as a result of the pedagogical intervention through the proposal of the methodology of ludocreative expression. And this was significantly higher than the performance presented by the control group. So, it can be affirmed that the purpose of this research has allowed, offering children the opportunity to experience, discover, shape their expectations on their own initiative, in order to develop their potential, develop own thinking and creative attitudes in dialogue with their classmates and those who have accompanied this exchange process through the proposal. There is no doubt that in this interim search is to recognize in each child a subject of expression and creation, so that it is recognized in its existence and in its possibilities of learning. Furthermore, being familiar with creativity, they affirm themselves in flexibility, spontaneity and originality, qualities that [11] mentions, they are necessary to insert themselves in a questioning way in a world characterized by the sense of efficiency and utility.

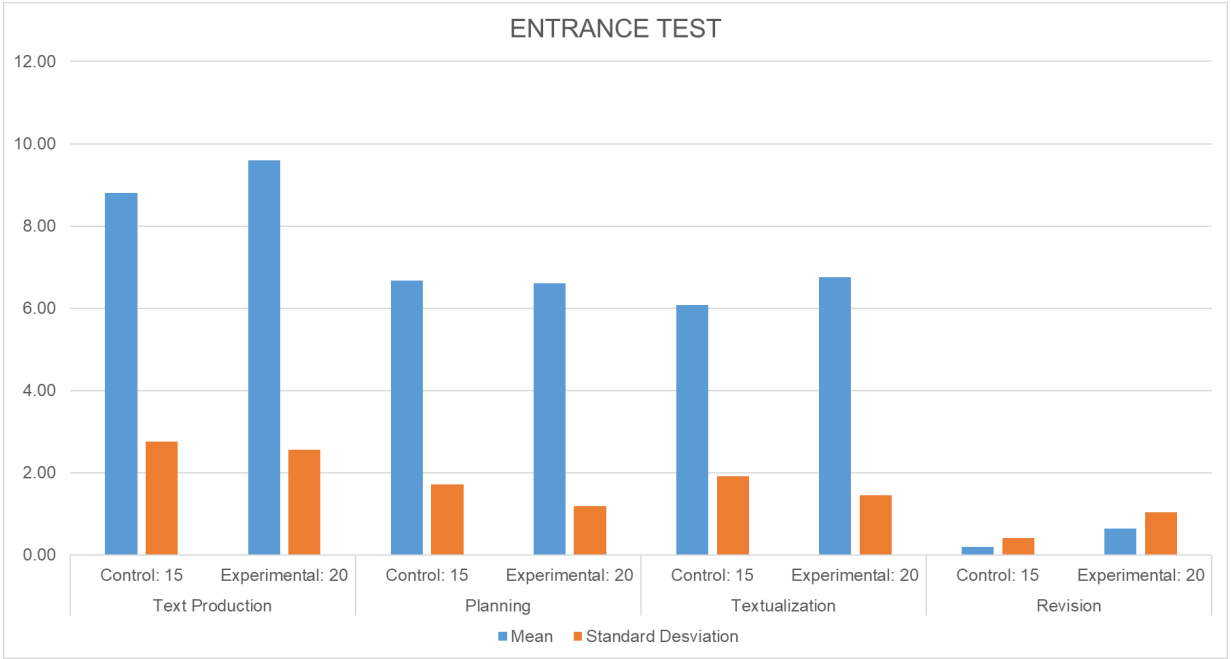
Creating an environment conducive to continued discovery [10] has been quite an assumed challenge, since it fosters open situations, an unusual situation in the classroom, since children are often used to following instructions and indications, often biasing their own initiatives or proposals, this methodology has allowed to open gaps to be considered as protagonists, discovering playful experiences and interacting with their classmates and materials. In addition, it has had the support of the teacher and classroom assistant who accompanied this process with their active participation through dialogues, questions, contributions of information, and openness to the various forms of art expression (painting, modeling, body expression, music, dramatization, building) to finally systematize children's opinions towards the objective to be achieved about the different types of text productions (messages, poetry, stories, riddles, among others) as stated by [8] the child with its fantasy, by imitation, begins to understand and use the symbols of communication that later allows him or her to consolidate a conceptual elaboration., in this case through the verbalization of the various texts that the child formulates, learning takes place with a natural sequence, which makes from curiosity to understanding. On the other hand, it should be noted that children concluded this process of text production with the craft publication of their own books, which, according to [11], enables an aesthetic perception and a physical relationship from the tactile, visual and olfactory aspects. Consequently, from the perspective of Education through Art, expression rather than a successful product is a process, which is coupled with respect to the identity and culture.

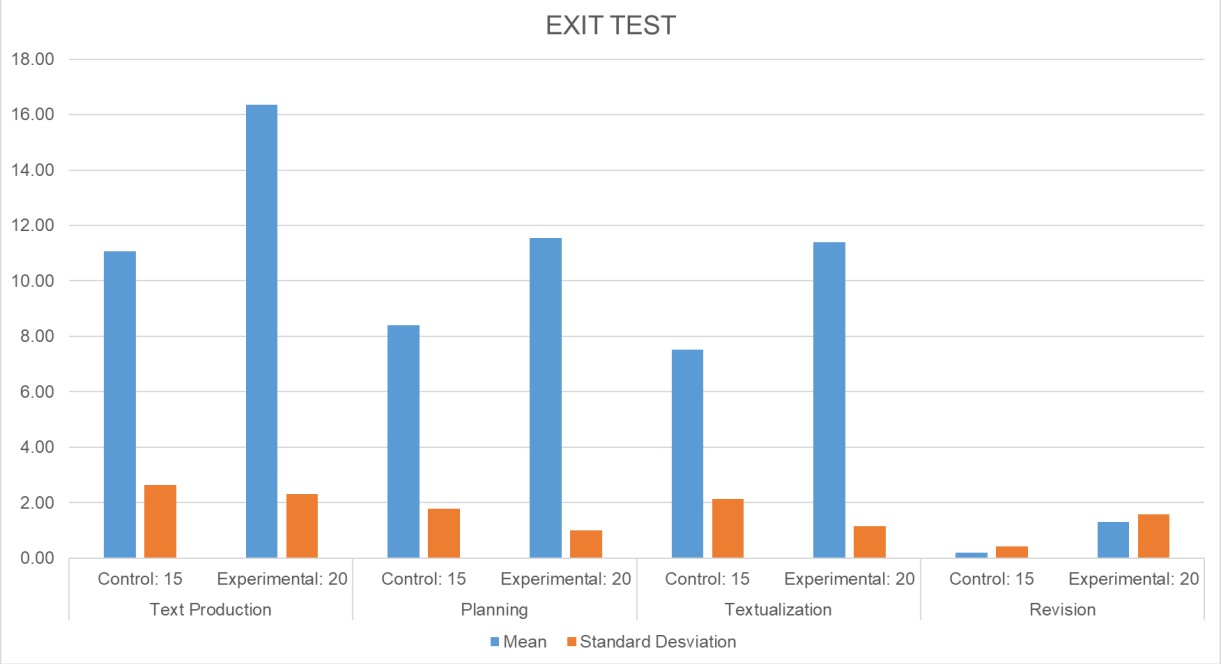
The results of the statistical analysis allow to verify that the application of the teaching-learning methodology based on the pedagogy of ludocreative expression significantly improves this

aspect, where the children of the experimental group (Inmaculada Concepción) get a higher score in the production of texts compared to the children of the control group (Nuestra Señora del Carmen), demonstrating that the planning of the texts by the 5-year-old children of IEI 555 Inmaculada Concepción in the district of Santiago de Surco significantly improves compared to IEI 086 Nuestra Señora del Carmen from the Santiago de Surco district, for this, the children participated through expression activities so that from that experience, they prepared to tell their emotions and ideas about themselves and the environment, intuitively using various techniques and materials, as stated by [12] thus giving the aspect of planning that answer the questions like: Who would you like to like to send this "x" (message, story, poetry) to? thus determining the recipient, what do I want to express? and why?, thus focusing on the subject and the purpose. From this perspective, the contributions of the ideas of the children that worked individually and in groups are visualized, contributions that can be sustained in a group debate through dialogue.

Regarding the textualization as shown in Table 8, the teaching-learning methodology based on the pedagogy of ludocreative expression significantly improves the textualization by 5-year-old children of IE 555 Inmaculada Concepción in the district of Santiago de Surco. In relation to this [13], points out that the expression of the narrative qualities makes mention of the attitudes towards the reproduction of information, demonstrating the rhetorical qualities of children in which they express their needs, emotions, interests, ideas and experiences using sentences understandable to others, varying the intonation according to their intention; organizing their ideas and asking what they did not understand, participating in oral communication situations, generally focusing on the subject and interpreting what other people say, identifying explicit information and making deductions, they also enjoy listening to texts of simple structure in which known words predominate and relate what was heard in their own words, the latter is evidenced in group productions.

In the production of texts, the revision that can see the effects achieved in the experimental group (Inmaculada Concepción) obtain a higher score although differences that are not significant with respect to the children in the control group (Nuestra Señora del Carmen) which it can be verified that the application of the teaching-learning methodology based on the ludocreative expression improves the revision of the production of texts by children of 5 years of age, although to a lesser degree compared to the other aspects of planning and textualization. In this sense, these data indicate that there were certain difficulties at the time of applying this aspect, due to it requires a more detailed evaluation, especially if it is developed individually. According to the approaches made by [13], it has to be analyzed from a perspective in which the study of the psychological and pedagogical conditions of learning are basic to understand the results of literacy and the results are important to understand the differences, precisely in the revision, particularities are observed in which more precise models of the processing and understanding of what is written must be reached, going beyond the description of interesting evolutionary situations. For this, the role of metacognition must be reevaluated by providing precise questions that allow them to question children about their own productions, originating a dialogue to contrast their initial hypotheses with new ideas that emerge from the rereading, based on this, the scope mechanism should be rethought to improve this process, also considering that the level of metacognition in 5-year-old children will go evolving as they grow and that is evident in "children's awareness of their purpose in reading, how to proceed to achieve those purposes and how to regulate the process through self-regulation of understanding. Metacognition is applied to reading when one is aware of the behavior during reading and the appropriate use of reading strategies to facilitate or remedy failures during its execution" [14].





The need for an explanation of individual differences both in excellence and regarding to difficulty cannot be ignored, in this sense it can be seen that children have proven to be so constructive in relation to writing and written language, starting with the orality, they have also become familiar with the different types of texts, recognizing their structure and particularities, so it should be perceived that after textualization, this aspect can be deepened in a particular way depending on what the child want communicate, remaining the main idea, identifying the repetitions or omissions, being necessary to promote other alternatives of mediation scope of work in the classroom and that can also be extended at home. On the other hand, it coincides with the proposal developed by [15] when he mentions that in the revision, the text is refined, and in which it would be convenient to verify or reject the existence of any difficulty, since in the case of children, it observes that several of them are in the process of making coherent texts both in the content and in the structure of the same, and there have also been cases in which children have not required to use this revision process because they have responded to their true intentions, in this sense, are varied communicative situations.

Finally, Figure 6 and Figure 7 show the bar graph of the mean and standard deviation of the entrance test and the exit test, respectively. It should be noted that in these diagrams the difference between the results of the control and experimental groups can be seen more clearly.

4. Discussion

This research confirms the importance of promoting playful activities to generate the production of texts in children, allowing to stimulate, develop and enrich the potential of oral and written language.

The application of the ludocreative expression methodology allowed the enrichment of the components of text production (messages, poetry, stories, riddles) in the children from IE 555 Inmaculada Concepción.

Text production is significantly increased by natural development, as was the case in the control group. However, after applying the ludocreative expression methodology, it was observed that almost all of the children exposed to it managed to achieve superior performance in the use of its components, considering the respective steps in the production of texts. As well as, statistically significant differences are shown before and after the application of the program in the experimental group.

Likewise, there are statistically significant differences in the children of the experimental group compared to the children of the control group, which is possible to visualize the effects of the activities of ludocreative expression in relation to the children belonging to the experimental group.

5. Conclusions

The application of the teaching-learning methodology based on the ludocreative expression significantly improves the production of texts, where it is evident that the control group obtained a score of 9.53 while the experimental group reached 24.35. Based on those results, the effect of the " Create and Have Fun" module is demonstrated.

Regarding planning, the control group has a score of 9.83, while the experimental group is 24.13, which shows a significant improvement in 5-year-old children from IE 555 Inmaculada Concepción compared to IE 086 Nuestra Señora del Carmen from the Santiago de Surco district.

Regarding textualization, the control group presents a score of 9.60, while the experimental group is 24.3, which shows that the experimental group has a greater and significant increase in relation to the control group.

The application of the teaching-learning methodology based on the ludocreative expression does not significantly improve the revision, which shows an average range of 14.20 in the control group, while in the experimental group a 20.85 is shown, which shows that it is necessary to implement this dimension to get better results.

The importance of new forms of teaching is important in Peru and is highlighted when it comes to children. Currently, the Ludocreativa education has been applied in few educational institutions in Peru, that is why in this study, the importance of applying this methodology will be corroborated, it would improve teaching in children in the majority and also that it would enhance their imagination. In this research work, the difference between the control and experimental groups is shown, as a conclusion there is a significant difference between the entrance and exit tests in the production of texts.

Conflict of Interest

The authors declare no conflict of interest.

Acknowledgment

We want to thanks to Dr. Raimundo Dinello, who opened up the possibility of growth on a personal and professional level through each of the exchanges of the ludocreative forums.

Also, we would like to thank IE 555 Inmaculada Concepción and IE 086 Nuestra Señora del Carmen, who, through their managers and teaching staff provided the best of logistical and pedagogical provisions for the implementation of this research.

References

[1] M. Izquierdo, Emilio o la educación (Rouseauu, trans), Editorial Verbum, 2019.

[2] L. Echavarría, Y. Rivera, and M. Segovia, "Ludoteca: Villa Kids. For the development of social skills of children from 4 to 7 years old at Colegio Gimnasio Moderno Villa del Norte," Bachellor Thesis, Universidad de Cartagena, 2016.

[3] M. Villena, "Action Plan "Create and Have Fun" based on playful strategies to raise the level of oral expression in 4-year-old children from J.N. N° 1861-9 de Octubre, Huamachuco Sánchez Carrión in the 2015," Magister Thesis, Universidad Nacional Pedro Ruiz Gallo, 2019.

[4] J. Piaget, B. Inhelder, Psicología del niño, Ediciones Morata, 2016.

[5] R. Pacheco, D. Mafla, "Ludo-creative strategies in the development of the oral language of girls and boys of the kirdengarten level 2 (3-4 years) of the child development center 'My Golden World Kids' in the period 2017 – 2018," Ph.D Thesis, Universidad Central de Ecuador, 2017.

[6] G. Zuccalá, "Producing texts at the beginning of schooling: the production of oral texts, dictated to an adult and written, in the 5th and 1st grade room. Comparison between different pedagogical approaches," Bachellor Thesis, Universidad Nacional de la Plata, 2015.

[7] E. L. Escalante, M. Coronell, V. Narváez-Goenaga, Juego y lenguajes expresivos en la primera infancia una perspectiva de derechos, Editorial Verbum, 2016.

[8] R. A. Dinello, Cuaderno de lúdica y sociología de la educación, Psicolibros Waslala, 2011.

[9] K. M. Silgado, L. C. Rey, "Improving reading comprehension through recreational activities in second grade students of the Nuestra Señora del Pilar Educational Institution," Magister Thesis, Fundación Universitaria Los Libertadores, 2017.

[10] C. Freinet, Los Metodos Naturales III : El aprendizaje de la escritura, Editorial Fontanella, 1972.

[11] M. Pantigoso, Educación por el arte. Hacia una pedagogía de la expresión, Instituto Nacional de Cultura, 1994.

[12] C. H. Ramirez, "Academic Audit on the Impact of the Administrative Process on the Achievement of Educational Quality Standards of the SISE Institute of San Juan De Lurigancho - 2017," Magister Thesis, Universidad Nacional Federico Villarreal, 2017.

[13] A. Teberosky and L. Tolchinsky, "Beyond initial reading and writing," J. Study Educ. Dev., **15**(58), 5–14, 1992.

[14] J. R. Reyes, Y. N. Villegas, "Metacognition in university education. A case study," Rev. Electrónica Psicol. Iztacala, **22**(2), 2277-2290, 2019.

[15] G. H. Chinga, J. A. Meza, "Production of narrative texts in students of the 5th cycle of primary education in a school in Pachacútec," Bachellor Thesis, Universidad San Ignacio de Loyola, 2012.

Annexure

Table 2: Text Production Steps Evaluation Chart (Original Version)

I. PASOS DE LA PRODUCCIÓN DE TEXTOS	**CRITERIOS**			
	C	P	S	O
PLANIFICACIÓN (PL) **La docente escribe textualmente lo que dice el niño**				
1 a. ¿A quién te gustaría escribirle?				
1 b. ¿Qué te gustaría escribirle?				
1 c. ¿Para qué le escribirías?				
TEXTUALIZACION (T) **La docente escribe textualmente lo que dice el niño**				
2 a. ¿Cuál es el mensaje que le quieres hacer llegar? (Darle las gracias, hacer algún pedido, u otro.)				
REVISIÓN (R) **La docente le vuelve a leer el texto producido para que el niño decida si quiere o no modificarlo.**				
3 a. ¿Dejamos así el mensaje o lo cambiarías?				
PUBLICACIÓN (P) **La docente escribe textualmente lo que dice el niño.** **Si tiene iniciativa de producir otra presentación del texto, se le brinda material fungible (colores, hojas, stickers.)**				
4 a. ¿Cómo harás llegar este mensaje a "x"? (amigo, padres u otro)				

Table 2. Story Creation Evaluation Chart (Original Version)

II. TIPO DE TEXTOS: LITERARIOS	**CRITERIOS**			
	C	P	S	O
A. CREACIÓN DE CUENTO **La docente presenta seis imágenes, el niño las organiza y elabora un cuento.** **La docente copia textualmente lo que dice el niño.**				
PLANIFICACIÓN (PL) Y TEXTUALIZACIÓN (T)				
1.¿Cómo crearías un cuento a partir de estas imágenes?				
2.¿Qué título le pondrías?				
REVISIÓN (R)				
3. ¿Cambiarías alguna parte del cuento?				
Si responde sí cambiaría, se le pregunta: 4. ¿Cuál?				

Table 3. Riddle Creation Evaluation Chart (Original Version)

B. CREACION DE ADIVINANZA	**CRITERIOS**			
	C	P	S	O
PLANIFICACIÓN (PL) Y TEXTUALIZACIÓN (T)				
1. ¿Cómo crearías una adivinanza a partir de este objeto?				
REVISIÓN (R)				
2. ¿Cambiarías alguna parte de la adivinanza?				
Si responde sí cambiaría, se le pregunta: 3. ¿Cuál?				

Table 4. Poetry Creation Evaluation Chart (Original Version)

C. CREACIÓN DE POESÍA	**CRITERIOS**			
	C	P	S	O
PLANIFICACIÓN (PL) Y TEXTUALIZACIÓN (T)				
1. ¿Cómo crearías una poesía para este títere?				
REVISIÓN (R)				
2. ¿Cambiarías alguna parte de la poesía?				
Si responde sí cambiaría, se le pregunta: 3. ¿Cuál?				

Advances in Science, Technology and Engineering Systems Journal Vol. 5, No. 5, 137-147 (2020)

www.astesj.com

Special Issue on Innovative Research in Applied Science, Engineering and Technology

ASTESJ

ISSN: 2415-6698

Towards Directing Convolutional Neural Networks Using Computational Geometry Algorithms: Application to Handwritten Arabic Character Recognition

Mohsine Elkhayati*, Youssfi Elkettani

Mathematics department, Faculty of Science, Ibn tofail university, Kenitra 14000, Morocco

ARTICLE INFO

Article history:
Received: 28 June, 2020
Accepted: 19 August, 2020
Online: 09 September, 2020

Keywords:
Convolutional neural network
Computational geometry
Gabriel's graph
Relative neighborhood graph
Appearance rate
Handwritten Arabic characters

ABSTRACT

Suppose we want to classify a query item Q with a classification model that consists of a large set of predefined classes L and suppose we have a knowledge that indicates to us that the target class of Q belongs to a small subset from L. Naturally, this filtering will improve the accuracy of any classifier, even random guessing. Based on this principle, this paper proposes a new classification approach using convolutional neural networks (CNN) and computational geometry (CG) algorithms. The approach is applied and tested on the recognition of isolated handwritten Arabic characters (IHAC). The main idea of the proposed approach is to direct CNN using a filtering layer, which reduces the set of possible classes for a query item. The rules of the relative neighborhood graph (RNG) and Gabriel's graph (GG) are combined for this purpose. The choice of RNG-GG was based on its great capacity to correctly reduce the list of possible classes. This capacity is measured by a new indicator that we call "the appearance rate". In recent years and due to strong data growth, CNNs have performed classification tasks very well. On the contrary, CG algorithms yield limited results in huge datasets and suffer from high computational time, but they generally reach high appearance rates and do not require any training phase. Consequently, the proposed approach uses an optimal architecture to exploit the advantages of the two techniques and overcome the computational time issue. Experiments carried out on the IFHCDB database have shown that the suggested approach outperforms a normal CNN and yield satisfactory results.

1. Introduction

Supervised classification aims to assign a new item to a class from a given set of classes according to its feature values and to a training set [1]. Supervised classification requires previously classified reference samples in order to train the classifier and subsequently classify unknown data [2]. Different supervised classification methods are available. The simplest methods do not require training but rather rely on the notions of proximity between pre-known samples and the unknown sample [2] such as Computational Geometry (CG) algorithms. Training-based algorithms such as decision trees and Neural Networks (NN) form a second set of methods. Many algorithms are widely used in the literature for classification tasks, including Support Vector Machine (SVM), artificial NNs, decision trees, and K-Nearest Neighbors (KNN). This paper proposes a new classification approach, which attempts to combine the robustness of a deep artificial NN, which is a Convolutional Neural Network (CNN), and the advantages of two CG algorithms, which are the relative neighborhood graph (RNG) and Gabriel's graph (GG). The approach is applied to the recognition of Isolated Handwritten Arabic Characters (IHAC).

Recently, deep learning algorithms have emerged and dominated many research areas. They have obtained excellent results and solved many difficult issues. Due to strong data growth, they have outperformed conventional classification algorithms and in some tasks, they have surpassed human capabilities. Deep learning is a sub-domain of machine learning that uses high-level hierarchy architectures to learn high-level abstractions in data [3]. Deep architecture models have been successfully implemented to solve many visual recognition problems such as image recognition [4], text recognition [5], and character recognition [6]. Deep learning generally relies on Deep Neural Networks (DNN). The main contrast between a NN and a

*Mohsine Elkhayati, Ibn tofail university, faculty of science, Kenitra, Morocco, +212-677343723 & MohsinElkhayati@gmail.com

DNN is the depth of the network, in other words, the number of hidden layers used in the system. DNNs can be classified into five different categories: Feedforward Neural Networks (FFNNs), Recurrent Neural Networks (RNNs), Radial Basis Function Neural Networks (RBFNNs), Kohonen Self Organizing Neural Networks (KSONNs), and Modular Neural Networks (MNNs) [7]. In FFNNs, the information flows in one direction, there is no looping or cycle. Unlike FFNNs, the units of RNNs form a cycle; the output of a unit becomes the input to itself. The hidden layer of an RBFNN includes a radial basis function and each unit represents a cluster center. KSONN organizes itself the network model in the input data using unsupervised learning. The MNN partition a huge network into smaller independent neural network modules [7]. CNN is an FFNN, and one of the most commonly used NNs in the literature, particularly in the area of pattern recognition. It is one of the most remarkable learning techniques where the network layers are trained with great robustness [8]. In general, CNNs are based on three main types of layers: convolutional layers (CLs), pooling layers (PLs), and fully connected layers (FCLs); each layer plays an important role in the CNN architecture.

Computational geometry consists of studying the algorithms that can be stated in terms of geometry, it is worth mentioning that there is a bunch of purely geometric problems that cannot belong to the computational geometry [9]. Several CG algorithms and techniques have been proposed to solve classification problems, such as GG, RNG, K-Nearest Neighbors (KNN), the Delaunay triangulation, the Voronoi diagram, the convex hull, and polygon triangulation. The most commonly used is KNN because of its simplicity and the no need for knowledge about the distribution of training data [10]. Unlike deep learning algorithms, CG algorithms have been effective in small databases, but with the strong growth in database sizes, the capacity and the computational complexity of these algorithms are problematic. Except for KNN, these algorithms have not been widely used in the literature, and to our knowledge; they have never been used for the classification of IHAC. However, based on certain experiences, it has been noticed that they obtain excellent results in terms of a new indicator that we call "Appearance Rate". A CG algorithm applies its proximity rules to connect between instances that can belong to different classes. The appearance rate is the probability that the query item is connected to at least one instance of its correct target class. This indicator assesses the ability of a CG algorithm to act as a class filter. This is an important indicator and is the main motivation behind the approach and behind the use of the hybridization of RNG and GG (RNG-GG). To our knowledge, the appearance rate indicator has never been considered before, and this paper is the first attempt to introduce it.

Suppose we have to classify a new item with a classification model that consists of a large set of classes L and suppose that we have information that confines the new item's correct target class to a small subset of L. Of course, this filtering will improve the accuracy of any classifier, even random guessing. Based on this principle, the idea of the approach is to use a filtering layer to direct CNN by reducing the set of possible classes for a new item. The filtering layer applies the rules of RNG-GG on the features extracted by the CLs of CNN in order to extract a list of possible classes. This list is then provided to the output layer of CNN. At this level, other classes are excluded from the classification and the class in the list with the maximum softmax value is considered the target class.

RNG and GG are computationally expensive when applied to huge datasets and high dimensional spaces, while CNNs work well when trained on huge datasets. This imposed itself as a real challenge. In this context, we adopted an optimal CNN architecture to reduce computational time without losing CNN's high performance. The architecture uses a reduced number of filters and many PLs to provide the smallest possible feature vectors to the filtering layer. In addition, in the filtering layer, we only apply the rules of RNG-GG against constructing full graphs. These two strategies avoided unrealistic execution time.

The approach has been tested on the recognition of IHAC using the IFHCDB database [11]. The results are satisfactory and outperform the normal CNN's performance by approximately 3%. These results give a new breath to CG algorithms, open another vision angle on the usefulness of these algorithms, and make us wonder about the benefits of directing robust classifiers using a class filtering. On the other hand, even the CG algorithms do not require a training phase and even if we adopted strategies that considerably reduce the computational time, the execution time of the proposed approach is even a little higher compared to that of a normal CNN in the classification phase. Generally, with powerful computers, this small difference in computing time becomes negligible.

The rest of the paper is organized as follows: Section 2 presents some recent works that have applied CNNs to IHAC recognition. Section 3 describes the proposed approach and the used algorithms. Section 4 Shows performed experimentations and obtained results. Finally, Section 5 concludes the paper.

2. Related works

Recently, supervised learning using CNNs has been very successful in image classification tasks, and this success is due mainly to the large scale labeled datasets [12]. An acceptable number of works have used CNNs for IHAC recognition. On the contrary and except KNN, CG algorithms have been rarely used in recent years and no attempt to use them for IHAC recognition in the literature to our knowledge. In this section, we will focus on the most recent works using CNNs for the recognition of IHAC and languages using the Arabic alphabet such as Urdu.

The IHAC recognition is a complicated task for several reasons: firstly, the Arabic alphabet contains characters that change their shapes depending on their position in the word: beginning, middle, final, or isolated [13] (see Figure 1). Secondly, there is a set of characters that have the same shape, the only difference between them is the number or the position of diacritical points [14], e.g. (ش, س) (د, ذ) (ح, خ, ج) (ب, ت, ث). Thirdly, 60% of the characters contain diacritical points; these diacritics are isolated and are written above or below the character. Sometimes, these points may be related to each other

or to the main body of the character due to writing errors or writing styles. The presence of these isolated or linked diacritics disturbs the features extraction process because they can modify the character shape, can be treated as noise or as an isolated character. Moreover, a set of characters have the same number of diacritics, which reduces the inter-character variability. Figure 1 shows the shape of the handwritten Arabic characters according to their position.

Name	Isolated	Start	Middle	End	Name	Isolated	Start	Middle	End
Alif	أ	أ	ـا	ـا	Daad	ض	ضـ	ـضـ	ـض
Baa	ب	بـ	ـبـ	ـب	TTaa	ط	طـ	ـطـ	ـط
Taa	ت	تـ	ـتـ	ـت	Dhaa	ظ	ظـ	ـظـ	ـظ
Thaa	ث	ثـ	ـثـ	ـث	Ayn	ع	عـ	ـعـ	ـع
Jim	ج	جـ	ـجـ	ـج	Ghayn	غ	غـ	ـغـ	ـغ
Haa	ح	حـ	ـحـ	ـح	Faa	ف	فـ	ـفـ	ـف
Khaa	خ	خـ	ـخـ	ـخ	Qaaf	ق	قـ	ـقـ	ـق
Dall	د	د	ـد	ـد	Kaaf	ك	كـ	ـكـ	ـك
Dhall	ذ	ذ	ـذ	ـذ	Laam	ل	لـ	ـلـ	ـل
Raa	ر	ر	ـر	ـر	Meem	م	مـ	ـمـ	ـم
Zayn	ز	ز	ـز	ـز	Noon	ن	نـ	ـنـ	ـن
Seen	س	سـ	ـسـ	ـس	Haa	ه	هـ	ـهـ	ـه
Sheen	ش	شـ	ـشـ	ـش	Waw	و	و	ـو	ـو
Saad	ص	صـ	ـصـ	ـص	Yaa	ي	يـ	ـيـ	ـي

Figure 1: Handwritten Arabic characters and their shape according to their position

In [15], the authors proposed a new approach to recognize offline Urdu handwritten characters and numerals using CNNs. The authors extract geometrical features of the characters and numerals first in order to embed them with pixel-based data that will be extracted by CNN. The proposed CNN model consists of 3 CLs, 2 PLs, and 2 FCLs. The authors suggested a local database on which they experimented with their approach. Regarding characters classification, they got 98.3% accuracy. It is worth mentioning that they reduced the number of classes into 10 by grouping similar characters into groups.

In [16], the authors proposed a hybridization between CNN and the multidimensional long short-term memory neural network (MDLSTM) to recognize Urdu characters written in Nastaliq font. CNN is used to extract the low level translational invariant features in characters. These features are fed to MDLSTM, which in turn extracts high order features and make the classification. The approach achieved 98.12% as recognition accuracy, which outperformed the state-of-the-art on the UPTI dataset [17].

In [18], the authors proposed an approach for IHAC recognition using a CNN architecture composed of 2 CLs, 2 PLs, and 2 FCLs. The Rectified Linear Unit (RELU) activation function was used after the CLs and the first FCL. The PLs had no overlapping regions, which down-samples the feature maps by 2 in each direction. The proposed model achieved 94.9% accuracy on a local database of 16,800 images.

Inspired by the success of the very deep model VGGNet, [19] proposed an alphanumeric VGGnet to recognize handwritten Arabic alphanumeric characters. They tried to reduce the overall complexity of VGGNet while maintaining high performance. The proposed model consists of 13 CLs, 2 PLs, and 3 FCLs. Dropout and augmentation techniques are adopted to prevent overfitting. The approach was tested on two databases, ADBase database for digits and HACDB for characters. An accuracy of 99.57% was obtained on ADBase and 97.32% on HACDB.

The authors in [20] suggested a hybridization of CNN and SVM to recognize IHAC. CNN is used to extract features from images and SVM for recognition. CNN architecture includes 2 CLs, 2 PLs, and 2 FCLs. Since the CLs do not contain a large number of parameters, dropout was applied only on FCLs to avoid overfitting. The outputs of the last FCL are then taken by SVM as a feature vector to continue the training process. The classification phase is done only with SVM. The approach has been tested with and without the dropout technique. The best accuracy (94.17%) was achieved using dropout.

The authors in [21] proposed an IHAC recognition approach using CNN and transfer learning strategies. The network architecture is built around AlexNet CNN, it consists of eight layers (5 CLs and 3 FCLs). Hidden layers are equipped with RELU and max-pooling is applied after the first, the second, and the fourth CL. The architecture was tested using three learning strategies; learning from scratch and two transfer learning strategies (CNN as feature extractor and fine-tune CNN). Experimentations have shown that learning from scratch brings better results compared to both transfer learning strategies and can reach a 100% accuracy in some conditions.

In [22], an automatic handwriting recognition model based on CNN was proposed. The model consists of 3 CLs, 3 PLs, and 4 FCLs. RELU activation function is used after each CL and 80% dropout is used in FCLs to combat overfitting. Besides this, the authors introduced a new database called Hijja, which included 47,434 Arabic characters. Therefore, the proposed model was evaluated on the new database and the AHCD [18] database. It achieved 88% accuracy on Hijja and 97% on AHCD. A comparison made in the paper showed that the proposed model outperformed the CNN-for-AHCD proposed by [18].

The othors of [23] trained a CNN holistically to recognize Arabic names. They proposed a CNN architecture composed of 4 CLs and 4 FCLs. Each CL is equipped with the RELU activation function. Max-pooling is used after the second and the fourth CL. The first FCL is equipped with RELU and the second with the softmax activation function. Batch normalization layers are used to normalize inputs and hence speed up the learning process. The dropout technique is used after the first FCL with a keep probability parameter of 0.2. The proposed CNN model obtained a 99.14% accuracy on the SUST-ARG names database [24]. The authors did not find many works in the literature that experimented with the same dataset. Therefore, they made a comparison with two works and their approach performances were much better compared to the two works.

A CNN model for handwritten Arabic characters recognition was designed in [25]. The architecture of the model consists of 3 CLs, an FCL of 200 neurons, and an output layer of 28 neurons (as the number of classes). Batch normalization, ReLU activation

function, and dropout of 0.5 follow each CL. Categorical Cross-Entropy [26] was used as a cost function. Experimental results showed that the proposed model was able to achieve an accuracy of 94.8% and 94.7% on the AIA9K [27] and AHCD datasets respectively.

3. Method

3.1. Material

3.1.1. Convolutional neural network

CNN is a feedforward neural network that uses CLs to extract high-level characteristics and properties included in the input data. It is a type of NNs, which has been used in many fields and has solved important problems. CNN is inspired by the biological mechanism of the animal cortex where the CLs play the role of receptive fields. CNN is generally trained with a back-propagation algorithm and can learn from high dimensional inputs, non-linear mappings of huge amounts of data [28]. CNN has many advantages; it automatically detects and extracts the invariant salient characteristics [29] and uses shared weights in CLs, which can reduce the number of parameters and improve performance [30].

Generally, CNN is based on three principal kinds of layers, which are CLs, PLs, and FCLs, each kind of layer plays an important role in the CNN architecture. In new deep learning libraries, another layer called Rectified Linear Unit (ReLU) [31] is considered to introduce the non-linearity in the network. Besides, dropout layers [32] are used in order to reduce overfitting. Figure 2 illustrates the general pipeline of CNN architecture.

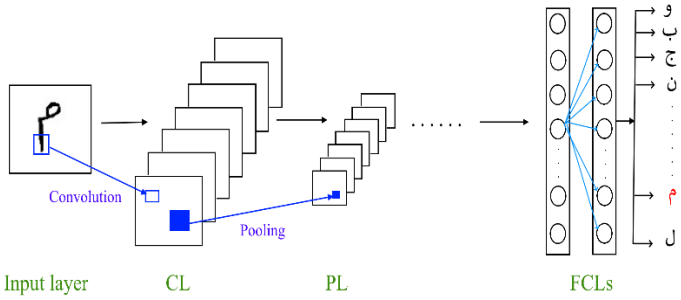


Figure 2: The pipeline of the general CNN architecture

CLs are feature extractors that use mathematical convolutions. Using some matrix filters, the CL tries to find features throughout the entire image. It generates various feature maps according to the number of filters; each filter is specified for a feature. The output of this layer is a set of filtered images [33].

The subsampling or PLs reduce the dimensionality of the CL's output images. They may be placed after CLs and they are translation-invariant because they take into account neighboring pixels as CLs do. The most widely used subsampling techniques are max pooling and average pooling [3]. The output of the PL has the same number of images with fewer pixels, but it retains important features.

FCLs are performed like a traditional NN, in which each neuron in a layer is connected to all neurons in the next layer. The input layer uses a 1D feature vector instead of the 2D matrix used by CLs and PLs. In the output layer, in most cases, a softmax function is used to assign a value between 0 and 1 to each neuron knowing that each neuron represents a class. The class with the maximum value is considered the predicted class. The FCLs represent the high-level reasoning of the network [18]. They contain around 90% of the parameters and aim to classify the input data in an appropriate class [3].

The ReLU layers are generally used to introduce non-linearity on the network. A ReLU layer converts the negative pixels of each feature map to 0 and maintains positive pixel values. This increases the non-linearity on the network without affecting the receptive fields of the CLs [31].

Dropout is a popular technique used in CNNs. The dropout layers aim to reduce the risk of overfitting and to speed up the training process [32]. The technique was proposed by [34] and explained in depth by [35]. The dropout layer randomly nullifies the weights and outputs of a number of units to disable their influence on the forward pass and backpropagation.

3.1.2. Relative neighborhood graph

In computational geometry, the relative neighborhood graph (RNG) is an undirected graph defined on a set of points of the Euclidean plane by the connection of two points P_i and P_j by an edge whenever there is no third point P_k closer to both points P_i and P_j, $1 \leq i, j, k \leq n$. This graphic was proposed by Godfried Toussaint [36] in 1980 as a means of defining a structure from a set of points [37].

Let $\Omega = \{P_1, P_2, \ldots\ldots, P_n\}$ be a set of n points in the m-dimensional space, and $d(P_i, P_j)$ denotes the distance between P_i and P_j. The RNG (Ω) connects all pairs of points (P_i, P_j), $(i \neq j)$ for which there is no other point P_k with the property that the greater of the two distances $d(P_i, P_j)$ and $d(P_j, P_k)$ is less than the distance $d(P_i, P_j)$ [38]. Which is expressed by the following formula:

$$d(P_i,P_j) \leq Max(d(P_i,P_k),d(P_j,P_k)), \forall P_k \in \Omega \setminus P_k \neq P_i,P_j \quad (1)$$

In other words, the two points P_i and P_j are neighbors if the lune in Figure 3 (a) obtained by the intersection of the hyperspheres of centers P_i and P_j, and of radius the length of the edge (P_i, P_j) does not contain any other point of Ω.

3.1.3. Gabriel's graph

Gabriel's graph (GG) [39] is a connected graph in which, if two points P_i and P_j are connected by an edge, then the hypersphere of diameter $\delta(P_i, P_j)$ does not contain any points of Ω.

If we call μ the center of the edge (P_i, P_j), the vertices P_i and P_j will be neighbors in the sense of Gabriel if and only if they verify the following property:

$$\delta(P_k,\mu) \geq \delta(P_i,\mu) = \delta(P_j,\mu) = \frac{\delta(P_i,P_j)}{2}, \forall P_k \in \Omega \setminus P_k \neq P_i,P_j \quad (2)$$

Since the hatched circle in Figure 3 (b) which has the diameter $\delta (P_i, P_j)$ is empty, the two points P_i and P_j are connected by an edge.

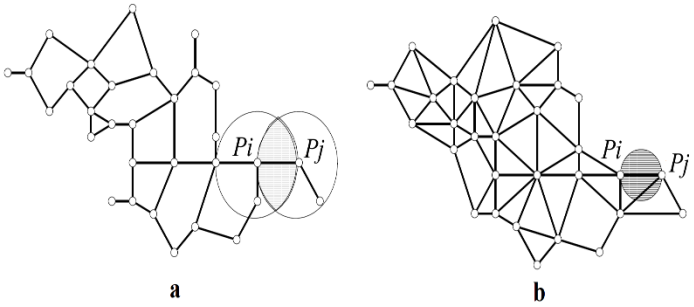


Figure 3: Diagram explaining RNG (a) and GG (b)

3.2. Architecture

Suppose we have prior knowledge that the correct target class of the query item *Q* belongs to a small subset of classes instead of the whole database's classes set. This will limit choices for a classifier and then increase the probability of having a correct decision. Based on this principle, the main idea behind the approach is to direct CNN by using a filtering layer that attempts to reduce the list of possible classes for *Q*. The filtering layer hybrids the rules of two CG algorithms (RNG and GG) to provide a reduced list of possible classes to CNN. CNN ignores other classes and attempts to classify *Q* based on the provided list. Figure 4 illustrates the proposed approach's architecture.

The performed CNN architecture consists of 3 CLs, 3 PLs, 1 Dropout layer, and 3 FCLs including an input layer, a hidden layer, and an output layer. The input layer of the network is a binary image of size (28×28×1). The first CL consists of 16 filters of 5×5×1 size. In the second CL, 24 filters of 3×3×1 are used, and in the third CL, 32 filters of 3×3×1 are used. In order to reduce the resolution of the images by the half, we use the max-pooling strategy with a 2×2 window and stride 2 in all PLs. The first FCL consists of the feature vector resulted from the last PL (512 values). The second FCL consists of 128 neurons and the output layer consists of *n* neurons as the number of classes (In our case it is 28 classes). The softmax activation function is used in the output layer. The ReLU activation function is used by all CLs. The dropout technique is used before the first FCL with a keep probability parameter of 0.5.

The filtering layer does not intervene in the training phase, but it just captures the features extracted by CNN in order to use them at the classification phase. The output of the last PL is 32 filtered images of 4×4×1 size, which will be transformed into a 1D feature vector (512 values). This vector will be fed to FCLs, and at the same time to a 512D space. Once the training phase is finished, we will get a trained CNN and a 512D space which includes the feature vectors of all training samples.

Since RNG/GG does not require a training phase, the filtering layer only intervenes during the classification phase. At this phase,the query item *Q* follows the same architecture and once its feature vector is introduced into the *512D* space, the rules of RNG-GG are applied to *Q*, which connects it to a certain number of instances. The list of classes of these instances is provided to the CNN output layer (In our example the list contains *C2*, *C3*, and *C5*). From this list and according to the assigned softmax values, the class with the maximum value is considered the target class of *Q* (In our example the target class is *C5* since it has the maximum softmax value from the list), while classes outside the list are definitively excluded from the classification.

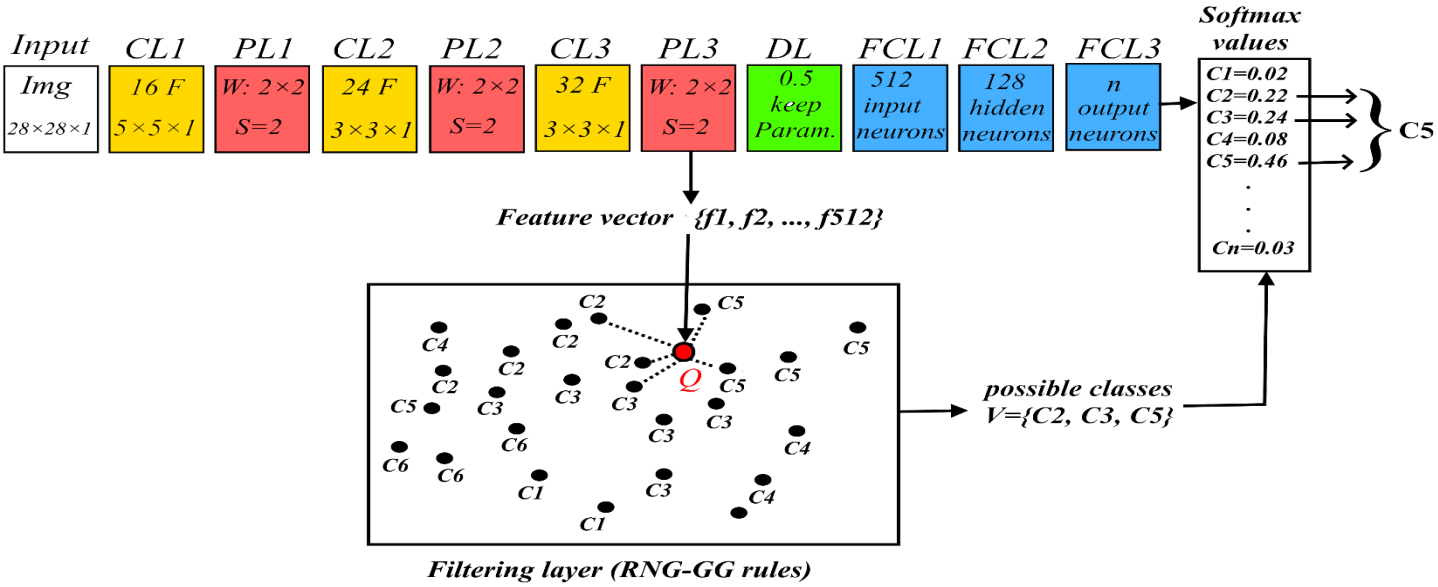


Figure 4: The proposed approach architecture

3.3. Filtering layer

As mentioned in the previous section, the filtering layer applies the rules of RNG-GG in order to provide a reduced list of possible classes to CNN. The motivation behind using this layer and the reasons for using RNG-GG are explained and discussed in this section. Our points of view are reinforced in the experiments and results section. CG algorithms such as RNG/GG generally give acceptable classification accuracies when applied to small datasets and low dimensional spaces. However, in the case of large datasets and high dimensional spaces, they are computationally expensive and do not give satisfactory results. In this section, we will discuss a new advantage of these algorithms, which we call appearance rate. We will introduce it, explain its importance, and discuss how to exploit it for a classification problem. After that, we will address the computational complexity issue. Finally, we will illustrate the hybridization technique between RNG and GG.

3.3.1. Appearance rate

CG algorithms are based on a simple technique for classifying new data. Once a query item *Q* is processed, it will be connected to a set of instances based on the proximity rules of the used algorithm. The classes of these instances will then pass to a voting system, in which the class with the maximum number of instances will be selected as the target class *Cq*. Based on some experiments, CG algorithms yield unsatisfactory classification accuracies, but it was noticed that *Cq* passes to the voting system with a high probability. This means that the problem of CG lies in the voting system. In other words, the prediction based on the number of connected instances does not bring good results. The probability that *Cq* appears in the voting system is what we call the appearance rate, i.e. the appearance rate is the probability that *Q* will be connected to at least one instance of *Cq*. More clarification, the appearance rate allows us to know the ability of an algorithm to detect the target class of *Q* (before the voting system), while the classification rate shows its ability to perform a final classification (after the voting system). As far as we know, the appearance rate indicator has not been considered before; therefore, this paper represents the first attempt to introduce it. This indicator is the key point of the approach and the main motivation for combining RNG-GG and CNNs. More directly, RNG-GG has approached 100% appearance rate (see **section 4.2**). This inspired us to use it to reduce the list of possible classes before making a final classification by CNN.

Overall, to classify *Q* using RNG/GG, we construct the graph based on their proximity rules and extract the classes' labels of the instances that are connected to *Q*. These labels are saved into a vector, *V= {C1, C2,…, Cn }*. Finally, a voting system is applied in which the most voted label of *V* is considered the target class of *Q*. We are not interested in the voting phase. However, to know the ability of an algorithm to connect *Q* with at least one instance of *Cq*, we introduced the appearance rate indicator (*AR*) which is calculated using the following formula.

$$AR = \frac{\sum_{q=1}^{TN} f(C_q)}{TN} * 100 \quad (3)$$

$$\text{with} \quad f(C_q) = \begin{cases} 1 & if \ C_q \subset V \\ 0 & Otherwise \end{cases}$$

Denotes *f(Cq)* is the appearance function of *Cq* in *V*; *TN* is the total number of test items.

The appearance rate is an important indicator because it gives us the possibility of confining *Cq* in a small defined list instead of the whole list of classes. If this indicator is high, it will help any classifier to make the right prediction because it reduces choices. Otherwise, if this indicator is weak, it will decrease the classification accuracy, consequently, the class filtering will not be useful.

3.3.2. Computational complexity

Unlike small datasets and low dimensional spaces, constructing RNG/GG graphs in the case of large datasets and large dimensional spaces is time-consuming and memory-intensive. The two parameters that complicate the RNG/GG calculations are the number of instances and space dimensionality. Constructing a graph on a space requires calculating all the distances between each instance and all the other instances of the space and checking the proximity rules each time. Consequently, the higher the number of instances and dimensions, the more the calculations increase. Generally, to perform the classification, RNG/GG is applied directly to the instances of the space and does not require a training phase. This is an advantage because it does not need time for training, but it is also a disadvantage because it takes a long time to construct a graph each time to classify a new item. We can think for example to introduce the new element into an already existing graph. This idea appears ideal to avoid reconstructing the graph each time, but actually, the introduction of a new item will change a significant number of edges (create new ones and delete existing ones), which will create a change in the entire structure of the graph. Once again, we find ourselves facing an obligation to reconstruct the graph from scratch.

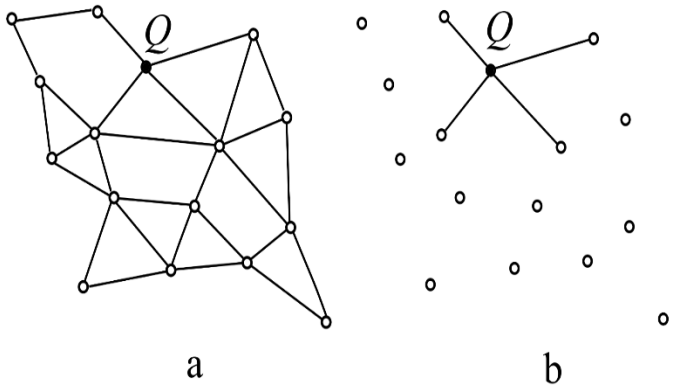


Figure 5: Illustration of the GG construction on a set of points; (a) full graph; (b) mini-graph

The good news is that our model only needs edges of the query item *Q*, while other edges in the graph are not necessary. On this basis, it is not necessary to construct the full graph because it does not add any benefit to the process. The idea is then to construct a mini-graph that consists only of the edges of *Q* instead of the full graph. Figure 5 shows the difference between the construction of a GG full graph (a) and the construction of a mini-graph (b). This strategy significantly reduced the computational time by ignoring unprofitable calculations (see **section 4.3**).

3.3.3. Hybridization

Our approach is based on the use of a robust CNN's architecture and a filtering layer including the rules of RNG and GG together. The hybridization between RNG and GG is applied as follows: Once a query item is introduced into the *512D* space, GG and RNG rules are applied to it at the same time, which produces a mini-graph composed of GG and RNG edges around the query item. The classes' labels of all the instances connected to *Q* are then stored in a vector *V*. Figure 6 shows an example of a constructed mini-graph based on the proposed hybridization.

Based on the example figured in Figure 6, the vector will contain the following labels, *V = {C2, C3}*. *V* will be provided then to the CNN output layer to perform classification. Other classes are ignored and the class with the maximum softmax value from *V* will be considered the target class *Cq*.

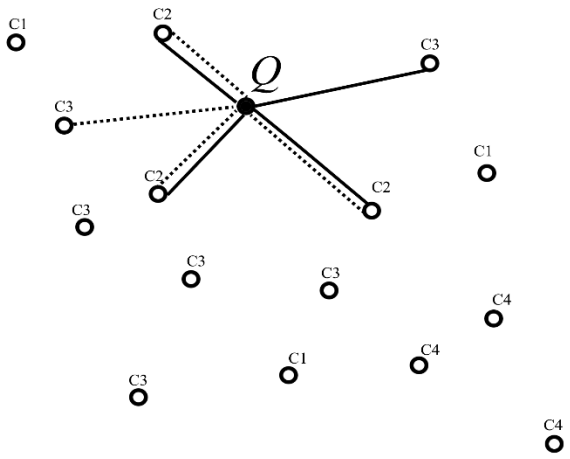


Figure 6: The constructed mini-graph from the hybridization of GG (solid edges) and RNG (dotted edges).

4. Experimentations and results

This section presents and discusses the results obtained from three experiments. Section 4.1 describes the database used in all the experiments. Section 4.2 Evaluates and compares the appearance rate of certain CG algorithms. This experiment aims to justify the choice of RNG-GG and to show the difference between the classification rate and the appearance rate of CG algorithms. In section 4.3, we compare the computational complexity of a mini-graph construction with a full graph construction. Finally, in section 4.4, we present and discuss the obtained results.

4.1. Dataset

To evaluate the performances of the proposed approach, we used the Isolated Farsi Handwritten Character Database (IFHCDB) [11]. The database contains 52,380 single characters and 17,740 digits. The distribution of characters is not uniform, which means that the number of samples is not the same for all characters. We are only interested in the 28 Arabic characters, which represent 97% of the characters in the database. Therefore, the experiments are carried out using a dataset from IFHCDB containing 35,989 characters for training and 15,041 for tests. All the presented experiments were carried out using this dataset.

4.2. Appearance rate results

In this section, we compare the appearance rate, the reduction rate, and the classification rate of four algorithms that are 9-NN, RNG, GG, and RNG-GG. The choice of KNN was due to its popularity and the choice of nine neighbors (9-NN) was due to the experiments carried out. The reduction rate concerns the percentage of ignored classes. Table 1 shows the results of the experiment.

Table 1: Comparison between the appearance rate, the classification rate, and the reduction rate of the studied algorithms

Classifier	9-NN	RNG	GG	RNG-GG
Appearance rate	69.2 %	74.5 %	91.3 %	99.1 %
Classification rate	65.6 %	59.4 %	58.5 %	64.2 %
Reduction rate	66.3 %	72.3 %	45.9 %	43.6 %

The results presented in Table 1 reinforce what was mentioned previously on the difference between the classification rate and the appearance rate of the studied algorithms. 9-NN did not show any significant change in the appearance rate compared to the classification rate; however, GG, RNG, and RNG-GG have shown great changes. This proves the idea that the problem of classification using RNG/GG lies in the voting system. RNG-GG yields an excellent appearance rate (99.1%). This result can be read as follows: in 99.1% of cases, the correct target class of the query item is detected by the algorithm and then passed to the next stage; on the other hand, the algorithm can reduce the number of classes that reach the final classification stage by a rate of 43%.

It is worth reminding that the idea of the proposed approach was born from the results of this experiment and the related conclusions. The high appearance rate obtained by RNG-GG encouraged us to consider using it as a filtering layer for a robust classifier such as CNN.

4.3. Computational complexity results

In this section, we compare the computational time of RNG and GG full graphs construction with mini-graphs construction. Feature vectors (512 values) of the training set (35,989 images) were extracted using CNN. Therefore, the graphs are constructed on a *512D* space of 35,989 training points.

The experiment was performed on a computer with an Intel Core i3-3110M processor with 2.40 GHz frequency, 4GB RAM, and Windows 10 64-bit operating system. Table 2 shows the results of the experiment.

Table 2: The computational time of full graphs and mini-graphs construction in a *512D* space of 35,989 points.

Algorithm	**GG**		**RNG**	
	Full graph	***Mini-graph***	***Full graph***	***Mini-graph***
Computational time	18.4 minutes	13.20 seconds	19.6 minutes	13.65 seconds

As shown in Table 2, the computational time of an RNG/GG mini-graph construction is too short than the full graph construction. Constructing a full graph every time we need to classify a new item has no benefit, is time-consuming and unrealistic. If for example, we want to classify words, paragraphs, or documents, it can take hours, even days and this is not realistic. However, the mini graph consumed about 80 times much less time than the full graph in this experiment and seems to be more realistic to some extent. Even both algorithms do not require a training phase, but they are computationally expensive and this remains the big drawback of these algorithms, especially when applied to huge databases. Indeed, the used strategy significantly reduced the computational time, but generally, the execution time of the approach is a little higher of a normal CNN since it consumes more time to make filtering, but this is can be negligible with the presence of powerful computers.

4.4. Accuracy results and discussion

4.4.1. Normal CNN against directed CNN

In this section, we compare the results obtained by a normal CNN with those obtained by the proposed directed CNN. The first experiment was performed using the proposed CNN architecture without the intervention of the filtering layer. The second experiment was performed with the intervention of the filtering layer. Both experiments were carried out using the same hyper-parameters. Table 3 compares the accuracies obtained by the two experiments.

Table 3: Comparison between the results obtained by normal CNN and directed CNN

Approach	**Normal CNN**	**Directed CNN**
Classification rate	94.2 %	97.4 %

From Table 3, we note that the use of RNG-GG as a filtering layer has improved the classification accuracy of CNN. Indeed, this strategy would not have succeeded if we did not have a strong filtering layer that provides reliable results; otherwise, the correct class could be rejected in the filtering layer, which would decrease the classification accuracy. Therefore, the obtained results are mainly thanks to the high appearance rate of RNG-GG.

Table 4: The confusion matrix of the proposed approach

	ا	ب	ت	ث	ج	ح	خ	د	ذ	ر	ز	س	ش	ص	ض	ط	ظ	ع	غ	ف	ق	ك	ل	م	ن	ه	و	ى	Accuracy
ا	297																						29						99.03 %
ب		291	8	6																3	1				3			3	92.38 %
ت		4	407	7																					4			4	95.53 %
ث			2	10																									83.33 %
ج					161	2	3											1	1										95.83 %
ح					4	354	7											4											95.93 %
خ						1	106												1										98.14 %
د								776	10	9	3																		97.24 %
ذ								2	10																				83.33 %
ر								4		128	17												10						97.65 %
ز									3	12	320																		95.52 %
س												693	12								2	4			3				97.05 %
ش												6	160																96.38 %
ص														138	2									1					97.87 %
ض														1	107														99.07 %
ط																60													100 %
ظ																	15												100 %
ع						4												248	9										95.01 %
غ																		1	41										97.61 %
ف																				265					10				96.36 %
ق																				10	131								92.90 %
ك																						192							100 %
ل	14									6													877	3					97.44 %
م														14				11						145		11			97.58 %
ن			8	5							9														112			6	97.56 %
ه																		6						10		738	5		97.23 %
و										7	4													8			389		95.34 %
ى		9	5	5																4	3				5			132	97.71 %
Total number of test images = 15041																													
Total number of correct classification = 14650 = 97.4%																													
Total number of miss-classification = 391 = 2.6%																													

4.4.2. Confusion matrix

Against printed / Latin languages, Arabic handwriting has many challenges and difficulties, which make the task of recognition very difficult for any classifier. The similarities between the characters and the writing style are the main factors responsible for the confusion between the characters and thus lead to miss-classifications. Table 4 shows the confusion matrix of the proposed approach.

From the confusion matrix, we can conclude that the majority of miss-classifications are due to the great similarity between some characters such as (س، ش), (ل ،ا), (ب، ت، ث، ن), etc. It is also worth mentioning that the distribution of the database is not uniform, some characters are represented with a large number of samples and some others are represented with a small number. This presents a great challenge for the classifier and negatively affects the classification accuracy. From Table 4, we also notice that the average of accuracies is not necessarily equal to the overall accuracy since the distribution is not uniform. We expect that normalizing the distribution by increasing the number of samples for small classes will generally improve the performance of the approach.

4.4.3. Comparison with recent approaches

This section compares the results of the proposed approach with other recent works in the literature. Table 5 shows the comparison results.

Table 5: A comparison between the obtained accuracy with other recent works

Reference	Method	Database	Accuracy
[20]	CNN based-SVM + Dropout	HACDB	94.17 %
[19]	Very deep NN	HACDB	97.32 %
[20]	CNN based-SVM + Dropout	IFN/ENIT	92.95 %
[18]	CNN	AHCD	94.90%
[27]	Windows-based descriptors	AIA9k	94.28 %
[25]	CNN	AIA9K	94.8 %
[40]	specificity and the singularity	IFHCDB	96.31 %
[41]	Modified Bitmap Sampling+ local binary pattern	IFHCDB	97.18 %
[42]	Derivative projection profile + Hamming Neural Network	IFHCDB	96.91 %
Proposed method	Directed CNN	IFHCDB	97.4 %

From Table 5, it appears that the proposed approach outperforms other approaches. Usually, this comparison is for internalization as it cannot be completely reliable for some reasons:

- The databases used are not the same;
- the splitting schemes used are not the same (Percentage of training, validation, and test data);
- Some works used untrained data for testing and others did not;
- Some works used pre-processing techniques to make the classifier's job easier, while others have not.

It must be reminded that this paper aims to show the importance of directing a robust classifier such as CNN by using a filtering layer. For this purpose, experiments were carried out on the IHAC recognition. Indeed, this work does not deal with specific characteristics or particular cases and does not use any particular treatment adopted to Arabic handwriting. Despite this blind application, the results were satisfactory and outperformed other approaches. Therefore, the authors of this article expect that an in-depth focus on the characteristics of the application domain will improve the performance of the approach.

Generally, the obtained results prove the effectiveness of the proposed approach and its ability to improve CNN's performance. This can open up a new avenue of research based on the direction of robust classifiers using class filtering. On the other hand, these results breathe new life into CG algorithms by thinking of using them as classifier helpers. This breath comes from the appearance rate indicator, which in turn is an important indicator that assesses the filtering capacity of algorithms.

5. Conclusion

In this paper, we presented a new classification approach based on CNN and RNG-GG. The approach was tested on the IHAC recognition. The main idea of the approach was to direct CNN by using a filtering layer, which limits the number of possible classes for a query item. This filtering layer relies on the rules of RNG-GG. The choice of RNG-GG was based on some experiments and conclusions that showed its high appearance rate. The appearance rate is a new indicator that we introduced in this paper. It evaluates the filtering capabilities of a CG algorithm. This indicator is very important and was the main motivation for using a filtering layer to direct CNN.

Generally, CNNs yield good classification accuracies on huge datasets. Conversely, CG algorithms face great challenges in computational time and classification accuracy when applied to huge databases, but as said before, they yield an excellent appearance rate, in particular, RNG-GG. On this basis, we have tried to propose an optimal architecture, which exploits the advantages of the used algorithms and overcomes their limits. Consequently, the proposed CNN architecture uses an optimal number of filters and three PLs in order to minimize the size of the feature vector, which will be fed to RNG-GG. This makes it possible to reduce the dimensionality of the space and then the computational time of RNG-GG. Besides this, we applied only the rules of RNG-GG on the query item against constructing full graphs, which significantly reduced the computational time.

Some experiments were carried out on the IFHCDB database to assess the performance of the proposed approach. The results were satisfactory and the approach outperformed a normal CNN and other recent approaches in the literature. Therefore, these results could open up new perspectives and impose new questions such as how directing a classifier through class filtering can be beneficial in terms of performance, and how to exploit the high appearance rate given by RNG-GG in classification tasks. Furthermore, the obtained results gave new life to CG algorithms as they have not been widely used for classification tasks in the

literature, especially in recent years due to their limitations on huge datasets. On the other hand, the proposed approach requires a little more execution time than a normal CNN. This time is consumed during class filtering. This issue becomes negligible with the presence of powerful computers, and despite that, we are trying to reduce it further.

In future work, we intend to find a more efficient solution for time complexity in order to have the freedom to improve the architecture of the network by adding more layers and more filters. Besides, we intend to try more combinations between other CG algorithms and other kinds of deep neural networks.

References

[1] G. M. Di Nunzio, A. Sordoni, "Picturing bayesian classifiers," in: Data Mining Applications with R, Academic Press, 35–61, 2014, doi:10.1016/B978-0-12-411511-8.00002-5.

[2] X. Ceamanos, S. Valero, "Processing hyperspectral images," in: Optical Remote Sensing of Land Surface, Elsevier, 163–195, 2016, doi:10.1016/B978-1-78548-102-4.50004-1.

[3] A. C. YanmingGuo, A. YuLiu, C. ArdOerlemans, C. SongyangLao, A. SongWu, S. Michael, A. C. Lew, "Deep learning for visual understanding: a review," Neurocomputing, **187**, 27–48, 2016, doi:/10.1016/j.neucom.2015.09.116.

[4] A. Krizhevsky, I. Sutskever, G. E. Hinton, "Imagenet Classification with Deep Convolutional Neural Networks," in NIPS'12: Proceedings of the 25th International Conference on Neural Information Processing Systems, Lake Tahoe, Nevada, 1097–1105 , 2012, doi:10.1145/3065386.

[5] T. Wang, D. J. Wu, A. Coates, A. Y. Ng, "End-to-End Text Recognition with Convolutional Neural Networks," in the 21st International Conference on Pattern Recognition (ICPR2012), Tsukuba, IEEE, 3304–3308, 2012.

[6] A. Coates, B. Carpenter, C. Case, S. Satheesh, B. Suresh, T. Wang, D. J. Wu, A. Y. Ng, "Text Detection and Character Recognition in Scene Images with Unsupervised Feature Learning," in International Conference on Document Analysis and Recognition, Beijing, IEEE, 440–445, 2011, doi:10.1109/ICDAR.2011.95.

[7] B. Koyuncu, H. Koyuncu, "Handwritten character recognition by using convolutional deep neural network: a review," International Journal of Engineering and Technologies-IJET, **5**(1), 1–6, 2019, doi:10.19072/ijet.528775.

[8] Y. Lecun, L. Bottou, Y. Bengio, P. Haffner, "Gradient-based learning applied to document recognition," Proceedings of the IEEE, **86**(11), 2278–2324, 1998, doi:10.1109/5.726791.

[9] M. Bundzel, T. Kasanický, "Using algorithms of computational geometry for pattern recognition and comparison to support vector machine," 2005.

[10] G. T. Toussaint, C. Berzan, "Proximity-graph instance-based learning, support vector machines, and high dimensionality: an empirical comparison," in: Machine Learning and Data Mining in Pattern Recognition, Springer, Heidelberg, 222–236 2012, doi:10.1007/978-3-642-31537-4_18.

[11] S. Mozaffari, K. Faez, F. Faradji, M. Ziaratban, S. M. Golzan, "A Comprehensive Isolated Farsi/Arabic Character Database for Handwritten OCR Research," in Tenth International Workshop on Frontiers in Handwriting Recognition, La Baule, France, Suvisoft, 385–389, 2006.

[12] Z. Chen, R. Ding, T. W. Chin, D. Marculescu, "Understanding the impact of label granularity on CNN-based image classification," CoRR, abs/1901.07012, 2019.

[13] J. Chen, Information Preserving Processing of Noisy Handwritten Document Images, Ph. D. Thesis, Lehigh University, 2015.

[14] N. Amara, F. Bouslama, "Classification of Arabic script using multiple sources of information: State of the art and perspectives," International Journal on Document Analysis and Recognition, **5**(4), 195–212, 2003, doi:10.1007/s10032-002-0092-6.

[15] M. Husnain, M. M. Saad, S. Mumtaz, M. Z. Jhanidr, M. Coustaty, M. Muzzamil Luqman, J. M. Ogier, G. S. Choi, "Recognition of Urdu handwritten characters using convolutional neural network," Appl. Sci., **9**(13), 2758–2778, 2019, doi:10.3390/app9132758.

[16] S. Naz, A. I. Umar, R. Ahmad, I. Siddiqi, S. B. Ahmed, M. I. Razzak, F. Shafait, "Urdu Nastaliq recognition using convolutional recursive deep learning," Neurocomputing, **243**, 80–87, 2017, doi:10.1016/j.neucom.2017.02.081.

[17] N. Sabbour, F. Shafait, "A segmentation-free Approach to Arabic and Urdu OCR," in: Document Recognition and Retrieval XX, SPIE, 8658, 215–226, 2013, doi:10.1117/12.2003731.

[18] A. El-Sawy, M. Loey, H. EL-Bakry, "Arabic handwritten characters recognition using convolutional neural network," WSEAS Trans. Comput. Res., **5**, 11–19, 2017.

[19] M. Mudhsh, R. Almodfer, "Arabic handwritten alphanumeric character recognition using very deep neural network," Information, **8**(3), 105–118, 2017, doi:10.3390/info8030105.

[20] M. Elleuch, R. Maalej, M. A. Kherallah, "New design based-SVM of the CNN classifier architecture with dropout for offline Arabic handwritten recognition," Procedia Comput. Sci., **80**, 1712–1723, 2016, doi:10.1016/j.procs.2016.05.512.

[21] C. Boufenar, A. Kerboua, M. Batouche, "Investigation on deep learning for off-line handwritten Arabic character recognition," Cognitive Systems Research, **50**, 180–195, 2018, doi:10.1016/j.cogsys.2017.11.002.

[22] N. Altwaijry, I. Al-Turaiki, "Arabic handwriting recognition system using convolutional neural network," Neural Comput & Applic, 2020, doi:10.1007/s00521-020-05070-8.

[23] M. E. Mustafa1, M. K. Elbashir, "A Deep learning approach for handwritten Arabic names recognition," International Journal of Advanced Computer Science and Applications (IJACSA), **11**(1), 678–682, 2020, doi:10.14569/IJACSA.2020.0110183.

[24] M.E. Musa, "Towards building standard datasets for Arabic recognition," International Journal of Engineering and Advanced Research Technology (IJEART), **2**(2), 16–19, 2016.

[25] K. Younis, "Arabic handwritten characters recognition based on deep convolutional neural networks," Jordan J Comput Inform Technol (JJCIT), **3**(3), 186–200, 2018.

[26] P. Golik, P. Doetsch, H. Ney, "Cross-Entropy vs. Squared Error Training: A Theoretical and Experimental Comparison," in 14th Annual Conference of the International Speech Communication Association, Lyon, France, 1756–1760, 2013.

[27] M. Torki, M. E. Hussein, A. Elsallamy, M. Fayyaz, S. Yaser, "Window-based descriptors for Arabic handwritten alphabet recognition: A comparative study on a novel dataset," arXiv preprint arXiv: 1411.3519, 2014.

[28] D. S. Maitra, U. Bhattacharya, S. K. Parui, "CNN Based Common Approach to Handwritten Character Recognition of Multiple Scripts," in 13th International Conference on Document Analysis and Recognition (ICDAR), Tunis, IEEE, 1021–1025, 2015, doi:10.1109/ICDAR.2015.7333916.

[29] H. C. Shin, H. R. Roth, M. Gao, M. Lu, Z. Xu, I. Nogues, J. Yao, D. Mollura, R. M. Summers, "Deep convolutional neural networks for computer-aided detection: CNN architectures, dataset characteristics and transfer learning," IEEE Transactions on Medical Imaging, **35**(5), 1285–1298, 2016, doi:10.1109/TMI.2016.2528162.

[30] J. Bai, Z. Chen, B. Feng, B. Xu, "Image Character Recognition Using Deep Convolutional Neural Network Learned from Different Languages," in 2014 IEEE International Conference on Image Processing (ICIP), Paris, 2560–2564, 2014, doi:10.1109/ICIP.2014.7025518.

[31] V. Nair, G. E. Hinton, "Rectified Linear Units Improve Restricted Boltzmann Machines," in the 27th International Conference on Machine Learning, 807–814, 2018.

[32] N. Srivastava, G. Hinton, A. Krizhevsky, I. Sutskever, R. Salakhutdinov, "Dropout: A simple way to prevent neural networks from overfitting," J. Mach. Learn. Res., **15**(1), 1929–1958, 2014.

[33] Y. LeCun, K. Kavukcuoglu, C. Farabet, "Convolutional Networks and Applications in Vision," in 2010 IEEE International Symposium on Circuits and Systems, Paris, 253–256, 2010, doi:10.1109/ISCAS.2010.5537907.

[34] G. E. Hinton, N. Srivastava, A. Krizhevsky, I. Sutskever, R. Salakhutdinov, "Improving neural networks by preventing co-adaptation of feature detectors," arXiv e-prints, abs/1207.0580, 2012.

[35] P. Baldi, P. J. Sadowski, "Understanding Dropout," in Proceedings of the NIPS, Advances in Neural Information Processing Systems 26, Curran Associates, Inc., 2814–2822, 2013.

[36] G. T. Toussaint, "The relative neighborhood graph of a finite planar set," Pattern Recognition **12**(4), 261–268, 1980, doi:10.1016/0031-3203(80)90066-7.

[37] F. Muhalenbach, Evaluation de la Qualité de Représentation de Fouille de Données, Ph. D. Thesis, University of Lumière Lyon II, 2002.

[38] J. Katajainen, O. Nevalainen, "An almost naive algorithm for finding relative neighborhood graphs in Lp metric," Theoretical Informatics and Applications, **2**(21), 199–215, 1987.
[39] K. R. Gabriel, R. R. Sokal, "A new statistical approach to geographic variation analysis," Systematic Biology **18**(3), 259–278, 1969, doi:10.2307/2412323.
[40] Y. Boulid, A. Souhar, M. Y. Elkettani, "Handwritten character recognition based on the specificity and the singularity of the Arabic language," International Journal of Interactive Multimedia and Artificial Inteligence, **4**(4), 45–53, 2017, doi:10.9781/ijimai.2017.446.
[41] Y. Boulid, A. Souhar, M. M. Ouagague, "Spatial and textural aspects for Arabic handwritten characters recognition," International Journal of Interactive Multimedia and Artificial Intelligence, **5**(1), 86–91, 2018, doi:10.9781/ijimai.2017.12.002.
[42] M. Askari, M. Asadi, A. Asilian Bidgoli, H. Ebrahimpour, "Isolated Persian/Arabic handwriting characters: Derivative projection profile features, implemented on GPUs," Journal of AI and Data Mining, **4**(1), 9–17, 2016, doi:10.5829/idosi.JAIDM.2016.04.01.02.

ASTES

Advances in Science, Technology and Engineering Systems Journal Vol. 5, No. 5, 148-153 (2020)

www.astesj.com

Special Issue on Multidisciplinary Innovation in Engineering Science & Technology

ASTESJ

ISSN: 2415-6698

Design of Purebred Dog Recommendation System Using MCDM Approach

Phie Chyan*

Department of Informatics, Atma Jaya University of Makassar, Makassar, 90224, Indonesia

ARTICLE INFO

Article history:
Received: 15 May, 2020
Accepted: 18 August, 2020
Online: 09 September, 2020

Keywords:
Dog Breed
Dog Adopter
Purebred Dog
Decision Support System
MCDM Approach

ABSTRACT

The dog is one of the first animals domesticated by human, and for thousands of years, it has been artificially bred into hundreds of types in order to provide certain traits that humans want. Nowadays, the selection of dogs by potential adopters has become a problem due to the availability of different type of breeds with their physical and mental characteristics. This study aims to design a decision support system through an analytical model that uses variety of data on the characteristics of purebred dogs obtained from different sources. Data from official sources is obtained from international purebred dog organizations that set the standards for each breed type, while data from unofficial sources is obtained from the dog lovers community, experts, and kennel owners. The result of the study provides appropriate recommendations to potential adopters in selecting a breed that suits their preferences and needs.

1. Introduction

This paper is an extension of work originally presented in **2018** International Seminar on Research of Information Technology and Intelligent Systems (**ISRITI**) [1]. According to the history recorded since 15 thousand years ago, Dogs were one of the first animals domesticated by humans in East Asia and then spread throughout the world and became involved in the long history of human culture and civilization. Through artificial selection, humans breed dogs into a new kind of breed by mating two species of dogs that have certain characteristics and traits to accentuate the desired combination of their traits [2]. Nowadays dogs have developed into hundreds of breeds with a total of 344 breeds officially recognized by FCI. Among the many types of breeds, the dog has divided into several breed groups with similar physical and psychological characteristics. Each breed group has certain characteristics that can support the role of the dog in social aspects with human's society [3]. Some types of dogs are used by humans to help in herding cattle, others are used as guard dogs to help law enforcement work as sniffer dogs.

The term dog refers to the dog domesticated by Canis lupus familiaris. Dogs were classified as Canis familiaris by Linnaeus in 1758 but in 1993 by the Smithsonian Institute and the American Mammal Experts Association, dogs were designated as subspecies of the gray wolf Canis lupus. Dogs are social animals, but the dog's personality and behavior can vary depending on the breed. In addition to genetic traits, the dog's personality and behavior also depend on the caring environment and treatment received from the dog's owner and people who interact closely with the dog.

Dogs as social animal have a vast variety of personality and are among the most high intelligence animals according to scientific research and field evidence. The level of intelligence of the dog depends on the race and each dog individually. According to Coren (2006), a dog psychologist who conducts dog intelligence studies on more than 100 breeds, the standard of intelligence of a dog is how quickly the dog can follow a new command given and how obedient the dog is to the commands it has learned [4]. Another proof is according to research at the University of Lincoln published, dogs have human-like intelligence who can psychologically recognize emotions and other human psychological states, and this ability is only demonstrated by dogs in interacting with humans, this shows the cognitive social abilities of a dog are more advanced than any other animal that is genetically closer to humans, and this ability is a genetic shift that distinguishes dogs from their wolf ancestors [5].

Based on the physical attributes dogs vary greatly in size, appearance, and behavior compared to other pets. Several of the important physical attribute of dogs highlighted as follows : Dogs have strong muscles, sturdy ankle bones, cardiovascular systems that support physical endurance and running speed, and teeth to catch and tear their prey. Dogs technically walk on tiptoes with toes. In term of sense of sight, research shows dogs can see several colors, although not as much and bright as can be seen by humans with a brightness level of approximately half of the accuracy of

*Corresponding Author: Phie Chyan, Email: Phie_chyan@lecturer.uajm.ac.id

human vision [6]. In sense of hearing aspect dogs can hear low-frequency sound range from 16 to 20Hz (humans only hear frequencies of 20-70 Hz), and high-frequency sounds range from 70 kHz to 100 kHz (humans only hear frequencies 13-20 kHz) and from the sense of smell Dogs have nearly 220 million olfactory cells that are sensitive to odors. According to research conducted by Michell (1999) on the age of various breeds of dogs, dog life expectancy depends on the breed with a median value between 10-13 years [7].

Breed standard is a set of guidelines which is used to ensure that the dog produced by a breeder or breeding facility conforms to the specifics of the standardized breed. Breed standards are devised by breed associations not by individuals and are written to reflect the use or purpose of the species and breed of the dog [8]. Breed standards help define the ideal dog of a breed and provide goals for breeders in improving stock. In essence, a breed standard is a blueprint for an dog fit for the function it was bred - i.e. herding, tracking etc. For that purposes purebred dogs have a non-profit organization/federation that aims to standardize and register purebred dogs that will improve the quality of breeding and use of purebred dogs whose health and physical characteristics meet the standards. Federation Cynologique Internationale(FCI) is the parent organization that oversees almost all organizations/kennels from various countries except the USA, Canada, and the United Kingdom. The American Kennel Club (AKC) is a registry of purebred dog pedigrees in the United States that also has an international reputation. At present, FCI and AKC are the world's largest breed of dog registration institutions that establish the standardization and grouping of purebred dogs, until now various dog organizations in the world use the standards issued by FCI and AKC as guidelines in identifying dog breeds.

Humans are faced with various problems in the selection of dog breed, there are so many breeds available with each of their feature and characteristics and should all of those have aligned with human needs as prospective adopters who also have their respective interests [9]. Selection of the breed that is not compatible can bring problems for both the dog itself and the adopter, a dog may not be well taken care of and even end up in the dog shelter only because of incompatibility with the expectations of the adopter, while the time and cost had wasted for the adopter. More criteria need to be considered by prospective dog adopters apart from physical form characteristics like body size and structure such as the average intelligence level of a breed, ease of care, innate traits, and more. So many criteria that must be considered by prospective adopters in choosing breed types makes decision making a complicated task because of the difficulty in analyzing the influence, interests, and relation between one criteria with another and coupled with many types of breeds available that make this problem requires Multi-Criteria Decision Making (MCDM) approach to handle it. The purpose of this study is to design a Decision Support System (DSS) that can provide analytical recommendations using MCDM approach for the problem of selecting a breed of dog that suit the needs and preferences of the potential adopters.

2. Methodology

2.1. Data Sources

Primary data for this study came from FCI and AKC's online knowledge base sources that contain information on officially recognized breeds, groupings, and their physical and psychological characteristics. Secondary data sources came from interviews conducted with the dog lovers community, dog experts, veterinarians, and kennel owners to find out the experience of the respondents according to their fields and expertise regarding how to choose, care, and handle the breed of dog to be adopted including obstacles encountered in dealing with various problems involving purebred dogs. Data collected from primary and secondary sources were then processed to become a knowledge base of the designed system.

2.2. Analytic Model

To support the developed system model, an MCDM based approach is needed in analyzing data sources to produce an appropriate analytical model [10]. The basic principles of developing an analytical model based on MCDM approach are :

- Decomposition : After defining the problem regarding the selection of dog breeds, then the main problem-solving process was carried out into more specific elements to support structure of the main problem, this process must be carried out until the most specific sub-elements are obtained and formed the hierarchical model.
- Comparative Judgment : Conduct an assessment of the elements relative importance in decision making for the selection of dog breeds at a certain level related to elements at a higher level. The assessment results would be presented in the form of pairwise comparison to get the relative weights among the elements.
- Synthesis of Priority : Each pairwise comparison matrix needs to compute to get local priority value since the pairwise comparison matrix exists at each level, then local priorities must be synthesized to obtain global priorities. Procedures for synthesizing differ according to the shape of the hierarchy. The ordering of elements according to relative importance through a synthesis procedure is called priority setting.

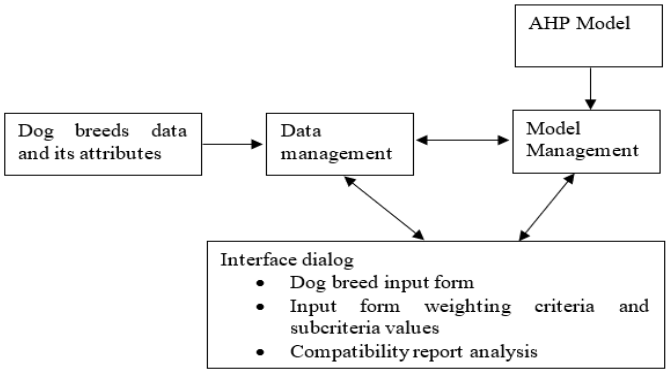


Figure 1: Architecture of DSS for Purebred Dog Selection

2.3. System Modelling

The proposed decision support system model consists of several subsystems, the first is a data management subsystem that utilizes structured data sources as a relational database model, the second is a management subsystem model that utilizes the developed analytic models [11,12]. This analytic model would provide to system an analytical capability by utilizing a

mathematical formula to generate recommendations for the user. Finally, the interface model subsystem is a system component that users used to communicate with the system through an intuitive interface. Figure 1 shows the architectural model of a decision support system for purebred dog selection.

2.4. Data Analysis and Analytic Model

Based on the developed analytic model by processing the data sources, several main criteria and sub-criteria have determined in the selection of dog breeds. These criteria and sub-criteria were obtained based on collected and processed data from a primary data source that was the dog kinology information from the FCI and AKC as the leading world dog registries to obtain standardization information on physical and psychological characteristics of each breed. The collected data was then compared with secondary data sources obtained from dog lovers communities, dog experts, veterinary and kennel owners to know their experience and preferences in selecting and caring for a purebred dog as a result, eight main criteria and seven sub-criteria were formulated with its degree of intensity used in decision making for the selection of purebred dogs as follows:

1. Intelligence: This criterion defines the ability of the dog to obey commands and its tendency to understand new commands. This criterion has two sub-criteria namely obedience and trainability, which defines how good the dog to obey the commands given by its owner at a given time and how good the dog to understand new commands in minimal repetition count, respectively.

a. Obedience

- High: The dog can obey 70 % or more of the command given every time.
- Medium : The dog can obey 30 % or more of the command given every time.
- Low: The dog can obey less than 30% of the command given every time.

b. Trainability

- High: The dog can understand new command with training frequency less than 16 reps.
- Medium: The dog can understand new command with traning frequency 16 to 40 reps.
- Low: The dog can understand new command with training frequency more than 40 reps.

2. Hygiene: This Criterion defines the level of frequency of a dog to produce natural waste that beyond its control like feather loss (shedding) and drooling. This criterion has two sub-criteria namely non-shedding and non-drooling.

a. Non-Shedding

- High: Feather loss rarely occurs.
- Medium: Feather loss occurs periodically/seasonally naturally.
- Low: Feather loss occurs most of the time naturally

b. Non-Drooling

- High: Drooling never or rarely happen..
- Medium: Drooling sometimes occur in certain condition..
- Low: Drooling occurs frequently.

3. Maintenance: This Criterion determines how necessary a specific dog according to the breed type requires special care outside of its daily care, the specific treatment like advanced grooming, specific nail care, and any other special treatment. The intensity degree for this criterion are:

- High: The dog do not need or only require minimal additional care like simple grooming
- Medium : The dog need moderate additional care like full grooming
- Low : The dog needs special care since that affects its hygiene and healthy body. the dog might need advanced grooming, nail trimming, and any other services.

4. Friendliness: This Criterion defines the aggressiveness level of a purebred dog naturally shown against the subject (humans and other animals). Excessive barking toward unfamiliar subject indicates mild aggressive behavior, and severe aggressive behavior has indicated by a tendency to attack the subjects. The intensity degree for this criterion are:

- High: The dog is friendly and generally does not bark if there is no provocative action from the subject.
- Medium: The dog might always bark at any unfamiliar subject.
- Low: The dog has tendency to engage in aggresive behavior including barking and attacking unfamiliar subject.

5. Adaptability: This Criterion defines the level of adaptability of dog breed toward human, other pet, and environment, good adaptability allows the dog to adjust well with the environment and made a good relationship with the adopter and other pets.

a. Adaptation to Human

- High: The dog can adapt well and easy to make new connection with human.
- Medium : The dog can still adapt well but need time to make a new relationship with a human.
- Low : The dog need much time to adapt and build new relationship with human and sometimes the dog may seem uncomfortable until they fully adapt with the human counterparts

b. Adaptation to other pets

- High: The dog highly adaptable and can live along with other pets without problems.
- Medium: The dog can adapt well with a certain pet usually with same species but can behave aggressively to the other one.
- Low: The dog does not like other animal and has a tendency to consider other dog as a rival.

c. Adaptation to environment

- High: The dog highly adaptable to various environmental conditions and has a high tolerance with weather changes.

- Medium: The dog can still adapt well with certain enviromental condition but sometimes need human to help the adaptability process.
- Low: The dog needs a certain environmental condition to live well and very dependant to human to help the adaptability process.

6. Popularity: This criterion defines how popular a breed based on the rankings released by AKC. AKC annually updates the most popular dog ranking data based on genealogy registration, contests, and surveys. For adopters to have a popular dog has benefits such as the ease of joining a large community of dog owners. The intensity degree for this criterion are:

- High: Very popular dog breed, which is a breed that ranks between 1 to 25 according to the latest AKC annual List.
- Medium: moderately popular dog breed, which is a breed that ranks between 26 to 100 according to the latest AKC annual List.
- Low: Less popular dog breed, which is a breed that ranks below 100 according to the latest AKC annual List.

7. Longevity: The life expectancy of a dog breed. According to research, each dog has a lifespan between 5 to15 years depending on the breed [13]. The intensity degree for this criterion are:

- High: The dog breed with an average lifespan above 12 years.
- Medium: The dog breed with an average lifespan between 9 to 12 years
- Low: The dog breed with an average lifespan below 9 years.

8. Impression: Adopters based criteria that express the level of their impression on the certain dog breed subjectively (usually about the dog physically attraction). The intensity degree for this criterion are:

- High: The prospective adopter has a great impression of the breed type.
- Medium: The prospective adopter has a good impression of the breed type.
- Low: The prospective adopter is less interested in breed type.

3. Result and Discussion

3.1. System Design and Evaluation

Based on the designed model, the data of all breeds that have been officially recognized by FCI and AKC were 193 breeds and have been recorded in the database. Table 1 shows some of the breeds available in the system.

Table 1: List of some dog breeds

001	Chihuahua
002	Pekingese
003	Pomeranian
004	Golden Retriever
005	Maltese
006	German Shepherd
007	Border Collie
008	Shih Tzu
009	Labrador Retriever
010	Chow-chow
011	Doberman Pinscher
012	Bulldog
013	Saint Bernard
014	Boxer
015	Bloodhound
016	Shiba Inu
017	Poodle (Toy)
018	Dalmatian

Then from the designed analytical model, each data criteria, sub-criteria, and intensity levels have been structured into the database as shown in table 2 to table 4, there were eight main criteria, which three of them have sub-criteria, finally, there were three degrees of intensity data that will be used for each criterion and sub-criterion.

Table 2: List of Criteria

ID Criteria	Criteria
1	Intelligence
2	Hygiene
3	Maintenance
4	Friendliness
5	Adaptability
6	Popularity
7	Longevity
8	Impression

Table 3: List of SubCriteria

ID SubCriteria	Criteria	Subcriteria
1	Intelligence	Obedience
2	Hygiene	Trainability
1	Maintenance	Non-Shedding
2	Friendliness	Non-Drolling
1	Adaptability	Human
2	Popularity	Animal
3	Longevity	Environment

Table 4: List of Intensity

ID Intensity	Intensity
1	Low
2	Medium
3	High

The system provided several preset (pre-configured set) options that can be used by the user as a prospective adopter for finding the right breed, Besides that users can manually configure the settings tailored to their needs. The preset provided by the system refers to collected data from the FCI and AKC knowledge base in their official website (http://fci.be) and (www.akc.org) plus collaboration with empirical data obtained from the dog lovers community, dog experts, and veterinary. Besides, each preset available will also take the subjective preferences of the user into account by giving the impression criterion certain weight value that will be used in computing to generate recommendations.

There were several pre-configured sets provided by the system that can be used by users in the selection of dog breeds. One

example of a preset provided by the system was namely working-dog preset. This preset was useful for finding dog breed recommendations that have the potential to support humans jobs. This preset has intended to provide recommendations to prospective adopters who need breed types that have great potential to be trained for specific works according to the needs of prospective adopters, for example, dogs that are planned to work as herding dogs for livestock, these dogs must meet the requirement needed as easy to train, independent, easily adaptable, and have good territorial awareness [14]. Another pre-configure set provided by the system wasthe Family-dog preset to help the user to find a dog who can be a great companion for its adopter. The dog expected to be friendly with all family members including children and to other pets such as cats and rabbits. The dogs that are suitable for this role were the dog whose main character is friendly, physically attractive, and have great adaptability to humans and other pets. Both preset certainly have different weighting values and criterion importance ranking, Working-dog preset has higher weighting values for intelligence and adaptability criteria (table 5), while family-dog presets prioritize impression criteria since it is primarily used by an adopter who chooses a dog as a family companion as same as the friendliness criteria which is the second most important criterion for this preset category (table 6). From the criteria weighting matrix, we can get a rank of each criterion based on the eigenvector value. Table 7 and table 8 shows the criteria ranking for working-dog presets and the criteria ranking for family-dog presets respectively.

Table 5: Weighting value matriks for working-dog preset

	Intelligence	Hygiene	Maintenance	Friendliness	Adaptability	Popularity	Longevity	Impression
Intelligence	1	7	4	9	2	5	8	6
Hygiene	0.14	1	0.33	2	0.22	0.5	2	0.5
Maintenance	0.25	3	1	5	0.33	2	4	3
Friendliness	0.11	0.5	0.2	1	0.14	0.25	0.5	0.33
Adaptability	0.5	5	3	7	1	3	6	4
Popularity	0.2	2	0.5	4	0.33	1	3	2
Longevity	0.13	0.5	0.25	2	0.16	0.33	1	0.5
Impression	0.16	2	0.33	3	0.25	0.5	2	1
Total	2.49	21	9.61	33	4.41	12.58	26.5	17.3

Table 6: Weighting value matriks for family-dog preset

	Intelligence	Hygiene	Maintenance	Friendliness	Adaptability	Popularity	Longevity	Impression
Intelligence	1	0.2	4	0.25	3	0.5	2	0.16
Hygiene	5	1	8	2	7	4	6	0.5
Maintenance	0.25	0.125	1	0.14	0.5	0.25	0.33	0.11
Friendliness	4	0.5	7	1	6	3	5	0.33
Adaptability	0.33	0.14	2	0.16	1	0.25	0.5	0.125
Popularity	2	0.25	4	0.33	4	1	3	0.2
Longevity	0.5	0.16	3	0.2	2	0.33	1	0.14
Impression	6	2	9	3	8	5	7	1
Total	14.8	4.38	38	7.08	31.5	14.33	24.83	2.56

Table 7: Criterion importance rank for working-dog preset

Criteria	Eigenvector value	Priority Rank
Intelligence	0.3862	1
Adaptability	0.2407	2
Maintenance	0.1329	3
Popularity	0.0892	4
Impression	0.0623	5
Hygiene	0.0489	6
Longevity	0.0342	7
Friendliness	0.0236	8
	Consistency ratio	2.63%

Table 8: Criterion importance rank for family-dog preset

Criteria	Eigenvector value	Priority Rank
Intelligence	0.3433	1
Adaptability	0.246	2
Maintenance	0.1762	3
Popularity	0.0872	4
Impression	0.0597	5
Hygiene	0.0399	6
Longevity	0.0272	7
Friendliness	0.0204	8
	Consistency ratio	3.69%

The next step after all the criteria and sub-criteria weights have obtained from the preceding process was to perform the computation on all of these weights value to each official breed stored in the database to get the compatibility score of each dog breed. The process of calculating the compatibility value of each alternative has done by weighting the intensity of each criterion and sub-criterion to each dog breed profile based on information stored in the data source. In this example, the subjective preference of prospective adopter was ignored by weighting the intensity of the impression criteria for each breed using the same value. The compatibility result of each breed for Working-dog presets and Family-dog presets were shown in Figure 2 and Figure 3, respectively.

ALTERNATIVE COMPATIBILITY SCORE

Weighting Result | | Summary

Alternative	Intelligence		Hygienity		Maintenance	Friendliness	Adaptability			Popularity	Longevity	Impression	SUM
	Obedience	Trainability	Non-Shedding	Non-Drooling			Human	Pet	Environment				
Pomeranian	0.2455	0.1227	0.0019	0.0368	0.0533	0.0095	0.0618	0.0618	0.0099	0.0892	0.0055	0.0623	**0.7602**
Golden Retriever	0.2455	0.1227	0.0049	0.0148	0.0533	0.0236	0.1541	0.0618	0.0247	0.0892	0.0137	0.0623	**0.8706**
German Shepherd	0.2455	0.1227	0.0049	0.0148	0.1329	0.0236	0.1541	0.0618	0.0247	0.0892	0.0137	0.0623	**0.9502**
Border Collie	0.2455	0.1227	0.0019	0.0059	0.1329	0.0095	0.0618	0.0248	0.0099	0.0358	0.0137	0.0623	**0.7267**
Labrador Retriever	0.2455	0.1227	0.0049	0.0148	0.1329	0.0236	0.1541	0.0618	0.0099	0.0892	0.0137	0.0623	**0.9354**
Doberman Pinscher	0.2455	0.1227	0.0121	0.0059	0.1329	0.0038	0.0618	0.0248	0.0247	0.0892	0.0137	0.0623	**0.8364**
Shiba Inu	0.2455	0.0197	0.0019	0.0148	0.1329	0.0236	0.0618	0.0618	0.0247	0.0358	0.0137	0.0623	**0.6615**
Poodle Toy	0.2455	0.1227	0.0121	0.0368	0.0313	0.0095	0.0618	0.0618	0.0247	0.0892	0.0342	0.0623	**0.7819**
Dalmatian	0.0985	0.1227	0.0019	0.0148	0.1329	0.0095	0.1541	0.0618	0.0247	0.0358	0.0137	0.0623	**0.6531**
Miniatur Schnauzer	0.2455	0.1227	0.0121	0.0368	0.0213	0.0095	0.0618	0.0618	0.0099	0.0892	0.0137	0.0623	**0.7466**
Miniatur Pinscher	0.0985	0.1227	0.0019	0.0368	0.1329	0.0038	0.0618	0.0618	0.0099	0.0358	0.0342	0.0623	**0.6624**
Pappilon	0.2455	0.1227	0.0049	0.0368	0.0213	0.0236	0.1541	0.0248	0.0099	0.0358	0.0342	0.0623	**0.7759**
Rottweiler	0.2455	0.1227	0.0121	0.0148	0.1329	0.0095	0.0618	0.0248	0.0247	0.0892	0.0137	0.0623	**0.814**

Figure 2: Breed compatibility result for working-dog preset

ALTERNATIVE COMPATIBILITY SCORE

Weighting Result | | Summary

Alternative	Intelligence		Hygienity		Maintenance	Friendliness	Adaptability			Popularity	Longevity	Impression	SUM
	Obedience	Trainability	Non-Shedding	Non-Drooling			Human	Pet	Environment				
Chihuahua	0.016	0.0032	0.0245	0.185	0.0204	0.0707	0.007	0.0028	0.0011	0.0872	0.0399	0.3433	**0.8011**
Pekingese	0.0064	0.0032	0.0245	0.185	0.0082	0.0707	0.0174	0.007	0.0011	0.035	0.016	0.3433	**0.7178**
Pomeranian	0.0398	0.0199	0.0098	0.185	0.0082	0.0707	0.007	0.007	0.0011	0.0872	0.0064	0.3433	**0.7854**
Golden Retriever	0.0398	0.0199	0.0245	0.0742	0.0082	0.1762	0.0174	0.007	0.0028	0.0872	0.016	0.3433	**0.8165**
Maltese	0.016	0.0032	0.061	0.185	0.0033	0.0707	0.0174	0.007	0.0004	0.0872	0.016	0.3433	**0.8105**
German Shepherd	0.0398	0.0199	0.0245	0.0742	0.0204	0.1762	0.0174	0.007	0.0028	0.0872	0.016	0.3433	**0.8287**
Border Collie	0.0398	0.0199	0.0098	0.0297	0.0204	0.0707	0.007	0.0028	0.0011	0.035	0.016	0.3433	**0.5955**
Shih Tzu	0.0064	0.0032	0.0245	0.185	0.0082	0.1762	0.0174	0.007	0.0011	0.0872	0.0399	0.3433	**0.8994**
Labrador Retriever	0.0398	0.0199	0.0245	0.0742	0.0204	0.1762	0.0174	0.007	0.0011	0.0872	0.016	0.3433	**0.8287**
Chow Chow	0.0064	0.0032	0.0098	0.0742	0.0033	0.0283	0.007	0.007	0.0011	0.035	0.0399	0.3433	**0.5585**
Doberman Pinscher	0.0398	0.0199	0.061	0.0297	0.0204	0.0283	0.007	0.007	0.0028	0.0872	0.016	0.3433	**0.6624**
Bulldog	0.0064	0.0032	0.0098	0.0742	0.0082	0.1762	0.0174	0.0028	0.0028	0.0872	0.0064	0.3433	**0.7379**
Saint Bernard	0.0064	0.008	0.0098	0.0297	0.0033	0.1762	0.0174	0.007	0.0011	0.035	0.0064	0.3433	**0.6436**
Boxer	0.016	0.008	0.0245	0.0297	0.0204	0.0707	0.0174	0.007	0.0028	0.0872	0.0064	0.3433	**0.6334**
Bloodhound	0.0064	0.0032	0.0245	0.0297	0.0204	0.0707	0.0174	0.007	0.0028	0.035	0.0064	0.3433	**0.5668**

Figure 3: Breed compatibility result for family-dog preset

Based on the results of the compatibility value, the system will display three dog breeds by the highest compatibility value to be used as recommendations for prospective adopters. Figure 4 and Figure 5 shows the three recommended dog breed by the system for working dog presets and family dog presets respectively.

Working Dog Recommendations

Picture	Dog Breed	Total Score
	German shepherd	0.9502
	Labrador retriever	0.9354
	Golden retriever	0.8706

Figure 4: Working-dog recommendation by system

Family Dog Recommendations

Picture	Dog Breed	Total Score
	Shih Tzu	0.8994
	Papillon	0.8882
	Siberian Husky	0.8752

Figure 5: Family-dog recommendation by system

4. Conclusion

Based on research conducted, researchers have designed an analytical model that uses multiple data sources to gather information regarding the physical and psychological characteristics of each dog breed for quantitative analysis without rule out the personal subjectivity of prospective dog adopters. The result was a decision support system that can assist prospective dog adopters in choosing the breed that suits their needs and preferences best by making recommendations based on the dog breed compatibility ranking towards their preference. The final decision remains the prerogative of prospective adopters with all the consequences.

Conflict of Interest

The authors declare no conflict of interest.

References

[1] P. Chyan, "Decision Support System for Selection of Dog Breeds," in 2018 International Seminar on Research of Information Technology and Intelligent Systems (ISRITI), 343–346, 2018, doi:10.1109/ISRITI.2018.8864327.

[2] S. Barnard, C. Passalacqua, A. Capra, S. Marshall-Pescini, E.P. Previde, P. Valsecchi, "Social behavioral profile of different dog breeds," Journal of Veterinary Behavior, **6**(1), 83–84, 2011, doi:https://doi.org/10.1016/j.jveb.2010.09.004.

[3] M. Nitzschner, A.P. Melis, J. Kaminski, M. Tomasello, "Dogs (Canis familiaris) evaluate humans on the basis of direct experiences only," PloS One, **7**(10), e46880–e46880, 2012, doi:10.1371/journal.pone.0046880.

[4] S. Coren, The Intelligence of Dogs: A Guide to Thoughts, Emotions, and Inner Lives of Our Canine Companions, Atria Books, 2006.

[5] S. Coren, How Dogs Think, First Free Press, Simon & Schuster, New York, 2004.

[6] A. Miklosi, Dog Behaviour, Evolution, and Cognition, 2nd Editio, Oxford University Press, 2016.

[7] A.R. Michell, "Longevit of British breeds of dog and its relationships with-sex, size, cardiovascular variables and disease," Veterinary Record, **145**(22), 625–629, 1999, doi:10.1136/vr.145.22.625.

[8] J. Anderson, M. Krieger, M. Safley, A comparative analysis of alpaca breed type and standards, Northwest Alpaca at Wayback Machine, 2009.

[9] C. Coile, Encyclopedia of Dog Breeds, Barron's Educational series, 2015.

[10] T.. Saaty, Fundamentals of Decision Making and Priority Theory with the Analytic Hierarchy Process, RWS Publication, 2000.

[11] P. Chyan, "Design of intelligent camera-based security system with image enhancement support," Journal of Physics: Conference Series, **1341**, 42009, 2019, doi:10.1088/1742-6596/1341/4/042009.

[12] P. Chyan, "Image Enhancement Based On Bee Colony Algorithm," Journal of Engineering and Applied Sciences, **14**(1), 43–49, 2019.

[13] E. Korec, O. Chalupa, M. Hančl, J. Korcová, M. Bydžovská, "Longevity of Cane Corso Italiano dog breed and its relationship with hair colour," Open Veterinary Journal, **7**(2), 170–173, 2017, doi:10.4314/ovj.v7i2.15.

[14] M.J. Dotson, E.M. Hyatt, "Understanding dog–human companionship," Journal of Business Research, **61**(5), 457–466, 2008, doi:https://doi.org/10.1016/j.jbusres.2007.07.019.

ASTES

Advances in Science, Technology and Engineering Systems Journal Vol. 5, No. 5, 154-166 (2020)

www.astesj.com

Special Issue on Multidisciplinary Innovation in Engineering Science & Technology

ASTESJ

ISSN: 2415-6698

Four-Dimensional Sparse Data Structures for Representing Text Data

Martin Marinov*, Alexander Efremov

Faculty of Automatics, Technical University of Sofia, 1000, Bulgaria

ARTICLE INFO

Article history:
Received: 12 July, 2020
Accepted: 24 August, 2020
Online: 10 September, 2020

Keywords:
Text Classification
Data Cleaning
Data Preparation
Sparse Representations

ABSTRACT

This paper focuses on a string encoding algorithm, which produces sparse distributed representations of text data. A characteristic feature of the algorithm described here, is that it works without tokenizing the text and can avoid other data preparation steps, such as stemming and lemmatization. The text can be of arbitrary size, whether it is a single word or an entire book, it can be processed in the same way. Such approaches to text vectorization are not common in the machine learning literature. This sets the presented encoder apart from conventional text vectorizers. Two versions of the encoding algorithm are described and compared - the initial one and an improved version. The goal is to produce a robust data preparation procedure, capable of handling highly corrupted texts.

1. Introduction

This paper describes a modification of a text encoding algorithm, presented at ICASC 2019. Since the conference proceedings paper [1] was written, there have been further developments and those will be presented here, but first a bit of backstory.

One of the most prolific research teams, who currently experiment with sparse distributed representations (SDR), are Jeff Hawkins, Subutai Ahmad [2] and the people working with them at the private company Numenta. The principle author of this paper found out about the concept of SDR from their work and drew inspiration from their research.

An important thing to note, is that the long term goal of the researchers at Numenta is to distance their developments from conventional machine learning and artificial neural networks. We do not share this goal, in fact we are merely trying to make solutions based on sparse information representation, which are complementary to classic machine learning.

Here we present a type of encoder for text data, which is not described in the research paper on sparse encoders, published by a member of Numenta [3]. Our solution is also different from the Cortical.io SDR text encoder, which is mentioned in point 6 of the Numenta paper (Webber, "Semantic Folding"). We follow the principles described in the conclusions of the Numenta research paper, but the algorithms and implementation are entirely our own. The data structures we use are not binary arrays, we use key-value data structures to implement the representations. Compared to other SDR text encoders, another notable difference in our approach is that we consider characters to be the basic building units of text, not abstract constructs such as words.

This paper focuses on a key enhancement made to our algorithm, presented at ICASC, and the potential benefits it offers. It also covers the development of a benchmark text classification problem, for evaluating the utility of our text encoding algorithms, by comparing them to conventional text vectorizers.

To avoid confusion, our initial algorithm will be referred to as CP (Current-Prior). The modified one, which is the focus of this paper, will be referred to as CPPP (Current-Position-Prior-Position). Their names hint at the way in which they transform strings into sparse distributed representations.

2. Comparing CP and CPPP sparse representations

In brief, CP encoding goes through strings character by character and uses only their sequencing to create a sparse representation of the strings in a two-dimensional encoding space. For a more detailed description of each step, please refer to the ICASC paper. The encoding space is an abstract concept and one of its key features is that the coordinate system uses non-numeric characters, to define the location of points within the space. As the CP encoder moves from character to character, it projects the last

*Corresponding Author, Martin Marinov, e-mail: mu_marinov@abv.bg

character it has read onto the horizontal axis, but it also uses the vertical axis to track prior characters. This is why the algorithm is called current-prior. The result is a specific pattern of points in the encoding space, which is highly dependent on the symbol arrangement of the strings being processed.

	-	a	b	c	d	e	f	g	h
-									
a									
b									
c									
d						de		dg	
e					ed	ee		eg	
f									
g						ge			
h									

Figure 1: edge (CP encoded)

		d						e						g					
		0	1	2	3	4	5	0	1	2	3	4	5	0	1	2	3	4	5
d	0																		
	1																		
	2											de					dg		
	3																		
	4																		
	5																		
e	0																		
	1			ed								ee					eg		
	2																		
	3																		
	4																		
	5																		
g	0																		
	1																		
	2																		
	3											ge							
	4																		
	5																		

Figure 2: edge (CPPP encoded)

The encoding patterns can be illustrated in various ways, with one of the more human-readable ones being tabular representation, as seen on Figure 1. If the representations are being processed by a computer program, however, there are more suitable data structures, which could be used. For example, the CP encoded word shown in Figure 1 can be stored as a set of character pairs: {' e', ' d', ' g', ' ', 'ed', 'eg', 'ee', 'e ', 'dg', 'de', 'd ', 'ge', 'g '}.

CPPP encoding works in a similar way, but in addition to character sequences it also factors in the position of the characters. In other words, the sparse encoding space has two additional sub-axes, which track the positions of the last read symbol and the position of prior symbols. Even though this defines a four-dimensional encoding space, it can still be represented in tabular form (Figure 2). This is the key modification to the CP algorithm and it is noted in the name (Current-Position-Prior-Position).

In theory, the readability of these tables does not diminish, because the encoded strings are sparse patterns by definition. The repetition of the sub-axes below the main axes doesn't make the tabular representation harder to interpret. It still looks like a grid with seemingly random non-empty elements scattered throughout. There is actually nothing random about the distribution of the non-empty elements, however. It is strictly based on the encoded string.

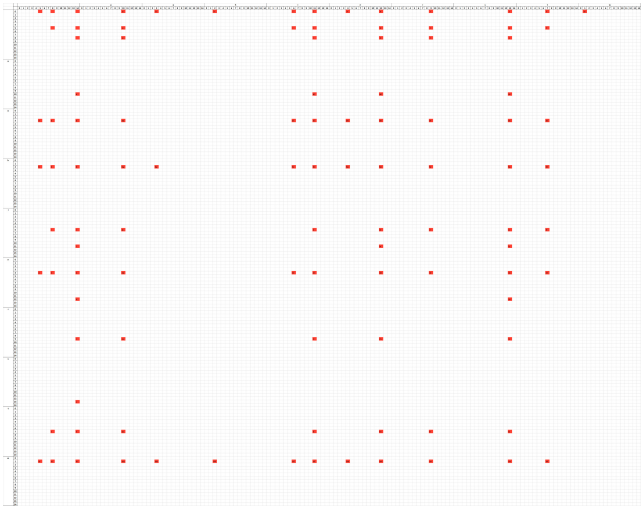


Figure 3: The phrase "when it rains", encoded with CPPP

Difficulties could arise in practice, because of the size of the string being encoded. The sparse representation is still logical and consistent, it is just not possible for a human to comprehend what it means at a glance (Figure 3).

However, these algorithms are meant to be utilized by computers, not people. Machines are far better at processing large amounts of information. The ability to represent the encodings in a human-readable format is useful mainly to the developers, as a debugging tool and a way to illustrate the working principles of these algorithms.

3. Pseudocode implementation

3.1. Input-output

strIn - The string which has to be transformed into a sparse representation. It can be of arbitrary length.

SR - The output from the encoding procedure, i.e. the sparse representation of the input. It is just a key-value data structure. We used python dictionaries, but any other dictionary-like data structures from other languages can be used to implement the algorithms.

winSize - A control parameter, which sets the maximum allowed distance between characters, when forming character pairs.

For example, when encoding an entire book, it would make little sense to form pairs from characters at the start of the book and characters at the very end of the book. That would just create more character pairs (points in the encoding space) than is necessary and significantly increase the size of the sparse representation.

We used winSize = 20, i.e. we told the program not to form points from characters, which were separated by more than 20 characters.

3.2. CP encoding algorithm

Algorithm 1: Current-Prior

```
Result: SR
Receive strIn;
Initialize dictionary object SR;
prior_pos = 0;
while prior_pos < length of strIn do
    current_pos = prior_pos + 1;
    while current_pos < length of strIn do
        chrPair = Concat(strIn[prior_pos], strIn[current_pos]);
        SR[chrPair] = 1;
        current_pos += 1;
    end
    prior_pos += 1;
end
```

3.3. CPPP encoding algorithm

The keys in the CPPP sparse representation key-value data structure are derived in the same way as the ones produced by CP encoding. However, the values are not just a single number. The values are lists of numbers, specifically the positions of the characters, which produced the keys of the dictionary.

Algorithm 2: Current-Position-Prior-Position

```
Result: SR
Receive strIn;
Initialize dictionary object SR;
prior_pos = 0;
while prior_pos < length of strIn do
    current_pos = prior_pos + 1;
    while current_pos < length of strIn do
        chrPair = Concat(strIn[prior_pos], strIn[current_pos])
        if chrPair not in keys of SR then
            SR[chrPair] = list(empty list, empty list);
            append current_pos to list SR[chrPair][0];
            append prior_pos to list SR[chrPair][1];
        end
        current_pos += 1;
    end
    prior_pos += 1;
end
```

4. Advantages and disadvantages of CPPP

When processing repeating syllables and characters, the CP algorithm projects them in the same points of the sparse encoding space. In contrast, CPPP ensures that each repeating symbol will be projected to a different point in the encoding space. A direct consequence of this is that CPPP encoding can handle strings with arbitrary lengths, whereas CP cannot.

It is possible to saturate the two-dimensional encoding space used by the CP algorithm, if a sufficiently long string is processed. CPPP can transform large strings, without decreasing the sparsity of their representations in the four-dimensional encoding space. The significant advantages of this are:

- **Reversible encoding**. It is possible to turn the sparse representations back into strings, without information loss.
- **No need for tokenization**. Text documents (data) can be processed as a single, long, uninterrupted sequence of characters. There is no need for splitting them by delimiters, such as whitespace, commas and such.
- **Increased capacity**. Due to the introduction of the two additional dimensions, for tracking character positions, it is possible to compare not only tokens (words), but entire sentences, phrases, paragraphs and documents.
- **Precise string comparison**. CPPP allows not only the quantification of similarity between strings, but it also makes it possible to determine which specific parts of the strings correspond to each other and which ones differ.

Despite the advantages, the modified algorithm has a notable drawback: the simple methodology for comparison of CP sparse representations is not applicable to CPPP encoded text.

To illustrate the reason, several words encoded by the two algorithms will be examined. The chosen words are **tree**, **trim** and **tree-trimmer**, because these words are short, some of them have double characters and the third one is a compound word, which includes the other two.

CP encoding (Figures 4 to 6) does not represent the following things properly:

- The double **e** in **tree** and the double **m** в **trimmer**. In both cases, the corresponding points for these characters in the encoding space overlap. For the word **tree**, the points are **re** and **te**. For **trimmer**, the points are **im**, **rm** and **tm**.
- The repetition of **tr** in **tree-trimmer** (Figure 6). Again, the representations of the two different instances of this character sequence overlap completely in the two-dimensional encoding space. This means that the initial string cannot be recovered, by using only its sparse representation.

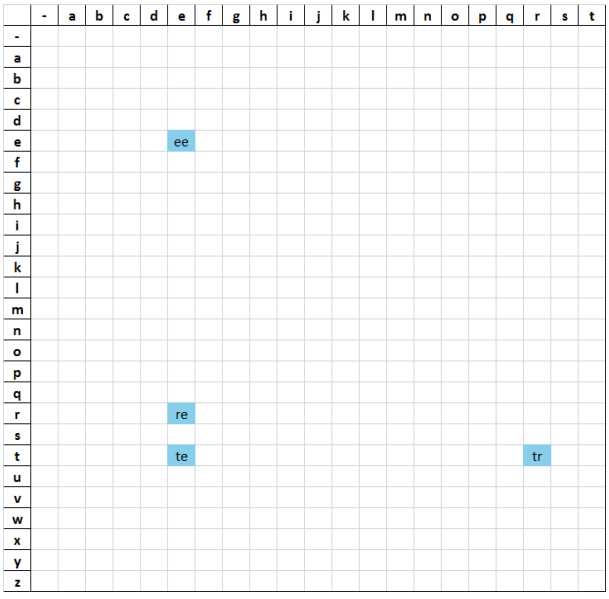


Figure 4: tree (CP encoded)

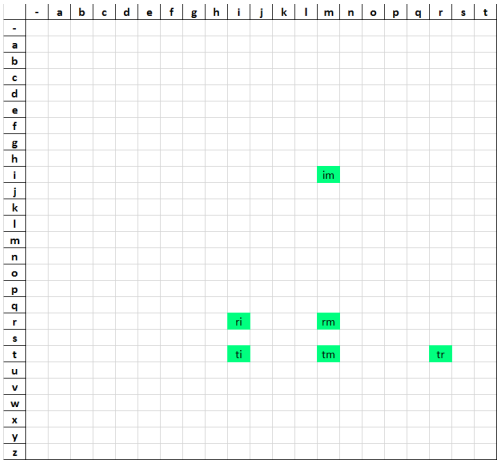


Figure 5: trim (CP encoded)

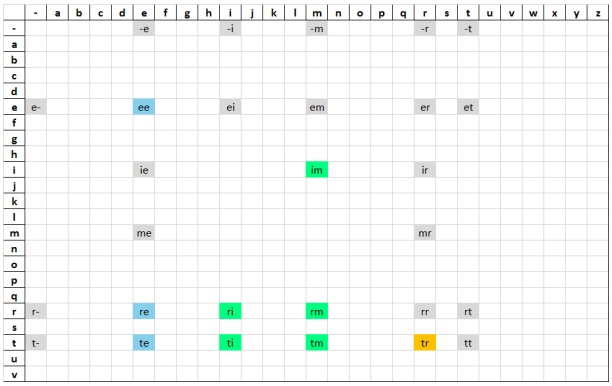


Figure 6: tree-trimmer (CP encoded)

On the other hand, CPPP encoding creates mirror points, when representing repeating character sequences. An example of this can be seen on Figure 7, arrows have been drawn to bring attention to the points in question. They indicate, that the letter **e** is present more than once in the word **tree**. The fact that sectors **re** and **te** have more than one non-empty value is informative, although the algorithmic processing of this information is not as trivial, as the procedure used to compare sparse patterns in CP encoded strings.

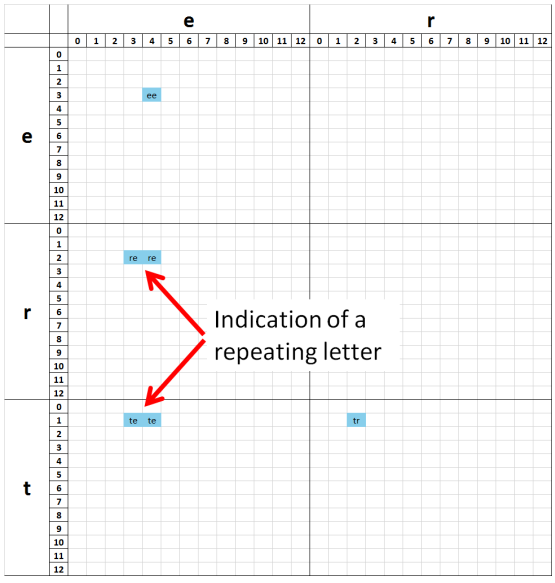


Figure 7: tree (CPPP encoded)

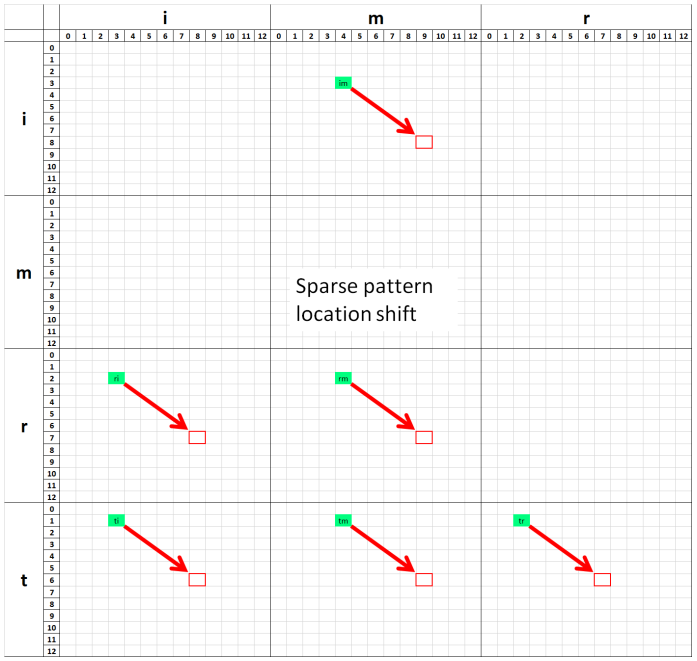


Figure 8: trim (CPPP encoded)

A second complication inherent in CPPP encoding is illustrated on Figures 8 and 9. The points which represent the word **trim** have shifted their positions in the sparse space. This is to be expected, in the third string there is another word before **trim**, which causes a translation of the sparse pattern to the right. This is logical and informative, but again, the algorithmic analysis and quantification of such relations is more complex than the one employed for CP sparse representations of text.



Figure 9: tree-trimmer (CPPP encoded)

These two characteristics of the modified encoding space (mirror points and non-stationary sparse patterns) are the things that give it the aforementioned advantages. However, there is no analogue for them in the two-dimensional encoding space, which means the comparison method developed for CP sparse representations is not applicable to four-dimensional encodings of strings. To utilize the full potential of CPPP encoding, other comparison techniques have to be used.

5. Methods for comparing CPPP sparse representations

In theory, it is possible to feed the encoded strings into artificial neural networks and have them learn to recognize the same types of patterns, which people can notice in small sparse representations. However, in recent years the European Union has begun to implement legal frameworks and guidelines for the use of artificial intelligence, which emphasize the need for algorithmic transparency (see the publications from 2019 by the EPRS, such as "A governance framework for algorithmic accountability and transparency").

It is the opinion of the authors, that the more society delegates decision making to machines, the more the legal regulations and requirements for decision transparency will increase. Conventional ANN are black-box approaches to modelling data and as such, the authors try to avoid relying on them, in favor of more algorithmically transparent models. In addition, it is possible to logically and methodically explain why each element of a CPPP sparse representation exists in the encoding space.

In order to make use of the encoded data, however, specialized procedures have to be developed, for quantifying similarities between encoded strings, as well as processing larger units of written information, such as documents, chapters in books etc. To be more specific, text classifiers based on the bag-of-words approach require accurate word/token counts, in order to build quality TF-IDF representations of textual data. Other machine learning approaches, such as n-gram modelling, require tracking of token sequences as well, in order to take into account the context in which individual words are used in the text.

The methods for distinguishing and locating words in CPPP encoded corpora are currently under development, their implementations could change. However, brief examples will be given, to showcase possible ways of carrying out basic operations with CPPP encoded text.

5.1. Basics of locating words in CPPP text representations

The text is CPPP encoded as a single, uninterrupted string. In addition, the computer has access to a machine-readable dictionary, which consists of separately encoded words. Note the different way of encoding the data and the dictionary. Unlike common practice, tokenization of the dataset is avoided, the text is kept intact and it is CPPP encoded as a whole. This is because it is not known which parts of the text correspond to which words, before some kind of analysis is done. This approach avoids the presupposition, that the text being processed is well formatted and can easily be parsed with a few simple delimiting characters.

The dictionary, however, is a collection of distinct words, by definition, so it is divided into separately encoded strings. It is also possible to curate the dictionary manually and ensure the entries are properly separated, something which usually isn't practicable with the dataset.

5.2. Word search based on maximizing pattern overlaps

For each element (word, token, phrase) in the machine-readable dictionary, the following steps are carried out: finding all potential locations of the search term within the text and filtering the possible results, to leave only the most consistent matches.

5.2.1. Initialization of a character weight vector W.

The purpose of W is to indicate which parts of the text correspond to the dictionary entry, which is under consideration during the entry enumeration. It is initialized as an all-zero vector, with a length equal to the number of characters in the text being analyzed. The first element of W indicates how many times the first character takes part in forming character pairs, which are common to both data and dictionary sparse representations. The second element of W indicates the same for the second character of the text. The third element covers the third character etc.

5.2.2. SPOQ procedure - pseudocode implementation.

The current implementation of the Sparse Pattern Overlap Quantification Procedure, or SPOQ for short, is described here (algorithm 3). It is used to find similar patterns in the encoded data. SR_1 is the sparse representation of the data, SR_2 is a sparse representation of a specific dictionary entry.

Algorithm 3: SPOQ

```
Result: W_SPOQ
Initialize W vector with all zero elements;
commonKeys = Intersection(keys of SR_1, keys of SR_2);
for each com in commonKeys do
    crnt_pos1 = SR_1[com][0];   prev_pos1 = SR_1[com][1];
    crnt_pos2 = SR_2[com][0];   prev_pos2 = SR_2[com][1];
    delta1 = crnt_pos1 - prev_pos1;
    delta2 = crnt_pos2 - prev_pos2;
    for each b in delta2 do
        proximity = abs(delta1 - b);
        W[ crnt_pos1[ index of min(proximity) ] ] += 1;
        W[ prev_pos1[ index of min(proximity) ] ] += 1;
    end
end
```

5.2.3. SPOQ example.

If we look at the sparse representations shown on Figures 8 and 9, their encoding spaces can be divided into sectors (denoted S_T and S_D respectively), by using the primary axes (the ones that track character sequencing). These sectors correspond to the common keys between the two sparse representation data structures. For those sectors, which are not empty and present in both representations, the distances Δp_T and Δp_D are calculated. They indicate how far apart specific pairs of characters are in both representations. For details, see Table 1.

The example shown in Table 1 assumes that the word **trim** is a word from the machine-readable dictionary and **tree-trimmer** is the text. The elements of the weight vector are incremented, based on the closest matches between Δp_T and Δp_D in each sector. This is why indices 6,7,8 and 9 of W will have the highest non-zero values. They correspond neatly to the location of the word **trim**, within the string **tree-trimmer**.

Note that this is a relatively simple procedure and it can produce false positives. The fact that index 1 and 2 also get incremented once is an example of the limitations of SPOQ. In addition, there is no guarantee that all relevant characters will be matched properly.

Table 1: Principle of operation of the SPOQ procedure

S_T	Δp_T	S_D	Δp_D	Incrementations of W
ri	3 – 2 = **1**	ri	8 – 2 = 6	
		ri	8 – 7 = **1**	W_8 += 1 and W_7 += 1
ti	3 – 1 = **2**	ti	8 – 1 = 7	
		ti	8 – 6 = **2**	W_8 += 1 and W_6 += 1
im	4 – 3 = **1**	im	9 – 8 = **1**	W_9 += 1 and W_8 += 1
		im	10 – 8 = 2	
rm	4 – 2 = **2**	rm	9 – 2 = 7	
		rm	9 – 7 = **2**	W_9 += 1 and W_7 += 1
		rm	10 – 2 = 8	
		rm	10 – 7 = 3	
tm	4 – 1 = **3**	tm	9 – 1 = 8	
		tm	9 – 6 = **3**	W_9 += 1 and W_6 += 1
		tm	10 – 1 = 9	
		tm	10 – 6 = 4	
tr	2 – 1 = **1**	tr	2 – 1 = **1**	W_2 += 1 and W_1 += 1
		tr	7 – 1 = 6	
		tr	7 – 6 = **1**	W_7 += 1 and W_6 += 1
		tr	12 – 1 = 11	
		tr	12 – 6 = 6	

5.2.4. *Filtration of weak matches*

The SPOQ search procedure described in points 5.2.2 and 5.2.3 is supposed to generate rough estimations of word positions, within a given text. False positives and overlaps between the weight vectors of multiple dictionary entries are to be expected. Currently, it is assumed that these can be handled with adequate filtration techniques.

Regarding how the filtration of each weight vector is done, the code for the SPOQ procedure was described in point 5.2.2, it is the one which produces the initial W vectors, denoted as W_{SPOQ}. Point 5.2.5 covers the code for the filtration steps, which further modify W_{SPOQ}.

5.2.5. *Pseudocode of the filtration procedures.*

Algorithm 4: Frequency filtration

```
Result: W_F
W = W_SPOQ;  #input
W[W == 1] = 0;
N = length of W – 2; cp = 1;
while cp <= N do
    if W[cp-1] == 0 and W[cp] != 0 and W[cp+1] == 0 do
        W[cp] = 0;
    end
    cp += 1;
end
```

Algorithm 5: Match length filtration

```
Result: W_L
W = W_F;  #input
likely_loc = integer sequence from 0 to length of W;
Keep only the elements of W where W > 0;
W_filtered = zero vector of length W;
i = 0;
j = 1;
while j < length of W do
    if likely_loc[j] - likely_loc[j-1] != 1 then
        substring_size = likely_loc[j-1] - likely_loc[i];
        if substring_size > 2 then
            # This substring is a good match, it is long enough
            W_filtered[ likely_loc[i]: likely_loc[j-1] ] = 1;
        else
            # Bad match, substring is too short
        end
        i = j
    end
    j += 1
end
```

5.3. *Visualization of SPOQ and W filtration.*

To visualize the values of the character weight vector, as it is altered by the filtration steps, we utilize custom plots. In addition to W, they display the actual text under evaluation, so that we can quickly determine if the values of W are as they should be.

The layout of the custom plots is described in Figure 10. For specific example with data, refer to Figures 11 to 14 and point 5.3.1, which describes what those figures illustrate.

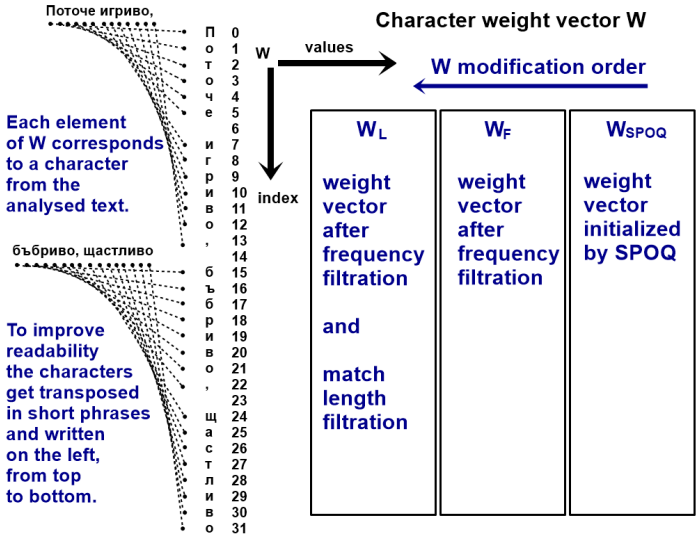


Figure 10: Description of custom plot layout

5.3.1. *Example of SPOQ and W filtration used on text*

To illustrate the filtration process, the Bulgarian poem "Поточе" (Stream), written by Elin Pelin, will be used as an example dataset. When searching for the word песни (songs), the SPOQ procedure is used to obtain an initial weight vector W_{SPOQ}, shown on Figure 11.



Figure 11: search for **песни**



Figure 12: search for **песен**

The largest peak in W_{SPOQ} is roughly equal in size to the length of the search word, about five in this case. As expected, the biggest peak is roughly where the word is in the poem, but there are many other smaller peaks scattered around it. This is why additional filtration steps are necessary.

Many of the individual elements in W_{SPOQ} are equal to 1 or are surrounded by zeros on both sides. Using the frequency filtration procedure, we zero-out all of these and get a clearer indication of where the search-word is, as shown on Figure 11, subplot W_F. Unfortunately, some false positives still remain.

An additional filtration step can be applied, this time targeting the lengths of the matches. Presumably longer sequences of non-zero values indicate better matches. If we zero-out all matches shorter than 2 characters, we obtain the result seen on Figure 11, subplot W_L. This is indeed where the word is in the document.

5.3.2. Necessary refinements to SPOQ and filtration.

There is a caveat to the simple filtrations described here. Their thresholds are static hyper-parameters, meaning they were set by a person at some point and are not necessarily a good fit in all possible word search cases.

For an example of this, refer to Figure 12, which shows the search for the word песен (song). This is the singular form of the word and a more likely entry in a properly curated dictionary. In this case, the match is weaker and a small increase in the threshold of the length filter (from 2 to 4) could zero-out the entire weight vector, thereby suppressing the one relevant match in the dataset.

The filtration thresholds have to be dynamically adjustable by an automated subroutine. Manual adjustment would not be practicable, considering the number of word searches and comparisons that have to be done in an adequately sized corpus.

A single search in the encoded text could produce multiple results, if the search-word is present in the data more than once, as seen on Figure 13. However, multiple results for a single search could also contain false positives, due to the nature of the algorithm.

Figure 14 shows an example of false positives making it through both filtration steps. The reason for this is that the search-word бистро (pure) is contained nearly unchanged in the word сребристо (silvery). This is why the filtered weight vector has 4 peaks, instead of just 2, which is the correct number of occurrences of the search-word. Finding similar character sequences is the intended behavior of the program, but they aren't always a correct match.

Work is still ongoing on the development of dynamic filtration, capable of resolving the issues caused by false positives and ambiguities arising from overlaps between the weight vectors of different dictionary entries. Formulating the problem as an optimization procedure is under consideration, the idea being that this way it will be possible to automatically reach a single interpretation of a given corpus. The aim is to produce a data preparation module, based on CPPP encoding. It should be capable of replacing conventional data preparation steps, such as tokenization, stemming, lemmatization, as well as give sufficiently accurate word counts and position estimations.

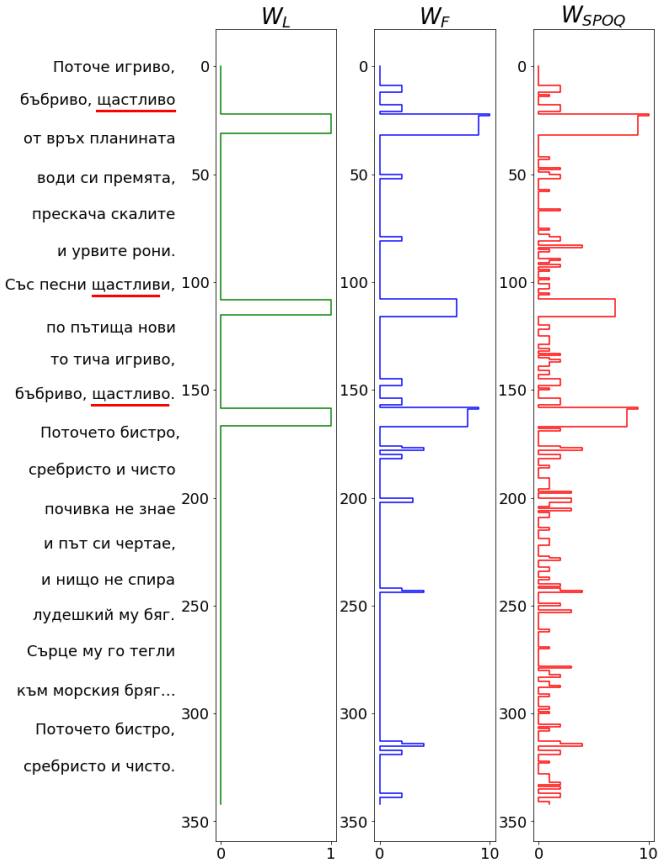


Figure 13: search for **щастливо**



Figure 14: search for **бистро**

6. Text classification benchmark

In order to conduct a more rigorous evaluation, of the performance and quality of CPPP data preparation, a classification problem has been defined, by using a dataset from the LSHTC challenges [4]. Specifically, the small wikipedia dataset from LSHTC3 was used, since it was the only challenge in which the raw text was provided.

The dataset has 456886 documents, each one containing only abstracts of wikipedia articles. The documents are labeled, although the labels are not human readable, they are merely integers representing a specific topic covered in each document. There is also a complex label hierarchy, however for the purposes of our benchmark problem, we do not take it into account. We only use a subset of the entire corpus, which contains documents with a single label. In addition, we alter the labels to reduce everything to a binary classification problem. This way we can train a simple model and focus on the data preparation part of the workflow. The aim is to make changes only in the data preparation stage, the text classifier itself will always be the same, with fixed hyper-parameters.

6.1. Subsetting the dataset and forming binary labels

Looking only at the documents with a single label, the top 10 most frequently occurring label codes are listed in Table 2. Next to the codes are descriptions, based on reading and evaluating a dozen of the documents associated with a given label.

Table 2: Top 10 most used labels

Label	Documents	Label Description
167593	5277	Movies
347803	1470	Businessmen and inventors
324660	1433	Historic buildings
283823	1359	Writers and journalists
284433	1310	Journalists
272741	1006	Film actors
395447	999	Screenwriters
114873	945	Plants
352578	846	Novelists
93043	762	Painters

Label 167593 was chosen as the positive class (the one we want to predict with the model). The decision was based solely on the number of documents tagged with 167593. To create the benchmark corpus, all documents with the chosen label were selected, and reassigned to class 1. An additional 4000 randomly chosen documents, from the remaining 451609 in the dataset, were assigned to class 0, regardless of what their labels were originally. This is how the initial classification of the documents was reduced to a binary classification problem.

In addition, a variable was added to the subset, which randomly separates it into two roughly equal in size parts. This is used to perform a training-validation split, for when the text classification model is trained on the subset.

The only preprocessing of the raw text was the removal of punctuation and the substitution of numbers with the placeholder <NUMBER>. Other preprocessing steps, such as named entity

recognition, have not been implemented, although they are under consideration.

Note that for statistical purposes, this procedure was repeated 30 times, to produce 30 distinct subsets, each with different documents assigned to the negative class 0 and different training-validation splits. The number 47 was used as a seed for generating 30 random numbers, which in turn were used as seeds when the subsets were created. This ensures repeatability of the process. The pseudocode for creating subsets is included (Algorithm 6).

Algorithm 6: Procedure for subsetting the LSHTC3 dataset

Result: Document subsets

```
# Parameters for subset generation
ran_stat = 47;              # keep constant, used as seed
num_of_subsets = 30;        # Can be varied
N_neg = 4000;               # Can be varied
train_test_ratio = 0.5;     # Can be varied

Load dataset (Dw)
Separate docs for positive and negative class (Dn and Dp);

# Generate a list of random integers
rand_int_list = generate_random_integers(
    max value = 1000000,
    length = num_of_subsets,
    seed = ran_stat
);

for each rand_int in rand_int_list do
    Randomly sample (seed = rand_int) N_neg documents
    from Dn;
    Append Dn_sample to Dp to get subset Ds;
    Remove punctuation in Ds;
    Replace numbers with <NUMBER> in Ds;
    Add train-test separation flag to Ds(seed = rand_int);
    Save the subset Ds as "subset_<rand_int>.csv";
end
```

6.2. Corrupting the text

In order to test whether CPPP encoding can provide more robust data preparation than conventional techniques, each of the created subsets had its documents subjected to varying degrees of text corruption. Note that this only affects the documents used for model validation, the training documents were untouched. The types of text corruption used are:

- D – character deletions. Example: **word** becomes **wrd**.
- I – character insertions. Example: **word** becomes **wyozrds**.
- B – character blurring. Repeating one or more character in the string many times. Example: **wworrrd**.

These three basic types of corruption can be combined together in 7 meaningful ways (___, __I, _D_, _DI, B__, B_I, BD_, BDI), if we allow for the possibility that one or more of them can be inactive. The inactive ones are indicated by an underscore.

In addition, it is possible to regulate the number of affected words in a document, as well as the severity of text corruption. Table 3 shows examples of the codes used to denote corruption type and severity and explains how to interpret them.

Table 3: Corruption code examples

Corruption code	Interpretation
___ 000 000 0011528	No corruption, use the subset derived from seed 11528.
__I 001 005 0367540	Insert extra characters, at most 1 per word, for 5% of the words in each document. Use the subset derived from seed 367540.
B_I 009 001 0815602	Blur and insert characters, at most 9 per word, for 1% of the words in each document. Use the subset derived from seed 815602.

Generating the corrupted subsets is done automatically by the benchmark application, which enables the systematic production of thousands of datasets, with varying degrees of corruption. This procedure has a longer code implementation than the algorithms described so far, which is why it has been split into two parts for ease of readability.

The inner word corruption procedure (Algorithm 8) is the one, which actually changes the words/tokens. The outer corruption procedure (Algorithm 7) is the one which tokenizes the documents and selects which words/tokens in which documents to corrupt. The outer corruption procedure also cycles through all test documents and generates different corruption possibilities, depending on three parameters:

- CT – corruption type (see the start of 6.2);
- NCA – number of characters to alter per word;
- NWD – number of words to alter per document.

Note that the user does not simply specify the values of these 3 parameters, the user provides several valid values for each of them. The benchmark application determines all relevant parameter combinations by itself.

Algorithm 7: Outer word corruption procedure

Result: Corrupted document subset

```
Load subset file;
Determine which documents are for training and testing;
Extract rand_int from the subset name, it will be used as a
seed for the random number generator;
ParamCombinations = VaryParameters(
    valid_values_for_CT,
    valid_values_for_NCA,
    valid_values_for_NWD
);
for each parameter combination in ParamCombinations do
    for each docTxt in documents for testing do
        Tokenize docTxt;
        indeces_of_words = randomly select words to alter;
        for each wrd_ind in indeces_of_words do
            Call the inner word corruption procedure;
        end
    end
end
```

Algorithm 8: Inner word corruption procedure

Result: A single corrupted word/token

```
Read parameters from the outer procedure;
Read docTxt and wrd_ind (indexes the target word);

Randomly select only one type of text corruption to use;

# Select positions in the word for corrupting randomly
max_index = length of doc_txt[wrd_ind] – 1;
wrd_seed = rand_int + max_index +
Unicode code point of first character +
Unicode code point of last character;
 if max_index == 0 do
   positions = list with one element (index 0);
 Else
   positions = generate_random_integers(
       from 0 to max_index,
       length = chars_to_alter,
       seed = wrd_seed
   );
 End

 if corruption_type is D do
    if length of positions > 1 do
       Leave only unique values in positions list;
       Sort positions list in descending order;
    End
    for each pos in positions do
       delete character at pos in doc_txt[wrd_ind];
    End
 End

 if corruption_type is I or B do
    if corruption_type is I do
       if length of positions > 1 do
          Sort positions list in descending order;
       End
       seed = wrd_seed;
       chars2ins_length = chars_to_alter;
       chars2ins = random Unicode code points (32 to 126);
    End

    if corruption_type is B do
       chars2ins = empty list
       for each pos in positions do
          Append Unicode code point of
          doc_txt[wrd_ind][pos] to chars2ins;
       End
    End
    i = 0
    while i < length of positions do
       insert chars2ins[i] into positions[i] of doc_txt[wrd_ind];
       i += 1
    End
 End
```

6.3. Predetermining computation requirements

If processing time or memory is an issue, the total number of corrupted datasets Dc can be calculated beforehand with an equation (1).

$$D_c = N_s(1 + CA_cA_w) \quad (1)$$

where:

- N_S – Number of initial subsets.
- C – The number of meaningful combinations of the basic types of text corruption.
- A_C – The number of character alteration levels.
- A_W – The number of word alteration levels.

As mentioned earlier, we prepared an example with 30 distinct subsets from the full corpus. If we want to alter 1, 3 and 9 characters per word for 1, 5, 20, 50, 80 and 95 percent of the words in each document, then:

$A_C = |\{1, 3, 9\}| = 3$

$A_W = |\{1, 5, 20, 50, 80, 95\}| = 6$

Thus, the application would produce 30*(1+7*3*6) = 3810 distinct subsets, all with varying types and severity of text corruption, within the desired ranges.

6.4. Training the text classifiers

The Python module scikit-learn was used, specifically the TfidfVectorizer object for feature extraction and the RandomForestClassifier object for creating the text classification models. A distinct model is trained on each of the subsets. Their hyper-parameters are fixed, so any change in prediction quality is due entirely to the dataset, nothing else. The feature extractor and model were trained only on the training data, the validation data was only used to generate class predictions.

The hyper-parameters of the TfidfVectorizer are as follows:

- stop_words = 'english'
- analyzer = 'word'
- vocabulary = None
- binary = True
- max_df = 1.0
- min_df = 1
- use_idf = False
- smooth_idf = False
- sublinear_tf = False

The hyper-parameters of the random forest classifier were the default ones, the only parameter we explicitly specified was random_state. This was set equal to the final number in the corrupted subset names (see Table 3). This number is the seed used to generate the subset. Using it as the seed for the model ensures that the random forest algorithm will produce consistentl results for each subset file, no matter how many times the benchmark is executed.

6.5. Evaluating the benchmark results

As expected, models evaluated with uncorrupted or lightly corrupted datasets perform very well, models tested with

moderately corrupted documents perform worse and the ones tested with text with severe corruption perform the worst of all.

The full table of classification results is 3810 rows, too large to be included in this paper. Only a snippet is included (Table 4) to show what the format of the output looks like. The full table is summarized with charts in point 6.6.

Table 4: Excerpt from the classification results table

CT	NCC	PWC	Seed	TP	TN	FP	FN
___	0	0	189191	2525	1891	107	95
BDI	3	1	265329	2543	1844	136	96
BDI	3	5	11528	2422	1800	213	169
BD_	1	20	265329	1303	1865	1376	75
BD_	1	50	11528	2387	1247	248	722
B_I	3	95	265329	269	1886	2410	54
B_I	9	1	11528	2520	1866	115	103
_D_	9	95	11528	2380	1436	255	533
_D_	9	5	889991	2513	1905	141	80
_D_	9	50	616169	1321	1880	1327	90
_DI	9	20	837510	1459	1889	1170	82
__I	1	5	998096	2482	1868	146	127
__I	1	20	11528	2348	1826	287	143

Table header descriptions:

- CT – text corruption type.
- NCC – Number of characters altered per word.
- PWC – Percentage of words affected in each test document.
- Seed – The random number generator seed, which was used to create the initial subset and to alter the text.
- T_P – true positives.
- T_N – true negatives.
- F_P – false positives.
- F_N – false negatives.

6.6. Visualizing the benchmark results

In order to visualize the classifier results in a more compact manner, two things were done with the full results table. First, all T_P, T_N, F_P and F_N were averaged and grouped by CT, NCC and PWC. This effectively combines the results for all of the 30 distinct seeds/subsets which were used. The aggregated results table is reduced to only 128 rows as a result of this summarization.

The second step is quantifying the quality of the classification models. Two metrics were calculated, the first one of which is the widely used F_1 score (4), which is just the harmonic mean of the Precision (2) and Recall (3) metrics. The other quality metric is the Matthews correlation coefficient MCC [5], which is specifically designed to give more reliable evaluations for binary classification results (5).

$$P = \frac{T_P}{T_P + F_P} \quad (2), \quad R = \frac{T_P}{T_P + F_N} \quad (3), \quad F_1 = 2\frac{PR}{P + R} \quad (4)$$

$$MCC = \frac{T_P T_N - F_P F_N}{\sqrt{(T_P + F_P)(T_P + F_N)(T_N + F_P)(T_N + F_N)}} \quad (5)$$

The resulting charts are shown on Figures 15 to 28. Note that the Percent of Words Changed per test document (PWC) is on the x-axis, the classification quality metrics are on the y-axis and there is a separate line for each of the 3 levels of word corruption used (1, 3 and 9 character alterations per word).

From the charts it is evident, that there is a consistent downward trend of model quality versus PWC, regardless of the way in which the datasets were corrupted. An interesting thing to note is that MCC is more sensitive than the F_1 score. This, combined with the fact that it gives reliable results, even when the class sizes are imbalanced, makes it the preferred model evaluation metric by the authors.

A detailed comparison between the many text corruption approaches is beyond the scope of this paper. What matters is that the overall trends are the same, regardless of the exact manner in which the test texts were damaged.

The intent here is to describe the benchmark classification problem, which will serve as an evaluation tool for the quality of the custom data preparation tools, based on CPPP encoding. The experimental setup might change (more granulated levels of PWC, more subsets etc.). Once the custom data preparation solution is more mature, it will be evaluated alongside the conventional feature extraction objects from the nltk package in Python.

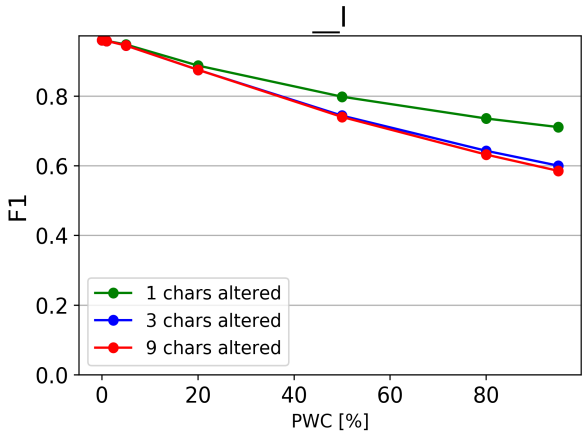


Figure 15: Effect of character insertions on classification quality

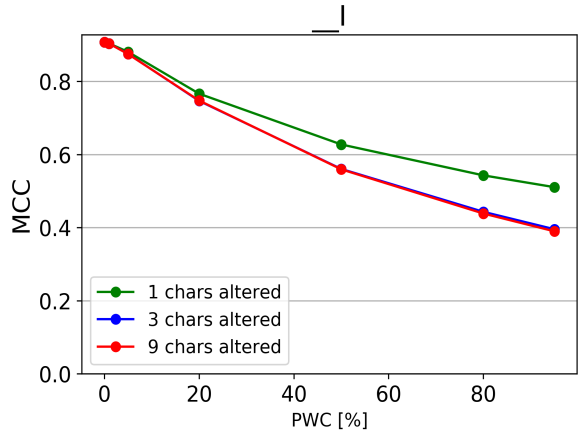


Figure 16: Effect of character insertions (MCC)

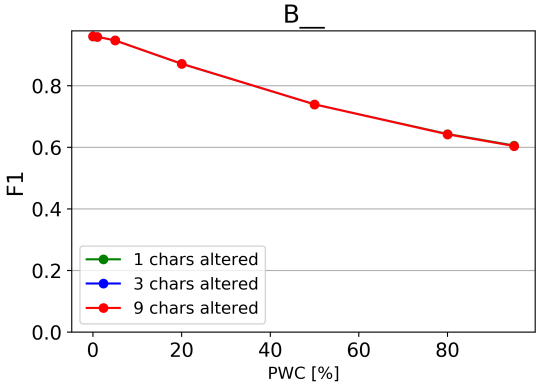


Figure 17: Effect of character repetitions on classification quality

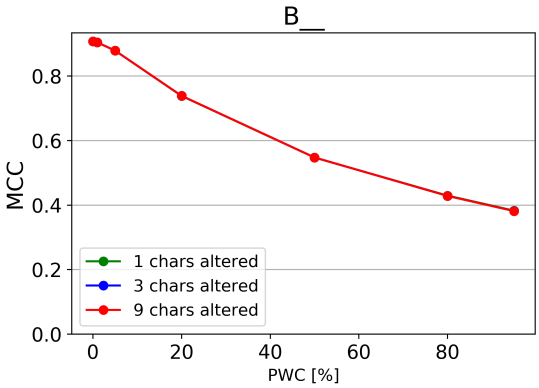


Figure 18: Effect of character repetitions (MCC)

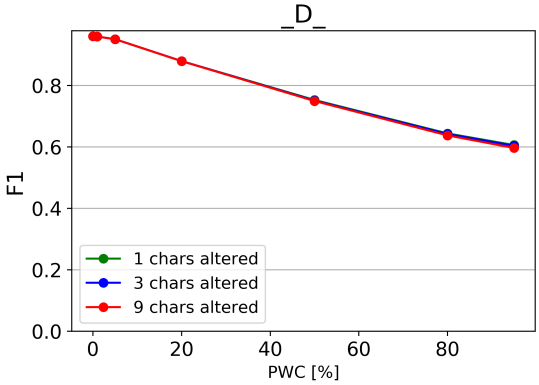


Figure 19: Effect of character deletions on classification quality

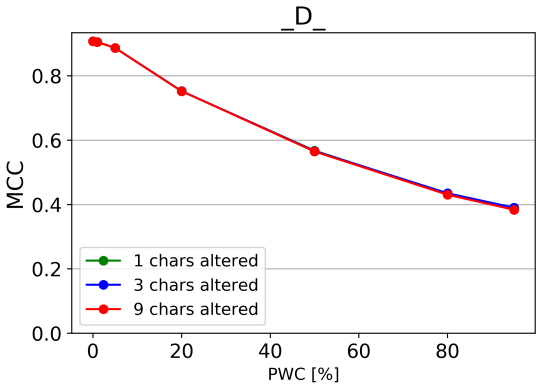


Figure 20: Effect of character deletions (MCC)

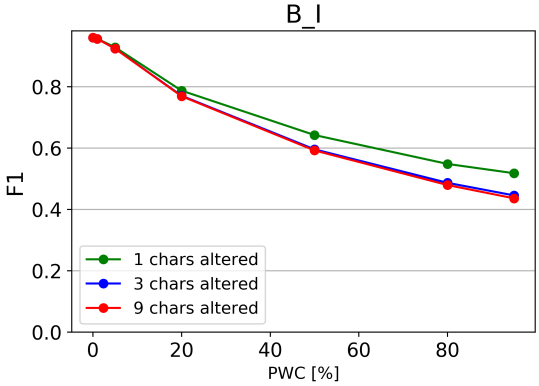


Figure 21: Effect of character repetition and insertion on classification quality

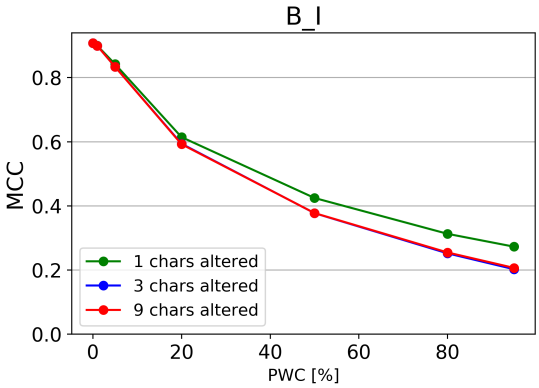


Figure 22: Effect of character repetition and insertion (MCC)

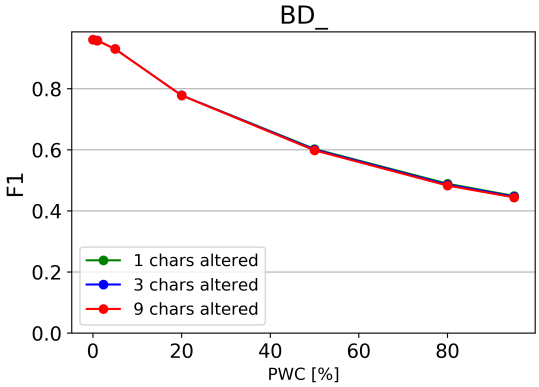


Figure 23: Effect of character repetition and deletion on classification quality

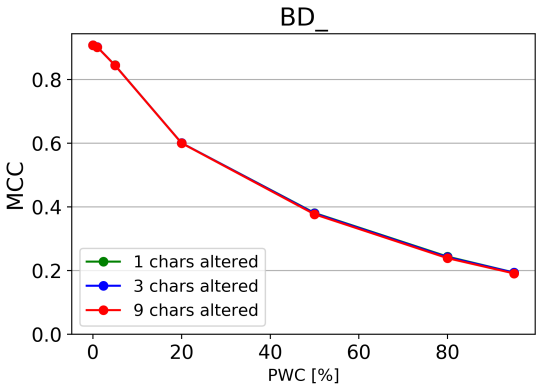


Figure 24: Effect of character repetition and deletion (MCC)

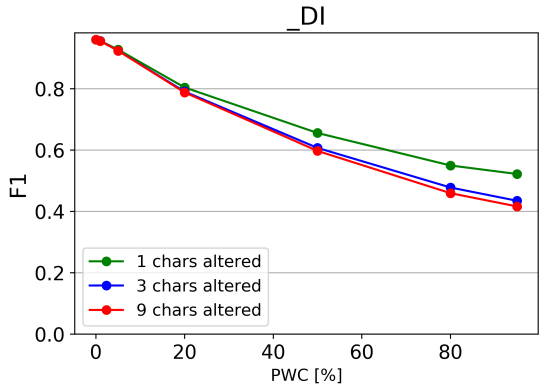


Figure 25: Effect of character deletions and insertions on classification quality

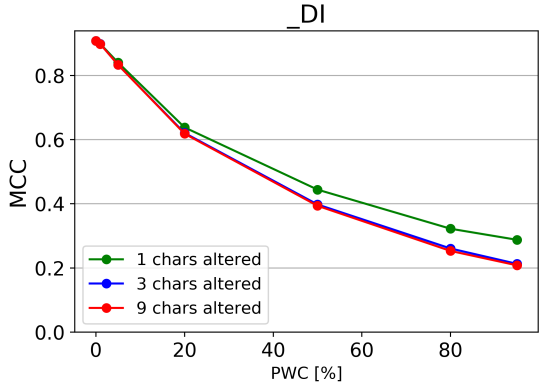


Figure 26: Effect of character deletions and insertions (MCC)

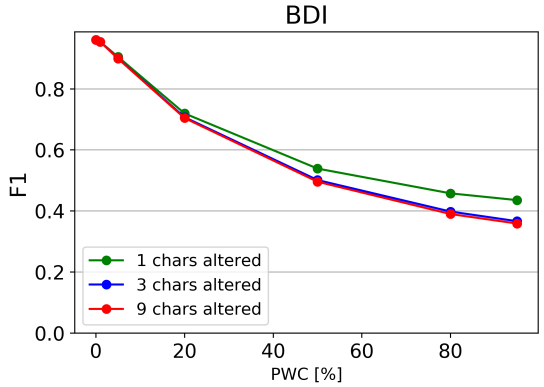


Figure 27: Effect of character repetition, deletion and insertions on quality

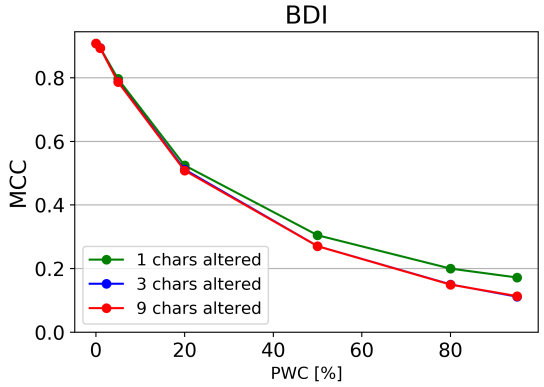


Figure 28: Effect of character repetition, deletion and insertions (MCC)

The CPPP text encoding algorithm has notable advantages over the initial CP algorithm. The significant ones are:

- drastically increased capacity of the encoding space;
- corpora don't have to be tokenized with delimiters;
- the ability to create sparse representations of words, phrases, sentences, paragraphs and even entire documents.

The CPPP algorithm also has advantages over conventional text vectorizers, which rely on tokenization, stemming and other rudimentary techniques of parsing out individual words in a text. The current versions of the string comparison subroutines (SPOQ and its associated filtrations) were presented in the paper. These will be developed further, in order to fully utilize the potential of the sparse representations, produced by the CPPP algorithm.

The benchmark classification problem, described at the end of the paper, will help guide the ongoing development effort. It will also enable comparisons to be made with conventional solutions for data preparation and feature extraction, by using widely known and reliable classification quality evaluation metrics.

Conflict of Interest

The authors declare no conflict of interest.

Acknowledgment

The authors would like to thank Technical University of Sofia – Research and Development Sector, for their financial support.

References

[1] M. Marinov and A. Efremov, "Representing character sequences as sets : a simple and intuitive string encoding algorithm for NLP data cleaning," in 2019 IEEE International Conference on Advanced Scientific Computing (ICASC), 1-6, 2019, https://doi.org/10.1109/ICASC48083.2019.8946281

[2] Subutai Ahmad, Jeff Hawkins, "Properties of Sparse Distributed Representations and their Application to Hierarchical Temporal Memory", Cornell University, 2015, arXiv:1503.07469

[3] Scott Purdy, "Encoding Data for HTM Systems", Cornell University, 2016, arXiv:1602.05925

[4] Ioannis Partalas, Aris Kosmopoulos, Nicolas Baskiotis, Thierry Artieres, George Paliouras, Eric Gaussier, Ion Androutsopoulos, Massih-Reza Amini, Patrick Galinari, "LSHTC: A Benchmark for Large-Scale Text Classification", Cornell University, 2015, arXiv:1503.08581

[5] Chicco, Davide, and Giuseppe Jurman. "The advantages of the Matthews correlation coefficient (MCC) over F1 score and accuracy in binary classification evaluation," BMC Genomics, **21**(6), 2020, https://doi.org/10.1186/s12864-019-6413-7

Advances in Science, Technology and Engineering Systems Journal Vol. 5, No. 5, 167-175 (2020)

www.astesj.com

Special Issue on Innovative Research in Applied Science, Engineering and Technology

ASTESJ

ISSN: 2415-6698

Convolutional Neural Network Based Classification of Patients with Pneumonia using X-ray Lung Images

Hicham Moujahid[1], Bouchaib Cherradi[1, 2,*], Oussama El Gannour[1], Lhoussain Bahatti[1], Oumaima Terrada[1], Soufiane Hamida[1]

[1]*SSDIA Laboratory, ENSET Mohammedia, Hassan II University of Casablanca, 28820, Mohammedia, Morocco.*

[2]*STIE Team, CRMEF Casablanca-Settat, provincial section of El Jadida, 24000, El Jadida, Morocco.*

ARTICLE INFO

Article history:
Received: 29 July, 2020
Accepted: 18 August, 2020
Online: 10 September, 2020

Keywords:
Convolutional neural network
Machine learning
Deep learning
Pneumonia detection
Chest x-ray images
COVID-19

ABSTRACT

Analysis and classification of lung diseases using X-ray images is a primary step in the procedure of pneumonia diagnosis, especially in a critical period as pandemic of COVID-19 that is type of pneumonia. Therefore, an automatic method with high accuracy of classification is needed to perform classification of lung diseases due to the increasing number of cases. Convolutional Neural Networks (CNN) based classification has gained a big popularity over the last few years because of its speed and level of accuracy on the image's classification tasks. Through this article, we propose an implementation a CNN-based classification models using transfer learning technique to perform pneumonia detection and compare the results in order to detect the best model for the task according to certain parameters. As this has become a fast expanding field, there are several models but we will focus on the best outperforming algorithms according to their architecture, length and type of layers and evaluation parameters for the classification tasks. Firstly, we review the existing conventional methods and deep learning architectures used for segmentation in general. Next, we perform a deep performance and analysis based on accuracy and loss function of implemented models. A critical analysis of the results is made to highlight all important issues to improve.

1. Introduction

Pneumonia is an infection inflaming air sacs in the lungs, it can be bacterial or viral including covid-19 virus, but symptoms are often similar independently of the factors causing the disease [1]. Doctors need additional analysis or X-ray imaging to identify the cause of the pneumonia. The X-ray imaging of the lungs allows them to identify only if a lung has pneumonia or not [2].

Many germs can cause pneumonia including viruses, bacteria, and fungi commonly collected from the air and can overpower the immune system which leads to critical health situations. Therefore, early diagnosis [3] based on X-ray image classification is very important at first in order to prevent complications and make treatment efficient. Then advanced diagnosis is needed to determine the type and the cause of the pneumonia using medical tests and X-Ray scans.

Manual classification of pneumonia disease still the most efficient way, usually used by radiologists. The principle inconvenient of this method is about the time-consuming, which is a very important factor in the case of a pandemic.

Nowadays, many researchers become very interested in applications of artificial neural networks (ANN), especially convolutional neural networks (CNN). This method is efficient for medical image classification tasks. It makes computers capable of solving many pattern recognition and object extraction problems using datasets of 2D or 3D images. In case of 3D MRI images classification task it requires a huge processing capacity which can be bypassed by adopting a parallel algorithms [4], [5]. In [6], an example of the above parallel approach where the authors propose a parallel c-mean algorithm applied to MRI images classification showing good time complexity on its results.

To overcome the constrain of execution time, using Graphical Processing Units (GPU) become crucial today in medical image processing applications, especially in a context of machine and deep learning algorithms. They can significantly accelerate parallel processing, therefore almost all works related to medical image processing in medical field uses GPUs as accelerators to achieve better and fast results [7], [8].

*B. CHERRADI, CRMEF Casablanca-Settat, provincial section of El Jadida, 24000, Email: bouchaib.cherradi@gmail.com

However, machine learning algorithms and convolutional neural networks (CNNs) models have gained a lot of attention for almost all diseases classification and prediction problematic including breast cancer detection [9], cardio vascular prediction and diagnosis [10], [11], diabetes mellitus prediction [12], [13], etc.

In this work, we make an implementation of some CNN models using transfer learning technique. We used these models to perform pneumonia detection. Results evaluation and comparison is made in order to adapt and select the best model for the task according to certain parameters.

The rest of this paper is organized as follows: In section 2, we present a brief overview of some different classification techniques on relevant related work used for the prediction of various human diseases, and we focused on studies conducted on the prediction of pneumonia disease from lung X-ray images. Section 3 present the used dataset and CNN models. In section 4, we present the models experimental results and discuss the performance evaluation measures. Section 5 concludes this article and presents some perspectives at this work.

2. Related work

In this section, we review some related and similar works that matches classification task for pneumonia diseases using different machine and deep learning models. These models are evaluated within different metrics and reached less or more important performances, depending on their architecture and conception.

Recently many researches published about the pneumonia disease detection, especially ANN based models achieving great results which are very suitable for this type of disease. Note that COVID-19 virus causes severe pneumonia disease.

In 2019, the authors in [14] published a work concerning pneumonia detection applying a combination of mRMR feature selection and machine learning models on the Chest X-ray images. Features extraction is performed using existing CNN models: AlexNet, VGG16 and VGG19 and then combining the results as an input features set to feed and train five different machine learning models: decision tree, k-nearest neighbors, linear discriminant analysis, linear regression, and support vector. The experiment shows the best results for linear discriminant analysis obtaining 99.41% accuracy.

In January of 2020, the authors published in [15] a model based on transfer learning technique for Chest X-ray images of pneumonia disease. This model consists of combining AlexNet, DenseNet121, InceptionV3, resNet18 and GoogleNet generating a new architecture and reaching 96.39% accuracy on test images. The dataset used in this work is from Guangzhou-women-and-Children's Medical Center dataset [16].

Lately, the authors in [17] published a work about another method of automatic pneumonia detection based also on chest X-ray images focusing this time on specific region of interest (ROI) to classify and segment images. The method was compared in this study with five different classifiers: Multilayer perceptron, sequential minimal optimization (SMO), random forest, Classification via regression and classification via logistic regression. The proposed study shows a higher accuracy on logistic regression classifier with accuracy of 95.63% on test dataset.

In [18], another work published about a machine learning algorithm for pneumonia classification. In this work, the authors built a CNN model from scratch in order to classify images of pneumonia disease based on X-ray chest images obtaining a validation accuracy of 93.7%; where an augmentation method was adopted to increase the dataset size. In table 1, we summarize main information's about these works.

Based on these works and others, we develop and compare in this paper some convolutional neural networks in the goal to enhance the test accuracy on pneumonia disease detection from Lung X-ray images. In fact, we will introduce only automatic methods related to deep learning techniques which are the most adapted for the task of classifying 2D images based of lung X-ray datasets.

3. Materials and methods

3.1. Dataset description

The original dataset used in this work is called "Labeled Optical Coherence Tomography (OCT) and Chest X-Ray images for Classification" version 3 [19]. Only Chest X-Ray part is used in experiments. All models developed in this paper are trained and tested on this part of dataset. The concerned lung X-ray database

Table 1: Summary of related works methods and results.

Reference	Year	Method	Number of tested models	Best model or classifier	Dataset	Number of classes	Best accuracy
[14]	2019	Complex of mRMR feature selection and machine learning models	5	Linear Discriminant Analysis	Guangzhou-women-and-Children's Medical Center dataset	2	99.41%
[15]	2020	Transfer learning-based approach	5	Ensemble transfer learning based	Guangzhou-women-and-Children's Medical Center dataset	2	96.39%
[17]	2020	Automatic pneumonia detection based on ROI for classification	5	Logistic Regression	NIH ChestX-ray14 dataset	2	95.63%
[18]	2019	CNN based model for pneumonia disease classification	1	-	Guangzhou-women-and-Children's Medical Center dataset	2	93.7%

Table 2: Dataset distribution over training, validation and testing sub sets.

Dataset	NORMAL	PNEUMONIA
Training subset	1108	2991
Validation subset	238	641
Testing subset	237	641
Total dataset	1583	4273

is composed of 2 types of images: Images for normal patients (NORMAL) and images for patients with pneumonia disease (PNEUMONIA). In table 2, we summarize the structure of the dataset (Training, validation and Testing).

Figure 1 present some samples of normal and pneumonia lung x-ray images.

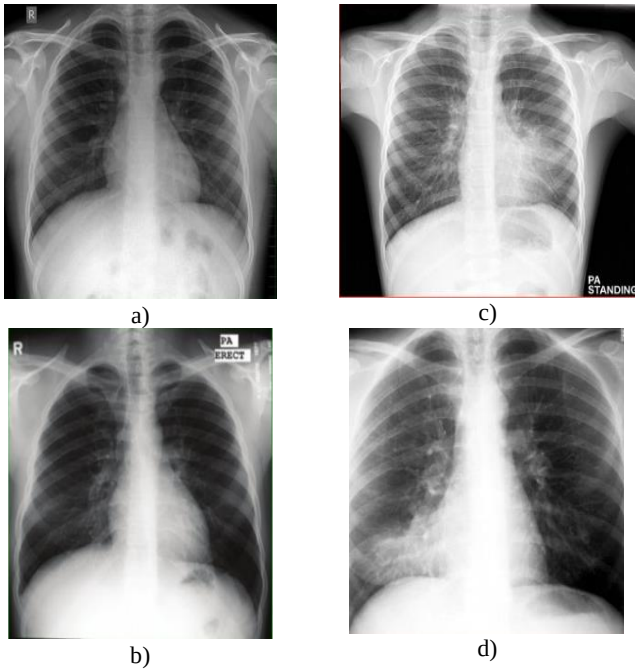


Figure 1: Example of Normal (a & b) and pneumonia (c & d) X-ray samples from the dataset.

3.2. Artificial Neural Network (ANN)

Artificial neural network (ANN) concept is inspired from the human brain being the smarter system that can process real data. The treatment ability came from connections between neurons of the brain. This structure forms a huge natural neural network able to resolve complicated operations in the real world. ANN is about superposing a lot of artificial neurons just like the natural neural network [20]. The elementary ANN (perceptron) is the simplest architecture of an artificial neural network, illustrated in figure 2.

The perceptron composed from input layer having a vector {xi} as inputs, sharable weights in the form of a vector $\{w_i\}$ too and a bias. $\{y_i\}$ presents the output of the perceptron in the form of a vector of probabilities of predictions.

3.3. Convolutional Neural Network (CNN)

Convolutional Neural Network (CNN) is an ANN network but the inverse is not true. CNN are most commonly applied to automatically process visual images. A CNN contains one or more convolution layer.

$$y_i = bias + \sum_{i=1}^{i=n} w_i . x_i = w_1 . x_1 + w_2 . x_2 + \cdots + w_n . x_n \quad (1)$$

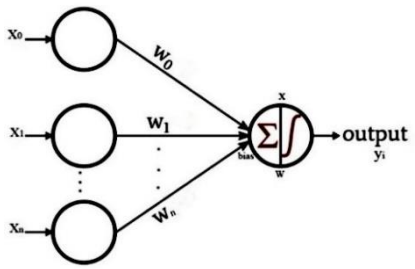


Figure 2: Architecture for a single layer perceptron.

The notion of CNN is old. This abstraction had been verified to work more accurately for recognition of hand written characters [21]. However, this type of networks loses the challenge to process large and heavy images. Therefore, this method was impractical because of the constraints of processing power, lack of memory and datasets availability. Nowadays, these limitations are relatively passed out, because of the technological evolution of storage, memory and methods optimization.

3.4. CNN Architecture

CNNs architecture consists of concatenating multiple types of layers successively which are input layers, convolutional layers and dense layers. In general, convolutional neural networks are based on its process on two principle factors: sharing weights and connectivity between neurons of each convolutional layer.

- Sharing weights: At each convolutional layer, every neuron has its weights that need to be shared to all neurons of the next layer. Those weights need also to be shared to all neurons in the previous layer in order to achieve back propagation process.
- Connectivity: All neurons of each layer are locally connected only to all neurons in the next layer. This connectivity conception reduces the complexity of the network.

Generally, to build a CNN network, an input layer is required with specific configuration including image shapes and patch. Then a convolutional layer's type must follow, also configured with specific number of neurons and specific function of optimization and activation. Each convolutional layer needs a pooling layer to follow with a specific filter of pooling. After that a number of Dense layers must be created before the output layer that requires a loss function to be configured [22].

3.5. Proposed methodology for lung pneumonia classification using CNN

The main steps for any image classification system are: image preprocessing, feature processing included in the convolution process, training the network and validating the resulted model. At the end testing the final CNN model.

Figure 3 shows the general architecture of a CNN model used to detect lung pneumonia containing input layer, convolution layers with *ReLU* activation function, pooling layers and fully connected layers.

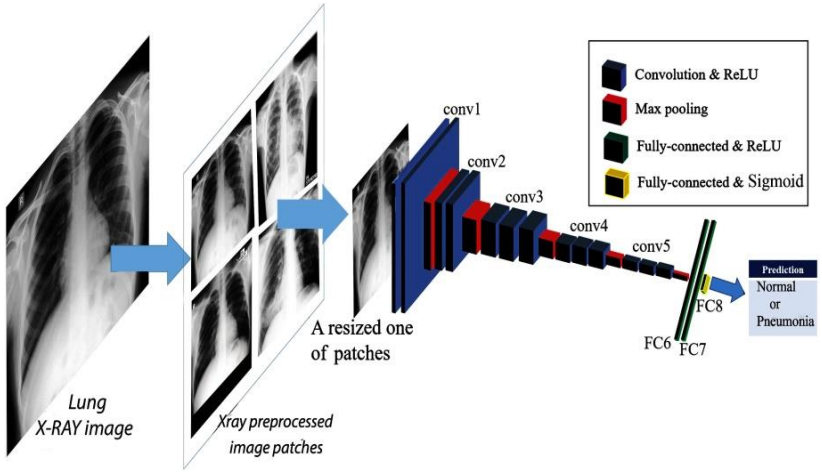


Figure 3: *Illustration of CNN architecture used for pneumonia detection on lung X-ray images.*

- **Dataset preprocessing:** it consists of preparing data to feed the network, this preparation is about reshaping and resizing images, dropping out unusable images and adapting contrast. Also converting raw data to victors and normalizing it [21]. The output of this process feeds a CNN network for training in order to become a pre-trained model, ready for the testing phase [23].

- **Features selection and extraction:** This step is included in the convolution layers, and consists of extracting useful features only, then converted to the adequate format.

  The selection part consists of selecting the most useful features to achieve the classification case of study [24].

- **Training:** At this phase the network is trained by updating weights of neurons across layers, it's called the learning process. This is done by minimizing the loss function and maximizing the accuracy rate of the validation part. If there is only two classes to predict, a sigmoid function is used for the loss optimization [24].

  The learning goal of the model is achieved using an optimizer from a huge scale of optimizers existing in the literature but the back-propagation algorithms are the most used in classification case [21].

- **Classification evaluation metrics**

  Almost all metrics to process the performance of a model are based on some primordial parameters to be calculated:

  True positive abbreviated by TP: Number of images accurately classified as pneumonia matching the ground truth.

  True negative abbreviated by TN: Number of images accurately classified as normal matching the true labels.

  False positive abbreviated by FP: CNN classifies images as containing pneumonia but that it's actually normal according to the ground truth.

  False negative abbreviated by FN: Number of images which the CNN classifies as not containing pneumonia but are actually containing pneumonia according to the ground truth labels [25].

  Based on those calculated parameters, we can compute the precision abbreviated as *P*, recall abbreviated as *R*, the F1 score and the accuracy as:

$$P = TP * \frac{1}{TP+FP} \quad (2)$$

$$R = TP * \frac{1}{TP+FN} \quad (3)$$

$$F1 = 2 * \frac{R*P}{R+P} \quad (4)$$

$$Accuracy = (TP + TN) * \frac{1}{TP+TN+FP+FN} \quad (5)$$

  F1 result is obtained by processing parameters in (Eq.2) and (Eq.3). The formula of this parameter is in (Eq.4).

- **Testing:** On this step we use test set as a different dataset and new one for the model. In order to well testing the model, the ground truth of the test set must be similar to the training set but not correlated. This makes the test more valid and accurate [26].

- **Classification:** This is the last step on the CNN model, it consists of affecting a label to each image from the input features with a specific confidence of decision:

  Initialization: Before to start the learning stage where the weights are updated over epochs. Those weights must have initiated by the initial values, in some cases those values are random. Otherwise those values are generated by a predefined function. The Xavier initialization is the usually used method of initialization [21].

  Activation function: This is the function representing the processing part of a neuron. It depends on the type a layer of the neural network. Most used activation function for layers in CNN network is *ReLU* function [27].

  Pooling: This phase consists of reducing the size of features by applying a filter and keeping only the most important elements. The most popular pooling method in CNN models is max pooling and average pooling. The max pooling consists of selecting only the maximum element in the filter and the average pooling consists of averaging all elements inside the filter [21].

  Regularization: This technic is about reducing over fitting problems and improving performance of the model. There are many methods to ensure regularization, and the most

popular method is dropout. The dropout method is based on eliminating the less important features on each iteration [27].

Loss Function: This hyper parameter defines the function that evaluates how much the trained model can fail predicting the affected task. Its value is reverse to the accuracy value. More the loss is minimal the more the accuracy must be maximal. The quadratic error is the most used for loss function in CNNs [28].

4. Results and discussion

CNNs models have proven interesting results in many applications lately. These models existed in literature differ in the network size, defined optimizers and the type of layers used.

Training task require a big processing capacity which leads us to choose a parallel architecture of processing, by adopting graphical processing unit (GPU), in the virtual environment to accelerate the training step offered by *KAAGLE* platform. In our experiment we used dual cores of CPU with 13 GB of RAM memory equipped with a GPU of 16 GB of RAM memory.

4.1. Building proposed CNN models using transfer learning approach

In our experiment, we build and compile five different models based on existing models in the literature using transfer learning technique.

Depending on the case, each model can succeed or fail the classification task. For our case of pneumonia detection problematic and after running many algorithms many times by trying at each different configuration, we select those architectures in figure 4. With given configurations relatively presenting better results in term of accuracy and loss taking in consideration the over-fitting and the under-fitting problems.

4.2. Compiling and training CNN models

In all models experimented in this work, we add two dropout layers and one dense layer with SOFTMAX activation at the output layer as a classifier. We used a logistic regression algorithm called "RMSProp" optimizer and categorical cross entropy accuracy as a metric during the model compilation.

Weights are initialized using image-net. We decide to not freeze any layer of the original model, because of the nature of pneumonia detection problematic compared to the originally trained dataset.

In order to reduce over fitting on training layers, we used a callback parameter specifying to stop training when no accuracy improvement happened within three successive iterations. That obliges the training process to stop at the epoch where no accuracy improvement happened.

4.3. Validation and testing the given CNN models

While training our proposed models, the validation process goal consists of checking the accuracy of the model in each epoch. Then update weights on the back-propagation process to use in the next epoch for learning. For this task, we used validation dataset as described in figure 1.

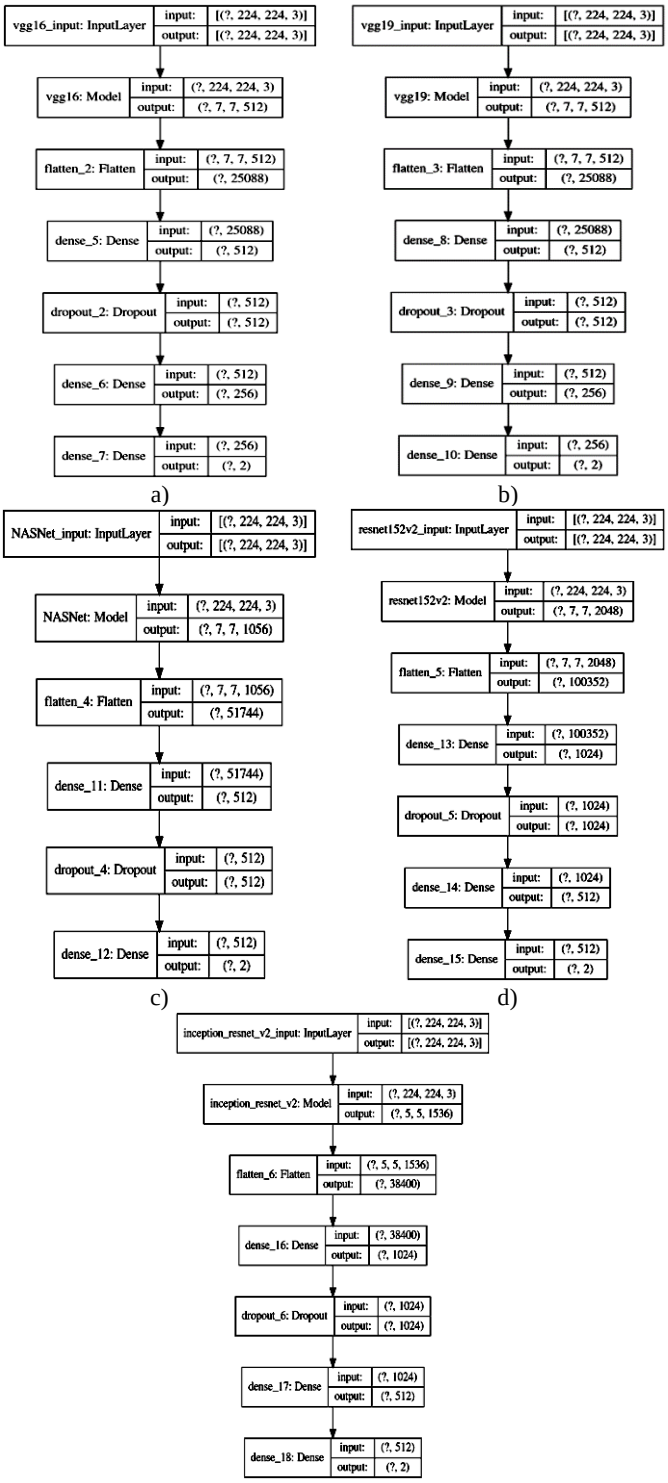


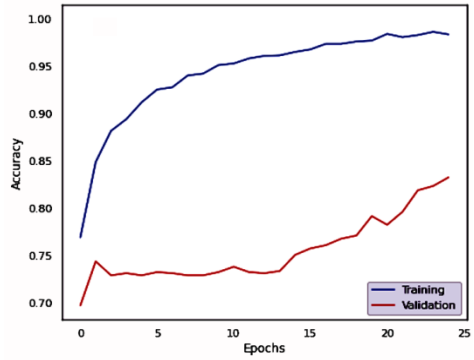
Figure 4: Architecture of proposed transfer learning-based models: (a) VGG16, (b) VGG19, (c) NasNetMobile, (d), ResNet152V2 (e) Inception-Resnet-v2.

In this step, we can get the performance and evaluation metrics for our models before trust them for real case classification.

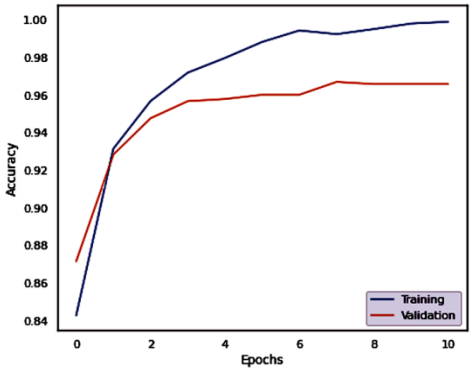
In general VGG16 gets good results in many cases for fine-tuning task [29], this is the mean reason of choosing this model at first for transfer learning to process pneumonia classification.

As shown in figure 5, for the VGG16 based transfer learning model we get the best accuracy and very interesting accuracy

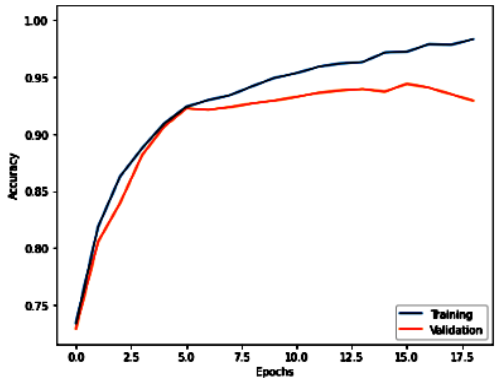
evolution over iterations compared to other tested models. The accuracy continues improving until the 30th epoch and the convergence between the validation and the training accuracy is very good, which makes this model the most adapted for our task. The first 10 epochs show a fast improvements and convergence of the accuracy then the next epochs converge very well but improves slowly without losing convergence aspect.



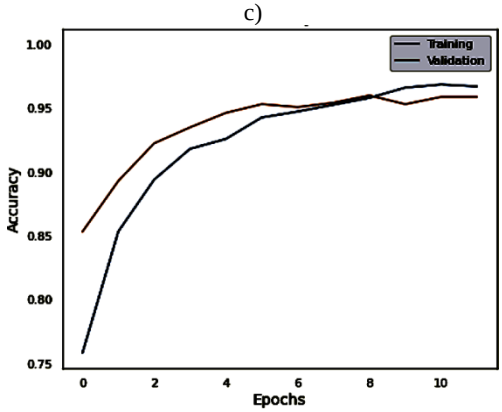
a)



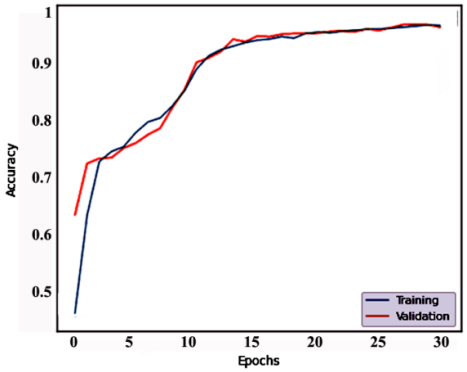
b)



c)



(d)



(e)

Figure 5: Evolution of training and validation accuracy over epochs for different models: a) NasNetMobile based model, b) ResNet152V2, c) Inception-Resnet-v2 based model, d) VGG19 based model, e) VGG16 based model.

From figure 6, it's clear that all well predicted features show probability over 80% (green aspect), and the only miss predicted feature (red aspect) here shows a 68% probability of confidence which is also a clear indication for experts to give more interest of verification and correction for non-confident classifications. Therefore, the model can be a good tool to help for pneumonia disease diagnosis. Time and effort for medical experts in diagnosing pneumonia cases specially in the case of COVID-19 can be saved. In fact, human visual system has many limitations about detecting the gray-scale resolutions even with high brightness and contrast, X-Ray images can present a large scale of gray-scale shades than the human eye could detect. This is another reason why the automatic diagnosis is primordial for improving the disease detection.

VGG19 based transfer learning model shows also good accuracy convergence, where the maximum value is achieved on the 10th epoch and relatively starts to stabilize for the next epochs, therefore the algorithm ends to avoid over-fitting.

Models: Inception-Resnet-v2 based model and ResNet152V2 based shows similar accuracy evolution results. Speed of convergence for the first one is performed after 18 epochs but for the second in just 10 epochs. That gives an advantage for the second one. The NasNetMobile based model shows a very bad accuracy results in term of convergence or accuracy values, which makes this model badly ranked for this task.

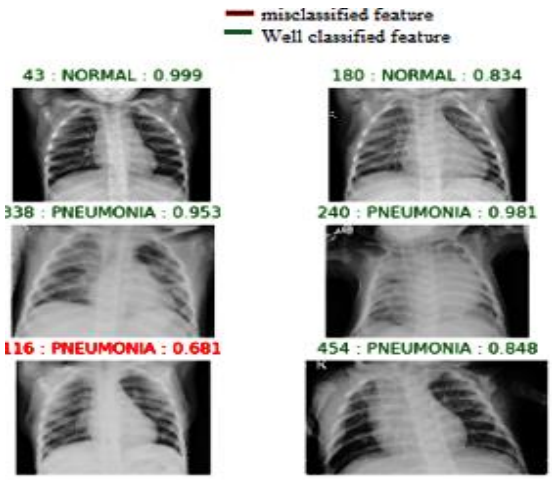
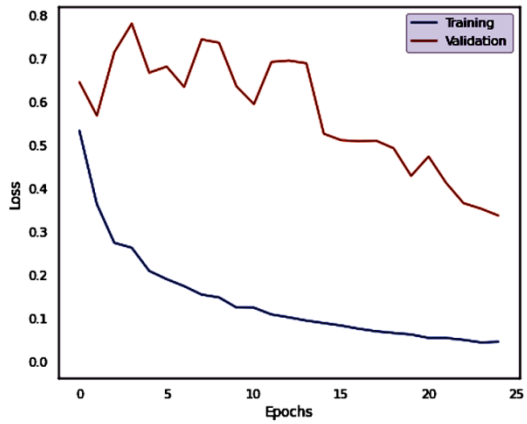


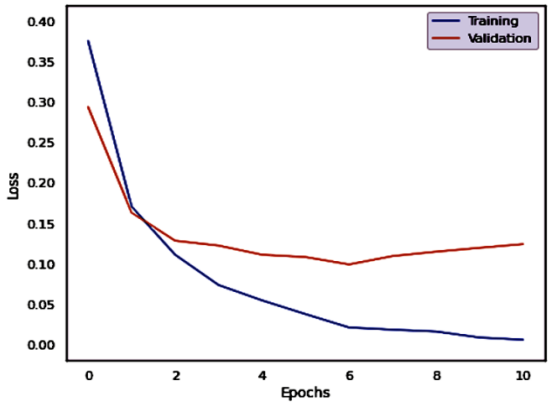
Figure 6: Example of predicted features using a VGG 16 based transfer learning model showing in the left the id number of the feature in the testing dataset and the probability of prediction in the right.

Loss curve is also an important tool to evaluate models just like the accuracy curve. In our experiment, results of loss functions are illustrated in figure 7.

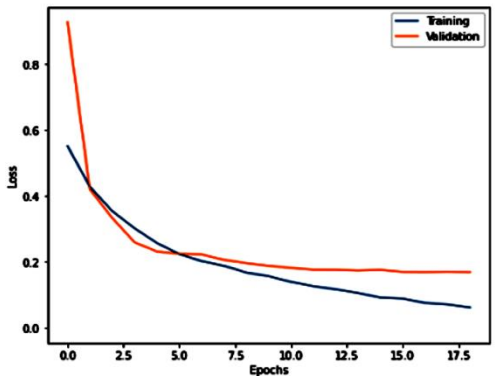
Similarly, to accuracy curve analysis, this tool confirms that VGG16 based model is the best model achieving pneumonia detection task. NasNetMobile based model shows again the worst results for this task. Regarding confusion matrix tool, our models shows the following results:



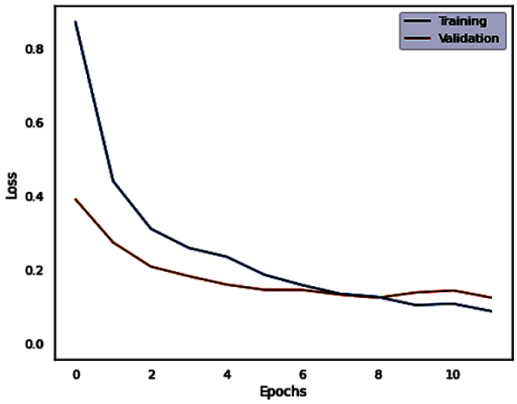
a) NasNetMobile based model



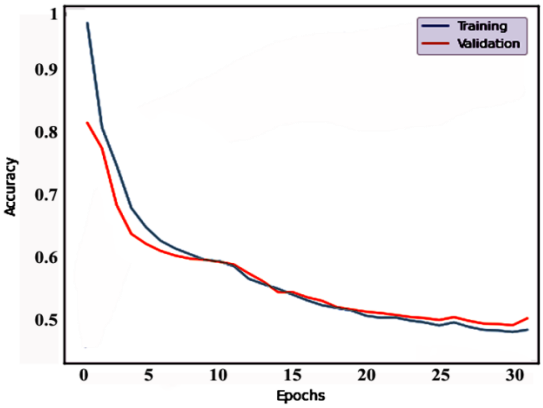
b) ResNet152V2



c) Inception-Resnet-v2 based model



d) VGG19 based model



e) VGG 16 based model

Figure 7: Evolution of training and validation loss over epochs for different models: a) NasNetMobile based model, b) ResNet152V2, c) Inception-Resnet-v2 based model, d) VGG19 based model, e) VGG16 based model.

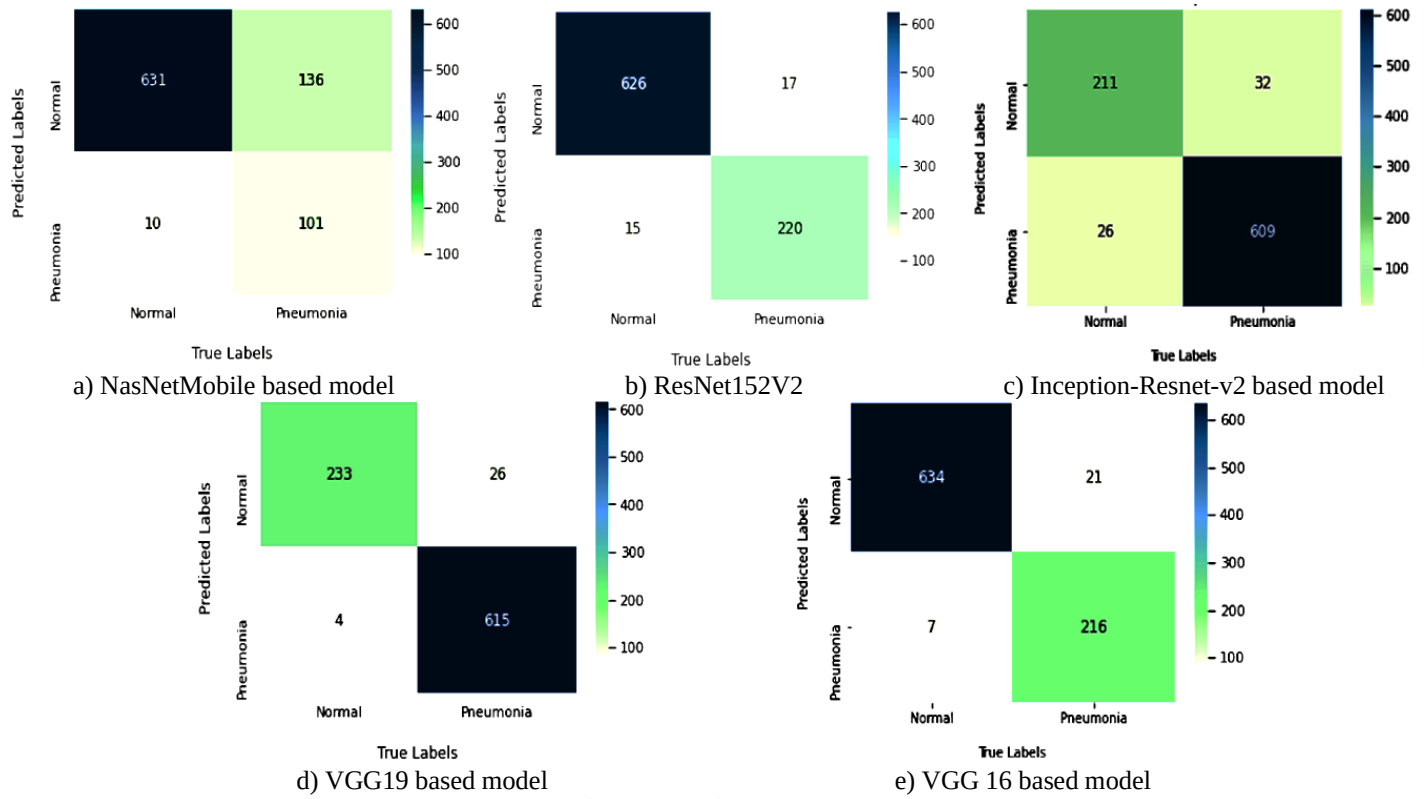
VGG19 based model failed on predicting the 26 case of pneumonia but succeed on predicting 615 of 641 features. The model also failed to predict normal for only 4 cases. In general, this is a good result regarding the total number of cases.

VGG16 based model fails detecting 21 pneumonia cases which make it better than VGG19 based model. But not efficient on detecting pneumonia cases compared to Resnet152V2 based.

However, ResNet152V2 based total fails of 32 predictions including normal and pneumonia cases. Which is more than VGG16 based model. Therefore VGG 16 based model presents the best confusion matrix results in this experiment. The other models in this experiment show fewer interesting results on their confusion matrix. Classification based on CNN methods for Medical images gets the better performance (accuracy) on fine-tuning the model VGG16 modeled by Google Company, showing the results of almost: 97% for pneumonia detection, 11.51% loss. It is clear that

Table 3: Comparison of different implemented CNN models.

Method	Epochs	Learning rate	Optimizer	Activation	Loss function	Accuracy	Loss	Precision	Recall	F1-score
VGG16 based	33	10^{-5}	RMSProp	Softmax	Categorical cross entropy	**96.81%**	**11.51%**	91%	97%	94%
VGG19 based	12	10^{-5}	RMSProp	Softmax	Categorical cross entropy	96.58%	14.43%	**96%**	**99%**	**98%**
NasNetMobile based	25	10^{-5}	RMSProp	Softmax	Categorical cross entropy	83.37%	36.13%	43%	91%	58%
ResNet152V2 based	11	10^{-5}	RMSProp	Softmax	Categorical cross entropy	96.35%	16.27%	93%	94%	93%
InceptionResNetV2 based	18	10^{-5}	RMSProp	Softmax	Categorical cross entropy	94.87%	17.18%	89%	90%	89%



a) NasNetMobile based model b) ResNet152V2 c) Inception-Resnet-v2 based model

d) VGG19 based model e) VGG 16 based model

Figure 1: Confusion matrix of all trained and tested models.

loss function of the model VGG16 based model is minimal; also, its accuracy presents the maximum of all trained models. VGG16 based model get into its maximum value of accuracy on epoch 33 with loss value of 11.51% and precision of 91%. VGG19 based model is very close to the VGG16 based one in term of accuracy, but the rest of the models as showed in table 3 presents relatively bad accuracy results to trust for our task.

ROC curve is a fundamental tool for model performance evaluation based on sensitivity/specificity reports or true positive rate and false positive rate, in this ROC graph each curve the sensitivity (true positive rate) is plotted as a function of a specificity value (false positive rate). Area under the curve (AUC) represents how well the model can distinguish between a normal and pneumonia image called.

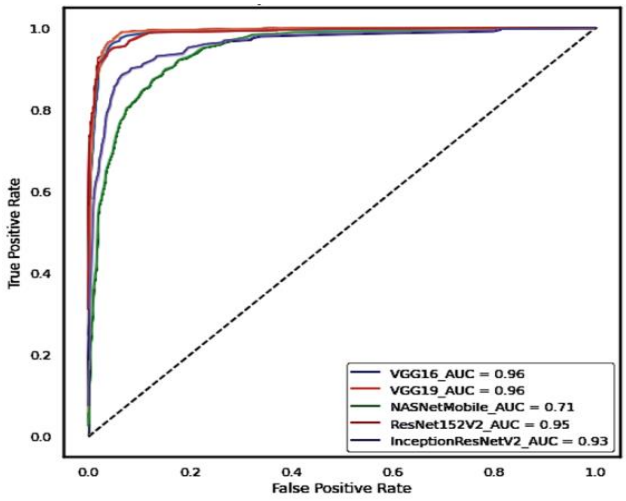


Figure 2: ROC curve comparison for all implemented models.

In general, more the area is big, more the curve is near to the left corner of the graph and more the represented model is better in terms of performance.

5. Conclusion and perspectives

Pneumonia disease classification is a primordial step for diagnosing lung infections which can be caused by several factors including covid-19.

Machine learning methodology especially convolutional neural networks are a very interesting techniques to automatically, efficiently and rapidly output results.

This method faces sense the beginning many problems like the leak of datasets in the world and algorithms complexities in time and processing.

To improve prediction accuracy more and more some extensions must be done, like increasing the dataset by combining multiple independent datasets to set a bigger database of samples that conduct us to use higher processing performances in order to train all the given dataset in a reasonable time and epochs, we need also to preprocess differently the input images by cropping and correcting contrast on X-Ray images based on processing concentration while training, and also proposing the best adapted optimizer on training.

Also, we plan in the future to make our conception of optimized novel model adapted specially for chest X-Ray images. Training stage takes relatively a lot of time depending on the complexity of the algorithm that must be optimized as much as possible and the capacity of available resources. Therefore, there is a lot of required work to achieve by researchers' efforts to take benefits of this magic field in our world.

Conflict of Interest

The authors declare no conflict of interest.

Acknowledgment

This work is a part of a project supported by co-financing from the CNRST (Centre National pour la Recherche Scientifique et Technique) and the Hassan II University of Casablanca, Morocco. The project is selected in the context of a call for projects entitled "Scientific and Technological Research Support Program in Link with COVID-19" launched in April 2020 (Reference: Letter to the Director of "Ecole Normale Supérieure de l'Enseignement Technique de Mohammedia" dated the 10th June 2020).

References

[1] S. Kang, W. Peng, Y. Zhu, S. Lu, M. Zhou, W. Lin, W. Wu, S. Huang, L. Jiang, X. Luo, M. Deng, "Recent progress in understanding 2019 novel coronavirus (SARS-CoV-2) associated with human respiratory disease: detection, mechanisms and treatment," International Journal of Antimicrobial Agents, 105950, 2020, doi:10.1016/j.ijantimicag.2020.105950.

[2] A. Jacobi, M. Chung, A. Bernheim, C. Eber, "Portable chest X-ray in coronavirus disease-19 (COVID-19): A pictorial review," Clinical Imaging, **64**, 35–42, 2020, doi:10.1016/j.clinimag.2020.04.001.

[3] J. Gong, J. Ou, X. Qiu, Y. Jie, Y. Chen, L. Yuan, J. Cao, M. Tan, W. Xu, F. Zheng, Y. Shi, B. Hu, "A Tool to Early Predict Severe Corona Virus Disease 2019 (COVID-19) : A Multicenter Study using the Risk Nomogram in Wuhan and Guangdong, China," Clinical Infectious Diseases, ciaa443, 2020, doi:10.1093/cid/ciaa443.

[4] H. Moujahid, B. Cherradi, L. Bahatti, Convolutional Neural Networks for Multimodal Brain MRI Images Segmentation: A Comparative Study, Springer International Publishing, Cham: 329–338, 2020.

[5] N.A. Ali, B. Cherradi, A. El Abbassi, O. Bouattane, M. Youssfi, "Parallel Implementation and Performance Evaluation of some Supervised Clustering Algorithms for MRI Images Segmentation," in Proceedings of the 4th International Conference on Big Data and Internet of Things, ACM, Rabat Morocco: 1–7, 2019, doi:10.1145/3372938.3373007.

[6] O. Bouattane, B. Cherradi, M. Youssfi, M.O. Bensalah, "Parallel c-means algorithm for image segmentation on a reconfigurable mesh computer," Parallel Computing, **37**(4), 230–243, 2011, doi:10.1016/j.parco.2011.03.001.

[7] N. Ait Ali, B. Cherradi, A. El Abbassi, O. Bouattane, M. Youssfi, "GPU fuzzy c-means algorithm implementations: performance analysis on medical image segmentation," Multimedia Tools and Applications, **77**(16), 21221–21243, 2018, doi:10.1007/s11042-017-5589-6.

[8] N.A. Ali, B. Cherradi, A. El Abbassi, O. Bouattane, M. Youssfi, "Modelling the behavior of the CPU and the GPU versus the clusters number variation for sequential and parallel implementations of BCFCM algorithm," ARPN Journal of Engineering and Applied Sciences, **12**(21), 6030–6038, 2017.

[9] S. Laghmati, A. Tmiri, B. Cherradi, "Machine Learning based System for Prediction of Breast Cancer Severity," in 2019 International Conference on Wireless Networks and Mobile Communications (WINCOM), IEEE, Fez, Morocco: 1–5, 2019, doi:10.1109/WINCOM47513.2019.8942575.

[10] O. Terrada, A. Raihani, O. Bouattane, B. Cherradi, "Fuzzy cardiovascular diagnosis system using clinical data," in 2018 4th International Conference on Optimization and Applications (ICOA), IEEE: 1–4, 2018.

[11] O. Terrada, B. Cherradi, A. Raihani, O. Bouattane, "Atherosclerosis disease prediction using Supervised Machine Learning Techniques," in 2020 1st International Conference on Innovative Research in Applied Science, Engineering and Technology (IRASET), IEEE, Meknes, Morocco: 1–5, 2020, doi:10.1109/IRASET48871.2020.9092082.

[12] O. Daanouni, B. Cherradi, A. Tmiri, "Predicting diabetes diseases using mixed data and supervised machine learning algorithms," in Proceedings of the 4th International Conference on Smart City Applications - SCA '19, ACM Press, Casablanca, Morocco: 1–6, 2019, doi:10.1145/3368756.3369072.

[13] O. Daanouni, B. Cherradi, A. Tmiri, "Diabetes Diseases Prediction Using Supervised Machine Learning and Neighbourhood Components Analysis," in Proceedings of the 3rd International Conference on Networking, Information Systems & Security, ACM, Marrakech Morocco: 1–5, 2020, doi:10.1145/3386723.3387887.

[14] M. Toğaçar, B. Ergen, Z. Cömert, F. Özyurt, "A Deep Feature Learning Model for Pneumonia Detection Applying a Combination of mRMR Feature Selection and Machine Learning Models," IRBM, S1959031819301174, 2019, doi:10.1016/j.irbm.2019.10.006.

[15] V. Chouhan, S. Singh, A. Khamparia, D. Gupta, P. Tiwari, C. Moreira, R. Damasevicius, V. Albuquerque, "A Novel Transfer Learning Based Approach for Pneumonia Detection in Chest X-ray Images," Applied Sciences, **10**, 559, 2020, doi:10.3390/app10020559.

[16] D.S. Kermany, M. Goldbaum, W. Cai, C.C.S. Valentim, H. Liang, S.L. Baxter, A. McKeown, G. Yang, X. Wu, F. Yan, J. Dong, M.K. Prasadha, J. Pei, M.Y.L. Ting, J. Zhu, C. Li, S. Hewett, J. Dong, I. Ziyar, A. Shi, R. Zhang, L. Zheng, R. Hou, W. Shi, X. Fu, Y. Duan, V.A.N. Huu, C. Wen, E.D. Zhang, et al., "Identifying Medical Diagnoses and Treatable Diseases by Image-Based Deep Learning," Cell, **172**(5), 1122–1131.e9, 2018, doi:10.1016/j.cell.2018.02.010.

[17] B.B. Chaudhuri, M. Nakagawa, P. Khanna, S. Kumar, Proceedings of 3rd International Conference on Computer Vision and Image Processing: CVIP 2018, Volume 1, Springer Nature, 2019.

[18] O. Stephen, M. Sain, U.J. Maduh, D.-U. Jeong, "An Efficient Deep Learning Approach to Pneumonia Classification in Healthcare," Journal of Healthcare Engineering, **2019**, 1–7, 2019, doi:10.1155/2019/4180949.

[19] D. Kermany, K. Zhang, M. Goldbaum, "Large Dataset of Labeled Optical Coherence Tomography (OCT) and Chest X-Ray Images," **3**, 2018, doi:10.17632/rscbjbr9sj.3.

[20] C. Senaras, M.N. Gurcan, "Deep learning for medical image analysis," Journal of Pathology Informatics, **9**(1), 25, 2018, doi:10.4103/jpi.jpi_27_18.

[21] Y. Lecun, L. Bottou, Y. Bengio, P. Haffner, "Gradient-based learning applied to document recognition," Proceedings of the IEEE, **86**(11), 2278–2324, 1998, doi:10.1109/5.726791.

[22] S. Srinivas, R.K. Sarvadevabhatla, K.R. Mopuri, N. Prabhu, S.S.S. Kruthiventi, R.V. Babu, An Introduction to Deep Convolutional Neural Nets for Computer Vision, Elsevier: 25–52, 2017.

[23] N. Tajbakhsh, J.Y. Shin, R.T. Hurst, C.B. Kendall, J. Liang, Automatic Interpretation of Carotid Intima–Media Thickness Videos Using Convolutional Neural Networks, Elsevier: 105–131, 2017.

[24] S. Miao, J.Z. Wang, R. Liao, Convolutional Neural Networks for Robust and Real-Time 2-D/3-D Registration, Elsevier: 271–296, 2017.

[25] H. Chen, Q. Dou, L. Yu, J. Qin, L. Zhao, V.C.T. Mok, D. Wang, L. Shi, P.-A. Heng, Deep Cascaded Networks for Sparsely Distributed Object Detection from Medical Images, Elsevier: 133–154, 2017.

[26] N. Srivastava, G. Hinton, A. Krizhevsky, I. Sutskever, R. Salakhutdinov, "Dropout: A Simple Way to Prevent Neural Networks from Overfitting," Journal of Machine Learning Research, **15**(56), 1929–1958, 2014.

[27] H.-I. Suk, An Introduction to Neural Networks and Deep Learning, Elsevier: 3–24, 2017.

[28] F.C. Ghesu, B. Georgescu, J. Hornegger, Efficient Medical Image Parsing, Elsevier: 55–81, 2017.

[29] S.S. Yadav, S.M. Jadhav, "Deep convolutional neural network based medical image classification for disease diagnosis," Journal of Big Data, **6**(1), 113, 2019, doi:10.1186/s40537-019-0276-2.

ASTES

Advances in Science, Technology and Engineering Systems Journal Vol. 5, No. 5, 176-192 (2020)

www.astesj.com

ASTESJ

ISSN: 2415-6698

Detailed Security Evaluation of ARANz, ARAN and AODV Protocols

Liana Khamis Qabajeh[1, *], Mohammad Moustafa Qabajeh[2]

[1]*Faculty of Information Technology and Computer Engineering, Palestine Polytechnic University, Palestine*

[2]*Faculty of Information Technology and Computer Engineering, Palestine Technical University Kadorie, Palestine*

ARTICLE INFO

Article history:
Received: 12 May, 2020
Accepted: 02 September, 2020
Online: 10 September, 2020

Keywords:
Position-based
Secure
Scalable
Routing protocol
Location service
Mobile Ad-Hoc networks
Security evaluation
ARANz
ARAN
AODV

ABSTRACT

Ad-Hoc networks are self-organized wireless networks. Finding a secure and efficient route leading from a specific source node to an intended destination node is one of the serious concerns in mobile Ad-Hoc networks. ARANz is one of the significant protocols that has been proposed for such networks. ARANz implements the authentication methods used with the original Authenticated Routing for Ad-Hoc Networks (ARAN) and enhance security and attain robustness by dividing the network into zones and introducing several local certificate authority servers. Using restricted directional flooding, ARANz reveals improved scalability and performance.

The purpose of this paper is to discuss in details the misbehavior detection system used with ARANz protocol, along with presenting a detailed simulated security and performance evaluation of ARANz and other existing protocols. Through extensive simulation using GloMoSim simulator, a detailed security evaluation has been conducted to evaluate ARANz and compare it with the original ARAN and Ad-Hoc On-demand Distance Vector (AODV). Simulation results confirm the effectiveness of ARANz in discovering secure routes within quite large networks including large number of moving nodes, while retaining the minimum packet routing load. Results also prove that ARANz has superior performance regardless malicious nodes percentage conducting different types of attacks such as modification, black hole, grey hole and fabrication. Hence, ARANz can be a good choice for Ad-Hoc networks established among students on a campus or peers at a conference, where pre-deployment of some keys and certificates is possible.

1. Introduction

Ad-Hoc networks are self-configurable and self-organized networks without centralized control. Unstable infrastructure, scarcity of resources and dynamic network topology are some Ad-Hoc networks properties that made efficient routing one of the important issues especially that routing is conducted in a multi-hop fashion and all nodes act as both hosts and routers. In addition, the concept and nature of Ad-Hoc networks result in making them exposed to attacks using modification, impersonation and fabrication [1], [2]. Hence, safe exchanging of data through the network has been a challenging task.

Managed-open environment might be found among students on a campus or peers at a conference. In such environments, there is an opportunity of using previously established infrastructure and pre-deployment of some keys and certificates [1], [2]. However, the approach that depends on a single centralized server is unfeasible for Ad-Hoc networks, as it might be the operation bottleneck [1]. Hence, the certificate authority and position service are supposed to be distributed among numerous servers. Moreover, the demand for scalable and energy-efficient routing protocols, along with the availability of small and low power positioning devices lead to adopting position-based routing in mobile Ad-Hoc networks.

A new distributed and secure position-based routing protocol, ARANz, has been proposed in our work in [1]. Adopting the original Authenticated Routing for Ad-Hoc Networks (ARAN) [2], ARANz seeks to enhance the routing protocol performance and distribute the routing load by dealing with the network as zones. Additionally, it looks for achieving robustness, enhancing security, solving the single point of failure and avoiding single point of attack via distributing trust among multiple certificate authority

*Corresponding Author: Liana Khamis Qabajeh, liana_tamimi@PPU.EDU

servers. Finally, ARANz utilizes restricted directional flooding to exhibit enhanced scalability, robustness and performance.

This paper is an expansion of our work in [1]. A detailed discussion of the ARANz protocol, security analysis of ARAN and ARANz protocols, along with simulated performance evaluation among Ad-Hoc On-demand Distance Vector (AODV) [3], ARAN and ARANz protocols have been conducted in [1]. This work, on the other hand, presents a detailed discussion of the Misbehavior Detection System used with ARANz protocol. Moreover, this paper presents a detailed simulated security and performance evaluation of AODV, ARAN and ARANz protocols. This paper also evaluates the effectiveness of these protocols in tackling security concerns considering different number of malicious nodes found in the network and perform diverse attacks such as modification, black hole, grey hole and fabrication. Hence, in this research, we propose a novel Misbehavior Detection System, integrate it with the ARANz protocol, and conduct detailed simulated security and performance evaluation of AODV, ARAN and ARANz protocols.

Through this research we are trying to answer the following research question; will identifying and isolating the malicious nodes in ARANz help in achieving high level of performance and security compared to the other two protocols? Hence, we can set out and try to prove our research hypotheses; that is, utilizing the proposed misbehavior detection system with ARANz will improve its performance and security.

Results prove that ARANz is able to find out secure routes effectively and is still able to have superior performance even with having large percentage of malicious nodes conducting different types of attacks. Moreover, ARANz maintained the minimum packet routing load in all conducted scenarios compared to AODV and ARAN protocols, which assures its scalability. The price of ARANz is a longer latency in route discovery due to the required time for authentication, packet processing together with obtaining the position of the destination.

The rest of the paper is structured as follows. Section 2 discusses Ad-Hoc networks routing protocols security and introduces AODV and ARAN protocols. Section 3 presents ARANz protocol including a detailed discussion of the proposed misbehavior detection system. Section 4 provides security analysis along with a simulated comparison among AODV, ARAN and ARANz protocols. Our findings are discussed in Section 5 and our work is concluded in Section 6. To conclude, future directions are presented in Section 7.

2. Background and Related Work

This section presents security issues and conducted efforts to ensure security in Ad-Hoc networks. Subsection 2.1 discusses Ad-Hoc routing protocols security issues; including different security requirements along with some attacks conducted to disrupt an Ad-Hoc network security. Subsection 2.2 discusses recent conducted efforts related to Ad-Hoc networks security. While, Subsections 2.3 and 2.4 introduce AODV and ARAN protocols since our protocol will be compared to them.

2.1. Ad-Hoc Routing Protocols Security

Ensuring Ad-Hoc network security requires satisfying many requirements [4]-[8]. One important requirement is confidentiality. *Confidentiality* ensures that sensitive data being sent through the network are kept secret; i.e., messages content may be interpreted merely by their source and destination. Another requirement is *integrity* which assures that a message sent over the network is not corrupted whether intentionally or accidentally. *Availability* means that network should stay operational and accessible to allow sending and receiving messages at any time. Additionally, the nodes identities assure that they are who they pretend to be; *authentication*. *Non-repudiation* assures that neither sender nor receiver should be able to deny sending or receiving a message. Moreover, *privacy* has become a key security issue and numerous efforts considering anonymous Ad-Hoc routing protocol have been proposed. The *anonymity* in an Ad-Hoc network assures that the identity of nodes, route paths information and location information must be unidentified not only by adversary nodes but also by other nodes in the network.

Routing is an essential operation in Ad-Hoc networks; so, it is a major target for attackers to disrupt an Ad-Hoc network. Many attacks [5], [9], [10] may be performed against Ad-Hoc networks. *Fabrication* attack is carried out by generating deceptive routing packets. These attacks are hard to be recognized as they appear as legitimate routing messages. *Modification* attack targets the routing computation integrity. By altering routing information, an attacker may result in network traffic dropping, or redirecting to another destination, or taking a longer path to the destination. In *Impersonation* attack, a malicious node may conduct various attacks and fake the network topology by pretending to be another legitimate node.

2.2. Recent Works in Ad-Hoc Networks Security

Recently, many research efforts have been conducted considering Ad-Hoc networks security. Some of them, such as [11]-[14], have discussed and elaborated a comprehensive analysis of Ad-Hoc networks security issues due to its special characteristics along with presenting the proposed defeating approaches against existing attacks.

Some other researchers conducted security assessment and evaluation of existing Ad-Hoc networks secure routing protocols. Authors in [15], for example, examined the performance of AODV routing protocol under numerous security attacks. They found that conducting diverse attacks results in lower throughput and packet delivery ratio. Additionally, authors in [16], studied the performance and security of AODV routing protocol and Secure Ad hoc On demand Distance Vector routing protocol [17] taking into account various attack types including replay and blackhole attacks.

Other researches proposed new security solutions to avoid specified Ad-Hoc networks attacks. In [18] and [19] new flooding attacks prevention routing protocols have been proposed. In [20] a triple factor architecture of a secured scheme has been suggested for environments considering reactive routing protocols such AODV. In this architecture, each node computes the trust considering the direct information then verifies the reputation via gathering information from its neighboring nodes and uses a cryptographic algorithm to ensure security. Integrating the proposed procedure at every node enhances the throughput and lowers the overhead even upon malicious nodes existence.

Authors in [2] proposed ARAN protocol to prevent a number of attacks such as modification, impersonation and fabrication exploits. In [21], authors proposed a quantitative trust model for Ad-Hoc networks those are integrated with Internet of Things (IoT). The proposed model combines both direct and indirect trust to calculate a node's final trust value. Diverse trust evidences along with direct trust have been taken into account. Moreover, only trusted nodes are chosen in the route between source and destination to ensure secure and reliable packets delivery. Detailed discussions of recent research work done on security solutions for Ad-Hoc networks can be found in [11]-[13], [22].

One protocol of interest is the ARAN protocol since it provides authentication of route discovery, setup and maintenance as well as message integrity and non-repudiation. Moreover, ARAN prevents a number of attacks such as modification, impersonation and fabrication exploits. ARAN is a secure extension of AODV. One advantage of reactive routing protocols, such as AODV, is that no periodic routing packets are required. In the following two subsections, AODV and ARAN protocols are further explained since our protocol has been proposed based on and will be compared to them.

2.3. Ad-Hoc On-demand Distance Vector (AODV)

Ad-Hoc On-demand Distance Vector (AODV) [3] is a reactive routing protocol, i.e. it uses flooding to detect routes on-demand. The query packet in AODV has a number-of-hop field which is incremented by all intermediate nodes. AODV forwards data packets based on next hop information maintained on the nodes involved in the route. Reactive routing protocols have the advantage that there is no need for periodic routing packets. On the other hand, they may have increased control overhead in high mobility and heavy traffic loads environments. Scalability is considered to be another weakness since they rely on blind broadcast to find routes. Broadcasting routing packets to the entire network leads to congestion and large routing overhead along with affecting the protocol's performance due to dropping data packets.

2.4. Authenticated Routing for Ad-Hoc Networks (ARAN)

Authenticated Routing for Ad-Hoc Networks (ARAN) [2] is similar to AODV, but provides authentication during different phases. The main intention of ARAN is to protect routing packets against attacks conducted by malicious nodes in a managed-open environment. Hence, it requires some security coordination before deployment. It assumes the existence of a trusted Certificate Authority (CA) server. All trusted nodes are aware of the public key of the CA. Each node requests a certificate from this CA before joining the Ad-Hoc network. ARAN uses cryptographic certificates to avoid most security attacks targeting Ad-Hoc routing protocols, including message integrity, authentication and non-repudiation.

ARAN consists of a preliminary certification step followed by a route discovery process. In a try to find a route in ARAN, source node broadcasts a Route Discovery Packet (RDP), which is responded to by a unicast REPly (REP) packet that is initiated by the intended destination, and forwarded along the reverse path towards the source. Routing packets are end-to-end authenticated and only authorized nodes participate in sending these packets. Consequently, each node that forwards a request or a reply signs it to enable the subsequent node to check the validity of the previous one.

Compared to original AODV, ARAN prevents numerous attacks including altering routing messages, misrepresenting node's identity (spoofing attack) and injecting into the network routing messages that have been previously captured (replay attack). Furthermore, simulations in [2] show that ARAN performance is equivalent to that of AODV in discovering and maintaining routes.

In contrast, in addition to scalability problem with the number of nodes (which is inherited from AODV) ARAN incurs additional packet overhead and longer route discovery latency due to signing each packet. Lastly, ARAN uses single certificate server which results in a need to keep it uncompromised. Depending on a centralized certificate authority in a physically insecure environment forms a single point of capture and compromise reducing protocol's availability and robustness against attacks.

3. ARANz Routing Protocol

In this section, our proposed protocol along with the proposed misbehavior detection system are presented. Section 3.1 shows our methodology and assumptions. Section 3.2 gives a basic presentation of ARANz phases, while Section 3.3 tackles a detailed discussion of the proposed misbehavior detection system.

3.1. Methodology and Assumptions

ARANz routing protocol [1] adopts ARAN protocol authentication steps along with dividing the network into virtual zones. In ARANz, cryptographic certificates are used to avoid most of the attacks threaten Ad-Hoc routing protocols and to discover irregular behavior. However, ARANz suggests a hierarchal routing model, aiming to improve routing protocol performance and share out load via dealing with the area as zones. Furthermore, ARANz aims to attain high level of security and robustness, solve the single point of failure and attack problems by distributing trust among several Local Certificate Authority (LCA) servers. Every zone has numerous LCAs collaborating together to issue certificates for the nodes residing currently within this zone.

Furthermore, ARANz tries to demonstrate improved scalability, performance and robustness against regular topological changes through applying restricted directional flooding concept. So, LCAs also play the role of position servers and nodes contact LCAs of their zones informing them about their new position upon movement. ARANz also proposed a misbehavior detection scheme to improve its security. Within this scheme, the procedure to identify misbehaving nodes, and the needed actions to be taken upon discovering them are proposed to mitigate service interruption.

ARANz assumes that nodes are arbitrarily distributed in a square-shape area and know their positions. Primary Certificate Authority (PCA) is a pre-chosen node having the required software to divide the area into zones and elect the preliminary LCAs. PCA possesses the network private key (K_{NET-}). All trusted participating nodes own a private/public key pair and the network public key (K_{NET+}).

3.2. ARANz Phases

ARANz consists of five phases. These phases are network setup, network maintenance, location service, route instantiation

and maintenance and lastly data transmission. PCA initiates *Network setup phase*, divides the area into zones and elects the initial LCAs. *Network maintenance phase* ensures preserving the network hierarchy considering some concerns including nodes certificates update, LCAs synchronization, nodes movements along with destroyed and corrupted nodes. Figure1 shows the network structure supposing that the entire area is divided into sixteen zones.

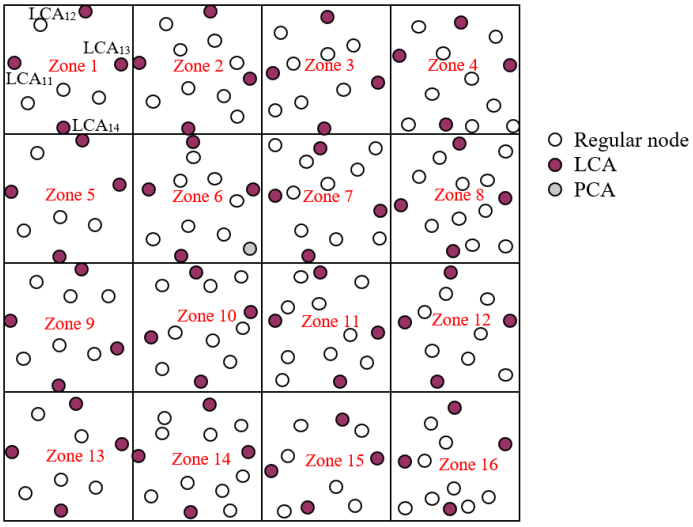


Figure 1: Network structure after electing initial LCAs

When a source has data to send to a specific destination; source should obtain the position of the destination before conducting the route discovery procedure. *Location service phase* allows the source to acquire the position of the destination via Position Discovery Packets (PDP) and Position REPly (PREP) packets.

After obtaining the destination position, *route instantiation and maintenance phase* is started using Route Discovery Packets (RDP), Route REPly (RREP) packets and ERRor (ERR) packets. After accomplishing route discovery and setup, the source starts *data transmission phase* and sends data to the intended destination via the selected route.

Table 1 summarizes the different phases in ARANz protocol. A detailed discussion of ARANz different phases, along with the packets sent during each phase can be found in our work in [1]. In the following subsection we concentrate on the details of the suggested Misbehavior system considering malicious nodes residing in the network and conducting different attacks such as modification, black hole, grey hole, and fabrication.

Table 1: ARANz protocol different phases

Phase	Explanation
Network setup	Consists of issuing certification, dividing network into zones, deciding on initial LCAs and informing each node about the initial role it will play in the network.
Network maintenance	Ensures maintenance of the network structure, considering updating nodes certificates, needed synchronization, as well as nodes movement, corrupting and distortion.
Location service	Allows source to obtain position of the destination by communications with its zone LCAs.
Route instantiation and maintenance	Includes sending a RDP via restricted directional flooding from source to destination, unicasting a RREP from the destination along the reverse path towards the source and maintaining the selected route using ERR packets to announce broken links in active paths.
Data transmission	Relaying data packets through the selected route during the route instantiation process until reaching the destination.
Misbehavior detection system	Helps in identifying malicious nodes and excluding them from future communications.

Let us define some notations and variables to be used in the forthcoming sections. Table 2 presents variables, notations and packet identifiers used with ARANz protocol. While, Table 3 shows the notation used to present the suggested misbehavior detection system.

Table 2: Variables, notations and packet identifiers for ARANz

Notation	Explanation	Notation	Explanation
PCA	Primary Certificate Authority	LCA_{zs}	Zone *z* Local Certificate Authority *s*
$LCAsZ_z$	Zone *z* LCAs identities and positions	IP_n	Node *n* IP address
N_n	Node *n* Nonce	$Cert_n$	Node *n* Certificate
K_{n-}	Node *n* Private key	K_{n+}	Node *n* Public key
K_{NET-}	Network Private key	K_{NET+}	Network Public key
$\underrightarrow{Rdf}$	Send packet using restricted directional flooding	$\underrightarrow{Fln}$	Flood packet to entire network
MNODE	Misbehaving NODE	CNODE	Compromised NODE
PDP	Position Discovery Packet	RDP	Route Discovery Packet
PREP	Position REPly packet	RREP	Route REPly packet
ERR	ERRor packet		

Table 3: Variables and notations for the proposed misbehavior detection system

Notation	Explanation	Notation	Explanation
Fd_{nm}	Number of dropped data packets by node m that it receives from node n	Fm_{nm}	Number of modified control packets sent from node m to node n
Nm	Number of packets received indicating the misbehavior of a node so that this node is considered as compromised	Sd_{nm}	Number of delivered data packets by node m that it receives from node n
Sm_{nm}	Number of unmodified control packets sent from node m to node n	$TrstVd_{nm}$	Node n trust value regarding node m considering dropping attacks
$TrstVf_{nm}$	Node n trust value regarding node m considering fabrication attacks	$TrstVm_{nm}$	Node n trust value regarding node m considering modification attacks
Thd	Dropping threshold	Thf	Fabrication threshold
Thm	Modification threshold	TT	Trust table

3.3. Misbehavior Detection System

Malicious nodes might conduct erratic actions such as using invalid certificates and inappropriately signed massages. ARANz responds to all erratic behaviors by dropping any packet showing any erratic behavior.

Malicious nodes, however, may cause more severe misbehaving actions and attacks, such as altering some fields in control packets, dropping data packets and fabricating error packets. In these cases, our protocol collaborates with a misbehavior detection system to help in detecting and isolating malicious nodes, such as the one proposed in this section.

The proposed system is powerful regarding flexibility and accuracy in managing trust and lightweight in terms of computation. Our system is flexible and can be used to protect against several attacks. The main concept is that each node has a trust table (TT) to maintain reputation information regarding neighboring nodes. In the TT, values about several events are stored. A node uses this value to evaluate its neighbor as misbehaving (malicious) or well-behaving node. Each node is responsible for gathering events from direct relations and computing its own trust values for its neighbors.

Section 3.3.1 discusses the process of collecting data about different trust metrics. After that, dealing with malicious and compromised nodes are explained in Sections 3.3.2 and 3.3.3, respectively.

3.3.1 Data Collection and Trust Metrics Calculation

Whenever a misbehaving action is detected, it triggers a response by the neighboring nodes. Hence, one important aspect of trust management systems is collecting data. Consequently, it is necessary to identify what events reflect a helpful feedback to the scheme and assist in making the proper decision.

Many trust metrics can be considered to disclose the cooperation willingness of nodes during route establishment and maintenance as well as data forwarding phases, however, as trade-off between implementation cost and intended security, a number of these metrics have been selected in this work. The behavior aspects that have been chosen for monitoring are:

- Control packet modification: nodes assemble trust information regarding their neighbors during interactions considering the try to modify some fields in PDP, PREP, RDP or RREP packets.
- Data packet dropping: nodes are evaluated concerning their sincerity and willingness in forwarding data packets, trying to reduce grey-hole and black-hole attacks. Readiness can be checked either based on link layer acknowledgements, or through overhearing [23].
- Error packet fabrication: to protect against fabricating ERR packets, each node keeps information about the number of ERR packets issued by each neighbor.

Let us now quantify these aspects. For the first two trust metrics, node A calculates trust values concerning node B considering modification attacks ($TrstVm_{AB}$) and dropping attacks ($TrstVd_{AB}$) using (1) and (2).

$$TrstVm_{AB} = \frac{Sm_{AB}}{Sm_{AB} + Fm_{AB}} \quad (1)$$

$$TrstVd_{AB} = \frac{Sd_{AB}}{Sd_{AB} + Fd_{AB}} \quad (2)$$

Where Sm_{AB} and Sd_{AB} consider the number of successful co-operations, whereas Fm_{AB} and Fd_{AB} consider the number of failed ones. In other words, for the first metric Sm_{AB} is the number of unmodified control packets and Fm_{AB} stands for the number of modified control packets received by node A from node B. For the second metric, Sd_{AB} stands for the number of delivered data packets and Fd_{AB} is the number of dropped data packets by node B that it already received from node A.

For the last trust metric, node A computes a trust value concerning neighbor B considering ERR packets fabrication attack ($TrstVf_{AB}$) by counting the ERR packets issued by B that passes through node A towards the source.

3.3.2 Malicious Nodes

Once $TrstVm_{AB}$ or $TrstVd_{AB}$ become less than a threshold Thm or Thd respectively, node A considers node B as a malicious node. Also, if $TrstVf_{AB}$ becomes higher than a threshold Thf, node A believes that node B is a malicious node. In these cases, node A excludes node B from upcoming communications. Moreover, node A sends a Misbehaving NODE (MNODE) packet to announce this misbehavior to its nearest zone LCA. This packet

is sent via Restricted directional flooding (Rdf). Suppose that the nearest LCA to node A is node I, then node A sends the following MNODE packet to node I:

$$A \xrightarrow{Rdf} I: [MNODE, IP_I, N_A, IP_B] K_{A-}, Cert_A$$

The MNODE packet contains a packet type identifier (MNODE), the nearest LCA IP address (IP_I), the sending node nonce (N_A) and the misbehaving node IP address (IP_B). The principle of the nonce is to distinctively identify a MNODE packet sent by a specific node. Every time A sends a MNODE packet, it adds up the nonce value. The packet is signed by the node private key (K_{A-}) and node certificate ($Cert_A$) is added to the packet to allow other nodes to authenticate the signature and ensure that A certificate is still active.

3.3.3 Compromised Nodes

From the reputation of a node, it can be identified as misbehaving, consequently, it may be eliminated from the routing process if it is proved to be a misbehaving node. In our scheme, if major part of LCAs in a specific zone have collected a pre-defined number (Nm) of MNODE packets indicating the misbehavior of a particular node, then they work together and send a Compromised NODE (CNODE) message to the entire network. Consequently, this node is excluded by other nodes until its certificate expires normally. Suppose that the nearest LCA to the compromised node is node I, then node I will broadcast the following CNODE packet:

$$I \xrightarrow{Fln} ALL: [CNODE, N_I, [IP_B] K_{NET-}] K_{I-}, Cert_I$$

The CNODE packet is sent using network flooding (Fln) technique. In network flooding, a packet is forwarded to all nodes existing currently in the network. Thus, each node upon receiving a packet continues broadcasting the packet to all its neighbors. The CNODE packet contains a packet type identifier (CNODE), the nonce of the sending node (N_I) and the IP address of the compromised node (IP_B). CNODE packets are signed by the private key of the node (K_{I-}) and node certificate ($Cert_I$) is appended to the packets to enable other nodes to validate signature and verify certificate freshness. To ensure that the node initiated the packet is truly one of the trusted LCAs, the compromised node IP address is signed by K_{NET-}.

Same procedure is appropriate if the misbehaving node is a LCA. Thus, if three LCAs of a specific zone received a pre-defined number of MNODE packets demonstrating the misbehavior of the fourth LCA, this LCA is taken out from the LCAs list ($LCAsZ_z$) of this zone, a CNODE packet is broadcast and a new LCA election procedure is initiated. Even before withdrawing the certificate from the misbehaving LCA, other LCAs can give certificates for trusted nodes in this zone even if the compromised LCA refused to initiate ACREP packets.

If two LCAs of the same zone are compromised simultaneously, neither the two compromised LCAs nor the trusted LCAs are able to issue certificates. This state may stay till the expiration of certificates of zone nodes. Accordingly, these nodes become unable to take part of any upcoming activity. This state may also end (before the expiration of nodes' certificates) by losing battery energy of one compromised LCA or its departure to a neighboring zone. At this point, a new LCA election is conducted to substitute the compromised LCA. Having a third well-behaving LCA, these LCAs can perform their tasks normally.

On the other hand, this state may end by replacing a trusted LCA with a compromised one (e.g. the trusted LCA moved to a neighboring zone and the newly elected LCA is compromised). Now, there are three compromised LCAs in this zone. Hence, the security of the entire network is compromised and these LCAs may work together to give certificates to misbehaving nodes.

3.3.4 Misbehavior Detection System Summary

This section has discussed the misbehavior detection system in details. Table 4 summarizes the packets sent during the misbehavior detection system phase.

Table 4: Packets sent during the misbehavior detection phase of ARANz

Pid	Stand for	Explanation
MNODE	Misbehaving NODE	• Sent to report the misbehavior of other nodes. • Sent using restricted directional flooding. • Sent from any regular node n to nearest LCA in its zone z.
CNODE	Compromised NODE	• Sent after collaboration of the majority of LCAs in zone z upon receiving the pre-defined number of MNODE packets for a specific misbehaving node. • Sent using network flooding. • Sent from LCAs of zone z to All nodes

4. Performance and Security Evaluation

Our next step is to study ARANz performance and security and compare it with existing protocols. Section 4.1 shows our simulation environment and methodology. Section 4.2 through Section 4.6 study the effect of the malicious node percentage conducting modification, black hole, grey hole, fabrication and multiple attacks, respectively.

4.1. Simulation Environment and Methodology

Our protocol should be compared with the basic ARAN protocol since our protocol is based on it. Additionally, AODV protocol is also considered since AODV is usually considered as a benchmark for Ad-Hoc routing protocols performance evaluation and as ARAN is proposed based on AODV. In the following subsections a detailed simulated performance and security evaluation of the three routing protocols is provided.

Evaluating the performance of AODV, ARAN and ARANz protocols is conducted using GloMoSim simulation tool. Nodes transmission range of 250m is simulated. The nodes initial positions are randomly chosen with node density of 60nodes/km^2. After that, nodes may travel regarding the random waypoint mobility model, i.e., every node moves to a randomly selected position at a specified speed and then pauses for a chosen pause time, before selecting another random position and repeating these steps.

Source and destination pairs are randomly chosen for both local and external communications. 802.11 MAC layer and Constant Bit Rate (CBR) traffic over User Datagram Protocol (UDP) are used. Five CBR sessions are conducted in all runs. Each session generates 1000 512-byte data packets at the rate of 4 packets per second. A percentage of 60% of local communication is considered, i.e., two of the five CBR sessions in each run are external and the others are local.

For simulating ARAN and ARANz, it has been assumed that the key distribution procedure has been completed. A 512-bit key and 16-byte signature are simulated [2].

For either protocol, a routing packet processing time of 1ms is simulated [3]. Moreover, a processing delay of 2.2 ms is added for the ARAN and ARANz cryptographic operations [2]. In order to minimize collisions, an arbitrary delay between 0 and 10ms is added before forwarding a broadcast packet.

The effect of malicious node percentage has been tested considering the following *performance metrics*:

1. Packet Delivery Fraction (PDF): fraction of the generated data packets by the source nodes that are received by intended destination nodes.
2. Average Path Number of Hops (APNH): average length of the discovered routes by a protocol. It is evaluated by averaging the number of hops needed by different data packets to arrive at their destinations.
3. Packet Network Load (PNL): resulted overhead packets to construct and maintain network structure along with updating certificates and positions of nodes. It is evaluated in ARANz as the total of all packets sent throughout the setup and maintenance phases. Alternatively, it is calculated in ARAN as the summation of transmitted packets to certify nodes. The forwarding at every hop along the routes is also considered in this metric calculation. Regarding AODV, it is an unsecure flat topology-based protocol; i.e., it has no network structure maintenance nor nodes positions or certificates update. Hence, PNL of AODV is not included in the figures.
4. Packet Routing Load (PRL): ratio of routing packets to delivered data packets. Routing packets include all packets sent throughout the location service, route instantiation and route maintenance phases. Retransmission at all hops along the path is also considered.
5. Average Route Acquisition Latency (ARAL): average time to discover a route to the destination. It is calculated in ARAN and AODV as the average delay from sending a route discovery packet by a source to receiving the first related route reply packet. Considering ARANz, it is calculated as the average time needed for both discovering the destination position and finding a route to it.

Each point in the following figures is an average of five simulation runs with similar configuration but different randomly generated numbers. Several scenarios have been conducted for numerous attacks with different number of attacking nodes. The effect of malicious nodes behavior is studied on a 2km×2km network containing 240 nodes and is divided into 4 zones. These nodes move at a maximum speed of 5m/s. Simulations are run with randomly chosen 0%, 10%, 20% and 40% malicious nodes.

To investigate the malicious node percentage effect, five scenarios have been simulated. Malicious nodes perform the following attacks towards data and/or control packets:

1. Modification attack: Malicious nodes performing modification attack selectively reset the hop count field to 0 in the route discovery and setup packets passing through them. By assigning the hop count field to 0, a malicious node makes other nodes believe that it is just one hop from the source or destination.
2. Black hole attack: Misbehaving nodes dump every data packet that they are supposed to forward.
3. Grey hole attack: Misbehaving nodes drop some data packets at random intervals.
4. Fabrication attack: Misbehaving nodes performing this attack periodically fabricate error packets with a specific probability.
5. Multi-attack: Malicious nodes carry out multiple attacks with a specific probability.

For these scenarios some or all the following *security metrics* have been added, as necessary, to the set of the studied performance metrics:

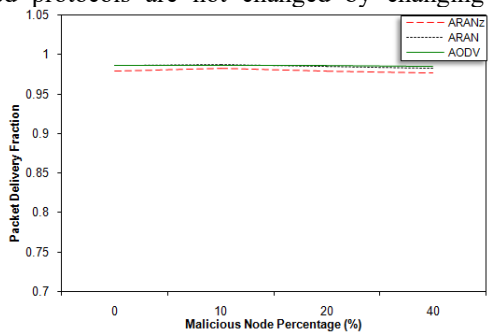
1. Malicious Route Percentage (MRP): portion of the selected routes that pass through malicious nodes. It is evaluated as the number of routes having misbehaving nodes within them over the number of all used routes.
2. Packet Loss Percentage (PLP): fraction of data packets that are abandoned by malicious nodes without any notification.
3. Fabricated Error Packets (FEP): number of error packets that are fabricated by misbehaving nodes.
4. Compromised Node Percentage (CNP): fraction of nodes that are treated as compromised due to recognizing their misbehavior.
5. Packet Malicious Load (PML): extra packets sent for the misbehavior detection system including MNODE and CNODE packets. The transmission at each hop is also considered in this metric calculation.

The last two metrics are only specified for ARANz since the other two protocols do not have misbehavior detection schemes. Some initial experiments have been carried out to choose the best values for modification threshold (Thm), dropping threshold (Thd), fabrication threshold (Thf) and the number of MNODE packets that LCAs should receive to consider a specific node as compromised (Nm). Different values for Nm are considered ranging from 1 to 3, also Thm and Thd are assigned values ranging from 0.3 to 0.7. Finally values of Thf range from 3 to 7. Results of these experiments show that a larger number of misbehaving nodes are really identified as compromised nodes upon setting Nm, Thm, Thd and Thf to 1, 0.5, 0.5 and 3, respectively. Accordingly, these are the values that are assigned for these parameters upon simulating different scenarios.

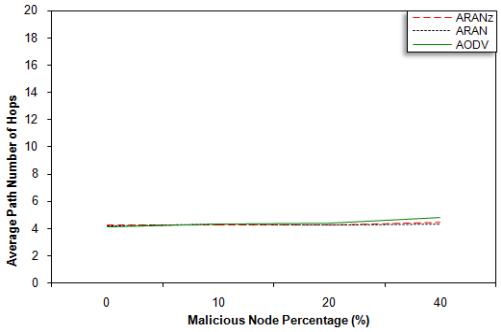
4.2. Malicious Node Percentage Effect Considering Modification Attack

In this scenario, the simulated malicious behavior represents the modification attack. Upon receiving a route discovery or reply, a malicious node chooses a random number between 0 and 1. If the chosen number is lower than 0.5, then the node illegitimately assigns the value of 0 to the hop count field, to convince other nodes that it is only one hop from the source or destination. If not, it forwards the control packet without modification.

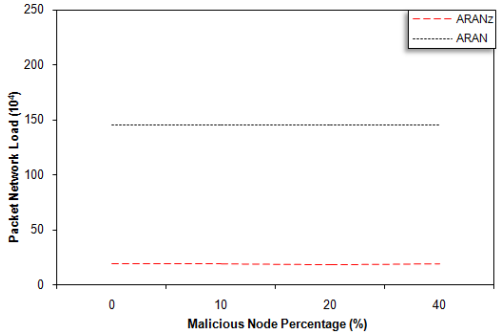
It is clear from Figure 2 (a through e) that the first five metrics of the three studied protocols are not changed by changing malicious node percentage, except APNH and ARAL for AODV. This fact indicates that the three protocols are able to deliver data while having acceptable routing load regardless the malicious nodes percentage. In case of ARAN and ARANz, data delivery is almost guaranteed without affecting either the time required to obtain the routes or the number of hops in the selected paths. In AODV, however, APNH and ARAL slightly increase with increasing malicious node percentage since AODV can be exploited by malicious nodes so that non-optimal routes are chosen, while such exploitation in ARAN and ARANz is unfeasible.



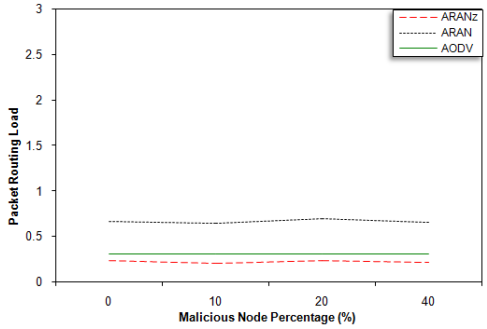
(a) Packet delivery fraction



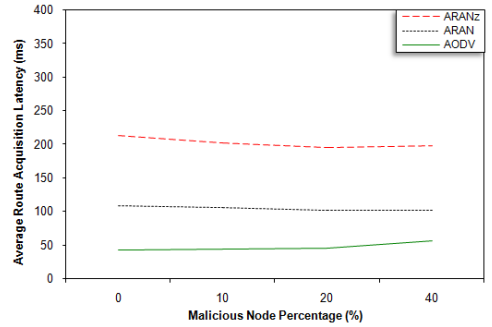
(b) Average path number of hops



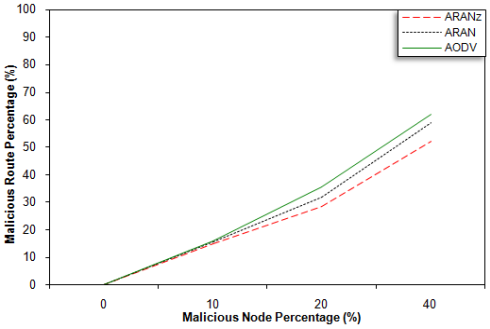
(c) Packet network load



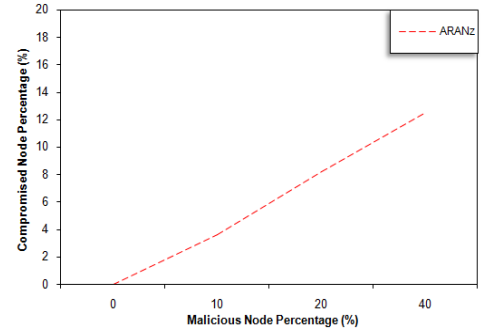
(d) Packet routing load



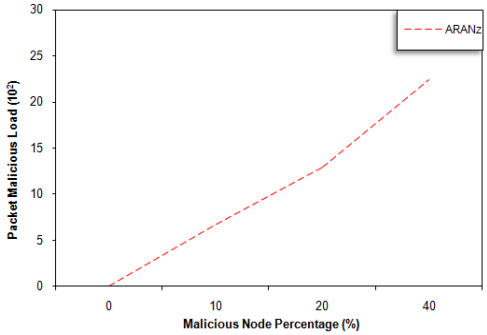
(e) Average route acquisition latency



(f) Malicious route percentage



(g) Compromised node percentage

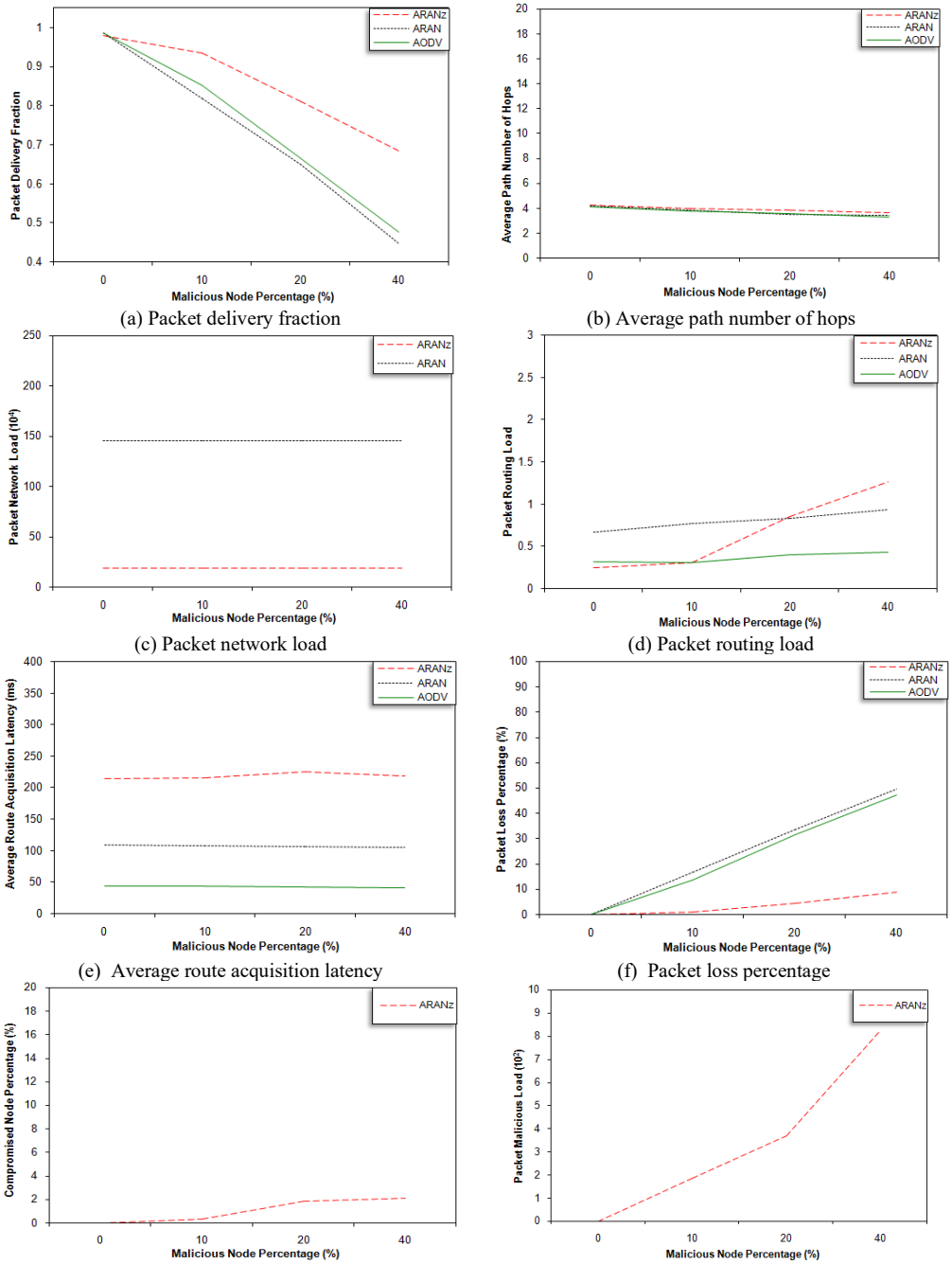


(h) Packet malicious load

Figure 2: Malicious node percentage effect considering modification attack

ARANz achieved the minimum PRL. In contrast to AODV and ARAN, ARANz does not send the RDP packets to the entire network, instead, these packets are forwarded using restricted directional flooding to the destination. AODV is superior in its ARAL as it has the shortest processing delay at each node. On the other hand, while processing routing control packets in ARAN and ARANz, each node has to validate the preceding node digital signature and replace old signature with its own signature, besides the usual packet processing done by AODV. This signature verification and generation result in additional delay at each hop, and so ARAL increases. Moreover, ARANz has the highest ARAL since it needs to carry out a destination position discovery step.

Figure 2 (f) shows that MRP significantly increases for the three protocols upon increasing the malicious node percentage. Yet, the figure shows that upon using AODV, more fraction of routes has malicious nodes within them. When the malicious node sets the value of hop count field as 0, it convinces nodes to select the route that passes through itself; because AODV chooses the shortest paths. ARAN and ARANz, on the other hand, are not exploited in such way. The chosen route may pass through a malicious node but not forced to do so. Referring to Figure 2 (g and h), it is apparent that CNP and PML for ARANz increase as the misbehaving nodes increase. This implies that ARANz is efficient in discovering modification attacks and confirms our research hypotheses; i.e., utilizing the proposed misbehavior detection system improve ARANz performance and security.



(a) Packet delivery fraction
(b) Average path number of hops
(c) Packet network load
(d) Packet routing load
(e) Average route acquisition latency
(f) Packet loss percentage
(g) Compromised node percentage
(h) Packet malicious load

Figure 3: Malicious node percentage effect considering black hole attack

4.3. Malicious Node Percentage Effect Considering Black Hole Attack

The black hole attack is considered in this scenario. In this attack, malicious nodes dump all data packets that they receive.

From Figure 3 (b, c and e), it is obvious that the APNH, PNL and ARAL for the three protocols are generally not affected by the simulated percentage of malicious nodes. The almost constant APNH and ARAL indicate that the three protocols are able to discover the shortest paths without affecting the time required to obtain the routes even with increasing the malicious node percentage. PNL for ARAN and ARANz protocols has almost fixed values for the reason that packets initiated to update nodes certificates and maintaining network structure are sent regardless of the number of nodes dropping data packets.

It is noticeable from Figure 3 (a) that PDF decreases for the three protocols upon increasing the malicious node percentage. The decrease in PDF is justifiable as the malicious nodes in this scenario perform the black hole attack, they drop the data packets they receive. However, the figure assures that the decrease in PDF is slower and insignificant in ARANz, suggesting that ARANz is capable of isolating the black hole attackers and confirms our research hypotheses.

By looking at Figure 3 (d), we can observe that PRL for AODV and ARAN is approximately not affected by misbehaving node percentage. For ARANz, this metric slightly increases as the malicious nodes number increases since detecting malicious nodes in ARANz causes reinitiating RDP packets in a try to find another secure route, i.e. slightly increasing the routing overhead.

Figure 3 (f) shows that PLP increases for the studied protocols as the misbehaving node percentage increases. However, when simulating ARANz the increase in PLP is much slower. This assures that ARANz is efficient in detecting black hole attacks and justifies the increase in CNP and PML for ARANz with increasing the malicious node percentage (refer to Figure 3 (g and h)).

4.4. Malicious Node Percentage Effect Considering Grey Hole Attack

In this scenario, the grey hole attack is considered. In such attack, a misbehaving node arbitrarily drops data packets. To simulate this attack, when a misbehaving node receives a data packet, an arbitrary number between 0 and 1 is drawn. When the number is lower than 0.5, the node drops the data packet. Otherwise, the data packet is sent to the successor node.

As in the previous scenario, Figure 4 (b, c and e) shows that APNH, PNL and ARAL for the evaluated protocols are somehow not affected by the percentage of malicious nodes existing in the network. Figure 4 (a) shows that PDF decreases for the three protocols as the number of malicious nodes dropping data packets is increased. However, the decrease in PDF is slower in ARANz implying that ARANz is efficient in detecting grey hole attackers.

Figure 4 (d) shows that PRL for AODV and ARAN is not affected by malicious node percentage. On the other hand, this metric for ARANz slightly increases with increasing the malicious node percentage. This increase in PRL is due to reinitiating RDP packets as a result of detecting malicious nodes.

Looking at Figure 4 (f), it is clear that upon increasing the malicious node percentage PLP increases for the three protocols. However, upon using ARANz, the increase in PLP is much slower, which is an evidence that ARANz is efficient in identifying grey hole attackers and helps us answer our research question. This also justifies the increase in CNP and PML for ARANz with increasing malicious node percentage (refer to (Figure 4 (g and h)).

In comparison with the previous scenario (black hole attack effect), results of the conducted experiments show that the increase in PRL, CNP and PML for ARANz is slower in this scenario. This means that discovering grey hole attackers is more difficult and requires a longer time compared to discovering black hole attackers because grey hole attackers drop only some of the data packets they receive, so it takes longer time to detect them. Another point to mention here is that even though discovering grey hole attackers is slower than discovering black hole attackers, black hole attackers drop all packets they receive. Consequently, the increase in PLP and the decrease in PDF are almost the same in both cases.

4.5. Malicious Node Percentage Effect Considering Fabrication Attack

This scenario is performed to examine the result of conducting the fabrication attack. In this attack, misbehaving nodes periodically fabricate ERR packets with a specific probability. To simulate this attack, malicious nodes existing in the route between the source and destination nodes periodically draws a number between 0 and 1. When the drawn number is lower than 0.5, they send an ERR packets along the path toward the source to report false broken links.

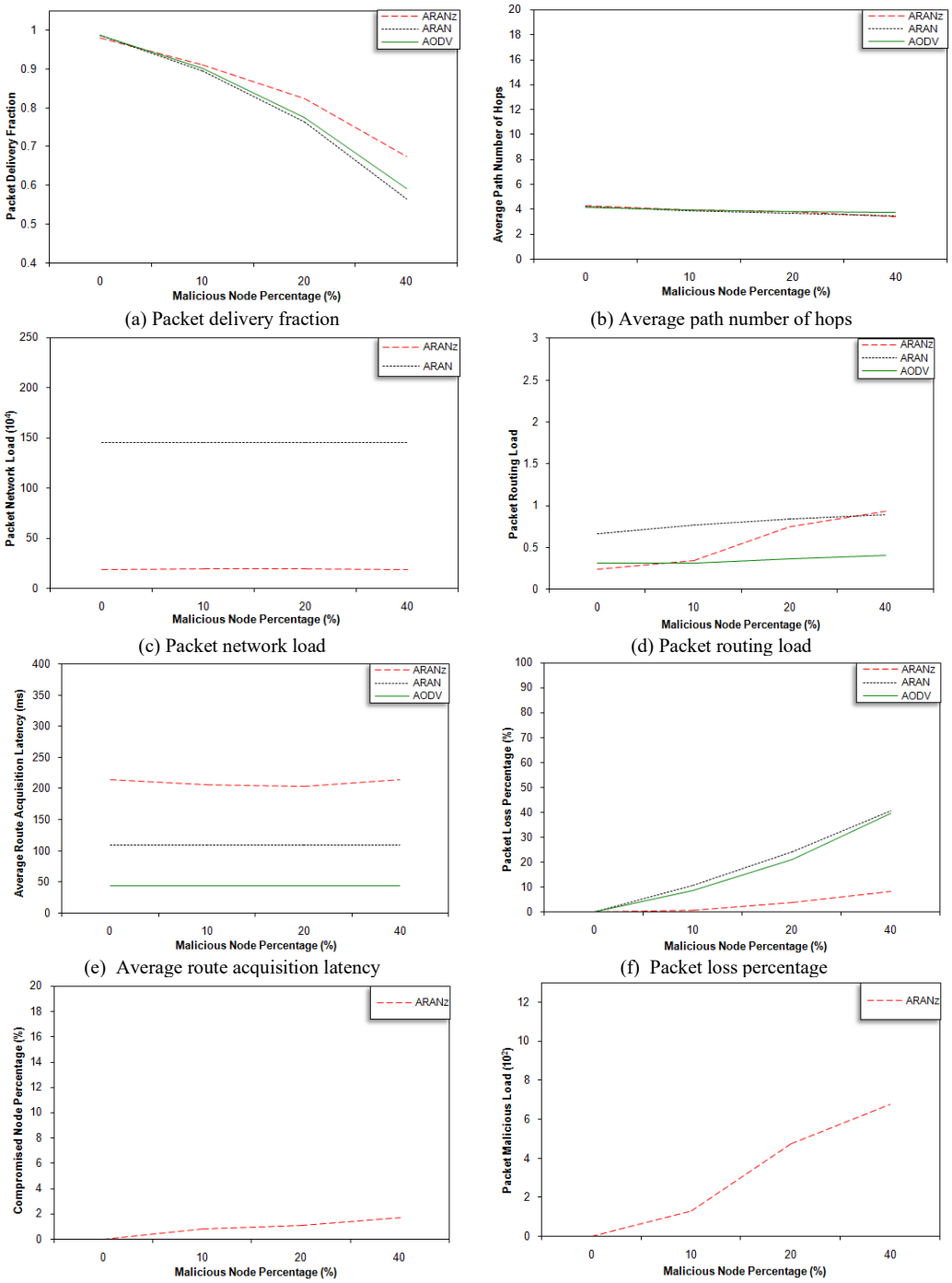
Figure 5(a) 5.93 shows that PDF decreases slightly for the three protocols as the malicious node percentage increases due to dropping some data packets as a result of receiving the fabricated ERR packets. However, the PDF for the three protocols is still above 90% even with the existence of large percentage of fabrication attackers.

As in the preceding three scenarios, Figure 5 (b and c) show that APNH and PNL for the evaluated protocols are, to some extent, not affected by attacking nodes percentage. This suggests that the three protocols are still able to discover the shortest paths even with the existence of some malicious nodes.

By looking at Figure 5 (d), it is noticeable that PRL for either protocol increases as the malicious node percentage increases. This increase in PRL is because of reinitiating RDP packets by the source node as a result of receiving the fabricated ERR packets.

Figure 5 (e) shows that ARAL for AODV and ARAN protocols is not affected by attacking nodes percentage. However, this metric for ARANz slightly increases with increasing the malicious node percentage. In ARANz, discovered malicious nodes are not included in future route selections which may result in choosing non-optimal paths that do not contain malicious nodes.

Figure 5 (f) shows that FEP increases for the three protocols upon increasing the malicious node percentage. But, the increase in FEP is much slower upon simulating ARANz, which indicates ARANz effectives in detecting and isolating nodes performing fabrication attack and answers our research question.



(a) Packet delivery fraction

(b) Average path number of hops

(c) Packet network load

(d) Packet routing load

(e) Average route acquisition latency

(f) Packet loss percentage

(g) Compromised node percentage

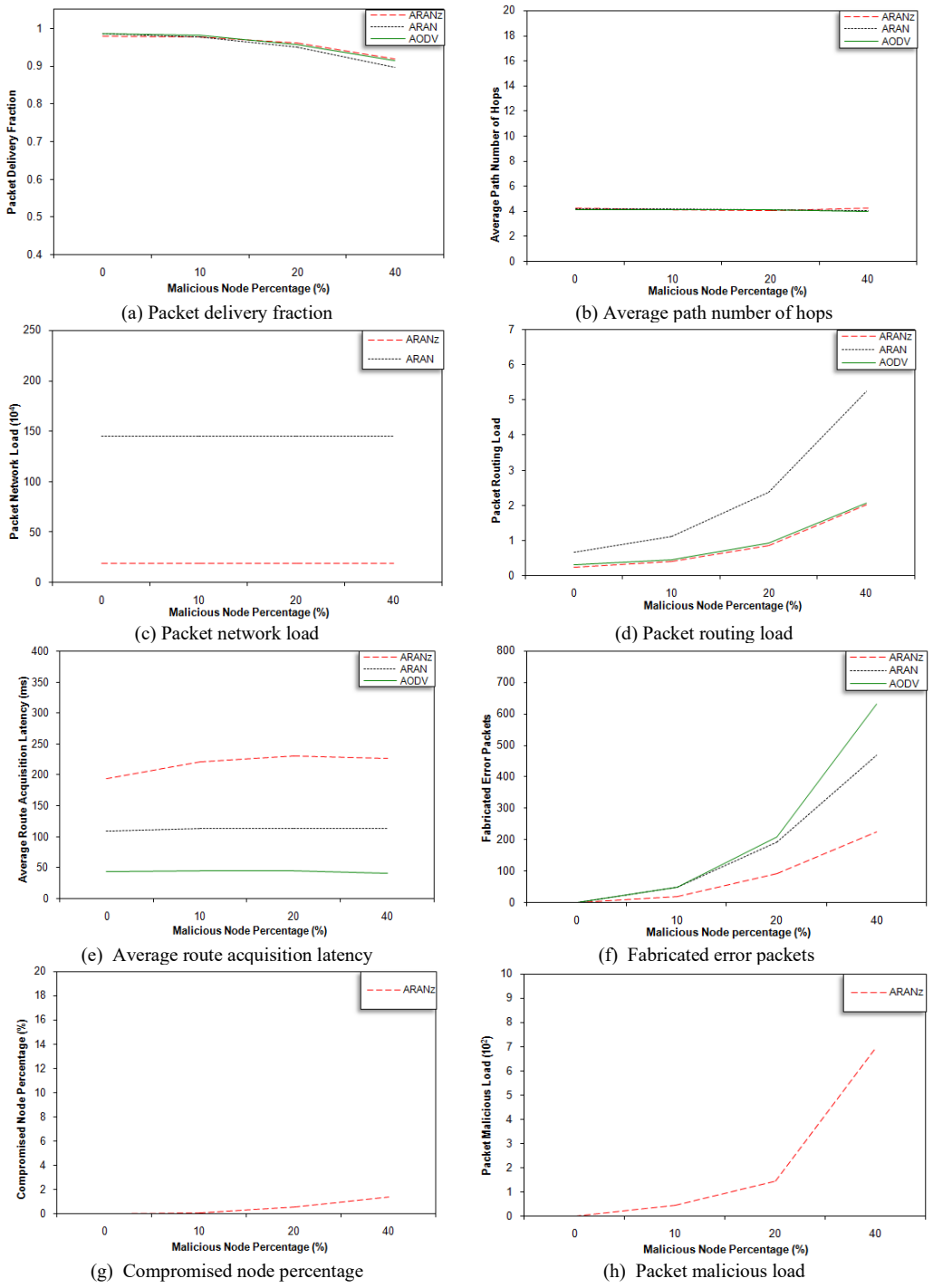
(h) Packet malicious load

Figure 4: Malicious node percentage effect considering grey hole attack

Figure 5 (g and h) show that CNP and PML increase as the malicious node percentage increases. In other words, as malicious node percentage increases ARANz demonstrates its effectiveness in distinguishing more and more malicious nodes.

4.6. Malicious Node Percentage Effect Considering Multi-Attack

In this scenario, the effect of multi-attack is studied. In this attack, malicious nodes perform multiple attacks with a specific probability. To simulate multi-attack, malicious nodes perform modification, grey hole and fabrication attacks. The same details used to simulate each attack separately in the previous scenarios are used to simulate multi-attack. In other words, malicious nodes performing multi-attack illegally reset the hop count field to 0 in a received route discovery or route reply, if a drawn number is less than 0.5. They also drop a received data packet if a drawn number is less than 0.5 and periodically fabricate ERR packet if a drawn number is less than 0.5.



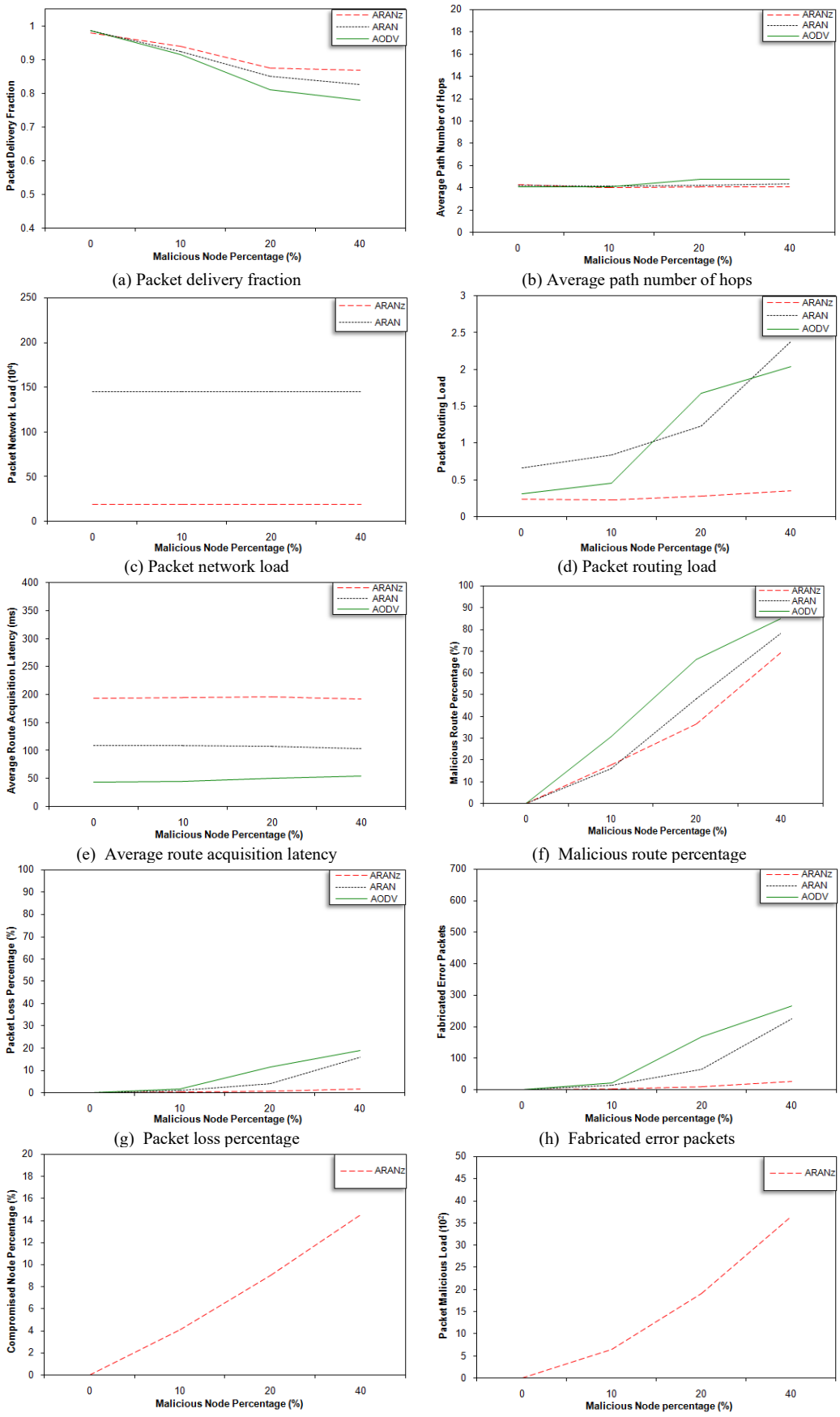
(a) Packet delivery fraction
(b) Average path number of hops
(c) Packet network load
(d) Packet routing load
(e) Average route acquisition latency
(f) Fabricated error packets
(g) Compromised node percentage
(h) Packet malicious load

Figure 5: Malicious node percentage effect considering fabrication attack

Referring to Figure 6 (a) it is clear that increasing malicious node percentage results in decreasing PDF for all protocols. This is mainly due to data packets dropped upon performing grey hole attack. The slower decrease in ARANz PDF is an indication that ARANz is effective in identifying and isolating multi-attack malicious nodes even if the simulated percentage is large.

Figure 6 (b) shows that APNH for AODV slightly increases upon increasing malicious node percentage. Misbehaving nodes can exploit AODV, via modification attack, so that non-optimal routes are chosen. ARAN and ARANz are not exploitable in this way.

It is conspicuous from Figure 6 (c) that malicious node percentage definitely does not affect PNL for ARAN and ARANz protocols. The reason behind the stable PNL is that updating nodes' certificates and positions is carried out regardless the number of existing malicious nodes.



(a) Packet delivery fraction

(b) Average path number of hops

(c) Packet network load

(d) Packet routing load

(e) Average route acquisition latency

(f) Malicious route percentage

(g) Packet loss percentage

(h) Fabricated error packets

(i) Compromised node percentage

(j) Packet malicious load

Figure 6: Malicious node percentage effect considering multi-attack

Figure 6 (d) reveals that PRL for all studied protocols increase upon increasing malicious node percentage. This increase in PRL is mainly due to reinitiating RDP packets by the source upon receiving the fabricated ERR packets. Also, it is apparent that ARANz attained the minimum PRL and ARANz has the slowest increase in PRL, which reflects ARANz effectiveness in detecting and isolating the fabrication attackers and assures our research hypothesis. Furthermore, it is clear that AODV is highly affected by the fabrication attack because the selected routes in AODV are forced to pass through malicious nodes via modification attack. After that, these malicious nodes start to fabricate ERR packets resulting in higher PRL. In ARAN and ARANz, however, routes are not forced to go through malicious nodes due to their robustness against the modification attacks.

Figure 6 (e) shows that ARAL for AODV slightly increases upon increasing malicious node percentage due to selecting non-shortest paths (since it is susceptible to modification attack). ARAL for ARAN and ARANz protocols is not affected by increasing attacking nodes percentage since they are robust against modification attacks.

Figure 6 (f) reveals that the MRP increases for the three protocols as the misbehaving nodes percentage increases. As the figure also shows, more routes with malicious nodes within them are used upon simulating AODV. When the attacker sets the hop count field to 0, it forces AODV to select the route passes through itself since AODV selects the shortest path.

Figure 6 (g) assures that the PLP increases upon increasing malicious node percentage due to dropping data packets via the grey hole attack. However, upon using ARANz, the increase in PLP is significantly slower indicating that ARANz is efficient in distinguishing grey hole attackers.

The FEP for the evaluated protocols increases upon increasing the malicious node percentage (as shown in Figure 6 (h)). However, the increase in FEP is much slower upon using ARANz, which illustrates that ARANz is effective in identifying and extracting nodes performing fabrication attack. Also, the increase in FEP is faster in AODV protocol since it is forced to use routes containing malicious nodes (via modification attack). Afterward, these nodes start sending fabricated ERR packets, resulting in higher FEP.

Figure 6 (i and j) show that as malicious node percentage increases ARANz demonstrates its effectiveness in detecting more and more malicious nodes, i.e. CNP and PML significantly increase as the percent of malicious nodes performing multi-attack increases.

5. Results Summary and Discussion

From the obtained simulation results, presented in the previous section, we can conclude that increasing malicious node percentage results in decreasing PDF and/or increasing PRL, MRP, PLP and FEP for the three protocols. In most cases, however, the decrease or increase in these metrics is much slower upon using ARANz. This assures ARANz efficiency in discovering and isolating the malicious nodes compared to the other two protocols due to the utilized misbehavior detection scheme. Consequently, this proves our research hypotheses; utilizing the proposed misbehavior detection system has really improved ARANz performance and security.

Table 5: Summary of the evaluated routing protocols

Protocol / Criterion	AODV	ARAN	ARANz
Approach	Topology-based (reactive)	Topology-based (reactive)	Position-based (restricted directional flooding)
Basic security	-	Timestamps and certificates	Timestamps and certificates
Proposal	Uses next hop information kept on each node in the least number-of-hop route.	• Provides route discovery, setup and maintenance authentication. • Prevents most attacks via using cryptographic certificates. • Routing packets are authenticated at each hop from source to destination and vice versa.	• Deals with area as zones and introduces several LCAs. • Involves initiating a PDP if destination position is unknown. • Prevents most attacks via using cryptographic certificates. • Control packets are authenticated at each hop from source to destination and vice versa.
Advantages	• No single point of failure. • High robustness against nodes failure.	Robustness against most security attacks.	• Robustness against most security attacks. • No single point of compromise and failure. • Reduced packet overhead. • High availability, robustness and scalability.
Disadvantages	• Relies on blind broadcasts to discover routes; resulting in higher control overhead and lower scalability. • May be exposed to security vulnerabilities.	• Single point of compromise and failure; low availability and robustness. • Scalability problem with the number of nodes inherited from AODV • Increased packet overhead and route discovery delay compared to original AODV due to the encryption/decryption procedures.	• Synchronization among LCAs. • Extra hardware (GPS). • Extra delay to obtain the destination position.

Table 6: Summary of the simulated performance and security evaluation

Metric \ Protocol	AODV	ARAN	ARANz
Packet Delivery Fraction (PDF)	High	High	High
Average Path Number of Hops (APNH)	Almost the same as other protocols	Almost the same as other protocols	Almost the same as other protocols
Packet Network Load (PNL)	-	High	Low
Packet Routing Load (PRL)	Medium	High	Low
Average Route Acquisition Latency (ARAL)	Low	Medium	High
Malicious Route Percentage (MRP)	High	Medium	Low
Packet Loss Percentage (PLP)	High	High	Low
Fabricated Error Packets (FEP)	High	High	Low
Compromised Node Percentage (CNP)	-	-	Increased as malicious nodes increase
Packet Malicious Load (PML)	-	-	Increased as malicious nodes increase

Moreover, as malicious node percentage increases, ARANz effectiveness in distinguishing and isolating malicious nodes is increasingly demonstrated by achieving higher CNP. This assures that ARANz is efficient in identifying and isolating malicious nodes performing modification attack against control packets, black hole and grey hole attacks against data packets, ERR packets fabrication attack as well as multi-attack against control and data packets. Discovering malicious nodes and excluding them from future routes may result in reinitiating RDP packets and choosing non-optimal paths that do not contain malicious nodes within them, hence, causing higher PML, PRL and ARAL.

Furthermore, results suggest that ARANz has accomplished scalability by retaining the minimum packet routing load even upon increasing the percentage of malicious nodes conducting different attacks. ARANz reduced packet routing load is a normal result of using restricted directional flooding to send RDP packets.

The price of ARAN and ARANz improved security is the increased routing load and latency in the route discovery process due to the performed cryptographic computations. Moreover, lower packet routing load of ARANz comes in the fee of increased latency in the route discovery due to destination position obtaining time.

Differing form ARAN, ARANz distributes load and trust by dealing with the area as zones and introducing several LCAs in each zone. ARANz has achieved robustness and high level of security and solved the single point of failure and attack problems by dealing with the area as zones and distributing trust among multiple LCAs. Accordingly, ARANz has achieved both security and scalability. Scalability has been assured by maintaining the minimum packet routing load within relatively large networks. This is a normal result of utilizing restricted directional flooding instead of broadcasting route discovery packets as in AODV and ARAN. Utilizing the misbehavior detection system helped ARANz to assure high level of security by identifying and isolating malicious nodes conducting different types of attacks. Hence, ARANz can be a good choice for Ad-Hoc networks established among students on a campus or peers at a conference, where pre-deployment of some keys and certificates is possible.

Table 5 highlights the key characteristics of the discussed protocols along with their advantages and disadvantages. Whereas Table 6 summarizes the main points concluded from the simulated evaluation.

6. Conclusions

One of the important issues to be tackled in Ad-Hoc networks is efficient routing since all nodes in the network act as both hosts and routers. Moreover, the nature of Ad-Hoc networks makes them prone to different attacks. AODV is an unsecure routing protocol, hence, its processing overhead is low. However, AODV broadcasts route discovery packets resulting in increasing packet overhead. Therefore, AODV scalability is low. ARAN is also a reactive protocol that sends the route discovery packet to all nodes in the network. Moreover, ARAN cryptographic certificates are utilized to detect erratic behaviors. However, using these certificates results in higher route acquisition latency as well as higher packet and processing overheads. This increase is due to the encryption/decryption procedures together with route request broadcast. The centralized trust and load are considered other problems of ARAN.

ARANz, on the other hand, proposes a hierarchal algorithm to improve the protocol performance and scalability through dealing with the area as zones. Via using several LCAs, ARANz achieves

robustness, enhances security and mitigates the single point of failure and attack problems. It also exhibits improved scalability and performance through the use of position-based routing.

In this research, a detailed discussion of the novel misbehavior detection system that has been integrated with ARANz protocol has been provided. Moreover, in this work a detailed performance and security evaluation has been conducted among AODV, ARAN and ARANz protocols. Our simulations show that ARANz is able to have superior performance even with having large percentage of malicious nodes conducting modification, black hole, grey hole and fabrication attacks. ARANz scalability has been proven through achieving the minimum packet routing load in all conducted scenarios. The expense is higher latency due to the required time for packet processing and authentication in addition to inquiring the destination position.

Accordingly, the obtained results confirm our research hypotheses; the proposed novel misbehavior detection system has certainly improved ARANz performance and security.

Hence, ARANz is considered a good choice for managed-open environments in which Ad-Hoc networks are established among students on a campus, peers at a conference, or even employees in a factory. In such environments, pre-deployment of some keys and certificates is possible. Moreover, the proposed misbehavior detection system can be incorporated into other existing non-secure routing protocols to help them protect the network and achieve security.

7. Future Works

The research presented in this work serves as a starting point for future research. First of all, more investigation is required in order to expansively evaluate ARANz protocol performance and security. For example, ARANz performance can be studied under different mobility models and different traffic generation applications. ARANz may also tested considering the case when nodes are not evenly geographically distributed. Moreover, ARANz security may be compared with other recent secure routing protocols.

Second, increased refinement and improvement of a routing protocol is always probable. ARANz may be modified to deal with different number and positions of LCAs in each zone, as well as using different zone shapes. One of the interested ideas that we are thinking of is extending our protocol to be implemented in 3-Dimensional environments such as buildings or war environments containing for example both vehicles and aircrafts.

As with other position-based routing protocols, there is a possibility of finding other techniques for nodes to be aware of their positions without using GPS. Additionally, on the subject of misbehavior mitigation, the proposed misbehavior detection system may be improved to detect other types of attacks. More attention may be given to authentication, key distribution and decreasing processing time and processing overhead of encryption approach.

Additionally, one of the important research limitations facing researchers in Ad-Hoc networks field is the difficulty to implement and test the network in real environment especially when the number of nodes is large. So, we look forward to implement and test our protocol via real implementation. However, this will require a large number of nodes and broad geographical areas to test its scalability.

Finally, this paper worked on one of the important Ad-Hoc network issues; i.e., security issue. However, there are still many open research concerns and challenges facing Ad-Hoc networks which worth exploring. These issues include, but not limited to, multicasting, energy-efficiency and provision of Quality-of-Service (QoS).

Conflict of Interest

The authors declare no conflict of interest.

References

[1] L. Qabajeh, M. Mat Kiah, M. Qabajeh, "A more secure and scalable routing protocol for mobile ad hoc networks," Security and Communication Networks, **6**(3), 286-308, 2013.

[2] K. Sanzgiri, D. LaFlamme, B. Dahill, B. Levine, C. Shields, E. Belding-Royer, "Authenticated routing for ad hoc networks," IEEE Journal on Selected Areas In Communications, **23**(3), 598-610, 2005.

[3] C. Perkins, E. Royer, "Ad hoc on-demand distance vector routing," 1999 IEEE Workshop on Mobile Computing Systems and Applications, New Orleans, USA, 90-100, 1999.

[4] M. Belgaum, Sh. Musa1, M. Su'ud, M. Alam, S. Soomro, Z. Alansari, "Secured approach towards reactive routing protocols using triple factor in mobile ad hoc networks," Annals of Emerging Technologies in Computing (AETiC), **3**(2), 2019.

[5] H. Moudni, M. Er-rouidi, H. Mouncif , B. Hadadi, "Secure routing protocols for mobile ad hoc networks," in 2016 International Conference on Information Technology for Organizations Development (IT4OD), 1-7, 2016.

[6] H. Shen, L. Zhao, "ALERT: an anonymous location-based efficient routing protocol in MANETs," IEEE transactions on mobile computing, **12**(6), 1079-1093, 2013.

[7] H. Chen, Y. Xiao, X. Hong, F. Hu, J. Xie, "A survey of anonymity in wireless communication systems," Security and Communication Networks, **2**(5), 427-444, 2009.

[8] S. Seys, B. Preneel, "ARM: anonymous routing protocol for mobile ad hoc networks," International Journal of Wireless and Mobile Computing, **3**(3), 145-155, 2009.

[9] B. Saoud, A. Moussaoui, "New routing protocol in ad hoc networks," in 2019 International Conference on Computer Networks and Inventive Communication Technologies ICCNCT, 443-452, 2019.

[10] A. Pirzada, C. McDonald, "Reliable routing in ad hoc networks using direct trust mechanisms," In Cheng M, Li D. Advances in Wireless Ad Hoc and Sensor Networks, 133-159, 2008.

[11] A. Dorri, S. Kamel, E. kheyrkhah, "Security challenges in mobile ad hoc networks: A survey," International Journal of Computer Science & Engineering Survey (IJCSES), **6**(1), 15-29, 2015.

[12] Sh. Thapara, S. Sharmab, "Attacks and security issues of mobile ad hoc networks," in 2019 International Conference on Sustainable Computing in Science, Technology & Management (SUSCOM), Jaipur, India, 1463-1470, 2019.

[13] Z. Khan, A. Sharma, "Security aspects of MANETs: A review," International Journal of Computer Science and Mobile Computing, **8**(7), 40-44, 2019.

[14] F. Abdel-Fattah, Kh. Farhan, F. Tarawneh, F. AlTamimi, "Security challenges and attacks in dynamic mobile ad hoc networks MANETs," in 2019 IEEE Jordan International Joint Conference on Electrical Engineering and Information Technology (JEEIT), Amman, Jordan, 28-33, 2019.

[15] M. Soni, B. Joshi, "Security assessment of routing protocols in mobile ad hoc networks," in 2016 IEEE International Conference on ICT in Business Industry & Government (ICTIBIG), 2016.

[16] M. Soni, B. Joshi, "Security assessment of SAODV protocols in mobile ad hoc networks," Data Science and Big Data Analytics, **16**, 347-355, 2018.

[17] J. Arshad, M. Azad, "Performance evaluation of secure on-demand routing protocol for mobile ad hoc networks," in 2006 IEEE Sensor and Ad Hoc Communications and Networks Conference (SECON), 2006.

[18] N. Luong, T. Vo, D. Hoang, "FAPRP: a machine learning approach to flooding attacks prevention routing protocol in mobile ad hoc networks,"

Wireless Communications and Mobile Computing, 2019. https://doi.org/10.1155/2019/6869307

[19] M. Abu Zant, A. Yasin, "Avoiding and isolating flooding attack by enhancing AODV MANET protocol (AIF_AODV)," Security and Communication Networks, 2019. https://doi.org/10.1155/2019/8249108

[20] M. Belgaum, Sh. Musa, M. Su'ud, M. Alam, S. Soomro, Z. Alansari, "Secured approach towards reactive routing protocols using triple factor in mobile ad hoc networks," Annals of Emerging Technologies in Computing (AETiC), **3**(2), 32-40, 2019.

[21] W. Alnumay, U. Ghosh, P. Chatterjee, "A trust-based predictive model for mobile ad hoc network in Internet of Things," Sensors, 2019. https://doi.org/10.3390/s19061467

[22] M. Boulaiche, "Survey of secure routing protocols for wireless ad hoc networks," Wireless Personal Communications, 2020. https://doi.org/10.1007/s11277-020-07376-1

[23] T. Zahariadis, P. Trakadas, S. Maniatis, P. Karkazis, H. Leligou, S. Voliotis, "Efficient detection of routing attacks in wireless sensor networks," in 2009 International Conference on Systems, Signals and Image Processing (IWSSIP), June, Chalkida, Greece; 1-4, 2009.

Advances in Science, Technology and Engineering Systems Journal Vol. 5, No. 5, 193-200 (2020)

www.astesj.com

ASTESJ

ISSN: 2415-6698

Evaluation of Disadvantaged Regions in East Java Based-on the 33 Indicators of the Ministry of Villages, Development of Disadvantaged Regions, and Transmigration Using the Ensemble ROCK (Robust Clustering Using Link) Method

Luluk Wulandari, Yuniar Farida*, Aris Fanani, Nurissaidah Ulinnuha, Putroue Keumala Intan

UIN Sunan Ampel Surabaya, Mathematics Department, Surabaya, 60237, Indonesia

ARTICLE INFO

Article history:
Received: 01 July, 2020
Accepted: 14 August, 2020
Online: 10 September, 2020

Keywords:
Disadvantaged region
Clustering of numeric data
Clustering of cathegorical data
Ensemble ROCK method
The Ministry of Villages
Development of Disadvantaged Regions
Transmigration (Indonesian: Kementerian Desa, Pembangunan Daerah Tertinggal, dan Transmigrasi)

ABSTRACT

East Java province is a large province in Indonesia, in which Surabaya is the second largest metropolitan city after Jakarta. Various problems of development inequality in East Java have caused East Java to be defined as a disadvantaged area in 2015. The determination of disadvantaged regions is carried out every 5 years using 6 criteria and 33 indicators that have been set by the Ministry of Villages, Development of Disadvantaged Regions, and Transmigration. However, from several studies that have been conducted on the determination of disadvantaged regions, there is no research applies 33 indicators as a whole. So in this study, an evaluation of the determination of disadvantaged regions will be carried out using 33 indicators that have been determined by The Ministry of Villages, Development of Disadvantaged Regions, and Transmigration. Criteria data used are the results of the 2014 and 2018 surveys. These data are in the form of numerical data and categorical data. The method used is ensemble Robust Clustering Using Link (ROCK), which is a clustering method that can accommodate mixed data both categorical and numerical, using the concept of distance to measure the similarity or closeness between a pair of data points. The best cluster results for evaluating the determination of disadvantaged regions in 2020 consist of 4 clusters with the smallest Sw and Sb ratio of 0.3873984 and the optimum threshold value of 0.04. The results of the clustering, place Trenggalek, Bondowoso, Situbondo, Probolinggo, Tuban, Pamekasan, Sumenep, Bangkalan, and Sampang regions as disadvantaged regions in East Java.

1. Introduction

Based on the Presidential Regulation of the Republic of Indonesia Number 131 the year 2015 concerning the Determination of Disadvantaged Regions in 2015-2019, East Java Province is one of the 21 Provinces that are lagging in Indonesia. Not only that, but East Java Province is also the only Province in Java which has several disadvantaged district or city. Therefore, a study needs to be carried out to evaluate various problems of development inequality that have left some regions in East Java behind.

Government Regulation number 78 of the year 2014 article 6 paragraph 1 states that the determination of disadvantaged regions is carried out every 5 years based on criteria and indicators established by the Ministry of Villages, Development of Disadvantaged Regions, and Transmigration. In this case, the last disadvantaged region was determined in 2015 listed in Presidential Regulation number 131 of the year 2015 and will be re-established in 2020. In this study, the criteria used are survey data in 2014 and 2018, which sources data were obtained from the Central Statistics Agency in the form of data on village potential, statistics on people's welfare and the profile of each province in a certain number of years. The data in 2014 are used as a comparison with government decisions related to the determination of disadvantaged regions in 2015. While the data in 2018 will be used as predictions for the determination of disadvantaged regions in 2020. The results of this study are expected to provide a relevant picture in which regions have the potential to be left behind in the future. Thus, the government of District/City can take policies towards their regions that are adjusted to the characteristics of each region to alleviate the region from being left behind.

In practice, the government determines disadvantaged regions based on Presidential Regulation Number 131 the Year 2015

*Corresponding Author: Yuniar Farida, UIN Sunan Ampel Surabaya, Indonesia, +62 81252347261, yuniar_farida@uinsby.ac.id

Article 6 Paragraph 2, using composite aspects and range values. Statistically, the two methods are only suitable for analyzing numerical data. While in reality, indicators to determine the status of disadvantaged regions do not only refer to numerical data. But several indicators are categorical. Thus, if the composite aspect and interval values are used as an analysis, it will not be able to accommodate 6 criteria consisting of 33 indicators. To overcome this, a special method is needed that can accommodate all types of data, both categorical and numerical. The statistical method that can be used for clustering mixed data is the ensemble method [1]-[3]. In this study, the ensemble method used is Robust Clustering Using Link (ROCK). Ensemble ROCK method is a clustering method that uses the concept of distance to measure the similarity or closeness between a pair of data points [4], [5]. The advantage of the ensemble ROCK method is it has better accuracy compared to the agglomerative hierarchy method with good scalability [6].

Ensemble ROCK method has proven to be optimal for conducting mixed data clustering in solving various cases [7], such as the research conducted by Shashi Sharma and Ram Lal Yadav, the research proved that ensemble ROCK method is more optimal when compared to the K-Means method for the cluster analysis process [8]. Similar to the research conducted by Dwi Harid Setiadi, in the application of ensemble ROCK method for mapping disadvantaged regions, it proved to be more optimal when compared to the SWFM ensemble method [9]. Then Alvionita compared the SWFM and ROCK methods for grouping orange accessions. In that study, it was found that the ROCK method had better grouping performance than the SWFM method [10]. Therefore, in this study, researchers will evaluate disadvantaged regions in East Java based-on indicators Ministry of Villages, Development of Disadvantaged Regions, and Transmigration using ensemble ROCK method.

2. Related Works

In the last few years evaluation of disadvantaged regions has been carried out, including Anik Djuridah in his research evaluating the status of disadvantaged regions using Discriminant analysis [11]. In that research, it was only determined the number of indicators that influence the determination of the status of being left behind from an area, without being known with certainty which regions are included in the group of disadvantaged regions and not. Similar to the research conducted by Satria, Herman, and Fajar who analyzed the development of disadvantaged regions in East Java using *Location Quotient dan Shift Share Esteban Marquillas analysis* [12]. In that study, it was only used the GRDP (Gross Regional Domestic Product) variable.

Furthermore, Dwi Hariadi Setiadi in his final project was mapping the District/City of disadvantaged regions using the *Ensemble Similarity Weight And Filter Method* (SWFM) and *Robust Clustering Using Link* (ROCK) [9]. In that study, researchers only used 5 criteria and 13 indicators. The five indicators are infrastructure, regional characteristics, economy, human resources (HR), and regional financial capacity, without including accessibility criteria. Whereas in the Government Regulation Ministry of Villages, Development of Disadvantaged Regions, and Transmigration listed in Law No. 78 of 2014 and explained in Presidential Regulation No. 131 of the year 2015 article 2 paragraph 1, 2 and 3 which states that the determination of disadvantaged regions uses six criteria (community economy, human resources, facilities and infrastructure, regional financial capacity, accessibility, and regional characteristics) consisting of 33 indicators used to determine the status of disadvantaged regions.

Based on several related studies mentioned above, no research evaluates disadvantaged regions using all the criteria and indicators that have been determined as a whole. So, in this study an evaluation of disadvantaged regions will be conducted based on all the criteria and indicators set by the Indonesia Ministry of Villages, Development of Disadvantaged Regions, and Transmigration.

3. Theoretical Framework

3.1. Factor Analysis

Factor analysis is a step to reduce research variables both numerical and categorical data using the Principal Component Analysis (PCA) method. The technique of this analysis is conducted by finding the relationship between the variables that were originally independent of each other, becoming a set of new variables that have a strong correlation and number fewer than the original variable [13]-[15]. The first step is to test the assumption of the adequacy of the variables to be processed using the Kaiser Meyer Olkin Measure of Sampling (KMO) and the Barlett Test. If the KMO value is more than 0.5, then it has fulfilled the variable adequacy requirements. So that the data is enough to be factored. While the Hypothesis test for the Barlett test is as follows:

H_0 : The partial correlation formed from the data is not enough to be factored

H_1 : The partial correlation formed from the data is enough to be factored

If $sig < \alpha(a = 0.05)$, then H_0 is rejected. So it can be concluded that the partial correlation formed from the data is sufficient to be factored [16], [17].

3.2. K-Means

K-Means Clustering method is a method that partition data into K groups, where K is the number of groups determined by the researcher. In this research, numerical data will be clustered using K-Means. The K-Means algorithm is as follows [17], [18]:

a. Determine the desired number of clusters

b. Determine the initial centroid randomly as much as k

c. Determine the closest distance from each observation object to the cluster center which is determined using euclidean distance as follows:

$$d(x_i, x_j) = \sqrt{\sum_{k=1}^{n} (x_{ik} - x_{jk})^2} \quad (1)$$

where

$d(x_i, x_j)$: Distance between two objects of i and j

x_{ik} : The value of i object in the k group
x_{jk} : The value of j object in the k group

d. Determine the average value of each cluster as follows:

$$T_{kj} = \frac{x_{1j} + x_{2j} + \cdots + x_{nj}}{n} \quad (2)$$

where

T_{kj} : The average value of the k cluster on the j variable
n : Amount of data

e. Determine the new centroid closest distance using euclidean distance using (1)

f. If it doesn't get the right result, then return to the calculation in step b

The optimum grouping validation uses R-Square and Pseudo F-statistic values. The optimum number of groups can be shown by the highest R-Square and Pseudo F-statistics values [19]. Pseudo F-Statistics values can be calculated by:

$$Pseudo\ F - Statistics = \frac{\left(\frac{R^2}{k-1}\right)}{\left(\frac{1-R^2}{n-k}\right)} \quad (3)$$

where the value of R^2 is

$$R^2 = \frac{SSB}{SST} \quad (4)$$

The R-Square calculation involves several diversity data calculations, they are total diversity, diversity within groups, and diversity between groups [10]. The value of diversity can be calculated by:

$$SSB = SST - SSW \quad (5)$$

$$SST = \sum_{j=1}^{m}\sum_{i=1}^{n}\left(x_{ij} - \bar{x}_j\right)^2 \quad (6)$$

$$SSW = \sum_{h=1}^{k}\sum_{j=1}^{m}\sum_{i=1}^{n_k}\left(x_{ijh} - \bar{x}_{jh}\right)^2 \quad (7)$$

where

SST : Sum of Square Total
SSW : Sum of Square Within Group
SSB : Sum of Square Between Group
m : The number of numerical variables in the observation
k : The number of groups
n : Total number of objects under observation
n_k : Number of members in the k group
x_{ij} : The value of i object in the j variable
$\bar{x}_j$: Average of all j variable
x_{ijh} : The value of i object in the j variable, and h group
$\bar{x}_{jh}$: Average of all j variable, and h group

3.3. K-Modes

K-Modes is the development of the K-Means method specifically used to handle categorical data type cases [20], [18]. This method has an efficient algorithm based on frequency to find modes [21], [18].

Several modifications to the K-Modes method are accommodated from the K-Means method, as follows:

a. The distance of two data points between X and Y is the number of features found in X and Y. Measuring the similarity between objects X and Y is given by:

$$d(x,y) = \sum_{j=1}^{e} \delta \in (X_j, Y_j) \quad (8)$$

where

e : Number of Features

$\delta \in (X_j, Y_j)$: Matching value, the value is based on:

$$\delta(X,Y) = \begin{cases} 0\ (X_j = Y_j) \\ 1\ (X_j \neq Y_j) \end{cases} \quad (9)$$

b. Change the means value (average) to mode value (modes)

c. In searching for mode values, data frequency is used. The centroid point is obtained from each feature's mode.

The validation method to find out the most optimum grouping in categorical data uses the calculation of the value of r is given by:

$$r = \frac{1}{n}\sum_{h=1}^{k} q_h \quad (10)$$

where

n : The number of observations
q_h : The highest number of objects (dominance) in the h-group with $(h = 1,2,\ldots,k)$.

3.4. Ensemble ROCK

The ensemble ROCK method uses the concept of a link that is used to measure the similarity and closeness that occurs at a pair of data points [22], [23] and [4]. Here are the steps of clustering data by using ensemble ROCK method:

a. Calculate $sim(X_i, X_j)$ as a measurement of similarity as folllows:

$$sim(X_i, X_j) = \frac{X_i \cap X_j}{X_i \cup X_j}, i \neq j \quad (11)$$

where

X_i : The i group observation group
X_j : The j group observation group

b. Determine Neighbors by calculating the link value as follows:

$$link(C_i, C_j) = \sum_{X_{i \in C_i}, X_{j \in C_j}} link(X_i, X_j) \quad (12)$$

c. Calculate the Goodness measure value $G(C_i, C_j)$ as follows:

$$G(C_i, C_j) = \frac{link(C_i, C_j)}{(n_i + n_j)^{1+2f(\theta)} - n_i^{1+2f(\theta)} - n_j^{1+2f(\theta)}} \quad (13)$$

where $link(C_i, C_j)$ are the number of links of all possible pairs of objects contained in C_i and C_j, and $f(\theta)$ is the threshold function obtained, with $f(\theta) = \frac{1-\theta}{1+\theta}$ where θ $(0 < \theta < 1)$ is a random threshold value determined by the researcher.

d. Compare the results of clustering from each threshold (θ) researchers have determined.

The validity of ensemble ROCK method can be derived from the ratio of S_w (sum within) and S_b (sum between), $\left(\frac{S_w}{S_b}\right)$. The better grouping performance of the cluster obtained by the smallest ratio of $\left(\frac{S_w}{S_b}\right)$ [18][24]. The value of S_w and S_b is:

$$Sw = [MSW]^{\frac{1}{2}} \quad (14)$$

$$Sb = [MSB]^{\frac{1}{2}} \quad (15)$$

where

$$MSW = \frac{SSW}{(n-k)} \quad (16)$$

$$MSB = \frac{SSB}{(k-1)} \quad (17)$$

SSW and SSB for categorical data can be formulated by:

$$SSW = \sum_{h=1}^{k} \left(\frac{n_{.h}}{2} - \frac{1}{2n_{.h}} \sum_{i=1}^{p} n_{ih}^2 \right) = \frac{n}{2} - \frac{1}{2} \sum_{h=1}^{k} \frac{1}{n_{.h}} \sum_{i=1}^{n} n_{ih}^2 \quad (18)$$

$$SSB = \frac{1}{2} \left(\sum_{h=1}^{k} \frac{1}{n_{.h}} \sum_{i=1}^{n} n_{ih}^2 \right) - \frac{1}{2n} \sum_{i=1}^{n} n_{i.}^2 \quad (19)$$

where

n_{ih} : The number of observations in the i category, and h group, with $h = 1,2,3, \ldots, k$

$n_{.h} = \sum_{i=1}^{n} n_{ih}$: The number of observations in the h group

$n_{i.} = \sum_{h=1}^{k} n_{ih}$: The number of observations in the i category

4. Research Method

4.1. Research data

The research data were obtained from the Central Statistics Agency (BPS) of East Java with the website address https://jatim.bps.go.id/. The data consists of survey data in 2014 and 2018. Data in 2014 as a comparison with the determination of disadvantaged regions in 2015 by the Ministry of Villages, Development of Disadvantaged Regions, and Transmigration. While the 2018 data will be used as predictions to provide an overview regarding the determination of disadvantaged regions next 2020.

This study consists of two types of variables used, namely alternative variables and criterion variables. The alternative variables in this study concern all District/City in East Java Province consisting of 29 District and 9 City according to the details in Table 1.

Table 1: Alternative Research Variables

Code	District/City	Code	District/City
01	Pacitan	20	Magetan
02	Ponorogo	21	Ngawi
03	Trenggalek	22	Bojonegoro
04	Tulungagung	23	Tuban
05	Blitar	24	Lamongan
06	Kediri	25	Gresik
07	Malang	26	Bangkalan
08	Lumajang	27	Sampang
09	Jember	28	Pamekasan
10	Banyuwangi	29	Sumenep
11	Bondowoso	30	Kediri City
12	Situbondo	31	Blitar City
13	Probolinggo	32	Malang City
14	Pasuruan	33	Probolinggo City
15	Sidoarjo	34	Pasuruan City
16	Mojokerto	35	Mojokerto City
17	Jombang	36	Madiun City
18	Nganjuk	37	Surabaya City
19	Madiun	38	Batu City

The criterion variable in this study consists of 6 criteria whose 33 indicators. These variables consist of numeric and categorical data. For criterion variables that are of numerical data type, the determination of disadvantaged regions has 27 indicator variables shown in Table 2.

Table 2: Variable Criteria for Numerical Data

Criteria	Indicator	Source
Regional economy	Percentage of poor population (x_1)	The Potential of East Java Village
	Population production per capita (x_2)	
Regional characteristics	Percentage of villages affected by the earthquake (x_3)	The Potential of East Java Village
	Percentage of villages affected by landslides (x_4)	
	Percentage of villages affected by floods (x_5)	
	Percentage of villages affected by other disasters (x_6)	
	Percentage of protected forest area (x_7)	
	Percentage of villages conserving critical land (x_8)	
	Percentage of villages in conflict (x_9)	
Human Resources	Life expectancy (x_{10})	Human Development Index
	Average school length (x_{11})	
	Literacy numbers (x_{12})	
Accessibility	Distance from District capital to provincial capital (x_{13})	East Java in Figures
	Number of villages with easy access to security services > 5 km (x_{14})	
Infrastructure	Number of villages with the widest asphalt road surface (x_{15})	Potential of East Java Village
	The largest number of villages on the road surface is hardened (x_{16})	
	Number of villages with the broadest road surface (x_{17})	
	Number of villages with the widest road surface (x_{18})	
	Number of market villages without permanent buildings (x_{19})	
	Number of health infrastructure per 1000 population (x_{20})	
	Number of doctors per 1000 population (x_{21})	
	Number of high schools per 1000 population (x_{22})	
	Percentage of household electricity users (x_{23})	
	Percentage of household telephone users (x_{24})	
	Percentage of households that use clean water (x_{25})	
Regional Finance	Degree of Fiscal Decentralization (x_{26})	
Characteristics of certain regions	Percentage of Disadvantaged Villages (x_{27})	Human Development Index

Next, for the criterion variable whose categorical data, the determination of disadvantaged regions has 6 indicator variables shown in Table 3.

Table 3: Categorical Data Criteria Variables

Criteria	Indicator	Criteria	Indicator
Characteristics of Specific Regions	Borderland (x_{28})	0:Not Borderland 1:Borderland	East Java in Figures
	Island existence (x_{28})	0: Own the island 1: Not an island	
	Post-tribal conflict regions (x_{30})	0: There are no conflicts 1: there is a conflict	
	Food insecure regions (x_{31})	0: Not a food-insecure area 1: Food insecure regions	Center for Data and Information on Development of Specific Regions of Food-Prone Regions
	Landslide (x_{32})	0: Nothing 1: medium 2: medium height	Regional Planning and Development Agency
	Flood (x_{33})	0: Nothing 1: Intermediate 2: Height	
	Earthquake (x_{34})	0: Nothing 1: Yes	
	Tsunami (x_{35})	0: Nothing 1: Medium 2: Large	
	Volcano eruption (x_{36})	0: Nothing 1: Yes	

4.2. Data analysis

In this study, data analysis using ensemble ROCK method was carried out with the following steps:

1. Separate categorical data and numeric data
2. Reduce research variables with factor analysis both numeric and categorical data
3. Analyze numerical data clusters using the K-Means method
4. Validate the optimum grouping using Pseudo F-statistics and R^2
5. Analyze categorical data clusters using the K-Modes method
6. Validate the optimum grouping using the calculation of the value of *r* (highest accuracy)
7. Analyze mixed data clusters (numeric and categorical) results using the ROCK method

5. Results and Discussion

5.1. Determination of Disadvantaged Regions in 2015

The first step of this research is to cluster data from survey results in 2014 that used as a determination of disadvantaged regions in 2015. For the data processing in this section (in 2014), we don't elaborate, but we provide detailed discussions for data processing in 2018 in the next sub-section.

The following results of regional clusters in East Java (the data processing in 2014) using the ROCK method can be shown in Table 4.

Based on Table 4, it is known that cluster in disadvantaged regions are Trenggalek, Jember, Banyuwangi, Bondowoso, Situbondo, Probolinggo, Bangkalan, Sampang, Pamekasan, Sumenep, and Probolinggo City, this is in line with the determination of disadvantaged regions conducted by the Government. Based on Presidential Regulation No. 131/2015, it is known that District/City in East Java Province included in

disadvantaged regions are Bangkalan, Sampang, Bondowoso, and Situbondo.

Table 4: Clusters of disadvantaged, developing, independent and developed regions

Cluster	District/City
Disadvantaged	Trenggalek, Jember, Banyuwangi, Bondowoso, Situbondo, Probolinggo, Bangkalan, Sampang, Pamekasan, Sumenep, Probolinggo City
Developing	Pacitan, Blitar, Kediri, Pasuruan, Ngawi, Kediri City, Tuban, Blitar City, Mojokerto City, Madiun City
Independent	Lumajang, Mojokerto, Jombang, Bojonegoro, Lamongan, Gresik, Pasuruan City
Developed	Ponorogo, Tulungagung, Malang, Sidoarjo, Nganjuk, Madiun, Magetan, Malang City, Surabaya City, Batu City

5.2. *Predicting* the Designation of Disadvantaged Regions in 2020

After the determination of disadvantaged regions in 2015, the next determination will carried-out in 2020. Based on data compiled from the 2018 survey, it can be predicted which regions are potentially designated as disadvantaged regions in East Java. To analyze this case, we use the ensemble ROCK method. In this section, we provide detailed discussions for its data processing.

The first step in the ROCK method is factor analysis. There are several assumption tests in factor analysis, including the adequacy of correlation data between variables using the KMO test and the dependency test between variables using the Barlett test. KMO test results $(0.524) > 0.50$ and Bartlett test obtain sig. $(0.000) < (\alpha = 0.05)$.They show that the research data has fulfilled the correlation and is sufficient to be factored. The results of the factor analysis of numerical data were obtained from the results of factoring and the biggest loading factors. The results of factor analysis for numerical data can be shown in Table 5.

Table 5: Results of numerical data factor analysis

Factor	Indicator	Loading Value
1	The average length of school (x_{11})	0.947
2	Number of high schools per 1000 population (x_{22})	0.784
3	Number of villages with the broadest road surface (x_{17})	0.251
4	Percentage of villages affected by the earthquake (x_3)	0.745
5	Number of villages with easy access to security services (x_{14})	0.745
6	Percentage of villages affected by flooding (x_5)	0.420
7	Number of villages with the widest road surface (x_{18})	0.322

The results of the factor analysis will be analyzed and clustered using the K-Means method. In this case, cluster analysis will be carried out into 2,3, and 4 clusters. The selection of an optimal number of clusters is obtained from the largest Pseudo F-statistics and R-Square values. Table 6 is the result of calculating the Pseudo F-statistic and R-Square values for each cluster.

Table 6: R-Square and Pseudo F-Statistic values for each clustering

Number of Cluster	*R-Square*	*Pseudo F-statistic*
2 Cluster	0.5680428	47.34160
3 Cluster	0.7443780	50.96045
4 Cluster	**0.8258974**	**53.76237**

Based on Table 6 it is known that the optimal number of clusters is 4 cluster. The results of clustering numerical data in the district/city of East Java can be shown in Table 7.

Table 7: Results of cluster using K-Means

District /City	Cluster Result	District /City	Cluster Result
Pacitan	4	Magetan	2
Ponorogo	2	Ngawi	2
Trenggalek	2	Bojonegoro	3
Tulungagung	2	Tuban	3
Blitar	2	Lamongan	1
Kediri	3	Gresik	1
Malang	3	Bangkalan	1
Lumajang	3	Sampang	3
Jember	3	Pamekasan	3
Banyuwangi	4	Sumenep	2
Bondowoso	2	Kediri City	3
Situbondo	2	Blitar City	2
Probolinggo	3	Malang City	3
Pasuruan	1	Probolinggo City	3
Sidoarjo	1	Pasuruan City	1
Mojokerto	1	Mojokerto City	1
Jombang	3	Madiun City	2
Nganjuk	3	Surabaya City	1
Madiun	2	Batu City	3

Then, factor analysis will be carried out for categorical data. The results of the KMO test and the Barlett test for categorical data indicate that the KMO test result $(0.683) > 0.50$ and Bartlett's test obtain sig. $(0.000) < (\alpha = 0.05)$. They show that the research data has fulfilled the correlation and is sufficient to be factored. The results of factor analysis for categorical data can be shown in Table 8.

Table 8: Results of categorical data factor analysis

Factor	Indicator	Loading Value
1	Landslide-prone regions (x_{32})	0.818
2	Post-conflict regions (x_{30})	0.874
3	Borderland (x_{28})	0.867

Next, the results of the factor analysis will be analyzed and clustered using the K-Modes method. In this case, cluster analysis will be conducted into 2,3, and 4 clusters. The selection of an optimal number of cluster is obtained from the highest r accuracy value. Table 9 is the result of calculating the accuracy value of r for each cluster.

Table 9: Comparison of the r values for each clustering

Number of Cluster	r
2 Cluster	0.6666667
3 Cluster	0.7894736
4 Cluster	**0.8245614**

Based on Table 9, it is known that the optimal number of clusters is 4 clusters. The results of clustering categorical data in the district/city of East Java can be shown in Table 10.

Table 10: Results of cluster using K-Modes

District /City	Cluster Result	District /City	Cluster Result
Pacitan	1	Magetan	1
Ponorogo	1	Ngawi	1
Trenggalek	1	Bojonegoro	3
Tulungagung	2	Tuban	3

Blitar	2	Lamongan	3
Kediri	2	Gresik	3
Malang	2	Bangkalan	1
Lumajang	1	Sampang	3
Jember	2	Pamekasan	3
Banyuwangi	2	Sumenep	3
Bondowoso	2	Kediri City	4
Situbondo	2	Blitar City	4
Probolinggo	1	Malang City	4
Pasuruan	1	Probolinggo City	1
Sidoarjo	2	Pasuruan City	1
Mojokerto	2	Mojokerto City	4
Jombang	2	Madiun City	4
Nganjuk	2	Surabaya City	1
Madiun	2	Batu City	4

After obtaining cluster of categorical and numerical data, the next step is to analyze a mixed data cluster using Ensemble ROCK. In this study, the mixed data will be clustered into 3 and 4 clusters. The threshold values *(θ)* that will be tested are 10 threshold *(θ)*, they are 0.1; 0.2; 0.3; 0.01; 0.02; 0.03; 0.04; and 0.05. Among the 10 thresholds used, a threshold value which produce the optimum cluster will be chosen by finding the smallest *Sw* and *Sb* ratio. The ratio of *Sw* and *Sb* from each threshold for grouping 3 and 4 clusters are as follows:

Table 11: *Sw* and *Sb* ratio values for each threshold for grouping 3 and 4 clusters

Threshold	3 Clusters	4 Clusters
0.1	0.7237014	0.855867
0.15	0.5414150	0.9331397
0.2	0.4737199	0.5209103
0.25	1.3563698	0.8428222
0.3	0.4157780	0.4938904
0.01	0.5260732	0.8196005

Based on Table 11, it is known that the smallest value of *Sw* and *Sb* ratio is owned by the 0.02 threshold with 4 clusters. The results of the mixed data cluster analysis in 4 clusters whose threshold value of 0.02 can be shown in Table 12.

Table 12: Results of the ROCK method cluster ($\theta = 0.02$)

Cluster	Cluster Member (District/City)
Cluster 1	Pacitan, Tulungagung, Blitar, Jember, Mojokerto, Jombang, Magetan, Blitar City, Madiun City, Probolinggo City.
Cluster 2	Kediri, Banyuwangi, Nganjuk, Madiun, Bojonegoro, Gresik, Kediri City, Pasuruan City, Mojokerto City.
Cluster 3	Trenggalek, Bondowoso, Situbondo, Probolinggo, Tuban, Bangkalan, Pamekasan, Sumenep, Sampang.
Cluster 4	Ponorogo, Malang, Lumajang, Pasuruan, Sidoarjo, Ngawi, Lamongan, Malang City, Surabaya City, Batu City.

Based on the Regulation of the Minister of Villages, Development of Disadvantaged Regions and Transmigration Number 3 of 2016 concerning Technical Guidelines for Determining Indicators in the Determination of Disadvantaged Regions Article 17 states that in Determining the Direction of Backwardness, it is measured based on positive and negative Composite Index whose values are between +1 and -1 on the criteria. A positive composite index means the higher index of a criterion, the worse condition of a region. Some examples of indicators included in the positive composite index are indicators of the percentage of poor people, the percentage of flooded villages, percentage of villages with critical land. The higher percentage value of those indicators, the worse situation of the region. Conversely, a negative composite index means the lower index of a criterion, the better condition of a region. One example of indicators included in the negative composite index is the average length of the school indicator, the lower value of that indicator, the better condition of the region.

Figure 1 is the percentage group of negative composite levels of each cluster results with the direction of each indicator lags.

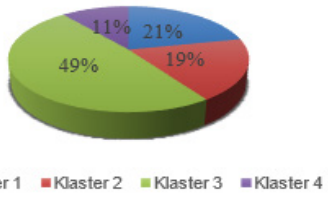


Figure 1: Percentage of Behind Each Cluster

Based on Figure 1, the percentage of negative composite level with the highest backwardness is cluster 3, then followed by cluster 1, cluster 4, and cluster 2. Each cluster result will be grouped successively into disadvantaged, independent, and developed regions. Table 13 is a cluster of disadvantaged, developing, independent, and developed regions.

Table 13: Clusters of Disadvantaged, developing, independent and developed regions

Cluster	Cluster Member (District/City)
Disadvantaged	Trenggalek, Bondowoso, Situbondo, Probolinggo, Tuban, Bangkalan, Pamekasan, Sumenep, Sampang.
Developing	Pacitan, Tulungagung, Blitar, Jember, Mojokerto, Jombang, Magetan, Blitar City, Kota Madiun, Probolinggo City.
Independent	Kediri, Banyuwangi, Nganjuk, Madiun, Bojonegoro, Gresik, Kediri City, Pasuruan City, Mojokerto City.
Developed	Ponorogo, Malang, Lumajang, Pasuruan, Sidoarjo, Ngawi, Lamongan, Malang City, Surabaya City, Batu City.

5.3. Discussion

Based on Table 13, it is known that regions designated as disadvantaged regions in East Java consist of Trenggalek, Bondowoso, Situbondo, Probolinggo, Tuban, Bangkalan, Pamekasan, Sumenep, Sampang. It is quite reasonable, some facts compiled from the online mass media reinforce the statement.

In the prediction of setting up disadvantaged regions in 2020, it is known that Tuban has entered into disadvantaged regions. This is because of the percentage of poor people at Tuban increased from the previous year. Based on the news in suarabanyuurip.com (accessed 30-May-2019), the poverty level of Tuban is ranked fifth out of all District/City in East Java [25]. In addition, the percentage of clean water user households in Tuban District is very low, similar to Trenggalek and Situbondo District. Here is a graph of 5 districts/cities that are pockets of poverty in East Java.

On the other hand, based on the Presidential Regulation of the Republic of Indonesia Number 63 the Year 2020 concerning Determination of Disadvantaged Regions in 2020-2024, it was found that East Java has been separated from the provinces with disadvantaged regions. This is possible because local

governments have conducted evaluations and various handling efforts to reduce the region of disadvantaged status. Nonetheless, this research result can provide an overview for district/city governments so that they can immediately anticipate and make policies that are adjusted to the characteristics of each region so that their region does not become disadvantaged again.

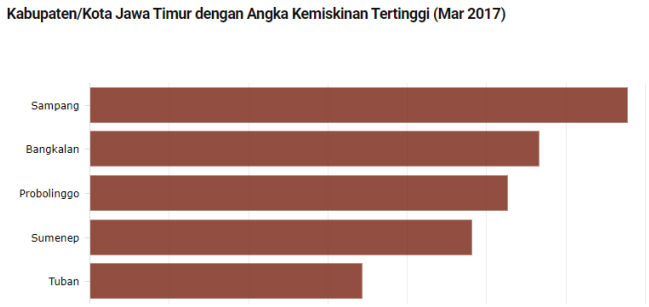


Figure 2: The top 5 poor districts/cities in East Java

Source: https://databoks.katadata.co.id/datapublish/2018/01/24/di-mana-kantong-kemiskinan-jawa-timur

6. Conclusion

The results of clustering using the ROCK ensemble method obtained cluster results for the prediction of disadvantaged regions in 2020 consist of Trenggalek, Bondowoso, Situbondo, Probolinggo, Tuban, Pamekasan, Sumenep, Bangkalan, and Sampang. The best cluster results for evaluating the determination of disadvantaged regions in 2020 consist of 4 clusters with the smallest *Sw* and *Sb* ratio of 0.3873984 and the optimum threshold value of 0.04.

The characteristics of each region that are determined as disadvantaged regions, need to be improved to alleviate the area from disadvantages including the level of fiscal decentralization, the percentage of poor population, life expectancy, the average length of schooling, number of health infrastructure, percentage of household electricity users, the percentage of telephone user households, the low percentage of households using clean water, access to the nearest service facility, and the low percentage of protected forest regions.

References

[1] T. Alqurashi, W. Wang, "Clustering ensemble method," International Journal of Machine Learning and Cybernetics, 2018, doi:10.1007/s13042-017-0756-7.

[2] S. Liu, B. Zhou, D. Huang, L. Shen, "Clustering Mixed Data by Fast Search and Find of Density Peaks," Mathematical Problems in Engineering, **1**, 1–7, 2017, doi:10.1155/2017/5060842.

[3] S. Vega-Pons, J. Ruiz-Shulcloper, "A survey of clustering ensemble algorithms," International Journal of Pattern Recognition and Artificial Intelligence, **25**(3), 337–372, 2011, doi:10.1142/S0218001411008683.

[4] K.S. Sudipo Guha, Rajeev Rastogi, "A robust clustering algorithm for categorical attributes," Information Systems, **25**(5), 345–366, 2000, doi:10.1016/S0306-4379(00)00022-3.

[5] M.F. Balcan, Y. Liang, P. Gupta, "Robust hierarchical clustering," Journal of Machine Learning Research, **15**, 4011–4051, 2014, doi:10.1184/r1/6476297.

[6] M.V.J. Reddy, B. Kavitha, "Clustering the Mixed Numerical and Categorical Datasets Using Similarity Weight and Filter Method," International Journal of Database Theory and Application, **5**(1), 121–133, 2012.

[7] J. Oyelade, I. Isewon, F. Oladipupo, O. Aromolaran, E. Uwoghiren, F. Ameh, M. Achas, E. Adebiyi, "Clustering Algorithms : Their Application to Gene Expression Data," Libertas Academica Freedom To Research, **10**, 237–253, 2016, doi:10.4137/BBI.S38316.TYPE.

[8] S. Sharma, Applied multivariate tecnhiques, John Wiley & Sons Inc, New York, 1996.

[9] D.H. Setiadi, Pemetaan Kabupaten/Kota di Jawa Timur Berdasarkan Indikator Daerah Tertinggal Dengan Metode Data Campuran Ensamble ROCK dan SWFM, Institut Teknologi Sepuluh Nopember, 2018.

[10] Alvionita, Sutikno, Suharsono, "Ensemble ROCK Methods and Ensemble SWFM Methods for Clustering of Cross Citrus Accessions Based on Mixed Numerical and Categorical Dataset," in IOP Conf. Series: Earth and Environmental Science, 1–10, 2017, doi:10.1088/1755-1315/5.

[11] A. Djuraidah, "Evaluasi Status Ketertinggalan Daerah Dengan Analisis Diskriminan," Seminar Nasional Matematika Dan Pendidikan Matematika Jurusan Pendidikan Matematika FMIPA UNY, 1–16, 2009.

[12] S. Wiratama, H.C. Diartho, F.W. Prianto, "Analisis Pembangunan Wilayah Tertinggal di Provinsi Jawa Timur," E-Journal Ekonomi Bisnis Dan Akuntansi, **5**(1), 16–20, 2018, doi:10.19184/ejeba.v5i1.7726.

[13] I. Simarmata, A.J.A. Arma, Arnita, "Aplikasi Analisis Faktor dengan Metode Principal Component Analysis dan Maximum Likelihood dalam Faktor-faktor yang Memengaruhi Pemberian Makanan Tambahan Pada Bayi Usia 0-6 Bulan di Desa Pematang Panjang Kecamatan Air Putih Kabupaten Batubara Tahun 2013," Jurnal Kebijakan, Promosi Kesehatan Dan Biostatistika, **5**, 1–10, 2013.

[14] H. Suriani, I. Norlita, W.J. Wan Yonsharlinawati, G. Khadizah, B. Kamsia, G. Darmesah, A.S. Asmar Shahira, "Using Factor Analysis on Survey Study of Factors Affecting Students ' Learning Styles," International Journal of Applied Mathematics and Informatics, **6**(1), 33–40, 2012.

[15] H. Schneeweiss, H. Mathes, "Factor Analysis and Principal Components," Journal of Multivariate Analysis, **55**, 105–124, 1995.

[16] A. Field, Factor Analysis Using SPSS, 1–14, 2005.

[17] R.A. Johnson, D.W. Wichern, Applied Multivariate Statistical Analysis Sixth Edition, Six, Person Prentice Hall, New Jearsey, 2007.

[18] C. Oktarina, K.A. Notodiputro, I. Indahwati, "Comparison of K-Means Clustering Method and K-Medoids on Twitter Data," Indonesian Journal of Statistics and Its Applications, **4**(1), 189–202, 2020, doi:10.29244/ijsa.v4i1.599.

[19] A.R. Orpin, V.E. Kostylev, "Towards a statistically valid method of textural sea floor characterization of benthic habitats," Marine Geology, **225**(1–4), 209–222, 2006, doi:10.1016/j.margeo.2005.09.002.

[20] Z. Huang, "Extensions to the k-Means Algorithm for Clustering Large Data Sets with Categorical Values Extensions to the k-Means Algorithm for Clustering Large Data Sets with Categorical Values," Data Mining and Knowledge Discovery, **2**(3), 283–304, 1998, doi:10.1023/A:1009769707641.

[21] P.S. Bishnu, V. Bhattacherjee, "A Modified K -Modes Clustering Algorithm," in International Conference on Intelligent Information Hiding and Multimedia Signal Processing, 60–66, 2013, doi:10.1109/IIH-MSP.2014.118.

[22] M. Dutta, A.K. Mahanta, A.K. Pujari, "QROCK: A quick version of the ROCK algorithm for clustering of categorical data," Pattern Recognition Letters, **26**(15), 2364–2373, 2005, doi:10.1016/j.patrec.2005.04.008.

[23] S. Guha, R. Rastogi, K. Shim, "Rock: a robust clustering algorithm for categorical attributes," Information Systems, **25**(5), 345–366, 2000, doi:10.1016/S0306-4379(00)00022-3.

[24] M.J. Bunkers, J. James R. Miller, A.T. DeGaetano, "Definition of Climate Regions in the Northern Plains Using an Objective Cluster Modification Technique," Journal of Climate, **9**(1), 130–146, 1996, doi:10.1175/1520-0442(1996)009<0130:DOCRIT>2.0.CO;2.

[25] N.S. Wisnujati, Laporan Pelaksanaan Penanggulangan Kemiskinan Daerah Kabupaten Tuban Tahun 2016, Universitas Wijaya Kusuma Surabaya, Surabaya, 2019

ASTES

Advances in Science, Technology and Engineering Systems Journal
Vol. 5, No. 5, 201-211 (2020)
www.astesj.com

ASTES Journal
ISSN: 2415-6698

A Review of RPL Objective Function based Enhancement Approaches

Ines Kechiche*, Ines Bousnina, Abdelaziz Samet

SERCOM Laboratory, Tunisian Polytechnic School, University of Carthage, La Marsa 2078, Tunisia

ARTICLE INFO

Article history:
Received: 24 July, 2020
Accepted: 02 September, 2020
Online: 14 September, 2020

Keywords:
RPL
LLNs
Routing
Objective function
Metric combination
Fuzzy logic

ABSTRACT

Since the release of of the IPv6 Routing protocol for Low-Power and Lossy Networks by the IETF ROLL working group, several enhancement schemes were proposed. In fact, They aim to extend the network lifetime, reduce congestion, mitigate end to end delay and moderate energy consumption. In fact, considering the vast area of Low-Power and Lossy Networks applications, the routing protocol was designed with a great deal of flexibility without dictating any specific routing metric/constraint to be used for building the routing topology. This paper presents a deep review of recent works on Routing Protocol for Low-Power and Lossy Networks and highlights Objective Function enhancements scheme. The objective is to provide an insight into relevant efforts such as novel metrics design and fuzzy logic techniques used for the Objective Function metric combination. The proposed enhancement schemes, highlight some limitations and give useful guidelines for future developments are also discussed.

1 Introduction

The IPv6 routing protocol for low-power and lossy networks (LLNs), was designed to achieve routing function for resource-constrained devices in industrial, home, and urban environments [1]. Since routing is of great apprehension in spoiling the resources in these devices, poor path selection may cause the scant assets to drain out quickly. Thus, RPL could achieve what traditional routing protocols such as OSPF, OLSR and AODV or DSR failed to do and overcome LLNS networking limitations, such as high loss rates, low data rates, and network instability [2].

RPL depends on objective function (OF) operations to choose a preferred parent for traffic forwarding. The OF considers a number of nodes/networks metrics and constraints to select the best path. Two OFs were dressed by the IETF ROLL working group, namely OF zero (OF0) [3] and Minimum Rank with Hysteresis Objective Function (MRHOF) [4]. The primitiveness of the standardized OFs have motivated OF refinement work to seek for enhancing network performance. Hence, many research works have tackled this issue and focused on OF and new metric calculation strategies that seek to improve network performances in terms of energy, reliability, latency and lifetime. Although the main line of OF optimization was multiple metrics combination many enhancement schemes resort to Cross-layer design to tap mac layer information and bring out the fitting measurements that would build the optimal OF.

1.1 Contribution of the Survey

Through this survey, the goal is to provide the research community with a solid piece of work that gathers all research efforts made for RPL OF enhancement. Our survey will help them get a deep vision on existing contributions and their shortcomings. Through enhancement strategies classifications, introduced nodes and networks metrics not specified in [5] are highlighted. Thus, researchers working on this issue will find at their disposal all the necessary information on already introduced metrics as well as combination techniques applied such as simple weighted or Artificial Intelligence (AI) based association in addition to the routing metrics taking part of these operations . As a matter of fact, in this survey, we do not settle for listing OF improvement work only but also classify them and outline plausible areas for follow-up research.

1.2 Organization of the Survey

This paper surveys substantial contributions brought by the research community to develop RPL routing in LLNs. An overview of various efforts done on optimizing the RPL OFs is presented. Our goal is to label the different approaches used to tackle this issue by stressing on introduced routing metric and presenting different metric combination techniques. This paper also brings out the fitting metrics that could result in RPL enhancement. This survey is organized as follows. First, section 2 recalls RPL basic knowledge and highlights relevant aspects of this protocol namely Destination-

*Corresponding Author: Ines Kechiche, Email: ines.kechiche@gmail.com

Oriented Directed Acyclic Graph (DODAG) construction process, communication pattern and OF operation. Then, section 3 focuses on main RPL OF based enhancement strategies. In section 4, the strengths and weaknesses of the aforementioned enhancement proposals, as well as relevant open issues and future work guidelines are discussed. Section 5 presents enhancement opportunities for future works. Finally, section 6 concludes the paper.

2 The IPv6 Routing Protocol for LLNS

RPL [1] is a distance-vector and a source routing protocol designed by the ROLL Working Group through RFC 6550 in order to meet specific requirements of LLNs. It is an IPv6 ready routing protocol based on a 6lowpan adaptation layer that allows micro devices to take part of the Internet of Things (IoT). Two basic components of RPL are the DODAG and the OF. Thus the RPL protocol purpose is to attenuate the cost of reaching the root node from any node in the network. This cost calculation is handled by RPL OF.

As it points collection-based networks, it supports three traffic patterns: multipoint-to-point traffic (MP2P), point-to-multipoint traffic (P2MP), and point-to-point (P2P) traffic.

2.1 DODAG Building Process

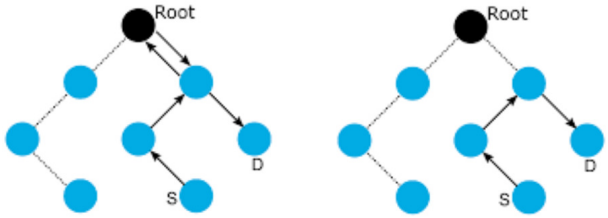
Rooted at an LLN border router (LBR), the DODAG provides RPL with an accurate vision of the network status and then it is easy to determine low cost paths to address any node from root. It is built on the basis of the parent selection process through what each node selects a preferred parent (best path) to transfer its packets toward the root node or other nodes. Thereby, both upward and downward traffic are enabled.

2.1.1 ICMPv6 messaging

When activated, RPL discards the IPv6 Neighbor Discovery process [6]. DODAG is then maintained through RPL ICMPv6 messages (i.) DAG Information Solicitation (DIS) used by non root nodes to persue an active RPL instance, (ii.) DAG Information Object (DIO) initially flooded by DAG root to advertise the creation of an RPL DAG and then relayed by nodes joining the DAG (iii.) Destination Advertisement Object (DAO) messages are used for parent selection, confirming or canceling processes. They allow reverse route information by keeping track of visited nodes along the upward path from leaf node to DODAG root. Thus, each node, except the DODAG root, sends a DAO message to populate the routing tables with prefixes of their children and to announce their addresses and prefixes to their parents. A Destination Advertisement Object Acknowledgment (DAO-ACK) is then sent as a response by the DAO recipient, i.e. the preferred parent.

2.1.2 Communication pattern

Basically RPL supports different Modes of OPeration (MOP) [1] namely (i) non-storing MOP without or with downward traffic, respectively MOP0 and MOP1, (ii) storing MOP without or with multicast support, respectively MOP2 and MOP3. Fig. 1 illustrates traffic forwarding in case of storing and non-storing modes. Storing mode makes nodes produce less networking overhead. However, the non storing mode is interesting since nodes with strict memory limitations could not store a large number of routing states. When non-storing mode (MOP 0) is enabled, intermediate routers (ie: non-BR nodes) do not keep track of available routes and downward routes are not maintained. However the LBR may resort to source routing whenever it needs to direct the traffic along a specific path. In (MOP 1), downward routes are enabled, hence P2P and MP2P communication is allowed. However, route calculation is performed at the DODAG root and subsequently forwarded to its destination. In (MOP 2), downward routes are also supported, but differently from MOP 1. Through DAO messages exchange, the intermediate nodes maintain, individually, a routing table and no longer resort to the root node to make downward traffic possible. Finally MOP 3 extends MOP 2 operation by the possibility of multicasting data. So far non-root are able to address enabled clusters of nodes through multicast DAOs. According to whether nodes are multicast ready or not, the MOP flag is set to 3 or 2 subsequently. For better comprehension of communication pattern related issues [7] is advised.



(a) RPL non-storing mode (b) RPL storing mode

Figure 1: P2P communication pattern for MOP 1 and MOP 2 [8]

2.1.3 Trickle algorithm

Since DIO messages exchange may lead to raising traffic overhead, an adaptive beaconing scheme is used for RPL routing signaling: the trickle algorithm [9, 10]. In trickle-based strategy, transmission of DIO messages is dynamically adjusted. When inconsistencies are detected (i.e. a node's data is incoherent with its neighborhood), the communication rate exponentially increases to resolve quickly the inconsistency. Otherwise, nodes slow down communication until reaching a predefined maximum value. However, this may affect RPL ability to swiftly respond to topology changes [6].

2.2 Objective Function Operations

RPL OF handles next hop selection issues. In fact, as depicted in Fig. 2, the OF defines, (i.) how to estimate the path cost, (ii.) how to pick out parents (when, who, how many), (iii.) how to estimate the rank and (iv.) how to propagate the path cost. To address the cited issues, the OF defines how a node transcribes one or more metrics into a rank value that represents the routing distance from a node to a LBR. Thus, the selected metrics evaluate path cost and hence decide about the best path. Some RPL implementations rely on a single metric while other ones merge various routing metrics and

constraints [10]. Depending on their features, the routing metrics are organized on link metrics and node metrics. They may reflect quality or quantity, and be static or dynamic. In addition to routing metrics OF parents may consider some routing constraints while taking routing decisions such as avoiding unreliable links or nodes with low power level battery. The arrangement of the aforementioned metrics and constraint may pertain to implementation needs.

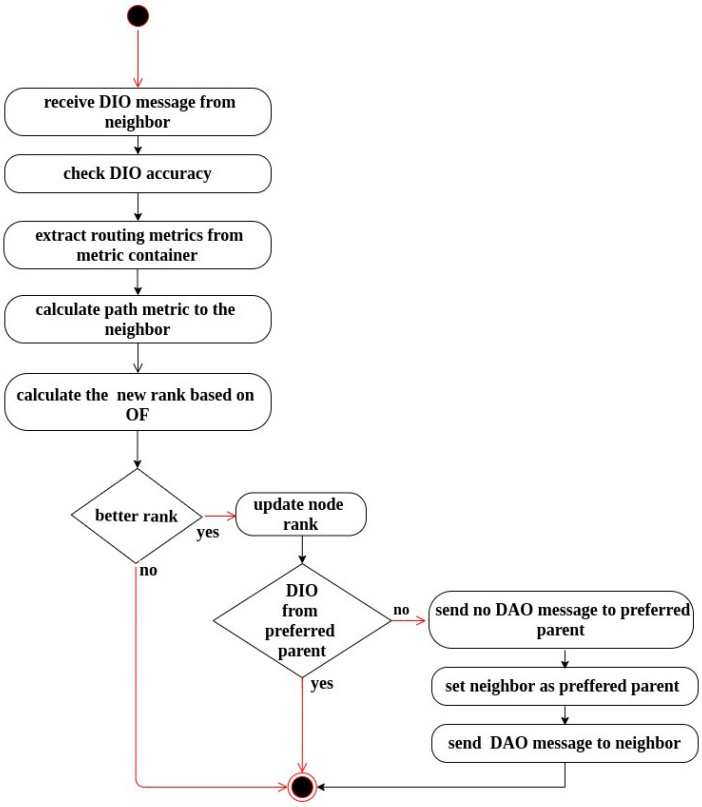


Figure 2: RPL OF main operations

3 The IPv6 Protocol for LLNs Objective Function Enhancement Strategies

Compelled by the challenging needs of LLNs, a collection of routing metrics with static or dynamic constraints [2], the IETF-ROLL working group designed RPL. However, the choice of the two settings; used metrics and constraints combinations and layer were left as an open issue for ulterior refinement work since RPL may have vast areas of applications. So far, depending on applications scenarios [11] and target environments requirements, many adaptation and improvement work have been made. Some of them are based on improving the metrics used for constructing the routes, others focused on MAC protocols overhaul. RPL built routes according to a parent selection process performed by an Objective Functions (OF). To supply different LLNs application requirements, a collection of routing metrics with static and dynamic constraint, have been introduced in [5]. Choice was left to the OF implementer to decide how to express each metric, to develop composite metrics or to define new ones. In the following, recent works in this direction are investigated. A summary of the reviewed OFs goals and specification is provided through tables 4 and 5.

3.1 Single Metric Based OF

Till now, only two basics OFs are published by the IETF Roll working group namely, OF0 [3], and MRHOF [4]. Rank calculation is based on Hop Count (HC) metric for OF0 and Expected Transmission Count (ETX) metric in the case of MRHOF. Nevertheless ETX and HC metrics seem clearly insufficient to deal with common networking issues such as throughput, energy saving and load balancing,

To deal with issues related to varying traffic patterns, ETX metric calculation method was revised in [12]. Bearing in mind that link quality estimation should not rely only on upward traffic, authors enable the parent node link quality information piggybacking through downward traffic. The proposed DT-RPL nodes will henceforth stabilize the ETX metric faster than with standard RPL nodes. Authors compared their scheme to standard RPL using different traffic patterns and demonstrate that they perform better in both Packet Delivery Ratio (PDR) and control overhead. In [13],authors proposed a mac -aware routing metrics namely R-metric and Q-metric. The R-metric can be used for reliability purpose and it measures end-to-end reliability regarding MAC layer measured back-offs and retransmissions. Thus, with R-metric the estimation of this probability is faster than the ETX estimation. The Q-metric is advised when it is a matter of improving the network lifetime by selecting the lightest parent, in terms of traffic load. The authors also boosted their proposed OF by adapting the corresponding MAC parameters so as to mitigate nodes energy consumption in the network. Unfortunately, for their proposed scheme evaluation, the author considered the back pressure protocol, a non RPL-protocol.

Authors in [14] substituted the ETX metric by another metric that decreases measured delay on path leading to root node. Their proposed Averaged Delay (AVG_DEL) metric gather all hop by hop measured delays along the path from a node towards the DAG root. Authors did some changes on MAC-layer to make learning neighbors wake-up phases possible and thus compute the AVG_DEL. Although promising performances against ETX based OF the proposed solution Simulation results did not present its impact on network scalability and energy consumption. Another delay based RPL OF enhancement approach was presented in [15]. First the authors developed a novel real-time and end-to-end delay EED estimation mechanism considering both path delays and node processing delays. According to the authors, the proposed EED is more accurate than the Expected Transmission Time ETT based. Afterwords, authors presented an RPL Adaptation for EEDEM (RA-EEDEM). They claim their proposed scheme enhanced slightly the Packet Reception Ratio PRR (14%) and measured Average EED by (12%).

A new routing metric, TXPFI, was introduced in [16]. It metric estimates the expected number of frame retransmission needed till data correct transmission. Author claims that applied to the

IETF RPL protocol, the novel metric achieves a low packet drop rate and proves its efficiency to get around non cooperative relays. Instead,authors in [17] tried to maximize the network lifetime by selecting next hop to DODAG root according to node remaining energy. Beginning from node energy, nodes add up time periods spent in each state or activity (transmit, receive, idle,sense, compute). Thus, the remaining energy capacity can be easily computed according to a formula specified in devices datasheet. The measured path cost will then correspond to the remaining energy of the weakest node on the path. According to the proposed OF, nodes will then select a neighbor for which path to root node held the best minimum lifetime value. The major inconvenience of this method is an observed degradation of the transmission reliability since inefficient routes with bad radio links may be used. In another work [18], authors proposed a new approach where they worked on increasing network reliability while maintaining a balanced energy consumption among network nodes. First, they tried to spot energy-bottleneck nodes and then balance traffic load between them. To this end, authors designed the Expected LifeTime (ELT) metric to estimate how much time a node has to live until its energy starvation. According to simulation results the proposed OF ensured a balanced energy consumption for topology nodes independently from their distance the DODAG Root. However, an additional latency is observed.

Different from previous works, authors in [19] and [20] tackled the problem of unbalanced traffic load by considering the number of children. In [19] a load balanced OF (LB-OF) that aims to balance workload distribution among all nodes in LLNs specially bottleneck nodes is proposed. To this end, authors substituted ETX metric by considering the children number for rank calculation and hence preferred parent selection. Compared to MRHOF, the proposed strategy helped to balance the number of children nodes for the overburdened nodes and thus ensure node lifetime maximization. However, authors did not study the proposed OF impact on PDR or end-to-end delay. Authors in [20] called their proposed solution Bounded Degree RPL(BD-RPL). Rather than considering the children number as a metric they used it as a constraint for DODAG construction by setting boundaries for the number of children a preferred parent could accept. Thus, the resulting DODAG is called a k-degree tree. Owing to authors the profit of the proposed scheme is the absence of any additional overhead compared to RPL. It is also independent from the radio link quality metric. According to authors, BD-RPL (with degree 3) achieved an improvement over standard RPL by an average of 10% in packet delivery, 50% in energy consumption, and 60% in delay. For load regulation purpose, authors in [21] introduced a new node metric for RPL based on the estimated node Queue Backlog in order to ensure better throughput performance while maintaining usual delay values and be suitable for different network appliances. Table 1. Provides a summary of the aforementioned enhancement schemes.

3.2 Metric Combination Based OF

Considering a single routing metric for the OF operations seems to be insufficient to fulfill LLN application requirements. For example, focusing only on network reliability enhancement may be harmful for the network expected life time and latency. Thus, to overcome these limitations, many researchers worked on associating new or existent routing metrics and constraints in order to achieve better networking performances. While some of the enhancement scheme focused on simple weighted combination of RPL usual metrics [21]–[25] specified by [5], others [26]–[31] resorted the Fuzzy Logic (FL) properties to address the choice of the best path making possible the combination of non additive metrics.

3.2.1 Additive metric based routing strategies

To deal with issues related to traffic load and congestion, the author in [21] presented also an enhanced version of their proposed queue backlog based OF where they resort to associate the Queue Backlog node metric to other metrics from those proposed in [5]. Thus, the node weight is a scalar association of a penalty function trading system queue occupancy that authors try to minimize and a link usage cost computed through ETX metric (as presented in [21]) or any other metric from those cited in [5] if needed. In the same way, authors in [22], presented a new RPL OF called Congestion-Aware OF (CA-OF). This OF implies in addition to ETX on a new RPL routing metric not introduced in [5] namely the Buffer Occupancy (BO). The aforementioned OF aims to enhance traffic reliability by selecting parents across less congested paths. The resulting additive metric applies adaptive weights to ETX and BO metrics depending on traffic intensity. Thus, in low traffic the proposed OF stands on the ETX metric to select a preferred parent. As soon as the network tends to be congested, the ETX metric is dismissed and the OF considers only the BO for the next hop election process. According to authors, CA-OF could achieve good network performance regarding reliability, energy consumption and throughput. In [23], authors worked on improving the end-to-end packet delivery performance by regulating the traffic load within the routing tree. Thus, they proposed QU-RPL, to deal with traffic congestion problems for parent selection, the authors introduced a novel metrics. The queue utilization (QU) coefficient measured for a node k ensures the network stability by avoiding inefficient parents changes authors worked on setting a threshold to recognize when the network is congested and consequently associate the QU factor to HC and ETX metric in order to designate a preferred parent.

Singh and Chen introduced a new OF for efficient routing (OF-ER) [24] based on a composite efficient routing (CER) metric used for best parent selection. The CER metric combines a set of weighted metrics, namely, the link quality ETX, packet loss due to queue occupation, node's remaining time to live, delay and observed bottlenecked nodes. Authors claim that OF-ER could not only reduce energy consumption and queue loss, but also expand node's expected lifetime. Unfortunately , the authors did not report the introduced metric impact on traffic overload nor its ability to support network scaling

Authors in [25] Improved RPL (I-RPL) where the OF relies on an LCI index for parent node selection. The LCI index is deducted from various metrics, for instance, link quality and node energy. Hence, for preferred parent selection, the next-hop with the largest LCI index is selected. However, I-RPL stores also a potential parent node that could be used to forward traffic if multi-path routing is needed to relieve congested nodes. According to the authors, the proposed scheme achieved promising results in terms of load

Table 1: Single metric based Objective Functions

Proposal	**Rank calculation metric**	**Metric nature**	**Traffic pattern**	**Evaluation tools**	**Reference OF**	**Evaluation Metrics**
DT-RPL [12]	ETX enhanced (through piggybacking)	Link metric	Upward and downward traffic	TestBed RPL(ETX)[1]	PDR Traffic overhead	Duty Cycle
Di Marco et al. [13]	R-metric Q-metric	Link metric	Upward traffic	Testbed	Back-pressure protocol [32]	Power consumption End-to-end reliability
Gonizzi et al.[14]	Average Delay	Link metric	Upward traffic	Cooja simulator[33]	RPL(ETX)[1]	Average per-node Delay Throughput Traffic overhead Parent change
RA-EEDEM[15]	End to end delay	Link & node metric	Upward traffic	Cooja simulator [33]	ETT based solution EEDEM [34]	Packet reception ratio
Karkazis et al [16]	TXPFI	Link metric	-	J-Sim network simulator[35] route simulator	Lex(PFI,ETX) Lex(HC,PFI)	Average packet loss rate
Kamgueu et al. [17]	Remaining energy	Node metric	-	Cooja simulator[33]	RPL(ETX)[1]	Remaining energy
Iova et al. [18]	Expected lifetime	Node metric	-	WSNet[36]	MRHOF[4] Remaining energy[17] Energy [37]	PDR End to end delay Parent change Consumed energy Expected lifetime
LB-OF [19]	Number of children	Node metric	-	Cooja simulator [33]	MRHOF[4] OF0[3]	Energy Consumption PDR Lifetime
BD-RPL[20]	Bonded Number of children	Node metric	Upwardtraffic downward traffic	Cooja simulator[33] FIT IoT-lab[38]	RPL[1]	Energy Consumption PDR Average Delay
Awad et al.[21]	Queue backlog	Node metric	-	-	-	-

Table 2: Weighted Metric Combination based OF enhancement schemes

Proposal	Link metrics used	node metrics used	metric combination	Evaluation tool	Reference OF	Evaluation metric
Awad et al.[21]	ETX	Queue backlog	Scalar addition	-	-	-
CA-OF [22]	ETX	Buffer Occupancy	Weighted Combination	Cooja simulator [33]	RPL(ETX) RPL(Energy) OF0	Buffer Overflow Loss packet Throughput Energy consumption Packet delivery ratio
Qu-RPL [23]	ETX	Hop Count Queue utilization	Weighted Combination	Real testbed	Tiny RPL	Packet delivery Routing overhead Parent change
En-RPL [24]	ETX Delay	Packet loss Lifetime queue utilization Number of bottlenecked nodes	Weighted Combination	Cooja simulator [33]	Standard RPL with qu-RPL congestion avoidance configuration	Queue loss ratio End to end delay Traffic overhead Energy consumption
IRPL[25]	ETX	Node Energy Data Throughput Data TX Rate	Weighted Combination	Cooja simulator [33]	RPL(ETX) RPL(Residual Energy)	Data delivery rate Residual Energy Parent changes End to end delay

balance, end-to-end delay and packet delivery.

The aforementioned enhancement schemes are summarized in Table 2.

3.2.2 Fuzzy logic based routing strategies

Fuzzy logic [26] is a heuristic method based on artificial intelligence process that was widely implemented to deal with complexity problems in communication and computer networks. In [27], authors employed fuzzy logic to gather heterogeneous routing metrics namely delay, ETX and energy into one neighbour quality value. Through a two stage fuzzification engine, they estimated first the quality of service (QoS) from delay and ETX. Then, they combined obtained QoS to energy in a second fuzzification stage to estimate neighbors' resulting quality. Authors claim that their proposed fuzzy logic based OF reduced packet loss and parents change than ETX based RPL. In [28], a designed QoS-aware fuzzy logic OF (OF-FL) is presented. Authors stressed out the profit of various metrics association to meet routing requirements and selected HC, end to end delay, ETX and battery level for their fuzzification engine. The proposed solution, performed better energy conservation and end to end delay than OF (ETX) especially for distant nodes. In [29], an OF based on a combined metric using fuzzy logic method OF-EC is proposed. Similar to [27], they selected ETX, HC and energy metrics as input for the fuzzy logic process but computed energy consumption differently. Thus, to determine the energy consumption they used both transmission and reception consumed power, processing power and both full and low power modes consumption. Authors claim that the proposed OF-EC showed satisfying performance for measured PDR, network lifetime, convergence time, latency, overhead, and energy consumption compared to other RPL OF namely OF-FUZZY [27], MRHOF and ENTOT [39].

Authors proposed in [30] the Composite Metric OF (CMOF) that combines weighted latency and ETX path metrics expecting to enhance both delay and PDR by selecting paths with good connectivity and less traffic. In fact, while ETX will grant the use of reliable links, latency will measure both traffic and contention at any given node by summing time packets spent in the transmit queue and the time taken to access the channel. Moreover, authors employed a power regulation scheme. CMOF stands apart from similar works by substituting default values used for fuzzy sets by new thresholds unlike [28]. Nevertheless, the authors did not defend the choice of these new values nor explain the accuracy of the used thresholds.

An extra scheme of metrics combination using fuzzy logic method is given in [31], the authors presented a holistic OF, OPP-FL, that combines several representative metrics to enhance best route selection namely ETX, HC and Children Number (CN) making use of the fuzzy logic approach.Through the proposed OF they tried to limit the impact of a node overload on routing performance and equilibrate the routing load between the different parent nodes while trying to stay closest to the root. Indeed, the number of children nodes attached to a parent can negatively affect the delay of data transmission in the network. The work focused on delay and reliability enhancement by promoting the selection of parents who are closer to the root and less burdened. Simulation results showed that OPP-FL outperformed the standard ETX based OF (MRHOF) and the fuzzy logic based OF OF-EC in terms of PDR and network latency in high network density topologies. Authors proposed in [40] a fuzzy-based mobility OF (FMOF) through which they apply fuzzy logic process to a hand-off enabled RPL mechanism , the mRPL [41], in order to reinforce mobility support in WSN networks. As input for the fuzzification engine, the authors selected three metrics namely HC, ETX, and Radio Signal Strength Indicator (RSSI). However, different from previous enhancement schemes, the authors tested different input weighted combinations. According to simulation results, the proposed scheme achieved good results in terms of reducing the handoff delay and PDR in case of low

Table 3: Fuzzy logic based OF enhancement schemes

Proposal	Link metrics used	Node mectrics used	Evaluation tool	Reference OF	Evaluation metric
Kamgueu et al.[27]	ETX Delay	Energy	Real indoor testbed	RPL(ETX)	Power consumption End to end delay Parent changes loss rate
OF-FL[28]	end to end delay ETX	Hop Count Battery level	Cooja simulator [33]	MRHOF [4] OF0 [3]	Power Consumption End to end delay Parent changes Average Hop count Loss rate
OF-EC [29]	ETX	Hop Count Energy consumption	Cooja simulator [33]	RPL(ETX) EN-TOT OF-Fuzzy [27]	Power consumption Traffic overhead Packet delivery ration
CMOF [30]	ETX	Packets latency	Cooja simulator [33]	MRHOF [4]	Per hop delay Packet delivery ratio
FMOF [40]	ETX RSSI	Hop count	Cooja simulator [33]	MRHOF [4] OF0 [3]	Hand-off delay Packet reception ratio Traffic overhead
OPP-FL [31]	ETX	Hop Count Children number	Cooja simulator [33]	MRHOF [4] OF-EC [29]	Average end to end delay Traffic overhead Packet delivery ratio

transmission rate. Table 3. Summarizes the surveyed fuzzy logic based OF enhancement schemes.

4 Discussion

The previous section reviewed relevant and recent approaches for OF based RPL enhancement strategies. According to the results presented in each work, the majority of aforementioned solutions could improve the PDR, reduce congestion and preserve energy consumption. Although these approaches aimed to improve the standard RPL, we deem that the ability of the proposed solution to supply to IoT application requirements is still to be proven, since the performances of the mostly proposed schemes were compared to standard RPL and there are still a need for further testbed validation. The following are some findings with regards to the reviewed enhancement schemes.

4.1 Metric Combinations Approach

Relying on a single metric for OF rank calculation seems to be deficient and in most cases ends up degrading others while ensuring interesting performances in terms of some network parameters. Our main purpose of reviewing single metric based OF was to point out novel metrics not yet cited in [5]. Nevertheless, metric combination could achieve promising results especially if we resort to cross-layer design. AI based techniques should be more exploited not only through fuzzy logic combination processes but also for weighted metric combination. Since it would be so helpful for researchers to decide for the most suitable metric weights values.

4.2 Energy Efficiency

Energy efficiency is among key considerations of the reviewed OF since it was oftenly present either as OF metric or as a node constraint. In fact, most of the reviewed enhancement schemes aimed at preserving energy while providing a good PDR. Simulations have shown that used as a single metric, the node energy is not that efficient and should be associated with other metrics to provide promising results.

4.3 Multipath Routing and Congestion Avoidance

Congestion avoidance was among main OF enhancement goals since it would affect both end to end delay and network reliability. Several research works resort to multipath routing to consolidate congestion avoidance efforts and decrease the number of bottlenecked nodes. Some of them triggered multipath routing for congestion problem remediation. More details of congestion control RPL based solutions is given in [32].

4.4 Design Complexity

Authors of the aforementioned RPL OF enhancement solutions approaches tried to overcome the standard RPL drawbacks. However, none of the concerned research works raised memory capacity purpose and the ability of the constrained node to support the final enhancement schemes complexity. In fact, the proposed solutions tend to be complex, due to its storage and processing capacity requirements. Resorting to multipath routing compels nodes to support larger routing tables including alternatives path in particular if

downward routing is enabled. Moreover, fuzzy logic based metric combinations require intensive memory capacity.

Table 4: Synthesis of enhancement schemes capabilities

Proposal	Cross layer design	Multipath routing	Mobility support	Scalability support	Security consid-eration
DT-RPL [12]	√	x	x	-	x
Di Marco et al. [13]	√	x	x	-	x
Gonizzi et al. [14]	√	x	x	-	x
RA-EEDEM [15]	√	x	x	-	x
Karkazis et al. [16]	√	x	x	√	√
Kamgueu et al. [17]	√	x	x	-	x
Iova et al. [18]	√	√	x	-	x
LB-OF [19]	√	x	x	√	x
BD-RPL [20]	√	x	x	x	x
CA-OF [22]	√	x	x	√*	x
Qu-RPL [23]	√	x	x	-	x
En-RPL [24]	√	√	x	x	x
IRPL [25]	√	√	x	x	x
Kamgueu et al. [27]	√	x	x	x	x
OF-FL [28]	√	x	x	√	x
OF-EC [29]	√	x	x	√*	x
CMOF [30]	√	x	x	x	x
FMOF [40]	√	x	√	x	x
OPP-FL [31]	√	x	x	√	x

*Slight variation of nodes number

4.5 Link Reliability and Security Purpose

Link reliability is a main concern in LLN usually addressed through cross layer design by invoking MAC metrics. However, packet loss is not entirely due to link propriety . It would be interesting to consider security related issues when seeking for PDR optimization. For instance, a non cooperative node may silently drop data instead of forwarding it. If such malicious nodes had a forward position among RPL tree, many of attached nodes can be discarded. In such cases relying only on RPL self-healing mechanisms is insuffisant. We recommend further studies to consider security purposes among major design factors such as application requirement and mobility. In [16] authors started working on combining security requirements (trustworthiness) and link reliability for OF design. More focus on the RPL security enhancement field is provided by [7].

4.6 Network Scalability

Scarce are research works that have efficiently addressed scalability concerns while validating their proposed OF through simulations. In fact, most proposed OF experimentation were made with networks topologies with under fifty nodes. Thus, the proposed schemes are likely to face genuine adaptability issues in bi-directional large-scale networks especially with LLNs rising areas of application and IoT. Furthermore, as recommendation for new schemes design, we subjoin thinking about devices heterogeneity and applications interoperability among different hardware configurations.

5 Opportunities and Future Work

Most of aforementioned enhancement schemes, were evaluated by referring only to the standard OF defined by the ROLL working group. Thus we face a panoply of objective functions without really having feedback on the effectiveness of one function in relation to another. At this stage, it would be more interesting to work on a new standard that takes into account these different approaches and facilitates their implementation. Thus future proposed OF will no longer have to refer to a very basic objective function i.e. MRHOF, but rather reinforce already established efforts.Moreover, it would be interesting in the new standard to update the structure of DIO messages so as to intuitively propagate information regarding widely used metrics that have proven their effectiveness such as the number of children attached to a node or the hop count. Thus the effort of research will be focused on calculation methods and optimization algorithms.

The use of AI, particularly Machine Learning (ML) techniques, could be very also interesting insofar as it will make it possible to merge different proposed routing schemes. Researchers can get through ML useful insights to understand which routing metric is more likely to affect network behaves and ensures better performances. Moreover, better adaptability of proposed algorithms to IoT specific applications would be achievable. The ML-based approach will also take advantage of the reduced cost of simulation compared to real test deployment and then allow large-scale networks testing.

In another case, the majority of improvement approaches focus on non-root nodes so it is high time to work on sink nodes by

Table 5: Synthesis of enhancement schemes achievements

Proposal	Reliability enhancement	Delay enhancement	Extending lifetime	Load balancing and congestion avoidance
DT-RPL [12]	√	-	√	-
Di Marco et al. [13]	√	-	√	√
Gonizzi et al. [14]	-	√	-	-
RA-EEDEM [15]	√	√*	-	-
Karkazis et al. [16]	√	-	-	-
Kamgueu et al. [17]	-	-	√	-
Iova et al. [18]	√*	x	√	√
LB-OF [19]	√h	-	√*	√*
BD-RPL [20]	√	√	√	√
CA-OF [22]	√	-	-	√
Qu-RPL [23]	√	-	-	√
En-RPL [24]	√	x	√	√
IRPL [25]	√	√*	√	√
Kamgueu et al. [27]	√	√*	√	-
OF-FL [28]	√	√	√	-
OF-EC [29]	√	-	x	-
CMOF [30]	√	√	-	√a
OPP-FL [31]	√c	√c	-	-
FMOF [40]	√b	√	-	-

*No or slight variation

[h] In case of high number of nodes

[a] enhanced through a TX power control mechanism

[b] only in low transmission rate

[c] Significant improve can be observed in case of random node deployment and high density networks

optimizing the placement of the collector nodes. Thereby, intermediate nodes can be relieved from complex algorithms involving considerable storage and processing capacity. Indeed the 6LBR is main-powered and benefits from a significant processing and storage capacity which will allow it to deploy quite relevant optimization solutions without worrying about the complexity of the processing involved. In the light of the obtained results, an update will be broadcast through the IPv6 control messages to large networks to invite the other nodes to adapt the new routing parameters promising better performance.

Another big challenge to be faced by RPL is to attest its willing to fit specific IoT application. Although, it has proven its efficiency in smart grid Advanced metering infrastructure (AMI) application, more work is to do in terms of security, reliability, and delay to meet other IoT applications requirements.

6 Conclusion

Through this work, we concentrated on RPL enhancement efforts made through the OF as the core of the RPL routing function. We gave an overview of enhancements work made till now to supply LLNS main applications requirements and overcome nodes limitation in terms of energy. First, we exposed a glimpse of the RPL protocol in terms of design, DODAG construction and different traffic patterns. Then, we highlighted researchers endeavor to enhance RPL protocol. Notably, we reviewed a set of literature works tackling major RPL OF improvements. In particular, our survey classified them to single metric based OF enhancement and metric combinations based OF enhancement schemes. For single metric based OF enhancement works, we focus on novel metrics not already tackled in [5]. For metrics combination based OF, which is the widespread technique, we presented weighted linear combination techniques and fuzzy logic based combination techniques. We have also noticed that besides cross-layer design approaches, multipath routing was widely used by a notable number of papers. We also emphasized the need for future research works to focus on the ability of the proposed schemes to apply for networks scalability purpose and real implementation and experiments.

Conflict of Interest

The authors declare no conflict of interest.

References

[1] T. Winter et al., “RPL: IPv6 routing protocol for low-power and lossy networks,” Internet Eng. Task Force, Fremont, CA, USA, RFC 6550, Mar. 2012.

[2] E.K. Pister , E.P. Thubert , S. Dwars , T. Phinney , “Industrial Routing Requirements in Low Power and Lossy Networks”, IETF Request for Comments : 5673, MARCH 2009.

[3] P. Thubert, ”Objective function zero for the routing protocol for low-power and lossy networks (RPL)”, IETF Request for comments: 6552,March 2012.

[4] O. Gnawali, P. Levis, The minimum rank with hysteresis objective function, IETF request for comments: 6719, September 2012.

[5] J. Vasseur , M. Kim , K. Pister , D. Barthel , ”Routing metrics used for path calculation in low-power and lossy networks”, RFC 6551, 1–12, 2012.

[6] E. Ancillotti, C. Vallati, R. Bruno, E.Mingozzi, ”A reinforcement learning-based link quality estimation strategy for RPL and its impact on topology management” Computer Communications, **112**(3), 1–13, 2017. https://doi.org/10.1016/j.comcom.2017.08.005

[7] P. O. Kamgueu, E. Nataf, T. D. Ndie, ”Survey on RPL enhancements:a focus on topology, security and mobility”, Computer Communications, **120**, 1-17, 2018. https://doi.org/10.1016/j.comcom.2018.02.011

[8] J. V. V. Sobral, J. J. P. C Rodrigues, R. A. L. Rabêlo, J. Al-Muhtadi, V. Korotaev, ”Routing Protocols for Low Power and Lossy Networks in Internet of Things Applications” Sensors, **19**(9), 21-44, 2019. https://doi.org/10.3390/s19092144

[9] P. Levis , T. Clausen , J. Hui , O. Gnawali , J. Ko , ”The Trickle algorithm”, IETF RFC 6206, 2011.

[10] P. Levis , N. Patel , D. Culler , S. Shenker , ”Trickle: a self-regulating algorithm for code propagation and maintenance in wireless sensor networks”, 1st conference on Symposium on Networked Systems Design and Implementation (NSDI), USA, 2004. https://doi.org/10.5555/1251175.1251177

[11] H. Kharrufa, H. A. A. Al-Kashoash and A. H. Kemp, ”RPL-Based Routing Protocols in IoT Applications: A Review,” in IEEE Sensors Journal, **19**(15), 5952-5967, August, 2019. https://doi.org/10.1109/JSEN.2019.2910881.

[12] H. S. Kim, H. Cho, H. Kim, S. Bahk, ”DT-RPL: Diverse Bidirectional Traffic Delivery through RPL Routing Protocol in Low Power and Lossy Networks” Computer Networks. , **126**, 150–161, 2017. https://doi.org/10.1016/j.comnet.2017.07.001

[13] P. Di Marco, C. Fischione, G. Athanasiou and P. Mekikis, ”MAC-aware routing metrics for low power and lossy networks,” IEEE INFOCOM, Turin, 13–14, 2013. https://doi.org/10.1109/INFCOM.2013.6566722.

[14] P. Gonizzi, R. Monica and G. Ferrari, ”Design and evaluation of a delay-efficient RPL routing metric” in 2013 9th International Wireless Communications and Mobile Computing Conference (IWCMC), Sardinia, 1573–1577, 2013. https://doi.org/10.1109/IWCMC.2013.6583790

[15] P. Pinto, A. Pinto and M. Ricardo, ”RPL modifications to improve the end-to-end delay estimation in WSN” in 2014 11th International Symposium on Wireless Communications Systems (ISWCS), Barcelona, 868–872, 2014. https://doi.org/10.1109/ISWCS.2014.6933475.

[16] P. Karkazis, I. Papaefstathiou, L. Sarakis, T. Zahariadis, T. Velivassaki and D. Bargiotas, ”Evaluation of RPL with a transmission count-efficient and trust-aware routing metric” in 2014 IEEE International Conference on Communications (ICC), Sydney, NSW, 550–556, 2014. https://doi.org/10.1109/ICC.2014.6883376.

[17] P. O. Kamgueu, E. Nataf, T. N. Djotio, O. Festor, ”Energy-based metric for the routing protocol in low-power and lossy network”, International Conference on Sensor Networks, Barcelona, Spain, 145-148, 2013. https://doi.org/10.5220/0004313401450148.

[18] O. Iova , F. Theoleyre , T. Noel , ”Using multiparent routing in RPL to increase the stability and the lifetime of the network”, Ad Hoc Netw,**29**,45–62, 2015. https://doi.org/10.1016/j.adhoc.2015.01.020

[19] M. Qasem, A. Al-Dubai, I. Romdhani, B. Ghaleb and W. Gharibi, ”A new efficient objective function for routing in Internet of Things paradigm” IEEE Conference on Standards for Communications and Networking (CSCN), Berlin, 1–6, 2016. https://doi.org/10.1109/CSCN.2016.7785168.

[20] F. Boubekeur, L. Blin, R. Leone, and P. Medagliani, ”Bounding Degrees on RPL” in 2015 ACM 11th Symposium on QoS and Security for Wireless and Mobile Networks (Q2SWinet), New York, USA, 123—130, 2015. https://doi.org/10.1145/2815317.2815339

[21] A. M. A. Awad, R. A. Rahim and A. H. A. Hashim, ”Queue Backlog as a Node Metric for RPL Protocol” in 2016 International Conference on Computer and Communication Engineering (ICCCE), Kuala Lumpur, 246–250, 2016. https://doi.org/10.1109/ICCCE.2016.61

[22] H. A. A. Al-Kashoash, Y. Al-Nidawi and A. H. Kemp, ”Congestion-aware RPL for 6L0WPAN networks” in 2016 Wireless Telecommunications Symposium (WTS), London, 1–6, 2016. https://doi.org/10.1109/WTS.2016.7482026.

[23] H. Kim, J. Paek and S. Bahk, ”QU-RPL: Queue utilization based RPL for load balancing in large scale industrial applications” in 2015 IEEE 12th Annual International Conference on Sensing, Communication, and Networking (SECON), Seattle, WA, 265–273, 2015. https://doi.org/10.1109/SAHCN.2015.7338325.

[24] P. Singh and Y. Chen, ”RPL Enhancement for a Parent Selection Mechanism and an Efficient Objective Function”IEEE Sensors Journal., **19**(21), 10054–10066, 2019. https://doi.org/10.1109/JSEN.2019.2927498

[25] Z. Wang, L. Zhang, Z. Zheng and J. Wang, "An Optimized RPL Protocol for Wireless Sensor Networks"in 2016 International Conference on Parallel and Distributed Systems (ICPADS), Wuhan, 294–299, 2016. https://doi.org/10.1109/ICPADS.2016.0047.

[26] L. A. Zadeh, "Fuzzy logic",Computer,**21**(4), 83-93,April 1988. https://doi.org/10.1109/2.53.

[27] P. Kamgueu, E. Nataf and T. Ndie Djotio, "On design and deployment of fuzzy-based metric for routing in low-power and lossy networks," IEEE 40th Local Computer Networks Conference Workshops (LCN Workshops), Clear water Beach, FL, 789-795, 2015. https://doi.org/10.1109/LCNW.2015.7365929.

[28] O. Gaddour, A. Koubâa, N. Baccour and M. Abid, "OF-FL: QoS-aware fuzzy logic objective function for the RPL routing protocol," 12th International Symposium on Modeling and Optimization in Mobile, Ad Hoc, and Wireless Networks (WiOpt), Hammamet, 365-372, 2014. https://doi.org/10.1109/WIOPT.2014.6850321.

[29] H. Lamaazi and N. Benamar, "RPL enhancement using a new objective function based on combined metrics," 13th International Wireless Communications and Mobile Computing Conference (IWCMC), Valencia, 1459-1464, 2017. https://doi.org/10.1109/IWCMC.2017.7986499.

[30] T. G. Harshavardhana, B. S. Vineeth, S. V. R. Anand and M. Hegde, "Power control and cross-layer design of RPL objective function for low power and lossy networks," 10th International Conference on Communication Systems & Networks (COMSNETS), Bengaluru, 214-219, 2018. https://doi.org/10.1109/COMSNETS.2018.8328200.

[31] I. Kechiche, I. Bousnina and A. Samet, "A novel opportunistic Fuzzy logic based objective function for the Routing Protocol for Low-Power and Lossy Networks," 15th International Wireless Communications & Mobile Computing Conference (IWCMC), Tangier, Morocco, 698-703, 2019. https://doi.org/10.1109/IWCMC.2019.8766691.

[32] S. Moeller, A. Sridharan, B. Krishnamachari, O. Gnawali, "Routing without routes: the backpressure collection protocol" in 2010 ACM/IEEE 9th conference on Information Processing in Sensor Networks (IPSN), New York, NY, USA, 279–290, 2010. https://doi.org/10.1145/1791212.1791246

[33] J. Eriksson, F. Österlind, N. Finne, N. Tsiftes, A. Dunkels, T. Voigt, R. Sauter, and P. Marrón,"COOJA/MSPSim: interoperability testing for wireless sensor networks" in 2009 International Conference on Simulation Tools and Techniques (ICSTT),Brussels, BEL, **27**, 2009. https://doi.org/2009.10.4108/ICST.SIMUTOOLS2009.5637

[34] P. Pinto, A. Pinto and M. Ricardo, "End-to-end delay estimation using RPL metrics in WSN" in 2013 IFIP Wireless Days (WD), Valencia, 1–6, 2013. https://doi.org/10.1109/WD.2013.6686524

[35] A. Sobeih et al., "J-Sim: a simulation and emulation environment for wireless sensor networks," IEEE Wireless Communications,**13**(4), 104–119, 2006. https://doi.org/10.1109/MWC.2006.1678171.

[36] E. Ben Hmida, "WSNet Simulator : An event-driven simulator for large scale wireless sensor networks", available online http://wsnet.gforge.inria.fr/download.html".

[37] L. Chang, T. Lee, S. Chen and C. Liao, "Energy-Efficient Oriented Routing Algorithm in Wireless Sensor Networks," in 2013 IEEE International Conference on Systems, Man, and Cybernetics, Manchester, UK 3813–3818, 2013. https://doi.org/10.1109/SMC.2013.651

[38] E.Fleury, N.Mitton, T.Noel, C.Adjih., "FITIoT-LAB: The Largest IoT Open Experimental Testbed" in ERCIM News, **14**, 2015. https://hal.inria.fr/hal-01138038

[39] F. Demicheli, G.Ferrari, P. Gonizzi, Design, Implementation and Evaluation of an energy RPL routing metric: Study of an energy efficient routing metric, LAP LAMBERT Academic Publishing, 2014.

[40] I. H. Urama, H. Fotouhi and M. M. Abdellatif, "Optimizing RPL Objective Function for Mobile Low-Power Wireless Networks," IEEE 41st Annual Computer Software and Applications Conference (COMPSAC), Turin, 678-683, 2017. https://doi.org/10.1109/COMPSAC.2017.185.

[41] H. Fotouhi, D. Moreira, and M. Alves, "mRPL: Boosting mobility in the Internet of Things," Ad Hoc Networks, **26**, 17–35, 2015. https://doi.org/10.1016/j.adhoc.2014.10.009

ASTES

Advances in Science, Technology and Engineering Systems Journal
Vol. 5, No. 5, 212-216 (2020)
www.astesj.com

ASTES Journal
ISSN: 2415-6698

Learning Tool for Kids on Android Platform

Gulam, Afan Galih Salman*, Bayu Kanigoro*

Computer Science Program, School of Computer Science, Bina Nusantara University, 11480, Indonesia

ARTICLE INFO

Article history:
Received: 16 June, 2020
Accepted: 25 August, 2020
Online: 14 September, 2020

Keywords:
Education
Mobile Application

ABSTRACT

The evolution of IT keeps growing worldwide, especially mobile technology. Today, mobile technology not only held by adults but also kids. The proportion of kids who used smartphones is increasing each year. The growing technology in mobile applications encourages developers to build educational apps to help kids learn to know alphabets, numbers, animals, and simple calculations in a fun way. This paper describes an educational "Homy Kid Lesson" as an Android-based application. The goal of this Homy Kid Lesson is helping children to know numbers, recognize letters, recognize animal names, and to perform simple calculations with an attractive interface. Research methods include data collection, design, and implementation. The development is done through the research literature, comparing it with similar apps, interviews, and questionnaires. Application design uses a storyboard. Its implementation refers to Extreme Programming (XP) model. The result is an educational application "Homy Kid Lesson" which can be a learning tool and as electronic media for learning with interest and fun concept. Contribution and novelty are increasing the ability of children to recognize letters and numbers early, increase the knowledge of animal names, introducing how to spell the letters and numbers to children also train the child's ability to simple counting and introduced the method of learning with electronic media.

1 Introduction

The development of information technology (IT) is more advanced and growing. It is also accompanied by the increasing needs of the community for technology and information. The information received is easily accessible from various locations, which can also be easily consumed by the community through technology. The development of multimedia technology also quickly offers a major change in the current human lifestyle [1]. Another supporting factor is the increasing use of smartphones, especially those based on Android. The Android operating system is an operating system on smartphones that are freely available for commercial or non-commercial use [2]. The Android operating system was introduced in 2008. Android continues to grow because it has advantages of open source and Android also offers many tools for building software that offers possibilities for application development [3].

Currently, the learning media for children in Android software is still limited such as learning letters, numbers, animals, and simple calculations for children. These apps usually offer only one learning material, such as an app for learning a letter or an app for learning numbers. Seeing these conditions would be better if learning materials are combined and used as a medium of learning for children, to facilitate the children learn letters, numbers, animals, and simple calculation [4]. Therefore the application built under the name "Homy Kid Lesson" by providing features with music and animation to help children recognize letters, numbers, and animal names in a fun way, and also do simple calculations (addition and subtraction) of course with interesting and interactive images. The goal of this Homy Kid Lesson application to help the children to know numbers, recognize letters, recognize animal names, and to perform simple calculations. The benefits of this application increase the ability of children to recognize letters and numbers early, increasing the knowledge of animal names, introducing how to spell the letters and numbers to children also train the child's ability to simple counting and introduced the method of learning with electronic media.

2 Methodology

Mobile learning in pre-school education has potential benefits suggested by Mike et. al [5]. With the implementation of a systematic study, researchers wanted a positive impact on the use of mobile devices and ICT (information and communication technology) in

*Corresponding Authors:
Afan Galih Salman, Jl. KH Syahdan No. 9, Kemanggisan, Jakarta Barat, DKI Jakarta, 11480, asalman@binus.edu
*Bayu Kanigoro, Jl. KH Syahdan No. 9, Kemanggisan, Jakarta Barat, DKI Jakarta, 11480, bkanigoro@binus.edu

kindergarten, not only of computers in the classroom but also on the technology used to assist teachers. The main concern is how to maximize the benefits of this instrument to improve the children's experience of ICT in education.

Mobile application for teaching mathematics has been proposed by Zaranis et. al [6] in kindergarten to helps students more active in learning and improve their initiative and opportunity for self-study. It shows that mobile application is very effective in increasing the motivation of kindergarten students for this is the position of kindergarten students to organize what, when, and where they learn. It becomes an easy platform for learning.

The basic functional requirements for mobile apps for children with special needs is proposed by Kraleva et. al [7]. This issue became very important in the last years because an increase in the number of children with special needs on a worldwide scale is observed and at the same time the increase in the use of mobile technologies.

Research design-based method proposed by Soykan et. al [8] developed for students and teachers in teaching concept skills to develop disabled students and to examine the process of developing software based on the infrastructure of operant conditioning theory. Their design-based research method developed for students and teachers in teaching concept skills to developmentally disabled students and to examine the process of developing software based on the infrastructure of operant conditioning theory.

Analysis of this type of application is done by analyzing similar apps that have been developed before. It gets an overview of these applications and gets additions so that apps can be made better. A comparison of these applications is shown in table 1.

Table 1: Comparison with Similar Applications

	ABC Sound Apps	Number Baby Flash Cards Apps	Animal 123 Apps	Homy Kid Lesson Apps
Learn Alphabet	✓	✗	✗	✓
Learn Number	✗	✓	✗	✓
Learn Animals	✗	✗	✓	✓
Animation	✗	✗	✗	✓
Learn Music	✗	✗	✗	✓

The development combines three different levels for the system integration, framework, and structure of the game. On a conceptual level, a game is considered as a system (i.e. a set of interrelated elements). A game is designed by specifying certain relevant factors, taking into account the two fundamental dimensions of space and time: the space dimension overs the static configuration of gaming locations (virtual) and includes associated objects, attributes, and relationships, and its evolution over time covers the game dynamics. On a technical level, the framework describes the basic architecture of the game development system which describes the system and its tools for developing the places, objects, actor roles, and scenarios of the video game. On a practical level, i.e. the structure of the game, the options offered to the players, and the multimedia representation of the game environment. The research method used in this study is shown in Figure 1.

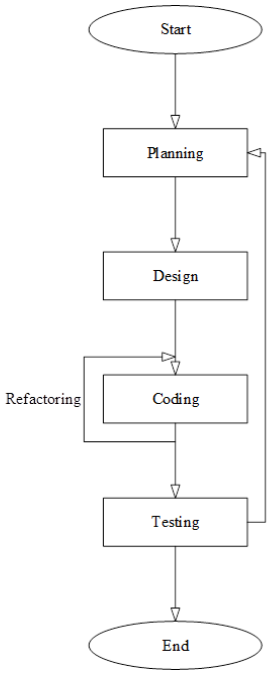


Figure 1: The research method used in this study.

The proposed app uses a model of Agile Extreme Programming (XP) [9], which has stages of development as follows: Planning, that focus to get an overview of the functions and application software through communication with the user. This phase consists of several parts: literature studies, questionnaires, interviews, and analysis of similar applications. Results of communication with the user later collected in an index of stories in which each point of the index is determined to build priorities. The design stage aims to build the pattern of the logic of a system based on a result of communication with the users. It provides a kind of design in the development of applications, namely the application design, system design using CRC maps are then formulated in UML9 also build user interface design using a storyboard. Coding, first make a unity check to test the system to be implemented and write application code on the XP model applies the concept of paired programming. Testing at this stage on XP also carried out at the coding stage is with unit tests. After each module in the unit test, the final process test this application by using Eight Golden Rules Theorem [10] as an acceptance test.

Based on the results of the questionnaire and the questionnaire obtained, several conclusions can be drawn. Most respondents agreed that the introduction of numbers, letters, and names of animals is important for young children. Most respondents agreed that early childhood children should be taught simple calculations (addition and subtraction). Some respondents answered that the method of learning while playing is very well used in providing educational insight to early childhood. Some respondents think

that the application of education can help in providing educational insight into early childhood. Respondents on average agree that the educational applications of mobile devices can increase interest in learning in young children. The average respondent said that the age range of 3-5 years is the ideal age to provide educational insight to early childhood because in this age range the child is experiencing growth and development which is often referred to as "Golden Age". Respondents said that to increase motivation to learn in young children must be done with an attractive and attractive environment as well as a supportive environment. Respondents gave positive responses to educational applications that could help in providing educational insight into early childhood. The app will add music and animation functions to make it easier for children to recognize the letters, recognize the numbers. It will add animation to introduce the names of the animals. The survey results showed that as many as 105 respondents answered that letter recognition is important for early childhood. With so many respondents assessing the importance of this, the application will present a letter recognition feature for toddlers. As many as 105 respondents answered that the recognition of numbers is important for early childhood. With a fairly dominant number of respondents, this application will present a number recognition feature for young children. The survey results showed that as many as 105 respondents answered that the recognition of animal names is important for early childhood. With the results obtained, the application will present the name recognition feature for early childhood. The survey results showed that 77 respondents answered that early childhood should be taught simple calculations. From the viewpoint of quite a lot of respondents, the application will present a simple calculation feature for young children. Figure 2 shows the use case for the application.

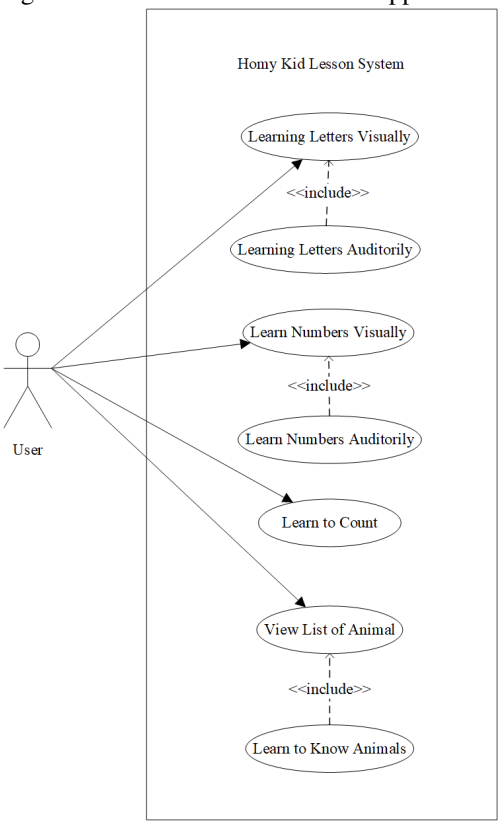


Figure 2: Use Case for "Homy Kid Lesson" app

3 Result

Here is the main page image of the educational app "Homy Kid Lesson". On the main page, there are four main features of the application: learn to know the letters, learn to know numbers, and learn to know the names of animals and make simple calculations, figure 3.



Figure 3: Home Menu

The feature screen, shown in figure 4, "ABC" contains alphabet letter keys from A to Z to learn to recognize letters. When one of the letters is selected, the page appears to learn the letter along with the spelling of the selected letter. There is also a feature to learn with music when the "music" button is pressed.

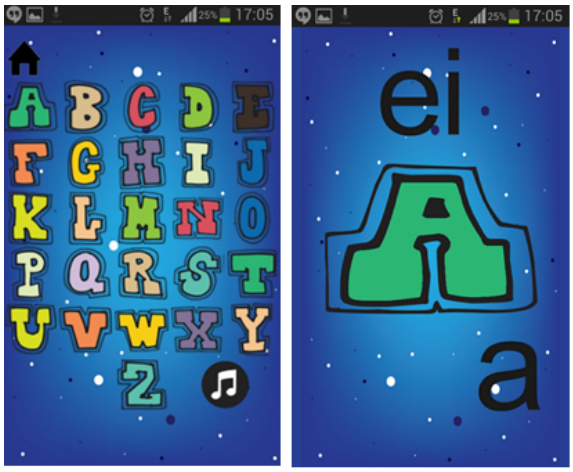


Figure 4: Learn to Know Letter

The feature screen "123", shown in figure 5, contains buttons of rows with numbers from 1 to 10, when user pressed then will show a page to learn numbers. There is also a function to learn music when the "music" button is pressed.



Figure 5: Learn to Know Number

The feature screen “Animals”, shown in figure 6, contains a list of images of animals, when user selected one of the animals then will display the physical shape of the animal with the sound of the selected animal.

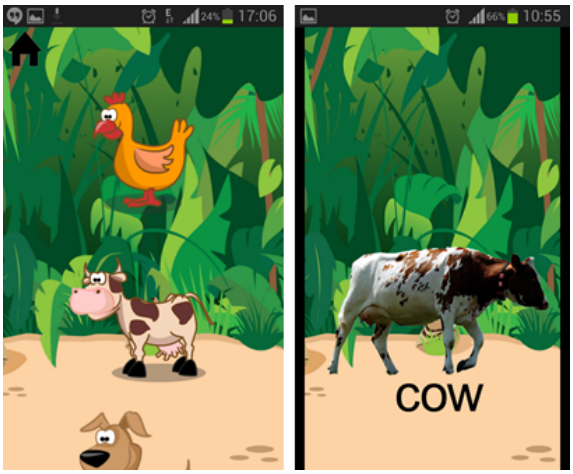


Figure 6: Learn to Know Animals

The feature screen “Count” contains two main menu plus (+) and minus (−). The plus (+) button is a function to perform addition mode and minus (−) functions to perform calculations in the subtraction mode. In this calculation menu, the user can try ten simple calculation questions see figure 7.

Table 2 shows questionnaire results of 52 respondents that have tried “Homy Kid Lesson” application.

Table 2: Questionnaire Results

Answer	Number of Respondents	Percentage
Very Attractive	30	58%
Attractive	22	42%
Less Attractive	0	0%
Not Attractive	0	0%

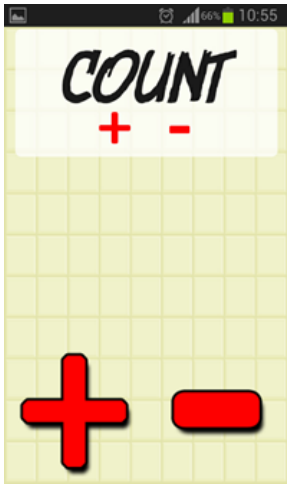


Figure 7: Learn to Know Calculation

As shown in table 2, all respondents said the educational application “Homy Kid Lesson” is very attractive to use. Application evaluation was carried out by giving questionnaires to 52 parents and teachers. They tried the educational application “Homy Kid Lesson” directly. This evaluation questionnaire includes questions relating to the eight golden rules and five measurable human factors by Shneiderman and Plaisant. Based on the evaluation results obtained, it can be concluded that the educational application ”Homy Kid Lesson” is interesting in terms of appearance design, learning features, instructions, and easy to use. Overall, the educational application ”Homy Kid Lesson” received a positive response so the application ”Homy Kid Lesson” could be an alternative learning media for children. This app increases the ability of children to recognize letters and numbers early, increasing the knowledge of animal names, introducing how to spell the letters and numbers to children also train the child’s ability to simple counting and introduced the method of learning with electronic media.

4 Conclusion

Educational applications “Homy Kid Lesson” can help children to learn about letters, numbers, and names of animals and to perform simple calculations. The educational application “Homy Kid Lesson” can help children learn to spell letters and words. The educational application “Homy Kid Lesson” becomes an alternative learning tool for children.

More features such as Bahasa as an add-on feature for recognizing letters and numbers. Add math material such as multiplication and division; add more objects or images for features to recognize animal names.

The contribution to this research is that this application acts as an alternative medium of learning for children. The learning method used in this application uses a fun playstyle approach.

References

[1] T. Vaughan, Multimedia: Making It Work, McGraw-Hill Osborne Media New York, 2010.

[2] L. D. Darcey, Android Application Development in 24 Hours, Sams Publishing Indiana, 2012.

[3] M. Gargenta, Learning Android: Develop Mobile Apps Using Java and Eclipse, O'Reilly Media USA, 2011.

[4] Sutomo, Android: Pemrograman Aplikasi Mobile Smartphone dan Tablet PC berbasis Android, Informatika Bandung, 2012.

[5] M. McCabe, S. Tedesco, "Using QR codes and mobile devices to foster an inclusive learning environment for mathematics education" International Journal of Technology and Inclusive Education (IJTIE), **1**(1), 37–43, (2012). https://doi.org/10.20533/ijtie.2047.0533.2012.0006

[6] N. Zaraniz, M. Kalogiannakis, S. Papadakis, "Using mobile devices for teaching realistic mathematics in kindergarten education" Creative Education, **4**(7), 1, (2013). https://doi.org/10.4236/ce.2013.47a1001

[7] R. Kraleva, Velin Kralev, "An evaluation of the mobile apps for children with special education needs based on the utility function metrics" International Journal on Advanced Science Engineering and Information Technology, **8**(6), 2269–2277, (2018). https://doi.org/10.18517/ijaseit.8.6.6309

[8] E. Soykan, Fezile Özdamlı, "Development process of instructional mobile application for special needs children" International Journal of Technology Enhanced Learning **11**,3, 259–278, (2019). https://doi.org/10.1504/ijtel.2019.10020449

[9] R. Pressman, Software engineering: a practitioner's approach, Palgrave macmillan, 2005

[10] B. Shneiderman, C. Plaisant, M. Cohen, S. Jacobs, N. Elmqvist, N. Diakopoulos, Designing the user interface: strategies for effective human-computer interaction, Pearson, 2016

ASTES

Advances in Science, Technology and Engineering Systems Journal
Vol. 5, No. 5, 217-223 (2020)
www.astesj.com
Special Issue on Innovative Research in Applied Science, Engineering and Technology

ASTES Journal
ISSN: 2415-6698

Thermal Performance Analysis of Parabolic Trough Solar Collector System in Climatic Conditions of Errachidia city, Morocco

Mohamed Hajjaj[*,1], Amine Tilioua[2], Abdellah Mellaikhafi[2], Abella Bouaaddi[1]

[1]*Laboratory Engineering Energy, Materials and Systems, Department of Physics, National School of Applied Sciences, Ibn Zohr University Agadir, 80000, Morocco*

[2]*Thermal and Applied Thermodynamics, Mechanics Energy Efficiency and Renewable Energies Laboratory, Department of Physics, Faculty of Sciences and Techniques Errachidia, Moulay Ismaïl University of Meknès, B.P. 509 Boutalamine Errachidia, Meknes, 50050, Morocco*

ARTICLE INFO

Article history:
Received: 03 July, 2020
Accepted: 19 July, 2020
Online: 14 September, 2020

Keywords:
Parabolic Trough Collector
Absober tube
Solar Domestic Heating Water
Direct Normal Irradiation
Temperature
Modelling

ABSTRACT

The water heating with parabolic trough solar collectors (PTC) is a very widespread and at the same time quite promising solar technology. However, PTC presents several problems in terms of the profitability of water heating. For this reason, our study of water heating with PTC collectors consists of two main parts. In the first part, we investigate the effect of direct normal irradiation in the absorber tube using the TRNSYS software of the Errachidia city. In the second part, the study is entirely focused on the heat balance of the absorber tube in order to estimate the fluid outlet temperature. Besides, a mathematical model is developed to simulate and control the fluid outlet temperature circulating through the absorber tube of the collector. The water outlet temperature prediction was carried out by a thermal performance study of the PTC in weather conditions of Errachidia city (Morocco) using TRNSYS software and Matlab Code in the year's typical days.

1 Introduction

A great deal of effort has been made, especially in the last decade to improve systems for converting solar energy into heat and particularly for electricity production. Parabolic trough reflector technology is the most common and is currently used by the most powerful solar power plants in the world and improving the efficiency of these concentrators is the concern of several researchers. The PTC offers the possibility to produce electricity and hot water from solar energy. The temperature of the fluid can be raised up to 500 ° C. The operating principle of this technology is based on the concentration of the sun's rays on a horizontal tube, where a heat transfer fluid circulates that will be used to transport the heat to the power plant itself. The parabolic-cylindrical collector is composed of a long mirror (usually with silver or polished aluminum plating), rectangular, parabolic cylinder shape and completed by a tube with a double vacuum envelope that runs along the entire length of the focal length line. The sun's rays are reflected by the mirror to converge on the tube. The absorber tube is the essential part of the concentrator, it is often made of copper covered with a selective layer, and it is surrounded by a transparent glass envelope. The parabolic shape of the mirrors allows the sun's rays to be concentrated throughout the tube. By circulating the heat-transfer fluid in the center of this tube, the fluid is heated and conducts the heat to the container with a determined flow rate. As with any concentrating collector, parabolic troughs need to follow the sun in order to concentrate direct solar radiation. As a line concentration collector, the parabolic cylinder has a single axis tracking system. Schematic of the solar PTC system with receiver is presented in Figure 1. Several studies have been conducted by researchers to improve the energy efficiency of parabolic trough systems. Cheng et al [1] examined the temperature distribution at the outer surface of the absorber tube of a CCP as a function of the surface radiation flux distribution using the Monte Carlo MCRT method. The authors have combined the MCRT method and the finite volume method via the Fluent ANSYS calculation code, elaborating a multitude of simulations and taking into account the dependence of the physical properties of the heat transfer fluid (Sylitherm 800 oil) with temperature. The results obtained were compared with previous experimental data [2] and it was noticed that there was a 2% difference in the temperature

[*]Corresponding Author: Mohamed Hajjaj, BP 607 Boutalamine, Errachidia 52000, Morocco. Email: med.hajjaj85@gmail.com

of the heat transfer fluid (HTF) at the absorber outlet. In addition, Kaloudiset al [3] performed a numerical study on the collector of a parabolic-cylinder concentrator system with nano heat transfer fluid, in order to simulate the SEGS LS2 type collector. The authors used four cases of boundary conditions for numerical simulation involving all heat transfer modes at the different tube interfaces.

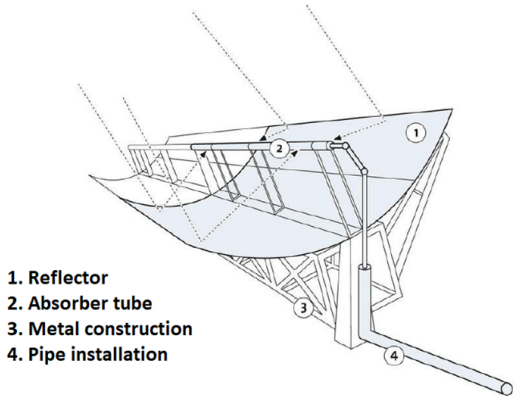


Figure 1: Schematic of the PTC system with receiver [4]

Besides, In [5], the authors have investigated the energy performance of a PTC solar in the climatic conditions of the Algerian Sahara. The authors performed a simple numerical simulation of the one-dimensional implicit finite difference method applied to the energy balance of solar collectors by dividing the absorber tube, the glass cover and the fluid in many segments. Both fluids were used, water and synthetic oil TherminolVP-1 in the simulation. However, simulation results showed that the thermal efficiency is approximately 69.73 and 72.24%, which decreases at higher temperatures of synthetic oil-based fluids but increases by 2% at lower water temperatures. Bellos et al [6] have studied three different types of parabolic cylindrical collectors (vacuum tube receptor, non-vacuum tube receptor and bare tube without cover) to improve the thermal margin with the implementation (Syltherm 800/Cu) in a systematic manner. The use of nanofluids improved performance in the bare tube with 7.16%, 4.87% for the non-evacuated receptor and 4.06% for the evacuated receptor at a flow-rate of 25 L/min. Zhao et al [7] have examinated the global performance of the PTC solar using three different tubes (one smooth and two internally finned tubes), the authors characterized the solar collector performance by energy efficiency, exergy efficiency and thermo-hydraulic efficiency. The results obtained showed that the output temperature of the solar air collectors depends on the solar irradiation, the air flow rate and the geometry parameters of the spindle fin. IPF#2 tubes have the highest collector efficiency and air temperature, while the STube without using pin fins has the lowest values.

In Morocco, the solar plan is part of the national energy strategy which aims at quantitatively assessing the level of security of a secure and sustainable, clean, green and accessible energy provision [8]. The idea is, therefore, to study the energy efficiency of a parabolic trough solar collector and the thermal behavior of an absorber tube to improve their efficiency. The simulation is divided into two steps, the first part includes the simulation using the TRNSYS software [9], on the entire cylindro-parabolic system whose aim is to control this system and especially its operation in Saharan environment, in order to provide hot water in collective buildings [10], and taking into account the specific climatic effects in the Errachidia city (South of Morocco). In the second part, we numerically investigate using a developed Matlab code the geometrical effect of absorber tubes in order to improve the energy efficiency of a parabolic trough solar collector.

2 Theoretical study

2.1 Optical performance of PTC

2.1.1 Concentration rate

The concentration rate is defined as the ratio of the opening surface to the receiver surface[11, 12].

$$C = \frac{S_O}{S_r} \tag{1}$$

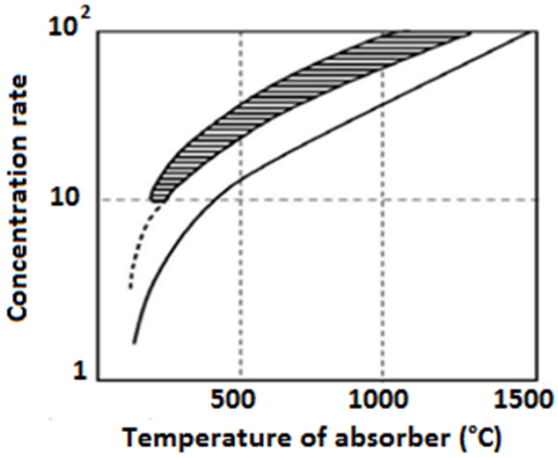


Figure 2: Concentration rate as function of the receiver temperature[11]

Figure 2 shows the variation in concentration rate as a function of absorber temperature.

- Low concentration:

  $1 < C < 10$ involved $T_C \approx 150$ °C

- Average concentration:

  $10 < C < 100$ involved $T_C \approx 1000$ °C

- High concentration:

  $C \geqslant 100$ involved $T_C \geqslant 1000$ °C

2.1.2 Radiation absorption

The radiation absorption is defined as follows [12]:

$$E = E_b.\rho.(\gamma.\tau).C \tag{2}$$

2.2 Thermal performance study of PTC

The thermal performance of PTC can be determined from different methods. The power received of PTC (Q_u) is determined from the quantities (F_R) and (U_L)[12].

2.2.1 Overall heat loss factor U_L (covered tube)

In the event that the tube receiver is covered by a glass selective surface (S_C), the irradiation coefficient in the glass to absorber region is dissimilar from the irradiation coefficient in the absorber to glass region, this coefficient is usually negligible [10]. The coefficient of heat loss is expressed by relationship:

$$F' = \frac{\frac{1}{U_L}}{\frac{1}{U_L} + \frac{D_e}{h_{fi} D_i (\frac{D_e}{2\lambda} \ln \frac{D_e}{D_i})} + \frac{1}{U_L}} \quad (3)$$

$$F_R = \frac{m_f . C_p}{S_r . U_L} . \left[1 - e^{\left(\frac{S_r . U_L . F'}{m_f . C_p}\right)}\right] \quad (4)$$

$$U_L = \left[\frac{S_r}{(h_v + h_{r,c-a}).S_r} + \frac{1}{h_{r,a-c}}\right] \quad (5)$$

$$h_{r,c-a} = \frac{\sigma(T_r^2 - T_c^2).(T_r - T_c)}{\frac{1-\varepsilon_r}{\varepsilon_r} + \frac{1}{F_{rc}} + \frac{(1-\varepsilon_c).S_r}{\varepsilon_c . S_c}} \quad (6)$$

$$h_{r,a-c} = 4.\sigma.\varepsilon.\bar{T}^3 \quad (7)$$

2.2.2 Useful heat (Q_u)

The useful heat is determined from the power recovered by the PTC at the focal line and it is expressed by the following relationship:

$$Q_U = F_R.[E.\rho.\tau.\alpha.\gamma.S_o - U_L.S_r(T_{out} - T_{inl})] \quad (8)$$

2.2.3 The outlet temperature T_{out} of HTF

The output temperature of HTF is determined from the following equation [13]:

$$T_{out} = T_{inl} + \frac{Q_U}{m_f . C_p} \quad (9)$$

2.2.4 Solar concentrator efficiency η

The efficiency of the PTC is given by the following relationship [14].

$$\eta = \frac{Q_U}{E.\gamma.S_o} \quad (10)$$

3 Numerical simulation

3.1 TRNSYS model

To evaluate the thermal efficiency of a solar PTC, we used the TRNSYS software. It allows users to specify the system components and to connect these components together. Each component (type) contains input and output parameters.

In the present study, a new numerical model is developed using the Matlab language to simulate the temperature evolution in the fluid, absorber and glass cover. Concerning the simulation by TRNSYS software, we used the different components such as a parabolic cylindrical collector (type 536) and a pump (type 3d). Other components used: weather (type 109), regulation (type 2b) ON/OFF differential controller, storage tank (type 4c) and online plotter (type 65a). The schematic of the TRNSYS model of the PTC system takes into account water as HTF in the weather conditions of Errachidia city, it is presented in Figure 3.

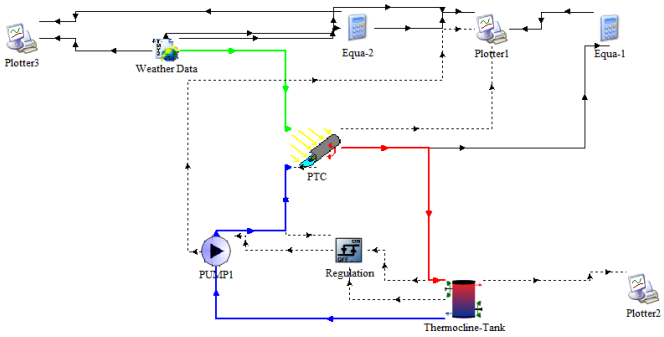


Figure 3: TRNSYS model of a solar PTC with Thermocline- Tank

3.2 Weather data of Errachidia city

Morocco's energy efficiency agency has proposed a new classification of climatic zones, each having different meteorological properties. In addition, the wind speed, ambient temperature, and total radiation on the inclined surface of the city under study are generated by the METEONORM software. According to this study's aims, which focuses on the thermal efficiency of a PTC tube for the Errachidia site. Geographical localization of Errachidia city (semi-arid climate) offers the ideal climatic conditions such as intense sunshine all year round, low humidity and precipitation. The ambient temperature variation all year round in the selected zone is shown in Figure 4. Besides, the estimation of the direct normal irradiation (DNI) throughout the year is shown in Figure 5. The evolution of the annual inlet and outlet temperature of the water is illustrated in Figure 6.

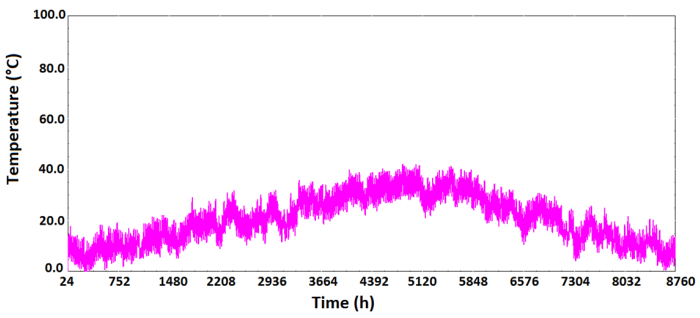


Figure 4: Ambient temperature evolution during one year at the Errachidia site

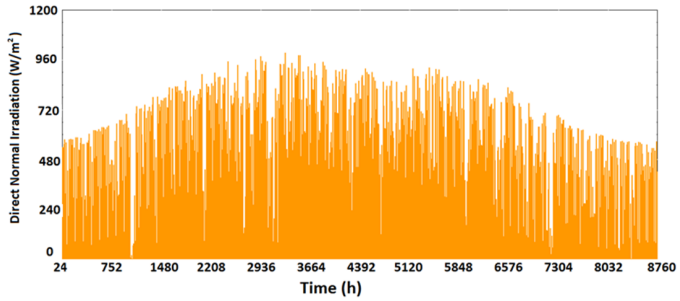


Figure 5: Annual direct normal irradiation in Errachidia city

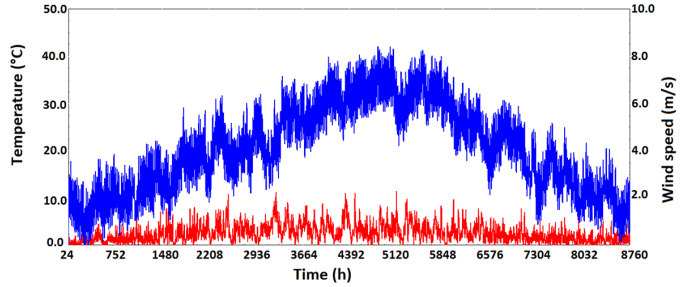


Figure 6: Variation of water inlet and outlet temperature for one year at Errachidia city

4 Results and discussion

The estimation of the amount solar radiation captured by the PTC is based on the method employed by [15]. For modelling the thermal behavior of PTC components in transient regime, we have taken into account the following assumptions :

- The sky is assumed to be a blackbody;
- Under climatic conditions, the physical properties of the glass and the absorber are supposed constant;
- Fluid velocity is supposed to be constant;
- The wind speed is 3.75 m/s;
- The physical properties of the fluid in the absorber are assumed to be temperature dependent;
- The air enclosed between the absorber and the glass is stagnant and transparent.

4.1 Geometrical and optical parameters of PTC

The main element of PTC system which allows receiving incident solar radiation is the absorber, also it allows to convert radiation in the form of heat and transmit it to the HTF. The incident solar radiation is not entirely absorbed and transmitted to the HTF, but part is dissipated as heat loss between the absorber and the cover glass. Figure 7 illustrates heat transfer of the absorber used, taking into consideration the different shares of energy, which were collected by the fluid and lost to the environment.

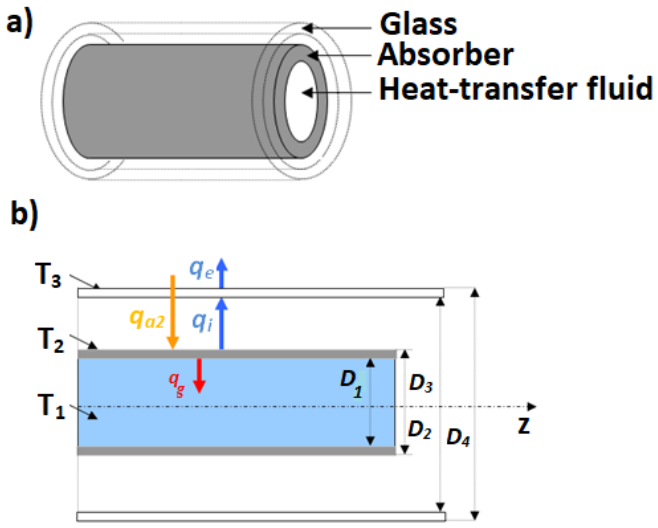


Figure 7: Thermal exchanges between the absorber tube and the other components of PTC

Tables 1 and 2 present the geometric and optical properties of the components of our PTC system. The physical properties of HTF (water) are shown in Table 3. The water temperature and the PTC components calculated from the energy balance [16], for the typical days of the year and for a HTF mass flow rate value of 0.0083 kg/s.

Table 1: Geometrical characteristics of the PTC elements

Geometric characteristics	**Value**
External diameter of the absorber, D_e	1.4 cm
Internal diameter of the glass cover, $D_{(c,i)}$	4.2 cm
External diameter of the glass cover, $D_{(c,e)}$	4.35 cm
Effective width of the mirror, W_{eff}	1 m
Element length, Δz	0.1 m
Collector absorber tube length, L_{tube}	2 m
Focal distance	0.235m

Table 2: Optical properties of materials used

Properties	**Value**
Absorption coefficient of the absorber tube, α	0.8
Glass transmission coefficient, τ	0.8
Reflectance of the mirror surface, ρ_m	0.85
Emissivity of the absorber tube, ε_r	0.12
Emissivity of the glass cover tube , ε_c	0.9

The thermal modelling of the absorber receiver of PTC is done by a calculation and programming procedure under Matlab by solving the energy balance equation. For this purpose, we have developed a calculation program to simulate the fluid temperature at the absorber outlet. The thermal model takes into account all heat transfers: convection in the receiver pipe, in the gap between the absorber and the glass cover, on the one hand, and between the glass cover and the ambient air, on the other hand. The thermal balance equation between the absorber and the HTF can be written :

$$\pi\rho_1 C_1 D_1 \frac{\partial T_1}{\partial t}(z,t) = -\rho_1 C_1 \phi \frac{\partial T_1}{\partial z}(z,t) + q_g(z,t) \quad (11)$$

The initial conditions and limits are given by following relationships:

$$T_1(z,0) = T_{amb}(0) \quad (12)$$

$$T_1(0,t) = T_e(t) \quad (13)$$

where T_e is the inlet temperature and T_{amb} is the ambient temperature.

Table 3: Properties of heat fluid (water)

Properties	Value
Heat capacity, C_f	4180 kJ.kg^{-1}.K^{-1}
Volume flow rate, D_f	30 l/h

Table 4: Comparison of parameter effects on PTC in the present study with other similar works.

Dimension of PTC	Mass flow rate Kg/s	Temperature of water	References
1 m x 2 m	0.0083	149 °C	Present study
1.25 m x 0.8 m	0.0117 - 0.0167	36.5 °C	[16]
1.49 m x 1.49 m	0.00111	104 °C	[17]
1.2 m x 1.5 m	0.0017	65 °C	[18]
1.82 m x 1.03 m	0.00111	50 °C	[19]
6 m x 2.3 m	0.55	165 °C	[20]
7.8 m x 5 m	0.345	47.24 °C	[21]

In order to produce hot water 90°C, for domestic and industrial applications. We have choose the right mass flow and the good PTC dimensions. Table 4 presents a comparison of parameter effects on PTC in the present study with other similar works. We noticed that when the mass flow rate and the opening radius of the collector increases the outlet temperature of the hot water rises. To produce a sufficient quantity of hot water, it is necessary to select parabolic cylindrical collector dimensions in relation to the outlet temperature of the water and the mass flow rate (Table 5).

Table 5: Hot water production in 90°C for different theoretical cases [22]

Dimension of PTC	Mass flow rate Kg/s	Quantity of hot water (L/day)
1.6 m x 1.8 m	0.0074	133.2
1.6 m x 3 m	0.0123	221.4
1.6 m x 6 m	0.0250	450.0
1.6 m x 10 m	0.0411	739.8
1.6 m x 15 m	0.0633	1139.4

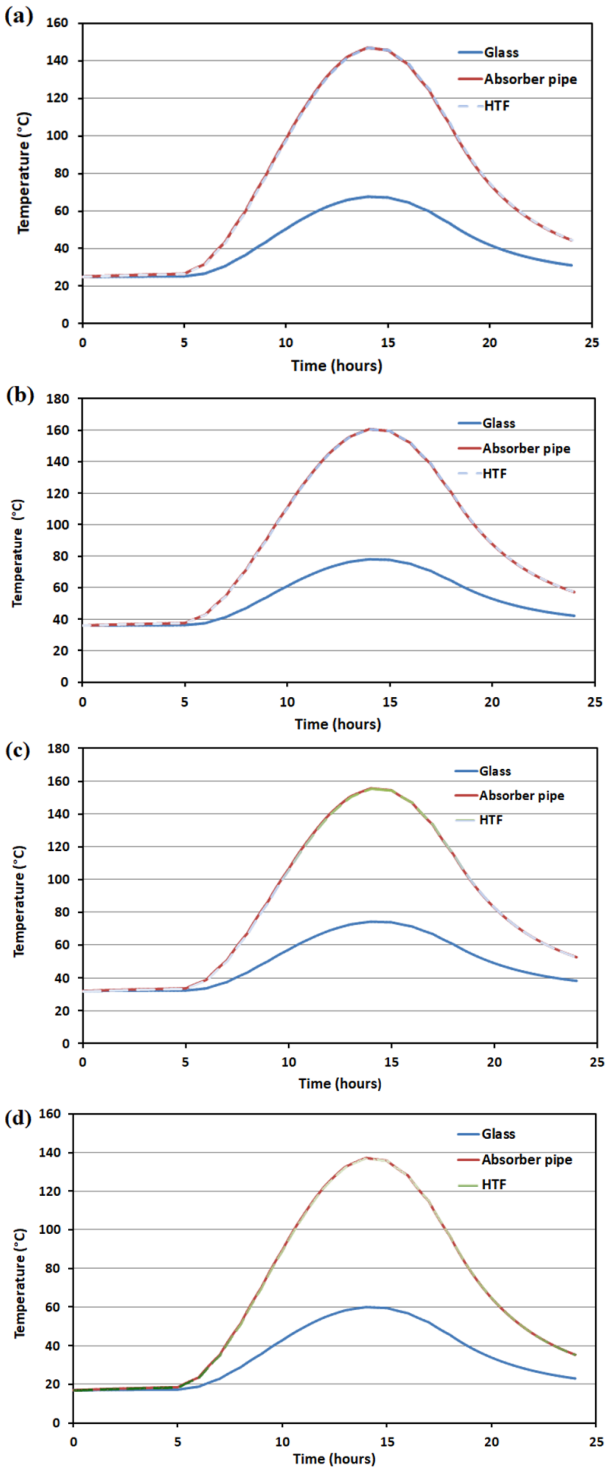


Figure 8: Outlet temperature evolution of fluid, absorber and glass for; (a) March 21, (b) June 21, (c) September 21 and (d) December 21

4.2 Temperature outlet evolution in typical days of year

Figure 8 shows the temperature evolution of the fluid, the absorber and the glass cover versus the time from March 21, June 21, September 21 and December 21, 2019 for the concentrator whose geometric properties are given in Table 1. We observed that the temperature variation depends on the climatic conditions of Errachidia, particu-

larly on the incident solar energy.

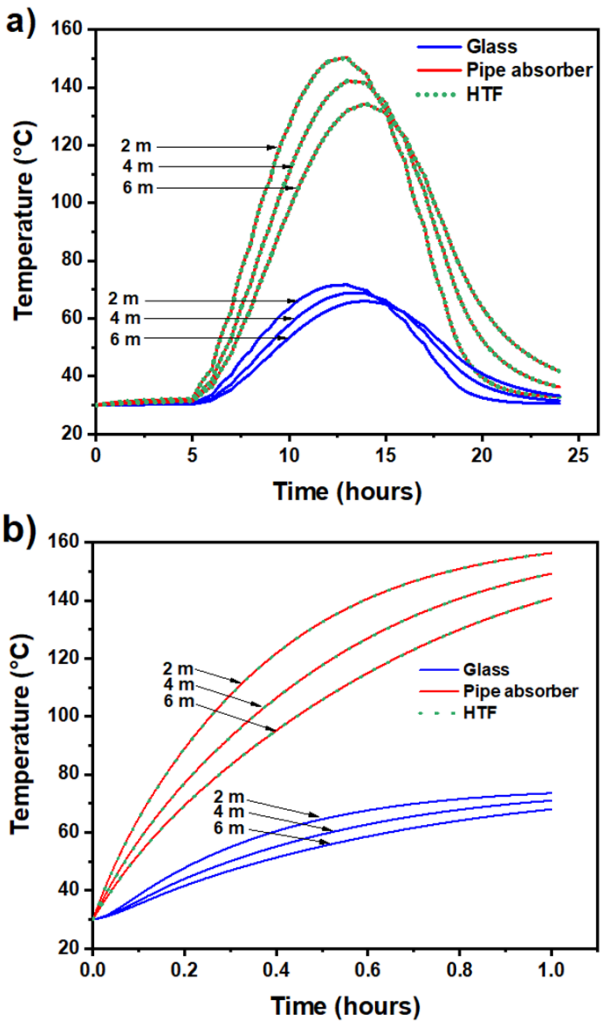


Figure 9: (a) Outlet temperature evolution of the glass, absorber and HTF for; 2 m, 4 m and 6 m of the length tube, (b) PTC temperature - stagnation conditions.

4.3 Absorber tube length effect

The thermal performance of PTC and the water heating requirements depend on the geometric properties of PTC solar. In the modeling we have chosen 3 different absorber lengths 2m, 4m and 6m, respectively. Excluding stagnation, we observe that the risk of overheating at the PTC level does not exist, the temperature of the absorber tube stays below 70°C using water as HTF. The daily variation of the fluid temperature, the absorber tube and the glass cover as a function of time is illustrated in Figure 9a. We noticed that when the receiver pipe length is small the efficiency of the system increases and the temperature of the absorber also increase. We observed that, in theory, the stagnation of the temperature of the absorber and fluid exceeds 158°C of water as HTF. The risk of deterioration of the system in the case of water HTF is important. We also observed that when the absorber tube length is small the temperature of the absorber also increases (Figure 9b).

4.4 Absorber tube thickness effect

Figure 10 shows the thickness effect of the receiver pipe on the fluid daily temperature, the receiver pipe and the glass cover versus of time for 1.5 mm, 2.5 mm and 3.5 mm respectively, for the concentrator whose geometric properties are given in Table 1. We observe that the thickness of the absorber has a small impact on the fluid temperature evolution and stagnation of the temperature compared to the tube length.

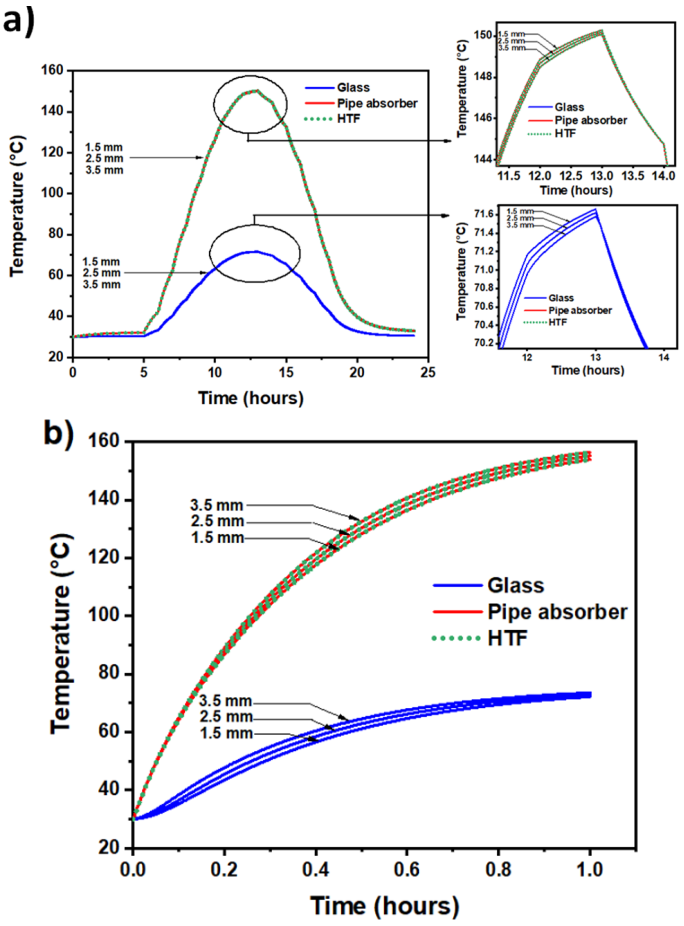


Figure 10: (a) Outlet temperature evolution of HTF, absorber and glass cover for different absorber tube thickness 1.5 mm, 2.5 mm and 3.5 mm; (b) PTC temperature stagnation conditions.

5 Conclusions

In this paper, the study of the water heating circulating in an absorber tube of a solar PTC is investigated. The heating process modeling of the fluid is performed. To verify the temperature of fluid, absorber and glass cover, a mathematical model is elaborated from the heat exchanges of the glass tube with the environment. The geometrical dimensions of the parabolic-cylindrical collector have been taken into account in the modeling. The results obtained in this study showed that there was a significant temperature difference between the inlet and the outlet of PTC for the test days considered. Excluding stagnation, the absorber tube length effect on the fluid temperature evolution was observed. However, the absorber tube thickness effect is very small on the temperature evolution. This

investigation offers multiple perspectives on the use and analysis of parabolic-cylindrical collector behavior such as the optical performance evaluation of the system or to test other heat transfer fluids. Finally, an economic study can be envisaged to evaluate the cost-effectiveness of the system.

Nomenclature

T_a	Ambient temperature (°C)
T_r	Absorber temperature
$\bar{T}$	Average irradiation temperature
T_C	Concentration temperature
T_c	Cover temperature (glass tube)
T_1	Heat transfer fluid temperature
C_p	Calorific power
C_1	Heat-transfer fluid specific heat
D_1	Internal diameter of the absorber
E_p	Incident radiation on the map opening
E	Incident solar radiation (W/m^2)
T_{inl}	Fluid inlet temperature
T_{out}	Fluid outlet temperature
F_{rc}	Form factor between the receiver and the cover, which is equal to 1
h_{fi}	Heat transfer coefficient at inside the absorber (W/(m^2.°C)
m_f	Mass flow
S_o	PTC opening area
S_r	Receiver surface (m^2)
D_e,D_i	Outside and inside diameter of the absorber
q_g	Amount of the energy gained by the heat transfer fluid

Greek Symbols

γ	Optical collector factor
ε_r	Emissivity of the surface of the absorber
λ	Thermal conductivity (W/(m.°C))
τ	Transmission factor
ρ	Reflection factor of the concentrator mirror
ϕ	Heat transfer fluid mass flow rate
ρ_1	Heat transfer fluid density
ε_c	Glass emissivity of the cover
$\tau\alpha$	Transmission-absorption coefficient

Physical constants

σ	Stefan-Boltzmann Constant ($5.667.10^{-8}$W/m^{2}K^4)

Conflict of Interest The authors declare no conflict of interest.

References

[1] Z.D. Cheng, Y.L. He, J. Xiao, Y.B. Tao, R.J. Xu, "Three-dimensional numerical study of heat transfer characteristics in the receiver tube of parabolic trough solar collector", International Communications in Heat and Mass Transfer **37**, 782–787, 2010.

[2] V.E. Dudley, G.J. Kolb, A.R. Mahoney, T.R. Mancini, C.W. Matthews, M. Sloan, D. Kearney, " Test results: SEGS LS-2 solar collector", Sandia National Laboratories, Albuquerque, 1994.DOI: 10.2172/70756

[3] E. Kaloudis, E. Papanicolaou, V. Belessiotis, "Numerical simulations of a parabolic trough solar collector with nanofluid using a two-phase model." Renewable Energy **97**, 218–229, 2016.https://doi.org/10.1016/j.renene.2016.05.046

[4] P. Hubert Wagner, "Thermodynamic simulation of solar thermal power stations with liquid salt as heat transfer fluid", Ph.D Thesis Technical University of Munich, 2012.

[5] Y. Marif, H. Benmoussa, H. Bouguettaia, M. M. Belhadj, M. Zerrouki, "Numerical simulation of solar parabolic trough collector performance in the Algeria Saharan region", Energy Convers. Manage. **85**, 521–529, 2014. https://doi.org/10.1016/j.enconman.2014.06.002.

[6] E. Bellos, C. Tzivanidis, Z. Said, "A systematic parametric thermal analysis of nanofluid-based parabolic trough solar collectors", Sustainable Energy Technologies and Assessments, **39**, 100714, 2020. https://doi.org/10.1016/j.seta.2020.100714

[7] Z. Zhao, F. Bai, X. Zhang, Z. Wang, "Experimental study of pin finned receiver tubes for a parabolic trough solar air collector ", Solar Energy, **207**, 91–102, 2020.

[8] S. Zafar, Africa, Renewable Energy, Solar Energy, Wind Energy, 2019. https://www.ecomena.org/

[9] M. Hajjaj, A. Mellaikhafi, A. Tilioua, C. Messaoudi, A. Bouaaddi, Numerical Investigation and Control The Thermal Storage System in A Single-Tank for CSP Plants,International Journal of Advance Science and Technology, **29**, 10s, 8378–8389, 2020.
http://sersc.org/journals/index.php/IJAST/article/view/24294

[10] Z. D. Cheng, Y. L. He, J. Xiao, Y. B. Tao, and R. J. Xu, "Three-dimensional numerical study of heat transfer characteristics in the receiver tube of parabolic trough solar collector." Int. Commun. Heat Mass Transf., **39**(7), 782–787, 2010. https://doi.org/10.1016/j.icheatmasstransfer.2010.05.002

[11] M. Hajjaj, A. Bouaaddi, A. Mellaikhafi, A. Tilioua, C. Messaoudi, "Simulation of the water outlet temperature in a solar Parabolic Trough Collector in the Errachidia site " in 2020IEEE 1st International Conference (IRASET), Meknes, Morocco, 2020. DOI: 10.1109/IRASET48871.2020.9092323.

[12] J.A. Duffie and W.A. Beckman, Solar Engineering of Thermal Processes, 2nd Edition, John Wiley & Sons Inc, 1991.

[13] W. Chekirou, N. Boukheit, T. Kerbache, "Analyse Thermique pour l'Absorbeur d'un Concentrateur Solaire Cylindro Parabolique", 12ème Journées Internationales de Thermique, 61–64, Morocco, 2005.

[14] M. Li and L.L. Wang, "Investigation of Evacuated Tube Heated by Solar Trough Concentrating System", Energy Convers. Manage., **47**, 3591–3601, 2006. https://doi.org/10.1016/j.enconman.2006.03.003

[15] ASHRAE Handbook, Fenestration Fundamentals, USA, 2001.

[16] A. Valan Arasu and T. Sornakumar, "Performance characteristics of Parabolic Trough Solar Collector system for hot water generation", International Energy Journal, **7**, 137–145, 2006. DOI: 10.2298/TSCI0602167V

[17] M. Rizwan, Md. A. R. Junaidi, M. Suleman and M. A. Hussain, "Experimental verification and analysis of Solar Parabolic Collector for water distillation", International Journal of Engineering Research, **3**, 588–593, 2014. DOI: 10.17950/ijer/v3s10/1008

[18] M. G. Tayade, R. E. Thombre and S. Dutt, "Performance evaluation of Solar Parabolic Trough", International Journal of Scientific and Research Publications, **5**, 1–5, 2015.

[19] K. H. Bhujangrao, "Design and development of prototype cylindrical parabolic solar collector for water heating application", Journal of Renewable Energy Development, **5**, 49–55, 2016. DOI: 10.14710/ijred.5.1.49-55

[20] M. Qu, D. H. Archer and S. V. Masson, "A linear parabolic trough solar collector performance model", Renewable Energy Resources and a Greener Future, VIII-3-3, 2006. DOI: 10.1115/ES2007-36052

[21] D. Sauceda, N. Velazquez, O. Garcia-Valladares and R. Beltran, "Numerical simulation and design of a parabolic trough solar collector used as a direct generator in a solarGAX cooling cycle", J. Mech. Sci. Technol., **25**, 1399–1408, 2011. https://doi.org/10.1007/s12206-011-0326-y

[22] M. E. Soudani, K. E. Aiadi, D. Bechki, "Water heating by Parabolic Trough Collector with storage in the Ouargla region of Algerian Sahara", Materials Today: Proceedings, **24**, 137–139, 2020. https://doi.org/10.1016/j.matpr.2019.07.707

ASTES

Advances in Science, Technology and Engineering Systems Journal
Vol. 5, No. 5, 224-236 (2020)
www.astesj.com
Special Issue on Multidisciplinary Innovation in Engineering Science & Technology

ASTES Journal
ISSN: 2415-6698

Applicability of Generalized Metropolis-Hastings Algorithm to Estimating Aggregate Functions in Wireless Sensor Networks

Martin Kenyeres[*,1], Jozef Kenyeres[2]

[1]*Institute of Informatics, Slovak Academy of Sciences, Dubravska cesta 9, 845 07 Bratislava 45, Slovak Republic*

[2]*Sipwise GmbH, Europaring F15, 2345 Brunn am Gebirge, Austria*

ARTICLE INFO

Article history:
Received: 09 July, 2020
Accepted: 25 August, 2020
Online: 14 September, 2020

Keywords:
Distributed computing
Data aggregation
Consensus algorithms
Wireless sensor networks
Metropolis-Hastings algorithm

ABSTRACT

Over the last decades, numerous distributed consensus-based algorithms have found a wide application as a complementary mechanism for data aggregation in wireless sensor networks. In this paper, we provide an analysis of the generalized Metropolis-Hastings algorithm for data aggregation with a fully-distributed stopping criterion. The goal of the implemented stopping criterion is to effectively bound the algorithm execution over wireless sensor networks. In this paper, we analyze and compare the performance of the mentioned algorithm with various mixing parameters for distributed averaging, for distributed summing, and for distributed graph order estimation. The algorithm is examined under different configurations of the implemented stopping criterion over random geometric graphs by applying two metrics, namely the mean square error and the number of the iterations for the consensus. The goal of this paper is to examine the applicability of the analyzed algorithm with the stopping criterion to estimating the investigated aggregate functions in wireless sensor networks. In addition, the performance of the algorithm is compared to the average consensus algorithm bounded by the same stopping criterion.

1 Introduction

This paper is an extension of work originally presented in the Proceedings of the EUROCON 2019 - 18th International Conference on Smart Technologies [1].

1.1 Wireless Sensor Networks

Wireless sensor networks (WSNs) are a technology formed by small-size autonomous low-cost sensor nodes equipped with three basic components - a sensing subsystem, a processing subsystem, and a wireless communication subsystem [2]–[4]. These subsystems enable the sensor nodes to concurrently sense the surrounding area, to process the measured data, and to communicate with each other via wireless transmission channels [2, 3]. Moreover, the sensor nodes are supplied by an energy source, allowing WSNs to execute the programmed tasks [3]. WSNs are required to obtain a lot of information about the observed physical phenomenon (e.g., light, motion, temperature, seismic events, humidity, pressure, etc.) and to effectively deliver the measured data to the end-users [3, 5]. Furthermore, they are self-organizing systems typically consisting of many sensor nodes (i.e., hundreds or even thousands) distributed over large-scale areas (either in a random fashion or manually) whereby large geographical territories can be cooperatively monitored with very high precision [2, 6]. As WSNs are generally built-up on an ad-hoc basis, the deployment of the sensor nodes is significantly simplified [7]. In many applications, the sensor nodes are required to operate under inhospitable environmental conditions and without any human interaction; therefore, the design of the algorithms for WSNs has to be affected by these facts [2]. So, WSN-based applications have to be viable and energy-efficient so that the robustness of WSNs to potential threads is high [2]–[4]. Over the last years, WSNs have found the application in various areas such as industrial monitoring, health care, localization, security, structural monitoring, military monitoring, etc. [8].

1.2 Consensus-based Algorithms for Data Aggregation

As the sensor nodes are vulnerable to numerous threats (e.g., temperature, radiation, pressure variations, electromagnetic noise, coverage problems, a high failure rate, etc.) and can measure highly correlated or even duplicated information, complementary algorithms for data

[*]Corresponding Author: Martin Kenyeres, E-mail: martin.kenyeres@savba.sk

aggregation are applied in many WSN-based applications in order to suppress these negative factors and to optimize the overall energy consumption (see Figure 1 for an example demonstrating the difference between WSNs with and without data aggregation) [9, 10]. In addition, data aggregation algorithms can optimize also routing mechanisms, thereby reducing the total energy requirements as well [11]. In the literature, one can find several papers concerned with how to effectively bound algorithms for data aggregation whereby the communication, computation, and energy requirements of WSNs can be optimized [12]–[14]. Note that data aggregation is an important process not only in WSNs but also in other industries [15]–[18].

Over the last decades, consensus-based algorithms for data aggregation have significantly gained the attention of the world-wide scientific community [13, 17, 19]. The problem of consensus achievement poses one of the most fundamental challenges in distributed computing [20]. In WSNs, the term consensus, in general, means the task of getting a group of the sensor nodes to agree on a common value determined by the initial states of all the sensor nodes in this group [21]. The consensus is achieved either asymptotically or in a bounded time interval due to iterative mutual interactions among these sensor nodes [21]. Eventually, each sensor node knows the exact value or an estimate of the wanted aggregate function. Gutierrez-Gutierrez et al. [22] define two categories of consensus-based algorithms for data aggregation, namely the deterministic and the stochastic algorithms. In the literature, one can find many deterministic approaches, e.g., the Maximum Degree weights algorithm, the Metropolis-Hastings algorithm (MH), the Best Constant weights algorithms, the Convex Optimized weights algorithm, etc. [1, 13, 19]. Probably, the most frequently quoted stochastic consensus-based algorithms are the Push-Sum algorithm, the Push-Pull algorithm, the Broadcast gossip algorithm, the Pairwise gossip algorithm, the Geographic gossip algorithm, etc. [14, 22]–[25]. As stated in [4], the algorithms differ from each other in many aspects such as the convergence rate, the robustness to potential threats, the initial configuration, the performance in mobile systems, etc.

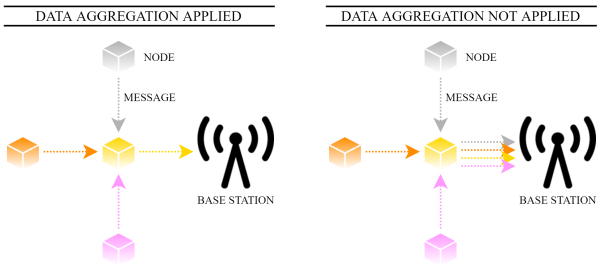


Figure 1: Comparison of WSN with/without data aggregation

1.3 Generalized Metropolis-Hastings for Data Aggregation

In this paper, we focus our attention on MH, which was proposed by Nicolas Metropolis et al. in the 1950s and extended by Wilfred Keith Hastings approximately twenty years later [1]. Since its definition, it has found the application in various areas, e.g., simulating multivariate distributions, block-at-a-time scans, acceptance-rejection sampling, etc. [1]. Lately, Schwarz et al. have defined its generalized variant (referred to as the generalized Metropolis-Hastings algorithm and labeled as GMH) and derived the convergence conditions over arbitrary graphs including critical topologies such as bipartite regular graphs [26]. This algorithm poses a multi-functional distributed linear consensus algorithm able to estimate various aggregate functions, namely the arithmetic mean, the sum, and the graph order. Its weight matrix is symmetric and doubly stochastic, and each graph edge is allocated a weight determined by the degrees of two linked vertices [1]. Thus, this algorithm represents a fully-distributed approach in contrast to many other distributed consensus-based algorithms for data aggregation that require global information for the optimal initial configuration and the proper operating (e.g., the maximum degree, the Laplacian spectrum, etc.) [19]. Therefore, this algorithm (including its original version) has significantly attracted the attention of the world-wide scientific community over the past years [1].

1.4 Summary of Contribution

In this paper, we extend the analysis from [1], where GMH for distributed averaging with the stopping criterion proposed in [27] is analyzed. The extension presented in this paper lies in an analysis of GMH also for distributed summing and distributed graph order estimation. Thus, we compare GMH for estimating different aggregate functions with a various mixing parameter and under various initial configurations of the implemented stopping criterion over 100 unique random geometric graphs (RGGs). In [1], it is identified that GMH can be applied to estimate the arithmetic mean, which motivates us to examine and to compare the applicability of GMH to estimating also other aggregate functions. In the case of distributed summing, we carry out two scenarios - either the initial inner states or the final estimates (i.e., the inner states after the consensus is achieved) are multiplied by the graph order. Thus, the experimental section consists of four scenarios. Finally, GMH for distributed summing and distributed graph order estimation is compared to our previous work where the average consensus algorithm is analyzed [8].

1.5 Paper Organization

The content of this paper is organized as follows:

- *Section 1*: is divided into five subsections:
  - *Section 1.1*: provides basic information about WSNs, i.e., a brief introduction about this technology, its purpose, constraints, and application.
  - *Section 1.2*: is concerned with consensus-based algorithms, i.e., a brief introduction into data aggregation/these algorithms, their purpose, classification, and examples.
  - *Section 1.3*: deals with GMH and introduces its history, application, purpose, and features.
  - *Section 1.4*: is focused on a summary of our contribution presented in this paper.
- *Section 2*: is concerned with a literature review focused on the application of GMH in (not only) WSNs.

- *Section 3*: provides a theoretical insight into the topic and is partitioned into two subsections:
  - *Section 3.1*: introduces the applied mathematical model of WSNs, the definition of GMH, its convergence conditions, and the analyzed functionalities of GMH.
  - *Section 3.2*: deals with the implemented stopping criterion, i.e., why to implement it, its parameters, and its principle.
- *Section 4*: is focused on the applied research methodology and the metrics for performance evaluation.
- *Section 5*: consists of the experimentally obtained results in Matlab2018b (32 figures in overall), an analysis of the depicted results, a comparison of various functionalities of GMH, and a comparison of GMH to the average consensus algorithm.
- *Section 6*: briefly summarizes the outcomes of the research presented in this paper.

2 Literature Review

In this section, we turn our attention to the applicability of MH for various purposes in (not only) WSNs.

In [29], the authors focus their attention on data acquisition in WSNs. They apply MH to determine the mixing time, which is the minimal length of a random walk to approximate a uniform stationary distribution. In the next paper [30], the authors propose an approach for estimating the model parameters for time synchronization in WSNs. Here, they apply MH in combination with Gibbs samples for estimating the parameters of the Bayesian model. The paper [31] is concerned with the tuning parameters of WSNs. In this case, MH is used to determine the acceptance probability. For higher values of the temperature, the algorithm accepts all the moves, meanwhile, stochastic hill-climbing is performed in the case of lower temperatures. The authors of [32] apply a random walk as a routing scheme and compressive sensing to recover raw data in order to optimize the communication costs and detection performance. MH is used to choose neighbors that receive a message. In [33], a novel approach based on MH that synthesizes safe reversible Markov chains is introduced. The authors of [34] propose an approach for evaluating the network loss probability of the mobile collectors for harvesting data in WSNs. As stated in the paper, the optimal movement strategy is achieved in the case of applying MH. In [35], the authors provide a Markov point process model to generate evolving geometric graphs capable of responding to external effects. In the presented model, the vertices can move according to MH-based rules, giving a random pattern of points whose distribution is similar to the Markov point process distribution. In [36], MH finds an application to obtaining a sequence of random samples from an arbitrary distribution. The biggest benefit of applying MH is that this algorithm is independent of the normalization factor. In the paper [37], a novel MH-based algorithm assumed to protect WSNs from internal attacks is proposed and analyzed. In this approach, MH is used to generate the samples from a stationary distribution. In [38], the authors propose a spatial-temporal data gathering mechanism based on MH with delayed acceptance. This approach allows harvesting compressive data by sequentially visiting small subsets of nodes along a routing path. In [13], MH is analyzed over WSNs with embedded computing and communication devices. A centralized stopping criterion based on the mean square error is applied to bound the algorithm execution in this paper. The authors of [39] propose a novel consensus-based algorithm for data aggregation over WSNs by combining MH with the convex optimized weights algorithm, thereby optimizing both the transient and the steady-state algorithm phase. In [40], MH is applied to target tracking in WSNs for surveillance tasks. The proposed approach is to convert binary detections into finer position reports by applying the spatial correlation. The mechanism for a node-specific interference problem appearing in heterogeneous WSNs is proposed in [41]. In this approach, MH is employed in its first step. In [42], it is stated that MH can be used to choose the next nodes in random walks. The paper [43] is focused on a modified MH for estimating the item, structural, and **Q** matrix parameters. In [44], the authors propose a TunaMH method based on MH (as its name evokes) for exposing a tunable tradeoff between its batch size and the convergence rate that is theoretically guaranteed. The authors of [45] propose a novel MH to provide large proposal transitions accepted with a high probability due to a significant increase in the complexity and in the dimension of the interference problems. The authors of [46] address the incipient fault detection problem, which is solved by the proposed two-step technique. In the second step, MH is used to perform the change point detection. In [47], the authors present a received signal strength-based inter-network cooperative localization approach utilizing MH. At the end of this section, as mentioned above, Schwarz et al. define the generalized variant of MH and analyze its convergence in [26].

Thus, it can be seen that our contribution is an analysis of GMH for estimating three aggregation functions with the fully-distributed stopping criterion from [27]. In none of the provided papers, such a deep analysis of GMH for data aggregation with a stopping criterion proposed primarily for WSNs is carried out.

3 Theoretical Background

3.1 Model of GMH for Estimating Average/Sum/Graph Order in WSNs

In this paper, WSNs are modeled as undirected simple finite graphs (with the graph order n) formed by two time-invariant sets, namely the vertex set **V** and the edge set **E** ($G = (\mathbf{V}, \mathbf{E})$), and so the graph order and the graph size are constant [1]. The vertex set **V** gathers all the graph vertices, which represent the sensor nodes in WSN and are distinguishable from each other by the unique index number, i.e., $\mathbf{V} = \{v_i : i = 1,2,...n\}$. The edge set **E** is formed by all the graph edges representing the direct connection between two vertices (v_i and v_j are linked by e_{ij}). Subsequently, the neighbor set of v_i, which is a set consisting of all the neighbors of the corresponding node, can be defined as follows [1]:

$$\mathcal{N}_i = \{v_j : e_{ij} \in \mathbf{E}\} \tag{1}$$

From a global view, GMH can be modeled as follows [26]:

$$\mathbf{x}(k+1) = \mathbf{W} \times \mathbf{x}(k) \tag{2}$$

From a local view, the formula (2) can be cast as follows [1]:

$$x_i(k+1) = [W]_{ii} \cdot x_i(k) + \sum_{j \in \mathcal{N}_i} [W]_{ij} \cdot x_j(k), \quad i = \{1, 2, ...n\} \tag{3}$$

Here, $\mathbf{x}(k)$[1] is a variant column vector containing the inner states of all the sensor nodes in WSN at the corresponding iteration, and $\mathbf{W}$ is the weight matrix defined for GMH as follows [26]:

$$[W]_{ij} = \begin{cases} \frac{1}{max\{d_i, d_j\}+\epsilon}, & \text{if } e_{ij} \in \mathbf{E} \\ 1 - \sum_{i \neq l} [W]_{il}, & \text{if } i = j \\ 0, & \text{otherwise} \end{cases} \tag{4}$$

Here, d_i poses the degree of v_i, and ϵ represents the mixing parameter, which has to take a value from the following interval for the convergence achievement [26]:

$$\epsilon \in [0, 1] \tag{5}$$

Note that the convergence is obtained for $\epsilon = 0$ only unless the underlying graph is bipartite regular [26]. As stated in [26], the adjacency matrix $\mathbf{A}$ of a bipartite graph has a block structure with zero diagonal in the case of $\epsilon = 0$, which implies:

$$\mathbf{W} = \frac{1}{d} \cdot \mathbf{A} = \frac{1}{d} \cdot \begin{pmatrix} 0 & \mathbf{A}_0 \\ \mathbf{A}_0^{\mathrm{T}} & 0 \end{pmatrix} \tag{6}$$

Thus, the sensor nodes are divided into two groups, and their inner states oscillate between two values equal to the arithmetic means determined by the inner states of the sensors nodes in these groups. The mixing parameter $\epsilon = 0$ causes the equality in $\rho(\widetilde{\mathbf{L}})^2 \leq 2$ in the case of the bipartite regular graphs, resulting in the divergence of the algorithm:

$$\rho(\widetilde{\mathbf{L}}) = 2 \implies \rho(\mathbf{W} - \frac{1}{n} \cdot \mathbf{1} \times \mathbf{1}^{\mathrm{T}}) = 1 \tag{7}$$

In Figure 14, we show the evolution of the inner states over a random bipartite regular graph for four values of the mixing parameter ϵ, including $\epsilon = 0$. From the figures, it can be seen that the inner states converge to the arithmetic mean except for $\epsilon = 0$, when the algorithm diverges.

Properly configured GMH operates in such a way that the inner state of each sensor node asymptotically converge to the value of the estimated aggregated function (which determines the value of the steady-state), i.e. [1]:

$$\lim_{k \to \infty} \mathbf{x}(k) = \lim_{k \to \infty} \mathbf{W}^k \times \mathbf{x}(0) = \frac{1}{n} . \mathbf{1} \times \mathbf{1}^{\mathrm{T}} \times \mathbf{x}(0) \tag{8}$$

Here, $\mathbf{1}$ poses an all-ones vector formed by n elements, and $\mathbf{1}^{\mathrm{T}}$ is its transpose. In the following part, examples of how the inner states evolve with an increase in the iteration number for each analyzed functionality of GMH are shown.

[1]Here, k is the label of an iteration, and $\mathbf{x}(k = 0)$ represents the initial inner states

[2]$\widetilde{\mathbf{L}}$ is the weighted Laplacian matrix

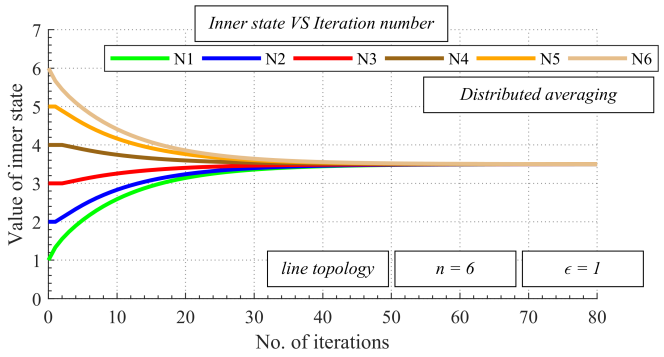


Figure 2: Inner states as function of number of iterations over line topology with graph order $n = 6$ - distributed averaging, mixing parameter $\epsilon = 1$

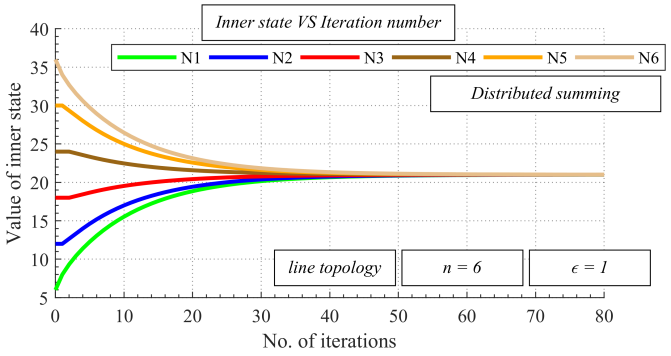


Figure 3: Inner states as function of number of iterations over line topology with graph order $n = 6$ - distributed summing, mixing parameter $\epsilon = 1$

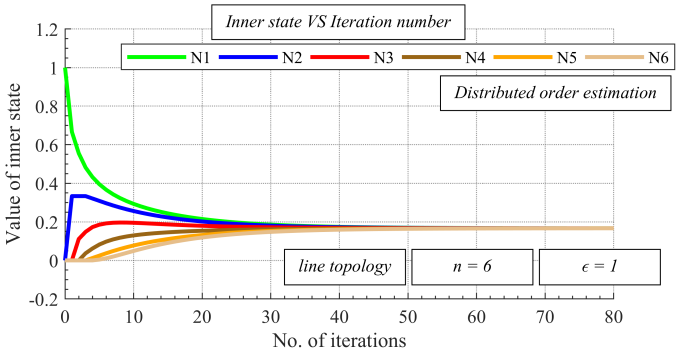


Figure 4: Inner states as function of number of iterations over line topology with graph order $n = 6$ - distributed graph order estimation, mixing parameter $\epsilon = 1$

The existence of the limit (8) is essential for GMH to operate correctly and is ensured, provided that these three convergence conditions are met [26]:

$$\mathbf{1}^{\mathrm{T}} \times \mathbf{W} = \mathbf{1}^{\mathrm{T}} \tag{9}$$

$$\mathbf{W} \times \mathbf{1} = \mathbf{1}, \tag{10}$$

$$\rho(\mathbf{W} - \frac{1}{n} \cdot \mathbf{1} \times \mathbf{1}^{\mathrm{T}}) < 1 \tag{11}$$

Here, $\rho(\cdot)$ is the spectral radius of the corresponding vector/matrix, and its value is equal to the largest eigenvalue in the absolute value from the corresponding spectrum, i.e.:

$$\rho(\cdot) = \max_i \{| \lambda_i(\cdot) |\} \tag{12}$$

Here, $\lambda_i(\cdot)$ is the i^{th} largest eigenvalue from the corresponding spectrum.

As mentioned earlier, GMH can estimate three various aggregate functions, namely the arithmetic mean, the sum, and the graph order. The values of the initial inner states are affected by the estimated aggregate function as follows:

- *Distributed averaging*: the initial inner states are equal to (for example) independent local measurements.
- *Distributed summing*: the initial inner states are equal to (for example) independent local measurements and multiplied by the graph order n - this multiplication is carried out either before the algorithm begins or after completing the algorithm.
- *Distributed graph order estimation*: one of the sensor nodes is selected as the leader, and its initial inner state is equal to "1". The other sensor nodes initiate their inner state with "0". Once the consensus is achieved, the sensor nodes determine the inverted value from the final estimates, which is equal to an estimate of the graph order n.

3.2 Distributed Stopping Criterion for WSNs

In this section, we introduce the implemented stopping criterion for bounding the execution of GMH. As mentioned earlier, an effectively stopped execution may significantly optimize the algorithm in terms of many aspects such as the overall energy consumption, the communication amount, etc., and therefore, a proper initial configuration of the implemented stopping criterion is essential especially in energy-constrained technologies such as WSNs. In this paper, we analyze the fully-distributed stopping criterion from [27], which is determined by two constants:

- *accuracy*
- *counter threshold*

Both constants are the same at each sensor node and have to be set before the algorithm begins. Also, each sensor node has its own *counter*, which is a variable initiated by "0" at each sensor node. The principle of the stopping criterion lies in a comparison of the finite difference between two subsequent inner states at each sensor node with pre-set *accuracy*. If the finite difference is smaller than *accuracy counter threshold*-times in the array, the algorithm is locally completed at the corresponding nodes, and this node does not participate in the algorithm anymore. If not, the value of *counter* is reset regardless of its current state. See Algorithm 1 for the formalization of GMH with the stopping criterion from [27].

Algorithm 1 GMH for distributed averaging/summing/graph order estimation with bounded execution

At the beginning of the algorithm (i.e., $k = 0$), every sensor node $v_i \in \mathbf{V}$ initiates its inner state (i.e., $x_i(0)$) with a scalar value according to the estimated aggregate function:

- *Distributed averaging*: the initial inner states are equal to (for example) independent local measurements.
- *Distributed summing*: the initial inner states are equal to (for example) independent local measurements and multiplied by the graph order n - this multiplication is carried out either before the algorithm begins or after completing the algorithm.
- *Distributed graph order estimation*: one of the sensor nodes is selected as the leader, and its initial inner state is equal to "1". The other sensor nodes initiate their inner state with "0". Once the consensus is achieved, the sensor nodes determine the inverted value from the final estimates.

Also, each sensor node $v_i \in \mathbf{V}$ sets its *counter* to "0". The parameters *counter threshold* and *accuracy* are constant during the algorithm execution and set to the same value at each sensor node. Each sensor node is considered to be active until it locally completes the algorithm.

At the next iterations (i.e., $k = 1, 2, ...$), every active sensor node repeats the following steps as long as it is active:

1. sends a broadcast message containing its current inner state to (1) as well as collecting the inner states from (1).
2. updates its inner state for the next iteration by applying the update rule (2)/(3).
3. verifies whether the finite difference between two subsequent inner states is smaller than *accuracy*, i.e., $|\Delta x_i(k)| < accuracy$. If it is true, it increments its *counter* by "1", otherwise, sets it to "0".
4. verifies the condition: *counter* = *counter threshold*. If it is valid, the corresponding sensor node considers GMH to be locally completed, and this sensor node becomes inactive. If it is invalid, the sensor node repeats the previous steps.

4 Research Methodology

This section is concerned with the applied research methodology and the metrics for performance evaluation.

As already mentioned in this paper, the weight matrix of GMH is modifiable by changing the value of the mixing parameter ϵ. As stated in [26], the convergence is ensured for ϵ taking value from (5) unless the underlying graph is bipartite regular. As it is not too likely that WSNs are bipartite regular [26], we do not include them in the experimental section - GMH diverges over these topologies, which may significantly skew the presented results. Therefore, we separately analyze these critical topologies in Section 3.1. In the experimental section, the mixing parameter ϵ takes the following four values:

- $\epsilon = \{1, 2/3, 1/3, 0\}$

As mentioned above, we apply the stopping criterion from [27] to bound the algorithm. In our experiments, its configuration is selected as follows:

- *accuracy* = $\{10^{-2}, 10^{-4}, 10^{-5}, 10^{-6}\}$
- *counter threshold* = {3, 5, 7, 10, 20, 40, 60, 80, 100}

As mentioned earlier, the performance of GMH with various initial configurations is tested over RGGs with the graph order $n = 200$ - see Figure 5 for their representatives. For the sake of high research credibility, we generate 100 graphs each with a unique topology where the algorithm is examined.

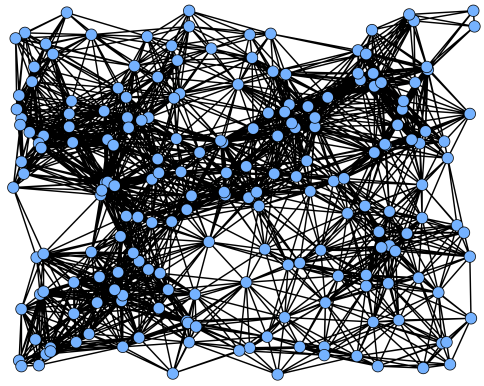


Figure 5: Representative of random geometric graphs

In the experimental part, we analyze GMH estimating three different aggregate functions, and therefore we partition the content of the experimental part into four scenarios as follows:

- ◇ *Scenario 1* - GMH estimates the arithmetic mean from all the initial inner states, which are independent and identically distributed random values of the standard Gaussian distribution, i.e.:

$$x_i(0) \sim N(0,1), \quad i = \{1, 2, ...n\} \tag{13}$$

- ◇ *Scenario 2* - the algorithm determines estimates of the sum calculated from all the initial inner states, which are IDD random values of the same distribution as in the previous scenario. The inner states are multiplied by the graph order n before GMH begins.
- ◇ *Scenario 3* - in this scenario, GMH also estimates the sum from all the initial inner states like in Scenario 2, compared to which the inner states are multiplied by the graph order n after the consensus is achieved.
- ◇ *Scenario 4* - the graph order n, i.e., the size of a network, is estimated in this scenario. One of the vertices is selected as the leader, whose initial inner state is equal to "1", meanwhile, the other ones initiate their initial inner state with "0" (in our analyses, the best-connected node is the leader), i.e.:

$$x_i(0) = \begin{cases} 1, & if\ v_i\ is\ the\ leader \\ 0, & if\ v_i\ is\ not\ the\ leader \end{cases} \tag{14}$$

The inverted value of the inner states is determined after the consensus is achieved.

To evaluate the performance of the algorithm, we apply two metrics:

- *Mean Square Error* (MSE): is used to quantify the precision of the final estimates and defined as follows [48, 49]:

$$\mathrm{MSE} = \frac{1}{n}.\sum_{i=1}^{n}\left(x_i(k_l) - \mathbf{1}^{\mathrm{T}} \times \frac{\mathbf{x}(0)}{n}\right)^2 \tag{15}$$

Here, k_l is the iteration when the consensus is achieved.

- *Convergence rate*: quantifies the algorithm speed (labeled as k_l) and is expressed as the number of the iterations for the consensus achievement among all the sensor nodes in WSN.

In all the shown figures, we depict and analyze the average of both metrics over 100 graphs for each *accuracy*, *counter threshold*, and the mixing parameter ϵ.

5 Experimental Section

In this section, we provide and discuss numerical experiments executed in Matlab2018b. As mentioned above, we extend the analysis of bounded GMH from [1], where this algorithm for distributed averaging is analyzed in terms of the estimation precision and the convergence rate. In this work, the extension lies in an analysis of GMH for distributed summing (either the initial inner states or the final estimates are multiplied by the graph order n) and GMH for graph order estimation. Also, GMH is compared to the average consensus algorithm. The experimental section consists of:

Table 1: List of figures provided in experimental section

Figure	Applied Metric	Scenario	Note
No. 6	MSE	No. 1	Cited from [1]
No. 7	Convergence rate	No. 1	Cited from [1]
No. 8	MSE	No. 2	
No. 9	Convergence rate	No. 2	
No. 10	MSE	No. 3	
No. 11	Convergence rate	No. 3	
No. 12	MSE	No. 4	
No. 13	Convergence rate	No. 4	

The first part is concerned with an MSE analysis of all the functionalities of GMH. From Figure 6, Figure 8, Figure 10, and Figure 12, it is seen that an increase in *counter threshold* and a decrease in *accuracy* result in a decrease in MSE, whereby the precision of the final estimates is increased in each scenario. Also, lower values of the mixing parameter ϵ ensure that the value of MSE is lower regardless of the estimated aggregate function. Furthermore, we can see that the algorithm achieves the highest precision in the case of estimating the graph order (i.e., in Scenario 4). The values of MSE, in this case, are from the range $[-110.7, -43.2]$[3]. The second highest precision is obtained when the arithmetic mean is estimated (Scenario 1). In this case, the values of MSE are from

[3]only MSE for $\epsilon = 0$ are provided - see Table 2 for the results obtained for the other values of the mixing parameter ϵ

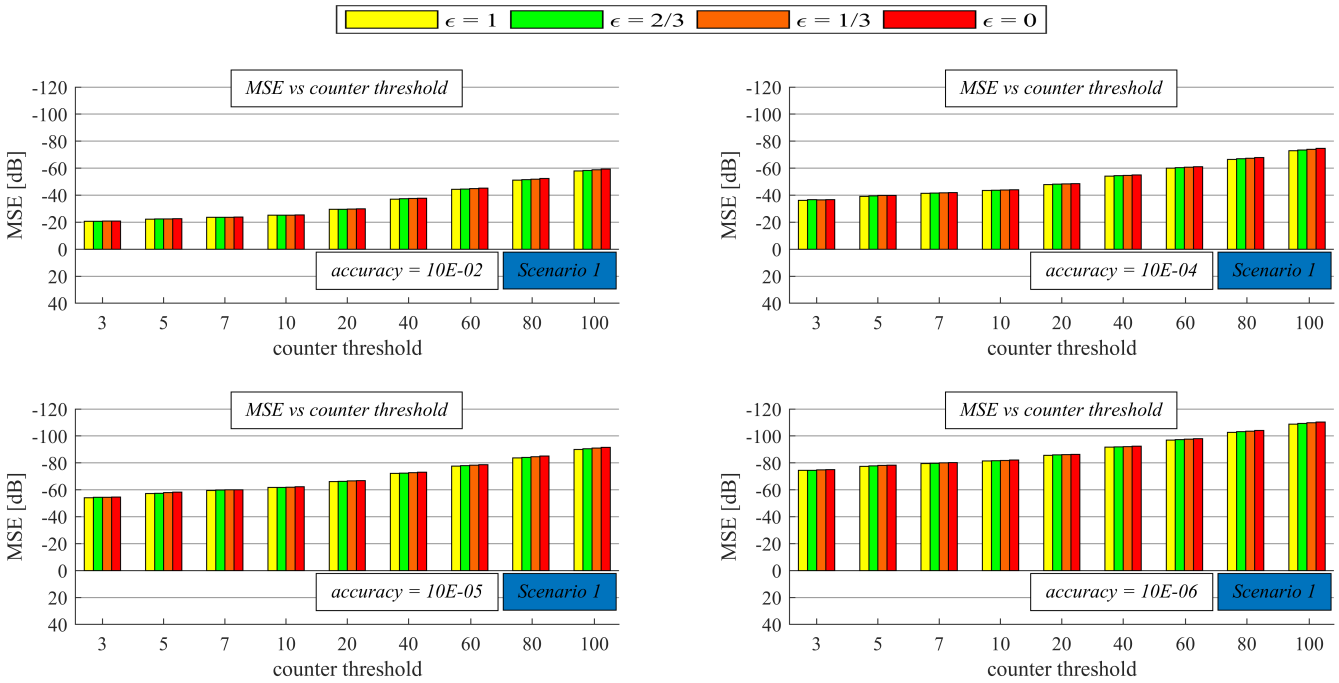


Figure 6: Estimation precision quantified by mean square error for various configurations of implemented stopping criterion and different mixing parameter – generalized Metropolis-Hastings for distributed averaging – Scenario 1

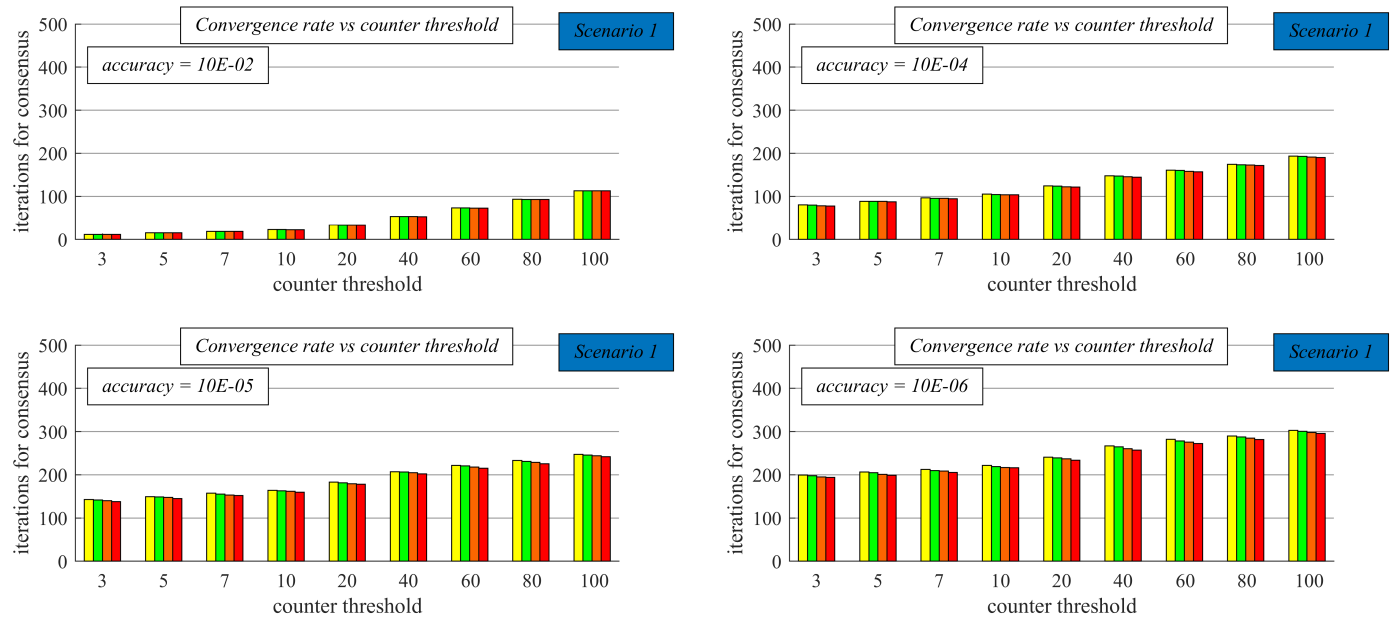


Figure 7: Convergence rate expressed as iteration number required for consensus achievement for various configurations of implemented stopping criterion and different mixing parameter – generalized Metropolis-Hastings for distributed averaging – Scenario 1

the range $[-110.4, -20.88]^3$. The worst estimation precision is observed in the case of sum estimation. Here, Scenario 2 (MSE is from $[-109.9, 4.288]^3$) outperforms Scenario 3 (MSE is from $[-64.36, 25.14]^3$), proving that multiplying the initial inner states with the graph order n ensures higher precision of the algorithm than multiplying the final estimates. As mentioned earlier, we analyze the average consensus algorithm for distributed summing and distributed graph order estimation in our previous work [8]. Compared to those results, it can be seen that GMH outperforms the average consensus algorithms for estimating both examined aggregate functions. For *counter threshold* = 100, *accuracy* = 10^{-6}, and ϵ ensuring the highest performance, GMH outperforms the average consensus algorithm by 12.78 dB in Scenario 2, by 77.31 dB in Scenario 3, and by 104.469 dB in Scenario 4. Moreover, an important fact

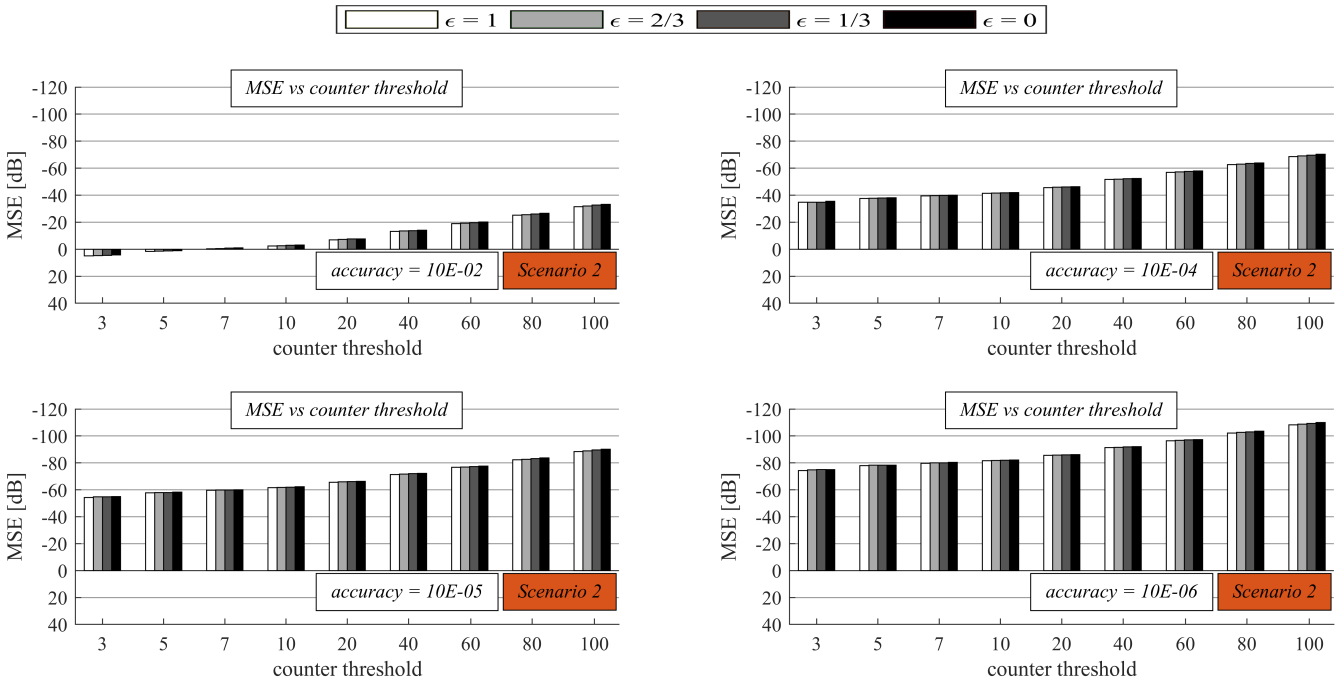


Figure 8: Estimation precision quantified by mean square error for various configurations of implemented stopping criterion and different mixing parameter – generalized Metropolis-Hastings for distributed summing – Scenario 2

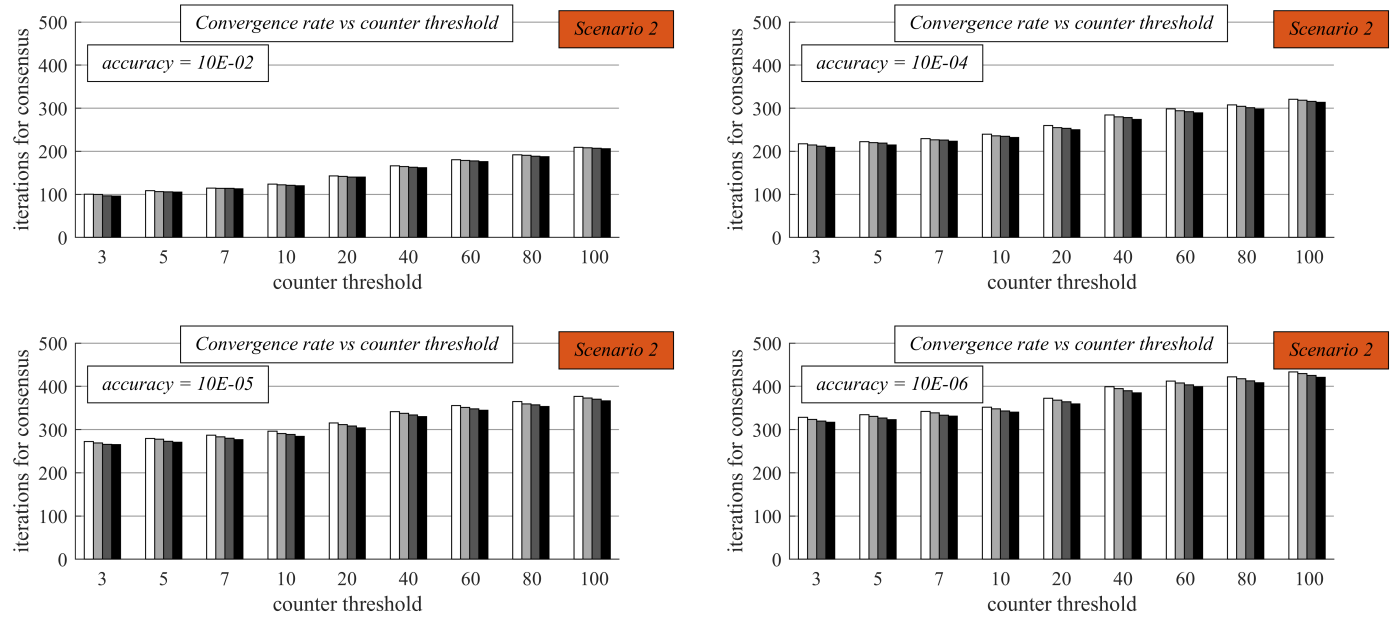


Figure 9: Convergence rate expressed as iteration number required for consensus achievement for various configurations of implemented stopping criterion and different mixing parameter – generalized Metropolis-Hastings for distributed summing – Scenario 2

identified in [8] is that the average consensus achieves a very low estimation precision for lower values of *counter threshold* and higher values of *accuracy* in the case of graph order estimation, making the algorithm unusable with these configurations of the stopping criterion. However, in this paper, we identify that this phenomenon is not visible in the case of GMH; therefore, this algorithm is much more appropriate for graph order estimation than the average consensus algorithm when the stopping criterion [27] is implemented. In addition, the value of the mixing parameter ϵ has a less intensive impact on MSE compared to the average consensus algorithm for distributed summing/distributed graph order estimation. In the following part, we turn our attention to the convergence rate of GMH expressed as the iteration number for the consensus achievement. From Figure 7, Figure 9, Figure 11, and Figure 13, we can

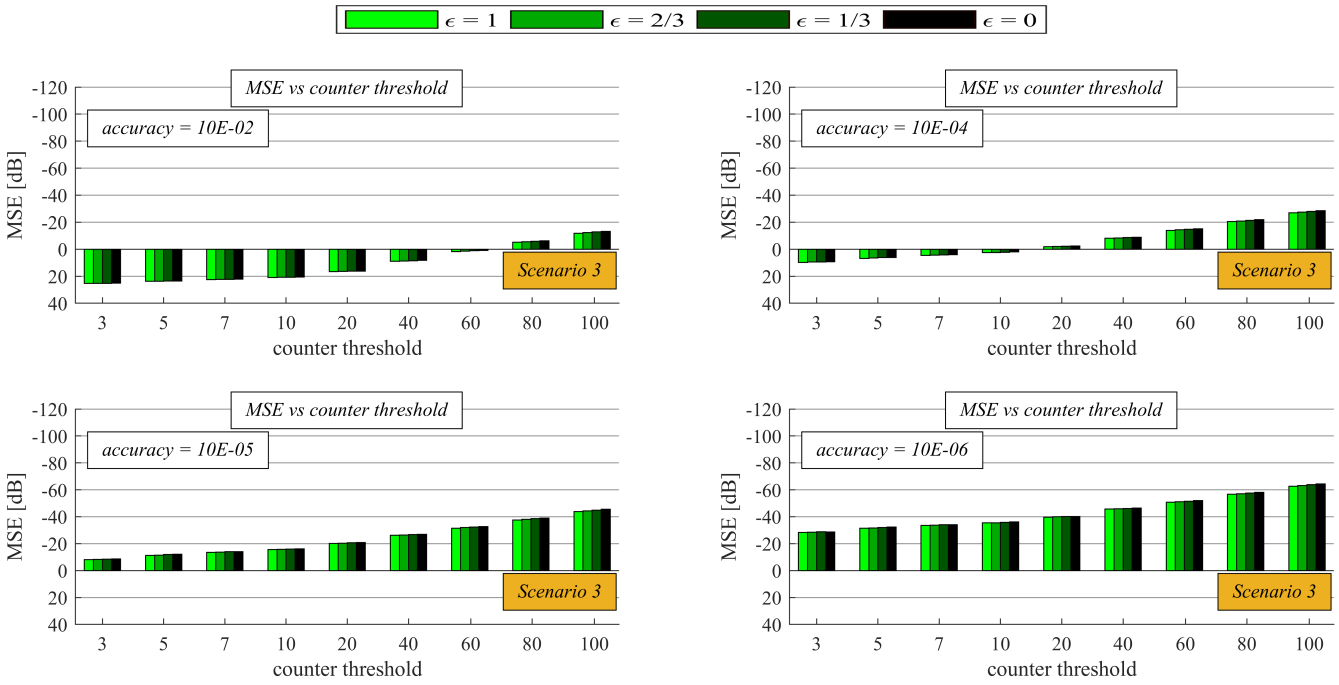


Figure 10: Estimation precision quantified by mean square error for various configurations of implemented stopping criterion and different mixing parameter – generalized Metropolis-Hastings for distributed summing – Scenario 3

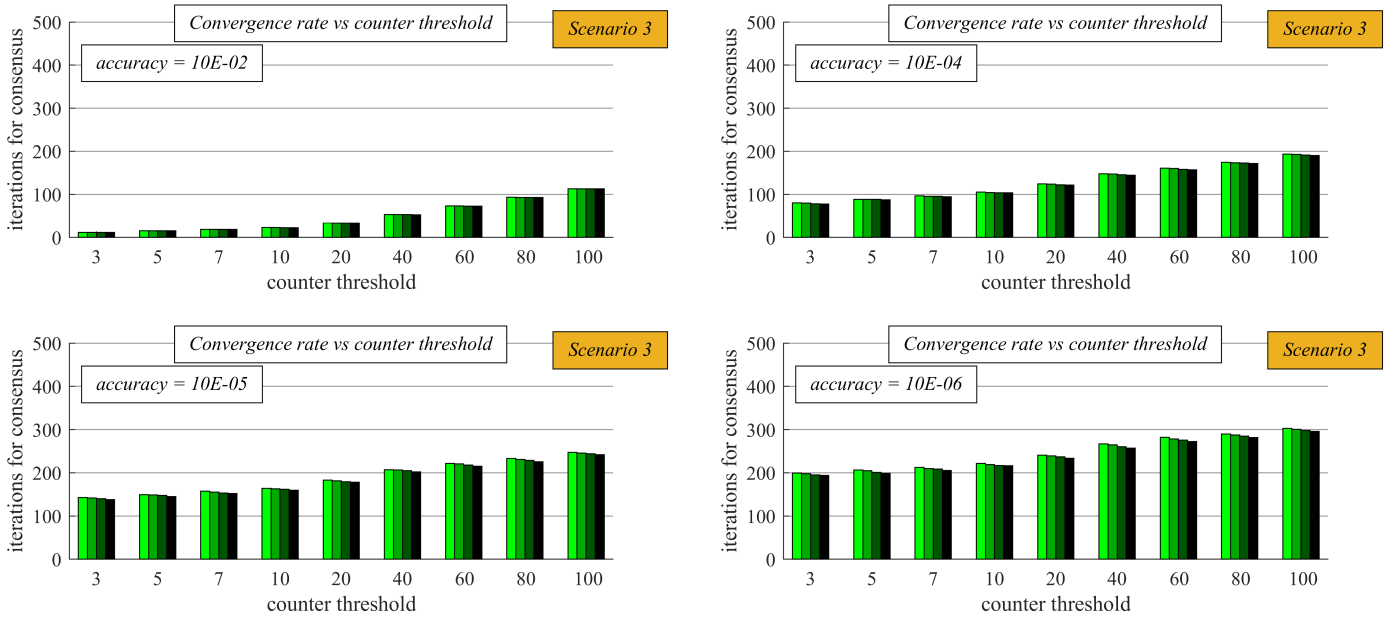


Figure 11: Convergence rate expressed as iteration number required for consensus achievement for various configurations of implemented stopping criterion and different mixing parameter – generalized Metropolis-Hastings for distributed summing – Scenario 3

see that an increase in *counter threshold* and a decrease in *accuracy* result in an increase in the number of the iterations required for the consensus; therefore, the convergence rate is decreased in each analyzed scenario. Again, a higher convergence rate in each scenario is obtained for lower values of the mixing parameter ϵ. Like in the previous analysis, Scenario 4 outperforms all three other scenarios also in terms of the convergence rate, and the convergence rate in this scenario is from the interval $[5, 240.5]^3$. As furthermore seen, the second-highest convergence rate is achieved by both Scenario 1 and Scenario 3 ($[11.55, 295.80]^3$); therefore, the number of the iterations for the consensus achievement is the same (with a few exceptions) in both scenarios. In contrast to the previous analysis, Scenario 2 ($[95.78, 420.9]^3$) is outperformed by Scenario 3, meaning that multiplying the final estimates ensures a higher convergence rate than multiplying the initial inner states. Compared to our pre-

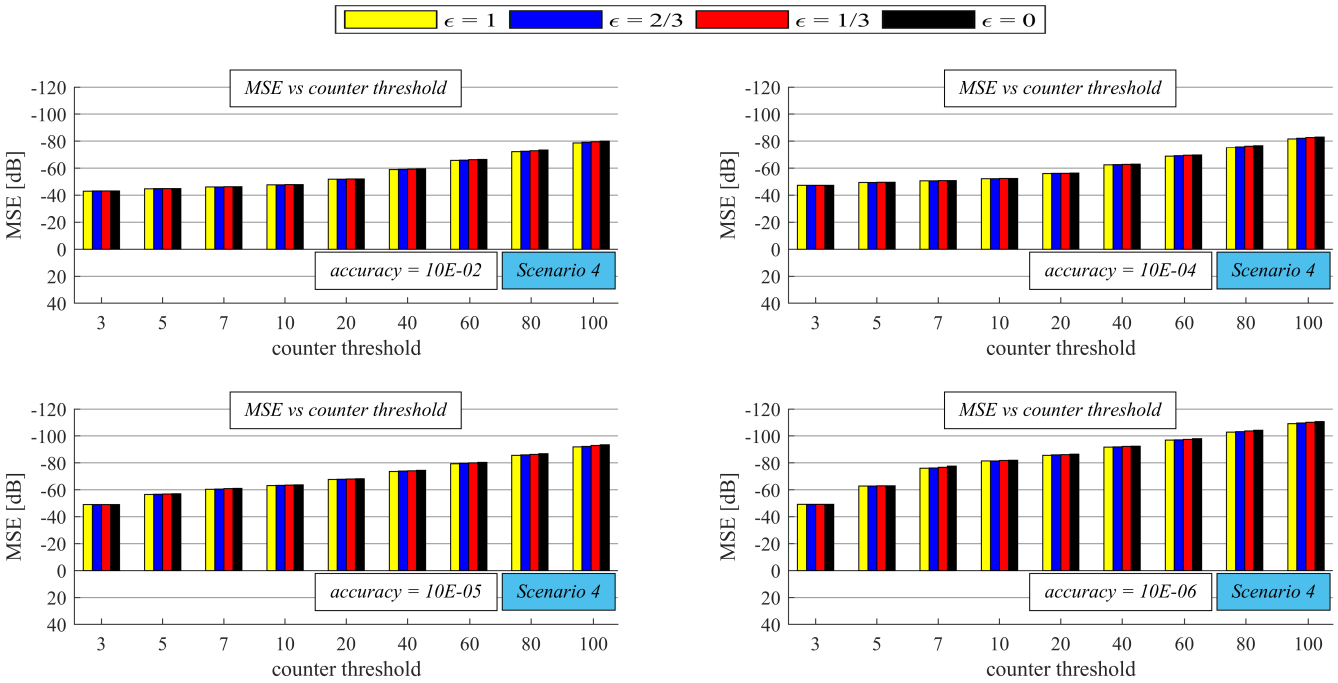


Figure 12: Estimation precision quantified by mean square error for various configurations of implemented stopping criterion and different mixing parameter – generalized Metropolis-Hastings for distributed graph order estimation – Scenario 4

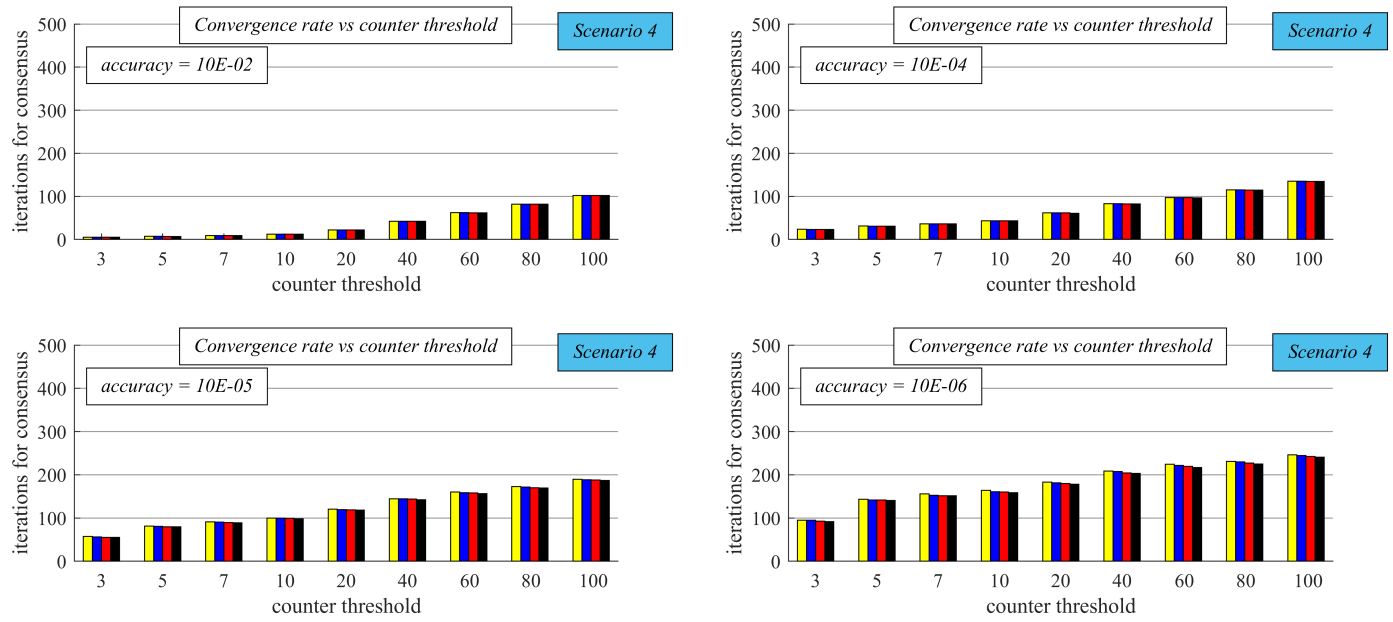


Figure 13: Convergence rate expressed as iteration number required for consensus achievement for various configurations of implemented stopping criterion and different mixing parameter – generalized Metropolis-Hastings for distributed graph order estimation – Scenario 4

vious work, GMH outperforms the average consensus algorithm also in terms of the convergence rate in both distributed summing and distributed graph order estimation. For *counter threshold* = 100, *accuracy* = 10^{-6}, and ϵ ensuring the highest performance, the convergence rate of GMH is greater than the convergence rate of the average consensus algorithm by 139.5 iterations in Scenario 2, by 87.3 iterations in Scenario 3, and by 52.5 iterations in Scenario 4. Also, like in the previous analysis, the value of the mixing parameter ϵ has only a marginal impact on the convergence rate in contrast to the average consensus algorithm examined in [8].

6 Conclusion

In this paper, we provide an extension of the analysis of GMH for distributed averaging over WSNs published in the conference proceedings of IEEE Eurocon 2019. The extension presented in this paper lies in an analysis of GMH for estimating also other aggregate functions, i.e., distributed summing and distributed graph order estimation. In our analyses, the algorithm with a different mixing parameter ϵ is bounded by a distributed stopping criterion with varied initial configurations (i.e., *counter threshold* takes the values (10^{-2}, 10^{-4}, 10^{-5}, 10^{-6}), and *accuracy* takes the values (3, 5, 7, 10, 20, 40, 60, 80, 100)). The experimental part consists of four scenarios (i.e., these functionalities are analyzed: distributed averaging, distributed summing - the initial inner states are multiplied by the graph order n, distributed summing - the final estimates are multiplied by the graph order n, a distributed graph order estimation). From the presented results, it is seen that an increase in *counter threshold* and a decrease in *accuracy* result in higher precision of the algorithm, however, the convergence rate expressed as the iteration number of the consensus achievement is decreased as a consequence. Thus, regardless of the estimated aggregate function, the highest precision of the final estimates and the lowest convergence rate is ensured for the configuration *accuracy* = 10^{-6} and *counter threshold* = 100, and vice versa the configuration *accuracy* = 10^{-2} and *counter threshold* = 3 results in the highest convergence rate and the lowest precision. Also, we identify that the optimal performance in terms of the estimation precision and the convergence rate is achieved for $\epsilon = 0$ (i.e., the lower bound of the mixing parameter ϵ), and an increase in ϵ causes lower precision and lower convergence rate. However, the value of the mixing parameter ϵ does not have an essential impact on the algorithm performance according to both applied metrics. In the experimental section, also the performances of GMH for estimating the arithmetic mean, the sum, and the graph order are compared to each other. The best performance is achieved in the case of graph order estimation in terms of both the estimation precision and the convergence rate (for $\epsilon = 0$, the values of MSE lie in $[-43.2, -110.7]$, and the convergence rate in $[5, 240.5]$). The second-best performance is achieved when the arithmetic mean is estimated (for $\epsilon = 0$, MSE is from $[-20.88, -110.4]$, and the convergence rate from $[11.55, 295.8]$). Thus, the lowest precision and convergence rate are achieved in the case of sum estimation. Here, multiplying the initial inner states instead of the final estimates ensures higher precision of the algorithm (for $\epsilon = 0$, MSE $[-109.9, 4.29]$, the convergence rate $[95.78, 420.9]$), meanwhile, multiplying the final estimates results in a higher convergence rate (for $\epsilon = 0$, MSE $[-64.36, 25.14]$, the convergence rate $[11.55, 295.8]$). The most important fact identified in this paper is that GMH achieves a high estimation precision regardless of the estimated aggregation function; therefore, this research identifies its applicability to estimating also two other aggregate functions in WSNs. In addition, we also compare GMH for distributed summing and distributed graph order estimation to the average consensus algorithm, thereby identifying that GMH is more appropriate for data aggregation over WSNs with the implemented stopping criterion than the average consensus algorithm in both applied metrics - the estimation precision and the convergence rate expressed as the iteration number necessary for the consensus achievement. GMH outperforms the average consensus (in the case that the performances of the most precise configurations are compared) by 12.78 dB and 139.5 iterations in Scenario 2, by 77.31 dB and 87.3 iterations in Scenario 3, and by 104.469 and 52.5 iterations in Scenario 4.

Thus, the final conclusion of the presented research is that the lower bound of mixing parameter ϵ ensures the highest performance in both the estimation precision and the convergence rate - so, in real-world implementations, $\epsilon = 0$ is recommended for use. Also, an increase in *counter threshold* and a decrease in *accuracy* cause the algorithm to be more precise but, on the other hand, decelerated regardless of the estimated aggregate function, meaning that the initial configuration of the stopping criterion has to be affected by the fact whether a WSN-based application requires more precise or faster data aggregation. The most important identified fact is that GMH is applicable to estimating all three examined aggregate functions in WSNs.

Conflict of Interest The authors declare no conflict of interest.

Acknowledgment This work was supported by the VEGA agency under the contract No. 2/0155/19 and by COST: Improving Applicability of Nature-Inspired Optimisation by Joining Theory and Practice (ImAppNIO) CA 15140. Since 2019, Martin Kenyeres has been a holder of the Stefan Schwarz Supporting Fund.

References

[1] M. Kenyeres, J. Kenyeres, "Applicability of Generalized Metropolis-Hastings Algorithm in Wireless Sensor Networks," in 18th International Conference on Smart Technologies (EUROCON 2019), 1–5, 2019, doi:10.1109/EUROCON.2019.8861554.

[2] A. Al-Karaki, A. E. Kamal, "Routing Techniques in Wireless Sensor networks: A Survey," Secur. Netw, **11**(6), 6–28, 2004, doi:10.1109/MWC.2004.1368893.

[3] G. Anastasi, M. Conti, M. Di Francesco, A. Passarella, "Energy conservation in wireless sensor networks: A survey," Ad Hoc Netw., **7**(3), 537–568, 2009, doi:10.1016/j.adhoc.2008.06.003.

[4] M. Kenyeres, J. Kenyeres, "Average Consensus over Mobile Wireless Sensor Networks: Weight Matrix Guaranteeing Convergence without Reconfiguration of Edge Weights," Sensors, **20**(13), 3677, 2020, doi:10.3390/s20133677.

[5] M. A. Mahmood, W. K. G. Seah, I. Welch, "Reliability in wireless sensor networks: A survey and challenges ahead," Comput. Netw., **79**, 166–187, 2015, doi:10.1016/j.comnet.2014.12.016.

[6] W. Ye, J. Heidemann, D. Estrin, "An energy-efficient MAC protocol for wireless sensor networks," in 21st Annual Joint Conference of the IEEE-Computer-and-Communications-Societies Location (INFOCOM 2002), 1567–1576, 2002, doi:10.1109/INFCOM.2002.1019408.

[7] B. Rashid, M. H. Rehmani, "Applications of wireless sensor networks for urban areas: A survey," J. Netw. Comput. Appl., **60**, 192–219, 2016, doi:10.1016/j.jnca.2015.09.008.

[8] M. Kenyeres, J. Kenyeres, "Distributed Network Size Estimation Executed by Average Consensus Bounded by Stopping Criterion for Wireless Sensor Networks," in 24th International Conference on Applied Electronics (AE 2019), 1–6, 2019, doi: 10.23919/AE.2019.8867009.

[9] D. Izadi, J. H. Abawajy, S. Ghanavati, T. Herawan, "A data fusion method in wireless sensor networks," Sensors, **15**(2), 2964–2979, 2015, doi:10.3390/s150202964.

[10] B. Yu, J. Li, Y. Li, T. Herawan, "Distributed data aggregation scheduling in wireless sensor networks," in 28th Conference on Computer Communications (IEEE INFOCOM 2009), 2159–2167, 2009, doi:10.1109/INFCOM.2009.5062140.

[11] L. Krishnamachari, D. Estrin, S. Wicker, "The impact of data aggregation in wireless sensor networks," in 22nd International Conference on Distributed Computing Systems Workshops (ICDCSW 2002), 575–578, 2002, doi:10.1109/ICDCSW.2002.1030829.

[12] N. Al-Nakhala, R. Riley, T. Elfouly, "Distributed algorithms in wireless sensor networks: An approach for applying binary consensus in a real testbed," Comput. Netw., **79**(14), 30–38, 2015, doi:10.1016/j.comnet.2014.12.011.

[13] G. Stamatescu, I. Stamatescu, D. Popescu, "Consensus-based data aggregation for wireless sensor networks," Control. Eng. Appl. Inf., **19**(2), 43–50, 2017, doi:10.1016/j.comnet.2014.12.011.

[14] D. Kempe, A. Dobra, J. Gehrke, "Gossip-based computation of aggregate information," in 44th Annual IEEE Symposium on Foundations of Computer Science (FOCS 2003), 482–491, 2003.

[15] K. Kenda, B. Kazic, E. Novak, D. Mladenic, "Streaming data fusion for the internet of things," Sensors, **19**(8), 1955, 2019, doi:10.3390/s19081955.

[16] G. B. Markovic, V. S. Sokolovic, M. L. Dukic, "Distributed hybrid two-stage multi-sensor fusion for cooperative modulation classification in large-scale wireless sensor networks," Sensors, **19**(19), 4339, 2019, doi:10.3390/s19194339.

[17] D. Merezeanu, M. Nicolae, "Consensus control of discrete-time multiagent systems," U. Politeh. Buch. Ser. A, **79**(1), 167–174, 2017.

[18] V. Oujezsky, D. Chapcak, T. Horvath, P. Munster, "Security testing of active optical network devices," in 42nd International Conference on Telecommunications and Signal Processing (TSP 2019), 9–13, 2019 doi:10.1109/TSP.2019.8768811.

[19] L. Xiao, S. Boyd, "Fast linear iterations for distributed averaging," Syst. Control. Lett., **53**(1), 65–78, 2004, doi:10.1016/j.sysconle.2004.02.022.

[20] M. J. Fischer, N. A. Lynch, M. S. Paterson, "Impossibility of Distributed Consensus with One Faulty Process," J. ACM, **32**(2), 374–382, 1985, doi:10.1145/3149.214121.

[21] Y. Zheng, Y. Zhu, L. Wang, "Consensus of heterogeneous multi-agent systems," IET Control. Theory Appl., **5**(16), 1881–1888, 2011, doi:10.1049/iet-cta.2011.0033.

[22] J. Gutierrez-Gutierrez, M. Zarraga-Rodriguez, X. Insausti, "Analysis of known linear distributed average consensus algorithms on cycles and paths," Sensors, **18**(4), 968, 2018, doi:10.3390/s18040968.

[23] S. S. Kia, B. Van Scoy, J. Cortes, R. A. Freeman, K. M. Lynch, S. Martinez, "Tutorial on Dynamic Average Consensus: The Problem, Its Applications, and the Algorithms," IEEE Control Syst., **39**(3), 40–72, 2019, doi:10.1109/MCS.2019.2900783.

[24] T. C. Aysal, M. E. Yildiz, A. D. Sarwate, A. Scaglione, "Broadcast gossip algorithms for consensus," IEEE Control Syst., **57**(7), 2748–2761, 2009, doi:10.1109/TSP.2009.2016247.

[25] J. C. S. Cardoso, C. Baquero, P. S. Almeida, "Probabilistic estimation of network size and diameter," in 2009 4th Latin-American Symposium on Dependable Computing (LADC 2009), 33–40, 2009, doi:10.1109/LADC.2009.19.

[26] V. Schwarz, G. Hannak, G. Matz, "On the convergence of average consensus with generalized metropolis-hasting weights," in 2014 IEEE International Conference on Acoustics, Speech, and Signal Processing (ICASSP 2014), 5442–5446, 2014, doi:10.1109/ICASSP.2014.6854643.

[27] J. Kenyeres, M. Kenyeres, M. Rupp, P. Farkas, "WSN implementation of the average consensus algorithm," in 17th European Wireless Conference 2011 (EW 2011), 139–146, 2011.

[28] M. Sartipi, R. Fletcher, "Energy-efficient data acquisition in wireless sensor networks using compressed sensing," in 2011 Data Compression Conference (DCC 2011), 223–232, 2011, doi:10.1109/DCC.2011.29.

[29] A.Chatterjee, P. Venkateswaran, "An efficient statistical approach for time synchronization in wireless sensor networks," Int. J. Commun. Syst., **29**(4), 722–733, 2016, doi:10.1002/dac.2944.

[30] A. Munir, A. Gordon-Ross, S. Lysecky, R. Lysecky, "Online algorithms for wireless sensor networks dynamic optimization," in 2012 IEEE Consumer Communications and Networking Conference (CCNC'2012), 180–187, 2012, doi: 10.1109/CCNC.2012.6181082.

[31] M. Nguyen, Q. Cheng, "Efficient data routing for fusion in wireless sensor networks," Signal, **1000**(8), 11–15, 2012.

[32] M. El Chamie, B. Açıkmeşe, "Safe Metropolis-Hastings algorithm and its application to swarm control," Syst. Control. Lett., **111**, 40–48, 2018, doi:10.1016/j.sysconle.2017.10.006.

[33] A. Vijayalakshmi, V. Bhuvaneswari, "Mobile agent based optimal data gathering in Wireless Sensor Networks," in 10th International Conference on Intelligent Systems and Control (ISCO 2016), 1–4, 2016, doi:10.1109/ISCO.2016.7726974.

[34] D. J. Irons, J. Jordan, "Geometric networks based on Markov point processes with applications to mobile sensor networks," in 2013 2nd International Conference on Mechanical Engineering, Industrial Electronics and Informatization (MEIEI 2013), 1–17, 2013.

[35] N. Ramakrishnan, N. Ertin, R. L. Moses, "Assumed density filtering for learning Gaussian process models," in 2011 IEEE Statistical Signal Processing Workshop (SSP 2011), 257–260, 2011, doi:10.1109/SSP.2011.5967674.

[36] M. R. Ahmed, H. Cui, X. Huang, "Smart integration of cloud computing and MCMC based secured WSN to monitor environment," in 2014 4th International Conference on Wireless Communications, Vehicular Technology, Information Theory and Aerospace and Electronic Systems (VITAE 2014), 1–5, 2014, doi:10.1109/VITAE.2014.6934449.

[37] H. Zheng, J. Li, X. Feng, W. Guo, Z. Chen, N. Xiong, "Spatial-temporal data collection with compressive sensing in mobile sensor networks," Appl. Soft Comput., **17**(11), 2575, 2017, doi:10.3390/s17112575.

[38] V. Schwarz, G. Matz, "Nonlinear average consensus based on weight morphing," in 2012 IEEE International Conference on Acoustics, Speech, and Signal Processing (ICASSP 2012), 3129–3132, 2012, doi:10.1109/ICASS.2012.6288578.

[39] S. Oh, P. Chen, M. Manzo, S. Sastry, "Instrumenting wireless sensor networks for real-time surveillance," in 2006 IEEE International Conference on Robotics and Automation (ICRA 2006), 3128–3133, 2006, doi:10.1109/ROBOT.2006.1642177.

[40] L. Martino, J. Plata-Chaves, F. Louzada, "A Monte Carlo scheme for node-specific inference over wireless sensor networks," in 2016 IEEE Sensor Array and Multichannel Signal Processing Workshop (SAM 2016), 1–5, 2016, doi:10.1109/SAM.2016.7569731.

[41] M. T. Nguyen, K. A. Teague, "Compressive sensing based random walk routing in wireless sensor networks," Ad Hoc Netw., **54**, 99–110, 2017, doi:10.1016/j.adhoc.2016.10.009.

[42] C. W. Liu, B. Andersson, A. Skrondal, "A Constrained Metropolis–Hastings Robbins–Monro Algorithm for Q Matrix Estimation in DINA Models," Psychometrika, **85**(2), 322-357, 2020, doi:10.1007/s11336-020-09707-4.

[43] R. Zhang, A. F. Cooper, C. De Sa, "Asymptotically Optimal Exact Minibatch Metropolis-Hastings," arXiv preprint arXiv:2006.11677, 2020.

[44] Y. Marnissi, E. Chouzenoux, A. Benazza-Benyahia, J. C. Pesquet, "Majorize-Minimize Adapted Metropolis-Hastings Algorithm," IEEE Trans. Signal Process., **68**, 2356–2369, 2020, doi:10.1109/TSP.2020.2983150.

[45] M. F. D'Angelo, R. M. Palhares, R. H. Takahashi, R. H. Loschi, L. M. Baccarini, W. M. Caminhas, "Incipient fault detection in induction machine stator-winding using a fuzzy-Bayesian change point detection approach," Appl. Soft Comput., **11**(1), 179–192, 2011, doi:10.1016/j.sysconle.2017.10.006.

[46] S. Büyükçorak, G. K. Kurt, A. Yongaçoğlu, "Inter-network cooperative localization in heterogeneous networks with unknown transmit power," in 28th Annual IEEE International Symposium on Personal, Indoor and Mobile Radio Communications (PIMRC 2017), 1–5, 2017, doi:10.1109/PIMRC.2017.8292505.

[47] V. Skorpil, J. Stastny, "Back-propagation and K-means algorithms comparison," in 8th International Conference on Signal Processing (ICSP 2006), 1871–1874, 2006, doi:10.1109/ICOSP.2006.345838.

[48] S. S. Pereira, A. Pages-Zamora, "Mean square convergence of consensus algorithms in random WSNs," IEEE Trans. Signal Processs, **58**(5), 2866–2874, 2010, doi:10.1109/TSP.2010.2043140.

Appendix

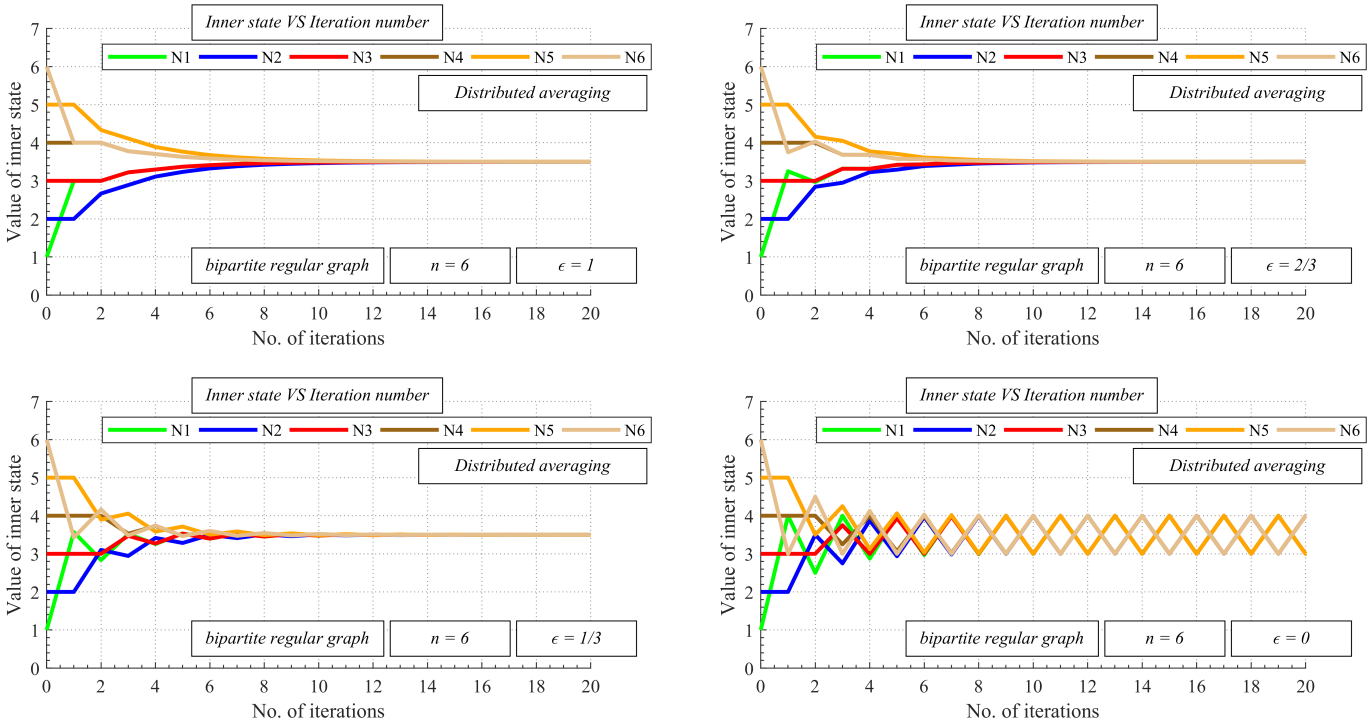


Figure 14: Evolution of inner states over bipartite regular graph for four values of mixing parameter ϵ

Table 2: Tables summarizing presented experimental results

Maximal and minimal precision of GMH quantified by MSE								
	Scenario 1		Scenario 2		Scenario 3		Scenario 4	
	Max	Min	Max	Min	Max	Min	Max	Min
$\epsilon = 1$	-108.7 dB	-20.69 dB	-108.3 dB	4.89 dB	-62.68 dB	25.33 dB	-109.1 dB	-43.03 dB
$\epsilon = 2/3$	-109.2 dB	-20.73 dB	-108.8 dB	4.68 dB	-63.22 dB	25.29 dB	-109.6 dB	-43.08 dB
$\epsilon = 1/3$	-109.8 dB	-20.8 dB	-109.4 dB	4.52 dB	-63.78 dB	25.22 dB	-110.2 dB	-43.14 dB
$\epsilon = 0$	-110.4 dB	-20.88 dB	-109.9 dB	4.29 dB	-64.36 dB	25.14 dB	-110.7 dB	-43.2 dB

Maximal and minimal convergence rate of GMH quantified by iteration number								
	Scenario 1		Scenario 2		Scenario 3		Scenario 4	
	Max	Min	Max	Min	Max	Min	Max	Min
$\epsilon = 1$	11.66 ite.	302.8 ite.	100.2 ite.	433.6 ite.	11.66 ite.	302.8 ite.	5.13 ite.	246 ite.
$\epsilon = 2/3$	11.61 ite.	300.5 ite.	99.87 ite.	429.6 ite.	11.61 ite.	300.5 ite.	5.09 ite.	244.5 ite.
$\epsilon = 1/3$	11.57 ite.	298.1 ite.	96.68 ite.	425.4 ite.	11.57 ite.	298.1 ite.	5.02 ite.	242.5 ite.
$\epsilon = 0$	11.55 ite.	295.8 ite.	95.78 ite.	420.9 ite.	11.55 ite.	295.8 ite.	5 ite.	240.5 ite.

ASTES

Advances in Science, Technology and Engineering Systems Journal
Vol. 5, No. 5, 237-244 (2020)
www.astesj.com
Special Issue on Multidisciplinary Sciences and Engineering

ASTES Journal
ISSN: 2415-6698

FPGA Acceleration of Tree-based Learning Algorithms

Haytham Azmi*

Microelectronics Department, Electronics Research Institute, Cairo, Egypt

ARTICLE INFO

Article history:
Received: 21 June, 2020
Accepted: 02 September, 2020
Online: 14 September, 2020

Keywords:
Acceleration
Machine learning
Decision tree
FPGA

ABSTRACT

Machine learning classifiers provide many promising solutions for data classification in different disciplines. However, data classification at run time is still a very challenging task for real-time applications. Acceleration of machine-learning hardware solutions is needed to meet the requirements of real-time applications. This paper proposes a new implementation of a machine learning classifier on Field Programmable Gate Arrays (FPGA). The proposed implementation utilizes the MicroBlaze soft-core processor on FPGA and uses the Advanced eXtensible Interface (AXI) bus to integrate the MicroBlaze with hardware peripherals. Experimental results shows that hardware-software co-design is a promising solution as it saves silicon area and provides a flexible configuration of decision tree algorithms at run time.

1 Introduction

The continuous growth of Internet of Things (IoT) applications that need real-time data analysis, such as video cameras in surveillance applications, live streaming videos on social media networks and sensor data from smart cities, is driving the demand for an efficient platform that can process this huge amount of data and discover hidden patterns.

When designers explore hardware options for big-data analysis, Graphics Processing Units (GPUs) and Field Programmable Gate Arrays (FPGAs) appear as two promising solutions for the implementation of machine learning applications. GPUs have been dominating the parallel computing market for a long time and their hardware solutions have been thoroughly tested in different industrial domains. However, FPGA solutions have been recently considered in many high performance Artificial Intelligence (AI) applications and showed an improved power consumption, compared to GPUs.

To choose the optimum implementation, designers need to answer several design questions and explore possible solutions at early design phases. Examples of these questions are: what is the maximum clock frequency that can be reached in the target hardware platform? How many General Purpose Input/Output (GPIO) pins that can be utilized by the target hardware platform? Does the target hardware platform support parallel processing and concurrency or not? what is the average power consumption of similar implementations on the target platform? etc. Designers must study these questions carefully at early deign phases. The choice of the hardware platform has a significant impact on the performance of the target applications.

FPGA-based implementations of machine learning classifiers provide an efficient solution for real-time applications that use deep learning algorithms for classification [1]. FPGA-based implementation helps system engineers design modular systems and execute several tasks concurrently, which helps in processing real-time data more efficiently. The implementation of machine learning classifiers on FPGA can be done in many different ways. This paper discusses these alternative implementation options and presents a case study of hardware implementation of a machine learning algorithm on FGPA.

This paper has two main contributions.

- First, we present a comparative analysis of different design approaches of machine learning classifiers in the literature. The paper discusses technical implementation challenges and proposes practical solutions that help designers better implement efficient classifiers.
- Second, we propose a hybrid implementation of a machine learning, tree-based classifier. The proposed implementation utilizes hardware-software co-design approach that integrates a soft-core microprocessor on FPGA. The soft-core is used along with other digital blocks to build an area-efficient machine learning classifier. As a proof of concept, we use a MicroBlaze Xilinx IP core on Virtex-UltraScale FPGA to run the main tree-based algorithm and report its implementation details.

The novelty of the proposed implementation is that it bridges the

*Corresponding Author: Haytham Azmi, Microelectronics Department, Electronics Research Institute, Cairo, Egypt, haitham@eri.sci.eg

Table 1: Some of the proposed work in the literature that discusses the hardware implementation of machine learning classifiers.

N	Dataset	Classification	Target Platform	Performance	Reference
1	IBM DataQuest Generator	Decision Tree (Gini calculation)	PowerPC	5.58 times	**[2]**
2	UCI repository	Adaboost algorithm	VHDL Generator	5 to 10 ns per decision	**[3]**
3	Spambase UCI repository	Decision Trees Majority voting	Xilinx Virtex 5 XC5VLX110T	N/A	**[4]**
4	EEG data in house	Soft Decision Tree	Xilinx Spartan 3	98.1%	**[5]**
5	From **[6]**	Decision Tree (image-based)	software tool	75 million samples per second	**[7]**
6	From **[8]**	C4.5 classifier	Xilinx Virtex-6 XC6LX670	97.92% accuracy	**[9]**

gap between hardware and software when dealing with machine learning classifier implementation. Our solution addresses several challenges related to creating a customized machine learning classifier on FPGA from a raw dataset file. We discuss these challenges in detail in this paper and explain how researchers can use our proposed implementation to build low-cost, high-performance classifier on FPGA.

The rest of this paper is organized as follows. Section 2 presents the related work in the literature. Section 3 discusses the hardware implementation of the decision tree algorithm. Section 4 presents the results of the experimental work. Section 5 draws our conclusions and suggests new directions for future work.

2 Related Work

Utilizing hardware solutions for machine learning classification has been a challenging task for many researchers and system engineers. Researchers targeted different platforms, such as microprocessor-based systems, FPGA-based designs and parallel computing techniques to design efficient hardware classifiers for real-time applications. Table 1 highlights some of the proposed work in the literature that discusses the hardware implementation of machine learning classifiers. In this section, we highlight examples of the related work in more details.

In [2], the authors used *Gini* score calculation to develop a decision tree model. Authors went through two phases to build a decision tree model. First, they chose the splitting attribute and a split index for the root. Then, they split the children records based on the the first phase's decision. The proposed implementation in [2] recursively repeated this process until a stopping criterion is met [2]. In practical applications, Conventional Neural Networks (CNN) are trained off-line using training datasets through the back-propagation process. Following that, the trained CNN models are used to recognize images using the feed-forward process. Since there is currently a trending approach in recognizing images in real-time applications, the execution time of the feed-forward process is the most significant factor when it comes to performance evaluation [10]. In [11], the authors presented a software tool that can automatically generate a tree classifier Verilog code from python scripts. Authors used SciKit-Learn machine learning library to build the trained model and calculate the threshold values for the tree nodes. Following that, the tool is used to generate a Verilog code for decision trees and random forests [11].

In [12], the authors presented an implementation of Q-learning with Artificial Neural Networks (ANN) on FPGA for real-time applications that have latency and power constraints. The proposed implementation reduced processing time by utilizing the parallel structure of FPGA logic units. In [12], the authors demonstrated the implementation of a single neuron Q-learning accelerator as well as Multilayer Perception (MLP) Q-learning accelerator on a Virtex 7 FPGA. The authors discussed the architecture of the implementation in their paper [12]. However, when they evaluated the performance, it was compared to a CPU-based implementation. The speedup in performance was completely expected because of the concurrency achieved by FPGA. The paper did not provide any information about the speedup in performance when compared to GPU implementation [12].

In [13], the authors proposed a method to optimize CNN by utilizing four techniques: 1) fixed-point quantization to minimize calculations, 2) approximation of activation function to reduce the complex mathematical operations, 3) pipelining and parallelization of loops and tasks to speedup execution time, and 4) memory reorganization to enhance fetch time. Authors targeted the LeNet-5 architecture, which is a neural network architecture for handwritten and machine-printed character recognition [14]. They implemented their proposed accelerator on a Xilinx FPGA and used Zynq-7000 platform. The paper reported an operating frequency at 166MHz, which is not a useful measure for high performance applications. However, the paper reported that the proposed implementation can reduce the consumed energy by 93.7% compared to a GPU implementation [13]. The authors in [15] designed a decision tree classifier to recognize letters and digits. Xilinx Zynq SoC is used by the authors as a target hardware platform and Vivado high level synthesis is used as a development tool with C/C++ synthesis. Authors verified the correctness of the generated HDL code using C/RTL co-simulation [15].

In [16], the authors proposed a pipelined design that is partitioned into two stages. The first stage of the proposed design determines the conditions of the decision tree for which the classification can be done. The second phase of the proposed design used a pipelined data path for parallel execution.

Other implementations have been also proposed in the literature. In [17], the authors presented an automatic modulation classifier to identify the signal modulation format for electronic applications. In [18], the authors presented a hybrid classification engine using CPU and FPGA shared memory.

Although there are several proposed solutions in the literature for the hardware implementation of machine learning classifiers, the FPGA design and implementation of such classifiers were not discussed in proper details. We try to address this gap in our paper to present a hardware-software co-design implementation of a machine learning classifier on FPGA.

3 Hardware Implementation of Decision Trees

Designers explored various ways to implement decision tree algorithms on hardware platforms. In this section, we first highlights the basic concepts of implementing a single node on FPGA and how the synthesis tool interprets the HDL model and convert it into logic gates. Then, we discuss the common methodologies used in hardware implementation of such algorithms.

Classifying instances based on a training dataset has been used extensively to mine hidden patterns within detests [19]. One of the most popular classification algorithms is the tree-based classifier, where the main goal is to construct a tree from a labeled training dataset. The decision tree consists of a root node and children nodes. Each node represents a test on a feature, whereas each branch represents the outcome of a test, and each leaf node represents a class label. Figure 1 shows an example of a decision tree.

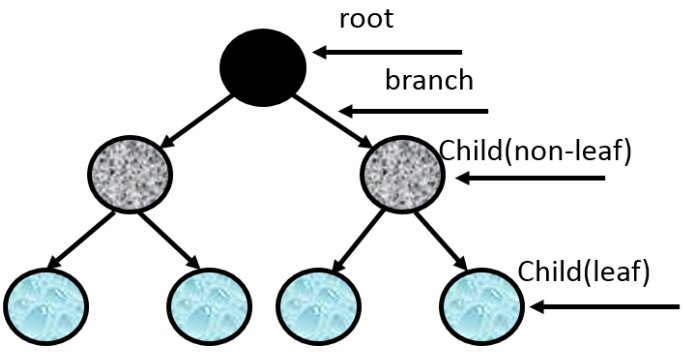


Figure 1: An example of a decision tree.

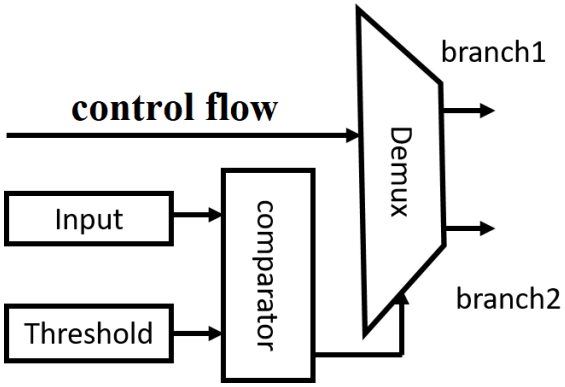
Decision trees can be constructed using different algorithms. The most critical design parameter is how to choose the feature at each node that best splits the dataset. The classification algorithms in the literature use different evaluation metrics to perform two design decisions.

1. Which feature should be used to split the dataset records at each node?
2. What is the the threshold value that should be used to split the dataset records at each node?

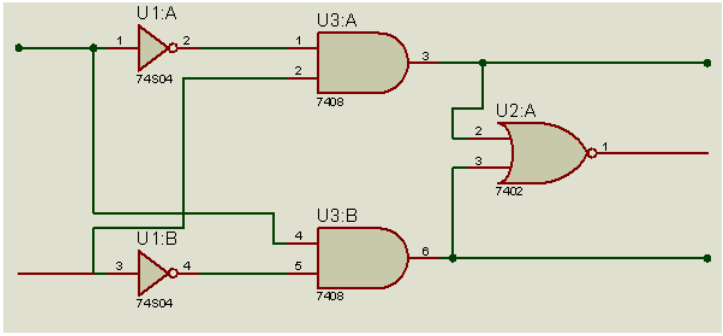
Examples of these evaluation metrics include using Gini index [20] and information gain, which is based on the concept of entropy [21]. Examples of decision tree algorithms include ID3, C4.5, CART, CHAID, and MARS [22]. ID3 is used in this paper as an example of a decision tree implementation. Other algorithms, such as C4.5 and CART, can be implemented using the same approach

A node in a decision tree algorithm represents a branching condition. If the input meets the condition, the flow of the tree goes through a certain path. Otherwise, a different path is selected. The tree can have a binary node or a multi-threshold node. Binary nodes branch out into two paths only, whereas multi-threshold nodes can branch out into more than two paths.

Figure 2 shows an example of the internal structure of a simple binary node. Figure 2a shows a block diagram of a branching circuit for a single node. The node first checks the input value and compares it to a given threshold value. The comparator then sends the result to a demultiplixer circuit that directs the flow of the control signals into one of two branches. A simple implementation of a one-bit comparator circuit is shown in Figure 2b. The comparator is usually designed to deal with n-bit values but Figure 2 is used here to simplify the concept.



(a) A block diagram of a branching circuit for a binary node



(b) Equivalent schematic of a branching circuit of a binary node

Figure 2: An example of a branching circuit of a binary node.

Since we are targeting Xilinx UltraScale architecture, we conducted an extensive study of the Configurable Logic Block (CLB) architecture of Xilinx UltraScale family. The CLB is the main building block that is used to implement all combinational and sequential logic of our proposed tree-base classifier. Each CLB unit consists of a group of logic elements along with an interconnect resource to connect all logic units. We followed the UltraScale Architecture Configurable Logic Block user guide in [23] to make sure that the synthesis tool will interpret the HDL code correctly and will generate an optimum logic design for the target application.

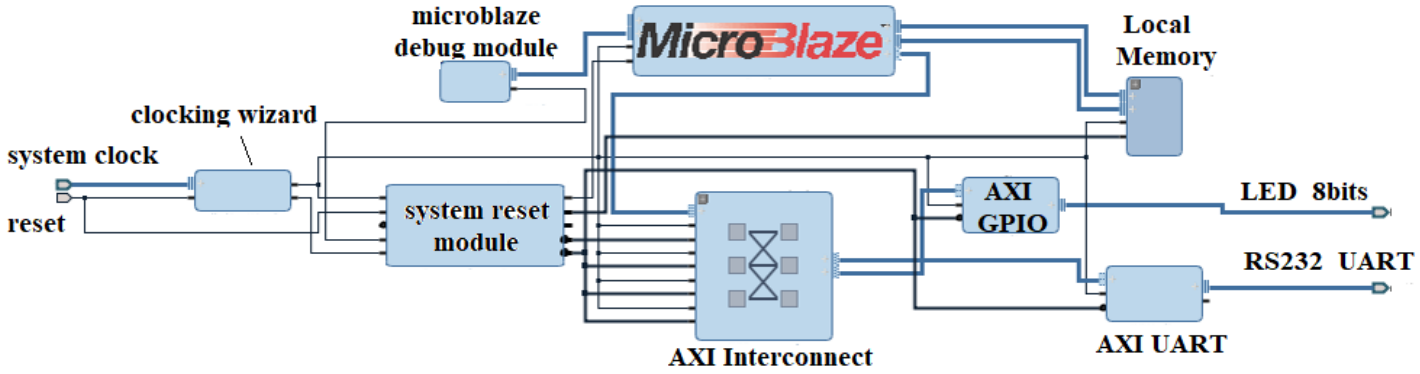


Figure 3: An example of a MicroBlaze interface circuit.

3.1 Implementation Challenges

Researchers utilized different techniques to implement machine learning algorithms on FPGA. Two common approaches are mostly cited in the literature. The first approach is writing the machine learning algorithm in a high level language, such as C, and then using a synthesis tool to convert from a high level language to a hardware description language. The second approach is targeting a structure-based design. Then, building all components in hardware and connecting these modules using port mapping. Each one of these two techniques has its advantages and disadvantages. Moreover, there are different implementation challenges associated with each approach. In this section, we discuss these challenges in details and explore different solutions to address them.

High Level synthesis (HLS) tools provide a mechanism to auto-generate HDL codes from high level languages, such as C, C++ and SystemC. HLS tools can save development time when implementing complex algorithms that can be easily represented in C language, for example. However, the majority of these tools do not provide complete support to generate recursion function in hardware description languages. Recursion comes with a difficult synthesis challenge by nature because the synthesis tool does not know when the exit condition will happen and hence can not predict the complexity of the hardware circuit that should be generated to implement the recursion function. For example, to generate a tree-based classifier, it is important that the synthesis tool knows the maximum depth of the tree. Otherwise, the tool can't support the generation process of the tree hardware logic at run time if the depth is unknown.

This limitation is blocking the usage of HLS tools in such scenarios. Researchers created various techniques to address this problem by developing recursive functions as an Embedded Domain Specific Language (EDSL) in C++ [24]. Authors in [24] addressed the recursion limitation by utilizing the C++ front-end of an HLS compiler [24]. However, this approach is not easy to integrate with HLS tools, such as Vivado, as the library needs to be re-customized every time the tool is used. This limitation makes it difficult to rely on this approach as a permanent solution, especially for real-time applications that require recursions to operate at run-time. Another proposed solution is having a maximum estimated depth of the tree and generating the digital logic for any tree-based classifier based on that maximum depth. However, this solution might fail if the target application requirements exceed the maximum depth. Moreover, if the requirements were within the maximum depth, the generated logic will have extra gates that are not used in the design, which causes an overhead area cost.

Another approach is utilizing structural implementation by dividing up the machine learning classifiers into separate blocks. These blocks are designed to deal with data-input, feature engineering, dataset training, and classification or prediction. For each block, designers write the hardware description code that implements the functionality of the intended block. The design is then connected together through port mapping as one complete design and used to process input data and solve machine learning problems.

This approach is proven to provide an optimized design for the target problem. However, the design process forces engineers to make very rigid design decisions to handle the target training set. For example, when generating a tree, designers can build a simple tree design and then re-instantiate this block through a pipeline structure. The challenge with this design method is that it causes a significant delay during the training phase because it executes the learning tasks sequentially. On the same context, designers can expand the tree to the required depth using hardware generators. This approach has a technology-based limitation as the maximum tree depth must be defined based on the target available silicon area.

3.2 Proposed Hardware/Software Co-design

Our proposed design aims at addressing the limitations of previous designs that are discussed earlier. We utilize the hardware-software co-design approach which gives designers the ability to execute several tasks in parallel while benefiting from the conventional implementation of complex recursive functions. This approach has been adopted previously by several researchers. The authors in [25] presented various implementations of decision trees using a sequence of universal nodes.

We explored soft and hard cores offered by Xilinx technology and we chose to use the the MicroBlaze IP core as our main processor [26]. MicroBlaze is built as a soft processor, RISC-based architecture, with a rich set of instructions that are optimized for embedded applications [27]. The MicroBlaze solution offers complete flexibility to select the needed peripheral, bus interfaces for memory and GPIO, and the ability to implement complex recursive functions that are needed in the machine learning training phase [27].

To complete the machine learning system design, we utilized other IPs to be able to train the network using different types of datasets. The soft-core is wrapped up by a Verilog code so that it can interact with the other components in the system. The soft-core is configurable in terms of number of ports, interrupt vectors, programmable timers, size of memory, and the maximum operating frequency.

Figure 3 shows a schematic diagram of the MicroBlaze interface circuit. The IP comes with default ports for interrupt, debug, clock , reset, DLMB, ILMB and AXI interfaces. Designers have several options when it comes to the configuration of the MicroBlaze interface. Designers can choose to integrate AXI or ACE bus and can also enable or disable the debug interface. To speed up the performance, designers can use instruction and data caches. The MicroBlaze is connected to its peripherals through an AXI interconnect.

Figure 4 shows that AXI interconnect can be configured in two different ways. First, the number of master/slave connections can be programmed to generate the required interfaces. Second, the interconnect optimization strategy can be set to minimize the area or maximize the performance, which gives the designer the ability to choose various strategies based on the application requirements.

Having a standard interface like AXI bus allows designers to easily integrate other hardware peripherals/IPs to the design easily. Since AXI is part of the Advanced Microcontroller Bus Architecture (AMBA) family, it will also easy to integrate any peripheral/IP that can be connected to AXI through bridges, such as APB, ACE, etc.

We conducted an extensive study of the architecture of the target FPGA to analyze the propagation delay through each LUT regardless of the function implemented, which is done for all classification functions.

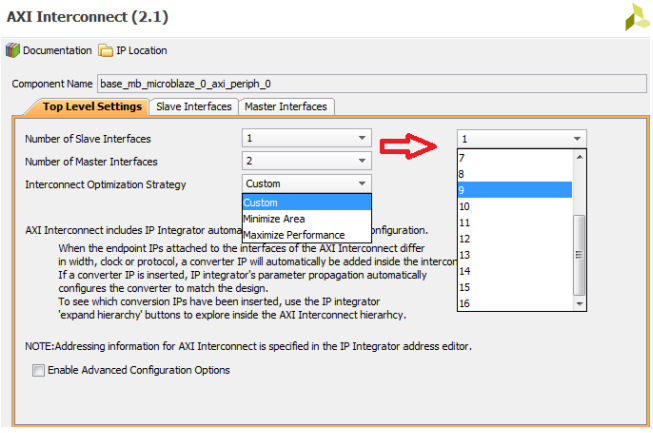


Figure 4: A programmable AXI interconnect control window from Xilinx.

To implement a hardware/software co-design on Virtex UltraScale, we use Vivado software tool. After completing the software programming in the Software Development Kit tool, we had to generate the .elf file and associate it with the MicroBlaze IP in Vivado to complete the integration process. The association process had several technical challenges. For example, the default block RAM size was one big limitation. We addressed this issue by allocating extra memory for the MicroBlaze software code.

The integration between hardware logic design and software code that runs on a microprocessor achieved several performance enhancement goals. First, the hardware logic of the entropy calculation and tree splitting is done using combinational logic gates that execute in parallel, which speeds up the processing of the tree generation during training and the classification during testing. The software code that runs on the MicroBlaze soft-core addressed the recursion task during the generation of the tree structure. Therefore, this integration was a major factor in improving the overall performance of the proposed design.

4 Experimental Work

The proposed system is designed to deal with different types of datasets that might need further processing. Figure 5 shows various data types that need to be considered before reading dataset for processing. Data can be qualitative or quantitative. Qualitative data includes

- nominal data, such as variables with no ranking sequence or inherent order like race and gender, etc.
- ordinal data, such as variable with an order like blood group, etc.
- binary data that has only two options, such as yes and no.

On the other hand, quantitative data includes

- discrete data, such as finite numbers of values that can not be classified meaningfully, etc.
- continuous data is information that can be measured on a scale and can be classified meaningfully, etc.

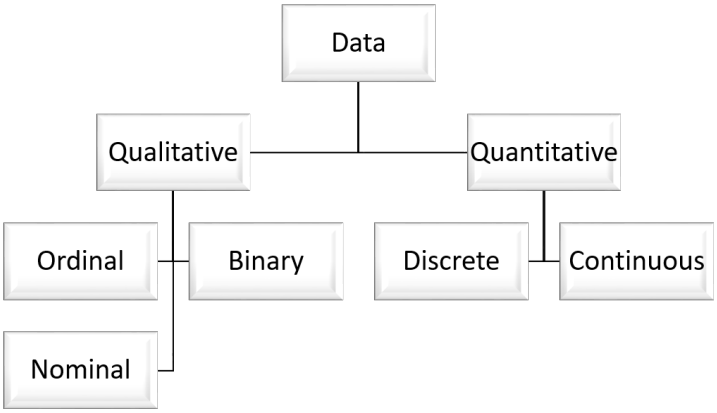


Figure 5: An explanation of the different data types that should be handled by the proposed design.

A pre-processing step must be executed first in order to convert the input data, into a standard format that is easy to process by the machine learning engine. One possible solution is to convert all various data types into binary format. This conversion is a very significant step to ensure that all input data types are converted to a machine-friendly format.

Figure 6 shows an example of the conversion process from nominal and numerical types of data to binary data type. The conversion

process is done as follows. First, each feature is examined to extract its list of all possible values. For example, the first column in Figure 6 (i.e. currency) can take three values: 1A, 5A and 6A. For each one of these values, we create a separate feature in the dataset in binary format. The new feature indicates whether each specific instance in the dataset has the currency set to that value or not. Since the currency feature has three values. Then, three new binary features are created to replace it. As shown in the example in Figure 6, the currency feature is replaced in the conversion by three binary features: currency(1), currency(5), and currency(6).

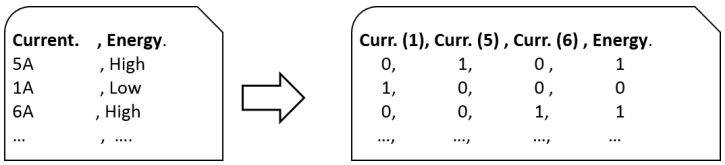


Figure 6: An example of converting nominal to binary format.

The number of features in Figure 6 for the output set will most likely increase based on how many nominal values are found in each feature. This conversion process helps researchers get an early estimation of the required memory blocks that should be allocated to host and process the training set.

4.1 Choosing the most significant feature

The most important decision in building a decision tree is choosing the root element that best distinguishes different patterns base on a certain threshold. The tree structure helps in building a model that classifies instances by navigating through various nodes in the tree until reaching one of the leaf nodes [28]. We use the information gain in this paper as our target evaluation metric so that the feature with the highest information gain is selected as the root element. The children nodes are then generated recursively. We continue to split the tree until we reach the decision nodes. The information gain calculations are based on the impurity level calculations in a set of samples. The formula used to calculate the entropy is given by [28]:

$$Entropy = -\sum_{i} P_i log_2 P_i \quad (1)$$

Where P_i is a probability of the class i relative to the total number of samples in the dataset.

The MicroBlaze processor is used to complete the calculations of the information gain as part of the software implementation of the target classifier. Feature selection plays a major role in improving the success rate of the decision tree classification. We conducted a comparative analysis to check which features are highly correlated and which features are causing overlaps that reduces the classification accuracy.

4.2 FPGA Implementation

FPGA implementation goes through various steps. First, we compile the code, then we simulate the design to make sure that the design functions correctly. Following that, we perform design synthesis to convert the design into equivalent logic gates. After synthesis, we perform post-synthesis simulation to ensure that the setup, hold, and propagation delays of the used gates don't affect the functionality of the design. Then, we perform the translation, mapping, place and route steps. Finally, we perform post-layout simulation and generate the bitstream file that is used to program the target FPGA.

Table 2 summarizes the results of the FPGA implementation of the proposed design. Due to the utilization of the MicroBlaze soft-core, we used limited resources from the target FPGA. Figure 7 presents a snapshot of the software tool that shows the placement and layout of the generated cells on the target FPGA. Figure 7 highlights the layout utilization percentage when implementing the proposed design in the target FPGA. The layout confirms the synthesis results that such a design doesn't require a lot of silicon area when implemented using the proposed SW/HW co-design approach. This is due to the utilization of the MicroBlaze software core, which saves a lot of silicon area during the implementation process. Figure 8 shows the statistics of on-chip components used from slice logic to implement the interface circuit with the MicroBlaze soft-core. It is clear from the figure that look-up-tables and registers constitute the majority components used from the slice logic in the FPGA.

Table 2: Implementation results

N	Item	Measure
1	Total On-Chip Power (W)	0.232
2	Dynamic (W)	0.154
3	Device Static (W)	0.151
4	Effective TJA (C/W)	1.7
5	Max Ambient (C)	84.5
6	Junction Temperature (C)	25.5
7	Slice Logic	3542
8	Block RAM	9
9	MMCM	2
10	I/O	14

We studied several implementations in the literature to compare the implementation of our proposed solution to previous implementations in the literature. We found out that it is difficult to make a one-to-one comparison due to three reasons. First, the target FPGA in the published work in the literature is different from ours. Therefore, the hardware utilization and used resources will not use the same base-reference to report the results, which makes it difficult to compare one implementation to another.

Second, there is no standard benchmark for dataset/classifier pair that is used across different implementations in the literature. Therefore, we could not implement a reference dataset/classifier pair to make a fair comparison. Third, the results are reported in different formats in the published papers. Few authors used utilization ratios, whereas others created their own cost unit formulas. Hence, the performance evaluation criteria are not the same across different publications. Although these factors affect the correctness and acc-

Table 3: Comparison with other implementation in the literature.

N	Implementation	Used Hardware	Implementation Main Finding	Reference
1	Gini-based decision tree	Xilinx Virtex-II Pro-based	31% minimum utilization	[29]
2	Hyper-rectangle hardware implementation	Xilinx Virtex (unknown version)	minimum 18 custom cost unit	[30]
3	Various architectures	Xilinx Virtex 5	SMpL needs 56% less resources	[31]
4	Multiple classifier systems,	Xilinx Virtex 5	95.8% accuracy - custom performance	[32]
5	Random Forest	GPU GeForce GTX 280	GPU implementation evaluates the forest in about 1% of the time compared to CPU	[33]
6	Random Forest	NVIDIA Tesla C2050	speed increases at least 300x compared to CPU	[34]
7	Proposed HW-SW co-design	Xilinx UltraScale	Less than 1% utilization of resources	This paper

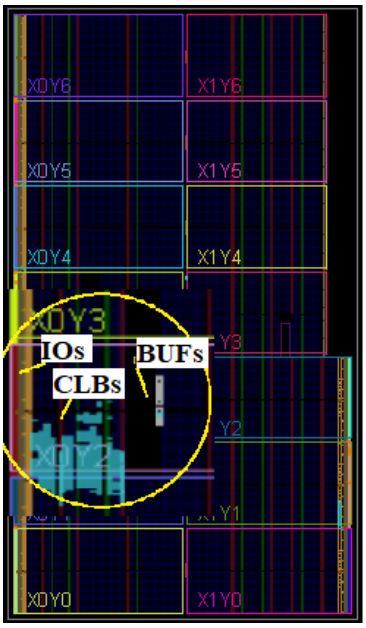


Figure 7: A snapshot of the FPGA placement and routing of the target design.

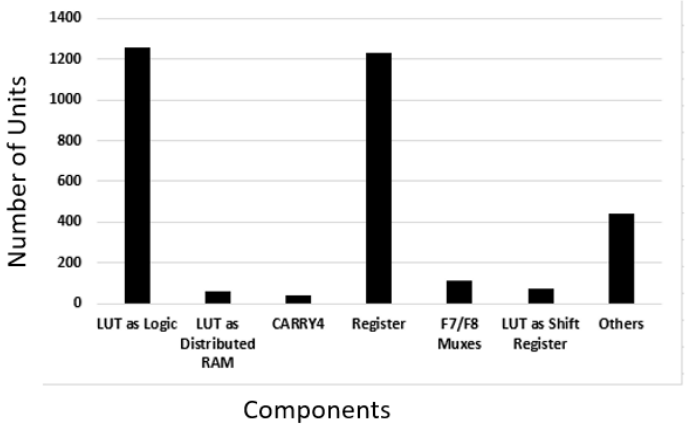


Figure 8: On-chip components used from slice logic.

curacy of the comparison, we reported the implementation results of various published work in Table 3. We presented these findings in Table 3 to show the different ways authors reported their implementation results of tree-based classifiers on FPGA. We also added GPU implementation results as examples of alternative hardware implementations. Experimental results show that the proposed design utilized less than 1% of the FPGA resources when implemented on Xilinx Virtex UltrScale FPGA.

5 Conclusion and Future Work

This paper presented a promising software-hardware co-design architecture for the implementation of machine learning algorithms. As a proof of concept, the paper discussed the implementation of a decision-tree algorithm based on ID3 implementation. The main functions of the ID3 algorithm ran on a MicroBlaze soft-core IP from Xilinx to utilize the processing units that are already available in the FPGA design flow. The integration of peripherals with the MicroBlaze is done through an AXI AMBA bus using a light weight version. Choosing AXI bus is an important design decision to make sure that the soft-core IP has a standard interface that simplifies the integration with other peripherals.

References

[1] A. Shawahna, S. M. Sait, A. El-Maleh, "FPGA-based Accelerators of Deep Learning Networks for Learning and Classification: A Review," CoRR, **abs/1901.00121**, 2019.

[2] R. Narayanan, D. Honbo, G. Memik, A. Choudhary, J. Zambreno, "An FPGA Implementation of Decision Tree Classification," in 2007 Design, Automation Test in Europe Conference Exhibition, 1–6, 2007, doi:10.1109/DATE.2007.364589.

[3] R. Narayanan, D. Honbo, G. Memik, A. Choudhary, J. Zambreno, "An FPGA Implementation of Decision Tree Classification," in 2007 Design, Automation Test in Europe Conference Exhibition, 1 – 6, 2007, doi:10.1109/DATE.2007.364589.

[4] M. Barbareschi, S. D. Prete, F. Gargiulo, A. Mazzeo, C. Sansone, "Decision Tree-Based Multiple Classifier Systems: An FPGA Perspective," International Workshop on Multiple Classifier Systems, 194–205, 2015.

[5] R.Harikumar, M.Balasubramani, "FPGA Synthesis Of Soft Decision Tree (SDT) For Classification Of Epilepsy Risk Level From Fuzzy Based Classifier Using EEG Signals," International Journal of Soft Computing and Engineering, **1**, 206–211, 2011.

[6] N. Dalal, B. Triggs, "Histograms of oriented gradients for human detection," in 2005 IEEE Computer Society Conference on Computer Vision and Pattern Recognition (CVPR'05), volume 1, 886–893 vol. 1, 2005, doi: 10.1109/CVPR.2005.177.

[7] M. FULARZ, M. KRAFT, "Hardware implementation of a decision tree classifier for object recognition applications," Measurement Automation Monitoring, **61**, 379–381, 2015.

[8] T. Traces, "TCP Statistic and Analysis Tool," http://tstat.tlc.polito.it/, accessed: 2019-08-06.

[9] K. K. M. Da Tong, Lu Sun, V. Prasanna, "High Throughput and Programmable Online Traffic Classifier on FPGA," Proceedings of the ACM/SIGDA international symposium on Field programmable gate arrays, 255–264, 2013.

[10] C. Zhang, P. Li, G. Sun, Y. Guan, B. Xiao, J. Cong, "Optimizing FPGA-based Accelerator Design for Deep Convolutional Neural Networks," in Proceedings of the 2015 ACM/SIGDA International Symposium on Field-Programmable Gate Arrays, FPGA '15, 161–170, ACM, New York, NY, USA, 2015, doi: 10.1145/2684746.2689060.

[11] T. Bhaaskar, K. Vishal, "Automatic generation of hardware Tree Classifiers," https://open.bu.edu/handle/2144/23688, 2017, accessed: 2020-09-07.

[12] P. R. Gankidi, J. Thangavelautham, "FPGA architecture for deep learning and its application to planetary robotics," in 2017 IEEE Aerospace Conference, 1–9, 2017, doi:10.1109/AERO.2017.7943929.

[13] Gan Feng, Zuyi Hu, Song Chen, Feng Wu, "Energy-efficient and high-throughput FPGA-based accelerator for Convolutional Neural Networks," in 2016 13th IEEE International Conference on Solid-State and Integrated Circuit Technology (ICSICT), 624–626, 2016, doi:10.1109/ICSICT.2016.7998996.

[14] Y. Lecun, L. Bottou, Y. Bengio, P. Haffner, "Gradient-based learning applied to document recognition," Proceedings of the IEEE, **86**(11), 2278–2324, 1998.

[15] R. Kulaga, M. Gorgon, "FPGA Implementation of Decision Trees and Tree Ensembles for Character Recognition in Vivado HLS," Image Processing and Communication, **19**, 71–82, 2015.

[16] F. Saqib, A. Dutta, J. Plusquellic, P. Ortiz, M. S. Pattichis, "Pipelined Decision Tree Classification Accelerator Implementation in FPGA," IEEE Transactions on Computers, **64**, 280–285, 2015.

[17] J. Grajal, O. Yeste-Ojeda, M. Sanchez, M. Garrido, M. Lopez-Vallejo, "Real-time FPGA Implementation of an Automatic Modulation Classifier for Electronic Warfare Applications," The 19th European Signal Processing Conference (EUSIPCO), 1514–1518, 2011.

[18] M. Owaida, H. Zhang, C. Zhang, G. Alonso, "Scalable Inference of Decision Tree Ensembles: Flexible Design for CPU-FPGA Platforms," 27th International Conference on Field Programmable Logic and Applications (FPL), 1–8, 2017.

[19] S. Surekha, "A Comparative Study of Rough Set Theoretic Decision Tree Induction Algorithms," in 2018 International Conference on Current Trends towards Converging Technologies (ICCTCT), 1–6, 2018, doi:10.1109/ICCTCT.2018.8550978.

[20] H. Liu, M. Zhou, X. S. Lu, C. Yao, "Weighted Gini index feature selection method for imbalanced data," in 2018 IEEE 15th International Conference on Networking, Sensing and Control (ICNSC), 1–6, 2018, doi: 10.1109/ICNSC.2018.8361371.

[21] B. Chen, L. Xing, B. Xu, H. Zhao, J. C. Príncipe, "Insights Into the Robustness of Minimum Error Entropy Estimation," IEEE Transactions on Neural Networks and Learning Systems, **29**(3), 731–737, 2018, doi:10.1109/TNNLS.2016.2636160.

[22] R. C. Barros, M. P. Basgalupp, A. C. P. L. F. de Carvalho, A. A. Freitas, "A Survey of Evolutionary Algorithms for Decision-Tree Induction," IEEE Transactions on Systems, Man, and Cybernetics, Part C (Applications and Reviews), **42**(3), 291–312, 2012, doi:10.1109/TSMCC.2011.2157494.

[23] "UltraScale Architecture Configurable Logic Block User Guide," *https://www.xilinx.com/support/documentation/user_guides/ug574-ultrascale-clb.pdf*, accessed: 2019-08-06.

[24] D. B. Thomas, "Synthesisable recursion for C++ HLS tools," in 2016 IEEE 27th International Conference on Application-specific Systems, Architectures and Processors (ASAP), 91–98, 2016, doi:10.1109/ASAP.2016.7760777.

[25] J. R. Struharik, "Implementing decision trees in hardware," in 2011 IEEE 9th International Symposium on Intelligent Systems and Informatics, 41–46, 2011, doi:10.1109/SISY.2011.6034358.

[26] H. Azmi, R. Sayed, "FPGA-based Implementation of a Tree-based Classifier using HW-SW Co-design," 2019 6th International Conference on Advanced Control Circuits and Systems (ACCS) & 2019 5th International Conference on New Paradigms in Electronics & information Technology (PEIT), 224–228, 2019.

[27] "Xilinx MicroBlaze Processor," *https://www.xilinx.com/products/intellectual-property/microblazecore.html*, accessed: 2020-08-26.

[28] Y. Zhong, "The analysis of cases based on decision tree," in 2016 7th IEEE International Conference on Software Engineering and Service Science (ICSESS), 142–147, 2016, doi:10.1109/ICSESS.2016.7883035.

[29] R. Narayanan, D. Honbo, G. Memik, A. Choudhary, J. Zambreno, "An FPGA Implementation of Decision Tree Classification," in 2007 Design, Automation Test in Europe Conference Exhibition, 1–6, 2007.

[30] J. Mitéran, J. Matas, J. Dubois, E. Bourennane, "Automatic FPGA based implementation of a classification tree," in SCS 2004 Signaux, Circuits et Systèmes Application to Informations Systems, IT 03, Workshop on Information Systems, 2004.

[31] J. R. Struharik, "Implementing decision trees in hardware," in 2011 IEEE 9th International Symposium on Intelligent Systems and Informatics, 41–46, 2011.

[32] M. Barbareschi, S. Del Prete, F. Gargiulo, A. Mazzeo, C. Sansone, "Decision Tree-Based Multiple Classifier Systems: An FPGA Perspective," in F. Schwenker, F. Roli, J. Kittler, editors, Multiple Classifier Systems, 194–205, Springer International Publishing, Cham, 2015.

[33] T. Sharp, "Implementing Decision Trees and Forests on a GPU," in D. Forsyth, P. Torr, A. Zisserman, editors, Computer Vision – ECCV 2008, 595–608, Springer Berlin Heidelberg, Berlin, Heidelberg, 2008.

[34] D. Marron, A. Bifet, G. D. F. Morales, "Random Forests of Very Fast Decision Trees on GPU for Mining Evolving Big Data Streams," in Proceedings of the Twenty-First European Conference on Artificial Intelligence, ECAI'14, 615–620, IOS Press, NLD, 2014.

ASTES

Advances in Science, Technology and Engineering Systems Journal Vol. 5, No. 5, 245-252 (2020)

www.astesj.com

Special Issue on Multidisciplinary Innovation in Engineering Science & Technology

ASTESJ

ISSN: 2415-6698

Assessing Heutagogical Elements in Learning of Engineering Education: Instrument Validation

Mimi Mohaffyza Mohamad[*,1], Alias Masek[1], Jailani Md Yunos[1], Maizam Alias[1], Nor Hidayah Hamdan[1], Andika Bagus Nur Rahma Putra[2]

[1]*Faculty of Technical and Vocational Education, Universiti Tun Hussein Onn Malaysia, Johor, 86400, Malaysia*

[2]*Department of Mechanical Engineering, Faculty of Engineering, Universitas Negeri Malang, Jl. Semarang No.5 Malang, 65145, Indonesia*

ARTICLE INFO

Article history:
Received: 12 May, 2020
Accepted: 11 August, 2020
Online: 14 September, 2020

Keywords:
Validation
Instrument
Heutagogy approach
Self-determined learning
Rasch Measurement Model

ABSTRACT

Practically level of design element (i.e., explore, sharing, connect) is an essential of heutagogical approach. The self-determined learning process can be at ease with the implementation of these elements, and the critical step is reliability to measure teaching and learning feedback. Although various instruments were proposed in the literature to assess heutagogy elements, the specific potential Rasch Measurement Model to determine the practicality levels of heutagogy element is less emphasized. This paper aimed to validate the research instrument (six constructs with 65 items). The instrument was administered to N=175 students for a pilot study. The Rasch model was conducted to examine reliability (0.93, 0.94) with α = 0.97, separation index (3.75, 4.01) for item and person, respectively. Besides, item fit (three-item dropped), polarity and standardized correlation residual (no overlapping items). The findings have shown that the instrument has high validity and reliability for use in measuring the practical level of heutagogy elements.

1. Introduction

Pedagogical or andragogical approach is generally related to the role of teachers and learners in the traditional education system. As the future of education has offered many new opportunities in the learning process, the continuous transfer of learning from pedagogy to andragogy and finally arriving in heutagogy shows that change must take place in the classroom compulsory [1]. With the rapid development of technology, the education system is increasingly shifting to a self-directed approach by heutagogical method [1,2,3]. From this trend, students can obtain valuable information from different sources and accessible from any platform (i.e., online or mobile system). Therefore, the heutagogy approach focuses on life-long learning and self-determined learning methods. There are multiple contexts of studies that have been discussed in the literature, such as related to necessity [4], practice [5,6,7] and teacher's training [8] of heutagogy learning approach. Most studies have found that the heutagogical approach can be an essential learning style for producing students who are well-prepared for the complexities of today's workplace.

In the context of measurement, evaluation of the heutagogical learning approach's implementation strategies in the teaching and learning process is a vital issue to be taken into account. Implementation and learning strategies need to be aligned with the design principle of the heutagogical learning environment (i.e., exploration, creation, reflection, connection, assessment and sharing) [9]. To date, a number of validation instruments, tests, experiments and studies have been developed to evaluate the effectiveness of the heutagogical learning from a different point of view [4, 6, 9]. The validation process consists of a systematic procedure, including a pilot study. The pilot study's main goal is to improve the quality of the item and increase confidence in the interpretation of the data [10]. While every student has a different style of preferred learning ways, a pilot study is required to determine the capability of the developed instrument to analyze the practicality of heutagogy data. During data analysis, the need to identify the element of heutagogical approach that best fits the different categories of student's profiles, especially in engineering education, arises as to the main issue

Based on the above premises, an instrument was developed in this study, involving the student's reflection to determine the practical level of heutagogical elements applied in learning, based

[*]Corresponding Author: Mimi Mohaffyza Mohamad, Tel: +6074534193, Email: mimi@uthm.edu.my

on the design elements proposed [9]. This research instrument was developed in the questionnaire form. It is a practical way to gather data, collect results easily, and gather information from a large number of respondents [11]. When involving a self–assessment test, the psychometric tests element must be considered during the instrument development to ensure the high reliability and validity of the instruments.

In this phase, a set of questionnaire with a Likert scale was used to obtain feedback from students. However, using only a descriptive analysis of the Likert scale data does not provide sufficient information and concrete findings [12], since the Likert scale is commonly ordinal data that categorizes the respondent's point in general (i.e., less accurate interoperation). The Rasch Measurement Model analysis was therefore conducted to improve response accuracy. The Rasch model analysis can convert the latent traits, either nominal or ordinal data into interval and ratio data by creating a logit scale. This can be useful and provide scientific measurement for this study. The objectives of the study are as follows:

- to identify the validity and reliability of the heutagogy elements in learning of engineering education using Rasch Measurement Model
- to identify the point measure correlation in the construct of the heutagogy elements in the learning of the engineering education which are in the acceptable range
- to identify the fit items in the construction of the items heutagogy elements within the acceptable range.

2. Literature Review

2.1. Heutagogy Learning Approach

Heutagogy, or the study of self-determined learning, has gained interest in the field of engineering education aimed at 21st-century skill requirements and industrial needs [9]. The increasing number of education institutions, for example, technical universities, have started to explore and implement a self-determined learning environment for their students. The main goal of heutagogy is to teach lifelong learning. Heutagogical approach differs from other traditional methods (i.e., pedagogy and andragogy). In comparison, these three learning approaches can be differentiated based on the teaching and learning environment and its implementation. Generally, figure 1 shows the progression of three teaching approaches.

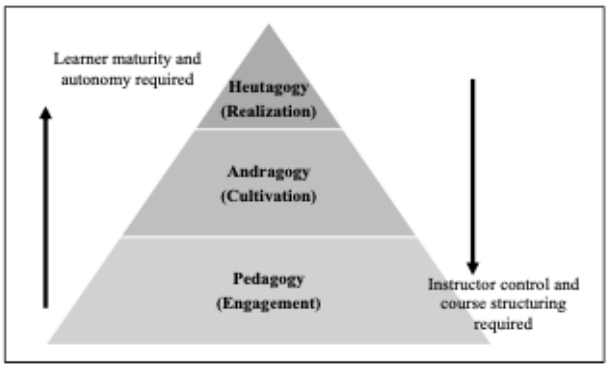


Figure 1: Progression of Learning Approach

At the first level, pedagogy is mainly focusing on teacher-led learning, where teachers have to decide on the overall learning content and process (i.e., what students will learn and how they will learn). In the first level, students depend on instruction from the teachers. In the second level, andragogy is taking place where teachers play an important role as a mentor in andragogical environments and cultivate the students' ability to self-directed learning. At the third level, entering at heutagogy learning level 3 encourages students to fully control the learning environment, where students solve their learning problems with their own decisions. Therefore, it is important for students as well to equip themselves with problem-solving skills [13]. In this case, the teacher is only preparing the learning context in general [1].

2.2. Heutagogical Study and Instrument

Heutagogy is an extension of the pedagogy and andragogy approach which places the learner, rather than the teacher or institution or even the curriculum, at the center of the learning process [9]. The goal of heutagogy is to prepare responsible, self-capable, proactive, competent students who are ready to face the actual workplace environment. Most heutagogical studies in engineering education, vocational education, and pre-service teacher professions have found that heutagogy is a credible response to the critical issues that learners face within the workplace and have designed their learning environments based on the approach. For example, within the vocational education, [14] the innovation of training module based on heutagogy has been developed as acceleration for increasing the pedagogical supremacy of professional education lecturers in the industrial revolution. The findings reported that heutagogy provides a learning framework that addresses the needs of vocational students, who must learn in an ever-changing environment that is both complex and helps them to become lifelong learners.

Table 1 summarizes the previous relevant heutagogical studies that can be categorized into two research directions; namely the category/principle and the type of environment. The category or principle perspective, in which heutagogy is defined as the center of the teaching and learning process and becomes an active agent of all learning experiences, from planning and execution to learning assessment [2, 9, 15]. The main goals of these studies are to understand the perceptions, needs and experiences of learners or their characteristics or to develop a learner-centered curriculum. There are previous study that have illustrated the finding of their small-scale study on heutagogy approach, which can be one of the key elements for enhancing the curriculum, encouraging students to determine what, how, when and where they learn and enabling educators to be more flexible in delivering their curriculum [16].

Next, the research also indicated several different types of the learning environment (i.e., traditional face-to-face), online, or a combination could support self-determined learning [9]. With the availability of an online platform, implementing self-determined learning activities can be more convenient as an online platform can connect, share, create, and collect more resources, that has been highlighted in several previous studies [17]. This has already been indicated in some of the research studies [18-20]. Critical thinking can be developed among students [21] to solve learning problems [22] and researcher found that reflective independent and critical thinking skills can be developed [3].

Table 1 : Summary of Related Works

Research Direction	Themes	Element focused	Instrument/ Methodology
Category/ Principle	Learner-centered and learner-determined learning	Perceptions [21]	Semi-structured group interviews
		Heutagogical needs and experiences of the learner [4]	Interviews, literature review, documentation, and observation
		Curriculum development [15,22]	Group discussion
			Semantics search and discussion
			Questionnaire survey
		Strategy and implementation [23]	Standardized and open-ended interviews
	Self-reflection	Motivation [2]	Phenomenological interviews
Type of environment	Online platform, mobile application	ICT literacy [19]	Questionnaires survey
		Practices [17]	Questionnaire, semi-structured interviews,
		Critical thinking MOOC [20]	Trello online discussion tool
	Blended Learning	Practices and technology adaptation [8,24]	Workshop
			Quasi-experimental design, semi-structured interview

in heutagogy learning program by using a blended approach. It is also noted that the affordance of mobile social media tools can facilitate student-determined learning experience (heutagogy) in authentic contexts [3].

On the other hand, interview questions were mostly used in the standard instruments, and the results encourage two-way communication. Besides, it allows participants (i.e., lecturer or students) to freely express their needs, perceptions and experiences in the implementation and practice of self-determined learning [21], the interview questions are useful in profoundly exploring the participants' attitude, experiences. For example, [19] selected 138 high school teachers to determine online learning competence through a heutagogy approach. The result indicated that all the heutagogy elements (i.e., exploration, creation, collaboration, connection, sharing and reflection of experience) were identified as important. However, one of the neglected remaining issues is on how the heutagogy approach instrument can be best validated? Therefore, this study was conducted to validate the proposed instrument used for heutagogy learning approach among engineering students.

3. Methodology

Figure 2 shows an overview of the validation process of heutagogical element in learning of engineering education. There are five main steps conducted, starting with the development of the questionnaire, data collection, data processing, data analysis, and reporting findings. First of all, the research instrument in the form of a questionnaire survey was developed. The questionnaire consists of two sections; Section A includes the students' Demographic profiles, and in Section B, a total of 65 items to gauge students' learning style. In section B, six main constructs/elements of heutagogical learning style have been evaluated namely, (a) explore, (b) create, (c) collaboration, (d) connect, (e) share and (f) reflection.

Furthermore, the questionnaire was distributed through the online platform and the student portal. Students have to rate items based on a scale ranging from 1 (never) to 5 (always). Students' response represents the percentage of the practice such as 1 (0 percent practice), 2 (1-20 percent practice), 3 (21 percent-50 percent practice), 4 (51 percent-80 percent practice) and 5 (>80 percent practice), respectively. Respondents were given approximately fifteen minutes to complete the questionnaire. A total of 175 students from University Tun Hussein Onn Malaysia, (UTHM) were randomly selected for research sampling. From the responses obtained, the collected data underwent a pre-processing process, such as determining the missing data and converting it to the appropriate format (i.e., convert excel to. prn text file). Next, the data analysis was performed using the Rasch measurement model, which focuses on four main analyses, including: (i) reliability and separation index; (ii) item fit and polarity. The flow of the data analysis was illustrated in figure 2.

3.1. Rasch Model in Measuring Heutagogical

Equation 1 shows the adaptation of the mathematics model underlying the Rasch measurement model [23,24,25]. This principle indicates that students have a higher probability of responding to the less difficult item and a lower probability of accurately responding to the more difficult item.

$$P_r\{X_{ni} = 1\} = \frac{e^{\beta_n - \delta_i}}{1 + e^{\beta_n - \delta_i}} \quad (1)$$

where β_n is the ability of student n and δ_i is the difficulty of heutagogy item *i*. Besides, $\beta_n - \delta_i$ is the probability of student's response for each heutagogy item. In this case, the $P_r\{X_{ni} = 1\}$ is the success probability or also known as logit value upon the interaction between the relevant students and the assessment item. Thus, this study has simply the Equation (1) into a logarithmic function, as shown in Equation (2).

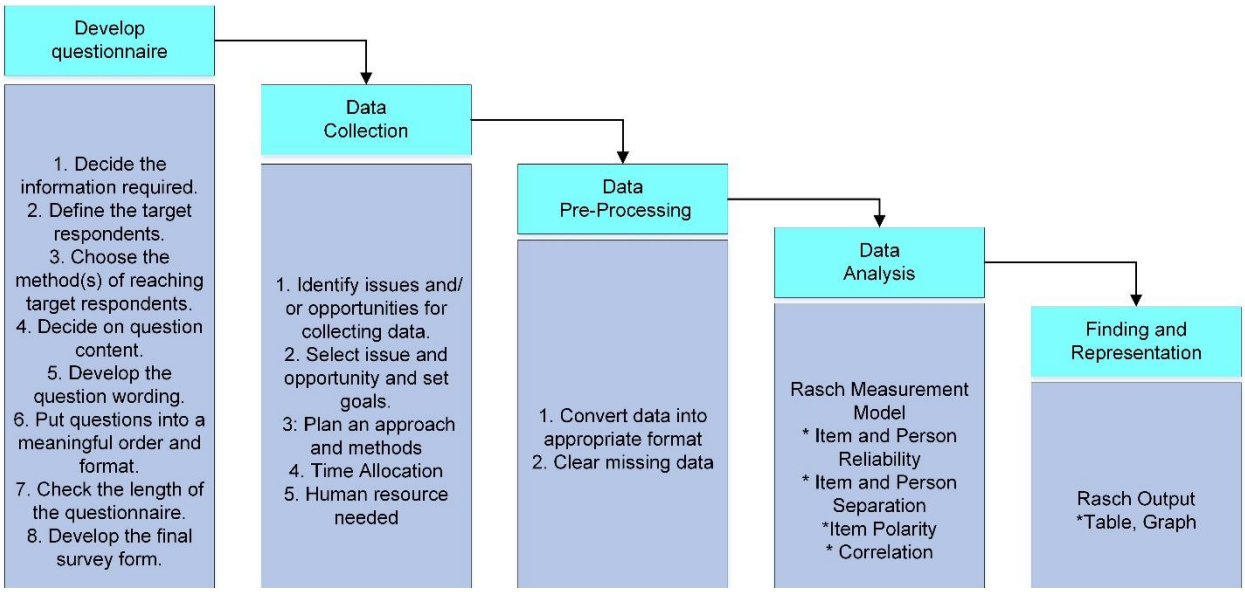


Figure 2: Data analysis flow

$$logit\left(\frac{P}{1-P}\right) = \beta_n - \delta_i \quad (2)$$

The probability of students' success for each heutagogical item demonstrates the relationship between students' ability and the difficulty of given items in the heutagogy element.

3.2. Analysis Using Rasch Measurement Model

Based on the aforementioned Rasch model analysis, Table 1 shows the summary of the statistical criteria and the acceptable value for further study. The following analysis in Table 2 was examined in order to assess the validity and suitability of the item in the Rasch Model.

a. Reliability and Separation Index. Reliability refers to the consistency of the measure, which can be obtained through the Cronbach Alpha values and the internal reliability index [26]. The value of Cronbach Alpha (α) is between 0 (no internal reliability) and 1 (perfect internal reliability) with a minimum score of 0.70 [27]. While the separation index indicates the statistically distinct measurement level of an item's difficulty or a person's ability [27].
b. Item polarity. Item polarity was evaluated by using a point–measure correlation coefficient (PTMEA CORR). The values of the high and positive items range from 0.3 to 0.8, representing items that are working in the right direction to measure each of the developed constructs [28]. However, the negative values or zero indicated a conflicted relationship between items within the construct. An item that exceeds the 0.3-0.8 interval is recommended for removal [29].
c. Item fit. In the Rasch model, item infit and outfit mean-square fit statistics (MNSQ) were commonly used to determine the item fit assessment. The infit statistics are inlier-sensitive fit statistics, which indicate the responses of items that are close to the person's ability level [30]. Outfit statistics are referred to as outlier-sensitive fit statistics, which represent unexpected responses to items outlying from the person's ability level. The item is considered to be consistent with the Rasch measurement when MNSQ reaches the expected value of 1 and always be positive.
d. The MNSQ optimal value of each item must be located within 0.5–1.5 [30]. The values of less than 0.5 or 1.5–2.0 do not bring efficiency to building measurements, but do not decline [31]. Therefore, any individual item with MNSQ more than 2.0 will be suggested for removal from the present study.

Table 2 : Summary of Statistical

Criteria	Statistical Info	Result	
		Value	Indicator
Item Misfit	Person & Item Reliability [26]	0.9-1.0	Very good and effective level of consistency
		0.7-0.8	Good and Acceptable
		0.6-0.7	Acceptable
		< 0.6	The item needs to be repaired
		< 0.5	The item needs to be dropped
	Separation [32]	Value ≥ 2	Acceptable
Item Validity	Item Polarity [26]	PTMEA CORR > 0	Acceptable
Item	Item Fit [26]	Total Mean Square infit and outfit in range 0.6-1.4	Acceptable
		Total Mean Square infit and outfit in range 0.6-1.5	Acceptable

e. Standardized measurement of the residual correlation value. This analysis was conducted to determine the overlapping of the items. High residual correlation for pair items indicated that item is not independent (i.e., items are the same characters or combination of the shared item). As for the pairing item's correlation, value that is greater than 0.7 indicates a high correlation value, and only one item must be maintained. In contrast, the other items should be dropped [32,33].

4. Results and Discussion

4.1. Demography Profile

Table 3 presented the demographic profile of the respondents. There are three main demographic profiles collected, such as gender, year of study, and faculty members. All the information was presented in the cross-tabulation output, which is faculty versus year of study and gender versus faculty. Gender information is included in this study as it is a way of looking at how heutagogy element impacts learning experiences between different groups of male and female students.

Table 3: Demography Profile

Criteria	Year of Study				Gender	
Faculty	1st	2nd	3rd	4th	Male	Female
FKAAS	0	1	0	0	0	1
FPTP	23	43	68	1	56	79
FPTV	9	2	17	11	13	106
Total	32	46	85	12	69	106

4.2. Reliability and Validity

Table 4 shows the statistical summary of the reliability and separation index of the survey instrument. The value of 0.97 obtained in this study indicates that the reliability of the instrument used was high and adequate. In item measurement, the reliability value of 0.93 indicates that items of the instrument are very sufficient to measure the learning heutagogical elements. The person's reliability indicates the probability of a person's response results of 0.94 when the same test is performed. Hence, this heutagogical learning instrument is at a high level of reliability. Meanwhile, for the separation index (SI), both item and person measurements were obtained acceptable value $\geqslant 2$, SIitem = 3.75, and SIperson = 4.01.

Table 4 : Reliability and Separation Index

TE	Item Measurement		Person Measure		α
	Reliability	Separation	Reliability	Separation	
65	0.93	3.75	0.94	4.01	0.97

4.3. Mean and Mean Logit

Table 5 shows the mean and mean logits for each construct in this developed instrument. The higher mean score is obtained for 'explore' construct, $\bar{x}$ = 4.018, which indicated that the students agreed that the explore item suggested is working well in their learning process. This is matter because the student needs to be provided with free and large opportunity to explore the variety of learning pathways, information, and resources during the learning process [9, 15]. However, the value of the connect construct means obtained, $\bar{x}$ = 3.804 still indicates the high level of student's agreement with the connecting element. This matters because the creation connections are comfortable with the affordance of an online platform (i.e., social media, video conferencing), which allows students to have the opportunity to share new knowledge with others who have the same interest [34].

On the other hand, the measure means were obtained to determine the item agreement among the students. The negative value item indicated that students were more comfortable to agree on the item. In this case, explore (- 0.24 logit) and share (- 0.03 logit) constructs were more comfortable obtaining a high degree of agreement among the students.

Table 5 : Mean and Mean Logit

No	Construct	TE	$\bar{x}$	SD	Mean Logit		
					Min	Max	Total
1	Explore	10	4.01	18.9	-0.54	0.31	-0.24
2	Create	11	3.87	52.5	-0.75	1.19	0.03
3	Collaboration	12	3.90	31.9	-0.61	0.72	0.00
4	Connect	10	3.80	45.9	-0.82	1.01	0.19
5	Share	12	3.92	28.2	-0.64	0.48	-0.03
6	Reflection	10	3.88	33.0	-0.45	1.00	0.05
	Total	65					

* TE- Total Item, SD - Standard Deviation, $\bar{x}$ = Mean

4.4. Correlation

Standardized measurement of the residual correlation value is to determine whether there are overlapping items. High residual correlation for the two items showed that the item is not independent, either because the item has the same characteristics among each other or because it combines several different dimensions that are shared. If the correlation value of the two items above 0.7 shows a high correlation value and only one item must be maintained [31]. In contrast, the other items should be dropped. Based on Table 6, no overlapping pairs have been found, and no items have been dropped.

Table 6 : Large standardized residual correlation used to identify the dependent item

Correlation	Entry Number	Item	Entry Number	Item
0.56	51	SH51	52	SH52
0.50	38	CN38	39	CN39
0.46	43	CN43	45	SH45
0.45	26	CL26	35	CN35
0.43	53	SH53	58	RF58
0.42	64	RF64	65	RF65
0.42	25	CL25	26	CL26
0.41	23	CL23	24	CL24
0.41	60	RF60	61	RF61
0.41	8	EX8	9	EX9

4.5. Item Fit and Item Polarity

Due to space limitation, Table 6 presented only the estimation of difficulty parameter and model fit estimations of misfit items. Mean square information (MNSQ) and the point measure correlation (PTMEA-CORR) aimed to determine the item's suitability for the developed instrument. For the MNSQ assessment, the list presented that MNSQ infit range is at 0.67 logit – 1.90 logit. As the MNSQ infit acceptable range is 0.50 logit – 1.5 logit, three items RF59 = 1.90 logit SH53, item SH44 = 1.58 logit, were found exceed the acceptable range.

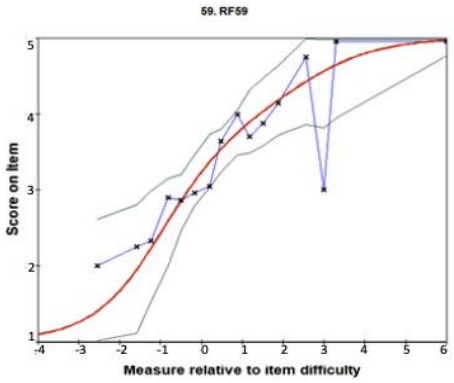


Figure 3: The ICC Curve for Misfitting Item, RF 59

Based on the output presented in Table 5, an example of the ICC curve for misfitting items was generated in Figure 3. The red curve is the expected ICC if the data fitted the Rasch model. The blue curve is the observed or empirical ICC. The grey line in the outskirts of the red curve is the confidence interval constructed from an estimate and its standard error. The empirical ICC for misfitting item RF59 has a slightly large deviation from the expected ICC. This fact is reflected in RF59 with a large outfit-MNSQs value of 2.02. However, Figure 4 presented a good-fit item, SH47, in which the outfit-MNSQs value, 0.90 was obtained and is within an acceptable range. In addition, PTMEA-CORR can also be used to accept or abolish the items tested. The acceptable range depends on the purpose of the instrument. However, the negative value of the PTMEA-CORR items does not measure what should be measured and should be dropped. In this study, all tested PTMEA-CORR items were positive (0.43 logit -0.63 logit) and were therefore retained.

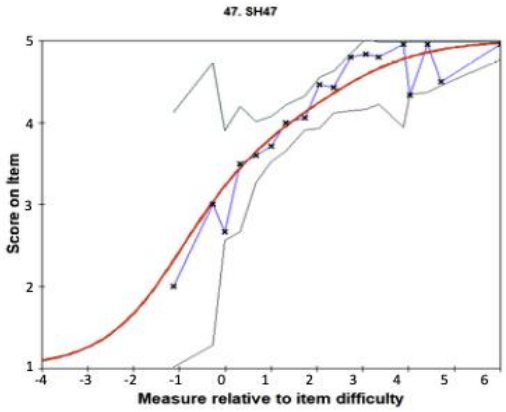


Figure 4: The ICC Curve for Good-fit Item,47

The detail of the item fit explained in Table 7, which shows fit index item that measured in infit/outfit, and items RF59, SH83, and SH44 are more than 1.4 logit values, and this item needs to revise.

4.6. Variable Map

Based on the above findings, this list of logit measurement information for each item is useful for understanding each item's position in the variable map. Figure 5 shows the distribution of the item's difficulty. In this case, item CR12 received a high measure of logit value, +1.99 indicating the most difficult item to respond to. In contrast, item CN35 indicated the easier item to be answered as the measured value obtained, - 0.82 logit.

Table 7 : Partially Outcome of Item Fit

Measure	Model S.E	Infit		Outfit		PT-Measure		Item
		MNSQ	ZSTD	MNSQ	ZSTD	CORR	EXP	
1.00	0.10	1.90	6.70	2.02	7.3	0.43	0.57	RF59
0.48	0.10	1.83	5.9	1.84	5.0	0.43	0.54	SH53
0.32	0.11	1.58	4.3	1.52	4.0	0.44	0.53	SH44
1.06	0.10	1.38	3.2	1.49	4.0	0.50	0.57	CR20
1.01	0.10	1.40	3.3	1.47	3.8	0.46	0.57	CN42
0.31	0.11	1.41	3.2	1.45	3.5	0.30	0.53	EX7
0.41	0.10	1.32	2.6	1.34	2.7	0.46	0.58	CN43
1.19	0.09	1.26	2.3	1.32	2.8	0.51	0.46	CR12
-0.75	0.12	1.30	2.4	1.23	1.9	0.44	0.53	CR13
0.38	0.11	1.30	1.7	1.17	1.4	0.53	0.52	SH45
0.11	0.11	1.20	0.9	1.19	1.6	0.43	0.49	CL31
-0.32	0.12	1.11	0.9	1.17	1.4	0.41	0.49	EX1
-0.30	0.12	1.06	0.7	1.15	1.3	0.46	0.51	EX3

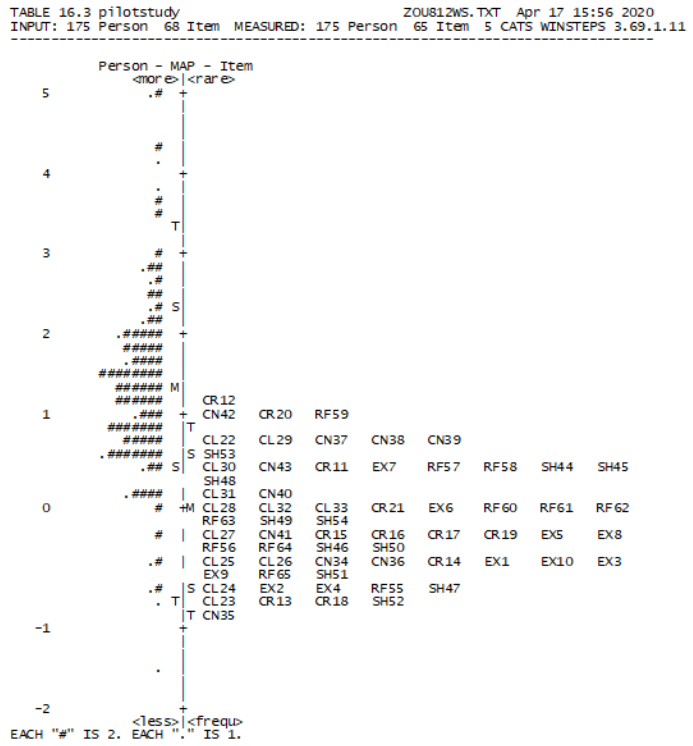


Figure 5 : Variable Map (Item – Person)

5. Conclusion

An instrument for gauging a heutagogy element in learning for the engineering education area was successfully developed and validated using the Rasch measurement model. Using this model, the validity and reliability of items have been proven using the data gathered from the pilot study, to fit the engineering education students. In this study, we have provided two implications of the findings based on The Rasch model framework provides systematics procedures for validating the developed instrument (e.g., Reliability, construct validity, item fit, separation index). Besides, the Rasch measurement model provides an impact on discovering the meaning of students' measure, which heutagogy element applied in students' learning using from the context of the instrument's items. The first contribution in this context, a huge implication, is probably on the potential for individual reflection and feedback practices. Practitioners in schools and teacher educators can be referred to the Wright Map/Variable Map that explicitly uses the heutagogy element in the learning process. Teachers can prepare the best strategies and implementation process for important aspects of the heutagogy element to students. Another implication from this study identified potential strategies for curriculum development and the teaching process. A total of 175 students can generally use the heutagogical elements at least by sharing information with other engineering or non-engineering students through an online platform. In this case, students can discover more learning experiences, learn new things, and identify mutual students with similar interests. This repeating process can lead to life-long learning and future collaboration. We are currently working on a test within the different categories of students, from pre and post-secondary subjects, using the developed instrument to explain the changes in the critical heutagogical elements. The findings will be reported in the subsequent publication.

Acknowledgment

The authors would like to thank all the associate editors and referees for their thorough reading and valuable suggestions, which led to the improvement of this paper. The Research Management Center (RMC), Universiti Tun Hussein Onn Malaysia and Ministry of Higher Education (MOHE) are acknowledged for the financial support received for this research (Research Fund: Development of Heutagogical Learning Module for Engineering Education Student , Grant Code K134, MyRIVET). Universitas Negeri Malang is recognized as a research collaborator and researchers from both universities Tee Tze Kiong, Yee Mei Heong, Lee Ming Foong, Razali Hassan, Haris Anwar Syafrudie, Ahmad Mursyidun Nidhom, Azhar Ahmad Smaragdina and research assistant Anies Faziehan Zakaria.

References

[1] J. Md. Yunos, H. A. Syafrudie, M. Alias, R. Hassan, M. H. Yee, "Heutagogical Teaching And Learning Activities Preferences For Malaysia Technical University Lecturer: Instrument Validation," International Journal of Advanced Science and Technology, **29(**4), 3875-3886, 2020.

[2] Blaschke L.M. Self-determined Learning (Heutagogy) and Digital Media Creating integrated Educational Environments for Developing Lifelong Learning Skills. In: Kergel D., Heidkamp B., Telléus P., Rachwal T., Nowakowski S. (eds) The Digital Turn in Higher Education. Springer VS, Wiesbaden. 129-140,2018. https://doi.org/10.1007/978-3-658-19925-810

[3] N. Canning, "Playing with heutagogy: Exploring strategies to empower mature learners in higher education," Journal of Further and Higher Education, **34**, 59-71, 2010. https://doi.org/10.1080/03098770903477102

[4] V. Narayan, J. Herrington, and T. Cochrane, "Design principles for heutagogical learning: Implementing student-determined learning with mobile and social media tools," Australasian Journal of Educational Technology, **35**, 2019. 2019. https://doi.org/10.14742/ajet.3941

[5] A. B. N. R. Putra, H. A. Syafrudie, J. M. Yunos, A. M. Nidhom, A. A. Smaragdina, and A. I. Sembiring, "Analysis of the Necessity for Heutagogical Approach Through 4Cs Skills as Innovation for Vocational Lectures in the Education 4.0," in 1st Vocational Education International Conference (VEIC 2019), 2019, 362-371.

[6] H. Praherdhiono, E. P. Adi, and R. N. Devita, "Understanding of Digital Learning Sources with the Heutagogy Approach using the K-Means and Naive Bayes Methods," in 2018 4th International Conference on Education and Technology (ICET), 2018, 23-27.

[7] K.-T. Wong, N. binti Abdullah, and A. Hamdan, "Mobile-Heutagogical Practices among Student Teachers: Its Pedagogical Affordances and Challenges," International Journal of Interactive Mobile Technologies (iJIM), 14, 130-143, 2020. https://doi/10.3991/ijim.v14i02.11819

[8] W. Kung-Teck and M. A. Yeop, "Modelling the Factor Influencing the Implementation of Mobile-Heutagogical Practices among Teachers: An Application of Invariance Multi-Group Structural Model," International Journal of Learning, Teaching and Educational Research, **18,** 1-16, 2019. https://doi/10.26803/ijlter.18.12.1

[9] A. S. Preece and P. K. Hamed, "Andra-Heutagogy: A New Approach For Teacher Training," International Journal of Education and Pedagogy, **2**, 98-105, 2020.

[10] L. M. Blaschke and S. Hase, "Heutagogy: A holistic framework for creating twenty-first-century self-determined learners," in The future of ubiquitous learning, ed: Springer, 25-40, 2015. https://doi/10.1007/978-3-662-47724-3

[11] Z. A. Hassan, P. Schattner, and D. Mazza, "Doing a pilot study: why is it essential?," Malaysian family physician: the official journal of the Academy of Family Physicians of Malaysia, **1**(70) 2006.

[12] E. M. Mitropoulou, I. Tsaousis, D. Xanthopoulou, and K. V. Petrides, "Development and Psychometric Evaluation of the Questionnaire of Ethical Leadership (QueL)," European Journal of Psychological Assessment, 2019.

[13] J. Arbuckle, "Amos (Version 7.0) SPSS, Chicago," IL,2006.

[14] T. K. Tee, S. Saien, F. Rizal, Sukardi, Risfendra, M. H. Yee, M. M. Mohamad, W. Othman, M. N. A. Azman and N. Azid, "Design And Technology Teacher In TVET: A View On Thinking Style And Inventive Problem-Solving Skill," Journal of Technical Education and Training, **12**(1),197-203, 2020. https://doi.org/10.30880/jtet.2020.12.01.021

[15] A. Putra, H. Syafrudie, A. Nidhom, A. Smaragdina, J. M. Yunos, and A. Sembiring, "The innovation of module training based heutagogy as an acceleration for increasing pedagogical supremacy of vocational education lecturers in the industrial revolution 4.0," in Journal of Physics: Conference Series, 012043, 2020. https://doi.org/10.1088/1742-6596/1456/1/012043
[16] S. Hase, "Learner defined curriculum: Heutagogy and action learning in vocational training," Southern Institute of Technology Journal of Applied Research, 1-10, 2011.
[17] M. Snowden and J. Halsall, "Exploring the application of a self-determined approach to learning," International Journal of Innovation and Learning, **22**, 293-303, 2017. https://doi.org/10.1505/IJIL2017.086730
[18] A. Chimpololo, "An analysis of heutagogical practices through mobile device usage in a teacher training programme in Malawi," 2019.
[19] J. Purnomo, "ICT literacy of high school mathematics teacher: online learning competence with heutagogical approach," in Journal of Physics: Conference Series, 2019
[20] M. Rathakrishnan and A. Raman, "Heutagogy Approach Using Trello Online Learning on the Critical Thinking Skills Amongst Students With Different Learning Styles," in Redesigning Higher Education Initiatives for Industry 4.0, ed: IGI Global, 41-55, 2019. http://doi.org/10.4018/978-1-5225-7832-1.ch003
[21] N. Azid, H. Ridzuan, T. K. Tee and M. H. Yee, "Malaysia and China Students' Feedback on the Implementation of Critical Thinking Pedagogy: A Case Study," International Journal of Advanced Science and Technology, **29**(3), 227-237, 2020.
[22] M. H. Yee, N. Hamdan, B. C. Kok, T. K. Tee, N. Azid, "Development of Integrated Creative and Critical Thinking Module in Problem-Based Learning to Solve Problems," International Journal of Scientific & Technology Research, **9**(3), 6567-6571, 2020.
[23] M. Gribbins and V. Cook, "Workshop: Emerging technologies and practices that promote student-centered learning," in Proceedings of the Twelfth Midwest Association for Information Systems Conference (MWAIS), Springfield, Illinois, 2017.
[24] T. G. a. F. Bond, C.M., Applying the Rasch model: Fundamental Measurement in the Human Sciences Second ed. New Jersey: Lawrence Erlbaum Associates., 2007.
[25] M. Gribbins and V. Cook, "Workshop: Emerging technologies and practices that promote student-centered learning," in Proceedings of the Twelfth Midwest Association for Information Systems Conference (MWAIS), Springfield, Illinois, 2017.
[26] G. Rasch, "Probabilistic Models for Some Intelligence and Attainment Tests. Chicago, IL: University of Chicago Press," 1960.
[27] H. Othman, N. A. Ismail, I. Asshaari, F. M. Hamzah, and Z. M. Nopiah, "Application of Rasch measurement model for reliability measurement instrument in vector calculus course," Journal of Engineering Science and Technology, vol. 10, pp. 77-83, 2015.
[28] A. M. Talib, F. O. Alomary, and H. F. Alwadi, "Assessment of Student Performance for Course Examination Using Rasch Measurement Model: A Case Study of Information Technology Fundamentals Course," Education Research International, vol. 2018. https://doi.org/10.1155/2018/8719012
[29] W. Fisher, "Rating Scale Instrument Quality Criteria. Rasch Measurement Transactions", **21**(1), 1095, ed, 2007.
[30] J. M. Linacre, "A user's guide to FACETS rasch-model computer programs,", **18**, 2018, 2014.
[31] M. B. Paulsen and L. W. Perna, "Higher Education: Handbook of theory and research" vol. 31: Springer, 2016.
[32] M. Illhan and G Nese, A Comparison of Difficulty Indices Culculated for Open-Ended Items According to Classical Test Theory and Many Facet Rasch Model. Eurasioan Journal of Educational Research **75**, 99-114, 2018. https://doi:10.14689/ejer.2018.75.6
[33] T. Bond and C. M. Fox, Applying the Rasch model: Fundamental measurement in the human sciences: Routledge, 2015.
[34] J. P. Meyer, Applied measurement with Metrik: Routledge, 2014.

ASTES

Advances in Science, Technology and Engineering Systems Journal Vol. 5, No. 5, 253-261 (2020)

www.astesj.com

Special Issue on Multidisciplinary Innovation in Engineering Science & Technology

ASTESJ

ISSN: 2415-6698

Differential Evolution based Hyperparameters Tuned Deep Learning Models for Disease Diagnosis and Classification

Sathyabama Kaliyapillai*, Saruladha Krishnamurthy

Computer Science and Engineering, Pondicherry Engineering College, Pondicherry, 605014, India

ARTICLE INFO

Article history:
Received: 21 June, 2020
Accepted: 05 August, 2020
Online: 14 September, 2020

Keywords:
Deep Learning
Disease Diagnosis
Feature Selection
Healthcare
Differential evolution
Parameter Tuning
LSTM.

ABSTRACT

With recent advancements in medical filed, the quantity of healthcare care data is increasing at a faster rate. Medical data classification is considered as a major research topic and numerous research works have been already existed in the literature. Presently, deep learning (DL) models offers an efficient method for developing a dedicated model to determine the class labels of the respective medical data. But the performance of the DL is mainly based on the hyperparameters such as, learning rate, batch size, momentum, and weight decay, which need expertise and wide-ranging trial and error. Therefore, the process of identifying the optimal configuration of the hyper parameters of a DL is still remains a major issue. To resolve this issue, this paper presents a new hyperparameters tuned DL models for intelligent medical diagnosis and classification. The proposed model is mainly based on four major processes namely pre-processing, feature extraction, classification and parameter tuning. The proposed method makes use of simulated annealing (SA) based feature selection. Then, a set of DL models namely recurrent neural network (RNN), gated recurrent units (GRU) and long short term memory (LSTM) are used for classification. To further increase the classification performance, differential evolution (DE) algorithm is applied to tune the hyperparameters of the DL models. A detailed simulation analysis takes place using three benchmark medical dataset namely Diabetes, EEG Eye State and Sleep stage dataset. The simulation outcome indicated that the DE-LSTM model have shown better performance with the maximum accuracy of 97.59%, 88.52% and 93.18% on the applied diabetes, EEG Eye State and Sleep Stage dataset.

1. Introduction

At present times, healthcare sector becomes more common where massive amount of medical data plays a major role. In this view, for instance, precision healthcare aims to assure the proper medication is offered to the appropriate patients promptly by considered different dimensions of patient's information, comprising variability in molecular trait, atmosphere, electronic health record (EHR) and standard of living [1]. The higher accessibility of medical details brought numerous chances and issues related to healthcare researches. Particularly, discover the interconnections between diverse set of data exist in dataset still remains a basic issue to design effective medicinal models using data driven techniques and machine learning (ML). Earlier studies have focused on linking many data sources for building joint knowledge bases which can be utilized for predictive analysis and discovery. Though former techniques exhibit noteworthy performance, prediction models using ML models are not mainly employed in healthcare sector [2]. Actually, it is not possible to completely utilize the available healthcare data due to its sparsity, high dimensional heterogeneity, temporal dependence, and irregularities. These problems become even more difficult by distinct medicinal ontologies employed for data generalization which frequently include disagreements and inconsistencies. In some cases, the identical clinical phenotype can be defined in several ways along the data [3].

For instance, in EHR, a patient affected by 'type 2 diabetes mellitus' could be detected by the use of laboratory test reports of haemoglobin A1C >7.0, occurrence of 250.00 ICD-9 code, 'type 2 diabetes mellitus' declared in the free text medical notes, etc. As a result, it is not trivial to harmonize every medical concept to develop a higher-level semantic structure and comprehend their relationships [4]. A widespread method in healthcare researches is to have medical experts for specifying the phenotypes to utilize

*Corresponding Author: Sathyabama Kaliyapillai, Email: sathii_manju@pec.edu

in an adhoc way. At the same time, the supervised description of the feature space performs poor scaling and ignores the chances of discovering effective patterns.

On the other hand, representation learning approaches permit automatic discovery of representations required to predict it from the actual data. Deep learning (DL) techniques are representation-learning approaches with many stages of representation, attained by integrating simpler but nonlinear models [5]. DL models exhibited better results and attained significant attention in natural language processing, computer vision, and speech recognition. DL models have been introduced in healthcare sector due to its better performance in various fields and fast developments of technical enhancements [6]. Several works have also been carried out on DL model for biomedical sector. For instance, Google DeepMind has initiated schemes to utilize its knowledge in medicinal field. In contrast, DL models have not been broadly validated for a wide range of medicinal issue which can get advantages from its abilities [7] . DL have several ways which can be supportive in healthcare, namely multi-modality data, capability of handling complex, superior performance, and end-to-end learning scheme includes characteristic learning etc. Stepping up these works, the entire DL research study should address many issues describing the features of healthcare info requires to upgrade the patterns and tools which allows DL to combine through healthcare workflows and medical decision support [8] . At the same time, the performance of the DL is mainly based on the hyper parameters such as, learning rate, batch size, momentum, and weight decay, which need expertise and wide-ranging trial and error. As a result, the procedure to determine the optimum configuration of the hyper parameters of a DL is still remains a major issue**.**

In this view, this paper presents a new hyperparameters tuned DL models for intelligent medical diagnosis and classification. The proposed model is mainly based on four major processes namely pre-processing, simulated annealing (SA) based feature extraction, recurrent neural network (RNN), gated recurrent units (GRU) and long short term memory (LSTM) based classification and differential evolution (DE) based parameter tuning. A detailed simulation analysis takes place using three benchmark medical dataset namely Diabetes, EEG Eye State and Sleep stage dataset.

2. Related Works

Numerous research methods apply DL to forecast diseases from the status of the patient [9]. Use a 4-layer CNN to identify block of heart failure and chronic obstructive pulmonary disease and demonstrate topmost beneficiary measures. RNN with word embedding, pooling and Long Short-Term Memory (LSTM) concealed unit were applied in Deep Care, an end-to-end deep dynamic network that conclude existing infection declare and calculates upcoming healthcare results. The authors planned to sense LSTM part with a degrade events in handling uneven timed actions (i.e. usually longitudinal EHR). Besides, they included medicinal involvement in the techniques to finding the shapes in a dynamic manner. DeepCare estimates the threat on diabetes in future and psychological healthcare of patient cohort, intervention recommendation, and modelling the evolution of disease [10].

RNN with Gated Recurrent Unit (GRU) are utilized by to design Doctor AI, an end-to-end model which make use of patient's record to calculate diagnose and medication for successive encounter. The valuation indicated notably higher recall compared to low baseline and good believes by adjusting the resulting method from one body to another without losing large accuracy rate [11]. In other aspects, [12] designed a model to study deep patient representation from the EHR via a 3-layer Stacked Denoising Autoencoder (SDA). They apply this novel version on disease to predict the risk by means of random forest as classification model. The validation have been implied on 76,214 patients comprise seventy eight diseases from various medical domains and temporal window (within 1 year). As a finally result, drastically the deep representation direct to better prediction than utilizing raw EHR or conventional representation learning algorithms (e.g. Principal Component Analysis (PCA), k-means). Likewise, they illustrated that result considerably gets better after accumulating a logistic weakening layer on top of the last AE to modify the whole supervised network.

Likewise, [13] use RBM to discover representation of EHR which exposed a novel concept and established an improved approach for predicting accuracy ratio on diseases count . DL was tested to model nonstop time signals, like laboratory result, towards the usual recognition of definite phenotype. For instance,[14] utilized RNN by LSTM to identify the pattern in multivariate time series of experimental dimensions. Especially, a technique has been trained to classify 128 diagnoses from 13 but unevenly sample experimental dimensions from patients in pediatric Intensive Care Unit (ICU). The result shows a major improvement comparing with some sturdy baselines includes multilayer perceptron skill on the hand-engineered type. Use SDA regularize with earlier facts based on ICD-9 for discovering a featured pattern of physiology in medical time sequence [15].

Use a 2-layer stack AE (without regularization) to design a longitudinal series of serum uric acid measurement to differentiate the uric-acid signature of gout and sharp leukemia [16]. Evaluate CNN and RNN with LSTM unit to foresee the beginning stage of disease only from lab-test measures, presenting enhanced output than logistic regression with handcrafted, medically related characteristics [17]. Neural language deep model are applied to EHR, specifically to study embedded representations of the medicinal proposal, equally as diseases, medication and laboratory test that can be used for testing and estimate. As a pattern, use RBM to find out abstraction in ICD-10 cryptogram on a cohort of 7578 logical health patients for forecasting risks of suicide [18]. A wide plan related to RNN obtains capable effects in eliminating protected health details from medical observations to influence the usual de-identification of free-text patient summary. The calculation for not planned patient readmissions after the discharge in recent times receives concentration as well. In this field, presented Deepr, an end-to-end architecture which supports on CNN, which detect and merge medical pattern in the longitudinal patient EHR for stratifying medicinal threats [19]. Deepr carried out fine in forecasting the readmission in six months and have ability to notice significant and interpretable clinical patterns.

3. Objectives

Differential Evolution (DE) is an optimization algorithm. This study aims to apply DE to tune hyper parameter settings of the

deep learning models. The convergence of DE algorithm is evaluated to select optimal hyperparameters on the basis of certain searching process such as crossover, mutation and selection. The enhancement of the accuracy and performance of the proposed model is also determined in comparison with Random search algorithm.

4. The Proposed Model

The working process of the presented model is shown in Figure 1. As shown in Figure, the input data undergoes pre-processing, feature extraction, classification and parameter optimization. Initially, the input data is pre-processed to remove the unwanted data and transform it to a compatible format. Then, SA-FS process takes place to select the useful subset of features. Then, DL models are applied to carry out the classification process. Finally, DE is applied for the parameter optimization of the DL models.

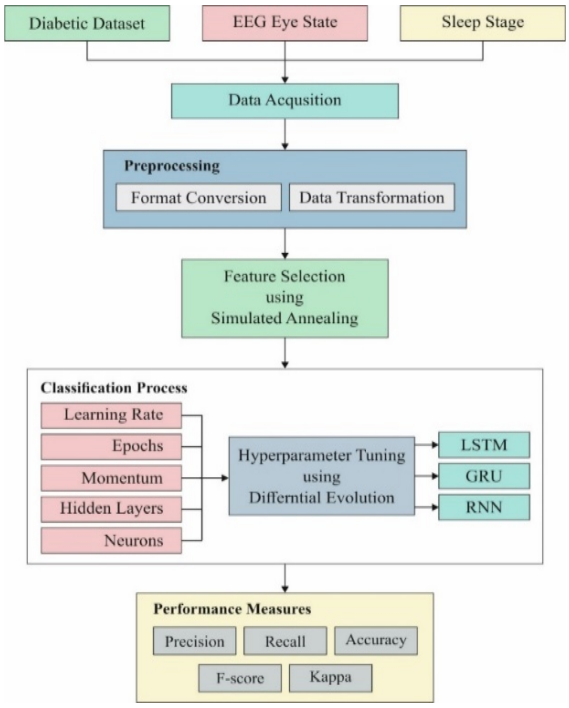


Figure 1: Block diagram of proposed method

4.1. Pre-processing

The major task of data pre-processing is converting the original input data into most intelligible format. As the practical input data is incomplete, there is maximum probability of having error filled data. Thus, data pre-processing is mainly used for transforming the actual data into understandable format which can be applied for next computation. In this approach, pre-processing is carried out in 2 phases such as, Format conversion as well as Data transformation. Initially, format conversion task is conducted when any kind of data type is transformed into .arff format. Then, data transformation is processed with diverse sub-processes as given in the following.

Normalization: This process is applied for scaling the data measures within the specific grade as (-1.0 to 1.0 or 0.0 to 1.0)

Attribute Selection: Novel attributes are obtained from the given set of variables which is applied for mining task in future.

Discretization: Actual measures of mathematical attributes would be interchanged by conceptual levels.

4.2. SA based Feature Selection Process

SA is defined as a processing model of annealing operation. For physical content, the premise should be filled with massive amount of energy and periodically during the cooling operation. When a solution is applied with minimum criterion value, then it is managed using a degree of minimization as well as a current temperature $T(q)$ for all $Q(1 \leq q \leq Q)$ iterations [20]. Followed by, the temperature is slowly reduced while limiting the likelihood of accepting inferior solutions. Some of main components of SA for FS are listed as follows.

- The method to generate initial subset;
- The selection of a temperature rank which is defined by $\text{maximum}\,T(1)$, $\text{minimum}\,T(Q)$, temperature, and cooling scheme.

5. Methodologies

In this section, three DL models namely RNN, GRU and LSTM which are applied for classification process has been discussed in the following subsections.

5.1. RNN based Classification Model

RNN belongs to the NN where the output from existing step is induced as input to the next step. In classical NN, every input and output are autonomous; however, the prediction of a data is processed using previous data and no requirement of memorizing the previous data. Hence, RNN is used to resolve these issues with the help of a hidden layer. The most remarkable feature of RNN is hidden state that saves few data regarding the sequence. RNN is composed of a “memory” that records every detail that has to be determined. It applies similar parameters for every input as it processes the similar operation on hidden layers and produces the better outcome. Finally, the difficulty of parameters is reduced on contrary to alternate NN. Here, NN performs the following operations such as RNN transforms the autonomous activations to dependent activations by generating the similar weights and biases for all layers, and minimize the complications of parameters and remember every existing output by providing the result as input to the subsequent hidden layer. Thus, 3 layers are combined where weights and bias of each hidden layer is identical, that forms an individual recurrent layer.

Training through RNN

The training process involved in RNN is listed as follows.

- A single time step of input is given to the network.
- Determine the present state with the help of recent input and existing states.
- The present h_t forms h_{t-1} for future time step.

- The same is repeated on the basis of problem and combine the data from previous states.
- After completing the last current state then it computes the attained result.
- Then result is related to original output where the desired result and an error are produced.
- The error undergoes back-propagation to the network and improves the weights so that RNN it trained.

5.2. LSTM based Classification Process

LSTM performs the learning operation over a range of prolonged time intervals. It solves the diminishing gradients problem by replacing periodical neuron using complex structural method named as LSTM unit. The LSTM consists of four neural network layer and three gates (input gate, forget gate and output gate) that are used to control the flow of information. These gates are employed using logistic function in order to calculate the values between 0 and 1. The key elements of LSTM are provided in the following and illustrated in Figure 2.

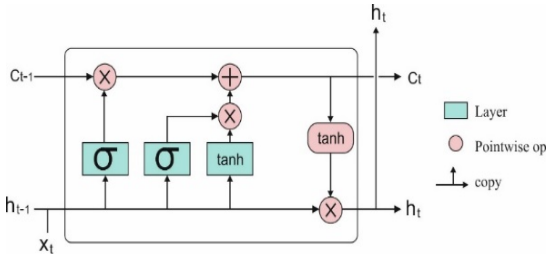


Figure 2: LSTM Model

Input Gate (i_t)

An input gate controls a new value flow into the memory.

Forget gate (f_t)

A forget gate removes the information from the cell state which is no longer required to process. It performs scaling on the internal state of the cell in prior to adding it as input to the cell through the self-recurrent connection of the cell, so adaptively forgetting or resetting the cell's memory

Output Gate (o_t)

It is also a multiplicative unit determines the next hidden state from the current cell state.

Cell State (c_t)

Cell state contains memory unit which maintains all relevant information required for processing. After the gates are closed, data is trapped inside a memory cell. It activates the error signals flowing over several time steps with no consideration of vanishing gradients. The equation of the LSTM units are given below.

$$z_t = tanh(W^z x_t + R^z h_{t-1} + b^z) \quad (1)$$
$$i_t = \sigma(W^i x_t + R^i h_{t-1} + b^i) \quad (2)$$
$$f_t = \sigma(W^f x_t + R^f h_{t-1} + b^f) \quad (3)$$
$$o_t = \sigma(W^o x_t + R^o h_{t-1} + b^o) \quad (4)$$
$$c_t = z_t \odot i_t + s_{t-1} \odot f_t \quad (5)$$
$$h_t = tanh(c_t) \odot o_t \quad (6)$$

5.3. GRU based classification model

The Vanishing-Exploding gradients issue can be solved using RNN. The major scheme is LSTM. A model with minimum popularity but highly productive variations is named as GRU. In contrast to LSTM, it has 3 gates which do not retain the Internal Cell State. The data saved in Internal Cell State in an LSTM recurrent unit is embedded into hidden state of GRU. The collected data is provided to the subsequent GRU. Some of the various gates of a GRU is defined in the following:

Update Gate (z)

It computes the previous knowledge that has to be conveyed to future processing. It is analogous to Output Gate in LSTM recurrent unit.

Reset Gate (r)

It evaluates the older knowledge which has to be discarded. It is analogous to the integration of the Input Gate and Forget Gate in an LSTM recurrent unit.

Current Memory Gate ($\bar{h}_t$)

It is highly applied for GRU process. It is combined into Reset Gate with Input Modulation Gate is a sub portion of Input Gate and applied to establish non-linearity into input and make the input Zero-mean. An alternate reason to make a sub-part of Reset gate is to limit the effect of existing data on recent information which is applied for next computation.

The fundamental task of GRU is related with RNN as defined with few variations between 2 models. Figure 3 shows the structure of GRU model. The inner working process of GRU has gates that change the recent input and existing hidden state. The working of GRU has been discussed as follows. Initially, the input as current input and older hidden state are assumed as vectors. Then, the measures of 3 various gates are computed as follows.

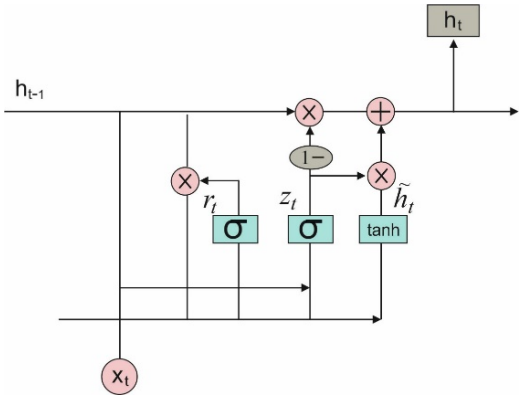


Figure 3: Structure of GRU model

Initially for all gates, determine the parameterized recent input and previous hidden state vectors by processing element-wise multiplication among the assumed vector and the respective

weights. Then, Use the concerned activation function for a gate element-wise on parameterized vectors. The list of gates is provided with the activation function. The task of calculating the recent Memory Gate is different from alternate process. Initially, the Hadamard product of Reset Gate as well as previous hidden state vector has been examined. Then vector undergoes parameterization and included to parameterize recent input vector.

$$\overline{h}_t = \tanh\left(W \odot x_t + W \odot (r_t \odot h_{t-1})\right) \quad (7)$$

The present hidden state is calculated by same vector and dimensions of input are defined. These vectors are indicated by 1. Then compute the Hadamard product of update gate and existing hidden state vector. Also, produces a novel vector by reducing the update gate from ones and determine the Hadamard product of vector present in recent memory gate. Consequently, include 2 vectors for reaching recent hidden state vector.

$$h_t = z_t \odot h_{t-1} + (1 - z_t) \odot \bar{h}_t \quad (8)$$

6. DE based Parameter Optimization Model

The main aim of DL classification model is to optimize the hyper-parameters namely epochs, learning rate, momentum, hidden layers, and neurons with the application of DE method and results in optimal medical data classification. Here, the parameters exist in these methods are Batch size and count of hidden neurons. The DE model is initialized from first solutions that is produced randomly and tries to enhance the accuracy of emotion classification. The Fitness Function (FF) of DL approach is applicable to perform the estimation and provide the accuracy of medical data classification [21]. DE approach was initially coined by Storn. Generally, DE is mainly applied for parameter optimization as well as real value functions. It is a population oriented searching that has been employed extensively for frequent searching process. Currently, the efficiency of DE is represented in various applications like strategy adaptation for global numerical optimization and FS for healthcare diagnosis. Similar to Genetic Algorithm (GA), DE models employs the crossover and mutation; however, the equation is improved in explicit manner. The optimization in DE is composed of 4 phases: initialization, mutation, crossover and selection.

Firstly, the primary population $S_i^t = \{s_{1,i}^t, s_{2,i}^t, , s_{D,i}^t\}, i = 1, .., Np$ has been produced randomly, in which Np implies the population size and t means the recent iteration, where initialization is 0. It is defined for all types of problem space with specific integer ranges constrained by upper as well as lower bounds: $s_j^{low} \le s_{j,i} \le s_j^{up}$, for $j = 1$, 2, D, where D denotes the dimension of problem space. The main objective of this model is to optimize the hyperparameters of RNN, GRU and LSTM networks, hence, the dimension of the problem is $2(D = 2)$. Every vector is combined and develops into candidate solutions$_i^t$, named as target vector, to the multi-dimensional optimization issue. Secondly, in mutation, there are 3 unique vectors $s_{j,p}^t, s_{j,r}^t, s_{j,q}^t$ from population S_i^t are decided arbitrarily to produce novel donor vector v with the help of mutation function

$$v_{j,i}^t = s_{j,p}^t + F_i * \left(s_{j,r}^t - s_{j,q}^t\right) \quad (9)$$

Where F_i depicts the constant lies between $[0, 2]$ defines the mutation factor. It is apparent that, the value of $v_{j,i}^t$ for all dimensions are measured adjacent to integer value. Then, in crossover, the trial vector has been determined for all D dimension of target vector s_i^t and every D dimension of donor vector v_i^t using binomial crossover. Here, the dimension of trial vector is managed by c_r , cross over rate, that is a user based constant from $[0, 1]$.

$$u_{j,i=}^t \begin{cases} v_{i,j}^t \; if \; r \le c_r \; or \; j = J_{rand} \\ s_{i,j}^t \qquad otherwise \end{cases} \quad (10)$$

where J_{rand} refers the even distributed random integer within $[1, D]$, and r_i represents the shared random value from $[0, 1]$. Finally, in selection, the target vector s_i is related with trial vector u_i , and maximum accuracy is elected and applied for future generation. It is clear that, the selection operation is attained using different deep learning technique, and a vector with effective fitness value is admitted for next iteration. Hence, the last 3 phases are repeated until meeting the termination condition. The entire process of DE based parameter tuning of DL models is provided in Algorithm 1.

Algorithm 1: Differential Evolution with Deep Learning Models (LSTM, GRU, RNN)
Initialization; Population Size (PS), Crossover Rate (CR), Scale Factor (SF), Termination Criteria (TC)

Begin Procedure
while (TC Not Met) **do**
For Each individual, target vector, in the PS;
Mutation: Choose three individuals from the PS arbitrarily and generate a donor vector using Eq. 9
Crossover: Calculate the trial vector for the i[th] target vector using Eq. 10
Selection: Apply LSTM, GRU, RNN Algorithm as fitness function f and evaluate

$$\text{If } f(s_i^t) \le f(u_i^t) \text{ then } s_i^{t+1} = u_i^t$$
$$\text{Else } s_i^{t+1} = s_i^t$$

End For
End While
End Procedure

7. Performance Validation

7.1. Dataset used

The performance of the proposed model undergo validation against three benchmark medical dataset namely diabetes, EEG EyeState (UCI Machine Learning Repository) and Sleep Stage dataset (physionet.org). The details of the dataset are shown in Table 1. The first diabetes dataset includes a total of 101766 instances with the existence of 49 features. Besides, the number of classes in diabetes dataset is two, where 78363 instances comes under positive class and remaining number of 23403 instances falls into negative class.

Table 1: Dataset Description

Dataset Type	Description	Values
Diabetes	Number of Instances	101766
	Number of Attributes	49
	Number of Class	2
	Number of Positive Samples	78363
	Number of Negative Samples	23403
	Data source	[UCI Repository]
EEG Eye State	Number of Instances	14980
	Number of Attributes	15
	Number of Class	2
	Number of Class 1	82527
	Number of Class 2	6723
	Data source	[UCI Repository]
Sleep Stage	Number of Subjects	25
	Sex Distribution Male	21
	Sex Distribution Female	4
	Average Age	50
	Average Weight	95
	Average Height	173
	Number of Class	5
	Name of the Class	Wake/S1/S2/SWS/REM
	Data source	[Physionet.org]

Next, the second EEG Eye Sate dataset comprises a total of 14980 instances with 15 features. Among the total number of instances, a set of 82527 instances comes under class 1 and the remaining 6723 instances falls into class 2. The duration time of every recording was 117 seconds. Next, diverse eye states monitored for each recording were added manually. Consequently, the corpus dataset was developed with 14980 instances. Every instance has 14 EEG features and an eye-state class (either 0 for open, or 1 for closed). Additionally, the count of instances with open-eye class in the corpus dataset is 8257 (55.12%), at the time of number of closed-eye type instances is 6723 (44.88%). Moreover, the dataset is applied in massive studies. Hence, 3 of the instances' (2 open states, and one closed state) values were outliers and it is applicable to remove from classification process. Finally, the Sleep stage dataset from UCI repository is composed of 25 instances, including 21 male and 4 female instances. It consists of the entire night PSG recordings of 25 persons with sleep-disordered breathing. Every individual recording has 2 EEG channels, two EOG channels, and one EMG channel as well as an annotation file with complete onset time and period of each hypopnea event.

7.2. Results analysis

Table 2 provides the feature selection results of the proposed SA model on the applied dataset. The table values indicated that the SA based model has chosen a collection of 16 features out of 49 features on Diabetes dataset and 9 features out of 15 features on the applied EEG Eye State dataset.

Table 2: Selected features of Simulated Annealing for Applied Dataset

Dataset	Selected Features
Diabetes	4,5,6,14,17,18,19,20,21,22,23,24,27,29,30,31
EEG Eye State	1,3,4,5,7,9,10,11,12

Table 3: Average epoch rate, learning rate, momentum, hidden layers, and neurons by DE and RS optimization models

Methods	Epochs	Learning Rate	Momentum	Hidden Layers	Neurons
DE	100 200 300	0.0001 0.001 0.01	0.0 0.5 0.9	2 4 6	32 64 128
Random Search	100 200 300	0.0001 0.001 0.01	0.0 0.5 0.9	2 4 6	32 64 128

Table 3 tabulates the different hyperparameters tuned by DE and Random Search (RS) optimization algorithms. The optimal hyperparameters determined by the proposed method are number of epochs: 100, learning rate: 0.001, momentum: 0.5, hidden layers: 4 and number of neurons: 64.

Table 4: Performance Analysis of Proposed Method for Applied Datasets

Methods	Measures	Precision	Recall	F-Measure	Accuracy	Kappa
DE-LSTM	**Diabetes**	97.46	96.20	97.23	97.59	92.40
	EEG Eye State	90.13	89.40	90.30	88.52	86.83
	Sleep Stage	92.94	91.65	92.31	93.18	89.58
RS-LSTM	**Diabetes**	96.15	95.62	96.29	95.89	90.39
	EEG Eye State	88.72	88.56	89.71	87.11	85.09
	Sleep Stage	90.63	89.73	90.66	91.49	87.48

Table 4 and Figure 4 (a) (b) (c) shows the classifier outcome of the DE-LSTM model on the applied three datasets to investigate the impact of parameter tuning process. The table values showed that the DE-LSTM model has attained better results over the RS-LSTM on the applied dataset. It can be ensured from the values that the DE-LSTM model has attained a higher accuracy of 97.59% on the applied diabetes dataset whereas the RS-LSTM model has reached to a lesser accuracy of 95.86%. Similarly, on the applied

EEG Eye State dataset, the proposed DE-LSTM model has exhibited better results with the accuracy of 88.52% whereas a slightly lesser accuracy of 87.11% has been achieved by the RS-LSTM model. Likewise, on the applied Sleep Stage dataset, the proposed DE-LSTM has shown its superior performance with the maximum accuracy of 93.18%. Figure 5 shows the loss graph of the RS and DE models on the applied diabetes dataset. The figure indicated the loss rate of the proposed model gets reduced with an increase in number of epochs.

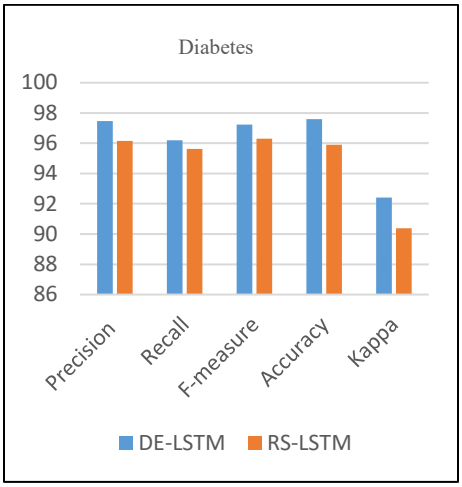


Figure 4 (a) Diabetes

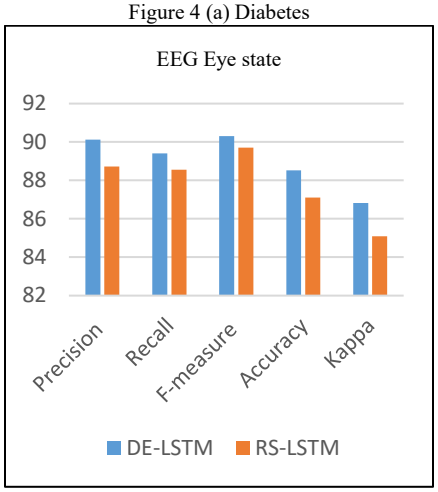


Figure 4 (b) Eye state

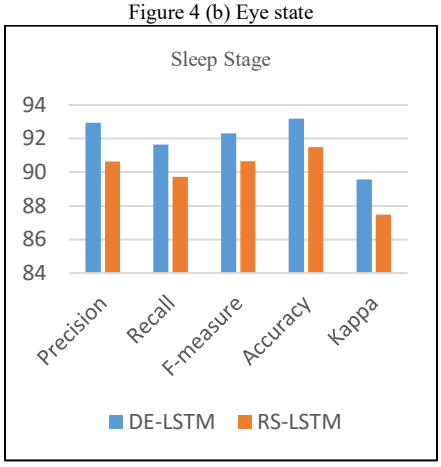


Figure 4 (c) Sleep stage dataset.

Figure 4. Classification results analysis of DE-LSTM and RS-LSTM models (a) Diabetes, (b) EEG Eye State and (c) Sleep stage dataset.

Table 5: Comparison of Proposed DE-LSTM with State of Arts for Diabetes Datasets in terms of Accuracy

Classifiers	Accuracy (%)
DE-LSTM	97.59
DE-GRU	96.34
DE-RNN	92.43
RS-LSTM	95.89
SA-LSTM	95.48
GRU	91.54
RNN	86.87
LSTM	91.75
MLP	81.90

Table 5 and Figure 6 offer a comparative analysis of the proposed models on the applied diabetes dataset in terms of accuracy. The

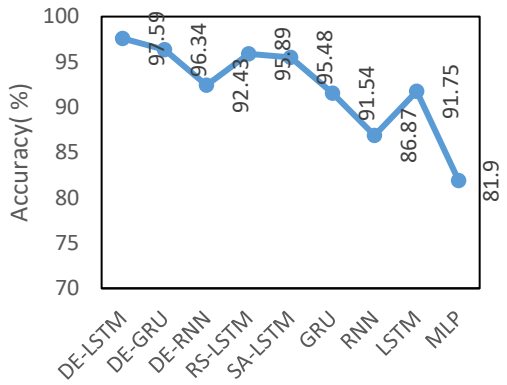


Figure 6. Accuracy analysis of various models on Diabetes Datasets

Table 6: Comparison of Proposed DE-LSTM with State of Arts for EEG Eye State in terms of Accuracy

Classifiers	Accuracy (%)
DE-LSTM	88.52
DE-GRU	87.14
DE-RNN	85.23
RS-LSTM	87.11
SA-LSTM	84.49
GRU	80.65
RNN	78.94
LSTM	81.78
Linear SVM	55.12
HMM	54.12

experimental values indicated that the RNN and MLP models have stated ineffective performance by attaining minimal accuracy values of 86.87% and 81.90% respectively. Next to that, the GRU and MLP models have reached to slightly higher and closer accuracy values of 91.54% and 91.75% respectively. Then, the DE-RNN model has accomplished better results with the accuracy of 92.43%. Simultaneously, the RS-LSTM and SA-

LSTM models have accomplished manageable results with the closer accuracy values of 95.89% and 95.48% respectively. On continuing with, the near optimal accuracy of 96.34% has been offered by the DE-GRU model. However, the DE-LSTM model has outperformed all the compared methods with the maximum accuracy of 97.59%.

Table 6 and Figure 7 provide a comparative analysis of the presented models on the applied EEG Eye State with respect to accuracy. The experimental values implied that the Linear SVM as well as HMM methods have shown inferior function by reaching lower and same accuracy values of 55.12%. Then, the RNN and GRU models have attained better and nearby accuracy values of 78.94% and 80.65% correspondingly. Followed by, the LSTM and SA-LSTM approaches have achieved manageable accuracy values of 81.78% and 84.49% respectively. At the same time, the DE-RNN and RS-LSTM models have obtained considerable results with the nearby accuracy values of 85.23% and 87.11% correspondingly. Along with that, the near optimal accuracy of 87.14% is provided by the DE-GRU model. Thus, the DE-LSTM model has performed well than other approaches with the higher accuracy of 88.52%.

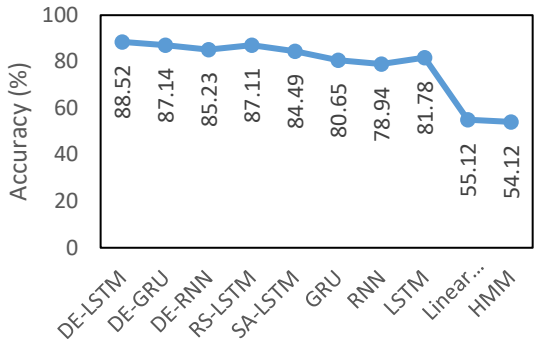


Figure 7: Accuracy analysis of various models on EEG Eye State

Table 7: Comparison of Proposed DE-LSTM with State of Arts for Sleep Stage Dataset in terms of Accuracy

Classifiers	Accuracy (%)
DE-LSTM	93.18
DE-GRU	91.57
DE-RNN	87.93
RS-LSTM	91.49
GRU	85.42
RNN	82.19
LSTM	86.45
CNN	78.23
5C-CNN	83.20
7C-CNN	87.50
9C-CNN	89.00
11C-CNN	90.12
DBN	72.20
SAE	77.70
RBF	81.70

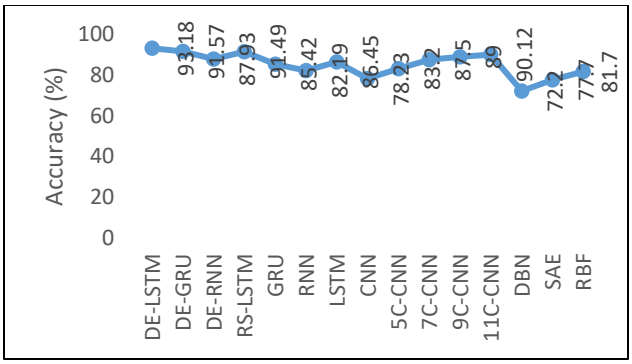


Figure 8: Accuracy analysis of various models on Sleep Stage Dataset

Table 7 and Figure 8 show a comparative analysis of the proposed method on the given Sleep Stage Dataset in terms of accuracy. The experimental values showcased that the DBN model has revealed poor performance by accomplishing lower accuracy values of 72.20%. Then, the SAE, CNN and RBF models have attained reasonable performance and closer accuracy values of 77.70%, 78.23% and 81.70% respectively. Next to that, the RNN, 5C-CNN and GRU methods have achieved appreciable results with the accuracy values of 82.19%, 83.20% and 85.42% respectively. Meantime, 7C-CNN, LSTM and DE-RNN frameworks have attained better results with the near accuracy values of 86.45%, 87.50% and 87.93% correspondingly. Concurrently, the 9C-CNN, 11C-CNN and RS-LSTM methodologies have performed better results with accuracy values of 89%, 90.12% and 91.49% respectively. In line with this, the closer and best accuracy of 91.57% has been provided by the DE-GRU model. Therefore, the DE-LSTM model functions an outstanding performance of related models with optimal accuracy of 93.18%. From the above mentioned tables and figures, it is evident that the proposed DE-LSTM model can be employed as an appropriate medical data classification model. Besides, it is ensured that the inclusion of hyper parameter tuning technique helps to improvise the classification performance.

8. Conclusion

This paper has presented a new hyperparameters tuned DL models for intelligent medical diagnosis and classification. The proposed model involves different processes namely pre-processing, feature extraction, classification, and parameter optimization. Initially, the input data is pre-processed to remove the unwanted data and transform it to a compatible format. Then, SA-FS process takes place to select the useful subset of features. Then, DL models are applied to carry out the classification process. Finally, DE is applied for the parameter optimization of the DL models. A detailed simulation analysis takes place using three benchmark medical dataset namely Diabetes, EEG Eye State and Sleep stage dataset. The simulation outcome indicated that the DE-LSTM model have shown better performance with the maximum accuracy of 97.59%, 88.52% and 93.18% on the applied diabetes, EEG Eye State and Sleep stage dataset. In future, the performance of the proposed models can be improved by the use of clustering techniques and learning rate scheduler.

Conflict of Interest

The authors declare no conflict of interest.

References

[1]. A. Gottlieb, G.Y. Stein, E. Ruppin, R.B. Altman, R. Sharan, "A method for inferring medical diagnoses from patient similarities," BMC Medicine, **11**, 194, 2013, doi:10.1186/1741-7015-11-194.

[2]. R. Miotto, F. Wang, S. Wang, X. Jiang, J.T. Dudley, "Deep learning for healthcare: Review, opportunities and challenges," Briefings in Bioinformatics, **19**(6), 1236-1246, 2017, doi:10.1093/bib/bbx044.

[3]. I. Tobore, J. Li, L. Yuhang, Y. Al-Handarish, A. Kandwal, Z. Nie, L. Wang, "Deep learning intervention for health care challenges: Some biomedical domain considerations," Journal of Medical Internet Research, **7**(8), e11966, 2019, doi:10.2196/11966.

[4]. R. Bellazzi, B. Zupan, "Predictive data mining in clinical medicine: Current issues and guidelines," International Journal of Medical Informatics,**77**(2), 81-97, 2008, doi:10.1016/j.ijmedinf.2006.11.006.

[5]. G. LeCun, Y., Bengio, Y., Hinton, "Deep learning. Nature," **521** (7553), 436–444, 2015, doi:10.1038/nature14539.

[6]. T. Young, D. Hazarika, S. Poria, E. Cambria, " Recent trends in deep learning based natural language processing [Review Article], " IEEE Computational Intelligence Magazine, **13**(3), 55-75, 2018, doi:10.1109/MCI.2018.2840738.

[7]. J. Powles, H. Hodson, "Google DeepMind and healthcare in an age of algorithms," Health and Technology, **7**(4), 351-367, 2017, doi:10.1007/s12553-017-0179-1.

[8]. A. Qayyum, J. Qadir, M. Bilal, A. Al Fuqaha, "Secure and Robust Machine Learning for Healthcare: A Survey," IEEE Reviews in Biomedical Engineering, 2020, doi:10.1109/RBME.2020.3013489.

[9]. Y. Cheng, F. Wang, P. Zhang, J. Hu, "Risk prediction with electronic health records: A deep learning approach," in 16th SIAM International Conference on Data Mining, 432-440, 2016, doi:10.1137/1.9781 611974348.49.

[10]. T. Pham, T. Tran, D. Phung, S. Venkatesh, "Predicting healthcare trajectories from medical records: A deep learning approach," Journal of Biomedical Informatics, 16, 218-229, 2017, doi:10.1016/j.jbi. 2017.04.001.

[11]. E. Choi, M.T. Bahadori, A. Schuetz, W.F. Stewart, J. Sun, "Doctor AI: Predicting Clinical Events via Recurrent Neural Networks.," JMLR Workshop and Conference Proceedings, 301-318, 2016.

[12]. R. Miotto, L. Li, B.A. Kidd, J.T. Dudley, "Deep Patient: An Unsupervised Representation to Predict the Future of Patients from the Electronic Health Records," Scientific Reports, 6(1), 1-10, 2016, doi:10.1038/srep26094.

[13]. Z. Liang, G. Zhang, J.X. Huang, Q.V. Hu, "Deep learning for healthcare decision making with EMRs," in Proceedings IEEE International Conference on Bioinformatics and Biomedicine(BIBM),556-559, 2014, doi:10.1109/BIBM.2014.6999219.

[14]. Z.C. Lipton, D.C. Kale, C. Elkan, R. Wetzel, "Learning to diagnose with LSTM recurrent neural networks," in 4th International Conference on Learning Representations, ICLR 2016 - Conference Track Proceedings, 2016.

[15]. Z. Che, D. Kale, W. Li, M.T. Bahadori, Y. Liu, "Deep computational phenotyping," in Proceedings of the ACM SIGKDD International Conference on Knowledge Discovery and Data Mining, 507-516, 2015, doi:10.1145/2783258.2783365.

[16]. T.A. Lasko, J.C. Denny, M.A. Levy, "Computational Phenotype Discovery Using Unsupervised Feature Learning over Noisy, Sparse, and Irregular Clinical Data," PLoS ONE, **8**(6), e66341, 2013, doi:10.1371/journal.pone.0066341.

[17]. D. Kollias, A. Tagaris, A. Stafylopatis, S. Kollias, G. Tagaris, "Deep neural architectures for prediction in healthcare," Complex & Intelligent Systems, 4(2),119-131, 2018, doi:10.1007/s40747-017-0064-6.

[18]. T. Tran, T.D. Nguyen, D. Phung, S. Venkatesh, "Learning vector representation of medical objects via EMR-driven nonnegative restricted Boltzmann machines (eNRBM)," Journal of Biomedical Informatics, **54**, 96-105, 2015, doi:10.1016/j.jbi.2015.01.012.

[19]. P. Nguyen, T. Tran, N. Wickramasinghe, S. Venkatesh, "Deepr: A Convolutional Net for Medical Records," IEEE Journal of Biomedical and Health Informatics, **21**, 22-30, 2017, doi:10.1109/JBHI.2016. 2633963.

[20]. R. Panthong, A. Srivihok, "Wrapper Feature Subset Selection for Dimension Reduction Based on Ensemble Learning Algorithm," in Procedia Computer Science, **72**, 162-169, 2015, doi:10.1016/j.procs. 2015.12.117.

[21]. B. Nakisa, M.N. Rastgoo, A. Rakotonirainy, F. Maire, V. Chandran, "Long short term memory hyperparameter optimization for a neural network based emotion recognition framework," IEEE Access, **6**, 49325-49338, doi:10.1109/ACCESS.2018.2868361.

ASTES

Advances in Science, Technology and Engineering Systems Journal Vol. 5, No. 5, 262-268 (2020)

www.astesj.com

Special Issue on Multidisciplinary Innovation in Engineering Science & Technology

ASTESJ

ISSN: 2415-6698

A Novel Demand Side Management by Minimizing Cost Deviation

Vikas Anand Vatul[1], Arputha Aravinth [1], Narayanan K[*,1], Gulshan Sharma[2], Tomonobu Senjyu[3]

[1]*EEE Department, SASTRA Deemed University, Thanjavur, Tamil Nadu, India*

[2]*Department of Electrical Power Engineering, Durban University of Technology, South Africa*

[3]*Power and Energy System Control Laboratory, University of the Ryukyus, Japan*

ARTICLE INFO

Article history:
Received: 20 July, 2020
Accepted: 01 September, 2020
Online: 17 September, 2020

Keywords:
Power Systems
Energy System
Demand Side Management
Aggregated Energy
Pricing Model
Smart Grid
Renewable Energy

ABSTRACT

In the recent times power shortage has been a major setback to deal for the effective operation of power systems. Bridging the gap between generation and demand is known as Demand Side Management (DSM). For an effective DSM strategy to be implemented, it is crucial that both utility and customers be involved. By DSM, the energy generated is used more effectively. This reduces the burden of the utility to invest on additional generation. In this work, a DSM strategy has been performed on two systems: (i) on RTS 24 bus system with wind energy sources distributed at some nodes of the system (ii) on an institutional load with installed solar power plant. A generic DSM strategy to effectively utilize the generated energy and to minimize the utility bills for the customer has been proposed. An instantaneous billing scheme has been proposed. By implementing the instantaneous billing scheme, customers can be persuaded to change their consumption behavior, matching the demand with available generation. The results obtained are promising, with a resulting flat load profile and reduced utility bills for the customer.

1. Introduction

Demand Side Management (DSM) has been in practice from the 20th century. Initially, DSM was implemented by replacing older equipment with a newer one for improved efficiency. DSM effectively reduces the gap between supply and demand with the help of various services. DSM is performed by suggesting adjustment in the electricity consumption of the customer to produce desired changes in the power distribution system. Some DSM strategies used to alter customers' load profiles involve load shedding, valley filling, peak clipping, flexible load shape, strategic load growth, strategic conservation and load shifting [1]. The final load profile for each system depends on the operational requirement of the system. Performing DSM has the same objective to minimise customers' utility bills and to reduce Peak to Average Ratio (PAR) by taking up different pricing models in many researches. By performing DSM, electrical infrastructure can be utilised effectively, and new investments on the same can be deferred. Price billing schemes are an important aspect of performing DSM. In recent times, instantaneous load billing scheme has been used to perform DSM. By implementing this billing scheme, the price at each hour can be changed depending on the aggregated load at that hour.

A quadratic cost function has been used with the motive of reducing the total cost and minimize PAR with a simple billing mechanism for the subsequent period is proposed in [2]. This does not consider peak classification during the day, making it unfair to the customer by billing them similar at all times of the day based only on energy consumption. Some pricing models have been introduced and mapping between retail users and wholesale electric prices is portrayed in [3]. The motive was to improve utilization of cumulative generated energy and reduce energy cost by wholesale mapping of energy requirement [3]. A polynomial cost function with time-dependent coefficients has been used in [4]. The focus was to find the aggregated energy consumption and the selfish customers would modify their energy consumption in order to reduce their energy prices. The time slots have been classified in [4] as on peak, mid-peak and off-peak. Coefficients are time-dependent and are assigned based on the peak

[*]Corresponding Author Narayanan. K, EEE Department, SASTRA Deemed University, Thanjavur, Tamil Nadu, India. Mob: +91-9790258910 Email: narayanan.mnit@gmail.com

classification. The coefficients are based on the currency used in the billing.

A system with industrial, commercial and residential loads have been considered to perform DSM in [5] and hourly costs were paralleled with the costs in [6]. In [5], a logarithmic pricing model was used to compute the energy consumption price and a load shifting based on average cost was devised to perform DSM. The hourly prices were lower when compared to the strategy by [6] which uses a heuristic algorithm to minimise utility costs. [2]-[6] are pivotal to this work as a mathematical pricing model for energy consumption is a significant element for performing DSM.

DSM using strategic conservation is portrayed in [7]. In the study, some customers with the presence of Distributed Generators (DGs) were considered. The key highlights of the study were bi-directional energy flow from customer to grid, incentives and balancing, mass-produced renewable energy. In [8], discharge of Plug-in Hybrid Electric Vehicle (PHEV) during peak demand was used for DSM. Since different utilities use different pricing methodologies, the concept of cost efficiency as a metric to determine the consumption efficiency is explained in [9]. Home Load Management Systems (HLM) used to achieve residential load management, without focusing on electricity pricing has been discussed in [10]. The concept of coordinated demand response of residential customers in a smart grid has been highlighted. A price model as a ratio of total connected load at that instant to the total aggregated load through all time slots is proposed in [11]. It emphasizes on analysing a realistic situation by considering realistic consumer behaviour to determine the participation of the consumer in DSM. Though the work mentions to account for the realistic situation, deviation of load demand from the forecasted data has been over looked while performing DSM.

A standalone, Hybrid energy source with a combination of wind and solar energy has been designed to electrify a village in India in the study performed in [12]. The design aspects included solar irradiation and wind speed and the objective was to optimize the size of the energy source without affecting the performance of the same. In [13], planning of distributed sources such as distributed generators and shunt capacitors to achieve objectives on technical, economical and societal levels are discussed. Expansion of a micro-grid due to increasing load demand are discussed in [14] with wind turbines, Solar energy source, and batteries. The expansion is carried out in an isolated micro-grid and load forecasting with uncertainties are considered in the research.

In this work, two systems are considered: (i) IEEE 24 bus Reliability Test System (RTS 24) with integrated Windmills [15] and (ii) an institutional energy consumption model with integrated solar panels. Any deviation in the load demand from the forecasted base load is taken into account in the proposed pricing model. This makes the proposed pricing model realistic and practical since load demands are dynamic and seldom match with the forecasts. A polynomial cost function in which coefficients are based on off-peak, mid-peak and on-peak hours from a previously referenced research is also considered and analysed. Load shifting algorithm has been developed to reduce the deviation of hourly load demand from the fixed base load. This has proved to reduce consumers aggregated energy cost for the day and to acquire a flat load profile. This will also reduce PAR and enhance the efficiency of the power system.

2. System Model

Two systems were considered to apply the proposed method. It has been assumed that all the consumers were equipped with HLMs (Home load management systems) or smart meters. IEEE 24-bus reliability test system (RTS 24) with wind energy source of 200MW at six different points in the grid is considered as system 1. Hourly load demand for System 1 is acquired from [15] and the wind scenarios are acquired from [16]. An institution in which a connected load of 4000kW and decentralised solar power plant of an installed capacity of 1.25MW is considered as system 2. Since, an institutional load is considered, all loads are assumed to be shift able during any period of the day.

The RTS – 24 bus system has been considered since it has installed wind energy, which is operational for the entire 24 hours of the day. Since load considered in the RTS 24 bus system is more flexible in contrast to the institutional load considered, it offered a better scope for analysis.

Assuming load demand for future 'm' operational periods has been forecasted to perform Demand Side Management. The consumption of energy for 'm' time slots can be formulated for any random customer 'j' as

$$p_j = (p_j^1, \ldots\ldots, p_j^m) \tag{1}$$

where p_j^m is the consumption of energy at the m^{th} hour by customer 'j'. The energy profile of the consumer is subject to a maximum and minimum constraint.

$$p_{min}^m < p^m < p_{max}^m \tag{2}$$

where p_{max}^m is the maximum energy consumption limit at hour 'm' and p_{min}^m is the minimum energy consumption limit at hour 'm'.

Energy generation from the renewable energy source is also assumed to be forecasted beforehand to perform DSM. The renewable energy output can be formulated as

$$g_j = (g_j^1, \ldots\ldots, g_j^m) \tag{3}$$

where g_j^m is the energy output from the installed renewable source at the m^{th} hour by customer 'j'. It is assumed that the solar plant installed in System 2 can generate energy only during the day time.

3. Problem Formulation

The aim of the study is to minimise energy consumption bills of the consumer without affecting their routine in terms of energy usage.

The suggested DSM considers systems with installed renewable sources. By considering generation from renewable sources, the effective demand from utility reduces. Thus, the cost will also reduce in this case. Energy consumption from the utility can be mathematically computed by

$$E_j^m = p_j^m - g_j^m \quad (4)$$

Where E_j^m is the energy requirement from the utility for customer 'j' at the m^{th} hour.

A pricing model has been proposed and is compared with a realistic polynomial pricing model [4]. The pricing models have been incorporated in the proposed Demand Side Management. The polynomial cost function [4] used was

$$Ch(Lh) = a(Lh^b) + c \quad (5)$$

where Lh is the hourly load in kWh or MWh, price parameters are given as

$$a > 0\ ;\ b \geq 1\ ;\ c \geq 0 \quad (6)$$

4. Proposed Price Model

The suggested pricing model is based on the fixed base load of the system for the particular day and deviation of hourly energy consumption from the base load at each time period. The suggested pricing model can be formulated as

$$\gamma(h) = x \times (\beta) + y \times (\delta) \quad (7)$$

$$\delta = p^m - \beta \quad (8)$$

$$x, y > 0 \quad (9)$$

where p^m is the energy consumption of the consumer at the m^{th} hour and 'x' & 'y' are the cost coefficients. 'y' is a time dependent factor and is assigned based on peak timings. 'δ' is the deviation of hourly energy consumption from the base load 'β'. This cost function is more appropriate for DSM, as utility bills of the consumers can be minimised by offsetting the deviation of the energy consumption at that time slot by different methods and services. This price model has been developed from the polynomial cost function and indicates energy consumption prices in cents per kWh or MWh used.

The proposed pricing model possesses important features that are essential for an energy pricing model to be used in DSM. It is a convex cost function; it rapidly increases with an increase in hourly energy consumption.

A generic DSM algorithm has been proposed for any system with forecasted energy generation from the renewable energy source, forecasted load demand at each time slot and a base load of the system.

5. Proposed DSM and Load Shifting Model

Proposed DSM includes energy generation from renewable source installed in the system. By doing so, energy consumption of the consumer from the utility will reduce. This will reflect on the utility bills of the customer for the same energy requirement. The above-discussed cost functions are incorporated to evaluate the utility bills for the customers against their energy usage. A load shifting algorithm has been developed to minimise the hourly deviations at certain time slots. Flowchart for the proposed DSM is shown in Figure 1.

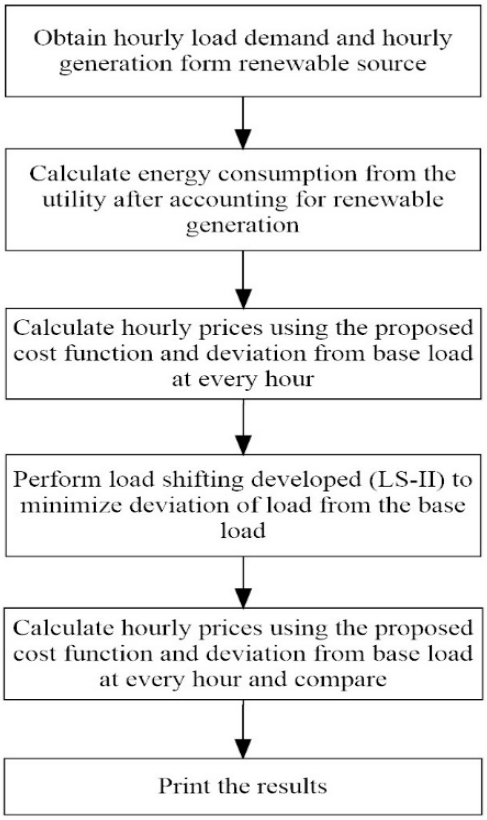


Figure 1: Proposed DSM

A load shifting method is developed to offset the deviation of the load demand from the fixed base load in the time slot under consideration. Load shifting is one among many DSM strategies, where loads from certain time slots of the day are shifted to other time slots to reduce peak demand without creating a new peak at a different time slot. Controllable and non-controllable (critical loads) loads are the two types of loads present in a system. Controllable loads are loads that can be shifted without any constraint and non-controllable loads are those that cannot be shifted [1].

Peaks timings are considered from [4] and each time in a day has been classified as On-peak, Mid-peak, and Off-peak based on the load forecast at that hour. The developed load shifting algorithm aggregates the loads exceeding the base load at each time slot within the peak timings and equally spreads the loads within the peak classifications.

Time slots at on-peak, mid-peak and off-peak is taken as m1, m2, m3 respectively. Fixed base loads at on peak, mid-peak and off-peak are assumed as B1, B2, B3 respectively. The aggregated load at on peak, mid-peak and off-peak periods are given as

$$S1 = \sum[p(m) - B1] \quad (10)$$
$$S2 = \sum[p(m) - B2] \quad (11)$$
$$S3 = \sum[p(m) - B3] \quad (12)$$

where S1, S2, S3 are the aggregated load that exceeds the base load in each peak period and $p(m)$ is the load demand of the consumer in m^{th} hour.

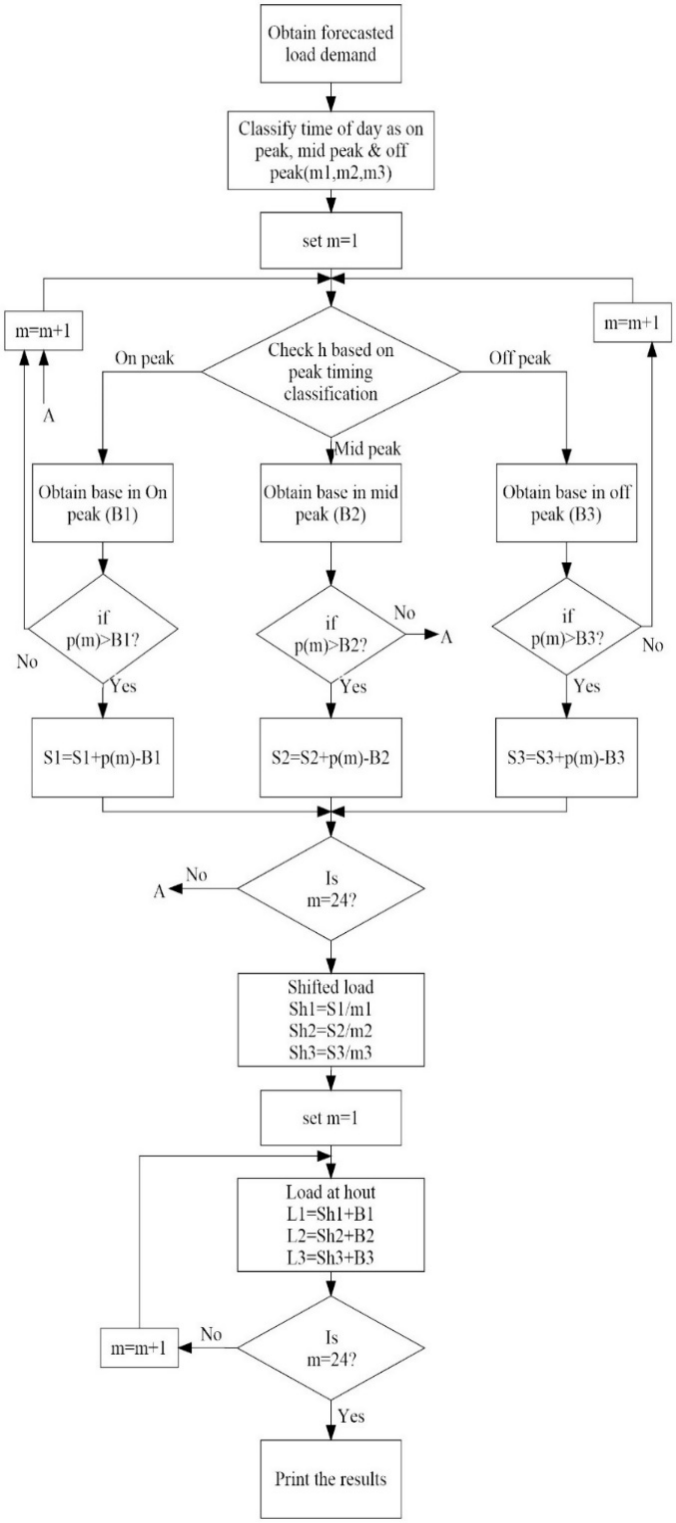


Figure 2: Load Shifting Algorithm

Load to be shifted from on-peak, mid-peak and off-peak can be formulated as

$$Sh1 = S1/m1 \quad (13)$$
$$Sh2 = S2/m2 \quad (14)$$
$$Sh3 = S3/m3 \quad (15)$$

where $Sh1, Sh2\ and\ Sh3$ depict the loads that needs to be shifted within on-peak, mid-peak and off-peak hours respectively. The load demand of the consumer at each peak period after performing the shifting can be formulated as

$$L1 = Sh1 + B1 \quad (16)$$
$$L2 = Sh2 + B2 \quad (17)$$
$$L3 = Sh3 + B3 \quad (18)$$

here, $L1, L2\ and\ L3$ represent the load demand at on-peak, mid-peak and off-peak hours after performing load shifting.

The developed load shifting algorithm is represented as a flowchart below in Figure 2.

6. Numerical Results

Numerical results of the proposed DSM are presented and are compared with polynomial pricing model [4]. The entire time frame under consideration has been classified into on peak, mid-peak and off-peak hours. 'a' in the polynomial cost function and 'y' in the proposed cost function is set as 0.003 from 12 Midnight to 7AM (Off-peak), as 0.004 from 7AM to 4PM & 10PM to 12 Midnight (Mid-peak) and 0.005 from 4PM to 10PM (On-peak), 'b' and 'c' are set as 1 and 0 respectively for all M∈m.

The proposed DSM has been carried out on System 1 (RTS 24). System data [15], Load management including the renewable generation and load shifting is shown in Figure 3.

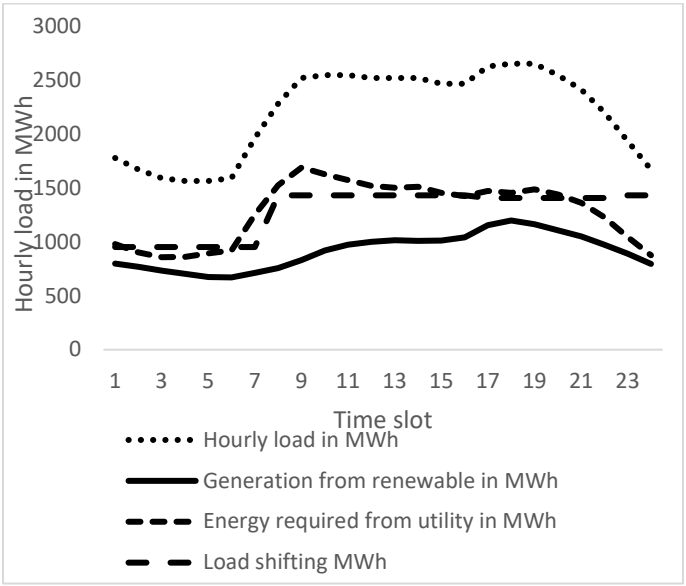


Figure 3: Proposed DSM on System 1

For System 2, peak timing has been classified in a slightly different manner taking into account the consumption pattern of the institutional load. Off-peak from 12 Midnight to 6 AM & 10PM to 12 Midnight; mid-peak from 9AM to 5PM and on-peak from 6AM to 9AM & 5PM to 10PM.

The proposed DSM was carried out on System 2. System data and Load management after including energy generation from the renewable source and load shifting are shown in Figure 4.

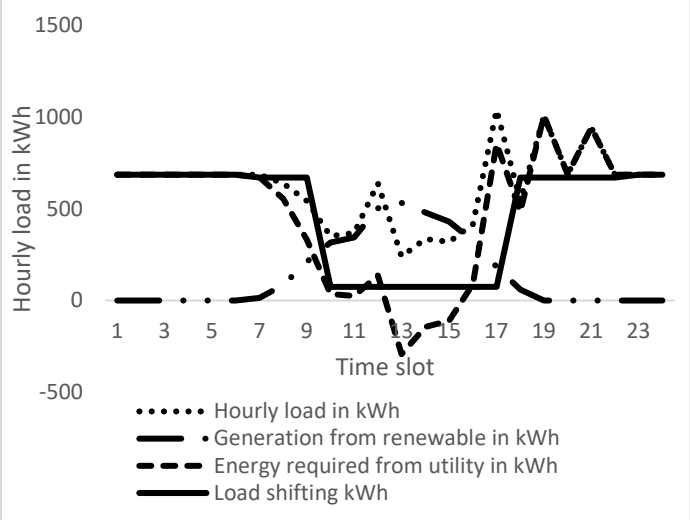


Figure 4: Proposed DSM on System 2

Hourly energy prices for System 1 and System 2 are calculated using the proposed pricing model and compared with the polynomial cost function [4]. Energy prices at each time slot for System 1 before and after load shifting, by polynomial and proposed cost functions are shown in Table 1.

Table 1: Hourly energy prices by polynomial and proposed cost function on System 1

Time slots	Hourly load in MWh	Polynomial cost function [4]		Proposed cost function	
		Before load shifting	After load shifting	Before load shifting	After load shifting
1	978.6	2.9358	2.8543	6.0634	4.7572
2	901.2	2.7036	2.8543	5.8312	4.7572
3	857.2	2.5717	2.8543	5.6993	4.7572
4	860.2	2.5807	2.8543	5.7083	4.7572
5	891.6	2.6748	2.8543	5.8024	4.7572
6	920.4	2.7612	2.8543	5.8888	4.7572
7	1250.8	3.7524	2.8543	6.88	4.7572
8	1524.4	6.0976	5.7223	7.6614	6.6738
9	1688.1	6.7525	5.7223	8.3163	6.6738
10	1625	6.4999	5.7223	8.0637	6.6738
11	1572.8	6.2911	5.7223	7.8549	6.6738
12	1519.6	6.0783	5.7223	7.6421	6.6738
13	1502.3	6.0092	5.7223	7.573	6.6738
14	1508.3	6.0332	5.7223	7.597	6.6738
15	1452.2	5.8087	5.7223	7.3725	6.6738
16	1424.1	5.6963	5.7223	7.2601	6.6738
17	1470.3	7.3516	7.0313	7.3516	7.0313
18	1453	7.2648	7.0313	7.2648	7.0313
19	1486.7	7.4337	7.0313	7.4337	7.0313
20	1437.5	7.1877	7.0313	7.1877	7.0313
21	1362.1	6.8107	7.0313	6.8107	7.0313
22	1227.9	6.1396	7.0313	6.1396	7.0313
23	1045	4.18	5.7223	5.7438	6.6738
24	874.8	3.499	5.7223	5.0628	6.6738
Total:	30834.1	125.1141	125.1132	164.2091	148.9

It can be observed from Table 1 that with the given cost function using the proposed DSM, hourly costs during on-peak periods are scaled to a price highest of the three followed by mid-peak and off-peak periods. This is detected because of the development of coefficients in the proposed cost function pertaining to peak timings. These coefficients influence the cost of electric power during a given time of the day.

Energy prices at each time slot for System 2 before and after applying the load shifting algorithm are given in Table 2.

Table 2: Hourly energy prices by polynomial and proposed cost function on System 2

Time slots	Hourly load in kWh	Polynomial cost function [4]		Proposed cost function	
		Before load shifting	After load shifting	Before load shifting	After load shifting
1	686.4	2.0592	2.0592	2.5392	2.2082
2	686.4	2.0592	2.0592	2.5392	2.2082
3	686.4	2.0592	2.0592	2.5392	2.2082
4	686.4	2.0592	2.0592	2.5392	2.2082
5	686.4	2.0592	2.0592	2.5392	2.2082
6	686.4	2.0592	2.0592	2.5392	2.2082
7	672.2	4.0335	4.0272	3.7935	3.9527
8	555.1	3.3304	4.0272	3.0904	3.9527
9	331.6	1.9898	4.0272	1.7498	3.9527
10	35.3	0.1412	0.2979	0.3812	0.3724
11	24.4	0.0976	0.2979	0.3376	0.3724
12	136.6	0.5465	0.2979	0.7865	0.3724
13	-292.9	-1.1714	0.2979	-0.9314	0.3724
14	-144.8	-0.5793	0.2979	-0.3393	0.3724
15	-109.6	-0.4382	0.2979	-0.1982	0.3724
16	90	0.3601	0.2979	0.6001	0.3724
17	856.8	3.427	0.2979	3.667	0.3724
18	484.2	2.9054	4.0272	2.6654	3.9527
19	1008	6.048	4.0272	5.808	3.9527
20	688	4.128	4.0272	3.888	3.9527
21	944	5.664	4.0272	5.424	3.9527
22	686.4	4.1184	4.0272	3.8784	3.9527
23	686.4	2.0592	2.0592	2.5392	2.2082
24	686.4	2.0592	2.0592	2.5392	2.2082
Total:	11456.5	51.0746	51.0744	54.9146	52.2664

It can be observed from Table 2 that renewable energy generation from the solar installations is higher than the load demand of 13th, 14th and 15th hour. By performing the proposed load shifting ensures effective usage of the generated renewable energy during all time slots in the day. The shiftable loads during other time slots avail the excess energy beyond the demand in these time slots.

It can be observed from Table 1 and Table 2, by the proposed pricing model, aggregated hourly cost after shifting is lesser than the aggregated hourly cost before shifting. The overall cost has been reduced by reducing the hourly deviation by load shifting at certain time slots.

Cost-benefit of the proposed cost function is depicted in Table 3. It is observed that there is a significant cost benefit with the proposed cost function after shifting during the mid-peak and off-peak hours in both the systems where as there is a meagre change in the aggregated cost on the on-peak hours.

It can be observed from Figure 3 and 4, by the proposed DSM, the energy requirement is not compromised, while it is being met efficiently. By performing the proposed DSM, a flat load profile can be obtained for certain timeslot thus improving Peak to Average Ratio.

It is a superior substitute to previously existing instantaneous energy billing models. The customers will not have to downsize their consumption but have to shift non-essential consumption to reap benefit in the proposed DSM. Participation of customers in DSM would increase, to minimize their deviation from the already predicted fixed base load with the knowledge of the deviation from base load from the HLM.

Table 3: Cost-benefit with the proposed Cost function on system 1 and 2

Cost-Benefit of proposed cost function on System 1		
Peak Classification	Before Load Shifting	After Load Shifting
On Peak	42.1881	42.1878
Mid Peak	80.1476	73.4118
Off Peak	41.8734	33.3004
Cost-Benefit of proposed cost function on System 2		
On Peak	30.2975	31.6216
Mid Peak	4.3035	2.9792
Off Peak	20.3136	17.6656

7. Conclusion

For a successful DSM, pricing model and billing mechanism are crucial. The proposed pricing model based on the deviation of hourly load demand from the fixed base load has been observed to be a better alternative over the other realistic polynomial cost function.

Renewable generation is unforeseeable and, in most cases, influenced by external factors. The generation from the renewable sources can be higher than the system requirements during some periods in a day and by performing load shifting, generation from renewables can be effectively utilised. By adopting the proposed algorithm, the energy requirement of the system from the utility decreases.

The total cost is reduced after load shifting is performed by the proposed cost function. This is due to the fact that by load shifting, the deviation of the hourly load demand from the fixed base load is reduced at certain time slots and increases in some to have a balanced shifting, but generated energy is effectively utilised. Therefore, the aim to reduce consumers' utility bills are met and peak to average ratio improves by incorporating the proposed DSM.

Conflict of Interest

The authors declare no conflict of interest.

Acknowledgment

The authors would like to thank SASTRA Deemed University for sharing their consumption data and energy generation from their installed solar power plant.

References

[1] B.R. Gupta, 'Generation Of Electric Energy' (S. Chand Limited, 2009)
[2] A.H. Mohsenian-Rad et al., "Autonomous Demand Side Management Based on Game-Theoretic Energy Consumption Scheduling for the Future Smart Grid," IEEE Trans. Smart Grid, **1**(3), 320–331, 2010, doi: 10.1109/TSG.2010.2089069
[3] P. Samadi et al., " Advanced Demand Side Management for the Future Smart Grid Using Mechanism Design," IEEE Trans. Smart Grid, **3**(3), 1170–1180, 2012, doi: 10.1109/TSG.2012.2203341
[4] H.H. Chen, "Autonomous Demand Side Management with Instantaneous Load Billing : An Aggregative Game Approach," IEEE Trans. Smart Grid, **5**(4), 1744–1754, 2014, doi: 10.1109/TSG.2014.2311122
[5] B. Saravanan, "DSM in an area consisting of residential, commercial and industrial load in smart grid," Front. Energy, **9**(2), 211–216, 2015, doi: https://doi.org/10.1007/s11708-015-0351-0
[6] T. Logenthiran et al., "Demand side management in smart grid using heuristic optimization," IEEE Trans. Smart Grid, **3**(3), 1244–1252, 2012, doi: 10.1109/TSG.2012.2195686
[7] I. Atzeni et al., "Demand-Side Management via Distributed Energy Generation and Storage Optimization," IEEE Trans. Smart Grid, **4**(2), 1–11, 2012, doi: 10.1109/TSG.2012.2206060
[8] B. Gao et al., "Game-theoretic energy management for residential users with dischargeable plug-in electric vehicles," Energies, **7**(11), 7499–7518, 2014, doi: https://doi.org/10.3390/en7117499
[9] J. Ma et al., "Residential Load Scheduling in Smart Grid: A Cost Efficiency Perspective," IEEE Trans. Smart Grid, **7**(2), 771–784, 2015, doi: 10.1109/TSG.2015.2419818
[10] A. Safdarian, "Optimal Residential Load Management in Smart Grids: A Decentralized Framework," IEEE Trans. Smart Grid, **7**, (4), 1836–1845, 2016, doi: 10.1109/TSG.2015.2459753
[11] Y. Wang et al., "Load Shifting in the Smart Grid: To Participate or Not?," IEEE Trans. Smart Grid, **7**(6), 2604–2614, 2016, doi: 10.1109/TSG.2015.2483522
[12] S. Rangnekar et al., "Sizing and performance analysis of standalone wind-photovoltaic based hybrid energy system using ant colony optimisation," IET Renew. Power Gener., **10**(7), 964–972, 2016, doi: 10.1049/iet-rpg.2015.0394
[13] N. Kanwar et al., "Optimal distributed resource planning for microgrids under uncertain environment," IET Renew. Power Gener., **12**(2), 244–251, 2018, doi: 10.1049/iet-rpg.2017.0085
[14] Z. Wang et al., "Optimal expansion planning of isolated microgrid with renewable energy resources and controllable loads," IET Renew. Power Gener., **11**(7), 931–940, 2017, doi: 10.1049/iet-rpg.2016.0661
[15] C. Ordoudis et al., "An Updated Version of the IEEE RTS 24-Bus System for Electricity Market and Power System Operation Studies," Technical University of Denmark. 2016.
[16] Data for Stochastic Multiperiod Optimal Power Flow Problem', https://sites.google.com/site/datasmopf/, accessed April 2018.

Appendix

System 2 under consideration was of an institution. The system demand was obtained from SASTRA deemed University on a working day. The renewable utilization from the installed solar plant was also obtained for the same day. It has a connected load of 4000kW and decentralised solar power plant with an installed capacity of 1.25MW.

Table 4 System Data for System 2

Hours	Hourly load in kW	Utilization from Solar plant in kW
1	686.4	0
2	686.4	0
3	686.4	0
4	686.4	0
5	686.4	0
6	686.4	0
7	686.4	14.155
8	640	84.94
9	544	212.36
10	352	316.706
11	368	343.592
12	640	503.37
13	240	532.86
14	336	480.83
15	320	429.56
16	416	325.974
17	1040	183.25
18	544	59.7733
19	1008	0
20	688	0
21	944	0
22	686.4	0
23	686.4	0
24	686.4	0

ASTES

Advances in Science, Technology and Engineering Systems Journal Vol. 5, No. 5, 269-277 (2020)

www.astesj.com

Special Issue on Innovative Research in Applied Science, Engineering and Technology

ASTESJ

ISSN: 2415-6698

Supervised Machine Learning Based Medical Diagnosis Support System for Prediction of Patients with Heart Disease

Oumaima Terrada[1], Soufiane Hamida[1], Bouchaib Cherradi[1, 2], Abdelhadi Raihani[1,*], Omar Bouattane[1]

[1]*Signals, Distributed Systems and Artificial Intelligence laboratory (LSSDIA), ENSET of Mohammedia, Hassan II University of Casablanca, Mohammedia, 28820, Morocco*

[2]*STIE Team, CRMEF Casablanca-Settat, provincial section of El Jadida, El Jadida, 24000, Morocco*

ARTICLE INFO

Article history:
Received: 20 July, 2020
Accepted: 01 September, 2020
Online: 17 September, 2020

Keywords:
Atherosclerosis
Machine learning techniques
Artificial intelligence

ABSTRACT

Application in the field of medical development has always been one of the most important research areas. One of these medical applications is the early prediction system for heart diseases especially; coronary artery disease (CAD) also called atherosclerosis. The need for a medical diagnosis support system is to detect atherosclerosis at the earlier stages to optimize the diagnosis, avoid the advanced cases, and reduce treatment costs. Earlier, the datasets are collected from specific medical sources and have evaluated against computer applications. In this paper, a supervised machine learning medical diagnosis support system (MDSS) for atherosclerosis prediction is presented that able to obtain and learn automatically knowledge from each patient's clinical data. Therefore, we used three Machine Learning (ML) classifiers for the proposed MDSS for atherosclerosis. Thus, this work is accomplished using databases collected from the UCI repository (Cleveland, Hungarian) and Sani Z-Alizadeh dataset. The performance metrics were computed utilizing Accuracy, Recall and Precision. Furthermore, F1-score and Matthews's correlation coefficient these measures were also calculated to greatly increase the proposed system performance. Additionally, 10-fold cross-validation methods have been used for proposed model performance evaluation that achieved 94% as the best accuracy average. Consequently, the proposed model can be used to support healthcare and facilitate large-scale clinical diagnostic of atherosclerosis diseases.

1. Introduction

As stated by the World Health Organization (WHO), heart disease is one of the leading causes of death when the heart is unable to pump oxygenated blood through the body [1]. There are other forms of Cardiovascular Disease (CVD), including coronary artery disease (CAD), also called atherosclerosis. This disease narrowed arteries and buildup of plaque caused by cholesterol in the blood. This ailment occurs due to narrowed or blocked blood vessels and coronary arteries because of the plaque accumulation. This plaque is made of cholesterol, calcium and other substances. As the buildup increases, the plaque reduces blood flow to the coronary arteries. Therefore, the flow in the myocardium decreases. This can cause symptoms such as angina. The pain can be in the chest, shoulder, abdomen, arms, and neck. During this pain, the oxygenated blood decreases. This situation called myocardial ischemia. When the coronary artery has near completely narrowed, the myocardium tissue dies and leading a heart attack (myocardial infarction) [2,3].

Here, it seems important to establish and develop a medical diagnostic support system (MDSS) to automate the classification and prediction of CVD. However, medical diagnostic research requires greater precision and efficiency to make the best clinical decisions. Although classical MDSS has proven its ability to solve most diagnostic problems, it offers a lower accuracy factor and is unable to make a correct diagnosis [4,5].

Recently, therapy systems and medical diagnostics using Machine Learning (ML) is a wide-ranging section of artificial intelligence (AI). These technologies have influenced scientific fields such as finance, applied sciences, biology and medical

*A. Raihani, University Hassan II of Casablanca, abraihani@yahoo.fr

applications [6–14]. Subsequently, several works have been proposed to develop (MDSS) in order to predict and classify patients with heart diseases to improve health care [15–23].

In this case, we propose a new MDSS using some selected ML algorithms. The main goal is to classify and predict the patient's health issue based on the principal chosen features by analyzing the heart disease databases. Atherosclerosis risk factors have been identified from the knowledge and the expertise of medical experts and doctors. These risk factors are known as uncontrollable risk factors and controllable risk factors. The identification of these factors is based on several features. Uncontrolled Atherosclerosis risk factors contain family history, age and gender [3].

The remainder of this paper is structured as follows: In the second part (Section II), we review some related work in the literature. In the third part (Section III), we have presented and explained our proposed system process. In particular, we present the global flowchart of the proposed MDSS and the selected machine learning algorithms; in addition to used CAD datasets. The fourth part (Section IV) describes the evaluation parameters used to assess and compare our MDSS performance with similar measures. In the fifth part (Section V), we showed the details of implementation and presented the results and discussions. The last part (Section VI) concluded this work and gave certain proposed perspectives.

2. Related work

In this part, we have presented several selected works from literature review on automatic heart disease diagnosis. These works used the same well-known databases and that we will consider later for the performance comparison.

In [15] , The authors applied neural network integration methods to build new models by linking predicted values from previous models. Compared to the ML algorithm, the accuracy rate presented 89.01%. Another work published in [16], the authors suggested a clinical decision support system (CDSS) using Weighted Fuzzy Rules (WFR) for predicting heart disease. They used two scenarios of evaluation; the first scenario automatizes the approach for the WFR generation while the second scenario develops a fuzzy rule-based CDSS. They tested their CDSS using the Cleveland's heart disease database. Compared to the system based on a neural network, the best precision value obtained by this method is 62.35%.

In [17], the authors applied Fast Decision Tree (FDT) and C4.5 tree pruning methods. This approach aims to integrate the machine learning analysis results in different CAD databases. The outcomes showed that the classification accuracy is 78.06% which is higher than the average classification accuracy of separate datasets of 75.48%. Recently in 2017, the authors in[18] proposed a Hybrid Neural Network-Genetic (HNNG) to improve the neural network by strengthening its initial weights based on a genetic algorithm. The highest accuracy rate is 93.85% using Z-Alizadeh Sani data set and the Cleveland's heart disease database.

Other approaches have covered the medical diagnosis issue of heart diseases. In [19], the authors have depicted the CDSS performances for heart failure risk prediction. This system based on two methods, Fuzzy Analytic Hierarchy Process (Fuzzy_AHP) and artificial neural network (ANN). The result shows that compared to the traditional ANN method, the average prediction accuracy of this method reaches 91.10%. More recently, in 2018 the authors of [20] presented the design and implementation of the MDSS for heart diseases. This system is developed using the Fuzzy_AHP method and Fuzzy Inference System (FIS). The results of the developed method indicate the possibility of having a heart disease. From the experimental results it has been proven that the AI and ML methods in the medical field have given good results. In [24], used ML methods, which are Naive Bayes (NB), Random Forest (RF), Support Vector Machine (SVM), ANN, and K-Nearest Neighbours (KNN) algorithms. These ML methods used to improve CAD diagnosis. The reached average accuracy is higher than 80%. As well, specificity and sensitivity results are around 70% to 90%.

Too recently in [22], the authors developed a new method, called Hybrid Feature Selection (2HFS) applying Gaussian Naive Bayes (GNB), Random Forest (RF), Decision tree (DT) and Gradient Boosting (XGBoost) classifiers. In this study, authors have used Nasarian CAD database and they have also tested this approach with Long Beach VA, Hungarian and Z-Alizadeh Sani databases to achieve accuracies of 83.94%, 81.58% and 92.58% respectively.

This work aims to propose a new MDSS for diagnosis of patients with atherosclerosis. The proposed approach is based on five some selected ML algorithms: ANN, RF, Adaptive Boosting (AdaBoost), DT, and XGBoost. The study simulates the execution of the different algorithms configurations in order to evaluate the performance of the resulted models, and then choose which the best was; using performance evaluation methods to improve each one. The actual work is an improvement of our earlier research [11–14].

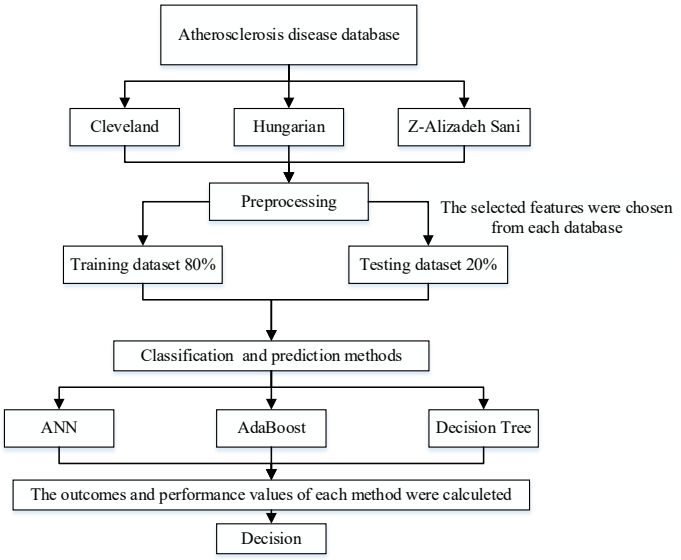


Figure 1: Flowchart of the proposed MDSS using ML algorithm.

3. Materials and methods

3.1. Global overview of the proposed MDSS

In this work, we proposed an MDSS using ML technique. This system based on three supervised ML algorithms. These classifiers have been applied to find the best prediction based on the chosen

important features by analyzing the atherosclerosis databases. Figure 1 shows the flowchart of the proposed work using ML algorithms.

3.1.1. Artificial Neural Network (ANN)

Artificial neural network (ANN) is inspired by the biological neural network to imitate human neurophysiology. At present, researchers have integrated statistical methods and numerical analysis into neural networks to give a mathematic model [25].

Where $\{x_1, x_2, \ldots, x_n\}$ represent the n inputs, ($W_{i,n}$) represents the weights and (y_i) are the outputs of the neural network using sigmoid function as a nonlinear activation function ($f(.)$) for each neuron. The activation function is given by equation (1):

$$f(x) = \frac{1}{1 + e^{-x}} \tag{1}$$

The ANN algorithm is achieved using the following equations

Network equation:

$$net_i = \sum_{j=1}^{m} w_{i,j} * x_i + b_i \tag{2}$$

Predicted outputs equation:

$$y_i = f_i(net_i) \tag{3}$$

Slope equation:

$$S_i = \frac{\partial f_i}{\partial net_i} \tag{4}$$

Error (e_i) using for the actual output (t_i) and the predicted output (o_i) equation:

$$e_i = t_i - o_i \tag{5}$$

The last step in the ANN algorithm is to check if the standard stop error is reached. This means that the actual error (e_{i+1}) is smaller than the last error and that the approximation of the total error function is valid.

3.1.2. Adaptive Boosting (AdaBoost)

Adaptive Boosting [26,27] as known AdaBoost, is an ML algorithm proved by Yoav Freund and Robert Schapire. This method can be used in combination with many ML algorithms to improve performance for binary classification. AdaBoost structure can be briefly defined as follows.

For each learner (t), AdaBosst calculated the weighted classification error as using the following equation:

$$e_t = \sum_{n=1}^{N} d_n^{(t)} II(y_n \neq h_t(x_n)) \tag{5}$$

With (y_n) is the true class label, (x_n) is predictor vector for observation (n), (h_t) is the hypothesis (learner predictor), ($d_n^{(t)}$) is the observation weight in step (t), (II) is the indicator function and the AdaBoost trains learners sequentially.

AdaBoost can increase weights for each misclassified observation and reduces weights for each observation correctly classified.

After training phase, AdaBoost computes prediction using the following equation:

$$f(x) = \sum_{t=1}^{T} \alpha_t h_t(x) \tag{6}$$

with:

$$\alpha_t = \frac{1}{2} log \frac{1-\varepsilon_t}{\varepsilon_t} \tag{7}$$

Where (α_t) are the weak hypothesis weights in the ensemble.

AdaBoost training step can be considered as the exponential loss minimization using the following equation.

$$\sum_{n=1}^{N} w_n e^{(-y_n f(x_n))} \tag{8}$$

Where the true class is $y_n \in \{-1, 1\}$, (w_n) is the weight normalized to add up to 1 and $f(x_n) \in (-\infty, +\infty)$ is the predicted classification score.

3.1.3. Decision Tree (DT)

Decision Tree (DT) is a supervised machine learning algorithm. This method is usually used in binary classification problems. The objective is to construct a set of choices in a tree graphic form consisting of nodes and branches based on each collected attribute[28].

The decision tree algorithm is achieved using the following equations:

Probability ($P(T)$) to estimate that an observation (j) is in node (n) is defined with the following expression:

$$P(T) = \sum_{j \in X} w_j \tag{9}$$

Information gain (G(T, X)) for each tree's node to classify all input data is defined with the following expression:

Where: (w_j) is weight of the observation (j).

$$G(T, X) = E(X) - E(T|X) \tag{10}$$

The entropy (E (T)) is defined with the following expression:

$$E(T) \equiv \sum_{i=1}^{c} -p_i log_2 p_i \tag{11}$$

Where: (p_i) is the probability of the class i with i = 1, …, c with (c) is the total number of classes. In the case of binary classification c=2.

3.2. Databases description

3.2.1. Cleveland dataset

Cleveland dataset is collected by David Aha for machine learning repository [29]. It is obtained from the Cleveland Clinic Foundation database of the University of California Irvine. This database consists of 76 attributes of which only 14 attributes are commonly used in most published researches: 13 inputs and one output. In this proposed work, only 270 instances are used from the 303 records patients owing to some missing values. It is noted that this dataset performs with 54% healthy subjects and 46% CAD patients. The healthy subjects are marked 0 while the unhealthy ones are designated by the value 1. Table 1 summarizes all used Cleveland Features.

Table 1: Cleveland dataset features and their descriptions.

No	Features	Description	Scale
1	Age	Age in years	29 - 77
2	GD	Gender	Female (0), Male (1)
3	CP	Chest pain type	Typical angina (1), Atypical angina (2), Non-angina pain (3), Asymptomatic (4)
4	trestbps	Resting blood pressure on admission to the hospital (mm/Hg)	94 - 200
5	chol	Serum cholesterol (mg/dl)	126 - 564
6	Fbs	Fasting blood sugar is greater than 120 mg/dl	No (0), Yes (1)
7	Restecg	Resting electrocardiographic results	Normal (0), Having ST-T wave abnormality (1), Showing probable or definite left ventricular hypertrophy by Estes' criteria (2)
8	Thalach	Maximum heart rate achieved (ppm)	71 - 202
9	Exang	Exercise induced angina	No (0), Yes (1)
10	Oldpeak	ST depression induced by exercise relative to rest	0 - 6,2
11	slope	The slope of the peak exercise ST segment	Up sloping (0), Flat (1), Down sloping (2)
12	ca	Number of major vessels colored by fluoroscopy	0-3
13	Thal	The heart status	Normal (3), Fixed defect (6), Reversible defect (7)
14	num	Diagnosis of heart disease	Healthy (0), Patient has heart disease (1)

3.2.2. Hungarian dataset

The Hungarian dataset is collected by Andras Janosi, at the Hungarian Institute of Cardiology, Budapest [29]. This database contains 10 features. Through the 294 dataset samples, 262 samples were commonly used, 34 simples have been rejected because of missing values. The Hungarian simples are segregated in 62.21% healthy subjects and 37.78% with heart disease.

3.2.3. Z-Alizadeh Sani dataset

The Z-Alizadeh Sani dataset is randomly collected at Tehran's Shaheed Rajaei Cardiovascular, Medical and Research Centre. This dataset is built for CAD diagnosis, containing 303 samples with 54 features for each patient. The selected features include the main data on the patient's physical examinations, echocardiograms (ECGs), physical examinations, laboratory tests, demographic characteristics, and symptoms [18,23].

Alizadehsani et al [23] have classified patients into two outputs classes: 71% of patients suffered from CAD and 29% healthy. This dataset also contains stenosis prediction outputs of three coronary arteries i.e., LAD, RCA, and LCX. In this study, we have manually selected 17 features as the most important features according to the atherosclerosis risk factor [2,30].

3.3. Features selection

During the preprocessing step that consist essentially of the dataset cleaning (Ignoring inputs with missing values), the prediction inputs are based on the features of each database. Atherosclerosis risk factors have been identified from the expertise of medical experts and doctors. These risk factors are known as uncontrollable risk factors and controllable risk factors. The suitable features are chosen from each dataset as input data based on the related literature [2,30].

The corresponding outputs used for prediction are the binary labels “Diagnosis of heart disease” which reflects the actual condition of the patient considered. These 2 classes are: a patient has atherosclerosis or healthy. Here, a value of 0 means that there is no atherosclerotic disease, this means that the reduction in diameter is less than 50%. A value of 1 indicates the presence of atherosclerotic disease, which means that the diameter is reduced by 50% according to the database collected by UCI data (Cleveland and Hungarian). Regarding the Z-Alizadeh Sani database, the output is divided into two category labels. Therefore, Category 0 specifies that there is no atherosclerotic disease, which means normal. Category 1 indicates the presence of atherosclerotic disease, which indicates CAD.

4. Performance evaluation metrics

In this work, we used many performance methods to improve our proposed MSSD of atherosclerosis disease. These methods represent as following:

- The Recall, the true positive rate (TRR) or the sensitivity calculates the degree of patients having correctly identified the disease.

$$Recall = \frac{TP}{TP + FN} \tag{12}$$

- Precision or Positive predictive value, this metric is the positive proportion result in diagnostic tests that is true positive results.

$$Precision = \frac{TP}{TP + FP} \tag{13}$$

- Accuracy (ACC) that computes the precision degree.

$$ACC = \frac{TP + FN}{TP + FP + FN + TN} \tag{14}$$

- Just like our case, the Matthews Correlation Coefficient (MCC) is a quality metric used for machine learning binary classification.

$$MCC = \frac{TP * TN - FP * FN}{\sqrt{(TN + FP) * (TN + FN) * (TP + FP) * (TP + FN)}} \tag{15}$$

- F1-score (FS) that shows the precision harmonic means.

$$FS = \frac{2 * TP}{2 * TP + FP + FN} \quad (16)$$

Where FN, TP, FP and TN are respectively false negative, true positive, false positive and true negative. In the ML field confusion matrix is also known as an error matrix. The matrix represents the performance of the algorithm, but it contains two types of information: the predicted value and the actual value. Table 2 explains the confusion matrix for the binary classification [31,32].

Table 2: Confusion matrix.

Predicted diagnostic outcome	**Actual diagnostic outcome**		
	Patient has the disease	**Patient has not the disease**	**Row total**
Negative	FN	TN	TN +FN (Negative test)
Positive	TP	FP	FP +TP (Positive test)
Column total	FN +TP (Patients number have the disease)	TN + FP (Patients number have not the disease)	TP + FP + FN + TN (Total Population)

5. Simulation results and performance comparison

To prove the effectiveness of our proposed classifiers and predictors, many experiments and simulation were performed to empirically identify the best ML models. In this way, three sets of atherosclerosis data are used, and various performance evaluation methods are used to summarize the experimental results in tables to assess the effectiveness of the proposed method. A comparison of the obtained results with previous work was also conducted.

5.1. ML design and implementation

For ANN technique and as any empirical work, many simulations were conducted to select the best hyper parameters. As will be showed later, the best performance is reached for the following architecture configuration presented in table 3.

The learning parameters and neural network architecture used in each dataset in this study relate to the hidden layer, the number of neurons, the value of the learning rate, and the type of activation function in each layer.

Table 3: The proposed ANN architecture specifications and training parameters.

Architecture				
Dataset name		Cleveland	Hungarian	Z-Alizadeh
The layers number		1	1	1
Weights and bias		Randomly initialized		
The neuron number	Input	13	10	17
	Hidden 1	8	8	6
	Output	2		
Activation functions	Input	Tangent-sigmoid (T-S)		
	Hidden 1			
	Output	Linear		
Learning rule		Backpropagation & Levenberg-Marquardt		
Learning rate		0.001		

In DT algorithm, the first step is to calculate the entropy of the output or the target using the equation (11). The next step we obtained the entropy for each branch. The last step, the dataset divided by its branches and repeat the process every branch until all data is classified.

In the second algorithm AdaBoost, we calculate the weighted classification error using equation (5) for each learner. Then we reduce weights for each observation correctly classified by learner t. after finished training, we calculate the prediction for the new obtained data using equation (6). Then we minimize the exponential loss using equation (8).

5.2. Classification and prediction performance evaluation results on testing datasets

The classification techniques described above were implemented to identify subjects with and without heart disease. Those algorithms were compared using standard evaluation metrics: accuracy (ACC), precision, recall, F1-score (FS), Matthews's correlation coefficient (MCC), confusion matrix and Receiver Operating Characteristic curve (ROC).

5.2.1. Confusion matrix results

The MDSS for atherosclerosis is made based on three ML techniques: ANN, AdaBoost and DT algorithms. To validate our model, three databases were used: Cleveland, Hungarian, and Z-Alizadeh Sani database consisting of 270, 262 and 303 patients' records respectively as shown in table 4.

Each database is split on two datasets using interleaved indices: 80% been used for training, and 20% for testing. Then we trained the three classifier algorithms were compared to select the best one. Table 4 shows the results of the confusion matrix obtained after testing 835 patients collected from the Cleveland, Hungary and Z-Alizadeh Sani databases using the ANN, AdaBoost and DT algorithms.

Table 4: Confusion matrix results.

Datasets	**Methods**	**TP**	**FP**	**FN**	**TN**
Cleveland	ANN	20	4	6	24
	DT	19	5	5	25
	AdaBoost	16	8	23	7
Hungarian	ANN	17	5	3	28
	DT	16	6	8	23
	AdaBoost	15	7	5	25
Z-Alizadeh Sani	ANN	40	1	5	12
	DT	41	9	8	3
	AdaBoost	40	4	5	12

5.2.2. Performance metrics results

During the testing phase, the outcomes are given to the proposed classification system to classify and predict patients with atherosclerosis. The achieved results are calculated using the standards performance metrics: ACC, precision, recall, FS, and MCC. To improve our atherosclerosis prediction system, two further machine learning metrics are used: FS as binary classification accuracy test and MCC as a binary classification quality measure.

The FS and MCC metrics should nearby 1 to assess on the system efficiency. Table 5 shows the obtained evaluation metrics

for ANN, AdaBoost and DT algorithms using Cleveland, Hungarian, and Z-Alizadeh Sani databases.

Table 5: the proposed system performance metrics.

Datasets	Methods	ACC	Precision	Recall	FS	MCC
Cleveland	ANN	**91.41%**	**79.67%**	**70.36%**	**0.75**	**0.60**
	DT	81.48%	79.17%	79.17%	0.80	0.46
	AdaBoost	72.22%	69.57%	66.67%	0.68	0.44
Hungarian	ANN	**90%**	**85%**	**78%**	**0.81**	**0.75**
	DT	73.58%	66.57%	72.73%	0.70	0.46
	AdaBoost	77.36%	75.00%	68.18%	0.71	0.53
Z-Alizadeh Sani	ANN	**94%**	**92.58%**	**97.73%**	**0.94**	**0.75**
	DT	81.97%	83.67%	93.18%	0.88	0.57
	AdaBoost	85.25%	88.89%	90.91%	0.90	0.63

5.3. Cross-validation

In this section, we present the analysis of system performance using the k-factor cross-validation technique. As a result, the databases are divided into k data sets. For each validation, one dataset is used as the test dataset and the rest of the datasets are used as the training dataset.

The principle of cross-validation is that we run a given model several times. In our case, ten times (K = 10), then we average the ten different tests, after that we average the test results of these K experiments. Obviously, this requires more computing time, as we have now conducted K separate learning experiments, but the evaluation of the learning algorithm will be more accurate. In other words, we use all the data for training and all the data for testing. In this case, we use the interleaved analysis method to divide each database into two parts: 80% of the training set and 20% of the test set.

When analyzing the Cleveland training dataset (graph shown in Figure. 2), The Cleveland database average accuracy computation, the ANN algorithm achieved 91.41% compared with the average accuracy of the other algorithms (AdaBoost and DT) are respectively 72.22% and 81.48% as shown in the graph.

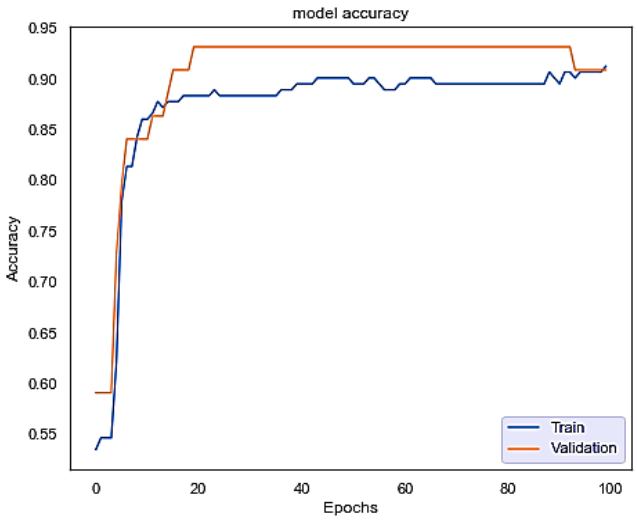


Figure 2: ANN Cross-validation analysis of Cleveland database

In Hungarian training dataset, the average accuracy achieved 90.00% with regard to the graph shown in figure 3. During this database analyze, the ANN algorithm produced a higher accuracy compared with the other algorithms.

Similarly, in Sani Z-Alizadeh training dataset, the ANN algorithm achieved a higher accuracy (94.00%) compared with the other algorithms. in addition, the ANN algorithm average accuracy computation increased nearly by 10% higher than the other algorithms (AdaBoost and DT) are respectively 85.25% and 82.00% (graph shown in Fig. 2).

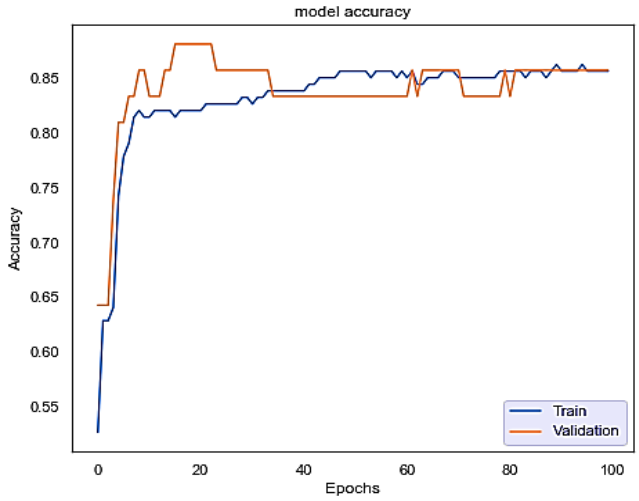


Figure 3: ANN Cross-validation analysis of Hungarian database.

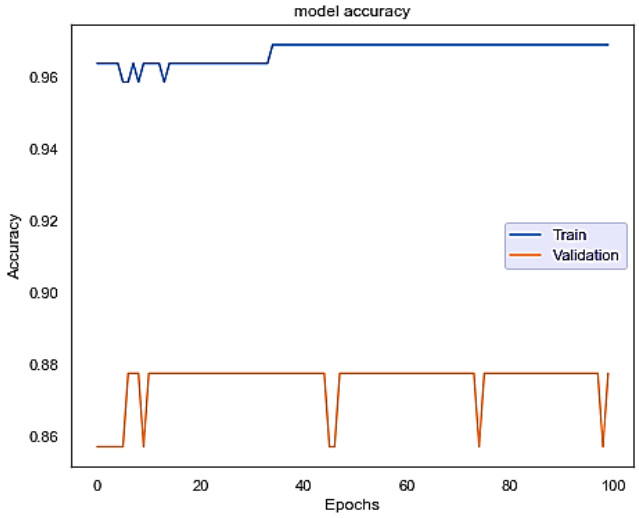


Figure 4: ANN Cross-validation analysis of Z-Alizadeh Sani database.

5.4. Receiver Operating Characteristic Curve (ROC)

In order to increase the prediction of healthy subjects and subjects with CAD, ROC assessment indicators are used to check the performance of our classifier. For each classifier, ROC will apply a threshold in the range [0, 1] to the output field.

In figure 5, the ROC analysis results for Cleveland testing dataset demonstrates that the ANN presents the better classification performance comparing to AdaBoost and DT algorithms. Where has 80% as recall value and the 70.36% as precision value. The ROC analysis results for the Hungarian

database, as shown in figure 6, prove that ANN reached the 85% as best precision with 90% as accuracy value.

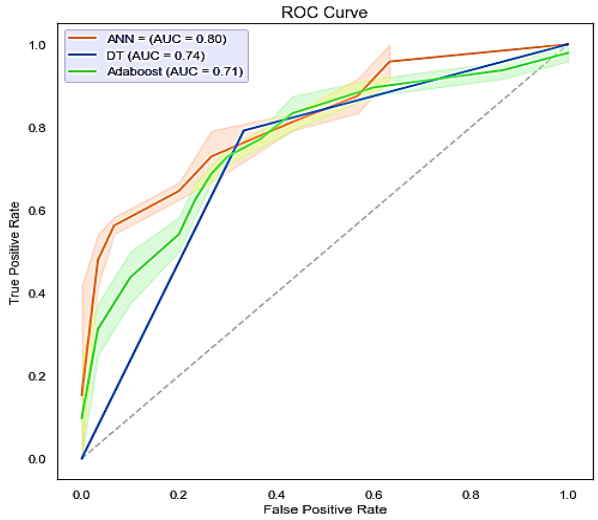


Figure 5: ROC Cleveland Database.

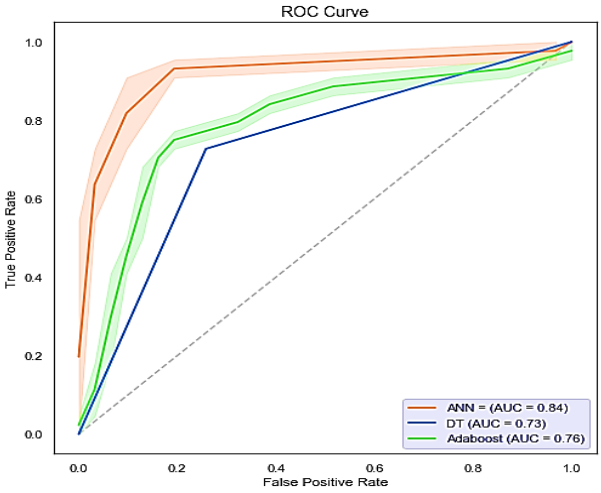


Figure 6: ROC Hungarian Database.

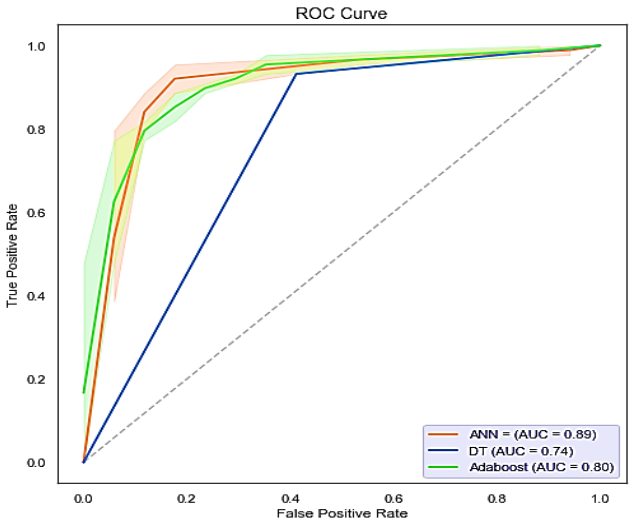


Figure 7: ROC Z-Alizadeh Sani Database.

The Z-Alizadeh Sani database as shown in figure 7, the ROC analysis showed that the ANN method reached 98% as the best recall while the AdaBoost and the DT methods reached respectively the best recall of 90.18% and 93.18%. However, the best results of ROC were obtained when using our proposed ANN method.

6. Discussion and performance comparison

To assess the effectiveness of our proposed method, we conducted experiments on the aforementioned Cleveland, Hungary and Z-Alizadeh Sani databases. We compare our results with some previous work as shown in Tables 6, 7 and 8. We can see from these tables that our proposed system has better prediction performance compared to other classifiers.

In Table 6, we present the results by comparing the accuracy of the proposed system with previous work using the Cleveland database.

Table 6: Classification Cleveland database accuracies.

Author and year	Method	Accuracy (%)
Anooj et al. (2012) [16]	Weighted fuzzy rules	62.35
El-Bialy et al. (2015) [17]	C4.5	78.54
	FDT	77.55
Arabasadi (2017) [18]	Neural Network	84.80
	HNNG	89.40
Das et al. (2009) [15]	Neural Networks Ensemble	89.01
Proposed method	**ANN**	**91.41**

In addition, we have used comparative study to show the performance of the proposed system. In the Cleveland analysis dataset, the proposed system showed that the ANN method can achieve a higher accuracy of 91.41% as shown in Table 6, while the accuracy of previous systems such as Weighted Fuzzy, C4.5, FDT, Neural Network, Set neural networks, HNNG, is 62.35%, 78.54%, 77.55%, 84.80%, 89.01% and 89.40%, respectively.

In the Hungarian database, the proposed system achieves a better precision of 90.00%, as shown in Table 7. Here, the previous systems (like the weighted fuzzy rules method) only obtained 46.93%, HNNG gained 87.10%. Table 7 lists the correctness of the classification of the Hungarian database.

Table 7: Classification Hungarian database accuracies.

Author and year	Method	Accuracy (%)
Anooj P.K.(2012)[16]	Weighted fuzzy rules	46.93
El-Bialy et al. (2015) [17]	C4.5	78.57
	FDT	78.23
Arabasadi (2017) [9]	Neural Network	82.90
	HNNG	87.10
Alizadeh (2018) [23]	SVM, Naïve Bayes, and C4.5	88.77
Proposed method	ANN	90.00

Similarly, when analyzing the Z-Alizadeh Sani dataset, our system obtained the best accuracy, as presented in Table 8. For the accuracy of HNNG achieved 93.85% compared to our system's accuracy of 94.00%. As shown in Table 8, compared to previous research, our proposed system works best for performing efficient classification and prediction.

Table 8: Classification Z-Alizadeh Sani database accuracies.

Author and year	Method	Accuracy (%)
Arabasadi et al. (2017) [18]	HNNG	93.85
	Neural Network	84.62
Abdar et al. (2019) [33]	SVC	92.45
	nuSVM	93.08
	LinSVM	92.09
Nasarian (2020)[22]	2HFS	92.58
Proposed method	**ANN**	**94.00**

7. Conclusion

In this work, we proposed an MDSS for the early prediction of atherosclerosis. Applied to datasets, the proposed system is based on three ML algorithms (ANN, AdaBoost and DT algorithms) to generate functionalities suitable for predicting patients with / without atherosclerotic disease. Using clinical data sets, a total of 835 samples were obtained from the databases in Cleveland, Hungarian and Z-Alizadeh Sani. The experimental results show that compared to other ML techniques, the ANN algorithm has better accuracy. In addition, the Accuracy, Precision, Recall and F1_Score indicators and the ROC graph are used to assess the performance of the proposed algorithm. Finally, a comparative predictive analysis is carried out between the experimental results and the different methods available in the literature (such as weighted fuzzy rules, HHNG and 2HFS). Based on common performance indicators, this comparison shows that our proposed system has the highest accuracy of 94% in predicting and classifying atherosclerosis. Like future research guidelines, the proposed system will include different methods and functions for other heart diseases to improve the accuracy of predictions.

Conflict of Interest

The authors declare no conflict of interest.

References

[1] Cardiovascular diseases (CVDs).

[2] R. Ross, "Atherosclerosis — An Inflammatory Disease," New England Journal of Medicine, **340**(2), 115–126, 1999, doi:10.1056/NEJM199901143400207.

[3] P. Libby, P.M. Ridker, G.K. Hansson, "Progress and challenges in translating the biology of atherosclerosis," Nature, **473**(7347), 317–325, 2011, doi:10.1038/nature10146.

[4] R.A. Miller, "Medical Diagnostic Decision Support Systems--Past, Present, And Future: A Threaded Bibliography and Brief Commentary," Journal of the American Medical Informatics Association, **1**(1), 8–27, 1994, doi:10.1136/jamia.1994.95236141.

[5] E. Shortliffe, Computer-Based Medical Consultations: MYCIN, Elsevier, 2012.

[6] O. Daanouni, B. Cherradi, A. Tmiri, Type 2 Diabetes Mellitus Prediction Model Based on Machine Learning Approach, Springer International Publishing, Cham: 454–469, 2020.

[7] S. Laghmati, A. Tmiri, B. Cherradi, "Machine Learning based System for Prediction of Breast Cancer Severity," in 2019 International Conference on Wireless Networks and Mobile Communications (WINCOM), IEEE, Fez, Morocco: 1–5, 2019, doi:10.1109/WINCOM47513.2019.8942575.

[8] S. Hamida, B. Cherradi, A. Raihani, H. Ouajji, "Performance Evaluation of Machine Learning Algorithms in Handwritten Digits Recognition," in 2019 1st International Conference on Smart Systems and Data Science (ICSSD), IEEE, Rabat, Morocco: 1–6, 2019, doi:10.1109/ICSSD47982.2019.9003052.

[9] S. Hamida, B. Cherradi, H. Ouajji, "Handwritten Arabic Words Recognition System Based on HOG and Gabor Filter Descriptors," in 2020 1st International Conference on Innovative Research in Applied Science, Engineering and Technology (IRASET), IEEE, Meknes, Morocco: 1–4, 2020, doi:10.1109/IRASET48871.2020.9092067.

[10] S. Hamida, B. Cherradi, H. Ouajji, A. Raihani, Convolutional Neural Network Architecture for Offline Handwritten Characters Recognition, Springer International Publishing, Cham: 368–377, 2020.

[11] O. Terrada, A. Raihani, O. Bouattane, B. Cherradi, "Fuzzy cardiovascular diagnosis system using clinical data," in 2018 4th International Conference on Optimization and Applications (ICOA), IEEE: 1–4, 2018.

[12] O. Terrada, B. Cherradi, A. Raihani, O. Bouattane, "A fuzzy medical diagnostic support system for cardiovascular diseases diagnosis using risk factors," in 2018 International Conference on Electronics, Control, Optimization and Computer Science (ICECOCS), IEEE, Kenitra: 1–6, 2018, doi:10.1109/ICECOCS.2018.8610649.

[13] O. Terrada, B. Cherradi, A. Raihani, O. Bouattane, "Classification and Prediction of atherosclerosis diseases using machine learning algorithms," in 2019 5th International Conference on Optimization and Applications (ICOA), IEEE, Kenitra, Morocco: 1–5, 2019, doi:10.1109/ICOA.2019.8727688.

[14] O. Terrada, B. Cherradi, A. Raihani, O. Bouattane, "Atherosclerosis disease prediction using Supervised Machine Learning Techniques," in 2020 1st International Conference on Innovative Research in Applied Science, Engineering and Technology (IRASET), IEEE, Meknes, Morocco: 1–5, 2020, doi:10.1109/IRASET48871.2020.9092082.

[15] R. Das, I. Turkoglu, A. Sengur, "Effective diagnosis of heart disease through neural networks ensembles," Expert Systems with Applications, **36**(4), 7675–7680, 2009, doi:10.1016/j.eswa.2008.09.013.

[16] P.K. Anooj, "Clinical decision support system: Risk level prediction of heart disease using weighted fuzzy rules," Journal of King Saud University - Computer and Information Sciences, **24**(1), 27–40, 2012, doi:10.1016/j.jksuci.2011.09.002.

[17] R. El-Bialy, M.A. Salamay, O.H. Karam, M.E. Khalifa, "Feature Analysis of Coronary Artery Heart Disease Data Sets," Procedia Computer Science, **65**, 459–468, 2015, doi:10.1016/j.procs.2015.09.132.

[18] Z. Arabasadi, R. Alizadehsani, M. Roshanzamir, H. Moosaei, A.A. Yarifard, "Computer aided decision making for heart disease detection using hybrid neural network-Genetic algorithm," Computer Methods and Programs in Biomedicine, **141**, 19–26, 2017, doi:10.1016/j.cmpb.2017.01.004.

[19] O.W. Samuel, G.M. Asogbon, A.K. Sangaiah, P. Fang, G. Li, "An integrated decision support system based on ANN and Fuzzy_AHP for heart failure risk prediction," Expert Systems with Applications, **68**, 163–172, 2017, doi:10.1016/j.eswa.2016.10.020.

[20] S. Nazari, M. Fallah, H. Kazemipoor, A. Salehipour, "A fuzzy inference-fuzzy analytic hierarchy process-based clinical decision support system for diagnosis of heart diseases," Expert Systems with Applications, **95**, 261–271, 2018, doi:10.1016/j.eswa.2017.11.001.

[21] M. Abdar, U.R. Acharya, N. Sarrafzadegan, V. Makarenkov, "NE-nu-SVC: A New Nested Ensemble Clinical Decision Support System for Effective Diagnosis of Coronary Artery Disease," IEEE Access, **7**, 167605–167620, 2019, doi:10.1109/ACCESS.2019.2953920.

[22] E. Nasarian, M. Abdar, M.A. Fahami, R. Alizadehsani, S. Hussain, M.E. Basiri, M. Zomorodi-Moghadam, X. Zhou, P. Pławiak, U.R. Acharya, R.-S. Tan, N. Sarrafzadegan, "Association between work-related features and coronary artery disease: A heterogeneous hybrid feature selection integrated with balancing approach," Pattern Recognition Letters, **133**, 33–40, 2020, doi:10.1016/j.patrec.2020.02.010.

[23] R. Alizadehsani, M.J. Hosseini, A. Khosravi, F. Khozeimeh, M. Roshanzamir, N. Sarrafzadegan, S. Nahavandi, "Non-invasive detection of coronary artery disease in high-risk patients based on the stenosis prediction of separate coronary arteries," Computer Methods and Programs in Biomedicine, **162**, 119–127, 2018, doi:10.1016/j.cmpb.2018.05.009.

[24] A. Cuvitoglu, Z. Isik, "Classification of CAD dataset by using principal component analysis and machine learning approaches," in 2018 5th International Conference on Electrical and Electronic Engineering (ICEEE), IEEE, Istanbul: 340–343, 2018, doi:10.1109/ICEEE2.2018.8391358.

[25] D. Hanbay, I. Turkoglu, Y. Demir, "An expert system based on wavelet decomposition and neural network for modeling Chua's circuit," Expert Systems with Applications, **34**(4), 2278–2283, 2008, doi:10.1016/j.eswa.2007.03.002.

[26] Y. Freund, M. Kearns, D. Ron, R. Rubinfeld, R.E. Schapire, L. Sellie, "Efficient Learning of Typical Finite Automata from Random Walks," Information and Computation, **138**(1), 23–48, 1997, doi:10.1006/inco.1997.2648.

[27] Y. Freund, R.E. Schapire, "Adaptive Game Playing Using Multiplicative Weights," Games and Economic Behavior, **29**(1–2), 79–103, 1999,

doi:10.1006/game.1999.0738.

[28] S.R. Safavian, D. Landgrebe, "A survey of decision tree classifier methodology," IEEE Transactions on Systems, Man, and Cybernetics, **21**(3), 660–674, 1991, doi:10.1109/21.97458.

[29] R. Detrano, A. Janosi, W. Steinbrunn, M. Pfisterer, J.-J. Schmid, S. Sandhu, K.H. Guppy, S. Lee, V. Froelicher, "International application of a new probability algorithm for the diagnosis of coronary artery disease," The American Journal of Cardiology, **64**(5), 304–310, 1989, doi:10.1016/0002-9149(89)90524-9.

[30] M. Rafieian-Kopaei, M. Setorki, M. Doudi, A. Baradaran, H. Nasri, "Atherosclerosis: process, indicators, risk factors and new hopes," International Journal of Preventive Medicine, **5**(8), 927–946, 2014.

[31] A.S. Glas, J.G. Lijmer, M.H. Prins, G.J. Bonsel, P.M.M. Bossuyt, "The diagnostic odds ratio: a single indicator of test performance," Journal of Clinical Epidemiology, **56**(11), 1129–1135, 2003, doi:10.1016/S0895-4356(03)00177-X.

[32] A.G. Lalkhen, A. McCluskey, "Clinical tests: sensitivity and specificity," Continuing Education in Anaesthesia Critical Care & Pain, **8**(6), 221–223, 2008, doi:10.1093/bjaceaccp/mkn041.

[33] M. Abdar, W. Książek, U.R. Acharya, R.-S. Tan, V. Makarenkov, P. Pławiak, "A new machine learning technique for an accurate diagnosis of coronary artery disease," Computer Methods and Programs in Biomedicine, **179**, 104992, 2019, doi:10.1016/j.cmpb.2019.104992.

ASTES

Advances in Science, Technology and Engineering Systems Journal Vol. 5, No. 5, 278-281 (2020)

www.astesj.com

ASTESJ

ISSN: 2415-6698

Proposal for a Control System to Optimize Water use in Households in Peru

Witman Alvarado-Diaz*, Brian Meneses-Claudio, Avid Roman-Gonzalez

Universidad de Ciencias y Humanidades (UCH), Image Processing Research Laboratory (INTI-Lab), Lima, Peru

ARTICLE INFO

Article history:
Received: 17 April, 2020
Accepted: 25 July, 2020
Online: 17 September, 2020

Keywords:
Water saving
Control
Water waste
Solenoid valves
Domestic shower
Environmental impact

ABSTRACT

Water is an important vital resource, and must be protected and saved. Unfortunately, millions of liters of water are wasted annually at the national level in Peru, one of the factors is the discomfort when people take a hot shower, because first the water is cold, which is contained in the pipes of domestic connections with the heating tank, the cold water is wasted by sending directly to the drain until the water to be in a pleasant temperature, that means about 5 liters of water are wasted. The technology within engineering has carried out a variety of innovations that respond and solve problems related to water saving, that's why, this paper proposes to create an automated system that saves the wasted water in domestic showers, the proposal is characterized by being sustainable, for its environmental and economic impact; solving in this way a latent problem of society as well as raising public awareness of the benefits of saving water. As a result, a preliminary prototype was obtained, which demonstrates the basic operation of the proposed system.

1. Introduction

The main problem focus in this work is the waste of water, which, according to the Autoridad Nacional Del Agua (ANA) in Peru, approximately 37% is wasted and 50% is wasted in urban areas, in addition to coastal areas only 17% of the water is used. The proposed technology will promote greater awareness of water conservation practices, thus helping to reduce drinking water consumption in homes.

In [1], a tank is built that saves the hot water for aquariums of fish, this water is collected from power plants, which normally throw the water into the sea causing thermal pollution. The main purpose of the project is to recycle the waste of hot water produced by the power plants, taking advantage of it for agriculture; in this way, it is possible to maintain the thermal equilibrium of the aquariums with fish.

In [2], they mention that in a common domestic water supply, the connection of water pipes with the water heater is usually long, whereby the water is trapped, which is at an uncomfortable temperature, so users waste this water by letting it flow down the drain until water has a pleasant temperature. It proposed to save the trapped water, allows the circulation of hot and cold water by introducing a new component called back box installed inside the domestic water supply, this allows the water to flow in the opposite direction to the pressure of the line, the simulation showed the viability and effectiveness of the new approach.

In [3], they show us that magnetic induction water heater is a new device that can be used to heat the shower water, making a saving of water and energy; this heater consumes less electricity and does not store hot water; they mention that the induction heater is a device that aims to solve environmental and energy problems.

In [4], they mention that water consumption is increasing as the population grows, and it is the hotels that contribute significantly to the consumption of water, even more those that do not monitor the use of water, which results in millions of liters of wasted water per year, so the paper of the reference has a low-cost, precise, small and low-power wireless device for monitoring water in hotel showers.

In [5], the main references regarding the management of water demand are reviewed, as a strategy for efficient use in urban aqueducts; in addition, a management process is generated from the housing level to higher levels; some measuring equipment and low consumption devices are described; finally, the social mechanisms for efficient water use are listed.

Section 2 presents the development of the water saving system, recognizing the current domestic connections and the proposals in

*Corresponding Author: Witman Alvarado-Diaz, Email: walvarado@uch.edu.pe

addition to the electronic control system. Section 3 contains the preliminary results obtained from the application of the preliminary water saving system. In section 4, the reader can find the respective discussions and in section 5 the conclusions for the present paper.

2. Methodology

First, it must know the scheme of standard domestic supply, in homes that have a hot water tank, which distributes it throughout the house. In Figure 1, the reader can see a basic diagram of connections corresponding to a tank and a shower, which has a system of keys, those allows to control and mix the water to obtain different temperatures and quantities.

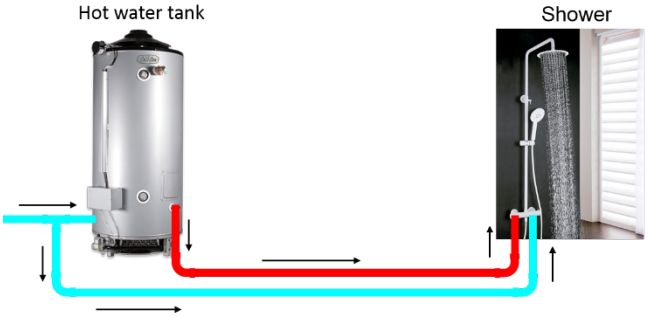


Figure 1: Diagram of the common connection of hot and cold-water pipes.

The aforementioned connections, it considers them to be inefficient, since to obtain a pleasant temperature, the cold water must be wasted until a pleasant temperature is obtained, which implies a huge waste of water, for which a new connection system is proposed, in addition of an electronic control system that saves water.

2.1. Connection Design

In order to save the cold water that accumulates in the hot water pipe, it is proposed to make the connections shown in Figure 2, where the reader can observe, following the flow of water that when opening the hot water key, all the cold water of the pipe enters to the connections using the activation of the “C” solenoid valve, this cold water enters a water container until the temperature sensor detects that the water is hot, at that moment, the solenoid valve closes "C" and solenoid valve "B" is activated allowing water to flow into the shower; the cold water contained in the container will periodically come out with the activation of the solenoid valve "A" and the pump, making the hot water mix with the cold water contained; people can control the temperature of the water by opening the cold water; at the end, when the hot and cold water keys are closed, the system will be deactivated, closing all the solenoid valves; in the event that only the cold water key is opened, the system must act normally until the container is filled, then an alarm will be activated and the solenoid valve “B” will be activated and the solenoid valve “C” deactivated, allowing cold water to flow the shower in addition to the process to get the container empty.

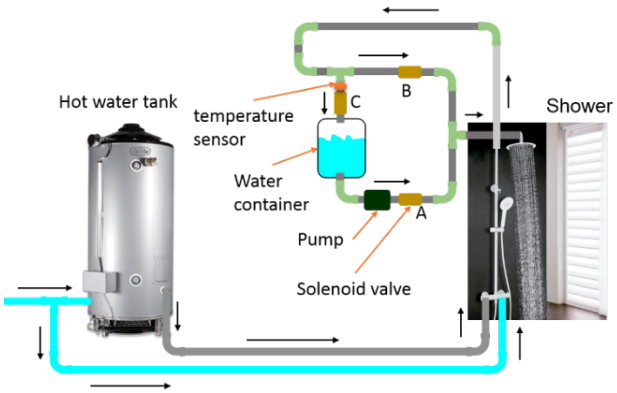


Figure 2: Proposal of connections for water saving.

2.2. Electronic Control

To carry out all the control of the aforementioned processes, an electronic test control system based on an Arduino nano is implemented, which is responsible for controlling relays, which can activate or deactivate the solenoid valves and the pump; for protection, the relays are connected a diode, a transistor and a resistor, as the reader can see in Figure 3.

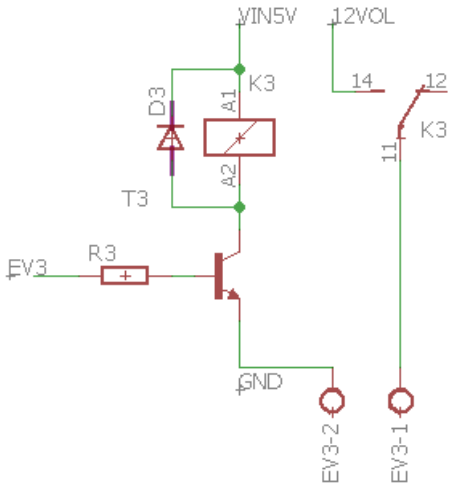


Figure 3: Relay connections.

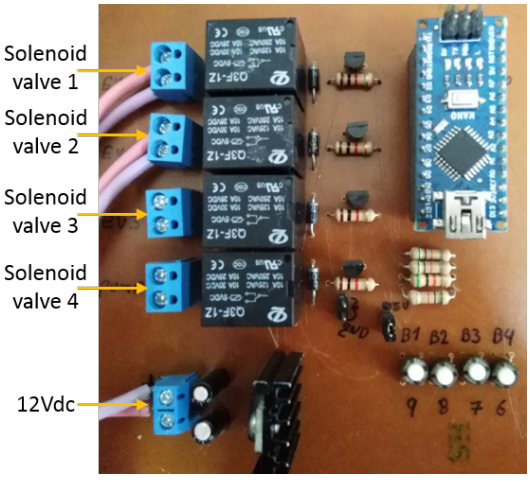


Figure 4: Electronic control board.

In figure 4, it can see the design of the control board, in which it can see the aforementioned relay, it can also see the connections of the Arduino nano, and its respective power supply also placed 4 buttons in order to make tests to the system, it is worth mentioning that the system designed is a preliminary system which tests are carried out to obtain a complete system in the future.

In Figure 5, it can see the basic programming scheme for the Arduino nano, in order to achieve the basic control of all components, and thus demonstrate its operation; as it can see with few instructions, it can make the system works in the same way as it was proposed at the beginning.

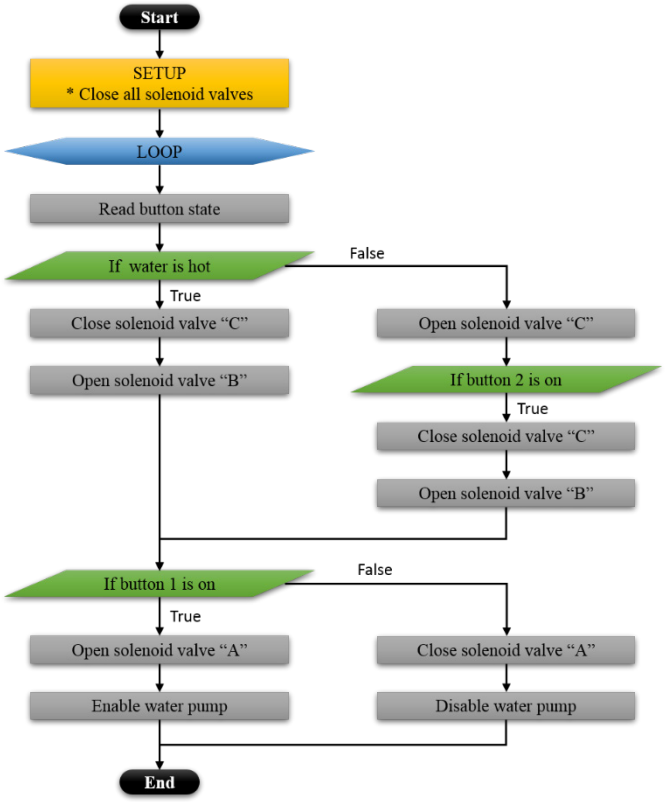


Figure 5: Programming diagram.

3. Results

As preliminary results, a model was built (Figure 6), in which the operation of the proposed system is demonstrated, this prototype has a similar operation, as proposed in the present investigation

Be aware that there are millions of people without access to drinking water and that its excessive use contributes to scarcity, water is a gift of nature that we must protect and share.

Around the world, there are commercial solutions that save water, however, none have alternative connections that divert water to a container, which saves it and spends it according to user requirements; the proposed system has this connection, to which add a control system, which together save water.

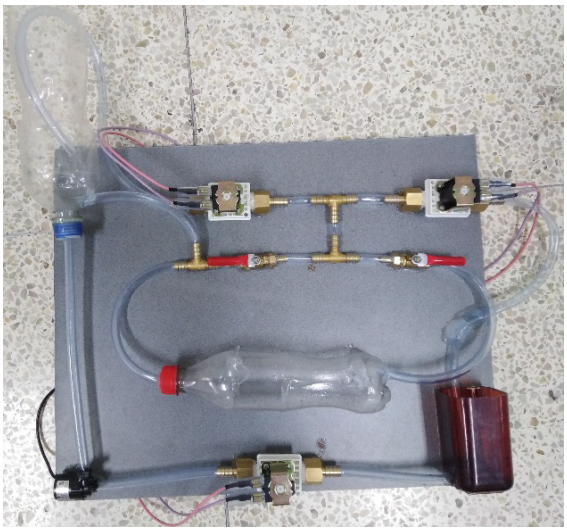


Figure 6: Test prototype.

Using the proposed system, it is possible to save in a family of 4 members, until 600 liters of water per month, which affects indirectly, reducing the amount to be paid for home water service. The 600 liters per month per family is calculated taking some minimum requirements, so the calculation of a single hot shower is performed, if it projects the calculation in a very long time, a very large saving of such a precious resource could be calculated.

Performing the respective calculations for the city of Lima, which has, according to the Instituto Nacional de Estadistica e Informatica del Perú (INEI), a total of 9 million 320 thousand inhabitants, considering only a saving of 4 liters per person, it could save approximately more than 37 million liters in just 1 day in Lima, therefore, monthly would mean a saving of more than approximately 1 billion liters of drinking water in the city of Lima.

4. Discussions

This project helps meet the sustainable development goals set by the United Nations (UN), explicitly helps with 6th and 12th Goal, which according to the UN in 2019 that 3 of 10 people do not have access to drinking water. In addition, it is mentioned that women and girls are responsible for collecting 80% of water in homes without access to water, which is a serious problem even more since being minors, they are exposed to various dangers. 40% of the world's population survive with water scarcity. An important fact to know is that less than 3% of the world's water is suitable for human consumption, of which 2.5% is frozen. Therefore, humanity has only 0.5% to cover all its needs. We must

Thanks to projects like ours, it is possible to save large amounts of water, as previously mentioned, this water would greatly benefit the poorest sectors of the city, since they are the ones who suffer from a worrying water shortage.

The test prototype has been simulated in the Proteus software (figure 7), in which it can demonstrate the correct operation of the prototype, thus evidencing that it is possible to build a system capable of allowing to save all the cold water that is normally

wasted, before taking a shower. In the future, it is planned to build a robust and complex system that allows to save as much water as possible.

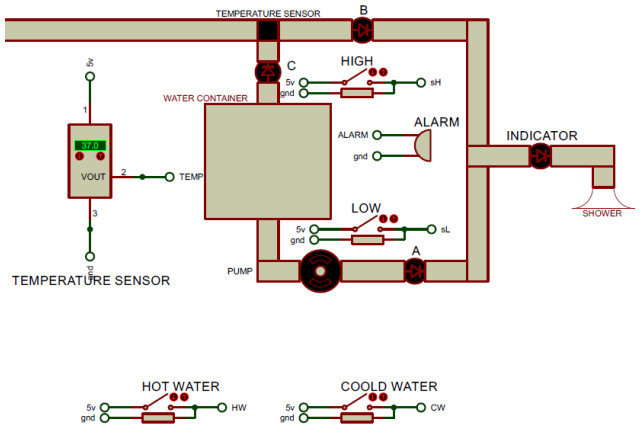


Figure 7: Simulation of the system

5. Conclusion

The designed control system contributes to the preservation of the environment and water saving by becoming a reliable device, contributing to the preservation of such a precious and limited resource. Using this type of projects, it will be able to achieve that the water reaches the neediest people and especially to the children of the whole world, since according to the UN, one of every four educational centers of primary level lacks water suitable for human consumption worldwide. In addition, another of the vulnerable populations are people living in rural areas, of which 80% use unsafe and unhealthy water sources. Finally, it is important to mention that approximately two thirds of the world's population (4,000 million people) suffer from severe water scarcity at least one month a year.

The present paper is an advance to a greater development of a system capable of optimizing the use of water in the homes of Lima Peru, a first advance is presented demonstrating that the project works and is applicable to save water in the showers of the houses that have a water heater tank, as well as in the hotel industry. The presentation of a prototype that simulates the functions that the final project could have is considered as a first step, in addition to the tests carried out in a circuit simulation, as a future vision, the development of an advanced electronic control system is proposed in order to save the maximum possible amount of water, in this way we contribute, so more people could have this important resource.

An important limitation that must be covered is security, since it is not raised in this research work, a security system must be developed to avoid possible current outflows that may affect users, in addition a control system must be added for the water flow, so that users can control it according to their preferences.

References

[1] A. Angani, K.B. Jun, Y.R. Musunuri, M. Akbar, K.J. Shin, "Development of Heat Storage and Delivery System Using Wasted Hot Water," in 2017 International Conference on Applied System Innovation (ICASI), 432–435, 2017, doi:10.1109/ICASI.2017.7988445.

[2] Y. Osais, M. Siddiqui, "A New Technique for Saving Water Trapped Inside Home Water Networks," in 2017 Intelligent Systems Conference (IntelliSys), 160–165, 2017, doi:10.1109/IntelliSys.2017.8324284.

[3] O.F. Rafael, M.C. Roberto, "Water heater by magnetic induction," in CONIELECOMP 2013, 23rd International Conference on Electronics, Communications and Computing, 192–197, 2013, doi:10.1109/CONIELECOMP.2013.6525784.

[4] P.J. Hawrylak, W. Nichols, X. Li, T. Johannes, R. Decook, K. Mongold, C. Cornell, L.A. Flint, A. Singh, "HydroSense : A Self-Powered Wireless Device for Monitoring Water Usage in Hotel Showers," in 2015 IEEE Global Humanitarian Technology Conference (GHTC), 2015, doi:10.1109/GHTC.2015.7343990.

[5] D. Gildardo, M. Silva, J.G. Erazo, "Eficiencia en el consumo de agua de uso residencial," Revista Ingenierías Universidad de Medellín, **11**(21), 23–38, 2012.

ASTES

Advances in Science, Technology and Engineering Systems Journal Vol. 5, No. 5, 282-287 (2020)

www.astesj.com

ASTESJ

ISSN: 2415-6698

BISINDO (*Bahasa Isyarat Indonesia*) Sign Language Recognition Using CNN and LSTM

Andi Aljabar*, Suharjito

Department of Computer Sciences, Bina Nusantara University, Jakarta, 11480, Indonesia

ARTICLE INFO

Article history:
Received: 16 May, 2020
Accepted: 07 July, 2020
Online: 17 September, 2020

Keywords:
Sign Language
BISINDO
CNN
RNN
LSTM

ABSTRACT

Sign language is one of the languages which are used to communicate with deaf people. By using it, they can communicate and understand each other. In Indonesia, there are two standards of sign language which are SIBI (Sistem Bahasa Isyarat) and BISINDO (Bahasa Isyarat Indonesia). Deep learning is a model that is used to apply to this topic. In this model, there are a lot of methods such as convolutional neural network, recurrent neural network, long-sort term memory, and each model has its characteristics. There are also some issues in deep learning by sign language recognition as the object such as data training, object position, pose, lighting, and the background of objects. This research will describe how to combine background subtraction and gaussian blur pre-processing, forwarding pre-processing background subtraction with CNN by using BISINDO, LSTM, and a combination between CNN and LSTM. In conclusion, this research shows that a combination between CNN and LSTM is the best model by explaining the accuracy and testing with sign language BISINDO as the object. The accuracy showed that for CNN 96%, LSTM 86%, and combination CNN and LSTM 96%, and the loss showed that for CNN 18%, LSTM 41%, and combination CNN and LSTM 17%.

1. Introduction

In recent years computer vision has been developed very rapidly, starting from its use in the robotic field, human interaction with computers, authentication of iris and fingerprints, face detection, and more. One popular topic at the moment is Sign Language Recognition (SLR). Sign language is a language that is used with deaf people communities to communicate with each other. In Indonesia, there are two standards of sign language, they are called SIBI (*Sistem Bahasa Isyarat Indonesia*) and BISINDO (*Bahasa Isayarat Indonesia*). There are many differences between SIBI and BISINDO, one of them was adopted from ASL (American Sign Language), this one calls SIBI [1]. However, both SIBI and BISINDO are still used in Indonesia. Nevertheless, SIBI has been approved by the government of Indonesia, and SIBI is used in schools and for studying, but most of the deaf people in Indonesia use BISINDO in their life activities more than SIBI [2].

Moreover, some research already studied this topic such as Leap Motion Controller (LMC), and HMM (Hidden Markov Model) vision base approach dan Microsoft Kinect dataset [3], [4]. For example, by using HMM and BISINDO object, the experiment got around 60% of accuracy [5]. It is because of how complex this system is. It is not only because of the method and model but also some aspects such as preprocessing. In preprocessing has some methods, one of them which will be experimented in this research is background subtraction and gaussian blur. One technique that will be used is how the system can distinguish the object's hand and the background.

Nevertheless, there are some issues about this topic in that data such as background image (data), lighting, and others [6]. As mentioned before, preprocessing is one of the important steps before the data entering the model. This research will use a black background. It will help the system to read the object easier than using a random background. Light and space between an object and camera are also important, which will influence the vectors matrix on the model and will affect the result.

In the earlier research about this machine learning and deep learning, the researcher using Generalized Learning Vector Quantization (GLVQ) and Kinnect as a dataset [2], [7]. As a rapid computer vision technology, especially for this topic, they will be applied with sign language. This topic has a lot increasing in its sectors. Such as Deep learning by using CNN (Convolutional Neural Network) and RNN (Recurrent Neural Network), they are

*Corresponding Author: Andi Aljabar, Bina Nusantara University, Jakarta, Tel: +62853-42622246 Email: andi.aljabar@binus.ac.id

used to manage image or video which is extracted in the frame than will translate the object to the text. The accuracy and loss of each own models are very dependent on some variables such as filter, pixel, and layers that are used. Filter, pixel, and layers are also a differentiator between the previous models such as Lipnet, Resnet, VGGnet, and others

In addition, All models have the same way to predict the sign [8]. Firstly, by preprocessing the data to be vectors matrix than doing processing by using the model, for the last the model giving the accuracy of recognition by doing training and validation to the data. In the pattern, the data must be divided into three parts, training, validation, and testing. The data training and validation will be used to make the model and data testing will be used to get the ability of the model that was created. The input from recognition sign language is an image or video (the combination of several images), the data processing requires a large bandwidth or low latency.

Furthermore, there are many types of researches that have each own positive and negative impact on this topic. According to some references by using deep learning in the neural network, this research will increase the accuracy and compare models CNN, LSTM, and a combination of CNN and LSTM.

2. Literature Review

2.1. Preprocessing

Preprocessing is the way to make data to be good to train. It means, preprocessing is a technique to improve the quality of image to remove the obstruction of the image and others [9]. *Preprocessing* is also used to smoothing the images for low frequencies. And also use to convert the image to the color that the model needed [10].

On the other hand, the mainframe of *preprocessing* is how the data can be normalized than that can be training as well to give the best result in accuracy [11]. Even it is text or image data. *Background subtraction* is one of the methods to subtract the image data in the *preprocessing* method. These three components in *background subtraction*, according to the color standard which is the RGB (Red, Green, Blue) [12]. By reducing and increasing the value of each own RGB, this can get the image result of *preprocessing*.

After *preprocessing*, data already normalize. Next, how the data will be matching with the models. In this research is using CNN and LSTM model to manage the data then get the result.

2.2. CNN (Convolutional Neural Network)

The convolutional neural network is a model that is used to process object recognition. In 2012, CNN is becoming a model that really important to support object recognition [13]. CNN also works well to do adaptive multi-modal and shows it's a great power on image recognition [13].

CNN is spreading the data to the layer frames. According to the upgrading, CNN has many changes such as VGG16, ResNet. Nowadays, 3D-CNN is a hot topic to study about. As mentioned before, 3D-CNN has become the model that can process 3D data

Figure 1 shows how CNN works [14]. The data will be converted to the layers which consist of *max pooling* and *fully connected* layers. It is also using high-resolution layers and low-resolution layers, it is depending on the dataset.

2.3. LSTM (Long Short-term Memory)

LSTM is a method that is used to process data sequentially and was developed by RNN. In LSTM, there is a new module which is called gates. That components are the input gate, neuron recurrent connection, forget gate, and output gate [15].

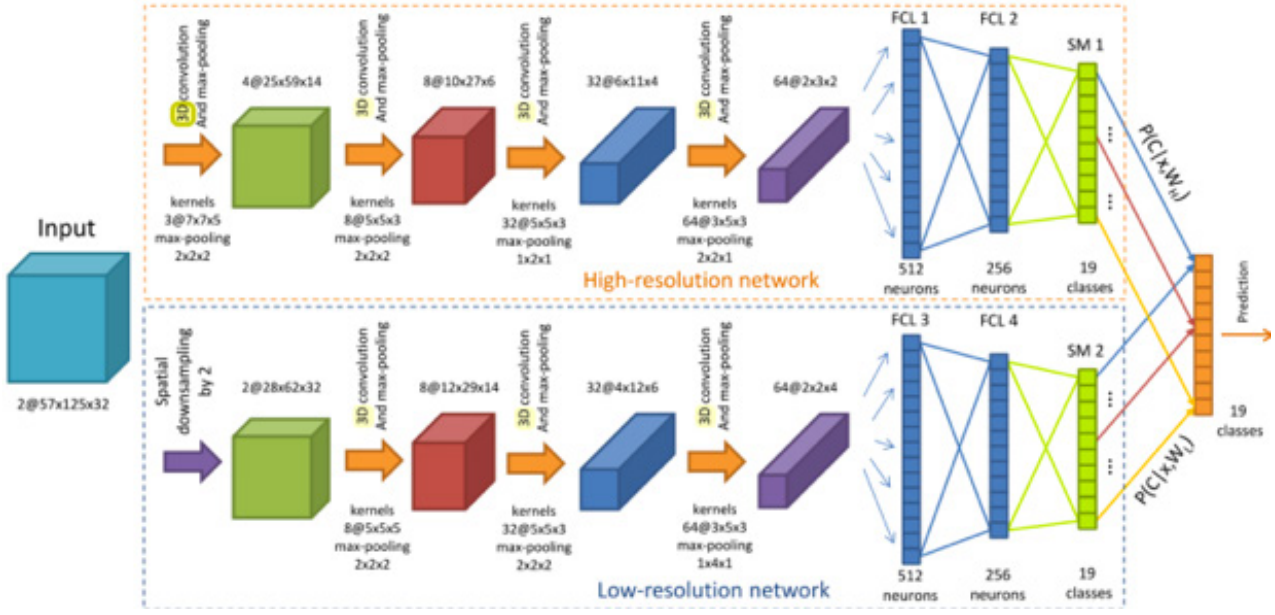


Figure 1: CNN Structure

RNN is used to the real sequential data which depends on time series data [7]. Both RNN and LSTM are parts of DNN [16]. It means DNN is increasing itself. Even the data is already learned, by using LSTM, the data will also be trained because of the sequential feature that it has. Therefore, LSTM is powerful to manage continuous recognition tasks. Figure 2 will show you how the LSTM works and the gate structure of it [17]

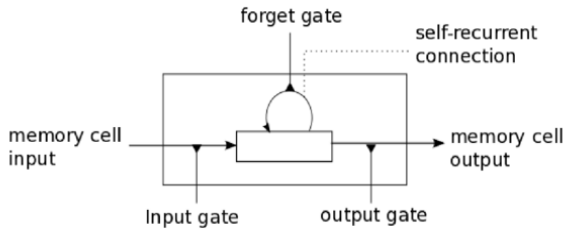


Figure 2: LSTM Structure

As shown in figure 2, the data will be stored in the memory cell. The data which is indicated as noise will be sent to the forget gate and the other data will continue to the self-recurrent. Furthermore, the forget gate will process the data again to the self recurrent connection than process the other data and the data from the forget gate to mark as the real data than send to the memory cell output to do the next steps.

In addition, it means to process image data there are three steps which are *preprocessing*, modeling, and testing model.

3. Methodology

Firstly, doing study literature about sign language recognition, then determine the background study and point of topic research. The next step was collecting the dataset which became the data training. The next step was doing *preprocessing* the data that was collected. To get a new result, the model was doing some interflow of layers in CNN, LSTM, and some combinations between CNN and LSTM. The last step was writing the paper and the result of this research.

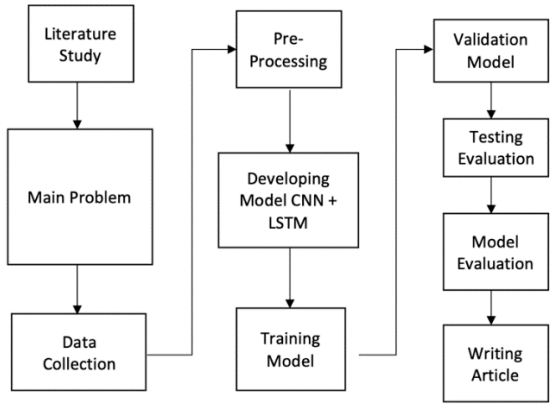


Figure 3: Research Method

As mentioned in [3] by using 9 frames in CNN than combine it with 1024 cells in LSTM showed the result accuracy and loss of CNN, LSTM, and combination CNN and LSTM, Especially for CNN used two types of model extraction, start from high to low and low to high. By using HMM (Hidden Markov Model), object BISINDO and both male and female as samples could get a 60-70% accuracy result [17]. Another research used four models of LipNet, 3 blocks of 3D-CNN. The first model was using 3 blocks of 3D-CNN, then the second was using one block of 3D-CNN, the third model was using eight blocks of CNN and last was using 2 blocks of B-RNN by using SIBI as objects. The result was by calculating the average of WER (Word Error Rate) equal to 88,79% and CER (Character Error Rate) equal to 65.33% [5].

Table 1: Research Comparison

Authors	Method & Dataset	Accuracy Result
[5]	HMM & BISINDO	accuracy 60-70%
[7]	CNN + B-RNN & SIBI	Average of word error rate 88.79%, average of character error rate 65.33%
[18]	C3D-CNN & EgoGesture	accuracy EgoGesture 91.04%, nVGesture 77.,39%
[19]	C3D-CNN & 3D dynamic skeletal data	accuracy 78%
[8]	CNN + LSTM & Chinese Sign Language	accuracy 96.52%
[20]	LSTM & Kinnect	accuracy 63.3%
[4]	CNN + LSTM & American Sign Language	Softmax Accuracy 91,5%, Pool Layer Accucary 56,5%

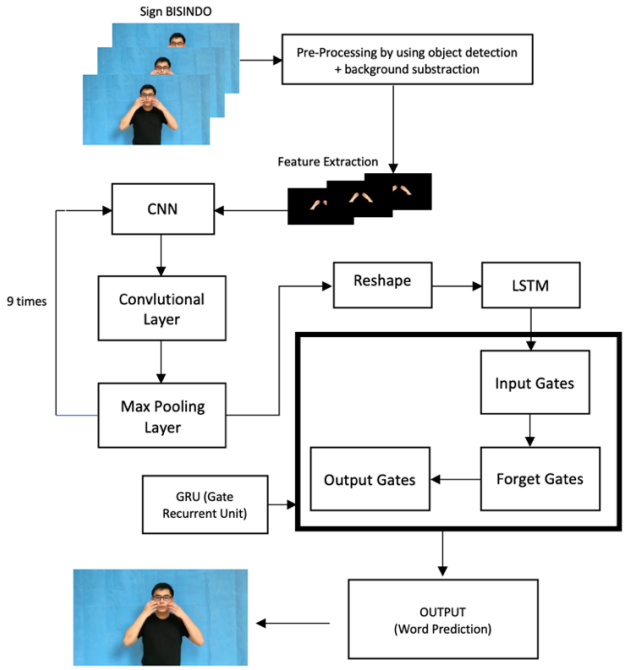
According to table 1, CNN, and LSTM were the best combinations to sign language by using such as kind of object sign language. Besides, by using HMM with BISINDO object had a high of error rating [17]. The result was used different dataset and still had a good accuracy by each own paper. By comparing the result of CNN, LSTM, and combination CNN and LSTM that this research showed the result of a good method for BISINDO object

3.1. Proposed Method

Before *preprocessing*, the data was created by 2 alphabets and 8 words of BISINDO (*A, Berapa (how many/much), Kamu (you), L, Nama (name), Sama-sama (your welcome), Saya (I), Sayang (love), Terimakasih (thank you), and Umur(age)*). After that normalizing the data. On the other hand, Inside the purpose model, the process was doing training, validation, and testing according to the dataset from *background subtraction*. The dataset became an input than did mapping from the real data. The data was converted to another kind of data. Pixel of data or images was transferred to the matrix number than gave the output data to recognize the gesture.

As imaged in fig. 4, it told how the rule from the model was used. The first, if the data is ready that will do *preprocessing* and

that *preprocessing* will produce all the images in black and white pictures. After that, the model was doing training data by using CNN and LSTM. On the other hand, after training, the model did the next process to produce hidden layers of CNN, refer to how many layers that were creating. Next steps, the output from CNN became processed in LSTM. According to LSTM, the data stored in the same gates of LSTM. The last step was doing validation data by doing *max pooling* and *fully connected* layer between both CNN and LSTM.



There are types of data, data training, and data validation. The model needs that because of the theory of validation. The model can validate the data if there is another data similar to datasets. Validation data is not an implementation mode, it is part of the model [21]. In the last, after getting the result of *preprocessing*, training and validation showed how the model worked together for implementation.

3.2. Dataset and Preprocessing

In preprocessing. The data was collected by using a camera around three feet and it has 720p HD. The camera recorded the object and direct it to save the object as the dataset by using the preprocessing method (*background subtraction and gaussian blur*). Data size was 100 x 89 pixels of each own image. Every single object had 1000 for training and 100 for validation. For the testing used a video for each object.

Figure 5 explains how the dataset was recorded and converted it to grayscale images by using *background subtraction.* However, preprocessing used *0.5 weight* and 7.0 gaussian blur. The first step is *preprocessing* using *background subtraction*. The videos or dataset converted to the gray object (hand object). After that made all the dataset in the same value, to do that, converting the image scale to the size 100x90 pixel. The dataset for training was 1000 images for each own object. And the data validation was 100 images for each own object. Figure 7 shows how the image became the vectors matrix.

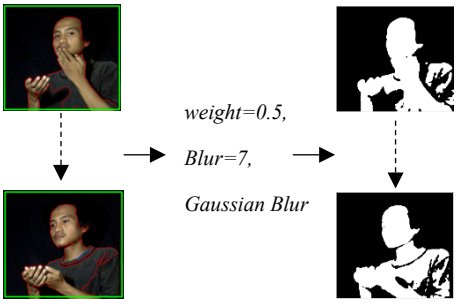


Figure 5: Dataset Recording

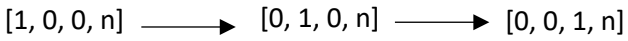


Figure 6: Image to vectors array

3.3. CNN (Convolutional Neural Network)

After *preprocessing*, the image had the same value capacity. After that converted again by translating the image gray to the array matrix. When the image pixel is found in white it will be given value 1 on the value matrix and if the image found black it will give value pixel as 0 and also the weight of data was 0.5. It showed in figure 6. Then, CNN processed the vectors matrix.

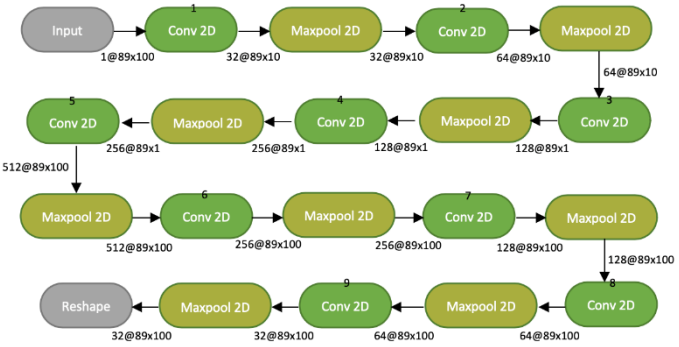


Figure 7: CNN Model

This research used the CNN model. Furthermore, this used 9 or more layers of CNN to training and validating the data. Figure 8 told how CNN worked with the matrix. The matrix processed in CNN using hidden layers. As mentioned before this used 9 hidden layers or more. Also, CNN 32 filters to 512 pixels filters of layers in the low to high then using 512 pixels to 32 in the high to low. CNN also used 89x100 pixels of each own layer including hidden layers. For each method was using 30 *epocs*.

In the CNN model after the last *maxpooling* 2D by 32@100x89 pixel, it used fully connected layers to produce the model of CNN. Therefore, in combination between CNN and LSTM using end to end training and validation, before the data entered the LSTM model, firstly it was reshaped then processed to the next step.

3.4. LSTM (Long Short-term Memory)

Figure 9 shown how LSTM worked with its gate. Next steps, the output from CNN processed more by using the LSTM model which had 1024 of cells. During the training process, LSTM or DNN model kept the data, then calculated all the data training. If the cache training did not clean the LSTM kept it in memory.

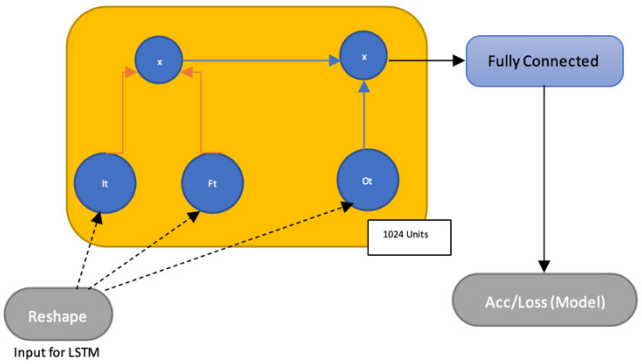


Figure 8: LSTM Model

LSTM worked with a sequential segment. The data sent to the gate. If the date had some noise than the data was sent to the forget gate. If the data was an input then the data stored to the cell. Before *max pooling* and *fully connected* layers, the LSTM system will call forget gate, afterward training the data more. After that give the result.

This research was used processor intel core i7 with 6 core of CPU, AMD Radeon R9 M370X of GPU, and 16GB for ram. The Training and validation took for CNN took more than 2 hours, LSTM took more than 3 hours, and the combination between CNN and LSTM took more than 3 hours.

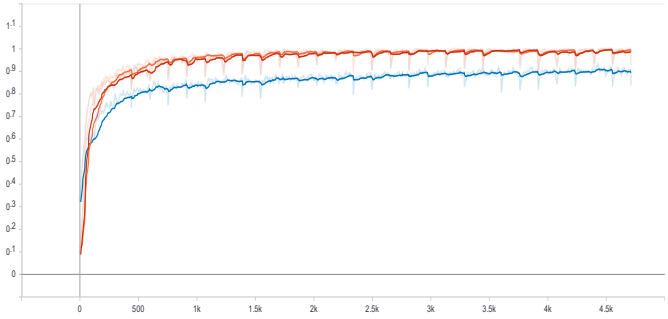


Figure 9: Training accuracy CNN, LSTM and CNNLSTM

4. Results

According to figure 10, orange for CNN, blue for LSTM, and red for CNNLSTM. The lowest score of accuracy training model is LSTM, and CNN also CNNLSTM almost the same.

Table 2: Accuracy and Loss Training

Medel	Acc	Loss
CNN	96%	18%
LSTM	86%	41%
CNN + LSTM	96%	17%

As shown in table 2, The lowest score of loss training model is CNNLSTM a point in the last result is 17% of loss, CNN has 18% of loss and LSTM has 41%. On the accuracy. CNN and LSTM have the same score which is 96%.

Table 3: Testing Result

Objek	CNN	LSTM	CNN LSTM
A	99%	98%	99%
Berapa (how much/many)	90%	75%	94%
Kamu (you)	99%	99%	99%
L	90%	94%	90%
Nama (name)	83%	66%	89%
Sama-sama (your welcome)	0%	75%	89%
Saya (I)	87%	73%	91%
Sayang (love)	88%	87%	88%
Terima Kasih (thank you)	92%	75%	90%
Umur (age)	0%	67%	71%
AVERAGE	73%	81%	90%

Table 3 shown the testing result of each own data object model CNN, LSTM, and CNN+LSTM. CNN got 73%, for LSTM got 81%, and combination CNN+LSTM got 90% of each own average.

5. Conclusion

With the rapid development in machine learning and deep learning, is expected to facilitate life. One of the benefits that develop a deep learning method to do hand predictions in sign language. By using the CNN, LSTM, and CNN + LSTM methods and focus on filtering, layers, and BISINDO object. According to the training, validation, and testing model, the best model to use in this object is CNN+LSTM. It got 96% for accuracy, 17% for loss, and 90% for testing.

Although this paper point explains the deferential between CNN, LSTM, and CNN+LSTM models, the dataset needs to add for all symbolic in sign language. For the future, it is also good to focus on the other part of sign languages such as expression detection, body gesture detection or mouth detection.

References

[1] M.A. Kumbhar, D.P. Bhaskar, "A Review on Motion Detection Techniques," International Journal of Trend in Scientific Research and Development, **-2**(1), 736–740, 2017, doi:10.31142/ijtsrd5928.

[2] R.A. Mursita, "Respon Tunarungu Terhadap Penggunaan Sistem Bahasa Isyarat Indonesa (SIBI) dan Bahasa Isyarat Indonesia (BISINDO) dalam Komunikasi," Inklusi, **2**, 221–232, 2015.

[3] R.K. Deepak, "Hand gesture recognition using Kinect," International Journal on Future Revolution in Computer Science & Communication Engineering, **4**(6), 59–62, 2012, doi:10.1109/icsess.2012.6269439.

[4] K. Bantupalli, Y. Xie, "American Sign Language Recognition using Deep Learning and Computer Vision," Proceedings - 2018 IEEE International Conference on Big Data, Big Data 2018, 4896–4899, 2018, doi:10.1109/BigData.2018.8622141.

[5] T. Handhika, R.I.M. Zen, D.P. Lestari, I. Sari, "Gesture recognition for Indonesian Sign Language," In Journal of Physics: Conf. Series, **1028**, 1–8, 2018, doi:10.1088/1742-6596/1028/1/012173.

[6] Y. Zhang, C. Cao, J. Cheng, H. Lu, "EgoGesture: A New Dataset and

Benchmark for Egocentric Hand Gesture Recognition," IEEE Transactions on Multimedia, **20**(5), 1038-1050_, 2018, doi:10.1109/TMM.2018.2808769.

[7] M.C. Ariesta, F. Wiryana, Suharjito, A. Zahra, "Sentence Level Indonesian Sign Language Recognition Using 3D Convolutional Neural Network and Bidirectional Recurrent Neural Network," 2018 Indonesian Association for Pattern Recognition International Conference (INAPR), 16–22, 2018, doi:10.1109/INAPR.2018.8627016.

[8] S. Yang, Q. Zhu, "Continuous Chinese sign language recognition with CNN-LSTM," Ninth International Conference on Digital Image Processing (ICDIP 2017), **10420**(100), 104200F, 2017, doi:10.1117/12.2281671.

[9] S. Perumal, T. Velmurugan, "Preprocessing by contrast enhancement techniques for medical images," International Journal of Pure and Applied Mathematics, **118**(18), 3681–3688, 2018.

[10] Y. Alginahi, "Preprocessing Techniques in Character Recognition," Intech, **10**, 1–21, 2010, doi:10.5772/9776.

[11] G. Hima Bindu, P.V.G.D. Prasad Reddy, M. Ramakrishna Murty, "Image preprocessing of abdominal CT scan to improve visibility of any lesions in kidneys," Journal of Theoretical and Applied Information Technology, **96**(8), 2298–2306, 2018.

[12] A. Solichin, A. Harjoko, "Metode Background Subtraction untuk Deteksi Obyek Pejalan Kaki pada Lingkungan Statis," Seminar Nasional Teknologi Informasi 2013, 1–6, 2013.

[13] A. Karambakhsh, A. Kamel, B. Sheng, P. Li, P. Yang, D.D. Feng, "Deep gesture interaction for augmented anatomy learning," International Journal of Information Management, **45**(October 2017), 328–336, 2019, doi:10.1016/j.ijinfomgt.2018.03.004.

[14] P. Molchanov, S. Gupta, K. Kim, J. Kautz, "Hand gesture recognition with 3D convolutional neural networks," In Proceedings of the IEEE Conference on Computer Vision and Pattern Recognition Workshops, 1–7, 2015, doi:10.1109/CVPRW.2015.7301342.

[15] T. Katte, "Recurrent Neural Network and its Various Architecture Types," International Journal of Research and Scientific Innovation, **V**(III), 124–129, 2018.

[16] D. Avola, M. Bernardi, L. Cinque, G.L. Foresti, C. Massaroni, "Exploiting Recurrent Neural Networks and Leap Motion Controller for the Recognition of Sign Language and Semaphoric Hand Gestures," IEEE Transactions on Multimedia, **21**(1), 234–245, 2019, doi:10.1109/TMM.2018.2856094.

[17] F. Beşer, M.A. Kizrak, B. Bolat, T. Yildirim, "Recognition of Sign Language using Capsule Networks," In 2018 26th Signal Processing and Communications Applications Conference (SIU), 1–4, doi:10.1109/SIU.2018.8404385.

[18] O. Köpüklü, A. Gunduz, N. Kose, G. Rigoll, "Real-time Hand Gesture Detection and Classification Using Convolutional Neural Networks," In 2019 14th IEEE International Conference on Automatic Face & Gesture Recognition, 1–8, 2019.

[19] C.R. Naguri, R.C. Bunescu, "Recognition of dynamic hand gestures from 3D motion data using LSTM and CNN architectures," Proceedings - 16th IEEE International Conference on Machine Learning and Applications, ICMLA 2017, 1130–1133, 2017, doi:10.1109/ICMLA.2017.00013.

[20] L. Tao, W. Zhou, L. Houqiang, "SIGN LANGUAGE RECOGNITION WITH LONG SHORT-TERM MEMORY," In 2016 IEEE International Conference on Image Processing (ICIP), 2871–2875, 2016, doi:10.1142/S0218127407017628.

[21] G. Devineau, W. Xi, F. Moutarde, J. Yang, G. Devineau, W. Xi, F. Moutarde, J. Yang, D. Learning, G. Devineau, W. Xi, F. Moutarde, J. Yang, "Deep Learning for Hand Gesture Recognition on Skeletal Data," In 2018 13th IEEE International Conference on Automatic Face & Gesture Recognition (FG 2018), 106–113, 2018.

Advances in Science, Technology and Engineering Systems Journal Vol. 5, No. 5, 288-294 (2020)

www.astesj.com

ASTESJ

ISSN: 2415-6698

A Didactic Balance to Solve Equations

Lhachimi Mohamed Younes[*,1], Mamouni My Ismail[2], Achtaich Naceur[1]

[1]*Team of Biomathematics, Laboratory of Analysis, Modelisation and Simulation, Department of Mathematics and Informatics, Hassan II University of Casablanca, Faculty of Sciences Ben M'sik, B.P. 7955, Bd Commandant Harti, Sidi Othmane, Casablanca 20700, Morocco*

[2]*Department of Didactics and Mathematics, Street Allal Al Fassi, Madinat Al Irfane, Rabat, 10000, Morocco*

ARTICLE INFO

Article history:
Received: 19 May, 2020
Accepted: 07 August, 2020
Online: 17 September, 2020

Keywords:
Mathematical education
One-degree equation
Educational games

ABSTRACT

Solving equations does not require only to well master the techniques but also to well understand the different underlying concepts and processes. Many of the mistakes made by the students are often due to misinterpretation of the concepts taught, especially the use of letters which the main conceptual obstacle that students have to overcome. We present here an educational game, in the form didactic balance which may help the students to master resolving equations of the first degree. In our conception, we were very aware to avoid that our balance becomes a calculating machine that solves the equations instead of the student. The balance was designed to develop inside the student the rigor of mathematical reasoning, one of the didactic objectives behind the introduction of the notion of the equation of the one-degree equations at this stage of the learning process, that of the middle-school learners. The novelty is to offer to both teachers and students a didactic tool that may replace the traditional method of solving equations.

1. Introduction

To solve the one-degree equations is the first learning situation where the students are asked to develop proper mathematical reasoning. In fact, their previous activities were almost of an algebraic computation nature, while resolving one-degree equations requires abstraction after modeling a real context into a mathematical problem. A survey on a sample of 1000 students how learners are disappointed while solving certain equations: they no longer know where to start, or what to find [1]. For example, to check that $x=3$ value is a solution to the equation "$17+2x=9x-4$":

- Only 35% of students think to substitute the value $x=3$ in the equation;
- More than 50% try first to solve the equation and secondly to check that the solution found is effective;
- 20% fail to give any answer,

*Corresponding Author: Lhachimi Mohamed Younes, Faculty of Sciences Ben M'sik, Hassan II University of Casablanca, +212609253075, youneslhachimi@gmail.com

The main difficulties in solving equations are: what are we looking for? How to find it and where to start? To overcome these difficulties, we propose didactic remediation, in the form of an educational game, whose main goal is to accompany the student in developing his strategic techniques and mathematical reasoning.

The bad representation of the use letters in mathematics is identified as a didactic obstruction while solving equations [2-5]. The second goal of our didactic balance is to help the students well understand the different roles that letters may help in mathematics.

The remainder of our paper is organized as follows. In a section, we will approach the theoretical framework of some concepts like the didactic obstruction, the one-degree equations, the literal arithmetic, the educational games. The section devoted to the educational game we propose is divided in two parts. In the first one, we will show how our didactic balance was designed in order to respect the norms and standards of educational games. In the second part, we propose a simulation of the game. Finally, we conclude by some interpretations and research perspectives.

2. Literature review

2.1. Motivation and novelty

Our interest in the one-degree equations is part of a general reflection on the teaching of algebra in middle school and more specifically on the role that algebraic equations can play to help middle school students in developing their algebraic reasoning. Indeed, the false apparent simplicity of the algebraic chapters in middle school and the symbolic way this chapter is proposed to justify the enormous difficulties encountered by middle school students in algebra [6, 7]. This challenges us to innovate the teaching techniques and tools in this mathematical area more precisely [8-11].

The originality of our game is to provide children with pedagogically-appropriate ideation scaffolding, as it incorporated one-degree equations resolution best strategies. Its novelty is to be open to the incorporation of newly invented methods, provided the new additions fit with its existing system components. We guided the children through a series of steps targeted at enabling them to model a real context into a one-degree equation and then resolve the equation. These steps are described next. Moreover, the game combines two major techniques used in serious games:

- **Competition:** when the learner tries to maintain the equilibrium of the balance while adding coins;
- **Strategy:** when the learner tries to maintain the equilibrium of the balance while distributing the city with buildings of the same floors.

2.2. The didactic obstruction

Historically, this terminology was the first one to be introduced [12] while analyzing some experiences in the physical sciences. The didactic obstruction was defined [12] as an obstacle between the concept studied and the learner's desire to learn. It is considered as an important and being interested "piece of knowledge" that unexpectedly became erroneous or unusual, or simply unsuitable [13]. They are seen as false representations of the learning task induced by previous learning, which hinders new ones [14]. They are obstinate to appear inside a given context by producing false answers. Three types are distinguished according to their origin [15]:

- The onto-genetic obstruction is related to the biological learner's development;
- The epistemological obstruction is related to the historical development of the concept studied;
- The didactic obstruction is related to the teaching process itself.

The traversal nature of these obstacles and their resistance to prompt the educational community to propose different remediation strategies.

For example, a certain flexibility is proposed that allows students to put in their own ideas and a rigidity that guarantees. The concept will not be losing insight to be constructed [16]. The first identify the origin of the didactic obstruction by analyzing the student answers and secondly to propose some alternative teaching activities that allow the students to overcome the identified obstruction [17].

2.3. One-degree equations

The one-degree equations

$$a.x + b = c.x + d \quad (1)$$

are the first taught ones by learners are those of the first degree. We distinguish different solving methods:

- *The substitution method*, very suitable for the reduced equations of the form

  $$e.x = f \quad (2)$$

  consists to try many numerical values until obtaining a solution. Using such methods opens up the learner on some classical mathematical reasoning, like true or false, the absurd or the cases distinction [18].

- *The overlap method*, which is an extended form of the substitution method, consists of replacing the unknown by an entire algebraic expression. For example, to solve the equation "*2(x-2)=2*", we expect that the student considers the expression "*x-2*" as an unknown, to deduce by substitution that "*x-2=1*", before concluding that "*x = 3*" is a solution. Looks at this method, a preparation of the student to recurrence and variables changes reasoning [19, 20].

- *The formal method:* consists to identify first the operations that have been applied in the equation (1) to the unknown, then recognize secondly the reciprocal operations, then finally apply a common operator to the two members of the equation in order to transform it into another reduced equation (2) that can be resolved by a substitution approach. For example, to solve the equation "*3x+6=12*", the student is asked to structure his strategy as follows:

Table 1: Example of operations and their opposite ones in the substitution method

Operations applied to the unknown	Reverse operations to find the solution
Operation 1: the unknown is multiplied by 3. Result 1= *3.x*	
Operation 2: we add 6 to Result 1. Result 2= *3x+6*	Opposite operation 2: we subtract 6 from the second member Opposite result 2 = *6*
	Opposite operation 1: we divide the opposite result 2 by 3. Solution = *3*

2.4. Literal arithmetic

This terminology was the first to be introduced and was defined [21] as any arithmetic operations on arbitrary quantities. it was rather seen as an a formal game involving writing [22]. It was pointed as the main origin of difficulties by many researches [23, 24, 25] that the students found in mathematics, especially in the algebra part. The results of the survey show us the non-mastery of the status of the letter when solving a mathematical problem in literal calculus. In a sample of 300 students, only one person correctly answered the following question: Which is the greater number n or w, if $7+n+22=109$ and $7+w+22=109$. For many others, w was greater than n, because it's lexicographic rank [11].

In fact, the students are generally confused about the role and nature that the letter can play in the literal arithmetic, since the rules change completely compared to those known in the numerical calculus [26]. For example, the equation "$4(2x+3)=2(4x+2)+6$" means implicitly that the relation is true for any real numbers. This is never specified and therefore not necessarily obvious for the student. Here, the letter plays the role of a variable, which can take any value. While, in the example, "$2x + 3 = 4$", the student is rather asked to find a value of x verifying the equality. This is not specified here either.

2.5. The educational games

In educational games were interested and have been pointed out how by many researches [27, 28, 29], they differ from the standard one by their contexts and objectives. However, their common point is that in both the player has to put up a strategy while dealing with a critical situation (for example, freeing prisoners in ordinary games or solving a one-degree equation in educational ones). One may ask why educational games (as a distraction tool) deal with mathematics (as a rigorous discipline). The answer is that in both, the player-learner is asked to resolve a problem, by taking initiatives, making choices, making decisions, anticipating solutions. In short, by putting up a logical and rigorous reasoning. In addition, the educational games help the player-learner to overcome his didactic and cognitive difficulties. Indeed, in the case of a failure situation in a classroom, the students prefer to make no additional effort. While the educational games lead the students to relax, to try again and again, to make mistakes. This is essential for the teaching-learning process [16]. We are recalled the social contribution of educational games, "a child who plays is a child who socializes"[30]. Indeed, in educational games, both adversaries and partners should respect the rules, if not this is synonymous with exclusion. This is a kind of socialization.

Furthermore, the official instructions in many educational systems recognize the educational value of the educational games by reaffirming their contribution in the teaching-learning process. We cite for example, the French official instructions which state that the educational games "lead to a multiplicity of sensory, motor, emotional, intellectual experiences ... It can be the starting point for many didactic situations proposed by the teacher... ".

3. The balance game

3.1. The theoretical approach

In subsection 2.3, we have discussed how the students fall into the situation, which was pointed out, in a failure one, their role is abandoned as learners [31, 32]. Since they think that in terms of didactic contract, it is the teacher's role to note, correct, and validate. In an educational game, the student-learner in a failure situation never gives up; motivated by surpassing himself he tries again and again.

Their difficulties have been pointed also in the literal arithmetic, as the main obstacle to resolve equations. In the educational game, we propose instead of considering the letter as an obstacle, it will be rather considered as an objective following the "objective-obstacle" approach [33]. The resolution method that has been adopted while implementing our game is the formal one.

On the other hand, students have a private and proper knowledge validation which is not generally get-at-able to the teacher [34]. In our balance game, the student can perform his computation capacities, his reflection, his reasoning ... In a failure situation, the game does not resolve the equation, but encourages the student to detect his error, to correct it, to formulate a new answer and then to validate it.

3.2. A simulation

Let us recall that the educational games are generally designed in several levels (or stages, or rounds,…) which generally correspond to the unity and signifies a progression, which symbolizes an achievement of a knowledge component for the student and an evaluation tool for the teacher. Our game is organized in four stages:

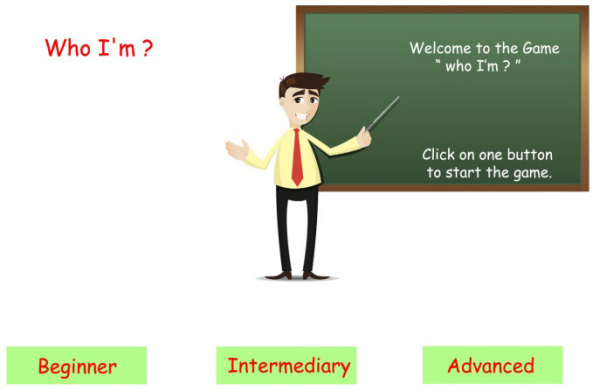


Figure 1: The starting point when the student choose his profile

Round 0: The Modeling step.

At this stage, the game asks the student to model a real situation, drawn from his daily life, in the form of a one-degree equation. He can click on the "Beginner" button which leads to a reduced equation of the form

$$a.x = b \qquad (3)$$

Or on the "Initiated" button which leads to that of the form :

$$a.x + b = c \quad (4)$$

While the "Advanced" button leads to equations of the form (1). We are thus in the approach to adapt the learning to the student profile [35-37].

Once done, the game proposes to the student an enigma and asks him to model it in a one-degree equation. He can change it or even change his profile at any time of the game.

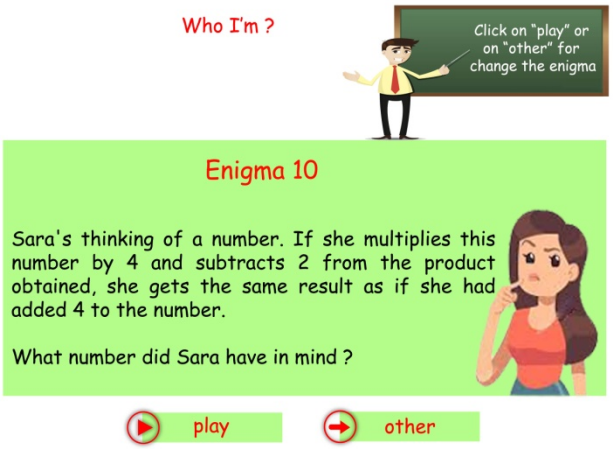


Figure 2: The starting point when the student choose his profile

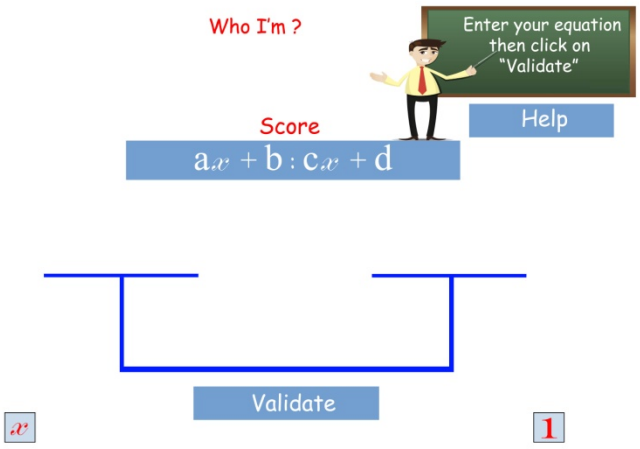


Figure 3:When the student is asked to enter the equation

Round 1: The Modeling step.

At this stage of the game, the student is asked to enter the one-degree equation he got after modeling the enigma proposed in the last level. The game does not propose the classic keyboard method to enter the equation but rather to drop coins in the both sides of the balance. Each side of the balance itself is divided in two areas: an area for the unknown where coins of the form «x» can be dropped and an area for the constants where he can drag that of the form «1». As in a building game, the balance is introduced here as an area with four buildings, where each one contains a given number of top and bottom floors. Dragging a coin somewhere, means adding a top or a bottom floor.

- Building A : the left panel of the left side of the balance;
- Building B : the right panel of the left side of the balance;
- Building C : the left panel of the right side of the balance;
- Building D : the right panel of the right side of the balance.

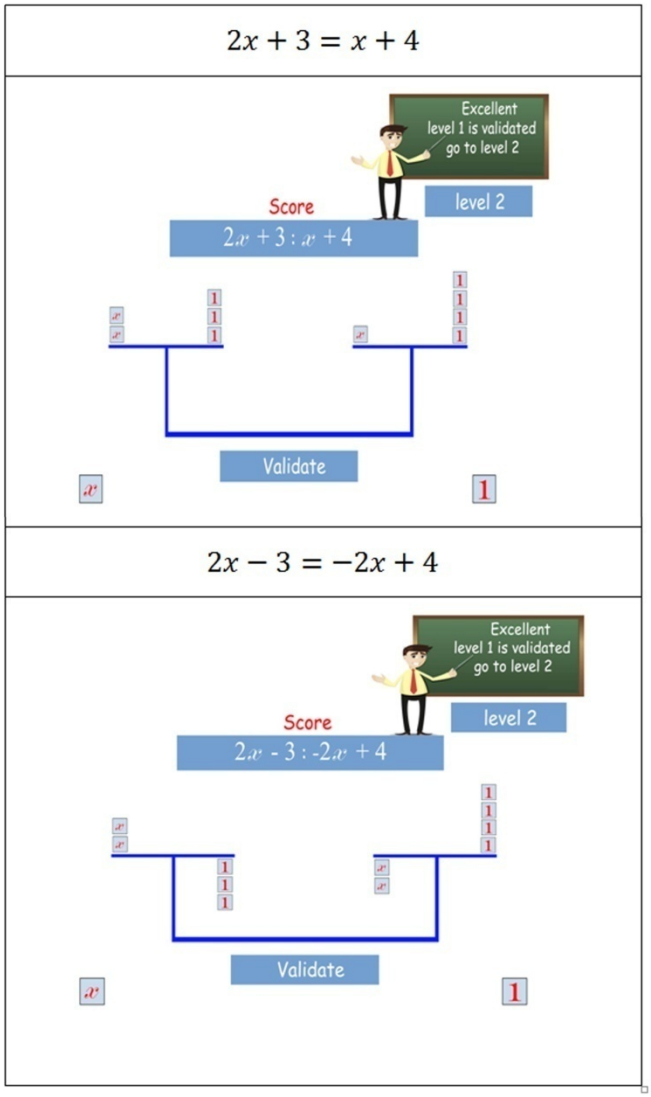


Figure 4: Example of the right way to enter equations

Table 2: Example of help tutorial

left side of the balance		right side of the balance	
Building A	Building B	Building C	Building D

Drop "a" times the coin «x» above when is positive and below when is negative.	Drop "b" times the coin «1» above when is positive and below when is negative.	Drop "c" times the coin «x» above when is positive and below when is negative.	Drop "d" times the coin «1» above when is positive and below when is negative.

A screen displays the equation obtained after each coin addition, thereby, the student feels himself in a game situation, like in a football match for example. Once the score displays the equation that has been modeled before, the game felicitates the student and invites him to press the "Validate" button. A "Help" button is incorporated in each phase of the game in any case for more technical instructions.

Round 2: The reduction step.

The task here is to reduce the inputted equation (1), into an equivalent one of the form (2). In a classroom blackboard, the student should apply the same additions and subtraction simultaneously on both members of the equation. In the screen game, he should drag-drop the same numbers of coins simultaneously in both sides and panels of the balance. While doing, he should respect these following strict rules of the algebraic and literal computations:

- Adding the same expression to each member of the equation should be done by adding the same number of coins in top appropriate panel and side of the balance;
- Subtracting the same expression to each member of the equation should be done by adding the same number of coins in the bottom appropriate panel and side of the balance.

If something was done wrong during the student manipulations, then an error message invites him to restore the broken equilibrium.

Table 3: The steps to follow while reducing the equation

	blackboard manipulations	game manipulations
Initial equation	*6x-4=3x+2*	comment 0
First manipulation	*6x-4+4=3x+2+4*	comment 1
Second manipulation	*6x=3x+6*	comment 2
Third manipulation	*6x-3x=3x+6-3x*	comment 3
Reduced form	*3x=6*	comment 4

- **Comment 0:** this manipulation was already done in level 1 when he enters the equation (1) he got after modeling the enigma of the level 0;
- **Comment 1:** he should add 5 coins of the form «1» in the right top panel of each side of the balance. If not well done, he got this "teacher" instruction: "the number of tops and bottom floors in your building B should be the same";
- **Comment 2:** normally, in such a blackboard classroom situation the student should erase the expression *-5+5* by himself. In the game a "delete" button is incorporated: when pressed, a window is opened and proposes to the student to enter a number (in our situation, he should enter the number *5*). Then, he is asked to press once in the top floors and again in top floors of the right building (here in the building B). We consider that a middle-school student has no problem in the addition, thus the operation *10+5=15* is automatically done by the game by adding automatically floors up or down the building when coins are added in a panel;
- **Comment 3:** he should add *3* coins of the form «x» in the left bottom panel of each side of the balance. If not well done, he got this "teacher" instruction: the number of tops and bottom floors in your building C should be the same. He should once again simplify the erase the expression "*3x-3x*" by using the "delete" button;
- **Comment 4:** finally, the player-learner gets his reduced equation and is felicitated and invited to go to the next level.

Round 3: The resolution step.

At this stage where the equation is reduced to the form (2), the building A contains "*e*" floors, the building D contains "*f*" floors, while the other ones are empty. Then, the game asks the student to redistribute the "*f*" floors of the building D, in many "*f*" floors sub-buildings. Once well done, the next game instruction is a window that invites the student to enter the value of "*x*", which is the number of the sub-buildings in panel D.

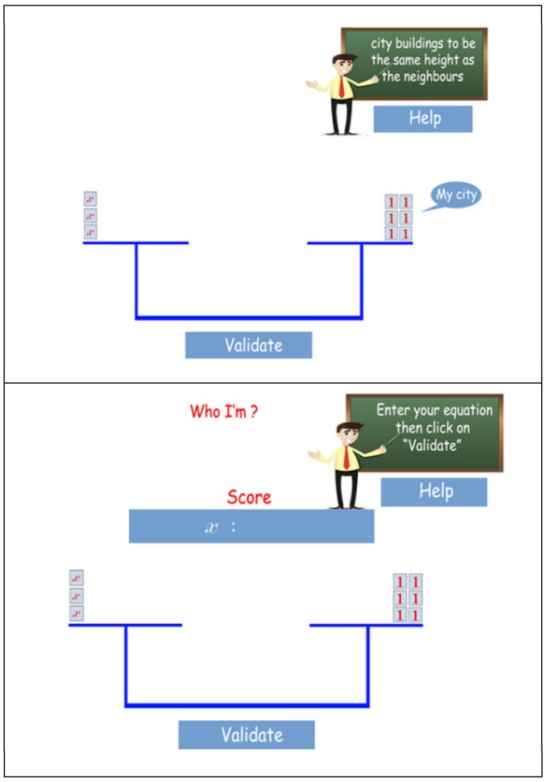


Figure 5: The final resolution step

The case when "*e*" and "*f*" are both positive, is an elementary case which will not pose great problems to the student. Otherwise, the game proposes an "Inverse" button which interprets the multiplication of one equation member by -1. Its effect in the game is inverse bottom floors to tops floors.

- If "*e*" or else "*f*" is negative, then the player should push the "Inverse" button and then click on the right panel. Then the game stores this information and will multiply by *-1* the value of "*x*" entered by the student when asked.
- If both "*e*" and "*f*" is negative, then the player repeats the inverse manipulation twice. The game will store this information and will not change the value of "*x*" entered by the student when asked.

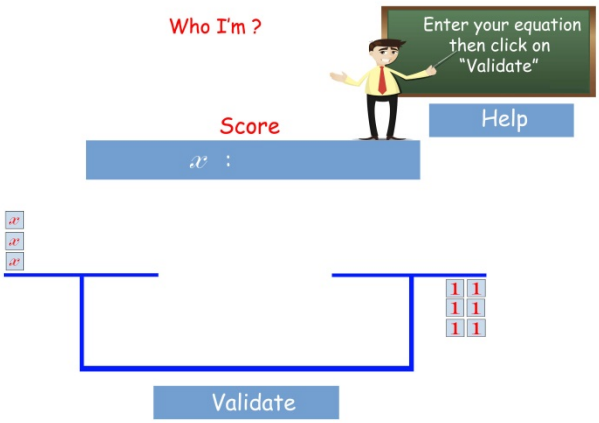


Figure 6: Simulation of the equation *3x=-6*

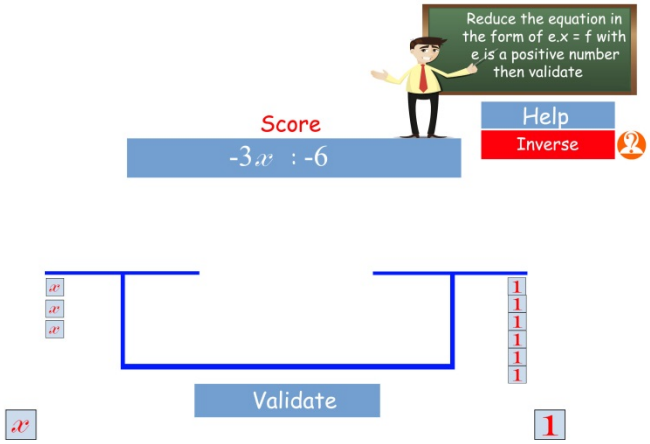


Figure 7: Simulation of the equation $-3x = -6$

4. Discussion

As early mentioned in this paper, our main goal is to help middle-school students to develop their rigor, logic, and mathematical reasoning while playing to solve one-degree equations. In its current state, the paper presents only the theoretical philosophy, the technical design, and a virtual simulation of the game. The future work on progress is to develop the "game", to experiment on a sample of middle-school students to know how they transpose their "gaming" skills to performance of solving equations on the blackboard. Thus, our discussion will be theoretical to argue that our didactic balance is beyond being an educational game maybe also a real and alternative teaching-learning activity.

Firstly, our game is an a-didactic situation (as shown by in Table 3), which is a teaching activity where the decisions were made by the learner based on his proper knowledge, without the teacher intervention [15].

We know also that in each learning situation, the students need to adjust their actions according to their own knowledge. Any teaching situation should offer flexibility doses which enable the learner to confront the persistent of his knowledge [16]. Our game fits into the same approach as he takes care to ensure this freedom area by limiting the teacher (illustrated by an interactive photo) interventions to only the cases of false technical manipulations.

Table 4: Example of steps to follow while reducing the equation

a-didactic situation moment	the associated game moment
Decentralization	When the game proposes an enigma.
Action	The moment preferred by the players, here when they drag and drop coins.
Formulation	When they decide to validate a manipulation.
Validation	When the click on a button validation.
Institutionalization	When the game felicitate the student and invite him to go to the next level.

Our game also deals with [38], who suggests assisting the student in any cognitive transition as must give up its initial system of action and adopting another different system of action. By proposing coins for both variables and numbers, the transition from numbers to letters should be smoothly easy.

On the other hands, resolving equations in mathematics involves two types of skills:

- the ability to model a real problem into a mathematical problem;
- the ability to establish a strategy to solve the underlying mathematical problem.

Our didactic balance agrees with [39] who deplores the fact that handbooks focus on the solving methods more than on the modeling philosophy and who suggest that both of these skills should be learned simultaneously.

As mentioned early in this paper (to resolve one-degree equations), we adopt the formal method. In [40], the author pointed out the possible negative effect of this method: the student finds himself in an out of context situation, when sometimes he loses the sense of what he was looking for. The game we propose is mindful to avoid this possible confusion, since as in a movie, the main goal (to find « x ») accompanies the student, during all the stages and levels of the game.

Finally, we can conclude that our educational game takes care to respect all these requirements: to contextualize the learning, to give the learner-player a free margin to make his proper initiatives and decisions, to allow the learner to overcome his didactic and cognitive obstructions, to accompany the student in a situation of failure.

5. Further work

The authors are aware to evaluate the game in practice by operating factual information and discussing its educational advantages. Indeed, the game conception is in progress and real simulations will be done by a sample of students. The data collected will be presented in a future work.

References

[1] J. VLASSIS and I. DEMONTY, La résolution des équations du premier degré à une inconnue, Cahiers du Service de Pédagogie Expérimentale de Université de Liège, 2000.

[2] A. Cortés and N. Kavafian, "Les principes qui guident la pensée dans la résolution des équations" Petit x, no. 51, 47-73, 1999.

[3] F. Chalancon, S. Coppé and N. Pascal, "Les vérifications dans les équations, inéquations et en calcul littéral" Petit x, no 59, 2002.

[4] G. Combier, J. C. Guillaume and A. Pressiat, Les débuts de l'algèbre au collège: au pied de la lettre!, Institut National de Recherche Pédagogique, 1996.

[5] J. Vlassis and I. Demonty, La résolution des équations du premier degré à une inconnue, Cahiers du Service de Pédagogie Expérimentale de Université de Liège, 2000.

[6] J. P. Drouhard, J. L. Dorier, L. Coulange and A. Robert, Enseignement de l'algèbre élémentaire: bilan et perspectives, La Pensée Sauvage, 2012.

[7] G. Gattegno, The Common Sense of Teaching Mathematics, Educational Solutions World, 2010.

[8] T.L. Kurz and I. Batarelo, "Using anchored instruction to evaluate mathematical growth and understanding" Journal of Educational Technology Systems, **33**(4), 421- 436, 2005. https://doi.org/10.2190/78JG-57N4-0702-XH25

[9] Y. Li and E.A.Sillver, "Can younger students succeed where older students fail? An examination of third graders solutions of a division-with-reminder (DWR) problem" Journal of Mathematical Behavior, **19**(2), 233-246, 2000. https://doi.org/10.1016/S0732-3123(00)00046-8

[10] J. Sharp and B. Adams, "Children's construction of knowledge for fraction division after solving realistic problems" The Journal of Educational Research, **95**(6),333-347, 2002.https://doi.org/10.1080/00220670209596608

[11] S. Wagner and C. Kieran, An agenda for research on the learning and teaching of algebra, Research issues in the learning and teaching of algebra, Routledge,220-237, 2018.

[12] G. Bachelard, La formation de l'esprit scientifique Contribution à une psychanalyse de la connaissance objective, Libraire Philosophique J. VRIN, Paris, 1938.

[13] J. Piaget, L'épistémologie génétique, Presses Universitaires de France, Paris, 1970.

[14] G. Brousseau, "Les obstacles épistémologiques et les problèmes en mathématiques" Recherches en Didactiques des Mathématiques, **4**(2), 164-198, 1983.

[15] G. Brousseau, " Obstacles épistémologiques, conflits socio-cognitifs et ingénierie didactique" in Actes du colloque international Obstacles épistémologiques, conflits socio-cognitifs et ingénierie didactique, Montréal, Canada, 1986.

[16] J. P. Astolfi, L'erreur, un outil pour enseigner, ESF éditeur, Paris, 1997.

[17] R. Berthelot and M. H. Salin, "L'enseignement des angles aux élèves de 10 à 13 ans: Identification d'un obstacle didactique" Revue des sciences de l'éducation, **22**(2), 417-442, 1996. https://doi.org/10.7202/031887ar

[18] J. Vlassis, "The balance model: Hindrance or support for the solving of linear equations with one unknown" Educational Studies in Mathematics, **49**(3), 341-359, 2002. https://doi.org/10.1023/A:1020229023965

[19] J. Vlassis, Sens et symboles en mathématiques: étude de l'utilisation du signe" moins" dans les réductions polynomiales et la résolution d'équations du premier degré à une inconnue, Peter Lang, 2010.

[20] A. H. Schoenfeld, Mathematical problem solving, Elsevier, 2014.

[21] O. Terquem, Manuel d'algèbre, ou Exposition élémentaire des principes de cette science, à l'usage des personnes privées des secours d'un maître, Paris, RORET, 1834.

[22] Y. Chevallard,"Le passage de l'arithmétique à l'algébrique dans l'enseignement des mathématiques au collège, Deuxième partie : Perspectives curriculaires : la notion de modélisation" Petit x, no 19, 43-72, 1989.

[23] D. Celik, G. Gunes, "Different Grade Students Use and Interpretation of Literal Symbols" Educational Sciences: Theory and Practice, **13**(2), 1168-1175, 2013.

[24] K. P. Christou and S. Vosniadou, " What kinds of numbers do students assign to literal symbols? Aspects of the transition from arithmetic to algebra" Mathematical Thinking and Learning, **14**(1), 1-27, 2012. https://doi.org/10.1080/10986065.2012.625074

[25] M. Zeljić, "Modelling the relationships between quantities: Meaning in literal expressions" EURASIA Journal of Mathematics, Science and Technology Education, **11**(2), 431-442, 2015. https://doi.org/10.12973/eurasia.2015.1362a

[26] D. Guerrier, M. Le Berre, C. Pontille and J. Reynaud-Fleury, Le statut logique des énoncés dans la classe de mathématiques. Éléments d'analyse pour les enseignants, IREM de Lyon, 2000.

[27] N. Pelay, "Jeu et apprentissages mathématiques: élaboration du concept de contrat didactique et ludique en contexte d'animation scientifique," Doctoral dissertation, Université Claude Bernard-Lyon I, 2011.

[28] L. Sauvé and D. Kaufman, Jeux et simulations éducatifs: Études de cas et leçons apprises, Presses de l'Université du Québec, 2010.

[29] T. M. Connolly, E. A. Boyle, E. MacArthur, T. Hainey and J. M. Boyle, "A systematic literature review of empirical evidence on computer games and serious games" Computers & education, **59**(2), 661-686, 2012. https://doi.org/10.1016/j.compedu.2012.03.004

[30] S. De Freitas, "Are games effective learning tools? A review of educational games" Journal of Educational Technology & Society, **21**(2), 74-84, 2018. http://www.jstor.org/stable/26388380

[31] Y. Chevallard, Sur l'analyse didactique. Deux études sur les notions de contrat et de situation, IREM d'Aix Marseille, 1988.

[32] G. Brousseau, "Fondements et méthodes de la didactique des mathématiques" Recherches en didactique des mathématiques, **7**(2), 1986.

[33] J. L. Martinand, Connaître et transformer la matière, Peter Lang, 1986.

[34] I. Shor, When students have power: Negotiating authority in a critical pedagogy, University of Chicago Press, 2014.

[35] S. Connac, La personnalisation des apprentissages: agir face à l'hétérogénéité, à l'école et au collège, ESF Sciences Humaines, 2018.

[36] A. Feyfant, Individualisation et différenciation des apprentissages, Dossier d'actualité de la VST, no 40, 2008.

[37] M. Romero, Jeux numériques et apprentissages, Editions JFD, 2016.

[38] H. Squalli, "La généralisation algébrique comme abstraction d'invariants essentiels" in 2015 Actes du congrès Espace Mathématique Francophone (EMF), Alger, 2015.

[39] J. Colomb, Combier Georges, Guillaume Jean-Claude, Pressiat André, Calcul littéral : Savoir des élèves de collège, Institut National de Recherche pédagogique, 1995.

[40] L. Not, Les pédagogies de la connaissance, Toulouse : Sciences de l'Homme, Privat, 1988.

ASTES

Advances in Science, Technology and Engineering Systems Journal Vol. 5, No. 5, 295-301 (2020)

www.astesj.com

ASTESJ

ISSN: 2415-6698

Arduino-Compatible Modular Kit Design and Implementation for Programming Education

Gyeongyong Heo*

Department of Electronic Engineering, Dong-eui University, Busan, 47340, Korea

ARTICLE INFO

Article history:
Received: 22 July, 2020
Accepted: 11 August, 2020
Online: 17 September, 2020

Keywords:
Arduino
Programming Education
Modular Design
FRUTO Kit

ABSTRACT

To cultivate creative talent, ways to learn creative problem-solving skills is needed, and one of them is programming. Arduino is a well-known tool used for programming education and the usefulness has been demonstrated in various case studies. However, there are several problems in existing Arduino-compatible kits as education tools, including the need for understanding hardware and the difficulty of expanding the kits with third-party hardware. In this paper, the design of an Arduino-compatible modular kit, called as FRUTO, is proposed that can be easily connected and conveniently programmed to overcome the problems. The structure and features of the FRUTO kit that implements the proposed design are also shown. The FRUTO kit consists of the FRUTO module that uses a unified connector for easy and intuitive connection and the FRUTO library that abstracts hardware-dependent code for easy programming. The FRUTO kit is easier to use and more scalable than existing kits. Even more, it can be used in various ways depending on the students' familiarity with hardware and programming. These strengths will make the kit to be an appropriate tool for various microcontroller-related education as well as programming education.

1. Introduction

In modern society, programming goes beyond creating programs that run on computers to include interacting with everyday environments through computers. This concept of programming is more important than ever in the context of the fourth industrial revolution and the internet of things. The importance of programming education is also evident in the inclusion of programming in curriculum, beginning in the United Kingdom in 2014. In Korea, programming education has been implemented gradually since 2018 following the curriculum revision in 2015 [1]. Accordingly, information course was designated as compulsory and physical computing was included as part of information course. Physical computing, designed to teach interactive design at Interactive Telecommunications Program at New York University, means building interactive physical systems by the use of software and hardware that can sense and respond to analog world [2], which can be extended to a creative framework for understanding human beings' relationship to digital world. The introduction of physical computing, not just computer-based programming, in information course reflects the assessment that programming education helps to develop problem-solving skills and improve logical thinking. The findings that hardware education has a positive impact on students' interest, motivation and learning attitudes also influenced this decision [3-4]. Physical computing can be beneficial for students who are not necessarily interested in pursuing computer programming but would like to gain a better understanding of technology and how it is shaping our world[5].

Arduino is one of the representative tools used for programming education[6-8]. Arduino began as an open-source microcontroller project for artists and has become one of the leading microcontroller projects for its ease of use. Arduino has been widely adopted as an educational tool in elementary, middle and high schools as well as universities, and various educational effects using Arduino have been reported [9-10]. In addition, various studies on the development of Arduino-compatible educational tools are also in progress [11-13]. However, one of the problems in using Arduino as an educational tool is that it requires knowledge of hardware. Besides, existing Arduino-compatible kits are designed without consideration of various applications and are limited in their use in ways that are not considered in design phase. These problems are from the fact that existing kits were designed for Arduino itself. The kit for programming education should be considered as a tool.

*Corresponding Author: Gyeongyong Heo, Department of Electronic Engineering, Dong-eui University, Busan, 47340 Korea, +82-51-890-1673, hgycap@deu.ac.kr

In this paper, the design of a modular Arduino-compatible kit, called as FRUTO, is proposed to overcome the problems mentioned, and its structure and features are shown that implement the proposed design. On the hardware side, the connection between modules is made easy and intuitive with a unified connector, while on the software side, the code for controlling modules uses common abstract functions to facilitate easy programming, which results in improved usability. The proposed design also improved scalability by allowing anyone to produce hardware and software modules using the proposed design. As a result, improved usability and scalability make the FRUTO kit a learning tool for students of various levels. The proposed design was recognized for its differentiation through patent registration [14-15], and the FRUTO kit that implements the design is undergoing a pre-launch test.

In the next section, Arduino-compatible kits used in programming education and their limitations are presented. Section 3 is devoted to propose a new kit design that solves the problems of existing kits, and section 4 describes the FRUTO kit that meets the proposed design. Conclusions and directions for further improvements are discussed in section 5.

2. Arduino as a Tool for Programming Education

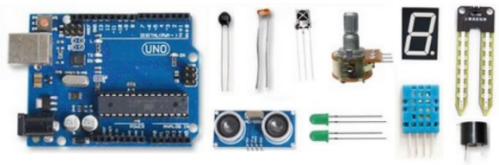
2.1. Programming Education using Arduino

As a leading physical computing platform, Arduino has been widely used for programming education as well as physical computing. In particular, Arduino is drawing attention as an alternative to overcome the limitations of the traditional programming education, as it places importance on the process of 'thinking by hand' through the prototyping process [16]. The use of Arduino for physical computing and programming education comes from the fact that it is highly accessible and usable as it is designed as a platform for artists and designers. The fact that Arduino is suitable for project-based learning (PBL) is another reason why Arduino is used as a tool for programming education. PBL has advantages such as getting structured and integrated knowledge for problem-solving beyond fragmentary knowledge and fostering active attitudes and confidence by searching for the knowledge required in problem-solving. The usefulness of PBL using Arduino in engineering subjects as well as programming education has been demonstrated in various case studies [17-19].

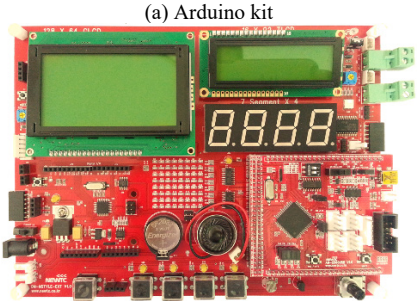
2.2. Problems with Existing Kits in Hardware

There are several Arduino-compatible kits used for programming education, which can be divided into three groups: (1) Arduino kit using the original Arduino board, (2) Arduino-compatible all-in-one board with built-in I/O devices, (3) Arduino-compatible kit with modular I/O devices and a unified connector.

The fundamental problem in using the original Arduino board as an educational tool is that students need to understand hardware. Since most I/O devices use different numbers of I/O pins and different data exchange methods, it is necessary to understand the hardware specification of each I/O device to obtain the desired operation. One way to solve the hardware dependency is to use an all-in-one board that contains all the necessary I/O devices as shown in Fig. 1-(b). All-in-one boards do not require a deep understanding of hardware, which can be seen as an advantage. On the other hand, it is difficult to use in ways that are not considered in the design, that is, it is poor in scalability. Moreover, programming education using an all-in-one board is almost the same with the conventional computer-only education.



(a) Arduino kit



(b) Arduino-compatible all-in-one board with built-in I/O devices



(c) Arduino-compatible kit with modular I/O devices

Figure 1: Arduino-compatible kits for programming education

The modular kit in Fig. 1-(c) uses a unified connector to make the connection easy. However, only simple I/O devices can be made in modules, and the position where the module can be connected to the main module is fixed. In addition, the control method varies from module to module in spite of the unified connector.

Table 1: Evaluation of existing Arduino-compatible kits

Type	Diversity	Connectivity	Independency
Arduino kit	○	×	×
All-in-one board	×	△	○
Modular kit	△	△	△

Table 1 summarizes the evaluation of existing kits based on the number of available I/O devices (Diversity), the degree of easy connection (Connectivity), and the degree of hardware-related knowledge required (Independency). Of the three types, modular kits can be used reasonably in all respects. However, modularity in software is not considered and hardware modularity is limited to some simple I/O devices. Therefore, there is a need for a new design that all modules can be connected easily and intuitively using a unified connector.

2.3. Problems with Existing Kits in Software

Two programming tools are mostly used to make programs for existing kits: Arduino and Scratch. Arduino uses C/C++ language to write a program, while scratch uses drag-and-drop blocks to build a program visually. It is not easy, however, to make complex code with the blocks given and the assembled blocks should be converted to C/C++ code before compilation. Therefore, only

C/C++ language under Arduino environment is considered in this paper.

Writing a program using C/C++ language under Arduino environment also has a similar problem with that on the hardware side. Since different I/O devices have different I/O control methods, it is also necessary to understand hardware to write the code for a specific I/O device. Most existing kits are based on Arduino environment. The Arduino library already provides an abstraction of low-level functions for AVR microcontrollers in Arduino boards, which makes it possible for different AVR microcontrollers to control a specific I/O device in the same way. That is, Arduino provides a microcontroller-independent library. However, as I/O devices are still controlled in different ways, the Arduino library is still hardware-dependent. Therefore, it is necessary to ensure hardware independence through a library that can control I/O devices with common abstract functions. This library should be based on the Arduino library for compatibility with Arduino.

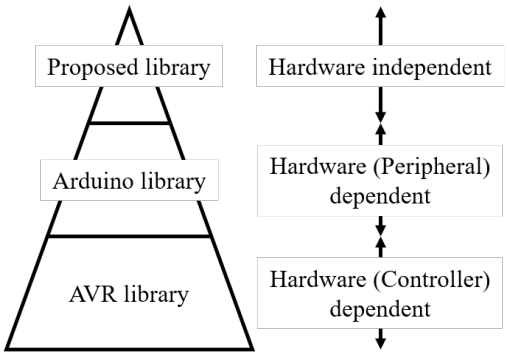


Figure 2: Hierarchical library structure

3. Proposed Kit Design

3.1. Requirements

The most important problem to be solved in a new design is the dependence on hardware. Most of the existing kits are for learning Arduino, not for learning programming or physical computing. As a kit for programming education should reduce hardware dependency as much as possible, the kit design proposed here has the following goals:

- a modular kit with easy and intuitive connection using a unified connector
- hardware-independent abstract functions to exchange data between modules
- scalability by adding third party or DIY(Do It Yourself) modules and corresponding libraries
- applicability in various microcontroller-related education

To achieve these goals, the followings are applied to the design.

- There are two kinds of modules: main module and expansion module with an I/O device.
- The Modules form a cascading connection with I2C(Inter-Integrated Circuit).
- The main module is compatible with Arduino and has one dedicated I2C connector for connecting an expansion module.
- Each expansion module includes a microcontroller that controls the I/O device and communicates with the main module.
- The microcontroller in each expansion module is one of the microcontrollers used in Arduino boards for compatibility.
- The expansion module has two dedicated I2C connectors to support cascading connection.
- The program for the main module consists of the code for I2C communication and system logic for overall system control.
- The program for the expansion module consists of the code for I2C communication and the code for I/O device control.
- Hardware-dependent code for I2C communication and I/O device control is provided through a dedicated library.
- I2C communication code in the main module uses common abstract functions in the library across all expansion modules.
- The dedicated library is based on the Arduino library to maintain the compatibility with Arduino.
- The module design is based on the published Arduino design and the proposed design is also open source.
- The dedicated library is also open source.

The core of this design and implementation is in the modularization of hardware and software. Hardware modularization enables easy and intuitive connection and software modularization allows students to focus on hardware-independent system logic.

All modules are compatible with Arduino, so the kit can be used in a variety of configurations, such as main and expansion modules together, main module only, and expansion module only. These configurations can be selected according to the student's prior knowledge of hardware and software, and used in various microcontroller-related education.

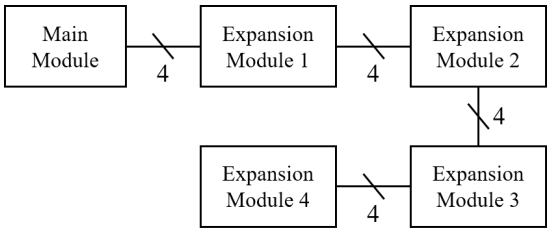


Figure 3: Cascading module connection

3.2. Hardware Design

The key in the proposed design is to enable cascading connection using a unified connector. In order to enable cascading connection, a communication method that can share a serial connection line and a dedicated controller for communication are required. There are many ways to share the serial connection line, and one of them is I2C communication[20], which is supported by Arduino by default. I2C communication allows cascading connection with four lines. In I2C communication, the main module acts as a master and the expansion modules act as slaves.

Fig. 3 shows an example of module cascading using I2C connection.

The controller in the expansion module is responsible for controlling I/O devices as well as I2C communication. The proposed design adopts ATmega328 as the microcontroller for all modules to maintain compatibility with Arduino UNO. Fig. 4 shows the basic configuration of the main and expansion module in the proposed design. The main module has one I2C connector as a starting point, and the expansion module has two I2C connectors to support cascading connection.

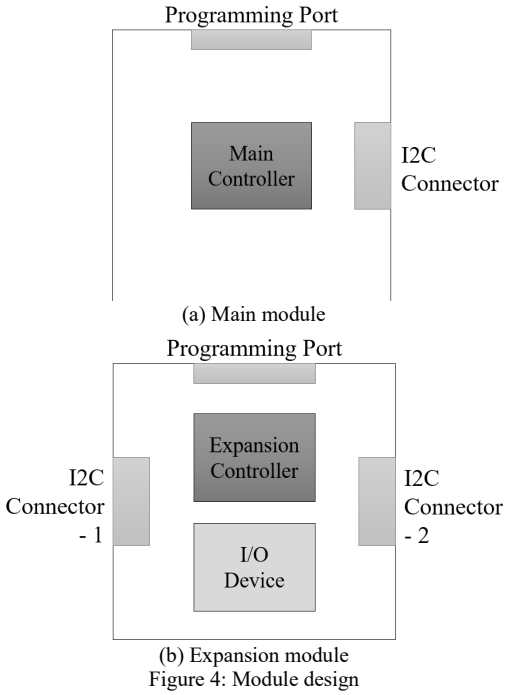


Figure 4: Module design

3.3. Software Design

In the proposed design, the library is also modular. The Arduino library is an abstraction of low-level microcontroller functions. However, the Arduino library is hardware dependent as it requires the understanding of I/O devices connected to an Arduino board. Therefore, the proposed design reduces hardware dependency by separating hardware-dependent and hardware-independent code.

Consider a system that uses a main module, a button module, and an LED module to represent button states to LEDs. In this configuration, three ATmega328s are used, and three programs for each ATmega328 are required. The button module requires a program to read the status of the buttons and send it to the main module through I2C communication, while the LED module requires a program to represent the data received from the main module to LEDs. That is, the program for the expansion module includes hardware-dependent code for controlling I/O devices and I2C communication. On the other hand, the program for the main module contains the code for I2C communication with the expansion modules and the hardware-independent code for controlling the overall system, called system logic. The emphasis in programming education should be on hardware-independent system logic.

In the proposed design, the library consists of a main (or master) library and expansion (or slave) libraries. The expansion library has I2C communication and I/O device control functions, and is pre-installed in the expansion module. The main library, on the other hand, provides common abstract functions for exchanging data through I2C communication with expansion modules. The main library is compiled with system logic and installed in the main module.

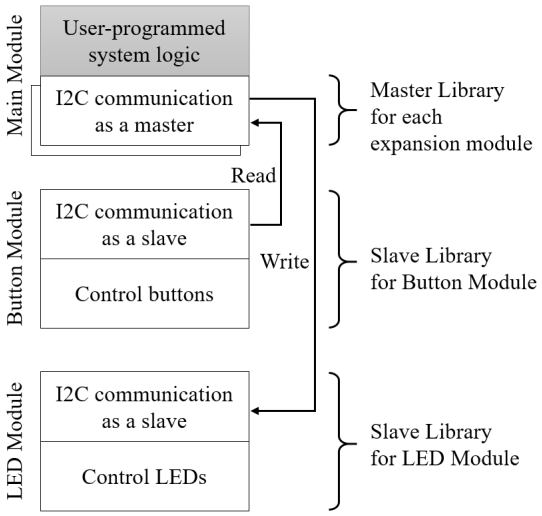


Figure 5: Program structure

In Fig. 5, each library contains hardware-dependent code, and system logic is hardware-independent code that is the only one students must write. Hardware-independent system logic allows students to develop logical thinking and problem-solving skills that are the goal of programming education.

4. FRUTO Kit

The FRUTO kit is a kit that satisfies the guide and consists of the FRUTO modules corresponding to hardware and the FRUTO library corresponding to software.

4.1. FRUTO Module

The FRUTO module can be a main module or an expansion module, and ATmega328 is used as the controller for each module. The main module follows the published design of Arduino UNO and has an additional I2C connector for cascading connection. On the other hand, an expansion module is composed of an expansion controller, I/O devices, and I2C connectors.

Fig. 6 shows the circuit diagram of an LED module. Unlike the main module, the expansion controller uses minimal circuit in the Arduino UNO design. Therefore the expansion module cannot fully operate as an Arduino UNO compatible board. However, in most cases, the expansion module uses the pre-installed program, and a custom program can be installed with an external programmer.

The modules are connected directly to each other by default, but a dedicated cable and a distribution module is also included in the FRUTO kit to enable flexible connection. Fig. 7 shows an example of connecting 4 modules using a distribution module and a dedicated cable.

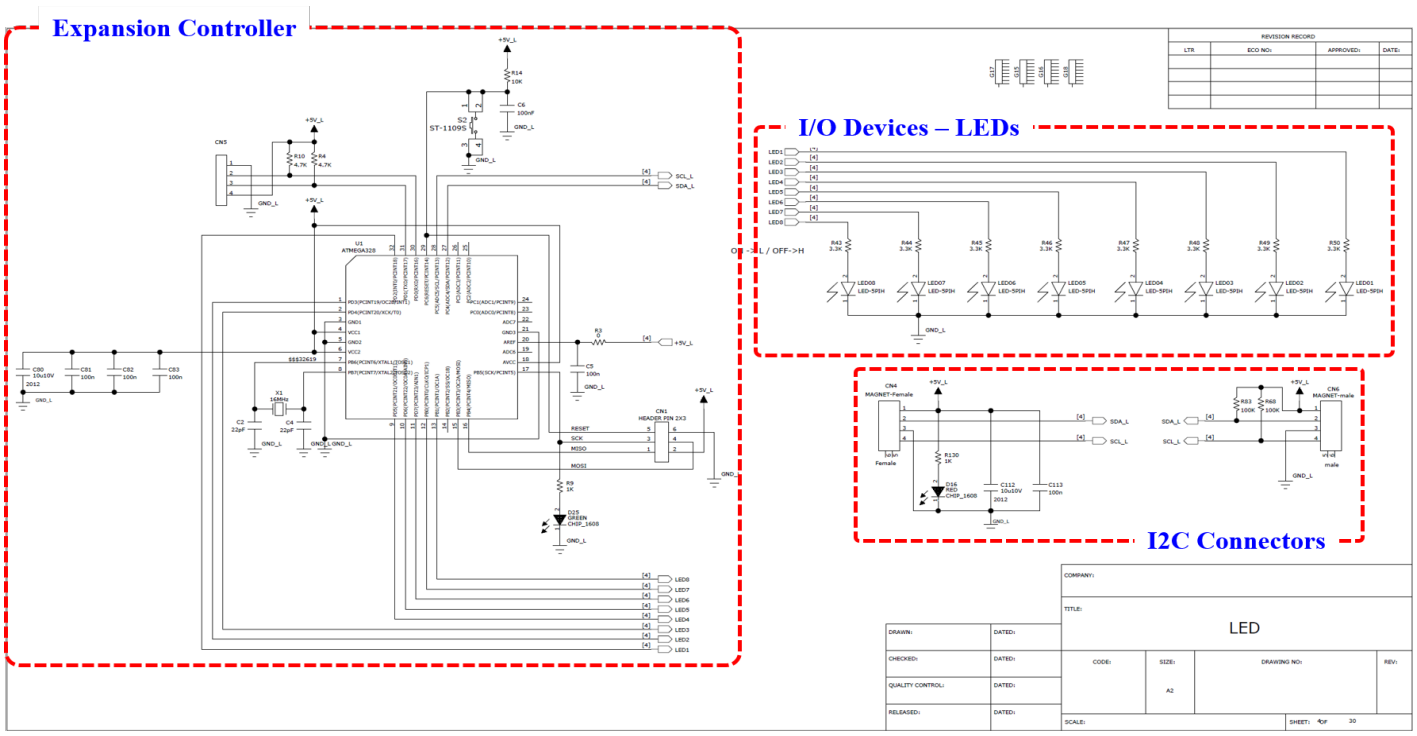


Figure 6: LED module circuit diagram

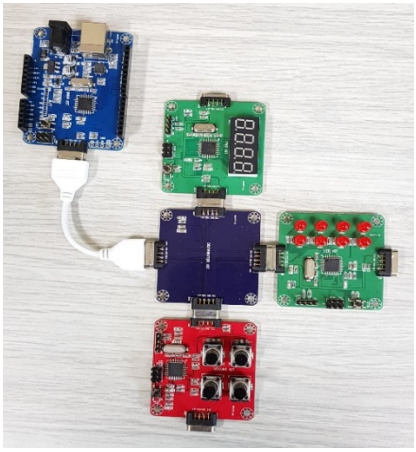


Figure 7: FRUTO module connection

4.2. FRUTO Library

As shown in Fig. 5 the programs needed for the FRUTO kit are a library for a master, libraries for slaves, and a main Arduino sketch. The master and slave libraries are provided as part of the FRUTO library, and students only need to make a master sketch for a main module. Fig. 8 shows a blink sketch that blinks the LEDs on the LED module at 1-second intervals.

```
#include <FRUTO.h>
void setup() {
    FRUTO.begin();
}
void loop() {
    Module_LED.on();                    // turn on 8 LEDs
    delay(1000);
    Module_LED.off();                   // turn off 8 LEDs
    delay(1000);
}
```

Figure 8: Master sketch

Fig. 8 does not look very different from Arduino's blink sketch. However, the FRUTO library is characterized by the fact that hardware-independent 'on' and 'off' are used instead of hardware-dependent 'digitalWrite', and that the 'on' and 'off' are based on the common abstract function 'write'.

```
#include "Module_LED.h"
void _Module_LED::on(void){             // turn on 8 LEDs
    write(0xFF);
}
void _Module_LED::off(void){            // turn off 8 LEDs
    write(0x00);
}
void _Module_LED::write(byte value){
    Wire.beginTransmission(MODULE_LED);
    Wire.write(value);
    Wire.endTransmission();
}
```

Figure 9: Master library for an LED module – Module_LED.cpp

```
#ifndef _MODULE_LED_
#define _MODULE_LED_
#include "Arduino.h"
#include <Wire.h>
#define MODULE_LED 11                   // I2C address
class _Module_LED {
    public:
        void on(void);                  // turn on 8 LEDs
        void off(void);                 // turn off 8 LEDs
        void write(byte value);         // send LED data
};
extern _Module_LED Module_LED;          // LED module instance

#endif
```

Figure 10: Master library for an LED module – Module_LED.h

The master library in Fig. 9 and 10 is a library defined differently according to each expansion module. Whereas the operations common to all modules are defined in the system library. Typical common operations included are to initiate I2C communication and to initialize each expansion module.

```
#include "FRUTO.h"

void _FRUTO::begin(void){
    Wire.begin();                          // start I2C as a master
}
```

Figure 11: FRUTO system library – FRUTO.cpp

```
#ifndef _FRUTO_
#define _FRUTO_

#include "Arduino.h"
#include <Module_LED.h>                    // initialize a module

class _FRUTO {
    public:
        void begin(void);
};

extern _FRUTO FRUTO;
#endif
```

Figure 12: FRUTO system library – FRUTO.h

Data sent to the expansion module using the master library is received and processed by the LED module. Fig. 13 and 14 show the slave library for an LED module, which receives one byte data and controls 8 LEDs accordingly. Since the slave library is the same as the sketch for Arduino, it is also possible to learn Arduino through the slave library. This can also be seen from the fact that the slave library has an INO extension.

```
#include <Wire.h>
#define MODULE_LED 11                      // I2C address
int LED_pins[] = { 2, 3, 4, 5, 6, 7, 8, 9 };
byte LED_status = 0;                       // LED state

void setup() {
    for (int i = 0; i < 8; i++) {
        pinMode(LED_pins[i], OUTPUT);
    }
    Wire.begin(MODULE_LED);                // start I2C as a slave
    // register data receive handler
    Wire.onReceive(receiveFromMaster);
    LED_control();
}
void loop() { }
// receive data from master
void receiveFromMaster(int bytes) {
    LED_status = Wire.read();
    LED_control();
}
void LED_control(void) {
    for (int i = 0; i < 8; i++){
        digitalWrite(LED_pins[i], ((LED_status >> i) & 0x01));
    }
}
```

Figure 13: Slave library for an LED module – Module_LED_slave.ino

Although the types of code presented seem diverse and complex, students can start by writing a main Arduino sketch for programming education. Table 2 summarizes the functions and features of each code.

4.3. FRUTO Kit

The FRUTO kit consists of modular hardware compatible with Arduino UNO and the FRUTO library for programming support. The biggest advantage of the FRUTO kit in hardware is that it is easy to add I/O devices. The hardware configuration is completed by simply connecting the module having the I/O devices required through a unified 4-pin connector. Observations of the course using the FRUTO kit showed that the time required for hardware configuration was less than one third compared to the course using other Arduino-compatible kit. The rest of the time could be spent on conceptual descriptions of the hardware and how it works.

The biggest advantage of the FRUTO kit in software is that the hardware-dependent code is provided as a library. Low-level hardware control tasks are handled in each expansion module, which allows students to build and test a system by writing only hardware-independent code for a main module. The hardware-independent code can be made in the same manner with the original sketch except that there is no hardware-controlling code. The length of the code required when using the FRUTO library is about 1/2 when controlling simple I/O device such as an LED module, and about 1/4 when controlling a complex I/O device such as an LED matrix module compared to the code using the Arduino library. Overall, it was less than one third. The rest of the time can be used to develop the logical procedures of the system.

In addition to simplifying hardware connection and programming, one of the advantages of the FRUTO kit is that it can be used as an educational tool for students of various levels. Table 3 shows an example of how to use the FRUTO kit depending on the students' level. For beginners, the biggest advantage is that it allows them to easily configure a system and write a program for it with minimal hardware knowledge. Intermediates can use the expansion modules and Arduino environment to learn Arduino and/or microcontrollers. Module DIY allows advanced students to design and implement an Arduino-compatible kit.

5. Conclusion

As the importance of programming education is being emphasized more than ever, the demand for an appropriate learning tool is also increasing. In addition, research findings that using Arduino can improve problem-solving and team-level collaboration, have led to various attempts to use Arduino for programming education. However, existing Arduino-compatible tools are limited in their use because of their hardware dependency. In this paper, the design of a modular Arduino-compatible kit, termed as FRUTO, that minimizes hardware dependency has been proposed, and its configuration and features are examined that implemented the proposed design. The FRUTO kit is easy to connect and program, and expandable in many directions, which makes it a versatile learning tool.

Table 2: Codes for the FRUTO kit

Name		Code Sample	Uploaded to	Function	Student Level	Remarks
Master Sketch		Fig. 8	Main Module	Control expansion modules with the master library	Beginner	
FRUTO Library	Master Library	Fig. 9, 10	(Main Module)	Exchange data with expansion modules	Expert	Used in conjunction with a master sketch
	System Library	Fig. 11, 12	(Main Module)	Initialize the system	Expert	
	Slave Library	Fig. 13	(Expansion Module)	Exchange data with a main module and control I/O devices accordingly	Intermediate	Pre-installed in each expansion module

Table 3: FRUTO kit utilization by level

Level	Hardware		Software		Remarks
	Used hardware	Hardware dependency	Programming area	Used library	
Beginner	FRUTO kit	LOW	Master sketch	FRUTO	Useful for rapid prototyping
Intermediate	Main or expansion module alone	MID	Slave library, Module test sketch	Arduino	Similar to using existing Arduino-compatible kits
Expert	Module DIY	HIGH	FRUTO library	Arduino	

Currently, the FRUTO kit has 10 expansion modules and is undergoing a pre-launch test in programming and microcontroller-related education. Although the FRUTO kit satisfies the design guide, developing a Scratch-like block programming tool is expected to increase the number of users. Securing compatibility with existing learning tools like Lego is also expected to contribute to user growth. The feedback collected during the test including the ones mentioned above might be incorporated into future modifications and revisions.

Conflict of Interest

The authors declare no conflict of interest.

References

[1] J. Choi, S. An, and Y. Lee, "Computing education in Korea-current issues and endeavors", ACM Transactions on Computing Education, **15**(2), 1-8, 2015. http://doi.org/10.1145/2716311

[2] D. O'Sullivan and T. Igoe, Physical Computing, Thomson, 2004.

[3] A. Khanlari, "Effects of educational robots on learning STEM and on students' attitude toward STEM," in 2013 IEEE 5th Conference on Engineering Education, Kuala Lumpur, Malaysia, 2013. http://doi.org/10.1109/ICEED.2013.6908304

[4] H. Aoki, J. M. Kim, Y. Idosaka, T. Kamada, S. Kanemune, and W. G. Lee, "Development of state-based squeak and an examination of its effect on robot programming education," KSII Transactions on Internet and Information Systems, **6**(11), 2880-2900, 2012. http://doi.org/10.3837/tiis.2012.11.008

[5] H. Bort, M. Czarnik, and D. Brylow, "Introducing computing concepts to non-majors: a case study in gothic novels," in the 46th ACM Technical Symposium on Computer Science Education, Kansas City, Missouri, USA, 2015. http://doi.org/10.1145/2676723.2677308

[6] M. Banzi and M. Shiloh, Getting Started with Arduino: The Open Source Electronics Prototyping Platform, Make Media, 2014.

[7] L. M. Herger and M. Bodarky, "Engaging students with open source technologies and Arduino," in 2015 IEEE Integrated STEM Education Conference, Princeton, NJ, USA, 2015. http://doi.org/10.1109/ISECon.2015.7119938

[8] Y. Jang, W. Lee, and J. Kim, "Assessing the usefulness of object-based programming education using Arduino," Indian Journal of Science and Technology, **8**(S1), 89-96, 2015. http://doi.org/10.17485/ijst/2015/v8iS1/57701

[9] J. H. Park and S. H. Kim, "Case study on utilizing Arduino in programming education of engineering," The Journal of Institute of Korean Electrical and Electronics Engineers, **19**(2), 276-281, 2015. http://doi.org/10.7471/ikeee.2015.19.2.276

[10] P. Mellodge and I. Russel, "Using the Arduino platform to enhance student learning experiences," in the 18th ACM Conference on Innovation and Technology in Computer Science Education, Canterbury, England, UK, 2013. http://doi.org/10.1145/2462476.2466530

[11] J. Sarik and I. Kymissis, "Lab kits using the Arduino prototyping platform," in 2010 IEEE Frontiers in Education Conference, Washington, DC, USA, 2010. http://doi.org/10.1109/FIE.2010.5673417

[12] K. Eom, Y. Jang, J. Kim, and W. Lee, "Development of a Board for Physical Computing Education in Secondary Schools Informatics Education," The Journal of Korean Association of Computer Education, **19**(2), 41-50, 2016. http://doi.org/10.32431/kace.2016.19.2.005

[13] A. Garrigos, D. Marroqui, J. M. Blanes, R. Gutierrez, I. Blanquer, and M. Canto, "Designing Arduino electronic shields: Experiences from secondary and university courses," in 2017 IEEE Global Engineering Education Conference, Athens, Greece, 2017. http://doi.org/10.1109/EDUCON.2017.7942960

[14] Tn1, Microcontroller Kit, Korean Patent 1017353010000 to Korean Intellectual Property Office, 2017.

[15] G. Heo and J. Jung, "Arduino Compatible Modular Kit Design for Educational Purpose", Journal of the Korea Institute of Information and Communication Engineering, **22**(10), 1371-1378, 2018. https://doi.org/10.6109/jkiice.2018.22.10.1371

[16] M. Rpzybylla and R. Romeike, "Physical computing and its scope – Towards a constructionist Computer science curriculum with physical computing," Informatics in Education, **13**(2), 241-254, 2014. http://doi.org/10.15388/infedu.2014.05

[17] P. Plaza, E. Sancristobal, G. Fernandez, M. Castro, and C. Perez, "Collaborative robotic educational tool based on programmable logic and Arduino," in 2016 Technologies Applied to Electronics Teaching, Seville, Spain, 2016. http://doi.org/10.1109/TAEE.2016.7528380

[18] P. Martin-Ramos, M. J. Lopes, M. M. L. da Silva, P. E. B. Gomes, P. S. P. da Silva, J. P. P. Domingues, and M. R. Silva, "First exposure to Arduino through peer-coaching: Impact on students' attitudes towards programming," Computers in Human Behavior, **76**, 51-58, 2017. http://doi.org/10.1016/j.chb.2017.07.007.

[19] S. J. Kim, "Project-based embedded system education using Arduino," The Journal of Korean Institute of Information Technology, **15**(12), 173-180, 2017. http://doi.org/10.14801/jkiit.2017.15.12.173

[20] X. Righetti and D. Thalmann, "Proposition of a modular I2C-based wearable architecture," in 2010 15th IEEE Mediterranean Electrotechnical Conference, Valletta, Malta, 2010. http://doi.org/10.1109/MELCON.2010.5475965

ASTES

Advances in Science, Technology and Engineering Systems Journal Vol. 5, No. 5, 302-307 (2020)

www.astesj.com

ASTESJ

ISSN: 2415-6698

Implementation of a Levitation System for the Visualization of the Magnetic Phenomenon

Zeila Torres Santos[1], Brian Meneses-Claudio[2,*]

[1]*Interdisciplinary Research Center Science and Society (CIICS), Universidad de Ciencias y Humanidades, 15314, Perú*

[2]*Image Processing Research Laboratory (INTI-Lab), Universidad de Ciencias y Humanidades, 15314, Perú*

ARTICLE INFO

Article history:
Received: 22 July, 2020
Accepted: 11 August, 2020
Online: 17 September, 2020

Keywords:
Magnetic Levitator
Electromagnet
Electronic Circuit
Differential Potential

ABSTRACT

The phenomenon of magnetic fields is affected depending on the polarity, the positive and negative poles will give a response of attraction and repulsion that can be easily observed. Being also important as an educational element where the theory materializes and is observed, which enriches all science. The objective of this work is to create a circuit that allows reaching the balance between the electronic components, making use of the fundamental electronics together with an LDR and a light sensor. Both generate a connection bridge in which the object that levitates to remain in the air fluctuates, achieving the objective of creating a levitator and being able to observe the nature of electronics and electromagnetism as a whole. As a result, it was obtained that there is a difference between the use of basic and advanced electronic circuits, in addition to identifying the variation in the voltage consumption between the coin and the screw, because the more voltage consumption, the greater the length of wave implying that the frequency decreases but the power intensifies. On the other hand, it should be noted that the use of a voltage generator to identify the voltage and power variations that were shown at the time of the different tests.

1. Introduction

The interaction of electric and magnetic fields produces a phenomenon called Electromagnetism; this phenomenon is a topic of physics that describes the response of charged particles with these fields. The movement of electric charges generates a magnetic field, this field is also associated with the force such as the magnets, being this force of repulsion or attraction, allowing these latter responses to phenomena such as levitation, these fields have as their unit of measurement the volts per meter [1].

It can be ensured that the theory is incomplete when it does not have the experimental part to observe these phenomena, being important to have both scientific experimentations equally. The fact of designing and implementing a levitator is of such importance, to generate interest in students who like science or not, can observe physical phenomenon [2], being through electronics the possibility of synthesizing the device with the electronic devices basics, without the need to use modern electronic devices such as Arduino or similar.

Basic concepts such as that of Electromagnetism, is explained to students of engineering, physical sciences, mathematics and similar careers and even to students in the last years of school. According to a report [3], they indicated that the quality of the infrastructure of the study centers of a public university and a private university was 75% to 51% respectively, that is, public universities focus their teaching more on the part theoretical than a practical definitions of physical phenomena, on the other hand, private universities focus on the general explanation of the physical sciences because they do not consider it of much relevance, being a very important factor due is in these spaces where the theory is applied, because many students allege that science laboratories are poorly implemented because they do not have adequate instrumentation for the development of scientific experimentation. A most recent results in the PISA evaluation [4], show that it still needs a greater improve in the learning process since the important points for the technological development of a country are at the base scientific.

In [5], the author mentioned that Oersted in 1820 discovered an electric current exerts a force on a magnet. This was the beginning to understand the electromagnetism phenomenon. The charged particles in movement are the mean actors to the electric and magnetic performances to induce a property of two bodies attract or repel each other. But it is important to note that there are

*Brian Meneses-Claudio, Sr, +51 1 950159924 & bmeneses@uch.edu.pe

bodies called permanent magnets therefore it is not necessary to induce a current to charge it because internally they have an atomic structure of alignment which creates a strong magnet.

The materials have different properties due to their response to the induced magnetic force, the same happening regarding the electric force because the internal atomic structure could be aligned in the same or opposite direction, in a weak or strong way, working internally with an intrinsic physical property called spin.

In [6], the author presents the design and construction of a magnetic repulsion levitator controlled by Arduino, also using metal structures to keep the coil at an adequate height and perform levitation, also used Hall sensors and a PI controller, the union of these circuits causes the current to remain stable and controlled by the Arduino, thus operate the magnetic levitation. This work confirms the use of programmable electronic devices for the operation of a magnetic levitator by attraction.

In [7], the authors propose an electronic circuit with an electronic transformer capable of converting alternating current to direct current for the supply of the electronic circuit, in addition to the current control and therefore the electromagnetic field, they used a loop PID control closed, it means that they used the feedback of the same system for self-regulation. In addition, it presents the simulation signals that they obtained in the MATLAB Simulink tool, obtaining stable signals when the electromagnetic field was created while maintaining an object attached to the coil and distortion signals when it had the electromagnetic field without any object in its area of radiation.

In [8], the authors propose a closed loop system for the operation of a magnetic levitator by attraction through the use of an infrared linear communication sensor between transmitter and receiver, the main function of the receiver is to decrease its resistance to allow the passage of the current and activate the electromagnetic field. The use of the sensors for the stabilization of the metallic object has to be calibrated due to the high transmission range of the infrared sensor; they also indicate that it is beneficial because the ambient light will not affect the resistance variation of the receiving infrared sensor.

The main idea of this research work is to contribute to teaching, but even more to give fundamental electronics a main role and create a device that can arouse curiosity by being able to visualize the physical phenomenon of the electric and magnetic fields, which even when carried out by a team of researchers, its creation and operation is made possible. Also, the simulations were made in the electronic laboratory where the phenomenon and the variation of the values were studied.

In section 2, the theory as well as the formulas is explained in detail, used to study the applied physical phenomenon. Then in section 3, the dimensions of the levitation system will be shown in detail, as well as the designs prior to its implementation. Later in section 4, the design of the electronic circuit for the magnetic levitation system will be shown, it should be noted that this design was made by constantly testing the electronic devices verifying their improvement. Also, in section 5, the magnetic levitation system already implemented in a circuital and structural way is shown, where it also has to be careful with the distribution of the cables so that they do not hinder the operation of the circuit. Also, in section 6, the results of the operation of the attraction levitation system, the visualization of the variation of the electrical signals emitted by the coil and captured by an electronic oscilloscope are presented, in addition to the separation distance between the metallic object and the coil. Then in section 7, the conclusions of the research work are presented, reinforcing the tests that were made with the operation of the magnetic levitation system and some observations that were obtained in the experimental part. Finally, in section 8, the discussion of the research work will be shown, in addition to some recommendations and errors of the implementation process when the magnetic levitation system was working.

The implementation of the levitator was based on the theory of electromagnetism; formulas will be presented to identify the stabilization and calibration of metallic objects, and the formulas combine mathematical equations will help to accurately discover the physical quantities of voltages, sensitivities, electronic units and other useful components in the process. The use of the theory, implementation and simulation makes the research work relevant for educational and teaching purpose.

2. Theory

A design that gives us an idea of the forces that occur is shown in Figure 1:

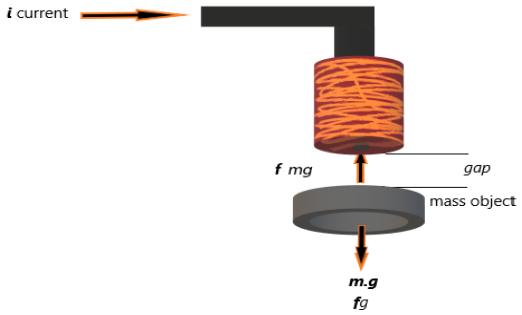


Figure 1: Simplify scheme of the magnetic levitator with forces acting

In equation (1) it has a mathematical expression related to Newton's equation of motion, in this particular case, the levitation forces will be related to the electric current, inductance and the distance or position of the object to be levitated, that is i, $\vec{L}$ and x. So, the equation is:

$$\vec{f}_{mg}(\vec{i},x)=\frac{i^2}{2}\frac{d\vec{L}}{dx} \tag{1}$$

In equation (2), it can see that the terms $\vec{f}_{mg}$ of the inductance are added to the force depending on the object, that is, $L_{i=0,1}$, being L_1 the inductance in the absence of the object to levitate and L_0 the inductance of the electromagnet in the equilibrium position x_0, that is, making a first expansion in L is: $L(x)=L_1-\frac{L_0 x_0}{x}$

$$\vec{f}_{mg}(\vec{i},x)=\frac{i^2}{2}\frac{d(L_1-\frac{L_0x_0}{x})}{dx} \quad (2)$$

If it makes a substitution to simplify using $k=\frac{L_0x_0}{2}$, so, the equation is:

$$\vec{f}_{mg}(\vec{i},x)=\frac{ki^2}{x^2} \quad (3)$$

According to Newtonian mechanics of a system, the sum of total forces exerted on an object that is with the effect of gravity must be equal to zero, that is, if it sees the object to be levitated in Figure 1, it can obtain the following equation:

$$\sum\vec{F}=m\vec{a}=m\ddot{y}=\vec{f}_{mg}(\vec{i},x)-\vec{f}_g=0 \quad (4)$$

Taking as reference the up direction as positive and the down direction as negative from the point of the object to levitate:

$$m\frac{d^2h}{dt^2}=mg-k\left(\frac{i(t)}{x}\right)^2 \quad (5)$$

Where h indicates the height of the object or gap.

Since the system indicates that it must apply Kirchhoff's law because it has an electric circuit and an inductor L, Ohm's law and Faraday's law for a closed RL circuit, it has again a differential equation:

$$v(t)=R.i(t)+L(x)\frac{d}{dt}i(t) \quad (6)$$

Thus, with equations (5) and (6), it will have a system of two equations that allow to understand the laws of motion of the object to be levitated. Which according to [2] it will be possible to construct equations of state in the state space according to the degrees of freedom of the system.

3. Structure Design of the Magnetic Levitation System

The system of Magnetic Levitation by Repulsion tends to have structures where the coil has an adequate height where in the lower part the metallic materials can be located so that they can be magnetized by the electromagnetic field generated by the coil.

For this reason, the structure for the system was designed in the SOLIDWORKS software, which gives us a broader view on the location of the components, in addition this design was sent to a laser cutter, for the manufacture in MDF material following characteristics shown in Table 1. These dimensions were specified and then sent to be laser cut.

The design of the structure was in a simple geometry, which allows the student to observe the internal configuration, such as the electronic circuit, the positions of the photoresistors, the copper coil and the possibility of reproducing it. It is shown in the next Figure 2, the necessary conditions for the location of the electronic devices that will be implemented later in section 5.

Table 1: Graph representations

	Dimensions (L, D, W)	Thickness
Base	32 x 29 x 2 cm	18 mm
Top Box	22 x 8 x 10 cm	4 mm
Side supports	1 x 8 x 21 cm	9 mm
Coil	2 x 2 x 4 cm	Coiling

It should be noted that the structure was built based on the dimensions of a Breadboard, this being useful for the initial test of electronic circuits, where all the components were located, in addition, a circular orifice was added in the front of the design structural for the location of the led as shown in Figure 2 (a), the response of this led will indicate with its lighting the exact time to generate the phenomenon of magnetic levitation. Also, in Figure 2 (c), the reader can see 2 circular orifices of 1 mm in size, where the positive and negative cables of the coil can be connected to the breadboard. Finally, 2 circular orifices were added at the left rear side as shown in Figure 4, these orifices were 3 mm in size to supply positive and negative voltage to the breadboard without the need to uncover the structure.

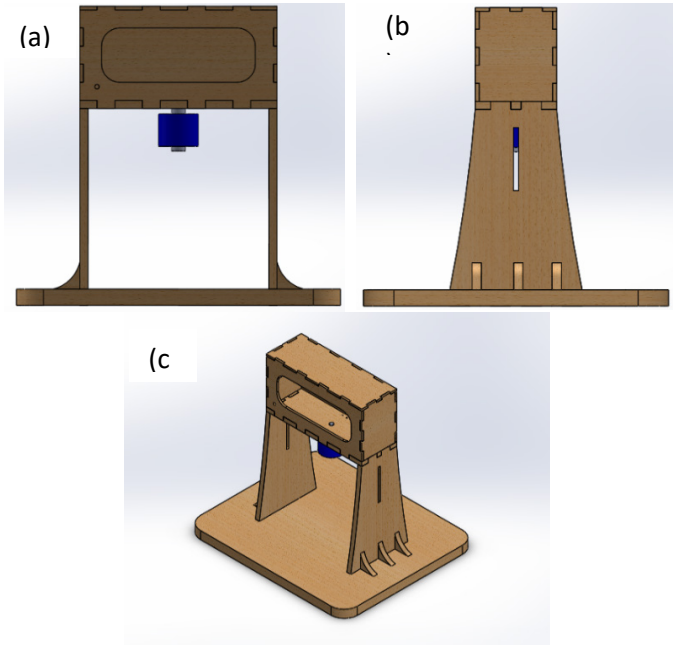


Figure 2: Design of the Structure of the Magnetic Levitator System by Attraction. (a) Front View. (b) Profile View. (c) Panoramic View.

4. Magnetic Levitation System Design

The design of an electronic circuit for a magnetic levitator [9] by attraction was proposed using an infrared sensor and an LED. These last two devices in the Proteus 8 software worked optimally but when it was implemented, errors were obtained with the sensors because the operating range did not adapt to the system, due to this it was changed to a photo-resistance and a red laser for current flow control.

The electronic components used for the design of the Levitation System are shown in the Table 2.

Table 2: Electronic Components

Resistors	• 1 x 330 Ω • 2 x 22 kΩ • 1 x 4.7 kΩ • 1 x 5.6 kΩ • 1 x 1.2 kΩ
Electric Capacitor	• 1000 µf (microfarad) • 4.7 µf (microfarad)
Led Diode	• 2x Diode Led
TRIAC or Triode	• IRF510
Rectifier Diode	• 1N5401
Coil	• 3 millihenries
Operational Amplifier	• LM358
Sensor	• Light Dependent Resistor (LDR) 1k Ω
Voltage Supply	• 12 volts and 2 Amperes • -12 volts and 2 Amperes

The electronic components were following the research work [2], in addition to the use of its equation but adding an LDR that is will serve as a sensor for the activation and deactivation of the levitation system.

As shown in Figure 3, the design of the previous research work was followed because this time with two different components that will be the sensors of our magnetic levitator circuit, in addition to indicating that it was verified that the consumption current of the electronic circuit was of 1 Ampere, this depended on the coil that was used.

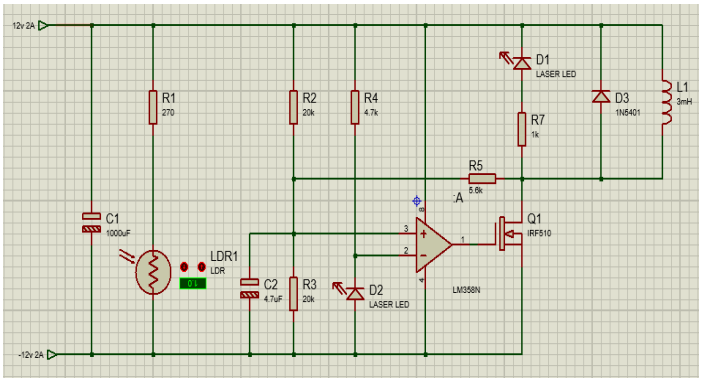


Figure 3: Design of the Electronic Circuit of the Levitation System.

Diode D3 is connected in reverse due to the requirement of the coil. In case of discharge, the diode can discharge the coil immediately, losing its magnetic field. Therefore, an immediate electric charge is required to levitate the metal object, the coil must be in constant operation of electric charge and discharge, depending on the sensors.

5. Magnetic Levitation System Implementation

After simulating the circuit in Proteus Software 8, the next step was the construction of the electronic circuit, a Protoboard was used for the location of all electronic components in addition to the correct voltage distribution. In addition, a stable voltage generator was used to know the power supply of the electronic circuit and to know its voltage and current variation when there is an object levitating and when there is nothing levitating.

The circuit implemented in a Breadboard and being powered by a voltage generator, as the reader can see the blue led light, this LED indicates that the circuit is working because it is connected close to the coil as shown in Figure 3. Also, in Figure 4, it is verified that the connection was tested near an aluminum plate and thus check the effect of its magnetic field. It should be noted that when using the iron, aluminum should be careful not to cross the cables.

Jumpers were used for interconnecting electronic devices because they are easy to use and reliable for optimal connection of electronic circuits. In addition, colors for positive and negative voltage supply were assigned to the various electronic devices that are polarized so as not to damage or burn them.

It is concluded that for the metallic object to remain levitated attracted by the magnetic field, the red-light pointer must have a minimum presence in the LDR so that it remains at a static point of levitation and current consumption by the circuit and the coil.

After the construction of the electronic circuit, it was placed in the upper part as shown in Figure 4. This space has an opening so that the circuit can be observed, then the sensor that is formed by the red-light laser must be calibrated and the photo resistor, both must be located at the same height face to face and below the level of the coil. The metallic object will fluctuate between the space of the coil and the sensors forming a gap.

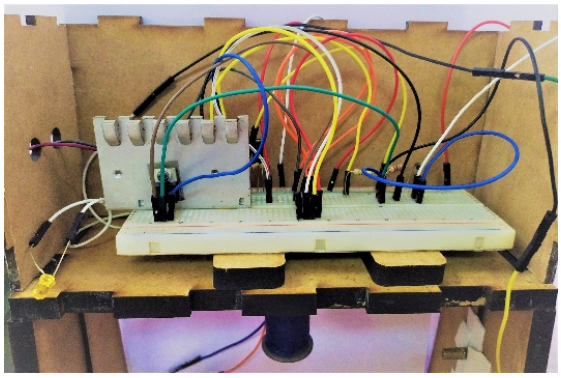


Figure 4: Electronic Circuit of the Levitation System.

A TRIAC heat-sink was placed because it is the electronic component through which all the electric force will pass and tends to heat up, and be prone to get worse.

During the implementation of the magnetic levitation system, tapes were used to hold the red laser pointer and the LDR, being a manual calibration, many tests had to be done to keep the metal objects levitating. These electronic devices had to be correctly placed one in front of the other to maintain the optimal current

consumption, achieving with this precision to visualize the phenomenon.

6. Results

After assembling all the components explained above, it will simulate if the system is capable of levitating metal objects, and if it is strong enough to levitate heavy metal objects. Figure 5 shows two images where in the first one, it is seen that a coin is levitating and in the second image, the reader can appreciate a levitating screw, implying that it not only serves for objects of lesser weight such as currency but also with a bit considerable weights like a screw.

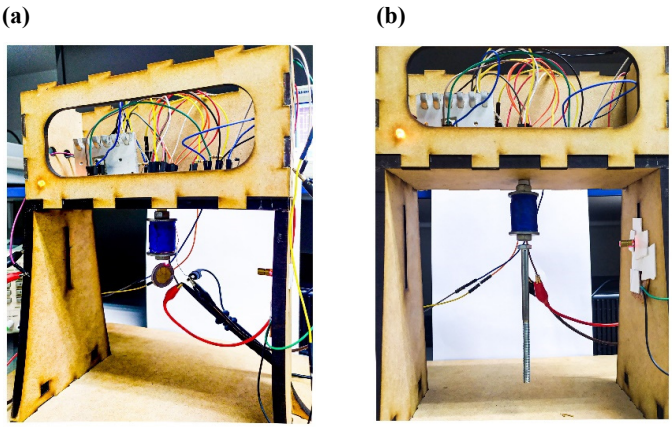


Figure 5: Magnetic Levitation System by Attraction (a) Levitation of a Coin (b) Levitation of a Screw.

It should be noted that for the levitation of metallic objects to work, the red light laser has to be in a small fraction in the photoresistor because there must be a voltage and current consumption by the coil to create a magnetic field capable of maintaining levitating to the metal object and it remains in balance.

The voltage variation was observed in the Voltage Source because when the metallic object is levitating as a result of the electromagnetic field generated by the coil, there was a higher current consumption; Figure 6 shows the use of a Voltage Source for the operation of the circuit to verify its variation.

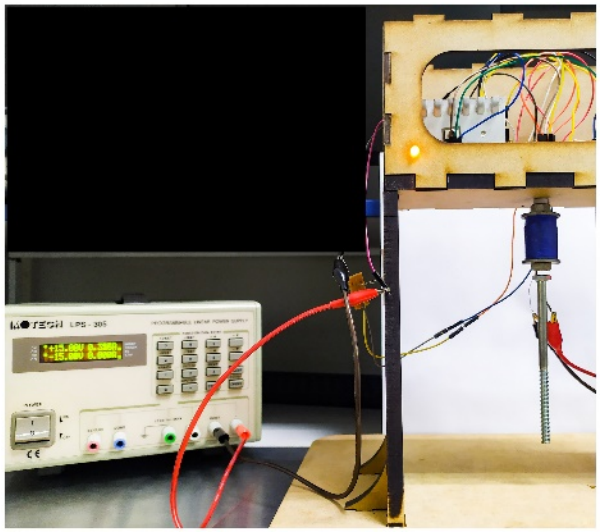


Figure 6: Response assembled prototype of a magnetic levitator system.

In addition, it was tried to verify the current flow that was going through the coil at that time, because it was wanted to know the variation that the signal presented in the coil at the time when it was with a metallic object levitating and when there was no metallic object in its area of operation. Because of this with the help of an electronic oscilloscope and probes, it was connected in the coil to know its electrical variation. As shown in Figure 7 (a) is the flow signal current when the coil was at rest, i.e. when there is no metal object in the magnetic field. Figure 7 (b) shows a square signal. This signal is when the coil has a metallic object in the operation area of levitation, but when the object moves away from the operation area of the coil then the square wave period increases until finally obtain an amorphous signal as the first one shown.

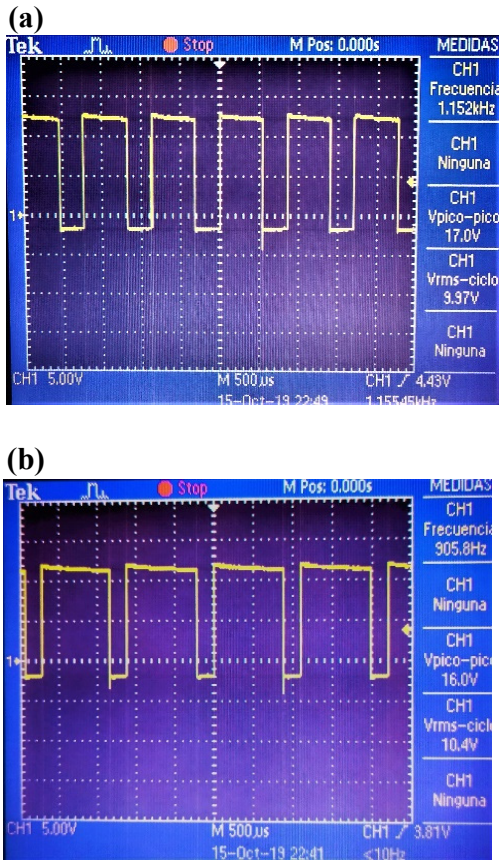


Figure 7: Signal of the Electric Flow of the Coil (a) Levitation of a Coin (b) Levitation of a Screw.

These signals, shown in Figure 7, show that the coil can reach stability when it has a metallic object levitating, in addition the period it presents is due to the fact that it is constantly charged and discharged from current.

7. Discussion

- To prevent the coil from overheating or reaching very high temperatures, many research studies indicate that the coil could be reinforced in the number of turns and the thickness of the coil so that it can dissipate heat, therefore, the circuit should also withstand more current because the coil will require.

- The implementation of the Magnetic Levitation System was tested after the design and construction of the structure because the positioning of all the elements was required for operation, prior to operation the level of power of the magnetic field was tested to attract metallic objects and control system presented by the red-light pointer and the LDR.
- The research work presents the implementation of a magnetic levitator based on the use of basic electronic components, it means that they are components known by students of first engineering cycles, thus enhancing the visualization of the phenomenon, disagreeing with the research work [10], where They use an ARDUINO for the implementation of a magnetic levitator, which is another implementation option but requires knowledge of programming languages for an educational environment, where students cannot visualize in detail the construction and location of each electronic component.
- The LDR electronic device is very sensitive to ambient light, that is why a previous calibration is required that covers the ambient light and can only receive the intensity of the red laser light, many investigations work on the design and implementation for that reason. A magnetic levitator indicates that the use of the infrared sensor is the best option.
- This research work, not only raises an educational-visual levitator of physical phenomena but also has the idea of future research, such as the union of two types of levitators such as repulsion and suspension. The subject of study of the magnetic fields is broad and very versatile, so we wonder what would happen if two types of levitators were joined, what characteristics these forces would have and how the levitating would object react as mention in [11], where they implemented a repulsion and suspension levitator with an analog regulator, but it must be with more knowledge in regulator and power electronic, it does not have educational focus but it has phenomenon visualization focus.
- Calibration complications arose because the red laser pointer and LDR must be correctly aligned, this calibration error and in addition to trial and error, generated vibrations, oscillations and even the malfunction of the magnetic levitation system. Calibration was manual because our main topic is to present this research work in the educational field for students to prove that with electronic circuits, magnetic fields and forces can be generated that allow the levitation of an object.
- The research team is sure that it will be of great use to take this device to schools or universities, as a study and inspiration, as it is a physical phenomenon that could be concluded and proved.

8. Conclusions

Creation has been made into the study of precision or control sensors, in this research work a red-light pointer and an LDR were used to control the system, based on these good results were obtained such as the levitation of metallic objects.

- The coil tends to heat due to the constant current consumption that is being induced, due to this it must be well placed at the base of the structure to prevent it from falling when it is in operation.
- The metallic object to remain levitated attracted by the magnetic field; must have a minimum presence in the intersection of the light sensor and the LDR so that it remains at a static point of levitation and current consumption by the circuit and the coil.

Conflict of Interest

The authors declare no conflict of interest.

References

[1] M. R. Khan, A. Raj, M. M. Hossain, S. Kumar, and A. Sharma, Distribution of electromagnetic field and pressure of single-turn circular coil for magnetic pulse welding using FEM. Singapore; New York: Springer, 2019.

[2] B. Meneses-Claudio, Z. Torres Santos, and A. Roman Gonzalez, "Study and design of a Magnetic Levitator System" International Journal of Advanced Computer Science and Applications, **10**(5), 426-430, 2019. http://doi.org/10.14569/IJACSA.2019.0100553

[3] P. Rojas, R. Andrade, and J. Saavedra, La Reforma del Sistema Universitario Peruano: Internacionalización, avance, retos y oportunidades. Perú; Lima: British Council, 2016.

[4] G. Moreano, A. Darcourt, W. Hernández, and S. Ramos, Competencia científica e interés en carreras de Ciencia y Tecnología según PISA 2015. Perú; Lima: MINEDU, 2019.

[5] M. Pérez de Landazábal and P. Varela Nieto, Oersted and Ampère: origins of electromagnetism. España; Madrid: Nivola, 2001.

[6] J. P. Borrás, "Diseño, estudio y contrucción de un levitador magnético con Arduino", Bachelor Thesis, Escuela Superior de Ingeniería Industrial, Universitat Politècnica de Catalunya, 2016.

[7] L. E Venghi, G. N. Gonzalez, and F. M. Serra, "Implementation and control of a magnetic levitation system," IEEE Latin America Transactions, **14**(6), 2651-2656, 2016. https://doi.org/10.1109/TLA.2016.7555233

[8] G. A. Marín and J. A. Garzón, Construcción de una plataforma de levitación electromagnética utilizando sensores infrarrojos, Ph. D. Thesis, Facultad de Tecnologías Eléctrica, Universidad Tecnológica de Pereira, 2015.

[9] S. Folea, C. I. Muresan, R. De Keyser, and C. Ionescu, "Theoretical Analysis and Experimental Validation of a Simplified Fractional Order Controller for a Magnetic Levitation System," IEEE Transactions on control systems technology, **24**(2), 1-7, 2015. https://doi.org/10.1109/TCST.2015.2446496

[10] J.P. Borràs Marne, "Diseño, estudio y contrucción de un levitador magnético con Arduino," Escola Tècnica Superior d'Enginyeria Industrial de Barcelona - Grau En Enginyeria En Tecnologies Industrials, 2016.

[11] J.A. Ortega Díaz, "Diseño y construcción de un sistema de levitación magnética gobernado por un regulador analógico," Escola d'Enginyeria de Barcelona Est - Grau en Enginyeria Electrònica Industrial i Automàtica, 2018.

ASTES

Advances in Science, Technology and Engineering Systems Journal Vol. 5, No. 5, 308-313 (2020)

www.astesj.com

Special Issue on Multidisciplinary Innovation in Engineering Science & Technology

ASTESJ

ISSN: 2415-6698

Economic and Environmental Analysis of Life Expectancy in China and India: A Data Driven Approach

Nittaya Kerdprasop*,1, Kittisak Kerdprasop[1], Paradee Chuaybamroong[2]

[1]*School of Computer Engineering, Suranaree University of Technology, Nakhon Ratchasima 30000, Thailand*

[2]*Department of Environmental Science, Thammasat University, Rangsit Campus 12120, Thailand*

ARTICLE INFO

Article history:
Received: 08 June, 2020
Accepted: 13 September, 2020
Online: 17 September, 2020

Keywords:
Data analysis
Life expectancy
Environment and economic
Web graph
Classification and regression tree

ABSTRACT

A data analytic approach presented in this work covers both data descriptive and predictive modeling with two main objectives: (1) discovering factors related to longevity of populations in the two most populated nations, China and India, and (2) generating life expectancy predictive models for both countries. Descriptive modeling methods to explore major environmental and economic factors anticipating to affect longevity patterns of people are web graph analysis and chi-squared automatic interaction detection (CHAID) techniques. Web graph analysis has been applied for the ease of visualization and CHAID is for discovering factors leading to longevity. From the analysis results, particulate emission including ozone pollution and PM2.5 concentrations are the most important factor threatening life of populations in both China and India. To predict number of years an individual is expected to live based on the available environmental and economic factors, several statistical and machine learning techniques are applied and it turns out that a linear regression model yields the most accurate prediction result.

1. Introduction

Longevity, education and income are the three main indicators that the United Nations Development Program (UNDP) has adopted for computing the human development index (HDI) to assess development level of each country [1]. The HDI captures three main essential aspects: a long and healthy life, an ability to have sufficient knowledge, and a decent standard of living. The health aspect is measured from life expectancy at birth, which is number of years a new-born baby is expected to live, averaging from the cohort. The knowledge aspect is measured from years of schooling. The standard of living aspect is measured from the gross national income per capita. The HDI is the geometric mean of all three aspects that have gone through the normalized process. This paper focuses on the longevity indicator through the life expectancy at birth measure, as it is considered [2], [3] a reflect for the good health of population.

The analysis of longevity trends within and across nations is of interest among many groups of researchers [4]-[7]. The number of years an individual is expected to live is also important to actuaries for making an optimal and economical insurance and pension plans [8]-[10]. Both positive and negative factors affecting longevity have been investigated by several researchers. For instance, Chinese researchers had explored the factors relating to energy consumption in daily life of Chinese people through the use of coal and electricity [11], [12]. The results are that coal usage relates to shorten life, whereas domestic electricity usage shows positive correlation to longevity. However, the choice of energy sources depends on the household income. Such economic and socio-economic factors had been proven by many researchers [13], [14], [15] that they can affect the long-life of population.

Exposure to polluted environment is also another important factor studied by various researchers [16], [17] to assess its impact against longevity. Environment factors reported to have negative impact toward shorten longevity includes carbon dioxide (CO2) emission [18], [19], particulate matter (PM10) and sulfur dioxide (SO2) concentrations [20], [21]. A poor climate condition also shows negative impact toward longevity of population [22], [23].

From the literature review, it can be noticed that most researchers study longevity by building a predictive model to forecast number of years the populations are expected to live using various methods including regression [24], autoregressive integrated moving average [25]-[27], and neural network algorithms [28], [29]. Some researchers [30] apply an ensemble method to make forecasting through a number of models and use the averaging scheme to predict the years of living.

*Corresponding Author Nittaya Kerdprasop, nittaya@sut.ac.th

In this work, we make our contribution to the demography as well as the environmental fields of research by proposing a different longevity analysis approach in which both numeric and categorical modeling are applied, instead of the sole numeric computation. Our data analytic method generates descriptive model through categorical computation to reveal life-threatening factors and also produces predictive model to make a numeric prediction toward number of years an individual is expected to live based on the available economic and environmental factors. The data source and our analysis methodology are explained in Section 2. Results from the data analytic approach are presented in Section 3. Performance evaluation of the predictive models is shown in Section 4. The conclusion is in Section 5.

2. Materials and Methods

The main purpose of our research is to present descriptive and predictive modeling methods to automatically discover major factors influencing good health of people living in the highly populated countries. We choose China and India to be our case study because the two countries are the most populated ones in the world (China = 1.43 billion, India = 1.36 billion [31]) and the trends of human development index (HDI) of the two countries are almost similar. The geographic location of China and India and the trend in HDI improvement from the years 1990 to 2018 are shown in Figures 1 and 2, respectively.

We focus the HDI analysis along the dimension of long and healthy life through the discovery of major factors affecting life expectancy at birth among populations in China and India. The life expectancy at birth together with other 16 economic and environmental indicators expecting to play some role on lifespan during 1960-2017 have been accessed from the World Bank database [32]. The summary of all attributes is listed in Table 1.

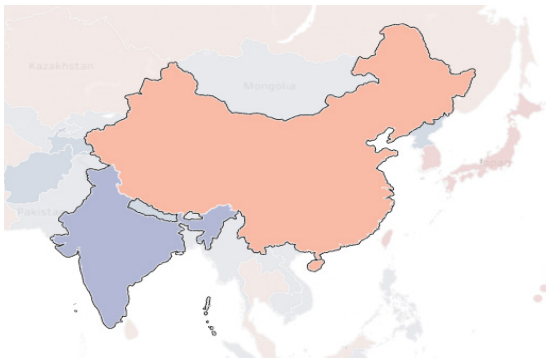


Figure 1: Location of China (above -- in orange) and India (below -- in grey) (image source: https://data.worldbank.org/country/)

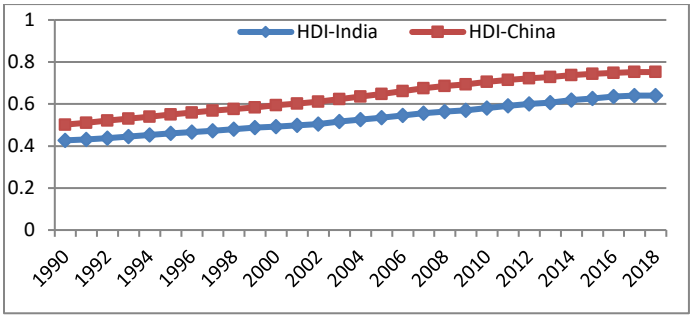


Figure 2: HDI improvement of China and India from the years 1990 to 2018 (data source: http://hdr.undp.org/en/data)

Table 1: Selected attributes for life threatening analysis

Attribute	Description	Unit
National_ income	Net national income per capita	annual % growth
Education_ expense	Education expenditure -- excluding investments in buildings and equipment	% of GNI
Forest_ depletion	Net forest depletion -- if growth exceeds harvest, this figure is zero	% of GNI
Particulate_ emis	Particulate emission damage -- calculated as foregone labor income due to premature death due to exposure to ozone pollution and indoor concentrations of $PM_{2.5}$ in households cooking with solid fuels	% of GNI
Agri_met_ emis	Agricultural methane emissions -- from animals, animal waste, rice production, agricultural waste burning	% of total
CO2_ emission	CO_2 emissions -- carbon dioxide produced during consumption of solid, liquid, and gas fuels and gas flaring	metric tons per capita
Electric_ power	Electric power consumption	kWh per capita
Energy_use	Energy use	kg of oil equivalent per capita
Exports	Exports of goods and services	% of GDP
Forest_area	Forest area -- excluding tree stands in agricultural production systems and trees in parks and gardens	% of land area
GDP_growth	GDP growth	annual %
GNI	GNI per capita growth	annual %
High-tech_exports	High-technology exports -- products with high R&D intensity, such as in aerospace, computers, pharmaceuticals, scientific instruments, and electrical machinery	% of manufactured exports
Imports	Imports of goods and services	% of GDP
Industry	Industry, value added -- industries correspond to ISIC divisions 10-45 and 15-37	% of GDP
Manufacturing	Manufacturing, value added -- industries belonging to ISIC divisions 15-37	% of GDP
Life	Life expectancy at birth -- the number of years a newborn infant would live if patterns of mortality at the time of its birth were the same throughout its life	years

Among all 17 numeric data attributes, life expectancy at birth is the target of our analysis. The main steps in the data-driven analytical approach are illustrated in Figure 3.

The first step is data extraction including the selection of data attributes from the World Bank database and the data preparation to be in a suitable format for further analysis steps. The next step is data exploration, which is the analysis of correlation among data attributes. The third step is the discovery of factors threatening life of population in China and India. This step needs the transformation from numeric to be categorical through the binning approach. The descriptive model to reveal important factors affecting lifespan is derived by the algorithm chi-squared automatic interaction detection, or CHAID [33]. This algorithm has been adopted because its model represented as a tree structure

has many advantages such as efficiency, interpretability and successful adoption to solve a wide range of problems [34],[35]. To visualize factor association, we adopt the web graph method.

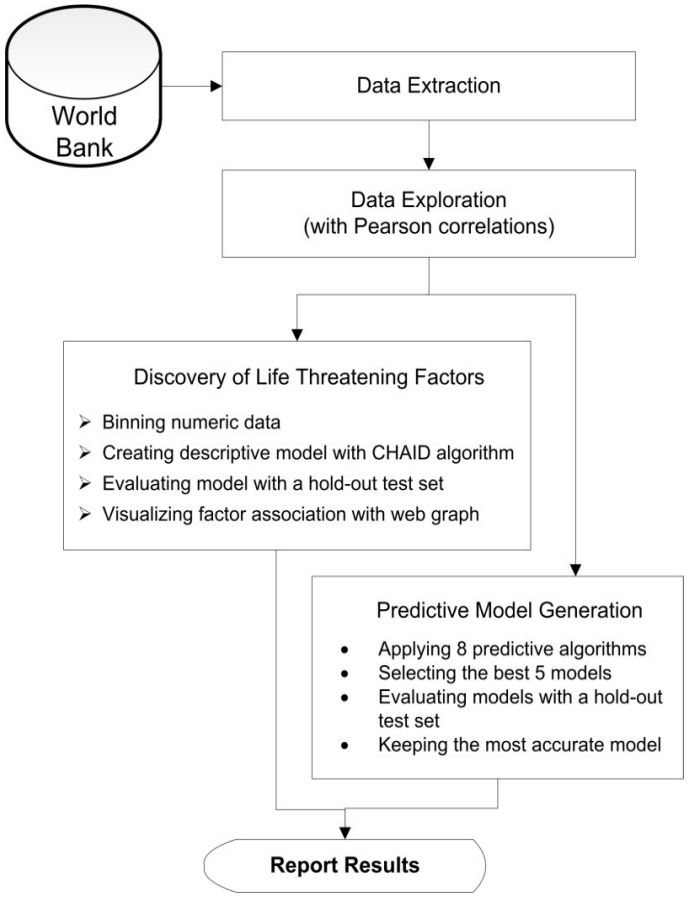


Figure 3: The main steps for data-driven analytical approach

The fourth and also the last step of our analytical method is the predictive model generation. We adopt 8 algorithms in this modeling step including regression, generalized linear model (GLM), k-nearest neighbors (kNN), support vector machine (SVM), classification and regression tree (CART), chi-squared automatic interaction detection (CHAID), artificial neural network (ANN), and linear.

The obtained models are evaluated for their performances observed during the training process. The best 5 models are then selected for further testing with the hold-out method in which the separated test dataset has been applied. In the training and testing steps, the total 48 records of data during the years 1960-2017 had been split as two separate subsets: training and testing. The training dataset comprises of 45 records, whereas the testing dataset contains 13 records.

After evaluating prediction performance of the best 5 models using the same set of test data, the most accurate model is kept as the final model. This model is to be used for forecasting the number of years an individual is expected to live. It is worth noting that forecasting model for one country may be different from another because the modeling is a data driven approach such that different set of training data may yield different modeling result, even though set of data attributes is the same.

3. Analytical Results

According to the design of our data analytical approach, there are three main steps of data analysis: data exploration, descriptive model creation, and predictive model generation. We thus present the results from these three main steps sequentially in the following three subsections.

3.1. Data Exploration Results

The results of Pearson correlation analysis is shown in Table 2. It can be noticed similarity between the two countries that source of energy and amount of energy usage have strong positive influence toward longevity. The values in terms of import, export and industry are also among the top-5 positive factors associating with longevity.

In case of correlation analysis to reveal negative factors to lifespan of population, we can notice that particulate emission is among the top-five factors associating to life shortening in both China and India. However, other factors such as forest depletion, forest area, the export of high-technology product, the expense in education and the national income per capita are also appeared as having negative influence toward longer life of population in the two countries. These results are preliminary data exploration. The next step is the in-depth analysis discovering only prominent factors relating to longevity of population.

Table 2: Pearson correlation between life expectancy at birth and economic and environmental factors

	Top-5 Positive Factors (correlation)	**Top-5 Negative Factors** (correlation)
China	Energy_use (0.856) Electric_power (0.837) Imports (0.800) Exports (0.767) Industry (0.734)	Forest_depletion (-0.862) Education_expense (-0.862) Particulate_emis (-0.709) High-tech_exports (-0.689) Forest_area (-0.672)
India	Electric_power (0.954) Energy_use (0.940) Industry (0.902) Exports (0.875) Imports (0.838)	High-tech_exports (-0.853) Particulate_emis (-0.848) Forest_area (-0.798) National_income (-0.739) Forest_depletion (-0.717)

3.2. Descriptive Modeling Results

Descriptive analytics refer to the process of applying statistical and other intelligent techniques to provide insight into the historical data to gain some understanding about the important factors, hidden patterns or concealed behavior. To understand characteristics of longevity pattern, we apply CHAID algorithm to reveal prominent factors affecting lifespan and display it as a tree structure as shown in Figure 4 (root of a tree is on the left hand side). It can be seen from the patterns that particulate emission damage is the most important environmental factor shortening lifespan of populations in both China and India.

A web graph to display association between economic and environmental factors and life expectancy at birth for each population group is also shown in Figure 5. The thickness of line linking each node in a graph represents strength of association. The thicker is the stronger. The web graph also shows the strong association between a short lifespan and a high level of particulate emission damage for both Chinese and Indian populations.

China

Particulate_emis in [0.27-0.34] => Lifespan in [74.29-76.41]

Particulate_emis in [0.35-0.75] => Lifespan in [69.93-74.28]

Particulate_emis > 0.75 => Lifespan in [67.61-69.92]

Particulate_emis is unknown

Exports in [2.49-8.32] => Lifespan in [59.08-67.60]

Exports in [8.33-17.91] => Lifespan in [67.61-69.92]

Exports in [17.92-36.03] => Lifespan in [59.08-67.60]

(Accuracy on test data = 100%)

India

Particulate_emis in [0.78-1.02] => Lifespan in [64.96-68.80]

Particulate_emis in [1.03-2.21] => Lifespan in [59.92-64.95]

Particulate_emis in > 2.22 => Lifespan in [54.71-59.91]

Particulate_emis is unknown

Industry in [21.41-26.16] => Lifespan in [47.72-54.70]

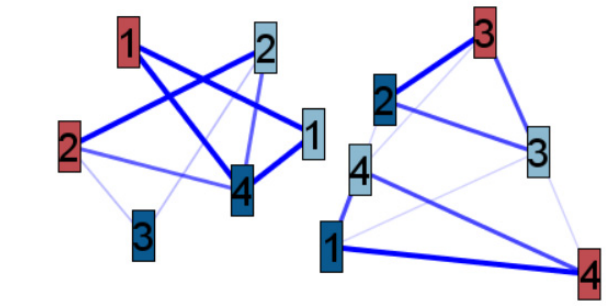
Industry in [26.17-27.84] => Lifespan in [54.71-59.91]

Industry in [27.85-31.13] => Lifespan in [47.72-54.70]

(Accuracy on test data = 84.62%)

Figure 4: Factors affecting lifespan of populations in China and India discovered by the CHAID algorithm

China



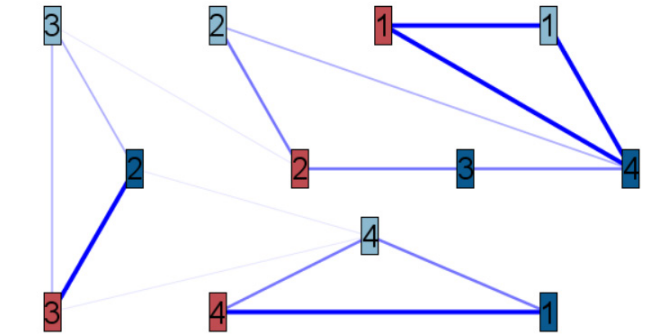
Life expectancy at birth (LE)

Particulate emission damage (PE)

Exports (EX)

LE: 1=[59.08-67.60], 2=[67.61-69.92],
3=[69.93-74.28], 4=[74.29-76.41]
PE: 1=[0.27-0.34], 2=[0.35-0.75],
3 = >0.75, 4 = unknown
EX: 1=[2.49-8.32], 2=[8.33-17.91],
3=[17.92-23.58], 4=[23.59-36.03]

India



Life expectancy at birth (LE)

Particulate emission damage (PE)

Industry (IN)

LE: 1=[47.72-54.70], 2=[54.71-59.91],
3=[59.92-64.95], 4=[64.96-68.80]
PE: 1=[0.78-1.02], 2=[1.03-2.21],
3 = >2.22, 4 = unknown
IN: 1=[21.41-26.16], 2=[26.17-26.72],
3=[26.73-27.84], 4=[27.85-31.13]

Figure 5: Factors contributing to longevity of populations displayed as a web graph

3.3. Predictive Modeling Results

Predictive modeling is the data analytical approach to generate a model with the main aim of using that model to forecast future event. We apply both statistical and machine learning methods to build a predictive model from the training dataset. From the model performance comparison, linear regression is a method yielding the most accurate result for both China and India cases. The linear regression models to predict lifespan of population in each country are presented in Figure 6. It can be noticed that education expense is among the first two factors appeared in the models and it shows positive influence toward long life of population in both countries.

China: *Life expectancy at birth*

= Education_expense * 6.195 +
Agri_methane_emission * 0.00005864 +
CO2_emission * -4.16 +
Electric_power_consumption * -0.008426 +
Energy_use * 0.03816 +
Exports * -0.07075 +
Forest_area * 0.0001171 +
GDP_growth * 0.01842 +
GNI * -0.00001071 +
Hi-tech-exports * -0.0002215 +
Imports * 0.3694 +

Industry * -0.2848 +
Manufacturing * 0.000447 + 48.7

India: *Life expectancy at birth*

= National_income * -0.02832 +
Education_expense * 2.28 +
Forest_depletion * -0.02815 +
Agri_methane_emission * -0.000006419 +
CO2_emission * 8.185 +
Electric_power_consumption * 0.02312 +
Energy_use * -0.04361 +
Exports * 0.2372 +
Forest_area * 0.00003288 +
GDP_growth * -0.2307 +
GNI * 0.3371 +
Hi-tech-exports * 0.00004354 +
Imports * -0.1426 +
Industry * 0.7558 +
Manufacturing * -0.173 + 35.8

Figure 6: Factors contributing to longevity of populations in China and India

4. Model Evaluation

We test performance of descriptive and predictive models with a separate set of test data. The descriptive model derived by CHAID algorithm to reveal longevity pattern of population in China with 100% of accuracy, whilst the accuracy of CHAID model drops to 84.62% when the algorithm tries to fit model with data from Indian training cases. The decrease in accuracy may occur from the low level of homogeneity in the training data.

To build a predictive model, we apply eight algorithms and then select the best five models to test performance on a hold-out dataset. The evaluation results for the case of China population are illustrated in Table 3, whereas the results of India population modeling assessment are shown in Table 4. The best predictive model from both population groups with the least mean absolute error is the one derived from the linear regression algorithm.

Table 3: Predictive model evaluation results for China

Algorithm	Correlation	Number of Factors	Mean Absolute Error
Regression	**0.977**	13	**0.602**
CHAID	0.972	7	0.769
CART	0.971	12	0.916
GLM	0.874	16	1.597
SVM	1.0	16	3.212

Table 4: Predictive model evaluation results for India

Algorithm	Correlation	Number of Factors	Mean Absolute Error
Regression	**0.996**	15	**0.544**
CHAID	**0.996**	16	0.562
CART	0.988	7	1.071
GLM	0.926	16	1.507
SVM	0.895	15	1.888

5. Conclusion

We present data analytical approach to create descriptive and predictive model with the two main aims: to discover threatening factors that may shorten lifespan and to predict the number of years on average an individual is expected to live based on the economic and environmental variables. The analytical approach is data driven in the sense that model is to be generated from the training data. Therefore, using different datasets can result in obtaining different models, even though the same data variables and the same learning algorithm have been applied.

To derive a descriptive model, we adopt the CHAID algorithm. The training data are World development indicators accessed from the World Bank database with two specific countries, China and India, and the target of analysis is life expectancy at birth which is one aspect that the UNDP applied for computing the human development index of a country. The models of China and India show one common finding that particulate emission damage due to the exposure to ambient ozone pollution and PM2.5 is the most important factor affecting shorter longevity. We also apply several learning algorithms to derive predictive models to forecast number of years an individual is expected to live based on the available economic and environment factors. The most accurate predictive model is the one built from the linear regression method.

Conflict of Interest

The authors declare no conflict of interest.

Acknowledgment

This work has been supported by grant from Suranaree University of Technology through the funding of Data and Knowledge Engineering Research Unit in which the first and second authors are principal researchers.

References

[1] UNDP, "Human Development Indices and Indicators: 2018 Statistical Update," http://hdr.undp.org/sites/default/files/hdr2018_technical_ notes.
[2] D. Dicker et al., "Global, regional, and national age-sex-specific mortality and life expectancy, 1950–2017: A systematic analysis for the Global Burden of Disease Study 2017," The Lancet, **392**(10159), 1684–1735, 2018.
[3] M. Kim, Y.H. Khang, "Why do Japan and South Korea record very low levels of perceived health despite having very high life expectancies?," SSRN Electronic Journal, article 3276420, 2018.
[4] L. Wang, Y. Li, H. Li, J. Holdaway, Z. Hao, W. Wang, T. Kraft, "Regional aging and longevity characteristics in China," Archives of Gerontology and Geriatrics, **67**, 153-159, 2016.
[5] S. Wang, K. Luo, R. Ni, Y. Tian, X. Gao, "Assessment of elemental background values and their relation with lifespan indicators: A comparative

study of Jining in Shandong Province and Guanzhong area in Shaanxi Province, northern China," Science of The Total Environment, **595**, 315–324, 2017.
[6] L.A. Johnston, "The economic demography transition: is china's 'not rich, first old' circumstance a barrier to growth?," Australian Economic Review, Jul., 1–21, 2019.
[7] R. Bai, J. Wei, R. An, Y. Li, L. Collett, S. Dang, W. Dong, D. Wang, Z. Fang, Y. Zhao, Y. Wang, "Trends in life expectancy and its association with economic factors in the belt and road countries—evidence from 2000–2014," International Journal of Environmental Research and Public Health, **15**(12), article 2890, 2018.
[8] E. Kurtbegu, "Replicating intergenerational longevity risk sharing in collective defined contribution pension plans using financial markets," Insurance: Mathematics and Economics, **78**, 286–300, 2018.
[9] E. Debonneuil, S. Loisel, F. Planchet, "Do actuaries believe in longevity deceleration?," Insurance: Mathematics and Economics, **78**, 325–338, 2018.
[10] L. Mayhew, D. Smith, D. Wright, "The effect of longevity drift and investment volatility on income sufficiency in retirement," Insurance: Mathematics and Economics, **78**, 201–211, 2018.
[11] S. Wang, K. Luo, "Life expectancy impacts due to heating energy utilization in China: Distribution, relations, and policy implications," Science of The Total Environment, **610–611**, 1047–1056, 2018.
[12] S. Wang, Y. Liu, C. Zhao, H. Pu, "Residential energy consumption and its linkages with life expectancy in mainland China: A geographically weighted regression approach and energy-ladder-based perspective," Energy, **177**, 347–357, 2019.
[13] W.C. Cockerham, Y. Yamori, "Okinawa: an exception to the social gradient of life expectancy in Japan," Asia Pacific Journal of Clinical Nutrition, **10**(2), 154–158, 2001.
[14] J. Jiang, L. Luo, P. Xu, P. Wang, "How does social development influence life expectancy? A geographically weighted regression analysis in China," Public Health, **163**, 95–104, 2018.
[15] C. Lee, M. Kim, "The relationship between internet environment and life expectancy in Asia," Review of Integrative Business & Economics, **8**(2), 70–80, 2019.
[16] K. Hassan, R. Salim, "Population ageing, income growth and CO2 emission: empirical evidence from high income OECD countries," Journal of Economic Studies, **42**(1), 54–67, 2015.
[17] J.C. Yeh, C.H. Liao, "Impact of population and economic growth on carbon emissions in Taiwan using an analytic tool STIRPAT," Sustainable Environment Research, **27**(1), 41–48, 2017.
[18] N. Kerdprasop, K. Kerdprasop, "Regression tree analysis of CO2 emissions and environmental factors to the survival rate of population in Thailand and China," in the International MultiConference of Engineers and Computer Scientists (IMECS), 286–290, 2016.
[19] N. Kerdprasop, K. Kerdprasop, "Association of economic and environmental factors to life expectancy of people in the Mekong basin," in the 12th IEEE Conference on Industrial Electronics and Applications (ICIEA), 1984–1989, 2017.
[20] L. Wang, B. Wei, Y. Li, H. Li, F. Zhang, M. Rosengerg, L. Yang, J. Huang, T. Kraft, W. Wang, "A study of air pollutants influencing life expectancy and longevity from spatial perspective in China," Science of The Total Environment, **487**, 57–64, 2014.
[21] W. Song, Y. Li, Z. Hao, H. Li, W. Wang, "Public health in China: An environmental and socio-economic perspective," Atmospheric Environment, **129**, 9–17, 2016.
[22] J. Lv, W. Wang, Y. Li, "Effects of environmental factors on the longevous people in China," Archives of Gerontology and Geriatrics, **53**(2), 200–205, 2011.
[23] J. Robine, F.R. Herrmann, Y. Arai, D.C. Willcox, Y. Gondo, N. Hirose, M. Suzuki, Y. Saito, "Exploring the impact of climate on human longevity," Experimental Gerontology, **47**(9), 660–671, 2012.
[24] G. Gulis, "Life expectancy as an indicator of environmental health," European Journal of Epidemiology, **16**, 161–165, 2000.
[25] T. Torri, J.W. Vaupel, "Forecasting life expectancy in an international context," International Journal of Forecasting, **28**(2), 519–531, 2012.
[26] K.J. Foreman et al., "Forecasting life expectancy, years of life lost, and all-cause and cause-specific mortality for 250 causes of death: Reference and alternative scenarios for 2016–40 for 195 countries and territories," The Lancet, **392**(10159), 2052–2090, 2018.
[27] M.D. Pascariu, V. Canudas-Romo, J.W. Vaupel, "The double-gap life expectancy forecasting model," Insurance: Mathematics and Economics, **78**, 339–350, 2018.
[28] M. Kanevski, R. Parkin, A. Pozdnukhov, V. Timonin, M. Maignan, V. Demyanov, S. Canu, "Environmental data mining and modelling based on machine learning algorithms and geostatistics," Environment Modelling & Software, **19**(9), 845–855, 2004.
[29] M. Leuenberger, M. Kanevski, "Extreme Learning Machines for spatial environmental data," Computers & Geosciences, **85**, 64–73, 2015.
[30] V. Kontis, J.E. Bennett, C.D. Mathers, G. Li, K. Foreman, M. Ezzati, "Future life expectancy in 35 industrialised countries: Projections with a Bayesian model ensemble," The Lancet, **389**(10076), 1323–1335, 2017.
[31] United Nations, Department of Economic and Social Affairs, Population Division, "World Population Prospects 2019: Data Booklet," https://population.un.org/wpp/Publications/
[32] The World Bank, "World Development Indicator," https://databank.worldbank.org/source/world-development-indicators
[33] G. Kass, "An exploratory technique for investigating large quantities of categorical data," Applied Statistics, **29**(2), 119–127, 1980.
[34] S. Jang, H. Choi, Y. Jung, E. Moon, T. Yoon, "A comparison of H1N1 and H3N2 viruses using decision tree and Apriori algorithm," International Journal of Machine Learning and Computing, **6**(1), 76–79, 2016.
[35] S. Boonamnuay, N. Kerdprasop, K. Kerdprasop, "Classification and regression tree with resampling for classifying imbalanced data," International Journal of Machine Learning and Computing, **8**(4), 336–340, 2018.

ASTES

Advances in Science, Technology and Engineering Systems Journal Vol. 5, No. 5, 314-331 (2020)

www.astesj.com

Special Issue on Multidisciplinary Innovation in Engineering Science & Technology

ASTESJ

ISSN: 2415-6698

ISR Data Processing in Military Operations

Ladislav Burita*, Ales Novak

Department of Informatics and Cyber Operations, University of Defence, Brno, 66210, Czech Republic

ARTICLE INFO

Article history:
Received: 17 June, 2020
Accepted: 31 August, 2020
Online: 17 September, 2020

Keywords:
ISR data processing
Business Intelligence
Data Mining
Big Data

ABSTRACT

This paper provides an overview of Intelligence, Surveillance, and Reconnaissance (ISR) data with respect on NATO standards and recommendations; further presents methods, tools, and experiences in ISR data processing in military operations. The steps of the Intelligence cycle and disciplines Business Intelligence (BI), Data Warehousing, Data Mining, and Big Data are presented in the introduction. The literature review is oriented to the analysis of intersections between ISR and BI methods. The next chapter describes the ISR data processing in detail; there are listed structures, formats, standards, and data from the operational point of view. The ISR operational picture is explained, and steps of the ISR data mart is completed. The last part is oriented to Big Data processing; NoSQL, in-memory and streaming databases. The last two chapters are focused on the description of research results in the processing of ISR data. The ISR data mart experiment processes the radio transmission data that consists of detected radio signals. Results are visualized in RapidMiner Studio. The Big Data experiment is realized in Apache Hadoop.

1. Introduction

This review paper is an extension of work originally presented in the 7th International Conference on Military Technologies [1]. Paper summarizes methods, tools, and experiences in ISR (Intelligence, Surveillance, and Reconnaissance) data and information processing in military operations.

The important focus in the paper is oriented on the NATO ISR data standards. The ISR data format includes in authors point of view: the structured data, unstructured (text) data and Big Data.

The ISR data processing mainly uses Business Intelligence (BI) techniques, which include data and text analysis, Data Mining (DM), Data Warehousing (DW) On Line Analytical Processing (OLAP), and Decision Support Systems (DSS).

1.1. The ISR Processes and Data

The Command and Control (C2) of the military units is mostly mentioned as OODA (Observe-Orient-Decide-Act) management cycle [2]. Each phase of the cycle can be supported by appropriate information technologies (IT). The most important phase is orientation, which affects both the creation of the right alternatives for decision and the method of observation and that functions are supported by IT. The Intelligence Cycle (IC) supports the orientation phase. The IC is defined as "The sequence of activities whereby information is obtained, assembled, converted into intelligence and made available for users." The IC goal is to solve commanders' problems related to the operational situation. It consists of four phases [3]: Direction, Collection, Processing and Dissemination.

The ISR process "A coordination through which intelligence collection disciplines, collection capabilities and exploitation activities provide data, information and single-source intelligence to address an information or intelligence requirement, in a deliberate, ad hoc or dynamic time frame in support of operations planning and execution" [4] is a part of data collection in IC.

The ISR activities consist of five phases: Task, Collect, Process, Exploit and Disseminate (TCPED). In the collection phase, by the NATO documents, data are obtained from heterogeneous sources and thus covers multiple intelligence disciplines:

- Human Intelligence (HUMINT) - information that is collected and provided by human sources.
- Acoustic Intelligence (ACINT) - the detection and utilization of acoustic signals or emissions.
- Imagery Intelligence (IMINT) - collection, processing and exploitation of image sequences.
- Measurement and Signature Intelligence (MASINT) – the source of information in scientific and technical area.

*Corresponding Author: Ladislav Burita, ladislav.burita@unob.cz

- Open Source Intelligence (OSINT) – information gathered from publicly available sources.
- Signals Intelligence (SIGINT) - collecting and exploiting electromagnetic signals.

The approach of NATO to ISR area is rapidly changing because of disrupting possibilities in technology and science. In the last years, the community of innovation in NATO has been in cooperation with the NATO Support and Procurement Agency (NSPA), prepared conditions for extensive changes in the AWACS (Airborne Warning and Control System) aerial survey and the method of exchanging information.

NATO is planning the next version of AFSC (NATO Alliance Future Surveillance and Control) as an ISR distributed network systems as opposed to a single platform. This is meaning as combination of technical and human resources that would provide more enhanced surveillance capability opposed a single complex and expensive platforms. [5]

1.2. Business Intelligence

Business Intelligence (BI) is including tools, technologies, and practices data collection, aggregation or integration, processing, analysis, and presentation of in the form of information to support decision-making tasks.

All sources of data including information systems (IS) for decision preparing contain the huge volume of data. It is not possible to obtain the awaiting information for the decision process directly from the data sources and it is unnecessarily time consuming and expensive.

It must be prepared many questions that lead to the desired result. Data are spread in many sources in a various format, and therefore obtaining information is very difficult.

Commanders or directors are able to prepare decision strategy quicker and better by BI; are able to simply prepare or modify company strategies or processes, which leads to competitive advantage in a military area.

BI is an approach that has an impact on the effective decision, and thus increases the quality of the organization and leads to an advantage in warfare.

BI infrastructure includes components that collects, stores, summarizes, aggregate, integrate and analyzes the data produced by an organization or military unit. It is a broad term that encompasses data mining, data warehousing, online analytical processing (OAP), performance benchmarking, descriptive analytics, business process reengineering (BPR) and reporting, see Figure 1.

1.3. The data Warehousing and OLAP

The data warehouse (DW) is prepared as a trusted and integrated data collection for analyze processes with outputs that are directed to the decision process in a company or a military unit. It helps users solve problems and preparation decision in business and military missions.



Figure 1: Business Intelligence [6]

Sources for DW are IS in business, Enterprise Resource Planning (ERP) systems, Customer Resource Management (CRM) data sources, and other data files, see Figure 2. The DW is preparing from data sources thru ETL (Extract – Transform – Load) processes.

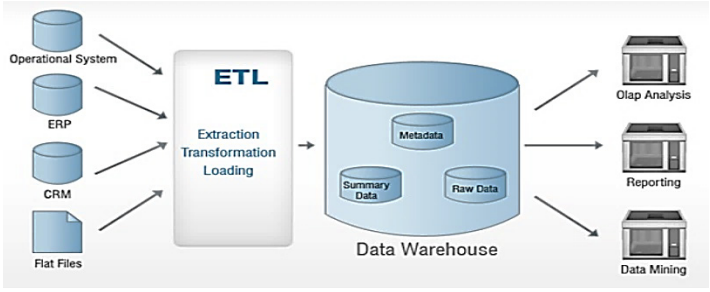


Figure 2: Data Warehousing [7]

The main reason of DW constitution is the possibilities of the IS of other data sources for decision-making support:

- Information systems have not a satisfactory performance in analysis, it takes too long, it is expensive and the historical data are usually missing.
- Data are spread in more inconsistent applications (production, commerce, human, finance, logistics, and other) resources.
- Database structure of the DW data sources are not optimal for decision-making elaboration.

OLAP (or OLAP Cube) is abbreviation of On Line Analytical Processing. It is a multidimensional memory whose dimensions form required view of data structure and many variants of detail view in information. The OLAP cube in gasoline industry consists of dimensions: Time, Product, and Measure, see Figure 3.

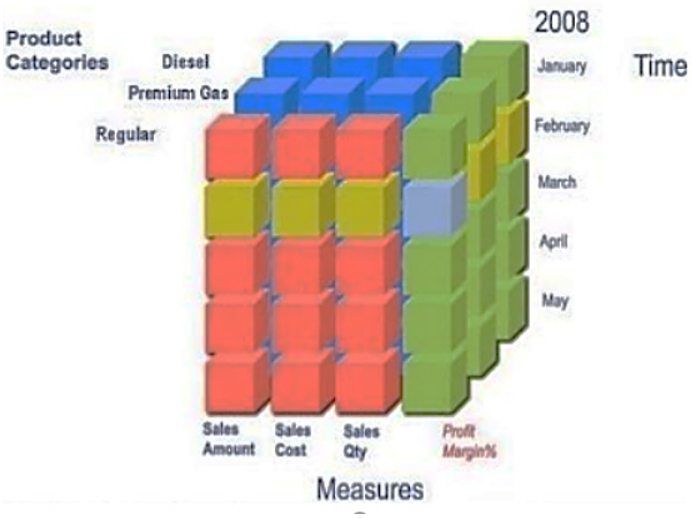


Figure 3: OLAP – the multidimensional memory [8]

Each node of the OLAP consists of product category, time, and sales results (amount, cost, quantity, and profit margin in %). In the prepared data structure, the results can be by managers good monitored from various directions.

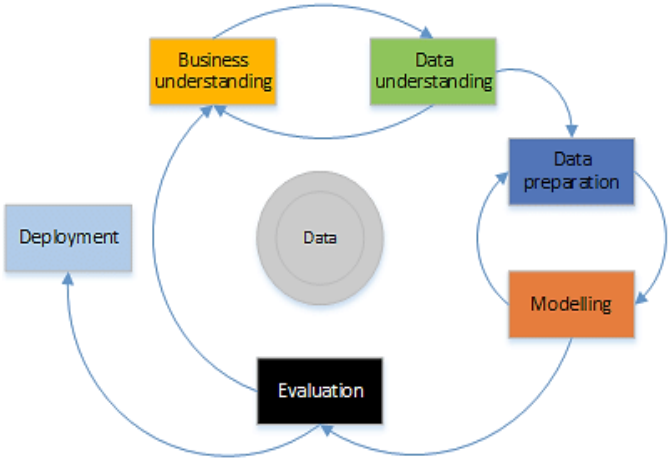


Figure 4: CRISP-DM methodology phases [9]

1.4. Data Mining, Methods and Tools

The mission of Data Mining (DM) is to find information, not known before, from databases. There are used modelling approach and statistical tools to gain knowledge from data. The usually used DM methodology is Cross Industry Standard Process (CRISP) that include processes of data acquisition, processing and transformation by application of DM method, evaluation, visualization, and presentation; see Figure 4.

The effectiveness and quality of the decision process depends on the reliable data; mistakes may lead to bad results. Mistaken data is a result of practical processing and data can be incomplete, inconsistent or should contain problems.

Set of actions in the data processing:

- Cleaning Data - completion the missing values, identify and remove boundary values, eliminate data inconsistency.
- Data Integration – various sources of data should be integrated.
- Data Transformation – aggregation, normalization and reduction makes data useful for analysis.
- Descriptive summarization of data – understanding of structure and properties of the data.
- Discretization - conversion of analogue format into digital form.

The often-used DM methods include decision trees (DT), neural networks (NN), statistical methods (SM), and genetic algorithm (GA). The popular method of DM is statistics: discrimination and regression analysis, and pivot tables.

In DT method is data divided into groups which represent the same class. The goal is to find the optimal tree by the principle that differentiate chosen attributes the best.

Method NN is based on set computational neurons with weighted connections. NN functions are set up by testing data.

GA is used if it is a problem to find the quick solution, and method is likened from the natural environment.

The most popular BI SW in the academic environment are products SAS Institute and IBM SPSS.

SAS is the statistical SW for data management, various kinds of analysis (multivariate, predictive, or statistical) for BI, a policy investigation. SW is able to process data from many sources, perform analysis on them, and makes available a graphical user interface for common user and developed solution using the special language for technical users.

The most extensive SAS solution offers for customer intelligence. It includes parts for marketing, social media and web analytics, is able to profile customers, predict their business steps, and provides optimal communication.

The SAS SW for enterprises and organizations is preparing for risk and compliance analysis, includes risk simulation, scenario building to reduce the risk and development of corporate policies.

The SAS supply-chain SW prepares forecasting for company development, solution of products distribution, inventory and optimal pricing. Exists also the SAS SW for environmental sustainability, economic and social consequences in causal relations between production and its impact on the eco-environment. The SAS has solution for government, industry, trade, and communications. [10]

The SPSS SW suite solves various kind of analysis (statistical, text, predictive), includes solution for artificial intelligence (machine learning algorithms).

SPSS offers open-source connections, integration with Big Data tools, and simply deployment into own applications.

The SPSS SW is prepared as flexible and ease to use for all categories of users (from common to advance).

SW is offered for all sizes and complexity of projects and can improve company or organization efficiency, minimize risk, and find opportunities [11].

1.5. Big Data

Big Data is a term that includes primarily theme with amount of data, its format, generation and changing of data, and processing. The first characteristics of big data is large *volume*. Simple example is possible to take from social media that millions users generate every second data that volume is constantly growing.

The next characteristics is *velocity* of generating and changing data. Simple example is possible to take from Internet of Things (IoT), which sensors generate data about your condition. Sometimes they are data streams, their processing cannot be performed by conventional analytical methods.

The third characteristics is dealing with *variety* of formats. Data can be standardized or unstandardized, formalized or structured (databases, files), unstructured or text (documents), web pages, pictures, schemas, graphs, etc.

The last two characteristics refers to the *veracity* refers to the credibility and reliability of the data, and the *value* is the importance given by company or military organization to use data. In a military environment, the reliability of data, for example when assessing the enemy's situation, is crucial.

The summary of Big Data definition concludes the five "V" specification: volume, velocity, variety, veracity and value. There are special means and techniques for big data processing, an overview of which is at Figure 5. They are divided into three groups, and 15 sub-groups:

1. Computing tools.
2. Storage tools.
3. Support technologies.

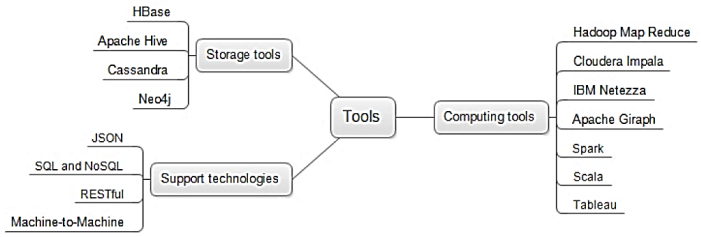


Figure 5: Mind map representation of Big Data tools [12]

As the variety, volume, veracity, value, and velocity of data is undergoing a rapid transformation and aggravating the cognitive burden on the Warfighter, armed forces require technologies to store, process, verify, and disseminate actionable intelligence at pace.

It is widely accepted that decision-making in the future information-dominated battlespace will depend on big data processing using artificial intelligence (AI) methods. It is important to address ways to gain and retain the information advantage through disruptive innovation and big data analytics, addressing cloud computing, the acquisition of data from disparate sources, data validation, visualization, accelerated and autonomous decision-making, and network resilience through cyber defense mechanisms. AI, big data technologies and ML will transform ISR and command and control (C2). [13]

2. The Literature Review

The aim of literary review is to map the interest of authors of articles, indexed on Scopus, in the topic published in the article. Information from the selected articles is oriented about the knowledge of the ISR area in relation to information technologies (IT). Overview of the selected relevant articles is listed in Table 1. The goal of individual queries was to find the relevant papers only in one area of interest. The queries were directed to all fields of the papers (the first version of the literature review, on March 26, 2020). The IT query found papers that correlate the query (BI and DW and DM and BigD) and in complex query was the result connected to ISR area. Only one paper [14] has met a complex selection requirement. The paper deals with the application of big data analytics in meteorological research.

Table 1: Number of relevant papers to the query - the first version

Query	ISR	BI	DW	DM	BigD
Individual	3 981	30 478	36 840	552 791	228 493
IT		619			
Complex	1				
ISR and DM	8 (open access, citated>0)				
ISR and BigD	9 (open access, citated>0)				

After the first version of the literature review was discovered that more than one-half of the found papers have keyword "ISR" matching only in references. Therefore, a second literature review was carried out (on April 2, 2020), where the queries were directed only to fields Title, Abstract, and Key-words of the papers. The overview of the selected relevant articles is listed in Table 2.

Table 2: Number of relevant papers to the query – the second version

Query	ISR	BI	DW	DM	BigD
Individual	1 697	7 503	12 849	169 113	81 292
IT		22			
Complex	0				
ISR and DM	15 (5, citated>0)				
ISR and BigD	12 (5, citated>0)				

The ten selected articles (see Table 3) were further analyzed in detail; see Table 3 that shows the areas of interest. Each paper was described by three themes – characteristics of the paper interest. Among the most, numerous characteristics of the analyzed papers are "military" and "data or information fusion", these themes integrate orientation and interest of most analyzed papers with connection to the theme "ISR data processing". This first conclusion of the analysis correlates completely with the focus and aim of the article.

Let us now get focus more closely on the analyzed articles. First, how data or information fusion is assumed in chosen articles and with what requirements is this operation connected? In addition, the second focus: Which artificial intelligence (AI) techniques, agent based, and knowledge approaches were used.

In [15], the author explains information superiority than can be achieved by application of the four RIGHT: information, time,

format, and people. However, it is only right when skilled commanders are able getting information use in praxis. Information superiority is possible only by intensive application of information and communication technologies that spread information in almost real time by remote access regardless of time and space. The condition of good cooperation on the battlefield is information interoperability and security in broaden contexts. That is why NATO is intensively developing standardization in the field of data exchange, which includes the concept Coalition Shared Data (CSD). It supports operational processes in NATO Joint ISR and by using the Intelligence Cycle.

Table 3: Areas of interest in the analyzed papers

Area of interest	Paper										Σ
	[15]	[16]	[17]	[18]	[19]	[20]	[21]	[22]	[23]	[24]	
Agent-based system		1			1						2
AI-Machine learning							1				1
AI-Neural network									1		1
Air Force						1					1
Cybersecurity										1	1
Data or information fusion	1	1	1	1					1		5
DNN architecture				1							1
GDPR								1			1
HPEC architecture						1					1
Information management	1										1
ISR mission support						1					1
Knowledge approach				1							1
Military	1	1	1		1	1	1		1	1	8
Navy					1					1	2
OSINT and BDA								1			1
Personal security								1			1
QuEST strategy							1				1
STACK model			1								1

Explanation to Table 3:

- AI-Artificial Intelligence
- BDA-Big Data Analytics
- DNN-Dual Node Network
- GDPR-General Data Protection Regulation
- HPEC-High Performance Embedded Computing
- OSINT-Open Source Intelligence
- QuEST-Qualia Exploitation of Sensor Technology
- STACT-Spatial, Temporal, Algorithm, and Cognition

In [16], the author presented elements to achieve integration of information (information fusion). The solution includes a distributed surveillance system and intelligence databases. Data sources comes from electronically situational awareness, controlled by military and civilian security operators and commanders in principle of ISR. The surveillance system works automatically; integrates data from aircraft systems, sensors, and background information into a military situational picture. Components for information fusion are agent-based mechanisms for integration and drawing using different reasoning techniques, knowledge modelling, information extraction and transformations.

The data fusion strategies for ISR missions, similar to previous paper, is presented in [17]. Extraction of sematic information from various set of sensors and its processing is based on new AI algorithms and computational power. Content of the project is bringing challenges for information fusion algorithms for moving targets, combination of image data with different temporal frequency, getting the contextual information by monitoring of mobile phones. Name of solution is STACK- Spatial, Temporal, Algorithm, and Cognition.

In [18], the author described the distributed fusion systems for integration. Solution includes adaptive methods that improve usefulness data sources. |The data processing cycle supports to find needed data, to develop models (situation modelling), and evaluate predictive characteristics of model (impact of prediction to success in mission). The goal of system is to improve availability, quality, variety, and actuality of data for information fusion. Machine learning techniques learn to find typical symptoms for integration data with fusion system and ontology. Extension of the Data Fusion & Resource Management Dual Node Network (DNN) architecture was applicate. The data mining methods are used to find models in data sources with help of automatically learn component behaviors by fusion procedure.

Project Albert is oriented to key areas that traditional modeling and simulation techniques often do not capture satisfactorily and uses two data management concepts, data farming and data mining, to assist in identifying areas of interest. The actual solution in Project includes four agent-based models that allow agents to interact with each other and produce emergent behaviors [19].

The Air Force Research Laboratory is developing new computing architecture, designed to provide high performance embedded computing solution to meet operational and tactical real-time processing intelligence surveillance and reconnaissance missions [20].

The achieved results in use of big data and relevant technologies, introduction of artificial intelligence (machine learning) learning are specified in [21]. The situation understanding is solved in collaboration human and machine using the Qualia Exploitation of Sensor Technology (QuEST). The QuEST is, in comparison to the limits of traditional big data processing, a completely progress and offer a higher-level system in situational awareness preparation.

Analyses, focused to open source intelligence and big data analytics with the emphasis on reconnaissance and how personal security is part of that entity. The main question is how privacy manifests itself as part of both mentioned data sources [22].

The big data from military sources are extensively multimodal and multiple intelligence, where numerous sensors along with human intelligence generate structured sensor and unstructured audio, video and textual ISR data. Data fusion at all levels remains a challenging task. While there are algorithmic stove-piped systems that work well on individual modalities. There is no system that can seamlessly integrate and correlate multi-source data; as textual, hyperspectral, and video content. It is not effective to solve integration of individual data sources gradually; better results can be achieved by integration at a higher level of the model by deep fusion of all data sources, while achieving accuracy of integration and obtaining the basic properties of signals [23].

US Navy is proposing emerging maritime strategy of command, control, communications, computers, intelligence, surveillance and reconnaissance with big data [24].

Summary in the sources of the literature review to the content of the manuscript: the one view is bringing similarities in data description and its processing and other view differences between analyzed papers and this manuscript in detail point of view at ISR data. The manuscript is specifying formats of ISR data as NATO standard (STANAG). ISR products are described and explained in relation to the command and control processes, management cycle and to the intelligence loop.

The common focus is in military area with ISR data processing, including even big data. The ISR data has sources from many various activitiers and is of different formats. Procedures of data processing are oriented primarily to data integration (fusion) and then to dissemination for military operations support.

In the manuscript are mentioned experiences and achievements of the Czech Armed Forces (CAF) in the described topic. It is also a comprehensive overview of the use of business intelligence tools.

The manuscript presents the results of research during the elaboration of the dissertation, too.

3. ISR Data Processing

3.1. ISR Data Overview

The Intelligence Cycle, the ISR process and its individual steps were introduced in previous chapters. In these individual steps, many heterogeneous sensor data and information are created, processed and managed. Military orders and tasks are issued to military units, civilian agencies and other cooperation organizations. Data are collected on gathering sensors platforms based on those orders. Operators and analysts process and exploit collected data and based on them they create ISR reports or other needed documents. Finally, ISR results are spread to its customers.

All sensor data, information and documents can be processed, stored and managed in many different ways. They are typically stored in the traditional File System or the Relational Database. This type of storage represents an easy way to store the data but in most cases are proprietary data formats used. There is a lack of interoperability because of proprietary data format utilization so it is difficult or even impossible to share proprietary data among different sensor platforms, units or even allies and nations. As a result, operators, analysts and commanders might not be able to understand gathered data so those data are not used in the decision preparation. NATO to reduce this interoperability lack introduced the concept of Coalition Shared Data (CSD).

CSD was standardized in STANAG 4559 as the NATO Standard ISR Interface (NSILI) [25] and its objective is to ensure interoperability for ISR documents exchange. NSILI defines the interface as a standard to search and access in ISR document libraries (IPL). CSD and NSILI are used as a synonym within NATO ISR community. For simplicity, the term NSILI will be used for the standard itself and the term CSD for its physical implementation in this article.

The CSD aims to ensure interoperable sharing of ISR products but NSILI is not designed and intended for user-friendly data querying, searching, reporting, data mining and analysis. NSILI does not specify client behavior; it is focused only on the server-side functionality and machine-to-machine interfaces, such as other CSDs, sensor platforms and exploitation stations. Moreover, NSILI data model is not universal military data model and therefore it does not cover all relevant military data formats so all ISR data and information cannot be stored in the CSD. NSILI also defines its own dissemination and synchronization mechanism, which affects data accessibility and availability on different nodes.

The operator and analyst needs to search relevant data efficiently regardless of their formats, storage or even CSD implementation details and limits. To achieve this goal, it is proposed to build a data warehouse on top of CSDs, sensor data databases and other military data sources. The data warehouse can help to solve some issues mentioned while other difficulties would remain. Those are connected with strict NSILI data model and streaming nature of some sensors data. The Big Data approach will be utilized to cope with those aspects.

3.2. ISR Data Formats

In the following paragraphs, will be introduced relevant ISR and military data formats, which will be later used as a base for building ISR data warehouse. Many data format standards are applied in a military environment to store ISR specific data. Those data format standards include common military data formats, ISR specific ones as well as common enterprise data formats such as PDF, Office formats, images formats, video formats etc. In the article is focus only on military data formats, both common and ISR specific ones.

3.3. Common Military Data Formats

Common military data formats relevant to ISR data include textual messages, operational pictures, blue force tracks etc. These data are widely used for the exchange and integration of military systems. Relevant data standards are already implemented and adapted in the CAF and its implementation in the CAF has been confirmed on many experiments, trials, etc. Some of those standards cover not only data formats but includes also transport protocol and mechanism of exchange.

Textual messages arte included in the APP-11 [26] message catalogue, which is NATO product, used in exercises and missions to exchange text as a structured information between allied military units. The messages are prepared upon the latest technical standard ADatP-3 that defines the rules of organizations and exchange of the messages. The actual version of the APP-11 message catalogue includes four hundreds messages ISR specific ones. All messages can be exchanged using the XML or slash-separated files.

Operational pictures utilize the NATO Vector Graphic (NVG) for coding and common using overlays. The NVG includes an XML data format for the coding battlespace elements into result messages and report for automated exchange of the overlays [27].

Blue Force Tracking (BFT) is the ability to track flawlessly with 100% accuracy the identification and location of own military forces in NATO missions, exercises and operations in almost real time. NATO C2 are equipped with this system and preparation for working with BFT is carefully required. NATO Friendly Force Information (NFFI) and NFFI in Message Text Format (FFI MTF) are two XML based message forms that are used by Blue Force Tracking capability [28].

3.4. ISR Specific Data Formats

The ISR community developed and adopted a wide set of data format standards for individual intelligence disciplines. The set of those ISR data standards is maintained by STANREC 4777 Ed. 2 - NATO ISR Interoperability Architecture (NIIA) [29]. Although NIAA lists about 25 key ISR standards, only the most significant for the CAF are mentioned in this article:

STANAG 4545 – NATO Secondary Imagery Format (NSIF) provides implementation guidance that is designed for the distribution, storage, and interchange of secondary imagery products.

STANAG 4559 – NATO Standard ISR Library Interfaces (NSILI) promotes interoperability of NATO ISR libraries and provides services for the exchange of shared ISR products.

STANAG 4609 – NATO Digital Motion Imagery Standard (NDMIS) guides the consistent implementation of Motion Imagery Standards to achieve interoperability in both the communication and functional use of Motion Imagery Data.

STANAG 4658 – Cooperative Electronic Support Measure Operations (CESMO) exists to enable the warfighter to rapidly share and receive electromagnetic spectrum threat information.

STANAG 5516 – Tactical Data Exchange - Link 16 provides guidelines on how to ensure interoperable use of Link 16 Tactical Data Links (TDL) to disseminate information.

The most important standard from a data integration perspective is already introduced STANAG 4559 NSILI, which will be evaluated in more details. NSILI defines architecture; use cases (publish, ingest, retrieve, synchronization); two service interfaces, modern web service interface and obsolete Common Object Request Broker Architecture (CORBA) interface; metadata model etc. NSILI covers two main functional areas, ISR Product Library and JISR Workflow.

ISR Product Library covers the first set of data managed by NSILI. It is specified as an AEDP-17 NATO STANDARD ISR LIBRARY INTERFACE. There are about 20 different types of ISR documents that are supported by standard AEDP-17.

They have format as ground moving target indication, tactical data link (TDL) reports, geographic area of interest and geospatial vector, intelligence information requirements, images and video, Microsoft office files, request for information (RFI), operational rules, organization structures (ORBAT), system specifications and assignments; chemical, biological, radiological and nuclear information; electronic order of battle, system deployment status, messages and tactical symbols.

AEDP-17 defines the following services:

- The service to metadata of query entries of ISR documents included within CSD servers.
- The publishing service to publish and modify the content of CSD servers.

The metadata set valid to all ISR products is specified by NSILI. This set contains ISR document status, source library, publisher, date and time of modification, security classification and ability for publication, product type, identifier of mission, used language, comments, related geographical data etc.

NSILI is defining as an additional group of metadata for each ISR document. The additional set of metadata extends the common set of metadata by attributes relevant only to given ISR product type; it is containing logical data model of metadata but it does not prescribe how it should be implemented on the physical level. Query and publish services defines XML based structure of metadata (Catalogue Entry Data Set) which can be exchanged among multiple CSDs.

JISR Workflow is covering the second set of data managed by NSILI. It is specified as an AEDP-19 NATO STANDARD ISR WORKFLOW ARCHITECTURE [30]. AEDP-19 defines Community of Interest (COI) services to manipulate following data entities: organization, requirement, priority, task, request and geographic area of interest (GAOI). COI services utilize underlying Simple Persistence Service (SPS++) to store entities.

SPS++ stores entities as XML artefacts in a content-agnostic way and allows easy synchronization among nodes. On the other hand, SPS++ does not allow efficient search, because the whole entity is stored as one (atomic) XML artefact without any auxiliary attributes.

Both sets of services, ISR product Publish/Query services and JISR Workflow services are intended for operational purposes mainly, not for data analyses. The support for efficient data searching is very limited because

IPL introduces its own specific query language, which enables to search ISR products according to the value of attributes, and its combination but extended data querying is limited. JISR WF services provide even only predefined business services without any extension mechanism available.

3.5. ISR Data from Operational Point of View

In the previous sub-chapter, selected data formats were described from a technology point of view. The following section will focus on its utilization in ISR operations from an operational point of view. The ISR tasks, sensors data, ISR products, and ISR operational pictures will be discussed.

3.6. ISR Tasks

The ISR task is a directive for the appropriate employment of ISR assets. There are software tools utilized to manage ISR tasks and visualize them in different perspectives (time, unit, GAOI) to depict ISR tasks decomposition, dependencies or conflicts. The main goal is to effectively coordinate and manage data gathering activities. [31]

In NATO operations, ISR tasks should be managed within the Information Request Management and Collection Management (IRM&CM) process [32].

IRM&CM process is corresponding with Task and Collect phases of the ISR process and it aims to decompose commanders' tasks in form of Request for Information (RFI) into the hierarchical structure of Priority Information Requirements (PIR), Specific Intelligence Requirements (SIR), Essential Elements of Information (EEI). ISR tasks may be refined into specific (proprietary) orders to allow automated tasking of ISR assets.

The overview lists and plans are created based on this decomposition and it consists o fa list of approved and prioritized ISR collection requirements, ISR tasks and dynamic re-tasking priorities. [33]

Those lists and plans include Intelligence Collection Plan (ICP), Collection Exploitation Plan (CXP) and Collection Tasking List (CTL), which are intended to track and monitor the operation of data collection.

It aims to assist in producing, completing and monitoring intelligence requirements, to indicate how each requirement is to be satisfied, to visualize tasks structure and de-conflict tasks.

The general structure of an ISR task includes identification of the task, name of the task, description of the task, associated geographic area, date and time of task validity, sensor or asset responsible for collecting activity according to organization structure (ORBAT), associated PIRs, SIRs, EEIs and other detailed parameters.

There are a lot of technology standards used to store ISR tasks:

- Structure of requirements, tasks and requests defined in AEDP-19, which should be the preferred option.
- Tasks format defined in AEDP-17.
- APP11 messages stored in the file system or the database.
- Intelligence discipline-specific formats, e.g. CESMO requests.
- Proprietary textual or binary formats stored as files.
- Proprietary database structures.
- Office documents (Word, Excel, PDF), and others.

It is not possible to create an overall overview of all tasks due to diversity of used data formats. To solve this issue data mart could be built on the top of multiple ISR tasks storages. Building this data mart is challenging due to the fact of a variety of data formats used. Tens or even hundred APP11 message types, individual disciplines data formats, office documents, AEDP-17 and AEDP-19 XML structures are in a place for the ETL phase. Due to the number of data sources and used data formats, implementation of ETL phase might include hundreds of transformation rules and its maintenance might be expensive. Also, rigid data structures of data mart might not be flexible enough, more flexible Big Data technologies could be utilized to build a data mart and mine the data.

3.7. Sensor Data

Sensor data are the main output of the Collection phase of the ISR process. Sensor data serves as input for the analyst's work. Although intelligence disciplines cover multiple data sources, this article and experiments focus, only on those sensors data formats which are used in the CAF, especially IMINT and COMMS-ESM ones.

COMMS-ESM data formats

Sensor data formats for COMMS-ESM includes detected activities, direction findings and geolocations. Detected activity (DA) is a logical data entity describing detected radio signals and its parameters. DA is produced by sensor platform based on (multiple) sensors (activity detectors) raw data.

DA consists of physical parameters such as carrier frequency, quality and level of the detected signal, date and time of the detection, transmission time, type of signal, type of the modulation and other technical information depending on the sensor and its capabilities. All parameters are the same within one detected activity, when one of the parameters changes, the new activity is automatically detected and recorded.

Direction finding (DF) is a logical data entity describing direction from an emitter (to the receiver) of the radio signal and its parameters. DF is produced by sensor platform based on (multiple) sensors (direction finders) raw data. DF consists of physical parameters such as direction, focus error, carrier frequency, quality and the level of detected signal, date and time of the detection, transmission time, and other technical information depending on the sensor and its capabilities. DF is associated with one or multiple DAs.

The geolocation is a logical data entity describing a position of the emitter and error ellipse. The geolocation can be produced on the sensor platform or commands post, it can be calculated automatically or set manually, both options are based on the intersection of DFs.

All mentioned entities (DA, DF, geolocation) are standardized in STANAG 4658 CESMO but proprietary formats are widely used on most sensor platforms, as captured physical parameters are always sensor specific. Gathered data are transformed into CESMO format in the case that sensors and assets are running CESMO operation and they are connected into the CESMO network.

CSD does not support those entities (DA, DF, geolocation) as they are in the scope of Electronic Warfare (EW) rather than in the scope of ISR. Due to this fact, EW and SIGINT data are stored in specific (proprietary) databases, which can be utilized for building ISR data mart. Due to the diversity, volume and streaming nature of the data, the Big Data approach can be considered in processing those data.

Imagery data formats

Imagery data formats are intended to store images (photos), video sequences and video streams. Many proprietary and standard-based data formats are used in this area to cover the complexity and diversity of image and video shooting. Imagery data formats contain not only imagery data itself but also image/video metadata such as a sensor position, heading and telemetry, camera technical details (field of view, lens parameters, etc.), camera type (electro-optical, infra-red, thermal, etc.), picture technical parameters (resolution, dimension, bands, encoding, etc.), video technical parameters (resolution, dimension, sampling frequency, encoding, etc.). Imagery analysts can utilize only a few of those metadata; the majority of them is rather technical.

Imagery data and video streams and clips are well supported in NSILI; however, this support is limited only to images compliant to STANAG 4545 NSIF and video clips and stream compliant to STANAG 4609 NDIMS. In the case that other picture or video formats are used, the data should be converted and enriched to

supported formats or it can be stored as a simple document type without taking advantage of imagery and/or video metadata.

STANAG 4545 NSIF is a container for images and its metadata. Imagery data and metadata are combined into one complex binary file. Industry based and proven image formats and codecs such as JPG, JPG2000, not compressed images etc. are utilized for images encoding. Common NSILI metadata set is extended for imagery products with parameters such as imagery category, cloud cover percentage, decompression technique, number of bands, number of rows, number of columns and title.

Common NSILI metadata set is extended for video products with parameters such as average bitrate, category, encoding schema, framerate, number of rows, number of columns, metadata-encoding scheme, MISM level, scanning mode, number of VMTI target reports and VMTI processed. Some of those parameters are very technical ones and they are not suitable for the operator to search and query.

Even in the case that industry data formats are used for imagery data, e.g. JPG captured by the digital camera, they can contain useful metadata stored in EXchangeable Image File Format (EXIF). EXIF is an industry data format for digital photography and enables to enrich raw imagery data by metadata such as geoposition, date, time, camera technical parameters such as pixel dimensions, ISO setting (equivalency of sensitivity of a film to light), aperture, white balance, lens used parameters etc.

Those metadata can be extracted and some of them could be transformed into NSIF or NSILI metadata however, none of those STANAGs support EXIF metadata directly.

STANAG 4609 NDIMS uses industry-based container architecture to store video, audio and metadata components of a video sequence. Industry-based data formats and codecs for video encoding are utilized so STANAG 4609 defines parameters for containers, data formats, codecs and its combination. It also defines a set of metadata using key-length-value (KLV) triples to encode camera position, sensor telemetry, video quality etc. KLV metadata should be extracted when video files or streams are published info CSD.

Not all imagery data are stored in the CSD due to the variety of formats and limited support in NSILI. Imagery data are rather stored directly in the file system, especially in the case that standard JPG pictures or MPEG videos are used. Naming conventions and directory hierarchy are typically used to capture basic metadata as date-time and position.

To build data mart on the top of imagery data, metadata defined in STANAG 4545 NSIF, STANAG 4609 NDIMS and STANAG 4559 NSILI, as well as KLV and EXIF metadata, should be considered in data mart design and they should be supported in the extract phase of ETL.

As was demonstrated in the previous paragraphs, the set of image and video metadata is quite wide and fuzzy which is difficult to maintain in relational databases but Big Data can handle it more appropriately.

Another reason to utilize Big Data technologies is managing a huge volume of multimedia files and geolocation metadata processing.

3.8. ISR Products

ISR products are the output of Processing and Exploitation phases of the ISR process. ISR products include sensor data, ISR reports and other documents created and evaluated by the analyst.

There are about 20 ISR product types with a set of common metadata and ISR product-specific ones defined in the NSILI as was showed in NSILI related chapters. The common structure of ISR report or product consists of the identification of the product, name of the report, associated geographic area, date and time of validity, capturing sensor or asset identification, associated task and other detailed parameters.

There are a lot of technology standards used to store ISR products:

- ISR products format defined in AEDP-17, which should be the preferred option.
- APP11 messages stored in a file system or database.
- Intelligence disciplines specific formats, e.g. COMS-ESM or IMIMT data formats introduced in the previous chapter.
- Proprietary textual or binary formats stored as files.
- Proprietary database structures.
- Office documents (Word, Excel, PDF), and others.

It is not possible to create an overall overview of all ISR products due to diversity of used data formats. To solve this issue data mart could be built on the top of multiple ISR products storages. Building this data mart would be challenging due to the fact of a variety of data formats used, similarly as in the case of ISR tasks data mart. Tens or even hundred APP11 message types, individual disciplines data formats, office documents, AEDP-17 XML structures, NVGs, etc. are in place for the ETL phase. Due to the number of data sources and used data formats, implementation of ETL phase might include hundreds of transformation rules and its maintenance might be expensive. In addition, rigid data structures of a data mart might not be flexible enough, more flexible Big Data technologies could be utilized to build data mart and mine the data.

3.9. ISR Operational Picture

ISR Operational Picture is a specific ISR product, a contribution of the ISR community to Common Operational Picture (COP). COP is [34] a single identical display of relevant operational information (e.g. position of own troops and enemy troops, position and status of important infrastructure such as bridges, roads, etc.) shared by more than one command.

NVG is used for encoding and sharing COPs. NVG standard includes a file format for the encoding of battlespace objects into overlays and protocol for the automated exchange of the overlays. NVG is an XML based format, the elements of NVG represent individual objects and its type (point, line, arrow, etc.), label, position, symbol code and other attributes, see the example in Figure 6.

The symbol code is uniquely defining associated graphic symbol from APP-6 symbology. The code is an alphanumerical sequence (e.g. SFGPUCR---EF***) where each character's

subsequence symbolizes [35] unit identity, dimension, status, function, size of the unit and additional information. There are several encoding standards for military symbology, NATO specific, USA specific and symbology for the dismounted soldier.

```
<?xml version="1.0"?>
<nvg
xmlns="https://tide.act.nato.int/schemas/2012/10/nvg"
version="2.0.0">
        <point label="CZE_ISR_BN_HQ" uri="da8eefcc-
1a3f-403d-9d12-e91f60a19693" modifiers="M:53;T:ISR"
symbol="app6c:SFGPUCR---EF***" y="53.1288105381945"
x="18.00605177595984"/>
        <point label="F_EB_coy_A_ISR" uri="22c7cc78-
e3a1-4bb9-81be-f2d4b3cac037" modifiers="M:ISR;T:A"
symbol="app6c:SFGPU------G***" y="50.20523308421297"
x="12.914633886152924"/>
</nvg>
```

Figure 6: Example of NVG data format

The operational picture represented in NVG format is intended for operational purposes, to visualize a tactical situation in overlays on the map. As its primary usage is visualization, qualitative aspects of the COP such as the size of covered area, count, status and types of units, etc., are not automatically processed or evaluated at all. Those quantitative aspects can be handled by data mart where those values could be extracted during the ETL phase. In fact, it is the task of data mining, because it is about digging hidden information from (source) data. Big Data technologies could be also for managing incoming changes of NVGs due to its streaming nature.

3.10. ISR Data Mart

As was discussed in previous paragraphs, ISR data are stored in multiple CSDs, APP11 messages and files, proprietary databases, proprietary data files, NVG files, office documents, images, videos etc. Although CSD is preferred way to store the ISR data, CSD does not cover all types of ISR products and common military data such as NVGs, NFFIs, APP11s, etc. so there is no central point to collect all ISR related data. Moreover, validation rules applied to the metadata are quite strict in the NSILI, which might conflict with wide and fuzzy nature of a sensor data. Finally yet importantly, as NSILI is focused on the interoperability mainly, it does not cover all requirements of a data analyst, especially requirements related to powerful queries, data analyses and data mining.

Building specific data marts for individual intelligence disciplines was proposed to enable operator and data analyst perform real data analyses on the ISR data. Following steps should be done to design ISR data mart: the identification of relevant data sources, the design of data model for data mart, the definition and implementation of ETL processes, the definition of analytical tasks etc. Data warehouse for all ISR data can be also built on the top of those ISR data marts but its design is out of the scope of this article.

3.11. Data Sources

The possible sources of ISR data presented in previous paragraphs include, but are not limited to:

- CSDs.
- NVG files and servers.
- APP11 messages stored in databases or file system.
- Proprietary databases/file systems for ISR task.
- Proprietary databases/file systems for reports.
- Proprietary ESM-COMMS data databases/file systems.
- Imagery files with NSIF or EXIF metadata.
- Video files with NDISM and/or KLV metadata.
- Office documents.
- CESMO network.
- NFFI network.

3.12. The Data Model for Data Marts

The design of a data model for individual data marts would be a straightforward generalization of logical data models introduced in previous chapters. Common metadata attributes should be added and those could be inspired by NSILI common metadata attributes such as date, time, geolocation, originator, type and security to list the most important ones. APP11 messages would be more challenging as there are about 400 messages types. Common header items could be generalized but individual content of the message should be analyzed with respect of corresponding intelligence discipline. Detail design of individual data marts is out of the scope of the article but some ideas are introduced in the practical part of the article.

There is only a very small subset of common metadata applicable to all individual data marts. The basic idea of its identification was introduced in the previous chapter. Generalization of common metadata applicable to a data warehouse level can be done in the next steps. The data warehouse will then consist of a very small number of common attributes (date, time, position) and a huge number of specific attributes for each database entry, there can be tens or even hundreds of attributes for sensor data. The huge number of attributes can lead to some implementation and performance issues. Columns are used in traditional databases to store attributes so there will be hundreds of mostly empty columns. It may not be effective concerning allocated disk space and memory. Big data technologies, especially column databases are designed and intended for this type of tasks.

3.13. The Extract Task

Extract tasks are to be run periodically; typical business intelligence process runs ETL during the night, which might not be sufficient in the military environment especially on the tactical level. The data extraction interval could be hours or online business intelligence should be employed. Big Data technologies, especially streaming databases are designed and intended for this type of tasks.

Data extraction details will be discussed in the next paragraphs:

CSDs

Data extraction from CSD can be implemented on the top of the AEDP-17 and AEDP-19 services. The query service specified in AEDP-17 uses Catalogue Entry Data Set, which can be used as

an input format for the extraction task. In that case, the extraction task will be universal for each standard based CSD. On the other hand, the web service interface is used so the extraction task does not have to be optimal from a performance perspective. Direct access into the underlying database should be much efficient but it will not be universal as an internal implementation of underlying CSD database differs.

The COI services specified in AEDP-19 to manipulate organization, requirement, priority, task, request and GAOI uses XML structures, which can be used as an input format for the extraction task; there are about 150 entities used. The extraction task will be universal for each standard based implementation as the underlying SPS++ service is content-agnostic. Direct database access is not an option in that case as SPS++ entities are not bound with its type and COI services must be used. On the other hand, AEDP-19 defines its own notification mechanism, which allows spreading out data extraction in the time and thus improving performance.

NSILI defines a synchronization mechanism so the server's topology must be taken into account in the extraction task. It must be specified from which CSDs are data extracted to avoid duplicities and unnecessary extraction of the data. Another approach would be to build a special instance of CSD, which will be synchronized with other CSDs as their copy in read-only mode. The extraction task will be run only on this specific instance so it can utilize direct access into the underlying database and thus provide optimal performance.

NVG

Operational Pictures are stored as NVG files on the file system or in the database and those can be read with the extraction task. The web service interface defined to publish and retrieve NVGs can be also utilized for the extraction task.

The extraction task needs to access NVGs from all the mentioned resources. There could be also built read-only NVG server, which will aggregate NVGs from different NVG sources (servers, files, databases) and notify the extraction task in the case of new or changed NVG.

APP11

An exchange mechanism is not defined for APP11 messages so they can be stored in files, databases or messaging queues. The extraction task needs to access all those storages and to handle the complexity of messages as standard defines more than 400 message types which can be stored in two different formats, XML and slash-separated file.

Proprietary databases and file systems

The standard database connector should be used to extract data from proprietary databases. The definition of the extraction task needs to be done for each individual data source by the source database definition. As the database definition is proprietary there might be legal, technology and other obstacles, which might make the extraction task more complicated or even impossible.

The extraction from the file system is a very similar task, significant difference would be that the parser of the file structure needs to be incorporated into the chain of ETL processes. Parsing of XML or CSV files is mostly trivial or similar to database extraction but there are more complex and/or binary data formats used.

Imagery and video databases and file systems

Imagery and video files are a good example of complex binary file formats where the complex parser needs to be employed. Common ETL tools mostly do not support binary formats such as NSIF or EXIF so user-specific code needs to be implemented. It needs to be considered that parsing of binary structures might be time-consuming.

CESMO network

The concept of CESMO is based on platforms, which periodically contribute to the sensor network. All assets connected into CESMO network are real sensor systems so the connection of read-only data consumers is not supported from the operational perspective although it is technically possible. For that reason, CESMO should not be connected directly to the extraction task; rather some ESM proxy system should be used. This proxy ESM system would collect, filter and aggregate raw ESM data and store them in the ESM database, which would be a source for the extraction task.

3.14. Transform and Load Tasks

Data extracted from different data sources need to be transformed into data mart data model (the transform task) and then loaded into data mart itself (the load task). Data from multiple data marts can be also processed into the overall ISR data warehouse. Transform and load tasks are standard functionality of data marts and data warehouses, so its analyses and design are out of the scope of the article, only a few notes are mentioned.

Many parameters for those tasks, such as time of jobs execution, frequency and period of jobs, error recovery policies, executed actions etc. should be allowed to be configured by a user.

The transform task is typically covered by mapping tool, which declarative prescribes mapping of input data structures to output structures. This mapping can be defined directly in the source code or industry standard based mapping such as eXtensible Stylesheet Language (XSLT) can be used. Datamart implementations utilize a combination of those approaches and powerful GUI enabling the visual mapping of data structures is available to users.

The duration of the load task might take a lot of time as huge volumes of the data are being stored. Some optimization can be implemented on the database level as well as time-intensity could be also covered on the organizational level. For example, spreading activities during the whole day can be considered.

3.15. Visualization Tools

The final step of a building data mart is the design of the presentational layer for end-user. Most BI tools provide this kind of functionality as an integral part of the toolset. Set of dashboards, tables, graphs are typically available to the end-user. The goal is to enable to visualize underlying data in user friendly and easy to understand manner. Some practical observations and experiences with selected tools are presented in the practical part of the article.

3.16. Data Marts and the Tactical Network Limits

Limits of the tactical network must be taken into account in the case that data mart implementation and topology is designed at the military environment. The tactical network cannot be expected as reliable and it could be limited by low bandwidth, high latency, communication windows and distributed topology; mash-up networks need to be also considered.

The data mart should be implemented only on that organizational level where it makes sense. A higher level of command would be an appropriate level, while sensor level would be probably inappropriate. Anyway, carefully evaluation of a data flow is needed for the proper design of data mart topology.

3.17. The Big Data Tools to Process ISR Data

Some issues remain even in the case of using BI tools for ISR data processing; those issues cover:

- Extract phase is typically run once a day, in a given time.
- Streaming nature of sensor data.
- Wide and fuzzy data sources.
- Multimedia data processing.
- The volume of the data.
- Office documents and other unstructured data.

The concept of Big Data can be used to deal with those issues. The nature of the ISR data and identified issues of its processing satisfies already mentioned characteristic of Big Data described by 5Vs. Following technologies can be utilized to mitigate listed issues: Not Only SQL databases (NoSQL), Map-Reduce algorithm, In-memory computing and Streaming databases.

3.18. NoSQL Databases

NoSQL databases are a wide set of technologies and approaches solving or improving selected issues of relational databases. One of the primary impulses for NoSQL movement was the beginning of massive distributed databases and applications on the internet. NoSQL databases include key-value databases, document databases, column databases, and graph databases to name the most significant ones.

NoSQL databases are employed by Big Data techniques or products as an underlying layer and enabler thus they are evaluated in the following chapter of the article.

3.19. Map Reduce

Map-Reduce represents a universal way to parallelize the computation. Map-Reduce is a combination of two functions, map and reduce. Input data are split into chunks based on key-value pairs. Those chunks are distributed to mapper components, mapper component execute given task, which is written in the map function. The output of the map function is collected and grouped by the controller according to keys in the key-value pair. Then reducer functionality is executed and finally, all values are combined into the result. [36]

Development with Map-Reduce principle means split code into map, reduce functionality, and define rules for distribution input data into chunks. Coordination and synchronization of execution map and reduce tasks, data distribution and collection of results is managed by appropriate Map-Reduce framework.

Apache Hadoop is an open-source implementation of Map-Reduce principle and it is intended to process, store and analyze a huge amount of distributed and non-structured data. Although is Hadoop the key technology for the Big Data, Hadoop and the Big Data are not equal. [37]

Hadoop ecosystem consists of more connected projects including Hadoop Distributed File System (HDFS), MapReduce framework, NoSQL storages Cassandra and HBase and other components. HDFS [38] is a distributed file system intended to utilize common (utility) hardware so it was designed to be fault-tolerant to HW and network faults. MapReduce framework is a computational layer enabling parallel execution of computation in each node. Results of the computation are aggregated and stored in the storage layer (HDFS). All those components form an ecosystem enabling vertical scaling; each layer is implemented in a specialized product, which can be easily replaced.

3.20. In-Memory Databases

In-memory databases offers very fast processing of data, over 100.000 operations per second on a single machine. The volume of processed data is limited by the size of RAM, another downside is that data can get lost between subsequent disk flushes (e. g. due to server crashes or by losing power supply). Due to those facts, in-memory databases are recommended to be used on the strategic or operational level, not on the tactical level, thus In-memory databases are out of the scope of the article [39].

3.21. Streaming Databases

Streaming databases are intended to process the data which are streamed continuously without the option of being available for long periods; so the query processor can only respond to queries that have been previously registered with it and can produce results for the data stream by looking at a portion of the stream available within a certain window. Another use case for streaming databases is a situation when the query is executed in parallel with incoming data processing so returned data does not contain data just received. [40]

An alternative to the streaming database could be streaming platform such as Apache Kafka. The streaming platform allows publish and subscribe to streams of records, similar to a message queue or enterprise messaging system, store streams of records in a fault-tolerant durable way and process streams of records as they occur. [41]

Some ISR data have streaming nature, especially COMMS-ESM data, TDL etc. Even so, streaming databases are out of the scope of this article.

4. Building Multiple ISR Data Marts

Selected ISR data and its main characteristic, BI principles and Big Data technologies were introduced in the previous chapters. In this chapter will be proposed how to utilize BI approach to build the ISR data mart. The universal ISR data warehouse will not be built, only specific data marts for each individual area with a focus on EW data, ISR products, ISR operational pictures and operational diary as an overview of ISR tasks.

Data marts were built with the utilisation of RapidMiner Studio, an open-source software platform for analytics teams. The

tool is used for data preparation, machine learning, and predictive model deployment. To achieve that functionality, the tool contains about 400 operators for data manipulation enabling load data from multiple sources, transform and process them and visualize the resulting output.

4.1. The Data Mart for Electronic Warfare Data

The physical nature of radio signal propagation and other factors such as reflections, terrain conductivity, time of day, weather, etc. make the processing of electronic warfare data difficult and challenging. Another challenge is that radio transmission or broadcasting on fixed frequency or band is not widely used as it is easy to monitor, jam and deception by the enemy so sophisticated methods such as frequency hopping, direct sequence, chirp, time-hopping etc. are used instead. Frequency hoping will be considered in the following experiments.

Frequency hopping is a method of transmitting radio signals by rapidly switching a carrier frequency among many frequencies using a pseudorandom sequence known to emitter and receiver only. In practice frequency hopping means separation of one (logical) radio transmission into a huge amount of very short (2-300 milliseconds) physical transmissions on different frequencies. The activity detector does not know parameters of the pseudo-random sequence so it is not possible to determine to which transmission the detected activity belongs, if any, or if it is burst, interference or disturbance. If the emitter, detector or both are moving, the detected frequency can be changed due to the Doppler Effect. [42]

Due to aspects of the real environment, an activity detector or direction finder will produce a lot of data including bursts, disturbances, interferences, reflected signals, fake signals etc. Captured data may look randomly on the first view so further analysis of data is needed. Physical aspects need to be taken into account for these analyses so an experienced operator is needed. Alternative methods based on data mart implementation will be evaluated to reduce the need for operator skills, one example could be employing histogram to analyse DFs [43].

Table 4: The sample of generated data.

Frequency	Quality	Level	Detection Start	Duration
64566928	80	88	2020-06-13 13:34:03.642	10
65449040	90	91	2020-06-13 13:34:03.652	10
66397251	3	92	2020-06-13 13:34:03.662	10
67477144	93	5	2020-06-13 13:34:03.672	10
64161124	83	92	2020-06-13 13:34:03.682	10

Following part of the experiment focus on analyses of detected activities. The first step of the building data mart is to define the data model as different sensors use different sets of attributes. The proposed data model for detected activities consists of (carrier) frequency, quality (of detected signal), level (of detected signal), date and time of the detection and duration of the transmission. A random set of activities was generated in a proposed logical data format, the sample of generated data is shown in Table 4.

The generated set of activities simulates multiple frequency hopping transmissions on different bands including bursts and disturbances. Multiple communication scenarios were tested, in the presented example are two frequency hopping broadcasts within one minute frame; one broadcast is in band 63-68 MHz with duration 10 milliseconds of one physical activity and the second one is in the band 66-73 MHz with duration 200 milliseconds of one physical activity.

Both transmissions partially overlap and random disturbances, noise and bursts are added in the band. The different activities/bursts ratio in the sample data were simulated, the number of activities, bursts and its ratio is shown in Table 5. The volume of generated data was limited to about 5000 to 10 000 thousand rows, which is the limit of a free version of RapidMiner Studio.

Those sets were loaded into RapidMiner Studio to be analyzed and visualized. Basic statistical analysis such as average of individual parameters (frequency, duration, quality) are not useful at all but histogram can be used for a basic overview of data distribution for quick identification of two bands with the most significant traffic as demonstrated in Figure 7.

Table 5: Activities/bursts ratio for a different set of data

Activities	Bursts	Sum	Burst/Activity Ratio
3170	32	3202	1,05%
3185	162	3347	5,1%
3148	320	3468	10,2%
3169	1578	4747	49,8%
3163	3243	6406	102,5%

On the other hand, as the number of bursts increases, activities/bursts ratio also increases and as a result, the histogram became much less clear as demonstrated in Figure 8 for 50% activities/bursts ratio.

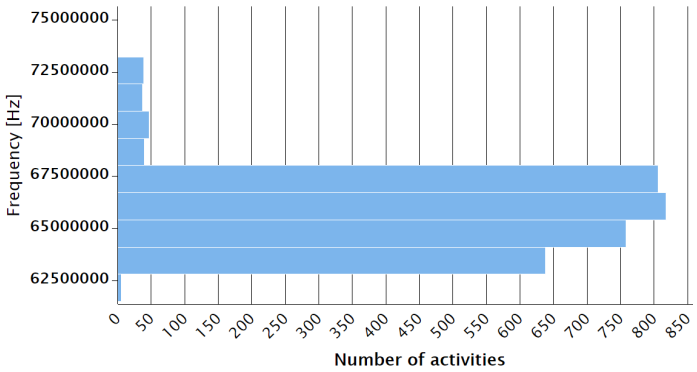


Figure 7: Frequency histogram for sample data with 1% activities/bursts ratio

Distribution of frequencies in the time can be seen on the scatter diagram, examples are shown in Figure 9, 10, and 11 for different activities/bursts ratio. The colour represents the duration of the activity, which can help to analyse data visually.

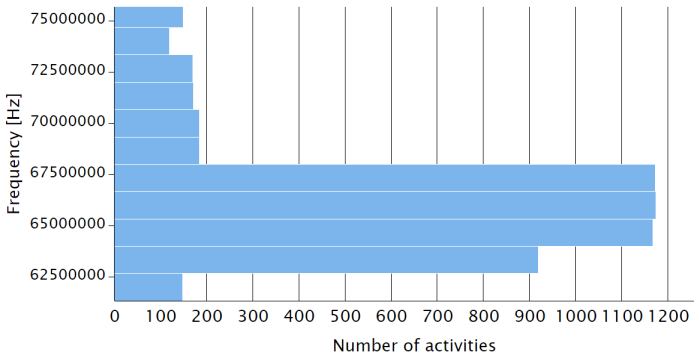


Figure 8 Frequency histogram for sample data with 50% activities/bursts ratio

The data with activities/bursts ratio higher than 10% are quite messy, so it must be filtered in the tool. All activities with quality or level lower than 70 are cut off, the result is in Figure 12 and the resulting picture is much clear to see the relevant activities.

Note: Despite all the data were generated randomly, the output seems to be quite regular and it will be expected that real data are less regular but real measurement data are classified. Similar kind of data analyses and visualization could be done for DF data where azimuth will be used as another dimension for visualization.

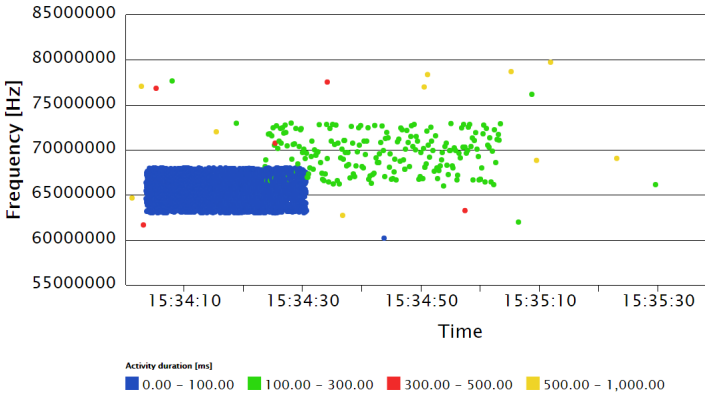


Figure 9: Scatter diagram for the original data with 1% activities/bursts ratio

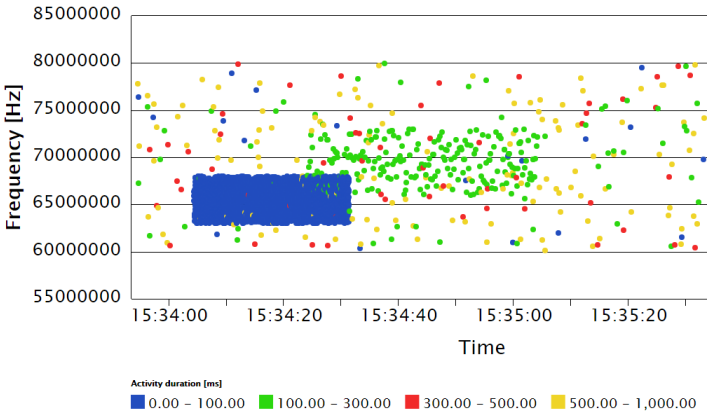


Figure 10: Scatter diagram for the original data with 10% activities/bursts ratio

The main benefit of the presented approach is its easy ability of the graphical presentation and visualization. Although the basic graphical overview of the radio spectrum is an integral part of a sensor controlling SW, its main purpose is to control the sensor, not to provide advanced data analyses.

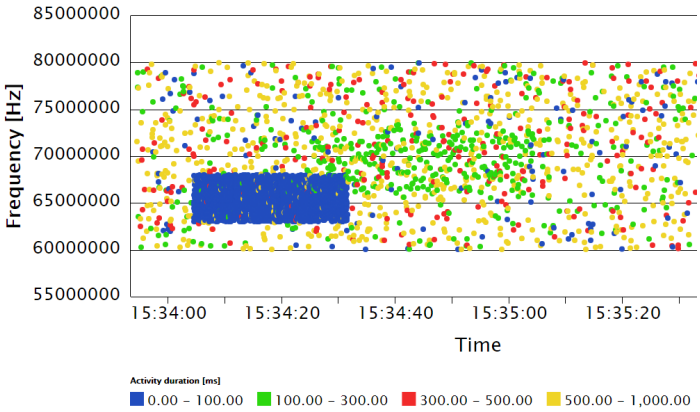


Figure 11: Scatter diagram for the original data with 50% activities/bursts ratio

Moreover, sensor controlling SW is typically tightly coupled with the sensor's data model (and capabilities) so it is hard, or even impossible, to utilize it for processing and visualization of data from different sensors.

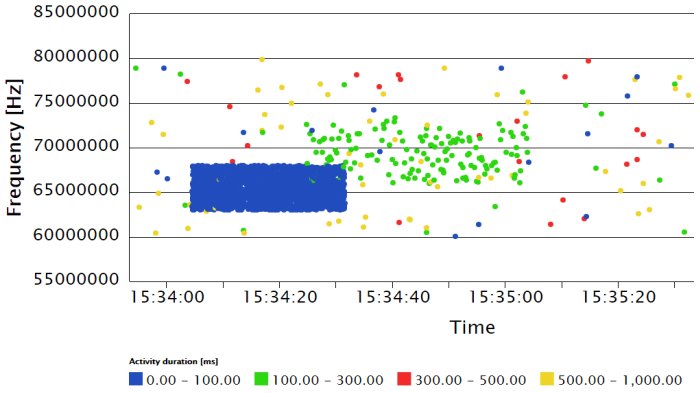


Figure 12: Scatter diagram for the filtered data with 50% activities/bursts ratio

Mentioned disadvantages could be eliminated by the implementation of the data mart and utilisation of its visualisation tools. Those tools enable to load the data from different sensors, to transform them into a unified data model, to clean and filter them and finally to visualize the results. It allows performing much complex data analysis then any sensor controlling SW can with lower effort. Visualisation tools are highly and easily configurable so a different view of the data is easy to achieve. On the other hand, all analyses must be done concerning the physical nature of detected activities and radio waves propagation as well as knowledge of the operational and tactical situation.

4.2. ISR Products Statistics

The common set of metadata for ISR products defined by NSILI includes: ISR product status, publisher, source library, date and time of modification, security (classification, release-ability), ISR product type, mission identifier, language, description, related geographical area (country code or geographic reference box) etc. There was generated a random set of metadata for ISR products in the experiment. Most of the generated ISR products were imagery products, the rest were random products. All mandatory attributes were generated, optional attributes were set optionally. Values of some attributes were set with typos to simulate real data.

The generated set of metadata was load into RapidMiner Studio and processed. In this case, unlike the previous experiment, basic statistics such as the total number of products and the number of different product types could be beneficial, see Figure 13. Note: Number of documents is in logarithmic scale in figure.

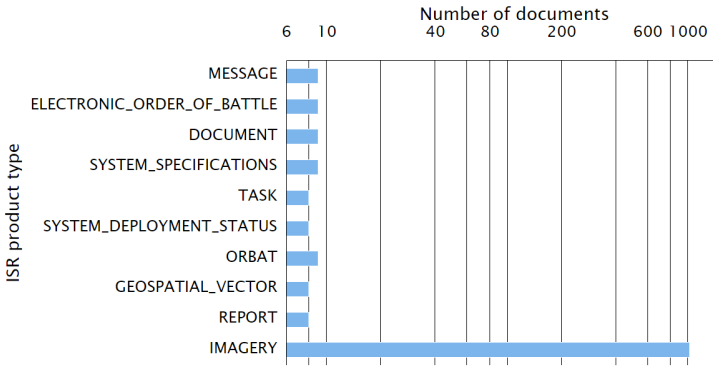


Figure 13: ISR Products types and its number

More advanced statistics were also evaluated, ISR products were grouped by Language and Type, the output is shown in Table 6. It can be easily seen that many imagery products have not set Language attribute, which could be an indicator of the low quality of input data. This observation is an example of how this kind of analyses could easily identify issues in the data and help to improve the process of data collection and processing.

Table 6: The example of grouping ISR products by Language and Type

Language	Type	Number of records
CZE	IMAGERY	511
null	IMAGERY	414
FRA	IMAGERY	37
ITA	IMAGERY	31
ENG	IMAGERY	31
CZE	EOB	7
CZE	DOCUMENT	7
CZE	MESSAGE	6
CZE	REPORT	5
CZE	GEOSPATIAL_VECTOR	5

Queueing three processes generated the report shown in Table 6: data load, aggregation and sort. The chain of data processes is shown in Figure 14, which demonstrate how is data processing managed within RapidMiner Studio.

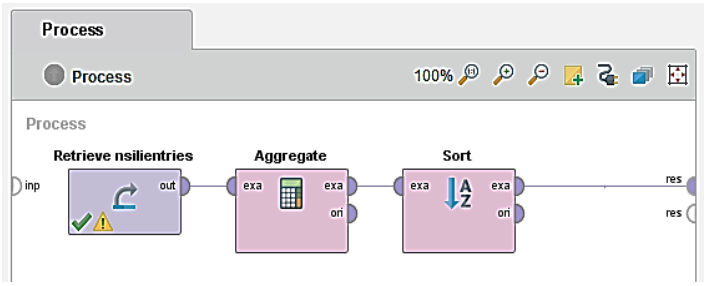


Figure 14: The example of processes design

The data mart built on top of ISR products can be used to generate ISR products statistics. Those statistics and reports to improve collecting tasks and their data quality. The missing data or incorrect values are easy to identify in reports such as in Table 6. The RapidMiner Studio allows drilling down the data to identify the original source of incorrect data. In contrast, NSILI defines the search functionality via its query language only and there is no standard way to see such qualitative and quantitative criteria.

Another benefit would be the improvement of collecting process based on the statistics. The most of ISR products in the shown example were originated from imagery intelligence, based on this simple statistic can commander request data from another intelligence discipline to verify or refute the information by another source.

4.3. The Operational Picture

The operational picture can contain tens or hundreds of battlespace objects such as friendly, enemy and neutral units. In this case, the data model of the data mart would be based on Position, Unit identity, Dimension, Status, Function, Size of the unit, additional modifiers and other attributes. The proposed set of attributes was created as a generalization of the data models of individual military symbology standards. Operational pictures can be load and transform into the data mart, only challenging operation during this step is parsing of military symbol codes. Following analyses, presentation and visualization would be based on the same or similar principles as already presented.

The benefit of BI approach in this scenario is a display of quantitative indicators derived from COP. Those quantitative indicators are not displayed in the COP graphical representation, so their explicit calculation brings new information to the operator. The issue here is that especially the enemy's situation is based on reconnaissance output so it might not correspond to reality.

4.4. The Operational Diary

The operational diary keeps track all activities of the unit and should contain all tasks, requests, and relevant reports. As a side effect, it enables to verify that all RFIs were answered in the given time, the reliability of the sensor can be tracked as well as a response time of the subordinate units, their efficiency etc.

The benefit of BI approach in this scenario is the ability to monitor the performance of units based on automatically tracked tasks and reports. The data model of a data mart would use attributes such as the task and report status, the date and time of creation, the expected time of reporting, the real-time of reporting, collecting platform etc.

The real tactical situation must be taken into account when the operational diary is evaluated. No relevant information might be tracked from tactical reasons or due to the communication infrastructure limitations and issues.

5. Big Data to Process ISR Data

Selected Big Data technologies were evaluated for ISR data processing, especially document databases for metadata storage and Hadoop for ISR data synchronization.

5.1. Document Database as NSILI Metadata Storage

Document databases are an evolution of simple key-value stores, which use the key-value tuples. The key is an identifier of record and the value is content of record that can be both structured

and unstructured. One logical entity can be stored multiple times, each one is optimized for a different type of a query which is very efficient for queries but leads to a rise of the volume of space needed. [44]

Document databases extend this approach with the possibility of structured document storage. Another advantage of a document database is its schema-less nature, which means that structure of stored documents is not validated on the database level so different data structures can be stored within one table.

The experimental CSD implementation with the document database as an underlying layer for AEDP-17 Publish/Query services and AEDP-19 SPS++ services was evaluated and discussed in [45]. The conclusion was that document database usage raised significantly flexibility of the solution as it enables to store any relevant document independently of its content and version. The implementation time and workload were also dramatically lower.

On the other hand, the disadvantage of NoSQL technologies is the fragmentation of its implementation where each particular product is specialized to its specific purpose and/or use case. There is also a lack of standardization so it is very difficult or even impossible to migrate from one NoSQL solution to another.

5.2. Hadoop for ISR Data Synchronization

CSD utilizes two technologies to share and disseminate ISR products and its metadata, CORBA and web service, both of them have some disadvantages.

CORBA as a technology is already obsolete, it is not supported in modern programming languages and it would become obsolete in the future edition of NSILI. Moreover, CORBA protocol is binary so security mechanism based on XML security labelling is not applicable. Real experiences show that CORBA implementation of data synchronization is slow as CORBA is an implementation of Object Request Broker with a lot of overhead functionality from the perspective of CSD.

Web services, in contrast, solve those issues but NSILI does not define all functionality, especially synchronization features are not defined. It is not a problem of web service technology rather of NSILI standard itself.

Although synchronization via Web services is not standardized, it is possible to utilize Web services for synchronization CSDs. Synchronization based on Web services must handle topology of CSDs network, data duplication etc. The use of Hadoop to manage this task is proposed. The basic idea is to export data via Query service to Hadoop File System, then to distribute it to different nodes and finally import the data into CSD via Publish service. Batch export and import need to be implemented which is an implementation detail.

Import or Publish services should handle duplicity. Circle synchronisation is forbidden in NSILI and according to the standard, it is a configuration issue. CSDs synchronisation is a directional point to point and the administrator is responsible for proper configuration and avoiding the circle dependencies. The same rule needs to be satisfied in the case of proposed Hadoop based synchronisation.

Hadoop would be used in the way, that all CSDs has the same data or the same subset of data exported by individual CSDs. One CSD would export for example only IMINT data and do not export EW data, so all CSD in the network will access IMINT data. The data would be separated to those, which should be synchronised with all participants of the CSD network and those data that should not be synchronised. The set of products can be easily configured by the query definition.

The advantage of Hadoop utilisation would be a much easier configuration of synchronisation network and synchronised products. The map-reduce mechanism is not used in that case, only advantages of a distributed file system are utilised. The synchronisation implemented in this way would be resistant to network or hardware failures which is provided by Hadoop itself. This type of the synchronisation over distributed file system would be applicable for other data distribution as well, including EW data etc. but limits of the tactical network need to be taken into account.

5.3. Map-Reduce for ISR Data

Processing of the ISR data can be seen as Map-Reduce task as data collected on sensor level are reduced and distributed to a higher level on command, where are combined with data from other sources, reduced and so on. Although the idea is similar, human interaction is expected, so the process is not fully automated to be understood as Map-Reduce task.

Based on experience, distributed computing is not ideal for the tactical network. The requirement is that systems should work even in the case that connection is lost, some nodes are temporary or permanently not available etc. Distributed computing and especially MapReduce is a specific approach to computation and only selected tasks can benefit from it, especially those which can be easily parallelised. The infrastructure for parallelisation and data distribution is needed which is not a case on the tactical level. Nevertheless, future research of utilisation MapReduce principles is recommended. Big Data principles are applicable for processing the data of individual intelligence disciplines while Map-Reduce principle seems to be not so beneficial on a tactical level due to infrastructure reasons.

6. Conclusion

The ISR process, principles of BI and Big Data technologies were introduced in this paper. Areas in ISR environment where BI and Big Data approach can be beneficial were identified and a way to build ISR data mart was proposed. Experimental data marts were built and loaded by data preparation (data from practice is not possible to get or it is not available due to security reason), but the possibility of data processing, analyses and presentation remain without problems. The utilisation of the document database for ISR products library implementation and Apache Hadoop for its synchronisation was proposed.

Some other promising Big Data technologies were identified and proposed for evaluation in future works. Those technologies include streaming databases and streaming platforms to process sensor data and MapReduce principles.

Proposed utilisation of Big Data technologies is also applicable to other intelligence disciplines, especially OSINT which is based on research on open sources such as newspapers, internet pages, television broadcast etc. would benefit of all aspects of Big Data technologies. Similarly, IMINT analyses would benefit from presented technologies. In any case, the limits of tactical networks must be taken into account when implementing Big Data technologies.

There were demonstrated an advanced BI business analyses that are not used in ISR systems; it is quite original solution. It was also shown that all proposed analyzes have to take into account the real data from military operations, exercises and missions. Regarding this result is awaiting that the domain experts, operators and the data analyst in military environment have sufficient knowledge not only in monitoring operations, but they are able also prepare appropriate results using BI, AI and other relevant technologies.

Acknowledgement

Mr. Novak was participating of development Integrated SoftWare Module for Command, Control, Communications, Computers, Intelligence, Surveillance, Targeting Acquisition and Reconnaissance (ISWM C4ISTAR) project in 2014-2016 focusing on ICT (Information and Communication Technology) support of JISR (Joint ISR) cycle and interoperability of ISR products through STANAG 4559 NSILI compatible implementation.

Mr. Burita presents the results of the research as a part of the project [46] at the Faculty of Military Technologies of the University of Defence, Department of Informatics, and Cyber Operations.

References

[1] A. Novak, L. Burita, "Business Intelligence and ISR Data Processing" in Proceedings of the International Conference on Military Technologies 2019 - (ICMT). Brno, Czech Republic: University of Defence, 1-8, 2019.
[2] OODA Loop [Online]. [Cit. 2020-03-12]. Available at https://www.toolshero.com/decision-making/ooda-loop/
[3] NATO Standardization Office, AJP-2 Allied joint doctrine for intelligence, counter-intelligence and security, 2016.
[4] NATO Standardization Office, AJP-2.7 Allied joint doctrine for intelligence, surveillance and reconnaissance, Edition A, version 1, 2016.
[5] The Global Airborne Intelligence and C2 Community's Annual General Meeting, The Hurlingham Club, London, UK, 2020 [Online]. [Cit. 2020-03-26]. https://www.defenceiq.com/events-airborneisr/
[6] Business Intelligence [Online]. [Cit. 2020-03-15]. Available at https://www.123rf.com/visual/search/9342840
[7] Data Warehousing Solution [Online]. [Cit. 2020-03-16]. Available at http://www.aspiretss.com/services/data-warehousing-solution
[8] OLAP Cubes in SQL Server [Online]. [Cit. 2020-03-17]. Available at https://www.sqlshack.com/olap-cubes-in-sql-server/
[9] CRISP-DM methodology phases [Online]. [Cit. 2020-03-18]. Available at https://www.researchgate.net/figure/CRISP-DM-methodology-phases-Adaptation-of-Chapman-P-3_fig1_318309402
[10] SAS Analytics SW and solutions [Online]. [Cit. 2020-03-20]. Available at https://www.sas.com/en_us/home.html
[11] IBM SPSS software [Online]. [Cit. 2020-03-22]. Available at https://www.ibm.com/analytics/spss-statistics-software
[12] F. L. F. Almeida, "Benefits, Challenges and Tools of Big Data Management", Journal of Systems Integration, **4**(8), 12-20, 2017, DOI: 10.20470/jsi.v8i4.311.
[13] International conference Big Data for Defence, June 23-25, 2020, London, UK.
[14] M.K. Hernandez, C. Howard, R. Livingood, and C. Calongne, „Applications of decision tree analytics on semi-structured north Atlantic tropical cyclone forecasts", International Journal of Sociotechnology and Knowledge Development, **11**(2), 31-531, 2019. DOI: 10.4018/IJSKD.2019040103.
[15] B. Essendorfer, A. Hoffmann, J. Sander, and A. Kuwertz, „Integrating coalition shared data in a system architecture for high level information management", in Proceedings of The International Society for Optical Engineering (SPIE): Counterterrorism, Crime Fighting, Forensics, and Surveillance Technologies II, Berlin, Germany, 10802, 2018. DOI: 10.1117/12.2501861.
[16] A. Kuwertz, D. Mühlenberg, J. Sander, and W. Müller, "Applying knowledge-based reasoning for information fusion in intelligence, surveillance, and reconnaissance", Lecture Notes in Electrical Engineering, 501, 119-139, 2018. DOI: 10.1007/978-3-319-90509-9_7.
[17] Z. Kira, A.R. Wagner, C. Kennedy, J. Zutty, and G. Tuell, "STAC: A comprehensive sensor fusion model for scene characterization", in Proceedings of SPIE, Multisensory, Multisource Information Fusion: Architectures, Algorithms, and Applications, 9498, 949804, 2015. DOI: 10.1117/12.2178494.
[18] C. Bowman, G. Haith, A. Steinberg, C. Morefield, and M. Morefield, "Affordable non-traditional source data mining for context assessment to improve distributed fusion system robustness", in Proceedings of SPIE, Multisensor, Multisource Information Fusion: Architectures, Algorithms, and Applications, 8756, 875603, 2013. DOI: 10.1117/12.2018386.
[19] G.E. Horne, E.A. Bjorkman, and T. Colton, "Putting agent based modeling to work: Results of the 4th international project albert workshop", in Proceedings of SPIE, 4716, 99-107, 2002. DOI: 10.1117/12.474904.
[20] M. Barnell, C. Raymond, C. Capraro, and D. Isereau, "Agile Condor: A scalable high performance embedded computing architecture", in 2015 IEEE High Performance Extreme Computing Conference, Waltham, United States, 2015. DOI: 10.1109/HPEC.2015.7322447.
[21] S. Rogers, J. Culbertson, M. Oxley, H. Clouse, B. Abayowa, J. Patrick, E. Blasch, and J. Trumpfheller, "The QuEST for multi-sensor big data ISR situation understanding", in Proceedings of SPIE: Ground/Air Multisensor Interoperability, Integration, and Networking for Persistent ISR VII, Baltimore, United States, 9831, 2016. DOI: 10.1117/12.2229722.
[22] J. Rajamäki, J. Simola, "How to apply privacy by design in OSINT and Big Data analytics", in 18th European Conference on Information Warfare and Security (ECCWS), Coimbra, Portugal, 2019, 364-371.
[23] S. Das, L. Jain, and A. Das, "Deep Learning for Military Image Captioning", in 21st International Conference on Information Fusion, Cambridge, United Kingdom, 8455321, 2165-2171, 2018. DOI: 10.23919/ICIF.2018.8455321.
[24] S.P. Wang, W. Kelly, "IT Professional Conference: Challenges in Information Systems Governance, Gaithersburg, United States, 70293032014, 2014. DOI: 10.1109/ITPRO.2014.7029303.
[25] NATO Standardization Office (NSO), AEDP-17: NATO Standard ISR Library Interface, Edition A Version 1, Brussels, 2016.
[26] APP-11 and ADatP-3. What is APP-11 (NATO Message Catalogue) and ADatP-3 (Allied Data Publication 3)? And what is the difference between the two? [Online]. [Cit. 2019-04-14]. Available from: https://systematic.com/defence/capabilities/c2/interoperability/app-11-and-adatp-3/
[27] ADatP-4733 NATO Vector Graphics Specification, NATO Standardization Office, 2017.
[28] Friendly Force Tracking, US-Army Stand-To [Online]. [Cit. 2019-04-16]. Available from: https://www.army.mil/standto/archive_2016-02-24
[29] AEDP-02 NATO Intelligence, Surveillance, and Reconnaissance (ISR) Interoperability Architecture (NIIA), Edition 1, Volume 1: Architecture Description.
[30] NATO Standardization Office (NSO), AEDP-19: NATO Standard ISR Workflow Architecture, Edition A Version 1, Brussels, 2018.
[31] NATO AJP-2.7 ALLIED JOINT DOCTRINE FOR JOINT INTELLIGENCE, SURVEILLANCE AND RECONNAISSANCE. [Online]. [Cit. 2020-06-01]. Available from: https://standards.globalspec.com/std/10031247/AJP-2.7
[32] Information Requirements Management and Collection Management. [Online]. [Cit. 2020-06-01]. Available from: https://moodle.unob.cz/pluginfile.php/46438/mod_resource/content/1/T3-1%20Information%20Requirements%20Management%20and%20Collection%20Management%20%28lecture%29.pdf
[33] Intelligence Studies: Types of Intelligence Collection. [Online]. [Cit. 2020-06-01]. Available from: https://usnwc.libguides.com/c.php?g=494120&p=3381426´
[34] Common Operational Picture Defined. [Online]. [Cit. 2020-06-01]. Available from: 34https://www.coolfiresolutions.com/blog/common-operational-picture-defined/
[35] NATO joint military symbology APP-6(C), NATO Standardization Office, 2011.
[36] What is Map Reduce? [Online]. [Cit. 2020-05-16]. Available from: https://www.ibm.com/analytics/hadoop/mapreduce
[37] What is Apache Hadoop? [Online]. [Cit. 2020-05-16]. Available from: https://www.ibm.com/analytics/hadoop
[38] HDFS Architecture Guide. Online]. [Cit. 2020-05-16]. Available from: https://hadoop.apache.org/docs/r1.2.1/hdfs_design.html
[39] In-Memory Database for Time and Mission-Critical Applications. [Online]. [Cit. 2020-05-20]. Available from: https://raima.com/in-memory-dbms-2/?gclid=CjwKCAjwh472BRAGEiwAvHVfGm2FqIjqdfL5ljAyoDD7JL8jeFJu_fIf1KJNjN2H90vWnma3qKwtuxoCgVoQAvD_BwE
[40] What Is a Streaming Database? [Online]. [Cit. 2020-05-20]. Available from: https://hazelcast.com/glossary/streaming-database/
[41] Apache Kafka® is a distributed streaming platform. [Online]. [Cit. 2020-06-01]. Available from: https://kafka.apache.org/intro
[42] Frequency Hopping. [Online]. [Cit. 2020-05-22]. Available from: https://www.sciencedirect.com/topics/physics-and-astronomy/frequency-hopping

[43] „Communication tools PR4G, Retia Company“, Proceedings of the C2 systems in Ministry of Defence Czech Republic, Brno, 2002.
[44] What is a Document Database? [Online]. [Cit. 2020-06-01]. Available from: https://www.mongodb.com/document-databases
[45] A. Novak, “The Comparison of STANAG 4559 NSILI Compliant Tactical Intelligence Database Implementation in Relational Database and NoSQL Database” in 2018 New Trends in Signal Processing Conference, Demanovska Dolina, Slovakia, 2018, 1-7, DOI: 10.23919/NTSP.2018.8524063.
[46] ZRO209, Project of departmental research: Development of systems C4I and cyber security, Brno, University of Defence, 2016-2020.

Advances in Science, Technology and Engineering Systems Journal Vol. 5, No. 5, 332-341 (2020)

www.astesj.com

Special Issue on Multidisciplinary Sciences and Engineering

ASTESJ

ISSN: 2415-6698

Design and Implementation of Reconfigurable Neuro-Inspired Computing Model on a FPGA

Basutkar Umamaheshwar Venkata Prashanth*,1, Mohammed Riyaz Ahmed[2]

[1]School of Electronics and Communication Engineering, REVA University, Bengaluru, 560064, India

[2]School of Multidisciplinary Studies, REVA University, Bengaluru, 560064, India

ARTICLE INFO

Article history:
Received: 23 July, 2020
Accepted: 12 September, 2020
Online: 17 September, 2020

Keywords:
Bio-Inspired Computing
FPGA
Neuron
Synapse
IP Core

ABSTRACT

In this paper we design a large scale reconfigurable digital bio-inspired computing model. We consider the reconfigurable and event driven parameters in the developed field-programmable neuromorphic computing system. The various Intellectual Property (IP) cores are developed for the modules such as Block RAM, Differential Clock, Floating Point, and First In First Out (FIFO) for the design of the neuron model in Xilinx ISE, with exploration of register transfer logic (RTL) and hardware synthesis using Verilog code. The architecture for design at device level offers the best possible design tradeoff for specific processor architectures and development choices. In this paper we perform algorithmic design of a large scale reconfigurable logical bio-inspired computing model. The proposed algorithm is implemented on Field Programmable Gate Array (FPGA) to develop a neuron model to be utilized in neuromorphic computing system.

1. Introduction

This research manuscript is an extension of work originally presented in *International Conference on Artificial Intelligence and Signal Processing* [1]. The bio-inspired computing is achieved with core building blocks of neuromorphic engineering which mainly constitute circuits and systems and is proposed as structures of spin devices [2].

The above direction opens a new path and induces a key approach for developing bio-inspired algorithms for implementations of bio-inspired algorithm based computing systems [3]. In nature the crucial role of learning and memory is achieved with help of synapses. The synapses which are plastic in nature, is formed with inter cellular connections of neurons, and the combination of these biological structures form the basic building blocks of neural networks [4]. Synapses can change their state based on the neural activity of coupled neurons. The functionality of neurons and synapses is mimicked in hardware by utilizing very large scale integration technology, plays a key role in design of neuromorphic computing systems [5]. The pathway to efficient neuromorphic systems is encoding the neural and synaptic functionalities in an electronic spin. It shows the potentials to exploit energy efficiency, performance, reliability, and magnetization using electric fields, and enhanced memory density of spintronic memory devices [6]. The bio-inspired computing systems is presented, with an aim to establish interaction framework, between two directions of natural system computation and artificial system computation [7]. In the in-memory computing for emerging memory devices, there is no separation between memory and logic, to overcome Von-Neumann bottleneck and also in-memory computing devices are designed with zero-off state power and due to this, they have a distinct advantage of the non-volatile state [8]. The in-memory computing is combined with a high gate or synapse density which enables forming of cross-bar array in the device, which can be easily integrated with CMOS with high density, operating with high current and voltage consuming high dynamic power, with In-memory computing device contains long switching time hence they operate with limited speed and have limited endurance, again the cross-bar in-memory computing is highly parallel, operate with low-power, low cost [9]. The verticals of Cross-bar in-memory computing are bio-inspired computing, deep learning, in-memory logic, chip/data security, architecture, device modeling [10]. The static random access memory latches and capacitors are utilized in a very large scale integrated devices, an architecture to implement strewed memory elements is embodied in this in-memory computing device as depicted in Figure 1 is aimed towards supporting the use of memristive devices as digital and synapse-like memory elements. The key contributions of the research manuscript are:

- Algorithmic design of a large scale reconfigurable logical bio-inspired computing model.
- Implementation of bio-inspired model on FPGA.

*Corresponding Author: B.U.V. Prashanth, prashanthbuv@reva.edu.in

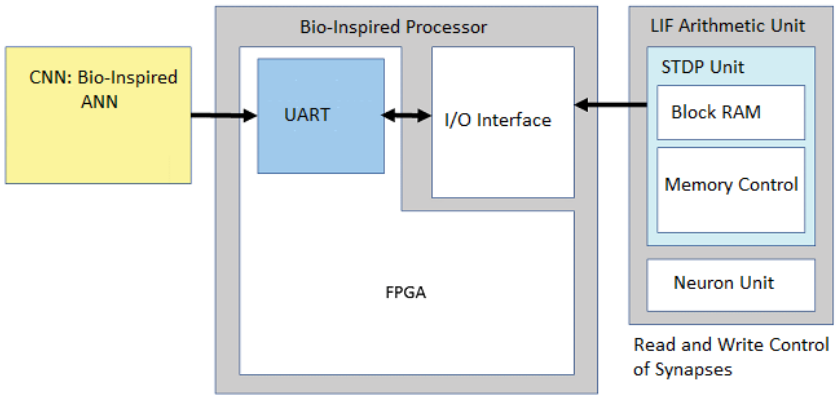


Figure 1: Block Diagram of FPGA based Bio-Inspired Computing System

2. Background

The emerging research architectures which support memory-based computing, exponential performance scaling, which enables mixed mode technology solutions. The problem of establishing the bridge between natural and artificial computation is one of motivation which illuminates the bio-inspired computation in artificial systems [11]. The paradox of programming a bio-inspired computer is the need to figure out the new class of algorithms, we are also missing out some very important basic concepts. The intelligent computational system are initially built with a Boolean logic or functions, next through logical phase, and into semiconductor technology phase, further into computational complexity phase and ends at an experimental computation phase [12]. The lesson learnt here is while dealing with intelligence the first stage is to probe into evolution, complexity, and also thermodynamics which is not an equivalent of a Boolean logic or functions, during the second stage new and novel electronics technology is required which is not an equivalent of electronics technology, which was defined during the computation phase, in the further stage the implementation complexity is not an equivalent to computational complexity, and the final stage is the practical intelligence stage which is also not an equivalent practical computation stage, defined during process of computation [13]. The factor synaptic plasticity, which accounts for the determination of the magnitude of the synaptic weights. The plasticity is also called as the learning of the synaptic junctions which probes the cognitive abilities to the bio-inspired architectures [14]. For analysis, if an experiment is performed considering the circuit with four access transistors to decouple read and write current paths, with the peripheral circuits for timing window, and aimed towards the spike-timing-dependent plasticity (STDP) implementation. Apart from these four transistors, one more transistor named as M_{STDP} is also connected to pre-charge line in the circuit, which is responsible to implement the STDP and this transistor is biased in the sub threshold saturation regime. The gate voltage of M_{STDP} transistor is called as PRE voltage, which starts increasing linearly as the pre neuron spikes [15]. As the post neuron is triggered, the POST signal is activated with the current flows through the device. The current is also known as the programming current , which is the 1 ns duration write current and is exponentially related with the magnitude to the delay factor of pre-neuron and post-neuron spikes. As the STDP measurements are taken between the % changes in the synaptic weights with respect to spike timing difference in (ms) , the synaptic weight is updated which depends on difference in the timing of post and pre neuron spikes[16].

3. Algorithm Design

In this section the design of algorithm is enumerated for a FPGA based large scale logical reconfigurable neuron model.

Algorithm 1: Algorithm for FPGA Top Level Module

```
Result: Top Level module of IP Block
Model initialization;
while Apply Clock Signal do
    Instantiate Clock Signal;
    if FSM Instantiation then
        Select RAM;
        Select MATMUL
    Else
        Compute:
        Communication Unit;
        Initialize UART;
        Initialize FIFO;
    End
    Emulate layer of network;
    Read Weight RAM;
    Load input RAM;
    Process data as perceptron;
End
```

To realize the spiking neural functionalities by utilizing the leaky-integrate magnetization dynamics [17]. To enable the abstraction of the magnetic functions as stochastic spiking neurons, the parameter required is the thermal noise which is prevalent in nano-magnets at certain temperatures which are not equal to zero [18]. The reconfigurable neuron model consists of two units such as finite state machine unit (FSM) unit and communication unit. The Algorithm 1 illustrates the abstract view of the top level model hierarchy. The IP core module as described in Figure 2(a) emulates the layer of the network and loads data (weight or input) and then process the data to obtain the synapse weight output as depicted in Figure 2(b). Further the flag signal is controlled in

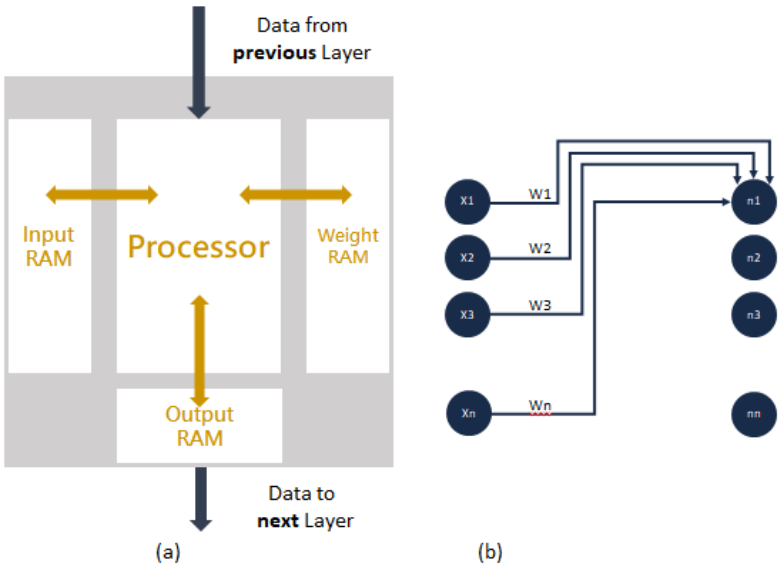


Figure 2: (a) IP-core module (b) Details of synapse weight information

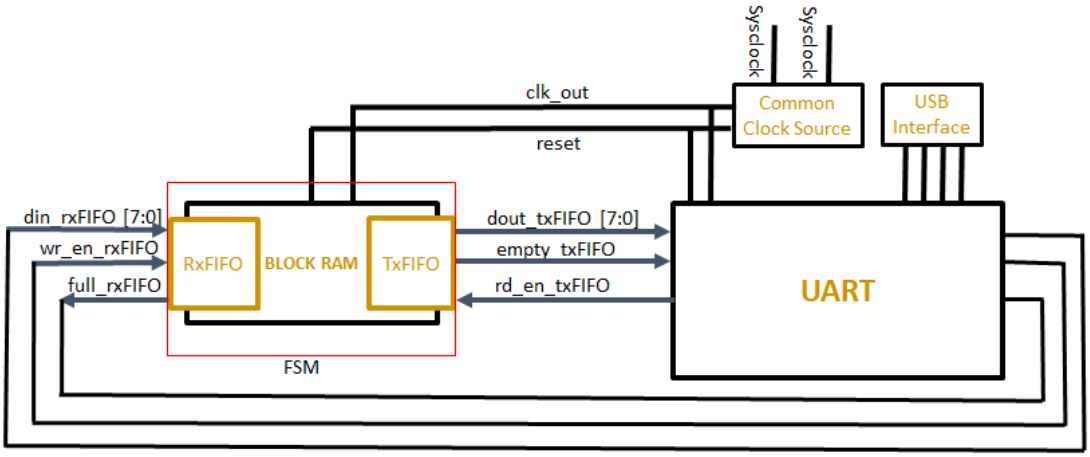


Figure 3: RTL schematic of Top Layer with sub-module Read/Write Memory

order to make the FSM to halt while the other sub programs are running [19]. The layer of the network is mimicked with reading the weight information from weight RAM, along with load input data from input RAM and processing the data as a simple neuron model [20]. The 8 bit parameter data width is applied as input to FPGA from data floating unit of USB module and from FPGA the parameter data is passed to FIFO block. The input data is further connected to din of input RAM, along with connecting row index to address of input RAM, and connection of read data to input of outgoing FIFO [21]. The outputs of last add operation is directly wired to the resultant RAM. The data packets are segmented at this stage and the information of data packets are available at the next stage. In the next stage the packet data is segmented into respective component registers. Write the input and weight data to padded variables when flag is high. The Figure 3 illustrates the above design process as sub-module read and write memory with FSM unit (with block RAM, Transmit FIFO, Receive FIFO) and universal asynchronous receiver and transmitter (UART) unit. Further also describes the communication link between FSM unit and the UART unit. Here the data sent from universal serial bus (USB) transforms to parallel data and is then sent to the FIFO for processing [22]. The Figure 3 can be considered as register transfer logic (RTL) schematic of the top layer module.

4. Implementation

In this section the implementation details of large scale reconfigurable digital bio-inspired computing model is described. The algorithm described is implemented on the hardware FPGA environment satisfying the requirement of hardware combined with the software co-design concept. The hardware used is FPGA ALTERA DE2 with a cyclone chip.

The Figure 4 represents the topology of the FSM of a RAM read/write process with FIFO pop data in sequence. The complete architecture of the bio-inspired computing system consists of system controller based on an advanced reduced instruction set computing (RISC) machine (ARM) processor, core-array of two dimensions, and a UART Controller. The interpretation of data is dependent of the order of popping the data. Sub-module MATMUL contains two dot product operations in parallel, which consists of floating point IPs as shown in Figure 5 in the form of

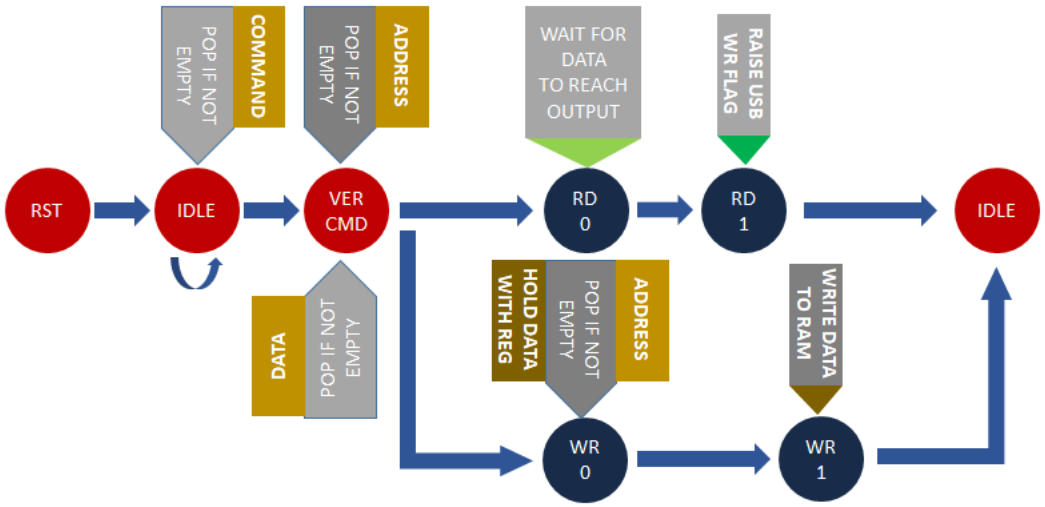


Figure 4: FSM Topology of Read/Write Process

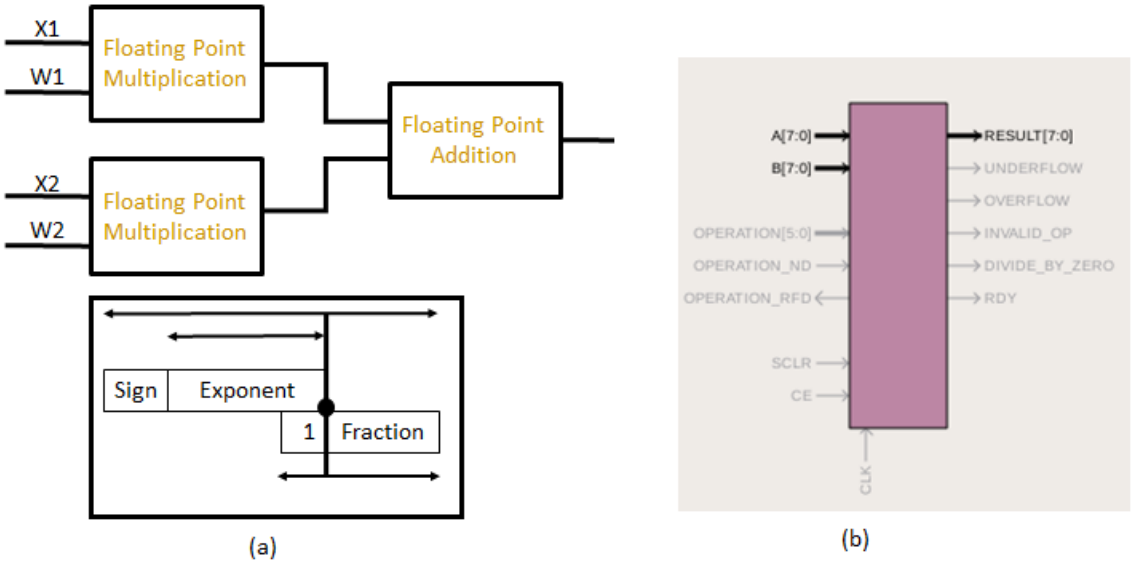


Figure 5: Submodule Dot Product Module/Process

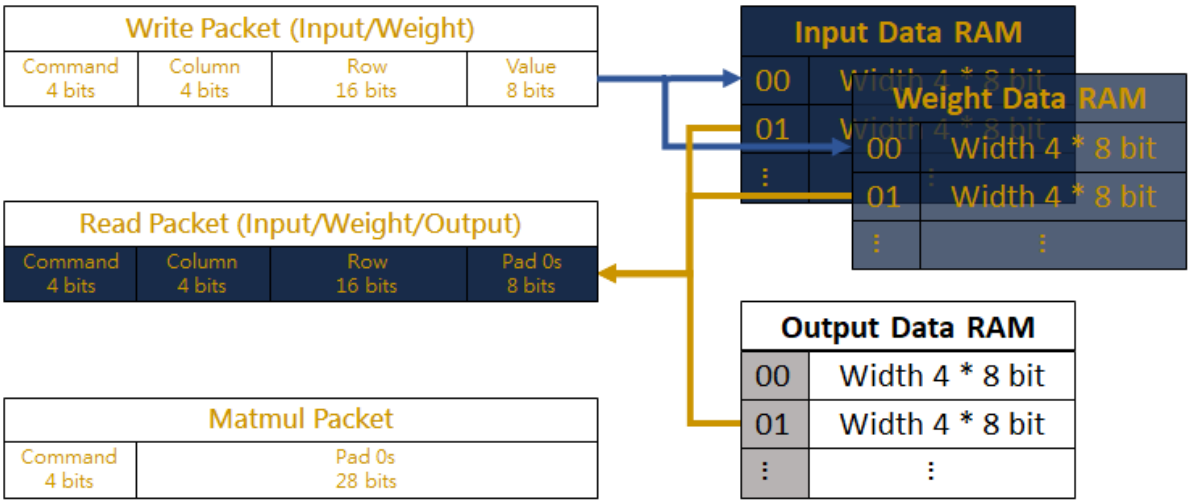


Figure 6: Information Transfer Packet

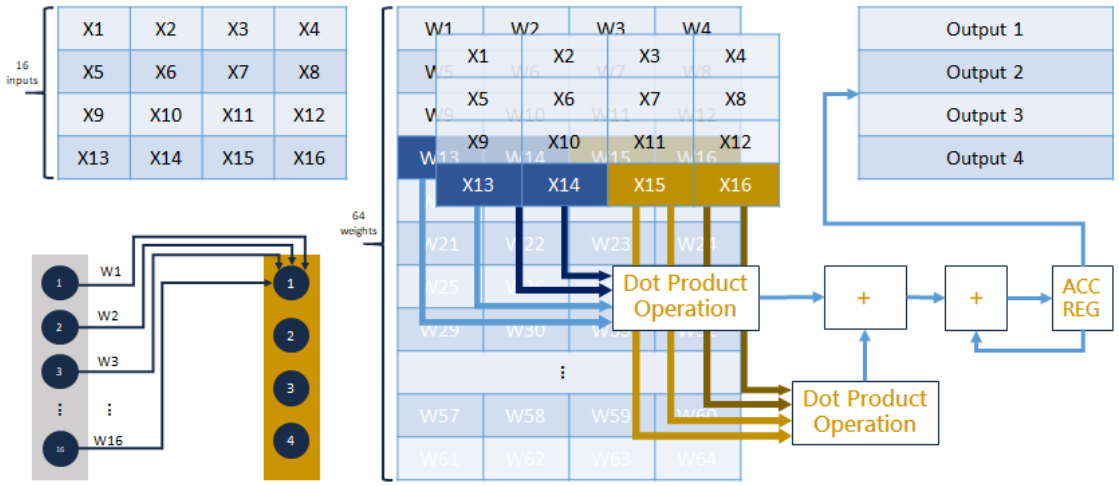
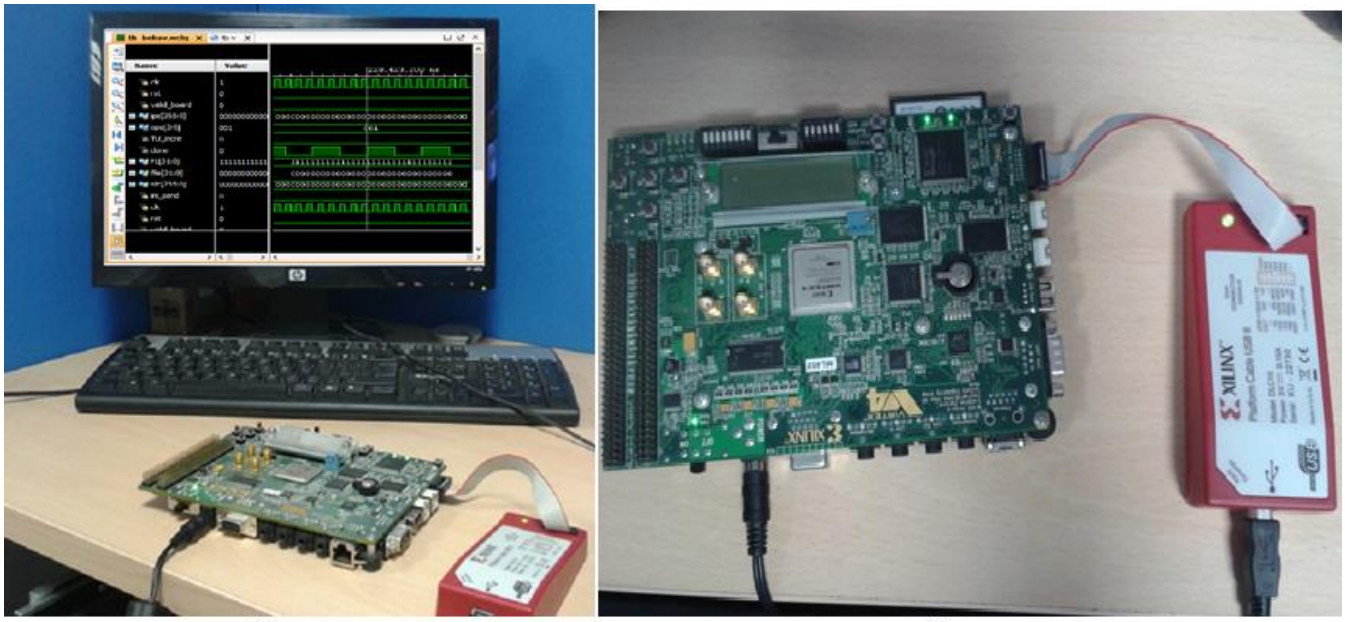


Figure 7: Implementation of a single core consists of 16 inputs and 4 outputs, implying that the weight RAM is 64 rows in depth.



(a) (b)

Figure 8: (a) The bio-inspired computing system setup (b) FPGA ALTERA DE2 Board setup with Xilinx JTAG adapter

The implementation of a single core consists of 16 inputs and 4 outputs, implying that the weight RAM is 64 rows in depth as described in Figure 7. The implementation of bio-inspired computing system is done on Altera Cyclone IV FPGA contained as a part of ALTERA DE2 Board. The VERILOG language was used to program the bio-inspired framework and compiled in Xilinx ISE platform with x86 64 bit CPU executing on Linux Ubuntu 16.04 operating system.

5. Results Obtained

In this section the results obtained with various Intellectual Property (IP) cores which are developed for the modules such as Block RAM, Differential Clock, Floating Point, and First In First Out (FIFO) for the design of the neuron model in Xilinx ISE, with exploration of register transfer logic (RTL) and hardware synthesis using Verilog code are presented.

The Figure 8(a) depicts the complete setup of bio-inspired computing system implementation and the Figure 8(b) represents JTAG adapter connection with FPGA ALTERA DE2 Board. The Figure 9 illustrates the behavioral simulation of developed reconfigurable bio-inspired computing is obtained in Xilinx ISE environment. We can look at output ram data out signal to double check if the data is correct in simulation. The execution is based on vector less activity propagation with peak memory and execution is carried out in Vivado-v-2014.2 FPGA has considerable static power consumption, but normally efficient power is measured as difference in idle state and real-time data processing for the machine.

The equation for obtaining the parameters is described in Equation (1).

% Synaptic Pruning = (Number of Neurons pruned) / (Size of Network x Accuracy x Energy) (1)

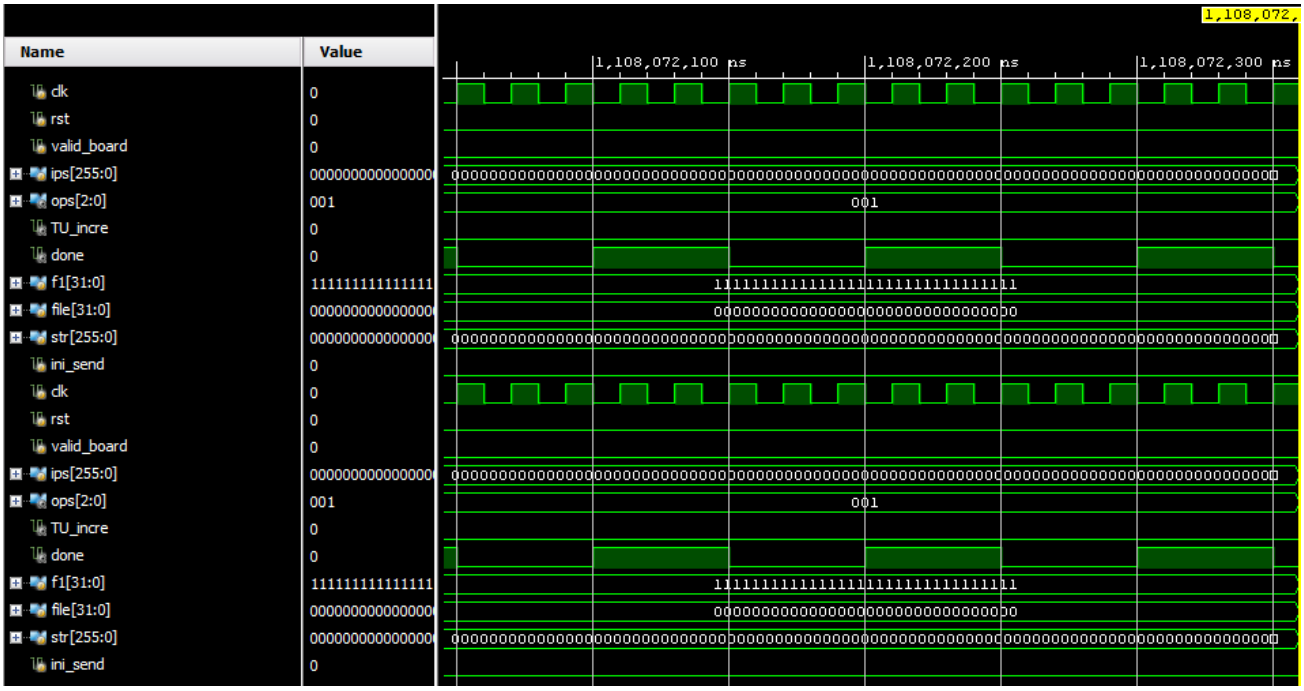


Figure 9: Behavioral simulation of the developed reconfigurable bio-inspired computing architecture

Table 1: Design Trade-off Parameters

Parameters [23], [24], [25]	Existing Neuron Model	Proposed Neuron Model	Efficiency Improvement	Performance Improvement
1. Computational Efficiency	2.3 x Enhanced	2 x Enhanced	0.36 %	89 %
2. Energy efficiency	2.8 x Enhanced	3.2x Enhanced	-	High
3. Throughput	High	High	-	-
4. Accuracy	90.02%	90.4%	1.69 %	90 %
5. Entropy	10% - 25% for 800 Neurons	12 % for 100 Neurons	-	2 %

On the other hand, a poor input output reflects the system glitch at which glue logic in FPGA DE2 board is affected in worst case, as the system changes the incoming events dynamically. The Table 1 depicts the architecture considerations for design at device level and offers the best possible design tradeoff for specific processor architectures and development choices. The parameters are described in Table 1 such as Computational Efficiency, Energy Consumption, Throughput, Accuracy, Entropy are compared with previous work with existing neuron model with the proposed neuron model. It is noteworthy that in the proposed design except LUT all other parameters have the same value for logic utilization post synthesis and post implementation, the reason behind this is the designed system is more of device specific. During Idle mode, the device does not process events and therefore there is no computation. The ADC14DS065/080/095/105 converts the analog data into 14 bit words, but it outputs the data on 1 or 2 serial data lines per channel. The digital output operates at LVCMOS voltage levels except for the serial signals and clock outputs LVDS signals.

These devices operate up to 65 million samples per second (MSPS) in a single lane mode while the higher data rates operate in a dual lane mode, each lane operates at half the data rate to keep the required clock frequencies from being excessive. Using this technique, the FPGA interface can support the highest data rate of 105 (MSPS) with a high throughput as shown in Table 1. The FPGA then will combine the two data streams appropriately to create the correct signals.

The serial data bus uses less board space for the signals, is easier to route and achieves similar data rates to a parallel interface with less wires for data bus. The parallel data bus from the ADC14155 can be connected to the FPGA using an I/O bank configured for 1.8 LVCMOS inputs. The data rate of this bus is 5-155 MHz, which is well within the I/O capabilities of the FPGA.

The designed FPGA module further consists of the blocks required for interfacing an ADC with the FPGA with 3.2x enhanced energy efficiency and 2x enhanced computational efficiency as described in Table 1.

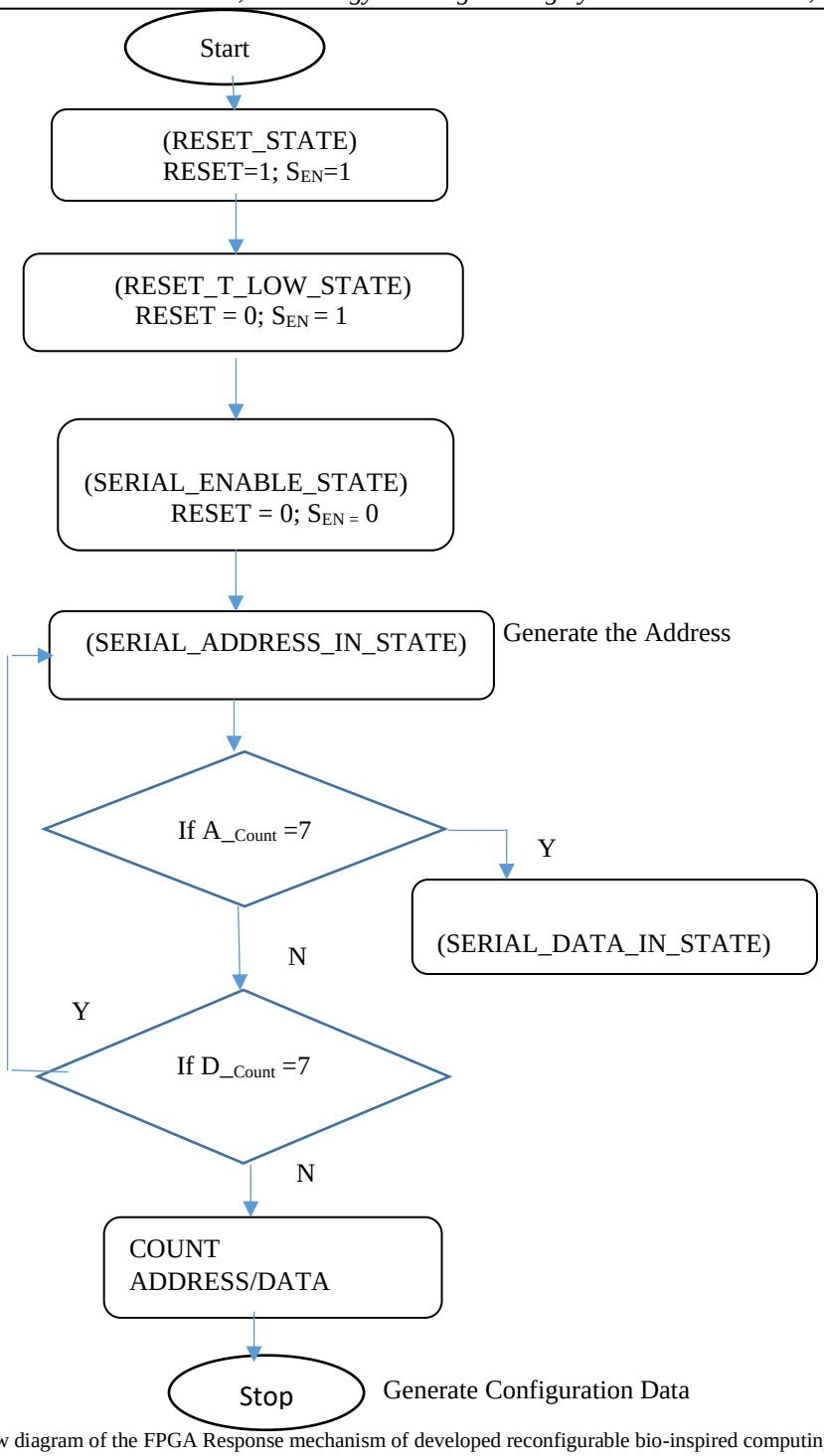


Figure 10: Flow diagram of the FPGA Response mechanism of developed reconfigurable bio-inspired computing architecture

The signals such as RESET and S_{EN} indicate the reset state and serial enable state respectively of FPGA device selected. The serial register reset pulse is greater than 10 ns. If RESET=1; S_{EN}=1 then the FPGA is in the reset state, if the signals RESET=0; S_{EN}=1 then the FPGA is RESET_T_LOW_STATE, and if RESET = 0; S_{EN}= 0, then the FPGA is in serial enable state. The Figure 10 illustrates the flow diagram which forms the basis for algorithm designed to implement a bio-inspired computing system. The $A_{_COUNT}$ is the address count for generating the address and $D_{_COUNT}$ is the data count to generate configuration data. To enable the serial interface of analog to digital converter (ADC), the serial registers were first reset to the default values and the RESET pin was kept low.

Serial enable (S_{EN}), serial data (S_{DATA}), and serial clock (S_{CLOCK}) function as serial interface pins in this mode were used to access the internal registers of the ADC. The registers were reset either by applying a pulse on the RESET pin or by setting RESET bit high.

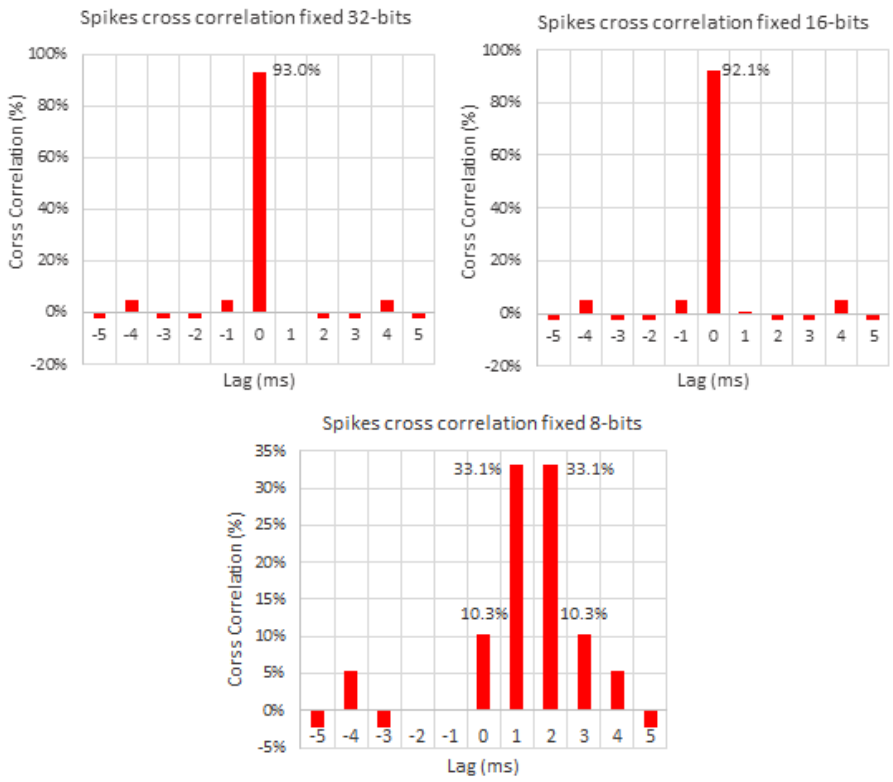


Figure 11: Spike Cross Correlation mechanism of developed reconfigurable bio-inspired computing architecture

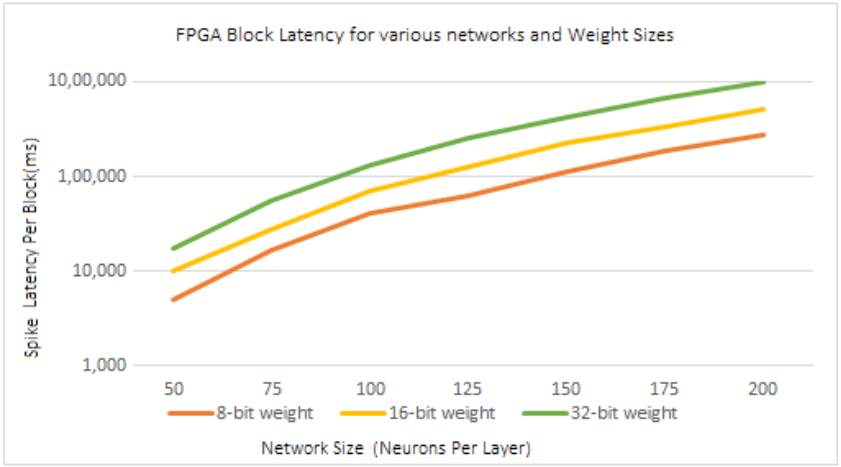


Figure 12: Rate of Change of BRAM generation in Cyclone-V FPGA Block Latency

For the increased flexibility, a combination of serial interface registers and parallel pin controls (CTRL1 to CTRL3) were used to configure the device. To enable this option, RESET pin was configured low. The parallel interface control pins CTRL1 to CTRL3 were available. After power up, the device is automatically configured according to the voltage settings on these pins. In the bus of ADC test for the CYCLONE-V FPGA device, the selected component bus is the 12 channel ADC_RAM component. The data captured through the single clock, the signals included are clock signals such as clk_p, clk_m, the reset signal and the 14 bit input and output data vector signals along with a data type register which is 14 bit vector. The timings of the spikes are analyzed, in a cross correlation of the spikes timings over the FPGA implementation. It is observed that 93% and 92% of the spikes are correlated in the 32 and 16-bits implementation respectively with the implementation with a zero lag delay. On the other hand, 8-bit implementation is slightly different, with 87% of the spike shifted between 0 and 3ms and centered in a 1.5ms shift average with entropy of ~12 % for 100 Neurons with ~2% of performance improvement as described in the Table 1. The analog to digital converter configuration through the serial mode with the signals as seen in spike cross correlation simulation result depicted in the Figure 11. The signals are clock, reset, serial clock, adc_ reset, serial data enable, serial data, and state of the system, the address data consists of a 16 bit vector and these parameters are calculated in terms of rate of change of Block-RAM generation in Cyclone-V FPGA as depicted in Figure 12 and with differential clock simulation time in FPGA based bio-inspired computing module is illustrated in Figure 13.

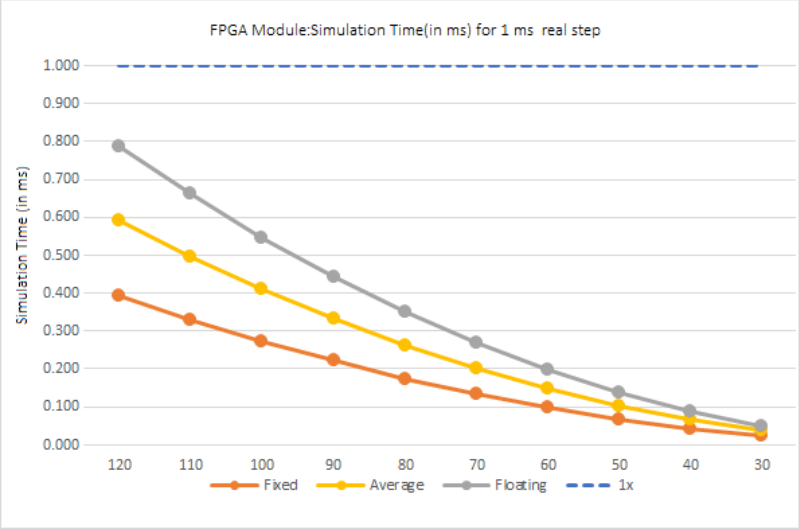


Figure 13: Differential Clock simulation time (in ms) for 1 ms real step in Cyclone-V

6. Conclusions

In this paper the FPGA based algorithmic design of a large scale reconfigurable logical bio-inspired computing model is carried out. The proposed algorithm is implemented on Field Programmable Gate Array to develop a neuron model to be utilized in neuromorphic computing system. The reconfigurable and event driven parameters are considered with the various Intellectual Property (IP) cores are developed for the modules such as Block RAM, Differential Clock, Floating Point, and First in First out (FIFO) for the design of the neuron model in Xilinx ISE, with exploration of register transfer logic (RTL) and hardware synthesis using Verilog code. The architecture for design at device level offers the best possible design tradeoff for specific processor architectures and development choices are summarized. This research paves a way for design of architecture that can be compatible for convolution neural network Artificial Neural Network (ANN).

Conflict of Interest

The authors declare no conflict of interest.

Acknowledgment

The Authors wish to thank School of ECE, REVA University, Bengaluru, India for providing necessary facilities in carrying out this research work.

References

[1] B.U.V. Prashanth, M.R. Ahmed, "FPGA Implementation of Bio-Inspired Computing Architecture Based on Simple Neuron Model," 2020 International Conference on Artificial Intelligence and Signal Processing (AISP), 1–6, 2020, doi:10.1109/AISP48273.2020.9073420.

[2] B.U.V. Prashanth, M.R Ahmed, "FPGA Implementation of Bio-inspired Computing Based Deep Learning Model," In Advances in Distributed Computing Machine Learning, Lecture Notes in Networks and Systems, **127**. Springer, doi: 10.1007/978-981-15-4218-3_24.

[3] R.K. Sarma, M.T. Khan, R.A. Shaik, J. Hazarika, "A Novel Time-Shared and LUT-Less Pipelined Arch. for LMS Adapt. Filter," IEEE Transactions on Very Large Scale Integration Systems, **28 (1)**, 188–197, 2020, doi:10.1109/TVLSI.2019.2935399.

[4] Mohammed Riyaz Ahmed B.K Sujatha, "Reinforcement Learning based on Computational Cognitive Neuroscience in Neuromorphic VLSI Chips," International Journal of Advanced Research in Computer Science and Software Engineering, **2** (8), 2013.

[5] B.U.V. Prashanth, M.R. Ahmed, "Design and performance analysis of artificial neural network based artificial synapse for bio-inspired computing," in Advances in Intelligent Systems and Computing, **1108,** 2020, doi:10.1007/978-3-030-37218-7_135.

[6] C. Pan, A. Naeemi, "Beyond-CMOS non-Boolean logic benchmarking: Insights and future directions," in Proceedings of the 2017 Design, Automation and Test in Europe, 2017, doi:10.23919/DATE.2017.7926971.

[7] X. Lou, Y.J. Yu, P.K. Meher, "Lower Bound Analysis and Perturbation of Critical Path for Area-Time Efficient Multiple Constant Multiplications," IEEE Transactions on Computer-Aided Design of Integrated Circuits and Systems, 2017, doi:10.1109/TCAD.2016.2584181.

[8] A. Agarwal, L. Bopanna, "Low Latency Area-Efficient D.A Based Multi-Rate Filter Architecture for SDR Receivers," Journal of Circuits, Systems and Computers, **27** (08), 2018, doi:10.1142/S0218126618501335.

[9] T. Xu, A. Fumagalli, R. Hui, "Efficient R.T Digital Subcarrier Cross-Connect (DSXC) Based on D.A DSP Algorithm," in Journal of Lightwave Technology, **38**(13), 3495-3505, 2020, doi: 10.1109/JLT.2019.2937787.

[10] D. Datta, P. Mitra, H.S. Dutta, "FPGA implementation of high performance digital down converter for SDR," Microsystem Technologies, 2019, doi: 10.1007/s00542-019-04579-w.

[11] B.K. Mohanty, P.K. Meher, "An Efficient Parallel DA-Based Fixed-Width Design for Approximate Inner-Product Comp," IEEE Transactions on Very Large Scale Integration (VLSI) Systems, **28** (5), 1221-1229, 2020, doi:10.1109/TVLSI.2020.2972772.

[12] M.R. Ahmed, B.K. Sujatha, "A review on methods, issues and challenges in neuromorphic engineering," in 2015 International Conference on Communication and Signal Processing, ICCSP 2015, 2015, doi:10.1109/ICCSP.2015.7322626.

[13] M. D'arco, E. Napoli, E. Zacharelos, "Digital circuit for seamless resampling adc output streams," Sensors (Switzerland), **20** (6), 2020, doi:10.3390/s20061619.

[14] H. Jiang, C. Liu, L. Liu, F. Lombardi, J. Han, "A review, classification, and comparative evaluation of approximate arithmetic circuits," ACM Journal on Emerging Technologies in Computing Systems, **13** (4), 1–34 2017, doi: 10.1145/3094124.

[15] Md Zahangir Alom, et al., "A state-of-the-art survey on D.L architectures," Electronics, **8** (3), 292, 2019, doi: 10.3390/electronics8030292

[16] S. Fukami, H. Ohno, "Magnetization switching schemes for nanoscale three-terminal spintronics devices," Japanese Journal of Applied Physics, **56**(8), 0802A1, 2017, doi:10.7567/JJAP.56.0802A1

[17] T. Jungwirth, et al., "The multi directions of antiferromagnetic spintronics," Nature Physics, **14** (3), 200, 2018, doi:10.1038/s41567-018-0063-6

[18] C. D. Schuman, et al., "A programming framework for neuromorphic systems with emerging technologies," 4th ACM International Conference on Nanoscale Comp. and Comm., ACM, 2017, doi: 10.1145/3109453.3123958
[19] G. Sanchez, et al., "A highly scalable parallel spike-based digital neuro architecture for high-order fir filters using LMS adaptive algorithm," Neurocomputing, **330**, 425-436, 2019, doi:10.1016/j.neucom.2018.10.029.
[20] M. Sharma, S.K. Singh, "New Tech. Peasant Multiplication for Efficient Signal Processing Applications", Indonesian Journal of Elect. Engineering Comp Science, **8** (3), 726-729, 2017, doi: 10.11591/ijeecs.v8.i3.pp726-729.
[21] W. Zhao et al., "A division-free and variable-regularized LMS-based generalized side lobe canceller for adaptive beamforming and its efficient hardware realization," IEEE Access, **6**, 64470–64485, 2018, doi: 10.1109/ACCESS.2018.2875409
[22] S. Dixit, D. Nagaria, "LMS Adaptive Filters for Noise Cancellation: A Review," International Journal of Electrical and Computer Engineering (IJECE), **7** (5), 2017, doi:10.11591/ijece.v7i5.pp2520-2529.
[23] A. Mahabub, "Design and implementation of cost-effective IIR filter for EEG signal on FPGA," Australian Journal of Electrical and Electronics Engineering, **17 (2)**, 83-91, 2020, doi:10.1080/1448837X.2020.1771662.
[24] B. Khurshid, R.N. Mir, "An Efficient FIR Filter Structure Based on Technology-Optimized Multiply-Adder Unit Targeting LUT-Based FPGAs," Circuits, Systems, and Signal Proc.,**36,** 600–639,2017, doi:10.1007/s00034-016-0312-9.
[25] W. Guo, H.E. Yantır, M.E. Fouda, A.M. Eltawil, K.N. Salama, "Towards efficient neuromorphic hardware: Unsupervised adaptive neuron pruning," Electronics (Switzerland), **9 (7)**, 2020, doi:10.3390/electronics9071059.

ASTES

Advances in Science, Technology and Engineering Systems Journal Vol. 5, No. 5, 342-347 (2020)

www.astesj.com

ASTESJ

ISSN: 2415-6698

Factors Influencing the Intention to Use Technology Services to Implement Self-Service Technology Case Study: Situation Pandemic Covid-19

Erick Fernando[1,*], Surjandy Surjandy[1], Meyliana Meyliana[1], Henry Antonius Wijadja[1], Desman Hidayat[2], Ary W Kusumaningtyas[3], Roni Heryatno[3]

[1]*School of Information Systems, Information Systems Department, Bina Nusantara University, Jakarta, 11480, Indonesia*

[2]*BINUS Entrepreneurship Center, Management Department, Bina Nusantara University, Jakarta, 11480, Indonesia*

[3]*BINUS Entrepreneurship Center, Global employability and entrepreneurship, Bina Nusantara University, Jakarta, 11480, Indonesia*

ARTICLE INFO

Article history:
Received: 03 July, 2020
Accepted: 16 August, 2020
Online: 17 September, 2020

Keywords:
Adoption technology
Self-Service Technology
Covid-19

ABSTRACT

This study aims to analyze a person's intention in using self-service technology (SST) services during the pandemic COVID-19. Where this time, raising problems one of the social distancing that affects a service provided, especially on services that use technology that applies SST. This study develops from previous research where the customer has satisfaction in using SST services. Still, this use does not know a person intention to use SST services, so it is necessary to develop with several factors the adoption of technology, namely influence that can make a person intention to use. The research framework of this research consists of several factors and indicators, namely efficiency (4 indicators), Reliability (4 indicators), security (3 indicators), Convenience (3 indicators), Ease of use (4 indicators). This study uses an online survey with google form for users of self-service technology services in 5 major cities in Indonesia. Dissemination of the survey for three months, and the obtained were 100 respondents valid. This research conducts testing using Smarpls v3.0. The results of this study found two factors that influence perceived usefulness, namely: efficiency and reliability, and found three factors that did not have an impact, namely Security factors, Convenience Factors, Perceived Ease of use, and Service Trust do not have an impact on perceived usefulness. This result is a very interesting finding because during the period pandemic COVID-19. These factors are no longer the top priority in the use of SST services and do not affect who intention to use a technology service. Thus, it can be concluded that whose intention at a certain level of the problem will prioritize the reliability and efficiency of the system for service. This factor can be the focus of the company in developing systems that adopt Self-service technology.

1. Introduction

During the pandemic COVID-19 disease that has adversely affected various sectors of human life in various countries, these sectors include the industrial sector, the education sector, the tourism sector and other sectors[1]-[3]. Adverse impacts are influenced by social distancing (giving social distance) between humans, thereby reducing services provided between people[2, 3]. Thus, various industrial sectors require a large technological role to help overcome the various problems that arise, with the development of industry 4.0, which is an integrated industry and provides a service system automation. Therefore, this automation service must use self-service technology services.

Self-service technology (SST) is a technology that provides independent services to customers without involving the assistance of services from people[4]-[6]. Services that use SST include the current banking industry very much from automated teller machine (ATM), mobile services and internet banking to current account opening services, trading industry including order services and self-purchase with web or mobile services namely e-commerce, the healthcare industry with automated consulting services, and other company services provided to customers in the form of customer relationship management [4].

The role of the current application of SST in the industry sector provides solutions to companies and provides benefits in reducing operational and labor costs. However, the application of SST in

*Corresponding Author: Erick Fernando, erick.fernando_88@yahoo.com

various industrial sectors must be able to know the factors that influence the intention to use it. The SST implementation must be able to be used correctly by the user continuously, so the developed technology must be able to increase the intention to use it.

In this article, we focus on discussing and analyzing the factors that influence intention to use in using technology that implemented SST. This article provides two very important contributions focuses. First, this study uses a technology acceptance model (TAM) [7] that is integrated with SST. Second, the construction of the model construct adds one independent variable, namely service trust. Because the service trust studied previously is very influential in the SST service [8]. The development of this model can provide usefulness and Ease of use as well as the intention of someone using it to broaden their understanding of SST acceptance and the mechanisms that must be prepared in the application of SST in various industrial sectors [8].

2. Literature

Self-service technology is an innovative technology that allows customers to take advantage of services without the involvement of service employees [4]. Self-service technology (SST) can also be interpreted as a business that uses a technology interface to provide the best communication to consumers in the transaction process of products or services provided by the company [9]. The application of SST to customers must provide satisfaction to customers from the experience of using SST and influence the desire of customers to return and intention to use [10]. Examples of SST transactions are : bank transactions through automated teller machines (ATM), SPBU, shopping via the internet, vending machines, internet banking, phone banking, making reservations and purchasing tickets through online kiosks [4].

The role of technology is very high in a service provided by a company or industry, especially SST. SST has a factor of perceived usefulness (PU) that has a very important role in people intention to use a service [5]. Thus, technology can hopefully be used to serve all the needs of users. Users of technology services, especially self-service, can be used for a small risk when using them. This gives a perfect sense of trust in a service. Therefore, the use of technology in SST is influenced by a sense of trust in SST to bring up people the intention to use it [11, 12]. User experience in the use of services with high trust can have a substantial impact on perceived usefulness[6,8,13]. The experience of using the services will be influenced by the Ease of use of the service, so it will indirectly affect people's intentions to use technology that implements SST.

The use of Self-Service Technology that is implemented must be able to improve service convenience and provide efficient service processes to customers. Therefore, SST must provide fast services with a shorter time to complete transactions that reduce activity costs. Then the development of SST must provide reliable system reliability to respond to all customer requests on the system. In addition, security in the use of systems that implementation SST to transaction data until the customer's personal data becomes an important thing that must be considered.

3. Conceptual Framework

This study develops from previous research by [14] where the customer has a satisfaction in using SST services, but this user does not know people intention to use SST services, so it is necessary to develop with several factors the adoption of technology [7] namely influence that can make people for intention to use this SST service that is perceived usefulness, perceived Ease of use, intention use. So the research framework developed as follows

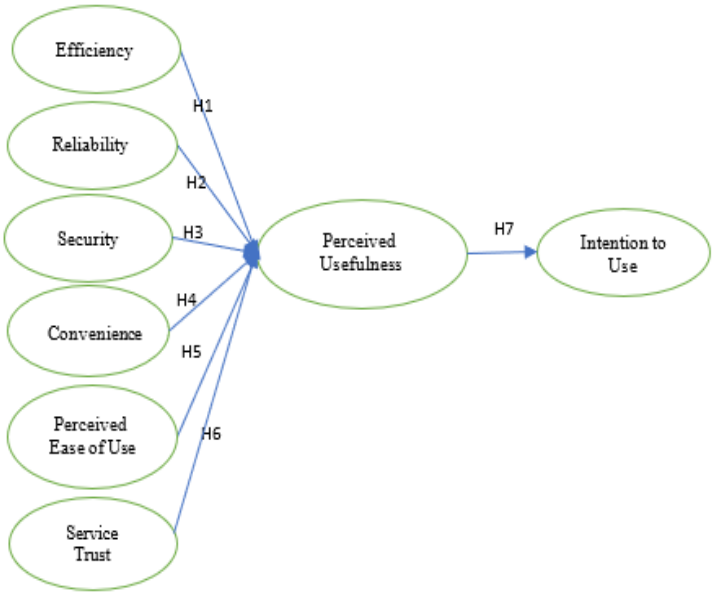


Figure 1: Research Framework

All of these things provide a positive user experience so that users intend to use it continuously and can also provide recommendations to other users. Therefore, the following hypothesis is proposed:

- H1. Efficiency in SST services has a positive impact on perceived usefulness.
- H2. Reliability in SST services has a positive impact on perceived usefulness.
- H3. Security in SST services has a positive impact on perceived usefulness.
- H4. Convenience in SST services has a positive impact on perceived usefulness.
- H5. Perceived Ease of use in SST services has a positive impact on perceived usefulness.
- H6. Service Trust in SST services has a positive impact on perceived usefulness.
- H7 perceived usefulness in SST services has a positive impact on intention to Use.

4. Methodology

4.1. Research Design

This study uses an online survey with Google form for users of self-service technology services in 5 major cities in Indonesia. Services used include ATM, internet banking, mobile banking, and independent check-in machines at airports, toll payments, service queue numbers, online shopping, gas stations, finding machines for food and beverages. Respondents taken have used one or more SST services. Dissemination of the survey for 3 months, and the respondents obtained were 100 people.

Table 1: Respondent characteristic

Characteristic	%
Gender	
- Male	65
- Female	35
Age	
- Less 20	15
- 21 – 25	25
- 26 – 30	37
- 31 – 35	18
- 36 – 40	3
- Over 40	2
Education	
- Student	18
- Bachelor	42
- Master	30
- PhD	10
Self-Service Technology Users	
- Self-check-in at airport	10
- ATM	25
- SPBU	8
- Tol Payment	20
- Internet Banking	10
- Mobile Banking	10
- Online Shopping	15
- vending machine	2

4.2. Development variable

Development of the instrument used in this study is the result of the adoption of several constructs that have been used in previous research. Constructs and indicators are modified to make the instrument in accordance with the current research context.

Table 2: Development Variable and instrument

Variable	Symbol	Instrument
Service Trust	ST1	I believe that the transaction system in the self-service technology service is secure (ex. Toll payment, E-commerce payment, bank print service, laundry service, and other services)
	ST2	I believe the transaction process and the results of the Self-service technology are correct (ex. Toll payments, E-commerce payments, bank print services, laundry services, and other services)
	ST3	I believe that the self-service technology available makes security increased
	ST4	I believe that the filling process carried out with self-service technology is easy to do
Security	S1	Overall, I am satisfied with the Self-service technology provided
	S2	I made the right decision to use self-service technology
	S3	I can easily recommend self-service technology to my friends and others
Convenience	C1	Self-service technology can be accessed at any time
	C2	Self-service technology provisions allow me to make transactions anywhere
	C3	Self-service technology is convenient to use
Perceived usefulness	PE1	It's easy to become an expert in using the Self-service technology provided
	PE2	Self-service technology has clear instructions
	PE3	The Self-service technology provided by is easy to use
	PE4	Interacting with the system does not require much mental effort
Reliability	R1	I get accurate and error-free services from self-service technology (ex. Toll payments, E-commerce payments, bank printing services, laundry services, and other services)
	R2	I can depend on the services provided through self-service technology (Expert insight)
	R3	The Self-service technology completes my selected transactions within the allotted time
	R4	Self-service technology is Reliable
Efficiency	EF1	Self-service technology provides fast service with shorter waiting times
	EF2	Self-service technology saves me time
	EF3	Self-service technology allows me to complete transactions quickly
	EF4	Self-service technology reduces the cost of my activities
Perceived of use	PU1	I think using services Self-service technology can make understanding more efficient
	PU2	I think using a self-service technology will not be limited by time and location, which is very helpful for me
	PU3	By using Self-service technology services, I realize the extraordinary development of technology
	PU4	I think I can get payment information quickly using the Self-service Technology service
	PU5	I think using the service Self-service technology can make life more comfortable

Variable	Symbol	Instrument
	PU6	Self-service technology helps me learn to operate the tool
	PU7	Self-service technology provided helped me to live more economically
Intention to Use	IU1	I want to use the self-service technology provided
	IU2	I want to use the Self-service technology service to link the payment and purchase information
	IU3	I continue to increase the frequency of use of self-service technology services
	IU4	I believe the frequency of use of self-service technology in the future will continue to increase
	IU5	I always re-use the Self-Service Technology
	IU6	I will use the Self-service technology whatever happens later

4.3. Measurement

This study modified the model developed [14], namely: efficiency (4 indicators), reliability (4 indicators), security (3 indicators), Convenience (3 indicators), Ease of use (4 indicators), adding one Important factor according to Hee-Dong Yang [8] are service trust (4 indicators) and with several factors of technology adoption developed [7], so that one can find out someone who intention to use this SST service namely perceived usefulness (7 indicators), perceived Ease of Use (4 indicators), intention use (6 indicators). This study uses a measurement scale point 6 with the type of interval data that aims to get a more specific response picture of the respondents.

5. Result

This research conducts testing using Smartpls v3.0 because the research framework has a latent construct. The test was initiated by testing the validity using a loading factor value greater than 0.5 and reliability using an average variance extracted (AVE) value greater than 0.5, composite reliability (CR) greater than 0.6, and Cronbach alpha greater than 0.6 [15].

Table 3: Reliability Test

	Cronbach'alpha	CR	AVE
Convenience	0.848	0.904	0.758
Efficiency	0.929	0.95	0.825
Intention use	0.939	0.953	0.772
Perceived ease of use	0.93	0.95	0.826
Perceived usefulness	0.936	0.948	0.725
Reliability	0.935	0.954	0.838
Security	0.926	0.953	0.871
Service trust	0.897	0.929	0.766

Table 4: Validity test

	Convenience	**Efficiency**	**Intention Use**	**Perceived Ease of use**	**Perceived usefulness**	**Reliability**	**Security**	**Service Trust**
C1	0.888							
C2	0.887							
C3	0.836							
EF1		0.922						
EF2		0.945						
EF3		0.942						
EF4		0.820						
IU1			0.927					
IU2			0.951					
IU3			0.935					
IU4			0.876					
IU5			0.664					
IU6			0.886					
PE1				0.862				
PE2				0.920				
PE3				0.934				
PE4				0.918				
PU1					0.911			
PU2					0.854			
PU3					0.897			
PU4					0.896			
PU5					0.894			
PU6					0.770			
PU7					0.718			

	Convenience	Efficiency	Intention Use	Perceived Ease of use	Perceived usefulness	Reliability	Security	Service Trust
R1						0.916		
R2						0.939		
R3						0.919		
R4						0.886		
S1							0.940	
S2							0.919	
S3							0.940	
ST1								0.907
ST2								0.949
ST3								0.833
ST4								0.804

A. Evaluate the model

Evaluate the model using the "coefficient of determination" value (R2) and the value of "Path coefficient", where the value according to the hair must be greater than 0.5. The results of the evaluation are the perceived usefulness of 0.911 and the intention to use 0.809 so that the model is a very fit model.

B. Hypotheses Test

Hypothesis testing using the standard p-value value, according to hair p-value, must be less than 0.005, then the hypothesis is accepted / significant while the opposite is rejected / not significant. Hypothesis test results are found, namely: Hypothesis 1 testing gets a p-value of 0,000, so it can be concluded that efficiency greatly affects the perceived usefulness. Testing Hypothesis 2 gets a p-value of 0.035 so that it can be concluded that reliability greatly affects the perceived usefulness. Testing Hypothesis 3 gets a p-value of 0.526, so it can be concluded that security has no impact on perceived usefulness. Testing Hypothesis 4 gets a p-value of 0.663, so it can be concluded that Convenience does not have an impact on perceived usefulness. Testing Hypothesis 5 gets a p-value of 0.626, so it can be concluded that the perceived Ease of use has no impact on perceived usefulness. Testing Hypothesis 6 gets a p-value of 0.735, so it can be concluded that Service Trust has no impact on perceived usefulness. Hypothesis 6 testing gets a p-value of 0.000, so it can be concluded that perceived usefulness has an impact on the Intention to Use.

6. Conclusion

The results of this study indicate that factors influence whether or not someone who intention in using SST services. The efficiency factor greatly affects perceived usefulness. This is in accordance with previous studies that describe that the efficiency of SST services is needed to make transactions carried out quickly so as to provide a reduction in costs and time required by customers [6,14,16]. So on its own, increasing its use will affect someone who intends to use it. The reliability factor greatly affects perceived usefulness. This is consistent with previous research, which states that a reliable system can improve services as much as the user wants, which requires precision, good consistency of a system. This directly increases to someone who intends to use SST services [10,14,17–19]. Security factors, Convenience Factors, Perceived Ease of use, and Service Trust do not have an impact on perceived usefulness. The findings of the study contradict the previous studies which stated that the safety, simplicity, and Ease of use of the system are highly considered by users when they want to use technology. Therefore, the results of this study make a very interesting finding because it happened during the Covid-19 pandemic that made these factors no longer a priority in the use of SST services and did not affect someone who intended to use technology services. Therefore, it can be concluded that someone whose intention is at a certain level of problem will give priority to the reliability and efficiency of the system for services. These factors may be the company's focus on developing a system that implements SST. Researchers in further research can develop discussions on automation factors in SST, if you can augment someone who intends to use SST services because this automation is a new part of Industry 4.0 needs.

Reference

[1]. M.P.A. Murphy, "COVID-19 and emergency eLearning: Consequences of the securitization of higher education for post-pandemic pedagogy," Contemporary Security Policy, **41**(3), 492–505, 2020, doi:10.1080/13523260.2020.1761749.

[2]. R. Vaishya, A. Haleem, A. Vaish, M. Javaid, "Emerging Technologies to Combat the COVID-19 Pandemic," Journal of Clinical and Experimental Hepatology, **10**(4), 409–411, 2020, doi:10.1016/j.jceh.2020.04.019.

[3]. M. Javaid, A. Haleem, R. Vaishya, S. Bahl, R. Suman, A. Vaish, "Industry 4.0 technologies and their applications in fighting COVID-19 pandemic," Diabetes and Metabolic Syndrome: Clinical Research and Reviews, **14**(4), 419–422, 2020, doi:10.1016/j.dsx.2020.04.032.

[4]. K. Kansana, A. Tripathi, D.- Issues, "Understanding Self Service Technologies," (September), 2019.

[5]. V. Ong, N.M. Yee, G.J. Hui, N. Kasim, I. Hizza, "The Impact of Service Automation on Customer Satisfaction and Customer Retention: An Empirical Study of Malaysian Rail Transportation," Proceedings of 4th Global Business and Finance Research Conference, (May), 2015.

[6]. M. Sedighimanesh, A. Sedighmanesh, N. Ashghaei, "The Impact Of Self-Service Technology On Customer Satisfaction Of Online Stores," International Journal of Scientific & Technology Research, **06**(07), 172–178, 2017.

[7]. F.D. Davis, "Perceived Usefulness, Perceived Ease of Use, and User Acceptance of," Information Technolog MIS Quarterly, **13**(3), 319--340., 1989, doi:10.2307/249008.

[8]. H.D. Yang, J. Lee, C. Park, K. Lee, "The adoption of mobile self-service technologies: Effects of availability in alternative media and trust on the relative importance of perceived usefulness and ease of use," International Journal of Smart Home, **8**(4), 165–178, 2014, doi:10.14257/ijsh.2014.8.4.15.

[9]. N. Taufik, M.H. Hanafiah, "Airport passengers' adoption behaviour towards self-check-in Kiosk Services: the roles of perceived ease of use, perceived usefulness and need for human interaction," Heliyon, **5**(12), 2019, doi:10.1016/j.heliyon.2019.e02960.

[10]. N. Robertson, H. McDonald, C. Leckie, L. McQuilken, "Examining customer evaluations across different self-service technologies," Journal of Services Marketing, **30**(1), 88–102, 2016, doi:10.1108/JSM-07-2014-0263.

[11]. L. Zeng, Factors influencing the adoption of self-service technologies: A study of the benefits and risks of self-service technologies and trust beliefs of service providers, 2016.
[12]. D.D. Dugar, "Public Self Service Technology (SST): Designing for Trust Factors enhancing user ' s trust towards a public," 2018.
[13]. H. Oh, M. Jeong, S. Baloglu, "Tourists' adoption of self-service technologies at resort hotels," Journal of Business Research, **66**(6), 692–699, 2013, doi:10.1016/j.jbusres.2011.09.005.
[14]. Gunawardana, D. Kulathunga, H.M.R.S.S. Perera, W.L.M.V., "Impact of Self Service Technology Quality on Customer Satisfaction: A Case ...: EBSCOhost," Gadjah Mada Intemational Joumal of Business, **17**(1), 1–24, 2015.
[15]. J.F. Hair Jr, G.T.M. Hult, C. Ringle, M. Sarstedt, A primer on Partial Least Squares Structural Equation Modeling (PLS-SEM), Sage Publications, Singapore, 2013.
[16]. C.K.M. Lee, Y. Ng, Y. Lv, P. Taezoon, "Empirical analysis of a self-service check-in implementation in Singapore Changi Airport," International Journal of Engineering Business Management, **6**(1), 33–44, 2014, doi:10.5772/56962.
[17]. H. Iberahim, N.K. Mohd Taufik, A.S. Mohd Adzmir, H. Saharuddin, "Customer Satisfaction on Reliability and Responsiveness of Self Service Technology for Retail Banking Services," Procedia Economics and Finance, **37**(16), 13–20, 2016, doi:10.1016/s2212-5671(16)30086-7.
[18]. P.S. Otieno, K. Govender, "Managing airport service quality – The impact of self-service technologies," Investment Management and Financial Innovations, **13**(3), 387–393, 2016, doi:10.21511/imfi.13(3-2).2016.11.
[19]. J.S.C. Lin, P.L. Hsieh, "Assessing the Self-service Technology Encounters: Development and Validation of SSTQUAL Scale," Journal of Retailing, **87**(2), 194–206, 2011, doi:10.1016/j.jretai.2011.02.006.

ASTES

Advances in Science, Technology and Engineering Systems Journal Vol. 5, No. 5, 348-355 (2020)

www.astesj.com

ASTESJ

ISSN: 2415-6698

Water Availability for a Self-Sufficient Water Supply: A Case Study of the Pesanggrahan River, DKI Jakarta, Indonesia

Ramadhani Yanidar[1,2], Djoko Mulyo Hartono[*,3], Setyo Sarwanto Moersidik[3]

[1]*Department of Civil Engineering, Faculty of Engineering, Universitas Indonesia, Depok, 16242, Indonesia*

[2]*Department of Environmental Engineering, Faculty of Architecture Landscape and Environmental Technology, Universitas Trisakti, Jakarta 11440, Indonesia*

[3]*Environmental Engineering Study Program, Department of Civil Engineering, Faculty of Engineering, Universitas Indonesia, Depok, 16242, Indonesia*

ARTICLE INFO

Article history:
Received: 03 July, 2020
Accepted: 16 August, 2020
Online: 17 September, 2020

Keywords:
Dependable flow
GIS
System dynamics
Water supply
Water demand

ABSTRACT

The research will explore the challenges of using local water sources inside the city for a self-sufficient urban water supply by developed a system dynamics model. This study aims to evaluate and understand the Pesanggrahan River appropriateness as a raw drinking water source through a conceptual model that can accurately represent the interactions between the water supply and demand system. A set of time series data for the monthly precipitation and river flow rates at two stations from 2002 to 2016 were used to calculate the 90% dependable river flow fluctuations over one year. The results showed that water availability becomes limited in July, August, and September. Simulation results demonstrated that the Pesanggrahan River could supply 450 liters/s. The water demand exceeded the supply if the average water consumption 150 liters/capita/day for 100% service coverage. However, they will balance when service coverage 66 %, but reducing water consumption to 99 liters/capita/day will increase service coverage to 100%. The average water consumption and service coverage forming a linear equation relationship $Y = 99.20x-0.99$ with a correlation factor $R^2 = 0.99$. This research contributes to enhancing the resilience of the water supply system. It provides a well-founded, flexible, and realistic approach to recognize and deal with challenges to local raw water resources limitation that inherent with uncertainties in water resources management.

1. Introduction

Freshwater is essential to sustain life, and its role is irreplaceable and of high value to its users. Water is vital, finite, and fugitive [1]. Although water is a renewable resource, its availability is limited. As a result of its volatile nature, it is quite challenging to determine the limits of water resources and assess flow variations. Climate change has various implications. The spatial variability of water due to climate change is quite large. For planning purposes, it is not realistic to rely on estimates of extreme rainfall across an entire city.

Therefore, local or decentralized raw water sources should be used as an alternative water supply for the betterment of the population [2]. Furthermore, independent diversification of water supplies can help overcome climate uncertainty and natural variability, which is a significant challenge for cities around the world [3]. For planning purposes, it is not realistic to rely on estimates of extreme rainfall across an entire city.

Currently, raw water resources for the centralized water supply mostly emphasize outside the cities, namely [4]-[7]. Studies on local raw water research have been proposed groundwater and treated wastewater for the landscape in the next decade [8]. However, the opportunities to use local river water that passes through cities are still rarely explored as raw water sources. In order to fill this gap, this research will explore the challenges of

[*]Corresponding Author: Djoko Mulyo Hartono, Department of Civil Engineering, Faculty of Engineering, Universitas Indonesia, Email: djokomh@eng.ui.ac.id

using local water sources inside the city for self-sufficient urban water supply by developed a system dynamics model.

The water supply services in DKI Jakarta, Indonesia, use centralized piped systems. The primary raw water sources are currently the reservoirs that are ± 70 km away from Jakarta, and the treated water primarily comes from Tangerang, which acts as a buffer city. The local water resources in DKI Jakarta only fulfill 5.7% of its current water demand. The service coverage has reached only 60.27%. Therefore, people still depend on groundwaters as alternative clean water sources. Over-abstraction of groundwater has sharpened inequalities in access to water within and beyond the centralized piped network [9]. Besides, variations of groundwater extraction caused land subsidence in Jakarta [10]. Consequently, it needs additional raw water resources for Greater Jakarta to improve the services of centralized piped systems and facilitate the reduction of groundwater use.

Thirteen rivers cross DKI Jakarta in Indonesia. These rivers have the potential to increase the raw water through rainwater runoffs, which are almost entirely discharged into the sea to prevent flooding. Pesanggrahan River is one of the raw water sources inside the DKI Jakarta area. Due to its water quality, it is adequate for use as a raw drinking water source [11]. However, it is necessary to prove that the quantity of its supply is sufficient for decentralized raw water services accommodating the inhabitants of the sub-basin of the Pesanggrahan River in the DKI Jakarta subregion.

Water availability is associated with the dependable flow of specific probabilities that determine the minimal river discharge characteristics. This analysis of the Pesanggrahan River was calculated based on a 90% dependable flow. The managing water supply systems need a deep understanding of all of the issues. Controlling the integrated system, which has a causal relationship with the different subsystems, requires appropriate strategies and policies. Therefore, this study utilized a system dynamics model to represent and understand the causal interaction between the quantity of raw water sources and the increase in its requirements

The dynamic feedback interaction between the available raw drinking water sources and the consumer population reflects the continually evolving problems in the system. Fortunately, researchers can formulate a feasible policy based on the estimation and simulation results provided by a system dynamics model. To meet its population's requirement for raw drinking water sources, DKI Jakarta must adopt a management strategy to balance the water supply and demand.

This study aims to evaluate and understand the Pesanggrahan River's appropriateness as a raw drinking water source through a conceptual model that can accurately represent the interactions between the water supply and demand system. This research will contribute to enhancing the resilience of the water supply system for inhabitants in DKI Jakarta

2. Material and Methods

This study developed a water availability model for a self-sufficient water supply using system dynamics. The water quantity variable was based on a historical hydrology data analysis of natural water flow from the upstream area. The simulation focused on water availability during one-year fluctuations based on dependable river flow and potential runoff.

Concerning [12]-[14], this study employed the main variables related to hydrology analysis—namely, monthly rainfall, monthly river discharge, basin area, sub-basin land cover, and rainfall-runoff. The variables in the model were based on the results of the Pesanggrahan River analysis, using the 90% dependable discharge data. Furthermore, the alternative sources of additional raw water included reused collected rainfall, which varied with the seasons.

2.1. Study Area and Data Sources

The study area was constrained to the sub-basin of the Pesanggrahan River in the DKI Jakarta subregion, which has several tributaries entering the main river flow to DKI Jakarta Province, Indonesia. The precipitation and river discharge data were obtained from the Ciliwung Cisadane Rivers Area Agency (BBWSCC). The Pesanggrahan River discharge data came from two different monitoring stations, namely Sawangan Station (2000–2016) and Kebun Jeruk Station (2002–2016). Sawangan station was the sole source of precipitation data for 2009 to 2016. The digital elevation model (DEM) used the 8m x 8m map sourced from the National Geospatial Information Center (INA-Geoportal).

2.2. Water Availability Analysis Method

The duration curve method was used for the water availability analysis, while the dependable flow was calculated using the Weibull probability formula [15] with a flow duration curve based on (1) :

$$P(X \geq x) = \frac{m}{n+1} 100\% \quad (1)$$

Where, P(X ≥ x) = the probability of the occurrence of variable X (discharge) being equal to or greater than x m3/s (the percentage probability), m = the data rating, the order number of the discharge n = the amount of data, the number of data X = the series data discharge, the dependable flow = the reliable discharge when the probability matches the allotment of the source of clean water, and P(X ≥ Q90%) = 0.9.

To calculate the potential runoff, we used the rational modification method based on the following equation (2) :

$$Q = \frac{\sum_{i=0}^{n} C_i x A_i}{\sum_{i=0}^{n} A_i} \; x \; R \; x \; \sum_{i=0}^{n} Ai_i \quad (2)$$

where Q = the potential runoff (m3/month), Ci = the land cover runoff coefficient, Ai = the area of land cover (Ha), R = the 90% dependable monthly rainfall at the Sawangan Station (mm/month), and A = the area of the sub-watershed of the Pesanggrahan River (Ha).

Figure 1 shows our concept for determining the potential runoff coefficient using a geographic information system (GIS) [16]. The spatial slope classification data used in the present study was the result of an analysis of national DEM data of 8m x 8m using GIS tools. A simple linear relationship between the potential runoff coefficients and the surface slope was used to calculate the potential runoff coefficient, as shown in (3) [17]:

$$C = C_0 + (1 - C_0)\frac{S}{S+S_0} \quad (3)$$

where C is the potential runoff coefficient for a surface slope S (%), S_0 (%) is a slope constant for different land use and silty clay soil combinations, and C_0 is the coefficient of the potential runoff representing the values belong to [17].

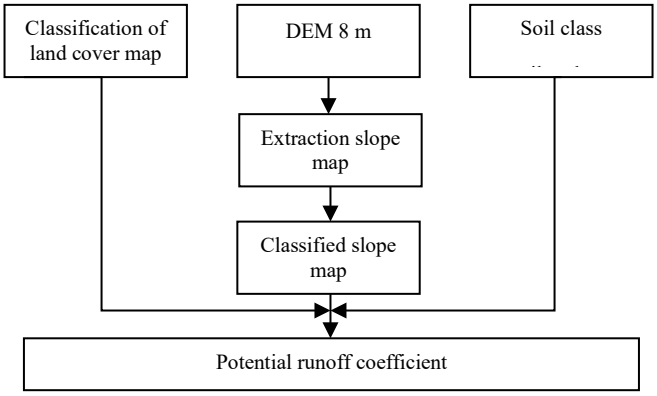


Figure 1: The concept of determining the potential runoff coefficient

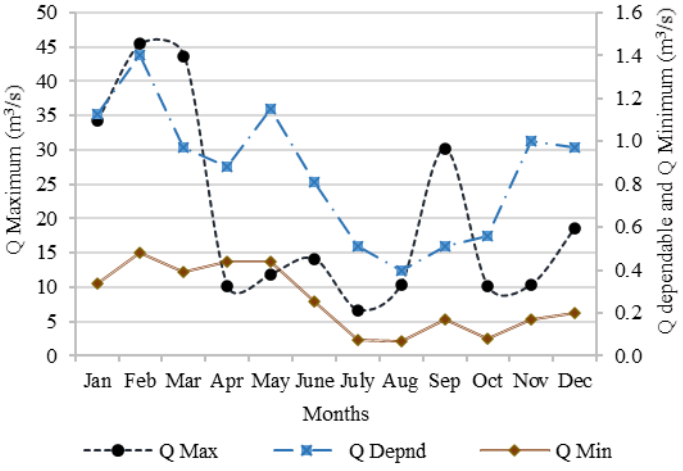
2.3. A System Dynamics Model for Water Availability

A system dynamics model development used the PowerSym tool. The model was developed based on a causal loop diagram (CLD) and stock-flow diagram (SFD) to represent and understand the causal interaction between the quantity of a raw water source and the increases in its requirements

3. Result and Discussion

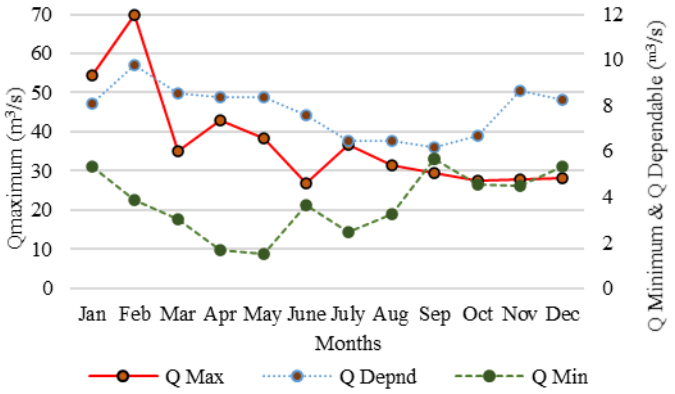
3.1. Dependable Flow of Pesanggrahan River

The maximum, minimum, and 90% dependable monthly river flow fluctuations at both the Sawangan Station and Kebun Jeruk Station are shown in Figure 2 and Figure 3.



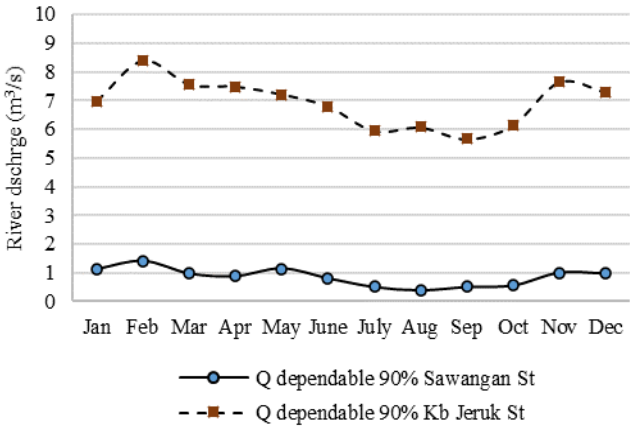
At the Sawangan Station, the minimum river flow varied between 0.07 m^3/s and 0.44 m^3/s, while the maximum river flow varied between 10.1 m^3/s and 45.4 m^3/s. With this data, a Stream's Regime Coefficient (KRS) of 103 to 144 was obtained, which indicated medium to poor conditions for water availability [18]. The 90% dependable monthly river flow ranged from 0.4 $m^3/$ sec to 1.4 m^3/s (Figure 2).

However, in the course of the river flow to Jakarta, the discharge significantly increased due to the additional flow of the Angsana River and Kali Putih River into the point W2 (6°18' 43.6" S 106°46'29.1" E) from a 5.122 ha sub-watershed and the flow of the Grogol River at point P (6°15'38.0"S 106°46'34.7" E) from a 360 ha sub-watershed. Therefore, the river flow measurement at the Kebun Jeruk Station in the downstream was significantly higher than the measurement at the Sawangan Station, as the minimum flow was 1.65 m^3/s to 5.66 m^3/s and the maximum flow was 26.7 $m^3/s$to 69.9 m^3/s. The KRS was 12.34 to 16.2, which indicated the right conditions for water availability [18]. Meanwhile, the dependable flow fluctuated from 6.18 m^3/s to 9.79 m^3/s (Figure 3).



This analysis required precipitation data from the same time, station, and interval as the river flow data series; however, the precipitation data was only available through the measurements taken at the Sawangan Station. Therefore, statistical analysis and visual comparison were required to compare the precipitation data at both monitoring station locations.

Figure 4 shows the measurements for the dependable monthly flow at both the Sawangan and Kebun Jeruk stations. The measurements at the two locations followed similar patterns. In addition, the relationship between the Pesanggrahan River flow patterns at Kebun Jeruk Station and Sawangan Station was R^2=90%, forming a linear regression model of Y = 3.42X + 4.85 (Figure 5). Therefore, there was no significant difference in precipitation measurements between the two stations. However, in the development of the model, it was assumed that the precipitation at the two locations had the same value and that the additional discharge of the Pesanggrahan River came from potential runoff on sub-watersheds [19]. Based on this model, there was a relationship between the dependable flow in the Pesanggrahan River and the precipitation data.



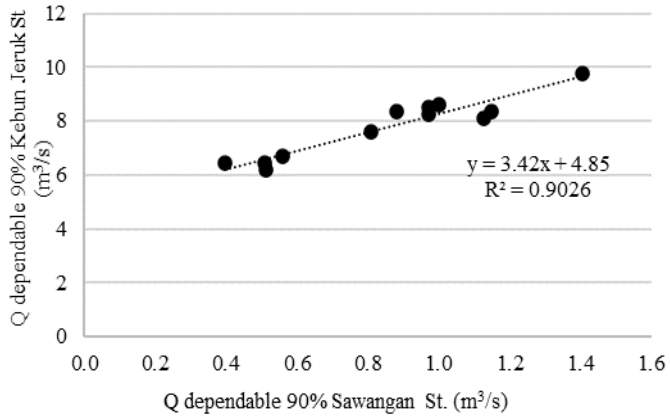
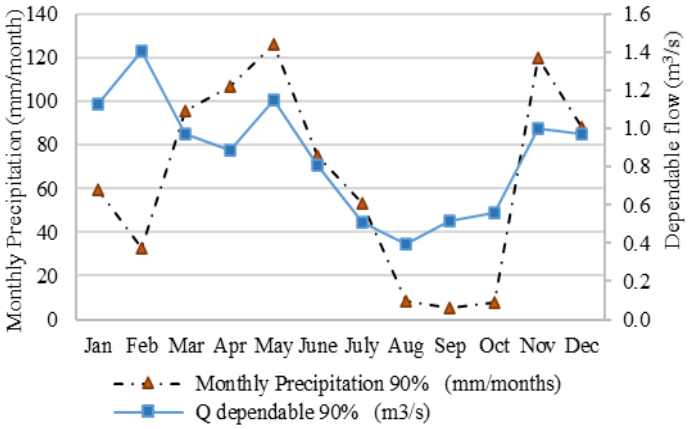


Figure 6 shows the monthly precipitation data at the Sawangan Station, with a 90% probability ranging from 5.5 mm/month in September to 125.8 mm/day in May. The discharge measurements ranged from 0.4 m^3/s in August to 1.4 m^3/s in February.

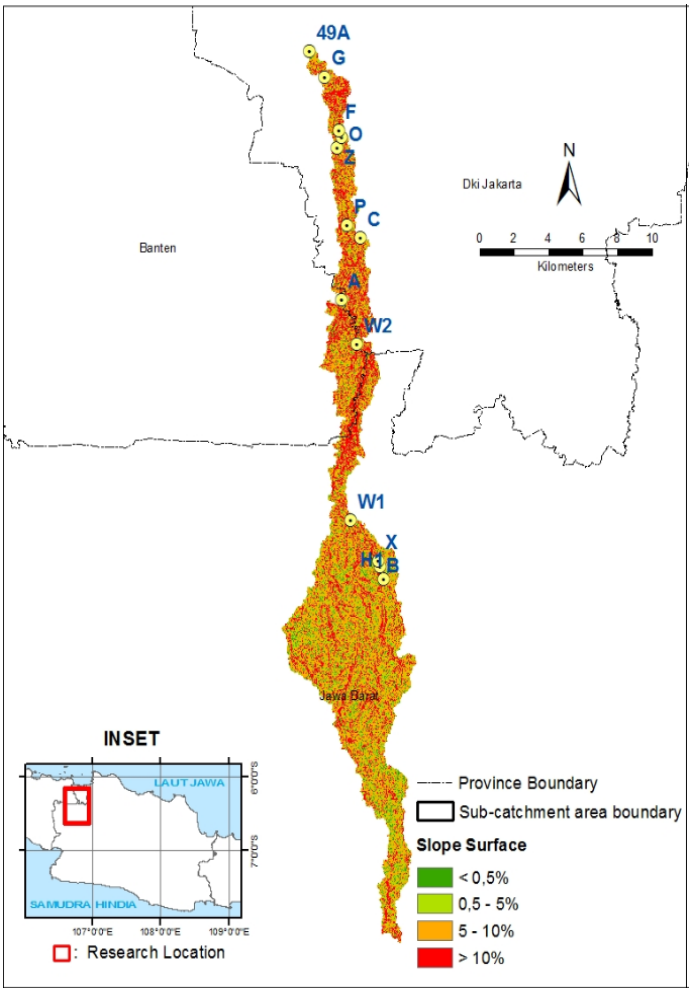


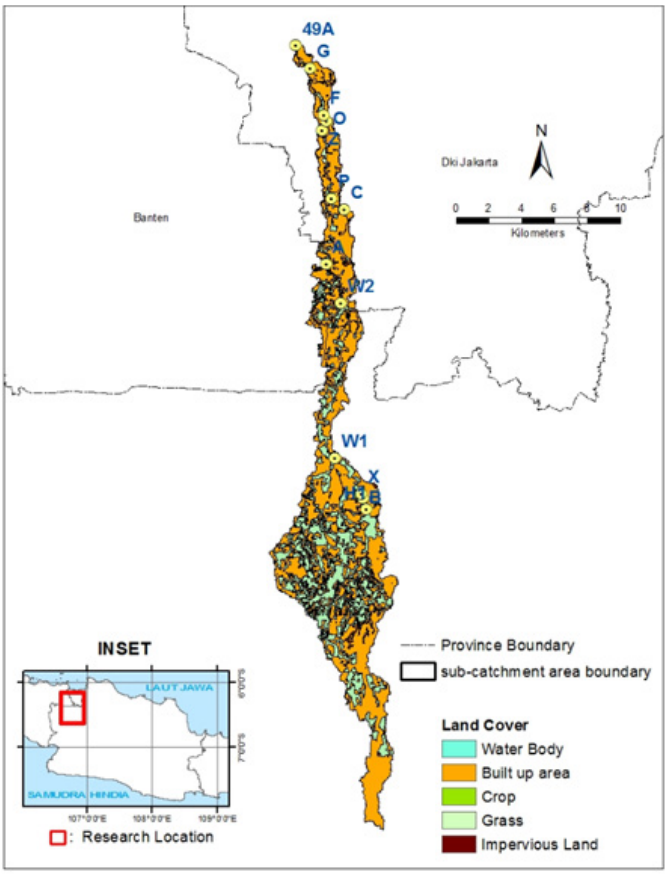
When developing the system dynamics model, the monthly precipitation and runoff fluctuation data are shown in Figure 6 was used as an auxiliary function for the available raw water sources that could serve as a self-sufficient water supply in DKI Jakarta.

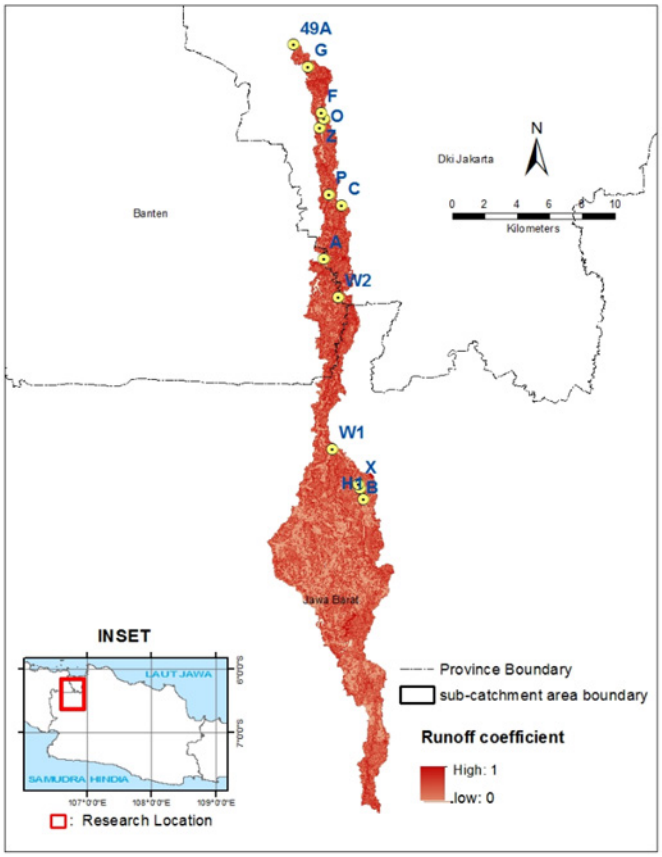
3.2. Potential Runoff Coefficient Identification

The potential runoff can be understood as the additional amount of water that increases the river water flow. Silty clay dominated the hydrology soil type in the sub-basin of the Pesanggrahan River in the DKI Jakarta subregion. The land cover, sloped surfaces, and hydrological soil groups were all taken into account in the potential runoff coefficients

A land cover map featuring water bodies, built-up land, grass, plants, and impervious land is shown in Figure 7. The DEM map processing generated a slope map with four classifications, as shown in Figure 8. A GIS overlay of the slope map (Figure 5) and land cover map (Figure 6) is also provided. A new field was added to the attribute table of the overlay. The results of Eq. (3) were entered into the new field, and then a potential runoff coefficient map was created, as shown in Figure 9.

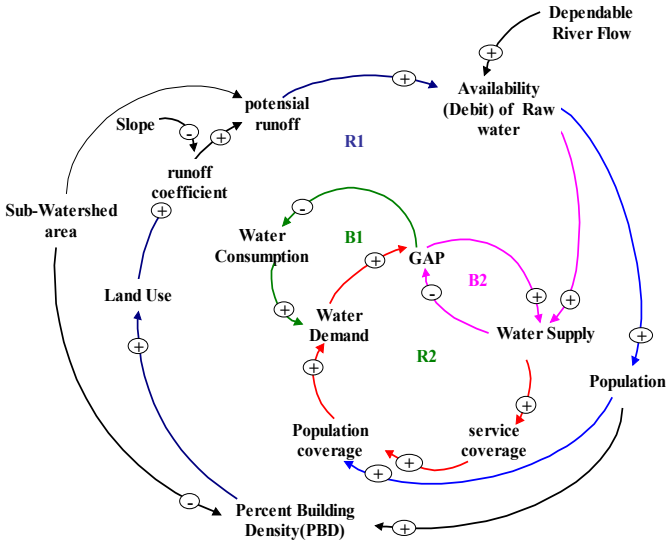






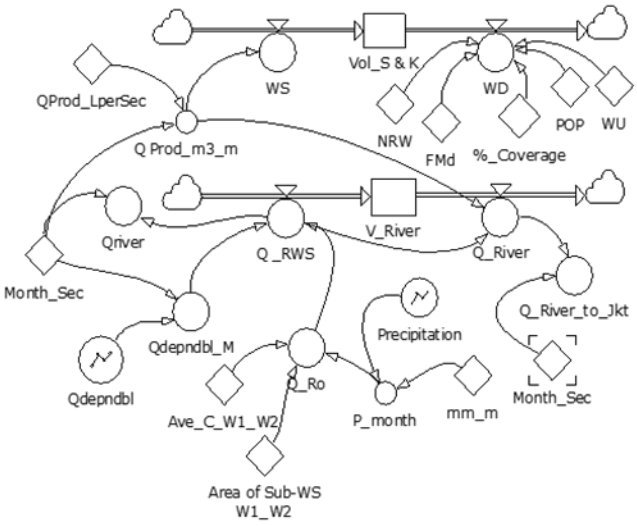
3.3. Model System Dynamics for the Pesanggrahan River Water Availability

The situation analysis provided by the CLD structure of the system dynamics model described the appropriateness of the Pesanggrahan River as a raw water source (see Figure 10).



The model was built by four loops of causal relationships between different components. Two of those loops were positive or reinforced loops (R): R1 and R2. The other two loops were negative loops (B), which modeled the relationships between the factors balancing the water supply (B1 and B2). Furthermore, the model showed various factors that were associated with increasing or decreasing the flow of raw water resources.

Based on the causal loop built above, an SFD was made for the water quantity availability model, as shown in Figure 11. The operational definitions of each component model are presented in Table 1.



Stock flow diagram (SFD) of the System Dynamics Model for Water Availability

Table 1: Operational Definitions of the Variables / Component Models

No	Variables	Operational Definition	Measurement unit
1	V_River	The volume of the river water	m^3
2	Q_RWS	Pesanggrahan River's inflow from the upstream (Bogor) to Sawangan Station, Depok	m^3/month
3.	Q_River	Inflow of the Pesanggrahan River from the sampling point W2, Cinere Depok	m^3/month
4	Q_Ro	Runoff discharge from the sub-watersheds of the river segment	m^3/month
5	Qdepndbl_M	The fluctuations of the 90% probability river flow per month	m^3/month
6	Precipitation	The fluctuations of the 90% probability precipitation	mm/day
7	Ave_C_W1_W2	C value of the average runoff coefficient of the river segment W1–W2	Ha
8	Area_of_Sub-WS_W1_W2	Area of the watershed river segment W1–W2	Ha
9	Vol_S&K	A gap of cumulative supply and demand	m^3
10	WS	The water production capacity plan	m^3/month
11	Q_Prod	Discharge of raw water in the river intake	m^3/month
12	WD	Water demand	m^3/month
13	POP	Quantity of the population served	population
14	WU	Average water consumption	Liters /capita /day
15	FMd	The maximum day factor for the water demand	
16	NRW	Non-revenue water factor	%

3.4. Simulation Results

Model simulations provided an overview of the Pesanggrahan River's water availability in a year. The analysis of the 90% dependable monthly discharge showed that there was a fluctuation in water quantity, with minimal availability in August. Initial simulations demonstrated a scenario involving raw water extraction at the upstream location (W2) of the Pesanggrahan sub-district of DKI Jakarta. The inflow of river water was assumed as the 90% dependable monthly discharge (Figure 4) at the Sawangan Station (W1), with an additional flow from the potential runoff of 5.112 Ha W1-W2 sub-watershed area (Figure 9). Furthermore, the simulation results showed that the Pesanggrahan River could supply raw water at a rate of 450 liters/s for the population in the Pesanggrahan River Basin of the DKI Jakarta subregion. Figure 12 shows that a constant supply of 450 liters/s would result in water demand exceeded the supply if the average water consumption was 150 liters/capita/day of 100% service coverage.

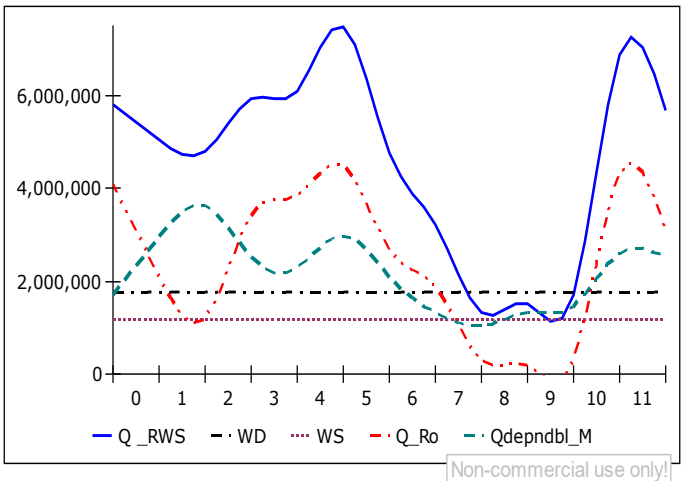


Figure 12: Results assuming 450 liters/s raw water uptake discharge and 150 liters/capita/day average water consumption

The simulation results of various water consumption scenarios produce the total water demand equal to total supply, which refers to the water availability of 450 m^3/s (Figure 13).

They showed variations in service coverage, with the average water consumption forming a linear equation relationship $Y= 99.202x^{0.986}$ with a correlation factor $R^2 = 0.99$ (Figure 14). The simulation model proves that self-sufficient water supply in the region will require increased awareness of the water scarcity crisis and changes to the perception and lifestyle of Jakarta's inhabitants.

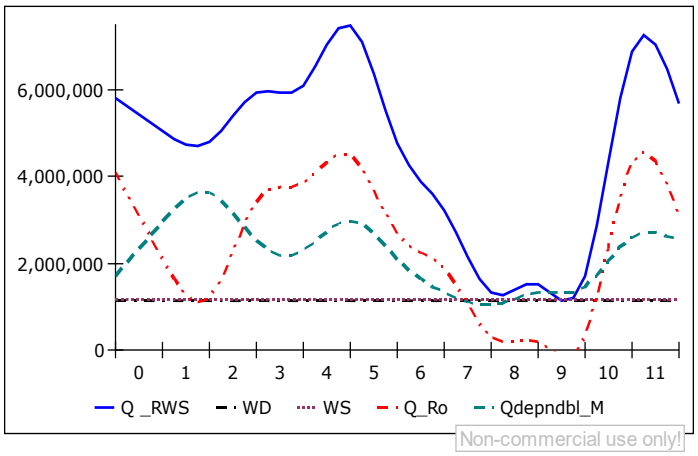


Figure 13: Results assuming 450 liters/s raw water uptake discharge of various water consumption scenarios that produce the total water demand equal to total supply

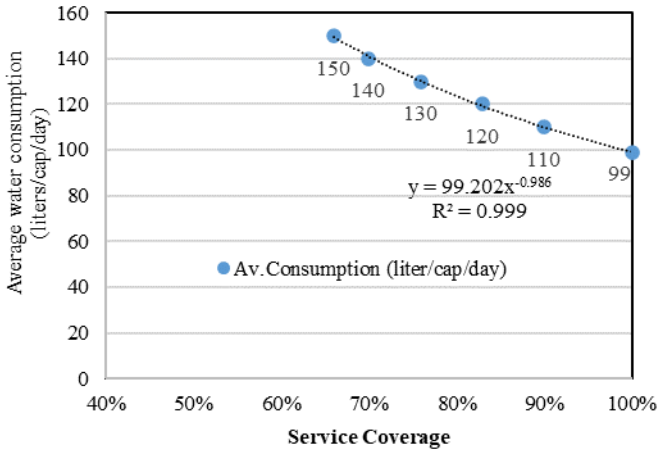


Figure 14: Simulation results of the service coverage policy based on average water consumption

A policy strategy for lowering water consumption is needed. One of the alternatives is to use prices as a policy instrument that can reduce water consumption [20],[21]. Eliminating water subsidies by gradually increasing prices is a more promising strategy than pushing up prices to match inflation [21]. Besides, price scenarios can be combined with technological interventions, such as water-saving taps and "Xeriscaping," as a strategy to reduce water consumption [22]. An impounding reservoir could be another option for increasing the water supply to overcome the minimum flow in July, August, and September. The results of our reliable discharge analysis showed a significant increase from the upstream of the Sawangan Station to the downstream of the Kebun Jeruk Station. Moreover, the downstream had a KRS indicating good conditions for water availability if selected as a raw water intake location. However, it should be noted that water quality deteriorated in the downstream location of the river. As a limitation of this study, our model did not include water quality as a variable. Hence, detailed computer simulations of the integrated water resource system should be performed to clarify the availability of drinking water in terms of quantity and quality [23].

The verification results of the model structure, the mathematical equations, and the interrelationships between the subsystems accurately reflect the real situation. Together, they represent a simplification of the entire process. However, due to its limitations, there are always differences from the actual reality [24]. Nevertheless, this model is useful as a decision support tool for water supply planning and management, because the availability of raw water is explained based on a minimum river flow with a probability of 90%.

4. Conclusion

The system dynamics model provides insight and an in-depth understanding of the water availability problems involved in creating a self-sufficient water supply in DKI Jakarta, Indonesia. The Pesanggrahan river could supply 450 liters/s where water extraction at the upstream of sub-district of DKI Jakarta. It will balance with the demand if the average water consumption 150 liters/capita/day when service coverage 66% or reducing water consumption to 99 liters/capita/day will increase service coverage to 100%. This study contributes to enhancing the resilience of the water supply system. It recognizes and deals with challenges to local raw water resources limitation that inherent with uncertainties in water resources management.

Though the water quality deteriorated at the downstream, the quantity of water increased. In future research, it needs to develop a model that includes water quality variables and more in-depth simulations to obtain the optimal location for water intake and a storage strategy that can meet the quantity and quality of drinking water needs for the region.

Conflict of Interest

The authors declare no conflict of interest.

Acknowledgment

This research was financially supported by the Research Grant of Doctoral Dissertation (PUTI Doktor), Universitas Indonesia, with Contract No NKB-658/UN2.RST/HKP.05.00/ 2020.

The authors would like to thank and give appreciation to Ardiansyah, ST, for his assistance in guiding and assisting data processing with GIS.

References

[1]. P. Van Der Zaag, H.H.G. Savenije, Principles of Integrated Water Resources Management, doi:10.1201/b13146-9.

[2]. P. Jaramillo, A. Nazemi, "Assessing urban water security under changing climate: Challenges and ways forward," Sustainable Cities and Society, **41**(November 2016), 907–918, 2018, doi:10.1016/j.scs.2017.04.005.

[3]. M.A. Renouf, S. Serrao-Neumann, S.J. Kenway, E.A. Morgan, D. Low Choy, "Urban water metabolism indicators derived from a water mass balance – Bridging the gap between visions and performance assessment of urban water resource management," Water Research, **122**, 669–677, 2017, doi:10.1016/j.watres.2017.05.060.

[4]. J. Yang, G. Li, L. Wang, J. Zhou, "An Integrated Model for Simulating Water Resources Management at Regional Scale," Water Resources Management, **29**(5), 1607–1622, 2015, doi:10.1007/s11269-014-0897-3.

[5]. L. Garrote, A. Granados, A. Iglesias, "Strategies to reduce water stress in Euro-Mediterranean river basins," Science of the Total Environment, 543, 997–1009, 2016, doi:10.1016/j.scitotenv.2015.04.106.

[6]. T. Li, S. Yang, M. Tan, "Simulation and optimization of water supply and demand balance in Shenzhen: A system dynamics approach," Journal of Cleaner Production, **207**, 882–893, 2019, doi:10.1016/j.jclepro.2018.10.052.

[7]. L. Yuan, W. He, D.M. Degefu, Z. Liao, X. Wu, M. An, Z. Zhang, T.S.

Ramsey, "Transboundary water sharing problem; a theoretical analysis using evolutionary game and system dynamics," Journal of Hydrology, 582(December 2019), 124521, 2020, doi:10.1016/j.jhydrol.2019.124521.
[8]. M.H. Ahmadi, M. Zarghami, "Should water supply for megacities depend on outside resources? A Monte-Carlo system dynamics simulation for Shiraz, Iran," Sustainable Cities and Society, 44(October 2018), 163–170, 2019, doi:10.1016/j.scs.2018.10.007.
[9]. M. Kooy, C.T. Walter, I. Prabaharyaka, "Inclusive development of urban water services in Jakarta: The role of groundwater," Habitat International, **73**, 109–118, 2018, doi:10.1016/j.habitatint.2016.10.006.
[10]. I. Abidin, H.Z., Andreas, H., Gumilar, "Land subsidence of Jakarta (Indonesia) and its relation with urban development.," Nat Hazards, **59**, 1753, 2011.
[11]. R. Yanidar, D.M. Hartono, S.S. Moersidik, "Water quality assessment for self-sufficient water resources for DKI Jakarta," in IOP Conference Series: Earth and Environmental Science, 2018, doi:10.1088/1755-1315/106/1/012056.
[12]. C.C. Yang, L.C. Chang, C.C. Ho, "Application of system dynamics with impact analysis to solve the problem of water shortages in Taiwan," Water Resources Management, **22**(11), 1561–1577, 2008, doi:10.1007/s11269-008-9243-y.
[13]. G. Wu, L. Li, S. Ahmad, X. Chen, X. Pan, "A Dynamic Model for Vulnerability Assessment of Regional Water Resources in Arid Areas: A Case Study of Bayingolin, China," Water Resources Management, **27**(8), 3085–3101, 2013, doi:10.1007/s11269-013-0334-z.
[14]. Y. Sun, N. Liu, J. Shang, J. Zhang, "Sustainable utilization of water resources in China: A system dynamics model," Journal of Cleaner Production, 142, 613–625, 2017, doi:10.1016/j.jclepro.2016.07.110.
[15]. F. Dixey, "Engineering hydrology," Journal of Hydrology, **27**(1–2), 169, 2003, doi:10.1016/0022-1694(75)90105-5.
[16]. S.H. Mahmoud, "Investigation of rainfall-runoff modeling for Egypt by using remote sensing and GIS integration," Catena, **120**, 111–121, 2014, doi:10.1016/j.catena.2014.04.011.
[17]. Y.B. Liu, F. De Smedt, "WetSpa Extension , A GIS-based Hydrologic Model for Flood Prediction and Watershed Management Documentation and User Manual," Documentation and User Manual, (March), 1–126, 2004.
[18]. Y. Lilis Handayani, Siswanto, B. Sujatmoko, G. Oktavia, "Stream's regime coefficient in upstream Rokan watershed of Riau Province," MATEC Web of Conferences, 276, 04013, 2019, doi:10.1051/matecconf/201927604013.
[19]. D.P. Loucks, E. van Beek, Water resource systems planning and management: An introduction to methods, models, and applications, Springer, 2017, doi:10.1007/978-3-319-44234-1.
[20]. K. Qaiser, S. Ahmad, W. Johnson, J. Batista, "Evaluating the impact of water conservation on fate of outdoor water use: A study in an arid region," Journal of Environmental Management, **92**(8), 2061–2068, 2011, doi:10.1016/j.jenvman.2011.03.031.
[21]. M. Goldani, H. Amadeh, "A System Dynamics Approach in Water Resource Management and Government Subsidy Policy: A Case Study of Tajan Basin in Iran ," Proceedings of the 29th International Conference of the System Dynamics Society, 1–18, 2011.
[22]. S. Ahmad, D. Prashar, "Evaluating Municipal Water Conservation Policies Using a Dynamic Simulation Model," Water Resources Management, **24**(13), 3371-3395., 2010, doi:10.1007/s11269-010-9611-2.
[23]. A. Mirchi, K. Madani, D. Watkins, S. Ahmad, "Synthesis of System Dynamics Tools for Holistic Conceptualization of Water Resources Problems," Water Resources Management, **26**, 2421–2442, 2012, doi:10.1007/s11269-012-0024-2.
[24]. J. Sterman, "System Dynamics; System Thinking and Modeling for a Complex World," 2002.

ASTES

Advances in Science, Technology and Engineering Systems Journal Vol. 5, No. 5, 356-363 (2020)

www.astesj.com

ASTESJ

ISSN: 2415-6698

Component of Trust for Developing Crowdwork System: A Systematic Literature Review

Sugiarto Hartono*[,1,2], Meyliana[1,2], Ahmad Nizar Hidayanto[1,3], Harjanto Prabowo[1]

[1]*Computer Science Department, Bina Nusantara University, 11480, Indonesia*

[2]*Information Systems Department, School of Information Systems, Bina Nusantara University, 11480, Indonesia*

[3]*Faculty of Computer Science Universitas Indonesia, 16424, Indonesia*

ARTICLE INFO

Article history:
Received: 09 July, 2020
Accepted: 07 August, 2020
Online: 17 September, 2020

Keywords:
Component
Trust
Crowdwork System

ABSTRACT

Crowdwork is a system that brings job providers and crowdworkers in a portal. Nowadays, many companies are turning to freelancing rather than hiring full-time employees. In addition, the workers have also switched to working as freelancers. New problems also arise in the crowdwork system. Trust is one of the main issues that arise in the crowdwork system. It happens because the job providers and workers do not meet each other on the crowdwork portal. This research aims to examine the components that affect trust in a crowdwork system. The benefit is that stakeholders can be aware of how to increase trust in the crowdwork system. The method used in this research is systematic literature review, by analyzing Scopus based journals related to trust in the crowdwork system. This research produces 11 components and 38 indicators. There are three components that needs concern to stakeholders who want to take advantage of crowdwork systems and focus on trust. These components are reciprocal voting, monetary reward, and cognitive effort. The platform should enable stakeholders to have reciprocal voting, less cognitive effort, as well as clean and clear monetary reward procedure.

1. Introduction

Crowdwork system is a portal that allows employers to find workers on a project-based online basis. Crowdworking is a socio-technical work system formed through a series of relationships that connect organizations, individuals, technology and work activities. Online crowdwork takes place in the online marketplace which allows companies to find workers and supports workers in finding work [1]. Through online crowdwork, workers will carry out performance activities through distributed crowdworkers and be financially funded by job providers (can be individuals, groups, or organizations). Crowdworking uses internet technology to answer the needs of the workforce digitally [2]. Crowdworking initially emerged using well-known concepts such as sharing economy and collaborative consumption. Crowdworking is an option to hire labor.

Freelancing is greatly helped by the crowdworking platform system. Crowdworking is growing nowadays and starting to be glimpsed by workers. Crowdworking can provide opportunities to be able to work flexibly through digital platforms. A survey shows that there are almost five million crowdworker workers in the UK [3]. 18% of Netherlands citizen have tried to find work through platforms digital [4]. Around 12% of the Swedish population work as gig workers [5]. According to Indonesian Central Statistics Agency (BPS) at the end of 2018, as many as 56.8% of Indonesians worked in the informal sector, which is accompanied by an increase in the number of workers who are entrepreneurs in Indonesia, including freelancers. In May 2019, there are 129.36 million workforces in Indonesia. Freelance took 4.55% or around 5.89 million people. This number increased 16% from 2018 (data is gained from Sribulancer, one of the Freelance Indonesia service providers). This increase is due to the fact that crowdworking facilitates connectivity in the global workforce search network and enables rapid scalability [6]. From the employer side, crowdworking can also change fixed costs into variable costs for employee cost.

Trust often linked to the someone reputation in a system. User reputation is the only method to identify trust. There are various perspectives to estimate trust. Trust is one kind of sciences widely explored in computer science. Trust value can be measured through subjective opinion, whereas trust assessment can be

*Corresponding Author: Sugiarto Hartono, shartono@binus.edu

calculated by combining user reputation with estimates from various sources [7]. Trust is also needed in the online labor system, such as crowdwork system.

The main problem related to trust in crowdwork system lies in the assessment of crowdworkers who are unfair, and the lack of transparency in the assessment given by the employer. This has an impact on job satisfaction and the continuous intention to participate in the crowdwork system. This is supported by Ye & Kankanhalli's research [8] which says that trust is an important factor in the participation of workers in a crowdwork system. Feller et al. [9] also said that trust is one of the critical factors in the success of crowdworking and it has an impact on worker participation. In an online environment, trust can encourage participation and can mediate the relationship between environmental conditions and subsequent participation [10,11]. Therefore, this research will identify component factor of trust for developing crowdwork systems especially online freelancing platforms using systematic literature review.

2. Theoretical Foundation

2.1. Crowdwork System

According to Howcroft and Kåreborn [12], crowdwork has 4 (four) typologies that are intended to answer future issue and challenge. It also help to understand the complex field of crowdwork. The purpose of typology is to reduce the complexity of various kinds of crowdwork.

1. Online task

Online task crowdwork provide paid work (as the worker interest) for a specific task. Actors who initiate processes of this type are employers. The tasks are modular, ranging from micro work to more complex work.

2. Playbour

'Playbour' (a combination of work and games) is based on unpaid work. 'Playbour' [13] is an ideological strategy that connects games, labor creativity, and autonomy [14]. This type of crowdwork is according to workers request. Workers have more sense to innovate. It also increase workers productivity, because there is no clear boundaries between work and pleasure.

3. Asset-Based services

This type is a type of crowdwork that involves asset-based employment services. This category is closely related to the idea of sharing economy [15]. The tasks managed digitally, are mostly carried out offline and depend on the use of workers' assets.

4. Profession-based freelance

This type is for professional-based freelance jobs. This type of crowdwork tends to have a more attention that needs high level skills and knowledge.

According to Kuek et al. [16], crowdwork can be divided into 2 types (microwork and online freelancing) which has diffentiation in terms of size and complexity of the work. Kuek et al. explains, microwork refers to simple work and no need more time to accomplish. The worker doesn't need special skills. Online freelancing needs high level skills and experience in big projects. It also needs more time to complete task in online freelancing. The example of microwork is logo design, while the example of online freelancing is system development project. More than 50% of online freelancers is bachelor's degree, while 33% of workers in microwork have them.

2.2. Trust

Trust is a major problem in the dynamics of group organizations, for example political and social organizations [17]. Trust is defined as an attribute carried out by people about the motives of group authority. If people have confidence in the authority of the group, it proves that the person cares about their needs. This authority group has genuine interests, cares about the person's way of thinking and point of view, and considers each person's opinion, and acts fairly to the person. Trust reflects the assessment that the motives of the authority are full of kindness and care. Groups that have authority are motivated to act in a way that considers the well-being of people in the group [18].

Dwyer and Oh [19] state that trust is the desire to achieve long-term goals. The biggest failure in building relationships between sellers and consumers is a lack of trust. There are two main topics of trust

a. Trust in partner's honesty, related to trust in the honesty of partners / companies
b. Trust in partner's benevolence, related to trust in the company's good intentions

3. Methodology

This research uses a systematic literature review method by analyzing research paper or literature related to component factor of trust to develop crowdwork system. The phases of this research are divided into several stages, such as: determining the source of research literature, determining the pattern of literature search keywords, determining the inclusion and exclusion criteria, extracting data, and analyzing findings to answer the research problem formulation.



Figure 1: Phases of Systematic Literature Review

Source: Adapted from Tranfield and Smart [20]

A. Determine Source of Research Literature

In this initial stage, the research literature source will be determined to find research articles related to the topic. Research Literature Sources used include:

a. SAGE
b. Science Direct
c. ACM Digital Library
d. Springer

Keywords to search for research article papers use the Boolean operator in order to obtain the appropriate search results. Boolean operators used are OR and AND. The keywords used are:

a. Trust AND (component OR Attribute) AND (framework OR model) AND (crowdwork OR crowdsource OR (crowdwork AND system) OR (crowdsource AND system))
b. Trust AND (component OR Attribute) AND (framework OR model) AND (crowdwork OR crowdsource)

The inclusion criteria for searching research articles consist of three stages. The first stage is the "Studies Found" process. Search results according to keywords will be categorized as "Studies Found". The next stage is "Candidate Studies". If the title and abstract of the research article in studies are found match to the research topic, then it is categorized as "Candidate Studies". The final stage of this research is "Selected Studies". If the paper on "Candidate Studies" answers the research problem statement, it will be included in "Selected Studies".

Exclusion criteria used in this study include:

a. The research article paper used in this study has a publication year for the past five years.
b. Research Paper has a complete writing structure, complete paper identities, and complete identity of the author.
c. If duplication occurs, it will be excluded in this literature study.

B. Data Extraction

This study analyzed 622 papers included in the Founded Studies and derived from 4 sources of literature and in accordance with the inclusion and exclusion criteria that have been set. Paper included in the Founded Studies is then re-analyzed the suitability between the title, abstract, and the research question, so that obtained 35 papers included in Candidate Studies. The paper included in Candidate Studies was then re-analyzed by reading the entire paper content and found 8 papers included in Selected Studies. Here are the findings of the literature from various sources:

Table 1: Result of Data Extraction

Source	Found	Candidate	Selected
Sage	51	8	3
Science Direct	392	15	3
Springer	7	2	1
ACM Digital Library	172	10	1
Total	622	35	8

4. Results and Discussion

This study aims to discover what components factors of trust that are needed to develop the Crowdwork System. This section will present demographic data and characteristic trends from the literature included in the Selected Studies category, such as publication sources, publication years, classification of trust component of crowdwork or crowdsource system components of the literature study. The following table shows the sources of journal publications consist of title, year, and type of publication. There are 7 journal papers used in this literature review. It can be concluded that crowdworking is more closely researched in the disciplines of strategic information systems and management.

There are 16 authors who have written 7 papers in total. The 16 authors are grouped into 8 departments. Authors who contribute research on trust component of crowdworking or crowdsourcing tend to write with research approaches. Most of them have academic background (87.5%, 14 authors) and 2 authors (12.5%) have industry background. The detailed of author name can be seen in table 3.

Table 2: Source of Literature and Paper Discipline

No	Title	Paper Discipline	Source	Year	Type
1	Crowdsourcing-Based Business Models [21]	Management	Sage	2015	Journal
2	Combining User Reputation [22]	Data and Information Quality	ACM	2016	Journal
3	Community building on crowdwork [23]	Political Economy	Sage	2020	Journal
4	The Future of Work: New Roles [24]	Human Resources	Sage	2018	Journal
5	Developing and maintaining clients' trust [25]	Strategic Information Systems	Science Direct	2018	Journal
6	Should You Really Produce [26]	Product Innovation Management	Springer	2017	Journal
7	Solvers' participation [27]	Strategic Information Systems	Science Direct	2017	Journal

Table 3: Author's Information

Author	Department	Author's Background	# of Author's Publication
Andreas Herrmann	Business Administration, Law and Economics	Academic	1
Archana Nottamkandath	Computer Science	Academic	1
Atreyi Kankanhalli	Computer Science	Academic	1
Christine Gerber	Computer Science	Academic	1

Author	Department	Author's Background	# of Author's Publication
Davide Ceolin	Computer Science	Academic	1
Hua (Jonathan) Ye	Computer Science	Academic	1
Ji-Ye Mao	Management Science & Engineering	Academic	1
Kevin Freitas	Human Resources	Industry	1
Paul Groth	Computer Science	Academic	1
Reto Hofstetter	Marketing and Communication Management	Academic	1
Suleiman Aryobsei	Management Business	Industry	1
Thomas Kohler	Law and Philosophy (Open Innovation & Crowdsourcing)	Academic	1
Valentina Maccatrozzo	Computer Science	Academic	1
Wan Fokkink	Computer Science	Academic	1
Wenyu (Derek) Du	Information Systems	Academic	1

The detailed data of institutions produced paper is listed on table 4. It can be seen that each university produced one paper each.

Table 4: List of Institution

Institutions	# of papers	%
A.T. Kearney	1	6.25
Beihang University, Beijing, China	1	6.25
Berlin Social Science Center	1	6.25
Boston College Law School	1	6.25
Dream11	1	6.25
Elsevier B.V.	1	6.25
National University of Singapore	1	6.25
Netherlands eScience Center	1	6.25
Renmin University of China, Beijing, China	1	6.25
The University of Auckland	1	6.25
Universita della Svizzera italiana	1	6.25
Universities of St. Gallen	1	6.25
VU University Amsterdam	4	25

Trust on crowdworking has been widely discussed over the past five years (2015, 2016, 2017, 2018, 2019, and 2020). There are 2 papers published on 2017, 2 papers published on 2018, 1 paper published on 2015, 1 paper published on 2016, 1 paper published on 2020.

According to 8 papers found in Selected Studies, there are 11 components and 38 indicators related to trust model on crowdwork platform. Reciprocal voting is described by project participation, project submitted, social ties, votes provided, votes received, worker's participation, worker's solution, and project duration. Open communication is described by community building, level of interaction, topics of interaction, purposes of interaction. Online testimonial is described by vividness, emotional absorption, and message-value congruency. Monetary reward is described by return of submission, submission, and financially rewarded. Cognitive effort is described by difficulty of understanding requirement, effort into understanding requirement, time and effort of task solving, time needed to solve problem. Loss of knowledge power is described by unique value, power base, respect to others, and unique knowledge. Initiating trust is described by escrow services, feedback system, and accreditation system. Augmenting trust is described by requirement analysis services and contract formation services.

Maintaining trust is described by periodical evaluation and harmonious conflict resolution. User reputation is described by author reputation and stereotype reputation. Trustworthiness reputation is described by evidence prior performance, stereotype reputation, and user reputation. The details of indicator for each component can be seen on table 5.

Table 5: Component, Definition, and Indicator of Crowdwork Systems

Component	Definition	Indicator
Reciprocal Voting	Based on cooperation and social influence theory, peer voting to competitive online environment (such as crowdwork/crowdsource system) may trigger cooperation among stakeholders through reciprocal voting. Cooperation may happen in competitions if there are two persons who meet and interact repeatedly [28, 29]. Reciprocity is a kind of cooperation in competition [30,31]. The objective of reciprocal voting used to vote ideas/solution in online system is to prevent social bias. The company can ignore that motive and allow vote to affect innovation process [32,33]. The better the result of screening innovation process, the more successful will get in innovation process [34, 35, 36]. So, the conception and knowledge for social bias in online system (such as crowdwork or crowdsource system) is very critical for open innovation.	Project Participation
		Project Submitted
		Social Ties
		Votes Provided
		Votes Received
		Worker's Participation
		Worker's Solution
		Project Duration
Open Communication	Management should provide open communication to make interaction decentralized. But, it will impact to critical comments. Management may choose to take preventive action (such as control to irresponsible autonomy). The persuasive effect of testimonials is based on heuristic thinking and cognitive shortcuts (availability and representative heuristics). [37,38]	Community Building
		Level of Interaction
		Topics of Interaction
		Purposes of Interaction
Online Testimonial	Testimonial includes description of personal experience or opinion. Some studies found that testimonials are more persuasive than factual information, but other studies found conversely. Testimonials are very efficient in public media because individual don't engage in extensive cognitive processing of media messages. [39,40,41,42]	Vividness
		Emotional Absorption
		Message-value congruency
Monetary Reward	Monetary reward includes on extrinsic motivation. It is provided as an incentive for crowdworker [43]. Crowdworker can expect reward for solution they give to job provider [44]. Monetary reward is the important factor for crowdworker to undertake the action in crowdwork system [45,46].Terwiesch and Xu did research on TaskCNPlatform [47]. They suggest that monetary reward will stimulate participation of crowdworker on platform. Based on social exchange theory, expectation of monetary reward should motivate crowdworker to choose to act [48,49,50].	Return of Submission
		Submission
		Financially Rewarded
Cognitive Effort	Cognitive effort is mandatory for problem solving on crowdworking platform. Cognitive effort will take part as a medium for solving the gap between past solution/knowledge and current problem. It's costly and will connect the expertise to the problem and develop solution for that problem. Crowdworker must leverage cognitive effort to identify, understand the requirement/problem, and propose the solution [51]. Crowdworkers are not likely to participate when they perceive high cognitive effort is needed for that participation. Crowdworkers expect the crowdwork platform can reduce cognitive effort, so it can build crowdworker's trust to platform. For example, platform must give feedback to the crowdworker if their solutions are not adapted [52,53]. By providing past solution, cognition effort will be reduced [54,55].	Difficulty of Understanding Requirement
		Effort Into Understanding Requirement
		Time and Effort of Task Solving
		Time Needed to Solve Problem

Component	Definition	Indicator
Loss of Knowledge Power	Loss of knowledge power is a barrier to knowledge sharing. In crowdwork platform, knowledge is a source of power by crowdworkers. Crowdworker have fear feeling when the job provider know their ideas or solution before they have rewarded. Job provider act opportunistically and not pay the crowdworker once they get the solution. It will impact trust crowdworkers on job provider and they are not participating in crowdwork platform [56]. Crowdworkers also may have feeling that crowdwork platform will misuse their solution and it also impact to crowdworker's trust to platform [57,58].	Unique Value
		Power Base
		Respect to Others
		Unique Knowledge
Initiating	In initiating trust, job provider get list of crowdworker and select one of them to work with. There are many concerns related to initiating trust, such as crowdwork opportunistic behaviors (for example crowdworker get monetary reward without properly delivering the solution), crowdworker can't fulfill job provider's requirement [57,58].	Escrow Services
		Feedback System
		Accreditation System
Augmenting	In augmenting trust, job provider negotiates with selected crowdworker about deliverables and prices of contract. The solution must be met with job provider's requirement. The requirements are often not fixed and unclear. Several job provider said that the result of task that needed identify requirement usually less predictable and not meet job provider's expectation [57,58].	Requirement Analysis Services
		Contract Formation Services
Maintaining	In maintaining trust, job provider feel uncertainty about commitment and project status progress. Young crowdworkers have enthusiasm and creativity, but they ignore professionalism. Job provider also have concern about crowdworkers commitment (especially during implementation phase) [57,58].	Periodical Evaluation
		Harmonious Conflict Resolution
User Reputation	User reputation is asset in social live that plays fundamental role to build online ecosystem, reputation can be used to increase recommendation in a system. [59, 60]	Author Reputation
		Stereotype Reputation
Trustworthiness Estimation	Trust estimation is procedure that the trust level for an artifact based on a combination of the reputation of the user who created the artifact and of the provenance stereotype to which the artifact belongs. Trust estimation also a procedure that to determines whether artifact is acceptable based on supplied test entries and background information. This is a form of probability to make decision ahead [59, 60].	Evidence Prior Performance
		Stereotype Reputation
		User Reputation

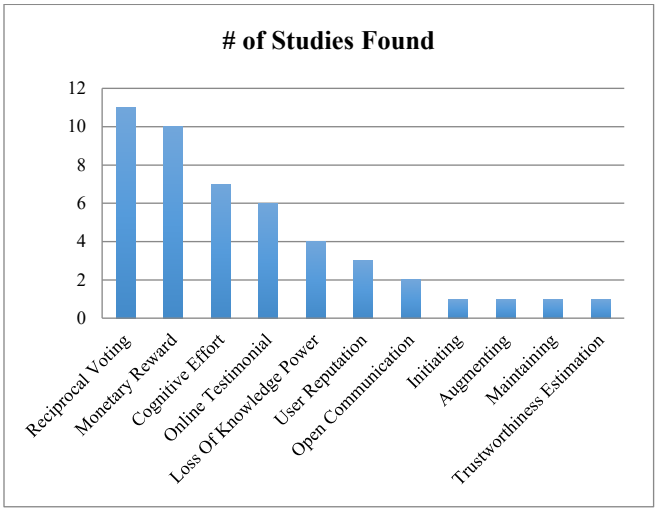


Figure 2: Relationship Between Number of Studies Found and Components
Source : Processed by the Author

Figure 2 describes the number of studies found from literature study. The top three most discussed components from the study are Reciprocal Voting, Monetary Reward, and Cognitive Effort.

5. Implication

This research has an impact on both academic and practice. Academically, the results of this study can be used as a reference for researchers who are concerned with crowdworking or crowdsourcing. There are 11 components and 38 indicators as result of the research can be used for those who are concern with trust component to develop a crowdwork system model. Practically, the company must pay good attention to these 11 components and 38 indicators, if they want to use crowdwork systems. The crowdwork platform must have a good technology aspect, clean and clear procedure about the system (from initiating, augmenting, and maintaining process), stakeholder voting, and reward procedure about the effort that provided by the crowdworker.

6. Conclusion & Future Research

Trust is critical factor to those who want implement crowdwork system. There are 11 components and 38 indicators of trust in crowdwork system as research result. This research will help the academic and practitioner related to crowdwork system. Stakeholders need to pay attention to these components and

indicators if they want to use crowdwork system, especially on reciprocal voting, monetary reward, and cognitive effort, since they are the most discussed component from literature study. The platform should allow the job provider and worker to do clean and clear reciprocal voting (more objective assessment) as well as monetary reward procedure. The platform also should provide the features that can minimalize cognitive effort to use the platform. By doing so, the issue of trust stated on introduction (unfair assessment and lack of transparency) can be overcomed.

The resulting components will be processed using quantitative methods (questionnaires) to be used as the basis for making trust system for crowdwork platform.

Conflict of Interest

The authors declare no conflict of interest during the research process.

Acknowledgment

This work is supported by Research and Technology Transfer Office, Bina Nusantara University.

References

[1] A. Kittur, et al., "The Future of Crowd Work. In Proc. CSCW (2013), 1301-18.
[2] J. Howe "The rise of crowdsourcing. Wired Magazine, **14**(6). Available at: http://www.wired.com/wired/archive/14.06/crowds_pr.html. (2006).
[3] U. Huws et al., "Crowd working survey: size of the UK's 'Gig Economy' revealed for the first time. FEPS. Available at: http://www.feps-europe.eu/assets/a82bcd12-fb97-43a6-9346-24242695a183/crowd-working-surveypdf.pdf. (2016c).
[4] U. Huws et al., Crowd working survey: new estimate of the size of Dutch 'Gig Economy'. FEPS. Available at: http://www.feps-europe.eu/assets/778d57d9-4e48-45f0- b8f8-189da359dc2b/crowd-working-survey-netherlands-finalpdf.pdf. (2016a).
[5] U. Huws et al., Crowd working survey: size of Sweden's 'Gig Economy' revealed for the first time. FEPS. Available at: http://www.feps-europe.eu/assets/3f853cec-1358-4fb4-9552-274b55e05ecf/crowd-working surveyswedenpdf.pdf. (2016b).
[6] A. Gawer "Bridging differing perspectives on technological platforms: toward an integrative framework. Research Policy **43**(7): 1239–1249. 2014.
[7] D. Ceolin et al., "Combining User Reputation and Provenance Analysis for Trust Assessment. Journal of Data and Information Quality, 7(1-2), 1–28. doi:10.1145/2818382. 2016.
[8] H. Ye, Solvers' participation in crowdsourcing platforms: Examining the impacts of trust, and benefit and cost factors. The Journal of Strategic Information Systems, **26**(2), 101–117. 2017. doi:10.1016/j.jsis.2017.02.001.
[9] J. Feller et al., 'Orchestrating' sustainable crowdsourcing: a characterisation of solver brokerages. J. Strateg. Inform. Syst. **21** (3), 216–232. 2012.
[10] D.J. Kim, A study of the multilevel and dynamic nature of trust in e-commerce from a cross-stage perspective. Int. J. Electron. Commer. **19** (1), 11–64. 2014.
[11] Porter, Constance & Donthu, Cultivating Trust and Harvesting Value in Virtual Communities. Management Science. **54**. 113-128. 10.1287/mnsc.1070.0765. 2008.
[12] D. Howcroft, Typology of Crowdwork Platforms. Work, Employment and Society, **33**(1), 21–38. https://doi.org/10.1177/0950017018760136. 2019.
[13] J. Kücklich, Precarious Playbour: Modders and the Digital Games Industry. Fibreculture Journal. 2005.
[14] Fuchs, Christian. Social Media: A Critical Introduction. London: Sage. ISBN 978-1-4462-5731-9 (pbk), 978-1-4462-5730-2 (hbk). 2014.
[15] S. Tom, What's Yours Is Mine: Against the Sharing Economy. 10.2307/j.ctt1bkm65n. 2016.
[16] S.C. Kuek et al., The global opportunityin online outsourcing, 2015.
[17] K. Cook, Trust and Governance (Braithwaite V. & Levi M., Eds.). Russell Sage Foundation. 1998. Retrieved July 3, 2020, from www.jstor.org/stable/10.7758/9781610440783
[18] K. Cook, Trust in Society. Russell Sage Foundation. 2001. Retrieved July 3, 2020, from www.jstor.org/stable/10.7758/9781610441322
[19] W. Kristof & O. Gaby. The Influence of Seller Relationship Orientation and Buyer Relationship Proneness on Trust, Commitment, and Behavioral Loyalty in a Consumer Environment. Journal for the Theory of Social Behaviour. **31** (1). 2012.
[20] D. Tranfield, D. Denyer, P. Smart, Towards a methodology for developing evidence-informed management knowledge by means of systematic review. British journal of management, **14**(3), 207-222, 2003.
[21] T. Kohler, Crowdsourcing-Based Business Models: How to Create and Capture Value. California Management Review, **57**(4), 63–84. 2015. doi:10.1525/cmr.2015.57.4.63
[22] C. Gerber, "Community Building on Crowdwork Platforms: Autonomy and Control of Online Workers?" Competition & Change, 2020. doi:10.1177/1024529420914472.
[23] K. Freitas, The Future of Work: New Roles and Capabilities for HR Thanks to Social Media. NHRD Network Journal, **11**(2), 35–43. 2018. doi:10.1177/0974173920180209
[24] W. Du, Developing and maintaining clients' trust through institutional mechanisms in online service markets for digital entrepreneurs: A process model. The Journal of Strategic Information Systems. 2018. doi:10.1016/j.jsis.2018.07.001
[25] R. Hofstetter, Should You Really Produce What Consumers Like Online? Empirical Evidence for Reciprocal Voting in Open Innovation Contests. Journal of Product Innovation Management, **35**(2), 209–229. 2017. doi:10.1111/jpim.12382
[26] H. Ye et al., Solvers' participation in crowdsourcing platforms: Examining the impacts of trust, and benefit and cost factors. The Journal of Strategic Information Systems, **26**(2), 101–117. [2017]. doi:10.1016/j.jsis.2017.02.001
[27] D.G. Rand, Human cooperation. Trends in Cognitive Sciences. **17** (8): 413–25. 2013.
[28] M.A. Nowak, Five rules for the evolution of cooperation. Science. **314** (5805): 1560–63. 2006.
[29] R.M. Axelrod, The evolution of cooperation. New York: Basic Books. 2006.
[30] R.L. Trivers, The evolution of reciprocal altruism. Quarterly Review of Biology. **46** (1): 35–57. 1971
[31] R.A. Clark, Global innovativeness and consumer susceptibility to interpersonal influence. Journal of Marketing Theory and Practice. **14** (4): 275–85. 2006.
[32] D.B. Wooten, Informational influence and the ambiguity of product experience: Order effects on the weighting of evidence. Journal of Consumer Psychology. **7** (1): 79–99. 1998.
[33] R. Cooper, Perspective: The Stage-GateVR idea-to-launch process—Update, what's new, and NexGen systems. Journal of Product Innovation Management. **25** (3): 213–32. 2008.
[34] R. Sethi et al., Stage-gate controls, learning failure, and adverse effect on novel new products. Journal of Marketing **72** (1): 118–34. 2008.
[35] C. Terwiesch, Innovation contests, open innovation, and multiagent problem solving. Management Science. **54** (9): 1529–43. 2008.
[36] J. Braverman, Testimonials Versus Informational Persuasive Messages. Communication Research, **35**(5), 666–694. 2008. doi:10.1177/0093650208321785
[37] H.B. Brosius, The utility of exemplars in persuasive communications. Communication Research, **21**, 48-78. 1994.
[38] P.R. Dickson, The impact of enriching case and statistical information on consumer judgments. Journal of Consumer Research, **8** (4), 398-406. 1982.
[39] E.J. Baesler et al., The temporal effects of story and statistical evidence on belief change. Communication Research, **21** (5), 582-602. 1994.
[40] M.C. Green et al., The role of transportation in the persuasiveness of public narratives. Journal of Personality and Social Psychology, **79**, 701-721. 2000.
[41] M.D. Slater, Value-affirmative and value-protective processing of alcohol education messages that include statistical evidence or anecdotes. Communication Research, **23**, 210-235. 1996.
[42] J. Howe, Crowdsourcing: why the power of the crowd is driving the future of business. Crown Bus. 2008
[43] N. Kaufman et al., More than fun and money: worker motivation in crowdsourcing- a study on Mechanical Turk. In: Americas Conference on Information Systems, Detroit, Michigan. 2011.
[44] D.C. Brabham, Moving the crowd at iStockphoto: the composition of the crowd and motivations for participation in a crowdsourcing application. First Monday. **13**. 2008

[45] D.C. Brabham, Moving the crowd at Threadless: motivations for participation in a crowdsourcing application. Inform., Commun. Soc. **13** (8), 1122–1145. 2010.
[46] H. Zheng, "Task design, motivation, and participation in crowdsourcing contests. Int. J. Electron. Commer. **15** (1), 57–88. 2011
[47] C. Terwiesch et al., Innovation contests, open innovation, and multiagent problem solving. Manage. Sci. **54** (9), 1529–1543. 2008
[48] L.D. Molm, " Coercive Power in Social Exchange. Cambridge University Press, New York. 1997.
[49] M.M. Wasko, Why should I share? Examining social capital and knowledge contribution in electronic networks of practice. MIS Quart. **29** (1), 35–57. 2005.
[50] G.W. Bock, R.W. Zmud, Behavioral intention formation in knowledge sharing: examining the roles of extrinsic motivators, social psychological forces, and organizational climate. MIS Quart. **29** (1), 87–111. 2005.
[51] Boudreau, K.J., Lakhani, K.R. How to manage outside innovation. MIT Sloan Manage. Rev. **50** (1), 69–76. 2009
[52] M. Boons et al., Feelings of pride and respect as drivers of ongoing member activity on crowdsourcing platforms. J. Manage. Stud. **52** (6), 717–741. 2015.
[53] A. Kankanhalli, Comparing potential and actual innovators: an empirical study of mobile data services innovation. MIS Quart. **39** (3), 667–682. 2015.
[54] R.E. Petty et al., The effects of group diffusion of cognitive effort on attitudes: an information-processing view. J. Pers. Soc. Psychol. **38** (1), 81–92.1980.
[55] E.C. Garbarino, Cognitive effort, affect, and choice. J. Consum. Res. **24** (2), 147–158. 1997.
[56] A. Afuah, C. Tucci, Crowdsourcing as a solution to distant search. Acad. Manage. Rev. **37** (3), 355–375. 2012.
[57] H.Ye, A. Kankanhalli, Investigating the antecedents of organizational task crowdsourcing. Inform. Manage. **52** (1), 98–110. 2015
[58] A. Kankanhalli et al., Contributing knowledge to electronic knowledge repositories: an empirical investigation. MIS Quart. **29** (1),113–143. 2005.
[59] T. Krishnaprasad, P. Anantharam, C. A. Henson, and A. P. Sheth. Comparative trust management with applications: Bayesian approaches emphasis. Future Generation Computer Systems. **31**. 182–199. 2014.
[60] J. Gao, Zhou, T. Evaluating user reputation in online rating systems via an iterative group-based ranking method. Physica A: Statistical Mechanics and Its Applications, **473**, 546–560. doi:10.1016/j.physa.2017.01.055. 2017.

ASTES

Advances in Science, Technology and Engineering Systems Journal Vol. 5, No. 5, 364-369 (2020)

www.astesj.com

ASTESJ

ISSN: 2415-6698

Modelling and Simulation of Reduce Harmonic Distortion in Non-linear Loads

Agus Junaidi[*,1], Rahmaniar[2], Rudi Salman[1], Joni Safrin Rambey[1], Baharuddin[1]

[1]*Department of Electrical Engineering, Faculty of Engineering, Universitas Negeri Medan, Medan, 20221, Indonesia*

[2]*Department of Electrical Engineering, Faculty of Engineering, Universitas Pembangunan Panca Budi, Medan 20122, Indonesia*

ARTICLE INFO

Article history:
Received: 27 July, 2020
Accepted: 29 August, 2020
Online: 17 September, 2020

Keywords:
Harmonics
Wave Defects
Non-linear Loads
Active Filter

ABSTRACT

Harmonic distortion is a problem that can be caused by the use of power electronic devices. The effect of harmonics has an impact on changes in the input voltage source waveform which is referred to as wave defects. This incident has an impact on electronic faults and overheating of the power transformer coil as a supplier. One cause of the emergence of harmonics is the use of non-linear loads on the electric power system. Utilization of non-linear loads such as arc fires (metal casting), welding, magnetic core in transformers and rotating machines, synchronous machines, adjustable speed drives, solid-state switches High voltage DC transmission and Photovoltaic invertors can produce input wave defects. The filter is modelled through a reference current which is used as a PWM pulse generator reference signal to trigger the inverter, further generating a filter current that is injected into the system. Inverter control uses the Propositional Integrator (PI) control approach. From the simulation test results using the Psim software, it is shown that the recorded input waves due to harmonic distortion can be corrected by placing an active filter into the power system.

1. Introduction

Modeling and simulation have been widely applied in the field of electric power systems, through modeling and simulation, being able to observe and analyze system performance like the actual system, this is done by simulation [1]. The use of various power electronic equipment such as power converters and other non-linear loads in the industry and by consumers at this time has an impact on an increase in damage to the electrical system voltage and distorted waveforms called harmonics. The presence of harmonics in the power grid results in greater power losses in distribution, disruptions in communication systems and the chance of failure of the operation of electronic equipment that has high sensitivity, including microelectronic control systems. Power quality problems that occur in consumers due to harmonics are a serious concern [2]. Power quality problems that occur to consumers due to harmonics are a serious concern. International standards on electric power quality (IEEE-519, IEC 61000, EN 50160) insist that electrical equipment and facilities should not produce harmonic content greater than the value specified, and also sets a distortion limit to the supply voltage. So that efforts to control harmonics can be done one of them by using active filters [3-5].

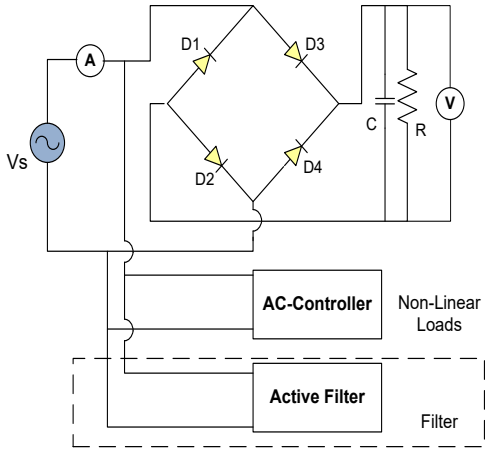


Figure 1: Non-Linear Loads System using Active Filter

Figure 1 shows a non-linear load consisting of a single-phase AC to DC converter with a C filter and a controlled AC load, which are two non-linear loads that cause harmonic generation.

[*]Corresponding Author: Agus Junaidi, Department of Electrical Engineering Faculty of Engineering, Universitas Negeri Medan, Indonesia 20221, agusjunaidi@unimed.ac.id

An active filter injects current output which will reduce harmonics due to the two non-linear loads. Problems from non-sinusoidal currents due to non-linear loads. The pulsed current has been discussed (corrected) using the "hight power factor pre-regulator" with an uncontrolled rectifier load with a boost converter, this has been discussed in [2]. Application of use for this system if used on a heater can change the system output (output). The processing power demand of a very large pre-regulator with AC control produces harmonics.

Harmonics are a series of current or voltage waves whose frequency is an integer multiple of the base frequency of the voltage or current itself [9]. The integer multiplier at the frequency of the harmonics is the order of n of the harmonics. For example, the basic frequency of an electrical system in Indonesia is 50 Hz, so the second harmonics are 2 x 50 Hz (100 Hz), the third is 3 x 50 Hz (150 Hz), and so on until the nth harmonics that have n x 50 Hz frequencies. Wave defects caused by interactions between the system's sinusoidal waveforms and other wave components are better known as harmonics, which are other wave components that have integer multiples frequencies from their fundamental components.

2. Inverter and Control Equivalent Models

A Circuit-equivalent Models for Current-controlled Inverters are used as a control circuit for Models for Three-Phase Inverters [10]. however, in this design, Single-phase inverters are used as active filters to reduce harmonics. Use of a single-phase full-bridge inverter as an active filter. The use of Fuzzy control has been recommended to minimize harmonics in single-phase inverters. In a conventional PWM inverter, a gate signal for the switching element in the first leg will be generated compared to a sinusoidal modulation signal via a triangle carrier wave. A phase shift signal of 180 ° from the first foot is applied to the second leg of the inverter. The gate signals for switches S1, S4 and S2, S3 are synchronized respectively [11]. Figure 2 shows the inverter used as an active filter.

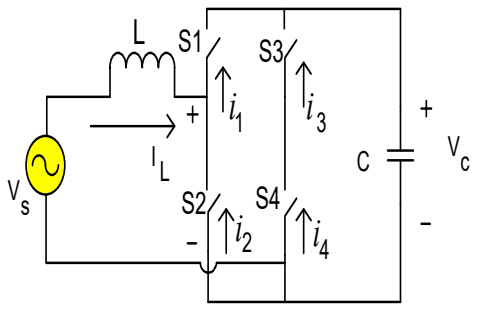


Figure 2: Single-Phase Inverters are Used as Active Filters

Figure 2 shows the active filter scheme, assuming that $Vc > |Vs|$. During the positive half-wave source voltage, i_L The value can be set to a positive value by making $Vx = 0$; I_L can be set near zero by making $Vx = Vc$, During the half-wave negative.

source voltage, iL will be negative by making $Vx=0$; iL can be set to zero by making $V_x = -V_c$. Specifically switches S_3 and S_4 can be used to strengthen $Vx \leq 0$ and $Vx \geq 0$, respectively, while switches S_1 and S_2 are used to activate I_L.

For modelling and control, assume the state of each inverter switch is.

$$u_x = \begin{cases} 1 \text{ if } S_x \text{ conduct} \\ 0 \text{ if } S_x \text{ open} \end{cases} \quad (1)$$

equation (1) Subscripts of x indicate the switch, as in

$$u_1 + u_2 = 1 \quad (2)$$

and,

$$u_3 + u_4 = 1 \quad (3)$$

A definition of u for other switches will be obtained, $V_x = [u_1 u_4 - u_2 u_3]Vc$. Or, using an equation $V_x = [u_1 + u_4 - 1]$ Vc, and $i_c = [u_1 + u_4 - 1]\ i_L$. With the above analysis, the equation for the inductor current and the capacitor voltage is obtained

$$\dot{i}_L = \frac{1}{L}[\text{Vs} - [u_1 + u_4 - 1]\text{ Vc}] \quad (4)$$

$$\dot{v}_c = \frac{1}{C}[u_1 + u_4 - 1]i \quad (5)$$

For active filter applications, we can define line currents, as in

$$i_s^* = k.v_s \quad (6)$$

where k is a scale factor based on the real power required by the load,

$$s = i_s - k.v_s = 0; \quad s\dot{s} \leq 0 \quad (7)$$

From equation (7) we can control $\dot{s}$ to control $\dot{i}_s$. Filters can make $\dot{i}_s$ positive or negative according to switch operation. Besides, the accuracy of this design ensures $|\dot{i}_s| > |k\dot{i}_s|$. From equation (7) we can control to control. Filters can make positive or negativity according to switch operation. Besides, the accuracy of this design ensures $|\dot{i}_s| > |k\dot{i}_s|$. for the u_1 value under the $i_s < k.v_s$ condition the filter control constant used is 0. Whereas for the u_1 value under the $i_s > k.v_s$ condition the filter control constant used is 1. for the u_3 value under the $i_s < k.v_s$ condition the filter control constant used is 0. whereas for the u_1 value under the $i_s > k.v_s$ condition the filter control constant used is 1. The active filter control value setting for a non-linear load is shown in table 1.

Table 1: The Nonlinear Control Setting Used in the Application of an Active Filter

Control setting	$i_s < k.v_s$	$i_s > k.v_s$
u_1	0	1
u_2	1	0
	$v_s < 0$	$v_s > 0$
u_3	1	0
u_4	0	1

3. Concept of Equivalent Control and Control design for Active Filters.

The concept of equivalent control is based on shift control. From Kirchhoff's law, the current at the source will be obtained,

$$i_s = i_L + i_{loads} \quad (8)$$

where I load is a combination of current from a nonlinear load, then,

$$\dot{s} = \dot{i}_s - k\dot{v}_s \tag{9}$$

for current (i_{loads}), as in

$$\dot{i}_{loads} + \frac{1}{L}[v_s - [u_1 + u_4 - 1]v_c] - k\dot{v}_s = 0 \tag{10}$$

From table 1 we get the equation,

$$u_4 = \frac{1+\text{sgn}(v_s)}{2} \tag{11}$$

where,

$$\text{sgn(x)} = \begin{cases} 1 & \text{for} \quad x > 0 \\ -1 & \text{for} \quad x < 0 \end{cases} \tag{12}$$

Equivalent control for S_1, as in

$$u_{1eq} = \frac{L}{v_c}\left[i_{loads} - k\dot{v}_s\right] + \frac{v_s}{v_c} + \frac{1-\text{sgn}(v_s)}{2} \tag{13}$$

Active filter circuit design based on Figure 2, then we can take the equation:

$$i_L = i_{\text{line}} - i_{\text{loads}} \tag{14}$$

and,

$$i_{\text{line}} = \frac{\sqrt{2}P_{loads}}{V_{rms}} \sin \omega t \tag{15}$$

$$q_c = [u_1 + u_4 - 1]\, i_L\, T \tag{16}$$

where T is the switching period. Whereas the current equation is,

$$i_c = \left[u_{1eq} - \frac{1}{2}\frac{\text{sgn}(v_s)}{2}\right] i_L \tag{17}$$

where T is the switching period. Whereas the current equation is

$$v_c = V_o + \frac{1}{\omega C}\int_0^{\omega t}\left[u_{1eq} - \frac{1}{2} + \frac{\text{sgn}(v_s)}{2}\right] i_L\, d(\omega t) \tag{18}$$

$$v_c = V_o + \sqrt{\frac{2}{C}\left\{\frac{1}{\omega}\int_0^{\omega t} v_s i_L\, d(\omega t) - \frac{1}{2}Li_L^2\right\}} \tag{19}$$

The inductance value of filter L is determined by equation (19). With u_{1eq} it is running from u_1. In this equation, the determination of the limit u1 is $0 \le u_{1eq} \le 1$. The PI control will be used to adjust the capacitor current. Changes in current capacitors will be related to changes in the magnitude of the line current and changes in the average power caused by nonlinear loads. Capacitor current is connected to the low-pass filter which produces an average capacitor current. $\bar{i}_c$ will be compared between the nominal capacitor current and the difference from the PI control. The PI control output, the comparison factor, k, is used to control the reference for the line current.

4. Simulation of a Non-linear Loads without Active Filter and using Active Filter

4.1. Non-linear Load Simulation without Active Filter

Figure 1 is used as a basis for simulating the use of active filters in non-linear loads, the system can be simulated with the Psim program. Where here will be compared the results of system simulations without using an active filter with a system that uses an active filter. The parameter values used in this simulation can be seen in table 2.

Table 2: Data for Simulation Tests

Name	Symbol	Value
AC Controller	R	30 Ω
Uncontrolled Rectifier	C	1250 µF
	R	33 Ω
Aktif Filter	L	1.75 mH
	C	1280 µF

Based on the parameters above, the system in the simulation with the Psim program can be seen in figure 3, where the system with two nonlinear loads without using an active filter.

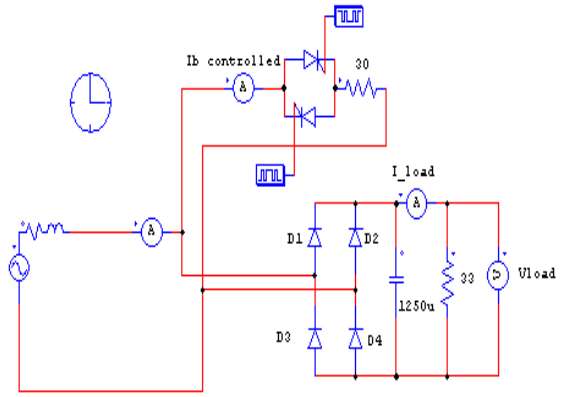


Figure 3: Simulation Non-Linear Loads without Active Filters

Figure 3, shows an electric circuit with multi-non-linear loads. The image is a reference in simulating the effect of non-linear loads. The circuit image consists of a single-phase rectifier with a C filter. On the other hand, a controlled AC load is also installed as assuming a non-linear multi-load. Input voltage 220 Volt with a frequency of 50 Hz as a source to supply non-linear load needs. A simulation device for measuring the input current waveform is mounted on the input and output loads. To see the effect of non-linear load performance. A single-phase rectifier uses a capacitor filter in parallel with another load that is a controlled AC load. Each load is connected to an AC voltage source of 220 V, 50 Hz. The simulation uses Psim software, with the simulation results shown in figure 4 a-d.

Figure 4.a shows the output waveform of a controlled rectifier as a non-linear load. Rectifier that converts an AC source to DC for a specific load requirement.

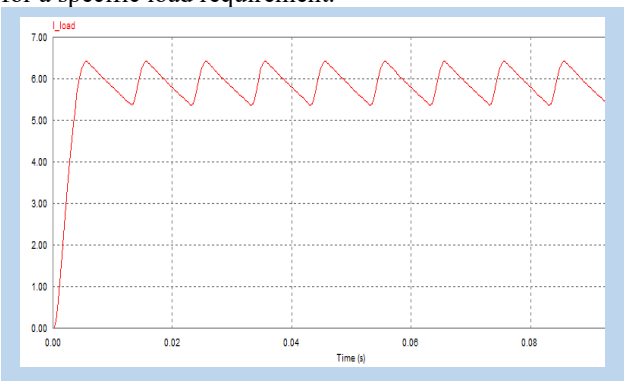


Figure 4.a: Load Current in Single-Phase Rectifier

The effect of ripple reduction in a rectifier using the C input filter causes the input current source to become distorted, as shown in figure 4.b

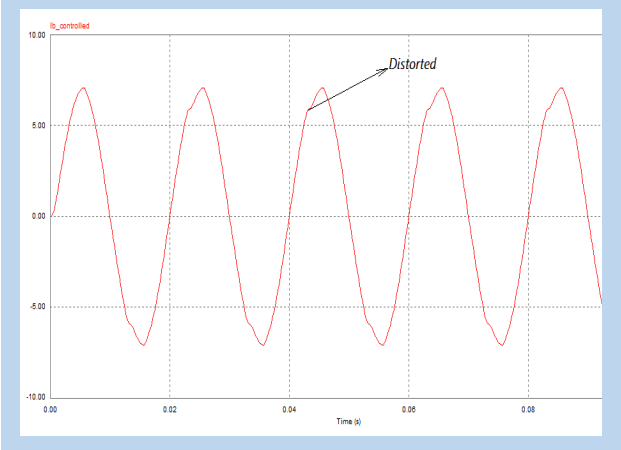


Figure 4.b: Input current at controlled AC load

The input current at a non-liner load without using a filter indicates that the input waveform has been distorted, such as the simulated display shown in figure 4.c

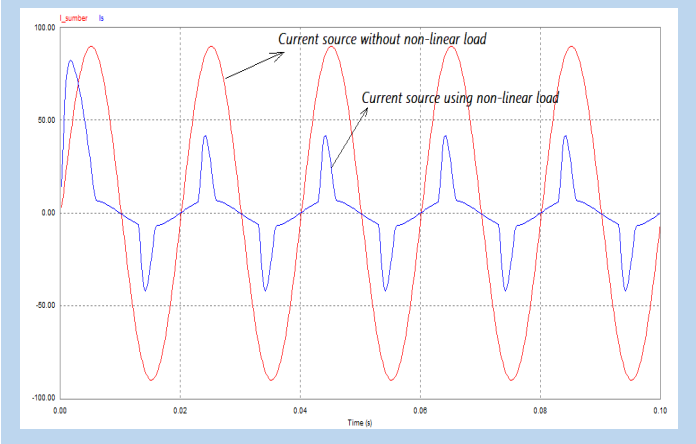


Figure 4.c: Current Source Using Non-Linear Loads and Current Source without Non-Linear Loads.

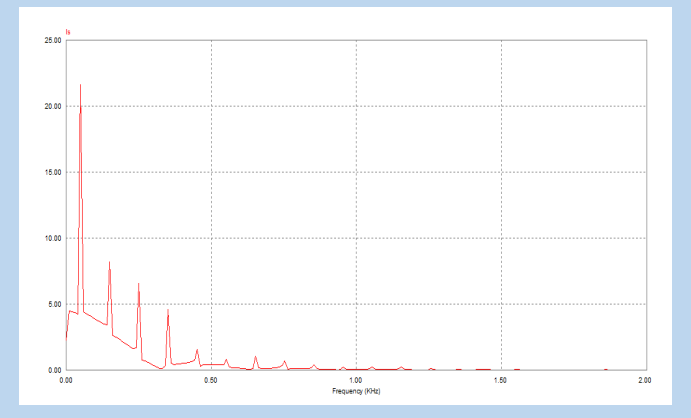


Figure 4.d: Harmonic Spectrum- FFT Input Current of Non-Linear Loads without Active Filters

Figure 4.a is the output of a single-phase wave rectifier with filter C. Filter C is intended to reduce the ripple in the need for a direct current source, generated by the rectifier. Figure 4.b is a display of input waves from a controlled AC load. From the picture, it can be seen that the waveform is not sine (distorted) this is due to the effect of the controlled AC load, Whereas Figure 4.c. shows the comparison of the source current when not yet burdened by non-linear loads, and after being burdened by non-linear loads. From the image display, there is a distortion in the source current wave. This is caused by the influence of two non-linear loads attached to the circuit. Furthermore, to see the amount of distortion caused by harmonics, the harmonic spectrum in Figure 4.d shows the suitability of the harmonics in the source current [12]. wave form the current in each phase is not pure sinusoidal, meaning that the system current has been distorted by harmonics due to non-linear loads. The simulation results for the current harmonic spectrum in Figure 4.d can be seen the THD Harmonics value as in Table 3.

Table 3. Harmonics Input Currents Without Active Filters

Harmonic components	Freq. (Hz)	Current (I_S)
Fundamental currents	50	19.0
3rd Harmonics (I_3)	150	6.78
5rd Harmonics (I_5)	250	5.65
7rd Harmonics (I_7)	350	4.02
The 9rd Harmonics (I_9)	550	1.51
Total Harmonic Distortion (THD) %		51.65

The harmonic distortion value in the harmonic spectrum simulated in Figure 4.d is 51.65%, while according to the IEEE 519-1992 standard it has been set that the allowable THD limit is 15%. From the calculation results, total harmonic distortion (THD) in table 3 has exceeded the standard. Harmonic improvement due to non-linear loads is carried out by installing active filters, to observe the effect of active filters in reducing harmonic distortion.

4.2. Simulation of a Nonlinear Loads using Active Filter

The filter design to reduce harmonics in this simulation uses active filters that are controlled using PI controls. The active filter is a new type of harmonic elimination filter device in the power system. This filter is composed of power electronic devices. The main components contained in the active filter area. Inverter The inverter is used as an active filter that is connected in parallel with the load voltage source to compensate for the harmonics. Controller The controller is used in an active filter circuit to reduce the error signal at the load voltage source. The non-linear load simulation design mounted on the active fist is shown in Figure 5.

The working principle of the shunt active filter is to compensate for the load current in a simple way, namely injecting harmonic currents whose phase is 180^0 different from that of the load generated, thereby eliminating each other. The active filter gets the input from the source voltage and load current which is used to obtain the harmonic reference current in the control system. Theory reactive active power (p-q) is used as a control to get reference current. The reference current will be used to reference the PWM generator which will be compared with the carrier signal which will generate pulses. The pulse is used to trigger the inverter which is then used to generate a filter current wave for injection. Use of VSI (Voltage Source Inverter) to allow the adjustment of harmonic currents in the active filter. This inverter uses a dc capacitor as supply and can perform a switching process at high

frequencies to produce a signal that is able to overcome the harmonic currents generated by non-linear loads. Proportional integral control (PI) with the input signal in the proportional integral control with a filter amplifier (LP) is the difference between the harmonic signal from the band pass filter, the inverter output signal is negative feedback, this PI control is used in the Voltage Source Inverter control as an active filter.

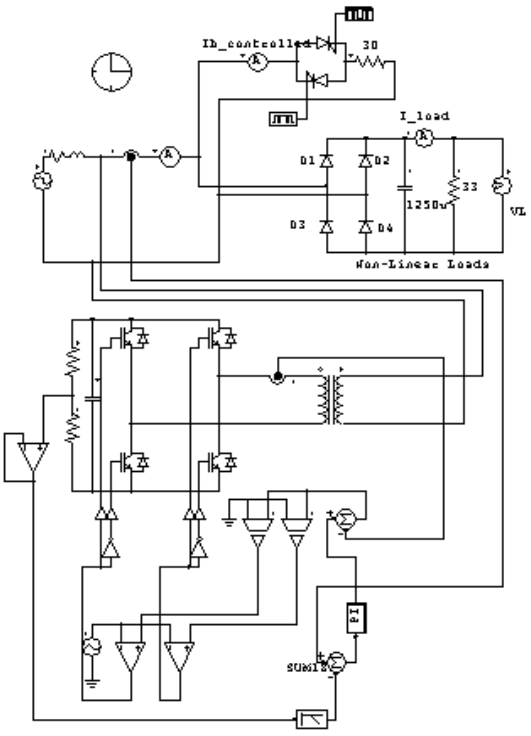


Figure 5: Simulation Circuit of Non-Linear Load using Active Filter

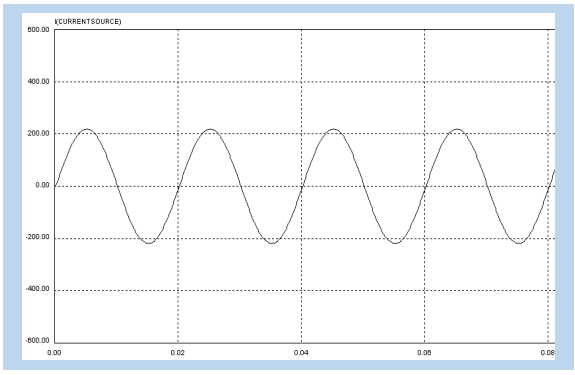


Figure 6. a: Source Current Waveform using Active Filter



Figure 6.b: Harmonic Spectrum-FFT Input Voltage

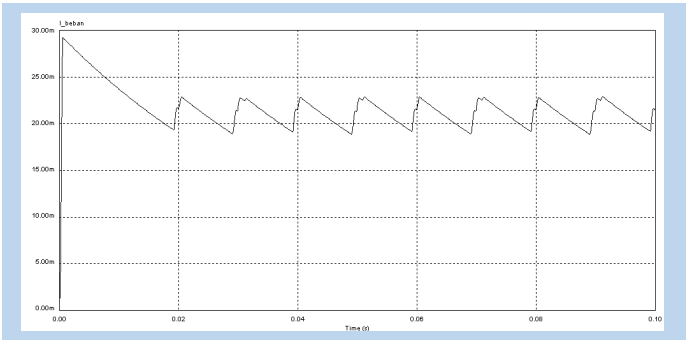


Figure 6.c: Load Current Waveforms

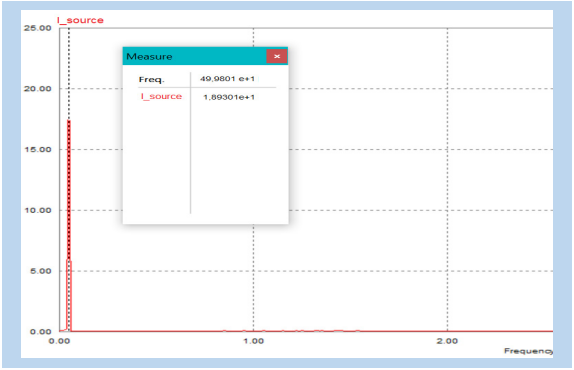


Figure 6.d: Harmonic Spectrum-FFT Input Current

Figure 5, shows a simulation of a non-linear load mounted on an active filter. Observation of simulation performance through the effect of filter installation on the input current. Without an active filter, it can be seen that there are harmonics in the input current due to the non-linear load. After installing the active filter, the simulation results are shown in Figure 6 (a-d).

Figure 6 a-d shows the simulation results of each non-linear load using an active filter. The response plot from the simulation results shows that wave defects in the input current arising from non-linear harmonic loads can be reduced using active filters using PI control.Figure 6.1 is a form of input current using an active filter with a DC voltage output from the load rectifier shown in Figure 6.c.

Figures 6.c and 6d show the harmonic spectrum for input voltage and input current using active filters, respectively. It can be seen from the observation that harmonics can be reduced using an active filter, so that the FFT of the spectrum in Figures 6.c and 6.d is only the fundamental voltage and current at the fundamental frequency of 50 Hz, shown in table 4.

Table 4. Harmonics Input Currents and Voltage Using Active Filters

Harmonic components	Freq. (Hz)	Current (I_S)
Fundamental current	49.9801	18.93
Fundamental Voltage	50.82	219.03

From these results it can be seen that the difference in harmonic improvement without using an active filter (table 3) and by using an active filter (table 4). From the two comparisons, the results show that the use of an active filter can improve the input current wave defects (system harmonics), based on the IEEE 519-1992 standard, the harmonics are less than 5%.

5. Results and Discussion

From the circuit simulation in Figure 3 with an unfiltered system and Figure 6. which illustrates the system using an active filter, the following results will be shown: When a single-phase source is connected to a multi-linear non-load system, the controlled rectifier and AC load driver causes the input side, the current to be distorted and contain harmonics as shown in Figures 4.b and 4c. The FFT of the input current containing harmonics is shown in Figure 4.d. showing non-sinusoidal current waves. Input currents have pulsating (wave vibrations) if the system is maintained with non-sinusoidal conditions that will affect the system's work and can damage the equipment. (heating of the winding and transformer core). The non-linear multi-load system is connected in parallel with a single-phase active filter as shown in figure (5). To keep producing a DC output like Figure 6.c, the rectifier is given a filter capacitor, as a result, a wave defect will occur. This wave defect is corrected with an active filter so that the current at the input side will return sinusoidal as shown in Figure 6.a. Simulation results for multi-load non-linear with active filter show the waveform on the input side (Source Side) again does not experience waveforms (distorted) spectrum harmonics (FFT) seen in Figure 6.b only fundamental harmonics only, this shows that the use of active filters reduces harmonics and corrects input current waveform defects.

6. Conclusion

Non-linear load simulation without active filter and using an active filter with PI control, it can be concluded:

- Non-linear load distorts the input current. The harmonics content in the input current through the FFT plot graph shows the harmonics 3, 5, 7 dan 9 have significant values.
- PI control system inputted on the inverter circuit as an active filter has a good function in reducing harmonics. The simulation results show that the input current FFT after using an active filter is only the fundamental current. This shows that harmonics have improved with the installation of an active filter.

Conflict of Interest

The authors declare that there is no conflict of interests regarding the publication of this paper.

Acknowledgement.

This research did not receive any specific grant from funding agencies in the public, commercial, or not-for-profit sectors. This paper was produced from the results of research activities supported by LPPM UNIMED

Reference

[1] A. Rahmaniar, A. Junaidi, Ganefri, A.Hamid K, N.Jalinus, J.Jama, " Modelling and Simulation: An Injection Model Approach to Controlling Dynamic Stability Based on Unified Power Flow Controller," Journal of Theoretical and Applied Information Technology, **97**(20), 2334-2345, 2019.

[2] M. Halpin, W.Xu, S Ranade, P.F. Ribeiro."Tutorial on Harmonics Modeling and Simulation", IEEE Power Engineering Society Harmonics Working Group, 1998

[3] F. Z. Peng, George W.O. Jr, D.J. Adams, "Harmonic and Reactive Power Compensation Based on the Generalized Instantaneous Reactive Power Theory for Three-Phase Four-Wire Systems," IEEE Transactions On Power Electronics, **13**(1), 1998. DOI**:** 10.1109/63.728344

[4] M. Rafiei, H. Toliyat, R.G. T. Gopalarathnam, "An Optimal and Flexible Control Strategy for Active Filtering and Power Factor Correction Under Non-Sinusoidal Line Voltages", IEEE Transactions On Power Electronics, **13**(16), 2001, DOI: 10.1109/61.915499

[5] K. Hemachandran, B.Justus, S.S. Darly, "Harmonic Mitigation In A Single Phase Non-Linear Load Using SAPF With PI Controller" Recent Advances in Electrical Engineering and Computer Science, 157-161, 2015, Doi: 10.13140/RG.2.1.2897.7365.

[6] Faiz J, Shahgholian G," Modeling And Simulation Of A Three-Phase Inverter With Rectifier-Type Nonlinear Loads", Armenian Journal of Physics, **2**(4), 307-316, 2009.

[7] J.R. Johnson, "Managing harmonics and resonance with active harmonic filters in an offshore ring main oil field," in 13th International Conference on Harmonics and Quality of Power, 2008, DOI: 10.1109/ICHQP.2008.4668749

[8] S.M. Adnaan, " Design And Simulation Of A Nonlinear Load Model Used to Simulate Voltage Notches And Harmonics Caused By A 6-Pulse Three-Phase Rectifier," International Journal of Science, Engineering and Technology Research, **06**(06), 984-995, 2017.

[9] E.H Mayoral, M. A. H López, E.R Hernandez, H.J.C. Marrero, J.R.D Portela, V.I.M Oliva, " Fourier Analysis for Harmonic Signals in Electrical Power Systems", InTech, 2017.

[10] B. Johnson, Minghui Lu, V.Purba, S.Dhople, "Circuit-equivalent Models for Current-controlled Inverters", IEEE, 2019, DOI: 10.1109/COMPEL.2019.8769670

[12] D. A. Torrey, A.M.A.Zamel, "Single-Phase Active Power Filters for Multiple Non-Linear Loads," IEEE Transactions on Power Electronics, **10** (3), 1995, DOI**:** 10.1109/63.387990.

[13] D. Shmilovitz, "On the Definition of Total Harmonic Distortion and Its Effect on Measurement Interpretation," IEEE Transactions On Power Delivery, **20**(1), 2005, DOI: 10.1109/TPWRD.2004.839744.

ASTES

Advances in Science, Technology and Engineering Systems Journal Vol. 5, No. 5, 370-375 (2020)

www.astesj.com

ASTESJ

ISSN: 2415-6698

Using Envelope Analysis and Compressive Sensing Method for Intelligent Fault Diagnosis of Ball Bearing

Khaldoon Fadhel Brethee*, Ghalib Rzayyig Ibrahim, Rashaq Abdullah Mohammed

Mechanical Engineering Department, Engineering College, University of Anbar, Al-Anbar, 10081, Iraq

ARTICLE INFO

Article history:
Received: 30 July, 2020
Accepted: 11 September, 2020
Online: 17 September, 2020

Keywords:
Ball bearing
Fault diagnosis
Vibration signal
Big data acquisition
Compressive sensing

ABSTRACT

Bearings are the key components of many rotating machines, in which serious failure or even major breakdown may occur due to their abnormal operation and defects. Thus, accurate fault diagnoses of bearing elements are essential for proactive predictive maintenance. However, the using of multiple sensors with high sampling rate reveal considerable shortages in the analysis of big data acquisition. Therefore, compressive sensing (CS) proposes in this study to overcome the aforementioned problems and support the fault diagnostic approach of ball bearing defects. The amount of data processed by CS technique can be significantly reduced to be more reliable for backup data. It can be a collaborative reconstruction method to compress the sampling data size and reliably exploiting similar sparsity structure of the acquired signal. Little attention has been paid for practically used sparseness of the CS converted signal in early fault detection of defects in ball bearing. Envelope analysis and CS technique are employed on experimental vibration data for fault detection in inner race and outer race of ball bearing. The results show that the reconstructed CS signal can characterize reliable features for bearing fault detection with some limitations in the range of compression ratio (up to 40%) and the selection of reconstructed sparse bandwidth. Hence, envelope analysis can provide optimal bandwidth to reconstruct the sparse modulated signal of ball bearing to overcome the limitation of the CS method.

1. Introduction

Ball bearing is widely used to support rotors in rotating machinery, in which its failure is one of the foremost causes of system breakdowns. The faults in bearing could inevitably cause serious failures or even catastrophic damages to the machinery. Fatigue fracture, flacking, crack and wear are the most common failure modes of bearing, which starts by spalling in the bearing raceway and becomes more severe over a period of time. This may result in extensive damage to the operating mechanism of the bearing and the system assembly. Proper operation of bearing can be achieved by careful handling and right usage operation. The lifespan is relatively long, and it may eventually fail due to overloading, which result in significant increase in noise and vibration. Therefore, it is important to monitor the condition of the rotating machine elements, which is often effective to indicate the condition of raised faults at early stages. However, the using of multi sensors with high rate data acquisition comprise considerable shortages in transferring, storage and processing the acquired data, which is a major challenge in the detection efficiency [1-2].

The signature of bearing fault is generally masked by noise and spread over a wide frequency band, which make difficulties in fault diagnosis. Thus, different techniques have been used in various studies to detect various bearing faults at the early stages [3]. This can help to avoid long-term breakdown of the machinery. Vibration analysis is an effective way for condition assessment and fault diagnostics of various mechanical equipment applications. It can be processed with wide diversity signal processing methods to give valuable information for early detection of the abnormality in the bearing structure [4]. Basically, time domain and frequency domain analyses are used for tracking machinery operating conditions. Hence, various studies aimed to detect and diagnose the existence of a localized defect in bearing by using efficient time and frequency domain methods. Envelope analysis or demodulation extraction is an effective technique used for the fault detection approach from the amplitude variation of modulated signal [5]. It is widely used for detecting harmonics from the spectrum of vibration signal based on high frequency resonance techniques [6]. The envelope analysis has increasingly used in monitoring the health condition of bearings due to its simplicity and strength [7]. However, making envelope analysis suitable for

*Corresponding Author: Khaldoon F. Brethee, University of Anbar, Iraq, khaldon77m@uoanbar.edu.iq

speed and load transients are constrained and the defect information is not obvious and the selection of optimal band is the most difficult task.

Online monitoring of machinery elements requires analyse of big data acquisition to simultaneously propose real time condition monitoring approach. The continuous data streams should be analysed without distortion or being affected by scalability, which may put a big challenge for integrating the predictive maintenance decision. The powerful analysis of big data provides reliable decision support to detect the abnormality within the system components and indicate its performance. However, sampling rate is the major limit for acquiring big data acquisition. To get a good balance between a big data acquisition and the limitations of sampling theory, compressive sensing (CS) is a new signal processing technique, which can be used in machine condition monitoring due to its ability to sample the signal below the Nyquist sampling rate [2, 8]. CS is widely used in various applications such as medical imaging, seismic imaging, communications and networks [9-11]. It can reduce the big data by a down-sample strategy with preserving reliable extraction of fault features [12]. The compression approaches can help the measuring of wireless transmission data by reducing its volume, hence significant reduction in energy consumption of wireless communication can be achieved [13-14]. The CS method can overcome the problem with the sampling, storage, transmission, and processing of big data acquisition.

The detection of bearing's fault feature can be extracted from the sparse samples of the vibration signal based on reconstruction compressive sensing signal. The CS can improve the condition monitoring approaches to be smaller, cheaper and efficient for used power in wireless devices [13]. It has the capability to develop useful information for condition monitoring of roller bearing with high level of accuracy [6, 8, 15-17], However, little attention has been paid for providing good sparseness of the CS converted signal, and apply it in fault diagnosis of ball bearing defects.

This study uses envelope analysis and CS method for monitoring and fault diagnosis of ball bearing defects, based on frequency shift and envelope analysis. These techniques has performed on vibration signal that acquired from experimental test of a ball bearing presented in an induction motor. It is expected that the CS approach achieves better classification accuracy for the purposed fault diagnosis from down sampling of the acquisition data.

2. Envelope Analysis

This method is mainly used to extract the periodic excitation in vibration signal of machinery, which can be used to detect and diagnose various defects in bearing. It has the ability to extract the amplitude modulated of vibration signal due to fault symptoms based on selected band pass filter. Figure1 shows the general steps of envelope analysis method for detecting process, which based on the following equations [5, 15-16]:

$$X(f) = \int_{-\infty}^{\infty} x(t) e^{-j\omega t} dt \tag{1}$$

$$x(n) = \frac{1}{N} \sum_{k=0}^{N-1} X(f)\, e^{-j\omega kn} \tag{2}$$

$$x_{env}(n) = \sqrt{x(n)\, x^*(n)} \tag{3}$$

$$X_{env}(k) = \sum_{k=0}^{N-1} x_{env}(n)\, e^{-j\omega kn} \tag{4}$$

where, X(f) is the fast Fourier transform of the raw vibration signal x(t). x(n) is the resampled signal based on the selected bandwidth with N number of samples. The analysed envelope signal is x_{env} and its envelope spectrum is X_{env}. The main advantage of the envelope analysis is reliable fault detection of wide frequency range within certain frequency bands, which gives high excitation related to the impact of fault frequency. However, the envelope analysis is often mixed with noise, which may add some difficulties for the effective extraction of fault features.

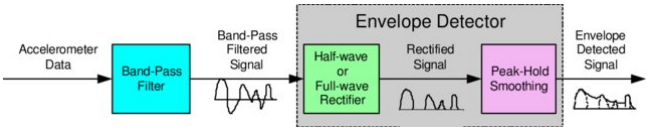


Figure 1: The general steps of envelope analysis method [18]

3. Theory of Compressive Sensing

In order to overcome the limitation of the sampling rate and processing of big data acquisition, compressive sensing method has been developed to resample the signal below the Nyquist sampling rate and express reliable sparse signal. The original signal, x(t) is reconstructed and multiplied by a sensing matrix to perform the compressed data, which denoted by y, as [6, 8-12]:

$$y = \Phi x \tag{5}$$

where, Φ is a random sensing matrix with size of $M \times N$. M is the length of compressed signal (y) with size of $M \leq N$.

The sparse components are produced with the dictionary of sparsifying transform Ψ by the following equation:

$$y = \Phi \Psi \eta \tag{6}$$

The proposed CS strategy is used for defecting bearing's fault from the representation η of the sparse signal x, which can be demonstrated in figure 2. Before resampled the vibration signal with the bandwidth, the frequency was shifting with an exponential function, $e^{-j2\pi ft}$ based on interest shift frequency. The resampled signal is then divided into multiple partitions and averagely calculate root mean square (RMS) for each divided segment. The RMS values are composed based on the length of the sensing matrix M $(M<N)$ and reconstruct the signal with sparse representation, η to determine its discrete Fourier transform. The extracted sparse representation of the signal can help to indicate the variation due to presence of defect. The defects existing in bearing elements are produced at a certain period and referred as bearing fault frequencies. Envelope demodulation technique is applied to the high-frequency band to extract the periodic

excitation in the vibration signal and the harmonics of fault frequency components.

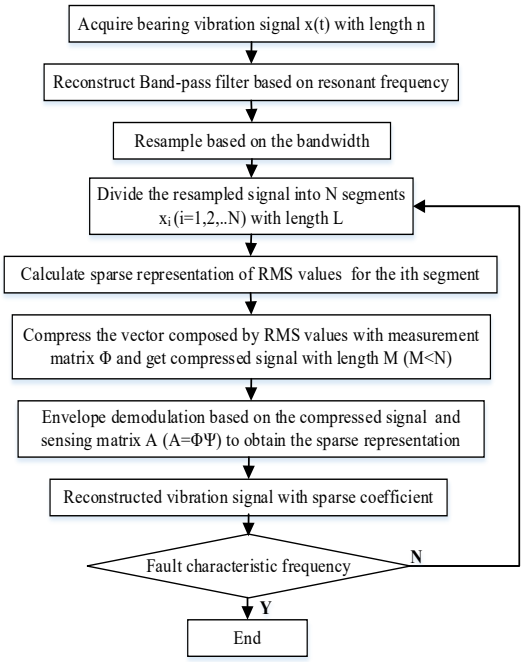


Figure 2: Fault detection strategy based on compressed sensing method

The determination of an optimal bandwidth to reconstruct the sparse signal of ball bearing imposes a severe challenge to apply the CS method. Due to modulation of the acquired vibration signal with the resonance frequency of the system or even with accelerometer, uncontrolled bandwidth could affect the performance analysis of the proposed method in a specific application. Hence, envelope analysis can give a clear indication to the effect of modulation within the measured vibration signal, which can help to overcome the limitation of the CS method.

4. Experiment test

Various experiments were performed with outer race and inner race faults in ball bearings to verify the effectiveness of using envelope analysis and the CS method. The experiment test was implemented in the laboratory to detect the seeded faults in ball bearings that used in an induction AC motor to drive a DC motor at various conditions. Figure 3 shows the construction of experiment test and the components of data acquisition system.

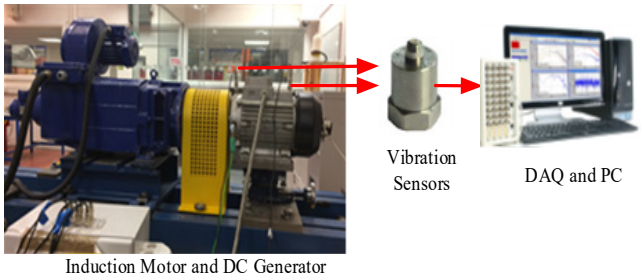


Figure 3: The Schematic diagram of experiment test system

In this experiment, three similar ball bearings have been used within the motor drive and their main operating parameters are detailed in Table 1.

Table 1: The description of ball bearing parameters

Component	Value
Pitch Diameter, D_p	46.4 mm
Ball Diameter, D_b	9.53 mm
Number of ball, N_p	9
Contact angle, β	0
Operating motor speed (shaft frequency, f_r)	1496rpm (24.94 Hz)

The three tested ball bearings are denoted as baseline (without fault) and the other two bearings are produced with inner race fault and outer race fault, respectively. The seeded bearing faults are shown in figure 4. The failures of inner race and outer race of bearing are very common defects that could happen due to improper installation, incorrect lubrication, overloading, etc. Furthermore, the defect at any rotating element of machinery transmits to the bearing races and presents in terms of spalling, smearing, wear and surface distress. As a result, higher level of vibration is excited, which can be sensitive indicator to the starting of bearing deterioration.


(a) Inner race fault (b) Outer race fault

Figure 4: The Photographs of simulated ball bearing's faults

The ball bearing characterises with a complex excited vibration can be extracted from the measured vibration signal by an accelerometer mounted on the bearing's housing in vertical and horizontal directions. The excitation of bearing vibration is proportional with the structural design parameters of the ball bearing and the defects in their elements. The bearing vibration is rich in multi frequency components that induced in wide frequency bandwidth. The characteristic frequencies of the bearing defects can be identified by analysing the relative motion between the bearing elements and the rotor frequency, f_r. Then, the defect characteristic frequencies of the ball bearing elements can be indicated based on:

$$\text{Outer race fault frequency: } f_o = \frac{N_b}{2} f_r \left(1 - \frac{D_b}{D_p}\cos\beta\right) \quad (7)$$

$$\text{Inner race fault frequency: } f_i = \frac{N_b}{2} f_r \left(1 + \frac{D_b}{D_p}\cos\beta\right) \quad (8)$$

where N_p is the number of rolled balls, D_b is the ball diameter, D_p is the pitch diameter of the bearing, and β is the contact angle.

The seeded defects in the inner race and outer race can be detected based on their identified frequencies, and denoted by fault frequency are evaluated in Table 2.

Table 2: Fault frequency of ball bearing

Parameter	Value (Hz)
Inner Race Fault Frequency, f_i	135.26
Outer Race Fault Frequency, f_o	89.16

5. Vibration Data Analysis

The vibration signal of ball bearing is mainly recorded in time domain for visual inspection, which is analysed by using advance signal processing methods. The analysis of vibration signal in time domain and frequency domain are obviously the two powerful techniques used for contemporary condition monitoring scheme. However, no clear impacts of the defects can be located and some frequency harmonics coincide and spread within wide waveform, and cause a lot of difficulties in the fault detection and diagnostic approaches [19]. Figure 5 and figure 6 show the time waveform and spectrum of vibration signal for three types of ball bearings (baseline (no fault), outer race fault and inner race fault).

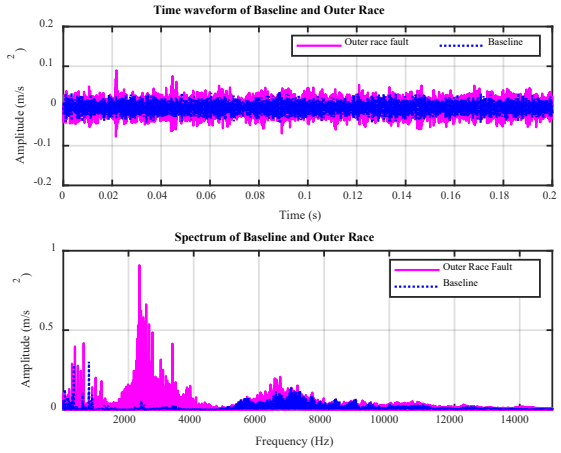


Figure 5: Vibration waveform and spectrum for baseline and outer race fault

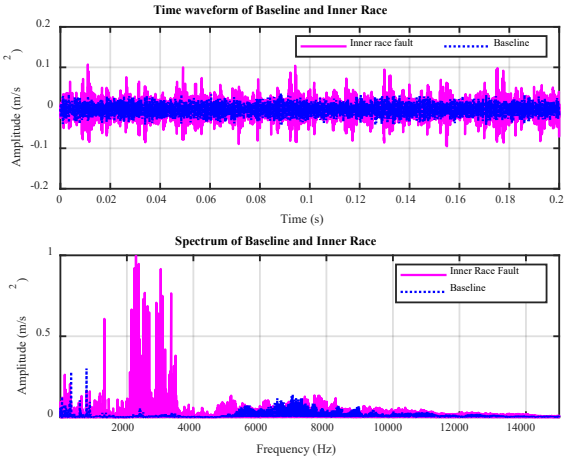


Figure 6: Vibration waveform and spectrum for baseline and inner race fault

The spectra of the bearings with outer race and inner race defects represents resonance around 3kHz. This excitation effect is probably due to resonate the natural frequencies of bearing elements or the accelerometer with the periodic impacts of the bearing defects. Figure 7 shows the spectra of the tested bearings at low frequency band (< 500Hz) includes characteristic frequencies of the bearing defects. The difference in the bandwidth of the ball bearing defect is belonged to the variation of the transmission path of the excited vibration from the bearing components to the transducer. The vibration from the bearing with outer race defect has shorter path as compared with the inner race defect, where the harmonics cannot be revealed distinctively.

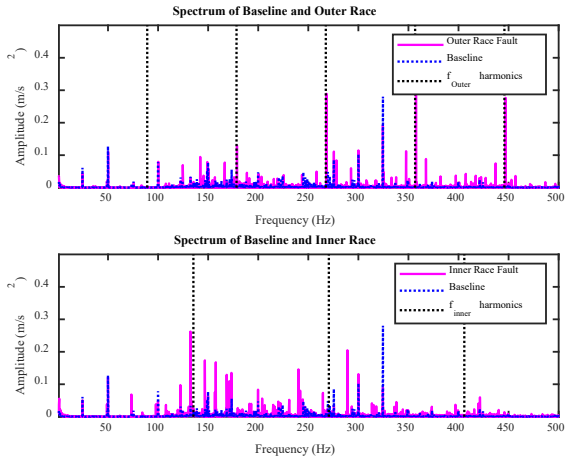


Figure 7: The spectra of the tested bearings at low frequency bands

5.1. Envelope Analysis

Amplitude modulation of vibration signal can be extracted from the envelope analysis in some specific bands. Figure 8 and figure 9 show the envelope analysis results of baseline, outer race fault and outer race fault bearings. The characteristic frequencies due to bearing defect and their harmonics (f_o=89.16 Hz and f_i=135.26 Hz) are significant, which are verified by using effective filter parameters. A band pass filter was used within the range of modulation bandwidth (1kHz – 5kHz). This range was chosen based on the higher amplitude of spectra shown in figures 5 and 6, where the bearing defects can be demodulated from the bearing natural frequencies. However, the determination of an optimal narrowband becomes poses a severe challenge for accurately employing envelope analysis.

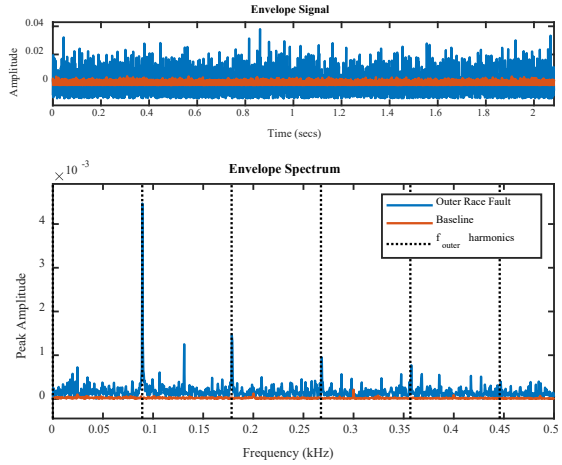


Figure 8: Envelope waveform and spectrum of baseline and outer race fault

5.2. Compressive Sensing Analysis

In order to overcome the problem with high sampling rate and big data acquisition, CS method can significantly reduce the

consumption energy and the volume of transmission data [13-17]. The sampling rate can be reduced with using frequency shifting that can move the sparse signal from the high frequency range to a lower bandwidth. An exponential function $e^{-j2\pi fot}$ was used to resample the ball bearing vibration signal with envelope resampling from the original sampling frequency 96kHz to 3kHz. Then, divide the resampled signal into segments averagely and calculate the RMS value for every segment. The RMS values composed by all *N* vector are compressed with a random sensing matrix to provide a reconstruct compressed signal with length *M (M<N)*. The RMS value was determined for every 5 points, thus the sampling frequency is compressed to 600Hz and the length of this vector is 2400 points and the CS process was repeated 10 times to acquire the average results of bearing faults, where random effects of measurement matrix can be reduced. Figure 10(a) shows the period of original RMS signal and the reconstructed RMS signal with CS for outer race bearing's fault, where the compression ratio *(M/N)* of this process is up to 30%.

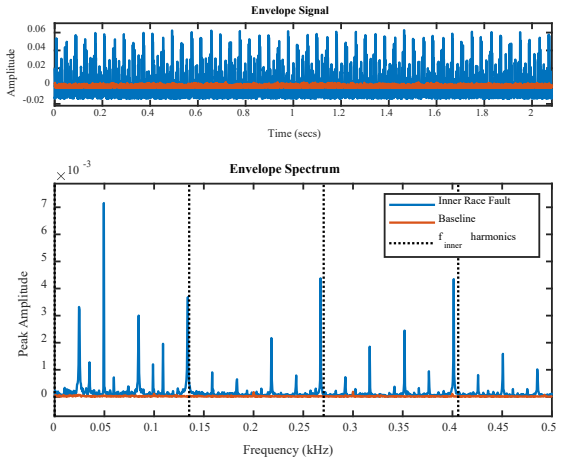


Figure 9: Envelope waveform and spectrum of baseline and inner race fault

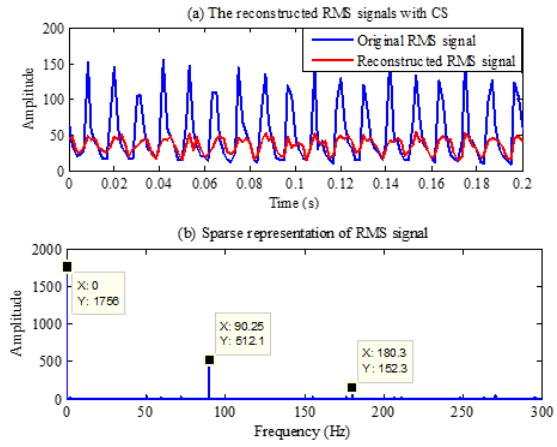


Figure 10: Reconstructed RMS signal and its sparse representation of vibration signal with outer race fault

It is clear that the amplitude of reconstructed signal is much smaller than that of the original RMS signal with maintaining good consistency so the fault frequency is not much affected, as demonstrated in figure 10(b). The sparse representation of the RMS signal is displayed at frequency 90.25Hz and its harmonics, which are closer to the outer race fault frequency. The deviation in the fault frequency f_o could result due to the variation in the rotor frequency f_r of the induction motor.

Similarly, the trends of the reconstructed RMS signal for the ball bearing with inner race fault is shown in figure 11(a), where same parameters of averaging and compression ratio were used. The reconstructed RMS signal shows good consistent with the original RMS signal. Thus, the inner race fault frequency is displayed clearly at frequency 134.8 Hz, as shown in figure 11(b). The frequency 50Hz is the second harmonic frequency of the shaft rotating frequency, which is modulated with the inner race fault frequency. Therefore, it can be concluded that CS method can be reliably used to extract and detect the outer race and inner race faults of ball bearings and can be used to classify the defect according to the damaged element.

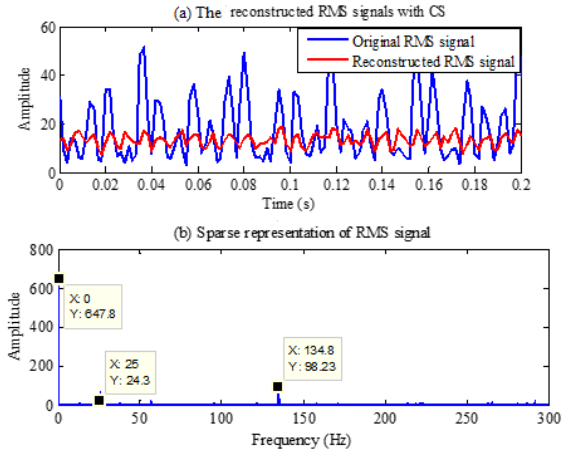


Figure 11: Reconstructed RMS signal and its sparse representation of vibration signal with inner race fault

The performance of the CS method was evaluated for various compression ratios *(M/N)* by measuring signal to noise ratio (SNR) of the compressed signal. SNR is related to the reconstructed compressed signal and the original measured data. Figure 12 shows a clear decreasing in the SNR with increasing the *M/N* ratio. It can be observed that the range of compression ratio between 30-40% provides an acceptable level of SNR, which is significantly decreased for further compression of the signal.

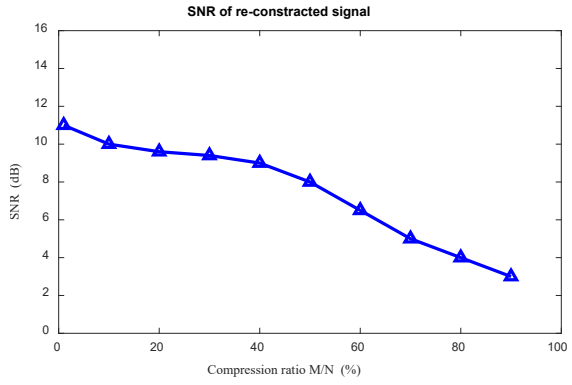


Figure 12: The evaluation of CS method for various compressions of the signal

Due to reduction in the sparse representation of the reconstructed signal, the diagnostic features of bearing defects are also influenced by the variation of the *M/N* ratios. Figure 13 shows

the variation in the amplitude peaks of the reconstructed sparse signal at the fault frequency features (f_o and f_i). The peaks of the fault frequency give clear indication for the sparse signal with the range of compression ratio up to 40%. However, the amplitude of the fault frequencies is decreased for higher compression ratios, which may influence the fault diagnostic approaches. Good fault detection accuracy can be found for the compression ratio between 20-40%, which can be evaluated based on the amplitude variation of bearing fault frequency. The higher accuracy of the CS method within the compression range was found for M/N=30%. The indication accuracy of bearing defects was found to be 94.7% for the 30% compressed signal as compared with the original signal. Moreover, the accuracy of the CS method was 91.8% for 40% compression ratio, which is relatively acceptable to reduce the data size and provide good indication of bearing defects.

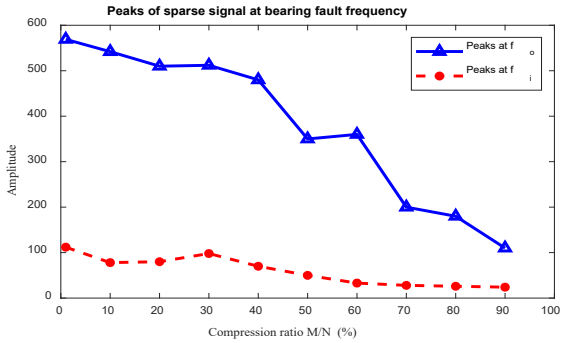


Figure 13: The amplitude peaks of the compressed signal at the diagnostic fault frequencies of inner race and outer race defects

6. Conclusion

This paper proposes the using of CS strategy as an approach for intelligent condition monitoring and fault detection of ball bearing. The CS method was applied based on frequency shifting of the high sparse response to a lower frequency band with applying envelope extraction at certain frequency bands, to overcome the problems of big data acquisition and the limitation of sampling theory. This process can help to significantly reduce the sampling rate with reliably extract the ball bearing's fault features, where sufficient information can be retrieved from the limited samples. Thereby, CS method can be reliably used to extract and detect ball bearing's faults, in which reliable fault detection can be extracted for compression ratio up to 40%. The limitation of applicable CS method on the bearing fault diagnosis is the selection of suitable reconstructed sparse bandwidth. Hence, the bearing vibration signal is a modulated signal with bearing resonance frequencies or even with accelerometer elements, which can be extracted from envelope analysis. However, the determination of an optimal narrowband poses a severe challenge to be employed. More evaluation of the proposed method in terms of accuracy and cost comparison with other methods will be addressed in the future work with considering of wireless transmission data for a large range of applications.

Conflict of Interest

The authors declare no conflict of interest.

Acknowledgment

The authors would like to acknowledge the University of Anbar, Iraq and the University of Huddersfield, UK.

References

[1] L. Liu, "Robust fault detection and diagnosis for permanent magnet synchronous motors," PhD Thesis, College of Engineering, The Florida State University, USA, 2006.

[2] M. Rani, S. Dhok, R. Deshmukh, "A Machine Condition Monitoring Framework Using Compressed Signal Processing," Sensors, **20**(1), 319, 1-15, 2020, doi:10.3390/s20010319.

[3] N. Tandon, A. Choudhury, "A review of vibration and acoustic measurement methods for the detection of defects in rolling element bearings," Tribology international, **32**(8), 469-480, 1999.

[4] C. K. Mechefske, "Machine condition monitoring and fault diagnostics," In Vibration and Shock Handbook. Boca Raton, FL: CRC Press, Taylor and Francis Group, **25**, 1-35, 2005.

[5] Y. T. Sheen, "An envelope analysis based on the resonance modes of the mechanical system for the bearing defect diagnosis," Measurement, **43**(7), 912-934, 2010, doi:10.1016/j.measurement.2010.03.011.

[6] G. Tang, W. Hou, H. Wang, G. Luo, J. Ma, "Compressive sensing of roller bearing faults via harmonic detection from under-sampled vibration signals," Sensors, **15**(10), 25648-25662, 2015, doi:10.3390/s151025648.

[7] D. Abboud, J. Antoni, S. Sieg-Zieba, M. Eltabach, "Envelope analysis of rotating machine vibrations in variable speed conditions: A comprehensive treatment," Mechanical Systems and Signal Processing, **84**, 200-226, 2017, doi:10.1016/j.ymssp.2016.06.033.

[8] H. O. Ahmed, M. D. Wong, A. K. Nandi, "Intelligent condition monitoring method for bearing faults from highly compressed measurements using sparse over-complete features," Mechanical Systems and Signal Processing, **99**, 459-477, 2018, doi:10.1016/j.ymssp.2017.06.027.

[9] S. Li, L. Xu, X. Wang, "Compressed sensing signal and data acquisition in wireless sensor networks and internet of things," IEEE Transactions on Industrial Informatics, **9**(4), 2177-2186, 2013, doi:10.1109/TII.2012.2189222.

[10] D. J. Holland, D. M. Malioutov, A. Blake, A. J. Sederman, L. F. Gladden, "Reducing data acquisition times in phase-encoded velocity imaging using compressed sensing," Journal of magnetic resonance, **203**(2), 236-246, 2010, doi:10.1016/j.jmr.2010.01.001.

[11] S. Qaisar, R. M. Bilal, W. Iqbal, M. Naureen, S. Lee, "Compressive sensing: From theory to applications, a survey," Journal of Communications and networks, **15**(5), 443-456, 2013, doi:10.1109/JCN.2013.000083.

[12] Y. Ma, X. Jia, H. Bai, G. Wang, G. Liu, C. Guo, "A new fault diagnosis method using deep belief network and compressive sensing," Journal of Vibroengineering, **22**(1), 83-97, 2020, doi:10.21595/jve.2019.20850.

[13] J. Beuchert, F. Solowjow, S. Trimpe, T. Seel, "Overcoming Bandwidth Limitations in Wireless Sensor Networks by Exploitation of Cyclic Signal Patterns: An Event-triggered Learning Approach," Sensors, **20**(1), 260, 1-19, 2020, doi:10.3390/s20010260.

[14] L. Yin, C. Liu, S. Guo, Y. Yang, "Sparse random compressive sensing based data aggregation in wireless sensor networks," Concurrency and Computation: Practice and Experience, **32**(3), e4455, 2020, doi:10.1002/cpe.4455

[15] E. Sejdić, I. Orović, S. Stanković, "Compressive sensing meets time–frequency: an overview of recent advances in time–frequency processing of sparse signals," Digital signal processing, **77**, 22-35, 2018, doi:10.1016/j.dsp.2017.07.016.

[16] X. F. Li, X. C. Fan, L. M. Jia, "Compressed sensing technology applied to fault diagnosis of train rolling bearing," In Applied Mechanics and Materials, Trans Tech Publications, **226**, 2056-2061, 2012, doi:10.4028/www.scientific.net/AMM.226-228.2056.

[17] X. Tang, Y. Xu, F. Gu, A. D. Ball, G. Wang, "Fault detection of rolling element bearings using the frequency shift and envelope based compressive sensing," In 2017 23rd International Conference on Automation and Computing (ICAC), IEEE, 1-6, 2017, doi:10.23919/IConAC.2017.8082063.

[18] M. Lebold, K. McClintic, R. Campbell, C. Byington, K. Maynard, "Review of vibration analysis methods for gearbox diagnostics and prognostics," In Proceedings of the 54th meeting of the society for machinery failure prevention technology, Virginia Beach, VA, May 1–4, 623–634, 2000.

[19] H. Saruhan, S. Saridemir, A. Qicek, I. Uygur, "Vibration analysis of rolling element bearings defects," Journal of applied research and technology, **12**(3), 384-395, 2014, doi:10.1016/S1665-6423(14)71620-7.

ASTES

Advances in Science, Technology and Engineering Systems Journal
Vol. 5, No. 5, 376-381 (2020)
www.astesj.com
Special Issue on Multidisciplinary Innovation in Engineering Science & Technology

ASTES Journal
ISSN: 2415-6698

Semiclassical Theory for Bacteria Motility Under External Electric Fields and Interactions with Nanodevices

Huber Nieto-Chaupis*

Universidad Autónoma del Perú, Panamericana Sur Km. 16.3, Villa el Salvador, Lima, Perú

ARTICLE INFO

Article history:
Received: 18 June, 2020
Accepted: 02 September, 2020
Online: 21 September, 2020

Keywords:
Bacteria
Classical Electrodynamics
Probability Amplitude

ABSTRACT

The accurate identification and characterization of microbiological species is a must that allows us to design engineered pharmacology to tackle down the diversity of diseases derived of them. This paper presents a study about the usage of both classical dynamical and electrodynamics in conjunction to the Feynman's path integral to describe as well as identify the displacement of bacteria in closed spaces. Our methodology consists in the in the usage of the usage of probability amplitude to investigate the theoretical motility of bacteria can be disturbed through electrical interactions from the fact that them contain ions in their biochemical composition.Our study yields that bacteria might exhibit a pattern of probabilities as function of space and time. It would be advantageous for an engineered nanodevice that would sense them uniquely through electrical interactions.

1 Introduction

It is well-known that some type of bacteria might be lethal in humans [1] moreover in the shortest times, so that their understanding with respect to physical and chemical interactions constitutes a must. Nowadays, notable advances to tackle down diseases caused by bacteria and virus have demanded to engineer precise pharmacology [2]. Furthermore, with the expected arrival of nanomedicine, one expects that the so-called nanodevices [3] can achieve an efficient task to defeat any intrusion of microbiological compound in humans. Thus, an accurate knowledge of bacteria's properties and biochemical characteristics turns out to be critic for the application of an accurate nano pharmacology, with the lowest cost-benefits fraction [4].

In this paper, theory of bacteria's response to electrical interactions derived from both classical electrodynamics and quantum mechanics path integrals is treated. Essentially, particular attention is paid on the probability amplitude. Commonly it is written as [5],

$$\mathcal{A} = \langle z_b|\mathbf{U}(t_b, t_a)|z_a\rangle\,.$$

with $\mathbf{U}(t_b, t_a)$ the quantum mechanics evolution operator,

$$\mathbf{U}(t_b, t_a) = \mathrm{Exp}\left[-i\left(\frac{\mathbf{P}^2}{2\mathrm{M}\hbar} + \frac{Q_J\mathbf{V}(\mathbf{R})}{|\mathbf{R}-\mathbf{R}_J|}\right)\right].$$

Although this equation is a pure quantum mechanics description of a compound electrically charged, the employment of distances at the order of nanometer leads us to implement this approach by which quantum effects cannot be discarded. Thus this paper has a target to present a scheme to identify bacteria through the measurement of the probability as function of time and spatial displacement. Because bacteria have a well defined ionic composition, it make them sensitive to electrical interactions. Therefore bacteria can be disturbed by electric fields and potentials, as consequence their dynamics is strongly affected. In this manner, chemotaxis and quorum among them are modified. Therefore, bacteria would exhibit patterns in according to their internal ionic composition. With this information, then is plausible their identification. The usage of quantum mechanics appears as a closed-form tool that would describe perturbed paths of bacteria. Thus, one can ask about the probability that an aggregation of bacteria is disabled in their main functions in presence of external electric fields. This paper has as purpose to answer this question.

The rest of this paper is as follows: in second section all the classic physics that would model bacteria and their spatial dynamics is presented. In third section, the implementation of the probability amplitude with the gained knowledge from the classical analysis is done. In fourth section, the implementation of integer-order Bessel's functions is done. This has as objective to extract the possible probabilities while a single bacterium is trapped in a closed space. Finally, conclusion of paper is presented.

*Corresponding Author: Huber Nieto-Chaupis, Email: hubernietochaupis@gmail.com

2 Bacteria in Classical Physics

As studied by Bechhold at 1904, bacteria are carriers of negative charges. At 1932 Leo Olitzki studied bacterial migration of cells under various values of pH [6]. After at 1932, Burke and Gibson analyzed electric reactions of bacteria observing spatial translation to the positive pole and demonstrating the negative charge composition of bacteria under fixed electrodynamic situations [7]. Therefore, it is possible to extract an exact dynamics to understand the response and behavior of bacteria or any microbiological aggregation in a scenario of electrical exposure.
Thus, by knowing the electric potential, the entire dynamics is derived from the Newton's equation given by: $\vec{\mathbf{F}} = Mvdv/ds = -Q\vec{\nabla}[\Phi(x,y,z) + \phi(x,y,z)]$ with $\phi(x,y,z)$ a noise that emerges in macro-biological scenarios. However in isolated environments $\phi(x,y,z) \approx 0$.

2.1 The Classical Dynamics Approach

Consider the Poisson's equation defined by an electric potential $\mathbf{U}(\mathbf{r})$ and charge volumetric density ρ written as:

$$\nabla^2\mathbf{U}(\mathbf{r}) = -\frac{\rho}{\epsilon_0} \tag{1}$$

and ϵ_0 the electrical permittivity. Then after an integration in both members of Eq.(1),

$$\nabla \int (\nabla \mathbf{U}(\mathbf{r}))\, dV = -\frac{1}{\epsilon_0}\int \rho(\mathbf{r}) dV$$
$$\int \nabla\cdot\mathbf{E} dV = \frac{1}{\epsilon_0}\int \rho(\mathbf{r}) dV \Rightarrow \mathbf{E}\int d\mathbf{A} = \frac{Q}{\epsilon_0} \Rightarrow,$$

with $\mathbf{E}$ the electric field one can arrive to:

$$\mathbf{E} = \frac{Q}{\epsilon_0 \int d\mathbf{A}}, \tag{2}$$

where the well-known Gauss's law is used. In this manner the electric force $\mathbf{F} = q\mathbf{E}$, onto a single bacterium of charge q due to the presence of an external total charge Q is written as $\mathbf{F} = q\mathbf{E} = \frac{qQ}{\epsilon_0\int d\mathbf{A}} \Rightarrow \int vdv = \int \frac{2qQ}{M\epsilon_0\int d\mathbf{A}} d\mathbf{s}$ yielding the displacement:

$$R(t) = \int_0^T dt \sqrt{\int \frac{2qQ}{M\epsilon_0\int d\mathbf{A}} d\mathbf{s}} = T\sqrt{\frac{2qQ}{M\epsilon_0}\int \frac{d\mathbf{s}}{\int d\mathbf{A}}}, \tag{3}$$

clearly the charge Q supposed to be the one that acts onto the bacterium is a finite sum of independent charges. Thus one gets:

$$R(t) = T\sqrt{\frac{2q\sum_j^J Q_j}{M\epsilon_0}\int \frac{d\mathbf{s}(t)}{\int d\mathbf{A}}}, \tag{4}$$

in the same logic, the displacement done by a compound of N bacteria due to the presence of Q charges is written as:

$$R(t) = T\sqrt{\frac{2\sum_n^N q_n \sum_j^J Q_j}{M\epsilon_0}\int \frac{d\mathbf{s}(t)}{\int d\mathbf{A}}}. \tag{5}$$

If all charges have same magnitude, then $\sum_n^N q_n = Nq$ and $\sum_j^J Q_j = JQ$. A toy model can be established from Eq.(5) in the sense that the net displacement for N bacteria and J external charges can be written as:

$$R(t) = T\sqrt{NJ}\sqrt{\frac{2qQ}{M\epsilon_0}\int \frac{d\mathbf{s}(t)}{\int d\mathbf{A}}}. \tag{6}$$

Integrations inside the square root can be carry out in a straightforward manner in according to the choice of coordinate system. For instance a choice is the cylindric system allows us to write $\int d\mathbf{A}$=$2\pi L\mathbf{r}(t)$. On the other hand while the electric force acts onto the radial direction then $d\mathbf{s}(t) \to d\mathbf{r}(t)$ therefore one obtains that:

$$R(t) = T\sqrt{NJ}\sqrt{\frac{2qQ}{2\pi\epsilon_0 ML}\int \frac{d\mathbf{r}(t)}{\mathbf{r}(t)}}$$
$$= T\sqrt{NJ}\sqrt{\frac{2qQ}{2\pi\epsilon_0 ML}\mathrm{Log}\left[\frac{\mathbf{r}(t)}{\mathbf{r}(0)}\right]}. \tag{7}$$

Clearly the classic physics establishes that the displacement is dictated by the inverse of the root square of product of ML. In this manner, when $ML >> NJ$ the net displacement might be negligible.

2.2 The Electrodynamics Classical Approach

A rigorous treatment about the dynamics of any ionic compound in an electrical scenario demands to use exact solutions of either Poisson or Laplace equations. By following the picture that a single bacterium is enclosed inside a cylindric system, it is possible to derive a closed-form formulation of the bacteria displacement. In fact, consider a charged object inside a finite cylindric shape, then the electric potential becomes the Jackson's potential [8] and it is written as:

$$\mathbf{U}(\mathbf{x},\mathbf{x}') = \frac{2Q}{\pi\epsilon_0 LR^2}\sum_{m,k,n}^{\infty} \mathrm{e}^{im(\phi-\phi')}\sin\left(\frac{k\pi z}{L}\right)\sin\left(\frac{k\pi z'}{L}\right)\times$$
$$\times\frac{J_m\left(\frac{x_{mn}r}{R}\right)J_m\left(\frac{x_{mn}r'}{R}\right)}{\left[\left(\frac{x_{mn}}{R}\right)^2+\left(\frac{k\pi}{L}\right)^2\right]J_{m+1}^2(x_{mn})}. \tag{8}$$

Thus, one can see that actually this full solution is the product of the individual solutions of the involved coordinates, so that one can state that the solution is separable as: $\mathbf{U}(\mathbf{x},\mathbf{x}') = \Phi(\phi,\phi')Z(z,z')R(\rho,\rho')$. While one can adopt the radial solution, it is explicitly dependent on the integer numbers m,k,n.
In this manner, the solution along the z coordinate appears as the one that exhibits tractability from the mathematical point of view, and that fits with the physics about the motility and spatial displacements of bacteria. Subsequently, for a fixed radius and polar angle, the Jackson's potential can be written in its simplified form as:

$$\mathbf{U}(\mathbf{z},\mathbf{z}') = \frac{2Q}{\pi\epsilon_0 LR^2}\sum_{k}^{\infty}\sin\left(\frac{k\pi z}{L}\right)\sin\left(\frac{k\pi z'}{L}\right). \tag{9}$$

With this one can estimate the electric field from $\mathbf{E} = -\nabla \mathbf{U}(\mathbf{z}, \mathbf{z}')$ created along the longitudinal coordinate turns out to be:

$$\mathbf{E} = -\hat{\mathbf{k}}\frac{\partial}{\partial z'}\mathbf{U}(\mathbf{z}, \mathbf{z}') = \frac{2kQ}{\epsilon_0 L^2 R^2}\sum_k^{\infty} \sin\left(\frac{k\pi z}{L}\right)\cos\left(\frac{k\pi z'}{L}\right)\hat{\mathbf{k}}. \quad (10)$$

When the difference $|z - z'| << 1$ the electric field depends on this so that the identity sin(2x)=2 sin(x)cos(x) is used. Thus, a single bacterium containing an ion of charge q inside the cylinder feels this field and it is going to experience a net electric force given by:

$$\mathbf{F}(\mathbf{z}) = q\mathbf{E}(\mathbf{z}) = \frac{-kqQ}{\epsilon_0 L^2 R^2}\sum_k^{\infty} \sin\left(2\frac{k\pi z}{L}\right)\hat{\mathbf{k}}. \quad (11)$$

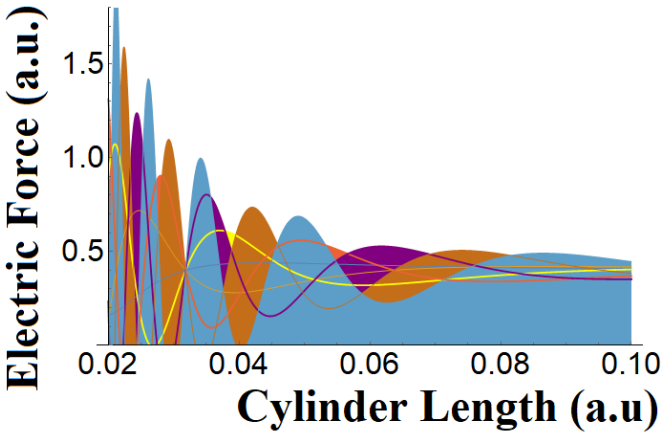


Figure 1: The intensity of electric force $\|\mathbf{F}(\mathbf{z})\|$ from Eq.(11) in the S.I system on a single bacterium as function of the length of cylinder L for values of k from 1 to 7. A noise field of 40% is attained.

3 The Probability Amplitude of Bacteria Displacement

3.1 Motivation

The prospective implementation of nano technologies through nano devices, would demand to employ accurate theoretical formulations that would have to encompass for example the nano biological scenarios. Under this view, emerges quantum mechanics as a robust theoretical frame that would describe the interactions through the language of probabilities.

In fact, commonly in quantum mechanics the probability amplitude $\mathcal{A}$ requires of the exact knowledge of the Green's function or the function that dictates the space-time propagation. For example, the propagation of a massive particle from the point t_a, z_a to t_b, z_b is given by:

$$\mathcal{A} = \langle z_b|\mathbf{U}(t_b, t_a)|z_a\rangle\,. \quad (12)$$

In the case of a free particle, the evolution operator is explicitly given by:

$$\mathbf{U}(t_b, t_a) = \mathrm{Exp}\left[\frac{iE(t_a - t_b)}{\hbar}\right] = \mathrm{Exp}\left[\frac{ip^2(t_a - t_b)}{2M\hbar}\right]. \quad (13)$$

In praxis one needs to employ the representation of momentum given by the completeness relation $\int dp\,|p\rangle\langle p| = \mathrm{I}$ on gets:

$$\mathcal{A} = \frac{1}{2\pi\hbar}\int dp \mathrm{Exp}\left[-i\left(\frac{p^2(t_b - t_a)}{2M\hbar} + \frac{p(z_a - z_b)}{\hbar}\right)\right]. \quad (14)$$

In order to evaluate the integral, it is required the explicit form of the initial and final states at the momentum representation. Thus, these states can be written as $\mathrm{Exp}(-i\frac{pz_a}{\hbar})$ and $\mathrm{Exp}(i\frac{pz_b}{\hbar})$ respectively with normalization constants for both states given by $\frac{1}{\sqrt{2\pi\hbar}}$, with the causal condition $t_a > t_b$ then the integration turns out to be in a straightforward manner resulting in (the reader can check that the square completion "trick" is used.):

$$\mathcal{A} = \sqrt{\frac{M}{i2\pi\hbar(t_a - t_b)}}\mathrm{Exp}\left[\frac{iM(z_b - z_a)^2}{2\hbar(t_b - t_a)}\right]. \quad (15)$$

Clearly Eq.(15) requires of an additional physics that by the which one can describe the displacement of bacteria in presence of external fields. Therefore, Eq.(15) can model all those trajectories with those intensities that are negligible and cannot to affect dynamics.

3.2 The Path Integral Scheme

The scheme of path integral invented by Feynman [9] inside the framework of quantum electrodynamics [10] emerged as an independent methodology to find probability amplitudes of elementary processes.

For instance, the case subject to a negligible external potential one could be treating the free particle containing kinetic energy. Therefore, the probability amplitude contains an infinite number of paths for a spatial displacement initialized at z_b, t_b arriving to z_a, t_a. In order to calculate the amplitude probability the employed time for carrying out such motility demands to assume that the whole employed time has N+1 slices in the form: $t_\ell = \epsilon\ell + t_a$ with the integer ℓ running from $\ell = 0, 1, ..., N, N+1$ so that the concrete problem consists in to evaluate the product of integrals from the general formulation:

$$< z_b, t_b|z_a, t_a >= \lim_{N\to\infty}\frac{1}{\sqrt{2i\pi\epsilon/m}}\times$$
$$\times\prod_{i=1}^{N}\int_0^L \frac{dz_i}{\sqrt{2\pi\epsilon/m}}\exp\left[i\sum_{i=1}^{N+1}\frac{m}{2\epsilon}(z - z_{i-1})^2\right]. \quad (16)$$

It should be noted that the kinematic part is denoted by the free-particle Lagrangian

$$\mathcal{L} \approx \sum_{i=1}^{N+1}\frac{m}{2\epsilon}(z - z_{i-1})^2\,. \quad (17)$$

Turning back on the bacteria displacement, one can apply the method given above to attack the problem of bacteria motility when it is subject to external potential. In fact, Janke and Kleinert [11] have demonstrated that the path integral of a free particle between two space points inside a box is actually the product of the well-known wave functions when these closed-form solutions of the Schrödinger's equation. Thus, Janke and Kleinert have found that

$< z_b, t_b|z_a, t_a >$ turns out to be a closed-form expression characterized by having a complex exponential, and reads:

$$< z_b, t_b|z_a, t_a >= \frac{2}{L}\sum_{q=1}^{\infty}\sin(\frac{\pi q z_b}{L})\sin(\frac{\pi q z_a}{L}) \text{Exp}\left[-i\frac{(\pi q)^2(t_b-t_a)}{2mL^2}\right]. \quad (18)$$

It is interesting to note that of product of two sin functions matches well to right-side of Eq.(9). In this manner, because the presence of the wave functions: $\Psi(\beta z_a) = \sqrt{\frac{2}{L}}\text{Sin}(\beta z_a)$ and $\Psi(\beta z_b) = \sqrt{\frac{2}{L}}\text{Sin}(\beta z_b)$, with $\beta = \frac{q\pi}{L}$, one can interpret that are solutions for a free particle in a cylinder. Furthermore, Eq.(18) can be also written in a simplified manner as:

$$< z_b, t_b|z_a, t_a >= \sum_{q=1}^{\infty}\Psi(\beta z_b)\Psi(\beta z_a)\text{Exp}\left[-i\frac{\beta^2(t_b-t_a)}{2m}\right], \quad (19)$$

thus for small displacements, $z_a \approx z_b$ so that Eq.(19) can be written in a compact form as:

$$< z_b, t_b|z_a, t_a >= \sum_{q=1}^{\infty}|\Psi(\beta z_a)|^2\,\text{Exp}\left[-i\frac{\beta^2(t_b-t_a)}{2m}\right], \quad (20)$$

exhibiting the square of wave function denoting the probability density. With the definition of $\gamma = \frac{2Q}{\pi\epsilon_0 L R^2}$ the Jackson's potential from Eq.(9) can be rewritten as:

$$\mathbf{U}(\mathbf{z_b}, \mathbf{z_a}) = \gamma\sum_{q}^{\infty}\sin(\beta z_b)\sin(\beta z_a). \quad (21)$$

Certainly, Q denotes the charge that generates the Jackson's potential inside and outside of cylinder of length L and radius a. Therefore, the quantum mechanics paths are contained inside the cylinder. It is noteworthy to remark that the geometry "seen" by the charge Q is a finite cylinder.

3.3 Bacteria in a Cylindrical Geometry

Consider now a negatively charged bacteria under circumstances as given in [**?**] with electric properties as studied and simulated in [**?**] with charge Q_B that can move along the surface of cylinder, then the force per unit of charge attained to a single bacterium can be derived in a straightforward manner as:

$$\frac{\mathbf{F}}{Q_B} = \mathbf{E} = \nabla\mathbf{U} = \frac{Q}{4\pi\epsilon a^2}\sum_{q=1}^{\infty}\text{Exp}\left(-i\frac{t\beta^2}{2M}\right)\nabla\left(\int < z_b, t_b|z_a, t_a > dt\right). \quad (22)$$

where the electric potential has been approximated to the probability amplitude. Under this assumption it is clear that Eq.(22) differs notable from the pure classic force. One can note that the quantity M and Q_B becomes the mass and charge of a single bacterium. The infinite sum gives account of the quantum paths. Aside, the term $\int < z_b, t_b|z_a, t_a > dt$ exhibits the character probabilistic since $< z_b, t_b|z_a, t_a >$ is understood as the density of probability.
It is interesting to note that from Eq.(22) the basic Coulomb force between the bacteria and test charge separated by a distance a each other can be derived, yielding:

$$\mathbf{F} = \frac{QQ_B}{4\pi\epsilon a^2}\sum_{q=1}^{\infty}\text{Exp}\left(-i\frac{t\beta^2}{2M}\right)\nabla\left(\int < z_b, t_b|z_a, t_a > dt\right),$$

and the classic Coulomb law is recovered yielding:

$$\mathbf{F}_{\text{CL}} = \frac{Q_B Q}{4\pi\epsilon a^2} \quad (23)$$

that would indicate that bacterium and a charge Q (as nano device for instance) are experiencing a Coulomb force each other along the quantum path (as seen at Fig.2) with a separation given by a distance a the cylinder radius.
In other words the single bacterium in a cylinder with $a << L$ is attained to be on the cylinder surface. In this manner, the charge Q generates a Coulomb-like force to a single bacterium.
In addition, the gradient of the probability $\int < z_b, t_b|z_a, t_a > dt$ provides the stochastic component to the dynamics of bacteria in presence of an external charge Q.

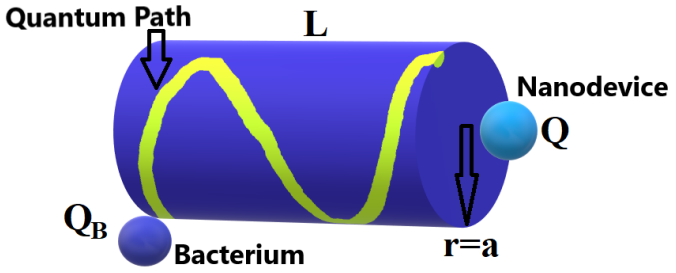


Figure 2: Sketch of the quantum path along the external area of cylinder indicating the constant radial distance between the bacterium and nanodevice.

The resulting hybrid force or semi-classical force might opt only of the real part with respect to the complex exponential, so that one gets that:

$$\mathbf{F} = \mathbf{F}_{\text{CL}}\sum_{q=1}^{\infty}\text{Cos}\left(\frac{t\beta^2}{2M}\right)\nabla\left(\int < z_b, t_b|z_a, t_a > dt\right). \quad (24)$$

Below in Fig.3 this force is plotted. For this end the quantity $\int < z_b, t_b|z_a, t_a > dt$ is assumed to be proportional to αz that means that the probability to find the bacteria inside the cylindric geometry increases with the longitudinal distance z. Despite of this, one can see that the electric force decreases with the bacterial mass or aggregation [12].

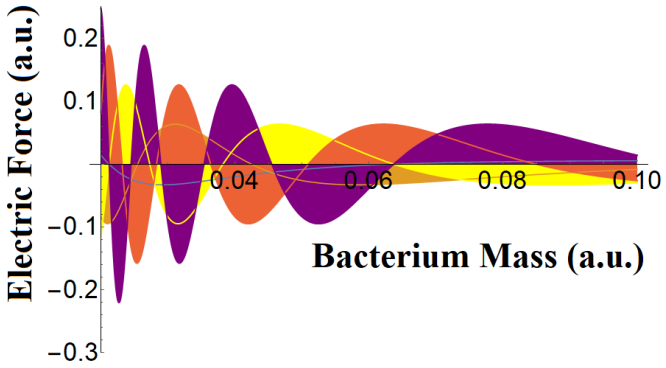


Figure 3: The electric force at the S.I as function of bacteria mass in according to Eq.(24). The force appears to be extenuated in up to a 40% of their top values as seen for a mass of 0.08 expressed in arbitrary units.

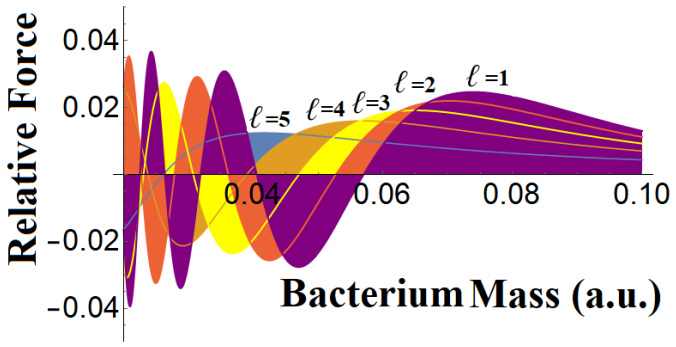


Figure 4: The relative electric force from Eq.(26) in the S.I up to for the first 5 orders of the Bessel function.

4 Bessel Shapes of Bacterium Paths

Turning back to Eq.(24), attention is paid on the complex exponential,

$$\mathbf{F} = \mathbf{F}_{\rm CL}\sum_{q=1}^{\infty}{\rm Exp}\left(-i\frac{t\beta^2}{2M}\right)\nabla\left(\int < z_b, t_b|z_a, t_a > dt\right). \tag{25}$$

by which the usage of the Bessel expansion appears to be feasible in this analysis through the implementation of

$${\rm Exp}\left(-i\frac{tq^2\pi^2}{2ML^2}\right) = {\rm Exp}\left(-i\frac{t}{2M}\sin\lambda\right) \tag{26}$$

where the change $\sin(\lambda) = \frac{q^2\pi^2}{L^2}$, therefore the direct application of the expansion then reads as:

$${\rm Exp}\left(-i\frac{t}{2M}\sin\lambda\right) = \sum_{\ell} J_\ell\left(\frac{t}{2M}\right){\rm Exp}(-i\ell\lambda), \tag{27}$$

so that the relative force reads:

$$\frac{\mathbf{F}}{\mathbf{F}_{\rm CL}} = \sum_{\ell} J_\ell\left(\frac{t}{2M}\right)\nabla\left(\int < z_b, t_b|z_a, t_a > dt\right). \tag{28}$$

In Fig.4, Eq.(28) the relative force was plotted up to for 5 orders of the Bessel function. For this end $\nabla\left(\int < z_b, t_b|z_a, t_a > dt\right)$ turned out to be proportional to $\mathrm{Cos}(z_b)$. The dominant distribution is for $\ell = 1$. In contrast to Fig.3, the relative force does not decreases for large values of bacterium mass. The fact that one can see small values, then it might correlated to the dominance of the classic of Coulomb force against the quantum description. It is fully coherent for large values of bacteria's mass that exhibits a small relative force indicating that that for large masses the Coulomb force governs the electrical interactions.

In order to include the probabilistic concept in Eq.(28) the relative force can be understood as the gradient of quantum mechanics probability in the sense of:

$$\left|\frac{\mathbf{F}}{\mathbf{F}_{\rm CL}}\right|_\ell = J_\ell\left(\frac{t}{2M}\right)\nabla\mathcal{P}(z_b) \tag{29}$$

with $\mathcal{P}(z_b)$ the probability of finding a single bacterium at z_b.

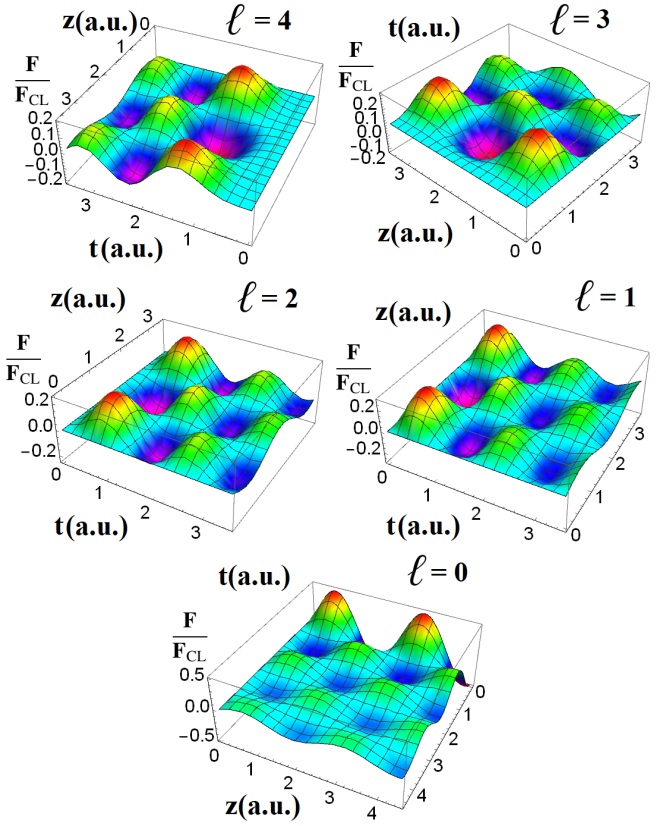


Figure 5: The relative electric force from bottom to top for the orders ℓ=0-4 as function of space and time (expressed in arbitrary units) for a fixed value of bacterium mas $M = 1$.

4.1 Probabilities as Electric Patterns of Bacteria

In Fig.5 up to 5 different 3D distribution of the Eq.28 at a fixed mass, and as function of the z coordinate and time are plotted.

Since the relative force is proportional to the gradient of probability $\nabla\left(\int < z_b, t_b|z_a, t_a > dt\right)$, then Fig.5 can be seen as the curves of probabilities.
In this sense the peaks that all surfaces are exhibiting would correspond to the best scenarios by which one can measure the mass leading to the identification of a particular specie. In bottom panel the case when ℓ=0 is shown. One can see that at $t = 0$ up to 2 maximum values for $z = 0.5$ and 3.0 are exhibited by the 3D curve. One clearly can see that the approximation of Eq.(28) might give a better interpretation of this curve in the sense that for $\ell = 0$ results in $\left|\frac{\mathbf{F}}{\mathbf{F}_{\rm CL}}\right|_\ell \nabla\mathcal{P}(z_b)$ exhibiting the important weight of the quantum mechanics probability that would be the cause for the apparition of peaks. In middle right panel, the relative force for $\ell = 1$ displays again two peaks (both curves in color red) for t=0.1, while at the left side the case for $\ell = 2$ again is exhibited two peaks for t=0.2. Therefore, the order of the Bessel function might be understood as the cause of a slight shift at time with a reduced relative force. This is analogue to the case of the wave packet whose amplitude is minimized with time. Therefore the relative force has actually a quantum behavior as consequence of the classical and quantum engagement through the Jackson's potential. However, the degradation of these surfaces of probabilities are balanced with the apparition of minor peaks as seen at left and right plots. In top left plot, the case when $\ell = 3$ is plotted. Here there are two peaks at $t = 1.5$ at $z = 1$ and $z = 3.5$. It is noteworthy as done in previous case, one can see the apparition of minor peaks. Again, the variation as to up and down of the relative force is entirely related to the quantum behavior. The drastic case is seen at the left panel where $\ell = 4$ whose peaks appear to be rather reduced in contrast to previous cases. In effect, at $t = 2$ and $z = 2.5$ is seen a hole resulting in a null probability and the electric interaction with a nano device [13] inside the cylinder is either lost or not enough to measure the tracking of bacterium under the assumption that **there multiple paths that bacterium would opt while is inside of a closed geometry.**

5 Conclusion

In this paper, the analysis of any microscopic biological specie such as a single bacterium or virus containing a ionic aggregation inside, has been treated through classical and quantum methodologies. The results, have shown that the path integral formulation might enclose the classical electrodynamics formulation dictated by the Jackson's potential. Thus, the relative force was defined as the ratio of the quantum mechanics over the Coulomb-like under the assumption that an engineered nano device [14] coexist inside the cylinder. The 3D plots (done with the package Wolfram [15] for figures 1-5) for different orders of Bessel function have exhibited that the bacterium acquires a pure quantum mechanics behavior. Further studies to understand this quantum and classical correspondence in a more general view are required to support the diverse transitions between the classical and quantum mechanics in nano systems subject to classical fields.

References

[1] A. F. Boggs, "Antibacterial resistance: who pays?" Expert Opinion on Therapeutic Patents, **13(8)**, 1107–1112, 2005, doi:10.1517/13543776.13.8.1107.

[2] L. Good, "Antisense antibacterials," Expert Opinion on Therapeutic Patents, **12(8)**, 1173–1179, 2002, doi:10.1517/13543776.12.8.1173.

[3] H. Nieto-Chaupis, "Macrophage-Like Nanorobots To Anticipate Bacterial Dynamics," in 2019 IEEE 9th Annual Computing and Communication Workshop and Conference (CCWC), 0873–08789, 2019, doi:10.1109/CCWC.2019.8666506.

[4] H. Nieto-Chaupis, "Bacteria Nano Communications Described by a Machine Learning Theory Based on the Feynman Path Integral," in 2019 IEEE 53th Annual Conference on Information Sciences and Systems (CISS), 1–4, 2019, doi:10.1109/CISS.2019.8692893.

[5] J. J. Sakurai, Modern Quantum Mechanics, Chapter II Section 2.5, Addison-Wesley, 2010.

[6] L. Olitzki, "Electrical Charge of Bacterial Antigens," The Journal of Immunology, **4**, 251–256, 1932, doi:10.1186/s11671-019-3005-z.

[7] V. Burke, F. O. Gibson, "The Gram Reaction and the Electric Charge of Bacteria," The Journal of Immunology, **2**, 211–214, 1932, doi:10.1186/s11671-019-3005-z.

[8] J. D. Jackson, Classical Electrodynamics, Third Edition, Chapter II, Problem 3.13, Wiley, 1999.

[9] R. P. Feynman, "Space-Time Approach to Quantum Electrodynamics," Physical Review, **76**, 769, 1949, doi:10.1103/PhysRev.76.769.

[10] R. P. Feynman, "Mathematical Formulation of the Quantum Theory of Electromagnetic Interaction," Physical Review, **80**, 440, 1950, doi:10.1103/PhysRev.80.440.

[11] W. Janke, H. Kleinert, "Summing Paths for a Particle in a Box," Lettere Nuovo Cimento, **25**, 297–300, 1979, doi:10.1007/BF02776259.

[12] M. M.-H. Hasnaa Fatehi, M. T. Figge, "Modelling cellular aggregation induced by chemotaxis and phototaxis," Mathematical Medicine and Biology: A Journal of the IMA, 373–384, doi:10.1093/imammb/dqq002.

[13] Y. W. Mingyu Wang, Z. Yang, "Cooperation Method of Symmetrically Distributed Multi-Nanorobotic Manipulators Inside SEM for Nanodevice Constructing," in 2018 IEEE 13th Annual International Conference on Nano/Micro Engineered and Molecular Systems (NEMS), 543–548, 2018, doi:10.1109/NEMS.2018.855.6984.

[14] Q. Xia, "Memristive nanodevices: CMOS compatibility and novel applications," in 2016 IEEE 18th Mediterranean Electrotechnical Conference (MELECON), 1–4, 2016, doi:10.1109/MELCON.2016.7495316.

[15] "Wolfram Mathematica https://www.wolfram.com," .

Advances in Science, Technology and Engineering Systems Journal Vol. 5, No. 5, 382-388 (2020)

www.astesj.com

ASTESJ

ISSN: 2415-6698

Creating a Website Scoring for High-Order Thinking Skills Game

Yogi Udjaja[1,*], Sasmoko[2], Jurike V.Moniaga[1], Millionsen Christ Lo[1]

[1]*Computer Science Department, School of Computer Science, Bina Nusantara University, Jakarta, 11480, Indonesia*

[2]*Primary Teacher Education Department, Faculty of Humanities, Bina Nusantara University, Jakarta, 11480, Indonesia*

ARTICLE INFO

Article history:
Received: 27 March, 2020
Accepted: 24 June, 2020
Online: 21 September, 2020

Keywords:
Website Scoring
HOTS Game
Website Development

ABSTRACT

There have been many activities to train the brain to remain active, one of its activities is by playing games. Games with the right presentation can train the brain as a whole. This research is focused on High-Order Thinking Skills (HOTS) in order to be able to train the brain's ability in players. Can be concluded that the Web scoreboard with Hypertext Prepocessor (PHP) and Structured Query Language (SQL) has been successfully developed. Web consists of three main menus namely the home menu, score menu, contact menu. unity code accessed to a web page to get data from a web server. This is a simple module for retrieving URL data.

1. Introduction

This is a quiz game focused on children which is a math problem that contains Creativity, Critical Thinking, and Problem Solving with the aim of helping develop and improve their skills. The player's character is a man seeking wealth in 3 regions of Indonesia, and each region will display cultures in their respective regions. To do that the character must solve the puzzle in each region that will give players direction to treasure.

This is one type of media used in providing teaching in the form of games with the aim of stimulating thinking power and increasing concentration through unique and interesting media. This understanding of course identifies that educational games aim to support the teaching and learning process with activities that are fun and more creative. Therefore, the game that is made must have features that are interesting and easy to understand so that players do not get bored easily and have difficulty in running the game. Because this game is made so that players can learn while playing

Now the HOTS game really needs a scoreboard because many players can see the score after playing to see how much value the player get. Therefore the idea came up with making a scoreboard on the website using the php programming language and the SQL database language. Games are very useful if used positively, such as games that function as edutainment media, for example media that distribute not education with entertainment or often called playing while learning. Then the researchers are interested in building an Android-based learning game for young children. Educational games allow for repeated drill and practice with nearly immediate feedback. In this type of games, facts are practiced over and over, but often in the context of an imaginary world, narrative, plot, or goal [1].

Games that are packaged simply and attractively are expected to be useful as an educational media that is educative for children, and can be an alternative medium for teachers and parents in stimulating children's creativity and fostering a child's passion for "learning while playing" early on interesting, fun, effective so that the child still gets joy when learning. The purpose of this research is to produce a game-based learning application [2].

2. Related Research

2.1. Game

The game is a problem solving activity, approached with a pleasant attitude, the game is also something we play and find pleasure in playing it [3 - 4]. A good game is a game that can make users actively participate and have the right amount of challenges, not too little or too much [5].

The attitude of people when playing a game, can be different from the person who is not playing a game, because when the person is playing a game then player will feel as if he is in the "world" that the game created [6]. The game certainly provides

*Corresponding Author: Yogi Udjaja, Jakarta, Indonesia 11480, +62 898 268 3399, udjaja.yogi@gmail.com, yogi.udjaja@binus.ac.id

problems and challenges to be faced by players, if the game does not provide a challenge then the game will be less fun to play. The game also provides a destination for the user, so the user has a goal in playing the game, if the game has no goals maybe the players will find that the game is boring [7].

In describing films or books, the term genre refers to the content of the work while in the game genre refers to the type of challenge that the game offers. In games, genre does not depend on content. An example of such a genre is "Puzzle Games", Specifically a frequently used puzzle game in these studies is Tetris. Arguably, the main cognitive demand in this game is mental rotation and spatial visualization [8].

2.2. MySQL

MySQL was originally created in 1979, by Michael "Monty" Widenius, David Axmark, and Allan Larson. The three of them later founded a company called MySQL AB in Sweden.

My Structured Query Language (MySQL) version 1.0 was released in May 1996 and its use was only limited among internal users. In October 1996, MySQL version 3.11.0 was released to the general public under an "Open but limited" license. With this license, anyone can view the original program and use the MySQL server for free for non-commercial activities. However, for commercial activities, the license must be paid.

MySQL is a Relational Database Management System (RDMS) that is fast and easy to use for various needs. Each user can freely use MySQL, but with the limitations that the software may not be used as a derivative product that is commercial. MySQL is actually a derivative of one of the main concepts in a pre-existing database. SQL (Structured Query Language) is a database operation concept, especially for the selection or selection and entry of data, which allows data operations to be done easily automatically [9].

1.) Make Table

Algorithm 1: Table structure

```
1. Create TABLE people (
2.  SELECT
3. DECLARE AN INTEGER CALLED NOT NULL
   AUTO_INCREMENT,
4. SET NAMA VARCHAR LENGTH 50,
5. DECLARE AN INTEGER CALLED Kalimantan,
6. DECLARE AN INTEGER CALLED Sulawesi,
7. DECLARE AN INTEGER CALLED Papua,
8. DECLARE AN INTEGER CALLED Score,
```

This is the sql table of the game hots in phpmyadmin when creating a table.

2.) Display Data

The command to display data stored in the table can be done with the command “select”.

Example: “SELECT * from people;”.

2.3. Hypertext Preprocessor

Hypertext Preprocessor (PHP) stands for PHP Hypertext Preprocessor, it is a scripting language that is placed on the server. The results of PHP are sent to the client where the user uses a browser. Specifically PHP is designed to form dynamic web applications. That is, it can form a view based on the latest requests. In principle, PHP has the same function as ASP (Active Server Page), Cold Fusion, or Perl. [10].

PHP is not limited to the output of HTML (HyperText Markup Language). PHP also has the ability to process images, PDF files, and flash movies. PHP can also produce text like XHTML and other XML files. One feature that can be relied on by PHP is its support for many databases, one of which is MySQL.

2.4. XAMPP

XAMPP is a web server software that can be used to accommodate the operating systems that you use (X), Apache (A), MySQL (M), PHP (P) and Perl (P) [11]. By installing XAMPP, you don't need to install the application server one by one because in XAMPP already has:

1.) Apache + open SSL

2.) MariaDb + PBXT engine

3.) PHP

4.) PHPMyAdmin

5.) Perl

6.) Filezilla FTP Server

7.) Mercury Mail Transport System.

2.5. C#

C# is a new programming language created by Microsoft (developed under the leadership of Anders Hejlsberg who incidentally has also created a variety of programming languages including Borland Turbo C++ and Borland Delphi). The C# language has also been standardized internationally by ECMA [12].

2.6. UNITY

Unity is a cross-platform game engine developed by Unity Technologies. This software was first launched in 2005 and is one of the many game engines used by many professional game developers in the world. Unity is a game developer tool with integrated rendering capabilities in it. By using the sophistication of its features and also the high work speed, Unity can create an interactive program not only in 2 dimensions, but also in 3 dimensions.

This Unity 3D application is a game engine or a graphics processing software, images, sounds and others are used to create games. Although it can be published to various platforms, Unity needs a license to be published on certain platforms. But Unity provides free users and can be published in a standalone form.

Features in Unity 3D [13]:

a. Hierarchy Tab, the tab functions to enter objects that will be displayed in this game.
b. Inspector Tab, a tab that functions to edit object properties that are clicked on the object component in the Hierarchy Tab, which is used to edit and add components to the object.
c. Project Tab, contains all the ingredients that we will use in making games, where various components such as folders, images, object3D, assets, materials and others will be used.
d. Console Tab, where the error message will appear in the project.
e. Scene Tab, window that is used to build games,view,and manage object in a scene.
f. Game Tab, where the game is being tested, can be run by clicking the play button.

2.7. The Scripting API

Although Unity ships with many built-in components, most games require additional game-specific behaviours.These behaviours can be implemented programmatically in special components called Scripts by using Unity's Scripting API. Scripts can be written in either C#, JavaScript or Boo. In this implementation, all Scripts were written in C#. The Scripting API is an IoC (Inversion of Control) framework, which means that the Scripts written by developers can't control the execution of the game. Rather, the developers have to implement certain methods in the Scripts and Unity will call those methods under certain conditions [14].

3. Research Method

3.1. Unity Sending Data to Server

Connect it using WWW in unity code accessed to a web page to get data from a web server. This is a simple module for retrieving URL data.

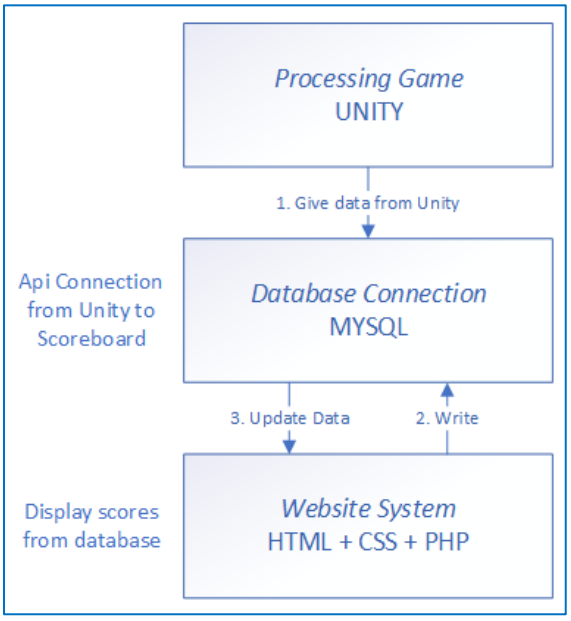


Figure 1: Architecture Transfer Data from Game to Website

3.2. Inserting Data into Database from Unity

Helper class to generate form data to post to web servers using the UnityWebRequest or WWW classes for api script. Create a new file to insert data by using the $ _POST Variable, taking the form data from unity:

Algorithm 2: WWWForm

1. PROCEDURE SubmitAnswer ()
2. BEGIN PROCEDURE
3. RECEIVE DATA WWWForm (newWWWForm)
4. SET FORM TO ["namaPost","kalimantanPost","sulawesiPost","papuaPost","skorPost",]
5. SEND CreateUserURL TO form
   END PROCEDURE

All use $ _post with a string and take names, Kalimantan, Sulawesi, Papua, and scores. Its like telling php someone is going to post something from somewhere so, whatever php post with this id assign it in to string in step 1 (give data from unity) look at Figure 1 when processing Unity Game. Unity Game.Server-side PHP Script to handle POST and GET requests,two scenes with two scripts GET and POST attached to each scene and use C# scripts for sending GET and POST request,that's the basic to make Unity C# communicates to PHP script.

3.3. Table Scoreboard Website

Website containing score table data that has 3 assessment columns, namely the Creativity, Critical Thinking, and Problem Solving columns. From the three columns will be automatically added to the score column. This creates a new php website file. To sort the data from the largest to the smallest using ORDER BY … DESC

Algorithm 3: WWWForm

1. DECLARE @servername,
2. DECLARE @server_username ,
3. DECLARE @server_password ,
4. DECLARE @dbName ,
5. CONNECTION(@servername, @server_username, @server_password, @dbName);
6. SHOW DATA FROM people SORT skor DESCENDING ORDER

It is necessary to determine if there is the same name so that there are no 2 same names here using IF ELSE. If there is the same name, then do an SQL update, If there is no same name then insert data using SQL insert like step 2 (write) look at Figure 1

connection from unity to scoreboard and sort the score from the largest to the smallest using ORDER BY … DESC.If there are more than zero rows returned,the function fetch_assoc() puts all the result into an associative array that can loop through.The while() loops through the result set and outputs the data from the no,nama,Kalimantan,Sulawesi,papua,and skor columns.

Algorithm 4: Insert Name

1. BEGIN
2. SHOW DATA FROM people INCLUDE nama = '$nama'";
3. UPDATE DATA FROM people (Kalimantan,Sulawesi,Papua)EXCEPT nama
4. ELSE
5. SEND people TO (nama,kalimantan,sulawesi,papua,skor)
6. END

From here it can be seen that an update and insert can be done as step 3(update data) look at figure 1 only if the name is the same will be updated automatically, not overrided. By using this it can also be used for websites even though they have been built in unity.

3.4. Make a Quiz

In the quiz there is an animated writing move up and down using anchored animation. There is also if true the phrase "congratulations you enter the next stage" will appear using animation.And to make the play button enter the main quiz by using the On Click. In the usernameAdd.SaveName section to fill in the player's name and click the button to start the game look figure 2.

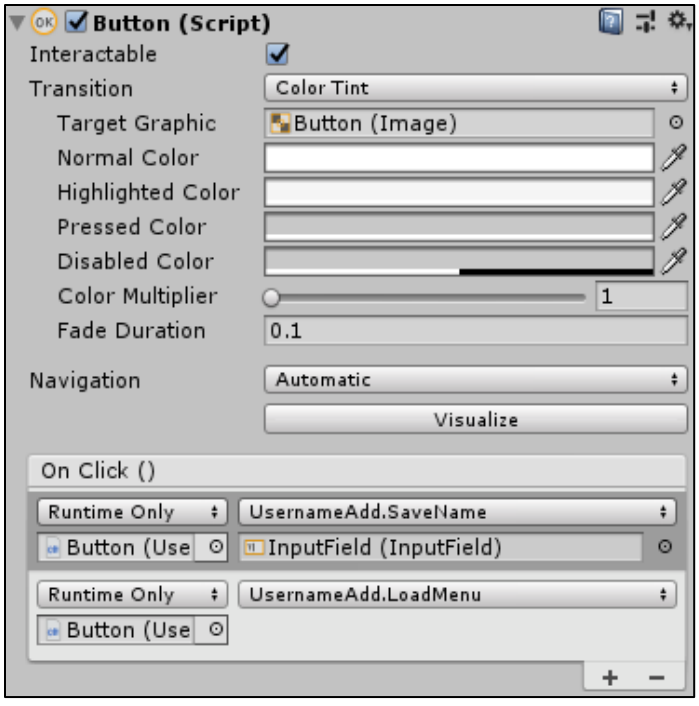


Figure 2: Button (Script)

3.5. Script Gameplay

For the gameplay part starts from void start to display the first time when you click on play.

Algorithm 5: Display Quiz Questions

1. PROCEDURE tampil_soal()
2. BEGIN PROCEDURE
3. SEND urutan_soal REPEAT
4. SET text_soal.text TO DISPLAY SOAL
5. END PROCEDURE

When the quiz question has been displayed, it is necessary use if else so that there are conditions where if it is true it will display an animated sentence and the score will increase by 1.

Algorithm 6: Gameplay.cs

1. PROCEDURE void jawab()
2. BEGIN PROCEDURE
3. If LevelLocation <= 9
4. THEN
5. if urutan_soal < soal.Length - 1
6. THEN
7. If input_jawaban.text = jawaban(urutan_soal) Then
8. feed_benar.SetActive(False)
9. feed_benar.SetActive(True)
10. feed_salah.SetActive(False)
11. AddScore1()
12. AddLoc()
13. SubmitAnswer()
14. input_jawaban.text = ""
15. tampil_soal()
16. Else
17. feed_benar.SetActive(False)
18. feed_salah.SetActive(False)
19. feed_salah.SetActive(True)
20. End If
21. If True Then
22.
23. If input_jawaban.text = jawaban(urutan_soal) Then AddScore1()
24. End If
25. End If
26. End If
27. End If
28. End PROCEDURE

The answer can be true or false, when the first problem is finished then the animation will be reset to proceed to the next problem.Skor+- to increase the score when its True. Every time you answer there will be a value addition.tampil_soal()every time the "question" has been answered then the next "question" must be displayed.

3.6. Void Update

Example: text_skor.text = skor.ToString ();

Skor.ToString use to send numbers to the text that is a string for adding scores when you have solved the next problem in void update and display text scores in the upper right corner:

Algorithm 7: Send Number to the text

```
1. Private Function update() As Void
2.  READ DATA skor.ToString()
3.  End Function
```

when the script has been created, the script will display like figure 3.



Figure 3: Gameplay (Script)

Drag "question" into "text_soal" the answers to “Input_jawaban, animation when False and True inserted into “Feed_benar” and “Feed_salah”. Processed again to be able to send all the data from the unity game can be displayed in the website menu.

In Figure 1 after completing the game, then the unity script is sent to the MYSQL. MySQL can be stored anywhere in the filesystem and set using the MySQL configuration. Also, it is a best practice is to ensure that the logs in the filesystem are not cluttered with other logs such as application logs.

4. Result and Discussion

The web-based HOTS scoreboard is made using the PHP programming language and the SQL.Web database consists of three main menus namely the home menu, score menu, contact menu.

4.1. Home Menu

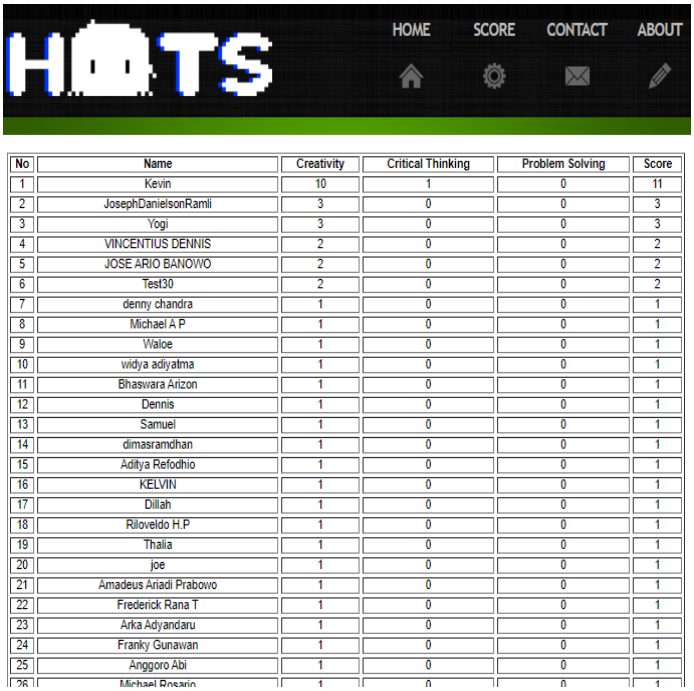
Home is the starting page or the first time when Hotsquiz is run.On this menu there is a slider and an explanation of what is meant by the HOTS game.

4.2. Score Menu.

The score menu functions to display the HOTS player’s data based on the name and sequence of scores from the largest to the smallest see figure 5.



Figure 4: Home Menu



No	Name	Creativity	Critical Thinking	Problem Solving	Score
1	Kevin	10	1	0	11
2	JosephDanielsonRamli	3	0	0	3
3	Yogi	3	0	0	3
4	VINCENTIUS DENNIS	2	0	0	2
5	JOSE ARIO BANOWO	2	0	0	2
6	Test30	2	0	0	2
7	denny chandra	1	0	0	1
8	Michael A P	1	0	0	1
9	Waloe	1	0	0	1
10	widya adiyatma	1	0	0	1
11	Bhaswara Arizon	1	0	0	1
12	Dennis	1	0	0	1
13	Samuel	1	0	0	1
14	dimasramdhan	1	0	0	1
15	Aditya Refodhio	1	0	0	1
16	KELVIN	1	0	0	1
17	Dillah	1	0	0	1
18	Riloveldo H.P	1	0	0	1
19	Thalia	1	0	0	1
20	joe	1	0	0	1
21	Amadeus Ariadi Prabowo	1	0	0	1
22	Frederick Rana T	1	0	0	1
23	Arka Adyandaru	1	0	0	1
24	Franky Gunawan	1	0	0	1
25	Anggoro Abi	1	0	0	1
26	Michael Rosario	1	0	0	1

Figure 5: Score Menu

This table is already connected to the unity game and every question that is successfully done will be sent directly to the scoreboard website.Extensive results carried out show that this ORDER by…DESC is working.

4.3. Game

The main view is the start page that will be accessed by the user. On this page, enter the username and press the play button.

4.4. Question Menu

On the Problem page, the user will do 1 of the 25 questions provided. Each correct answer will be worth 1 and if wrong is 0.



Figure 6: Game Start



Figure 7: Questions

And this is the Display Notification When the User is Right in Choosing Answers.



Figure 8: Answer Question

After working on the correct problem, the value will automatically be entered into the scoreboard on the website. If you see the score on Unity, it will display the status in the pause menu or when in the Island selection menu.

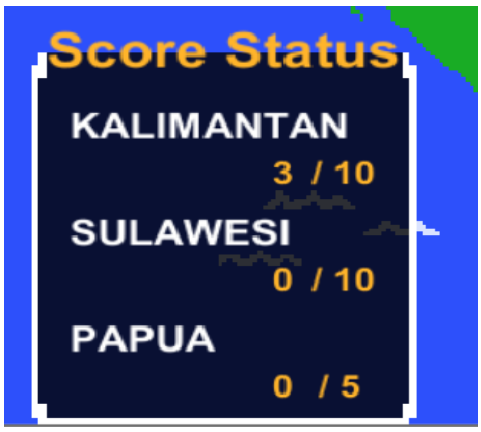


Figure 9: Score Status

Based on the problems above, the processing time needed to solve the problems in Kalimantan is 3 minutes, for Sulawesi Island the processing time is 5 minutes, and for Papua Island the processing time is 7 minutes. when the score is displayed there is a submit button to send scores of Papua, Kalimantan, Sulawesi to the scoreboard website using the $_POST Variable and automatically sort the numbers.

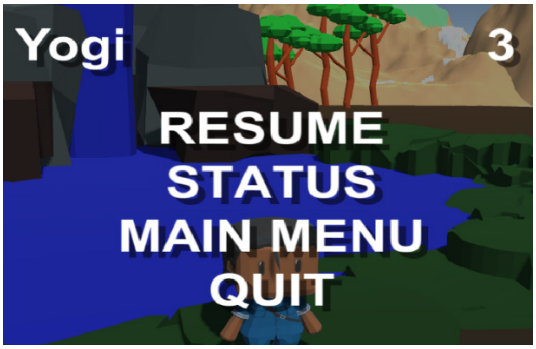


Figure 10: Pause Menu

5. Conclusion

Based on the research and discussion in the previous chapters, it can be concluded that the Web scoreboard with PHP and SQL has been successfully developed. This system is able to manage scores and can be updated automatically both to insert data and update data. Sending data from unity to php can already be done.

HOTS Game Educational Game Development uses Unity 3d game engine software with math problems. HOTS Game educational game runs on the android platform and has a genre of quiz and puzzle. This game has 3 different levels, namely creativity, critical thinking and problem solving. This game also has the highest value feature and a value recap which is useful for summarizing the result of player's answers in each game session.

Maybe there is a need for buttons on the options menu still not available because the buttons have different types, namely toggle buttons and regular buttons. The toggle button in question is the music and sound settings button, while the regular button is the value and help button. Music and sound toggle buttons can be moved to the main menu of the game. Thus, the music or sound settings button can be used as the first setting for the player and added game levels with different levels of difficulty from the previous level.

References

[1] A. Baytak, S. Land, "A case study of educational game design by kids and for kids" in 2010 Procedia – Social and Behavioral Sciences,2010. https://doi.org/10.1016/j.sbspro.2010.03.853

[2] F. Ke, "An implementation of design-based learning through creating educational computer games: A case study on mathematics learning during design and computing". Computers and Education,2014. https://doi.org/10.1016/j.compedu.2013.12.010

[3] Y. Udjaja, "Gamification assisted language learning for Japanese language using expert point cloud recognizer" International Journal of Computer Games Technology, 2018. https://doi.org/10.1155/2018/9085179

[4] Y. Udjaja, Renaldi, Steven, K. Tanuwijaya, I. K. Wairooy, "The Use of Role Playing Game for Japanese Language Learning" in 2019 Procedia Computer Science, ***157***, 298-305,2019. https://doi.org/10.1016/j.procs.2019.08.170

[5] J. Schell, The art of game design: A book of lenses. In The Art of Game Design: A Book of Lenses,2008.

[6] D. P. Kristiadi, Y. Udjaja, B. Supangat, R. Y. Prameswara, H. L. H. S. Warnars, Y. Heryadi, W. Kusakunniran, "The effect of UI, UX and GX on video games" In 2017 IEEE International Conference on Cybernetics and Computational Intelligence (CyberneticsCom) (158-163). IEEE,2017. https://doi.org/10.1109/cyberneticscom.2017.8311702

[7] Y. Udjaja, V. Guizot, N. Chandra, "Gamification for Elementary Mathematics Learning in Indonesia" International Journal of Electrical and Computer Engineering, **8**(5), 3859, 2018. https://doi.org/10.11591/ijece.v8i5.pp3859-3865

[8] A. Oei, M. Patterson, "Playing a puzzle video game with changing requirements improves executive functions" Computers in Human Behavior,2014. https://doi.org/10.1016/j.chb.2014.04.046

[9] F. Kromann, "Beginning PHP and MySQL", In Beginning PHP and MySQL, 2018.

[10] P. Kroll, P. Kruchten, "The Rational Unified Process Made Easy", In Rational Unified Process Made Easy: A Practitioner's Guide to the RUP,2003.

[11] M. Sangeetha, "Smart supply chain management using internet of things", International Journal of Systems, Control and Communications,2018. https://doi.org/10.1504/ijscc.2018.090754

[12] S. Lydford, C# Primer. In Building ASP.NET Web Pages with Microsoft WebMatrix,2011. https://doi.org/10.1007/978-1-4302-4021-1_3

[13] D. Polancec, I. Mekterovic, " Developing MOBA games using the Unity game engine" in 2017 40th International Convention on Information and Communication Technology, Electronics and Microelectronics, MIPRO , 2017. https://doi.org/10.23919/mipro.2017.7973661

[14] C. Bell, "MySQL for the Internet of Things", In MySQL for the Internet of Things,2016.

ASTES

Advances in Science, Technology and Engineering Systems Journal Vol. 5, No. 5, 389-394 (2020)

www.astesj.com

ASTESJ

ISSN: 2415-6698

Sentiment Analysis on Utilizing Online Transportation of Indonesian Customers Using Tweets in the Normal Era and the Pandemic Covid-19 Era with Support Vector Machine

Jajam Haerul Jaman*, Rasdi Abdulrohman, Aries Suharso, Nina Sulistiowati, Indah Purnama Dewi

Fakultas Ilmu Komputer, Universitas Singaperbangsa Karawang, Karawang, 41361, Indonesia

ARTICLE INFO

Article history:
Received: 27 March, 2020
Accepted: 24 June, 2020
Online: 21 September, 2020

Keywords:
Support Vector Machine
Covid-19 Era
Sentiment Analysis
Text Mining

ABSTRACT

Online transportation in Indonesia is a new trend of transportation that is currently used among the lower to upper society. The change in behavior began in 2011 and is growing to this day, the comments that are growing on social media are very important for the online transportation company the negative comments lower the level of users while the good comments increase the users' level. Thus, the comments influence the overall trust of their customers. Among social media, Twitter is a place where many people convey feelings of pleasure and displeasure timely, especially at a time when the COVID-19 pandemic is becoming a serious outbreak. Through these "tweets," many customers express their experience with the service. In this paper, we aim to analyze the experience of online transportation consumers using Support Vector Machine. The data were taken in two periods, i.e. April 2019 ("the normal era") and June 2020 ("the COVID-19 pandemic outbreak. Class logging is done based on 3 categories namely positive, negative and normal, while in mining the data we labeled with the keywords @grabID and @gojekindonesia, 1618 data were obtained with a ratio of 1183 is normal era data and 435 data in the era of COVID-19 pandemic, The highest accuracy results occurred in the normal era with a ratio of 10% as test data and 90% as its training data on linear and sigmoid kernels of 0.8060 while the COVID-19 era only got the highest accuracy of 0.59 in linear kernels with a ratio of 60:40. This is a sign that the COVID-19 pandemic does not contribute to decreasing trust in the service.

1. Introduction

Online transportation in Indonesia began to operate in early 2011 and continues to develop since 2015. It is now one of the most in-demand service needs in Indonesia [1] which is prominently run by two large companies. Despite the in-app review, many customers choose to post their responses or suggestions even disappointment in social media, such as Twitter.

Sentiment analysis is part of data mining which uses text as the object of analysis. Simply stated, it describes a concept of knowledge capture obtained by appraising opinions or sentiments that are incurred from the expression with text as an object.

Some scholars also refer to sentiment analysis as opinion mining. People give their reviews in the form of unstructured formats through blogs, forums, etc. These unstructured reviews have been processed to extract opinions from them and these opinions can be positive, negative, or neutral [2].

The purpose of this paper is to unravel the underlying online transportation review on Twitter or tweets and compare them in two periods: the normal era and the Covid-19 pandemic era. The data was analyzed using vector machine support with the python language.

2. Related Work

Several papers explain the use of SVM with its performance. In previous studies [3], the author explains of the 800 data obtained by being divided into two 500 sections for test data and 300 for data testing, the results obtained were quite high at 0.80. However, this research possesses a weakness on the side of its features so that it can be calcified. Another study was conducted In the paper [4] the author purposed who compared the performance of SVM and Naïve Bayes algorithms with the following stages in the preprocessing data set converted into structured reviews to then converted back to numerical using the lexicon-based approach, this preprocessing approach uses feature selection and semantic analysis, here are the word cutting, POS bar tagging and

*Corresponding Author: Jajam Haerul Jaman, Tel: +62 8158 5339 743 & Email: jajam.haeruljaman@staff.unsika.ac.id

calculating sentiment scores with the stone dictionary from SentiWorldNet. These were then put into the classification process using both SVM and Naïve Bayes. The result was that from 3 data sets tested (Gold, Film, and Twitter) achieved performance for a naïve bay of 69.10%, 74.55%, and 76.67%, for SVM gained 72.74%, 74.73%, and 76.92%, apart from two comparison algorithms also performed using the RBF kernel where the result was 73.56%, 74,745 and 78.18%. Further analysis resulted in the highest accuracy value by RBF kernel, so the use of the RBF kernel is highly recommended. In another paperm it is presented a sentiment analysis of regional head candidates using an SVM algorithm to build the model. The data sets were taken from news documents about regional heads in East Java 2018, i.e. Kompas, JPNN, Republika, and Detik, The result was that Gus Ipul as a candidate for regional head number two has precision value, remember, and AUC as many 0.940, 0.948 and 0.890 respectively. Models built on the data resulted in a good performance with accurate estimation.

While sentiments regarding the use of transportation are presented in the following papers. The paper introduced SVM and nonnegative matrix factorization in the stock market prediction process using Twitter and historical data. The stock exchange dataset used LQ 45 from August 2018 to January 2019. This feature consists of closing price, volume, percentage of topics, and sentiment. The price and volume were taken from yahoo finance data, while topics and sentiments were retrieved from the comments of every stock market in LQ45. The result obtained 60.16% accuracy.

The second in [5], the author presented also showed that SVM provides a fairly good level of accuracy from 1183 data to 90% training data and 10% data testing, the result is linear use 0.8, RBF 0.78, Sigmoid 0.8, and polynomial 0.77.

The author performs conducted a review of his comments from Twitter related to the use of transportation managed by the government of DKI Jakarta namely "TransJakarta" algorithm used is Convolutional Neural Network, architecture testing using VGG, ResNet, and GoogleNet, consisting of 16 layers, ResNet 34 layers, and GoogleNet 22 layers, the results obtained from the Resnet 34 layer architecture model provide the best F-Score 98.11%, better than VGG which has the highest F-Score score of 96.74% and GoogleNet 96.80%.

The author presented a paper with the title "Exploring the Performance Characteristics of the Naïve Bayes Classifier in the Sentiment Analysis of an Airline's Social Media Data," the purpose is to know comments of airline operator users on Twitter using Naïve Bayes its architectural model, The dataset obtained was a negative sentiment of 37.47% and positive by 65.53%, They highlighted that the large training data set is potential to improve the accuracy of classifier classification.

3. Material and Method

3.1. Data Collecting / Methods and Technique

In the early stages of this paper is limited to the two largest online transportation companies in Indonesia namely GoJek Indonesia and GrabId, following the retrieval of data taken from [5] in April 2019 then continued the process of crawling data using twitter APIs in April to June 2020 where this era is referred to as the era of COVID-19 pandemic.

3.2. Research Planning

The planning of the research consists of 5 stages as follows:

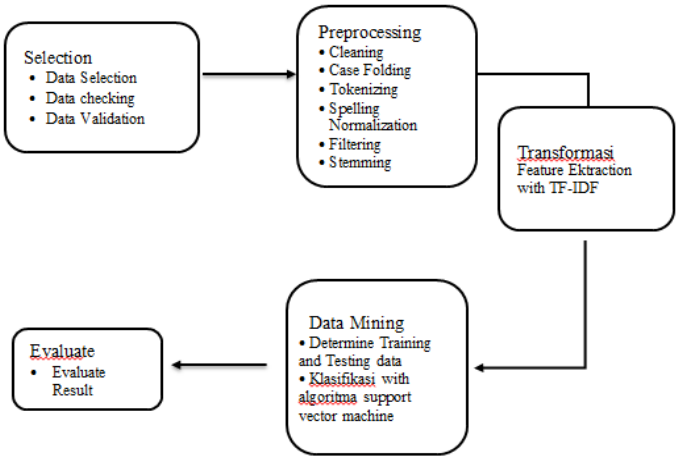


Figure 1: Research Planning [5]

3.2.1. Data Selecting

Data retrieval was carried out in the data crawling process. The content of the data was customer key access is as the entry key into Twitter APIs, Access Tokens, and access token secrets for the final stage of data crawling. The keyword, i.e. @grabid and @gojekindonesia was used and tweets published in April 2019 until June 2020 were selected. The data were randomly retrieved so that not all days were taken. Then the data was examined using the help of the Indonesian dictionary in the literary package as standardization of Natural Language Processing (NLP) to be then labeled, The data was validated by a team of Indonesian language experts in the language center building at Universitas Singaperbangsa Karawang.

3.2.2. Preprocessing

- Cleaning

This stage is the process by which the data is cleaned, while some of the writings that must be cleaned between others are writings in the form of @ symbols like "@", "#" and characters "!$%^&*()_", the purpose of which is to make the data readable clearly.

	text_cleaning
0	AT_USER min mau lapor tadi saya beli grabfood ...
1	AT_USER AT_USER LGSG AKU BUKA LOH SKRG! ngaruh...
2	kurang setia apa coba? :') AT_USER URL
3	Udah ditelp kasih petunjuk keberadaan eh drive...
4	AT_USER Setahun lbh memakai js gojek,baru kali...

Figure 2: Text Cleaning Process

- Cse folding

Case folding is a stage where data is standardized. The letters, words, or sentences that sentence case, upper case,

capital each word, and toggle case were changed into lowercase so that the uniformity of the data is maintained.

- Tokenizing

Tokenization is a process in which sentences are cut into tokens. Some punctuation marks such as commas, dots, and others were limited. Tokens will be read into words according to Indonesian language grammar.

```
import re
def tokenize(text):
    tokens = re.findall('\w+',text)
    return tokens
data['text_tokenization']=
data['text_cleaning'].apply(lambda
x:tokenize(x.lower()))
showtext_tokenizing
=pd.DataFrame(data,columns=['text_tokenization'])
showtext_tokenizing.head()
```

	text_tokenization
0	[at_user, min, mau, lapor, tadi, saya, beli, g...
1	[at_user, at_user, lgsg, aku, buka, loh, skrg,...
2	[kurang, setia, apa, coba, at_user, url]
3	[udah, ditelp, kasih, petunjuk, keberadaan, eh...
4	[at_user, setahun, lbh, memakai, js, gojek, ba...

Figure 3: Source Code and Result Tokenization Text

- Spelling and Normalization

To be able to read more clearly, the spelling was normalized so the words are in proper spelling, Also, many abbreviations were normalized such as min being admin, telp to telephon (make/made a phone call).

	text_normalization
0	[at_user, admin, mau, lapor, tadi, saya, beli,...
1	[at_user, at_user, langsung, aku, buka, loh, s...
2	[kurang, setia, apa, coba, at_user, url]
3	[udah, telephon, kasih, petunjuk, keberadaan, ...
4	[at_user, setahun, lebih, memakai, jasa, gojek...

Figure 4: Normalization Text

- Filtering Process

The step was to remove unused words, this process is also called Stop Word.

	text_stopwordremove
0	[admin, mau, lapor, tadi, saya, beli, grabfood...
1	[langsung, aku, buka, loh, sekarang, ngaruh, t...
2	[kurang, setia, apa, coba]
3	[udah, telephon, kasih, petunjuk, keberadaan, ...
4	[setahun, lebih, memakai, jasa, gojek, baru, k...

Figure 5: Filtering Text

- Stemming

A Steaming is done to retrieve the main words of each sentence. The things to note in this process are the removal of all affixes, prefixes, endings, or both.

	text_stemmed
0	[admin, mau, lapor, tadi, saya, beli, grabfood...
1	[langsung, aku, buka, loh, sekarang, ngaruh, t...
2	[kurang, setia, apa, coba]
3	[udah, telephon, kasih, tunjuk, ada, eh, drive...
4	[tahun, lebih, pakai, jasa, gojek, baru, kali,...

Figure 6: Steaming Process

3.3. Data Transformation

After the preprocessing phase is completed, the transport process in which the term used is TF-IDF (Term Frequencies - Inverse Document Frequency) which is a step of changing from categorical values to numerical values. The data is then extracted into values.

3.4. Text mining with SVM

The next step is data mining with SVM as the model, Positive, Negative, and Neutral were the 3 classes used, as follows:

Table 1: Scenario

Scenario	Training	Testing
S1	0.5	0.5
S2	0.6	0.4
S3	0.7	0.3
S4	0.8	0.2
S5	0.9	0.1

3.5. Evaluation

The evaluation was carried out to see the performance of SVM performance, accuracy being the benchmark for performance, accuracy will determine how well the initial data is obtained, preprocessing, and transformation.

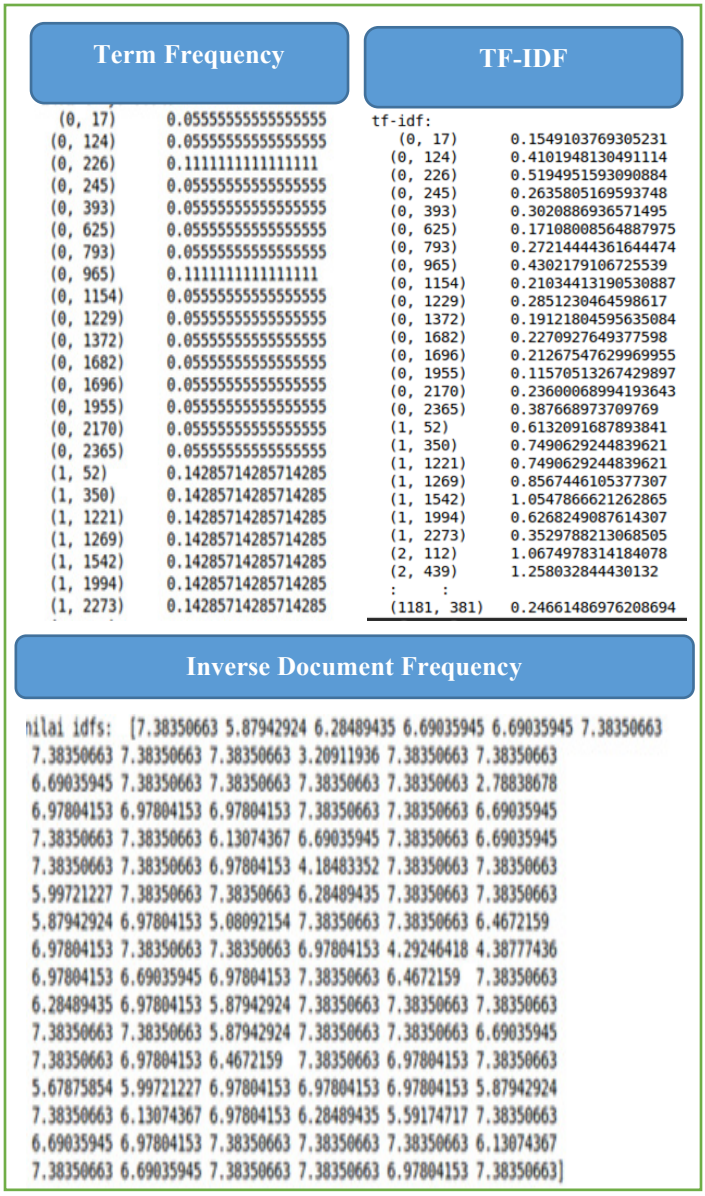


Figure 7: Transformation

4. Result

There are more than 3,000 data gained in the crawling process. The data was then preprocessed and resulted in much as 1618 for the normal era and 435 for the Covid-19 eras.

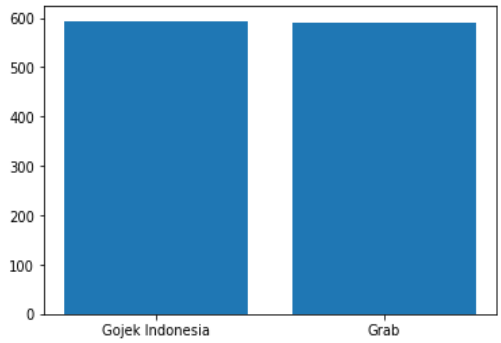


Figure 8: Comparison of objects on data in normal eras.

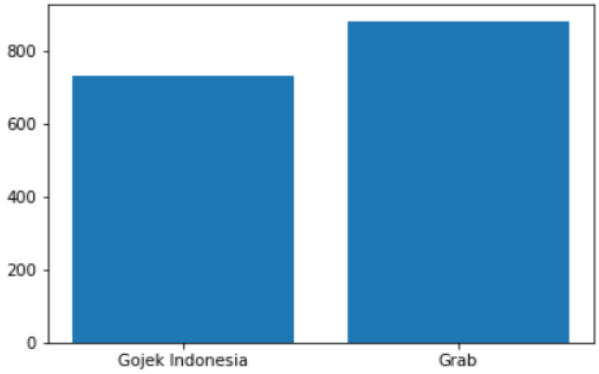


Figure 9: Comparison of objects on data with Covid-19 eras

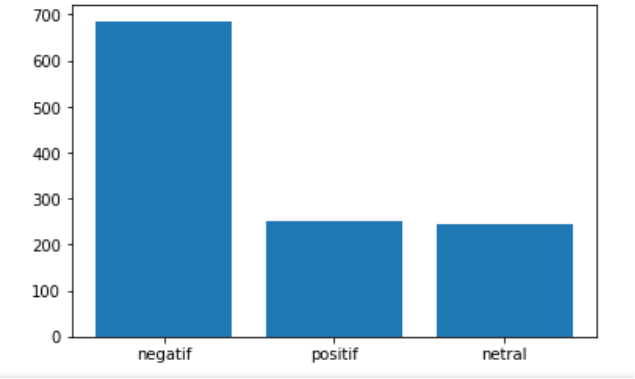


Figure 10: Sentiment Comparation in the normal eras.

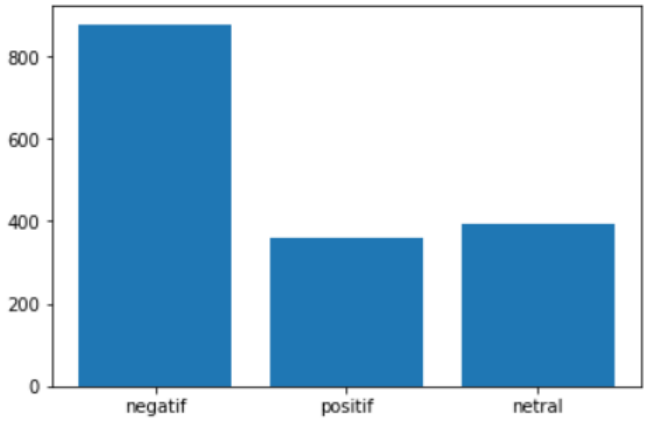


Figure 11: Sentiment Comparation With Covid-19 eras

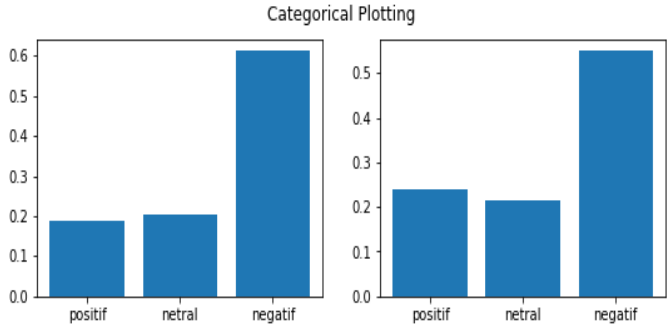


Figure 12: Categorical Plotting normal eras

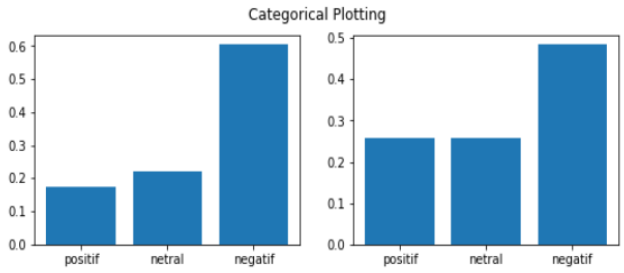


Figure 13: Categorical Plotting with Covid-19 eras

In Figure 12 the data is separated into categories based on the object, for Gojek Indonesia 733 data was generated while for Grab ID 885 data was generated. Each category was then revealed the pattern as shown in Table 3 during the normal era and Table in the pandemic era.

Table 2: Indonesia Linguists Validation Result in the normal eras

Data	Gojek Indonesia	GrabID
Total	733	885

Table 3: Indonesia Linguists Sentiment Validation Result in the normal eras

Sentiment	Gojek Indonesia	Grab ID
Positive	111	140
Negative	363	323
Neutral	120	126

Table 4: Indonesia Linguists Sentiment Validation Result with Covid-19 eras

Object	Gojek Indonesia	Grab ID
Positive	127	226
Negative	443	429
Neutral	163	225

Table 4 shows that there is a significant increase in the sentiment of online transportation in the Covid-19 era

Table 5: Presentation of data increase after coupled with COVID-19 era

Object	Positive	Negative	Neutral
GojekIndonesia	0,14	0.22	0.36
Grab ID	0.61	0.33	0.79

Table 6: Result of Various Kernel Accuracy in Normal Eras

Scenario	Kernel			
	Linear	RBF	Sigmoid	Poly
50:50	0.64	0.59	0.63	0.59
60:40	0.77	0.74	0.75	0.75
70:30	0.66	0.64	0.61	0.61
80:20	0.76	0.74	0.70	0.71
90:10	0.80	0.78	0.80	0.77

Tables 6 and 7 show that following the additional data from the COVID-19 era, there is a decrease in inaccuracy. Hence, this is very poor data with which high accuracy is rather difficult to achieve. It is assumed that the trend is heavily influenced by the transportation policies, both from the Government and company in the pandemic era, such as health protocols on online transportation partners that make the performance of the online transportation decrease.

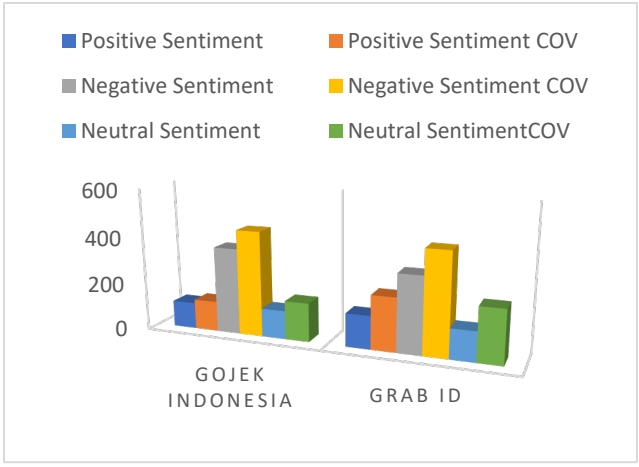


Figure 14: Increased of sentiment in the Covid-19 era

Table 7: Result of Various Kernel Accuracy with Additional data Covid-19 Era

Kernel	Scenarios				
	50:50	60:40	70:30	80:20	90:10
1. Linear	0.58	0.59	0.51	0.54	0.55
2. Rbf	0.55	0.56	0.51	0.50	0.50
3. Sigmoid	0.57	0.57	0.49	0.53	0.53
4. Poly	0.52	0.53	0.47	0.47	0.47

5. Conclusion

This study aimed to compare sentiment analysis toward online transportation service in pre-and whilst COVID-19 pandemic era by VMS. It is found that the performance in every kernel in the pandemic era decreased. In the normal era, the highest accuracy obtained is in the linear kernel, and sigmoid with a ratio of 90:10 results in an accuracy of 0.8. Meanwhile, in the pandemic era, the highest accuracy is only found in linear kernels with a ratio of 50:40 which is 0.59. The accuracy likely declined due to several factors, such as poor and unstructured initial data and the costumers' reluctance to adopt the health protocol which contributes to the raise of displeased with the service.

Conflict of Interest

The trend of transportation service is to continue to develop and attract various research in the field. However, this study is neither attributive nor sponsored by any company mentioned in the research.

References

[1] F.Y. Kristo, Awal Mula Transportasi Online Menjamur di Indonesia, Detik.Com, 2017.

[2] A.S.H. Basari, B. Hussin, I.G.P. Ananta, J. Zeniarja, "Opinion mining of movie review using hybrid method of support vector machine and particle swarm optimization," in Procedia Engineering, 453–462, 2013, doi:10.1016/j.proeng.2013.02.059.

[3] D.G. Nugroho, Y.H. Chrisnanto, A. Wahana, "Analisis Sentimen Pada Jasa Ojek Online ... (Nugroho dkk.)," 156–161, 2015.

[4] B. Jadav, V. Vaghel, "Sentiment Analysis using Support Vector Machine based on Feature Selection and Semantic Analysis," International Journal of Computer Applications, **146**(13), 26–30, 2016.

[5] J.H. Jaman, R. Abdulrohman, "Sentiment Analysis of Customers on Utilizing Online Motorcycle Taxi Service at Twitter with the Support Vector Machine," in ICECOS 2019 - 3rd International Conference on Electrical Engineering and Computer Science, Proceeding, 231–234, 2019, doi:10.1109/ICECOS47637.2019.8984483.

ASTES

Advances in Science, Technology and Engineering System Journal Vol. 5, No. 5, 395-400 (2020)

www.astesj.com

ASTESJ

ISSN: 2415-6698

Multi-Objective Optimization when Surface Grinding the 3X13 Steel by Combining the General Reduced Gradient Algorithm and Harmonic Mean Method

Nhu-Tung Nguyen, Dung Hoang Tien, Do Duc Trung *

Faculty of Mechanical Engineering, Hanoi University of Industry, Hanoi, 100000, Vietnam

ARTICLE INFO

Article history:
Received: 10 August, 2020
Accepted: 11 September, 2020
Online: 21 September, 2020

Keywords:
Surface Grinding
3X13 Steel
Surface Roughness
Vibration
GRG Algorithm
Harmonic Mean method

ABSTRACT

In this paper, the multi-objective optimization process was applied for the surface grinding process of 3X13 steel using an aluminum oxide grinding wheel (WA46J7V1A). For each experiment, three cutting parameters, including the workpiece velocity, feed rate, and the depth of cut, were controlled to change according to the experimental matrix. At each experiment, surface roughness and vibrations of the technology system in three directions (X, Y, and Z) were measured and analyzed. The surface roughness and vibration amplitudes were modeled as a quadratic function of workpiece velocity, feed rate, and the depth of cut. The General Reduced Gradient (GRG) algorithm and Harmonic Mean (HM) method were combined to solve the multi-objective optimization problem about the surface grinding process of 3X13. The optimized values of surface roughness and vibration amplitudes (in X, Y, Z directions) were 0.901 µm, 0.815 µm, 1.594 µm, and 0.599 µm, respectively. These results that were determined at the cutting conditions were workpiece velocity of 14.428 m/min, the feed rate of 5.789 mm/stroke, and cutting depth of 0.013 mm. By conducting the grinding process at the optimal values of grinding conditions, the experimental results of surface roughness and system vibration amplitudes were quite close to that one of the predicted results. This proposed approach can be applied to improve the machining quality of the surface grinding process of 3X13 steel.

1. Introduction

Surface roughing of a part when machined by the grinding method, has a great influence on the workability and life of the product. Therefore, it is often selected as one of the most important factors for evaluating the efficiency of the grinding process. The vibration of the technology system also has a great influence on the accuracy and quality of the part surface. Therefore, researching solutions to limit the vibration amplitude of the technological system also plays an important role in grinding technology. To obtain the small values of the surface roughness and vibrations of the technological system to ensure the requirements of the product quality, determining the optimum value of the cutting parameters that needs to be done for each specific case.

The response surface method (RSM) was used to determine the optimum values of the cutting depth, feed rate, and the dressing depth. This method was applied in grinding process of AISI 1080 steel by using the A60V5V grinding wheel to obtain the minimum value of machined surface roughness [1]. RSM was applied to determine the optimum value of the grinding wheel speed, feed rate, and cutting depth when using the AA46/54 K5V8 grinding wheel to grind the EN 8 steel. The purpose of the optimization process in this study was an assurance that the surface roughness has the lowest value with the highest material removal rate [2]. To obtain the minimum value of surface roughness, RSM was used to determine the optimum values of traverse speed, depth of the cut, and the number of passes in the grinding process of Inconel 718 alloy [3]. RSM was applied to determine the optimum value of wheel speed, work speed, depth of cut, abrasive mesh, and grinding direction (up and down grinding) to ensure the minimum value of surface roughness when grinding Inconel 625 alloy [4]. RSM was applied to determine the optimal value of the cutting depth, the number of grinding strokes, and wheel grade to ensure a minimum surface roughness, maximum surface hardness, and maximum flatness when grinding spheroidal graphite cast iron using the green silicon carbide grinding wheel [5].

To ensure the smallest surface roughness, Taguchi method was applied to determine the optimum value of the coolant concentration and flow of the cooling fluid, feed rate, workpiece velocity, and cutting depth when grinding 9CrSi steel by using

*Corresponding Author: Do Duc Trung, Faculty of Mechanical Engineering, Hanoi University of Industry, Vietnam, doductrung@haui.edu.vn

Cn46TB2GV1,300.32,127.30 m/s grinding wheel (Hai Duong grinding wheel, Vietnam) [6]. Taguchi method and RSM were combined to determine the optimum values of grinding grain size, the cutting depth, and the feed rate when grinding the AISI 1035 steel. The purpose of this study is also to ensure that the surface roughness of the machined part has a minimum value [7]. The WA36G5VBE grinding wheel was used to perform experiments with three materials, including mild steel, cast iron, and carbon steel (three different hardness levels). In this study, the Taguchi method was applied to determine the optimum values of the workpiece hardness, workpiece velocity, and the depth of cut to obtain the minimum value of surface roughness [8].

Taguchi method was applied to investigate the influence of cutting parameters on the system vibrations when grinding the C9rSi steel alloy. The obtained results showed that the cutting parameters have a significant influence on the system vibrations [9]. Taguchi method was applied to determine the optimum values of the grinding wheel speed, workpiece speed, and the feed rate to ensure that the vibration amplitudes of the grinding wheel have the smallest values. In this study, the 1-A-355-38-127-C-46-J-7-V grinding wheel was used to grind the S45C steel [10].

Taguchi-gray method was applied to determine the optimum values of the grinding wheel speed, workpiece speed, and feed rate when grinding OCR12VM tool steel using A80QV grinding wheel. The purpose of this study is to ensure that the surface roughness, vibration in the X direction, and vibration in the Z direction have the smallest values [11].

Although the studies to determine the optimal values of the cutting parameters to ensure the surface roughness and vibrations of the technological system having the smallest value, that has been carried out in many studies. However, the studies that were performed for the surface grinding process of the 3X13 steel have been not mentioned. Meanwhile, 3X13 stainless steel is often used to make the machine parts with high precision, working in extreme conditions (such as valves of air compressors, etc.). For these parts, the surface grinding method is often chosen as the final machining method for important surfaces. So, it is necessary to study the surface roughness and vibrations of the technological system when surface grinding this steel.

On the other hand, in the previous studies, when determining the optimal values of cutting parameters in the surface grinding process, two popular methods were often used that were the response surface method and the Taguchi method. The studies that applied the combination of the GRG algorithm and the HM method to solve the optimization process of surface grinding processes have not been mentioned. Therefore, the combination of the GRG algorithm and the HM method to determine the optimal value of the workpiece velocity, the feed rate, and the cutting depth when grinding 3X13 steel is to ensure that both surface roughness and vibration amplitudes in the three directions X, Y, Z having the small values that will contribute to the novelty of both the method and the research objects in the grinding technology.

2. Experimental Method

2.1. Experimental Grinding Wheel and Machine

The grinding wheel was used in this work, which had the symbol of WA46J7V1A–180'13'31.75 as described in Figure 1. The experiments were carried out in the surface grinding machine APSG-820/2A.



Figure 1: Experimental grinding wheel

2.2. Experimental Workpiece

The experimental workpiece material is 3X13 steel that was made by Russia. The chemical compositions of the workpiece are listed in Table 1. The equivalent sign of 3X13 steel, according to several Standard are described in Table 2. The properties of 3X13 steel were listed in Table 3. The workpieces dimensions are the length of 60 mm, the width of 40 mm, and the height of 10 mm, as shown in Figure 2.

Table 1: Chemical Composites of 3X13 Steel

Element	C	Si	Mn	Cr	S
(%)	0.42	1.00	1.00	13.00	0.005

Table 2: Equivalent Symbol of 3X13 Steel of According Several Standard

Russia	United States	Germany	Japan	France	England	Europe	Italy	Spain	China	Sweden	Finland	Czech
GOST	SAE	DIN	JIS	AFNOR	BS	EN	UNI	UNE	GB	SS	PN	CSN
3X13	420	1.4028	SUS420J2	410F21	420S45	1.4028	GX30Cr13	F.3403	3Cr13	2304	3H13	17023

Table 3: The Properties of 3X13 Steel

Density, g/cm^3	7.8
Melting point, °C	1450 - 1510
Specific heat capacity, J/kg	460 at 0 – 100^{0}C
Electrical resistivity, μΩ·m	0.55 at 20^{0}C
Elastic modulus, MPa	200
Thermal conductivity, W/m	24.9 at 100^{0}C
Coefficient of thermal expansion, μm/m	10.3 at 0 – 100^{0}C
	10.8 at 100 – 315^{0}C
	11.7 at 315 –538^{0}C

2.3. Measurement System

MITUTOYO-Surftest SJ-210 surface roughness tester was used to measure the machining surface roughness of the product (Figure 2). The evaluation length was fixed at 0.8 mm. The surface roughness was measured perpendicular to the cutting velocity direction and repeated three times following three repeated times

of each cutting test. The average value of surface roughness in three consecutive times was used for analysis and evaluation.

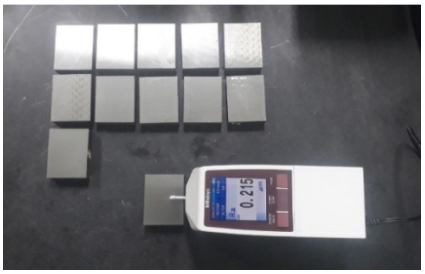
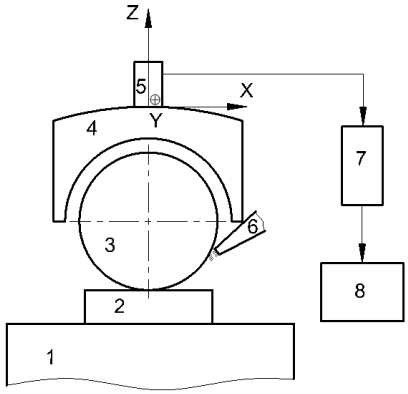


Figure 2: The experimental workpiece and surface roughness tester

The block diagram of the experimental system was described in Figure 3. The vibration measurement system that included the acceleration sensor Type 4525-B-001, the data processing box, and the PULSE software was used to measure the system vibrations. For each experiment, the vibrations of the system were measured simultaneously in three directions (X, Y, Z). The detail is illustrated in Figure 4.



1. Magnetic table; 2. Workpiece; 3. Grinding wheel; 4. Wheel guard; 5. Acceleration sensor; 6. Nozzle; 7. Data processing box; 8. PC and software

Figure 3: Block diagram of the experimental system



Figure 4: Setup of vibration measurement

2.4. Experimental Matrix

The experimental matrix was designed according to the Box-Behnken form. Figure 5 presents the Box-Behnken experimental diagram with three variables (including workpiece velocity, feed rate, and depth of cut). By this form, each cutting parameter has three levels corresponding to the three coding values (-1, 0, and 1), which were described in Table 3. In Figure 5, each point represents an experiment. C is the central experiment point. In the central experiment point, the workpiece velocity, feed rate, and depth of cut were the average values of each parameter (10 m/min, 6 mm/stroke, and 0.015 mm, respectively). The number of experiments at the central point is three times. The experimental matrix was described in Table 5.

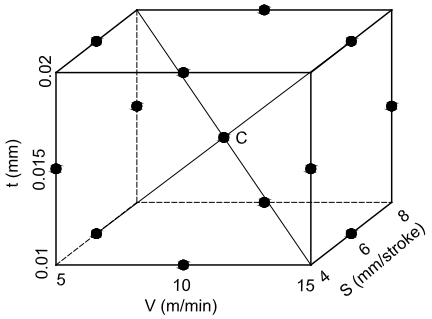


Figure 5: Box-Behnken experimental design with three variables

Table 4: Input Factors and The Their Values at the Coded Levels

Factors	Symbol	Unit	The values at the coded levels		
			-1	0	1
Workpiece velocity	V	m/min	5	10	15
Feed rate	S	mm/stroke	4	6	8
Depth of cut	t	mm	0.01	0.015	0.02

Table 5: Experimental Matrix and Results

No.	Cutting Conditions			Surface Roughness	Vibration Amplitudes		
	V (m/min)	S (mm/ stroke)	t (mm)	Ra (μm)	Ax (μm)	Ay (μm)	Az (μm)
1	10	4	0.01	0.332	0.191	0.277	0.212
2	15	6	0.01	0.377	0.206	0.297	0.333
3	15	8	0.015	1.128	0.977	1.960	1.215
4	10	8	0.01	1.068	0.560	0.839	0.693
5	5	8	0.015	0.508	0.443	0.687	0.599
6	5	4	0.015	0.490	0.199	0.160	0.242
7	15	6	0.02	0.761	0.291	0.324	0.36
8	15	4	0.015	0.799	0.18	0.232	0.272
9	10	8	0.02	1.263	0.571	0.968	0.581
10	5	6	0.02	0.886	0.277	0.343	0.387
11	10	6	0.015	1.229	0.282	0.449	0.419
12	10	4	0.02	1.107	0.217	0.313	0.322
13	10	6	0.015	1.192	0.338	0.502	0.45
14	5	6	0.01	1.164	0.193	0.233	0.32
15	10	6	0.015	1.176	0.341	0.499	0.459

2.5. Machining Conditions

The experiments were conducted in the grinding conditions as following: Grinding wheel velocity: 26 (m/s). Cooling fluid: emulsion 10%, overflow irrigation method, the volume flow rate

of 5 (lit/min). Dressing conditions: dressing depth 0.01 (mm), dressing feed rate: 100 (mm/min).

3. Experimental Results and Discussions

The experimental results of surface roughness and vibration amplitudes in three directions (X, Y, Z) were stored and described in Table 5 and Figure 6.

It seems that the tendencies of vibration amplitudes were the same. When the system vibration amplitude in one direction increased, the vibration amplitudes in other directions also increased, and vice versa. The phenomenon can be explained that the vibrations in the machining process caused by many factors such as the stiffness of the system, the damping ratio of the system, cutting forces, etc. In all parameters, cutting forces have a significant effect on the vibrations. When cutting forces increase, the vibrations will increase. Besides, in the grinding process, the cutting forces were formed in all directions (X, Y, Z), and when cutting forces increases, the vibrations will increase in all directions. So, the tendencies of vibration amplitudes were the same in different directions.

Figure 6 also showed that the tendency of the surface roughness was also quite the same as the tendency of vibration amplitudes. The phenomenon can be explained that when the vibrations were encreased in X and Y direction, it made the machining surface wave also increasing. Besides, when the vibration in Z direction increased, the cutting depths of the cuts of grinding grains leaving on the surface of the part increased. So, when the vibrations increase, in most cases, the surface roughness also increases.

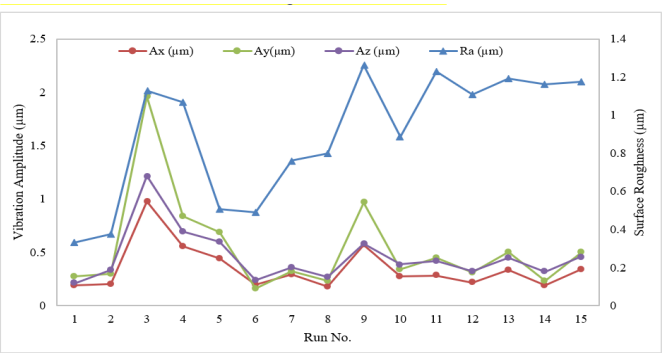


Figure 6: The relationship between surface roughness and vibration amplitudes

In all experiments, the surface roughness was smallest at the experiment number 1 (Ra = 0.332 µm). At this experiment, the vibration amplitude in Z direction was also the smallest (Az = 0.212 µm), while the vibration amplitudes in X and Y directions were not the smallest. In the X direction, the smallest vibration amplitude was 0.18 (µm) that was obtained at experiment number 8, while in the Y direction, the smallest vibration amplitude was 0.1608 (µm) that was obtained at experiment number 6. These results can be explained as follows: vibration components and surface roughness are not only dependent on the cutting parameters but also dependent on the interaction between those parameters, as well as dependent on other factors in the machining process. The complex influence of the factors on the vibration and surface roughness components has different roles and degrees. It is not easy to explain these phenomena. Therefore, more experimental studies are needed to clearly explain these phenomena. It means that it is impossible to determine the value set of V, S, t to obtain the smallest values of all the objective functions (Ra, Ax, Ay, and Az). It is only possible to determine the value set of V, S, t to obtain the small harmonic values of Ra, Ax, Ay và Az. So, it is necessary to solve the multi-objective optimization problem. This issue was presented in the next section.

4. Multi-Optimization by Using General Reduced Gradient Algorithm and the Harmonic Mean Method

4.1. Surface Roughness and Vibration Amplitude Models

From the experimental results in Table 5, the surface roughness and vibration amplitudes in three directions (X, Y, Z) were modeled as a quadratic function of workpiece velocity, feed rate, and depth of cut as expressed by (1) to (4). These equations were the basis to solve the multi-objective optimization problem when surface grinding of 3X13 steel. The factor of machining conditions (V, S, t) will determine by solving the multi-objective optimization problem when considering all 4 of these models simultaneously.

$$R_a = -3.0561 + 0.1001 * V + 0.7001 * S + 162.4333 * t$$
$$-0.0123 * V^2 - 0.0402 * S^2 - 3824.4444 * t^2 \quad (1)$$
$$+0.0078 * V * S + 6.62 * V * t - 14.50 * S * t$$

$$A_x = 0.7965 - 0.0641 * V - 0.4313 * S + 93.50 * t$$
$$-0.0003 * V^2 + 0.0341 * S^2 - 2871.6667 * t^2 \quad (2)$$
$$+0.0138 * V * S + 0.0020 * V * t - 0.3750 * S * t$$

$$A_y = 1.6054 - 0.1237 * V - 0.9833 * S + 208.715 * t$$
$$-0.0005 * V^2 + 0.0721 * S^2 - 6892.6667 * t^2 \quad (3)$$
$$+0.030 * V * S - 0.8360 * V * t + 2.3250 * S * t$$

$$A_z = -0.0377 - 0.081 * V - 0.2977 * S + 137.290 * t$$
$$+0.0008 * V^2 + 0.0302 * S^2 - 4454.8333 * t^2 \quad (4)$$
$$+0.0146 * V * S - 0.4060 * V * t - 5.550 * S * t$$

4.2. General Reduced Gradient Algorithm

The GRG algorithm was used to solve nonlinear problems. The basic principles and ways to solve the problem by the GRG algorithm have been detailed in several studies [12] and [13]. Currently, the GRG algorithm has also been integrated into the solver tool of Microsoft Excel. Using Microsoft Excel to solve problems with the GRG algorithm has the advantage of being non-programming and convenient even for people who are not specialized in mathematics or computer science.

4.3. Harmonic Mean Method

The HM method was introduced the first time in 1999 [14]. This is the new approach method to solve the multi-objective optimization problems in the case without enough information on the evaluation criteria. In the multi-objective optimization problems, there is not enough information about the weight number of the objective functions. This method can be solved the

problems most harmoniously. According to this method, the minimum of the overall function can be expressed by (5) [15].

$$\{f(x_1), f(x_2), \dots f(x_3)\} \to min \quad (5)$$

where f(xi) is the individual objective functions

And then, the optimization problem can be rewritten by (6).

$$F(x) = \{\frac{1}{f(x_1)} + \frac{1}{f(x_2)} + \frac{1}{f(x_3)}\}^{-1} \to min \quad (6)$$

4.4. Optimization Process and Results

To solve the multi-objective optimization problem for surface roughness and vibration amplitudes in X, Y, Z directions, the constraints of objective functions and input parameters (workpiece velocity, feed rate, and depth of cut) must be determined. The regression models of surface roughness and vibration amplitudes were built based on the experimental matrix and data, so the constraints of cutting conditions and objective functions were determined by (7) and (8).

$$\begin{cases} 5\left(\frac{m}{min}\right) \le V \le 15\left(\frac{m}{min}\right) \\ 4\left(\frac{mm}{stroke}\right) \le S \le 8\left(\frac{mm}{stroke}\right) \\ 0.01\ (mm) \le t \le 0.02\ (mm) \end{cases} \quad (7)$$

$$\begin{cases} Ra > 0 \\ Ax > 0 \\ Ay > 0 \\ Az > 0 \end{cases} \quad (8)$$

According to the MH method, the multi-objective function was rewritten by (9).

$$F'(V,S,t) = \left\{\frac{1}{Ra} + \frac{1}{Ax} + \frac{1}{Ay} + \frac{1}{Az}\right\}^{-1} \to min \quad (9)$$

Applying the GRG algorithm to solve (9) with the constraints as by (7) and (8). The optimal values of the input parameters and the objective functions were obtained and listed in Table 7.

Using the optimal values of cutting parameters (V, S, t) from Table 7, the grinding tests were conducted to verify the optimal values of the objective function. The tested results were stored in Table 8.

Table 7: The Optima Values of the Parameters and Objective Functions

V (m/min)	S (mm/ stroke)	t (mm)	Ra (µm)	Ax (µm)	Ay (µm)	Az (µm)
14.428	5.789	0.013	0.826	0.316	0.496	0.010

Table 8: Verified Results of Optimal Values of Grinding Cutting Parameters

Test No.	V (m/min)	S (mm/ stroke)	t (mm)	Ra (µm)	Ax (µm)	Ay (µm)	Az (µm)
1	14.428	5.789	0.013	0.8442	0.349	0.502	0.011
2				0.8453	0.352	0.519	0.011
3				0.8258	0.365	0.522	0.011
Average				0.838	0.355	0.514	0.011
The difference with the optimal values				0.012	0.039	0.018	0.001

The tested results were compared with the optimized results. The tested results were quite close to the optimized results. The difference in percentage between the optimizing process and testing process of surface grinding was 1.43% for surface roughness, 10.99% for vibration amplitude in the X direction, 3.50% for vibration amplitude in the Y direction, 9.09% for vibration amplitude in the Z direction. Table 9 presents the comparison results of surface roughness deviation between calculated results and experimental results according to the optimum values of the cutting parameters in different studies. Deviations between calculated values and experimental values of vibration components were not included in this table. The reason is that until now, it seems that there have not been any studies on the surface grinding process with the optimization of all three parameters Ax, Ay, and Az, then conducting experiments to verify the optimal results as the done works of this study.

Table 9: Comparison of the deviations of different studies

Method	Combining the GRG algorithm and the HM method	Taguchi method	Response surface method	Taguchi method with Grey Relational Analysis
Source	This study	Reference [6]	Reference [3]	Reference [16]
Deviation %	1.43	7.18	9.85	5.3

The results from Table 9 showed that, although it must ensure the harmony between the surface roughness criteria and the vibration component criteria, the deviation in surface roughness between calculated results and the experimental results in this study was still much smaller than that of some other methods. This result has shown outstanding advantages in solving the multi-objective optimization problem by combining the GRG algorithm and the HM method. So, the optimal value of cutting parameters in this study can be used to improve the surface grinding process of 3X13 steel.

5. Conclusions

In this study, the surface roughness and vibration amplitudes in X, Y, Z directions was modeled as a quadratic function of workpiece velocity, feed rate, and depth of cut in the surface grinding process of 3X13 steel. The GRG algorithm and MH method were successfully combined to solve the multi-objective optimization problem. The optimized values of surface roughness and vibration amplitudes (in X, Y, Z directions) were 0.838 µm, 0.355 µm, 0.514 µm, and 0.011 µm, respectively. These results that were determined at the cutting conditions were workpiece velocity of 14.428 m/min, the feed rate of 5.789 mm/stroke, and cutting depth of 0.013 mm. The optimization results of the surface grinding process were successfully verified by the tested results.

References

[1]. S. Periyasamy, M. Aravind, D. Vivek, Dr. K. S. Amirthagadeswaran, "Optimization of Surface Grinding Process Parameters for Minimum Surface Roughness in AISI 1080 Using Response Surface Methodology", Advanced Materials Research, **984**, 118-123, 2014, doi: https://doi.org/10.4028/www.scientific.net/AMR.984-985.118.

[2]. B. Dasthagiri, Dr. E. Venu Gopal Goud, "Optimization Studies on Surface Grinding Process Parameters", International Journal of Innovative Research in Science, Engineering and Technology, **4**(7), 6148- 6156, 2015, doi: 10.15680/IJIRSET.2015.0407166.

[3]. N.A. Yaakob, Hema Nanthini Ganesan, Nurul Hatiqah Harun, Raja Lzamshah, Mohd Shahir Kasim, Jaharah A. Ghani, C. H. Che Haron, "Influence of grinding parameters on the surface finish of Inconel 718", Journal of Mechanical Engineering, **3**(2), 199-209, 2017.

[4]. R. SouzaRuzzi, Rosemar Batistada Silva, Leonardo Rosa Ribeiroda Silva, Álisson RochaMachado, Mark JamesJackson, AmauriHassui, "Influence of grinding parameters on Inconel 625 surface grinding", Journal of Manufacturing Processes, **55**, 174-185, 2020, doi: https://doi.org/10.1016/j.jmapro.2020.04.002.

[5]. C. S Sumesh, Harikrishna S, Harikrishnan S Nair, Mahesh V, Ramkumar R, "Experimental Investigation and Optimization of Surface Grinding of Spheroidal Graphite Cast Iron Using Response Surface Methodology", Journal of Mechanical Engineering Research and Developments, **43**(2), 305-321, 2020, doi: https://jmerd.net/02-2020-322-335/.

[6]. L. Tung, Vu Ngoc Pi, Do Thi Thu Ha, Le Xuan Hung, Tien Long Banh, "A Study on Optimization of Surface Roughness in Surface Grinding 9CrSi Tool Steel by Using Taguchi Method", Lecture Notes in Networks and Systems, **63**, 100–108, 2019, doi: https://doi.org/10.1007/978-3-030-04792-4_15.

[7]. M. Aravind, Dr. S. Periyasamy, "Optimization of Surface Grinding Process Parameters By Taguchi Method And Response Surface Methodology", International Journal of Engineering Research & Technology, **3**(5), 1721-1727, 2014.

[8]. S. Talapatra, I. Islam, "Optimization of Grinding Parameters for Minimum Surface Roughness using Taguchi Method", International Conference on Mechanical, Industrial and Energy Engineering, ICMIEE-PI-140191, 1-6, 2014.

[9]. T. Nguyen, N. Nguyen, Long Hoang, "A study on the vibrations in the external cylindrical grinding process of the alloy steels", Modern Physics Letters B, **2040150**, 1-6, 2020, doi: https://doi.org/10.1142/S0217979220401505.

[10]. C. Wang, Xin-Xiang Zhuo, Yong-Quan Zhu, "Optimization Analysis of Vibration for Grinder Spindle", Sensors and Materials, **32**(1), 407–416, 2020, doi: https://doi.org/10.18494/SAM.2020.2603

[11]. H. Jumianto, Suhardjono, Sampurno, M.Khoirul Effendi, "Multi-response optimization on vibration and surface roughness of the process parameter surface grinding of OCR12VM using Taguchigrey method", AIP Conference Proceedings, **2187**(030015), 1-8, 2019, doi: https://doi.org/10.1063/1.5138319.

[12]. H. Lee, S. Chen, He-Yau Kang, "A Study of Generalized Reduced Gradient Method with Different Search Directions", Measurement Management Journal, **1**(1), 25-38, 2004.

[13]. L.S. Lasdon, Richard L. Fox, Margeryw. Patner, "Nonlinear optimization using the generalized reduced gradient method", Revue française d'automatique, informatique, recherche opérationnelle. Recherche opérationnelle, **8**(3), 73-103, 1974, doi: http://www.numdam.org/item/?id=RO_1974__8_3_73_0.

[14]. D. Xia, S. Xu, and Feng Qi, "A proof of the arithmetic mean-geometric mean-harmonic mean inequalities", RGMIA Research Report Collection, **2**(1), 85-87, 1999.

[15]. N. Van Hieu, "A new approach to solving a multi-criteria decision problem with partial information about criteria", The Journal of Science and Technology of Danang University, **1**(74), 99-102, 2014.

[16]. L. Tung, V. Ngoc Pi, Vu Thi Lien, Tran Thi Hong, Le Xuan Hung, Banh Tien Long, "Optimization of dressing parameters of grinding wheel for 9CrSi tool steel using the Taguchi method with grey relational analysis", IOP Conf. Series: Materials Science and Engineering, **635**(012030), 1-8, 2019, doi:10.1088/1757-899X/635/1/012030.

ASTES

Advances in Science, Technology and Engineering Systems Journal Vol. 5, No. 5, 401-413 (2020)

www.astesj.com

ASTESJ

ISSN: 2415-6698

Strain–Displacement Expressions and their Effect on the Deflection and Strength of Plate

Onyeka Festus[1,*], Edozie Thompson Okeke[2,*], Wasiu John[1]

[1]*Department of Civil Engineering, Edo University, Iyamho, Edo State, 312102, Nigeria*

[2]*Department of Civil Engineering, University of Nigeria, Nsukka Enugu State, 410101, Nigeria.*

ARTICLE INFO

Article history:
Received: 10 August, 2020
Accepted: 11 September, 2020
Online: 21 September, 2020

Keywords:
CSCS and SCFS rectangular plate
Shear deformation theory
Strain-displacement expression
Variation calculus
Critical lateral imposed load

ABSTRACT

This paper studied the bending analysis of an isotropic rectangular plate for the effects of aspect ratio, shear and deflection on the critical lateral load of the plates using the polynomial shear deformation theory (PSDT). One of the plate is clamped at opposite edge clamped and the other opposite edge simply supported (CSCS). The other of the plate is simply supported at the first and fourth edge, clamped at second edge and free of support at the third edge (SCFS). Direct variational method of analysis was adopted using strain-displacement expressions to obtain the direct governing equations for the determination of the coefficient of deflection and shear deformation along the direction of x and y coordinate. From the established equation, a new model for determination of the critical lateral imposed load of the plate is developed. The study revealed that: (i) as the specified thickness of the plate increases, the value of critical lateral imposed load increase (ii) the critical lateral imposed load decrease as the plates span increases. Numerical comparison was conducted to verify and demonstrate the efficiency of the present theory. The result obtained are in good agreement with those in the literature.

1. Introduction

Plates are widely used as the main structural components of the hull of ships, automobiles, gate dams, aircrafts, bridges, etc., because they possess interesting structural characteristics. For instance, when they are subjected to transverse loading (loading perpendicular to their fiber direction), they transit from their stable state of equilibrium to the unstable one. Such transition is normally referred to as bending or structural instability. During this transition, a critical point exists where an infinitesimal increase in load can cause the plate surface to bend.

The load at this critical point defines the bending and shear strength of the plate, or the critical load. Increase in load beyond the critical load leads to collapse [1].

Meanwhile, it is proven that when the critical load is lesser than the value of allowable load of the structure, the structure will remain on the straight or limited deflection. When the critical load exceeds the design load of the structure, it will be in deflecting position [1]. Therefore, there is need to determine the critical load.

Due to enormous application of plate and their relevant in engineering, various theories for plate analysis have been developed using linear strain-displacement expressions. It is proven from previous studies that results obtained using linear strain-displacement expressions may be unreliable for nonlinear stress and bending analyses [2, 3].

Isotropic plates refer to plates whose material properties in all directions at a point are same while anisotropic or orthotropic plates refer to plates whose material properties are direction dependent [4, 5]. They can also be classified according to their shapes as rectangular, circular, triangular, skew and elliptical plates. Isotropic thick plates are being widely used in structures subjected to uniformly distributed load, which produce a very large stresses on it [6, 7]. In order to describe the correct bending response of any type of plates, including shear deformation effects, refined theories are required.

In classical plate theory, it is assumed that line which is normal to the neutral surface before deformation remain straight and normal on the neutral surface after deformation. This assumption results in under-estimation of deflection [8-10].

First order shear deformation theory (FSDT) has been employed by many researchers to analyze thick plates. The theory,

[*]Corresponding Author: Okeke Thompson Edozie, University of Nigeria Nsukka, Nigeria, Email: edozie.okeke@unn.edu.ng
Onyeka, Festus; Edo University Iyamho, Edo State, Nigeria, Email: onyeka.festus@edouniverity.edu.ng

unlike the classical plate theory (CPT) took account of the shear deformation by introducing shear correction factor to satisfy the constitutive relations for transverse shear stresses and shear strains. The authors in [11], adopted FSDT in their work by employing a stress and displacement based approach respectively, which incorporates the effect of shear deformation. FSDT is discovered to have assumed transverse shear stress to be constant through the thickness of the plate, which violates the shear stress free surface conditions on the top and bottom surfaces of the plate [11-13]. The errors in deflection and stresses, the importance of the shear effect in plate bending was realized and the higher order theories were developed which take transverse stresses and strains into account. Higher order theories aim at improving the accuracy by incorporating transverse strains/stresses in the formulation without shear correction factor.

Results obtained in [6, 7, 14, 15] using the above theories [Exponential, hyperbolic and Trigonometric shear deformation function] often shows slight errors in predicting responses of the lateral load on the structures because tedious nature and not too sure of ones works using Fourier series to analyze thick plate. In this present work, the polynomial shear deformation function is used.

In the present paper, nonlinear strain–displacement expressions are employed for the analysis of rectangular plates subjected to uniform distributed loads to suggest a more reliable, refined plate theory that satisfies the continuity of all of the transverse stress components. This theory, which is based on traditional fourth-order shear deformation plate is presented and applied in a bending analysis of rectangular thick plates using the direct variational energy method. The investigation involves two case studies. One of the plate has an opposite edge clamped and the other opposite edge simply supported (CSCS). The other on the plate has simply supported at the first and fourth edge, clamped at second edge and free of support at the third edge (SCFS). Furthermore, derivation of three simultaneous governing equations for the plate and numerical solutions for deformations and stress distributions of different points of the plate with a uniformly distributed mechanical load for various boundary conditions is presented.

The aim of this study is to determine bending analysis of an isotropic rectangular plate for the effects of aspect ratio and deflection on the critical lateral load of the plates. The study sought to achieve the aim through the following objectives:

- To formulate the potential energy of a thick rectangular plate in line with the work of author in [17].
- To perform general variation of the total potential energy and obtain the solution of resulting three simultaneous governing equations.
- To perform a direct variation of the total potential energy and obtain formulas to calculate coefficients of deflection and shear deformation rotation in both x and y axes.
- To determine the values of stiffness coefficients (k) using polynomial displacement functions.
- To obtain the in-plane and out of plane displacement and stresses of the rectangular thick plate.
- To determine the critical lateral imposed load before deflection reaches the maximum specified limit (q_{iw}) and its corresponding critical lateral imposed load before the plate reaches an elastic yield stress (q_{ip}).

2. Previous Works

The authors in [7], applied a new hyperbolic shear deformation theory for the bending and free vibration analysis of isotropic, functional graded laminated plate. Hamilton principle was applied using a Navier procedure to obtain the deflection and stresses in the rectangular plate.

In [10], the authors developed a mathematical model that is based on direct variation procedures and potential energy principle, and applied to thin rectangular Plates with two opposite edges clamped and other opposite edges simply supported and thin rectangular plates with one edge clamped and the three other sides simply supported. Their result clearly shows that the direct variational method circumvents the tedious and rigorous procedures involved in the classical and numerical methods.

In [12, 13], the authors used a first order shear deformation theory which was applied in the analysis of thick rectangular plates clamped at opposite edge clamped and the other opposite edge simply supported (CSCS). They determined the centroidal deflection of the plate. The authors in [11] unlike [12] improved by using a generalized Levy solution approach in the analysis of thick rectangular plates, clamped at opposite edge clamped and the other opposite edge simply supported (CSCS). Both did not take into account effect of transverse shear deformation.

In [15], the authors used a trigonometric shear deformation theory (TSDT) was for the analysis of isotropic plate, taking into account transverse shear deformation effect is presented. The theory which was built upon the classical plate theory uses the virtual work principle to determine the displacement and stress in a thick rectangular plate with four edges simply supported plate. They got the results of stresses for static flexural analysis of simply supported thick isotropic plates for uniformly distributed load.

The authors in [16], used polynomial shear deformation theory (PSDT) for the analysis of rectangular plates. Their theory incorporates the effect of transverse shear stress and shear deformation in the analysis. Results obtained using the theories did not introduce much error and easier to apply in the analysis, but it ended up determining the displacements, moments and stresses that may occur due to the applied load without obtaining the critical lateral load in predicting responses of the applied load which can lead to failure on the structures.

The authors in [17, 18] have used PSDT for the analysis of rectangular plates. They obtained the expression for critical lateral load in predicting responses of the applied load determined to solve bending problem of rectangular plates with all four edges clamped (CCCC) and plate with free of support at third edge and the other edges clamped (CCFC) using third order shear deformation theory for rectangular thick plate respectively. They [17] did not check the effect of shear stress and [18] did not solve for order boundary condition.

Apart from the distinctiveness of the present study with respective individual previous works, there exists an aspect of distinctiveness of the present study over the previous works put

together. This lies in exponential functions, hyperbolic functions, trigonometric and polynomial displacement function. The present work unlike the previous works which assumed the displacement function, perform general variation of the total potential energy in order to get a close form (exact) polynomial displacement function from first principle. They also went ahead to determine the critical lateral impose load used in predicting the flexural characteristics for an isotropic rectangular CSCS and SCFS plate, a feat previous work did not achieve.

3. Methodology

3.1. Assumptions

Considering the following assumptions, the total potential energy of a thick rectangular plate will be formulated. They includes:

- The material of the plate is homogeneous and isotropic.
- The plate material is elastic and obeys Hooke's law.
- The deflection **(w)** is less than one-fifth of the thickness.
- The stress normal to **x-y** plane is so small that it can be neglected. That is to say those, the in-plane displacements, u and v are differentiable in x, y and z coordinates, while the out-of-plane displacement (deflection), w is only differentiable in x and y coordinates.
- The effect of the out-of-plane normal stress on the gross response of the plate is small when compared with other stresses.
- The vertical line that is initially normal to the middle surface of the plate before bending is no longer straight nor normal to the middle surface after bending.

3.2. Kinematics and Constitutive Relations

The kinematics in the structural mechanics sense mean the relationship between the engineering strains and displacement. The three displacements of thick place assumed to involve the deflection, w(x,y) and the two inplane displacements, u(x,y,z), and v(x,y,z) was used to establish the constitutive equations of the rectangular plate. The values of deflection (w), inplane displacement along x and y axis (u and v) as was gotten from the assumption made in the previous section as:

$$u = \frac{zdw}{dy} + F.\theta_{sx} \tag{1}$$

Similarly,

$$v = \frac{zdw}{dy} + F.\theta_{sy} \tag{2}$$

The normal strain along x, y and z axis are ε_x, ε_y and ε_z respectively. That is:

$$\varepsilon_x = \frac{du}{dx} \tag{3}$$

Similarly reasoning in y direction, gives:

$$\varepsilon_y = \frac{dv}{dy} \tag{4}$$

Similarly reasoning in z direction, gives:

$$\varepsilon_z = \frac{dw}{dz} \tag{5}$$

The curvature in x-z plane is defined as:

$$\gamma_{xy} = \frac{du}{dy} + \frac{dv}{dx} \tag{6}$$

The curvature in x-z plane is defined as:

$$\gamma_{xz} = \frac{du}{dz} + \frac{dw}{dx} \tag{7}$$

The curvature in x-z plane is defined as:

$$\gamma_{yz} = \frac{dv}{dz} + \frac{dw}{dx} \tag{8}$$

Shear deformation profile of the thick rectangular section of plate $F(z)$ used in this study is given as [17]:

$$F(z) = \frac{5z}{3}\left(z^3 - \frac{2z}{t^3}\right) \tag{9}$$

Where;

θ_{Sx} and θ_{Sy} =shear deformation rotation along x and y axis.

The constitutive equations for five stress and strain components are:

$$\varepsilon_x = \frac{\sigma_X - \mu\sigma_Y}{E} \tag{10}$$

$$\varepsilon_y = \frac{\sigma_Y - \mu\sigma_X}{E} \tag{11}$$

$$\gamma_{xy} = \frac{2(1+\mu)\tau_{xy}}{E} \tag{12}$$

$$\gamma_{xy} = \frac{2(1+\mu)\tau_{xz}}{E} \tag{13}$$

$$\gamma_{yz} = \frac{2(1+\mu)\tau_{yz}}{E} \tag{14}$$

The constitutive equations for five stress and strain components becomes:

$$\sigma_x = E\varepsilon_x + \mu\sigma_y \tag{15}$$

$$\therefore \sigma_x = \frac{E\left(\varepsilon_x + \mu\varepsilon_y\right)}{1-\mu^2} \tag{16}$$

Similarly reasoning in y direction, gives:

$$\sigma_y = \frac{E\left(\varepsilon_y + \mu\varepsilon_x\right)}{1-\mu^2} \tag{17}$$

Similarly reasoning in z direction, gives:

$$\sigma_z = \frac{E(\varepsilon_z + \mu\varepsilon_x)}{1-\mu^2} \tag{18}$$

Rearranging equation 12, 13 and 14, the shear stress along (x-y), (x-z) and (y-z) respectively becomes:

$$\tau_{xy} = \frac{E}{2(1+\mu)}.\gamma_{xy} \tag{19}$$

$$\tau_{xz} = \frac{E}{2(1+\mu)}.\gamma_{xz} \tag{20}$$

$$\tau_{yz} = \frac{E}{2(1+\mu)}.\gamma_{yz} \tag{21}$$

3.3. Total Potential Energy

The total potential energy functional (Π) of thick rectangular isotropic plate were derived [19] from the constitutive relations and presented as;

$$\Pi = U + V \tag{22}$$

The strain energy equation, U is presented as:

$$U = \frac{1}{2}\iiint_{-\frac{t}{2}}^{\frac{t}{2}} (\sigma_x\varepsilon_{x+}\sigma_y\varepsilon_{y+}\tau_{xy}\gamma_{xy} + \tau_{xz}\gamma_{xz} + \tau_{yz}\gamma_{yz})dxdydz \tag{23}$$

Substituting appropriately, gave:

$$U = \frac{D}{2}\iint \left[\left| g_1\left(\frac{d^2w}{dx^2}\right)^2 - 2g_2\left(\frac{d^2w}{dx^2}.\frac{d\theta_{Sx}}{dx}\right) + g_3\left(\frac{d\theta_{Sx}}{dx}\right)^2\right| + \left|2g_1\left(\frac{\partial^2 w}{\partial x\partial y}\right)^2 - 2g_2\left(\frac{\partial^2 w}{\partial x\partial y}.\frac{d\theta_{Sx}}{dy}\right) - 2g_2\left(\frac{\partial^2 w}{\partial x\partial y}.\frac{d\theta_{Sy}}{dx}\right)\right| + \left|(1+\mu)g_3\left(\frac{d\theta_{Sx}}{dy}\right)\left(\frac{d\theta_{Sy}}{dx}\right)\right| + \frac{(1-\mu)}{2}\left|g_3\left(\frac{d\theta_{Sx}}{dy}\right)^2 + g_3\left(\frac{d\theta_{Sy}}{dx}\right)^2\right| + \left|g_1\left(\frac{d^2w}{dy^2}\right)^2 - 2g_2\left(\frac{d^2w}{dy^2}.\frac{d\theta_{Sy}}{dy}\right) + g_3\left(\frac{d\theta_{Sy}}{dy}\right)^2\right| + \left|\frac{(1-\mu)}{2}g_4(\theta_{Sx})^2 + \frac{(1-\mu)}{2}g_4\left(\theta_{Sy}\right)^2\right|\right] dxdy \quad (24)$$

and the potential energy is presented as:

$$V = -\int_0^a\int_0^b qw(x,y)\partial x\partial y \quad (25)$$

By substituting Equation 24 and 25 into 22, gives:

$$\Pi = \frac{Et^3}{24(1-\mu^2)a^4}\int_0^1\int_0^1 \left[\left| g_1{A_1}^2\left(\frac{\partial^2 h}{\partial R^2}\right)^2 - 2g_2A_1A_2\left(\frac{\partial^2 h}{\partial R^2}\right)^2 + g_3{A_2}^2\left(\frac{\partial^2 h}{\partial R^2}\right)^2\right| + \left|2g_1\frac{{A_1}^2}{\propto^2}\left(\frac{\partial^2 h}{\partial R\partial Q}\right)^2 - 2g_2\frac{A_1A_2}{\propto^2}\left(\frac{\partial^2 h}{\partial R\partial Q}\right)^2 - 2g_2\frac{A_1A_3}{\propto^2}\left(\frac{\partial^2 h}{\partial R\partial Q}\right)^2\right| + \left|(1+\mu)g_3\frac{A_2A_3}{\propto^2}\left(\frac{\partial^2 h}{\partial R\partial Q}\right)^2\right| + \frac{(1-\mu)}{2}\left|g_3\frac{{A_2}^2}{\propto^2}\left(\frac{\partial^2 h}{\partial R\partial Q}\right)^2 + g_3\frac{{A_3}^2}{\propto^2}\left(\frac{\partial^2 h}{\partial R\partial Q}\right)^2\right| + \left|g_1\frac{{A_1}^2}{\propto^4}\left(\frac{\partial^2 h}{\partial Q^2}\right)^2 - 2g_2\frac{A_1A_3}{\propto^4}\left(\frac{\partial^2 h}{\partial Q^2}\right)^2 + g_3\frac{{A_3}^2}{\propto^4}\left(\frac{\partial^2 h}{\partial Q^2}\right)^2\right| + \left|\frac{(1-\mu)}{2}\rho^2 g_4{A_2}^2\left(\frac{\partial h}{\partial R}\right)^2 + \frac{(1-\mu)}{2}.\frac{\rho^2 g_4{A_3}^2}{\propto^2}\left(\frac{\partial h}{\partial Q}\right)^2\right|\right] ab\partial R\partial Q - \int_0^1\int_0^1 qA_1h\, ab\partial R\partial Q \quad (26)$$

Where; breathe aspect

$$D = \frac{Et^3}{12(1-\mu^2)} \quad (27)$$

$$x = aR \text{ and } y = bQ \quad (28)$$

The length to breadth aspect ratio, $\propto = \frac{b}{a}$ (29a)

The span to thickness ratio, $\rho = \frac{a}{t}$ (29b)

Let:

$$w = A_1.h \quad (30)$$

$$\theta_{Sx} = \theta_{Sxx}.\theta_{Sxy} = \left[\frac{dh}{dR}\right][A_2] \quad (31)$$

And;

$$\theta_{Sy} = \theta_{Syx}.\theta_{Syy} = \left[\frac{dh}{dQ}\right][A_3] \quad (32)$$

Where:

h is the plate shape function.

w, θ_{Sx}, and θ_{Sy} are the deflection , shear deformation along x axis and shear deformation along y axis respectively while,

A_1, A_2 and A_3 are the coefficient of the deflection , shear deformation along x axis and shear deformation along y axis respectively.

3.4. Governing Energy Equation

The elastic plate presented plate in Figure 1 and 2 under bending subjected to uniformly distributed load was used to obtain the displacement – strain relationships in terms of curvatures.

3.4.1. General Governing Equation

The total potential energy shall be minimized with respect to the deflection w, shear deformation along x axis, θ_{Sx} and shear deformation along y axis, θ_{Sy}. Minimizing or differentiating total potential energy equation with respect to w, θ_{Sx}, and θ_{Sy} is said to be the direct variation.

$$\frac{\partial\Pi}{\partial w} = \frac{\partial\Pi}{\partial\theta_{Sx}} = \frac{\partial\Pi}{\partial\theta_{Sy}} = 0 \quad (33a)$$

By solving the resulting three simultaneous governing equation the actual deflection w, shear deformation along x axis, θ_{Sx} and shear deformation along y axis, θ_{Sy} was gotten as:

$$w = \left(a_0 + a_1R + \frac{a_2R^2}{2} + \frac{a_3R^3}{6} + \frac{qa^4}{D}\left(\frac{n_1}{w_3}\right).\frac{R^4}{24}\right) \times \left(b_0 + b_1Q + \frac{b_2Q^2}{2} + \frac{b_3Q^3}{6} + \frac{qa^4}{D}\left(\frac{n_1}{w_3}\right).\frac{Q^4}{24}\right) \quad (33b)$$

The general polynomial shear deformation function (Rotation equation for y-axis) of a rectangular plate as was obtained and presented:

$$\theta_{Sx} = \left(a_4 + a_5R + \frac{a_6R^2}{2} + \frac{qa^3}{D}\left(\frac{n_4}{g_2\emptyset_3}\right).\frac{R^3}{6}\right) \times \left(b_7 + b_8Q + \frac{b_9Q^2}{2} + \frac{b_{10}Q^3}{6} + \frac{b_{11}Q^4}{24}\right) \quad (34)$$

The general polynomial shear deformation function (Rotation equation for y-axis) of a rectangular plate as was obtained and presented:

$$\theta_{Sy} = \left(a_7 + a_8R + \frac{a_9R^2}{2} + \frac{a_{10}R^3}{6} + \frac{a_{11}R^4}{24}\right) \times \left(b_4 + b_5Q + \frac{b_6Q^2}{2} + \frac{qa^3}{D}\left(\frac{\propto^3 n_5}{g_2\emptyset_1}\right).\frac{Q^3}{6}\right) \quad (35)$$

The following type of plate with their respective support conditions are in consideration.

The following type of plate with their respective support conditions are in consideration.

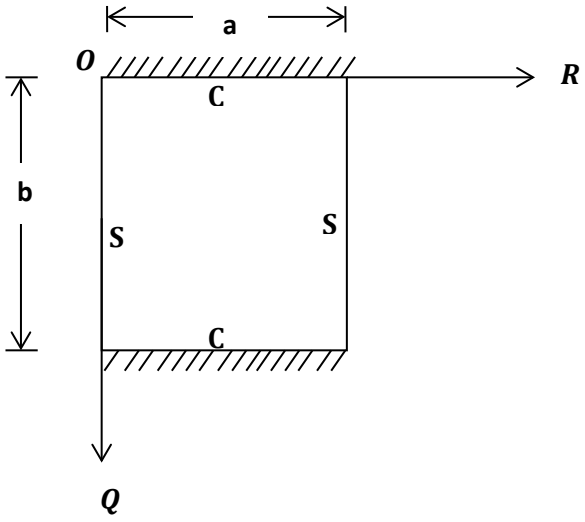


Figure 1: CSCS Rectangular Plate

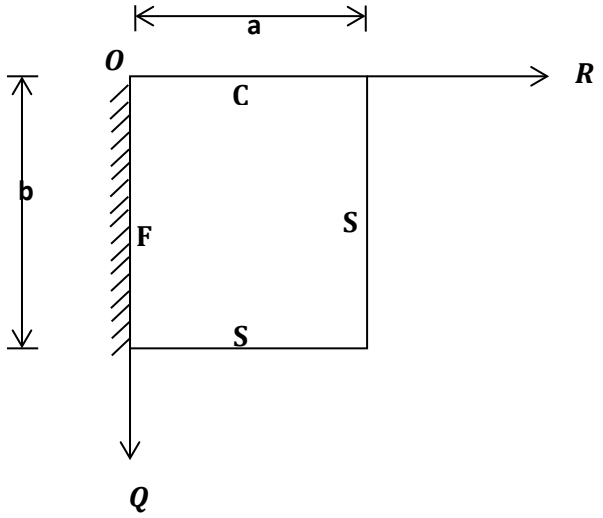


Figure 2: SCFS Rectangular Plate.

3.4.2. Direct Governing Equation

The total potential energy shall be minimized with respect to the coefficient of the deflection A_1, shear deformation along x axis A_2 and shear deformation along y axis A_3. Minimizing or differentiating total potential energy equation with respect to A_1, A_2, and A_3 is said to be the direct variation.

$$\frac{\partial \Pi}{\partial A_1} = \frac{\partial \Pi}{\partial A_2} = \frac{\partial \Pi}{\partial A_3} = 0 \tag{36}$$

This gives:

$$\begin{bmatrix} r_{11} & r_{12} & r_{13} \\ r_{21} & r_{22} & r_{23} \\ r_{31} & r_{32} & r_{33} \end{bmatrix} \begin{bmatrix} A_1 \\ A_2 \\ A_3 \end{bmatrix} = \frac{qa^4}{D} \begin{bmatrix} k_f \\ 0 \\ 0 \end{bmatrix} \tag{37}$$

Let:

$$r_{11} = g_1\left(k_a + \frac{2}{\propto^2}k_b + \frac{1}{\propto^4}k_c\right) \tag{38}$$

$$r_{12} = -g_2\left(k_a + \frac{1}{\propto^2}k_b\right) \tag{39}$$

$$r_{13} = -g_2\left(\frac{1}{\propto^2}k_b + \frac{1}{\propto^4}k_c\right) \tag{40}$$

$$r_{21} = -g_2\left(k_a + \frac{1}{\propto^2}k_b\right) \tag{41}$$

$$r_{22} = \left(g_3 k_a + \frac{(1-\mu)}{2 \propto^2} g_3 k_b + \frac{(1-\mu)}{2}\rho^2 g_4 k_d\right) \tag{42}$$

$$r_{23} = g_3 \frac{(1+\mu)}{2 \propto^2} k_b \tag{43}$$

$$r_{31} = -g_2\left(\frac{1}{\propto^2}k_b + \frac{1}{\propto^4}k_c\right) \tag{44}$$

$$r_{32} = g_3 \frac{(1+\mu)}{2 \propto^2} k_b \tag{45}$$

$$r_{33} = \left(g_3 \frac{(1-\mu)}{2}\left(\frac{1}{\propto^2}k_b + \frac{1}{\propto^4}k_c\right) + g_4 \frac{(1-\mu)}{2 \propto^2}\rho^2 k_e\right) \tag{46}$$

$$S_b = \frac{r_{21}.r_{33} - r_{23}.r_{31}}{r_{22}.r_{33} - r_{23}.r_{32}} \tag{47}$$

$$S_c = \frac{r_{21}.r_{32} - r_{22}.r_{31}}{r_{23}.r_{32} - r_{22}.r_{33}} \tag{48}$$

Therefore;

$$A_1 = \frac{qa^4}{D}\left(\frac{k_f}{r_{11}S_1 - r_{12}S_2 - r_{13}S_3}\right) \tag{49}$$

That is:

$$A_1 = \frac{qa^4}{D}.k \tag{50}$$

Also;

$$A_2 = S_2 A_1 \tag{51}$$

$$A_3 = S_3 A_1 \tag{52}$$

Let:

$$k = \frac{k_f}{k_T} \tag{53}$$

where,

$$k_T = k_a + \frac{2}{\propto^2}k_c + \frac{1}{\propto^4}k_d \tag{54}$$

And, $S_1 = 1$

$$k_a = \int_0^1 \int_0^1 \left(\frac{d^2h}{dR^2}\right)^2 dRdQ \tag{55}$$

$$k_b = \int_0^1 \int_0^1 \left(\frac{d^2h}{dRdQ}\right)^2 dRdQ \tag{56}$$

$$k_c = \int_0^1 \int_0^1 \left(\frac{d^2h}{dQ^2}\right)^2 dRdQ \tag{57}$$

$$k_d = \int_0^1 \int_0^1 \left(\frac{dh}{dR}\right)^2 dRdQ \tag{58}$$

$$k_e = \int_0^1 \int_0^1 \left(\frac{dh}{dQ}\right)^2 dRdQ \tag{59}$$

$$k_f = \int_0^1 \int_0^1 h.dRdQ \tag{60}$$

3.5. Displacement and stress analysis

By incorporating the established expression for deflection and shear deformation coefficients the deflection, and the two inplane displacement and stresses of the plate is presented as:

$$w = A_1.h \tag{61}$$

$$u = [-\overline{A_1}s + \overline{A_2}F(s)]\frac{dh}{dR}\left(\frac{tqa^3}{D}\right) \tag{62}$$

$$v = \frac{1}{\propto}[-\overline{A_1}s + \overline{A_3}F(s)]\frac{dh}{dQ}\left(\frac{tqa^3}{D}\right) \tag{63}$$

$$\sigma_x = \frac{Et}{a^2(1-\mu^2)}\left[[-\overline{A_1}s + \overline{A_2}F(s)]\frac{d^2h}{dR^2} + \frac{\mu}{\propto^2}[-\overline{A_1}s + \overline{A_3}F(s)]\frac{d^2h}{dQ^2}\left(\frac{qa^4}{D}\right)\right] \tag{64}$$

$$\sigma_y = \frac{Et}{a^2(1-\mu^2)}\left[\mu[-\overline{A_1}s + \overline{A_2}F(s)]\frac{d^2h}{dR^2} + \frac{1}{\propto^2}[-\overline{A_1}s + \overline{A_3}F(s)]\frac{d^2h}{dQ^2}\left(\frac{qa^4}{D}\right)\right] \tag{65}$$

$$\tau_{xy} = \frac{Et(1-\mu)}{2a^2(1-\mu^2)}\left[-2\overline{A_1}s + \overline{A_2}F(s) + \overline{A_3}F(s).\frac{1}{\propto}\right]\frac{d^2h}{\partial R\partial Q} \tag{66}$$

$$\tau_{xz} = \frac{E(1-\mu)}{2(1-\mu^2)}\overline{A_2}\frac{dF(z)}{dz}\frac{dh}{dR}\left(\frac{qa^4}{D}\right) \tag{67}$$

$$\tau_{yz} = \frac{E(1-\mu)}{2(1-\mu^2)}\overline{A_3}\frac{dF(z)}{dz}\frac{1}{\propto}\frac{dh}{dQ}\left(\frac{qa^4}{D}\right) \tag{68}$$

Where;

z = st

3.6. Formulation of Expression for the Critical Imposed Load Before Deflection Reaches Specified Maximum Limit, q_{iw}

The maximum critical lateral load on the plate before its deflection reaches allowable value will be determined [17]. This is to ensure that deflection does not exceed specified maximum limit.

Therefore:

$$w = A_1\mathrm{h} < \mathrm{w_a} \tag{69}$$

$$\frac{12(1-\mu^2)qa^4}{Et^3}.k.\mathrm{h} < \mathrm{w_a} \tag{70}$$

where,

$\mathrm{w_a}$ = Allowable deflection

Also,

$$q = \gamma + q_{iw} \tag{71}$$

This gives:

$$q_{iw} < Et^3\frac{\mathrm{w_a}}{(1-\mu^2)12.k.\mathrm{h}a^4} - \gamma \tag{72}$$

where;

γ = Self weight of the plate

and,

q_{iw} = Critical Imposed load of the plate

Where;

i = specific thickness

3.7. Formulation of Expression for the Critical Load before Plate Reaches Elastic Yield Stress, q_{ip}

The critical lateral imposed load on the plate before it reaches yielding point is determined [18], to ensure that the stress due to the applied stress on the plate does not exceed elastic yield point.

Recall that;

$$U = \frac{1}{2}\iiint_{-\frac{t}{2}}^{\frac{t}{2}} \cap dxdydz \tag{73}$$

where;

$$\cap = \sigma_x\varepsilon_x + \sigma_y\varepsilon_y + \tau_{xy}\gamma_{xy} + \tau_{xz}\gamma_{xz} + \tau_{yz}\gamma_{yz} \tag{74}$$

Substituting values of $\varepsilon_x, \varepsilon_y, \gamma_{xy}, \gamma_{xy}, and\ \gamma_{yz}$ 10 to 14 into Equation 74 gives:

$$\cap = \frac{1}{E}\left[{\sigma_x}^2 - \mu\sigma_x\sigma_y - \mu\sigma_x\sigma_y + {\sigma_y}^2 + 2(1+\mu){\tau_{xy}}^2 + 2(1+\mu){\tau_{xz}}^2 + 2(1+\mu){\tau_{yz}}^2\right] \tag{75}$$

To ensure that the critical lateral load the plate is determined before it reaches yielding;

$$\cap = \frac{1}{E}\left[{\sigma_x}^2 - \mu\sigma_x\sigma_y - \mu\sigma_x\sigma_y + {\sigma_y}^2 + 2(1+\mu){\tau_{xy}}^2 + 2(1+\mu){\tau_{xz}}^2 + 2(1+\mu){\tau_{yz}}^2\right] < \cap_0 \tag{76}$$

Where;

$\cap_0$ = yielding point of the plate.

For a bar,

$$let\ \sigma_x = fy\ and\ \sigma_y = \tau_{xy} = \tau_{xz} = \tau_{yz} = 0 \tag{77}$$

Therefore;

$$\cap < \cap_0 > \frac{fy^2}{E} \tag{78}$$

Substituting Equation 76 into 78 gives:

$$\frac{1}{E}\left[{\sigma_x}^2 - 2\mu\sigma_x\sigma_y + {\sigma_y}^2 + 2(1+\mu){\tau_{xy}}^2 + 2(1+\mu){\tau_{xz}}^2 + 2(1+\mu){\tau_{yz}}^2\right] < \frac{fy^2}{E} \tag{79}$$

Let,

$$\sigma_y = n_1\sigma_x \equiv n_1 = \frac{\sigma_Y}{\sigma_x} \tag{80}$$

$$\tau_{xy} = n_2\sigma_x \equiv n_2 = \frac{\tau_{xy}}{\sigma_x} \tag{81}$$

$$\tau_{xz} = n_3\sigma_x \equiv n_3 = \frac{\tau_{xz}}{\sigma_x} \tag{82}$$

$$\tau_{yz} = n_4\sigma_x \equiv n_4 = \frac{\tau_{yz}}{\sigma_x} \quad (83)$$

Therefore, substituting Equations 80, 81, 82 and 83 into 79 gives:

$$\sigma_x{}^2 - 2\mu n_1\sigma_x{}^2 + n_1{}^2\sigma_x{}^2 + 2(1+\mu)n_2{}^2\sigma_x{}^2 + 2(1+\mu)n_3{}^2\sigma_x{}^2 + 2(1+\mu)n_4{}^2\sigma_x{}^2 < fy^2 \quad (84)$$

This gives:

$$\sigma_x < \frac{fy}{\sqrt{[1 - 2\mu n_1 + n_1{}^2 + 2(1+\mu)n_2{}^2 + 2(1+\mu)n_3{}^2 + 2(1+\mu)n_4{}^2]}} \quad (85)$$

Simplifying Equation 64, gives:

$$\sigma_x = \frac{Est\mathrm{A}_1}{(1-\mu^2)\propto^2}\left(\frac{d^2h}{dR^2} + \frac{\mu}{\propto^2}\frac{d^2h}{dQ^2}\right) \quad (86)$$

Thus:

$$\sigma_x = s\left(\frac{d^2h}{dR^2} + \frac{\mu}{\alpha^2}\frac{d^2h}{dQ^2}\right)\frac{qa^2}{t^2}.12k \quad (87)$$

Equating 85 and 87, gives:

$$\frac{12.qa^2.k.s}{t^2}.\beta_2 < \frac{fy}{\beta_3} \quad (88)$$

where;

$$\beta_2 = \left(\frac{d^2h}{dR^2} + \frac{\mu}{\propto^2}\frac{d^2h}{dQ^2}\right) \quad (89)$$

and,

$$\beta_3 = \sqrt{[1 - 2\mu n_1 + n_1{}^2 + 2(1+\mu)n_2{}^2 + 2(1+\mu)n_3{}^2 + 2(1+\mu)n_4{}^2]} \quad (90)$$

From Equation 88, expression for q was gotten as:

$$q < \frac{fyt^2}{12.a^2.k.s.\beta_2.\beta_3} \quad (91)$$

Let;

$$q = q_{\,d} + q_{\,ip} \quad (92)$$

This gives:

$$q_{\,ip} < \frac{fyt^2}{12.a^2.k.s.\beta_2.\beta_3} - q_{\,d} \quad (93)$$

This gave:

$$q_{\,ip} < \frac{fyt^2}{12.a^2.k.s.\beta_2.\beta_3} \quad (94)$$

This gave:

$$q_{\,ip} < \beta_4 t^2 - \gamma t \quad (95)$$

where;

$$\beta_4 = \frac{fy}{12.a^2.k.st.\beta_2.\beta_3} \quad (96)$$

$q_{\,ip}$ = critical imposed lateral load before plate reach yield stress; fy = strength

i = specific thickness

$q_{\,d}$ = Self weight of the plate

4. Results and Discussions

4.1. Results

The numerical analysis of CSCS and SCFS rectangular plate at various span-thickness ratios are presented in Figure 2 to 10 and Figure 11 to 19 respectively.

A fourth order polynomial displacement function for the analysis CSCS plate was derived as presented in Equation 97:

$$w = \frac{F_{a4}.F_{b4}}{576}(R - 2R^3 + R^4) \times (Q^2 - 2Q^3 + Q^4) \quad (97)$$

Let the amplitude,

$$A = \frac{1}{576}(F_{a4} \times F_{b4}) \quad (98)$$

And shape function;

$$h = (R - 2R^3 + R^4) \times (Q^2 - 2Q^3 + Q^4) \quad (99)$$

Also, a third order polynomial displacement function for SCFS plate was derived for the analysis as presented in Equation 100:

$$w = \frac{F_{a4} \times b_5}{17280}(1.5R^2 - 2.5R^3 + R^4) \times \left(\frac{7Q}{3} - \frac{10}{3}Q^3 + \frac{10}{3}Q^4 - Q^5\right) \quad (100)$$

Let the amplitude,

$$A_1 = \frac{1}{17280}(F_{a4} \times b_5) \quad (101)$$

And shape function;

$$h = (1.5R^2 - 2.5R^3 + R^4) \times \left(\frac{7Q}{3} - \frac{10}{3}Q^3 + \frac{10}{3}Q^4 - Q^5\right) \quad (102)$$

The values stiffness coefficient obtained from the above expression is presented in Table 1. Table 3 presents the result of the comparison made with previous work [11, 12 and 20] for non-dimensional center deflection multiplied by $\mathrm{D/qa^4}$ of CSCS square rectangular thick plate at various aspect ratios while Table 4 presents the corresponding percentage difference between the values of centroidal deflection.

Figure 3 contains a graph of the critical lateral imposed load versus length to breadth aspect ratio of CSCS plate for a span (a) of 1000mm at allowable deflection, ($\mathrm{w_a}$) of 1.0mm. A length to breadth aspect ratio of 1.0 through 2.0 was used at an interval of 0.1 with a specified thickness (i) of 5mm, 10mm and 15mm. Figure 4 contains a graph of the critical lateral imposed load versus length to breadth aspect ratio of CSCS plate for a span (a) of 1000mm at allowable deflection, ($\mathrm{w_a}$) of 3.0mm. A length to breadth aspect ratio of 1.0 through 2.0 was used at an interval of 0.1 with a specified thickness (i) of 5mm, 10mm and 15mm. Figure 5 contains a graph of the critical lateral imposed load versus length to breadth aspect ratio of CSCS plate for a span (a) of 1000mm at allowable deflection, ($\mathrm{w_a}$) of 5.0mm. A length to breadth aspect ratio of 1.0 through 2.0 was used at an interval of 0.1 with a specified thickness (i) of 5mm, 10mm and 15mm. Figure 6 contains a graph of the critical lateral imposed load

versus length to breadth aspect ratio of CSCS plate for a span (a) of 3000mm at allowable deflection, (w_a) of 1.0mm. A length to breadth aspect ratio of 1.0 through 2.0 was used at an interval of 0.1 with a specified thickness (i) of 5mm, 10mm and 15mm. Figure 7 contains a graph of the critical lateral imposed load versus length to breadth aspect ratio of CSCS plate for a span (a) of 3000mm at allowable deflection, (w_a) of 3.0mm. A length to breadth aspect ratio of 1.0 through 2.0 was used at an interval of 0.1 with a specified thickness (i) of 5mm, 10mm and 15mm. Figure 8 contains a graph of the critical lateral imposed load versus length to breadth aspect ratio of CSCS plate for a span (a) of 3000mm at allowable deflection, (w_a) of 3.0mm. A length to breadth aspect ratio of 1.0 through 2.0 was used at an interval of 0.1 with a specified thickness (i) of 5mm, 10mm and 15mm. Figure 9 contains a graph of the critical lateral imposed load versus length to breadth aspect ratio of CSCS plate for a span (a) of 5000mm at allowable deflection, (w_a) of 1.0mm. A length to breadth aspect ratio of 1.0 through 2.0 was used at an interval of 0.1 with a specified thickness (i) of 5mm, 10mm and 15mm. Figure 10 contains a graph of the critical lateral imposed load versus length to breadth aspect ratio of CSCS plate for a span (a) of 5000mm at allowable deflection, (w_a) of 3.0mm. A length to breadth aspect ratio of 1.0 through 2.0 was used at an interval of 0.1 with a specified thickness (i) of 5mm, 10mm and 15mm. Figure 11 contains a graph of the critical lateral imposed load versus length to breadth aspect ratio of CSCS plate for a span (a) of 5000mm at allowable deflection, (w_a) of 5.0mm. A length to breadth aspect ratio of 1.0 through 2.0 was used at an interval of 0.1 with a specified thickness (i) of 5mm, 10mm and 15mm. Figure 12 depicts a graph of the critical lateral imposed load versus length to breadth aspect ratio of SCFS plate for a span (a) of 1000mm at allowable deflection, (w_a) of 1.0mm. A length to breadth aspect ratio of 1.0 through 2.0 was used at an interval of 0.1 with a specified thickness (i) of 5mm, 10mm and 15mm. Figure 13 depicts a graph of the critical lateral imposed load versus length to breadth aspect ratio of SCFS plate for a span (a) of 1000mm at allowable deflection, (w_a) of 3.0mm. A length to breadth aspect ratio of 1.0 through 2.0 was used at an interval of 0.1 with a specified thickness (i) of 5mm, 10mm and 15mm. Figure 14 depicts a graph of the critical lateral imposed load versus length to breadth aspect ratio of SCFS plate for a span (a) of 1000mm at allowable deflection, (w_a) of 5.0mm. A length to breadth aspect ratio of 1.0 through 2.0 was used at an interval of 0.1 with a specified thickness (i) of 5mm, 10mm and 15mm. Figure 15 depicts a graph of the critical lateral imposed load versus length to breadth aspect ratio of SCFS plate for a span (a) of 3000mm at allowable deflection, (w_a) of 1.0mm. A length to breadth aspect ratio of 1.0 through 2.0 was used at an interval of 0.1 with a specified thickness (i) of 5mm, 10mm and 15mm. Figure 16 depicts a graph of the critical lateral imposed load versus length to breadth aspect ratio of SCFS plate for a span (a) of 3000mm at allowable deflection, (w_a) of 3.0mm. A length to breadth aspect ratio of 1.0 through 2.0 was used at an interval of 0.1 with a specified thickness (i) of 5mm, 10mm and 15mm. Figure 17 depicts a graph of the critical lateral imposed load versus length to breadth aspect ratio of SCFS plate for a span (a) of 3000mm at allowable deflection, (w_a) of 5.0mm. A length to breadth aspect ratio of 1.0 through 2.0 was used at an interval of 0.1 with a specified thickness (i) of 5mm, 10mm and 15mm. Figure 18 depicts a graph of the critical lateral imposed load versus length to breadth aspect ratio of SCFS plate for a span (a) of 5000mm at allowable deflection, (w_a) of 1.0mm. A length to breadth aspect ratio of 1.0 through 2.0 was used at an interval of 0.1 with a specified thickness (i) of 5mm, 10mm and 15mm. Figure 19 depicts a graph of the critical lateral imposed load versus length to breadth aspect ratio of SCFS plate for a span (a) of 5000mm at allowable deflection, (w_a) of 3.0mm. A length to breadth aspect ratio of 1.0 through 2.0 was used at an interval of 0.1 with a specified thickness (i) of 5mm, 10mm and 15mm. Figure 20 depicts a graph of the critical lateral imposed load versus length to breadth aspect ratio of SCFS plate for a span (a) of 5000mm at allowable deflection, (w_a) of 5.0mm. A length to breadth aspect ratio of 1.0 through 2.0 was used at an interval of 0.1 with a specified thickness (i) of 5mm, 10mm and 15mm. Figure 21 is a curve that showed the comparison made with previous work [20] for non-dimensional center deflection of SCFS rectangular thick plate at 1.5 length to width ratios.

4.2. Discussion

It is seen from the Figure 3 to 20 that as the specified thickness (t) of plate increases, the value of critical lateral imposed load (q_{iw} and q_{ip}) increases. This implies that increase in the thickness of the plate ensures safety in the plate structure.

More so, from the tables that as the specified deflection (w_a) increases, the value of critical lateral imposed load (q_{iw}), while the critical imposed load (q_{ip}) remains constant. This implies that increase in the allowable deflection value required for the analysis of the plate reduces the chances of failure of structural member. Meanwhile, this does not affect critical imposed load (q_{ip}).

From the results of CSCS plate presented in Figure 3 to 11, it shows that the values of critical lateral imposed load q_{iw} and q_{ip} decrease as the length-width ratio increases, this continues until failure occurs. This means that an increase in plate length increases the chance of failure in a plate structure.

Figure 3 to 11 presents the result of CSCS plate with span of 1000mm, 3000mm and 5000mm at allowable deflection of 1mm, 3mm and 5mm at 5mm, 10mm and 15mm specified thickness. From the result, the value of q_{iw} and q_{ip} is between $-0.3846\ \mathrm{N/mm}$ to $154.288\ \mathrm{N/mm}$ and $-0.0120\ \mathrm{N/mm}$ to $193.825\ \mathrm{N/mm}$ been the highest and lowest value at respectively. From that table it is observed that the value of q_{ip} if greater than that of q_{iw}, this is because the failure of plate in q_{ip} means total failure but that of q_{iw} is like a warning requesting maintenance.

Looking closely at Figure 3 to 5 (CSCS plate with span of 1000mm at allowable deflection (w_a) value between 1mm to 5mm). It finds that failure on q_{iw} only occur at between length to width ratio of 1.6, 1.8, 1.9 and 2 with a value of -0. 0183N/mm, -0. 0556N/mm, -0. 0847N/mm, -0.1078 and -0. 1264N/mm in thickness of 5mm with value.

Looking closely at Tables 6 to 11 (CSCS plate with span between 1000mm and 5000mm at allowable deflection (w_a) value between 1mm to 5mm). It finds that failure on q_{iw} only occurs at all length to width ratio (1 to 2) between value of -1.1215N/mm and -0.0036N/mm at all thickness. The negative value of critical lateral imposed load q_{iw} (and positive value of q_{ip}) only reveals that the plate fails in q_{iw} for the entire plate w_a

(1mm to 5mm) and span of 1000mm to 5000mm. This means that the plate structure is not safe and required maintenance.

Meanwhile, from Figure 9 to 11, it is observed that total failure occurs at length to breadth ratio of 2 with specified thickness of 5mm at value of -0.3846N/mm and -0. 012N/mm for q_{iw} and q_{ip} respectively. This means that the failure cannot be maintained.

From the results of SCFS plate presented in Figure 12 to 20, it shows that the values of critical lateral imposed load q_{iw} decrease as the length-width ratio increases, this continues until failure occurs. This means that an increase in plate length increases the chance of failure in a plate structure. Meanwhile the values of critical lateral imposed load q_{ip} increase as the length-width ratio increases, this continues until safety is ensured.

Figure 12 to 20 presents the result of SCFS plate with span of 1000mm, 3000mm and 5000mm at allowable deflection of 1mm, 3mm and 5mm at 5mm, 10mm and 15mm specified thickness. From the result, the value of q_{iw} and q_{ip} is between -1.1331N/mm to 80.0504N/mm and 0.1328N/mm to 183.365N/mm been the highest and lowest value at respectively. From that tables it is observed that the value of q_{ip} if greater than that of q_{iw}, this is because the failure of plate in q_{ip} means total failure but that of q_{iw} is like a warning requesting maintenance.

Looking closely at Figure 15 to 20 (SCFS plate with span between 1000mm and 5000mm at allowable deflection (w_a) value between 1mm to 5mm). It is seen that failure on q_{iw} only occurs at all length to width ratio (1 to 2) between value of -1.1331N/mm and -0.1525N/mm at all thickness. The negative value of critical lateral imposed load q_{iw} (and positive value of q_{ip}) only reveals that the plate fails in q_{iw} for the entire plate w_a (1mm to 5mm) and span of 1000mm to 5000mm. This means that the plate structure is not safe and required maintenance.

The positive value of critical lateral imposed load q_{iw} *and* q_{ip} for other types of plate reveals that the plate neither fail in q_{iw} nor in q_{ip} for plate all span at allowable deflection, w_a of 1000mm to 5000mm for the two boundary conditions into consideration. This means that the plate structure is safe.

However, the value of stiffness coefficient is higher with the structure with free support than that with simple support and clamped. Consequently, the value of q_{iw} *and* q_{ip} are higher in the CSCS plate than SCFS plate, this shows that the capacity of the plate to resist bending is higher in the SCFS plate than that of CSCS plate.

The result from comparison made in Table 2, 3 and Figure 3, shows that the average percentage difference between the present study and that of [12] and [13] is 9.2% and 16.6% the difference is higher than that of [20] because the latter is a higher shear deformation theory whose value is closer to the exact as it did not require a shear correction factor for the analysis. Meanwhile, the result of the three equally validates these polynomial displacement functions for rectangular plate's analysis. Though the disparity between the values in bending is obvious. It does not invalidate the results, since the values of the present solution are upper bound results, which will not put the structure being designed in danger. Hence, the approximating function according to polynomial function can be used reliably for analysis of a plate with all edges clamped and simply supported at opposite edge. They present good interpretations of the two results. From Table 3 and Figure 3, it can be seen that the results obtained in this work agree very well with those from the previous work [12, 13 and 20]. The disparity between the three values or total average percentage difference of 10.6% is very negligible. Hence, the approximating function according to the polynomial function can be used with confidence for analysis of deflection on a plate with such configurations.

5. Conclusion

A displacement based, refined shear deformation theory includes the effects of transverse shear deformations. The constitutive relations are satisfied in respect of in-plane stress and transverse shear stress. The theory obviates the need of a shear correction factor. The governing differential equations and associated boundary conditions obtained are variationally consistent and can be used with confidence in the analysis of isotropic rectangular.

Furthermore, it can be concluded that the values of critical lateral load obtained by this theory achieve accepted vertical shear stress to the thickness of plate variation and satisfied the transverse flexibility of condition at the top and bottom faces of the plate while predicting the flexural characteristics for an isotropic rectangular CSCS and SCFS plate. The deflection and stresses obtained by present theory are in good agreement with the other order theories. This validates the efficacy and credibility of the present polynomial shear deformation theory.

Hence, the effect of deflection and crack in a mild steel rectangular plate can be managed in the analysis and design of structures. This approach overcomes the challenges of the conventional practice in the structural analysis/design which involves checking of deflection and shear; the process which is proved unreliable.

6. Recommendation of Future Scope of Studies

This lies in the establishment of higher order orthogonal polynomial shear deformation/displacement function for free vibration and buckling analysis of rectangular or circular thick plate. Then determining the critical buckling load parameters for the plate using virtual work principles.

Table 1: Values of Stiffness Coefficient, k for Various Support (boundary conditions)

Type	Plate	k_1	k_2	k_3	k_4	k_5	k_6
1	cscs	0.007	0.009	0.039	0.008	0.009	0.007
2	scfs	1.509	0.182	0.028	0.072	0.016	0.062

Table 2: Percentage difference between the values of centroidal deflection from present and past studies

$$\%\text{Diff} = \frac{\text{Absolute difference betwee present and pasr value}}{\text{Past value}}$$

$\rho = \frac{a}{t}$	Present	[11]	[12]	[20]
5	0.0024	17.447	28.511	13.3448
10	0.0021	0.9479	4.7393	3.7168
20	0.0020	-	-	1.0830
Average % Difference		9.20	16.63	6.05
Total % Difference	10.62			

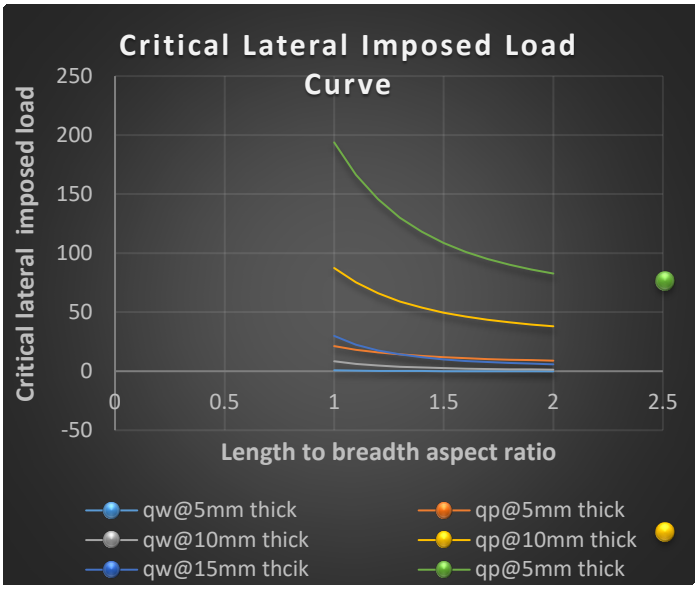


Figure 3: Graph of critical lateral imposed load versus length to breadth ratio of CSCS plate for span, a = 1000mm at w_a = 1.0mm

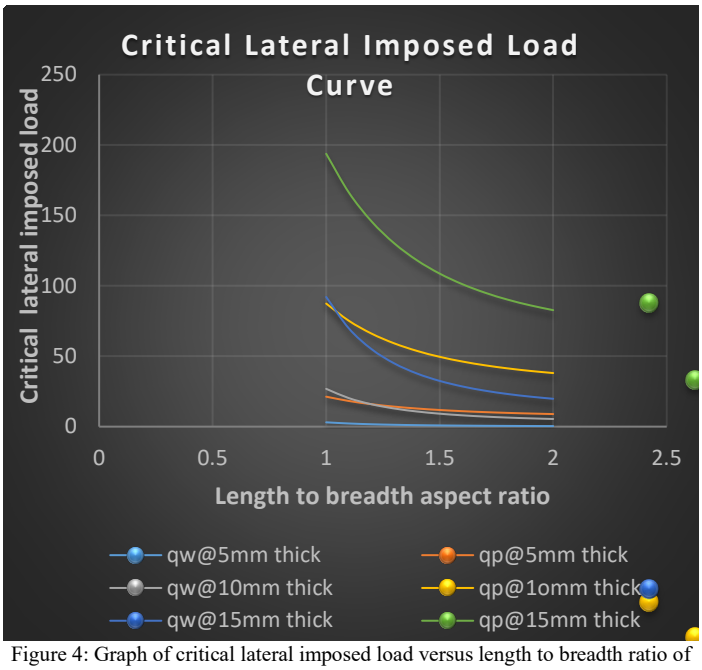


Figure 4: Graph of critical lateral imposed load versus length to breadth ratio of CSCS plate for span, a = 1000mm at w_a = 3.0mm

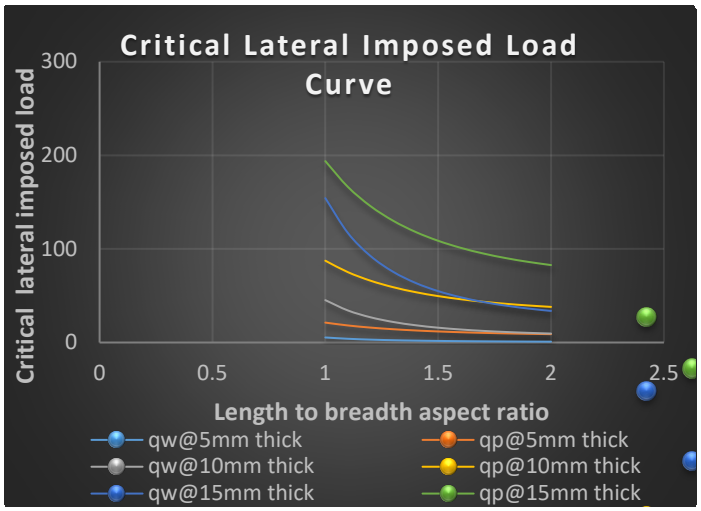


Figure 5 Graph of critical lateral imposed load versus length to breadth ratio of CSCS plate for span, a = 1000mm at w_a = 5.0mm

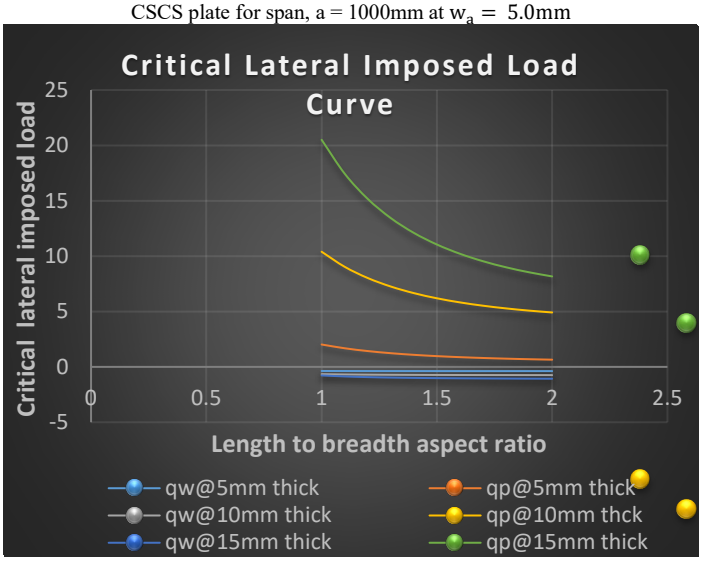


Figure 6: Graph of critical lateral imposed load versus length to breadth ratio of CSCS plate for span, a = 3000mm at w_a = 1.0mm

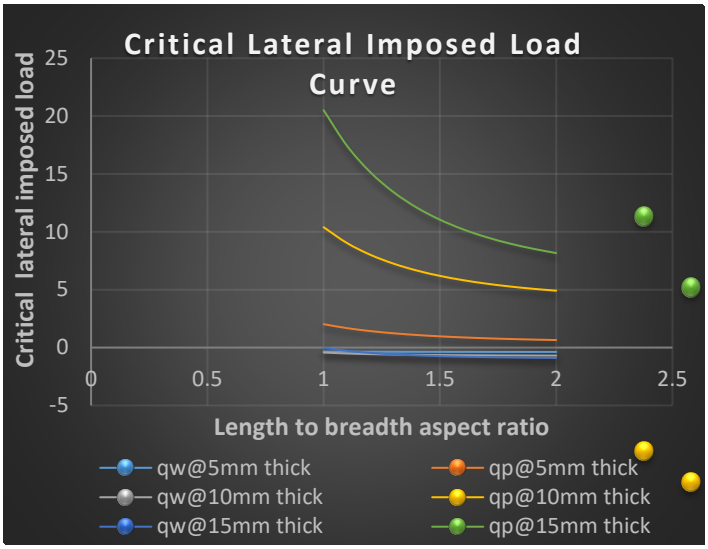


Figure 7: Graph of critical lateral imposed load versus length to breadth ratio of CSCS plate for span, a = 3000mm at w_a = 3.0mm

Table 3: Comparison of values of non-dimensional center deflection multiplied by D/qa^4 of CSCS square and 1.5 aspect ratio rectangular thick plate obtained herein with those from [12], [13] and [20] respectively.

$\rho = \frac{a}{t}$	Present (ρ = 1.0)	[12] (ρ = 1.0)	[13] (ρ = 1.0)	Present (ρ = 1.5)	[20] (ρ = 1.5)
5	0.0024	0.0028	0.0030	0.0061	0.0069
10	0.0021	0.0021	0.0022	0.0057	0.0059
20	0.0020	-	-	0.0055	0.0056

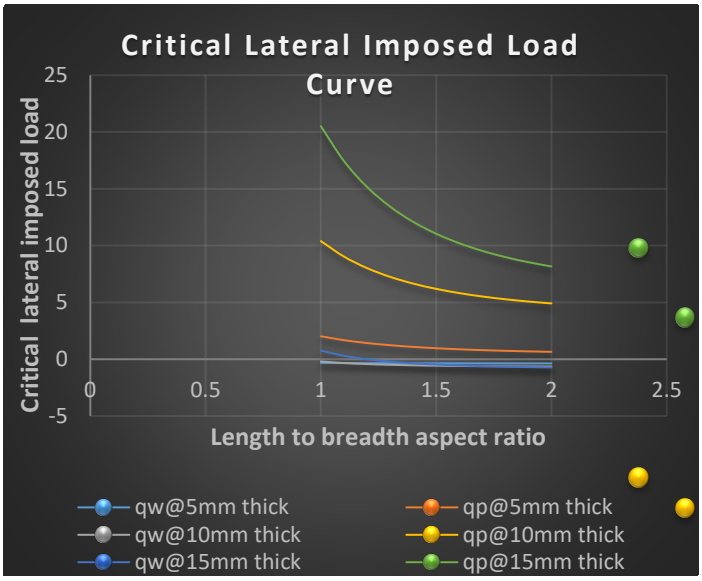


Figure 8: Graph of critical lateral imposed load versus length to breadth ratio of CSCS plate for span, a = 3000mm at w_a = 5.0mm

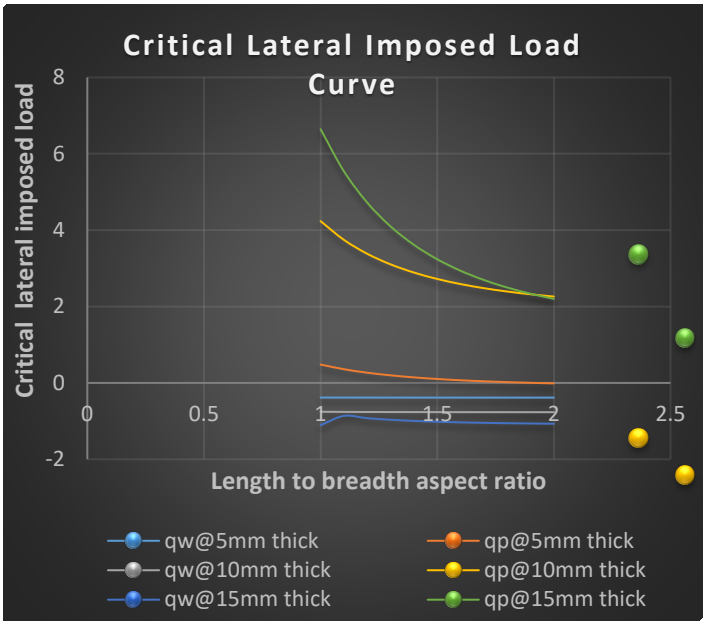


Figure 9: Graph of critical lateral imposed load versus length to breadth ratio of CSCS plate for span, a = 5000mm at w_a = 1.0mm

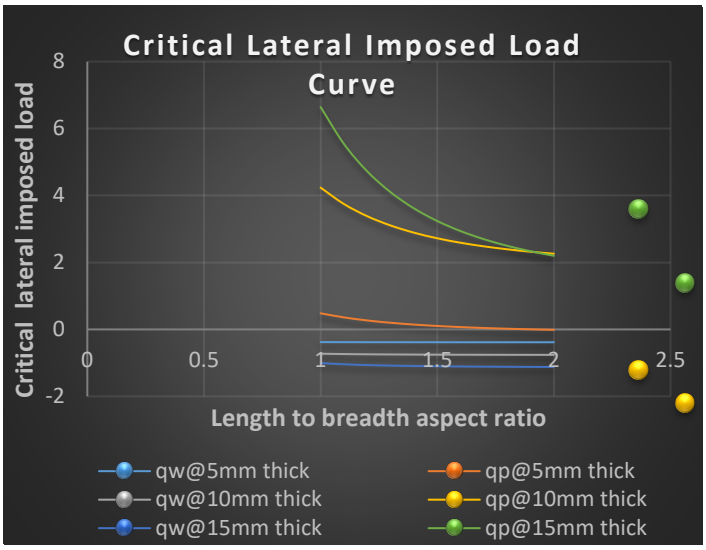


Figure 10: Graph of critical lateral imposed load versus length to breadth ratio of CSCS plate for span, a = 5000mm at w_a = 3.0mm

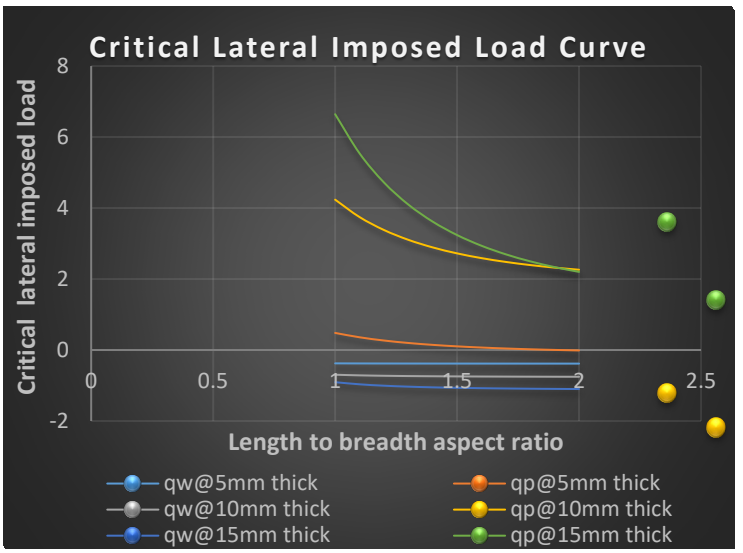


Figure 11: Graph of critical lateral imposed load versus length to breadth ratio of CSCS plate for span, a = 5000mm at w_a = 5.0mm

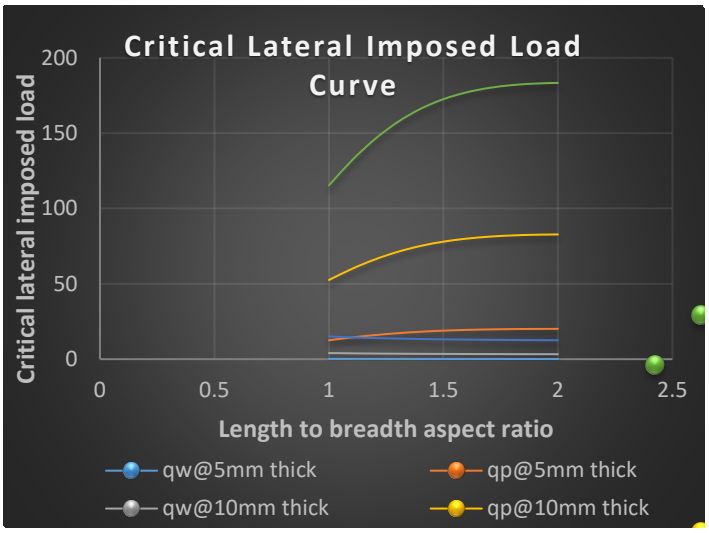


Figure 12: Graph of critical lateral imposed load versus length to breadth ratio of SCFS plate for span, a = 1000mm at w_a = 1.0mm

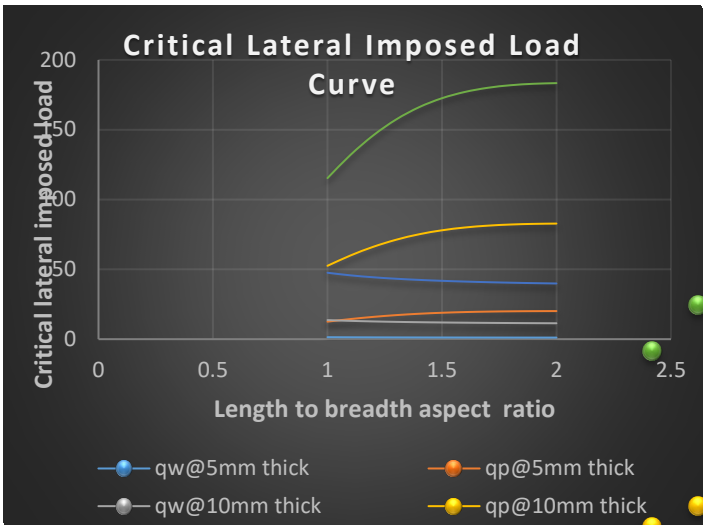


Figure 13: Graph of critical lateral imposed load versus length to breadth ratio of SCFS plate for span, a = 1000mm at w_a = 3.0mm

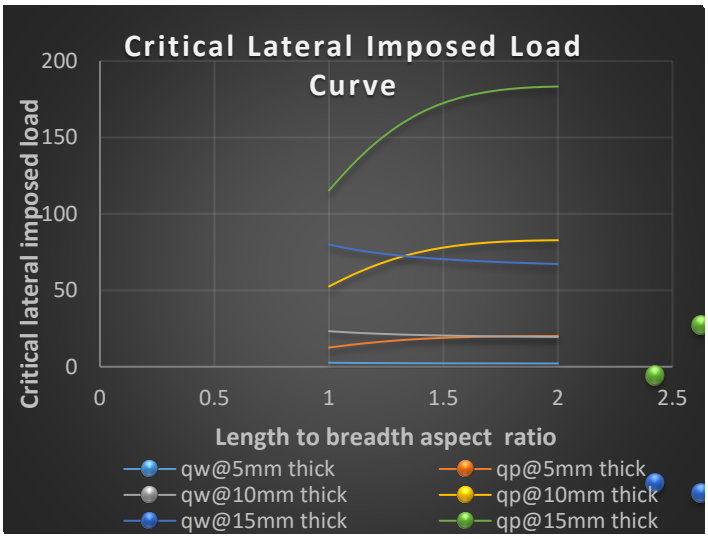


Figure 14: Graph of critical lateral imposed load versus length to breadth ratio of SCFS plate for span, a = 1000mm at w_a = 5.0mm

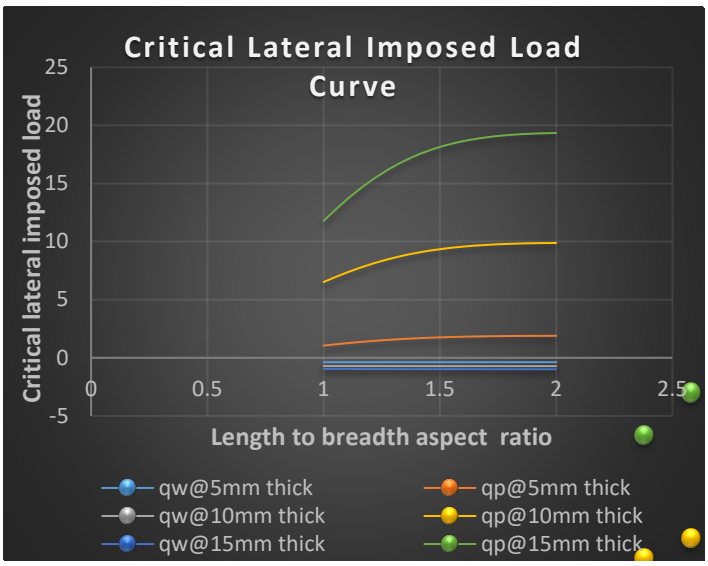


Figure 15: Graph of critical lateral imposed load versus length to breadth ratio of SCFS plate for span, a = 3000mm at w_a = 1.0mm

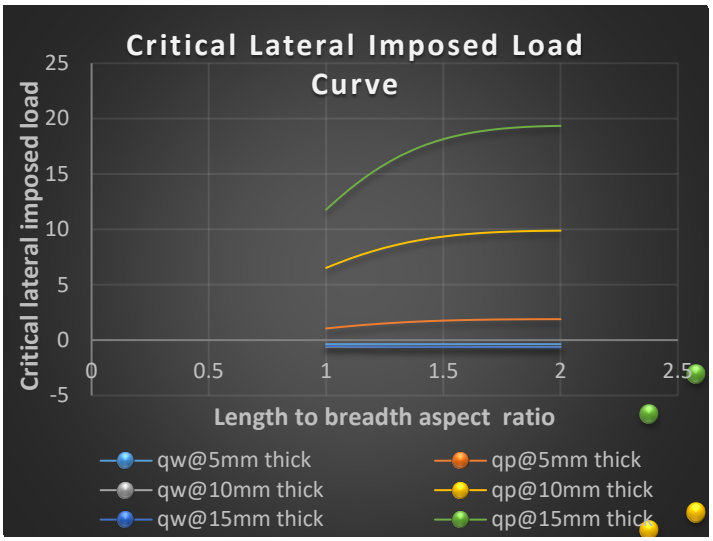


Figure 16: Graph of critical lateral imposed load versus length to breadth ratio of SCFS plate for span, a = 3000mm at w_a = 3.0mm

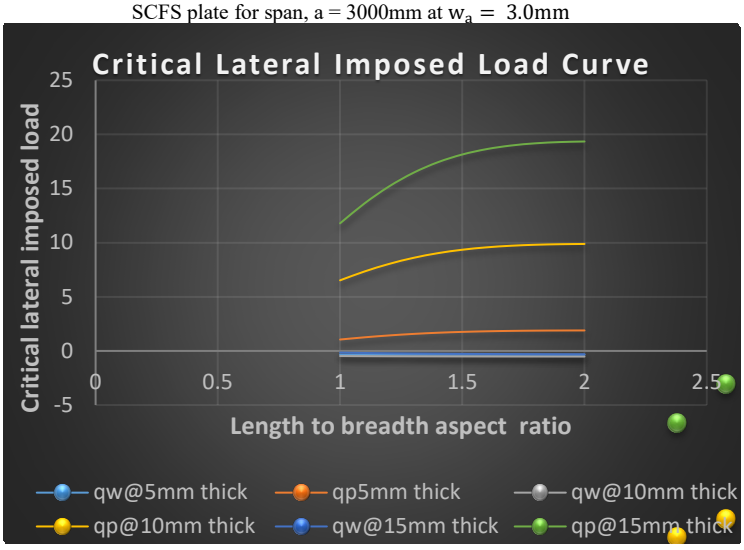


Figure 17: Graph of critical lateral imposed load versus length to breadth ratio of SCFS plate for span, a = 3000mm at w_a = 5.0mm

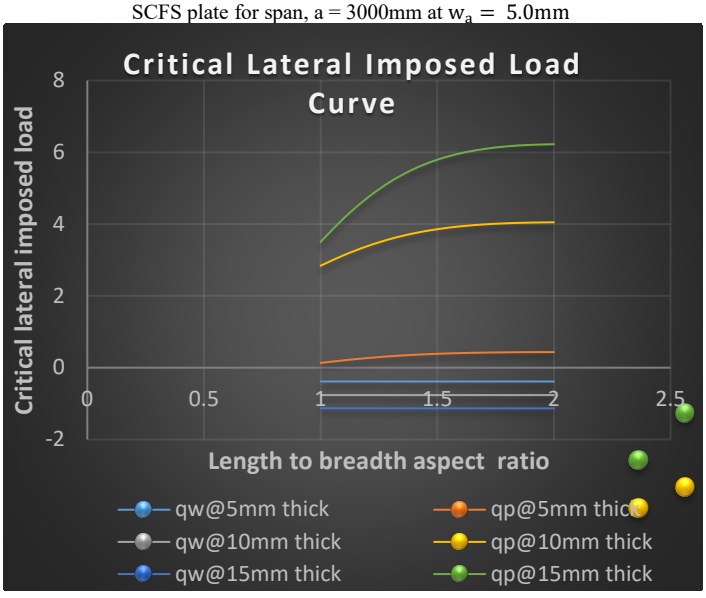


Figure 18: Graph of critical lateral imposed load versus length to breadth ratio of SCFS plate for span, a = 5000mm at w_a = 1.0mm

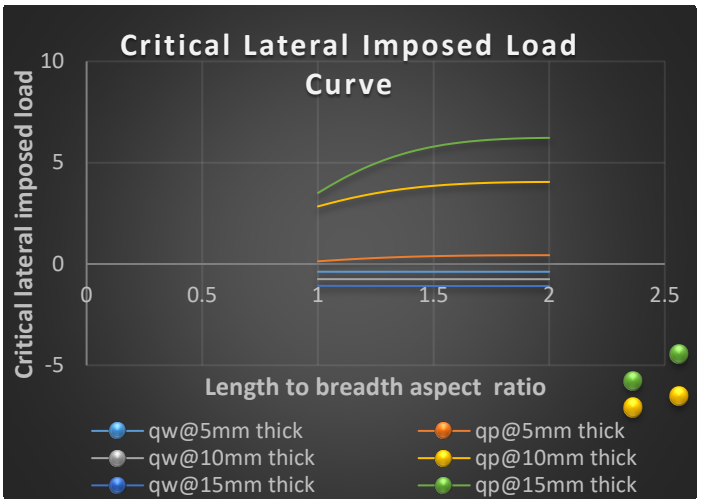


Figure 19: Graph of critical lateral imposed load versus length to breadth ratio of SCFS plate for span, a = 5000mm at w_a = 3.0mm

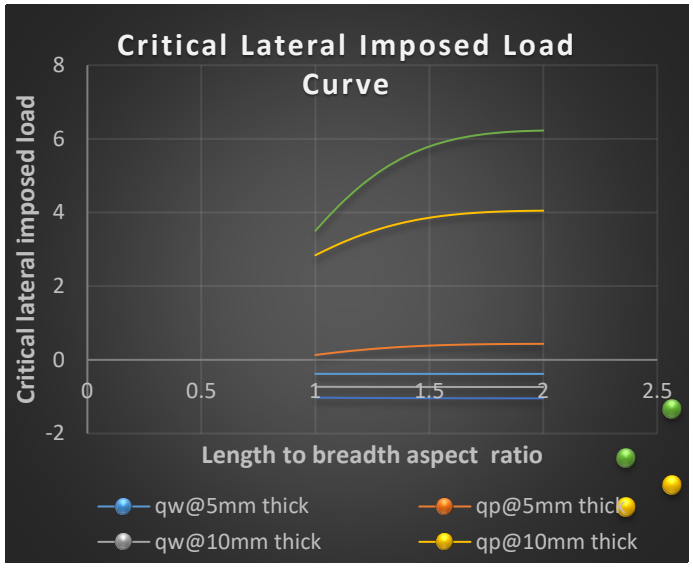


Figure 20: Graph of critical lateral imposed load versus length to breadth ratio of SCFS plate for span, a = 5000mm at w_a = 5.0mm

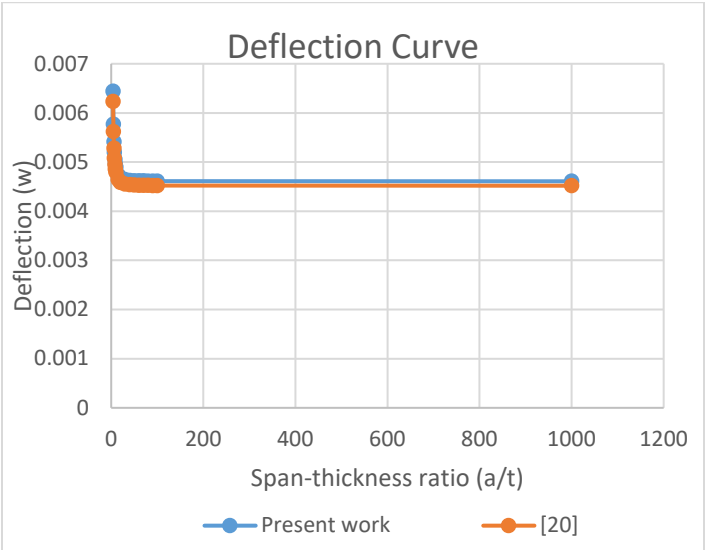


Figure 21: Comparison of values deflection of SCFS rectangular thick plate with 1.5 span-thickness ratio obtained herein with those from [20]

Conflict of Interest Statement

On behalf of all authors, I Okeke Thompson Edozie the corresponding author hereby state that there is no conflict of interest.

References

[1] Bert Louis Smith, "Critical load for a rectangular plate simply supported on three edges, built in on the fourth edge, and compressed on two opposite-simply supported edges by a load in the plane of the plate," A master's degree thesis submitted to the School of Mines and Metallurgy of the University of Missouri, Rolla, Missouri, 1960.

[2] K. P. Soldatos, "On certain refined theories for plate bending," ASME Journal of Applied Mechanics, **55**: 994–995, 1988.

[3] Li Rui, Xiaoqin Ni, Gengdong Cheng, "Symplectic superposition method for benchmark flexure solutions for rectangular thick plates," J. Eng. Mech., **10,** 1-17, 2014.

[4] I.I. Sayyad, S.B. Chikalthankar, and V.M. Nandedkar, "Bending and free vibration analysis of isotropic plate using refined plate theory, " Bonfring International Journal of Industrial Engineering and Management Science, Vol. 3(2): 40-46, 2013.

[5] A.S. Mantari, C. Oktem, Guedes Soares, "A new trigonometric shear deformation theory for isotropic, laminated composite and sandwich plates," Int. J. Solids and Struc, **49**: 43-53, 2012.

[6] E. I. Adah, D. O. Onwuka, O. M. Ibearugbulem, "Development of polynomial based program for pure bending analysis of SSSS rectangular thin isotropic plate," International Journal of Science, Engineering and Technology Research (IJSETR), Vol. **5**(7): 2290-2295, 2016.

[7] F. O. Okafor, O. T. Udeh, "Direct method of analysis of an isotropic rectangular plate using characteristic orthogonal polynomials," Nigerian Journal of Technology (NIJOTECH), Vol. **34**(2): 232 – 239, 2016.

[8] C. H. Aginam, C. A. Chidolue, C. A. Ezeagu, "Application of direct variational method in the analysis of isotropic thin rectangular plates," ARPN Journal of Engineering and Applied Sciences, **7**(9):1128-1138, 2012.

[9] E. Reissner, "A note on bending of plates including the effects of transverse shearing and normal strains," ZAMP: Zeitschrift fur Angewandte Mathematik und Physik, **32**: 764–767, 1981.

[10] D. W. Cooke, M. Levinson, "Thick rectangular plates- II, the generalized Levy solution," International journal of Mechanical Sciences, **25**: 207-215, 1983.

[11] C. M. Wang, J. N. Reddy, K. H. Lee, "Shear deformable beams and plates. Relationship between classical plate theories," Elsevier science ltd, Uk, 2000.

[12] A. S. Sayyad, Y. M. Ghugal, "Bending and free vibration analysis of thick isotropic plates by using exponential shear deformation theory," Applied and Computational Mechanics, **6**(1): 65–69, 2012.

[13] Amale Mahi, El Abbs Adda Bedia, Abdalouahed Tausi, "A new hyperbolic shear deformation theory for bending and free vibration analysis of an isotropic, functionally graded, sandwich, laminated composite plate," Applied mathematical modelling, **25**: 2489-2508, 2015.

[14] Y. M. Ghugal, A. S. Sayyad, "Free vibration of thick isotropic plates using trigonometric shear deformation theory," J. Solid Mech. **3**(2): 172-182, 2011.

[15] I. I. Sayyad, S. B. Chikalthankar, V. M. Nandedkar, "Trigonometric shear deformation theory for thick plate analysis," International Conference on Recent Trends in engineering & Technology – 2013 (ICRTET'2013) Organized By: SNJB's Late Sau. K. B. Jain College of Engineering, Chandwad.

[16] O. M. Ibearugbulem, F. C. Onyeka, "Moment and stress analysis solutions of clamped rectangular thick plate," European Journal of Engineering Research and Science, **5**(4): 531-534, 2020.

[17] F. C. Onyeka, F.C, "Direct analysis of critical lateral load in a thick rectangular plate using refined plate theory," International Journal of Civil Engineering and Technology Vol. **10**(5): 492-505, 2019.

[18] F. C. Onyeka, O. M. Ibearugbulem, "Load analysis and bending solutions of rectangular thick plate. International journal on emerging technologies," **11**(3): 1103–1110, 2020.

[19] F. C. Onyeka and F. O. Okafor, H. N. Onah,, "Application of exact solution approach in the analysis of thick rectangular plate," International Journal of Applied Engineering Research, **14**(8): 2043-2057, 2019.

[20] Gwarah, Ledum Suanu, "Application of shear deformation theory in the analysis of thick rectangular plates using polynomial displacement functions. A published PhD. thesis presented to the school of postgraduate studies in civil engineering, federal university of technology, Owerri, Nigeria, 2019.

Advances in Science, Technology and Engineering Systems Journal Vol. 5, No. 5, 414-425 (2020)

www.astesj.com

Special Issue on Multidisciplinary Innovation in Engineering Science & Technology

ASTESJ

ISSN: 2415-6698

A Hybrid Model for Coronary Heart Disease Prediction in Thai Population

Chalinee Partanapat*, Chuleerat Jaruskulchai, Chanankorn Jandaeng

Management of Information Technology, School of Informatics, Walailak University, Nakhon Si Thammarat 80161, Thailand

ARTICLE INFO

Article history:
Received: 14 July, 2020
Accepted: 08 September, 2020
Online: 21 September, 2020

Keywords:
Data Mining
Feature Selection
Coronary Heart Disease
Socioeconomic Status
Rediscretization on Clinical Values

ABSTRACT

The ability to verify the critical risk factors related to an effective diagnosis is very crucial for improving accuracy on coronary heart disease prediction. The objective of this research is to find the best predictive model for coronary heart disease diagnosis. Three approaches are set up to achieve the goals (1) investigating the classifier algorithms that are most suitable for the Thai heart disease dataset in this study (2) exploring features analyzed to be the significant risk factors in the predictive model, both major risk factors, and socioeconomic status and (3) rediscretizing the predefined clinical values on certain major risk factors. In order to achieving the optimal model before incorporating with feature selection process, several classifier approaches are conducted in this experiment. The study shows that the most effective classifiers ranked from the highest accuracy are Support Vector Machine, Naïve Bayes, Decision Tree, and Multi Layer Perceptron. Support Vector Machine produces the highest accuracy of 88.18%, with respect to both major risk factors and socioeconomic factors. Moreover, when adjusted thirteen major risk factors and five socioeconomic factors altogether, the accuracy is proved to be better than conducting each one alone. To investigate the better predictive performance of our study, feature selection methods of both filter and wrapper groups are employed with exploring the hybrid models to identify the most relevant features for Thai coronary heart disease. Relief Attribute Evaluation with Bayes Theorem is proved to be the best one with the accuracy of 92.59%, classified by SVM. To prove the accuracy enhancement, we perform rediscretization model on predefined medical values to examine different physical and personalized information of each person which can be incurred the coronary heart disease in different situation. The findings found that equal-depth rediscretization values on 7 major risk factors as Obesity, Hypertension, age, LDL, HDL, Fasting Blood Sugar, and Triglyceride, influences and improves with the better accuracy than predefined values of 95.50% classified by SVM. Thus, this finding shows that the proposed technique definitely outperforms predefined values from medical field.

1. Introduction

Coronary Heart Disease (CHD) is a chronic and fatal disease that is appeared to become the major health problem in Thailand. The most critical major risk factors causing such disease include Hypertension, HDL, LDL, Triglyceride, or diabetes. Base on literature reviews, many researchers attempted to utilize data mining techniques to enhance prediction ability on heart disease, which it was mostly based only on the major risk factors (MRF). Nevertheless, the factors related to socio-economic parts, called as socioeconomic status (SES), can also be influenced as one of crucial factors affecting on coronary heart disease. These factors can be found in various developing countries as well as in Thailand. The SES, like age and sex, can be mentioned after empirical demonstration that it can be a powerful predictor discovering the heart disease for Thai people [1]. Commonly, the high death rates from heart disease happened in Thailand can be caused by stress, hard works, and others. But even low SES can recently be found as influential factors related to heart disease problems for Thai patient [2]. In addition, the factors such as high blood pressure level, obesity, and smoking, lower education level, occupation as well as unhealthy life-styles can also affect heart disease [3]. Although previous researchers conducted experiment SES for heart disease prediction, they merely used statistical

*Corresponding Author: Chalinee Partanapat, Department of MIT, WU, Nakhon Si Thammarat 80161, Thailand, Email: joepooh14@gmail.com

methods to derive the study result. However, there have been few studies utilizing the data mining techniques. Thus, we need to find out which major or biological risk factors and SES factors that are the critical risk factors for Thai population. This study applied data mining techniques task as supervised machine learning methods via various feature selection models. Moreover, the rediscretization approaches are also used to find patterns that are hidden in the datasets to explore which risk factors can be the significant ones in prediction coronary heart disease for Thai population. In the last phase of this study, we proposed rediscretized methods for transforming the predefined medical values to novel rediscretized values to investigate the better accuracy for Thai heart study. The purposes of this research are to (1) explore the critical major and SES risk factors analyzed to be critical for Thai population (2) to rediscretize the predefined medical values on some of major risk factors.

2. Literature Review

For the last few years, many researchers have been attempting to employ advanced data mining technique approaches for prediction in medical field. In this study, the literature review is categorized into 3 paradigms. Firstly, explore heart disease prediction applying SES independently. The predictive model by applying Logistic Regression methods with Linear Regression using Statistical Software as SAS was conducted [4]. The result implied that gender and age are correlated with income levels and education, which is critical for incurring Coronary Heart Disease. Furthermore, the correlation between Risk of All-Cause Cardiovascular Mortality and Socioeconomic Status was performed [5]. The authors conducted the experiment by applying Twenty-Three risk factors. They employed association among socioeconomic status to evaluate the performance by Cox proportional hazard models using SAS Statistical Software. This research explored the correlation between lower social-economic status (SES) and worse conditions of health were directly related to the heart disease. The result revealed that each of the 23 socioeconomic status conducted was critically correlated, especially when assigning age with income.

Secondly, classification is applied in this study in order to classify Thai people who are healthy and who can be taken in to the consideration of heart disease. In [6], the authors developed a research on Effective Heart Disease Prediction by employing feature selection as association algorithm. They used Maximal Frequent Itemset Algorithm (MAFIA) classified by Non Linear Integrals to obtain the effective result. Further study of a predictive methodology on heart disease patient diagnosis based on decision tree J48 and Bagging Algorithms was presented [7]. Feature selection algorithms as Information Gain, GINI, and Gain Ratio were employed generated as ranking of most significant features. The highest performance is assessed on the basis of accuracy as 84.1%. Additionally, heart disease prediction applying j48, Bayes Net, SMO, and Multilayer perception with 10-fold cross validation using WEKA software was proposed [8]. SMO produced the highest accuracy of 89%. The heart disease prediction focusing on non- linear classification algorithm has also been developed [9]. They conducted with big data tool as Hadoop Distributed File System (HDFS) along with SVM for optimizing the set of feature. The research compared the performance of different data mining techniques. SVM in parallel fashion was executed as the best performance of prediction with 85% of accuracy.

Finally, discretization has been developed as applying for the first step in classification process in data mining approaches. In [10], the authors developed a discretization method and Information Gain on Naïve Bayes to diagnose heart disease. The authors used the heart disease dataset recruited from the UCI dataset composing of 270 instances and 14 features. The experiment was conducted with 10 fold cross validation. The results of the application showed that the accuracy of Naïve Bayes classifier was 85.18% while Naïve Bayes with discretization and information gain obtained the increased accuracy of 85.56%. Further study was conducted on the experiment of Heart Disease Prediction proposing different types of Decision along with discretization [11]. They evaluated the performance of alternative of decision trees by calculating sensitivity, specificity, and accuracy. The result showed that nine voting Equal Frequency Discritization with Gini Index Decision Tree produced the best accuracy with 85.3%, when compared with other methods without discretization.

3. Major Contribution of the Work

This study has the usefully applicable contribution both for data mining and medical field as (1) the effective performance of a hybrid model for coronary heart disease prediction for Thai population, which explores novel strategy achieved by combining feature selection approaches for choosing the most relevant attributes and rediscretization model, can be utilized for public health personnel as a primary prevention tool; and (2) a rediscretization model of this heart disease prediction system can be applied to the other diseases that have the same risk factors as stroke [12].

4. Proposed Method

This study proposed the hybrid models of feature selection methods and rediscretization on predetermined clinical values of major risk factors to prove the better performance on predictive accuracy on heart coronary disease. We firstly conducted hybrid of feature selection models to explore the most relevant attributes or risk factors that strongly related to the coronary heart disease. In the final of the study, the rediscretization on medical values was proposed to investigate the enhanced performance on prediction and to prove the strongly robust risk factors that can be the significant indicators for coronary heart disease in Thai population. In this phase, the stage of the proposed method includes data gathering, research framework, proposed hybrid models of prediction, and experiment process. Then, the algorithms of feature selectors chosen to develop the model for measuring the performance are described. Finally, the results from both hybrid predictive model and rediscretization model are compared for observing the prediction accuracy and are analyzed in discussions.

4.1. Dataset Collection

The dataset used in this work was recruited from Ramathibodi Hospital, Bangkok, Thailand. This Thai heart disease dataset

consisted of 20,000 records, composing of 11,240 male and 8,760 female. Additionally, this data set contains 1,205 record with CHD. There are two types of attributes, first is 13 major risk factors (attributes) and the other type is 5 SES. Detail values of each attribute and their corresponding predefined values by medical field are listed in Table1 and Table 2. The full dataset of participants were conducted in this research to explore the best fit classifiers for dataset in this study. We then performed the analysis on the dataset to determine the relation between baseline major risk factors and SES to incur CHD. The 13 major risk factors applied for the experiment are age, gender, HDL, LDL, Fasting Blood Sugar, Hypertension, Exercise, Smoking, Alcohol intake, Diabetes, Obesity, Hereditary, and Triglyceride. The 5 socioeconomic status used in the experiment are income, education, Occupation, Jobs, and Living Conditions.

The 13 major risk factors (attributes), which have the corresponding predefined values of medical field are listed in Table 1.

Table 1: Description of each attribute for major risk factors

No.	Attributes	Descriptions	Values
1	Gender	Male or Female	0: Female 1: Male
2	Age	Age in years	Continuous
3	HDL	Good cholesterol (mg/dl)	0: >= 40 1: < 40
4	LDL	Bad cholesterol (mg/dl)	0: <= 130 1: >130
5	fbs	Fasting Blood Sugar (mg/dl)	0: <= 120 1: >120
6	hp	Hypertension	0: No 1: Yes
7	Exercise	Physical Activity	0: No Exercise 1: Less Than 3d/wk 2: Greater or Equal than 3d/wk
8	Smoke	Smoking Habit	0: Non-Smoking 1: Smoking
9	Alcoholic	Alcoholic Habit	0: Non-Drinker 1: Drinker
10	Diabetes	Diabetes Mellitus	0: No 1: Yes
11	Obesity	Measured By BMI	0: No 1: Yes
12	Hereditary	Family Member Diagnosed with HD	0: No 1: Yes
13	Tg	Triglyceride (mg/dl)	0: 0 – 200 1: >200

The additional five risk factors related to socioeconomic status are employed to assess in the prediction analysis in order to derive improved result as well as effective prediction. Moreover, the result generated from the study can provide the identification on whether correlated with the major risk factors to cause the coronary heart disease. The factors concerning socioeconomic status and their representing values are detailed in Table 2.

4.2. Experiment settings

In this work, WEKA was used as a tool for preprocessing and classifying CHD dataset. For preprocessing step, Weka was facilitated on feature selection, both traditional and designed hybrid model, and was employed for discretization. Finally, classifier algorithms were used for prediction analysis.

Three experiments were conducted for this study. The experiment performance was assessed by Confusion Matrix, which it was the standard metrics to measure the accuracy. In the meantime, the performances derived from the classifiers were also compared in order to see the different views of the results.

The experiment that had been done in the first time had the objective to identify the classification algorithms that can effectively investigate the most relevant dataset of Thai heart disease. In this stage, the study incrementally studied and separately evaluated 13 factors related to biological (MRF) perspectives and 5 factors about the socioeconomic status (SES). Next step, both MRF and SES were assessed together. The predictive performance as accuracy in this designed experiment was examined the effective measurement between conducting MRF and SES separately and adjusting both of them. Lastly, the comparison for both scenarios on the derived result was also conducted.

Table 2: Description of each attribute of socioeconomic risk factors

No.	Attributes	Descriptions	Values
14	Income	Income levels (THB)	0 = <=10,000 1 = >10,000 - 20,000 2 = >20,000 - 50,000 3 = >=50,000
15	Edu	Education Levels	0 = Secondary 1 = Vocational 2 = Bachelor 3 = Higher than Bachelor
16	Occupation	Occupation Levels	0 = Manager 1 = Intermediate 2 = Self-Employed 3 = Technical
17	Jobs	Employment status	0 = Unemployed 1 = Employed
18	liv. cond.	Living condition	0 = Rented 1 = Owner

The second experiment focused on applying various feature selection models to CHD dataset. This experiment was designed to evaluate the efficiency of classification by examining performance of filter and wrapper approaches, including proposed hybrid models pioneered from combined feature selector methods to improve the classification accuracy. In this section, 10 filter algorithms and wrapper approach were applied. Furthermore, the hybrid models generated from combined feature selectors were developed. All of filter algorithms were classified by 4 classifiers and the accuracy of each were compared. For wrapper approaches, and the hybrid ones, were proposed to investigate the

enhancement of predictive performance. Feature selection methods employed in this study are as followings:-

- Correlation Based Feature Selection (CFS): Typically, CFS algorithm evaluates strong features subsets containing features that are highly correlated with the class [13]. We mainly performed both CFS and CFS with other three feature selection approaches in this study. 18 risk factors were used to identify the robust and relevant factors. The factors that executed the value highly related to the class selected by CFS were age, gender, LDL, hypertension, smoking, diabetes, obesity, triglyceride, income, and education.
- Bayes Theorem: based on statistical technique describing the usage of the Theory of conditional probability, which assume with possible causes for a given observed event. It can be computed from the knowledge that has already been occurred. It identifies the relation between event and probability [14]. Applying Bayes' theorem, assume that one would like to investigate whether the prospective participants have a chance to get the heart disease by knowing their triglyceride. Triglyceride is the critical causes of CHD, the participants' triglyceride information can be determined the probability of CHD occurrence.
- CFS and Bayes Theorem: A novel hybrid feature selection model generated from CFS with Bayes Theorem combination was proposed. The features selected by CFS algorithm will be assigned to Bay's theorem for conclusively better reduction. Correspondingly, the insignificant features will be removed. Bay's theorem selects the feature with the highest conditional probability. In this study, CFS with Bayes Theorem is proved to give the better accuracy than the single selector approach.
- Chi-squared attribute evaluation: A Chi-squared feature selection is normally applied to test the independence of two variables or features. The aim of this feature selection is to select the features which are significantly dependent on the other feature or the response. When two features are significantly different, the chi-square value will be smaller, and it can be implied that features are not related to each other as it is not dependent on the response [15]. In this study, we focused on exploring the critical risk factors that are correlated with CHD for Thai people.
- Random Tree: Algorithms used for selecting features by randomized method. It works effectively on large dataset as having the greatest solving problem in impurity, while reducing time for training model and achieving accuracy improvement [16]. This selector algorithm produced the highest accuracy when combined with CFS to determine the critical risk factors of Thai CHD.
- Info Gain Attribute Evaluation: An algorithm proposed for feature ranking and feature reduction evaluated by Entropy, which characterizes the impurity of a collection of examples [17]. In this study, the risk factors selected by this method are reduced to 8 factors with higher accuracy than without feature selection.
- SVM Attribute Evaluation: This approach evaluates the features, which are ranked with respect to the square of coefficients as linear using SVM classification algorithm [18].
- Wrapper Subset Evaluation: A learning algorithm that are applied to evaluate the feature subsets and use the predictive model to score them due to the accuracy to detect the possible relationships between variables [19]. In this study, we applied wrapper approach including Genetic Algorithm and Sequential Search to solve the problem of performing of intensive calculation.

The third experiment was developed to assess and to compare the new rediscretized values with the predefined medical values. In this experiment, we proposed rediscretization model on 7 major risk factors (MRF) that have continuous and predefined categorical values. The new rediscretized values are automated binning by WEKA, starting from 2 to 10 bins, before feeding to the best feature selector from the previous experiment. Lastly, the accuracy of rediscretized values of each risk factor will be compared with the corresponding predefined medical values.

4.3. Designed Framework

The framework designed for this research was proposed focused on hybrid feature selection approaches for predicting coronary heart disease, which assembled numerous methods of attribute selectors via classification task to enhance the accuracy of prediction. The various hybrid feature selection models were combined from two different attribute selectors. All of these hybrid models, proposed to prove the improvement in accuracy, were generated into prospective classifiers to compare the predictive performance. Rediscretization was conducted at the last step to investigate the highest accuracy. The steps of designed framework were detailed and portrayed in Figure 1.

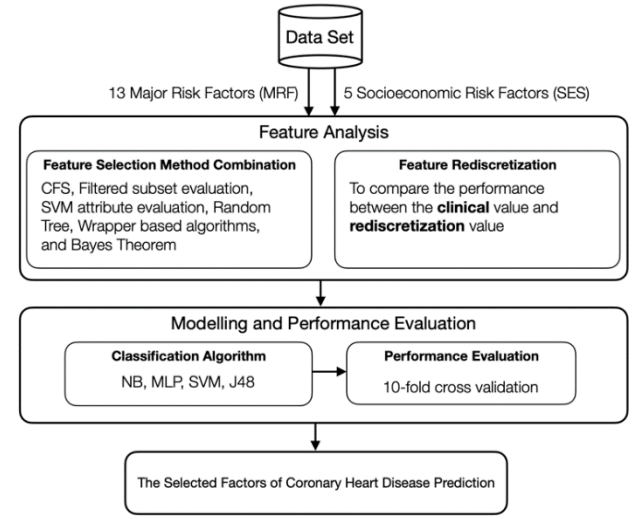


Figure 1: Proposed Framework of Predictive Model for CHD

In the phase of feature analysis, the In the phase of feature analysis, the research employed 18 feature selection models, including 10 filter approaches, wrapper models, and hybrid models in order to attain the significant attributes. The number of relevant or critical attributes drawn by these feature selector approaches would be fed into 4 classifiers, consisting of Naïve Bayes [20], Decision Tree J48 [21], Multilayer Perceptron (MLP), and Support Vector Machine (SVM) [22]. These 4 classifiers were proved to be the best ones resulting from the first study stage. Accordingly, the performance evaluation of different classification algorithms for each feature selector approach was compared and analyzed. Nevertheless, several significant MRF derived from attribute selection methods related to lifestyle such as no exercise, eating discipline, or personalization were

discovered to have the different effect on each individual. Hence, the study employed rediscretization model for predefined clinical values regarding MRF in order to investigate the improved predictive performance.

4.4. Experimental Results

The experimental result was divided into 3 parts corresponding to the experimental set up, which can be demonstrated as followings

4.4.1. Experiment 1

Before feature selection, we conducted 6 classifiers to find the best fit for our dataset, which were Naïve Bayes, K-Nearest Neighbor (KNN), J48, Neural Network (NN), MLP, and SVM, and we found that KNN and NN gave the accuracy less than 80% for every type of risk factors. Finally, only 4 classifiers were selected, due to predictive performance higher than 80%. Also the performance evaluation as accuracy was compared on 5 factors of socioeconomic status (SES) with 13 major risk factors (MRF). The experimental result obtained clearly revealed that that the entire 13 MRF produced much better accuracy performance than only socioeconomic factors. Classification algorithm as SVM obviously executed as the highest classifier compared with the other three. Accordingly, predicting heart disease considering only SES in Thai people, the predictive performance cannot be accepted due to low accuracy. The comparison of predictive performance of these four classifiers between all MRF and SES factors are shown in Table 3.

Table 3: Comparison of accuracy between all major risk factors (MRF) and all socioeconomic risk factors (SES)

Classifiers	Accuracy (%)		
	MRF	SES	MRF+SES
Naïve Bayes	86.70	47.33	86.14
J48	83.17	43.33	84.88
MLP	82.50	54.68	83.66
SVM	86.88	56.78	**88.18**

From Table 3, the result showed that after adjusting all MRF and SES together, the predictive performance is a little better than that of MRF itself. It indicates that when considered Socioeconomic status (SES) as a predictor of coronary heart disease independently of the major risk factors as gender, age, diabetes, hypertension, smoking, physical activity, cholesterol, and body weight, SES itself is not a powerful determinant for health problem even it is inversely associated with risk for CHD. For example, low education or low income can be proved to have a chance of occurrence of CHD but not directly contributed to CHD without analyzing the major risk factors together. Accordingly, this finding found that consideration of SES with major risk factors would address more CHD risk. The performance of all 18 risk factors and each type of risk factors are compared and are evaluated by four classifiers. The comparison of results is represented in table 3.

According to Table 3, the result confirmed that adjusting major risk factors with SES provides the better accuracy. The above result was performed before process of feature selection, SVM classifier produced the best accuracy of 88.18%. The result examined the relationship between major risk factors and SES that when these two types of risk factors were assessed together, they affect the accuracy more than considered SES alone. Low education was defined as a low SES. If considered with major risk factors, it is strongly related with smoking [23].

4.4.2. Experiment 2

After achieving the performance evaluation before feature selection, the number of irrelevant attributes was minimized by exploring four feature selector approaches, including CFS, Filtered Subset Evaluation, SVM Attribute Evaluation, and Random Tree respectively. The critical relevant attributes obtained from each attribute selector approach were presented in Table 4.

Based on the results given in Table 4, among 4 feature selector approaches, Random Tree produced the minimum number of risk factors, which decreased to 7 factors. The factors including gender, age, smoking, LDL, and education were then accounted as the critical factors influencing CHD incurrence for Thai people. Accordingly, the finding discovered that all classifiers produced the higher accuracy after removing irrelevant attributes.

Subsequently, we proposed three hybrid feature selection approaches, which were developed from combining CFS with Filtered subset evaluation, CFS with SVM attribute evaluation, and CFS with Random Tree. Accordingly, the study proved that the three proposed hybrid models produced the better predictive accuracy. The relevant attributes or the critical risk factors achieved from three proposed hybrid feature selection models were shown in Table 5.

From the result given in Table 5, the best performance measurement yielded to SVM classifier with the highest accuracy of 90.55%, selected by CFS with Random Tree attribute selector approaches.

As a result displayed in Table 4 and Table 5, we observed the finding and found that the combination of two feature selection approaches called hybrid models produced the better accuracy than applying a single feature selector. Furthermore, Education which is the SES factors is appeared in every selector approach, both a single selector method and hybrid models. Thus, the result in this phase can be implied that low education level is considered as a critical risk factor related to SES and has the direct effect on CHD in Thai people. Consequently, Thai people with less education have more chance to raise CHD.

The findings indicated that classifiers give the improved accuracy after utilizing the hybrid feature selector approaches. The crucial factors including age, gender, LDL, smoking and low education can raise CHD of Thai people. Additionally, diabetes was found that it can also have an effect on Thai heart disease related with age, sex, cholesterol and smoking.

After results of hybrid feature selectors conducted in filter group were shown in Table 5, there were other feature selection in another group as wrapper subset evaluation of wrapper group was also implemented. Herewith, other five feature selections including wrapper subset evaluation (WSE), information gain attribute evaluation (IGAE), qui-squared attribute evaluation (CAE), gain ratio attribute evaluation (GRAE), one attribute evaluation (OAE), and relief attribute evaluation (RAE) had been employed as they were accepted to investigate the enhanced accuracy of prediction of factors affecting CHD occurrence in Thailand. The reduced selected factors are displayed in the Table 6.

Table 4: Number of selected attributes by each attribute selection method and attributes selected

Selection Method	Selected Attributes	Accuracy (%)				
		Naïve Bayes	J48	MLP	SVM	Average
CFS subset evaluation	10 (1, 2, 4, 6, 8, 10, 11, 13, 14, 15)	87.70	85.14	84.74	88.00	85.14
Filtered subset evaluation	8 (1, 2, 3, 6, 8, 10, 13, 15)	87.14	83.60	80.88	85.60	83.38
SVM attribute evaluation	8 (1, 2, 5, 8, 10, 14, 15)	88.00	85.74	85.50	88.74	85.94
Random Tree	7 (1, 2, 3, 4, 6, 8, 15)	88.18	86.00	87.11	**89.66**	**86.59**

Table 5: Selected features by CFS with Filtered subset evaluation, CFS with SVM attribute evaluation, and CFS with Random Tree

Selection Method	Selected Attributed	Accuracy (%)				
		Naïve Bayes	J48	MLP	SVM	Average
CFS	10 (1, 2, 4, 6, 8, 10, 11, 13, 14, 15)	87.70	85.14	84.74	88.00	85.14
CFS + Filtered subset evaluation	8(1, 2, 4, 6, 8, 10, 13, 15)	88.18	85.62	88.62	86.00	85.63
CFS + SVM attribute evaluation	7(1, 2, 4, 5, 8, 10, 15)	86.18	88.91	88.14	89.91	87.12
CFS + Random Tree	6(1, 2, 4, 8, 10, 15)	88.92	89.14	89.71	**90.55**	88.39

Table 6: The selected attributes by attribute selection methods

Selection Method	Selected Attributes	Accuracy (%)				
		Naïve Bayes	J48	MLP	SVM	Average
Wrapper Subset Evaluation	7(1, 2, 4, 8, 10, 15)	87.50	85.82	84.86	88.54	86.93
Info Gain Attribute Evaluation	8(1, 2, 4, 5, 8, 10, 13, 15)	87.00	85.18	84.66	87.74	86.15
Chi-squared Attribute Evaluation	9(1, 2, 3, 4, 5, 6, 8, 10, 13, 15)	83.70	81.66	82.88	85.50	83.44
Gain Ratio Attribute Evaluation	8(1, 2, 4, 6, 8, 10, 13, 15)	87.00	84.70	85.18	87.50	86.10
One Attribute Evaluation	8(1, 2, 4, 5, 8, 10, 13, 15)	87.50	85.18	86.88	88.00	86.89
Relief Attribute Evaluation	7(1, 2, 4, 8, 10, 15)	88.89	85.97	87.50	**89.50**	**87.97**

Table 6 displayed the result of selected attributes from feature selection algorithms mentioned above. There are 5 crucial biological factors as age, sex, LDL, diabetes, smoking, and socioeconomic factors as education accepted as the crucial factors as picked in every selector approach. This study implies that gender, age, LDL, diabetes, smoking and levels of education are the critically related factors causing CHD for Thai population.

In addition, the study revealed that Triglyceride was appeared to show the impact on prediction and could have the critical effects on Thai Heart Disease, associated with age, sex, cholesterol and smoking and diabetes.

The selected attributes were picked into classification algorithms to investigate the prediction accuracy. The accuracy of related factors towards CHD can be seen in the Table 6, demonstrating comparative results.

From Table 6, after performing the hybrid feature selector approaches, classifiers produced the enhanced accuracy. Relief attribute evaluation method (RAE) classified by the SVM produced best accuracy as of 89.50%, indicating that age, sex, LDL, smoking, diabetes, and low education can affect CHD occurrence. Further analysis on the study result from six methods indicated that the diabetes can be one of crucial factors influencing coronary heart disease for Thais.

After using feature selection from filter group, we attempted to use other wrapper feature selections to study the related factors influencing CHD and then compare its performance evaluation with feature selectors in filter group. The studied wrapper models are then conducted and explained. First, the wrapper algorithms that have been conducted together with Baysian classifier were calculated to work out on average accuracies. Furthermore, the other two wrapper models as Forward Selection (FS) wrapped methodologies were experimented on feature subsets to assess the prediction performance about the coronary heart disease factors. The first one uses the Best First Search (BFS) which is the search algorithm that explores the graph by expanding the promising node with the best score [24]. The second one we generate the subset of features using the Sequential Floating Forward Search

(SFFS) [25]. The principle of such technique is to add one or more attributes progressively. For SFFS, after each step forward, backward steps would be applied to improve the efficiency of wrapper selector. The proposed wrapper with GA approach is also compared with four classifiers.

The finding suggested that gender, age, LDL, diabetes, smoking and education are the critical factors as they were selected in every feature selection method, and Triglyceride was also significantly involved as the major cause of CHD.

The list of features or risk factors for heart disease dataset generated by each of wrapper approach, which are Genetic Algorithm [26], Best First Search, Sequential Forward Floating Search, and without feature selection, is shown in Table 7.

Table 7: The Selected Features by different wrapper Techniques

	Feature	Selected Features					
		GA				BFS	SFFS
		NB	SVM	MLP	J48	NB	NB
1	Gender	✓	✓	✓	✓	✓	✓
2	Age	✓	✓	✓	✓	✓	✓
3	HDL	✓	✓		✓		
4	LDL	✓		✓		✓	✓
5	FBS		✓	✓		✓	
6	Hypertension		✓	✓	✓		
7	Exercise	✓		✓			
8	Smoke	✓	✓		✓	✓	✓
9	Alcoholic	✓	✓	✓			
10	Diabetes	✓	✓	✓	✓		
11	Obesity		✓				
12	Hrd.	✓	✓				
13	Tg	✓	✓		✓		
14	Income	✓	✓	✓			
15	Edu		✓	✓	✓	✓	✓
16	Ocp.						
17	Jobs		✓			✓	✓
18	Liv.Cond						

As the consequence of employing the wrapper feature selection method, the Table 8 displays the results related to the accuracy that has been derived by implementing 10-fold cross validation. Applying GA wrapper generated with BN yields the highest effective prediction accuracy as of 89.50%, which is accounted as the most accurate value compared to other feature selection methods. It is interpreted that the GA wrapper operated with Genetic Algorithm classified by Naïve Bayes can explore the most relevant and strongest features. In addition, the accuracy of classification algorithms with different wrapper feature selection are also mentioned and displayed in the Table 8.

As the result shown from wrapper feature selection group in Table 8, it can be again confirmed that the GA wrapper with BN classifier can produce the highest predictive accuracy of CHD as 89.50%. After investigating with wrapper methods, the other filter feature selectors were applied to reduce the irrelevant risk factors.

After that, the six-inconsequence hybrid models with Bayes theorem, which include CFS, Info Gain Attribute Evaluation, Chi-squared Attribute Evaluation, Gain Ratio Attribute Evaluation, One Attribute Evaluation and Relief Attribute Evaluation, have been experimented and their results obtained the improved predictive accuracy. The attributes attained from these selection methods are shown in the Table 9.

Table 8: The performance evaluation of wrapper-based feature selection algorithms

Wrapper Method	Accuracy (%)			
	Naïve Bayes	J48	MLP	SVM
GA Wrapper	**89.50**	88.82	85.60	84.55
BFS Wrapper	87.50	84.53	83.50	84.18
SFFS Wrapper	88.18	87.17	81.89	83.50
Without FS	86.50	84.50	80.88	80.12

Referring to the hybrid feature selection models in Table 9, the numbers of attributes deducted after applying Chi-squared attribute evaluation is 9, One attribute evaluation is 8, Gain Ratio attribute evaluation is 8, and Relief attribute evaluation is 7, respectively. These selected risk factors are processed into Bayes Theorem. The CFS method with Bayes Theorem generates 6 attributes. The info gain attribute evaluation method with Bayes theorem produces 7 attributes. The chi-squared attribute evaluation method with Bayes Theorem gives 8 attributes. The gain ratio attribute evaluation method with Bayes Theorem generates 7 attributes. The one attribute evaluation method with Bayes Theorem executes 7 attributes. And lastly, the relief attribute evaluation method with Bayes Theorem produces 6 attributes. The results also indicated that critical factors influencing CHD for Thai people can count on gender, age, LDL, smoking, and education. Nevertheless, this chosen dataset achieved from the hybrid models is summarily proved in accuracy improvement classified by four classification algorithms. The comparison of classifiers accuracy with deducted attributes is presented in Table 9.

As a result obtained in Table 9, when adjusting Bayes with these six feature selectors, the predictive accuracy is absolutely proved an improved performance. Relief attribute evaluation (RAE) with the attribute selector Bayes Theorem classified by SVM yields the highest accuracy of 92.59%. The attributes including age, sex, LDL, smoking, and low education are counted as the significant factors affecting the coronary heart disease for Thai people. Beyond this, the diabetes is revealed to be one of the critical factors conclusively associated with age, sex, cholesterol and smoking raising the CHD for Thai population.

4.4.3. Experiment 3

In the last step of our study, according to the values of some risk factors are continuous values or have the predefined range of value from the medical theory, which is not well suitable for nowadays lifestyle of Thai people. For example, attribute such as age, is shown in the clinical value as continuous, which is inappropriate for predictive analysis in medical domain and have no meanings to be the input for heart disease prediction. In this section, we propose the rediscretization method to improve the accuracy on predictive model for CHD of prediction. The proposed methodology involved systematically testing discretization techniques.

Discretization is one of the preprocessing techniques that is used for transforming the different continuous attributes, variables to discrete or nominal attributes [27]. In addition,

Table 9: The selected attributes by hybrid selection methods **with Bayes Theorem**

Selection Method With Bayes Theorem	Selected Attributed	Accuracy (%)				
		Naïve Bayes	J48	MLP	SVM	Average
CFS	6(1, 2, 4, 8, 10, 15)	89.88	86.60	87.11	**90.94**	88.63
Info Gain Attribute Evaluation	7(1, 2, 4, 8, 10, 13, 15)	88.50	86.88	87.50	89.88	88.19
Chi-squared Attribute Evaluation	8(1, 2, 4, 5, 8, 10, 13, 15)	85.92	83.29	84.07	87.50	85.20
Gain Ratio Attribute Evaluation	7(1, 2, 4, 8, 10, 13, 15)	88.00	85.88	86.50	88.67	87.26
One Attribute Evaluation	7(1, 2, 3, 4, 6, 8, 15)	88.18	86.50	87.88	89.50	88.02
Relief Attribute Evaluation	6(1, 2, 4, 8, 10, 15)	90.50	86.87	88.50	**92.59**	89.62

Table 10: Comparison of accuracy between Equal Width Binning and Equal Depth Binning with Age Attribute

No. of Bins	Accuracy (in%)	
	Equal Width Binning	Equal Frequency Binning
2	89.50	88.18
3	**91.00**	**95.33**
4	90.55	94.00
5	88.50	93.66
6	87.18	90.28
7	85.33	87.33
8	84.10	85.50
9	81.18	83.70
10	79.88	81.28

Table 11: Discretization on continuous and some of numeric factors of 7 risk factors

No.	Attributes	Descriptions	Clinical Value	Discretized Value
2	Age	Age (years)	Continuous	0: 0 – 37 1: 38 – 50 2: >= 51
3	HDL	Good cholesterol (mg/dl)	0: >= 40 1: < 40	0: >= 60 1: 50 – 59 2: 40 - 49 3: < 40
4	LDL	Bad cholesterol (mg/dl)	0: <= 130 1: >130	0: <= 100 1: 100 – 130 2: 130 – 160 3: >= 160
5	fbs	Fasting Blood Sugar (mg/dl)	0: <= 120 1: > 120	0: <= 125 1: >125
6	hp	Hypertension (mm/hg)	0: No 1: Yes	0: <= 125 1: 121 – 150 2: > 150
11	Obesity	Measured By BMI	0: No 1: Yes	0: 19-22 1: 23-25 2: 26-30 3: > 30
13	Tg	Triglyceride (mg/dl)	0: 0 – 200 1: > 200	0: 0 – 130 1: > 130-179 2: ≥180 – 259 3: > 259

several classifiers entail that some would work better on discretized or binarized data as the valuable meanings in the new range of values.

At the earlier stage of this experiment, we performed the simplest unsupervised discretization methods on prospective risk factors based on equal width and equal frequency discretization. Hence, the methodology of the research work is equal width binning and equal frequency binning to investigate which one produced the better accuracy for our heart disease dataset. The primarily results showed that equal frequency gave the higher accuracy than equal width. Thus, in this study, the equal depth (Equal Frequency) discretization was selected to conduct the experiment to help improving the predictive performance. To confirm the result, attribute "Age" was exemplified. The equal width method divided the range into the user-defined number of approximately equal size of intervals.

The equal frequency method divides the values into k groups and each group contains approximately the same number of training values [28]. The new discretized value of each factor will be automated binning. The number of bins was generated by WEKA tool. We tried 9 numbers of bins starting from 2 bins to 10 bins. Table 10 contains the measurement of accuracy regarding to the number of bins generated.

This study specifies the parameter by the number of bins and how many values should be included in each bin or each interval. According to the result shown in Table 10, Equal Frequency discretization approach gave the better accuracy and the bin that achieved the highest accuracy was selected to perform rediscretization on the final experiment. Rediscretization on medical values designed to 7 attributes or risk factors is shown in Table 11.

According to the Table 11, first four major risk factors, which are age, HDL, LDL, and fasting blood sugar has been rediscretized. The rediscretized values of attribute "Age" was categorized as followings: the range of 0-37 years old contains 6,132 people, which is accounted for 31%. The range of 38-50 years old contains 8,258 people, which is accounted for 41%. The range of age more than 50 years old contains 5,610 people, which is accounted for 28%. This range of rediscretized values of attribute "Age" gives the best accuracy when compared with any other number of bins. We tried 2 to 10 bins of discretization and the number of 3 bins produced the best performance. Thus, the rediscretized values of 3 bins were selected for the study. The attribute "HDL" was rediscretized into 4 ranges. The range of more than or equal to 60 mg./dl contains 3,232 people, which is accounted for 16%. The range of 50-59 mg./dl contains 5,162 people, which is accounted for 26%. The range of 41-49 mg./dl contains 6,221 people, which is accounted for 31%. The range of less than or equal to 40 mg./dl contains 5385 people, which is accounted for 27%. Similar to attribute age, we tried rediscretization from 2 bins to 10 bins and the selected 4 bins gave the best accuracy. The attribute "LDL" was categorized into 4 bins of new range of values. The range of less than or equal to 100 mg./dl contains 3,657 people, which is accounted for 18%. The range of 101-130 mg./dl contains 4,953 people, which is accounted for 25%. The range of 131-160 mg./dl contains 5,745 people, which is accounted for 29%. The range of less than or equal to 40 mg./dl contains 5,645 people, which is accounted for 28%. Similar to attribute age, we tried rediscretization from 2 bins to 10 bins and the selected 4 bins produced the best performance evaluation. The attribute "Fasting Blood Sugar" was rediscretized to the new range of values as 2 bins. We selected this bin as the best accuracy. The first range is less than or equal to 125 mg/dl, which involves 12,240 people. Another range is more than 125 mg/dl, which involves 7,760 people.

Furthermore, as the experiment conducted in the phase of feature selection, hypertension is one of the critical risk factors for incurring the chance of occurrence for CHD. Thus, this study applied additional risk factor as hypertension for rediscretization. Many previous researches defined and divided the range of systolic blood pressure (SBP) in different range of values due to the purpose and the main idea of their researches. Generally, Hypertension was categorized according to blood pressure readings and the examination by physician is usually performed under the multivariate period of time [29]. Hypertension is considered related to several factors, such as age, body mass index, blood pressure, smoking, family history, and physical inactivity [30]. In our study, the blood pressure determination used for experiment is Systolic Blood Pressure (SBP), and the SBP that we obtained is categorized in to class "Yes" and "No", and the rediscretized values from predefined ones, which has been chosen as the best accuracy from the bins explored from 2 to 10 bins. The rediscretized values selected in the new range can be categorized in to 3 bins, which are less than or equal to 120 mm/hg, 120 – 150 mm/hg, and more than 150 mm/hg. Systolic blood pressure with our participant's characteristics is shown in Table 12.

Table 12: Characteristics of Participants with rediscretized values of hypertension

Systolic Blood Pressure (mm/hg)		Hypertension	
		Men (%)	Women (%)
Normal	$\leq$ 120	43	52
High Normal	>120 – 150	41	34
Hypertension	> 150	16	14

As a result shown in Table 12, the finding found that there were relatively few participants at the higher stage of hypertension. Approximately half of the participants for each gender had blood pressure level in the normal range. After rediscretizing to the new range of blood pressure levels, in addition to the first four factors, the predictive accuracy is proved to more efficient and to have a better performance.

At initial examination of the feature selection phase, obesity is one of the relative risks but not selected by the selection models. Nevertheless, obesity was found to be relative associated with coronary heart disease. Thus, this study also explored the rediscretization task on obesity risk factors as the sixth factors to investigate the better accuracy in prediction, by adding to five factors above. The percentages of each interval of attribute obesity can be summarized in the Table 13.

As a result, presented in Table 13, most of participants have the normal or a little bit overweight. In the medical value, people would be detected to be critical overweight or have the obesity when they must have the value of obesity of more than 25. In our

study, you can be detected to be risky to have a chance of coronary heart disease occurrence when you have a value of BMI ranged from 23 to 25. Therefore, if people take the discretized value of obesity as consideration, they can have a primary prevention for avoiding overweight, which might finally lead to coronary heart disease.

Table 13: The ratio of Participants with rediscretized values of Obesity

Discretized Values	Participants (%)
19-22	22
23-25	36
26-30	26
>30	16

Referring to the phase of feature selection, triglyceride was explored to be the critical risk factors for CHD, because it was appeared in every attribute selection methods. Thus, it indicates that triglyceride is the significant major risk factors for Thai people. Triglycerides, usually considered as having levels higher than 200 mg/dl., are a type of fat stored in human's blood, which are derived from consuming fat and high calories food. In this research, triglyceride is one of the major risk factors to be rediscretized the medical values to test the better classification performance due to difference of individuals on the basis of both physical and behavioral issues.

Normally, triglyceride is considered adjusting with HDL, and LDL. Accordingly, this study considered to examine the better accuracy by rediscretizing the attribute of triglyceride, in addition to rediscretized five factors conducted earlier. Triglyceride has been tried rediscretizing from 2 to 10 bins similar to other discretized factors, and has been chosen a 4-bin as the best accuracy for our dataset.

Table 14: Characteristics of Participants with rediscretized values of triglyceride

Triglyceride (mg/dl)		Participants (%)
Normal	0 – 130	36
Normal to borderline High	131 – 179	26
Borderline High to High	180 – 259	25
High	> 259	13

According to Table 11, the rediscretized values of triglyceride were categorized into 4 bins, due to the best accuracy ranged from 2 to 10 bins. The new range of triglyceride values was divided starting from 0 – 130 mg/dl, 130 – 179 mg/dl, 180 – 259 mg/dl, and more than 259 mg/dl. Compared with the predefined clinical value, which was categorized into only 2 classes with the criteria of 0 -200 and more than 200 mg/dl., the new rediscretized values can provide more details. Cutoffs for discretized values of triglyceride provided some characteristics of participants, was shown in Table 14.

As seen in the Table 14, the people who has triglyceride in the range of 0 – 130 mg/dl is accounted for 36%, in the range of 131 – 179 mg/dl is accounted for 26%, in the range of 180 – 259 mg/dl is accounted for 25%, and in the range of more than 259 mg/dl is accounted for 13%. The finding found that most of participants in this study ware categorized in the normal to borderline high level. Additionally, the experimental result of this finding provided some significant information for people who were in the normal to borderline high level. In this level, there are 5225 participants involved. Within 5,225 people, there are 311 of them that has the heart disease, and 12 of them has the triglyceride less than 150 mg/dl. Furthermore, in the level of borderline high to high triglyceride value, 4,950 people were categorized in this level and 543 of them had the heart disease. With this number, there were 114 participants that have triglyceride value less than 200 mg/dl. Therefore, the rediscretization in this study can help as an early warning for people who look healthy but actually, they can have a chance to get the CHD, even they have the triglyceride value less than 200 mg/dl or even less than 150 mg/dl. They can have the primary prevention for being aware of eating food, exercise, and other positive behavior that will inverse with incurring a chance of CHD.

Consequently, rediscretization on the seventh major risk factor which is triglyceride is proved to produce the better predictive accuracy. The performance evaluation of comparative 7 rediscretized major risk factors conducted on the experiment is shown in Table 15.

Table 15: Comparison of the accuracy of different algorithms between with feature selection, without feature selection and Discretization, and with discretization and feature selection for 7 major risk factors

		Accuracy (%)			
		NB	J48	MLP	SVM
no discretization no feature selection		83.18	81.67	80.67	85.55
no discretization but feature selection with RAE		88.82	87.55	83.59	90.92
discretization + RAE	4 Factors	90.90	88.82	87.59	91.92
	5 Factors	91.33	89.02	90.55	92.58
	6 Factors	92.05	90.67	91.89	93.10
	7 Factors	93.47	92.18	92.57	**95.50**

According to Table 15, the full dataset of 20,000 instances are employed for rediscretization. As the empirical studies in the earlier experiment proved that RAE with Bayes is the best hybrid model for selecting the relevant risk factors, rediscretization task in this phase is conducted and classified applying RAE with Bayes, based on accuracy measurement. Table 15 demonstrates the accuracy comparison of 4 different classifiers, which are Naïve Bayes, J48, MLP, and SVM, between without feature selection and without discretization, without discretization and feature selection by RAE, and with feature selection by RAE and with discretization for 4, 5, 6, and 7 risk factors respectively.

From the result shown in Table 15, the comparison of 3 experimental setting is shown. The predictive performance of CHD dataset for Thai people classified by 4 classifiers is presented without feature selection and without discretization in the first row. The second row presents critical risk factors associated with CHD are pioneered by feature selection but not fed into discretization method, which are classified by 4 classifiers. The last section demonstrates predictive accuracy of rediscretization method with RAE feature selection approach for

4, 5, 6, and 7 risk factors respectively. Rediscretization is set up on medical values, which is divided in 4 rounds. For the first round, we rediscretized on four major risk factors as age, Fasting Blood Sugar, Obesity and Triglyceride. In the second round, hypertension is added as the fifth major risk factors for rediscretization with the first four factors conducted in the first round. For the third round, LDL is the sixth factors included for rediscretization with the five factors performed in the second round. Finally, HDL is the last factors added on for rediscretization including the six factors performed earlier. As seen in all of the performance measurement, the results can be summarized that the proposed method explored and designed applying rediscretization produces the better predictive performance than classifying without rediscretization. Accordingly, the finding can be implied that all classifiers is achieved the improved accuracy when performing rediscretization. Additionally, rediscretization approach with RAE feature selection on 7 risk factors for Thai heart disease dataset classified by SVM produces the highest accuracy of 95.50%, when compared with predefined clinical value conducted in the experimental setup with no feature selection and with no rediscretization as 85.55%, and 90.92% as with the process of hybrid feature selection model but no rediscretization applied. Thus, the finding can infer that the more numbers of risk factors rediscretized, the more predictive accuracy are produced.

Finally, according to the result of rediscretization on clinical values shown above, we describe the characteristic of data of each rediscretized major risk factors in context. Thus, the example of data which are rediscretized from clinical values, categorized by men and women are demonstrated in Table 16.

Table 16: Comparison of Data Characteristics of Rediscretized values from major risk factors categorized by gender

	No CHD (n = 18,795)		With CHD (n = 1,205)	
	Male	Female	Male	Female
	10,436	8,359	804	401
HDL (mg/dl)				
>= 60	2,738	2,407	228	110
>=50 - 59	3,167	2,608	241	124
>=40 - 49	2,627	2,163	206	103
<40	1,724	1,361	129	64
LDL (mg/dl)				
<=100	1,932	1,536	146	73
>100 - 130	2,582	2,039	245	118
>130 - 160	2,987	2,515	230	115
>160	2,935	2,269	226	113
Obesity (BMI)				
19 - 22	2,288	1,848	176	88
23 - 25	3,744	3,024	288	144
26 - 30	2,704	2,184	208	104
>30	1,664	1,344	128	64
Triglyceride (mg/dl)				
0 - 130	3,644	2,293	263	119
>130 – 179	2,704	2,284	192	100
>179 – 259	2,536	2,315	185	93
>259	1,552	1,647	164	89

5. Conclusion and Discussion

The findings of this research can be implied that Education is the significant SES indicator that can incur CHD associated with the major risk factors. Support vector machine (SVM) is the best classifier for our dataset due to the best accuracy in every feature selection methods, and for the whole study. The proposed hybrid models of feature selection were explored to produce the better accuracy for CHD prediction on Thai people. Additionally, the objective of the research also concentrates on identifying SES factors and individual biological factors strongly associated with CHD by discovering the critical risk factors from both types which are significantly predictable for raising CHD. SES factors as education has been found as a significant indicator for raising CHD, after adjusting with major risk factors. Furthermore, SES factors as income is also revealed to be a significant predictor that have the great impact for causing CHD for Thai citizens, as well as the biological factors as gender, age, cholesterol, smoking, and diabetes.

Finally, this study proposed rediscretization approaches, which are confirmed to enhance the predictive accuracy of classifiers on CHD diagnosis. Equal Frequency Discretization with attribute selected by RAE and Bayes is proved to produce the accuracy improvements, as higher than the traditional classifiers conducted without feature selection and without rediscretization. SVM gives the highest predictive performance of 95.50% accuracy. After employing the rediscretiztion method in order to convert the predefined clinical values to the new boundaries of values with different number of intervals, we found that age, triglyceride, obesity, LDL, HDL, and hypertension are appeared to be significantly correlated with CHD. In addition, the finding can be implied that the proposed rediscretization method is proved to achieve the higher accuracy of predictive model, compared with the predefined values from medical field. Equal Frequency Discretization pioneered with attribute selection by RAE combined with Bayes generates the higher accuracy than the classification without rediscretization and with no feature selection, which indicates that the novelty of proposed rediscretization model is obviously superior to the predefined medical values. Nevertheless, in general, each individual country has its own individual characteristics, different physical conditions, lifestyles and environment. Thus, the similar parameter values are able to be measured and applied in alternative approaches for best suitable prediction incorporating with risk factors to derive the best performance measurement in predictive model.

References

[1] S. Dedkhar, “Risk factors of cardiovascular disease in rural Thai women,” The University of Arizona, https://repository.arizona.edu/handle/10150/195629, 2006.

[2] P. Vathesatogkit, P. Sritara, M. Kimman, B. Hengprasit, T. E-Shyong, HL. Wee, M. Woodward, "Associations of lifestyle factors, disease history and awareness with health-related quality of life in a Thai Population," pone, **7**(11), 2012, https:/doi.org/10.1371/0449921.

[3] G.M. Egeland, A. Tverdal, R.M. Selmer, H.E. Meyer, "Socioeconomic status and coronary heart disease risk factors and mortality: Married residents, three countries, Norway," The Norwegian Journal of Epidemiology, **13**(1), 155 – 162, 2003.

[4] R.V. Luepker, D. Rosamond, R. Murphy, J.M. Sprafka, A.R. Folsom, P.G. McGovern, H. Blackburn, "Socioeconomic Status and Coronary Heart Disease Risk Factor Trends : The Minnesota Heart Survey," 2172-2179, 2015, https:// doi:10.1161/01.CIR.88.5.2172.

[5] J.W. Lynch, G.A. Kaplan, R.D. Cohen, J. Tuomilehto, J.T. Salonen, "Do Cardiovascular Risk Factors Explain the Relation between Socioeconomic Status, Risk of All-Cause Mortality, Cardiovascular Mortality, and Acute Myocardial Infarction?," in 1996 CRPIT 9th proceeding of the Australian Data Mining Conference in Research and Practice in Information Technology, **144**(10), 934 – 942, 1996.

[6] S. Saravanakumar, S. Rinesh, "Effective Heart Disease Prediction using Frequent Feature Selection Method," International Journal of Innovative Research in Computer and Communication Engineering, **2**(1), 2767 – 2774, 2014.

[7] M. Shouman, T. Turner, R. Stocker, "Using Decision Tree for Diagnosing Heart Disease Patients," in 9th proceedings of Australian Data Mining Conference in Research and Practice in Information Technology (CRPIT), **121**, 23-29, 2011.

[8] M. Sultana, A. Haider, "Heart Disease Prediction using WEKA tool and 10-Fold cross-validation," The Institute of Electrical and Electronics Engineers, March 2017.

[9] R. Sharmila, S. Chellammal, "A conceptual method to enhance the prediction of heart diseases using the data techniques," International Journal of Computer Science and Engineering, **6**(4), 21-25, 2018.

[10] T.F. Mubaroq, E. Sugiharti, I. Akhlis, "Application of Discretization and Information Gain on Naïve Bayes to Diagnose Heart Disease," Journal of Advances in Information Systems and Technology, **1**(1), 75-82, 2019, https://doi: 10.5121/csit.2013.3305.

[11] M.M. Kirmani, S.I. Ansarullah, "Prediction of Heart Disease using Decision Tree a Data Mining Technique," International Journal of Computer Science and Network (IJCSN), **5**(6), 885-892, 2016.

[12] C. Partanapat, C. Jandaeng, C. Jaruskulchai, A Hybrid Model for Coronary Heart Disease Prediction in Thai Population, Ph.D. Thesis, Walailak University, 2019.

[13] A. Hall Mark, "Correlation-based feature selection for machine learning," The University of Waikato, 1999.

[14] K. Mani, P. Kalpana, "An Efficient Feature Selection based on Bayes Theorem, Self Information and Sequential Forward Selection," International Journal of Information Engineering and Electronic Business, **6**, 46-54, 2016, https://doi.org/10.5815/ijieeb.2016.06.06.

[15] S. Ravichandran, V.B. Srinivasan, C. Ramasamy, "Measuring Accuracy of Classification Algorithms for Chi-Square Attribute Evaluator in MCDR," in 28th Advances in Engineering and Technology Convergence, Bangkok, Thailand, 2019.

[16] S.L. Pundir, S. Amitra, "Feature Selection using Random Forest in intrusion detection system," International Journal of Advances in Engineering & Technology, **6**(3), 1319-1324, 2013.

[17] A. Hall Mark, A. Smith Lloyd, "Practical feature subset selection for machine learning," Springer, 1998.

[18] C. Arunkumar, M.P. Souraj, S. Ramakrishnan, "A Comparative Performance Evaluation of Supervised Feature Selection Algorithms on Microarray Datasets," in 7th International Conference on Advances in Computing & Communications (ICACC), 209-217, 2017, https:// doi.org/10.1016/j.procs.2017.09.127.

[19] R. Kohavi, G.H. John, "Wrapper Subset Evaluation," Artificial Intelligence, 273-324, 1997.

[20] B. K. Bhardwaj, S. Pal, "Data Mining: A prediction for performance improvement using classification," International Journal of Computer Science and Information Security (IJCSIS), **9**(4), 136-140, 2011.

[21] D. N. Bhargava, G. Sharma, D. R. Bhargava, M. Mathuria, "Decision Tree Analysis on J48 Algorithm for Data Mining," International Journal of Advanced Research in computer Science and Software Engineering, **3**(6), 1114-1119, 2013.

[22] S. Bhatia, P. Prakash, G.N. Pillai, "SVM based decision support system for heart disease classification with inter-coded genetic algorithm to select critical features," in 2008 Proceedings of the World Congress on Engineering and Computer Science (WCECS), San Francisco, USA, 2008. http://www.iaeng.org/publication/WCECS2008.

[23] E. Ferdousy, M. Islam, M. Matin, "Combination of Naïve Bayes Classifier and K-Nearest Neighbor in the Classification Based Predictive Models," Computer and Information Science, **6**(3), 48-56, 2013, https://doi:10.5539/cis.v6n3p48.2013.

[24] B. Abdullah, I. Abd-Alghafar, G. I. Salama, A. Abd-Alhafez, "Performance evaluation of a genetic algorithm based approach to network intrusion detection system," in 13th international conference on aerospace sciences and aviation technology, Military Technical College, Kobry Elkobbah, Cairo, Egypt, 1-17, 2009. https:// doi: 10.21608/asat.2009.23490.

[25] J. Anil, Z. Douglas, "Feature selection: Evaluation, application, and small sample performance," in 1997 IEEE transactions on pattern analysis and machine intelligence, **19** (2), 153-158, 1997.

[26] M.A. Jabbar, B.L. Deekshatulu, P. Chandra, "Heart disease prediction using lazy associative classification," in 2013 International Multi-Conference on Automation, Computing, Communication, Control and Compressed Sensing (iMac4s), 40-46, 2013.

[27] H. Liu, R. Setiono, "Feature selection via Discretization," in 1997 IEEE Transactions on Knowledge and Data Engineering, **9**(4), 642-645, 1997. https://doi.org/10.1109/69.617056.

[28] A. Rajalakshmi, R. Vinodhini, K. Fathima Bibi, "Data Discretization Technique Using WEKA Tool" International Journal of Computer Science & Engineering Technology (IJCSET), **6**(8), 293-298, 2016.

[29] P.W. Wilson, R.B. D'Agostino, D. Levy, A.M. Belanger, H. Silbershatz, W.B. Kannel, "Prediction of Coronary Heart Disease Using Risk Factor Categories," American Heart Association, **97**(18), 1837-1847, 1998, doi.org/10.1161/01.CIR.97.18.1837.

[30] R.S. Vasan, M.G. Larson, E.P. Leip, W.B. Kannel, D. Levy, "Assessment of frequency of progression to hypertension in non-hypertensive participants in the Framingham Heart Study: a cohort study," Lancet, **358**, 1682–1686, 2001, doi: 10.1016/S0140-6736(01)06710-1.

ASTES

Advances in Science, Technology and Engineering Systems Journal Vol. 5, No. 5, 426-433 (2020)

www.astesj.com

Special Issue on Innovative Research in Applied Science, Engineering and Technology

ASTESJ

ISSN: 2415-6698

Shape Optimization of Planar Inductors for RF Circuits using a Metaheuristic Technique based on Evolutionary Approach

Imad El Hajjami[*,1], Bachir Benhala[1], Hamid Bouyghf[2]

[1]*Faculty of Sciences, Moulay Ismail University, Meknes, 50050, Morocco*

[2]*FSTM Mohammedia, Hassan II University, Casablanca, 20000, Morocco*

ARTICLE INFO

Article history:
Received: 14 July, 2020
Accepted: 08 September, 2020
Online: 21 September, 2020

Keywords:
Optimization
Integrated Inductors
Evolutionary Algorithms
Quality Factor
RF Circuits

ABSTRACT

In this article, we concentrate on the use of a metaheuristic technique based on an Evolutionary Algorithm (EA) for determining the optimal geometrical parameters of spiral inductors for RF circuits. For this purpose, we have opted for an optimization procedure through an enhanced Differential Evolution (DE) algorithm. The proposed tool allows the design of optimized integrated inductors not only with a maximum quality factor(Q), but also with a maximum self-resonant frequency (SRF), and a minimum surface area, in addition to being adapted to any model of any technology. This paper presents also a comparison between performances of the optimized inductors (inductor square shape and inductor circular shape), in terms of the quality factor, SRF, and circuit size. For the purpose of mitigating the impact of parasitic effects, design basics have been taken into consideration. Then, in order to investigate the efficacy of evaluated results, an (EM) simulator has been employed.

1. Introduction

Integrated Inductors are of paramount importance elements, layout-optimization for spiral inductors has been the focus issue of several studies for the last few years, as for application, the four main characteristics that are required for the design of spiral inductors are: high inductance, high current capability, energy density, and low losses, with the inductors properties being identified by its geometrical and technological parameters [1].

For the sizing of spiral inductors, the designer should consider three main parameters [2], [3], the inductance value which is one of the most sensitive parameters, then, the quality factor (Q), and finally the self-resonant frequency (SRF).

Many works have been conducted for the sake of modeling and optimizing of spiral inductors. Formulation, modeling, and implementation remain the main steps for designing an integrated inductor [4], [5]. However, to ameliorate the optimization, the operation could be repeated many times till an acceptable solution is found.

Metaheuristic's techniques are especially applied to the optimal sizing of analog circuits [6], such techniques have proven to be efficient in solving difficult problems because they necessitate less time to converge and yield better solutions.

In this field, the methods mostly used are EA: 'Evolutionary Algorithms ' [7], such as the Differential Evolution (DE) Algorithm [8], and the Genetic Algorithm (GE) [9], [10], but in the last two decades, a new group of nature-inspired heuristic optimization algorithms have been introduced as SI: 'Swarm Intelligence Techniques', such as Ant Colony Optimization (ACO) [11], [12], Gravitational Search Algorithm (GSA) [13], Artificial Bee Colony (ABC) [14], Dragonfly Algorithm (DA) [15], Particle Swarm Optimization (PSO) [16], Grey Wolf Optimizer (GWO) [17], and Bacterial Foraging Optimization (BFO) [18].

Nevertheless, for the sake of achieving the optimal sizing of the (RF) spiral inductors, the Differential Evolution (DE) is to be the focus technique in this paper since it has been widely used in circuit design in the last decade.

In order to design circular and square spiral inductors for operating frequencies around 2.5 GHz, the inductor π-model has been embedded in the improvement device.

The next sections of the paper layout introduce as follows: Section 2 is devoted to the descriptions of the inductor π-model used, afterward, section 3 provides the synopsis of the DE

[*]Corresponding Author: Imad El hajjami, i.elhajjami@edu.umi.ac.ma

algorithm, while the optimal values of DE parameters have been determined by a proposed technique. Then, section 4 highlights the inductor sizing-optimization method, the technological parameters, and the design constraints as well, besides, the optimization results are presented, where analytical results obtained with DE are investigated by ADS momentum simulation software. Last and not least, the conclusion is offered in section 5.

2. Planar Spiral Inductors

All the shapes of spiral inductor known by four main geometrical parameters, the spacing between lines (s), the number of turns (n), the line width (w), and the outer length of a side (d_{out}), while the inner length of a side (d_{in}) defined by: $d_{in} = (d_{out} - 2.(n .(s + w) - s))$.

There are other important geometry parameters such the inductor length, while: $L = 4.n.d_{avg}$ for the square shape, and $L = 4.n.d_{avg}$ for the circular shape, then, the inductor area: $A=d_{out}^2$, and finally, the average diameter: $d_{avg} = 0.5.(d_{out} + d_{in})$.

Layouts of the circular and the square inductor have been showing respectively in Figure 1 and Figure 2 [19].

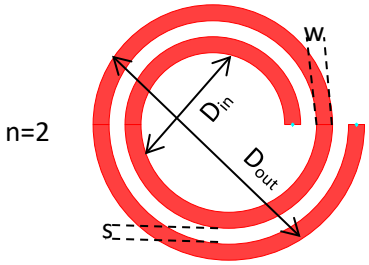


Figure 1: Layout of the Circular Integrated Inductor

2.1. The electrical Model of Integrated Inductors

It is important, thus, to present the expressions of the electrical model components for the inductor π-model, Figure 3 presented the electrical circuit for this type, while, C_s, C_{si}, C_{ox}, R_s, and R_{si} are respectively the substrate capacitance, the series capacitance between the spiral and the metal underpass, the substrate-oxide capacitance, the series resistance, and the substrate resistance, these parameters are determined by equations (1 2,3,4,5,6,7,8, 9):

$$C_{ox} = \frac{l.\omega.\varepsilon_{ox}}{2.t_{ox}} \quad (1)$$

$$C_s = \frac{(n.\varepsilon_{ox}).w^2}{t_{ox,m1-m2}} \quad (2)$$

$$C_{si} = \frac{C_{sub}.l.w}{2} \quad (3)$$

$$C_{sub} = \frac{\varepsilon_{sub}}{h_{sub}} \quad (4)$$

$$R_{si} = \frac{2}{(G_{sub}.l.w)} \quad (5)$$

$$G_{sub} = \frac{\sigma_{sub}}{h_{sub}} \quad (6)$$

$$R_s = \frac{l}{\sigma_m.\delta.\omega\left(1 - \exp\left(-\frac{t}{\delta}\right)\right)} \quad (7)$$

$$\delta = V\frac{2}{\omega.\mu.\sigma} \quad (8)$$

$$\sigma_m = \frac{1}{t.R_{sh}} \quad (9)$$

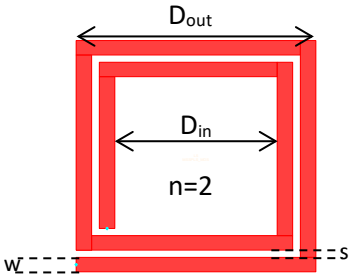


Figure 2: Layout of the Square Integrated Inductor

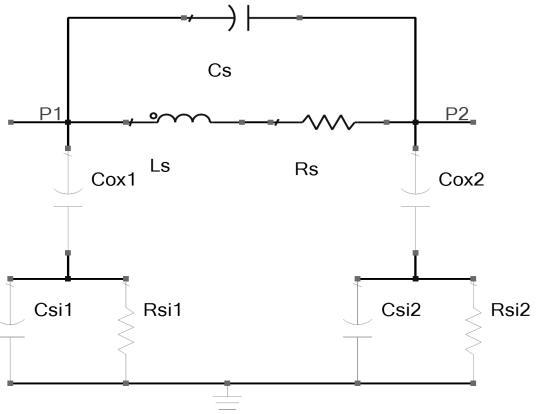


Figure 3: Integrated Inductor Electrical π -Model

where (t) is the turn thickness, (t_{ox}) is the oxide thickness between the spiral and the substrate, (σ_m) is the conductivity of the metal, (ω) is the frequency, ($t_{ox, M1-M2}$) is the oxide thickness between the spiral and the under-pass, (ε_{ox}) is the oxide permittivity, (G_{sub}) is the substrate conductance per unit area, (C_{sub}) is the substrate capacitance per unit area, (h_{sub}) is the substrate height, (σ_{sub}) is the substrate conductivity, (δ) is the skin depth, (μ) is the magnetic permeability of free space, and finally, (R_{sh}) is the sheet resistance.

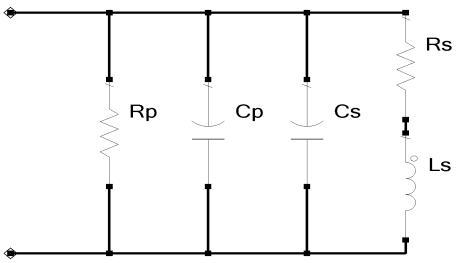


Figure 4: The Parallel π-Equivalent Circuit of Integrated Inductors

A similar inductor model has been shown in Figure 4, the quality factor (Q) was calculated by equations (10) and (11), where (C_p) is the shunt capacitance, and (R_p) is the shunt resistance.

$$Rp = \frac{1 + (\omega . Rsi(Csi + Cox))^2}{Rsi . \omega^2 . Cox^2} \quad (10)$$

$$Cp = \frac{(\mathrm{Cox} + Rsi^2 . \omega^2 (\mathrm{Csi} + \mathrm{Cox}) \mathrm{Csi} . \mathrm{Cox})}{1 + (Rsi . \omega (Csi + Cox))^2} \quad (11)$$

2.2. Inductance Ls

The model of the inductance L_s for the square inductor is expressed [19], [20] in equation (12):

$$Ls = \beta . dout^{\alpha 1} . w^{\alpha 2} . davg^{\alpha 3} . n^{\alpha 4} . s^{\alpha 5} \quad (12)$$

$\beta = 0.00166, \quad \alpha 2 = -0.125 \quad \alpha 4 = 1.83$
$\alpha 1 = -1.33, \quad \alpha 3 = 2.50, \quad \alpha 5 = -0.022$

The expression of the inductance L_s for the circular inductor is given in equation (13) [21]:

$$Ls = \frac{\mu_0 . n^2 . d_{avg} . c_1}{2} \left(\ln \left(\frac{c_2}{\rho} \right) + c_3 . \rho + c_4 . \rho^2 \right) \quad (13)$$

$c_1 = 1.00 \quad c_3 = 0.00$
$c_2 = 2.46 \quad c_4 = 0.20$

The coefficients c_i, β, and α_i are not depending on the technology but on the structure of the inductor. With ρ is the fill ratio, inductances in nH, and dimensions in µm.

The expression of the inductance for a given frequency (f) for two ports [20] defined as follow:

$$L = \left(\frac{1}{2\pi f} \right) . imag \left(\frac{1}{-Y(2,1)} \right) \quad (14)$$

2.3. The Quality factor (Q)

The quality factor is presented as follows:

$$Q = 2\pi * Energy\ stored / energy\ dissipated \quad (15)$$

The Q-Factor can be formed as:

$$Q = \left(\omega . \frac{Ls}{Rs} . \frac{2 . Rp}{2 . Rp + Rs . \left(\left(\omega . \frac{Ls}{Rs} \right)^2 + 1 \right)} \right) \times \left(1 - (Cs + 0{,}5 . Cp) . \left(\frac{Rs^2}{Ls} + \omega^2 . Ls \right) \right) \quad (16)$$

An ideal inductor has an infinite Quality factor [19].

When the peak magnetic energy is the same as the electric energy, the Q-Factor is equal to zero, this phenomenon is defined as the self-resonant frequency phenomena.

The energy stockpiled in the inductor is attached to the imaginary part of the input admittance (Y_{in}), whereas the real part of (Y_{in}) is proportional to the energy dissipated in resistances, with this approach is abridged to [20]:

$$Q = \frac{imag(-Y(1,1))}{Real(Y(1,1))} \quad (17)$$

3. The Differential Evolution Algorithm

It is possible to say that the DE algorithm, as is the genetic algorithm, is a population-based using identical operators' mutation, crossover, and selection. However; what makes the genetic algorithms yield a better solution is the fact that it builds on the crossover operation while the DE builds on the mutation one [8].

At the beginning of the DE process, the population of the n-pop solution vectors is randomly selected. This population is then ameliorated by stratifying mutation, crossover, and selection operators. First, the algorithm uses the mutation process as its search mechanism. Then, the DE uses crossover (recombination) operators, and the child vector that takes parameters from one parent more than the other. Afterward, a selection process is carried out in order to change the parent vectors if their fitness is less than of the newly generated child vectors. This three-stage process is repeated until a better solution is found [22].

The principal steps of the DE algorithm are defined mathematically as follows:

3.1. Mutation

For each objective vector $x_{j,k}$,a mutant vector is generated by (18):

$$v_{j,k+1} = x_{r1,k} - \beta \times (x_{r2,k} - x_{r3,k}) \quad (18)$$

where $j, r_1, r_2, r_3 \in \{1, 2, \ldots, NP\}$ are arbitrary chosen and must be different from each other. In equation (18), *(β)* is the scaling factor which affects the difference vector $(x_{r2,k} - x_{r3,k})$.

3.2. Crossover

The trial vector is produced by the mixture of the parent vector with the mutated vector:

$$u^i_{j,k+1} = v^i_{j,k+1} \quad if \quad (rand \leq Pc) \quad (19)$$
$$u^i_{j,k+1} = x^i_{j,k} \quad if \quad (rand > Pc)$$

where (P_c) is the crossover probability parameter.

3.3. Selection

The comparison between a parent and its identical offspring called the selection and can be expressed as:

$$x_{j,k+1} = u_{j,k+1} \quad if\ g(u_{j,k+1}) \leq g(x_{j,k}) \quad (20)$$
$$x_{j,k+1} = x_{j,k} \quad for\ Otherwise$$

where $g_{(x)}$ is the objective function value of the trial vector. The DE algorithm can be declared in 1:

3.4. The DE Algorithm Parametrization

To determine the optimal values of DE parameters, the Ackley function presented in equation (21) was investigated for 100 population and 1000 number of iterations.

Algorithm 1: Differential Evolution Algorithm

Begin
T=0;
Generate the initial population of individuals N;
Evaluate $g\ (x_{j,\ k})$
For *each individual i in the population* **do**
Choose r_1, r_2, r_3 within the range [1, N] randomly;
For *each parameter j* **do**
Generate the mutant vector with equation (18) ;
Generate a new vector with equation (19);
end for
if $g\ (u_{j,\ k+1}) \leqslant g\ (x_{j,\ k})$ **then**
$x_{j,k+1} = u_{j,k+1}$
else
$x_{j,k+1} = x_{j,k}$
end if
end for
T=T+1;
end

$$f(x) = -20.e^{-0.2\sqrt{\frac{\sum_{i=1}^{n} x_i^2}{n}}} + e^{\frac{\sum_{i=1}^{n}(\cos(2\pi x_i))}{n}} + 20 + e^1 \quad (21)$$

The Ackley function has one global minimum at: f (x_j) = 0; for x_j = (0 , … , 0).

The function evaluated on $x_j \in [-32, 32]$ for all (j = 1 , … , 32) .

Figure 5 displays the variation of fitness convergence according to the crossover probability P_c and the upper bound of the scaling factor $beta_{max}$ (with the lower bound of the scaling factor-beta $_{min}$ equal to 0,1). The cost function versus the number of iterations presented in Figure 6.

From Figure 5, the values of DE parameters that gave the best convergence are presented in Table 1.

4. Inductors Sizing

In the following section, we aim to maximize the Q-Factor for a specific value of the inductance for two structures, square and circular, by combining the inductor π-model and the DE optimization procedure. Afterward, simulations with ADSEM are adopted.

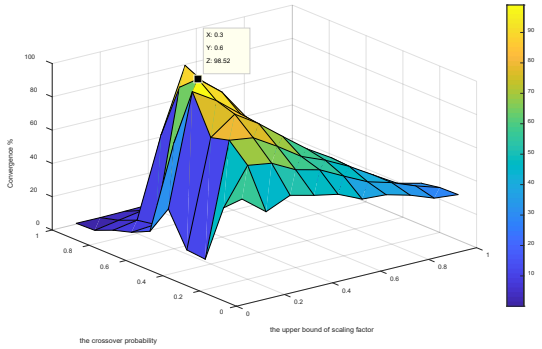


Figure 5: Convergence Rate versus the Crossover Probability and the Upper Bound of the Scaling Factor, with $beta_{min}$=0.1.

4.1. Constraints of the study

To minify the parasitic phenomena [20], [23], the liaison between geometry parameters in (22) is well respected as a sort of included design-rules [20], [23].

$$0.2 \leq \frac{din}{dout} \leq 0.8, \qquad 5w \leq din \quad (22)$$

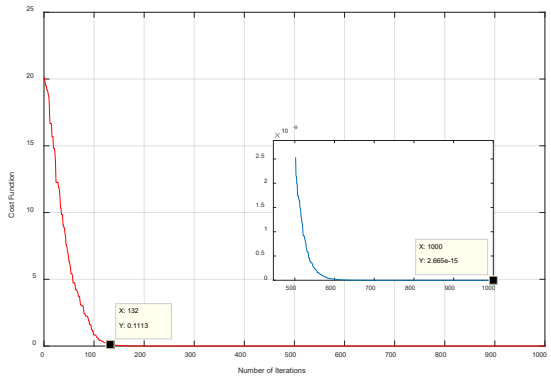


Figure 6: The Cost Function versus the Number of Iterations for the Ackley Function.

Table 1: Parameters Values of the Differential Evolution Algorithm.

Parameter	Value
The crossover probability	0.6
The lower bound of the scaling factor	0.1
The upper bound of the scaling factor	0.3
Population size	100
The number of iterations	500

• *The SRF Constraint*

The condition for a minimum self-resonant frequency which SRF ≥ SRF_{min} can be formed as [20]:

$$\left((2\pi SRF_{Min})^2.Ls.(Cp+Cs) + \frac{(Rs^2.(Cs+Cp))}{Ls}\right) \leq 1 \quad (23)$$

4.2. Optimization Procedure

The goal of this optimization is to find the optimum geometrical parameters of the spiral inductor to get a higher value of Q-Factor, the problem can be formulated as follows:

Find: $D = (Dout, w, s, n)$ (24)
To maximize: Q
Subject to:

$$g_1(x) = Ls = Ls_{req}$$
$$g_2(x) = Q \geq Q_{Min}$$
$$g_3(x) = SRF_{Min} \leq SRF$$
$$g_4(x) \leq 0, g_5(x) \leq 0, g_6(x) \leq 0, g_7(x) \leq 0$$
$$g_8(x) = n_{Min} \leq n \leq n_{Max}$$
$$g_9(x) = s_{Min} \leq s \leq s_{Max}$$
$$g_{10}(x) = w_{Min} \leq w \leq w_{Max}$$
$$g_{11}(x) = Dout_{Min} \leq Dout \leq Dout_{Max}$$

The objective function for the DE was defined as the following:

$$Fcost(x) = \left(\frac{1}{Q} + 10^9(L - Lsreq)\right).P(x) \quad (25)$$

Where :

$$P(x) = \prod_{i=3}^{i=7} Pi(x) \quad (26)$$

Or

$$Pi(x) = 1 + s_i \quad if\ g_i(x) > 0 \quad (27)$$
$$Pi(x) = 1 \quad for\ otherwise$$
$$s_3 = s_4 = s_5 = s_6 = s_7$$

where (s_i) is the penalty coefficient, and P(x) is the sum of constraints.

Constraints $g_8(x)$, $g_9(x)$, $g_{10}(x)$, and $g_{11}(x)$ are boundary constraints, as result, they can be examined, while the DE was not allowed to generate a candidate vector farther these limitations.

Equations of constraints $g_4(x)$, $g_5(x)$, $g_6(x)$, and $g_7(x)$ have been shown in Table 2.

4.3. Results and Discussions

In the following, we will be adopting a sizing of square and circular inductors, with distinct values of the inductance Ls_{req} in the field beyond 2.5 GHz, as shown in Table 3 the technological and physical parameters have been well presented, while Table 4 represents the geometry parameter boundaries.

The details of the optimization have been presented in Table 5 and Table 6. On aim to verify our procedure, Figure 7 gives the cost function versus the number of iterations for square inductors, in this case, the constraint for minimum self– resonant frequency is added as SRF_{min}=22 GHz. The optimization results of the maximum Q-Factor and area (A) for both circular and square inductors versus the inductance obtained using the DE algorithm are presented in Figure 8.

The Q-Factor versus frequency for each value of the inductance has been shown in Figure 9 and Figure 10. The simulation using momentum software has also been shown in Figure 11, Figure 12, Figure 13, and Figure 14.

The comparison between optimization results and simulations is presented in Table 7 and Table 8.

Table 2: Equations of Constraints.

Constraint	Equation
$g_4(x)$	(D_{in}/D_{out})-0.8
$g_5(x)$	0.2-(D_{in}/D_{out})
$g_6(x)$	(2.n+1).(s+w)-D_{out}
$g_7(x)$	(5.w-D_{in})

Table 3: The values of technological parameters.

Symbol	Parameter	Value
t	Metal thickness	2.8 µm
σ	Metal conductivity	4×10^7 Ω/m
ρ	Substrate resistivity	0.2 Ω.m
t_{sub}	Substrate thickness	600 µm
t_{ox}	The thickness of the oxide	6.42 µm
ε_r	The relative permittivity of the silicon	11,9
µ	The magnetic permeability of free space	$4\pi \times 10^{-7}$ H/m
$t_{ox_m1\text{-}m2}$	Oxide thickness between spiral and underpass	0.66 µm
ε_r	The relative permittivity of the Oxide	4
ε_0	Permittivity of vacuum	8.85×10^{-12} F/m

Table 4: Sizing Variables and their Allowable Ranges.

Sizing variable	Lower bound	Upper bound
w	1 µm	12 µm
d_{out}	140 µm	280 µm
s	2 µm	2.5 µm
n	1.50	12.00

Table 5: Optimization Results of Circular Inductors using the DE Algorithm.

Ls_{req}	Ls_{An}	D_{out}	w	s	n	Q
1.00	1.00	166.12	12.00	2.38	3.50	8.26
3.00	3.00	220.00	12.00	2.32	5.50	11.44
5.00	5.00	238.85	11.30	2.03	7.00	12.91
7.00	7.00	261.11	11.10	2.00	8.00	13.34
9.00	9.00	268.03	10.13	2.00	9.00	12.90
11.00	11.00	265.34	8.81	2.00	10.00	12.16
13.00	13.00	280.00	8.60	2.00	10.50	11.57
15.00	15.00	273.35	7.66	2.00	11.50	11.13

Table 6: Optimization Results of Square Inductors using the DE Algorithm.

Ls_{req}	Ls_{An}	D_{out}	w	s	n	Q
1.00	1.05	140.00	12.00	2.00	2.50	9.74
3.00	2.97	201.00	11.99	2.00	3.50	13.13
5.00	4.99	230.00	10.14	2.00	4.00	13.22
7.00	7.00	240.00	8.37	2.00	4.50	12.48
9.00	9.00	250.20	7.69	2.00	5.00	12.28
11.00	11.00	260.00	7.45	2.00	5.50	12.21
13.00	13.00	267.00	7.24	2.00	6.00	12.01
15.00	15.00	272.00	7.01	2.00	6.50	11.69

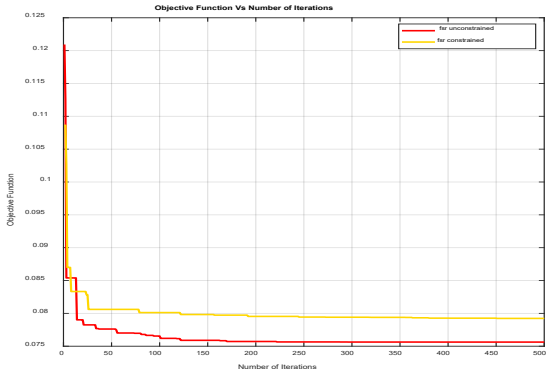


Figure 7: The Objective Function versus Iterations Number for a Square Inductor.

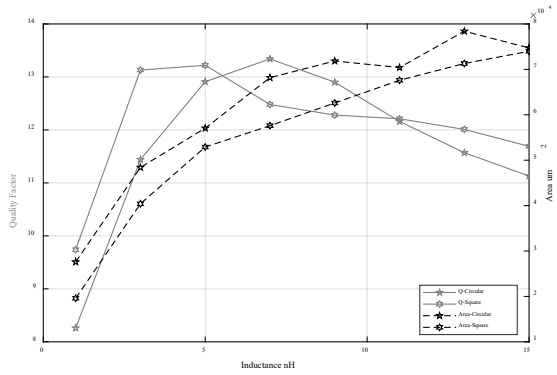


Figure 8: The Quality Factor and Inductors Area versus Inductance.

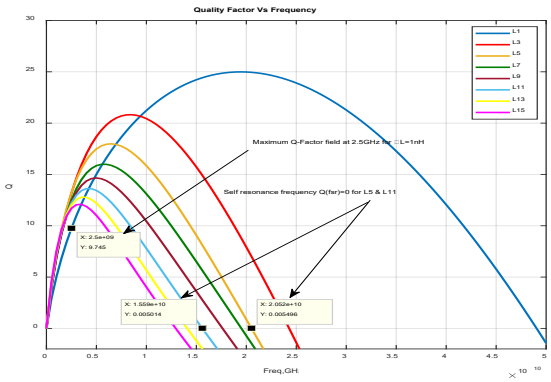


Figure 9: The Quality Factor of Square Inductors versus Frequency.

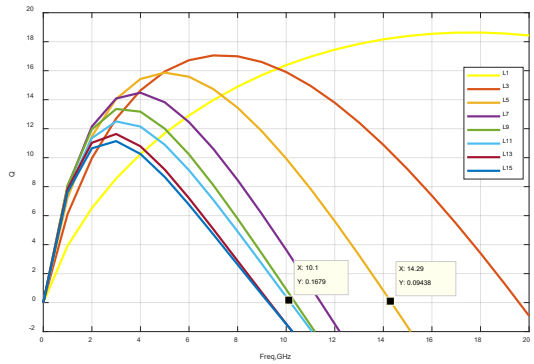


Figure 10: The Quality Factor of Circular Inductors versus Frequency.

What the results show is that when the inductance value increases, the quality factor decreases, and the self-resonant frequency decreases as well.

However, the results are very good in terms of the circuit's size, and the constraints are very robust.

The DE algorithm provides better results concerning the circuit's size and has a faster convergence as shown in the results.

We can notice that the simulation of square inductors is very accurate, with an error below 8.50% for the inductance value, and 5.21% for the quality factor for L_s less than 11 nH. It is possible to explain the increase of the error when the value of inductance is greater than 11 nH, in that we have taken similar limits of geometrical parameters for all values of the inductance, when the value of L_s has augmented, the number of turns became higher and D_{out} increased with a small percentage, in such circumstances, the quality factor decreases owing to the parasitic phenomena effects, this problem can be solved by increasing the parameters of the allowable range in the proportion of the outer diameter.

As for the circular inductor, generally, the error is below than 5.66% for inductance value, and 21.56% for the quality factor, Although, this type has the shortest perimeter, and with a circular configuration, a higher quality factor (Q) is obtained. Yet, this type shows a response to the parasitic phenomena effects.

We notice through the simulation that the circular inductor is not significantly affected by parasitic phenomena in terms of the self-resonant frequency. From Figures 10 and 13, we observe that the inductor of L_s equal to 11 nH reaches its maximum of Q-Factor when $f_{max} \sim 2$ GHz, the area on the left of f_{max}, is an area where the Q-Factor is fundamentally affected by the magnetic induced losses, skin and proximity effects, and the DC resistance [24],[25]. On the opposite side of f_{max}, in addition to the preceding effects, the Q-Factor is also affected by the substrate noise coupling [23]. The evaluated SRF equal to 10.1 GHz, and the SRF obtained via simulation equal to 8.5 GHz, at this time, the Q-Factor is equal to 0, starting from this point, the peak magnetic energy is less than the electric energy, due to the perturbation of this last because of the parasitic phenomena.

The layout constraints for circular inductors required extensive research, in order to mitigate the parasitic phenomena effects.

Moreover, the degradation of the Q-Factor can be seen more clearly for square inductors, from Figures 9 and 11, for L_s equal to 11 nH, the Q-Factor equal to 0 when the evaluated SRF equal to 15.59 GHz and the SRF obtained via simulation equal to 7 GHz, we conclude that this type is extremely influenced by the parasitic phenomena.

Table 7: Comparison between Optimization Results and Momentum Simulations for Circular Inductors.

Ls_{An}	Ls_{EM}	ϵ%	Q_{AN}	Q_{EM}	ϵ%
1.00	1.25	25.00	8.26	9.20	11.80
3.00	2.96	1.33	11.44	10.82	5.41
5.00	4.81	3.80	12.91	11.34	12.16
7.00	6.72	4.00	13.34	10.94	16.50
9.00	8.49	5.66	12.90	11.29	12.48
11.00	11.32	2.90	12.16	9.86	18.91
13.00	13.28	2.15	11.57	9.40	18.75
15.00	15.35	2.33	11.13	8.73	21.56

Table 8: Comparison between Optimization Results and Momentum Simulations for Square Inductors.

Ls_{An}	Ls_{EM}	ϵ%	Q_{AN}	Q_{EM}	ϵ%
1.05	0.96	8.50	9.74	10.09	3.59
2.97	2.78	6.39	13.13	13.65	3.96
4.99	4.74	5.01	13.22	13.66	3.32
7.00	6.78	0.80	12.48	13.97	4.25
9.00	8.72	3.14	12.28	13.12	5.21
11.00	10.79	1.90	12.21	12.15	0.49
13.00	12.74	2.00	12.01	10.81	10.00
15.00	14.85	1.00	11.69	9.67	17.27

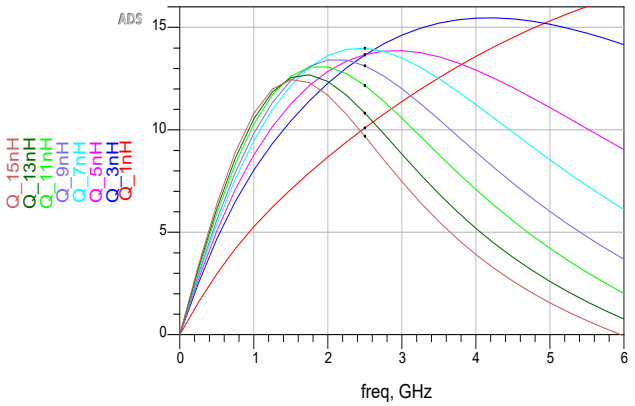


Figure 11: Simulation of the Quality Factor versus Frequency in Momentum for Square Inductors.

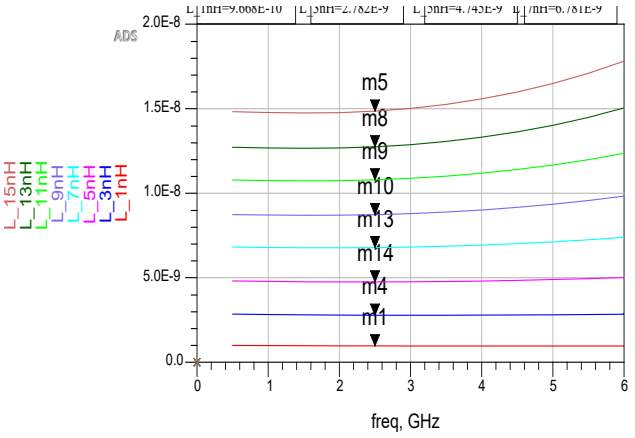


Figure 12: Simulation of the Inductance versus Frequency in Momentum for Square Inductors.

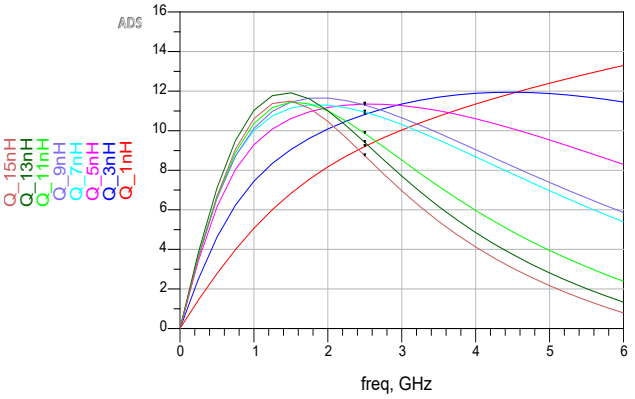


Figure 13: Simulation of the Quality Factor versus Frequency in Momentum for Circular Inductors.

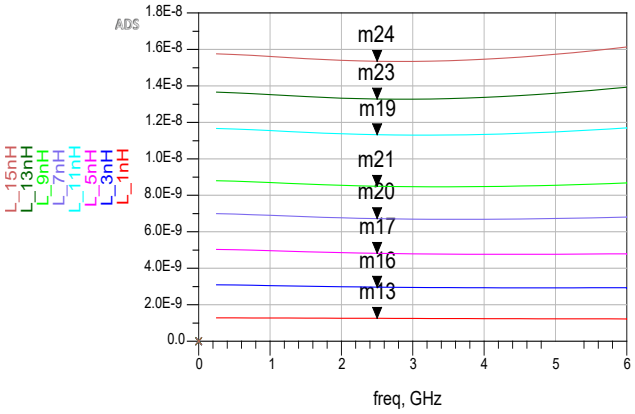


Figure 14: Simulation of the Inductance versus Frequency in Momentum for Circular Inductors.

5. Conclusion

For dealing with the optimal sizing of spiral inductors for (RF) circuits, we proposed on this paper an application of the Differential Evolution (DE) algorithm. Two inductor structures have been optimized i.e. shape square and shape circular, with a maximum Q-Factor, a maximum self-resonant frequency (SRF), and a minimum surface area. The performances of optimized inductors showed good results in terms of the Q-Factor, with the square inductor presenting a higher SRF and a smaller area (A) than the circular one.

The π-model does not allow for the assimilation of noises parasitic effects in a good way, leading to a lower SRF value, that is why we are focusing on using the double π-model, instead, for the integrated inductors optimal sizing.

References

[1] J. M. Lopez-Villegas, J. Samitier, C. Cane, P. Losantos, J. Bausells, "Improvement of the quality factor of RF integrated inductors by layout optimization," IEEE Transactions on Microwave Theory and Techniques, **48**(1), 76–83, 2000, https://doi.org/10.1109/22.817474

[2] H. M. Hsu, K. Y. Chan, H. C. Chien, H. C. Kuan, "Analytical design algorithm of planar inductor layout in CMOS technology," IEEE Transactions on Electron Devices, **55**(11), 3208–3213, 2008, https://doi.org/10.1109/TED.2008.2004248

[3] J. N. Burghartz, B. Rejaei, "On the design of RF spiral inductors on silicon," IEEE Transactions on Electron Devices, **50**(3), 718–729, 2003, https://doi.org/10.1109/TED.2003.810474

[4] Y. Yorozu, M. Hirano, K. Oka, Y. Tagawa, "Improvement of the quality factor of RF integrated inductors by layout optimization," IEEE Transactions on Microwave Theory and Techniques, **48**(1), 76–83, 2000, https://doi.org/10.1109/22.817474

[5] S. Abi, H. Bouyghf, A. Raihani, B. Benhala, "Swarm intelligence optimization techniques for an optimal RF integrated spiral inductor design," in 2018 International Conference on Electronics, Control, Optimization and Computer Science (ICECOCS), Kenitra, Morocco, 1–7, 2018, https://doi.org/10.1109/ICECOCS.2018.8610524

[6] P. Siarry, Z. Michalewicz, Advances in metaheuristics for hard optimization, Natural Computing Series, Springer, 2008.

[7] M. Crepinsek, S. H. Liu, M. Mernik, "Exploration and exploitation in evolutionary algorithms: A survey," ACM Computing Surveys, **45**(3), Article 35, 2013, https://doi.org/10.1145/2480741.2480752

[8] R. Storn, K. Price, "Differential evolution: A simple and efficient heuristic for global optimization over continuous spaces," J. Global Optimization, **11**(4), 341–359, 1997, https://doi.org/10.1023/A:1008202821328

[9] A. El Beqal, B. Benhala, I. Zorkani, "A Genetic algorithm for the optimal design of a multistage amplifier," International Journal of Electrical and Computer Engineering, **10**(1), 129–138, 2020, http://doi.org/10.11591/ijece.v10i1.pp129-138

[10] M. Mitchell, An introduction to genetic algorithms, The MIT Press, 1998.

[11] B. Benhala, "Sizing of an inverted current conveyors by an enhanced ant colony optimization technique," in 2016 Conference on Design of Circuits and Integrated Systems (DCIS), Granada, Spain, 1–5, 2016, https://doi.org/10.1109/DCIS.2016.7845271

[12] L. Kritele, B. Benhala, I. Zorkani, "Ant Colony Optimization for Optimal Low-Pass Filter Sizing," in: E. G. Talbi, A. Nakib. (Eds.), Bioinspired Heuristics for Optimization, Studies in Computational Intelligence, Springer, Cham, 283–299, 2019, https://doi.org/10.1007/978-3-319-95104-1_18

[13] E. Rashedi, H. Nezamabadi, S. Saryazdi, "GSA: A gravitational search algorithm," Information Sciences, **179**(13), 2232–2248, 2009, https://doi.org/10.1016/j.ins.2009.03.004

[14] C. J. Lin, M. L. Huang, "Modified artificial bee colony algorithm for scheduling optimization for printed circuit board production," Journal of Manufacturing Systems, **44**(1), 1–11, 2017, https://doi.org/10.1016/j.jmsy.2017.04.006

[15] S. Mirjalili, "Dragonfly algorithm: A new meta-heuristic optimization technique for solving single-objective, discrete, and multi-objective problems," Neural Computing and Applications, **27**(4), 1053–1073, 2016, https://doi.org/10.1007/s00521-015-1920-1

[16] B. Benhala, P. Pereira, A. Sallem, Focus on swarm intelligence research and applications, Nova Science Publishers, 2017.

[17] S. Mirjalili, S. M. Mirjalili, A. Lewis, "Grey wolf optimizer," Advances in Engineering Software, **69**, 46–61, 2014, https://doi.org/10.1016/j.advengsoft.2013.12.007

[18] K. M. Passino, "Biomimicry of bacterial foraging for distributed optimization and control," IEEE control systems Magazine, **22**(3), 52–67, 2002, https://doi.org/10.1109/MCS.2002.1004010

[19] C. P. Yue, C. Ryu, J. Lau, T. H. Lee, S. S. Wong, "A physical model for planar spiral inductors on silicon," in International Electron Devices Meeting, Technical Digest, San Francisco, USA, 155–158, 1996, https://doi.org/10.1109/IEDM.1996.553144

[20] S. S. Mohan, M. del Mar Hershenson, S. P. Boyd, T. H. Lee, "Simple accurate expressions for planar spiral inductances," IEEE Journal of Solid-State Circuits, **34**(10), 1419–1424, 1999, https://doi.org/10.1109/4.792620

[21] B. Rejaei, J. L. Tauritz, P. Snoeij, "A predictive model for si-based circular spiral inductors," in Topical Meeting on Silicon monolithic integrated circuits in RF systems, Ann Arbor, 148–154, 1998, https://doi.org/10.1109/SMIC.1998.750210

[22] D. Karaboga, B. Akay, "A comparative study of Artificial Bee Colony algorithm," Applied Mathematics and Computation, **214**(1), 108–132, 2009, https://doi.org/10.1016/j.amc.2009.03.090

[23] P. Pereira, M. H. S. Fino, F. V. Coito, M. V. Neves, "RF integrated inductor modeling and its application to optimization-based design," Analog Integrated Circuits and Signal Processing, **73**, 47–55, 2011, https://doi.org/10.1007/s10470-011-9682-x

[24] J. Aguilera, R.Berengue, Design and test of integrated inductors for RF applications, Dordrecht: Kluwer Academic Publishers, 2004.

[25] Y. Cao , R. A. Groves, X. Huang, N. D. Zamdmer, and al, "Frequency-independent equivalent-circuit model for on-chip spiral inductors," IEEE Journal of Solid-State Circuits, **38**(3), 419–426. 2003, https://doi.org/10.1109/JSSC.2002.808285

ASTES

Advances in Science, Technology and Engineering Systems Journal Vol. 5, No. 5, 434-443 (2020)

www.astesj.com

Special Issue on Innovative Research in Applied Science, Engineering and Technology

ASTESJ

ISSN: 2415-6698

New Algorithm for the Development of a Musical Words Descriptor for the Artificial Composition of Oriental Music

Mehdi Zhar*, Omar Bouattane, Lhoussain Bahatti

SSDIA Laboratory, Ecole Normale Supérieur de l'Enseignement Technique (ENSET), Mohammedia, 28810, Morocco

ARTICLE INFO

Article history:
Received: 14 July, 2020
Accepted: 08 September, 2020
Online: 21 September, 2020

Keywords:
Artificial Intelligence
Music
Musical Grammar
Alphabets
¼ de ton
Filtering

ABSTRACT

The Music Composition Library of the great composers constitutes an intellectual heritage. This article introduces an algorithm of artificial Oriental composing music based on the descriptors determined on a large learning base to automatically write Oriental music as the logic identical to any composer. Musical words are called a grammatical alphabet. Each word derived is created with the descriptors through its very own alphabet by crossing a number of filters removing all improper combinations and maintaining the features correctly responding with each filtering process while honoring the grammar of oriental music. A musical word is a combination of a rhythmic word and a symbolic word.

1. Introduction

Over the last years, Methods of experimental studies applied to the musical field have improved considerably. Only think of an ever-increasing amount of music sites that stream. There are nearly as many options to catalog and label music recordings as there are websites today. What features may be used to execute these processes though? What elements of the song will be taken into consideration when deciding descriptors used and What is the essence of music composing?

There is currently no method or rationale for an artificial arrangement for oriental music in a composer's style and manner. In comparison, numerous analyses have been established in the sense of occidental music.

Musical composition is an art based on the learning baggage that the composer learns implicitly by listening to a varied set of musical styles, we suppose that in the human being there are natural algorithms that allow in a very intelligent way to analyze, calculate and measure the stored data on a natural learning basis in effort to allow new creations and innovations, and we suppose that is the case of composer who produces new musical phrases.

Based on this idea that our work will reposition itself. The oriental music artificial by appealing to the ideas and thoughts of the great composers of history such as Mohammed ABDELWAHAB, Farid el ATTRACHE and others.

We present here a profound model of the algorithmic composition of the monophonic oriental melodies centered on a description from musical scores in alphabet form controlled by a number of compositional rules allowing for the production of words to constitute musical pieces. We extend the previous model to two distinct tasks: quantifying attributes and writing derivative words, which constitutes a song. The remainder of the paper is structured as follows: In section 2, we discuss the prior works as state-of-the-art on the collection of artificial music composition. Section 3 is devoted to our method modeling. The algorithm in question is developed in section 4. Section 5 is dedicated to Test and validate results. Finally, in section 6, we conclude this article and propose future work related to it.

2. State of the Art

The first studies of mathematical description for compositional music are related according to the literature to (Pierre Barbaud) [1]. From 1957 on, this style of music often referred to like electronic music or automated composition, brought the technical fascination that the Illiac String Quartet Suite created by both the author Lejaren Hiller and also the theorist Leonard M Isaacson, a work produced at the University of Illinois using the Illiac IV (Illinois Accumulator) computer [2]. Many plays consequently in display throughout the day. Use of Markov chains and stochastic processes by combining different theoretical properties that lead to composition [3]-[5]. According to [6], Single process systems will not appear to be successful, a network which is writing songs with harmonic attachment and other models of music composition has

*Corresponding Author Mehdi ZHAR, Email: mehdi.zhar@gmail.com

been presented in [7]-[11]. In the Blues style [12] we find an approach that helps producing monophonic songs of chord progression. Another idea is outlined in a device that produces F0 contour dynamically whenever a partition is provided out of an automated learning frame. This is expressed as a mathematical black box forming a contour of F0 with required characteristics like naturalness & expressiveness [13]. Using the well-established uniform distance from compression as a reference feature, which genetic algorithms can use to produce music automatically in a known style [14]. Neural networks in the thinking process might be helpful [15]-[20]. Neural networks in the thought process could help with more specifics [21]-[25]. A model considers melody and rhythm in tandem when modeling the relation among these two features, this method allows for the creation of fascinating full melodies or suggests alternative a series have broken harmony in accordance with the features of the splitting itself [26]. The classification of the oriental notes was suggested in [27] for identification by a system for modeling a musical sound by collecting a set of harmonic features representing the greatest knowledge found in this sound. Another method of audio classification was described in [28] enhancing the extraction of features using of constant transformation model, including initial musical context-related to audio features where notes occur. The simulation of a lute's sounds is discussed in [29]. Another model that considers notes as abstract functions, we find in [30], an eastern note and a quarter-tone scale pattern. In [31], an automated composition process of eastern music, which allows the generation of derived terms, based on the original features of a selected composer. In [32], the studies highlighted functionalities of SVM on a common songs database of 409 sounds of 16 groups, a comparison of SVM-based distinction Guo was established with other traditional methods, while proposing a new audio recovery criterion, called Boundary Deviation (DFB). [33] work on automated singer identification by distinguishing instrumental and singing sounds using audio information such as timbre parameters, pitch level, mel frequency cepstral coefficients (MFCC), linear predictive coefficients (LPC) and Indian video songs (IVS) audio signal loudness. In [34], an examination of the influence of texture choice on the identification of automated music genres and a novel K-Means-based texture filter aimed at distinguishing different sound textures in each album. The results indicate that the capture of texture heterogeneity within songs is necessary in order to improve the classifier accuracy and also reveal that the K-Means texture selection is capable of achieving substantial improvements over all the baseline using fewer textures per track than that of the other texture selectors examined and that the use of multiple texture representation makes for more possibilities. In [35] authors suggest a new paradigm for the classification of songs, integrating a Bidirectional Recurrent Neural Network dependent attention system. It also incorporates two focus-based models (serial focus and parallel attention). Compared to sequential attention, the parallel focus becomes more robust and the studies yield better results. In [36] an algorithm that illustrates a hierarchical structure from a series of discrete signs by replacing the repeated sentences with a grammatical method generating the sentence. In [37] a study of language identification in the field of artificial intelligence. In [38] a vertical partitioning model based on the Decision Tree mechanism for rhythmic music.

3. Modeling

To grasp the composer's logic composition of opera, symphony or something similar of Arabic musical art, it seems impossible to research a musical score as a whole, although our concept is to research the form and logic of which each word of the partition was composed, recognizing that there are N bars in the piece (play). measures are taken as words and word series forms a musical phrase. Original terms contain some amount of specific information that could be used in artificial compositions as input features. with more precision, our concept is based on the study of the word belonging to a musical piece, the word can contain relevant information forming a thought of the composer that we can decipher using the descriptors, this will allow us to reuse these parameters in order to artificially compose music while respecting the laws applied to the original word

3.1. Originality of Arabic Music

Students learn repertoire and technical methods through oral practice conveyed by a teacher. He evolves after some mastery of those components and places himself in the improvisation game and in the art of making music. He builds on the background of the components conveyed to him as well combine them so according to his desires, or even from that he creates variations that enrich a common repertoire. That oral tradition stays one of the most important elements of the understanding and pedagogy of Eastern music. Hence it is essential to have clear control of rhythmic and melodic structures to compose and analyze Eastern music. Students study melodic parts and never present them precisely as originally recorded. Professional Arabic musicians, like Indian professional musicians and American Jazz musicians, add musical innovations or improvisations to established pieces. Improvisations may be pretty long, converting 10-minute song into one-hour presentations, and often have nothing in common with the initial model. Carries different understanding of what constitutes a specific artist (in the last century, the older aesthetic frame lived side by side with a new aesthetic of modernization and creativity, leading to new combinations and fusions). One could sum up the traditional aesthetics as follows: A professional musician is required to memorize a vast repertoire of tunes, musical words, ornamental techniques, etc., while rarely playing the same song the same manner. Individuality and originality are important-but it can only be appreciated to the degree that it generates and expands hereditary awareness.

3.2. The Alphabet

We consider in our method two alphabets, one rhythmic alphabet, and one symbolic alphabet.

3.2.1 The Symbolic Alphabets

There are seven basic notes (C, D, E, F, G, A, B, S) in both Western and Arabic music plus (S) silence, which is known as a tone. But the peculiarity of the Oriental world comes from the fact that a quarter-tone is present, a note can be assigned to one of five states instead of one of three as in occidental music.
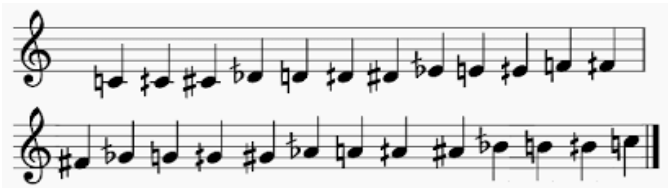


Figure 1: Notes states

Name of notes in traditional Arab vocabulary:

Table 1: Arabic Note Name

Name of Common Arabic Notes	Name of Occidental Notes
ELYAKAH	G (low)
ELTIK YAKAH	G+
ELQARAR ELHISAR	G#/ Ab
ELQARAR ELTIK HISAR	G#+/ Ab-
ELOUCHAÏRAN	A
ELQARAR ELNIM ADJAM	A+
ELQARAR ELADJAM	Bb
ELIRAQ	Bb+
ELQAOUACHT	B
ELTIK ELQAOUACHT	B+
ELRAST	C
ELNIM ELZIRKOULAH	C+
ELZIRKOULAH	C#/Db
ELTIK ELZIRKOULAH	C#+/Db-
ELDOUKAH	D
ELNIM ELKOURDI	Eb-/D+
ELKOURDI	Eb
ELSIKAH	Eb+
ELBOUZALIK	E
ELTIK ELBOUZALIK	E+/F-
ELDJAHARKAH	F
ELNIM ELHEDJAZ	F+/Gb-
ELHEDJAZ	F#/Gb
ELTIK ELHEDJAZ	G-/F#+
ELNAOUA	G (medium)

Bearing in mind the infinity of tones, we inferred infinity of musical notes. Human ear hears frequencies varying between 20 Hz (weakest frequency) to 20,000 Hz (maximum frequency), music culture artists defined this principle in a representation of musical keys.

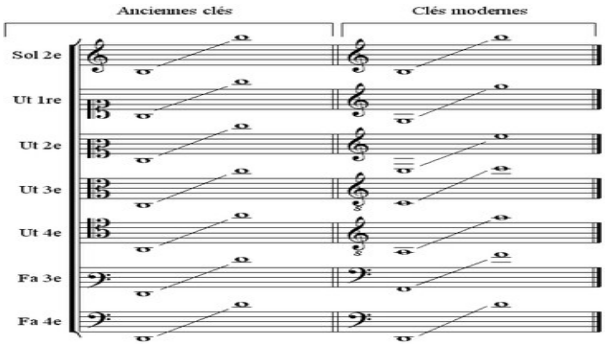


Figure 2: Note range

For this post, for each note, we'll find five states and seven different pitches.

Symbolic Alphabet Matrix:

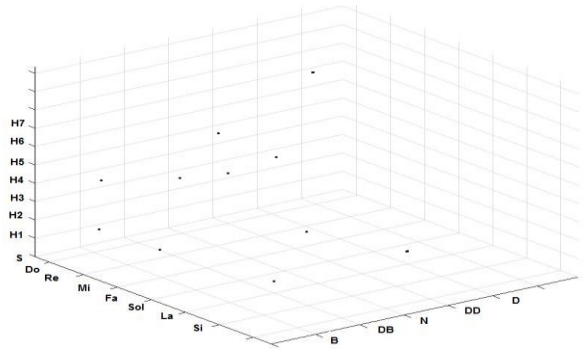


Figure 3: Matrix of the symbolic alphabet

3.2.2 *Ranges Representation*

A scale represents a subset of the alphabet consisting of seven notes of its derivatives plus the (S) silence. We may identify each spectrum at a 49-symbol height representing the terms and their heights. Finally, we have a number of symbols equal to 50.

Maqam:

Improvisation is not a free-for-all of Arabic literature. It must express a specific musical mode (known as maqam), that further means even more than playing on a given scale; so every maqam has a large vocabulary of idiomatic harmonic phrases as well as ornaments which the performer must perfect. Therefore, modulations are required (mood and scale changes), and melodies are required to be opened and closed, for some improvisation in a specific maqam.

Maqam is the term applied to the Eastern music scales, that title means the set of tonal intervals of the seven fundamental notes (as well as five notes in the sense of Eastern pentatonic scales). Scales are named by a note which even the sound was interrupted. oriental Maqam is different from the occidental ones as they are composed of a quarter of a tone while they are still smooth and sharp.

Example of Maqam RAST:
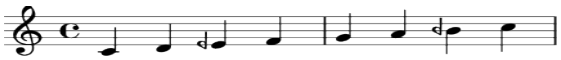


Figure 4: RAST Maqam

In Arabic, Maqam Rast is the title of a maqam (musical mode) and associated music systems. Rast is a Persian term that signifies "true" or "correct." Rast is known as the fundamental maqam in both Iranian and Eastern music, in the very same manner as major scale in occidental music, but in detail, it is unique from the major scale (the big scale is actually kind of like Ajam Maqam). Rast includes a third half flat with a seventh-scale half flat degree.

Tone Interval of Main Maqam:

This table contains our own work to define the interval of oriental maqam.

Table 2: The Interval of Maqam

Rast Genre	Tone Interval of Maqam
Rast	1 - 3/4 - 3/4 - 1 - 1 - 3/4 - 3/4
Kirdane	3/2 - 1/4 - 3/4 - 1 - 1 - 3/4 - 3/4
Sazkar	3/2 - 1/4 - 3/4 - 1 - 1 - 3/4 - 3/4

Suznak	1 - 3/4 - 3/4 - 1 - 1/2 - 3/2 - 1/2
Nairuz	1 - 3/4 - 3/4 - 1 - 3/4 - 3/4 - 1
Yakah	1 - 3/4 - 3/4 - 1 - 3/4 - 3/4 - 1
Dalanshine	1 - 3/4 - 3/4 - 1 - 1 - 3/4 - 3/4
Suzdalara	1 - 3/4 - 3/4 - 1 - 1 - 1/2 - 1
Mahur	1 - 3/4 - 3/4 - 1 - 1 - 1 - 1/2
Bayati Genre	
Bayati	3/4 – 3/4 - 1 - 1 - 2/1 - 1 - 1
Bayati Shuri	3/4 - 3/4 - 1 - 1/2 - 3/2 - 1/2 - 1
Husayni	3/4 - 3/4 - 1 -1 - 3/4 - 3/4 - 1
Muhayyar	3/4 - 3/4 - 1 - 1 - 1/2 - 1 - 1
Nikriz Genre	
Nikriz	1 - 2/1 - 1,5 - 2/1 - 1 - 2/1 - 1
Nawa Athar	1 - 2/1 - 1,5 - 2/1 - 2/1 - 1,5 - 1/2
Athar Kurd	1/2 - 1 - 3/2 - 1/2 - 1/2 - 3/2 - 1/2
Nahawand Genre	
Nahawand	1 - (1/2) / 1 - 1-1 - (1/2) / 1 - 1,5 - 2/1
Farahfaza	1 - 1/2 - 1 - 1 - 1/2 - 3/2 - 1/2
Nahawand Murassa	1 - 1/2 - 1 - 1/2 - 3/2 - 1/2 - 1
Ushaq Masri	1 - 1/2 - 1 - 1 - 3/4 - 3/4 - 1
Hijaz Genre	
Hijaz	1/2 - 1,5 - 1/2 - 1-2 - 1/2 - 1 - 1
Hijazkar	1/2 – 3/2 - 1/2 - 1 - 1/2 - 3/2 - 1/2
Shadd Araban	1/2 – 3/2 - 1/2 - 1 - 1/2 - 3/2 - 1/2
Shahnaz	1/2 – 3/2 - 1/2 - 1 - 1/2 - 3/2 - 1/2
Suzidil	1/2 – 3/2 - 1/2 - 1 - 1/2 - 3/2 - 1/2
Zanjaran	1/2 - 1 - 1/2 - 1 - 3/2 - 1/2 - 1
Kurd Genre	
Kurd	2/1 - 1 - 1 - 1 - 2/1 - 1 - 1
Hijazkar Kurd	1/2 - 1 - 1 - 1 - 1/2 - 1 - 1
Sikah Genre	
Sikah	3/4 - 1 - 1 - 4/3 - 4/3 - 1 – 3/4
Houzam	3/4 - 1 - 2/1 - 1,5 - 1/2 - 1 – 3/4
Rahat al-Arwah	3/4 - 1 - 2/1 - 1,5 - 1/2 - 1 – 3/4
Iraq	3/4 - 1 - 3/4 - 3/4 - 1 - 1 - 3/4
Awj Iraq	3/4 - 1 - 1/2 - 3/2 - 1/2 - 3/2 - 1/4
Bastanikar	3/4 - 1 - 3/4 - 3/4 - 1/2 - 3/2 - 1/2
Mustaar	5/4 - 1/2 - 1 - 1/2 - 1 - 1 - 3/4
Ajam Genre	
Ajam	1 - 1 - 2 - 1 - 1 - 1 - 1/2
Ajam Ouchayrane	1 – 1 - 1/2 - 1 - 1 - 1 - 1/2
Shaouq Afza	1 - 1 - 1/2 - 1 - 1/2 - 3/2 - 1/2
Independents Maqam	
Maqam Jiharkah	1 - 1 - 1/2 - 1 - 1 - 3/4 - 3/4
Maqam Lami	1/2 - 1 - 1 - 1/2 - 1 - 1 - 1
Maqam Saba	3/4 – 3/4 - 2/1 - 1,5 - 2/1 - 1 - 1
Maqam Saba Zamzam	1/2 - 1 - 1/2 - 3/2 - 1/2 - 1 - 1/2
Maqam Sikah Baladi	3/4 - 1 - 3/4 - 1/2 - 1/2 - 3/4 - 1

The scale reduces the number of available alphabets; also, every scale does have its own alphabet specified by the tonal intervals by considering the silence S also as a note into account.

Standard range: A{s, q1; q2; q3; ...; q49} pentatonic range: A{s, q1; q2; q3; ...; q35}.

3.2.3 The Rhythmic Alphabet

A musical note's shape-or number-defines its duration, and it shapes the musical rhythm by integrating the various durations. There are many types of note and specific silences or figures: Round, White, Black, Eighth, Sixteenth, Sixteenth, Triple Eighth, Quadruple Eighth, dotted notes, etc.

Example:

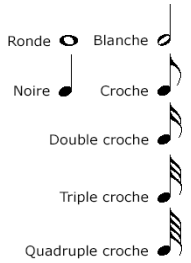


Figure 5: Rhythmic alphabet

Every note pattern's rhythm has always been worth twice as much as that which follows. We should find, in our analysis, the following set of durations (1/16, 3/32, 7/64, 1/48.1/48.1/48, 1/8, 3/16, 7/32, 1/24.1/24.1/24, 1/4, 3/8, 7/16, 1/12.1/12.1/12, 1/2, 3/4, 7/8, 1/6.1/6.1/6, 1, 3/2, 7/4, 1/3.1/3.1/3, 2, 3, 7/2, 2/3.2/3.2/3, 4, 6, 7, 4/3.4/3.4/3)

Every musical word is a mixture of symbols belongs to a symbolic alphabet and also has a length belongs to a rhythmic alphabet; the construction of musical words refers to the concatenation of a number of symbolic alphabets aligned to their rhythmic alphabet.

4. Proposed Algorithms

We suggest two algorithms: the first feeds a research base with calculated descriptors and second produces measurements involving derived terms that, while taking into account the grammar of western music, follow the same constraints as the original words in the study base.

4.1. Learning Steps

We will present a learning algorithm in this section, based on descriptors we described before. Those descriptors constitute the necessary details about a score's musical metric. 11 information's piece of fundamental for extracting from the initial term while respecting laws of Eastern musical grammar, condition of distance among the notes shall be regulated by scale, note and, note figures.

The measure in the first sense is a segmentation of the interval between musical discourse. In other words, measure is the separation of a musical piece into equal parts of the same duration.

Vertical bars on the staff show this section named measuring bars. This is determined by a certain number of periods-times being units for period calculation. Furthermore, the metric should be used as a broader unit of measurement that requires multiple periods in this respect.
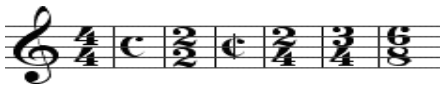


Figure 6: The Measure

A bar includes two kinds of information, essential information describing the form of the music (rhythm, harmony, polyphony), and details of expression called nuances. In Western music, nuance is a symbol indicating the relative strength of note, a phrase, or a whole passage of a musical composition. During their performance, the nuances permit the musician to reproduce the dynamics of the work.

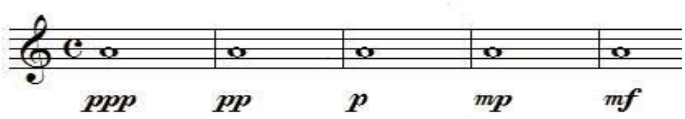


Figure 7: The Nuances

In comparison, the use of variations is almost absent in Arabic music. The peculiarity of oriental music lies with the fact that, in an ensemble, each musician will perform the same song but with different nuances. For this reason, nuances are excluded from this work.
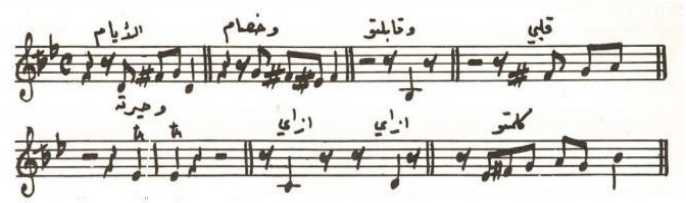


Figure 8: The Absence of Nuances

4.1.1 Proposed Learning Algorithm

The proposed algorithm consisting of browsing a piece of music from an entered score, determining the descriptors, and then feeding a chronologically ordered learning base. This will allow us to have a database containing calculated features preventing initial words, the parameters stored in different tables constitute the thoughts of the composers but it is presented in a mathematical way including for each musical piece: the composer, the chosen scale, the chosen rhythm, the number of notes in a word, the sum of the intervals detected, the largest interval between two consecutive notes, and the smallest interval between two consecutive notes, the greatest duration of a note referring to the word concerned, the smallest duration of a note belonging to the word in question, the greatest pitch of note pertaining to the word and the smallest pitch of a note which belongs to that word and the pitch of the first note referring to the word concerned.

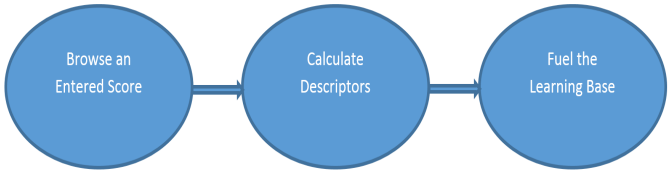


Figure 9: The Learning Algorithm

4.1.1.1 Representation of Descriptors

We identified eleven descriptors:

- **Nnote:** Notes numbers.
- **Gnote:** Maqam (indicated on armor, taken on consideration alterations the first and the last note of partition).
- **Snote:** Sum of tonal intervals among notes (depending on Maqam).
- **Gd:** Largest tonal interval among two notes (in terms of the Maqam).
- **Pd:** Smallest tonal interval among two notes (in terms of the Maqam).
- **R:** Rhythm
- **Dnote:** Longest note duration (in terms of the Maqam).
- **Pnote:** Shortest note duration (in terms of Rhythm)
- **Hnote:** First note pitch of the term.
- **Gh:** Highest height of the word.
- **Ph:** Lowest height of the word.

4.1.1.2 Browse an Entered Score

The algorithm beginning checks the score's first/last notes to determine the scale's main note then checks the rhythm (R) and starts measuring each note's length consecutively and as per the specified time unit. When sum of durations of note achieves the rhythm, the system Sees the previous sequence as a term, and then goes on to next one.

R = Rhythm

I = duration note for I = 0 to I = R → I=in + in+1

When terminal segmentation is complete, the system moves to descriptor estimating.

4.1.1.3 Calculation of the descriptors of each word:

The Algorithm for each segmented term:

1. Calculate the Nnote number.
2. checks the presence on the basis of the main note previously mentioned of the seven deferential notes constituting the Maqam, and measures distances (tonal interval) among them to conclude the Maqam
3. Calculates for each term, sum of the intervals tones among notes.
4. For each sentence, the system calculates the larger Gd, and between two sentences, the smallest tonal interval Pd.
5. For each term the system determines, largest duration Dnote and smallest one Pnote.

4.1.1.4 Power supply for the learning base

The algorithm takes each word to be a sequence (Gh, Ph, Note, Pnote, Hnote, Gnote, R, Dnote Snote, Pd, Gd). Feeding takes place on a learning base, which comprises the structure as follow:

1. Symbolic terms matrix table of heights.

2. Rhythmic alphabet table.
3. Ranges table.
4. Table of composers.
5. Pieces table
6. Descriptors and words table
7. Worktables.

4.2. Composition

The proposed model aims to create derivative words automatically in terms of the music descriptors contained in the database. First, the method starts by splitting the rhythmic word from symbolic word and by milking each one in a particular way. A collection of rules for calculating distance and filtering is implemented to create derived terms, then the system proceeds to a concatenation operation at the end, the entire process is rebooted N times to produce a similar musical song in the chosen composer's style of composition. It is sort of a continuation of the composer's thinking.

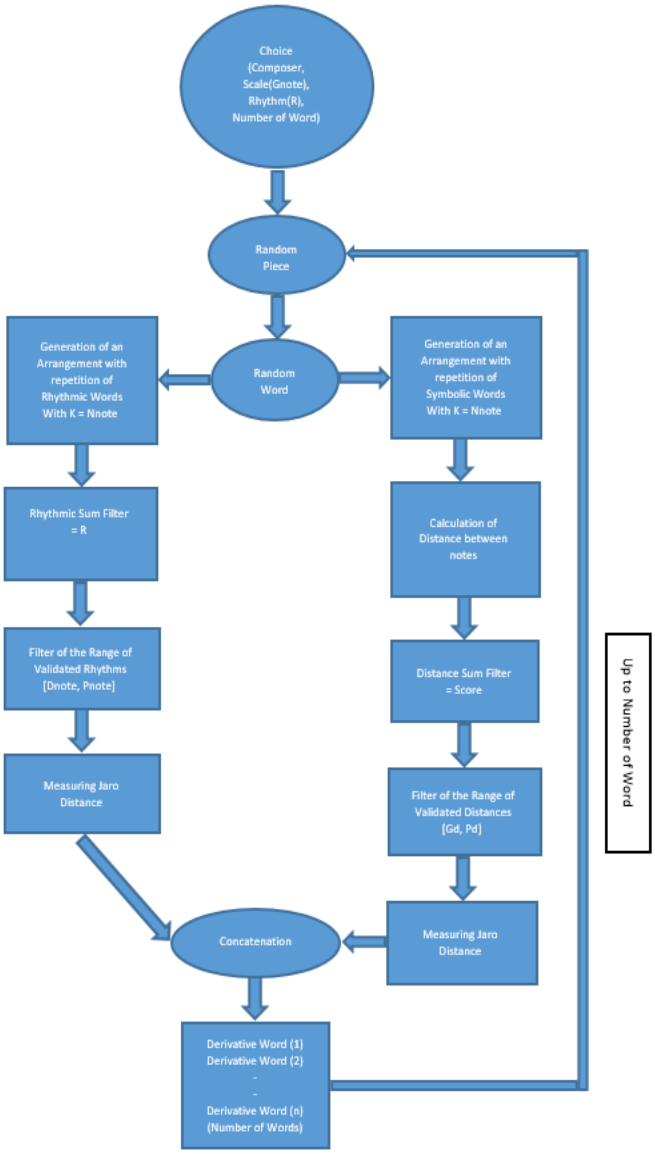


Figure 10: The Composition Algorithm

Option of (composer, scale, rhythm): In effort to create derived words, three essential elements (composer, scale, rhythm) should be filling at the beginning. the selection of Maqam will decide the rules applied to both the measure and the rhythm and will determine the size of measures.

RANDOM Piece: Randomly the algorithm selects a piece from among many pieces selected by a filter (composer, scale, rhythm).

RANDOM Measurement: Randomly the algorithm selects a measurement then retrieves its descriptors from multiple measurements of same piece.

4.2.1 The Symbolic Word

Generation repetition arrangement: All combinations are generated by the algorithm: n^k with k = Gnote scale note and specified by [Gh and Ph].

Calculation of distances between notes: Each of the 2 successive notes represents a distance, and the algorithm measures each distance by the scale concerned.

Filter on sum of distances = Score: If the distances between notes have been determined, the algorithm calculates the sum of all distances that constitute the term. All terms including Snote (word-derived) ! = Snote (original word) are excluded.

Filter of the range of validated distances [Gd, Pd]: The algorithm holds the terms [Gd, Pd] valued by distances.

Filtering by Measuring the Jaro Distance: In effort to choose words which is much less similar than the initial symbolic word, all words produced honoring all conditions and rules must be placed in competition.

The Jaro Similarity simj of two given strings

$$sim_j = \begin{cases} 0 & \text{if } m = 0 \\ \frac{1}{3}\left(\frac{m}{|s_1|} + \frac{m}{|s_2|} + \frac{m-t}{m}\right) & \text{otherwise} \end{cases} \quad (1)$$

where:

- |Si| is the length of sting Si;
- m is the number of matching characters
- t is half the number of transpositions

Two characters from S1 and S2 become considered matching even if they are similar and not further than the:

$$\left\lfloor \frac{\max(|s_1|, |s_2|)}{2} \right\rfloor - 1. \quad (2)$$

4.2.2 Rhythmic word

Generation of an arrangement with repetition: The method generates all different variations in rhythm as the same method as symbolic terms: n^k with k = Nnote.

Rhythm sum filter = R: The algorithm calculates sum of all distances which make up the term. All terms including R (word derivative)! = R (original word) are excluded.

Filter of the range of validated rhythms [Dnote, Pnote]: The system preserves terms whose letters respect [Dnote, Pnote].

Filtering by Measuring the Jaro Distance: All the words produced that comply with all laws and conditions should be placed in competition to prioritize terms that are less similar to the initial rhythmic word

Concatenation of *Symbolic word* and *Rhythmic word:*

Concatenation: The system randomly selects a derived word from the list of preserved terms and derived rhythmic term from the list of preserved rhythmic terms and combines the two.

The system reboots many times up to the **No** words.

5. Process Implementation

In this section, we are interested in generating a musical score by respecting laws and rules defined before. We have chosen to compose music by appealing to the thoughts of Mohammed ABDELWAHAB and this through his musical words that he composed before. all the musical libraries of different composing artists are considered intellectual heritage. in our algorithm, we try to create derived words from initial words.

Generation of pieces:

1. four words: Composer = Mohammed ABDELWAHAB; Maqam = Nahawand ; R = 4/4.
2. six words: Composer = Mohammed ABDELWAHAB; Maqam = Bayati ; R = 4/4.
3. Two words: Composer = Mohammed ABDELWAHAB; Maqam = Nahawand; R = 4/4.

5.1. Table of original words randomly selected from the learning base

Table 3: Original Words Randomly Selected from the Learning Bases

Composers	R	Maqam	Songs	Initial words
Mohammed abdelwahab	C	ELNAHAWAND	Al Fan	2do(2)1sib(2)1sol(2)
			Elfantazy	3/2mib(2)1/2re(2)3/4mib(2)1/4 re(2)3/4mib(2)1/4re(2)
			Elfan	1/2sib(2)1/2do(2)1/2re(2)1/ 2mi b(2)2fa(2)
			Elfan	3/2mib(3)1/2re(3)1st(3)1/4 re(3)1/4re(3)1/4mib(3)1/4fa(3)1/4s ol(2)
			Limta Zaman	1sol(2)2sol(2)2sol(2)1fa(3)
			Elfantazy	1/2re(2)1/2mib(2)1/2fa(2)1/2fa (2)1/2sol(1)3/4mib(2)1/4re(2)1/ 2do(2)1/2re(2)
			Limta Zaman	1sol(2)1/2lab(2)1/2sib(2)1lab(2)1sol(2)
		ELBAYATI	Elfantazy	3/2sol(1)1/2fa(2)3/2lab(1)1/2so l(1)
			Ya mousafir Wahdak	1/2sol(2)1/2do(2)1/2sib(2)1/2la db(2)1sol(2)1st(2)
			Manaa Sali	1sib(2)1ladb(2)1/2sib(2)1/2sib(2)1/2do(2)1/2sib(2)1/2ladb(2)
			Ya mousafir Wahdak	1/2re(2)1/2mib(2)1/2re(2)1/2re (2)1/2do(2)1/2sib(2)1/2do(2)1/ 2do(2)1/2sib(2)1/2ladb(2)
			Manaa Salie	1s(0)1do(2)1sib(2)1do(2)
			Manaa Salie	3/2re(2)1/2do(2)1sib(2)1ladb(2)
			Ya mousafir wahdak	1sol(2)1ladb(2)1sib(2)1do(2)
		ELNAHAWAND	Elfantazy	1/4lab(1)1/4sol(1)1/2fa(2)1/4fa (2)1/4fa(2)1/2mib(2)1/4fa(2)1/ 4fa(2)1/4mib(2)1/2re(2)1/4mib (2)1/2do(2)
			Alfan	2sib(2)1lab(2)3/4sol(2)1/4lab(2)

5.2. Table of Calculated Descriptors

Table 4: Calculated Descriptors

	Calculated Descriptors								
Initial Words	Nnote	Snote	Gd	Pd	Dnote	Pnote	Hnote	Gh	Ph
2do(2)1sib(2)1sol(2)	3	2,5	1,5	1	2	1	2	2	2
3/2mib(2)1/2re(2)3/4mib(2)1/4re(2)3/4mib(2)1/4re(2)	6	2,5	0,5	0,5	1,5	0,25	2	2	2
1/2sib(2)1/2do(2)1/2re(2)1/2mib(2)2fa(2)	5	3,5	1	0,5	2	0,5	2	2	2
3/2mib(3)1/2re(3)1re(3)1/4re(3)1/4mib(3)1/4fa(3)1/4sol(2)	7	3	1	0	1,5	0,25	3	3	2
1sol(2)2sol(2)1fa(3)	3	1	1	0	2	1	2	3	2
1/2re(2)1/2mib(2)1/2fa(2)1/2sol(1)3/4mib(2)1/4re(2)1/2do(2)1/2re(2)	8	7	2	0,5	1,5	0,25	2	2	1
1sol(2)1/2lab(2)1/2sib(2)1lab(2)1sol(2)	5	3	1	0,5	1	0,5	2	2	2
3/2sol(1)1/2fa(2)3/2lab(1)1/2sol(1)	4	3	1,5	0,5	1,5	0,5	1	2	1
1/2sol(2)1/2do(2)1/2sib(2)1/2ladb(2)1sol(2)1re(2)	6	8,5	3,5	0,75	1	0,5	2	2	2
2sib(2)1lab(2)3/4sol(2)1/4lab(2)	4	2	1	0,5	2	0,25	2	2	2
3/2mib(2)1/2re(2)3/4mib(2)1/4re(2)3/4mib(2)1/4re(2)	6	2,5	0,5	0,5	1,5	0,25	2	2	2
1sib(2)1ladb(2)1/2sib(2)1/2do(2)1/2sib(2)1/2ladb(2)	6	4,25	1	0,75	1	0,5	2	2	2
1/2re(2)1/2mib(2)1/2re(2)1/2do(2)1/2sib(2)1/2do(2)1/2sib(2)1/2ladb(2)	8	5,75	1	0,5	0,5	0,5	2	2	2
1s(0)1do(2)1sib(2)1do(2)	4	2	1	1	1	1	2	2	2
3/2re(2)1/2do(2)1sib(2)1ladb(2)	4	2,75	1	0,75	1,5	0,5	2	2	2
1/4lab(1)1/4sol(1)1/2fa(2)1/4sol(1)1/4fa(2)1/2mib(2)1/4fa(2)1/4mib(2)1/2re(2)1/4mib(2)1/4re(2)1/2do(2)	12	9	1	0,5	0,5	0,25	1	2	1
1sol(2)1ladb(2)1sib(2)1do(2)	4	2,5	1	0,75	1	1	2	2	2

5.3. Generation of an Arrangement with Repetition of Symbolic Words with k=Nnote

Table 5: Generation of arrangement with repetition of symbolic words with k=Note

Generation of 3375 symbolic term with n = 15, k=3, Gh=3 and Ph=2			
DO2,DO2,	DO2,RE	DO2,FA	DO2,LAB2,L
DO2,DO2	2,SOL3	2,RE3	AB2,LAB2
DO2,DO2,	DO2,RE	DO2,FA	DO2,LAB2,S
DO2,RE2	2,LAB3	2,MIB3	IB2
DO2,DO2,	DO2,RE	DO2,FA	DO2,LAB2,D
DO2,MIB2	2,SIB3	2,FA3	O3
DO2,DO2,	DO2,MI	DO2,FA	DO2,LAB2,R
DO2,FA2	B2,DO2	2,SOL3	E3
DO2,DO2,	DO2,MI	DO2,FA	DO2,LAB2,MI
DO2,SOL2	B2,RE2	2,LAB3	……

5.4. Example of Symbolic Derived Words Meeting the Conditions for the Original Word 1sol(2)2sol(2)1fa(3)

Table 6: Example of Symbolic Derived word

	W1	W2	W3
Word1	RE2	DO2	S
Word2	RE2	DO2	DO2
Word3	RE2	RE2	DO2
Word4	RE2	MIB2	RE2

All features generated respect the rule: Distance Sum Filter = Score; Filter of the Range of Validated Distances [Gd, Pd], and the Measuring of Jaro Distance to choose the derived word with the least similarity to the original word.

In the end, operation of RANDAM is executed to choose a single word among the words respecting all the conditions and this to reduce the probability of falling on the same word the next iteration.

5.5. Generation of an arrangement of rhythmic words with k=Nnote

Table 7: Generation of Arrangement of Rhythmic Words with K=Nnote

Generation of 125 rhythmic term with n = 5, k =3, Dnote=2 and Pnote=1			
1;1;1,5	1;2;1,5	1,5;1;1,5	1,75;1,75;1,5
1;1;1,75	1;2;1,75	1,5;1;1,75	1,75;1,75;1,75
1;1;1	1;2;1	1,5;1;1	1,75;1,75;1
1;1;2	1;2;2	1,5;1;2	1,75;1,75;2
1;1,5;1	1,5;1;1	1,5;2;1	1,75;1;1
1;1,5;1,5	1,5;1;1,5	1,5;2;1,5	1,75;1;1,5
1;1,5;1,75	1,5;1;1,75	1,5;2;1,75	1,75;1;1,75
1;1,5;1	1,5;1;1	1,5;2;1	1,75;1;1
1;1,5;2	1,5;1;2	1,5;2;2	1,75;1;2
1;1,75;1	1,5;1,5;1	1,75;1;1	1,75;2;1
1;1,75;1,5	1,5;1,5;1,5	1,75;1;1,5	1,75;2;1,5
1;1,75;1,75	1,5;1,5;1,75	1,75;1;1,75	1,75;2;1,75
1;1,75;1	1,5;1,5;1	1,75;1;1	1,75;2;1
1;1,75;2	1,5;1,5;2	1,75;1;2	1,75;2;2
1;1;1	1,5;1,75;1	1,75;1,5;1	1;1;1
1;1;1,5	1,5;1,75;1,5	1,75;1,5;1,5	1;1;1,5
1;1;1,75	1,5;1,75;1,75	1,75;1,5;1,75	1;1;1,75
1;1;1	1,5;1,75;1	1,75;1,5;1	1;1;1
1;1;2	1,5;1,75;2	1,75;1,5;2	1;1;2
1;2;1	1,5;1;1	1,75;1,75;1	……

5.6. Example of rhythmic derived words meeting the conditions for the original word 1sol(2)2sol(2)1fa(3)

Table 8: Example of Symbolic Derived Words

Filtering with R = 4		
W1	W2	W3
1	1	2
1	3/2	3/2
1	2	1
3/2	1	3/2
3/2	3/2	1
2	1	1

5.7. Filtering with Jaro Distance

Table 9: Filtering Based on Jaro Distance

Filtering With Jaro Distance		
W1	W2	W3
1	1	2
1	3/2	3/2
1	2	1
3/2	1	3/2
3/2	3/2	1
2	1	1

5.8. Concatenation of Symbolic Word and Derived Word

The last operation consists of concatenating respectively the derived symbolic words with the derived rhythmic words.

Table 10: Example of Concatenated Word

Concatenated Word		
3/2	1	3/2
RE2	MIB2	RE2
3/2RE(2)	1MIB(2)	3/2RE(2)

5.9. Partition generated
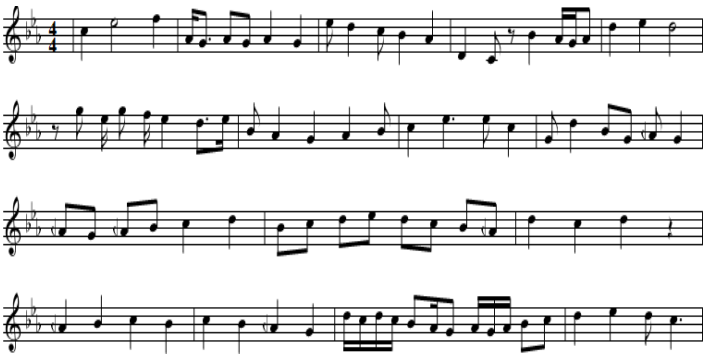


Figure 11: Automatic Generated Music

6. Conclusion and Future Works

The proposed algorithm permitted us to produce musical words that constitute parts from the descriptors we described, each word generated through its own alphabet according to the laws relating to this term by crossing a collection of filters that held only the correct words. We have been attempting to address the theory of the composition of known Arabic music composers. The result obtained and demonstrated in an artificially and automatically generated and written piece of music, shows that the machine can be an artist and we can guarantee the continuity of the composer's thoughts, On the other hand, this area of artificial composition of oriental music still needs to be developed, we suggest the incorporation of the principle of alterations identified by the existence in a word of a foreign text, The meaning of an immediate change of scale, taking into account the relations between the terms and the introduction of the patterns of the ranges according to their definition, taking into account the unique changes in each range.

Conflict of Interest

The authors declare no conflict of interest.

Acknowledgment

The H2020 Project SybSPEED, N 777720, supports this work.

References

[1] P. Barbaud, R. Philippe, "L'ordinateur et la musique," Communication & Langages, **3**(1), 17–25, 1969, doi:10.3406/colan.1969.3744.

[2] C.A. Wamser, C.C. Wamser, "Lejaren A. Hiller, Jr.: A Memorial Tribute to a Chemist-Composer," Journal of Chemical Education, **73**(7), 601, 1996, doi:10.1021/ed073p601.

[3] C. Ames, "The Markov Process as a Compositional Model: A Survey and Tutorial," Leonardo, 22(2), 175–187, 1989, doi:10.2307/1575226.

[4] K. Jones, "Compositional Applications of Stochastic Processes," 1981, doi:10.2307/3679879.

[5] D.P. Kingma, J. Ba, "Adam: A Method for Stochastic Optimization," ArXiv:1412.6980 [Cs], 2017.

[6] G. Papadopoulos, G. Wiggins. "Ai methods for algorithmic composition: A survey, a critical view and future prospects," In AISB Symposium on Musical Creativity, pages 110-117, Edinburgh, UK, 1999, doi.org/10.1080/17513472.2012.738554.

[7] J.D. Fernandez, F. Vico, "AI Methods in Algorithmic Composition: A Comprehensive Survey," Journal of Artificial Intelligence Research, **48**, 513–582, 2013, doi:10.1613/jair.3908.

[8] P.M. Todd, "A Connectionist Approach to Algorithmic Composition," Computer Music Journal, **13**(4), 27–43, 1989, doi:10.2307/3679551.

[9] K.M. Kitani, H. Koike, ImprovGenerator : Online Grammatical Induction for On-the-Fly Improvisation Accompaniment, Proceedings of the International Conference on New Interfaces for Musical Expression, 469–472, 2010, doi:10.5281/zenodo.1177827.

[10] P. Worth, S. Stepney, "Growing Music: Musical Interpretations of L-Systems," in: Rothlauf, F., Branke, J., Cagnoni, S., Corne, D. W., Drechsler, R., Jin, Y., Machado, P., Marchiori, E., Romero, J., Smith, G. D., and Squillero, G., eds., in Applications of Evolutionary Computing, Springer, Berlin, Heidelberg: 545–550, 2005, doi:10.1007/978-3-540-32003-6_56.

[11] M.C. Mozer, "Neural Network Music Composition by Prediction: Exploring the Benefits of Psychoacoustic Constraints and Multi-scale Processing," Connection Science, **6**(2–3), 247–280, 1994, doi:10.1080/09540099408915726.

[12] D. Eck, J. Schmidhuber, "Finding temporal structure in music: blues improvisation with LSTM recurrent networks," in Proceedings of the 12th IEEE Workshop on Neural Networks for Signal Processing, 747–756, 2002, doi:10.1109/NNSP.2002.1030094.

[13] J. Franklin, "Computational models for learning pitch and duration using lstm recurrent neural networks". In Proceedings of the Eighth International Conference on Music Perception and Cognition (ICMPC8), Adelaide, Australia. Causal Productions, 2004. doi: 10.1007/978-3-319-55750-2.

[14] M. Alfonseca, M. Cebrián, A. Ortega, "Evolving computer-generated music by means of the normalized compression distance," in Proceedings of the 5th WSEAS international conference on Simulation, modelling and optimization, World Scientific and Engineering Academy and Society (WSEAS), Stevens Point, Wisconsin, USA: 343–348, 2005.

[15] S. Hochreiter, "The Vanishing Gradient Problem During Learning Recurrent Neural Nets and Problem Solutions," International Journal of Uncertainty, Fuzziness and Knowledge-Based Systems, **06**(02), 107–116, 1998, doi:10.1142/S0218488598000094.

[16] F.A. Gers, J. Schmidhuber, F. Cummins, "Learning to Forget: Continual Prediction with LSTM," Neural Computation, **12**(10), 2451–2471, 2000, doi:10.1162/089976600300015015.

[17] A. Graves, A. Mohamed, G. Hinton, "Speech recognition with deep recurrent neural networks," in 2013 IEEE International Conference on Acoustics, Speech and Signal Processing, 6645–6649, 2013, doi:10.1109/ICASSP.2013.6638947.

[18] J. Chung, C. Gulcehre, K. Cho, Y. Bengio, "Empirical evaluation of gated recurrent neural networks on sequence modeling," NIPS 2014 Workshop on Deep Learning, December, 2014.

[19] K. Cho, B. van Merriënboer, C. Gulcehre, D. Bahdanau, F. Bougares, H. Schwenk, Y. Bengio, "Learning Phrase Representations using RNN Encoder–Decoder for Statistical Machine Translation," in Proceedings of the 2014 Conference on Empirical Methods in Natural Language Processing (EMNLP), Association for Computational Linguistics, Doha, Qatar: 1724–1734, 2014, doi:10.3115/v1/D14-1179.

[20] R. Jozefowicz, W. Zaremba, I. Sutskever, "An empirical exploration of recurrent network architectures," in Proceedings of the 32nd International Conference on International Conference on Machine Learning - **37**, JMLR.org, Lille, France: 2342–2350, 2015.

[21] Y. LeCun, Y. Bengio, G. Hinton, "Deep learning," Nature, **521**(7553), 436–444, 2015, doi:10.1038/nature14539.

[22] J. Schmidhuber, "Deep Learning in Neural Networks: An Overview," Neural Networks, **61**, 85–117, 2015, doi:10.1016/j.neunet.2014.09.003.

[23] I. Sutskever, O. Vinyals, Q.V. Le, "Sequence to sequence learning with neural networks," in Proceedings of the 27th International Conference on Neural Information Processing Systems - **2**, MIT Press, Cambridge, MA, USA: 3104–3112, 2014.

[24] A. Graves, "Generating Sequences With Recurrent Neural Networks," ArXiv:1308.0850 [Cs], 2014.

[25] T.J. Sejnowski, "The unreasonable effectiveness of deep learning in artificial intelligence," Proceedings of the National Academy of Sciences, 2020, doi:10.1073/pnas.1907373117.

[26] F. Colombo, S.P. Muscinelli, A. Seeholzer, J. Brea, W. Gerstner, "Algorithmic Composition of Melodies with Deep Recurrent Neural Networks," ArXiv:1606.07251 [Cs, Stat], 2016, doi:10.13140/RG.2.1.2436.5683.

[27] L. Bahatti, M. Zazoui, O. Bouattane, A. Rebbani, "Short-Term Sinusoidal Modeling of an Oriental Music Signal by Using CQT Transform," Journal of Signal and Information Processing, **04**(01), 51, 2013, doi:10.4236/jsip.2013.41006.

[28] L. Bahatti, O. Bouattane, M. Zazoui1, A. Rebbani, Fast Algorithm for In situ transcription of musical signals : Case of lute music, ResearchGate, 2020.

[29] L. Bahatti, A. Rebbani, O. Bouattane, M. Zazoui, "Sinusoidal features extraction: Application to the analysis and synthesis of a musical signal," in 2013 8th International Conference on Intelligent Systems: Theories and Applications (SITA), 1–6, 2013, doi:10.1109/SITA.2013.6560805.

[30] B. Marzouki, Application of Arithmetic and Cyclic Groups to Music, First International conference on mathematics and applications. Department of Mathematics and Informatics Faculty of Sciences Oujda, 2013.

[31] M. Zhar, O. Bouattane, L. Bahatti, "New Algorithm For The Development Of A Musical Words Descriptor For The Artificial Synthesis Of Oriental Music," in 2020 1st International Conference on Innovative Research in Applied Science, Engineering and Technology (IRASET), 1–8, 2020, doi:10.1109/IRASET48871.2020.9092157.

[32] Y. Zhu, Z. Ming, Q. Huang, "SVM-Based Audio Classification for Content-Based Multimedia Retrieval," in: Sebe, N., Liu, Y., Zhuang, Y., and Huang, T. S., eds., in Multimedia Content Analysis and Mining, Springer, Berlin, Heidelberg: 474–482, 2007, doi:10.1007/978-3-540-73417-8_56.

[33] T. Ratanpara, N. Patel, "Singer identification using perceptual features and cepstral coefficients of an audio signal from Indian video songs," EURASIP Journal on Audio, Speech, and Music Processing, **2015**(1), 16, 2015, doi:10.1186/s13636-015-0062-9.

[34] J.H. Foleis, T.F. Tavares, "Texture selection for automatic music genre classification," Applied Soft Computing, **89**, 106127, 2020, doi:10.1016/j.asoc.2020.106127.

[35] Y. Yu, S. Luo, S. Liu, H. Qiao, Y. Liu, L. Feng, "Deep attention based music genre classification," Neurocomputing, **372**, 84–91, 2020, doi:10.1016/j.neucom.2019.09.054.

[36] C.G. Nevill-Manning, I.H. Witten, "Identifying Hierarchical Structure in Sequences: A linear-time algorithm," Journal of Artificial Intelligence Research, **7**, 67–82, 1997, doi:10.1613/jair.374.

[37] E.M. Gold, "Language identification in the limit," Information and Control, **10**(5), 447–474, 1967, doi:10.1016/S0019-9958(67)91165-5.

[38] S. Guggari, V. Kadappa, V. Umadevi, A. Abraham, "Music rhythm tree based partitioning approach to decision tree classifier," Journal of King Saud University - Computer and Information Sciences, 2020, doi:10.1016/j.jksuci.2020.03.015.

ASTES

Advances in Science, Technology and Engineering Systems Journal, Vol. 5, No. 5, 444-451 (2020)

www.astesj.com

ASTESJ

ISSN: 2415-6698

Newton-Raphson Algorithm as a Power Utility Tool for Network Stability

Lambe Mutalub Adesina[1,*], Ademola Abdulkareem[2], James Katende[3], Olaosebikan Fakolujo[4]

[1]*Kwara State University Malete, Dept. of Electrical and Computer Engineering, Faculty of Eng'g and Technology, 241104, Nigeria*

[2]*Covenant University Sango Ota, Dept. of Electrical and Information Engineering, College of Engineering, 112233 Nigeria*

[3]*University of Namibia, Department of Electrical and Computer Engineering, Faculty of Technology, 13301 Namibia*

[4]*University of Ibadan, Dept. of Electrical and Electronics Engineering, Faculty of Technology, 200284 Nigeria*

ARTICLE INFO

Article history:
Received: 28 July, 2020
Accepted: 28 August, 2020
Online: 21 September, 2020

Keywords:
National power reform
Network reliability
Newton – Raphson Software
Operational parameters
Revenue generation
System collapse
Utility feeder network

ABSTRACT

Nigerian power utility companies particularly the distribution and generation aspects were recently in the process of national power reform converted from public to private service by privatization. Prior to these development, power utility companies' performance is low due to poor operational style that leads to inadequate revenue generation. Thus, the task before the privatized companies includes autonomy, high reliability operation and brake-even management. To achieve these goal, frequent outages and system collapses must be minimized. One of the methods of achieving this is using power flow to improve the reliability of power system which will subsequently improve other lacking factors. A developed software for Newton-Raphson power flow was tested with a known solution network and the results obtained are accurate and reliable. Therefore, this paper presents an application of this software on real-time transmission network. Nigerian 330kV transmission grid is considered as case study. The power flow analysis of this grid was carried out and the network operational parameters were obtained. These results are stated and carefully analyzed. In practice, power utility distribution network of medium voltage of 11kV feeder was also tested with this NR-Software in ascertaining network reliability and in the course of adding public transformers to utility feeder network.

1. Introduction

This paper is an extension of work originally presented in IEEE Nigeria Computer Conference, where a computer software package was developed using Newton-Raphson power flow algorithm [3]. The package was tested with a known solution network and the obtained results are accurate and reliable[3, 8]. Nigerian population is exponentially increasing with the attendant increase in demand for electric power supply proportionally. This becomes a serious task for the power utility companies in the country to meet the huge energy or power demand of the consumers continuously and safely. Also, power utility companies need to minimize the cost of running the network whether distribution or transmission for smooth, economical and profitable operation of the system. Adding equipment such as generators, lines, buses etc makes the network more prone to faults [3, 4, 8]. Thus, power system network could be interpreted as an interconnection of generators, buses, transformers and lines to give electricity supply to load at several points on the system[3, 4, 8, 11]. However, regardless of the number of load points on the system, the faults should be minimized and the load be made to operate at maximum efficiency with safety so as minimize losses. Therefore, power flow study is employed to study the power system network, and its behavior when it is subjected to any expansion or upgraded for any system.

Power flow studies are tools that are significantly used in system planning and design of power system. It is also used in future expansion and optimization of the existing systems in enhancing reliable performance. The main parameters obtained from typical power flow study include the magnitude and phase angle of the bus bars' voltages as well as the active and reactive power flowing between the buses [5, 9, 10]. Power flow equations when solved gives the steady state condition of every bus bar

*Corresponding Author: Lambe Mutalub Adesina, Nigeria, +2348033207586 lambe.adesina@kwasu.edu.ng

voltage of the network. The problem associated with these power flow equations is their non-linearity and difficulty in obtaining solution by mathematical calculation. These non-linear equations are normally solved by iteration techniques [5, 11, 12]. Therefore, power flow solution problems are an iterative process which involves assigning assumed values to the unknown bus bar voltages and subsequent calculation of new voltage values for the bus bars from assumed values for the remaining bus bars with the specified active power and reactive power or voltage magnitude. New set of voltage values for the bus bars are obtained which are eventually used to determine new set of bus bar voltages by a pre-defined algorithm. This iteration process is updated until the voltage changes between the last and just preceding iteration is less than a specified tolerance value for all the bus bars [3, 4, 8, 11]. From literature, most algorithms often result to high number of iterations and hence take long time to complete the required iterations. For a large network, high number of iterations is expected depending on the type of power flow technique and algorithm used. Several iterative techniques are used in power flow studies which include Gauss, Gauss Seidel, Newton Raphson (NR), Fast Decoupled, etc [3, 8]. Many research papers on related topic had been written and published using the above mentioned techniques but their iteration level is high resulting to long period of convergence [3, 8, 9, 12]. Thus, a software package in this regards is predicted to improve the convergence period.

2. Newton – Raphson Algorithm

The technique illustrates a vector $x \in IR^N$ such that,

$$F(x) = 0 \tag{1}$$

where,

F = Set of 'N' Nonlinear equations.

In Newton-Raphson (NR) Techniques, the vector of state variable is determined by performing an expansion of equation (1) by Taylor's series, assuming an initial estimate X (0). Neglecting error in higher order terms of Taylor series; solution for x is obtained using equation (2),

$$x^{(k)} = x^{(k-1)} - J^{-1} F(x^{(k-1)}) \tag{2}$$

where,

k = iteration,

J = A square matrix of same dimension as x and F, and its entries are partial derivatives defined as[3,4,6],

$$J_{pq} = \partial F_p / \partial x_q \,|_{x^{(k-1)}} \tag{3}$$

where,

p, q = Buses.

J_{pq} = Jacobian matrix of equation (1).

When this mathematical expression is related to power flow solution, then power mismatch is forced to zero via the derivatives of mismatch of the power flow equations. Thus, bus p equation is defined as [1,3],

$$P_p + jQ_p = E_p I_p^* \tag{4}$$

where

$$I_{P=} \sum_{K=1}^{NB} Y_{pk} \; E_k \tag{5}$$

Then,

$$P_p + jQ_p = E_p \sum_{K=1}^{NB} Y_{pk} E_k^* = |E_p|^2 Y_{pp}^* + \sum_{\substack{K=1 \\ K \neq p}}^{NB} Y_{pk}^* E_p E_k^* \tag{6}$$

For p= 1, 2, 3 …… NB, excluding the slack bus.

In starting iteration, initial voltages often assumed and used. The active power P and reactive power Q evaluated from equation (6) is deducted from the scheduled active power P_2 and reactive power Q_s at the bus. The difference is considered as errors stored. Polar co-ordinates are often used for voltage evaluations. In this approach, the voltage magnitudes and phase angles are treated separately as different variables. Consequently, bus injection equations are differentiated with respect to all variables at each bus. Therefore, the power mismatch for each of the buses are evaluated using equations (7) and (8) [2,7].

$$\Delta P_p = \sum_{k=1}^{NB} \frac{\partial P_p}{\partial \theta_k} \Delta\theta_k + \sum_{K=1}^{NB} \frac{\partial P_p}{\partial |E_{k|}} \Delta |E_k| \tag{7}$$

$$\Delta Q_p = \sum_{K=1}^{NB} \frac{\partial Q_p}{\partial \theta_k} \Delta\theta_k + \sum_{K=1}^{NB} \frac{\partial Q_p}{\partial |E_k|} \Delta |E_k| \tag{8}$$

The resulting partial differentials from equations (7) and (8) are put in a Jacobian matrix format so that these equations (7) and (8) are representable in matrix vector form as written in equation (9),

$$\begin{bmatrix} \Delta P_1 \\ \Delta P_{NB-1} \\ - - \\ \Delta Q_1 \\ \Delta Q_{NB-1} \end{bmatrix} = \left[\begin{array}{ccc|ccc} \frac{\partial P_1}{\partial \theta_1} & \cdots & \frac{\partial P_1}{\partial \theta_{NB-1}} & \frac{\partial P_1}{\partial |E_1|} & \cdots & \frac{\Delta P_1}{\Delta |E_{NB-1}|} \\ \frac{\partial P_{NB-1}}{\partial \theta_1} & \cdots & \frac{\partial P_{NB-1}}{\partial \theta_{NB-1}} & \frac{\partial P_{NB-1}}{\partial |E_1|} & \cdots & \frac{\Delta P_{NB-1}}{\partial |E_{NB-1}|} \\ - & - & - & - & - & - \\ \frac{\partial Q_1}{\partial \theta_1} & \cdots & \frac{\partial Q_1}{\partial \theta_{NB-1}} & \frac{\partial Q_1}{\partial |E_1|} & \cdots & \frac{\Delta Q_1}{\partial |E_{NB-1}|} \\ \frac{\partial Q_{NB-1}}{\partial \theta_1} & \cdots & \frac{\partial Q_{NB-1}}{\partial \theta_{NB-1}} & \frac{\partial Q_{NB-1}}{\partial |E_1|} & \cdots & \frac{\Delta Q_{NB-1}}{\partial |E_{NB-1}|} \end{array}\right] \begin{bmatrix} \Delta\theta_1 \\ \Delta\theta_{NB-1} \\ - - \\ \Delta |E_1| \\ \Delta |E_{NB-1}| \end{bmatrix} \tag{9}$$

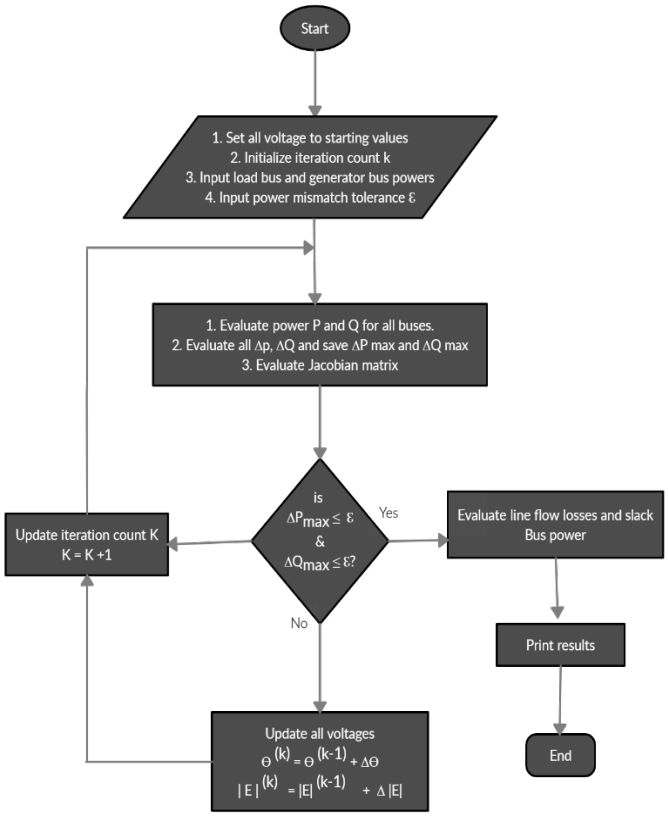
To fasting convergence, multiply voltage corrections by a constant called acceleration factor at each iteration end [3,8,12] as;

$$Q_p^{(k)}(\text{Accel}) = Q_p^{(k-1)} + \propto \Delta Q_p^{(k-1)} \tag{10}$$

$$|E_p|^{(k)}(\text{Accel}) = |E_p|^{(k-1)} + \propto \Delta |E_p|^{(k-1)} \tag{11}$$

where, $\propto$ = acceleration Factor, $0.7 < \propto > 1.4$

The common procedures of Newton-Raphson power flow solution are displayed in flowchart shown in Figure 1.



2.1 Developed NRPF Software Package

In solving power flow solution problem using the Newton-Raphson Technique, some computer programs were written to create the software package. The developed NRPF package was implemented for a small power system network using a personal computer (PC) in the paper presented at IEEE Nigeria Computer Conference [3]. The interface of package and it users are interactively designed. The arrangement of the package was done to limit the PC core memory and made possible by overlaying technique.

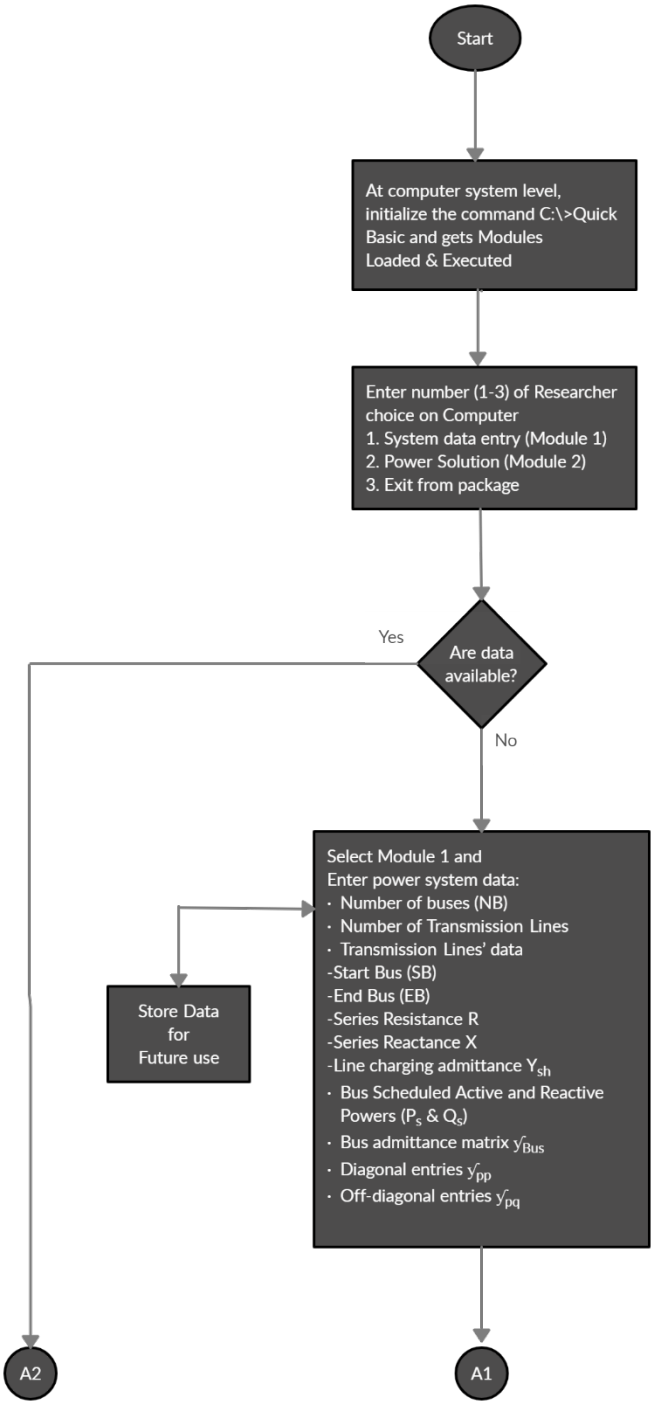
Overlaying reduced the working memory of the computer and allows the package to be put into modules. With this overlaying, the package operation is in 3 steps and named as;

1. NRPF Supervising module
2. ADESINA 1 Power system data entry and Management
3. ADESINA 2 NR power flow solution.

Only one out of the three modules are allowed to resident in core memory of computer at a time. The Quick Basic language command is used to interface the supervising module (NRPF) to each of the other two modules. Computer programs are coded in Microsoft's Quick Basic. These two modules are with their respective complete subroutine procedures.

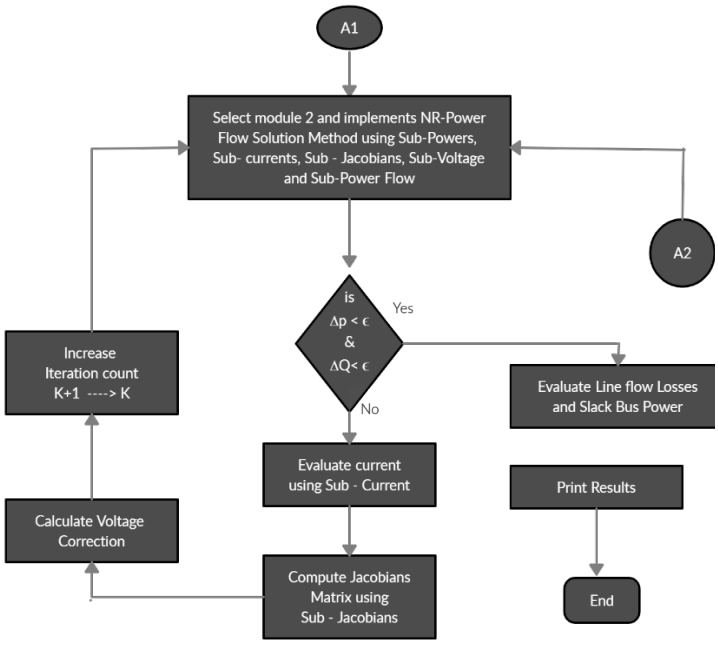
A. Supervising Module (NRPF)

NRPF is more or less act as Controller of the package structure because it allows the user to select which of the two modules is to be executed. At the starting point on computer, the command is C: \>Quick Basic NRPF. This implies loading the module into memory of computer and executes the process. Having activated the module, the computer displays the contents in block 3 of the flow chart in Figure 2



B. System Data Entry Module (ADESINA 1)

This module permits operational or network data input into computer by the user. It loads and executes the selected option on NRPF's menu. The Personal computer (PC) interactively ask for the under listed items.



1. Number of buses (NB) in the network
2. Number of transmission lines (NL)
3. Transmission line data
   - Start bus, (SB)
   - End Bus, (EB)
   - Series resistance, R
   - Series reactance, X
   - Line charging admittance, Y_{sht}
4. The bus scheduled active power P_S and reactive powers Q_S. Bus admittance matrix, Y_{bus}, are formulated. The non – availability of in – built complex arithmetic functions in Quick Basic, the real and imaginary parts of Y_{bus} are calculated separately. The admittance matrix, Y_{bus}, building algorithms are presented as follows;

The diagonal elements (Y_{PP}) of the Y_{bus} matrix is calculated by adding lines' admittances and line charging admittance.

The off-diagonal elements (Y_{pq}) are the negatives of the admittance buses p and q. Where there are no transmission lines between bus p and bus q, then the off-diagonal element is zero.

The aforementioned data above which already entered as module 1 are stored in data files for future use. This means module 1 do not needs calling since the data are already in memory and kept in data files. Exiting from module 1, the NRPF module is reloaded into memory and executed.

C. Power Flow Solution Module (ADESINA 2)

ADESINA 2 module implements the power flow solution technique. It is loaded into memory and executed provided the data files (ADESINA 1) earlier created had been inputted. When it is noticed that the data files are not in memory then computer gives error signal to show that file data is not yet in computer memory. This imply that, in running this module, the user must ascertain that system data entry module has been executed.

However, it is mentioned earlier that Quick Basic programming language have no in – built complex arithmetic library functions. Due to this lack, power flow solution would need reformulation in rectangular co-ordinates so that parameters in complex form can be effectively manipulated. The module is divided into a main programme and five under listed subroutines.

1. Sub Powers
2. Sub Currents
3. Sub Jacobian
4. Sub Voltage
5. Sub Power flows

The flow process of the program's logic is illustrated in Figure 2.

3. Description of Nigerian 330kVTransmission Grid

The Nigerian transmission grid is shown in figure 3. The grid consists of thirty-two buses including nine generator buses and thirty – four transmission lines. There are three power transformers which are usually the power regulation type. These transformers are usually the power regulation type. Each generation station, depending on its installed generation capacity has a number of generators. Some of the generators in the station are made to supply to the grid, while the remaining ones are considered as reserves. The company's installed generation capacities are shown in Table 2 [13] . Table 3 [13] shows the number of units of generators found in each station together with corresponding company's power factor specification. The generating stations have their installed generation capacity and has a number of generator units. Part of installed generators in the station give supply to the grid, while the remaining ones provides the spinning reserves. Available data shows that the total installed generation capacity is 3860MW.

Table 1: Names and Symbols of Buses

Bus No	Bus Name	Bus Symbol
1	Sapele	SPG
2	Osogbo	OS
3	Aiyede	AY
4	Ikeja West	IK
5	Akangba	AK
6	Benin	BN
7	Sapele (L)	SPL
8	Onitsha	ON
9	Enugu	EN
10	Alaoji	ALO
11	Akure	AKR
12	Benin-B	BNB
13	Delta (G)	DTG
14	Ajaokuta	AJ
15	Egbin (G)	EGBG
16	Afam (G)	AFG
17	Portharcourt	PT
18	Aladja	AL
19	Makurdi (G)	MKG
20	Ikom (G)	IKG
21	New-haven	NH

Table 2: Company's Instilled Generation Capacities [13]

Bus No.	Station Name	Installed Capacity (MW)	Type of Station
1.	Sapele	1020	Thermal
13.	Delta	820	Thermal
15	Egbin (G)	1320	Thermal
16.	Afam (G)	700	Thermal
19.	Makurdi (G)	0	Proposed
20.	Ikom	0	Proposed
Total installed Generation		3860	

Table 3: Generator Power Factor Specification for Generation Companies [13]

Substation Location	Number of Units	Power Factor (PF)
Afam I	2	0.80
Afam II	4	0.80
Afam III	4	0.80
Afam IV	6	0.80
Delta I	2	0.80
Delta II	6	0.80
Delta III	6	0.80
Sapele I	4	0.90
Sapele II	4	0.80
Egbin	6	0.80

Table 4: Bus Power and Voltage Specifications in per unit (p.u) [13].

BUS No	P_g(MW)	Q_g(MVAr)	P_{sp}(MW)	Q_{sp}(MVAr)	V(kV)
1	10.2	7.6	0	0	1.0
2	0	0	1.008	0.487	-
3	0	0	1.922	0.897	-
4	0	0	4.55	2.19	-
5	0	0	13.2	5.865	-
6	0	0	2.40	0.75	-
7	0	0	5.10	2.55	-
8	0	0	1.234	0.695	-
9	0	0	2.53	1.226	-
10	0	0	1.638	0.784	-
11	0	0	0.451	0.208	-
12	0	0	1.856	0.896	-
13	8.2	6.15	0	0	1.0
14	0	0	2.20	0.96	-
15	13.2	9.9	0	0	1.0
16	7	5.25	0	0	1
17	0	0	3.39	1.64	-
18	0	0	1.397	0.579	-
19	0	0	0	0	1
20	0	0	0	0	1
21	0	0	0.14	0.57	-

Table 5: Impedance and Shunt admittance of the Transmission Lines in per unit [13]

S/No	SB	EB	Z	YSHT
1	1	7	0 + j 0.0109	0
2	2	3	0.0041 + j 0.0349	0.437
3	2	4	0.0042 + j 0.0344	1.8
4	2	11	0.0037 + j 0.028	0.377
5	3	4	0.0049 + j 0.0416	0.521
6	4	5	0.0003 + j 0.0023	0.13
7	4	6	0.0025 + j 0.0195	4.648
8	4	15	0.0011 + j 0.0086	0.514
9	6	7	0.0005 + j 0.0035	0.832
10	6	8	0.0024 + j 0.0203	1.042
11	6	11	0.0053 + j 0.0483	0.577
12	6	12	0. + j 0.04	0
13	6	14	0.0035 + j 0.028	1.49
14	7	18	0.0011 + j 0.0095	0.478
15	8	9	0.0148 + j 0.01826	0
16	8	10	0.0023 + j 0.0199	1.048
17	8	21	0.0034 + j 0.0292	0.365
18	9	19	0.0018 + j 0.0139	0.208
19	9	20	0.0015 + j 0.0123	0.616
20	10	16	0.0005 + j 0.0035	0.208
21	12	13	0.0054 + j 0.0173	0.612
22	13	18	0.0011 + j 0.0088	0.135
23	16	17	0.0007 + j 0.0049	0.25

Table 6: Bus Power and Voltage Specifications in per unit

BUS NO	Pg (MW)	Qg (MVAr)	Ps(MW)	Qs(MVAr)	V(KV)
1	10.2	7.6	0	0	1.0
2	0	0	1.008	0.487	-
3	0	0	1.922	0.897	-
4	0	0	4.55	2.19	-
5	0	0	13.2	5.865	-
6	0	0	2.4	0.75	-
7	0	0	5.1	2.55	-
8	0	0	1.243	0.695	-
9	0	0	2.53	1.226	-
10	0	0	1.638	0.784	-
11	0	0	0.451	0.208	-
12	0	0	1.856	0.896	-
13	8.2	6.15	0	0	1.0
14	0	0	2.2	0.96	-
15	13.2	9.9	0	0	1.0
16	7.0	5.25	0	0	1.0
17	0	0	3.39	1.64	-
18	0	0	1.397	0.579	-
19	0	0	0	0	1.0
20	0	0	0	0	1.0
21	0	0	1.140	0.570	-

3.1. Software Application to Sub-Nigerian Transmission Grid.

In this section, the developed software is applied to a Sub-Nigerian Transmission Grid which covers the southern region of the country. This grid network is shown in Figure 3. Per unit impedance and Shunt admittance of the transmission lines in the network diagram of this figure 3 are shown in Table 5. Other parameters required in data input into computer includes;

$$Number\ of\ Buses\ =\ 21$$
$$Number\ of\ Lines\ =\ 23$$
$$Slack\ Bus\ Number\ =\ 1$$
$$Slack\ Bus\ Voltage\ =\ 1.0\ +\ j\ 0$$
$$Power\ mismatch\ tolerance\ \epsilon\ =\ 0.001\ per\ unit.$$

The bus scheduled powers for all non-generator buses are already shown in Table 3 above.

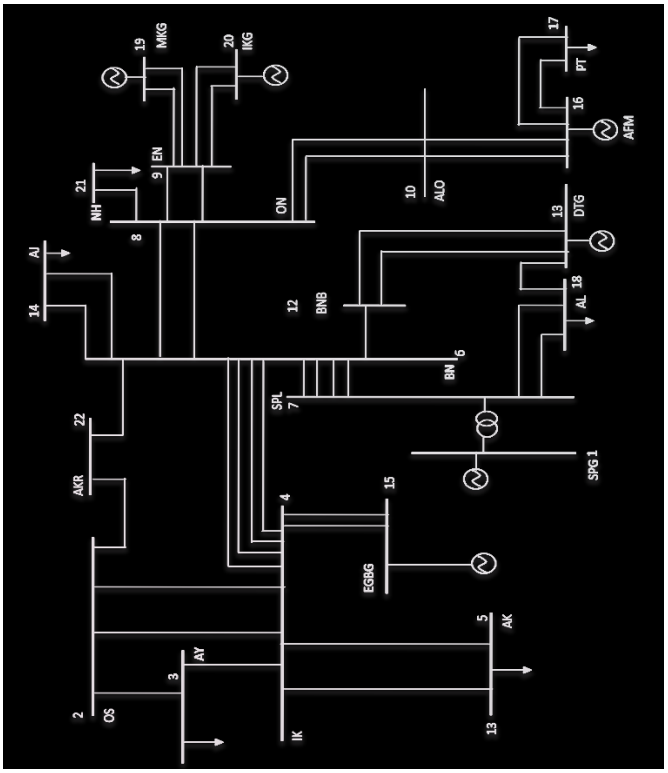


Figure 3: Nigerian 330kV Transmission[3,13]

ADESINA 1 module input data and store in computer memory. These data include; Number of bus bars, Number of transmission lines, Send-end bus bars number, Receiving-end busbar number, Line impedance, Line Susceptance, Bus scheduled active power P_{sp} and reactive power Q_{sp}. It is followed by the formulation of bus admittance matrix. ADESINA 2 module executes the bus voltage calculations which is initialized by slack bus bar assumed voltage, V = 1.00 + j 0 p.u. The system solution converged in third iteration with mismatched power tolerance, ϵ = 0.001 per unit. The power flow solution of this case study is shown in Table 7 to Table 9.

Table 7: Calculated Bus Voltages of the Network in per unit

Bus	Voltage (per unit)
1	1.0+ j 0
2	1.057 + j 0.062
3	1.051 + j .055
4	1.043 + j .045
5	1.043 + j .045
6	1.027 + j .025
7	1.021 + j .019
8	1.031 + j .029
9	1.047 + j .048
10	1.032 + j .029
11	1.046 + j .049
12	1.024 + j .022
13	1.0 + j 0
14	1.027 + j .026
15	1.0 + j 0
16	1.0 + j 0
17	1.032 + j .029
18	1.022 + j .019
19	1.047 + j .048
20	1.047 + j .048
21	1.031 + j .03

Table 8: Evaluated Bus Voltage Magnitudes, Phase Angles, Active and Reactive Powers

Voltage (per unit)			Power (per unit)	
Bus No	Magnitude	Phase Angle (degree)	Active (MW)	Reactive (MVAr)
1	1	0	0	0
2	1.059	3.357	0	2.203
3	1.052	2.996	0	0.479
4	1.044	2.471	0	3.806
5	1.044	2.471	0	0.065
6	1.027	1.395	0	4.294
7	1.021	1.066	0	0.656
8	1.031	1.611	0	1.228
9	1.048	2.625	0	0.724
10	1.032	1.61	0.001	0.628
11	1.047	2.682	0	0.477
12	1.024	1.231	0	0.306
13	1	0	0	0
14	1.027	1.45	0	0.745
15	1	0	0	0
16	1	0	0.001	0
17	1.032	1.61	0	0.125
18	1.022	1.065	0	0.306
19	1.048	2.625	0	0.416
20	1.048	2.625	0	0.308
21	1.031	1.667	0	0.182

Table 9: Calculated Power Flows between the Buses

Buses		Power Flow (per unit)	
From	To	Active	Reactive
1	7	1.746	-1.93
7	1	-1.746	2.004
2	3	-0.221	0.495
3	2	0.221	0.157
2	4	-0.545	0.721
4	2	0.544	-0.063
2	11	-0.516	0.704
11	2	0.514	-0.047
3	4	-0.264	0.744
4	3	0.263	0.37
4	5	0	0.518
5	4	0	0.518
4	6	-1.136	1.278
6	4	1.132	-0.226
4	15	-5.834	5.222
15	4	5.778	-3.786
6	7	-1.936	2.477
7	6	1.933	-0.568
6	8	0.219	0.768
8	6	-0.219	1.14

6	11	0.539	0.592
11	6	-0.541	1.364
6	12	-0.075	1.029
12	6	0.075	0.866
6	14	0.036	0.953
14	6	-0.036	0.946
7	18	0.01	0.09
18	7	-0.01	0.303
8	9	0.112	0.193
9	8	-0.112	0.374
8	10	0.004	0.226
10	8	-0.004	0.329
8	21	0.035	0.28
21	8	-0.035	0.274
9	19	0	0.071
19	9	0	0.071
9	20	0	0.071
20	9	0	0.071
10	16	-9.375	10.947
16	10	9.307	-5.622
12	13	-1.571	0.958
13	12	1.553	-0.902
13	18	2.434	-1.451
18	13	-2.445	3.069
16	17	6.714	-5.047
17	16	-6.768	6.503

4. Discussion of Results

Sapele generating station (Bus 1) of the power system network of figure 3 was chosen as the Slack bus for this analysis. This is because it is one of the sources of supply to the grid. The voltage of generator buses is constrained to 1.0 < 0 per unit.

In Table 8, the magnitude of the bus voltages varies from 1.021 to 1.059 per unit, apart from generator buses that are having 1.00 per unit as constraint value. The bus bar voltages of 0.95 and 1.05 per unit are recognized as the minimum and maximum voltage values for a standard power system grid [1, 2]. Therefore, buses that are having voltage magnitude whose values falls above 1.05 per unit are regarded as overloaded buses[3,8]. From Table 8, buses 2 (Osogbo) and 3 (Aiyede) falls in to this category of overloaded buses. Apart from these 2 bus bars, the calculated voltages of other bus bars in the grid are within the allowable range and therefore such bus bars are not overloaded. Overloaded busbars are often experienced due to high electricity demand as well as long distance between the busbars and the supply sources (generating stations). However, it is explicit in the study that two generation sources are not presently existing in the Nigerian power utility 330kV grid, but they are proposed for future expansion. These generation sources are Makurdi (MKG) and Ikom (IKG).

Table 9 shows the network flow pattern of the power flow solution results. It could be seen that these results justified a steady state condition of the grid because the transmission lines are not overloaded. Giving a clear picture, Table 9 illustrates the flow of active and reactive power from bus bar 2 (Osogbo) to bus bar 3 (Aiyede) measured at Aiyede are - 0.221MW and 0.495MVAr per unit respectively. But measuring the returns at Osogbo, the active and reactive powers are 0.221MW and 0.157MVAr per unit respectively which shows that the active power loss on the line is negligible. While lesser reactive power flow is measured at Osogbo, signifying losses.

Also, from Table 9, the Total Power Loss is obtained to be - 0.220 + j27.054 per unit while Table 2 shows that the total generation installed capacity is 3860MW. However, it's rare to have generation companies operating at an installed generation capacity. Therefore, it is assumed in this study that 75% of installed generation capacity is the generation level of the grid network for Nigeria. Consequently, 2895MW being 75% of installed generation capacity and of course the country generation level. From the above, total active power loss is 0.22 per unit which implies 22MW energy loss. Base on this value and generation capacity, the percentage energy loss in this network becomes 0.76%. This mean that energy lost in the network is very little and negligible. The results in table 9 indicates that the slack bus power S_1 is 1.746 + j2.004 per unit at Sapele Generating station while the power S_2 at bus just immediately after the generation bus termed Sapele load bus is 1.934 + j0.658 per unit. It is observed that S_2 is greater than S_1 because power S_1 has already been stepped up due to the applied step-up transformer that jacked the generated voltage up for transmission purposes.

In addition, the power utility data shown in table 2 shows that the installed generation capacities (active power) in Megawatts for bus bar 1 (the slack bus) is 1020MW (or10.20 per unit). While, the power flow solution results shows that the slack bus power (active) is 1.746 per unit, which of course is lower than the installed generation capacity of 10.20 per unit. This, however, confirms that the use of bus 1 as the slack bus is realistic. The power flow solution converged at eight iterations and the results obtained are quite reasonable, interpretable and reliable. This makes the software package better compared to previous research works where power flow solution either converged at high iteration level or the system did not converge at all leading to no solution.

It was observed that the following transmission lines are either having high reactive power than the active power or both powers are having almost the same values. The affected lines include; line 1-7, 2-4, 2-11, 4-6, 6-7, 10-16, 13-18 and 16-17. This condition is not tolerated in power system as it causes system instability. Therefore, installation of Capacitor bank or other means of absorbing reactive power on those lines is highly recommended to power utility management.

5. Conclusion

This paper presents an application of the developed NR software package to the power flow analysis of Nigerian 330 kV regional power utility grid. The grid consists of 21 buses and 23 transmission lines. Often, a bus bar, preferably a generator bus bar is used as slack bus. Consequently, bus bar 1 (Sapele bus bar) was chosen as the slack bus and its voltage is 1.0 < 0 per unit for this analysis. The voltage of the voltage controlled bus bars (or generator) were also constrained to 1.0 < 0 per unit. The results of the analysis converged at the third iteration. This early convergence of the NR solutions satisfied the theoretical reports of Newton – Raphson iterative algorithm. In addition, early

convergence may not also be unconnected with the use of real life power system grid having reliable operational parameters or data. The results of the power flow analysis for this Nigerian 330kV regional transmission grid are presented and discussed. These results are accurate and reliable. The transmission lines with high reactive power will deserves an installation of equipment that could reduce or control the reactive power on the lines. On the same note, the bus bars with voltage values not fall within the specified range would require the special attention of the power utility company; in this case, Transmission Company of Nigeria (TCN). Furthermore, the package can also be applied to determine the stability of medium voltage distribution feeders.

Conflict of Interest

The authors declare no conflict of interest.

Acknowledgment

The authors sincerely appreciate the Transmission Company of Nigeria (TCN) for providing the data used in this research work.

References

[1] A. Abdulkareem, Power Flow Analysis of Abule-Egba 33-kV Distribution Grid System with real network Simulations., IOSR J. Electr. Electron. Eng. **9,** 67–80, 2014.
[2] I.A. Adejumobi, G.A. Adepoju, K.A. Hamzat, Iterative Techniques for Load Flow Study: A Comparative Study for Nigerian 330kv Grid System as a Case Study, Int. J. Eng. Adv. Technol. **3,** 153–158, 2013.
[3] L.M. Adesina, J. Katende, G.A. Ajenikoko, Development and Testing of Q-Basic Computer Software for Newton-Raphson Power Flow Studies, in: 2019 2nd Int. Conf. IEEE Niger. Comput. Chapter, 1–6, 2019.
[4] R. Alqadi, M. Khammash, An Efficient Parallel Gauss-Seidel Algorithm for the Solution of Load Flow Problems, Int. Arab J. Inf. Technol. **4**, 148–152, 2007.
[5] J. Chakavorty, M. Gupta, A New Method of LoadB_ Flow Solution of Radial Distribution Networks, in: 2011.
[6] H.-C. Kim, N. Samaan, D.-G. Shin, B.-H. Ko, G.-S. Jang, J.-M. Cha, A New Concept of Power Flow Analysis, J. Electr. Eng. Technol. 2, 2007.
[7] M.A. Kusekwa, Load Flow Solution of the Tanzanian Power Network Using Newton-Raphson Method and MATLAB Software, Int. J. Energy Power Eng. **3,** 277, 2014.
[8] L.M. Adesina, O. Ogunbiyi, G. Ajenikoko, Newton-Raphson Algorithm for Power Flow Solution and Application, **9**, 1–17, 2020.
[9] V.K. Shukla, A. Bhadoria, Understanding Load Flow Studies by using PSAT, in: 2013.
[10] S. Singh, Optimal Power Flow using Genetic Algorithm andParticle Swarm Optimization, IOSR J. Eng. **2**, 46–49, 2012.
[11] S. Singh, Load Flow Analysis on Statcom Incorporated Interconnected Power System Networks Using Newtonraphson Method, IOSR J. Electr. Electron. Eng. **9,** 61–68, 2014.
[12] M. Syai'm, A. Soeprijanto, Improved Algorithm of Newton Raphson Power Flow using GCC limit based on Neural Network, Int. J. Electr. Comput. Sci. **12,** 7–12, 2012.
[13] Transmission Company of Nigeria, Line parameters, Bus specified power and voltages, Annu. Mag. Natl. Grid. 2014.

ASTES

Advances in Science, Technology and Engineering Systems Journal
Vol. 5, No. 5, 452-459 (2020)
www.astesj.com

ASTES Journal
ISSN: 2415-6698

Comparative Study of Cryptocurrency Algorithms: Coronavirus Towards Bitcoin's Expansion

Fatma Mallouli[*,1], Aya Hellal [1], Fatimah Abdulraheem Alzahrani[1], Abdulsalam Ali Almadani[2], Nahla Sharief Saeed[3]

[1] *Computer Department, Deanship of Preparatory Year and Supporting Studies, Imam Abdulrahman Bin Faisal University, Dammam 31441, Saudi Arabia*

[2]*Information System Department, College of Computer and Information Sciences, Al Imam Mohammad Ibn Saud Islamic University, Riyadh 13318, Saudi Arabia*

[3]*Computer Department, Community College, Imam Abdulrahman Bin Faisal University, Dammam 31441, Saudi Arabia*

ARTICLE INFO

Article history:
Received: 12 June, 2020
Accepted: 05 September, 2020
Online: 24 September, 2020

Keywords:
Corona virus (COVID−19)
Cryptocurrency
Blockchain
Asymmetric

ABSTRACT

The widespread presence of Corona virus (COVID-19) is causing organizations and individuals major economics downsizing. The way this virus is transmitted from one individual to another is the real cause of the problem. For that, researchers in different fields started seriously looking for touch-less and contact-less exchange. Particularly in the finance world, cash transactions and key pad based transactions are becoming obsolete because they are some of the major causes of the spread of this virus (and other viruses and bacteria). Cryptocurrency could be one of the solutions to the above mentioned situation. This novel money is based on Blockchain technology, which is based on cryptography algorithms for the safety and the security of the transactions. This paper exhibits a comparative study of the asymmetric cryptography algorithms. This helps the user to best choose the most secure, safe and reliable method to encrypt/decrypt the transactions created in the Blockchain.

1 Introduction

Over the last eight months, the number of corona patients has increased dramatically all over the world. The direct impact on world economy was a major decrease of financial development in numerous countries. The spread of this contagious disease is caused by the direct contact or by touching humans , objects like Credit cards, physical wallets, and cash money, or by the use of contact code ATM and other machines. The wide spread of the current epidemic caused significant losses to organizations, individuals, and governments which made the corona prevention a hot subject for all researchers. This quick corona spread forced everybody to adopt virtual and contact less applications to ensure safe and secure financial transactions. Our topic is simply one of the possible solutions that can help the finance world to adopt the Blockchain technologies for the creation of new coins called cryptocurrency. These currencies could, in the near future, take a portion of the financial transactions currently governed by banks. Our research is on how to best secure these transactions, or in other words, how to choose the best methods/algorithms to encrypt/decrypt messages while creating the Blockchains. This research is an extension of work originally presented in a conference named "International Conference on Cyber Security and Cloud Computing, CSCloud 2019". In order to introduce the new epidemic corona virus that changed the concept of dealing with physical money and lead people and investors to use innovative technology such us BlockChain and Bitcoin [1] as a preventive and safe way to cope with corona virus epidemic. The corona virus (COVID-19) flare-up in late 2019 involves a genuine danger around the globe [2]–[3]. The seriousness of the plague was enormous to such an extent that the World Health Organization(WHO) was firm to announce that corona virus (COVID-19) is a pandemic, around a month after the first apparition. The corona spread disabled all kind of vital economic [4] drivers like airports, [5] and transportation industry, education, tourism and related fields, government agencies, etc. The world started looking for alternative solutions to keep economy going while keeping a distance between the person and anything surrounding him/her. Particularly in the finance world, the correlation between Bitcoin and the equities market has obviously increased [6, 7]. The rest of this article is organized as follows. section 2 introduces corona virus dis-

[*]Corresponding Author: Fatma Mallouli, Imam Abdulrahman Bin Faisal University, Dammam 31441, Saudi Arabia, fmmallouli@iau.edu.sa

ease and its impact on the wold economies and finances. Section 3 introduces, summarizes, and explains cryptography and its different branches in the first three subsections; then focuses on introducing BlockChain/Bitcoin and their terminologies [8]–[9]. Section 4 explains the RSA asymmetric algorithm while Section 5 does the same for El Gamal asymmetric algorithm. Section 6 presents a brief comparison between RSA and El Gamal. Section 7 explains the Elliptic Curve (ECC) asymmetric algorithm, where Section 8 presents a comparison between RSA and ECC. Finally, in Section 9, we conclude and present some promising future directions in this field .

2 Coronavirus Disease (COVID-19)

By the end of the year 2019, a new Corona virus disease appeared known as SARS-CoV-2 has resulted in the outbreak of a respiratory disease called COVID-19 [10]. It is a contagious epidemic caused by a newly discovered corona virus. People who got infected with the COVID-19 epidemy will experience fever and respiratory problems. Until today recovering do not require special treatment which is not found yet also, vaccination is not available yet. Corona virus is so dangerous specially while attacking older people, and those with underlying medical problems like cardiovascular disease, diabetes, chronic respiratory disease, and cancer. Corona virus caused many deaths in several countries. During this early period, researchers scientists exploring the main cause of this novel epidemic by investigating clinical manifestation and diagnosis. Thus, all of them agree that the causes are still not known yet, but they all agree that prevention is the only way to be safe from this danger. In fact, exchanging cash money hand to hand is one of the major causes of the rapid spread of covid-19 virus [11]. When possible it's a good idea to use contact less payments. Based on the fact that prevention is the safe procedure therefore people run away from cash money to use the digital money transactions. One of the newest applications of digital money is the Blockchain- based-cryptocurrency [12]. Are we going to see our planet without cash, without ATM-machines and without third party financial institutions?

2.1 Cryptography

In a simple way, defining Cryptography [13] is systematically hiding information. By doing so, only the authorized parties on both ends of the communication link can access the right information. The process can be considered as an art, however, it is actually a science. Broadly, Cryptosystems are classified into two main categories, the asymmetric (Figure 3) and the symmetric (Figure 2). This classification is based on the concepts of the key used.

2.2 Concepts Used in Cryptography

In the coming paragraph, we described some of the cryptography concepts [14]–[15].

Cryptography: also termed as "secret writing" is a science of concealing information so that only the intended parties can have access to the private information. It protects the privacy and modification of data which may occur due to active and passive attacks in the channel. *Encryption:* Transforming a message written in plain text into a cipher text message is the encryption process.

Decryption: The decryption process is writing back a cipher text message into its original plain text message.

Plain Text: The plain text is nothing but the raw message communicated orally or in writing using any human language. It takes the form of plain text. the plain text could be read or heard then understood by the sender, the recipient, or by any third party that has accessed the transmitted message.

Cipher Text: Cipher [16] simply the secret message or the coded message. When applying a suitable scheme to codify a plain text, the output message is named a cipher text.

Key: the most important part of the process of the encryption and decryption is the choice of the key. It is the base of security in the cryptography process. The type of the key chosen defines the class (Symmetric or asymmetric).

Symmetric key: also known as secret key cryptosystem [17]. We only use one key to encrypt and to decrypt.

Asymmetric key: also known as public key cryptosystem. contrary to the Symmetric [18] , the Asymmetric needs two keys: one to encrypt and one to decrypt.

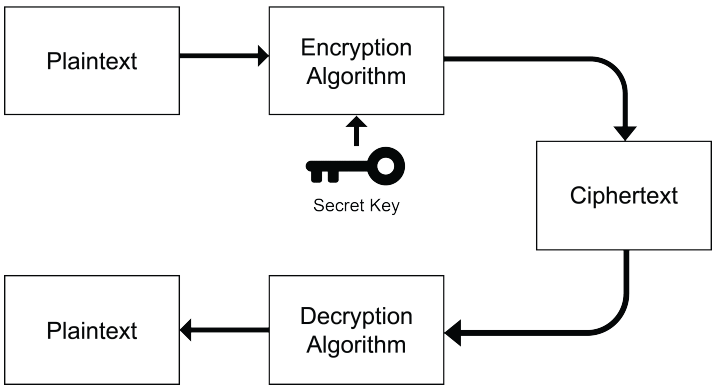


Figure 1: Symmetric Encryption

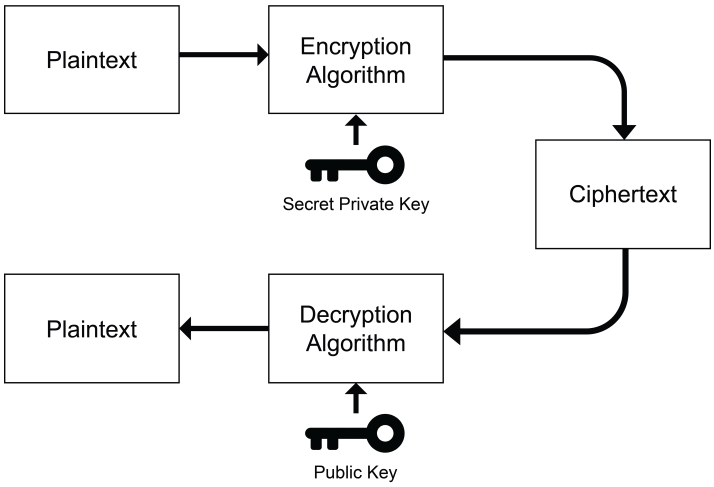


Figure 2: Asymmetric Encryption

Encryption Standard (DES)Algorithm: In 1977, IBM invented a symmetric key bloc and named it Data Encryption Standard (DES). It uses a 64-bits block size and a 56-bits key size (in which the parity bits are 8 bits) to encrypt any plain text of 64 bit in size.

Triple Data Encryption Standard (3DES): In 1978, IBM modified DES Algorithm and created a new version of it called 3DES or Triple Data Encryption Standard. The 3DES is meant to enhance the security of the data. 3DES uses a 64-bits block size and a 56-bits key size just like the DES, but it performs the same DES algorithm 3 times to every block of the data. The 3DES is definetely more secure than the DES, but it is vulnerable to brute force attack [19].

Advanced Encryption Standard (AES): Developed by the National Institute of Standard and Technology (NIST) to replace the two prior algorithms listed above after defining the weak points of the DES and the 3DES. AES-128, AES-192 and AES-256 make up the 3 block ciphers of AES. The difference between the 3 blocks is in the key size and the number of rounds. While AES-128 has a 128-bits key length and consists of 10 rounds, AES-192 has a 192-bits key length and consists of 12 rounds, and AES-256 has a 256-bits key length and consists of 14 rounds. Every round goes through a series of steps. For example: Substituting a Byte, or Shifting a row, or Mixing columns, or Adding Round Key, etc... AES Algorithm is much more secure when compared to DES or 3DES.

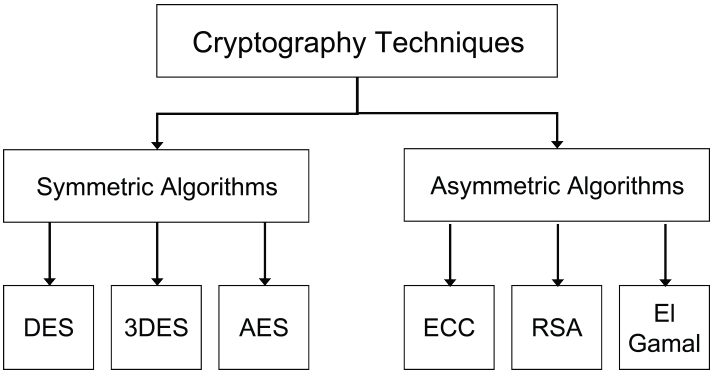


Figure 3: Cryptography Technique

There are many cryptography algorithms used to secure information divided in two groups, symmetric and asymmetric [20]. symmetric algorithms such as DES, 3DES, AES, and Asymmetric such as RSA, El Gamal and ECC [21]. Each algorithm has its own advantages and disadvantages. Therefore, the challenge is how to define the best alternative in terms of security and running time. This work is meant to focus only on comparing the asymmetric algorithms: RSA,ElGamal and ECC which will be presented and defined in the coming sections.

2.3 Need of Cryptography

Cryptography is used to achieve many goals [22], and some of the goals are listed below:

- Access Control: Only the confirmed authenticated person or group is eligible to log into the received message.
- Data Integrity: The guarantee that no change or modification has occurred to the message while in transit.
- Non-Repudiation: The sender cannot deny sending the message, and the receiver cannot deny the reception of the delivered message.
- Authentication: is identifying a special person or group to access special resources using keys.
- Confidentiality: is the fact that only the end link (receiver) is the owner of the cipher key. This is the major or the ultimate objective of cryptography.

2.4 Overview Of BlockChain Terminology and its main application: Bitcoin

Blockchain was first introduced in the early nineties of the twentieth century, but was not used in any application till 2008. The first appearance of Blockchain was to introduce the first cryptocurrency: Bitcoin. From its name, Blockchain is simply a series of blocks of information connected together like a chain [13]. The information in each block is a digital ledger (see Fig.1) linked in a database that is distributed to all users. An important feature of Blockchain is the fact that it is so hard to remove a piece of information added to the ledger. Since the base of the Blockchain is exchanging information peer-to-peer, then there is no need for a third party interference. Therefore, Blockchain is a decentralized exchange of information. The question now is why all this enthusiasm for Blockchain? and the answer is simply because of the qualities tied to this technology. Blockchain focuses on anonymity, on security, and on data integrity without having an outsider (third party such as a bank) in charge of the exchange transaction.

During this research, and while looking into different scientific papers, we noticed that over 80% of the papers concentrate on cryptocurrency like the Bitcoin framework, and less than 20% focused on other Blockchain applications like the Smart Contracts and Licensing. The researches in this field also concentrate on improving the technology of Blockchain in terms of security and privacy. Our paper in its comparison of the different algorithms used for cryptography proposes and exhibits the better performance of utilizing the elliptic curve algorithm in the creation of the digital signature associated with the Bitcoin. Digital signature is the key parameter used to identify the users (end links) and to recognize any unapproved changes occurred to the transaction [17, 23]. The digital signature within the Blockchain technology is The part that guarantees the authentication, and the non-repudiation as well as the integrity of the messages (blocks). It is an electronic verification to the beneficiary of the identity of the sender, and the integrity of the information stored in the delivered block. Technically, digital signatures use a mix of hash functions and public key cryptography. First, a hash function is applied to digest the message. Then, encoding is applied to the message digest to create the signature using the endorser's private key. Any receiver can use the public key and a similar hash function to check the transmitted signature. Up to date, most cryptocurrency frameworks have utilized an Elliptic Curve Digital Signature Algorithm (ECDSA).

2.5 Main terminology of BlockChain and Bitcoin

2.5.1 BlockChain

It is a growing list of records (blocks) linked together using cryptography. Every block is composed of:

1. Hashing
    - The hash of the prior block Hashing is the procedure that a miner on a Proof-of-Work Blockchain constantly repeats in order to find an eligible signature (aka a proof of work). In other words; it is the procedure of repeatedly inserting a random string of digits into a hashing formulae until finding a desirable output.
2. A time stamp
3. Transaction data:
    - By design, the Blockchain is an open distributed ledger that is very resistant to modification of data.
    - There is no need for a third-party approval of any transaction: decentralized.
    - The BlockChain is managed by peer-to-peer network: distributed ledger
4. Block
    - found in the Bitcoin Blockchain. Blocks connect all transactions together. Transactions are combined into single blocks and are verified every ten minutes through mining. Each subsequent block strengthens the verification of the previous blocks, making it impossible to double spend bitcoin transactions (see double spend below).

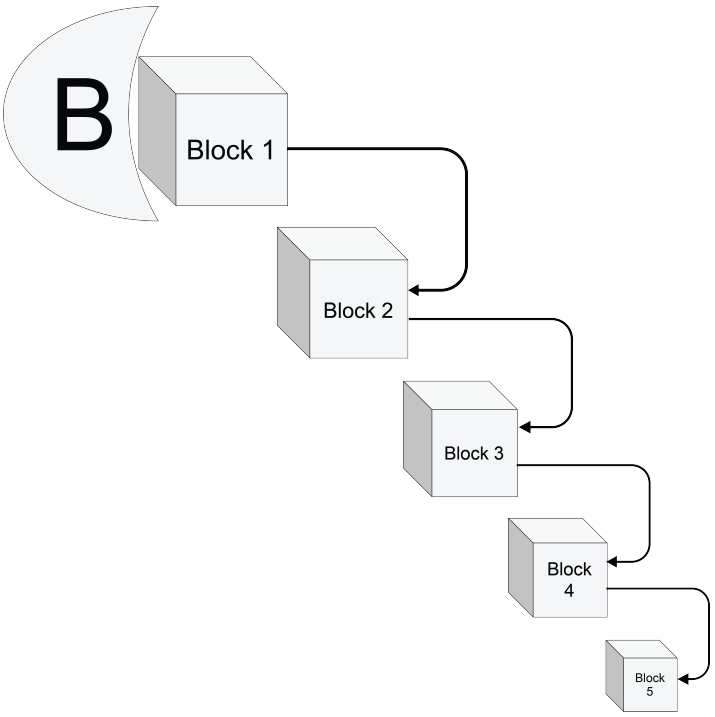


Figure 4: BlockChain System

2.5.2 Bitcoin Blockchain

Bitcoin Blockchain is a public ledger recording bit coin transactions. Blocks are created every ten minutes and distributed to all [24, 25].

1. Mining: record keeping service (using computer power)
2. Decentralized: use of public/private key is the basis of decentralization
    - No central storage (the bit coin ledger is distributed)
    - Ledger is public: any body can store it on their personal computer
    - There is no single admin: the ledger is maintained by equally privilege minors
    - Any body can become a minor
    - Issuance of bit coins is decentralized: they are issued as a reward for the creation of a new block.

3 RSA Algorithm

In 1978, and in one of MIT labs in Massachusetts, the professors Leonard Adleman ,Adi Shamir, and Ron Rivest invented the encryption algorithm RSA abbreviated from the three names of the inventors [7]. RSA is classified as an asymmetric type of encryption in which two keys are needed: the first is public and it is available to all users to encrypt their messages. The second key is private and it is used in the decoding procedure of the encrypted message. While symmetric encryption uses just one key to code and to decode the raw information, asymmetric uses two various keys. The major advantage of the asymmetric algorithm over the symmetric is the strong encryption that makes the decryption process much more complicated for hackers to interfer in the process and cause any damage to the raw message or to the signatures.

Implementing the RSA algorithm on a plain text requires several steps summarized by Adki and Hatkar as follows: first, select two prime numbers p and q.Then, a modulus n is picked for the public key and the private keys to be the product of p and q [26, 27]. The next step is to select a public key named e where e cannot be a factor of $(p-1)(q-1)$. The step after is to calculate the private key d using the following formula $(d * e) \bmod (p-1)(q-1) = 1$. The next step is to calculate the encrypted cipher text using the following formula C= Me mod n, where C is the output text, and M is the raw message text. Finally, using the same variables as the prior step M and C to calculate the decryption using the following $M = Cd \bmod n$. Note that the size of the key must be greater than 1024 bits to guarantee a high level of security, and to make it difficult for hackers to identify [13]. Example1 is a good illustration of the process.

Example 1: The following example is an excellent illustration of how the RSA public key encryption algorithm works. In this example, we picked two small prime numbers p and q to be 5 and 7 respectively. Then, using the two parameters given, we generated the public key and the private keys as follows:

- Given 5 to represent p
- Given 7 to represent q

- Computation of the modulus n: $n = p * q : n = 5 * 7 = 35$
- Compute $m = (p-1) * (q-1) : m = 4 * 6 = 24$
- Select e, so that e and m are co-prime numbers:
- $e = 5$
- Compute the private key d, so that d*e mod m = 1: d = 29
- The public key $\{n, e\}$ is = $\{35, 5\}$
- The private key $\{n, d\}$ is = $\{35, 29\}$
- With the public key of $\{35, 5\}$, encryption of a raw text M represented as number 23 can be illustrated as:
- Given public key $\{n, e\}$ as $\{35, 5\}$
- Given raw text M represented in number as 23
- Divide B into blocks: 1 block is enough in our example
- Compute encrypted block $C = M \wedge e \bmod n$:

$C = 23 \wedge 5 \bmod 35 = 6436343 \bmod 35 = 18$ The cipher text C represented in number is 18 With the private key of 35, 29, decryption of the cipher text C represented as number 18 can be illustrated as: Given private key n,e as 35,29 Given cipher text C represented in number as 18 Divide C into blocks: 1 block is enough Compute encrypted block:
$M = C \wedge d \bmod n$:
$M = 18 \wedge 29 mod 35 = 18 * 18 \wedge 28 \bmod 35$
$= 18 * (18 \wedge 4) \wedge 7 \bmod 35$
$= 18 * (104976) \wedge 7 \text{mod} 35$
$= 18 * (104976 \bmod 35) \wedge \bmod 35$
$= 18 * (11) \wedge 7 \bmod 35$
$= 18 * 19487171 \bmod 35$
$= 350769078 \bmod 35$
$= 23$
The raw text M represented in number is 23.

4 EL GAMAL Algorithm

The El Gamal method is an asymmetric cryptosystem algorithm [28]. It is so incredible as far as coding and decoding. This algorithm presents a similar structure while encrypting within the public key and private key models. Subsequently, encryption is not the same as signature check . signature creation relies upon the El Gamal signature method. The principle weaknesses of El Gamal algorithm are first the requirement for randomness, and the slow speed during coding and decoding. The primary disadvantage of this algorithm is that during encryption, the message is extended by a factor of two. This leads to having an expanded cipher text which is twice the length of the raw text. On a positive note, such message development is insignificant if the cryptosystem is utilized uniquely for secret keys exchange.

4.1 El Gamal Encryption Algorithm

begin: *Initialisation:Domainparameters (p,q,g); recipient's public key B; encoded message m in range* $0 < m < p - 1$. *OUTPUT: Ciphertext (c1,c2).*

1: Choose a random $k$in the range $1 < k < p - 1$
2: Compute $c_{1=}g^{k} \bmod p$
3: Compute $c_{2=}m * B \bmod p$
4: Return ciphertext (c_1, c_2)

The ciphertext is the pair (c1,c2), which are both about p bits long. Neal Koblitz [KOB94] describes c2 as the message m "wearing a mask" and c1 as a "clue" which can be used to remove the mask, but only by someone who knows the secret key b.

4.2 El Gamal Decryption Algorithm

begin: *Initialisation: Domain parameters* (p, q, g)*; recipient's private key b; cipher text* $(c1, c2)$. *OUTPUT: Message representative, m.*

1: Compute $m = c_1^{p-b-1} c_2 \bmod p$
2: Compute $c_{2=}m * B \bmod p$
3: Return m

Note that ,$c_1^{p-b-1} = (c_1^b)^{-1}$, since for any, $c \in \mathbb{Z}_p^* Z.c^{p-b-1} = c^{-b}.c^{p-1} = c^{b^{-1}}.1$ as $c^{p-1} = 1$

5 Comparison EL GAMAL Algorithm and RSA Algorithm

El Gamal algorithm isn't automatically secure. it can not exclusively be utilized in data encryption, however in numeric signature and the security depends on the issue of divergence logarithm in finite domains [28]. The procedure steps in El Gamal algorithm to RSA starts by picking a prime number p, and two random numberg, x, where $g < p$ and $x < p$, calculate $Y = g \wedge x(\bmod p)$, of which Y, g, and p are the public Comparison of El Gamal and RSA models has been done based on security and time utilization for coding and decoding. RSA is reliable and can be utilized for application in remote system on account of its efficient running time speed, and high security level. This research examines that El Gamal algorithm is safer when contrasted with RSA method on the grounds that it generates much collocated cipher text and it was likewise moderate because when we encode and decode it, it produces more than one public key. In [29], the author demonstrates that El Gamal digital signature security is continually being tested and increasingly becoming in-genuine. An improved El Gamal comparison is proposed. Despite the fact that, El Gamal algorithm is considered secure and efficient and It has the benefit of making the equivalent plain text that gives an alternate cipher text, every time during encryption. Meanwhile, it has its own burdens. The fundamental issue that only one random number is utilized. Likewise examinations and researchers demonstrated another major disadvantage: the cipfer text is twice the length of the plain text. El Gamal Algorithm slightly different to RSA as appeared in Table 1.

Table 1: Summary Table On Asymmetric Algorithms Of RSA And El Gamal

S.NO	Factors	RSA	El-Gamal
1	Developed	1978	1985
2	Key Length Value	>1024 bits	1024 bits
3	Type of Algorithm	Asymmetric	Asymmetric
4	Security Attacks	Timing Attack	Meet-in-The middle Attack
5	Simulation Speed	Fast	Fast
6	Scalability	No Scalability occurs	Good scalability
7	Key Used	Different key used for Encrypt and Decrypt Process	Different key used for Encrypt and Decrypt Process
8	Power Consumptin	High	Low
9	Hardware and Software Implementation	Not very efficient	Faster and efficient

6 ELLIPTIC CURVE Algorithm

Independently and in two different years (1985 and 1987), Neal Koblitz and Victor S. Miller introduced Elliptic Curve Cryptography (ECC) [30]. Elliptic curve cryptography was a smart way of transforing a mathematical problem into an applicable computer algorithm. In general, The notion of public key cryptography is what brings complexity into any asymmetric cryptosystem. Elliptic Curve cryptography (ECC) is based upon the algebraic structure of elliptic curves over a finite field. Figure 6 is a graph illustration of the elliptic curve, and the following example 2 is a numeric illustration of the elliptic curve as well.

Example 2: $(p = 7, n = 2, a = 1, b = 6)$
$y^2 = x^3 + x + 6$
(Note:$4 + 27 * 36 = 976 = 3$ mod7)
There are 49 integer points on this "curve"
Ex: $(3, 6) \rightarrow 3 \wedge 3 + 3 + 6 = 36 \bmod 7 = 1 = 6 \wedge 2 \bmod 7$
$(4, 2) \rightarrow 4 \wedge 3 + 4 + 6 = 74 \bmod 7 = 4 = 22 \bmod 7$
$(6, 5) \rightarrow 6 \wedge 3 + 6 + 6 = 228 \bmod 7 = 4 = 52 \bmod 7$
Points on the "curve" for which there are solutions: $(1, 1), (1, 6), (2, 3), (2, 4), (3, 1), (3, 6), (4, 2), (4, 5), (6, 2), (6, 5)$
Note: $(3, 1), (2, 3), (6, 2)$ are on the same line.
$y = 2x + 7, y = x/3$ are the same line
(7 mod 7 = 0, 1/3 is the inverse of 3 which is - 2).

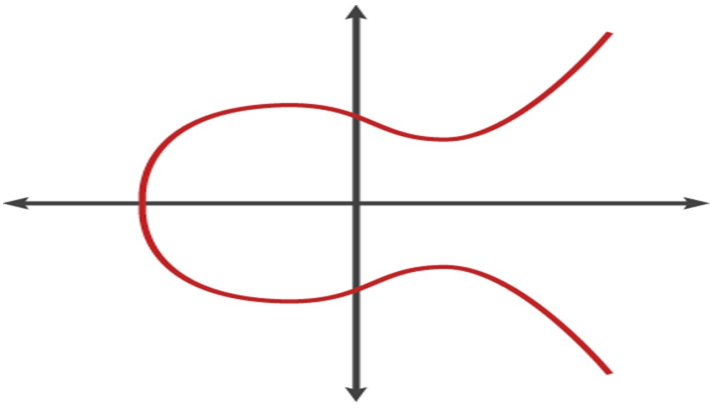


Figure 5: elliptic-curve-cryptography

7 Comparison between ECC and RSA Algorithms

While transmitting the encrypted text using RSA, the private key is not attached to the message. This feature is a primary advantage of RSA over other algorithms since it makes it impossible for a hacker to know the private key. Another very powerful feature of RSA is providing a digital signature by the public key [14]. The importance of the online digital signature comes from the fact that it solves two major security issues. The first is that the message could only be sent to the required person with no changes, and second, it guarantees the identity of the sender [31, 32]. The listed advantages eventually cause the RSA algorithm to be slow in processing, which is the major disadvantage of RSA [14].

Compared to other double key algorithms, ECC lies over a mathematical structure : elliptic curves over a finite field. The algebraic model gives this algorithm a set of advantages over RSA. The primary and most important feature is the length of the key. For the same security level, if RSA requires 1024 bit key, ECC would only require 160 bit key. This gives ECC the advantage to be very appropriate for wireless communications. Actually, in practice ECC became the number one choice for networks and for communication devices due to the size and the efficiency benefits. Today's 'devices that are accessing networks and services are small in size and with minimal power use: this had given ECC cryptography the edge because of the use of tiny key sizes and because of the computational efficiency tied to Elliptic Curve Cipher.

Process wise, Elliptic curve cryptography is more complicated than RSA. While in RSA, only one coding algorithm is used; in ECC, different ways of encryption are applied. When confidentiality is the objective, ECC uses arithmetic algorithms for high-level security functions, and if authentication is the objective ECC implements the digital signature processes. ECC can either be implemented in hardware or in software. ECC applies very generic procedures, therefore if a group of users agree on publicly known data, then every user can generate their own keys (private key and public key) [13, 33, 31, 30, 34, 35]. As shown in Table 2, and compared to RSA, Elliptic Curve Cryptography is clearly more efficient and can provide higher security.

Table 2: Comparison between RSA and ECC

Security bit level	RSA	ECC
80	1040	160
112	2048	224
128	3072	256
192	7680	384
256	15360	512

8 Conclusion

counting more than 200,000 detailed passings. The fear of this as of late recognized illness has closed businesses and grounded thousands of flights. When the syndrome (covid-19) virus hit the world economy in 2020, lots of people lost their jobs and business. Investors start very pessimistic about the dramatic harmful economic consequences. To rebound the market slowly within this contagious epidemic seems like a problematic situation. The new deadly corona virus is a detrimental effect on the global economy. This lead people and investors to use Bitcoin and get a way from cash money contact. the concentration on Bitcoin which is the Blockchain main application remain us to focus on the popular algorithms used in the cryptography world . Innovative technologies such as Blockchain and its major bitcoin application have interfered as promising solutions for fighting effects of corona virus epidemic on cryptocurrency. This paper presents a comparative study of different key algorithms like :RSA, El Gamal and ECC. in this study we have compared RSA, El Gamal and Elliptic Curve algorithms to demonstrate the performance of Elliptic Curve algorithm. We have shown that the elliptic curve crypto-schemes offer the highest security per bit ratio compared to any other currently known public-key cryptosystem. This is a plus point for cryptography system during corona virus epidemic where the future of Bitcoin is a hot subject. To ensure high security levels for cryptocurrency system , Elliptic Curve Cryptography is highly recommended. the pandemic of covid-19 has a negative impact on business meanwhile this disruption is a challenge to the technologies to take over the classical procedures. during the world crises of the corona virus, Blockchain help in economy Recovery and it is a pivotal engine to accelerate financial transactions. Bitcoin plays an important role in world finance transactions. it is becoming very useful today while corona epidemic drives for accelerating the use of digital money.This paper might helps the user to use the most efficient method to encrypt/decrypt the transactions created in the Blockchain. However, Elliptic curve crypto-schemes offer a lot of promise in terms of security and memory requirement than any other present crypto-schemes. more research is needed in this field for better understanding and effective correlation of bitcoin and ECC.

References

[1] F. Mallouli, A. Hellal, N. S. Saeed, F. A. Alzahrani, "A Survey on Cryptography: Comparative Study between RSA vs ECC Algorithms, and RSA vs El-Gamal Algorithms," 2019 6th IEEE International Conference on Cyber Security and Cloud Computing (CSCloud)/ 2019 5th IEEE International Conference on Edge Computing and Scalable Cloud (EdgeCom), 173–176, 2019, doi:10.1109/CSCloud/EdgeCom.2019.00022.

[2] E. Livingston, K. Bucher, "Coronavirus disease 2019 (COVID-19) in Italy," Jama, **323**(14), 1335–1335, 2020, doi:10.1001/jama.2020.4344.

[3] R. E. Ferner, J. K. Aronson, "Chloroquine and hydroxychloroquine in covid-19," 2020, doi:10.1136/bmj.m1375.

[4] M. Kumar, S. Srivastava, "Image authentication by assessing manipulations using illumination," Multimedia Tools and Applications, **78**, 12451–12463, 2018.

[5] Z. Allam, D. S. Jones, "On the coronavirus (COVID-19) outbreak and the smart city network: universal data sharing standards coupled with artificial intelligence (AI) to benefit urban health monitoring and management," in Healthcare, volume **8**, 46, Multidisciplinary Digital Publishing Institute, 2020, doi:10.3390/healthcare8010046.

[6] P. S. S. H. Vikrant M. Adki, "A Survey on Cryptography Techniques," International Journal of Advanced Research in Computer Science and Software Engineering, **6**, 2016.

[7] V. K. Mitali, A. Sharma, "A Survey on Various Cryptography Techniques," International Journal of Emerging Trends & Technology in Computer Science, **3**, 2014.

[8] G. Brown, R. Whittle, Algorithms, Blockchain & Cryptocurrency: Implications for the Future of the Workplace, Emerald Group Publishing, 2020.

[9] A. Hachicha, F. Hachicha, "Analysis of the bitcoin stock market indexes using comparative study of two models SV with MCMC algorithm," Review of Quantitative Finance and Accounting, 1–27, 2020.

[10] R. a. Vishvkarma, "The Dedicated Databases for COVID-19 Research," GMJ Medicine, **4**(1), 2020, doi:10.29088/GMJM.2020.256.

[11] H. Aldawsari, A. Alnagada, "Coronavirus Economic Effects on the Seven Largest Advanced Economies in the World (G7)," 2020, doi:10.2139/ssrn.3613725.

[12] J. Bouoiyour, R. Selmi, "Coronavirus Spreads and Bitcoin's 2020 Rally: Is There a Link?" 2020, doi:10.13140/RG.2.2.16003.86561.

[13] S. K. G. Omar G. Abood, "A Survey on Cryptography Algorithms," International Journal of Scientific and Research Publications, **8**, 2018, doi:10.29322/IJSRP.8.7.2018.p7978.

[14] A. Kahate, Cryptography and Network Security, McGraw Hill Education, 2013.

[15] A. Shah, M. Engineer, "A survey of lightweight cryptographic algorithms for iot-based applications," in Smart Innovations in Communication and Computational Sciences, 283–293, Springer, 2019.

[16] M. M. Hammood, K. Yoshigoe, A. M. Sagheer, "RC4-2S: RC4 stream cipher with two state tables," in Information Technology Convergence, 13–20, Springer, 2013.

[17] R. L. Rivest, A. Shamir, L. Adleman, "A Method for Obtaining Digital Signatures and Public-key Cryptosystems," Commun. ACM, **21**(2), 120–126, 1978, doi:https://doi.org/10.1145/359340.359342.

[18] S. A. Ritu Tripathi, "Comparative Study of Symmetric and Asymmetric Cryptography Techniques," International Journal of Advance Foundation and Research in Computer, **1**, 2014.

[19] R. K. Hussein, A. Alenezi, H. F. Atlam, M. Q. Mohammed, R. J. Walters, G. B. Wills, "Toward confirming a framework for securing the virtual machine image in cloud computing," Advances in Science, Technology and Engineering Systems, **2(4)**, 44–50, 2017, doi:doi:10.25046/aj020406.

[20] D. Jost, U. Maurer, J. L. Ribeiro, "Information-Theoretic Secret-Key Agreement: The Asymptotically Tight Relation Between the Secret-Key Rate and the Channel Quality Ratio," in A. Beimel, S. Dziembowski, editors, Theory of Cryptography — TCC 2018, volume **11239** of *LNCS*, 345–369, Springer International Publishing, 2018.

[21] A. Poojari, H. Nagesh, "A Comparative Analysis of Symmetric Lightweight Block Ciphers," in Emerging Technologies in Data Mining and Information Security, 705–711, Springer, 2019.

[22] K. N. Jassim, A. K. Nsaif, A. K. Nseaf, A. H. Hazidar, B. Priambodo, E. Naf'an, M. Masril, I. Handriani, Z. P. Putra, "Hybrid cryptography and steganography method to embed encrypted text message within image," Journal of Physics: Conference Series, **1339**, 012061, 2019, doi:10.1088/1742-6596/1339/1/012061.

[23] U. M. Christian Badertscher, B. Tackmann, "On Composable Security for Digital Signatures," in Public-Key Cryptography, volume **10769** of *LNCS*, 494–523, Springer, 2018.

[24] S. Underwood, "Blockchain beyond Bitcoin," Communications of the ACM, **59**, 15–17, 2016, doi:10.1145/2994581.

[25] U. M. D. T. Christian Badertscher, Juan Garay, V. Zikas, "But Why does it Work? A Rational Protocol Design Treatment of Bitcoin," 2018.

[26] X. Meng, X. Peng, L. Cai, A. Li, Z. Gao, Y. Wang, "Cryptosystem based on two-step phase-shifting interferometry and the RSA public-key encryption algorithm," Journal of Optics A: Pure and Applied Optics, **11**(8), 085402, 2009, doi:10.1088/1464-4258/11/8/085402.

[27] M. Kumar, "Advanced RSA cryptographic algorithm for improving data security," in Cyber Security, 11–15, Springer, 2018.

[28] R. Ansah, E.-P. Samuel, D. Attuabea, B. Adjei, B.-R. K Bawuah, P. Antwi, "Relevace of Elliptic Curve Cryptography In Modern-Day Technologie," **3 (2)**, 1–10, 2018.

[29] R. Ansah, R. Boadi, W. Obeng-Denteh, A. Y Omari-Sasu, "Review of the Birch and Swinnerton-Dyer Conjecture," 182–189, 2016, doi:10.5923/j.ajms.20160604.07.

[30] A. U. Hardik Gohel, "Study of Cyber Security with Advance Concept of Digital Signature," International Journal of Advanced Research in Computer Science, **6**, 2015.

[31] H. Adki, V. M., "A Survey on Cryptography Techniques," International Journal of Advanced Research in Computer Science and Software Engineering, **6**, 2016.

[32] Z. Xi, L. Li, G. Shi, S. Wang, "A comparative study of encryption algorithms in wireless sensor network," in Wireless Communications, Networking and Applications, 1087–1097, Springer, 2016.

[33] X. Sun, M. Xia, "An Improved Proxy Signature Scheme Based on Elliptic Curve Cryptography," in 2009 International Conference on Computer and Communications Security, 88–91, 2009.

[34] D. M. Behrouz A Forouzan, Cryptography and Network Security, McGraw-Hill Education, 2011.

[35] G. Shen, B. Liu, "Research on Efficiency of Computing kP in Elliptic Curve System," in 2010 6th International Conference on Wireless Communications Networking and Mobile Computing (WiCOM), 1–4, 2010.

ASTES

Advances in Science, Technology and Engineering Systems Journal
Vol. 5, No. 5, 460-468 (2020)
www.astesj.com
Special Issue on Multidisciplinary Innovation in Engineering Science & Technology

ASTES Journal
ISSN: 2415-6698

Bayes Classification and Entropy Discretization of Large Datasets using Multi-Resolution Data Aggregation

Safaa Alwajidi[*,1,2], Li Yang[2]

[1]*Department of Computer Science, Western Michigan University (WMU), Kalamazoo, MI 49008, USA*

[2]*Department of Mathematics and Computer Science, University of North Carolina at Pembroke (UNCP), Pembroke, NC 28372, USA*

ARTICLE INFO

Article history:
Received: 21 May, 2020
Accepted: 10 July, 2020
Online: 24 September, 2020

Keywords:
Big data analysis
Data reduction
Data aggregation
Multi-resolution
Entropy discretization

ABSTRACT

Big data analysis has important applications in many areas such as sensor networks and connected healthcare. High volume and velocity of big data bring many challenges to data analysis. One possible solution is to summarize the data and provides a manageable data structure to hold a scalable summarization of data for efficient and effective analysis. This research extends our previous work on developing an effective technique to create, organize, access, and maintain summarization of big data and develops algorithms for Bayes classification and entropy discretization of large data sets using the multi-resolution data summarization structure. Bayes classification and data discretization play essential roles in many learning algorithms such as decision tree and nearest neighbor search. The proposed method can handle streaming data efficiently and, for entropy discretization, provide sufficient information to find the optimal split variable and the optimal split value.

1 Introduction

Big data analysis offers new discovery and values in various application areas such as industrial sensor networks [1], finance [2], government information systems [3], and connected health [4]. Big data is redundant, inconsistent, and noisy. Machine learning algorithms face extreme challenges to analyze big data precisely and quickly.

Volume and velocity are the primary characteristics of big data. The massive size of data being accumulated consumes storage and leads to management shortcomings [5]. According to a IDC report [6], the volume of data may reach 40 Zettabytes (10^{21} *bytes*) by 2020. In addition, big data often come in the format of complex data streams. For example, in Wide-area Sensor Network (WSN), autonomous sensors generate a huge amount of data from the environment and transmit the data through the network to the backend servers for further processing and analysis.

Big data analysis is challenging to computing power and resources [7]. Analysis algorithms need to scan the data at least once, leading to a time complexity of $O(N)$, where N is the number of data records. Yet many algorithms use iterative computations that require multiple passes of data access. For example, Support Vector Machine (SVM) is a well-known algorithm that requires multiple scans of the dataset with time complexity $O(N^3)$. For processing of big data, accessing data point by point is a prohibitive process.

One idea to solve the problem is to summarize the data and use the summarized data for data processing. The summarization aggregates data points into a hosting structure that can be used by most mining and learning algorithms for efficient and effective analysis. The hosting structure should: (i) require one scan of the original data for its construction; (ii) hold representative statistical measures of the original data that satisfy requirements of most of the mining and learning algorithms; (iii) update the statistical measures incrementally to deal with streaming data; and (iv) organize the statistical measures at multiple resolutions. The multiresolution view of data gives us the flexibility to choose the appropriate level of summarization that fits the available resources.

In our previous work [8], we have developed an effective technique to create, organize, access, and maintain a tree summarization structure for efficient processing of large data sets. The developed tree structure is incrementally updated and provides the necessary information for many data mining and learning algorithms. This paper is a continuation of the previous work by developing data mining and learning algorithms. Namely, this research develops algorithms for Bayes classification and entropy discretization of large data sets using the multi-resolution data summarization structure.

[*]Corresponding Author: Safaa Alwajidi, +19105216517, safaa.alwajidi@uncp.edu

Bayes classification and data discretization play essential roles in many learning algorithms such as decision tree and nearest neighbor search. The proposed method can handle streaming data efficiently and, for entropy discretization, provide sufficient information to find the optimal split variable and split value for continuous variables. Data discretization for continuous variable plays a central role in learning algorithms such as decision trees.

The rest of the paper is divided into five sections. Section 2 summarizes existing data reduction techniques. Section 3 introduces the multiresolution structure and discusses its implementation, updating, and performance. Bayes classification and entropy discretization are introduced in Section 3 and Section 4 respectively. The last section concludes the paper.

2 Techniques for Data Reduction

For efficient and effective management, transmission and processing of large data sets, many techniques have been proposed. One straightforward way to reduce data size is data compression. Data compression reduces storage, I/O operations [9, 10] and network bandwidth [11], and also helps to accelerate data transmission [12]. One problem with data compression is the overhead of compression and decompression [13]. While it preserves the complete dataset, the method does not reduce the complexity of data processing, which needs to access the original data anyway.

The size of relational data can be reduced in two ways: either to reduce the number of attributes or to reduce the number of data records. One technique to reduce the number of attributes is dimensionality reduction [14]. One example algorithm for dimensionality reduction is principal component analysis (PCA) [15], which is an expensive process. Most machine learning algorithms require multiple scans of the dataset with time complexities based on the number of data records, therefore, reducing the number of data records seems to be the way to go for big data analysis.

One example technique to reduce the number of data records is sampling. Sampling is a statistical subset technique in which a small number of data points are randomly chosen to produce an unbiased representation of the dataset. A recent study [16] shows that random sampling is the technique commonly used to gain insights in big data. However, it is difficult to quickly extract a representative random sample. A critical problem is how to handle the selection bias due to issues such as class imbalance [17, 18] and nonstationary values of data [19]. A systematic method of sampling that mediates the tensions between resource constraints, data characteristics, and the learning algorithms accuracy is needed [20]. Intricate methods to subset the big data, such as instance selection [21] and inverse sampling [22], are computationally expensive [23, 24] because of the inefficient multiple preprocessing steps. Furthermore, newly added data points change data statistical measures and require re-sampling. Moreover, sampling is not appropriate in some application areas. For example, epidemiologic research involves systematic biases due to great enthusiasm in the sampling of people in EHRs (Electronic Health Records) systems and there are often biases in the way information is obtained and recorded. A large sample size cannot overcome these problems [25].

One powerful way to reduce the number of data records is to aggregate the data records. Data aggregation is a reduction technique that considers all points in the dataset. It preserves enough information from the dataset while combining similar data records into one which summarizes the data records into representative statistical measures. Data aggregation is used in privacy preservation [26] and Wireless Sensor Networks (WSNs) to reduce the volume of data traffic [27]. However, few studies have been conducted to aggregate and summarize big data for data analysis.

One of the early methods to use aggregated data to support advanced analysis and decision making is On-line Analytical Mining (OLAM) [28]. OLAM integrates mining models on top of a multidimensional data cube and OLAP engine. It has been used in many applications to provide efficiency and scalability for data mining and knowledge discovery such as association rules [29]. The multidimensional data cube uses a conceptual hierarchy in each categorial dimension to aggregate data in a multi-resolution format. However, many big data sets are not in relational databases and contain continuous attributes with no concept hierarchy.

A tree index structure is one of the major techniques that can be used to aggregate data at multiple resolutions [30]. Regions in multi-resolution aggregation need to be grouped and linked for quick reference. Many variations of tree structures have been used to save data for fast access such as CF tree used in BIRCH [31], R* tree used in DBSCAN [32, 33], KD-tree [34], aR-tree [35], and R+-tree [36]. However, these trees do not meet all of our requirements such as hosting aggregated data, query independence, simple creation, and incremental updates.

3 Multi-Resolution Tree Structure for Data Aggregation

We are given a dataset of size $N \times d$, where N is the number of data points, d is the number of variables, and $N \gg 2^d$. These variables take continuous numeric values. Continuous data are common such as the data generated from sensors like temperature, air pressure, gyroscope, accelerometer, GPS, gas sensors, water sensors and vital data from patients. Aggregating the dataset into a multi-resolution hierarchical structure is not a straightforward process. Continuous data lacks concept hierarchy.

We propose a hierarchical multilevel grid summarization approach to aggregate the data. Similar method has been used in spatial data mining [37] and robotic mapping [38]. In this method, each dimension in the dataset is divided into a limited number of equal width and nonoverlapping regions (intervals). Each region stores the summarization information of the raw data points falling inside it. We labeled each region by giving it a number to distinguish between them. The multilevel structure aggregates data at multiple granularities, where multiple regions at a lower level are grouped to form one region at the next higher level. We assume each level is summarized into a half number of regions in the immediate beneath level. This method provides a concept hierarchy for continuous data.

The hierarchical multilevel grid can be assumed as a multidimensional data cube. However, regions in multi-resolution aggregation need to be linked for quick references. We propose a tree index structure to host the aggregated data in the multidimensional data cube.

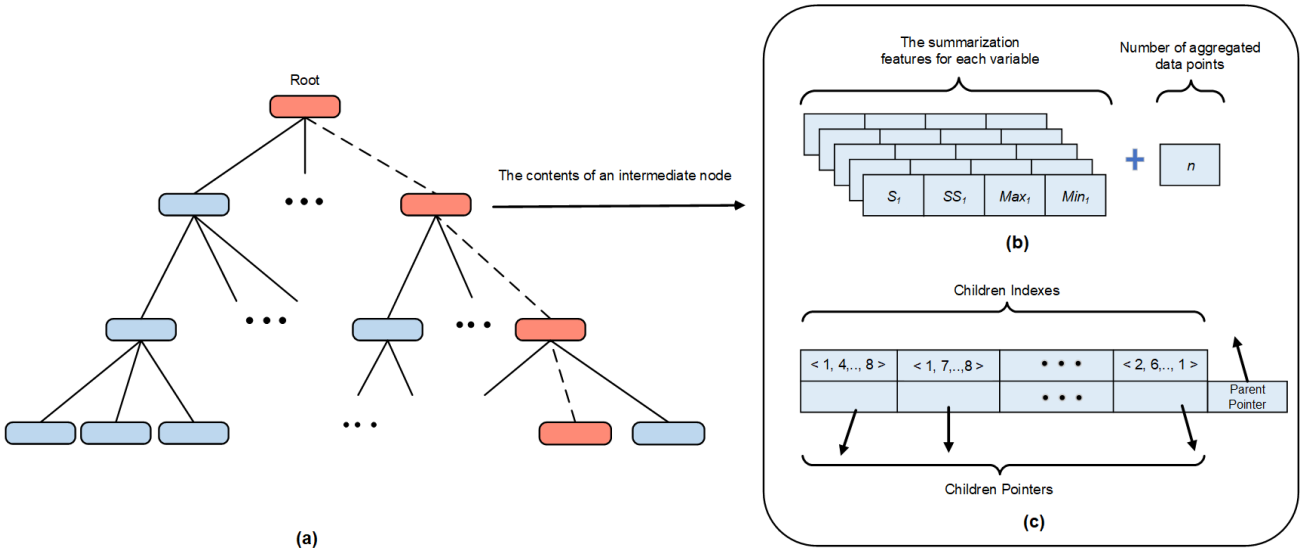


Figure 1: The multi-resolution structure (a) Updating the multi-resolution tree (b) The summarization features (c) The mapping table

The tree is an efficient structure in which summarization features at high levels can be computed from features at low levels without rescanning the original raw data. This is useful for incremental updating. Also, the tree provides quick reference links between its levels to support multiresolution aggregation. Searching the tree structure is faster than searching the massive raw dataset.

All data records are aggregated at each level of the tree. Aggregations are performed on all variables at the same time. This multi-resolution aggregation reduces the number of tree nodes and provides the trade-off between efficiency and accuracy. The user can choose the appropriate level of aggregation. Typically, navigation is a top-down process from the top to lower levels.

Each intermediate node holds a mapping table and a set of summarized statistical measures. The mapping table, Fig.1(c), contains a set of entries that hold node indexes along with their corresponding pointers and is used for linking a node with its parent and children nodes. The mapping tables helps to reduce the I/O operations. For instance, to access a desired child node from its parent, we start by searching the parent's mapping table to check if the index of the desired child is available.

3.1 Tree Node Index and Mapping between Nodes

A tree node is a hyperrectangular area that is specified by an interval in each dimension. Each interval has a unique index number that distinguishes it from other intervals. Consequently, each node has a set of index numbers corresponding to its intervals in all dimensions. We call this set a node index. The node index is used to identify the exact nodes in the tree to be called and uploaded to the main memory.

A mapping function, $f(\{v_1, v_2, ..., v_d\}) = \{name_l\}_{l=1}^{h}$ is used to generate the node index from incoming data point $\{v_1, v_2, ..., v_d\}$, where v_i is the value of variable i, and $name_l$ is the node name at level l. Each name is a tuple of the form $\langle l, I_1, I_2, \ldots, I_d \rangle$, where l is the tree level and I_i is the region number of variable i. The availability of the node names for incoming data point along with mapping tables, which consist of child nodes indexes, helps to assign the incoming data point to its corresponding nodes without searching the tree. Instead, it uploads only the required nodes for updating. See section III (c) for the detailed procedure.

3.2 Sufficient Statistical Measures

Multiple statistical measures can be collected on data points aggregated in a region. The set of statistical measures should be expressive enough to answer most data queries. Since each data mining algorithm needs different statistical measures, we need to find common statistical measures for all or most of the algorithms to ensure that the proposed structure can be used by these algorithms. Extracting sufficient statistical measures of the aggregated data is crucial to provide information to data analysis algorithms. In addition, efficient analysis of streaming data requires incrementally updating of these statistical features.

For each data node, we collect number of data points, sum of data values, sum of squared data values, as well as minimum and maximum values along each variable $(n, S_p, SS_p, Min_p, Max_p)$ in this node. We collected these measures inspired by BIRCH [31]. These five statistical measures are small in size and can be incrementally updated.

Basic statistics like mean, variance, and standard deviation can be incrementally and directly computed from these statistical features. Other features such as variables correlation and variable distribution can also be computed. We assume that the data is uniformly distributed inside each region of the variable.

These measures provide enough information to compute cluster means, sizes, and distances in different modes. In addition, Euclidean, Manhattan, L1 and L2 distances between cluster centers, and average inter-cluster distances can also be computed. This information is useful for clustering algorithms and similarity-based learning. As we will discuss in Sections IV and V on learning algorithms, other measures such as likelihood, conditional probability, and dynamic splitting can be calculated using the collected

statistical measures.

3.3 Implementation and Performance Analysis

The proposed multi-resolution structure is a tree like structure. Its implementation and updating is a top-down process, starting from the root node towards the leaf nodes. Algorithm 1 explains the procedure of implementing and updating the multi-resolution structure. Inputs to the algorithm are the desired number h of levels in the resulted tree structure, expected maximum and minimum values for each variable along with a matrix W of region width for each variable at each level in the tree.

The implementation requires a single scan of the training dataset. To insert a new data record, the algorithm uses the index keys generated by the mapping function and starts at the root node to find an entry that matches the first index key. If the entry is found, the algorithm updates the corresponding node statistical features. In case the entry is not found, the algorithm creates a new entry in the root mapping table to hold the index key. The algorithm then creates a new node, associate it with the newly created entry, and initialize the node statistical features. The algorithm repeats this process until it reaches the leaf node.

The worst performance of the proposed structure occurs when the tree has the maximum number of nodes. We assume that the number of regions for each variable at a level in the tree doubles in the next beneath level. In this case, each node has a maximum of 2^d child nodes. The total number of nodes in the tree with h levels and one root node is:

$$N_{Tree} = 1 + \left\lfloor \sum_{l=1}^{h} \frac{\prod_{p=1}^{d} \left(max_p - min_p\right)/w_{ph}}{2^{(h-l)(d-1)}} \right\rfloor \quad (1)$$

where $w_{ph} \in W$, is the regions width for variable p at level h. The values max_p and min_p are the maximum and minimum values of variable p respectively.

The proposed multi-resolution tree is an efficient structure since it avoids uploading and searching all tree nodes during insertion and updating. Insertion one data points calls only $(h + 1)$ nodes. Empirically for streaming data, the consecutive data points fall within the same range of values which means that they will be aggregated into the same nodes. Therefore, disk caching helps to reduce disk operations. Implementing the multi-resolution tree does not create empty nodes with no data.

To analysis the worst case to implement the multi-resolution structure, we assume the data of N points is scattered all over the regions and no region left empty. In this case, each node has the maximum number of children and thus the multi-resolution structure has the maximum number of nodes. The implementation of such case costs $O\left(Nd(R + (h-1)2^d)\right)$ where R is the number of entries in the root's map table, and $\left((h-1)2^d\right)$ is the cost to search the map tables of visited nodes. Since h is relatively small value, the cost become $O\left(Nd(R + 2^d)\right)$.

Fig. 1 (a) illustrates how Algorithm 1 works. To insert a data record, only the red nodes, one at each level of the tree, are visited and uploaded. The dotted links represent the algorithm traverse and progress from the root to a leaf node.

Algorithm 1: Implementing and Updating the Multi-Resolution Tree

```
Input  : N × d dataset, h number of levels, and W matrix of regions width
Output : T the Multiresolution structure with h levels
foreach O_i ∈ N do
    // The data point O_i is a tuple {v_1i, v_2i, ..., v_di}
    for l ← 1 to h do
        foreach Variable p ∈ d do
            Index[l, p] ← [v_pi − min_p]/W_pl ;
        end
    end
    if T.root is Null then
        Create the root node ;
    else
        CurrentNode ← root ;
        UPDATE(Index, CurrentNode, O_i);
    end
    for l ← 2 to h − 1 do
        UPDATE(Index, CurrentNode, O_i);
    end
end
Procedure UPDATE
  Input Index, CurrentNode, O_i(datarecord)
  Output UPDATED T
  if Index not in CurrentNode.MapTable then
      Create a new entry iEntry in CurrentNode.MapTable;
      iEntry ← Index;
      Create a new node e;
      Create a new entry cEntry in CurrentNode.children;
      cEntry ← e ;
      e.parent ← CurrentNode;
      CurrentNode ← e;
      Initialize CurrentNode statistical features and entries based ;
  else
      CurrentNode ← Child node corresponding to the Index entry
                    in the CurrentNode.MapTable;
      Update CurrentNode statistical features based on O_i values;
  end
  end procedure
```

4 Bayes Data Classification

Class probabilities are essential for Bayesian classifiers, hidden Markov model (HMM), and in defining entropy, gain ratio, and Gini index for decision trees. Naive Bayes is a classification model based on conditional probability. By including class attribute as a regular attribute in building the multi-resolution tree, we can calculate conditional class probabilities from the multi-resolution tree without accessing individual points in the training dataset.

The class attribute, also called the response variable, is a categorical attribute that has a finite number of labels (values). We can divide the class attribute into regions where each region is a unique class label. There is no aggregation applied on the class attribute and it maintains the same set of regions at all levels in the multi-resolution tree. Unlike continuously values variables, no numbers assigned for its regions. Those regions are indexed by their labels.

Given a $N \times d$ dataset with the class attribute $C = \{c_1, c_2, \ldots, c_m\}$, where m is the number of distinct values of class labels, the number of leaf nodes at level h is:

$$N_h = \left\lfloor \prod_{p=1}^{d-1} [\left(max_p - min_p\right)/w_{ph}] \times m \right\rfloor \quad (2)$$

All data points that are aggregated in a leaf node belong to a single class. Aggregating data points from different classes in one node leads to reduce the number of nodes in the multi-resolution tree and then reduce the storage needed for the tree. However, it consumes more memory and increases the number of I/O disk operations. For example, if parent node aggregates data points that belong to two classes A and B, there is a chance that only one child node has the data points of class A and the rest child nodes have data points belong to class B. Consequently, accessing child node of class A requires to upload all child nodes to memory to find that node of class A.

Computation of class probability from the proposed tree structure requires a single scan of the tree. The highest level in the tree maintains the same information of other levels but it is the most aggregated and compact level. The number of child nodes of the root is much less than the number of data points in the training dataset. Thus, the computation of class probabilities from the highest level in the multi-resolution tree consumes less memory and more efficient than working on the very large training datasets.

Given $E = \{e_1, e_2, ..., e_k\}$, a set of child nodes of root in the multi-resolution tree that aggregates dataset with the class attribute $C = \{c_1, c_2, ..., c_m\}$. The probability of a class c_j, $c_j \in C$ and $1 \leq j \leq m$ can be computed by :

$$P(c_j) = \frac{\sum_{i=1}^{k} [n_i \times \mathcal{F}\left(y_i = c_j\right)]}{\sum_{i=1}^{k} n_i} \quad (3)$$

n_i, y_i are the number of aggregated data points and class label of node e_i, $\mathcal{F}$ takes value 1 if $y_i = c_j$ and 0 otherwise.

Naive Bayes, Eq. (4), uses class probability for classification. It requires scanning all data points in the training dataset to classify one unknown point, under the assumption that the variables are independent. Suppose continuous variables are normally distributed, it requires to computes the likelihood for a continuous variable using Eq.(5). Then, finds the estimated class label $\hat{y}$ based on the Bayes theorem that computes class probability $P(C)$ for all classes and assigns the class label c_j with the highest posterior probability to unclassified point x.

$$\hat{y} = \underset{j \in \{1,...,m\}}{\operatorname{argmax}} P(c_j) \prod_{p=1}^{d} P(x_p|c_j) \quad (4)$$

$$P(x_p|c_j) = \frac{1}{\sigma_{pj}\sqrt{2\pi}} e^{\frac{-(x-\mu_{pj})^2}{2{\sigma_{pj}}^2}} \quad (5)$$

The likelihood requires a scan of all points in the training dataset to find the conditional mean, variance and standard deviation to classify a single unknown point. The proposed multi-resolution structure provides an efficient way to compute the conditional mean, variance, and standard deviation of continuous variable p. It requires to scan the nodes of the highest level in the tree only once to compute these conditional features for each class c_j separately, as shown in Table I.

Table 1: Conditional Features Computation for Variable p and class j

Feature		Comments
μ_{pj}	$\frac{S_{pj}}{n_j}$	Conditional mean
${\sigma_{pj}}^2$	$\frac{SS_{p_j} - \frac{\left(S_{p_j}\right)^2}{n_j}}{n_j}$	Conditional variance
σ_{pj}	$\sqrt{{\sigma_{pj}}^2}$	Conditional standard deviation

Consequently, any classification algorithms based on this computation of class probability can work efficiently without loss in accuracy to cope with the large scale data and streaming data. The multi-resolution Naive Bayes algorithm, which accepts the multi-resolution tree as input, has been implemented using Java JDK 13. We have tested the algorithm on eight artificially generated datasets, each set has two continuous variables and binary class label. The multiresolution structured implemented from the training set, 80% of the raw dataset, and the remaining 20% used as a testing set. We have compared the results of applying the multiresolution Naive Bayes on the root level of the multiresolution structure with the results of applying the traditional Naive Bayes algorithm on the raw datasets. Experimental results are given in figure 2. The results show that the multi-resolution Naive Bayes is 25% faster on average than the algorithm that works on raw data sets while keeping the same accuracy of classification.

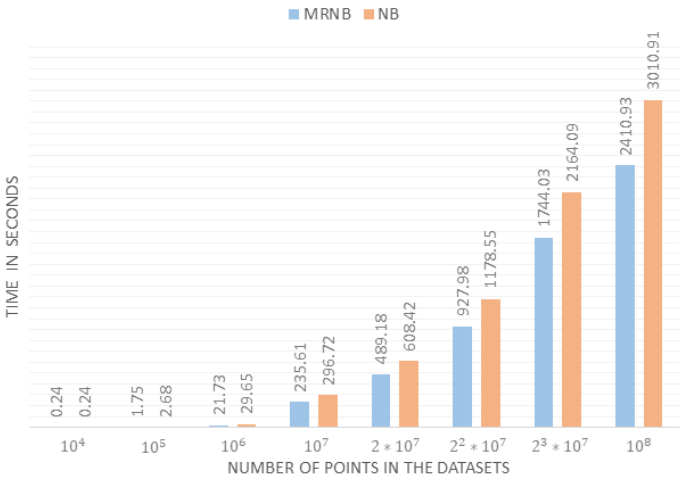


Figure 2: Comparison of the computation time between multiresolution Naive Bayes (MRNB) and raw data Naive Bayes (NB) algorithms for eight datasets

5 Entropy Discretization Overview and Challenges

We present another application to speed up learning algorithms that sort and search the dataset multiple times to produce an optimal solution. In this section, we propose a high speed and incremental technique for entropy discretization of continuous variables using

the multi-resolution structure. The high speed, representative, and incrementally updated structure helps to generate entropy discretization efficiently and effectively for big data and streaming data.

5.1 The Motivation

Several miming and learning logarithms iteratively split the dataset as part of their learning models. Examples of these algorithms are Bayes Belief Network (BBN) classification for continuous data [39], KD-tree used in nearest neighbor (NN) search [40, 41], and conventional decision tree [42] used for classification. The splitting procedure sorts the variable values and then seeks for the best value to split the variable based on a specific criterion. This procedure is repeated for each variable to find the best point and best variable to split the dataset.

The continuous variable has a vast number of values that make sorting and testing of its values during the splitting procedure a complicated task. Entropy discretization converts the continuous variable into a categorical variable by dividing it into a minimal set of non-equal width regions with minimal loss of information. Applying the splitting procedure iteratively on the small number of regions resulted from entropy discretization is more efficient than the iterative scan of the vast number of data points in the dataset. However, entropy discretization is a computationally expensive and memory consuming technique. It needs to search and test all the variable values to divide it into regions. Consequently, entropy discretization is a prohibitive task on big data as well as on streaming data and requires a fast incremental discretization to cope with updating when new data arrives.

5.2 Entropy Discretization Overview and Challenges

Entropy discretization divides the continuous variable based on entropy. Entropy is a measure of information. Higher entropy means less information loss. It is computed by using the frequency-probability distribution in Eq.(6).

$$H(X) = \sum_{x \in X} P(x) \log_2 P(x) \tag{6}$$

where x is a value in the continuous variable X.

Dividing the continuous variable into several regions affects entropy in a way that the entropy increases when the number of regions increases. To decide the optimal number of regions, there is a comprise between keeping information and keeping performance. Choosing a large number of regions seems reasonable to ensure high entropy and better representation of the distribution in such data. However, there is a danger of an over discretization where too many regions can be dispensable because it slows the performance. Hong [43] proposed a method to find the optimal number of regions with minimal loss of information. The relationship between the entropy and the number of regions is curve. If we draw a straight line from the origin of the graph to the maximum entropy and the maximum number of regions, the curve will be always above the line. Hong showed that when the curve is most apart from the line, we reach the optimal number of regions. This point is called the Knee point.

Ellis [39] uses Hong method to discretize continuous variables and feeds them to the Bayes Belief Network algorithm. His method starts with dividing the continuous variable into regions and sorting them. Each region has a distinct value of the continuous variable. The method then merges two adjacent regions with the smallest difference of frequency (number of aggregated data points). The process of merge continues until reaching the maximum height point on the curve (Knee point). The Knee point is reached when the change in the number of regions becomes greater than the change in the entropy of the regions. This relation is explained in Eq.(7) in the next section. However, when the number of distinct values is very big, this method of entropy discretization is computationally prohibitive. The time complexity of this method for d continuous variables is $O(d(m(log_2 m + m^2)$, where m is the number of distinct values. The number of distinct values is very big in some applications like sensor data, human activity recognition, and health care data, where m approaches the number of data points N.

5.3 Proposed Algorithm

We propose a fast entropy discretization technique by using the multi-resolution structure. The proposed technique finds the optimal number of non-equal width entropy regions based on the equal width regions in the multi-resolution structure. The multi-resolution structure has properties such as the hierarchical organization of aggregated data which makes the proposed technique more efficient than working on the massive number of data points in the training dataset to generate the regions of entropy discretization.

The multi-resolution structure discretizes each continuous variable into non-overlapping equal-width regions, each resides on a separate node of the same tree level. The proposed algorithm optimizes this discretization of the variable by merging its regions from two different nodes into one region repeatedly until reaching to Knee point.

Algorithm 2 explains the proposed entropy discretization technique for a dataset of d continuous variables. For each variable, the algorithm starts working on the parents of the leaf nodes (it can easily be adapted to work on any other level except root and leaves). For each parent, the algorithm merges the adjust regions in the sibling leaves. The new resulted regions are saved into a local file associate with the parent node. This pass is called the local mode. Then, in the global mode, the algorithm uses regions from all local files and merge the adjacent regions from nodes belong to different parents. The final result of the global mode is a set of optimal entropy regions that are saved into a global file for each variable, as shown in figure 4.

The region is represented by its boundary (cut point) and the number of its aggregated data points (frequency). This information is obtained from the statistical features of the node that hosts the region. The statistical features Max maximum value of the region is used as a cut point while n the number of aggregated data points inside the node is used as frequency. To deal with multiple regions, the algorithm uses a list to save the cut points of that regions combined with a corresponding list of their frequencies.

The merge procedure in algorithm 2, that is used in both local and global modes, is iterative. It sorts the regions based on their cut points and runs the following steps:

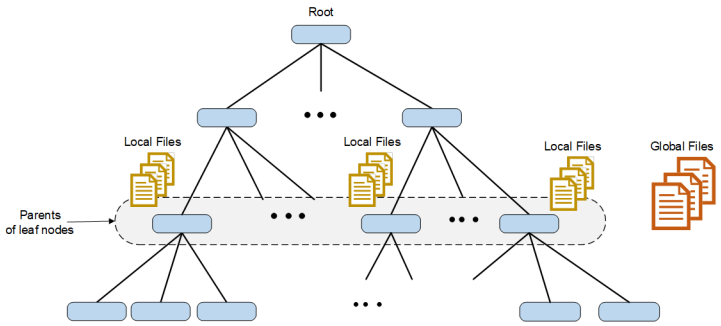


Figure 3: The multi-resolution structure with local and global files, one local file for each variable on every parent node and one global file for each variable

- Compute the entropy, *Entr*, for current K regions using Eq.(6). In this case, x is a region in variable X. The regions frequencies are used to compute the probability.

- Find two adjacent regions with a minimum frequency difference and merge them. The new cut point of the new region is the greatest cut point of the two merged regions while the new frequency for the new region is the sum of the frequencies of the two merged regions.

- Compute the entropy, *newEntr*, for resulted $K-1$ regions after the merge.

- Compute the rate of change in the number of regions to the change in their entropy using Eq.(7).

$$Rate = (newEntr \times K) - (Entr \times (K-1)) \tag{7}$$

The Knee point is proportional to this rate and is reached just before the decrease in this rate. If the rate is decreased, the algorithm stops the merge procedure. Otherwise, the algorithm updates the cut point and frequency lists by replacing the cut points and frequencies of the two merged regions by the cut point and frequency of the new region. The algorithm repeats the last three steps until the rate starts to decrease.

Although the local mode may lead to a little loss in the information due to missing a merge of regions from different parents, the local mode is still important to improve the performance in building and updating entropy discretization. Local mode reduces the sort to only nodes belong to the same parent because these nodes are neighbors to each other and there is a high possibility to merge them. The local mode helps to trigger the global mode only if it is needed, as summarized in Fig 5. After updating the multi-resolution structure due to the arrival of new data points, the local modes are triggered only for the parents of the updated leaves. The local modes for other parent nodes are ignored. If any of the triggered local modes achieves a merge, the global mode will be triggered. Otherwise, the algorithm terminates without global mode because the new data point has not effected the entropy discretization.

Algorithm 2: Build Entropy Discretization

Input : E the set of parent nodes of leaves in the multiresolution tree
Output : *GlobalFiles* set of files, each contains the entropy discretization for a single variable

```
// Main Program
foreach Variable p ∈ d do
    // Local Mode
    foreach e ∈ E do
        Children ← child nodes of e ;
        Cuts ← Max_p values from all Children;
        Freqs ← n values from all Children;
        LCuts, LFreqs ← MergeRegions(Cuts, Freqs);
        LocalFile ← LCuts and LFreqs ;
        AllCuts ← AllCuts ∪ LCuts;
        AllFreqs ← AllFreqs ∪ LFreqs;
    end
    // Global Mode
    GCuts, GFreqs ← MergeRegions(AllCuts, AllFreqs);
    GlobalFile ← GCuts and GFreqs ;
end
```

```
procedure MergeRegions(Cuts, Freqs)
Output : Updated Cuts and Freqs lists after iterative merge of regions
    Sort Cuts and Freqs based on values of Cuts ;
    Initializing the number of regions: K, baseK ← |Cuts|;
    Entr ← calculate entropy for K regions;
    oldRate ← 0 ;
    Flag ← TRUE ;
while (Flag) do
        R1, R2 ← two adjacent regions in Cuts with minimum Freqs difference;
        Merge R1 and R2 into one region ;
        newEntr ← calculate entropy after merge for (K − 1) regions ;
        newRate ← (newEntr × baseK) − (Entr × (K − 1));
    if newRate > oldRate then
        // Apply the merge of R1 and R2
            Update Cuts and Freqs;
            K ← K − 1 ;
            oldRate ← newRate ;
    else
        // Decline the merge of R1 and R2
            Flag ← False;
    end
end
return Cuts, Freqs;
end procedure
```

Finally, the algorithm outputs a set of global files. The global file contains the optimal number of entropy regions that represent the distribution of a single continuous variable. The set of global files can be used to feed the mining and learning algorithms for efficient and effective learning.

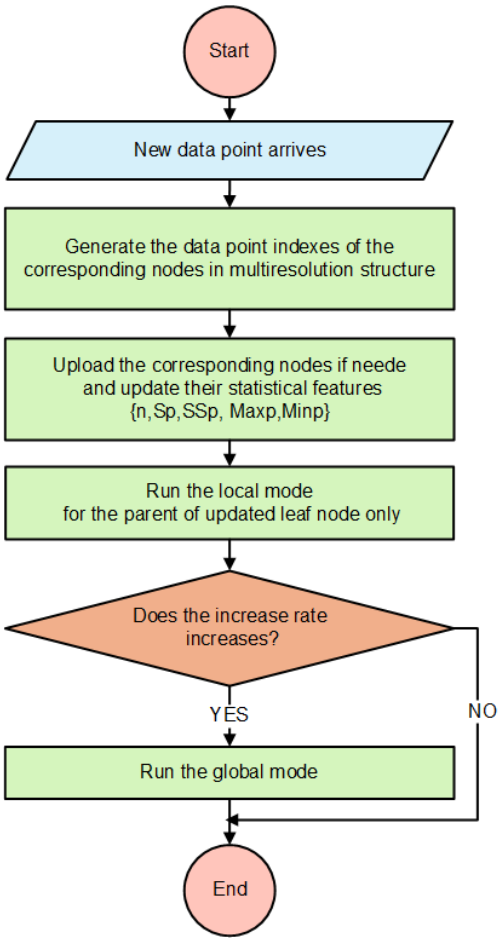


Figure 4: Updating process of multi-resolution structure and entropy discretization

6 Conclusions

In this paper, we have studied fast Bayes classification and entropy discretization of continuous variables using a multi-resolution data aggregation structure for mining and processing of large datasets. The proposed Bayes classification works by getting required conditional probabilities directly from aggregated statistical measures. Entropy discretization works in local and global modes to find the optimal number of non-equal width entropy regions with minimal loss of information based on the equal-width regions of the multi-resolution structure. The multiresolution structure makes the proposed technique more efficient to generate entropy discretization regions than working on the massive number of data points in the big dataset. The resulted entropy discretization regions are saved into files linked to leaf nodes and their parents for fast updates of these regions to cope with streaming data. These files are useful to find the best split point and best split variable for continuous variables that are essential for several learning algorithms that iteratively seek for the optimal variable and value to split the dataset. These algorithms include Bayes Belief Network (BBN) classification for continuous data, KD-tree data structure used in fast nearest neighbor search, and conventional decision trees used for classification.

References

[1] L.-M. Ang, K. P. Seng, "Big Sensor Data Applications in Urban Environments," Big Data Research, **4**, 1–12, 2016, doi:https://doi.org/10.1016/j.bdr.2015.12.003.

[2] B. Fang, P. Zhang, "Big Data in Finance," in S. Yu, S. Guo, editors, Big Data Concepts, Theories, and Applications, 391–412, Springer International Publishing, Cham, 2016, doi:10.1007/978-3-319-27763-9_11.

[3] G.-H. Kim, S. Trimi, J.-H. Chung, "Big-data applications in the government sector," 2014.

[4] L. A. Tawalbeh, R. Mehmood, E. Benkhlifa, H. Song, "Mobile Cloud Computing Model and Big Data Analysis for Healthcare Applications," IEEE Access, **4**, 6171–6180, 2016, doi:10.1109/ACCESS.2016.2613278.

[5] H. Zhang, G. Chen, B. C. Ooi, K.-L. Tan, M. Zhang, "In-Memory Big Data Management and Processing: A Survey," IEEE Transactions on Knowledge and Data Engineering, **27**(7), 1920–1948, 2015, doi:10.1109/TKDE.2015.2427795.

[6] R. Kune, P. K. Konugurthi, A. Agarwal, R. R. Chillarige, R. Buyya, "The anatomy of big data computing," Software: Practice and Experience, **46**(1), 79–105, 2016, doi:10.1002/spe.2374.

[7] M. H. ur Rehman, C. S. Liew, A. Abbas, P. P. Jayaraman, T. Y. Wah, S. U. Khan, "Big Data Reduction Methods: A Survey," Data Science and Engineering, **1**(4), 265–284, 2016, doi:10.1007/s41019-016-0022-0.

[8] S. Alwajidi, L. Yang, "Multi-Resolution Hierarchical Structure for Efficient Data Aggregation and Mining of Big Data," in 2019 International Conference on Automation, Computational and Technology Management (ICACTM), 153–159, 2019, doi:10.1109/ICACTM.2019.8776717.

[9] B. H. Brinkmann, M. R. Bower, K. A. Stengel, G. A. Worrell, M. Stead, "Large-scale electrophysiology: Acquisition, compression, encryption, and storage of big data," Journal of Neuroscience Methods, **180**(1), 185–192, 2009, doi:10.1016/j.jneumeth.2009.03.022.

[10] H. Zou, Y. Yu, W. Tang, H. M. Chen, "Improving I/O Performance with Adaptive Data Compression for Big Data Applications," in 2014 IEEE International Parallel Distributed Processing Symposium Workshops, 1228–1237, 2014, doi:10.1109/IPDPSW.2014.138.

[11] A. A. Abdellatif, A. Mohamed, C.-F. Chiasserini, "User-Centric Networks Selection With Adaptive Data Compression for Smart Health," IEEE Systems Journal, **12**(4), 3618–3628, 2018, doi:10.1109/JSYST.2017.2785302.

[12] Q. Han, L. Liu, Y. Zhao, Y. Zhao, "Ecological Big Data Adaptive Compression Method Combining 1D Convolutional Neural Network and Switching Idea," IEEE Access, **8**, 20270–20278, 2020, doi:10.1109/ACCESS.2020.2969216.

[13] A. Oussous, F.-Z. Benjelloun, A. Ait Lahcen, S. Belfkih, "Big Data technologies: A survey," Journal of King Saud University - Computer and Information Sciences, **30**(4), 431–448, 2018, doi:10.1016/j.jksuci.2017.06.001.

[14] D. M. S. Arsa, G. Jati, A. J. Mantau, I. Wasito, "Dimensionality reduction using deep belief network in big data case study: Hyperspectral image classification," in 2016 International Workshop on Big Data and Information Security (IWBIS), 71–76, 2016, doi:10.1109/IWBIS.2016.7872892.

[15] M. A. Belarbi, S. Mahmoudi, G. Belalem, "PCA as Dimensionality Reduction for Large-Scale Image Retrieval Systems," 2017, doi:10.4018/IJACI.2017100104.

[16] J. A. R. Rojas, M. Beth Kery, S. Rosenthal, A. Dey, "Sampling techniques to improve big data exploration," in 2017 IEEE 7th Symposium on Large Data Analysis and Visualization (LDAV), 26–35, IEEE, Phoenix, AZ, 2017, doi:10.1109/LDAV.2017.8231848.

[17] T. Hasanin, T. Khoshgoftaar, "The Effects of Random Undersampling with Simulated Class Imbalance for Big Data," in 2018 IEEE International Conference on Information Reuse and Integration (IRI), 70–79, 2018, doi:10.1109/IRI.2018.00018.

[18] C. K. Maurya, D. Toshniwal, G. Vijendran Venkoparao, "Online sparse class imbalance learning on big data," Neurocomputing, **216**, 250–260, 2016, doi:10.1016/j.neucom.2016.07.040.

[19] W. Song, P. Liu, L. Wang, "Sparse representation-based correlation analysis of non-stationary spatiotemporal big data," International Journal of Digital Earth, **9**(9), 892–913, 2016, doi:10.1080/17538947.2016.1158328.

[20] G. Cormode, N. Duffield, "Sampling for big data: a tutorial," in Proceedings of the 20th ACM SIGKDD international conference on Knowledge discovery and data mining, KDD '14, 1975, Association for Computing Machinery, New York, New York, USA, 2014, doi:10.1145/2623330.2630811.

[21] M. Malhat, M. El Menshawy, H. Mousa, A. El Sisi, "Improving instance selection methods for big data classification," in 2017 13th International Computer Engineering Conference (ICENCO), 213–218, 2017, doi:10.1109/ICENCO.2017.8289790, iSSN: 2475-2320.

[22] J. K. Kim, Z. Wang, "Sampling Techniques for Big Data Analysis," International Statistical Review, **87**(S1), S177–S191, 2019, doi:10.1111/insr.12290.

[23] S. García, S. Ramírez-Gallego, J. Luengo, J. M. Benítez, F. Herrera, "Big data preprocessing: methods and prospects," Big Data Analytics, **1**(1), 2016, doi:10.1186/s41044-016-0014-0.

[24] S. García, J. Luengo, F. Herrera, "Instance Selection," in Data Preprocessing in Data Mining, volume 72, 195–243, Springer International Publishing, Cham, 2015, doi:10.1007/978-3-319-10247-4_8.

[25] R. M. Kaplan, D. A. Chambers, R. E. Glasgow, "Big Data and Large Sample Size: A Cautionary Note on the Potential for Bias," Clinical and Translational Science, **7**(4), 342–346, 2014, doi:10.1111/cts.12178.

[26] Y. Liu, W. Guo, C.-I. Fan, L. Chang, C. Cheng, "A Practical Privacy-Preserving Data Aggregation (3PDA) Scheme for Smart Grid," IEEE Transactions on Industrial Informatics, **15**(3), 1767–1774, 2019, doi:10.1109/TII.2018.2809672.

[27] M. Tamai, A. Hasegawa, "Data aggregation among mobile devices for upload traffic reduction in crowdsensing systems," in 2017 20th International Symposium on Wireless Personal Multimedia Communications (WPMC), 554–560, 2017, doi:10.1109/WPMC.2017.8301874, iSSN: 1882-5621.

[28] J. Han, "Towards on-line analytical mining in large databases," ACM Sigmod Record, **27**(1), 97–107, 1998.

[29] T. Ritbumroong, "Analyzing Customer Behavior Using Online Analytical Mining (OLAM)," 2015, doi:10.4018/978-1-4666-6477-7.ch006.

[30] B. W. F. Pan, D. R. Y. Cui, Q. D. W. Perrizo, "Efficient OLAP Operations for Spatial Data Using Peano Trees," in Proceedings of the 8th ACM SIGMOD workshop on Research issues in data mining and knowledge discovery, 28–34, San Diego, California, 2003.

[31] T. Zhang, R. Ramakrishnan, M. Livny, "BIRCH: an efficient data clustering method for very large databases," in ACM Sigmod Record, volume 25, 103–114, ACM, 1996.

[32] M. Ester, H.-P. Kriegel, J. Sander, X. Xu, "A Density-Based Algorithm for Discovering Clusters in Large Spatial Databases with Noise," in Proceedings 2nd International Conference on Knowledge Discovery and Data Mining, 226–231, 1996.

[33] K. Mahesh Kumar, A. Rama Mohan Reddy, "A fast DBSCAN clustering algorithm by accelerating neighbor searching using Groups method," Pattern Recognition, **58**, 39–48, 2016, doi:10.1016/j.patcog.2016.03.008.

[34] Y. Chen, L. Zhou, Y. Tang, J. P. Singh, N. Bouguila, C. Wang, H. Wang, J. Du, "Fast neighbor search by using revised k-d tree," Information Sciences, **472**, 145–162, 2019, doi:10.1016/j.ins.2018.09.012.

[35] Y. Hong, Q. Tang, X. Gao, B. Yao, G. Chen, S. Tang, "Efficient R-Tree Based Indexing Scheme for Server-Centric Cloud Storage System," IEEE Transactions on Knowledge and Data Engineering, **28**(6), 1503–1517, 2016, doi:10.1109/TKDE.2016.2526006.

[36] L.-Y. Wei, Y.-T. Hsu, W.-C. Peng, W.-C. Lee, "Indexing spatial data in cloud data managements," Pervasive and Mobile Computing, **15**, 48–61, 2014, doi:10.1016/j.pmcj.2013.07.001.

[37] M. Huang, F. Bian, "A Grid and Density Based Fast Spatial Clustering Algorithm," in 2009 International Conference on Artificial Intelligence and Computational Intelligence, 260–263, IEEE, Shanghai, China, 2009, doi:10.1109/AICI.2009.228.

[38] A. Hornung, K. M. Wurm, M. Bennewitz, C. Stachniss, W. Burgard, "OctoMap: an efficient probabilistic 3D mapping framework based on octrees," Autonomous Robots, **34**(3), 189–206, 2013, doi:10.1007/s10514-012-9321-0.

[39] E. J. Clarke, B. A. Barton, "Entropy and MDL discretization of continuous variables for Bayesian belief networks," International Journal of Intelligent Systems, **15**(1), 61–92, 2000, doi:10.1002/(SICI)1098-111X(200001)15:1⟨61::AID-INT4⟩3.0.CO;2-O.

[40] H. Wei, Y. Du, F. Liang, C. Zhou, Z. Liu, J. Yi, K. Xu, D. Wu, "A k-d tree-based algorithm to parallelize Kriging interpolation of big spatial data," GIScience & Remote Sensing, **52**(1), 40–57, 2015, doi:10.1080/15481603.2014.1002379.

[41] B. Chatterjee, I. Walulya, P. Tsigas, "Concurrent Linearizable Nearest Neighbour Search in LockFree-kD-tree," in Proceedings of the 19th International Conference on Distributed Computing and Networking, ICDCN '18, 1–10, Association for Computing Machinery, Varanasi, India, 2018, doi:10.1145/3154273.3154307.

[42] A. Bifet, J. Zhang, W. Fan, C. He, J. Zhang, J. Qian, G. Holmes, B. Pfahringer, "Extremely Fast Decision Tree Mining for Evolving Data Streams," in Proceedings of the 23rd ACM SIGKDD International Conference on Knowledge Discovery and Data Mining, KDD '17, 1733–1742, Association for Computing Machinery, Halifax, NS, Canada, 2017, doi:10.1145/3097983.3098139.

[43] S. J. Hong, "Use of contextual information for feature ranking and discretization," IEEE Transactions on Knowledge and Data Engineering, **9**(5), 718–730, 1997, doi:10.1109/69.634751.

ASTES

Advances in Science, Technology and Engineering Systems Journal
Vol. 5, No. 5, 469-477 (2020)
www.astesj.com
Special Issue on Multidisciplinary Sciences and Engineering

ASTES Journal
ISSN: 2415-6698

Interpretation of Machine Learning Models for Medical Diagnosis

Nghia Duong-Trung*,[1], Nga Quynh Thi Tang[2], Xuan Son Ha[1]

[1]*Software Engineering Department, FPT University, Can Tho city, 94000, Vietnam*

[2]*National Taiwan University of Science and Technology, Taipei city, 106335, Taiwan*

ARTICLE INFO

Article history:
Received: 13 August, 2020
Accepted: 18 September, 2020
Online: 24 September, 2020

Keywords:
Interpretable Machine Learning
Medical Diagnosis
Black-box Model Selection
Mobile Application

ABSTRACT

Machine learning has been dramatically advanced over several decades, from theory context to a general business and technology implementation. Especially in healthcare research, it is obvious to perceive the scrutinizing implementation of machine learning to warranty the rewarded benefits in early disease detection and service recommendation. Many practitioners and researchers have eventually recognized no absolute winner approach to all kinds of data. Even when implicit, the learning algorithms rely on learning parameters, hyperparameters tuning to find the best values for these coefficients that optimize a particular evaluation metric. Consequently, machine learning is complicated and should not rely on one single model since the correct diagnosis can be controversial in a particular circumstance. Hence, an effective workflow should effortlessly incorporate a diversity of learning models and select the best candidate for a particular input data. In addressing the mentioned problem, the authors present processes that interpret the most appropriate learning models for each of the different clinical datasets as the foundation of developing and recommending diagnostic procedures. The whole process works as (i) automatic hyperparameters tuning for picking the most appropriate learning approach, and (ii) mobile application is developed to support clinical practices. A high F1-measurement has been achieved up to 1.0. Numerous experiments have been investigated on eight real-world datasets, applying several machine learning models, including a non-parameter approach, parameter model, bagging, and boosting techniques.

1 Introduction

This paper is an extension of work initially presented in IEEE ACOMP 2019 [1] as an invited paper.

The advancement in clinical and healthcare practice today is due to the vast database explosion. Hospitals, health professionals, and treatment centers disclose medical data to the community to call for mutual support and benefit. The data availability is expanding in many forms, both the number of known attributes and the number of new observations [2]. We can see an excellent example from the widely published new coronavirus (COVID-19) data [3]. However, due to privacy concerns, medical data is abundant, but it is also very sparse, which we only have on specific individuals. A country's medical data may not be relevant to develop solutions for the same disease in another country. That creates challenges and difficulties for traditional medical diagnosis because many observations are lost due to a lack of information. The central issue is that health data is characterized by the considerable complexity of detecting new symptoms and sparsely presenting diseases due to insufficient data collection across a population or community. As an added difficulty, medical data exists in many different structures. For example, numbers, categories, text, images, and time-series make medical diagnosis even more difficult. However, from the benefit of big data to health care, leveraging medical data collection offers an excellent opportunity to improve the efficiency of healthcare provider [4, 5]. Current challenges in health practice include information overload, confounding attributes, and noise data in different populations, making manual analysis of experts ultimately difficult [6, 7]. The cost of using medical professionals to examine multiple clinical cases accumulated over time is very high. From a medical diagnosis, one can argue that there is an urgent need to work with a wide variety of data, leverage useful knowledge, and recommend a system that can make the most of information from that data.

Classification is an essential task in health diagnostic systems. We use observed metrics to classify samples into different diseases, or separate degrees of the same illness [8, 9]. Clinicians are trained

*Corresponding author: Nghia Duong-Trung, Software Engineering Department, FPT University, Can Tho city, 94000, Vietnam. Contact No. (+84)0939.657.063. Email: duong-trung@ismll.de

and have the solid knowledge to classify diseases based on sample data accurately. We can agree that correctly distinguish the right disease is one of the fundamental bases for effective treatment of the disease. However, as more data appears in clinical fields, the existing manual diagnostic process that relies on expert expertise cannot be applied quickly and effectively. As a result, the course of treatment may have to be done more slowly or eliminated. Addressing mentioned problems lies in the interactions between healthcare and automation decisions based on machine learning, applying to the classification problem. Thus, one can argue that the classification design is an iterative process between machine learning and available clinical sources to demonstrate the implications of a medical diagnostic procedure. Consequently, the authors turn our attention to proposing processes that automatically select the most suitable machine learning models for each of the different types of data as the foundation of building and recommending diagnostic procedures.

The classic definition of machine learning is "A computer program is said to learn from experience E with respect to some class of tasks T and performance measure P, if its performance at tasks in T, as measured by P, improves with experience E". It was initially described as a computer program that learns to automatically perform a required task or make a decision from data without explicitly programmed. This definition is comprehensive and can cover almost any set of data-driven approaches. Machine learning has been dramatically advanced over several decades, from theory context to a general business and technology implementation. Especially in healthcare research, it is obvious to perceive the scrutinizing implementation of machine learning to warranty the rewarded benefits in early disease detection, service recommendation, and patient-oriented information offering [10]–[13]. There are two substantially interrelated questions in medical diagnosis: How can computer scientists build machine learning programs that automatically improve through experience, e.g., through data? How can practitioners and clinical experts incorporate with these machine learning programs? The first question can be addressed by marriage between machine learning models and vast medical data. The more data we feed into the learning algorithms, the more accurate the prediction is. Whatever the machine learning models are used, the fundamental expectation is to generalize the knowledge from training data to unseen observations. It is the generalization capacities of learning approaches on how robust they are to their modeling assumptions or the errors in the test set. However, many practitioners and researchers have eventually recognized that there is no absolute winner approach to all kinds of data. The reasons can be broken down into many considerations. The prediction accuracy is diminished when the quantity and quality of clinical data are incomplete.

Different regions expose unique characteristics of a particular disease, which may affect the generalization capacities of learning models [13]. The privacy of medical records also subtracts the high availability of data for research. It is inadvertently possible that racial biases might be built into healthcare systems [14]. The reason might be placed at the characteristics of machine learning models themselves. Even when implicit, the learning approaches generally reply to learn parameters, hyperparameters tuning to find the best values for these coefficients that optimize a particular evaluation metric. Consequently, the use of machine learning is complicated and should not rely on one single model since the correct diagnosis in a particular circumstance can be controversial. Hence, an effective workflow should effortlessly incorporate a diversity of learning models and select the best candidate for a particular input data. It comes to the design idea of black-box models [15] in unintended consequences of machine learning in medicine. The workflow should work with various types of input data and transparently amalgamate diverse models. In that setting, different learning approaches for medical diagnosis are evaluated to select the most accurate one. More importantly, the result's interface should also be attractive to enhance hospital experts and end-users' incorporation.

Today, smartphones are one of the most ubiquitous communication devices and the fastest growing technology industry sectors. An increasing number of mobile applications have been developed to perform a comprehensive spectrum of daily tasks and entertainment. Its impact on medical treatment has already been significant on a global scale. In this paper, the authors deploy an Android mobile application to illustrate how the proposed workflow integrates with hospital experts and patients as end-users. Mobile health is a new concept that describes services supported by mobile communication devices such as smartphones, tablets, smartwatches, patient monitoring devices. However, the discussion of mobile health is out of our research scope. Interesting readers might refer to several mindful papers in the literature [16]–[18].

To be the best of our knowledge, the authors have made several contributions as follows:

- We sharp the connection between the automatic selection of machine learning models for classification in medical diagnosis.
- We extend the pool of machine learning models, including a single approach, bagging algorithm, and advanced boosting technique. We prove that there is no winner model to address medical data sources.
- We extend the background of machine learning algorithms in much more details.
- We extend the experiments section where we carefully describe experimental results, reproducibility, and mobile app development.

The rest of the paper is organized as follows. Section 2 gives a general idea of how our proposed workflow works and how the best learning model is selected. Then in Section 3, the authors introduce required machine learning materials and methodology that need to comprehend the experiments. More specifically, we discuss several well-known machine learning models and evaluation metrics. Our intensive comparison is then discussed in Section 4 in which we go through data collection, experimental results, reproducibility, and mobile app development. Finally, several final thoughts are presented in Section 5.

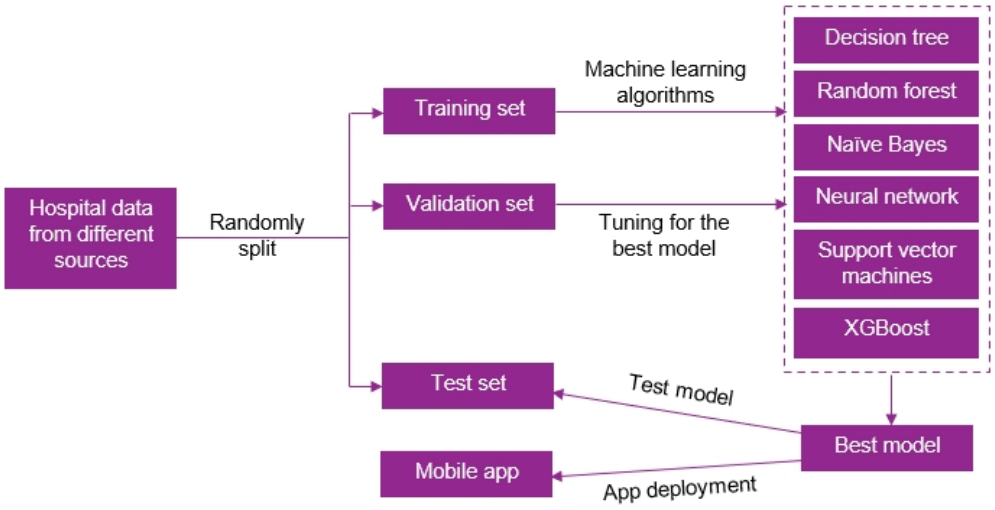


Figure 1: Automatic Selection of Machine Learning Models.

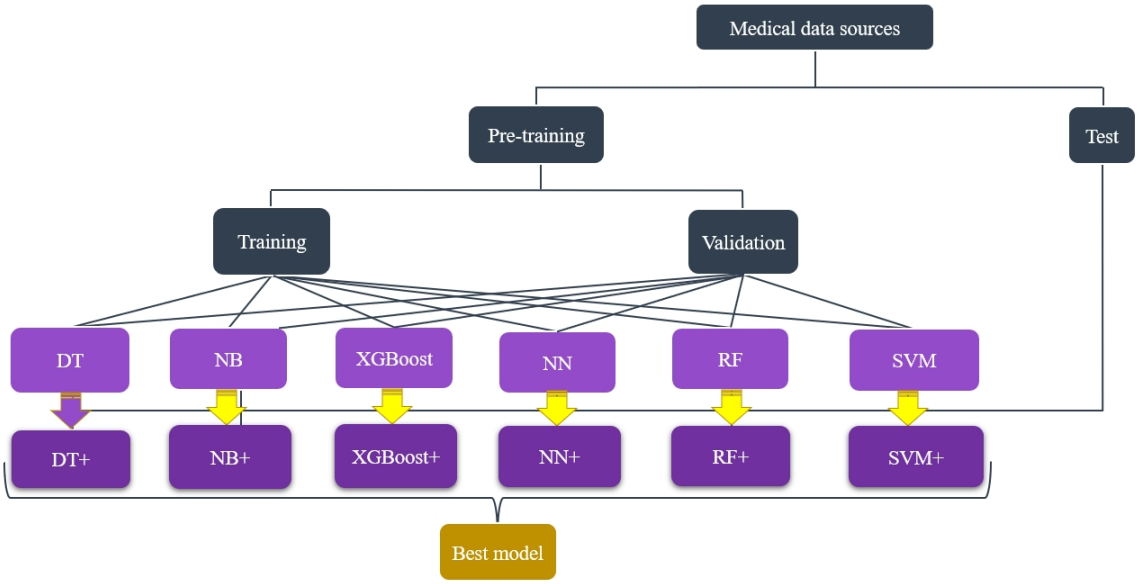


Figure 2: Hyperparameters tuning for picking the most appropriate learning approach.

2 Interpretation of Machine Learning Models

As mentioned in the previous discussion, the authors propose processes that interpret the most appropriate learning models for each of the different clinical datasets as the foundation of developing and recommending diagnostic procedures. The whole process works as (i) hyperparameters tuning for picking the most appropriate learning approach, and (ii) a mobile application is developed to support clinical practices, see Figure 1. Here, clinical experts might not need to understand the technical part because it is done automatically. Experts feed hospital data from different sources to the system. First, data preparation starts with splitting sources into training-validation-test schemes. The training and validation sets are feed into a black box of several predefined learning models. The best model is selected based on an evaluation metric's optimization, performing on the validation set. Finally, the instances that are considered as unseen data belong to the test dataset. Figure (3) illustrates a practical splitting protocol in machine learning. This selection mechanism is described in Figure (2). The authors apply decision trees (DT), naïve Bayes (NB), artificial neural networks (NN), random forest (RF), support vector machines (SVM), and extreme gradient boosting (XGBoost).

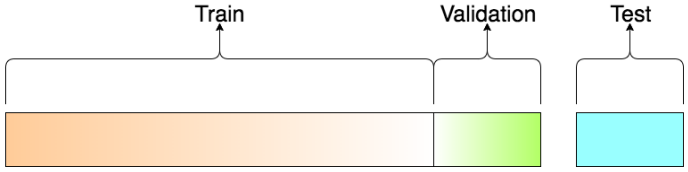


Figure 3: A visualization of the dataset splitting.

3 Materials and Methodology

In this section, the authors briefly present the implemented machine learning approaches. We do not pretend that our discussion will be an overview of models. Interesting readers might refer to several textbooks for further self-learning and comprehension [19]–[22]. Furthermore, other interesting papers that connect the gap between machine learning and medical research can be found at [23]–[26].

3.1 Support Vector Machines

SVM constructs a hyperplane in a high dimensional space. Assuming that the linear model is $v^T x$, then the following constraints need to be satisfied in case of the data points are linearly separable:

$$y_i(v^T x_i + b) \geq 1. \tag{1}$$

SVM seeks to find a good hyperplane where the margin to different classes' data points is maximum. Hence, SVM optimizes:

$$\min \frac{1}{2}\|v\|^2 \tag{2}$$

In case of non-linear separation, the constraints cannot be fulfilled. Then, soft margin is applied. The optimization in Equation 2 becomes

$$\begin{aligned} &\min \frac{1}{2}\|v\|^2 + C\sum_i \sigma_i, \\ &\text{subject to } y_i(v^T x_i + b) \geq 1 - \sigma_i\ , \sigma_i \geq 0. \end{aligned} \tag{3}$$

The Lagrangian is calculated as follows:

$$L = \frac{1}{2}\|v\|^2 - \sum_i \beta_i(y_i(v^T x_i + b) - 1 + \sigma_i). \tag{4}$$

Setting the respective derivatives to 0, then the dual form of the optimization is as follows:

$$\begin{aligned} &\max \sum_i \beta_i - \frac{1}{2}\beta_i\beta_j y_i y_j x_i^T x_j, \\ &\text{subject to } \sum_i \beta_i y_i = 0, \beta_i \geq 0. \end{aligned} \tag{5}$$

where the ranking model $v = \sum_i \alpha_i y_i x_i$ is achieved by solving the quadratic programming. The optimality in Equation 5 is applied by the Karush-Kuhn-Tucker (KTT) conditions. Then we get:

$$\beta_i = 0 \quad \Rightarrow \quad y_i(v^T x_i + b) \geq 1, \tag{6}$$

$$0 < \beta_i < C \quad \Rightarrow \quad y_i(v^T x_i + b) = 1, \tag{7}$$

$$\beta_i = C \quad \Rightarrow \quad y_i(v^T x_i + b) \leq 1. \tag{8}$$

3.2 Naïve Bayes

Due to its easy implementation and high performance, many machine learning practitioners consider Naïve Bayes is a simple but effective machine learning model [27]. We denote a vector $\mathbf{x}$, a set τ and $y = s$ as model's parameters and accompanying label respectively. Then, we can define a generative model $\mathbf{x}$ as follows:

$$P(y = s|\mathbf{x}, \tau) = \frac{P(y = s|\tau)P(\mathbf{x}|y = s, \tau)}{\sum_{s'} P(y = s'|\tau)P(\mathbf{x}|y = s', \tau)}\ , \tag{9}$$

where $P(\mathbf{x}|y = s, \tau)$, $P(y = s|\mathbf{x})$ are class-conditional density and class posterior. $P(y = s)$ is class prior. Equation (9) can be proportionally calculated as follows:

$$P(y = s|\mathbf{x}, \tau) \propto P(y = s|\tau)P(\mathbf{x}|y = s, \tau). \tag{10}$$

Then, the class-conditional density in Equation (9) is estimated as follows:

$$P(\mathbf{x}|y = s, \tau) = \prod_{i=1}^{D} P(x_i|y = s, \tau_{is})\ , \tag{11}$$

which is the Naïve Bayes classifier. Because it is not expected that the features should be independent, Equation (11) can be re-written depending on each feature's type, e.g. binary, real-valued, or categorical attributes. Specifically, in case of binary attributes, the Bernoulli distribution can be utilized as follows:

$$P(\mathbf{x}|y = s, \tau) = \prod_{i=1}^{D} \mathcal{B}(x_i|\mu_{is})\ , \tag{12}$$

where μ_{is} means the probability of attribute i objected to class s. In case of real-valued attributes, the Gaussian distribution can be computed as follows:

$$P(\mathbf{x}|y = s, \tau) = \prod_{i=1}^{D} \mathcal{N}(x_i|\mu_{is}, \sigma_{is}^2)\ , \tag{13}$$

where μ_{is} and σ_{is}^2 mean the probability of attribute i objected to class s and its variance respectively. In case of categorical attributes, multinoulli distribution is used as follows:

$$P(\mathbf{x}|y = s, \tau) = \prod_{i=1}^{D} \mathcal{C}(x_i|\mu_{is}, \sigma_{is})\ , \tag{14}$$

where $x_i \in \{1, \ldots, K\}$ is categorical attributes and σ_{is} is a histogram over K.

In our research, disease classification is basically to classify input vector into different categories. Depending on the representation as a binary or real-valued matrices, Equation (12 or 13) is applied to make prediction.

3.3 Artificial Neural Networks

We apply Multilayer Perceptrons as the version of artificial neural networks applied in the experiments. We form the the model as follows:

$$p(y|x, \theta) = \mathcal{N}(y|\mathbf{w}^T\mathbf{g}(\mathbf{x}), \sigma^2)\ , \tag{15}$$

where $\mathbf{g}(\mathbf{x})$ is called the hidden layer. It is defined as follows:

$$\mathbf{g}(\mathbf{x}) = f(\mathbf{V}x) = \left[f(\mathbf{1}^T\mathbf{x}), \ldots, f(\mathbf{v}_H^T\mathbf{x})\right] , \tag{16}$$

where H is the number of hidden units, f is a logical function. $\mathbf{V}$ is the weight matrix from the inputs to the hidden nodes, while $\mathbf{w}$ is the weight vector from the hidden nodes to the output. In our experiments, we deploy an artificial neural network with 2 hidden layers due to the hardware constraints. A sigmoid function is activated on the output if the classification is binary.

$$p(y|x, \theta) = \mathcal{B}(y|\text{sigmoid}(\mathbf{w}^T\mathbf{g}(x))) . \tag{17}$$

Regarding multi-class classification, sum-to-one constraint is applied:

$$p(y|\mathbf{x}, \theta) = C(y|\mathcal{S}(\mathbf{W}\mathbf{g}(\mathbf{x}))) . \tag{18}$$

3.4 Decision Trees

We denote R as the number of regions, w_r is the weight response in the r region. A decision tree is formed as follows.

$$f(x) = \sum_{r=1}^{R} w_r \phi(\mathbf{x}, \mathbf{v}_r) , \tag{19}$$

where $\mathbf{v}_r$ is the choice of variable to split on.

To find the best partitioning of the input data, the greedy procedure is used in common. There is progress that measures the quality of a split in the classification setting. Given a threshold t, we fit a multinoulli model to the data that satisfies the condition $X_j < t$ by estimating the class-conditional probabilities as follows:

$$\hat{\pi}_c = \frac{1}{|L|} \sum_{i \in L} \mathbb{I}(y_i = c) , \tag{20}$$

where L is the data in the leaf. Then the misclassification rate is calculated as follows:

$$\frac{1}{|L|} \sum_{i \in L} \mathbb{I}(y_i \neq \hat{y}) = 1 - \hat{\pi}_{\hat{y}}. \tag{21}$$

Note that the most probable class is $\hat{y}_c = \text{argmax}_c\, \hat{\pi}_c$. Moreover, the Entropy can be measured as follows:

$$\mathbb{H}(\hat{\pi}) = -\sum_{c=1}^{C} \hat{\pi}_c \log \hat{\pi}_c . \tag{22}$$

We leave the Entropy as the default setting for the decision tree in our experiments.

3.5 Bagging Aggregation with Random Forest

Although DT is one of the most effective and speedy models, it is highly variable due the the splitting. At first, DT is trained on a complete dataset. Then that dataset is split into two portions. DT is applied on the two portions and interestingly, they return different results. The idea of bagging technique helps to reduce the variance in any model [28]. An example of bagging is the generation of many decision trees in parallel. We can train T different trees on different subsets of the data, chosen randomly with replacement, and then compute the ensemble as follows:

$$f(x) = \sum_{t=1}^{T} \frac{1}{T} f_m(x) , \tag{23}$$

where f_t is the t'th tree. This helps reduce the variance of the predictions.

3.6 Boosting Technique with XGBoost

XGBoost, see Figure 4, is a popular and efficient machine learning implementation of the gradient boosted trees [29]. It has been widely applied in some data competitions. The general idea of gradient boosting is to predict a class by combining several weak learners. XGBoost used a regularized objective function (L1 and L2) that combines a convex loss function (emerging from the difference between the ground-truth and prediction) and a penalty term for controlling model complexity. A gradient descent algorithm is used to minimize the loss when adding new learners. The training proceeds iteratively, adding new trees that predict the prior trees' residuals associated with previous trees to perform the final prediction. Regularization is included to reduce overfitting. The authors denote the i-th instance with an associated label as $x_i \in \mathbb{R}^d$, $\hat{y}$ as the prediction given x_i. T is the number of trees. Then we define:

$$\hat{y}_i = \sum_{t=1}^{T} f_t(x_i) , f_t \in \mathcal{F} . \tag{24}$$

Machine learning is basically the procedure of learning parameters $\theta = \{w_j | j = 1, \ldots, d\}$. The objective function is follows:

$$H(\theta) = L(\theta) + \Omega(\theta) , \tag{25}$$

where $L(\theta)$ is the training loss and $\Omega(\theta)$ is the regularization configuration. Optimizing $L(\theta)$ results in high prediction accuracy, while optimizing $\Omega(\theta)$ balances the simplicity of model. For each iteration j, we define the XGBoost objective function by expanding Equation (25).

$$H^{(j)} = \sum_{i=1}^{n} l(y_i, \hat{y}_i^{j-1} + f_j(x_i)) + \Omega(f_j) . \tag{26}$$

We can see that we cannot optimize Equation (26) by using traditional optimization methods because XGBoost objective is a function of functions. However, we can transform the original objective function to the Euclidean domain by Taylor approximation [30].

$$f(x + \Delta x) \simeq f(x) + f'(x)\Delta x + \frac{1}{2} f''(x)\Delta x^2 . \tag{27}$$

The first order gradient statistics is defined as $g_i = \partial_{\hat{y}^{t-1}} l(y_i, \hat{y}^{t-1})$, while the second order gradient statistics of the loss function is defined as $h_i = \partial^2_{\hat{y}^{t-1}} l(y_i, \hat{y}^{t-1})$:. Hence, Equation (26) can be rewritten as follows:

$$H^{(j)} = \sum_{i=1}^{n} [g_i f_j(x_i) + \frac{1}{2} h_i f_j^2(x_i)] + \Omega(f_j) \tag{28}$$

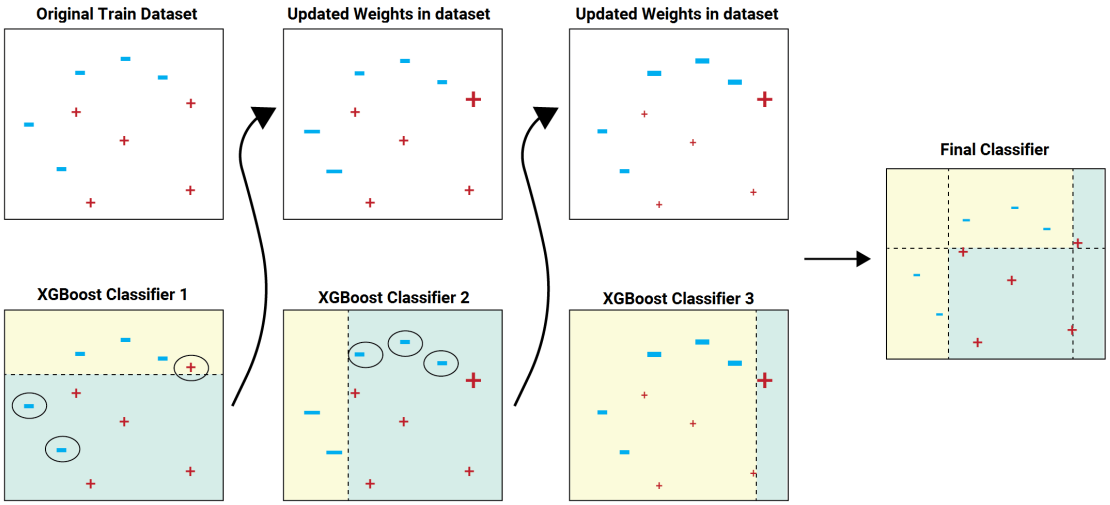


Figure 4: The sequential ensemble methods in XGBoost.

4 Experiments

4.1 Evaluation Metrics: F1-measure

We denote TrueP, FalseP, and FalseN as true positive, false positive, and false negative. With the classification problem where the classes' data sets are very different from each other, there is a logical operation commonly used as Precision-Recall. First of all, consider the problem of binary classification. We also consider one of the two classes to be positive and the other to be negative. With a way of determining a class to be positive, precision (Pre) is defined as the ratio of the number of true positive points to those classified as positive (TrueP + FalseP). The recall (Rec) is defined as the ratio of the number of true positive points to positive (TrueP + FalseN). Mathematically, Precision and Recall are two fractions with equal numerators but different denominators:

$$\text{Pre} = \frac{\text{TrueP}}{\text{TrueP} + \text{FalseP}} \tag{29}$$

$$\text{Rec} = \frac{\text{TrueP}}{\text{TrueP} + \text{FalseN}} \tag{30}$$

We combine Equations 29 and 30 to compute F1-measure as follows:

$$\text{F1-measure} = 2\frac{\text{Pre} \times \text{Rec}}{\text{Pre} + \text{Rec}} \tag{31}$$

4.2 Dataset Collection

In this paper, eight datasets related to medical data are selected from the UCI Machine Learning Repository. More specifically, the experimental datasets are Breast Cancer Data[1], Heart Disease Data[2], Dermatology Data[3], Vertebrae Data[4], Hepatitis Data[5], Cervical cancer (Risk Factors) (RF) Data[6], Autism Adolescent Data[7], and Diabetes Data[8]. The authors prudentially select several categorization datasets that are suitable for the research's scope. Categorical attributes are converted into numerical representation using a one-hot encoding process. Data imbalance is accepted as the native characteristics of classification data sources. The eight experimental datasets are shown in Table (1).

Table 1: Hospital data from different sources

#	Dataset	Prediction Type	# Samples	# Attributes
1	Breast Cancer	Binary	286	9
2	Dermatology	Multi class	365	22
3	Heart Disease	Multi class	303	13
4	Hepatitis	Binary	155	19
5	Vertebrae	Multi class	310	6
6	Cervical Cancer (RF)	Binary	858	32
7	Autism Adolescent	Binary	768	20
8	Diabetes	Binary	104	8

In the experiments, the authors set up the splitting scheme by the following ratios. First, we randomly split without replacement the dataset into 70% and 30% for the pre-training and test parts respectively. Next, the pre-training portion is randomly split without replacement into 80% and 20% for the training and validation

[1] https://archive.ics.uci.edu/ml/datasets/Breast+Cancer
[2] https://archive.ics.uci.edu/ml/datasets/Heart+Disease
[3] https://archive.ics.uci.edu/ml/datasets/Dermatology
[4] https://archive.ics.uci.edu/ml/datasets/Vertebral+Column
[5] https://archive.ics.uci.edu/ml/datasets/Hepatitis
[6] https://archive.ics.uci.edu/ml/datasets/Cervical+cancer+(Risk+Factors)
[7] https://archive.ics.uci.edu/ml/machine-learning-databases/00420/
[8] https://archive.ics.uci.edu/ml/datasets/diabetes

portions respectively. The role of these sets is introduced above, see Figure (2).

4.3 Experimental Results

As mentioned above, the model's performance is judged by its ability to predict unseen data accurately. Hence, the best scores are considered on the test sets. The F1-measure of experimental models performing on datasets are summarized in Table (2). Overall, there is no absolute best approach. However, the random forest model achieves remarkable performance on four different datasets, e.g., Breast Cancer, Cervical Cancer, Autism, and Diabetes. The neural network approach gets the least performance since it does not win any best prediction.

One interesting point to note is that Naïve Bayes algorithm achieves the F1-measure of 1.0 on the Dermatology data. Meanwhile, XGBoost gains the F1-measure of 0.94 on the Diabetes dataset. RF is the best models performing on four different data, namely Breast Cancer, Hepatitis, Cervical Cancer (RF), and Autism Adolescent. Observing all experimental datasets, Vertebrae is the most challenging. Even the best model, e.g., SVM, only achieves the F1-measure of 0.54. Statistics in Table (1) show that Cervical Cancer has the most instances and the most attributes, e.g., 858 and 32, respectively. Even though Cervical Cancer has the most observations, one can argue that only partial representations of properties might not be enough to learn coefficients for 32 attributes. The performance of XGBoost is not stable. While it is the winner performing on Diabetes dataset, the prediction capacity is much more insufficient than other models on other datasets.

Table 2: The report of F1-scores. The best scores are in **bold**.

#	Dataset	Pool of Learning Models					
		DT	RF	XGBoost	NB	NN	SVM
1	Breast Cancer	0.76	**0.79**	0.26	0.75	0.77	0.75
2	Dermatology	0.95	0.96	0.18	**1.00**	0.90	0.91
3	Heart Disease	**0.63**	0.61	0.49	0.58	0.52	0.58
4	Hepatitis	**0.80**	**0.80**	0.21	**0.80**	0.70	0.74
5	Vertebrae	0.50	0.52	0.38	0.53	0.51	**0.54**
6	Cervical Cancer (RF)	**0.94**	**0.94**	0.11	0.93	0.91	0.87
7	Autism Adolescent	0.59	**0.93**	0.15	0.87	0.90	0.87
8	Diabetes	0.61	0.92	**0.94**	0.53	0.63	0.50

4.4 Reproducibility

A grid search strategy on tuning models' hyperparameters is provided for the ease of reproducing the experimental results. The number of estimators and the allowable depth of the trees are investigated regarding tree-based models. We investigate the performance of Gaussian and Bernoulli Naïve Bayes algorithms. Regarding the neural network, the authors examine the effect of the number of units in its hidden layers. We take into account the effect of C and kernel configuration for SVM. Other hyperparameters leave default settings by scikit-learn library [31]. The experimental environment is as follows: windows 10, CPU Intel Core i5-2410M, 2.30GHz, and 8GB of RAM. Table (3) presents our hyperparameters setttings. Hyper-parameters are parameters that are not directly learned within estimators. They are passed as the constructor's arguments of the estimator classes. The best hyperparameters' combination for each machine learning model, and the total search time is presented in Table (4).

Table 3: Hyperparameters space.

Models	Hyperparameters	Settings
DT	Max depth (Max)	$1 \rightarrow 101$
	Min samples leaf (Min)	$1 \rightarrow 101$
RF	Max	$1 \rightarrow 51$
	N estimators (N)	$1 \rightarrow 51$
	Min	$1 \rightarrow 51$
NB	Algorithm (A)	Gaussian (G), Bernoulli (B)
XGBoost	Max	$1 \rightarrow 101$
	gamma (Gm)	$0.1 \rightarrow 0.9$
	# of Parallel trees (Nt)	$1 \rightarrow 51$
	# of jobs (Nj)	$1 \rightarrow 51$
	Sketch Eps (Ep)	$0.1 \rightarrow 0.9$
NN	Hidden layer size (S)	$(1 \rightarrow 101, 1 \rightarrow 101)$
SVM	Kernel (K)	Linear (Li), Poly, RBF
	C	$1 \rightarrow 101$

4.5 Mobile App Development

A mobile application, named Medical Diagnosis, is developed for disease diagnosis in the clinic. The app supports several preliminary features such as disease information and input questions for inspection. Currently, the application runs on the Android mobile operating system and works on a client-server architecture. Machine learning approaches are trained on a regular laptop, which acts as a server. After training the models on a server, the most current classifiers are updated into the client devices. Android Studio 3.2 is used as the IDE to develop the mobile application. The emulation and debugging are done on Genymotion version 5.4.2. The proposed interpretation procedure automatically selects the best model for an investigated input dataset. Then, the models are saved as pickle classifiers[9] [32, 33].

The client is an Android mobile device that is equipped with saved pickle classifiers. A friendly graphical user interface (GUI) provides questions to get input from users on the client-side; either they type in the required information or select from pre-defined options. The main components of the GUI are designed as follows. Textview is used to display messages, comments, and headings. Gridview is used to create a list of two image columns to choose diseases that need an easy diagnosis. Listview creates a list of histological properties for the user to select. The display of symptoms for users to choose on Listview helps users conveniently review the selected symptom. HorizontalScrollView is used to display the properties that the user has selected or entered. Besides, on this screen, the user can copy or delete the selected properties. Toast in Android helps users recognize the entered or selected properties, showing errors connected to the API. The properties are described clearly for the convenience of the user entering and selecting information using Dialog. Each disease's attribute is handled separately with different Dialogs depending on the value of the feature that the user enters or selects. The Dialog can also be used to provide diagnostic

[9] https://docs.python.org/3.6/library/pickle.html

Table 4: The best hyperparameters combination.

Dataset	Learning Models																			
	DT			RF				XGBoost						NB		NN		SVM		
	Ma	Mi	Search time	Ma	N	Mi	Search time	Ma	Gm	Nt	Nj	Ep	Search time	A	Search time	S	Search time	K	C	Search time
Breast Cancer	11	1	35s	1	2	23	3h03m	1	0.1	1	1	0.1	1h06m	G	8s	(8,13)	3h17m	Li	6	1m22s
Dermatology	6	1	50s	4	10	1	3h20m	1	0.1	1	1	0.1	1h35m	B	7s	(49,39)	56m	Li	1	1m47s
Heart Disease	4	5	50s	8	18	2	3h22m	1	0.1	1	1	0.1	2h03m	B	4s	(32,28)	31m	Li	1	2m41s
Hepatitis	1	1	40s	5	11	1	3h07m	1	0.3	20	44	0.2	1h12m	B	2s	(43,72)	45m	Li	1	1m05s
Vertebrae	1	1	20s	2	47	22	3h08m	1	0.3	20	14	0.2	1h33m	G	3s	(7,90)	1h15m	Li	3	3m38s
Cervical Cancer (RF)	5	1	9s	1	1	1	2h05m	1	0.1	1	1	0.1	2h05m	B	8s	(37,33)	50m	Li	2	2m30s
Autism Adolescent	3	28	44s	1	8	1	2h54m	1	0.1	1	1	0.1	0h43m	B	3s	(73,53)	1h19m	Li	1	1m09s
Diabetes	4	48	58s	12	7	3	3h17m	1	0.3	20	5	0.2	1h15m	G	3s	(34,14)	57m	Li	2	2m18s

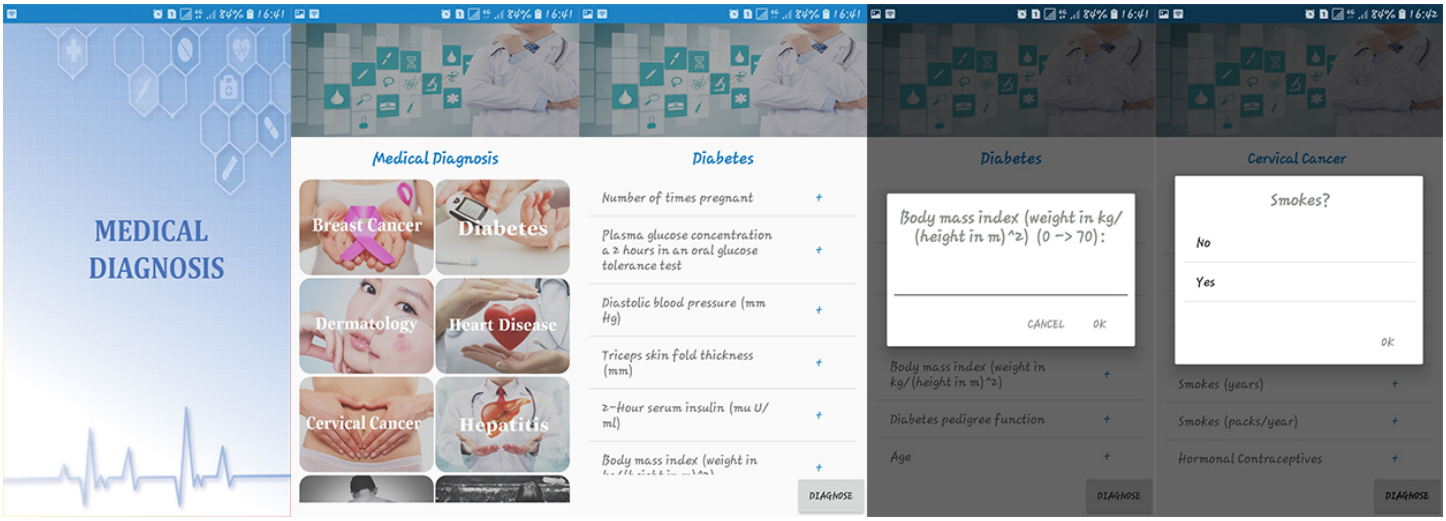


Figure 5: Several screenshots of our mobile application.

returns or report missing symptoms of the user. The application is designed to suit all types of screens of different mobile phones. The application can run on Android OS 5.0.0 and above.

The server holds an up-to-date trained model, configuration, a database, and complete Android packages that are really to install and update to the client. When this paper is conducted, the authors merely develop a mobile application for Android only. Several screenshots of our mobile application are shown in Figure (5).

5 Conclusion

In this research, the authors have described the interpretation of machine learning models for the task of classification in medical diagnosis. We propose processes that interpret the most appropriate learning models for each of the different clinical datasets as the foundation of developing and recommending diagnostic procedures. The whole process works as (i) hyperparameters tuning for picking the most appropriate learning approach, and (ii) a mobile application is developed to support clinical practices. We also explain an urgent need to optimize medical processes and regular experts' workflows to support healthcare services while reducing investment costs and improving efficiencies. The experimental results, interpretation of models, and reproducibility are thoughtfully discussed. A mobile application is also developed. We believe that our work has substantially extended our previous paper has encouraged further research machine learning, healthcare, and medical diagnosis.

References

[1] N. Duong-Trung, X. N. Hoang, T. B. T. Tu, K. N. Minh, V. U. Tran, T.-D. Luu, "Blueprinting the Workflow of Medical Diagnosis through the Lens of Machine Learning Perspective," in 2019 International Conference on Advanced Computing and Applications (ACOMP), 23–26, IEEE, 2019, doi: 10.1109/ACOMP.2019.00011.

[2] W. H. Crown, "Potential application of machine learning in health outcomes research and some statistical cautions," Value in health, **18**(2), 137–140, 2015, doi:10.1016/j.jval.2014.12.005.

[3] C. Cheng, J. Barceló, A. S. Hartnett, R. Kubinec, L. Messerschmidt, "COVID-19 Government Response Event Dataset (CoronaNet v. 1.0)," Nature Human Behaviour, **4**(7), 756–768, 2020, doi:10.1038/s41562-020-0909-7.

[4] Y. Wang, N. Hajli, "Exploring the path to big data analytics success in healthcare," Journal of Business Research, **70**, 287–299, 2017, doi:10.1016/j.jbusres.2016.08.

[5] C. H. Lee, H.-J. Yoon, "Medical big data: promise and challenges," Kidney research and clinical practice, **36**(1), 3, 2017, doi:10.23876/j.krcp.2017.36.1.3.

[6] M. Swan, "The quantified self: Fundamental disruption in big data science and biological discovery," Big data, **1**(2), 85–99, 2013, doi:10.1089/big.2012.0002.

[7] A. Holzinger, I. Jurisica, "Knowledge discovery and data mining in biomedical informatics: The future is in integrative, interactive machine learning solutions," in Interactive knowledge discovery and data mining in biomedical informatics, 1–18, Springer, 2014, doi:10.1007/978-3-662-43968-5_1.

[8] R. Freeman, L. Frisina, "Health care systems and the problem of classification," Journal of Comparative Policy Analysis, **12**(1-2), 163–178, 2010, doi:10.1080/13876980903076278.

[9] K. A. Wager, F. W. Lee, J. P. Glaser, Health care information systems: a practical approach for health care management, John Wiley & Sons, 2017.

[10] T. B. Murdoch, A. S. Detsky, "The inevitable application of big data to health care," Jama, **309**(13), 1351–1352, 2013, doi:10.1001/jama.2013.393.

[11] H. M. Krumholz, "Big data and new knowledge in medicine: the thinking, training, and tools needed for a learning health system," Health Affairs, **33**(7), 1163–1170, 2014, doi:10.1377/hlthaff.2014.0053.

[12] Z. Obermeyer, E. J. Emanuel, "Big data, machine learning, and clinical medicine," The New England journal of medicine, **375**(13), 1216, 2016, doi:10.1056/NEJMp1606181.

[13] M. Chen, Y. Hao, K. Hwang, L. Wang, L. Wang, "Disease prediction by machine learning over big data from healthcare communities," Ieee Access, **5**, 8869–8879, 2017, doi:10.1109/ACCESS.2017.2694446.

[14] D. S. Char, N. H. Shah, D. Magnus, "Implementing machine learning in health care—addressing ethical challenges," The New England journal of medicine, **378**(11), 981, 2018, doi:10.1056/NEJMp1714229.

[15] F. Cabitza, R. Rasoini, G. F. Gensini, "Unintended consequences of machine learning in medicine," Jama, **318**(6), 517–518, 2017, doi:10.1001/jama.2017.7797.

[16] S. R. Steinhubl, E. D. Muse, E. J. Topol, "The emerging field of mobile health," Science translational medicine, **7**(283), 283rv3–283rv3, 2015, doi:10.1126/scitranslmed.aaa3487.

[17] A. Jutel, D. Lupton, "Digitizing diagnosis: a review of mobile applications in the diagnostic process," Diagnosis, **2**(2), 89–96, 2015, doi:10.1515/dx-2014-0068.

[18] C.-K. Kao, D. M. Liebovitz, "Consumer mobile health apps: current state, barriers, and future directions," PM&R, **9**(5), S106–S115, 2017, doi:10.1016/j.pmrj.2017.02.018.

[19] K. P. Murphy, Machine learning: a probabilistic perspective, MIT press, 2012.

[20] I. H. Witten, E. Frank, M. A. Hall, C. J. Pal, Data Mining: Practical machine learning tools and techniques, Morgan Kaufmann, 2016.

[21] M. Mohri, A. Rostamizadeh, A. Talwalkar, Foundations of machine learning, MIT press, 2018.

[22] N. Duong-Trung, Social Media Learning: Novel Text Analytics for Geolocation and Topic Modeling, Cuvillier Verlag, 2017.

[23] Y.-Y. Song, L. Ying, "Decision tree methods: applications for classification and prediction," Shanghai archives of psychiatry, **27**(2), 130, 2015, doi:10.11919/j.issn.1002-0829.215044.

[24] D. Walk, "Using Random Forest Methods to Identify Factors Associated with Diabetic Neuropathy: A Novel Approach," 2017, doi:10.1093/pm/pnw311.

[25] X. Liu, H. Zhu, R. Lu, H. Li, "Efficient privacy-preserving online medical primary diagnosis scheme on naive bayesian classification," Peer-to-Peer Networking and Applications, **11**(2), 334–347, 2018, doi:10.1007/s12083-016-0506-8.

[26] P. Naraei, A. Abhari, A. Sadeghian, "Application of multilayer perceptron neural networks and support vector machines in classification of healthcare data," in 2016 Future Technologies Conference (FTC), 848–852, IEEE, 2016, doi:10.1109/FTC.2016.7821702.

[27] T. Li, J. Li, Z. Liu, P. Li, C. Jia, "Differentially private Naive Bayes learning over multiple data sources," Information Sciences, **444**, 89–104, 2018, doi:10.1016/j.ins.2018.02.056.

[28] A. M. Prasad, L. R. Iverson, A. Liaw, "Newer classification and regression tree techniques: bagging and random forests for ecological prediction," Ecosystems, **9**(2), 181–199, 2006, doi:10.1007/s10021-005-0054-1.

[29] T. Chen, C. Guestrin, "Xgboost: A scalable tree boosting system," in Proceedings of the 22nd acm sigkdd international conference on knowledge discovery and data mining, 785–794, ACM, 2016, doi:10.1145/2939672.2939785.

[30] A. Guzman, Derivatives and integrals of multivariable functions, Springer Science & Business Media, 2012.

[31] F. Pedregosa, G. Varoquaux, A. Gramfort, V. Michel, B. Thirion, O. Grisel, M. Blondel, P. Prettenhofer, R. Weiss, V. Dubourg, J. Vanderplas, A. Passos, D. Cournapeau, M. Brucher, M. Perrot, E. Duchesnay, "Scikit-learn: Machine Learning in Python," Journal of Machine Learning Research, **12**, 2825–2830, 2011, doi:10.1016/j.patcog.2011.04.006.

[32] M. Lutz, Learning python: Powerful object-oriented programming, O'Reilly Media, Inc., 2013.

[33] J. Avila, T. Hauck, Scikit-learn cookbook: over 80 recipes for machine learning in Python with scikit-learn, Packt Publishing Ltd, 2017.

ASTES

Advances in Science, Technology and Engineering Systems Journal
Vol. 5, No. 5, 478-484 (2020)
www.astesj.com
Special Issue on Innovative Research in Applied Science, Engineering and Technology

ASTES Journal
ISSN: 2415-6698

Contextual Word Representation and Deep Neural Networks-based Method for Arabic Question Classification

Alami Hamza[*,1], Noureddine En-Nahnahi[1], Said El Alaoui Ouatik[1,2]

[1]*LISAC Laboratory, Faculty of Sciences Dhar El Mahraz, Sidi Mohamed Ben Abdellah University, PO Box 1796, Fez 30003, Morocco*

[2]*Laboratory of Engeneering Sciences, National School of Applied Sciences, Ibn Tofail University, Kenitra, Morocco*

ARTICLE INFO

Article history:
Received: 01 July, 2020
Accepted: 05 September, 2020
Online: 24 September, 2020

Keywords:
Arabic Question Classification
Contextual Word Representation
ELMo
RNN
CNN

ABSTRACT

Contextual continuous word representation showed promising performances in different natural language processing tasks. It stems from the fact that these word representations consider the context in which a word appears. But until recently, very little attention was paid to the contextual representations in Arabic question classification task. In the present study, we employed a contextual representation called Embeddings from Language Models (ELMo) to extract semantic and syntactic relations between words. Then, we build different deep neural models according to three types: Simple models, CNN and RNN mergers models, and Ensemble models. These models are trained on Arabic questions corpus to optimize the cross entropy loss given questions representations and their expected labels. The dataset consists of 3173 questions labeled according the Arabic taxonomy and an updated version of the Li & Roth taxonomy. We performed various comparisons with models based on the widely known context-free word2vec word representation. These evaluations confirm that ELMo representation achieves top performances. The best model scores up to 94.17%, 94.07%, 94.17% in accuracy, macro $F1$ score, and weighted $F1$ score, respectively.

1 Introduction

Question Answering Systems (QAS) have become one of the most popular information retrieval applications. These systems enable automatic answering to natural questions. This involves several parts functioning jointly to extract exact response, considering a user's question. A typical QAS is composed of three main components: 1) Question processing performs Question Classification (QC) and keywords extraction; 2) Passage retrieval apply information retrieval techniques to extract the passages that most probably contains the answer; 3) Answer processing processes the extracted passages and formulate the answer in natural language. A proper QC method enhances the performance of QAS by omitting insignificant answer candidates. In [1], the authors showed that 36.4% of errors made by QAS are associated to the QC. Despite the progress in different English natural language processing domains due to machine learning models, Arabic questions classification must address countless challenges owing to the lack of labeled corpora and difficulties associated to the complex morphology of this language, such us the absence of capital letters, the presence of diacritical marks, and its inflectional and derivational nature.

A typical QC method based on machine learning is composed of three main steps: 1) question preprocessing; 2) question representation; and 3) question classification. Previous works [2] represented words with term frequency-inverse document frequency (TF-IDF) method. This latter neglects relationships between words inside a question resulting in poor question representation. This restrictions led the authors [3] to use a continuous distributed word embeddings model [4]. This word representation ignores the context word yet it has the up side of considering both semantic and syntactic relations between words.

In this paper, we build question embedding by using a contextual representations namely Embeddings from Language Models (ELMo) [5]. Unlike the well known word2vec [4] representation that not consider the context, ELMo representation is able to compute word representation considering the word's context. In addition, we build various models according to three types: Simple models, CNN and RNN mergers models, and Ensemble models. The simple models are based on global max pooling, CNN, and RNN without any CNN/RNN combination. The CNN and RNN mergers models combine CNN and RNN layers to extract automatically more features from word representations. The Ensemble models predict

[*]Corresponding Author: Alami Hamza, Sidi Mohammed Ben Abdellah University, Morocco hamza.alami1@usmba.ac.ma

the probability of class labels by mixing the probability scores from different models. Our evaluations confirm that contextual representations show a good effects on Arabic question classification, and ensemble models based on word2vec and ELMo representations achieves top performances since they scored up to 94.17%, 94.07%, 94.17% in regards to accuracy, macro $F1$ score, and weighted $F1$ score.

The rest of the paper is structured as follows: Section 2 provides a brief overview of the previous works on Arabic question classification; Section 3 reveals our method for Arabic question classification which is based on contextual word representation; Section 4 presents the performance evaluations and the comparison results of various models; Finally, Section 5 concludes and gives future works and perspectives.

2 Related works

Numerous researches proposed methods for Arabic question classification. We introduce some of these methods in the following paragraphs.

In [6], the authors created a question answering system particularly for the holy Quran. Questions are represented by a set of terms, every term comprises both a part of speech tag and a stem of a word. They introduced a new taxonomy especially for classifying the question associated to the holy Quran. A support vector machine (SVM) classifier was trained on 180 training questions and tested with 3-folds cross validation on 50 questions. The obtained accuracy was about 77.2%.

In [7], the authors pursued a rule based approach to build their Arabic question classifier. The authors employed the NOOJ [1] tool to develop the Arabic linguistic rules that characterize question. They prepared a set of 200 questions for training questions and a set of 200 questions for test. They observed recall and precision are 93% and 100%, respectively.

In [2], the authors performed a comparison between two well known algorithms, SVM and Multinomial Naive Bayes, for Arabic question classification. In order to represent questions into vector space model, the TF-IDF method was applied. They trained the models with 300 training questions and tested on 200 questions. The best results were achieved by the SVM model which scored 100%, 94%, and 97% on precision, recall, and F1-measure.

In [3], the authors suggested a new Arabic taxonomy motivated from Arabic linguistic rules. They applied the continuous distributed word representation proposed in [4, 8, 9] to represent words. This representation captures semantic and syntactic relations between words. Various models including SVM, XGBoost, logistic regression were trained to classify questions given their words vectors. They built a dataset that contains 1041 questions for training and 261 questions for testing. The best performances were scored with the SVM model. It achieved 90%, 91%, 90%, and 90% on accuracy, precision, recall, and F1 score.

These works added on the progress of Arabic question classification methods. Nevertheless, the sizes of the datasets used in these studies were relatively small. Also, the TF-IDF representation has several drawbacks such us the word representation is sparse and huge, the semantic and syntactic relations between words can not be captured. What's more, the enriched word2vec representation calculates static word vectors neglecting the context were a word appears. Thus, a word with multiple meaning (polysemy phenomena) is misrepresented. Finally, the method based on linguistic rules proposed by [7] is highly impacted by the dataset used to extract rules and demands greater time and rules to consider additional Arabic question types.

[1] http://www.nooj-association.org/

3 Method

Our method is composed of three main steps including preprocessing, question representation, and questions classification.

3.1 Preprocessing

Our preprocessing pipeline is composed of two main steps: 1) punctuation and non Arabic words removal; 2) questions tokenization. Unlike standard pipelines of text preprocessing which perform stop words removal, we keep these words since they contain valuable information and are involved during the question classification. For instance, the words *Why* and *Who* are essential to identify the question type.

3.2 Question representation

To represent questions into a vector space format, we use the ELMo representation introduced in [5, 10]. All the words included into a question are passed to a neural network that is composed of two main layers: 1) one dimensional convolutional neural network with different filter sizes that computes word embeddings based on its character level embeddings; 2) a stack of two Bidirectional LSTM (BiLSTM) layers. The network is trained with large textual corpora to optimize language model objective. Thus, the ELMo representation of a word k, given by $\mathbf{ELMo}_k$, is calculated by the next equation:

$$\mathbf{ELMo}_k = \frac{1}{3}\sum_{j=0}^{2} \mathbf{h}_{k,j}^{(LM)} \quad (1)$$

where $\mathbf{h}_{k,j}$ is the output of the hidden layers j of the neural network. Figure 1 depicts the overall design of the ELMo technique. In order to calculate contextual word representation, we used the pre-trained word representation presented by [10, 11]. The model is trained with a set of 20-million-words data randomly picked from the Arabic Wikipedia corpus. Every word in represented by an 1024 dimension vector.

A question Q, that is a succession of l words, is modeled by the later matrix:

$$\mathbf{Q} = [\mathbf{ELMo}_{word_1}, ..., \mathbf{ELMo}_{word_l}] \quad (2)$$

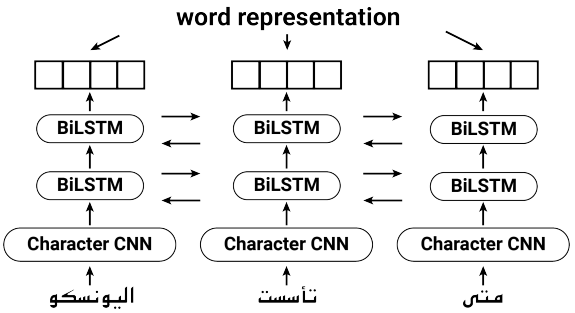


Figure 1: The overall architecture of Embeddings from Language Models

3.3 Questions classification

We constructed several neural network models on top of ELMo embeddings for Arabic questions classification. The goal is to investigate the behavior of contextual representation with diverse neural network architectures. In the course of training, the parameters of the ELMo model are fixed and the remainder of the parameters are optimized according the categorical cross entropy loss denoted by the equation:

$$J(\theta) = -\frac{1}{T}\sum_{t=1}^{T}\left[y_t \log \hat{y}_t + (1 - y_t)\log\left(1 - \hat{y}_t\right)\right] \tag{3}$$

where y_t is the true class label, $\hat{y}_t$ is the predicted class label, and T is the count of a taxonomy's classes.

3.3.1 ELMo with global max pooling

Our primary model consists of a pile of layers including input layer, global max pooling layer and a softmax layer. The input layer represents the input features which are questions embeddings calculated with the ELMo model. The global max pooling catches the more important characteristics. The softmax layer maps these features to a vector of probabilities. Figure 2 depicts the explained architecture.

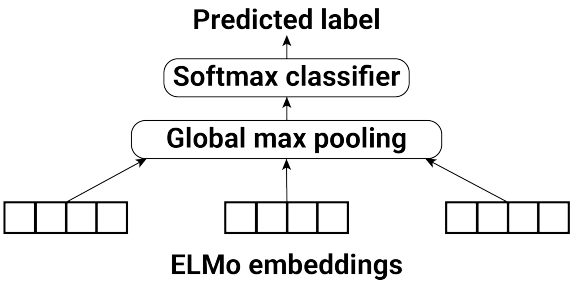


Figure 2: ELMo with global max pooling model

3.3.2 ELMo with global max pooling and dense layer

Based on the model described in the previous subsection 3.3.1 and with the purpose of extracting more features, we included a dense layer among the softmax layer and the global max pooling layer. Figure 3 illustrates the described architecture.

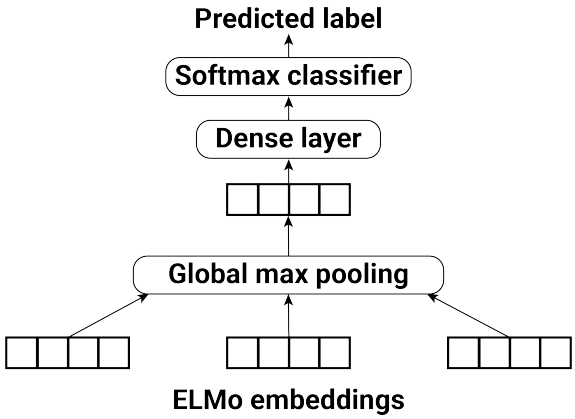


Figure 3: ELMo with global max pooling and dense layer model

3.3.3 ELMo with last hidden state of a GRU layer

To extract additional features, we included a Gated Recurrent Unit (GRU) layer that can handle sequential data and extract helpful information. Let denote Q a question represented by $Q = [w_1, w_2, ...w_k]$ where k the number of word vectors within Q and w_i is the i-th word vector of the question. GRU processes the data word-by-word according to the time-step from the past to the future. At each time step the current hidden state is computed as follows:

$$r_t = \text{sigmoid}\left(W_r \cdot [h_{t-1}, w_t]\right) \tag{4}$$

$$z_t = \text{sigmoid}\left(W_z \cdot [h_{t-1}, w_t]\right) \tag{5}$$

$$\tilde{h}_t = \tanh\left(W_{\tilde{h}} \cdot [r_t \odot h_{t-1}, w_t]\right) \tag{6}$$

$$h_t = (1 - z_t) \odot h_{t-1} + z_t \odot \widetilde{h}_t \tag{7}$$

The output of the final hidden state is passed to the softmax layer to compute the probabilities of belonging to each class label. Figure 4 presents the described architecture.

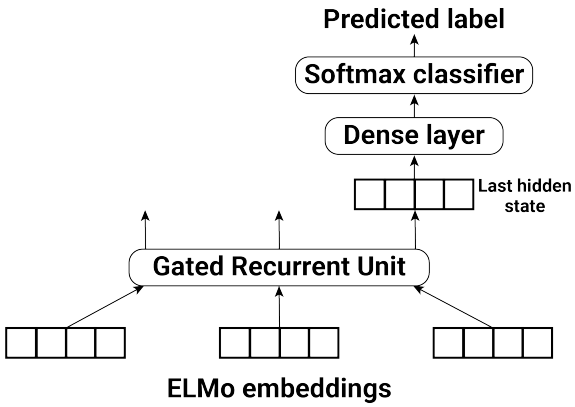


Figure 4: ELMo with last hidden state of a GRU layer model

3.3.4 ELMo with GRU and global max pooling

This model considers all the time steps from the GRU layer. It applies a global max pooling to extract the most important features

from every words within a question. The architecture of the model is illustrated in Figure 5.

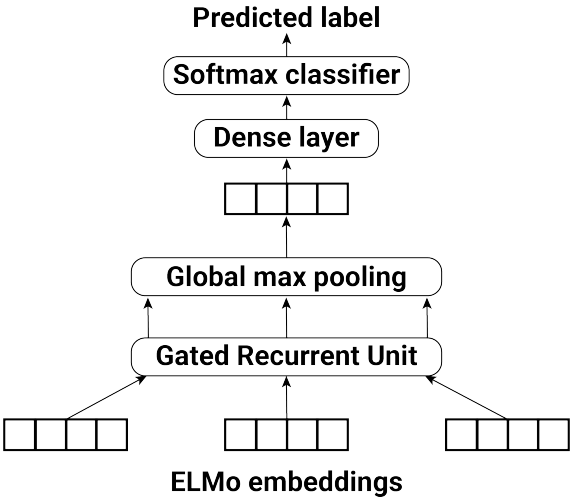


Figure 5: ELMo with GRU and global max pooling model

3.3.5 ELMo with CNN and global max pooling

Convolutional Neural Networks (CNN) proved good performances in both computer vision and NLP fields. These models extract new features applying 1 dimensional convolution on word neighbours. Figure 6 illustrates the model architecture. Let $w_i \in \mathbb{R}^p$ the p dimensional word representation corresponding to the i-th word in the question. A question of length k, which is padded when necessary, is represented by the following equation:

$$Q = [w_1, w_2, ...w_k] \tag{8}$$

where Q the question matrix. New features $m \in \mathbb{R}^{k-n+1}$ are produced by applying a convolution to each window of n words. The window size n vary between 2 to 5 thus we compute for each widow size a feature map. We then apply global max pooling [12] to capture the most important features. We concatenate these features and apply a softmax layer to classify the question.

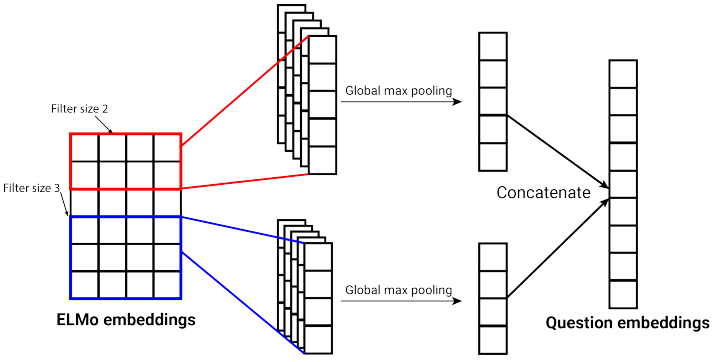


Figure 6: Multiple filters CNN with global max pooling

3.3.6 ELMo with CNN, GRU, and global max pooling

This model apply a convolution filters on top of ELMo embeddings. This operation results in a number of features maps equals to the number of filters used. Next, each features map is passed to GRU layers. The question embeddings is then the concatenation of the outputs of a set global max pooling functions applied on top of each hidden states of GRU layers. Finally, a softmax function is applied to classify the question. Figure 7 illustrates the architecture of this model.

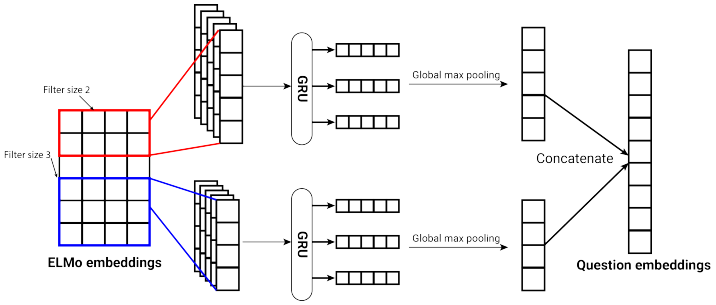


Figure 7: Multi filters CNN and GRU layers

3.3.7 ELMo with GRU, CNN, and global max pooling

The architecture of this model is similar to the architecture described in section 3.3.6. The only change is we apply first a GRU layer then convolution operations with different filter. Figure 8 presents the general architecture of this model. Various convultions with filter size between 2 to 5 are applied to the hidden states of the GRU layer. Next, a global max pooling is applied to extract the most important features for each filter features. Finally, the outputs of the global max pooling functions are concatenated to build the question embeddings.

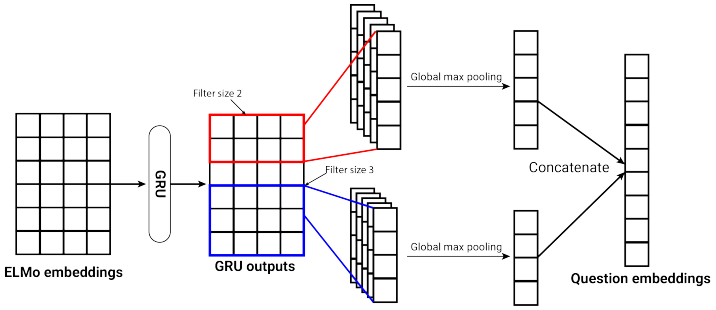


Figure 8: GRU and multi filters CNN model

3.3.8 Ensemble Models

An ensemble model aggregates the prediction of diverse models results in once final prediction for unseen data. We applied two ensemble models including mean scores-based ensemble and max scores-based ensemble. The mean scores-based model computes the average of the probability scores predicted by each model the class label with the highest probability score is assigned to the question. The max scores-based model pick the class label with the highest probability across all the predicted scores from different model.

4 Experimental results

4.1 Questions Classification Dataset

The dataset consists of 3173 Arabic questions. These questions are manually labeled with an application created by our team. We picked randomly 80% (2538) of questions as training set and 20% (635) of questions as testing set. Table 1 and Table 2 show the distribution of the class labels.

Table 1: Distribution of classes in the Arabic questions dataset

Classes	#	Classes	#
(Human...) العاقل	602	(Entity...) غير العاقل	1084
(Status...) حال الشيء و هيئته	121	(Location) المكان	450
(Time) الزمان	318	(Numbers) العدد	304
(Yes/No) التصديق	294		

Table 2: Distribution of classes in the Arabic questions dataset

Classes	#	Classes	#
Abbreviation	22	Description	709
Entity	468	Human	627
Location	453	Numeric	600
Yes/No	294		

4.2 Experimental settings

Considering that we deal with a multi-class classification problem, we use three measures to evaluate every model. The measures contain accuracy, macro F1 score and weighted F1 score. We employed widely known libraries including Scikit-learn, Tensorflow 2.0 and Keras libraries to construct and evaluate every single model [13, 14]. In the interest of reducing the internal covariate shift and the training time, we utilize layer normalization [15]. We fixed the batch size at 32 questions and the epochs at 1000 iterations for each model. We retained the model that achieves the optimal loss on training set. Our experiments are completely carried out in Google Colaboratory[2].

4.3 Simple models evaluation

We segment the proposed models into three sets including simple models, CNN and RNN mergers, ensemble models. The first set contains simple models that are composed with global max pooling, convolutions, and recurrent neurones layers. These model do not contain any type of combination between convolutions and recurrent neurones layers. The second set is named CNN and RNN mergers where convolutions and recurrent features are merged. The last models apply ensemble methods to build the question classification performance.

We evaluate our simple models with two different word representation: 1) The context-free word representation, designated by enriched word2vec with subword information [16], which embeds a word into a 300 dimensional vector. This technique possesses the capability to catch semantic and syntactic relationships among words. At the same time, it do not take into account the word in context; and 2) The contextual word representation ELMo [5] which calculates a 1024 dimensional vector for each word. This representation regards the context of word resulting in an enhanced question embeddings. Table 3 and Table 4 shorten the achieved performances with both the Arabic taxonomy and the updated Li & Roth taxonomy. In the event of the Arabic taxonomy, the ELMo representation surpasses the enriched word2vec representation in regards to accuracy, macro F1 score, and weighted F1 score. Nonetheless, this come at the expense of the lower size of the words' vectors. Lastly, the model which consists of ELMo embeddings, GRU layer, and global max pooling layer achieves the best performances outlined by 93.86%, 93.37%, and 93.84% on accuracy, macro F1 score, and weighted F1 score. In the event of the updated Li & Roth taxonomy, word2vec based models handle better the imbalanced dataset problem. The model that have word2vec embeddings as inputs and composed of GRU and global max pooling achieves 87.24% in terms of macro F1 score. The model composed of ELMo embeddings, CNN, and global max pooling scored top results in terms of accuracy and weighted F1 score.

Table 3: Performance measures (accuracy, macro F1 score, and weighted F1 score) of simple models with Arabic taxonomy

	Accuracy	*macro F1 score*	*weighted F1 score*
W2V + Global max pooling	78.74%	78.38%	78.64%
W2V + Global max pooling + dense	82.99%	82.86%	82.92%
W2V + Last hidden state of GRU	92.44%	92.74%	92.45%
W2V + GRU + Global max pooling	92.76%	92.96%	92.75%
W2V + CNN + Global max pooling	90.55%	91.00%	90.56%
ELMo + Global max pooling	86.77%	88.25%	86.83%
ELMo + Global max pooling + dense	88.03%	89.03%	88.11%
ELMo + Last hidden state of GRU	91.97%	92.12%	91.96%
ELMo + GRU + Global max pooling	**93.86%**	**93.37%**	**93.84%**
ELMo + CNN + Global max pooling	90.70%	91.12%	90.65%

Table 4: Performance measures (accuracy, macro F1 score, and weighted F1 score) of simple models with the updated Li & Roth taxonomy

	Accuracy	*Macro F1 score*	*Weighted F1 score*
W2V + Global max pooling	76.54%	65.61%	76.32%
W2V + Global max pooling + dense	81.73%	70.51%	81.68%
W2V + Last hidden state of GRU	91.65%	85.50%	91.56%
W2V + GRU + Global max pooling	92.13%	**87.24%**	92.05%
W2V + CNN + Global max pooling	89.13%	85.87%	88.97%
ELMo + Global max pooling	80.94%	71.87%	80.52%
ELMo + Global max pooling + dense	84.72%	76.51%	84.86%
ELMo + Last hidden state of GRU	91.50%	82.31%	91.69%
ELMo + GRU + Global max pooling	91.97%	82.67%	92.03%
ELMo + CNN + Global max pooling	**92.28%**	82.78%	**92.33%**

4.4 CNN and RNN mergers evaluation

We test out CNN and RNN mergers with the word2vec and ELMo word representations. These models have the ability to extract more valuable features from raw data. Table 5 presents the results of the CNN and RNN mergers with the Arabic taxonomy. The model that takes ELMo embeddings as inputs and apply GRU then CNN achieves the best scores 94.01%, 93.60%, and 93.98% in terms of accuracy, macro F1 score, and weighted F1 score. Besides, Table 6 shows that the word2vec word representation with Li & Roth taxonomy scored the best results 91.81% accuracy, 88.32% macro F1 score, and 91.84% weighted F1 score. However, the model

[2]https://colab.research.google.com/

architecture remains the same. Thus, the evaluation confirms that applying GRU layer followed by CNN layer is better than applying CNN layer then GRU layer for Arabic question classification.

Table 5: Performance measures (accuracy, macro F1 score, and weighted F1 score) of the CNN and RNN mergers with the Arabic taxonomy

	Accuracy	*Macro F1 score*	*Weighted F1 score*
W2V+CNN+GRU+Global Max Pooling	90.71%	90.91%	90.68%
W2V+GRU+CNN+Global Max Pooling	92.44%	92.47%	92.43%
ELMo+CNN+GRU+Global Max Pooling	91.02%	90.96%	91.03%
ELMo+GRU+CNN+Global Max Pooling	**94.01%**	**93.60%**	**93.98%**

Table 6: Performance measures (accuracy, macro F1 score, and weighted F1 score) of the CNN and RNN mergers with the updated Li & Roth taxonomy

	Accuracy	*Macro F1 score*	*Weighted F1 score*
W2V+CNN+GRU+Global Max Pooling	91.02%	86.16%	90.92%
W2V+GRU+CNN+Global Max Pooling	**91.81%**	**88.32%**	**91.84%**
ELMo+CNN+GRU+Global Max Pooling	90.87%	81.24%	90.86%
ELMo+GRU+CNN+Global Max Pooling	91.65%	84.87%	91.75%

4.5 Ensemble models evaluation

Finally, we evaluate the ensemble models based on the mean scores and the max scores obtained by classifier models with the best performances. Table 7 and Table 8 present the result of the ensemble model based on the GRU + CNN + Global Max Pooling model with Arabic and Li & Roth taxonomies, respectively. We notice that the ensemble method surpasses simple models and CNN and RNN mergers in the case of Arabic taxonomy. However, for Li & Roth taxonomy the mean scores-based ensemble model achieved the best results in terms of accuracy and weighted F1 score. The GRU + Global Max Pooling achieves the best performance according to the macro F1 score.

Table 7: GRU + CNN + Global Max Pooling ensemble model with Arabic taxonomy

	Accuracy	**Macro F1 score**	**Weighted F1 score**
Mean scores-based Ensemble	94.17%	94.07%	94.17%
Max scores-based Ensemble	94.17%	94.07%	94.17%

Table 8: GRU + CNN + Global Max Pooling ensemble model with Li & Roth taxonomy

	Accuracy	**Macro F1 score**	**Weighted F1 score**
Mean scores-based Ensemble	**92.60%**	**86.52%**	**92.69%**
Max scores-based Ensemble	92.44%	86.39%	92.54%

4.6 Discussion

From the one hand we discuss the obtained results for the Arabic taxonomy. The ELMo contextual word representation performs better than the word2vec context free word representation. The simple models evaluation shows that the GRU a recurrent neural network architecture is more appropriate than CNN for Arabic question classification. The CNN and RNN mergers evaluation confirms that the stack GRU/CNN achieves better results than the stack CNN/RNN. Besides, the ensemble models build with the word2vec and ELMo embeddings impact positively the performance of the Arabic question classification task. On the other hand, the classifiers trained with Li & Roth taxonomy shows different behaviors. The simple models evaluation reveals that the ELMo representation with CNN + Global Max Pooling model has top performances in terms of accuracy and weighted F1 score while the word2vec representation with GRU + Global Max Pooling model has the top performance in terms of macro F1 score. Thus, the latter model is able to handle imbalanced data problem more appropriately. The CNN and RNN mergers evaluation supports that word2vec with the stack GRU/RNN model is better than ELMo embeddings with RNN/GRU model. Finally, ensemble models improve the accuracy and the weighted F1 score but not the macro F1 score.

To conclude, the Arabic taxonomy works well with contextual representation ELMo and ensemble models while the model choice with Li & Roth taxonomy is related to the performance, e.g., if the objective is to optimize the accuracy of the question classification task then the ensemble model is more appropriate.

5 Conclusion

In this work, we built various Arabic question classifier based on simple models, CNN and RNN mergers and Ensemble methods. We trained these models with both context free word representation word2vec [4, 16] and contextual word representation ELMo [5, 10]. The latter has the upside to compute, for a word, a vector that catch semantic and syntactic meaning by considering its context. Ability that the enriched wor2vec model can not perform. We compared the performances of the proposed models with two different question taxonomies including Arabic taxonomy and Li & Roth taxonomy. From the one side, the experiments on questions labeled with Arabic taxonomy showed that contextual representation achieved promising results 94.01% accuracy, 93.60% macro F1 score and 93.98% weighted F1 score. Along with, ensemble methods improve the results slightly since it scored the top performances 94.17% accuracy, 94.07% macro F1 score and 94.17% weighted F1 score. On the other side, for questions labeled with Li & Roth taxonomy the top classifier in terms of macro F1 score (87.24%) was built based on word2vec and GRU + Global Max Pooling model. The mean score-based ensemble model scored 92.60% accuracy and 92.69% weighted F1 score which are the best obtained results in terms of accuracy and weighted F1 score. Thus, the the model choice with Li & Roth taxonomy is related to the performance the classifier needs to optimize more

As perspectives, we arrange to expand this work by building other Arabic question answering system components including the passage retriever and the answer processing modules. First, we plan to construct a module that aims to retrieve the most similar passages to a question based on contextual representation. Next, We intend to integrate these context aware representations in the answer processing module. Finally, we project to build an Arabic question answering system based on components that integrate contextual word embeddings, which have the capabilities of extracting syntactic and semantic relation of a word considering its context, to enhance further their performances.

Conflict of Interest The authors declare no conflict of interest.

References

[1] D. Moldovan, M. Paşca, S. Harabagiu, M. Surdeanu, "Performance issues and error analysis in an open-domain question answering system," ACM Transactions on Information Systems, **21**(2), 133–154, 2003, doi:10.1145/763693.763694.

[2] W. Ahmed, B. A. P, "CLASSIFICATION OF ARABIC QUESTIONS USING MULTINOMIAL NAIVE BAYES." International Journal of Latest Trends in Engineering and Technology Special Issue SACAIM, 82–86, 2016.

[3] A. Hamza, N. En-Nahnahi, K. A. Zidani, S. E. A. Ouatik, "An arabic question classification method based on new taxonomy and continuous distributed representation of words," Journal of King Saud University - Computer and Information Sciences, 2019, doi:https://doi.org/10.1016/j.jksuci.2019.01.001.

[4] P. Bojanowski, E. Grave, A. Joulin, T. Mikolov, "Enriching Word Vectors with Subword Information," Trans. Assoc. Comput. Linguistics, **5**, 135–146, 2017.

[5] M. E. Peters, M. Neumann, M. Iyyer, M. Gardner, C. Clark, K. Lee, L. Zettlemoyer, "Deep Contextualized Word Representations," in M. A. Walker, H. Ji, A. Stent, editors, Proceedings of the 2018 Conference of the North American Chapter of the Association for Computational Linguistics: Human Language Technologies, NAACL-HLT 2018, New Orleans, Louisiana, USA, June 1-6, 2018, Volume 1 (Long Papers), 2227–2237, Association for Computational Linguistics, 2018, doi:10.18653/v1/n18-1202.

[6] H. Abdelnasser, M. Ragab, R. Mohamed, A. Mohamed, B. Farouk, N. El-Makky, M. Torki, "Al-Bayan: an arabic question answering system for the holy quran," in Proceedings of the EMNLP 2014 Workshop on Arabic Natural Language Processing (ANLP), 57–64, 2014.

[7] H. M. Al Chalabi, S. K. Ray, K. Shaalan, "Question classification for Arabic question answering systems," in Information and Communication Technology Research (ICTRC), 2015 International Conference on, 310–313, IEEE, 2015.

[8] T. Mikolov, I. Sutskever, K. Chen, G. S. Corrado, J. Dean, "Distributed Representations of Words and Phrases and their Compositionality," in C. J. C. Burges, L. Bottou, Z. Ghahramani, K. Q. Weinberger, editors, Advances in Neural Information Processing Systems 26: 27th Annual Conference on Neural Information Processing Systems 2013. Proceedings of a meeting held December 5-8, 2013, Lake Tahoe, Nevada, United States, 3111–3119, 2013.

[9] T. Mikolov, K. Chen, G. Corrado, J. Dean, "Efficient Estimation of Word Representations in Vector Space," in Y. Bengio, Y. LeCun, editors, 1st International Conference on Learning Representations, ICLR 2013, Scottsdale, Arizona, USA, May 2-4, 2013, Workshop Track Proceedings, 2013.

[10] W. Che, Y. Liu, Y. Wang, B. Zheng, T. Liu, "Towards Better UD Parsing: Deep Contextualized Word Embeddings, Ensemble, and Treebank Concatenation," in D. Zeman, J. Hajic, editors, Proceedings of the CoNLL 2018 Shared Task: Multilingual Parsing from Raw Text to Universal Dependencies, Brussels, Belgium, October 31 - November 1, 2018, 55–64, Association for Computational Linguistics, 2018, doi:10.18653/v1/k18-2005.

[11] A. Kutuzov, M. Fares, S. Oepen, E. Velldal, "Word vectors, reuse, and replicability: Towards a community repository of large-text resources," in Proceedings of the 58th Conference on Simulation and Modelling, 271–276, Linköping University Electronic Press, 2017.

[12] R. Collobert, J. Weston, L. Bottou, M. Karlen, K. Kavukcuoglu, P. P. Kuksa, "Natural Language Processing (Almost) from Scratch," J. Mach. Learn. Res., **12**, 2493–2537, 2011.

[13] M. Abadi, A. Agarwal, P. Barham, E. Brevdo, Z. Chen, C. Citro, G. S. Corrado, A. Davis, J. Dean, M. Devin, S. Ghemawat, I. Goodfellow, A. Harp, G. Irving, M. Isard, Y. Jia, R. Jozefowicz, L. Kaiser, M. Kudlur, J. Levenberg, D. Mané, R. Monga, S. Moore, D. Murray, C. Olah, M. Schuster, J. Shlens, B. Steiner, I. Sutskever, K. Talwar, P. Tucker, V. Vanhoucke, V. Vasudevan, F. Viégas, O. Vinyals, P. Warden, M. Wattenberg, M. Wicke, Y. Yu, X. Zheng, "TensorFlow: Large-Scale Machine Learning on Heterogeneous Systems," 2015, software available from tensorflow.org.

[14] M. Abadi, P. Barham, J. Chen, Z. Chen, A. Davis, J. Dean, M. Devin, S. Ghemawat, G. Irving, M. Isard, M. Kudlur, J. Levenberg, R. Monga, S. Moore, D. G. Murray, B. Steiner, P. Tucker, V. Vasudevan, P. Warden, M. Wicke, Y. Yu, X. Zheng, "TensorFlow: A system for large-scale machine learning," in Proceedings of the 12th USENIX Symposium on Operating Systems Design and Implementation (OSDI '16), 265–283, 2016.

[15] L. J. Ba, J. R. Kiros, G. E. Hinton, "Layer Normalization," CoRR, **abs/1607.06450**, 2016.

[16] E. Grave, P. Bojanowski, P. Gupta, A. Joulin, T. Mikolov, "Learning Word Vectors for 157 Languages," in N. Calzolari, K. Choukri, C. Cieri, T. Declerck, S. Goggi, K. Hasida, H. Isahara, B. Maegaard, J. Mariani, H. Mazo, A. Moreno, J. Odijk, S. Piperidis, T. Tokunaga, editors, Proceedings of the Eleventh International Conference on Language Resources and Evaluation, LREC 2018, Miyazaki, Japan, May 7-12, 2018, European Language Resources Association (ELRA), 2018.

ASTES

Advances in Science, Technology and Engineering Systems Journal Vol. 5, No. 5, 485-492 (2020)

www.astesj.com

ASTESJ

ISSN: 2415-6698

Review of Orange Juice Extractor Machines

Ugwu Benedict Nnamdi[*,1], Chime Thompson Onyejiuwa[2], Chime Rufus Ogbuke[3]

[1]*Mechanical & Production Engineering Department, Enugu State University of Science and Technology, 400001, Nigeria*

[2]*Chemical EngineeringDepartment, Enugu State University of Science and Technology, 400001, Nigeria*

[3]*Mechanical Engineering Department, Institute of Management and Technology, 400001, Nigeria*

ARTICLE INFO

Article history:
Received: 11 June, 2020
Accepted: 26 August, 2020
Online: 24 September, 2020

Keywords:
Juice extractor
Masticator
Triturating juicer
Twin gear
Extraction efficiency

ABSTRACT

There is some agricultural equipment for post harvesting of Orange fruit Juice, all the machine is geared towards extraction of the fruit juice. Fruit juice extraction is the act of wringing out the juice content of fruits by way of an effective processing and storage which enhance reduction in wastage. Fruit juices which literally have high antioxidants help in increasing serum capacity of the body and at the same time balances the oxidative stress and discomfort normally caused by high-fatty and sugar meals. The history of juice extraction dates back to the nineteenth century. The extraction of juice from its fruit has progressed tremendously from the old tedious method of squeezing to an automated juice extracting machine across the world, making it an essential tool for citrus farmers. Juice extractor machine are classified broadly into four types centrifugal, masticating, Triturating and Press juicers which may be operated manually or electrically. Many attempts have been made to extract oranges using both manual and mechanized means. Traditionally the task of extraction of orange is easy but time consuming. The manual still requires the operator to remove the pulps and the seeds while the mechanized is a whole automated process made easy.

Both mechanized and manual fruit juice machines discussed in this work is developed to provide an affordable and user-friendly machine. These machine models exist all over the world with very few becoming popular while the rest got fizzle out due to their limitations. Then simple portable machines that squeeze the juices from the orange are to be reviewed in this work for better and healthy juice extraction.

1. Introduction

A juicer is a machine that has the capacity of producingjuice from fruits, leafy green and vegetables. Several kinds of fruits or vegetables extracted are dependent on the type of fruit juicer developed [1]. A juice extractor is an implement that can extract juice from both fruits and vegetables. A juice extractor is a machine designed and fabricated to snap out fluid (juice) from the fruit, either by squeezing, pressing or crushing for the purpose of drinking. The juice extractors are classified into different types based on their mode of operation.

Fruit juice extractor is an enhanced agricultural device which uses the pressing mechanism to extract juices from some fruit [2]. The fruit juice extraction unit operational processes are: sorting, grading, rinsing, peeling, cutting, juice formulation, clarification, storage and packaging [2].

This practice of squeezing, pressing and crushing of fruits just to obtain the juice and reduce the draw-back of waste and pulp is referred to as fruit juice extraction. The orange fruit can be eaten raw, or possibly extract its juice or fragrant peel as produce. Approximately 70% of citrus productions in 2012 were as a result of sweet oranges. In 2014, countries like California and Florida in United States of America with Brazil have ubiquitous rate of production of oranges with 70.9 million metric tons of oranges grown worldwide. Orange extraction started with hand extraction of juice which is rather slow, tedious and unhygienic, the use of machine came into being as the demand for juice consumption increased [3]. The benefits of using machine for extraction are: saves time, improves efficiency, increase capacity and reduced

[*]Corresponding Author: Ugwu Benedict Nnamdi, Engineer, Contact No: (+234) 8037888550, E-Mail: bnugwu@yahoo.com

spoilage and waste [4]. Physical operated juice extractors have been developed for home use but it has limited output [5]. Generally, electric powered juice extractors have accessories like electric motor, switch, belt, pulley, gears and bearings and components parts like a hopper which introduces the fruit to the machine compressing chamber, a housing unit (compressing chamber) which incorporates an array of pressersexceptionally arranged, a strainer (for sieve off waste), a juice collector container and a waste bin built-in for the orange waste (pulps, skin and seeds) disposal.

As there are no better ways to preserving this orange fruits, preservation of the orange fruits through extraction of the juice has been established as the most effective technique so far. With this extraction mechanism fruit juices can be stored and preserved for months or even years before expiration [2].

A simple machine produced from locally sourced materials for extraction of juice from the orange fruits effectively and efficiently at an affordable price so as to encourage a healthy living through consumption of fruit juice and longer preservation of the fruit during its harvest was necessary.

2. Juice extractor and its classification

A juice extractor also known as a juicer, is an implement used for extracting juice from fruits, leafy greens and other types of vegetables in a practice referred to as juicing [6]. It crushes squeezes and grinds the juice out from its fleshy tissue [7].They are different types ofjuice extractors; each works best for some variety of fruits and vegetables. Presently, juice extractors are classified into four essential types**:** masticator, centrifuge, triturating juicers (twin gear), and press juicer [8].

2.1. Centrifugal Juicer

Centrifuges designed as the fastest and most affordable of all motorized fruit juice extractor has mesh chamber where sharp blades rotate at a super-sonic speed to slice the fruits and extract the juice from the pulp [9]. These machines have advanced features that can process juice within seconds. Normally with a large feeding chute it can chow down larger volumes of fruit items even without pre-processing, this juicer reduces time sent on preparation work. Due to their very high speed noise, heat, and oxidation of the juice are observed. The heat generated breaks down certain enzymes and nutrients, while plenty air introduced oxidizes the juice their by causing a loss of nutrient thus reducing the juice quality as well as the shelf life. The basic component parts are plunger, top cover, top latch assembly, top blade, bottom blade, basket, juice bowl and mesh screen Centrifugal juicers are produced by Breville, Omega, Hamilton, Black and Decker. They have speedy, short prepping, juicing, and cleaning time as advantage.They are simple to assemble/disassemble, compact for processing and also affordable.

2.2. Masticating Juicer (Cold Press Juicers)

A masticating juicer has a screw worm shaft that works to press and crush the orange into lesser bit before pressing it against the juice extraction compartment for juicing [9]. Masticating juicers are also referred to as single auger juicers or slow juicer, since it takes long time to produce fruit juice and vegetable juice as weighed alongside centrifuges. These machines are in two main varieties namely vertical and horizontal masticating juicers. Vertically configured models have larger auger and feeding chute while the horizontal juicers have feeding chute with smaller footprints, but are prone to blockage due to the placement of the pulp ejector. To avoid these small chutes problems which emanates pre-cutting of every produce before feeding is paramount. Masticators serve a multifunctional purpose of a grocery processor and grinder. Mostly found in kitchens as juice maker and grain mills. Even with their slow speed, they perform very well on both hard and soft agricultural produce of kale and orange; with exceptional juice quality occasioned by heat absences which naturally destroy both the enzymes and antioxidants in the juice. Masticators are seen as the best juicers for leafy greens. Basic components of masticating juicers are pusher, hopper, auger, perforated screen, spinning brush and silicon brush. They have high juice yield with improved juice quality. They function with tough and yielding materials but are generally costly.

2.3. Triturating Juicer

The triturating juicer comprises of two gears coupled closer to each another, with the intention of crushing, grinding and extracting juice from the agricultural produce using a low speed [9]. The extracted juices are smooth, pulsating, and excellent in nutrients.These machines have a knob that you can adjust to achieve the necessary back pressure which gives more control over different ranges of produce with varying firmness as to making it more efficient at extracting a lot of juice. Triturating juicer is similar to single-gear juicers, with additional functions like it has separate kits for noodles making, nuts and seeds grinding, and chopping vegetables while in other juicers they are all incorporated as a single unit.Triturating juicers are mostly heavy and bulky, mainly desired for commercial activities.

2.4. Press Juicer (Citrus Juicer)

Citrus juicers are of several types: vertical hand-press type, pneumatic or hydraulic juice press type, press bowl type, and spinning bowl type, with others not mentioned. They are produced both as manual and electric juicer at different prices, categorized in every shapes, sizes, and materials.Citrus juicers are mainly preferred for orange juice processing, but a good number of juicers can also process lime, lemon, grapefruit, and even pomegranate. This citrus juicer requires the fruits to be cut into half across the middle and then place on the juicer. Manual citrus juicers some of them have handle for pressing of the fruit and squeeze out the juice, while others have a cone like cup for pressing the fruit until it extracts the juice. The juicer can be considered as cold-pressed processing in absence of heat, even though they are motorized machine [10]. These juicers most of them have detachable parts, which make them very easy to couple, dismantle, and tidy up. They are the more preferred juicer among families that make their own fresh orange juice because it takes them less than 3minutes to process and even clean up the mess

from the juice. Omega, Black and Decker are the renowned manufacturers of this juicer.

3. Manual citrus juice extractor operational assessment

3.1. Hand presser/squeezer

The manual Juicers classified as hand juicing presser, are usually built with a rigid corrugated cone which presses down on half of any fruit be it orange, lime, lemon, tomato or other citrus fruit to extract its juice. This juicer requires your own muscle to squeeze the juices out from the fruits, but if it does not add heat to the juice, the result is a juice that is very nutrient-dense.



Figure 1: [a] Image of lever action Hand juicer; [b] Image of hand squeeze Juicer [8]

Hand Juice Press is a commercial grade juicer with a heavy-duty cast iron body and a 304 stainless steel strainer. It has a long, lightweight handle with a comfortable rubber grip to reduce any stress on your hand. This handle is in an upright position moving vertically downward at 90 degrees with a sturdy base that ensures no slipping or tilting during use. It has provided a safety hat to lock it into place so that it will not fall on you accidentally. This juicer is super-easy to use. It only takes three steps to process the fresh juice. First, cut your fruit into half, place the flat side down on the pressing plate, and press down the handle. The fruit juice is collected effortless. The strainer and funnel are both removable from the unit, making the units clean-up a breeze. This juicer leaves a lot of pulp in your juice. The overall dimensions are (220 x 180 x 370) mm and container diameter 120mm. See fig 3.1

3.2. Hand Squeeze Juicer

The Stainless-Steel orange squeezer is a heavy, 378grams, stainless steel juicer with superior strength. It has the right size of cup for any small citrus fruit to fit into. Larger oranges and grapefruit are too big for this unit. We noticed that the cup showed some pitting after minimal use. This unit has long, thick, silicone-bonded handles to ensure the best comfort for your hand, and give you the best leverage to get the most quantity of juice. There is an issue with the handles, though. This orange squeezer is safe for easy cleaning, but the rubber on the handles is not molded on. That means if you throw it in the dishwasher, water will get in under the rubber coating and allow it to slip off. Juice squeezer has several models. See fig 1b.

3.3. Hand- held Juicer

It is a 71-gram unit with its own measuring cup, and a strainer built into the reamer. The reamer fits on the top of the measuring cup, but it does not lock in its position very well. You may have to help hold it in place with the same hand you are using to hold the cup. The measuring cup has a drip-free pour spout, so you can transfer your juice into whatever container you like without making a mess. The measuring cup and reamer is both Bisphenol A -free for your good health. The reamer can be removed from the cup for easy cleaning. The reamer is a bit easy to clean, but the cup takes a little more effort. This juicer is pretty small, not leaving a whole lot of room for your hand to fit into. What makes it even more challenging is that the cup has a slightly narrowed neck, which makes the opening even smaller. It can still be named oxo good grip citrus juicer which is manufacturers' trade name.



[a] Image of Hand –held citrus juicer; [b] Component parts of dome shape hand juicer [11]

3.4. Dome shape juicer

This juicer has multiple functions. If the reamer is facing up, it's suitable for juicing lemons, oranges, and other citrus fruits. When you flip the reamer over and have it pointing downward, it does excellently at juicing watermelon, pomegranate, and large fruits. The juice is caught in a cup that holds one cup of liquid. It is consisted of middle seat, Juice cup and upper cover. This juicer is easy to assemble and take apart to clean, but it does have a lot of pieces to keep. See Fig 2b

3.5. Cup Hand- held citrus Juicer

It is not a standard juicer. The top cup helps to hold your fruit, while you can use the collection container for drinking of juice. The lid can be flipped over, so that it stores neatly inside the cup, but it can also act as an egg separator when in this inverted position. The unit consists of two different sizes of reamers, one 12-tooth reamer developed to extract juice optimally by fully pressing each lemon, lime or any other smaller citrus fruit; and the other is one 3-claw large reamer for juicing bigger fruits and orange. There is also a large 476gram capacity cup for collection of juice. At times referred to as manufacturer of the product like sunhanny orange squeezer.

3.6. An orange juice Extractor

A designed and constructed orange juice extractormachine with diameter of 160 mm and a height of 350 mm have small blades sharpened that is coupled to a shaft which rotates with the bevel gear drive mechanism to actualize the fruit extraction [12]. Theturning of the handle rotates the machine designed for high efficiencyand ease of operation, which combine the extraction and

beating often by macerating. The orange juice extractorencompasses of two main component parts a goblet and a physically operated mechanism. The physically operated mechanism contains a pair of bevel gear, two bearings and two shafts all in a casing. The following components were fastened to make up the drive mechanism, handle, Small sharpened blades, impeller shaft, bearing, dynamic seal and the goblet for leak proof. The performance test of the extractor machine showedthat about 180-220 oranges were extracted per hour.



Figure 3: (a) Illustrating the Cup hand-held citrus juicer operation (b) component parts of a cup hand-held citrus juicer [11]

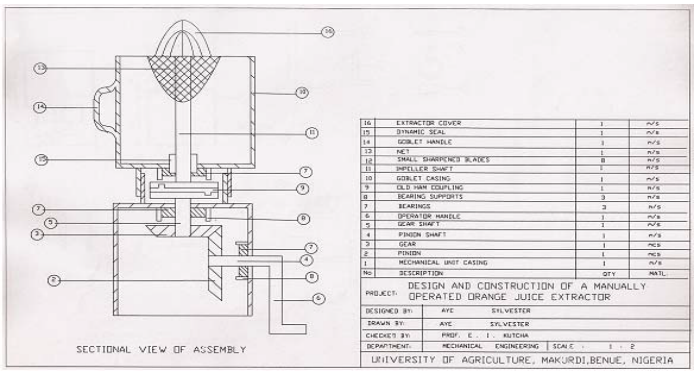


Figure 4: Diagram of Manualorange juice extractor with the component parts as shown in the legend [12].

4. Electric power operated orange Juice Extractors

4.1. Masticating machines

The mass of juice in waste product was ascertained using the technique of American Society of Agricultural Engineers (1982), which involved oven drying the chaff at 130˚C until a constant weight was reached. A stop watch and weighing balance were both used to obtain the time of extraction and measure the mass of the extracted fruit and chaff. The experiment was replicated five time using orange, while for multipurpose extraction machine it is replicated thrice for each fruit. The test was carried out at different extraction speeds with the aid of gear arrangement. The juice yield, extraction efficiency and extraction loss of these machines were calculated using equations (4.1 – 4.3) as stated below

Juice yieldequation

$$J_Y = \left(\frac{M_{JE}}{M_{JE}+M_{RW}}\right) \times 100 \quad (1)$$

Extraction efficiency equation

$$E_F = \left(\frac{M_{JE}}{XM_{FS}}\right) \times 100 \quad (2)$$

Extraction loss equation

$$E_L = \left(\frac{M_{FS}-(M_{JE}+M_{RW})}{M_{FS}}\right) \times 100 \quad (3)$$

where:

M_{JE} = Mass of Juice extracted (kg)

M_{RW} = Mass of Residual waste/dry pulp (kg)

M_{FS} = Mass of Feed sample (kg)

J_Y = Juice yield (%)

E_F = Extraction efficiency (%)

E_L = Extraction loss (%)

The juice constant was calculatedby getting the ratio of the sum of massesof juice extracted and juice in chaff to the mass of fruit feed sample.
Juice constant of Orange fruit

$$X = \left(\frac{M_{JE}+M_{JC}}{M_{FS}}\right) \quad (4)$$

where:

x = Juice constant of fruit (decimal)

M_{JC} = Mass of Juice in the chaff

4.1.1 Juice pulping machine

A juice pulping machine is an electrically powered juicer [13]. It consists of an auger-sieve combination placed above an aluminum frame, a handle for manual operation and produces juice free of seed and skin. The fruit press consists of a crusher mounted on components like screw-thread, crusher and slated cage. The machine is a lever operated press that grinds and crushes in one operation with an output of about 25 litres of juice per hour when operated by one person. The machine is using a masticating process.



Figure 5: Image of Juice pulping machine [13]

4.1.2. Juice Extractor machine

The juice extractor machine has a power requirement of 1.17 kW and is operated by a 1420 rpm electric motor [14]. Both the extraction capacity and extraction efficiency of the extractor

machine were performed. With an average juice extraction capacity for orange as 5.10 kg/hr and its extraction efficiency as 78.78% while that of grape is 2.79 kg/hr and 75.66 % respectively. 280 % of the manual extraction approach was reported as orange juice extraction capacity while 304 % of the values obtained were activated by using a domestic extraction cup. The manual extraction method accounted for 220 % grape juice extraction, with 180 % of the value obtained necessitated by the use of the extraction cup. The straight auger introduced as a replacement for tapered one resulted in an increase in the juice extraction efficiency of 89.2% and juice extraction capacity of 15.8 kg/h for sweet orange. The shaft speeds of the machine were studied with sorted grades of fruits according to its size and thickness with respect to extraction efficiency and capacity using regression analysis. The various fruit thickness used for the test was 20, 40, and 60 mm with extractor shaft speeds of 300, 400, 500 and 600 rpm. Three categorical sizes of pineapple and orange fruits studied showed that juice extraction efficiency and capacity have very strong quadratic relationships with speed. An exceptional linear relationship exists between extractor shaft speed and its capacity for 60 mm apple thickness.

4.2. Juice Extractor machine

Juice Extractor machine has been developed with the performance evaluation conducted as a function of its extraction efficiency [15]. The extractor components parts are as follows: screw jack, screw connecting rod, pressing mechanism, frame, interlock, hopper, and discharge mechanism. The performance evaluation tests showed an improved juice yield of 76%, with extraction efficiency of 83% and low extraction loss of 3%. It is a masticating machine with the same basic component parts.

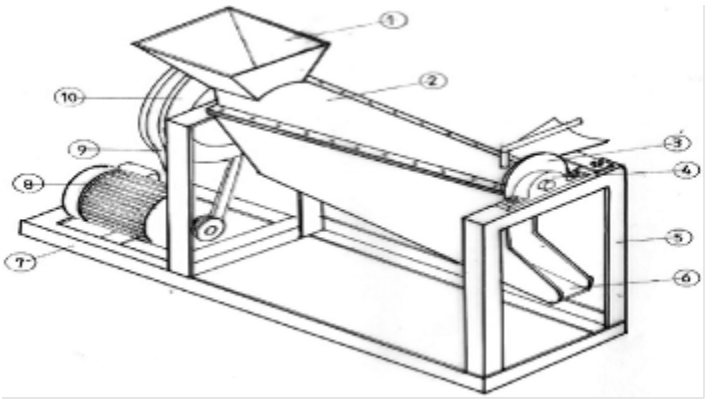


Figure 6: Mini orange juice extractor with component parts as follows 1 - Hopper; 2 – Extraction compartment; 3 – Disc plate; 4 – Bearing housing; 5 – Frame support; 6 – Juice conveyor; 7 – Base stand; 8 – Electric motor; 9– Transmission belt; 10 – Pulley [16]

4.3. Mini Orange juice extractor

Mini orange juice extractor was constructed with locally available fabrication materials for a small scale processing [16]. The mastication machine components parts includes hopper for feeding in orange, a lid cover, auger shaft, strainer, juice conveyor, trash outlet, transmission belt, frame support, pulleys and bearings. During processing, the auger shaft transmits, compresses, squashes and constrict the fruit to extort the juice which in turn passes through the juice sieve for filtration and then to the juice conveyor while the remaining waste is pushed to a trash bin. An average juice yield of 41.6 % and juice extraction efficiency of 57.4 % were recorded. The machine has a 2 horse power electric motor with juice extraction capacity of 14 kg/h. See figure 6.

4.4. A motorized Fruit Juice Extractor

A motorized fruit juice extractor machine was developed with the orange fruits washed and weighed (as 1kg, 1.5kg and 2kg respectively) of fruit sliced into 8 and 16 parts using the extractor to process the juice [17]. The juice yield, extraction loss and extraction efficiency of the machine were obtained using equations 4.1- 4.3 above. Normal juice yield of 64.6 % extraction efficiency of 68.2 % and corresponding extraction loss of 7.05 % were obtained from the 16 slice lengths of orange fruit. From the test result carried out using the juice extractor and the hand squeezing method, it was obvious that the rate of extraction increases as the weight of fruit increases with a corresponding increase in the juice yield and extraction efficiency. The juice extraction efficiency average and capacity were 57.70 % and 25.83 % respectively. This study reveals that juice yield and extraction efficiency reduces while extraction loss rises with amplified size of fruit slices. Juice yield, extraction efficiency and extraction loss from 16 slice lengths oranges ranged between 48.90 – 64.60 %, 50.00 – 68.20 % and 0.6 –7.35 % respectively. The higher extraction efficiency (mean value) of 57.70 % of the juice extractor reported the extraction rate to be more proficient than that of the hand squeezing method which has extraction efficiency (mean value) of 28.5 %. The motorized juice extractor components includes Hopper, Transmission Belt, Power Shaft coupling, Bearing, residual Outlet, Juice conveyor, Shaft housing, Seal, Cylindrical Drum, Electric Motor, Bolt, Adjustable Port and Frame Support

4.5. A Multi-Fruit Juice Extractor

Multi-fruit juice extractor design and construction with performance evaluation on fruits of pineapple, orange and melon were conducted [15]. The extractor functions on the principle of compressive and shear squeezing force wielded through an auger transmission system. The associated component parts consists of a tool frame, collection channel, gear box, juice extraction chamber, tapered auger shaft, perforated screen base, and electric motor. The components design analysis provided the parameters incorporated in the sizing, fabrication and coupling of the machine. Performance evaluation of peeled or unpeeled fruits of pineapple, orange and water melon indicated percentage juice yield of 79.1, 68.7 %, and 77 or 69.2 %, 89.5 and 89.7 % respectively, while extraction efficiency of 96.9 %, 94.3%, and 96.6 % for peeled pineapple, oranges and water melon respectively and 83.6 %, 84.2 %, and 97.1 % respectively for unpeeled and extraction losses of peeled and unpeeled fruits of pineapple, oranges and water melon are 2.1 and 2.7 % , 2.1 and 2.5 %, and 2.9 and 2.6 % respectively. The machine is recommended for households and

local fruit juice vendors because its operation is simple, easy and maintenance friendly.See figure 7.



Figure 7: Image of a multi Fruit juice Extractor [15]

4.6. Mechanized Fruit Juice Extracting

This extractor machine serves as both slicer and extractor of fruits and vegetable [18] with the assistance of the slicing blade, screw conveyor shaft, hopper, electric motor, gear train, conical resistor, juice collector, waste collector, barrel and ball bearings it exerts contact shear and compressive force. The fruits fed into the machine are continuously crushed by a metal crusher against the metal surface that separates the juice from the waste which then is collected through a unique channel while the wastes are pushed to the trash bin. The efficiency of the machine is 67% output and the throughput of 4.8 litres per Minute. It is a masticating machine with a robust construction and convenient design. It appears as table top machine with the dimensions as 500mm x 300mm, therefore there are available for domestic and commercial activities.

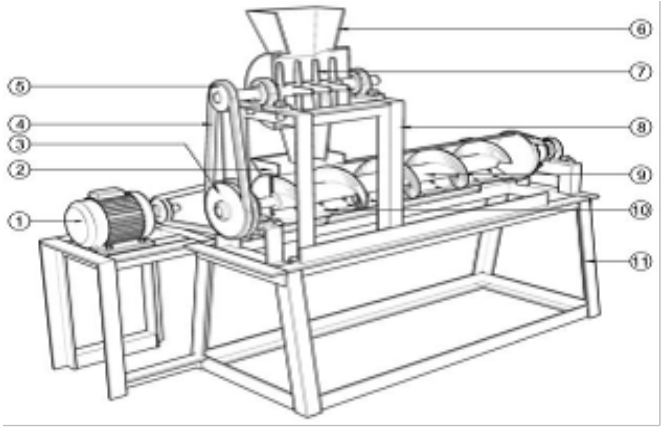


Figure 8: Image of Fruit juice extractor machine [19]

4.7. Fruit juice extractor machine

This machine is divided into two basic compartments: the chopping and the juice extracting compartments [19]. The performance evaluation results reported a typical juice yield of pineapple, orange and ginger were 74 %, 72 % and 34 % respectively; while juice extraction efficiencies of 84 %, 80 % and 71 % respectively; and juice extraction losses of 18 %, 16 % and 9 % respectively at optimum machine speed of 335 rpm for pineapple and oranges whereas 476 rpm is for ginger. This Extractor with 3hp electric motor has the capacity of process 30 litres/hr of oranges. See figure 8.

4.8. Modified Fruit juice Machine

A manual fruit juice machine fabricated by Onyene was modified by the addition of electric motor [20]. Then performance evaluation to ensure that the already existing extraction parts can work well with the new amount of power that the motor produces when compared with human power. The auger transmits, crushes, presses and constricts the fruits to extract the juice. The juice extract passes through the sieve for filtration and collection in the juice collector while the waste is trashed into the basket. When tested for freshly harvested orange and pineapple fruits, results show that the normal juice yield for orange and pineapple were respectively 23.20% and 24.75 % as against 17.47% and 17.50% of the manual extractor; juice extraction efficiencies were respectively 60.22% and 65.76% as against 50.32% and 53.76% of the manual extractor; and juice extraction losses were respectively 12.86% and 14.04% as against 12.06% and 11.34% of the manual extractor at 1.2kg/min feed rate. The modified machine was calculated to be 21.04% more efficient than the manual operated machine. This extractor is powered by a 3hp electric motor with a process capacity of 16.2 litres/hr of orange. See figure 9.



Figure 9: Image of Hand modified Fruit juice Extractor [20]

4.9. Motorized Juice Extractor machine

A motorized juice extractor machine was developed and evaluated [21] with the results of the evaluation of fruit yield for orange, pineapple and golden melon as 38.00, 51.43 and 39.67% respectively, with extraction efficiencies of 65.47, 83.94 and 53.17% respectively while the juice extraction loss of 6, 9 and 28% respectively for the three fruits mentioned above. This extractor component parts includes the hopper, slicing chamber, extracting chamber, frame support and channels for juice and waste discharge. The juice extraction machine is powered by 2 horse power electric motor. See figure 10.

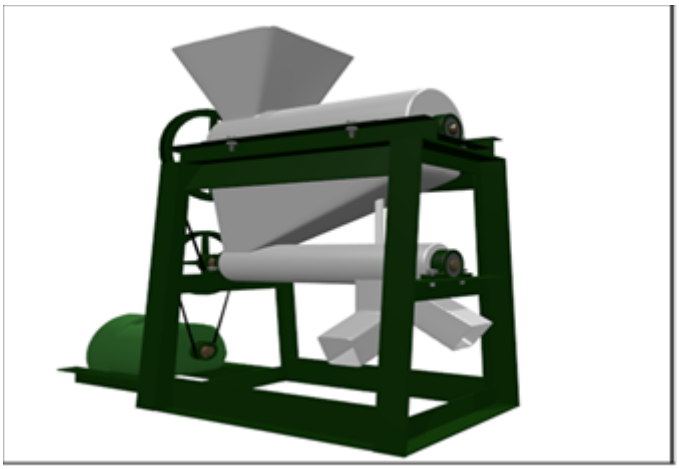


Figure 10: Image of a motorized juice extractor [21]

4.10. Centrifuge juice extractor machine

4.10.1. Centrifugal Beach Juicer Machine

It is a Centrifugal machine with a 76mm Big Mouth Feed Chute, power capacity 800W. The units comprises of orange reamer, strainer, knob, bumper, cup and its support kits, gear rack, under counter pulp chute, and micro mesh metal strainer and blade set.



Figure 11: Image of a centrifugal juice extractor [22]

4.11. Triturating and Citrus orange extractor machine

4.11.1. Automatic orange juice extractor

An Automatic orange juice extractor is a 120 watt electric juicer which processes an astounding 22 to 30 oranges per minute. It weighs between 44kg - 46 kg as durable machine with the dimensions 508 x 890 x 508 mm, and is enclosed in a corrosion resistant, stainless steel housing. Although it is an 'orange' juicer, but can still be used for your other citrus fruits extraction, such as limes, grapefruit or succulent lemons for lemonade. This juicer has a strainer that collects the pulps and seeds as well as filter for your fresh juice, giving you the juice, and keeping the rest in a waste basket. This juicer has a very easy operational and cleaning approach with a safety cut-off switch. In operation, fruits are introduced into the machine through the hopper. They are received by the orange collector and sliced into two halves by means of a knife placed between the two collectors. Each half of the orange enters the collector is then pressed by the rotary balls. Thus, the machine transports, slices and presses the fruit inside the extraction chamber until juice is pressed out of the fruit. The juice extracted is drained through the perforation provided at the bottom of the extraction chamber. The halved squeezed orange residual waste is thrown out through the pulp outlet on both sides of the machine. The component parts of this machine included gear drive, Reamers (knaggy balls), Remaining collectors, knife, sieve, hopper, waste bucket and electric motor.



Figure 12: Image of an automatic orange juice extractor machine [23]

5. Conclusion

The orange juice extraction machines have existed for a very long time now but the limitations associated with the once in use have raised concern for a review and best way to harness the fruits available during its season. Orange juice extraction is still a serious issue that desires attention, since a greater percentage of the fruit turns as waste during its season. In Nigeria for instant there is a large-scale cultivation of orange fruits, which requires a suitable mechanism to be identified and developed for the fruit optimal harvest. Several attempts have been made in the past to mechanize the extraction of orange juice. Those attempts produced both manually and electrically operated machines. Some of the machines were gigantic, uneconomical, time and energy consuming. There is a great need to explore these existing mechanisms which apparently would be both economical and satisfactory to end users. Depending upon the needs of farmers and consumers, a suitable mechanism must to be selected.

Conflict of Interest

The authors declare no conflict of interest.

Acknowledgment

We wish to acknowledge the management of Enugu State University of Science and Technology (ESUT) Enugu, Nigeria. More especially the staff and students of Mechanical and Production Engineering for their support and resilience.

References

[1] M. Mushtaq "Fruit Juices Extraction, Composition, Quality and Analysis" Academic press, 131-159 2018. https://doi.org/10.1016/B978-0-12-802230-6.00008-4.

[2] E. R Farnworth, M. Lagace , R. Couture, V. Yaylayan, B. Stewart. "Thermal

processing,storage conditions, and the composition and physical properties of orange juice" .Food Res Int **34**, 25–30, 2001. https://doi.org/10.1016/s0963-9969(00)00124-1
[3] X. Jiang "Design and Research on Multi-function Juice Extractor" Advance Journal of Food Science and Technology **6**(6), 774-779, 2014. https://doi.org/10.19026/ajfst.6.109
[4] T. D. Boylston "Temperate Fruit Juice Flavors" Handbook of Fruit and Vegetable Flavors 451-462, 2010. https://doi.org/10.1002/9780470622834.ch24
[5] A. Eyeowa, B. Adesina, Diabana, O. A Tanimola. "Design, fabrication and testing of a manual juice extractor of small scale applications". Current Journal of Applied Scienceand Technology **22**(5), 1-7,(2017). https:// DOI: 10.9734/CJAST/2017/33360
[6] www.foodterms.com. "juicer : Encyclopedia : Food Network". Retrieved 13 January 2017.
[7] P. R. Ashurst, "Production and Packaging of Non-Carbonated Fruit Juices and Fruit Beverages" Springer Science and Business Media New York 1999. https://doi.org/10.1007/978-1-4757-6296-9
[8] https://www.google.com/search?q=manual orange juice extractor
[9] https://healthykitchen101.com/types-of-juicers/
[10] https://www.goodnature.com/blog/types-of-juicers/
[11] https://www.amazon.com/Sunhanny-Squeezer-Anti-Slip-Rotation-Transparent
[12] S. A. Aye, , & A. Ashwe, "Design and Construction of an Orange Juice Extractor". Proceedings of the World Congress on Engineering Volume III WCE 2012, July 4 - 6, 2012, . London, U.K. ISBN: 978-988-19252-2-0; ISSN: 2078-0958 (Print); ISSN: 2078-0966 (Online).
[13] Emelike, N., & Ebere, C, "Effect of packaging materials, storage conditions on the vitamin C and pH value of cashew-apple (Anacardium occidentale L.) juice. Journal of Food and Nutrition Sciences, **3**(4), 160-165, 2015. https://doi.org/10.11648/j.jfns.20150304.14
[14] B.A. Adewumi, "Development Of A Manual Fruit Juice Extractor". Nigerian Food Journal **22**(1), 2005 . https://doi.org/10.4314/nifoj.v22i1.33585.
[15] M. M Odewole, K. J Falua, S. O Adebisi, K. O Abdullahi, "Development and performance evaluation of a multi fruit juice extractor". FUOYE Journal of Engineering and Technology **3**(1) 2018. https://doi.org/10.46792/fuoyejet.v3i1.171
[16] A. M. Olaniyan, "Development of a small scale orange juice extractor". Journal of Science and Technology, **47**(1), 105-108. 2010 https://doi.org/10.1007/s13197-010-0002-8.
[17] C. S. Bamidele, "Design, Fabrication And Evaluation Of A Motorized Fruit Juice Extractor" B.Eng Thesis, Department Of Agricultural And Environmental Engineering, University Of Agriculture, Makurdi 2011.
[18] A. I. Gbasouzor, C A. Okonkwo, "Improved Mechanized Fruit Juice Extracting Technology For Sustainable Economic Development In Nigeria"Proceedings of the World Congress on Engineering and Computer Science 2014 Vol II WCECS 2014, 22-24 October, 2014, San Francisco, USA. ISBN:978-988-19253-7-4, ISSN: 2078-0958(Print); ISSN: 2078-0966 (Online) https://doi.org/10.1007/978-94-017-7236-5_32
[19] N. A. Boih, "Design, development and performance evaluation of a fruit Juiceextraction machine", Unpublished M. Eng. Mechanical Engineering Project Report, Department of Mechanical Engineering, Ahmadu Bello University, Zaria, Nigeria, 2015.
[20] M. C. Nwoke, "Modification & Performance Evaluation of An Existing Fruit Juice Extraction Machine, 2017. https://www.academia.edu/,
[21] M.J. Omoregie, T.I. Francis-Akilaki, T.O. Okojie "Design And Construction Of A Motorised Juice Extractor" Journal of Applied Sciences and Environmental Management **22**(2), 207 2018. https://doi.org/10.4314/jasem.v22i2.9
[22] https://juicerkings.com/different-types-of-juicers/
[23] https://rainmachine.en.made-in-china.com/product/China-Commercial-Electric-Orange-Juicer-Extractor-Automatic-Slow-Lemon-Squeezer.html

ASTES

Advances in Science, Technology and Engineering Systems Journal Vol. 5, No. 5, 493-499 (2020)

www.astesj.com

ASTESJ

ISSN: 2415-6698

Knowledge Mapping of Virtual Academic Communities: A Bibliometric Study Using Visual Analysis

Chunlai Yan[1], Hongxia Li[*,1,2]

[1]*Rattanakosin International College of Creative Entrepreneurship, Rajamangala University of Technology Rattanakosin, Phutthamonthon, 73170, Thailand*

[2]*School of management Science and Engineering, Chongqing Technology and Business University, Chongqing, 400067, China*

ARTICLE INFO

Article history:
Received: 26 May, 2020
Accepted: 14 August, 2020
Online: 24 September, 2020

Keywords:
Virtual academic communities
Bibliometric
Knowledge map
Document co-citation analysis
Burst detection

ABSTRACT

This study aims to provide a systematic and complete knowledge map for researchers in the field of virtual academic communities (VACs) and to help them quickly understand the key knowledge, evolution trends and research frontiers. This paper adopts the bibliometric method, with the help of bibliometric analysis software Citespace and VOSviewer quantitative analyze the retrieved literature data, and the analysis results are presented in the form of tables and visualization maps. Analysis of 372 literature data related to VACs from the Web of Science database shows that: the development of research in this field has gone through three stages and produced a number of representative key scholars and highly cited literature; the document co-citation knowledge map and keyword clustering map show the research hotspots in VACs; the results of burst detection and disciplinary overlay analysis reveal the research frontier, development trend and disciplinary coverage in VACs.

1. Introduction

The development of internet technology has made significant changes in the way people exchange information. The U.S. Statista survey data shows the rapid growth in global social network users in 2010-2015, with 2.72 billion users expected by 2021 [1]. Facebook, WeChat, Instagram, and other social networks have more than 100 million active users. With the development of new knowledge communication carriers, the mode of academic exchange has also changed, and more scientific research scholars share their knowledge and collaborate in scientific research through online academic exchange platforms. The advancement of Web2.0 technology makes it possible for researchers from different nations to work together with the support of online collaborative platforms, such as virtual academic communities (VACs) [2]. With the coming era of big science and the globalization of science and technology, the internet has gradually become a vital platform for people to participate in social activities and promote intellectual changes in the way of scholar interaction. VACs such as ResearchGate, Academic.edu, Mendeley, and muchong.com have gradually become the sites for researchers to exchange knowledge and share information. The collaboration of researchers based on the VACs has also increased day by day. The VACs are online learning communities for users to exchange academic-related views and resources, and it break through the traditional style of interpersonal communication and improve the efficiency of interaction so that knowledge exchange is not limited by time, space and location [3]. The rise of virtual academic communities has prompted a large number of researchers to become interested in the topic, but it is not easy for researchers to obtain a panoramic view of the knowledge structure, evolution and key nodes in the field. Before the advent of bibliometric tools, researchers mainly rely on peer-reviewed articles or collections of essays to obtain a panoramic view of a discipline or research field. This method lacks of objectivity because of the research peers' knowledge vision and subjective judgment, and often does not reveal the key literature and emerging research hotspots in this field completely and comprehensively, and is easily controversial. The emergence of bibliometric analysis tools provides another possibility for researchers, that is, from simple subjective judgment to subjective judgment combined with objective measurement. This study is guided by this idea.

Bibliometric method is a quantitative analysis method, which takes scientific and technological literature as the research object, and uses mathematical and statistical methods to describe, evaluate and predict the current situation and development trend of each research field. This paper uses two common bibliometric analysis

* Corresponding author: Hongxia LI, No. 19, Xuefu Ave, Nanan District, Chongqing, P.R.China 400067 +8602362769587, lihongxia@ctbu.edu.cn

software, Citespace and VOSviewer, to study the critical path of knowledge evolution in the field of VACs, to reveal the important knowledge inflection point in this field, and to analyze the potential dynamic mechanism of evolution and the frontier of exploration development through the drawing of a series of visual maps.

2. Data Source and Research Method

2.1. Data source

Web of Science (WOS) is used as a data source in this paper. WOS contains the Science Citation Index (SCI), the Social Sciences Citation Index (SSCI), the Art &Humanities Citation Index (A&HCI), and the CPCI-SSH, which is the deepest and most complete database of citation index data available worldwide. Compared with other large databases such as EBSCO, Springer, Wiley-Blackwell, WOS database covers all SSCI source journals, and its sub-database has high authority in academia [4].This paper retrieves the Web of Science by the search formula (TS=("virtual communit*") OR(TS= "online communit*") OR (TS= "academic blog") OR (TS="question and answer network") OR (TS="social networking sites")) and then filtered the proposed topic by the keyword "academic" and sift through the duplicate literature. Finally, 372 papers are sorted out for this proposed research, which are highly related to the topic of VACs.

2.2. Research Methodology

VOSviewer is a JAVA based knowledge mapping software developed by the center for science and technology research at Leiden university in the Netherlands. It presents the structure, evolution, cooperation and other relationships of the knowledge field for literature data [5]. By using VOSviewer, this paper makes statistical analysis of the age and key words of the literature related to the VACs, and combines the synonymous key words to count the high frequency key words. CiteSpace V knowledge visualization software is a multi-dimensional, temporal and dynamic knowledge plotting tool developed by Professor Chen (2006) of Drexel University, USA [6]. The software can convert abstract data into graphic expression (Chen & Liu, 2005), so that the users can visually see relevant information in the corresponding research field and grasp structural relationship, evolution law and other features of knowledge in the research field by analyzing and understanding the graphs [7]. CiteSpace version 5 is used to analyze the selected literatures in this paper. Firstly, we use the co-citation analysis to sort out the key node literature, and use the clustering and burst detection to analyze the research hotspots and frontier of the VACs; Secondly, we draw the knowledge map to analyze the evolution trend of the research in the field of VACs. Finally, we use the coupling relationship of the literature to analyze the internal relationship between the disciplines involved in the literature.

3. Data Analysis

3.1. General Analysis of Literature

The annual number of publications in a VACs research area shows the importance of the research results in the VACs field, and the changing trend can measure the overall development of the research field. Table 1 shows the annual number of publications in the VACs field. It can be observed from Table 1 that the annual number of publications in VACs field shows a rising trend, and the whole process gone through three stages: initial development (1995-2007), climbing period (2008-2014), and rapid development period (2015-2020). The number of publications in the period of rapid development shows "well blowout" growth. The above analysis shows that the focus on the VACs is increasing gradually, and with the rapid development of internet technology, this focus is becoming more and more intense.

Table 1: The annual number of publications related to VACs

Year	Amount of publications	Year	Amount of publications
1995	2	2008	12
1996	0	2009	17
1997	3	2010	20
1998	2	2011	24
1999	1	2012	20
2000	0	2013	26
2001	1	2014	26
2002	1	2015	42
2003	0	2016	40
2004	2	2017	39
2005	7	2018	38
2006	6	2019	30
2007	8	2020	5

3.2. Research hotspot analysis

The keywords are brief summaries of the topics and contents of the literature research. It is helpful to know the essential research contents of the literature via correct analysis of the keywords and capable of knowing the hot topics of the subjects, institutions, and research knowledge in a certain period by measuring the number of the keywords [8]. Based on the software called "Citespace V" and the keywords of the publishing, the research on the VACs is visualized. This paper selects the period of 1995-2020 with a time slice of 3 years and the top 50 frequent keywords in each stage for visualization, adopts the Minimum Spanning Tree (MST) to adjustment the graph, and finally the clusters results and extracts them with k (keyword) as the label to obtain Figure 1.Table 2 is the specific clustering information obtained using the "Cluster Export" function and Table 3 is the high-frequency keyword statistics of the VACs.

The node in the cluster map is the keywords, and its circle area represents the frequency of its appearance. The connection between node and node represents the co-occurrence relationship between keywords, and its thickness indicates the co-occurrence intensity. The structure of Citespace clustering are mainly determined by two indicators: modularity (Q-value for short) and average silhouette (S-value for short). The larger the Q-value, the

better the clustering of the network; moreover, the Q-value interval is [0,1]; Q>0.3 indicates the clustering network structure

is significant. The S-value can be used to measure the homogeneity of the clustering graph; when it is approaching to 1, the homogeneity is higher; when it is above 0.5, it is considered that the clustering result is reliable. As Q=0.5761 and S=0.685 in Figure 1, it shows that the clustering structure obtained in this study is reliable.

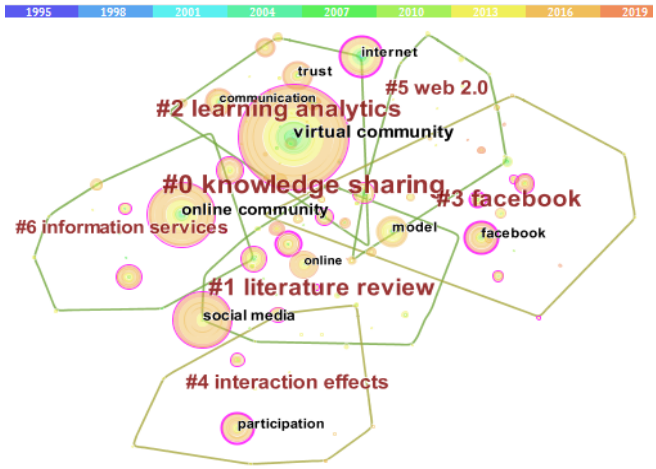


Figure 1: Keyword Clustering Graph of VACs

Table 2: Keyword clustering information of VACs

Cluster ID	Term	Size	Silhouette	Mean （year）
0	Knowledge sharing	22	0.757	2010
1	Literature review	19	0.717	2012
2	Learning analytics	19	0.645	2012
3	Facebook	18	0.673	2014
4	Interaction effects	14	0.841	2013
5	Web 2.0	14	0.78	2012
6	Information services	12	0.887	2011

Table 3: High-frequency keywords for VACs ,1995-2020

S/N	Keyword	Freq	Centrality
1	Virtual community	87	0.17
2	Online community	53	0.18
3	Social media	46	0.12
4	Internet	32	0.2
5	Model	26	0.03
6	Facebook	25	0.22
7	Participation	24	0.22
8	Trust	24	0.05
9	Communication	23	0.07
10	Online	23	0.05
11	Technology	21	0.19
12	Community	20	0.1
13	Behavior	19	0.16
14	Knowledge	18	0.25
15	Education	17	0.14
16	word of mouth	16	0.04
17	engagement	15	0.19
18	network	14	0.06
19	impact	13	0.06
20	information	13	0.03
21	motivation	13	0.11
22	satisfaction	12	0.12
23	student	11	0.28
24	antecedent	10	0.11
25	knowledge sharing	10	0.03
26	social network	10	0.05
27	web 20	9	0.09
28	academic library	9	0.17
29	higher education	9	0.01
30	management	9	0.1

From Table 3, it can be observed that the research scope of the VACs is comprehensive. The frequency of social media and the internet appeared 46 and 32 times, respectively, which is the most critical keyword studied by scholars in research community. The keyword such as model, Facebook, participation, trust, communication, technology, and knowledge are researched many times. The keywords such as student (0.28), knowledge (0.25), participation (0.22), and Facebook (0.22) have high centrality, which indicates that the nodes corresponding to these keywords are in a relatively leading position in the given map. The research focus of the VACs can be seen from Figure 2 and Table 2, which contains seven topics: knowledge sharing, literature review, learning analytics, Facebook, interaction effects, web 2.0 and information services.

3.3. Document co-citation analysis

The concept of document co-citation was proposed in 1973 by Marshakova and Henry, which refers to the co-citation relationship formed by the simultaneous citation of two or more documents by the third article [9]. Document co-citation analysis (DCA) can be used to identify key literature and research frontiers in a research field. The "cited Reference"" was used as the node in the citespace, set LBY=-1(no limitation of retroactivity) , timeslice=3 years, and top N=30. The document co-citation map of the VACs was obtained by using Pathfinder pruning and displaying in a time-zone mode, which is shown in figure 2. According to Figure 2, it can be seen that the co-citation relationship in the field of VACs in 1995-2020 is very close, while the high citation contribution is more concentrated in the period 2004-2010. Of these, there were Fishbein and Ajzen, Davis and Bagozzi two high cited documents before 1995, which were cited 20 times [10-11]; between 1995 and 2003, there were five high cited documents, mainly Nahapiet, Preece, which were cited 67 times [12-14]; during 2004-2010, there were six high cited documents, such as Chiu et al, Hsu et al, Wasko and Faraj, which were cited 100 times [15-17]. After 2010, the number of references to relevant research literature in VACs was relatively low. In order to better study the theoretical results in this field, the first five cited literatures in this field are listed, which is shown in Table 4 below.

3.4. Frontier and Trend Analysis

The Burst Detection Algorithm was proposed by Kleinberg in 2002, He believes the term high burst has an intelligence function, and can reflect the frontier of research field [18]. According to the literature retrieved by WOS, we click Burstness

button and set the Minimum duration to 1 year for Burst Detection. The first 11 mutation keywords were obtained, and they reveal different stages and future trends in VACs. Keywords in the graph represent the corresponding keywords, year indicates the first time in the retrieval record, strength indicates the strength of the mutation, beginning indicates when the mutation started, ending means the end time. The start and end time of the year corresponds to a small red rectangular block.

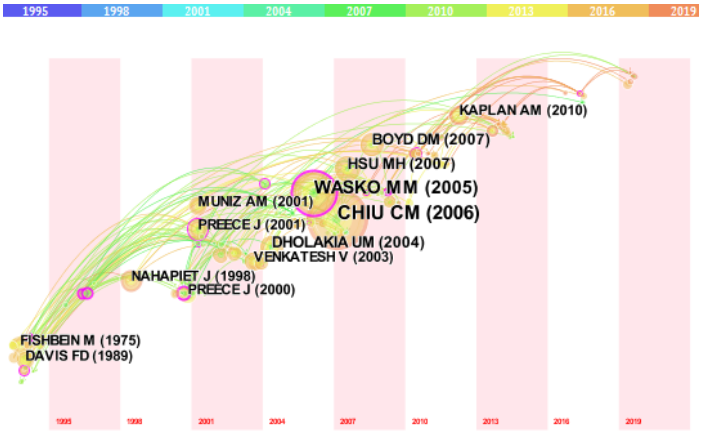


Figure 2: Map of Document Co-citation Time Zones

Table 4:. High frequency citations literature

S/N	Title of the literature	Main Authors	Name of Journal	Frequency of citations
1	Understanding knowledge sharing in virtual communities: An integration of social capital and social cognitive theories	Chiu C M	Decision Support Systems	33
2	Why Should I Share? Examining Social Capital and Knowledge Contribution in Electronic Networks of Practice	Wasko M M	MIS Quarterly	24
3	Knowledge sharing behavior in virtual communities: The relationship between trust, self-efficacy, and outcome expectations	Hsu M H	International Journal of Human-Computer Studies	15
4	Social Network Sites: Definition, History, and Scholarship	Boyd D M	Journal of Computer-Mediated Communication	14
5	A social influence model of consumer participation in network- and small-group-based virtual communities	Dholakia U M	International Journal of Research in Marketing	13

Top 11 Keywords with the Strongest Citation Bursts

Keywords	Year	Strength	Begin	End	1995 - 2020
internet	1995	4.3644	1995	2008	
virtual community	1995	4.6258	2006	2010	
web 20	1995	3.577	2008	2012	
information	1995	2.8433	2008	2009	
model	1995	2.443	2013	2015	
user acceptance	1995	2.4296	2014	2014	
social networking site	1995	2.3699	2016	2018	
social media	1995	3.1078	2016	2018	
trust	1995	3.8335	2017	2017	
engagement	1995	3.1123	2019	2020	
impact	1995	2.5947	2019	2020	

Figure 3: Burst Detection of Keywords

Figure 3 shows that during the period 1995-2020, virtual community and internet had the strongest burst intensities, and were respectively concentrated in the period 1995-2008 and 2006-2010. Model, user acceptance, social networking site, social medica, and trust have a certain degree of burst After 2010, which illustrates the research hotspots and frontiers in this stage focused on social networking sites, acceptance, models in the VACS. while Engagement (participation) and impact burst intensities were 3.1123 and 2.5947 respectively from 2019 to 2020.

3.5. Disciplinary Overlay Analysis

Disciplinary overlay analysis can use the coupling relation of the literature to analyze the internal relation between the discipline involved in the literature [19]. Figure 4 is obtained by using the Z-scorce algorithm to superposition and simplify the literature data of the VACs, in which the thickness of the lines indicates the degree of connection between the disciplines. The Part1 area in the figure is constructed by the discipline relationship of the citing literature, and the Part2 area is constructed by the discipline relationship of the cited literature.

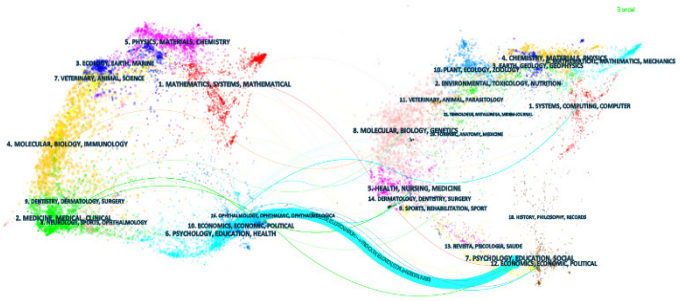


Figure 4: Disciplinary Overlay Map of VACs

Figure 4 shows that the research on VACs in the Part1 focuses on psychology, education, health, and economics, and these disciplines provide a developing knowledge base for research of VACs. Part2 shows that the research literature of VACs has been cited in psychology, education, society, environmental science and

biomolecules. Research in economics, which is less distributed, is more often cited in computer science.

4. Findings and Discussion

4.1. Findings

This paper uses the bibliometric method, with the help of bibliometric analysis software Citespace and VOSviewer, to analyze the annual publish amount, key authors, keywords and citations of the literature, and uses the Document Xo-citation Analysis， the Keywords Clustering Algorithm, the Burst detection algorithm and the Z-scorce algorithm to analyze the research hot spots, research frontiers and evolution trends in the field of VACs to provide key knowledge reference for related researchers.

According to the statistics of the trend of the number of papers, the development of the research field of virtual academic community has experienced three stages. They are initial development (1995-2007), climbing period (2008-2014), and rapid development period (2015-2020). The document co - cited analysis shows that, Fishbein、 Davis、 Nahapiet、 Preece、 Wasko、 Chiu、 Hsu are the high frequency cited authors of the VACs fields. “Understanding knowledge sharing in virtual communities ： An integration of social capital and social cognitive theories”, “Act Why Should I Share? Act Examining Social Capital and Knowledge Contribution in Electronic Networks of Practice”, and “Knowledge sharing behavior in virtual communities: The relationship between trust, self-efficacy, and outcome expectations” are the high frequency cited articles of VACs fields. Based on co-citation statistics and knowledge maps, researchers can quickly master the important knowledge in this field.

Research hotspots and cutting-edge surveys show that the research results, the research contents of virtual academic community mainly include knowledge sharing, literature review, learning analytics, Facebook, interaction effects, web 2.0 and information services and so on. Burst detection results show that Model, user acceptance, social networking site, social medica, trust, engagement, and impact is the latest frontier topic in this field. The key nodes of central screening show the evolution path of domain development, and further reveal the trend of domain development, which provides researchers with panoramic view of VACs.

4.2. Discussion

The following is a discussion of research topics in the field of VACs and the views of major scholars. Keywords Clustering map in figure 1 show that the research subjects of VACs mainly focus as follow.

- knowledge sharing and exchange in VACS and their influencing factors. It can be concluded by analyzing related literatures that many factors influence the behavior of knowledge sharing and exchange in the VACs. From the individual members of the community, psychological state, self-efficacy, social status and the degree of trust between each other are the main influencing factors; from the social environment, the influence of internet technology and cultural factors is more significant; from the community itself, the influence of connectivity and learning perception are more significant.
- The practice and influence of social media in academia. Some researchers conduct a comprehensive literature review of academic social media for the first time, which help to understand better the influencing factors of using social media [20]. Many scholars put forward the views related to academic social media, summarized as follows: Social media can be used as a new way to evaluate academic work, which is considerable to significance the academic researchers and stakeholder [21]. Social media plays a vital role in promoting collaboration and networking in global virtual communities [22]. Social networks are increasingly influential in teenagers [23]. The most comprehensive research review of social media scholarship shows that Facebook has a massive advantage in social networking academic research and more scholars should conduct academic research on social media [24]. The study of teachers using social networks in 22 medical colleges found a total of 40 social media tools, of which the most popular platforms are considered as Facebook by 9 institutions, Twitter by 8 institutions, and blogs by 8 institutions. In conclusion, the trend of social media use in academia is gradually increasing, especially among the young student groups, but there are still a series of problems such as private security, mental health issues are increasing day by day [25].
- The Theoretical Model basis of VACs. On the basis of social capital theory, social cognition theory, social network theory, collective action theory, planning behavior theory and technology acceptance model, researchers have gradually perfected the theoretical framework of VACs. Some scholars use the theory of social capital to construct the influencing factor model of virtual community knowledge sharing with the variables of interaction relationship, trust, reciprocity norm, identity, shared vision and shared language. This literature has the highest citation frequency in the statistical backtracking period, which provides a reference for many researchers [15]. Another study shows how individual motivation and social capital influence knowledge contribution behavior based on the theory of collective action in electronic networks, which argues that personal reputation, experience, and sense of belonging have a positive impact on knowledge sharing, and this literature has also received extensive attention from researchers [16]. A model based on the theory of social cognition shows the relationship between trust, self-efficacy and expectation of results, and considers environmental factors as future research directions [17]. The social impact model of VACs points out that group norms and social identity are two key factors of community participation [26]. The technology acceptance and community factors affect the behavior of participating in virtual communities of

practice, and the participants' domain knowledge has the most significant influence on the quality of their collaborative results [27]. "Quality of online discussion" is a measure to evaluate the results of virtual community interaction, which is influenced by network interaction, social identity, and social connectivity [28].

5. Conclusions and limitations

Combine the keyword burst detection result and the analysis of important literature, we can conclude that participation and social impact research is an important frontier trend in VACs. In addition, the participation behavior and social impact of VACs in different disciplines are different, and quantitative comparative research can be done in the future to provide reference for the overall development of VACs.

The way of knowledge exchange has changed in the era of great science, and the emergence of VACs provides a new platform for knowledge sharing and research cooperation. The existing research on VACs has obtained rich results, and generates a number of representative key researchers and theoretical literature. But the analysis of the evolution and trend of the field shows that the scope of research in this field needs to be expanded, and there are still many controversies about the theoretical model, concept, and structural dimension, which are the directions that researchers need to further study. The research of VACs is a multidisciplinary field, which involves behavioral science, psychology, education, economics information science and so on. Researchers can further expand the field of interdisciplinary research, and enrich the research in this field with the help of the research methods, research perspectives and research paths of different disciplines.

Bibliometrics is a scientific and effective research method of statistics, description and prediction of academic status and development trend. Its analysis of the research field relies on the quantity and quality of the downloaded literature. Based on the database of the core collections included in the WOS, the research results have strong objective impartiality. However, due to the limitations of the database, and some databases do not support the download, so the results may be biased. Future research can consider using data mining technology to expand the scope of source data collection and improve the quantity and quality of literatures.

Conflict of Interest

The authors declare no conflict of interest.

Acknowledgment

This study was substantially supported by a project (70901080) from the National Natural Science Foundation of China. The research was substantially supported by a project (19SKGH091) from the Chongqing Education Commission of China and project from the Open Fund of Research Centre of Enterprise Management. This study was also substantially supported by a project (2053002) from Chongqing Technology and Business University of China.

References

[1] Statista. “Number of social network users world- wide from 2010 to 2021（ in billions” [EB / OL]. https://www.statista.com/topics/1164/social-net-works/. [2018-12-05].

[2] F. Berdun, M. G. Armentano, “Modeling users collaborative behavior with a serious game” IEEE Transactions on Games, **11**(2), 121-128, 2018. https://doi.org/10.1109/tg.2018.2794419

[3] H. F. Lin, “Effects of extrinsic and intrinsic motivation on employee knowledge sharing intentions” Journal of Information Science, **33**(2), 135-149, 2007. https://doi.org/10.1177/0165551506068174

[4] R. F. Ma, X. J. Liang, Y. P. Jiang, “Evolution of academic groups and hotpots of the western cultural and creative industry research institute” World Regional Studies, **24**(2), 96-104, 2015. DOI: 10.3969/j.issn.1004-9479.2015.02.011

[5] N. J. V. Eck, L. Waltman, “Software survey: VOSviewer, a computer program for bibliometric mapping” Scientometrics, **84**(2), 523, 2010. https://doi.org/10.1007/s11192-009-0146-3

[6] C. Chen, “Cite Space II: detecting and visualizing emerging trends and transient patterns in scientific literature” Journal of the American Society for Information Science and Technology, **57**(3), 359-377, 2006. https://doi.org/10.1002/asi.20317

[7] Y. Chen, Z. Y. Liu, “Quietly rising scientific knowledge graph” Studies in Science of Science, **(23)**2, 149-154, 2005. DOI: 10.16192/j.cnki.1003-2053.2005.02.002

[8] J. F. Zhao, F. Jiang, “Study on bibliometrics and scientific knowledge graph in modern college education” University Education Science, **111**(1), 115-123, 2014. DOI: 10.3969/j.issn.1672-0717.2014.01.018

[9] H. Small, “Co-citation in scientific literature: a new measure of the relationship between publications” Journal of the America Society of Information Science, **24**(4), 265-269, 1973. https://doi.org/10.1002/asi.4630240406

[10] R. J. Hill, M. Fishbein, I. Ajzen, “Belief, attitude, intention and behavior: An introduction to theory and research” Contemporary Sociology, **6**(2), 244, 1977. https://doi.org/10.2307/2065853

[11] F. D. Davis, R. P. Bagozzi, P. R. Warshaw, “User acceptance of computer technology: A comparison of two theoretical models” Management Science **35**(8), 982-1003, 1989. https://doi.org/10.1287/mnsc.35.8.982

[12] J. Nahapiet, S. Ghoshal, “Social Capital, Intellectual Capital, and Organizational Advantage” Academy of Management Review, **23**(2), 242-266, 1998. https://doi.org/10.1016/b978-0-7506-7222-1.50009-x

[13] J. Preece, “Online communities: Designing usability and supporting Socialbilty” John Wiley & Sons, Inc., Hoboken. **100**(9),459-460, 2000. https://doi.org/10.1108/imds.2000.100.9.459.3

[14] J. Preece, “Sociability and usability in online communities: determining and measuring success” Behavior and Information Technology, **20**(5):347-356, 2001. https://doi.org/10.1080/01449290110084683

[15] C. M. Chiu, M. H. Hsu, T. G. Wang, “Understanding knowledge sharing in virtual communities: An integration of social capital and social cognitive theories” Decision Support Systems, **42**(3), 1872-1888, 2006. https://doi.org/10.1016/j.dss.2006.04.001

[16] M. M. Wasko, S. Faraj,”Why should I share? Examining social capital and knowledge contribution in electronic networks of practice” MIS Quarterly, **29**(3), 35-57, 2005. https://doi.org/10.2307/25148667

[17] M. H. Hsu, T. L. Ju, C.-H. Yen, C. M. Chang, “Knowledge sharing behavior in virtual communities: The relationship between trust, self-efficacy, and outcome expectations” International Journal of Human-Computer Studies, **65**(2), 153-169,2007. https://doi.org/10.1016/j.ijhcs.2006.09.003

[18] J. Kleinberg, “Bursty and Hierarchical Structure in Streams”. Proceedings of the 8th ACM SIGKDD International Conference on Knowledge Discovery and Dala Mining. Edmonton. Alberta. Canada：ACM Press, 02, 91-101, 2002. https://doi.org/10.1145/775047.775061

[19] C. Chen, “Scarching for intellectual turning points: progressive knowledge domain visualization” Proc Natl Acod Sci USA, **101**(1):5303-5310, 2004. https://doi.org/10.1073/pnas.0307513100

[20] E. W. T. Ngai, S. S. C. Tao, K. K. L. Moon, “Social media research: Theories, constructs, and conceptual frameworks” International Journal of Information Management, **35**(1), 33-44, 2015. https://doi.org/10.1016/j.ijinfomgt.2014.09.004

[21] C. Lamberton, A. T. Stephen, “A thematic exploration of digital, social media, and mobile marketing: Research evolution from 2000 to 2015 and an agenda for future inquiry” Journal of Marketing, **80**(6), 146-172, 2016. https://doi.org/10.1509/jm.15.0415

[22] I. Hussain, “A study to evaluate the social media trends among university students” Procedia - Social and Behavioral Sciences, **64**(9):639-645, 2012. https://doi.org/10.1016/j.sbspro.2012.11.075

[23] J. Ahn, “The effect of social network sites on adolescents social and academic development: Current theories and controversies” Journal of the American

Society for Information Science and technology, **62**(8), 1435-1445, 2011. https://doi.org/10.1002/asi.21540
[24] E. Stoycheff, J. Liu, K. A. Wibowo, D. P. Nanni, "What have we learned about social media by studying Facebook? A decade in review" New Media & Society, **19**(6), 968-980, 2017. https://doi.org/10.1177/1461444817695745
[25] P. S. Cahn, E. J. Benjamin, C. W. Shanahan, "'Uncrunching' time: medical schools' use of social media for faculty development" Medical Education Online, **18**(1), 20995, 2013. https://doi.org/10.3402/meo.v18i0.20995
[26] U. M. Dholakia, R. P. Bagozzi, L. K. Pearo, "A social influence model of consumer participation in network- and small-group-based virtual communities" International Journal of Research in Marketing, **21**(3), 241-263,2004. https://doi.org/10.1016/j.ijresmar.2003.12.004
[27] N. Nistor, B. Baltes, M. Dascălu, D. Mihăilă, G. Smeaton, Ş. Trăuşan-Matu, "Participation in virtual academic communities of practice under the influence of technology acceptance and community factors. A learning analytics application" Computers in Human Behavior, **34**, 339-344, 2014. https://doi.org/10.1016/j.chb.2013.10.051
[28] H. P. Shih, E. Huang, "Influences of web interactivity and social identity and bonds on the quality of online discussion in a virtual community" Information Systems Frontiers, **16**(4), 627-641,2014. https://doi.org/10.1007/s10796-012-9376-7

ASTES

Advances in Science, Technology and Engineering Systems Journal Vol. 5, No. 5, 500-505 (2020)

www.astesj.com

Special Issue on Multidisciplinary Sciences and Engineering

ASTESJ

ISSN: 2415-6698

Simulated Annealing for Traveling Salesman Problem with Hotel Selection for a Distribution Company Based in Mexico

Raúl Jiménez-Gutiérrez*, Diana Sánchez-Partida, José-Luis Martínez-Flores, Eduardo-Arturo Garzón-Garnica

Department of Logistics and Supply Chain Management, UPAEP University, 17 Sur 901, Barrio de Santiago, CP 72410 Puebla, Puebla, México

ARTICLE INFO

Article history:
Received: 16 July, 2020
Accepted: 29 August, 2020
Online: 24 September, 2020

Keywords:
TSP
TSPHS
TSP-HOBS
Simulated Annealing
Metaheuristic

ABSTRACT

A distribution company in Mexico covers the travel expenses for 21 sales representatives. Currently, the routes they follow are not established clearly, which can lead to high costs in this subject. A reduction of such cost is sought after, by optimizing the routes for each one of them. The following research finds an improvement on the routes for the sales representative of a distribution company in Mexico. It was done by using the Traveling Salesman Problem with Hotel Selection or Base selections via a Simulated Annealing algorithm. The results show an improvement in a reasonable timeframe by using the Simulated Annealing. It also shows that the maximum process time was of 156.63 minutes, and the least amount of improvement was 24.44% over the current route selection. Applying this model will be beneficial for the company as the company is trying to reduce costs related to the sales representatives such as; fuel cost, hotel cost, and travel expenses.

1. Introduction

For the agro-industry, to satisfy the specific demands of customers using different strategies in product and service has proven successful in an increasingly competitive global market.

Logistics has been an essential part of the success of the companies. Nowadays, there is more focus on how companies can optimize their resources and do more with less, a perfect balance between efficiency and customer service. According to [1] logistics are vital because it creates value, for customers and suppliers of the firm, and value for the firm's stakeholders. Value in logistics is expressed in terms of time and place.

Logistics have several improvement methods that could be implemented, not only in the logistics areas of the companies but also in commercial areas. Mexico is not an exception where TSP models can be helpful as the lack of road infrastructure and the long distances, besides the facts mentioned there some companies trying to make savings by reducing the sales force and extending the region coverage of the sales representatives.

As an example, we can find the Traveling Salesman Problem (TSP), where rapid growth of the companies raises the need to implement commercial strategies to visit their clients with the highest possible efficiency and quality but with the least cost. It is at this point is where mathematical models show up to create a clear vision and achieve such goals. Moreover, in the case of the TSP, it can help the companies to reduce the fixed costs for the sales representative such as:

1. Fuel costs.
2. Pay toll costs.
3. Maintenance costs.
4. Accommodation costs.
5. Meal expenses.
6. GPS costs.
7. Other travel expenses.

To develop study cases related to having route efficiency is essential for the companies established in Mexico. According to the National Association of supermarkets and department stores, during 2019, Mexico has grown 7.7% [2]. Furthermore, part of this growth is due to the effort of the sales force.

Therefore, for the current research, a variant for the TSP will be implemented, the Traveling Salesman Problem with Hotel Selection (TSPHS) with Simulated Annealing. The main objective for a TSPHS is to have an efficient route, including the stops where the sales representative will rest after their work shifts as they need, in many cases, to visit several clients.

*Corresponding Author: Raúl Jiménez-Gutiérrez, 15 pte 317, +52 2212673274, Raul.jimenez02@upaep.edu.mx

2. Problem Description

A distribution company based in Mexico is responsible for delivering products to a nationwide authorized dealer's network. Goods are sent using established couriers, and the distribution center is based in the central region of the country. All sales are made through authorized dealers to assure the quality of service. The company tries to keep a high level of service for the dealers and has several sales representatives throughout the country. The role of each sales representative is to establish a sales plan with each dealer, take orders, assure such orders have been fulfilled, and present the dealers with technical information and training, both for existing products as well as new products. The company decided to divide the country's sales territory into eleven commercial zones to have an efficient approach, and to know and cover the needs of the dealer's network. Fig. 1 shows the current zones within the country, the distribution company provided the information as part of its current structure of commercial zones.



Figure 1: Sales Representative Zones

Each commercial zone has a sales representative in charge. The sales representative, the primary task is to visit each dealer of the zone he is in charge of and know the needs of each dealer. He must provide feedback about the sales plan that the dealer has for the year, as well as other tasks that include a demonstration of new products, special deliveries (this term is used when a sales representative brings support to the final user and explains how to assemble, use and give maintenance) and training.

It is worth to mention that the company covers the travel expenses for the route or the visits that they need to do. It means that the company covers the gasoline, toll payment, hotels, meals, and other possible expenses that the sales representative incurs during the visits in its entirety. The sales representative needs to make all of the visits as traveling during his working hours, which are set to nine working hours per day. The information provided by the company did not include the time each sales representative spends with the dealer/client. However, the variation in travelling time between the calculated average and the real one was found to be enough to cover the time of the visit. It was decided to leave the visit time out of the calculations, to ease the solving of the model.

Despite the facts above, there is no specific route for the sales representative. Therefore, the order in which to drive to each dealer store to make their visits is entirely up to the sales representative. In several cases, they pass through the same point twice. Being inefficient on the route design could increase the expenses for the company. As an example, the sales representative in charge of the south region is in charge of 19 dealers. Back in 2019, he drove 57081 km, equivalent to MXN 98,011.00 in gasoline expenses only.

The main objective of this research is to find an improvement in the efficiency of the routes that each sales representative travel among their specific commercial zones, using a well-known combinatorial optimization problem, the Traveling Salesman Problem with hotel selection (TSPHS) solved by a simulated annealing method, focused on finding the following objectives:

- Improvement of the routes.
- Find the hotel that allows the sales representative to rest or, in some cases, go back to their homes but still being efficient on the route.

As part of the improvement strategy to have better routes, the distribution company conducted and applied a survey to the sales representatives to know their preferences about staying in a hotel or at their home. All sales representatives agreed that they prefer to get back to their homes, but they know that, in most cases is not possible to return to their homes due to the long distances that they need to drive.

Table 1: Hotel and Base Data

ZONE	HOTEL	HOME
M11	7	1
M12	5	1
M13	3	1
M14	7	1
M21	5	1
M22	5	1
M23	3	1
M24	13	1
M31	4	1
M32	2	1
M33	5	1

The sales representatives commented as well that, in some cases, they suffer from stressful situations, as there are several times when they do not have the chance to get back to their homes, and when they try to book a hotel, there are no available rooms. According to [3], sales representatives are susceptible to stress by the nature of their job. Therefore, this research includes the hotel and the home of the sales representative that for this purpose is called *base*.

The results of the aforementioned internal survey were compiled into a table with the number of hotels commonly used in each zone. The table is the following:

It is worth to mention that, the agent has a list of authorized hotels that the company selected previously. All of those hotels are in the same price range; therefore, the sales representative can choose either one, without it representing a considerable difference in cost.

Hence the limitations for the research will be to stablish the routes for each sales representative.

3. Literature Review: Travelling Salesman Problem with Hotel Selection and Simulated Annealing.

The problem of this research has been studied in several research cases, and it is well described in the literature. The TSP is one of the most well-known combinatorial optimization problems, where the main idea is to find an optimal solution to avoid passing the same point twice. Over the years, several methods based on deterministic or probabilistic heuristics have been proposed to solve the known problem. The method includes branch-and-bound, particle swarm optimization, neural network, and simulated annealing [4].

In simple words, the TSP consists of determining a minimum distance circuit passing through each vertex once and only once. Such a circuit is known as a tour or Hamiltonian circuit [5].

A formal definition of TSP, according to [6]:

Let $K_n = (V_n, E_n)$ be the complete undirected graph with n = [Vn[nodes and $m = |E_n| = \binom{n}{2}$ edges. An edge e with endpoints i and j is also denoted by ij, or by (i,j). We denote by $\mathbb{R}^{E_n}$ the space of real vectors whose components are indexed by the elements of E_n. The component of any vector $z \in \mathbb{R}^{E_n}$ indexed by the edge $e = ij$ is denoted by Z_e, z_i, or $z(i,j)$.

Now, considering that the salesperson, in some cases, needs to travel long distances, the need for a hotel stay arises. Such stay is an everyday activity, to end his daily route and start his route the next day to visit another dealer. Selecting a hotel to end/rest/start the route converts the research into a traveling salesman problem with hotel selection.

According to this research, there are several cases where the Traveling Salesman Problem with Hotel Selection (TSPHS) has been studied; Vansteenwegen [7] introduced the concept of TSPHS, the difference between TSP and TSPH, the last one is where a mobilized entity (salesman) cannot visit all locations (customers) at once without taking any break (break at a hotel location). It is because the salesman has limited working hours; the target at the end is to reduce the total travel time.

The TSPHS can be defined [7] on a complete graph $G = (V, A)$ where V is the set of vertices and $A = \{(k,l) \mid k,l \in V, k \neq l\}$ is the set of arcs. There are s available hotels (which are indexed through $k = 1 \ldots s$) and n customers (which are indexed through $k = (s+1) \ldots (S+n)$) In the set V. Each customer k is assigned service or visiting time T_k where T_k is $k = 0, \forall = 1, \ldots,$. The time kl_c needed to travel between locations k and l is known for all $(k,l) \in A$.

Several examples of TSPHS can be found in the literature as well as new heuristics solution methods. As it is mentioned in [8] that the TSPHS is a difficult optimization problem that arises in many practical situations, in this case, the authors gather the data into four sets:

Table 2: Customer and Hotels Data

Set	Number of Customers	Number of hotels
1	48-288	6
2	10	2
	15	
	30	
	40	
3	52 - 1002	3
		5
		10
4	52 - 1002	10

As can be seen, it is similar to the distribution company based in Mexico, but instead of having four sets, it has eleven commercial zones with a specific number of customers and hotels.

The new metaheuristic that they implemented is a two-phase multi-start procedure that combines a simple GRASP (Greedy randomized adaptive search procedures) and a variable neighborhood descent to improve the solution. They find that for smaller instances, the method was able to find either optimal solutions or best solutions, but also that the difficulty increases if the number of hotels grows.

Another example of solving the TSPHS with a new metaheuristic solution can be found with a Migrating Bird Algorithm (MBO) [9], and the solution approach is based on the flight formation of migrating birds, using this method it is shown that it is efficient for solving the problem in a reasonable computational time. Furthermore, in this paper, it is mentioned that simulated annealing was run, and it got results in a reasonable timeframe as well. For the TSPHS with Migration Bird Algorithm, the result shows that the gap between the MBO and the exact solution is acceptable.

Other methods available include Particle Swarm Optimization [10], [11], Artificial Bee Colony [12], Ant Colony [13], Crow Search Optimization [14], Cat Swarm Optimization [15], Grey Wolf Optimization [16], Whale Optimization [17]. The advantages/disadvantages of these methods are all well documented in literature. Some of these methods have successfully been used to solve TSP [12], [13], [16]. And even some have been applied in combination with Simulated Annealing [11]. In previous (unpublished) work by the authors, the Simulated Annealing algorithm was programmed and tested. The advantages and disadvantages of applying each of the aforementioned methods were evaluated. But the largest consideration was still the cost of implementing, or programming, such algorithms. In all the cases, the cost, expressed mainly in programming time, of implementing the newer algorithms was higher than:

1. The available time the authors could allocate for the research.
2. The deadline the company had to respect.

Both these factors resulted in a cost that was higher than the benefits of implementing a newer algorithm, even if it would eventually yield better results. Still, an improvement could be obtained by implementing a simpler, cheaper (in this case) to apply, method.

A simple example of solving the TSPHS [18] that was formulated as a mixed-integer linear programming (MILP).

$$\min \sum_{d=1}^{m} \sum_{k=0}^{s+n} \sum_{l=0}^{s+n} x_{k,l,d}\, C_{k,l} \tag{1}$$

$$s.t. \sum_{l=0}^{s} x_{0,l,1} = \sum_{k=0}^{s+n} x_{k,0,m} = 1 \tag{2}$$

$$\sum_{h=0}^{s} \sum_{k=0}^{s+n} x_{k,h,d} = \sum_{h=0}^{s} \sum_{l=0}^{s+n} x_{h,l,l} = 1, \qquad d = 1, \dots, m \tag{3}$$

$$\sum_{k=0}^{s+n} x_{k,h,d} = \sum_{l01}^{s+n} x_{h,l,d+1,}\ d = 1, \dots, m-1\ ; h = 0, \dots, s \tag{4}$$

$$\sum_{d=1}^{m} \sum_{k=0}^{s+n} x_{k,i,d} = 1, \qquad i = (s+1), \dots, s+n \tag{5}$$

$$\sum_{k=0}^{s+n} x_{k,i,d} = \sum_{l=0}^{s+n} x_{i,l,d}\ \ d = 1, \dots, m; i = s+1, \dots, s+n \tag{6}$$

$$\sum_{k=0}^{s+n} \sum_{l=0}^{s+n} x_{k,l,d}\, (c_{k,l} + T_l) \le C, \qquad d = 1, \dots, m \tag{7}$$

$$u_i - u_j + 1 \le n-1) \left(1 - \sum_{d=1}^{m} x_{i,j,d}\right)\ i = s+1, \dots, s+n; j = s+1, \dots, s+n \tag{8}$$

$$x_{ijd} \in 0,1, \qquad d = 1, \dots, m;\ i = 0, \dots, s+n;$$

$$j = 0, \dots, s+n \tag{9}$$

$$u_i \in 1, \dots, n, \qquad i = s+1, \dots, s+n \tag{10}$$

The objective function (1) minimizes the total travel time. As mentioned above, the number of trips, m, is not a decision variable in this formulation, but a given parameter of the problem. An alternative formulation could be to minimize the number of trips first and then minimize the travel time. Constraint (2) guarantees that the tour starts and ends in the first starting hotel 0. Constraints (3) ensure that each trip starts and ends in one of the available hotels $(0, \dots, s)$. Constraints (4) guarantee that, if a trip ends in a given hotel, the next trip starts in the same hotel. Constraints (5) ensure that every customer is visited once, and constraints (6) verify the connectivity inside each trip. Constraints (7) limit the time budget of each trip, and constraints (8) are required to prevent sub tours.

For this instance, [18] the goal of the TSPHS is to determine a tour of minimal length that visits all n customers. The tour is composed of connected trips with limited length, and every trip should start and end in one of the available hotels. The hotels that are selected determine to a great extent, the length of the total tour.

Combining the TSPHS with another strategy can yield an advantage, in recent research, it can be found that the simulated annealing as a complementary for effective results. In [19] can be found that Kirkpatrick introduced the implementation of simulated annealing. The process begins by considering a solution space $\boldsymbol{S}$ of an exclusive tour through the set of given cities or points $\mathbf{1}, \mathbf{2}, \dots, \boldsymbol{n}$, with a set of updated solutions $\boldsymbol{x_1'}$ created by randomly switching the orders of two cities. The energy function, or fitness function, which represents the length of the route $\boldsymbol{x_i}$, is denoted by $\boldsymbol{f(x_1)}$. The relative change Δ in cost $\boldsymbol{f}$ between $\boldsymbol{x_i}$ and $\boldsymbol{x_i'}$ is expressed as $\Delta \boldsymbol{f} = \frac{f(x_i') - f(x_i)}{f(x_i)}$.

Besides, it is mentioned in [20] that using the potential usefulness of a fixed temperature algorithm is considered suitable for small problem instances. On the same document [20], where they implement a Simulated Annealing (SA) to solve a TSP, the optimal fixed temperature is chosen experimentally by running simulated annealing many times at each of several fixed temperatures and determining which temperature is best, according to an appropriate optimality criterion. As a result, they see that fixed-temperature simulated annealing tends to outperform the use of a fast cooling schedule, but for TSP instances of size less than 150 cities [20].

4. Solution Approach

The only information the authors had in hand was the list of coordinates of the clients, hotels, and base of each zone. However, a detailed record of the agents' travels was not available. As the travel time was to be limited, because of the maximum work time, and to be able to know at which moment a hotel had to be selected, some kind of transformation was needed. The geographical data had to be converted to travel time. The process is explained next.

A sample set of location pairs, covering as many zones as possible, was selected. For each pair of locations, the traveling time was sought, using Google Maps®. Also, the Euclidean distance for that pair was computed. For all pairs, the relationship between the Euclidean distance, the Google Maps® distance, and the travel time was set up in a table. The traveling time varied between 3 minutes and 917 minutes. The Google Earth distance varied between 650 meters and 1,153,000 meters. The Euclidean distance varied between 413 meters and 954,496 meters. The proportion varied between 0.0006 and 0.007 and averaged 0.0013. Therefore, multiplying the Euclidean distance by the proportion's average should yield an approximation to the travel time between both locations.

A simulated annealing method was implemented instead of getting an exact solution due to the fact - that previous research shows that simple TSP models with 50 locations take too much time to get a solution or, even worse, do not get a solution using currently available computing equipment. Additional to this, using metaheuristics yields a result reasonably close to those of the exact methods [21]. As the solution requires the addition of

the hotel selection, which adds even more complexity to the model solving, a quicker solving method was needed. Such is the reason for the use of heuristics instead of trying to obtain an exact solution.

As was already mentioned, a Simulated Annealing algorithm was used. It was programmed in GNU Octave®. The objective of such an algorithm was to find an improvement in the total time of travel for each sales agent. It was, therefore, improving the operating costs of the company. Some considerations had to be taken to achieve such a goal.

If the agent has to choose a hotel and the travel time from his current location to the nearest hotel is larger than the time to his base, including a 30-minute tolerance, the agent will return to his base.

The sum of all the distances traveled, including the times the traveler returns to his base, were considered to evaluate the objective function. According to [22], SA simulates a collection of atoms in equilibrium at a set temperature. SA starts with an initial state. A random change is made to this state, and the change in energy, ΔE, is calculated. If the new state has lower energy than the previous state, i.e.

$$\Delta E \leq 0$$

the new state is carried into the next iteration. However, if the new state has high energy, it is accepted with probability $P(\Delta E) = \exp(-\Delta E / K_B T)$ where T is the temperature and K_B it is Boltzmann's constant. This acceptance of an uphill move (a move with $\Delta E \geq 0$) is analogous to a higher energy molecule knocking lose a molecule trapped in a state of excess energy Determining the cooling (annealing) schedule in step 3(f) of SA is crucial to the success of the algorithm. The chance of accepting an energy-increasing move is inversely proportional to ΔE and proportional to T, which decreases with time.[22]

The following steps were taken into account in order to generate a new solution,

- The current best solution is obtained, and the hotels and returns to the base are removed. The remaining list includes only client locations.
- Two points are obtained randomly, and an exchange, or flip, is performed.
- The base is added at the beginning and end of the route.
- Each leg is traveled, calculating the travel time through the previously obtained time-distance relationship.
- When the accumulated time to arrive at the next client exceeds the maximum journal duration, a hotel or base is added. It is done by obtaining the middle point between both clients and finding the hotel or base closest to such point. If the travel time to the base is lesser than to a hotel, or even if it is more extensive, up to a tolerance of 30 minutes, the base is selected. Then the resting point is added, and the journal time reset.

5. Problem Solution

The first solution was considered as the order in which each client appears in the database. The SA model was run for each zone, finding an improvement in each case. A graph showing the behavior of the model in one of such runs is shown in Figure 2. Improvements were found for all the zones, the execution time and improvement of all the zones can be observed in Table 3.

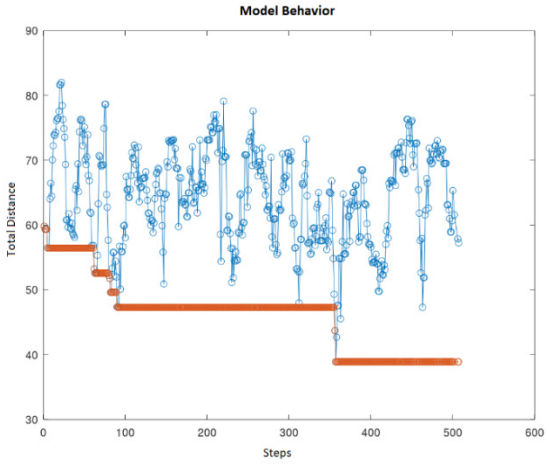


Figure 2: Model Behavior

Table 3: Results of the model's execution

Zone	Init OF	Final OF	Improvement	Runtime (minutes)
M11	54.3782	38.4468	29.29%	114.77
M12	76.8986	56.0846	27.06%	113.06
M13	34.2869	19.4949	43.14%	63.25
M14	102.632	73.683	28.20%	231.82
M21	39.8978	18.2448	54.27%	69.53
M22	41.5431	22.5259	45.77%	89.24
M23	18.4146	12.1156	34.20%	77.32
M24	130.139	84.894	34.76%	266.01
M31	54.583	41.2396	24.44%	156.63
M32	28.2553	14.4192	48.96%	68.57
M33	75.500	48.4674	35.80%	177.82

An example of the resulting routes is shown in Figure 3, where the return of the agent to his base can be appreciated. To ease the reading of this document and to avoid disclosing information that could lead to the identifying of the company or disclosing its clients, the other tables and routes will not be shown.

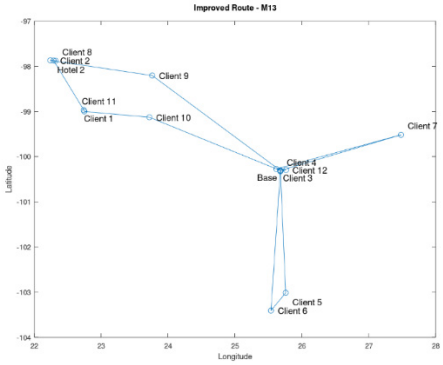


Figure 3: Sample Route

The model was run on a laptop PC. Intel® Core i5, 8Gb RAM. As shown in table 3, the execution times varied from 63.25

minutes to 266.01 minutes, or from roughly one hour to a close to four and a half hours. The full execution of the model for all zones did not take more than two full days. An attempt to solve the model precisely by the use of a linear solver was also made, but the execution took more than 100 hours without results, so the SA results were the only ones available.

6. Conclusions

An improvement in the travel time and hotel stays of the sales representatives for the distribution problem of an international company with a presence in Mexico was sought. The scope of the problem included all the Mexican territory, divided into eleven commercial zones. A Simulated Annealing method was selected to try and find better results than the current ones in a reasonable time frame.

The only information available was the location of each client, hotel, and base, but the problem needed a way to relate those to travel times. A relationship was obtained by calculating the travel time within a small number of locations. In this way, the relationship between Euclidean Distance and Travel Time was obtained.

A Travelling Salesman Problem with Hotel or Base Selection was implemented, using the aforementioned Simulated Annealing method, for each of the commercial zones. The model was run, and new routes were obtained for each zone. The maximum process time was of 156.63 minutes, and the least amount of improvement shows a 24.44% improvement over the current route selection.

6.1. Scope for future research

Using more precise mathematic models to find the relationship between the distance and the travel time can improve the efficiency of the calculation of travel time when only the coordinates are known. It could mean that more straightforward calculations would yield more precise results when travel time is needed.

References

[1] R.H. Ballou, "Business logistics: importance and some research opportunities," Gestão & Produção, **4**, 117–129, 1997, doi:10.1590/s0104-530x1997000200001.

[2] ANTAD, Annual report, Nov. 2019, Accessed on May 2, 2020. [Online]Available on: https://www.antad.net/informeanual/2019/estadisticas.html

[3] J.K. Sager, "A structural model depicting salespeople's job stress," Journal of the Academy of Marketing Science, 1994, doi:10.1177/0092070394221007.

[4] X. Geng, Z. Chen, W. Yang, D. Shi, K. Zhao, "Solving the traveling salesman problem based on an adaptive simulated annealing algorithm with greedy search," Applied Soft Computing Journal, 2011, doi:10.1016/j.asoc.2011.01.039.

[5] G. Laporte, "The traveling salesman problem: An overview of exact and approximate algorithms," European Journal of Operational Research, 1992, doi:10.1016/0377-2217(92)90138-Y.

[6] M. Jünger, G. Reinelt, G. Rinaldi, Chapter 4 The traveling salesman problem, Handbooks in Operations Research and Management Science, 1995, doi:10.1016/S0927-0507(05)80121-5.

[7] C.A. Gencel, B. Keçeci, "Traveling salesman problem with hotel selection: Comparative study of the alternative mathematical formulations," in Procedia Manufacturing, 2019, doi:10.1016/j.promfg.2020.01.270.

[8] C. Marco, S. Kenneth, Vansteenwegen, Pieter, Goos Peter, "A Simple Grasp+VND For The Travelling Salesperson Problem with Hotel Selection," University of Antwerp Faculty of Applied Economics BE Tech. Rep. out, 1-16,2012. https://repository.uantwerpen.be/docman/irua/f171bd/1c42703e.pdf

[9] K. Amirhossein, B. Mahdi, "A Migration Birds Algorithm for the travelling salesperson problem with hotel selection," Shahed University, 2015, **8**, 283-286, 2015 http://confnews.um.ac.ir/images/41/conferences/or8/237_2.pdf

[10] N. Supattananon and R. Akararungruangkul, "The Modified Particle Swarm Optimization for a Special Case of the Assignment Problem: A Case Study in Chicken Transportation," Math. Probl. Eng., **2020**, 1–15, 2020, doi:10.1155/2020/5716985.

[11] T. Bui, T. Nguyen, H.M. Huynh, B. Vo, J. Chun-Wei Lin, T.-P. Hong, "Multiswarm Multiobjective Particle Swarm Optimization with Simulated Annealing for Extracting Multiple Tests," Scientific Programming, 2020, doi:10.1155/2020/7081653.

[12] I. Khan, M.K. Maiti, K. Basuli, "Multi-objective traveling salesman problem: an ABC approach," Applied Intelligence, 2020, doi:10.1007/s10489-020-01713-4.

[13] B.P. Silalahi, N. Fathiah, P.T. Supriyo, "Use of Ant Colony Optimization Algorithm for Determining Traveling Salesman Problem Routes," Jurnal Matematika "MANTIK," 2019, doi:10.15642/mantik.2019.5.2.100-111.

[14] M. Jain, A. Rani, V. Singh, "An improved Crow Search Algorithm for high-dimensional problems," Journal of Intelligent and Fuzzy Systems, 2017, doi:10.3233/JIFS-17275.

[15] A.M. Ahmed, T.A. Rashid, S.A.M. Saeed, Cat Swarm Optimization Algorithm: A Survey and Performance Evaluation, Computational Intelligence and Neuroscience, 2020, doi:10.1155/2020/4854895.

[16] M.L. Taha, B. Al-Khateeb, Y.F. Hassan, O.M.M. Ismail, O.A. Rawash, "Solving competitive traveling salesman problem using gray wolf optimization algorithm," Periodicals of Engineering and Natural Sciences, 2020, doi:10.21533/pen.v8i3.1462.g617.

[17] M.M. Mafarja, S. Mirjalili, "Hybrid Whale Optimization Algorithm with simulated annealing for feature selection," Neurocomputing, 2017, doi:10.1016/j.neucom.2017.04.053.

[18] P. Vansteenwegen, W. Souffriau, K. Sörensen, "The travelling salesperson problem with hotel selection," Journal of the Operational Research Society, 2012, doi:10.1057/jors.2011.18.

[19] A.E.S. Ezugwu, A.O. Adewumi, M.E. Frîncu, "Simulated annealing based symbiotic organisms search optimization algorithm for traveling salesman problem," Expert Systems with Applications, 2017, doi:10.1016/j.eswa.2017.01.053.

[20] M. Fielding, "Simulated annealing with an optimal fixed temperature," SIAM Journal on Optimization, 2000, doi:10.1137/S1052623499363955.

[21] E.A. Garzón-Garnica, D.P. Cruz-Benítez, O.D. Badillo-Valenzuela, D. Sánchez-Partida, J.L. Martínez-Flores, "Automated data acquisition for a large scale Capacitated Vehicle Routing Problem," in IFAC-PapersOnLine, 2015, doi:10.1016/j.ifacol.2015.06.281.

[22] J.W. Pepper, B.L. Golden, E.A. Wasil, "Solving the traveling salesman problem with annealing-based heuristics: A computational study," IEEE Transactions on Systems, Man, and Cybernetics Part A:Systems and Humans., 2002, doi:10.1109/3468.995530.

ASTES

Advances in Science, Technology and Engineering Systems Journal Vol. 5, No. 5, 506-511 (2020)

www.astesj.com

Special Issue on Multidisciplinary Innovation in Engineering Science & Technology

ASTESJ

ISSN: 2415-6698

Growth Models and Age Estimation of Rice using Multitemporal Vegetation Index on Landsat 8 Imagery

Abdi Sukmono*, Arief Laila Nugraha, Arsyad Nur Ariwahid, Nida Shabrina

Department of Geodetic Engineering, Faculty of Engineering, Diponegoro University, Semarang, 50275, Indonesia

ARTICLE INFO

Article history:
Received: 16 July, 2020
Accepted: 29 August, 2020
Online: 24 September, 2020

Keywords:
Age of Rice
Growth Model of Rice
Multitemporal EVI

ABSTRACT

Age and growth are two essential rice biophysics parameters used to determine the health parameters and production rate. The spatial data of both parameters can utilize remote sensing technology, which in turn makes use of several vegetation indices to achieve accurate estimation. However, due to the rapid changes in rice plants' characteristics, it is essential to study vegetation index utilization using a multitemporal method to improve its accuracy. Therefore, this research uses a multitemporal Enhanced Vegetation Index (EVI) to estimate rice's age and growth model. The multitemporal EVI patterns were observed to estimate the Time Early Planting (TEP) and the maximum EVI value of rice in an area. The results showed that the maximum EVI value in the rice fields of Demak Regency has a class range of 0.4 to more than 0.9. The highest value is in the class of 0.80 - 0.85 covering 12023.28 ha, followed by 0.75 - 0.80 at 11834.19 ha. Furthermore, the multitemporal EVI method on Landsat 8 images was used to estimate the rice age with accuracy or RMSE of 7.7 days. The result also showed that this value is good enough because the RMSE is still in the same range of paddy growth phases.

1. Introduction

Rice is the essensial food for about half of the world's population. It is supply 20 % of the calories consumed worldwide [1]. Almost 90 % the global rice is produced in Asia, Africa and America Latin [2]. Most of country in thats region used rice as the staple food, especiaally in Indonesia. According to Saliem [3], close to 100% of the Indonesian population consume this product, thereby making it a staple food, with significant economic importance. The continuous increase in population leads to a rise in rice demand, therefore, an essential management strategy, such as the rice intensification system, to boost production [4].

The intensification and management of rice cultivation are inseparable from high-tech approaches due to its ability to monitor biophysical parameters such as the growth phase closely. Detailed information on the growing phase is needed to evaluate rice development [5],[6]. Furthermore, the biophysical monitoring of these parameters is valuable for the growth model and prediction of rice production [7], [8]. This growth phase model is also closely related to rice's age and used to obtain predictable information related to future harvest time.

*Corresponding Author: Abdi Sukmono, Diponegoro University, +62 85733065477, sukmono35@gmail.com

Spatial data is needed to monitor rice growth and age models for proper distribution and analysis using remote sensing technology. Several approaches are used to estimate the rice-growing phase, such as the Vegetation Index value approach, as stated in a research carried out by [9] and [10]. However, this study utilizes the Normalized Difference Vegetation Index (NDVI) to estimate rice growth. NDVI is a method occasionally used to monitor vegetation growth from space [11], [12]. Furthermore, various vegetation index techniques were developed to improve their accuracy and efficiency. Therefore, rice plants with a fast-changing level of green sensitivity utilized various combinations of techniques. The multitemporal data technique is one of the methods that can provide a solution [13]. Generally, indices such as NDVI show the growth status of green vegetation, therefore plant monitoring can be realized using remote sensing with time series or multitemporal data [14].

The utilization of this technique was carried out by [15] to detect rice biological parameters with NDWI and multitemporal EVI on Modis imagery, which is good for growth monitoring because of its daily temporal resolution. However, this method has a low spatial resolution, therefore it is only intended for regional plant growth studies. NDVI also affects soil and atmospheric reflection [16]. This tends to affect rice plants that have background soil types and diverse vegetation densities. [17] carried out a research to modify modified NDVI and ensure the

canopy background and atmospheric noise are minimized to Enhanced vegetation Index (EVI). Therefore, this study aims to utilize multitemporal Enhanced vegetation Index (EVI) techniques on Landsat 8, which has a moderate spatial resolution that is sufficiently resolved to natural change from local to global scale [18]. Landsat 8 imagery needs to be assessed to determine its use in monitoring growth models and estimating the rice age due to its efficiency, medium spatial resolution, and freedom of usage. Therefore, this study's results can be used to estimate the growth model and age of rice in a cheap, efficient, and accurate method.

2. Method

2.1. Description of Study Area

This study was conducted in all rice fields in Demak Regency, Central Java province, Indonesia. This region is the second-largest rice producing region in Central Java Province. In 2019, rice fields were 106 629.56 hectares (ha) with the production of 666 141, 30 Metric Ton (MT) of dry grain [19]. Demak is located adjacent to the Capital of Central Java Province, making it the major food supplier to Semarang City. The rice fields in this province have similar characteristics in terms of shape, function, and varieties. The paddy has a large plot above 100 m x 100 m, thereby making it suitable for analysis using pixel-based satellite image data, where the pixel size of the Landsat image is 30 m x 30 m. The majority of the Paddy fields in Demak are irrigated and dominated by Ciherang and Mekongga rice types, with some comprising of IR 64 during the dry season. When the same rice varieties varieties are planted, it allows for a fairly balanced analysis to estimate its growth model. The study areas in this study are shown in Figure 1.

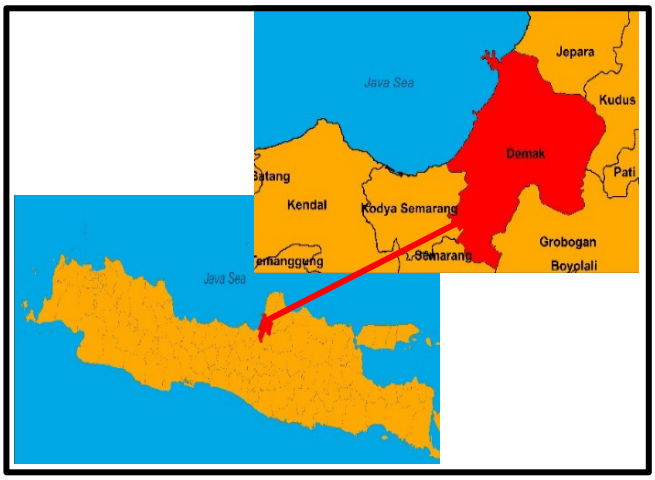


Figure 1: Location of Study Area

Paddy in Demak Regency is planted twice a year, namely season 1 (March - June) and season 2 (September-December). This study was conducted from March –June 2019, also known as planting season 1.

2.2. Preparation and Preprocessing Data

Data were obtained from Landsat 8 OLI multi-temporal acquisition images on March 4, 2019, March 20, 2019, April 5, 2019, April 21, 2019, May 8, 2019, May 24, 2019, June 9, 2019, and June 25, 2019. Therefore, the acquisition images were obtained for 4 months with a range of 16 days. Furthermore, supporting data was also prepared, using the Indonesian Topographic Map in Demak Regency for geometric tests and rice field map for cropping images at a scale of 1: 25,000.

Image preprocessing was carried out to determine the quality of images from geometric, radiometric, and atmospheric errors. In this study, Landsat 8 OLI imagery was tested for geometric accuracy using the image to map method. This test used 20 test points (Independent Control Points) extracted from Topographic Map data on a scale of 1: 25,000 and distributed in the study area. This study's geometric accuracy-test requirements need to meet Circular Error 90 (CE 90) using a map accuracy of 1: 25,000. This was followed by determining the geometrical quality and radiometric calibration process. The result of accuracy test of geometric has the RMSE 24.9 m. So it meets the requairement of the map accuracy 1 : 25.000. This research also converted the pixel value of DN (Digital Number) and image data to the BoA (Bottom of Atmospheric) reflected value. This was carried out using the second simulation of a satellite signal in the solar spectrum-vector (6SV) algorithm. Furthermore, it also utilized the sun's azimuth angle at the time of image recording. The final image preprocessing stage was used to carry out the cloud removal by the BQA (Band Quality Assessment) method before the image is cropped with the Rice Field Area of Interest in Demak Regency for effective and efficient processing.

2.3. Growth of Rice Modelling Method

Rice growth models were obtained using multitemporal vegetation index values at 30 sampling points to obtain a chart value. The rice growth pattern in the graph is polynomial and shows the level of the greenness of plants from one time to another. Healthy plants have a high maximum vegetation index value on the graph.

This study utilized the EVI (Enhanced Vegetation Index), which is an improvement from the previous algorithm, known as NDVI (Normalized Difference Vegetation Index). This Algorithm is sensitive to the "red" band channel that absorbs the canopy, with lower optical penetration depth, thereby, enabling it to absorb more quickly in high biomass areas. EVI is becoming increasingly sensitive to NIR bands on moderate to high amounts of vegetation with greater optical depth penetration into the canopy. Therefore, it is better to describe variations in biophysical canopies' structure and fails to absorb in areas with high biomass [20], [21].

EVI is derived from the soil-adjusted vegetation index (SAVI) and atmosphere-resistant vegetation index. It is an optimized combination of blue, red, and NIR channels, based on Beer's law of canopy radiation transfer, designed to extract its greenness, regardless of soil background and atmospheric aerosol variations [21] as shown in equation 1.

$$EVI = \mathrm{G} * \frac{NIR - RED}{(\mathrm{L} + NIR + C1\ RED + C2\ BLUE)} \quad (1)$$

Where L value is a calibration factor of the canopy and soil effect, G is a scale factor, with the EVI value in the range between -1 to 1. Furthermore, C1 and C2 are the weight of aerosol resistance. The variable and values of the equation coefficients above are L = 1, C1 = 6, C2 = 7.5, and G = 2.5 [22].

2.4. Age of Rice Estimation Method

The rice plants' growth profile is determined using the Landsat 8 imagery, which has a multi-temporal 16-day recording time using the EVI algorithm. The beginning of planting was marked by an EVI value lower than the harvest time and vacant land. Based on vegetation index changes, it is used to determine the spatial distribution of age (HST) and rice growth at a certain time or period [15].

The early growth phase of rice had EVI values lower than at harvest time (100-120 days) with vacant land. The Time Early Planting (TEP) can be spatially estimated when the maximum EVI is obtained. It can be calculated using the modified equation from [15], as shown in equation (2).

$$TEP = T_{-EVI}Max - \frac{1}{2} * (\frac{LP}{Period}) \quad (2)$$

Where $T_{-EVI}Max$ is the time when the maximum EVI value is obtained with the unit in Julian date, LP is the planting time for rice plants, and the period is the temporal resolution of Landsat 8. When the TEP value is obtained, the age of the rice at the time of image acquisition is determined by calculating the difference in the acquisition date with TEP. So the equation modified become equation 3.

$$TEP = T_{-EVI}Max - \frac{1}{2} * (\frac{110}{16}) \quad (3)$$

Equation 3 was modified the band in EVI and Landsat 8 period or temporal resolution with the rice planting time in study area is 110 days.

2.5. Limitation of The Study

This research was conducted in a research area characterized by irrigated rice fields during the dry season. rice varieties in the study area were homogeneous, most of which planted medium time planting rice. So that the rice planting time (LP) is assumed to be homogen, that is 110 days.

3. Result and Discussion

3.1. Growth Model of Rice Result

The development of rice growth models is obtained by arranging a multitemporal EVI pattern (March 4 2019, March 20 2019, April 5 2019, April 21 2019, May 8 2019, May 24 2019, June 9 2019, and June 25 2019) to produce its graphical representation. In this study, 25 sampling points were chosen to determine the multitemporal EVI pattern in the study area with the graph shown in figure 2.

Figure 2 shows more than one whole wave (one peak and one trough) on the multitemporal EVI graph. This is used to illustrate the model of rice growth patterns in the study area. It also means that there is more than one planting season in the study area. The minimum EVI value (trough) indicates that the land was vacant at that time, and the maximum value indicates that the rice was at the peak greening phase.

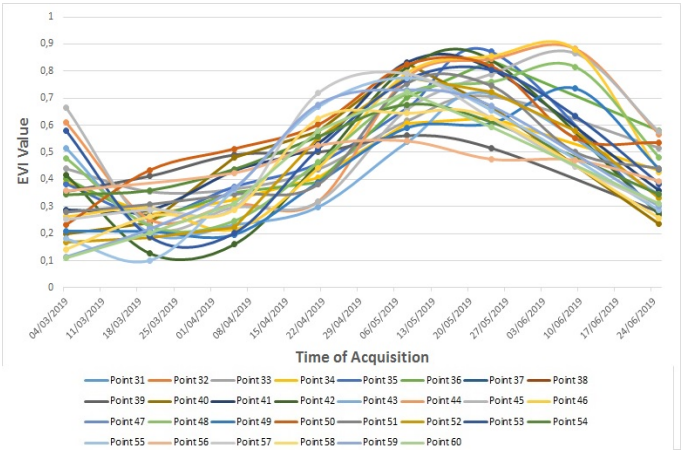


Figure 2: Graph of multitemporal EVI patterns at sample points

In general, the rice growth pattern shows the EVI value moves up towards the peak and decreases with the plant turning yellow when the rice has passed the flowering phase. This is influenced by rice flowers' effects and continues to decline because the seeds start maturing while drying the stems. A maximum EVI image is needed to determine the image with the highest value at each pixel. It is necessary because the highest pixel values among all multitemporal images represent the phase with the highest greenish level at 60-64 days after planting (HST), also known as the flowering phase. The maximum EVI that has been obtained is classified into 11 classes with an interval of 0.05, as shown in Figure 3.

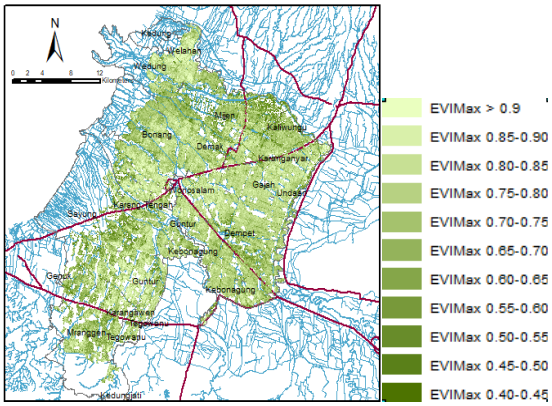


Figure 3: Maximum EVI classification results in Demak Regency

Figure 3 shows the spatial distribution of EVI max for each rice field area. This EVI class shows that the higher the value, the healthier the plants in the rice fields. This classification can be recapitulated in each class area shown in Table 1 and the graph in Figure 4.

Table 1 and Figure 4 show each EVI Max class area, which indicates that the EVI Max rice in Demak Regency in the first Planting Season of 2019 is the widest at 0.80-0.85 covering 12023.28 ha, followed by 0.75-0.80 ha at 11834 ha. Figure 4 shows that more than 70% of rice fields in Demak Regency in the planting season 1 of 2019 have an EVI Max above 0.70. Based on [16], the high EVI and NDVI represent the healthy vegetation. Therefore, the pattern of rice growth in the first planting season is healthy,

with the greenness of rice (chlorophyll), which is closely related to crop health.

Table 1: Area of each EVI Max class in Demak Regency rice field

Class of EVI Max	Area (ha)
EVIMax 0.4-0.45	961.02
EVIMax 0.45-0.50	1299.42
EVIMax 0.50-0.55	1800.99
EVIMax 0.55-0.60	2617.92
EVIMax 0.60-0.65	3781.71
EVIMax 0.65-0.70	5665.05
EVIMax 0.70-0.75	8542.08
EVIMax 0.75-0.80	11834.19
EVIMax 0.80-0.85	12023.28
EVIMax 0.85-0.90	7320.6
EVIMax > 0.9	2731.32

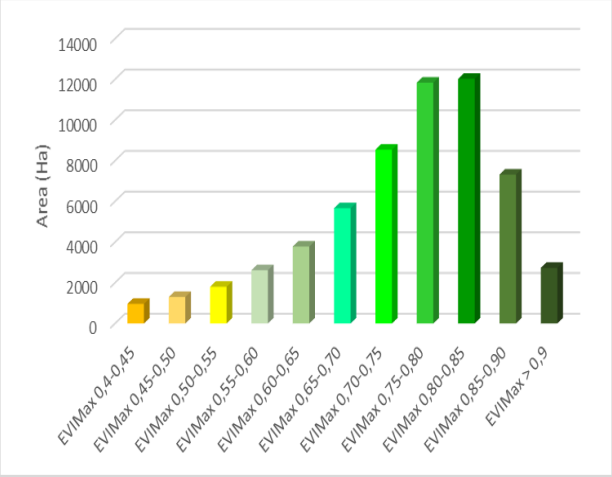


Figure 4: Graphic of Area in each EVI Max class of Rice field in Demak Regency from March – June 2019

3.2. Age Estimation of Rice Result

In this study, the age of rice was calculated using the Time Early Planting (TEP) estimation approach. This was obtained by running equation 1 on the EVI Max image, which was previously extracted from the time when EVI Max occurred on the Julian Date unit. Age estimation results are obtained from the difference between the time of acquisition or observation with TEP. The results of processing Time Early Planting and Age Estimation of rice in Demak Regency as of July 26, 2019 are shown in Figure 5 and Table 2.

Figure 5 and Table 2 show the results of Time Early Planting (TEP) and Age Estimation of Rice in Demak Regency on July 26, 2019. The widest TEP and Age Estimation was obtained on March 20, 2019 (Age of 99 Days) covering 8482, 245 Ha, followed by March 4, 2019 (Age of 115 Days) at 7088, 355 Ha and March 21, 2019 (Age of 67 Days) at 6846, 277 Ha. It shows that the rice field in Demak Regency on July 26, 2019, was dominated by Ripening's growing phase. The harvesting time estimation is obtained by adding the Time Early planting (TEP) with the Long Period (LP). It is the planting time for rice in the study area. Most of the rice varieties in Demak in planting season II were medium rice types (aged after planting 110 days). So that the harvesting time can be obtained by adding 110 days to TEP.

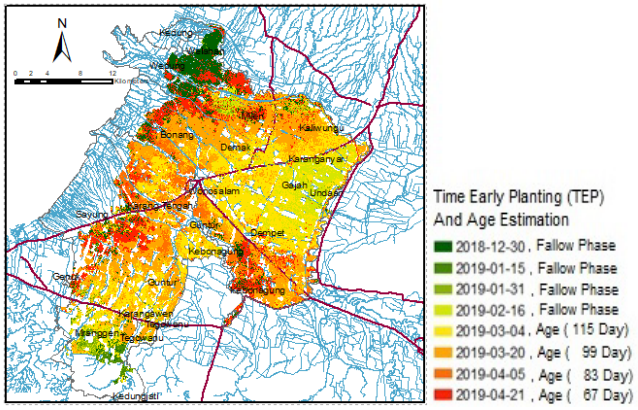


Figure 5: Time Early Planting and Age Estimation as of July 26, 2019

Table 2: Time Early Planting estimation result

Time Early Planting Estimation	Time Harvesting Estimation	Area (ha)
2018-12-30	2031-11-30	4718.604
2019-01-15	2021-04-21	827.056
2019-01-31	2021-11-16	1020.586
2019-02-16	2030-09-13	4227.501
2019-03-04	2038-07-30	7088.355
2019-03-20	2042-06-09	8482.245
2019-04-05	2029-01-31	3589.963
2019-04-21	2038-01-17	6846.277

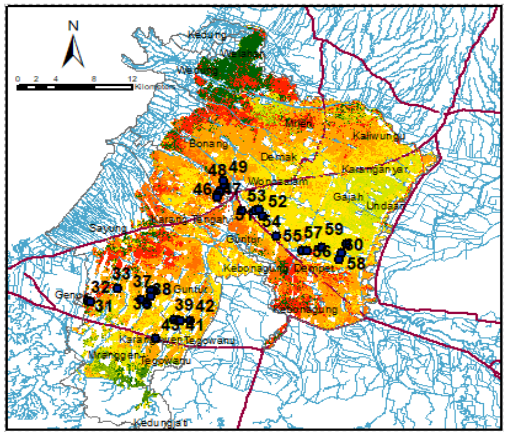


Figure 6: Spatial distribution of the validation sample point

3.3. Validation

Validation is used to determine the accuracy of rice's estimated age with the Time Early Planting (TEP) approach of EVI

Multitemporal Landsat 8. In this study, this process was carried out at 25 points distributed in the study area, as shown in Figure 6. This was carried out by field observations and interviews with farmers in order to obtain the actual age of rice. The validation was carried out on July 26, 2019.

The distributed validation test sample points also considered the representation of each rice age estimation results using the proportional random sampling technique. It aims to ensure that the validation is sufficient to meet the existing population. The results of this validation are shown in Table 3.

Table 3: Validation result of rice age estimation

Sample Point	Age of Rice In Situ	Age of rice Estimation	Error (Days)
31	48	67	19
32	59	67	8
33	95	99	4
34	96	99	3
35	104	99	5
36	104	99	5
37	97	99	2
38	106	99	7
39	104	115	11
40	117	115	2
41	109	115	6
42	98	99	1
43	104	99	5
44	97	83	14
45	97	83	14
46	95	83	12
47	95	83	12
48	82	83	1
49	87	83	4
50	107	115	8
51	107	115	8
52	107	115	8
53	92	99	7
54	112	115	3
55	112	115	3
56	114	115	1
57	117	115	2
58	112	115	3
59	117	115	2
60	107	115	8
		RMSE	7.698

The Root Mean Square Error (RMSE) or the accuracy of the multitemporal EVI method is obtained to estimate the rice age by 7.698 days. This is sufficient when compared to the Landsat 8 temporal resolution of 16 days. Furthermore, this method is quite effective for identifying vegetative, reproductive, and ripening phases. This value is good enough because the RMSE is in the same range of growth phases of rice. Another study by [23] using time series MODIS data with the method wavelet and fourier transform in EVI graphic to estimate phenological age of rice. The result of this method has the RMSE of 12.1 day. Then [24] also used the MODIS time series data to estimate phenological stage. They used savitky golay transform in EVI multitemporal graphic. It has RMSE of 10 days. The last study propose by [25] used the machine learning in one time Landsat 8 imagery to clasification the growth phases of rice. The result of this study show that SVM radial data has the overal accuracy 70,5 % in classification of growth phase of rice. Therefore multitemporal EVI using the TEP method of Landsat 8 that has a RMSE of 7.698 days, was appropriate to estimate the age of rice..

4. Conclusion

The following conclusions were made based on the research analysis:

In conclusion, the multitemporal EVI from Landsat 8 imagery can describe rice growth models with the ability to provide information on the number of growing seasons in the study area and the health level of rice from the maximum EVI value. Furthermore, more than 70% of rice fields in the Demak Regency in the planting season 1 of 2019 have an EVI Max above 0.70, therefore it is in the quite healthy category.

The study also showed that the multitemporal EVI method of Landsat 8 Imagery can estimate rice age using the Time Early Planting (TEP) approach. It has an RMSE accuracy of 7.7 days and sufficient for monitoring the rice age because the RMSE value is still in the same growth phase range.

Conflict of Interest

The authors declared no conflict of interest.

Acknowledgment

The authors are grateful to the Faculty of Engineering – Diponegoro University for funding this research through the 2020 Strategic Research grant. This article publication is suported by World Class University (WCU) Program from Diponegoro Univeristy. We are also grateful to all those that supported this research.

References

[1] M. Kubo, M. Purevdorj. The Future of Rice Production and Consumption, Journal of Food Distribution Research **35**(1), 129-142, 2004.

[2] Bandumula, N. Rice Production in Asia: Key to Global Food Security. Proc. Natl. Acad. Sci., India, Sect. B Biol. Sci. **88**, 1323–1328, 2018. https://doi.org/10.1007/s40011-017-0867-7

[3] H. Saliem, N. Hermanto, E. Suryani, R. Suhaeti, & M. Arian. The Dynamics of Indonesian Consumption Patterns of Rice and Rice-Based Food Eaten Away From Home. Analisis Kebijakan Pertanian, [S.l.], **17**(2), 95-110, dec. 2019. ISSN 2549-7278. doi: http://dx.doi.org/10.21082/akp.v17n2.2019.95-110

[4] H. Maridjo, Y. Mudayen, & A. Prihantoro. Increased productivity and technical efficiency of rice farming with the System of Rice Intensification (SRI) method in Purworejo District, Central Java. Journal of Economics, Business, & Accountancy Ventura, [S.l.], **19**(1), 49-58, july 2016. doi: http://dx.doi.org/10.14414/jebav.v19i1.535

[5] J. R. Porter, M. A. Semenov . Crop responses to climatic variation. Phil. Trans. R. Soc. B **360**: 2021–2035. 2005. doi: http://doi.org/10.1098/rstb.2005.1752

[6] S. FUKUI, Y. ISHIGOOKA, T. KUWAGATA, T. HASEGAWA. A methodology for estimating phenological parameters of rice cultivars utilizing data from common variety trials. Journal of Agricultural Meteorology, **71**(2), 77-89. 2015. https://doi.org/10.2480/agrmet.D-14-00042

[7] W. Koppe, M. L. Gnyp, C. Hut, Y. Yao, Y. Miao, X. Chen, G. Bareth. Rice monitoring with multi-temporal and dual-polarimetric TerraSAR-X data. Int

J Appl Earth Obs Geoinformation **21**, 568–576. 2012. https://doi.org/10.1016/j.jag.2012.07.016

[8] R. Nurtyawan, A. Saepuloh, A. G. Harto, K. Wikantika, A Kondoh. Satellite Imagery for Classification of Rice Growth Phase Using Freeman Decomposition in Indramayu, West Java, Indonesia. HAYATI Journal of Biosciences, **25**(3), 126-137, 2014. https://doi.org/10.4308/hjb.25.3.126

[9] K. L. Liu, Y. Z. Li, H. W. Hu. Predicting ratoon rice growth rhythm based on NDVI at key growth stages of main rice. Chilean J. Agric. Res. **75(**4), 410-417 Chillán dic. 2015. http://dx.doi.org/10.4067/S0718-58392015000500005.

[10] R Rosle, N. N. Che'Ya, N. A. Roslin, R. M. Halip, M. R. Ismail. Monitoring Early Stage of Rice Crops Growth using Normalized Difference Vegetation Index generated from UAV. IOP Conf. Series: Earth and Environmental Science **355**, 2019. 012066. doi:10.1088/1755-1315/355/1/012066

[11] P. Santos, A. J. Negri. A Comparison of the Normalized Difference Vegetation Index and Rainfall for the Amazon and Northeastern Brazil. J. Appl. Meteor. (1997) **36** (7): 958–965. 1997. https://doi.org/10.1175/1520-0450(1997)036<0958:ACOTND>2.0.CO;2

[12] C. J. Trucker, P. J. Sellers. Satellite remote sensing of primary production. Int. J. Remote Sens., **7**, 1395–1416. 1986. https://doi.org/10.1080/01431168608948944

[13] C. Yonezawa, M. Negishi, K. Azuma, M. Watanabe, N. Ishitsuka, S. Ogawa, G. Saito. Growth monitoring and classification of rice fields using multitemporal RADARSAT-2 full-polarimetric data. Int. J. Remote Sens., **33**(18), 2012. https://doi.org/10.1080/01431161.2012.665194

[14] Jiang, D., Wang, N., Yang, X. et al. Study on the interaction between NDVI profile and the growing status of crops. Chin. Geograph.Sc. **13**, 62–65. 2003. https://doi.org/10.1007/s11769-003-0086-4

[15] D. D. Domiri. The method for detecting biological parameter of rice growth and early planting of paddy crop by using multi temporal remote sensing data. IOP Conf. Series: Earth and Environmental Science **54**(2017) 012002. 2018. doi:10.1088/1755-1315/54/1/012002

[16] J. Xue, B. Su. Significant Remote Sensing Vegetation Indices: A Review of Developments and Applications. Journal of Sensors **2017**, Article ID 1353691, 17 pages. https://doi.org/10.1155/2017/1353691

[17] H. Q. Liu and A. Huete, "Feedback based modification of the NDVI to minimize canopy background and atmospheric noise," IEEE Transactions on Geoscience and Remote Sensing, **33**(2), 457–465, 1995.

[18] D. P. Roy, M. A. Wulder, T. R. Loveland, C. E. Woodcock, R. G. Allene, M. C. Anderson. Landsat-8: Science and product vision for terrestrial global change research. Remote Sensing of Environment, **145**, 154-172. 2014. https://doi.org/10.1016/j.rse.2014.02.001

[19] BPS. 2020. Central Java In Figure. BPS-Statistics of Central Java Province, 2020.

[20] X. Gao, A. Huete, W. Ni, T. Miura. Optical-biophysical relationships of vegetation spectra without background contamination. Remote Sens Environ **74**, 609–620. 2000. https://doi.org/10.1016/S0034-4257(00)00150-4

[21] A. Huete, K. Didan, W. V. Leeuwen, T. Miura, E. Glenn. MODIS Vegetation Indices. In: Ramachandran B., Justice C., Abrams M. (eds) Land Remote Sensing and Global Environmental Change. Remote Sensing and Digital Image Processing, **11,** 2010 Springer, New York, NY. https://doi.org/10.1007/978-1-4419-6749-7_26

[22] B. D. Wardlow, S. L. Egbert. Analysis of time series MODIS 250m Vegetation index Data for Crop Calssification in the U.S Central Great Plains. Remote Sensisng of Environment, **83**, 97-111. https://doi.org/10.1080/01431160902897858

[23] T. Sakamoto, M. Yokozawa, H. Toritani, M. Shibayama, N. Ishitsuka, H. Ohno. A crop phenology detection method using time-series MODIS data. 2004. Remote Sensing of Environment **96**(3–4), 366-374, 2005. https://doi.org/10.1016/j.rse.2005.03.008

[24] L. Shihua, X. Jiangtao, N. Ping, Z Jing, W Hongshu, W. Jingxian. Monitoring paddy rice phenology using time series MODIS data over Jiangxi Province, China. Int J Agric & Biol Eng, 2014; **7**(6): 2 — 36. DOI: 10.3965/j.ijabe.20140706.005

[25] F. Ramadhani , R. Pullanagari , G. Kereszturi, J. Procter, Mapping of rice growth phases and bare land using Landsat-8 OLI with machine learning, International Journal of Remote Sensing, **41**(21), 8428-8452, 2020. DOI: 10.1080/01431161.2020.1779378

ASTES

Advances in Science, Technology and Engineering Systems Journal Vol. 5, No. 5, 512-525 (2020)

www.astesj.com

Special Issue on Multidisciplinary Innovation in Engineering Science & Technology

ASTESJ

ISSN: 2415-6698

Genetic Organization and Evolution of Electromechanical Objects with Adaptive Geometry of Active Zone

Vasyl Shynkarenko[1], Ali Makki[2], Viktoriia Kotliarova[1,*], Anna Shymanska[1], Pavlo Krasovskyi[1]

[1]*Department of Electromechanics, National Technical University of Ukraine "Igor Sikorsky Kyiv Polytechnic Institute", Kyiv, 03056, Ukraine*

[2]*KEEP'MOTION Company, Luzinay, 38200, France*

ARTICLE INFO

Article history:
Received: 12 August, 2020
Accepted: 01 September, 2020
Online: 24 September, 2020

Keywords:
Electromechanical object
Active zone
Variable geometry
Electromagnetic chromosome
Genetic code
Macrogenetic program
Synthesis
"Elastic" electromechanics
Functional evolution

ABSTRACT

The paper is devoted to the presentation of a new methodological approach (new philosophy) to the formulation and solution of directed search and synthesis of electromechanical objects for a given function problems. The object under the study is a class of electrical machines and electromechanical devices which operation is carried out with a variable structure or geometry of the active zone. The research is relevant due to the characteristic trend in the evolution of modern technology which is associated with the creation of complex technical systems with the ability to change the structure and spatial geometry of the executive body in accordance with changing of external factors. The novelty of the synthesis methodology is determined by genetic nature of the technical evolution of electromechanical objects and by genetic programs of structure formation using. According to the results of research the genetic principles and macrogenetic programs of electromechanical objects with variable spatial geometry of active parts have been determined for the very first time. The area of existence and results of genetic synthesis of "elastic" electromechanics objects are presented. The reliability of genetic models, genetic programs and the results of the electromechanical objects with adaptive spatial geometry of the active zone synthesis is confirmed by the results of evolutionary experiments.

1. Introduction

One of the current trends in the development of mobile technical systems is associated with the transition from classical rigid forms and monostructures to spatially distributed structures with adaptive spatial geometry which functioning is as close as possible to natural analogues. This trend is relevant due to the growing demands of improving the dynamic characteristics and mass and size dimensions, increasing energy efficiency and reliability of technical systems based on the use of the latest materials and the widespread introduction of digital technologies. In the process of interaction between the object and external environment, the energy characteristics of the whole system change which is accompanied by a changing of the parameters and physical state of its elements. Factors of external influence often determine the necessity of the spatial geometry and structure of the system adaptation in the area of their direct interaction. Spatially adaptive systems and technologies are already used in modern aviation, space and military technics, electronics, automotive, robotics, machine-building and other science-intensive technical fields [1]-[5]. The latest direction of technology development has not yet received an unambiguous definition and occurs under various terminological names: "elastic mechanics", "machines with adaptive morphology", "soft robotics", "flexible electronics", "reconfigured systems", "objects-transformers", etc.

Analysis of the functional and technical evolution of electromechanical converters of energy (EMCE) shows a great variety of electrical machines and electromechanical devices, which operation of which is directly related to changes in the structure and geometry of their active zone in space and time. In the concept of structural-system approach, these electromechanical objects (EM-objects) and devices belong to the class of genetically organized systems (GOS) which structural diversity is determined by the relevant genetic programs and their development is regulated by systemic laws of genetic evolution [6].

The object of research is the functional classes of modular EMCE which operating routines are realized with a change in the spatial geometry and structure of the active parts. An

*Corresponding Author: Viktoriia Kotliarova, sharik_2004@ukr.net

informational sources review shows the absence of a systematic analysis of the structural organization and technical evolution of these objects and is currently limited to describing only their known technical implementations. The tasks of determination the principles of structure formation of EM-objects with variable geometry of the active zone and their genetic programs and of analysis the directions of their structural and functional evolution.

2. Genetic Organization of Electromagnetic Systems

The genetic approach in modern science acquires a key role in understanding of the fundamental principles of structural organization and laws of complex systems developing which opens the possibility of implementing scenarios for predicting and managing heredity in the generalized language of genetic information not only in biological systems but also in systems of anthropogenic origin [7], [8]. General system principles of hierarchical structural organization of complex systems, interdisciplinary structural isomorphisms and homologies indicate that the class of GOS includes not only systems of natural origin (biological, chemical, crystallographic) but also technical, musical, linguistic, mathematical and other anthropogenic systems. Evolutionary alive and anthropogenic systems regardless of their level of complexity have two alternative properties: heredity and variability. Heredity is manifested in the fact that an arbitrary object, population or species as a whole, retain in a number of generations their inherent genetic characteristic and properties. The property of variability predetermines a variety of options for the implementation and ways of development of hereditary structures by adapting them to changing environmental conditions.

The theoretical basis of GOS are interconnected system principles of structural organization and information heredity which predetermine the diversity and development of systems of different physical nature. The principles of structure formation and the genetically acceptable diversity of GOS objects are determined through the genetic information of the elemental basis, which is ordered by genetic classifications (GC) of the natural type. Periodic genetic classifications in the concept of GOS perform the function of generative systems. The category of generating systems includes the periodic classification of chemical elements, the classification of 230 groups of crystals symmetry, the classification of geographical zoning, the periodic classification of natural numbers and others. Genetic organization and evolution are determined by a system of interrelated principles and laws, the form of presentation of which is the generative system – the Periodic Genetic Classification (Table 1). The absence of certain invariant principles in GOS of a certain physical nature should be considered as a temporary phenomenon which is explained by the unevenness of structural and systemic studies or the lack of genetic classifications (generative systems) of the corresponding elemental basis. The biological science is particularly at the level where the theoretical basis operates on almost all system-wide principles of genetic evolution except its own generative periodic table the search for which is continued today [9].

As for the electromechanics principles are shown in Table 1 were absent in the classical theory of electric machines, and became known only after the discovery and analysis of the invariant properties of GC (Figure 1). Analysis of intersystem isomorphisms, after some time, revealed the principles of invariance of GOS also in the system of natural numbers [10].

Table 1: System-wide Principles of Invariance in Genetically Organized Systems of Different Physical Nature (Fragment)

Invariants of GOS	Biology	Music	Linguistics	Chemistry	Electro-mechanics	Natural numbers
Own elements base	+	+	+	+	+	+
Generative periodic system of elements	?	+	?	+	+	+
Universal genetic code	+	+	?	+	+	+
The principle of symmetry saving	+	+	+	+	+	+
The principle of topological invariance	+	+	+	+	+	+
The principle of genetic information saving	+	+	+	+	+	+
Structures genetic memory	+	+	+	+	+	+
The principle of parity	+	+	+	+	+	+
Homology	+	?	+	+	+	+
Isotopy	+	+	+	+	+	+
Isomerism	+	+	+	+	+	+

+ discovered or have been investigated;
? currently missing or need to be clarificated.

Electromagnetic field is a fundamental physical property of material and natural phenomena. The magnetic field was formed in the early stages of the evolution of the universe and is primary comparatively with chemical and biological evolution.

The information which accompanies magnetic fields has exceptional importance for studying the evolution of different physical nature systems. The discovery of the Genetic Classification of primary sources of the electromagnetic field have established that EMCE as systems of both natural and anthropogenic origin belong to the category of genetically organized systems [6]. The elemental basis of the GC is represented by the primary sources of the electromagnetic field (electromagnetic chromosomes) which perform the role of the original elementary structures in the tasks of combinatorial and topological synthesis of structures in arbitrary level of complexity. The position and invariant properties of an arbitrary primary source of field in the structure of the GC are determined by its genetic information which is represented by a universal genetic code. Electromagnetic, topological and geometric properties of the primary structures of the GC are determined by the system-wide principles of electric charge, symmetry and topology stability.

Elemental and information basis of the first large period of GC is represented by 36 oriented field sources (electromagnetic chromosomes) of the basic level, the location and genetic information of which unambiguously determine their belonging to the corresponding geometric class of active surfaces (Genus taxonomic category), their connectivity and orientation (Homological series), genetic code (Species category) and the principle of parity (Twin-species category). There is a deterministic connection between the elemental basis of GC and EM-objects-descendants which is determined by the principles of genetic structure and information stability. Therefore, an arbitrary EM-object is a carrier of genetic information which recognizes its location in the subject area of the generative system as well as determines the taxonomic status and the corresponding genetic programs of structure and its relationship with other elements of the system.

The structure of the GC is a form of presenting the fundamental principles the structure and information stability as well as the integral periodic law.

According to the results of genetic analysis and numerous evolutionary experiments it is established that the structural diversity and properties of electromagnetic and electromechanical objects were created by many generations of specialists are endowed with highly ordered system connections recognized by universal genetic codes of elemental GC basis.

The set of these provisions is a system basis for setting and solving fundamentally new problems including problems of determining and decoding of genetic programs of arbitrary functional classes of electromechanical systems (EM-systems), implementation of structural prediction and genetic synthesis technologies, development of genetic data banks and knowledge bases.

3. Spatial Geometry and Topology of Electromagnetic Structure

Spatial geometry and topology in the evolution of structures are fundamental problems in the theory of genetically organized systems of arbitrary physical nature. “The problem of the inheritance of forms is one of the most important problems of the human mind. Any form, any state of a certain process is a product of the union or intersection of elementary forms (atoms) that have similarity, indivisibility and immutability... Any evolution comes down to changes in the relative position, organization of these elementary forms” [11]. “…In modern physics it is assumption that the set of elementary forms and functions of matter is limited, and new forms and functions appear only as a result of combinations and transformations of basic forms and functions” [12]. These provisions are necessary conditions for the development of GOS.

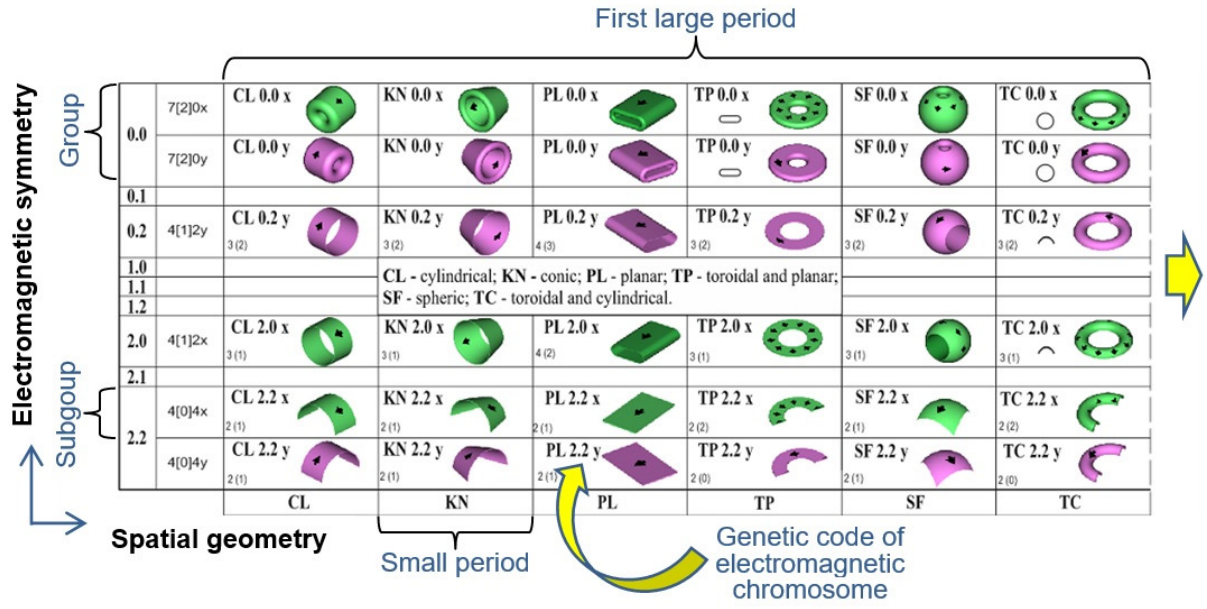


Figure 1: Generative System − Genetic Classification of Primary Sources of Electromagnetic Field (the First Large Period)

Spatial geometry, electromagnetic symmetry and topology of primary sources of electromagnetic field (electromagnetic chromosomes) define the concept of genetic information and play the role of invariants in the structure of arbitrary Species of EMCE. In the structure of the universal genetic code, spatial geometry is encoded by the first component of genetic information which determines the Genus affiliation of objects-descendants. The structural equivalent of the spatial geometry of the primary field source is the active surface of the corresponding EM-object. The geometry of the active zone, electromagnetic symmetry and topological properties of the electromagnetic structure determine the principles of structure formation of EM-objects at all levels of their structural organization, starting from the level of electromagnetic chromosomes and ending with complex systems created in the process of evolution (Figure 2).

Changing of the spatial geometry and parameters of the secondary environment is a necessary condition for the functioning of the vast majority of EMCEs designed for direct implementation of technologies (magnetic and electrodynamic separators, electromechanical disintegrators, magnetohydrodynamic converters, etc.). So their analysis is a separate task. In this study structures with only variable spatial orientation and geometry of the primary active part (stator, armature, inductor, poles, etc.) are analyzed.

4. Macrogenetic Programs

The limits of arbitrary functional classes of EMCE existence and the quantitative composition of genetically acceptable Species are determined by their macrogenetic programs [13]. Macrogenetic programs are carriers of systematized information on the Species diversity of structures, including structural representatives of known Species and Species that are not involved yet in the technical evolution of the functional class. The problem of determining the genetic program will be considered on the example of a class of EM-objects the which functioning is carried out with a variable spatial orientation (OZ-rotation) of the active parts (Figure 3).

The integrated search function F_{OZ} is determined by a set of the following partial requirements:

- the presence of a solid secondary part (C_2);

- the possibility of OZ-rotation ($\beta = 0 \div \pi$) of the primary part relatively to the *OZ*-normal;

- invariability of the air gap ($\delta \approx const$);

- ensuring the maximum area of overlap of the active zone ($S_a = max$).

Then the vector of the integral function F_{OZ} in the multidimensional search space R^n takes the following form:

$$F_{OZ} = \{C_2, (\beta = 0 \div \pi), (\delta \approx const), (S_a = max)\} \subset R^n. \quad (1)$$

The search space is limited by the elemental basis of the first large period of GC (excluding sources-isotopes). This set of requirements is met by electromagnetic chromosomes of three Genuses: Spherical (SF), Flat (PL) and Toroidal Flat (TP) primary sources of the electromagnetic field. The results of genetic analysis show that the electromagnetic chromosomes of the Spherical and the Flat Genuses are endowed with the greatest tendency to rotational symmetry of the *OZ*-type

$$Q_{SF} = (SF0.0y;\ SF0.0x;\ SF0.2y;\ SF2.0x;\ SF2.2y;\ SF2.2x); \quad (2)$$

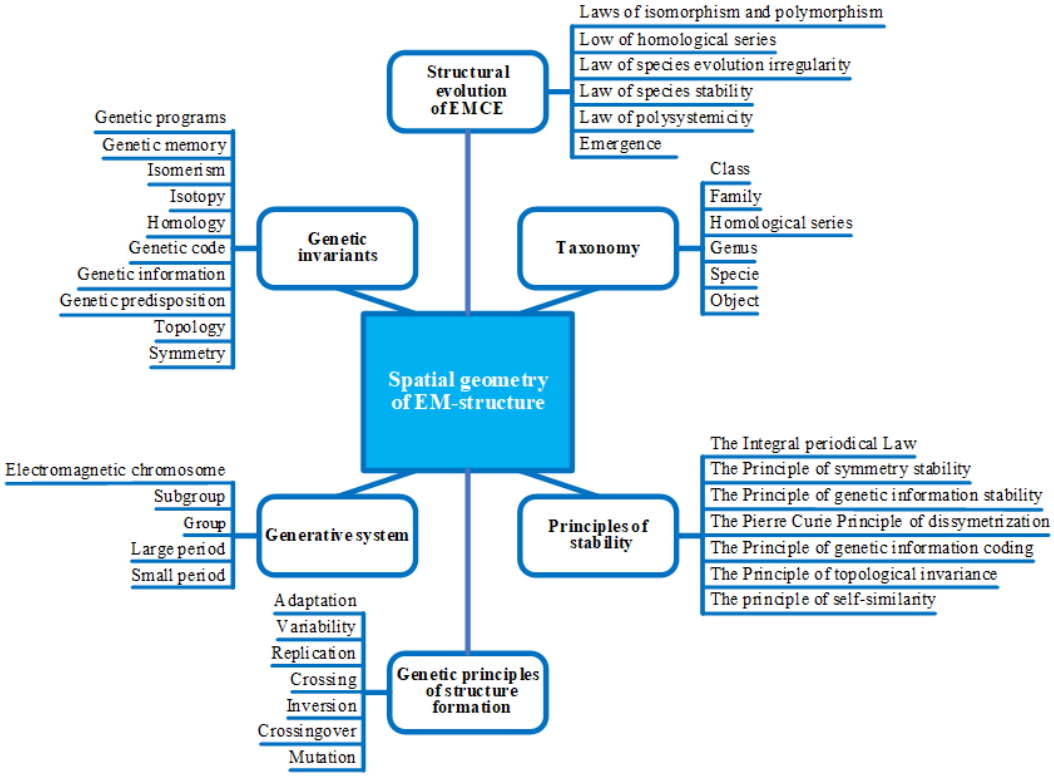


Figure 2: Ontology of the Category "Spatial Geometry of Electromagnetic Structure" in the Theory of Genetic Evolution of Electromechanical Converters of Energy

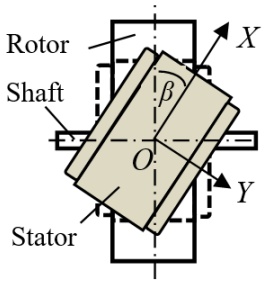


Figure 3: The Model of Electric Machine with OZ-rotary Stator

$$Q_{PL} = (PL0.0y;\ PL0.0x;\ PL0.2y;\ PL2.0x;\ PL2.2y;\ PL2.2x), \quad (3)$$

as well as two chromosomes of the Toroidal Flat Genus

$$Q_{TP} = (TP2.2y;\ TP2.2x). \quad (4)$$

Spatial OZ-rotation is also allowed by hybrid electromagnetic chromosomes of the intraspecific level:

$$Q_H = \{(PL2.2x,y)_1 \times (CL)_2;\ (PL2.2x,y)_1 \times (TP)_2;\ (PL2.2x,y)_1 \times (SF)_2;\ (TP2.2x,y)_1 \times (PL)_2\}. \quad (5)$$

The finite set of electromagnetic chromosomes (2–5) is generalized by the concept of macrogenetic program of structure formation of a functional class of objects with *OZ*-rotating active parts. The macrogenetic program contains information about the genetically acceptable elemental basis, which determines the Species diversity of both known and potentially possible EM-objects with a rotary inductor of the *OZ*-type.

Analysis of the spatial geometry and topology of paired electromagnetic chromosomes of the first large GC period shows that asymmetric field sources of group 2.2 with x-y topological invariance are endowed with the maximum genetic predisposition to change the spatial orientation. Such topological properties (provided that the value of the air gap $\delta \approx const$ is unchangeable) occur only in two primary sources of the electromagnetic field with genetic codes:

$$PL\ 2.2y = PL\ 2.2x;\ SF\ 2.2y = SF\ 2.2x, \quad (6)$$

as well as at the level of their electromechanical pairs:

$$(PL\ 2.2y)_1 \times (PL)_2 = (PL\ 2.2x)_1 \times (PL)_2; \quad (7)$$

$$(SF\ 2.2y)_1 \times (SF)_2 = (SF\ 2.2x)_1 \times (SF)_2. \quad (8)$$

The spatial geometry of the active zone of the descendant structures which are synthesized on the basis of chromosomes (6) is not "sensitive" to changes in the orientation of the active surfaces relative to the *OZ*-normal. But the change of the orientation of the active parts significantly affects the electromagnetic, electromechanical and functional properties of EM-structures-descendants. Genetic principles of mutation and structural replication determine the principles of structural synthesis of multi-element electric machines and electromechanical devices of modular design [14], [15], [16].

The relationship between genetic codes and the tendency to relative rotation at the level of paired electromagnetic chromosomes is evidence that electromechanical structures (EM-structures) with variable active zone geometry will occur at all other levels of structural complexity of a genetically organized EM-system: chromosomal (combinatorial space of paired electromagnetic chromosomes), elemental (active sections of windings, poles, moving active elements), object (inductors, armatures, rotors) and systemic (electromechanical systems with spatially distributed and active parts, etc.) levels.

5. Principles of Structure Formation of Objects with Adaptive Geometry of the Active Surface

In the theory of genetic synthesis electromagnetic structures with a violation of proportions, geometric relationships, or a violation of the electromagnetic symmetry of the active parts belong to the class of genetically mutated [6]. The system-wide principle of mutation is one of the most productive and least studied mechanisms of structure formation in GOS both of natural and of anthropogenic origin. In the methodology of genetic synthesis the corresponding group of homeomorphic transformations is matched to the mutation operator *M*. The genetic operator of the mutation changes the genetic information of an arbitrary structure, generating a sequence of homologous structures within a given topological space R^T:

$$M\,(S) \rightarrow (S_{M1}, S_{M2}, \ldots, S_{Mn}) \subset R^T, \overline{1, \infty}. \quad (9)$$

The topological equivalent of mutational transformations is volume or surface deformations of active elements or surfaces as well as changes in the spatial geometry and orientation of their relative position. The most well-known representatives of genetically mutated EM-objects are electric machines with beveled grooves, functional classes of electric motors with a rolling rotor, EM-objects with rotary stators and variable geometry of the active surface and so on. Topological model (9) indicates the unique role of mutations in understanding the mechanisms of intraspecific, interspecific and intergeneric structural relationships and transformations. Analysis of the mechanisms of mutagenesis in technical objects opens the possibility of structural prediction and synthesis of fundamentally new structural varieties.

In applied tasks of genetic synthesis, the operator *M* is matched with a group of continuous spatial deformations, compression, tension, shear, rotation, torsion and others. In procedures for the synthesis of multi-element EM-structures the mutation operator forms a stable combination with the replication operator and isomeric compositions the structural equivalents of which are spatially distributed modular structures.

In the general case for the replication coefficient $k_r \geq 2$ the mutated structure S_M allows *N* variants of spatial isomeric compositions in R^3 the number of which will increase with increasing value of k_r.

$$M(S_M) \rightarrow k_r\ s \in K_i \subset R^3,\ i = \overline{1 \div N}, \quad (10)$$

where: S_M – electromagnetic mutant chromosome; k_r – replication rate; R^3 – three-dimensional space of existence of isomeric compositions K_i.

The basis of the structure formation of EM-structures classes which allow spatial elastic deformation of the active surface is the fundamental principle of topological invariance which determines the structure and properties of primary elements within an arbitrary subgroup of periodic GC. From the point of genetic information topologically equivalent chromosomes form the corresponding horizontal series of homologous EM-structures which are subject to the realization of elastic deformation of the active zone provided the electromagnetic structure and topology stability. In the structure of the first large period of the GC there are six such series

$$T = (H_{00y}, H_{00x}, H_{02y}, H_{20x}, H_{22y}, H_{22x}). \quad (11)$$

According to the criterion of maximum adaptation to changes in the spatial geometry of the active surface of EM-objects the highest level of genetic predisposition is endowed with electromagnetic chromosomes of group 2.2. Within the first large period of GC the genetic information of the sources of group 2.2 is represented by two horizontal homologous series

$$T_{22y} = (CL\ 2.2y;\ KN\ 2.2y;PL\ 2.2y;\ TP\ 2.2y;\ SF\ 2.2y;\ TC\ 2.2y); \quad (12)$$

$$T_{22x} = (CL\ 2.2x;\ KN\ 2.2x;PL\ 2.2x;\ TP\ 2.2x;\ SF\ 2.2x;TC\ 2.2x). \quad (13)$$

For electric machines with solid secondary parts which implement rotational or translational spatial motion the range of generating structures is limited by the chromosome set of the subgroup T_{22y}. It si known that the changing in the spatial geometry of homologous electromagnetic chromosomes is related to the homeomorphism relation:

$$H_{22y} = (\ldots \leftrightarrow CL \leftrightarrow KN \leftrightarrow PL \leftrightarrow TP \leftrightarrow SF \leftrightarrow \leftrightarrow TC \leftrightarrow \ldots)2.2y \subset R^3. \quad (14)$$

In synthesis algorithms the homeomorphism of chromosomes (14) is realized by procedures of intergeneric chromosomal mutations which leads in changing of the Generic geometry of the corresponding chromosome within a given topological space. The genetically admissible set of intergeneric chromosomal mutations is theoretically determined by the combinatorial space of chromosomes of group 2.2 and is practically limited by their possibility of technical realization of structures-descendants. Paired chromosomal mutations ($N_1 = 2$) will be of the greatest practical value within subgroup 2.2y whose genetic predisposition is sensitive both to changes in the spatial orientation of active parts and to changes in the geometry of the active surface. These chromosomal mutations have a deterministic relationship with the spatial geometry of the active surface and the type of spatial motion of objects-descendants (Table 2).

Systematized information which is presented in Table 2 can be considered as a system basis for the structure formation of objects of "elastic electromechanics" of subgroup 2.2y for the combinatorial space $N_1 = 2$.

The invariant component of the genetic code (*2.2y*) indicates a common topological space within homeomorphic transformations are allowed. Changing the geometry of an arbitrary chromosome of a series (14) is carried out using a genetic mutation operator (9). Homeomorphism of primary sources of the electromagnetic field indicates the practical possibility of "elastic" formation at the level of electromagnetic twin structures which elemental basis is determined in the periodic structure of GC by isotope sources [17].

Table 2: Relationship between Intergeneric Chromosomal Mutations, Active Surface Geometry and the Type of Spatial Motion of EM-objects-descendant (Subgroup T_{22y})

Intergeneric chromosomal mutations	Type of spatial deformation	Structural formula of mutated chromosome	Type of spatial motion of objects-descendant
$PL \leftrightarrow CL$	M_{OY}	$2.2y(PL \leftrightarrow CL)_1$	Progressive (V_{OX}) ↔ rotational (ω_{OY})
$PL \leftrightarrow TP$	M_{OZ}	$2.2y(PL \leftrightarrow TP)_1$	Progressive (V_{OX}) ↔ rotational (ω_{OZ})
$PL \leftrightarrow SF$	$(M_{OY} \leftrightarrow M_{OX})_R$	$2.2y(PL \leftrightarrow SF)_1$	Progressive (V_{OX}) ↔ rotational (ω_{OY})
$CL \leftrightarrow SF$	M_{OX}	$2.2y(CL \leftrightarrow SF)_1$	Rotational (ω_{OY})
$PL \leftrightarrow KN$	$M_{OZ} \leftrightarrow M_{OY}$	$2.2y(PL \leftrightarrow KN)_1$	Progressive (V_{OX}) ↔ rotational (ω_{OY})
$TP \leftrightarrow KN$	M_{OY}	$2.2y(TP \leftrightarrow KN)_1$	Rotational (ω_{OZ}) ↔ (ω_{OY})
$CL \leftrightarrow KN$	M_{OZ}	$2.2y(CL \leftrightarrow KN)_1$	Rotational (ω_{OY})
$KN \leftrightarrow SF$	$(M_{OX} \leftrightarrow M_{OY})_R$	$2.2y(KN \leftrightarrow SF)_1$	Rotational (ω_{OY})
$TP \leftrightarrow SF$	$(M_{OX} \leftrightarrow M_{OY})_R$	$2.2y(TP \leftrightarrow SF)_1$	Rotational (ω_{OZ}) ↔ (ω_{OY})
$CL \leftrightarrow TP$	$M_{OY} \leftrightarrow M_{OZ}$	$2.2y(CL \leftrightarrow TP)_1$	Rotational (ω_{OY}) ↔ (ω_{OZ})
$CL \leftrightarrow TC$	$[M_{OY} \leftrightarrow (M_{OX})_{R1} \leftrightarrow (M_{OZ})_{R2}]$, where $(R_2 > R_1)$	$2.2y(CL \leftrightarrow TC)_1$	Rotational (ω_{OY}) ↔ (ω_{OZ})
$PL \leftrightarrow TC$	$[(M_{OX})_{R1} \leftrightarrow (M_{OZ})_{R2}]$, where $(R_2 > R_1)$	$2.2y(PL \leftrightarrow TC)_1$	Progressive (V_{OX}) ↔ rotational (ω_{OZ})
$KN \leftrightarrow TC$	$[(M_{OZ})_{R2} \leftrightarrow (M_{OX})_{R1}]$, where $(R_2 > R_1)$	$2.2y(KN \leftrightarrow TC)_1$	Rotational (ω_{OY}) ↔ (ω_{OZ})
$SF \leftrightarrow TC$	$[(M_{OX})_{R1} \leftrightarrow (M_{OZ})_{R2}]$, where $(R_2 > R_1)$	$2.2y(SF \leftrightarrow TC)_1$	Rotational (ω_{OY}) ↔ (ω_{OZ})

This pattern of interspecific topological formation is also characteristic of some biological species which was first noticed by the Scottish biologist and mathematician D'Arcy Thompson in 1917 [18]. The use of a group of topologically equivalent transformations (continuous deformations) allows the transition from the spatial geometry of the structure of one Genus to the spatial forms of other Homologous Genus. Therefore, the procedures for the synthesis of homologous EM-structures according to model (14) acquire the status of intergeneric mutations which are directly related to the change of the first component of the genetic information of the genetic code. This once again confirms the conclusion about the structural evolution of electromechanical objects occurs not only on the principle of heredity (i.e. within vertical Homologous Series) but also largely through the horizontal exchange of information within horizontal Homologous Series.

6. Genetic Synthesis

The homeomorphism of the primary structures of subgroups opens the possibility of the synthesis of EM-objects which are endowed with the property of changing their own spatial geometry within a genetically determined topological space. For example genetic information for a structure whose active surface can change geometry within three topologically equivalent geometric shapes ($N_G = 3$) for subgroup H_{22} can be represented as the result of a local intergeneric mutation

$$S_M = (H_{CL} \leftrightarrow H_{PL} \leftrightarrow H_{TP})2.2y \subset H_{22}. \quad (15)$$

Formula (15) corresponds to the model of a mutated EM-structure the geometry of the active surface of which can alternately exist in one of three generic forms flat, cylindrical or toroidal flat (Figure 4).

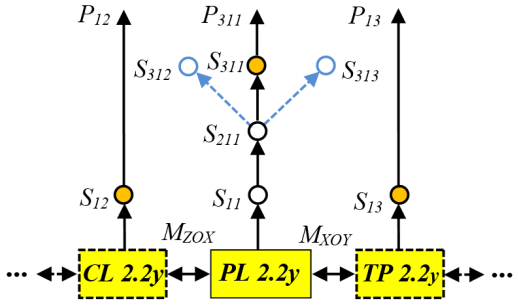


Figure 4: Genetic Model of Intergeneric Mutated EM-structure ($N_G = 3$) with Variable Geometry of Active Surface Synthesis

The results of the microgenetic program decoding confirm the dominant role of the mutation operator (M_i) in the procedures of formation of EM-objects with variable geometry of the active surface (Table 3).

The results of genetic analysis of the model allow to obtain the structural formula of the integrated mutated chromosome S_{M3}

$$S_{M3} \rightarrow (PL2.2_y)_1 \rightarrow \begin{Bmatrix} M_{ZOX} \rightarrow (CL2.2_y)_1 \times (CL2.2_y)_2 \\ M_{OZ} \rightarrow [(PL2.2y): M_{XOY}]_2 \\ M_{XOY} \rightarrow (TP2.2_y)_1 \times (TP2.2_y)_2 \end{Bmatrix} \quad (16)$$

Technical implementation of the synthesized on the basis of the S_M chromosome structure is possible if two opposite requirements are provided: providing of elastic deformation and maintaining the required mechanical stiffness of the active surface of the inductor. Modern polymers and composites allow to implement these requirements. One of the possible technical solutions involves the implementation of a hybrid design of the inductor, in which U-shaped magnetic conductors with concentrated windings, mechanically combined into a monolithic structure using a polymer-reinforced filler with a high coefficient of elasticity (Figure 5).

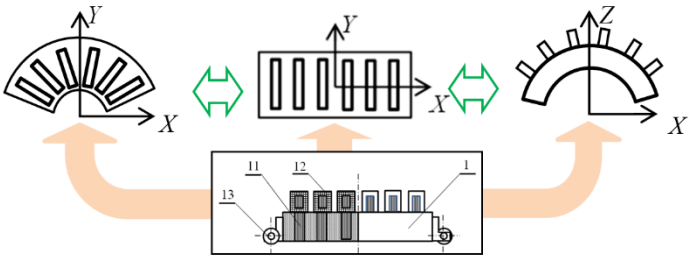


Figure 5: Multifunctional Inductor Module with Spatially Adaptive Active Surface (Chromosomal Mutation $CL2.2y \leftrightarrow PL2.2y \leftrightarrow TP2.2y$) Was Synthesized on the Basis of the Electromagnetic Chromosome S_{M3}

Genetically synthesized inductor is endowed with a unique ability to function with the ability to sequentially change the geometry of the core (cylindrical *CL* ↔ flat *PL* ↔ toroidal flat *TP*), which opens the possibility of implementing both translational and rotational motion of the moving part. Electromechanical objects with such properties can be generalized to the concept of objects of "elastic" electromechanics.

Table 3: The Results of Decoding of the Electromagnetic Chromosomes Local Intergeneric Mutation Microgenetic Program ($N_G = 3$)

Chromosomal code	Structural formula of synthesized chromosome	Chromosomal status	Weighting factor
PL 2.2y	*PL 2.2y*	Parental	–
	$[(PL\ 2.2y):M_{ZOX}]_1 \rightarrow (CL\ 2.2y)_1$	Parental mutated	–
	$[(PL\ 2.2y):M_{XOY}]_1 \rightarrow (TP\ 2.2y)_1$	Parental mutated	–
S_{11}	$(PL2.2y)_1 \times (PL2.2y)_2$	Electromagnetic double, informational	–
S_{12}	$(CL2.2y)_1 \times (CL2.2y)_2$	Electromagnetic double, generative	0.3
S_{13}	$(TP2.2y)_1 \times (TP2.2y)_2$	Electromagnetic double, generative	0.6
S_{211}	$[(PL2.2y):M_{OZ}]_1 \times (PL2.2y)_2$	Mutated (*OZ*-rotative), informational	–
S_{311}	$[(PL2.2y):M_{OZ}]_1 \times [(PL2.2y):M_{XOY}]_2$	Mutated $(M_{XOY})_2$, generative	0.8
S_Σ	$(S_{12} \leftrightarrow S_{13} \leftrightarrow S_{311})$	Integral, generative	1.0

7. Practical Implementation

One of the urgent tasks is to create modern technological complexes designed for technological preparation and processing of rolled steel and large diameter steel pipes. The problem of synthesis will be considered on the example of creating a traction spatially adaptive EM-system of a robotic technological complex for processing large diameter steel pipes. The initial information for the synthesis of a genetic model is a set of requirements for the desired structure of the EM-system and the results of the analysis of its macrogenetic program.

The integral function of F_S synthesis must satisfy the following set of partial requirements:

1) To provide the possibility of functioning with steel products of both cylindrical and flat spatial shape (G_{2CL}, G_{2PL}) which simultaneously perform the function of the secondary part of the EM system;
2) To implement progressive, rotational and complex spatial motion of the technological object ($\omega \times V$);
3) To minimize the number of functional modules of the EM system ($M_I \rightarrow min$);
4) To provide ability of quick changing of the spatial layout and number of active inductor modules in the structure of the manipulator ($N_I \rightarrow var$).

Taking into account these partial requirements, the vector of the integral synthesis function in the search space R^n takes the form:

$$F_S = [(G_{2CL}, G_{2PL}); (\omega \times V); (M_I \rightarrow min); (N_I \rightarrow var)] \subset R^n. \quad (17)$$

Requirement 3 is provided by changing the spatial orientation of the elementary inductor module relative to the surface of the process object (*OZ*-rotation) and changing the spatial geometry of the active surface of the inductor module under the action of magnetic gravity whith condition to provide constantally of the air ($\delta_{OZ} \rightarrow const$).

The multilevel genetic model of the divergent type is corresponds to given search function (17) (Figure 6).

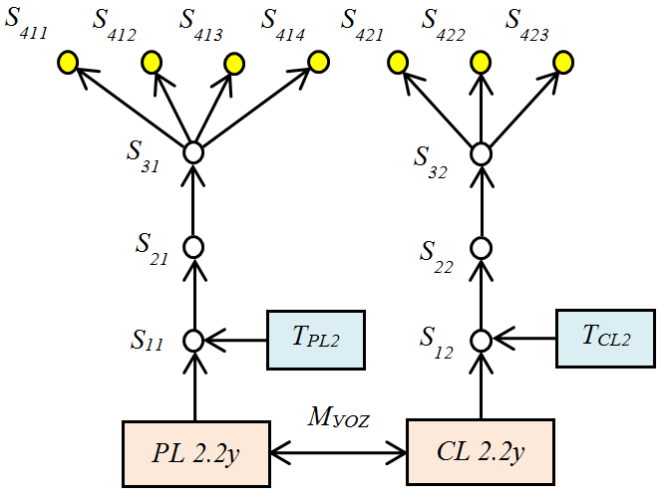


Figure 6: Genetic Model of Spatially Distributed Modular EM-system with Adaptive Geometry of Active Zone

The structure of the model contains five levels of genetic complexity which are represented by: the parent electromagnetic chromosome *PL 2.2y* of the dominant type of EM-structures (zero level); parallel sequences of genetically modified electromagnetic chromosomes of information type (S_{11}–S_{32}) which determine the trajectory of synthesis of the desired EM-structure (levels 2-4); isomeric spatial compositions of generating electromagnetic chromosomes (S_{411}–S_{414}; S_{421}–S_{423}) which satisfy the given function of synthesis and model the spatially distributed structure of the modular EM-system (level 5).

A characteristic feature of the genetic model (Figure 6) is determined by the homeomorphism of the parent chromosomes *PL 2.2y* and *CL 2.2y* which can coexist in two geometric forms of the active surface through the operator of the intergeneric mutation (M_{YOZ})

$$M_{YOZ}\,[2.2y\,(PL \leftrightarrow CL)_{ZOX}]_1 \subset T_{22Y}. \quad (18)$$

Another type of mutation is represented by chromosomes S_{21} and S_{22} which simulate their ability to implement the relative *OZ*-rotation of the active parts. These chromosomal mutations determine the procedure of synthesis of the EM-structure which is able to alternately implement the function of a flat inductor of progressive motion or an arc cylindrical inductor of rotational motion which depends on the type of secondary chromosome which simulates the spatial geometry of the object. Variants of the spatial geometry of the active surface of the technological object (requirement 1) in the model are represented by secondary transit chromosomes T_{PL2} and T_{CL2}. The results of decoding the microgenetic program are given in Table 4.

The results of the analysis of the microgenetic program (Table 4) confirm the dominant role of mutation (M_i) and replication (R_i) operators in the formation procedures of isomeric compositions which determine the genetic nature of the structure of modular EM-objects with variable structure and active zone geometry. The structural formulas of isomeric chromosomal compositions S_{411}–S_{414} (for functioning with flat objects) and S_{421}–S_{423} (for functioning with cylindrical objects) which have the status of generative satisfy the given F_S function. Each of these isomeric compositions is associated with a specific structural equivalent of the generic geometry, spatial location and orientation of the inductor modules.

Genetic synthesis procedures reproduce the deterministic relationship between genetic synthesis operators and isomeric compositions of electromagnetic chromosomes on the one hand and the pattern of inductor modules and the type of spatial motion on the other. Structural isomerism is a systemic property of genetically organized systems of arbitrary physical nature with a multi-element $(N \geq 2)$ structure, to form N_i variants of spatial compositions. The phenomenon of isomerism of primary sources of electromagnetic fields was first discovered and described in the analysis of invariant properties of the system model − Genetic Classification of primary sources of electromagnetic fields [6]. The synthesized isomeric compositions allow to determine the spatial layout schemes of inductor modules and the corresponding types of spatial motion of the technological object depending on its type and spatial geometry (Table 4).

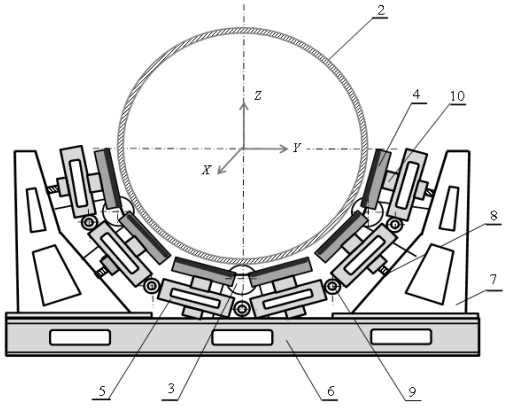
Table 4: The Results of a Modular EM-system with Variable Spatial Structure and Active Zone Geometry Structure Formation Microgenetic Program Decoding

Chromo-somal number	Structural formula of synthesized chromosome	Chromosomal status
PL2.2y	*PL 2.2y*	Parental
	$[(PL\ 2.2y){:}M_{ZOY}]_1 \rightarrow (CL\ 2.2y)_1$	Parental, intergeneric mutant
S_{11}	$(PL2.2y)_1 \times (T_{PL})_2$	Electromagnetic double, informational
S_{21}	$[(PL2.2y){:}M]_1 \times (T_{PL})_2$	Mutated, informational
S_{31}	$[(PL2.2y){:}M{:}R]_1 \times (T_{PL})_2$	Replicated, informative
S_{411}	$[(PL2.2y){:}M{:}R_{XOY}{:}V_{OX}]_1 \times (T_{PL})_2$	Isomer (*OX*-oriented), generative
S_{412}	$[(PL2.2y){:}M{:}R_{XOY}{:}V_{OY}]_1 \times (T_{PL})_2$	Isomer (*OY*-oriented), generative
S_{412}	$[(PL2.2y){:}M{:}R_{XOY}{:}\omega_{OZ}]_1 \times (T_{PL})_2$	Isomer (*OZ*-rotative), generative
S_{413}	$[(PL2.2y){:}M{:}R_{XOY}{:}V_{OX}:V_{OY}:\omega_{OZ}]_1 \times (T_{PL})_2$	Isomer $(V, \omega)_{XOY}$, generative
S_{12}	$(CL2.2y)_1 \times (T_{CL})_2$	Electromagnetic double, informational
S_{22}	$[(CL2.2y){:}M]_1 \times (T_{CL})_2$	Mutated, informational
S_{32}	$[(CL2.2y){:}M{:}R]_1 \times (T_{CL})_2$	Replicated, informative
S_{421}	$[(PL2.2y){:}M{:}R_{ZOY}{:}V_{OX}]_1 \times (T_{CL})_2$	Isomer (*OX*-oriented), generative
S_{422}	$[(CL2.2y){:}M{:}R_{ZOY}{:}\omega_{OX}]_1 \times (T_{CL})_2$	Isomer (*OX*-rotative), generative
S_{423}	$[(PL2.2y){:}M{:}R_{ZOY}{:}V_{OX}) \leftrightarrow (CL2.2y){:}M{:}R_{ZOY}:\omega_{OX}]_1 \times (T_{CL})_2$	Isomer $(V, \omega)_{OX}$, generative

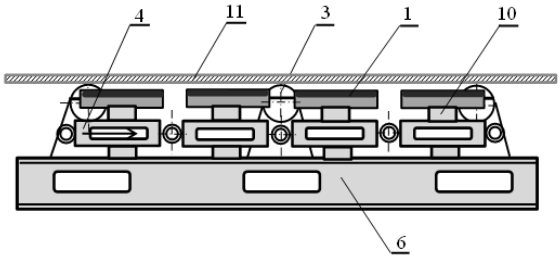
Technical implementation of a multifunctional EM-system with spatially distributed inductors carried out on a unified module with variable spatial geometry which is synthesized by a genetic formula

$$S_{M2} \rightarrow \left(PL2.2_y\right)_1 \rightarrow \begin{Bmatrix} M_{OZ} \rightarrow [(PL2.2y){:}\, M_{XOY}]_2 \\ M_{ZOX} \rightarrow \left(CL2.2_y\right)_1 \times \left(CLP2.2_y\right)_2 \end{Bmatrix} \quad (19)$$

Elastic deformation of the active surface of the modules is carried out under the action of electromagnetic gravity which allows to use one module to operate both steel pipes of different diameters and rolled steel sheets (Figure 7). The function of *OZ*-rotation of modules relative to the surface of the object of operation provides the implementation of various types of spatial motion of the technological object (progressive, rotating, helical, plane-parallel or complex programmable motion).



a)



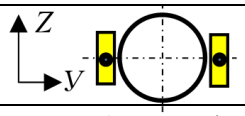
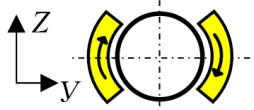
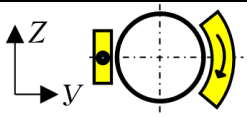
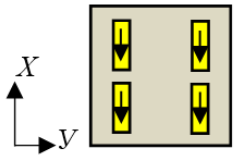
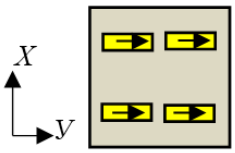
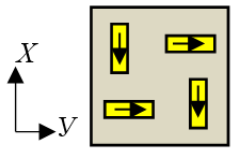
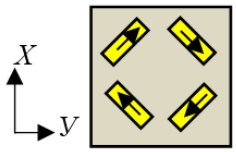
b)

Figure 7: Multifunctional Electromechanical System Based on Unified Adaptive Inductor Modules (S_{M2}) for Technological Manipulator of Steel Pipes (a) and Rolled Steel (b)

Systematized variants of spatial configurations of inductor modules (Table 5) perform the function of a genetic catalog to select the modes of operation of the spatially distributed EM-system of the technological manipulator. The results of the analysis are also the source of information for the development of algorithms for automated process control.

The speed of the object is regulated by the changing the spatial orientation of the inductor modules using frequency or amplitude-phase control. The modular structure of inductors and unification of units of the technological manipulator at the minimum expenses of time provides adaptation of spatial structure and geometry of EM-system under the given technological process. The spatial structure of the system also provides the ability to operate the number of active modules which allows to implement energy-saving algorithms for controlling the modes of operation of objects with different dimensions and weight.

Table 5: Relationship between Genetic Information of Isomeric Compositions, the Spatial Arrangement of Active Inductor Modules and the Type of Spatial Motion of the Technological Object

Type of spatial motion	Structural formula of isomeric compositions	Geometry and spatial arrangement of inductor modules*
The technological object is a steel pipe		
Progressive: $\pm (V_{OX})$;	$4(PL\ 2.2x)_{XOY}$	
Rotative: $\pm (\omega_{OX})$;	$4[(CL\ 2.2y):M_{OZ}(\pi/4):M_{ZOY}]_{ZOY}$	
Rotative-progressive (helical): $\pm (V_{OX} \times \omega_{OX})$;	$2(PL\ 2.2x)_{XOY} \times 2[(CL\ 2.2y):M_{OZ}(\pi/4)]_{ZOY}$	
The technological object is a steel sheet		
Progressive: $\pm (V_{OX})$;	$4(PL\ 2.2x)_{OX}$	
Progressive: $\pm (V_{OY})$;	$4[(PL\ 2.2y):M_{OZ}(\pi/4)]_{OY}$	
Flat-parallel: $\pm (V_{OX} \times V_{OY})$;	$2(PL\ 2.2x)_{OX} \times 2[(PL\ 2.2y): M_{OZ}(\pi/4)]_{OY}$	
Rotative: $\pm (\omega_{OZ})$;	$(PL\ 2.2y): M_{OZ}\ [(-\pi/4) \times (\pi/4) \times (3\pi/4) \times (5\pi/4)]_{XOY}$	

*For $N_I = (2\times2)$

8. Genetic Evolution

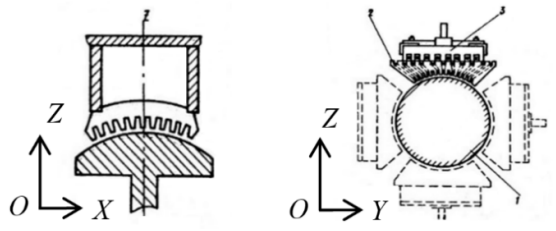
The results of genetic programs decoding were verified by carrying out of evolutionary experiments. The main task of the evolutionary experiment is to determine the deterministic correspondence between the genetic information of the elemental basis of genetic programs and the genetic codes of the real diversity of EM-objects-descendants that have historically emerged in the process of technical evolution [19].

The first structural representatives of objects with a change in the orientation of the active parts were induction electric machines with a rotating stator. The term "rotary stator" became known in the technical literature in the late eighteenth century after the publication of the French engineer P. Boucher [20]. But the concept of "rotary stator" turned out to be broader and ambiguous as its structural identification is associated with the specification of the spatial orientation of the axis of rotation relative to the axis of rotation or direction of movement of the moving part which in general case could be unconformitive. According to this feature electrical machines and electromechanical devices with the function of the relative orientation of their active parts can be divided into two subclasses:

- EMCE with the possibility of rotation of the active parts relative to the axis of rotation (*OY*-rotation);

- EMCE with the possibility of rotation of the active parts relative to normal (*OZ*-rotation).

In electromechanical objects the normal vector is perpendicular to the active surface of the converter. The rotation of the stator relative to the axis *OZ* allowed to implement one of the ways of non-contact speed control of the induction motor with the possibility of reversing. Such engines were patented in the late 40's of last century (Figure 8) [21], [22].



a) b)

Figure 8: The First Electric Machines with Rotary OZ-symmetry: a) Asynchronous Motor of the Spherical Genus (SF 2.2y); b) Induction Electric Machine of the Cylindrical Genus with a Hybrid Design of Rotary Stators (4PL 2.2y).

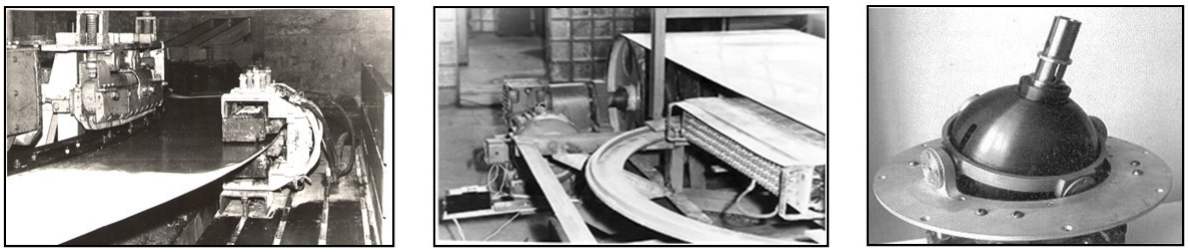
The historical stage of the genetic evolution of EMCE with variable spatial geometry of active parts is represented by a wide variety of electrical machines and electromechanical devices for different functional purposes. In 1966–1969 the first traction linear asynchronous motors (LAM) with a capacity of 5, 10 and 40 kW for driving experimental and full-scale cars of passenger overpass electric vehicles were designed, created and tested at the Special Design Bureau of Linear Electric Motors in Kyiv [23]. One of the projects involved the development of a motor with a could change the geometry of a flat active surface into a curved (arc) which significantly reduced the turning radii. In fact it was the first structural representative of traction linear motors in the design of which the principle of spatial deformation of the active surface of a moving inductor is implemented which is matched by an intergeneric mutation

$$M_2(S_M) \rightarrow 2[(PL2.2y) \leftrightarrow (CL2.2y)]_1 \subset H_{22}. \quad (20)$$

For dynamic tests of full-scale traction linear asynchronous motors a ring-type stand with an active part of 9.74 m diameter was put into operation at the Special Design Bureau of Linear Electric Motors (Kyiv). The design of the stand was implemented according to the formula of an intraspecific hybrid $(PL2.2x)_1 \times (TP0.2y)_2$. Dynamic tests of traction induction motors were carried out on the stand with the possibility of changing both the parameters of the secondary part and changing the geometry and power of their inductors (Figure 9, a). The development of space technology and autonomous robotic complexes have had significant affect on the intensity of research and development of spatially adaptive multi-coordinate electromechanical systems based on spherical electric machines (Figure 9, c) [24], [25], [26].

The current stage in the evolution of modular objects of spatially adaptive electromechanics is characterized by the use of new polymer and composite electromagnetic materials, printing technologies for magnetic circuits and windings as well as the capabilities of additive technologies of 3D- and 4D-printing. These technologies and the widespread use of magnetoelectric excitation systems have stimulated the development of technical solutions related to the implementation of the modular principle at all levels of the EM-object organization (Figure 10).

Thus the development of electromechanics is in accordance with the systemic laws of genetic evolution. The species diversity of EM-objects which determines the structural potential of a certain functional class is gradually expanding which is clearly illustrated by the dynamics of macroevolution of EM-objects with adaptive spatial geometry (Figure 11). The trajectory of macroevolutionary events reproduces the relationship of the elemental basis of Genetic Classification (Generative System) with real historical events of the appearance of structural representatives with the corresponding genetic codes which confirms the validity of the theory and practice of genetic evolution.



a) b) c)

Figure 9: Examples of EM-objects with Variable Spatial Orientation and Geometry of Active Parts: a) Universal Stand (Diameter 9.74 m) for Dynamic Tests with the Possibility of Changing the Geometry of Traction Linear Induction Motors; b) Electrodynamic Separator with Flat OZ-rotary Inductor (Specie PL 2.2y) [22]; c) Three-coordinate Synchronous Motor with a Rotary Stator for Orientation Systems (Representative of the Spherical Genus) [26].

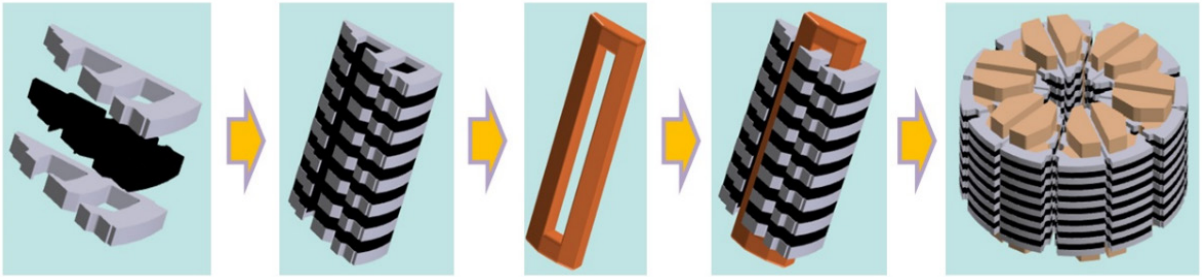


Figure 10: Multilevel Implementation of the Modular Principle in the Genetic Design of Linear Electric Motors with Transverse Magnetic Flux (Representative of the Specie CL 2.0x) by the Technology of KEEP'MOTION Company

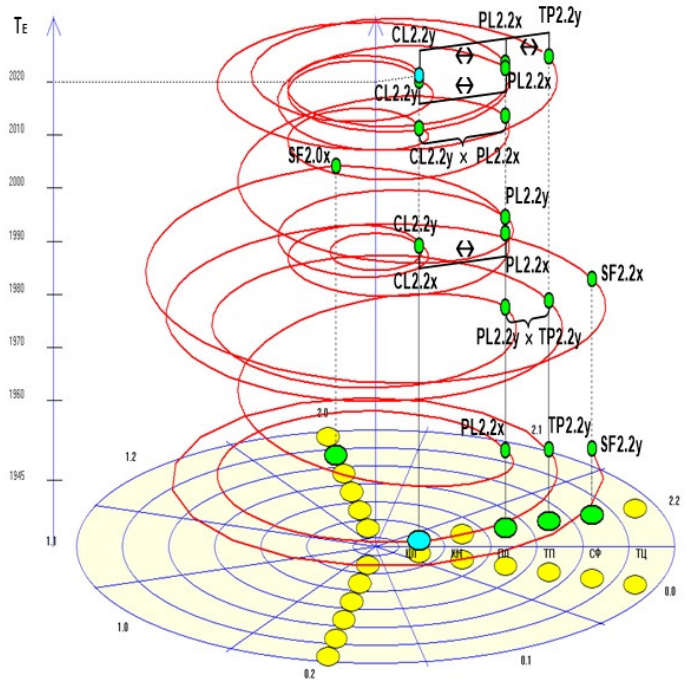


Figure 11: Macrogenetic Evolution of Species Diversity of Electric Machines with Adaptive Spatial Geometry of the Active Zone (T_E = 75 years)

The current stage of functional evolution of spatially adapted modular EM-systems is represented by a wide variety of EM-objects for different purposes (Figure 12). Modern EM-systems combine the functions of executive bodies with elements of spatial self-organization and artificial intelligence. Examples of such systems are robotic complexes with reconfigured structures [27], spatially distributed electromechanical systems of cableless passenger elevators of the MULTI series, implemented by MAGLEV technology [28], electromechanical systems of branched 3D networks-conveyors, grips and manipulators of anthropomorphic robotic systems, machining centers [5] and others. A promising area of practical use of EM-objects of elastic electromechanics are inductor systems of magnetic therapy equipment and implanted artificial life support systems in medicine [29].

The results of genetic analysis of the directions of functional evolution confirm the reliability of genetic programs and form the basis for the tasks of structural prediction and innovative synthesis of their new structural varieties. The technical evolution of spatially adaptive electromechanics in the nearest future will be largely determined by advances in materials science, genetic electromechanics, additive technologies and artificial intelligence.

9. The New Philosophy of Synthesis

The presence of the Generative Periodic System of primary sources of the electromagnetic field and the methodology of deciphering the structural information potential of genetic programs open the possibility of transition to the fundamentally new philosophy of creating complex technical systems with the ability to predict and discover new types and functional classes of EMCE. Such tasks are directly related to the theory of genetic Specie formation of EM-systems and the formulation of the corresponding prognostic-evolutionary experiment. The concept of Species is fundamental in the evolution of GOS as only through the category of Species it became possible to explain the mechanisms of micro- and macroevolution of EM-systems, determine genetic programs of structure formation and develop principles of genetic taxonomy of EMCE.

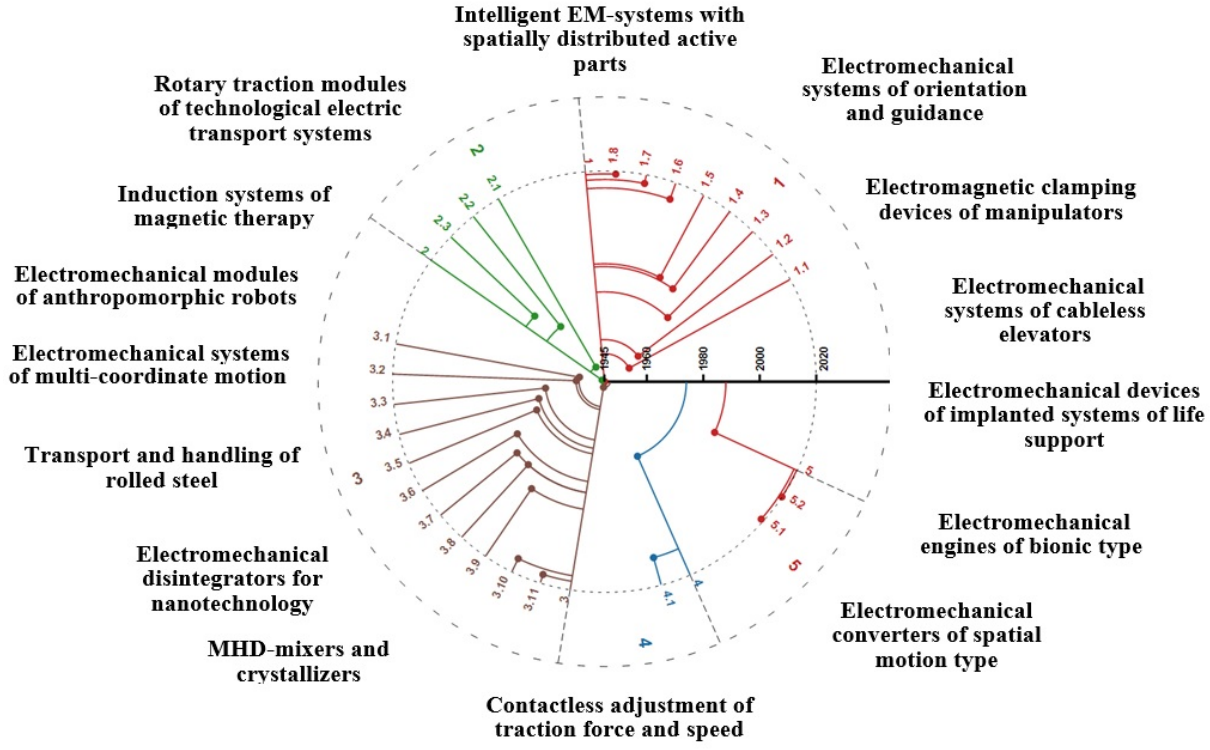


Figure 12: The Main Directions of Functional Evolution of EMCE with Variable Structure and Spatial Geometry of Active Parts

Until recently the discovery of new Species was considered the prerogative of biological science the systemic foundation of which is biological taxonomy. The discovery of the Biological Species is a landmark scientific event of international level. In the concept of GOS the concept of Species is a natural and necessary component in the hierarchy of interrelated levels of genetic complexity of electromagnetic systems: "Electromagnetic gene" → "Electromagnetic chromosome" → "Electromagnetic structure" → "Population of structures" → "Species" → "Genus" → "Functional class of EM-objects". But the establishment of the relationship and logical sequence of these categories became possible only after the discovery of the Periodic Table of primary sources of the electromagnetic field in 1991 (Figure 1) [6].

The reliability of the theory of genetic Specie formation is confirmed by evolutionary experiments the results of deciphering dozens of macrogenetic programs [30] and the creation of technology for genetic prediction of new types of EM-objects [31].

The genetic concept of Specie formation establishes a deterministic relationship between the information of the elemental basis of GC and the Species diversity of EM-objects, between the processes of macro- and microevolution of electromechanical objects and between the history of electromechanics and its future.

Opposite to the problem of biological Species which has been remainding controversial since Darwin due to the lack of their generating system the diversity of electromagnetic Species is strictly regulated by the periodic structure of genetic classification where information on both species involved in technical evolution and currently absent stored in the form of appropriate genetic codes. This sets a precedent for setting fundamentally new intellectual tasks – the prediction, discovery and introduction into technical evolution of new Species of EMCE.

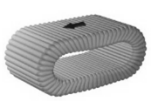
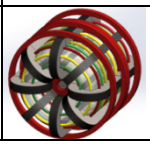
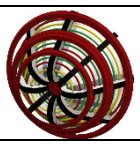
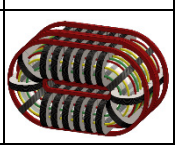
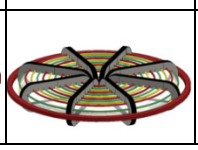
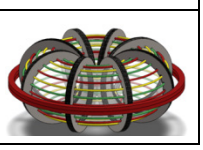
The task of new Species discovering is directly related to the synthesis and technical implementation of their first structural representatives. As an example, consider the problem of finding EM-objects with the maximum use of active volume (V_A) of an electric machine or electromechanical device. According to the results of the analysis of electromagnetic symmetry and topology of electromagnetic chromosomes of the first large period of GC (Figure 1) it is established that only electromagnetically symmetric chromosomes of group 0.0 are endowed with the maximum genetic predisposition to the criterion ($V_A \rightarrow max$). The geometry and topology of the active surfaces of the zero group is limited by the elemental basis of two topologically equivalent subgroups (y- and x-orientation) with Betty number β (S) = 2. At the level of multiphase windings such topology and symmetry can be provided only by magnetic systems with ring-distributed windings and the internal location of the active zone.

The reliability of the results of genetic prediction is confirmed by the results of group synthesis of representatives of a new structural class of electromechanical disintegrators (EMD) which designed for direct implementation of nanotechnologies (fine and ultrafine grinding, intensive mixing, preparation of homogeneous powder mixtures and compositions, enrichment technologies, etc.). Implementation of contradictory requirements (V_A = 100 %) while providing technical access to the internal working chamber during operation, was ensured by implementing the modular principle with variable spatial geometry of the external electromagnetic system of EMD (Table 6).

The development of technical solutions for EMD and their subsequent group patenting simultaneously proved the discovery and introduction into technical evolution of 6 new Species of EMCE which structural representatives were absent in the history of structural electromechanics. It should be noted that in the real evolution of technology the introduction into the evolution a new Specie occurs once every 30–40 years.

Actually, genetic electromechanics has accumulated experience in solving a number of unique problems which formulation were impossible a few years ago. It becomes obvious that the new understanding of synthesis is based on a rethinking and widespread use of systemic principles of structural and informational heredity. In each system it is possible to allocate as a building brick the elementary structures underlying technology of genetic synthesis. It is an atom in nanotechnology, a gene in biotechnology, a bit in information technology, a neuron in cognitive technology. Such system of interconnected initial structures is invariant to the time of evolution, the level of complexity of objects-descendants and their functional purpose. The transition to genetic technologies is a natural way to unity and harmony with nature, discovery and rational use of the hidden structural potential of genetic programs, creation of multifunctional integrated systems of natural-anthropogenic type, synthesized by genetic codes and models of living nature.

Table 6: Synthesized Structures of New Species of Electromechanical Disintegrators with Variable Geometry of Electromagnetic System and with 100% Using of the Active Volume for Direct Implementation of Nanotechnologies

Genus geometry	Cylindrical	Conical	Flat type	Toroidal flat	Spherical	Toroidal cylindrical
Genetic code	*CL 0.0x*	*KN 0.0x*	*PL 0.0x*	*TP 0.0x*	*SF 0.0x*	*TC 0.0x*
Electromagnetic chromosome						
3D-model of EMD structure						

10. Conclusions

The main results of the research can be summarized as follows:

- for the first time it is established that the principles of genetic structure formation of spatially distributed modular EM-systems with adaptive geometry of active zone are determined by electromagnetic symmetry and topological properties of generative sources of the electromagnetic field;

- for the first time macrogenetic programs of genetically admissible basic Species of EM-structures with variable orientation of active parts (18 Species) and objects of «elastic» electromechanics (12 Subspecies) which allow changing of spatial geometry of active surface are defined;
- it is established that in the algorithms of spatially adaptive systems synthesis the dominant role belongs to the operators of replication (modularity) and mutation ("elasticity") which determine the structure of modularity and "elasticity" of the synthesized structures;
- for the first time genetic programs are defined and algorithms of intergeneric mutation are developed, which determine the principles of structure formation of "elastic" electromechanics modular objects, which functioning is carried out with variable geometry of the active surface;
- the presence of a deterministic relationship between the elemental basis of the Periodic system of primary sources of the electromagnetic field (genetic program), isomeric chromosomal compositions, the spatial arrangement of active inductor modules and the type of spatial motion of the technological object is established;
- the reliability of genetic models, programs and synthesized structures is confirmed by the results of evolutionary experiments;
- practical implementation of research results is carried out on the example of project development of a competitive modular EM-system with adaptive spatial structure which is the part of a robotic technological complex designed for processing steel pipes and rolled products.

The results of research form the basis for the problems solving of innovative synthesis of new structural varieties of modular EM-systems with adaptive spatial structure of active elements and using of "elastic" electromechanics innovative technology.

Conflict of Interest

The authors declare no conflict of interest.

References

[1] A.N. Knaian, K.C. Cheung, M.B. Lobovsky, A.J. Oines, P. Schmidt-Neilsen, N.A. Gershenfeld, "The Milli-Motein: A self-folding chain of programmable matter with a one centimeter module pitch," in 2012 IEEE/RSJ International Conference on Intelligent Robots and Systems, 1447–1453, 2012, doi:10.1109/IROS.2012.6385904.

[2] I.-C. Cheng, S. Wagner, Overview of Flexible Electronics Technology, Springer, Boston, MA: 1–28, 2009, doi:10.1007/978-0-387-74363-9_1.

[3] E. Tsihosh, Supersonic aircrafts. Reference manual. Translation from Polish, Mir, Moscow, 1983.

[4] V. Shikhirin, "Elastic machines and mechanisms of the future," The Summary of Technologies, **2**(6), 37–42, 2001.

[5] Y.N. Kuznetsov, G.J.A. Hamuyela, T.O. Hamuyela, Morphological synthesis tools and mechanisms: Monograph, Ltd "Gnosis," Kiev, 2012.

[6] V.F. Shynkarenko, Fundamentals of the Theory of Evolution of Electromechanical Systems, Naukova Dumka, Kyiv, 2002.

[7] V. Shynkarenko, V. Kotliarova, A.N. Al-Husban, "Genetical Modeling, and Experimental Analysis of the Functional Evolution of Electromechanical Energy Converters," Journal of the Technical University of Gabrovo, **49**, 15–20, 2015.

[8] M. Zagirnyak, V. Prus, V. Shynkarenko, "The assessment of the processes of aging of the electric machines with structural unit defects using the genetic approach," Przegląd Elektrotechniczny, **95**(1), 145–148, 2019, doi:10.15199/48.2019.01.37.

[9] S.G. Inge-Vechtomov, "The search for a periodic system… in evolution," Science First Hand, **2**(3), 20–25, 2004.

[10] V.F. Shynkarenko, "Isomorphisms of generative systems (on the example of electromagnetic and numeric)," Electromechanical and Energy Saving Systems, **1**(45), 46–55, 2019, doi:10.30929/2072-2052.2019.1.45.46-55.

[11] R. Thom, Structural stability and morphogenesis, Logos, Moscow, 2002.

[12] A. Lima-de-Faria, Evolution without Selection: Form and Function by Autoevolution, Mir, Moscow, 1991.

[13] V. Shynkarenko, Iu. Gaidaienko, A.N. Al-Husban, "Decoding and functional analysis of genetic programs of hybrid electromechanical structures," Modern Applied Science, **8**(2), 36–48, 2014, doi:10.5539/mas.v8n2p36.

[14] V. Shynkarenko, A. Makki, V. Kotliarova, A. Shymanska, "Modular Principle in the Structural organization and Evolution of Electromechanical Objects," in 2019 IEEE International Conference on Modern Electrical and Energy Systems (MEES), 162–165, 2019, doi:10.1109/MEES.2019.8896446.

[15] V. Shynkarenko, A. Makki, A. Shymanska, V. Kotliarova, "Genetic Synthesis of Electromechanical Objects of the Modular Type," in 2019 IEEE International Conference on Modern Electrical and Energy Systems (MEES), 166–169, 2019, doi:10.1109/MEES.2019.8896596.

[16] V. Shynkarenko, V. Kotliarova, P. Krasovskyi, N. Misan, "Principles of structural construction of spatially adaptive electromechanical systems with variable structure and geometry of the active surface," Bulletin of NTU "KhPI", Series: "Electric Machines and Electromechanical Energy Conversion," **3**(1357), 62–70, 2020, doi:10.20998/2409-9295.2020.3.11. (In Ukrainian)

[17] V. Shynkarenko, V. Kotliarova, "Twin-objects and double-objects in the structural evolution of electromechanical energy converters," in 2017 International Conference on Modern Electrical and Energy Systems (MEES), IEEE: 116–119, 2017, doi:10.1109/MEES.2017.8248865.

[18] N. Witkovski, The Sentimental History of Science. Translation from French, CoLibri, Moscow, 2007.

[19] V.F. Shinkarenko, I.A. Shvedchikova, V.V. Kotlyarova, "Evolutionary Experiments in Genetic Electromechanics," in Proc. 13th Anniversary International scientific Conference "Unitech'13," 289–294, 2013.

[20] K.I. Shenfer, Asynchronous machines, Gosizdat, Moskow–Leningrad, 1929.

[21] P.A. Fridkin, "A new type of arc stator for an electric drive with low and adjustable rotation speeds," Electricity, **1**–**2**, 22–23, 1945.

[22] O.N. Veselovsky, M.N. Godkin, Induction motors with open magnetic circuit, Informelectro, Moskow, 1974.

[23] V.F. Shynkarenko, "Developments of Special Design Bureau of Linear Electric Motors and their place in evolution of new types of electric transport," Collection of Scientific Works "Research on the History of Technology," **3**, 8–31, 2003.

[24] D. Martínez Muñoz, Spherical machines: a literature review, 2005.

[25] O. Saßnick, Application of the Spherical Induction Motor to Dynamically Stable Robots. Marshall Plan Scholarship Research Report, 2015.

[26] A.E. Antonov, Electric machines of magnetoelectric type. Fundamentals of the theory and synthesis, IED NASU, Kiev, 2011.

[27] I.M. Makarov, V.M. Lokhin, S.V. Manko, M.P. Romanov, M.V. Kadochnikov, "Knowledge processing technologies in control problems of autonomous mechatronic-modular reconfigurable robots," Information Technologies, **8**, 2–29, 2010.

[28] J. Condliffe, World's First Cable-Free Elevator Zooms Horizontally and Vertically Using Maglev Tech, MIT Technology Review, 2017.

[29] N.I. Kulikov, A.D. Kupriyanov, "Implantable auxiliary blood circulation system based on a controlled valve motor integrated with a diaphragm-type blood pump," Biotekhnosfera, **4**(16), 9–14, 2011.

[30] A.A. Avgustynovych, Theoretical bases of electric machines Species genetic systematics creation, PhD Thesis, IED NASU, 2008. (In Ukrainian)

[31] V.F. Shinkarenko, "Genetic Foresight as System Basis is in Strategy of Management Innovative Development Technical Systems," Proceedings of the Tavria State Agrotechnological University, **4**(11), 3–9, 2011.

ASTES

Advances in Science, Technology and Engineering Systems Journal Vol. 5, No. 5, 526-535 (2020)

www.astesj.com

Special Issue on Innovative Research in Applied Science, Engineering and Technology

ASTESJ

ISSN: 2415-6698

Multi Closed-loop Adaptive Neuro-Fuzzy Inference System for Quadrotor Position Control

Halima Housny[1], El Ayachi Chater[*,2], Hassan El Fadil[1]

[1]*Electrical Engineering, National School of Applied Sciences, Ibn Tofail University, Kénitra 14000, Morocco*

[2]*Electrical Engineering, Higher School of Technology, Mohammed V University, Salé 11060, Morocco*

ARTICLE INFO

Article history:
Received: 01 August, 2020
Accepted: 15 September, 2020
Online: 26 September, 2020

Keywords:
Adaptive neuro-fuzzy inference system
Quadrotor system UAVs
Intelligent control
Integral control

ABSTRACT

This paper deals with a multi closed-loop adaptive neuro-fuzzy inference system (ANFIS) design for the under-actuated quadrotor systems. First, the training data set for the fuzzy inference system is obtained using a proportional integral derivative controller. Then, an initial ANFIS controller is designed, where the integral control action is preserved in the multi-closed-cloop ANFIS for each quadrotor system state. Thereafter, scaling gains are added to the controller inputs/outputs, and a multidimensional PSO algorithm is used to tune all the control parameters. Besides, using a simulation example, the aerial vehicle performances are investigated in the presence of an unknown payload mass parameter. Specifically, the position tracking performances of the proposed multi closed-loop PSO-based ANFIS plus integral control strategy is compared with the classical PID, conventional ANFIS, and non-optimized ANFIS plus integral controllers. Thus, using the conducted simulation results, it results that the multi closed-loop PSO-based ANFIS plus integral can achieve perfect translational trajectory-tracking and ensure better attitude stabilization despite unknown quadrotor payload mass parameter. Therefore, the proposed new multi closed-loop PSO-based control strategy may be considered as an efficient controller when considering an arbitrary trajectory-tracking problem for the quadrotor system.

1. Introduction

In recent years, a growing number of researchers have been interested in quadrotor aerial vehicles as a result of their vertical take-off and landing (VTOL) ability, accurate hovering, good behavior even in case of severe maneuverability, and low cost. Then, the growing utilization of these unmanned aerial vehicles (UAV) has begun for all types of tasks. For instance, these aerial vehicles are commonly utilized in smart farming [1], real-time mapping while exploring confined spaces such as tunnels and mines [2], and air travel [3]. However, although the quadrotor has become a successful UAV, this aerial robot is an underactuated and coupled system. Thus, to control this nonlinear system, several approaches have been presented. However, designing an efficient control strategy for this aerial vehicle is still a difficult task. In the literature, different methods have been used to ensure the quadrotor flight stabilization. First, prominent control approaches for quadrotor attitude stabilization and trajectory-tracking control include the proportional-integral-differential (PID) controller [4]. However, despite this control approach could ensure flight stabilization for hovering state, it cannot stabilize the quadrotor in presence of external disturbances. Also, using a simplified dynamic model, the position control could be achieved using a nested loop based backstepping control strategy [5]. Furthermore, the backstepping technique was combined with integral control, which allows bringing together the backstepping robustness against disturbances, with the integral control robustness against model uncertainties (see *e.g.* [6], [7], and [8]). The result was an integral backstepping control (IBC) scheme that could be used for attitude stabilization as well as for trajectory tracking control. However, although the altitude control objective was ensured, the vehicle hovering still shows attitude oscillations (see *e.g.* [9]).

Besides, as a powerful tool for controlling nonlinear systems, many (integral) sliding mode controllers were designed for stabilizing the quadrotor attitude (see *e.g.* [10]). However, a persistent shattering effect was observed on the vehicle attitude, although the stable hovering was achieved. Therefore, due to its switching control behavior, which is not acceptable by quadrotor

[*]Corresponding Author: El Ayachi Chater, EST-UM5 Avenue Prince Heritier BP 227, Tel: +212-663318151; Email: elayachi.chater@um5.ac.ma

dynamics, perfect autonomous quadrotor flight cannot be ensured using a sliding mode control strategy. Then, to compensate for parameter uncertainty, many adaptive control strategies are also proposed for controlling the quadrotor position (see *e.g.* [11]), with satisfactory results despite the yaw angle was poorly stabilized.

Interestingly, several fuzzy logic controllers (FLC) are also proposed for the autonomous quadrotor flight control (see *e.g.* [12], [13]). Indeed, to achieve the attitude stabilization as well as position tracking control, fuzzy logic control is usually utilized. To test the proposed fuzzy control performances, a few results have shown that efficient position control may are obtained for smooth trajectory tracking, despite poor vehicle attitude stabilization. Roughly, using only fuzzy logic controllers, the quadrotor attitude and its vertical position control problem could be solved using a reduced intelligent fuzzy-based controller (see *e.g.* [14]). Specifically, combining the two above controllers with a metaheuristic optimization tool permits obtaining better performances. For instance, a PID-like structure consists of using a fuzzy controller that utilizes the error, its derivative, and its integral as input signals. Interestingly, each input is applied through a block whose gain is adjustable. Moreover, the control action (*i.e.* the controller output) may also be applied through a block whose gain could be tuned. Thus, using an optimization algorithm, all the scaling-gains could be independently adjusted, which allows improving the controller performances. Namely, the provided simulation results show good attitude stabilization and stable reference trajectory tracking for the (*x,y,z*)-position and ψ-yaw rotation (see *e.g.* [15] [16]). However, the robustness of the proposed controllers was not sufficiently highlighted. Besides, artificial neural networks (ANN) have shown their effectiveness in controlling unmanned aerial vehicles [17]. Specifically, the fuzzy logic controller utilizes expert knowledge in establishing the rule-base [18], while artificial neural networks learn system operations utilizing neurons in almost a similar way the human beings do [19]. Interestingly, a new control strategy denoted adaptive neuro-fuzzy inference system (ANFIS) has appeared, which allows benefiting from FLC as well as ANN control approaches. For instance, using quadrotor tests, the ANFIS was shown to be as good as a type-2 fuzzy controller [20]. Then, compared to conventional proportional-integral-differential control, a multi-disturbance simulation scenario has shown that the ANFIS controller can enhance the quadrotor trajectory-tracking performances [21]. Indeed, to implement its inner fuzzy inference subsystem, the ANFIS approach can construct its knowledge utilizing training data from any classical controller. Interestingly, while designing the ANFIS controller, adding (input-output) scaling-gains can improve the control system robustness, which necessitates using an optimization or teaching-learning algorithm [22]. Especially, the particle swarm optimization still proves its high efficiency in ANFIS design, whether for tuning the membership functions [23] or for tuning the rule base of the inference mechanism [24].

Considering the above presentation, this work presents the ANFIS design steps for controlling a quadrotor UAV whose payload mass parameter is assumed to be unknown during the aerial vehicle flight. Thus, we first present the learning ANFIS controller design step, where the necessary training data set is collected from a classical proportional-integral-differential controller. Then, the other ANFIS design steps are described in detail. Specifically, this work presents an improved structure of the ANFIS control strategy, namely the multi closed-loop ANFIS plus integral control action, where an additional integral control action is shown to be improving the quadrotor control system performances. Roughly, as the steady-state operation of a quadrotor is hovering, it results that an integral control can compensate for unmodeled dynamics and parameter deviations. For this reason, the initial integral control action is maintained as an additional component in the proposed ANFIS, which makes the proposed control strategy a new multi closed-loop control structure [25]. Then, to improve the ANFIS performances, the state error signals are applied to the controller inputs through linear blocks whose scaling factors could be optimized. Besides, after the optimization process, the resulting control system performances are compared to those obtained using a classical PID and the conventional (non-optimized) ANFIS controllers. It turns out that the multi closed-loop PSO-based ANFIS plus integral controller can show better tracking control performances and better compensation for external disturbances.

It is worth noticing that the ingredients of the proposed idea have been presented in previous authors' work [26]. However, the main idea of the present paper is fully rewritten to make the proposed control strategy concisely designed with a complete quadrotor system model, without using the small-angle assumption. Besides, to show the robustness and the effectiveness of the proposed multi closed-loop ANFIS plus integral control strategy, both internal, as well as external disturbances, are here taken into account and shown to be compensated for.

This work comprises five sections. First, the quadrotor mathematical model is described in section 2. Then, in section 3, the PSO-based adaptive neuro-fuzzy inference system plus integral design steps are described. To show the effectiveness of the enhanced ANFIS control strategy, a simulation example is provided and commented in section 4. Finally, a concluding summary ends the paper.

2. Quadrotor Mathematical Model

The main actuation of a quadrotor is based on the rotors that are equidistant from the vehicle center of gravity (COG). Thus, this aerial vehicle motion is usually controlled utilizing the relative speed of its four actuators. However, the three rotations around the (φ, θ, ψ) Euler angles, and the linear motions along the (x, y, z) three axes, make the quadrotor a six-degree-of-freedom (6DOF) system. For this reason, the quadrotor is said under-actuated because it has only four control inputs.

2.1. Quadrotor kinematic model

The quadrotor is a symmetrical structure, which can rotate around its three axes. Then, studying its dynamics involves two frames. First, the body-fixed frame $\boldsymbol{\mathcal{F}}_B = \left(G, e_{bx}, e_{by}, e_{bz}\right)$, where G is the vehicle center of gravity. Then, the inertial frame $\boldsymbol{\mathcal{F}}_E = \left(O, e_{ix}, e_{iy}, e_{iz}\right)$, where O is an arbitrarily chosen origin in the space (see Figure 1).

Thus, w.r.t $\boldsymbol{\mathcal{F}}_E$ -frame, let $\boldsymbol{\xi} \coloneqq [x \quad y \quad z]^T$ denote the absolute vehicle CoG position, and $\boldsymbol{\eta} \coloneqq [\varphi \quad \theta \quad \psi]^T$ denote the vehicle attitude and orientation, where (φ , θ , ψ) denote respectively the roll, pitch, and yaw Euler angles. However, to

avoid the gimbal lock problem, let us consider the following usual assumption:

A1. $-\pi/2 < \varphi < \pi/2\,, -\pi/2 < \theta < \pi/2$

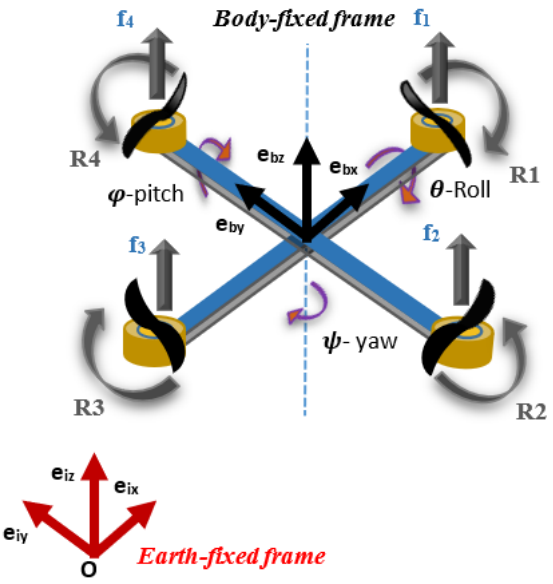


Figure 1: Quadrotor X-structure and frames

Now, let us notice that the well-known rotation matrix from $\boldsymbol{\mathcal{F}_B}$-frame to $\boldsymbol{\mathcal{F}_E}$-frame is given by [27]:

$$\boldsymbol{R}(\eta) = \begin{bmatrix} c_\theta c_\psi & s_\varphi s_\theta c_\psi - c_\varphi s_\psi & c_\varphi s_\theta c_\psi + s_\varphi s_\psi \\ c_\theta s_\psi & s_\varphi s_\theta s_\psi + c_\varphi c_\psi & c_\varphi s_\theta s_\psi - s_\varphi c_\psi \\ -s_\theta & s_\varphi c_\theta & c_\varphi c_\theta \end{bmatrix} \quad (1)$$

with $c_\alpha := cos(\alpha)\,, s_\alpha := sin(\alpha)$. This means that

$$\dot{\boldsymbol{\xi}} = \boldsymbol{R}(\eta)\boldsymbol{V_b} \quad (2)$$

where $\dot{\boldsymbol{\xi}} := [v_x \quad v_y \quad v_z]^T$ and $\boldsymbol{V}_b := [u \quad v \quad w]^T$ denote respectively the earth-fixed and body-fixed vehicle linear velocities.

Now, concerning angular velocities, the transformation matrix from the $\boldsymbol{\mathcal{F}_E}$-frame to the $\boldsymbol{\mathcal{F}_B}$-frame is denoted the transfer matrix and is given by [27]

$$\boldsymbol{T}(\eta) = \begin{bmatrix} 1 & 0 & -s_\theta \\ 0 & c_\varphi & s_\varphi c_\theta \\ 0 & -s_\varphi & c_\varphi c_\theta \end{bmatrix} \quad (3)$$

Then, it follows that

$$\boldsymbol{\Omega}_b = \boldsymbol{T}(\eta)\dot{\boldsymbol{\eta}} \quad (4)$$

where $\dot{\boldsymbol{\eta}} := [\dot{\varphi} \quad \dot{\theta} \quad \dot{\psi}]^T$ denotes the Euler angles rates, and $\boldsymbol{\Omega}_b := [p \quad q \quad r]^T$ denotes the body-fixed angular velocity.

2.2. Quadrotor dynamic model

Assuming that the quadrotor rotors do rotate at ω_i $(i = 1 \ldots 4)$, it results that each quadrotor actuator generates a thrust force that is given by $f_i := k{\omega_i}^2, (k > 0)$, w. r. t $\boldsymbol{\mathcal{F}_B}$. Thus, the total upward thrust writes:

$$\boldsymbol{F}_b := [0 \quad 0 \quad T]^T \quad (5)$$

where $T := k\sum_{i=1}^{4} {\omega_i}^2$. Then, considering the $\boldsymbol{\mathcal{F}_E}$-earth-fixed frame, and using solid mechanics, the total upward thrust writes:

$$\boldsymbol{F}_e := \boldsymbol{R}(\eta)\boldsymbol{F}_b \quad (6)$$

Thus, using Newton formalism for translational motions, the quadrotor translational dynamics are described by:

$$m\ddot{\boldsymbol{\xi}} = \boldsymbol{F}_e - \boldsymbol{W}_g \quad (7)$$

where m denotes the aerial vehicle total mass, and $\boldsymbol{W}_g$ denotes the quadrotor weight vector, which is given by:

$$\boldsymbol{W}_g := [0 \quad 0 \quad mg]^{\mathrm{T}} \quad (8)$$

where g stands for the gravity acceleration.

Now, to describe the aerial vehicle rotation motion, let us recall that the above thrust forces do also produce the following torques:

$$\boldsymbol{U}_\eta := [\tau_\varphi \quad \tau_\theta \quad \tau_\psi]^T, \quad (9)$$

with

$$\begin{bmatrix} \tau_\varphi \\ \tau_\theta \\ \tau_\psi \end{bmatrix} := \begin{bmatrix} kl(-{\omega_2}^2 + {\omega_4}^2) \\ kl(-{\omega_1}^2 + {\omega_3}^2) \\ d(-{\omega_1}^2 + {\omega_2}^2 - {\omega_3}^2 + {\omega_4}^2) \end{bmatrix} \quad (10)$$

where l denotes the distance between each rotor and the quadrotor center of mass. $(d > 0)$ denotes the drag constant.

Thus, using Newton formalism for rotational motions, the aerial vehicle rotation dynamics are described by:

$$\boldsymbol{J}\dot{\boldsymbol{\Omega}}_b = \boldsymbol{U}_\eta - \boldsymbol{\Omega}_b \times \boldsymbol{J}\boldsymbol{\Omega}_b \quad (11)$$

where $\boldsymbol{J} := diag(j_x, j_y, j_z)$ denotes the inertia matrix, and $\boldsymbol{\Omega}_b$ denotes the above body-fixed angular velocity defined in (4).

Then, let us notice that, using the following vectors:

$$\begin{cases} \boldsymbol{U} := [T \quad \tau_\varphi \quad \tau_\theta \quad \tau_\psi]^T \\ \boldsymbol{\Omega}_s := [{\omega_1}^2 \quad {\omega_2}^2 \quad {\omega_3}^2 \quad {\omega_4}^2]^T \end{cases} \quad (12)$$

and considering the following actuation matrix:

$$\mathbf{M}_a := \begin{bmatrix} k & k & k & k \\ 0 & -kl & 0 & kl \\ -kl & 0 & kl & 0 \\ -d & d & -d & d \end{bmatrix} \quad (13)$$

it results that the control distribution from the actuating motors may be described by:

$$U = \mathrm{M}_a \Omega_s \tag{14}$$

Ultimately, according to (4), (7), and (11), the quadrotor dynamics can be summarized as follows:

$$\begin{cases} \dot{x} = v_x \\ \dot{y} = v_y \\ \dot{z} = v_z \\ \dot{v}_x = (c_\varphi s_\theta c_\psi + s_\varphi s_\psi)\frac{T}{m} \\ \dot{v}_y = (c_\varphi s_\theta s_\psi - s_\varphi c_\psi)\frac{T}{m} \\ \dot{v}_z = (c_\varphi c_\theta)\frac{T}{m} - g \\ \dot{\varphi} = p + q\, s_\varphi t_\theta + r\, c_\varphi t_\theta \\ \dot{\theta} = q c_\varphi - r s_\varphi \\ \dot{\psi} = q\frac{s_\varphi}{c_\theta} + r\frac{c_\varphi}{c_\theta} \\ \dot{p} = \frac{\tau_\varphi}{j_x} + \frac{j_y - j_z}{j_x} qr \\ \dot{q} = \frac{\tau_\theta}{j_y} + \frac{j_z - j_x}{j_y} pr \\ \dot{r} = \frac{\tau_\psi}{j_z} + \frac{j_x - j_y}{j_z} pq \end{cases} \tag{15}$$

Now, considering the above quadrotor dynamics, and using enhanced fuzzy control strategies, our objective is guaranteeing the tracking-control of arbitrary ξ_{des} position for any ψ_{des} -yaw orientation, and ensuring the stabilization of (φ, θ) attitude angles, in presence of unknown aerial vehicle payload mass parameter.

3. Multi Closed-loop PSO-based ANFIS plus Integral Controller

3.1. Problem statement

From the above objective, let us design the system inputs, namely the vector $\boldsymbol{U} := [T \quad \tau_\varphi \quad \tau_\theta \quad \tau_\psi]^T$, which allows ensuring the tracking of $(x_{\mathrm{des}}, y_{\mathrm{des}}, z_{\mathrm{des}})$-reference trajectory for arbitrary ψ_{des} -yaw orientation, and the stabilization of (φ, θ) quadrotor attitude, despite random payload mass change during the vehicle flight, which also means a change of the matrix inertia. More concisely, we aim to stabilize the quadrotor system while tracking a position reference trajectory with the constraint to keep small overshoot and small rise and settling times, despite the presence of external disturbances. Then, it is worth noticing that because of quadrotor under-actuation, the control system structure may be designed using two control subsystems. Namely, an upstream control subsystem whose role is to ensure the reference trajectory tracking, and a downstream control subsystem whose role is stabilizing the vehicle attitude.

3.2. PSO-based ANFIS plus integral algorithm

Now, we briefly describe the proposed PSO-based adaptive neuro-fuzzy inference system plus integral (ANFIS+I) control strategy that is based on a Multi-Closed-loop ANFIS controller, where the additional control scaling gains are optimized using a multidimensional PSO algorithm. For clarity, algorithm 1 enumerates the main steps of the code to implement using a simulation tool (*e.g.* Matlab). For clarity, the methodology of the PSO-based ANFIS+I control design may be summarised using algorithm 1.

Algorithm 1: PSO-based ANFIS+I control algorithm

Collect training data
Generate ANFIS controller
ANFIS Enhancement with integral control
ANFIS+I scaling factors optimization using PSO

3.3. ANFIS architecture

The adaptive neuro-fuzzy inference system (ANFIS) algorithm was firstly introduced by Jang in 1993 [28], which was considered as an intelligent hybrid algorithm based on the benefits of both fuzzy logic control (FLC) and artificial neural network (ANN) approaches. The idea started from the fact that to design a suitable FLC for the considered plant, we need a minimum of knowledge upon the system functioning, which allows us to define the fuzzy rules of the controller. Then, we should define the membership function type and degree. For this reason, the design of this control is considered a complicated task despite the wide use of the FLC system in control engineering [29]. Thus, to compensate for the disadvantages of the FLC system, the artificial neural network (ANN) is also used. Roughly, the ANN algorithm may be utilized during the learning process, which can approximate an unknown function from the system inputs and outputs data set, using a multitude of neurons in a similar way of a human-being brain.

Indeed, through five layers of the ANN algorithm, the system output y is computed from $(x_1,\ x_2)$ inputs using several inference system parameters such as the fuzzy rules number and the membership function type and degree. For clarity, Figure 2 shows the ANFIS architecture model.

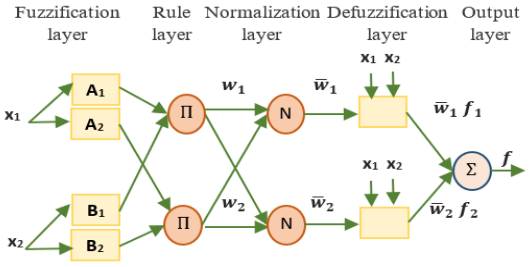


Figure 2: ANFIS architecture with two membership function

Now, the learning process of the ANFIS algorithm may be described as follows:

First, in the fuzzification layer, the output of each node is computed from the following equation:

$$\begin{cases} O_i^1 = \mu_{A_i}(x_1) \\ O_i^1 = \mu_{B_i}(x_2) \end{cases} \tag{16}$$

where (x_1, x_2) are the inputs, $(A_i\ ,\ B_i)$ are the node linguistic label, where i varies from 1 to the membership function number.

Then, to compute the output node of the second layer, we use the product of each input entering into the node as follows:

$$\begin{cases} O_j^2 = w_j \\ w_j = \mu_{A_i}(x_1) * \mu_{B_i}(x_2) \end{cases} \quad (17)$$

where j varies from 1 to the fuzzy rule number n and w_j is a rule-coefficient that stands for the firing strength.

Now, to compute the value of each node in the normalization layer, each firing strength is divided by the sum of all firing strength, which is denoted by the normalized firing strength according to the following equation:

$$\begin{cases} O_j^3 = \bar{w}_j \\ \bar{w}_j = \frac{w_j}{\sum_{j=1}^{9} w_j} \end{cases} \quad (18)$$

where j varies from 1 to n

Then, in the defuzzification layer, using the normalized firing strength $\bar{w}_j$ and the consequent parameters $\{p_j, q_j, r_j\}$, we compute a weighted value of each fuzzy rule using the following equation:

$$\begin{cases} O_j^4 = \bar{w}_j f_j \\ \bar{w}_j f_j = \bar{w}_j (p_j x_1 + q_j x_2 + r_j) \end{cases} \quad (19)$$

Thus, the final unique node value obtained in the output layer is computed by adding the incoming inputs according to the following equation:

$$O_1^5 = \sum_{j=1}^{n} \bar{w}_j f_j \quad (20)$$

3.4. ANFIS algorithm design

To design the ANFIS controller, the first step is the collection of learning data. Indeed, this learning process is very important while designing the ANFIS controller. In this work, we choose to select the training data set from a proportional-integral-differential controller. Then, benefiting from the symmetrical structure, to control the six-state quadrotor system, namely $(x, y, z, \varphi, \theta, \psi)$, only four P(I)D controllers are necessary. Roughly, similar PD controllers are used for the horizontal positions x and y, similar controllers are used for the attitude Euler angles φ and θ, a PID control structure is used for the quadrotor altitude z, and for controlling the ψ-yaw quadrotor orientation (see Figure 3). Then, to get the necessary training data for the ANFIS controller, the responses of the four P(I)D controllers are collected. Especially, in this work, the training data is a 3-dimensional vector, namely, the $(e, \dot{e})$ controller inputs and the y-controller output. Roughly, two steps are needed during the design of the ANFIS controller: the training and the testing process. Moreover, the initial training data is arbitrarily separated into a training data V_{train} (70% of initial data) and the testing data V_{test} (30% of initial data). Then, to transform the $(e, \dot{e})$-inputs into the y-output, we should select several parameters of the ANFIS algorithm.

Moreover, to approximate the fuzzy inference system (FIS) from the initial data set, the type and degree of the input-output membership functions (MFs) should be defined.

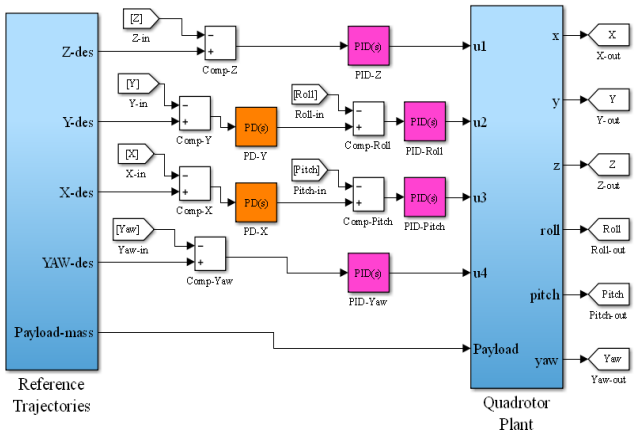


Figure 3: Quadrotor system controlled by the PD plus integral controllers

However, it is worth noticing that the choice of the membership functions degree significantly affects the necessary computational time for designing the controller. This means that choosing a small MFs degree is beneficial to the controller computing time. Then, in the proposed ANFIS controller, only three inputs MFs and three output MFs, are configured to implement each fuzzy inference system (FIS) of the controller. Furthermore, compared to other MFs types such as the trapezoidal, triangular, and bell, the Gaussian MFs type is characterized by the less complexity and high precision (see *e.g.* [30], and [31]). Thus, the (Gaussian) MFs that are chosen as inputs MFs type are defined by:

$$\mu_{A_i}(x) = e^{-\frac{(c_i - x)^2}{2\sigma_i^2}} \quad (21)$$

where $c_i(\sigma_i), (i = 1, 2, 3)$, are the center(width) of the fuzzy set for each MF. Finally, the other inference parameters are chosen as shown in Table 1:

Table 1: Inference system parameters

Fuzzy type	Defuzzification method	Inference engine
Takagi-Sugeno	*weighted average (wtaver)*	*prod-max*

Indeed, to design the ANFIS controller, we should select additional ANFIS parameters such as training epoch number n_{ep}, training error goal E_{train} and optimization method. Practically, we used the parameter values that are given in Table 2.

Then, in quadrotor system control, the trained ANFIS controller is used instead of the above controllers (see Figure 3).

3.5. Integral control action for ANFIS controller

Each of the four resulting ANFIS controllers has two inputs (the error, and its derivative $\dot{e}$) as shown in Figure 4. Then, the steady-state error cannot be removed because of the non-existence of internal integral control. For this reason, we associate each ANFIS controller with an integral control action to combine the benefits of the ANFIS controller and the integral control, which allows obtaining an enhanced and robust controller that is denoted ANFIS+I.

Table 2: ANFIS algorithm parameters

Training epoch number n_{ep}	Training error goal E_{train}	Optimization method
20	0	Last-squares and back-propagation gradient descent

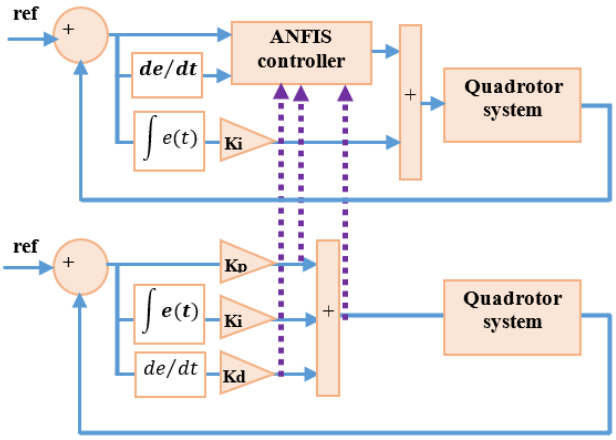


Figure 4: Selection of training data set for ANFIS controller

For this reason, two inputs of each initials controllers (error e , and its rate $\dot{e}$) are used to design the ANFIS controller while the integral action ($\int e(t)$) is maintained in the designed ANFIS controller with the same parameter K_i. Thus, due to the additional integral control, the controller results in a multi closed-loop control structure, which permits obtaining better performance for the quadrotor control system [25].

Furthermore, to enhance the performance of the ANFIS+I controller, three inputs and output scaling gains are added as shown in Figure 5. Then suitable values should be determined for each scaling gain. Specifically, as three scaling parameters should be simultaneously tuned for each ANFIS+I state-controller, in the next subsection, the multidimensional particle swarm optimization (PSO) algorithm is proposed.

3.6. Multidimensional PSO algorithm description

Based on the observation of birds flying, the particle swarm optimization (PSO) metaheuristic algorithm was initiated by J. Kennedy and R. C. Eberhart in 1997 [32]. Thus, the theory of this algorithm is based on the arbitrary choice of particles to design the initial population in a fixed search space [16]. Then, at each new iteration, a different population is selected according to the position and velocity of each particle.

Therefore, as stated by the next equations, the best values of the local and global fitness parameters are computed as follows:

$$\begin{cases} v_{ij}(\mathrm{t}+1) = w\, v_{ij}(\mathrm{t}) + \mathrm{c}_1 r_1 \left(\chi_{1,ij}(\mathrm{t}) - \chi_n(\mathrm{t})\right) \\ \qquad\qquad + \mathrm{c}_2 r_2 \left(\chi_{2,ij}(\mathrm{t}) - \chi_{ij}(\mathrm{t})\right) \\ \chi_{ij}(\mathrm{t}+1) = \chi_{ij}(\mathrm{t}) + v_{ij}(\mathrm{t}+1) \end{cases} \quad (22)$$

where $i = 1 \ldots n$ denotes the particle number of populations, $j = 1 \ldots m$ assigns the parameter to tune in dimension m. c_1 and c_2 denote the cognitive and social constants, respectively. r_1 and r_2 are arbitrary scalars in the interval [0,1]. w is the inertia weight that is used to balance the effect of the previous velocity to the actual value. Thus, at each specific time t, for each particle i in each dimension j, several parameters are to consider: the velocity v_{ij}^t, the position χ_{ij}^t, the local best fitness $\chi_{1,ij}^t$, and the global best fitness $\chi_{2,ij}^t$. Then, to design the four PSO-based ANFIS+I controller, a code was developed using Matlab Environment. The main steps of this code are presented in Algorithm 2.

Algorithm 2: Multidimensional PSO algorithm steps

Result: Optimum parameters

Set the search space, the particles number n, the number of iteration n_{iter};

Repeat:

Generate a random population

Evaluate the objective function

Evaluate the local and global best fitness

Compute the velocity and position of particles according to equation (22)

Until the maximum number of iterations (n_{iter}) is reached

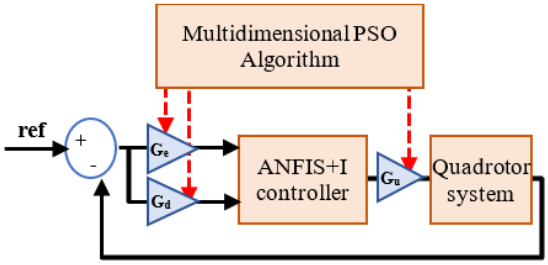


Figure 5: ANFIS+I controller scaling gains tuning using multidimensional PSO algorithm

The objective is to find the optimal values of the PSO-based ANFIS+I scaling gains for each controlled state (x, z, φ, and ψ) (see Figure 5). Then, the optimization algorithm starts by selecting the multidimensional PSO parameters such as the population number (n), the tune dimension (m), the maximum iterations number (n_{iter}), and the search space.

In this work, to reduce the tuning dimension using the multidimensional PSO algorithm, we utilize the same PSO-based ANFIS+I controller for the horizontal position x and y as well, and for the attitude angle φ and θ as well, which permits simplifying the optimization dimension to three scaling factors G_e, G_d and G_u for only four ANFIS+I controllers. Thus, dimension m could be reduced to twelve parameters. Besides, we choose 500 as the population number, 5 as the maximum number of iterations, and [0.1 , 5] as bounds of the search space.

Then, the optimization process starts by initializing a random population p_{ij}, where i ($1 \le i \le n$) represents a population particle, and j ($1 \le j \le m$) denotes the number of tuned parameters. Then, at each iteration k ($1 \le k \le n_{iter}$), the algorithm generates a new population p_{ij} after evaluating the best local and global fitness, which is based on computing two parameters: position and velocity of each particle according to equation (22). Of course, these computations are repeated until the

maximum of iteration number ($i.e\ n_{iter}$) is reached and the smallest value of the objective function criterion is obtained. Thus, the algorithm ends and provides the suitable scaling gains that correspond to an optimal ANFIS+I controller.

3.7. Objective function criterion choice

As described in the above subsection, the multidimensional PSO algorithm role is to optimize the scaling gains of the (four) ANFIS+I controllers, which ends by obtaining a minimum value of an objective function criterion. For this reason, several criteria can be used such as the overshoot (Mp), the settling time (Ts), the rise time (Tr) [20], the integral of absolute error (IAE), the integral of squared error (ISE), the integral of time-weighted squared error ($ITSE$), and the integral of time-weighted absolute error ($ITAE$) [33]. However, IAE and ISE objective function criteria do ignore the time when computing the difference between the desired signal and the actual signal (*i.e,* error e), which could result in high settling time and unacceptable overshoot [34], while $ITAE$ and $ITSE$ objective function criteria do compute the error through the time and allow improving the system performances.

Therefore, in this work, we use the well-known $ITAE$ objective function criterion. Then, for each state, to evaluate the ANFIS+I scaling gains, we consider the $ITAE$ criterion that is defined by:

$$ITAE = \int_0^\infty t|e(t)|\,dt \qquad (23)$$

4. Simulation Results

In this section, the simulation tests are provided to show the efficiency of the proposed PSO-based ANFIS+I controller. For clarity, the quadrotor system parameters are given in Table 3 [4].

To check the robustness of the proposed control strategy, four different controllers are implemented for controlling the quadrotor system.

Table 3: Quadrotor system parameters

Symbol	Description	Value
g	Gravitational acceleration	9.81 m.s^{-2}
m	Quadrotor mass	0.65 Kg
l	Distance from center to motor	0.23 m
j_x	Moment of inertia about x-axis	7.5 10^{-3} Kg.m^2
j_y	Moment of inertia about y-axis	7.5 10^{-3} Kg.m^2
j_z	Moment of inertia about z-axis	1.3 10^{-2} Kg.m^2
k	Propeller force constant	3.13 10^{-5} N.s^2
d	Propeller torque constant	7.5 10^{-7} N.s^2

First, we collect the training data set that is used to design the fuzzy inference system. Thus, the first simulation scenario consists in controlling the quadrotor system by the classical PID control approach. For simplicity, for each quadrotor state ($\varphi, \theta, \psi, x, y, z$), the suitable control parameters are determined using the Matlab PID Tuner. These parameters are summarized in Table 4.

Thereafter, the ANFIS controller is implemented using the data collected from the quadrotor system dynamic response when it is controlled by the PID control approach. In this step, an initial ANFIS controller is designed using the generated fuzzy inference system. Roughly, two MATLAB functions are available: *genfis1*, which returns the initial membership functions set, and *anfis*, which gives the fuzzy inference system.

Table 4: Parameters of PID controller

	x	y	z	φ	θ	ψ
k_p	0.011	-0.011	3.09	0.4	0.4	3.7
k_i	0	0	1.5	0.15	0.15	7.5
k_d	0.12	-0.12	4.5	0.11	0.11	0.56

Then, to improve the ANFIS controller, we kept the initial integral control action in the designed controller, which allows guaranteeing more robustness to the closed-loop system.

In the next step, to improve the quadrotor control system performances, we use the multidimensional PSO algorithm to optimize the ANFIS+I scaling gains ($i.$e G_e, G_d , and G_u). Table 5 gives the value of the obtained scaling gains for each quadrotor state after the optimization process.

Table 5: ANFIS+I scaling gains tuned by multidimensional PSO algorithm

	x	y	z	φ	θ	ψ
G_e	4.82	-4.82	2.21	4.56	4.56	4.26
G_d	0.73	-0.73	1.26	0.36	0.36	2.66
G_u	4.4	-4.4	2.31	0.95	0.95	2.21

For comparison purposes, Table 6 shows the performance results of the four control strategies: classical PID, ANFIS (without the integral control, (non-optimized) ANFIS+I, and multidimensional PSO-based ANFIS+I controllers.

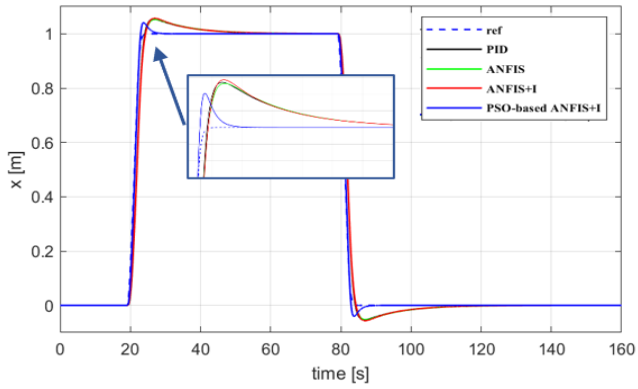


Figure 6: x-state tracking control response

Figures 6, 7, and 8 show the simulation results for x, y, and z quadrotor system states, respectively. The comparison of the four control strategies permits claiming that the PSO-based ANFIS+I controller can provide better control performances than the other control strategies. Except for the altitude (z) rise time, the proposed controller gives the smallest overshoot and the minimum rise and settling times.

For simplicity, the ψ-yaw reference trajectory was chosen to be null. Then, from Figures 9, 10, and 11, it is shown that quadrotor Euler angles, namely (φ, θ, ψ) are very small, which means that the three quadrotor rotational motions are well stabilized.

Table 6: Performances of the PID, ANFIS, ANFIS+I, and PSO-based ANFIS+1

		PID	ANFIS	ANFIS+I	PSO-based ANFIS+I
x	$M_p(\%)$	5.17	5.05	5.47	4.08
	$T_r(s)$	2.9	3.006	3.02	2.4
	$T_s(s)$	26.5	26.7	26.5	15.24
	$ITAE$	1.003	0.99	1.01	0.15
y	$M_p(\%)$	5.17	5.04	5.47	4.08
	$T_r(s)$	2.9	3.006	3.02	2.4
	$T_s(s)$	26.5	26.79	26.5	15.24
	$ITAE$	1.49	1.49	1.5	0.24
z	$M_p(\%)$	6.95	4.04	7.008	0.61
	$T_r(s)$	1.68	1.75	1.68	1.8
	$T_s(s)$	8.23	8.11	8.24	6.05
	$ITAE$	0.47	0.35	0.47	0.10

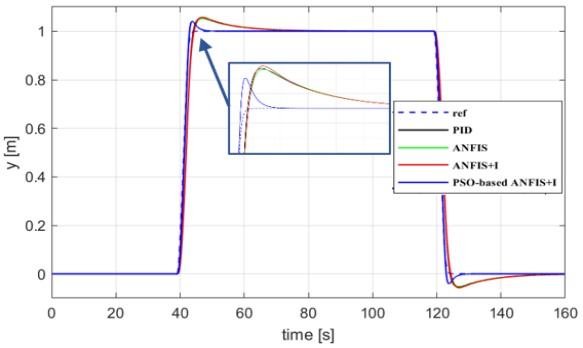


Figure 7: y-state tracking control response

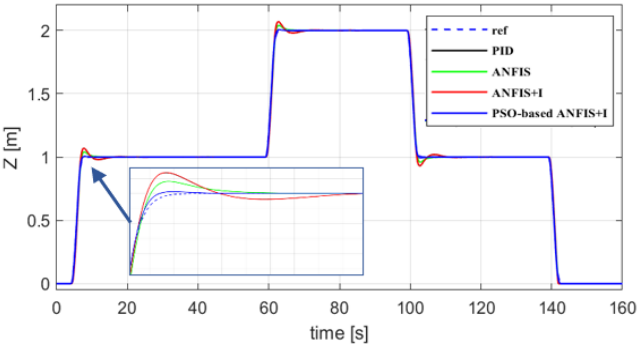


Figure 8: z-state tracking control response

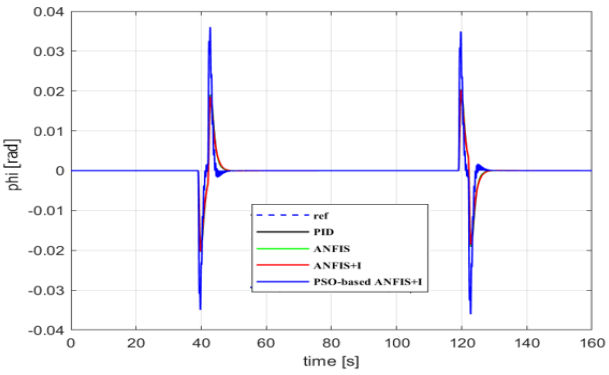


Figure 9: φ-state tracking control response

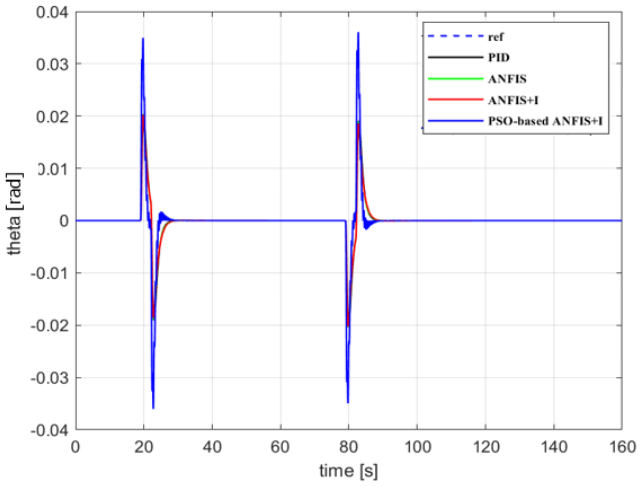


Figure 10: θ-state tracking control response

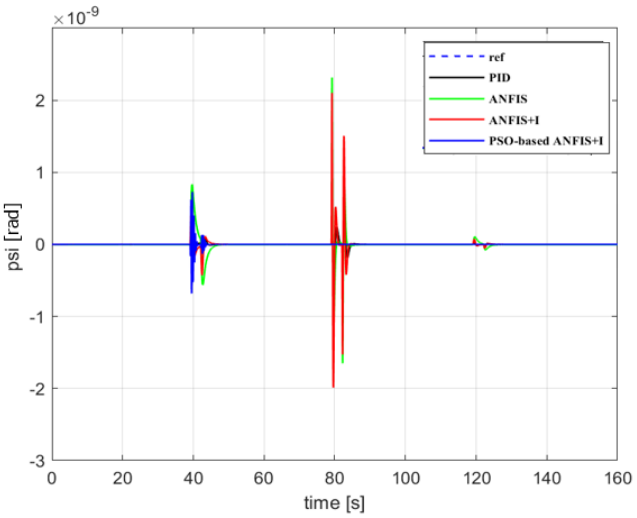


Figure 11: ψ-state tracking control response

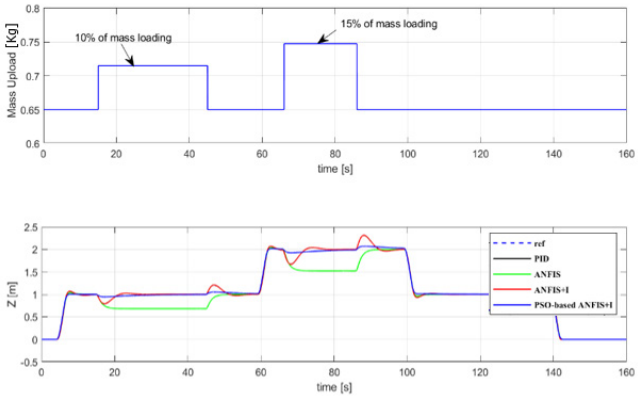


Figure 12: Mass payload disturbance rejection

Besides, additional simulation tests have been performed to evaluate the robustness of the proposed control strategy for the quadrotor system trajectory-tracking. Specifically, a payload mass has been added to the quadrotor system as an (unknown) external disturbance. Then, Figure 12 shows the effects on the quadrotor altitude z of 10% and 15% of total mass change, respectively. It is clearly shown that, in the case of the proposed controller, the fact

that the aerial vehicle's total mass could be modified during the air travel has almost no effect upon the tracking quality. This means that the proposed controller can efficiently compensate for external static-like disturbances.

Then, from the above simulation examples, it results that the multi closed-loop PSO-based ANFIS+I control strategy can ensure the best control performances in comparison with the other control strategies, namely it generates the smallest overshoot and the smallest rise and settling times as well.

5. Conclusion

In this paper, a PSO-based adaptive neuro-fuzzy inference system plus integral (ANFIS+I) control is proposed as a new intelligent controller for the quadrotor trajectory tracking control problem. First, to collect the necessary training data set, a classical PID (tuned) controller is implemented for the quadrotor system. Then, to achieve good robustness, the (initial) integral control action is preserved in the control structure in addition to the generated ANFIS controller. Moreover, scaling gains are added to the ANFIS inputs-output, and optimized using the minimization of the $ITAE$ objective function criterion. Thus, the new control strategy denoted multidimensional PSO-based ANFIS plus integral is designed. To show the effectiveness of the proposed controller, several simulation tests are provided. Namely, in comparison with the traditional PID, the ANFIS controller, ANFIS plus integral control, it is shown that the proposed control strategy can ensure better time-domain performances in case of trajectory tracking problem for the quadrotor system. Particularly, the proposed controller can efficiently compensate for unknown mass modification with the smallest overshoot and good attitude stabilization. Therefore, the multi closed-loop ANFIS+I controller, where the scaling gains are optimized using the multidimensional PSO-algorithm, can be considered as an additional control strategy to solve the position tracking problem for the quadrotor system.

References

[1] U.R. Mogili, B. Deepak, "Review on application of drone systems in precision agriculture," Procedia Computer Science, 133, 502–509, 2018. doi:10.1016/j.procs.2018.07.063.

[2] E. Kaufman, K. Takami, Z. Ai, T. Lee, "Autonomous Quadrotor 3D Mapping and Exploration Using Exact Occupancy Probabilities," in 2018 Second IEEE International Conference on Robotic Computing (IRC), IEEE: 49–55, 2018. doi:10.1109/IRC.2018.00016.

[3] X. Liang, Y. Fang, N. Sun, H. Lin, "Dynamics analysis and time-optimal motion planning for unmanned quadrotor transportation systems," Mechatronics, 50, 16–29, 2018. doi: 10.1016/j.mechatronics.2018.01.009.

[4] S. Bouabdallah, Design and control of quadrotors with application to autonomous flying, Ph. D Thesis, Epfl, 2007.

[5] E. de Vries, K. Subbarao, "Backstepping based nested multi-loop control laws for a quadrotor," in 2010 11th International Conference on Control Automation Robotics & Vision, IEEE: 1911–1916, 2010. doi: 10.1109/ICARCV.2010.5707890.

[6] S. Bouabdallah, R. Siegwart, "Full control of a quadrotor," in 2007 IEEE/RSJ International Conference on Intelligent Robots and Systems, IEEE: 153–158, 2007. doi: 10.3929/ethz-a-010039365.

[7] A. Poultney, P. Gong, H. Ashrafiuon, "Integral backstepping control for trajectory and yaw motion tracking of quadrotors," Robotica, **37**(2), 300–320, 2019. doi: 10.1017/S0263574718001029.

[8] E. Chater, H. Housny, H. El Fadil, "Robust Control Design for Quadrotor Trajectory Path Tracking," in 2019 8th International Conference on Systems and Control (ICSC), IEEE: 21–26, 2019. doi: 10.1109/ICSC47195.2019.8950509.

[9] J.F. Guerrero-Castellanos, N. Marchand, A. Hably, S. Lesecq, J. Delamare, "Bounded attitude control of rigid bodies: Real-time experimentation to a quadrotor mini-helicopter," Control Engineering Practice, 19(8), 790–797, 2011. doi: 10.1016/j.conengprac.2011.04.004.

[10] M. Herrera, W. Chamorro, A.P. Gómez, O. Camacho, "Sliding mode control: An approach to control a quadrotor," in 2015 Asia-Pacific Conference on Computer Aided System Engineering, IEEE: 314–319, 2015. doi: 10.1109/APCASE.2015.62.

[11] M. Huang, B. Xian, C. Diao, K. Yang, Y. Feng, "Adaptive tracking control of underactuated quadrotor unmanned aerial vehicles via backstepping," in Proceedings of the 2010 American Control Conference, IEEE: 2076–2081, 2010. doi: 10.1109/ACC.2010.5531424.

[12] S.A. Raza, W. Gueaieb, "Fuzzy Logic based Quadrotor Flight Controller.," ICINCO-ICSO, 9, 105–112, 2009.

[13] E. Kayacan, R. Maslim, "Type-2 fuzzy logic trajectory tracking control of quadrotor VTOL aircraft with elliptic membership functions," IEEE/ASME Transactions on Mechatronics, **22**(1), 339–348, 2016. doi: 10.1109/TMECH.2016.2614672.

[14] M. Santos, V. Lopez, F. Morata, "Intelligent fuzzy controller of a quadrotor," in 2010 IEEE international conference on intelligent systems and knowledge engineering, IEEE: 141–146, 2010. doi: 10.1109/ISKE.2010.5680812.

[15] H. Housny, H. El Fadil, "New Deterministic Optimization Algorithm for Fuzzy Control Tuning Design of a Quadrotor," in 2019 5th International Conference on Optimization and Applications (ICOA), IEEE: 1–6, 2019. doi: 10.1109/ICOA.2019.8727622.

[16] H. Housny, H. El Fadil, "Fuzzy PID Control Tuning Design Using Particle Swarm Optimization Algorithm for a Quadrotor," in 2019 5th International Conference on Optimization and Applications (ICOA), IEEE: 1–6, 2019. doi: 10.1109/ICOA.2019.8727702.

[17] S. Bansal, A.K. Akametalu, F.J. Jiang, F. Laine, C.J. Tomlin, "Learning quadrotor dynamics using neural network for flight control," in 2016 IEEE 55th Conference on Decision and Control (CDC), IEEE, Las Vegas, NV, USA: 4653–4660, 2016, doi:10.1109/CDC.2016.7798978.

[18] F. Soares, J. Burken, T. Marwala, "Neural network applications in advanced aircraft flight control system, a hybrid system, a flight test demonstration," in International Conference on Neural Information Processing, Springer: 684–691, 2006. doi: 10.1007/11893295_75.

[19] A. Abraham, "Beyond integrated Neuro-fuzzy systems: reviews, prospects, perspectives and directions," School of Computing and Information Technology, Monash University, Victoria, Australia, 2002.

[20] P. Ponce, A. Molina, I. Cayetano, J. Gallardo, H. Salcedo, J. Rodriguez, "Experimental Fuzzy Logic Controller Type 2 for a Quadrotor Optimized by ANFIS," IFAC-PapersOnLine, **48**(3), 2435–2441, 2015, doi:10.1016/j.ifacol.2015.06.453.

[21] S. Rezazadeh, M.A. Ardestani, P.S. Sadeghi, "Optimal attitude control of a quadrotor UAV using Adaptive Neuro-Fuzzy Inference System (ANFIS)," in The 3rd International Conference on Control, Instrumentation, and Automation, IEEE, Tehran, Iran: 219–223, 2013, doi:10.1109/ICCIAutom.2013.6912838.

[22] O. Ghorbanzadeh, H. Rostamzadeh, T. Blaschke, K. Gholaminia, J. Aryal, "A new GIS-based data mining technique using an adaptive neuro-fuzzy inference system (ANFIS) and k-fold cross-validation approach for land subsidence susceptibility mapping," Natural Hazards, **94**(2), 497–517, 2018, doi:10.1007/s11069-018-3449-y.

[23] H.M.I. Pousinho, J.P.S. Catalao, V.M.F. Mendes, "Wind power short-term prediction by a hybrid PSO-ANFIS approach," in Melecon 2010-2010 15th IEEE Mediterranean Electrotechnical Conference, IEEE: 955–960, 2010. doi: 10.1109/MELCON.2010.5475923.

[24] J.P. da S. Catalão, H.M.I. Pousinho, V.M.F. Mendes, "Hybrid wavelet-PSO-ANFIS approach for short-term electricity prices forecasting," IEEE Transactions on Power Systems, **26**(1), 137–144, 2010. doi: 10.1109/TPWRS.2010.2049385.

[25] H. Housny, E. Chater, H. El Fadil, "Multi-Closed-Loop Design for Quadrotor path-Tracking Control," in 2019 8th International Conference on Systems and Control (ICSC), IEEE: 27–32, 2019. doi: 10.1109/ICSC47195.2019.8950659.

[26] H. Housny, H. El Fadil, "PSO-based ANFIS for quadrotor system trajectory-tracking control," in 2020 1st International Conference on Innovative Research in Applied Science, Engineering and Technology (IRASET), IEEE: 1–6, 2020. doi: 10.1109/ICSC47195.2019.8950659.

[27] R. Mahony, V. Kumar, P. Corke, "Multirotor Aerial Vehicles: Modeling, Estimation, and Control of Quadrotor," IEEE Robotics Automation Magazine, **19**(3), 20–32, 2012, doi:10.1109/MRA.2012.2206474.

[28] J.-S. Jang, "ANFIS: adaptive-network-based fuzzy inference system," IEEE Transactions on Systems, Man, and Cybernetics, **23**(3), 665–685, 1993. doi: 10.1109/21.256541.

[29] L.A. Zadeh, Fuzzy sets and applications, 1987.

[30] N. Talpur, M.N.M. Salleh, K. Hussain, "An investigation of membership functions on performance of ANFIS for solving classification problems," IOP Conference Series: Materials Science and Engineering, 226, 012103, 2017, doi:10.1088/1757-899X/226/1/012103.
[31] A. Sadollah, Introductory Chapter: Which Membership Function is Appropriate in Fuzzy System?, InTech, 2018, doi:10.5772/intechopen.79552.
[32] J. Kennedy, R.C. Eberhart, "A discrete binary version of the particle swarm algorithm," in 1997 IEEE International conference on systems, man, and cybernetics. Computational cybernetics and simulation, IEEE: 4104–4108, 1997. doi: 10.1109/ICSMC.1997.637339.
[33] T.K. Priyambodo, A. Dharmawan, O.A. Dhewa, N.A.S. Putro, "Optimizing control based on fine tune PID using ant colony logic for vertical moving control of UAV system," in AIP Conference Proceedings, AIP Publishing: 170011, 2016. doi: 10.1063/1.4958613.
[34] R.A. Krohling, J.P. Rey, "Design of optimal disturbance rejection PID controllers using genetic algorithms," IEEE Transactions on Evolutionary Computation, **5**(1), 78–82, 2001. doi: 10.1109/4235.910467.

Advances in Science, Technology and Engineering Systems Journal Vol. 5, No. 5, 536-549 (2020)

www.astesj.com

ASTESJ

ISSN: 2415-6698

Malware classification using XGboost-Gradient Boosted Decision Tree

Rajesh Kumar *, Geetha S

School of Computer Science & Engineering, VIT University, Chennai campus, 600128, India

ARTICLE INFO

Article history:
Received: 31 July, 2020
Accepted: 06 September, 2020
Online: 26 September, 2020

Keywords:
Malware
Machine learning
Gradient boost decision tree
XGBoost

ABSTRACT

In this industry 4.0 and digital era, we are more dependent on the use of communication and various transaction such as financial, exchange of information by various means. These transaction needs to be secure. Differentiation between the use of benign and malware is one way to make these transactions secure. We propose in this work a malware classification scheme that constructs a model using low-end computing resources and a very large balanced dataset for malware. To our knowledge, and search the complete dataset is used the first time with the XGBoost GBDT machine learning technique to build a classifier using low-end computing resources. The model is optimized for efficiency with the removal of noisy features by a reduction in features sets of the dataset by domain expertise in malware detection and feature importance functionality of XGboost and hyperparameter tuning. The model can be trained in low computation resources at less time in 1315 seconds with a reduction in feature set without affecting the performance for classification. The model gives improved performance for accuracy with the tuning of the hyperparameter and achieve higher accuracy of 98.5 and on par AUC of .9989.

1. Introduction

Most of the cybersecurity issues are related to malware. Malware is malicious software. The first malware, "Morris worm" which is also a virus appeared in 1989-90. Malware is used to collect personal, financial data of a user and give control of ICT (Information Communication Technology) devices mobiles, computers, and systems to command and control centers managed by hacker groups. Malware is at the helm of the cybersecurity issue. The goal of hacker groups or hackers is to make the malware reach the system, network gear, and then use it for their ulterior motives. It may cost millions of dollars if one malware goes undetected [1]. As society becomes increasingly dependent on the computing system, it is important to detect malicious software (Malware). Specific code sequences, signature, executed by a virus are used by antivirus to detect the malware. Finding such code sequences is not matching with the speed at which new malware is being generated with greater use of ICT systems in varieties of areas ranging from individual, business, industrial. Nowadays with the Internet of Things (IoT), Industry 4.0, the use of ICT has grown at a very large rate and so has the attraction of hackers to hack them by use of malware, software with disingenuous intention, such as virus, worm, rootkit, key logger, Trojan horse, ransomware, spyware, etc. To detect this malware using traditional methods such as using a signature base [2] will leave much malware undetected, resulting in security issues. A signature-based approach is used in antivirus software. A signature is set with static and/or dynamic analysis manually to identify the malware. Malware authors keep the same functionality but polymorph the malware. Such polymorphed malware cannot be detected by antivirus as the signature is different. This problem is currently rampant. New polymorphed malware can be detected by a machine learning approach. The signature-based approach is insufficient as millions of new malware appear almost on an everyday basis. A technique needs to be developed that generalizes to new malware. Hence, detection of malware using machine learning is the right choice. Efficient automated malware detectors are required to classify software, application as malware, or benign.

The dataset for malware research is not available publicly due to privacy concerns. Few online databases of malware [3] allow limited use of data. Many malware detection research is done using unbalanced data, the number of malware is very high compared to benign software. There may be discrepancies in malware data collected and that may be possible in a real environment. For effective malware research, one needs the large, balanced recent, and right mix of families of malware database [4]. With a large database with many attributes related to malware, one needs to use

*Corresponding Author: Rajesh Kumar; Email: rajesh.kumar@vit.ac.in

expensive, complex, and high-end computing machines. In this research, we plan to use one such large database [5], which is shared publicly and low computing resources to build a matching or better malware detection system. Here we aim at extracting low dimension, effective features that contribute to learning and result in effective classifiers to detect malware. XGboost using Gradient Boost Decision Tree (GBDT) algorithm is used to extract few effective features from a large database with large attributes. To our knowledge, the complete dataset is not used with the XGboost GDBT algorithm. We use this combination to extract the features, which can be used with low-end computing resource to build effective malware classifier. This paper is organized with a background related to malware detection in section 2, the literature survey in section 3, methodology in section 4, experiments, and results in section 5, and conclusion in section 6.

2. Background

For malware, detection features may be extracted from the file format they are packed in. The executable, libraries, objects are packed using Common Object File Format (COFF). For the Windows operating system, it is Portable Executable 32/64 (PE32/64) [6,7]. It may also be possible to find file agnostic features such as histogram of bytes in the program, byte entropy of various parts of a program [8], or strings available in the program [9]. The string may include URL accessed, registry accessed, deleted, modified, or files accessed, deleted or modified or IP address accessed, files accessed, created, deleted and modified, registry created, modified, and deleted. It may be possible to find a set of features for the detection of malware. A neural network can help achieve a higher-level representation of malware. The sequence classifier takes n bytes, n-gram, as input in [10]. However, it is limited to a few bytes or kilobytes. However, for malware, it may have to take millions of bytes, as the size of executable programs. The efficient extraction of features leads to efficient malware detection. Deep learning models use a complete executable without the need for features from domain knowledge [11]. It takes high-end computing resources and a large amount of time.

2.1. Portable executable

Windows binary consists of PE header [6], code, data, and resource part. The PE header has a COFF Header, optional header, and section tables. Each of these has subparts and further subparts. COFF header consists of 24 bytes and has signature 0x50450000, Machine, Number of sections, TimeDate. The Optional header has a standard COFF field of 28 bytes, windows specific field of 68 bytes, and data directories of 144 bytes data directories. The standard COFF consists of magic, major, minor linker version, size of code, initialized data, uninitialized data, address of entry point, the base of code, data, etc. Windows-specific field consists of image base, section, file alignment, major, minor OS version, major, minor image version, major, minor subsystem version, win32 version value, size of image, header, checksum, subsystem, DLL characteristics, size of stack reserved, commit, size of heap reserve, commit, loader flags, number of RVA and sizes. The data directory consists of various table and size of tables such as location and size Export table, Import table, Resource table, Exception table, Certificate table, Base relocation table, Debug, architecture data, TLS table, Load Config, Bound Import, Import Address Table (IAT), Delay import descriptor, CLR runtime header, Global ptr. Each of the section tables consists of 40 bytes and contains information such as name, Virtual size, and address, location, and size of Raw data, Number of relocations, Number of line number, characteristics. There may be more than one section. Name of sections are .text, .rdata, .data, .idata, .rsro, .rsrc etc. There are several methods to extract these fields. The technique employed here is to use LIEF (Library for Instrumenting Executable Files) [12].

2.2. Techniques used for malware detection

Malware can be detected using a static or dynamic detection method. The Static method [13,14] identifies the malware before the execution of the file and serves as a critical defense mechanism. Static malware detection does not execute the malware and uses the structural information as file format [6, 15] available in applications. One has to identify efficient features to be used to build malware detection systems. If we get information from a binary program using techniques such as Portable Executable 32/64 (PE32/64) header information for windows program. Polymorphic, Metamorphic malware is created by malware authors with minor changes to avoid detection by antiviruses, which uses signature-based detection. In Polymorphism, the malware authors use a combination of data prepend, data append, and encryption, decryption to generate malware in large numbers. In metamorphism, the malware themselves change code by a combination of dead code, code transposition, register reassignment, and instruction substitution can generate a large amount of malware. As the signature changes in polymorphic malware, the antivirus is unable to detect malware. As malware authors use various means to avoid detection such as obfuscated code [16], convoluted systems library calls, detection of malware has a limitation. At times, code is obfuscated by non-standard, private methods [7,16] to make the detection more difficult even by domain experts. Such complexity in detection may be avoided by dynamic malware detection [17-19].

In dynamic malware detection, the application is allowed to run in a protected virtual environment. The application unfolds all the obfuscation, convoluted means of making systems call, and the effects of malware can be observed. For dynamic analysis, the malware cannot be executed on a normal system, as it will infect the system. It has to be run in a sandbox or special customized virtual environment to restore the system to a previous state when the malware was not run. The computational needs are high in a virtual environment or machine. Malware author builds features in malware to detect such a virtual machine environment. Once the malware detects such a virtual environment, the malware changes its behavior and behaves as normal benign software. There have been efforts to avoid the detection of the virtual environment by malware [20, 21]. An expert may declare such malware as benign, which causes unprecedented destruction, loss in a real normal working environment. The dynamic malware detection uses effects caused by malware such as files created, modified, deleted, or registries created, modified, deleted, or network connection set up to specific IP addresses to command and control centers of malware authors or to download next set of malware. It is time-consuming to run the malware in a virtual environment and observe the effects of each malware. Doing this exercise for a large number of malware generated these days due to polymorphism and metamorphism requires a large time and a large number of domain experts. In addition to the challenge of changing the behavior of malware on detection of the virtual environment, both time and domain experts are not available.

Hence, it emphasizes the use of deep learning and machine learning techniques for malware detection.

Deep learning [11, 22-25] and machine learning [5,10, 26-29] has been used to make automated detectors to identify the malware and the family of malware. In most cases dataset used [26] are not available, unbalanced or detectors work with an unavailable specific setting and specific datasets. A private emulation environment is required to overcome challenges imposed by dynamic analysis. It also makes it difficult, as a private, non-public environment is not available. As the data and the parameters used for building models are not available, it is not possible to compare the results, accuracies across the works. Our work uses the open dataset [5]. It is a balanced dataset with 300k malware, 300k benign applications with 2351 hashed features [28,30] derived using LIEF [12] and portable executable file format [6] for training and separate 100k malware and 100k benign software with the same number of hashed feature sets for testing. The statistical summary of benign files is used to reduce the privacy concern. SVM with nonlinear kernel needs O(N**2) multiplication for one iteration. N is the number of samples in the dataset. K-NN needs not only computation at the same level but also all the labels in memory. Hence, these methods are not scalable. Scalable alternatives are the neural network, ensemble decision tree. The ensemble algorithm has been effective with large samples and features. Gradient Boosting Decision Tree (GBDT) algorithm used in XGboost [31, 32], LightGBM [33,34] will be more effective for large dataset with large feature sets. There are multiple times, maybe twenty-plus, improvement in the training process.

3. Literature survey

In [17] author used a list of Dynamic Link Library (DLL) from the PE header and list of functions imported from those DLL as features. Besides, they used few more PE header features as well on a dataset of 4206 samples. It had 3265 malware. They achieved a 97.76 % detection rate. In [13], PE Miner framework, author used 189 features consisting of section size, features from the COFF section, resource table, and import of DLL as binary features. All the features were derived from the PE header. Specific DLL group's functions used for a specific purpose and import of DLL indicates the intent of the software. They achieved the Area Under Curve (AUC) of .991 and False Positive (FP) rate < 0.5% for on dataset of 15000 samples. In [35] author used a dataset of 116000 samples consisting of 100000 malware and remaining benign software. They started with 100 features from the PE header and iterated to finalize of 7 most influencing features. It is also termed as Adobe malware classifier. They achieved a TP rate of 98.56% and an FP rate of 5.68% on 1/5th of the dataset using tenfold cross-validation. The High FP rate is also reported in [5] by using the specified 7 features from the PE header. In [36], SAVE (Static Analyzer of Vicious Executables), author use the API calling sequence of specific identified packed obfuscated malware to find similarity measures with other samples to detect malware. They use Euclidean distance to generate similarity report and detect new malware as one of the families of malware compared with. They use a 32-bit vector consisting of DLL name as 16 bit and each API in a DLL as another 16 bits.

In [37] author extract the behavior attributes of 10 different families of ransomware aggregating to 150 samples. Three different machine learning algorithms J48 Decision tree, KNN, Naive Bayes are used for classification. They use Virustotal [3] to get the behavioral report of each ransomware sample. It is like getting features and their value using the dynamic analysis. They achieve a classification accuracy of 78% by reducing the number of attributes to 12 from 27. In [18] author extract API calls of malware by dynamic analysis method and use fours step methodology to determine suspicious behavior. The suspicious behavior is identified by copy, delete, search, move, read, write, and change attributes operations on a file. They use calling sequence and statistical analysis to identify the malware. 386 samples are used of which 77% were packed using Armadilo, UPX, PE lock, Upack, KKrunchy. In [38] author use Hidden Markov Model using API calls and opcode. All combinations of static and dynamic analysis for the training phase and test phase are experimented such as static analysis data for training and static analysis data for testing, static analysis data for training, and dynamic analysis data for testing. They use 745 malware samples from 6 families of malware and report various AUC-ROC and AUC-PR (Area Under Curve - Precision-Recall) results. In [24], MtNet (A multi-task neural network), author use an anti-malware engine to extract the sequence of API and parameters used in those API and null-terminated objects from system memory. They believe the majority of null-terminated objects are unpacked strings and indicate a code fragment of malware. Many events to one event mapping are performed considering multiple API achieve the same results. Besides API trigram is made for three API calls. 50,000 feature sets are reduced to 4,000 and random projection is used to further reduce the training time of the neural network. Very large size database of 6.5 Million samples used in this project. It has a training data sample of 4.5 million consisting of 1.3 Million malware from 98 families, 1.55 Million generic malware, and 3.65 benign software. The test data is separate 2 Million samples. They experiment with the effects of hidden layers on accuracy and report an accuracy of 99.51% and low FP and FN rate. In [39] author uses dynamic analysis and CNN to build classifiers using 9 families of malware, each with 1000 malware. They achieve 99% Precision, Recall, and F1 score and FPR of 1%. Malware variants of one family have the same type of API calling sequence. Hence, feature image build using color-coding resembles and this similarity of the image is detected using CNN.

In [40] author uses malware image fingerprints using the concept of GIST – Global Image Descriptor to compact image features and store malware in a large database of 4.3 million malware. New malware is pre-processed to compact image features as done with each of the malware in the database and search the database for in 3 seconds to find the matching image. In [41] author used 8 bits of a byte of executable a vector for building a greyscale image of fixed width. Image visualization of the binary value of executable gives more information about different sections and structures of malware. Even change in small code from polymorphed, meta morphed malware may also be identified as some pattern, change in the pattern of the image. They achieved 98% malware family classification accuracy using a dataset of 9,458 samples of 25 different malware families. Signal processing techniques are used to get noise-free signals in other areas of electronics. In [42] author use these techniques to get a noise-free signature of polymorphic malware to detect malware. They have used 1.2 Million samples consisting of

packed and unpacked malware and good ware. The trained model is used for recent daily malware. They can detect 50% malware with 99.5% accuracy. In [43] author observes the malware can be hidden by steganography in image or audio files. Such images, audio, maybe part of many websites. 2019 Symantec threat intelligence report identifies one in 10 websites as malicious. A Hybrid of image visualization and dynamic analysis feature is used in [44]. Features of images from packed malware are extracted using a pre-trained CNN model and visualized using t-Distributed Stochastic Neighbor Embedding (t-SNE). Besides, API calls sequences derived from the deobfuscated program code of each sample are used to compute eight different distance metrics such as Manhattan, Cosine, Bray-Curtis, Canberra, Hamming, Euclidean, Correlation, and Chebyshev. SVM with four different kernels uses the distance computed between known and unknown samples to detect malware. They report 98.6% accuracy.

In [25] author attempts deep learning for features extracted using dynamic analysis. The malware family is identified using 60 kernel APIs and a sequence of calls as a feature from dynamic analysis. Convolution and LSTM were used for malware detection.

A comparison with the n-gram model is a suboptimal approach [26] as the malware author may manipulate the n-grams and it will make the feature disappear. Just a single byte change can make the feature disappear from consideration in the model. The model is built on a PE header and there was a difference in performance. It is explained as a feature used across the model was different, resulting in a difference in performance.

Whole program files as malware or benign are used as input in [11] and referred to as Malconv. Malware as an executable is very large data to feed in a deep learning model compared to other uses of deep learning. It does it to prove that the required features will be extracted using deep learning without domain expertise. The architecture of Malconv uses Convolution Neural Network architecture (CNN). The malware may have high positional variation at the PE32 header information, location variance due to macro-level reordering of function at code section leading to macro-level reordering in binary to polymorph the malware or to avoid detection of malware. The architecture of Malconv takes care of a high amount of positional variations and location variance in a file by a mandatory combination of CNN architecture and global max pooling. Global max pooling is an enhancer of CNN. For independent feature location, global max pooling is done before a fully connected convolution layer. It can make a model regardless of the location of features in the file. Hence, it addresses the activation of features irrespective of the location of features. Raff observed batch normalization made the model not to learn due to discontinuity at function level and missing correlation across large ranges. It uses a wider breadth of input patterns with embedding and shallow CNN.

Deep learning has dramatically improved the state of art in object classification. It infers the most useful features representation for the task such as by raw images, text, or speech waveforms as input to the machine-learning model. However, image processing, signal processing techniques in machine learning cannot be applied to the malware domain. CNN is used to be in line with a high level of location in variations. The holes in dilated convolution can be interpolated for spatially consistent image processing, but does not apply to or can be interpolated for malware detection. This error signal is easily missed with the nature of malware available in real life.

However, handcrafted features continue to give improved results for malware detection as per publish literature [5] and we also find the same. There is a constant emergence of new malware in large numbers by minor changes in existing malware. Besides, new techniques are discovered to use the vulnerabilities of hardware and software at different levels. These new techniques and vulnerability at different levels in hardware and software require the expertise of domain knowledge and difficult to fulfill by deep learning. The structured format of PE continues to make handcrafted features as relevant even if state or art shifts to end deep learning in the future. It will be good to combine the use of broad handcrafted features and deep learning.

There is a lack of public datasets for comparison with other machine learning techniques used. Hence, the results obtained remain applicable to that study and cannot be extended to other datasets. A comparison has been done in [5] and the J48 adobe malware model [35] to get an 8% False Negative Rate (FNR) and 53% False Positive Rate (FPR).

4. Methodology

We select XGBoost [32], a GBDT implementation, and a publicly available dataset [5] to build the classifier that can operate on a low complexity computation machine to give matching or better results.

Ember dataset is large data with a separate training set and test set. Both the training and test set have balanced (equal) malware and benign software. Each sample in the dataset has a large number of features from PE header which are file form type. The data has file form agnostic features also. These file form agnostic features are derived from the whole file and non-PE header part. We use XGBoost to extract useful features that contribute to building an efficient model for malware classification. These selected, reduced feature sets bring down the complexity of computation. These reduced feature sets are used to build a classifier using the XGBoost algorithm. A comparison is performed to demonstrate the performance of such a classifier.

4.1. Gradient Boosted Decision Tree (GBDT)

Boosting is a process in which a weak learner can be modified to become better. It makes a poor hypothesis into a very good hypothesis. The focus is on developing new weak learner that can handle remaining difficult observations. New weak learner focusses on training difficult to classify instances, patterns and get added to the previous weak learner. Weak learners are used successively, equation (1) to get a series of hypotheses. Each hypothesis is focused on the sample examples that have not been covered by the previous hypothesis or have been misclassified the sample. Hence, a weak learner is better than a random choice. The boosting has it's beginning in adaptive boosting that puts more weight on data points that are not classified, misclassified, or hard to predict. It puts less weight on instances already classified. The weak learners are sequentially added to classify the unclassified patterns. In other words, difficult instances keep on getting higher

$$z_i^{(0)} = 0$$

$$z_i^{(1)} = f_1(x_i) = z_i^{(0)} + f_1(x_i)$$

$$z_i^{(2)} = f_1(x_i) + f_2(x_i) = z_i^{(1)} + f_2(x_i)$$

$$z_i^{(t)} = \sum_{k=1}^{t} f_k(x_i) = z_i^{(t-1)} + f_t(x_i) \quad (1)$$

$$obj^{(t)} \simeq \sum_{i=1}^{n} \left[l\left(y_i, z_i^{(t-1)}\right) + g_i f_t(x_i) + \frac{1}{2} h_i f_t^2(x_i) \right] + \Omega(f_t) + c \quad (2)$$

where

$$g_i = \partial_{z(t-1)} l(y_i, z^{t-1}), h_i = \partial^2_{z(t-1)} l(y_i, z^{t-1})$$
$$\Omega(f_t) + c \quad (3)$$

$$\Omega(f_t) = \gamma T + \frac{1}{2}\lambda \sum_{j=1}^{T} \omega_j^2 \quad (4)$$

weightage until it is classified. It follows an accurate prediction by using a moderately inaccurate rule of rough and moderate heuristics. Adaptive boosting is upgraded to Adaptive, Reweighing, and Combine (ARC) algorithm. It re-computes the classifier and weighted inputs. Next, this was put into a statistical framework for numerical optimization to minimize the loss model by adding the weak learner and using the gradient descent procedure to make a gradient boosting machine. As one weak learner is added at a time there are two approaches, Stage wise additive model and Stepwise additive model. In the stage-wise additive model, the weak learner remains unchanged, frozen as new weak learners are added.

In the stepwise approach, the previous weak learners are readjusted on the entry of new weak learners. A decision tree is used as a weak learner in gradient boosting. It may have decision stumps or larger trees going up to 4 to 8 levels. The weak learners are constrained by the maximum layer, number of nodes, maximum number of splits, maximum number of leaf nodes. It follows a stage-wise additive approach in which existing trees are not changed and one tree is added at a time greedily. The best split points are divided on the gain index or to minimize the loss. A gradient descent model minimizes the loss while adding the trees. In general, the gradient descent is used to minimize a set of parameters e.g. the coefficient of a regression equation or weights in a neural network. The loss or error is computed and the weights are updated to minimize the error. Various differentiable loss functions such as classification error, an area under curve, logarithmic loss, mean square error, mean error, etc. may be used for binary or multiclass classification. Here we have the weak learner as sub-models in place of parameters. After calculating error or loss add a tree to reduce the error. This adds a tree to reduce error is like applying gradient descent boost procedure. This is done by parametrizing the tree. The parameters of the tree are modified to reduce the loss function. This is called gradient descent with function or functional gradient descent.

Gradient descent in functional space is used to find the weighted combination of classifiers. The type of problem guides the use of a loss function. One can select a loss function depending on the problem under consideration.

The function must be differentiable. The loss functions selected for this problem are classification error, area under curve, logarithmic loss. A new boosting algorithm is not required for each loss function. The framework is generic such that any differentiable loss function can be used. Area Under Curve (AUC) [45] is a good parameter for comparison in machine learning performance and is used here. It is invariant to the classification threshold, giving quality of prediction irrespective of the threshold chosen. Besides, it is scale-invariant. Predictions are made by majority votes of weak learners and weighted by individual accuracy. Another parameter used for the performance efficiency of the classifier is logloss. Logloss is one of the performance parameters used in [27].

Gradient boosting is a greedy algorithm. The dataset can quickly overfit the model. Regularization method equation (3) penalizes various parts of the algorithm and improves performance by reducing overfitting. It makes the model more general. The weight of the leaf node may be regularized using regularization functions such as L1 (linear average), L2 (squared mse) regularization of weights. This additional regularization helps smooth the final learned weight to avoid overfitting.

4.2. XGboost GBDT

XGboost, Extreme Gradient boosting, uses a gradient boosting decision tree algorithm. XGboost is designed for speed and performance. It has an engineering goal to push the limits of computational resources, for boosted tree algorithms. There are a variety of interfaces to access XGboost such as C++, Python, R, Java, Scala, etc. In this work, we have used the python interface. Data structure and algorithms use cache optimization for better efficiency. The algorithm uses the efficiency of computation time and memory resources. It makes the best uses of resources to train the model. It automatically handles the missing values in the dataset but not applicable to the dataset used here. We can further boost the existing model with new data by further training. It is fast compared to other implementation of gradient boosting benchmarking random forest implementation. It is memory efficient, fast, and of high accuracy.

Existing models are boosted with a new model to reduce the error made by the existing model. The sequence of addition continues until the error is reduced to the required level or the number of addition in the model has reached the constraint set. In gradient boosting machine, new models are added for using residual or error data points to make final predictions.

In Equation (1) symbol z_i is the prediction for i th input. In the beginning, round 0, there is no prediction. In round 1 equation (1) prediction is by $f_1(x_i)$ [32, 46]. More trees are required in a model if there are more constraints for trees. Similarly, less constraint on trees requires less number of trees. For a good model,

$$obj(t) \simeq \sum_{1}^{n} \left[g_i f_t(x_i) + \frac{1}{2} h_i f_t^2(x_i) \right] + \gamma T + \frac{1}{2}\lambda \sum_{j=1}^{T} \omega_j^2 \quad (5)$$

$$obj^{(t)} \simeq \sum_{j=1}^{T} \left[\left(\sum_{i \in I_j} g_i \right) \omega_j + \frac{1}{2} \left(\sum_{i \in I_j} h_i + \lambda \right) \omega_j^2 \right] + \gamma T \quad (6)$$

$$obj^{(t)} \simeq \sum_{j=1}^{T} \left[A_j\, \omega_j + \frac{1}{2}\left(B_j + \lambda\right)\omega_j^2 \right] + \gamma T, \quad (7)$$

$$here\ A_j = \sum_{i \in I_j} g_i\ , B_j = \sum_{i \in I_j} h_i$$

there must be a weak learner with skills but should remain weak. The model over fits as more and more trees are added. Hence, trees should be added only until no further improvement in the model is there. Shorter trees in depth are preferred, as deeper trees make the weak leaner stronger and they are no weaker. Several nodes constraint the size of the tree. The tree is not symmetric if other constraints are used. Another constraint on adding a tree may be a minimal improvement to loss function at any split added to a tree. The learning rate of trees can be set by weight assignment to each tree which finally leads to predictions. The combination of each tree can be weighted and added for predictions. There is a trade-off between the learning rate and the number of trees. If the learning rate is low, more trees need to be added, and take longer to train the model. The shrinkage, learning rate, reduce the influence of each tree so that in future better trees can be added. It gets name gradient boosting because it uses a gradient descent algorithm to reduce the loss to a minimum when adding a new model. With each addition of a new model, the prediction keeps on improving. From (1) using Taylor expansion the objective of the gradient descent model in a boosted tree is given in (2). (2) Includes the regularization (3) for generalization of the tree [36, 49]. In XGboost, the regularization objective will select a model that has simple prediction functions. Equation (5) is derived from (3). Equation (6) is concerning the number of trees. Equation (8) gives the roots of (7). Using the roots solution of (7) is in (8). As we split the tree on the left and right side, it can be written as (10). A_L, B_L are weights of the leaves on the left side of the tree, and A_R, B_R is weights of the leaves in the right [46]. To optimize the cost of the final output of the model, the output of the new tree is added to the output of the existing sequence of trees. This process is followed until the loss reaches to required one or keeps adding the member of trees until the maximum number of add is reached. The loss keeps reducing as more and more trees are added and stops at the maximum number of trees are reached. It is also described in Algorithm1.

$$\omega_j^* = -\frac{A_j}{B_j + \lambda} \tag{8}$$

$$f(obj) = -\frac{1}{2}\sum_{j=1}^{T} \frac{A_j^2}{B_j + \lambda} + \gamma T \tag{9}$$

$$Gain = \frac{1}{2}\left[\frac{A_L^2}{B_L + \lambda} + \frac{A_R^2}{B_R + \lambda} + \frac{(A_L + A_R)^2}{B_L + B_R + \lambda}\right] - \gamma \tag{10}$$

Algorithm1: XGBoost GBDT Algorithm

Input: Dataset

Output: XGBoost GBDT Model

1. Each iteration adds a tree. Start with a tree of depth 0.
2. Compute g_i, h_i from (2) A_j, B_j from (7)
3. Add a split for tree
   A. Rules for split finding and adding split
   B. Enumerate over all the features
   C. For each node, Enumerate over all the features
   D. For each feature, sort the instances by the feature value
   E. Use a linear scan to decide the best split along with the feature
   F. Take the best split solution along with all the features by Computing the gain as in (10)
4. Stop if the gain is negative
5. Continue the steps to max depth = 3 (default)
6. $z_i^{(t)} = z_i^{(t-1)} + f_t(x_i)$
7. $y_i^{(t)} = y_i^{(t-1)} + \varepsilon f_t(x_i)$
8. $\varepsilon = .1$ Learning rate or shrinkage by a tree, one weak learner

Repeat the steps 1-6 for adding more tree until n_estimator = 100 (default)

4.3. Time Complexity

For GBDT time complexity is O(nfd log n). O(n log n) is time complexity to sort n samples. There are several features and levels of depth of the tree. This needs to be done for each feature and depth level. The default max_depth in XGBoost GBDT is 3. Using GBDT it can be further optimized using approximation or caching the sorted features. Hence, it can scale to a very large dataset and features. In machine learning, nonlinear SVM kernel needs O(N**2) multiplication during each iteration, and with a large dataset pursuing the method brings resource constraints in terms of computation, memory, and time taken to train the model. K-NN needs not only computation but storage of all the label samples during prediction and not scalable.

5. Experiments and results

5.1. Dataset

We use the EMBER [5] dataset consisting of 1.1 million entries with a label for malware, benign, and some parts left as unknown. The Dataset has a training set for 900K samples and an exclusive separate test set for 200K samples. The training data set is balanced with 300K malware, 300k benign, and 300k entries left as unlabelled. The test data set has 100k malware and 100k benign entries. The equal number of malware and benign in training and test makes this dataset a balanced dataset for building a good classifier to classify the malware. The balanced test set further adds to good testing. Many datasets used in malware classification are unbalanced and prone to erroneous results. Each of the entries has 2351 feature sets taken from software that may be malware or benign. The features are from PE header (General

Table 1: Data Set Used

Sl n.	Label type	Malware	Benign	Unknown/Unlabelled
1	Training data set	300K	300K	300K
2	Test data set	300K	100K	0

(COFF), Optional header, and sections), API called by them from various DLLs. Some of the features are from file agnostic such raw byte histogram, byte entropy, and strings embedded in the software. Table 1 summarizes the datasets.

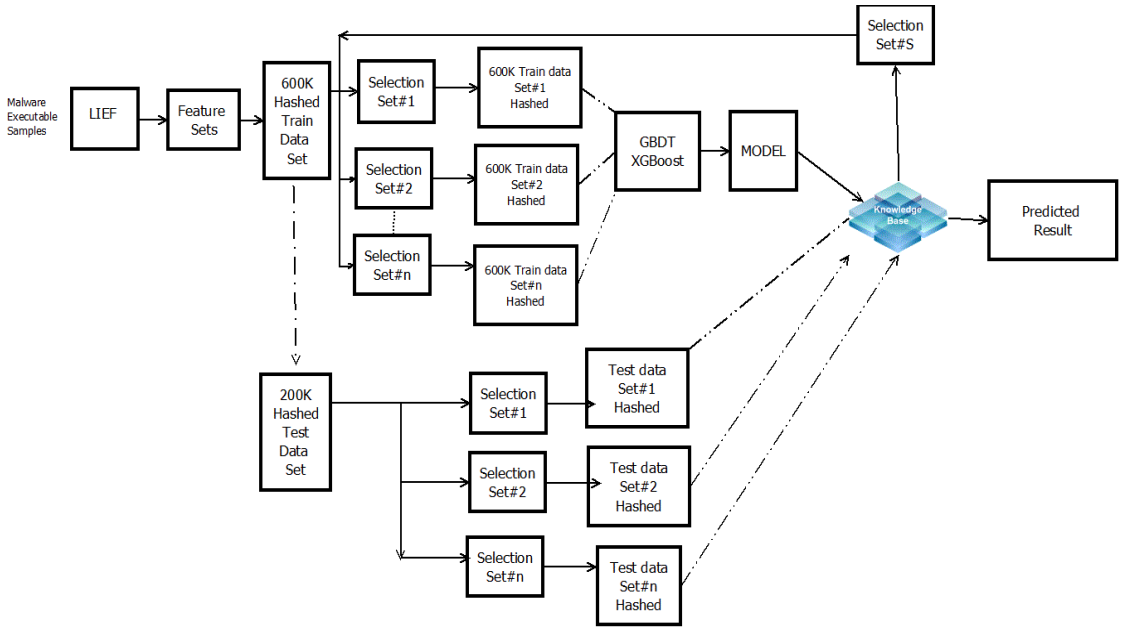


Figure 1: Systems Block for selection data

5.2. Experiment design

The objective of the proposed work is to build a classifier with low computing resources and achieve improved or comparable accuracy, AUC using XGBoost classifier for the large data set. We tried to reduce the features in using the following four experiments.

- Experiment Part1: Subdivide the feature sets based on a few parts of the PE header.
- Experiment Part2: Subdivide the features sets based on file form agnostic part.
- Experiment Part3: Use domain knowledge to eliminate a few features.
- Experiment Part4: Feature importance associated with building the GBDT.

Low-end compute machine with an i5 processor, 8 GB RAM with Windows 10 is used for various training and testing.

Experiment design Part1, Part2

Figure 1 shows the block diagram for this research. Feature sets can be derived from executable of any operating system in various formats using the LIEF library. The features sets include API calls, DLLs, and PE header fields. More file form agnostic features may be added. If the number of features for a part is very large in number. They can be hashed or one hot encoded as may be required. All these hashed, hot encoded make 2351 features in the dataset[1]. All the features are categorized and identified in many sets such as set#1, set#2, … set#n. The Dataset has 600K samples training sets and separates 200K samples in the test set. These samples are balanced for malware and benign software. For each sample in the training dataset and test, dataset identified features are used to make a sub dataset. These sub-datasets are used with the XGBoost algorithm to build a model and to build the knowledge base. Test sub-datasets are used for testing the model and compare the results.

Table 2: datasets for selection set#1 to set#6

Sl. no	Description	Train	Test	No. of features
1	Rawbyte histogram	300k Malware 300K Benign	100k Malware 100K Benign	256
2	Byte entropy	300k Malware 300K Benign	100k Malware 100K Benign	256
3	Strings,	300k Malware 300K Benign	100k Malware 100K Benign	104
4	Strings, General(COFF),Optional Header, Section	300k Malware 300K Benign	100k Malware 100K Benign	431
5	Imports_of_-API with DLL	300k Malware 300K Benign	100k Malware 100K Benign	1280
6	Exports_of API	300k Malware 300K Benign	100k Malware 100K Benign	128

The feature sets in the dataset [5] are broadly divided into information from the file format of executable and file format agnostic features of executable. The file format for executable is from PE header [6-7, 15, 47]. They are having five groups General (COFF), Optional Header, Sections, API Imports, and API Exports. The file format agnostic features are in three groups such as raw byte histogram, byte entropy histogram, and string extraction. Each of the groups is hashed into a fixed number of bins. The groups have been identified to eliminate noisy features. A significant amount of domain expertise is required to perform the feature engineering. The contribution of various features in the detection of malware will be divided into six parts as per the PE header, and file form agnostic part. Three of these will be based on file form agnostic parts and three will be based on the PE header part. The regrouping is selected based on domain knowledge of malware. In [23] author has used entropy for building classifiers. Besides, [8] were the motivation to use group 1 and 2. The strings features alone can give a better classifier. Hence, one, group#3 is made for strings alone. In [39] author had

used 7 features from the general and header part of the PE header. These features were used in [5] and did not give good performance in their experiment. Hence, another group of larger features is made of strings, General (COFF) part of PE header, optional header, and section part from PE header. Many researchers have used imports of API along with DLL [18, 26, 50]. The malware tends to export its API rather than using the API from standard DLL. This aspect prompted us to use group#6. Datasets will be reorganized as per groups identified. The regrouping is done to build an efficient classifier model for predictions considering the computation power, low memory. This will generate multiple datasets as a subgroup of original datasets. The model needs to be built for each selectionset# of a dataset for comparison. The datasets are reorganized as following and details in Table 2.

1. Raw byte histogram
2. Byte entropy
3. Strings extracted
4. Strings Extracted, General(COFF), Optional Header, Sections
5. Imports of API with DLL
6. Exports of API

Each group identified above are selectionset#1, selectionset#2, selectionset#3, selectionset#4, selectionset#5, selectionset#6. This sub section covers the first two bullets identified in the methodology section.

Experiment design Part3

Each of the executable, applications has MZ as the signature in the first word of PE header as per PE format. There should be only one MZ in an executable. If there is more than one MZ string in an executable, it may indicate the executable has embedded more application or program as obfuscated code and indicate a malware. Hence, it was predicted that the feature that represents more than one "MZ" signature string in a dataset, the feature will contribute to efficient malware prediction.

Experiment design Part 4

XGboost gives feature importance while building the model. The relative importance of a feature is higher if it used more time to make key decisions in building a gradient boosted decision tree. This attribute can be ranked and compared with each other. There is an explicit calculation for each feature in the dataset for a model made using XGboost. There are more ways in which feature importance may be computed such as improvement in performance measure at each split point, and many rows, samples, covered at each split point. The performance measure is averaged for all the decision trees in the XGboost model. Figure 2 shows the block diagram for building a classifier model using the selected features that contribute to building the tree in previous experiment part 1, and 2. The selected features, contributing to building the model, will be used to make separate the train and test select datasets. The dataset will have only the important features identified while building the XGBoost model in the previous experiment. This updated dataset will be used to build the XGBoost GBDT model again and the performance will be compared. It is expected that this updated model build using selected features should be more efficient in terms of computation resources, faster and yield higher performance results.

The feature importance of the model made using the base data set was compared and it was found that only 276 features among 2351 hashed features contribute to making the model. The rest of the hashed feature 2351 – 276 = 2075 features do not contribute to making the model. A new select dataset was constructed using the 276 hashed feature that contributes to the building model. The remaining 2075 hashed features with zero contribution, representing noise, were excluded from the select dataset. Table 3 shows the dataset built using block model as in Figure 2 and used for experiment part 4.

Table 3: Datasets for Selected Important Features

Description	Train	Test	Number of features
Selected Important Features	300k Malware 300K Benign	100k Malware 100K Benign	276

Table 4 lists all the 276 important features derived from experiment part 1 and experiment part2. The file form agnostic features Histogram of bytes in the executable, 2-dimensional byte entropy for executable, and the string are hashed. Hence the index of these three features is listed in the table. The COFF features, Optional header features that could be identified along with their indexes had been identified and named in the table. Few of the PE header section features are identified which are not hashed. The API imported and API exported are hashed and specific API and DLL cannot be identified. Among the 276 features that contribute to making an efficient model, there were features from all groups. But there was no feature from the export group of feature sets.

All the 128 hashed features derived from the export group of features were noisy. It also confirms the observation as in Table 2 for Set #6 feature which represents export system call features in a hash bin.

5.3. Experimental results

Results Experiment part1, part2

Models are built using XGboost for each regrouped datasets and compared for prediction efficiency. The prediction efficiency is measured in terms of accuracy, area under curve, and logloss. The results are tabulated in Table 5.

It was expected that group4 with strings extracted, general(COFF), header, and section regrouped dataset will be highly efficient as these parameters contribute more to the identification of malware in manual static analysis. This proved to be true with the experimental results is given in Table 2. The AUC is very close to the overall AUC of the base dataset and the accuracy part is less than 3% down from the base dataset with the number of features reduced to 431 from 2351. With all 2351 features with XGBoost, the accuracy was 97.09. Compare this with 431 selected features the accuracy is down <2%. It demonstrates the subgroup of features was nearly equal to the full features of the dataset. The performance of the model using the exports part of the regrouped dataset was very poor and was excluded from further experiments. Group#4 with Strings, General(COFF), Optional Header, and Sections have the highest accuracy among all the groups of regrouped feature sets.

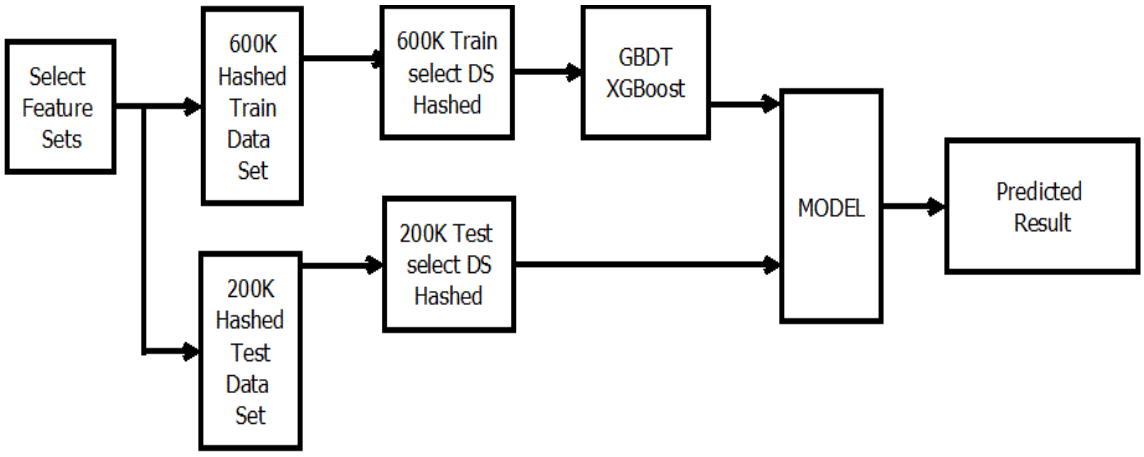


Figure 2: Model Block diagram using XGBoost feature importance

Table 4: Index of Selected 276 Import Features

Description	Number of features	Index number of features
Raw byte histogram	66	1, 2, 3, 6, 10, 15, 19, 21, 22, 27, 29, 31, 32, 33, 35, 37, 40, 41, 43, 45, 46, 50, 54, 63, 64, 65, 66, 68, 69, 74, 76, 88, 89, 90, 93, 95, 105, 106, 107, 111, 112, 113, 116, 123, 125, 128, 131, 133, 135, 181, 182, 196, 198, 199, 204, 209, 214, 217, 218, 219, 223, 231, 239, 245, 253, 255
Byte Entropy	46	256, 303, 312, 318, 326, 328, 335, 338, 357, 360, 362, 372, 373, 375, 377, 378, 385, 386, 388, 389, 392, 396, 399, 401, 410, 411, 413, 417, 426, 431, 447, 456, 457, 464, 466, 470, 472, 494, 498, 499, 502, 504, 508, 509, 510, 511
Strings	34	512, 515, 521, 529, 530, 531, 532, 533, 534, 543, 551, 552, 553, 554, 558, 562, 570, 578, 583, 588, 589, 596, 597, 600, 601, 602, 604, 605, 606, 611, 612, 613, 614, 615
General (COFF)	6	616(size), 617(v size), 618(has debug), 619(exports), 620(imports), 623(has signature)
Optional Header,	16	626(Time Stamp),632(Machine), 637(characteristics), 640, 654(subsystem), 655, 658(DLL characteristics), 660, 677, 678, 679, 680, 681, 682, 683, 685,
Sections	27	688(name of section),689(size), 691(v size), 692(properties), 693(section size), 707, 712, 734, 736, 748(section entropy hash), 770, 771, 775, 784, 785, 786, 797(section v size hash), 798, 803, 825, 827, 834, 836, 843, 906, 930, 940
Imports of API with DLL	81	951, 954, 986, 994, 1011, 1043, 1060, 1073, 1162, 1190, 1197, 1225, 1254, 1263, 1303, 1309, 1312, 1316, 1342, 1343, 1360, 1362, 1366, 1377, 1387, 1388, 1396, 1399, 1404, 1445, 1451, 1455, 1476, 1482, 1484, 1505, 1526, 1545, 1546, 1597, 1629, 1656, 1663, 1685, 1689, 1693, 1704, 1712, 1724, 1756, 1773, 1775, 1799, 1807, 1815, 1836, 1886, 1892, 1901, 1949, 1969, 1973, 1991, 2004, 2006, 2018, 2034, 2047, 2052, 2078, 2083, 2097, 2110, 2114, 2125, 2140, 2159, 2180, 2184, 2188, 2210
Exports of API	0	

It was used for further enhancement by hyperparameter tuning of n_estimator. n_estimator hyperparameter in XGboost is cunt of trees to fit. It is also number epochs the algorithm is run to add a tree until the number of trees reaches n_estimator count to further improve the accuracy[14,36] of the model. The default value of n_estimators is 100. For group 4, Figure 3 shows classification error, Figure 4 shows area under the curve for n_estimator =100 and Figure 5 log loss with n_estimator=100. It shows that the model is not overfitting and has room for improvement. Hence, further hyperparameter tuning is done for group4, selectionset#4, with n_estimators = 200, 300, and thereafter with 400.

Table 5: Comparison of Prediction Efficiency for Regrouped Data

Sl no.	Name of datasets	Accuracy	AUC
1	Raw byte histogram	93.28%	.978743
2	Byte Entropy	90.69%	.967944
3	Strings	92.2845%	.97618
4	Strings, General, Optional Header, Sections	95.4405%	.992099
5	Imports of API with DLL	92.05%	.977229
6	Exports of API	58.8985	.597902
7	Base dataset with LightGBM[1]	98.162%	.999112
8	With All features as in Base dataset	97.09	.99571

Table 6: Group 4 Performance Parameter

Sl n.	n_estimator	Accuracy	AUC	logloss	Classification error
1	200	96.537%	.995015	.10523	.03462
2	300	97.07%	.996472	.08768	.02713
3	400	97.49%	.997261	.07675	.02445

Table 6 shows the improvement in performance parameters for accuracy, AUC, and logloss. The accuracy and AUC for group4 with merely 431 features are comparable to the performance of the base dataset with 2351features. Figure 6 shows classification error, Figure 7 shows AUC, and Figure 8 shows log loss for n_estimator=400. Table 6 shows the accuracy and AUC for n_estimator 200, 300, 400. The accuracy for just 431 features is 97.495 higher than the accuracy with all the 2351 features 97.09 %

using XGBoost with n_estimator = 400. Further feature selection has been done that matches the performance of the base dataset or improves in some performance parameters for classification.

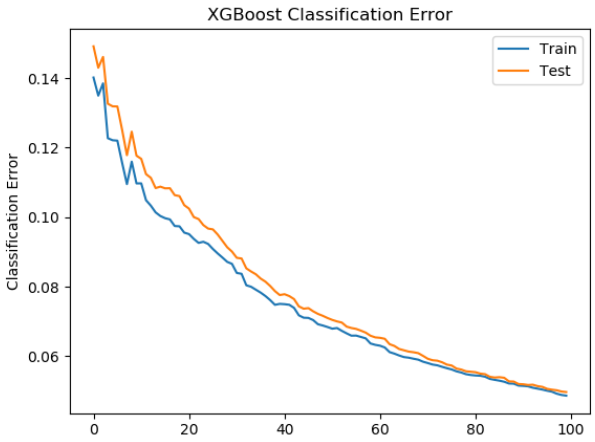


Figure 3: XGBoost classification Error for n_estimator = 100

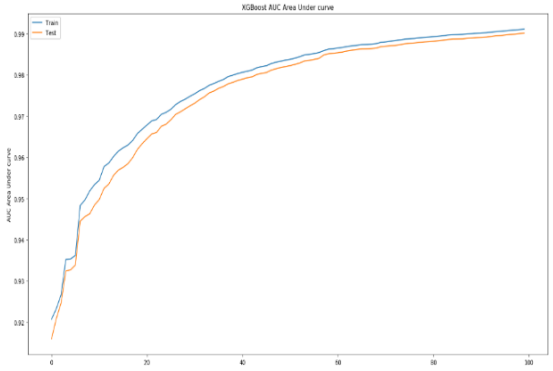


Figure 4: XGBoost AUC for n_estimator = 100

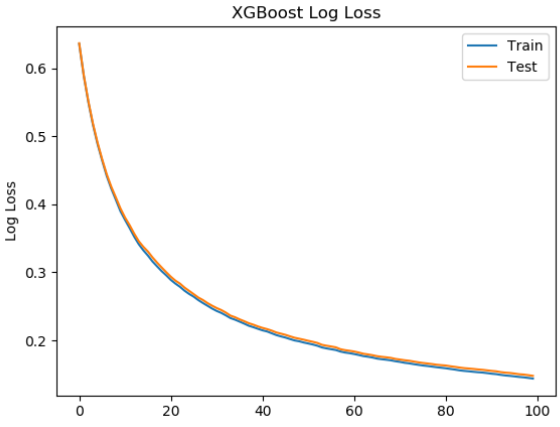


Figure 5: XGBoost Logloss for n_estimator = 100

Results Experiment part3

Inclusion or exclusion of features representing more than one MZ had no effects on prediction efficiency. On further investigation using the SHA-256 signature at virustotal [3], it was found that benign application may package up to 32 executable for software upgrade purposes

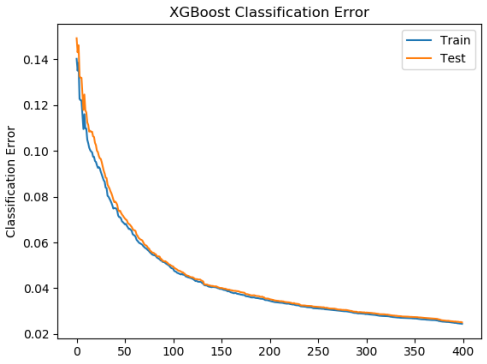


Figure 6: XGBoost classification Error for n_estimator = 400

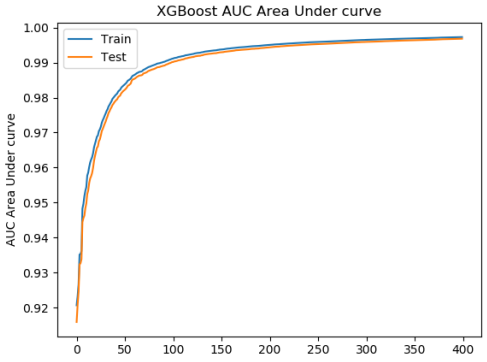


Figure 7: XGBoost AUC for n_estimator = 400

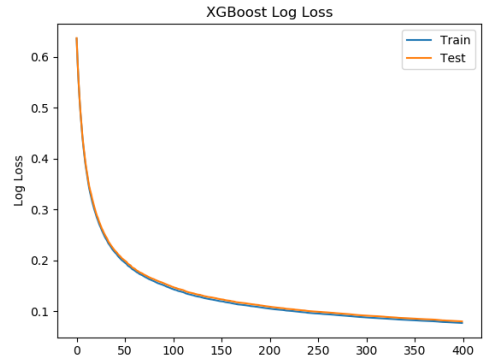


Figure 8: XGBoost logloss for n_estimator = 400

Results Experiment part4

A model was built with these selected 276 features and prediction efficiency were explored. The accuracy, AUC, and logloss parameters for the n_estimators 600 are tabulated in Table 5 and compared with base datasets. The accuracy has given a 1% increase compared with only subset#4 in Table 7. It has exceeded the accuracy of all the features in the base dataset by 1.41% (98.5% vs 97.09%). It has also exceeded the accuracy compared to the base set at 98.2% as reported by author in [5]. The AUC value is marginally less .999112 vs .99872.

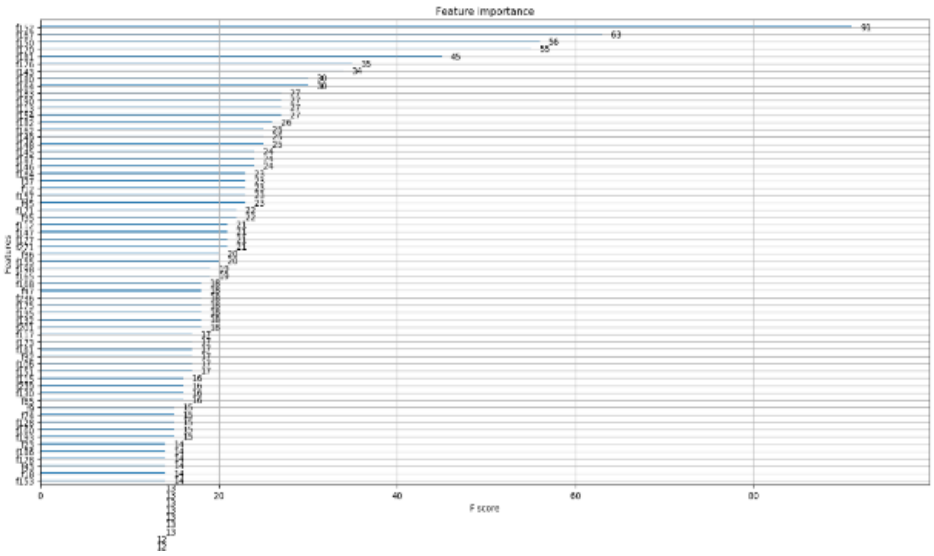


Figure 9:Feature importance selected 276 features, number times called

Table 7: Accuracy, Auc for Base Dataset and 276 Features as Per Feature Importance

Sl no.	n_estimator	Accuracy	AUC	logloss	Classification error
1	Base dataset [1] using LightGBM	98.162%	.999112	NA	NA
2	With All features as in Base dataset	97.09	.99571	NA	NA
3	Select 276 feature sets, n_estimator=600	98.5%	.998972	.046314	.014157
4	Group4 feature sets, n_estimator=600	97.49%	.997261	.076753	.024453

5.4. Further reduction in important *features*

The feature importance of these selected 276 is further studied. It was found that all the selected features contributed to building the classifier model. Unlike with base dataset, in which there were 2075 features were noisy and did not contribute to building the model. None of the selected 276 falls into the category which does not contribute to building the model using XGboost.

Figure 9 gives how many times a feature is used for generating the GDBT model using the XGboost method. The actual figure is not legible due to the 276 feature. Hence, the only top part of the results of the feature is shown in each figure.

5.5. Hyperparameter tuning with learning rate

We tried to optimize the model with a change in the learning rate. The default learning rate in XGBoost is 0.1. We tried with a learning rate of 0.01 and n_estimator=600. The model build gave slow movement to performance parameters as in the default learning rate. We used learning rate of 0.15 and .2 with n_estimators = 600. It indicates that the model gives the same efficiency but at a different rate. Hence, performance parameters are not affected at n_estimator = 600 for various learning rates. There was no improvement in performance parameters.

Table 8: Performance of XGBoost with other classification algorithm

Models	Accuracy (%)	Precision	Recall	F-score	Time in Second
Gaussian Naïve Bayes	51.82	0.43	0.10	0.17	470.37
KNN	56.38	0.52	0.88	0.65	307.66
Linear SVC	49.98	0.48	0.99	0.65	115.62
Decision Tree	89.62	0.85	0.94	0.89	177.43
AdaBoost	89.24	0.87	0.91	0.89	105.06
Random Forest	93.6	0.9	0.98	0.93	141.54
ExtraTrees	94.68	0.92	0.98	0.94	47.62
GradientBoosting	93.16	0.89	0.98	0.93	72.83
XGBoost	93.04	0.89	0.98	0.93	106.89
XGB with trained model 1	97.72	0.98	0.97	0.98	63.24
XGB with trained model 2	98.22	0.99	0.98	0.98	61.44

5.6. Comparison with other classification algorithm

Eight other classification algorithms were compared with the XGBoost classification algorithm on a sub dataset of 5000K Training and 5000k test datasets with selected 276 features. The performance of these algorithms is listed in table 8. XGBoost indicates classification performance without hyperparameter

tuning, XGB with trained model 1 is the tuned model with n_estimator = 400 and XGB with trained model 2 is the tuned model with n_estimator = 600. It indicated the performance score of XGB with trained model 2 is best among all the classification algorithm. XGBoost is better than Gaussian naïve Bayes, K-Nearest Neighbour (KNN), Linear SVC, Random forest, and Decision tree in terms of the time to make model and test for sub dataset. Extratrees, GradientBoosting, Adaboosts are better than XGBoost in terms of time to train and test the model for the identified sub dataset.

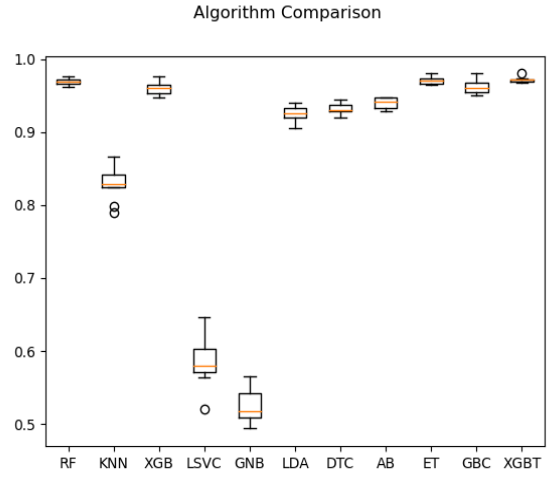


Figure 10: Algorithm comparison with Accuracy with 10-fold cross validation

5.7. K-fold Cross-validation of algorithms

Cross-validation is a statistical method to validate the classification algorithm. 10 fold cross-validation was done with the same sub data set as above with 5000 K training data set with selected 276 features and eight different classification algorithms. Figure 6 displays a whisker and box plot for the accuracy of eight different classification algorithms and a trained XGBoost model. The XGBT is the label for the trained XGBoost model. The cross-validation for the model makes the smallest box in the Figure 10. It means the model does not have much variation for the accuracy while performing the 10 fold cross-validation. It indicates the model is optimized well with hyperparameter tuning.

5.8. Comparison with other works

Table 9 compares the result of this research with other similar work, identified with reference in the column, which have used either the dataset given in [5] in part or full or other very large datasets for building malware classifier. The accuracy is marginally low compared to [48] as they have used 1/3 of the samples. It is also low compared to author using deep convolution malware classifier in [49, 50]. They have used high-end computing resources with 1711 features. In [50] author saves computation time by detecting malware during the static analysis and prevent dynamic analysis of malware in the Security Operation Center. Such work to use the large dataset with low-end computing is not available at this time and is one of the contributions. We have achieved higher accuracy using low computing resource of intel i5 processor and reduced 276 number of features compared other works which use high-end computing.

Table 9: Comparison with Other Works

	Robust intelligent MWD using DL[48]	**Ember [5]**	**Malconv[11]**	**The Need for speed, Brazillian MWC[26]**	**DEEP CONVOLUTIONAL MALWARE CLASSIFIERS [49]**	**Static PE Malware Detection[50]**	**XGBoost**	**A hybrid static tool for dynamic detection of MW [51]**
Size of Data	70148 Benign, 69860 malware Static Analysis part	800K	2 Million	21116 Benign 29704 Malware	20 Million	800K	800K	195,255 Benign, 223,352 malware
Results - Accuracy	98.9 highest by DNN	98.2	92.2	98	97.1	99.394	98.5	98.73%
AUC	Not Specified	0.99911	0.99821	Not Specified	76.1 for interval 0-.001	0.999678	0.998972	Not Specified
Processor Used	Intel Xeon	Intel i7	Not Specified	Not Specified	Not Specified	24 v CPU Google Compute Engine	Intel i5	Not Specified
No of features	Not Specified	2351	not applicable	25 PE header + 2 hash	538, 192	1711	2351, (276)	4002 features from static analysis. 4594 features from dynamic analysis
GPU	Yes,	NO	8 x DGX-1	Not Specified	Not specified	NO	NO	Not specified
Train Data	42140 Benign 41860 Malware	300K Benign 300K Malware	2 Million	.5x21116 Benign .5x29704 Malware	20 Million	300K Benign 300K Malware	300K Benign 300K Malware	Not specified
Time	Not available	20 Hours	25 hours /Epoch 250 Hours	Not available	Not available	5 minutes	1315 seconds without hyper parameter tunning	Not specified

6. Conclusion

Dataset had been regrouped into various groups with domain expertise in malware detection to build efficient models with low computational resources without GPUs. The regrouped data with strings extraction, general, header, section with just 431 feature sets compared to 2351 gives comparable efficiency in prediction performance at n_estimator=400. The model is further improved considering the feature importance as given by XGBoost and selected 276 features from 2351 features in base original data. Selected features are used to generate models using XGboost, with low-end computing resources compared to other similar work. The model with the selected feature gives improved prediction performance. The features learned can be widely useful if the performance parameters are the same across datasets. All the hashed feature derived from the export function group did not contribute to build an efficient model and to predict the malware.

Although the open base dataset is very large and balanced, the malware in datasets may not be exporting the API Calls or private APIs for malware activities. Hence, the export part of the features of the dataset did not contribute to building the model. However, this may not be always true. Shared biases are minimized if the data is from different sources. The sources of data for base datasets are not known. It also gives an upper and lower bound of accuracy.

Ember dataset is for windows executable. Using LIEF methodology in [12], we can generate datasets for other operating systems such as Linux, Mac os Android, etc. The challenge remains to get the malware samples for other OS. The techniques described here can be used to generate a model using low computational resources that can predict malware efficiently. Further, the study may be possible to determine which exact features from the PE format of application or file agnostic features are part of the selected feature.

To our knowledge, this research is one of its kind that uses a full dataset with the XGBoost GBDT algorithm to get matching or higher accuracy with a low computing resource. The basic model using the XGBoost classification algorithm was trained using low computation resources in 1315 seconds with a reduction in the feature set. The hyperparameter tuned model gives improved performance for accuracy of 98.5 and on par AUC of .9989.

Conflict of Interest

The authors declare no conflict of interest.

References

[1] V. Blue, RSA: Brazil's "Boleto Malware" stole nearly $4 billion in two years, https://www.zdnet.com/article/rsa-brazils-boleto-m.

[2] F. Cohen, "Theory and Experiments," 6, 22–35, 1987. https://doi.org/10.1016/0167-4048(87)90122-2

[3] https://www.virustotal.com

[4] C. Rossow, C.J. Dietrich, C. Grier, C. Kreibich, V. Paxson, N. Pohlmann, H. Bos, M. Van Steen, "Prudent practices for designing malware experiments: Status quo and outlook," Proceedings - IEEE Symposium on Security and Privacy, (June 2014), 65–79, 2012, doi:10.1109/SP.2012.14.

[5] H.S. Anderson, P. Roth, "EMBER: An Open Dataset for Training Static PE Malware Machine Learning Models," 2018. https://arxiv.org/abs/1804.04637

[6] M. Pietrek, Inside windows-an in-depth look into the win32 portable executable file format, MSDN Magazine, 2002. https://docs.microsoft.com/en-us/previous-versions/bb985992(v=msdn.10)?redirectedfrom=MSDN

[7] D. Devi, S. Nandi, "PE File Features in Detection of Packed Executables," International Journal of Computer Theory and Engineering, (January), 476–478, 2012, doi:10.7763/ijcte.2012.v4.512.

[8] D. Baysa, R.M. Low, M. Stamp, "Structural entropy and metamorphic malware," Journal in Computer Virology, 9(4), 179–192, 2013, doi:10.1007/s11416-013-0185-4.

[9] M. Sebastián, R. Rivera, P. Kotzias, J. Caballero, Avclass: A tool for massive malware labeling, 230–253, 2016, doi:10.1007/978-3-319-45719-2_11.

[10] E. Raff, R. Zak, R. Cox, J. Sylvester, P. Yacci, R. Ward, A. Tracy, M. McLean, C. Nicholas, "An investigation of byte n-gram features for malware classification," Journal of Computer Virology and Hacking Techniques, **14**(1), 2018, doi:10.1007/s11416-016-0283-1.

[11] E. Raff, J. Barker, J. Sylvester, R. Brandon, B. Catanzaro, C. Nicholas, "Malware Detection by Eating a Whole EXE," 2017, doi:10.13016/m2rt7w-bkok.

[12] Quarkslab, LIEF: library for instrumenting executable files, https://lief.quarkslab.com/.

[13] M.Z. Shafiq, S.M. Tabish, F. Mirza, M. Farooq, "PE-miner: Mining structural information to detect malicious executables in realtime," Lecture Notes in Computer Science (Including Subseries Lecture Notes in Artificial Intelligence and Lecture Notes in Bioinformatics), 5758 LNCS, 121–141, 2009, doi:10.1007/978-3-642-04342-0_7.

[14] A. Moser, C. Kruegel, E. Kirda, "Limits of static analysis for malware detection," Proceedings - Annual Computer Security Applications Conference, ACSAC, 421–430, 2007, doi:10.1109/ACSAC.2007.21.

[15] M.Z. Shafiq, S.M. Tabish, F. Mirza, M. Farooq, "PE-miner: Mining structural information to detect malicious executables in realtime," Lecture Notes in Computer Science (Including Subseries Lecture Notes in Artificial Intelligence and Lecture Notes in Bioinformatics), 5758 LNCS, 121–141, 2009, doi:10.1007/978-3-642-04342-0_7.

[16] F. Guo, P. Ferrie, T.C. Chiueh, "A study of the packer problem and its solutions," Lecture Notes in Computer Science (Including Subseries Lecture Notes in Artificial Intelligence and Lecture Notes in Bioinformatics), 5230 LNCS, 98–115, 2008, doi:10.1007/978-3-540-87403-4_6.

[17] M.G. Schultz, E. Eskin, E. Zadok, S.J. Stolfo, "Data mining methods for detection of new malicious executables," Proceedings of the IEEE Computer Society Symposium on Research in Security and Privacy, (February 2001), 38–49, 2001, doi:10.1109/secpri.2001.924286.

[18] M. Alazab, S. Venkataraman, P. Watters, "Towards understanding malware behaviour by the extraction of API calls," Proceedings - 2nd Cybercrime and Trustworthy Computing Workshop, CTC 2010, (July 2009), 52–59, 2010, doi:10.1109/CTC.2010.8.

[19] M. Egele, T. Scholte, E. Kirda, C. Kruegel, "A survey on automated dynamic malware-analysis techniques and tools," ACM Computing Surveys, **44**(2), 2012, doi:10.1145/2089125.2089126.

[20] M. Carpenter, T. Liston, E. Skoudis, "Hiding virtualization from attackers and malware," IEEE Security and Privacy, 5(3), 62–65, 2007, doi:10.1109/MSP.2007.63.

[21] T. Raffetseder, C. Kruegel, E. Kirda, "Detecting system emulators," Lecture Notes in Computer Science (Including Subseries Lecture Notes in Artificial Intelligence and Lecture Notes in Bioinformatics), 4779 LNCS, 1–18, 2007, doi:10.1007/978-3-540-75496-1_1.

[22] R. Pascanu, J.W. Stokes, H. Sanossian, M. Marinescu, A. Thomas, "Malware classification with recurrent networks," ICASSP, IEEE International Conference on Acoustics, Speech and Signal Processing - Proceedings, **2015-August**, 1916–1920, 2015, doi:10.1109/ICASSP.2015.7178304.

[23] J. Saxe, K. Berlin, "Deep neural network based malware detection using two dimensional binary program features," 2015 10th International Conference on Malicious and Unwanted Software, MALWARE 2015, 11–20, 2016, doi:10.1109/MALWARE.2015.7413680.

[24] W. Huang, J.W. Stokes, "MtNet: A multi-task neural network for dynamic malware classification," Lecture Notes in Computer Science (Including Subseries Lecture Notes in Artificial Intelligence and Lecture Notes in Bioinformatics), 9721, 399–418, 2016, doi:10.1007/978-3-319-40667-1_20.

[25] B. Kolosnjaji, A. Zarras, G. Webster, C. Eckert, "Deep learning for classification of malware system call sequences," Lecture Notes in Computer Science (Including Subseries Lecture Notes in Artificial Intelligence and Lecture Notes in Bioinformatics), 9992 LNAI, 137–149, 2016, doi:10.1007/978-3-319-50127-7_11.

[26] F. Ceschin, F. Pinage, M. Castilho, D. Menotti, L.S. Oliveira, A. Gregio, "The Need for Speed: An Analysis of Brazilian Malware Classifers," IEEE Security and Privacy, **16**(6), 31–41, 2019, doi:10.1109/MSEC.2018.2875369.

[27] R. Ronen, M. Radu, C. Feuerstein, E. Yom-Tov, M. Ahmadi, "Microsoft Malware Classification Challenge," http://arxiv.org/abs/1802.10135, 2018.

[28] J. Jang, D. Brumley, S. Venkataraman, "BitShred: Feature hashing malware for scalable triage and semantic analysis," Proceedings of the ACM Conference on Computer and Communications Security, 309–320, 2011, doi:10.1145/2046707.2046742.
[29] J.Z. Kolter, M.A. Maloof, "Learning to detect malicious executables in the wild," KDD-2004 - Proceedings of the Tenth ACM SIGKDD International Conference on Knowledge Discovery and Data Mining, 7, 470–478, 2004, doi:10.1145/1014052.1014105.
[30] K. Weinberger, A. Dasgupta, J. Langford, A. Smola, J. Attenberg, "Feature hashing for large scale multitask learning," ACM International Conference Proceeding Series, 382, 2009, doi:10.1145/1553374.1553516.
[31] Jason Brownlee, XGBoost with Python Gradient Boosted Trees with XGBoost and sci-kit learn. Edition: v1.10
[32] https://xgboost.readthedocs.io/en/latest/python/python_api.html
[33] https://lightgbm.readthedocs.io/en/latest/Python-Intro.html
[34] Ke, G., "LightGBM: a highly efficient gradient boosting decision tree." In: Advances in Neural Information Processing Systems, 3149–3157 (2017). http://papers.nips.cc/paper/6907-lightgbm-a-highly-efficient-gradient-boosting-decision-tree
[35] K. Raman, "Selecting Features to Classify Malware," InfoSec Southwest 2012, 1–5, 2012.
[36] A.H. Sung, J. Xu, P. Chavez, S. Mukkamala, "Static Analyzer of Vicious Executables (SAVE)," Proceedings - Annual Computer Security Applications Conference, ACSAC, (January), 326–334, 2004, doi:10.1109/CSAC.2004.37.
[37] H. Daku, P. Zavarsky, Y. Malik, "Behavioral-Based Classification and Identification of Ransomware Variants Using Machine Learning," Proceedings - 17th IEEE International Conference on Trust, Security and Privacy in Computing and Communications and 12th IEEE International Conference on Big Data Science and Engineering, Trustcom/BigDataSE 2018, 1560–1564, 2018, doi:10.1109/TrustCom/BigDataSE.2018.00224.
[38] A. Damodaran, F. Di Troia, C.A. Visaggio, T.H. Austin, M. Stamp, "A comparison of static, dynamic, and hybrid analysis for malware detection," Journal of Computer Virology and Hacking Techniques, **13**(1), 2017, doi:10.1007/s11416-015-0261-z.
[39] M. Tang, Q. Qian, "Dynamic API call sequence visualisation for malware classification," IET Information Security, **13**(4), 367–377, 2019, doi:10.1049/iet-ifs.2018.5268.
[40] L. Nataraj, D. Kirat, B. Manjunath, G. Vigna, "SARVAM: Search And RetrieVAl of Malware," Ngmad, (January), 2013.
[41] L. Nataraj, S. Karthikeyan, G. Jacob, B.S. Manjunath, "Malware images: Visualization and automatic classification," ACM International Conference Proceeding Series, 2011, doi:10.1145/2016904.2016908.
[42] D. Kirat, L. Nataraj, G. Vigna, B.S. Manjunath, "SigMal: A static signal processing based malware triage," ACM International Conference Proceeding Series, (March 2016), 89–98, 2013, doi:10.1145/2523649.2523682.
[43] S. Geetha, N. Ishwarya, N. Kamaraj, "Evolving decision tree rule based system for audio stego anomalies detection based on Hausdorff distance statistics," Information Sciences, **180**(13), 2540–2559, 2010, doi:10.1016/j.ins.2010.02.024..
[44] S. Venkatraman, M. Alazab, "Use of Data Visualisation for Zero-Day Malware Detection," Security and Communication Networks, **2018**, 2018, doi:10.1155/2018/1728303..
[45] A.P. Bradley, "The use of the area under the ROC curve in the evaluation of machine learning algorithms," Pattern Recognition, **30**(7), 1145–1159, 1997, doi:10.1016/S0031-3203(96)00142-2.
[46] T. Chen, Introduction to Boosted Trees.. http://homes.cs.washington.edu/~tqchen/pdf/BoostedTree.pdf
[47] E. Raff, J. Sylvester, C. Nicholas, "Learning the PE header, malware detection with minimal domain knowledge," AISec 2017 - Proceedings of the 10th ACM Workshop on Artificial Intelligence and Security, Co-Located with CCS 2017, 121–132, 2017, doi:10.1145/3128572.3140442.
[48] R. Vinayakumar, M. Alazab, K.P. Soman, P. Poornachandran, S. Venkatraman, "Robust Intelligent Malware Detection Using Deep Learning," IEEE Access, **7**, 46717–46738, 2019, doi:10.1109/ACCESS.2019.2906934.
[49] M. Krčál, O. Švec, O. Jašek, M. Bálek, "Deep convolutional malware classifiers can learn from raw executables and labels only," 6th International Conference on Learning Representations, ICLR 2018 - Workshop Track Proceedings, (2016), 2016–2019, 2018.
[50] H. Pham, T.D. Le, T.N. Vu, Static PE Malware Detection Using Gradient, Springer International Publishing, 2018, doi:10.1007/978-3-030-03192-3.
[51] D. Kim, D. Mirsky, A. Majlesi-Kupaei, R. Barua, "A Hybrid Static Tool to Increase the Usability and Scalability of Dynamic Detection of Malware," MALWARE 2018 - Proceedings of the 2018 13th International Conference on Malicious and Unwanted Software, 115–123, 2019, doi:10.1109/MALWARE.2018.8659373.

ASTES

Advances in Science, Technology and Engineering Systems Journal Vol. 5, No. 5, 550-553 (2020)

www.astesj.com

Special Issue on Innovative Research in Applied Science, Engineering and Technology

ASTESJ

ISSN: 2415-6698

The Newtonian Model of the Smolensk Catastrophe

Józef Pawelec*

The European University in Warsaw, Warsaw, 03-199, Poland

ARTICLE INFO

Article history:
Received: 23 April, 2020
Accepted: 02 September, 2020
Online: 27 September, 2020

Keywords:
Suspicious fog
Misleading radar
3D model of crash

ABSTRACT

The pre-reason of the Smolensk catastrophe was a dense fog. The pilots took three trials to find the proper way to airfield. Each case the tower communicated: you are on the curse and path. Pilots, however, resigned. In third critical trial the co-pilot prolonged the response second ring to 8 seconds and the engines could not already take the plane up. It collided with a thick tree and made an upside down. Next it crashed on the ground and left a bloody trace of merely ~100 m long. This means that a mean acceleration at initial speed of 100 m/s and linear braking reached -50 m/s^2. The real values could be even higher as the peak slowdown is always higher the mean. The clue of the Smolensk crash was then a fog and high azimuth error of radar. If it was correct but the ceiling too low, the plane could lose the under-carriage but avoided the upside down and the bloody crash.

1. Introduction

The Smolensk catastrophe took 96 victims: the Polish chief political and military leaders including the current President Lech Kaczynski and the President on Exile - Richard Kaczorowski. The reasons of this tragic event are still under investigations. The Poland claims it was assassination [1]-[3], while the Russia rejects it [4]. So, our statements – although math-physically correct – should be recognized as some hypothesis. The final verdict waits for an international legal process. The plane crashes in civil transport occur one per a million of flights and they are caused by the pilot faults, the engine failures or the foggy weather. It is obvious that Polish Side has chosen the best crew for this high rank visit: the high educated and experienced pilots, familiar with Tu-154. They knew the airfield and speak Russian. Also, the plane has undergone to the major overhaul 2 years ago. So, the technical problems or the pilot faults seem to be unlikely.

2. The Weather

In UTC 10:40:52 of 10-th April 2010 at 2 km to the airport the crew was informed by the tower: *you are in the curse and path!* [3], [4]. The Tu-154 in that moment was 90 m over the local terrain but merely 30 m over the far airfield plane, Fig.1. The speed was 78 m/s and the descent rate –6.2 m/s. Hence, the proper level should be

$$h_{proper} = \left(\frac{2000}{78}\right) * 6.2 = 160\ m,\ h_{choosen} = 30m \quad (1)$$

Moreover, the curse of flight was ~8^0 left the runway. It is defined by the airfield tower and the collision point to come. The direction error was more dangerous than the low level of flight because the last one causes usually the loss of the undercarriage, while the false direction results in dangerous collisions with trees or buildings. And Tu-154 just collided with a birch of 40 cm thick and has lost ~6 m of the left wing! This caused the plane to upside down within several seconds and to crash in half-backside position 425 m before and 150 m aside the airfield in a hostile environment, Fig.1. We will show that the speed of hitting the ground could reach 100 m/s. The crater was also ~100 m long. Hence, at linear braking the negative acceleration reached -50 m/s^2. The real cases are always non-linear and bring higher values, so none could survive.

If there was no directional error, some accident could also take place, but it would surely draw less victims - if any – thanks to the braking action and normal position of plane.

So, we claim that main determining factors of the Tu–154 crash in Smolensk were the extremely foggy conditions and the high directional error of the radar reaching -8^0!

The visibility along the horizon line was ~300 m, so in case of an obstruction there was a few seconds for an escape. In such conditions the Head Command was not entitled to give the permission for landing at all!

It is probably the historical precedence that the plane with President on board was taken down in dense fog with the radar of an angular inaccuracy reaching ±8^0.

*Corresponding Author: Józef Pawelec; Email: k.kosmowski@wil.waw.pl

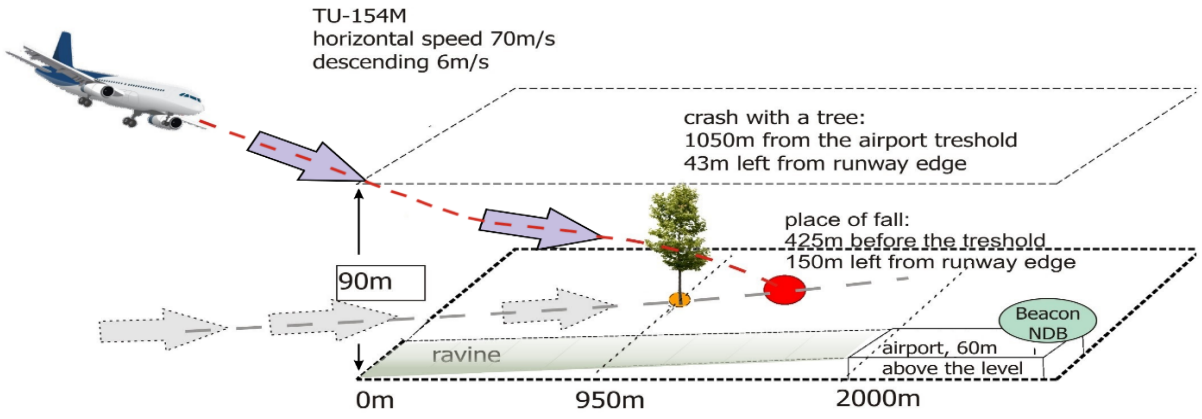


Figure 1: An illustration of the Tu-154 catastrophe: the plane flies much steep and much left the runway

The parts of crash have been dispersed over the area of ~300x300 m. This gave rise to some suspicious theories of assassination. The question is, however, who and when arranged a plot and put an explosive material on the board? So, we will trust further on the physical basis. The mass of Tu-154 reached 90 ton and the landing speed approached 100 m/s due to engines and gravity. If the collision is resilient, the reflection distance is given by eq. (2) [5], [6]

$$h = v^2 \sin(2\alpha)\,/2g \qquad (2)$$

where v – the speed, α – angle to the ground, g – acceleration.

For v = 100 m/s and $\alpha = 15^0$ this distance reaches h≈250 m.

If the collision is not resilient, the body is crashed but the maximal distance of parts dispersion reaches the comparable or even higher values (±).

For live beings the critical parameter is the negative acceleration. According to the witness reports the length of the landing crater reached ~100 m. The initial speed was also ~100 m/s due to the engines and gravitation. Assuming linear decreasing of speed, we obtain the mean of ~50 m/s and the time to run over the crater – 2s. However, at the beginning the speed decreases much higher than in the end, so we will use the total time to run only **1** s. Hence the maximal acceleration reached

$$a = \frac{\Delta V}{\Delta t} \approx -100\,\frac{m}{s} : 1s = -100\,\frac{m}{s^2} \approx -10G \qquad (3)$$

The real values could be even greater, while 3 G is already dangerous.

How these physical phenomena can be transferred onto the live body? The most sensitive is usually the heart. It can tolerate the acceleration up to 3 G. The level of 10 G is usually the lethal one.

4. Modelling of The Up-Side Down

The up-side down turnover played the critical role in all the catastrophe. We will model it using the Newtonian's theory.

The most important role in this theory plays the transversal distribution of the masses m_i along the wings line. If the mass m_i is at the distance r_i from the centre of turning, then – in case of breakdown – the energy and movement increases proportionally to $m_i r_i^2$. We could observe such scenes during the war if a plane tears a part of its wing in a battle. Then, it spins down and crashes in blow of fire.

The Tu-154 has lost one third of the wing in a crash with big tree (40 cm). This was the very dangerous disturbance. We should take into account that 90% of the plane masses are gathered in its very centre (±2 m), so in case of loss of a distant part, the plane is turned very quickly by ~180^0. We will calculate this turn-over using the real data.

The inertial moments will be defined for two mass distributions: the linear and exponential one. Next, we will take a mean. Below, the eq. (4) defines the square of the linear inertial moment k^2_l, while eq.(5) – the exponential moment k^2_e [5], [6]

$$k_l^2 = \frac{1}{M}\sum_{i=14}^{0} m_i r_i^2 = \frac{1}{45}\begin{pmatrix} 4*14^2 + 8*10^2 + \\ 12*6^2 + 16*2^2 + 0 \end{pmatrix} \approx \frac{2100}{45} \qquad (4)$$

hence $k_l \approx \sqrt{\frac{2100}{45}} \approx 6.8\ m$

The symbols used in eq. (4) mean:

M – the half mass of the plane body [45 000 kg =45 t],

m_i – its digitalized part at the distance of r_i

r_i – the arm from the middle of plane to m_i

k – the resultant arm of inertia [m].

The similar expressions for the exponential distribution of the wing masses bring the following results

$$k_e^2 = \frac{1}{M}\sum_{i=14}^{0} m_i e^{-r_i} = \frac{1}{45}\begin{pmatrix} 4e^{-14} + 8e^{-12} + \\ 16e^{-2} + \cdots \end{pmatrix} \approx 0.53 \qquad (5)$$

hence $k_e \approx 0.73\ m$.

Finally, we have chosen the square mean between (4)-(5) k_l=6.8 m, k_e=0.73 m; hence, square mean $k \approx 2\ m$.

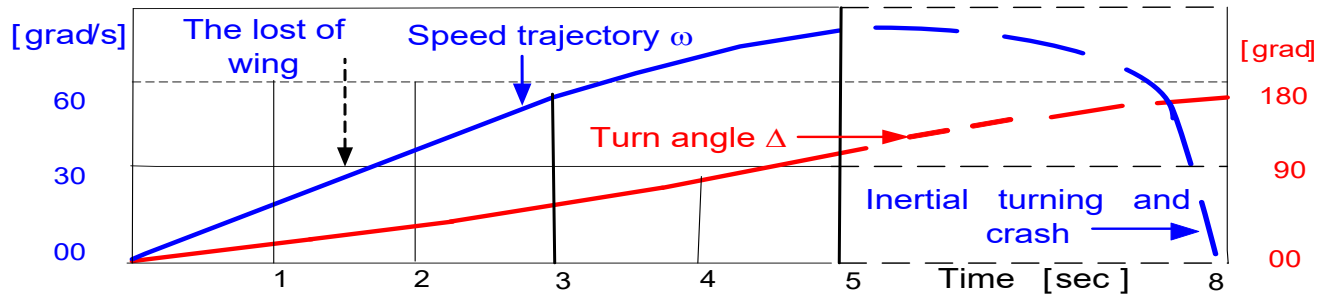


Figure 2: The simulated axial speed ω and the turn angle Δ of the Tu-154 plane after its collision with the tree vs. time

The angular frequency ω and the acceleration α of any rotation body is given by the following equations [5], [6]

$$\omega = Frt/Mk^2 \qquad (6)$$

ω – the angular speed of a body [degrees/s], t – the running time [s].

5. The Axial Turning

The force F, eq. (6), is the result of unbalance caused by the loss of a wing part and - next - the loss of total wing. We will take its mean as 10% of the gravitation force, $F=0.1*M$. Hence, for the shortened wing of r=13 m and the square of an inertial moment k^2 = 4 m^2, we obtain the approximated equation for the orbital speed ω in the first seconds, see (6)

$$\omega(t) = \left(\frac{F}{M}\right) * \left(\frac{r}{k^2}\right) t = 0.1 * \left(\frac{13}{4}\right) t = 0.33t \qquad (8)$$

This means that in the first second the plane turns around by 0.33 of radian, i.e. ~20^0!

One can observe in Fig.1 that a birch and the fall down points are distant away by 525 m. The plane used to cover it ~8 s, Fig.2. So, the mean speed was ~65 m/s and the max value could easily reach 100 m/s.

The red line shows the plane angle Δ relative to the horizon. We can see it is near 180^0.

6. The Discussion

The Russia accuses the Polish pilots for the crash [4]. This has no grounds. These pilots were the most experienced officers. They landed safely in extremely conditions, also on this same airfield and same plane and have made 3 trials preceding the crash! It is not excluded that a reason of the tragedy was an artificial fog and some falsification of the radar system without the knowledge given to the tower staff. No planes used this radar. The Putin's plane used modern ILS system.

The crashes in forests bring usually the fatal toll. Only in Poland there were two big ones: in Kabaty near Warsaw and in Miroslaviec. Nobody survived! The extensive literature on Tu-154 crash is given in [7-19].

In Smolensk crash, the large masses of Tu-154 were located in the very centre (±2 m), while the strange force appeared much outside (~13 m). These caused the plane to turn backside in ~8 sec. and in next few seconds it crashed on the freeze woody ground without any control by the crew. As we have shown the speed obtained ~100 m/s due to the engines and the gravity.

Such a crash could be compared – within the energy domain (10^9 kgm) – with the point collision of 4 trucks at a traffic circle, each of 22 t and the speed of 180 km/h. Who can risk to stand inside such a circle?

Why the crashes in the air are so dangerous in comparison with the land crashes? This is because in the last case the cars have the support in the ground, while the planes are hanging in free space. If one engine is damaged, the pilot can use the power of the second one, but if the wing is damaged, especially its ending part, the pilot is helpless.

The second wing could not replace the first one, because its role is just contrary to the action of the first.

7. Conclusions

The math-physical model of the Smolensk catastrophe has been given. It takes into account the distribution of masses, the values of forces, their directions and the resulted movement of a plane in pseudo 3D space. This approach is based on the Newtonian theory. It explains while the plane has made an upside down and why it crashed on hundred parts over the area of ±300m. This analysis suggests also the pre-reasons of the crash: the dense fog (artificial?), the radar having no valid certifications (?) and the tower staff not informed about (?) These charges should be investigated in the further legal process.

Conflict of Interest

The author declares no conflict of interest.

Acknowledgment

The author is obliged to phd K. Kosmowski and Mr B. Grochowina for their valuable discussions and help in preparation the paper.

References

[1] J. Pawelec, "The Smolensk Catastrophe in the Light of Physics Lows", WORLDS4, London , July 30/31, 2019.
[2] J. Pawelec, "Misguidance under the Polish Tu-154 Crash", International Journal of Computers and Information Technology, September, 2018.
[3] The Ministry of Home Office, Poland, *The Final Report of Tu-154 Crash,*

Warsaw, July 31, 2011.
[4] The Interstate Aviation Committee, *The Final Report of Tu-154 Crash,* Moscow, February 29, 2012.
[5] D. Halliday at al., *Fundamentals of Physics,* John Wiley and Sons 2000.
[6] M. Jeżewski, *Physics,* Gov. Science. Ed., Warsaw 1991.
[7] Polish Pilots Saw Crash Coming, BBC News, 16.04.10
[8] Smolensk Air Disaster (Polish AF Tu-154 Crash), 2011
[9] Landing System Incompatibility Caused the Crash, 2012
[10] The Polish Pilots Asked for Russian Navigator, 2013
[11] N. Ojewska, Poland Polarized on Plane Crash, 2013
[12] P.Witakowski, Conferences on Smoleńsk Crash, 2013
[13] RiaNovosti: Polish Pilot was advised not to land, 2014
[14] The Tower Didn't Speak Eng., Rec. not landing, 2015
[15] Black Box Recording Made Public, *TV-Novosti,* 2015
[16] Apelblat M., British Experts Call for Future Inv.,.2015
[17] Poland to Russia over Withholding Wreckage, 2015
[18] Polish President Duda on Smolensk Crash, 30.11.2015
[19] Poland Re-open Investigations on Smolensk, 2016

ASTES

Advances in Science, Technology and Engineering Systems Journal
Vol. 5, No. 5, 554-558 (2020)
www.astesj.com

ASTES Journal
ISSN: 2415-6698

Butterfly Life Cycle Algorithm for Measuring Company's Growth Performance based on BSC and SWOT Perspectives

Kerin Augustin, Natasia, Ditdit Nugeraha Utama*

Computer Science Department, BINUS Graduate Program – Master of Computer ScienceBina Nusantara University, Jakarta, Indonesia 11480

ARTICLE INFO

Article history:
Received: 29 May, 2020
Accepted: 02 September, 2020
Online: 05 October, 2020

Keywords:
Butterfly life-cycle algorithm
Balanced scorecard
SWOT analysis
Company growth
Strategic planning models

ABSTRACT

Previous study of butterfly life-cycle algorithms (BLCA) has been done to construct a novel algorithm by impersonating the life-cycle of a real butterfly. The algorithm was tested in measuring the company's growth performance using a balanced scorecard (BSC) strategic planning model. This paper is proposed to continue the previous study by expanding the concept in measuring company growth, not only using BSC but also SWOT analysis as the strategic planning model and then to develop its application through coding procedure and more focused to code the assessment of BLCA. Then, we build the application using Java programming language. As a result, the model could be applied in companies to measure company's growth performance by comparing those two strategic planning models.

1 Introduction

Company is an organization that makes money by producing goods or services. In economics point of view, company growth can be measured in many ways, such as sales, number of employments, and asset growth. In a company, age and size of a company are found to be relevant to a growth determinant. Financial and productivity also found that it could influence the potential of a company's growth [1]. The importance of knowing company growth may influence the future for a company, which determines their planning decision to improve the quality of their company.

There have been many studies that have conducted research based on natural phenomena. For example, there are ant colony optimization, artificial bee colony, genetic algorithm, particle swarm optimization [2], and butterfly life cycle algorithm (BLCA) [3, 4]. In the previous study of BLCA, butterfly was chosen as one of the objects to be researched because of its perfect metamorphosis. Thus, each life-cycle of this butterfly can represent the growth of a company from start-ups to a mature company. By applying BLCA to a balanced scorecard (BSC) strategic planning model, the model is constructed to measure the company growth performance [3, 4].

By analyzing the butterfly life cycle, various algorithms are constructed. One of those are optimization algorithms for soft computing and localization [5, 6]. There is also a research that creates an algorithm to measure the company's growth by impersonating butterfly life cycles. Assuming the company as butterfly, the five stages of company (inception, survival, growth, expansion and maturity) are defined as five stages of butterfly life cycle, which are egg, caterpillar, instar, chrysalis, and butterfly [3, 7], where each stages have a different parameter that affects the growth.

While the previous study are using BSC to create the parameters, we conclude that the parameters could be gained from analyzing the company SWOT. SWOT analysis is a strategic planning model to help a company or organization to define their strengths, weaknesses, opportunities, and threats. This model is usually used as a qualitative method to analyze the internal and external environments of an organization. In this paper, we will assume qualitative outcomes of SWOT analysis to define the setting of quantitative targets, so we could measure the company's growth performance by using the result value of the SWOT analysis model.

Therefore, the contribution of this paper is to continue the previous study by expanding the concept in measuring company growth, not only using BSC but also SWOT analysis as the strategic planning model and then to develop its application through coding procedure and more focused to code the assessment of BLCA. Testing and reviewing the result of BSC and SWOT analysis strategic planning models to measure the company's growth is also part of this study. This study is composed of four stages including: literature

*Corresponding Author: Ditdit Nugeraha Utama, Computer Science Department, BINUS Graduate Program - Master of Computer Science, Bina Nusantara University, Jakarta, Indonesia 11480, +81289614291 & ditdit.utama@binus.edu

review, algorithm deep analysis, model constructing, and model testing. The details about the stages will be described in the research methodology section.

2 Literature Study

2.1 Related Works

Constructing algorithms based on natural phenomena has been a common thing. Algorithms that have been made are applied to solve real life problems. For example, ant colony optimization (ACO) for finding path, artificial bee colony (ABC) for swarm intelligence [2]. There is also a study about that inspired by the natural phenomenon of chameleon's safeguarding behavior. By observing chameleon's nature behavior, the studies produced a novel mechanism to assess a company resilience potency [8]. Also, after observing and studying butterfly life cycle, the study is conducted to create butterfly life-cycle algorithm (BLCA) for performance evaluation [4].

2.2 Butterfly Life Cycle Algorithm (BLCA)

The previous study of BLCA has been done with constructing a novel algorithm by impersonating the life-cycle of a real butterfly. The algorithm was tested in measuring the company's growth performance, where all indicator parameters of company growth performance were analogized from parameters of the constructed BLCA [3]. BLCA introduces the first 2 steps in butterfly for assessing company performance, where the first step is egg state, which contains three parameters and neutral conditions. Next step is caterpillar and instar stage, containing 4 parameters (with neutral condition) and the quality of egg [4].

In egg state, egg quality is affected by temperature [9, 10], humidity [10, 11], predator [12] and neutral conditions [4], which occur when all parameters are in good condition. The probabilities for positive condition are 0.20, 0.25, 0.25, 0.30 (neutral, temperature, humidity, predator). In negative condition, the probabilities are 0, 0.25, 0.25, 0.50 [4]. By using a roulette wheel, it acquires a value of condition index [13].

The five stages of company growth are inception, survival, growth, expansion and maturity [14]. These stages are analogous to the five stages of the butterfly life cycle (egg, caterpillar, instar, chrysalis, and butterfly) [3].

2.3 Balanced Scorecard (BSC)

BSC is a strategic management system that provides basics of business vision and strategic plan which contains feedback about both internal and external business processes. There are four different perspectives to measure company performance, those are financial, customer, internal business process, and innovation and learning, as in Figure 1.

The financial perspective is used to examine the whole company finance area, customer perspective used to determine sources of the current company's market position and examines customer satisfaction, the internal business perspective is used to determine the most effective action, and the innovation and learning is used to examine company availability for innovative changes. The goal of BSC is to direct, manage, and change in support of the longer-term strategy in order to manage performance of a company [15].

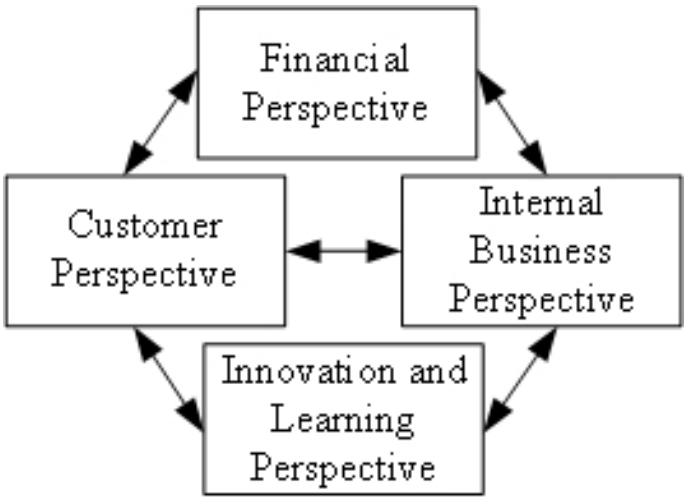


Figure 1: BSC Perspectives [16]

BSC concept found helpful to listing financial and non-financial performance measures [17]. BSC itself is usually used by companies to measure their business strategy, such as: passenger transport companies performing at Polish Market [16] and increase the banks performance in service quality [18].

2.4 SWOT Analysis

SWOT Analysis is a strategic planning model used to help a person or organization identify strengths, weaknesses, opportunities, and threats, as in Figure 2. SWOT analysis is divided into two dimensions of factor: internal factor and external factor. The internal factors are identified by examining the company environment, while external factors are identified by examining the elements outside its environment [19].

In conducting a SWOT analysis, there are several steps that must be carried out, those are: data collection, weight distribution, giving a rating, weight multiplying, score calculation, and analysis [20]. Data collection can be described as a process to search, identify, and determine each internal and external factors of an organization. Weight distribution considered as giving weight of each factor which the more important factor will weigh more. Giving a rating means, positive rating will be given to strengths and opportunities and negative rating will be given to weaknesses and threats. Weight multiplying means multiplying each weight to the given rating. Score calculation will show how an organization should react to certain factors, both internal and external factors. And last is analysis, which is the step to analyzing all the internal and external factors.

The use of SWOT aims to analyze the condition of the company which later with SWOT can provide the best corporate strategy design [21]. SWOT analysis can be considered as a growth strategy that the strategy utilizes the company's internal strength to get opportunities that exist in the external environment in order to increase the company's growth.

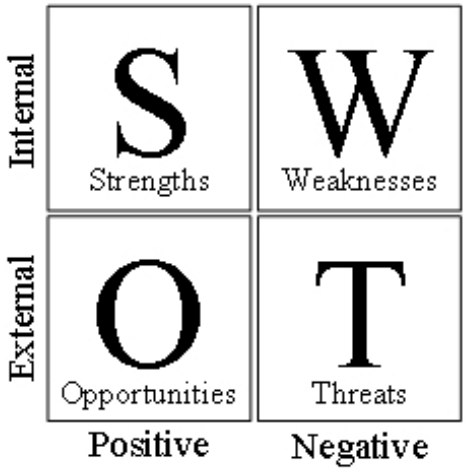


Figure 2: SWOT Analysis Diagram [20]

3 Research Methodology

In Figure 3, it can be shown that there are four stages of study to conduct this research. The basic idea of this research was referring to the butterfly life cycle algorithm (BLCA) [3, 4] that has been made before. Through the first stage, the concept of butterfly is reviewed and several ideas about the method to use is discovered. In the BLCA research [4], a balanced scorecard (BSC) is chosen to be applied as a method to measure company growth. Furthermore, this research will show comparison between the BSC and SWOT analysis method that refers to BLCA to measure the company's growth.

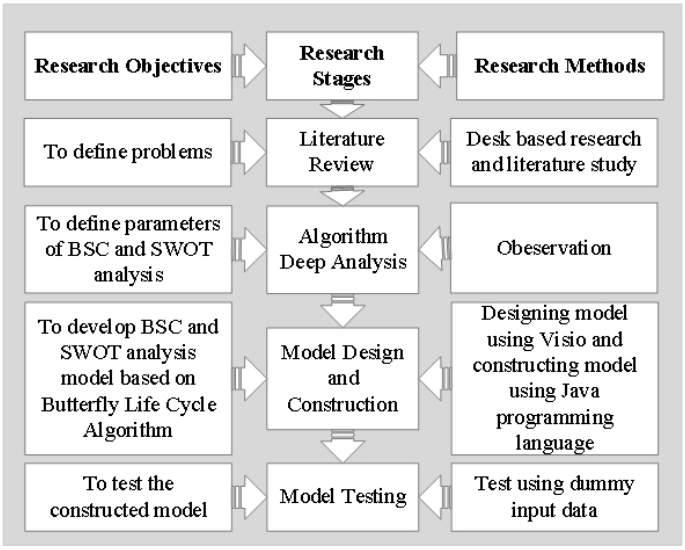


Figure 3: Research Methodology Block Diagram

In the algorithm deep analysis stage, the states are divided into five stages: egg, caterpillar, instar, chrysalis and butterfly [3]. These stages are illustrated as 5 stages of business growth, which are inception, survival, growth, expansion and maturity [14]. By using the BSC and SWOT analysis, the models are formed, where all indicator parameters of company growth performance were analogized from parameters of the BLCA [3, 4].

In the model design and construction stage, we use Microsoft Visio Professional 2016 to create the Unified Modeling Language (UML). By using that tools, class diagram and component diagram is constructed as the initial stage in constructing the model. Furthermore, the models are developed through coding procedure using Java programming language.

In the testing stage, dummy data will be employed to test the model that has been constructed. The dummy data [4] will be randomized in the system for the testing purpose.

4 Result and Discussion

In this part, through four stages of study, the model for the study is constructed. The egg's quality is determined by using equation (1), where α signifies as egg quality, and α_{st} denotes as egg's quality standard ρ_j embodies a roulette-wheel conception for j-th parameter's effect probability, θ_j is an occurrence states for j-th parameters and n denotes day summation in egg state (should be 4) [4]. The formula to calculate accumulate average (AA, for both AA for BSC in AA_{BSC} and AA for SWOT in AA_{SWOT}) are determined using equations (2) and (3) respectively, where equation (2) used to calculate using BSC method and equation (3) for SWOT method (those are one of contributions of this study). In the equations (2) and (3), F symbolized as finance, C presented as customer, BP defined as business process, and L signified as learning. We assume finance, customer and business process as external factors and learning as internal factor.

The weights of internal and external factor are considered as equals value. The internal value in BLCA are defined into one parameter, where external value are defines into three parameters, which detailed in equation (3).

$$\alpha = \alpha_{st} \sum_{i=1}^{n} \frac{\sum_{j=1}^{1} \rho_{ij}\theta_{ij}\rho_i}{n} \tag{1}$$

$$AA_{BSC} = \left(\frac{F + C + BP + L}{4}\right) \tag{2}$$

$$AA_{SWOT} = \left(\frac{\left(\frac{2(F+C+BP)}{3}\right) + 2L}{4}\right) \tag{3}$$

The company growth calculation is starting from egg state, where the company's age is below or equals to four years. The caterpillar state will start when the company's age is between five and seventeen years inclusively. These phenomenons are analogized from life cycle of butterfly's metamorphosis [3, 4]. In this paper, we conduct the company growth calculation only until the caterpillar state. The pseudo-code of this code procedure can be seen in Algorithm 1. It is a part of whole algorithm to embed two methods BSC and SWOT into BLCA [3, 4]. It is one of contributions from this

study.

Algorithm 1: Company Growth Calculation

```
Result: company performance
Initialize environment;
Calculate accumulate average;
Generate external factor;
Calculate contribution;
Initialize current year = 1;
while current year < 14 do
    if current year < 5 then
        Initialize i = 0;
        while i ≤ current year do
            Add Q for BSC with accumulate average;
            Add Q for SWOT with accumulate average;
            company performance = Q - contribution;
            Increment i;
        end
    else
        Initialize i = 0;
        while i ≤ current year do
            Add Q for BSC with accumulate average;
            Add Q for SWOT with accumulate average;
            Increment i;
        end
        Add Q with averageEggQModel;
        Divide Q with (current year - 4);
        while i ≤ current year do
            Q = Q - negative contribution;
            Q = Q + positive contribution;
            company performance = Q;
            Increment i;
        end
    end
    Increment current year;
end
```

Each environment has four components which are inputted and initialized in environment class. The components are normalized into one value by averaging all components. AA of BSC model are detailed in equation (2) and the SWOT model are detailed in equation (3). These equations describe two different models that commonly used to measure the company's growth, including its economic strength. In SWOT model, the environments are divided into two factors (internal and external) [19].

The external factor is generated randomly based on the selection in the roulette wheel. There are three components which are involved in the egg stage, those are temperature, humidity, and predator. However, the neutral condition is able to occur when all parameters are in good condition. The threshold are detailed in equations (4).

$$\begin{aligned} 0.00 \leq \rho_{neu} &\leq 0.20 \\ 0.20 < \rho_{temp} &\leq 0.45 \\ 0.45 < \rho_{hum} &\leq 0.70 \\ 0.70 < \rho_{pred} &\leq 1.00 \end{aligned} \tag{4}$$

Clear design of the application could be seen in the Figure 4 and Figure 5 as it represents the component diagram and class diagram of the constructed algorithm. The interface of input dashboard and output graph of BSC and SWOT analysis calculation result for the company growth performance are shown in Figure 6 and Figure 7.

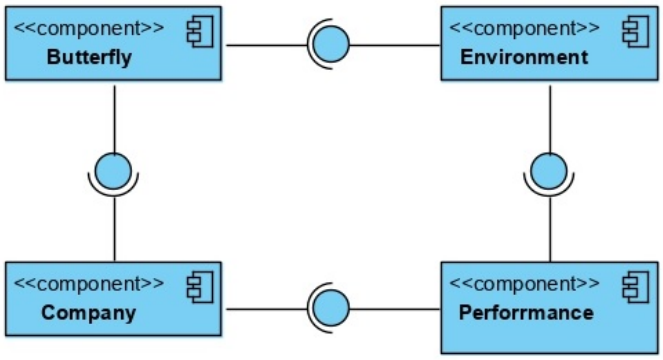


Figure 4: Component diagram of the constructed model

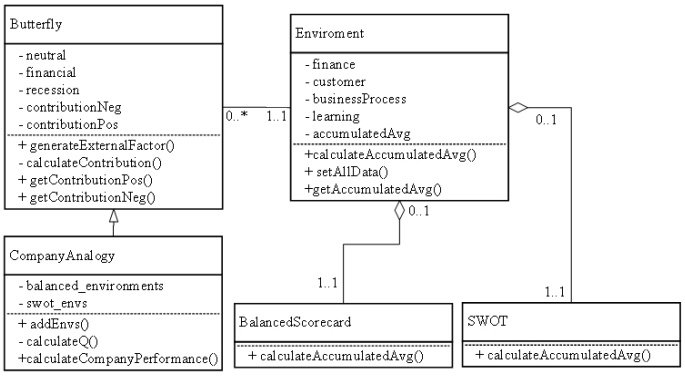


Figure 5: Class diagram of the constructed model

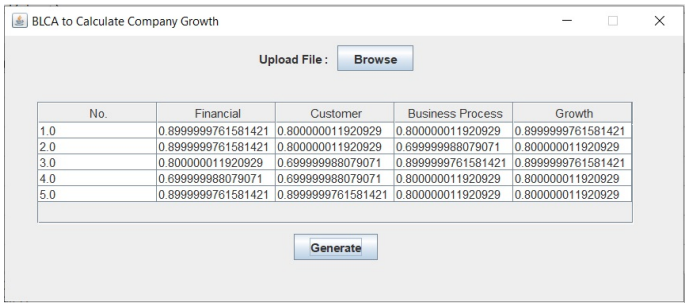


Figure 6: Input Dashboard

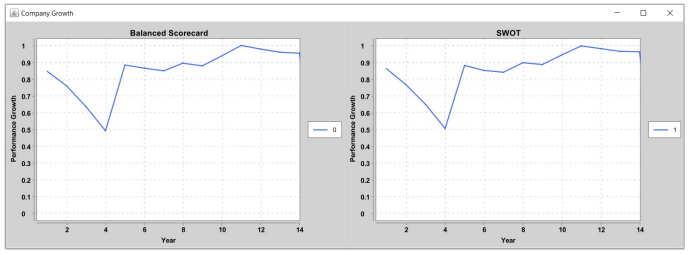


Figure 7: Output Graph

Based on Figure 7, the difference of result using BSC and SWOT analysis may not be noticeable. However the exact value of the result's average is different. The average result of BSC is 0.8604 and SWOT is 0.8558, which the value difference is 0.0046.

5 Conclusion and Further Works

Through four stages of study, two strategic planning models to measure company growth performance are constructed. Those are BSC and SWOT analysis models which are represented by butterfly life cycle. The model are developed through coding procedure to make an application so users can use it to measure their own company growth. This paper also expands the conception in measuring company growth, not only using BSC but also SWOT analysis where all the parameters are constructed and analogized from butterfly life-cycle. The result shows that there is a slightly different value between the two models that has been constructed. The value difference is 0.0046, which means that BSC and SWOT analysis might result in a similar value when both of parameters that are used are the same.

For the improvement of BLCA, the further study should be performed. For example, analyze the butterfly in the next stage for the growth by reviewing the other references or try making different parameters for the two strategic planning models, so users can really see the company growth's performance from two different strategic planning models. Furthermore, by developing BLCA into other organizations such as a university's growth could also be interesting.

References

[1] M. Zekić-Sušac, N. Šarlija, A. Has, A. Bilandžić, "Predicting company growth using logistic regression and neural networks," Croatian Operational Research Review, **7**(2), 229–248, 2016, doi:10.17535/crorr.2016.0016.

[2] X.-s. Yang, Nature-Inspired Optimization Algorithms, March, 2014.

[3] D. N. Utama, A. Mitchell, B. Fieri, H. Richard, "A Simple Butterfly Lifecycle Algorithm for Measuring Company's Growth Performance," IOP Conference Series: Materials Science and Engineering, **598**, 012041, 2019, doi:10.1088/1757-899x/598/1/012041.

[4] D. N. Utama, "An Enhanced-BLCA for Assessing Performance of Company ' s Growth," 5–8.

[5] S. Arora, S. Singh, "Butterfly optimization algorithm: a novel approach for global optimization," Soft Computing, **23**(3), 715–734, 2019, doi:10.1007/s00500-018-3102-4.

[6] S. Arora, S. Singh, "Node Localization in Wireless Sensor Networks Using Butterfly Optimization Algorithm," Arabian Journal for Science and Engineering, **42**(8), 3325–3335, 2017, doi:10.1007/s13369-017-2471-9.

[7] D. G. James, D. Nunnallee, "Life histories of Cascadia butterflies," Life Histories of Cascadia Butterflies, **86**(2), 1–447, 2011.

[8] D. N. Utama, B. K. Noveta, G. P. Warman, J. C. Setyono, N. Wikamulia, R. L. Tatulus, "A Simple Novel Mechanism for Company Resilience Measurement based on Life-Resilience Behavior of Chameleons (LRebeaCh)," (July), 1–5, 2019, doi:10.1109/icts.2019.8850929.

[9] K. Gotthard, S. Nylin, C. Wiklund, "Individual state controls temperature dependence in a butterfly (Lasiommata maera)," Proceedings of the Royal Society of London. Series B: Biological Sciences, **267**(1443), 589–593, 2000, doi:10.1098/rspb.2000.1042.

[10] M. Klockmann, K. Fischer, "Effects of temperature and drought on early life stages in three species of butterflies: Mortality of early life stages as a key determinant of vulnerability to climate change?" Ecology and Evolution, **7**(24), 10871–10879, 2017, doi:10.1002/ece3.3588.

[11] K. Fischer, M. Kirste, "Temperature and humidity acclimation increase desiccation resistance in the butterfly Bicyclus anynana," Entomologia Experimentalis et Applicata, **166**(4), 289–297, 2018, doi:10.1111/eea.12662.

[12] S. Le Hesran, T. Groot, M. Knapp, T. Bukovinszky, J. E. Nugroho, G. Beretta, M. Dicke, "Maternal effect determines drought resistance of eggs in the predatory mite Phytoseiulus persimilis," Oecologia, **192**(1), 29–41, 2020, doi:10.1007/s00442-019-04556-0.

[13] A. Lipowski, D. Lipowska, "Roulette-wheel selection via stochastic acceptance," Physica A: Statistical Mechanics and its Applications, **391**(6), 2193–2196, 2012, doi:10.1016/j.physa.2011.12.004.

[14] M. Scott, R. Bruce, "Five stages of growth in small business," Long Range Planning, **20**(3), 45–52, 1987, doi:10.1016/0024-6301(87)90071-9.

[15] u. Lesáková, K. Dubcová, "Knowledge and Use of the Balanced Scorecard Method in the Businesses in the Slovak Republic," Procedia - Social and Behavioral Sciences, **230**(May), 39–48, 2016, doi:10.1016/j.sbspro.2016.09.006.

[16] A. Tubis, S. Werbińska-Wojciechowska, "Balanced Scorecard use in Passenger Transport Companies Performing at Polish Market," Procedia Engineering, **187**, 538–547, 2017, doi:10.1016/j.proeng.2017.04.412.

[17] H. A. Akkermans, K. E. Van Oorschot, "Relevance assumed: A case study of balanced scorecard development using system dynamics," Journal of the Operational Research Society, **56**(8), 931–941, 2005, doi:10.1057/palgrave.jors.2601923.

[18] H. Dinçer, S. Yüksel, L. Martínez, "Analysis of balanced scorecard-based SERVQUAL criteria based on hesitant decision-making approaches," Computers and Industrial Engineering, **131**(March), 1–12, 2019, doi:10.1016/j.cie.2019.03.026.

[19] E. Gurel, M. TAT, "SWOT ANALYSIS: A THEORETICAL REVIEW," The Journal of International Social Research, **10**(51), 2017, doi:http://dx.doi.org/10.17719/jisr.2017.1832.

[20] H. Bahari, E. Leksono, E. Ismiyah, "Pendekatan Risk Management & Analisis Swot Untuk Mengantisipasi Penurunan Laba Di Ecos Minimart Gresik," Matrik, **XVIII**(2), 23–40, 2018, doi:10.350587/Matrik.

[21] S. P. Ramadhan, Qurtubi, M. S. Ragil, W. Sutrisno, "Performance Measurement Analysis Using SWOT and Balanced Scorecard Methods," Journal of Modern Manufacturing Systems and Technology, 2019, doi:10.1016/j.eng.2018.07.020.

ASTES

Advances in Science, Technology and Engineering Systems Journal
Vol. 5, No. 5, 559-562 (2020)
www.astesj.com

ASTES Journal
ISSN: 2415-6698

Wideband and High-Gain Aperture Coupled Feed Patch Array Antenna for Millimeter-Wave Application

Dat Vuong[1], Nam Ha-Van[2], Tran The Son[*1]

[1] *Vietnam-Korea university of information and communication technology, Information Technology, Danang, 550000, Vietnam*

[2] *Soongsil University, Department of Information Communication, Materials, and Chemistry Convergence Technology, Seoul, 100011, Korea*

ARTICLE INFO

Article history:
Received: 14 July, 2020
Accepted: 16 September, 2020
Online: 05 October, 2020

Keywords:
Aperture coupled feeding patch (ACFP)
Array antenna
Millimeter-wave
Wide bandwidth

ABSTRACT

Millimeter-wave (mmW) antenna is one of the most important parts of the fifth-generation (5G) systems because of its advanced characteristics, for example, wideband and high transmission rate. In this paper, an mmW 4x1 array antenna with high gain and wideband based on an aperture coupled feeding patch (ACFP) antenna is presented. The proposed array antenna operates at 28-GHz frequency. The antenna has a wide operating bandwidth of around 12.6 % at -10 dB bandwidth that covers 26.65 GHz to 30.35 GHz. The peak gain of the array antenna is approximately 13 dBi at 28 GHz and kept maintained in all interested frequency band. The proposed antenna is designed using a 0.127-mm thick Duroid 5880 substrate with a compact substrate of dimensions of 25 mm x 48 mm x 0.754 mm.

1 Introduction

Fifth-generation (5G) communication system has recently drawn increased attention for supporting tens to hundreds of times more capacity compared to the current 4G cellular network [1]–[4]. A bigger system capacity with wide bandwidth and high frequency is required to mitigate the higher path loss at mmW frequencies for a 5G system [5]. Furthermore, the shorter wavelengths of mmWs from installation perspectives are conducive to the reduction of antenna size that allows the incorporation of multiple patches or arrays in compact devices. Therefore, wide bandwidth and high transmission gain are two popular problems of mmW antenna design.

Several types of antenna have been recently proposed for mmW 5G system, such as dielectric-loaded planar inverted-F antenna [6, 7], microstrip leaky-wave antenna (LWA) [8]–[10], arrays of half-width microstrip LWA [11, 12], etc. In most cases, the bandwidth is narrow. In this paper, an aperture coupled feeding patch (ACFP) antenna is proposed to improve the bandwidth of the microstrip antenna. The ACFP antenna is an indirectly feeding method for the resonant patch that includes two substrates separated by a ground plane [13, 14]. To increase the transmission gain, a 4x1 array ACFP antenna is designed to obtain around 13 dBi gain at 28 GHz frequency with a compact size of 25 mm x 48 mm x 0.754 mm.

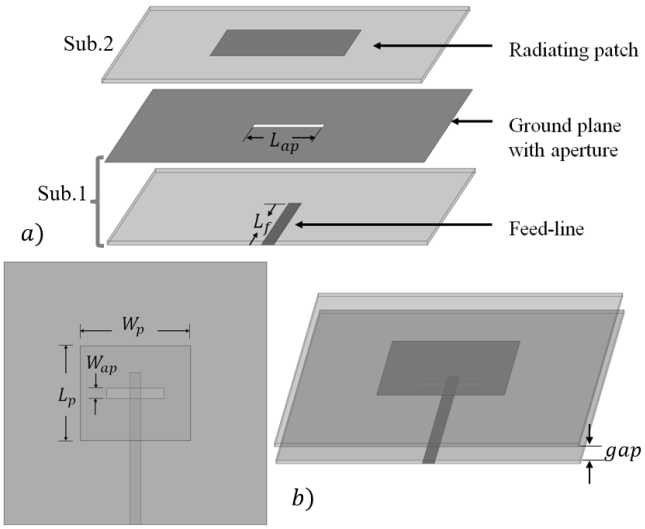


Figure 1: Single ACFP antenna structure: (a) separated components view; (b) top view and perspective view.

The organization of this paper is presented as follows. The proposed antenna's structure is described in Section II. The fabrication

*Corresponding Author: Tran The Son, Email: ttson@vku.udn.vn

and experimental results are presented in Section III.

2 Array Antenna Structure Design

Figure 1(a) shows the single ACFP antenna structure that has two substrates separated from each other. The top substrate has the radiating patch antenna element with a dimension of L_p = 3.6 mm and W_p = 4.2 mm, and the bottom substrate has a transmission feed line with a thickness of 0.4 mm and a length L_f = 4.5 mm. A small aperture is slotted in the ground plane to create coupling from the open-circuited feed line to the radiating patch. A rectangular aperture is generally placed in the patch central to maximize the coupling and generate the symmetric radiation pattern, which has a length L_{ap} = 2.2 mm and width W_{ap} = 0.4 mm. In this design, two substrates are separated by a ground plane and a small *gap* of 0.5 mm that can enhance the bandwidth and reduce the interference from the feed network to the main radiation pattern. A tapered line feed network is designed to array four ACFP antenna elements with small mutual coupling and internal reflections. With a conventional array antenna, radiating elements are normally separated by smaller half-wavelength. If the element spacing between two adjacent antennas is larger than a half-wavelength, the antenna gain decreases, and the grating lobe increases [15]. However, the element patch width is usually used in the order of 0.4-0.5 λ_0, which is conducive to a small remaining distance between the adjacent elements. This small distance would cause high mutual coupling. With the ACFP array antenna, the distance between the adjacent patch elements is chosen to be higher than a half wavelength [16]–[18].

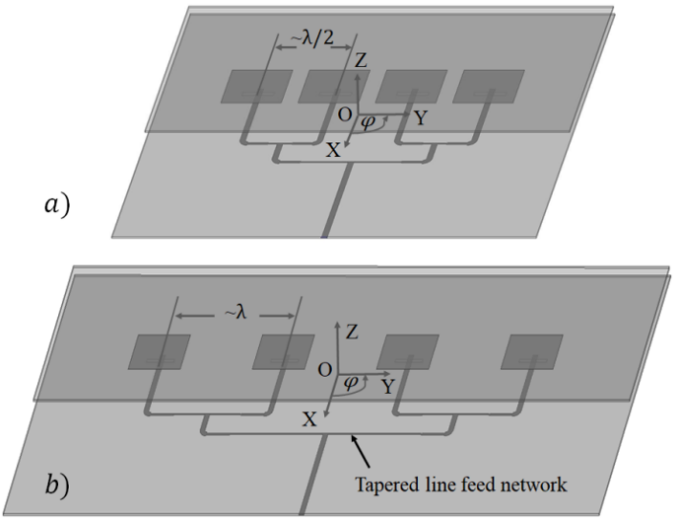


Figure 2: 4x1 ACFP array antenna with a tapered line feed network: a) 4x1 half wavelength spacing (HWS) array antenna; b) proposed 4x1 array antenna.

In this paper, a 4x1 half-wavelength spacing (HWS) array antenna is considered to verify the performance. Besides, a proposed 4x1 array antenna is optimized and compared to the performance with the 4x1 HWS array antenna. The 4x1 HWS array antenna and the proposed 4x1 array antenna are illustrated in Figure 2. Both antennas are designed using Duroid 5880 with the permittivity ε of 2.2 and the thickness of 0.127 mm for both layer substrates. The ANSYS HFSS software (ANSYS Inc. Canonsburg, PA, USA) was used to design, simulate, and optimized the antenna. The return loss S_{11} parameters, radiation patterns, and antenna gains in the simulation for the single antenna, the 4x1 HWS array antenna, and the proposed 4x1 array antenna are shown in Figure 3. The -10 dB bandwidth of the antennas cover the 28-GHz frequency band with almost higher than 12 % bandwidth that is shown in Figure 3(a). The bandwidth of the array antenna is a bit larger and shifted up than the single antenna.

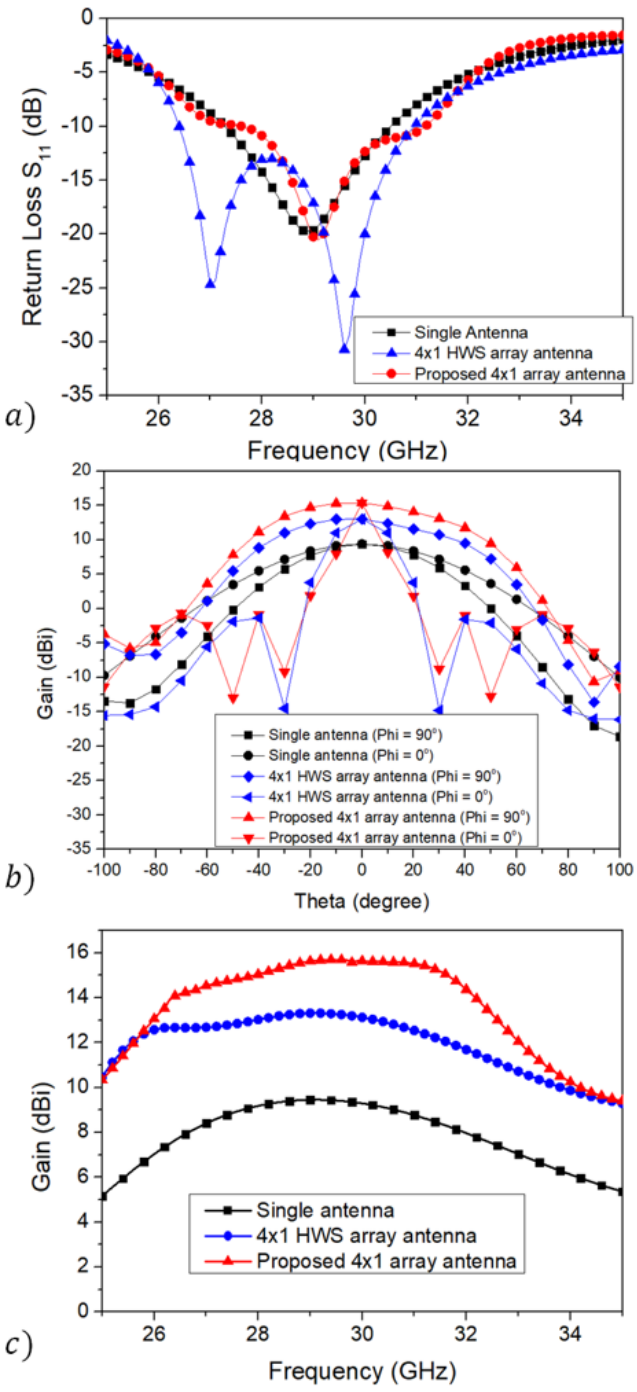


Figure 3: Simulation results of the single ACFP antenna, the 4x1 HWS array antenna, and the 4x1 array antenna: a) S_{11} parameters; b) radiation patterns; c) antenna gains.

A comparison of the radiation pattern and the realized gain between the single antenna, the 4x1 HWS array antenna, and 4x1 array antenna was demonstrated in Figure 3(b) and Figure 3(c) with the single antenna gain of around 9.45 dBi, the HWS array antenna of 13 dBi and the array antenna gain of 15.37 dBi. Because the tapered line feed network presented a good power divider with a small reflection, then the array can obtain a significant gain enhancement compared to the single. However, the radiation pattern of the array antennas is sharper and thinner at the plane of Phi = 0^o than the one of the single antenna. Normally, an HWS array antenna presents a better side lobe level (SLL) compared to a larger spacing array antenna. However, the SLL of the 4x1 HWS array antenna shows a worse value than the one of the optimal 4x1 array antenna with the element spacing around wavelength. In detail, the SLL of the HWS array antenna is -14.34 dB, while the SLL of the proposed optimal array antenna is -16.54 dB. Furthermore, the antenna gains on the overall interested frequency band of the optimal array antenna are significantly higher than the one of the HWS array antenna with almost 2dB on overall frequency band as shown in Figure 3(c).

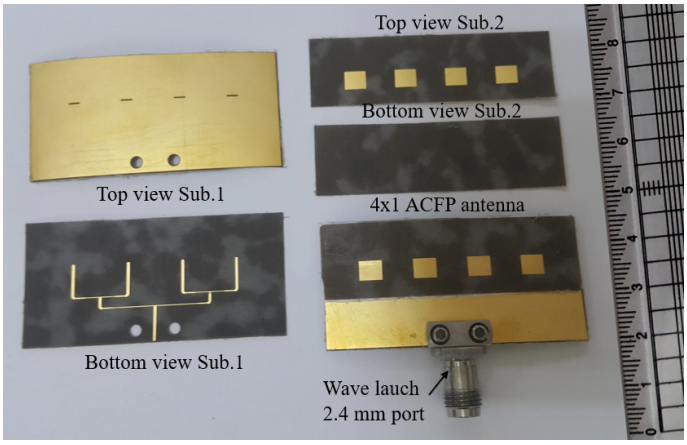


Figure 4: Fabrication of the 4x1 array antenna with the top view and bottom view of each layer substrate.

3 Array Fabrication and Measurement Results

Based on the analysis and design of the above section, the proposed array antenna was fabricated and measured to validate the performance, as demonstrated in Figure 4. The proposed antenna is printed on a 0.127-mm thick Duroid 5880 substrate. The bottom substrate contains a tapered line feed network on the bottom side and a ground plane with four aperture slots on the top side of the substrate, and the size is 25 mm x 48 mm. The top substrate has four radiating patches on the top side of the substrate. There is a small gap of 0.5 mm between two substrates that is an important factor to enhance the bandwidth of the antenna. A thin Styrofoam material was inserted between two layers to straight the antenna and fix the small gap between them. The antenna was connected to a Wave launch 2.4 mm port that can work at 28 GHz frequency band with low loss, wideband, and the terminal impedance of 50 Ω. This port has two screws to firm the antenna with the port. Therefore, two small holes are drilled nearby the feeding network, as shown in the view of Sub. 1. The radiation pattern and antenna gain were measured in a far-field chamber with the configuration setup as shown in Figure 5. The return loss was measured using an 8510C Vector Network Analyzer. The measured S_{11} parameter of the 4x1 array antenna is shown in Figure 6(a). The -10 dB bandwidth for the antenna frequency covers 26.65 GHz to 30.35 GHz, which is slightly different from the one in the simulation result. However, the proposed antenna still covers the interested frequency band. The radiation pattern of the proposed antenna at 28 GHz frequency is shown in Figure 6(b). There is a good agreement between the simulation and measurement results of the radiation pattern. The antenna gain at 28 GHz frequency in the measured result is slightly lower than the simulated gain because of the fabricated tolerance and losses in the measurement process. From the measured radiation pattern, the antenna presents a good performance with the side lobe level (SLL) of approximately -13.2 dB. The antenna gain is also measured in the overall wideband from 26 GHz to 30 GHz, which is depicted in Table 1. It can see that the antenna gain is kept unchanged around 13 dBi on all frequency bands. A comparison between the proposed array antenna and the related works in some important factors, such as overall size, the -10 dB bandwidth, and antenna gain are presented in Table 2. Both array antennas in [16, 17] were based on the ACFP structure which was arrayed 4x1 in series. From this Table, it is obvious that the proposed array antenna is significantly compact size, wider bandwidth, and higher gain compared with the referred antennas.

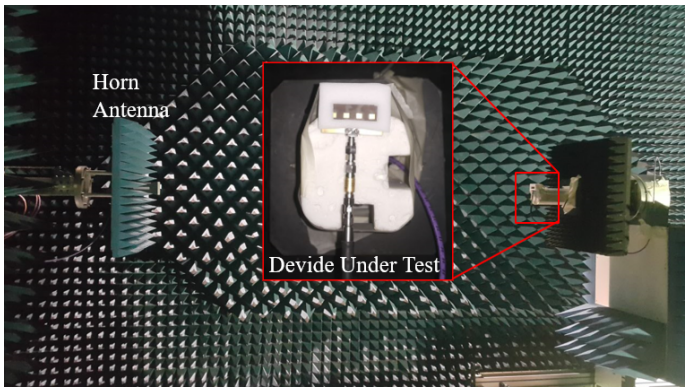


Figure 5: Configuration setup of the proposed array antenna for the measurement process.

Table 1: The measured antenna gain in the interested frequency band.

Freq. (GHz)	26.5	27	27.5	28
Gain (dBi)	12.2	12.86	13.03	13.06
Freq. (GHz)	28.5	29	29.5	30
Gain (dBi)	13.32	13.3	13.69	13.34

4 Conclusions

In this paper, a 4x1 array antenna using an ACFP antenna structure has been presented. The proposed antenna has a compact size of 25 mm x 48 mm x 0.754 mm and is printed on a Duroid 5880 substrate with a thickness of 0.127 mm for both layer substrates. A

wideband and high gain of the antenna is obtained with around 12.6 % bandwidth and approximately 13 dBi, respectively.

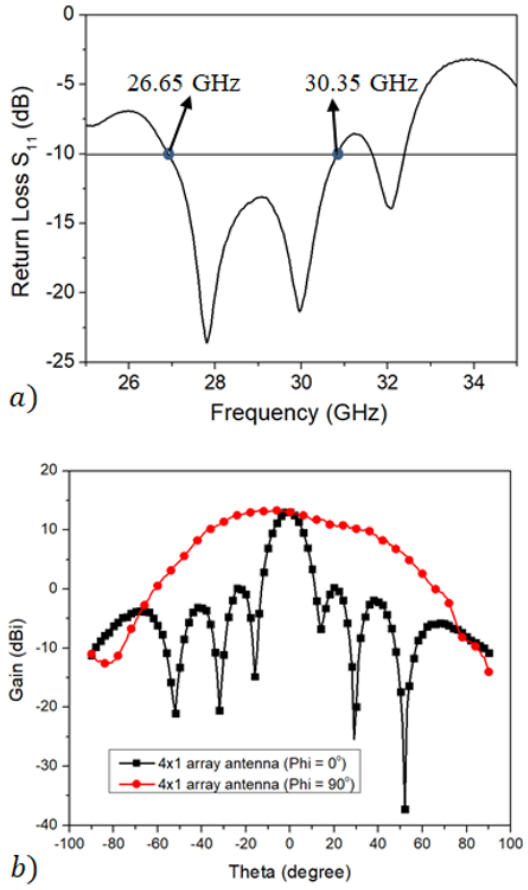


Figure 6: Measured results of the 4x1 array antenna: a) S_{11} parameter; b) radiation pattern and gain at 28 GHz frequency.

Table 2: Comparison of the proposed antenna with those of related works.

Ref.	Substrate	Overall Size (λ_0)	BW (%)	Gain (dBi)
[16]	0.127 mm thick Rogers 6002 28 GHz	2.8 x 0.93 x 0.088	~ 7.1	13.5
[17]	0.127 mm thick Rogers 5880 60 GHz	5 x 3 x 0.076	~ 6.7	12.5
This work	0.127 mm thick Rogers 5880 28 GHz	2.33 x 4.48 x 0.07	~ 12	13.69

References

[1] J. G. Andrews, S. Buzzi, W. Choi, S. V. Hanly, A. Lozano, A. C. K. Soong, J. C. Zhang, "What Will 5G Be?" IEEE Journal on Selected Areas in Communications, **32**(6), 1065–1082, 2014.

[2] T. S. Rappaport, S. Sun, R. Mayzus, H. Zhao, Y. Azar, K. Wang, G. N. Wong, J. K. Schulz, M. Samimi, F. Gutierrez, "Millimeter Wave Mobile Communications for 5G Cellular: It Will Work!" IEEE Access, **1**, 335–349, 2013.

[3] N. Ha-Van, C. Seo, "A Single-Feeding Port HF-UHF Dual-Band RFID Tag Antenna," J Electromagn Eng Sci, **17**(4), 233–237, 2017, doi:10.26866/jees.2017.17.4.233.

[4] Z. Pi, F. Khan, "An introduction to millimeter-wave mobile broadband systems," IEEE Communications Magazine, **49**(6), 101–107, 2011.

[5] S. Rangan, T. S. Rappaport, E. Erkip, "Millimeter-Wave Cellular Wireless Networks: Potentials and Challenges," Proceedings of the IEEE, **102**(3), 366–385, 2014.

[6] K. M. Morshed, K. P. Esselle, M. Heimlich, D. Habibi, I. Ahmad, "Wideband slotted planar inverted-F antenna for millimeter-wave 5G mobile devices," in 2016 IEEE Region 10 Symposium (TENSYMP), 194–197, 2016.

[7] K. M. Morshed, K. P. Esselle, M. Heimlich, "Dielectric loaded planar inverted-F antenna for millimeter-wave 5G hand held devices," in 2016 10th European Conference on Antennas and Propagation (EuCAP), 1–3, 2016.

[8] D. K. Karmokar, K. P. Esselle, T. S. Bird, "Wideband Microstrip Leaky-Wave Antennas With Two Symmetrical Side Beams for Simultaneous Dual-Beam Scanning," IEEE Transactions on Antennas and Propagation, **64**(4), 1262–1269, 2016.

[9] D. K. Karmokar, Y. J. Guo, P. Qin, K. P. Esselle, T. S. Bird, "Forward and Backward Beam-Scanning Tri-Band Leaky-Wave Antenna," IEEE Antennas and Wireless Propagation Letters, **16**, 1891–1894, 2017.

[10] M. Garcia-Vigueras, J. L. Gomez-Tornero, G. Goussetis, A. R. Weily, Y. J. Guo, "Enhancing Frequency-Scanning Response of Leaky-Wave Antennas Using High-Impedance Surfaces," IEEE Antennas and Wireless Propagation Letters, **10**, 7–10, 2011.

[11] D. K. Karmokar, K. P. Esselle, T. S. Bird, "An Array of Half-Width Microstrip Leaky-Wave Antennas Radiating on Boresight," IEEE Antennas and Wireless Propagation Letters, **14**, 112–114, 2015.

[12] D. K. Karmokar, K. P. Esselle, S. G. Hay, "Four-branch microstrip leaky-wave antenna array for radiation towards broadside," in 2014 International Workshop on Antenna Technology: Small Antennas, Novel EM Structures and Materials, and Applications (iWAT), 96–99, 2014.

[13] G. Kumar, K. P. Ray, Broadband microstrip antennas, Artech House Inc., 2003.

[14] N. N. Yoon, N. Ha-Van, C. Seo, "High-gain and wideband aperture coupled feed patch antenna using four split ring resonators," Microwave and Optical Technology Letters, **60**(8), 1997–2001, 2018, doi:10.1002/mop.31284.

[15] T. Suda, T. Takano, Y. Kazama, "Grating lobe suppression in an array antenna with element spacing greater than a half wavelength," in 2010 IEEE Antennas and Propagation Society International Symposium, 1–4, 2010.

[16] K. Phalak, A. Sebak, "Aperture coupled microstrip patch antenna array for high gain at millimeter waves," in 2014 IEEE International Conference on Communication, Networks and Satellite (COMNETSAT), 13–16, 2014.

[17] I. Mohamed, A. R. Sebak, "High-gain series-fed aperture-coupled microstrip antenna array," Microwave and Optical Technology Letters, **57**(1), 91–94, 2015, doi:10.1002/mop.28792.

[18] M. . Li, S. Kanamaluru, K. Chang, "Aperture coupled beam steering microstrip antenna array fed by dielectric image line," Electronics Letters, **30**(14), 1105–1106, 1994.

ASTES

Advances in Science, Technology and Engineering Systems Journal
Vol. 5, No. 5, 563-577 (2020)
www.astesj.com

ASTES Journal
ISSN: 2415-6698

Advances in Optimisation Algorithms and Techniques for Deep Learning

Chigozie Enyinna Nwankpa*

Design Manufacturing and Engineering Management, University of Strathclyde, Glasgow, G1 1XJ, UK

ARTICLE INFO

Article history:
Received: 25 August, 2020
Accepted: 24 September, 2020
Online: 05 October, 2020

Keywords:
Deep learning
Optimisers
Optimisation algorithms
Deep learning optimisers
Deep learning optimisation
Neural network optimisers

ABSTRACT

In the last decade, deep learning(DL) has witnessed excellent performances on a variety of problems, including speech recognition, object recognition, detection, and natural language processing (NLP) among many others. Of these applications, one common challenge is to obtain ideal parameters during the training of the deep neural networks (DNN). These typical parameters are obtained by some optimisation techniques which have been studied extensively. These research have produced state-of-art(SOTA) results on speed and memory improvements for deep neural networks(NN) architectures. However, the SOTA optimisers have continued to be an active research area with no compilations of the existing optimisers reported in the literature. This paper provides an overview of the recent advances in optimisation algorithms and techniques used in DNN, highlighting the current SOTA optimisers, improvements made on these optimisation algorithms and techniques, alongside the trends in the development of optimisers used in training DL based models. The results of the search of the Scopus database for the optimisers in DL provides the articles reported as the summary of the DL optimisers. From what we can tell, there is no comprehensive compilation of the optimisation algorithms and techniques so far developed and used in DL research and applications, and this paper summarises these facts.

1 Introduction

Optimisation algorithms and techniques have recently become a vast research area with the increasing availability of large datasets for DL research. Optimisation involves systematically choosing an appropriate set of values from a defined range of parameter set. These algorithms and techniques have witnessed remarkable breakthroughs in research aimed at performance improvement in applications. They are used in modelling NN to obtain better performance results by updating model parameters during the training, usually referred to as cost function in machine learning(ML). Optimisers are vital parameters when developing and deploying NN based models and help to ensure that models do not oscillate as well as preventing slow convergence [1]. Perhaps, modelling challenges have been driven research in optimisation to obtain appropriate parameters especially the assumptions made during the modelling problems as being convex functions, ill-conditioning of gradients, local minima, saddle points, plateau and flat regions, inexact, exploding gradients and cliffs, long term dependencies, theoretical limits of optimisation and poor correspondence between global and local structures [2].

To address these challenges and obtain efficient parameter learning as well as improve the performance of these learning algorithms, [3] outlined that there are three key areas to consider which include; to improve the model, to obtain better features, and lastly to improve the model inference. For large scale datasets, these improvements are necessary most importantly, to use the entire datasets for training and to obtain useful features for the learning model as well as to control the speed of learning (learning rate) of the model during the training process [4]. These large scale datasets involve massive data points and features that are used as decision variables in modelling. Some application areas that require some form of optimisation include ML, data analytics, natural language processing (NLP), among many others [5]–[6].

Cost functions have the inherent property of being convex; thus, there is always a line segment between two points on the graph of the cost function that lies on or above the chart [2]. This is achieved by reducing the difference between the predicted and actual outputs. Selecting optimal parameters for these models are difficult to achieve, with model parameters including learning rate, weights and biases, among others. The heuristic process of parameters optimisation including learning rate, weights and biases improves training stability, speed of convergence as well as a model generalisation but not currently achievable for all parameters. However, this calls for the need to review possible approaches to achieve optimal parameters. Optimisation models are used to minimise or maximise the objective function, usually referred to as the error function, cost

*Corresponding Author: Chigozie Enyinna Nwankpa, DMEM, University of Strathclyde Glasgow, +44 (0) 141 574 5194 & chigozie.nwankpa@strath.ac.uk

function or loss function in literature [2]. These terms will be used interchangeably in this paper. This error function is a crucial mathematical function which depends on the model's learnable parameters used for computing the target output from a set of inputs. The general training of NNs involves an iterative process of minimising the loss function given by

$$min_{\theta} J(\theta), \theta \epsilon \mathbf{R}^{d} \tag{1}$$

Where θ is a trainable parameter of the NN.

Conversely, as the internal parameters of the models are essential for the efficient training of the deeper architectures, which contains multiple hidden layers in their designs. The optimisation process helps the model to calculate and obtain optimal values as well as update the model parameters, thereby aiding effective learning of the features and patterns in the data. This makes the optimisation process, an essential part of model development for DL applications. This research provides a comprehensive overview of optimisation algorithms and techniques used in DL.

The remaining parts of the paper are organised as follows; Section 2 provides a brief introduction of deep learning, alongside the role of optimisers in DL research. Section 3 discusses the research method and motivation. Section 4 discusses the optimisation techniques used in DL research. Section 5 provides a brief discussion, and Section 6 presents the conclusion and future work.

2 Deep Learning

Deep learning is a sub-field of ML, where high levels of abstraction are learned from data [7]. This learning process is an iterative process that involves propagating the weights and biases of the network from input to output and vice versa. The DNNs are organized in layers, and these layers are arranged in a chain structure, with each layer being a function of the preceding layer. In this way, the overall output of the NN is obtained by computing the outputs of the successive layers from the input layer through the subsequent layers, with the output.

For a given system with $n-$ dimensional initial inputs of X, $k-$ layers, $W-$ weights and $b-$ biases ,

$$X = \begin{bmatrix} x_1 \\ x_2 \\ \vdots \\ x_n \end{bmatrix}, W = \begin{bmatrix} w_{11} & w_{12} & \dots w_{1n} \\ \vdots & \ddots & \\ w_{k1} & w_{k2} & w_{kn} \end{bmatrix}, b = \begin{bmatrix} b_1 \\ b_2 \\ \vdots \\ b_n \end{bmatrix}$$

the output of each layer is obtained by the computing the dot product of weights and inputs, with the model fitting bias term given by

$$y^{[1]} = \alpha((W^{[1]T} \cdot X) \ + b^{[1]}) \tag{2}$$

Where y^1 = first output layer, X = inputs to the model, α^1 = layer activation function (AF), W^1 = weight coefficient at layer, and b^1 = layer bias coefficients, are the parameters of the DNN. From the single layer model of equation 2, the n^{th} depth architecture is represented using numeric layer superscripts that shows the position of the parameters of the NN architecture, to obtain the overall output y of the very DNN as

$$y = \alpha((W^{[n]T} \cdot y^{n-1}) \ + b^{[n]}) \tag{3}$$

Pictorially, we can visualise this NN, assuming five inputs, three hidden layers and an output layer is depicted in Figure 1. As the input signals are received, the hidden layers perform different transformations on the signal before propagating the signal to the output layer, where the non-linear sum of the inputs signal is obtained. This output becomes the reference output for further processing and back propagation.

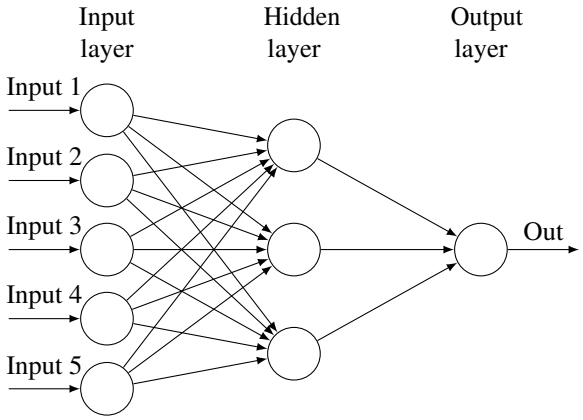


Figure 1: Neural network showing five input, three hidden and one output layer.

Conversely, the NN models consist of different architectures which are dependent on the components, arrangement, and the number of layers cascaded together, like in Figure 1. As the layers of the NN are cascaded together, more and more parameters are introduced into the network, thereby making the architecture deeper and the learning process more complicated. These models provide some distinct characteristics, mostly its scalability with increasing data and generalisation on unseen data[8].

To train these complex architectures, gradient descent is one of the most common approaches. It involves computing the minimum of a given function, by taking steps proportional to the negative of the gradient of a function at its current point [9]. During training, the inputs are forward propagated to the hidden layers and finally the output, producing a scalar cost function. This output cost is then made to flow backwards to obtain the gradient. This backward flow is known as backpropagation[10], and it involves repeated application of chain rule, across all possible paths in a NN, to obtain the gradient of each weight with respect to the corresponding output. The gradient descent would be discussed in details in the following section. Besides, as DL models depend on large amounts of data, finding the underlying patterns in the data will involve iteratively passing the data to the model until the entire examples are seen by the model, for some specified number of times, usually referred to as epochs. This entails that the models will adjust the weight and bias parameters until it attains optimal values. This adjustment process is often referred to as optimisation, and the role of these optimisation algorithms, to achieve proper learning in DNNs are outlined.

2.1 Role of Optimisers in Deep Learning

The training of DNN architectures requires the propagation of gradients to and fro the layers of the deep architectures. These gradients

and their initialisation have been studied extensively alongside their propagation behaviours during the training of the learning models. Majority of these models require some optimisation to obtain the appropriate parameters. The backpropagation algorithm is one of the foremost algorithms used to compute the reverse order of computation for NNs using chain rule [10]. The backpropagation algorithm is the partial derivative of the cost function C with respect to any weights w or biases b, represented as $\frac{\partial C}{\partial w}$ or $\frac{\partial C}{\partial b}$. It works by calculating the gradient of the cost function with respect to the respective weights and biases using the chain rule, while iterating backwards from the output layer, through each of the individual layers, to the inputs.

After the output is obtained by forward pass, the NN calculates the loss L, which quantifies the difference between the desired output and the actual output.The overall idea is to update the weight vectors to reduce the loss factor L. The gradient descent is used to update the weights by moving it to the opposite direction of the loss. This gradient of the loss with respect to the weights is given by

$$\frac{\delta L}{\delta w} = \frac{\delta L}{\delta y} \cdot \frac{\delta y}{\delta w} = \frac{\delta L}{\delta y} \cdot \frac{\delta y}{\delta z} \cdot \frac{\delta z}{\delta w} \tag{4}$$

where z is the inner product, obtained by $z = x^T w$ and $y = f(z)$. The update is performed in the opposite direction of the forward propagation beginning from the last layer to the first layer. This process is known as backward propagation or backpropagation. In [11], the authors highlighted that back-propagated gradients values decreases as they move from the output layers to the inputs. This causes the gradients to almost vanish at some point for very deep architectures [12], thereby requiring some optimisation to achieve an adequate learning, without dead signals. These optimisers modify the weights, biases, learning rate and other vital parameters of a model to improve the performance by reducing the losses. The numerous optimisers used to evaluate and update optimal values in these deep architectures.

3 Research Methodology and Motivation

A search of optimisers of DL was performed on the Scopus database using the keywords "optimisers" OR "optimizers" AND "deep learning", with the filter criteria outlined in Table 1. A total of 117 papers were obtained. Besides reading the titles, abstracts, and keywords, only 42 relevant articles were selected, in addition to some other articles added through cross-citation. The search results suggest that DL optimisation algorithms in literature have not been significantly explored. However, different authors have performed research on the comparison of different optimisation algorithms without a documented summary of the DL optimisers in the literature.

Nevertheless, the motivation behind this research is based on the trends observed in research publications where researchers discuss and compare the relevant DL optimisers while there is no documented research on the DL optimisers. This is evident in very recently published research where authors outlined the use of different optimisers in their research analysis including Adam, Stochastic Gradient Descent (SGD), AdaDelta, AdaGrad, RMSProp [13, 14], and many other applications outlined in the literature[15].

Table 1: Article Search Criteria

Criteria	Filter
Restriction	Title, abstract and Keywords
Language	English
Document Type	Articles
Keywords	Optimisers, Optimisation, DNN, DL, NN

Conversely, other authors considered the DNN optimisers as a tool to improve model design [16] and also to test the model performance of different applications including sign language recognition[17], optimising car crash detection [18], prediction of water leakage using Adam, RMSProp and AdaDelta [19], SGD, Adam, AdaGrad, AdaDelta, Nadam, RMSProp for bushfire prediction [20] among others. This article provides a comprehensive compilation of optimisers used in DL research. A search of the Scopus database reveals that there is considerable interest in optimisation techniques in DL with more and more researchers investigating these challenges with significant improvements since 2017, as shown in Figure 1.

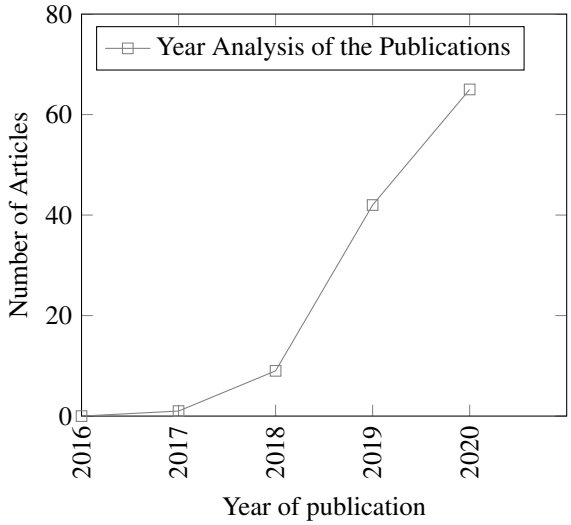


Figure 2: Scopus recent research interest for DL optimisers

However, another prominent trend in optimisation research is that it is not field-specific as authors from different fields are exploring these techniques to enhance their model performances. This is evident in Figure 3, showing the various areas of researchers investigating optimisers for DL, with computer science and engineering providing more than half of the optimisation research publications.

4 Optimisation Techniques

The numerous optimisation algorithms and techniques used in DNN design and applications are outlined. Due to the popularity of DL, a considerable amount of research has investigated and proposed new optimisation techniques, aimed at enhancing the model performances. These improvements outline the progress made in specific approaches and provide an entry point for discussing the current SOTA research in optimisation. Firstly, a brief outline of

weight initialisation is presented since the majority of the optimisation techniques involves adjusting weights and learning rate of a model, to obtain the best features from the data. Also, the first, and second-order optimisers, the swarm intelligence optimisers, alongside parallel computing, are discussed as the other techniques of optimising DNN found in the literature results.

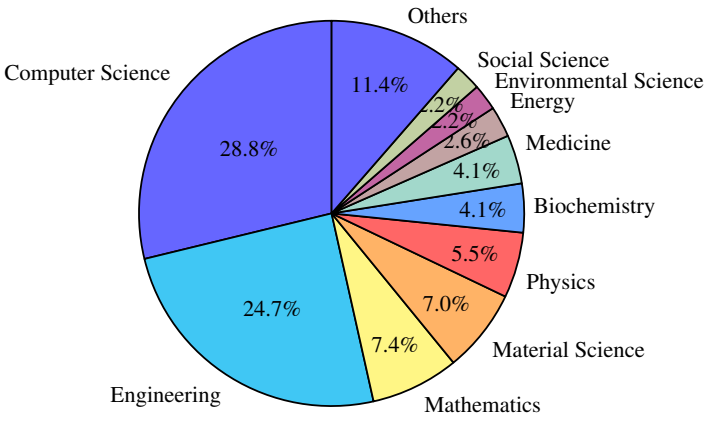


Figure 3: Scopus field of publication analysis.

4.1 Weight Initialisation

The initialisation process is a crucial optimisation approach for training DNNs. It specifies how fast the learning model converges and are used to define the starting point of a training process [21, 22], especially during the forward pass, thereby avoiding vanishing and exploding gradients. The DNNs inherently have a significant amount of parameters with a non-convex loss function response, which makes them challenging to train in real-time. To train these DNNs to achieve fast convergence while avoiding vanishing gradient problems, a careful and proper network initialisation is necessary [22, 23]. Although, it is worthy of highlighting that a proper initialisation ensures to avoid magnifying or reducing the magnitudes of a given signal exponentially [24]. While weights and biases are the key parameters to initialise, the initialisation should be able to break symmetry within the hidden units of the network.

Early weight initialisation techniques include the sparse initialisation where each unit is initialised to a constant non-zero value [25]. This approach provides more diversity in time initialised units but becomes a problem for larger Gaussian values and models with a very significant number of filters. Besides, other researchers performed initialisation differently, by initialising from Gaussian distribution with a standard deviation of 0.01, with the biases set to 1 [21], nevertheless, this technique suffers from poor convergence[24]. Other initialisation techniques include initialising with an orthonormal matrix with a carefully selected scale factor that accounts for non-linearity [26], with researchers suggesting that this technique performed better than the Gaussian distribution-based initialisation. Furthermore, the layer-sequential unit-variance(LSUV) initialisation uses the orthonormal matrices approach to pre-initialise weights of each convolution layer, with the variance of the output from the first layer normalised to 1, up to the last layer [27], in a deep CNN application.

Besides, another vital weight initialisation technique include the Xavier initialisation techniques[28], which uses a scaled uniform distribution and assumes that the activations are solely linear in all applications, thereby maintaining variance across each layer [24]. Perhaps, this is not true when the rectified activations are used in a model. This becomes a limitation for the Xavier initialisation as well as the poor convergence on very deep architectures with over thirty layers [24]. Other initialisation techniques for further exploration include the identity matrix technique, constant technique, orthogonal techniques, and variance scaling approach [26].

For proper initialisation, researchers suggest that the choice of the uniform or Gaussian distribution does not matter much but the scale of the initial distribution is a vital factor in the model optimisation [2], with the larger initial weights providing higher symmetry-breaking effect, avoidance of signal loss during forward and backwards passes, and a risk of exploding gradients. Conversely, the selection of optimal weight parameters alone cannot guarantee optimal performance especially as the behaviour of a model during the learning process is dynamic and the model parameters are not only the weights, although they are among the critical factors for the improved performance of DNNs.

4.2 Biases

The biases are vital parameters of the hidden layers of the NN. They are useful and allows for the shifting of the activation of a given NN to fit the incoming signals. It can move either left or right, thereby acting as an offset, to influence the output of the model. A crucial property of the biases is that they do not interact with the original inputs of the model as depicted in Figure 4. The initialisation of these biases is usually set to 0; however, it might be set to non-zero values in practice as researchers suggest, and that bias initialisation should not be from a random walk initialisation [29].

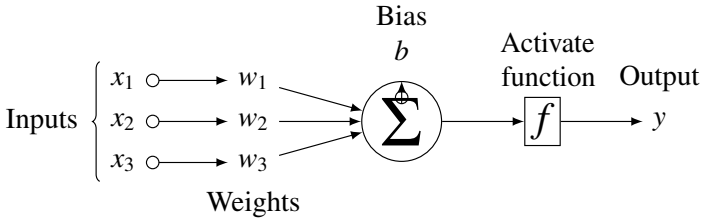


Figure 4: Typical neural network showing the positions of Weights and biases.

Conversely, initialising with high biases produces a very high output while using very low values, tends to make the signal disappear, thereby causing vanishing gradient problems. However, different architectures require different initialisation techniques; for example, the LSTM investigation have researchers suggesting to set the bias to 1, on the forget gate [30]. Another bias initialisation technique is to start with very small values, such that it would not cause massive saturation at the start especially when the rectified activations are involved [2].

Initialising the weight and bias parameters of a NN is a heuristic process and setting the bias to very small values for architectures with rectified activation is recommended while setting it to 0 for the linear activation is the standard practice. However, [2] suggest that setting biases to 0 is very compatible with the majority of the weight

initialisation techniques. Perhaps, where resources permit, setting these parameters as a hyperparameter is recommended, for scales are chosen by parameter search, thereby enhancing performance. Finally, to obtain the ideal model parameters for the weights and biases involves optimisation and these optimisation techniques are presented in the subsequent sections.

4.3 First Order Optimisers (FOO)

The FOO is the dominant class of optimisers used in DL research. These models try to minimise or maximise the error function (Ex) using gradient values with respect to other parameters in the network [31, 21]. Generally, the gradient is the rate at which parameters change with time. The minimised or maximised function is usually denoted by superscript *. The error function is given by [2]

$$x^* = argmin f(x). \tag{5}$$

Gradient descent tells when the function is increasing or decreasing at a particular point. The first order gradient produces a line tangential to a position on the error surface and is easy to compute, less time consuming and converges fast on large datasets. The variants of the first-order optimisation algorithms including batch, stochastic and mini-batch gradient descent, stochastic gradient descent with momentum as well as with warm restarts, Nesterov accelerated gradient, AdaGrad, AdaDelta, RMSProp, Adam, AdaMax, Nadam, AMSGrad, Radam and the Lookahead optimisers. These first-order algorithms are discussed in details subsequently.

4.3.1 Batch Gradient Descent (BGD)

This variant of gradient descent computes the gradient of the loss function with respect to the parameters θ for the whole training examples and update accordingly. The BGD is the default gradient descent algorithm, and it is given by

$$\theta = \theta - \eta \cdot \nabla_\theta J(\theta) \tag{6}$$

As this update is performed once, the BGD is inherently slow as well as not suitable when the entire examples cannot fit the computer memory, thereby not ideal for very DNN. The BGD does not guarantee to converge to some global minimum for convex surface errors alongside a local minimum for non-convex surfaces [32].

4.3.2 Stochastic Gradient Descent (SGD)

The SGD technique is one of the foremost approximation techniques found in the literature. It was first proposed as an approximation method of gradient optimisation by [33] and has witnessed diverse variants of optimisation to suit different applications. The stochastic gradient descent algorithm was proposed as a solution to manage the memory and speed of the BGD optimisation. The SGD solved these problems by randomly selecting the next set of examples that will update the trainable parameters, thereby improving the training speed. For a simple randomly selected examples $x^{(t)}, y^{(t)}$, the SGD is given by the relationship [34]

$$\theta_{t+1} = \theta_t - \eta_t \nabla_\theta \iota \left(\theta_t; x^{(t)}, y^{(t)}\right) \tag{7}$$

The advantage of SGD as outlined by [35] is that it performs better than the adaptive optimisers at very prolonged training time for effective hyperparameter tuning. However, some significant drawbacks exist for the SGD optimiser, which includes that there is no adaptive way for finding the optimal learning rate for the training process and the SGD has the gradients tending to zero at some point (saddle point), thereby making it difficult to continue alongside it's poor convergence speed. Furthermore, other authors highlighted that the SGD does not scale well with huge datasets as well as underfitting the data for very deep architectures [36]. These drawbacks inspired further research into improving the SGD optimisation technique.

4.3.3 Mini-Batch Gradient Decent (MGD)

The MGD is an optimiser that performs an update on every batch of the training examples. The MGD offers numerous advantages which include a reduction in the variance parameter updates, thereby leading to better convergence. MGD is fully optimised for training NNs, and it is computed by [31]

$$\theta = \theta - \eta \cdot \nabla_\theta J(\theta; x^{(i:i+n)}; y^{(i:i+n)}) \tag{8}$$

The limitation of MGD is that it does not guarantee excellent convergence speed as well as the difficulty of choosing the appropriate learning rate for the algorithm, which should ideally be a parameter of the dataset being considered.

4.3.4 Stochastic gradient Descent with Momentum (SGDM)

The SGDM was proposed to speed up the optimisation process of the training per dimension [37]. The process involves accelerating the process in line with the direction where the gradient points to, as well as slowing the process in the direction where the sign of the inherent gradient is changing. The classical SGDM update is given by the relationship [34]

$$v_{t+1} = \gamma v_t - \eta_t \nabla_\theta \iota \left(\theta_t; x^{(t)}\ y^{(t)}\right)\ ;\ \theta_{t+1} = \theta_t - v_{t+1} \tag{9}$$

Where v_{t+1} = current velocity vector, γ = momentum term which is usually set as $\gamma = 0.9$. Alternatively, the SGDM could also be achieved by keeping track of the previous parameter updates using an exponential decay function given by

$$\Delta x_t = \rho \Delta x_{t-1} - \eta g_t \tag{10}$$

Where ρ is the decay constant controlling the previous parameter updates. The drawback for the SGDM is that the learning rate is still manually optimised, and this makes it dependent on expert judgement when trying to optimise an SGDM based model.

4.3.5 Stochastic Gradient Descent with Warm Restarts (SGDR)

The SGDR is another variant of the gradient descent optimisation that uses warm restarts instead of learning rate annealing to accelerate the training of deep neural networks. In every restart, the learning rate is initialised to a value which is scheduled to decrease. A key property of the warm restart is that the optimisation does not start from the beginning but from the parameters of the model at the

last step of convergence. The decrease in learning rate is obtained using a schedule of aggressive cosine annealing given by [38]

$$\eta_t = \eta^i_{min} + \frac{1}{2}(\eta^i_{max} - \eta^i_{min})\left(1 + cos(\frac{T_{cur}}{T_i}\pi)\right) \quad (11)$$

Where η^t_{min} and η^t_{max} represents learning rate ranges and T_{cur} represents the number of epochs since the last restart. The T_i is the total epochs performed while i is the index of the iteration or run. The SGDR is used to deal with multi-modal functions, and these warm restart improves the rate of convergence in accelerated gradient schemes and has been successful in deep learning-based applications.

4.3.6 Nesterov Accelerated Gradient (NAG)

The Nesterov's accelerated gradient is another first-order optimisation method that provides better convergence than gradient descent based optimisers under certain conditions [22]. The NAG optimiser was inspired by Polyak classical momentum technique of accelerating gradient descent that accumulates a velocity vector in the direction of continuous decreasing objective function [33]. Typically, given an objective function $f(\theta)$ for minimisation, the classical momentum is obtained by

$$v_{l+1} = \mu v_t - \epsilon \nabla f(\theta_t) \quad ; \quad \theta_{t+1} = \theta_t + v_{l+1} \quad (12)$$

Where $\epsilon > 0$ = learning rate, $\mu \in [0, 1]$ = momentum coefficient and $\nabla f(\theta_t)$ = gradient at θ_t. The NAG optimiser and update rule is obtained using the relationships

$$v_{t+1} = \gamma v_t - \epsilon \nabla f\left(\theta_t + \mu v_t\right) \quad ; \quad \theta_{t+1} = \theta_t - v_{t+1} \quad (13)$$

The NAG computes gradient known as θ_{t+1} and approximates the subsequent steps for choosing optimal step size. The NAG first moves in the direction of past accumulated gradients γv_t, computes the current gradient and updates the gradient. However, the NAG and most of the gradient-based optimisers have the same general limitation of having hand-fixed learning rate. This limitation inspires the adaptive learning-based optimisation techniques, where the learning rates may be a learnable hyperparameter. The adaptive optimisers are discussed as follows.

4.3.7 AdaGrad

The AdaGrad optimiser is an adaptive gradient algorithm proposed by [1], and it represents another vital optimiser which has adaptive parameter specific learning rates that are updated relative to the frequency of parameter updates during training. The lower learning rates implies more parameter updates during training and vice versa. The main features of the AdaGrad include fast convergence, and it considers every parameter when selecting learning rates when compared to the gradient descent techniques where one single learning rate is used for all features. This creates the flexibility of increasing or decreasing the learning rate depending on the considered feature properties.

The AdaGrad algorithm update formulation is obtained first by defining the parameters, where g_t = gradient at a time step of t, When the partial derivative of the loss function with respect to parameter θ_i, at time step t, is given by $g_{t,i}$, we can deduce the following update relationships for AdaGrad

$$gt, i = \Delta_\theta J(\theta_{t,i}) \quad ; \quad \Delta x_t = -\frac{\eta}{\sqrt{\sum_{r=1}^{t} g_\tau^2}} \cdot gt \quad (14)$$

Where η is a global learning rate shared by all dimensions, and the denominator computes an ι_2 norm of all the past gradients on each dimensional basis. $g(t, i)$ = the gradient of the loss function with respect to parameter $\theta_{(i)}$ at t time step.

Generally, AdaGrad modifies the general learning rate η at every iteration of time step t for all parameters $\theta_{(i)}$ based on the past computed gradients for $\theta(i)$. The main identified limitations of AdaGrad includes fixing the global learning rate to a default value, the continued drop or decaying of the learning rate throughout the learning process [39] as well as the AdaGrad not been optimised for non-convex functions [2].

4.3.8 AdaDelta

The AdaDelta is another robust adaptive learning based optimiser proposed mainly to address a significant limitation of AdaGrad by reducing the aggressiveness of AdaGrad through reduction of the optimiser learning rate. The AdaDelta optimiser uses restricted windows of past gradients, to a fixed size w, to update the learning rates rather than accumulating all the past gradients in the network [39]. Rather than storing all the inefficient previous squared gradients w, it uses the sum of exponentially decaying average of the squared gradients. At time t, the running average $E[g^2]_t$ is given by

$$E[g^2]_t = \rho E[g^2]_{t-1} + (1 - \rho) g_t^2 \quad (15)$$

Where ρ is the decay constant. The update is given by

$$\Delta x_t = -\frac{RMS\,[\Delta x]_{t-1}}{RMS\,[g]_t} \cdot gt \quad (16)$$

Where Δ is the sum of the numerator term, t = time, and g = gradient. The authors enumerated the benefits of AdaDelta to include the elimination of manual fixing of learning rates, different dynamic learning rates per dimension of the parameters, less computation compared to gradient descent, robust to large gradients noise and architectures among other benefits. The author further highlighted that the hyperparameters do not require tuning, which makes the AdaDelta optimiser, a more straightforward algorithm to implement. The AdaDelta has recently been used in the design of a CNN architecture for automated image segmentation[40].

4.3.9 Root Mean Square Propagation (RMSProp)

The RMSProp is the root mean square optimisation technique which can be viewed as a modification of AdaGrad, that is optimised to perform on the non-convex setting by altering the gradient accumulation into a weighted exponential moving average. The RMSProp splits the learning rate by using an exponentially decaying average of squared gradients, and this optimiser is obtained by [2, 31]

$$E[g^2] = \gamma E[g^2]_{t-1} + (1 - \gamma)\, g_t^2\,;\, \theta_{t-1} = \theta_t - \frac{\eta}{\sqrt{E\,[g^2]_t + \epsilon}} \cdot gt \quad (17)$$

Where the appropriate values of $\gamma = 0.9$ and the learning rate $\eta = 0.001$. The RMSProp works well in stationary and online settings

[31] but suffers similar drawback like most of the non-adaptive optimisers as the learning rates are manually fixed or handcrafted. An advantage provided by RMSProp is that it requires less tuning compared to the SGD[35]. Besides, the RMSProp has been used in different DL architectures including to optimise the parameters of a combined deep CNN and LSTM for classifying protein structures[41] as well as the design of a new deep convolutional spiking neural network for time series classification[42].

4.3.10 Adam

Adam coined from adaptive moment estimation is another first-order gradient optimisation algorithm for stochastic objective functions based on adaptive estimates of moments of lower-order degrees. Adam is well suited for large-scale parameters and data as well as offering improved computational efficiency, improved memory requirement and invariant to the diagonal rescaling of gradients [31]. The Adam optimiser is designed to combine the properties of RMSProp and AdaGrad optimisers to obtain the first and second moments estimates which represent the mean and uncentred variance of respective gradients using

$$\hat{m}_t = \frac{m_t}{1-\beta_1^t} \quad ; \quad \hat{v}_t = \frac{v_t}{1-\beta_2^t} \tag{18}$$

Where $\hat{m}_t$ is the gradient and $\hat{v}_t$ is the squared gradient and β_1, β_2 are hyperparameters that control the exponential decay rate of these moving averages, typically $\beta_1, \beta_2 \in [0, 1]$. The gradient updates are estimated directly from running average of this first and second moment of a gradient to produce the update rule as

$$\theta_{t+1} = \theta_t - \frac{\eta}{\sqrt{v_t} + \epsilon}\hat{m}_t \tag{19}$$

The authors outlined that the appropriate values of the parameters β_1 and β_2 are 0.9 and 0.999 respectively, while $\varepsilon = 10^{-8}$. Furthermore, they highlighted that Adam performs well in practice and compares favourably with stochastic based optimisation techniques. It also converges fast and provided a solution for the majority of the challenges faced by different optimisers which include slow convergence and vanishing gradients. The Adam optimiser has been used in the design of a new gated branch neural network for an advanced driver assistance system[43] as well as been the most used optimiser in the recent DL model developments and has been used across diverse industrial applications[44, 45].

4.3.11 AdaMax

The AdaMax optimiser is a variant of Adam with infinity norm. The velocity parameter of the algorithm scales the gradient inversely to the ι_2 norm of the previous gradients through the v_t and current gradient $| g_t |^2$ terms. The gradient is obtained by the relationship [32]

$$v_t = \beta_2 v_{t-1} + (1-\beta_2) \mid g_t \mid^2 \tag{20}$$

The AdaMax convergence of the gradient with ι_∞ norm is

$$v_t = \beta_2^\infty v_{t-1} + (1-\beta_2^\infty) \mid g_t \mid^\infty = \ max(\beta_2 \cdot v_{t-1}, \mid g_t \mid) \tag{21}$$

The final update rule for the AdaMax is computed as

$$\theta_{t-1} = \theta_t - \frac{\eta}{u_t}\hat{m}_t \tag{22}$$

Where u_t depends on the max operation. Default values for $\eta = 0.002, \beta_1 = 0.2$ and $\beta_2 = 0.999$. The AdaMax has been incorporated in the design of a deep CNN based Light Detection and Ranging (LiDAR) system application [46].

4.3.12 Nesterov accelerated Adaptive Moment Estimation (NAdam)

The NAdam optimiser combines the properties of Adam optimiser and NAG optimiser to obtain an improved optimiser. It modifies the momentum term $\hat{m}_t$, and instead of adding the momentum term twice, the gradient is updated as *gt* alongside updating the parameters θ_{t-1}. The Nadam new update rule is written in the following form [47]

$$\hat{m}_t \leftarrow (1-\mu_t)g_t + \mu_{t+1}m_t \quad ; \theta_t \leftarrow \theta_{t-1} - \eta\frac{\hat{m}_t}{\sqrt{v_t}+\epsilon} \tag{23}$$

The Nadam optimiser was tested successfully on MNIST dataset, and it showed remarkable results [47].

4.3.13 AMSGrad

The AMSGrad combines the benefits of Adam and RMSProp as a moving average optimiser to guarantee convergence of learning systems. It uses lower learning rates when compared to Adam alongside incorporating slowly decaying gradients on the learning rate [48]. It also uses the maximum of past squared gradients instead of the commonly used exponential averages, to update the parameters of the optimiser where this maximum past gradient is obtained by

$$\hat{v}_t = max(\hat{v_{t-1}}, \hat{v}_t) \tag{24}$$

The new update rule for the AMSGrad becomes

$$\theta_{t-1} = \theta_t - \frac{\eta}{\sqrt{\hat{v}_t}+\epsilon}m_t \tag{25}$$

The authors outlined that the results from the testings of this AMSGrad outperformed the Adam optimiser in most cases; however, to see the practical performance of AMSGrad on more difficult datasets is still not proven. The AMSGrad has been successfully implemented for optimising the weights of deep Q-learning(DQL) used in the energy management of some hybrid electric vehicles[49].

4.3.14 Rectified Adam (RAdam)

The RAdam optimisation approach was proposed to address the large variance problem in the early stages of the adaptive learning rates by reducing the variance of the network parameters. This is achieved by rectifying the variance of the adaptive learning rate [50]. The rectified variance term is given by

$$r_t = \sqrt{\frac{(p_t-4)(p_t-2)p_\infty}{(p_\infty-4)(p_\infty-2)p_t}} \tag{26}$$

The value of p_∞ should be $p_\infty \leq 4$. The authors outlined that RAdam can obtain better accuracy or an accuracy identical to Adam, with a fewer number of epochs compared to the standard Adam optimiser. The RAdam showed excellent prospects and was tested on large scale datasets to highlight the performance.

4.3.15 Lookahead

The Lookahead optimiser is another optimiser that iteratively updates two sets of weights. The unique property of the Lookahead optimiser is that it works alongside another optimiser. It updates by choosing a search direction by looking ahead at some sequence of fast weights produced by another optimiser [51]. The fast weight update rule is

$$\theta_{t,i+1} = \theta_{t,i} + A(L, \theta_{t,i-1}, d). \tag{27}$$

Where A = optimisation algorithm, L = objective function, and d = current mini-batch training example. The authors outlined the new benefits provided by the Lookahead optimiser to include that it improves learning scalability and lowers variance with some little memory and computation cost.

4.4 Second-Order Optimisers (SOO)

The SOO uses second-order derivatives to improve model optimisation. These derivatives often referred to as Hessian matrix approximations of Hessian is useful to obtain optimal parameters during the training of NNs. These second-order models are inherently faster when the second-order derivative is known but are always costly and slower to compute in terms of memory and time. Some of the different SOO techniques used in DL are discussed in the following sections.

4.4.1 Newton's Method

This is a second-order optimisation technique that uses second-order Taylor series expansion to approximate $J(\theta)$ near some point θ_0 while ignoring the higher-order derivatives. The approximation relationship gives Newton's method optimisation as

$$J(\theta) \approx J(\theta_0) + (\theta - \theta_0)^T \nabla_\theta J(\theta_0) + \frac{1}{2}(\theta - \theta_0)^T H(\theta - \theta_0) \tag{28}$$

Where H is the Hessian of J with respect to θ computed at θ_0. The update rule is obtained by solving the critical point of this function given by

$$\theta^* = \theta_0 - H^{-1} \nabla_\theta J(\theta_0) \tag{29}$$

From the update rule, it is evident that Newton's method involves two stages which includes computing the inverse Hessian and secondly, updating the other parameters accordingly using the iteratively computed inverse Hessian. However, this method can only work when the Hessian is positive, and this is not the case for DNNs that have built-in non-convex objective functions with saddle points, that Newton's method cannot manage effectively without modification. A modification of Newton's method to include a regularisation term on the Hessian is a possible solution [2]. This is achieved by adding a constant along the diagonal of the Hessian thereby changing the update rule to

$$\theta^* = \theta_0 - [H(f(\theta_0)) + \alpha I]^{-1} \nabla_\theta f(\theta_0) \tag{30}$$

This strategy works well as long as the negative eigenvalues of the Hessian remain very close to zero. Some authors have pointed out that the use of this method for training DNNs imposes a huge computational burden. By implication, it possible to train networks with a small number of parameters in practical case using Newton's method [2], but limited in deep learning application.

4.4.2 Quasi-Newton's Methods (QNM)

The QNM is another second-order optimisation technique used in nonlinear programming applications where Newton's method of optimisation is difficult to use due to implementation timing constraints. They are used to find the global minimum of twice differentiable functions. The QNM requires only the gradient of the objective function to be computed during each iteration. The method is computationally cheaper and faster than the original Newton's method approach as it does not require the computation of the inverse Hessian as well as solving systems of linear equations. The Broyden-Fletcher-Goldfarb-Shannon (BFGS) algorithm is one of the popular QNM optimisation algorithms that approximate Newton's update rule as [2]

$$\theta^* = \theta_0 - H^{-1} \nabla_\theta J(\theta_0) \tag{31}$$

Where H is the Hessian of J with respect to θ computed at θ_0. The BFGS algorithm approximates the inverse of a matrix M_t, and once the inverse Hessian is updated, the direction of the descent ρ_t is determined by the relationship

$$\rho_t = M_t g_t \tag{32}$$

A line search in the direction of the descent is performed to determine the step size ϵ^* , with the final update rule as

$$\theta_{t+1} = \theta_t + \epsilon^* \rho_t \tag{33}$$

The need to store the Hessian matrix results makes the use of the BFGS algorithm computational expensive and unrealistic for deep learning models having millions of parameters for computation during training [2]. However, more recent research using the QNM approach has been applied successfully to train DNNs on large-scale datasets[52].

4.4.3 Sum of Functions Method

The sum of functions is another second-order optimisation approach that combines the SGD and BFGS algorithms to provide improved optimisation of DNNs [52]. The authors presented a method of minimising the sum of functions that combines the efficiency of SGD with the second-order curvature information used in QNM, thereby maintaining an independent Hessian approximation, for each contributing function in the sum, for computational traceability. This optimisation approach works with mini-batches of data, alongside the deep architectures with the approximation of the series function $G^t(x)$, defined by the intended approximate relationship

$$G^t(x) = \sum_{i=1}^{N} g_i^t \tag{34}$$

Where t = learning iteration, $g_i^t(x)$ = quadratic approximation corresponding to $f_i(x)$. For a vector x_t obtained by minimising the approximate objective function $G^{t-1}(x)$, we have that

$$x^t = argmin_x G^{t-1}(x) \tag{35}$$

We also know that $G^{t-1}(x)$ = sum of quadratic functions $g_i^{t-1}(x)$, Thus, the function can be minimised using a Newton's step given by

$$x^t = x^{t-1} - \eta^t (H^{t-1})^{-1} \frac{\delta G^{t-1}(x^{t-1})}{\delta x} \tag{36}$$

Where H^{t-1} is the Hessian of $G^{t-1}(x)$ and step length $\eta^t = 1$. Therefore, the update rule becomes

$$g_i^t(x) = \begin{cases} g_i^{t-1}(x) \text{ for } i \neq j \text{ and } g_i^t(x) = \\ \begin{bmatrix} f_i(x^t) \\ +(x - x^{tT} f_i(x^t) \\ +\frac{1}{2}(x - x^{tT} H_i^t (x - x^t) \end{bmatrix} \text{ for } i = j \end{cases} \tag{37}$$

Where the quadratic term H_i^t is set using the BFGS algorithm. The sum of function optimiser was successfully used to train large datasets.

4.4.4 Conjugate Gradient Methods

The conjugate gradient is a Hessian free second-order optimisation technique. It avoids the use of second-order Hessian matrix in optimising gradient computation by iteratively descending conjugate directions. Though this optimisation technique is an old optimisation technique, modified versions have been successfully applied in DL research [25]. The conjugate gradient minimises the objective function with respect to parameter θ and iteratively updates the approximation of each step is given by

$$M_{\theta_n} = f(\theta_n) + f'(\theta_n)^T \delta_n + \delta_n^T B \delta_n / 2 \tag{38}$$

Where B is the Gauss-Newton matrix and δ_n represents the search direction for updating the parameter θ_n.[36] The conjugate gradient method finds a search direction that is conjugate to the previous line search direction and during the training iteration t, the new search direction takes the form [2]

$$d_t = \nabla_\theta J(\theta) + \beta_t d_{t-1} \tag{39}$$

Where β_t = coefficient that controls how much direction of d_{t-1} that is added to the current search direction. The value of β_t can be computed using different techniques among the major ones include Polak-Ribieri and Fletcher-Reeves algorithms. The computation formula of these respective techniques is given by [2]

$$\beta_t = \frac{(\nabla_\theta J(\theta_t) - \nabla_\theta J(\theta_{t-1}))^T \nabla_\theta J(\theta_t)}{\nabla_\theta J(\theta_{t-1})^T \nabla_\theta J(\theta_{t-1})} \quad \approx$$

$$\beta_t = \frac{\nabla_\theta J(\theta_t)^T \nabla_\theta J(\theta_t)}{\nabla_\theta J(\theta_{t-1})^T \nabla_\theta J(\theta_{t-1})} \tag{40}$$

An important note is that for a quadratic surface, the conjugate direction ensures that the magnitude of the gradient along the previous direction does not increase. However, some researchers suggested that the second-order optimisers generally do not favour DL applications [38], and the authors highlighting the following as the reasons for that assertion about the second-order models.

- The stochastic nature of $\nabla f_t(x_t)$.
- The ill-conditioning of parameter f.
- The presence of saddle points caused by the geometric structure of the parameter space.

This makes the first-order optimisation algorithms and techniques more useful when considering deep learning-based model parameter optimisation.

Nevertheless, another technique to improve DL model training is regularisation where dropout, dropconnect and norm regularisation techniques are used to reduce the computational cost of the model. More detailed discussions on these regularisation techniques are described in the literature[34]. Besides, other optimisation techniques include the second-order Newton's Method, Conjugate Gradient, and Quasi-Newton's Method (QNM), as well as the' parallel computing, and sum of functions. These techniques aim to improve the convergence speed of large-scale machine learning datasets. Conversely, these second-order optimisers are not always used in DL applications because of the computational burden it causes for large networks with a significant number of parameters, making them difficult for DL models having millions of parameters for computation during training [2]. However, they are gaining attention recently with researchers exploring the QNM approach to train a DNN on large-scale datasets successfully[52].

4.5 Swarm Intelligence Optimisers (SIO)

The swarm intelligence (SI) optimisers are generally computational techniques for solving distributed problems inspired by biological behavioural examples of ants, honey bees, wasps, termites, birds flocking, and many others. The SIO provides fast and reliable techniques for finding solutions on numerous real and complex problems[53]. Typical examples of SIO include ant colony optimisation, particle swarm optimisation, firefly algorithms, artificial fish swarm optimisation and many others. A very detailed survey of these dynamic SIO and algorithms can be found in this literature [54]. However, our focus lies in these optimisers that have been implemented in DL research.

4.5.1 Grey Wolf Optimiser (GWO)

The GWO is a SI optimiser that has recently been applied to DL research where the GWO was used to optimise the number of hidden layers and weights of the neural network [55]. It is proposed by [56], and it mimics the grey wolves internal leadership hierarchy in-which four key categories of wolves including alpha, beta, omega and delta was used to represent the best individual as alpha, the second-best individual as beta, the third-best individual is recorded as delta, and the remaining individuals are considered as omega. The hunting is guided by alpha, beta and delta [53]. The positions of the wolves are obtained using optimisation relationships

$$\vec{D} = |\vec{C} \cdot \vec{X_P}(t) - \vec{X(t)}|$$

$$\vec{X}(t+1) = \vec{X_P}(t) - \vec{A} \cdot \vec{D} \tag{41}$$

where $\vec{A}$ and $\vec{C}$ are the coefficient vector, t represents the $t-th$ iteration, $\vec{X}$ is the wolf vector position and $\vec{X_P}$ is the prey vector position. The vectors $\vec{A}$ and $\vec{C}$ is obtained by

$$\vec{A} = 2a \cdot \vec{r_1} - \vec{a}$$

$$\vec{C} = 2 \cdot \vec{r_2} \tag{42}$$

where $\vec{r_1}$ and $\vec{r_2}$ are random vectors located in the slope of [0, 1] and the value of $\vec{a}$ lies between $0 and 2$.

The GWO has been recently applied in optimising flight models, especially to identify the flight state using CNNs [57] as well as modifying the hidden parameters of the SAE architecture[55]. Researchers suggest that the GWO is simple in design, fast with very high search precision, thereby making it easy to realise and implement in practical engineering applications[53]. The GWO was applied to the stacked auto-encoder (SAE) architecture for sorting different kinds of cotton [55] as well as for classifying extracted features of diabetic retinopathy dataset[58]. The GWO exploration has provided numerous improved versions, with the first being the improved Grey Wolf Optimiser (IGWO), proposed[53], as well as the multi-objective criteria version named multi-objective grey wolf optimizer (MOGWO) for DL application. The MOGWO was implemented in the long short term memory (LSTM) architecture on time series data to develop hybrid forecasting systems. Also, the use Harris hawk optimisation, which is a nature-inspired population-based optimiser, and GWO is combined based on the mutation and hierarchy properties to produce a hybrid SI optimiser named MH-HOGWO and applied in the multi-step ahead short-term forecasting of wind speeds [59].

4.5.2 *Multi-swarm particle swarm optimizer and Improved Firefly Algorithm (MSPSO-ImFFA)*

The MSPSO is another SI optimiser that has a modified version applied in DL research. This new adaptive MSPSO includes the improved firefly algorithms(ImFFA) that help the DNN to overcome the global and local minima as well as avoidance of premature converging during training. The MSPSO-ImFFA derivations and code can be found in the original paper[60]. The algorithms were used to train a DL backpropagation neural network (DLBPNN) for detecting and classifying lungs cancer nodules.

4.5.3 *Particle Swarm Optimisers (PSO)*

The PSO optimiser is another SI optimisation technique that has the ability to control the search by changing standard deviation (SD) and mean of a Gaussian distribution where the search area is linked to its SD. It uses a specific set of candidate solutions denoted by particles, that make-up the swarm population of the entire search space[61]. The improved ladder and long-tail (LLT) denoted as LLT-PSO is designed to cater for the internal setting as well as the external part of the multi-view fusion of the model. However, the model has two convolutional, and two fully-connected layers in all might not represent a typical deep architecture. The PSO has also been improved by [62] with the Adaptive Cooperative Particle Swarm Optimisation (ACPSO) proposed, which incorporates a learning automata to adaptively split the sub-population of cooperative PSO, thereby making the decision variables with strong coupling connection to enter the same sub-population. Conversely, other SI based optimisers explored for DL include the salp-swarm optimiser [63], harmony search optimiser on variational stacked autoencoders[64], whale optimisation algorithm(WOA) using bidirectional RNN [65], the Artificial Bee Colony (ABC) for optimizing hyperparameters for LSTM models, the AC-Parametric WOA (ACP-WOA) [66] for predicting biomedical images, symbiotic organisms search (SOS) algorithm [67], lion swarm optimiser(LSO) [68], and many others. Nevertheless, a comparison of the performance of these genetic algorithms shows that the GWO convergence rate is fastest compared to the Genetic Algorithm (GA), and PSO [69]. However, there is no holistic comparison of the performance of these SI optimisers found in the literature.

4.6 *Parallel Computing Optimisation*

Parallel computing is another optimisation approach aimed at improving the convergence speed of large-scale machine learning datasets. A popular SGD parallelised method was proposed by [70] where multi-core setting with tight coupling of the processing units ensures low latency between processors used in computing gradient updates. The parallel optimisation approach includes the synchronous and asynchronous techniques where the computation in the synchronous machines are affected by slow computers and machines on the networks causing delays [70], the asynchronous does not and it is the design model for most parallel connected devices. The parallelised SGD optimisation improves the standard SGD optimisation for application in deep learning [71]. The parallelised SGD optimiser is given by

$$vi = SGD(c^1, ...c^m, T, \eta, w_0) \quad \text{for} \quad i \in 1, ..., k \tag{43}$$

Where T = number of instances per machine. The overall sum of all gradients provide the aggregate from all computers as

$$v = \frac{1}{k} \sum_{i=1}^{k} V_i \tag{44}$$

The asynchronous process speeds up the training process by distributed processing with many central processing units (CPU) and graphics processing unit (GPU); however, the combination of the multiple GPU with asynchronous SGD accelerated the training process hugely [72], with the improvements in speed put at 3.2 times for four GPU's compared to single GPU [73]. The parallelised optimisation approach has become the default approach for training very DNNs for large datasets in recent time. Conversely, the SGD has also explored the high-performance computing cluster (HPCC) for distributed and parallelised DL applications and has been successfully implemented and tested on standard DL libraries [74].

5 Discussion

Optimisers and optimisation techniques have witnessed tremendous and advanced research results, of which there are observable trends. These trends in methods and algorithms show that there is no single

existing optimiser or optimisation technique that can be used as a stand-alone optimiser for all DL research application. To achieve a holistic optimisation, the use of multiple optimisation approaches at different stages of the development and deployment of DL based models is necessary and this aligns with the no free lunch theorem that no single meta-heuristic optimisation technique can satisfy all cases and applications [75]. In a typical DL model, which involves five key stages, as shown in Figure 5. Research has shown that each of these specific stages can be optimised in one way or another. However, some of the techniques involve optimising the model design using weight initialisation, gradients, and parallel computing, as well as other model improvement techniques not discussed which include data augmentation, regularisation, dropout, batch normalisation among other methods for DL.

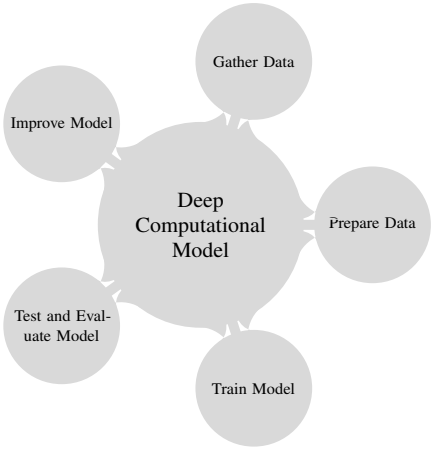


Figure 5: Typical deep learning model

The current application of these optimisation algorithms and techniques cuts across different industries that use neural networks to develop and deploy applications. For the stochastic gradient descent based optimisers, convergence may not be attainable when the performance of the model stops improving. A remedy to this challenges is early stopping in the case where the optimisation process is halted based on the performance of the validation set during training[76]. A proper early stopping criterion guarantees that the model training process continues as long as the network generalisation ability is improved and overfitting is avoided.

Perhaps, the current practices in the use of optimisers adopt multiple optimisation techniques where there are batch normalisation, weight and bias initialisation, data augmentation, mini-batch gradient descent, parallel computing and many other optimisation techniques involved in training a single DNN architecture. This makes most of the applications complex for development and deployment.

5.1 Application Areas

The application areas where the new optimisers are tested spans across image recognition, text classification, NLP, neural machine translation (NMT), regression-based problems. A summary table of the application areas of these optimisers are outlined. Besides, the most recent application trend is the use of SI optimisers in DL. This optimisation approaches represent the new research direction for improving DL model performances. The summary of these optimisers alongside the test dataset are outlined in Table 2, showing the original test datasets for these optimisers.

From Table 2, it is evident that ImageNet, MNIST and CIFAR-10/100 datasets rank among the most dormant datasets used in testing the new optimisation algorithms. This is as a result of the CNN architectures used for recognition applications. Although this trend is quite impressive, other datasets have also been used for NLP, and regression-based models like PT, NMT, EEG recordings and word2vec.

5.2 Model Testing Architectures

The DL architecture used in testing these novel optimisers is outlined, which include the CNN, SAE, DBN, RNN, and multi-layer neural networks (MLP), among other DNN architectures. The specific test per optimiser is presented in Table 3.

A remarkable trend in the architectures shows that major recent optimisers are tested on CNN architectures while the earliest optimisers were tested both on the MLP architectures. Also, the SI optimisers have found applications in RNN and SAE architectures, with some architectures not explicitly outlined by the authors of the original papers.

However, the use of optimisers among researchers has witnessed different researchers, selecting other datasets for testing the performance of new and ground-breaking development results. Testing these new and emerging optimisers with the same datasets or the down-sampled versions would present a reasonable and level approach to ascertain the reported results of the latest algorithm improvements. A gold standard for image recognition has been the ImageNet dataset, which one would suggest maybe the best for testing optimisers for image-based datasets alongside using the full dataset or the down-sampled versions which were used by some researchers to test their algorithm performances. A suggestion that new optimisation research and tests should use these four primary datasets including the ImageNet, MNIST and CIFAR-10/100 datasets for image-based analysis, alongside standard text and speech datasets, which will harmonise reporting of new ground-breaking results.

Conversely, comparing the SI optimisers alongside the adaptive and gradient-based optimisers is a future research mostly importantly to compare these optimisers on similar datasets. This is because most of the biological optimisers were tested on different datasets compared to the gradient-based optimisers, which were tested on mostly the four primary standard datasets.

5.3 Choosing An Optimiser

The choice of an optimiser for a specific application is a very challenging task; however, the choice is dependent on how well the model traverses or fits on a particular task. An approach to choosing one is to consider the model architecture, the shape of the expected loss function, and picking an optimiser that can appropriately fit the data on the function. Another important consideration is the notable trade-off on the speed of convergence, training, and generalisation. These considerations were also outlined by [2], as being essential for effective optimisation. A fast convergent model that

Table 2: Application areas of the various optimisation algorithms

Optimiser	Application Area / Datasets
SGDM [21]	ImageNet
SGDR [38]	EEG, ImageNet, CIFAR-10/100
AdaGrad [1]	ImageNet, MNIST, RCVI, UCI
AdaDelta [39]	NLP, MNIST,
Adam [31]	ImageNet
AMSGrad [48]	MNIST, CIFAR-10
RAdam [50]	NLP, ImageNet and CIFAR-10
Nadam [47]	MNIST, word2vec, Penn Treebank(PT)
Lookahead [51]	ImageNet, CIFAR-10/100, NMT, PT
GWO [56]	-
MOGWO [77]	Electrical power and Wind speed.
MSPSO-ImFFA [60]	LIDC and clinical datasets
LLT-PSO [61]	Left ventricle and mammography

Table 3: Architectures for testing the developed optimisation algorithms

Optimiser	CNN	RNN	SAE	DBN	MLP
SGDM [21]	*				
SGDR [38]	*				
AdaGrad [1]	-	-	-	-	-
AdaDelta [39]				*	*
Adam [31]	*				*
AMSGrad [48]					*
RAdam [50]	*	*			
Nadam [47]	*	*			
Lookahead [51]	*	*			
GWO [56]			*		
MOGWO [77]		*			
MSPSO-ImFFA [60]					*
LLT-PSO [61]	*				

cannot generalise is not very useful, therefore finding that balance between convergence and generalisation is critical. If the training speed is the most important factor, then the Adam optimiser ranks amongst the fastest optimisers, with reasonable generalisation capability. Perhaps, if the model can train for a longer time, the SGDM can provide better convergence.

Nevertheless, the use of the SI optimisers has not been tested on the very large datasets like ImageNet and therefore, we cannot say that the SI optimisers can perform optimally on huge datasets. This limits the proposition of the most appropriate and ideal optimiser suitable for every application. An excellent approach is to test the different optimisers heuristically. This approach guarantees that the best optimiser is selected for an application.

6 Conclusion and Future Work

The DL research has witnessed a remarkable breakthrough in the development of optimisers for improving the training process of DNNs. The different optimisers used in DL research have been presented, including gradient, adaptive, hessian, and swarm-based optimisers amongst the various optimisation techniques discussed. Besides, we outlined the different test application of these optimisers, alongside the datasets and architectures used for testing most of the discussed optimisers.

The use of compound optimisation techniques is an emerging trend in SI based optimisation research. It looks to be a future research direction while the approach might improve the gradient-based optimisation techniques. Among the investigated optimisers, first-order optimisers, especially Adam, has been the dominant optimiser, used for most DL research. It is the best performing optimiser for training very DNN architectures as validated by numerous researchers[78, 79]. However, the gradient descent-based optimisers and other adaptive optimisers have also performed remarkably in different application areas. For sparse datasets, the adaptive optimisers perform better compared to the SGD based optimisers alongside the accelerated optimisers like NAG and momentum-based optimisers. Besides, new research advances in DNN optimisation, more optimisation algorithms and techniques are being developed and with the most recent optimisers focusing on the challenges of the current optimisation algorithms.

In the future, the testing and comparing the gradient-based, adaptive, hessian and swarm optimisation techniques in DNN application will be performed to analyse and present the overall performance of

these optimisers in deep learning.

References

[1] J. Duchi, E. Hazan, Y. Singer, "Adaptive subgradient methods for online learning and stochastic optimization," Journal of Machine Learning Research, **12**(Jul), 2121–2159, 2011.

[2] I. Goodfellow, Y. Bengio, A. Courville, Y. Bengio, Deep learning, volume 1, MIT press Cambridge, 2016.

[3] J. Turian, J. Bergstra, Y. Bengio, "Quadratic features and deep architectures for chunking," in Proceedings of Human Language Technologies: The 2009 Annual Conference of the North American Chapter of the Association for Computational Linguistics, Companion Volume: Short Papers, 245–248, Association for Computational Linguistics, 2009.

[4] M. Kolbæk, Z.-H. Tan, S. H. Jensen, J. Jensen, "On loss functions for supervised monaural time-domain speech enhancement," IEEE/ACM Transactions on Audio, Speech, and Language Processing, **28**, 825–838, 2020, doi:10.1109/TASLP.2020.2968738.

[5] A. Cassioli, A. Chiavaioli, C. Manes, M. Sciandrone, "An incremental least squares algorithm for large scale linear classification," European Journal of Operational Research, **224**(3), 560–565, 2013, doi:10.1016/j.ejor.2012.09.004.

[6] V. Cevher, S. Becker, M. Schmidt, "Convex optimization for big data: Scalable, randomized, and parallel algorithms for big data analytics," IEEE Signal Processing Magazine, **31**(5), 32–43, 2014, doi:10.1109/MSP.2014.2329397.

[7] Y. LeCun, Y. Bengio, G. Hinton, "Deep learning," nature, **521**(7553), 436, 2015, doi:10.1038/nature14539.

[8] S. V. Albrecht, J. W. Crandall, S. Ramamoorthy, "Belief and truth in hypothesised behaviours," Artificial Intelligence, **235**, 63–94, 2016, doi:10.1016/j.artint.2016.02.004.

[9] A. Cauchy, "Méthode générale pour la résolution des systemes d'équations simultanées," Comp. Rend. Sci. Paris, **25**(1847), 536–538, 1847.

[10] D. E. Rumelhart, G. E. Hinton, R. J. Williams, et al., "Learning representations by back-propagating errors," Cognitive modeling, **5**(3), 1, 1988, doi:10.1038/323533a0.

[11] D. Bradley, Learning in modular systems, Ph.D. thesis, The Robotics Institute, Carnegie Mellon University, 2009.

[12] C. Nwankpa, W. Ijomah, A. Gachagan, S. Marshall, "Activation functions: Comparison of trends in practice and research for deep learning," CoRR, abs/1811.03378, 2018.

[13] E. Okewu, P. Adewole, O. Sennaike, "Experimental comparison of stochastic optimizers in deep learning," in International Conference on Computational Science and Its Applications, 704–715, Springer, 2019, doi:10.1007/978-3-030-24308-1_55.

[14] S. Reddy, K. T. Reddy, V. ValliKumari, "Optimization of Deep Learning Using Various Optimizers, Loss Functions and Dropout," Int. J. Recent Technol. Eng, **7**, 448–455, 2018.

[15] P. Kanani, M. Padole, "Deep Learning to Detect Skin Cancer using Google Colab," International Journal of Engineering and Advanced Technology Regular Issue, **8**(6), 2176–2183, 2019, doi:10.35940/ijeat.F8587.088619.

[16] J. Howard, S. Gugger, "Fastai: A layered API for deep learning," Information, **11**(2), 108, 2020, doi:10.3390/info11020108.

[17] A. Wadhawan, P. Kumar, "Deep learning-based sign language recognition system for static signs," Neural Computing and Applications, 1–12, 2020, doi:10.1007/s00521-019-04691-y.

[18] S. Mothe, A. Teja, B. Kakumanu, R. Tata, "A Model for Assessing the Nature of Car Crashes using Convolutional Neural Networks," International Journal of Emerging Trends in Engineering Research, **8**(3), 859–863, 2020, doi:10.30534/ijeter/2020/41832020.

[19] P. Arunsuriyasak, P. Boonme, P. Phasukkit, "Investigation of Deep Learning Optimizer for Water Pipe Leaking Detection," in 2019 16th International Conference on Electrical Engineering/Electronics, Computer, Telecommunications and Information Technology (ECTI-CON), 85–88, IEEE, 2019, doi:10.1109/ECTI-CON47248.2019.8955355.

[20] M. N. Halgamuge, E. Daminda, A. Nirmalathas, et al., "Best optimizer selection for predicting bushfire occurrences using deep learning," Natural Hazards: Journal of the International Society for the Prevention and Mitigation of Natural Hazards, 1–16, 2020, doi:10.1007/s11069-020-04015-7.

[21] A. Krizhevsky, I. Sutskever, G. E. Hinton, "Imagenet classification with deep convolutional neural networks," in Advances in neural information processing systems, 1097–1105, 2012.

[22] I. Sutskever, J. Martens, G. Dahl, G. Hinton, "On the importance of initialization and momentum in deep learning," in ICLR, 1139–1147, 2013.

[23] D. Mishkin, J. Matas, "All you need is a good init," CoRR, abs/1511.06422, 2015.

[24] K. He, X. Zhang, S. Ren, J. Sun, "Delving deep into rectifiers: Surpassing human-level performance on imagenet classification," in Proceedings of the IEEE international conference on computer vision, 1026–1034, 2015.

[25] J. Martens, "Deep learning via hessian-free optimization." in ICML, volume 27, 735–742, 2010.

[26] A. M. Saxe, J. L. McClelland, S. Ganguli, "Exact solutions to the nonlinear dynamics of learning in deep linear neural networks," CORR, abs/1312.6120, 2013.

[27] D. Mishkin, J. Matas, "All you need is a good init," in Proceedings of the ICLR, 2016.

[28] X. Glorot, Y. Bengio, "Understanding the difficulty of training deep feedforward neural networks," in Proceedings of the 13th international conference on artificial intelligence and statistics, 249–256, 2010.

[29] D. Sussillo, L. Abbott, "Random walks: Training very deep nonlinear feedforward networks with smart initialization," CoRR, abs/1412.6558, **287**, 300–302, 2014.

[30] R. Jozefowicz, W. Zaremba, I. Sutskever, "An empirical exploration of recurrent network architectures," in International conference on machine learning, 2342–2350, 2015.

[31] D. P. Kingma, J. Ba, "Adam: A method for stochastic optimization," in ICLR, 2015.

[32] S. Ruder, "An overview of gradient descent optimization algorithms," CoRR, abs/1609.04747, 2016.

[33] H. Robbins, S. Monro, "A stochastic approximation method," The annals of mathematical statistics, 400–407, 1951.

[34] J. Gu, Z. Wang, J. Kuen, L. Ma, A. Shahroudy, B. Shuai, T. Liu, X. Wang, G. Wang, J. Cai, et al., "Recent advances in convolutional neural networks," Pattern Recognition, **77**, 354–377, 2018, doi:10.1016/j.patcog.2017.10.013.

[35] C. Garbin, X. Zhu, O. Marques, "Dropout vs. batch normalization: an empirical study of their impact to deep learning," Multimedia Tools and Applications, 1–39, 2020, doi:10.1007/s11042-019-08453-9.

[36] S. Sigtia, S. Dixon, "Improved music feature learning with deep neural networks," in 2014 IEEE international conference on acoustics, speech and signal processing (ICASSP), 6959–6963, IEEE, 2014, doi:10.1109/ICASSP.2014.6854949.

[37] N. Qian, "On the momentum term in gradient descent learning algorithms," Neural networks, **12**(1), 145–151, 1999, doi:10.1016/S0893-6080(98)00116-6.

[38] I. Loshchilov, F. Hutter, "Sgdr: Stochastic gradient descent with warm restarts," in ICLR, 2017.

[39] M. D. Zeiler, "ADADELTA: an adaptive learning rate method," CORR, abs/1212.5701, 2012.

[40] R. Hemke, C. G. Buckless, A. Tsao, B. Wang, M. Torriani, "Deep learning for automated segmentation of pelvic muscles, fat, and bone from CT studies for body composition assessment," Skeletal Radiology, **49**(3), 387–395, 2020, doi:10.1007/s00256-019-03289-8.

[41] S. Zhou, H. Zou, C. Liu, M. Zang, T. Liu, "Combining Deep Neural Networks for Protein Secondary Structure Prediction," IEEE Access, **8**, 84362–84370, 2020, doi:10.1109/ACCESS.2020.2992084.

[42] A. Gautam, V. Singh, "CLR-based deep convolutional spiking neural network with validation based stopping for time series classification," Applied Intelligence, **50**(3), 830–848, 2020, doi:10.1007/s10489-019-01552-y.

[43] Y. Dou, Y. Fang, C. Hu, R. Zheng, F. Yan, "Gated branch neural network for mandatory lane changing suggestion at the on-ramps of highway," IET Intelligent Transport Systems, **13**(1), 48–54, 2018, doi:10.1049/iet-its.2018.5093.

[44] K. Gopalakrishnan, S. K. Khaitan, A. Choudhary, A. Agrawal, "Deep convolutional neural networks with transfer learning for computer vision-based data-driven pavement distress detection," Construction and Building Materials, **157**, 322–330, 2017, doi:10.1016/j.conbuildmat.2017.09.110.

[45] S. Das, S. Mishra, "Advanced deep learning framework for stock value prediction," International Journal of Innovative Technology and Exploring Engineering, **8**(10), 2358–2367, 2019, doi:10.35940/ijitee.B2453.0881019.

[46] F. H. Nahhas, H. Z. Shafri, M. I. Sameen, B. Pradhan, S. Mansor, "Deep learning approach for building detection using lidar–orthophoto fusion," Journal of Sensors, **2018**, 2018, doi:10.1155/2018/7212307.

[47] T. Dozat, "Incorporating nesterov momentum into adam," in ICML, 2016.

[48] S. J. Reddi, S. Kale, S. Kumar, "On the convergence of adam and beyond," in ICLR, 2018.

[49] G. Du, Y. Zou, X. Zhang, T. Liu, J. Wu, D. He, "Deep reinforcement learning based energy management for a hybrid electric vehicle," Energy, 117591, 2020, doi:10.1016/j.energy.2020.117591.

[50] L. Liu, H. Jiang, P. He, W. Chen, X. Liu, J. Gao, J. Han, "On the variance of the adaptive learning rate and beyond," in ICLR, 2020.

[51] M. R. Zhang, J. Lucas, G. Hinton, J. Ba, "Lookahead Optimizer: k steps forward, 1 step back," CoRR, abs/1907.08610, 2019.

[52] J. Sohl-Dickstein, B. Poole, S. Ganguli, "Fast large-scale optimization by unifying stochastic gradient and quasi-Newton methods," in ICML, 604–612, 2014.

[53] J.-S. Wang, S.-X. Li, "An improved grey wolf optimizer based on differential evolution and elimination mechanism," Scientific reports, **9**(1), 1–21, 2019, doi:10.1038/s41598-019-43546-3.

[54] M. Mavrovouniotis, C. Li, S. Yang, "A survey of swarm intelligence for dynamic optimization: Algorithms and applications," Swarm and Evolutionary Computation, **33**, 1–17, 2017, doi:10.1016/j.swevo.2016.12.005.

[55] C. Ni, Z. Li, X. Zhang, X. Sun, Y. Huang, L. Zhao, T. Zhu, D. Wang, "Online Sorting of the Film on Cotton Based on Deep Learning and Hyperspectral Imaging," IEEE Access, **8**, 93028–93038, 2020, doi:10.1109/ACCESS.2020.2994913.

[56] S. Mirjalili, S. M. Mirjalili, A. Lewis, "Grey wolf optimizer," Advances in engineering software, **69**, 46–61, 2014, doi:10.1016/j.advengsoft.2013.12.007.

[57] X. Chen, F. Kopsaftopoulos, Q. Wu, H. Ren, F.-K. Chang, "A self-adaptive 1D convolutional neural network for flight-state identification," Sensors, **19**(2), 275, 2019, doi:10.3390/s19020275.

[58] T. R. Gadekallu, N. Khare, S. Bhattacharya, S. Singh, P. K. R. Maddikunta, G. Srivastava, "Deep neural networks to predict diabetic retinopathy," J. Ambient Intell. Humaniz. Comput, 2020, doi:10.1007/s12652-020-01963-7.

[59] W. Fu, K. Wang, J. Tan, K. Zhang, "A composite framework coupling multiple feature selection, compound prediction models and novel hybrid swarm optimizer-based synchronization optimization strategy for multi-step ahead short-term wind speed forecasting," Energy Conversion and Management, **205**, 112461, 2020, doi:10.1016/j.enconman.2019.112461.

[60] M. Revathi, I. J. S. Jeya, S. Deepa, "Deep learning-based soft computing model for image classification application," Soft Computing, 1–20, 2020, doi:10.1007/s00500-020-05048-7.

[61] K. Lan, L. Liu, T. Li, Y. Chen, S. Fong, J. A. L. Marques, R. K. Wong, R. Tang, "Multi-view convolutional neural network with leader and long-tail particle swarm optimizer for enhancing heart disease and breast cancer detection," Neural Computing and Applications, 1–20, 2020, doi:10.1007/s00521-020-04769-y.

[62] G. Xiao, H. Liu, W. Guo, L. Wang, "A hybrid training method of convolution neural networks using adaptive cooperative particle swarm optimiser," International Journal of Wireless and Mobile Computing, **16**(1), 18–26, 2019, doi:10.1504/IJWMC.2019.097418.

[63] K. Mahmoud, M. Abdel-Nasser, E. Mustafa, Z. M Ali, "Improved Salp–Swarm Optimizer and Accurate Forecasting Model for Dynamic Economic Dispatch in Sustainable Power Systems," Sustainability, **12**(2), 576, 2020, doi:10.3390/su12020576.

[64] K. Chen, Z. Mao, H. Zhao, Z. Jiang, J. Zhang, "A Variational Stacked Autoencoder with Harmony Search Optimizer for Valve Train Fault Diagnosis of Diesel Engine," Sensors, **20**(1), 223, 2020, doi:10.3390/s20010223.

[65] E. M. Hassib, A. I. El-Desouky, L. M. Labib, E.-S. M. El-kenawy, "WOA+ BRNN: An imbalanced big data classification framework using Whale optimization and deep neural network," soft computing, **24**(8), 5573–5592, 2020, doi:10.1007/s00500-019-03901-y.

[66] A. S. Elsayad, A. I. Eldesouky, M. M. Salem, M. Badawy, "A Deep Learning H2O Framework for Emergency Prediction in Biomedical Big Data," IEEE Access, 2020, doi:10.1109/ACCESS.2020.2995790.

[67] D. Prayogo, M.-Y. Cheng, Y.-W. Wu, D.-H. Tran, "Combining machine learning models via adaptive ensemble weighting for prediction of shear capacity of reinforced-concrete deep beams," Engineering with Computers, 1–19, 2019, doi:10.1007/s00366-019-00753-w.

[68] Z. Yang, C. Wei, "Prediction of equipment performance index based on improved chaotic lion swarm optimization–LSTM," Soft Computing, 1–25, 2019, doi:10.1007/s00500-019-04456-8.

[69] D. D. Chakladar, S. Dey, P. P. Roy, D. P. Dogra, "EEG-based mental workload estimation using deep BLSTM-LSTM network and evolutionary algorithm," Biomedical Signal Processing and Control, **60**, 101989, 2020, doi:10.1016/j.bspc.2020.101989.

[70] M. Zinkevich, J. Langford, A. J. Smola, "Slow learners are fast," in Advances in neural information processing systems, 2331–2339, 2009.

[71] M. Zinkevich, M. Weimer, L. Li, A. J. Smola, "Parallelized stochastic gradient descent," in Advances in neural information processing systems, 2595–2603, 2010.

[72] T. Paine, H. Jin, J. Yang, Z. Lin, T. Huang, "Gpu asynchronous stochastic gradient descent to speed up neural network training," CoRR, abs/1312.6186, 2013.

[73] Y. Zhuang, W.-S. Chin, Y.-C. Juan, C.-J. Lin, "A fast parallel SGD for matrix factorization in shared memory systems," in Proceedings of the 7th ACM conference on Recommender systems, 249–256, ACM, 2013, doi:10.1145/2507157.2507164.

[74] R. K. Kennedy, T. M. Khoshgoftaar, F. Villanustre, T. Humphrey, "A parallel and distributed stochastic gradient descent implementation using commodity clusters," Journal of Big Data, **6**(1), 16, 2019, doi:10.1186/s40537-019-0179-2.

[75] D. H. Wolpert, W. G. Macready, "No free lunch theorems for optimization," IEEE transactions on evolutionary computation, **1**(1), 67–82, 1997, doi:10.1109/4235.585893.

[76] Y. Yao, L. Rosasco, A. Caponnetto, "On early stopping in gradient descent learning," Constructive Approximation, **26**(2), 289–315, 2007, doi: 10.1007/s00365-006-0663-2.

[77] D. Wei, J. Wang, K. Ni, G. Tang, "Research and Application of a Novel Hybrid Model Based on a Deep Neural Network Combined with Fuzzy Time Series for Energy Forecasting," Energies, **12**(18), 3588, 2019, doi:10.3390/en12183588.

[78] M. N. Khan, M. M. Ahmed, "Trajectory-level fog detection based on in-vehicle video camera with TensorFlow deep learning utilizing SHRP2 naturalistic driving data," Accident Analysis & Prevention, **142**, 105521, 2020, doi:10.1016/j.aap.2020.105521.

[79] S. Remya, R. Sasikala, "Performance evaluation of optimized and adaptive neuro fuzzy inference system for predictive modeling in agriculture," Computers & Electrical Engineering, **86**, 106718, 2020, doi:10.1016/j.compeleceng.2020.106718.

ASTES

Advances in Science, Technology and Engineering Systems Journal
Vol. 5, No. 5,578-591 (2020)
www.astesj.com
Special Issue on Innovative Research in Applied Science, Engineering and Technology

ASTES Journal
ISSN: 2415-6698

Numerical Study of Gas Microflow within a Triangular Lid-driven Cavity

Youssef Elguennouni[*,1], Mohamed Hssikou[2], Jamal Baliti[3], Mohammed Alaoui[1]

[1]*Moulay Ismail University of Meknes, Faculty of Sciences, Morocco*

[2]*University of Ibn Zohr, Faculty of Sciences, Agadir, Morocco*

[3]*University of Sultan Moulay Slimane, Polydisciplinary Faculty, Beni Mellal, Morocco*

ARTICLE INFO

Article history:
Received: 03 August, 2020
Accepted: 26 September, 2020
Online: 05 October, 2020

Keywords:
SRT-LBM
MRT-LBM
DSBC
BSBC
lid-driven
micro-cavity
Knudsen number
vortex

ABSTRACT

A rarefied gas flow is modeled inside two cases of triangular lid-driven microcavity using single (SRT) and multi-relaxation time (MRT) lattice Boltzmann approaches. In the first one, the right angle is in the top-left corner and the upper wall moves with positive horizontal velocity. However, in the second case, the right angle is in the bottom-left corner and the bottom wall moves with negative horizontal velocity. Unlike the classical form of square cavities, widely treated in the literature, the triangular form has a diagonal wall that affects the flow motion. At the moving wall, diffuse scattering boundary condition (DSBC) is employed while at the stationary sides, a combination of bounce-back and specular reflection boundary conditions (BSBC) is used. The computations are primarily performed in the slip and early transition regimes. The rarefaction effect, given by the Knudsen number (Kn) value, on the profiles of velocity components, is examined for both approaches. This study proves that for the higher values of Kn, the SRT-LBM approach cannot provide accurate results, particularly, near the inclined wall. However, the MRT-LBM approach confirms its validity even in the transition regime. A comparison with Direct Simulation Monte Carlo (DSMC) results for horizontal velocity contours shows the efficiency of the MRT-LBM approach than the SRT-LBM one which breaks down for rarefied flows.

1 Introduction

A complete description of gas microflows involved in the micro/nano-electro-mechanical systems (MEMS/NEMS) [1] remains a challenge for many researchers during the last decades. Lid-driven cavity flow is one of the classical benchmark problems of computational fluid dynamics (CFD) [2–5]. Such flow has been analyzed by various computational methods like the Navier-Stokes-Fourier equations (NSF) [6, 7], Direct Simulation Monte Carlo (DSMC) [7–10] and moment equations approach [6, 10, 11].

In micro-devices, gaseous flows undergoe non-equilibrium or rarefaction effects. The gas flow rarefaction degree is, usually, given by the Knudsen number (Kn) which is the ratio of gas-molecules mean free path (λ) and the characteristic length of the system (l) (see Fig. 1). The particle/wall collisions cease to be negligible against the particle/particle ones in the transition regime and the gas becomes rarefied. This situation takes place in many microfluidic and vacuum applications [12, 13].

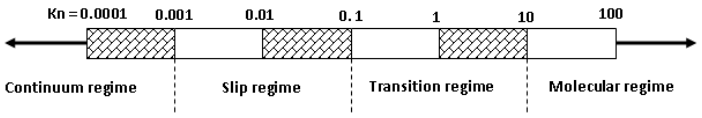


Figure 1: Flow regimes according to the Knudsen number.

To describe this kind of flows a kinetic based approach is needed. In order to save the computational time, the lattice boltzmann method (LBM) is used. This method was, first, inspired by the lattice gas automata (LGA) method for which the fluid is moving along the lattice. For both methods, the time, space, and velocities of the particles are discrete. The LGA model uses a six-speed hexagonal lattice, however, in LBM, the most used model for two-dimensional (D = 2) geometries is D2Q9 which is a square grid with nine discrete velocities (Q = 9). In recent years, LBM has become a promising alternative to simulate fluid flows and heat transfer problems. Unlike the classical CFD approaches, the LBM is a mesoscopic approach which combines the classical computational fluid

[*]Corresponding Author: Youssef Elguennouni, y.elguennouni@edu.umi.ac.ma

dynamics (CFD) and the kinetic description based on the Boltzmann equation. The method, therefore, ensures a relation between the macro and the microscopic descriptions of flow. Only a few studies that have investigated the effectiveness of this method and extend its ability to model hydrodynamic and rarefied flows [14–20]. However, the study of such flows requires a good choice and implementation of the boundary conditions (BC), which is a key step in the LBM simulation process. In the literature different BC are tested for various problems in order to capture non-equilibrium effects near the walls [21–25]. To solve the lattice Boltzmann equation (LBE), we used the well-known kinetic model of Bhatnagar–Gross–Krook (BGK) [26] which is the simplest and most widely used collision operator for the LBE. This operator is represented by a linear discretization of the relaxation of particle distribution function toward the Maxwell equilibrium state.

Application of LBM, under rarefaction conditions, to describe gas microflows is still a new field needing improvement to extend its applicability to this kind of flows. This study aims to simulate lid-driven gas flow in triangular micro-cavity. The results obtained by both approaches of LBM, SRT and MRT, are compared with those obtained by the DSMC method in the slip regime, usually encountered in MEMS devices [27]. The main simulation parameters are the Knudsen number (Kn) and the tangential momentum accommodation coefficient σ (TMAC). Unlike the DSMC method which needs a long computation time to give satisfactory results [28] and the extended macroscopic theory, like regularized 13 moment (R13), which the range of validity is limited [6, 29], the MRT-LBM proved its effectiveness for rarefied gas simulation.

2 Problem statement

In the current simulation, an isosceles right-angled triangular prism micro-cavity is considered with a large cross-sectional aspect ratio, the flow properties are independent of z-coordinate. In this study, the effect of any external body force is neglected. The gas flow can be considered within a two-dimensional enclosure of length scale $H = L$. According to the position of the moving wall, with a constant velocity U_0, two cases of the isosceles right triangle are considered in this study. In the first one, the right angle is in the top-left corner and the upper wall moves towards positive x-direction. However, in the second case, the right angle is in the bottom-left corner and the bottom wall moves in the negative x-direction (see Figs. 2).

3 Lattice Boltzmann models and boundary conditions

3.1 Boltzmann equation

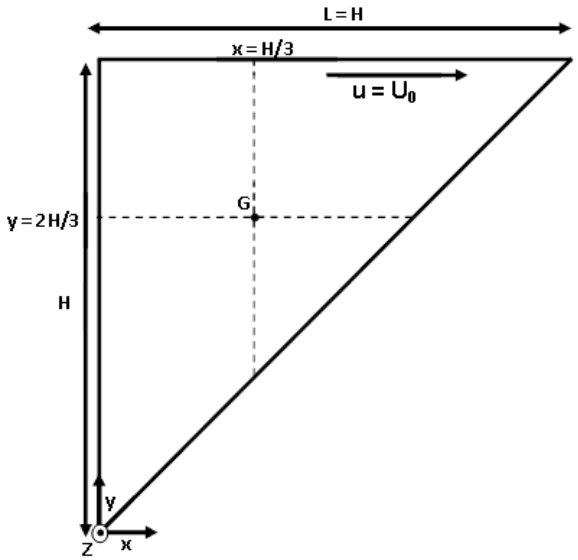
In absence of external force, the behavior of gas flow is governed by the Boltzmann equation given by

$$(\partial_t + \mathbf{c}.\nabla_r) f = \Omega(f). \quad (1)$$

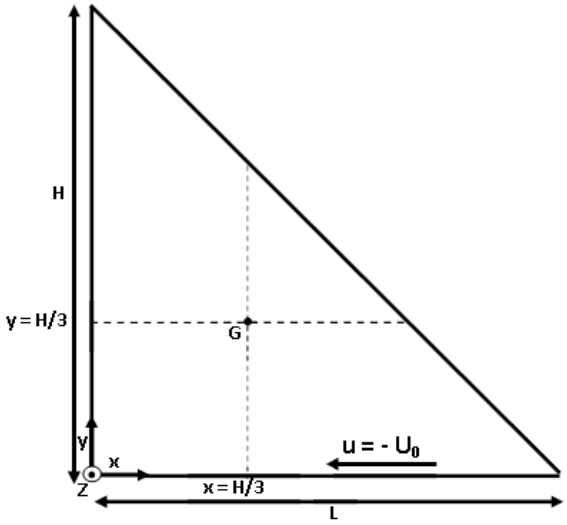
Where f is the distribution function and $\Omega(f)$ is the collision operator which represents the particles microscopic collision dynamics. In the BGK model, this operator is given by

$$\Omega(f) = -\frac{1}{\tau}(f - f^{eq}). \quad (2)$$

In which τ represents the relaxation time and f^{eq} is the Maxwell distribution function at the equilibrium state.



(a) Case (1)



(b) Case (2)

Figure 2: Studied domain configuration.

3.2 Single relaxation time lattice Boltzmann method (SRT-LBM)

For distribution function density f a D2Q9 model with square grid is used in this study. According to the BGK model, the governing, lattice Boltzmann equation, for this distribution function, is written as

$$f_k(\mathbf{x} + \mathbf{c}_k\Delta t, t + \Delta t) = f_k(\mathbf{x}, t)(1 - \frac{\Delta t}{\tau}) + \frac{\Delta t}{\tau} f_k^{eq}(\mathbf{x}, t). \quad (3)$$

The Maxwell distribution function f_k^{eq} at the equilibrium state is written in the Taylor expansion as

$$f_k^{eq} = w_k \rho \left[1 + 3\frac{\mathbf{c}_k.\mathbf{u}}{c^2} + \frac{9}{2}\frac{(\mathbf{c}_k.\mathbf{u})^2}{c^4} - \frac{3}{2}\frac{\mathbf{u}^2}{c^2}\right]. \quad (4)$$

Where the weight factors w_k are $w_0 = 4/9$, $w_{1-4} = 1/9$, $w_{5-8} = 1/36$, and c is the lattice speed given by: $c = \frac{\Delta x}{\Delta t} = \frac{\Delta y}{\Delta t}$. The discrete scheme D2Q9 is characterized by

$$\begin{bmatrix}\mathbf{c}_{k,x}\\ \mathbf{c}_{k,y}\end{bmatrix} = c\begin{bmatrix}(0 & 1 & 0 & -1 & 0 & 1 & -1 & -1 & 1)\\ (0 & 0 & 1 & 0 & -1 & 1 & 1 & -1 & -1)\end{bmatrix}, \quad k = 0-8$$

The macroscopic values of density ρ and velocity $\mathbf{u} = (u, v)$, are computed by the following relations:

$$\rho = \sum_{k=0}^{8} f_k, \quad (5a)$$

$$\rho\mathbf{u} = \sum_{k=0}^{8} f_k \mathbf{c}_k. \quad (5b)$$

For rarefied flows, the ratio of the mean free path λ and the mean thermal velocity $\langle v\rangle = \sqrt{\frac{8RT}{\pi}}$ is equivalent to the relaxation time τ given by

$$\tau = \frac{\lambda}{\langle v\rangle} = \lambda\sqrt{\frac{\pi}{8RT}}. \quad (6)$$

In microfluidic devices, gas flows are characterized by their rarefaction degree given by the Knudsen number $Kn = \frac{\lambda}{H}$, where H is the total number of lattice nodes in the y-direction. Usually, we set $c = \sqrt{3RT} = 1$ for D2Q9 model, therefore [22]

$$\tau = \sqrt{\frac{3\pi}{8}}\lambda \cong KnH. \quad (7)$$

3.3 Multi-relaxation time lattice Boltzmann method (MRT-LBM)

The collision operator in the multi-relaxation time lattice Boltzmann method (MRT-LBM) is given by

$$M^{-1}\mathbf{S}\left[\mathbf{m}(\mathbf{x}, t) - \mathbf{m}^{eq}(\mathbf{x}, t)\right]. \quad (8)$$

Thus, the eq. (3) becomes,

$$f_k(\mathbf{x} + \mathbf{c}_k\Delta t, t + \Delta t) - f_k(\mathbf{x}, t) = -\mathbf{M^{-1}S}[\mathbf{m}(\mathbf{x}, t) - \mathbf{m}^{eq}(\mathbf{x}, t)]. \quad (9)$$

Where $\mathbf{m}(\mathbf{x}, t)$ is a vector of moments and $\mathbf{m}^{eq}(\mathbf{x}, t)$ is the corresponding one at the equilibrium state. The passage from the velocities space to the moments space and vice versa is obtained by the following linear transformations:
$\mathbf{m} = \mathbf{M}f$ and $f = \mathbf{M^{-1}m}$.
For D2Q9 scheme, the transformation matrix $\mathbf{M}$ is given by

$$M = \begin{bmatrix} 1 & 1 & 1 & 1 & 1 & 1 & 1 & 1 & 1\\ -4 & -1 & -1 & -1 & -1 & 2 & 2 & 2 & 2\\ 4 & -2 & -2 & -2 & -2 & 1 & 1 & 1 & 1\\ 0 & 1 & 0 & -1 & 0 & 1 & -1 & -1 & 1\\ 0 & -2 & 0 & 2 & 0 & 1 & -1 & -1 & 1\\ 0 & 0 & 1 & 0 & -1 & 1 & 1 & -1 & -1\\ 0 & 0 & -2 & 0 & 2 & 1 & 1 & -1 & -1\\ 0 & 1 & -1 & 1 & -1 & 0 & 0 & 0 & 0\\ 0 & 0 & 0 & 0 & 0 & 1 & -1 & 1 & -1 \end{bmatrix}$$

The moments vector $\mathbf{m}$ is:

$$|\mathbf{m}\rangle = \begin{pmatrix}\rho & e & \varepsilon & \rho u & q_x & \rho v & q_y & p_{xx} & p_{xy}\end{pmatrix}^T.$$

Where e is the energy, ε is the square of energy, $\mathbf{j} = (\rho u, \rho v)$ is the momentum of density, and $\mathbf{q} = (q_x, q_y)$ is the vector of heat flux. The stress tensor components are also p_{xx}, and p_{xy}.
The moments vector at the equilibrium state $\mathbf{m}^{eq}(\mathbf{x}, t)$ is given by

$$\mathbf{m^{eq}} = \begin{cases} m_0^{eq} = \rho\\ m_1^{eq} = -2\rho + 3(j_x^2 + j_y^2)\\ m_2^{eq} = \rho - 3(j_x^2 + j_y^2)\\ m_3^{eq} = j_x\\ m_4^{eq} = -j_x\\ m_5^{eq} = j_y\\ m_6^{eq} = -j_y\\ m_7^{eq} = j_x^2 - j_y^2\\ m_8^{eq} = j_x j_y \end{cases} \quad (10)$$

In the moment space the collision matrix $\mathbf{S}$ is the diagonal matrix,

$$\mathbf{S} = \begin{pmatrix}1 & 1.4 & 1.4 & 1.0 & 1.2 & 1.0 & 1.2 & s_7 & s_8\end{pmatrix}.$$

Where $s_7 = s_8 = 1/\tau$. Note that by taking $s_k = 1/\tau, k = 0{-}8$, the MRT model is reduced to the SRT one.

3.4 Stationary and moving walls boundary conditions

Boundary conditions implementation plays a crucial role in gas flow simulation within micro-geometries. In the present study, a combination of bounce-back and specular boundary conditions (BSBC) is used at the stationary walls, however, diffuse scattering boundary conditions (DSBC) are imposed at the moving wall.

- *Combination of bounce-back and specular boundary conditions*

The BSBC is adopted by using the coefficient of the tangential momentum accommodation σ (TMAC) expressed by [30]

$$\sigma = \frac{M_i - M_r}{M_i - M_w}. \quad (11)$$

Where $M_{i,r,w}$ are the tangential momentum of molecules related, respectively, to the incident, reflected molecules, and wall. This coefficient ranges from 0 for pure specular reflection, to 1 which corresponds to the pure bounce-back one.

At the inclined wall, the boundary conditions using TMAC are as follows (see Fig. 3):

$$f_6 = f_8, \quad (12a)$$

$$f_2 = \sigma \times f_4 + (1 - \sigma) \times f_1, \quad (12b)$$

$$f_3 = \sigma \times f_1 + (1 - \sigma) \times f_4. \quad (12c)$$

- *Diffuse scattering boundary condition*

The DSBC is used to simulate fluid interactions at solid interfaces written as [31]

$$|(\mathbf{c}_k - \mathbf{u}_\mathbf{w}).\mathbf{n}|f_k = \sum_{(\mathbf{c}_{k'} - \mathbf{u}_\mathbf{w}).\mathbf{n}<0} |(\mathbf{c}_{k'} - \mathbf{u}_\mathbf{w}).\mathbf{n}|\Re_f(\mathbf{c}_{k'} \to \mathbf{c}_k) f_{k'}. \quad (13)$$

Where

$$\Re_f(\mathbf{c}_{k'} \to \mathbf{c}_k) = \frac{A_n}{\rho_\mathbf{w}} ((\mathbf{c}_k - \mathbf{u}_\mathbf{w}).\mathbf{n}) f_k^{eq}|_{\mathbf{u}=\mathbf{u}_\mathbf{w}}, \quad (14)$$

where k and k' refer to the reflected and incident directions of molecules, respectively, and $\mathbf{n}$ is the unit normal vector inward of the wall, and $\Re_f(\mathbf{c}_{k'} \to \mathbf{c}_k)$ is the scattering probability from the direction $\mathbf{c}_{k'}$ to $\mathbf{c}_k$. By satisfying zero normal flux condition across the wall, the coefficient of normalization A_n can be obtained by the following relation:

$$A_n = \rho_\mathbf{w} \frac{\sum_k |(\mathbf{c}_k - \mathbf{u}_\mathbf{w}).\mathbf{n}|f_k}{|(\mathbf{c}_k - \mathbf{u}_\mathbf{w}).\mathbf{n}|f_k^{eq} \sum_{k'} |(\mathbf{c}_{k'} - \mathbf{u}_\mathbf{w}).\mathbf{n}|f_{k'}}. \quad (15)$$

At the top wall, the unknown distribution functions are $f_{k=4/7/8}$ (see Fig. 3) can be determined from the known ones $f_{k=2/5/6}$ and $f_{k=4/7/8}^{eq}$ as shown in the DSBC (Eqs. (13)–(15)) by

$$f_{k=4/7/8} = \frac{A_n}{\rho_\mathbf{w}} f_{k=4/7/8}^{eq}(\rho_\mathbf{w}, \mathbf{u}_\mathbf{w})(f_2 + f_5 + f_6). \quad (16)$$

For the D2Q9 model, the coefficient A_n takes the value 6 [24].

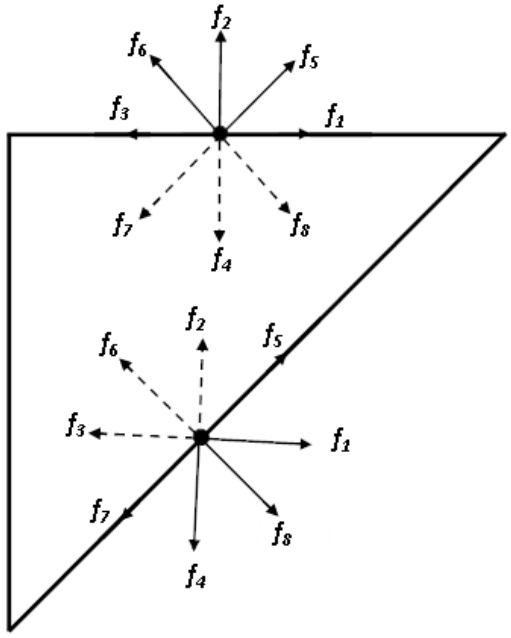


Figure 3: Gas-surface interaction at the top and inclined walls.

4 Results and discussion

All present simulations are carried out using a developed Fortran code. The SRT-LBM and MRT-LBM approaches are used to simulate lid-driven gas microflow in two configurations of triangular right micro-cavity isosceles (see Figs. 2). In the literature, the simulation of fluid microflows was made a lot for a square-section cavity [14–20]. However, a few studies were focused on the geometries with inclined sides [32–38]. Unlike most of these papers, based on the Reynolds number (Re), the rarefaction degree is expressed in this study according to the Knudsen number value (Kn).

4.1 Mesh independence study

For $Kn = 0.01$ and $\sigma = 0.5$, Table 1 shows mesh size effect on the x-velocity component at the center of the moving wall, while Figure 4 shows their effect on the profiles of u-velocity along the vertical line $x/H = 1/3$ and v-velocity along the horizontal line $y/H = 2/3$ for the case (1) using the SRT-LBM approach. Similarly, Figure 5 shows the profiles of u and v along the lines $x/H = 1/3$ and $y/H = 1/3$, respectively, for the case (2) by using the MRT-LBM approach. As shown, the grid size 300×300 is enough to offer good and reliable results.

Table 1: Effect of the mesh on the x-velocity component at the center of the moving wall for $Kn = 0.01$ and $\sigma = 0.5$.

Mesh	200×200	300×300	400×400
SRT-LBM for case (1)	0.9120	0.9116	0.9115
MRT-LBM for case (2)	-0.9057	-0.9061	-0.9062

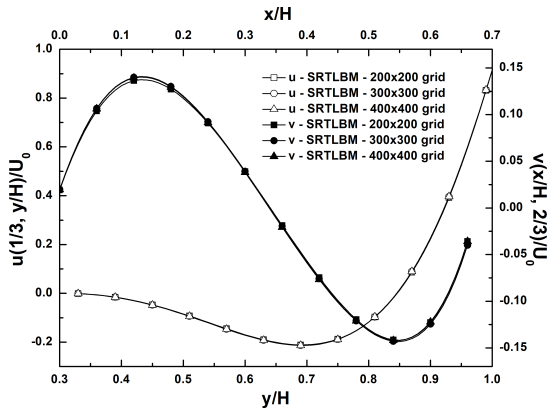


Figure 4: Profiles of u and v-velocity components along the lines $x/H = 1/3$ and $y/H = 2/3$, respectively, obtained by SRT-LBM for case (1).

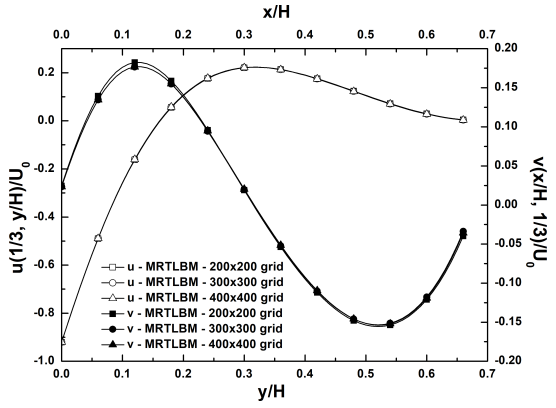


Figure 5: Profiles of u and v-velocity components along the lines $x/H = 1/3$ and $y/H = 1/3$, respectively, obtained by MRT-LBM for case (2).

4.2 Validation test

In order to ensure the validation of these models, a comparison is made with previous studies according to the widely used TMAC value ($\sigma = 0.7$) [14–16, 20] for both validation cases (square micro-cavity and a triangular micro-cavity (case(2)). At first, the profile of $u-$velocity for $Kn = 0.01$ and $Kn = 0.1$ along the vertical centerline are compared with the findings reported by Perumal et al. [14, 15] and Rahmati et al. [16] for a square micro-cavity (see Fig. 6a). Table 2 shows the location of the primary vortex center for $Kn = 0.01$ and $Kn = 0.1$. The results of the current study align well with those of Rahmati et al. [16, 17], and Tang et al. [18]. In the second validation case, u-velocity contours inside a triangular micro-cavity (case (2)) are confronted with those obtained by the DSMC method [38], the most confident and powerful method to study of such flows. Figures 6b and 7 show, respectively, the u-velocity component profiles for $x/H = 1/3$ and the u contours for $Kn = 0.01$ and $Kn = 0.1$. Table 3 shows the location of the primary vortex center according to the Knudsen number values $Kn = 0.01$ and $Kn = 0.1$. It is shown that MRT-LBM results are acceptable and approximate well, those of Roohi et al. [38], for which $U_0 = 100m/s$.

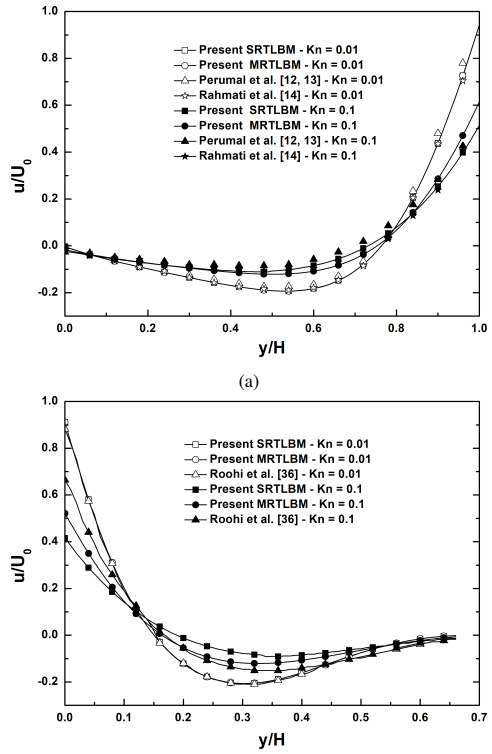


Figure 6: Profile of x-velocity for $Kn = 0.01$ and $Kn = 0.1$ (a) along the vertical centerline for square micro-cavity and (b) along the line $x/H = 1/3$ case (2) with a positive velocity $+U_0$.

4.3 Numerical results and analysis

In this work, the lid-wall moves with a fixed horizontal velocity $U_0 = 0.1$ for all simulations. To compare with and reproduce the results of Roohi et al. [38], the TMAC is taken $\sigma = 0.7$. Using the SRT-LBM and MRT-LBM methods, Figures 8 and 9 show the Knudsen number effect on the horizontal and vertical velocities profiles, respectively, for case (1) and case (2). The slip effect at the moving wall is more pronounced [14–17, 20, 38]. As predicted by the kinetic theory, the velocity slip vanishes at the continuum limit ($Kn = 0.007$), the gas-molecules velocity is almost equal the lid-velocity U_0. To evaluate both effects of rarefaction degree and TMAC value, Tables 4 and 5 show that as Kn and σ increase, the effects of non-equilibrium impact on the flow motion and the velocity slip evolve more importantly. For the first case, since the moving wall velocity is positive then the horizontal velocity component decreases to take negative values near the inclined wall, then increases to take positive values with y-coordinate beyond the primary vortex position. In that case, the lowest value of u/U_0 is located at $y/H = 0.7$ for $Kn = 0.007$ (see Figs. 8(a-b)). Similar and opposite behavior of u-component velocity is observed in the second case. The highest values of u/U_0 is located at $y/H = 0.32$ for $Kn = 0.007$ (see Figs. 9(a-b)). The vertical velocity-slip increases when Kn increases and it is more prominent by the SRT-LBM approach than by the MRT-LBM one [16, 20] (see Figs. 8(c-d) and 9(c-d)). The MRT-LBM method maintains its stability near the walls and the vertical slip-velocity can be captured even at the center of the inclined plane on the right (see Figs. 10b and 10d). However, for the SRT-LBM method, when the value of Kn increases fluctuations appear on and near the inclined wall. These fluctuations have a significant influence, especially for $Kn = 0.1$ (see Figs. 10a and 10c). For $Kn = 0.01$, 0.05, and 0.1, Table 6 shows the position of the primary and secondary vortices inside the micro-cavity for the first case. For both approaches, by increasing Kn, the primary vortex moves from right to left in the direction of x and from top to bottom in the direction of y. However, the secondary vortices at the bottom of the micro-cavity vanish and it cannot be captured using the SRT-LBM method while the MRT-LBM method retains their presence and these vortices undergo the same motion as the primary ones with Kn (see Figs. 12). For the value of TMAC $\sigma = 0.7$, these vortices are slightly shifted to the right with respect to the $\sigma = 0.5$ case. Table 7 presents the location of flow vortices in the second case. The primary vortex with Kn for both approaches moves from left to right in the direction of x and from bottom to top in the direction of y. But, SRT-LBM cannot retain its horizontal x-direction movement for $Kn = 0.1$. As in the case (1), unlike the SRT-LBM approach, the secondary vortices are well captured by MRT-LBM. These vortices move as the primary one along y-direction but in the opposite x-direction. Thus, unlike in the square-cavity, in the presence of an inclined wall, the flow stagnation points undergo two motion under rarefaction effects. For $\sigma = 0.7$, both types of vortices are moved in downward direction and shifted to the right with respect to the $\sigma = 0.5$ case. For different Knudsen numbers, the flow stagnation which corresponds to u/U_0 profiles intersection point remains the same (see Table 8, Figs. 8 (a-b) and Figs. 9(a-b)). The density ρ is also sensitive to the rarefaction degree and its value increases with Kn. An expected density has a great value near the upper-right and lower-left corners, for the cases (1) and (2), respectively (see Fig. 11a). To examine the required run time for both approaches, the profiles of velocity components at the gravity center of the micro-cavity (1) ($x = H/3, y = 2H/3$) are plotted as a function of the number of time steps for $Kn = 0.01$ and $\sigma = 0.7$. After approximately 10000-time steps number the velocity hits the steady-state (see Figs. 11b and 11c). Developed codes SRT-LBM and MRT-LBM are run on

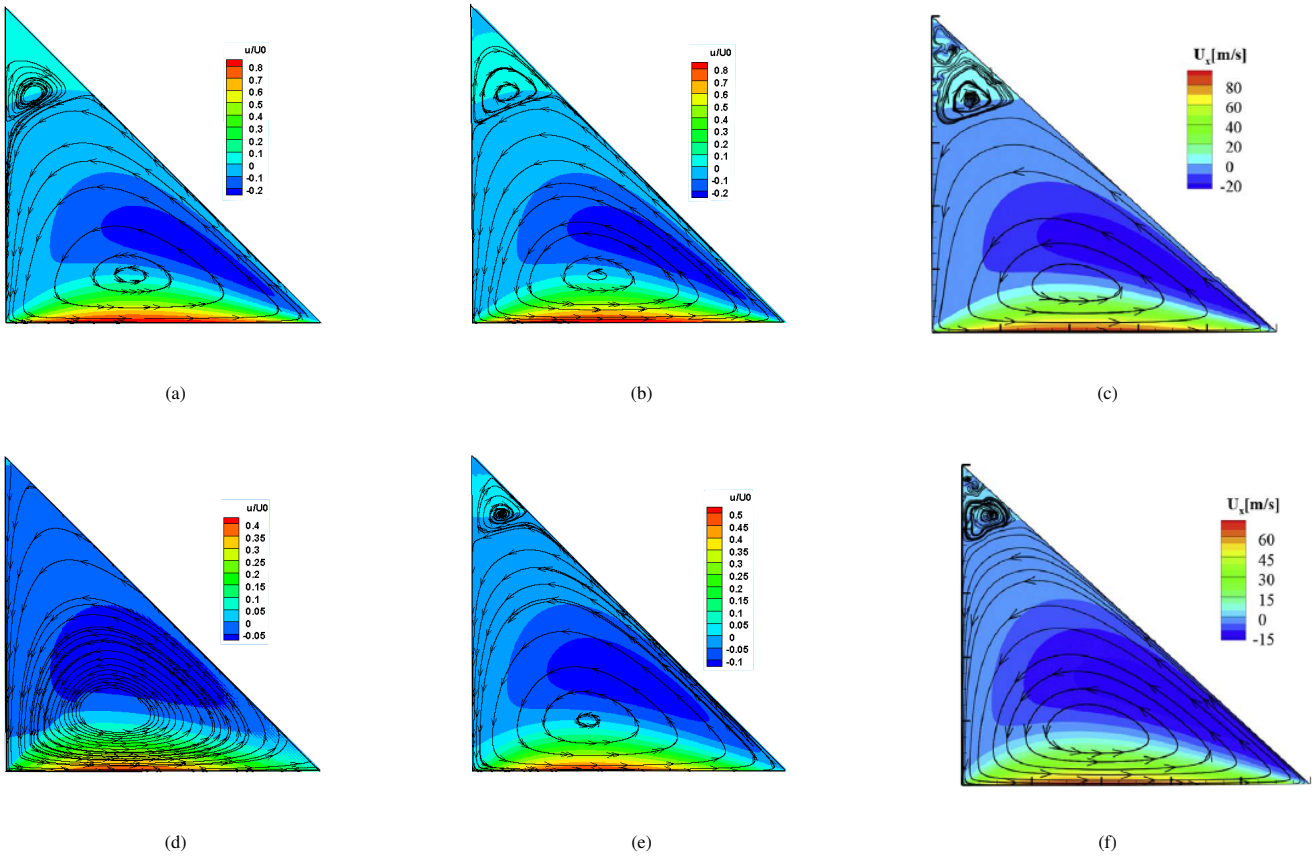


Figure 7: x-velocity streamlines and contours for $\sigma = 0.7$ - case (2) with a positive velocity $+U_0$. (a) SRT-LBM $-Kn = 0.01$ (b) MRT-LBM $-Kn = 0.01$ (c) Roohi et al. [38] $-Kn = 0.01$ (d) SRT-LBM $-Kn = 0.1$ (e) MRT-LBM $-Kn = 0.1$ (f) Roohi et al. [38] $-Kn = 0.1$.

Table 2: Primary vortex center locations for a square micro-cavity.

Kn	SRT-LBM	MRT-LBM	Rahmati et al. [16]	Rahmati et al. [17]	Tang et al. [18]
0.01	(0.5009, 0.7638)	(0.5030, 0.76378)	(0.5017, 0.7637)	(0.5022, 0.7663)	(0.5, 0.7633)
0.1	(0.5001, 0.7316)	(0.5041, 0.75336)	(0.5020, 0.7240)	(0.5023, 0.7570)	(0.5, 0.72)

Table 3: Primary vortex center locations for the triangular micro-cavity (case (2)).

Kn	SRT-LBM	MRT-LBM	Roohi et al. [38] - Monatomic	Roohi et al. [38] - Diatomic
0.01	(0.3979, 0.1525)	(0.3974, 0.1523)	(0.4209, 0.1520)	(0.4119, 0.1520)
0.1	(0.3529, 0.1888)	(0.3678, 0.1624)	(0.3799, 0.1659)	(0.3780, 0.1670)

the Intel (R) Core (TM) i5-3340 M CPU laptop @ 2.7 GHz and RAM 8.00 GB. To obtain accurate findings the MRT-LBM requires more processing time than the SRT-LBM [16, 20] due to the higher number of moments hired in the calculation to capture the effects of non-equilibrium (see Table 9). In Figures 12(a-i) the flow streamlines and u-velocity contours are plotted for $Kn = 0.007$, 0.05, 0.1, 1 and 3, respectively for $\sigma = 0.7$. As the increase in the Knudsen number, the streamlines take the wall shape and the secondary vortices observed for the lower Knudsen numbers vanish at the bottom of the micro-cavity (1) [14–16, 20]. In addition, the primary vortex undergoes a slight downward, and right-to-left movement with Kn growth. Also, u-velocity is sensitive to the degree of rarefaction and its value decreases as Kn increases. Figures 13 describe the flow streamlines, u and v-velocities contours for $Kn = 0.007$ and $Kn = 0.1$, respectively, by combining the cavity of case(1)/case(2) with their corresponding anti-symmetric cases. The segments connecting the primary and secondary vortices centers intersect at the center of the square micro-cavity, respectively (see Figs. 13(a-b)). The plots of the velocity components distributions, Figures 13(c-f), confirm the data anti-symmetric variation with respect to the square cavity center and their sensitivity to the rarefaction effect. So, by studying the two cases (1) and (2) we can deduce the characteristics of the gas flow in their corresponding anti-symmetrical forms.

Finally, it is shown that SRT-LBM loses its validity in the

transition regime while the results of the MRT-LBM method still remain convincing. To summarize the MRT-LBM method imposes itself as a good alternative for simulating the gas microflows usually encountered in the micro-devices.

Table 4: Slip effects on the x-velocity component $\frac{u(H/2,H)}{U_0}$ at the center of the moving wall - case (1).

Approaches	*Kn*	0.007	0.01	0.05	0.1
SRT-LBM	$\sigma = 0.5$	0.9372	0.91165	0.64171	0.41041
	$\sigma = 0.7$	0.93674	0.91076	0.63227	0.39725
MRT-LBM	$\sigma = 0.5$	0.93739	0.91214	0.67381	0.51394
	$\sigma = 0.7$	0.93692	0.91126	0.66554	0.50135

Table 5: Slip effects on the x-velocity component $\frac{u(H/2,0)}{U_0}$ at the center of the moving wall - case (2).

Approaches	*Kn*	0.007	0.01	0.05	0.1
SRT-LBM	$\sigma = 0.5$	-0.93045	-0.90587	-0.63838	-0.41238
	$\sigma = 0.7$	-0.92999	-0.90498	-0.62877	-0.39784
MRT-LBM	$\sigma = 0.5$	-0.93042	-0.90617	-0.67291	-0.51524
	$\sigma = 0.7$	-0.92998	-0.90531	-0.66484	-0.50287

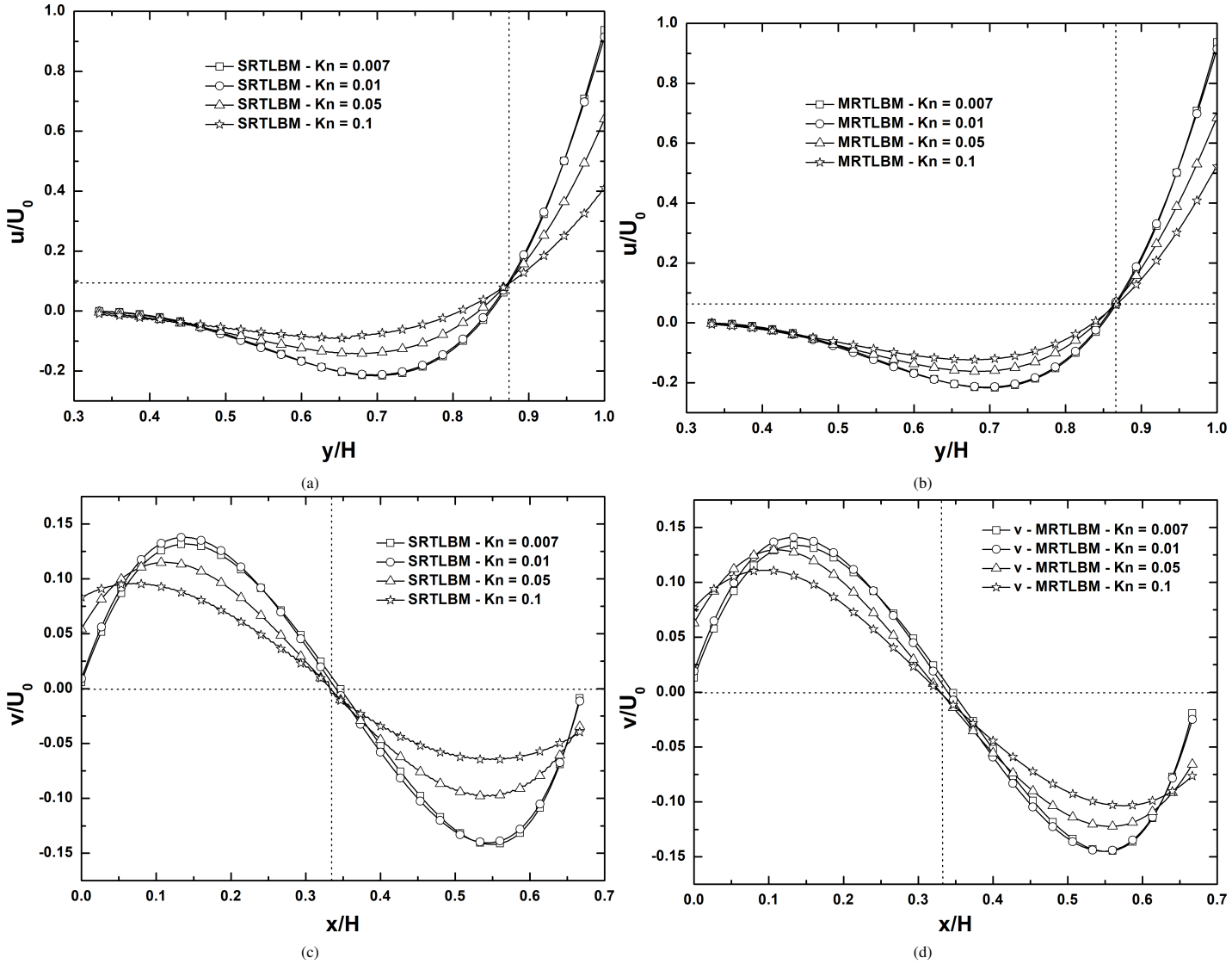


Figure 8: (a)-(b) x-velocity profile along the vertical line $x/H = 1/3$ and (c)-(d) profile of y-velocity along the horizontal line $y/H = 2/3$ at different Knudsen numbers for $\sigma = 0.7$ - case (1).

Table 6: Primary and secondary vortices locations for different values of Kn and σ - case (1).

Approaches \ Kn		0.01	0.05	0.1
SRT-LBM ($\sigma = 0.5$) **MRT-LBM**	Primary vortex	(0.3939, 0.8455)	(0.3697, 0.8298)	(0.3493, 0.8035)
	Secondary vortex	(0.0770, 0.2711)	– – – – –	– – – – –
	Primary vortex	(0.3933, 0.8458)	(0.3681, 0.8360)	(0.3660, 0.8298)
	Secondary vortex	(0.1101, 0.2572)	(0.0884, 0.1807)	– – – – –
SRT-LBM ($\sigma = 0.7$) **MRT-LBM**	Primary vortex	(0.3944, 0.8471)	(0.3713, 0.8351)	(0.3526, 0.8106)
	Secondary vortex	(0.0783, 0.2821)	– – – – –	– – – – –
	Primary vortex	(0.3938, 0.8473)	(0.3702, 0.8416)	(0.3681, 0.8377)
	Secondary vortex	(0.1124, 0.2669)	(0.1018, 0.2293)	(0.0910, 0.1878)

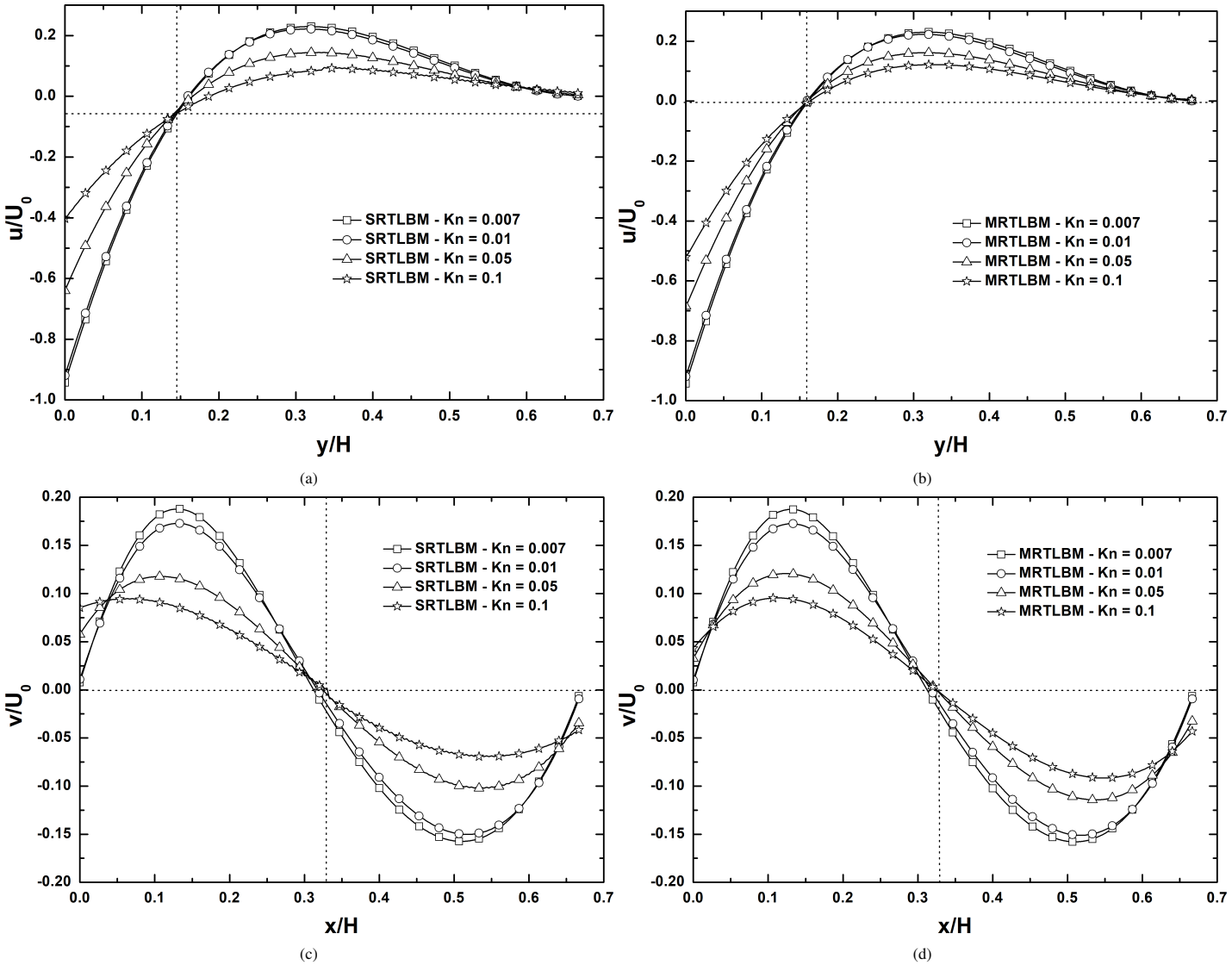


Figure 9: (a)-(b) x-velocity profile along the vertical line $x/H = 1/3$ and (c)-(d) profile of y-velocity along the horizontal line $y/H = 1/3$ at different Knudsen numbers for $\sigma = 0.7$ - case (2).

Table 7: Primary and secondary vortices locations for different values of Kn and σ - case (2).

Approaches \ Kn		0.01	0.05	0.1
SRT-LBM ($\sigma = 0.5$)	Primary vortex	(0.3275, 0.1616)	(0.3514, 0.1709)	(0.3379, 0.1944)
	Secondary vortex	(0.0871, 0.7438)	– – – – –	– – – – –
MRT-LBM	Primary vortex	(0.3272, 0.1612)	(0.3508, 0.1653)	(0.3537, 0.1709)
	Secondary vortex	(0.1069, 0.7517)	(0.0879, 0.8217)	– – – – –
SRT-LBM ($\sigma = 0.7$)	Primary vortex	(0.3296, 0.1597)	(0.3539, 0.1653)	(0.3404, 0.1870)
	Secondary vortex	(0.0896, 0.7329)	– – – – –	– – – – –
MRT-LBM	Primary vortex	(0.3293, 0.1594)	(0.3536, 0.1596)	(0.3555, 0.1630)
	Secondary vortex	(0.1098, 0.7417)	(0.1020, 0.7727)	(0.0912, 0.8133)

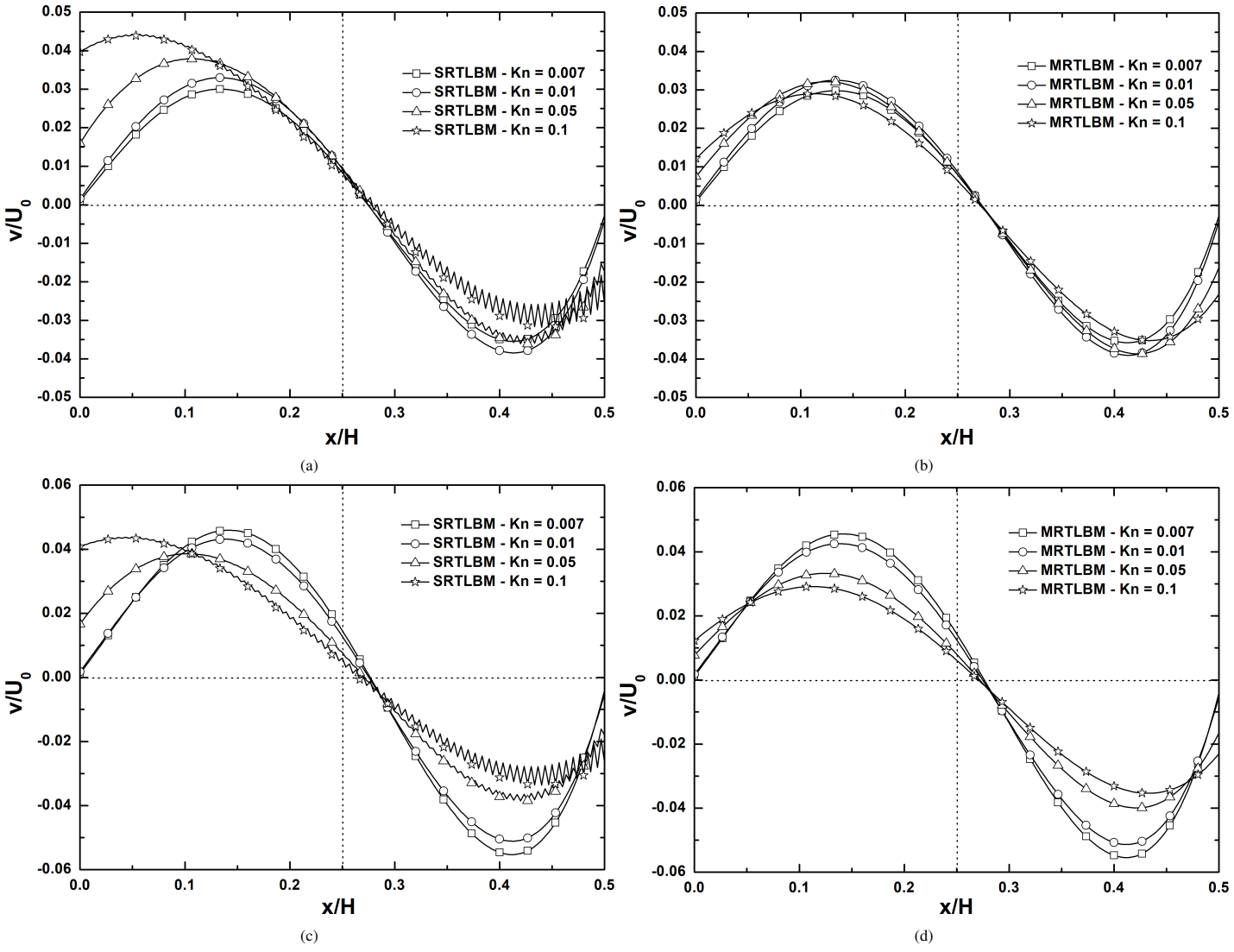


Figure 10: Profile of y-velocity along the horizontal line $y/H = 0.5$ at different Knudsen numbers for $\sigma = 0.7$ (a) SRT-LBM - case (1) (b) MRT-LBM - case (1) (c) SRT-LBM - case (2) and (d) MRT-LBM - case (2).

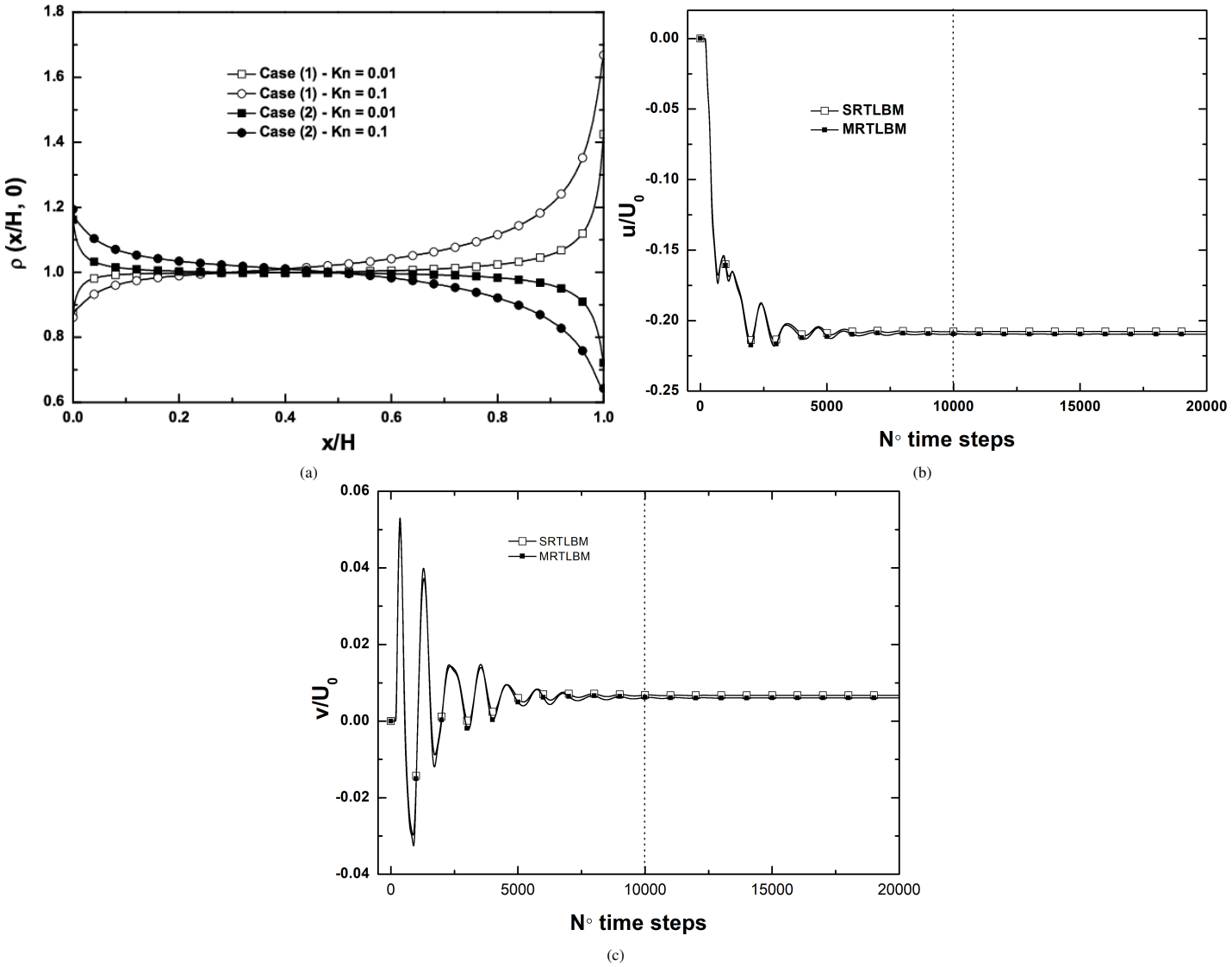


Figure 11: For $\sigma = 0.7$. (a) Density along the moving wall for $Kn = 0.01$ and $Kn = 0.1$ for both cases by using the MRT-LBM method and (b)-(c) Evolution of x and y-velocities at the center of gravity of the micro-cavity as a function of time for $Kn = 0.01$ by using both methods - case(1).

Table 8: Coordinates $(y/H, u/U_0)$ of the common intersection points at the line $x/H = 1/3$ for $\sigma = 0.7$.

Approaches \ Cases	Case (1)	Case (2)
SRT-LBM	(0.874, 0.094)	(0.145, −0.005)
MRT-LBM	(0.866, 0.064)	(0.159, −0.004)

Table 9: Execution time for 1000 iterations.

Approaches \ Mesh	**200 × 200**	**300 × 300**	**400 × 400**
SRT-LBM	10.4s	21.4s	37.3s
MRT-LBM	30.8s	65.4s	113.3s

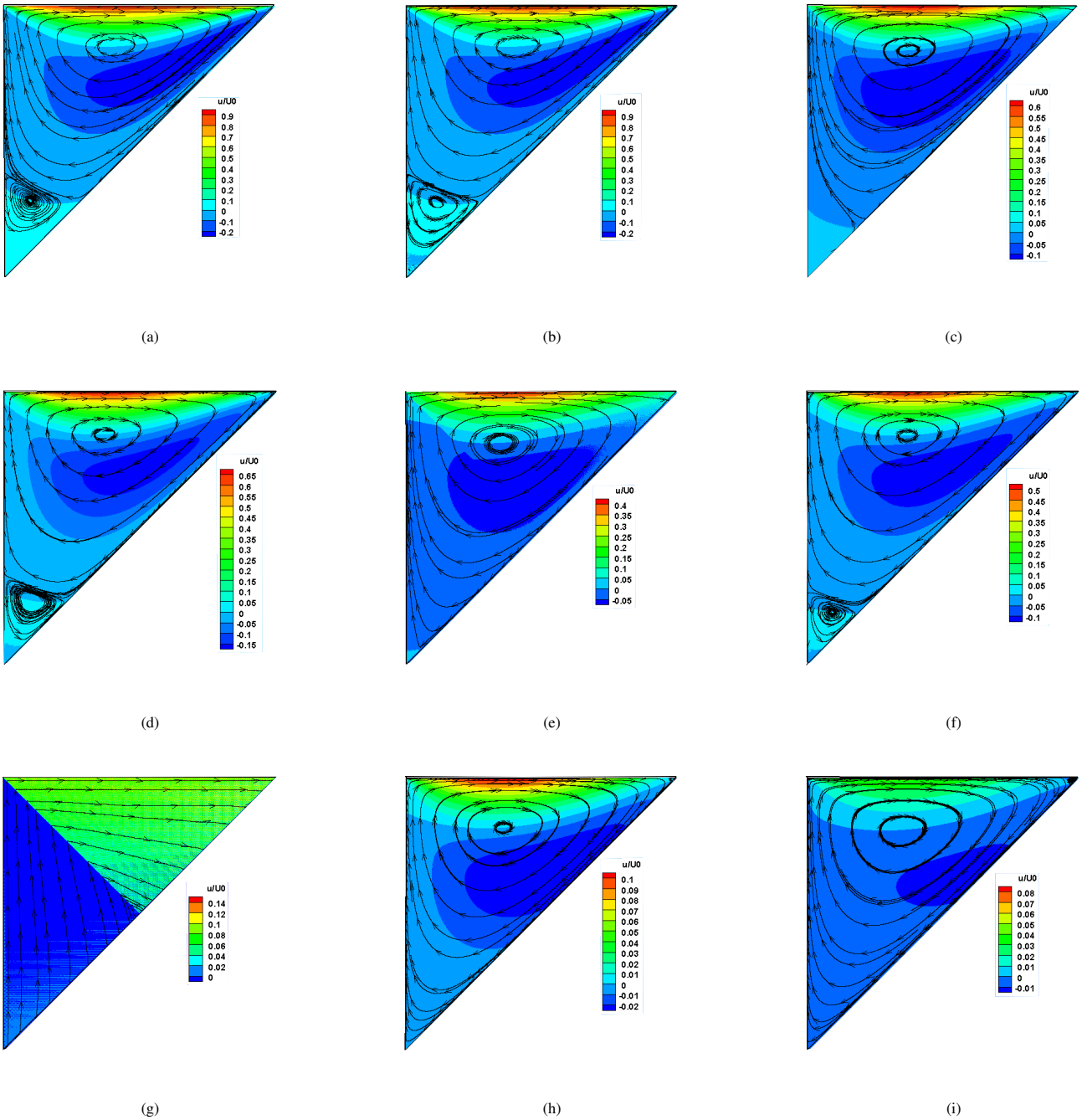
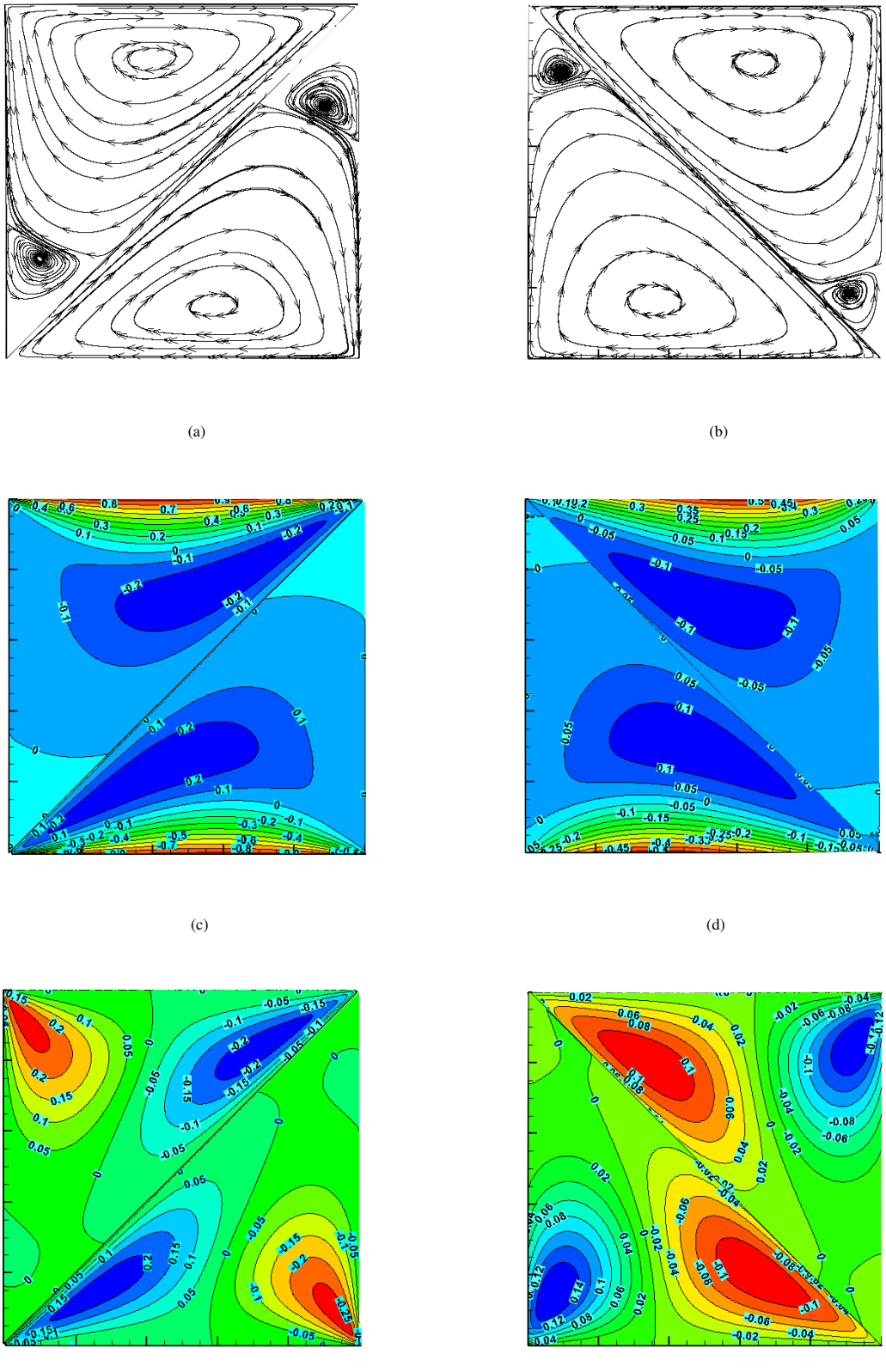


Figure 12: The flow streamlines and x-velocity contours for $\sigma = 0.7$ (case (1)) (a) SRT-LBM $-Kn = 0.007$ (b) MRT-LBM $-Kn = 0.007$ (c) SRT-LBM $-Kn = 0.05$ (d) MRT-LBM $-Kn = 0.05$ (e) SRT-LBM $-Kn = 0.1$ (f) MRT-LBM $-Kn = 0.1$ (g) SRT-LBM $-Kn = 1$ (h) MRT-LBM $-Kn = 1$ and (i) MRT-LBM $-Kn = 3$.



(a) (b)

(c) (d)

(e) (f)

Figure 13: The flow streamlines, x and y-velocities contours for $\sigma = 0.7$, respectively. (a, c and e) SRT-LBM $-Kn = 0.007$ (case (1) with its corresponding anti-symmetric shape) and (b, d and f) MRT-LBM $-Kn = 0.1$ (case (2) with its corresponding anti-symmetric shape).

5 Conclusion

In the current paper, a comparison between SRT-LBM and MRT-LBM confirms MRT-LBM method's ability to simulate rarefied gas flows. A lid-driven flow inside an isosceles triangular cavity is investigated numerically. The range of Knudsen numbers discussed is from the slip to the early transition regime. To capture non-equilibrium effects near the walls slip boundary conditions are used. It is clear that the SRT-LBM loses its validity with increasing the rarefaction degree while the MRT-LBM findings approximate well with those obtained by the DSMC method. To sum up, this research reveals many interesting characteristics of micro lid-driven microflows. In the slip regime, for small values of the Knudsen number, the results demonstrate that both methods are good alternatives, but in the transition regime, only MRT-LBM shows its capability to describe the gas microflows usually found in the MEMS/NEMS devices.

Nomenclature

H, L	Cavity height and length
t	Time
Kn	Knudsen number
Re	Reynolds number
R	Gas constant
c	Lattice speed
c_s	Speed of sound
$\mathbf{c}_k$	Lattice velocity vector
$\mathbf{u}$	Velocity vector
U_0	Velocity of the moving wall
f	Density distribution function
f_{eq}	Equilibrium density distribution function
w_k	Weight factors in the equilibrium distribution
M	Transformation matrix for D2Q9 scheme
$\mathbf{m}$	Moment vectors
$\mathbf{m}^{eq}$	Equilibrium moment vectors
S	Collision matrix
Greek Symbols	
λ	Mean free path
Δt	Time step
Δx, Δy	Lattice spacing in x and y directions
τ	Momentum relaxation time
σ	Tangential Momentum Accommodation Coefficient (TMAC)
ρ	Density

Conflict of Interest

The authors declared no potential conflicts of interest with respect to the research, authorship and publication of this article.

Acknowledgments

The authors wish to express their cordial thanks to the Editors and Reviewers for their valuable suggestions and constructive comments whish have served to improve the quality of this paper.

Funding

The authors received no financial support for the research, authorship and publication of this article.

References

[1] M. Gad-El-Hak, "The fluid mechanics of microdevices—the freeman scholar lecture," Journal of Fluids Engineering, Transactions of the ASME, **121**(1), 5–33, 1999, doi:10.1115/1.2822013.

[2] U. Ghia, K. N. Ghia, C. Shin, "High-Re solutions for incompressible flow using the Navier-Stokes equations and a multigrid method," Journal of computational physics, **48**(3), 387–411, 1982, doi:10.1016/0021-9991(82)90058-4.

[3] K. Ghasemi, M. Siavashi, "Three-dimensional analysis of magnetohydrodynamic transverse mixed convection of nanofluid inside a lid-driven enclosure using MRT-LBM," International Journal of Mechanical Sciences, **165**, 105199, 2020, doi:10.1016/j.ijmecsci.2019.105199.

[4] A. Bo, F. Mellibovsky, J. Bergadà, W. Sang, "Towards a better understanding of wall-driven square cavity flows using the lattice Boltzmann method," Applied Mathematical Modelling, **82**, 469–486, 2020, doi:10.1016/j.apm.2020.01.057.

[5] T. Huang, H.-C. Lim, "Simulation of Lid-Driven Cavity Flow with Internal Circular Obstacles," Applied Sciences, **10**(13), 4583, 2020, doi:10.3390/app10134583.

[6] J. Baliti, M. Hssikou, M. Alaoui, "Rarefaction and external force effects on gas microflow in a lid-driven cavity," Heat Transfer—Asian Research, **48**(1), 80–99, 2019, doi:10.1002/htj.21369.

[7] S. Mizzi, D. R. Emerson, S. K. Stefanov, R. W. Barber, J. M. Reese, "Effects of rarefaction on cavity flow in the slip regime," Journal of computational and theoretical nanoscience, **4**(4), 817–822, 2007, doi:10.1166/jctn.2007.2374.

[8] A. Mohammadzadeh, E. Roohi, H. Niazmand, "Simulation of Rarefied Gas Flow in Micro/Nano Cavity Using DSMC," in 10th Iranian Aerospace Society Conference, 2011.

[9] B. John, X.-J. Gu, D. R. Emerson, "Investigation of heat and mass transfer in a lid-driven cavity under nonequilibrium flow conditions," Numerical Heat Transfer, Part B: Fundamentals, **58**(5), 287–303, 2010, doi:10.1080/10407790.2010.528737.

[10] A. Mohammadzadeh, A. Rana, H. Struchtrup, "DSMC and R13 modeling of the adiabatic surface," International Journal of Thermal Sciences, **101**, 9–23, 2016, doi:10.1016/j.ijthermalsci.2015.10.007.

[11] A. Rana, M. Torrilhon, H. Struchtrup, "A robust numerical method for the R13 equations of rarefied gas dynamics: Application to lid driven cavity," Journal of Computational Physics, **236**, 169–186, 2013, doi:10.1016/j.jcp.2012.11.023.

[12] G. A. Bird, J. Brady, Molecular gas dynamics and the direct simulation of gas flows, volume 5, Clarendon press Oxford, 1994.

[13] F. Sharipov, Rarefied gas dynamics: fundamentals for research and practice, John Wiley & Sons, 2015.

[14] D. A. Perumal, G. V. Kumar, A. K. Dass, "Application of Lattice Boltzmann Method to Fluid Flows in Microgeometries." CFD letters, **2**(2), 2010.

[15] D. A. Perumal, V. Krishna, G. Sarvesh, A. K. Dass, "Numerical Simulation of Gaseous Microflows by Lattice Boltzmann Method," International Journal on Production and Industrial Engineering, **2**(1), 11, 2011.

[16] A. Rahmati, S. Niazi, "Application and comparison of different lattice Boltzmann methods on non-uniform meshes for simulation of micro cavity and micro channel flow," Computational Methods in Engineering, **34**(1), 97–118, 2015, doi:10.18869/ACADPUB.JCME.34.1.97.

[17] A. Rahmati, S. Niazi, "A multi relaxation time lattice Boltzmann method for simulation of flow in micro devices," in Proc. 19th Annual Int. Conf. on Mechanical Engineering, Birjand, Iran, 2011.

[18] G. Tang, W. Tao, Y. He, "Lattice Boltzmann method for gaseous microflows using kinetic theory boundary conditions," Physics of Fluids, **17**(5), 058101, 2005, doi:10.1063/1.1897010.

[19] G. Tang, W. Tao, Y. He, "Simulating two-and three-dimensional microflows by the lattice Boltzmann method with kinetic boundary conditions," International Journal of Modern Physics C, **18**(05), 805–817, 2007, doi:10.1142/S0129183107010577.

[20] Y. Elguennouni, M. Hssikou, J. Baliti, R. Ghafiri, M. Alaoui, "SRT-LBM and MRT-LBM comparison for a lid-driven gas microflow," in 2020 1st International Conference on Innovative Research in Applied Science, Engineering and Technology (IRASET), 1–6, IEEE, 2020, doi:10.1109/IRASET48871.2020.9092233.

[21] X. Nie, G. D. Doolen, S. Chen, "Lattice-Boltzmann simulations of fluid flows in MEMS," Journal of statistical physics, **107**(1-2), 279–289, 2002, doi:10.1023/A:1014523007427.

[22] C. Lim, C. Shu, X. Niu, Y. Chew, "Application of lattice Boltzmann method to simulate microchannel flows," Physics of fluids, **14**(7), 2299–2308, 2002, doi:10.1063/1.1483841.

[23] G. Tang, W. Tao, Y. He, "Thermal boundary condition for the thermal lattice Boltzmann equation," Physical Review E, **72**(1), 016703, 2005, doi:10.1103/PhysRevE.72.016703.

[24] X. Niu, C. Shu, Y. Chew, "Numerical Simulation of Isothermal Micro Flows by Lattice Boltzmann Method and theoretical analysis of the Diffuse scattering boundary condition," International Journal of Modern Physics C, **16**(12), 1927–1941, 2005, doi:10.1142/S0129183105008448.

[25] Q. Zou, X. He, "On pressure and velocity boundary conditions for the lattice Boltzmann BGK model," Physics of Fluids, **9**(6), 1591–1598, 1997, doi:10.1063/1.869307.

[26] P. L. Bhatnagar, E. P. Gross, M. Krook, "A model for collision processes in gases. I. Small amplitude processes in charged and neutral one-component systems," Physical review, **94**(3), 511, 1954, doi:10.1103/PhysRev.94.511.

[27] G. Karniadakis, A. Beskok, N. Aluru, Microflows and nanoflows: fundamentals and simulation, volume 29, Springer Science & Business Media, 2006.

[28] M. Hssikou, J. Baliti, Y. Bouzineb, M. Alaoui, "DSMC method for a two-dimensional flow with a gravity field in a square cavity," Monte Carlo Methods and Applications, **21**(1), 59–67, 2015, doi:10.1515/mcma-2014-0009.

[29] M. Hssikou, J. Baliti, M. Alaoui, "Extended macroscopic study of dilute gas flow within a microcavity," Modelling and Simulation in Engineering, **2016**, 2016, doi:10.1155/2016/7619746.

[30] Y. Zhang, R. Qin, Y. Sun, R. Barber, D. Emerson, "Gas flow in microchannels–a lattice Boltzmann method approach," Journal of Statistical Physics, **121**(1-2), 257–267, 2005, doi:10.1007/s10955-005-8416-9.

[31] S. Ansumali, I. V. Karlin, "Kinetic boundary conditions in the lattice Boltzmann method," Physical Review E, **66**(2), 026311, 2002, doi:10.1103/PhysRevE.66.026311.

[32] E. Erturk, O. Gokcol, "Fine grid numerical solutions of triangular cavity flow," The European Physical Journal Applied Physics, **38**(1), 97–105, 2007, doi:10.1051/epjap:2007057.

[33] F. Munir, N. A. Che Sidik, M. Rody, H. Zahir, M. Tahir, "Numerical simulations of shear driven square and triangular cavity by using Lattice Boltzmann scheme," World Academy of Science, Engineering and Technology, **70**, 190–194, 2010.

[34] F. A. Munir, M. I. M. Azmi, M. R. M. Zin, M. A. Salim, N. A. C. Sidik, "Application of lattice Boltzmann method for lid driven cavity flow," International Review of Mechanical Engineering, **5**(5), 856–861, 2011.

[35] M. Idris, C. Nor Azwadi, N. N. Izual, "Vortex structure in a two dimensional triangular lid-driven cavity," in AIP Conference Proceedings, volume 1440, 1078–1084, American Institute of Physics, 2012, doi:10.1063/1.4704323.

[36] M. Nazari, "LBM for modeling cavities with curved and moving boundaries," Modares Mechanical Engineering, **13**(5), 117–129, 2013.

[37] B. An, J. M. Bergadà Granyó, "Numerical study of the 2D lid-driven triangular cavities based on the Lattice Boltzmann method," in Proceedings of the 3rd Annual International Conference on Mechanics and Mechanical Engineering:(MME 2016), 945–953, Atlantis Press, 2016, doi:10.2991/mme-16.2017.133.

[38] E. Roohi, V. Shahabi, A. Bagherzadeh, "On the vortical characteristics and cold-to-hot transfer of rarefied gas flow in a lid driven isosceles orthogonal triangular cavity with isothermal walls," International Journal of Thermal Sciences, **125**, 381–394, 2018, doi:10.1016/j.ijthermalsci.2017.12.005.

ASTES

Advances in Science, Technology and Engineering Systems Journal
Vol. 5, No. 5, 592-600 (2020)
www.astesj.com
Special Issue on Multidisciplinary Innovation in Engineering Science & Technology

ASTES Journal
ISSN: 2415-6698

Review of Pedagogical Principles of Cyber Security Exercises

Mika Karjalainen*, Tero Kokkonen*

Institute of Information Technology, JAMK University of Applied Sciences, 40100, Jyväskylä, Finland

ARTICLE INFO

Article history:
Received: 10 August, 2020
Accepted: 15 September, 2020
Online: 05 October, 2020

Keywords:
Cyber Security Exercise
Expert Performance
Simulation Pedagogy

ABSTRACT

Modern digitalized cyber domains are extremely complex ensemble. Cyber attacks or incidents against system may affect capricious effects for another system or even for physical devices. For understanding and training to encounter those effects requires an effective and complex simulation capability. Cyber Security Exercises are an effective expedient for training and learning measures and operations with their outcomes in that complex cyber domain. Learning in cyber security exercises is relevant for different level actors in organisation hierarchy. Technical experts are able to train the technical capabilities whereas decision makers are able to train the decision-making capabilities under hectic cyber incident. In this paper, the pedagogical aspects of cyber security exercises are discussed in accordance with the law of the lifecycle of the cyber security exercise: planning phase, implementation phase, and feedback phase.

1 Introduction

This research is an extension of work originally presented in 2019 workshop on Cyber Range Technologies and Applications (CACOE 2019) organized in conjunction with 2019 IEEE European Symposium on Security and Privacy (EuroS&P 2019) [1]. This research is expanded from the original as follows: discussion about pedagogical theories and cyber-arena concept for complex environment simulation with the more detailed extended analysis of pedagogical aspects of the cyber security exercises and assessment of the exercise target audience.

Global digitalisation and networked systems have raised new threats. Modern digitalised cyber domains are extremely complex and forms incalculable reliance. That change in digital environment has reflected to the requirements of training and education. Traditionally, exercises are used in a military context to gain better performance for certain tasks. In the cyber domain and especially in the context of cyber resilience, the most valuable assets are personal skills. Those skills are trained efficiently with cyber security exercises.

Cyber security strategy of Finland [2] states that in the critical cyber competence areas, the high level of required training is confirmed by both national and international exercises. The significance of cyber security exercises is also observed in the cyber strategy of the United States of America [3] and the cyber security strategy of the European Union [4]. In addition, cyber security exercises are recognized as an important part of personnel training in commercial organisations, especially in the critical infrastructure organisations, for example, electricity companies [5]. There are several different cyber security exercises conducted globally, for example, the report [6] consists of a dataset of more than 200 cyber security exercises and the NATO Cooperative Cyber Defence Centre of Excellence (CCDCOE) highlights several exercises they organise or contribute [7].

There exist frameworks categorizing the required skills of personnel in organisations . National Institute of Standards and Technology (NIST) has published document called National Initiative for Cyber security Education (NICE) Cyber security Workforce Framework (NICE Framework) as a reference structure that designates the complex essence of the knowledge, skills, and abilities (KSAs) required in the different roles and tasks of the work within cyber security [8, 9]. There are also frameworks for curricula of education: Computing Curricula 2020 (CC2020) forms a guideline for academic degree programs in computing) [10]. When discussing cyber security, the CC2020 refer to the Cyber security Curricula 2017 (CSEC2017) that form curriculum guidelines for degree programs in cyber security [11].

Simulations have been widely used for study experts [12]. Education in the engineering sciences relies heavily on hands-on training, i.e. applying learned phenomena in practice. In that sense, different learning environments, simulators and test-beds have a remarkable role in the engineering education. When discussing cyber security exercises, the extremely important component is the exercise platform that simulates the cyber domain. Traditionally that kind of platform is called cyber range. Cyber range is executed as a technical platform for exercises that mimic the required networks and systems. As exercise platform, a cyber range, is required

*Corresponding Authors: Mika Karjalainen, mika.karjalainen@jamk.fi and Tero Kokkonen, tero.kokkonen@jamk.fi

to be closed and totally controlled to allow risk free usage of real attacks and intrusions [13]–[14]. The term cyber range originates from the similarity of the kinetic ranges with potential to improve competence or capability with weapons, operations, tactics and techniques [15]. As stated in [16], there exist several diverse cyber ranges globally that vary from enormous virtual-Internets to simple laboratory based test-beds. Because the spectrum of cyber ranges is so multifarious, authors of [16] introduced the concept of Cyber Arena for the simulation of realistic complex cyber-physical domain with unexpected dependencies between networks and systems.

JYVSECTEC (Jyväskylä Security Technology) is JAMK University of Applied Sciences Institute of Information Technology based cyber security focused research, development and training center that offers information and cyber security services [17]. JYVSECTEC has extensive experience for organising cyber security exercises for both national security authorities and private companies of critical infrastructure. Since 2013, Finland's national cyber security exercise has been organised annually by JYVSECTEC [18]. JYVSECTEC has also been Finland's representative in the Cyber Defence Pooling & Sharing Project of European Defence Agency (EDA) [19]–[20].

JAMK University of Applied Sciences has organised several different cyber security exercises. During those exercises, more than 1,500 experts have been involved in those learning experiments. In addition, there is an annual course of cyber security exercise for the cyber security students of bachelor's and master's programs of JAMK University of Applied Sciences. The data for this research of multiple-case design originates from observations, notes and questionnaires collected from the numerous cyber security exercises organised by JAMK University of Applied Sciences. The focus of this research is to characterize pedagogical principles of cyber security exercises as the educational framework for understanding the complex and interdependent cyber domain in the individual or organisational level.

Albeit, the importance of the cyber security exercises is widely recognized, there is a deficiency in the research of pedagogical aspects, especially in the viewpoint of competence development. In high level, cyber security exercise is a three-phase process consisting of different components of exercise life-cycle: planning phase, implementation phase and feedback phase. Those three phases can be divided into smaller steps of process. This study presents a competence development oriented view on that lifecycle of cyber security exercises. As part of that competence development oriented view, those three different components of exercise life-cycle are explored with the perspective of learning outcomes.

2 Cyber Security Exercises and the Pedagogical Principles

In recent years, cyber security exercises have established their position as a tool for developing the skills of cyber security professionals and as an operating environment for teaching. As business environments and the using of ICT in business have evolved, they have also become more complex at the same time. Consequently, the requirements for teaching environments have also changed.

In order to be able to teach skills that meet the needs of working life, it is necessary to understand the needs and be able to teach them in such a way that teaching builds skills that are needed in working life [21]. According to Ericsson's deliberated practices (DP) theory, the development of specialist skills must take into account the need to set well-defined learning objectives for students and the need to take into account the level of students' existing skills [22]. According to the deliberated practice theory, students do not benefit from the training if the tasks are at a level that they can perform routinely or if the goal setting of competence development has not been done with sufficient accuracy to mirror the student's level of competence.

Modern ICT teaching must therefore be able to mirror the changes in the operating environment to the change in competence requirements. When a modern cyber range is used in a cyber security exercise, the aim must be to make the operating environment as realistic as possible. The comprehensiveness and complexity of the teaching environment places demands on the student's level of competence. Thus, if cyber security training is used as a pedagogical tool for competence development, it should be noted that according to the Miller pyramid, the student's level of competence should be at the top of the pyramid [23]. This argument is supported by the andragogy, known as a theory of adult learning. According to andragogy theory an adult as a learner is often motivated, capable of self-direction and reflection on one's own existing competence [24]. Thus, for the adult learner learning experiment should be able to cause cognitive dissonance that allows the learner to update existing knowledge with new knowledge created in the learning event [25]. It must be possible to build a path of competence development, where in accordance with the constructive methodology, the student's developing competence enables the student to achieve new levels of competence through developing cognitive abilities [26]. Constructive methodology identifies problem-based learning as one of the key learning methods, in which the student develops his or her own skills by solving problems that lead to the learner's new knowledge [27].

The cyber security exercise can be seen as a complex problem field where the student solves the problems ahead and thus generates new knowledge for himself. This theory is supported also by experiential learning theory [28]. A key element in cyber security practice is working as a member of a team. This models real-life work where a person acts as part of, for example, a security operation team (SOC). In the exercise, all individuals are placed as a member of Teams (Blue Team) whose job is to defend and sustain the business in the operating environment assigned to them. The student can also act as part of a red team functionality that simulates threat activities. This role is to train, for example, the skills required for penetration testing. In the exercise, learners act in the role assigned to them, and communicate as part of a team of events that they perceive in their own operating environment. Thus, students share knowledge, solve problems and build new knowledge collectively.

To sum up, the cyber security exercise combines several pedagogical theories. The pedagogical framework of the cyber security exercises is shown in Figure 1. The exercise is also demanding from the point of view of pedagogical implementation and often requires a significant investment in pre-exercise planning, where the operating environment is constructed so that the required technical elements can be modeled and operational functionalities are designed so that pedagogical objectives can be achieved.

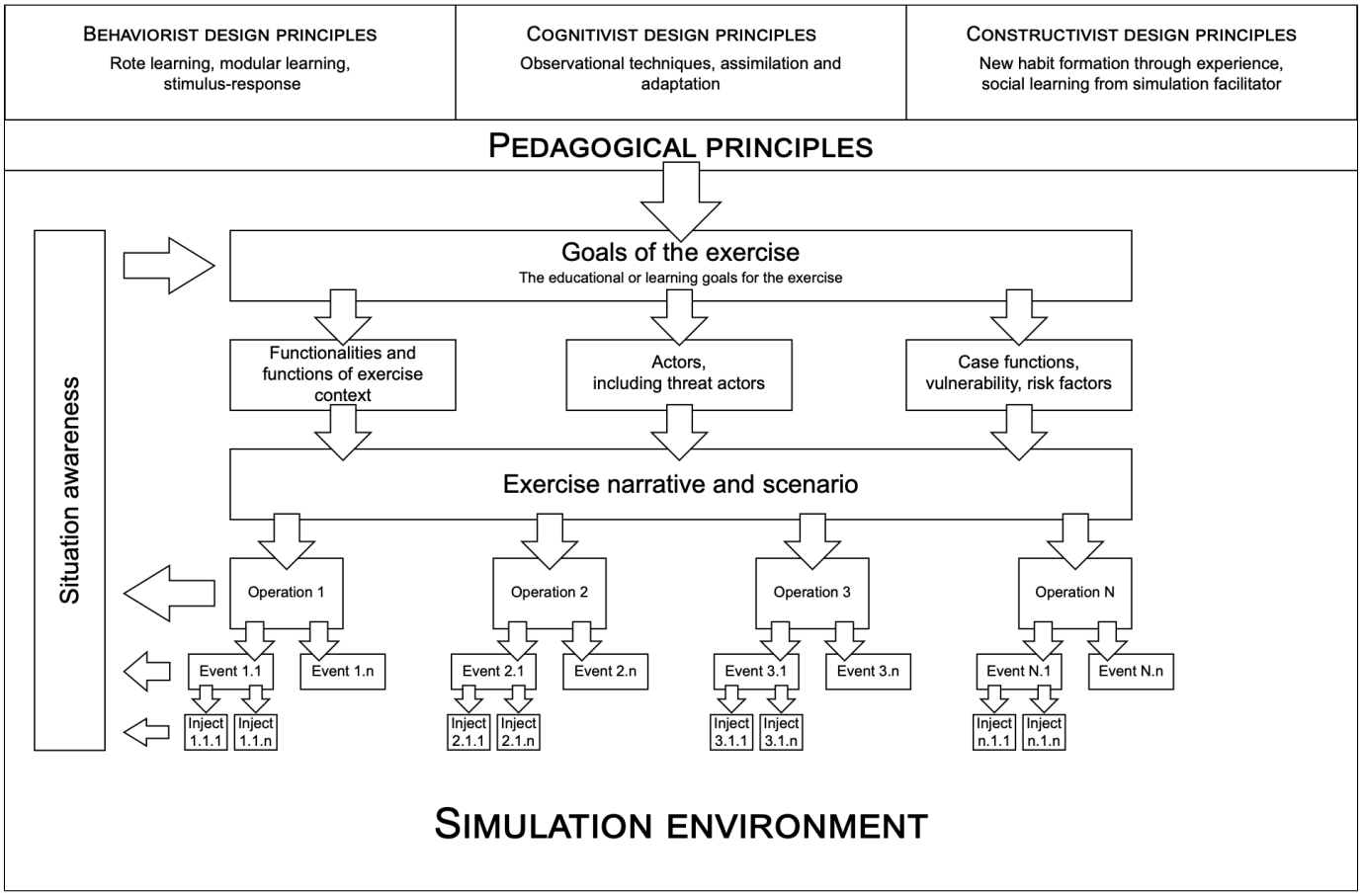


Figure 1: Pedagogical framework of the cyber security exercises [1]

2.1 Cyber Arena

According to complexity thinking, it should be possible to form an understanding of the functionality or entity under investigation as a whole, which is more than the sum of its parts [29]. The operating environment of cyber security can be seen as a complex entity consisting of different parts that interact with each other. Interaction takes place at different levels, such as in the technical operating environment, at the level of activities and processes, and as human interaction. The interconnection between different parts of the operating environment is partly defined and partly undefined. The key elements of complexity thinking are the recognition of the unpredictability of the environment, the difficulty of predicting cause consequences, and the self-organisation of the operating environment [30]. It is thus a matter of utilizing complexity thinking in accordance with the neo-reductionist school to model and simulate the subordination laws of the research object [31].

When the above is applied to the cyber environment, it is noteworthy to recognize the difficulties of applying traditional legislation, technological incompatibilities and the very rapid technical renewal of the environment. Thus, the student should be able to develop an understanding of unpredictability of the environment, unpredictable cause-and-effect relationships, and the risks of misuse of the technological element. In order for this entity to be embodied as part of cyber security education, a sufficiently realistic learning environment should be in place, such as Cyber Arena the overall high-level presentation of which is shown in Figure 2. It can be seen from the figure that the environment extensively models the cyber security domain. In order to be able to implement sufficient realism and the understanding of complexity, the teaching environment should model key functions and entities, as well as the interdependencies between the functions and or entities. In accordance with the authentic learning environment theory [32], the environment implements an operating environment in which the skills and competencies learned in cyber security practice will be applied.

3 Exercise Life-cycle

There are different definitions for the phases of cyber security exercise life-cycle. Wilhelmson and Svensson introduce three phases; planning, implementing and processing feedback, which are divided into into ten steps (exercise preparations, the master plan, the mission statement, exercise planning, practical preparations, implementation, evaluation, feedback, reporting, and the after action review) [33]. Consistently, MITRE describes three stages (Exercise Planning, Exercise Execution and Post Exercise) [34]. Vykopal et al. defines five stages for exercise; preparation, dry run, execution, evaluation, and repetition [35]. The Homeland Security Exercise and Evaluation Program (HSEEP) that provides a set of foundational concepts for exercise programs defines the management cycle with four stages: exercise design and development, exercise conduct, ex-

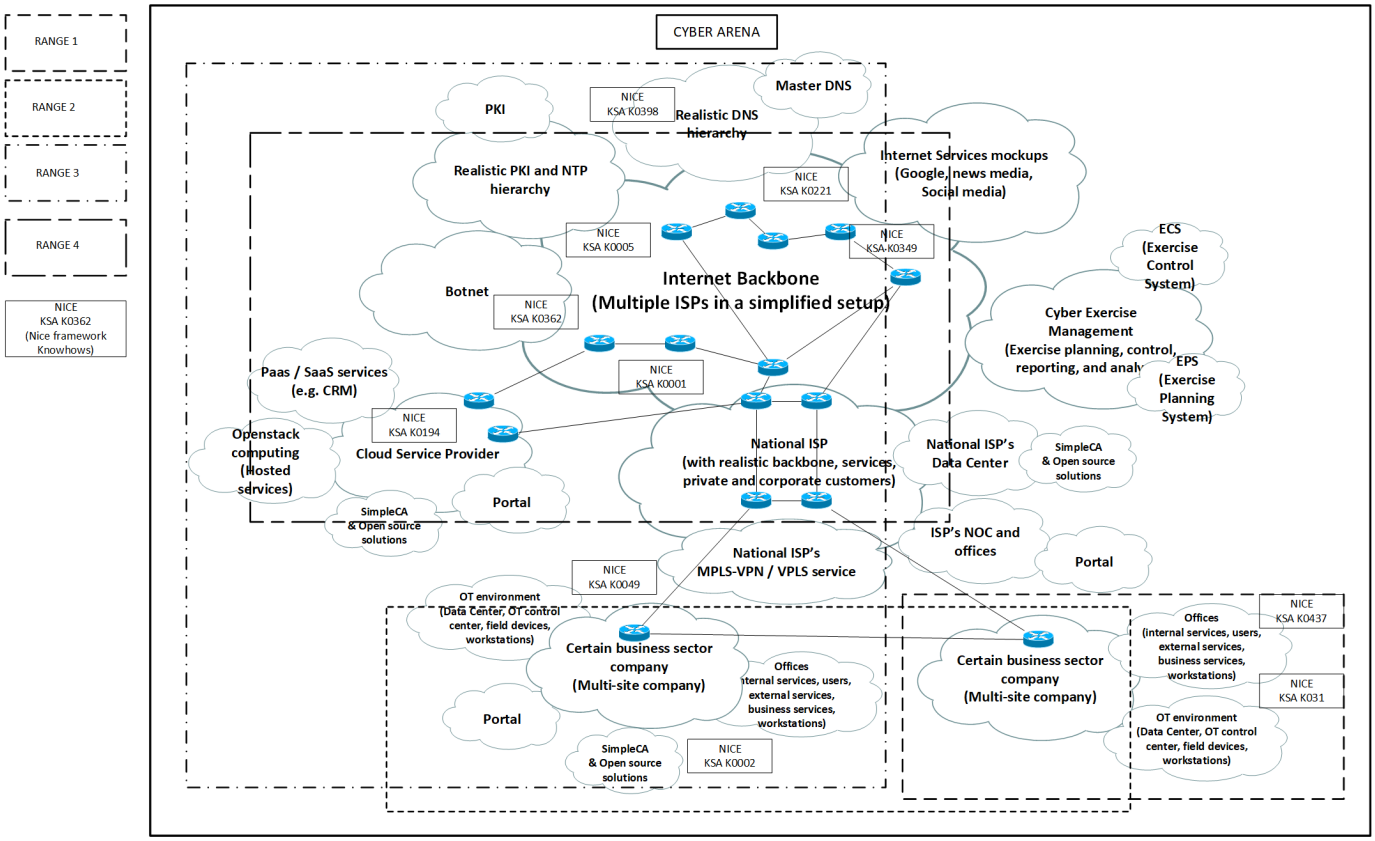


Figure 2: Comprehensive Cyber Arena [16]

ercise evaluation, and improvement planning [36]. As an integration of different definitions and a viewpoint for pedagogical aspects of this research the following three phases are selected *(i) planning phase, (ii) implementation phase, and (iii) feedback phase*. The extended view for pedagogical aspects of the cyber security exercises is shown in Figure 3. It illustrates whole process from planning phase to the implementation of the exercise.

3.1 Planning Phase

The first step of exercise life-cycle is the planning-phase. It is an extremely critical phase, because it determines the effectiveness of the whole exercise. From the viewpoint of competence development, the content of the exercise e.g. scenario, actors, and events shall be fitted to the requirements of the exercise target audience.

Based on the required learning outcomes and the target organisation, exercise parameters are derived including simulated operational environment of scenario for example technical functionalities, threat actors, risks and vulnerabilities. That scenario encompasses discrete events and injects of exercise describing the totality of simulated activities. If the scenario created during the planning phase includes obscurities, the exercise including technical environment may not increase the performance of the exercise target audience or organisation. All the elements mentioned supports the achievement of the set learning objectives. The learning objectives can be seen at several levels, the goals can be set from the perspective of organisational competence development, on the other hand, learning objectives can be set from the perspective of individual competence development. When learning goals are set from an organisational perspective, an individuals learning goals should be set so that they put the organisations goals into practice. In Figure 3, the goals of the exercise phase are opened, allowing us to look at an example of what kind of practical sections or tasks in the planning phase should be planned in order to be able to achieve the set goals in the exercise.

3.2 Implementation Phase

There are several differences between the phases of the exercise life-cycle. The most hectic phase is the implementation phase where the exercise target audience is acting in a simulated complex cyber domain under cyber deviation actions (attacks and intrusions). When acting under hectic and stressful cyber deviation circumstances, there is a requirement to maintain the understanding (situation awareness, SA) of the valuable assets' status in cyber domain. According to Endsley [37] *"Situation awareness is the perception of the elements in the environment within a volume of time and space, the comprehension of their meaning, and the projection of their status in the near future"*. The expertise of the individual has a remarkable outcome for the SA [38]. In this context, the term situation awareness refers to both, the understanding of the progress of the operational situation in the exercise, and the understanding of the monitoring and evaluation of the pedagogical objectives of the exercise.

During the exercise, also the decision making has a remarkable role in what incident handling actions shall be done and how to

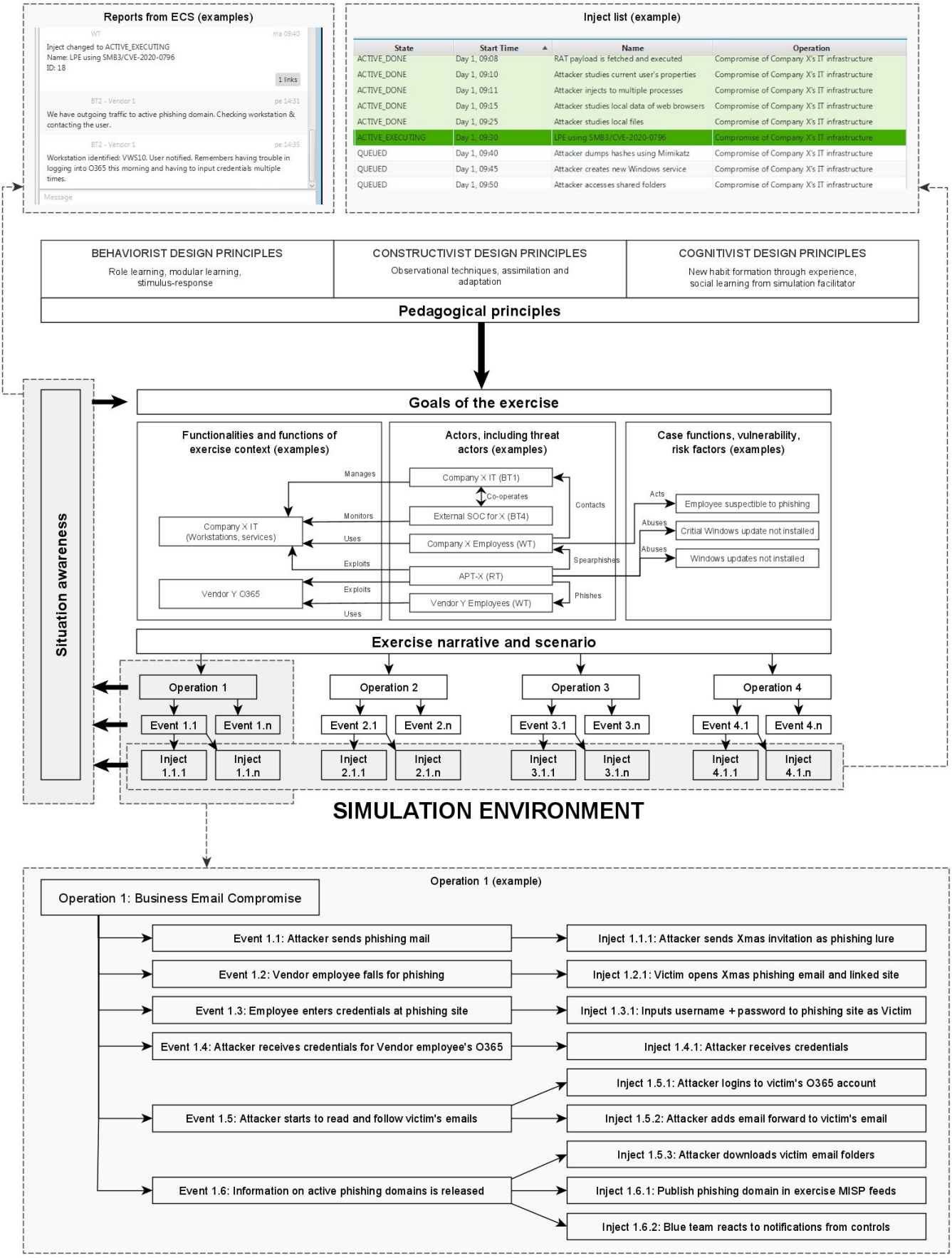


Figure 3: Detailed pedagogical framework of the cyber security exercises

categorize order of the required actions. Mostly, those decisions are based on SA as comprehension on two models of decision making cycle; Gartner's Adaptive Security Architecture (Predict-Prevent-Detect-Respond) [39] and OODA-loop (Observation-Orientation-Decision-Action) [40, 41].

Figure 3, illustrates that the operation line according to the exercise scenario, is opened to illustrate the practical actions of one operation performed during the exercise. The operation includes a series of events that are divided into injects with which the exercise is practically carried forward according to a planned scenario. An inject list has also been opened in the figure to show how in the practice the exercise proceeds with injects. The exercise management team (white team, WT) can use the information obtained through information systems to assess the situation, but it is often also necessary to monitor visually and interview students. This will ensure that the exercise proceeds as planned and that the set learning objectives can be achieved. If the WT notices that students are taking actions that are not realistic or the focus of the exercise begins to shift from the set goal, the WT should guide the course of the exercise. This can be done through information system injections or verbally by instructing students.

3.3 Feedback Phase

From the perspective of the development of an individual's competence, the feedback phase is the most important part of the exercise. Scheduling the feedback phase should be planned carefully with too long an interval of exercise and feedback may cause a decrease in learning intensity for the individual. The emotions and experiences raised by the exercise are alleviated and learning outcomes may suffer as a result. In the feedback phase, the pedagogical goals of the exercise are recalled and the events of the exercise are reflected against them by reviewing all operations performed and related events and injects in the exercise. This happens so that all operations performed in the exercise, related events and injects are reviewed. By doing so, the student can reflect the experience they have had during the exercise and thus deepen their own learning. It is also important to tie individual events through operations into an exercise scenario. This allows the student to increase the understanding of the bigger picture, for example, the threat actors' motive and the tools used for the attack. This is important and enables in the future the exercise event to be reflected in real situations of working life.

It is a good to set aside time for the feedback session so that the interaction between students and teachers can be enabled as widely as possible. Normally, each defensive team (blue team, BT) has the opportunity to open up their own observations and experiences in this section. This enables collegial and collaboratively learning. The offensive team (RT) also goes through its own operations, thus allowing BT to reflect its own observations in relation to the operations that took place.

4 Assessing Performance and Results

The Kirkpatrick four-level assessment framework can be used for the assessment of the exercise. Kirkpatrick divides assessment into four levels: (i) reaction, (ii) learning, (iii) behaviour, and (iv) results [42]. The Kirkpatrick framework is useful in assessing a larger entity such as an organisation or team, but it can also be used for the individual experience of learning in exercise. In the Kirkpatrick framework, the goals for the development of individual competence are set at level one and two. At level one the reactions caused by the exercise are assessed. At level two, the learning that has achieved by the individual is assessed. Kirkpatrick et al. recommends the use of control groups and tests for assessing the learning. The goals set for organisational competence development utilize the Kirkpatrick assessment model's, level three, which assesses the change in individual behaviour through the achieved learning outcomes, and level four which assesses the effects and implementation of advanced competence on organisational performance. Kirkpatrick model is a widely used evaluation model, the study [43] presents a framework for competence development and assessment in hybrid cyber security exercises, and the authors of [44] introduce one adoption of the Kirkpatrick Model.

Other methods for evaluating exercise can also be used, the authors of [45] have monitored communication during the cyber security exercise for understanding the behaviour of the exercise target audience. Their conclusion is that communication monitoring can be used as a resource in measuring the performance during the cyber security exercise.

When focusing on assessing the learning of an individual who has participated in the exercise, Brown and Pickford [46], have created a model that looks at the assessment of learning event as a whole. Brown and Pickford divide the assessment into the following subsections the significance and implementation of these sections should be planned in advance: why, what, how, who, when.

Why- why the assessment is made? What is the purpose of assessment in this particular learning event? In the context of a cyber security exercise, the aim of assessment is in some respects to control the individual's performance, facilitate the student's adaptation to the exercise, be able to assess the student's motivation, measure the competence, skills and know-how and to provide the student information about mistakes and inappropriate practices.

What- what are we assessing? In a cyber security exercise the processes of work, individual performance and success of team work can be assessed. In the exercise, the assessment should be performed at all stages of its life cycle.

How- how are we assessing? As discussed, Figure 3 illustrates the role of the situation awareness and all the inputs where the information for assessing will be collected. So, part of the information for the assessment can be collected via information systems and the reports from the BT that they are delivering to exercise control system. In addition to this, the teacher must monitor classroom activities. In this way, information can be obtained, for example, about an individual's performance in a specific role as part of a team. Visual observation can also provide information about the team's internal activities and role support and its possible functioning.

Who- who is suitable for making the assessment? In the exercise, students often work as a part of a team throughout the exercise. This provides an opportunity to implement the evaluation as a peer review, whereby the internal functionalities and inclusions of the team become more clearly assessed. In education leading to a degree, students are also often asked to have a learning diary in which the student can make a self-assessment of the exercise throughout its

life cycle. The role of teachers in the assessment may therefore be more aggregate.

When- when should assessment take place? In the cyber security exercise the assessment needs to be done in all phases of exercise. This is because the assessment plays a very important role as a function of guiding learning. The importance of formative or guiding assessment in cyber security exercises is emphasized. The theory of formative evaluation has been built specifically by Scriven [47]. According to Scriven, the concept of formative assessment became conceptualized. Formative assessment emphasizes that assessment should take place at all stages of the teaching and learning, and not just at the end. Several studies verify that learning outcomes are significantly improved when formative assessment that guides learning is included in the assessment as well as summative assessment. Thomas et. al [48] and Leahy et. al [49] have stated that learning outcomes improve when assessment includes formative assessment that guides learning in addition to the assessment learned skills.

Formative assessment emphasizes the importance of feedback. According to Hattie [50], the purpose of the feedback can be divided into three sections: *Feed up, feed back* and *feed forward* sections. The feed up gives the learner an answer to the question of where he or she is going. The purpose of feed up feedback is to continuously clarify and specify the learning objectives. Feed up feedback also aims to engage and motivate the learner to pursue to the set goals. A feed back, tells to the learner where he or she is at the moment. The feed back feedback is used to provide the student the information on how he or she has progressed in relation to the set learning objectives. In order to give exact feedback on the learner's position, the learning objectives must be precisely defined, also so that the prerequisites for progressive learning are perceptible and acceptable. Feed forward feedback, tells the learner what he or she should do next. In practice, guidance can be sought, for example, through questions that broaden the student's understanding, or with advice and tips on, for example, new ways for approaching to the set goals.

According to Hattie, each feedback question works on four levels: level of the task, level of process, level of self-regulation and level of person. The level of the task, i.e. how well the learner understands the set tasks and how he or she performs them. In practice, for example, feedback indicates whether an individual task has been solved correctly or incorrectly. Feedback should also be directed to correcting any malfunctions or performing the task correctly. Level of process indicates the process required to understand and perform a given task in the context of a cyber exercise, for example, what kind of operation is needed to bring an into the exercise so that the student learns the methods and technology used for a phishing campaigns. Level of self-regulation guides the learner to self-assessment and self-direction of action. At this level, feedback can also be used to guide the learner's motivation and adaptation to the teaching environment used. The level of the person includes assessments of the learner. This section often contains elements for assessing and providing feedback on a learners personality traits. In a cyber exercise, guidance can be given, for example, on a persons participation and activity as part of a team, what is a key part of a persons performance in the exercise.

The purpose of the feedback is to reduce the gap between existing competence and the target competence. Due to the complexity and scope of the cyber security exercise, special attention should be paid to the continuous feedback throughout the exercise life cycle.

5 Conclusion

There are elements in the cyber security operating environment in line with complexity thinking, however, it is a philosophical question of whether the cyber security environment is ultimately a complex entity. There is complexity in the operating environment. According to the definition of complexity, the phenomena are intertwined and the whole cannot be understood by disassembling the whole into parts and looking at the parts one by one. Unlike complex entities, the cyber operation environment can be controlled, although there may also be self-directed elements in the operation environment. When implementing cyber security education, the complexity of the operating environment should be taken into account. Therefore, the teaching environment should be a Cyber Arena style operating environment mimicking realistic operative cyber domain. In the Cyber Arena, several functional entities are combined forming an ensemble with complex cause-and-effect relationships manifested. Pedagogically, however, the constructive construction of competence development must be taken into account, in which case teaching starts from the parts or details of the operating environment and culminates the teaching for understanding the whole environment, including the interdependences of different entities.

As presented, the pedagogical objectives of the exercise should be taken into account at all stages of the life cycle. In the planning phase, goals are set for competence development. In education leading to a degree, the objectives are defined in the curriculum. In the exercise for the other target audience, the goals of competence development should be defined together with the representatives of the organisation. In this way, the objectives of the exercise are adapted to the current maturity and operations of the organisation. In the implementation phase, the realization of the goals must be monitored and, if necessary, the focus of the exercise must be directed towards the set goals. In the feedback phase, participants in the exercise are given the opportunity to interact through the exercise, in which the operations performed in the exercise are opened in detail. To support post-practice learning, it is also important to provide material to be distributed that allows students to return to the details of the exercise afterwards.

Generally accepted content frameworks, such as the NICE framework,can be used to design the content's learning objectives. This makes it possible to set structured teaching goals, through which the exercise scenario can be constructed in such a way that the technical functions do not remain separate events without causal relationships. The student who has done this is are able to form an entity from the exercise, at the latest at the feedback stage, through which he or she can learn about the effectiveness of the sub-entities of the operating environment as a whole.

Exercise evaluation is a challenging whole consisting of evaluating an individual, as well as evaluating the performance of an organisation or part of it. In order for assessment to serve the set competence development goals as well as possible, formative assessment that guides learning should be used where possible. In this way, the evaluation of the activities serves as a guiding element of the exercise, helping to ensure that the set learning objectives

are achieved. With regard to formative assessment, the importance of feedback is emphasized. It should be possible to deliver it at all stages of the exercise life cycle. Feedback should take into account interactivity and, where possible, make use of peer feedback from learners.

Future research should build on the understanding of the pedagogical requirements of cyber security exercise in relation to the teaching environment and individual learning gained in this and other studies and move towards assessing the development of organisational competence in cyber security exercise.

Conflict of Interest

The authors declare no conflict of interest.

Acknowledgment

This research is funded by the *Cyber Security Network of Competence Centres for Europe (CyberSec4Europe)* project of the Horizon 2020 SU-ICT-03-2018 program.

References

[1] M. Karjalainen, T. Kokkonen, S. Puuska, "Pedagogical Aspects of Cyber Security Exercises," in "2019 IEEE European Symposium on Security and Privacy Workshops (EuroS&p)," 103–108, 2019, http://dx.doi.org/10.1109/EuroSPW.2019.00018.

[2] Secretariat of the Security Committee, "Finland's Cyber security Strategy, Government Resolution 3.10.2019," https://turvallisuuskomitea.fi/wp-content/uploads/2019/10/Kyberturvallisuusstrategia_A4_ENG_WEB_031019.pdf, 2019.

[3] The White House, signed by President Donald J. Trump, "National Cyber Strategy of the United States of America," https://www.whitehouse.gov/wp-content/uploads/2018/09/National-Cyber-Strategy.pdf, 2018.

[4] European Comission, "Cybersecurity Strategy of the European Union: An Open, Safe and Secure Cyberspace," https://eur-lex.europa.eu/legal-content/EN/TXT/PDF/?uri=CELEX:52013JC0001&from=EN, 2013.

[5] FINGRID magazine, "Cyber security is ensured with genuine exercises," https://www.fingridlehti.fi/en/cyber-security-ensured-genuine-exercises/, 2017, Accessed: 12 May 2020.

[6] B. Uckan Färnman, M. Koraeus, S. Backman, "The 2015 Report on National and International Cyber Security Exercises : Survey, Analysis and Recommendations," Technical report, Swedish Defence University, CRISMART (National Center for Crisis Management Research and Training), 2015, http://dx.doi.org/10.2824/627469.

[7] The NATO Cooperative Cyber Defence Centre of Excellence, CCDCOE, "Exercises," https://ccdcoe.org/exercises/, Accessed: 12 May 2020.

[8] K. Saharinen, M. Karjalainen, T. Kokkonen, "A Design Model for a Degree Programme in Cyber Security," in "Proceedings of the 2019 11th International Conference on Education Technology and Computers," ICETC 2019, 3–7, Association for Computing Machinery, New York, NY, USA, 2019, http://dx.doi.org/10.1145/3369255.3369266.

[9] W. Newhouse, S. Keith, B. Scribner, G. Witte, National Initiative for Cybersecurity Education (NICE) Cybersecurity Workforce Framework, 2017, http://dx.doi.org/10.6028/nist.sp.800-181.

[10] Association for Computing Machinery (ACM) and IEEE Computer Society (IEEE-CS), "Computing Curricula 2020, CC2020, Paradigms for Future Computing Curricula (Draft, Version 36)," https://cc2020.nsparc.msstate.edu/, 2020.

[11] Association for Computing Machinery (ACM) and IEEE Computer Society (IEEE-CS) and Association for Information Systems Special Interest Group on Information Security and Privacy (AIS SIGSEC) and International Federation for Information Processing Technical Committee on Information Security Education (IFIP WG 11.8), "Cybersecurity Curricula 2017, (CSEC2017), Curriculum Guidelines for Post-Secondary Degree Programs in Cybersecurity (Version 1.0)," https://www.acm.org/binaries/content/assets/education/curricula-recommendations/csec2017.pdf, 2017, Accessed: 12 May 2020.

[12] P. Ward, A. M. Williams, P. A. Hancock, Simulation for Performance and Training, 243–262, Cambridge University Press, New York, NY, US, 2006, http://dx.doi.org/10.1017/CBO9780511816796.014, iD: 2006-10094-014.

[13] P. Nevavuori, T. Kokkonen, "Requirements for Training and Evaluation Dataset of Network and Host Intrusion Detection System," in Á. Rocha, H. Adeli, L. P. Reis, S. Costanzo, eds., "New Knowledge in Information Systems and Technologies," 534–546, Springer International Publishing, Cham, 2019.

[14] B. Ferguson, A. Tall, D. Olsen, "National Cyber Range Overview," in "2014 IEEE Military Communications Conference," 123–128, 2014, http://dx.doi.org/10.1109/MILCOM.2014.27.

[15] Z. Tian, Y. Cui, L. An, S. Su, X. Yin, L. Yin, X. Cui, "A Real-Time Correlation of Host-Level Events in Cyber Range Service for Smart Campus," IEEE Access, **6**, 35355–35364, 2018, http://dx.doi.org/10.1109/ACCESS.2018.2846590.

[16] M. Karjalainen, T. Kokkonen, "Comprehensive Cyber Arena; The Next Generation Cyber Range," in "2020 IEEE European Symposium on Security and Privacy Workshops (EuroS&P)," , 2020.

[17] JAMK University of Applied Sciences, Institute of Information Technology, JYVSECTEC, "Jyväskylä Security Technology," https://www.jyvsectec.fi, Accessed: 12 May 2020.

[18] Ministry of Defence Finland, "Kansallinen kyberturvallisuusharjoitus KYHA18 järjestetään Jyväskylässä, Official Bulletin 11th of May 2018," https://www.defmin.fi/ajankohtaista/tiedotteet/2018?9610_m=9314, 2018, Accessed: 12 May 2020.

[19] European Defence Agency, EDA, "Cyber Ranges: EDA's First Ever Cyber Defence Pooling & Sharing Project Launched By 11 Member States," https://www.eda.europa.eu/info-hub/press-centre/latest-news/2017/05/12/cyber-ranges-eda-s-first-ever-cyber-defence-pooling-sharing-project-launched-by-11-member-states, 2017, Accessed: 12 May 2020.

[20] European Defence Agency, EDA, "EDA Cyber Ranges Federation project showcased at demo exercise in Finland," https://www.eda.europa.eu/info-hub/press-centre/latest-news/2019/11/07/eda-cyber-ranges-federation-project-showcased-at-demo-exercise-in-finland, 2019, Accessed: 12 May 2020.

[21] H. Collins, R. Evans, A Sociological/Philosophical Perspective on Expertise: The Acquisition of Expertise through Socialization, 21–32, Cambridge Handbooks in Psychology, Cambridge University Press, 2 edition, 2018, http://dx.doi.org/10.1017/9781316480748.002.

[22] K. Anders Ericsson, "Deliberate Practice and Acquisition of Expert Performance: A General Overview," Academic Emergency Medicine, **15**(11), 988–994, 2008, http://dx.doi.org/10.1111/j.1553-2712.2008.00227.x.

[23] G. E. Miller, "The assessment of clinical skills/competence/performance," Academic medicine, **65**(9), S63–7, 1990.

[24] S. B. Merriam, L. L. Bierema, Adult learning: Linking theory and practice, John Wiley & Sons, 2013.

[25] M. S. Knowles, Designs for adult learning: Practical resources, exercises and course outlines from the father of adult learning., Alexandria, Va: American Society for Training & Development, 1995.

[26] S. Lindblom-Ylänne, A. Nevgi, "The effect of pedagogical training and teaching experience on approach to teaching," in "11th EARLI conference, Padua," , 2003.

[27] J. R. Savery, T. M. Duffy, "Problem based learning: An instructional model and its constructivist framework," Educational technology, **35**(5), 31–38, 1995.

[28] D. A. Kolb, R. E. Boyatzis, C. Mainemelis, et al., "Experiential learning theory: Previous research and new directions," Perspectives on thinking, learning, and cognitive styles, **1**(8), 227–247, 2001.

[29] T. Hanén, "Faced with the Unexpected - Leadership in Unexpected and Dynamic Situations: an Interpretation Based on Complexity Theory (Orig: Yllätysten edessä: kompleksisuusteoreettinen tulkinta yllättävien ja dynaamisten tilanteiden johtamisesta)," Ph.D. thesis, National Defence University, 2017, http://urn.fi/URN:ISBN:978-951-25-2870-7.

[30] R. Geyer, S. Rihani, Complexity and public policy: a new approach to twenty-first century politics, policy and society, Routledge, 2010.

[31] K. A. Richardson, "MANAGING COMPLEX ORGANIZATIONS: COMPLEXITY THINKING AND THE SCIENCE AND ART OF MANAGEMENT," Corporate Finance Review, **13**(1), 23–29, 2008, https://search-proquest-com.ezproxy.jyu.fi/docview/198834948?accountid=11774.

[32] J. Herrington, R. Oliver, "An instructional design framework for authentic learning environments," Educational Technology Research and Development, **48**(3), 23–48, 2000, http://dx.doi.org/10.1007/BF02319856.

[33] N. Wilhelmson, T. Svensson, Handbook for planning, running and evaluating information technology and cyber security exercises, The Swedish National Defence College, Center for Asymmetric Threats Studies (CATS), 2014.

[34] J. Kick, "Cyber Exercise Playbook," The MITRE Corporation https://www.mitre.org/sites/default/files/publications/pr_14-3929-cyber-exercise-playbook.pdf, 2014, Accessed: 12 May 2020.

[35] J. Vykopal, M. Vizvary, R. Oslejsek, P. Celeda, D. Tovarnak, "Lessons learned from complex hands-on defence exercises in a cyber range," in "2017 IEEE Frontiers in Education Conference (FIE)," 1–8, 2017.

[36] The U.S Department of Homeland Security, "Homeland Security Exercise and Evaluation Program (HSEEP)," https://www.fema.gov/media-library-data/1582669862650-94efb02c8373e28cadf57413ef293ac6/Homeland-Security-Exercise-and-Evaluation-Program-Doctrine-2020-Revision-2-2-25.pdf, 2020, Accessed: 12 May 2020.

[37] M. Endsley, "Toward a Theory of Situation Awareness in Dynamic Systems," Human Factors, **37**(1), 32–64, 1995, http://dx.doi.org/10.1518/001872095779049543.

[38] M. R. Endsley, Expertise and Situation Awareness, 633–652, Cambridge Handbooks in Psychology, Cambridge University Press, 2006, http://dx.doi.org/10.1017/CBO9780511816796.036.

[39] R. van der Meulen, "Build Adaptive Security Architecture Into Your Organization," https://www.gartner.com/smarterwithgartner/build-adaptive-security-architecture-into-your-organization/, 2017, accessed: 3 April 2020.

[40] G. L. Rogova, R. Ilin, "Reasoning and Decision Making under Uncertainty and Risk for Situation Management," in "2019 IEEE Conference on Cognitive and Computational Aspects of Situation Management (CogSIMA)," 34–42, 2019, http://dx.doi.org/10.1109/COGSIMA.2019.8724330.

[41] B. Brehmer, "The Dynamic OODA Loop: Amalgamating Boyd's OODA Loop and the Cybernetic Approach to Command and Control," in "10th International Command and Control Research and Technology Symposium, The Future of C2," , 2005.

[42] D. L. Kirkpatrick, J. D. Kirkpatrick, Evaluating Training Programs, Berrett-Koehler Publishers, Inc., San Francisco, 2006.

[43] A. Brilingaitė, L. Bukauskas, A. Juozapavičius, "A framework for competence development and assessment in hybrid cybersecurity exercises," Computers & Security, **88**, 101607, 2020, http://dx.doi.org/10.1016/j.cose.2019.101607.

[44] A. Ahmad, C. Johnson, "A Cyber Exercise Post Assessment: Adoption of the Kirkpatrick Model," Advances in Information Sciences and Service Sciences (AISS), **7**(2), 2015.

[45] T. Kokkonen, S. Puuska, "Blue Team Communication and Reporting for Enhancing Situational Awareness from White Team Perspective in Cyber Security Exercises," in O. Galinina, S. Andreev, S. Balandin, Y. Koucheryavy, eds., "Internet of Things, Smart Spaces, and Next Generation Networks and Systems," 277–288, Springer International Publishing, Cham, 2018.

[46] S. Brown, R. Pickford, Assessing skills and practice, Routledge, 2006.

[47] M. Scriven, "SOCIAL SCIENCE EDUCATION CONSORTIUM. PUBLICATION 110, THE METHODOLOGY OF EVALUATION." , 1966.

[48] L. Thomas, C. Deaudelin, J. Desjardins, O. Dezutter, "Elementary teachers' formative evaluation practices in an era of curricular reform in Quebec, Canada," Assessment in Education: Principles, Policy & Practice, **18**(4), 381–398, 2011.

[49] S. Leahy, D. Wiliam, "From teachers to schools: scaling up professional development for formative assessment," Assessment and learning, **2**, 49–71, 2012.

[50] J. Hattie, "Teachers Make a Difference, What is the research evidence?" , 2003.

ASTES

Advances in Science, Technology and Engineering Systems Journal Vol. 5, No. 5, 601-606 (2020)

www.astesj.com

Special Issue on Multidisciplinary Sciences and Engineering

ASTESJ

ISSN: 2415-6698

CNN-LSTM Based Model for ECG Arrhythmias and Myocardial Infarction Classification

Lana Abdulrazaq Abdullah[*, 1, 2, 3], Muzhir Shaban Al-Ani[1]

[1]*Department of Information Technology, College of Science and Technology, University of Human Development, Sulaymaniyah,46001, Iraq*

[2]*Department of Computer, College of Science, University of Sulaimani, Sulaymaniyah, KRG, 46001, Iraq*

[3]*Department of Applied Computer, Health and Applied Science, Charmo University, Sulaymaniyah, KRG, 46001, Iraq*

ARTICLE INFO

Article history:
Received: 11 July, 2020
Accepted: 15 September, 2020
Online: 05 October, 2020

Keywords:
ECG classification arrhythmia
Convolutional neural network
Long Short Term Memory
Myocardial Infarction

ABSTRACT

ECG analysis is commonly used by medical practitioners and cardiologists for monitoring cardiac health. A high-performance automatic ECG classification system is a challenging area because there is difficulty in detecting and clustering various waveforms in the signal, especially in the manual analysis of electrocardiogram (ECG) signals. In this paper, an accurate (ECG) classification and monitoring system are proposed using the implementation of 1D Convolutional Neural Networks (CNNs) and Long Short Term Memory (LSTM). The learned features are captured from the CNN model, and then fed to the LSTM model. No handcraft features are required for the model for the ECG classification. The result of the CNN-LSTM model has demonstrated superior performance than several state-of-the-arts that cited in the result section. The proposed models are evaluated on MIT-BIH arrhythmia and PTB Diagnostics datasets. Based on the obtained results, the CNN-LSTM method can improve the accuracy rate, such that 98.1 % and 98.66 % on Myocardial Infarction (MI) and arrhythmia classification, respectively.

1. Introduction

One of the most crucial organs in the human body is the heart, and monitoring of the heart has become a necessary diagnosis to the health of the human being. The electrical activity of the heart is well known as ECG, and Abnormality in ECG may cause symptoms of heart disease, such as persistent ventricular tachycardia, low blood pressure, rapid atrial fibrillation, and persistent ventricular tachycardia. These mentioned diseases are dangerous for human life and desire an urgent treatment [1]. The most significant information about the state of the heart can be observed from the ECG analysis, which can be monitored manually and automatically [2]. Due to the fact that there are various morphologies in the ECG signal, manual diagnosis is found difficult. Therefore, an automatic system of the ECG diagnosis has been interested in. Both feature extraction and classification approaches are the critical successes of any automatic ECG classification. There are plenty of applications that ECG analysis and classification involve, such as ischemic heart disease, arrhythmia, and myocardial infarction [3].

Feature extraction process is a viral area in ECG classification, and many approaches have been developed for this purpose as the feature has a significant impact on any machine learning system. Nowadays, there are numerous approaches for extracting features from ECG signals such as Discrete Wavelet Transform (DWT), Wavelet Transform (WT), and Mel Frequency Coefficient Cepstrum (MFCC).The DWT has been widely adopted in ECG classification as an effective feature, for instance, Desai at el. in [4], proposed system-based approach for computer-assisted detection of five classes of ECG arrhythmia beats by adopting DWT as a feature to train Support Vector Machine (SVM). In [5] developed a comprehensive model based on random forest techniques and discrete wavelet for arrhythmia classification. The authors in [6]used the DWT to capture features from the ECG signal based on ST-segment elevation and inverted T wave logic.

The MFCC was used as a handcrafted, which was extracted from the ECG signal directly, then the artificial neural network (ANN) was fed by the MFCC features [7]. The authors in [8] developed a hybrid features, which was merged MFCC and DWT after that the proposed feature was classified by k Nearest

[*]Corresponding Author: Lana Abdulrazaq Abullah, Sulaymaniyah, KRG, Iraq: lana.abdulrazaq@gmail.com

Neighbor (kNN). In addition, The WT was conducted to take features out from ECG signal for classifying four cardiac types such as healthy (N), Paced beats (P), right bundle branch block (RBBB), and left bundle branch block (LBBB). Then ANN and SVM were used to classify the extracted features [9].

The handcrafted feature is not always the best candidate feature for the ECG application, as it is a time-consuming and boring task [10]. Therefore, a featureless model like CNN has been interested in classifying the ECG analysis. CNN has been conducted into two forms, such as one dimensional and two-dimensional forms, for instance, Zubair at el. in [11] proposed the raw data fed a model-based 1D-CNN for classifying ECG signals into some classes that were suggested by the Association for Advancement of Medical Instrumentation (AAMI) and the model. Wang in [12] developed a model based on 1D CNN and modified Elman neural network (MENN),which was consisted of the 11-layers neural network, and the non-transform ECG signal also fed the model. While some researchers proposed their CNN model for ECG analysis based on two-dimensional forms, for instance, Zheng at el in [13] converted the one dimensional ECG signal into two-dimensional images and then fed to the CNN model. Yildirim at el. developed a model for detecting a diabetic subject by adopting pre-trained 2D-CNN model with frequency spectrum images, which were obtained from heartbeat signals [14].

In this paper, a hybrid model, which is composed by CNN and LSTM, is developed. No handcrafted feature requires the model as the CNN part is responsible for obtaining the feature. The learned features are given to the LSTM model to learn a deep pattern in the learned feature and classify into healthy and abnormal ECG signals, where the health ECG signal is chosen as the absolute normal ECG pattern template. According to our experimental result, LSTM can improve the classification rate, as shown in the result section. The rest of the paper is organized as follows: Section 2 explained a concise background area of the proposed model, Section 3 methodology. Results and discussion are addressed in Section 4. Finally, the conclusion section is given in Section 5.

2. Background

A representation of the cardiac activity of the heart is known as the ECG signal. The automatic monitoring system of the ECG signal has been focused area as it is related to the human health condition. Feature extraction and classification are the primary processes in any automatic monitoring system. In this paper, the suggested model is a fusion model, which consists of CNN and the LSTM model, as shown in Figure 1. A brief background of CNN and LSTM is addressed in the below section as CNN is used to extract the learned features, and LSTM is conducted to classify the learned features.

2.1 Convolution Neural Networks

The CNNs also known as the feature learner has excellent potential to extract useful features automatically from input raw data. The CNNs are normally comprised of two parts and each part has different function. Feature extractor is the first part of the CNNs and which is normally responsible to extract features automatically. The second part is classifier which is called a fully connected multi-layer perceptron (MLP). The fully connected part performs classification depend on the learned features from the first part. The feature extraction's part includes some layers namely; convolution layer and pooling layer. Any convolutional layer can take feature maps out from the previous layer. convolutional layer contains several convolution kernels (filters), added by bias, and then put throughout the activation function to generate a feature map for the next layer [15].

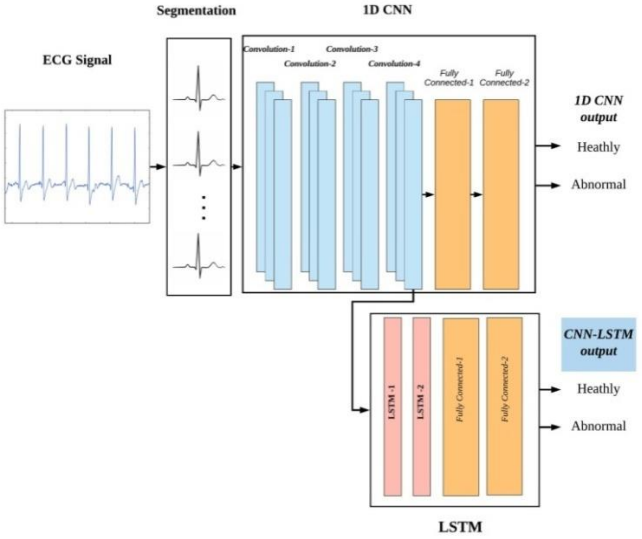


Figure 1: proposed CNN_LSTM scheme.

One of the common sub layers in feature extraction's part is called pooling layer. There are some types of the pooling layer which are Max, Min and Average pooling. Pooling layer can shrink the resolution of the feature maps. Max-pooling operation is used in the proposed model, which calculates the maximum value in a set of nearby inputs [11].There is difference between the both parts in term of complexity. The feature extraction's part, which is primary layer, performs more computations including feature extraction and feature selection compare to the fully connection layers [16].

Many similarities can be seen between the CNN structure the ANN with an input, hidden, and output layers. On the other hand, unlike NN, CNN is an enhanced version of the ANN, which is both translational and shift invariant. Typically, the CNNs comprise of various types of layers such as input, convolution, max pooling, average pooling, drop layer, and Softmax layer, etc. and play a specific role in the model [17].

2.2 Long Short-Term Memory

RNN is one of the types of network architectures, which is specifically designed to deal with the sequential problem, and it is commonly used in sequence classification. A well-known improvement of RNN was introduced by Hochreiter and Schmidhuber in 1997 [18], which is called Long Short Term Memory (LSTM). Plenty of applications of LSTM has been published recently [19]–[23]. The LSTM unit comprises a cell; a forget gate, an output gate, and an input gate[19]. The cell unit is in charge of remembering values at every time interval. The rest unit gates manage the flow of information into and out of the unit. In the memory block structure, a simple one-layer neural network

controls the forget gate. The functionality of this gate is formulated as Eq (1) [24].

$$f_t = \delta(w[x_t, h_{t-1}, c_{t-1}] + b_f) \quad (1)$$

where, x_t is the sequence of input; c_{t-1} is the previous LSTM block memory; h_{t-1} is the earlier block output; b_f is the bias vector; δ is the logistic sigmoid function, and W symbolizes separate weight vectors for every input. An input gate is a unit where the new memory is formed by the previous memory block effect and a simple NN with an activation function which is tanh. These operations are calculated by Eq (2) and (3)[25].

$$i_t = \delta(w[x_t, h_{t-1}, c_{t-1}] + b_i) \quad (2)$$

$$c_t = f_t . c_{t-1} + i_t . \tanh(w[x_t, h_{t-1}, c_{t-1}] + b_i) \quad (3)$$

The output gate is an output of the current LSTM block and can be formulated using Eqs (4) and (5) [19].

$$\delta_t = \delta(w[x_t, h_{t-1}, c_t] + b_0) \quad (4)$$

$$h_t = \delta_t . \tanh(c_t) \quad (5)$$

Where, b_i and b_i are the outputs of previous memory block;These mentioned units are linked to each other, as illustrated in Figure 2, which permit information to cycle between steps of adjacent time and also construct an inner feedback state which the network to the temporal feature in the given data [26].

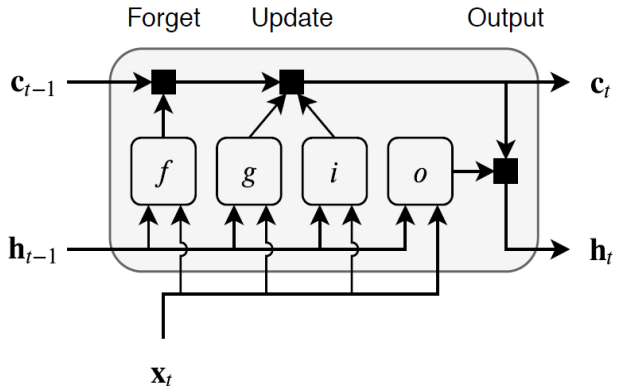


Figure 2: Connection LSTM units, where (i) is Input gate, (g) is Cell candidate, (f) is Forget gate, and (o) is Output gate [26].

3. Methodology

This section is divided into; data description, preprocessing, and experimental design.

3.1 Data description

3.1.1 MIT-BIH Arrhythmia Database

In this study, one of the examined database is a gathering of annotated ECG recordings that achieved by the Arrhythmia Laboratory of Boston's Beth Israel Hospital, known as the MIT-BIH Arrhythmia Database [27]. It comprises 48 half-hour excerpts of two-channel ambulatory ECG recordings, which were obtained from 47 subjects, and the dataset was recorded in the BIH Arrhythmia Laboratory between 1975 and 1979. The recordings are obtained with a frequency of 360 Hz; this means each record approximately consists of 30 *360 = 10800 samples and contains recordings from two leads: one is ML2, and the other is one of $V1, V2, V3, V4, V5,$ or $V6$. Two or more cardiologists independently annotated each record for a total of 110,000 annotations covered with the database: it is worth to mention that each annotation is placed in correspondence to the R peak of a single beat so that we have totally solved for this particular case the beat discovery problem. The MIT-BIH Arrhythmia database is split into two classes healthy and abnormal.

3.1.2 The Physionet PTB Diagnostic ECG database

The second examined database, which is used in this paper, was recorded by the Department of Cardiology at Benjamin Franklin University in Berlin, Germany. The dataset consists of 290 subjects and include 549 records (aged 17 to 87, mean 57.2; and 81 women, mean age 61.6 and 209 men, mean age 55.5). One to five records were observed from each subject. The dataset was split into two sections namely, healthy signals and different cardiac diseases such as myocardial infarction, bundle branch block, arrhythmia, cardiomyopathy/heart failure, myocardial hypertrophy, etc. Each record includes 15 simultaneously measured signals: the conventional 12 leads $(i, ii, iii, avr, avl, avf, V1, V2, V3, V4, V5, V6)$ together with the 3 Frank lead ECGs (vx, vy, vz)[8].

3.2 Preprocessing

In the MIT-BIH database, the beats are labeled based on the R position. The authors segment each record sample intoa separated beat and take samples from both sides of R waves. Each heartbeat consists of 130 sample points (65 samples before the R-peak and 64 samples after the peak), which is the smallest length ever been used for ECG classification. As showed in Figure. 3, the balanced dataset was created; the number of healthy beats is 86456 and 11230 beats of the abnormal beat.

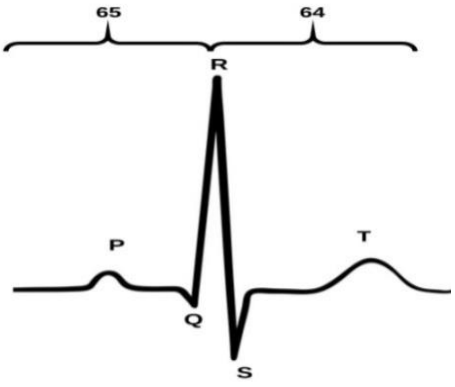


Figure 3: ECG signal.

Feature from the raw signal and eliminate noise from the ECG signals. The LSTM section can deal with the characteristics of ECG related to time series properly and able to predict the future QRS complexes using the previous QRS complexes. The 1D CNN structure contains 19 layers, including four convolution layers, two Dropout layers with half percent drop, and two fully-connected layers.

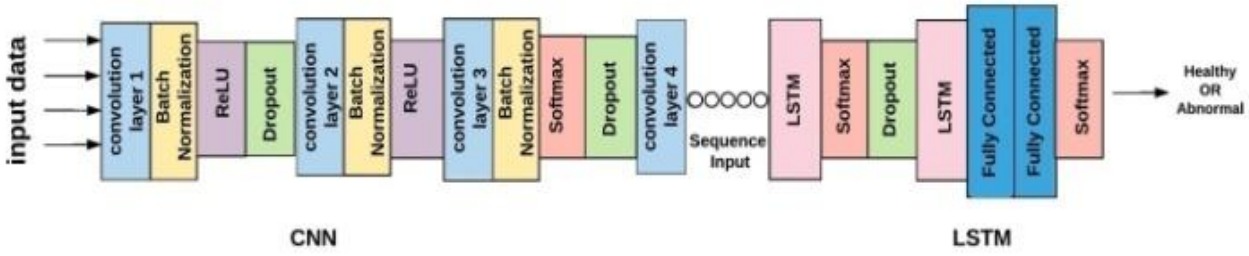


Figure 4: Structure of CNN-LSTM model.

Some parameters of the model such as number of convolution layer, filters and epochs are tuned based on cross validation methods. The description of the CNN-layers,are set out in Table 1.The spatial and local feature map is well extracted from the thirteenth layers of the CNN model, which is the convolutional layer with ten filters. The filters act to identify different features present in an ECG signal like edges, vertical and horizontal lines. Then, the features are fed to the LSTM model. For MIT-BIH Arrhythmia Dataset, the length of the learned features is ten times of the original signal thus the length of the feature is equal to 1300.Then; the learned feature is divided into ten separated beats and later merged them into a cell to be input to the LSTM model. In terms of the PTB Diagnostic ECG Dataset, the length of the ECG signal and the length learned features is 187.

Table 1: Description of 1D CNN model.

No. layer	Name	Description
1.	Input	Depend on the input with 'zero center' normalization
2.	Convolution Layer 1	20 7x7 convolutions with stride [1 x 1] and padding “same”
3.	Batch Normalization1	Batch normalization
4.	Clipped ReLU	Clipped ReLU with ceiling 5
5.	Dropout	50% dropout
6.	Convolution Layer 2	20 9x9 convolutions with stride [1 x 1] and padding “same”
7.	Batch Normalization2	Batch normalization 2
8.	Leaky ReLU	Leaky ReLU with scale 0.01
9.	Convolution Layer 3	30 5x5 convolutions with stride [1 x 1] and padding “same”
10.	Batch Normalization3	Batch normalization
11.	Softmax	Softmax
12.	Dropout	50% dropout
13.	Convolution Layer 4	10 3x3 convolutions with stride [1 x 1] and padding “same”
14.	Batch Normalization4	Batch normalization
15.	ReLU	ReLU
16.	Fully Connected1	60 fully connected layer
17.	Fully Connected2	Two fully connected layer
18.	Softmax	Activation function for the last Fully Connected layer
19.	Classification	Output cross-entropy

3.3 Experimental design

In the current study, a cross-learning method based on deep learning is proposed for automatically classifying healthy and abnormal of the ECG signal. The proposed model is developed by integrating CNN and LSTM, which consists of 19 layers,as illustrated in Figure 4,where the CNN section is responsible for capturing the locally

The implemented LSTM structure contains two lstmlayers, dropout layers, and two fully-Connected layers, as it is shown in Table 2. The output of the proposed model is two classes, which are healthy and abnormal Arrhythmia for MIT-BIH Arrhythmia Database and healthy and Myocardial Infarction for the PTB Diagnostic ECG Database.

Table 2: Description of LSTM model.

No. layer	Name	Description
1.	Input	Sequence input with input dimensions
2.	LSTM Layer 1	LSTM with 120 hidden units
3.	Softmax	Softmax
4.	Dropout	30% dropout

5.	LSTM Layer 2	LSTM with 120 hidden units
6.	Fully Connected1	Ten fully connected layer
7.	Fully Connected2	Two fully connected layer
8.	Softmax	Softmax
9.	Classification	Output cross-entropy

4. Result and discussion

2.3 MIT-BIH arrhythmia database

Nowadays, machine learning has been adopted for many applications, such as arrhythmia classification. One of the well-known datasets is the MIT-BIH arrhythmia dataset that has been adopted by a mounting number of researchers in ECG research. Table 3 shows the result of the proposed methods and some state of arts who have studied a model for detecting ECG arrhythmias. Inspire of these state of arts, ten-fold cross-validation is utilized to evaluate the proposed model. Although the proposed CNN-LSTM model is fed by the shortest length of the ECG signal ever, the result demonstrates higher classification accuracy than other related studies. However, the result of 1D CNN does not exceed the state of arts. Moreover, the performance of our proposed model exceed the performance of a CNN-LSTM model which was conducted by [28]. However, the structure of their model (11 layers) is simplest than our model (19 layers).

Table 3: Result of arrhythmia classification.

Study	Number of Classes	Classifier	Signal Length	Accuracy (%)
Andersen et al. 2019 [25]	2	CNN +RNN	360 , 250	97.80%
Wang 2020[12]	2	CNN+MENN	360	97.40%
Lih Oh[28]	5	CNN+LSTM	1000	98.48%,
Proposed method	2	CNN	130 sample	94.70%
	2	CNN+LSTM	130 sample	**98.66%**

2.4 MI Classification

Another well-known datasets are the PTB Diagnostics dataset that is used to evaluate the proposed methods. MI classification is an application of using the PTB Diagnostics dataset, and the MI can be treated as two classes' problem with infracted and non-infracted classes. The length of the signal 14552 samples and divided by 4046 infracted and 10506 non-infracted. Based on relevant researches in the literature, ten-fold cross-validation is adopted to weigh the proposed method. The experimental result in Table 4 shows a significant improvement in the classification accuracy. Moreover, the percentage of precision and recall are improved compared to the existing approaches available in the literature.

Table 4: MI classification result.

Study	Percentage (%)		
	Accuracy	Precision	Recall
Kachuee et al. [29]	95.90	95.20	95.10
Achary el al. [30]	93.5	92.80	93.70
Safdarian et al.[31]	94.70	-	-
Scratched 1D-CNN proposed	97.55	96.00	97.51
CNN-LSTM proposed	98.13	96.80	98.00

5. Conclusion

Detecting heart abnormalities using ECG signals is very challenging area. An accurate model to detect the abnormal ECG signals leads to offer correct treatment to the patients in the earlier stage of disease. In this paper, an effective arrhythmias and myocardial classification method that combines 1-D CNN and LSTM model. The proposed CNN-LSTM model is applied to the computerized recognition of abnormal ECG signals. According to our experimental result, the learned features from CNN can be useful features for a time series approach like LSTM.

Moreover, the LSTM can find out a better pattern in the learned feature compare to the fully-connection layer itself. Consequently, the classification result by LSTM has outperformed the states of arts. The authors recommend to use the proposed model to classify multiclass of arrhythmias and myocardial instead of binary class.

Conflict of Interest

The authors declare no conflict of interest.

Acknowledgment

The authors would like to thank assistant professor Mr, Zrar Kh Abdul for his support during the preparation of this work. Many thanks for the reviewers for their valuable comments and suggestions on the manuscript which improve the presentation of the paper.

References

[1] E. J. Benjamin et al., Heart Disease and Stroke Statistics—2017 Update, **135**(10), 2017.
[2] S. Saechia, J. Koseeyaporn, and P. Wardkein, "Human identification system based ECG signal," IEEE Reg. 10 Annu. Int. Conf. Proceedings/TENCON, 2007, 2–5, 2005, doi: 10.1109/TENCON.2005.300986.
[3] M. A. Serhani, H. T. El Kassabi, H. Ismail, and A. N. Navaz, "ECG Monitoring Systems: Review, Architecture, Processes, and Key Challenges," Sensors, 2020, doi: 10.3390/s20061796.
[4] U. Desai, R. J. Martis, C. G. Nayak, K. Sarika, and G. Seshikala, "Machine

intelligent diagnosis of ECG for arrhythmia classification using DWT, ICA and SVM techniques," 12th IEEE Int. Conf. Electron. Energy, Environ. Commun. Comput. Control (E3-C3), INDICON **2015**, 2–5, 2016, doi: 10.1109/INDICON.2015.7443220.

[5] G. Pan, Z. Xin, S. Shi, and D. Jin, "Arrhythmia classification based on wavelet transformation and random forests," Multimed. Tools Appl., **77**(17), 21905–21922, 2018, doi: 10.1007/s11042-017-5225-5.

[6] P. Kora, C. U. Kumari, K. Swaraja, and K. Meenakshi, "Atrial Fibrillation detection using Discrete Wavelet Transform," in Proceedings of 2019 3rd IEEE International Conference on Electrical, Computer and Communication Technologies, ICECCT 2019, 1–3, 2019. DOI: 10.1109/ICECCT.2019.8869498.

[7] M. Boussaa, I. Atouf, M. Atibi, and A. Bennis, "ECG signals classification using MFCC coefficients and ANN classifier," Proc. 2016 Int. Conf. Electr. Inf. Technol. ICEIT, 2016, 480–484, 2016. DOI: 10.1109/EITech.2016.7519646.

[8] S. A. A. Yusuf and R. Hidayat, "MFCC feature extraction and KNN classification in ECG signals," 2019 6th Int. Conf. Inf. Technol. Comput. Electr. Eng. ICITACEE, 2019, 1–5, 2019. DOI: 10.1109/ICITACEE.2019.8904285.

[9] S. Sahoo, B. Kanungo, S. Behera, and S. Sabut, "Multiresolution wavelet transform based feature extraction and ECG classification to detect cardiac abnormalities Multiresolution wavelet transform based feature extraction and ECG classification to detect cardiac abnormalities," 55–66, 2017. DOI: 10.1016/j.measurement.2017.05.022.

[10] Ö. Yıldırım, U. B. Baloglu, and U. R. Acharya, "A deep convolutional neural network model for automated identification of abnormal EEG signals," Neural Comput. Appl., 10–20, 2018. doi: 10.1007/s00521-018-3889-z.

[11] M. Zubair, J. Kim, and C. Yoon, "An automated ECG beat classification system using convolutional neural networks," in 2016 6th International Conference on IT Convergence and Security, ICITCS 2016. doi: 10.1109/ICITCS.2016.7740310.

[12] J. Wang, "A deep learning approach for atrial fibrillation signals classification based on convolutional and modified Elman neural network," Futur. Gener. Comput. Syst., **102**, 670–679, 2020, doi: 10.1016/j.future.2019.09.012.

[13] Z. Zheng, Z. Chen, F. Hu, J. Zhu, Q. Tang, and Y. Liang, "An automatic diagnosis of arrhythmias using a combination of CNN and LSTM technology," Electron., **9**(1), 1–15, 2020, doi: 10.3390/electronics9010121.

[14] O. Yildirim, M. Talo, B. Ay, U. B. Baloglu, G. Aydin, and U. R. Acharya, "Automated detection of diabetic subject using pre-trained 2D-CNN models with frequency spectrum images extracted from heart rate signals," Comput. Biol. Med., **113**, 103387, Oct. 2019, doi: 10.1016/j.compbiomed.2019.103387.

[15] W. Yin, X. Yang, L. Zhang, and E. Oki, "ECG Monitoring System Integrated with IR-UWB Radar Based on CNN," IEEE Access, **4**, 6344–6351, 2016, doi: 10.1109/ACCESS.2016.2608777.

[16] J. Li, Y. Si, T. Xu, and S. Jiang, "Deep Convolutional Neural Network Based ECG Classification System Using Information Fusion and One-Hot Encoding Techniques," Math. Probl. Eng., 2018. doi: 10.1155/2018/7354081.

[17] U. R. Acharya et al., "Automated identification of shockable and non-shockable life-threatening ventricular arrhythmias using convolutional neural network," Futur. Gener. Comput. Syst., **79**, 952–959, 2018. doi: 10.1016/j.future.2017.08.039.

[18] S. Hochreiter and J. Urgen Schmidhuber, "Long Shortterm Memory," Neural Comput., **9**(8), p. 17351780, 1997.

[19] C. Chen, Z. Hua, R. Zhang, G. Liu, and W. Wen, "Automated arrhythmia classification based on a combination network of CNN and LSTM," Biomed. Signal Process. Control, **57**, 101819, 2020, doi: 10.1016/j.bspc.2019.101819.

[20] X. H. Le, H. V. Ho, G. Lee, and S. Jung, "Application of Long Short-Term Memory (LSTM) neural network for flood forecasting," Water (Switzerland), **11**(7), 2019, doi: 10.3390/w11071387.

[21] E. Balouji, I. Y. H. Gu, M. H. J. Bollen, A. Bagheri, and M. Nazari, "A LSTM-based deep learning method with application to voltage dip classification," Proc. Int. Conf. Harmon. Qual. Power, ICHQP, 2018-May, 1–5, 2018, doi: 10.1109/ICHQP.2018.8378893.

[22] F. Weninger et al., "Speech enhancement with LSTM recurrent neural networks and its application to noise-robust ASR," Lect. Notes Comput. Sci. (including Subser. Lect. Notes Artif. Intell. Lect. Notes Bioinformatics), 9237, 91–99, 2015, doi: 10.1007/978-3-319-22482-4_11.

[23] F. Liu et al., "An Attention-based Hybrid LSTM-CNN Model for Arrhythmias Classification," Proc. Int. Jt. Conf. Neural Networks, 2019-July, 1–8, 2019, doi: 10.1109/IJCNN.2019.8852037.

[24] Ö. Yildirim, "A novel wavelet sequences based on deep bidirectional LSTM network model for ECG signal classification," Comput. Biol. Med., **96**(March), 189–202, 2018, doi: 10.1016/j.compbiomed.2018.03.016.

[25] R. S. Andersen, A. Peimankar, and S. Puthusserypady, "A deep learning approach for real-time detection of atrial fibrillation," Expert Syst. Appl., **115**, 465–473, 2019, doi: 10.1016/j.eswa.2018.08.011.

[26] J. Cheng, L. Dong, and M. Lapata, "Long short-term memory-networks for machine reading," EMNLP 2016 - Conf. Empir. Methods Nat. Lang. Process. Proc., 551–561, 2016.

[27] G. B. Moody and R. G. Mark, "The impact of the MIT-BIH arrhythmia database," IEEE Engineering in Medicine and Biology Magazine, **20**(3), 45–50, 2001, doi: 10.1109/51.932724.

[28] S. L. Oh, E. Y. K. Ng, R. S. Tan, and U. R. Acharya, "Automated diagnosis of arrhythmia using combination of CNN and LSTM techniques with variable length heart beats," Comput. Biol. Med., **102**, 278–287, 2018, doi: 10.1016/j.compbiomed.2018.06.002.

[29] M. Kachuee, S. Fazeli, and M. Sarrafzadeh, "ECG heartbeat classification: A deep transferable representation," Proc. - 2018 IEEE Int. Conf. Healthc. Informatics, ICHI 2018, 443–444, 2018, doi: 10.1109/ICHI.2018.00092.

[30] U. R. Acharya et al., "A deep convolutional neural network model to classify heartbeats," Comput. Biol. Med., **89**, 389–396, 2017, doi: 10.1016/j.compbiomed.2017.08.022.

[31] N. Safdarian, N. J. Dabanloo, and G. Attarodi, "A New Pattern Recognition Method for Detection and Localization of Myocardial Infarction Using T-Wave Integral and Total Integral as Extracted Features from One Cycle of ECG Signal," J. Biomed. Sci. Eng., **07**(10), 818–824, 2014, doi: 10.4236/jbise.2014.710081.

ASTES

Advances in Science, Technology and Engineering Systems Journal Vol. 5, No.5, 607-612 (2020)

www.astesj.com

Special Issue on Innovative Research in Applied Science, Engineering and Technology

ASTESJ

ISSN: 2415-6698

Experimental and Numerical Study of the Mechanical Behavior of Bio-Loaded PVC Subjected to Aging

Abdelghani Lakhdar*, Aziz Moumen, Laidi Zahiri, Mustapha Jammoukh, Khalifa Mansouri

SSDIA Laboratory, Hassan II University of Casablanca, ENSET of Mohammedia, 28830, Morocco

ARTICLE INFO

Article history:
Received: 10 July, 2020
Accepted: 19 September, 2020
Online: 05 October, 2020

Keywords:
PVC
Aging
Numerical modeling
Recycling
Coconut fibers
Cow horn fibers

ABSTRACT

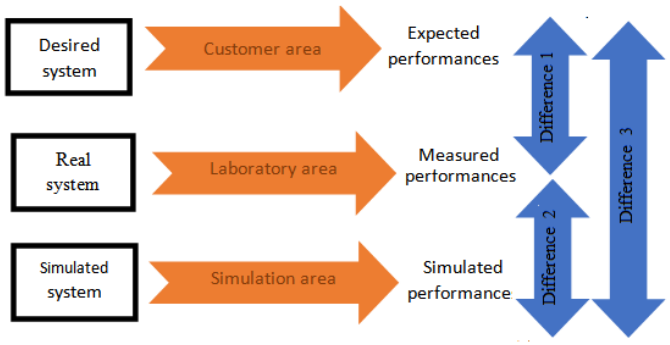
Increased recycling of PVC has become a requirement in industrial and scientific research level. Several studies will be realized. To confirm and check the recycled materials performance, it will be important to go through numerical modeling, which consists not only in validating the results of the experiments, but also in predicting what happens when the material is loaded. PVC material is more used in different fields, that ultimately means, after service life, an increase in waste requiring a high recycling rate. This article presents an approach validating the aging model as well as a numerical analysis predicting the mechanical properties of PVC after aging. The analysis samples (rigid and flexible) PVC which are subject to two types of accelerated aging, allows to obtain an aging model. Numerical modeling of PVC after aging is carried out using the finite element method and has been able to confirm the results obtained experimentally. Predicting the mechanical properties of rigid PVC after aging loaded with coconut and cow horn fibers after a first recycling is made by the finite element method, Mori-Tanaka and Double inclusion models. The obtained results have showed an improvement in the mechanical characteristics of the PVC studied using this natural bio-loading with these two fibers which respect the environment and have a lower cost and more lightness.

1. Introduction

The waste of plastic products continues to increase due to increased use in recent years. Among these materials we find PVC which covers all sectors of economic activity [1–5]. It's the second position after polyethylene. The PVC tonnages recycled under Vinyl Plus between 1 January and 31 December 2016 by the initiatives of the EuPC Sector Groups, Sector Associations and Recovinyl [6] are growing, in particular for window profiles, flexible PVC and cables, which involve industrial and scientific research to study the actions of recycled PVC.

The recycling of PVC is becoming a current necessity in the industry in order to upgrade it. However, this process requires the addition of fillers on the aged PVC to improve the mechanical characteristics. Before attempting this process based in the difference method consisting in proposing and validating a model from tests by evaluating the difference between the performances measured experimentally and the performances simulated numerically as shown in the figure 1.

This method also makes it possible to check the expected performances by evaluating the difference between a specification and the tests, and to predict the performances from the models, by evaluating the difference between the simulated performances and the performances expressed in the experimental specifications. In this context, an artificial aging model was carried out experimentally and numerically validated by the finite element modeling.



Currently, the recycling of PVC requires loading in order to ameliorate its mechanical characteristics. A variety of studies are focused on the bio loading of materials in view of the requirements in terms of sustainable development and the environment

*Corresponding Author: Abdelghani Lakhdar, lakhdarabdelghani11@gmail.com

In this study and using three numerical models, finite elements, Mori-Tanaka and Double inclusion [8, 9]. We will predict the behavior of bio-loaded PVC after aging. The fillers used are coconut and cow horn fibers.

The aim of the present study is to validate the aging model of PVC material experimentally and numerically, and to predict by a numerical modeling, the mechanical behavior of this material bio loaded.

2. Study of the PVC aging model

2.1. Description of the adopted aging model

2.1.1. Types of aging

Two types of aging are adopted. The Rigid and flexible PVC samples as illustrated in figure 2.

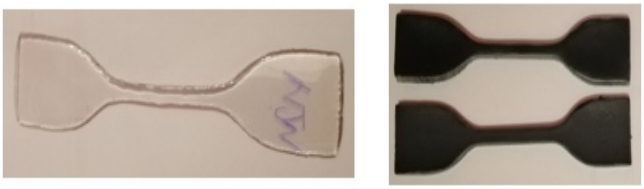


Figure 2: Flexible and rigid PVC specimen [3]

We took two configurations, accelerated artificial and under normal conditions aging at an average Moroccan temperature [3]. The figure 3 below shows the two types of aging

a) Aging by a constant temperature oven of 328.15 K
b) Aging by solar energy for 10h at average temperature T_{mean}= 300.15 K



Figure 3: aging configuration [3]

Table 1 illustrate that mean reference temperature is 300.15 K.

Table 1: Mean reference temperature in Morocco [3]

OUARZAZATE	Average temperature for 60 years	Maximum average temperature	Minimum average temperature	Record maximum temperature	Record minimum temperature	Average precipitation
unit	°K	°K	°K	°K	°K	°K
year	299.15	300.15	284.15	319.15	265.15	283.65
January	281.15	291.15	294.15	299.15	268.15	273.95
February	284.15	293.15	276.15	304.15	268.15	273.65
March	288.15	296.15	279.15	312.15	271.15	274.45
April	291.15	300.15	283.15	314.15	272.15	273.65
May	295.15	304.15	286.15	318.15	276.15	273.45
June	299.15	309.15	290.15	322.15	281.15	273.45
July	303.15	313.15	293.15	323.15	287.15	273.45
August	302.15	311.15	293.15	320.15	316.15	273.65
September	298.15	306.15	289.15	316.15	283.15	274.65
October	292.15	300.15	284.15	306.15	276.15	274.65
November	287.15	295.15	280.15	303.15	271.15	274.65
December	282.15	290.15	275.15	301.15	265.15	274.45

2.1.2. Results and discussion

After a tensile test carried out by the EZ-20 tensile machine (figure 4) and a numerical analysis using the finite element method, which is known for its strong ability to predict the behavior of more complex materials [10–19], on the flexible and rigid PVC samples after and before aging, the results obtained from the test are grouped together in the figures 5 and 6 and table 2.

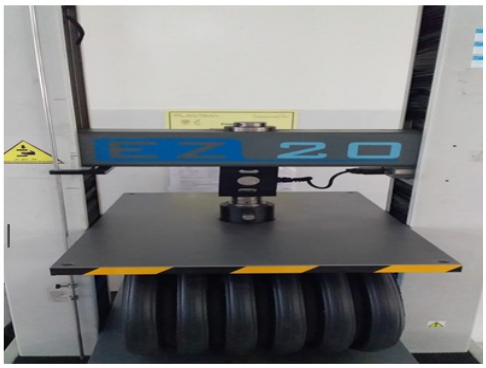


Figure 4: Tensile Testing machine EZ-20

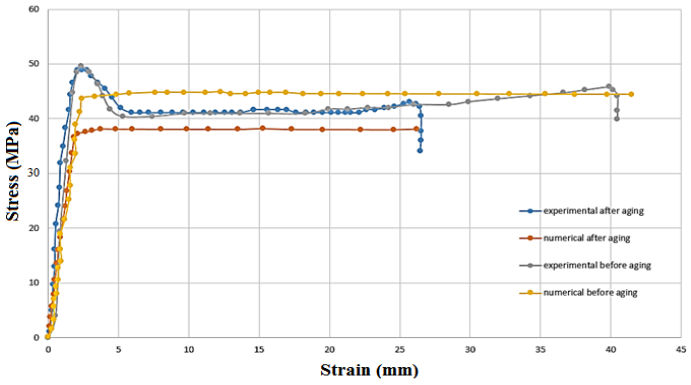


Figure 5: Tensile curves of rigid PVC before & after aging

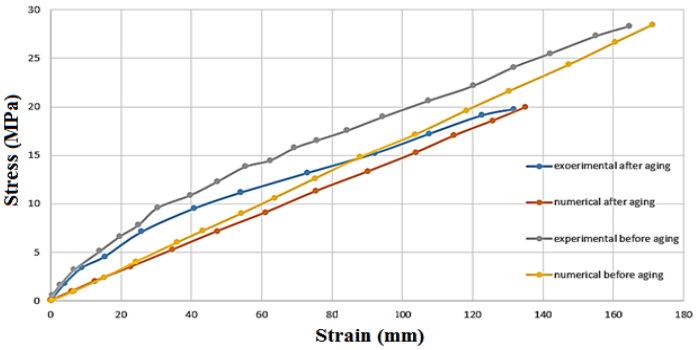


Figure 6: Tensile curves of flexible PVC before & after aging

Table 2: Experimental and numerical results

	Experimental Stress at break (MPa)	Numerical Stress at break (MPa)	Experimental Strain at break (mm)	Numerical Strain at break (mm)
Rigid PVC before aging	40	44	42	42
Rigid PVC after aging	34	37,5	26	26
Flexible PVC before aging	28	28	168	169
Flexible PVC after aging	20	20	135	135

We note that the stiffness of rigid PVC has changed slightly after aging and this is due to the inclination of the slope towards the elastic region. Its deformation potential before breaking has also been reduced. The flexibility of the flexible PVC is decreased at the elongation stage and become more rigid, its elastic limit is decreased.

Results of the analysis obtained numerically reveals that the numerical finite element modeling supports the findings already reported experimentally and that it is able to predict the mechanical behavior of more complex materials. The deformation ability of rigid PVC after aging has decreased, the stress at break for flexible PVC has decreased and the rigidity has increased because the deformation after aging is much less than before this process.

In order to return these products to their reference characteristics after many recycling, we have tried to establish a reference model for potential recycling studies.

Experimental research and numerical modeling were carried out using the finite elements approach on flexible and rigid PVC before and after aging.

Heat and ultraviolet rays are the key requirements for modifying the mechanical and thermal parameters of PVC, because the sensitivity of rigid PVC to these two conditions for 15 days, and 7 days for flexible PVC has been able to modify its mechanical characteristics.

3. Numerical Study of the Bio Loaded PVC

3.1. Numerical Models

3.1.1. Finite elements

This analysis is founded on the division of the bio composite by a good mesh and bringing together the sub-domains thereafter.

We will use the quadratic elements due to their efficiency of computation and the simplicity of convergence.

3.1.2. Mori-Tanaka

The mathematical model of this model is presented as follows:

$$\epsilon(x)= \xi(I,C_0) : \epsilon^*, \forall\ x \in (I) \qquad (16)$$

$\xi(I,C_0)$: Eshelby tensor

ϵ^* : The deformation acting the Eshelby volume.

The strain concentration tensor: $B^{\epsilon}= H^{\epsilon}(I,C_{fibers},C_{PVC})$ (17)

With:

$$H^{\epsilon}(\ I,\ C_{Fibers}\ ,\ C_{PVC}\ )= \{I +\ \xi(I,\ C_{Fibers}\ ):\ C^{-1}_{\circ Fibers}\ ):[\ C_{PVC} - C_{Fibers}]\}^{-1} \qquad (18)$$

H^{ϵ} : The fibers strain concentration tensor.

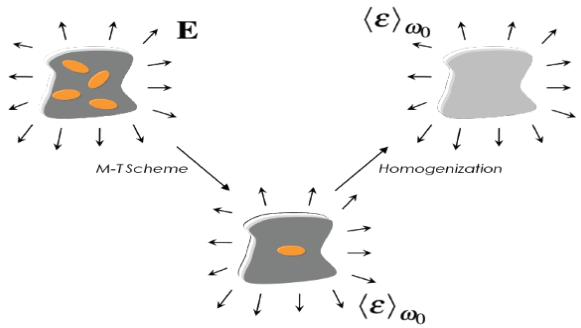


Figure 7: The Mori Tanaka model [8]

3.1.3. Double Inclusion

The strain concentration tensor in Coconut and cow horn fibers to its contour on the PVC matrix is presented by the following equation.

$$B^{\epsilon}= [(1-\xi(\upsilon_1))\ ((B_l^{\xi})^{-1} +\xi(\upsilon_1)(\ (B_v^{\xi})^{-1}]^{-1} \qquad (19)$$

With : $$\xi(\upsilon_1)=\frac{1}{2}\upsilon_1(1+\upsilon_1) \qquad (20)$$

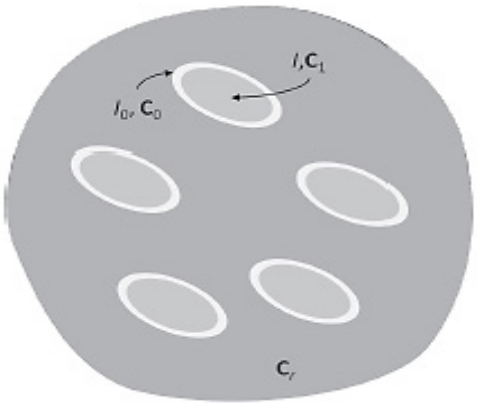


Figure 8: The Double inclusion model [9]

3.2. Bio loads

The loads used are from animal and natural origin, having a light density and a lower cost unlike classical loads affecting the environment. We will be interested in two types of loads in order to know their effect on the performance of PVC materials after aging

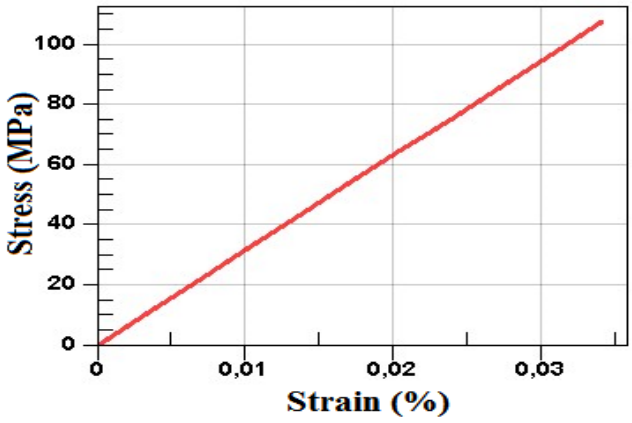


Figure 9: Tensile curve of the cow horns

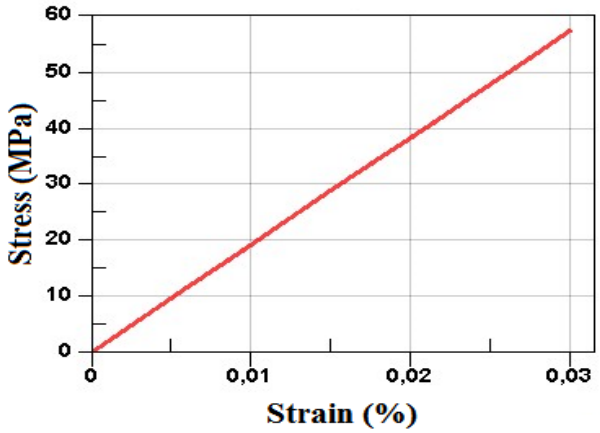


Figure 10: Tensile curve of the coconut

The two bio loads behave elastically with good values of the stresses at break and Young modulus as presented in the table 3.

Table 3: Numerical properties of cow Horns fibers in MPa

	Stress at break	Young modulus
Horn fibers	106.92	3148.4
Coconut fibers	57	1920

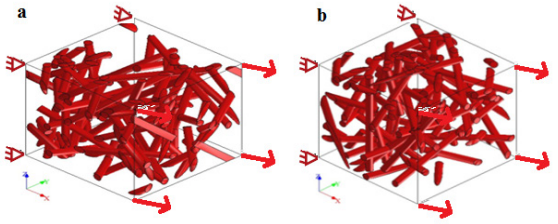
3.3. Results and Discussion

We studied in the previous chapter that the performances of PVC were modified after an accelerated aging which simulates reality. Before starting a first experimental recycling we will carry out a numerical modeling to predict what will happen.
The procedure consists in taking around10% of the two bio loads (cow horns and coconut), and adding it to PVC and comparing the results to see the improvements or degradations of the PVC material.

The idea is to find the material that will improve the performance of PVC and then use it as a bio load to improve recyclability. In what follows, we will simply choose rigid PVC as an object of this study

3.3.1. Internal Structure of the Bio loaded PVC

In this modeling, we choose a random distribution of coconuts and cow horns fibers in the PVC presented in figure 11 below



a) PVC bio laded by Coconuts b) PVC bio loaded by cow horns

Figure 11: internal structure of bio loaded PVC

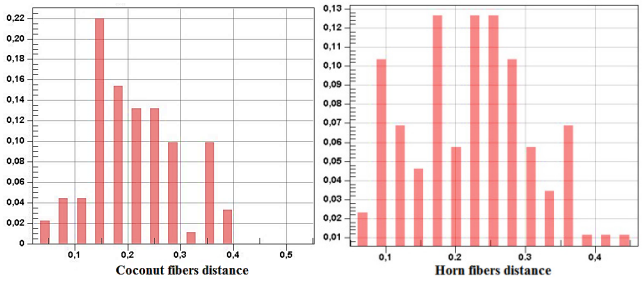


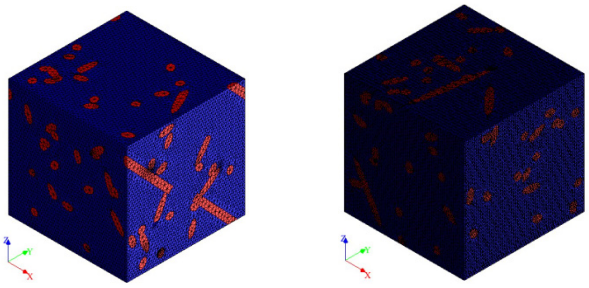
Figure 12: Ccoconut and horn fibers distance

The following table shows the statistical distance for the coconuts and cow horn fibers in PVC.

Table 4: coconuts and cow horn fibers distance

	Mean	Min	Max	Std dev
PVC bio loaded by Coconut	0.212	0.026	0.545	0.093
PVC bio loaded by Cow Horns	0.22	0.0538	0.455	0.0899

The meshes obtained by the numerical modeling of the coconut and cow horns are illustrated in Figure 13.



PVC bio laded by Coconuts PVC bio loaded by cow horns

Figure 13: PVC bio loaded mesh

The following table shows the parameters of mesh used in the present modeling.

Table 5: parameters of mesh

	Elements	Nodes	Size	Min size
PVC bio loaded by Coconut	330731	507283	0.029181	0.0058362
PVC bio loaded by Cow Horns	1449438	2182774	0.029181	0.0058362

We can deduce that the optimal percentage of the bio fillers in rigid PVC leading to better mechanical properties is 9.3Wt% for Coconut and 9.5 Wt% for Horn fibers.

Table 6: Number of fibers used and optimal content of bio loads

	Number of fibers	Content (Wt%)
PVC bio loaded by Coconut	31	9.3
PVC bio loaded by Cow Horns	32	9.5

We used two Rho and Gamma indicators for the two charging forms to check the consistency of the mesh, which are often used between 0 and 1 with better stability and convergence far from null.

We note that for Gamma it is between 0.6 and 1, whereas Rho is between 0.4 and 0.8, so they are far from 0 which verifies the mesh quality. Figures 14 and 15 demonstrate how those two indicators are distributed

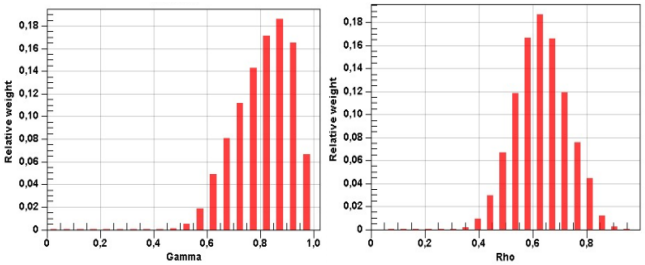


Figure 14: Gamma and Rho distribution of PVC bio loaded by Coconut

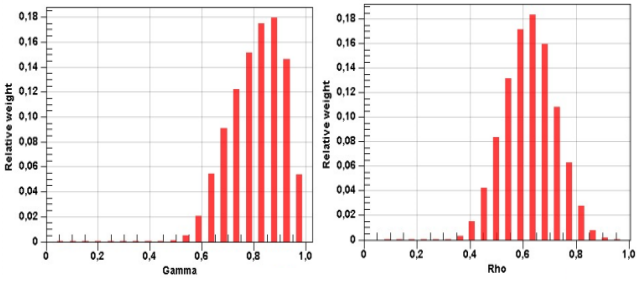


Figure 15: Gamma and Rho distribution of PVC bio loaded by Cow horns

Table 7 presents the average values obtained for Gamma and Rho criterion

Table 7: Average values of Gamma and Rho criterion

	Gamma criterion	Rho criterion
PVC bio loaded by Coconut	0.813	0.632
PVC bio loaded by Cow Horns	0.81	0.626

3.3.2. Effect of Bio loading on Rigid PVC

The three numerical models, finite elements, Mori-Tanaka and double inclusion illustrated in figures 16, 17 and 18 presents almost the same results as summarized in the table 8 and 9.

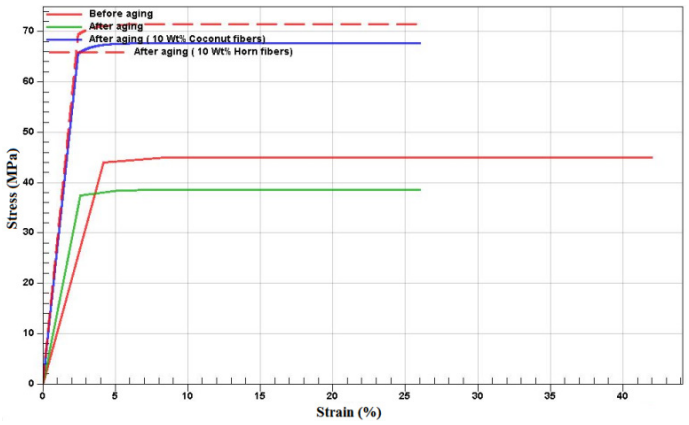


Figure 16: Tensile curve with the Finite element model

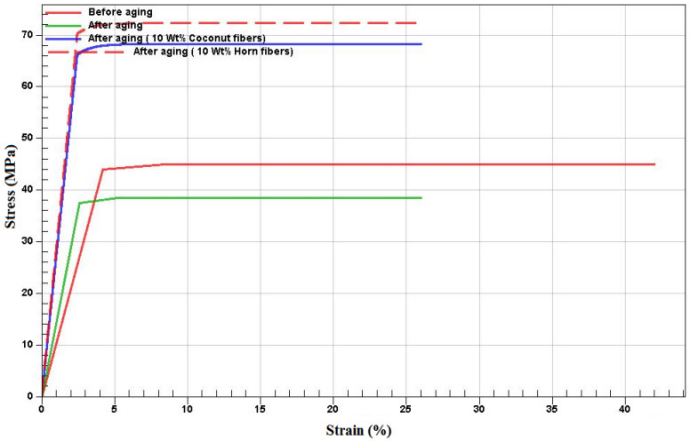


Figure 17: Tensile curves with the Mori-Tanaka model

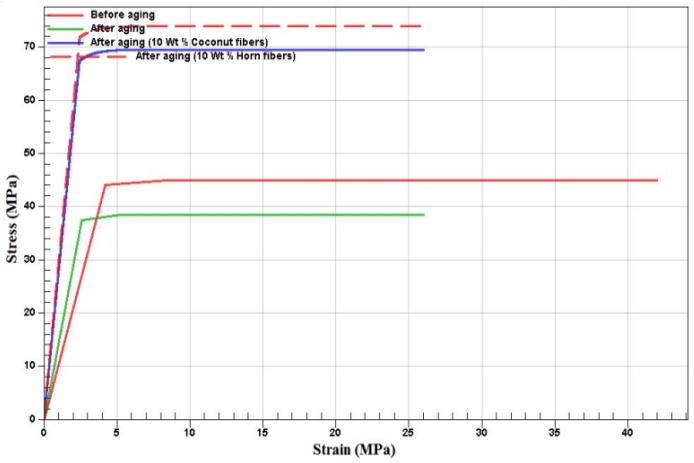


Figure 18: Tensile curves with the double inclusion model

Table 8: Numerical Stress at break in MPa obtained by different models for different content of Coconut fibers

Model	Content (Wt%)	Stress at break at
Mori-Tanaka	0	37.5
	10	68.521
Double inclusion	0	37.5
	10	69.799
Finite element	0	37.5
	9.3	68

Table 9: Numerical Stress at break in MPa obtained by different models for different content of Horn fibers

Model	Content (Wt%)	Stress at break at
Mori-Tanaka	0	37.5
	10	72.433
Double inclusion	0	37.5
	10	74.2
Finite element	0	37.5
	9.5	71.75

The analysis of the results obtained numerically for the different bio composites after a first aging show that the stresses at breakage improve by adding the two types of bio-loads compared to pre and post aging as shown in figures 16, 17, 18 and the tables 8 and 9.

Horn fibers have given better mechanical properties than coconut fibers. These results are validated by the different numerical models used. The numerical results show that the optimal percentages of Cow horns and Coconut fibers are 10 Wt% obtained by Mori-Tanaka and Double inclusion models and 9.3 Wt% obtained by the Finite element method for Coconut and 9.5 Wt% for cow horns fibers.

4. Conclusion

In this study, the mechanical behavior of flexible and rigid PVC pre and post aging was experimentally simulated and validated numerically. The submission of these PVCs to ultra violet rays and heat has caused the degradation of its performance. We then proceeded to bio loading rigid PVC after aging in order to compare its behavior with the pure state.

The modeling of these homogenizations are made by three numerical models, the finite element, Mori-Tanaka and Double inclusion models which have shown a power to predict the behavior of the bio loaded PVC after aging. The fillers used are Coconut and Cow horn fibers, resulting in an improvement in the performance characteristics of PVC after aging for an optimum percentage of around 10 percent Wt.

Cow horns fibers have given better mechanical properties than coconut fibers. These results are validated by the different numerical methods used.

Hence the improvement of the mechanical properties of rigid PVC after aging using this natural bio loading by these two fibers friendly to the environment and presenting a lower cost and more lightness.

In future works, we will opt for other numerical methods by simulating other natural bio loads and in different orientations of fibers in order to search for bio composites with better mechanical characteristics.

References

[1] E.T. Abdullah, S.M. Hasan, A.N. Naje, "Optical properties of PVC-MWCNT nano composites," 2013.

[2] A.M. El Sayed, W.M. Morsi, "Dielectric relaxation and optical properties of polyvinyl chloride/lead monoxide nanocomposites," Polymer Composites, **34**(12), 2031–2039, 2013.

[3] A. Lakhdar, M. Jammoukh, L. Zahiri, K. Mansouri, A. Moumen, B. Salhi, "Numerical and Experimental Study of the Behavior of PVC Material Subjected to Aging," in 2020 1st International Conference on Innovative Research in Applied Science, Engineering and Technology (IRASET), IEEE: 1–6, 2020.

[4] W. V Titow, Stabilisers: general aspects, Springer: 255–333, 1984.

[5] I. Janajreh, M. Alshrah, S. Zamzam, "Mechanical recycling of PVC plasticwaste streams from cable industry: A case study," Sustainable Cities and Society, **18**, 13–20, 2015.

[6] C.D.E.S. Activités, L. De Vinylplus, "RAPPORT D ' AVANCEMENT 2017," 2017.

[7] J.-L. Martinand, "La didactique des sciences," Revue Française de Pédagogie, **91**(1), 114–117, 1990.

[8] A. Moumen, M. Jammoukh, L. Zahiri, K. Mansouri, "Study Of The Optimal Micromechanical Behavior Of A Polymer Reinforced By Snail Shell Particles Using The Mori-Tanaka Numerical Model," in 2020 IEEE International conference of Moroccan Geomatics (Morgeo), 1–6, 2020, doi:10.1109/Morgeo49228.2020.9121908.

[9] S. Nemat, M. Hori, Micromechanics: overall properties of heterogeneous materials, 1993.

[10] A. Moumen, M. Jammoukh, L. Zahiri, K. Mansouri, "Numerical modeling of the thermo mechanical behavior of a polymer reinforced by horn fibers," International Journal of Advanced Trends in Computer Science and Engineering, **9**(4), 6541–6548, 2020, doi:10.30534/ijatcse/2020/342942020.

[11] P. Marimuthu, C. Kumar, "Finite element modelling to predict machining induced residual stresses in the end milling of hard to machine Ti6Al4V alloy," Periodicals of Engineering and Natural Sciences, **7**(1), 1–11, 2019.

[12] Ö.Y. Bozkurt, İ.C. Dai, Ö. Özbek, "The finite element analysis and geometry improvements of some structural parts of a diesel forklift truck," Periodicals of Engineering and Natural Sciences, **5**(2), 2017.

[13] S. Komurcu, A. Gedikli, "Numerical modelling of the in-plane loaded homogenized masonry walls," Periodicals of Engineering and Natural Sciences, **5**(3), 2017.

[14] J.J. Lee, E. Piersanti, K.-A. Mardal, M.E. Rognes, "A mixed finite element method for nearly incompressible multiple-network poroelasticity," SIAM Journal on Scientific Computing, **41**(2), A722–A747, 2019.

[15] M. Ghalandari, S. Bornassi, S. Shamshirband, A. Mosavi, K.W. Chau, "Investigation of submerged structures' flexibility on sloshing frequency using a boundary element method and finite element analysis," Engineering Applications of Computational Fluid Mechanics, **13**(1), 519–528, 2019.

[16] S.-F. Yin, S.-L. Xue, B. Li, X.-Q. Feng, "Bio–chemo–mechanical modeling of growing biological tissues: Finite element method," International Journal of Non-Linear Mechanics, **108**, 46–54, 2019.

[17] Y. Hong, Y. Yan, Z. Tian, F. Guo, J. Ye, "Mechanical behavior analysis of 3D braided composite joint via experiment and multiscale finite element method," Composite Structures, **208**, 200–212, 2019.

[18] J. Naveen, M. Jawaid, A. Vasanthanathan, M. Chandrasekar, Finite element analysis of natural fiber-reinforced polymer composites, Elsevier: 153–170, 2019.

[19] P. SPITERI, "Variational Approach for The Finite Element Method," AF503 V1, 2012.

ASTES

Advances in Science, Technology and Engineering Systems Journal Vol. 5, No.5, 613-619 (2020)

www.astesj.com

Special Issue on Multidisciplinary Innovation in Engineering Science & Technology

ASTESJ

ISSN: 2415-6698

A Typological Study of Portuguese Mortality from Non-communicable Diseases

Ana Paula Nascimento[1,*], Cristina Prudêncio[2], Mónica Vieira [3], Rui Pimenta [4], Helena Bacelar-Nicolau[5]

[1]*Biomatemática, Bioestatística e Bioinformática, Escola Superior de Saúde-Instituto Politécnico do Porto (ESS-IPP), Centro de Investigação em Saúde e Ambiente da Escola Superior de Saúde do Instituto Politécnico do Porto (CISA), Porto, 4000, Portugal*

[2]*Ciências Químicas e das Biomoléculas, Escola Superior de Saúde-Instituto Politécnico do Porto (ESS-IPP), Instituto de Investigação e Inovação em Saúde da Universidade do Porto (i3S), Centro de Investigação em Saúde e Ambiente da Escola Superior de Saúde do Instituto Politécnico do Porto (CISA), Porto, 4000, Portugal*

[3]*Ciências Químicas e das Biomoléculas, Escola Superior de Saúde-Instituto Politécnico do Porto (ESS-IPP), Centro de Investigação em Saúde e Ambiente da Escola Superior de Saúde do Instituto Politécnico do Porto (CISA), Instituto de Investigação e Inovação em Saúde da Universidade do Porto (i3S), Porto, 4000, Portugal*

[4]*Biomatemática, Bioestatística e Bioinformática, Escola Superior de Saúde-Instituto Politécnico do Porto (ESS-IPP), Centro de Estudos e Investigação em Saúde da Universidade de Coimbra, Porto, 4000, Portugal*

[5]*Faculdade de Psicologia da Universidade de Lisboa (FPUL), Instituto de Saúde Ambiental da Faculdade de Medicina da Universidade de Lisboa (ISAMB/FMUL), Lisboa, 1000, Portugal*

ARTICLE INFO

Article history:
Received: 10 July, 2020
Accepted: 19 September, 2020
Online: 05 October, 2020

Keywords:
Public Health
Non-communicable diseases
Date visualization
Cluster analysis

ABSTRACT

The most common non-communicable diseases, such as cardiovascular diseases and cancer, are a problem in global and national growth. The World Health Organization considers it a priority to study the specific causes of these diseases for trend monitoring. The aim of this paper is to identify a hierarchy of clusters of Portuguese mortality by non-communicable diseases using the agglomerative hierarchical cluster analysis. The Euclidean distance with complete linkage and average linkage criteria are used. These methods identify six clusters with both criteria, indicating some order of disease severity in the way clusters joint together. Special attention should be given to diseases in the last two clusters, where the last one is formed by ischemic heart disease, cerebrovascular diseases and larynx / trachea / bronchi and lung malignant tumor, all for males. In fact, these clustering results show that male gender seems to be a risk factor for at least two groups of the non-communicable diseases. Other suggested risk factors and / or pathophysiological mechanisms that in a direct or indirect way may enhance the common development of the pathologies found in the clusters arising from this study should also be an object of priority study.

1. Introduction

An important challenge of Public Health in Portugal is to decrease the number of deaths from Non-communicable diseases. In order to generate additional information in this domain, this paper is an extension of work originally presented in 14th Iberian Conference on Information Systems and Technologies [1].

According to the World Health Organization (WHO), the number of people who will suffer from the most common non-communicable diseases, including cardiovascular disease, cancer, or chronic respiratory diseases, will increase [2]. Non-communicable diseases are a worldwide and national problem and Public Health concerns [2], [3]. The study of non-communicable diseases is a matter of major importance in the world and in particular in Portugal [4], [5]. According to the Directorate General for Health (DGS) cardiovascular diseases and major cancers are mostly responsible for the lost years of life in the Portuguese population aged 35 and over [6]. The mortality rates of lung tumor malignant and rectal tumor malignant are increasing in Portugal

*Corresponding Author: Ana Paula Nascimento, ananascimento@ess.ipp.pt

[6]. Decreasing mortality from cancer is the biggest challenge for the next generations because cancer is the leading cause of early mortality [7]. The decrease in early mortality is relevant due to its individual and social impact [2]. Thus, according to WHO, it is of great importance to generate additional knowledge on the specific causes of these diseases, in order to monitor their trends [4]. Therefore, different studies are fundamental to analyze diseases evolution that might help to formulate hypotheses about risk factors and / or common pathophysiological mechanisms that, directly or indirectly, may enhance the common development of pathologies found in clusters, resulting from the hierarchy of non-communicable disease partitions, as this may be a working tool in health [8][9]. Unsupervised data analysis, namely cluster analysis, then can be useful to raise hypotheses about clusters of non-communicable diseases to be studied.

The development of the clustering analysis methodology is truly interdisciplinary. Taxonomists, social scientists, health scientists, psychologists, biologists, statisticians, mathematicians, engineers, medical researchers, computer scientists and others all contribute to the development of this methodology [10], [11]. Clustering analysis is a set of exploratory multivariate data analysis methods for identifying natural clusters in the data, based on a coefficient of similarity or dissimilarity between individuals or between variables, or more generally between statistical units of data [12]-[14]. This methodology aims to find homogeneous groups of statistical units in the data, where similarities between statistical units belonging to the same group are high and similarities between statistical units belonging to distinct groups are low [10], [12]-[14]. Hierarchical cluster analysis algorithms, both agglomerative and divisive, provide a hierarchy of partitions. Agglomerative hierarchical classification analysis methods are the most used [14][15]. These methods usually start with all statistical units separated into single-element groups (unit set - singletons), forming a cluster partition where the number of clusters is equal to the number of statistical units, and successively grouping together the most similar groups (according to the measure of similarity or dissimilarity between statistical units and the criterion of aggregation between groups) in the same cluster, until it forms a partition of a single cluster. It is recognized that agglomerative hierarchical cluster analysis can give different results for the same data, depending on the choice of the measure of comparison between statistical units and the aggregation criterion between groups [13], [16], [17]. One of the most used measures between individuals is the Euclidean distance. Moreover, the most commonly used aggregation algorithms are the farthest neighbor (or complete linkage) and the nearest neighbor (or single linkage) ones [10][12]. The complete linkage algorithm produces compact clusters, but is sensitive to outliers [16]-[18]. The single linkage algorithm is censored because it may disregard the structure of clusters, and it has the tendency to construct hierarchical partitions with chain effect [13], [16]-[18]. The average linkage method produces more balanced hierarchies, with no chain effect. This algorithm is an intermediate method between the two previously mentioned, and furthermore uses more data information [13], [16]-[18]. Therefore, the three aggregation criteria are often used over the same data sets, with the aim of knowing about clustering results robustness. Each agglomerative hierarchical cluster analysis is usually based on information concerning some "relative best partitions" of the hierarchy, namely immediately preceding relative maximum levels of increase / decrease in cluster dissimilarities [13], [19]. Moreover, by choosing a cut-off where there is the largest increase / decrease in cluster dissimilarities [13], it allows us to find an "absolute best partition". This suggests that, at the stage where the greatest increase / decrease occurs, the joining clusters are comparatively far apart. Therefore, the best number of groups in the data should be the number of groups present in the immediately preceding step [13], [16], [17].

Goal: The aim of this study is to obtain a hierarchy of cluster partitions of Portuguese mortality from non-communicable diseases, using agglomerative hierarchical cluster analysis, in order to identify clusters of diseases associated to different degrees of severity as well as clusters of diseases explicitly associated with gender. Clustering results might help either to identifying or to searching for common causes or risk factors to improve preventive medicine.

2. Materials and Methods

2.1. Data

The classification of diseases in this paper is according to the Tenth Revision International Classification of Diseases (ICD-10). This classification makes it possible for countries compile comparable national mortality [20].

Table 1: Non-communicable diseases (ICD-10)

Non-communicable diseases	Code
Lip/mouth and pharynx malignant tumor for males	1
Esophageal malignant tumor for males	2
Stomach malignant tumor for males	3
Colon malignant tumor for males	4
Rectal and anus malignant tumor for males	5
Liver / biliary / intrahepatic malignant tumor for males	6
Pancreatic malignant tumor for males	7
Larynx / trachea / bronchi and lung malignant tumor for males	8
Skin malignant tumor for males	9
Breast malignant tumor for males	10
Kidney malignant tumor for males	11
Bladder malignant tumor for males	12
Lymphatic tissue malignant tumor for males	13
Ischemic heart disease for males	14
Other heart diseases (I30-I33) for males	15
Other heart diseases (I39-I52) for males	16
Cerebrovascular diseases for males	17
Pneumonia for males	18
Chronic lower respiratory diseases for males	19
Asthma for males	20
Lip/mouth and pharynx malignant tumor for females	21
Esophageal malignant tumor for females	22
Stomach malignant tumor for females	23
Colon malignant tumor for females	24
Rectal and anus malignant tumor for females	25
Liver / biliary / intrahepatic malignant tumor for females	26
Pancreatic malignant tumor for females	27
Larynx / trachea / bronchi and lung malignant tumor for females	28
Skin malignant tumor for females	29
Breast malignant tumor for females	30
Kidney malignant tumor for females	31
Bladder malignant tumor for females	32
Lymphatic tissue malignant tumor for females	33

Ischemic heart disease for females	34
Other heart diseases (I30-I33) for females	35
Other heart diseases (I39-I52) for females	36
Cerebrovascular diseases for females	37
Pneumonia for females	38
Chronic lower respiratory diseases for females	39
Asthma for females	40

The non-communicable diseases used here are listed in Table 1. In this paper, it is presented an evolution of a previous work presented at [1]. In fact, a results analysis is performed considering diseases separated by gender. Table 2 displays the shorts names of the diseases, where M represents male gender and F represents female gender.

Table 2: Short names of non-communicable diseases

Short names of non-communicable diseases	Code
Lip_M	1
Esophageal_M	2
Stomac_M	3
Colón	4
Rectal_M	5
Liver_M	6
Pancreatic_M	7
Lung_M	8
Skin_M	9
Breast_M	10
Kidney_M	11
Bladder_M	12
Lymphatic_M	13
Ischemic_M	14
I30-I33_M	15
I39-I52_M	16
Cerebrovascular_M	17
Pneumonia_M	18
Chr.lowerrespiratory_M	19
Asthma_M	20
Lip_F	21
Esophageal_F	22
Stomac_F	23
Colon_F	24
Rectal_F	25
Liver_F	26
Pancreatic_F	27
Lung_F	28
Skin_F	29
Breast_F	30
Kidney_F	31
Bladder_F	32
Lymphatic_F	33
Ischemic_F	34
I30-I33_F	35
I39-I52_F	36
Cerebrovascular_F	37
Pneumonia_F	38
Chr.lowerrespiratory_F	39
Asthma_F	40

Data were requested from Statistics Portugal. Non-communicable diseases separate by gender are considered as individuals and annual age-standardized mortality rates in Portugal from 1994 to 2012 for non-communicable diseases are considered as variables. Annual age-standardized mortality rates are given by the ratio of the total number of deaths expected in the specific region for a given gender for a given disease over a year and the number of standard populations per 100 000 inhabitants. In theory any standard population could be used but frequently are used the Segi world, the European or the WHO world standard populations. Here it is used the European standard population. Age-standardized mortality rates enable comparisons to be made between populations that have different age structures. More details on methods of standardizing mortality rates can be found in [21], [22]. The mortality rates considered are based on individuals up to 65 years of age.

2.2. Methodology

In this paper agglomerative hierarchical cluster analysis of non-communicable diseases is applied. The age-standardized mortality rates for each of the years from 1994 to 2012 are used as variables to perform the analysis and the non-communicable diseases separated by gender are used as individuals. Since annual standardized mortality rates are quantitative variables, the Euclidean distance to measure disease dissimilarity is used. Euclidean distance depends less from the magnitude of values than the quadratic Euclidean distance, used in [1]. As aggregation criteria the three methods mentioned above were used. The clustering results were very similar, so in this presentation are only considered the average linkage and the complete linkage criteria.

3. Results

For all diseases listed in Table 1 in the case of male gender are presented in Table 3 the mean, standard deviation, minimum and maximum of annual age-standardized mortality rates between 1994 and 2012.

Table 3: Statistics summary of annual age- standardized mortality rates between 1994 a 2012 given by non-communicable diseases for males

Diseases	Mean	Standard Deviation	Min.	Max.
Lip_M	7.06	0.57	6.00	8.20
Esophageal-M	4.83	0.41	4.20	5.60
Stomac_M	10.48	1.49	8.50	12.90
Colon_M	6.33	0.34	5.50	6.80
Rectal_M	3.17	0.25	2.60	3.60
Liver_M	3.74	0.62	2.80	5.10
Pancreatic_M	3.84	0.37	3.30	4.60
Lung_M	25.21	0.91	23.60	27.60
Skin_M	0.86	0.21	0.50	1.20
Breast_M	0.15	0.05	0.10	0.20
Kidney_M	1.36	0.19	1.10	1.70
Bladder_M	1.81	0.26	1.40	2.30
Lymphatic_M	6.85	0.70	5.60	8.10
Ischemic_M	24.62	6.91	13.80	33.60
I30I33_M	0.44	0.11	0.30	0.60
I39I52_M	6.44	1.77	4.10	8.90
Cerebrovascular_M	20.54	6.55	12.10	30.30
Pneumonia_M	6.04	1.55	4.00	9.00
Chr.lowerrespiratory_M	4.22	1.42	2.40	6.80
Asthma_M	0.49	0.32	0.20	1.30

As shown in Table 3 the individuals of male gender died more by larynx / trachea / bronchi and lung malignant tumor, ischemic

heart disease and cerebrovascular diseases in Portugal between 1994 and 2012. Note that the standard deviation of annual age-specific standardized mortality rates in the case of larynx / trachea / bronchi and lung malignant tumor is very low so the mean is well representative of the mortality rates over the years. The standard deviation of annual age-specific standardized mortality rates in the cases of ischemic heart disease and cerebrovascular diseases is bigger than in all other cases. In fact, the mortality rates in these cases presented a decrease over the years while in the case of larynx / trachea / bronchi and lung malignant tumor the mortality rates are very similar. It can also be seen that in every other disease the standard deviation is low, so that does not exist a great difference between the mortality rates over the years. Table 4 presents the statistics summary in case of female gender.

Table 4: Summary statistics of annual age-standardized mortality rates between 1994 a 2012 given by non-communicable diseases for females

Diseases	Mean	Standard Deviation	Min.	Max.
Lip_F	0.64	0.14	0.40	0.90
Esophageal_F	0.34	0.12	0.10	0.50
Stomac_F	4.72	0.76	3.60	6.20
Colon_F	4.11	0.26	3.80	4.70
Rectal_F	1.74	0.15	1.40	2.00
Liver_F	0.95	0.15	0.70	1.20
Pancreatic_F	1.70	0.21	1.40	2.30
Lung_F	4.13	0.70	3.00	5.60
Skin_F	0.68	0.12	0.60	1.00
Breast_F	13.78	1.74	11.60	17.30
Kidney_F	0.48	0.08	0.40	0.70
Bladder_F	0.32	0.10	0.10	0.50
Lymphatic_F	4.56	0.58	3.60	5.50
Ischemic_F	6.13	2.05	3.00	9.40
I30I33_F	0.17	0.07	0.10	0.30
I39I52_F	2.82	1.08	1.40	4.40
Cerebrovascular_F	10.39	3.83	5.40	16.00
Pneumonia_F	2.18	0.59	1.30	3.40
Chr.lowerrespiratory_F	1.38	0.57	0.70	2.40
Asthma_F	0.32	0.20	0.00	0.80

As shown in Table 4, female gender individuals died more by breast malignant tumor, cerebrovascular diseases and ischemic heart disease in Portugal between 1994 and 2012. Note that the annual age-specific standardized mortality rates in the case of breast malignant tumor presents a decrease until 2004 while their values are very similar after that year. In the case of cerebrovascular diseases the mortality rates present a decrease until 2006 and are very similar after. For ischemic heart disease the mortality rates decrease over the years, nevertheless cerebrovascular diseases and ischemic heart disease seem to have a much higher mortaly rate in male than in female. In other cases the standard deviation of annual age-specific standardized mortality rates is very low, showing stability of mortality rates.

From the application of the agglomerative hierarchical cluster algorithms, the following results were obtained.

3.1. Agglomerative hierarchical cluster analysis with Euclidean distance and average linkage criterion

Table 5 contains the aggregation order matrix from the application of the agglomerative hierarchical cluster analysis with the Euclidean distance and average linkage aggregation criterion between groups. In Table 5 the columns Cluster 1 and Cluster 2 indicate the disease groups aggregating at each stage. The aggregation coefficient value in each step is noted by “Aggr. Coef.” and the increasing aggregation coefficient between successive steps is noted by “Dif.”.

Table 5: Aggregation order matrix of the cluster analysis with the Euclidean distance and average linkage aggregation criterion

Stage	Cluster1	Cluster2	Aggr. Coef.	Dif.
1	10	35	,332	-------
2	15	31	,592	0,260
3	22	32	,721	0,129
4	21	29	,775	0,54
5	15	22	,797	0,22
6	15	40	,901	0,104
7	10	15	1,124	0,223
8	25	27	1,140	0,016
9	12	25	1,289	0,149
10	9	21	1,334	0,045
11	10	20	1,490	0,156
12	9	26	1,499	0,009
13	23	33	1,982	0,483
14	11	12	2,011	0,029
15	9	10	2,220	0,209
16	7	24	2,486	0,266
17	6	28	2,516	0,03
18	16	34	3,013	0,497
19	11	39	3,081	0,068
20	6	7	3,204	0,123
21	11	38	3,838	0,634
22	1	4	3,878	0,04
23	2	23	4,184	0,306
24	5	6	4,196	0,012
25	1	13	4,553	0,357
26	2	5	5,439	0,886
27	9	11	5,542	0,103
28	16	18	5,854	0,312
29	19	36	6,519	0,665
30	2	19	7,273	0,754
31	1	16	8,281	1,008
32	3	37	10,544	2,263
33	1	2	12,334	1,79
34	3	30	16,129	3,795
35	1	9	18,145	2,016
36	14	17	19,928	1,783
37	8	14	32,412	13,132
38	1	3	39,753	7,341
39	1	8	89,941	50,188

Figure 1 presents the dendrogram associated to Euclidean distance and average linkage aggregation criteria.

From Table 5 and Figure 1 it may be observed the dendrogram has 39 levels. Reading the tree from top to bottom we find six well separated groups of diseases. The first group includes breast malignant tumor for males, other heart diseases (I30-I33) for females and males, kidney malignant tumor, esophageal malignant

tumor, bladder malignant tumor and asthma for females, asthma for males, lip/mouth and pharynx malignant tumor, as well as skin malignant tumor for females, skin malignant tumor for males and liver / biliary / intrahepatic malignant tumor for females. Thus the first group includes a mixture of diseases, where some paired diseases for females and males appear.

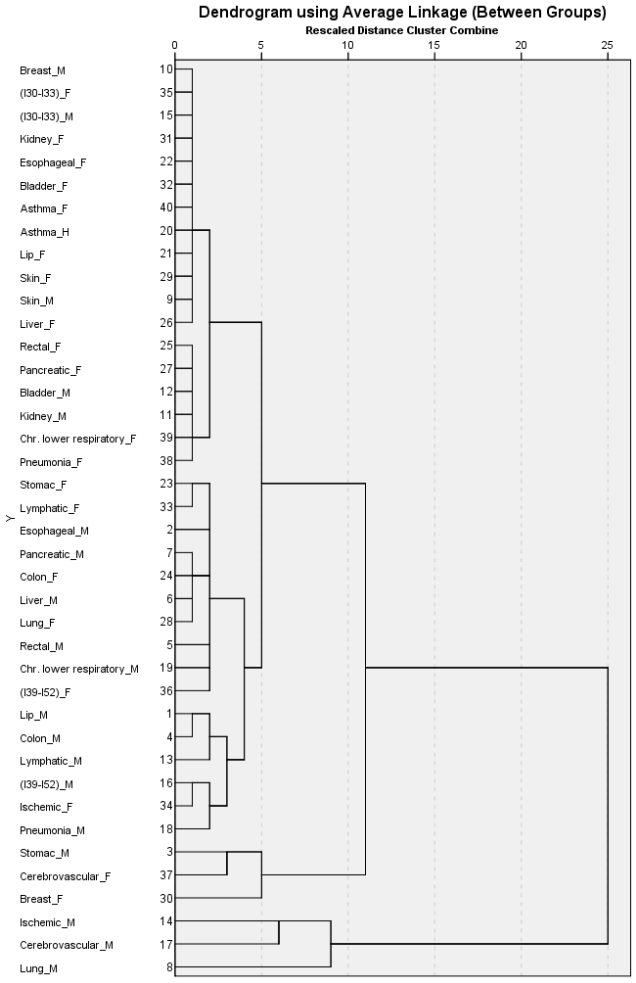


Figure 1: Dendrogram with Euclidean distance and average linkage aggregation criterion

The second cluster comprises: rectal and anus malignant tumor as well as pancreatic malignant tumor for females, bladder malignant tumor and kidney malignant tumor for males and chronic lower respiratory diseases and pneumonia for females. Note that the large cluster resulting from the union of these two groups mainly consists of diseases for females. The third group contains: stomach malignant tumor and lymphatic tissue malignant tumor for females, esophageal malignant tumor and pancreatic malignant tumor for males, colon malignant tumor for females, liver / biliary / intrahepatic malignant tumor for males, larynx / trachea / bronchi and lung malignant tumor for females, chronic lower respiratory diseases for males, other heart diseases (I39-I52) for females and rectal and anus malignant tumor for males. The fourth group contains: lip/mouth and pharynx malignant tumor, colon malignant tumor, lymphatic tissue malignant tumor, other heart diseases (I39-I52) and pneumonia, all for males and ischemic heart disease for females. Thus, this group is mainly constituted by diseases in male individuals. The fifth group contains: stomach malignant tumor for males, cerebrovascular diseases and breast malignant tumor for females. Finally, the sixth group includes: ischemic heart disease, cerebrovascular diseases and larynx / trachea / bronchi and lung malignant tumor, all for males.

3.2. Agglomerative hierarchical cluster analysis with Euclidean distance and complete linkage criterion

Figure 2 presents the dendrogram associated to Euclidean distance and complete linkage aggregation criterion.

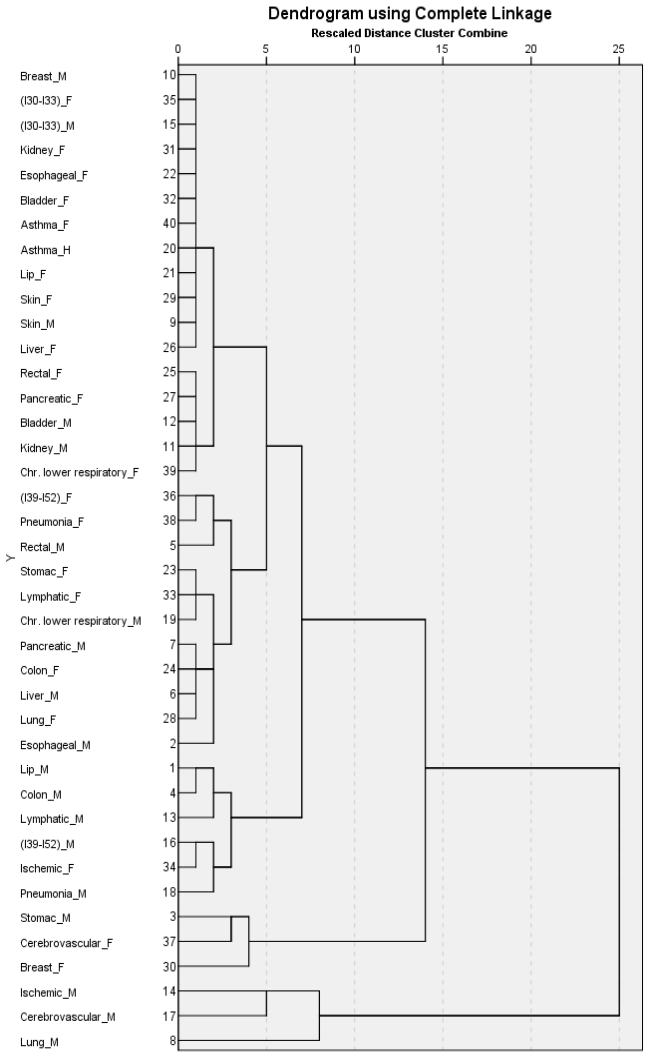


Figure 2: Dendrogram with the Euclidean distance and complete linkage aggregation criterion

As we point out above, the aggregation complete linkage and average linkage criteria gave very similar clustering results over our data. Comparing Figure 1 and Figure 2, it can be seen they both display dendrograms with 39 levels, showing six well separated clusters of diseases, grouped following a similar order in the hierarchy. Moreover, reading the tree from top to bottom in Figure 2, and comparing each cluster to the corresponding cluster in Figure 1, we find that: the first group is the same obtained with the average linkage aggregation criterion; the second group differs from the corresponding in average linkage criterion only because it doesn't include the pneumonia for females; the third group contains all the diseases included in the third cluster of average

linkage criterion plus the pneumonia for females; the last three groups are the same obtained with the average linkage criterion.

4. Discussion

Let's point out again that for analyzing and understanding clustering results obtained from hierarchical agglomerative methods based on Euclidean distance applied to diseases, it is expected that: 1- diseases in the same cluster will have similar mortality rates and similar behavior of the mortality rates over the years; 2- clusters of diseases indicate that the order of magnitude of mortality rates and the behavior over the years of mortality rates show larger differences between diseases in different clusters than diseases inside each cluster. Both aggregation criteria produce similar hierarchies with six well separated clusters (differing only by the classification of pneumonia for females), joining in same way. If one refers to the average linkage aggregation criterion the first group is formed at level 15, the second one at level 21, the third one at level 30, the fourth group at level 31 the fifth at level 34, and the six group at level 37, corresponding to some kind of chain effect in the dendrogram, indicating some order of disease severity in the way clusters joint together. The cut-off occurs at level 38, where the sixth cluster is separated from the cluster of every other diseases. Reading the tree from top to bottom, the first three groups include diseases with lower mortality rates and the last three put together the diseases with highest mortality rates. Then the diseases that seem to need more attention are the diseases in clusters four to six. Looking at Figures 1 and 2 it is clear that groups formed by diseases with lower mortality mainly occur for females while groups formed by diseases with higher mortality tend to be associated to male gender, so male gender appears to be a risk factor in many of listed diseases. The fourth cluster reveals that lip/mouth and pharynx malignant tumor, colon malignant tumor, lymphatic tissue malignant tumor, other heart diseases (I39-I52) in male gender, ischemic heart disease for females, and pneumonia for males need the same attention by health organizations in Portugal since they are in the same cluster. This suggests that may be there are common causes for these diseases that affect more the male gender than female gender. Looking again at Figure 1 and Figure 2, it can be seen that the diseases that cause more deaths are found in fifth and sixth clusters. In the case of breast malignant tumor and stomach malignant tumor, mortality rates have been decreasing [6], possibly due to preventive measures; however, it can be seen in the fifth cluster that the stomach malignant tumor for males provoke so many deaths like cerebrovascular diseases and breast malignant tumor for females and they come together with high values of mortality rate. Note that in the case of breast malignant tumor being woman is a risk factor. Diet and obesity possibly being risk factors for the diseases in the fifth cluster more preventive measures are necessary in that direction. The sixth cluster, very well separated from all the other clusters, includes ischemic heart disease, cerebrovascular diseases and larynx / trachea / bronchi and lung malignant tumor for male gender, diseases which present the largest mortality rates, showing that they deserve special attention. This cluster also appears very well separated from all the other clusters in previous work [1]. The results shown in the present work, point that the male gender may be a risk factor for some clusters of diseases. One explanation may be habits more associated to the male gender as smoking. Additionally, the role of hormonal and metabolic characteristics of the male versus female gender is yet to understand. The results confirm that mortality rates of the respiratory tract malignant tumors and cerebrovascular diseases are the highest and it is necessary to reinforce preventive measures in case of these diseases even that Portugal is significantly better than the mean of the high-middle Socio-Demographic Index group for ischemic heart disease and lung cancer [6]. The fact that ischemic heart diseases and cerebral vascular diseases are in the same cluster it is expected. In both pathologies there are common underlying causes such as the formation of atheromatous plaques and their relationship with obesity and hypercholesterolemia. The similarity of these pathologies to malignant tumors of the respiratory tract is may be related with the known increase of thromboembolic events secondary to tumors but this requires further studies to understand and elucidate this result. However, risk factors such as smoking are common to the three pathologies which may further relate those pathologies [23].

5. Conclusion

Public Health as a science for studying and preventing diseases, prolonging life and improving quality of life through organized efforts and informed choices needs to analyze the factors of health of a population [24]. Unsupervised data analysis can introduce new knowledge allowing organizations to take measures to provide the best health warranties of the general population.

The aim of this study was to search for an agglomerative hierarchical cluster analysis of Portuguese mortality from non-communicable diseases, in order to first of all identify clusters of diseases associated to different degrees of severity as well as clusters of diseases explicitly correlated with gender.

The obtained hierarchy provides six main clusters of diseases. Moving up the hierarchy it is found that these clusters are sequentially formed, some increasing order of disease severity appearing correspond to the increasing order of levels. The first groups include diseases with lower mortality rates while the last ones put together diseases with higher mortality rates.

Special attention should be given to the last three clusters since they contain diseases showing high degrees of mortality rates compared with other clusters. Moreover, the fourth cluster mainly includes diseases in male individuals and the sixth one, grouping the highest severe diseases, refers only to males. Thus, male gender seems to be a risk factor for these two clusters of diseases. Other suggested risk factors and / or pathophysiological mechanisms that in a direct or indirect way may enhance the common development of the pathologies found in the clusters arising from this study should also be an object of priority study.

Note that taking gender in account in the present study clearly improve results obtained in previous work [1]. Clustering results might help either to identifying or to searching for common causes or risk factors to improve preventive medicine.

One limitation of this work is the fact that the time period for study does not include data from recent years yet. It happens the work is included in a larger project and it is important to get these results. In future, recent data will be added, as well as countries comparison and other multivariate data analysis (e. g., factor analysis and other cluster analysis methods, like fuzzy hierarchy techniques). Data collection is in process.

Conflict of Interest

The authors declare no conflict of interest.

Acknowledgment

Authors would like to thank Professor J. Pereira Miguel for introducing us to the analysis of these data, highlighting the importance of its study in preventive medicine and public health. The authors would also like to acknowledge Professor Brígida Mónica Faria for her comments and suggestions that greatly valued this work.

Authors would like to acknowledge Escola Superior de Saúde – P.Porto and Centro de Investigação em Saúde e Ambiente da Escola Superior de Saúde do Instituto Politécnico do Porto (CISA).

References

[1] A.P. Nascimento, C. Prudêncio, M. Vieira, R. Pimenta, H. Bacelar-Nicolau, "Cluster analysis of noncommunicable diseases in Portugal," in Iberian Conference on Information Systems and Technologies, CISTI, 2019, doi:10.23919/CISTI.2019.8760798.

[2] WHO, World Health Statistics 2012, 2012.

[3] R. Beaglehole, R. Bonita, R. Horton, C. Adams, G. Alleyne, P. Asaria, V. Baugh, H. Bekedam, N. Billo, S. Casswell, M. Cecchini, R. Colagiuri, S. Colagiuri, T. Collins, S. Ebrahim, M. Engelgau, G. Galea, T. Gaziano, R. Geneau, A. Haines, J. Hospedales, P. Jha, A. Keeling, S. Leeder, P. Lincoln, M. McKee, J. Mackay, R. Magnusson, R. Moodie, et al., "Priority actions for the non-communicable disease crisis," The Lancet, **377**(9775), 1438–1447, 2011, doi:https://doi.org/10.1016/S0140-6736(11)60393-0.

[4] A. Alwan, T. Armstrong, M. Cowan, et al, Noncommunicable Diseases Country Profiles 2011, 2011.

[5] WHO, Noncommunicable Diseases Country Profiles 2014, 2014.

[6] Direção-Geral de Saúde, Portugal : The Nation's Health 1990 – 2016. An overview of the Global Burden of Disease Study 2016 Results, Seatle, WA, 2018.

[7] Direção-Geral de Saúde, A Saúde dos Portugueses 2016, 2017, doi:ISSN: 2183-5888.

[8] T.N. Haregu, F.M. Wekesah, S.F. Mohamed, M.K. Mutua, G. Asiki, C. Kyobutungi, "Patterns of non-communicable disease and injury risk factors in Kenyan adult population: A cluster analysis," BMC Public Health, **18**(Suppl 3), 2018, doi:10.1186/s12889-018-6056-7.

[9] G. Pistolla, P. Prastacos, N. Tzanakis, A. Philalithis, "Clustering of mortality rates in Greeces prefectures," Scientific Research and Essays, **7**(45), 3860–3876, 2012, doi:10.5897/SRE11.1754.

[10] A.K. Jain, "Data clustering: 50 years beyond K-means," Pattern Recognition Letters, **31**(8), 651–666, 2010, doi:10.1016/j.patrec.2009.09.011.

[11] H. Bacelar-Nicolau, F.C. Nicolau, A. Sousa, L. Bacelar-Nicolau, "3rd Stochastic Modeling Techniques and Data Analysis International Conference," in: Skiadas, C. H., ed., in One Cluster Analysis of Complex and Heterogeneous Data, International Society for the Advancement of Science and Technology (ISAST), Lisboa: 99–108, 2014.

[12] M.G.H. Omran, A.P. Engelbrecht, A. Salman, "An overview of clustering methods," Intelligent Data Analysis, **11**, 583–605, 2007, doi:10.3233/IDA-2007-11602.

[13] H. Bacelar-Nicolau, F. Nicolau, Á. Sousa, L. Bacelar-Nicolau, "Measuring similarity of complex and heterogeneous data in clustering of large data sets," Biocybernetics and Biomedical Engineering, **29**(2), 9–18, 2009.

[14] H. Bacelar-Nicolau, F.C. Nicolau, Á. Sousa, L. Bacelar-Nicolau, "Clustering of variables with a three-way approach for health sciences," TPM - Testing, Psychometrics, Methodology in Applied Psychology, **21**(4), 435–447, 2014, doi:10.4473/TPM21.4.5.

[15] F. Murtagh, P. Contreras, "Algorithms for hierarchical clustering: An overview," Wiley Interdisciplinary Reviews: Data Mining and Knowledge Discovery, **0**, 86–97, 2011, doi:10.1002/widm.53.

[16] C. Chatfield, A.J. Collins, Introduction to Multivariate Analysis, Chapman & Hall/CRC, 2018.

[17] B.S. Everitt, Cluster Analysis, 5th ed., Wiley, 2011, doi:10.1007/BF00154794.

[18] F. Murtagh, L. Pierre, "Ward's Hierarchical Agglomerative Clustering Method: Which Algorithms Implement Ward's Criterion?," Journal of Classification, **31**, 274–295, 2014, doi:10.1007/s00357.

[19] O. Silva, A. Sousa, H. Bacelar-Nicolau, F.C. Nicolau, "Encontro Nacional da Sociedade Portuguesa de Matemática, Probabilidades e Estatística," in: Antunes, N., ed., in Comparação de pares de particões em análise classificatória, Sociedade Portuguesa de Matemática: 175–178, 2012.

[20] H. Quan, V. Sundararajan, P. Halfon, A. Fong, "Coding algorithms for defining comorbidities in ICD-9-CM and ICD-10 Administrative Data," Medical Care, **43**(11), 2005.

[21] R. Beaglehole, R. Bonita, T. Kjellstrom, Basic Epidemiology, WHO, Geneva, 1993.

[22] S.K. Lwanga, C.Y. Tye, O. Ayeni, Teaching health statistics: lesson and seminar outlines, 1999.

[23] M. Palmer, J. Sutherland, S. Barnard, A. Wynne, E. Rezel, A. Doel, L. Grigsby-Duffy, S. Edwards, S. Russell, E. Hotopf, P. Perel, C. Free, "The effectiveness of smoking cessation, physical activity/diet and alcohol reduction interventions delivered by mobile phones for the prevention of non-communicable diseases: A systematic review of randomised controlled trials," PLoS ONE, **13**(1), 1–18, 2018, doi:10.1371/journal.pone.0189801.

[24] Elena Andresen, E.D. Bouldin, eds., Public Health Foundations: Concepts and Practices, John & Son, 2010.

ASTES

Advances in Science, Technology and Engineering Systems Journal Vol. 5, No.5, 620-629 (2020)

www.astesj.com

Special Issue on Multidisciplinary Innovation in Engineering Science & Technology

ASTESJ

ISSN: 2415-6698

The Design Process in the Improvement of The Experience Between a Brand and its Target Audience Through a Digital Product: The Lexus Portugal's used Car Website Case Study

Nuno Martins[1,*], Juan-Ramon Martin-Sanroman[2], Fernando Suárez-Carballo[2]

[1]*Polytechnic Institute of Cavado and Ave / ID+, Barcelos, 4750-810, Portugal*

[2]*Facultad de Comunicación de la Universidad Pontificia de Salamanca, Salamanca, 37007, Spain*

ARTICLE INFO

Article history:
Received: 24 July, 2020
Accepted: 21 September, 2020
Online: 05 October, 2020

Keywords:
Design Process
Lexus Portugal
UI & UX Design
Digital Design
Communication Design

ABSTRACT

The study aims to demonstrate how the use of the design process can align a brand's strategy with the interests of its target audience through a digital product based on a case study. Currently, Lexus internal studies show that there is a possibility to meet the needs of new audiences, beyond the traditional ones (men, 50+). In order to achieve this goal, the following objectives have been defined: communicate the brand and its cars' main values and philosophy, namely ecology, economy, safety and comfort; promote its services and products; and design an interface that guarantees users easy, pleasant and attractive navigation. The work process consisted of identifying the brand's strategy and values, identifying users, analyzing the main competing brands in the market, and designing a prototype within the framework of User-Centered Design, for which it had to address crucial issues such as the application of character models, UX and UI design, the creation of wireframes and user flows, interface design and the development of usability tests. The results demonstrate that it is possible to align the strategic interests of brands with the needs, objectives and expectations of users in a context of increasing global concerns of citizens related to reuse and sustainability. In this sense, it is vitally important that brands adopt Design processes in order to converge their own brand interests with people's demands.

1. Introduction

The research arose from a proposal by the Salvador Caetano Group (official representative of the Lexus brand in Portugal) for developing an official website meant specifically for promoting pre-owned Lexus cars in the Portuguese market.

According to Lexus Portugal, its clientele is mainly males, aged 50 and above. However, studies done by the brand regarding the used cars sector in the Portuguese market show that Lexus products and services have a high potential for growth in new market segments such as women and youth, aging 30 and above. This potential is associated with certain intrinsic factors of the brand, namely:

- Hybrid Technology: in the first half of 2020, 99% of Lexus used cars available for sale had hybrid engine technology. Cars with this technology are all equipped with an automatic gearbox, which facilitates the driving experience and ensures better safety. This technology also results in low pollutant emissions, thereby having a reduced impact on human health. These attributes are valued by the identified market segments (women and youth) that are typically more conscious about environmental concerns.
- The "Lexus Safety System" available on a significant sample of used cars: this system avoids a considerable volume of accidents through alerts and direct intervention in the driving process. Safety is an attribute particularly valued by women and families that have children.
- The reliability of the cars: there is a proven low probability of breakdown, especially of the type that renders the car non-functional and non-operable. The reliability factor in the used car sector specifically appeals to younger clients who have a greater probability of acquiring pre-owned cars at more accessible price points.

Additionally, certain extrinsic factors also affect purchase decisions, such as:

*Corresponding Author: Nuno Martins, nunomartins.com@gmail.com

- Lexus' main competitors in the premium segment (BMW, Mercedes-Benz, Audi, and Volvo) do not have a specific focus on the female audience in their used-vehicle programs. Therefore, there lies an opportunity for gaining advantage through leveraging a differentiating element.
- Citizens tend to be more aware of the more environment friendly motorizations (hybrid and electric). The supply of competing engines in their used-vehicle programmes is predominantly diesel, and there is little to no supply of more eco-friendly engines.

For this set of factors, Lexus Portugal has considered it timely and pertinent to develop a communication strategy that caters specifically to women and youth.

The current official Lexus Portugal website, in this regard, is presently the only source for accessing pricing and availability rated information of pre-owned Lexus vehicles. However, it does not provide the user with a pleasant and properly informed brand experience. According to Lexus Portugal, this has been a restrictive factor in its approach to the new market segments, and has, therefore, affected used car sales targets.

The research has accordingly required multidisciplinary skills and expertise to develop a communication strategy that answers to the concerns and expectations as outlined by to Lexus Portugal. The study took into account not only internal studies made available by Lexus Portugal, but also references related to car sales and drivers' consumption habits [1–3].

2. General and specific objectives

The main objective is to verify if the design process can make the users' needs converge with the brands' strategic lines by developing a digital platform through a case study.

To achieve the general objective, a further number of specific tasks were listed:

- To make an integrated list of the objectives proposed by Lexus for the new online platform, and systematize the entire work process to be developed — Together with the teams of Lexus Portugal and Portugal-based advertising agency Caetsu (responsible for advertising and communication at Lexus Portugal), a workplan was created to analyse all information and define the research aims and the stages of the development process.
- To develop a comparative analysis of the main online reference platforms in order to make a note of good solutions and potential problems. The objective of this analysis was to contribute to a better understanding of the identified market and to arrive at a starting set of guidelines towards designing the new solution.
- To use a design methodology that, close to the User-Centred Design framework, allows to design an online platform capable of aligning the interests defined from the brand strategy and the user experience in general terms.

3. Methodologies

The methodology adopted aimed to apply key practices associated with process design, namely UX and UI Design, the application of persona models, the creation of *wireframes* and *user flows*, the design of interfaces, and the development of usability tests [4–6]. The process consisted of analysis, discussion and resolution making in a collaborative manner among the various stakeholders regarding the different problems associated with the design and development of the online platform [7, 8]. The research process involved, besides the researchers (from the Digital Design area), teams from Lexus Portugal (namely, the General Management, the Marketing team and the Sales team), and the advertising agency Caetsu, alongside a select number of test users [9, 10].

Towards initiating the design process, the research team met with executives from Lexus Portugal and Caetsu with the purpose of: comprehending the philosophy of the Lexus brand; discussing the objectives of the new online platform to be developed; discerning the market and the target audience; and defining the strategies and the work process [11–13].

In order to better understand the respective market, a comparative analysis was developed taking into consideration the online platforms belonging to Lexus's main competitors such as Mercedes-Benz, BMW, Audi, and Volvo, alongside websites of multi-brand vendors such as StandVirtual and CarNext. This made it possible to map the brand's territory, and gain an understanding of the communication that has been developed with audiences online.

Later on, a further set of meetings were held with Lexus Portugal and Caetsu for presenting the analysis results and defining the structure of the information architecture pertaining to the online platform [14].

Correspondingly, the third phase of the project, saw the design of the online platform being supported through the building of an extensive collection of visual elements, in order to expedite the development of the project. Subsequently, visual prototypes were developed, wherein, the interface design incorporated concepts and graphic language previously defined by Lexus [15].

The last phase of the research was dedicated to the development of a high-fidelity prototype, and to carrying out usability tests in order to observe user behavior, detect problems, and make the required improvements towards guaranteeing the best possible experience [16].

4. Comparative analysis of the online platforms of the main competing brands

In order to arrive at an effective overview of the main competing brands' strategic approach, an analysis of the respective online platforms was first conducted. The platforms of Mercedes-Benz, BMW, Audi, and Volvo were hence analysed, alongside with two premier multi-brand used car platforms in Portugal, StandVirtual and CarNext.

The goal was to study the strengths and weaknesses of each of the online platforms, with the objective of obtaining relevant knowledge to be later applied in the development of the new Lexus online platform [17,18].

The development process began with an analysis of the navigation structure and the identification of the various functionalities of each of the online platforms. As can be seen in

Table 1, BMW's online platform was found to be the most complete in terms of functionalities and it also had the most extensive communication strategy. The brand's website was not limited to only providing search tools for its wide range of cars, but also provided the possibility of accessing further detailed information about its services – which was illustrated and animated with photos and videos, that were emotionally engaging, and emphasized the brand's core values and philosophy.

Table 1: Identification of the functionalities of the online platforms of competing brands (January, 2020). Source: own elaboration

Features	Mercedes -Benz	BMW	Audi	Volvo	Stand Virtual	Car Next
Login/Logout	X				X	
Favorites		X		X	X	
Comparator		X		X		
Configurator	X	X	X	X	X	X
News		X			X	X
Product Highlights		X	X	X	X	X
Testimonies						X
Image Galleries	X	X	X	X	X	X
Videos/ Animations		X				
Languages						X
Prices	X	X	X	X	X	X
Product Promotion		X			X	X
Contacts for + info.	X	X	X		X	X
Content sharing (email / social media)		X		X		
Contact directly by email		X		X	X	X
Responsive website	X	X	X	X	X	X

Such 'emotional' communication strategy alignment with brand values was also adopted by Volvo, although not emphasized to the same degree as BMW. Volvo's used-vehicle website was mainly designed around car search and selection tools, and it was careful to present the information in an appealing way through presenting eye-catching images and titles, wherein some of the brand's concepts and values were conveyed. Another interesting feature of Volvo's website was the use of thumbnails of car models in the configurator tool on the main page. This detail helps the user to perform an easier and more informed search. The least positive point of this website was the detailed presentation of each selected car, which revealed certain inconsistencies with the information organization and hierarchy.

Hallmark of Mercedes-Benz's used car website, on the other hand, was the simplicity of the search process, however, weaknesses pertaining to the content were apparent, particularly in terms of the lack of information about the advantages of acquiring a used car at the brand's official dealers. In addition, there was a lack of information about the brand's mission and vision, as well as images and graphics that could connect users emotionally to the brand's values and principles.

Of all the examples analysed, Audi's website was clearly the least interesting. The search tools were not optimally functional, and represented an obstacle in accessing information. In both the mobile and desktop versions of the website, several poorly distributed and organized information text blocks made it difficult to read the content. The website interface was also noticingly unattractive, replete with monochrome tones and outdated graphics. The photography of the vehicles though was of high quality which somewhat accentuated their perceived value.

Furthermore, the websites of *Stand Virtual* and *CarNext* were analyzed. These represent the largest and most popular online portals in Portugal for buying and selling used cars from most major brands. They were primarily directed at private entities and individuals.

Although the communication strategy of Stand Virtual and CarNext was different from what is intended by the Lexus group, they were considered important references since they dominate the used car sales market. Unlike Lexus, the target audience of the two companies is eclectic, seeking a diverse variety of cars from different brands.

Overall, both websites had a well-structured homepage with good content hierarchy. They did not have spaces dedicated to lifestyle concepts, wellness, or promotional texts. Both websites focused on two objectives: product search through filters, strategically positioned at the beginning of the page and easy to navigate; and inviting the user to make their product available for sale on the respective online platform. There was also a 'testimonials' section in CarNext's platform, which augmented the credibility of the service. This feature was considered a good reference and was correspondingly adopted in the development of the new Lexus platform.

In summary, it was found that, with the exception of BMW, the websites of the competitors were mainly limited to working as online platforms for searching and promoting vehicles available for sale.

BMW's website was the one that proved to be the closest to the intended solution for Lexus Portugal, providing relevant information about the brand and its services; and exploring images and videos with a more emotional outlook. However, the website's graphic and image component was not as refined as the brand's main website (bmw.pt), for the Portuguese market.

In accordance, the proposed prototype for Lexus Portugal intends to create a greater degree of integration between the main website of Lexus Portugal and its pre-owned division, presenting coherent solutions with the same level of graphic and image quality.

Following this competitor review, the corresponding developed work focused on the design and development of the Lexus used car online platform that was presented.

5. Online platform development

The design process of the online platform was developed along the following phases, in conjunction with regular feedbacks from the Lexus Portugal and Caetsu teams:

5.1. Interviews and definition of the Personas

The concept of *personas* was created to define the target audience of the digital solution under study. *Personas* are fictional personalities that can characterize potential users, representing the aspirations and attributes of a target group that a brand entity seeks to communicate with. Such idealization process can help understand the needs, experiences, behaviors, and ambitions associable with the target users. *Personas* are meant to simplify the design process, from the point of view that all processes are developed from the perspective of the user in order to ensure the best user experience for the target audience [19–21].

In order to define the *personas* and to generate a better understanding of the overall context of Lexus's used car market segment, including the aims and aspirations of the brand and its customer segment, a set of interviews was conducted with Lexus Portugal executives (CEO, Sales Manager, Brand and Product Director, and Digital Marketing Manager) and the creative lead from Caetsu responsible for Lexus' communication and advertising. The interviews were of a structured type, previously scripted, and consisted of open questions.

Through these interviews it was found that the Lexus client is mainly male, over 50 years old, and is positioned in the upper to upper-middle class social bracket. However, the brand's goal is to extend its target audience to younger age groups, from the age of 30 onwards, and particularly to the female public. It was also found that Portuguese customers are still unclear about the main advantages of hybrid technology. Moreover, when the customer visits a dealer of the brand, the vast majority have no knowledge about the available after-sales services or customization options for used cars.

These results reinforce our conviction about the need to develop an online platform that is not simply a search tool for used cars available for sale. Decision making when buying a car is increasingly influenced by previous online searches, before even visiting the physical sales stands [22]. For this reason, it is essential to make the complete information set available online: not only about the products, but also about the brand, the offered services, the sales conditions, and technological specifications, among other related data.

The *personas* were developed with the support of the Lexus Portugal's and Caetsu's teams. In defining the *personas* (as shown in Table 2), the research thus took into account not only the type of usual customer, but also the youth and female target segments that Lexus also wants to reach out to.

Three types of *personas* were defined, two female and one male. The majority are female, contrary to the results on the type of visitors that Lexus Portugal has had on its website (www.lexus.pt). In 2020, the majority of visitors to Lexus Portugal's website (approximately 65%) were male, with an average age of close to 45 years.

Table 2: Analysis grid of different *personas*.

JOÃO 45 years old	**LEONOR** 28 years old	**SOFIA** 55 years old
Architect in a studio in Lisbon and a technology lover.	Team coordinator, in an information technology company.	Medical specialist at a Coimbra Hospital
Features: João feels the need to buy a car that promotes safe, pleasant driving and, if possible, with a low environmental impact. He is looking for an excellent driving experience, but above all he wants a good deal. During his research, João realized that there are several technological solutions that cover sustainability concerns, and economic and technological consumption, without giving up comfort and luxury. Despite finding various platforms for car sales, and looking for the best price, he prefers to invest in a safe purchase. Besides all issues related to the product, João has doubts regarding the choice of the car brand and, for that, he tries to research the benefits and conditions offered by the various brands in their proprietary websites.	**Features:** Leonor lives far from her job and her old car is beginning to show the need for replacement with a more modern option that is safe and comfortable. As her everyday commutation is long, she is looking for an economical and durable solution. These constraints encourage Leonor to search for brands that have low maintenance cost, extended warranty services, and which offer excellent after-sales customer service. Beyond these concerns, Leonor is also aware that this is an important purchase and should be very well considered, which leads her to research, systematically and carefully, in trying to rationalize the choices as much as possible.	**Features:** Sofia usually leaves work late, and at the end of the day, enjoys her ride home relaxing in a car that offers unmatched comfort and luxury. She is looking to upgrade from her present one and promptly searches on her phone for the best deals available. She immediately quits from websites that feel clunky or too complicated, and gives clear preference to websites that are easy to navigate on her phone, and which provide the most relevant information upfront. Sofia considers it fundamental that the contents made available on the website are presented in a language and style that is simple, direct and easy to understand, and which does not get too technically complex. She knows the Lexus brand well as it is a frequent choice of her family members.

This type of majority audience is represented in the *persona* identified with the name João. This persona is also close to the type of Lexus customer, which is characterized by its focus on economy, the environment, security, reliability and technology.

However, the brand aims to change this trend and ensure that the younger and female audiences who visit the website do so successfully. The *personas* Leonor and Sofia intend to represent these customers' segments.

The *persona* Leonor represents the younger age group, which generally has less purchasing power. For this reason, buying a semi-new or used car can be a good option. They are people who buy cars for a long period of time and therefore prefer to make a slightly higher investment in the purchase in order to guarantee that it is a safe and reliable investment. Therefore, they prefer cars with high reliability, low maintenance costs and safety.

The *persona* Sofia represents the oldest age group, which usually has little availability and patience to seek information, especially in digital media. For this reason, it is fundamental to

have an online platform with good usability and that presents in a direct and brief way the main attributes of the brand's products and services. Although the typical client of the brand is male and above 50 years, the female gender is also important. According to internal Lexus Portugal studies, the female gender usually has a high influence on the purchasing decision of a relative, namely the partner (boyfriend or husband).

5.2. Information architecture

According to Garrett [23], the success of the user experience depends upon the designer's consideration of the following set of assumptions in the construction of information architecture [24, 25]:

- Strategy: represents what the user expects from the digital product.
- Objectives: requirements and specifications of functionalities that the product should meet.
- Structure: definition of hierarchies and content organization.
- Survey of technical limitations and usability of the product.
- Skeleton: design of the organization of the elements that will constitute the interface.
- Surface: corresponds to the final phase of the digital product, what the user interacts with.

In accordance with the needs as outlined by the Caetsu and Lexus team, a set of features and sections were defined for the digital product. The navigation experience was first established for the online platform to be well structured. During this initial stage, difficulties and possible obstacles regarding the user´s experience was also anticipated [26].

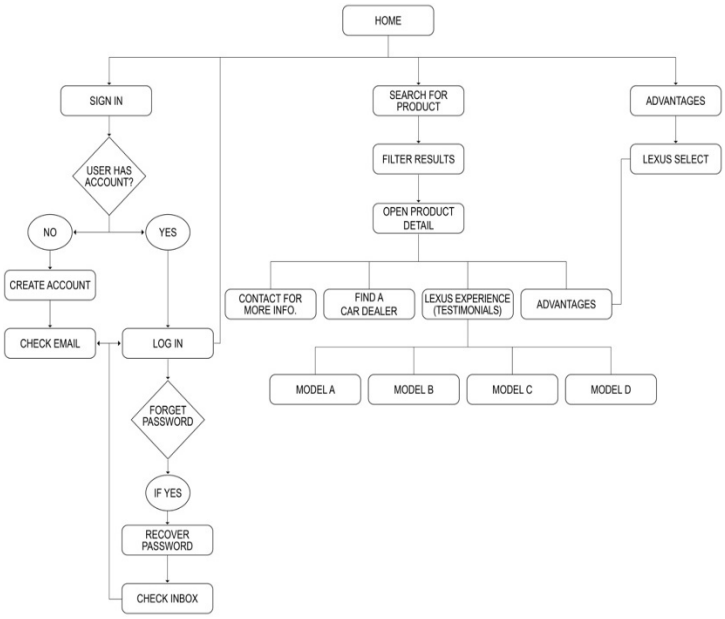


Figure 1: User flow diagram

5.3. Wireframes and user flows

After characterizing the *personas* and defining their main needs, the first low fidelity sketches, or *wireframes*, were created. These sketches were made by means of basic representation through shapes, with the objective of studying the disposition of contents and the functionality of each page. The sketches were at first drawn manually and then transferred digitally, allowing the skeleton of the online platform to be visualized.

Further on, in order to study the sequence of steps for the user to accomplish a certain task, *user flows* (as shown in Figure 1) were developed towards establishing performance parameters for each task. *User flows* are considered fundamental for the organization of *wireframes* in order to understand step by step the user's navigation intentions. For the development of the *user flows* the Sketch software was used, allowing to test the interaction between the different *wireframes* through simple graphic representations.

After this first phase, the first screens were designed, and later on, a set of detailed drawings, typography, icons, buttons, and other interactive elements were added, which completed the navigation paths and the linking between pages and sections.

5.4. Interface design

It was deemed fundamental for the interface to incorporate a visually pleasant layout, which could help users to read, concentrate, and perform tasks without hinderances. The interface was also finetuned to generate predictable user behavior and provide the user a sense of control when using the product.

When an interface has a nice layout, it helps users to read, concentrate, perform tasks better and increase real and perceived usability [27, 28]. The interface should generate predictable user behavior and give the user a sense of control when using the product.

5.4.1. Grid

Grids are practical tools in the structuring process and are responsible for the consistency and visual organization of the design and the elements that build the interface, and were thus considered essential in the design of the website [29].

Later on, a number of concepts linked with Responsive Web Design were used in order to create an interface that would be capable of adapting to various mobile devices, in accordance with the individual/situational preference of each user [30]. This was also done to create a cohesive, harmonious and balanced visual composition, towards ensuring optimal adaptability and to follow a structured logic throughout the procedure.

Due to the multiplicity of screen sizes, it was decided to define, in the desktop version, the current most used resolution in Portugal: 1366 pixels wide [31].

The grid used to build the desktop version of the platform was divided into twelve columns, each sixty pixels wide, with twenty pixels column gaps. At the end of each page, a margin corresponding to ten pixels was also incorporated.

In order to ensure a responsive layout that would adapt seamlessly to the interface format, similar parameters were considered: a screen width of 360 pixels (most prevalent locally), and a grid divided into twelve columns, each twenty-seven pixels wide and with a column gap of four pixels.

5.4.2. Color Palette

The design process in urderlined by the notion that the selection of the chromatic palette, during the UI Design process,

does not depend squarely on aesthetic sense, but on the intention behind the application of each element. This could be so in terms of capturing viewer attention to certain points, transmitting certain sensations; improving navigation; or creating a sense of harmony between all the elements that make up the interface [32].

Color, however, is a fundamental part of communicating Lexus' history. The selected color set (as shown in Figure 2) mainly emphasized on bringing softer tones in order to convey the brand's luxury positioning and subtle refinement. A predominance of neutral colors was also meant to highlight the contextual photographs of environment and lifestyle in conjunction with products of the brand. More luminous colors were additionally used in some details to highlight the aspect of technological contemporaneity in the brand, and capture the user's attention to certain informative or interactive elements.



Figure 2: Brand Lexus Colour Palette

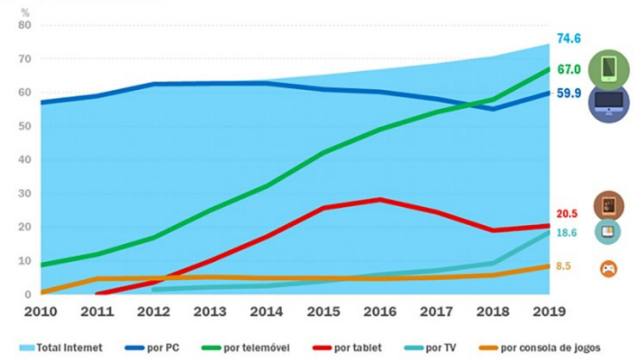
5.4.3. *Typography*

Bahat [33] views the use of the right typography as fundamental to guaranteeing readability, accessibility, hierarchy, and graphic balance. In digital products typography strongly influences the overall usability of the interface.

It is also one of the defining elements of a brand's visual identity. In the platform, the typographic family adopted was "Nobel" by Adobe Fonts, designed by Tobias Frere-Jones. It is a Sans Serif font, with several typographic styles and is suited to work correctly on digital media.

5.5. *Design of the online platform screens for the mobile and desktop versions*

According to Marketest [34], in the last 10 years, the use of the Internet through mobile devices has registered substantial growth in Portugal, especially through smartphones. As can be seen in Graph 1, in 2018 Internet use through smartphones surpassed desktop access. This trend has been determined to continue [34].



Graph 1: Internet use by platforms. Source: Marktest (2019)

For this reason, the design of the different screens of the platform focused on a mobile first approach and was then adapted to the desktop version. The strategic decisions that guided the design process behind the different screens were as follows:

- Homepage: Since it would be the first page that the user would have access to when visiting the website, the information and tools considered most relevant for the Lexus' target audience were highlighted, such as information on the advantages of the Lexus Select Service; information about the Lexus' experience (including access to testimonials from Lexus customers); and the possibility of searching immediately for available semi-new cars. As can be seen in figure 3, on the homepage there is a predominance of photographs and graphics that are positioned to accentuate the environment and the identity of the Lexus brand. In this way, the above mentioned objective of designing an online platform that reflected the Lexus philosophy and a user-friendly experience, was addressed.

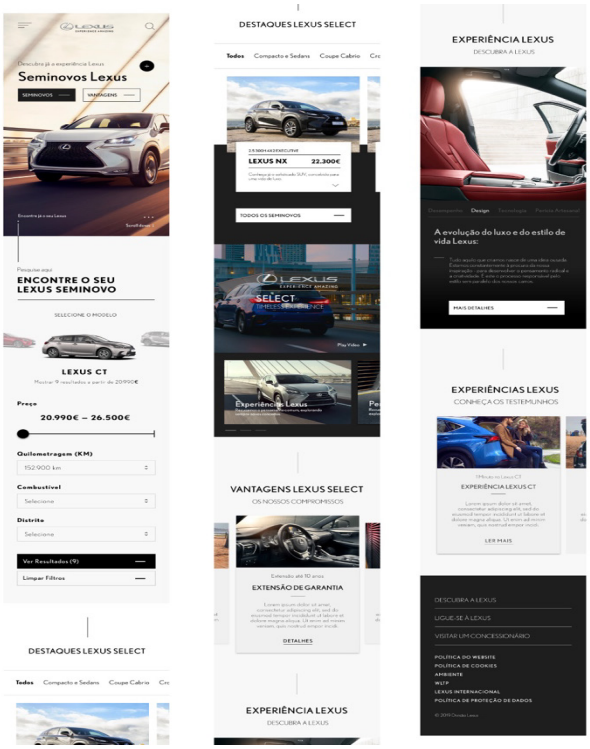


Figure 3: Lexus Homepage (mobile version)

- Configurator: Represented by the search and filter section of the homepage, the configurator was incorporated in a subtle manner, and not emphasized, with a view to provide the user greater freedom of choice in navigation. In the configurator the images of the car models were highlighted, allowing an easier, faster and more informed search.
- Testimonials: The "Testimonials" section was created with the aim of reaching out through personal narratives, towards building trust and empathy between the user and the brand. In this section testimonials from Lexus vehicle owners were presented, alongside promotional videos and informative texts about the cars.
- "Start" buttons: In the introduction to the "Lexus Advantages" page, ignition-style start buttons (similar to those found physically on Lexus cars and used to actually start the car's engine) were strategically applied. Through this type of elements, the intention was to involve the user with the visual ethos of the brand and its cars.
- Dark Mode: The introduction of a view mode with a predominance of dark tones was applied on pages such as "Lexus Select Advantages" and "Testimonials", towards ensuring eye comfort, and for garnering greater concentration in reading on higher text density sections.
- Quiz: on the online platform a Quiz component was created (as shown in Figure 4), entitled "Discover the ideal Lexus for you", with the aim of bringing communication between the user and the brand closer. In this section, the users have an option to answer a small questionnaire in order to identify and share their main preferences. Upon obtaining the users' inputs, the website employs a set of algorithms to suggest the most suitable car model. The analysis of the inputs also provides real-time availability of suggested options, and the respective store locations with available stock. The results that do not directly match the user's needs, are displayed towards the end of the search page. This strategy was intended to contribute to increasing empathy between the users and the brand.

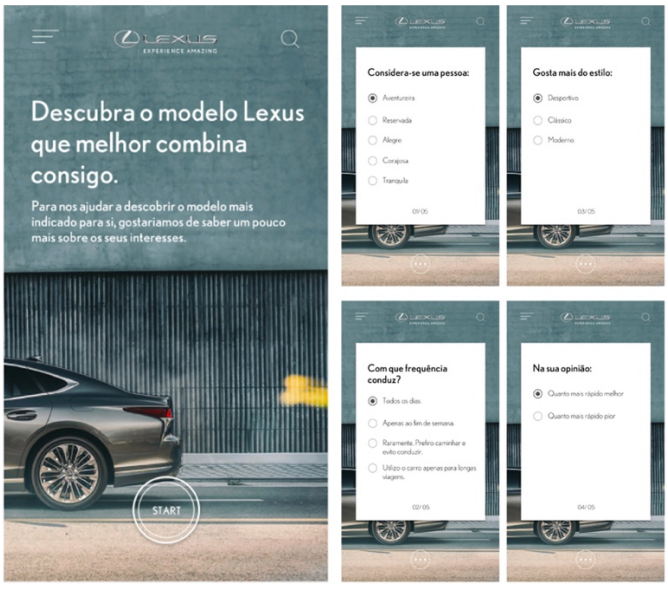


Figure 4: Quiz section (mobile version)

- Product listing: In this area the main characteristics of each car is presented, providing relevant information to viewers with illustrated icons that allow for an easier and faster reading experience. Also incorporated in the section are images of the respective cars, that are aligned to a predefined presentation standard, in order to ensure consistency and good image quality. Additionally, information pertaining to test-drive locations nearby is included.

As mentioned earlier, the mobile version of the platform was designed first, and then ported to the desktop version (as shown in Figure 5).

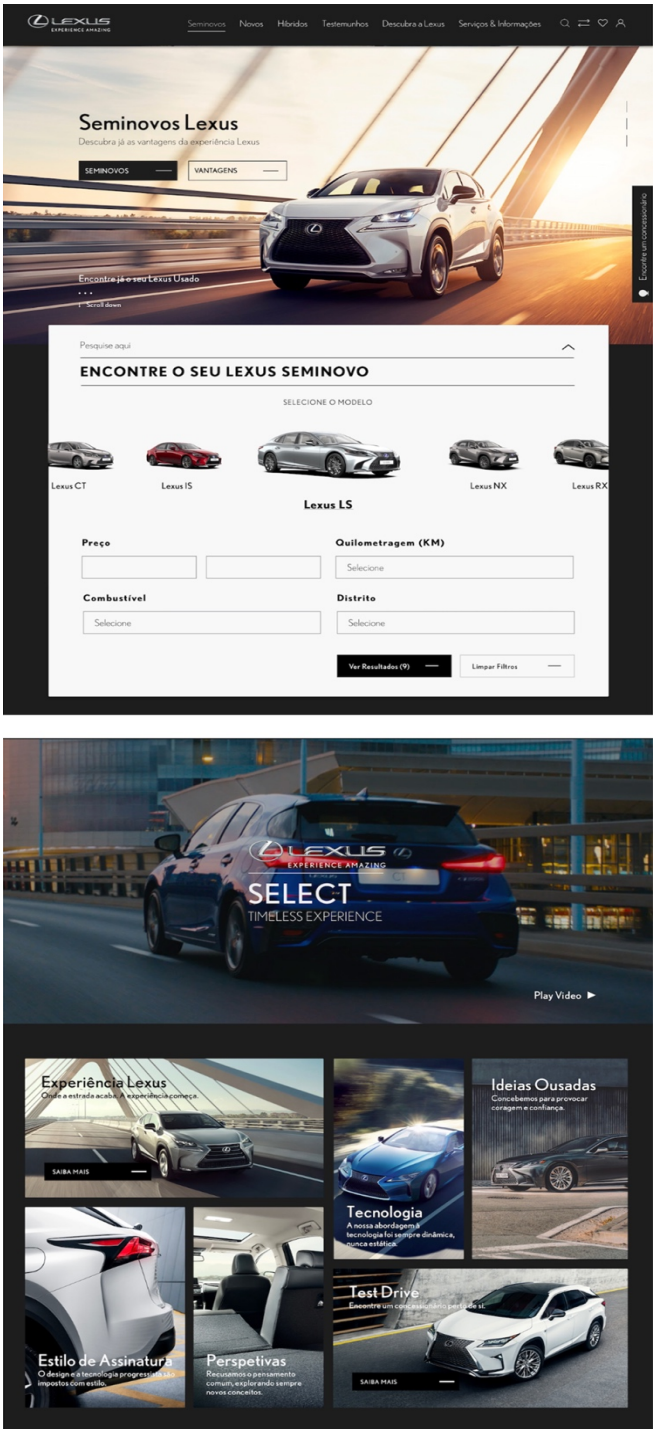


Figure 5: Homepage details (desktop version)

5.6. Prototype

Upon concluding the designing of each screen of the mobile and desktop versions in the 'Sketch' application, the software 'Invision' was used to prototype the online platform. Through this software, animations and transitions between screens were produced and applied. This allowed a better understanding of the flow and navigation of the website, before moving on to the usability testing phase of the prototype.

5.7. Usability tests

The usability tests were composed of a series of actions that were aimed to evaluate and verify the user's ease of use of the interface. The tests were conducted with users representing each persona for whom the product was being developed. The participants carried out a list of tasks and objectives, while being analyzed to provide observations on behavioral data [35].

There are several methods to study and evaluate usability. According to Nielsen [16], through 5 users, 85% of the usability problems of the product or service can be detected.

Throughout the development of the online platform several usability tests were performed in order to obtain a constant feedback from users and make the necessary improvements accordingly. This process helped reach the last phase of the work with a reduced number of errors and inconsistencies in the interface design.

For the last usability tests, towards attaining further rigor in the analysis method, six individuals (two for each of the three defined *personas*), men and women aged between 27 and 58, were selected for the sample.

The tests consisted of observing and evaluating user behavior in performing the following tasks:

- Enter the website and find the car configurator.
- Select a car and find the respective data sheet.
- Take the test to find out which car is right for you and ask for more information about it.
- Create a user account on the website.
- Find out more about Lexus Select and its benefits.
- Go to the testimonials page of former Lexus vehicle owners.

Users were also asked to indicate the difficulties, indecisions and doubts they encountered.

The tests lasted an average of 12 minutes per individual. According to the observations made, the following findings stood out:

- All users were able to accomplish the proposed tasks without demonstrating difficulty in finding the intended goal. However, in task 3, there was some indecision on the part of two of the users to start their task (by clicking on the button "The Lexus for you"). Taking this result into account, it was considered necessary to further highlight this functionality on the website, and subsequently improve it.
- The icons designed for the presentation of the car's technical data were highlighted by five users. These users considered this option an important aid in reading the contents.
- Older users took more time than newer users in performing the tasks. However, the difference was small.

After the usability tests, the same users were also asked to answer a short questionnaire towards assessing the level of satisfaction they experienced while using the online platform. The questionnaire was set to examine key areas such as the interaction, the perception of the information, the usefulness factor, and an overall impression of the website. In Table 3 the questions that have been asked to users are presented.

Table 3: The questions asked to users to evaluate the level of satisfaction experienced while using the online platform.

QUESTIONS
Perception and quality of the information
All the information on the website was readable?
Did you understand all the content of the website?
Is the information on the website well organized by the different parts of the website?
Usefulness
Has the website enabled you to become more enlightened about the brand's products?
Did the website clearly conveyed the advantages of buying a Lexus used car?
Has the website aroused your interest in getting to know the brand and its services better?
Interaction
Was the interaction with the website easy?
Did you find what you wanted easily?
Was the navigation through the website easy or did you ever felt lost?
Overall assessment
What is your overall assessment of the website?
Is there anything you would improve on the website?
If you answered "Yes", what would that be?

The results of these tests were reasonably positive. The tests demonstrated a high success rate in the overall fulfillment of tasks, identifying only minor problems that were correspondingly solved. The level of user satisfaction, based on the feedback obtained through the questionnaire, was high and thus determinative of the prototype's market-readiness.

6. Conclusions

As for the first of the specific objectives, the joint work with Lexus and the Caetsu agency allowed, in the first instance, to identify that the brand's strategy, beyond a better conversion ratio of the digital platform, was interested in promoting values related

to the circular economy, sustainability and responsible use of natural resources, which was a fully consistent action with offering a new life to used cars, even more so when these vehicles are almost entirely hybrid vehicles. Secondly, it allowed, in line with its strategy, to identify and model typical users based on the research data that the brand already had.

Secondly, the study concluded that, with the exception of BMW, the websites of the competing brands were mainly limited to serving as search tools for their respective used cars available for sale. The analysis of the competing brands, together with the collaborative research actions developed with the Lexus Portugal and Caetsu teams, provided a comprehensive understanding of the second-hand car segment in Portugal, and gave an idea of Lexus' target audience.

Regarding the third secondary objective, the methodological foundations of the design and development process of the online platform facilitated the realization of a viable solution by strictly adhering to the key principles of UX and UI design to achieve cohesion between the different elements of the process, such as the application of character models, information architecture, the creation of *frameworks* and *user flows* and the conceptualization of appropriate interfaces.

In addition, usability tests were conducted to evaluate user acceptance and identify areas for improvement. Once the necessary changes had been made, the prototype was submitted to the management of Lexus Portugal, which subsequently approved it and granted permission to move on to the execution phase, with a view to making it public in the coming months.

Thus, the results presented allow to claim that the online platform designed in this research can align the strategic interests of Lexus with those of its users, allowing Lexus Portugal to have a distinctive and even more complete solution compared to competing brands and entities, and to provide users with a solution more suited to their needs, goals and motivations.

Although user studies indicate a good result in terms of usability and user experience, in the future it's necessary to carry out further testing of the implemented product, in order to iteratively add improvements to it.

Based on the results, it is understood that the process employed in this research can be used in those cases where the strategic interests of the brands are to be aligned with those of the previously identified target audiences.

The process used in this research is intended to be the basis of a model that helps brands to align their strategic interests with the needs, expectations and objectives of their potential users. All of this is done from a design perspective and with the aim of turning their audience (potential customers) into satisfied users.

Conflict of Interest

The authors declare no conflict of interest.

Acknowledgements

This work is financed by national funds through the FCT – Fundação para a Ciência e a Tecnologia, I.P., under the scope of the project UIDB/04057/2020.

References

[1] G. Pedros-Perez, P. Martínez-Jiménez, P. Aparicio-Martinez, "The potential of car advertising in pursuing transport policy goals: Code of good practices in the Spanish context" Transportation Research Part D: Transport and Environment, **72**, 312-332, 2019. https://doi.org/10.1016/j.trd.2019.05.010

[2] A. Boelhouwer, A.P. van den Beukel, M.C. van der Voort, C. Hottentot, R.Q. de Wit, M.H. Martens, "How are car buyers and car sellers currently informed about ADAS? An investigation among drivers and car sellers in the Netherlands" Transportation Research Interdisciplinary Perspectives, **4**, 2020. https://doi.org/10.1016/j.trip.2020.100103

[3] Paulo Dinis, Fernando Moreira da Silva, "The Passenger Car in Portugal: Features of Functional Modules" Procedia Manufacturing, **3**, 312-332, 2015. https://doi.org/10.1016/j.promfg.2015.07.313

[4] Z. Kahraman, "Using user-centered design approach in course design" Procedia - Social and Behavioral Sciences, **2**(2), 2071-2076, 2010. https://doi.org/10.1016/j.sbspro.2010.03.283

[5] J. Braga, "Is human-centered Design broken?". UX Collective, 2019. [Online]. Available: https://uxdesign.cc/is-human-centred-design-broken-cac130eecc48. [Accessed: 28-Aug-2019]

[6] A. Chammas, M. Quaresma, C. Mont'Alvão, "A Closer Look on the User Centred Design" Procedia Manufacturing, **3**, 5397-5404, 2015. https://doi.org/10.1016/j.promfg.2015.07.656

[7] J. Liedtka, "Why Design Thinking Works". Harvard Business Review, 2018. [Online]. Available: https://hbr.org/2018/09/why-design-thinking-works.

[8] C. F. Llema, C. M. Vilela-Malabanan, "Design and Development of MLERWS: A User-Centered Mobile Application for English Reading and Writing Skills" Procedia Computer Science, **161**, 1002-1010, 2019. https://doi.org/10.1016/j.procs.2019.11.210.

[9] C. Abras, D. Maloney-Krichmar, J. Preece, User-Centered Design. In Bainbridge, W. Encyclopedia of Human-Computer Interaction. Thousand Oaks: Sage Publications, 2004.

[10] D. A. Noman, The Design of everyday things, New York: Basic Books, 2013.

[11] N. Martins, D. Brandão, D. Raposo (Eds.), Perspectives on Design and Digital Communication: Research, Innovations and Best Practices, Cham: Springer, 2021. https://doi.org/10.1007/978-3-030-49647-0.

[12] D. Raposo, "From Brand Mark to Corporate Visual Identity Systems" Convergências Journal, **2**(3), 2009. Retrieved from journal URL: http://convergencias.esart.ipcb.pt/?p=article&id=40

[13] J. Park, "Developing a knowledge management system for storing and using the design knowledge acquired in the process of a user-centered design of the next generation information appliances" Design Studies, **32**(5), 482-513, 2011. https://doi.org/10.1016/j.destud.2011.05.001

[14] D. Brown, "Chapter 2 - Agile Methods + UX = Agile UX" In Diana DeMarco Brown (Eds.), Agile User Experience Design: A Practitioner's Guide to Making It Work. 39-69, 2013. https://doi.org/10.1016/B978-0-12-415953-2.00002-9

[15] M. Kouprie, F. Sleeswijk Visser, "A framework for empathy in design: stepping into and out of the user's life" Journal of Engineering Design, **20**(5), 437-448, 2009. https://doi.org/10.1080/09544820902875033

[16] J. Nielsen, "Enhancing the explanatory power of usability heuristics" in Proceedings of the SIGCHI Conference on Human Factors in Computing Systems (CHI '94). Association for Computing Machinery, New York, NY, USA, 152–158, 1994. https://doi.org/10.1145/191666.191729

[17] N. Martins, M. Lemos, D. Brandão, D. Raposo, J. Neves, J. Silva, "Lexus used-vehicle online platform: comparative analysis of major competing brands' websites" in Advances in Design, Music and Arts: Proceedings of the 7th Meeting of Research in Music, Arts and Design, EIMAD 2020, May 14-15, 2020.Springer Series in Design and Innovation, **9**. Springer, Cham, 243-255, 2021. https://doi.org/10.1007/978-3-030-55700-3_17.

[18] D. Lachapelle, "A Designer's Guide to Competitor Research". Wayfair Experience Design, 2017. [Online]. Available: https://medium.com/wayfair-design/a-designers-guide-to-competitor-research-914b0deee25a. [Accessed: 23-Jul-2019]

[19] R. Dam & T. Siang, "Personas: A Simple Introduction". Interaction Design Foundation. [Online]. Available: https://www.interaction-design.org/literature/article/personas-why-and-how-you-should-use-them.

[20] A. Cooper, R. Reimann, D. Cronin, About Face 3: The essentials of interaction design. Information Visualization, **3**, Canada: Wiley Publishing, Inc, 2007.

[21] F. Anvari, D. Richards, M. Hitchens, M. Ali Babar, H. Tran, P. Busch, "An empirical investigation of the influence of persona with personality traits on conceptual design" Journal of Systems and Software, **134**, 324-339, 2017. https://doi.org/10.1016/j.jss.2017.09.020

[22] A. Teixeira, "Como está a evoluir o E-Commerce em Portugal em 2020". Digitalks, 2020. [Online]. Available: https://digitalks.pt/artigos/a-evolucao-do-e-commerce-em-portugal.

[23] J. J. Garret, The elements of the user experience. Berkeley: New Riders, 2003.

[24] R. Hartson, P. Pyla, "Chapter 16 - Designing the Ecology and Pervasive Information Architecture" In Rex Hartson & Pardha Pyla (Eds.), The UX Book (Second Edition). 341-358, 2019. https://doi.org/10.1016/B978-0-12-805342-3.00016-3

[25] A. Grilo, "O que é Arquitetura da Informação e como ela influencia a UX do seu produto". Comunidade UX Design Natal, 2016. [Online]. Available: https://medium.com/ux-design-natal/o-que-%C3%A9-arquitetura-da-informa%C3%A7%C3%A3o-e-como-ela-influencia-a-ux-do-seu-produto-b4f20881b2b4.

[26] F. Santana, "Arquitetura de Informação e o seu propósito". Coletivo UX, 2017. [Online]. Available: https://coletivoux.com/arquitetura-de-informação-e-o-seu-propósito-29cd278ebdfe.

[27] K. Kashimura, M. Kurosu, "Apparent usability vs. inherent usability: experimental analysis on the determinants of the apparent usability" in CHI '95: Conference Companion on Human Factors in Computing Systems. 292–293, 1995. https://doi.org/10.1145/223355.223680

[28] N. Tractinsky, A.S. Katz, D. Ikar, "What is beautiful is usable" Interacting with Computers, **13**(2), 127–145, 2000. https://doi.org/10.1016/S0953-5438(00)00031-X

[29] M. Soegaard, "The Grid System: Building a Solid Design Layout". Interaction Design Foundation, 2019. [Online]. Available: https://www.interaction-design.org/literature/article/the-grid-system-building-a-solid-design-layout.

[30] E. Marcotte, Responsive web design, Paris: Eyrolles, 2011

[31] StatCounter GlobalStats, "Screen Resolution Stats Portugal (Nov 2018 - Nov 2019)". StatCounter, 2019. [Online]. Available: https://gs.statcounter.com/screen-resolution-stats/all/portugal.

[32] T. Schlatter, D. Levinson, "Chapter 6 - Color" In Tania Schlatter, Deborah Levinson (Eds.), Visual Usability: Principles and Practices for Designing Digital Applications. 171-211, 2013. https://doi.org/10.1016/B978-0-12-398536-1.00006-1

[33] N. Bahat, "Improving UI Design Through Better Typography". Awwwards, 2015. [Online]. Available: https://www.awwwards.com/improving-ui-design-through-better-typography.html.

[34] Marktest, "Acesso à internet em Portugal é cada vez mais Mobile". Grupo Marktest, 2019. [Online]. Available: https://www.marktest.com/wap/a/n/id~2555.aspx.

[35] J. Nielsen, "Disruptive Workflow Design". Nielsen Norman Group, 2012. [Online]. Available: https://www.nngroup.com/articles/disruptive-workflow-design.

Advances in Science, Technology and Engineering Systems Journal Vol. 5, No. 5, 630-636 (2020)

www.astesj.com

Special Issue on Innovative Research in Applied Science, Engineering and Technology

ASTESJ

ISSN: 2415-6698

Sustainable Development Practices in the Moroccan Small and Medium Enterprise: by What Means and for What Purpose?

Keltoum Rahali[*,1], Abdelaziz Chaouch[1], Elmahjoub Aouane[2], Sami Chbika[2], Abderrazzak Khohmimidi[3], Mustapha Kouzer[1], Abdellatif Elouali[3]

[1]*Department of Chemistry, IBN TOFAIL University, Kenitra, 14000, Morocco*

[2]*Department of Biology, IBN TOFAIL University, Kenitra, 14000, Morocco*

[3]*Sciences of Management, Mohamed V University, Rabat, 10090, Morocco*

ARTICLE INFO

Article history:
Received: 24 July, 2020
Accepted: 23 August, 2020
Online: 05 October, 2020

Keywords:
Management
SME
Sustainable development

ABSTRACT

The objective of this article is to highlight the relationship between the integration of sustainable development practices in Moroccan Small and Medium Enterprises (Smes) and the challenge sought by managers in order to ensure competitiveness and sustainability. Indeed, present-day Smes are operating in a world where economic, social, societal or environmental constraints are constantly evolving. The Sme has to face, on a daily basis, new challenges such as economic stability and sustainability alongside the major structures because the challenge of any company is to be able to differentiate itself by adding its own trace promoting a more stable positioning in a fairly hostile environment. The investigation is carried out on a sample 30 Smes in the city of Kénitra due to the importance that this city holds in terms of both geographical dimension and economic inputs on the regional scale, 13.6% of the jobs generated by the SME according to the report of the high Planning Commission (HCP 2017). The results obtained reveal that the major concern of the managers of the Moroccan Sme is a purely commercial concern and that the integration of the various practices related to sustainable development in their managerial vision is only a means and does not constitute an objective to ensure the expected survival and sustainability.

1. Introduction

Most of the researches on Sustainable Development (SD) were focused, for the majority of them and until recently only on large structures. That being said, we believe that our study on Smes will be very useful as it provides us with the opportunity to analyze the means deployed by managers and the objective sought through the integration of sustainable development practices. In fact, Ashton, Russell and Futch [1] find that the majority of Smes in the United States of America are driven primarily by cost and competitiveness concerns, rather than by the implementation of green practices in their managerial practice. It is, in this sense, the merits of this study that will allow us to touch the why of the Why the integration of sustainable development practices in Moroccan Small and Medium Enterprise and by what means?

In [2], the author found that Smes represent approximately 90% of international organizations, Bank Al Maghreb identified a percentage that is close to 95% [3] with a 50% contribution to job creation, a rate which is very significant at national level. It should be noted that these structures also play a significant role in negatively impacting their environment [4]-[6]

Indeed, all the literature research shows that Smes, by their rather particular features, translate differently the integration into their systems of management of Sustainable Development (SD) practices than large structures i.e. often working in a different way in terms of their involvement in this process. Although the term of sustainable development is differently defined by several authors, we have retained the Brundtland's report definition (1987) "Our Common Future" [7] which defines it as a development that must meet the needs of the present without compromising the ability to meet those of future generations. This is not about stopping economic growth, on the contrary."

It is with this in mind that our investigation focused on the concern behind the introduction of this concept of SD through all its facets (certification, social responsibility, societal responsibility, green projects, etc..) within the company as well as the means used by managers in terms of environmental management and training to establish and convey their SD culture in their managerial vision. A vision that positions

[*]Keltoum RAHALI, IBN TOFAIL University Kenitra, +212676975725, rahkel@hotmail.fr

commercial concern as a priority sought through these SD practices.

The aim is to present the results of an investigation that was carried out in the city of Kénitra, a city possessing considerable assets giving it a place and a promising situation in the new regionalization. Our approach will show a methodological approach with a presentation of the main results we have achieved.

2. Methodology

We opted to conduct this investigation for a quantitative study through the development of different headings that fed our questionnaire in order to approach the well-basis on the perception and adoption of the multiple practices of sustainable development in management that aims at corporate citizenship in order to clarify the why of the implementation of this model in Smes operating in the city of Kénitra. We pre-tested our questionnaire on a sample of 5 Managers operating within Smes and 4 university teachers-researchers in the field of sustainable development to check its fluidity, the flow of questions, the respondent's understanding of all the sections of the questionnaire as well as the veracity of the answers that will allow us to obtain an overview of the concept of sustainable development and the implementation of its tools within Smes through a kind of management that we can refer to as responsible [8].

The components of this study can be summarized in the following axes:

- Identification of the SME and the manager,
- The SME managers perception of the concept of sustainable development,
- The means employed by the company to ensure its environmental and/or social involvement,
- The place of training and communication of SD practices in the managerial vision and in the integration of a culture within the SME.

For each explored axis, we matched either closed questions with the possibility of a yes or no answer, or questions with a range of answers ranging from one to several checkboxes. For more suggestions from respondents such as directors, managers, or project managers, whose functional quality is interesting, we have suggested an open question that could be used to push them forward in order to collect more information that can help us to better develop our interpretation.

We have conducted our investigation on 30 Smes (This data gathering phase coincided with the confinement). The choice is often made depending on the number of employees and turnover [9] [10]; as far as our investigation is concerned, only the workforce criterion will be used, a permanent workforce between (10 and 200) employees according to the 2002 Charter classification1. This classification, which corresponds to the quantitative approach, integrates two other qualitative parameters, namely its location in the kénitra region and the type of activity that is part of the industrial sector.

It is important to note that our sample includes Smes in this region whose activity is in the secondary sector, which is considered as strategic because it provides engineering jobs and research and development work for service companies of the tertiary sector [11], while focusing on the most widespread fields where technical progress remains moderate [12].

The city of Kénitra covers, according to the HCP, a total area of 3,052 km², or 17.37% of the entire region of Rabat-Salé-Kénitra (RSK) which is one of the 12 regions of Morocco, created by the new territorial division of the regions of 2015 in application of the Decree No. 2-15-40 of the Official Bulletin of 05 March 2015.

Our choice has settled on this city because it benefits from an economic array that allows it to appropriate a fairly important place in terms of production and job creation in its region. Its environmental aspect allows it to own a special natural heritage that can be negatively impacted by the establishment of the Atlantic Free Zone and industrial districts (Bir Rami, ...) which are often accompanied by strong urbanization. Our sample size included 30 Smes with 10 to 200 employees who wanted to actively contribute in this survey while providing face-to-face interviews over a period of January 25 to March 30, 2020 which coincided with the confinement's end.

3. Results synthesis

The study population's target and the respondents' profiles: By referring to the first results we have obtained after the questionnaires' analysis, we confirm that the degree of interest of Smes in the theme of sustainable development and its perception as a concept are significant. Indeed, this observation allows us to confirm that the association of the concept with the trilogy (economy, environment, and social) represents a particular interest for Smes with 66.7% (Figure 2). This situation remains verified among all those who were interviewed, irrespective of their academic training, and the field of activity of the SME. At this level, we tackle the profile of respondents, whose specifications are inserted in Tables 2 and 3.

As for the field of activity of Smes that we have approached, it remains diversified within the economic activity spectrum of Kénitra city and we note thus the strong weight of the construction sector with 26.6% which is explained by the strong urban activity in this city.

The second parameter that we mobilized to clarify the profile of respondents is the function of the respondent within the SME. It was found that the distribution of the population remains fairly balanced with a dominance of the executives (Project Managers) who totalize a score equal to 33%; the second population is represented by the managers (of sites, factory or a management function) with 23.4% and managers operating in the quality field with a score of around 16.7%.

Table 1: Field of activity

Fields of Activity	Number	Weight
Construction and Public Works	8	26,6%
Plastics industry	6	20,0%
Agri-Food / Agribusiness	6	20,0%
Piping and annexed equipment	3	10,0%
Lumber and Wood industry	3	10,0%
Clothing industry	2	6,7%
Metalic and mechanical industries	2	6,7%
Total	**30**	**100,0%**

[1] SME/SMI 2002 Charter, Dahir n° 1-02-188 du 12 joumada I 1423 (23 july 2002) Official Bulletin n° 5036 of 15/09/2002

Table 2: The respondent's positions

Occupation	Number	Weight
Manager (Project supervisor)	10	33,4%
Director	7	23,4%
Quality manager	5	16,7%
Administrative manager	3	10,0%
Team leader	2	6,7%
Operations support agent	2	6,7%
Others	1	3,3%
Total	**30**	**100,0%**

Taking these results into account, we can advance that sustainable development is seen as the concern of all the company's staff since the focus on this issue is shared by the different functions that structure the companies we have visited. This situation confirms the integration of horizontal management led by top management and which must be at the initiative of the environmental policy and the implementation of responsible management with the aim of defining a citizenship and responsibility SME environment with the attribute of vertical management [13] which brings together the various hierarchical levels of the company. A second factor to take into account in the identification of the respondent's level of education.

As shown in Table 3, nearly 40% of the population we surveyed has an engineering level while the remaining respondents are dispatched between different levels of training ranging from Bachelor's to MBA which explains the strong adherence of this profile to the many facets of the sustainable development at a rate of 66,7% (Figure 2) concerning the definition of this concept while linking it with its three fundamental axes: economic, environmental and social.

Table 3: The education level

Education level	Number	Weight
Engineer	12	40,0%
Baccalaureate	10	33,3%
Bachelor	4	13,3%
Mba	3	10,0%
Others	1	3,3%
Total	**30**	**100,0%**

Based on the three dominant criteria of the Material Data Sheet (business sector, function, and level of training of the respondent), we end up with representativeness of each modality that is not null and that is ensured by a value exceeding 2%. Through the heading «Perception of the term sustainable development», we want to raise the level of knowledge of this concept among respondents in order to assign it the connotation that stands against the perceived image and this through the strategic orientation and internal communication that is mobilized by the «awakened SME» to be able to highlight the interest and usefulness of a sustainable development approach within the structure.

As shown in Figure 1, the results from flat sorting, the awareness of the concept of sustainable development remains positive to the extent of 77% of the people we interviewed are familiar with the concept of sustainable development; it is necessary to deal with this percentage with caution since we had not assigned a definition to this concept but rather we propelled the spontaneous notoriety that stipulates the terminological knowledge of the concept of sustainable development without insisting on its understanding, its definition or even its axes to be set up within the company.

This awareness of the notion of sustainable development that is sometimes associated with corporate social responsibility [14] through the application of responsible management [15] by developing a vision of citizenship [16] can be acquired through internal information within the structure or through the environment or through the various media that deal with the subject especially in this era of Information and Communication Technologies (ICT) dominance.

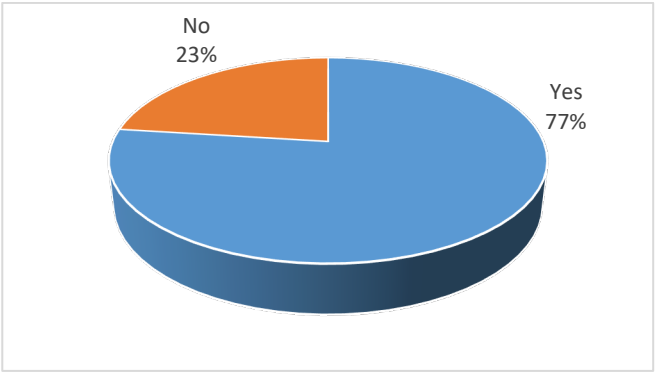


Figure 1: Sustainable development concept Notoriety

After identifying the awareness of the concept of sustainable development among the various companies that we were able to touch and whose score is of the order of 77%; we were interested in delimiting the definition of this concept in the image of each SME. At first glance, as shown in Figure 2, 66% of the population has recognized the concept of sustainable development associates it with the economic, social and environmental trilogy translated by T. Bansal [17] by the "3P" Profit, People and Planet.

Thus, SD can only be achieved through the three principles of economic efficiency, social equity and accountability; therefore, we can assume that the majority of people familiar with sustainable development have taken the time to document this concept either as a result of professional requirements or as a personal interest in the topic or in civic action since their definition falls under the common design adopted in 1987 at the Earth Summit and following the preparation of the first report of (G.H. Brundtland) which was carried out at the initiative of the United Nations and which identified the problem by associating it among other things with ecology, biodiversity and global warming...

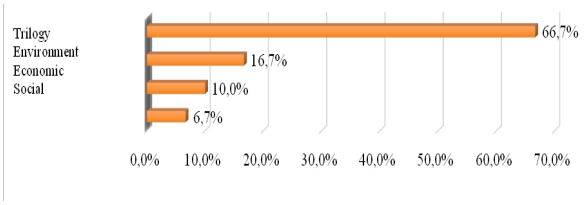


Figure 2: « Sustainable development » definition axes

Two parameters make it possible to justify the interest of the concept of sustainable development according to the perception of the respondents, namely the global necessity with 53,3% and that stipulates the preservation of natural resources with exploitation that will not alter that of future generations and this by the setting up of equipment aimed at the use of renewable energies and also promoting the optimization of the water

management (intelligent watering systems, featuring awareness regarding drinking water, etc.) and by adopting, each SME in its own way, responsible models to decrease the pollution that can arise during the exercise of their activities by putting in place an ecological vision within their operating method in terms of waste management, paper mining, moving more and more towards the concept of "zero paper" [18], without excluding, of course, the rationalization of their production systems.

Originating from the respondents, this vision shows their responsibility, regardless of their functions within the structure and activity they carry out. The second wave, represented by a total of 46,7%, is distributed with fairly close rates and emphasizes the competitiveness and the need for the implementation of sustainable development policies that will allow them to adjust into the new economic models as they are required by globalization.

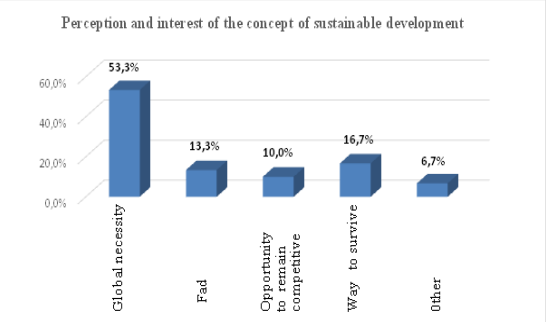


Figure 3: Perception and interest of the concept of sustainable development

3.1. *Interest and commitment of Smes in a sustainable development policy*

More than half of the Smes we interviewed, meaningly 56.7%, have an environmental policy as shown in Table 4. A policy initiated within the framework of sustainable development and characterized by the foundations of responsible management. Moreover, we note that European and Canadian Smes [19] increasingly integrate management practices in favour of Corporate Social Responsibility (CSR) and are more likely to opt for certifications that are closely related to the environment or sustainable development because several studies [20] point out that SME owners claim to have started integrating sustainable development into their management practices and that 20.8% of a population of future leaders declare that they intend to do so according to the survey conducted in 2010 by the Entrepreneurship Foundation (EF). This only shows the growing commitment and involvement of Moroccan SME managers in policies stemming from sustainable development with an awareness of this concept especially following the organization of the 22nd Conference of parties held in November 2017 at Marrakech, Morocco (COP22) in Morocco.

This environmental policy is quite often associated with certification, as shown in Figure 4. Indeed, the majority of Smes with 46,7% are certified in the quality management system, which is the result of the production system, that guarantees they conquer new markets, especially foreign markets, when they post a reference to a standardization label for their production process, which ranges from the purchase of the raw material, storage, production and supply chain management. Thus, we can observe that this initiative is more a commercial requirement than an environmental one. On the other hand, the company's affiliation to a Corporate Social Responsibility certification is only 6.7% which allows us to deduce that the Social responsibility is much more a state of mind and that environmental certification, which translates into 26.7% is more sought after by the Moroccan manager.

Table 4: Existence of environmental policy within the SME

Existence Of An A Environmental Policy In The Sme	Number	Weight
Yes	17	56,7%
No	13	43,3%
Total	**30**	**100,0%**

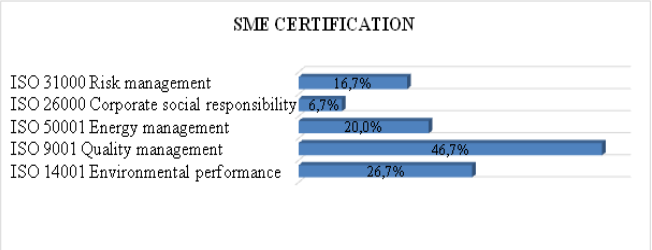


Figure 4: SME certification

Regarding the management and management methods within the SME, they must be able to lead, when implementing an environmental policy, a responsible act that aims to mobilize all staff around a collective vocation such as respect for the environment and the company's citizenship towards its stakeholders. We note in Figure 5, that the implementation of an environmental management plan is quite often the result of a 40% certification whereas the CSR approach is only 13,3%, a gap that remains significant due to the level of social involvement in Smes that remains relatively small compared to large enterprises.

Sharma, S [21] points out, financial constraints of an SME as opposed to a large enterprise that is more comfortable investing in a CSR business and has the ability to absorb fixed costs and ease of access to capital and other resources. It should also be stressed that when a certification project is set up, an accompanying system is put in place to standardize all production processes, the information system, the training of teams and all staff and the production platform which must meet in a manner that complies with a specification and a requirement of the chapters of the standard in relation to the (HSE) which refers to the safety and optimization of the quality system throughout the production process; therefore, the implementation of an environmental management plan is an indispensable act in the global certification chain (ISO 9001 version 2015).

At this level, the implementation of this plan by Smes is not necessarily voluntary but rather compulsory to obtain their certification that will allow them to open up to the foreign market. This is more of a purely commercial strategic act than an awareness of respect for and protection of the environment.

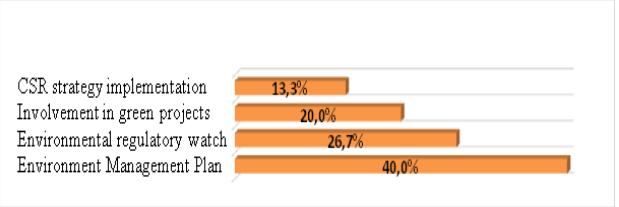


Figure 5: Management mode derived from sustainable development

3.2. Integration of sustainable development in the Smes managerial mode

The operational integration of sustainable development through the adoption of a management approach that takes into account the efficient use of natural resources (Figure 6), reveals that nearly 67% of the Smes we interviewed adopt a policy that optimizes their natural resources. This figure is quite encouraging and allows us to confirm the orientation of the SME of Kénitra city towards a green economy, thus promoting the setting up of a mindset that goes in a parallel way with respect for the environment while associating economic profit of the SME with its social and environmental dimensions.

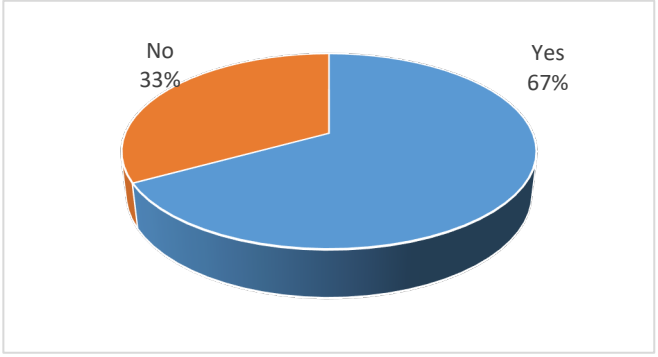


Figure 6: The efficient use of natural resources

It was necessary to stress this question, which concerns natural resources, by identifying the various means used by the SME to meet the challenge of sustainable development through the adoption of an environmental policy that must be based on the managers' actions and which represents their day-to-day activities as shown in Figure 7. It should be noted that all the answers must be stratified between the requirement of a certification process which has as its objective a commercial fact and the personal initiative which emerges more from the awareness of the mobilization and the individual commitment of everyone with regard to the environment.

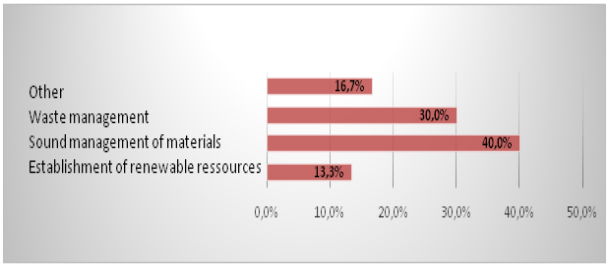


Figure 7: Means deployed to ensure efficient use of natural resources

The rational management of materials represents the largest part of the optimization of natural resources with a rate equal to 40 % and which often directly impacts the decrease of the expenses of the Smes monthly bill, followed by waste management which represents 30%. From this perspective, we can also deduce that the environmental policy adopted by Smes, which results in optimized management of natural resources, is more linked to the production process than to the specificity of the SME's activity. A production which, the more optimized it is, the more profit it will generate in the company's annual balance.

In addition, the implementation of renewable resources represents 13.3% although the latter allows to reduce costs considerably and to guarantee a low nuisance to the ecosystem. On the other hand, the investment cost of its implementation risks slowing down the environmental project of Smes and hinders the continuity of the sustainable development axes hoped by the manager. Through these results, we were able to highlight the importance of the implementation of environmental policy within Smes to ensure continuity, competitiveness indispensable in this era of globalization of markets especially with the outsourcing of activities from developed countries to emerging or developing countries through structures that demonstrate their support for sustainable development because the more the manager reveals its environmental involvement, the more he will gain responsible management and the more the market shares will increase. This brings us back to the fact that the implementation of this type of management requires a serious collective and individual awareness with the adoption of true corporate culture.

In the same line of thought and following the results inserted in figure 8, which represent the contribution of sustainable development to Smes, we point out that the overall trend in responses focused on seeking a competitive advantage and minimizing costs. While the reduction of the environmental impact and the production with the eco-label that allow to model own production come last; this trend of response allows us to confirm that Smes have more a commercial concern and consider, thus, sustainable development as an opportunity to label their production process (the process most targeted by the customer) in order to be able to integrate an international standardization that guarantees their acquisition of competitive advantage [22] and a referral to all their clients, subcontractors who are, quite often, already engaged in environmental policies.

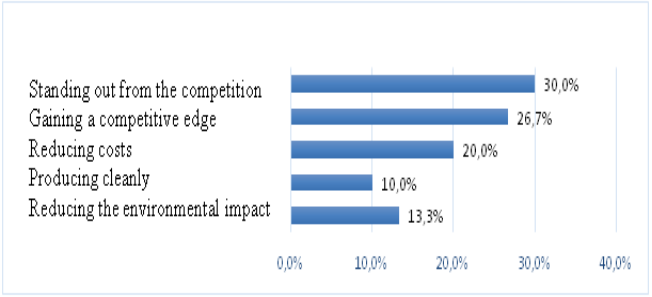


Figure 8: Contribution of sustainable development to Smes

3.3. The role of training and communication in the managerial perspective derived from sustainable development

In any management system qualified as performing, staff training constitutes a crucial axis in the implementation of either environmental or social policies. In fact, this is why we found that practically all the respondents were able to take a training course which is largely in the form of a conference with 40%, seminars 33.3% and internships in Morocco or abroad with respectively 10% and 16.7%.

Note, for example, that according to the survey that was conducted by the association for the sustainable Development practices (Apdd) [23], SME executives attended only 50% of conferences or seminars on sustainable development and wanted 33% more information on the various actions related to sustainable development. The observation that allows us to point out that the definition of this concept has undergone a marked evolution within the Moroccan SME which shows itself, aware of the impact of this type of training on the achievement of the goals of sustainable development as a whole.

Table 5: Kinds of contributions to sustainable development

Kinds of contributions to sustainable development	Number	Weight
Conferences	12	40,0%
Seminars	10	33,3%
Symposiums	5	16,7%
Internship Abroad	5	16,7%
Internship Inside Morocco	3	10,0%
Total	**30**	**100,0%**

Nearly 40% of the population took a training course focused on environmental management, followed by responsible management with a rate of 33.3%. The other topics are also related to environmental matters, such as sustainable development, the green economy and the management. The importance of these training actions is to demonstrate to what extent they enable participants to better perceive the concepts of implementing an environmental policy within the SME and to be able to customize their actions according to the sector and the process within which they operate.

It should be mentioned that our investigation has focused particularly on the themes that affect directly sustainable development while deliberately excluding the other themes that are oriented towards the Quality Management System, internal audit, communication, languages, etc. which are often planned either on the initiative of the manager or the staff.

Table 6: Sustainable development training topics

Sustainable Development Training Topics	Number	Weight
Environmental Management	12	40,0%
Sustainable Development	6	20,0%
Green Economy	7	23,3%
Eco-Management	5	16,7%
Responsible Management	10	33,3%
Total	**30**	**100,0%**

We conclude that the training of staff in the various topics related to the environment and Corporate Social Responsibility makes it possible to successfully integrate the practices of sustainable development within the company and therefore, increase awareness of the SME towards its social, social and environmental responsibility. This action mobilizes internal customers (the company's staff) and promotes the external SME's image towards all its stakeholders as well as its suppliers, which will enable it to evolve in terms of productivity and profitability, or its customers, which will ensure its successful positioning in an increasingly competitive market.

4. Discussion

The integration of sustainable development into the way of managing within Smes remains voluntary and expresses the company's commitment to its environment and stakeholders. With the emergence of this new concept that evolves in a framework marked by the economic demands that keep changing the world especially after the financial crisis of 2008, the political wave of 2011 (year of the new constitution in Morocco), the growing interest in environmental, social equity and human rights requirements; the adoption of more and more new management methods within companies and, particularly within Smes [24] who represent a significant share in the global economic weight, becomes a compulsory requirement in order to guarantee certain sustainability through the consecration of an economic asset which must be combined with environmental and social requirements. This new approach dictates that human capital is and will be for a long time to come to the cornerstone of any economy. Hence, its awareness, its training and support represents the optimal solution for Smes that want to go towards the acquisition of a sustainable competitive advantage.

Consequently, according to Torugsa, N.A [25], a social responsibility strategy can bring significant value to the market performance of an SME and can have a very significant impact on its financial performance. In addition, Lin, L et al, [26], consider that the corporate social responsibility (CSR) has presently become an essential aspect in a company's strategy and it is closely linked to its reputation because positive reputations generally lead to very positive financial results and performance.

During this survey, we were able to demonstrate that the concept of sustainable development through a few facets remains fairly well introduced within the Moroccan SME (77%); most often associated with the quality process or certification, it converges towards the same goal, namely, increasing competitiveness, resisting new changes in world trade and establishing an opportunity for referencing with all external stakeholders [27] that are very demanding and very committed in environmental policies.

References

[1] W. Ashton et al., "The Adoption of Green Business Practices Among Small US Midwestern Manufacturing Enterprises" J. Environ. Plan. Manag. 2017.

[2] C.M. Parker et al., "A review of interventions to encourage SMEs to make environmental improvements" Environmental and Planning C, 2009.

[3] Bank-Al-Maghreb, Rapport annuel, 285p, 2013.

[4] F. Labelle et al., "la responsabilité sociétale des petites et moyennes entreprises ou la RSPME" une analyse de la littérature des dix dernières années. 2010.

[5] L. Temri, "Partage des bonnes pratiques de développement durable" le cas des PME agroalimentaires du Languedoc-Roussillon, Innovations, **1**, 2009.

[6] H. Jenkins, "A critical of conventional CSR theory" An SME Perspective, journal of General Management, **29**, 2004.

[7] G.H. Brundtland, "Notre avenir à tous, Commission mondiale de l'environnement et du développement, Edition du Fleuve, 1987.

[8] J.C. Dupuis, "management responsable : vers un nouveau comportement des entreprises ? La Revue des Sciences de Gestion, n° 211-212, 2007. https://www.cairn.info/load_pdf.php article=rsg_247

[9] C. Blais, "Indicateur et tableau de bord de gestion : Mesure de la performance des PME en développement durable. Mémoire de maîtrise, Université de Sherbrooke, Sherbrooke, 2011.

[10] K. Delchet, "Développement durable, l'intégrer pour réussir, 2007.

[11] C. Clark, Les conditions du progrès économique, Paris, P.U.F., I960. https://www.universalis.fr/encyclopedie/colin-clark/

[12] J. Fourastié, préface de l'édition du Grand Espoir du XXe siècle, 1989.

[13] S. Ghoshal, "Changing the Role of Top Management : Beyond Structure to Processes", la Harvard Business Review, 1995

[14] E. Reynaud, "Impact de la protection de l'environnement sur la gestion des coûts, Responsabilité Sociale de l'Entreprise et Performance, éd. : d'organisation, Paris, 2004.

[15] R. Perez, "La revue des sciences de gestion, Direction et Gestion, n°211-212- RSE, Quelques réflexions sur le management responsable, le développement durable et la responsabilité sociale de l'entreprise, 2002

[16] Turcotte et al, Comprendre la responsabilité sociétale de l'entreprise et agir sur les bases de la norme ISO 26 000, 2011

[17] T. Bansal, "le développement durable en entreprise, Le développement durable en entreprise, c'est contribuer à la prospérité économique, à la santé des écosystèmes et au pouvoir des communautés, 2012.

[18] A. Bernillon, "Implanter et gérer la qualité totale, Les Éditions d'Organisation, 1988.

[19] M. Doucet, "le développement durable dans les PME au Québec : outil de diagnostic de facteurs d'influence et des pratiques mises en œuvre, 2012, https://www.usherbrooke.ca/environnement/fileadmin/sites/environnement/documents/Essais_2013/Doucet_M. 15-10-2012.pdf

[20] J. Rollin, Comment les entrepreneurs québécois jonglent-ils avec

l'intégration des principes de développement durable ? Site de la fondation de l'entrepreneurship, http://www.entrepreneurship.qc.ca/developpement_durable
[21] S. Sharma, Managerial Interpretations and Organizational Context as Predictors of Corporate Choice of Environmental Strategy. Acad. Manag. J.**43**, 681–697, 2000.
[22] C. Martinet, "Entreprise durable, finance et stratégie, 2004, https://www.cairn.info/revue-francaise-de-gestion-2004-5-page
[23] S. Lagarde-Dupraz, Questionnaire réalisé par l'Association pour les Pratiques du Développement Durable Apdd, 2000.
[24] D. Lebegue, l'ORSE – (Observatoire sur la Responsabilité Sociétale des Entreprises), 2003.
[25] N.A. Torugsa, O'Donohue,W.; Hecker, R. Capabilities, Proactive CSR and Financial Performance in SMEs:Empirical Evidence from an Australian Manufacturing Industry Sector. J. Bus. Ethics, **109**, 483–500, 2012.
[26] L. Lin et al., Financial performance and corporate social responsibility: Empirical evidence from Taiwan. Asia Pac. Manag. Rev, **24**, 61–71, 2019
[27] R. Freeman, Divergent Stakeholder Theory, Academy of Management Review, **4**, 1999.

Advances in Science, Technology and Engineering Systems Journal Vol. 5, No. 5, 637-644 (2020)

www.astesj.com

Special Issue on Multidisciplinary Sciences and Engineering

ASTESJ

ISSN: 2415-6698

Overcome Discrimination: A Logistic Regression with 10-year Longitudinal Investigation of Emo Kids' Facebook Posts

Proud Arunrangsiwed[1,*], Yothin Sawangdee[2]

[1]Faculty of Management Science, Suan Sunandha Rajabhat University, Bangkok, 10300, Thailand

[2]Institute for Population and Social Research, Mahidol University, Nakhon Pathom, 73170, Thailand

ARTICLE INFO

Article history:
Received: 29 July, 2020
Accepted: 25 September, 2020
Online: 05 October, 2020

Keywords:
Emo subculture
Facebook
Logistic regression

ABSTRACT

This study primarily aims to identify the factors that helped emo kids in 2010 move through the emo-identity discrimination and be able to obtain a certain level of achievement. Facebook is the social network that allows users to track friends' posts back over 10 years. Content analysis was conducted by using two coders to rate 1,432 Facebook posts published during 2010 until 2019, based on the variables: (1) emo-related content, (2) emotion expression, (3) being a part of fandom, (4) the group of fandom, (5) friend(s) and (6) family appearance. The results from logistic regression analysis reveal that past emo kids' Facebook posts are increasing in the contents about friends, family, and fan objects over time. However, the number of posts with emo music or emo fan object was reduced. Having social support and belonging to social group, like fandom, might help past emo kids overcome the hard time that they had got prejudiced. Future studies should develop a model or existing theory to explain the complexity of individuals' overlapping identities blended in social networking profiles.

1. Introduction

Emo is a subculture and a music genre being popular for teenagers in the first decade of 2000s [1]. It was linked to negative deviant behaviors, such as suicide and self-harm [2], [3]. The members of subculture or "emo kids" in those days currently become young adults [4]. However, these people initially experienced music-taste-based discrimination, and they are negatively stereotyped by people in mainstream culture [5], [6]. This study aims to track their social network posts to see the transformation of their identity and the evolution of relationship with family and peers. These would help identify the factors that save these subculture members from unfair prejudice, which result in their well-being in society.

Emo is considered as a subculture because it has its own values, norm, belief, sets of behaviors, and communication patterns [1], [7]. This subculture was spread via online media, such as Facebook, Myspace, and YouTube. The members shared common interest toward emo, punk music, and artists, such as Fall Out Boy, We the Kings, The Academy Is…, Dashboard Confessional, My Chemical Romance, Paramore, Mayday Parade, Taking Back Sunday, Panic! At the Disco, The All-American Rejects, Boys Like Girls, etc. They would not just perform as fans of these artists, but they also need to be able to identify with their music [1], [8]. These fans believe that their favorite songs can help them with difficult life event regarding school and parents. Their common apparels were black T-shirt and skinny jeans, and they usually applied black eyeliner with dyed black hair covering one eye [9], [10]. Emotional expression is acceptable for both female and male ones, e.g., subculture members would comfort a crying emo boy, rather than blaming him regarding the lack of masculinity. As the result of these characteristics, emo boys were often stereotyped by outsiders as gay men, which could cause serious cyberbullying.

Other than the mentioned practices, suicide and self-injury are perceived as important norms of emo subculture [11], [12]. After the suicide of two Australian female students, Jodie Gater and Stephanie Gestier, in 2017, emo kids were not viewed only as subculture members or fans of modern punk music, but folk devils [13], [14]. They used social network and allowed emo texts to alter their thoughts to associate with self-injury and suicidal idea [8], [15]. This contradiction against social norm is the cause that public marked them as deviants rather than a subculture [16], [17]. Mass media have played an important role to create moral panic regarding the link between music taste and anti-social behaviors

*Corresponding Author: Proud Arunrangsiwed, Suan Sunandha Rajabhat University, email: proud.ar@ssru.ac.th, parunran@nyit.edu

[18] as they connected the case of Columbine school shooting to metal music [19], [20], and the suicide of two female teenagers to emo music fandom [1], [21]. Although metal fans were initially judged by public that their music taste was related to aggression [19], [22], this group of fans discriminate against emo kids based on similar stereotypes [19], [23]. Metal fans also differentiate themselves from emo teens that they were stronger and more masculine than emo kids [24]. Whether emo boys were straight or had an LGBT identity, they were often prejudiced as gay [23]-[26]. On the other hand, as a part of punk music genre [27], punk musicians, fans, and subculture members have displayed their feminine aesthetic by applying cosmetics and female clothing for long time before the birth of emo music [28], [29]. In other words, how people viewed emo kids as gay or problematic is a kind of the discrimination toward a group.

2. Hypotheses Construction

In aforementioned section, emo is both music genre and subculture, some members or fans of which engage self-mutilation and suicide, while public stereotyped them -as a whole- to be folk devils with aggression against self [30], [31]. Problem music, whether punk, emo, or metal, has been targeted as the cause of negative behaviors [32]. Later, it was found that low self-esteem, not problem music, could directly bring about self-harm [33], and there is no relationship found between problem music use and low self-esteem [34], [35]. This implies that emo music may not be the cause of teens' suicide and self-harm, but it might be a part of coping process that pushes them through their actual initial life problem, that had diminished their self-esteem or had led them to self-mutilation [36].

While people outside subculture understand that teenagers are reinforced with suicidal thought and self-injury by emo music, emo fan scholars reported that these fans stopped cutting themselves after being coped by such the music [21], [37]. To identify with sad music is a part of coping skills that help people accept and make sense with negative event in their life [38], [39]. Sad emo songs were easily used as coping tools by their fans, since the lyrics are about problems with friends, family, heartbreaking, and loneliness [27], [40], [41]. Moreover, a part of subculture norm is to express emotion and identify with emotional emo songs [1], [8]. This helps construct the hypotheses that prior emo kids may continuously listen to emo music or being emo after the age of emo boom (2010), and they have been likely to express their emotion in their social network posts. Hence, the following hypotheses were formulated.

H1: Emo kids have posted emo-related texts on their social network (Facebook) profile since 2010 (roughly the last year that emo subculture was popular) until 2019.

H2: Emo kids have expressed their emotion in their social network posts since 2010 until 2019.

Although emo music helps teenagers cope with personal troubles, they may not avoid negative stereotype constructed by public. Therefore, it is important to identify the factors that help them walk through this discrimination. Racial discrimination could result in lower self-esteem and higher depression [42], [43]. Parents should not only help their children prepare for being discriminated at school [44], but should also teach them coping skills after ad hominem attack [45]. Other family members and people with similar identity as the victims could also help reduce stress from discrimination and find the way to solve such the problem for the victims [46] – [48]. The above literature could indicate that family and peers might be an important part that saved emo kids from the discrimination. This means emo kids may have lived with their family and communicated with their friends during 2010 to 2019. The particular evidence eventually entails the following hypotheses.

H3: Emo kids have posted texts (alphabetic text, image, or video) about their friends since 2010 until 2019.

H4: Emo kids have posted texts about their family since 2010 until 2019.

However, Strauss [49] stated that self-harm in emo kids was rooted from their lack of social and family support, and this is opposite from H3 and H4. If these adolescents were negatively stereotyped, low in self-esteem, and have lack of social support; being a part of fandom or fanship might be the factor that heightens their self-esteem [50], [51], and allows them to healthily grow up as well as people in mainstream culture [52]. Joining fan community could provide fans with sense of belonging and that brings about self-esteem [53]-[55]. While fans listen to their favorite songs, the music could stimulate their self-esteem [35], especially for metal music fans who extremely believe in ones' own authenticity [56]. Authenticity refers to having realness value, or freedom of expression regardless others' attitude or hegemony [57]. Eminem's authenticity, for instance, is scorn and crudeness [58]. Hall [29] found that emo musicians and also fans accepted their difference apart from outsiders in mainstream culture. This is close to the term of self-concept clarity toward group identity, which is associated with having self-esteem [59], [60]. Recently, it was found that emo fans could earn fan-related self-esteem during attending emo-punk concert [61]. These could derive a hypothesis that emo kids have been part of fandom or fanship whether it is directly about emo music or other objects of interest.

H5: Emo kids have posted texts related to any kind of fandom or fanship from 2010 until 2019.

Because identity can be changed over time [62], [63], to track Facebook posts of past emo kids could help understand their identity transformation related to their fan identification, emotion expression as subculture value, and how they obtain family and peer support. This may help explain how they overcome the discrimination and can live normally as well as general adults.

3. Method

The current study built on the previous study, which reported that emo kids who engaged in emo online community in past 10 years could handle the emo-identity discrimination and grow up and work in proper careers [64]. The current study would track the social network posts of the same group of past emo kids in mentioned study to seek for the factors that may allow them to move pass through the discrimination, and consequently, they could reach their life achievement.

Based on the reviewed articles [37], [46], [48], [51], fan identity, family and peers, and emo music consumption could be the important factors that help emo kids overcome the

discrimination and other life problems. Hence, the major variables that would be explored are (1) emo music or emo-subculture-related content in the Facebook post, (2) the level of emotion expression in the post, (3) being fan or being a part of fandom, (4) the group of fandom that the samples belong to, (5) friend(s) and (6) family appearance in Facebook post.

3.1. Samples

Because emo subculture was risen and grown in the Internet [14], data collection of the current study would be done online, as well as earlier studies of Overell [1], and Zdanow and Wright [8]. The cases of these researchers were prepared in the time that emo subculture and music were popular, or around 2006-2010, but for the current study, the data collection was done in 2019. The samples needed to be active social network users since 2010 until 2019. Because people could change their identities over time, to use the continuous-active users could help confirm their original identification as a part of emo subculture.

Therefore, the first researcher of the present study used one's own Facebook friend list containing emo kids in 2010 as the site for data collection. The majority of samples were white and yellow. Few were from Africa, Middle East, and India. This recruitment method might be the only way to ensure that these users had had emo identity during 2010. Other strategies to recruit the cases might be impossible, because it is hard to know the exact date that users like an emo-related Facebook page or join in a group. For Myspace, although it was the major social network considered as social capital for emo kids in those days, most users have now been inactive [1], [14], [24], [41].

The mentioned friend list had contained more than 300 users, but in 2019, the number of users left in this list is 273. The users who did not post any new post in the latest two months were excluded from the study. Only 62 users were active and selected as the samples. After 62 active users were added into the codesheet, we prepared the codesheet by listing the randomly selected timeline (wall) posts. Twenty-nine posts were chosen from each user. Three posts were selected each year, from 2010 until 2019. The only year with 2 selected posts is 2019, because the data collection was done in July, 2019. The process of the randomization was that each selected post in each year had equally gap of time, which was about 4 months. For instance, if the first selected post was published in early January, the next selected posts would be published in early May and early September, respectively. Therefore, the possible highest number of cases is 1,798. Because some users did not post anything in some month(s), the number of valid cases left for the analysis is 1,432. The 366 cases, which were blank, got removed from the final codesheet.

3.2. Data Collection

Data collection of the present study was done in Facebook. The raters needed to gather the information from "About" section of profile, and the selected posts in main timeline or wall. These posts could be in many forms, such as text, image, video, link from other websites, and mixing between two or more mentioned types. After codesheet preparation, two raters coded 7 variables as follows:

- Gender. Raters could look for this information in "about" part of Facebook profile. Female was coded as 0, and male was coded as 1.
- Emo-music-or-subculture-related content in the post. Raters could consider adding the value into this variable based on text, image, or video in each post. If the media contain emo music, music video, emo apparels, emo facial makeup, and hairstyle, the particular post would be marked as emo-related. Some phases or signs in text were also associated with emo-style discourse, e.g., xoxo, rawr, etc. This variable is for checking if users still have the same identity as they had had 10 years ago. If the post applied to the given condition, the raters would code 1, and 0 for not applied.
- The level of emotion expression in the post. Unlike the previous items, this variable is not dichotomous. If the user did not display any emotion at all, both verbally and nonverbally (use photos, sticker, Facebook mood, or emoticon), the raters would code the post as 0. The small, moderate, and extreme amount of emotion expression were coded as 1, 2, and 3, respectively.
- Friend(s) appearance in Facebook post. If friend(s)' name(s) was mentioned or tagged in the post, or friend(s)' photo(s) was published, the raters would code that post as 1. On the contrary, if the post was not related to any friend, it would be coded as 0.
- Family appearance in Facebook post. The coding rule was similar with the previous item. If there are one or more family members in the post, it would be coded as 1, and if not, it would be coded as 0.
- Being fan or being a part of fandom. Whether the user displayed oneself as emo fan or fan of other media object, the post would be coded as 1, and if the post has nothing to do with any fandom or idol, it would be coded as 0. It might be important to note that fandom-related posts could be a shared official post by their favorite artist, photos of artists, album cover, shared news, and also fan art or fan Photoshop manipulation.
- The group of fandom that the samples (each of their posts) belong to. If the previous item, "being fan or being a part of fandom," were coded as 0, the raters would leave this part of codesheet blank. If the raters found that the post was related to emo fandom, it would be coded as 0. If metal, death metal, or melodic death metal music was found in the post, it would be coded as 1. If the post was about pop or R&B music, it would be coded as 2. If the post was about sport, movie, Japanese anime/manga, games, and politic or government, it would be coded as 3, 4, 5, 6, and 7 respectively. Posts about politics and government could be considered as fandom-related posts, because it consists of the acts of fan and anti-fan, to support or to protest against some policy. Moreover, Bronstein [65] discovered that many people treated politicians the same way as they treated celebrities, and vice versa. Politicians could post non-politic-related photos, such as vacation with their family, and their supporters also commented and shared the posts.

Another variable is the number of month(s) counted from the beginning of 2010. This variable is the major predictor in all regression models. If the post was published in March, 2010, for instance, the value of this variable would be 3. If the post was published in February, 2011, the value will be 14. Hence, the smallest possible value is 1 month, and the highest is 115 (9 years and 7 months).

Case ID	year	month	Gender	Friend	Family	Emotional Expression Level	Fandom-related	Emo-subculture-related	Type of fandom	Month Pass Counted from Jan 2010
115	2018	Sep	0	0	1	2	0	0		105
116	2019	Feb	0	1	0	2	0	0		110
117	2019	July	0	0	1	2	0	0		115
118	2010	Sep	0	1	0	2	1	0	3	9
119	2011	Feb	0	0	0	3	1	0	3	14

Figure 1: Codesheet preparation

3.3. Analysis

Most parts of the data were presented using descriptive statistics. Logistic regression analysis was used to understand the probability of the variables, emo-music-or-subculture-related contents, being a part of fandom or fanship, friend(s), and family appeared in posts over time during 2010 to 2019. This implies that in the analysis, independent variable is the number of month counted from the beginning of 2010, and the dependent variables are all 4 mentioned dichotomous variables. At the same time, linear regression analysis was used to understand the effect of passing time on the level of emotion expression in social network post.

Because logistic regression analysis was employed for data analysis, the rated values of dichotomous variables cannot be averaged. There were 24 cases with disagreement, so the values of one rater were chosen to paste in final codesheet.

4. Findings

To answer if these past emo kids still listen to emo music or having emo identity (H1), the findings show that there are 341 posts related to emo music and emo subculture from 2010 until 2019. These are 23.8 percent of all post (n=1432), as presented in Table 1. However, lately, the number of this kind of post had been slightly decreased (Odds Ratio=.995; p=.006), especially in last 4 years (2016-2019).

According to Table 1. it is noticeable that some groups of variables are overlapping, and the most overlapping cases are between the groups, fandom and emo-related posts (n=150), and following by the overlapping of fandom, emo-related posts, and friend appearance in posts (n=33).

As shown in Figure 2., both male and female tracked emo kids have similar decreasing tendency in posts related to emo music and subculture, and women generally have higher numbers of this kind of posts than men. It was interesting to look into the demographic data regarding gender. After checking carefully in these 62 selected users, there are only two genders appearing which are female and male. Based on these 1432 cases, 570 cases were posts by female users, and 862 cases were posts by male users. This offers an opportunity for future researchers to understand more about emo masculinity. Men, who are emo or were previously emo, may not have an LGBT identity, but with the subculture value, it allows men to display their feminine characteristics.

Table 1: Frequency of, and friend-and-family-related posts, fandom-related post, and emo-related posts

Friend Appearance	Family Appearance	Fandom-related	Emo-related	n	percent
✓	-	-	-	154	10.75%
-	✓	-	-	83	5.80%
✓	✓	-	-	13	0.91%
-	-	✓	-	343	23.95%
✓	-	✓	-	27	1.89%
-	✓	✓	-	8	0.56%
✓	✓	✓	-	1	0.07%
-	-	-	✓	122	8.52%
✓	-	-	✓	22	1.54%
-	✓	-	✓	4	0.28%
-	-	✓	✓	150	10.47%
✓	-	✓	✓	33	2.30%
-	✓	✓	✓	5	0.35%
✓	✓	✓	✓	5	0.35%
-	-	-	-	462	32.26%
255	119	572	341	1432	100%
17.81%	8.31%	39.94%	23.81%	100%	

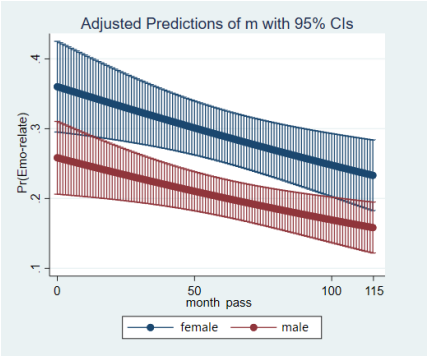


Figure 2: Margins plots for emo-related posts

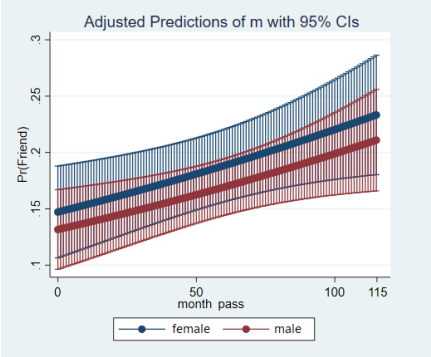


Figure 3: Margins plots for friend-related posts

Although emo media consumption and identification toward subculture were somewhat reduced, they still have emo core value, which is vulnerability (H2). Many posts were high in emotion expression until 2019 (Mean=1.661; S.D.=1.129). The linear

regression reveals no difference in the level of emotion expression in the post over time (F=3.595; R2=.003; Beta=-.050), but with small decreasing lately.

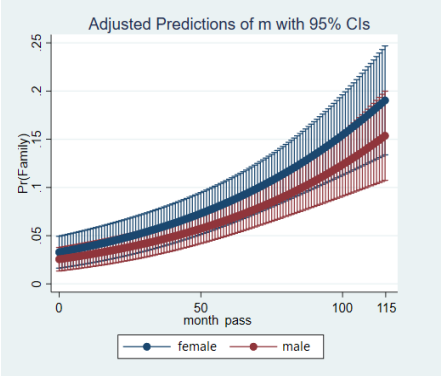


Figure 4: Margins plots for family-related posts

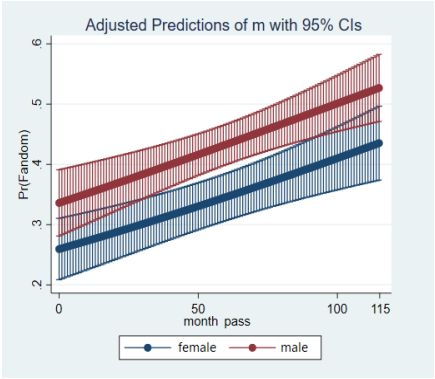


Figure 5: Margins plots for fandom-related posts

Unlike the expectation (H3, H4), these tracked emo kids rarely posted text and photos about their family and friends. Table 1. shows that there are only 17.8 percent of posts containing text, image, or video related to friend(s), and only 8.3 percent related to family. Based on the results of logistic regression in Table 2., only small increasing in friend-related posts was found (OR=1.005; p=.022), while there is a strong significant increasing of family-related posts (OR=1.017; p=.000). As seen in Figure 3. and 4., there is an actual increasing of friend and family contents in their Facebook posts. Women are higher in these types of posts them men. This could be because women have more willingness to disclose personal information in social network than men [66]. This might be related to gender norm and social acceptance that women can freely display their friendship, intimacy, and relationship with their family and peers.

Table 2: Univariate logistic regression
with the number of month counted from the beginning of 2010 as the predictor.

Dependent Variables	Emo-Related	Friend(s)	Family	Fandom
Overall OR (95%CI)	.995** (.991-.998)	1.005* (1.001-1.009)	1.017*** (1.011-1.023)	1.007*** (1.004-1.010)
Female OR (95%CI)	.996 (.990-1.001)	1.006 (.999-1.012)	1.014** (1.005-1.024)	1.011*** (1.006-1.017)
Male OR (95%CI)	.994* (.989-.999)	1.004 (.999-1.010)	1.019*** (1.010-1.028)	1.004* (1.000-1.008)
Overall OR (95%CI) Controlled by Gender	1.005** (1.002-1.009)	.995* (.991-.999)	.983*** (.977-.989)	1.445*** (1.159-1.800)

*p<.05; **p<.01; ***p<.001, n=1,432, n_{female}=570, n_{male}=862

The examples of family members found during the coding are wife, husband, grandmother, and uncle. The later marriage might be the reason that the number of family-related posts are lately greater. After reviewing the actual data, it could also be noticed that some who were married often changed their music taste and group of fandom to match their life partner.

For the fifth hypothesis (H5), these past emo kids belong to groups of fandom, whether it is emo music or other kind of media object fandom. This means that these people have had their fan identity for entire 10-year period tracked in the current study. The frequency of posts related to each group of fandom was presented in Table 3.

Table 3: Frequency of the posts
shown the groups of fandom which the cases belong to

Belonging to fandom	Number of Posts	Percent
Emo music	266	46.50
Metal/Death Metal	20	3.50
Pop or R&B	140	24.48
Sport	66	11.54
Movie	62	10.84
Japanese anime/manga	48	8.39
games	63	11.01
politic or government	37	6.47
Total (with overlapping cases)	702	112.73[1]
Total (all fandom-related post)	572	100.00

[1] The percentage is over 100, because some posts contained more than one type of fandom-related content.

Around 2013-2019, they posted texts and images about their fan objects more frequent than the first 3 years, as shown in Figure 5. Most of them still prefer emo music and bands until 2019, but they have also belonged to more groups of fandom. Like, after the first year, 2010, many of them started to listen to softer music, like pop and R&B. At the same time, some of them were interested in games, and Japanese comics and animation. Some showed that they have started to watch sport matches since 2015, such as soccer and American football. Similarly, some began to be interested in famous movies and Hollywood actors in 2015. In late 4 years, 2016-2019, some turned themselves to be the fans of politic. These past emo kids might increase their online civic engagement because they got older.

5. Discussion and Suggestion

As shifting away from the findings and suggestions of various studies that family plays an important role to solve the problem regarding discrimination in teenagers and students [45], [46], [48], the current study indicates that family and friends may not be a prominent factor that helps emo kids overcome the discrimination. This is because there had been lack of family-and-friend-related Facebook posts, especially at the beginning of the tracked period, 2010-2019. It is necessary to note that emo-identity discrimination had been peak at the beginning of the time period. One observation that can be explained this issue is that at the time that they got discriminated or cyberbullied, they may get lack of family support. Therefore, this part of findings suggests that it was other factor(s) that helps them overcome the discrimination.

Since the current study was conducted with content analysis and the cases were the public posts on Facebook, it might yield some imprecise data. Many emo kids, back in those days, were teenagers, and most of them might live with their parents and

communicate with them, but they might not need to show the photos of their parents in online space where other members of emo subculture would see. Like, middle school students do not want their parents to show up at school, because they may want to look independent and confident [67]. Therefore, these samples, with high-school age (around 2010), may not want to show their family on Facebook, too. To choose only one right conclusion among the finding (H3, H4) and this assumption that emo kids might live with parents in early 2010s, the in-depth interview should be employed in future studies.

Supported by numerous fan studies [50], [51], [56] and psychological studies [52], [68], these tracked emo kids may be able to move pass though the obstruction regarding discrimination, because they have been a part of fandom(s) (H5). Because fan activities [69], fans' media consumption [50], and sense of belonging in fan community [55] have a significant impact on fans' self-esteem, these emo kids may obtain the self-esteem from these fan-related factors. To have high self-esteem, people will be low in depression, and high in many positive life outcomes [52], [70].

Listening to emo music and identifying with it is also a kind of coping skills [21], [37]. Emo kids who faced negative life events were mentally healed by listening to emo music [21], [37]. The result of this study reveals that the tracked emo kids have continuously consumed emo music and expressed their emo identity (H1). Emo music might be the factor that helps them overcome the discrimination. It might be unusual to conclude that emo fans were prejudiced because of their music taste, and they could overcome the discrimination because of listening to emo music. An alternative suggestion is that fans used emo music as a part of coping process according to serious event in their real life. To be discriminated online might become small issue compared to the main problem they had had. This could be supported by the finding of Hall [29] that emo artists understood and showed the difference between emo subculture members and outsiders. Moreover, listening to ones' favorite music could help heighten self-esteem [35], so if emo fans were high in self-esteem strongly toward music and their subculture, the external factor might not be able to harm them.

Because emo kids have not only communicated with only people in the same subculture, it is still important to understand how they communicated with other people. Emo music and its fandom have been great parts of emo subculture. Fan communication may be able to help explain the practice in emo subculture. Fans normally communicated to 4 groups of people regarding their fan object and identity, which are (1) in-group members with the same identity, (2) hegemony, – or in this case is emo artists and emo bands, – (3) general out-group members, e.g. the friends and parents, and (4) out-group members who are their enemy, like people who discriminated against them [71].

To explain emo subcultural identity and their communication pattern might be somewhat complex. In Facebook or other social networking system (SNS) blends together many contexts people live in, in their real life. A Facebook friend might be an in-group member of emo subculture, but one might be an out-group member of workplace context. Future researchers may try to use social identities theory to explain all these complexities of the way many identities of an individual are mixed and blended in single SNS profile.

In the current study, the findings allow us to see the transformation of the identity from one to the others, from emo fans to other types of fandom, from young adolescents to adults with family and larger group of friends, and especially from vulnerable teenagers to stronger mature people.

Engaging in fandom might be the most important factor that helps emo kids move forward the discrimination, while the overall result could suggest that the way they move on and the transformation of their identity may be developed alongside with one another. Social network does not only help scholars to understand a subculture, but it actually helps and individual to see their developing identity, help them to understand themselves better, and that might be a part of how they move forward from discrimination, too.

An unexpected finding beside the major part of hypothesis testing is that many emo kids in 2010 had left their Facebook accounts, which causes a lot of missing cases in the present data sheet. Burke [72] found that many graduate students left their Facebook profile and signed up for other SNS such as LinkedIn because they need to look more professional, and some needed to switch to use other SNS to match their colleagues' choice.

The identity as an emo subculture member cannot be considered as a professional. Instead of editing the existing Facebook profile, some may choose to create a new profile. With the same group of samples but earlier study [64], many of them have worked in professional occupation such as, teachers, lecturers, engineers, designers, and some are entrepreneur of real estate business. In other words, while some people decided to leave their Facebook profile, some chose to continue using the same profile, but they turned it from an emo profile to be an expert one.

Even though the data of this study may consist of selection bias, we could learn that social network is an important part to spread, support, and maintain many subcultures, and one of these is emo subculture. We could see emo kids through their social network profiles that they have grown up to be young adults, used social capital in order to overcome the discrimination, coped with possible depression, and finally adjusted their life as subculture members to fit into the world complex society. Future study should continue looking at these emo kids' identity development and communication pattern through their adulthood and older adult ages. This way could help understand the strategies to achieve the long-term well-being of people who had experienced taste-and-identity-based discrimination.

6. Limitations

The major limitation of the present study is the small number of samples, which is 62 users. This may not be comparable to the actual population or emo kids before 2010. Moreover, these 62 users are the researcher's online friend, which might not represent general emo kids. Additionally, the data collection was content analysis done in online space, Facebook, where people may construct another identity such as ideal-self.

To solve this issue, researchers of future studies should hire computer experts to recruit more prior emo kids in 2010 who are

still active on social networking today. This would help increase sample size and strengthen the statistical conclusions of the current study. It is also important to note that many genders are available for Facebook users to choose. Therefore, samples with LGBT identity and asexual should be also included in future studies. As a result of this, the particular research would achieve a better generalization.

References

[1] R. Overell, "Emo online: networks of sociality/networks of exclusion," Perfect Beat, **11**(2), 141–162, 2010, doi: 10.1558/prbt.v11i2.141.

[2] M. Definis-Gojanović, D. Gugić, D. Sutlović, "Suicide and Emo youth subculture–a case analysis," Collegium antropologicum, **33**(2), 173–175, 2009.

[3] R. Young, N. Sproeber, R.C. Groschwitz, M. Preiss, P.L. Plener, "Why alternative teenagers self-harm: exploring the link between non-suicidal self-injury, attempted suicide and adolescent identity," BMC psychiatry, **14**(1), 137, 2014, doi: https://doi.org/10.1186/1471-244X-14-137.

[4] K. Moulton, Dashboard Confessional's Chris Carrabba Refuses to Age Out of Emo. Westword, (2018). Retrieved from https://www.westword.com/music/dashboard-confessionals-chris-carrabba-wont-age-out-of-emo-10161529

[5] S.J. Minton, Alterophobic bullying and violence. in J.L. Ireland, P. Birch, C.A. Irland, (eds.), The Routledge International Handbook of Human Aggression: Current Issues and Perspectives, Routledge, 2018, ISBN: 978-1-315-61877-7.

[6] D. Hernández-Rosete, "Bullying of emos in Mexico City: an ethnographic analysis," Cadernos de Saude Publica, **33**(12), 2017, doi: 10.1590/0102-311x00080116.

[7] T.D. Baker, S. Smith-Adcock, V.R. Glynn, "The Ghost of Emo: Searching for Mental Health Themes in a Popular Music Format," Journal of School Counseling, **11**(8), 1–35, 2013.

[8] C. Zdanow, B. Wright, "The representation of self-injury and suicide on emo social networking groups," African Sociological Review/Revue Africaine de Sociologie, **16**(2), 81–101, 2012.

[9] M. Heřmanský, There and Back Again: Linking Online and Offline Spaces in/of Czech Emo Subculture. in Hebdige and Subculture in the Twenty-First Century (pp. 169-205), Palgrave Macmillan, Cham, 2020.

[10] C.U. Gielis, It's not a fashion statement. An exploration of masculinity and femininity in contemporary emo music, Master thesis, Radboud University, 2018.

[11] P. Arunrangsiwed, R. Arunrangsiwed, Stereotyped Emo Kids: A literature review. in The 4th Technology Innovation Management and Engineering Science International Conference (TIMES-iCON), IEEE, 2019, doi: 10.1109/TIMES-iCON47539.2019.9024586.

[12] C. Partridge, Suicide, Angst, and Popular Music, Coward-Gibbs, M. (Ed.) Death, Culture & Leisure: Playing Dead (Emerald Studies in Death and Culture), Emerald Publishing Limited, 189-208, 2020, https://doi.org/10.1108/978-1-83909-037-020201020.

[13] M. Phillipov, "Just emotional people? Emo culture and the anxieties of disclosure," M/C Journal: A Journal of Media and Culture, **12**(5), 2009.

[14] M. Phillipov, "Generic misery music? Emo and the problem of contemporary youth culture," Media International Australia, **136**(1), 60–70, 2010, doi: doi.org/10.1177/1329878X1013600109.

[15] R. Trnka, M. Kuška, K. Balcar, P. Tavel, "Understanding death, suicide and self-injury among adherents of the emo youth subculture: A qualitative study," Death studies, **42**(6), 337–345, 2018, doi: 10.1080/07481187.2017.1340066.

[16] M.D. Daschuk, It's not a fashion statement, it's a death wish: subcultural power dynamics, niche-media knowledge construction, and the emo kid folk-devil, Master's thesis, University of Saskatchewan, 2009.

[17] S.F. Williams, "A walking open wound: Emo rock and the "crisis" of masculinity in America," in F. Jarman-Ivens (Ed.), Oh Boy! Masculinities and Popular Music (pp. 153–168). Taylor & Francis Group, 2013.

[18] R. Burns, C. Crawford, "School shootings, the media, and public fear: Ingredientsfor a moral panic," Crime, law and social change, **32**(2), 147–168, 1999.

[19] M.A. Miernik, "The evolution of emo and its theoretical implications," Polish Journal for American Studies, **7**, 175–188, 2013.

[20] G.W. Muschert, "Frame-changing in the media coverage of a school shooting: The rise of Columbine as a national concern," The Social Science Journal, **46**(1), 164–170, 2009, doi: 10.1016/j.soscij.2008.12.014.

[21] R. Haydn, My Chemical Romance: This Band Will Save Your Life, Plexus Publishing, 2015.

[22] C. Baker, B. Brown, "Suicide, self-harm and survival strategies in contemporary heavy metal music: a cultural and literary analysis," Journal of medical humanities, **37**(1), 1–17, 2016, doi: 10.1007/s10912-014-9274-8.

[23] R.L. Hill, "Is Emo Metal? Gendered Boundaries and New Horizons in the Metal Community," Journal for cultural research, **15**(3), 297–313, 2011, doi: 10.1080/14797585.2011.594586.

[24] K. Schmitt, Exploring dress and behavior of the emo subculture. Master's thesis, Kennesaw State University, 2011.

[25] H.T. Sternudd, A. Johansson, The girl in the corner: Aesthetics of suffering in a digitalized space, in L.G. Guerra, and J.A. Nicdao (Eds.), Narrative of Suffering: Meaning and Experience in a Transcultural Approach (pp. 105–115). Inter-Disciplinary Press, 2014.

[26] B.M. Peters, "Emo gay boys and subculture: Postpunk queer youth and (re) thinking images of masculinity," Journal of LGBT Youth, **7**(2), 129–146, 2010, doi: 10.1080/19361651003799817.

[27] B. Bailey, Emo Music and Youth Culture. in S. Steinberg, P. Parmar, B. Richard (Eds.), Encyclopedia of Contemporary Youth Culture, Greenwood Press, 2005.

[28] C.A. Aberle, Serious is Bad: A Queer Reading of Punk, Midwest Emo, and Connecticut DIY, Honors thesis, Wesleyan University, 2019.

[29] N. Hall, Representations of the Outsider in David Bowie's Glam Period and its Continuation through Punk, Goth, and Emo: Thematic, Aesthetic, and Subcultural Considerations, Master's thesis, University of Ottawa, 2015.

[30] M. Chęć, A. Potemkowski, M. Wąsik, A. Samochowiec, "Parental attitudes and aggression in the Emo subculture," Psychiatria polska, **50**(1), 19–28, 2016, doi: 10.12740/PP/36316.

[31] M.A. Hughes, S.F. Knowles, K. Dhingra, H.L. Nicholson, P.J. Taylor, "This corrosion: A systematic review of the association between alternative subcultures and the risk of self-harm and suicide," British journal of clinical psychology, **57**(4), 491–513, 2018, doi: 10.1111/bjc.12179.

[32] J. Lozon, M. Bensimon, "Music misuse: a review of the personal and collective roles of problem music," Aggression and Violent Behavior, **19**(3), 207–218, 2014, doi: 10.1016/j.avb.2014.04.003.

[33] A.C. North, D.J. Hargreaves, "Problem music and self-harming," Suicide and life-threatening behavior, **36**(5), 582–590, 2006, doi: 10.1521/suli.2006.36.5.582

[34] E. Bodner, M. Bensimon, "Problem music and its different shades over its fans," Psychology of Music, **43**(5), 641–660, 2015, doi: 10.1177/0305735614532000

[35] J. Kneer, D. Rieger, "The memory remains: How heavy metal fans buffer against the fear of death," Psychology of Popular Media Culture, **5**(3), 258, 2016, doi: 10.1037/ppm0000072.

[36] L. Meono, Using music-based interventions with adolescents coping with family conflict or parental divorce: A resource manual, Ph.D. Thesis, Pepperdine University, 2015.

[37] R. Hill, Emo saved my life: challenging the mainstream discourse of mental illness around My Chemical Romance, in Can I Play With Madness? Metal, Dissonance, Madness and Alienation (143–153), Inter-Disciplinary Press, Oxford, 2011.

[38] A.J. van den Tol, "The appeal of sad music: A brief overview of current directions in research on motivations for listening to sad music," The Arts in Psychotherapy, **49**, 44–49, 2016, doi: 10.1016/j.aip.2016.05.008.

[39] A.J. van den Tol, J. Edwards, N.A. Heflick, "Sad music as a means for acceptance-based coping," Musicae Scientiae, **20**(1), 68–83, 2016, doi: 10.1177/1029864915627844.

[40] T. Kelley, L. Simon, Everybody hurts: An essential guide to Emo culture. Harper Collins, 2007.

[41] R.A. Tanjung, The Commodified Emo Subculture In America Through The Used's Music Videos, Ph.D. thesis, Sebelas Maret University, 2011.

[42] E.H. Mereish, H.S. N'cho, C.E. Green, M.M. Jernigan, J.E. Helms, "Discrimination and depressive symptoms among Black American men: Moderated-mediation effects of ethnicity and self-esteem," Behavioral Medicine, **42**(3), 190–196, 2016, doi: 10.1080/08964289.2016.1150804.

[43] T. Yip, "The effects of ethnic/racial discrimination and sleep quality on depressive symptoms and self-esteem trajectories among diverse adolescents," Journal of youth and adolescence, **44**(2), 419–430, 2015, doi: 10.1007/s10964-014-0123-x.

[44] C.D. Presseau, Racial Discrimination and Mental Health for Transracially Adopted Adults: The Roles of Racial Identity and Racial Socialization, Ph.D. thesis, Lehigh University, 2016.

[45] S.M. Schires, N.T. Buchanan, R.M. Lee, M. McGue, W.G. Iacono, S.A. Burt, "Discrimination and ethnic-racial socialization among youth adopted from South Korea into white American families," Child development, **91**(1), e42–

e58, 2020, doi: 10.1111/cdev.13167.
[46] M. Banerjee, J.S. Eccles, Perceived racial discrimination as a context for parenting in African American and European American youth, in H.E. Fitzgerald, D.J. Johnson, D.B. Qin, F.A. Villarruel, and J. Norder (Eds.), Handbook of Children and Prejudice (233–247), Springer, 2019.
[47] L.A. Leslie, J.R. Smith, K.M. Hrapczynski, D. Riley, "Racial socialization in transracial adoptive families: Does it help adolescents deal with discrimination stress?," Family Relations, **62**(1), 72–81, 2013.
[48] M. Svetaz, "Tips to help teen patients deal with discrimination," Family practice management, **23**(4), 44, 2016.
[49] E. Strauss, Early adolescent boys' perceptions of the Emo youth subculture, Ph.D. Thesis, North-West University, 2012.
[50] J. Phua, "Consumption of sports team-related media: Its influence on sports fan identity salience and self-esteem," in Annual Meeting of the International Communication Association **21**, 2008.
[51] Y.C. Rhee, J. Wong, Y. Kim, "Becoming sport fans: Relative deprivation and social identity," International Journal of Business Administration, **8**(1), 118–134, 2017, doi: 10.5430/ijba.v8n1p118.
[52] U. Orth, R.W. Robins, K.F. Widaman, "Life-span development of self-esteem and its effects on important life outcomes," Journal of personality and social psychology, **102**(6), 1271–1288, 2012, doi: 10.1037/a0025558.
[53] P. Arunrangsiwed, C.S. Beck, "Positive and Negative Lights of Fan Culture," Suan Sunandha Rajabhat University Journal of Management Science, **3**(2), 40–58, 2016.
[54] H. Jenkins, Textual poachers: Television fans and participatory culture, Routledge, 2012, ISBN: 9780203114339.
[55] D.L. Wann, J. Hackathorn, M.R. Sherman, "Testing the team identification–social psychological health model: Mediational relationships among team identification, sport fandom, sense of belonging, and meaning in life," Group Dynamics: Theory, Research, and Practice, **21**(2), 94–107, 2017, doi: 10.1037/gdn0000066.
[56] R.E.S. Breen, We Mean It Maaan: Deconstructing Authenticity in the Punk and Metal Discourse, Master's thesis, Wesleyan University, 2017.
[57] M. Corciolani, "How do authenticity dramas develop? An analysis of Afterhours fans' responses to the band's participation in the Sanremo music festival," Marketing Theory, **14**(2), 2014, doi: 10.1177/1470593114521454.
[58] E.G. Armstrong, "Eminem's construction of authenticity," Popular Music and Society, **27**(3), 335–355, 2004, doi: 10.1080/0300776041000173317O.
[59] J.D. Campbell, P.D. Trapnell, S.J. Heine, I.M. Katz, L.F. Lavallee, D.R. Lehman, "Self-concept clarity: Measurement, personality correlates, and cultural boundaries," Journal of personality and social psychology, **70**(1), 141–156, 1996.
[60] J. Wu, D. Watkins, J. Hattie, "Self-concept clarity: A longitudinal study of Hong Kong adolescents," Personality and Individual Differences, **48**(3), 277–282, 2010, doi: 10.1016/j.paid.2009.10.011.
[61] P. Arunrangsiwed, P. Lekyan, "Being Unique does not make an Identity Conflict: A Narcissistic Fan of Mayday Parade," in The 6th International Conference on Management Science, Innovation and Technology, 2019.
[62] B.R. Johnson, G. Duwe, M. Hallett, J. Hays, S.J. Jang, K.R. Kerley, Faith and Service: Pathways to Identity Transformation and Correctional Reform. in K. R. Kerley (Ed.), Finding Freedom in Confinement: The Role of Religion in Prison Life (pp. 3–23), ABC-CLIO, 2018.
[63] N.L. Young, "Identity trans/formations," Annals of the International Communication Association, **31**(1), 250–299, 2007, doi: 10.1080/23808985.2007.11679068.
[64] P. Arunrangsiwed, K. Utapao, P. Bunyapukkna, K. Cheachainart, N. Ounpipat, "Emo Myth: 10-Year Follow-Up Stereotype Test of Emo Teens in 2000s," in International Conference on Innovation, Smart Culture and Well-Beings (ICISW2018), Bangkok, Thailand, 2018.
[65] J. Bronstein, "Like me! Analyzing the 2012 presidential candidates' Facebook pages," Online Information Review, **37**(2), 173-192, 2013, doi: 10.1108/OIR-01-2013-0002.
[66] N.R. Raselekoane, T.J. Mudau, P.P. Tsorai, "Gender differences in cyber-bullying among first-year University of Venda students," Gender and Behaviour, **17**(3), 13848-13857, 2019, ISSN: 1596-9231.
[67] L. Bailey, "Parental Involvement and Student Achievement: A Review of the Literature," Culminating Experience Action Research Projects, **6**, 19-44, 2004, doi: 10.1007/978-3-319-28064-6_2.
[68] J.F. Sowislo, U. Orth, "Does low self-esteem predict depression and anxiety? A meta-analysis of longitudinal studies," Psychological bulletin, **139**(1), 213–240, 2013, doi: 10.1037/a0028931.
[69] K. Bahoric, E. Swaggerty, "Fanfiction: Exploring in-and out-of-school literacy practices," Colorado Reading Journal, **26**, 25–31, 2015.
[70] A.A. Gardner, C.A. Lambert, "Examining the interplay of self-esteem, trait-emotional intelligence, and age with depression across adolescence," Journal of adolescence, **71**, 162–166, 2019, doi: 10.1016/j.adolescence.2019.01.008.
[71] P. Arunrangsiwed, R. Komolsevin, C.S. Beck, "Fan Activity as Tool to Improve Learning Motivation," Suan Sunandha Rajabhat University Journal of Management Science, **4**(2), 16–32, 2017.
[72] V.C. Burke, Email is Alive: How to Communicate with Graduate College Students, Doctoral thesis, UNLV, 2019.

ASTES

Advances in Science, Technology and Engineering Systems Journal Vol. 5, No. 5, 645-651 (2020)

www.astesj.com

Special Issue on Multidisciplinary Innovation in Engineering Science & Technology

ASTESJ

ISSN: 2415-6698

Finding Association Patterns of Disease Co-occurrence by using Closed Association Rule Generation

Panida Songram*, Phattanaphong Chompowiset, Chatklaw Jareanpon

POLAR Lab, Department of Computer Science, Faculty of Informatics, Mahasarakham University, 44150, Thailand

ARTICLE INFO

Article history:
Received: 03 August, 2020
Accepted: 25 September, 2020
Online: 05 October, 2020

Keywords:
Disease co-occurrence
Association disease
Association pattern of disease
Frequent disease
Closed itemset mining
Closed association rule mining

ABSTRACT

This paper proposes a closed association rule generation technique to investigate the association patterns of diseases that are frequent co-occurrence. Diseases records of 5,000 patients are studied to find the association patterns of disease co-occurrence. The CHARM algorithm is adapted to find frequent diseases that can cover all-important patterns with a small number. Then the association patterns of disease co-occurrence are created in a form of association rules from the frequent diseases. The rules represent diseases associated with other diseases. Accuracy and prediction ratio are defined to evaluate the generated association patterns. From the experimental results, the generated association patterns give 79.76% of accuracy and 84.03% of prediction ratio although the number of generated association patterns is small. Moreover, the top-10 association patterns of disease co-occurrence are investigated. Besides, the 5 most frequent diseases are found to deeply study the other related diseases of them. From the investigation, we found that diabetes mellitus, metabolic disorders, and renal failure are highly related to hypertensive diseases with 88.81% of confidence. In addition, we found that influenza and pneumonia, plastic and other anemias are highly related to metabolic disorders.

1. Introduction

The death of people is mostly caused by diseases. Diseases are social and economic problems in the world. A lot of money is paid for treating diseases. If a disease is early detected, people can prevent themselves from the disease. Detecting a disease can be found from other related diseases. Finding association patterns among these diseases is very challenging work in the domains of biology and medicine. The study of the association of diseases not only helps people to understand the relation of diseases but also leads to improvement in clinical manifestation, etiology, pharmacology, and epidemiology. Many techniques were proposed to study the association of diseases, such as network techniques, graph theory, network science, statistical methods, and mathematical modeling. They are studied based on microbes, disease-related genes, microRNAs (miRNA), disease-related metabolic reactions, and electronic medical records. [1].

Association rule mining is a technique that has been widely used in the clinical domain. It is applied to find association patterns of diseases, such as finding the relation of metabolic syndrome and other diseases [2], finding the relation of the disease and medicines [3], and finding the relation of factors and disease [4].

Unlike the previous works, we propose to investigate association patterns of disease co-occurrence based on closed association rule mining that will generate a small number of patterns with coverage of all-important patterns. The association patterns of disease co-occurrence are investigated from electronic medical records in Thailand. First, frequent diseases are generated based on closed itemset mining. Then they are used to generate closed association rules for representing association patterns of disease co-occurrence. Moreover, the sorting method is presented to select the top-k association patterns of disease co-occurrence for investigating diseases that are highly related to each other. Also, the most frequent diseases are found and explored other diseases that are related to them.

The rest of this paper is organized as follows: Section 2 mentions to related works. Section 3 gives the concept of closed association rule mining. Section 4 explains the overall proposed methodology. Section 5 gives the details of the experimental setup and experimental results. Finally, the conclusion is provided in Section 6.

2. Related Work

Finding the association of diseases has been widely studied in the domains of biology and medicine. It is investigated with

*Corresponding Author: Panida Songram, Email:panida.s@msu.ac.th

different datasets and different techniques, such as network techniques, graph theory, network science, statistical methods, and mathematical modeling. For example, in [5] proposed a microbe-based human disease network based on the text mining process. The network is constructed from the microbe-disease association dataset. It is investigated to find relationships between microbes and disease genes, symptoms, chemical fragments, and drugs. Cosine similarity is employed to identify the similarity between two diseases. In [6] proposed a disease-related gene mining method based on a weekly supervised learning model. The method consists of two parts, First, the differentially expressed gene set is screen based on the weakly supervised learning model. Second, a support vector machine is adopted to predict the disease-related genes in the differentially expressed gene set. The method verified the validity and accuracy of the method. In [7] proposed similarity computations to predict the associations between miRNAs and diseases. The similarity among miRNAs is computed based on the sequence and function information of miRNAs. The similarity among diseases is computed based on the semantic and function information of disease. Then the data sources are integrated by using the kernelized Bayesian matrix factorization method to infer potential miRNA-disease associations. The unknown miRNA-disease associations were effectively predicted from the method.

Association rule mining is a popular technique that was exploited in the medical domain. For example, in [2] adopted association rule mining to study metabolic syndrome that is related to other diseases and to understand the strength of association between diabetes mellitus, hypertension, and hyperlipidemia on patient's records in Taiwan. From the study, it was found that diabetes mellitus is related to oral diseases and blear eyes. Patients with metabolic syndrome have a higher connection with liver diseases than patients with diabetes mellitus. In [3] analyzed patient prescriptions to identify the relationship between the disease and medicines that are used to treat the patient's illness. The patient prescription datasets in 2015 and 2016 from two hospitals are collected to find the relationship. First, the top 10 diseases are clustered by the K-means algorithm. Next, the Apriori algorithm is applied to find the relationship between diseases and medicines. In [4] applied association rule mining to detect factors that contribute to heart disease for males and females on the UCI Cleveland dataset. Three algorithms, Apriori, Predictive Apriori, and Tertius, are investigated to identify the factors. From the investigation, females are at higher risk than males to be heart disease.

From previous works, association patterns of diseases are studied based on numerous factors such as genetics, metabolites, microbes, and miRNAs. In the real world, those factors are hard to understand and to access for people who are not in the domains of biology and medicine. Finding association patterns of diseases from a disease dataset is an easy way. The disease dataset can find out from the electronic medical records of patients. Besides, studying association patterns from medical records of patients in each area may get different knowledge. In this paper, association patterns of disease co-occurrence are investigated on a disease dataset that is retrieved from electronic medical records in Thailand. A closed association rule generation technique is proposed to investigate the association patterns of disease co-occurrence.

3. Closed Association Rule Mining

Association rule mining is a popular technique in data mining and has been widely used in many applications with several domains. It discovers the relationship between items in a large dataset. The basic definition of association rule mining can be explained as follows.

Let $I = \{i_1, i_2, \ldots, i_m\}$ be a finite set of items in a database and $D = \{d_1, d_2, \ldots, d_m\}$ be a set of transactions in the database, where each transaction represents a set of items. X and Y are itemsets, where $X, Y \subseteq I$. The support of X is the number of transactions containing X, denoted as $supp(X)$. The length of X is the number of items in X. An association rule r: $X \rightarrow Y$ is a relationship between itemset X and Y, where $X \cap Y = \varnothing$. X is called the antecedent of rule and Y is called the consequent of rule. The support of association rule r is defined as $supp(X \cup Y)$. The confidence of association rule r is defined as $conf(r) = supp(X \cup Y)/supp(X)$. The problem of association rule mining is to find all association rules passing minimum support threshold (*min_supp*) and minimum confidence threshold (*min_conf*).

The process for mining association rules consists of two main steps. The first step is to mine frequent itemsets having support no less than the minimum support threshold. The second step is the generation of association rules. Association rules are generated from frequent itemsets having length≥2. Frequent itemset X having length l will be possibly generated 2^l-2 rules that is the number of subsets of X. For example, X = (ACF). The length of X is 3 and the set of subsets of X is {A, C, F, AC, AF, CF}. Therefore, the number of association rules is $2^3 - 2 = 6$. They are A→CF, C→AF, F→AC, AC→F, AF→C, and CF→A. The confidence value of each rule will be calculated and a rule having confidence no less than the minimum confidence threshold will be selected as an interesting rule.

The important step of association rule mining is frequent itemset mining. Many algorithms were proposed for finding frequent itemsets, such as Apriori [8], FP-Growth [9], Ecat [10], DFIN [11], NegFIN [12]. However, a large number of frequent itemsets may be generated if a low minimum support threshold is given or a large dataset is mined. Then a large number of association rules are also generated. Closed itemset mining was proposed to reduce the number of frequent itemsets. It mines frequent itemset having no superset with the same support. Closed frequent itemsets are sufficient to mine association rules. All non-redundant association rules will be found from closed itemsets and cover the rules generated from frequent itemsets [13]. Thus, many redundant rules can be eliminated. The concept of closed itemset is based on the two following functions f and g as defined in Eq. (1) and Eq. (2).

$$f(T) = \{i \in I \mid \forall t \in T, i \in t\} \quad (1)$$

$$g(X) = \{t \in D \mid \forall i \in I, i \in t\} \quad (2)$$

Function f returns the set of itemsets included in all the transactions in T, where $T \subseteq D$

itemset if $c(X) = f(g(X)) = X$. The set of closed itemsets is defined as Eq. (3), where FI is a set of frequent itemsets.

$$CI = \{X \mid X \in FI \wedge \nexists Y \in FI, X \subset Y \wedge supp(X) = supp(Y)\} \quad (3)$$

For example, if a set of frequent itemset is FI = {(D):2, (FD):2, (B):2, (F):3, (AF):2, (CF):2, (ACF):2, (C):3, (AC):3, (A):3}. The set of closed itemset is CI = {(FD):2, (B):2, (F):3, (ACF):2, (AC):3} because (D):2 is subset of (FD):2 with the same support, so it is not a closed itemset. (AF):2 and (CF):2 are subsets of (ACF):2 with the same support, so they are not closed itemsets. (C):3 and (A):3 are subsets of (AC):3 with the same support, so they are not closed itemsets. In conclusion, closed itemsets are non-redundant patterns and cover all important patterns. Many algorithms were proposed to find closed itemsets, such as CHARM [14], DCI_CLOSED [15], and LCM [16].

4. Proposed Methodology

4.1. Data Collection and Preparation

The dataset is collected from a hospital database, Thailand. It is retrieved from disease records of patients who are over 30 years olds. The dataset consists of ICD-10 codes of 5,000 patients. Each transaction is ICD-10 codes of a patient. To reduce various ICD-10 codes, ICD-10 codes are grouped [17] and represented by numbers according to Table 1. For example, A00-A09 are grouped in the same category and represented as 1. The dataset is represented as number format because it is easily cleaned and computed for finding association patterns. The dataset is cleaned by removing duplicated numbers of each transaction. After the cleaning process, each transaction contains unique numbers that represent the disease occurrence of a patient. Finally, the characteristic of the dataset is shown in Table 2. An example dataset is shown in Figure 1.

Table 1: ICD-10 Category

ID	ICD-10	Meaning
1	A00-A09	Intestinal infectious diseases
2	A15-A19	Tuberculosis
3	A20-A28	Certain zoonotic bacterial diseases
4	A30-A49	Other bacterial diseases
5	A50-A64	Infections with a predominantly sexual mode of transmission
6	A65-A69	Other spirochetal diseases
…	…	…
222	Y90-Y98	Supplementary factors related to causes of morbidity classified elsewhere

Table 2: The Characteristic of the Dataset

Characteristic	Count
The total number of diseases	202
The total number of patients	5,000
The maximal number of diseases that occurs in a patient	56
The minimal number of diseases that occurs in a patient	6
The average number of diseases that occurs in a patient	11

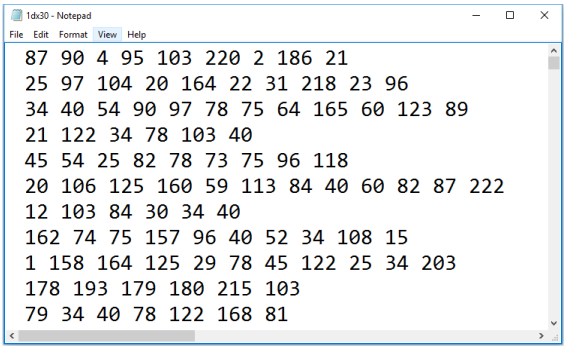


Figure 1: An Example Dataset

4.2. Finding Frequent Diseases

Closed itemset mining is adopted to find frequent diseases because it can generate non-redundant diseases with long disease co-occurrence and coverage of all-important patterns. The diseases with a certain frequency will be selected. The minimum support threshold is used as a filter to select interesting patterns of disease co-occurrence. A disease is considered as an item. All frequent diseases are found based on the CHARM algorithm [14] because CHARM can generate non-redundant frequent diseases with effective of computation time. It uses both itemsets and transaction ids to reduce the search space. Moreover, diffsets and a hash-based approaches are quickly exploited to remove redundant frequent diseases.

The CHARM algorithm firstly constructs an IT-tree that each node is represented by a pair of an itemset and a set of transaction ids. Then it performs a bottom-up depth-first search on the tree to find frequent itemsets. As soon as a frequent itemset X is generated, a set of transaction ids of X is compared with those of other itemsets having the same parent. If the set of transaction ids of X includes the set of transaction ids of the other itemsets, X and the other itemsets are merged to be closed itemsets because they are the same equivalence class. The idea for generating closed itemsets and eliminating non-closed itemsets is based on the following properties.

- If $g(X) = g(Y)$ *then* $c(X) = c(Y) = c(X \cup Y)$. This property implies that X can be replaced by $X \cup Y$ and Y is removed from further consideration.
- If $g(X) \subseteq g(Y)$ *then* $c(X) \neq c(Y)$ *but* $c(X) = c(X \cup Y)$. This property implies that very occurrence of X can be replaced by $X \cup Y$ but Y cannot be removed because it will generate a different closed itemset.
- If $g(X) \supset g(Y)$ *then* $c(X) \neq c(Y)$ *but* $c(Y) = c(X \cup Y)$. This property implies that very occurrence of Y can be replaced by $X \cup Y$ but X cannot be removed because it will generate a different closed itemset.
- If $g(X) \neq g(Y)$, X and Y are not the same equivalence class so that they will be considered to generate closed itemsets.

4.3. Finding Association Patterns of Disease co-occurrence

After finding all frequent diseases, frequent diseases having length no less than two will be used to find the association patters

of disease co-occurrence. An association pattern of disease co-occurrence is in form rule $X \rightarrow Y$, where X and Y are frequent diseases. The minimum confidence threshold is used to filter interesting association patterns. The association patterns of disease co-occurrence are discovered based on the Faster algorithm [8]. The idea of the Faster algorithm is trying to avoid the generation of rules that do not meet the minimum confidence threshold. If a rule $(I - X) \rightarrow X$ passes the minimum confidence threshold then all rules $(I - Y) \rightarrow Y$ will also pass the minimum confidence threshold, where $Y \subset X$. If a rule $(I - Y) \rightarrow Y$ does not pass the minimum confidence threshold, the rule $(I - X) \rightarrow X$ will not pass the minimum confidence threshold. This is because $supp(I - X) \geq supp(I - Y)$ and then the confidence of $(I - X) \rightarrow X$ is not more than the confidence of $(I - Y) \rightarrow Y$. For example, AC→F does not pass the minimum confidence threshold. A→CF and C→AF will not pass the minimum support threshold because of F⊂CF and F⊂AF. Therefore, A→CF and C→AF do not need to generate and compute their confidence.

4.4. Finding Top-k Association Patterns of Disease co-occurrence

After finding all association patterns that pass the minimum confidence threshold, the association patterns will be sorted and selected the top-k association patterns of disease co-occurrence. Given two association patterns, r_i and r_j, r_i has higher precedence than r_j if the following conditions hold:

- $conf(r_i) > conf(r_j)$; or
- if $conf(r_i) = conf(r_j)$, but $supp(r_i) > supp(r_j)$; or
- if $supp(r_i) = supp(r_j)$, but $size(r_i) > size(r_j)$, i.e., length of antecedent of r_i is larger than r_j.

The confidence value is considered as the first priority because it shows how much diseases are related to other diseases. High confidence shows that disease(s) Y is strongly related to disease(s) X. The support value is considered as the second priority because it shows how many patients occur an association pattern of disease co-occurrence. High support shows diseases that occur together in many patients. Next, the length of association pattern is considered as the third priority. The long pattern gives more information than the short one.

4.5. Evaluation Matrix

This paper aims to find association patterns of disease co-occurrence. To evaluate association patterns generated from the proposed method, the dataset is divided into a training set and a testing set by using the 10-fold cross-validation. For each fold, the training set is used to create a predictor that consists of association patterns, represented as rules. The consequent of the rule is considered as predicted diseases. The testing set is used to evaluate the predictor. Two matrixes, prediction ratio and accuracy, are defined to evaluate the effectiveness of the generated association patterns.

A prediction ratio is defined as $Predict = |P|/|A|$, where $|P|$ is the number of predicted diseases correctly and $|A|$ is the total number of the antecedent of rules appears in the testing set. Accuracy is defined as $Accuracy = |C|/|T|$, where $|C|$ the number of matching rules in the testing set and $|T|$ is the number of transactions in the testing set.

5. Performance Evaluation

5.1. Experiment Setup

To investigate the association patterns of disease co-occurrences on electronic medical records, four experiments are conducted. All experiments are implemented by JAVA and use the library in SPMF[18]. The details of the experiments are explained as follows.

The first experiment is conducted to compare the performance of CHARM with a well-known algorithm, call FP-Growth, when generating frequent diseases on the whole dataset with different minimum support thresholds. The minimum support thresholds are set from 1% to 10%. Both algorithms are evaluated by using the number of frequent diseases and computation time.

The second experiment is conducted to investigate the number of association patterns, accuracy, and prediction ratio when using different minimum support thresholds and different minimum confidence thresholds. To reliable results in the medical domain, the minimum support thresholds are set to 10%, 20%, 30%, and the minimum confidence thresholds are set to 60%, 70%, 80%, 90%. The dataset is divided into a training set and a testing set by using the 10-fold cross-validation. The number of association patterns, accuracy, and prediction ratio are reported on average.

The third experiment is conducted to discover the top-10 association patterns of disease co-occurrences from the whole dataset. The minimum support threshold is set to 10%. Then the top-10 association patterns of disease co-occurrences are selected by using the sorting method as explained in section 4.4. The fourth experiment is conducted to find the 5 most frequent diseases in the whole dataset. Then top-3 association patterns are selected to investigate other related diseases of the 5 most frequent diseases.

5.2. Experimental Results

Table 3 reports the number of frequent diseases that are generated on the dataset by using CHARM and FP-Growth. It shows that CHARM gives a smaller number of frequent diseases than FP-Growth when minimum support is set to 1%. Both algorithms generate the same frequent diseases when the minimum support threshold is more than 1%. However, the computation time of CHARM outperforms FP-Growth and almost steady although the minimum support threshold is small as shown in Figure 2. Therefore, the CHARM algorithm is selected for finding frequent diseases in our work.

Table 3: Comparing the Number of Frequent Diseases

min_supp(%)	The number of frequent diseases	
	CHARM	FP-Growth
1	7,015	7,025
2	1,885	1,885
3	861	861
4	502	502
5	327	327

6	216	216
7	158	158
8	128	128
9	105	105
10	81	81

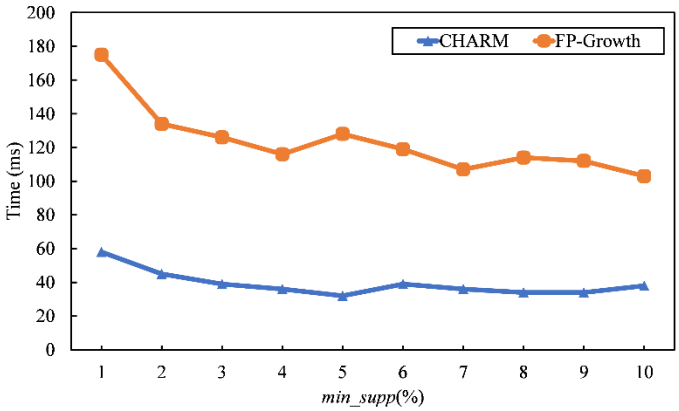


Figure 2: Computation Time of CHARM and FP-Growth

In Table 4, it reports the number of association patterns when different minimum support thresholds and different minimum confidence thresholds are given. The number of association patterns is reduced when the minimum support thresholds and the minimum confidence thresholds are increased. No association pattern is found when minimum confidence threshold is set to 90% so the accuracy and prediction ratio are not evaluated with 90% of minimum support threshold. Table 5 reports the accuracies. It shows that the highest accuracy is 79.76% when minimum support threshold and minimum confidence threshold are set to 10% and 60%, respectively. When minimum support threshold and minimum confidence threshold are increased, the accuracies will be reduced because the number of association patterns is also reduced and then the number of matching patterns in the testing set is small. In Table 6, the most prediction ratios are high although the number of association patterns is very small because the association patterns are created from the most frequent diseases that are strongly related together.

Table 4: The Number of Association Patterns of Disease Co-occurrence

min_supp(%) \ *min_conf(%)*	60	70	80	90
10	59	38	19	0
20	12	9	3	0
30	4	3	1	0

Table 5: Accuracy (%)

min_supp(%) \ *min_conf(%)*	60	70	80
10	79.76	74.32	56.82
20	71.42	71.20	41.26
30	59.23	58.08	34.03

Table 6: Prediction Ratio (%)

min_supp(%) \ *min_conf(%)*	60	70	80
10	81.04	80.03	82.56
20	77.53	82.77	79.30
30	69.70	84.03	80.58

Table 7: Top-10 Association Patterns of Disease Co-occurrence

Rank	Association pattern	No. of patients	Confidence (%)
1	Diabetes mellitus, Metabolic disorders, Renal failure ==> Hypertensive diseases	683	88.81
2	Diabetes mellitus, Renal failure ==> Hypertensive diseases	800	87.62
3	Hypertensive diseases, Influenza and pneumonia ==> Metabolic disorders	526	86.22
4	Diabetes mellitus, Hypertensive diseases, Renal failure ==> Metabolic disorders	683	85.37
5	Aplastic and other anemias, Diabetes mellitus ==> Metabolic disorders	584	85.25
6	Aplastic and other anemias, Hypertensive diseases, Renal failure ==> Metabolic disorders	504	85.13
7	Aplastic and other anemias, Renal failure ==> Metabolic disorders	640	84.76
8	Diabetes mellitus, Renal failure ==> Metabolic disorders	769	84.22
9	Diabetes mellitus, General symptoms and signs ==> Metabolic disorders	555	84.09
10	Aplastic and other anemias, Diabetes mellitus ==> Hypertensive diseases	574	83.79

Table 8: The 5 Most Frequent Diseases and Related Diseases

Disease	No. of patients	Association pattern
Metabolic disorders	3,288	1. Hypertensive diseases, Influenza and pneumonia ==> Metabolic disorders (support = 526, confidence = 86.22%) 2. Diabetes mellitus, Hypertensive diseases, Renal failure ==> Metabolic disorders (support = 683, confidence = 85.37%) 3. Aplastic and other anemias, Diabetes mellitus ==> Metabolic disorders (support = 584, confidence = 85.25%)
Hypertensive diseases	2,599	1. Diabetes mellitus, Metabolic disorders, Renal failure ==> Hypertensive diseases (support = 683, confidence = 88.81%) 2. Diabetes mellitus, Renal failure ==> Hypertensive diseases (support = 800, confidence = 87.62%) 3. Aplastic and other anemias, Diabetes mellitus ==> Hypertensive diseases (support = 574, confidence = 83.79%)
Diabetes mellitus	1,953	1. Metabolic disorders, Hypertensive diseases, Renal failure ==> Diabetes mellitus (support = 683, confidence = 74.72%) 2. Hypertensive diseases, Renal failure ==> Diabetes mellitus (support = 800, confidence = 71.49%) 3. Metabolic disorders, Renal failure ==> Diabetes mellitus (support = 769, confidence = 63.92%)
General symptoms and signs	1,734	1. Other diseases of the respiratory system ==> General symptoms and signs (support = 321, confidence =55.15%) 2. Metabolic disorders, Other diseases of the respiratory system ==> General symptoms and signs (support = 274, confidence =57.44%) 3. Influenza and pneumonia, Renal failure ==> General symptoms and signs (support = 252, confidence = 52.39%)
Renal failure	1,500	1. Aplastic and other anemias, Metabolic disorders, Hypertensive diseases ==> Renal failure (support = 504, confidence = 71.59%) 2. Aplastic and other anemias, Hypertensive diseases ==> Renal failure (support = 592, confidence = 68.91% 3. Metabolic disorders ==> Renal failure (support = 640, confidence = 60.09%)

Table 7 shows the top-10 association patterns of disease co-occurrence. From the top-10 association patterns of disease co-occurrence, most of top-10 association patterns are similar. For example, the first rank shows that if a patient has diabetes mellitus, metabolic disorders, and renal failure, then the patient has a chance to be hypertensive diseases with 88.81% of confidence. The second rank shows that if a patient has diabetes mellitus and renal failure, then the patient has a chance to be hypertensive diseases with 87.62% of confidence. We can conclude that diabetes mellitus, metabolic disorders, renal failure and hypertensive diseases are highly related together. In addition, we found that influenza and pneumonia, plastic and other anemias are highly related to metabolic disorders.

Table 8 shows the 5 most frequent diseases and other related diseases that are represented in association patterns. The 5 most frequent diseases are metabolic disorders, hypertensive diseases, diabetes mellitus, general symptoms and signs, and renal failure. The most frequent disease is metabolic disorders. 3,288 patients or 65.76% of the dataset have metabolic disorders. Hypertensive diseases, influenza and pneumonia, diabetes mellitus, renal failure, and aplastic and other anemias are highly related to metabolic disorders with more than 85% of confidence.

6. Conclusion

In this paper, we proposed a technique to find the association patterns of disease co-occurrence based on closed association rule mining. Closed itemset mining is applied to find frequent diseases. Then the frequent diseases are used to create association patterns of disease co-occurrence. The association patterns are sorted to select top-10 association patterns of co-occurrence. Moreover, the 5 most frequent diseases and other related diseases are discovered. From experiment results, they show that the association patterns of disease co-occurrence give high accuracy if the number of association patterns is large. The prediction ratio is high although the number of association patterns is very small because the association patterns are created from the most frequent diseases that are metabolic disorders, hypertensive diseases, diabetes mellitus, and renal failure. From the investigation of association patterns, we found that diabetes mellitus, metabolic disorders, and renal failure and hypertensive diseases are highly related together. Moreover, influenza and pneumonia, plastic and other anemias are highly related to metabolic disorders.

Acknowledgment

This research project was financially supported by Faculty of Informatics, Mahasarakham University 2020. We would like to thank Mahasarakham hospital for the dataset.

References

[1] Z. Batool, M. Usman, K. Saleem, M. Abdullah-Al-Wadud, F.-e. Amin, and A. Al-Eliwi, "Disease–disease association using network modeling: challenges and opportunities," Journal of Medical Imaging and Health Informatics, **8**, 627-638, 2018. https://doi.org/10.1166/jmihi.2018.2342

[2] C. Chan, C. Chen, and B. Liu, "Discovery of association rules in metabolic syndrome related diseases.", in IEEE International Joint Conference on Neural Networks (IEEE World Congress on Computational Intelligence), 856-862, 1-8 June 2008. https://doi.org/10.1109/IJCNN.2008.4633898
[3] M. Harahap, A. M. Husein, S. Aisyah, F. R. Lubis, and B. A. Wijaya, "Mining association rule based on the diseases population for recommendation of medicine need," Journal of Physics: Conference Series, **1007**, 1-11, 2018. https://doi.org/10.1088/1742-6596/1007/1/012017
[4] I. T. T. K. S. Nahar Jesmin, and Y.-P. Phoebe Chen, "Association rule mining to detect factors which contribute to heart disease in males and females," Expert Systems with Applications, **40**(4), 1086 - 1093, 2013. https://doi.org/10.1016/j.eswa.2012.08.028
[5] W. Ma, L. Zhang, P. Zeng, C. Huang, J. Li, B. Geng, J. Yang, W. Kong, X. Zhou, and Q. Cui, "An analysis of human microbe-disease associations," Briefings in bioinformatics, **18**, 85-97, 2017. https://doi.org/10.1093/bib/bbw005
[6] H. Zhang, X. Huo, X. Guo, X. Su, X. Quan, and C. Jin, "A disease-related gene mining method based on weakly supervised learning model,", BMC Bioinformatics , **20**, 169-174, 2019. https://doi.org/10.1186/s12859-019-3078-9
[7] W. Lan, J. Wang, M. Li, J. Liu, F. Wu, and Y. Pan, "Predicting microRNA-disease associations based on improved microRNA and disease similarities," IEEE/ACM Transactions on Computational Biology and Bioinformatics, Vol. 15, No. 6, 1774-1782, 2018. https://doi.org/10.1109/TCBB.2016.2586190
[8] R. Agrawal, and R. Srikant, "Fast algorithms for mining association rules," in 20th International Conference Very Large Data Bases VLDB, **1215**, 487-489, 2000. https://doi.org/10.1007/BF0294884
[9] J. Han, J. Pei, Y. Yin, and R. Mao, "Mining frequent patterns without candidate generation: a frequent-pattern tree approach," Data Mining and Knowledge Discovery, **8**(1), 53-87, 2004. https://doi.org/10.1023/B:DAMI.0000005258.31418.83
[10] M. J. Zaki, "Scalable algorithms for association mining," IEEE Transactions on Knowledge and Data Engineering, **12**(3), 372-390, 2000. https://doi.org/10.1109/69.846291
[11] Z.-H. Deng, "DiffNodesets: An efficient structure for fast mining frequent itemsets," Applied Soft Computing, **41**, 214-223, 2016. https://doi.org/10.1016/j.asoc.2016.01.010
[12] N. Aryabarzan, B. Minaei-Bidgoli, and M. Teshnehlab, "negFIN: An efficient algorithm for fast mining frequent itemsets," Expert Systems with Applications, **105**, 129-143, 2018. https://doi.org/10.1016/j.eswa.2018.03.041
[13] M. Zaki, "Closed itemset mining and non-redundant association rule mining," Encyclopedia of Database Systems, 365-368, 2009. https://doi.org/10.1007/978-0-387-39940-9_66
[14] M. Zaki, and C.-J. Hsiao, "CHARM: An efficient algorithm for Closed Itemset Mining," in the 2002 SIAM International Conference on Data Mining, 457-473, 2002. https://doi.org/10.1137/1.9781611972726.27
[15] C. Lucchese, S. Orlando and R. Perego, "Fast and memory efficient mining of frequent closed itemsets," IEEE Transactions on Knowledge and Data Engineering, **18**(1), 21-36, 2006. https://doi.org/10.1109/ TKDE.2006.10
[16] T. Uno, M. Kiyomi, and H. Arimura, "LCM ver. 2: Efficient mining algorithms for frequent/closed/maximal itemsets," in Proceeding of IEEE ICDM Workshop on Frequent Itemset Mining Implementations, Brighton, UK, November 1, 1-11, 2004. https://doi.org/10.1.1.108.155
[17] W. H. Organization, "ICD-10 Version:2019," International Statistical Classification of Diseases and Related Health Problems, 2019.
[18] P. Fournier-Viger, J. C.-W. Lin, A. Gomariz, T. Gueniche, A. Soltani, Z. Deng, and H. T. Lam, "The SPMF Open-Source Data Mining Library Version 2," Machine Learning and Knowledge Discovery in Databases, Lecture Notes in Computer Science, vol. 9853, 36-40, 2016. https://doi.org/10.1007/978-3-319-46131-1_8

ASTES

Advances in Science, Technology and Engineering Systems Journal Vol. 5, No. 5, 652-659 (2020)

www.astesj.com

Special Issue on Innovative Research in Applied Science, Engineering and Technology

ASTESJ

ISSN: 2415-6698

Investment of Classic Deep CNNs and SVM for Classifying Remote Sensing Images

Khalid A. AlAfandy[*,1], Hicham Omara[2], Mohamed Lazaar[3], Mohammed Al Achhab[1]

[1]*ENSA, Abdelmalek Essaadi University, Tetouan, 93002, Morocco*

[2]*FS, Abdelmalek Essaadi University, Tetouan, 93002, Morocco*

[3]*ENSIAS, Mohammed V University in Rabat, 10000, Morocco*

ARTICLE INFO

Article history:
Received: 08 August, 2020
Accepted: 21 September, 2020
Online: 05 October, 2020

Keywords:
Remote Sensing Images
ResNet
VGG
DenseNet
CNN
SVM
Deep Learning
Machine Learning

ABSTRACT

Feature extraction is an important process in image classification for achieving an efficient accuracy for the classification learning models. One of these methods is using the convolution neural networks. The use of the trained classic deep convolution neural networks as features extraction gives a considerable results in the remote sensing images classification models. So, this paper proposes three classification approaches using the support vector machine where based on the use of the ImageNet pre-trained weights classic deep convolution neural networks as features extraction from the remote sensing images. There are three convolution models that used in this paper; the Densenet 169, the VGG 16, and the ResNet 50 models. A comparative study is done by extract features using the outputs of the mentioned ImageNet pre-trained weights convolution models after transfer learning, and then use these extracted features as input features for the support vector machine classifier. The used datasets in this paper are the UC Merced land use dataset and the SIRI-WHU dataset. The comparison is based on calculating the overall accuracy to assess the classification model performance.

1. Introduction

With the growth of communication especially using satellites and cameras, the remote sensing images was appeared with the importance of processing and dealing with this type of images (remote sensing images). One of these substantial image processing is classification which done using machine learning technology. Machine learning is one of the artificial intelligence branches that based on training computers using real data which result that computers will have good estimations as an expert human for the same type of data [1]. Deep learning is a branch of machine learning that counts on the Artificial Neural Networks (ANNs) which can be utilized in the remote sensing image classification [2]. In the recent years, which the latest satellites versions and its updated cameras with high spectral and spatial resolution are released, the very high resolution (VHR) remote sensing images are appeared. As logical results, the VHR remote sensing images have redundancy pixels that can cause an over-fitting problem through training process with using the ordinary machine learning or ordinary deep learning in classification. So it must optimize the ANNs and extract convenient features from remote sensing images as a preprocessing before training [3]. The convolution neural networks (CNNs) are derived from the ANNs who haven't fully connected layers as the ANNs layers; it have an excited rapid advance in computer vision [4]. It is based on some blocks can enforced on images as filters and then extracting a convolution object features from the input images which solving many of computer vision problems, one of these problems is classification [5]. The need of dealing with the huge data, that be contained in the VHR remote sensing images, produced the need of specific CNNs deep networks architectures that can generate an elevated accuracy in the classification problems. So, the classic networks are appeared. Many of classic networks are mentioned by researchers in their research papers. In this paper we use three widely used classic networks as features extraction in our proposed approaches. These classic networks are; the DenseNet 196, the VGG 16, and the ResNet 50 models. There are many researchers used these networks in their researches that related to the remote sensing images classification. In [6], authors proposed a new model to improve the classification accuracy using the DenseNet model. In [7], authors built dual channel CNNs for the remote sensing images using the DenseNet as features extraction. In [8],

[*]Corresponding Author: Khalid A. AlAfandy, +212635549566, khalid_yuosif@yahoo.com

authors built small number of convolutional kernels using dense connections to achieve large number of reusable feature maps. It was lead them to propose a convolutional network based on the DenseNet for the remote sensing images classification. In [9], authors used the VGG and the ResNet models to propose the RS-VGG classifier for classifying the remote sensing images. In [10], authors were built a combination between CNNs algorithms outputs, the VGG model is one of these algorithms, so a representation of the VHR remote sensing images understanding were established by their proposed method. In [11], authors used the remote sensing images classification to distinguish the airplanes by using the pre-trained VGG model. In [12], authors built a classifier model that classifying the high spatial resolution remote sensing images by using a fully convolution network that based on the VGG model. In [13], authors proposed the use of the ResNet model to extract the VHR remote sensing images features, then concatenated with low level features to generate a more accurate model using the SVM. In [14], authors used the ResNet to extract the 3-D features by transfer learning. They proposed a classification method for the hyper-spectral remote sensing images. In [15], authors proposed a method for classifying forest tree species using high resolution RGB color images that captured by a simple grade camera mounted on an unmanned aerial vehicle (UAV) platform. They used the ResNet in their proposed. In [16], authors proposed aircraft detection methods that based on the deep ResNet and super vector coding. In [17], authors combined edge and texture maps to propose a remote sensing image usability assessment method based on the ResNet. In [18], authors presented a comparative study that discussed the difference between the using of the SVM and the deep learning in classifying the remote sensing images. In [19], authors proposed a remote sensing image classification method that based on the SVM and sequential classifier. In [20], authors proposed a remote sensing images classifier using the genatic algorithm (GA) and the SVM.

The problem that attended by this paper is the difficulty of reaching a high accuracy assessment in the VHR remote sensing images classification models. Many researchers proposed solutions for this problem in their researches but they depend on the deep learning only or the machine learning only. Few of them are proposed hybrid classification techniques that consist of combination of the deep learning and the machine learning such as [13] and [20]. The deep learning and the machine learning combination can lead to considerable results.

The aim of this paper is to propose a combination of a classic network and the SVM to build a novel remote sensing images classifier. In this paper, the desired classic networks that combined with the SVM classifier are the DenseNet 169, The VGG16, and the ResNet 50 models. We used the ImageNet pre-trained weights with these mentioned models, transfer learning, and then extract features. These extracted features are considered as input features for the SVM classifier which trained to achieve the desired performance classification models. A comparative study is done for the use of the mentioned three convolution models as features extraction that combined with the SVM classifier, as proposed in this paper, to determine the performance of using each model. This comparison is based on calculating the overall accuracy (OA) to determine the performance of each model as a features extraction. There are two used datasets in this study; the UC Merced land use dataset and the SIRI-WHU dataset.

The rest of this paper is organized as follow. Section 2 gives the methods. The experimental results and setup are shown in section 3. Section 4 presents the conclusions followed by the most relevant references.

2. The Methods

In this section the proposed models will explained with its structures. The classic networks that used in these proposals and the SVM will illustrate in brief as a literature review, ending with how to measure the learning model performance.

2.1. The Proposed Models

The features extraction from the remote sensing images is provided an important basis in the remote sensing images analysis. So, in this paper the classic networks outputs can considered as the features that extracted from the remote sensing images. Where the train of a new model of the CNNs requires large amount of data, so in these three models, we used the ImageNet pre-trained weights, transfer learning, and then extract the desired features, then use these features as input features in training the SVM classifier. In the DenseNet 169 model, we transfer learning to the last hidden layer, before the output layer, that had 1664 neurons. Its outputs considered as the input features for the SVM classifier. In the VGG 16 model, we transfer learning to the last hidden layer, before the output layer, that had 4096 neurons. Its outputs considered as the input features for the SVM classifier. In the ResNet 50 model, we transfer learning to the last hidden layer, before the output layer, that had 2048 neurons. Its outputs considered as the input features for the SVM classifier.

2.2. The Convolution Neural Networks (CNNs)

The CNNs are possessed from the ANNs with exclusion that it is not fully connected layers [21]. The CNNs considered as the magic solution for much computer vision problems. The CNNs depend on some of filters that reduce the image height and width and increase the number of channels, then processing the output with full connected (FC) neural network layers [21, 22]. Figure 1 shows one of the CNNs model structures [22].

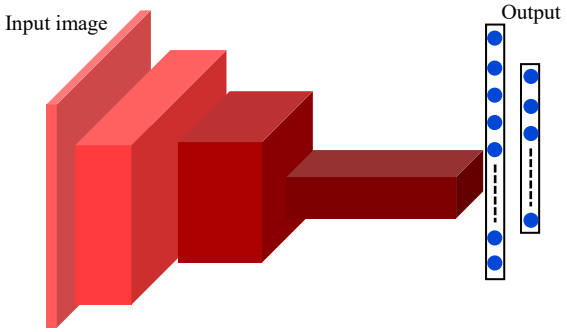


Figure 1: One of the CNNs model structures [23]

2.3. The DenseNet Model

In 2017, the DenseNets was proposed in the CVPR 2017 conference (Best Paper Award) [23]. The start point was from endeavored to construct a deeper convolution network that contains shorter connections between its layers close to the input and those close to the output, this deep convolution network can be more accurate and efficient to train. It is different from the

ResNet which has skip-connections that bypass the nonlinear transformation, the DenseNet add a direct connection from any layer to any subsequent layer. So the l^{th} layer receives the feature-maps of all former layers x_0 to x_{l-1} as (1) [23].

$$x_l = H_l([x_0, x_1, \dots, x_{l-1}]) \quad (1)$$

where $[x_0, x_1, \dots, x_{l-1}]$ refers to the spectrum of the feature-map produced in the layers $0, 1, 2, \dots, l-1$. Figure 2 shows the 5-layers dense block architecture. Table 1 shows the DenseNet 169 model architecture with the ImageNet pre-trained weights [23].

Table 1: the DenseNet 169 model architectures for ImageNet [23]

Layers	Output Size	DenseNet 169
Convolution	112×112	7×7 conv, stride 2
Pooling	56×56	3×3 max pool, stride 2
Dense Block (1)	56×56	$\begin{bmatrix} 1\times1 \text{ conv} \\ 3\times3 \text{ conv} \end{bmatrix} \times 6$
Transition Layer (1)	56×56	1×1 conv
	28×28	2×2 average pool, stride 2
Dense Block (2)	28×28	$\begin{bmatrix} 1\times1 \text{ conv} \\ 3\times3 \text{ conv} \end{bmatrix} \times 12$
Transition Layer (2)	28×28	1×1 conv
	14×14	2×2 average pool, stride 2
Dense Block (3)	14×14	$\begin{bmatrix} 1\times1 \text{ conv} \\ 3\times3 \text{ conv} \end{bmatrix} \times 32$
Transition Layer (3)	14×14	1×1 conv
	7×7	2×2 average pool, stride 2
Dense Block (4)	7×7	$\begin{bmatrix} 1\times1 \text{ conv} \\ 3\times3 \text{ conv} \end{bmatrix} \times 32$
Classification Layer	1×1	7×7 global average pool
	1000	1000D fully-connected, softmax

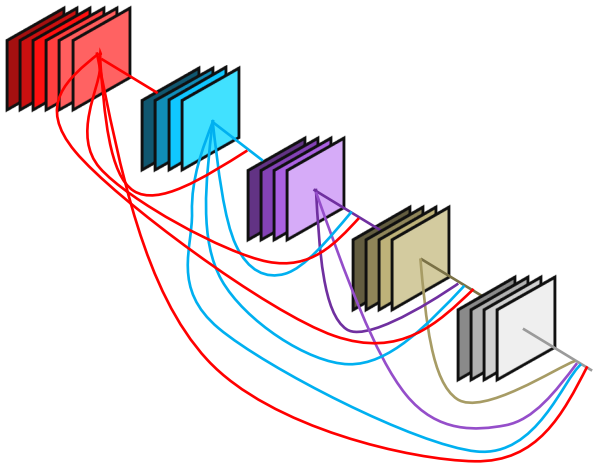


Figure 2: The 5 layers Dense block architecture [23]

2.4. The VGG Model

In 2015, the VGG network was proposed in the ICLR 2015 conference [24]. The start with inspected the effect of the convolution network depth on its accuracy with using the large-scale images. Through they rectified the deeper networks architecture using (3×3) convolution filters, they showed that an expressive growth on the prior-art configurations can be achieved by pushed the depth to 16-19 weight layers. The VGG model is a deeper convolution network that trained on the ImageNet dataset. Table 2 shows the VGG 16 model architecture with the ImageNet pre-trained weights [24].

Table 2: The VGG 16 model architectures for ImageNet [24]

Block	Layers	Output Size	VGG 16
Input		224×224×3	
Block 1	Convolution	224×224×64	3×3 conv 64, stride 1
	Convolution	224×224×64	3×3 conv 64, stride 1
	Pooling	112×112×64	2×2 max pool, stride 2
Block 2	Convolution	112×112×128	3×3 conv 128, stride 1
	Convolution	112×112×128	3×3 conv 128, stride 1
	Pooling	56×56×128	2×2 max pool, stride 2
Block 3	Convolution	56×56×256	3×3 conv 256, stride 1
	Convolution	56×56×256	3×3 conv 256, stride 1
	Convolution	56×56×256	3×3 conv 256, stride 1
	Pooling	28×28×256	2×2 max pool, stride 2
Block 4	Convolution	28×28×512	3×3 conv 512, stride 1
	Convolution	28×28×512	3×3 conv 512, stride 1
	Convolution	28×28×512	3×3 conv 512, stride 1
	Pooling	14×14×512	2×2 max pool, stride 2
Block 5	Convolution	14×14×512	3×3 conv 512, stride 1
	Convolution	14×14×512	3×3 conv 512, stride 1
	Convolution	14×14×512	3×3 conv 512, stride 1
	Pooling	7×7×512	2×2 max pool, stride 2
FC		4096	
FC		4096	
Output		1000, softmax	

The input images of this network is $(224 \times 244 \times 3)$. This network consists of five convolution blocks, each block containing convolution layers and pooling layer, then ending with two FC hidden layers (each layer has 4096 neurons), then ending with the output layer with softmax activation (1000 classes) [24].

2.5. The ResNet Model

In 2016, the ResNet was proposed in the CVPR 2016 conference [25]. They concerted the degradation problem by presenting a deep residual learning framework. Instead of intuiting, each few stacked layers directly fit a desired underlying mapping. The ResNet is based on skip connections between deep layers. These skip connections can skipping one or more non-linear transformation layers. The outputs of these connections are added to the outputs of the network stacked layers as (2) [25].

$$H(x) = F(x) + x \quad (2)$$

where H(x) is the final block output, x is the output of the connected layer, and F(x) is the output of the stacked networks layer in the same block. Figure 3 shows the ResNet one building block and tables 3 shows the ResNet 50 model architecture for the ImageNet [25].

Table 3: the ResNet 50 model architectures for ImageNet [25]

Layers	Output Size	ResNet 50
Conv 1	112×112	7×7 conv 64, stride 2
Conv 2_x	56×56	3×3 max pool, stride 2
		$\begin{bmatrix} 1\times1 \text{ Conv } 64 \\ 3\times3 \text{ Conve } 64 \\ 1\times1 \text{ Conv } 256 \end{bmatrix} \times 3$
Conv 3_x	28×28	$\begin{bmatrix} 1\times1 \text{ Conv } 128 \\ 3\times3 \text{ Conv } 128 \\ 1\times1 \text{ Conv } 512 \end{bmatrix} \times 4$
Conv 4_x	14×14	$\begin{bmatrix} 1\times1 \text{ Conv } 256 \\ 3\times3 \text{ Conve } 256 \\ 1\times1 \text{ Conv } 1024 \end{bmatrix} \times 6$
Conv 5_x	7×7	$\begin{bmatrix} 1\times1 \text{ Conv } 512 \\ 3\times3 \text{ Conve } 512 \\ 1\times1 \text{ Conv } 2048 \end{bmatrix} \times 3$
Classification Layer	1×1	7×7 global average pool
	1000	1000D fully-connected, softmax

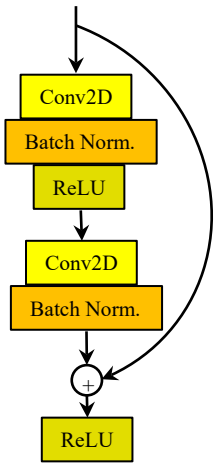


Figure 3: The ResNet building block[25]

2.6. The Support Vector Machine (SVM)

The SVM is a machine learning algorithm can act as a classifier or regression. It is based on small sample statistic theory that establishes optimal hyper-planes from the training data. These hyper-plans separate the different classes by building margins between classes. Maximizing these margins between classes, specially the nearest classes, on both sides of hyper-planes is the target for achieving the optimal SVM classifier [26, 27]. Figure 4 shows the possible and the optimal hyper-planes in the SVM model [26, 27].

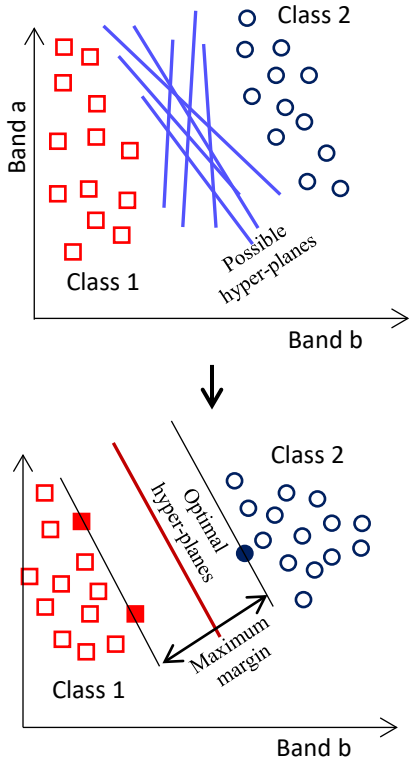


Figure 4: The possible and the optimal hyper-planes in the SVM model [26, 27]

2.7. The Performance Assessment

There are many matrices for gauge the performance of the learning models. One of them is the overall accuracy (OA). The OA is the main classification accuracy assessment [28]. It is measure the percentage ratio between the corrected estimation test data objects and all the test data objects in the used dataset. The OA is calculated using (3) [28, 29].

$$OA = \frac{Number\ of\ Correctly\ Estimations}{Total\ number\ of\ Test\ Data\ Objects} \times 100 \quad (3)$$

3. Experimental Results and Setup

This section will illustrate the experiments setup of the proposed algorithms, and then presents a comparative study for using each convolution model in our proposed. This comparison is based on calculating the OA for each model. The UC Merced land use dataset and the SIRI-WHU dataset are the used datasets. The details of these datasets will introduce in this section and then the experiments setup and results.

3.1. The UC Merced Land Use Dataset

The UC Merced Land use dataset is a collection of remote sensing images which has been prepared in 2010 by the University of California, Merced [30]. It is consists of 2100 remote sensing images divided into 21 classes with 100 images per each class. The

images were manually extracted from large images from the USGS National Map Urban Area Imagery collection for various urban areas around the USA. All images in this dataset are Geo-tiff RGB images with 256×256 pixels resolution and 1 square foot (0.0929 square meters) spatial resolution [30]. Figure 5 shows image examples from the 21 classes in the UC Merced land use dataset [30].



Figure 5: Image examples from the 21 classes in the UC Merced land use dataset [30]

3.2. The SIRI-WHU Dataset

The SIRI-WHU dataset is a collection of remote sensing images which the authors of [31] used this dataset in their classification problem research in 2016. This dataset consists of two versions that must complete each other. The total images in this dataset are 2400 remote sensing images divided into 12 classes with 200 images per each class. The images were extracted from Google Earth (Google inc.) and mainly cover urban areas in China. All images in this dataset are Geo-tiff RGB images with 200×200 pixels resolution and 2 square meters (21.53 square foot) spatial resolution [31]. Figure 6 shows image examples from the 12 classes in the SIRI-WHU dataset [31].

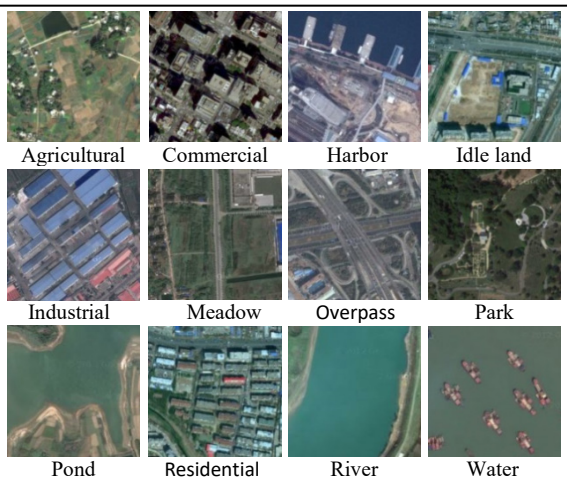
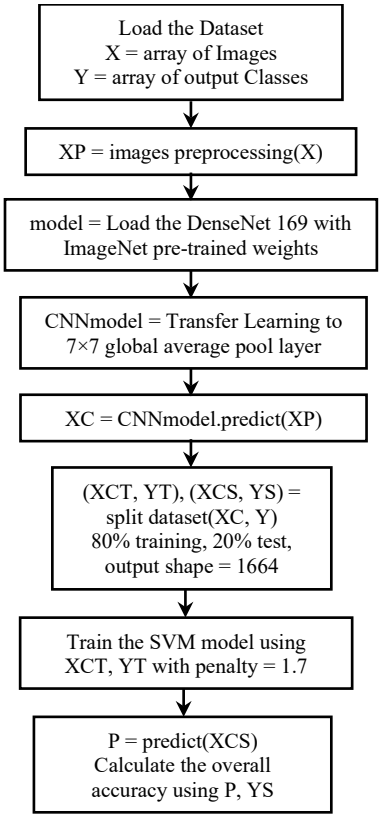


Figure 6: Image examples from the 12 classes in the SIRI-WHU dataset [31].

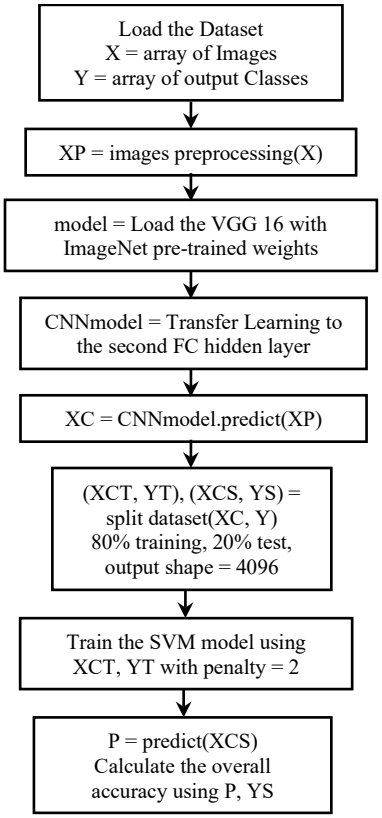
3.3. The Experimental Setup

All tests were performed using Google-Colab. The Google-Colab is a free cloud service hosted by Google inc. to encourage machine learning and artificial intelligence researches [32]. It is acts as a virtual machine (VM) that using 2-cores Xeon CPU with 2.3 GHz, GPU Tesla K80 with 12 GB GPU memory, 13 GB RAM, and 33GB HDD with Python 3.3.9. The maximum lifetime of this VM is 12 hours and it will be idled after 90 minutes time out [33]. Performing tests has been done by connecting to this VM online through ADSL internet line with 4Mbps communication speed. This connection was done using an Intel® coreTMi5 CPU M450 @2.4GHz with 6 GB RAM and running Windows 7 64-bit operating system. This work is limited by used the ImageNet pre-trained weights because the train of new convolution models needs a huge amount of data and more sophisticated hardware, this is unlike the lot of needed time consumed for this training process. The other limitation is that the input images shape is mustn't less than 200×200×3 and not greater than 300×300×3 because of the limitations of the pre-trained classic networks. The preprocessing step according to each network requirements is necessary to get efficient results; it must be as done on ImageNet dataset through these models were trained and produced the ImageNet pre-trained weights. The ImageNet pre-trained weights classic networks that used in this paper have input shape (224, 224, 3) and output layer with 1000 neurons according to the ImageNet classes (1000 classes) [34, 35]. So, it must perform transfer learning as stated in section 2.1. The used datasets were divided into 80% training set and 20% testing set before training the SVM model. It is must be notice that the SVM penalty value were determined by iterations and self-intuition. To extract the convolution features, the normalization preprocessing must done before extract features using the DenseNet 169 model, then using these features as input features to train the SVM model with penalty = 1.7. Where the BGR mode convertion is the desired preprocessing before extract features using the VGG 16 and the ResNet 50 models, then using its outputs as input features to train the SVM model with penalty = 2 for the VGG 16 extracted features and penalty =20 for the ResNet 50 extracted features. Figure 7 shows the flow charts of the proposed algorithms in this paper; figure 7.a. for using the DenseNet 169 model as features extraction, figure 7.b. for using the VGG 16 model as features extraction, and figure 7.c. for using the ResNet

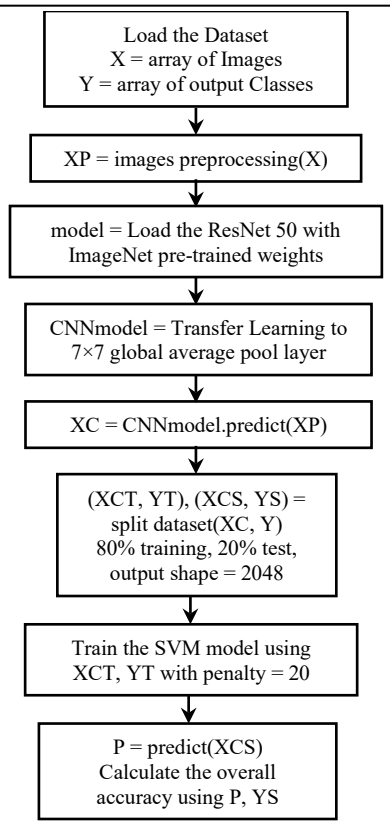
50 model as features extraction, and then training the SVM classifier.



a: Using the DenseNet 169 model



b: Using the VGG 16 model



c: Using the ResNet 50 model

7: The flow charts of the proposed algorithms in this paper

3.4. The Experimental Results

This section presents the results of the proposed algorithms with the used datasets in this paper. Through the training process we used the training data (80% from the used dataset) and then calculate the OA using the predictions of the test data (20% from the used dataset) to assess the performance of each model. Table 4 and figure 8 show the OA for the using of each model to extract features that act as the input features to train the SVM classifier using the both datasets.

Table 4: The OA for the use of the convolution models with the SVM classifier using the both datasets

	The DenseNet-SVM	The VGG-SVM	The ResNet-SVM
The UC Merced land use Dataset	0.902	0.881	0.926
The SIRI-WHU Dataset	0.94	0.942	0.958

As shown from these results, the ResNet–SVM model had the higher OA in this study where the VGG–SVM model had the lowest OA. In the other hand the DenseNet–SVM model had higher OA than the VGG–SVM model when using the UC Merced land use dataset and had very little lower OA than the VGG–SVM when using the SIRI-WHU dataset. The use of the SIRI-WHU dataset had higher OA than the use of the UC Merced land use dataset. These results illustrated that the OA had an opposite relation with the dataset image resolution and the dataset number

of classes, so the use of the SIRI-WHU dataset which has 12 classes, image resolution 200×200 pixels, and spatial resolution 2 square meters gave higher OA than the use of the UC Merced land use dataset which has 21 classes, image resolution 256×256 pixels, and spatial resolution 0.0929 square meters (1 square feet). Extracting features using the deeper convolution networks gave considerable accuracy but the connections between layers may have another influence. The VGG–SVM model, that has deeper network without any layers connections, gave a good OA so it had an efficient result. In the other hand the ResNet–SVM model, that has skip layers connections, and the DenseNet–SVM, that has full layers connections, gave higher OA but still the ResNet–SVM gave the highest OA in this comparison. If keeping in mind the penalty values that used in training the SVM classifier using the three models as features extraction, we saw that the VGG–SVM and the DenseNet–SVM had normal penalty to give its OA in this comparison, where the ResNet–SVM had a high penalty value and given the highest OA in this comparison. The ResNets are based on the skip layers connections so the layer connections can raise the classification accuracy. The DenseNets may have more connections but still the use of the ResNets has the higher OA. As a total the deeper convolution networks may give better accuracy but the deeper networks that have layers connections may give the more better accuracy. The convolution models that have skip connections can give the better OA than the convolution models that have full layers connections. A high penalty value is needed for training the SVM models when using input features that extracted from the skip connection convolution models. For the SVM classifiers, extracting features from the high resolution remote sensing images are preferred with the use of deep convolution models that have layers connections where extracting features from the low resolution remote sensing images are preferred with the use of deep convolution models that haven't layers connections.

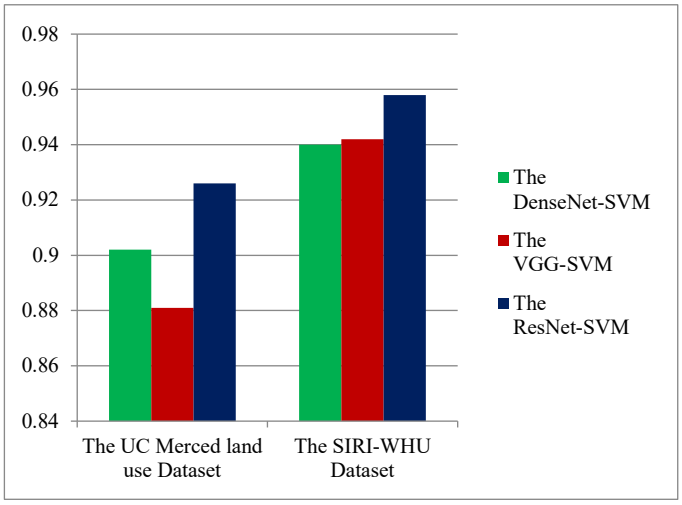


Figure 8: The OA for the use of the convolution models with the SVM classifier using the both datasets

4. Conclusions

This paper proposed remote sensing images classification approaches using the SVM classifier. The proposed approaches were based on using the deep convolution models classic networks as features extraction. The used classic networks in these approaches were the Densenet 169, the VGG 16, and the ResNet 50 models. The remote sensing images convolution features were extracted from these convolution models using the ImageNet pre-trained weights, which used as input features to train the SVM classifier. This paper also presented a comparison between the uses of the mentioned convolution models with the SVM classifier as proposed in this paper. This comparison was based on calculating the OA for using each model with the SVM classifier. There were two used datasets in this study; the UC Merced land use dataset and the SIRI-WHU dataset. This comparison illustrated that the ResNet–SVM model was more accurate than the other models that mentioned in this paper, which the OA of the DenseNet–SVM model was higher than the VGG–SVM model for using the UC Merced land use dataset and very little lower than the VGG–SVM using the SIRI-WHU dataset. The overall accuracy had an opposite relation with the remote sensing images resolution (pixel or spatial) and the number of dataset classes. For the SVM classifiers, it is preferred to use the deep networks without layers connections as features extraction with the low resolution remote sensing images where the deep networks that have layers connection are the preferred with the high resolution remote sensing images.

Conflict of Interest

The authors declare no conflict of interest.

References

[1] M. Bowling, J. Furnkranz, T. Graepel, and R. Musick, "Machine Learning and Games", Machine Learning, Springer, **63**(3), 211-215, 2006. http://doi.org/10.1007/s10994-006-8919-x

[2] K. Hwan Kim and S. June Kim, "Neural Spike Sorting Under Nearly 0-dB Signal-to-Noise Ratio Using Nonlinear Energy Operator and Artificial Neural-Network Classifier", IEEE Transactions on Medical Engineering, **47**(10), 1406-1411, 2000. http://doi.org/10.1109/10.871415

[3] M. Nair S., and Bindhu J.S., "Supervised Techniques and Approaches for Satellite Image Classification", International Journal of Computer Applications (IJCA), **134**(16), 1-6, 2016. http://doi.org/10.5120/ijca2016908202

[4] W. Rawat, and Z. Wang, "Deep Convolutional Neural Networks for Image Classification: A Comprehensive Review", Neural computation, **29**(9), 2352-2449, 2017. http://doi.org/10.1162/NECO_a_00990

[5] A. Khalid et al., "Artificial Neural Networks Optimization and Convolution Neural Networks to Classifying Images in Remote Sensing: A Review", in The 4th International Conference on Big Data and Internet of Things (BDIoT'19), 23-24 Oct, Rabat, Morocco, 2019. http://doi.org/10.1145/3372938.3372945

[6] Y. Tao, M. Xu, Z. Lu, and Y. Zhong, "DensNet-Based Depth-Width Double Reinforced Deep Learning Neural Network for High-Resolution Remote Sensing Images Per-Pixel Classification", Remote Sensing, **10**(5), 779-805, 2018. http://doi.org/10.3390/rs10050779

[7] G. Yang, B. Utsav, E. Ientilucci, Micheal Gartley, and Sildomar T. Monteiro, "Dual-Channel DenseNet for Hyperspectral Image Classification", in IGARSS 2018 - 2018 IEEE International Geoscience and Remote Sensing Symposium, 05 Nov, Valencia, Spain, 2595-2598, 2018. http://doi.org/10.1109/IGARSS.2018.8517520

[8] J. Zhang, C. Lu, X. Li, H. Kim, and J. Wang, "A Full Convolutional Network based on DenseNet for Remote Sensing Scene Classification", Mathematical Biosience and Engineering,, **6**(5), 3345-3367, 2019. http://doi.org/10.3934/mbe.2019167

[9] X. Liu, M. Chi, Y. Zhang, and Y. Qin, "Classifying High Resolution Remote Sensing Images by Fine-Tuned VGG Deep Networks", in IGARSS 2018 - 2018 IEEE International Geoscience and Remote Sensing Symposium, 22-27 Jul, Valencia, Spain, 7137-7140, 2018. http://doi.org/10.1109/IGARSS.2018.8518078

[10] S. Chaib, H. Liu, Y. Gu, and H. Yao, "Deep Feature Fusion for VHR Remote Sensing Scene Classification", IEEE Transactions on Geoscience and Remote Sensing, **55**(8), 4775-4784, 2017. http://doi.org/10.1109/TGRS.2017.2700322

[11] Z. Chen, T. Zhang, and C. Ouyang, "End-to-End Airplane Detection Using Tansfer Learning in Remote Sensing Images", Remote Sensing, **10**(1), 139-153, 2018. http://doi.org/10.3390/rs10010139
[12] G. Fu, C. Liu, R. Zhou, T. Sun, and Q. Zhang, "Classification for High Resolution Remote Sensing Imegery Using a Fully Convolution Network", Remote Sensing, **9**(5), 498-518, 2017. http://doi.org/10.3390/rs9050498
[13] M. Wang et al., "Scene Classification of High-Resolution Remotely Sensed Image Based on ResNet", Journal of Geovisualization and Spatial Analysis, Springer, **3**(2), 16-25, 2019. http://doi.org/10.1007/s41651-019-0039-9
[14] Y. Jiang et al., "Hyperspectral image classification based on 3-D separable ResNet and transfer learning", IEEE Geoscience and Remote Sensing Letters, **16**(12), 1949-1953, 2019. http://doi.org/10.1109/LGRS.2019.2913011
[15] S. Natesan, C. Armenakis, and U. Vepakomma, "ResNet-Based Tree Species Classification Using UAV Images", International Archives of the Photogrammetry, Remote Sensing & Spatial Information Sciences, **XLII**, 2019. http://doi.org/10.5194/isprs-archives-XLII-2-W13-475-2019
[16] J. Yang et al., "Aircraft Detection in Remote Sensing Images Based on a Deep Residual Network and Super-Vector Coding", Remote Sensing Letters, Taylor & Francis, **9**(3), 229-237, 2018. http://doi.org/10.1080/2150704X.2017.1415474
[17] L. Xu and Q. Chen, "Remote-Sensing Image Usability Assessment Based on ResNet by Combining Edge and Texture Maps", IEEE Journal of Selected Topics in Applied Earth Observations and Remote Sensing, **12**(6), 1825-1834, 2019. http://doi.org/10.1109/JSTARS.2019.2914715
[18] P. Liu et al., "SVM or Deep Learning? A Comparative Study on Remote Sensing Image Classification", Soft Computing, Springer, **21**(23), 7053–7065, 2016. http://doi.org/10.1007/s00500-016-2247-2
[19] Y. Guo et al., "Effective Sequential Classifier Training for SVM-Based Multitemporal Remote Sensing Image Classification", IEEE Transactions on Image Processing, **27**(6), 3036-3048, 2018. http://doi.org/10.1109/TIP.2018.2808767
[20] C. Sukawattanavijit et al., "GA-SVM Algorithm for Improving Land-Cover Classification Using SAR and Optical Remote Sensing Data", IEEE Geoscience and Remote Sensing Letters, **14**(3), 284-288, 2017. http://doi.org/10.1109/LGRS.2016.2628406
[21] Y. Chen et al., "Deep Feature Extraction and Classification of Hyperspectral Images Based on Convolutional Neural Networks", IEEE Transactions on Geoscience and Remote Sensing, **54**(10), 6232-6251, 2016. http://doi.org/10.1109/TGRS.2016.2584107
[22] E. Maggiori et al., "Convolutional Neural Networks for Large-Scale Remote-Sensing Image Classification", IEEE Transactions on Geoscience and Remote Sensing, **55**(2), 645-657, 2017. http://doi.org/10.1109/TGRS.2016.2612821
[23] G. Huang, Z. Liu, L. Maaten, and K. Q. Weinberger, "Densely Connected Convolutional Networks", in 2017 IEEE Conference on Computer Vision and Pattern Recognition (CVPR), 21-26 Jul, Honolulu, HI, USA, 2261-2269, 2017. http://doi.org/10.1109/CVPR.2017.243
[24] K. Simonyan and A. Zisserman, "Very deep convolutional networks for large-scale image recognition", in International Conference on Learning Representations (ICLR 2015), 7-9 May, San Diego, USA, 2015. https://arxiv.org/abs/1409.1556
[25] K. He, X. Zhang, S. Ren, and J. Sun, "Deep Residual Learning for Image Recognition", in 2016 IEEE Conference on Computer Vision and Pattern Recognition (CVPR), 27-30 Jun, Las Vegas, NV, USA, 770-778, 2016. http://doi.org/10.1109/CVPR.2016.90
[26] G. Mountrakis, J. Im, and C. Ogole, "Support vector machines in remote sensing: A review", ISPRS Journal of Photogrammetry and Remote Sensing, Elsevier, **66**(3), 247-259, 2011. http://doi.org/10.1016/j.isprsjprs.2010.11.001
[27] B.W. Heumann, "An Object-Based Classification of Mangroves Using a Hybrid Decision Tree-Support Vector Machine Approach", Remote Sensing, **3**(11), 2440-2460, 2011. http://doi.org/10.3390/rs3112440
[28] G. Banko, "A Review of Assessing the Accuracy of Classifications of Remotely Sensed Data and of Methods Including Remote Sensing Data in Forest Inventory", in International Institution for Applied Systems Analysis (IIASA), Laxenburg, Austria, IR-98-081, 1998. http://pure.iiasa.ac.at/id/eprint/5570/
[29] W. Li et al, "Deep Learning Based Oil Palm Tree Detection and Counting for High-Resolution Remote Sensing Images", Remote Sensing, **9**(1), 22-34, 2017. http://doi.org/10.3390/rs9010022
[30] Y. Yang and S. Newsam, "Bag-Of-Visual-Words and Spatial Extensions for Land-Use Classification", in the 18th ACM SIGSPATIAL international conference on advances in geographic information systems, 2-5 Nov, San Jose California, USA, 270-279, 2010. http://doi.org/10.1145/1869790.1869829
[31] B. Zhao et al., "Dirichlet-Derived Multiple Topic Scene Classification Model for High Spatial Resolution Remote Sensing Imagery", IEEE Transactions on Geoscience and Remote Sensing, **54**(4), 2108-2123, 2016. http://doi.org/10.1109/TGRS.2015.2496185
[32] E. Bisong, "Building Machine Learning and Deep Learning Models on Google Cloud Platform: A Comprehensive Guide for Beginners", Apress, Berkeley, CA, 2019.
[33] T. Carneiro et al., "Performance Analysis of Google Colaboratory as a Tool for Accelerating Deep Learning Applications", IEEE Access, **6**, 61677-61685, 2018. http://doi.org/10.1109/ACCESS.2018.2874767
[34] O. Russakovsky and L. Fei-Fei, "Attribute Learning in Large-Scale Datasets", in European Conference on Computer Vision, 6553, Springer, Berlin, Heidelberg, 10-11 Sep, Heraklion Crete, Greece, 1-14, 2010. http://doi.org/10.1007/978-3-642-35749-7
[35] J. Deng et al., "What Does Classifying More Than 10,000 Image Categories Tell Us? ", in The 11th European conference on computer vision, 6315, Springer, Berlin, Heidelberg, 5-11 Sep, Heraklion Crete, Greece, 71-84, 2010. http://doi.org/10.1007/978-3-642-15555-0

ASTES

Advances in Science, Technology and Engineering Systems Journal Vol. 5, No. 5, 660-668 (2020)

www.astesj.com

Special Issue on Multidisciplinary Sciences and Engineering

ASTESJ

ISSN: 2415-6698

Issues in File Caching and Virtual Memory Paging with Fast SCM Storage

Yunjoo Park, Hyokyung Bahn*

Department of Computer Science & Engineering, Ewha Womans University, 03760, South Korea

ARTICLE INFO

Article history:
Received: 09 August, 2020
Accepted: 21 September, 2020
Online: 05 October, 2020

Keywords:
Storage-Class Memory (SCM)
File Caching
Virtual Memory Paging

ABSTRACT

Storage-Class Memory (SCM) like Optane™ has advanced as a fast storage medium, and conventional memory management systems designed for the hard disk storage need to be reconsidered. In this article, we revisit the memory management system that adopts SCM as the underlying storage medium and discuss the issues in two layers: file caching and virtual memory paging. Our first observation shows that file caching in the SCM storage is profitable only if the cached data is referenced more than once, which is different from the file caching in hard disks, where a single hit is also beneficial. Our second observation in virtual memory paging shows that the page size in the SCM storage is sensitive to the memory system performance due to the influence of memory address translation and storage access cost. Our simulation studies show that the performance of paging systems can be improved by adjusting the page size appropriately considering application characteristics, storage types, and available memory capacities. However, the page size will not be a significant issue in mobile platforms like Android, where applications are killed before the memory space is exhausted, making situations simpler. We expect that the analysis shown in this article will be useful in configuring file caches and paging systems with the emerging SCM storage.

1. Introduction

With the large performance gap between hard disk drive (HDD) and dynamic random-access memory (DRAM), the main purpose of memory management in computing systems has been the minimization of disk I/Os [1, 2]. The access latency of hard disks is more than tens of milliseconds, which is five to six orders of magnitude larger than DRAM's access latency. Meanwhile, due to the rapid improvement of storage access time by the adoption of flash-based solid state drive (SSD) and storage-class memory (SCM), the extremely large performance gap has been decreased [3-5]. The access latency of the flash storage is less than fifty milliseconds, and hence the performance gap of storage and memory becomes less than 3 orders of magnitude. Such trends have been speeded up by the commercialization of SCM whose access latency is just 1 or 2 orders of magnitude slower than DRAM [6, 7].

A lot of patents related to the detailed architectures and algorithms of SCM management have been suggested, and Intel manufactured the commercial product of SCM, called Optane™ [8, 9]. Owing to its desirable features like high performance, low energy consumption, and long write endurance, SCM is anticipated to be adopted in the storage systems like flash SSD and hard disks [10-13].

SCM can also be adopted in the main memory system because it allows byte-accesses like DRAM but consumes less energy because it is a non-volatile medium [14]. However, the access latency of SCM is longer than that of DRAM, and hence it is now considered as high-end storage or additional memory that can be used together with DRAM. Although SCM may be used as either memory or storage, this article focuses on storage. Since the performance gap of storage and memory becomes small by adopting SCM, memory management systems targeting at slow hard disk storage need to be revisited.

In this article, we quantify the performance of systems based on SCM storage and analyze a couple of issues in the management of main memory under the SCM-based storage. In particular, this article analyzes two memory management hierarchies affected by the acceleration of storage devices, *file caching* and *virtual memory paging*.

File caching preserves file data read from the storage to the main memory area called the file cache and services requests for the same data from the cache without accessing storage. The

*Corresponding Author: H. Bahn, 52, Ewhayeodae-gil, Seodaemun-gu, Seoul 03760, Republic of Korea, +82-2-3277-4247, bahn@ewha.ac.kr.

purpose of file caching is to minimize the storage access frequency. However, since the storage access latency is fast enough by making use of SCM, it is questionable whether file caching is still needed. To validate this, we investigate the condition that file caching is effective according as the storage access latency is varied. Our preliminary study exhibits that a storage access takes about 30% more latency than a cache access even though the same data is accessed and the access latency of storage and cache is identical. This is because there exists heavy software stack to passing through the storage media. By observing this result, our finding is that file caching is still needed for SCM-based storage if the data in the cache is requested more than once after inserted into the cache. That is, since file caching needs additional time for inserting the requested data into the cache, more than a certain cache hits are necessary for caching to be profitable, and we show that this is at least twice for SCM storage. Note that low-end storage media like hard disks require only a single hit for caching to gain.

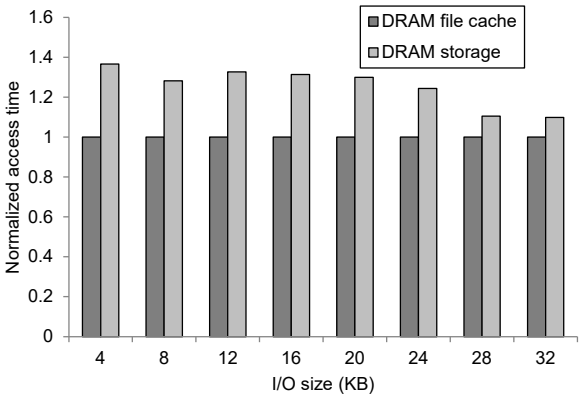


Figure 1: Latency of accessing data from the file cache and the DRAM-based storage.

Our second observation focuses on virtual memory paging if SCM is made use of as storage media. Similar to file caching, the purpose of virtual memory paging is the minimization of storage accesses, which is also called page faults, when storage is hard disk. Since the storage medium becomes fast enough, we observe that page fault handling may not be the main performance bottleneck of virtual memory paging. In particular, as the latency of storage access becomes small by adopting SCM, the bottleneck of the page access latency may be shifted to memory address translation. Note that to access a memory page, translating the address should be done first and then the data in the page is accessed from either memory or storage. As the data access is accelerated by the reduced storage access cost, the address translation process may be a new bottleneck by accessing page tables.

This article quantifies what will be the main bottleneck of virtual memory paging as the storage performance and the page size are changed. Based on our analysis, we discover the following two phenomena. First, a small page is not efficient in terms of the page fault rate but it performs well in terms of the data access latency. The reason is that a page fault handling latency is strongly related to the page size when the storage is SCM, which does not need seek movement. Second, even though a small page is efficient with respect to the latency of data access, it degrades the latency of address translation by increasing TLB miss counts. Due to this reason, deciding a page size needs to consider the trade-off relation of the data access latency and the address translation latency.

Our simulation results exhibit that the performance of virtual memory paging can be improved by adjusting the page size appropriately considering application characteristics, storage types, and available memory sizes. However, the page size will not be a significant issue in mobile platforms like Android, where applications are killed before memory space is exhausted, making situations simpler. We expect that the analysis shown in this article will be useful in configuring file caches and paging systems with the emerging SCM storage.

The remaining part of this article is organized as follows. In Section 2, we quantify the performance implication of file caching as the storage medium changes from hard disk to SCM. Section 3 anatomizes the virtual memory paging performances with high-performance SCM storage particularly focusing on page sizes. Section 4 presents the experimental results through conducting simulation experiments to observe the implications of SCM storage based memory management systems. Section 5 discusses the adoption of our model to the mobile application environments. Finally, we present the conclusion of this article in Section 6.

2. File Caching for SCM Storage

This section quantifies the efficiency of file caching as the storage medium changes from hard disk to SCM. To this end, we measure the latency of file system operations when DRAM is used as storage. Note that DRAM is volatile, but we use a certain area of DRAM as a storage partition just to see the effect of fast storage media. Note also that this situation implies the optimistic performance of SCM storage. We added a profiler to Ext4 for measuring the latency of directly accessing data from the DRAM storage and the latency of accessing data in the DRAM file cache.

Figure 1 depicts the access latency of DRAM storage and DRAM file cache as the size of data accesses changes. In this graph, we measure each case 10 times and plot their average. As can be seen in the graph, the access latency from DRAM storage is 30% longer than accessing the same data from DRAM file cache. Although the same DRAM is used for cache and storage, the performance gap occurs due to the existence of software I/O stack. When considering these results, file caching can be still necessary to buffer the latency gap between storage and memory although their access latencies are identical. However, as the gap is very small, some conditions need to be met for file caching to be beneficial.

When we use file caching, the accessed data should be stored into the cache, which requires additional latency. The access latency of DRAM storage shown in Figure 1 does not include this latency, and hence the accessed data is delivered directly to the user memory. If we use file caching, the accessed data is firstly stored in the file cache and then transferred to the user memory. The overhead of this additional copy operation in memory is not negligible when SCM storage is used because the time overhead to perform a memory copy is similar to that of a storage access. Thus, the gain of file caching is small or there are no profits at all because of this trade-off. Due to this reason, file caching is beneficial only when the benefit of subsequent cache hits is larger than the cost of

the additional memory copy operation. That is, cache hits are important for a cached data to gain, which differs from low-end storage media like hard disk drives where a single hit of data is sufficient for caching to gain. To quantify this, we measure the data access time t from the file cache, storage access time T, and time to access storage including the file caching cost T_m. Then, we evaluate the condition of caching to be beneficial with respect to the cache hit counts. The following equations represent the latency to access data with file cache T_c and without file cache T_x, respectively.

$$T_c = T_m + (n-1)\,t \quad (1)$$

$$T_x = n\,T \quad (2)$$

where n is the total access count for the data. File caching gains when T_c is less than T_x as follows.

$$n > (T_m - t) / (T - t) \quad (3)$$

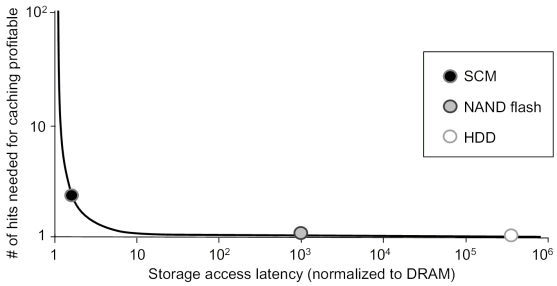
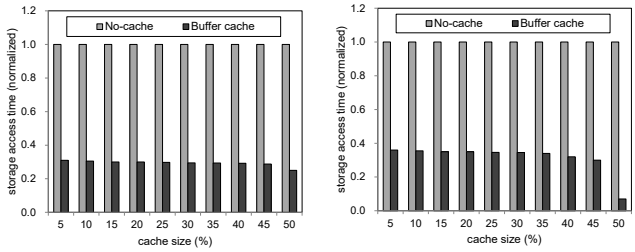


Figure 2: Hit counts necessary for a cached item to be beneficial as a function of the latency for accessing the storage media.

Based on Expression (3), we estimate the cache hit counts needed for caching to be beneficial. Figure 2 depicts the required hit counts when the storage media is flash memory, hard disk, and SCM. As plotted in the figure, the cache hit count necessary for caching to be profitable increases significantly as the performance gap of storage and memory is small. In the case of SCM storage whose access latency is only 30% slower than memory, the cache hit count necessary for caching to be profitable is two while resident in the cache. Hence, if a storage data is requested now and it will not be reused at least twice in the future, it would be better not to store it in the cache for performance improvement.

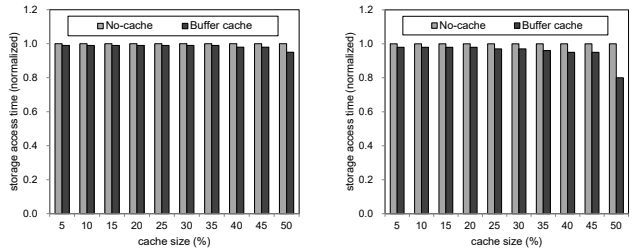
To quantify the influence of file caching in practical situations, we collect file request traces during the execution of two popular storage benchmarks, and replay them as the storage media is varied. The captured traces are web server and proxy server. We investigate the storage access latency with/without file caching under the two workload conditions. For the cache eviction algorithm, we use the least-recently-used (LRU), the most commonly adopted algorithm in file caching. LRU selects the data that was accessed the oldest among all data in the file cache and evicts it if there are no cache spaces to insert new data items.

Figure 3 depicts the storage access time with/without file caching when hard disk storage is used as the size of cache changes. Note that the cache size of 100% means that the cache size is equal to the total footprint of workloads, implying that the eviction algorithm is not necessary. This is not a realistic situation and in practical environments, the cache size is less than 50%. As can be seen from this figure, the effectiveness of file caching is significant in case of the hard disk storage. Specifically, file caching accelerates the storage performance by 70%, which is possible because hard disk is very slower than the file cache, and hence decreasing the disk I/O access counts by file caching is effective.



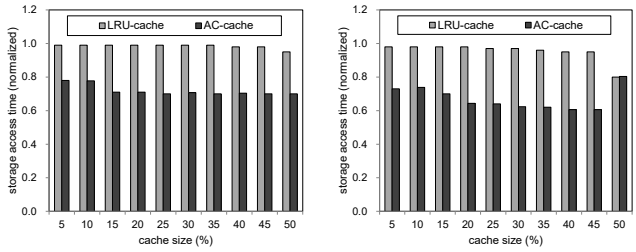
(a) Proxy (b) Web

Figure 3: Effectiveness of file caching under hard disk storage.



(a) Proxy (b) Web

Figure 4: Effectiveness of file caching under SCM storage.



(a) Proxy (b) Web

Figure 5: Performance of file caching with/without admission-controll (AC) under SCM.

Figure 4 depicts the storage access time without/with file caching when the storage medium is SCM. As can be seen from this figure, the effectiveness of file caching is insignificant in case of the SCM storage. In particular, the performance improvement by using file caching is less than 3% with the SCM storage. This apparently exhibits that the effectiveness of file caching decreases significantly as the performance gap of storage and memory becomes small. However, we conducted some new experiments, and show that file caching can be still effective by judicious management.

Figure 5 depicts the storage access time with file caching when the SCM storage is used, but we differentiate the result with two management policies. In particular, LRU-cache adopts the same configuration of Figure 4, which stores all data requested in the file cache and evicts the least-recently-used data if free cache space is necessary. The other graph, denoted by AC-cache (admission-controlled cache), is plotted by allowing the insertion of data into the file cache only if it is used more than once. This allows only

data used multiple times to be cached, thereby filtering out useless single-accessing data. Even though this is a simple technique, the effectiveness of AC-cache is significant as shown in Figure 5. The performance improvement ranges 20-40%. The implication of this result is that file caching is still useful when SCM storage is used, but management policies should be appropriately devised in order to get effective results.

3. Virtual Memory Paging for SCM Storage

This section presents the simulation results of virtual memory paging when we use SCM as storage.

3.1. Access Latency of a Virtual Memory Page

To use a memory page in virtual memory systems, translation of memory addresses between logical address and physical address needs to be conducted. This is done by referencing the page table, which is located at main memory. To improve the address translation performances, a certain part of the page table is cached in the Translation Look-aside Buffer (TLB), which is faster than main memory [15]. When a memory page is requested, address translation by TLB is tried first. The page table is referenced if address translation by TLB misses. Then, the memory data is accessed with the translated physical address. However, if the data does not reside in memory, storage should be accessed, which is called a page fault. Assume that the cache miss rate of TLB is R_T, and the page fault rate is R_F. Then the memory access time T_{TOTAL} can be denoted by

$$T_{TOTAL} = T_{ADDR} + T_{DATA} \quad (4)$$

$$T_{ADDR} = (1 - R_T) * t_\varepsilon + R_T * (t_\varepsilon + t_\tau) \quad (5)$$

$$T_{DATA} = (1 - R_F) * t_\tau + R_F * (t_\tau + T_{PF}) \quad (6)$$

where T_{ADDR} is the time required for performing address translation, T_{DATA} is the latency required for data access, t_ε is the latency required for TLB access, t_τ is the latency for accessing main memory, and T_{PF} is the latency for page fault handling including storage access time.

3.2. Eviction Policies

Since the size of TLB entries is fixed, adding an address translation data to TLB requires the eviction of a certain entry when no TLB entry is available. To choose an eviction victim, we adopt the least-recently-used (LRU) eviction policy, which is a representative algorithm adopted in TLB entry eviction [15].

Because the size of free pages in main memory is fixed, another eviction policy is necessary. Specifically, if the page requested is not in memory and should be loaded from storage, but there is no free page in memory, eviction of a page from memory is necessary. We use the second-chance algorithm, which is a popular eviction policy used in virtual memory systems, in our experiments [14].

The second-chance algorithm investigates if a page has been used recently or not by utilizing the reference bit of each page. When a page is used, the reference bit of that page becomes one. If a free page frame is needed, the second-chance algorithm investigates the reference bits of all pages in memory sequentially, and discards the page firstly found with its reference bit of zero. For each page whose reference bit is one while investigation processes, the second-chance algorithm resets the bit to zero, instead of discarding the page from memory. Thus, if a page is not accessed until the next investigation of the second-chance algorithm, it is evicted.

With this basic configurations, we conduct our simulations to quantify the efficiency of memory management systems when we use SCM-based storage.

3.3. Page Size and Prefetching

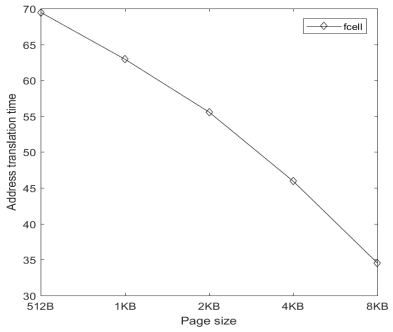
The current operating systems usually manage virtual memory by the unit of *page*. The size of a page is commonly set to 4 kilobytes, which is also the default page size of Linux. However, operating systems also allow the prefetching option, which loads maximum 128 pages together from the secondary storage when a page requested is not in memory. The rationale of this is to consider the characteristics of hard disk, which requires the basic cost for each access consisting of seek latency and rotational latency, accounting for the main part of storage access latency irrespective of the size of data loaded. This implies that loading large data in each request is efficient in case of hard disk based storage. Recent operating systems also support a huge page whose size is up to 4MB. This is also for hard disk storage systems, but it will not be efficient for SCM, in which the page size should be small because storage is fast and there are no seek time or rotational latency.

Nevertheless, it is not feasible to decrease the page size because memory address translation will be efficient with a large page size. That is, TLB with a large page size covers more memory address spaces, leading to improved address translation latency. Then, we need to decide the page size for SCM-based storage by considering the overall effect of storage access and address translation.

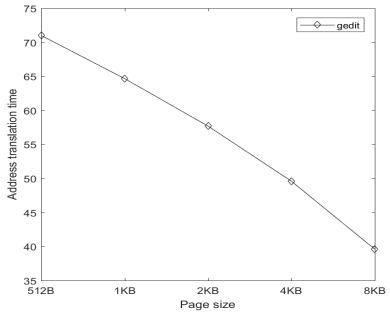
Also, the latency of SCM should be considered, which is optimistically as fast as DRAM, but can be up to 100 or 1000 times slower than DRAM. Due to the variance of performance gap between storage and memory, the relative impact of memory address translation compared to storage access is also varied. In particular, as the performance of SCM approaches that of DRAM, memory address translation incurs relatively more cost. On the contrary, as the performance gap of DRAM and SCM increases, the relative overhead of a storage access will be large. The relation of storage access and address translation will be analyzed in the next section as the performance of SCM is varied.

4. Performance Analysis

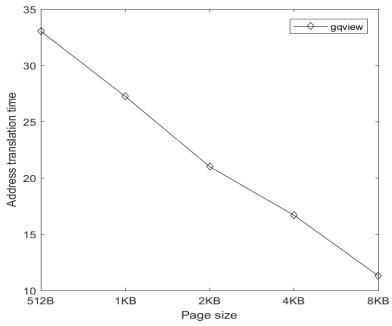
We conduct various simulations to investigate the efficiency of memory management subsystem as SCM storage is adopted. In particular, the impact of the page size on memory performance is investigated. The minimum page size is set to 512 bytes because the size of a page should be at least the block size of the last-level cache memory. We use the virtual memory reference traces captured by the Cachegrind tool of the Valgrind [16, 17]. We collect the virtual memory reference traces from five desktop workloads as listed in Table 1 [18-22].



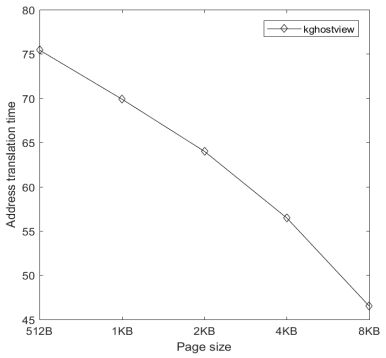
(a) freecell



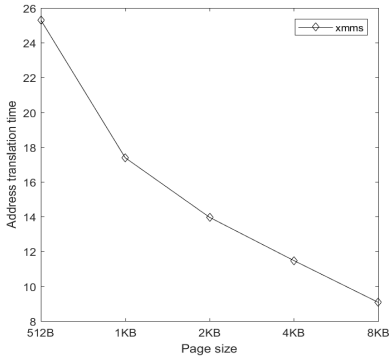
(b) gedit



(c) gqview

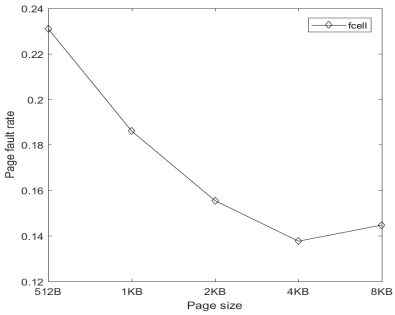


(d) kghostview

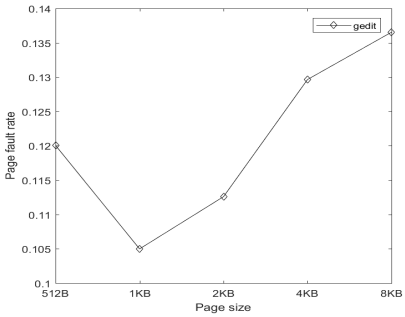


(e) xmms

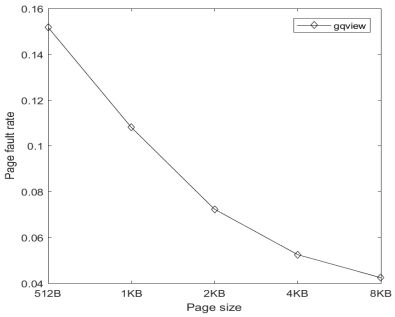
Figure 6: Memory address translation time of desktop workloads as the page size changes.



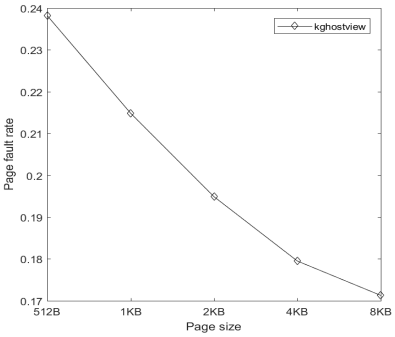
(a) freecell



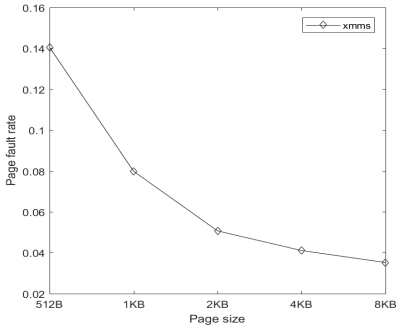
(b) gedit



(c) gqview

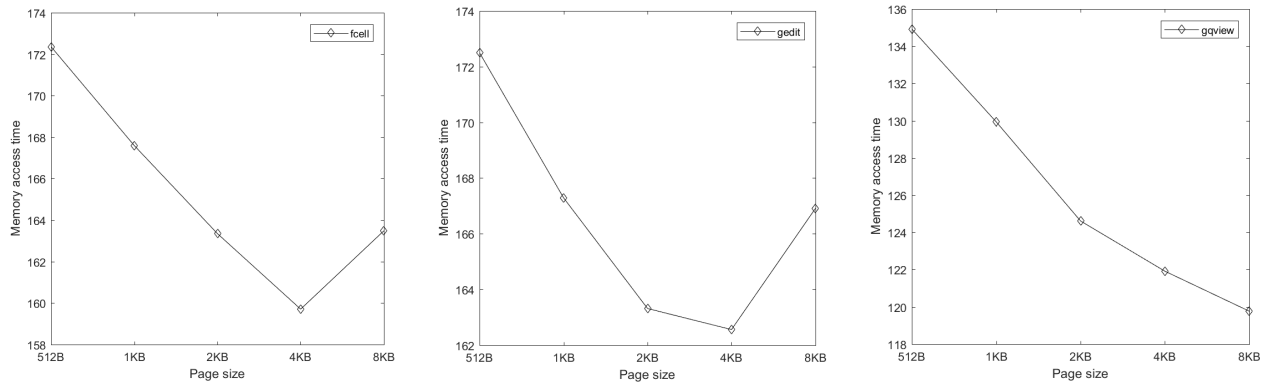


(d) kghostview

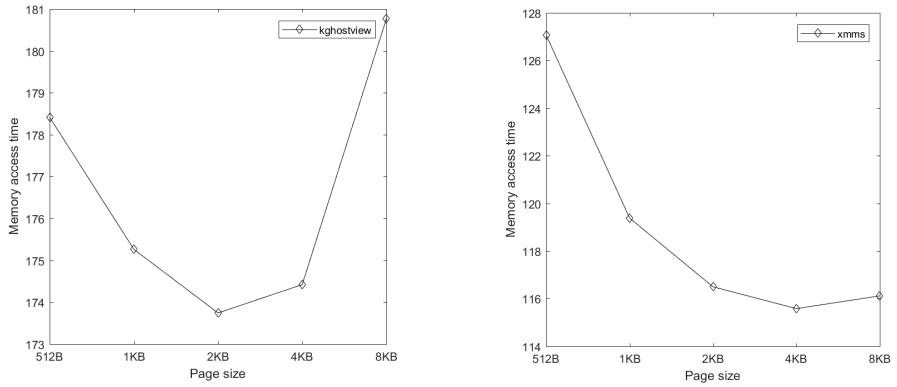


(e) xmms

Figure 7: Page fault rate of desktop workloads as the page size changes.

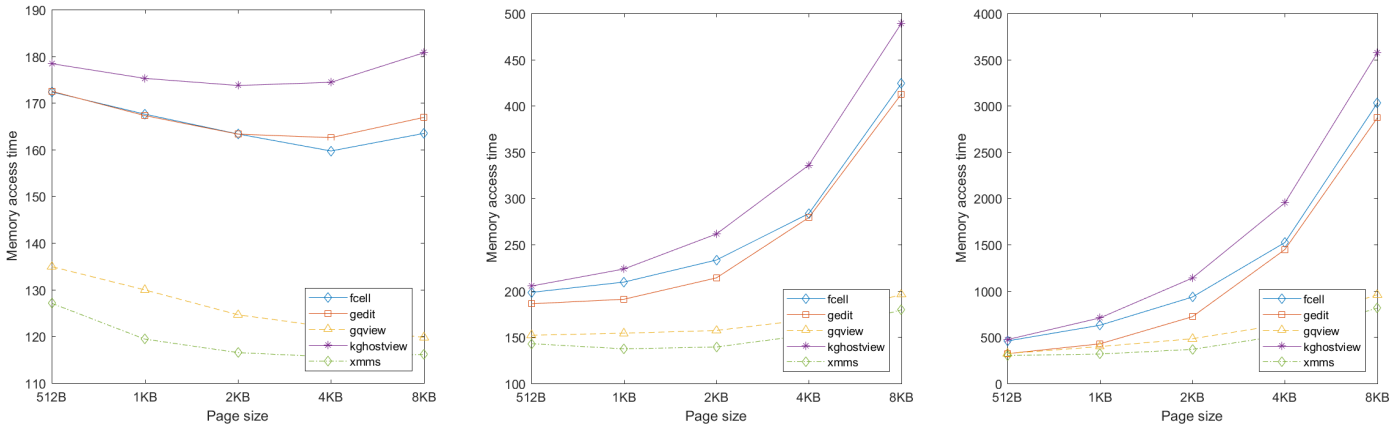


(a) freecell (b) gedit (c) gqview



(d) kghostview (e) xmms

Figure 8: Memory access time of desktop workloads as the page size changes.



(a) 1x of DRAM (b) 10x of DRAM (c) 100x of DRAM

Figure 9: Total memory latency of desktop workloads as the page size and storage access latency change.

4.1. Memory Address Translation

This section discusses the influence of the page size on the performance of memory address translation. Figure 6 depicts the memory address translation latency while running five desktop applications as the page size is changed. As the figure depicts, the latency of memory address translation decreases according as the page size grows. The reason is that the fixed TLB entries account for the address translations of wider memory spaces if the page size becomes large. An increased hit rate of TLB leads to the decreased latency of memory address translation by reducing the number of page table references. Nevertheless, it is known that the hit rate of TLB cannot increase any more when the page size is larger than a certain threshold [23]. Thus, the conclusion of this experiment is that a large page will perform well in terms of the memory address translation, but the page size does not need to be increased any longer after a certain large size.

Table 1: Characteristics of desktop workload

Application	Memory footprint (MB)	Memory access counts		
		Write	Read	Total
freecell [18]	9.84	60,040	430,135	490,175
gedit [19]	14.12	132,822	1,600,941	1,733,763
Gqview [20]	7.26	645,399	265,286	610,685
kghostview [21]	16.98	103,540	1,442,595	1,546,135
xmms [22]	7.86	978,242	190,697	1,168,939

4.2. Storage Access Frequency

This section discusses the impact of the page size on the storage access frequency. Figure 7 depicts the page fault rate of the five applications as the page size changes. As the figure shows, the best page size is not identical for different applications we considered. In most cases, a large page improves the page fault rate. In particular, the page size of 8 kilobytes exhibits the best results for gqview, kghostview, and xmms. On the contrary, the page size that exhibits the best result is 1 kilobytes for gedit and 4 kilobytes for freecell, respectively. The best page size relies not only on the application's characteristics but also on the free memory situation of the total system. When the memory size is insufficient for the given workload environment, decreasing the page size will perform well to retrieve only the data requested at that time. In contrast, when the available memory is sufficient, increasing the page size will be a better choice in terms of the storage access frequency. Also, when the workload is composed of sequential reference patterns, increasing the page size can reduce the number of storage accesses by retrieving large successive data together.

4.3. Total Memory access time

As hard disk requires large seek overhead for each storage access irrespective of the data size, decreasing the storage access frequency can lead to the improvement of data access latency. However, in case of SCM storage, as the data size becomes large, a storage access requires more time to load data. Assume a storage reference stream that is composed of sequential patterns and let us think of the storage access frequency for virtual memory paging that makes use of a large page size and a small page size. It is clear that a large page size is efficient in terms of the storage access frequency, but it does not essentially lead to the enhancement of data access latency because the storage access time becomes large for each I/O with SCM. Hence, instead of improving the storage access frequency, our aim is to reduce the data access latency. In other words, the page fault rate is not a fair performance index for SCM-based virtual memory paging, but the data access latency can be an alternative metric for SCM-based storage.

Unlike the page fault rate case, address translation latency has almost linear relation with the TLB miss rate because the access latency of a page table entry incurred by each TLB miss is identical though the page size is different.

Figure 8 depicts the total memory access latency of the desktop applications we considered as the page size changes. As the figures show, the best page size is not the same for different applications, and is also different from the results of Figure 7 that plots the page fault rate. From this result, we can see that the storage access frequency is not the primary factor of performance in case of SCM storage media. Also, this figure shows that the address translation latency can be another significant factor that influences the memory access time in case of fast SCM storage even though the effectiveness of address translation is smaller than the actual data access. Because a trade-off relation exists between data access and address translation in deciding an appropriate page size, we cannot simply conclude the page size as small or large but a judicious management is necessary for deciding the page size with given environments.

4.4. Relative Storage Performance

Figure 9 depicts the total memory latency for each application as the access latency of storage media changes. Specifically, Figures 9(a), 9(b), and 9(c) represent the total memory latency when the relative access latency of SCM is identical to DRAM, 10 times that of DRAM, and 100 times that of DRAM, respectively. As this figure shows, the page size that performs the best is not the same for each case as the access latency of storage media changes. If the performance of SCM is similar to DRAM as shown in Figure 9(a), the address translation latency becomes important, and hence increasing the page size performs relatively well. In other words, the role of TLB becomes significant in such environments, and the memory access time is improved with the page size of 4KB or 8KB. We cannot determine the best page size for all workloads as it depends on the total memory capacity as well as the workload characteristics. Figures 9(b) and 9(c) plot the total memory latency when the access latency of SCM media is 10 times and 100 times slower than DRAM, respectively. As these two figures show, the memory access time becomes better when we decrease the page size as small as possible. The reason is that the data access latency affects significantly if the storage becomes slow and thus the address translation procedure is less important. The best memory access time can be obtained if we set the page size to 512B for all cases.

Table 2: Characteristics of mobile workload.

Application	Memory footprint (MB)	Memory access counts		
		Write	Read	Total
facebook [24]	198.66	2,045,716	11,607,339	13,653,055
angrybirds [25]	76.94	3,822,479	14,368,068	18,201,717
youtube [26]	68.64	3,162,229	15,034,275	18,196,504
farmstory [27]	53.74	2,101,818	13,122,852	15,224,670
chrome [28]	259.86	4,104,436	16,895,563	20,999,999

When considering these overall situations, we can obtain the best memory access time not by fixing the page size to a constant but by varying relying on the application and storage characteristics. Hence, the common page size of 4KB will not be a good choice for all cases and needs to be changed appropriately if we use the SCM-based fast storage media.

5. Adopting the Model to Android Mobile Applications

In this section, we adopt our model to Android mobile applications to see the effect of the page size in SCM-based storage. To investigate a wide spectrum of Android applications, we collect virtual memory reference traces from five Android applications, namely, facebook a social network service [24], angrybirds a game [25], youtube an online streaming service [26], farmstory an online game [27], and chrome a web browser [28]. Table 2 lists the characteristics of the workloads.

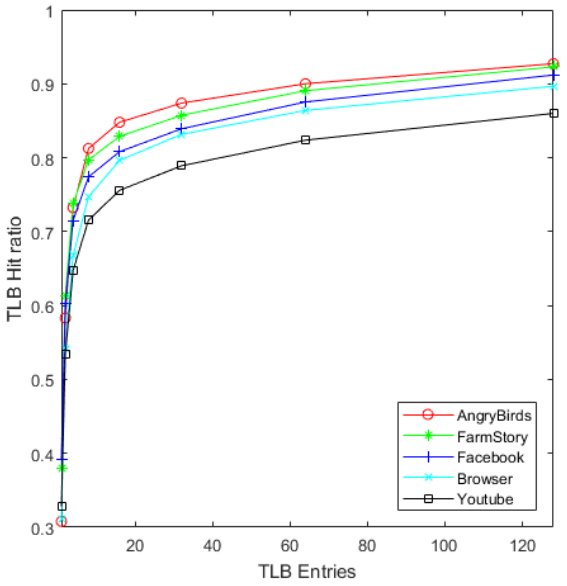


Figure 10: TLB hit rate of mobile workloads as the TLB size changes.

With these memory reference traces, we conduct extensive simulations, and analyze them similar to the desktop system cases in the previous section. Figure 10 depicts the TLB hit rate while executing five mobile applications as a function of the TLB size. As can be seen from the figure, the TLB hit rate is improved significantly as the TLB entries increase. The five applications show similar curve trends. Specifically, the TLB performance is improved sharply when the number of TLB entries is less than 20 and the slope of the curve becomes gradual after that point. Figure 11 depicts the TLB hit ratio as the page size changes. As can be seen from this figure, the TLB hit rate improves according as the page size increases. The reason is that the fixed number of TLB entries account for address translations of more memory capacity as the page size becomes large. An increased hit rate of TLB eventually leads to the decreased latency of memory address translation by reducing the number of page table references. However, the improvement of the TLB hit rate slows down when the page size is larger than a certain threshold. Thus, increasing the page size will perform well in terms of the performance of memory address translation, but it is not sensitive after a certain large page size.

Figure 12 depicts the page fault rate of the five Android applications as the page size changes. As can be seen from the figure, the page fault rate decreases as the page size increases for all applications we considered. Unlike desktop cases that do not exhibit the same trends for different applications, all mobile applications show similar results. The best page size relies on the application's characteristics in desktop cases, but a large page commonly improves the page fault rate of all mobile applications we considered. If the memory space is not sufficient for the given workload environment, large pages will not perform well due to retrieving the data not requested now. However, our Android application experiments show that the memory space is not exhausted in any applications. This is because Android does not use swap but kills applications if free memory space becomes small.

Figure 13 depicts the average memory access time (AMAT) of the five Android applications we considered as the page size changes. This graph separately represents the AMAT when the relative latency of SCM is identical to DRAM, 10 times that of DRAM, 100 times that of DRAM, and 1000 times that of DRAM, respectively. In the previous section, the page size that performs the best in desktop environments is not identical for each case as the performance of storage media is varied. If the performance of storage is similar to that of DRAM, increasing the page size performs relatively well, but if SCM becomes slow, decreasing the page size works well in desktop environments. However, as shown in Figure 13, the best results in mobile environments are obtained when the page size becomes large, and there are no significant differences in memory performances when the page size is larger than 1 kilobytes. This is also related to the memory management policies of Android, in which applications are killed before memory space is exhausted, and thus increasing the page size does not incur problems like desktop environments.

In summary, our conclusion is that the page size will not be a significant issue in mobile environments although fast SCM is used as the storage media.

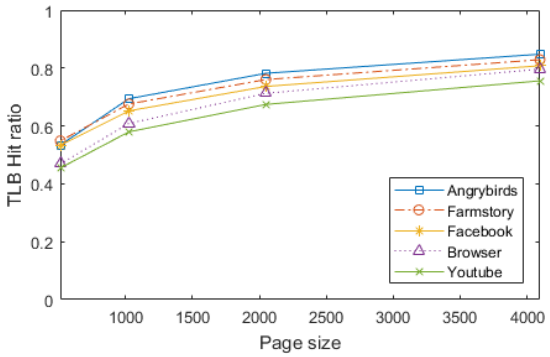


Figure 11: TLB hit rate of mobile workloads as the page size changes.

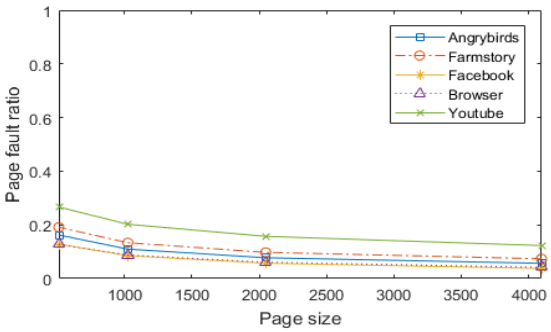


Figure 12: Page fault rate of mobile workloads as the page size changes.

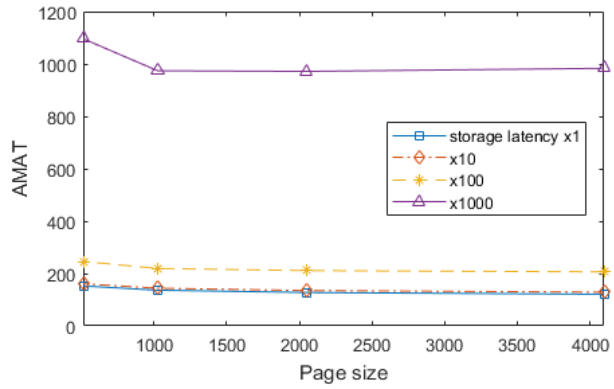


Figure 13: Average memory access time (AMAT) of mobile workloads as the page size and storage latency change.

6. Conclusion

In this article, we considered the effectiveness of traditional memory management systems and configurations if fast storage such as SCM is used as the storage media. Our study discussed the implication of SCM storage with respect to the two important memory/storage subsystems, file caching and virtual memory paging. The analysis results with respect to the file caching showed that caching file blocks is effective if the blocks retrieved from SCM storage is used more than once after loading to memory. Thus, the admission of file blocks to the cache should be controlled for managing the file cache appropriately in SCM-based storage media. In the case of virtual memory paging, our study showed that the number of storage accesses may not be the most important performance index, but the memory address translation process will also become important. In particular, our analysis showed that a common page size of 4 kilobytes is not a good choice for all cases when SCM storage is adopted, and determining the page size by decreasing or increasing it is needed because of the trade-off relation in storage access and memory address translation. However, we also showed that the page size is not a significant issue in mobile platforms like Android, where applications are killed before memory space is exhausted, making situations simpler. We expect that the findings in this article will be meaningful for emerging memory and storage management systems that make use of fast SCM media. In the future, we will perform the evaluation of our strategy with the complete system configurations consisting of the commercialized SCM products.

Conflict of Interest

The authors declare no conflict of interest.

Acknowledgment

This paper is an extension of work originally presented in the 6th IEEE Int'l Conf. on Information Science and Control Engineering [1]. This work was supported by the National Research Foundation of Korea (NRF) grant funded by the Korea government (MSIP) (No. 2019R1A2C1009275) and also by the ICT R&D program of MSIP/IITP (2019-0-00074, developing system software technologies for emerging new memory that adaptively learn workload characteristics).

References

[1] Y. Park, K. Cho, and H. Bahn, "Challenges and Implications of Memory Management Systems under Fast SCM Storage," in 2019 IEEE International Conference on Information Science and Control Engineering, 190-194, 2019. https://doi.org/10.1109/ICISCE48695.2019.00046
[2] S. Ng, "Advances in disk technology: performance issues," Computer, **31**(5), 75-81, 1998. http://doi.org/10.1109/2.675641
[3] C. Evans, "Flash vs 3D Xpoint vs storage-class memory: which ones go where?" Computer Weekly, **3**(9), 23-26, 2018.
[4] M. Stanisavljevic et al., "Demonstration of Reliable Triple-Level-Cell (TLC) Phase-Change Memory," in 2016 IEEE International Memory Workshop, 2016. https://doi.org/10.1109/IMW.2016.7495263
[5] S. Hyun, H. Bahn, and K. Koh, "LeCramFS: an efficient compressed file system for flash-based portable consumer devices," IEEE Trans. Consumer Electron., **53**(2), 481-488, 2007. https://doi.org/10.1109/TCE.2007.381719
[6] M. K. Qureshi, V. Srinivasan, and J. A. Rivers, "Scalable high performance main memory system using phase-change memory technology," ACM SIGARCH Computer Architecture News, **37**(3), 24-33, 2009. https://doi.org/10.1145/1555815.1555760
[7] E. Lee, J. Jang, T. Kim, and H. Bahn, "On-demand snapshot: an efficient versioning file system for phase-change memory," IEEE Trans. Knowledge Data Engineering, **25**(12), 2841-2853, 2013. https://doi.org/10.1109/TKDE.2013.35
[8] R. K. Ramanujan, R. Agarwal, and G. J. Hinton, "Apparatus and Method for Implementing a Multi-level Memory Hierarchy Having Different Operating Modes," US Patent 20130268728 A1, Intel Corporation, 2013.
[9] B. Nale, R. Ramanujan, M. Swaminathan, and T. Thomas, "Memory channel that supports near memory and far memory access," PCT/US2011/054421, Intel Corporation, 2013.
[10] E. Lee, S. Yoo, and H. Bahn, "Design and implementation of a journaling file system for phase-change memory," IEEE Trans. Comput., **64**(5), 1349-1360, 2015. https://doi.org/10.1109/TC.2014.2329674
[11] S. Eilert, M. Leinwander, and G. Crisenza, "Phase change memory: A new memory enables new memory usage models," in 2009 IEEE International Memory Workshop, 2009.
[12] E. Lee, J. Kim, H. Bahn, S. Lee, and S. Noh, "Reducing Write Amplification of Flash Storage through Cooperative Data Management with NVM," ACM Transactions on Storage, **13**(2), 2017. https://doi.org/10.1145/3060146
[13] E. Lee, H. Bahn, S. Yoo, S. H. Noh, "Empirical study of NVM storage: an operating system's perspective and implications," in 2014 IEEE International Symposium on Modeling, Analysis, and Simulation of Computer and Telecommunication Systems, 405-410, 2014. https://doi.org/10.1109/MASCOTS.2014.56
[14] S. Lee, H. Bahn, and S. H. Noh, "CLOCK-DWF: a write-history-aware page replacement algorithm for hybrid PCM and DRAM memory architectures," IEEE Trans. Comput., **63**(9), 2187-2200, 2014. https://doi.org/10.1109/TC.2013.98
[15] B. Anita, J. B. Chen, and N. P. Jouppi, "A simulation based study of TLB performance," in 1992 Int. Symp. Computer Architecture, 114-123, 1992.
[16] Valgrind, http://valgrind.org/
[17] N. Nethercote and J. Seward, "Valgrind: a program supervision framework," Electronic Notes in Theoretical Computer Science, **89**(2), 2003. https://doi.org/10.1016/S1571-0661(04)81042-9
[18] Freecell, https://en.wikipedia.org/wiki/FreeCell
[19] Gedit, https://wiki.gnome.org/Apps/Gedit
[20] Gqview, http://gqview.sourceforge.net
[21] Kghostview, https://linuxappfinder.com/package/kghostview
[22] Xmms, https://www.xmms.org/
[23] P. Weisberg and Y. Wiseman, "Using 4KB page size for virtual memory is obsolete," in 2009 IEEE International Conference on Information Reuse & Integration, 262-265, 2009. http://doi.org/10.1109/IRI.2009.5211562
[24] Facebook, https://www.facebook.com/
[25] Angrybirds, https://www.angrybirds.com/
[26] Youtube, https://www.youtube.com/
[27] Farmstory, https://play.google.com/store/apps/details?id=com.teamlava.farmstory
[28] Chrome, https://www.google.com/chrome/

Advances in Science, Technology and Engineering Systems Journal Vol. 5, No. 5, 669-673 (2020)

www.astesj.com

Special Issue on Multidisciplinary Innovation in Engineering Science & Technology

ASTESJ

ISSN: 2415-6698

Investigation of Dielectric Properties of Indigenous Blended Ester oil for Electric System Applications

D.M. Srinivasa[1,*], Usha Surendra[2], V.V. Pattanshetti[3]

[1]*Department of E&E Engineering, PES College of Engineering, Mandya, 571401, India*

[2]*Department of E&E Engineering, School of Engineering & Technology, Christ (Deemed to be University), Bangalore - 560074, India*

[3]*Central Power Research Institute, Bangalore, 560074, India*

ARTICLE INFO

Article history:
Received: 12 August, 2020
Accepted: 19 September, 2020
Online: 05 October, 2020

Keywords:
Antioxidants
Degasification
Indigenous oil

ABSTRACT

The insulation condition of a transformer decides the longevity of the equipment. The unpredicted failure of power transformer will lead to major disaster in the distribution network and it affects both environment and public safety. Nowadays synthetic oil and natural esters are alternatives to transformer oil because of the biodegradable nature. In this paper, investigations were carried out to study the performance of the blended ester. The different properties investigated were viscosity, breakdown voltage, flash point, dielectric dissipation factor and moisture content. Comparisons of the properties were made between mineral oil, vegetable oil without additives and with additives. Further Investigation was carried out to study the impact of antioxidants and degasification. The results indicated that the addition of antioxidants and degasification of the vegetable oil improve significantly its voltage withstanding capacity. The Indigenous oil is code named as DM; Indigenous oil with DBPC is codenamed as DM1, Indigenous oil with BHA is codenamed as DM2. The results have been tabulated and found to be satisfactory.

1. Introduction

The life of insulating medium is investigated by comparing the Breakdown strength and Viscosity of different oil in its pure form with that of the contaminated oil and to find the alternative for mineral oil. The presence of moisture content in the mineral oil compared to vegetable oil would be the main cause for failure of insulation. Vegetable oils which are reliable, cost-effective and environmentally friendly [1]. The evaluation of dielectric properties of Nomex-910 and thermally upgraded Kraft (TUK) paper is being investigated in soya-based natural ester oil by performing accelerated thermal ageing (at 1200C, 1500C and 1800C as per modified ASTM D1934) [2].

The waste cooking oil (WCO) acts as a potential alternative to the existing transformer insulating oil. The use of WCO promotes the optimal consumption of plant-based resources and more efficient waste management. Trans esterification method is performed to eliminate the free fatty acids in the WCO and to reduce viscosity. The trans esterification process is based on the chemical modification reaction between WCO, methyl alcohol (methanol) and sodium hydroxide (NaOH) catalyst lye that produces waste cooking oil methyl ester (WCOME). Chemical and electrical properties of the developed WCOME are compared with the existing WCO [3]. The analysis has been carried out to investigate the critical parameters in different vegetable oil before and after the inclusion of an aging derivative of 2–furfuraldehyde (2-FAL) [4]. The survey has been made to present recent research progress and also for future research. The research scenarios related to the performance of ester fluids versus mineral oils, miscibility, and retro filling of insulating fluids are discussed along with challenges and future aspects on the investigation to enhance the knowledge of ester fluids [5].

The impact of electrical and physicochemical properties of different vegetable oils with different ageing has been studied [6]. Due to lack of oxidative stability, the vegetable oils are less exposed as dielectric in transformer application [7]. The dielectric properties and partial discharge of mineral oil, natural ester and FR3 have been investigated. The suitability in practical use of oils is verified with impregnation of pressboard insulation [8]. The dielectric property of pongamia pinnata oil (PPO) under thermally aged condition has been investigated. [9]. Comparative study of five different types of natural ester liquid under a variation of temperature has been made with respect to different properties. [10]. A study has been carried out to explore the performance of coconut oil as an insulator [11]. Investigation of different properties of Palm Oil (PO) and Coconut Oil (CO) has been carried out under open thermal ageing condition [12]. The analysis of breakdown strength and

*Corresponding Author D. M. Srinivasa, dmsrinivasa.pesce@gmail.com, srinivasa.dm@res.christuniversity.in

physical characteristics of extra virgin olive oil and castor oil under unaged and thermally aged conditions is performed and compared the results with mineral oil with respect to same aging process [13]. The natural ester-based oils are investigated to analyse the suitability of it as better insulating medium with respect to their properties. Further analysis is carried out to on the fatty acid content and cost of vegetable oil [14]. Different vegetable oils and their blends are considered to investigate their dielectric properties with thermal ageing for about120 hours [15]. Neem oil, sunflower oil and mahua oil are blended with antioxidants plus nano powders to measure various properties. To minimize the oxidation stability, Synthetic antioxidants such as Beta Carotene and TBHQ (Tert-Butyl Hydro Quinone) and selenium are preferred as natural antioxidants [16].

Many a times vegetable oils develop bad odour due to oxidation and also rendered unfit for edible applications. These oils can be used effectively reconditioned for applications such as dielectrics by removal of the undesirable products.

In this research paper experiments have been carried out to determine the physical and electrical properties of Indigenous oil which is initially rancid in nature. This oil has chemically treated to bring to status of edible oil and then investigated for different properties. In this paper, section I explained the introduction and its related works. Section II, indicated the methodology and experimental procedure. Results and discussions have been given in section III and Section IV reserved for conclusion.

2. Experimental Procedure

The different physical and electrical characteristics of vegetable oil require special considerations. Due to the presence of oxygen, the degradation of the fluid takes place. So, the dielectric properties are investigated for the smooth operation of transformers.

2.1. Experimental Procedure

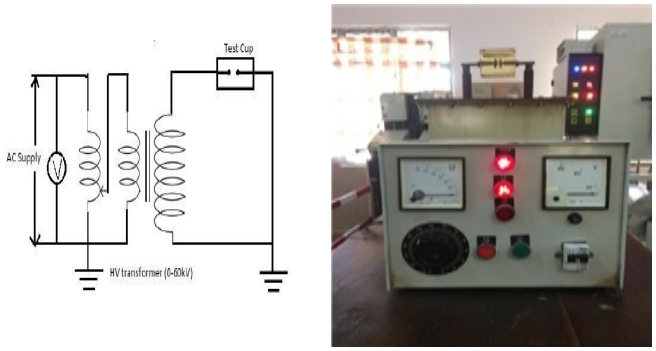
The process of refinement adopted in the present work has been given below.

- The vegetable oil was mixed with hot water (70˚C), shaken for 10 minutes and allowed to cool for 30 minutes. The separated supernatant was again mixed with hot water (60-70˚C) and stirred for 30 minutes. This process helped to remove the gums, waxes and other water soluble components from the oil.
- Removal of free acids: Oil has been mixed with equal volume of 5% Sodium Hydroxide solution and stirred for 20 minutes by treating with dilute caustic soda (5% solution). Free fatty acids reacted with caustic soda result in sodium soap. These acids can be coagulated by heating. Allow the soaps to settle and separate them from filtration.
- Removal of bad odour: Vegetable oil has bubbled with steam in the oil for 1 hour to remove the low volatile oxidised products. Supernatant oil layer has been taken out, leaving behind the condensed water.
- Removal of Pigments and Polar contaminants: Oil has been subsequently passed through an adsorbent column of korvi earth wherein pigments and other polar contaminants will be adsorbed leaving the clean oil ready for use as dielectric fluid.
- Removal of dissolved oxygen and removal of trace moisture and other polar components: Oil has been bubbled with hot nitrogen gas in a controlled manner to strip any dissolved oxygen, carbon dioxide, traces of moisture for almost 24 hours. The process has been used to reduce the moisture.
- Sample preparation: Mineral oil (Electrol-IS335), Indigenous oil and a quantity of 1108 ml of Indigenous oil mixed with 9 grams of DBPC (2,6-di-tert-butyl-p-cresol) and also 9 grams of BHA(Butylated hydroxyl Anisole) is mixed with 1108ml of Indigenous oil is magnetically stirred to ensure complete dissolution are the samples considered for investigation of physical and electrical properties. Samples prepared with indigenous oil without antioxidant has been named as DM, the indigenous oil with DBPC has named as DM-1and the indigenous oil with BHA has named as DM-2.

The following test has been conducted to investigate both electrical and physical properties.

2.2. Breakdown Voltage Conduction Test (BDV)

As per IEC standard, electrodes of spherical in shape has been placed at a distance of 2.5 mm and the liquid specimen filled test cup were used to carry out the test as per Figure 1. Repeatedly conducted the test for 6 times and noted the values for analysis purpose. AC high voltage supply varied gradually till its breakdown at a step of 2kV/sec. BDV test has been conducted as per IEC 60156 standards.



(a) (b)

Figure 1: (a). Circuit diagram for breakdown voltage measurement (b) Breakdown voltage test.

2.3. Kinematic Viscosity

Cannon-Fensken viscometer (Figure 2 and Figure 3) is used for the viscosity test. The test specimen has been filled in the tube up to the level indicated in the bulb. By maintaining a constant temperature of 40 degree centigrade, recorded the time taken by the test specimen to flow in a vertical direction from higher point to lower point of the bulb. Viscosity has been calculated by considering the calibration constant.

Kinematic Viscosity (centistokes-cSt) = (time in seconds) × (viscometer constant)

2.4. Flash Point

The ground level temperature at which flame causes the fire in the form of a flash under specified conditions is called the flash point. Flash point is measured using PENSKY MARTEN'S closed setup as shown in Figure 4. The procedure to identify the flash point has given as follows:

- To heat the oil, the liquid has been filled up to the specified level given in the flash point apparatus.
- External fire has been injected at regular time interval until the flash over occurs. Note the temperature at which flash occurs. Flash point=Recorded temperature at which flash occurs.



Figure 2: Cannon –Fensken viscometer



Figure 3: Viscometer tube.



Figure 4: Pensky martens.

2.5. Dielectric Dissipation factor

Dielectric dissipation factor is measured as per IEC-60247 standards using Eltel model-ADTR-2K Capacitance - Tan δ bridge.

2.6. Degasification Method

Oxidation stability is important to measure the quality and life time of liquid dielectrics. Moisture in oil will degrade the insulation. Transformer failure occurs due to the presence of moisture as well as heat, oxidation, and electrical stresses. Moisture has a significant effect on the dielectric strength. Improvement in the oxidation stability and reduction of moisture content level is achieved by adding antioxidants and also by degasification.

Indigenous oil with DBPC (DM-1) and BHA (DM-2) is considered for degasification with nitrogen gas to remove oxygen and also to reduce moisture content present in the Indigenous oil to investigate improvement in breakdown voltages.

3. Result and Discussion

Experiments have been conducted on DM, DM-1 and DM-2 to identify their breakdown voltage, viscosity, flash points, dielectric dissipation factor and moisture content.

3.1. Standard Values

The ranges of the various characteristics of liquid dielectrics as per IEC62770 standards, has been indicated in the table 1. After experimentation, results of MO, DM, DM-1and DM-2 has been compared with standard values and found out that, the values comes under with in the acceptance limits of IEC62770-2013.

Table 1: IEC62770-2013 standard ranges of liquid dielectrics

Characteristics	Acceptable limits	Mineral oil (MO)	Indigenous oil without Antioxidants(DM)	Indigenous oil with DBPC(DM-1)	Indigenous oil with BHA (DM-2)
Breakdown voltage, kV	30(min)	32	29	37	43
Dielectric dissipation factor	0.05(max)	0.00064	0.038	0.034	0.0511
Kinematic Viscosity, cSt @40 ˚C	50(max)	13.74	46	44	42
Water content, ppm	200(max)	11	501	454	340
Flash point, ˚C	250(min)	152	256	251	245

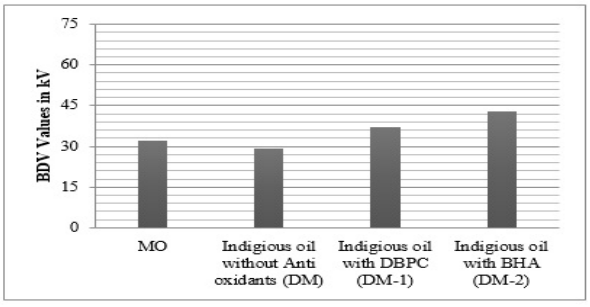


Figure 5: BDV Values of oils.

From Fig 5. BDV of DM-1 is higher than MO and DM. This indicates breakdown voltage of DM-2 is more than MO and DM and DM-1. As the BDV of Indigenous oil is high, this results in higher breakdown strength of Indigenous oil than MO.

Figure 10 indicated the Dielectric dissipation factor of MO, DM and DM-1 oils and the value has been observed and found out that it has well within the 0.05 of standard limits. But the DDF of DM-2 is slightly more than the standard limits. The desired low dissipation factor of oil has been achieved and also it indicated the low power factor.

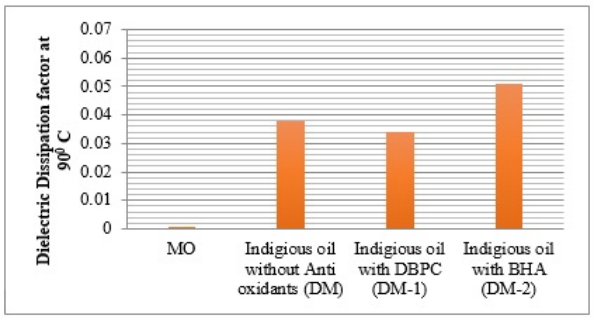


Figure 6: Comparative chart of dielectric dissipation factor of oils.

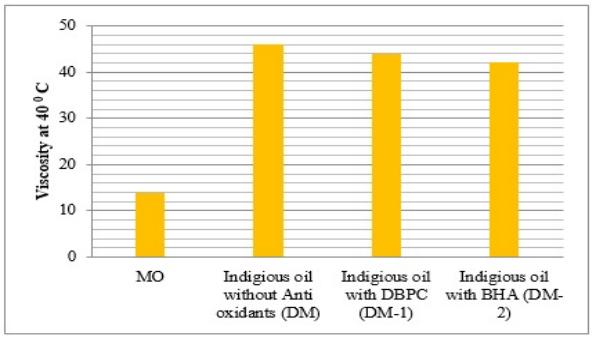


Figure 7: Viscosity of oils

From Figure 7 Viscosity of both DM, DM-1and DM-2 is higher than MO. For better cooling capability, the insulating liquid should have low viscosity. Still the value of viscosity of DM, DM-1and DM-2 will be reduced by reducing the moisture content.

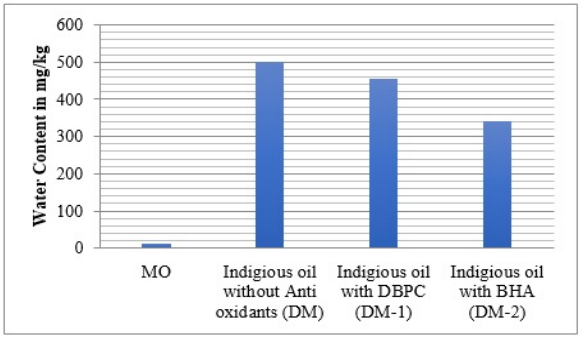


Figure 8: Water content of oils

From Figure 8 Water content is more in DM, DM-1 and DM-2 compared to MO. Reducing the water content in the oil enhances the properties, can be reached by adding antioxidants and also by degasification.

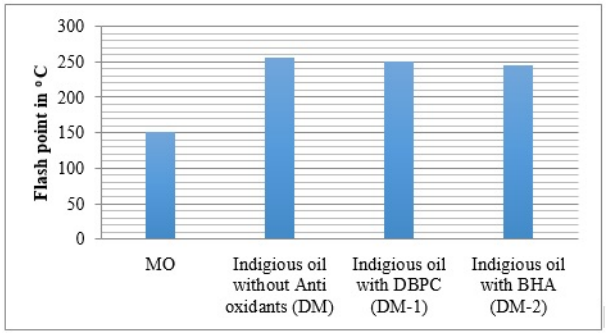


Figure 9: Flash point of oils.

From Figure 9. Flash points of DM, DM-1and DM-2 is very much higher than MO. This indicates higher withstanding capacity of Fire.

3.2. Improvement in BDV Values

Figure 10 indicates that there is a reduction in the moisture content of DM-2 after nitrogen bubbling.

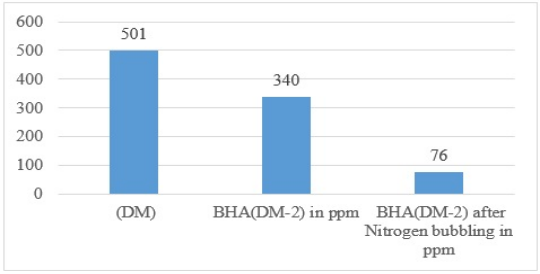


Figure 10: Reduction of Moisture content in DM-2(ppm)

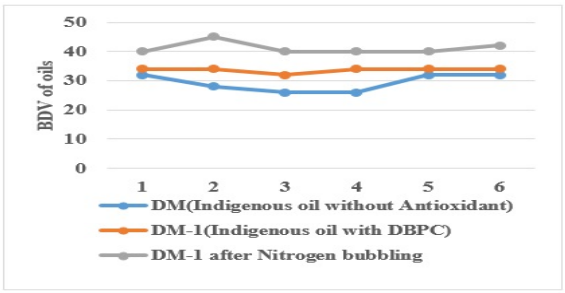


Figure 11: Comparison of breakdown voltage of oils

Figure 11 and 12 indicates that average breakdown voltage is increased in DM-1 after nitrogen bubbling compared with DM (Indigenous oil without Antioxidant) and DM-1(Indigenous oil with DBPC)

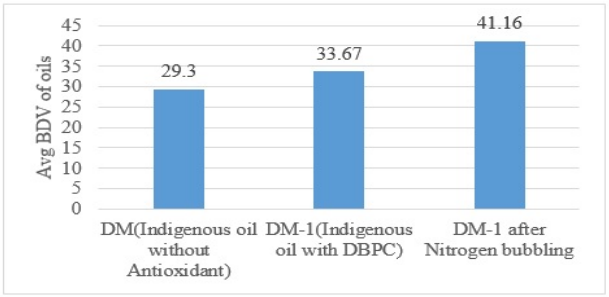


Figure 12: Average breakdown voltage of oils

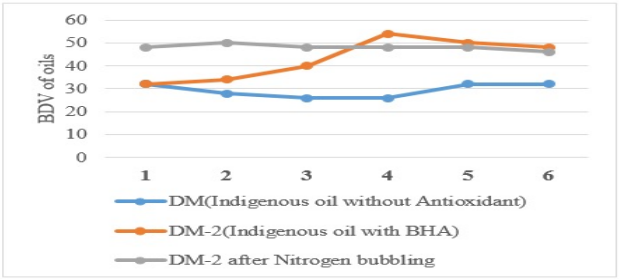


Figure 13: Comparison of breakdown voltage of oils

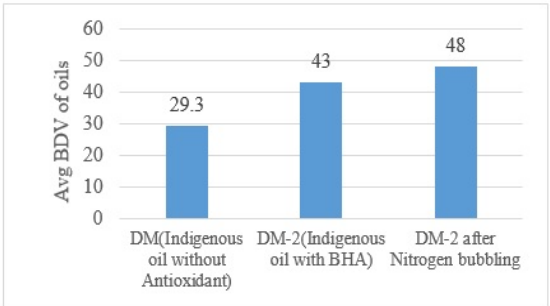


Figure 14: Average breakdown voltage of oils

Figure 13 &14 indicates that average breakdown voltage is increased in DM-2 after nitrogen bubbling compared with DM (Indigenous oil without Antioxidant) and DM-2(Indigenous oil with BHA).

4. Conclusion

Insulation property will be acted as the prime active portion of the high voltage equipment's. The cooling of the transformer depends on the viscosity of the insulating oil and governed by convection. Higher the flash point which in turn reduces the risk of transformer explosions and fire catching criteria and protect the environment.

After adding antioxidants, voltage withstanding capacity of Indigenous oil has been enhanced. It was observed that flash point of the DM, DM-1 and DM-2 is higher than that of mineral oil. In the similar manner, break down voltage (BDV), Dielectric Dissipation factor and Viscosity of DM, DM-1and DM-2 has been observed and found out that their values were well within the range of IEC62770-2013 standard values.

Further Breakdown voltage is enhanced due to addition of Anti-oxidants and also due to degasification.

In case of equipment failure or spillage, vegetable oil decomposition is very slow. The above experimental results justified that, the antioxidants blended indigenous oil can be treated as alternate oil for transformer applications in power system and also it is environmental supportive by means of biodegradation. As the flash point of Indigenous oil is better compared to Mineral oil and results in high fire withstanding capacity. Further this work can be extended by considering Indigenous oil with different antioxidants. The other properties can also be investigated by reducing the moisture content by adopting nitrogen bubbling method and also by other method.

References

[1] D M Srinivasa and Usha Surendra **"**Comparative study of Breakdown Phenomena and Viscosity in Liquid Dielectrics**"** 2019 Innovations in Power and Advanced Computing Technologies (i-PACT), 2019 Vellore, India https**:**//doi.org/: 10.1109/i-PACT44901.2019.8960134.

[2] Ankit Chouhan, Raj Kumar Jarial, and U. Mohan Rao "Thermal Performance of Nomex-910 and TUK Insulating Papers in Soya based Natural Ester Oil" International Journal on Electrical Engineering and Informatics, **12**(1), March 2020. https://doi.org/: 10.15676/ijeei.2020.12.1.5.

[3] Muhammad Nazori Deraman, Norazhar Abu Bakar, Nur Hakimah Ab Aziz, Imran Sutan Chairul,Sharin Ab Ghani "The Experimental Study on the Potential of Waste Cooking Oil as a New Transformer Insulating Oil" Journal of Advanced Research in Fluid Mechanics and Thermal Sciences **69**(1), 74-84, 2020, https://doi.org/10.37934/arfmts.69.1.7484.

[4] C. Subalaksmi, M. Bakrutheen, M. Willjuice Iruthayarajan "Influence of Aging Derivatives on Properties of Natural Ester Oil" International Journal of Innovative Technology and Exploring Engineering (IJITEE), **9**(4), February 2020, https://doi.org/: 10.35940/ijitee.D2031.029420.

[5] M. Rao, I. Fofana, T.Jaya, Esperanza Mariela Rodriguez-Celis, Jocelynalbert and Patrick Picher "Alternative Dielectric Fluids for Transformer Insulation System: Progress, Challenges, and Future Prospects" IEEE Access, **7**, 2019, 10.1109/ACCESS.2019.2960020.

[6] S.Senthil Kumar, A. Arul Marcel Moshi, S.R.Sundara Bharathi, K.Karthik Kumar "Optimization of Various Natural Ester Oils Impregnated Nomex Paper Performance in Power Transformer Applications under Different Ageing Conditions", International Journal of Recent Technology and Engineering (IJRTE), **8**(3), September 2019, https://doi.org/: 10.35940/ijrte.C5832.098319.

[7] K.Sindhuja, M.Srinivasan, N.Niveditha "Natural Esters as an Alternative to Mineral oil in Transformer Applications", International Journal of Pure and Applied Mathematics, **118**(20), 723-732,2018, http://www.ijpam.eu.

[8] K. Jariyanurat, S. Maneerot, P. Nimsanong, P. Kitcharoen, P. Chaisiri, N. Pattanadech "Dielectric Properties of Mineral oil compared with Natural Ester", 19th IEEE International Conference on Dielectric Liquids (ICDL), Manchester, United Kingdom, 25 – 29 June, 2017, https://doi.org/: 978-1-5090-4877-9/17.

[9] T. Mariprasath and V. Kirubakaran "Thermal degradation analysis of pongamia pinnata oil as alternative liquid dielectric for distribution transformer", Indian Academy of Sciences, **41**(9), 933–938 , September 2016, https://doi.org/: 10.1007/s12046-016-0529-0.

[10] M. H. A. Hamid, M. T. Ishak, M. F. Md. Din, N. S. Suhaimi, N. I. A. Katim, "Dielectric Properties of Natural Ester Oils Used for Transformer Application Under Temperature Variation", IEEE 6th International Conference on Power and Energy (PECON 2016), 2016, Melaka, Malaysia, https://doi.org/: 10.1109/PECON.2016.7951472.

[11] N. A. Muhamad and S. H. M. Razali, Electrical and Chemical Properties of New Insulating Oil forTransformer Using PureCoconut Oil", Journal of Advanced Research in Materials Science, **25**(1). 1-9, 2016, ISSN (online): 2289-7992.

[12] Nur Aqilah Mohamad, Norhafiz Azis, Jasronita Jasni, Mohd Zainal Abidin Ab Kadir, Robiah Yunus, Mohd Taufiq Ishak and Zaini Yaakub, "Investigation on the Dielectric, Physical and Chemical Properties of Palm Oil and Coconut Oil under Open Thermal Ageing Condition", J Electr Eng Technol; **11**(3): 690-698,2016, https://doi.org/: 10.5370/JEET.2016.11.3.690.

[13] S.Banumathi, S.Chandrasekar "Analysis of Breakdown Strength and Physical Characteristics of Vegetable Oils for High Voltage Insulation Applications" Journal of Advances in Chemistry, **12**(16), 4902-4912, 2016.

[14] S. Senthil Kumar, Dr. M. Willjuice Iruthayarajan, M. Bakrutheen "Analysis of Vegetable Liquid Insulating Medium for Applications in High Voltage Transformers", In 2014 International Conference on Science Engineering and Management Research (ICSEMR), 1-5. IEEE, 2014.

[15] M. S. Ahmad Kamal,N. Bashir, N. A. Muhamad "Insulating Properties ofVegetableOilsandTheirBlends", 2013 IEEE 7th International Power Engineering and Optimization Conference (PEOCO2013), Langkawi, Malaysia, 3-4 June, 2013. https://doi.org/: 978-1-4673-5074-7/13.

[16] Uma Devi Sankarasubbu and Senthil Kumar Suburaj Examining the Properties of Neem Oil, Sunflower Oil and Mahua Oil with Antioxidants and Nano Powders for Power Transformer" American Journal of Electrical and Computer Engineering, **3**(1), 20-29, 2019. doi: 10.11648/j.ajece.20190301.13

ASTES

Advances in Science, Technology and Engineering Systems Journal Vol. 5, No. 5, 674-679 (2020)

www.astesj.com

ASTESJ

ISSN: 2415-6698

Multi-layered Security Design and Evaluation for Cloud-based Web Application: Case Study of Human Resource Management System

Gautama Wijaya*, Nico Surantha

Computer Science Department, BINUS Graduate Program – Master of Computer Science, Bina Nusantara University, Jakarta 11480, Indonesia

ARTICLE INFO

Article history:
Received: 05 May, 2020
Accepted: 23 September, 2020
Online: 05 October, 2020

Keywords:
Multi-layered Security
NGFW
WAF
SQL Injection
Malicious File Injection

ABSTRACT

Cloud computing is the development of information technology to provides resources that can be accessed through network. Security and privacy in cloud computing are major concern for companies. Therefore, cloud computing architecture strategy and design are needed to reduce costs and ensure the security of company assets in cloud computing. In this study, we are using multi-layered security strategy that contain of Next-Generation Firewall and Web Application Firewall technologies. We conducted an evaluation on the design by using the SQL injection and malicious file injection method. The results of the evaluation show that the cloud computing architecture design that we proposed manage to prevent SQL injection and malicious file injection threats.

1. Introduction

Security and privacy are two major issues for companies that are adopting cloud computing [1]. Hence, companies are unwilling to move their assets to cloud computing [2], [3]. We need the right strategy and architecture design to reduce costs and ensure the security of the (applications and data) in cloud computing [4]. Therefore, we need to pay attention to this issue and the availability of security technology. Cloud computing architecture design is important to secure company assets. Most importantly, company assets in cloud computing are crucial for a company.

In this research, we conducted a case study on a company's cloud-based web application service that they provide for their human resources management. The main problem of this company is the security of their cloud-based web application. In cloud computing, the company uses only the security technology provided by the cloud service. Even more, the technology is not equipped with the ability to analyze and detect threats [5], which can endanger the company assets.

In this research, we use the System Development Life Cycles (SDLC) design method in the top-down network design to increase security for the company assets in cloud computing. We use a top-down network design because this method is considered the company's business goals and technical goals. Hopefully, our design can help companies to achieve business goals and technical goals [6], [7]. In this research, we are using multi-layered security by combining 2 security technologies, which are, Next-Generation Firewall and Web Application Firewall. We use multiple layers of security to increase protection against threats and create a safe cloud environment for the company [8]. Each layer of security has its technology, functions, and role to detect and prevent threats to enter the cloud environment.

The paper is organized, as follows; In part 2, we will discuss the basic concept of top-down network design using SDLC, multi-layered security, and the literature review from other researchers about secure cloud environment. In part 3, we will discuss the detailed method of the top-down network design using SDLC on the company. In section 4, we will discuss how the multi-layered security design is implemented and secure the cloud environment. In part 5, we will conclude the whole research.

2. Literature Review

2.1. Top-Down Network Design

Cloud computing architecture design is the way that companies use to ensure the efficiency, cost, and security control on the applications and cloud environments that they are using [9].

*Corresponding Author: Gautama Wijaya, Binus University, gautama.wijaya@binus.ac.id

Top-down network design is a method to make designs, ranging from the top layer of the OSI (application layer) to the bottom layer of the OSI (physical layer) [7].

In the design making process, we are using the top-down network design, which is divided into several stages. The following are the 4 (four) main stages that we took to create a cloud computing architecture design [6].

- Analyzing the requirements: We translated the business goal and technical goal that we are going to implement in the cloud computing architecture design. We also analyze the cloud computing architecture that they used recently to look for possible threats in the company's cloud computing environment.
- Developing logical design: We made a logical design of cloud computing architecture that we are going to use to secure the company's cloud environment.
- Developing physical design: We chose the security technology that we are going to implement on the logical design that we have made previously.
- The final stage: in the final stages, we implement the design that we have made, create a prototype, evaluates the security, and make documentation on the design.

2.2. Multi-layered security

A security strategy is needed to prevent threats and protect the cloud environment. Multi-layered security is one of many security strategies that can secure company asset. It is because each layer of security has function, role, and technology that can detect and prevent threats [8]. By layering security technology, as seen in figure 1, it can maximize the security of company assets.

In this study, we use the Next-Generation Firewall and Web Application Firewall security technologies to protect the company assets in cloud computing. These are the explanation of each security layer.

1. Layer 1, we use the Next-Generation Firewall (NGFW) as security technology. There are many features found in the Next-Generation Firewall (NGFW). Here are the features that we use in the first layer of the cloud computing architecture design [10]:

- IPS (Intrusion Prevention System)
- DPI (Deep Packet Inspection)
- TLS/SSL Encrypted Traffic Inspection
- Antivirus Inspection

2. Layer 2, we use the Web Application Firewall (WAF) as security technology, because it focuses on the security process at the application layer and analyzes each packet for any suspicious activity [11]. There are many features in the Web Application Firewall, so we utilize these features for our design. Here are the features that we use to secure cloud-based web application:

- SQL Injection and XSS
- CSRF Prevention
- Inspect HTTPS
- Traffic Encoded Traffic
- Virus Protection
- DOS Protection
- Data Theft Protection
- Brute Force Approach

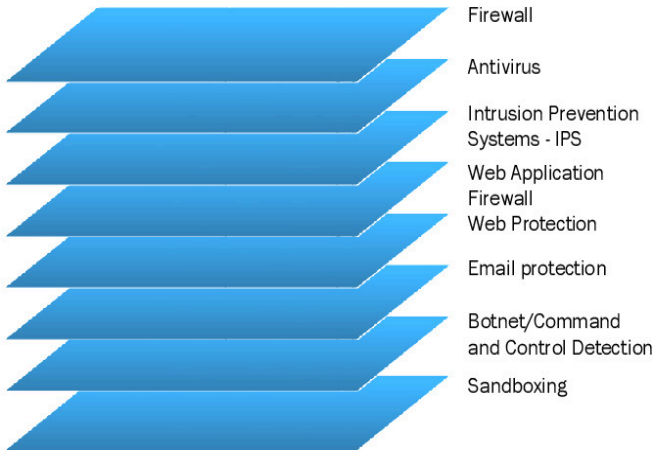


Figure 1: Multi-layered security by [8]

2.3 Previous Research to Secure Cloud-based Service

Here are some studies related to the design and security in cloud computing. The first study is titled "Towards Achieving Data Security with the Cloud Computing Adoption Framework" [12], and the research title is "Cloud computing adoption framework: A security framework for business clouds" [13]. Cloud computing architecture is a process of adopting cloud computing in a company. Making the right cloud computing architecture design can maximize the company's efficiency, cost, and service quality. Besides, a cloud computing architecture design is useful to improve the security of services and environments by ensuring that all data stored in the cloud are safe from attacks and threats. In this study, the authors made a cloud computing architecture design using the Cloud Computing Adoption Framework (CCAF). The framework creates 3 (three) layers of security that are used to protect data. The authors created the following layers of security: 1) Access Control and Firewall Layer, 2) Intrusion Detection System (IDS) and Intrusion Prevention System (IPS), dan 3) Encryption / Decryption Control Layer.

Multi-layered security is a strategy implemented to protect the environment. Based on Artur Rot and Boguslaw Olszewski's research, multiple layers of security can protect the environment from Advanced Persistent Threat (APT) threats. The results prove that it can improve cloud environment security. It is because each layer has its role, function, responsibility, and technology to protect the environment [8]. Based on a research from Mouna Jouini and Latifa Ben Arfa Rabai, there are 3 (three) requirements

to secure a cloud computing environment, which are Availability, Integrity, and Confidentiality.

Therefore, the authors use research methods that refer to research [12], [13], and [8], which made of a combination between Next-Generation Firewall (NGFW) and Web Application Firewall (WAF) technologies to secure cloud-based web application services a company made for human resource management.

3. Research Methodology

In this part, we will explain the process of creating an architecture design using the SDLC method in the top-down network design that we have mentioned previously in section 2. Here are the following steps:

3.1. Analyze Requirement

In this step, we do an analysis and identification on the company needs. There are 2 (two) stages carried out in this initial step:

1. Business Purpose Analysis: understanding the company's goals and limitations are important in the design process. For this reason, we conducted interviews with the supervisor and the company's management. The results are:

- Providing IT solution services for companies
- Increase satisfaction by using the cloud-based HRM services provided
- Increase the level of service provided

2. Technical analysis: In the second stage, we were doing technical analysis. The purpose is to recommend one or two technologies that we were going to use in making the design. To reach this technical goal, we have to analyze the business objectives of the company. Then we mapped it to suit the company's technical purpose. We can adjust the technical purpose to suit the company's business objectives. The company's main problem is the security technology that they have been using was unable to secure the company's assets and service. Therefore, we need a design that can improve the security and support the business goal of the company. Several technologies can be used to secure cloud-based web applications, such as Next-Generation Firewall and Web Application Firewall. Both technologies are able to support security at OSI layer 7.

3.2. Creating a Logical Design

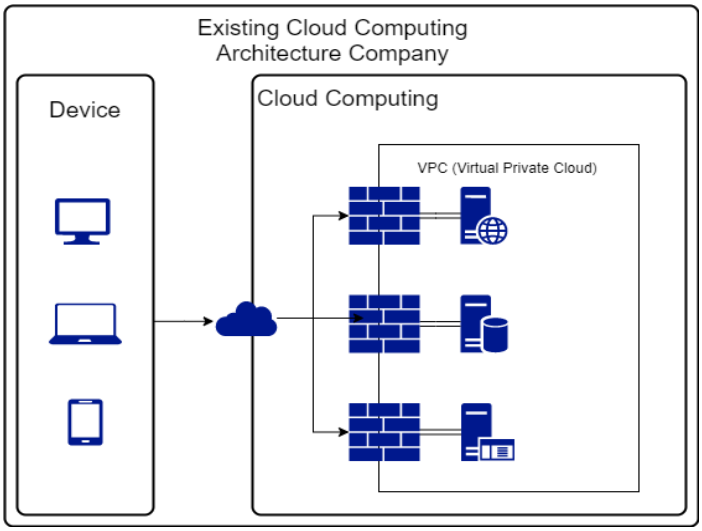


Figure 2: Existing Cloud Architecture at Company

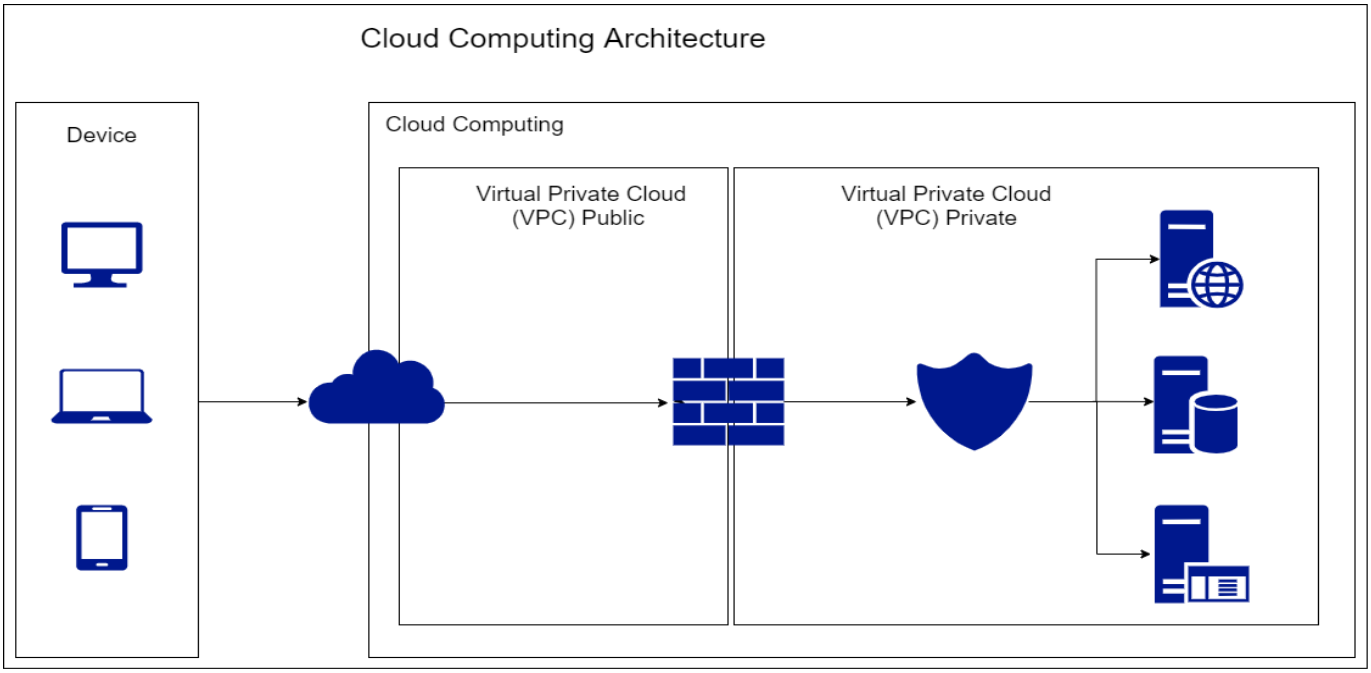


Figure 3: Propose Cloud Computing Architecture

In designing cloud-computing architecture, we need to know what kind of technology the company uses in providing services such as, operating systems, storage, servers, and other supporting services. After finding out the technology, we can make the design that meets their need.

Figure 3 is the logical design that we propose to improve the security of the company assets. We use a multi-layered security strategy by combining the Next-Generation Firewall and Web Application Firewall security technologies to secure the company assets. In our proposed design, we also take advantage of Virtual Private Cloud (VPC) technology. We separate between public and private networks using VPC so that the company assets cannot be accessed directly through the public network.

3.3. Creating Physical Design

After the logical design is complete, the next step is making the physical design. At this point, we had to determine which security technology that we were going to implement in each security layer. Here are the security technologies that we were using in each layer of security.

1. Next Generation Firewall Server: In the first layer, we used Next-Generation Firewall technology with 2vCPU server specifications, 8 GB of memory, SSD 1 = 10 GB, SSD 2 = 30 GB, whereas the Next Generation Firewall is using 2 NICs.
2. Web Application Firewall: The second layer is the Web Application Firewall with 2vCPU server specifications, 8 GB of memory, SSD 1 = 10 GB, SSD 2 = 30 GB.

To increase cloud-based web application services security provided by companies, we chose both technologies mentioned above. In cloud computing, we can use Pay as You Go (PAYG) services. So, companies do not have to purchase licenses to use the technologies.

4. Result and Discussion

In this chapter, we are going to evaluate our proposed cloud computing architecture to find out their capabilities. There will be 2 steps, the first step is to determine the cloud computing architecture design that is being used. Second, we create a prototype based on our cloud computing architecture design. We are doing the penetration testing by using the SQL injection and malicious file injection testing methods to evaluate the design. These are the test scenario by using the penetration testing method:

1. We use the SQLMAP tool to execute 3 (three) SQL command scripts, which can be seen in table 3 to attack the cloud-based web application.
2. We use the upload feature on the company's web application to send 200 Malicious Files to the cloud environment.

After the penetration testing process is complete, we collected logs and reports from each security layer. Afterward, we analyze the logs and reports. The results of the SQL injection can be seen in table 3 and the results of the malicious file injection can be seen in figure 7.

4.1. SQL Injection

The first penetration testing method that we use was SQL Injection using SQLMAP tools. According to [14], SQL Injection is a method to test web application security by sending malicious code to the server. We did this practice in order to prevent any threat in the future because every client's personal data are stored in the cloud-based web application. Table 2 is a comparison between using firewall security provided by the Cloud Service Provider (CSP) and multi-layered security cloud computing architecture.

Table 2 shows that the firewall that the company currently using unable to prevent or detect SQL Injection threats. This confirms that the database server and cloud computing environments are in danger.

Table 1: SQL Injection Script

NO	SQL Injection Script
1	Python sqlmap.py -u "https://apps.gautamaawijaya.com/Login.aspx?ReturnUrl=%2f" --risk=2 --dbs --dbms= MySQL -- randmon-agent
2	Python sqlmap.py -u "https://apps.gautamawijaya.com/Login.aspx?ReturnUrl=%2f"--data="log=test&pwd=test&wp-submit=Log+in" --dbs --level=3 --risk=2 --dbms=MySQL -- randmon-agent
3	python sqlmap.py -u "https://apps.gautamawijaya.com/Login.aspx?ReturnUrl=%2f" --data="log=test&pwd=test&wp-submit=Log+in" --dbs --level=3 --risk=2 --dbms=MySQL -- randmon-agent --tamper=between,charencode,charunicodeencode,equaltolike,greatest,multiplespaces,percentage,randomcase,sp_password,space2comment,space2dash,space2mssqlblank,space2mysqldash,space2plus,space2randomblank,uionalltounion

Table 2: Comparison of Result

No	Firewall	Cloud Computing Multi-layered Security
1	Pass	Block
2	Pass	Block
3	Pass	Block

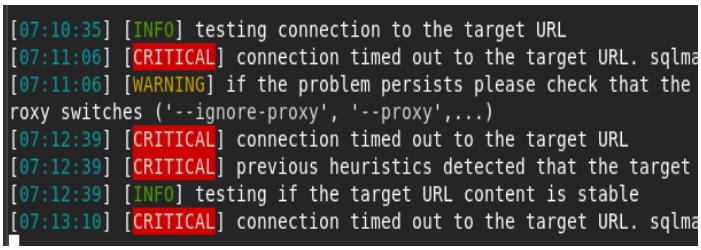


Figure 4: SQL Injection using SQL Map Tools

Figure 4 gives details of the SQL injection process using SQLMAP tools. The figure shows that "CRITICAL connection time out to the target URL". The message appears because the Next-Generation Firewall and Web Application Firewall have blocked the requests to SQLMAP tools.

Table 3: SQL Injection Result

Command	Layer 1	Layer 2
1	Block	-
2	Block	-
3	Pass	Block

Table 3 gives an overview on the ability of each layer to detect SQL injection threats. As explained in the test scheme before, in table 1, there are 3 SQL injection scripts used to evaluate the cloud computing design that we have proposed. The first layer, which is the Next-Generation Firewall, successfully prevent the SQL injection attack script 1 and 2 with the IPS features. Whereas the injection attack script 3 pass the first layer but successfully prevented by the second layer, which is the Web Application Firewall using SQL Injection and XXS features.

4.2. Malicious File Injection

The second method that we use to evaluate the cloud computing architecture design is Malicious File Injection. This method attacks the cloud computing architecture design by sending Malicious Files that have been infected by malware [15]. This method will attack the weakest part of the company's cloud-based web applications. Vulnerability was found in the photo upload feature which can be seen on figure 6. In those features, various types of file extensions can have access. Therefore, we take advantage of this weakness by uploading 200 malicious files.

In the attack process, we download 200 malware sample from the malware-sample-library, malware-sample, the Zoo, and Malware Database-master source. After the download process is complete, we verify 200 files that we are going to use in the evaluation. We confirm the malicious files and upload it to www.virustotal.com.

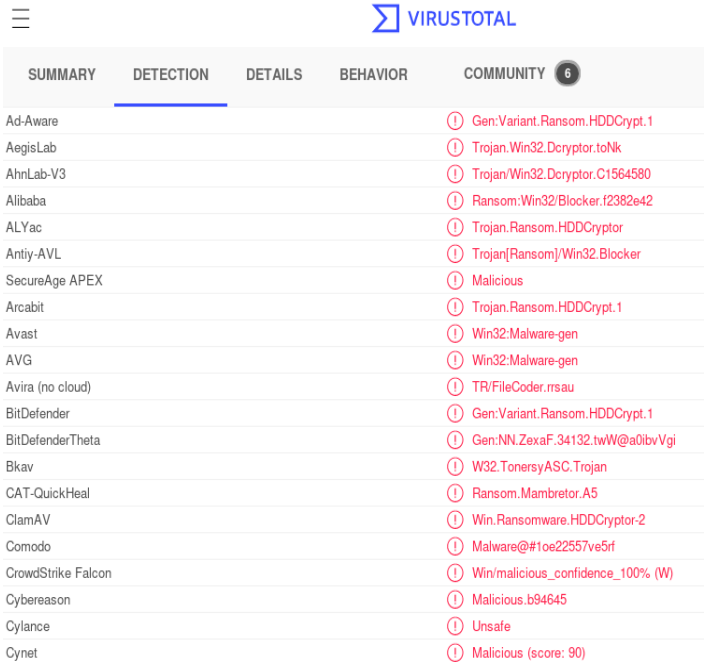


Figure 5: Virus Total Result

Figure 5 is the test result for one of the Malicious Files that we use. After the verification process complete, we begin the malicious file injection process.

We do the injection process to the weakest part of the photo upload feature. Figure 6 shown the photo upload feature that we used as a test.

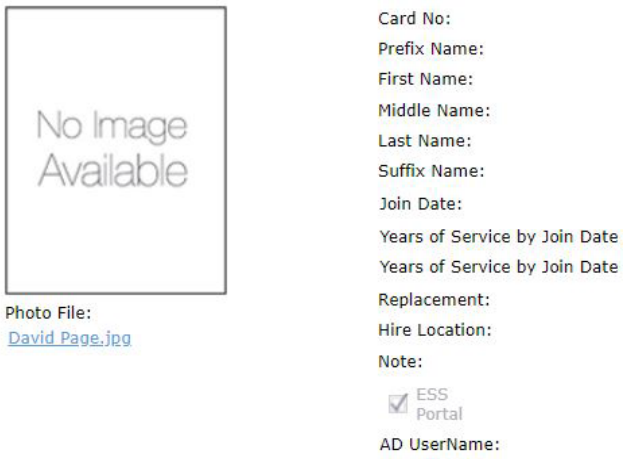


Figure 6: Feature of Cloud-based Web Application

In these features, we upload 200 malicious files that we have verified before. We repeat the process until all 200 malicious files are successfully uploaded.

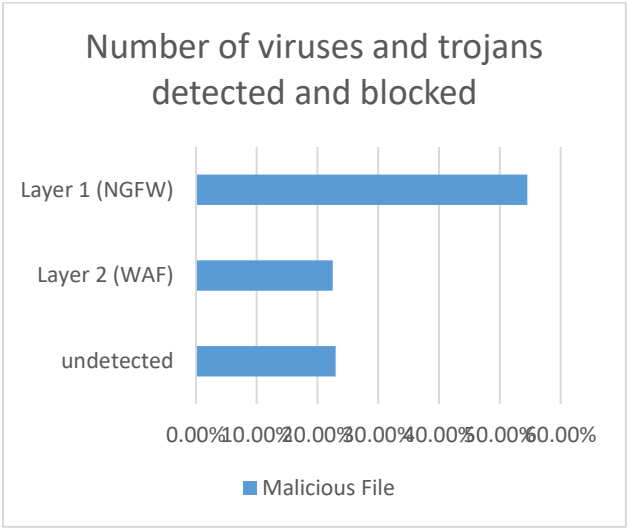


Figure 7: Number of viruses, trojans detected, and blocked

After the attack process is complete, we collect the logs and report from each layer. The logs and reports contain action information on how each layer detect and prevent threats. Figure 7 shows us information about the ability of each layer to identify malicious files. Next-Generation Firewall manage to identify 54.5% of threat on layer one, while at layer 2, the Web Application Firewall manage to detect 22.5% of threat. The total amount detected from this multi-layer security cloud computing architecture is 77%. While there are still 23% of malicious files that are not successfully identified by this architecture.

Table 4 shows the evaluation result using the malicious file injection method. In this evaluation, we divided the type of malware into 4 (four) categories shown in table 4. There is 23% undetected malware pass our proposed cloud computing architecture. To identify the malware, layers 1 and 2 use information from the malware signature database located in each layer. Therefore, the availability of malware information is important to be able to identify malware threats.

Table 4: File Injection Result

Virus Type	Total	L1	L2	detected	Undetected
Ransomware	38	23	7	30	8
Trojan	129	67	34	101	28
Worm and Virus	16	11	3	14	2
Other (Adware, Riskware, Backdoor and EXE infector)	17	8	1	9	8
Total	200	109	45	154	46

Evaluation using penetration testing with malicious file injection provides an overview on the ability of each layer to detect and prevent malicious files from reaching the environment through the application layer. The following is the comparison between firewall security provided by the Cloud Service Provider (CSP) and multi-layer security. The result shows that the firewall cannot detect and prevent malicious file threats. In comparison, multi-layer security manages to detect and prevent 154 file threats, equivalent to 77% of malicious files that have been identified and blocked.

5. Conclusion

Based on the evaluation and testing results, multi-layer security cloud computing architecture can protect company's cloud-based web applications. By using multi-layered security cloud computing, it is proven that it improves the security of cloud-based human resource management services.

Table 5: Comparison Security

NO	Evaluation Method	Existing Security	Multi-Layered Security
1	SQL Injection	PASS	Block
2	Malicious File Collection	PASS	Block

Table 5 is the comparison between security used by company and cloud computing multi-layer security. The current technology used by the company cannot optimally protect company assets. This makes the application, database, and the company's environment is under threat because it cannot detect and prevent threats.

In conclusion, it is important to create a cloud computing design that meets the needs of the company, because the design is going to be implemented to the company as well. Using the System Development Life Cycle (SDLC) method, the author is able to identify the needs, goals, technology, and problems experienced by the company. To improve the security of cloud-based web applications, the authors use multi-layer security architecture by creating several layers of security that can increase security for services provided by companies. The advantages of multi-layer security are each layer can cover its weaknesses in preventing and detecting threats. The result can be seen in our evaluation using the SQL Injection and Malicious File Injection methods. Assessment using these two methods provide an overview on how the multi-layer security architecture secures cloud-based web applications.

The result of this paper is to describe how to secure cloud-based web applications using multiple layers of security methods. Combining the Next Generation Firewall (NGFW) and Web Application Firewall (WAF), can maximize cloud-based web applications security as well. Many security technologies can be combined to secure cloud-based web applications.

Acknowledgment

The research publication is fully supported by Bina Nusantara University.

References

[1] H. Takabi, J.B.D. Joshi, G.J. Ahn, "Security and privacy challenges in cloud computing environments," IEEE Security and Privacy, **8**(6), 24–31, 2010, doi:10.1109/MSP.2010.186.

[2] M. Almorsy, J. Grundy, I. Müller, "An Analysis of the Cloud Computing Security Problem," International Surgery, **47**(3), 288–290, 2016, doi:arXiv:1609.01107.

[3] E. Abdurachman, F.L. Gaol, B. Soewito, "ScienceDirect ScienceDirect Survey on Threats and Risks in the Cloud Computing Environment Survey on Threats and Risks in the Cloud Computing Environment," Procedia Computer Science, **161**, 1325–1332, 2019, doi:10.1016/j.procs.2019.11.248.

[4] M. Jouini, L.B.A. Rabai, "A Security Framework for Secure Cloud Computing Environments," International Journal of Cloud Applications and Computing, **6**(3), 32–44, 2016, doi:10.4018/ijcac.2016070103.

[5] G.I.P. Duppa, N. Surantha, "Evaluation of network security based on next generation intrusion prevention system," Telkomnika (Telecommunication Computing Electronics and Control), **17**(1), 39–48, 2019, doi:10.12928/TELKOMNIKA.v17i1.9191.

[6] P. Oppenheimer and T.-D. N, Top-Down Network Design Top-Down Network Design, 2010.

[7] M. Wairisal, N. Surantha, "Design and Evaluation of Efficient Bandwidth Management for a Corporate Network," Proceedings of 2018 International Conference on Information Management and Technology, ICIMTech 2018, (September), 98–102, 2018, doi:10.1109/ICIMTech.2018.8528162.

[8] A. Rot, B. Olszewski, "Advanced Persistent Threats Attacks in Cyberspace. Threats, Vulnerabilities, Methods of Protection," in Position Papers of the 2017 Federated Conference on Computer Science and Information Systems, 113–117, 2017, doi:10.15439/2017f488.

[9] N. Khan, A. Al-Yasiri, "Cloud Security Threats and Techniques to Strengthen Cloud Computing Adoption Framework," International Journal of Information Technology and Web Engineering, **11**(3), 50–64, 2016, doi:10.4018/ijitwe.2016070104.

[10] J. Surana, K. Singh, N. Bairagi, N. Mehto, N. Jaiswal, "Survey on Next Generation Firewall," IJEDR - International Journal of Engineering Development and Research, **5**(2), 984--988, 2017.

[11] C, "Web application firewall using XSS," International Journal of Engineering & Technology, **7**(2.7), 941, 2018, doi:10.14419/ijet.v7i2.7.11429.

[12] V. Chang, M. Ramachandran, "Towards Achieving Data Security with the Cloud Computing Adoption Framework," IEEE Transactions on Services Computing, **9**(1), 138–151, 2016, doi:10.1109/TSC.2015.2491281.

[13] V. Chang, Y.H. Kuo, M. Ramachandran, "Cloud computing adoption framework: A security framework for business clouds," Future Generation Computer Systems, **57**, 24–41, 2016, doi:10.1016/j.future.2015.09.031.

[14] A. Hasan, D. Meva, "Web Application Safety by Penetration Testing," 4TH International Conference on Cyber Security (ICCS), (January), 159–163, 2018.

[15] K. Pooj, S. Patil, "Understanding File Upload Security for Web Applications," International Journal of Engineering Trends and Technology, **42**(7), 342–347, 2016, doi:10.14445/22315381/ijett-v42p261.

ASTES

Advances in Science, Technology and Engineering Systems Journal Vol. 5, No. 5, 680-691 (2020)

www.astesj.com

ASTESJ

ISSN: 2415-6698

Enterprise Architecture Institutionalization for Health Information Exchange (HIE) Cloud Migration

Kofi Osei-Tutu*, Yeong-Tae Song

Department of Computer and Information Sciences, Towson University, Towson MD, 21022, USA

ARTICLE INFO

Article history:
Received: 01 August, 2020
Accepted: 11 September, 2020
Online: 05 October, 2020

Keywords:
Enterprise Architecture
Enterprise Architecture Framework
Health Information Exchange
Cloud Technology

ABSTRACT

The functional priority of Health Information Exchanges (HIEs) is to ensure a timely transference of health data. Because of the frequency at which health records are transferred and the variety of health data HIEs receive, there are major challenges in efficiently accomplishing this. Cloud technology has become a generally accepted solution to remediate data transference issues but for HIEs, there are usually no clear paths to adoption.

Enterprise Architecture (EA) is a tool that can ensure the smooth adoption and implementation of technologies. This paper is an extension of a proposal originally presented in the 14th International Conference on Ubiquitous Information Management and Communication (IMCOM). In that article, an enterprise architecture that supports an HIE migration to a cloud architecture was proposed. This paper presents an EA migration plan and proposes an institutionalization framework, highlighting how the proposed EA can be applied to an HIE. A validation framework is provided as a means of testing the implementation of the HIE migration EA.

1. Introduction

Enterprise Architecture (EA) at its core can be defined as a blueprint for allocating IT resources for the ultimate support of business goals. When applied successfully, EA becomes a tool that enterprise architects and decision-makers can use to understand an organization's current state. Organizations can also use EA to pinpoint future goals and map a way of achieving them.

To successfully leverage EA, architects must be able to understand and diagram their organization's IT architecture, identify and understand business architecture as-is, and determine what future organizational business goals are (to-be). Once goals are outlined, a gap analysis can be performed to determine how IT can support the realization of organizational goals.

Enterprise architecture allows organizations to achieve great performance by ensuring there is a seamless flow of information and services throughout the organization. This requires that processes and systems are well integrated, and a high level of connectivity is maintained.

For an HIE to achieve great performance, there needs to be a bi-directional flow of data and processes between the HIE and the health institutions it serves. A smooth bi-directional flow is evidenced in an organization's computing resources' ability to seamlessly share data and information.

Health Information Exchange (HIE) organizations and technologies have become an essential component of well-developed healthcare environments. In the United States, federal health policies have been enacted to encourage the establishment of HIEs as a healthcare solution. The 21st Century Cures Act in 2016 and the Health Information Technology for Economic and Clinical Health Act (HITECH Act) in 2009 allowed HIEs to serve as a solution for healthcare interoperability [1], [2].

There are two general forms of HIEs: query-based and directed-data serving. Query-based HIEs function as an informational hub for healthcare providers, health institutions, and related organizations who have opted-in to access and edit patient records. Directed-data serving HIEs transfer data directly to opted-in institutions and organizations. With this solution, HIEs functioning as a data transfer point through which records are transmitted. Both HIE solutions utilize health data standards like Continuity of Care Document (CCD), DIRECT Secure Messaging, and other "push" triggered transmissions to ensure records are transferred [3].

Although HIE solutions, operations, and technologies are well established, challenges still exist in scenarios where records need to be urgently transferred or made available. These challenges

* Corresponding Author: Kofi Osei-Tutu, 7800 York Rd., Towson MD, koseitutu@towson.edu

stem from the complex data intake and transference workflows HIEs manage [4,5].

Well established HIEs serve multiple health institutions and deal with a wide variety of health records. Some of these records include demographic information, lab results, image reports, transfer summaries, radiology reports, and much more. Successful management of health data and ensuring that records are retrieved on-demand require a well-designed architecture and robust computing capabilities.

While current solutions allow health institutions to forward data to other care providers, data is not always readily available when needed. In emergency scenarios, access to patients' complete health records on-demand will greatly assist emergency caregivers in making better decisions and preventing medical errors.

Most HIEs and health institutions are addressing data transfer challenges by migrating from an on-premises environment to cloud-based computing and storage solutions. Private cloud sharing systems [6] and cloud computing technologies like IoT [7] have been researched and implemented. In healthcare, cloud-based health data exchange services and electronic health record (EHR) systems have become extremely popular. To smoothly transition from an on-premises HIE environment to a cloud-leveraged solution, it is necessary to architecturally account for all aspects of the migration. All the work involved in the project and the impact of every change must be taken into consideration. Enterprise architecture provides a valuable tool in that regard.

The rest of this paper is organized as such: section two discusses enterprise architecture concepts and introduces the three main enterprise architecture frameworks (EAFs) utilized to develop the proposed solution. Section two also provides an overview of HIEs and Cloud technologies. Section three provides a literature review of work done in this field. In section four, a cloud migration plan is proposed and an EA institutionalization framework for applying the architecture is presented. An architectural validation mapping and a means of testing the architecture is provided. Section five concludes the paper with a summary of the proposed solution, potential future work, and acknowledgments.

2. Background

2.1. Health Information Exchange (HIE)

As technology has improved over the past few decades, there have been great leaps in patient data recording and storage. These improvements brought about the development of Electronic Health Record (EHR) systems as a means of digitally recording and storing health data.

Before the introduction of HIEs, patient data like immunization records, lab test results, allergies, admission and checkup information, etc. were digitally managed on hospital EHR systems and health data was only accessible to the organization that recorded it. The inability to transfer health records among multiple health institutions limits healthcare coordination and produces unneeded costs, both to healthcare institutions and patients. The introduction of HIEs addressed those limitations and provided continuous care improvement and provisioning to patients.

Health Information Exchanges are collaborative health organizations established to provide a smooth transference of patient records between health institutions (i.e. Hospitals and Clinics) in a geographic location. The geographic location where an HIE resides is dependent on the local government's determination and the HIE's ability to accommodate data transference.

Depending on the government's influence on healthcare, health institutions like clinics, hospitals, etc., may not be mandated to participate in an HIE [2]. In any scenario, institutions that participate in an HIE environment expect their EHR systems and HIE technologies to be well integrated. These expectations mean that HIEs must accommodate heterogeneous EHR infrastructures, handle a variety of data formats, and be able to transfer records to different network architectures. For this reason, government agencies invest a lot of resources to ensure that necessary HIE operations are in place for EHR communication. Sometimes, government agencies are established and well-funded to support, promote, and monitor the success of HIE institutions. For instance, in 2010, the United States Department of Health and Human Services awarded over $548 million through the State HIE Cooperative Agreement Program [4] to several state HIEs throughout the country.

2.2. Enterprise Architecture (EA)

Enterprise Architecture is derived from the words, enterprise and architecture. An enterprise refers to organizations, businesses, or large corporations. Architecture is usually defined as a logical representation or design of a physical system. Combined, EA is defined as the complete expression of an organization's business, information systems, and technology strategies. EA also includes the process of identifying business processes, pinpointing business functions, and determining the impact of Information Technology (IT) on it.

Developing an enterprise architecture involves utilizing generally accepted EA principles, standards, and techniques to collect and document an organization's business strategies, processes, principles, and practices into understandable artifacts. The business artifacts are then married with already documented IT processes and assets. The purpose of accomplishing this is to facilitate the realization of organizational goals.

Once successfully applied, enterprise architecture provides a sense of clarity for organizational decision-makers. Using EA principles and practices, decision-makers can automate and streamline processes to better accomplish tasks. EA can also be used as a tool that facilitates the accomplishment of goals and the realization of technologies. Using an as-is architecture coupled with a to-be architecture, architects can perform a gap analysis to map a path to reach goals.

High-Performing healthcare organizations like Mayo Clinic in Minnesota, US and Lafayette General Health System (California, US) have engaged in these strategies and tactics to drive technical performance and improvement [8].

An enterprise architecture framework (EAF) is a predesigned architecture template used to develop enterprise architecture. Because EA combines a wide array of disciplines ranging from business management and organizational development to IT

architecting, EAFs serve as a tool to define how an EA can be designed and applied to enterprises. EAFs provides guidelines on how to create an architecture and can provide best practices in architectural design and development.

The process of applying an EA framework to an enterprise is termed institutionalization [9]. To apply or create an EA, enterprise architecture frameworks provide a set of well-defined guidelines and procedures that must be followed. The solution presented in this paper utilizes three EAFs: The Patient Demographic Data Quality Framework (PDDQ), the Zachman EA Framework, and The Open Group Architecture Framework (TOGAF).

The Open Group Architecture Framework (TOGAF)

TOGAF is the most well-adopted and applied EAF. TOGAF is made up of five key components, the Architecture Development Method (ADM), the ADM Guidelines and Techniques, Architecture Content Framework (ACF), Enterprise Continuum, and Architecture Capability Framework. These five pieces provide a comprehensive approach to enterprise architecture. As technology has evolved, the framework has been improved and revised [10]. The most current release of TOGAF is at version 9.2.

The ADM contains phases of the TOGAF EA design and implementation. Following the ADM phases step-by-step, organizations can develop an enterprise architecture. The phases are, Preliminary, Architecture Vision, Business Architecture, Information Systems Architectures, Technology Architecture, Opportunities and Solutions, Migration Planning, Implementation Governance, Architecture Change Management, and Architecture Requirements Management. The ADM also provides a set of guidelines and techniques that can be used to design and implement the framework [10].

The ACF provides a collection of artifacts that be utilized as building blocks for the design and implementation of architecture. With the ACF, architects have a tool that helps define how artifacts relate to each other, its importance, and how they fit into the development of an EA. Artifacts are also categorized in different TOGAF ADM phases so that architecture development and implementation is facilitated.

Enterprise Continuum provides practices and tools to classify and group architecture artifacts during the institutionalization process [10].

Zachman Enterprise Architecture Framework

The Zachman Enterprise Architecture Framework is an EA classification scheme of descriptive representations that can be utilized to design and develop an enterprise architecture [11].

At its core, the Zachman Framework is an ontological representation of systems and projects. For enterprise architects, Zachman provides a logical structure that can be emulated to categorize, arrange, and depict system/organizational artifacts in a detailed manner. The framework can be used to support healthcare institutions in the development, design, integration, and management of information systems.

Zachman is a matrix of representations that categorize actors, their roles, and their contributions to a system or an enterprise. The framework provides illustrations that describe actors' viewpoints to a system/organization based on their concerns. The matrix contains six columns: data, function, network, people, time, and motivation. The rows are comprised of the different stakeholders and their needs. For each matrix, there are a set of artifacts that contribute to the creation of architecture.

Patient Demographic Data Quality Framework (PDDQ)

The Office of the National Coordinator for Health Information Technology (ONC) of the United States government worked with the Capability Maturity Model Integration (CMMI) Institute to develop a framework that healthcare organizations can use to measure their patient data management capability. In 2015, The PDDQ Framework was derived from the Data Management Maturity model as a module to support the development of health systems, HIEs, and other health institutions alike.

The PDDQ is comprised of nineteen process areas across five categories. The five categories of the framework are Data Governance, Data Quality, Data Operations, Platforms and Standards, and Supporting Processes. These process areas provide a list of best practices needed to develop a sustainable healthcare data management organization/system so that patient data quality is improved and maintained [12].

2.3. Cloud Technologies

Cloud technologies, commonly termed Cloud Computing, provides a wide array of on-demand computing resources and services to its customers with great availability. The provisioning of these computing resources can greatly improve the development of IT in the support of their organization's goals. As cloud services are provided to an organization, IT has the responsibility of ensuring that the right services are acquired and resources are utilized to their full capacity [13].

Generally, cloud technologies service providers provide computing resources to its clients virtually from remote facilities (the cloud). Resources are categorized into three major services, Software as a Service (SaaS), Platform as a Service (PaaS), and Infrastructure as a Service (IaaS).

Software as a Service

Software as a Service is a cloud computing delivery model by which software is distributed to enterprises and organizations. SaaS software is usually procured on a subscription or license-based model and is accessed through the internet. Maintenance and the management of SaaS products are handled by the cloud computing service provider.

From an HIE perspective, software as a service can be leveraged for the organization's internal processes and functions. Organizational activities like HR and legal, finance and accounting, and sales and customer relationship management can benefit greatly when software can be delivered virtually. Architecturally, IT support and maintenance costs can be alleviated when there are fewer in-house applications to manage. The role of IT in these scenarios is to ensure that robust governance standards and policies are established and practiced by all users. IT must also provide resources that end users can use to access SaaS software and applications.

Platform as a Service

With Platform as a service, application platforms and development tools are provided to enterprises. Using cloud

technologies, organizations can leverage these services to provide its stakeholders with the hardware and software environments required to develop and deploy enterprise-level tools.

PaaS services are quickly becoming the most widely leveraged cloud computing technology resource because of the flexibility it provides to organizations to plan, build, and test quickly. PaaS provides computing platform resources like development tools and management services, computing middleware and frameworks, collaboration tools, and other integrated development services.

Because the value proposition of HIEs is to provide an environment where health data can be transferred across health institutions seamlessly, it is imperative that HIE IT departments quickly adjust to its customers' (health institutions) changing technology requirements. As EHR systems are upgraded or modified, HIE may require modifications to its transfer software codebase so that patient health records are transferred consistently. PaaS can provide HIE IT development teams with the resources needed to effectively perform its development activities.

Infrastructure as a Service

Infrastructure as a Service provides organizations and businesses with the computing infrastructure required to perform day to day business functions. Some of the infrastructure services IaaS provides include virtualized computing, storage, and networking.

Although PaaS provides organizations with a level of computing, storage, and network capabilities, IaaS encompasses the outsourcing of infrastructure components. Using the internet, organizations can access complete computing infrastructure components like servers, data centers, etc. from the cloud.

For HIEs, IaaS allows IT to outsource the complexities that result from managing computing infrastructures inhouse. On-premises architectures require major planning for backups, disaster recovery, and fault tolerance. However, with the introduction of IaaS, organizations can shift their focus to improving their technological provisioning while cloud service providers handle major infrastructure undertakings [13].

3. Related Work

Several HIE-related solutions have been proposed, developed, and implemented in the past decade. These solutions either seek to improve the level of interoperability in health data exchange or enhance HIE architecture.

Proposed solutions that address health data exchange interoperability have focused on interoperability architecture frameworks, cross-organizational standards (ex. HL7, SNOMED-CT), open source APIs to facilitate plug and play development solutions, complete middleware software applications, or a combination of the above.

For enterprise architecture focused solutions, S. In [14], the author highlighted successful EA implementations, discussed some of their characteristics, and presented the factors that lead to a successful EA implementation. A. In [15], the author also discussed successful implementations and recommended methods of assessing architecture institutionalizations. Although both papers address broad EA challenges, their proposals do not specifically target the development and implementation of a cloud migration architecture. A. In [7], the author provided an EA implementation template but did not identify specific methodologies and building blocks for creating an architecture. Although D. In [16], the author provided general guidelines for EA development in public sector organizations, the recommendations are general and do not specifically apply to HIE migrations to a cloud architecture. F. In [17], the author proposes a healthcare-specific EA but only focuses on the technology and infrastructure domains of architecture.

HIE Architecture solutions can be classified into four domains, Business, Data, Application, and Infrastructure. The subsections below introduce related solutions and discuss how previous work fits into the four domains of architecture.

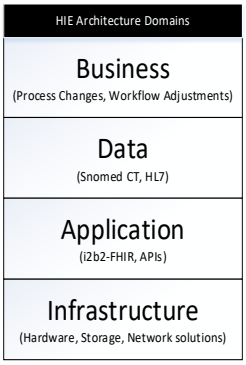


Figure 1: HIE Architecture Domains

In enterprise architecture, The Business Domain represents HIE and health institution organizational activities and goals. A combination of the Data, Application, and Infrastructure Domains represents IT. Within IT, the combination of application and data domains of architecture is referred to as Information Systems. The infrastructure domain is usually referred to as the Technology domain. Below is a breakdown of each architectural domain.

3.1. Business Domain

The Business Domain represents an aspect of architecture where business (healthcare) processes occur. To ensure HIEs are successful, organizational standards must be communicated and documented. Processes and activities must also be streamlined with effective documentation, practice, and governance.

Several articles identify useful references for developing interoperability on a business process level [8,18]. In [19], the author proposed business-focused enterprise architecture approaches for enhancing healthcare interoperability. Most of the related work proposed in this domain do not address items from other domains in detail.

3.2. Data Domain

At the Data Domain, health data collection, formatting, and management are at the forefront of all activities. HIEs must ensure that data security is enforced, and unauthorized individuals are prevented access to data. HIE organizations must also work to ensure a smooth transference and storage of health data. Lastly, HIEs should strive to maintain a high level of data interoperability in this domain.

Health data standards like Health Level 7 (HL7), Digital Imaging and Communications in Medicine (DICOM), and Systematized Nomenclature of Medicine (SNOMED CT) has been established to facilitate the storage, transference, and management of health records. Several articles have proposed solutions to leverage the HL7 standard, SNOMED CT, etc. [14], but very few have dealt with data management in a context where all four domains of architecture are addressed.

3.3. Application Domain

The application domain is a highly researched field that focuses on all software and application related tools used to enhance HIE operations.

Most interoperability-focused solutions are developed in this domain. Health data storage, sharing, and analysis solutions are also developed here. Some of these solutions include EHR and data sharing applications like Fast Health Interoperability Resources (FHIR), Integrating Biology and the Bedside (ib2b), and its corresponding APIs [20]. The introduction of blockchain-based healthcare solutions have been generally application and data domain-specific but is also greatly improving the quality of health data management.

3.4. Infrastructure Domain

At the infrastructure domain, system, network, and physical operational solutions are implemented. The purpose of this domain is to support the development and utilization of healthcare applications. The infrastructure domain provides the technology on which the rest of architecture is developed. Although application-based solutions are generally visible to stakeholders, infrastructure components may not always be visible.

HIE infrastructure solutions focuses on network connectivity, physical hardware components, server OS capabilities, storage hardware efficiency, etc. To ensure that the infrastructure domain is well built, HIEs must collaborate with health provider IT representatives and third party multi-disciplinary teams to create integration processes, support activities, and system administration.

4. HIE Enterprise Architecture for Cloud Migration

Enterprise Architecture can be leveraged as a tool for the adoption of technology. As described in section two, cloud technology addresses on-premises HIE challenges by ensuring the timely transfer of data to and from health providers. The HIE Enterprise Architecture presented in this section can be utilized to streamline the adoption of cloud technologies.

A complete enterprise architecture highlighting business level processes, information systems functions, and technology components are discussed in the institutionalization framework. A cloud migration architecture is proposed in section 4.2 and a validation framework is presented in 4.3.

4.1. EA Institutionalization Framework

This section presents how the proposed migration enterprise architecture can be leveraged as a tool for HIE cloud migration.

EA institutionalization requires the following steps to be followed:

1. Understanding an HIE's major business processes, functions, and policies.
2. Understanding the HIE's IT, its information systems, and its guiding processes/policies.
3. An understanding of the relationships between business and IT and how technology is constructed to support the HIE.
4. Designing and mapping an organization's architecture based on the information gathered in Steps 1,2 and 3.
5. Planning a feasible and realistic strategy to attaining future goals.

As discussed in previous sections, the primary step in developing an enterprise architecture is understanding business processes, functions, and activities and developing a robust business architecture.

Once that is completed an IT architecture must be built to fit the business architecture. The goal of EA is to design Information Technology to complement business goals and objectives.

Business Level Processes

The diagram below represents an overview of HIE business processes.

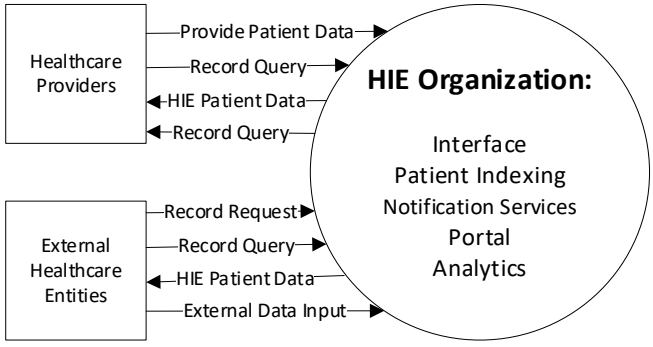


Figure 2: HIE Business Processes

The context diagram presents the five major processes and functions of HIEs.

- Interface – The interface process is the intermediary communication mechanism between an HIE and health institutions. It processes all incoming and outgoing data/records.
- Patient Indexing – Patient indexing comprises of the patient record mapping processes at the HIE level. HIEs must be able to understand incoming data from other health institutions.
- Notification Services – Notification processes are needed to initiate updates to health records in real-time. This process ensures that health records are updated on time without compromising data integrity.
- Portal – The portal process is the means by which HIE data can be accessible to healthcare institutions and other health providers.

Analytics – Using the analytics process, HIEs can provide a means of converting health data to health information. This process includes query creation and custom reports generation.

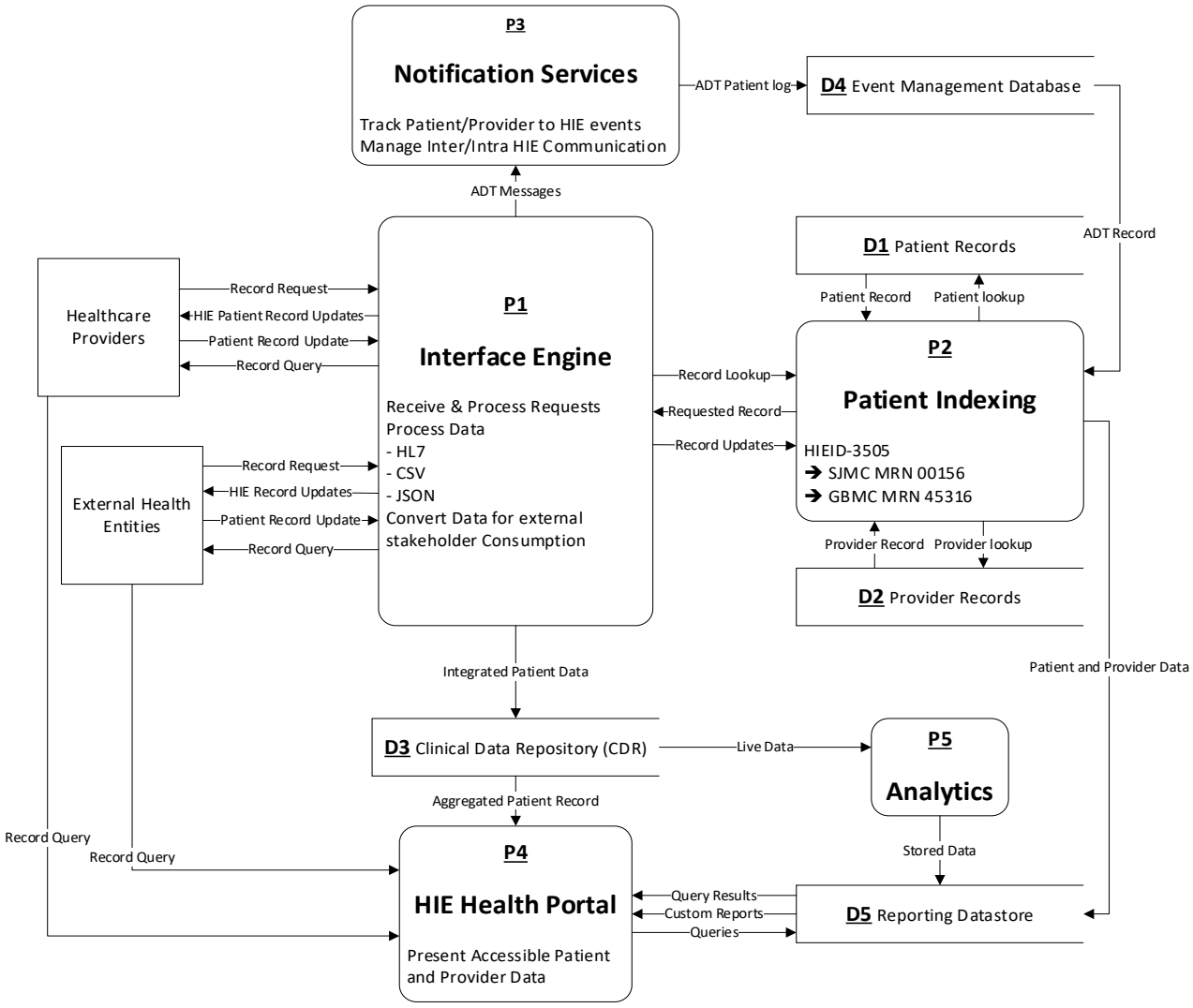


Figure 3: HIE Process and Information Systems Flow Diagram

HIEs have two main external stakeholders. These stakeholders are External Healthcare Entities and Healthcare Providers. External healthcare entities are healthcare institutions that may not directly provide health services but function to help improve health results. These institutions may include research institutions, other HIEs, or other health entities. Healthcare providers in this illustration represent partner hospitals and clinics.

External stakeholders usually have similar interactions with their HIEs. Flows include requests for data and updates to healthcare records.

Information Systems Architecture

Figure 3 is an excellent artifact for developing a comprehensive EA. It can be used to illustrate HIE business processes with corresponding application systems. Application systems are then mapped to potential data stores. The Information Systems Flow diagram, also referred to as a Data Flow Diagram is used to represent the relationship between the data domain and application domain of HIE IT architecture.

An understanding of HIE stakeholder relationships, internal application processes, and its relationship with data components can help organizational decision-makers understand the impact of information system changes. A breakdown of the relationships between HIE application systems (processes), external stakeholders, and data stores as portrayed above is as follows.

1. Interface Engine

The interface engine is referred to as the intermediary process between an HIE and its external stakeholders. This process serves as the communication hub for automated data transactions between HIE systems and external systems. Subsystems that reside within the interface engine process are:

- Request Receiving and Processing: This system focuses on receiving and processing external entity requests. This system queries external entities for data as when needed. Figure 3 highlights incoming and outgoing requests from external organizations to the Interface Engine.
- Data Conversion: As health data is received from external parties, tools and services are needed on the interface engine to perform data conversion. Since different health institutes may need to send data in different formats, the data conversion process is required to translate data as it enters the HIE

environment for consumption. Some examples of generally accepted health data formats accept are HL7, CSV, and JSON. Data is usually sent back to external entities in a similar format.

- Data Transference: After health data is converted, the interface engine forwards data to the patient indexing subsystem for processing. Health data is forwarded, processed, and shared with internal subsystems using the interface engine.

The interface engine system interacts with a clinical data repository (CDR) data store directly. The interface engine also interacts with notification service processes to ensure health records are automatically transported to and from clinical entities.

2. *Patient Indexing*

The patient indexing system ensures that patient records are properly maintained within the HIE. Indexing processes interact with interface engine systems to ensure received health data is reconciled with internal HIE records and that there are no redundancies. As seen in process two (P2) in figure 3, a patient's records may exist in different institutions and different EHR databases. Once a record update is received, the indexing process maps those records into a singular HIE record ID (HIEID-####).

The patient indexing system interacts with both provider and client data stores to ensure updates are stored. The indexing system receives record update messages like Admit Discharge Transport (ADT) alerts from notification systems.

Once records are updated, the indexing system transfers records to the reporting data store for data analytics reporting.

3. *Notification Services*

The notification services system ensures that records, alerts, and messages are transported to the right systems. This system tracks patient record updates and HIE events as they occur and logs them into the event management data store.

Depending on the system design, notification services processes may manage communications between both internal and external data stores. As previously explained, notification services systems communicate ADT and other update messages to the patient indexing and interface engine systems.

4. *HIE Health Portal*

The HIE Health Portal serves as a landing system for internal and external stakeholders. The portal also provides a means of communicating with external stakeholders.

As interface engine and reporting services processes append CDR data store, updates are delivered to the Health Portal for authorized user consumption. In special use cases, external health entities and health providers can provide their employees with the authorization to access this customer-facing system as a hub for complete health records access.

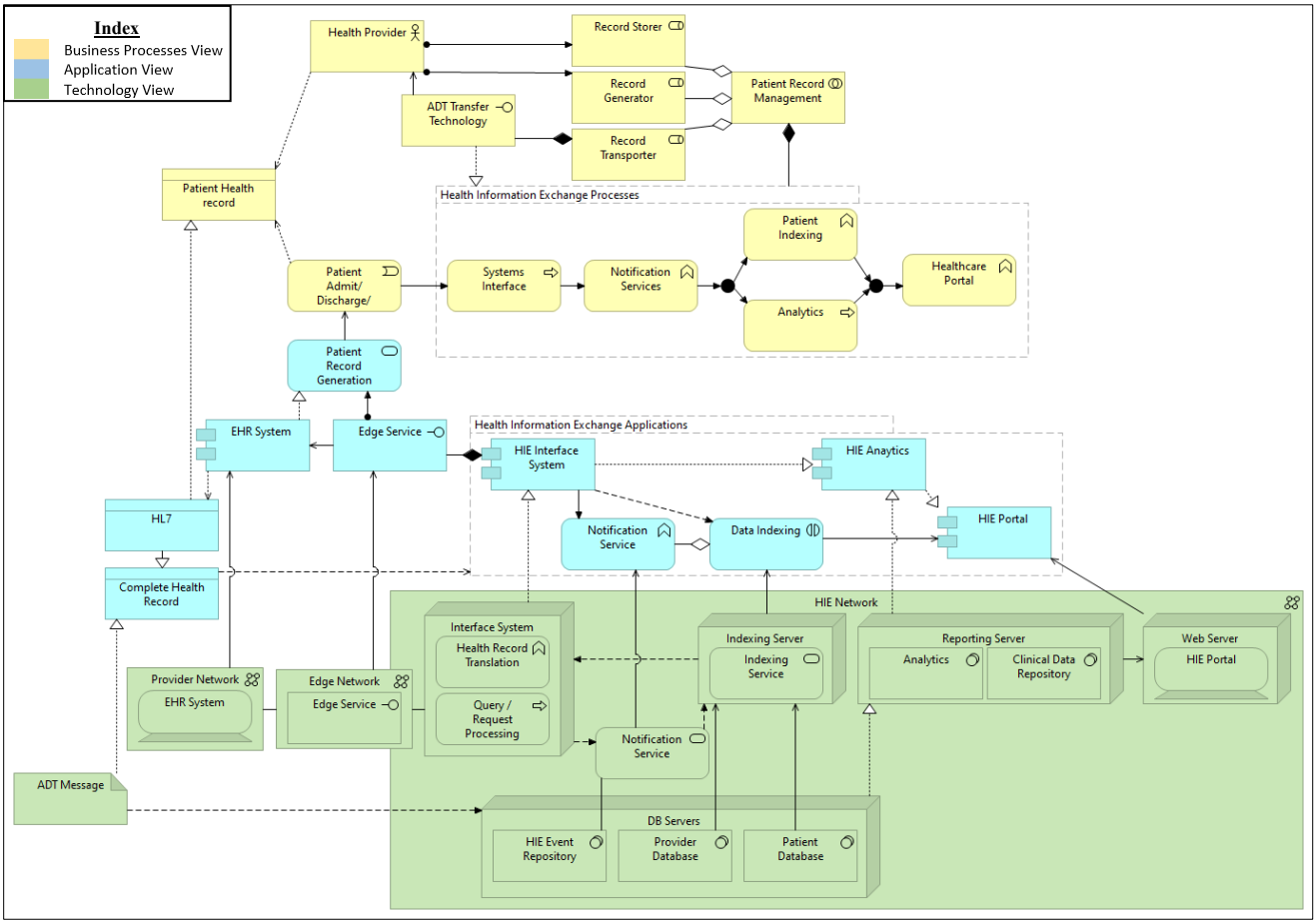


Figure 4: HIE Enterprise Architecture Integration

5. HIE Analytics

In our design, Analytics serves more as an ad-hoc system more than it does, a process. HIE Analytics can work in conjunction with the health portal system to provide comprehensive knowledge through queries and reports to all stakeholders.

The analytics system will interact with both the CDR's real-time data store and the reporting data store to generate relevant dashboards, reports, and queries. It should also be able to portal users with the ability to generate custom queries as needed.

Information Technology Integration Architecture

An EA integration artifact is an essential component of any enterprise architecture. Because the goal of enterprise architecture is to depict a holistic ontology of an organization or business, integration artifacts are essential to show how different layers and domains of architecture relate to each other.

Using ArchiMate, an enterprise architecture modeling language developed by The Open Group, architects can construct different views using its supported toolkit to demonstrate how organizations function. Because ArchiMate was developed based on the IEEE 1471 standard, the language is relatable to most professionals and can be easily adapted to other designing tools and languages.

Figure 4 presents a cross-layered integration of the four HIE architecture domains. Using ArchiMate, three views, Business, Information Systems, and Technology (Infrastructure) are mapped to show how the different layers of architecture interact with each other. This artifact shows how the business layer of architecture in an HIE is affected by data and application components. It also shows how the information systems layer (data and application domains) and its corresponding technology components relate to each other.

As seen in the artifact above the business layer is presented in yellow building blocks. Application and data components are represented in blue building blocks and technology components are represented in green building blocks. At the technology layer, ArchiMate is used to illustrate specific infrastructure components like physical nodes, computing devices, system software, network communications devices, and physical services.

4.2. HIE Cloud Migration Architecture

Executing a cloud migration is beneficial because HIEs can have access to greater computing capability, enhanced security, improved connectivity, and better storage capacity. A successful migration to the cloud requires a phased approach to ensure that no cloud competencies are compromised during migration. An unplanned migration can lead to data loss, systems outages, and cause significant downtime. This section proposes a phased migration plan and an information systems-focused migration architecture.

Phased Migration Architecture

ArchiMate is used with TOGAF ADM's Phases E, F, and G to illustrate how an implementation architecture will look like. Using the migration architecture in figure 4 as a blueprint, an HIE can transition to leveraging cloud technologies.

The proposed migration architecture breaks the cloud migration plan into three main phases: planning, computing migration, and storage migration.

In this artifact, work packages are broken into a cloud computing migration program and a cloud storage migration program. The cloud computing migration program is triggered by a planning project and the cloud storage migration program is triggered by the computing migration program. Both computing and storage programs are made up of projects (work packages). Storage and computing programs are mapped to deliverables and deliverables are used to perform a gap analysis. Gaps represent the difference between the "as-is" state of an architecture and its associated end-goals (plateau).

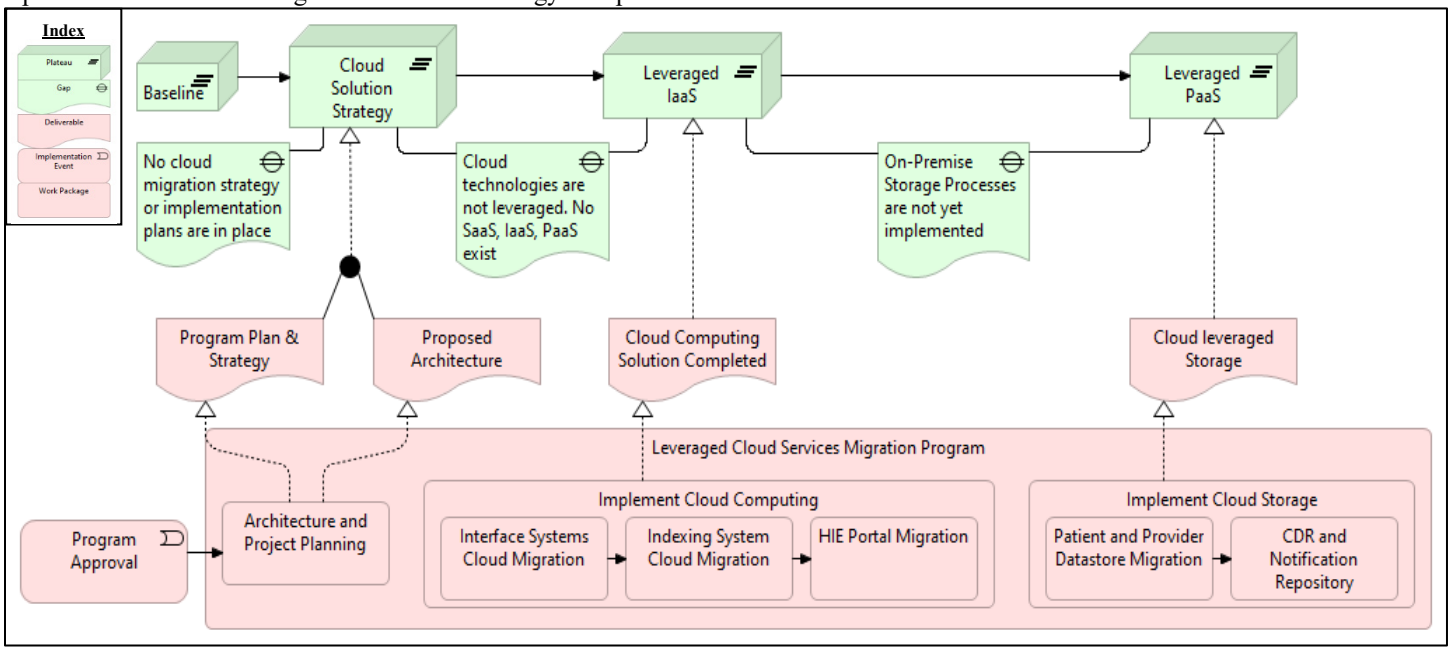


Figure 5: HIE Cloud Implementation and Migration View

Mapping all aspects of an enterprise architecture is essential to ensuring that phases of a migration do not affect other architectural building blocks. Below are detailed implementation steps as proposed above.

All technology adoption steps begin with a project proposal and approval. Implementation events are triggers to commence project work. Thus, an HIE cloud migration will begin with an implementation event that shows executive approval of cloud migration. Once an implementation initiative is started, thorough planning must be performed by enterprise architects, program and project managers, and their executive boards.

After the planning work packages have been completed, project plans, program achievement strategies, and to-be architectures must be provided. These two deliverables are required for implementation steps to continue.

Once project plans and future (to-be) architectures have been provided, a compute migration is the first step to cloud migration.

It is important to keep computing systems online during and after the migration is completed. Keeping both on-premises and cloud computing services online will allow on-premises applications to serve as a backup if needed. This strategy can be used for data storage as well.

The work packages specified in this program are interface system cloud migration project, indexing system migration project, and an HIE portal migration project. It must be noted that during the indexing system migration, work should be done to ensure that notification services systems and data store components are functional.

A cloud leveraged computing migration is the first adoption of IaaS. As discussed in 2.3, IaaS includes the provisioning of storage, network, and computing capabilities from a cloud technologies service provider. This plateau marks the first realization state in the migration implementation after planning is completed.

After the computing migration program is implemented, a major gap involving the utilization of PaaS solutions and a cloud leveraged storage service remains.

The storage migration program involves migrating data related components to the Cloud. This begins with the migration of patient and provider databases to a cloud storage service. Once completed, notification services and its related repositories can be migrated. Afterward, other cloud relevant data stores can be migrated as needed.

CDR data should be migrated only after both patient and provider databases are confirmed to be stable in the cloud environment because its data is more mission-critical data. It is also important to note that persistent data like patient and provider data stores should be fully migrated and confirmed to be stable before real-time data like the CDR and notification services are migrated.

Once all HIE data stores have been migrated and storage services are confirmed to be functional, steps can be taken to decommission on-premises systems.

Application and Data Migration Architecture

In scenarios where applications and data stores need to be migrated to a new environment, application and data migration artifacts can be used to demonstrate the high-level processes required for a successful migration. Application and Data Migration Diagrams are usually used alongside as-is and to-be architectures to ensure application and data components are well accounted for. The diagram below highlights the high-level processes required to ensure that an HIE's Interface System data and applications are well migrated from an on-premises system to a cloud-based environment. Using similar steps, architects can design other HIE information systems migration diagrams.

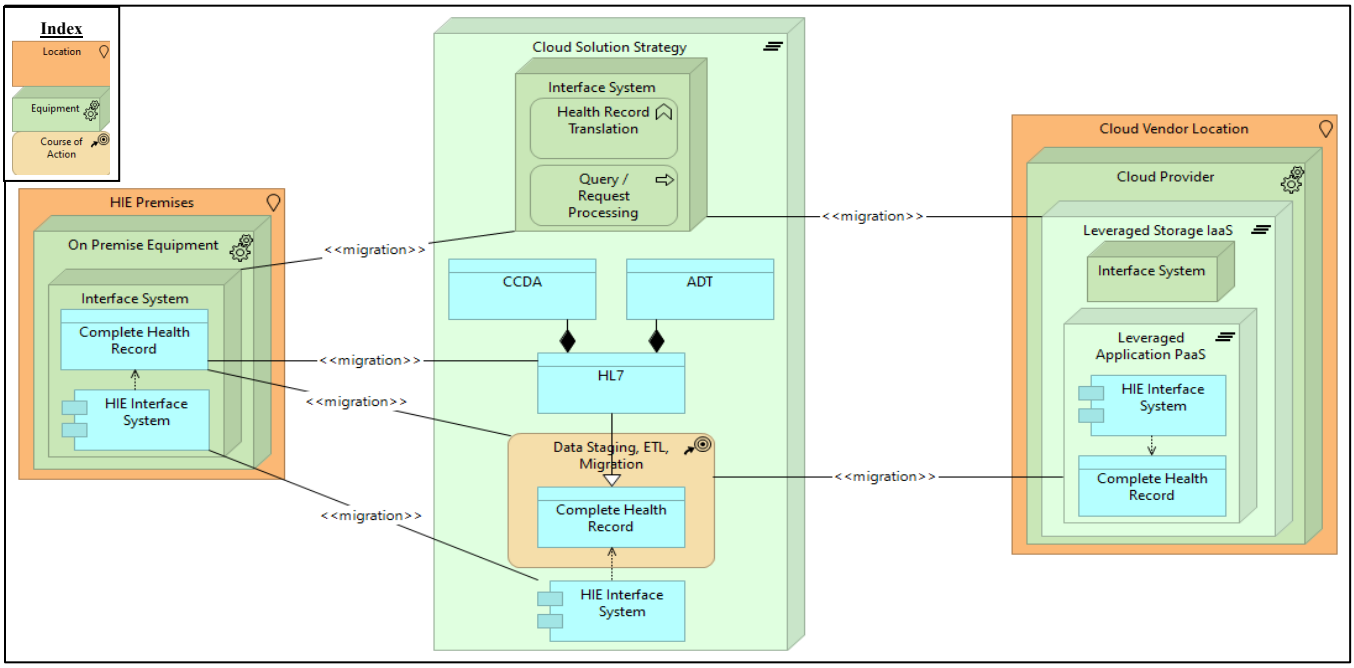


Figure 6: HIE Interface System Data and Application Migration

Using the Interface System Data and Application Migration artifact, architects can view an HIE's Interface System as-is architecture (HIE premises illustration on the left) and a to-be architecture with a cloud leveraged solution (Cloud Provider illustration the right). Once both viewpoints are presented, an architect can analyze and plan a migration path for both data and applications (Cloud solution strategy in the middle).

As seen in Figure 6, the migration strategy for a Cloud leveraged Interface system is developed in the Cloud Solutions Strategy plateau introduced in Figure 5. At this step, application and data components are broken down into manageable pieces and arranged to ensure a successful migration.

Both HIE Premise and Cloud Vendor locations are highlighted to distinguish an on-premises infrastructure from cloud vendors. Both on-premises and cloud leveraged equipment are also highlighted to show infrastructural ownership in an on-premises solution versus an IaaS or a PaaS solution.

Using the processes and artifact presented in this section, other applications and data migration views can be created for the other systems described in this article.

Architectural Impact on Information Exchange

The exchange of information is an integral function of HIEs. An HIE cloud migration facilitates data flow and streamlines the exchange of health information. The introduction highlights two ways HIEs share information. From a business processes standpoint, an HIE's value proposition and key activities are not greatly altered after a cloud migration. However, the architecture prescribed in our approach ensures that data flow is greatly improved regardless of whether an HIE is query-based or directed-data serving.

HIEs implementing a directed-data serving solution can benefit from a cloud-based solution because of the level of versatility provided when transferring different types of data across an HIE.

The utilization of an IaaS-based Interface System that leverages Platform-as-a-Service (PaaS) storage features with high computing capabilities will ensure that various data types, formats, and sizes can seamlessly flow through an HIE to external stakeholders. The proposed enhancement does not only exist at the infrastructure domain of an HIE architecture but the application domain as well. Specifically, during implementation, DIRECT Secure Messages applications and related CCD/HL7 APIs will need to be modified or migrated to a cloud computing system. Although Business processes will not need to be altered or modified, stakeholders will reap the benefits of this enhanced architecture as health record transfers are improved.

In a query-based solution, HIEs can use enhanced cloud technology to implement different application stacks to improve performance and enhance an HIE's value proposition. Query-based HIEs provide an informational hub for its users and transfer data from/to health institutions as needed. The utilization of a cloud-based clinical data repository will allow HIEs to perform better real-time health data analytics. Improved transfer of health records from external stakeholders to the HIE will greatly improve how quickly data can be made available in emergency scenarios.

A cloud migration in a query-based HIE can affect all domains of architecture. Once an HIE cloud migration is completed, the use of ADT messages can be used as a trigger to real-time analytics. The improved infrastructure (technology) layers can birth improvements to application and business domains. Although major changes may not be required for the business layers, HIEs can be presented with more functionality. HIEs can adopt enhanced cloud capabilities and tools to develop applications and tools for its customers. For example, an HIE can use the enhanced processing power leveraged by cloud technologies to develop predictive reporting to external stakeholders using artificial intelligence and machine learning frameworks.

4.3. HIE EA Validation Framework

This section provides a validation framework for the migration architecture. Using the validation mapping and architecture evaluation plan presented below, architects are provided with a means of ensuring that HIE Enterprise Architecture for Cloud Migration is well implemented.

Architecture Validation Mapping

TOGAF and Zachman offer artifact templates that can be used to build an EA. The PQQD, as explained in the background section is a means of certifying that an HIE is adequately managing health data. To ensure that an HIE's EA is well applied, the Validation Mapping Framework below has been proposed.

The diagram below shows a mapping of the three EA frameworks and presents artifacts types and process areas that can be used to determine if an implemented architecture is well applied.

PDDQ Process Areas	Architectural Layers (TOGAF & Zachman)
Governance Management	**Business** (Motivation, Organization, Behavior) **Representation**: Scope (Contextual) Enterprise Model (Conceptual) System Model (Logical)
Business Glossary	
Data Requirement Definition	
Process Management	
Process Quality Assurance	
Data Management Function	**Information Systems** - Data & Application layers - Logical | Physical Components **Representation**: Scope (Contextual) Enterprise Model (Conceptual) System Model (Logical)
Metadata Management	
Data Quality Planning	
Data Profiling	
Data Quality Management	
Data Cleansing & Improvement	
Data Lifecycle Management	
Data Standards	
Historical Data, Archiving & Retention	
Data Management Platform	**Technology** (Services, Logical, Physical Components) **Representation**: Scope (Contextual) Technology (Physical)
Communications	
Data Provider Management	
Data Integration	
Measurement & Analysis	

Figure 7: HIE EA Validation Mapping

Using TOGAF as a core of the validation framework, we align other frameworks to the business, information systems, and technology categorizations of the TOGAF ADM. The TOGAF ADM Guidelines Techniques can be used if an HIE needs to better implement a domain of architecture discussed in this sub-section.

Since Zachman is primarily a classification framework, an HIE can use its structure to organize artifacts in each layer of architecture. Zachman can be used to simplify the creation of EA artifacts provided by the TOGAF ACF.

The PDDQ framework was originated to ensure that patient data is prioritized [12]. For the presented validation mapping, process areas have been re-arranged to fit layers of the TOGAF ADM. For each layer of architecture, process areas are provided to measure an HIE's patient data management capability. To validate that an HIE is appropriately managing patient data after cloud migration, process area requirements for each layer of architecture should be measured.

Below is a breakdown of three architectural layers presented in the EA validation mapping.

Business: The Business layer represents stage B of the TOGAF ADM. The layer focuses on business strategy, organizational processes, and the day to day functions of a healthcare institution. In this validation framework, the business layer corresponds to the business domain of HIE architecture provided in section three. The Zachman framework recommends contextual, conceptual, and logical artifacts for this layer.

To ensure that an HIE has successfully implemented architecture from the business viewpoint, the following business-related processes from the PDDQ framework have been mapped: Governance Management, Business Glossary, Requirements Definition, Process Management, and Process Quality Assurance. These process areas were intricately studied and found to be related to the business layer.

Information Systems: The Information Systems layer is made up of a combination of the data and application domains in HIE architecture. Using the Zachman framework, Conceptual, Contextual, and Logical artifacts for scope, enterprise model, and system model are recommended.

HIEs can validate the architecture and its implementation with the following PDDQ process areas: Measurements and Assistance, Metadata management, Data Standards, Data profiling, Data Cleansing and improvements, Data lifecycle Management, and Data Provider Management.

Technology: At the lowest level of architecture, the technology layer deals with the network, hardware, infrastructure, and other physical operational components that support the management of business and information systems. The technology layer corresponds to the Infrastructure domain as discussed in the previous sections.

For Technology management, the PDDQ recommends the following process areas: Historical Data Archiving and Retention, Data Management Platform, and Data Integration. The Zachman framework recommends contextual (scope) and physical technology representation artifacts to create architecture.

HIE Enterprise Architecture Evaluation

An evaluation of traceability, reachability, and dependability is necessary to ensure that an enterprise architecture adequately aligns information technology to business.

Traceability is signified by how closely related components from different layers of architecture fit together to ensure interoperability [21]. Traceability traces how changes within a sector of an architecture propagate throughout other components within the same architecture [10]. An architecture's robustness is best measured by its reachability. Dependability is a measure of how dependent each artifact and architecture building block is to one another.

An enterprise architecture traceability test is used to ensure that an IT department's service offerings meet organizational goals. This means that there should be artifacts in place that clearly connect business components to information systems components and technology components, vice versa. The utilization of an IT portfolio is highly recommended by TOGAF. Measuring an IT portfolio with organizational operation metrics like costs, responsiveness, functionality, etc. is a great way to measure traceability. Also, mapping relationships between Business Process Modeling (BPM) diagrams, system design specifications, and use case diagrams are also a great means of evaluating traceability. An EA artifact like a Business Footprints Diagram can also be used to evaluate traceability.

Reachability is a test to ensure that information successfully traverses through an organization's architecture. When evaluating an HIE's level of architectural reachability, it is important to test how changes made at one layer of architecture propagates to other layers. For the proposed EA, utilizing architectural tools to simulate technology traversal is crucial. Structured modeled representations like sequence diagrams can be used to depict an architecture's level of reachability.

Composite dependability is the underlying goal of EA. While components of architecture should be interconnected, failure within sectors or layers of the EA should not cause the whole complete failure. Impact analyses and related evaluations can be used to perform a dependability assessment. Scenarios where changes within a function or artifact greatly affect the entire architecture should be addressed to strengthen the dependability of the enterprise architecture.

5. Conclusion

As discussed in previous sections, the adoption of cloud technology provides a greater level of availability, scalability, and flexibility to HIEs. HIE systems that reside in a cloud-based environment can efficiently and quickly improve its data transference capabilities as needed by throttling computing and network throughputs.

Enterprise Architecture is a tool that facilitates the adoption and implementation of technologies. For HIEs, EA provides an overarching view of its business and IT architecture. Once a complete view of the HIE's architecture is developed, a pathway for the realization of desired future goals can be easily created.

The biggest drawback of an EA approach centers around organizational planning and architecting. Without oversight and governance, HIE enterprise architects can be found focusing more on architecture planning and modeling processes than EA implementation and institutionalization. This can lead to delays and project cost overruns.

However, once the EA is implemented, HIEs can achieve strategic alignment between business capabilities, application services, and enterprise systems [22]. An alignment of HIE business functions to organizational goals, enterprise strategy, IT operations, and IT systems becomes more apparent once EA is applied.

In this paper, an enterprise architecture that supports an HIE's migration to the cloud for the facilitation of timely health data sharing is re-proposed. An EA institutionalization framework highlighting strategies and artifacts required to leverage the proposed architecture is presented. An HIE cloud migration architecture, providing a migration plan from an architectural standpoint is also presented. Finally, a validation framework that includes an evaluation plan and an architecture mapping is proposed to ensure that the HIE EA is well applied.

5.1. Future Work

As future work, an implementation of the proposed EA will prove important. An evaluation phase should be performed once the EA has been implemented. During the EA evaluation process, the proposed architecture's dependability, reachability, and traceability will be tested. The HIE EA Validation Mapping introduced in section four can also be used to ensure that the cloud-based HIE is well implemented.

Acknowledgment

The authors would like to thank Maryland's HIE Chesapeake Regional Information System for our Patients (CRISP) for their help and support in this research endeavor.

References

[1] K. Osei-Tutu, Y.T. Song, "Enterprise Architecture for Healthcare Information Exchange (HIE) Cloud Migration," in Proceedings of the 2020 14th International Conference on Ubiquitous Information Management and Communication, IMCOM 2020, 2020, doi:10.1109/IMCOM48794.2020.9001677.

[2] L. MELLO, MICHELLE M.; ADLER-MILSTEIN, JULIA; DING, KAREN L .; SAVAGE, "Legal Barriers to the Growth of Health Information Exchange—Boulders or Pebbles?," Lighting Design and Application: LD and A, **48**(5), 26–28, 2018.

[3] J.R. Vest, M.A. Unruh, J.S. Shapiro, L.P. Casalino, "The associations between query-based and directed health information exchange with potentially avoidable use of health care services," Health Services Research, 981–994, 2019, doi:10.1111/1475-6773.13169.

[4] H. Wu, E.M. LaRue, "Linking the health data system in the U.S.: Challenges to the benefits," International Journal of Nursing Sciences, **4**(4), 410–417, 2017, doi:10.1016/j.ijnss.2017.09.006.

[5] Y. Yang, X. Li, N. Qamar, P. Liu, W. Ke, B. Shen, Z. Liu, "Medshare: A Novel Hybrid Cloud for Medical Resource Sharing among Autonomous Healthcare Providers," IEEE Access, **6**, 46949–46961, 2018, doi:10.1109/ACCESS.2018.2865535.

[6] I.I. Systems, "Applying Modular Design in Architecting Interorganizational Information Systems Development in Shanghai," **2019**(September 2008), 175–190, 2019, doi:10.17705/2msqe.00015.

[7] A. Haghighathoseini, H. Bobarshad, F. Saghafi, M.S. Rezaei, N. Bagherzadeh, "Hospital enterprise Architecture Framework (Study of Iranian University Hospital Organization)," International Journal of Medical Informatics, **114**(February 2017), 88–100, 2018, doi:10.1016/j.ijmedinf.2018.03.009.

[8] R. Klischewski, "Information Integration or Process Integration? How to Achieve Interoperability in Administration," 57–65, 2004, doi:10.1007/978-3-540-30078-6_10.

[9] H. Song, Y.T. Song, "Enterprise architecture institutionalization and assessment," Proceedings - 9th IEEE/ACIS International Conference on Computer and Information Science, ICIS 2010, 870–875, 2010, doi:10.1109/ICIS.2010.127.

[10] O.G. Standard, T.O. Group, "Open Group Standard The Open Group," The TOGAF® Standard, Version 9.2, 1–181, 2013.

[11] J. a Zachman, "The Zachman Framework For Enterprise Architecture, Primer for Enterprise Engineering and Manufacturing," CA Magazine, **128**(9), 15, 2003, doi:10.1109/CSIE.2009.478.

[12] C. Institute, Patient Demographic Data Quality (PDDQ) Framework, Patient Demographic Data Quality Framework, 2018.

[13] M. Lnenicka, J. Komarkova, "Developing a government enterprise architecture framework to support the requirements of big and open linked data with the use of cloud computing," International Journal of Information Management, **46**(June 2018), 124–141, 2019, doi:10.1016/j.ijinfomgt.2018.12.003.

[14] S. Lee, S. Oh, K. Nam, "Transformational and Transactional Factors for the Successful Implementation of Enterprise Architecture in Public Sector," Sustainability, **8**(5), 456, 2016, doi:10.3390/su8050456.

[15] N.A.A. Bakar, S. Harihodin, N. Kama, "Assessment of Enterprise Architecture Implementation Capability and Priority in Public Sector Agency," Procedia Computer Science, **100**, 198–206, 2016, doi:10.1016/j.procs.2016.09.141.

[16] D.D. Dang, S. Pekkola, D. Duong Dang, "Systematic Literature Review on Enterprise Architecture in the Public Sector," **15**(2), 132–154, 2017.

[17] F. Chitsa, T. Iyamu, "Towards enterprise technical architecture for the implementation of the South African NHI," Advances in Science, Technology and Engineering Systems, **5**(2), 724–729, 2020, doi:10.25046/aj050290.

[18] J.C. Henderson, H. Venkatraman, "Strategic alignment: Leveraging information technology for transforming organizations," IBM Systems Journal, **32**(1), 472–484, 1993, doi:10.1147/sj.382.0472.

[19] P. DePalo, Y.-T. Song, "Healthcare interoperability through enterprise architecture," Proceedings of the 6th International Conference on Ubiquitous Information Management and Communication - ICUIMC '12, 1, 2012, doi:10.1145/2184751.2184837.

[20] A. Boussadi, E. Zapletal, "A Fast Healthcare Interoperability Resources (FHIR) layer implemented over i2b2," BMC Medical Informatics and Decision Making, **17**(1), 1–13, 2017, doi:10.1186/s12911-017-0513-6.

[21] L. Chung, N. Subramanian, "Bridging the gap between enterprise architectures and software architectures," Science of Computer Programming, 2007, doi:10.1016/j.scico.2006.12.001.

[22] P. Bhattacharya, "Modelling Strategic Alignment of Business and IT through Enterprise Architecture: Augmenting Archimate with BMM," Procedia Computer Science, **121**, 80–88, 2017, doi:10.1016/j.procs.2017.11.012.

ASTES

Advances in Science, Technology and Engineering Systems Journal Vol. 5, No. 5, 692-697 (2020)

www.astesj.com

ASTESJ

ISSN: 2415-6698

Smartphone Influence Factor of University Student's Academic Achievement

Surjandy[1,*], Meyliana[1], Kristianus Oktriono[2], Mika Milenia Catherine[1], Chutiporn Anutariya[3], Erick Fernando[1]

[1]*School of Information Systems, Information Systems, Bina Nusantara University, 11480, Indonesia*

[2]*Language Center, Tourism Department, Faculty of Humanities, Bina Nusantara University, 11480, Indonesia*

[3]*School of Engineering and Technology, Asian Institute of Technology, Pathumthani, Thailand*

ARTICLE INFO

Article history:
Received: 09 August, 2020
Accepted: 27 August, 2020
Online: 05 October, 2020

Keywords:
Smartphone
Explanatory Research
University Student
Social Network Activity

ABSTRACT

The smartphone is a phenomenal device or tool that recently transform the habit of people. In this part, the smartphone serves not only as a communication device but also more complex functionality. The early research reported that smartphones are used by university students to support their social and academic activities. However, the research report that explores how much influence factor of smartphone for educational university student activities is scarce, especially for academic achievement index. Therefore, this explanatory research examines the exploration of the smartphone influence factor with university student background (such as gender, achievement index), academic, and social activities. This study applied SPSS tools with the Correlation Bivariate technique to investigate the influence factor and successfully obtained 17 essentials correlation or relationship between factors.

1. Introduction

Smartphone has been popular because of the integration of technology in a portable device and the adoption of advance features. In this line, the users are engaged with the capability and personal management. The features of smartphones keep developing day by day, from the communication device to communicate using voice, picture/image, and video, for gaming single or multi player [1], or social activities. Arguably, it centralized the element of connectivity and global access. However, the previous study reported that smartphones are used by university students not only for social network activities but also for academic activities[2], [3]. As stated, the usage of smartphones for educational activities will assist a university student to fulfil the academic assignment[4]-[6]. In the other hand, previous research state that smartphone is not suitable for student [7].

Thus, this study explores how strong the influence of smartphones for social and academic activities. The study used explanatory or causal method research that explores the significance between two factors. The factors consist of student backgrounds such as achievement index, gender, smartphone screen width, and activities that use a smartphone. In this research, the Correlation Bivariate technique is used to describe how significant the influence of smartphones used by a university student for academic and social network activities. At the end of this study, it obtains 17 essential factors that explain the gender, age, and screen width. In this sense, achievement index is an influencing factor to university student academic and social network activities. The result of this study brings another insight into smartphone development in the feature and positive habit of a university student that uses the smartphone to gain a better achievement index.

Hypotheses for this study are:

- The university student backgrounds (for example age, gender) influence achievement index.
- The university student's smartphone feature (for example screen width) influences achievement index.

H0 where there is no influence between factors. H1 where there is influence between factors.

2. Literature Review

2.1. Smartphone

The smartphone is a device that has many features such as a communication device and can be used for any application

*Corresponding Author: Surjandy, Jl. K.H.Syahdan No.9 Jakarta, Indonesia, surjandy@binus.ac.id

https://dx.doi.org/10.25046/aj050585

installation purposes such as for FinTech payment, online transportation [7], e-book reading [8], and sending text/video/image message [2].

2.2. University Student Social network activities

The social network activities are an activity conducted by university student using a smartphone to communicate with other persons or group to access a social network, such as Instagram, Pinterest, Facebook, access to the website, playing a game, watching movie or film such as on YouTube [2].

2.3. University Student Academic activities

This term means that university students use a smartphone to support academic activities such as searching for content or information on learning, discussion with others in correlation with learning content [2].

2.4. The Explanatory or Causal Research

The explanatory or causal research is a method of analysis that mostly used in marketing to look for activity influence factor[9]. The study used causal or explanatory method aiming to look for the influence between factors of university student background, smartphone features, and university student daily activity that is performed by using smartphone [2].

3. Result and Discussion

This study uses explanatory/causal method research. In this part, the method is used for marketing research to look for routine activities. In a closer look, a university student is a primary respondent as the most active user that facilitates smartphone to support their academic and social network activities.

Table 1: Respondent

No	Description	Total
1	Gender (1Gn) See figure 1 for detail	419 (100%)
2	Age (2Ag) Below 17 years' old Between 18 – 25 years old Between 26 – 30 years old Above 30 years old	419 (100%) 3 (0.7%) 409 (97.6%) 4 (1.0%) 3 (0.7%)
3	Screen Width (3Sc) See figure 2 for detail	419 (100%)
4	Achievement Index (4Ai) Less than 2.0 2.00 – 2.50 2.51 – 2.99 Greater than 3.0	419 (100%) 19 (4.5%) 26 (6.2%) 85 (20.5%) 288 (68.7%)

Table 1 described the characteristics of the 419 respondents — the age of respondents is mostly between 18 to 25 years old or the age of university students from several universities in Indonesia. Based on APJII (Indonesia internet provider) report, it showed that university student is the most active user that use internet or social media with around 127 million users [10]; therefore, the respondents are representative for the population.

Figure 1 exhibits the respondent by gender, where 258 (61.6%) respondents are female and 161 males (38.4%). Figure 2 exhibits the smartphone used by the university student, with details of 8 university students used screen width below 3 inches (1.9%), 119 (28.4%) between 3 to 4 inches, 276 (65.9%) between 5 to 6 inches, and 16 (3.8%) used a smartphone with greater than the 7-inch screen width.

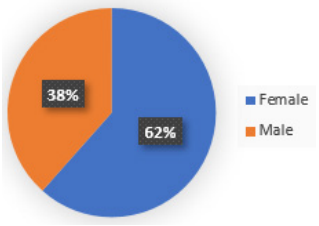


Figure 1: Respondent by Gender

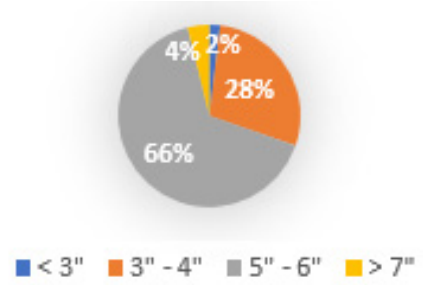


Figure 2: Smartphone Screen Width

Table 2: Validity Test

No	Description	Corrected Item-Total Correlation	Status
1	Smartphones used to access social media (FC1)	0.282	Valid
2	I have the knowledge needed to use a Smartphone (FC2)	0.410	Valid
3	Smartphones help provide solutions to face difficulties in the academic field (FC3)	0.527	Valid
4	Smartphones help in finding information about learning when needed (FC4)	0.530	Valid
5	Smartphone used to facilitate all access to information (FC5)	0.582	Valid

Table 2 described the validity result process of questioners. The validation is processed by comparing the value of Corrected item-total Correlation (CI-TC), and r table value. In this study, the r table value for 400 samples is 0.0978. The questioner is valid if CI-TC higher than 0.0978. It means that all questions are valid.

Table 3: Reliability Test

No	Description	Cronbach's Alpha	Status
1	FC1	0.721	Reliable
2	FC2	0.682	Reliable
3	FC3	0.629	Reliable
4	FC4	0.611	Reliable
5	FC5	0.610	Reliable

Table 3 described the consistency of the questioner. The result shows that Cronbach's Alpha is significant (more than 0.6) and reliable [11]. The following process of this study uses SPSS tools and the Bivariate technique to examine the correlation between academic background, respondent, background, and usage of

smartphone activities factors. Table 4 describes 36 relations result based on the calculation of the Correlation Bivariate technique.

The hypotheses result described in Table IV can be interpreted as follows:

- There is a correlation or relationship between the factor of hypothesis 0 (where there is no relation between factors) rejected, and hypothesis 1 (where there is a relationship between factors) accepted.
- There is no correlation or no relationship between factors where hypothesis 0 is accepted, and the hypothesis 1 is rejected.

Table 4: Hypothesis Result

No	Description	Pearson Correlation	H0	H1
1	1Gn – 2Ag	NC	Accepted	Rejected
2	1Gn – 3Sc	NC	Accepted	Rejected
3	1Gn – 4Ai	r -0.440** 0.000	Rejected	Accepted
4	1Gn – FC1	NC	Accepted	Rejected
5	1Gn – FC2	NC	Accepted	Rejected
6	1Gn – FC3	NC	Accepted	Rejected
7	1Gn – FC4	NC	Accepted	Rejected
8	1Gn – FC5	r -0.147** sig 0.003	Accepted	Rejected
9	2Ag – 3Sc	NC	Accepted	Rejected
10	2Ag – 4Ai	NC	Accepted	Rejected
11	2Ag – FC1	r -0.231** sig 0.000	Rejected	Accepted
12	2Ag – FC2	NC	Accepted	Rejected
13	2Ag – FC3	NC	Accepted	Rejected
14	2Ag – FC4	NC	Accepted	Rejected
15	2Ag – FC5	NC	Accepted	Rejected
16	3Sc – 4AI	NC	Accepted	Rejected
17	3Sc – FC1	r 0.135** sig 0.006	Rejected	Accepted
18	3Sc – FC2	NC	Accepted	Rejected
19	3Sc – FC3	NC	Accepted	Rejected
20	3Sc – FC4	NC	Accepted	Rejected
21	3Sc – FC5	NC	Accepted	Rejected
22	4Ai – FC1	NC	Accepted	Rejected
23	4Ai – FC2	NC	Accepted	Rejected
24	4Ai – FC3	r 0.137** sig 0.005	Rejected	Accepted
25	4Ai – FC4	r 0.106* sig 0.030	Rejected	Accepted
26	4Ai – FC5	r 0.195** sig 0.000	Rejected	Accepted
27	FC1 – FC2	r 0.296** sig 0.000	Rejected	Accepted
28	FC1 – FC3	r 0.197** sig 0.000	Rejected	Accepted
29	FC1 – FC4	r 0.122* sig 0.012	Rejected	Accepted
30	FC1 – FC5	r 0.210** sig 0.000	Rejected	Accepted
31	FC2 – FC3	r 0.311** sig 0.000	Rejected	Accepted
32	FC2 – FC4	r 0.224** sig 0.000	Rejected	Accepted
33	FC2 – FC5	r 0.349** sig 0.000	Rejected	Accepted
34	FC3 – FC4	r 0.519** sig 0.000	Rejected	Accepted
35	FC3 – FC5	r 0.421** sig 0.000	Rejected	Accepted
36	FC4 – FC5	r 0.591** sig 0.000	Rejected	Accepted

The detail explanation of Table 4 is as follows:

3.1. Explanation H1 & H0 from Table IV with Pearson sig value indicator

The hypothesis result is described with Pearson sig value indicator. If the Pearson sig indicator is lower than 0.05, it signifies hypothesis 0 or no correlation. In other words, it means that H0 is rejected, and hypothesis 1 is accepted. Conversely, if it is greater than 0.05, hypothesis 0 is accepted and hypothesis 1 is rejected.

3.2. Explanation of Bivariate Correlation between factors

This section explains all the factors that have a relationship with other factors.

There is a relationship between 1Gn with 4Ai where the Pearson r value is -0.440, sig 0.000, and alpha 99%. It indicates that the female (because of minus sign) is more likely having high index achievement compare to the male university student.

There is a relationship between 1Gn with FC5 where the Pearson r value is -0.147, sig 0.003, and alpha 99%. It signifies that the female (because of minus sign) is more likely using the smartphone to facilitate all access to information. However, males tend to the less-used smartphone to facilitate all access to information.

There is a relationship between 2Ag with FC1 where the Pearson r value is -0.231, sig 0.000, and alpha 99%. It represents that the younger age (because of the minus sign) is more likely using smartphones to access social media. However, the older generation tends to less-used smartphones to access social media.

There is a relationship between 3Sc with FC1 where the Pearson r value is 0.135, sig 0.006, and alpha 99%. It denotes that the bigger screen size, the user is more likely to use smartphones to access social media. However, the smaller screen size, the user tends to less use the smartphones to access social media.

There is a relationship between 4Ai with FC3 where the Pearson r value is 0.137, sig 0.005, and alpha 99%. It shows that the higher achievement index, the user is more likely using smartphones to provide solutions in encountering difficulties in the academic field. However, the user with lower achievement index, one tends to fewer use smartphones in providing solutions to meet the challenges in the educational area.

There is a relationship between 4Ai with FC4 where the Pearson r value is 0.106, sig 0.030, and alpha 95%. It states that the university student that has a higher achievement index is more likely using smartphone in finding information about learning when needed.

There is a relationship between 4Ai with FC5 where the Pearson r value is 0.195, sig 0.000, and alpha 99%. It describes that the university student that has a higher achievement index is

more likely using the smartphone to facilitate all access to information. However, the university students with lower achievement index, they tend to less use the smartphone to facilitate all access to information.

There is a relationship between FC1 with FC2 where the Pearson r value is 0.296, sig 0.000, and alpha 99%. It expresses that the university student that has more frequent in using a smartphone to access social media, they are more likely to have more knowledge (familiar) needed to use a smartphone.

There is a relationship between FC1 with FC3 where the Pearson r value is 0.197, sig 0.000, and alpha 99%. It points out that the university student who has more frequent use of a smartphone to access social media, one is more likely to use the smartphone to find solutions to face difficulties in the academic field. However, university students that have less frequent use of the smartphone to access social media, they tend to less use the smartphone to find solutions in the academic field.

There is a relationship between FC1 with FC4 where the Pearson r value is 0.122, sig 0.012, and alpha 99%. It implies that the university student that has more frequent use of a smartphone to access social media, one is more likely to use the smartphone to finding information about learning when needed. However, university students that have less frequent use of the smartphone to access social media, they tend to less use the smartphone to find information about education when required.

There is a relationship between FC1 with FC5 where the Pearson r value is 0.210, sig 0.000, and alpha 99%. It depicts that the university student that has more frequent use of a smartphone to access social media, one is more likely to use the smartphone to facilitate all access to information. However, the university student that less frequently use the smartphone to access social media, one tends to less use smartphone to facilitate all access to information.

There is a relationship between FC2 with FC3 where the Pearson r value is 0.311, sig 0.000, and alpha 99%. It clarifies that the university student that has more knowledge needed to use a smartphone, one is more likely using the smartphone to find solutions in the academic field. However, university student that has less experience required to use a smartphone, one tends to less use a smartphone to find solutions and to meet the challenges in the educational area.

There is a relationship between FC2 with FC4 where the Pearson r value is 0.224, sig 0.000, and alpha 99%. It indicates that the university student that has more knowledge needed to use a smartphone is more likely to use a smartphone to help in finding information about learning when required. However, university student that has less experience required to use a smartphone tends to less use smartphone to assist in finding information about education when required.

There is a relationship between FC2 with FC5 where the Pearson r value is 0.347, sig 0.000, and alpha 99%. It reveals that the university student that has more knowledge needed to use a smartphone, one is more likely using a smartphone to facilitate all access to information. However, university student that has less experience required to use a smartphone, one tends to less use smartphone to facilitate all access to information.

There is a relationship between FC3 with FC4 where the Pearson r value is 0.519, sig 0.000, and alpha 99%. It symbolizes that the university student that has to use the smartphone to find solutions in the academic field, one is more likely using a smartphone to find information about learning when needed. However, a university student who has a less-used smartphone to find solutions in the academic field, one tends to less use a smartphone in finding information about learning when needed.

There is a relationship between FC3 with FC5 where the Pearson r value is 0.421, sig 0.000, and alpha 99%. In this part, the university student who uses smartphone more frequent to encounter difficulties in the academic field, one is more likely using the smartphone to facilitate all access to information. However, a university student who less frequent uses smartphone to find solutions in the academic field, one tends to less use smartphone to facilitate all access to information.

There is a relationship between FC4 with FC5 where the Pearson r value is 0.591, sig 0.000, and alpha 99%. In this context, the university student who uses smartphone more frequent to find information about learning when needed, one is more likely using the smartphone to facilitate all access to information. However, a university student who uses the smartphone less frequently to find information about education when needed, one tends to fewer use smartphones to facilitate all access to information.

3.3. Strength correlation tension between factors

The strength correlation tension can be measured by examining the Pearson r value converted into absolute Pearson r or | r |. In this part, the percentage of strength value originates from the percentage square of absolute Pearson r value. Technically, strength correlation tensions are divided into 3 group values. The first represents the absolute r or |r| between 0.1 and 0.3 with the indication of the strong correlation tension is small. Following that, the strong correlation tension is medium in the range of between 0.3 and 0.5. Finally, the strong correlation tension is substantial with the value is higher than 0.5 [12]. Table 5 represents the strength correlation tension in detail.

Table 5: Strength Correlation Tension

No	Description	| r |	Strength	| r |^2	%
1	1Gn – 4A1	0.440	Medium	0.194	19.4%
2	1Gn – FC5	0.147	Small	0.022	2.2%
3	2Ag – FC1	0.231	Small	0.053	5.3%
4	3Sc – FC1	0.135	Small	0.018	1.8%
5	4Ai – FC3	0.137	Small	0.019	1.9%
6	4Ai – FC4	0.106	Small	0.011	1.1%
7	4Ai – FC5	0.195	Small	0.038	3.8%
8	FC1 – FC2	0.674	Strong	0.454	45.4%
9	FC1 – FC3	0.679	Strong	0.461	46.1%
10	FC1 – FC4	0.661	Strong	0.437	43.7%
11	FC1 – FC5	0.616	Strong	0.379	37.9%
12	FC2 – FC3	0.674	Strong	0.454	45.4%
13	FC2 – FC4	0.224	Small	0.050	5.0%
14	FC2 – FC5	0.349	Medium	0.122	12.2%
15	FC3 – FC4	0.519	Strong	0.269	26.9%
16	FC3 – FC5	0.421	Strong	0.177	17.7%
17	FC4 – FC5	0.591	Strong	0.349	34.9%

Table 5 presents the detail of relation, strength relation, and % of the influence. Figure 3 exhibits the percentage of the tension of influence.

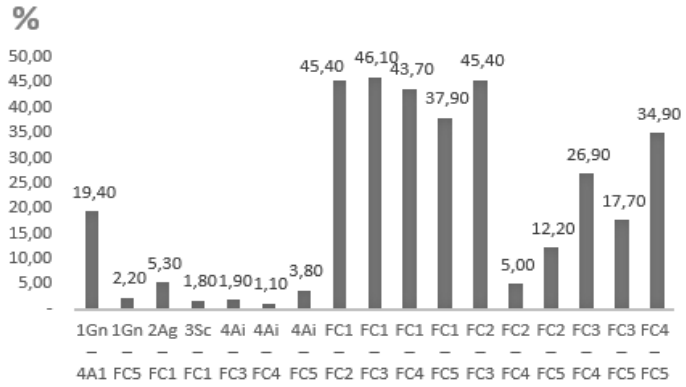


Figure 3: Percentage of Tension Correlation

The explanation of Table 5 and Figure 1. is as follows:

For 1Gn – 4Ai, it indicates that 19.4% (medium influence) gender factor influences on achievement index.

For 1Gn – FC5, it states that 2.2% (small influence) gender factor influences on the use of a smartphone to facilitate all access to information.

For 2Ag – FC1, it describes that a 5.3% (small influence) age factor influences on the use of a smartphone to access social media.

For 3Sc – FC1, it denotes that a 1.8% (small influence) screen width factor influences on the use of a smartphone to access social media.

For 4Ai – FC3, it states that a 1.9% (small influence) achievement index influences on using a smartphone to provide solutions in the academic field.

For 4Ai – FC4, it means that a 1.1% (small influence) achievement index influences on the use of smartphones to find information about learning when needed.

For 4Ai – FC5, it denotes that a 3.8% (small influence) achievement index influences on the use of a smartphone to facilitate all access to information.

For FC1 – FC2, it implies that a 45,4% frequent use of a smartphone to access social media influences strongly on a university student who has more knowledge needed to use a smartphone.

For FC1 – FC3, it expresses that a 46.1% frequent use of smartphones to access social media influences strongly on using a smartphone to provide solutions in the academic field.

For FC1 – FC4, it means that a 43.7% frequent use of the smartphone to access social media influences strongly on using a smartphone to find information about learning when needed.

For FC1 – FC5, it presents that a 37.9% frequent use of the smartphone to access social media influences strongly on using a smartphone to facilitate all access to information.

For FC2 – FC3, it signifies that 45.4% of university students who have the knowledge needed to use smartphone influences strongly on using a smartphone to find solutions in the academic field.

For FC2 – FC4, it describes that 5% (small influence) university students who have the knowledge needed to use smartphone influences on using a smartphone to find information about learning when required.

For FC2 – FC5, it states that 12.2% (medium influence) university students who have the knowledge needed to use a smartphone influence the using of the smartphone to facilitate all access to information.

For FC3 – FC4, it underlines that 26.9% (strong influence) smartphone provides solutions in the academic field. It influences the using of a smartphone to assist students in finding information about learning when needed.

For FC3 – FC5, it emphasizes that 17.7% (strong influence) smartphone assists students to find a solution in the academic field and influence on using a smartphone to facilitate all access to information.

For FC4 – FC5, it asserts that 34.9% (strong influence) smartphone assists the students in finding information about learning when needed. In this case, it influences on using a smartphone to facilitate all access to information.

3.4. Debatable result of Discussion

The early research reported that there is no influence of smartphones with academic achievement[5]. However, this study revealed that university student's smartphone has a relationship or influence on academic achievement index and higher academic achievement index. In this line, it tends to maximize the use of smartphones for academic activities.

4. Conclusion

This research obtains an essential result that accentuates the university student background such as gender, age, achievement index, screen width smartphone. In another part, debatable results were found from the early study [5] with this study. In this sense, this study indicates that there is a relation or influence of smartphones with university student achievement index. This contributes to the university in creating attractive content for learning. Moreover, the result is expected to engage the student in digital learning and increase their performance. The research also states that habit activities of using the smartphone improve the learning achievement index.

Conflict of Interest

The authors declare no conflict of interest.

References

[1] A. Surjandy, Y. U. Chandra, "The Smartphone for Disseminating of Fake News by the University Students Game Player", in 2017 International Conference on Information Management and Technology (ICIMTech), Yogyakarta, Indonesia, 14–18, 2017. https://doi.org/10.1109/ICIMTech.2017.8273503

[2] Surjandy, Julisar, "Is social media used as social activities or academic activities? (Study for college student's subject in information technology)", in *Proceedings of 2016 International Conference on Information Management and Technology, ICIMTech 2016*, Bandung, Indonesia, 130–134, 2017. https://doi.org/10.1109/ICIMTech.2016.7930316

[3] A. Lepp, J. Li, J. E. Barkley, S. Salehi-esfahani, "Computers in Human Behavior Exploring the relationships between college students ' cell phone use , personality and leisure", Computers in Human Behavior, **43**, 210–219, 2015. http://doi.org/10.1016/j.chb.2014.11.006

[4] J. Gikas, M. M. Grant, "Mobile computing devices in higher education: Student perspectives on learning with cellphones, smartphones & social media", The Internet and Higher Education, **19**, 18–26, 2013. https://doi.org/10.1016/j.iheduc.2013.06.002

[5] M. Samaha, N. S. Hawi, "Relationships among smartphone addiction, stress, academic performance, and satisfaction with life", Computers in Human Behavior, **57**, 321–325, 2016. https://doi.org/10.1016/j.chb.2015.12.045

[6] S. So, "Mobile instant messaging support for teaching and learning in higher education", The Internet and Higher Education, **31**, 32–42, 2016. https://doi.org/10.1016/j.iheduc.2016.06.001

[7] S. Hadad, H. Meishar-Tal, I. Blau, "The parents' tale: Why parents resist the educational use of smartphones at schools?", Computers & Education, **157**, 103984, 2020. https://doi.org/10.1016/j.compedu.2020.103984

[8] Surjandy, Julisar, "Do College Students use E-Book with Smartphone ? (Study for College Student's Subject in Information Technology)", in *Proceedings of the International MultiConference of Engineers and Computer Scientists 2017*, **II**, 15–18, 2017.

[9] H. Oppewal, 'Causal Research', in *Wiley International Encyclopedia of Marketing*, Chichester, UK: John Wiley & Sons, Ltd, 2010. https://doi.org/10.1002/9781444316568.wiem02001

[10] APJII, 'BULETINAPJIIEDISI23April2018.pdf', *APJII*, 1–7, 2018.

[11] UCLA, 'What does Cronbach's alpha mean?', *stats.idre.ucla.edu*, 2019. [Online].https://stats.idre.ucla.edu/spss/faq/what-does-cronbachs-alpha-mean/

[12] K. Yeager, 'LibGuides: SPSS Tutorials: Pearson Correlation', *kent.edu*, 2019. [Online]. https://libguides.library.kent.edu/SPSS/PearsonCorr

ASTES

Advances in Science, Technology and Engineering Systems Journal Vol. 5, No. 5, 698-708 (2020)

www.astesj.com

ASTESJ

ISSN: 2415-6698

Prototype for the Management of Engineering Companies and the ICT to Improve the Quality of Services

Segundo Moisés Toapanta Toapanta[*,1], Emmanuel Alejandro Narváez Picon[1], Luis Enrique Mafla Gallegos[2]

[1]*Department of Computer Science, Universidad Politécnica Salesiana (UPS), Guayaquil, 090150, Ecuador*

[2]*Faculty of Systems Engineering, Escuela Politécnica Nacional (EPN), Quito, 17-01-2759, Ecuador*

ARTICLE INFO

Article history:
Received: 10 August, 2020
Accepted: 11 September, 2020
Online: 05 October, 2020

Keywords:
Prototype
Quality of Services
Business management
Information technologies
Engineering and ICT Companies

ABSTRACT

Information on alternative technologies or new prototypes was analyzed to help improve the quality of business management services. The problem is the lack of application of new technologies that improve the quality of service and reduce disagreements in the management of organizations. The objective is to present a prototype for the management of engineering and ICT companies to improve the quality of services. The deductive method and exploratory research were used to analyze the information. The result was a mixed conceptual model of quality of service approach, a dual-security architecture for business management, control of algorithms with processes for quality of service and control of algorithms with information filter. It was concluded that an information filter with Blockchain is considered a fundamental alternative to provide control, reliability, immutability and improved quality of service.

1. Introduction

With the rapid development of IT technology the types of decision-making in business management depend on several IT information systems. The systems fail or crash business management risks and negative impacts are continually increasing [1].

Globalization and information technologies help the external commercialization of goods and services. The importance in the management of foreign trade are priority properties such as: Handling of goods, costs and administrative failures [2].

Knowledge Management is a scientific area related to the organizational value of knowledge and is understood as a multidisciplinary research field. The notions and practices that emerged and incorporated into organizations in different areas of IT service management the environment is unstable characterized by uncertainties and changes and technology changes rapidly. Competitors multiply products or services that quickly become obsolete and management is increasingly focused on knowledge of user management. Information systems aligned with existing corporate knowledge management and intellectual capital aims to explicitly represent and manage the different dimensions of organizational knowledge and competencies [3].

The objective of this document is to prototype the management of engineering and ICT companies to improve the quality of services.

Why is it necessary to make a prototype for management of engineering and ICT companies to improve the quality of services?

To manage the products and services of engineering and ICT companies with quality, effectiveness and efficiency.

The related and revised articles used for research are as follows:

A CPS-Based Intelligence-Awareness Platform for IT Service Management [1]. A Hyperledger Technology Approach to Mitigate the Risks of the Database in Foreign Trade Management [2]. A Knowledge Management Architecture for Information Technology Services Delivery [3]. A model to improve quality of service (QoS) in cloud based Virtual lab framework [4]. A Strategy for Server Management to Improve Cloud Service QoS [5]. A Study on R&D Organization Management of Japanese ICT Companies Using Patent Information [6]. Achieving agility and quality in product development - an empirical study of hardware startups [7]. Overview of Additive Manufacturing Informatics: "A Digital Thread" [8]. Adoption of Information and Communications Technology in the Turkish Forest Products Industry: A Case Study [9]. An Adaptive Framework for Improving Quality of Service in Industrial Systems [10]. Analysis

[*]Corresponding Author: Segundo Moisés Toapanta Toapanta, & Email: stoapanta@ups.edu.ec

Methods for Improving Quality of Service Metrics in Flying Ad Hoc Networks [11]. Analysis to Predict Cybercrime Using Information Technology in a Globalized Environment [12]. A Versatile Software Defined Smart Grid Testbed: Artificial Intelligence Enhanced Real-Time Co-Evaluation of ICT Systems and Power Systems [13]. Basics of Forming an Integrated Management System [14]. Cluster Content Caching: An Energy-Efficient Approach to Improve Quality of Service in Cloud Radio Access Networks [15]. Definition of an ICT Management Model to Mitigate Cyberbullying Risk in Social Networks [16]. Elimination of Losses in Information Services Based on Approaches of IT-Service Management [17]. Enabling Enhanced Data Security for Aquaculture Management Services [18]. Quality-of-Service based Energy Trading Mechanism for Microgrids in a Distribution Network [19]. Quality of Service Evaluation of VoIP over Wireless Networks [20]. Exploring the Different Combinations of Technological Capability and Technology Management Capability in Different Stages of New Product Development [21]. Modeling Equipment Hierarchy and Costs for ICT solutions [22]. An Improved Quality-of-Service Performance Using RED's Active Queue Management Flow Control in Classifying Networks [23]. Improved Quality of Service in ZigBee Network with Statistical Modeling [24]. Quality of Service Enhancement in Wireless LAN: A Systematic Literature Review [25]. Improving Quality of Experience of Service-Chain Deployment for Multiple Users [26]. Quality Improvement in Web Services Using function Replication [27]. Systems and software engineering — Engineering and management of websites for systems, software and services information [28]. Work in Progress: Management of technological development projects in the engineering undergraduate – A knowledge management approach and interdisciplinary [29]. Novel User-Placement Ushering Mechanism to Improve Quality-of-Service for Femtocell Networks [30]. Prototype of an alignment model of the Ministry of Telecommunications and the Information Society to a public organization in Ecuador [31]. Intelligent Quality of Service Aware Traffic Forwarding for Software-Defined Networking/Open Shortest Path First Hybrid Industrial Internet [32]. Quality of Service Provisions for Maritime Communications Based on Cellular Networks [33]. Role of Information and Communication Technology in Green Supply Chain Implementation and Companies' Performance [34]. Service Quality Evaluation by Exploring Social Users' Contextual Information [35]. Strategic Management for IT Services Using the Information Technology Infrastructure Library (ITIL) Framework [36]. The Influence of IT Service Management Performance Measurement To Customer Satisfaction [37]. The Study of e-Government Implementation in Improving the Quality of Public Services [38]. Trust-Based Service Management for Mobile Cloud IoT Systems [39]. Using Bayesian Network to estimate the value of decisions within the context of Value-Based Software Engineering [40].

It uses the deductive method and technique of exploratory research that allows us to work and study the information of the articles presented.

The results are primarily criteria for information security in systems that prioritize data integrity and security through encryption and security protocol. An algorithm with flowchart techniques to mitigate data security and thus achieve quality improvement as an end goal the prototype made can be used as a reference for other ICT engineering and management companies to improve the quality of services.

Turned out a mixed conceptual model of quality-of-service approach, a dual-security architecture for business management, algorithm control with processes for quality of service and information filter algorithm control.

It is concluded that a Blockchain-secure information filter is considered a critical option to provide control, reliability, immutability and improvement in quality of service.

2. Materials and Methods

2.1. Materials

The authors proposed an IT service management platform based on the cyber physical system to improve the process and build a smart industry. They identified companies with resources for software, hardware and troubleshooting programs. They analyzed the lower efficiency and quality of service to provide a good service with a degree of difficulty especially in the physical condition of the business management facilities. Results promote IT service efficiency and provide advance notice in the life cycle management process of IT department resources [1].

In this article the authors proposed a Blockchain system as an architecture and model applied to different areas to increase the level of information security. Determined the little diversity of proposals applied in Hyperledger to the commercialization area. They generated an architecture based on Hyperledger to mitigate the risks of information in the management of foreign trade. A comprehensive management model in exports and imports based on Hyperledger was proposed as a collaboration platform in the company's areas [2].

In organizations with a field in which researchers develop new innovations and improvements for the provision of service to users and clients. The authors analyzed IT business as unstable due to increased competition in technological development and as a result products became obsolete. Research provides a structure that produces good results so that service delivery can be improved [3].

The authors proposed the use of the cloud for better dynamics in education in universities for the use of e-learning materials. They obtained improvements in response time in accordance with the relevant restrictions so that resources are used appropriately and in a timely manner in the company [4].

The authors proposed an analysis of the cloud as data storage services on the network using a device. Identified a problem in the servers in the cloud when the servers stopped working and caused high power losses. As a result they identified typical solutions to save energy without causing loss of information and resources while the server is idle without affecting the quality of service [5].

The authors carried out a study about the difficult situation that companies go through due to poor management by managers. An investigation was carried out on the core of the company's staff on the basis of the comparisons made between Japanese and foreign technology development companies focused on ICT. As a result the area of technological development was verified as one of the Japanese ICT societies with greater central rigidity than foreign ones [6].

The authors proposed an implementation of an initialization system for companies that have a great possibility of growth in order to seek growth. Conducted user tests in order to improve the system in accordance with the innovative prototypes installed to improve the quality of service. As a result of the implementation the attention of users was improved to obtain growth and the business was scalable and profitable [7].

In this article the authors analyzed manufacturing processes in companies to improve service in the supply chain through digitization. They captured information throughout the product lifecycle to analyze cost reduction and delivery times to improve efficiency. As a result of the research the information is managed during the program process through complete maintenance with individual processes to create the final part [8].

The authors proposed an analysis of the experimentation of change in business interactions and operations in the ICT department. They conducted an investigation of the factors that affected the use of computers and the Internet in forests. As a result companies improved the ICT service for electronic commerce in which they used to do electronic business more effectively [9].

The authors proposed a flaw detection system to improve the quality of service in real-time multimedia applications. A memory mirroring system was implemented to limit the overhead on the system and the installation of virtual machines to improve the quality of service. As a result methods were applied to access additional memory in real time [10].

The authors proposed an analysis of data transmissions to improve efficiency according to the scenarios applied in the system. Reviewed quality of service metrics on multiple data transactions at different levels. As a result they obtained a level of efficiency in the retransmission of lost data through the application of a network of analytical calculations; this system was adapted to the source nodes in the system [11].

The authors proposed a data tree technique to mitigate cyber-attacks on the network. They applied data mining to identify vulnerabilities in the Blockchain network with the use of trees. As a result a robust system was obtained with detection of threats in the network and provided reliability in the system [12].

The authors proposed a versatile platform that exposes an application-provided Smart Grid benchmark architecture. They incorporated real-world wireless technology with an artificial intelligence algorithm to facilitate real-time tested design requirements. As a result a better evaluation potential was obtained in the systems implemented in the company [13].

The authors proposed a design management system for the use of procedures and policies to provide efficient filing of company processes. They opted for integrated management systems to allow greater efficiency at lower costs to grow competitively. As a result a management system was obtained that works autonomously without affecting the general direction [14].

The authors proposed a network architecture with connection to mobile devices over a network to provide high-speed services. An exchange of data from an origin to destination point was identified that caused high energy consumption and a low quality of service. As a solution a storage management system was implemented for centralized processing in order to improve and obtain performance gains in the system [15].

The authors proposed an ICT management model to moderate the situations of non-compliance to which users are exposed. They used logical research as a methodology to analyze information on the rates of users of social networks in Ecuador. They also established a conceptual model related to the development of digital skills in a qualitative description in the management of digital content by children and adolescents [16].

The authors proposed an information services loss elimination system based on IT service management approaches in an effective way. They implemented a system that benefits several companies in different countries. As a result of the implementation the activities in the IT departments were optimized that allowed reducing the consumption of resources [17].

The authors proposed a method to avoid some kind of private data transfer over the network. They scrambled sets of random numbers to make encryption keys in a client-server system to provide information security [18].

The authors proposed a microgrid system with power generation techniques that work autonomously; with the implementation of microgrids better service is provided to customers to provide reliability compared to a distribution network. As a result the cost of energy supply of the microgrids was analyzed for the verification of implementation costs to improve the system [19].

The authors proposed an analysis of the performance of IP voice in wireless networks to determine the problems that exist in the loss of voice packets. In the analysis communication models were obtained through the Internet according to the bandwidth established by an installed protocol. The set of resources and restrictions that caused a weak signal in a user's communication was identified [20].

The development and quality of new products determine the current positions that are in the market of companies that use long-range positive impacts in the implementation in future companies. Benchmarking is used to explore technology capacity and management to drive high performance to capture new markets and provide opportunities for product innovations [21].

The authors made a comparison between information systems and modeling approaches to have a limited level of detail and provide a more generic solution for equipment cost modeling. This method ensures that models can be easily communicated shared and reused by generating a great advantage over the use of sheet models and calculations [22].

The authors designed a scheduling algorithm to improve buffering performance. An algorithm was implemented to improve the packet drop that solved the usage savings due to the slowness of the bandwidth. As a result it was self-tuning and network traffic was managed to produce increased stability in storage parameters [23].

The authors proposed a system to optimize performance more efficiently to improve the quality of service in network parameters. They implemented sensor nodes to facilitate the performance in

the connections with the devices that affected the overall performance of the network [24].

The authors performed an analysis of users that require a network service in their homes and workplaces as a necessity to perform different activities. Increased numbers of wireless network users and devices were identified at a reasonable cost of implementation at the time to provide good product service [25].

Service optimization has been a latent issue so it affects the product service to solve this problem: An algorithm was created with that it was experimented and as a result it was obtained that reduced the delay time and at the same time reduced rejections [26].

The authors proposed an improvement in the network service to achieve better efficiency and reliability of the system. A coupling was implemented according to the measure used in the most common services to increase independence. Process replication processes were carried out to reduce the rate of errors in the system. They grouped functions by groups to generate new relationships in order to improve large-scale processes [27].

The authors analyzed websites for commercial marketing and social media purposes that reflect different interests and media choices for those websites that offer ICT reference information. The objective of this method is to improve the usability of informational websites and the ease of maintenance of monitored web operations in terms of locating relevant and timely information [28].

The authors proposed a technological development for the creation or improvement of products according to the design and implementation of a program. They improved product quality for Peruvian universities that were forced by the saturation of the workforce in the standardization of processes for higher education [29].

In this document they offer a real-time application for the final product that is critical for mobile applications through wireless channels. With product maintenance in a wireless environment it is very difficult based on limited resources. The proposed method was a two-dimensional map for users to help locate the desired location with the positioning system [30].

The authors proposed a prototype to improve the quality of service in users belonging to the administrative of state department in accordance with technological advances. As a result an alignment model was obtained for the Ministry of Telecommunications for the use of a methodology that allowed to know the management and strategies [31].

The authors conducted an analysis on the use of resources to improve the use of smart manufacturing technology. Compliance requirements were identified to acquire better service quality indices according to remote surveillance parameters or anomaly detection. As a result an emerging software-defined network architecture for network heterogeneity and traffic congestion has been proposed to improve system reliability [32].

The authors proposed a communication architecture centralized in the user for the distribution of antennas. Used a mathematically modified cellular technique oriented network scenario in the open ocean and processes should be used to improve traceability and packet transfers for better communication between two points [33].

Currently companies are looking for a way to make technological updates that do not affect our environment and that in turn give us very good benefits. Today environmental care has become very popular among companies, suppliers and customers by not taking care of the environment they have a negative impact. As a result customers or consumers lean towards other companies that do respect and help take care of our planet. Currently taking care of the environment is no longer an option if not an obligation companies have taken advantage of the use of good strategies to supply consumers [34].

The authors analyzed the impact of the use of social networks as a means of communication for the use of professional and daily life. They identified that the product service is very fundamental for users who prefer to share their experiences of an application or a visited place; the majority of companies publish publications to promote their product and thus the message reaches more people according to the appeal of the publication. We would use entropy to calculate the trust of users. We would review the rating of emotional characteristics and a unification to calculate an overall trust [35].

The authors proposed a system for telecommunications equipment to store, retrieve, transmit and manipulate data to improve the strategies and services of the information technology department. They identified strategic changes in IT planning and services as a complex system; they obtained an improvement in the efficiency of the system to handle the different processes for file management. As a result standards were obtained that provide a better IT service with a methodology focused on the customer and commercial service they guaranteed a quality service [36].

This study aims to see the problems that exist with the customer in the IT service through surveys to evaluate customer satisfaction. Measurement according to customer satisfaction levels is to improve performance through performance evaluations. Performed statistical tests to test correlation analysis and enterprise-level performance appraisal method design [37].

The authors conducted a study on electronic governments as a problem according to UNU surveys. The purpose of this study is to measure public perception of the implementation of e-government in the Bandung region society using the MMR method that combines quantitative methods through surveys and a qualitative method with complex processes. As a result it was achieved that in most dimensions an improvement such as: Availability costs, technology, reputation and support should be implemented while the benefit and content are good. Therefore before they can be implemented efforts should be considered in the quality of public products [38].

The management of hierarchical services allows the client to let us know his experience of quality of service through a report and consultation. An application containing smart city travel services, air pollution detection and response exceeds service management protocols. Most IoT devices are mobile and they connect through the internet depending on where you are and the power status device management trust is necessary as not all devices will be trusted and others may be malicious to the cloud service [39].

With the application of Bayesian networks today decision making in software engineering with a competitive, innovative and growth approach for the company. Therefore they need to make changes in the paradigms of values where a study was carried out taking into account the characteristics which are stored in a database. Where an estimated model was obtained with the use of Bayesian networks which have created a positive result within companies in their software products [40].

2.2. Methods

Considerations

We propose to use a technique to store information securely and permanently with tracking functions such as: Blockchain we also propose to use a quality-of-service prototype combining these two new proposals in the management of companies we will have a prototype to improve the desired quality of service.

Comparative table

In Table 1 we have a better view of the references what presents the technology on that the authors were based and a description of the proposal.

Table 1: Article Comparison

Ref.	Technology	Method or process	Security/Efficiency
[1]	Cyber system environment.	Providing quality service to promote effective information technology service.	Promote early alarm in IT resource lifecycle management, process optimization and IT resource service.
[2]	Secure Information Block Architecture.	Provides an architecture for mitigating management.	Moderate information risks through secure information block and Hyperledger-based foreign trade management.
[3]	Service technology delivery model.	Develop and innovate technological advancement to increase competitiveness.	Storage of important data that improved security and service to users with increased contribution to IT service delivery.
[4]	E-learning model.	Enable user interaction with material in a fast, reliable and cost-effective manner.	Cloud data storage such as the use of computing resources properly and thus provide efficiency to improve quality of service.
[5]	Management architecture for the server.	Effective three-state strategy for servers.	Reduced power consumption to prevent loss of information handled through the cloud get a quick response from servers and improve quality of service.
[6]	Information Platform Architecture.	Adaptive framework that prevents attacks and threats to protected data.	Data rigidity by computer means and social media platforms with foreign companies. Building core capabilities with changes in market competitiveness and data rigidity.
[7]	Agility structure and quality of startups.	Data collection through interviews and documentation.	Developing innovative new products help achieve growth by making a business scalable.
[8]	Digital application of manufacturing innovation.	In the applications data is stored of the services offered with respective evaluations for the quality of service.	Integrated tools are given parts for reliable playback and ensures smooth response timely process evaluation.
[9]	Adaptation of information technology in the industry.	Analysis of the environment of company to make use in business through information technology.	Business productivity, exchange of data or information with customers and facilitations of banking transactions.
[10]	Adaptive optimization service model.	Automatic detection device for the final product in real time.	Application to access memory in real time to offer good product quality in real time.
[11]	Data relay method.	Analyze the network with data in order to relay lost data applicable on different nodes.	Multiple transmission that was only adaptable on source nodes but also on various source nodes.
[12]	Data mining software.	Identify and detect cyberattacks using a data tree.	Data mining was applied when using mining software in the implementation of the decision tree technique for the detection of cyberattacks.
[13]	Neural search algorithm.	A test bench is displayed in that wireless technology is incorporated.	Software that incorporates wireless technology that has an AI algorithm to show a potential for Smart Grid test assessments.
[14]	Integrated system stage modeling.	Integrated system for quality management and training of the management system.	Management systems are opted as it helps to grow competitively and thus offers greater efficiency.
[15]	Accuracy method of performance results.	Use maximum cache storage and signal processing.	Improved performance gain and centralized processing was demonstrated through caching.

[16]	Conflict management model.	Analyze management information to solve problems.	Moderation of non-conformance situations that users are exposed to.
[17]	Structure of production processes and tools.	Optimize operating costs and achieve the objectives of information technology services provided.	The use of Lean helps to optimize activities and allows a considerable reduction in resource consumption.

Table 1 provides a brief description of the most relevant articles that were taken as a reference for the analysis of new technologies; in this way the processes are visualized in short detail together with their method and in turn the safety and effectiveness to complement the decision-making based on the proposed results.

3. Results

The results we have proposed for this phase based on studies to improve the quality of service, security and technologies that were implemented are:

- Mixed Conceptual Model of Quality of Service Approach.
- Dual-security architecture for business management.
- Control of algorithms with processes for the quality of services.
- Control of algorithms with information filter.

3.1. Mixed Conceptual Model of Quality of Service Approach

The presented model of new prototypes for the management of engineering and ICT companies to improve the quality of services is represented in Figure 1.

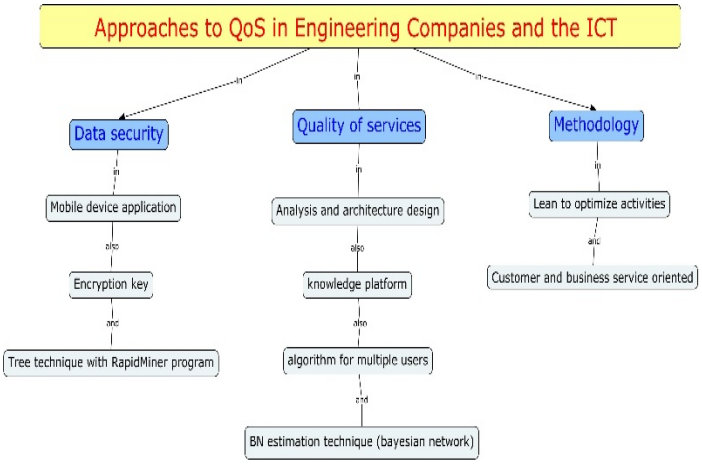


Figure 1: Conceptual model

Figure 1 shows the conceptual model segmentation in prototypes that have been referenced in three sectors called data security, quality of services and methodologies. There are different application scenarios, keys and techniques in that analyses and designs are applied with knowledge platforms and an algorithmic to optimize customer-oriented activities and improve service according to the management of company engineering.

The mathematical basis for measuring the conceptual model presented is expressed in the following formula (1):

$$Mmc = 1\frac{ADB}{ADMC + ACO + AIOC + AIB} \quad (1)$$

here:

ADMC is the amount of reliance on managed companies.

ADB is the number of direct beneficiaries.

ACO is the number of control offices.

AIOC is the number of reports per control office.

AIB is the number of indirect beneficiaries.

Formula (1) is applied to measure the conceptual model: Six scenarios were identified in the implementation according to business management; in the first scenario agricultural engineering was established with a measure of 97.62%; for systems engineering you have a measure of 82.99%; industrial engineering has a measure of 98.77%; electrical engineering has a measurement of 94.34%; in mechanical engineering a measure of 84.03% was obtained and in electronic engineering a measure of 90.03% is available.

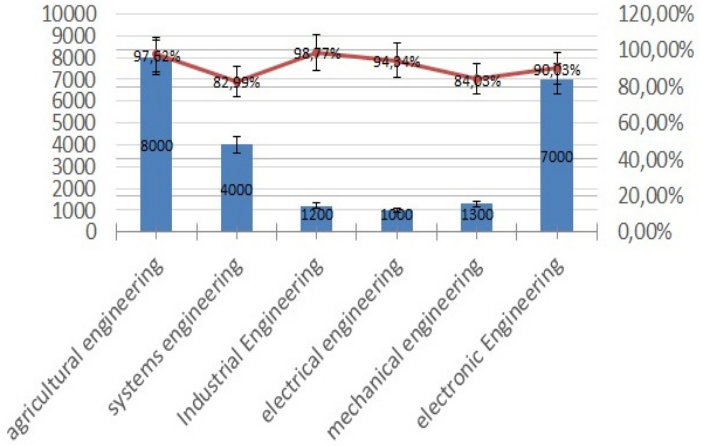


Figure 2: Measuring the conceptual model

Figure 2 shows the percentages of measurement of the management of engineering companies taking into account certain value indicators. Results allow you to have a view of the percentage-level comparisons of each engineering segmentation by approach to each management.

3.2. Dual-security architecture for business management

We proposed an architecture for business management in this case in the field of engineering. The participation of actors such as: Parent company, entity, branches and suppliers is established. Participants have an individual role according to process management, configuration management, control and supervision in the exchange process.

Figure 3 shows the architectural proposal for business management consists of the following parts: Information platform, application, matrix, distribution, protocol filter and evaluation with information risk calculation.

The Blockchain architecture we propose is established according to immutable information, audited information and

encrypted data. Consensus among participants that update the information. Participants have an authentication certificate.

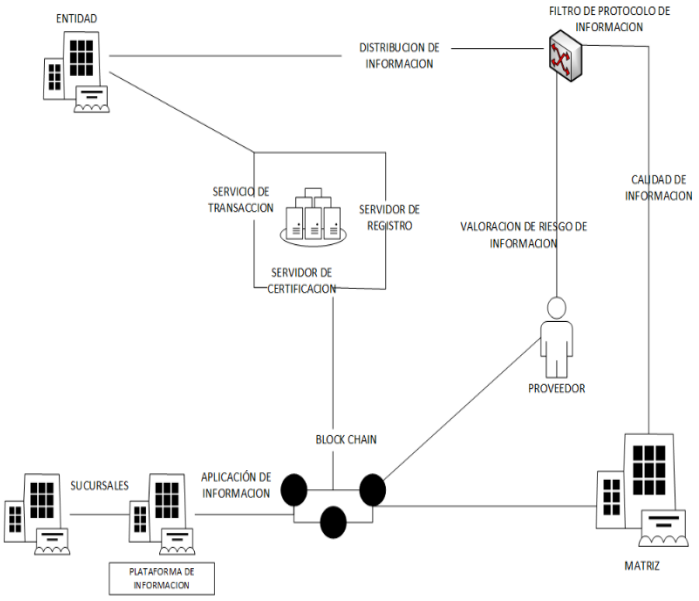


Figure 3: Dual-security architecture for business management

All actors will have a copy of the information in the Blockchain and localities are authorized to enter information related to the management of their area. In the operation of the management model branches have a general identifier for querying data.

We propose that the Blockchain be on the platform in order to intervene between the matrix and the corresponding entities; the model establishes authentication to determine network entry and update information if necessary; these actors aim to give their consent to update the data to form the consensus.

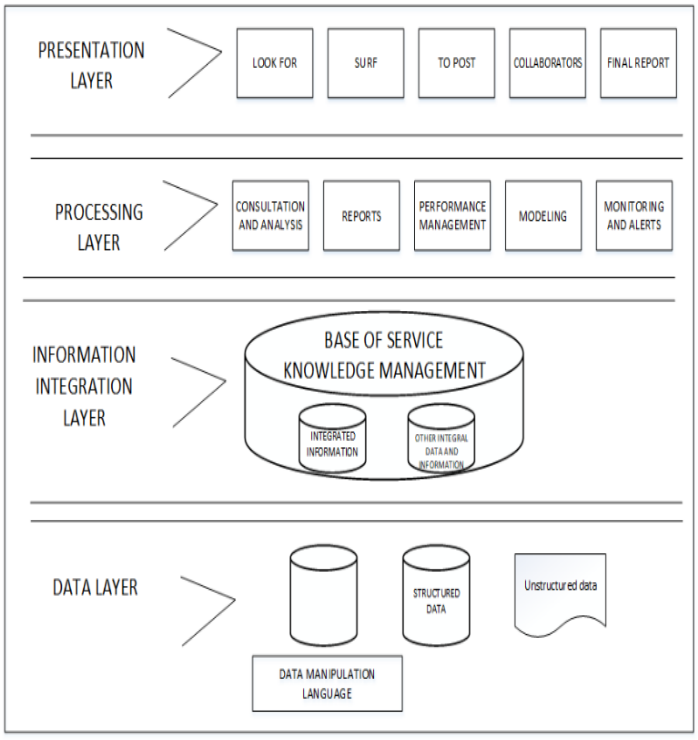


Figure 4: Four-layer architecture model

Figure 4 shows a layered architecture consisting of four levels to perform a successful process with data exchange with the company address.

Presentation layer is assigned the search, navigation, publication, collaboration and preparation of a final report.

Processing layer query and analysis processes, report management, performance management, modeling, monitoring and alerts are established.

Information integration layer is the foundation of service knowledge management, integrated information and other data with integrated information.

Data layer are databases for data manipulation, structured data and unstructured data all data is stored here.

3.3. Control of algorithms with quality of service processes

We proposed an algorithm as a guide in the process of new prototypes for the management of engineering and ICT companies to improve the quality of services; the algorithm aims to improve the steps of the methodology to avoid risks in information.

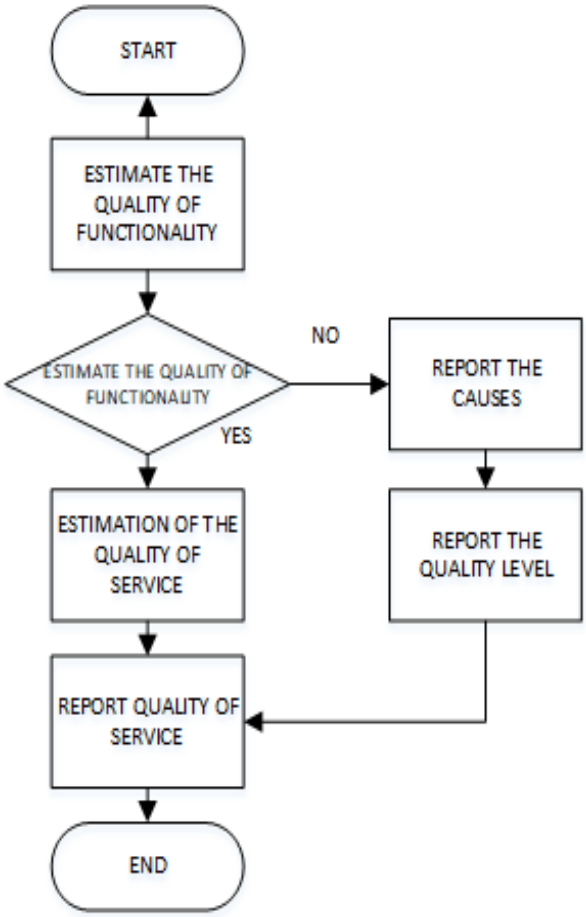


Figure 5: Information control algorithm

Figure 5 shows the application steps of the Quality of Service algorithm as a start to estimating the quality of functionality. The algorithm values the process of managing the operation of parameters. The system validates the quality of service condition and estimates under an internal range to report the quality of the

service. If the system does not meet the requirements the causes are reported and the level is validated to the appropriate quality standards; after the transaction is successful the system generates a report on the quality of the final product.

The mathematical basis for measuring the improvement in the quality of service as a final product is expressed in the formula (2):

$$CS = 1 - \frac{(LF)}{AS + AM + AA + AC} \quad (2)$$

here:

CS is the quality of services.

AS is the number of surveys.

AM is the amount of tracking.

AA is the number of alerts.

AC is the number of collaborators.

LF is the level of functionality.

For the measurement of the algorithm an example was made and the formula (2). Was applied the following example shows the use of the formula. For the improvement of the data a 31% was obtained; for the improvement of satisfaction you have a measurement of 25%. For the improvement of efficiency was obtained 17% and for the measurement of the productivity improvement 29% was obtained.

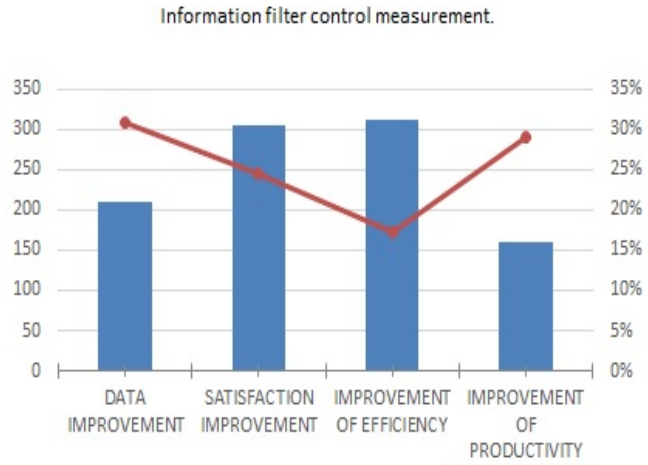


Figure 6: Information filter control

Figure 6 shows the measurement percentages of the improvement in quality of service in order to propose a prototype focused on different areas of engineering. You get an increase in data improvement by 31% over existing quality within the company and also improves satisfaction, efficiency and productivity. This was achieved through data collection through surveys, partner tracking and the level of functionality.

3.4. Control of algorithms with quality of service processes

We proposed an algorithm for engineering and ICT company management processes to improve the quality of services. The algorithm aims to improve the steps of the methodology to avoid risks in the control of information.

A process is maintained in that filters based on information and communication technologies are adopted to have greater control of the database. In the execution of this network of filters could be estimated an improvement in the process and obtain an increase in the quality of service. Information is partitioned into four stages such as blocking, processing, storing and exchanging it.

It should be noted that the algorithm process we have in mind can be applied to several management engineering companies in order to obtain an increase in favor of the data collected before obtaining it. This refers to that after applying the established algorithm could be reference to great power of quality information since in this way the results obtained can be measured more reliably.

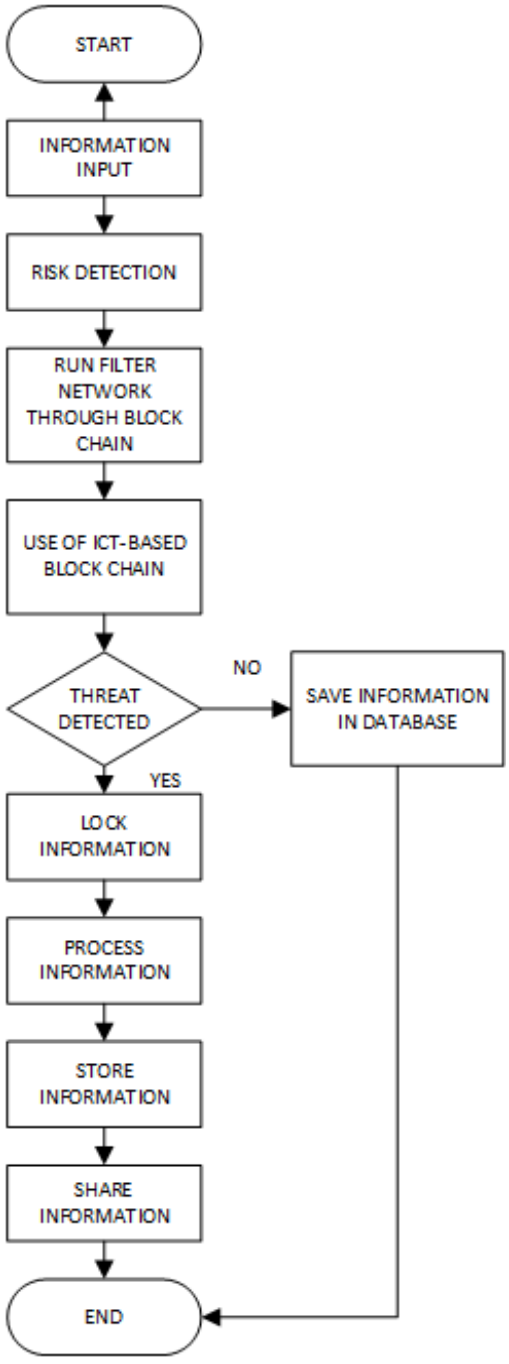


Figure 7: Control algorithm for information

Figure 7 shows the implementation steps of the control algorithm for information. First we have the input of information here is the input of all the parameter information. Risk detection finds the process of detecting anomalies in the data. In the process of a filtering network runs through Blockchain and its ICT-based use to analyze threats. A threat detection process is executed if the system detects the information is blocked then the information is processed according to the parameters the information is stored and shared. If the condition is met the information if the system does not detect a threat on the network is saved in a database engine and the process ends.

The mathematical basis for measuring control for the information presented is expressed in the formula (3):

$$Cfi = 1 - \frac{AUP}{AIE - ARD - AFN} \quad (3)$$

Here:

AUP is the amount of ICT-based Blockchain usage process.

AIE is the amount of information entered.

ARD is the amount of risk detected.

AFN is the amount of filter on the network.

Formula (3) was used for the measurement of the information control algorithm; for blocked information a measure of 71% was established; for the information processed the measure was 7%; for stored information a measure of 33% was established and for shared information a measure of 13%.

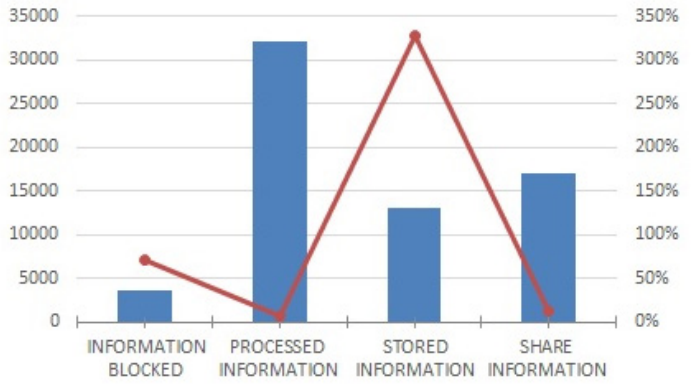


Figure 8: Filter control measurement information

Figure 8 shows the measurement percentages of the information filter control taking into account certain value indicators. This allows you to have a glimpse of the filtration process via Blockchain.

4. Discussion

To propose the results of this research we adopt Blockchain technology [2] to give a higher level of security consistency to the information that is generated and to avoid malicious actions in the handling of information. We also adopt architecture and reference information [3]. We even take quality management models [14] and along with modeling the quality of services [19]. Collecting future relevant data through the established prototype.

The results obtained were mainly criteria for the security of company management in systems that prioritize data security. Quality of services through encryption and protocol.

In the research process an algorithm scheme was determined they used flowchart techniques as an option for information control in business management; the manufactured prototype can be used as a reference for other quality of service management companies. A second algorithm scheme was obtained using flowchart techniques as a process option to obtain the quality of services as a final product.

5. Future Work and Conclusions

In the future we proposed that the integration of the Engineering Companies and the ICTs be carried out to improve the quality of the services of internal and external users. The results obtained in this investigation are considered as an alternative.

It was concluded that Blockchain is determined as a fundamental option to provide greater control, as well as robustness in the face of malicious failures and attacks. The reliability of the information serves to get a better detail of the report along with the availability that handles a data rate and thus its immutability and security would obtain an improved final product.

It was concluded that Blockchain is determined a fundamental option to provide greater control, robustness in the face of failures and malicious attacks. The reliability of the information serves to get a better detail of the report along with the availability that handles a data rate and thus its immutability and security would obtain an improved final product.

With the obtained indicators applied to the processes downtime was avoided. In this way the integrity and accessibility of information in the management of the security processes of technology companies have a higher priority and option of protection against the improvement of services.

It should be noted that the protocols followed in our experiment are fully applicable in other investigations. These applications need to delve into the issue of new prototypes for the management of engineering and ICT companies to improve the quality of services.

Conflict of Interest

The authors declare no conflict of interest.

Acknowledgment

The authors thank to Universidad Politécnica Salesiana del Ecuador to the research group of the Guayaquil Headquarters “Computing, Security and Information Technology for a Globalized World” (CSITGW) created according to resolution 142-06-2017-07-19 and Secretaría de Educación Superior, Ciencia, Tecnología e Innovación (Senescyt).

References

[1] Y. Zhao, Y. Rao, “A CPS-based intelligence-awareness platform for IT service management,” Proceedings - 2017 Chinese Automation Congress, CAC 2017, **2017-Janua**, 6668–6673, 2017, doi:10.1109/CAC.2017.8243978.

[2] S.M. Toapanta Toapanta, L.E. Mafla Gallegos, M.G. Guaman Villalta, N.S. Mora Saltos, "A hyperledger technology approach to mitigate the risks of the database in foreign trade management," Proceedings - 3rd International Conference on Information and Computer Technologies, ICICT 2020, (March), 313–319, 2020, doi:10.1109/ICICT50521.2020.00055.

[3] T. Almeida, J.B. De Vasconcelos, G. Pestana, "A knowledge management architecture for information technology services delivery," Iberian Conference on Information Systems and Technologies, CISTI, **2018-June**, 1–4, 2018, doi:10.23919/CISTI.2018.8399202.

[4] P. Tamang, A. Alsadoon, C. Withana, L.S. Hoe, A. Elchouemi, "A model to improve Quality of Service (QoS) in cloud based Virtual lab framework," 2015 International Conference and Workshop on Computing and Communication, IEMCON 2015, 1–5, 2015, doi:10.1109/IEMCON.2015.7344519.

[5] B.M. Nguyen, D. Tran, Q. Nguyen, "A strategy for server management to improve cloud service QoS," Proceedings - 2015 IEEE/ACM 19th International Symposium on Distributed Simulation and Real Time Applications, DS-RT 2015, 120–127, 2016, doi:10.1109/DS-RT.2015.14.

[6] I. Nakaoka, H. Fujino, Y. Park, Y. Chen, H. Akaoka, S. Masuyama, "A study on R&D organization management of Japanese ICT companies using patent information," Proceedings - 2017 International Conference on Advanced Informatics: Concepts, Theory and Applications, ICAICTA 2017, 2017, doi:10.1109/ICAICTA.2017.8090976.

[7] V. Berg, J. Birkeland, A. Nguyen-Duc, I.O. Pappas, L. Jaccheri, "Achieving agility and quality in product development - an empirical study of hardware startups," Journal of Systems and Software, **167**, 2020, doi:10.1016/j.jss.2020.110599.

[8] D. Mies, W. Marsden, S. Warde, "Overview of Additive Manufacturing Informatics: 'A Digital Thread,'" Integrating Materials and Manufacturing Innovation, **5**(1), 114–142, 2016, doi:10.1186/s40192-016-0050-7.

[9] T. GEDİK, İ. DURUSOY, "Adoption of Information and Communications Technology in the Turkish Forest Products Industry: A Case Study," Kastamonu Üniversitesi Orman Fakültesi Dergisi, **20**(1), 38–48, 2020, doi:10.17475/kastorman.705835.

[10] G. Jia, G. Han, D. Zhang, L. Liu, L. Shu, "An Adaptive Framework for Improving Quality of Service in Industrial Systems," IEEE Access, **3**, 2129–2139, 2015, doi:10.1109/ACCESS.2015.2496959.

[11] I.A. Kaisina, A. V. Abilov, A. V. Chunaev, M. Aiman Al Akkad, V. V. Khvorenkov, "Analysis Methods for Improving Quality of Service Metrics in Flying Ad Hoc Networks," Moscow Workshop on Electronic and Networking Technologies, MWENT 2020 - Proceedings, 2020, doi:10.1109/MWENT47943.2020.9067430.

[12] S.M. Toapanta Toapanta, L.E. Mafla Gallegos, B.E. Cisnero Andrade, M.G. Tandazo Espinoza, "Analysis to predict cybercrime using information technology in a globalized environment," Proceedings - 3rd International Conference on Information and Computer Technologies, ICICT 2020, (March), 417–423, 2020, doi:10.1109/ICICT50521.2020.00073.

[13] M. You, X. Zhang, G. Zheng, J. Jiang, H. Sun, "A Versatile Software Defined Smart Grid Testbed: Artificial Intelligence Enhanced Real-Time Co-Evaluation of ICT Systems and Power Systems," IEEE Access, **8**, 88651–88663, 2020, doi:10.1109/ACCESS.2020.2992906.

[14] Y. V. Velmakina, S. V. Aleksandrova, V.A. Vasiliev, "Basics of Forming an Integrated Management System," Proceedings of the 2018 International Conference "'Quality Management, Transport and Information Security, Information Technologies'", IT and QM and IS 2018, 77–78, 2018, doi:10.1109/ITMQIS.2018.8524955.

[15] Z. Zhao, M. Peng, Z. Ding, W. Wang, H.V. Poor, "Cluster content caching: An energy-efficient approach to improve quality of service in cloud radio access networks," IEEE Journal on Selected Areas in Communications, **34**(5), 1207–1221, 2016, doi:10.1109/JSAC.2016.2545384.

[16] R. Maciel, E. Mafla, "Definition of an ICT Management Model to Mitigate Cyberbullying Risk in Social Networks," (July), 2020.

[17] O. V. Efimova, N.P. Tereshina, N. V. Tereshina, V. V. Zhakov, "Elimination of Losses in Information Services Based on Approaches of IT-Service Management," Proceedings of the 2019 IEEE International Conference Quality Management, Transport and Information Security, Information Technologies IT and QM and IS 2019, 128–131, 2019, doi:10.1109/ITQMIS.2019.8928331.

[18] D. Piplani, D.K. Singh, R. Sharma, M. Aleembaig, "Enabling enhanced data security for aquaculture management services," Proceedings of the 2017 3rd Conference on Mobile and Secure Services, MOBISECSERV 2017, 2017, doi:10.1109/MOBISECSERV.2017.7886563.

[19] W. Zhang, T. Meng, Y. Luo, "Quality-of-Service based Enegy Trading Mechanism for Microgrids in a Distribution Network," IEEE Power and Energy Society General Meeting, **2018-Augus**, 7–11, 2018, doi:10.1109/PESGM.2018.8586265.

[20] K. Alalawi, H. Al-Aqrabi, "Quality of service evaluation of VoIP over wireless networks," 2015 IEEE 8th GCC Conference and Exhibition, GCCCE 2015, 1–4, 2015, doi:10.1109/IEEEGCC.2015.7060070.

[21] Y. Liu, W. Wu, P. Gao, K. Liu, "Exploring the Different Combinations of Technological Capability and Technology Management Capability in Different Stages of New Product Development," IEEE Access, **7**, 181012–181021, 2019, doi:10.1109/ACCESS.2019.2959207.

[22] J. Spruytte, M. Van der Wee, S. Verbrugge, D. Colle, "Modeling equipment hierarchy and costs for ICT solutions," Transactions on Emerging Telecommunications Technologies, **30**(3), 2019, doi:10.1002/ett.3583.

[23] A.M. Alkharasani, M. Othman, A. Abdullah, K.Y. Lun, "Improved Quality-of-Service Performance Using RED's Active Queue Management Flow Control in Classifying Networks," IEEE Access, **5**, 24467–24478, 2017, doi:10.1109/ACCESS.2017.2767071.

[24] N. Islam, M.J.H. Biddut, A.I. Swapna, S. Asaduzzaman, "Improved Quality of Service in ZigBee network with statistical modeling," Proceedings of 2015 3rd International Conference on Advances in Electrical Engineering, ICAEE 2015, 174–177, 2016, doi:10.1109/ICAEE.2015.7506824.

[25] M.H. Sanan, K.A. Alam, M.Z. Rafique, B. Khan, "Quality of Service Enhancement in Wireless LAN: A Systematic Literature Review," MACS 2019 - 13th International Conference on Mathematics, Actuarial Science, Computer Science and Statistics, Proceedings, 2019, doi:10.1109/MACS48846.2019.9024827.

[26] I.C. Wang, C.H.P. Wen, H.J. Chao, "Improving Quality of Experience of Service-Chain Deployment for Multiple Users," 2018 IEEE/ACM 26th International Symposium on Quality of Service, IWQoS 2018, **1**, 2019, doi:10.1109/IWQoS.2018.8624167.

[27] M.J. Amiri, M. Koupaee, "Quality improvement in web services using function replication," 2016 2nd International Conference on Web Research, ICWR 2016, 72–77, 2016, doi:10.1109/ICWR.2016.7498449.

[28] F.O.R. Standardization, D.E. Normalisation, "Systems and software engineering — Engineering and management of websites for systems, software, and services information," **1987**, 1987.

[29] J.E.Q. Rojas, J.E.Q. Tuesta, "Management of technological development projects in the engineering undergraduate-A knowledge management approach and interdisciplinarity," EDUNINE 2019 - 3rd IEEE World Engineering Education Conference: Modern Educational Paradigms for Computer and Engineering Career, Proceedings, (28740), 2–5, 2019, doi:10.1109/EDUNINE.2019.8875798.

[30] C. Wang, S.H. Fang, H.C. Wu, S.M. Chiou, W.H. Kuo, P.C. Lin, "Novel User-Placement Ushering Mechanism to Improve Quality-of-Service for Femtocell Networks," IEEE Systems Journal, **12**(2), 1993–2004, 2018, doi:10.1109/JSYST.2016.2635158.

[31] S.M.T. Toapanta, M.J.M. Canales, J.G.O. Rojas, L.E.M. Gallegos, "Prototype of an Alignment Model of the Ministry of Telecommunications and the Information Society to a Public Organization in Ecuador," Proceedings of the 2020 the 4th International Conference on Information System and Data Mining, (May), 58–64, 2020, doi:10.1145/3404663.3404676.

[32] Y. Bi, G. Han, C. Lin, Y. Peng, H. Pu, Y. Jia, "Intelligent Quality of Service Aware Traffic Forwarding for Software-Defined Networking/Open Shortest Path First Hybrid Industrial Internet," IEEE Transactions on Industrial Informatics, **16**(2), 1395–1405, 2020, doi:10.1109/TII.2019.2946045.

[33] Y. Xu, "Quality of Service Provisions for Maritime Communications Based on Cellular Networks," IEEE Access, **5**, 23881–23890, 2017, doi:10.1109/ACCESS.2017.2763639.

[34] J.R. Mendoza-Fong, J.L. García-Alcaraz, E.J. Macías, N.L. Ibarra Hernández, J.R. Díaz-Reza, J.B. Fernández, "Role of information and communication technology in green supply chain implementation and companies' performance," Sustainability (Switzerland), **10**(6), 2018, doi:10.3390/su10061793.

[35] G. Zhao, X. Qian, X. Lei, T. Mei, "Service Quality Evaluation by Exploring Social Users' Contextual Information," IEEE Transactions on Knowledge and Data Engineering, **28**(12), 3382–3394, 2016, doi:10.1109/TKDE.2016.2607172.

[36] H. Gunawan, "Strategic Management for IT Services Using the Information Technology Infrastructure Library (ITIL) Framework," Proceedings of 2019 International Conference on Information Management and Technology, ICIMTech 2019, (August), 362–366, 2019, doi:10.1109/ICIMTech.2019.8843711.

[37] A.N. Fajar, D.R. Andini, "The Influence of IT Service Management Performance Measurement to Customer Satisfaction," Proceedings of 2018 International Conference on Information Management and Technology, ICIMTech 2018, (September), 109–113, 2018,

doi:10.1109/ICIMTech.2018.8528195.

[38] Ariwiati, S.F. Ristekawati, R. Febriliantina, Zakiah, "The study of e-Government implementation in improving the quality of public services (A study on society in Bandung region)," 2016 International Conference on ICT for Smart Society, ICISS 2016, (July), 105–110, 2016, doi:10.1109/ICTSS.2016.7792858.

[39] I.R. Chen, J. Guo, D.C. Wang, J.J.P. Tsai, H. Al-Hamadi, I. You, "Trust-Based Service Management for Mobile Cloud IoT Systems," IEEE Transactions on Network and Service Management, **16**(1), 246–263, 2019, doi:10.1109/TNSM.2018.2886379.

[40] E. Mendes, M. Perkusich, V. Freitas, J. Nunes, "Using Bayesian Network to estimate the value of decisions within the context of Value-Based Software Engineering," ACM International Conference Proceeding Series, **Part F1377**(June), 2018, doi:10.1145/3210459.3210468.

ASTES

Advances in Science, Technology and Engineering Systems Journal
Vol. 5, No. 5, 709-716 (2020)
www.astesj.com
Special Issue on Multidisciplinary Innovation in Engineering Science & Technology

ASTES Journal
ISSN: 2415-6698

Newton-Euler Based Dynamic Modeling and Control Simulation for Dual-Axis Parallel Mechanism Solar Tracker

Sarot Srang[*,1], Sopagna Ath[2], Masaki Yamakita[2]

[1]*Institute of Technology of Cambodia, Industrial and Mechanical Engineering Department, 12150, Cambodia*

[2]*Tokyo Institute of Technology, Systems and Control Engineering Department, 152-8552, Japan*

ARTICLE INFO

Article history:
Received: 24 July, 2020
Accepted: 25 September, 2020
Online: 05 October, 2020

Keywords:
Parallel Mechanism
Kinematic Constrained
Euler Parameters
Cartesian Coordinate System
Algebraic Differential Equations

ABSTRACT

Dynamic modeling has been a crucial study in many areas of the engineering field. In this paper, we apply the Newton-Euler equation of motion to a two-DOF parallel mechanism solar tracker which is a close loop mechanism. The aim of this study is to show a simulation of the dynamical model with feedback control using a PD controller to orientate the solar panel perpendicular to the sun rays. The mechanism is modeled in the form of a system of algebraic differential equations. First, kinematic constraint equations were constructed in the form of algebraic equations to specify the dynamic interactions at joints. We use the Baumgarte stabilization method, a constraint violation method to eliminate computational error incurred by numerical approximation. Then, the dynamic equations of the system were formulated using the Newton-Euler equation of motion. To describe the translation and rotation motions, we apply Cartesian coordinates and Euler parameters. Simulation of driving the solar panel to reach the desired configuration is made, and the result shows that the PD controller provides good performance of the mechanism regardless of the complexity of the dynamic behavior of the mechanism.

1 Introduction

This paper is an extension of work originally presented in *2019 IEEE/ASME International Conference on Advanced Intelligent Mechatronics (AIM). IEEE, 2019* [1]. Solar energy has been a major current research in the electricity generation field because of its unlimited resource and environmental friendly behavior. The efficiency of solar energy can be improved by implementing a tracking mechanism which keeps the solar panel perpendicular to the sun rays. There exists two main types of tracking mechanism, a single and dual axis solar tracker [2]. Energy gain from a single axis solar tracker was reported to be 20% [3] while energy gain from a dual axis solar tracker was 30-40% [4].

Dual axis solar tracker has been of an interest research topic for many researchers, [3], [5]–[7], because of its outperformance over single axis solar tracker. Many researches on energy gain from solar tracking systems compared to the tilted fixed panel had been done both theoretically and experimentally [5]. In [7], the author proposed a two-axis decoupled solar tracking system based on parallel mechanism and showed that the tracker requires less driving torque, thus less power dissipation than the conventional serial tracker does. Furthermore, the tracking system does not need reducer with large reduction ratio. Therefore, complexity and weight of the system are also reduced. The parallel mechanism solar tracker can be implemented by mounting on either a fixed or moving platform to produce electrical energy. For instance, aerial vehicles, boats, land vehicles are considered as moving platform. Assuming that the parallel mechanism solar tracker is attached to an aerial vehicle, the dynamic effect must be taken into account. The scope of this study is limited to a fixed platform.

Various methods for dynamic modeling for mechanical systems have been widely developed, and each one has its own advantages and disadvantages. In general, dynamic modeling using generalized coordinate (e.g. Lagrange's dynamic equation) yields the smallest number of differential equations and, therefore, computational efficient. However, the order of nonlinearity is high, and derivation of equation in expanded form of multibody system with loops of connected links is very tedious. For parallel mechanism, derivation can be done by virtually decomposing the system as open loop mechanism with some kinematic constraint forces by the other

[*]Corresponding Author: Sarot Srang, Department of Industrial and Mechanical Engineering, Institute of Technology of Cambodia, Russian Federation Blvd., P.O.Box 86, Sangkat Tuek L'ak 1, Khan Tuol Kouk, Phnom Penh, Cambodia. srangsarot@itc.edu.kh

parts of the system. For a system with more than one loop like the tracker we are considering, the derivation is even more difficult, and only partial reaction (or constraint) forces can be determined. With cartesian coordinates in global and body-fixed frames and Euler parameters for describing rotation, dynamic modeling using Newton's method is much simpler, and systematic generation of kinematic constraints at all joints and dynamic equations can be derived easily [8]. The method yields system equations of algebraic-differential equations. Reaction forces and the coordinates describing motion of a system are obtained from solving the equations. The reaction force has an advantage for mechanical structure design. A high-performance computer can realize the simulation modeled in detail including the reaction force effect in this case. However, the analysis of reaction forces is not reported in this work.

The remaining contents of this paper are organized as follows. In section 2, the parallel mechanism is explained on configuration, and its kinematic is described by using Cartesian coordinate. Dynamic equations for unconstrained and constrained body which are described in Cartesian coordinate and using Euler parameters are given in section 3. For constrained body, the resulted equation is in the form of system algebraic-differential equations. In section 4, the controller design is covered by using PD controller. Section 5 presents the results and discussion. We conclude our paper in section 6.

2 Kinematic Constraint

Cartesian coordinate is used to describe the system configuration, and constraint equations are obtained from individual joints. Figure 1 shows the coordinate system, where $(Oxyz)$ is global frame and $(O_i\xi_i\eta_i\zeta_i)$ is body-fixed frame attached on body i with the center of mass O_i. A point P on the body has coordinate as a vector in body-fixed frame and global frame defined by $s_i'^P$ and r_i^P respectively. Figure 2 shows a parallel mechanism which is used as dual axis solar tracker. The body numbers are labeled as seen in the figure. The mechanism consists of 7 connected rigid bodies. It has a global coordinate $(Oxyz)$, and each body has its own body-fixed frame as explained in Figure 2. Body 7 is connected with body 5 and 6 via 2 spherical joints and with body 4 via a universal joint. Body 6 is connected with body 2 via a revolute joint. Body 5 is connected to body 3 via a universal joint. Body 4 is connected to body 1 (ground) via another revolute joint. Body 3 is connected with body 1 via a translational joint. Body 2 is connected with body 1 via another translational joint. Two linear actuators are attached at the translational joints. The actuators exert forces on body 2 and 3 along vertical axes.

Denote $q_i = \left[r^T, p^T\right]_i^T = [x, y, z, e_0, e_1, e_2, e_3]_i^T$ as a coordinate vector of the body i, where r_i is position vector of the center of mass of the body as illustrated in Figure 1, and $p_i = \left[e_0, e^T\right]_i^T = [e_0, e_1, e_2, e_3]_i^T$ is Euler parameters.

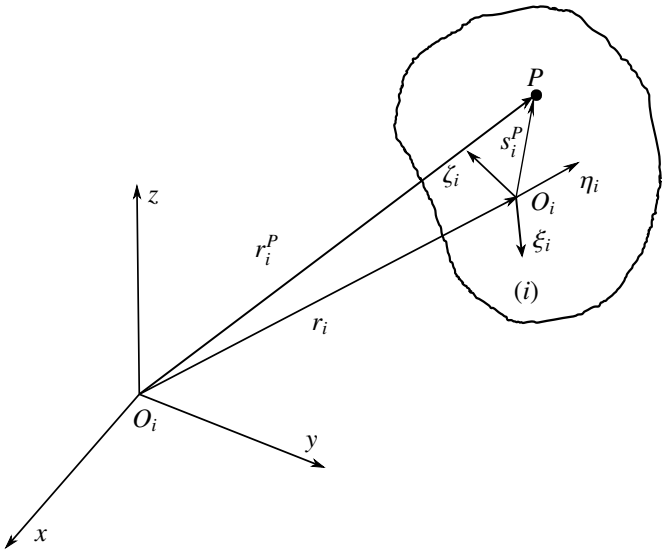


Figure 1: Cartesian Coordinate System

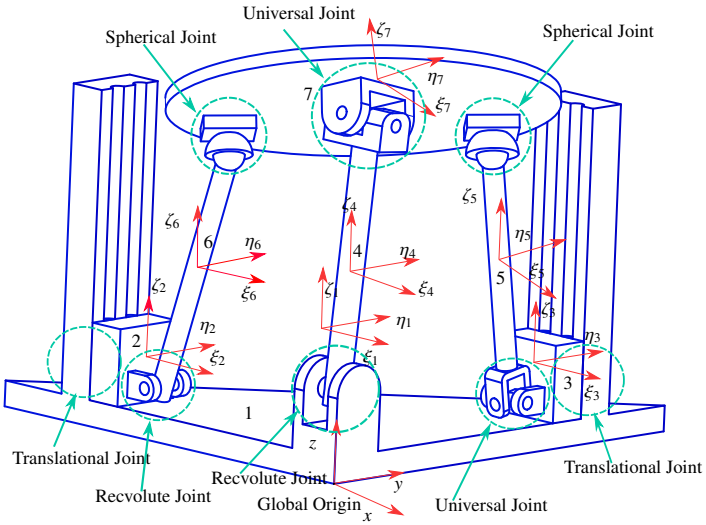


Figure 2: Global and Local coordinates of the parallel mechanism at the initial configuration

The parameter satisfies a mathematical relationship,

$$p_i^T p_i - 1 = 0. \tag{1}$$

The second time derivative of (1) is

$$p_i^T \ddot{p}_i + \dot{p}_i^T \dot{p}_i = 0. \tag{2}$$

Denote R_i as a rotational matrix of body i, and a pair of 3×4 matrices G_i and L_i defined as $G_i = [-e, \tilde{e} + e_0 I]_i$ and $L_i = [-e, -\tilde{e} + e_0 I]_i$. Then $R_i = G_i L_i^T$,[8] . The global coordinate of the point P illustrated in Figure 1 can be defined by

$$r_i^P = r_i + R_i s_i'^P = r_i + G_i L_i^T s_i'^P, \tag{3}$$

where $s_i'^P = \left[\xi^P, \eta^P, \zeta^P\right]_i^T$ is body-fixed coordinate of the point P.

Denote $q = \left[q_1^T, q_2^T, q_3^T, q_4^T, q_5^T, q_6^T, q_7^T\right]^T$ as coordinate vector for describing the configuration of the mechanism, and its respective first and second time derivative, $\dot{q}$ and $\ddot{q}$, for describing the motion of the mechanism. The number of coordinates of the system is $n = 7 \times 7 = 49$, and the number of Euler parameters relationship (or mathematical constraint) is 7.
Denote

$$\Phi \equiv \Phi(q) = 0 \tag{4}$$

as kinematic equation derived from kinematic constraints which have 34 equations. The compact form of the kinematic equation for each joint is given in Appendix A. The first and second time derivative of (4) are written as

$$\begin{aligned} \Phi_q \dot{q} &= 0, \\ \Phi_q \ddot{q} + \left(\Phi_q \dot{q}\right)_q \dot{q} &= 0 \\ \text{or } \Phi_q \ddot{q} &= \gamma, \end{aligned} \tag{5}$$

where $\gamma = -\left(\Phi_q \dot{q}\right)_q \dot{q}$ is called the right side of the kinematic acceleration equation and can be found in [8]. We adopt the constraint violation stabilization methods from [9], another similar technique can also be found in [10, 11].
Consider the following closed loop system,

$$\ddot{D} + K_P \dot{D} + K_D D = 0, \tag{6}$$

where K_P and K_D are constant and defined in Appendix B. Due to the fact that there exists numerical errors in using numerical method to solve the differential equations (5), we use the positive constraint violation stabilization method to obtain a stable response. So (5) is modified such that the kinematic constraint equations are satisfied by ensuring the shrinking of the computation error.
First time derivative of constraint equation is obtained as

$$\Phi_q \dot{q} = \dot{D} \tag{7}$$

Second time derivative of the constraint equation is given as

$$\begin{aligned} \Phi_q \ddot{q} + (\Phi_q \dot{q})_q \dot{q} &= \ddot{D} \\ &= -K_D \dot{D} - K_P D \\ &= -K_D(\Phi_q \dot{q}) - K_P \Phi(q) \end{aligned} \tag{8}$$

Thus,

$$\Phi_q \ddot{q} = \gamma - K_D(\Phi_q \dot{q}) - K_P \Phi(q). \tag{9}$$

The equation (9) is used for simulation and the performance is discussed in section 5.

3 Dynamic Modeling for Unconstrained and Constrained Bodies

Newton-Euler equations of motion is used to derive the equations of motion for multi-rigid bodies of the parallel mechanism. Prior to having the equations of motion for a set of interconnected bodies by kinematic joints which is known as constrained body, the equations of motion for body with no contact to other bodies which refers as an unconstrained body are written.

3.1 Dynamic Equations for Unconstrained Bodies

From Newton's method, an unconstrained body i with mass m_i and moment of inertia J_i' with respect to its center of mass exerted by external force f_i and moment τ_i' has dynamic equation of motion as

$$\begin{aligned} N_i \ddot{r}_i &= f_i \\ J_i' \dot{\omega}_i' + \tilde{\omega}_i' J_i' \omega_i' &= n_i', \end{aligned} \tag{10}$$

where $N_i = diag\left(\begin{bmatrix} m & m & m \end{bmatrix}\right)_i$ and ω_i' is the angular velocity defined in body-fixed frame. The equation of rotational motion in (10) is transformed by using the following relationships [8].

$$\begin{aligned} \omega' &= 2L\dot{p} \\ \dot{\omega}' &= 2L\ddot{p}. \end{aligned} \tag{11}$$

$$\widetilde{L_i \dot{p}_i} = L_i \dot{L}_i^T \tag{12}$$

Equation (10) becomes

$$\begin{aligned} 2J_i' L_i \ddot{p}_i + 4\widetilde{L_i \dot{p}_i} J_i' L_i \dot{p}_i &= n_i' \\ 2J_i' L_i \ddot{p}_i + 4L\dot{L}^T J_i' L_i \dot{p}_i &= n_i' \\ 2J_i' L_i \ddot{p}_i + L_i H_i \dot{p}_i &= n_i', \end{aligned} \tag{13}$$

where $H_i = 4\dot{L}_i^T J_i^T L_i$. The dynamic equations of motion for an unconstrained bodies are written as

$$\begin{aligned} N_i \ddot{r}_i &= f_i \\ 2J_i' L_i \ddot{p}_i + L_i H_i \dot{p}_i &= n_i' \\ p_i^T \ddot{p}_i + \dot{p}_i^T \dot{p}_i &= 0. \end{aligned} \tag{14}$$

In matrix form, (14) is rewritten as

$$\begin{bmatrix} N_i & 0 & 0 \\ 0 & 2J'L_i & 0 \\ 0 & p_i^T & 0 \end{bmatrix} \begin{bmatrix} \ddot{r}_i \\ \ddot{p}_i \\ 0 \end{bmatrix} + \begin{bmatrix} 0 \\ L_i H_i \dot{p}_i \\ \dot{p}_i^T \dot{p}_i \end{bmatrix} = \begin{bmatrix} f_i \\ n_i' \\ 0 \end{bmatrix}. \tag{15}$$

3.2 Dynamic Equations for Constrained Bodies

Bodies are interconnected to form a system of constrained bodies via kinematic joints which create constraint reaction forces and moments. When applying the constraint reaction forces and moments to (14), the dynamic equations of motion for a constrained bodies are written as

$$\begin{aligned} N_i \ddot{r}_i &= f_i + f_i^{(c)} \\ 2J_i' L_i \ddot{p}_i + L_i H_i \dot{p}_i &= n_i' + n_i'^{(c)} \\ p_i^T \ddot{p}_i + \dot{p}_i^T \dot{p}_i &= 0. \end{aligned} \tag{16}$$

A constrained body i is additionally exerted by reaction forces and moments $\left[f^{(c)}, n'^{(c)}\right]_i^T$ from joints. These forces and moments can be transformed to coordinate system consistent with q denoted by $\left[f^{*(c)}, n^{*(c)}\right]_i^T$ and defined by

$$\begin{bmatrix} f^{*(c)} \\ n^{*(c)} \end{bmatrix}_i = \begin{bmatrix} \Phi_r^T \\ \Phi_p^T \end{bmatrix}_i \lambda \tag{17}$$

To be used with the formulation (16), the moment in (17) is transformed to be

$$\begin{aligned} n'^{(c)} &= \frac{1}{2} L_i n'^{*(c)} \\ &= \frac{1}{2} L_i \Phi_{p_i}^T \lambda \end{aligned} \tag{18}$$

where $\lambda = [\lambda_1, \ldots, \lambda_{34}]$ is known as Lagrange Multipliers, and $\left[\Phi_{ri}, \Phi_{pi}\right] = \Phi_{qi}$ is Jacobian Matrix of the kinematic constraint $\Phi \equiv \Phi(q)$ with respect to q_i. Therefore, the dynamic equations of motion for the mechanism are given in compact form as

$$\begin{bmatrix} N_i & 0 & \Phi_{ri}^T \\ 0 & 2J'L_i & \frac{1}{2}L_i\Phi_{pi}^T \\ 0 & p_i^T & 0 \end{bmatrix} \begin{bmatrix} \ddot{r}_i \\ \dot{p}_i \\ -\lambda \end{bmatrix} + \begin{bmatrix} 0 \\ L_i H_i \dot{p}_i \\ \dot{p}_i^T \dot{p}_i \end{bmatrix} = \begin{bmatrix} f_i \\ n'_i \\ 0 \end{bmatrix}. \tag{19}$$

$$\begin{bmatrix} M & B^T \\ P & 0 \end{bmatrix} \begin{bmatrix} \ddot{q} \\ -\lambda \end{bmatrix} + \begin{bmatrix} b \\ c \end{bmatrix} = \begin{bmatrix} g \\ 0 \end{bmatrix}, \tag{20}$$

where

$$M = \begin{bmatrix} N_1 & 0 & \ldots & 0 & 0 \\ 0 & 2J'_1 L_1 & \ldots & 0 & 0 \\ \vdots & \vdots & \ddots & \vdots & \vdots \\ 0 & 0 & \ldots & N_7 & 0 \\ 0 & 0 & \ldots & 0 & 2J'_7 L_7 \end{bmatrix}$$

,

$$B = [\Phi_{r_1}, \frac{1}{2}\Phi_{p_1} L_1^T, \ldots, \Phi_{r_7}, \frac{1}{2}\Phi_{p_7} L_7^T]$$

,

$$P = \begin{bmatrix} 0^T & p_1^T & \ldots & 0^T & 0^T \\ \vdots & \vdots & \ddots & \vdots & \vdots \\ 0^T & 0^T & \ldots & 0^T & p_7^T \end{bmatrix}, b = \begin{bmatrix} 0 \\ L_1 H_1 \dot{p}_1 \\ \vdots \\ 0 \\ L_7 H_7 \dot{p}_7 \end{bmatrix}, c = \begin{bmatrix} \dot{p}_1^T \dot{p}_1 \\ \vdots \\ \dot{p}_7^T \dot{p} \end{bmatrix},$$

$$g = \begin{bmatrix} f_1 \\ n'_1 \\ \vdots \\ f_7 \\ n'_7 \end{bmatrix}, \text{ and } \ddot{q} = \begin{bmatrix} \ddot{r}_1{}^T & \ddot{p}_1{}^T & \ldots & \ddot{r}_7{}^T & \ddot{p}_7{}^T \end{bmatrix}^T =$$

$[\ddot{x}, \ddot{y}, \ddot{z}, \ddot{e}_0, \ddot{e}_1, \ddot{e}_2, \ddot{e}_3]_i^T, \quad (i = 1, 2, ...7).$

Equation (19) consists of 49 equations with 83 variables, therefore 34 constraint equations are appended with (19) to solve for coordinate vectors q and Lagrange multiplier λ. A system of algebraic differential equation is obtained as follow

$$\begin{bmatrix} M & B^T \\ P & 0 \\ \Phi_q & 0 \end{bmatrix} \begin{bmatrix} \ddot{q} \\ -\lambda \end{bmatrix} + \begin{bmatrix} b \\ c \\ 0 \end{bmatrix} = \begin{bmatrix} g \\ 0 \\ \gamma - K_D(\Phi_q \dot{q}) - K_P \Phi(q) \end{bmatrix}. \tag{21}$$

Equation (21) were solved for the coordinate vectors q by using state equations as follow:

$$x_1 = q = [x_1, y_1, z_1, [e_0, e_1, e_2, e_3]_1, \ldots, x_7, y_7, z_7, [e_0, e_7, e_7, e_7]_7]$$
$$x_2 = \dot{q} = [\dot{x}_1, \dot{y}_1, \dot{z}_1, [\dot{e}_0, \dot{e}_1, \dot{e}_2, \dot{e}_3]_1, \ldots, \dot{x}_7, \dot{y}_7, \dot{z}_7, [\dot{e}_0, \dot{e}_1, \dot{e}_2, \dot{e}_3]_7]$$

$$\dot{x}_1 = x_2 = \dot{q}$$
$$\dot{x}_2 = \ddot{q} = \begin{bmatrix} [I] & [0] \end{bmatrix} \begin{bmatrix} M & B^T \\ P & 0 \\ \Phi_q & 0 \end{bmatrix}^{-1} \begin{bmatrix} g - b \\ -c \\ \gamma - K_D(\Phi_q \dot{q}) - K_P \Phi(q) \end{bmatrix} \tag{22}$$

4 PD Controller

The desired value of actuator's displacement is obtained from the 3D model such that the solar panel reach the position as shown in Figure 4 where the desired value of the two actuators are $z_{2d} = 0.046m$, $z_{2d} = 0.046m$. The actual displacement of the two actuators labeled as body number 2 and body number 3 are denoted as z_2 and z_3 respectively. Figure 3 illustrates a common feedback controller known as proportional derivative (PD) controller that is used to obtain the desired response, and has a form as follow:

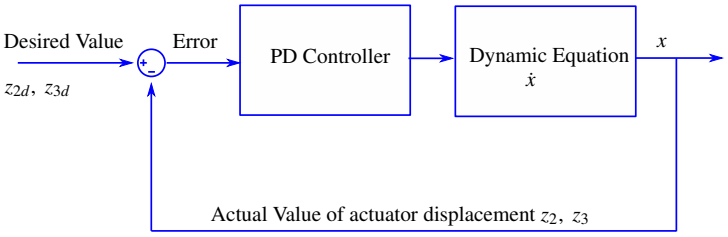


Figure 3: Block Diagram for PD Controller

$$u = K_p e_z + K_d \dot{e}_z, \tag{23}$$

where $u = \begin{bmatrix} f_{2z} \\ f_{3z} \end{bmatrix}$, $e_z = \begin{bmatrix} z_2 - z_{2d} \\ z_3 - z_{3d} \end{bmatrix}$ and $\dot{e}_z = \begin{bmatrix} \dot{z}_2 - \dot{z}_{2d} \\ \dot{z}_3 - \dot{z}_{3d} \end{bmatrix}$ are the position error and velocity error. K_p and K_d are 2 by 2 positive definite diagonal matrix. K_p plays a role as a spring that tries to keep the position error decreasing. K_d is considered as a damper which maintains the velocity error $\dot{e}$ decreasing.

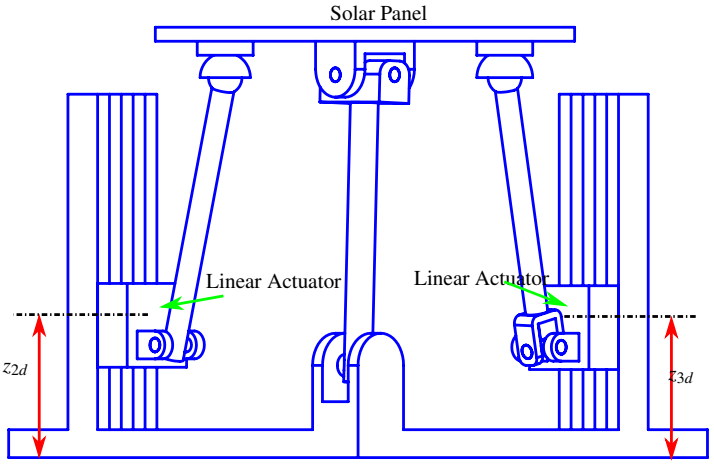


Figure 4: Desired configuration of the solar panel

5 Results and Discussion

PD control law is applied to drive the parallel mechanism from its initial configuration to the desired configuration with $K_p = \begin{bmatrix} 50 & 0 \\ 0 & 50 \end{bmatrix}$, and $K_d = \begin{bmatrix} 20 & 0 \\ 0 & 25 \end{bmatrix}$ as shown in Figure 1 and Figure 4. The control input $u = \begin{bmatrix} f_{2z} & f_{3z} \end{bmatrix}^T$ is exerted to the two actuators by assigning the external forces in the vector $g = \begin{bmatrix} f_1^T & n_1'^T & \dots & f_7^T & n_7'^T \end{bmatrix}^T$ containing

$$\begin{aligned} f_2 &= \begin{bmatrix} 0 & 0 & f_{2z} \end{bmatrix}^T \\ f_3 &= \begin{bmatrix} 0 & 0 & f_{3z} \end{bmatrix}^T, \end{aligned} \tag{24}$$

while keeping the remaining components in g to be zero. Other parameters used in this paper are shown in Appendix C. As can be seen in the Figure 5, the two actuators reach the desired position quickly. The movement of the solar panel can be observed in Figure 7. It appears that the parallel mechanism can be easily controlled such that it is practically possible to move the solar panel directed to the sunlight, and thus more energy could be produced. It is evident that the desired orientation of the solar panel is with its coordinate system ($\xi_7\eta_7\zeta_7$) is parallel to the global coordinate system (xyz). In this case, the euler parameters is expected to be equal to $\begin{bmatrix} \cos\frac{\phi}{2} & 0 & 0 & \sin\frac{\phi}{2} \end{bmatrix}^T$ [8], where ϕ is the rotation angle around ζ axis, and is reported true by Figure 8. Figure 9 illustrates the mathematical relationship of euler parameters of the solar panel as described in (1) which satisfies $p_7^T p_7 = 1$. When the euler parameters are used to describe a rotational coordinate, it is important to ensure that (1) is satisfied because the four quantities of euler parameters are not independent.

6 Conclusion

Our study provides the frame work for modeling any mechanism by obtaining the algebraic differential equations of motion derived from Newton-Euler equation of motion and kinematic constraint equations. This technique can be applied to a wide range of simulation applications, especially for a close loop mechanism. Moreover, our result confirms the usefulness of the Baumgarte stabilization method that deals with numerical error when solving system of algebraic differential equations with mathematical constraint of Euler parameters. The control simulations using PD controller was to drive the solar panel to reach the desired configuration with a good performance.

Future work should focus on applying a model based controller that could provide a better control result, especially for tracking control. If the same modeling approach is applied to a system that requires fast response, an investigation on computation time should be made.

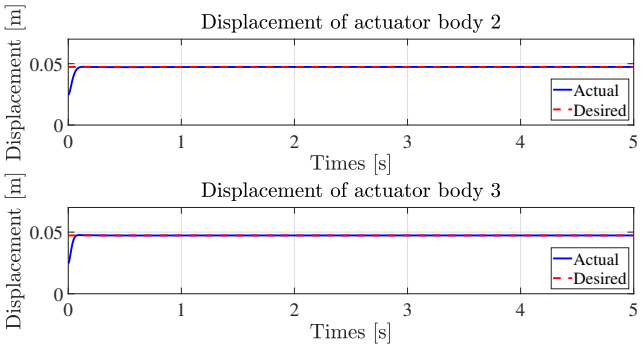


Figure 5: Response of Actuator's Displacement

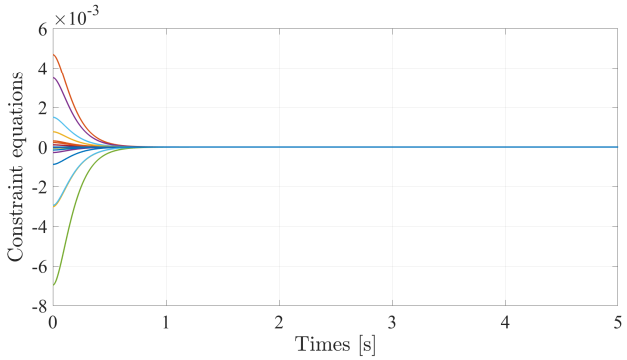


Figure 6: Kinematic constraint

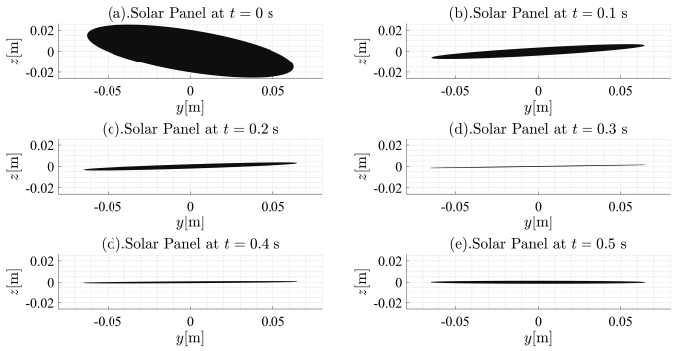


Figure 7: Orientation of Solar Panel

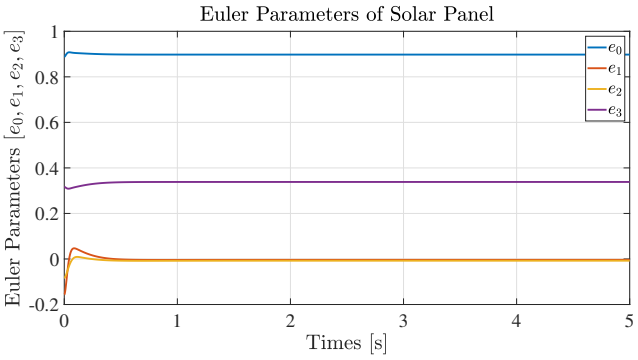


Figure 8: Euler Parameters Describing the Orientation of Solar Panel

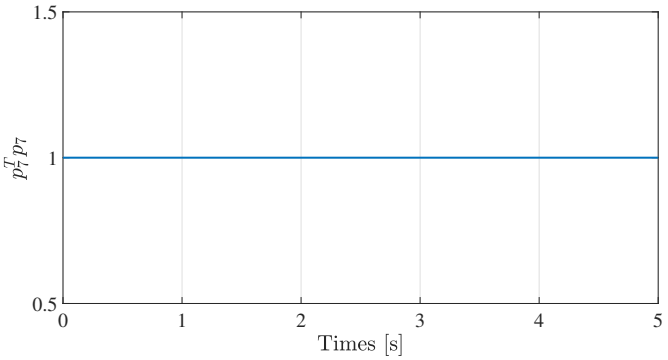


Figure 9: Mathematical Relationship of Euler Parameters of Solar Panel

APPENDIX A

For the parallel mechanism, by following the concept of relative constraints between two bodies from [8], the 34 constraint equations are obtained as follows:

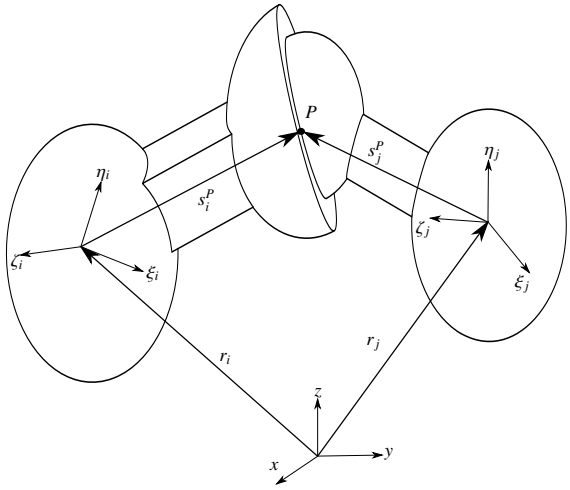


Figure 10: Spherical Joint

• Three equations for each Spherical joint between body (5,7) and (6,7).

$$\Phi^{(s,3)} \equiv r_i + A_i s_i'^P - r_j - A_j s_j'^P = 0, \tag{25}$$

where $s_i'^P = [\xi^P, \eta^P, \zeta^P]$ is body-fixed coordinate of the point P.

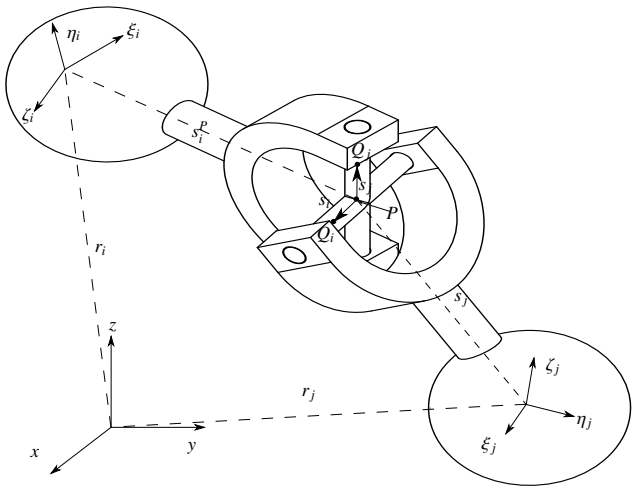


Figure 11: Universal Joint

• Four equations for each Universal joint between body (3,5) and (4,7).

$$\begin{aligned} \Phi^{(s,3)} &\equiv r_i + A_i s_i'^P - r_j - A_j s_j'^P = 0 \\ \Phi^{(n1,1)} &\equiv s_i^T s_j = 0, \end{aligned} \tag{26}$$

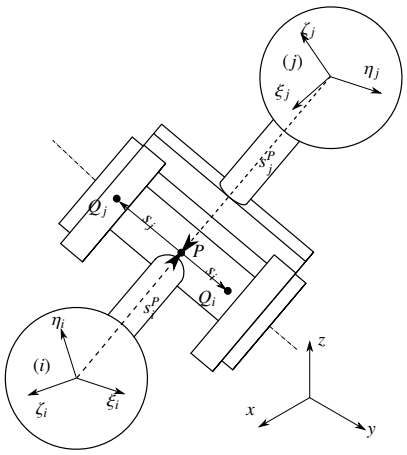


Figure 12: Revolute Joint

• Five equations for each Revolute joint between body (1,4) and (2,6).

$$\begin{aligned} \Phi^{(s,3)} &\equiv r_i + A_i s_i'^P - r_j - A_j s_j'^P = 0 \\ \Phi^{(p1,2)} &\equiv \tilde{s}_i s_j = 0, \end{aligned} \tag{27}$$

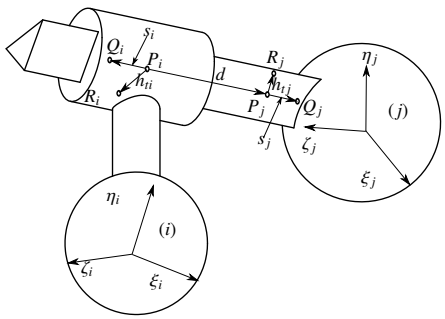


Figure 13: Translational Joint

• Five equations for each Translational joint between body (1,2) and (1,3).

$$\begin{aligned}\Phi^{(p1,2)} &\equiv \tilde{s}_i s_j = 0\\ \Phi^{(p2,2)} &\equiv \tilde{s}_i d = 0\\ \Phi^{(n1,1)} &\equiv h_{ti}^T h_{tj} = 0,\end{aligned} \tag{28}$$

APPENDIX B

Consider the following mass spring damper equation of motion

$$\ddot{D} + 2\zeta\omega_n\dot{D} + \omega_n^2 D = 0, \tag{29}$$

where ζ is a critical damping constant, and ω_n denotes a natural frequency. From (6) and (29), we can write

$$\begin{aligned}\ddot{D} + K_D\dot{D} + K_P D &= 0\\ \ddot{D} + 2\zeta\omega_n\dot{D} + \omega_n^2 D &= 0\end{aligned} \tag{30}$$

$$\begin{aligned}\zeta &= \frac{K_D}{2\omega_n} = \frac{K_D}{2\sqrt{K_P}}\\ \omega_n &= \sqrt{K_P}\end{aligned} \tag{31}$$

In the case of critically damped system, $\zeta = 1$ ensures a fast response with no overshoot. Therefore, we choose $K_D = 2\alpha$ and $K_P = \alpha^2$, where α is a positive constant and taken to be 10.

APPENDIX C

Table 1: Mass of body $i, i = 1, 2, \cdots, 7$.

Symbols	Value	Unit
m_1	475.09×10^{-3}	Kg
m_2	189.7×10^{-3}	Kg
m_3	189.7×10^{-3}	Kg
m_4	104.45×10^{-3}	Kg
m_5	53.25×10^{-3}	Kg
m_6	54.4×10^{-3}	Kg
m_7	890.5×10^{-3}	Kg

Table 2: Position vector of center of mass of body i at initial position, $i = 1, 2, \cdots, 7$

Symbols	Value	Unit
r_1	$10^{-3} \times [-63.93, 63.93, 30.41]^T$	m
r_2	$10^{-3} \times [-123.99, 15, 24.6]^T$	m
r_3	$10^{-3} \times [-15, 123.99, 24.6]^T$	m
r_4	$10^{-3} \times [-11.50, 18.37, 99.21]^T$	m
r_5	$10^{-3} \times [-12.99, 98.33, 68.84]^T$	m
r_6	$10^{-3} \times [-92.31, 15, 66.27]^T$	m
r_7	$10^{-3} \times [-34.28, 42.89, 136.56]^T$	m

Table 3: Euler parameters of body i at initial position,$i = 1, 2, \cdots, 7$

Symbols	Value
p_1	$[1, 0, 0, 0]^T$
p_2	$[1, 0, 0, 0]^T$
p_3	$[1, 0, 0, 0]^T$
p_4	$[1, 0, 0, 0]^T$
p_5	$[1, 0, 0, 0]^T$
p_6	$[1, 0, 0, 0]^T$
p_7	$[0.89043, -0.19791, -0.10481, 0.39619]^T$

Table 4: Moment of Inertia of body i,$i = 1, 2, \cdots, 7$

Symbols	Value	Unit
J_1'	$10^{-4} \times \begin{bmatrix} 20 & 8 & -1 \\ 8 & 20 & 1 \\ 1 & 1 & 26 \end{bmatrix}$	Kg m^2
J_2'	$10^{-4} \times \begin{bmatrix} 0.2774 & 0 & -0.0102 \\ 0 & 0.2015 & 0 \\ -0.0102 & 0 & 0.1987 \end{bmatrix}$	Kg m^2
J_3'	$10^{-4} \times \begin{bmatrix} 0.2015 & 0 & 0 \\ 0 & 0.2774 & 0.0102 \\ 0 & 0.0102 & 0.1987 \end{bmatrix}$	Kg m^2
J_4'	$10^{-3} \times \begin{bmatrix} 0.1217 & 0.0000 & 0 \\ 0.0000 & 0.1248 & 0 \\ 0 & 0 & 0.0054 \end{bmatrix}$	Kg m^2
J_5'	$10^{-4} \times \begin{bmatrix} 0.5827 & 0 & -0.0824 \\ 0 & 0.5940 & 0 \\ -0.0824 & 0 & 0.0172 \end{bmatrix}$	Kg m^2
J_6'	$10^{-4} \times \begin{bmatrix} 0.6242 & 0 & 0 \\ 0 & 0.6231 & -0.0000 \\ 0 & -0.0000 & 0.0058 \end{bmatrix}$	Kg m^2
J_7'	$10^{-4} \times \begin{bmatrix} 12 & 0 & 1 \\ 0 & 12 & 0 \\ 1 & 0 & 24 \end{bmatrix}$	Kg m^2

Acknowledgment This material is based upon work supported by the Air Force Office of Scientific Research under award number FA2386-17-1-0148.

References

[1] S. Srang and S. Ath, "Dynamic Modeling and Simulation for 2DOF Parallel Mechanism Solar Tracker," 2019 IEEE/ASME International Conference on

Advanced Intelligent Mechatronics (AIM), Hong Kong, China, 283-288, 2019. https://doi.org/10.1109/AIM.2019.8868501

[2] C.S. Chin, A. Babu, W. McBride, "Design, modeling and testing of a standalone single axis active solar tracker using MATLAB/Simulink", Renewable Energy, **36**(11), 3075-3090, 2011. https://doi.org/10.1016/j.renene.2011.03.026

[3] Yingxue Yao, Yeguang Hu, Shengdong Gao, Gang Yang, Jinguang Du, "A multipurpose dual-axis solar tracker with two tracking strategies", Renewable Energy, **72**, 88-98, 2014. https://doi.org/10.1016/j.renene.2014.07.002

[4] P. Y. Vorobiev, J. Gonzalez-Hernandez and Y. V. Vorobiev, "Optimization of the solar energy collection in tracking and non-tracking photovoltaic solar system," (ICEEE). 1st International Conference on Electrical and Electronics Engineering, 2004., Acapulco, Mexico, 310-314, 2004. https://doi.org/10.1109/ICEEE.2004.1433900

[5] Hossein Mousazadeh, Alireza Keyhani, Arzhang Javadi, Hossein Mobli, Karen Abrinia, Ahmad Sharifi, "A review of principle and sun-tracking methods for maximizing solar systems output", Renewable and Sustainable Energy Reviews, **13**(8), 1800-1818,2009. https://doi.org/10.1016/j.rser.2009.01.022

[6] T. Zhan, W. Lin, M. Tsai and G. Wang, "Design and Implementation of the Dual-Axis Solar Tracking System," 2013 IEEE 37th Annual Computer Software and Applications Conference, Kyoto, 276-277, 2013. https://doi.org/10.1109/COMPSAC.2013.46

[7] J. Wu, X. Chen and L. Wang, "Design and Dynamics of a Novel Solar Tracker With Parallel Mechanism," in IEEE/ASME Transactions on Mechatronics, **21**(1), pp. 88-97, Feb. 2016. https://doi.org/10.1109/TMECH.2015.2446994

[8] Nikravesh, Parviz E. Computer-aided analysis of mechanical systems, Prentice-Hall, Inc., 1988.

[9] Neto, M.A., Ambrósio, J. "Stabilization Methods for the Integration of DAE in the Presence of Redundant Constraints". Multibody System Dynamics **10**, 81–105 (2003). https://doi.org/10.1023/A:1024567523268

[10] Flores, P., Machado, M., Seabra, E., and Tavares da Silva, M. (October 13, 2010). "A Parametric Study on the Baumgarte Stabilization Method for Forward Dynamics of Constrained Multibody Systems." ASME. J. Comput. Nonlinear Dynam. January 2011; **6**(1): 011019. https://doi.org/10.1115/1.4002338

[11] Flores P., Pereira R., Machado M., Seabra E. (2009) "Investigation on the Baumgarte Stabilization Method for Dynamic Analysis of Constrained Multibody Systems". In: Ceccarelli M. (eds) Proceedings of EUCOMES 08. Springer, Dordrecht.https://doi.org/10.1007/978-1-4020-8915-2_37

ASTES

Advances in Science, Technology and Engineering Systems Journal
Vol. 5, No. 5, 717-726 (2020)
www.astesj.com
Special Issue on the Economic Impact of COVID-19 on Companies and Consumers

ASTES Journal
ISSN: 2415-6698

An Empirical Comparison of Different Two-Factor Models in the Context of Portfolio Optimisation

Jamal Agouram[*,1], Mouncif Harabida [2], Bouchra Radi[2] , Ghizlane Lakhnati[3]

[1]*Laboratory of Studies and Applied Researches in Economic Sciences (LERASE), Faculty of Law, Economics and Social Sciences, Ibn Zohr University, Agadir, 80000, Morocco*

[2]*Entrepreneurship, Finance and Audit Research Laboratory (LAREFA), National School of Business and Management (ENCG), Ibn Zohr University, Agadir, 80000, Morocco*

[3]*Laboratory of industrial engineering and informatics (LGII), National School of Applied Sciences (ENSA), Ibn Zohr University, Agadir, 80000, Morocco*

ARTICLE INFO

Article history:
Received: 04 September, 2020
Accepted: 21 September, 2020
Online: 05 October, 2020

Keywords:
COVID-19
Gini coefficient
Lower Partial Moments
Mean Absolute Deviation (MAD)
Mean-Gini (MG)
Mean-Variance (MV)

ABSTRACT

The crisis linked to the COVID-19 and the uncertainty it generates in the unprecedented health, societal, economic and financial fields have had a strong impact on the stock markets. Indeed, in such a climate of very high uncertainty, it is to be expected that the excessive stock market price movements will continue, with both declines and technical rebounds, and that the resulting volatility will remain particularly high. In order to cope with this crisis, investors and portfolio managers must mobilize all portfolio selection strategies. In particular, portfolio management and construction are based on the concepts of return and risk. This couple has been at the center of all the concerns of managers and investors in portfolio optimization issues since the introduction of the mean-variance model by Markowitz. However, many studies have proposed different measures of risk to overcome the drawbacks of variance. The objective of this paper is to present and compare the portfolio compositions and performance of four different portfolio optimization models using different risk measures, including variance, Mean Absolute Deviation, Gini coefficient and Lower Partial Moments (LPM). The results of this study show that the Mean-Lower Partial Moments (MLPM) model outperforms other models. The Mean-Lower Partial Moments (MLPM) model is suitable for investors during the crisis period (COVID-19) in the Moroccan financial market.

1 Introduction

During a financial crisis, it is crucial for investors and portfolio managers to implement the best portfolio selection model that takes into account investors' risk and return preferences. Several studies have evaluated and compared different portfolio management strategies according to their return and risk characteristics. The portfolios are made up of financial assets such as shares, bonds, credits, and options. A fundamental question in the management of asset portfolios is the choice of valid investment objectives. In the context of risk, individuals make decisions based on two fundamental parameters (return and risk).

Return[1] and risk[2] are two associated concepts in finance. Indeed, in the case of an investment in a risky financial asset, an investor will demand a higher return or a lower risk and investment decisions boil down to finding an optimal compromise between return and risk. So an investor who wishes to improve the return on his portfolio must accept to take more risk.

The notion of risk derives from changes in the prices of financial assets and their negative impact on the total financial value of the portfolio.

Therefore, the risk is a very important component in portfolio management. While the return is easy to assess, risk has not received consensus on what constitutes its fair measurement. Risk can be considered as variance (e.g., Markowitz [1], [2] [2], [3]; Tobin [4]; Sharpe [5]; Lintner [6], [7]; Mossin [8]; semi-variance Markowitz [3]; partial lower moments (e.g. Bawa [9], Bawa and Lindenberg [10], Fishburn [11] and Harlow and Rao [12], the so-called Value at

[*]Corresponding Author: Jamal Agouram, +212661653888 & jamal.agouram@edu.uiz.ac.ma
[1]Return is an indicator that measures the relative appreciation or depreciation of the value of a financial asset or portfolio of assets over a given period.
[2]The notion of risk derives from changes in the prices of financial assets and their negative impact on the total financial value of the portfolio.

Risk Morgan [13], Jorion [14], Grebeck [15].

So the risk and return couple will be very central terms in our analysis and it is essential that we understand the meaning of each term and how portfolios with different structures can be compared. To this end an overview of performance measures will be used to compare the performance of portfolios, providing investors with useful information on the capacity of managers and providing tools to assess the risk taken by the manager based on the different two-factor models.

In what follows, we will first briefly review the literature on two-factor models. The second section is devoted to the application of these models to real data from the Moroccan financial market. Portfolio performance measures will be used in the third section to compare the models.

2 Literature review

The advent of the Covid-19 pandemic, which includes both the Severe Acute Respiratory Syndrome (SARS) virus and the Middle East Syndrome (MOS), has led to major disruptions in world economies and particularly in financial markets. In fact, the financial markets reacted negatively to the growth of the cases confirmed by Covid-19 by posting abnormal negative returns on listed equities, reflecting investors' aversion to the pandemic. This crisis, like previous crises in the world's financial markets, has placed risk control at the center of the concerns of investors and portfolio management companies. Moreover, each of these crises is an opportunity to advance the risk measurement and management tools proposed by theorists and researchers in this field. In a risky environment, investors make decisions based on their selection criteria. Consequently, decision theory has been used as a basis for investment choice theory and portfolio management.

Indeed, many economists and financial theorists have used the fundamental contributions of decision theory since the middle of the 20th century to evaluate investment opportunities. The theory that has dominated risk studies since its emergence in 1944 is the theory of expected utility. The latter has become widely accepted in all areas of economic theory incorporating the risk factor. Parallel to this, Harry Markowitz [1] proposed his famous Mean-Variance model and gave the starting signal for modern portfolio choice theory. Indeed, the use of utility functions is often complex and does not lead to analytical solutions. This is why Markowitz simplified the problem of choice in uncertainty in order to solve it in a simple and explicit way. His idea was to measure the risk affecting a wealth by its variance.

The investor is then presumed to make decisions based on only two parameters: the first reflects the return on the investment measured by the expected return desired and the second reflects the risk measured by the variance. Markowitz asserts the strength of the relationship between return and risk because he has shown that, under certain conditions, investors can manage to balance their hopes of obtaining portfolios that have both the best possible return and a minimum of risk.

This approach leads to the theory of efficient portfolios, which suggests combining appropriate proportions of assets in a portfolio. A little later, Treynor [16], [17], Sharpe [5], Lintner [6], and Mossin [8] developed the Financial Asset Equilibrium Model (CAPM) which, under certain assumptions, leads to an equilibrium return for any stock. Later, Ross [18] developed an alternative to CAPM called Price Arbitration Theory (PAT) based on multifactorial models. The Markowitz, CAPM, and APT models form the core of classical portfolio theory.

The latter has revolutionized the way portfolio management is conceived and its contributions have become absolutely essential even today. However, the application of the Mean-Variance (MV) model in portfolio selection is questionable because this model is only valid if returns are normally distributed or if the investors have quadratic preferences. However, several researches have shown that returns on financial assets are not normally distributed. Similarly, Ballestero [19], Bond and Satchell [20], [21], Estrada [22], and Unser [23] have pointed out that variance is a dubious measure of risk because it treats above-average and below-average returns in the same way, whereas investors associate risk with returns below the target rate of return.

The restrictive nature of variance as a measure of risk in the Markowitz model has motivated a large number of studies to seek more appropriate risk measures. Markowitz [3], Fishburn [11], and Bawa and Lindenberg [10] have proposed the use of Lower Partial Moments.

To remedy the imperfections of the Mean-Variance approach, Shalit and Yitzhaki [24] introduced the Mean-Gini model in portfolio management as an alternative to the mean-variance model. The Mean-Gini model (MG) uses the Gini coefficient as the risk parameter rather than variance. Thus, the concept proposed by Shalit and Yitzhaki [24] is similar to Markowitz's [1], because it is based on two parameters. In addition, the Mean-Gini strategy can circumvent assumptions about the normality of the distribution of returns, and of the quadratic function of the utility function. Yitzhaki [25] showed also that the Gini coefficient satisfies the stochastic dominance of the second degree, which makes the Mean-Gini model compatible with the theory of expectation of utility.

Later, Shalit and Yitzhak [24] [26] presented the Generalised Mean-Gini (GMM) as a model that provides a measure to embody the preferences of different investors regarding their degree of risk aversion. As a result, this model can better reflect the perceived risk of an individual investor, as highlighted in the recent study by Cardin et al [27]. For these reasons, this theory is seen as an alternative to the traditional approach that has been dominant in financial theory for more than half a century. While Konno and Yamazaki [28], in contrast to Markowitz's quadratic model, proposed the first linear model by replacing the variance with the mean absolute deviation (MAD) as a measure of risk.

2.1 The Mean-Variance of Markowitz

The Mean-Variance model offers the investor a set of efficient portfolios, i.e. those with the lowest risk for a possible overall return[3] , and vice versa. This method uses only the concepts of mean for the expected return and variance[4] for the uncertainty associated with this return, hence the name Mean-Variance[5] associated with Markowitz analysis.

The variance of a portfolio combination of securities is equal to the weighted average covariance[6] of the returns on its individual securities:

$$Var(r_p) = \sigma_p^2 = \sum_{i=1}^{N}\sum_{j=1}^{N} x_i x_j Cov(r_i, r_j) \tag{2}$$

Markowitz's[2] model may be written as the following non-linear quadratic programming model:

$$min \sum_{i=1}^{N}\sum_{j=1}^{N} x_i x_j Cov(r_i, r_j) \tag{3}$$

$$s.t : \sum_{i=1}^{N} x_j r_j \geq w_0 \tag{4}$$

$$\sum_{i=1}^{N} x_j = 1 \tag{5}$$

$$0 \leq x_j \leq u_j, j \in N \tag{6}$$

The first constraint simply says that the expected return on the portfolio should equal the target return determined by the portfolio manager (w_0). The second constraint says that the weights of the securities invested in the portfolio must sum to one. The last constraint stipulates that asset weights must be positive, i.e. short sales are not allowed.

Since its appearance, the Markowitz model has taken a very important place in the evolution of modern finance and has achieved great success with its contribution to portfolio management. But with recent adjustments, this model has found several limitations raised by several practitioners of financial theory. As with any model, the limitations are generally focused around these assumptions[7] as well as on the estimation of these parameters.

2.2 The Mean-Lower Partial Moment Model

This concept was introduced by Bawa [9] and Fishburn [11] and Nawrocki [30]–[32] to define measures of downside risk in general. Since the variance takes into account all negative as well as positive deviations, lower partial moments only take into account negative deviations. Semi-variance is a special case of a class of asymmetric measures proposed by Markowitz [3] in the case where the investor is indifferent between two or more securities after having calculated the variance, i.e. the variance is sometimes insufficient to make the right decision. Semi-variance is a type of measure known as a measure of downside risk. This type of measure focuses primarily on losses. Unlike variance, no assumptions are made about the statistical distribution of asset returns. Thus, the lower partial moments represent, in a way, the standard deviation of returns below a target return. They do not penalize returns above a target return and differentiate between risk, returns below a minimum return, uncertainty and variability of returns. Bawa and Lindenberg [10], Lee and Rao [33], and Harlow and Rao [12] have developed lower partial mean-moment models (LPMM), and have shown their advantages over the Mean-Variance (MV) model. Despite these efforts, few studies have empirically examined these advantages.

Bawa (1975) developed the concept of downside risk by lower partial moments (MPM) of order n with a target rate of return τ[8] defined in continuous time by:

$$LPM_\alpha(\tau, R_i)^\alpha = \int_{-\infty}^{\tau} (\tau, R)^\alpha dF(R) \tag{7}$$

Where R, F, τ, and n denote respectively the rate of return of a security or portfolio, the probability distribution of that return, the target rate of return, and the degree of the moment.

Under these conditions, the portfolio choice problem according to the Mean-Lower Partial Moment Model criterion consists in solving the following optimization problem:

$$min \sum_{t=1}^{\tau} p_t z_t^2 \tag{8}$$

$$z_t \geq \sum (r_{jt} - r_j) x_j, t = 1, 2, \ldots, T \tag{9}$$

$$z_t \geq 0, t = 1, 2, \ldots, T \tag{10}$$

[3]In practice, the statistical parameters are often estimated at Based on time series (such as historical data from the financial markets), and after that they are somehow adjusted. Given any set of risky assets and a set of weights that describe how the portfolio investment is split, the general formula of expected return for n assets is:

$$E(r_p) = \sum_{j=1}^{N} x_j r_j \tag{1}$$

where: N the number of securities; x_j is the proportion of the funds invested in security j; r_j are the return on ith security j and portfolio p; and $E()$ is the expectation of the variable in the parentheses.

[4]As long as the assets are supposed to be characterized by distributions symmetrical, the variance or standard deviation are good measures because any normal distribution is fully described by its mean value and its variance (or standard deviation) (see, for example, Artzner et al [29]). Variance is not a good measure of risk if we are dealing with financial assets that are characterized by unsymmetric gains.

[5]Although the mean-variance approach proposed by Markowitz has been used extensively in practice, it has several limitations (computational load, the non-linear (quadratic) nature of the risk measure, the perception of non-symmetrical risk, the normal distribution of returns, and many others).

[6]High covariance indicates that an increase in one stock's return is likely to correspond to an increase in the other. A low covariance means the return rates are relatively independent and a negative covariance means that an increase in one stock's return is likely to correspond to a decrease in the other.

[7]As with any model, Markowitz-style portfolio selection is based on several assumptions about individual behaviour and the context of uncertainty.

[8]In the case where t is the mean of the return distribution, we find the traditional semi-variance as introduced by Markowitz.

$$\sum_{i=1}^{N} x_j = 1 \tag{11}$$

$$0 \leq x_j \leq u_j, j \in N \tag{12}$$

In order to test the Mean-Lower Partial Moment Model, we chose to place ourselves in a semi-variance context.

2.3 The Mean Absolute Deviation

The alternative presented by Konno and Yamazaki [28] suggests that Markowitz-type portfolio optimisation could be replaced or even improved by a model using the mean absolute deviation (MAD[9]) as a measure of risk to overcome the weaknesses of Markowitz's [2] non-linear model. The DSM results in a linear programming model, which proves to be equivalent to the Markowitz model and easier to compute. The DSM linear programming model, proposed by Konno & Yamazaki [28], can be posed as follows:

$$min \sum_{t \in T} p_t y_t \tag{14}$$

s.t: "Markowitz" constraints (2)-(3)

$$y_t + \sum_{j \in N} (r_{jt} - r_j) x_j \geq 0, t = 1, 2, \ldots, T \tag{15}$$

$$y_t - \sum_{j \in N} (r_{jt} - r_j) x_j \geq 0, t = 1, 2, \ldots, T \tag{16}$$

$$0 \leq x_j \leq u_j, j \in N \tag{17}$$

2.4 The Mean-Gini (MG) model

The Mean-Gini (MG) model was originally developed by Yitzhaki [25]. Then, it was applied in finance by Shalit and Yitzhaki [24] as an alternative model to the Mean-Variance model to assess risk and construct optimal portfolios that are consistent with the theory of utility expectation and stochastic dominance. The Mean-Gini (MG) model shows strong results when the mean-variance model is doomed to failure, particularly when assets are not normally distributed.

The Mean-Gini (MG) approach in finance is used by Bey and Howe [34] in portfolio analysis, Okunev [35] to evaluate the performance of mutual funds, Shalit and Yitzhaki [24] and agouram & lakhnati [36] [37] [38] to obtain optimal portfolio selection, Cheung et al. [39] to examine the effectiveness of hedging options and futures contracts, and Berkhouch et al. [40] introduced and applied the Tail Extended Gini functional and the Extended Gini Shortfall on daily returns for the MASI index.

Recall that the Gini coefficient is equal to:

$$\Gamma_p = 2cov(R_p, F(R_p)) \tag{18}$$

where R_p is the portfolio return and $F(R_p)$ is is the cumulative distribution function. Thus, the mathematical optimization problem is presented as follows:

$$min\Gamma_p = 2cov(R_p, F(R_p)) = 2 \sum_{i=1}^{N} x_i cov(R_i, F(R_p)) \tag{19}$$

$$s.t : \sum_{i=1}^{N} x_j r_j \geq w_0 \tag{20}$$

$$\sum_{i=1}^{N} x_j = 1 \tag{21}$$

$$0 \leq x_j \leq u_j, j \in N \tag{22}$$

where Γ_p is the Gini coefficient of the portfolio, x_j is the weight of asset j, r_j is the expected return on asset j per period, w_0 is the minimum rate of return required by the investor.

3 Data and Methodology

Our study focuses on a sample of securities of the MADEX Index for which we collected daily prices over the period from September 7, 2015 to August 28, 2020. The MADEX Index groups the values of 45 securities according to their capitalization and volumes traded. The index is therefore representative of the most capitalized and liquid securities listed on the Casablanca Stock Exchange.

The data will be used as follows:

- First of all, we will use the first 1113 daily returns, corresponding to the period from September 7th 2015 to February 28th 2020 (the date of appearance of the first positive case in Covid-19), for the composition of the four portfolios.
- Next, we will estimate the performance measures of the four portfolios in order to compare them. To calculate the performance of these portfolios, we use the following three performance measures : Sharpe Ratio, Treynor Ratio, Jensen Alpha. To be more precise, we will use the risk-adjusted Sharpe ratio of each model. We will use the following formulas:

$$S_P = \frac{E(R_P) - r_f}{R_{measure}} \tag{23}$$

Where S_P is the Sharpe ratio, $E(R_P)$ is the portfolio return, r_f is the return on risk-free assets and $R_{measure}$ is the risk measure of each model.

$$T_P = \frac{E(R_P) - r_f}{\beta_P} \tag{24}$$

[9]The mean absolute deviation is defined as the mean of the absolute values of the differences between the observations and their mean :

$$MAD(R) = \frac{1}{n} \sum_{i=1}^{n} |R_i - \bar{R}| \tag{13}$$

Where n is the number of observed values, $\bar{R}$ is the mean of the observed values and R_i are the individual values.

Absolute mean deviation is a more robust scale estimator relative to standard deviation and more resistant to outliers in a data set. For a larger mean absolute deviation, the risk is high.

where T_P is the Treynor Ratio, $E(R_P)$ is the portfolio return, r_f is the return on risk-free assets and β_P is is the beta of the portfolio.

$$\alpha = E(R_P) - (r_f + \beta_P(E(R_m) - r_f) \quad (25)$$

where S_P is the Jensen Alpha, $E(R_P)$ is the portfolio return, r_f is the return on risk-free assets and β_P is is the beta of the portfolio.

Table 1: Summary of datasets used

Stocks	Mean	Standard Deviation	Max	Min	Skewnes	Kurtusis	Jarque-Bera Test Statistic	P-Value Jarque-Bera
ADH	-0.0008	0.0230	0.0998	-0.0999	-0.0723	5.2333	1268.78	0.0000
ADI	0.0004	0.0333	0.2075	-0.1087	0.4387	3.0088	454.71	0.0000
ALM	0.0014	0.0308	0.0995	-0.1172	-0.1525	0.4731	14.67	0.0007
ATH	0.0002	0.0224	0.0999	-0.0999	-0.0115	2.0090	186.86	0.0000
ALT	0.0004	0.0197	0.0998	-0.0777	0.2459	2.7947	372.75	0.0000
ATW	0.0004	0.0099	0.0425	-0.0489	0.2240	2.7070	348.50	0.0000
BCI	0.0002	0.02892	0.0997	-0.2014	-0.2243	2.7009	347.00	0.0000
BCP	0.0002	0.0111	0.0685	-0.0925	-0.0133	8.1582	3081.04	0.0000
BOA	-0.0001	0.0130	0.0997	-0.0801	0.8456	8.2679	3296.83	0.0000
CIH	0.0001	0.0189	0.0820	-0.0754	0.2327	2.4187	280.83	0.0000
CMA	0.0012	0.0226	0.0994	-0.0993	0.0608	1.6813	131.53	0.0000
CMT	0.0004	0.0217	0.1000	-0.1146	-0.2687	4.7220	1045.55	0.0000
COL	0.0007	0.0290	0.2001	-0.2050	0.0516	4.8696	1098.20	0.0000
CRS	0.0010	0.0309	0.1000	-0.0997	0.2107	1.1873	73.47	0.0000
CTM	0.0015	0.0252	0.2553	-0.1522	1.2173	14.2007	9609.58	0.0000
DHO	0.0005	0.0232	0.0997	-0.0909	0.2774	2.3334	266.30	0.0000
DLM	-0.0009	0.0383	0.1231	-0.2189	-0.4775	2.1645	259.10	0.0000
DWY	0.0007	0.0251	0.1448	-0.0999	0.4550	3.2230	519.21	0.0000
FBR	-0.0003	0.0403	0.1415	-0.1550	0.0178	0.3493	5.70	0.0576
GAZ	0.0013	0.0286	0.0998	-0.0997	0.0523	0.7583	27.12	0.0000
HPS	0.0026	0.0283	0.1000	-0.1577	-0.0732	1.6319	124.27	0.0000
IAM	0.0003	0.0086	0.0582	-0.0752	-0.5511	12.7913	7630.40	0.0000
IBC	-0.0015	0.0424	0.1909	-0.2186	0.0141	1.5426	110.18	0.0000
INV	0.0006	0.0369	0.1238	-0.1150	0.0913	0.4477	10.82	0.0045
JET	0.0005	0.0288	0.1000	-0.1364	0.1825	1.9568	183.42	0.0000
LBV	0.0010	0.0257	0.0990	-0.0997	0.0424	1.4843	102.32	0.0000
LES	0.0007	0.0194	0.0993	-0.0877	0.4733	2.7353	387.82	0.0000
LHM	0.0004	0.0209	0.0997	-0.0997	-0.0274	2.4867	286.38	0.0000
LYD	0.0007	0.0275	0.0952	-0.0998	0.0352	0.8244	31.68	0.0000
M2M	0.0015	0.0344	0.1000	-0.1000	0.2485	0.3014	15.63	0.0004
MDP	0.0001	0.0390	0.2091	-0.3126	0.0467	4.5041	939.52	0.0000
MIC	0.0016	0.0273	0.0999	-0.0963	0.2107	1.0399	58.27	0.0000
MNG	0.0002	0.0290	0.2109	-0.0996	0.3517	4.0247	772.74	0.0000
NKL	0.0002	0.0280	0.0982	-0.0997	-0.0110	1.6414	124.73	0.0000
RDS	-0.0009	0.0235	0.0999	-0.0999	0.0537	2.1790	220.32	0.0000
RIS	0.0000	0.0289	0.1000	-0.0998	0.1481	1.1046	60.53	0.0000
S2M	0.0005	0.0277	0.1937	-0.1357	0.2211	3.2267	491.01	0.0000
SAH	0.0005	0.0280	0.0997	-0.0999	0.0060	1.8116	151.93	0.0000
SID	-0.0009	0.0285	0.1000	-0.1005	0.1213	1.6771	132.92	0.0000
SLF	0.0005	0.0212	0.0979	-0.1264	-0.2940	4.2780	863.19	0.0000
SMI	0.0008	0.0320	0.0908	-0.1334	-0.0988	0.2294	4.24	0.1199
SNP	0.0019	0.0331	0.1000	-0.1000	0.3789	1.4434	123.02	0.0000
STR	-0.0013	0.0422	0.1000	-0.1900	-0.0111	0.6210	17.87	0.0001
TQM	0.0007	0.0155	0.0758	-0.0656	0.1101	2.0392	194.73	0.0000
WAA	0.0005	0.0276	0.0989	-0.0998	0.0771	0.8688	36.03	0.0000

4 Empirical Results and Discussion

This study begins with an analysis of the characteristics of the 45 selected stocks that will enable us to build our portfolios according to the Mean-Variance (MV), Mean-Absolute Deviation (MAD), Mean-Lower Partial Moments (MLPM) and Mean-Gini (MG) strategies. Descriptive statistics are presented in Table 1. The normality test (Jarque-Bera) for each stock led us to reject the null hypothesis of the normality test at the 99% confidence level. This non-normality of returns does not seem to make the Mean-Variance test relevant (Amato et ali, 1999 [39]),we assume that in the context of our data, the Mean-Variance strategy is the least appropriate. These results indicate a property already observed in the financial data series that returns are generally not normally distributed. In addition, other properties of risky assets were found in the data series such as skewness and kurtosis. Figures 1, 2, 3 and 4 represent the daily returns of the different strategies during the crisis period from February 28, 2020 to August 28, 2020.

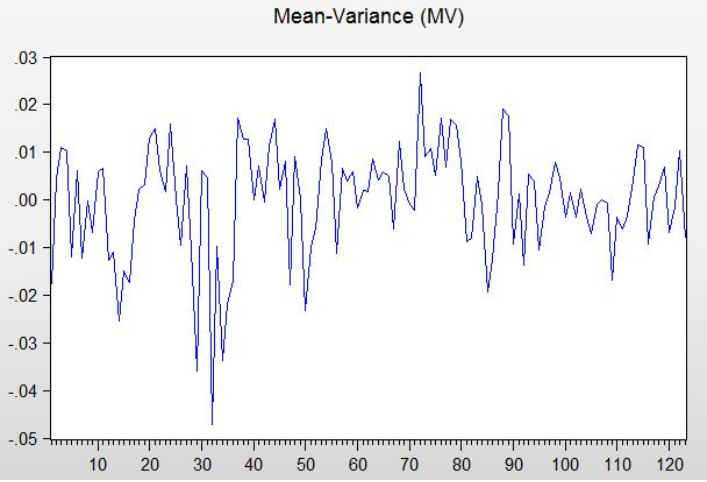


Figure 1: Graphical representation of return (Mean-Variance (MV)).

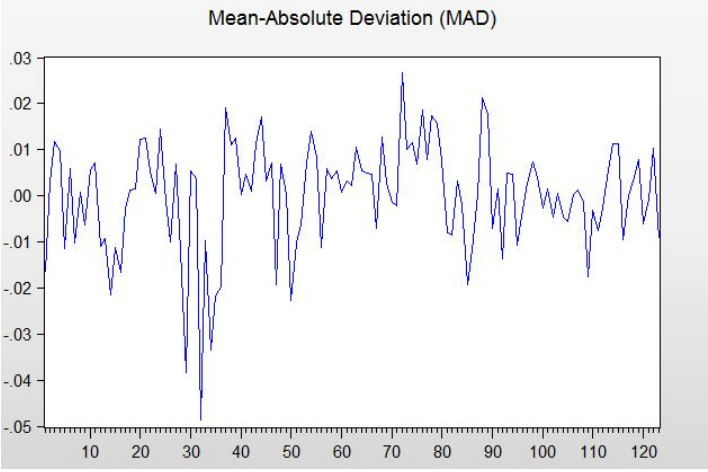


Figure 2: Graphical representation of return (Mean-Absolute Deviation (MAD)).

Table 2: Composition of the different portfolios

	Mean-Variance	Mean-Abslute Devaiation	Mean-Semivariance	Mean-Gini
ALM	7.73%	8.19%	3.97%	7.83%
CMA	2.40%	4.12%	2.61%	3.06%
CTM	11.40%	12.92%	11.14%	11.54%
GAZ	3.53%	2.70%	4.38%	3.77%
HPS	39.94%	41.27%	39.14%	40.51%
M2M	6.60%	5.50%	7.33%	6.05%
MIC	13.56%	13.06%	14.69%	13.30%
SNP	14.84%	12.25%	16.73%	13.94%

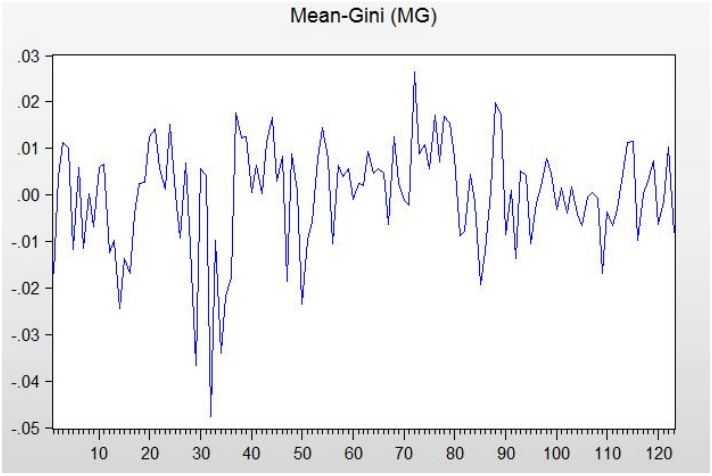


Figure 3: Graphical representation of return (Mean-Gini (MG)).

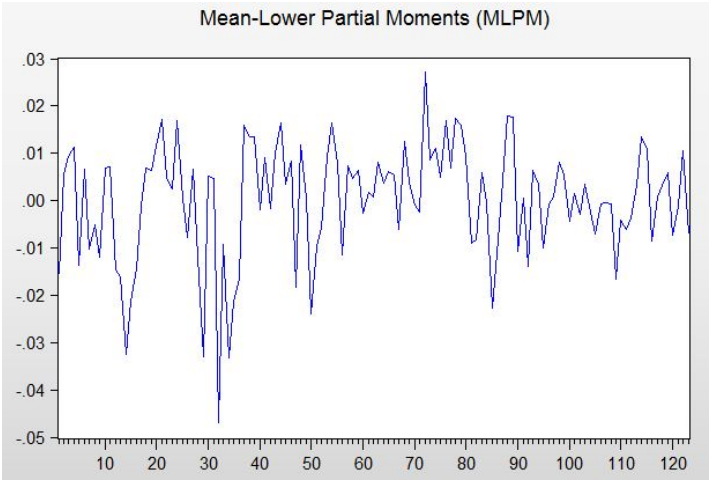


Figure 4: Graphical representation of return (Mean-Lower Partial Moments (MLPM)).

Table 2 above gives the proportions of each share in the optimal portfolios. The results show that the compositions are different as each portfolio has its own composition of shares but with the same assets (ALM, CMA, CTM, GAS, HPC, M2M, MIC, SNP) as the objective return for the period was 0.002 while the majority of the assets have negative returns. For the Mean-Variance strategy,

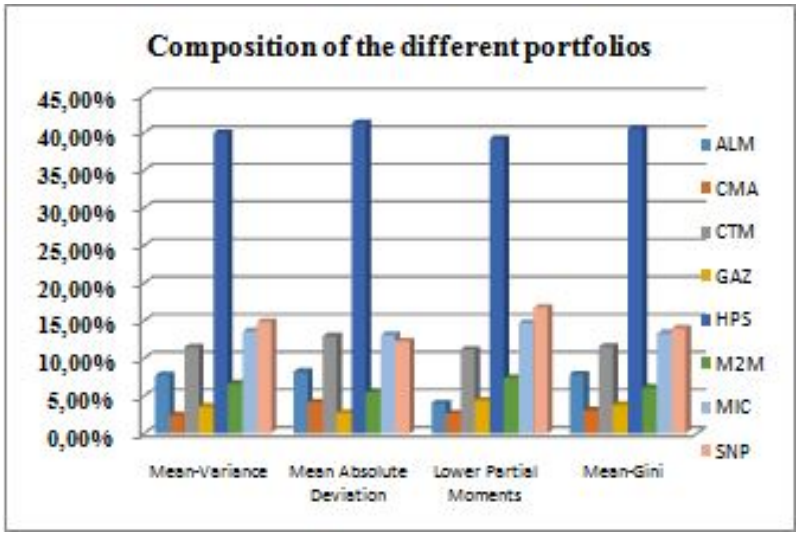


Figure 5: Composition of the different portfolios

HPS is in first place with 39.94, followed by SNP with 14.84, and CMA in last place with 2.40, while the other shares are not part of the composition. Figure 5 provides a detailed overview of the composition of each portfolio. Then, the summary statistics of the optimal portfolios obtained by the resolution of the optimisation programmes are presented in the table 3.

To compare the four stages over the crisis period, i.e. from the appearance of the first case of COVID-19 in Morocco Financial Market until now, we will use the Sharpe ration adjusted by each risk measure (Variance, Absolute Deviation (MAD), Lower Partial Moments (LPM) and Gini Coefficient). The results are presented in Table 4. These results show that the Mean-Lower Partial Moments (MLPM) strategy is the most efficient during this period of crisis compared to other strategies at the time. As shown in Figure 6 and 7, the Mean-Lower Partial Moments (MLPM) model is the one that represents the maximum performance of the Sharpe ratio adjusted by the different risk measures used. Whereas the two models Mean-Gini (MG) and Mean-Absolute Deviation (MAD) are in second position. Finally, the Mean-Variance (MV) model occupies the last position. In general, a higher Treynor Ratio indicates superior performance, and vice versa. In our case and based on the table 4 data, the Mean-Absolute Deviation (MAD) model is the best performing model, followed by Mean-Variance (MV) model which slightly outperforms the other two models: Mean-Lower Partial Moments (MLPM) and Mean-Gini (MG). The results for the Jensen Alpha show that the Lower Mean Partial Moment Model (MLPM) is the one that represents the maximum performance of the Jensen Alpha. Followed by the Mean-Absolute Deviation Model (MAD). While the Mean-Gini model (MG) takes third place. Finally, the Mean-Variance (MV) model occupies the last position.

5 Conclusion

In this paper, we have assessed the contribution of the theoretical approach of Mean-Variance (MV), Mean-Absolute Deviation (MAD), Mean-Lower Partial Moments (MLPM) and Mean-Gini (MG) to the resolution of portfolio management problems in extreme periods within the Casablanca financial center . Empirical application on a

Table 3: Descriptive statistics of portfolio

	Mean-Variance	Mean-Abslute Deviation	Mean-Semivariance	Mean-Gini
Mean	-0.00011	-0.00011	-0.00010	-0.00013
Median	0.00141	0.00175	0.001757	0.00164
Maximum	0.02676	0.02656	0.02712	0.02665
Minimum	-0.04877	-0.04763	-0.04697	-0.04720
Std. Dev.	0.01182	0.011768	0.01216	0.01181
Skewness	-0.99321	-0.98486	-0.92523	-0.94871
Kurtosis	5.18704	4.94169	4.41719	4.76167
J-Bera	44.7365	39.2064	27.8424	34.3566
Probability	0.00	0.00	0.00	0.00
MAD	0.898%	0.888%	0.936%	0.890%
Semivariance	0.949%	0.957%	0.970%	0.951%
Gini	0.7406%	0.7416%	0.7416%	0.7402 %

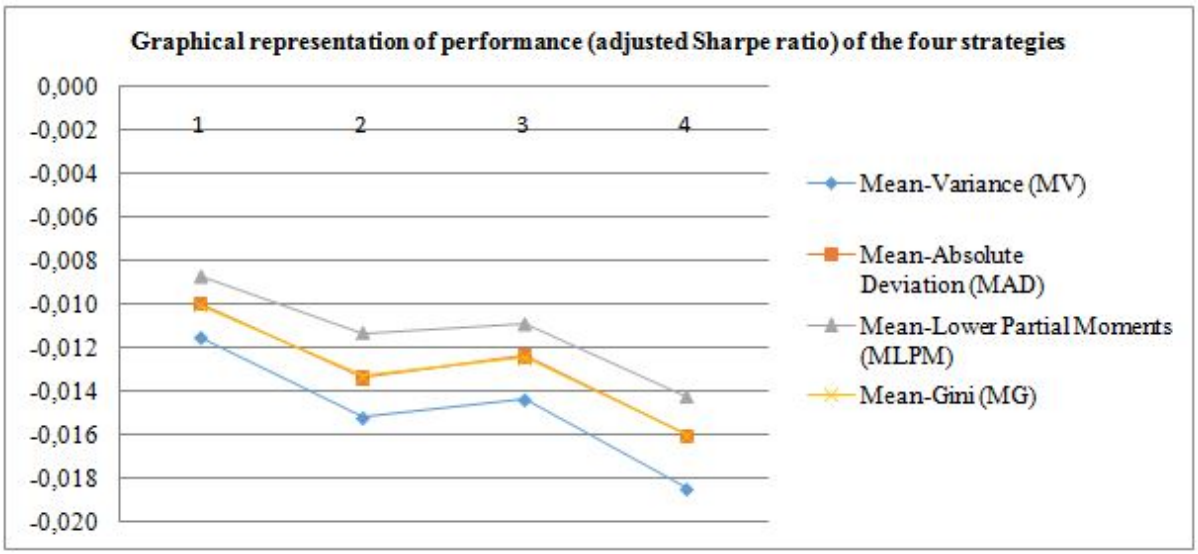


Figure 6: Graphical representation of performance (adjusted Sharpe ratio) of the four strategies.

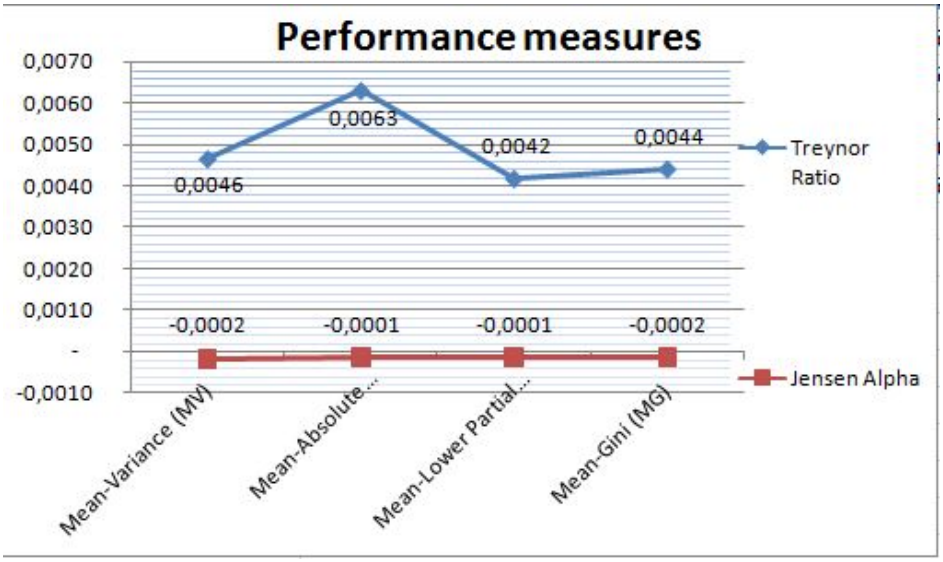


Figure 7: Graphical representation of performance (Treynor Ratio & Jensen Alpha) of the four strategies.

sample of stocks belonging to the MADEX index allowed the selection of four performing portfolios with a better risk/return ratio over the period before COVID-19. The main results show the superiority of the Mean-Lower Partial Moments (MLPM) model over other models based on the results of the adjusted Sharpe ratio. This comparison has been made on the period of the onset and amplification of the COVID-19 pandemic in Morocco. Also note the inferiority of

Table 4: Performance measures (Sharpe ratio,Treynor Ratio and Jensen Alpha) adjusted by each risk measure (Variance, Absolute Deviation (MAD), Lower Partial Moments (LPM) and Gini Coefficient)

performance measures		Mean-Variance (MV)	Mean-Absolute Deviation (MAD)	Mean-Semivariance	Mean-Gini (MG)
Sharpe ratio adjusted	Return/Standard deviation	-0.0116140	-0,0100686	-0,0087240	-0,0100996
	Return/Absolute Deviation	-0.0152826	-0.0134055	-0.0113376	-0.0133471
	Return/Lower Partial Moments	-0.0144509	-0.0124426	-0.0109366	-0.0124972
	Return/Gini	-0.0185225	-0.0160531	-0.0143108	-0.0160553
Treynor Ratio		0.0046469	0.0063047	0.0041626	0.0043972
Jensen Alpha		-0.0001810	-0.0001471	-0.0001440	-0.0001590

the mean-variance (MV) model in terms of performance measured by the adjusted Sharpe ratio since the different series of returns composing our portfolios are volatile, leptokurtic and asymmetric. They lead to a rejection of the Jarque-Bera normality test. As a result, the distribution of daily returns of Moroccan equities deviates from the normal distribution. Similarly, the results for the Jensen Alpha show that theMean-Lower Partial Moments (MLPM) is the model that represents maximum performance, followed by the Mean-Absolute Deviation (MAD) and the Mean-Gini Model (MG) in third place. Finally, the Mean-Variance (MV) model comes in last place. On the other hand, the Mean-Absolute Deviation (MAD)) model is the best performing, followed by the mean variance (MV) model which slightly outperforms the other two models: the Mean-Lower Partial Moments (MLPM) and the mean Gini (MG) based on the treynor ratio results. The results for the Jensen Alpha show that the Lower Mean Partial Moment Model (MLPM) is the model that represents the maximum performance of the Jensen Alpha. This is followed by the Mean-Absolute Deviation (MAD). While the Mean-Gini Model (MG) is in third place. Finally, the Mean-Variance (MV) model occupies the last position.

Through these results, we conclude that the best model available to investors in the Moroccan financial market is the Mean-Lower Partial Moments model (MLPM) since it is the most appropriate model for our financial market and its characteristics.For that and despite the use of the Mean-Variance model in the optimization and management of portfolios by the majority of managers, we underline the inadequacy of this model to the reality of the Moroccan financial center. Indeed, this model is built on the assumption of normality of returns. However, the reality of the financial markets is far from approaching normal distribution law, as several works have pointed out (Agouram and Lakhnati [41].

Conflict of Interest The authors declare no conflict of interest.

Acknowledgment We would like to thank our professor, Lakhnati Ghizlane of the National School of Applied Sciences (ENSA), Ibn Zohr University, Agadir who has helped us a lot in this research.

References

[1] H. Markowitz, "The Utility of Wealth," Journal of Political Economy, 1952, doi:10.1086/257177.

[2] H. Markowitz, "Portfolio analysis," Journal of Finance, **8**, 77–91, 1952.

[3] H. M. Markowitz, "Portfolio Selection, Cowles Foundation Monograph 16," New York, New York: JohnWiley and Sons, 1959MarkowitzPortfolio Selection: Cowles Foundation Monograph, **161959**, 1959.

[4] J. Tobin, "Estimation of Relationships for Limited Dependent Variables," Econometrica, 1958, doi:10.2307/1907382.

[5] W. F. Sharpe, "Capital Asset Prices: A Theory of Market Equilibrium under Conditions of Risk," The Journal of Finance, 1964, doi:10.2307/2977928.

[6] J. Lintner, "SECURITY PRICES, RISK, AND MAXIMAL GAINS FROM DIVERSIFICATION," The Journal of Finance, 1965, doi:10.1111/j.1540-6261.1965.tb02930.x.

[7] J. Lintner, "The Valuation of Risk Assets and the Selection of Risky Investments in Stock Portfolios and Capital Budgets," The Review of Economics and Statistics, 1965, doi:10.2307/1924119.

[8] J. Mossin, "Equilibrium in a Capital Asset Market," Econometrica, 1966, doi:10.2307/1910098.

[9] V. S. Bawa, "Optimal rules for ordering uncertain prospects," Journal of Financial Economics, **2**(1), 95–121, 1975.

[10] V. S. Bawa, E. B. Lindenberg, "Capital market equilibrium in a mean-lower partial moment framework," Journal of Financial Economics, 1977, doi:10.1016/0304-405X(77)90017-4.

[11] P. C. Fishburn, "Condorcet Social Choice Functions," SIAM Journal on Applied Mathematics, 1977, doi:10.1137/0133030.

[12] W. V. Harlow, R. K. S. Rao, "Asset Pricing in a Generalized Mean-Lower Partial Moment Framework: Theory and Evidence," The Journal of Financial and Quantitative Analysis, 1989, doi:10.2307/2330813.

[13] J. P. Morgan, Reuters Ltd, RiskMetrics - Technical Document, 1996.

[14] P. Jorion, "Risk management lessons from long-term capital management," European Financial Management, 2000, doi:10.1111/1468-036X.00125.

[15] M. Grebeck, S. Rachev, "Stochastic programming methods in asset-liability management," Investment Management and Financial Innovations, 2005.

[16] J. L. Treynor, "Market Value, Time, and Risk (revised manuscript)," Unpublished manuscript dated 8/8/61, 1961, doi:10.2139/ssrn.2600356.

[17] J. L. Treynor, "Author : Jack L . Treynor Fall , 1962 (Revised 12 / 28 / 02 , with minor edits by Craig William French) TOWARD A THEORY OF MARKET VALUE OF RISKY ASSETS," **1**(2), 15–22, 1962.

[18] S. A. Ross, "The arbitrage theory of capital asset pricing," Journal of Economic Theory, 1976, doi:10.1016/0022-0531(76)90046-6.

[19] E. Ballestero, "Mean-semivariance efficient frontier: A downside risk model for portfolio selection," Applied Mathematical Finance, 2005, doi:10.1080/1350486042000254015.

[20] S. A. Bond, S. E. Satchell, "Statistical properties of the sample semi-variance," Applied Mathematical Finance, 2002, doi:10.1080/1350486022000015850.

[21] S. A. Bond, S. E. Satchell, "Asymmetry, loss aversion, and forecasting," Journal of Business, 2006, doi:10.1086/503649.

[22] J. Estrada, "Mean-semivariance behavior: Downside risk and capital asset pricing," International Review of Economics and Finance, 2007, doi:10.1016/j.iref.2005.03.003.

[23] M. Unser, "Sampling - 50 years after Shannon," Proceedings of the IEEE, 2000, doi:10.1109/5.843002.

[24] H. Shalit, S. Yitzhaki, "Mean-Gini, Portfolio Theory, and the Pricing of Risky Assets," The Journal of Finance, 1984, doi:10.2307/2327737.

[25] S. Yitzhaki, "Stochastic Dominance, Mean Variance, and Gini's Mean Difference," American Economic Review, 1982, doi:10.2307/1808584.

[26] H. Shalit, S. Yitzhaki, "The mean-Gini efficient portfolio frontier," Journal of Financial Research, 2005, doi:10.1111/j.1475-6803.2005.00114.x.

[27] M. Cardin, B. Eisenberg, L. Tibiletti, "Mean-extended Gini portfolios personalized to the investor's profile," Journal of Modelling in Management, 2013, doi:10.1108/17465661311311978.

[28] H. Konno, H. Yamazaki, "Mean-Absolute Deviation Portfolio Optimization Model and Its Applications to Tokyo Stock Market," Management Science, 1991, doi:10.1287/mnsc.37.5.519.

[29] P. Artzner, F. Delbaen, J.-M. Eber, D. Heath, "Coherent measures of risk," Mathematical finance, **9**(3), 203–228, 1999.

[30] D. N. Nawrocki, "Optimal algorithms and lower partial moment: Ex post results," Applied Economics, 1991, doi:10.1080/00036849100000021.

[31] D. N. Nawrocki, "The characteristics of portfolios selected by n-degree Lower Partial Moment," International Review of Financial Analysis, 1992, doi:10.1016/1057-5219(92)90004-N.

[32] D. N. Nawrocki, "A Brief History of Downside Risk Measures," The Journal of Investing, 1999, doi:10.3905/joi.1999.319365.

[33] W. Y. Lee, R. K. S. Rao, "Mean Lower Partial Moment Valuation and Lognormally Distributed Returns," Management Science, 1988, doi:10.1287/mnsc.34.4.446.

[34] R. P. Bey, K. M. Howe, "Gini's Mean Difference and Portfolio Selection: An Empirical Evaluation," The Journal of Financial and Quantitative Analysis, 1984, doi:10.2307/2331094.

[35] J. Okunev, "MEAN GINI CAPITAL ASSET PRICING MODEL: SOME EMPIRICAL EVIDENCE," Accounting & Finance, 1989, doi:10.1111/j.1467-629X.1989.tb00155.x.

[36] J. Agouram, G. Lakhnati, "A Comparative Study of Mean-Variance and Mean Gini Portfolio Selection Using VaR and CVaR," Journal of Financial Risk Management, 2015, doi:10.4236/jfrm.2015.42007.

[37] A. Jamal, L. Ghizlane, "Mean-Gini portfolio selection: Forecasting VaR using GARCH models in Moroccan financial market," Journal of Economics and International Finance, 2015, doi:10.5897/jeif2014.0630.

[38] J. Agouram, G. Lakhnati, "Mean-gini and mean-extended gini portfolio selection: An empirical analysis," Risk Governance and Control: Financial Markets and Institutions, 2016, doi:10.22495/rcgv6i3c1art7.

[39] C. S. Cheung, C. C. Kwan, P. C. Yip, "The hedging effectiveness of options and futures: A Mean-Gini approach," Journal of Futures Markets, **10**(1), 61–73, 1990.

[40] M. Berkhouch, G. Lakhnati, M. B. Righi, "Extended Gini-type measures of risk and variability," Applied Mathematical Finance, **25**(3), 295–314, 2018.

[41] J. Agouram, J. Anoualigh, G. Lakhnati, "Capital Asset Pricing Model (CAPM) Study in Mean-Gini Model," International Journal of Applied Economics, Finance and Accounting, **6**(1), 57–63, 2020.

ASTES

Advances in Science, Technology and Engineering Systems Journal Vol. 5, No. 5, 727-741 (2020)

www.astesj.com

Special Issue on Multidisciplinary Sciences and Engineering

ASTESJ

ISSN: 2415-6698

Modeling and Implementation of Quadcopter Autonomous Flight Based on Alternative Methods to Determine Propeller Parameters

Gene Patrick Rible[*,1], Nicolette Ann Arriola[1], Manuel Ramos Jr.[1]

[1]*Electrical and Electronics Engineering Institute, College of Engineering, University of the Philippines, 1101, Philippines*

ARTICLE INFO

Article history:
Received: 18 August, 2020
Accepted: 22 September, 2020
Online: 10 October, 2020

Keywords:
Aerial Systems
Propellers
Quadcopter Modeling
Flight Control

ABSTRACT

To properly simulate and implement a quadcopter flight control for intended load and flight conditions, the quadcopter model must have parameters on various relationships including propeller thrust-torque, thrust-PWM, and thrust–angular speed to a certain level of accuracy. Thrust-torque modeling requires an expensive reaction torque measurement sensor. In the absence of sophisticated equipment, the study comes up with alternative methods to complete the quadcopter model. The study also presents a method of modeling the rotational aerodynamic drag on the quadcopter. Although the resulting model of the reaction torque generated by the quadcopter's propellers and the model of the drag torque acting on the quadcopter body that are derived using the methods in this study may not yield the true values of these quantities, the experimental modeling techniques presented in this work ensure that the derived dynamic model for the quadcopter will nevertheless behave identically with the true model for the quadcopter. The derived dynamic model is validated by basic flight controller simulation and actual flight implementation. The model is used as basis for a quadcopter design, which eventually is used for test purposes of basic flight control. This study serves as a baseline for fail-safe control of a quadcopter experiencing an unexpected motor failure.

1. Introduction

This paper is an extension of work originally presented in the 6th International Conference on Control, Automation and Robotics [1].

Multicopters as unmanned aerial vehicles (UAVs) are gaining massive attention in research because of their broad military and civilian applications [2]. Compared with other flying vehicles, multicopters have unique capabilities such as static hovering, vertical take-off and landing (VTOL) [3], and the ability to switch between any two arbitrary directions very quickly any time [4]. The simplest, most efficient, and most economical multicopter is the quadcopter since it contains the minimum number of propellers required to fully control its attitude and position. The quadcopter's dynamic model is used as a basis in designing and adjusting controllers for best flight performance. This new work presents cheaper, alternative methods to model the quadcopter using only basic mechanical tools and electrical measuring devices. The simpler alternative modeling methods presented in this paper can be used to successfully operate the quadcopter in basic flight or even in dynamic fail-safe flight mode. In fact, the modeling methods in this paper were employed in another study [1] on fail-safe control if a motor failure were to occur. The complete methods presented in this work are able to capture the effect of air resistance and propeller torque on the quadcopter dynamics without requiring expensive equipment such as a reaction torque sensor. This work is thus very useful to small-scale researchers who have limited equipment but who nevertheless wish to perform research works on quadcopters.

2. Background Information

2.1. Quadcopter Kinematics

In geometry, a coordinate is a set of values that locates a point. A coordinate frame is a system that uses a minimum of n coordinates to uniquely determine the position of points of geometric objects in an n-dimensional manifold such as the 3-dimensional Euclidean space. This is done by assigning an n-tuple of values to every point on the manifold. One coordinate frame is

[*]Corresponding Author: Gene Patrick Rible, 0889 Lim Extension, Digos, PH +63 956 257 2997, gsrible@up.edu.ph

linearly transformed into another through rotations and translations [5]. Thus, every rotation and translation of a coordinate frame is a transformation into another coordinate frame and because the operations involved in this transformation are linear, this transformation may be completely captured by matrix multiplication for the rotation and matrix addition for the translation.

In this paper, characters in **boldface** are vector or matrix quantities. Consider now the quadcopter kinematic diagram in Figure 1.a. There are three rotation angles ϕ, θ, ψ and three axial coordinates $\boldsymbol{x}$, $\boldsymbol{y}$, $\boldsymbol{z}$. Four propellers are arranged symmetrically about the quadcopter's center of mass (COM). Propellers 1 and 3 rotate opposite to the rotation of propellers 2 and 4. Three coordinate axes $\boldsymbol{x}$, $\boldsymbol{y}$, $\boldsymbol{z}$ are drawn along the quadcopter arms and with origin at the COM. The direction of roll, pitch, and yaw angles and their corresponding body frame angular velocity components are indicated by rotation arrows along the coordinate axes.

Since the motion of the Earth is relatively very slow compared with the motion of the quadcopter in flight, a non-rotating Earth may be assumed. Moreover, since the radius of curvature of the Earth at any point on its surface is very large in comparison with the distances traveled by a quadcopter in flight, a flat Earth may be further assumed.

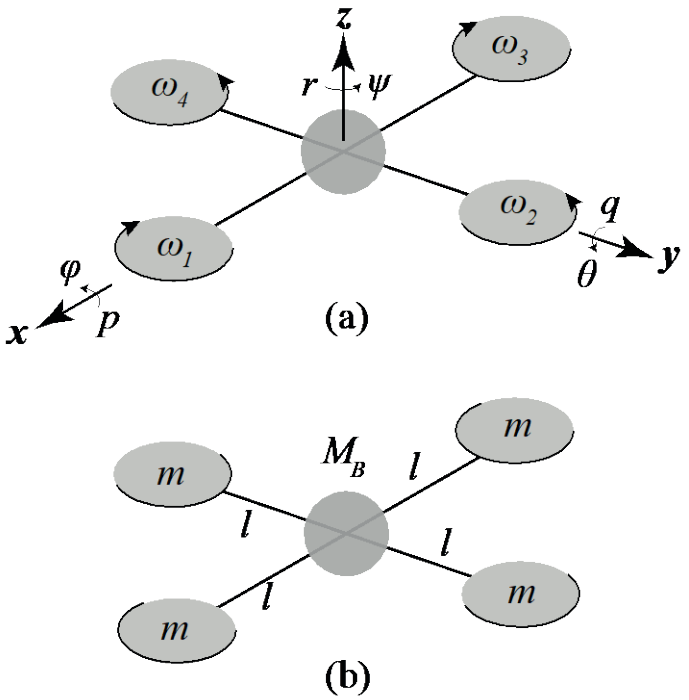


Figure 1: Quadcopter's (a) Kinematic [1] and (b) Dynamic Model

In this paper, a superscript indicates the coordinate frame with which an entity is defined. A rotation matrix that rotates C^a to C^b will be denoted by $\boldsymbol{R}_a^b$. Note that for a rotation matrix [5],

$$\boldsymbol{R}_b^a=\boldsymbol{R}_a^{bT}=\boldsymbol{R}_a^{b-1} \tag{1}$$

The quadcopter state variables are listed in Table 1. To control a quadcopter, state space readings are required. Under basic flight conditions, a state space that completely specifies the six degrees of freedom of a quadcopter and may be used for dynamic computations is (ϕ, θ, ψ, p, q, r, x, y, z, $\dot{x}$, $\dot{y}$, $\dot{z}$).

Table 1: Quadcopter State Variables [1]

x	inertial position along $\hat{\boldsymbol{x}}^i$ in C^i
y	inertial position along $\hat{\boldsymbol{y}}^i$ in C^i
z	altitude along $\hat{\boldsymbol{z}}^i$ in C^i
u	body frame velocity along $\hat{\boldsymbol{x}}^b$ in C^b
v	body frame velocity along $\hat{\boldsymbol{y}}^b$ in C^b
w	body frame velocity along $\hat{\boldsymbol{z}}^b$ in C^b
ϕ	roll angle in C^{v2}
θ	pitch angle in C^{v1}
ψ	yaw angle in C^v
p	roll angular velocity about $\hat{\boldsymbol{x}}^b$ in C^b
q	pitch angular velocity about $\hat{\boldsymbol{y}}^b$ in C^b
r	yaw angular velocity about $\hat{\boldsymbol{z}}^b$ in C^b

A generally accepted quadcopter dynamic model is shown in Figure 1.b. The four motors and propellers are assigned a mass m centered at a distance l from the quadcopter's geometric center such that all masses m are 90° apart from each other with respect to the quadcopter's geometric center. The remaining body mass of the quadcopter excluding the four motors and propellers is M_B which is centered at the quadcopter's geometric center. The centers of the four masses m and of mass M_B are assumed to be coplanar. The total mass of the quadcopter is thus

$$M=M_B+4m \tag{2}$$

Since the quadcopter's dimensions are negligibly small in comparison with the Earth's radius of curvature, it is safe to assume that the center of gravity of any part of the quadcopter coincides with the object's COM.

2.2. Moment of Inertia

Using the orthonormal $\boldsymbol{x}$, $\boldsymbol{y}$, $\boldsymbol{z}$ axes in Figure 1.a, a symmetric inertia matrix may be defined as follows:

$$\boldsymbol{J}\triangleq\begin{bmatrix} J_{xx} & -J_{xy} & -J_{xz} \\ -J_{yx} & J_{yy} & -J_{yz} \\ -J_{zx} & -J_{zy} & J_{zz} \end{bmatrix}$$

$$\triangleq\begin{bmatrix} \int(y^2+z^2)dm & -\int(xy)dm & -\int(xz)dm \\ -\int(yx)dm & \int(x^2+z^2)dm & -\int(yz)dm \\ -\int(zx)dm & -\int(zy)dm & \int(x^2+y^2)dm \end{bmatrix} \tag{3}$$

The diagonal components correspond to the axial moment of inertias (MOIs) of the quadcopter. The non-diagonal elements represent any inertial coupling that may be present between two axes of rotation. For a quadcopter that is symmetric about all three axes, the non-diagonal components of the inertia matrix are zero:

$$\boldsymbol{J}=\begin{bmatrix} J_{xx} & 0 & 0 \\ 0 & J_{yy} & 0 \\ 0 & 0 & J_{zz} \end{bmatrix} \tag{4}$$

2.3. Drag Torque

Due to air resistance, the drag vector $\boldsymbol{\tau}_d \triangleq \boldsymbol{\tau}_d{}^b = (0, 0, \tau_d)$ acting about $\hat{\boldsymbol{z}}^b$ may further be added into the model especially since the quadcopter will exhibit spinning about this axis after losing one or more propellers as implemented in this project. This drag vector is experimentally modeled in [6] as linearly increasing with the yaw angular velocity:

$$\tau_d = \gamma r \tag{5}$$

where γ is the drag coefficient. However, this is only true when the angular speed is very low and there is no turbulence [7]. In this work, it was experimentally found out that the drag torque is better approximated by

$$\tau_d = \left(\gamma_1 r^2 + \gamma_2\right)\mathrm{sgn}(r) \tag{6}$$

where "sgn" denotes the signum function. The approximately quadratic relationship provided by γ_1, especially for high angular speeds, is theoretically supported [8]. Meanwhile, if the quadcopter is tied to a bearing, γ_2 is an offset provided by the rotational kinetic friction after the bearing's rotational static friction has been overcome. Without the bearing, γ_2 is simply set to zero.

2.4. Rotational Dynamics

The complete rotational dynamic model for the quadcopter is [5]

$$\dot{\boldsymbol{\omega}}_{b/i} = \boldsymbol{J}^{-1}\left(\boldsymbol{\tau} - \boldsymbol{\omega}_{b/i} \times \left\{\boldsymbol{J}\boldsymbol{\omega}_{b/i} + \boldsymbol{J}^P \boldsymbol{\Omega}\right\} - \boldsymbol{\tau}_d\right) \tag{7}$$

which in simplified matrix form is [1]

$$\begin{bmatrix} \dot{p} \\ \dot{q} \\ \dot{r} \end{bmatrix} = \begin{bmatrix} \frac{1}{J_{xx}}\tau_\phi \\ \frac{1}{J_{yy}}\tau_\theta \\ \frac{1}{J_{zz}}\tau_\psi \end{bmatrix} - \begin{bmatrix} \frac{J_{zz}-J_{yy}}{J_{xx}} qr \\ \frac{J_{xx}-J_{zz}}{J_{yy}} pr \\ \frac{J_{yy}-J_{xx}}{J_{zz}} pq \end{bmatrix} - \begin{bmatrix} \frac{J_{zz}^P}{J_{xx}} q\Omega \\ \frac{J_{zz}^P}{J_{yy}} p\Omega \\ 0 \end{bmatrix} - \begin{bmatrix} 0 \\ 0 \\ \frac{1}{J_{zz}}\tau_d \end{bmatrix} \tag{8}$$

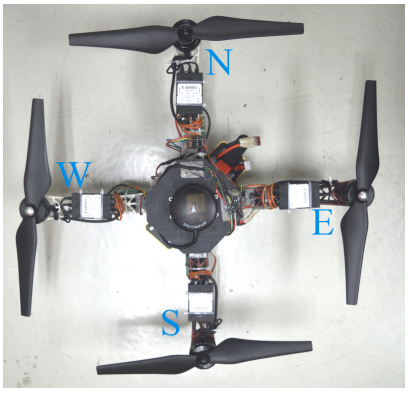
where the algebraic sum of the propeller angular speeds is denoted by [9, 10]

$$\Omega = \sum_{i=1}^{4} (-1)^i \omega_i \tag{9}$$

3. Experimental Methods

3.1. Hardware Design

The quadcopter's skeletal body is the DJI Flame Wheel 450 with the commercial DJI E600 propulsion system [11]. The electronic speed controllers (ESCs) of this propulsion system work by current control and, as with most ESCs in the industry [12], vary the speed of the propellers depending on the on-time of the sent commands and not on the duty cycle. Thus, twice the duty cycle at twice the frequency would result in the same effective on-time and thus, the same propeller speed. This sets a limit on the maximum allowable frequency for the ESCs as the period of the signal sent must be greater than the minimum on-time required to turn on the propellers. The DJI E600 ESCs can receive motor signals between 30 Hz and 450 Hz. Note that this limit on the actuation frequency also sets a limit on the effectivity of the flight controller since even if the controller loop frequency is increased, a constant delay in the actuation will persist. In this project, the target loop frequency of the controller was set at 450 Hz.



A top view of the quadcopter for this project is shown in Figure 2. The letters N, E, W, and S indicate the designated North, East, West, and South directions respectively along the quadcopter's body frame axes. Since cross configuration is used in this paper, $\boldsymbol{x}^b$ is assigned to point along the North; $\boldsymbol{z}^b$ is assigned to point towards the reader; and $\boldsymbol{y}^b$ completes a right-handed coordinate frame. Note that the quadcopter is not symmetric about the $\boldsymbol{x}^b\boldsymbol{z}^b$ plane nor is it symmetric about the $\boldsymbol{y}^b\boldsymbol{z}^b$ plane. However, the quadcopter is symmetric about the $\boldsymbol{x}_1{}^b\boldsymbol{z}_b$ and $\boldsymbol{y}_1{}^b\boldsymbol{z}^b$ where $\boldsymbol{x}_1{}^b$ is $\boldsymbol{x}^b$ rotated 45° about $\boldsymbol{z}^b$ and $\boldsymbol{y}_1{}^b$ is $\boldsymbol{y}^b$ rotated 45° about $\boldsymbol{z}_b$. An axis formed by any plane, the $\boldsymbol{x}^b\boldsymbol{y}^b$ plane for example, and any plane orthogonal to $\boldsymbol{x}^b\boldsymbol{y}^b$ that bisects the body symmetrically is an *axis of symmetry* while such a bisecting plane is a *plane of symmetry*. If more than one axis of symmetry exists, then the intersection of any two axes of symmetry will be the body's *origin*. Assuming that the body's mass is evenly distributed and placing $\boldsymbol{x}^b\boldsymbol{y}^b$ such that $\boldsymbol{x}^b\boldsymbol{y}^b$ passes through the body's COM, the existence of one plane of symmetry means that rotation of the body about an axis created by any other plane orthogonal to $\boldsymbol{x}^b\boldsymbol{y}^b$ and passing through the origin will be as if the body is rotating about an axis of symmetry. This means that for this quadcopter, even though $\boldsymbol{x}^b$ and $\boldsymbol{y}^b$ are not axes of symmetry, rotating about $\boldsymbol{x}^b$ and $\boldsymbol{y}^b$ will be as if they are axes of symmetry and so Equation (4) will still hold using C^b.

3.2. Quadcopter Modeling

Methods to obtain the propeller parameters and subsequently complete the quadcopter's dynamic model are discussed in this section.

3.2.1. Propeller Parameters

Typically, a force sensor and a reaction torque sensor are necessary to come up with the propeller thrust-torque and thrust–

pulse width modulation (PWM) relationships [13, 14]. However, these sophisticated sensors are highly expensive and not readily available. It is also extremely difficult, if not impossible, to find any force sensor or torque sensor product that will readily couple with a commercial UAV propeller to establish a working setup with enough airflow space for propeller modeling purposes. With these considerations in mind, an alternative setup was designed in this work to obtain such relationships for the model. The setup is shown in Figure 3.

The microcontroller sends PWM command to the propeller. As the propeller spins, a weighing scale measures the thrust while a tachometer measures the propeller angular speed. The reaction torque is computed from the voltage and current used to power the spinning propeller.

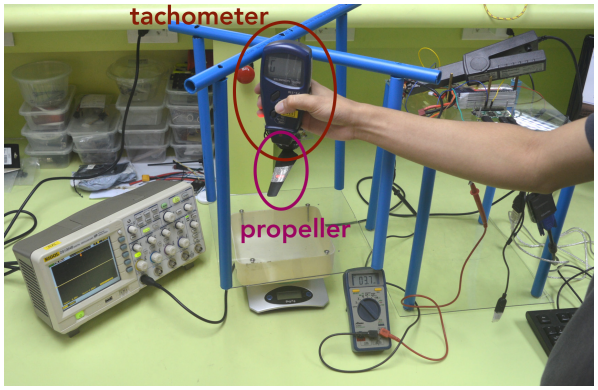


Figure 3: Alternative Propeller Modeling Method

The succeeding discussion on reaction torque appears in [1]. For every rotating propeller i, the produced thrust magnitude f_i, reaction torque magnitude τ_i, and angular speed ω_i are related by [15]

$$f_i=k_f\omega_i^2 \tag{10}$$

$$\tau_i=k_\tau\omega_i^2 \tag{11}$$

$$f_i=k\tau_i \tag{12}$$

where k_f, k_τ, k are positive constants. At steady state, electrical torque τ_e equals mechanical torque τ_m [16]. The propeller exerts a torque in a direction opposite its sense of rotation [17]—a part of this is the reaction torque τ_ψ exerted by the spinning propeller onto the body frame while the remaining is dissipated by aerodynamic drag $\tau_{d_{prop}}$. Thus, at steady state,

$$\tau_e=\tau_m=\tau_\psi+\tau_{d_{prop}} \tag{13}$$

From [15],

$$\tau_\psi=k_\tau\omega^2 \tag{14}$$

where k_τ is a positive scalar. It was also shown in [18] that

$$\tau_{d_{prop}}=k_d\omega^2 \tag{15}$$

where k_d is also a positive scalar. Since τ_ψ and $\tau_{d_{prop}}$ behave similarly with respect to ω, it is impossible to distinguish between the two. We can set $\tau_{d_{prop}}=0$ so that

$$\tau_\psi=\tau_e \tag{16}$$

$\tau_{d_{prop}}$ is lumped together with the drag torque τ_d on the body frame via experimental modeling. This effectively eliminates whatever excess torque allotment that went into τ_ψ.

3.2.2. *Axial Moments of Inertia*

The axial MOIs of the quadcopter were obtained by suspending the quadcopter on three different axes as shown in Figure 4. The MOI of the quadcopter about the axis located at the pivot point is

$$J_P=Mgr\left(\frac{T}{2\pi}\right)^2 \tag{17}$$

where T is the measured period of oscillation and r is the distance between the COM and the pivot point; Equation (17) is derived in [19]. Note that r is equal to the quadcopter arm length plus possibly a small additional length from the rope that tied the quadcopter to the pivot point. Using parallel axis theorem, the MOI of the quadcopter about the body frame axis passing through the quadcopter's COM is

$$J_C=J_P-Mr^2 \tag{18}$$

To accurately measure T, the quadcopter is filmed while swinging freely at 240 fps. The measured time intervals between 16 complete swings since the start of filming are averaged to yield an estimate of T. This is repeated three times. The average of the three trials is the assumed value for T. This averaging is important to protect the data from measurement errors. With this value, the quadcopter axial MOIs are then obtained using Equation (17) and Equation (18).

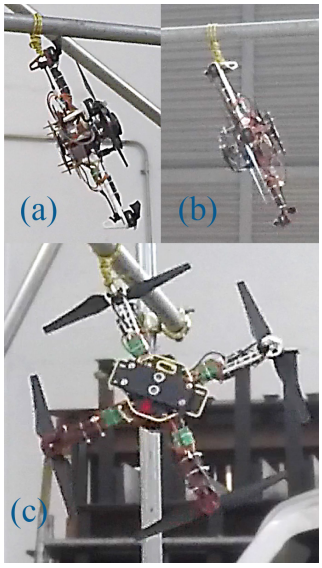


Figure 4: Measuring the Quadcopter MOI About (a) $\hat{x}^b$, (b) $\hat{y}^b$, and (c) $\hat{z}^b$

Meanwhile, to obtain the MOI of the motors and propeller blades about their axis of rotation, they were first weighed. Assuming that the propeller blade is a circular disk with an evenly distributed mass m_b and radius r_b, its axial MOI can be shown to equal

$$J_{z,b}=\frac{1}{2}m_b r_b^2 \tag{19}$$

Assuming that the motor is a solid cylinder with an evenly distributed mass m_m and radius r_m, its axial MOI can be shown to equal

$$J_{z,m}=\frac{1}{2}m_m r_m^2 \tag{20}$$

Since the propeller blade and motor have the same axis of rotation, their MOIs add up so that the propeller MOI about its axis of rotation is simply

$$J_{zz}^P=J_{z,b}+J_{z,m} \tag{21}$$

These were the same methods used in [6] to obtain J_{zz}^P. Since there are four propellers, four J_{zz}^P were computed. Since the propellers are manufactured to be identical, their J_{zz}^P values were averaged and the average value was taken as the J_{zz}^P of any of the propellers. Again, this averaging was done since the motors and propellers are manufactured to be identical; this averaging would protect from experimental errors and remove biases.

3.2.3. Drag Coefficients

The behavior of the drag torque due to air resistance may be experimentally determined by allowing the quadcopter body to rotate about $\hat{z}^b$ and applying different torques along the clockwise or counterclockwise direction. Increasing the applied torque will accelerate the rotation of the quadcopter about $\hat{z}^b$ until the drag torque due to the quadcopter's angular speed equals the applied torque, in which case the quadcopter's rotation about $\hat{z}^b$ reaches its steady state angular speed. Thus, different applied torques will correspond to different steady state angular speeds about $\hat{z}^b$ and the relationship of the applied torques (which become equal to the drag torques at steady state) with respect to the measured steady state angular speeds will determine the behavior of the drag torque due to air resistance. This behavior will be described by a quadratic equation consisting of drag coefficient(s). The same curve-fitting method based on experimental data plot, albeit using a simpler linear assumed model equation, was employed in [6].

Since air's viscosity increases with greater pressure and lower temperature, the air resistance will decrease with higher temperature and higher elevation (which lowers air pressure). It is possible to model the variation of the air resistance with respect to temperature and pressure if both the pressure and temperature of the environment can be controlled and maintained. However, without a closed room facility and equipment that maintains temperature and pressure, it is impossible to keep the temperature and pressure constant throughout the modeling of the air resistance versus angular velocity relationship. Moreover, a changing set of drag coefficients would imply a changing plant—this means that the periodic equilibrium solutions and controller decisions should also be dependent on temperature and pressure. Due to the lack of the aforementioned facility and equipment, and to simplify the problem, the air resistance versus the angular speed relationships were assumed constant and invariant to changes in pressure and temperature; this was also assumed in [6]. In a similar way, temperature and pressure could also affect the PWM to thrust relationship of the propellers. However, due again to the lack of the required facility and equipment to control ambient temperature and pressure and to simplify the problem, the PWM to thrust relationship was assumed constant and invariant to changes in pressure and temperature; this was also assumed in [13].

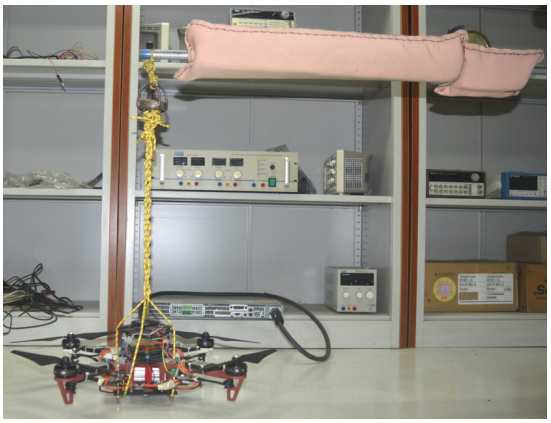


Figure 5: Rope and Bearing Setup for Air Resistance Characterization [1]

The drag torque on the quadcopter's body due to the air resistance was modeled by suspending the quadcopter along a bearing with a single axis of rotation as shown Figure 5. For the air resistance characterization setup, U-shaped metal rods were welded onto a circular bearing, resulting in an axially rotating pivot point. The quadcopter is made to rotate about $\hat{z}^b$ by commanding propellers 1 and 3 to exert a certain torque of the same value while disabling propellers 2 and 4. Each torque value will correspond to a steady state yaw angular velocity: the higher the torque value, the greater the magnitude of the steady state angular velocity of the quadcopter will be. The parametrization of the plot of the combined torque versus the steady state angular velocities will give the coefficients for the drag torque.

Because of metal welding, the metal junction areas expanded, making it hard for the bearing to rotate; this problem was solved using a rubbing compound to scrape off the expanded junction areas. A spherical ball bearing would allow for an omnidirectional rotation and would appear to be more preferable but under the same setup in Figure 5, the rotational friction it yielded was too high that it failed to rotate because of the weight of the quadcopter. In the end, the circular bearing was retained. Ideally, the rotational friction of the bearing would be unaffected by the mass that it carries. However, in reality, the heavier the mass, the greater the rotational kinetic and static friction. Dry lubricant was applied onto the bearing's interior to reduce the rotational friction.

3.3. Simulation of Basic Flight Controller with the Model Derived

The proportional–integral–derivative (PID) controller output is

$$u(t)=k_p\left(y_d(t)-y(t)\right)+k_d\frac{d}{dt}\left(y_d(t)-y(t)\right)$$
$$+k_i\int\left(y_d(t)-y(t)\right)dt \quad (22)$$

where $u(t)$ is the control output; $y(t)$ is the state variable to be controlled; $y_d(t)$ is the desired reference value; k_p, k_d, and k_i are non-negative constants to be tuned before running the controller. Implementing Equation (22) in a microcontroller or computer will result in a controller output that updates in discrete instances according to the controller loop frequency wherein the integral term becomes a running sum. Examining Equation (22), a sharp impulse called *derivative kick* can saturate the actuator and push away the system from the linear zone whenever a task requires $y_d(t)$ to change from one constant value to another [20]. Because of this, most of PID architectures use the derivative of $y(t)$ only. Thus,

$$u(t)=k_p\left(y_d(t)-y(t)\right)-k_d\frac{d}{dt}\left(y(t)\right)+k_i\int\left(y_d(t)-y(t)\right)dt \quad (23)$$

$$u(t)=k_p\left(y_d(t_k)-y(t_k)\right)-k_d\frac{y(t_k)-y(t_{k-1})}{t_k-t_{k-1}}$$
$$+k_i\sum_{j=1}^{k}\left(\left[y_d(t_j)-y(t_j)\right]\left[t_j-t_{j-1}\right]\right) \quad (24)$$

where Equation (24) is the discretized control law version of Equation (23) that can be implemented in microcontrollers.

The simulations were done at a controller frequency of 450 Hz; the higher the controller frequency, the closer Equation (24) will be to Equation (23). This frequency is chosen since it is the maximum signal frequency that can be sent to the motor ESCs.

The differential reference values used in tuning the basic flight controller in the simulations were ±2 m for the altitude, ±5° for the roll and pitch, and ±30° for the yaw. Furthermore, the settling period was set to 3 s; the desired number of oscillations for the altitude was set to 1; the desired number of oscillations for the yaw was set to 2; the desired number of oscillations for the roll and pitch was set to 11. The greater the desired number of oscillations for a variable, the stronger its proportional controller, the higher the variable overshoots, and the faster the system response will be for the variable.

In tuning the PID gains, k_i is initially set to zero. Afterwards, k_p is manually increased until the desired number of oscillations is reached. Then k_d is manually increased until no oscillation remains. The allowable error was set to 1 cm for the altitude and 0.1° for the angles. Note that in this PID tuning method, a single initial overshoot in $y(t)$ is allowed. k_i may be introduced in the end if steady state errors are to be removed. This tuning procedure was employed for the PID controllers of ϕ, θ, ψ, and z with controller outputs u_ϕ, u_θ, u_ψ, and u_z. For the quadcopter,

$$\begin{bmatrix}f_1\\f_2\\f_3\\f_4\end{bmatrix}=\begin{bmatrix}B\\B\\B\\B\end{bmatrix}+\begin{bmatrix}u_z\\u_z\\u_z\\u_z\end{bmatrix}+\begin{bmatrix}0\\u_\phi\\0\\-u_\phi\end{bmatrix}+\begin{bmatrix}-u_\theta\\0\\u_\theta\\0\end{bmatrix}+\begin{bmatrix}u_\psi\\-u_\psi\\u_\psi\\-u_\psi\end{bmatrix} \quad (25)$$

where B is the base weight which is set to $\frac{1}{4}Mg$ or one-fourth the total weight of the quadcopter; this is to ensure equal sharing of load among the four motors at hover. u_z, before being used in Equation (25), is first rescaled by dividing it by $\hat{z}^b\cdot\hat{z}^i=\cos(\phi)\cos(\theta)$ or the directional cosine between the quadcopter's body frame z-axis and the direction pointing opposite to gravity in order to take into account the quadcopter tilt which reduces the lift force [1].

4. Results and Discussion

4.1. Quadcopter Model and Simulation

The obtained parameters of the quadcopter used in this project are listed in Table 2. The standard acceleration due to gravity value is assumed for g. The rest of the parameters were obtained using methods in Section 3.

Table 2: Parameters of the Quadcopter

Parameter	Value	Unit
M	1.645	kg
l	0.2475	m
g	9.80665	m/s^2
J_{xx}	0.014002764	kg m^2
J_{yy}	0.014267729	kg m^2
J_{zz}	0.029487252	kg m^2
J_{zz}^P	2.66838E–04	kg m^2
γ_1	4.86291E–04	(N m)/(rad/s)^2
γ_2	1.22958E–03	N m

For the propeller characteristics, the following models were experimentally obtained:

$$f_i=h_1(P_i-h_2)^2 \quad (26)$$

$$f_i=c_1\omega_i^2 \quad (27)$$

$$\tau_i=(g_1f_i+g_2)\mathrm{sgn}(f_i) \quad (28)$$

where f_i is the force value in N, P_i is a command value from 0 to 255 with 0 corresponding to 0% duty cycle and 255 corresponding to 100% duty cycle, τ_i is the torque value in N m, and ω_i is the propeller speed in $^{\mathrm{rad}}/_{\mathrm{s}}$ of propeller i. Note that Equation (27) and Equation (28) are based on Equation (10) and Equation (12).

Following the alternative method designed, as described in Section 3, the propeller thrust to PWM, propeller thrust to angular speed, and propeller thrust to torque relationships were obtained. This final set of parameters was also used in computing the total torque exerted by the propellers for the drag coefficients. Figure 6, Figure 7, and Figure 8 show plots of these combinations. The plots in yellow correspond to the final model whose parameters are the average of those of the obtained models for the four propellers.

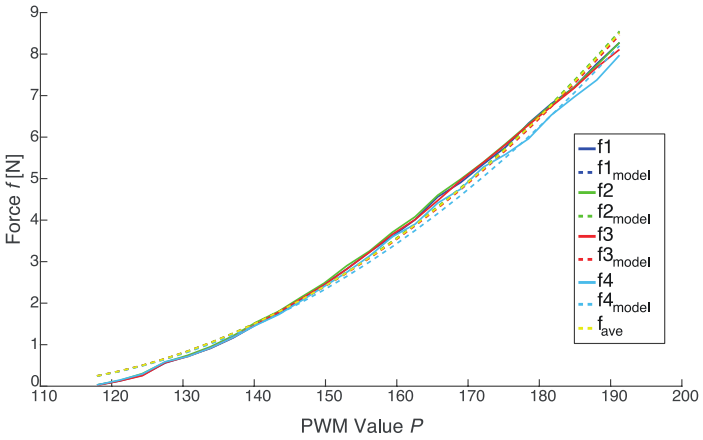


Figure 6: Propeller Thrust as a Function of PWM Command Value

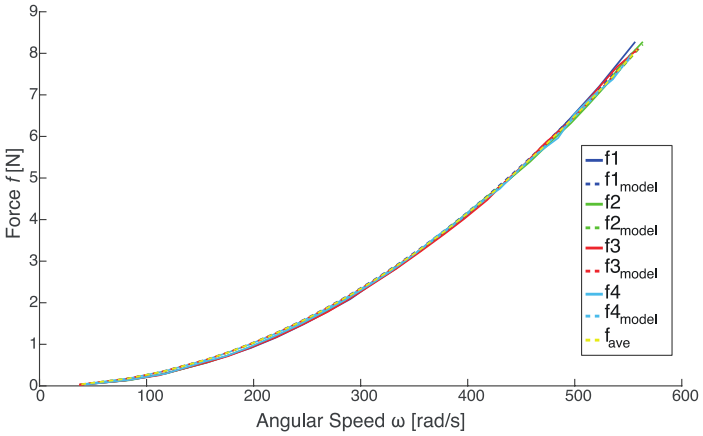


Figure 7: Propeller Thrust as a Function of Propeller Angular Speed

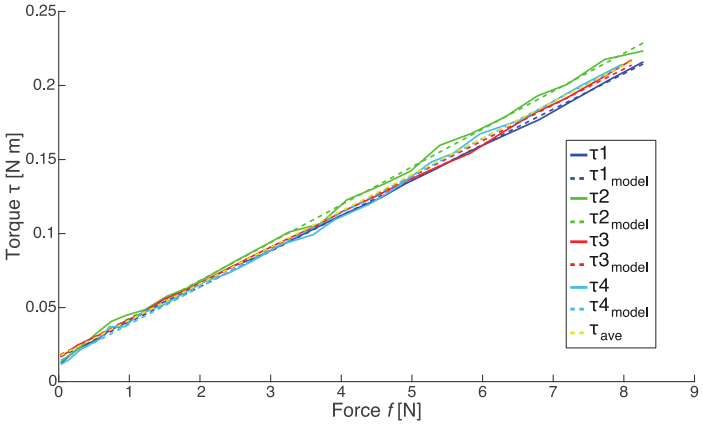


Figure 8: Reaction Torque as a Function of Propeller Thrust

The values of h_1, h_2, c_1, g_1, and g_2 were estimated from experimental data using the setup in Section 3.2.1. In particular, h_1 and h_2 were used to convert thrust commands into motor command values. The numbers from 0 to 255 were scaled to 40000 which was the limit of the microcontroller used. It was eventually found out after tuning the fail-safe flight controller in a different work [1] that this improves quadcopter performance. This reduced the discretization of thrust commands by two orders of magnitude and resulted in a highly smoothened or less shaky flight.

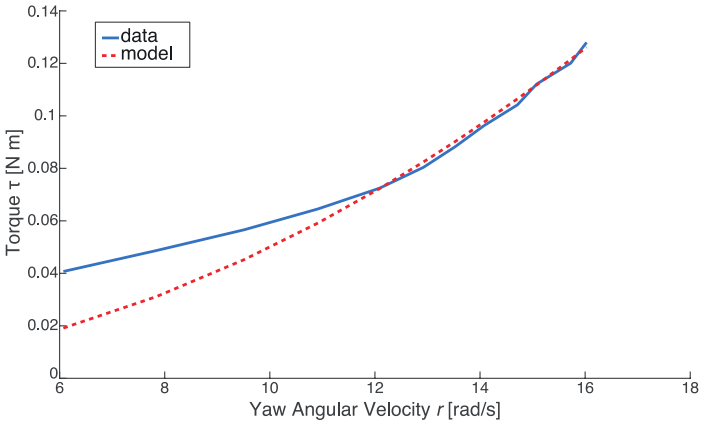


Figure 9: Steady State Yaw Angular Velocities of the Quadcopter Body as a Function of Propeller Torque

Figure 9 shows a plot of steady state angular velocities of the quadcopter body about $\hat{z}^b$ achieved at particular torque values exerted by propeller 1 and propeller 3 as well as a plot of the torque values predicted by the drag coefficients γ_1 and γ_2 in Table 2. Notice that the model for the drag is more accurate at higher angular velocities. This property proved useful in fail-safe mode [1] where the quadcopter's yaw rate would exceed normal operation values.

4.2. Basic Flight Controller

Figure 10 shows the breakdown of the basic flight controller to various sub-algorithms with their execution times. In the Main Loop, the Timing part updates the time parameters for the PID controller and for the flight instructions. The SPI Angles is the part where angles-related information is requested and received in a buffer. An Adjustable Delay is inserted to control the loop frequency. The Decode Angles part converts the information stored in the buffer into angular information that can be accessed in the code. The Basic Flight Control part is where the PID control law is computed. The Flight Instructions part is where certain flight decisions are made and where the PWM commands are sent to the motors.

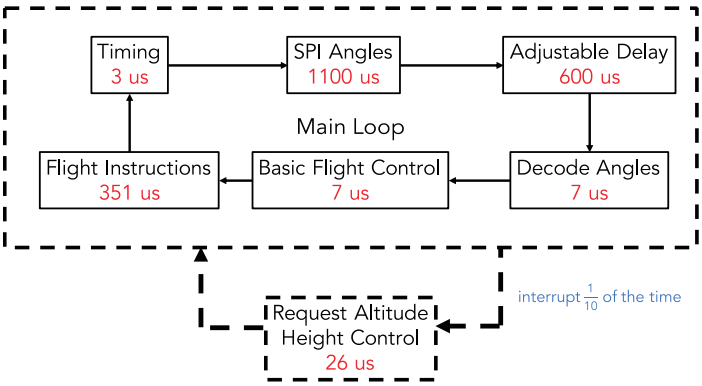


Figure 10: Basic Flight Control

The Main Loop is interrupted every $\frac{1}{10}$ of the time by the Request Attitude part where a function triggers the ultrasonic sensor to begin altitude measurement. Consequently, a Height Control part interrupts every $\frac{1}{10}$ of the time to calculate the

requested altitude reading and corresponding altitude PID output. The Main Loop's total execution time was 2068 µs corresponding to a 483.56 Hz frequency while the execution time of the altitude interrupts was 26 µs which occurred at a frequency of around 45 Hz.

The formula for computing the average execution time of the algorithms will now be discussed. Consider algorithm 1 with execution time T_1 interrupted by algorithm 2 with execution time T_2 every t_0 as illustrated in Figure 11.

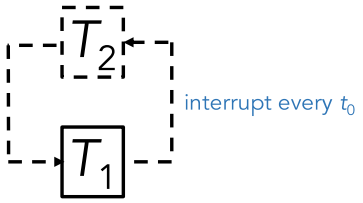


Figure 11: Algorithm 1 Interrupted by Algorithm 2 Every t_0

Then the processes can happen as demonstrated in Figure 12.

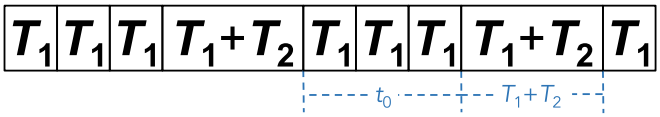


Figure 12: An Example of an Execution of the Processes in Figure 11

The average loop execution time is thus

$$T_{loop}=\frac{t_0}{t_0+T_1+T_2}T_1+\frac{T_1+T_2}{t_0+T_1+T_2}(T_1+T_2) \quad (29)$$

Using Equation (29) with $t_0=\frac{1}{45\text{ Hz}}$, T_1=2068 µs, and T_2=26 µs, the average loop period is 2070.23899911 µs so that the average loop frequency of the basic flight controller will be 483 Hz. The observed 450 Hz to 470 Hz main loop frequency in the implementation was due to intermittent drops in the clock frequency of the Raspberry Pi's processor.

4.3. Basic Flight Simulation

This section documents the simulation of basic flight for the modeled quadcopter. As shown in Table 3, the PID outputs were capped based on the characteristic quantity B discussed in Section 3.3.

Table 3: Limits of Output Variables for Basic Flight

Output Variable	Minimum	Maximum
f_1	0	$2B$
f_2	0	$2B$
f_3	0	$2B$
f_4	0	$2B$
u_z	$-B$	B
u_ϕ	$-B$	B
u_θ	$-B$	B
u_ψ	$-B$	B

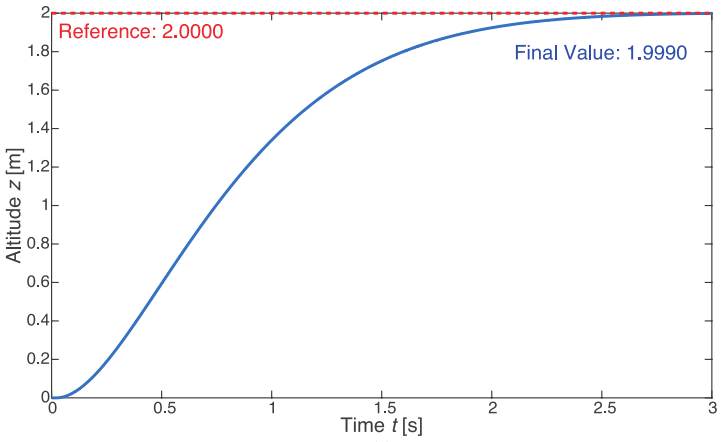
The basic flight simulations were done through MATLAB R2017a's ode45() solver using the parameters modeled and the experimentally determined drag coefficients in Table 3. In the absence of the bearing system that was later used in the fail-safe implementation [1], the rotational kinetic friction contribution of the bearing γ_2 was set to zero. These parameters corresponded to the quadcopter implemented.

The state variables of interest are ϕ, θ, ψ, and z. The tuned PID gains of the quadcopter in the simulation are listed in Table 4. The second symbol in the subscript indicates the variable to control. Since for this project's basic flight requirement, small steady state errors are of no concern, the integral gain was zeroed out for all variables to avoid unwanted system oscillations. The altitude was first tuned with the remaining variables' PID controllers disabled. Then with only the tuned altitude controller enabled, the roll and pitch controllers were separately tuned. Finally, the yaw controller was tuned with the rest of the tuned controllers enabled.

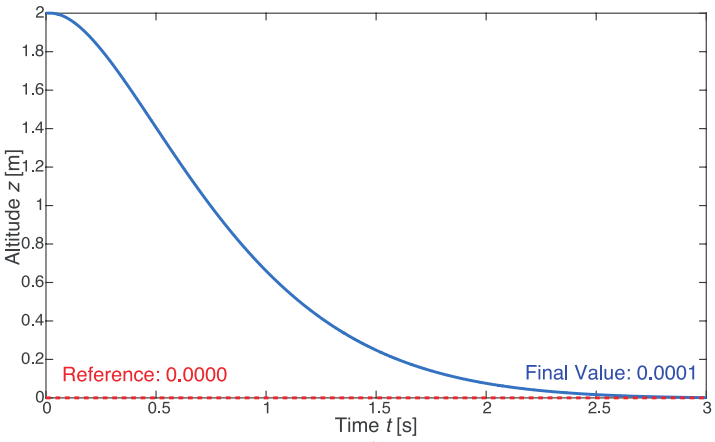
Table 4: Tuned PID Gains for Basic Flight Simulation

PID Parameter	Value	Unit
$k_{p,z}$	1.9	N/m
$k_{d,z}$	1.6	(N s)/m
$k_{p,\phi}$	17.1	N/rad
$k_{d,\phi}$	1.3	(N s)/rad
$k_{p,\theta}$	17.2	N/rad
$k_{d,\theta}$	1.3	(N s)/rad
$k_{p,\psi}$	7.7	N/rad
$k_{d,\psi}$	2.7	(N s)/rad

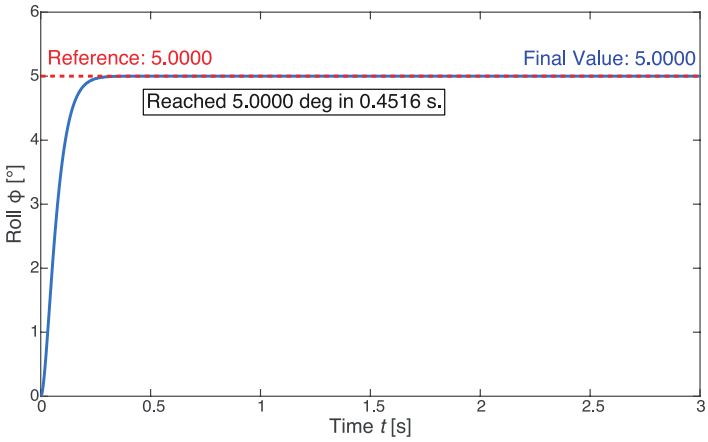
Results of the simulation with the tuned PID gains are shown in Figure 13, Figure 14, Figure 15, and Figure 16. Figure 13 demonstrates the quadcopter's stability and altitude response to ascent and landing commands. Figure 14 demonstrates the roll, pitch, yaw, and altitude stability of the modeled quadcopter as it accomplishes a positive roll command. The model was also tested for negative roll, and behaved similarly stable. Figure 15 demonstrates the quadcopter's stable response to a negative pitch command. The model was also tested for positive pitch and behaved similarly stable. The quadcopter remains stable and achieves the desired values as expected. Finally, Figure 16 demonstrates both positive and negative yaw responses. As expected, the positive and negative responses in all variables are symmetric, and the attitude and altitude controls are capable of maintaining stability upon a command change in a single flight parameter.


Reference: 2.0000
Final Value: 1.9990
Altitude z [m]
Time t [s]

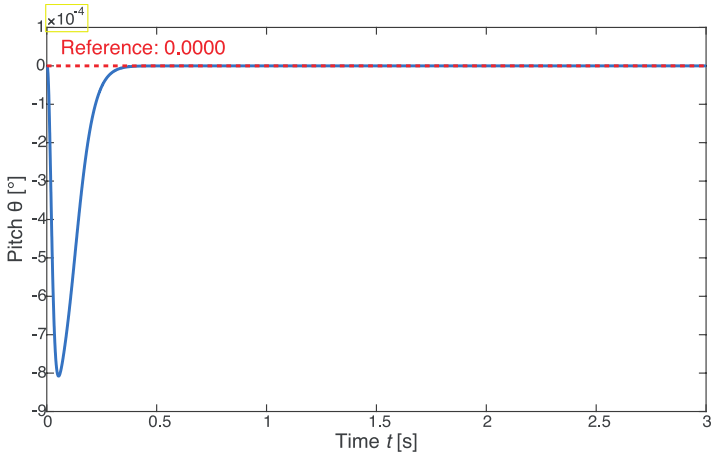
(a)


Reference: 0.0000
Final Value: 0.0001
Altitude z [m]
Time t [s]

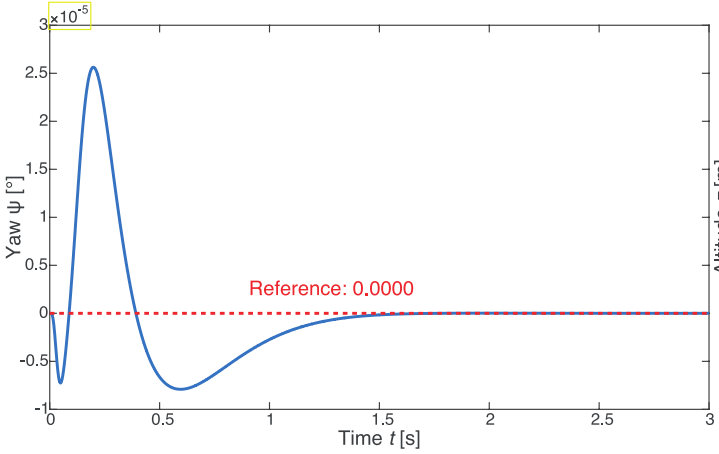
(b)


Reference: 5.0000
Final Value: 5.0000
Reached 5.0000 deg in 0.4516 s.
Roll ϕ [°]
Time t [s]

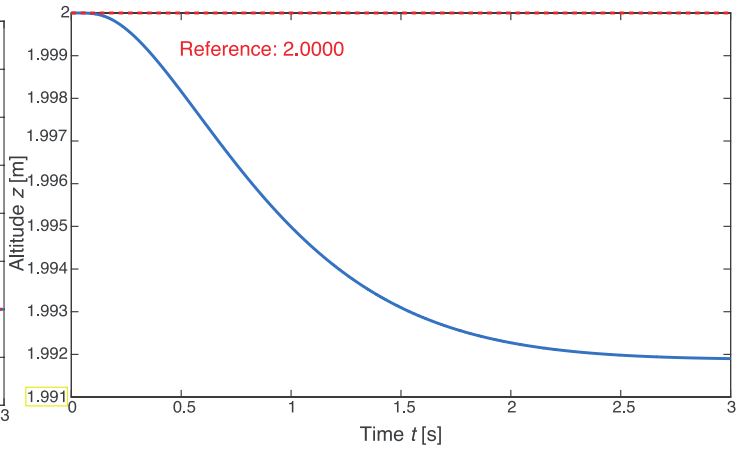
(a)


×10^-4
Reference: 0.0000
Pitch θ [°]
Time t [s]

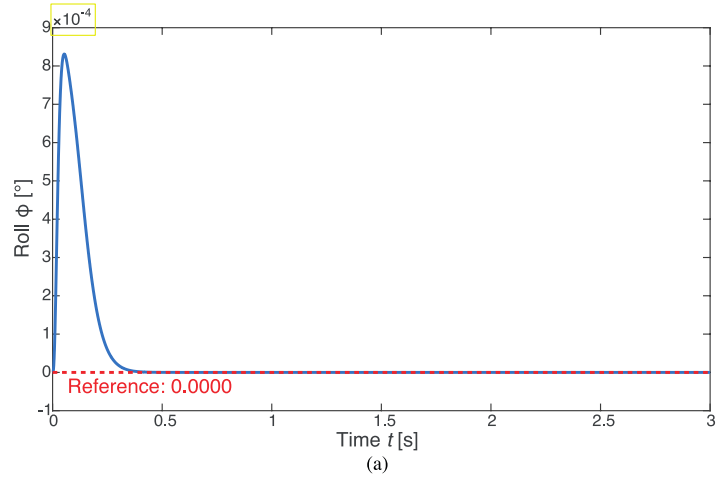
(b)


×10^-5
Reference: 0.0000
Yaw ψ [°]
Time t [s]

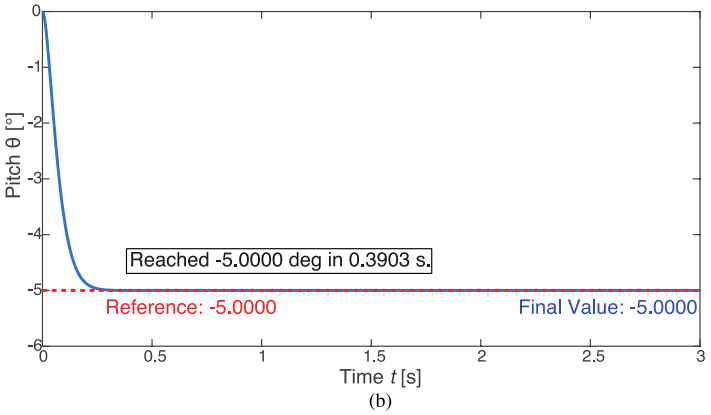
(c)


Reference: 2.0000
Altitude z [m]
Time t [s]

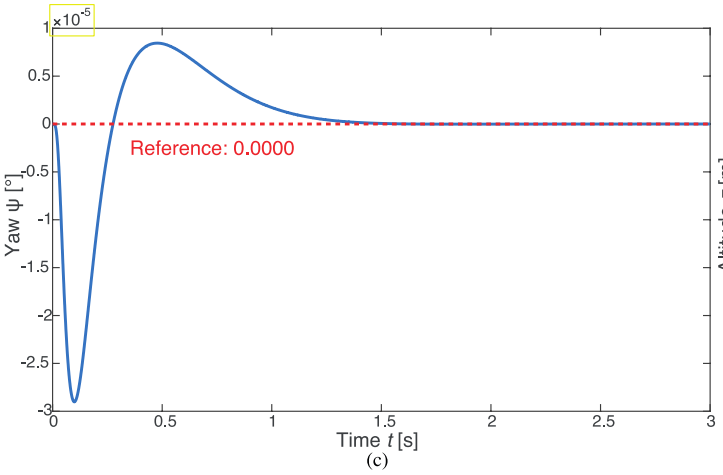
(d)


x10^-4
Roll ϕ [°]
Reference: 0.0000
Time t [s]

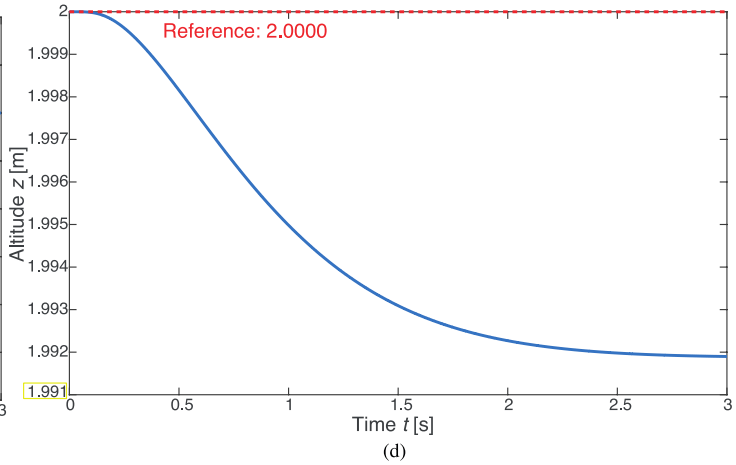
(a)


Pitch θ [°]
Reached -5.0000 deg in 0.3903 s.
Reference: -5.0000
Final Value: -5.0000
Time t [s]

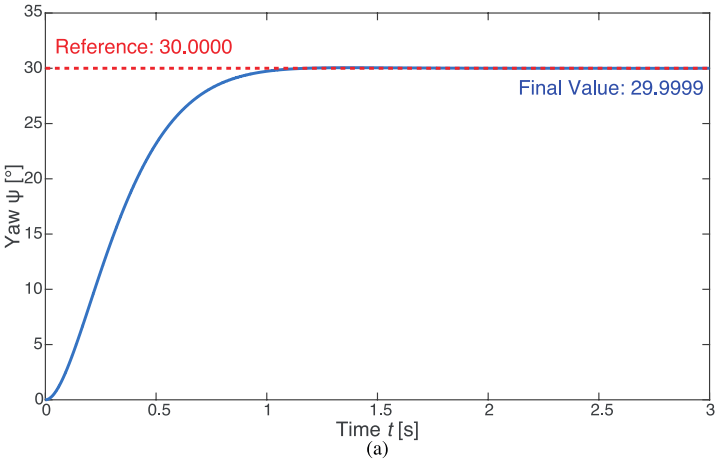
(b)


x10^-5
Yaw ψ [°]
Reference: 0.0000
Time t [s]

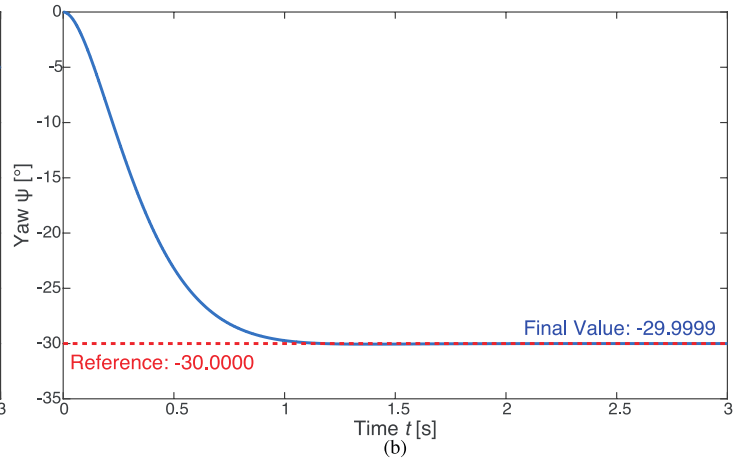
(c)


Reference: 2.0000
Altitude z [m]
Time t [s]

(d)


Reference: 30.0000
Final Value: 29.9999
Yaw ψ [°]
Time t [s]

(a)


Final Value: -29.9999
Reference: -30.0000
Yaw ψ [°]
Time t [s]

(b)

4.4. Basic Flight Implementation

This section documents the simulation of basic flight for the modeled quadcopter.

4.4.1. Control and Actuation Frequency

As simulated, the average loop frequency of the basic flight controller was around 450 Hz with the altitude controller interrupting every $\frac{1}{10}$ of the time. This was found to work well with the ultrasonic proximity sensor having a working frequency of 40 Hz in its datasheet [21]. The frequency used in the motor commands for the basic flight was 449 Hz since the ESC command frequency limit was 450 Hz.

4.4.2. Sensor Fusion Technique

The roll and pitch of the quadcopter can be extracted from the x, y, and z accelerometer axial readings using [22]

$$\phi=\arctan\left(\frac{accel_y}{accel_z}\right) \tag{30}$$

$$\theta=\arctan\left(\frac{-accel_x}{\sqrt{accel_y{}^2+accel_z{}^2}}\right) \tag{31}$$

while the yaw can be extracted from the x, y, and z magnetometer axial readings together with the estimates for the roll and the yaw using [23, 24]

$$\psi=\arctan\left(\frac{magnet_z\sin(\phi)-magnet_y\cos(\phi)}{magnet_x\cos(\theta)+magnet_y\sin(\theta)\sin(\phi)+magnet_z\sin(\theta)\cos(\phi)}\right) \tag{32}$$

Although these are absolute information about the attitude, these are very noisy estimates because of the noisy accelerometer and magnetometer readings. The gyroscope readings which are used to compute $\dot{\phi}$, $\dot{\theta}$, and $\dot{\psi}$ are less noisy but they can only give differential estimates for the angles. To get accurate and clean enough attitude estimates, complementary filter may be used to fuse the absolute but noisy estimates with the less noisy but differential estimates according to the weighting equation:

$$\phi=(1-\alpha)\phi_{accel,mag}+\alpha\phi_{gyro} \tag{33}$$

$$\theta=(1-\alpha)\theta_{accel,mag}+\alpha\theta_{gyro} \tag{34}$$

$$\psi=(1-\alpha)\psi_{accel,mag}+\alpha\psi_{gyro} \tag{35}$$

with α as the parameter.

The result is a low-pass filtering of the accelerometer and magnetometer's absolute estimates to remove the noise and a high-pass filtering of the gyroscope's differential estimates to remove the drift which worsens with each iteration. The time constant $\tau=\frac{\alpha dt}{1-\alpha}$ is for both filters for a loop frequency given by dt [25]. The tuning of α was done based on the value of τ which was adjusted in powers of 2 of the average loop period dt [1].

4.4.3. EMA Filter for Gyroscope

Using the smoothing factor, α_{EMA}, an exponential moving average (EMA) filter was applied on the gyroscope readings p, q, and r in order to remove noise according to the formula

$$p_i=\alpha_{EMA,p}p_i+(1-\alpha_{EMA,p})p_{i-1} \tag{36}$$

$$q_i=\alpha_{EMA,q}q_i+(1-\alpha_{EMA,q})q_{i-1} \tag{37}$$

$$r_i=\alpha_{EMA,r}r_i+(1-\alpha_{EMA,r})r_{i-1} \tag{38}$$

The time constant of an exponential moving average is the amount of time for the smoothened unit step response to reach $1-1/e\approx63.2\%$. The relationship between this time constant, τ_{EMA}, and α_{EMA} is given by

$$\alpha_{EMA}=1-e^{\frac{-dt}{\tau_{EMA}}} \tag{39}$$

where dt is the iteration frequency [26].

4.4.4. Sensor Tuning

The exponential smoothing of p, q, r were done first before performing the sensor fusion technique [1]. The α_{EMA} for each gyroscope reading was tuned while the quadcopter was being held mid-air. The tuning of α_{EMA} was done based on the value of τ_{EMA}, in powers of 2 of the average loop period dt [1]. τ_{EMA} for each of the variables was doubled until the amplitude of oscillations in p and q were within 0.01 $\frac{\text{rad}}{\text{s}}$. The same α_{EMA} was adopted for r. Since the r readings of the sensor was inherently less noisy, the amplitude oscillations in r using the same α_{EMA} in p and q were within 0.006 $\frac{\text{rad}}{\text{s}}$.

After tuning the value of α_{EMA}, the quadcopter was made to sit still on a flat surface for 1 minute. The gyroscope readings along each rotation axis for the minute were averaged to get the gyroscopic axial bias which must be subtracted from the future p, q, r readings of the gyroscope. The corresponding angular values from the accelerometer readings for the minute were also averaged to get the biases on the estimates of ϕ and θ; these must be subtracted from the future accelerometer estimates of ϕ and θ prior to sensor fusion. Meanwhile, the α value for the complementary filters in the roll, pitch, and yaw were increased until the amplitude of the oscillations were within $\pm0.1°$. Table 5 lists the filter values.

Table 5: EMA and Complementary Filter Values

Gyroscopic Axis	α_{EMA}
p	0.007782062
q	0.007782062
r	0.007782062
Angular Variable	α
ϕ	0.992248062
θ	0.992248062
ψ	0.984615385

4.4.5. PID Tuning

A lot of non-idealities that appeared in the actual implementation of basic flight were not captured in the simulation. These include irregular and intermittent delays in the processor, ESCs, and actuation of motors in addition to sensor noise and possibly slight modeling discrepancies. Thus, although implementing the simulated controller gains worked for the quadcopter's basic flight, its performance was improved by altering the simulated tuned controller gain values to better adapt to these non-idealities. Using the simulated gains in Table 4 as the starting point, the basic flight controller PID gains were retuned to the values listed in Table 6. Note that small integral gains for the roll and pitch angles, which were zeroed out in the simulation, became necessary in the implementation to ensure that the quadcopter did not drift from the reference command values over time, since drifting along the roll and pitch axes would quickly accelerate the quadcopter to dangerously high translational speeds.

Table 6: Tuned PID Gains for Basic Flight Implementation

PID Parameter	Value	Unit
$k_{p,z}$	2.4	N/m
$k_{d,z}$	0.14	(N s)/m
$k_{p,\phi}$	4.48	N/rad
$k_{d,\phi}$	0.221	(N s)/rad
$k_{i,\phi}$	0.0045	N/(rad s)
$k_{p,\theta}$	4.12	N/rad
$k_{d,\theta}$	0.13	(N s)/rad
$k_{i,\theta}$	0.0045	N/(rad s)
$k_{p,\psi}$	7.55	N/rad
$k_{d,\psi}$	0.248	(N s)/rad

To avoid external airflow disturbances such as wind gusts during the implementation of basic flight, the quadcopter was flown indoors. The hovering test produced the altitude, roll, pitch, and yaw response in Figure 17. In the following plots, the actual response is shown in blue whereas the reference command is shown in red. As expected, because of the aforementioned non-idealities, more jitter is present in the actual quadcopter response than in the ideal simulation results, but the settling of each parameter emphasizes the correct controller design which in turn verifies the quadcopter model derived.

Compared with the obtained altitude response using the flight controller in this work, the altitude control performance of typical modern UAVs [27] are more than twice as jittery. Moreover, the altitude tracking error of modern quadcopters using a similar ultrasonic sensor [28] can be more than 20 times worse than that in Figure 17. Although quadcopters using more sophisticated sensors like laser radar [29] can reduce altitude tracking error to almost one order of magnitude better than the altitude response presented in this paper, the controller in this work nevertheless performs more smoothly and with an almost equal fluctuation in the altitude.

Moreover, the graph responses for positive and negative banking along the roll and pitch directions are shown in Figure 18 and Figure 19. The quadcopter was set to hover at the beginning of both tests, and upon achieving stability, commanded to bank before returning to hover mode. In both plots, the quadcopter was able to find and settle around the command values in each change of state. The yaw responses to positive and negative rotation commands as shown in Figure 20 also demonstrate quick stabilization in either direction.

In terms of attitude control, the roll, pitch, and yaw responses of the quadcopter system developed in this work are typically more jittery compared with the responses of quadcopters using popular firmware systems like ArduPilot [30] and Pixhawk [31, 32] but the developed system can nonetheless achieve a lower average tracking error in the roll and pitch angles.

5. Summary and Conclusion

The study came up with alternative methods to determine thrust vs. PWM command, thrust vs. angular speed, and reaction torque vs. thrust relationships of the quadcopter's propellers as well as the coefficients of the aerodynamic drag acting on the quadcopter, thereby completing a dynamic model for the quadcopter. With the specific model, the study extended into designing and simulating a basic flight controller. The simulation led to determining PID values and limits which served as starting points for the actual controller implemented. Plots of the simulated responses to thorough actual tests demonstrated the expected stable flight of the quadcopter. These results further verified the completeness and correctness of the model obtained. This method was repeated for multiple versions of quadcopter with a completely different set of motors, ESCs, and propellers. Using the same methodology, corresponding values were obtained and similar behavior was demonstrated.

The quadcopter implemented in this paper was used in another work [1] which is the implementation of a fail-safe controller for a quadcopter that experiences a motor failure. A working basic flight controller is a stepping stone to solving the motor failure problem.

Conflict of Interest

The authors declare no conflict of interest.

Acknowledgment

This project was supported in part by grants from the UP Engineering Research & Development Foundation, Inc. Publication of this paper was made possible by the Engineering Research and Development for Technology program of the Department of Science and Technology in the Philippines.

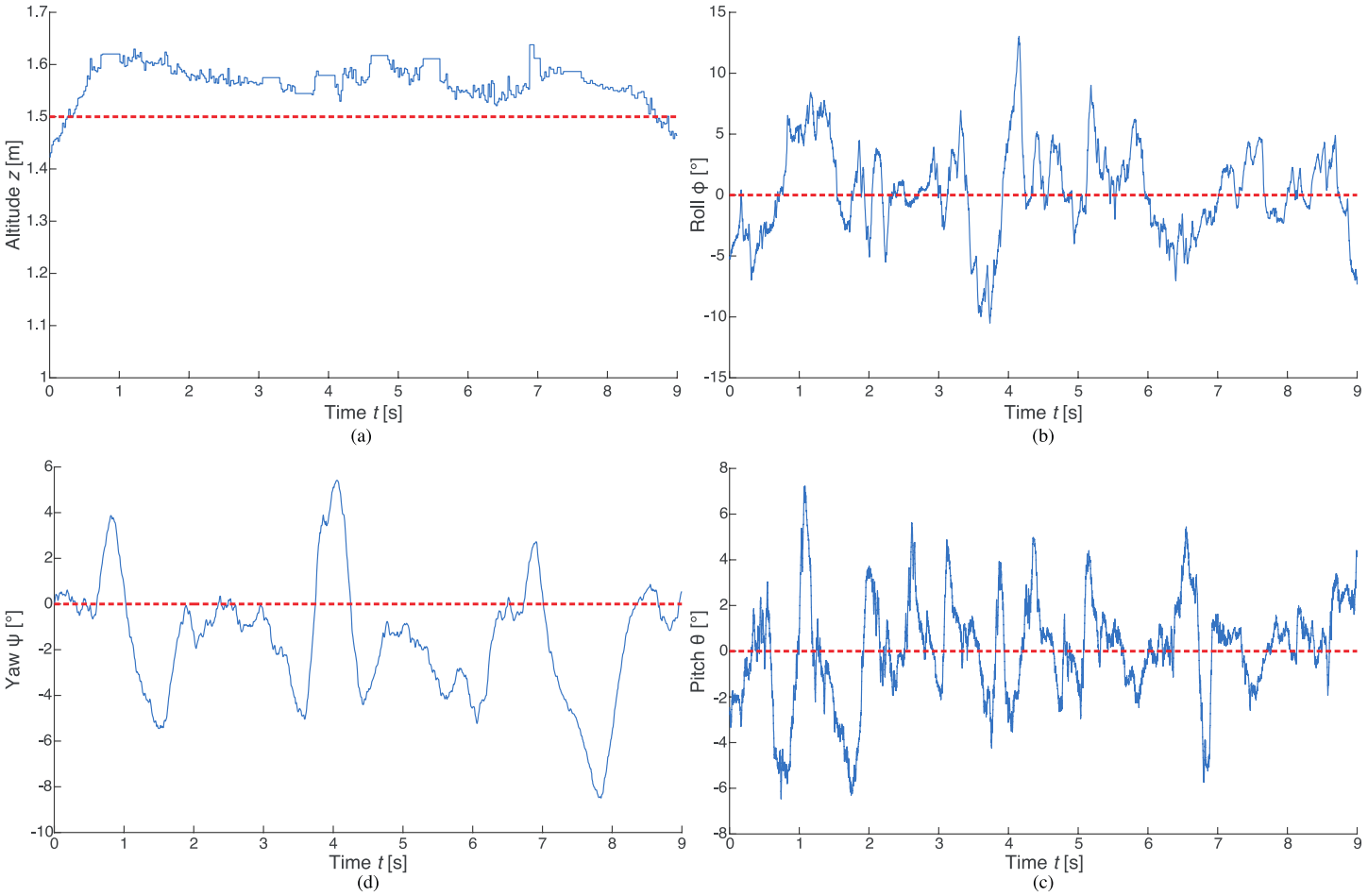


Figure 17: Quadcopter Hover Response. In (a), the quadcopter's altitude remains stably close to the 1.5 m reference value with time. In (b), the quadcopter's roll angle remains stably close to the 0° reference value with time. In (c), the quadcopter's pitch angle also remains stably close to the 0° reference value with time. In (d), the quadcopter's yaw angle remains similarly stable and close to the 0° reference value with time.

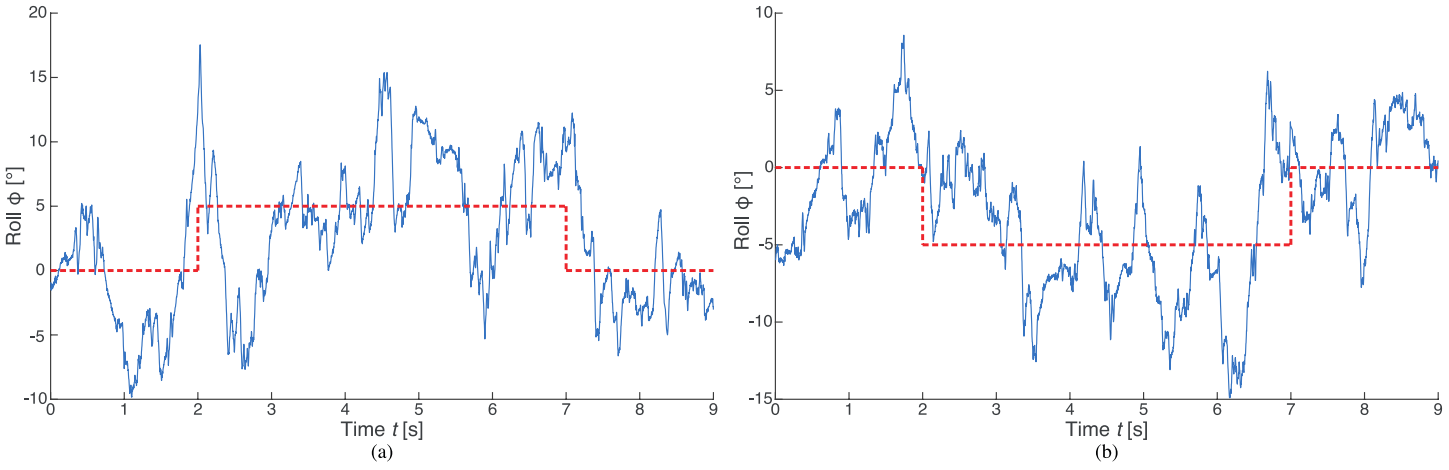


Figure 18: Quadcopter Roll Response to Positive and Negative Banking Commands. In (a), the quadcopter's roll angle, initially 0°, achieves a +5° command for 3 s before returning to 0°. In (b), the quadcopter's roll angle, initially 0°, achieves a –5° command for 5 s before returning to 0°. The quadcopter's pitch, yaw, and altitude were not significantly affected during banking.

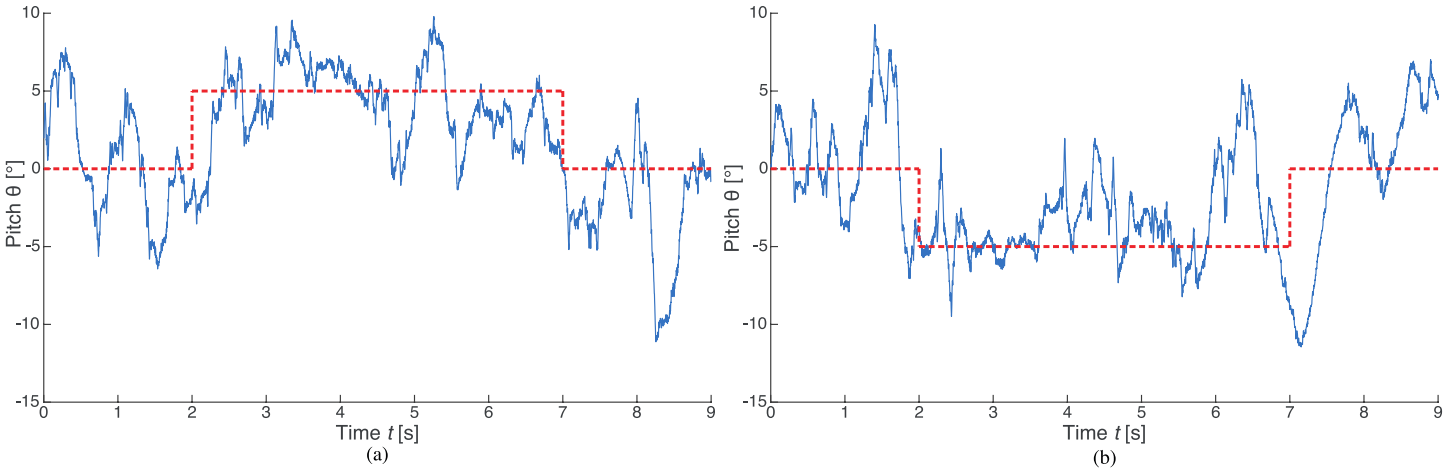


Figure 19: Quadcopter Pitch Response to Positive and Negative Banking Commands. In (a), the quadcopter's pitch angle, initially 0°, achieves a +5° command for 3 s before returning to 0°. In (b), the quadcopter's pitch angle, initially 0°, achieves a –5° command for 5 s before returning to 0°. The quadcopter's roll, yaw, and altitude were not significantly affected during banking.

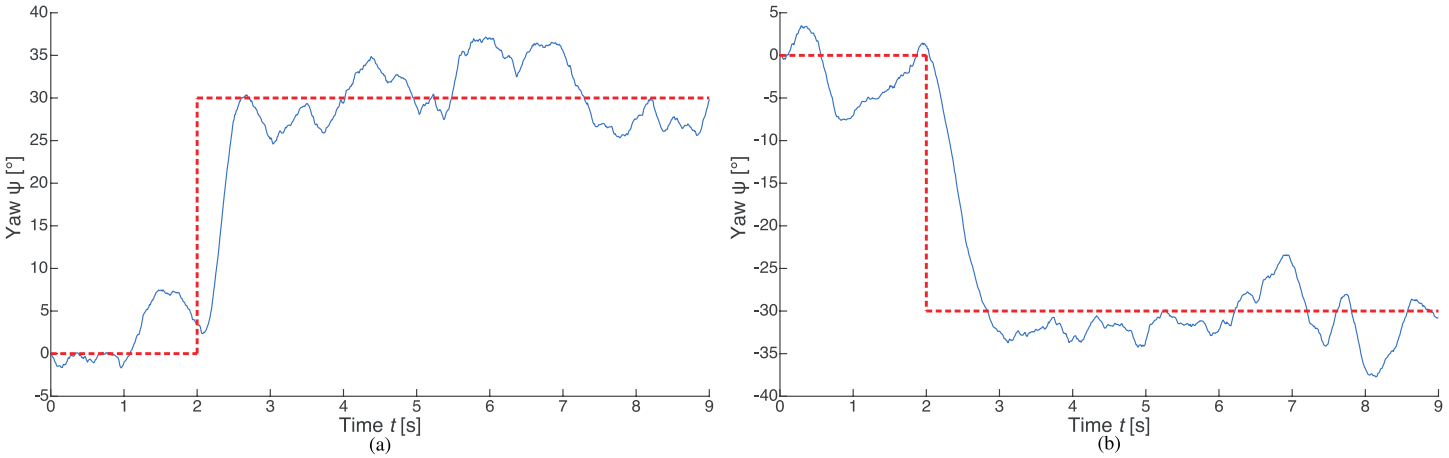


Figure 20: Quadcopter Yaw Response to Positive and Negative Rotation Commands. In (a), the quadcopter's yaw angle, initially 0°, achieves the +30° command. In (b), the quadcopter's yaw angle, initially 0°, achieves the –30° command. The quadcopter's roll, pitch, and altitude were not significantly affected during rotation.

References

[1] G. P. S. Rible, N. A. A. Arriola, M. C. Ramos, "Fail-Safe Controller Architectures for Quadcopter with Motor Failures" in 2020 6th International Conference on Control, Automation and Robotics (ICCAR), Singapore, 2020. https://doi.org/10.1109/ICCAR49639.2020.9108038

[2] B. Fan, J. Sun, Y. Yu, "A LQR controller for a quadrotor: Design and experiment" in 2016 31st Youth Academic Annual Conference of Chinese Association of Automation (YAC), Wuhan, Hubei, China, 2016. https://doi.org/10.1109/YAC.2016.7804869

[3] J. Qiao, Z. Liu, Y. Zhang, "Gain scheduling PID control of the quad-rotor helicopter" in 2017 IEEE International Conference on Unmanned Systems (ICUS), Beijing, China, 2017. https://doi.org/10.1109/ICUS.2017.8278414

[4] Y. Sen, W. Zhongsheng, "Quad-Rotor UAV Control Method Based on PID Control Law" in 2017 International Conference on Computer Network, Electronic and Automation (ICCNEA), Xi'an, Shaanxi, China, 2017. https://doi.org/10.1109/ICCNEA.2017.24

[5] R. W. Beard, "Quadrotor Dynamics and Control," Tech. Rep., Brigham Young University, 2008.

[6] M. W. Mueller, R. D'Andrea, "Stability and control of a quadrocopter despite the complete loss of one, two, or three propellers" in 2014 IEEE International Conference on Robotics and Automation (ICRA), Hong Kong, China, 2014. https://doi.org/10.1109/ICRA.2014.6906588

[7] G. K. Batchelor, An Introduction to Fluid Dynamics, Cambridge University Press, 2000.

[8] Y. Nakayama, R. Boucher, "9 - Drag and lift" in Introduction to Fluid Mechanics, Butterworth-Heinemann, 1998.

[9] A. Nagaty, S. Saeedi, C. Thibault, M. Seto, H. Li, "Control and Navigation Framework for Quadrotor Helicopters" J. Intell. Robot. Syst., **70**(1-4), 1–12, 2013. https://doi.org/10.1007/s10846-012-9789-z

[10] H. t. M. N. ElkHoly, "Dynamic Modeling and Control of a Quadrotor Using Linear and Nonlinear Approaches," MS Thesis, The American University in Cairo, 2014.

[11] DJI E600 Multirotor Propulsion System, User Manual V1.04, DJI Technology Co., Ltd., 2014.

[12] M.-G. Yoon, "On Driving Signal of Electronic Speed Controller for Small Multi-Rotor Helicopter" Int. J. Eng. Res. Technol., **4**(11), 2278–0181, 2015. https://www.ijert.org/on-driving-signal-of-electronic-speed-controller-for-small-multi-rotor-helicopter

[13] D. M. Filatov, A. V. Devyatkin, A. I. Friedrich, "Quadrotor parameters identification and control system design" in 2017 IEEE Conference of Russian Young Researchers in Electrical and Electronic Engineering (EIConRus), St. Petersburg, Russia, 2017. https://doi.org/10.1109/EIConRus.2017.7910684

[14] D. M. Filatov, A. I. Friedrich, A. V. Devyatkin, "Parameters identification of thrust generation subsystem for small unmanned aerial vehicles" in 2017 IEEE II International Conference on Control in Technical Systems (CTS), St. Petersburg, Russia, 2017. https://doi.org/10.1109/CTSYS.2017.8109574

[15] T. Bresciani, "Modelling, Identification and Control of a Quadrotor Helicopter," MS Thesis, Lund University, 2008.

[16] A. Hughes, Electric Motors and Drives: Fundamentals, Types and Applications, 3rd ed., Elsevier Science/Newnes, 2005.

[17] H. Young, R. Freedman, University Physics with Modern Physics, 14th (Global) ed., Pearson Education, 2016.

[18] Y. Nakayama, R. Boucher, Introduction to Fluid Mechanics, Butterworth-Heinemann, 1998.

[19] J. Shigley, J. Uicker, Theory of Machines and Mechanisms, International ed., McGraw-Hill, 1980.

[20] A. H. Ahmed, A. N. Ouda, A. M. Kamel, Y. Z. Elhalwagy, "Attitude stabilization and altitude control of quadrotor" in 2016 12th International Computer Engineering Conference (ICENCO), Cairo, Egypt, 2016. https://doi.org/10.1109/ICENCO.2016.7856456

[21] Ultrasonic Ranging Module HC - SR04, User's Manual, ElecFreaks, n. d.

[22] M. Pedley, "Tilt Sensing Using a Three-Axis Accelerometer," Freescale Semiconductor Application Note, **1**, 2012–2013, NXP Semiconductors N.V., 2013.

[23] H. Vathsangam, "Magnetometer - My IMU estimation experience," 2010. https://sites.google.com/site/myimuestimationexperience/sensors/magnetometer

[24] "3-Axis Compass Sensor Set HMC1055" in Sensing Earth's magnetic field: Compassing, Magnetometry and Dead Reckoning Solutions, Magnetic Sensors Product Catalog, Honeywell Solid State Electronics Center, 2001. https://stevenengineering.com/Tech_Support/PDFs/31MAGSEN.pdf

[25] S. Colton, "The Balance Filter," White Paper, 2007. https://d1.amobbs.com/bbs_upload782111/files_44/ourdev_665531S2JZG6.pdf

[26] G. Stanley, "Exponential Filter," 2010-2020. https://gregstanleyandassociates.com/whitepapers/FaultDiagnosis/Filtering/Exponential-Filter/exponential-filter.htm

[27] W. Liu, C. Yu, X. Wang, Y. Zhang, Y. Yu, "The Altitude Hold Algorithm of UAV Based on Millimeter Wave Radar Sensors" in 2017 9th International Conference on Intelligent Human-Machine Systems and Cybernetics (IHMSC), Hangzhou, Zhejiang, China, 2017. https://doi.org/10.1109/IHMSC.2017.106

[28] D. J. Esteves, A. Moutinho, J. R. Azinheira, "Stabilization and Altitude Control of an Indoor Low-Cost Quadrotor: Design and Experimental Results" in 2015 IEEE International Conference on Autonomous Robot Systems and Competitions, Vila Real, Vila Real District, Portugal, 2015. https://doi.org/10.1109/ICARSC.2015.30

[29] J. Zhao, Y. Li, D. Hu, Z. Pei, "Design on altitude control system of quad rotor based on laser radar" in 2016 IEEE International Conference on Aircraft Utility Systems (AUS), Beijing, China, 2016. https://doi.org/10.1109/AUS.2016.7748029

[30] Ö. Elbir, A. U. Batmaz, C. Kasnakoğlu, "Improving quadrotor 3-axes stabilization results using empirical results and system identification" in 2013 9th Asian Control Conference (ASCC), Istanbul, Turkey, 2013. https://doi.org/10.1109/ASCC.2013.6606281

[31] E. A. Niit, W. J. Smit, "Integration of model reference adaptive control (MRAC) with PX4 firmware for quadcopters" in 2017 24th International Conference on Mechatronics and Machine Vision in Practice (M2VIP), Auckland, New Zealand, 2017. https://doi.org/10.1109/M2VIP.2017.8211479

[32] S. Sakulthong, S. Tantrairatn, W. Saengphet, "Frequency Response System Identification and Flight Controller Tuning for Quadcopter UAV" in 2018 Third International Conference on Engineering Science and Innovative Technology (ESIT), North Bangkok, Thailand, 2018. https://doi.org/10.1109/ESIT.2018.8665114

ASTES

Advances in Science, Technology and Engineering Systems Journal
Vol. 5, No. 5, 742-749 (2020)
www.astesj.com

ASTES Journal
ISSN: 2415-6698

Student's Belief Detection and Segmentation for Real-Time: A Case Study of Indian University

Chaman Verma[*,1], Zoltán Illés[1], Veronika Stoffová[2]

[1]*Department of Media and Educational Informatics, Faculty of Informatics, Eötvös Loránd University , Budapest, 1117, Hungary*

[2]*Department of Mathematics and Computer Science, Faculty of Education, Trnava University, Trnava, 91843, Slovakia*

ARTICLE INFO

Article history:
Received:05 August, 2020
Accepted:06 September, 2020
Online:12 October, 2020

Keywords:
ANOVA
Belief
Clustering
Real-Time
Squared Euclidean Distance
Technology

ABSTRACT

This paper has explored the technology beliefs of university students considering four parameters. We have proposed an automatic belief identification system for academic institutions. For this, we used two different clustering algorithms to segment the student group with different beliefs about the technology. In the Hierarchical Clustering (HC), the Agglomerative approach was followed. The beliefs were segmented with Ward's method and Squared Euclidean Distance (SED). The HC method recommended a maximum of three and a minimum of two optimal clusters. Later, we applied K-Means clustering on 37 features to validate the initial cluster solution. Based on ANOVA's results, we select 20 significant features that contributed most to detect dissimilarity in students' beliefs. The findings of the paper proved that suggested features stabilized clustering as compared to all features. The novel features provided three clusters: cluster 1 with 27.61% ; cluster 2 with 34.36%; cluster 3 with 38.04% students with similar beliefs about the technology. Based on the results provided, we found the high (mean>3.5), undecided (mean:1.73-3.63), and hybrid (mean:1.34-4.68) beliefs towards the technology available at university. We also recommended the selected features to be used as predictors for the online belief detection system. The university administration needs to cure students belonged to undecided groups.

1 Introduction

Nowadays, artificial intelligence is most prevalent in every sector of our life. Not even the education domain stays untouched. To explore the hidden data patterns, the use of machine learning techniques play a vital role [1]. For this, two major types (supervised and unsupervised) of machine learning algorithms were used to solve various problems. The supervised machine learning classifiers are used appropriately in the education domain [2].

In the unsupervised machine learning algorithms, a variety of clustering algorithms are available. Cluster Analysis (CA) is an exploratory approach to organize raw data into a significant segment based on combinations. To structured vast amounts of data into the same type of similar groups is called CA, and these groups are also called clusters [3]. It is a mathematical tool in data mining to realize the hidden structure or specific patterns in a data set [4]. The CA's main objective is to scatter a finite set of N items into C clusters to explore the homogeneity within items in a single cluster. It also ensures the heterogeneity among the cluster relationships [4], [5]. According [6], the general mathematical notation of clustering shown in equation(1).

$$X = C_1 \cup ...C_i \cup C_n; \quad C_i \cap C_j = \phi(i \neq j) \tag{1}$$

where X denotes the original data set, C_i, $_j$ are clusters of X, and n is the number of clusters [7].

This paper used unsupervised machine learning algorithm *i.e.* HC methods having no idea of input. But we can have determined the output with the results provided. It makes an initial cluster solution to give a rough idea to decide the number of clusters. We used the agglomerative algorithm (Bottom-up) appropriate for small data samples. It has the complexity of $O(n^3)$ [4], and the applied agglomerative HC algorithm is well described.

The K-Means cluster algorithms have been using in the academic domain to analyzes the samples from different aspects. It has been used to select a thesis topic for students as a decision support system [8]. It also helped in the management of ideological and political education in the academic institutions [9], [10]. The academic performance of students was also segmented using it [11]. Several

[*]Corresponding Author: Chaman Verma, Faculty of Informatics, Eötvös Loránd University, Budapest, 1117, Hungary, +36-306178577 & chaman@inf.elte.hu.

significant factors explored that affected the student's enrollment in Indian institutions [12]. An online programming error detection system was also proposed based on three factors [13]. With the filtered content, the undergraduate thesis report clustered based on the theme [14]. A social network system was presented to connect newcomer students at college for coordination and support [15]. The automatic segmentation of test questions was proposed based on the correctness, incorrectness, modified times, and the difficulty level [16]. The reading behavior of university students was segmented using library loan records [17].

2 Research Contribution

The studied literature shown that the clustering algorithms had supported appropriate in the research for education informatics. Further, we did not find any technology beliefs segmentation with feature selection technique research. This paper applied unsupervised learning algorithms (clustering) on real-data. We have identified the likeness, and disagreement of students towards the technology provided, which is most important to focused object. Firstly, we implement the HC approach that provided initial cluster solution, and thereafter same three cluster solution implemented and validated with K-Means clustering inclusive ANOVA method. Using the combined approach, we have proposed 20 significant technology features that contributed most to detect dissimilarity in students beliefs. Further, the technology belief detection system could be helpful the university administration to analyze the likes and dislikes of students towards the technical facility provided. Therefore, this paper encourage the future researcher, and web developer to make automate real-time belief identification system that may helpful to the institute, and for the student himself or herself.

3 Research Organization

The rest of the paper is structured into five sections. Section 4 elaborates on the research methodology in detail. Section 5 about the experiments 6 concludes the paper with major findings. Section 7 enlightens the shortcomings of the paper. Section 8 discusses the future scope with recommendations.

4 Research Method

4.1 Purpose of the Study

The present study is a preliminary investigation to propose the new features identifying homogeneity and heterogeneity of technology beliefs among university students. Besides, students' responses need to be determined based on their perceptions. Assumed it as the main objective, the present study implemented two clustering algorithms with a feature selection approach.

4.2 Research Design

Figure1 displays the conceptual view of the present paper. We conducted a technology awareness survey to divide a group of students having similar nature using the segmentation. Firstly, a hierarchical clustering is applied to obtain initial cluster solution. In this, the agglomerative cluster formation algorithm is used with the SED cluster interval approach. The results of initial clusters displayed with agglomeration schedule, membership, dendrogram, and scatter plots, etc.,

Secondly, we applied non hierarchical clustering K-Means with ANOVA as a feature selection approach. The results are displayed with ANOVA table, membership of cluster, final cluster centre, final clusters, graphs, and scatter plots.

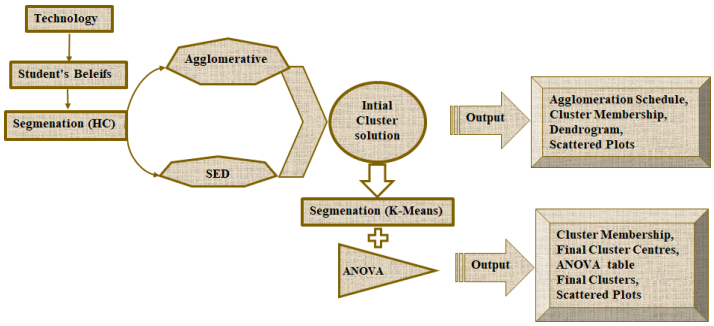


Figure 1: Technology Belief Detection and Segmentation.

4.3 Dataset Preprocessing

This paper used 163 primary data samples from one of A+ grade private institutions (Chandigarh University) in north India. Using the google form, We asked technology-based questions to the bachelor and master students of the university. The survey response rate was 100%. Samples were collected from 137 male students and 26 female students. Four major Features (F) of the Google Form was: Development-Availability (DA) with 16 questions; Usability (U) with 06 questions; Attitude (AT) with 06 questions; and Educational Benefit (EB) with 09 questions. We also calculated the mean score of recorded instances for these attributes. Dut to hybrid data metrics, all instances re-scaled on 0-1. Excellent reliability of 163 samples calculated 0.857 with Cronbach's Alpha method using equation(2).

$$\mu = \frac{N.\bar{c}}{\bar{v} + (N - 1.\bar{c})} \tag{2}$$

where N is the number of F. $\bar{c}$ is the average covariance between F-pairs, and $\bar{v}$ is the average variance.

4.4 Feature Selection

The analysis of variance with F statistics is appropriate to select the best contributors in clustering and has been used to compare the efficiency of supervised learners [18]. R.A. Fisher founded the ANOVA in 1920, and Snedecor founds F-distribution. We used both to select the most prominent features that participated significantly in the segmentation of beliefs. It provides vital features that contributed the most to the cluster solution.

$$TSS = \sum (x_i)^2 - C \tag{3}$$

The equation(3) calculated the total sum of square (TSS) using correlation factor C

$$DF = K - 1; DF = N - K; \tag{4}$$

The equation(4) shows the way to estimate the Degree of Freedom (DF), where K is number of cluster groups, and N is total number of cases in clusters.

$$CMS_a = \frac{SS_a}{K-1}; CMS_b = \frac{SS_b}{N-k} \tag{5}$$

The equation(5) calculated the cluster Mean Square (CMS) between the clusters and within the clusters.

$$F = \frac{CMS_a}{CMS_b} \tag{6}$$

The equation(6) calculated the F value based on the mean square of cluster values. Where CMS used for between (a) and within (b) cluster variances. The F statistic calculated with dividing CMS_a by CMS_b.

Table 1: Feature selection using ANOVA.

F1	3.1	0.5	6.6	0.002
F2	29.7	0.7	41.4	0.000
F3	30.8	0.6	51.3	0.000
F4	30.4	0.7	43.2	0.000
F5	44.4	0.6	71.3	0.000
F6	44.7	0.7	65.9	0.000
F7	9.3	0.9	10.5	0.000
F8	34.1	0.8	42.4	0.000
F9	25.2	1.2	21.7	0.000
F10	40.4	0.8	21.3	0.000
F11	17.1	0.81	21.3	0.000
F12	41.5	0.5	88.0	0.000
F13	30.0	0.41	73.0	0.000
F14	26.0	0.4	64.0	0.000
F15	29.3	0.5	55.6	0.000
F16	22.1	0.5	46.5	0.000
F17	34.7	0.3	107.1	0.000
F18	27.8	0.5	61.4	0.000
F19	29.9	0.4	74.2	0.000
F20	25.8	0.4	59.4	0.000

Table 1 displays the results of the ANOVA table with Feature Code (FC). We selected 20 significant features (F1-F20) having significant P value less than 0.05 with CMS, Error Mean Square (EMS) corresponding F, and P. We found that all features have large F values for providing the greatest separation between clusters.

5 Experiment, Results and Discussion

This section discusses the experimental results provided with the HC method, and K-Means.

5.1 Hierarchical clustering

We used the HC technique to ensure the initial clusters of students' beliefs towards technology. We used the Agglomerative, also called the bottom-up structure of cluster formation in the IBM SPSS Statistics 25. The solution range minimum value is 2, and the maximum value is 4 during the HC clustering. Each observation starts in its cluster, and pairs of clusters merged as one moves up the hierarchy. In this, we applied Ward's method [19] to form the cluster [20] and interval estimated with the SED approach that is deriving the Euclidean distance (d) between two data points involves computing the square root of the sum of the squares of the differences between corresponding values.

$$D_{K_L} = B_{K_L} = \frac{\left\|\bar{X}_K - \bar{X}_L\right\|^2}{1/N_K + 1/N_L} \tag{7}$$

Above equation(7) shows the applied ward's method having distance between two clusters (D and B). Manhattan distances used to generalized Ward's method [21]

$$d(x, y) = (1/2)|x - y|^2 \tag{8}$$

If equation (8) satisfies, then the combinatorial formula is given below in equation(9).

$$\begin{aligned} DJM = [((NJ + NK)DJK + (NJ + NL) \\ DJL - NJDKL)/(NJ + NM)] \end{aligned} \tag{9}$$

$$d(x, y) = \sqrt{\sum_{i=1}^{n} (x_i - y_i)^2} \tag{10}$$

In equation(10), d is SED estimated between the data points x, and y.

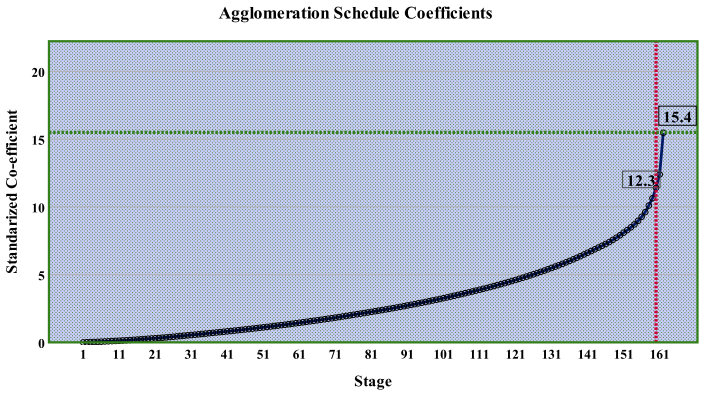


Figure 2: Cluster Stag and Co-efficient.

Figure2 visualizes the total number of cluster stages on the x-axis calculated by the HC and the estimated standardized Co-efficient across the y-axis. We see no significant difference among the stages up to 31. A considerable minor difference observed between stage 31 to 161 stages. The drastic updates (red vertical bar) noted in the HC coefficients after stage 161 spotted with a vertical reference line, and the value of the coefficient is 12.3. The green reference line as an x-axis reference proved the maximum standardized coefficient value is 15.4.

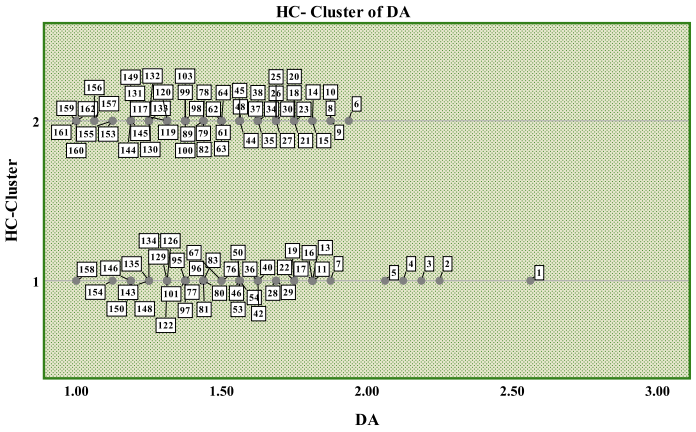


Figure 3: Development-Availability Belief Segmentation.

Figure3 visualizes the cluster belonged to the technology development and availability at university. We found both student groups seem different, but they have identical beliefs. One-hand, 51 students in one cluster, and on the other hand, 36 students remained in the second cluster. Student's responses are near the mean value of 1 and 2, proving that their university equipped with the latest technology. A very few students found unsure.

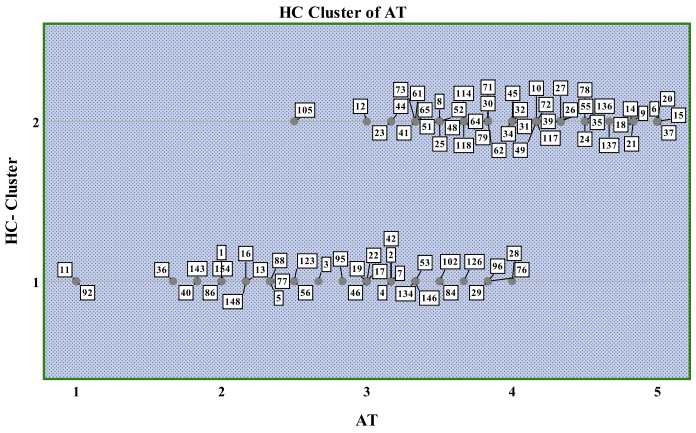


Figure 4: Attitude Belief Segmentation.

Figure4 shows the different two clusters with heterogeneous beliefs of students towards the attitude variable. We observed 45 students' beliefs firmer than the mean value of 3, and it proved that these students have a positive attitude towards technology. Only two students (11, 92) found negative only, which is near to mean 1. We also found 34 students are near to the mean values 2 to 4. Therefore, the majority of students' beliefs towards the agreement statements.

Figure5 demonstrates the cluster related to the use of technology at the university campus. The density of beliefs bowed towards a mean score 3 to 5 that depicted the agreement about the usability of technology. Therefore, they are using technology at university campus often or every time. Only 4 students strongly agreed at mean value 5 in cluster 1, and 2 agreed in cluster 2 who are using technology all the time.

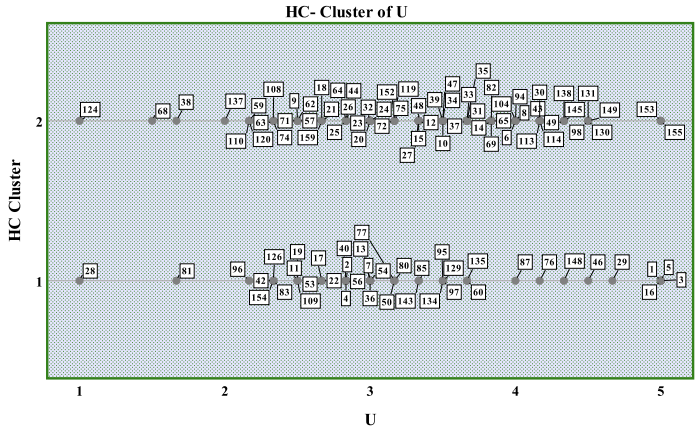


Figure 5: Usability Belief Segmentation.

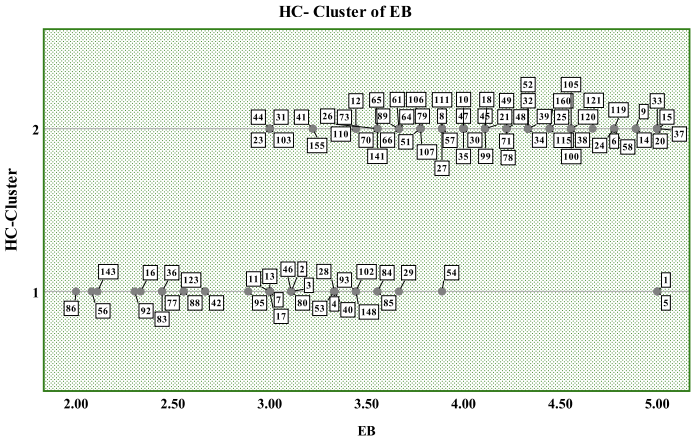


Figure 6: Usability Belief Segmentation.

Figure6 visualizes the formation of response clusters about the benefits of technology. We found one group of students convinced with the technology benefits, and the second group looks not satisfied with the benefits of technology. A total of 11 students disagreed with the benefits, and 9 students were undecided.

5.2 K-Means Clustering

To classify the student's beliefs towards the technology, we applied the K-Means cluster analysis algorithm in the IBM SPSS statistics tool. It assigns the cases to a fixed number of groups (clusters) whose characteristics are not yet known but are based on a set of specified variables. This paper used the K-Means algorithm [22], [23], where k=3, n=37, and t=10. This algorithm is very easy to use and implement. It's time complexity is O(nKt) K<=n, t<=n [10].

Addition, the Euclidean distance [13] (d) in equation(11) applied to estimate the closest point to the centroid that they helped to check the homogeneity among beliefs. where v is variable, and p is individual belief score.

$$d = \sqrt{\sum_{i=1}^{v}(p1_i - p2_i)^2} \tag{11}$$

Algorithm 1: Algorithm:K-MEANS

Input: The number of cluster k, no. of features n, no. of iteration t.

Output: A set of k clusters that minimizes the squared-error criteria.

initialization;

1. arbitrarily choose features as the initial cluster centers **repeat**
   2. re-assign each feature to the cluster to which the feature is the most similar;
   3. based on the mean value of the features in the cluster;
   4. update the cluster means, i.e., calculate the mean value of the features for each cluster;

until *no change*;

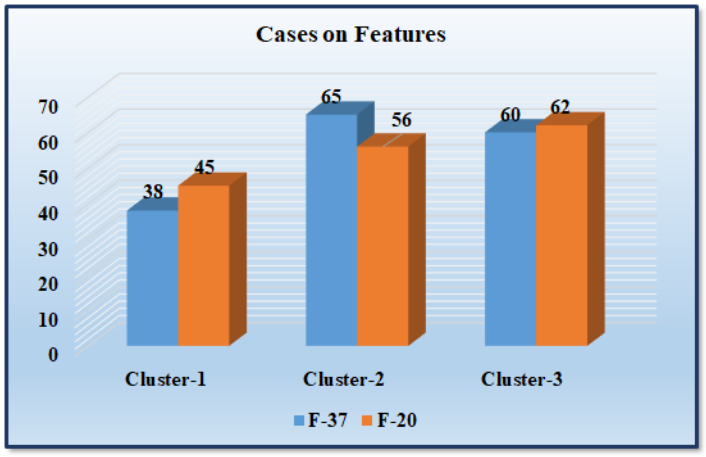


Figure 7: Feature based case count.

Figure7 displays a segmented count of beliefs that belonged to the respective cluster. With all features (F-37), cluster-1 has 38, cluster-2 has 65, and cluster-3 has 62. After the reduction of features, we see all three clusters segmented stable.

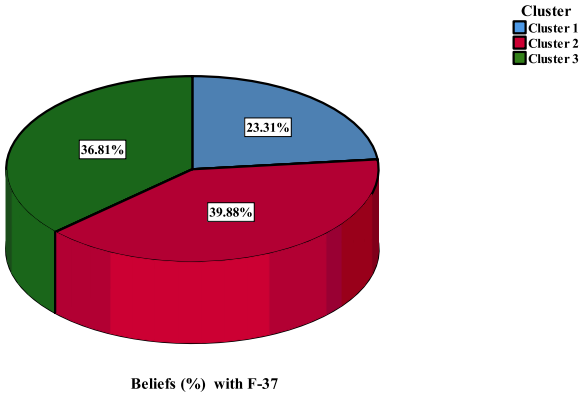


Figure 8: Student's Beliefs clustered with F-37.

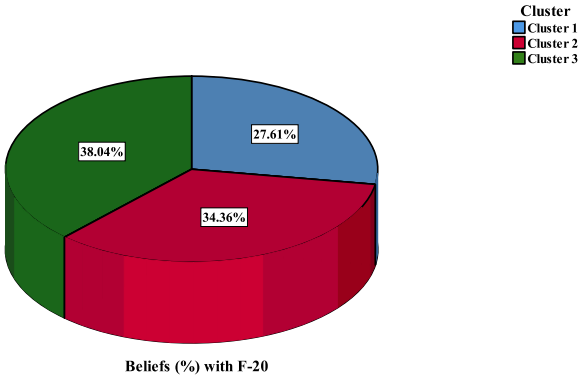


Figure 9: Student's Beliefs clustered with F-20.

Figure8 shows the percentage of beliefs comes under the belonging cluster with all considered features (F-37). It observed that the Cluster 2 has 39.88% beliefs, and Cluster 3 has 36.81%, which seems maximum. Cluster 1 holds the 23.31% beliefs, i.e., lowest count. Hence, this unstable segmenting improved with reduced features (F-20) shown in Figure9. We noted that the beliefs clustered appropriately.

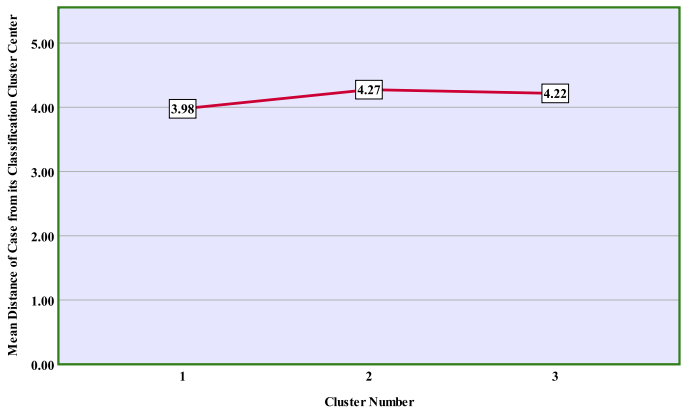


Figure 10: Mean Distance of individual case from centre with F-37.

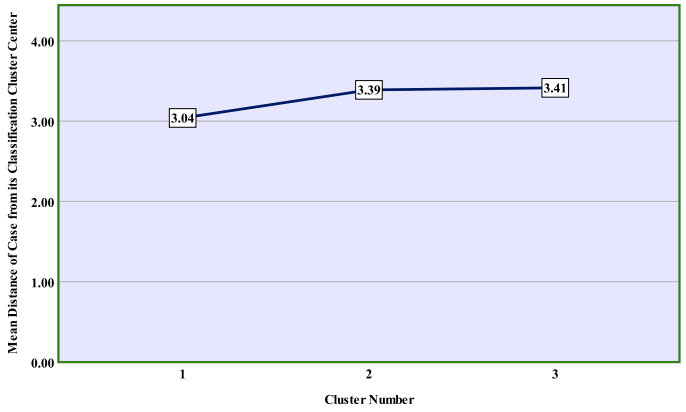


Figure 11: Mean Distance of individual case from centre with F-20

Figure10 shows the individual case mean distance from the clus-

ter center with all features (F-37). We observed unstable distances (3.98, 4.27, 4.22) between cluster 1 and cluster 2. The reduced data set features (F-20) made stable distance among three clusters depicted in Figure11.

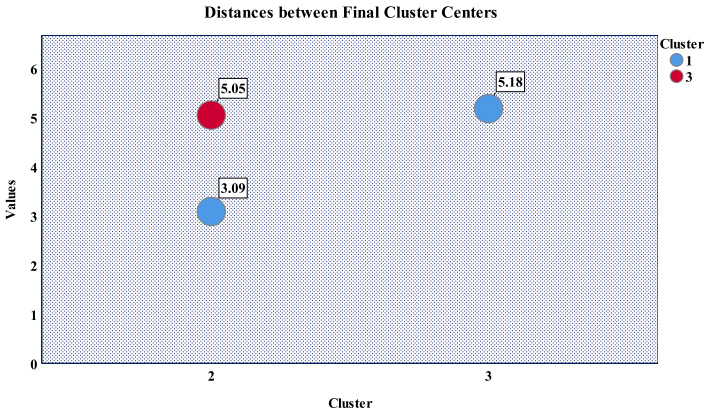


Figure 12: Distance between cluster.

Figure12 visualize the distance between the final cluster centers. The distance of cluster 1 from cluster 3 is measured by 5.05. We can see the lowest distance of cluster 1 from cluster 2. On this basis, We identified the beliefs in clusters 1 and 2 are mostly positive and high. Further, the beliefs belong to cluster 1, and cluster 2 are heterogeneous type.

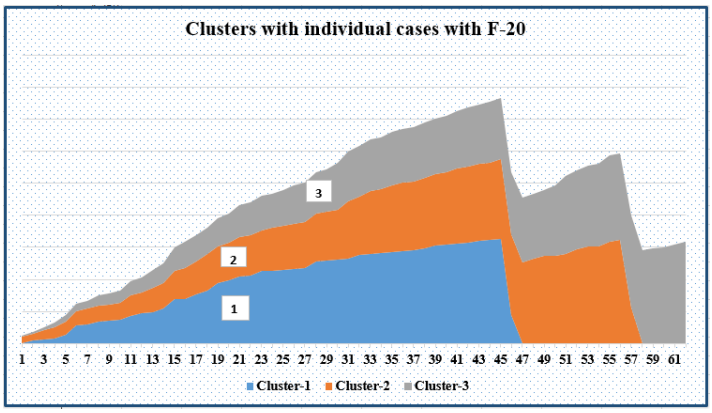


Figure 13: Individual cases under cluster.

Figure13 shows the individual case belong to the respective cluster. It is transparent that cluster 3 holds the highest number of instances 61. The cluster 2 holds the 58 cases, and the cluster 1 stores the minimum cases of 47. Thus, no significant difference was observed in the segmentation process.

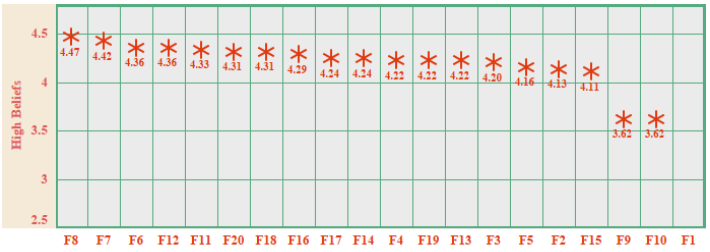


Figure 14: Detection of High Student's Belief

Figure14 depicts the student's beliefs nearer the highest mean values, and the features also found significant to make their thinking optimistic about university technology. It can be seen that the mean values are more generous than 3.5. Hence, we named it the high belief segment.

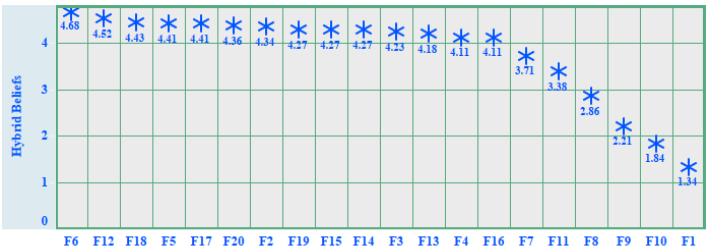


Figure 15: Detection of Hybrid Student's Belief.

Figure15 visualizes the mixed type of student's beliefs comes under the mean range of 1.34 to 4.68. For the five features (F1, F8, F9, F10, F11), the mean values are less than 3.5. Therefore, we entitled it a hybrid belief cluster.

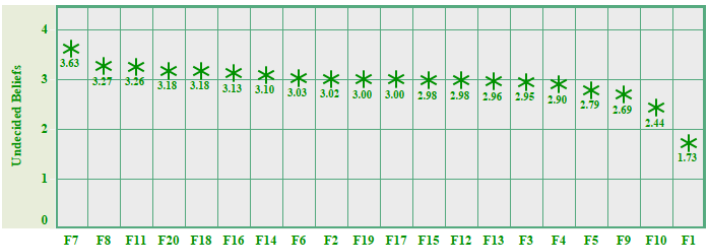


Figure 16: Detection of Undecided Student's Belief.

Figure.16, displays the beliefs within the mean range of 1.73 to 3.6. All the selected features (F1-F20) have the mean values of less than 3.5. Thus, we named the undecided beliefs cluster.

6 Conclusion

This study used the HC analysis to apply the segmentation of the similar beliefs of Indian students towards the technology. Using the HC approach, we observed two clusters with 100% covered observations. The paper's results proved that the 50% observations from samples are covering while framing 3 clusters. From the Agglomeration schedule, a drastic change was seen in the HC coefficients

after stage 161. We observed almost of students' agreed towards the available technology at university and found the rapid development in the latest technology. Further, one group of students uses technology appropriately, and the second group uses technology moderate. One group thinks the technology highly benefiting his or her education, and other group remain unsure or opposite the benefits.

Further, few more experiments were performed with the K-means algorithm to explore student's beliefs about the technology. Firstly, it considered all features (F-37) for the clustering and provided acceptable cluster groups. Later, we used significant features (F-20) based on the ANOVA in Table 1. The significance of used features shown with the validation statement (df=162,P<0.05). These features provided three stable dissimilar belief clusters. Based on these clusters, we scattered beliefs in high, hybrid, and undecided clusters.

7 Shortcomings

This paper used a small number of data samples from a specific university. The selected institution was private. The present research approach is confined to the HC analysis with the specific Wards' method and SED clustering distance measures. We used only the Agglomerative hierarchical procedure. Further, only ANOVA was used as a feature selection method with the K-Means analysis.

8 Future Suggestions

Future work recommended testing the HC algorithm with various cluster formation methods such as Between Group Linkage, Nearest Neighbour, Centroid, and Median.

Future recommendations are provided to apply more feature filter methods such as gain ratio, info gain, correspondence analysis principal components, info-gain [24]. The proposed approach could also be feasible to the public universities with sample enhancement. The results of the paper suggested the target university to focus more on the students who came under the undecided cluster in Fig. 16. Additionally, the target university can also automate this beliefs detection system [1] [2].

Also, We planned to compare the similarity of Indian and Hungarian students' beliefs towards the latest technology provided using hierarchical and non-hierarchical CA approaches. We also give a significant suggestion to develop real-time automation of homogeneity and heterogeneity in the responses.

Conflict of Interest The authors declare no conflict of interest.

Acknowledgment The work of Chaman Verma and Zoltán Illés was sponsored by the Hungarian Government and Co-financed by the European Social Fund under the project "Talent Management in Autonomous Vehicle Control Technologies (EFOP-3.6.3-VEKOP-16-2017-00001)

References

[1] C. Verma, V. Stoffová, Z. Illés, S. Tanwar, N. Kumar, "Machine Learning-based Student's Native Place Identification for Real-Time," IEEE Access, **8**, 130840–130854, 2020, doi:10.1109/ACCESS.2020.3008830.

[2] C. Verma, Z. Illés, V. Stoffová, V. Bakonyi, "Opinion Prediction of Hungarian Students for Real-Time E-Learning Systems: A Futuristic Sustainable Technology-Based Solution," Sustainability, 1–16, doi:10.3390/su12166321.

[3] S. Patel, S. Sihmar, A. Jatain, "A study of hierarchical clustering algorithms," in 2015 2nd International Conference on Computing for Sustainable Global Development (IEEE-INDIACom), 537–541, 2015, doi:https://ieeexplore.ieee.org/document/7100308.

[4] K. Sasirekha, P. Baby, "Agglomerative Hierarchical Clustering Algorithm-A Review," International Journal of Scientific and Research Publications, 1–3, doi:http://www.ijsrp.org/research-paper-0313.php?rp=P15831.

[5] M. Yang, "A Survey of hierarchical clustering," International Journal of Scientific and Research Publications, 1–16.

[6] R. Abe, S. Miyamoto, Y. Endo, Y. Hamasuna, "Hierarchical clustering algorithms with automatic estimation of the number of clusters," in 2017 Joint 17th World Congress of International Fuzzy Systems Association and 9th International Conference on Soft Computing and Intelligent Systems (IFSA-SCIS), 1–5, 2017, doi:10.1109/IFSA-SCIS.2017.8023241.

[7] M. K. Rafsanjani, Z. A. Varzaneh, N. E. Chukanlo, "A survey of hierarchical clustering algorithms," The Journal of Mathematics and Computer Science, 229–240, doi:10.22436/jmcs.05.03.11.

[8] E. Daniati, "Decision Support System to Deciding Thesis Topic," in 2017 International Seminar on Application for Technology of Information and Communication (iSemantic), 52–57, 2017, doi:10.1109/ISEMANTIC.2017.8251843.

[9] L. Huang, "Teaching Management Data Clustering Analysis and Implementation on Ideological and Political Education of College Students," in 2016 International Conference on Smart Grid and Electrical Automation, 308–311, 2016, doi:10.1109/ICSGEA.2016.61.

[10] L. Jing, "Ideological and Political Education Management Research based on Improved K-means Clustering," in 2016 International Conference on Robots & Intelligent System, 213–216, 2016, doi:10.1109/ICRIS.2016.114.

[11] J. Jamesmanoharan, S. H. Ganesh, M. L. P. Felciah, A. K. Shafreenbanu, "Ideological and Political Education Management Research based on Improved K-means Clustering," in 2014 World Congress on Computing and Communication Technologies, 200–202, 2014, doi:10.1109/WCCCT.2014.75.

[12] R. Ahlawat, S. Sahay, S. Sabitha, A. Bansal, "Analysis of factors affecting enrollment pattern in Indian universities using k-means clustering," in 2014 World Congress on Computing and Communication Technologies, 321–326, 2016, doi:10.1109/INCITE.2016.7857639.

[13] M. Cao, Q. Zhang, "A Empirical Study of Programming Behaviours on Large Scale Online Learning," in 2019 14th International Conference on Computer Science & Education (ICCSE), 889–894, 2019, doi:10.1109/INCITE.2016.7857639.

[14] R. Saptono, H. Setiadi, T. Sulistyoningrum, E. Suryani, "Examiners Recommendation System at Proposal Seminar of Undergraduate Thesis by Using Content-based Filtering," in 2018 International Conference on Advanced Computer Science and Information Systems (ICACSIS), 265–269, 2018, doi:10.1109/ICACSIS.2018.8618224.

[15] G. Shidhaganti, A. Patil, "Unsupervised Techniques to Develop a Social Networking Platform in an Educational Institute," in 2019 IEEE Tenth International Conference on Technology for Education (T4E), 246–247, 2019, doi:10.1109/T4E.2019.00057.

[16] H. Sun, Z. Shao, "Research on the Application of Students'Answered Record Analyze Model and Question Automatic Classify Based on K-Means Clustering Algorithm," in 2019 10th International Conference on Information Technology in Medicine and Education (ITME), 494–497, 2020, doi:10.1109/ITME.2019.00116.

[17] Y. Zhu, S. Gao, "A Study of the Reading Behavior of University Students," in 2018 9th International Conference on Information Technology in Medicine and Education (ITME), 357–361, 2018, doi:10.1109/ITME.2018.00086.

[18] C. Verma, V. Stoffová, Z. Illés, "Prediction of students' awareness level towards ICT and mobile technology in Indian and Hungarian University for the real-time: preliminary results," Heliyon, 1–9, doi:10.1016/j.heliyon.2019.e01806.

[19] G. Ward, J. J. H., "Hierarchical Grouping to Optimize an Objective Function," Journal of the American Statistical Association, 236–244, doi:10.22436/jmcs.05.03.11.

[20] "SAS, url = https://v8doc.sas.com/sashtml/stat/chap23/sect12.htm, urldate = 2020-07-21, year = 2020," .

[21] T. Strauss, M. J. von Maltitz, "Generalising Ward's Method for Use with Manhattan Distances," PLOS ONE, 1–21, doi:10.1371/journal.pone.0168288.

[22] L. Ye, C. Qiu-ru, X. Hai-xu, L. Yi-jun, Y. Zhi-min, "Telecom Customer Segmentation with K-means Clustering," in The 7th International Conference on Computer Science & Education (ICCSE 2012), 648–651, 2012, doi:10.1109/ICCSE.2012.6295158.

[23] H. Jia-wei, M. Kamber, Data mining-concepts and techniques, Higher education press, 2001.

[24] C. Verma, V. Stoffová, Z. Illés, "Prediction of residence country of student towards information, communication and mobile technology for real-time: preliminary results," Procedia Computer Science, 224–234, doi:10.1016/j.procs.2020.03.213.

ASTES

Advances in Science, Technology and Engineering Systems Journal Vol. 5, No. 5, 750-756 (2020)

www.astesj.com

Special Issue on Multidisciplinary Innovation in Engineering Science & Technology

ASTESJ

ISSN: 2415-6698

Johnson Noise and Optical Characteristics of Polymer Nanocomposites based on Colloidal Quantum Dots and *in-situ* Nanoparticles Formation

Fatin Hana Naning[*,1], S. Malik[2], Lee Feng Koo[1], Tze Jin Wong[1], Pang Hung Yiu[1]

[1]*Department of Basic Science and Engineering, Faculty of Agriculture and Food Sciences, Universiti Putra Malaysia Bintulu Campus, 97008 Bintulu, Sarawak, 93010, Malaysia*

[2]*Physics Department, Faculty of Science, Universiti Pendidikan Sultan Idris, 35900 Tanjong Malim, Perak, 31400, Malaysia*

ARTICLE INFO

Article history:
Received:10 August, 2020
Accepted: 11 September, 2020
Online: 12 October, 2020

Keywords:
Johnson Noise
Polymer Nanocomposite
Cadmium sulfide

ABSTRACT

Electrical and optical properties of polymer nanocomposite thin films have been analyzed to study their reliability and competency as a component for optoelectronic devices such as LED and solar cells. Polymer nanocomposite encounters various challenges, such as the dispersion of nanoparticles in the matrix that hinders their efficiency for potential devices. In this paper, two types of polymer nanocomposites have been fabricated, and their Johnson noise, current density-voltage, and optical have been measured. The first type of nanocomposite produced through an in-situ method, that is by impregnating CdS or CdSe nanoparticles in conjugated polymer, P3HT (NP-CdX:P3HT). The nucleation of the nanoparticles was done using gas exposure. The second type is by directly adding CdS or CdSe quantum dots into P3HT (QD-CdX:P3HT). Both kinds of polymer nanocomposite thin films were fabricated using modified Langmuir-Blodgett technique. Results showed that for frequency above 10 Hz, the Johnson noise was less than 1×10^{-27} A2/Hz, regardless of the quantity of quantum dots or nanoparticles. The J-V results show (NP-CdX:P3HT) electrical performance compared with QD-CdX:P3HT. High polymer crystallization of NP-CdX:P3HT thin films is revealed by UV-Vis absorbance spectra. The quantum confinement effect is evidence through peak shifting and depreciation of absorption. The photoluminescence intensity of thin films decreased when they were exposed to the gas. It can be concluded that the NP-CdX:P3HT nanocomposites can be further studied as they have greater potential to be exploited in optoelectronic devices.

1. Introduction

Polymer nanocomposites can be prepared through various methods, including physical adsorption, ligand-metal interaction, or by blending nanoparticles with the desired polymers. The inability of nanoparticles to spread uniformly in matrices is one of the key obstacles in the development of polymer nanocomposites for optoelectronic devices. Besides the size of the nanomaterials, the degree of mixing of the materials influences the polymer nanocomposites characteristics. If the nanomaterials are poorly dispersed, the mechanical properties of the thin films may degrade [1]. The nanomaterials blend affects the movement of electrons and the transport of holes. Current and holes motion cause excess noise in all conducting materials. Various types of electrical noises are present in an electronic system such as Johnson noise, 1/*f* noise, and generation-combination noise.

Johnson noise, also referred to as thermal noise, is caused by the movement of electrons in a material that produces a fluctuating electromotive force (emf) [2]. The electron scattering creates noise in terms of small net current flow. As the temperature and resistance of the material increases, the noise increases as well.

Johnson noise theory derived by Johnson and Nyquist by stating

$$S_V(f) = 4kRhfN(f,T) \quad (1)$$

*Corresponding Author: Fatin Hana Naning, UPM Bintulu Sarawak Campus, fatinhanaz@upm.edu.my

where $S_V(f)$ is the power spectral density (PSD) of the voltage noise, k is Boltzmann constant, R is the resistance, h is Planck constant, and f is the frequency. $N(f,T)$ is Planck number representing the energy quanta hf, at frequency f and temperature, T [3,4]. It can also be expressed as,

$$N(f,T) = kT/hf \quad (2)$$

The noise-voltage power spectral density under open-circuit condition is given by

$$S_V(f) = 4k^2TR \quad (3)$$

Alternatively, the noise-current power spectral density $S_I(f)$ can be calculated using

$$S_I(f) = 4k^2T/R \quad (4)$$

Equations (3) and (4) valid for frequency below tens of gigahertz over a wide range of temperatures [5].

Johnson noise arises from the random motion of free electrons that leads to temporary electrons agglomeration and voltage fluctuation [6]. The noise can be estimated by analysing the power spectral density (PSD) obtained from low-frequency electrical noise measurement. It is a conventional technique used to study the reliability and quality of electronic devices as the procedure is able to differentiate failed devices. Usually, the impaired devices hold excess noise [7] because PSD of noise increases with stress and damage [8]. Deterioration process of Organic Light Emitting Diode (OLED) utilizing noise measurement has been studied by Rocha et al. and Carbone [9, 10]. Both concluded that noise increases with damage level. Another research group reports that the intrinsic transport mechanism greatly influences low-frequency noise [11].

Polymer nanocomposites are commonly prepared by mixing the polymer with the nanomaterials through various tedious steps. The small introduction of nanomaterials into conjugated polymer matrices causes the modification in the polymers' properties due to the substantial surface-area-to-volume ratio of nanoparticles [12]. Researches showed that mechanical and optical properties of the polymer were altered as well [13, 14].

However, this method has some drawbacks that hamper the efficiency of the thin film due to the presence of ligand that inhibits charge transfer. Furthermore, the usage of cosolvent to mix the nanomaterials and polymer negatively affect the orientation of the polymer [15]. One way to impede these issues is by growing the nanomaterials *in-situ* in the matrices.

In the present study, we used poly(3-hyexylthiophene) (P3HT) as the polymer matrix, and the nanomaterials were cadmium sulfide (CdS) and cadmium selenide (CdSe). The nanocomposites were prepared by directly adding CdS or CdSe quantum dots (QD-CdX:P3HT) into P3HT, or by impregnating CdS/CdSe nanoparticles in the polymer matrix *in-situ* (NP-CdX:P3HT).

Poly(3-hyexylthiophene) is one of the well-studied conjugated polymers. It possesses a relatively strong absorption coefficient, low energy band gap, consequently high absorption even in very thin films [16]. P3HT also has greater hole mobility as compared to poly(phenylene vinylene) (PPV), another material that widely used for solar cells and LED [17]. P3HT is based on thiophene rings (four carbon atoms and one sulfur) and highly soluble in common organic solvents. Studies showed that regio-regular P3HT (rr-P3HT) has a higher degree of polymer chain ordering and electrical conductivity as compared with regio-random P3HT (rra-P3HT) [18, 19]. The CdS and CdSe were chosen because they possess lower HOMO (Highest Occupied Molecular Orbital) and LUMO (Lowest Unoccupied Molecular Orbital) than that of poly(3-hexylthiophene) [20].

The computation of Johnson noise engaged low-frequency electrical noise measurement (LFeNM), and the analysis was done at 25 ºC. LFeNM is a method generally employed to verify the reliability of any electronic devices. The relationship of Johnson noise to *J-V* and optical characteristics will be discussed as well.

2. Experimental Setup

This research involved four types of polymer nanocomposite thin film. The films were composed of II-VI semiconducting materials, CdX (CdS or CdSe), and conjugated polymer Poly(3-hexylthiophene) (P3HT).

2.1. Materials and Sample Preparation

Modified Langmuir-Blodgett method has been adopted to fabricate two types of thin films. The first type is the *in-situ* method, made by nucleating cadmium sulfide (CdS) and cadmium selenide (CdSe) nanoparticles (NP) directly in the P3HT matrice (NP-CdS:P3HT and NP-CdSe:P3HT). The second type of thin film was made by adding CdS and CdSe quantum dots (QDs) into P3HT (QD-CdS:P3HT and QD-CdSe:P3HT). Before these QDs were incorporated into P3HT, they were treated by refluxing them for 15 minutes in hexanoic acid at 115 ºC to remove trioctylphosphine oxide (TOPO) that capped the QDs. All materials were purchased from Sigma Aldrich. The solvent used to dissolve P3HT and stearic acid is chloroform (Mallinckrodt). The substrates used were ITO coated glass (5 Ω/sq) from Nanocs. ITO coated glass also acts as an electrode for electrical characterization. All materials used were as-received unless stated otherwise.

The first type of nanocomposite, NP-CdX:P3HT thin films were prepared by dispensing 0.4 ml P3HT solution (0.2 g/l) and 0.1 stearic acid solution (0.14 g/l) on water subphase that contained 0.5 mM cadmium (II) chloride ($CdCl_2$). Stearic acid possesses amphiphilic properties; hence it acts as a stabilizer to P3HT because P3HT is a non-amphiphilic material, thus not suitable for LB deposition. The stearic acid mixture will lessen the domination of the hydrophobic part of P3HT, and reduce the likelihood of supermonolayer structures formation. It also functioned as a capping agent of a divalent cation, cadmium ion, into its headgroup structure (COOH).

The films were deposited when the Langmuir layer surface pressure is continuously at 27 mN/m at an angle of 45º. The modified LB technique allows us to construct large-area polymeric thin films in a controlled order. After every deposition, each transferred layer was put in the oven for 15 s to dry the film and induce cross-linking in the polymer. The temperature of the oven was 50 ºC. Thirteen layers of film (~20 nm) were deposited on the ITO coated glass substrate. After the last film was transferred and

dried, the film was put in the chamber of hydrogen sulfide (H_2S), or hydrogen selenide (H_2Se) for 6 hours. This process was done to nucleate nanoparticles - CdS or CdSe, within polymer layers. Finally, the exposed films were annealed for 10 minutes in an oven at 120 ºC.

The second type of nanocomposite, QD-CdX-P3HT thin films, the QDs were added at 25 wt% or 50 wt% of P3HT solution (0.2 mg/ml). The solution was then carefully injected onto the surface of water subphase. Solid-phase optimized for the film 17 mN/m. Similar to the *in-situ* method, thirteen layers of film were deposited and dried. However, immediately after the last transfer, the film was straight put into an oven for annealing process. All samples were prepared in the cleanroom ISO 6 environment. Samples that will be tested for electrical characteristics were deposited with 150 nm of aluminum layer that serves as an electrode.

2.2. Measurement

Johnson noise measurement utilized current-to-voltage low-noise/low input impedance preamplifier (Signal Discovery), 35670A Dynamic Signal Analyser (Agilent). An interference shield box was used to encase the specimen in order to protect them from external wave or oscillation. The gain of the measurement has been set at 10^{-8} low noise (LN). The low-level noise signal measured from the sample was then fed to an amplifier, which converts the current power (A^2) to voltage power (V^2). The amplifier output would later become the DSA input and processed using LabView. The noise current power spectral density, *SI(f),* was evaluated within the 10 Hz to 1000 Hz frequency range. The noise reading was repeated 200 times.

Keithley 2636A source measure unit (SMU) was used to measure current density-voltage (*J-V*) characteristics. The SMU was attached to a four-point probe and a solar simulator with a light density of 100 mW/cm^2 that complies with the AM 1.5G spectrum. The measurement was carried out by continuously sweeping the feed voltage from -1.5 to +1.5 V.

The spectral absorption measurements were performed using JASCO V570 UV-Vis (Ultraviolet-visible) spectrophotometer operated at a resolution of 1 nm. Perkin Elmer LS 55 Fluorescence Spectroscopy was used to study the PL characteristic of the samples. The samples were excited at 430 nm, and the excitation slit was set at 10 nm, while the laser emission slit was 15 nm. Scan speed was 500 mm/min. The parameters were determined by optimizing the value of a reference sample.

3. Results and Discussion

Figure 1 (a) and (b) show the Johnson noise of NP-CdS:P3HT and NP-CdSe:P3HT, respectively. The unexposed film has the greatest resistance expressed as the highest noise level compared to the films exposed to H_2S or H_2Se gas environment.

The unexposed films are highly resistive due to the presence of stearic acid in the P3HT matrix. Stearic acid hinders efficient electrons movement. However, exposure of the thin film to H_2S or H_2Se gas, causing nanoparticles to nucleate in between P3HT layers. These nanoparticles facilitate the flow of electron, thus lowering the spectral density of noise. The high noise fluctuation for NP-CdS:P3HT thin film indicates that there could be an aggregation of the charges resulting in more substantial resistance at high frequency [21].

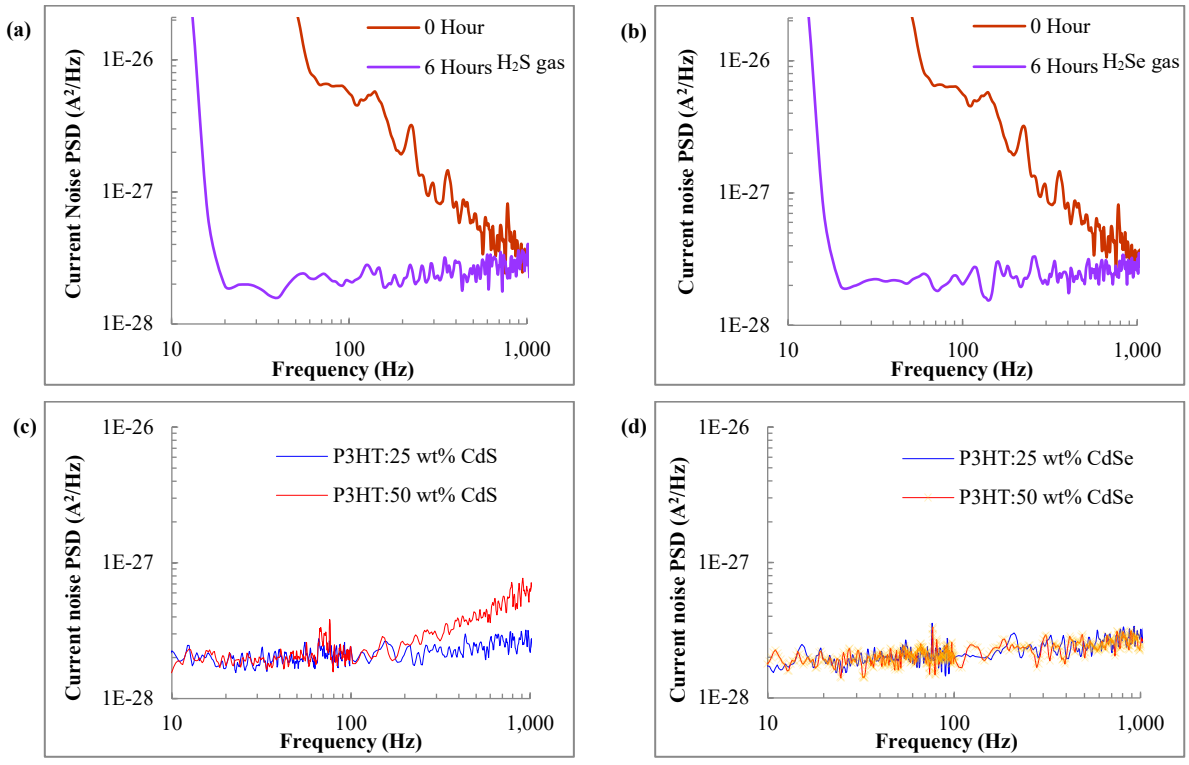


Figure 1: Johnson noise current spectral density of (a) NP-CdS:P3HT (b) NP-CdSe:P3HT (c) QD-CdS:P3HT (d) QD-CdSe:P3HT

On the other hand, as shown in Figure 1 (c) and (d), QD-CdX:P3HT has lower Johnson noise as compared with NP-CdX:P3HT thin films. Among the benefits of thin films formed by directly combining quantum dots with P3HT is that both elements are an exceptional conductor. Therefore the noise for this device is substantially low and stable irrespective of the amount or types of quantum dots. Nonetheless, QD-CdX:P3HT thin films display a growing increase in noise spectra at a frequency greater than 100 Hz, suggests that the thin film is prone to high-frequency degradation.

The noise results were supported by current density-voltage (*J-V*) measurement. The electrical properties studied were open-circuit voltage (V_{oc}), short-circuit current density (J_{sc}), fill factor (FF), and maximum power output (P_{max}). The fourth quadrant of *J-V* graphs for NP-CdX:P3HT thin films under illumination were plotted in Figure 2. Excitons are created when incident photons are absorbed in thin films. Then, the excitons dispersed inside the polymer matrix until they reached the interface between polymer/nanoparticles and disassociated into electrons and holes [22]. Consequently, the electric field formed at the boundary layer, pushing electrons and holes to the opposite sides. The nanoparticle's HOMO and LUMO energy is relatively lower than P3HT. The electrons will then be transported to the cathode while the holes are transferred to the anode, producing photocurrent [23].

The thin films exposed to the gas environment demonstrated greater J_{sc} as compared to film not treated with gas. When no current is supplied or $J = 0$ A, V_{oc} can be determined. Figure 2 demonstrated that the value of V_{oc} for the exposed films was twice as large as compared with unexposed thin films. NP-CdSe:P3HT gives the highest V_{oc} , 0.72 V, while the other films are in the range of 0.2 – 0.6 V. Even the principle of V_{oc} is not yell well known, Brabec et al. suggest that it depends heavily on the ionization potential of the donor and the electron affinity of the acceptor; hence the amount energy offset [24]. Meanwhile, Qi et al. show V_{oc} is determined by the composition of the elementals' mixture even it is not a straightforward relationship [25]. Thus it justifies the low V_{oc} value for thin films before gas treatment due to underdeveloped nanoparticles nucleation in the film matrices.

Short-circuit current density, J_{sc}, occurs when the current flow through the external circuit without connecting to a voltage source, $V = 0$ V. Low J_{sc} value for entire samples imply limited photon absorption by the films. Transportation of the charge is associated with Fill Factor or FF. High charge mobility is desired to prevent significant losses due to recombination [26, 27]. However, calculation shows FF values are small for all samples indicating the considerable recombination level occurs in thin films. The results are as corroborated by low J_{sc} value. The "squareness" of the FF is contributed by maximum power output, P_{max}, that is when the current and the voltage of the device are at maxima, or:

$$P_{max} = J_{MPP} \times V_{MPP} \quad (5)$$

where V_{MPP} and J_{MPP} are the values of voltage and current density at the maximum power point (MPP). Electronic devices must be operated at the maximum power point to generate maximum energy efficiency and minimize losses. In order to achieve maximum energy performance and, at the same time, reduces losses, the electronic appliances are desired to be operated at the highest power point [28].

The exposure of H_2S or H_2Se gas nucleated approximately 9% of nanoparticles. Hence the improvements in P_{max} for the exposed film were insignificant. Thin films mixed with 50 wt% quantum dots, however, posses even smaller P_{max} value. This is contrary to the study by Lek et al. that reports a rise in the weight ratio of nanoparticles would improve electrical performance [29]. Nonetheless, the improvement can only be observed until a certain weight percentage is reached. Whilst the study shows a low amount of quantum dots or nanoparticles causes inefficient pathways for electrons transportation [30], too high nanomaterials loading causing limited mobility of the holes, leading to lower device's performance. The summary of the *J-V* analysis is as tabulated in Table 1. The overall results demonstrated that NP-CdSe:P3HT nanocomposite the most reliable performance in both Johnson noise and J-V evaluation of all thin films.

Table 1: The electrical properties of thin films from *J-V* measurement

	V_{oc} (V)	J_{sc} (mA/cm^2)	FF	P_{max} (mW)
NP-CdS:P3HT	0.2	1.2×10^{-3}	0.18	1.2×10^{-4}
NP-CdSe:P3HT	0.72	1.2×10^{-3}	0.15	1.3×10^{-4}
QD-CdS:P3HT	0.32	1.1×10^{-4}	0.14	4.8×10^{-6}
QD-CdSe:P3HT	0.2	7.5×10^{-5}	0.21	3.2×10^{-6}

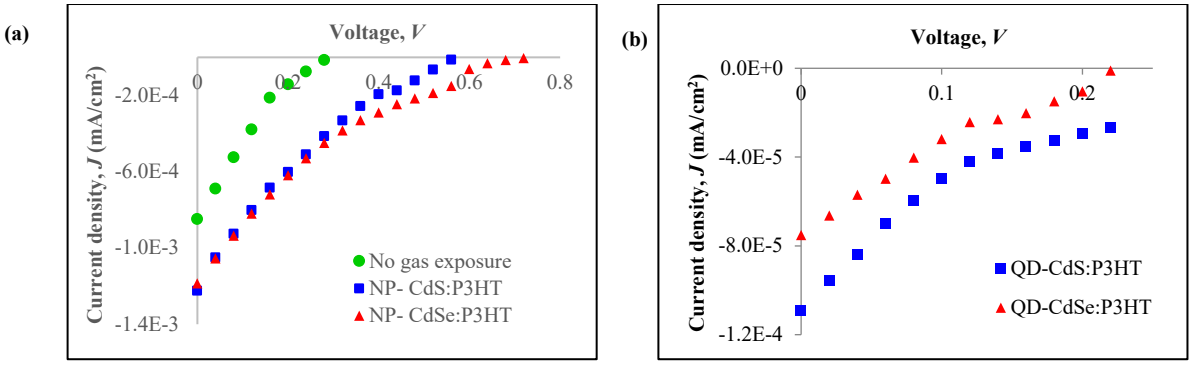


Figure 2: *J-V* graphs for thin films (a) unexposed sample, sample exposed to H_2S gas (NP- CdS:P3HT) and H_2Se gas (NP-CdSe:P3HT), and (b) QD-CdS:P3HT and QD-CdSe:P3HT

Figure 3 (a) displays the absorption spectra of pristine P3HT thin film, thin films before gas exposure, and after exposure to H_2S gas and H_2Se gas. Conjugation system in P3HT causes two peaks at 522 and 556 nm and a shoulder at 605 nm to appear in the UV-Vis graph. A similar result has been obtained by the Liao research group [31]. The peaks attribute to π-π* transition or the order of intermolecular chains of the polymer, while the shoulder is due to crystallization of polymer [32, 33]. When P3HT were mixed with stearic acid, the absorption spectra are lower than that of pristine P3HT, and its peak shifted towards the red spectrum at 529 and 560 nm, and the shoulder becoming less distinguishable. The shift indicates the presence of Cd^{2+} ion capped in the stearic acid matrices, as well as reduced P3HT π-conjugation length.

Before the thin films were exposed to the gas, the observable peak is at 560 nm. Nonetheless, exposure to H_2S gas environment for 6 hours caused the peak to shift to 556.5 nm. The blue shift of the peaks inkling the quantum confinement effect due to CdS nanoparticles formation in the thin film [34, 35]. The shoulder at 605 nm is more perceptible compared with an unexposed thin film. This shoulder is usually due to an increased crystallization of intra-chain interactions. The exposure to H_2S gas causing the absorption intensity to become lesser. This is due to the reaction of cadmium stearate with H_2S gas:

$$(CH_3(CH_{12})_{16}COO)_2Cd + H_2S \rightarrow 2H(CH_3(CH_{12})_{16}COO) + CdS \quad (6)$$

Similar to H_2S gas exposure, the absorption intensity of thin films exposed to H_2Se gas ambiance decreased compared with the unexposed thin film. One possible reason that contributes to such a profile is the shape and amount of CdSe nanoparticles created. The aspect ratio of CdSe nanoparticles is high, in which it resembles rod-like, and some of the nanoparticles agglomerate, creating a larger cluster.

Photoluminescence (PL) is a process of spontaneous light emission from the material under optical excitation. Ideally, the PL spectrum mirroring the image of the absorption spectrum, hence it clearly can be observed from Figure 3(b) the PL spectra resemble the UV-Vis absorption spectra. PL measurement is an indicator of excitons dissociation and its efficiency to transfer charge in the composite materials. The intensity of PL decreased when exposed to H_2S and H_2Se gas. The gas exposure caused the peak shifted towards the blue region, from 720 nm to 718 nm and 714 nm, respectively. The deviation suggested the reduction in P3HT aggregation, causing the PL to quench.

The occurrence of PL depends on the distance from the excitons formed to the donor/acceptor interface [36]. If the distance is lesser than the excitons' diffusion length, charge transfer to the nanoparticle is anticipated, hence the PL is quenched [37]. The more significant range caused recombination to take place. From literature, exciton diffusion length for P3HT is around 8 nm [38]. However, FESEM images in Figure 3 (c) – (e) showed that the distance between nanoparticles was considerably large, ranging from 100 to 150 nm. The number of nanoparticles impregnated in the thin film was small, causing the exciton that is further from the donor/acceptor interface to recombine before reaching the interface.

The UV-Vis spectra when the CdS / CdSe quantum dots were physically mixed into P3HT polymer as shown in Figure 4 (a) and (b). The absorption of pristine P3HT is comparable to the thin film with 25 wt% CdS and CdSe QDs. However, for QD-CdS:P3HT, the absorption is lower when the amount of QDs is doubled. This may be due to a smaller amount of P3HT in the composite [39]. The peaks and shoulders remain at the same wavelength as pristine P3HT. The absence of the CdS QDs absorption band is likely due to the overlapping with the P3HT absorption. While at 50 wt% of CdSe, the absorption is higher, and the shoulder is less distinguishable. The peaks are poorly shifted to red, 524 and 557.5 nm indicating the polymer chains are less crystallized due to QDs added. Both QD-CdS:P3HT and QD-CdSe:P3HT show no significant in amplitude variation with the increment of QDs wt%, comparable to the results reported for P3HT:CdSe TBPO-capped at different weight percentage [40].

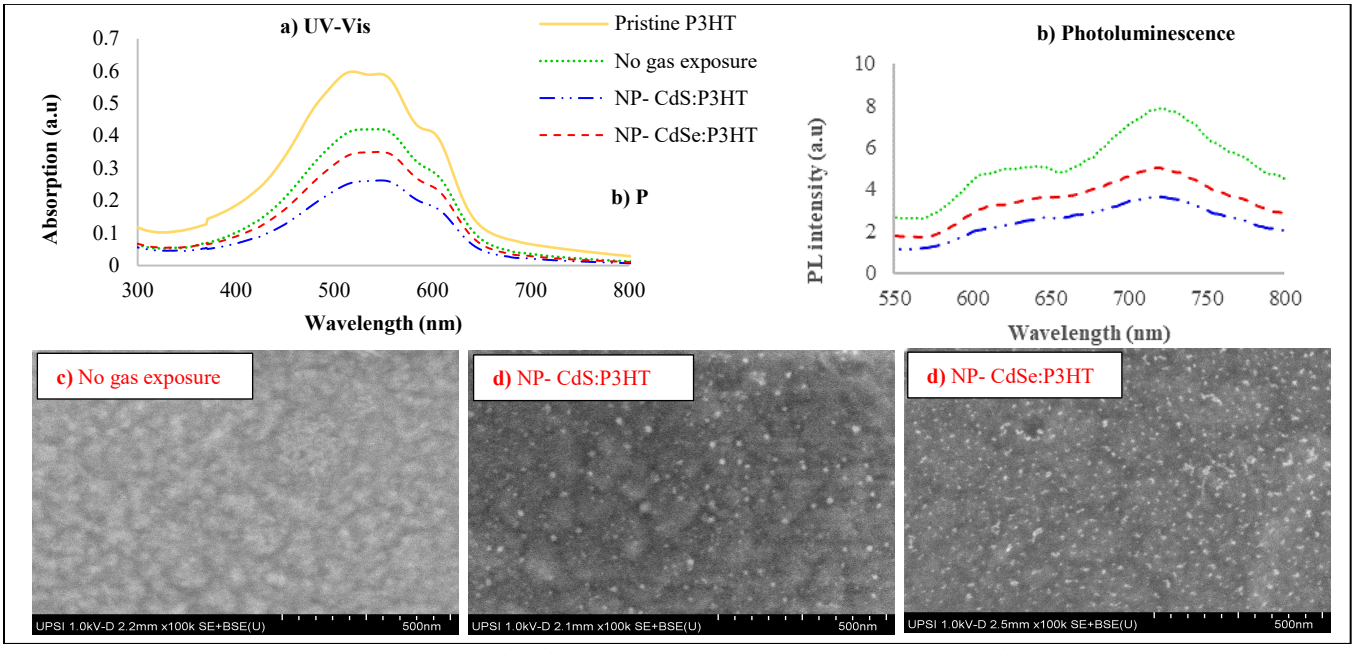


Figure 3: (a) UV-Vis absorption spectra, (b) photoluminescence spectra and (c) FESEM images for thin films not exposed to any gas, (d) exposed to H_2S gas (NP- CdS:P3HT), and (e) H_2Se gas (NP-CdSe:P3HT)

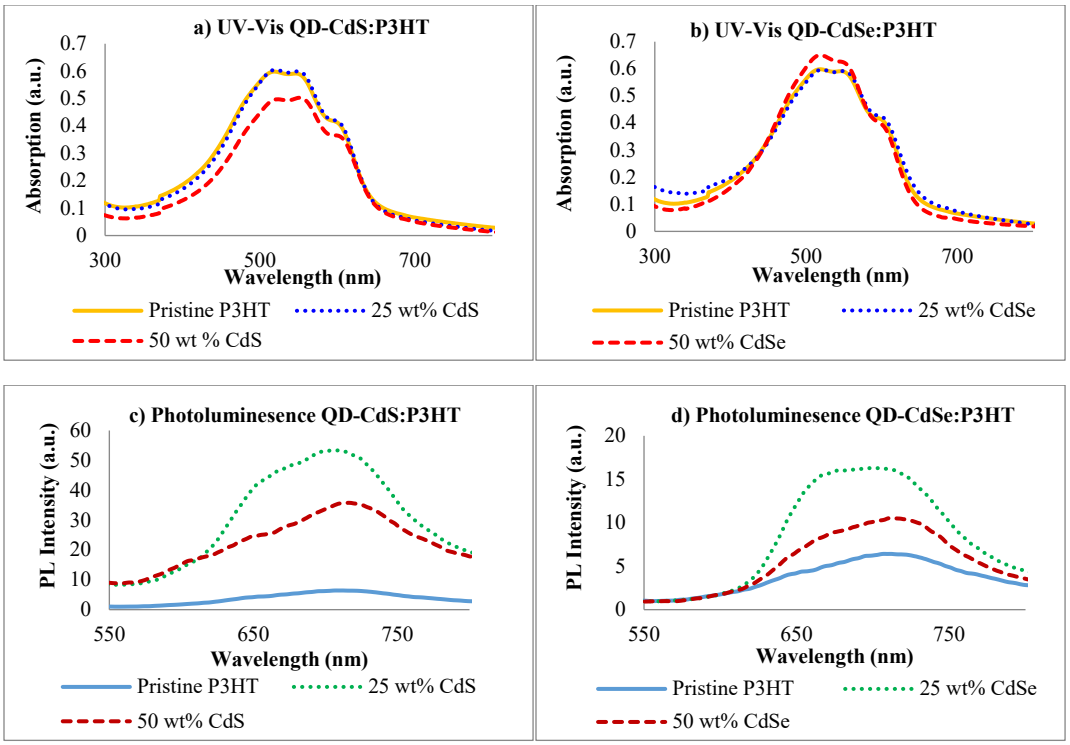


Figure 4: UV-Vis absorption spectra and photoluminescence of QD-CdS:P3HT and QD-CdSe:P3HT

On the other hand, photoluminescence spectra for QD-CdS:P3HT and QD-CdSe:P3HT are shown in Figure 4 (c) and (d), respectively. Both types of thin-film displayed similar characteristics, in which a higher amount of QDs (50 wt%) mixed into P3HT cause the film to quench stronger as compared to films with 25 wt% QDs. The quenching indicates a reduction in the domain size of P3HT blended with nanoparticles [41]. The decrease is owing to a shorter distance for the excitons to travel to the donor/acceptor interface when the weight percentage of nanoparticles in the polymer is doubled. The PL quenching also possibly due to the π-π interaction of P3HT with the nanoparticles [42], creating a new decaying pathway for excitons [43]. Higher excitons dissociation can be justified for better device performance.

Nonetheless, the PL intensity of P3HT:CdS QDs is higher and has a narrower peak than that of P3HT:CdSe QDs. The P3HT:25 wt% CdS has a maximum at 704 nm, while for P3HT:50 wt% CdS, the peak shifted to longer wavelength, 713.5 nm. The shift is also known as Stokes-shift. The redshift implies the increment in polymer aggregation, which can be achieved by the incorporation of QDs into the polymer matrix, as have also been observed by others [44].

4. Conclusion

The analysis has been done on the nanocomposite thin films prepared via two approaches – direct impregnation of nanoparticles in P3HT matrix (*in-situ*), and by physically mixing quantum dots with P3HT (*ex-situ*). Results show that QD-CdX:P3HT thin films possess low Johnson noise due to intrinsic properties of quantum dots and P3HT as an excellent conductor. Consequently, the noise is considerably small and stable for this system regardless of the weight percentage or types of quantum dots. However, the increment of noise can be observed at a frequency above 100 Hz for QD:CdX-P3HT thin films. This signifies the thin film is vulnerable to high-frequency degradation. For nanocomposite produced through the *in-situ* technique, the presence of stearic acid the P3HT matrix curb the free flow of electrons movement.

It can be concluded NP-CdSe:P3HT nanocomposite displayed more reliable performance in both Johnson noise and *J-V* measurement. Absorbance spectra show higher polymer crystallization NP-CdX:P3HT. The quantum confinement effect due to nanoparticles formation is translated by the shift of peaks and depreciation of absorption intensity. The PL intensity decreased when exposed to the gas. Both the thin films fabricated ex-situ displays similar spectra profile even when the amount of quantum dots was doubled. While the amount of quantum dots did not affect the absorbance significantly, the PL intensity decreased with increment of quantum dots' weight percentage. Overall, NP-CdX:P3HT showed better performance compared to QD:CdX-P3HT nanocomposite. Such findings have provided a bright prospective to study the nucleation of nanoparticles through gas exposure technique for optoelectronics applications.

Conflict of Interest

The authors declare no conflict of interest.

Acknowledgment

Authors are grateful to Universiti Putra Malaysia for the financial support through IPM Putra research grant 9674000.

References

[1] R. E. Gorga, R. E. Cohen, "Toughness Enhancements in Poly(Methyl Methacrylate) by Addition of Oriented Multiwall Carbon Nanotube"

J.Polym.Sci. Polym. Phys., **42**(14), 2690–2702, 2004. https://doi.org/10.1002/polb.20126
[2] H. Darabi, Radio Frequency Integrated Circuits and Systems, Cambridge University Press, 2015.
[3] J. B. Johnson, "Thermal Agitation Of Electricity in Conductors" Phy. Rev., 32, 97-109, 1928. https://doi.org/10.1103/PhysRev.32.97
[4] H. Nyquist, "Thermal Agitation of Eelectric Charge in Conductors" Phy. Rev., 32, 110-113, 1928. https://doi.org/10.1103/PhysRev.32.110
[5] X. Zhang, D. Chen, "An Integrated Circuit Solution to Johnson Noise Thermometry Using Low-Cost and Fast CMOS Technology" IEEE Sens. J., **19**(9), 3240-3251, 2019. https://doi.org/10.1109/JSEN.2019.2893241
[6] G. Vasilescu, Electronic Noise and Interfering Signals: Principles and Application, Springer-Verlag Berlin Heidelberg, 2005.
[7] L. K. J. Vandamme, "Noise as a Diagnostic Tool for Quality and Reliability of Electronic Devices," IEEE Trans. on Electron Dev., **41**(11), 2176 – 2187, 1997. https://doi.org/10.1109/16.333839
[8] Z. Chobola, L. Hasse, Z. Růžička, "Measurement of Low Frequency Noise of Monocrystalline Silicon Solar Cells," in XVII IMEKO World Congress, Croatia, 2003.
[9] P. R. F. Rocha, H. L. Gomes, L. K. J. Vandamme, D. M. de Leeuw, S. C. J. Meskers, P. van de Weijer, "Low-frequency Noise as a Diagnostic Tool for OLED reliability," in 22nd International Conf. on Noise and Fluctuations, 2013.
[10] A. Carbone, B. K. Kotowska, D. D. Kotowski, "Space-Charge- Limited Current Fluctuations in Organic Semiconductors" Phy. Rev. Lett., **95**, 236601-236605, 2005. https://doi.org/10.1103/PhysRevLett.95.236601
[11] L. Ke, X. Y. Zhao, R. S. Kumar, S. J. Chua, "Low Frequency Optical Noise from Organic Light Emitting Diode" Solid-State Electron., **52**(1), 7-10, 2008. https://doi.org/10.1016/j.sse.2007.07.004
[12] J. J. Luo, I. M. Daniel, "Characterization and Modelling of Mechanical Behaviour of Polymer/Clay Nanocomposites" Composites Science and Technology, **63**(11) 1607–1616, 2003. https://doi.org/10.1016/S0266-3538(03)00060-5
[13] C. L. Wu, Q. Zhang, M. Z. Rong, K. Friedrich, "Tensile Performance Improvement of Low Nanoparticles Filled-Polypropylene Nanocomposites" Compos. Sci. Technol., **62**(10-11), 1327-1340, 2003. https://doi.org/10.1016/S0266-3538(02)00079-9
[14] M. Haridas, S. Srivastava, J. K. Basu "Tunable Variation of Optical Properties of Polymer Capped Gold Nanoparticles" Eur. Phys. J. D, **49**, 93–100, 2008. https://doi.org/10.1140/epjd/e2008-00135-x
[15] Hung-Chou Liao, San-Yuan Chen, and Dean-Mo Liu. "In-Situ Growing CdS Single-Crystal Nanorods via P3HT Polymer as a Soft Template for Enhancing Photovoltaic Performance" Macromol. **42**(17), 6558–6563, 2009. https://doi.org/10.1021/ma900924y
[16] H. Hoppe, "Nanomorphology – efficiency Relationship in Organic Bulk Heterojunction Plastic Solar Cells," Ph.D Thesis, Johannes Kepler University Linz, 2004.
[17] J. Hou, X. Guo, Active Layer Materials for Organic Solar Cells. In W. C. H. Choy (Ed.), Organic solar cells: Materials and Device Physics, Springer-Verlag, 2012.
[18] H. Tang, F. Zhao, F. Zhang, "Investigation on an Optically-Controlled Phase-Shifter Based Organic Semiconductor Poly-(3-hexylthiophene) (P3HT)" J. Phys. Conf. Ser., **276**(1), 012092, 2011. https://doi.org/10.1088/1742-6596/276/1/012092
[19] E. O. Sako, H. Kondoh, I. Nakai, A. Nambu, T. Nakamura, T. Ohta, "Reactive Adsorption of Thiophene on Au(111) from Solution" Chem. Phys. Lett., **413**(4-6), 267-71, 2005. https://doi.org/10.1016/j.cplett.2005.07.086
[20] Y. Zhou, M. Eck, M. Krüger, M. Organic-Inorganic Hybrid Solar Cells: State of The Art, Challenges and Perspectives. In L. A. Kosyachenko (Ed.), Solar Cells - New Aspects and Solutions. IntechOpen, 2011.
[21] F.H. Naning, "Surface Pressure-Area Isotherm, Optical And Electrical Properties Of P3HT/Nanoparticles Thin Films By Modified Langmuir-Blodgett Technique" Ph.D Thesis, Universiti Pendidikan Sultan Idris, 2017.
[22] B. Kippelen, J. L. Bredas, "Organic Photovoltaics" Energy Environ. Sci., **2**, 251–261, 2009. https://doi.org/10.1039/B812502N
[23] N. S. Sariciftci, L. Smilowitz, A. J. Heeger, F. Wudl, "Photoinduced Electron Transfer From a Conducting Polymer to Buckminsterfullerene," Science, **258**(5087), 1474-1476, 1992. https://doi.org.10.1126/science.258.5087.1474
[24] C. J. Brabec, G. Zerza, G. Cerullo, S. De Silvestri, S. Luzzati, J. C. Hummelen, S. Sariciftci, "Tracing Photoinduced Electron Transfer Process in Conjugated Polymer/Fullerene Bulk Heterojunctions in Real Time" Chem. Phy. Lett., **340**(3-4), 232-236, 2001. https://doi.org/10.1016/S0009-2614(01)00431-6
[25] B. Qi, Q. Zhou, J. Wang, "Exploring the Open-Circuit Voltage of Organic Solar Cells Under Low Temperature" Sci. Rep., **5**, 11363, 2015. https://doi.org/10.1038/srep11363
[26] J. A. Bartelt, D. Lam, T. M. Burke, S. M. Sweetnam M. D. McGehee, "Charge-Carrier Mobility Requirements for Bulk Heterojunction Solar Cells with High Fill Factor and External Quantum Efficiency >90%" Adv. Energy Mater., **5**, 1500577, 2015. https://doi.org/10.1002/aenm.201500577
[27] I. Riedel, V. Dyakonov, "Influence Of Electronic Transport Properties of Polymer-Fullerene Blends on the Performance of Bulk Heterojunction Photovoltaic Devices" Phys. Status Solidi A, **201**, 1332–1341, 2004. https://doi.org/10.1002/pssa.200404333
[28] D. Bartesaghi, I. D. Pérez, J. Kniepert, S. Roland, M. Turbiez, D.N. L. J. A. Koster, "Competition Between Recombination and Extraction of Free Charges Determines the Fill Factor of Organic Solar Cells" Nat. Commun., **6**, 7083, 2015. https://doi.org/10.1038/ncomms8083
[29] J. Y. Lek, Y. M. Lam, J. Niziol, M. Marzec, "Understanding Polycarbazole-Based Polymer:CdSe Hybrid Solar Cells," Nanotechnology, **23**(31), 315401, 2012. https://doi.org/10.1088/0957-4484/23/31/315401
[30] Y. Zhou, M. Eck, C. Men, F. Rauscher, P. Niyamakom, S. Yilmaz, …M. Krüger, "Efficient Polymer Nanocrystal Hybrid Solar Cells by Improved Nanocrystal Composition," Sol. Mat. Sol. Cells, **95**(12), 3227-3232, 2011. https://doi.org/10.1016/j.solmat.2011.07.015
[31] H. C. Liao, N. Chantarat, S. Y. Chen, C. H. Peng, "Annealing Effect on Photovoltaic Performance of Hybrid P3HT/In-Situ Grown CdS Nanocrystal Solar Cells" J. Electrochem. Soc., **158**(7), 5251-5455, 2011. https://doi.org/10.1149/1.3585668
[32] U. Farva, M. A. Khan, C. Park, Effect of Post Annealing on the Performance of CdSe/P3HT Bulk Hetero-Junction Solar Cells. In Photovoltaic Specialist Conference, San Diego, USA, 2008.
[33] P. J. Brown, D. S. Thomas, A. Köhler, J. S. Kim, C. M. Ramsdale, H. Sirringhaus, R. H. Friend, "Effect of Interchain Interactions on the Absorption and Emission of Poly(3-hexylthiophene)" Phys. Rev. B, **67**(6), 064203, 2003. https://doi.org/10.1103/PhysRevB. 67.064203
[34] R. R. Prabhu, M. A. Khadar, "Characterization of Chemically Synthesized CdS Nanoparticles" Pramana J. Phys., **65**, 801-807, 2005. https://doi.org/10.1007/BF02704078
[35] P. Sonar, K. P. Sreenivasan, T. Madddanimath, K. Vijayamohanan, "Comparative Behavior of CdS and CdSe Quantum Dots in Poly(3-hexylthiophene) Based Nanocomposites" Mater. Res. Bull., **41**(1), 198-208, 2006. https://doi.org/10.1016/j.materresbull.2005.07.032
[36] B. Freisinger, "Investigation of P3HT/PCBM Particle-Based Solar Cells," Ph.D Thesis, Johannes Gutenberg-Universität Mainz, 2013.
[37] A. J. Ferguson, N. Kopidakis, S. E. Shaheen, G. Rumbles, "Quenching of Excitons by Holes in Poly(3-hexylthiophene) Films" J. Phys. Chem., **112**(26), 9865- 9871, 2008. https://doi.org/10.1021/jp7113412
[38] B. Annalisa, D. L. Tiziana, B. Carmela, V. Fulvia, H. Saif, M. Carla, "Exciton Dynamics in Hybrid Polymer/QD Blends", Energy Procedia, **44**, 167-175, 2014. https://doi.org/10.1016/j.egypro.2013.12.024.
[39] P. E. Shaw, A. Rusecka, I. D. W. Samuel, "Exciton Diffusion Measurements in Poly(3-hexylthiophene)" Adv. Mater. **20**(18), 3516-3520, 2008. https://doi.org/10.1002/adma.200800982
[40] D. Loubiri, Z. Ben Hamed, S. Ilahi, M. A. Sanhoury, F. Kouki, N. Yacoubi, "Effect of TBPO-Capped CdSe Nanoparticles Concentration on Sub-Bandgap Absorption in Poly(3-hexylthiophene) Thin Films Studied by Photothermal Deflection Spectroscopy" Synth. Met,, **206**, 1-7, 2015. https://doi.org/10.1016/j.synthmet.2015.04.018.
[41] A. J. MacLachlan, T. Rath, U. B. Cappel, S. A. Dowland, H. Amenitsch, A. C. Knall, … S. A. Haque, "Polymer/Nanocrystal Hybrid Solar Cells: Influence of Molecular Precursor Design on Film Nanomorphology, Charge Generation and Device Performance" Adv. Funct. Mater., **25**, 409–420, 2015. https://doi.org/10.1002/adfm.201403108
[42] H. C. Liao, S. Y. Chen, D. M. Liu, "In-Situ Growing CdS Single-Crystal Nanorods via P3HT Polymer as a Soft Template for Enhancing Photovoltaic Performance" Macromolecules, **42**(17), 6558-6563, 2009. https://doi.org/10.1021/ma900924y
[43] M. T. Khan, R. Bhargav, A. Kaur, S. K. Dhawan, S. Chand, "Effect of Cadmium Sulphide Quantum Dot Processing and Post Thermal Annealing on P3HT/PCBM Photovoltaic Device" Thin Solid Films, **519**(3), 1007-1011, 2010. https://doi.org/10.1016/j.tsf. 2010.08.032.
[44] S. N. Sharma, T. Vats, N. Dhenadhayalan, P. Ramamurthy, A. K. Narula, "Ligand-Dependent Transient Absorption Studies of Hybrid Polymer:CdSe Quantum Dot Composites" Sol. Energy Mater. Sol., **100**, 6–15, 2012. https://doi.org/10.1016/j.solmat.2011.10.020

ASTES

Advances in Science, Technology and Engineering Systems Journal Vol. 5, No. 5, 757-764 (2020)

www.astesj.com

Special Issue on Multidisciplinary Innovation in Engineering Science & Technology

ASTESJ

ISSN: 2415-6698

Transient Response & Electromagnetic Behaviour of Flexible Bow-Tie Shaped Chip-less RFID Tag for General IoT Applications

Muhammad Usman Ali Khan*, Raad Raad, Javad Foroughi

School of Electrical Computer and Telecommunication Engineering, University of Wollongong, Wollongong NSW, 2522, Australia

ARTICLE INFO

Article history:
Received: 11 June, 2020
Accepted: 23 July, 2020
Online: 12 October, 2020

Keywords:
Chipless RFID
Bow-tie
Polymer Substrate
FSS
RCS
PET
SEM
Coupling coefficients
IoT Applications

ABSTRACT

This paper is an extension of Novel Flexible Chip-less Bow-Tie RFID tag in which we presented the design, testing and fabrication of the tag and compared the results with Octagonal Chipless RFID tag. The chipless RFID tag was designed by using simulation software CST microwave studio and fabricated by using laser etching technique on a flexible polymer substrate Polyethylene Terephthalate (PET). The tag operates at frequency ranging from 8 to 18 GHz uses the Frequency Selective Surface (FSS) approach. A series of experiments are performed to measure the Radar Cross Section (RCS) in an anechoic chamber. The tag design is composed of six concentric Bow-Tie shaped loop resonators with one unitary element. In this paper, we demonstrated the Singularity Expansion Method (SEM) based circuit modelling and the transient behaviour of the RFID tag is performed. The coupling coefficients and the induced currents over the surface of Bow tie shaped rings are evaluated. The maximum read range is evaluated and the Bow-Tie RFID tag is proved to be more accurate and efficient with the variation of distance up to 1.8m at 0dBm which is extendable to 2.14m for higher input power. This range is maximum to our knowledge for such a high-frequency range of 8-18GHz. The 4-bits Bow-Tie Chipless RFID tag design is compact and can be deployed commercially for general IoT applications.

1. Introduction

This paper is an extension of work originally presented in the 19th International Symposium on Communications and Information Technologies (ISCIT) 2019 [1].

The Internet of Things (IoT) relies on smart environments comprises of wireless sensor networks [2] and personal area networks [3], [4] in which one interacts with IoT infrastructure must be uniquely identified. However, one big challenge is a need to commence seamless integration of IoT solutions with surroundings and with people [5]. Flexible materials for various IoT applications require a high level of integrity of components and mechanical robustness with repeated rolling and bending capabilities. In particular, flexible smart fitness watches, RFID tags and wearable sensors are good examples of applications that use flexible material. Besides, Elasticity and stretch-ability of materials are the key properties required by electronic devices that require large and reversible deformation. These bendable devices will also need to be versatile and may require the ability to store energy, operate with low power, and integrated with other devices and Internet of Things (IoT) applications [6]-[8].

The growth of wearable technology and the success of wearable devices has been hampered by limits such as the lack of materials and manufacturing techniques for seamless integration with electronic parts [9], the robustness in washing, drying and moulding [10], [11]. To address these challenges flexible polymer-based chipless RFID tag can be a good candidate.

In recent years, the research on wearable wireless communication and flexible devices has increased rapidly due to its usability and applications in personal communication systems [12]. For examples; Flexible antennas and Radio Frequency Identification (RFID) tags are used to keep track of several daily-routine activities, such as heartbeat and blood pressure measurement, the distance walked, the steps are taken and the calories burnt [13].

RFID Technology is growing rapidly and has significant importance in various medical, industrial and commercial applications [13], [14] such as UHF RFID tags, Chipless RFID

* Corresponding Author: Muhammad Usman Ali Khan, Email: muak803@uowmail.edu.au

tags and Near Field Magnetic Coupled tags are being in used in various commercial applications and medical applications [15]. In the traditional RFID technology, the backscattered field from the tags are used to transmit information by using time-variant loading or scatterer modulation [16]-[19] however, this technique requires the physical movement of the object which needs to be coded by using inductive coupling or the impedance modulation. Besides, the conventional RFID tags are active circuit, carrying a small near field chip including a power source and a memory at the centre of the body. Whereas the chipless RFID technology doesn't require memory or a chip to save codes, instead, it uses the physical aspects of the body such as geometry and the shape to send the data [13]. The primary principle of the chipless technology is to get the resonance from the body and to encode the backscattered signal at the receiver, without additional circuitry or communication protocols [20]. Various techniques have been proposed but generally, the chipless RFID technology can be categorised into two groups. The first one is the time domain-based also called time-domain reflectometry-based designs, Surface Acoustic Wave (SAW) is an example of this. The second group is frequency domain-based RFID tags sometimes known as spectral-based tags, Frequency Selective Surface (FSS) is an example of this technique. The SAW-based chipless RFID tags are primarily worked by piezoelectricity, in which Interdigital Transducer (IDT) on the surface of piezoelectric materials are used to convert the electromagnetic wave into the acoustic wave. The acoustic waves generate the identification code while propagating through the metallic surfaces of the tag separated by a certain distance and stored on the tag [21], [22]. The SAW RFID tags are commercially available but some important issues such as the reduction in the size, increase in the read range and the data capacity needs to address 15. Besides, the FSS based frequency domain chipless RFID technique is quite promising, in which an incident electromagnetic wave is completely or partially reflected from the surface of the resonators and matches with the resonance frequency, based on the nature and the shape of the elements. The chipless RFID tags are known as passive tags as no additional power is required to operate, which make these tags promising for general IoT applications.

Passive chipless RFID tags have gained much importance as a good candidate for IoT applications because of no additional circuitry, small size, increased lifetime and the cost-effectiveness [23]. As compared to conventional RFID tags, passive tags have many significant advantages such as they are extremely cheap and can be printed over a piece of paper simple as barcodes. Moreover, the wearable applications in which washing and heating will affect the energy source, the absence of the battery and the electrical circuits make these tags promising [24].

The general structure of a chipless RFID system is an adaptive version of the Ultra-Wide Band (UWB) frequency radar [25], in which an incident electromagnetic wave from a transmitter strikes at the surface of the tag and reflect toward the reader and decoder, see Figure 1. When an incident wave E^i on the surface of the conductive element, a current is induced at the resonant frequency, 9.2GHz in the case of chipless Bow-Tie RFID tag, see Figure 1.

In this paper, a 4-bit Bow-tie shaped chipless RFID tag is designed and the transient behaviour by the application of ElectroMagnetic (EM) wave is explained. In this design, the polarization feature of non-periodic bow-tie shaped cells is taken into account to get destructive and constructive interferences. The projection of the incidents wave and reflected field and decoded in terms of bits assigned to Radar Cross Sections (RCS) [26]. The RCS is a parameter to describe the level of scattering of a target object, in this case, a tag is the target object.

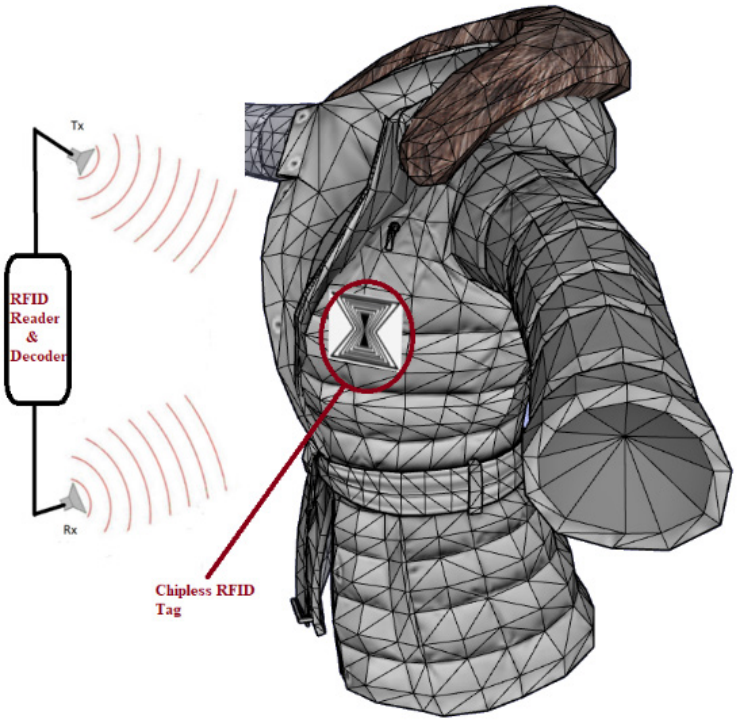


Figure 1: Structural diagram of Bow-Tie chip-less RFID system

This paper employs a simple equivalent model of the tag by using SEM-based circuit modelling. Furthermore, the coupling coefficients and the induced currents over the rings are evaluated and transient response of the Bow-Tie RFID tag is analysed. Finally, the maximum read range is calculated which is 1.8m for 0dBm and extendable to 2.14m for higher incident power, which is maximum to our knowledge for high frequencies of the range 8 to 18GHz.

The rest of the paper is organised as follows: Section II and Section III presents the tag design and its working principle, the material characterisation and optimised designs. Section IV presents the RCS measurements, which further describes the experimental verification of codes, on body RCS measurements, bending analysis and discussion. Finally, the conclusion is presented in Section V.

2. Design and Operation of Bow-Tie Chipless RFID Tag

The Bow-Tie shaped chipless RFID tag proposed in [1] is based on conventional Bow-tie shape which is opted as it has the most intense current flow on the edges of the resonating elements [27], hence cause a more intense backscattered signal. Another reason to opt this design is the fact that it provides more flexibility in designing at higher frequencies unlike octagonal [26], square [28], circular [29] and triangular [30] designs. Moreover, in Bow-tie chipless RFID tag the asymmetrical shape of the tag in which

the distance between the resonators is not constant, it diminished the mutual coupling as compared to the symmetrical surfaces, placed very close to each other [31]. In this paper, a 4-bit Bow-tie chipless RFID tag is proposed and the transient behaviour of the tag is presented. The robust tag is comprised of a periodic pattern of six Bow-tie shaped cells applicable for general IoT and wearable applications.

2.1. Working Principle

The resonant frequency of the tag depends on the inductance and the capacitance between the concentric metallic bow-tie shaped elements [32]. Therefore, when an EM wave strikes at the surface of the tag it induces currents and the corresponding capacitance and the inductances are changed. The extent of the reflected or transmitted wave after falling on the surface, depends upon the placement and the geometry of the rings. Aa results, surface currents (J_{in}) and (J_{out}) are induced on the inner and outer bow-tie shaped rings, respectively, as shown in Figure 2.

In this case, the whole structure including all the surrounding bow-tie rings, interact with each other and cause the creation of the standing waves. The standing waves produced the same polarization with an odd multiple of the difference of π phase by these surface currents which are approximately equal but opposite in phase. Hence, destructive interference results in backscatter wave (Es) and create a specific frequency response. Figure 2. represents the surface current distribution over the elementary cell and all periodic bow-tie shaped rings which tends to be minimum at the inner side of the tag, at the base and ceiling while maximum and almost constant in all vicinities of the Bow-Tie tag. The area of the tag showing minimum concentration correspond to capacitive behaviour and the area where the surface current is intensive corresponds to the inductive behaviour of the tag, see Figure 2.

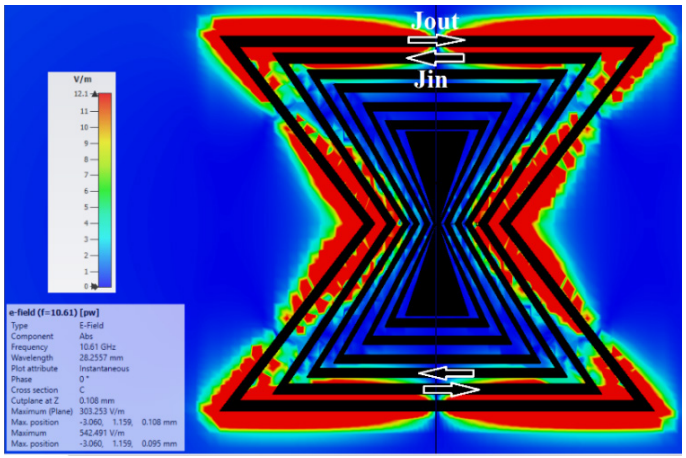


Figure 2: E-Field distribution and the directions of induced surface current (J)

3. Electromagnetic Behaviour of the Bow-Tie RFID Tag

The circuit model of the Bow-Tie chipless RFID tag provides insight into the electromagnetic response of the circuit when an incident EM wave strike at the tag and the induced current re-radiate the scattered fields. The current induced on the tag can be evaluated in different ways. One method is based on Singularity Expansion Method (SEM) in which the current induced on the tag is expanded in terms of the singularity poles of the tag. The concept of SEM has been widely used in circuit theory for a long time. Later on, this technique was used in evaluating EM response and designing of chipless RFID tags [33],[34],[35].

3.1. SEM-Based Equivalent Circuit of Chipless RFID Tag

In this paper, the SEM-based equivalent circuit of the octagonal chipless RFID tag is presented where the solution is evaluated as a collection of poles (Sn), coupling coefficient (Rn) and the entire function (Fe) in the complex frequency domain. The scattering analysis is performed by representing the chipless RFID tag with an equivalent circuit representation, see Fig. For electromagnetic response, the RFID scatterer assumed to be Perfectly Electric Conductor (PEC) in free space. Let's N be a total number of scatterers and an incident electric field E^i strike at the surface of the tag and E^s are scattered electric field with polarization vectors $\hat{a}_i$ and $\hat{a}_s$, respectively. The E^i causes an induced current (J_n) on the surface and the global resonances are demonstrated in the time domain as damped sinusoidal analogous to the Complex Natural Response (CNR) of the scatterer with some weighting residue as coupling coefficients (R_N). The distance between the two scatterers is optimised in such a way that the coupling between one and the alternative scatterer is very small to be negligible. Hence, the coupling between the two scatterers only at a time and ignored the effects of the others on them.

The SEM-based circuit equivalent model of the octagonal chipless RFID tag is presented in Figure 3. where, R_1, R_2…..R_N, L_1, L_2,…..L_N define the resistances and the inductances and C_1, C_2,… C_N is the inductance between two consecutive scatterers for N number of resonators.

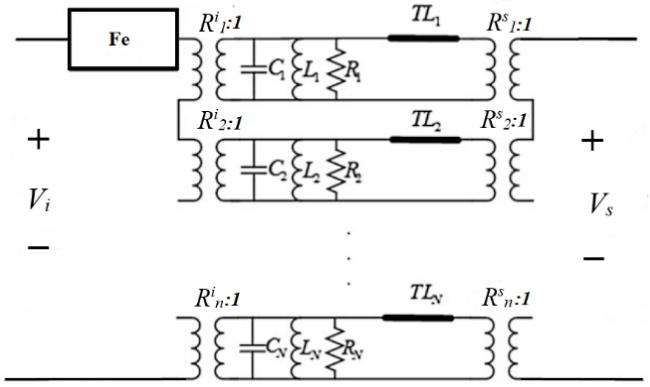


Figure 3: SEM-based equivalent circuit of Bow-Tie RFID Tag with N number of resonators

3.2. Transient Response of Bow-Tie Chipless RFID Tag

The E^i coupled to CNR's by coupling coefficients R^i_1, $R^i_{2,\ldots}$ R^i_n which depends on the direction and the polarization of incident electric filed, whereas R^i_1, $R^i_{2,\ldots}$ R^i_n denotes the coupling coefficients corresponding to E^s. The CNR of the model is presented by a parallel RLC circuit in series with delay line (TL) which designate the turn-on time of CNR, and Fe shows the early time response of the tag. Whereas, the input Vi and output voltages Vs are defined at the transmitting and receiving antennas ports, respectively.

Figure 4. shows the geometry of the Octagonal tag, when E^i strikes at the surface of the tag and E^s electric field is scattered with polarization vectors $\hat{a}_i$ and $\hat{a}_s$ assuming the incident electric field as

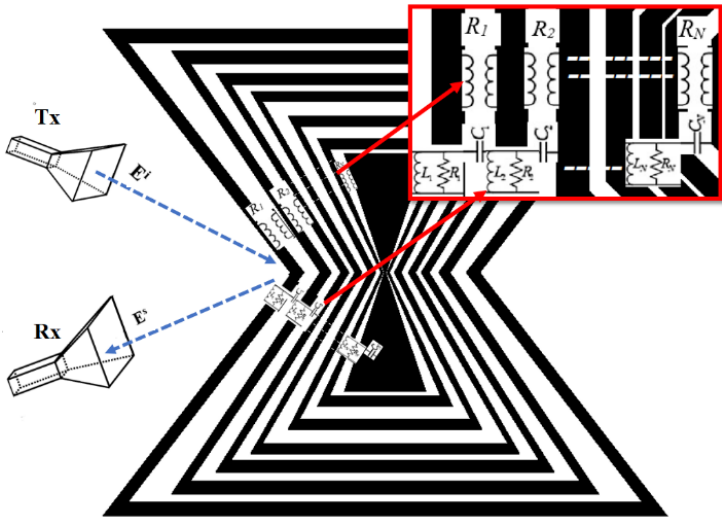


Figure 4: The geometry and the internal circuit modelling of the Bow-Tie RFID Tag Illuminated by an Incident Field Ei

a Dirac-delta function then the transfer function of the tag in the complex s-plane is defined as [15]

$$H_t(\hat{a}_i,\hat{a}_s;s)=\frac{E^s(r;s)}{E^i(r;s)} \tag{1}$$

After some mathematical manipulation, the transfer function in terms of early-time response $H_e(s)$ and late time response $H_1(s)$ with CNR's can be written as [15]

$$H(s)=H_e(s)+H_1(s)$$

$$=H_e(s)+\sum_{n=1}^{N}\left[\frac{A_n}{s-s_n}+\frac{A_n^*}{s-s_n^*}\right] \tag{2}$$

where

$$A_n=\frac{C}{2}\left(1+j\frac{1+\alpha_n}{\omega_n}\right)$$ and CNR's of the circuit is described by

$$s_n=\alpha_n+j\omega_n \tag{3}$$

$$\alpha_n=-\frac{\omega_0}{2Q} \quad \text{and} \quad \omega_n=\frac{\omega_0}{2}\sqrt{4-\frac{1}{Q^2}} \tag{4}$$

where Q represents quality factor which is kept below 0.5 and the RFID first resonator resonates at $f_1=\omega/2\pi$.

3.3. Evaluation of Surface Current Distribution (Jn) and the Coupling Coefficients (Rn).

The current distribution over the first resonator, the outermost octagonal ring is I_1 and V_1 is the induced voltage due to incident fields corresponding to the impedance Z_1 of the resonator then the current distribution over the octagonal scatterers can be evaluated by discretizing the length of the ring into N number of segments [15] as

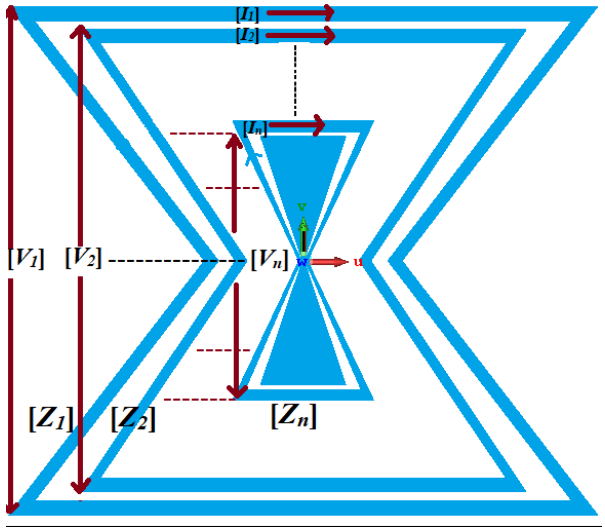


Figure 5: The induced voltages and currents distribution over the surface of the tag

$$[I_1]=[Z_1]^{-1}[V_1] \tag{5}$$

where $[Z_1]$ corresponds to N×N matrix referred to as system impedance matrix, $[I_1]$ and $[V_1]$ are the response vector of N×1corressponding to the incident field, see Figure 5.

The CNR's for the first scatterer is calculated from

$$[Z_1(S_n)][I_1(S_n)]=0$$

$$\Delta_1(S_n)=\det[Z_1(S_n)]=0 \tag{6}$$

The CNR's for the first resonator is obtained by expending $\Delta_1(s_n)$ in complex Taylor series.

$$\Delta_1(s_n)=\Delta_1(s_0)+\Delta_1'(s_0)\,(s-s_0)+\ldots \quad =0 \tag{7}$$

By keeping the first two terms of the equation and ignoring the rest of values the CNR, s_n, is obtained from

$$s_n=s_0-\frac{\Delta 1(s0)}{\Delta 1'(s0)} \tag{8}$$

where s_0 is the initial guess of resonant frequency, by repeating this procedure more accurate values can be evaluated for the first scatterer. For Bow-Tie design, the first resonance was calculated at approximately 9.2 GHz.

The equation (5) is modified to get current distribution for the first resonator of octagonal chipless RFID tag as

$$[I]=\sum_n\frac{R_n}{s-s_n}[J_n] \tag{9}$$

where R_n the residue of nth pole and J_n is the surface current distribution over the surface of the scatterer, which is evaluated in the next section. Also, The time-domain response can be obtained by applying inverse Laplace transform to (9).

To study the mechanism of scattering by a 4-bit octagonal chipless RFID tag, the surrounding medium is supposed as a free space with permittivity ε_0 and permittivity μ_0, the scatterer is PEC and the thickness of the tag is very small hence considered to be zero. Consider an incident field E^i strikes and the induced current over the surface of the tag is (J_n) then the scattered field E^s from the tag is either obtained from Electric Field Integral Equation (EFIE) or Magnetic Field Integral Equation (MFIE) [36]. The EFIE is used which is represented in Laplace form [37].

$$E^s(r;s) = \mu s \iint_A \left[\left(\vec{I} - \frac{1}{k^2} \nabla\nabla \right) G_0(r,r';s) \right] J(r,r';s) dS' \quad (10)$$

where A represents the surface area of the octagonal chipless RFID tag, $\vec{I} = \hat{x}\hat{x} + \hat{y}\hat{y} + \hat{z}\hat{z}$, k represents the propagation constant k=s/c in the complex frequency domain and G_0 defines the scalar Green's function in the free space.

$$G_0(r,r';s) = \frac{e^{-jk|r-r'|}}{4\pi |r-r'|} \quad (11)$$

The coupling coefficients are then evaluated by using the equations

$$R_n(s_n) = -\frac{\left\langle J_n(r), E^i{}_t(r;s_n) \right\rangle_r}{\left\langle \left\langle J_n(r), \left\langle \frac{\partial \vec{G}(r,r';s)}{\partial s}\bigg|_{s=s_n}, J_n(r') \right\rangle_{r'} \right\rangle_r} \quad (12)$$

This equation shows that the coupling coefficient depends upon E^i and natural modes $J_n(r)$ at the resonant frequency.

$$\left\langle J_n(r), E^i{}_t(r;s_n) \right\rangle_r = 0 \quad (13)$$

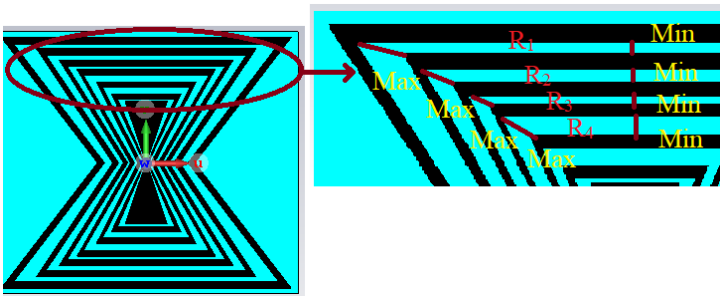


Figure 6: The variation of the distances between consecutive Bow-Tie shaped rings

The evaluation of coupling coefficients (R_1 to R_4) was not easy in the case of chipless Bow-tie RFID. This is because the distance between the two consecutive bow-tie shaped rings is not constant and hence mutual coupling varies, see Figure 6. Therefore, coupling coefficients are evaluated for the values of the maximum and the minimum distances between two consecutive rings at corresponding resonance, see Table 1. The values of coupling coefficients between the first two consecutive rings are -0.010 and -0.021 calculated for the maximum and the minimum spacing of 1.2mm and 0.23mm, respectively for 9.2GHz frequency, see Table 1. Similarly, all values are calculated for corresponding resonant frequencies of 11.3, 14 and 16.9 GHz. The maximum value of R_n from the table is -0.021 which is a sufficiently low value that assures reliable reading of the coded information. To reduce the mutual coupling the average spacing between the resonators can be increased, therefore the size of the tag would be significantly increased.

Table 1: Coupling Coefficients for Corresponding Resonances

n	Resonant Frequency F_{0n} (GHz)	Spacing Between Resonators Min to Max (mm)		Coupling Coefficients Minimum Rn	Coupling Coefficients Maximum Rn
		D_{min}	D_{max}		
1	9.2	0.23	1.2	-0.010	-0.021
2	11.3	0.35	0.9	-0.012	-0.017
3	14	0.17	0.6	-0.009	-0.014
4	16.9	0.52	1.1	-0.014	-0.020

4. Flexibility and Bending Analysis

The Bow-Tie tag is designed on 13.44×11.56mm2 PET substrate of 70µm thickness with conductive gold rings varied in thickness [1].

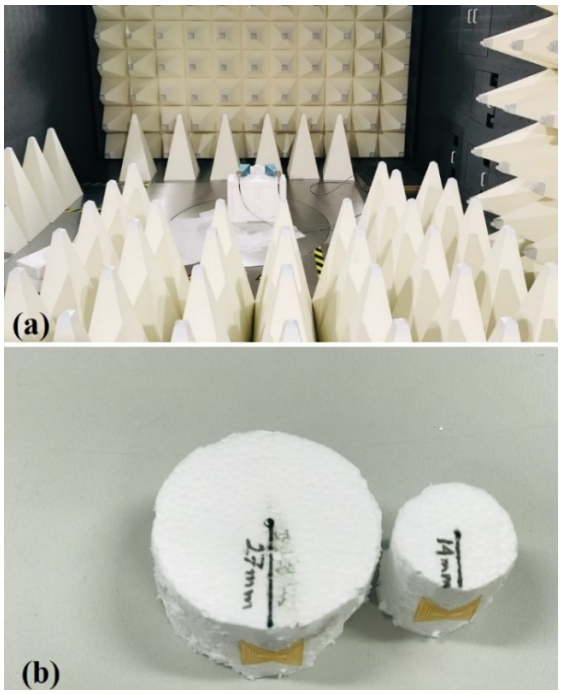
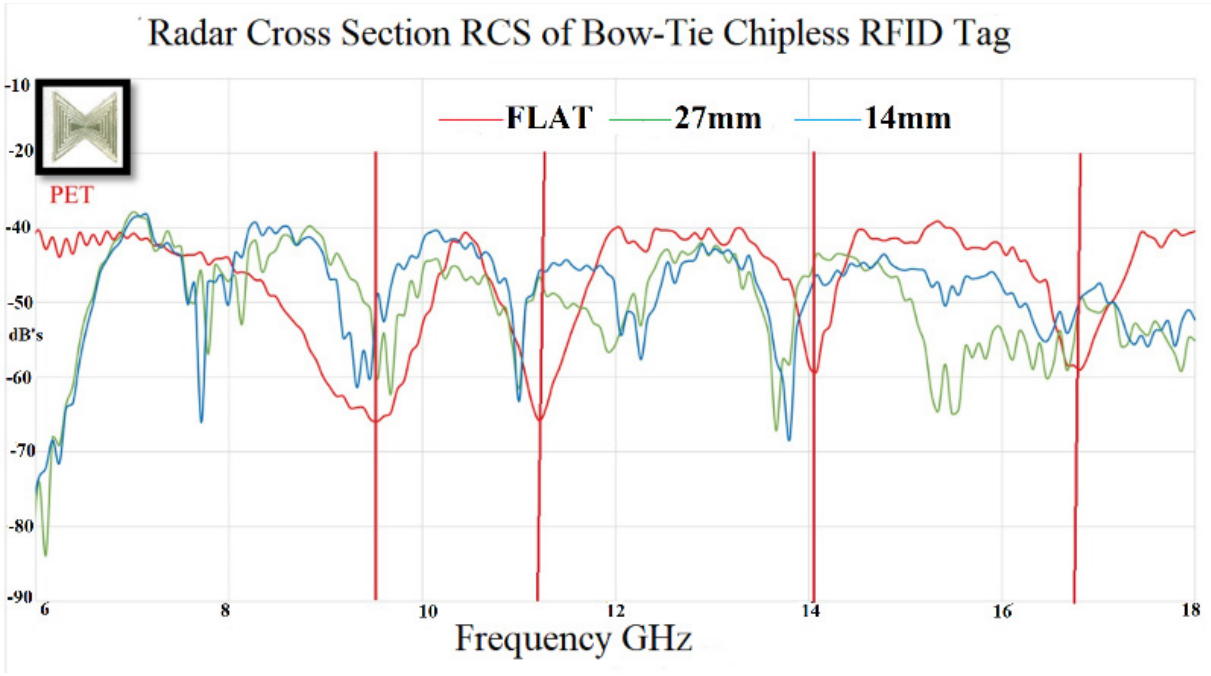


Figure 7: Chipless Bow-Tie RFID tags a) Experimental set-up in chamber b) Bending aspects of fabricated Chip-less RFID Tags at 27mm and 14mm

4.1. Experimental Setup and RCS Results

The chipless Bow-tie RFID tag is printed on a PET substrate by using Universal Laser Systems (ULS). The measurements of



the RCS obtained by the reflections from the tag are analysed by Vector Network Analyser (VNA). For this purpose, Keysigth VNA series E5063A is used with two similar horn antennas operating at 4-18GHz frequencies. To conduct the measurement, the testing is performed in the FRANKONIA anechoic chamber, having a frequency range of 30 MHz to 40 GHz. The compact Bow-Tie RFID tag design is highly flexible and the bit codes are successfully obtained up to the bending radius of 14mm [38]. The Bow-Tie RFID tag undergoes bending for the following cases of curvatures, flat, 14mm and 27mm, see Figure 7 (b).

The Passive Bow-tie RFID tag is placed in the horizontal (H) position to perform the bending analysis for the following cases flat, 14mm and 27mm. All the testing was performed in the Frankonia anechoic chamber. One of the impacts of bending is the signal strength degradation of the backscattered waves and the significant shift in the resonant frequency. In other words |RCS| is lowered while tag undergoes bending. In this case, since the distance of the tag from the reader, is kept very small about 12cm from the transmitter, so a very small reduction in the signal strength is obtained at 0dBm power. However, the percentage shift in the resonant frequency is quite prominent especially at a higher level of bending at 14mm, see Figure 8.

Figure 8. depicts the impact of bending on the RCS obtained in the chamber. A shift of 4% from the resonant frequency is obtained, when a PET substrate-based chipless Bow-tie RFID tag undergoes bending curvature 27mm for the lower range of the frequencies 8-14 GHz, whereas, more than 10% shift is observed for higher range of frequency up to 18GHz. Hereafter, there is no noticeable reduction of the signal strength is observed because of the small distance of tag from the reader. Hence, the experimental results depict that the RCS obtained and encode in frequency signature, from the bent chip-less RFID tag fabricated on the flexible PET substrate.

5. Maximum Read Range Estimation

This section provides the maximum read range of Bow-Tie Chipless RFID tag. The complex RCS feature (σ^{Tag}) of octagonal chipless RFID designs can be obtained by the following equations which are described in [39].

$$\sigma^{Tag} = \left[\frac{S_{21}^{Tag} - S_{21}^{No-Tag}}{S_{21}^{Ref} - S_{21}^{No-Tag}}\right]^2 \sigma^{Ref} \quad (14)$$

Where S_{21}^{No-Tag} is associated with the measurement taken in the empty chamber, S_{21}^{Ref} corresponds to reference value taken from define setup which could be any conductive surface, In this case, a copper square of 50mm x 50mm is taken. σ^{Ref} is associated with the simulation results for the same reference. The results achieved for all the tags show a good agreement between the measured and simulated designs.

The radar equation is used [40] to evaluate the maximum read range of the RFID tag. For this, numerically calculated RCS are considered by using the equation is follows:

$$= \sqrt[4]{\frac{G_T\, G_R \lambda^2 \sigma^{Tag} P_T}{(4\pi)^3 P_{min}}} \quad (15)$$

Where G_T and G_R are the gains of the transmitting and receiving horn antennas, P_T is the power transmitted by VNA to measure RCS, λ is the wavelength. P_{min} is the minimum power receive by receiving antenna and σ^{Tag} is the experimental values of RCS obtained from (14). For maximum read range calculations σ^{Tag} is taken for 1111bit codes, see Figure 8. flat case. The average RCS is obtained from a series of experiments [1] is around 0.02 m^2. The maximum read range is evaluated for -10, -3 and 0dBm transmitted power from VNA and the maximum range observed is 1.80m and extendable to 2.15m for 3dBm power. Hence, a robust Bow-tie chipless RFID tag with transient analysis

is successfully designed fabricated and tested, which is applicable for the IoT applications and the read range of the tag and bit capacity can be increased in future by using the asymmetrical property of the tag.

Table 2: Maximum Read Range Estimation

P_{min}(dB)	G_T (dBi) G_R (dBi)	λ^2 (m)	σ^{Tag} (m^2)	P_T (dB)	R (m)
-70	10	1.06 x 10^{-3}	0.02	-10	1.01
				-3	1.52
				0	1.80
				3	2.15

6. Conclusion

This paper is an extension of Novel Bow-Tie Chipless RFID tag which studies SEM-based circuit modelling of the bow-tie-shaped tag. The electromagnetic response of the tag is presented and coupling coefficients are obtained by transient analysis. The behaviour of the RFID tag is completely studied and experimentally verified for different patterns of bitstreams measured in terms of RCS. The coupling coefficients measured in this analysis evaluated for the values of the maximum and the minimum distances between two consecutive rings at corresponding resonance of 9.2, 11.3, 14 and 16.9 GHz. The maximum value of R_n from the table is -0.021 which is a adequately low value that would not impact the reliable coding of the information. Furthermore, the bending on Flexible Chip-less Bow-Tie RFID tag operating within the range of 8-18GHz are described up to the maximum bend of 14mm and the information stored on a bent chip-less RFID tag made of PET is successfully recovered. Finally, the maximum read range for the RFID tag is evaluated which is 1.8m for 0dBm power but extendable to 2.15m for higher powers. This range is maximum to our knowledge for such a high-frequency range of 8-18GHz.

Conflict of Interest

The authors declare no conflict of interest.

Acknowledgement

I would like to acknowledge the great contribution of my research colleague Panagiotis Ioannis Theoharis, for helping me in the measurements and the fabrications of the tags.

References

[1] M.U.A. Khan, R. Raad, J. Foroughi, F.E. Tubbal, J. Xi, "Novel Bow-Tie Chip-less RFID Tag for Wearable Applications," in 2019 19th International Symposium on Communications and Information Technologies (ISCIT), IEEE: 10–13, 2019, https://doi.org/10.1109/iscit.2019.8905208.

[2] M. Younan, E.H. Houssein, M. Elhoseny, A.A. Ali, "Challenges and recommended technologies for the industrial internet of things: A comprehensive review," Measurement, **151**, 107198, 2020, https://doi.org/10.1016/j.measurement.2019.107198.

[3] A. Čolaković, M. Hadžialić, "Internet of Things (IoT): A review of enabling technologies, challenges, and open research issues," Computer Networks, **144**, 17-39, 2018, https://doi.org/10.1016/j.comnet.2018.07.017

[4] E. Jovanov, "Wearables Meet IoT: Synergistic Personal Area Networks (SPANs)," Sensors, **19**(19), 4295, 2019, https://doi.org/10.3390/s19194295

[5] T.M. Fernández-Caramés, P. Fraga-Lamas, "Towards the Internet of smart clothing: A review on IoT wearables and garments for creating intelligent connected e-textiles," Electronics, **7**(12), 405, 2018, 2018. https://doi.org/10.3390/electronics7120405

[6] Y. Leterrier, "Mechanics of curvature and strain in flexible organic electronic devices," Handbook of Flexible Organic Electronics: Materials, Manufacturing and Applications, 1, 2014, https://doi.org/10.1016/b978-1-78242-035-4.00001-4

[7] N.L. Pira, "Smart integrated systems and circuits using flexible organic electronics: Automotive applications," Handbook of Flexible Organic Electronics: Materials, Manufacturing and Applications, 345, 2014, https://doi.org/10.1016/b978-1-78242-035-4.00014-2

[8] R. Anwar, L. Mao, H. Ning, R. Atakan, H.A. Tufan, S. uz Zaman, C. Cochrane, S.K. Bahadir, V. Koncar, F. Kalaoglu, B.A. Auld, C.E. Baum, D. Betancourt, K. Haase, A. Hübler, F. Ellinger, A.T. Blischak, M. Manteghi, A. Čolaković, L. Corchia, G. Monti, E. De Benedetto, A. Cataldo, L. Angrisani, P. Arpaia, L. Tarricone, F. Costa, S. Genovesi, A. Monorchio, et al., "The internet of things: How the next evolution of the internet is changing everything," IEEE Transactions on Antennas and Propagation, **59**(12), 1–4, 2014, https://doi.org/10.7551/mitpress/10277.003.0004

[9] L. Corchia, G. Monti, E. De Benedetto, A. Cataldo, L. Angrisani, P. Arpaia, L. Tarricone, "Fully-Textile, Wearable Chipless Tags for Identification and Tracking Applications," Sensors, **20**(2), 429, 2020, https://doi.org/10.3390/s20020429

[10] L. Corchia, G. Monti, L. Tarricone, "Durability of wearable antennas based on nonwoven conductive fabrics: Experimental study on resistance to washing and ironing," International Journal of Antennas and Propagation, **2018**, 2018, https://doi.org/10.1155/2018/2340293

[11] R. Atakan, H.A. Tufan, S. uz Zaman, C. Cochrane, S.K. Bahadir, V. Koncar, F. Kalaoglu, "Protocol to assess the quality of transmission lines within smart textile structures," Measurement, **152**, 107194, 2020, https://doi.org/10.1016/j.measurement.2019.107194

[12] Y. Wang, L. Li, B. Wang, L. Wang, "A body sensor network platform for in-home health monitoring application," in Proceedings of the 4th International Conference on Ubiquitous Information Technologies & Applications, IEEE: 1–5, 2009, https://doi.org/10.1109/icut.2009.5405731

[13] K. Finkenzeller, RFID handbook: fundamentals and applications in contactless smart cards, radio frequency identification and near-field communication, John Wiley & Sons, 2010, https://doi.org/10.1002/9780470665121

[14] D.K. Klair, K.-W. Chin, R. Raad, "A survey and tutorial of RFID anti-collision protocols," IEEE Communications Surveys & Tutorials, **12**(3), 400–421, 2010, https://doi.org/10.1109/surv.2010.031810.00037

[15] R. Rezaiesarlak, M. Manteghi, CHIPLESS RFID, Springer, 2016, https://doi.org/10.1007/978-3-319-10169-9_3

[16] J.P. Vinding, Interrogator-responder identification system, 1969.

[17] O.E. Rittenbach, Communication by radar beams, 1969, https://doi.org/10.1002/sce.3730530262

[18] R.M. Richardson, Remotely actuated radio frequency powered devices, 1963.

[19] R.F. Harrington, "Field measurements using active scatterers (correspondence)," IEEE Transactions on Microwave Theory and Techniques, **11**(5), 454–455, 1963, .https://doi.org/10.1109/tmtt.1963.1125707

[20] H. Khaleel, Innovation in wearable and flexible antennas, Wit Press, 2014, https://doi.org/10.2495/978-1-84564-986-9/008

[21] D.P. Morgan, "History of SAW devices," in Proceedings of the 1998 IEEE International Frequency Control Symposium (Cat. No. 98CH36165), IEEE: 439–460, 1998, https://doi.org/10.1109/freq.1998.717937

[22] B.A. Auld, Acoustic fields and waves in solids, Рипол Классик, 1973.

[23] V.D. Hunt, A. Puglia, M. Puglia, RFID: a guide to radio frequency identification, John Wiley & Sons, 2007.

[24] J. Foroughi, T. Mitew, P. Ogunbona, R. Raad, F. Safaei, "Smart Fabrics and Networked Clothing: Recent developments in CNT-based fibers and their continual refinement," IEEE Consumer Electronics Magazine, **5**(4), 105–111, 2016, https://doi.org/10.1109/mce.2016.2590220

[25] N.C. Karmakar, R. Koswatta, P. Kalansuriya, E. Rubayet, Chipless RFID reader architecture, Artech House, 2013.

[26] D. Betancourt, K. Haase, A. Hübler, F. Ellinger, "Bending and folding effect study of flexible fully printed and late-stage codified octagonal chipless RFID tags," IEEE Transactions on Antennas and Propagation, **64**(7), 2815–2823, 2016, https://doi.org/10.1109/tap.2016.2559522

[27] A.C. Durgun, C.A. Balanis, C.R. Birtcher, D.R. Allee, "Design, simulation, fabrication and testing of flexible bow-tie antennas," IEEE Transactions on Antennas and Propagation, **59**(12), 4425–4435, 2011, https://doi.org/10.1109/tap.2011.2165511

[28] F. Costa, S. Genovesi, A. Monorchio, "A chipless RFID based on

multiresonant high-impedance surfaces," IEEE Transactions on Microwave Theory and Techniques, **61**(1), 146–153, 2013, https://doi.org/10.1109/tmtt.2012.2227777

[29] M. Martinez, D. van der Weide, "Compact slot-based chipless RFID tag," in 2014 IEEE RFID Technology and Applications Conference (RFID-TA), IEEE: 233–236, 2014, https://doi.org/10.1109/rfid-ta.2014.6934234

[30] S. Rauf, M.A. Riaz, H. Shahid, M.S. Iqbal, Y. Amin, H. Tenhunen, "Triangular loop resonator based compact chipless RFID tag," IEICE Electronics Express, 14.20161262, 2017, https://doi.org/10.1587/elex.14.20161262

[31] M.A. Riaz, H. Shahid, S.Z. Aslam, Y. Amin, A. Akram, H. Tenhunen, "Novel T-shaped resonator based chipless RFID tag," IEICE Electronics Express, 14.20170728, 2017, https://doi.org/10.1587/elex.14.20170728

[32] R. Anwar, L. Mao, H. Ning, "Frequency selective surfaces: a review," Applied Sciences, **8**(9), 1689, 2018, https://doi.org/10.3390/app8091689

[33] A. Blischak, M. Manteghi, "Pole residue techniques for chipless RFID detection," in 2009 IEEE Antennas and Propagation Society International Symposium, IEEE: 1–4, 2009, https://doi.org/10.1109/aps.2009.5172097

[34] A.T. Blischak, M. Manteghi, "Embedded singularity chipless RFID tags," IEEE Transactions on Antennas and Propagation, **59**(11), 3961–3968, 2011, https://doi.org/10.1109/tap.2011.2164191

[35] R. Rezaiesarlak, M. Manteghi, "Complex-natural-resonance-based design of chipless RFID tag for high-density data," IEEE Transactions on Antennas and Propagation, **62**(2), 898–904, 2013, https://doi.org/10.1109/tap.2013.2290998

[36] C.E. Baum, The singularity expansion method, Springer: 129–179, 1976, https://doi.org/10.1007/3540075534_8

[37] J.-M. Jin, Theory and computation of electromagnetic fields, John Wiley & Sons, 2011, https://doi.org/10.1002/9780470874257

[38] M.U.A. Khan, R. Raad, J. Foroughi, F. Tubbal, P.I. Theoharis, M.S. Raheel, "Effects of Bending Bow-Tie Chipless RFID Tag for Different Polymer Substrates," in 2019 13th International Conference on Signal Processing and Communication Systems (ICSPCS), IEEE: 1–4, 2019, https://doi.org/10.1109/icspcs47537.2019.9008594

[39] A. Vena, E. Perret, S. Tedjini, "High-capacity chipless RFID tag insensitive to the polarization," IEEE Transactions on Antennas and Propagation, **60**(10), 4509–4515, 2012, https://doi.org/10.1109/tap.2012.2207347

[40] I.Y. Immoreev, "-Signal Waveform Variations in Ultrawideband Wireless Systems: Causes and Aftereffects," Ultrawideband Radar: Applications and Design, 71–104, 2012, https://doi.org/10.1201/b12356-4

ASTES

Advances in Science, Technology and Engineering Systems Journal Vol. 5, No. 5, 765-769 (2020)

www.astesj.com

Special Issue on Multidisciplinary Sciences and Engineering

ASTESJ

ISSN: 2415-6698

Brain Tumor Classification Using Deep Neural Network

Gökalp Çınarer[1,*], Bülent Gürsel Emiroğlu[2], Recep Sinan Arslan[1], Ahmet Haşim Yurttakal[1]

[1]*Bozok University, Computer Technologies Department, Yozgat-66100, Turkey*

[2]*Kırıkkale University, Computer Engineering Department, Kırıkkale-71451, Turkey*

ARTICLE INFO

Article history:
Received: 13 July, 2020
Accepted: 15 September, 2020
Online: 12 October, 2020

Keywords:
Brain Tumor
Classification
Deep Neural Network

ABSTRACT

Brain tumors are a type of tumor with a high mortality rate. Since multifocal-looking tumors in the brain can resemble multicentric gliomas or gliomatosis, accurate detection of the tumor is required during the treatment process. The similarity of neurological and radiological findings also complicates the classification of these tumors. Fast and accurate classification is important for brain tumors. Computer aided diagnostic systems and deep neural network architectures can be used in the diagnosis of multicentric gliomas and multiple lesions. In this study, the Deep Neural Network classification model with Synthetic Minority Over-sampling Technique pre-processing was used on the Visually Accessible Rembrandt Images dataset. The proposed model for the classification of brain tumors consists of 1319 trainable parameters and the proposed method has achieved 95.0% accuracy rate. Precision, Recall, F1-measure values are 95.4%, 95.0% and 94.9% respectively. The proposed decision support system can be used to give an idea to doctors in the detection of glioma type tumors.

1. Introduction

Brain tumors are tumor types located in the brain. The mortality rate is high. There are two different types: benign and malignant. Benign brain tumors, which have a slow growth rate, are easily separable from brain tissue. Malignant brain tumors grow faster and can damage nearby brain tissue[1]. There have been many successful studies in which computer were used in medical applications in recent years. Skin cancer [2], breast cancer [3], thyroid nodules [4] are some of these studies.

In addition, tumors originating from brain tissue are called primary brain tumors, while tumors formed by the splashing of cancerous cells that appear elsewhere in the body are called secondary brain tumors. The most common (65%) and most malignant brain tumor is glioblastoma [5]. Glioblastoma multiforme (GBM) is one of the deadliest cancer types and is a common type of malignant glioma in the central nervous system. With the development of computed tomography and magnetic resonance imaging (MRI), it has become increasingly clear that gliomas may have a multifocal or multicentric [6]. Although the diagnosis of multiple lesions becomes easier with the introduction of computed tomography into the field, the differential diagnosis of multiple cerebral lesions still remains a problem. In multifocal lesions, the lesions are localized in more than one part of the brain and there is a macroscopic or microscopic level relationship between them. In multicentric gliomas, there is neither macroscopic nor microscopic level relationship between lesions. The propagation path of multicentric lesions is unclear, but this situation is slightly different in multiple lesions. Multiple lesions create multiple cerebral areas using a systematic propagation pathway [7]. The correct detection of this condition is very important in the treatment of the disease.

Early diagnosis of brain tumors can change the course of the disease and save lives. On the other hand, computers perform complex operations in a very short time. Computers are used in many areas of life, especially in health, as it produces automatic, fast and accurate results. For this reason, computer-aided diagnostic (CAD) systems are frequently used today. CAD systems analyze the complex relationships in medical data and assist the doctor in decision making [8]. Salvati divided multifocal gliomas into four different categories. These are diffuse, multicentric, multiple and multi-organ. In addition, in his study, he divided his patients into multicentric and multifocal tumor groups and found that there was no significant difference between patients [9]. In a spike case, as malignant glial tumors damage nerve cells, it seems possible that the multicentricity of gliomas may also accompany multiple sclerosis [10]. DNN can learn quickly,

* Corresponding Author: Gökalp Çınarer, gokalp.cinarer@bozok.edu.tr

automatically identify features, and can be successfully applied in computer learning systems. Besides that, DNNs are also used in some medical image analysis. It can be preferred especially in brain tumor segmentation and classification. It is designed the DNN model to segment brain separate gray and white matter from cerebrospinal fluid and analyzed the segmentation accuracy with DNN [11]. Similarly DNN model for the segmentation of brain tumors is proposed [12].

In this study, Deep Neural Network (DNN) architecture was proposed to classify the MR brain image features as n/a, multifocal, multicentric and gliomatosis. Synthetic Minority Over-sampling Technique (SMOTE) was used as a pre-processing. It has been determined that the pre-processing has a significant effect on the classification success.

2. Material and Methods

2.1. Dataset

In the study, The Repository of Molecular Brain Neoplasia Data (REMBRANDT) dataset [13] was used. The REMBRANDT dataset is a dataset of The Cancer Imaging Archive (TCIA) database shared by the National Cancer Institute. TCIA is an accessible archive containing medical images [14]. This data set contains images of 33 patients. Each patient has an average of 20 MR images, on separate axial, sagittal and coronal planes. For each patient, there are feature key values provided by 3 different neuroradiologists from Thomas Jefferson University (TJU) Hospital. This feature set is called VASARI (Visually Accessible Rembrandt Images). VASARI dataset was used in the classification process.

2.2. SMOTE

SMOTE is a method used in unbalanced data. Every minority class sample is taken and synthetic samples are created by looking at any or the sample's entire k neighbour. Thus, the minority class is over-sampled [15]. The main difference from other sampling methods is the production of synthetic samples by looking at their neighbours, instead of copying and reproducing the minority class samples. Thus, it realizes class distribution without providing additional information.

2.3. Deep Neural Networks (DNN)

Machine learning technologies potentiate many technologies in the modern world. People use these technologies in many areas such as webcams, e-commerce activities, and mobile devices. In addition, it offers good results in complex problems. These are identifying objects from images, converting speech to text and matching web contents with the interests of the users. Traditional ML techniques have some limitations in processing raw data. Extracting features representing data in the raw form and converting them into feature vectors used as input for classifier is a difficult process that requires expertise [16].

Deep learning allows abstract representation of data by creating simple but nonlinear modules. In this way, it is possible to learn very complex functions. This structure reveals the distinguishing features between classes for classification problems. Deep learning produces successful results for many problems that cause problems in the advancement of artificial intelligence methods. It is used in many areas such as image recognition [17-19], speech processing [20, 21], and gene mutation prediction [22]. It is thought that DNN will make faster progress thanks to the new neural network structures proposed with an increase in computation capacity and amount of data [16].

Deep neural network structure is shown in Figure 1.

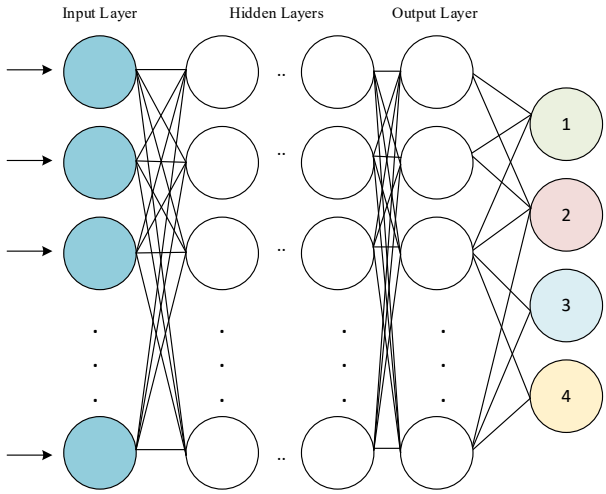


Figure 1: Deep Neural Network Schema [16]

The development of computer hardware structure and the widespread use of GPU architecture facilitates and speed up the training of the complex and multi-layered neural networks as shown in Figure 1. In this way, more outstanding [23].

The mathematical model used in the neural network training stage is shown in Eq-1.

$$f_{output} = af(m_n af(m_{n-1} \dots af(m_1 x))) \quad (1)$$

According to Equation, m_n represents the weight matrix in the nth layer and af is activation function. This structure gives better results than single-layer networks [24].

In this study, a deep neural network design with 1 input, 1 output and 2 hidden layer was designed.

The increasing of software technologies shaped under three specialized topics such as artificial intelligence, machine learning and deep learning has caused an increase in interest in these three subjects. Deep Neural Networks finds the relationship between a range of inputs and outputs. Successful results in many areas such as image processing, natural language processing, voice recognition [25].

3. Results

The application was carried out on the open source Python program. Tensorflow and Keras libraries were used. The count plot of the data to be classified into classes is given in Figure 2.

All images included in the Rembrandt data set consist of axial, sagittal and coronal image planes with an average of 20 images per plane for a total of 33 patients. In the data set, 30 different features were obtained from each tumor brain MR image. Rembrandt images (VASARI) were analyzed by three TJU radiologists and features of the images were extracted. In this way, a data set

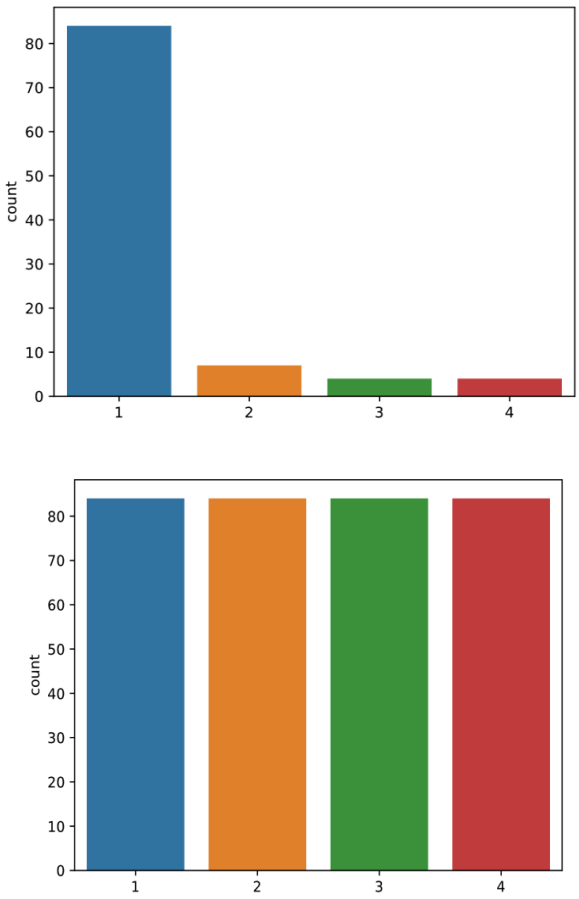


Figure 3: Count plot of data after SMOTE

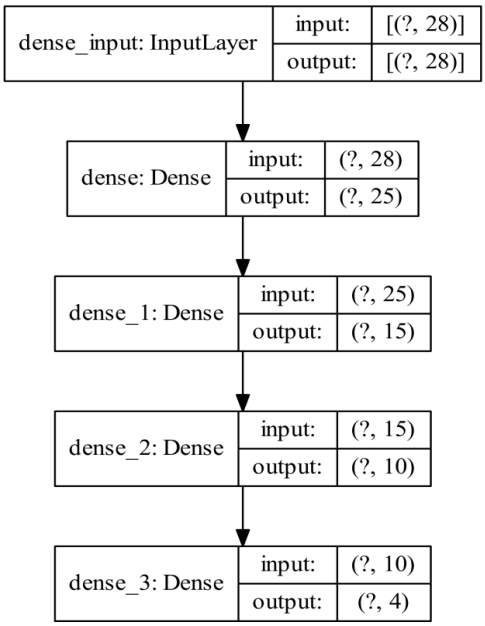


Figure 4: Proposed DNN Model

consisting of 99 patients and 30 different characteristic features used in the study. The data were classified according to n/a, multifocal, multicentric and gliomatosis. The data appears to be unbalanced. (84 n/a patient, 7 multifocal patient, 4 multicentric patient and 4 gliomatosis patient). For this reason, SMOTE pre-treatment was applied. Figure 3 shows the count plot after the SMOTE pre-processing.

The proposed DNN model is given in Figure 4. There are 3 hidden layers in the model, having 25, 15, and 10 filters, respectively. Model includes 1319 trainable parameters.

The activation function used in hidden layers is ReLu. The activation function used in the output layer is SoftMax. The optimizer who used the error back propagation phase is Adam. In this study, the data set was formed as 70% training and 30% test group. Figure 5 shows the change in accuracy on training and test data over 100 epochs.

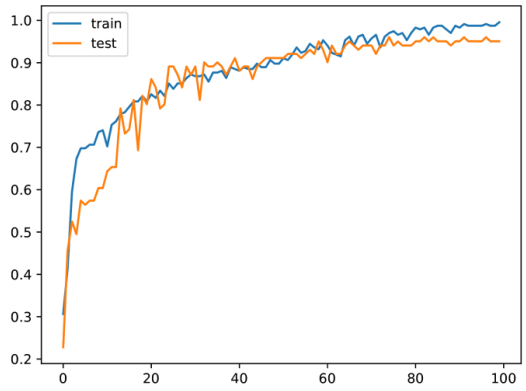


Figure 5: Accuracy graph

As can be seen from the graphic, the proposed method has overcome the over-fitting problem. Figure 6 shows confusion matrix.

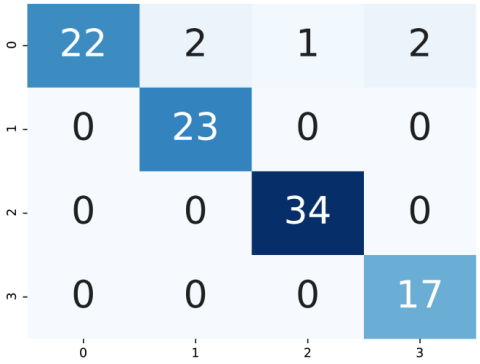


Figure 6: Confusion matrix

DNN model was used to categorize brain tumors into four classes (n / a, multifocal, multicentric and gliomatosis). Four basic measurement indicators were used when evaluating the classification results. The proposed DNN classifier knew the opinion of radiologists with 95% accuracy. The success rate of the model was also examined with other performance metrics such as precision recall and F1. Respectively Precision, Recall, F1-measure values are 0.954, 0.950 and 0.949.

4. Discussion

Deep learning methods are used in many research fields of medical image analysis, from image recording, radiomic feature

selection, segmentation and classification. Estimating the type of brain tumors is quite difficult and troublesome in the medical field.The aim of this study is to classify MR images of brain tumors as n/a, multifocal, multicentric and gliomatosis. In this study, unlike other studies, multiple cerebral lesions were classified. These lesions can have similar features and are difficult to classify. Studies in the literature determine tumor levels or predict whether the tumor is benign or malignant. Kumar and Vijay Kumar classified brain images as tumors and non-tumors using the Feed Forwarded Artificial neural network-based classifier and reached 91.17% accuracy with the ensemble classifier [26]. Glioblastoma and low-grade gliomas using logistic regression algorithm is classified with 0.88 accuracy [27]. Mahajani classified the MRI brain image as normal or abnormal with Back Propagation Neural Network (BPNN) and K Nearest Neighbor (KNN) algorithms. 70% accuracy using the KNN classifier and 72.5% accuracy using the BPNN classifier [28]. In the literature this dataset was tested with KNN, Random Forest (RF), Support Vector Machines (SVM), Linear Discriminant Analysis (LDA) machine learning algorithms. SVM algorithm with 90% accuracy rate was found to be better compared to other algorithms [29]. As seen in the examples, machine learning algorithms are commonly used approaches in classification. However, since deep learning models can analyze complex relationships effectively, it has gained an important place in machine learning in recent years. In another study, VGG-19 architecture used to classify brain tumors grades (I, II, III and IV) and achieve 0.90 accuracy and 0.96 average precision [30]. Also, in the other study it is classified the grades of glioma tumor using Convolutional Neural Networks (CNN) with an accuracy of 91.16% [31]. Compared to other algorithms, it has been seen that the applied method has advantages over traditional classifier algorithms. The complexity of the brain structure in the analysis of the brain image and the lack of imaging standards prevent the correct application of computer-aided learning systems in classifying brain tumors. Therefore, radiologist views come to the fore in determining these criteria. Table 1 shows some deep learning studies in the literature.

Table 1: Deep learning approaches for brain tumor classification

Aim and Method	Accuracy
Tumor Segmentation-DNN[32]	0.88
Brain Tumour, CNN[33]	91.43
Brain Tumour, Capsule Network[34]	86.56
Brain Tumoru, DNN[35]	90.66

In addition, proposed classification model can be tested with different parameters and radiomic features. Obtaining the data by experienced radiologists and determining the radiologist views with high accuracy is an indicator of the success of the algorithm. The Deep Learning approach facilitates researchers and trains the model using its own hyper parameters without specifying many features beforehand. But it is very important to apply the correct parameters to the model. In this study, the deep learning model was used and high accuracy was obtained with the correct parameters applied.

5. Conclusion

In the article, multifocal, multicentric and gliomatosis classification of brain tumors with SMOTE pre-processing of the DNN model were examined. The results show that the proposed method is very successful. The proposed method gives automatic, fast and accurate results. It can give an idea as a second look when doctors are unstable.

Conflict of Interest

The authors declare no conflict of interest.

Acknowledgment

No funding,

References

[1] J.C. Buckner, P.D. Brown, B.P. O'Neill, F.B. Meyer, C.J. Wetmore, J.H. Uhm, "Central nervous system tumors," in Mayo Clinic Proceedings, 2007, doi:10.4065/82.10.1271.

[2] N. Razmjooy, M. Ashourian, M. Karimifard, V. V. Estrela, H.J. Loschi, D. do Nascimento, R.P. França, M. Vishnevski, "Computer-Aided Diagnosis of Skin Cancer: A Review," Current Medical Imaging Formerly Current Medical Imaging Reviews, 2020, doi:10.2174/1573405616666200129095242.

[3] J.Y. Kim, J.J. Kim, L. Hwangbo, H.B. Suh, S. Kim, K.S. Choo, K.J. Nam, T. Kang, "Kinetic heterogeneity of breast cancer determined using computer-aided diagnosis of preoperative MRI scans: Relationship to distant metastasis-free survival," Radiology, 2020, doi:10.1148/radiol.2020192039.

[4] D. Fresilli, G. Grani, M.L. De Pascali, G. Alagna, E. Tassone, V. Ramundo, V. Ascoli, D. Bosco, M. Biffoni, M. Bononi, V. D'Andrea, F. Frattaroli, L. Giacomelli, Y. Solskaya, G. Polti, P. Pacini, O. Guiban, R. Gallo Curcio, M. Caratozzolo, V. Cantisani, "Computer-aided diagnostic system for thyroid nodule sonographic evaluation outperforms the specificity of less experienced examiners," Journal of Ultrasound, 2020, doi:10.1007/s40477-020-00453-y.

[5] H. Ohgaki, P. Kleihues, Epidemiology and etiology of gliomas, Acta Neuropathologica, 2005, doi:10.1007/s00401-005-0991-y.

[6] C.G. Patil, P. Eboli, J. Hu, Management of Multifocal and Multicentric Gliomas, Neurosurgery Clinics of North America, 2012, doi:10.1016/j.nec.2012.01.012.

[7] R.P. Thomas, L.W. Xu, R.M. Lober, G. Li, S. Nagpal, "The incidence and significance of multiple lesions in glioblastoma," Journal of Neuro-Oncology, 2013, doi:10.1007/s11060-012-1030-1.

[8] T.R. Jensen, K.M. Schmainda, "Computer-aided detection of brain tumor invasion using multiparametric MRI," Journal of Magnetic Resonance Imaging, 2009, doi:10.1002/jmri.21878.

[9] M. Salvati, L. Cervoni, P. Celli, R. Caruso, F.M. Gagliardi, "Multicentric and multifocal primary cerebral tumours. Methods of diagnosis and treatment," Italian Journal of Neurological Sciences, 1997, doi:10.1007/BF02106225.

[10] L.C. Werneck, R.H. Scola, W.O. Arruda, L.F.B. Torres, "Glioma and multiple sclerosis: case report.," Arquivos de Neuro-Psiquiatria, 2002, doi:10.1590/S0004-282X2002000300024.

[11] P. Moeskops, M.A. Viergever, A.M. Mendrik, L.S. De Vries, M.J.N.L. Benders, I. Isgum, "Automatic Segmentation of MR Brain Images with a Convolutional Neural Network," IEEE Transactions on Medical Imaging, 2016, doi:10.1109/TMI.2016.2548501.

[12] P. Dvořák, B. Menze, "Local structure prediction with convolutional neural networks for multimodal brain tumor segmentation," in Lecture Notes in Computer Science (including subseries Lecture Notes in Artificial Intelligence and Lecture Notes in Bioinformatics), 2016, doi:10.1007/978-3-319-42016-5_6.

[13] L. Scarpace, A.E. Flanders, R. Jain, T. Mikkelsen, D.W. Andrews, "Data From REMBRANDT," The Cancer Imaging Archive, 2015, doi:10.7937/K9/TCIA.2015.588OZUZB.

[14] K. Clark, B. Vendt, K. Smith, J. Freymann, J. Kirby, P. Koppel, S. Moore, S. Phillips, D. Maffitt, M. Pringle, L. Tarbox, F. Prior, "The cancer imaging archive (TCIA): Maintaining and operating a public information repository," Journal of Digital Imaging, 2013, doi:10.1007/s10278-013-9622-7.

[15] N. V. Chawla, K.W. Bowyer, L.O. Hall, W.P. Kegelmeyer, "SMOTE: Synthetic minority over-sampling technique," Journal of Artificial Intelligence Research, 2002, doi:10.1613/jair.953.

[16] W. Liu, Z. Wang, X. Liu, N. Zeng, Y. Liu, F.E. Alsaadi, "A survey of deep neural network architectures and their applications," Neurocomputing, 2017, doi:10.1016/j.neucom.2016.12.038.
[17] H. Fujiyoshi, T. Hirakawa, T. Yamashita, Deep learning-based image recognition for autonomous driving, IATSS Research, 2019, doi:10.1016/j.iatssr.2019.11.008.
[18] G. Hu, C. Yin, M. Wan, Y. Zhang, Y. Fang, "Recognition of diseased Pinus trees in UAV images using deep learning and AdaBoost classifier," Biosystems Engineering, 2020, doi:10.1016/j.biosystemseng.2020.03.021.
[19] M. Trokielewicz, A. Czajka, P. Maciejewicz, "Post-mortem iris recognition with deep-learning-based image segmentation," Image and Vision Computing, 2020, doi:10.1016/j.imavis.2019.103866.
[20] A.L. Maas, P. Qi, Z. Xie, A.Y. Hannun, C.T. Lengerich, D. Jurafsky, A.Y. Ng, "Building DNN acoustic models for large vocabulary speech recognition," Computer Speech and Language, 2017, doi:10.1016/j.csl.2016.06.007.
[21] J. Novoa, J. Fredes, V. Poblete, N.B. Yoma, "Uncertainty weighting and propagation in DNN–HMM-based speech recognition," Computer Speech and Language, 2018, doi:10.1016/j.csl.2017.06.005.
[22] M.K.K. Leung, H.Y. Xiong, L.J. Lee, B.J. Frey, "Deep learning of the tissue-regulated splicing code," Bioinformatics, 2014, doi:10.1093/bioinformatics/btu277.
[23] A. Yiğit, "İŞ SÜREÇLERİNDE İNSAN GÖRÜSÜNÜ DERİN ÖĞRENME İLE DESTEKLEME," Trakya Üniversitesi, Fen Bilimleri Enstitüsü, Yayınlanmış Yüksek Lisans Tezi, 2017.
[24] G.E. Dahl, T.N. Sainath, G.E. Hinton, "Improving deep neural networks for LVCSR using rectified linear units and dropout," in ICASSP, IEEE International Conference on Acoustics, Speech and Signal Processing - Proceedings, 2013, doi:10.1109/ICASSP.2013.6639346.
[25] Y. Zhang, M. Pezeshki, P. Brakel, S. Zhang, C. Laurent, Y. Bengio, A. Courville, "Towards end-to-end speech recognition with deep convolutional neural networks," in Proceedings of the Annual Conference of the International Speech Communication Association, INTERSPEECH, 2016, doi:10.21437/Interspeech.2016-1446.
[26] P. Kumar, B. Vijay Kumar, "Brain tumor MRI segmentation and classification using ensemble classifier," International Journal of Recent Technology and Engineering, 2019.
[27] K.L.C. Hsieh, C.M. Lo, C.J. Hsiao, "Computer-aided grading of gliomas based on local and global MRI features," Computer Methods and Programs in Biomedicine, 2017, doi:10.1016/j.cmpb.2016.10.021.
[28] P.P.S. Mahajani, "Detection and Classification of Brain Tumor in MRI Images," International Journal of Emerging Trends in Electrical and Electronics, 2013.
[29] G. Cinarer, B.G. Emiroglu, "Classificatin of Brain Tumors by Machine Learning Algorithms," in 3rd International Symposium on Multidisciplinary Studies and Innovative Technologies, ISMSIT 2019 - Proceedings, 2019, doi:10.1109/ISMSIT.2019.8932878.
[30] M. Sajjad, S. Khan, K. Muhammad, W. Wu, A. Ullah, S.W. Baik, "Multi-grade brain tumor classification using deep CNN with extensive data augmentation," Journal of Computational Science, 2019, doi:10.1016/j.jocs.2018.12.003.
[31] S. Khawaldeh, U. Pervaiz, A. Rafiq, R.S. Alkhawaldeh, "Noninvasive grading of glioma tumor using magnetic resonance imaging with convolutional neural networks," Applied Sciences (Switzerland), 2017, doi:10.3390/app8010027.
[32] M. Havaei, A. Davy, D. Warde-Farley, A. Biard, A. Courville, Y. Bengio, C. Pal, P.M. Jodoin, H. Larochelle, "Brain tumor segmentation with Deep Neural Networks," Medical Image Analysis, 2017, doi:10.1016/j.media.2016.05.004.
[33] J.S. Paul, A.J. Plassard, B.A. Landman, D. Fabbri, "Deep learning for brain tumor classification," in Medical Imaging 2017: Biomedical Applications in Molecular, Structural, and Functional Imaging, 2017, doi:10.1117/12.2254195.
[34] P. Afshar, A. Mohammadi, K.N. Plataniotis, "Brain Tumor Type Classification via Capsule Networks," in Proceedings - International Conference on Image Processing, ICIP, 2018, doi:10.1109/ICIP.2018.8451379.
[35] D. Nie, H. Zhang, E. Adeli, L. Liu, D. Shen, "3D deep learning for multi-modal imaging-guided survival time prediction of brain tumor patients," in Lecture Notes in Computer Science (including subseries Lecture Notes in Artificial Intelligence and Lecture Notes in Bioinformatics), 2016, doi:10.1007/978-3-319-46723-8_25.

ASTES

Advances in Science, Technology and Engineering Systems Journal Vol. 5, No.5, 770-780 (2020)

www.astesj.com

Special Issue on Multidisciplinary Innovation in Engineering Science & Technology

ASTESJ

ISSN: 2415-6698

Using Classic Networks for Classifying Remote Sensing Images: Comparative Study

Khalid A. AlAfandy[*,1], Hicham Omara[2], Mohamed Lazaar[3], Mohammed Al Achhab[1]

[1]*ENSA, Abdelmalek Essaadi University, Tetouan, 93002, Morocco*

[2]*FS, Abdelmalek Essaadi University, Tetouan, 93002, Morocco*

[3]*ENSIAS, Mohammed V University in Rabat, 10000, Morocco*

ARTICLE INFO

Article history:
Received: 12 August, 2020
Accepted: 25 September, 2020
Online: 12 October, 2020

Keywords:
Remote Sensing Images
ResNet
VGG
DenseNet
CNN
NASNet
Deep Learning
Machine Learning

ABSTRACT

This paper presents a comparative study for using the deep classic convolution networks in remote sensing images classification. There are four deep convolution models that used in this comparative study; the DenseNet 196, the NASNet Mobile, the VGG 16, and the ResNet 50 models. These learning convolution models are based on the use of the ImageNet pre-trained weights, transfer learning, and then adding a full connected layer that compatible with the used dataset classes. There are two datasets are used in this comparison; the UC Merced land use dataset and the SIRI-WHU dataset. This comparison is based on the inspection of the learning curves to determine how well the training model is and calculating the overall accuracy that determines the model performance. This comparison illustrates that the use of the ResNet 50 model has the highest overall accuracy and the use of the NASNet Mobile model has the lowest overall accuracy in this study. The DenseNet 169 model has little higher overall accuracy than the VGG 16 model.

1. Introduction

With rapid development of communication sciences especially satellites and cameras, the remote sensing images appeared with the importance of processing and dealing with this type of images (remote sensing images). One of these important image processing is classification which done by machine learning technology. Machine learning is one of the artificial intelligence branches that based on training computers using real data which result that computers will have good estimations as an expert human for the same type of data [1]. In 1959 the machine learning had a definition that "The machine learning is the field of study that gives computers the ability to learn without being explicitly programmed", this definition was made by Arthur Samuel [2]. Where the declaration of machine learning problem was known as "a computer program is said to learn from experience E with respect to some task T and some performance measure P", this declaration was made by Tom Mitchell in 1998 [3]. Deep learning is a branch of machine learning that depends on the Artificial Neural Networks (ANNs) which can be used in the remote sensing images classification [4]. In the recent years, with the appearance of the latest satellites versions and its updated cameras with high spectral and spatial resolution, the very high resolution (VHR) remote sensing images appeared. The redundancy pixels in the VHR remote sensing images can cause an over-fitting problem through training process where used the ordinary machine learning or ordinary deep learning in classification. So it must optimize the ANNs and have a convenient feature extraction from remote sensing images as a preprocessing before training the dataset [5-6]. The convolution Neural Networks (CNNs) is derived from the ANNs but its layers are not fully connected like the ANNs layers; it has an excited rapid advance in computer vision [7]. It is based on some blocks can applied on an image as filters and then extract convolution object features from this image, these features can be used in solving many of computer vision problems, one of these problems is classification [8]. The need of processing the huge data, which appeared with the advent of the VHR remote sensing images and its rapid development, produced the need of CNNs deep architectures that can produce a high accuracy in classification problems. It caused the appearance of the classic networks. There are many classic networks that are mentioned in the research papers which are established by researchers. However, this paper will inspect four of the well-known classic networks; the DenseNet

[*]Corresponding Author: Khalid A. AlAfandy, +212635549566, khalid_yuosif@yahoo.com

169, the NASNet Mobile, the VGG 16, and the ResNet 50 models. These four network models are used in the classification researches for the remote sensing images in many research papers. In [9], authors used the DenseNet in their research to propose a new model for improved the classification accuracy. In [10], authors used the DenseNet model to build dual channel CNNs for hyper-spectral images feature extraction. In [11], authors proposed a convolutional network based on the DenseNet model for remote sensing images classification. They build a small number of convolutional kernels using dense connections to produce a large number of reusable feature maps, which made the network deeper, but did not increase the number of parameters. In [12], authors proposed a remote sensing image classification method that based on the NASNet model. In [13], authors used the NASNet model as a feature descriptor which improved the performance of their trained network. In [14], authors proposed the RS-VGG classifier for classifying the remote sensing images which used the VGG model. In [15], authors proposed a combination between the CNNs algorithms outputs, one of these algorithms outputs is the outputs of the VGG model, and then constructed a representation of the VHR remote sensing images for resulting VHR remote sensing images understanding. In [16], authors used the pre-trained VGG model to recognize the airplanes using the remote sensing images. In [17], authors performed a fully convolution network that based on the VGG model for classifying the high spatial resolution remote sensing images. They fine-tuned their model parameters by using the ImageNet pre-trained VGG weights. In [18], authors proposed the use of the ResNet model to generate a ground scene semantics feature from the VHR remote sensing images, then concatenated with low level features to generate a more accurate model. In [19], authors proposed a classification method based on collaborate the 3-D separable ResNet model with cross-sensor transfer learning for hyper-spectral remote sensing images. In [20], authors used the ResNet model to propose a novel method for classifying forest tree species using high resolution RGB color images that captured by a simple grade camera mounted on an unmanned aerial vehicle (UAV) platform. In [21], authors proposed an aircraft detection methods based on the use of the deep ResNet model and super vector coding. In [22], authors proposed a remote sensing image usability assessment method based on the ResNet model by combining edge and texture maps.

The aim of this paper is to compare the using of the deep convolution models classic networks in classifying the remote sensing images. The used networks in this comparison are the DenseNet 196, the NASNet Mobile, the VGG 16, and the ResNet 50 models. This comparative study is based on inspecting the learning curves for the training and validation loss and training and validation accuracy through training process for each epoch. This inspection is done to determine the efficient of the model hyper-parameters selection. It is based also on calculating the overall accuracy (OA) of these four models in remote sensing images classification to determine the learning model performance. There are two use datasets in this comparative; the UC Merced Land use dataset and the SIRI-WHU dataset.

The rest of this paper is organized as follow. Section 2 gives the methods. The experimental results and setup are shown in section 3. Section 4 presents the conclusions followed by the most relevant references.

2. The Methods

In this section the used models, in this comparative study, will explained with its structures. The classic networks that used in this study will illustrated in brief as literature review, ending with how to assess the performance of the learning models.

2.1. The Used Models

The feature extraction of remote sensing images is provided an important basis in remote sensing images analysis. So, in this study the deep classic convolution networks outputs considered as the main features that extracted from the remote sensing images. In these four networks, we used the ImageNet pre-trained weights because the train of new CNNs models requires a large amount of data. We transfer learning, add full connected (FC) layers with the output layer containing neurons number that equal the dataset classes number (21 for the UC Merced land use dataset and 12 for the SIRI-WHU dataset), and then train these (FC) layers.

In the DenseNet 169 model we transfer learning to the last hidden layer before the output layer (has 1664 neurons) and get the output of this network with the ImageNet pre-trained weights, then adding FC layer (output layer) with softmax activation.

In the NASNet Mobile model we transfer learning to the last hidden layer before the output layer (has 1056 neurons) and get the output of this network with the ImageNet pre-trained weights, then adding FC layer (output layer) with softmax activation.

In the VGG 16 model we transfer learning to the output of last max pooling layer (has shape 7, 7, 512) in block 5 that before the first FC layer and get the output of this network with the ImageNet pre-trained weights, then adding FC layer (output layer) with softmax activation.

In the ResNet 50 model we transfer learning to the last hidden layer before the output layer (has 2048 neurons) and get the output of this network with the ImageNet pre-trained weights, then adding FC layer (output layer) with softmax activation.

2.2. The Convolution Neural Networks (CNNs)

The CNNs are taken from the ANNs with exception that it is not fully connected layers. The CNNs are the best solution for computer vision which based on some of filters to reduce the image height and width and increase the number of channels together, then processing the output with full connected neural network layers (FCs) which reduce the input layer neurons, reduce training time, and increase the training model performance [23-25]. These filters values are initialized with many random functions which can be optimized.

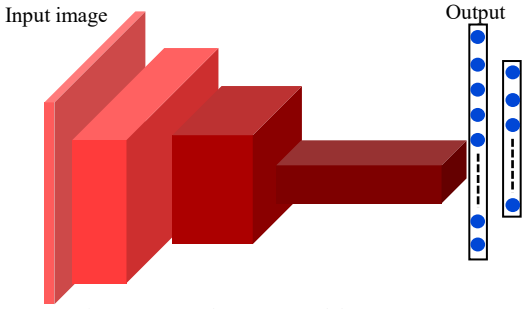


Figure 1: One of a CNNs model structures [25]

The filters design is based on the use of self-intuition as with ANNs structure design and learning hyper-parameters coefficient choice, which increasing the difficulty to reach the best solution for the learning problems [25]. Figure 1 shows an example of a CNNs model structure [24].

2.3. The DenseNet Model

In 2017, the DenseNets was proposed in the CVPR 2017 conference (Best Paper Award) [26]. They started from attempted to build a deeper network based on an idea that if the convolution network contains shorter connections between its layers close to the input and those close to the output, this deep convolution network can be more accurate and efficient to train. Other than the ResNet model which adds a skip-connection that bypass the nonlinear transformation, the DenseNet add a direct connection from any layer to any subsequent layer. So the l^{th} layer receives the feature-maps of all former layers x_0 to x_{l-1} as (1) [26].

$$x_l = H_l([x_0, x_1, \dots, x_{l-1}]) \quad (1)$$

where $[x_0, x_1, \dots, x_{l-1}]$ refers to the spectrum of the feature-map produced in the layers $0, 1, 2, \dots, l-1$.

Figure 2 shows the 5-layers dense block architecture and Table 1 shows the DenseNet 169 architectures for ImageNet. [26].

Table 1: the DenseNet 169 model architectures for ImageNet [26]

Layers	Output Size	DenseNet 169
Convolution	112×112	7×7 conv, stride 2
Pooling	56×56	3×3 max pool, stride 2
Dense Block (1)	56×56	$\begin{bmatrix}1\times1\text{ conv}\\3\times3\text{ conv}\end{bmatrix}\times 6$
Transition Layer (1)	56×56	1×1 conv
	28×28	2×2 average pool, stride 2
Dense Block (2)	28×28	$\begin{bmatrix}1\times1\text{ conv}\\3\times3\text{ conv}\end{bmatrix}\times 12$
Transition Layer (2)	28×28	1×1 conv
	14×14	2×2 average pool, stride 2
Dense Block (3)	14×14	$\begin{bmatrix}1\times1\text{ conv}\\3\times3\text{ conv}\end{bmatrix}\times 32$
Transition Layer (3)	14×14	1×1 conv
	7×7	2×2 average pool, stride 2
Dense Block (4)	7×7	$\begin{bmatrix}1\times1\text{ conv}\\3\times3\text{ conv}\end{bmatrix}\times 32$
Classification Layer	1×1	7×7 global average pool
	1000	1000D fully-connected, softmax

2.4. The NASNet Model

In 2017, the NASNet (Neural Architecture Search Net) model was proposed in the ICLR 2017 conference [27]. They used the recurrent neural networks (RNNs) to generate the model description of the neural networks and trained the RNNs with reinforcement learning to improve the accuracy of the generated architectures on a validation set. The NASNet model is based on indicting the previous layers that elected to be connected by adding an anchor point which has N-1 content-based sigmoid using (2). Figure 3 shows one block of a NASNet convolutional cell [27].

$$P(Layer\ j\ is\ an\ input\ of\ layer\ i) = sigmoid(v^T \tanh(W_{prev} * h_j + W_{curr} * h_i)) \quad (2)$$

where h_j refers to the hidden state of the controller at anchor point for the j^{th} layer and $j = [0, 1, 2, \dots, N-1]$.

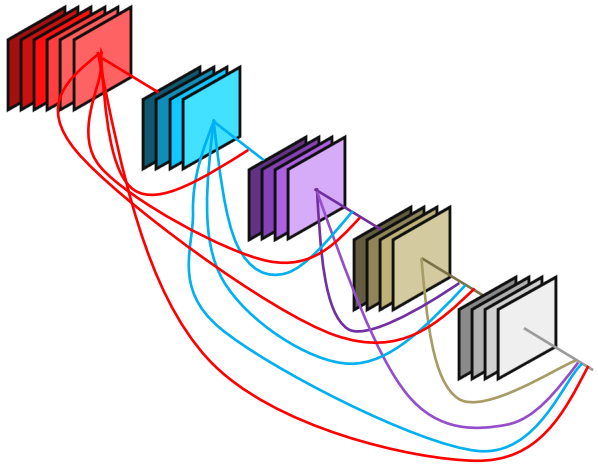


Figure 2: The 5 layers Dense block architecture [26]

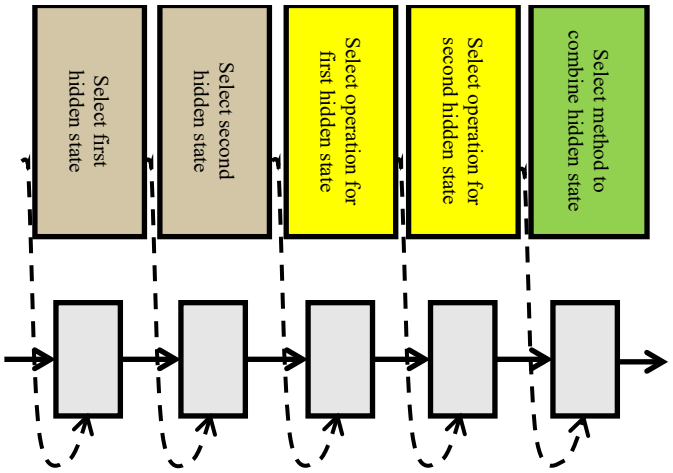


Figure 3: One block of a NASNet convolutional cell [27]

2.5. The VGG Model

In 2015, the VGG network was proposed in the ICLR 2015 conference [28]. They began with investigated the effect of the convolution network depth on its accuracy in the large-scale images. Through they evaluated the deeper networks architecture using (3×3) convolution filters, they showed that an expressive growth on the prior-art configurations can be achieved by pushed the depth to 16-19 weight layers. Table 2 shows the VGG 16 model architectures for the ImageNet [28].

Table 2: The VGG 16 model architectures for ImageNet [28]

Block	Layers	Output Size	VGG 16
Input		224×224×3	
Block 1	Convolution	224×224×64	3×3 conv 64, stride 1

	Convolution	224×224×64	3×3 conv 64, stride 1
	Pooling	112×112×64	2×2 max pool, stride 2
Block 2	Convolution	112×112×128	3×3 conv 128, stride 1
	Convolution	112×112×128	3×3 conv 128, stride 1
	Pooling	56×56×128	2×2 max pool, stride 2
Block 3	Convolution	56×56×256	3×3 conv 256, stride 1
	Convolution	56×56×256	3×3 conv 256, stride 1
	Convolution	56×56×256	3×3 conv 256, stride 1
	Pooling	28×28×256	2×2 max pool, stride 2
Block 4	Convolution	28×28×512	3×3 conv 512, stride 1
	Convolution	28×28×512	3×3 conv 512, stride 1
	Convolution	28×28×512	3×3 conv 512, stride 1
	Pooling	14×14×512	2×2 max pool, stride 2
Block 5	Convolution	14×14×512	3×3 conv 512, stride 1
	Convolution	14×14×512	3×3 conv 512, stride 1
	Convolution	14×14×512	3×3 conv 512, stride 1
	Pooling	7×7×512	2×2 max pool, stride 2
FC		4096	
FC		4096	
Output		1000, softmax	

The VGG network is a deeper convolution network that trained on the ImageNet dataset. The input images of this network is (224×244×3). This network consists of five convolution blocks, each block is containing convolution layers and pooling layer, then ending with two FC layers (each layer has 4096 neurons) then the output layer with softmax activation. The VGG network doesn't contain any layers connections or bypasses such as the ResNet, the NASNet or the DenseNet models, and at the same time gives high classification accuracy with the large scale images [28].

2.6. The ResNet Model

In 2016, the ResNet was proposed in the CVPR 2016 conference [29]. They combined the degradation problem by introducing a deep residual learning framework. Instead of intuiting each few stacked layers directly fit a desired underlying mapping. The ResNet is based on skip connections between deep layers. These skip connections can skipping one or more layers. The outputs of these connections are added to the outputs of the network stacked layers as (3) [29].

$$H(x) = F(x) + x \quad (3)$$

where H(x) is the final block output, x is the output of the connected layer, and F(x) is the output of the stacked networks layer in the same block.

Figure 4 shows the ResNet one building block. Tables 3 shows the ResNet 50 network architectures for the ImageNet [29].

Table 3: the ResNet 50 model architectures for ImageNet [29]

Layers	Output Size	ResNet 50
Conv 1	112×112	7×7 conv 64, stride 2
Conv 2_x	56×56	3×3 max pool, stride 2
		$\begin{bmatrix} 1\times1 \text{ Conv } 64 \\ 3\times3 \text{ Conve } 64 \\ 1\times1 \text{ Conv } 256 \end{bmatrix} \times 3$
Conv 3_x	28×28	$\begin{bmatrix} 1\times1 \text{ Conv } 128 \\ 3\times3 \text{ Conv } 128 \\ 1\times1 \text{ Conv } 512 \end{bmatrix} \times 4$
Conv 4_x	14×14	$\begin{bmatrix} 1\times1 \text{ Conv } 256 \\ 3\times3 \text{ Conve } 256 \\ 1\times1 \text{ Conv } 1024 \end{bmatrix} \times 6$
Conv 5_x	7×7	$\begin{bmatrix} 1\times1 \text{ Conv } 512 \\ 3\times3 \text{ Conve } 512 \\ 1\times1 \text{ Conv } 2048 \end{bmatrix} \times 3$
Classification Layer	1×1	7×7 global average pool
	1000	1000D fully-connected, softmax

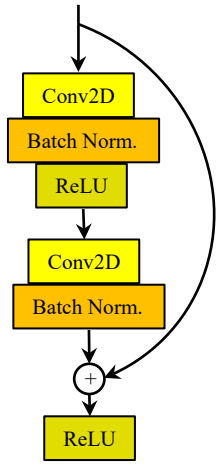


Figure 4: The ResNet building block [29]

2.7. The Performance Assessment

There are many matrices for gauge the performance of the learning models. One of these is the OA. The OA is the main classification accuracy assessment [30]. It is measure the percentage ratio between the corrected estimation test data objects and all the test data objects in the used dataset. The OA is calculated using (4) [30, 31].

$$\mathrm{OA} = \frac{Number\ of\ Correctly\ Estimations}{Total\ number\ of\ Test\ Data\ Objects} \times 100 \qquad (4)$$

The learning curves for the loss and the accuracy are very important indicator for determining the power of learning models through training process by using the corrected hyper-parameters [32]. By using these curves, you can determine if a problem exist on your learning model such as the over-fitting or the under-fitting problems. These curves represent the calculation of the loss and the accuracy values for the learning model at each epoch through the training process using training and validation data [32, 33].

3. Experimental Results and Setup

This comparative study is based on calculating the OA and plotting the learning curves to determine the power of the used hyper-parameter to achieved the better learning model performance. The UC Merced Land use dataset and the SIRI-WHU dataset are the used datasets in this study. The details of these datasets will introduce in this section and then the experiments setup details and the results.



Figure 5: Image examples from the 21 classes in the UC Merced land use dataset [34]

3.1. The UC Merced Land Use Dataset

The UC Merced Land use dataset is a collection of remote sensing images which has been prepared in 2010 by the University of California, Merced [34]. It consists of 2100 remote sensing images divided into 21 classes with 100 images for each class. These images were manually extracted from large images from the USGS National Map Urban Area Imagery collection for various urban areas around the USA. Each image in this dataset is Geo-tiff RGB image with 256×256 pixels resolution and 1 square foot (0.0929 square meters) spatial resolution [34]. Figure 5 shows image examples from the 21 classes in the UC Merced land use dataset [34].

3.2. The SIRI-WHU Dataset

The SIRI-WHU dataset is a collection of remote sensing images which the authors of [35] used this dataset in their classification problem research in 2016. This dataset consists of two versions that must complete each other. The total images in this dataset are 2400 remote sensing images divided into 12 classes with 200 images for each class. These images were extracted from Google Earth (Google inc.) and mainly cover urban areas in China. Each image in this dataset is Geo-tiff RGB image with 200×200 pixels resolution and 2 square meters (21.528 square foot) spatial resolution [35]. Figure 6 shows image examples with 12 classes in the SIRI-WHU dataset [35].

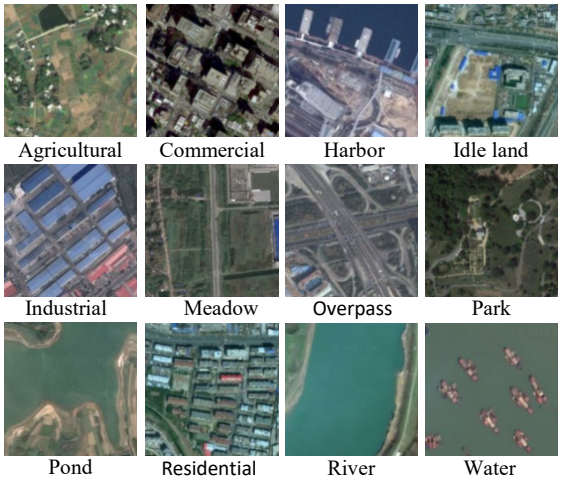


Figure 6: Image examples from the 12 classes in the SIRI-WHU dataset [35].

3.3. The Experimental Setup

The aim of this paper is to present a comparative study of using the classic networks for classifying the remote sensing images. This comparison is based on plotting the learning curves for the loss and the accuracy values, with every epoch, that be calculated through training process for the training and the validation data to determine the efficiency of the hyper-parameters values. The comparison is also based on the OA to assess each model performance. The used datasets in this study are the UC Merced land use dataset and the SIRI-WHU dataset where their details are stated in sections 3.1 and 3.2. All tests were performed using Google-Colab. The Google-Colab is a free cloud service hosted by Google inc. to encourage machine learning and artificial intelligence researches [36]. It is acts as a virtual machine (VM) that using 2-cores Xeon CPU with 2.3 GHz, GPU Tesla K80 with 12 GB GPU memory, 13 GB RAM, and 33GB HDD with Python 3.3.9. The maximum lifetime of this VM is 12 hours and it will be idled after 90 minutes time out [37]. Performing tests has been done by connecting to this VM online through ADSL internet line

with 4Mbps communication speed. This connection was done using an Intel® core™i5 CPU M450 @2.4GHz with 6 GB RAM and running Windows 7 64-bit operating system. This work is limited by used the ImageNet pre-trained weights because the train of new CNNs models needs a huge amount of data and more sophisticated hardware, this is unlike the lot of needed time consumed for this training process. The other limitation is that the input images shape is mustn't less than 200×200×3 and not greater than 300×300×3 because of the limitations of the pre-trained classic networks. The preprocessing step according to each network requirements is necessary to get efficient results; it must be as done on ImageNet dataset before training the models and produce the ImageNet pre-trained weights. The ImageNet pre-trained weights classic networks that used in this paper have input shape (224, 224, 3) and output layers 1000 nodes according to the ImageNet classes (1000 classes) [38, 39]. So, it must perform modifications on the learning algorithms that used these networks to be compatible with the used remote sensing images datasets as stated in section 2.1. The data in the used datasets were divided into 60% training set, 20% validation set, and 20% test set before training the last FC layers in each network model. The training process, using the training set and the validation set, is done for the model with a supposed number of epochs to determine the number of epochs that achieved the minimum validation loss. Thus, we consider that the assembling of the training set and the validation set are the new training data and then retrain the model with this new training set and the predetermined number of epochs that achieved the minimum validation loss. Finally test the model using the test set. It must be notice that, the learning parameters values, such as learning rate and batch size, were determined by intuition with taking in consideration the learning parameters values that used through training these models with the ImageNet dataset through producing the ImageNet pre-trained weights [26-29], where the used optimizer, the number of epochs, the additional activation and regularization layers, and the dropout regularization rates were determined by iterations and intuition. The classifier models are built using python 3.3.9, in addition to the use of the Tensorflow library for the preprocessing step and the Keras library for extracting features, training the last FC layers, and testing the models.

- In the DenseNet 196 model, the image resizing was done on the dataset images to have shape (224, 224, 3) to be compatible with the pre-trained DenseNet 196 model input shape, perform transfer learning to the 7×7 global average pooling layer that above the 1000D FC layer, and then add a FC layer, which has number of neurons equal to the used dataset classes, with softmax activation layer. The last layer weights were retrained with learning rate = 0.001, Adam optimizer and batch size = 256 with 100 epochs. The normalization preprocessing must be done on the dataset images before using on the DenseNet 169 model. Figure 7 shows the flow chart of the experimental algorithm that used the DenseNet 169 model.
- In the NASNet Mobile model, the image resizing was done on the dataset images to have shape (224, 224, 3) to be compatible with the pre-trained NASNet Mobile model input shape, perform transfer learning to the 7×7 global average pooling layer that above the 1000D FC layer, add a ReLU activation layer, dropout regularization layer with rate 0.5, and then adding a FC layer, which has number of neurons equal to the used dataset classes, with softmax activation layer. The last layer weights were retrained with learning rate = 0.001, Adam optimizer, and batch size = 64 with 200 epochs. The normalization preprocessing must be done on the dataset images before using on the NASNet Mobile model. Figure 8 shows the flow chart of the experimental algorithm that used the NASNet Mobile model.

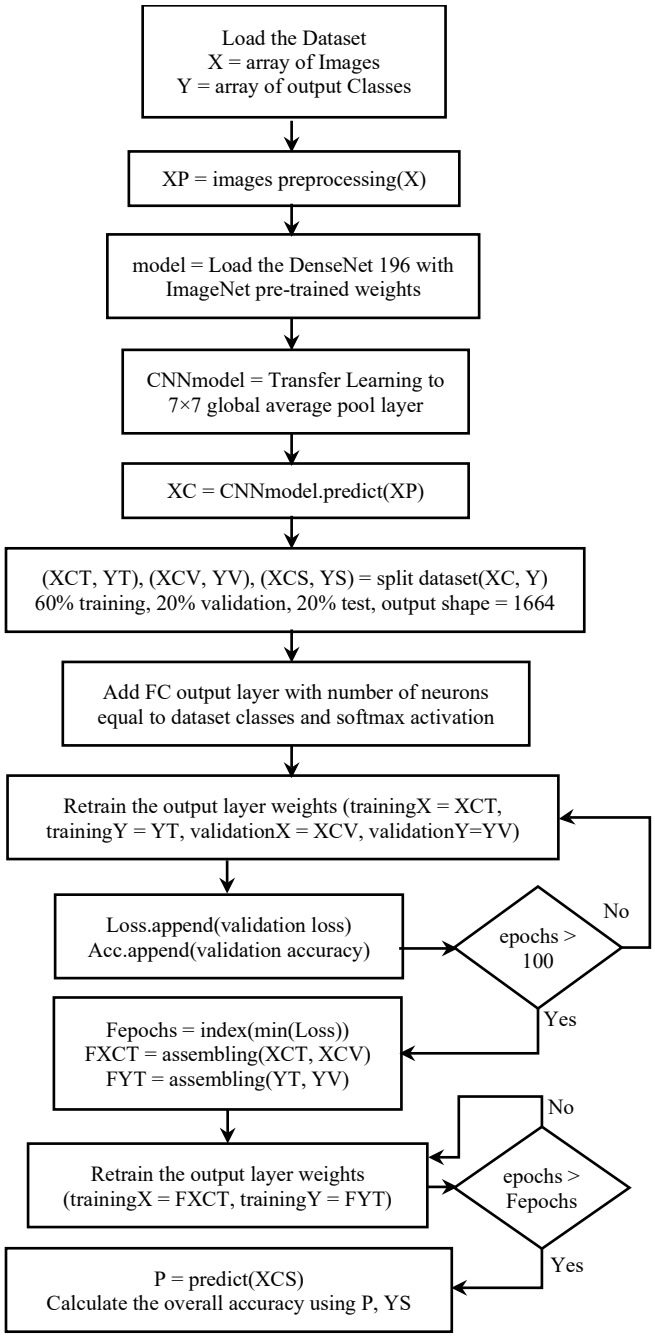


Figure 7: The flow chart of the experimental algorithm that used the DenseNet 169 model

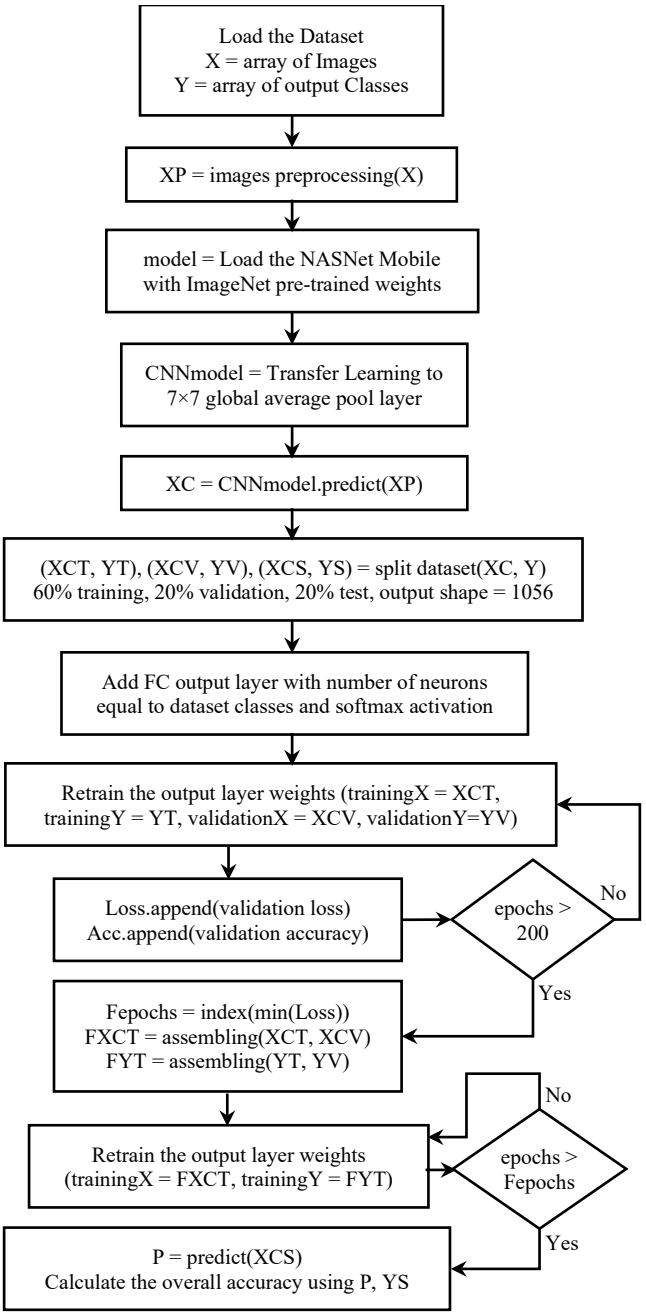


Figure 8: The flow chart of the experimental algorithm that used the NASNet Mobile model

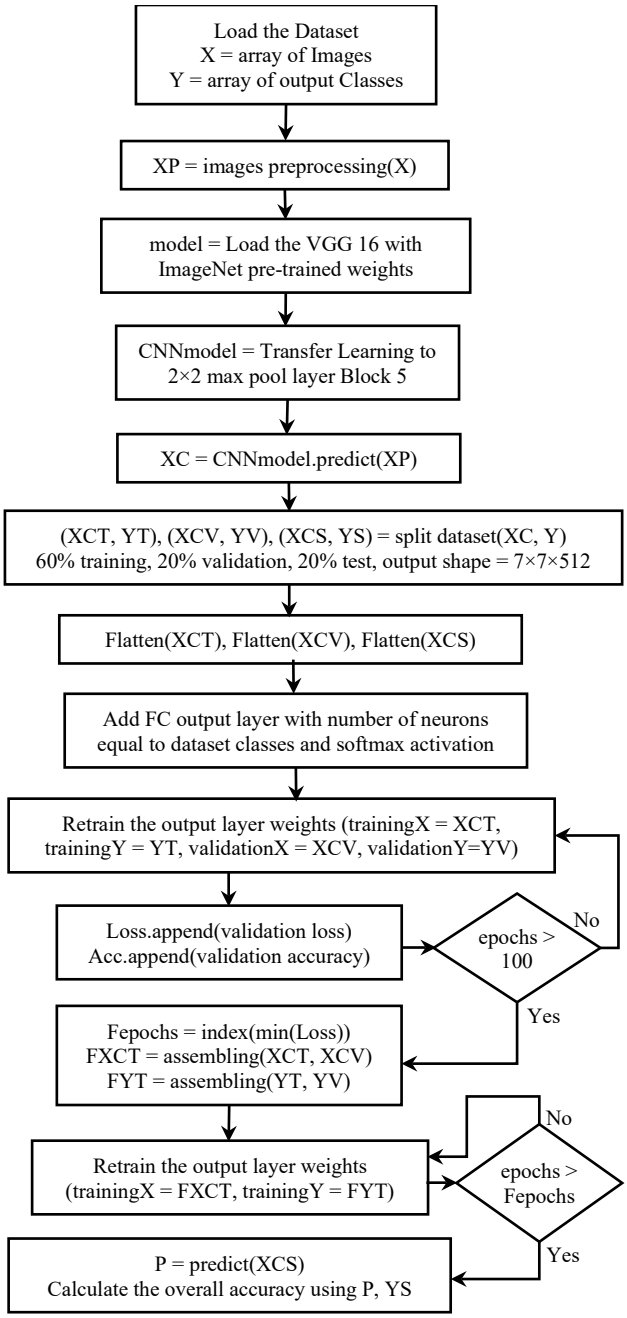


Figure 9: The flow chart of the experimental algorithm that used the VGG 16 model

- In the VGG 16 model, the image resizing was done on the dataset images to have shape (224, 224, 3) to be compatible with the pre-trained VGG 16 model input shape, perform transfer learning to the 2×2 max pooling layer in block 5, flatten the pooling layer output, add a ReLU activation layer, dropout regularization layer with rate 0.77, and then add a FC layer, which has number of neurons equal to the used dataset classes, with softmax activation layer. The last layer weights were retrained with learning rate = 0.001, Adam optimizer, and batch size = 64 with 100 epochs. The image conversion to the BGR mode preprocessing must be done on the dataset images before using on the VGG 16 model. Figure 9 shows the flow chart of the experimental algorithm that used the VGG 16 model.

- In the ResNet 50 model, the image resizing was done on the dataset images to have shape (224, 224, 3) to be compatible with the pre-trained ResNet 50 model input shape, perform a transfer learning to the 7×7 global average pooling layer that above the 1000D FC layer, and then add a FC layer, which has number of neurons equal to the used dataset classes, with softmax activation layer. The last layer weights were retrained with learning rate = 0.1, Adam optimizer, and batch size = 64 with 200 epochs. The image conversion to the BGR mode preprocessing must be done on the dataset images before using on the ResNet 50 model. Figure 10 shows the flow chart of the experimental algorithm that used the ResNet 50 model.

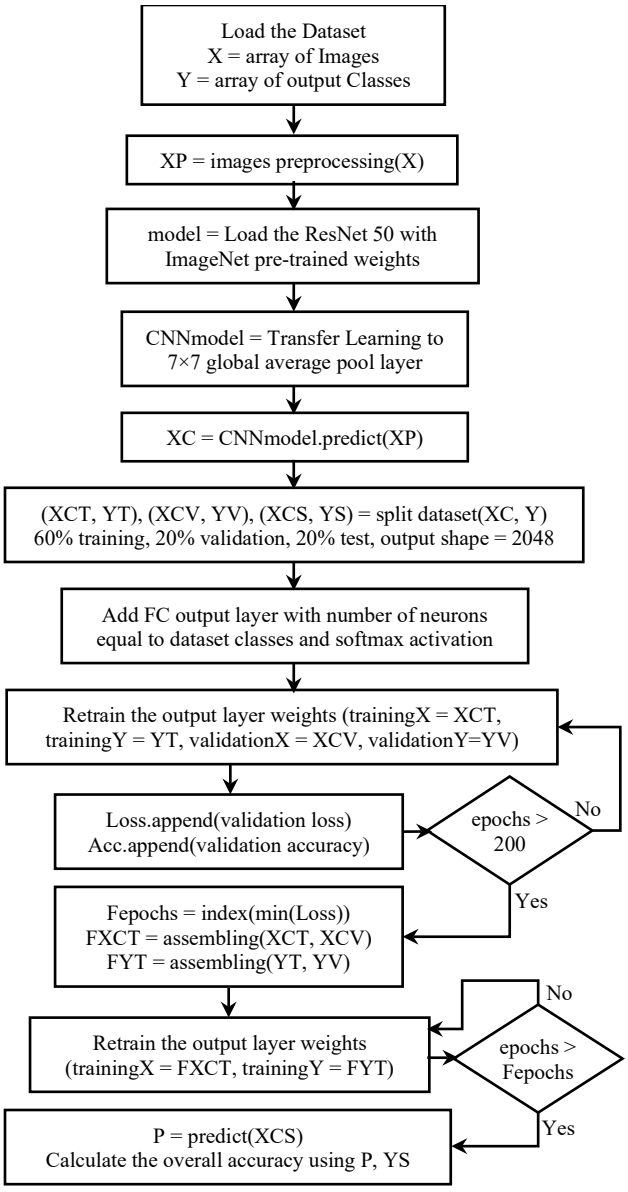
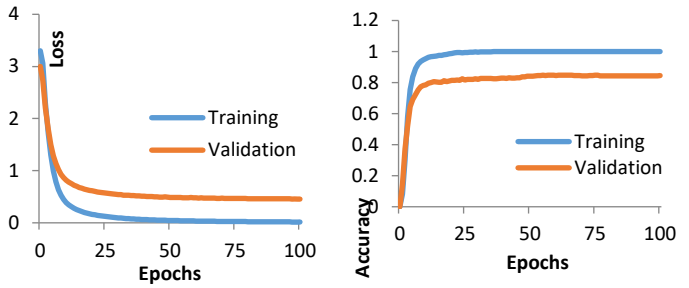
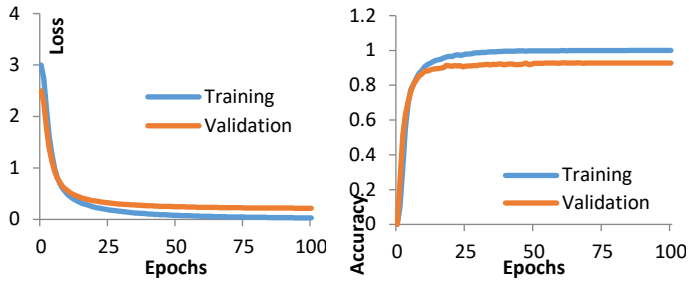


Figure 10: The flow chart of the experimental algorithm that used the ResNet 50 model

With the use of the stated convolution models in this study for classifying remote sensing images, through the training process we used the training data (60% from the used dataset) and the validation data (20% from the used dataset). Figure 11 shows the loss and the accuracy learning curves respectively for training the DenseNet 169 model, (a) for using the UC Merced land use dataset and (b) for using the SIRI-WHU dataset. Figure 12 shows the loss and the accuracy learning curves respectively for training the NASNet Mobile model, (a) for using the UC Merced land use dataset and (b) for using the SIRI-WHU dataset. Figure 13 shows the loss and the accuracy learning curves respectively for training the VGG 16 model, (a) for using the UC Merced land use dataset and (b) for using the SIRI-WHU dataset. Figure 14 shows the loss and the accuracy learning curves respectively for training the ResNet 50 model, (a) for using the UC Merced land use dataset and (b) for using the SIRI-WHU dataset.

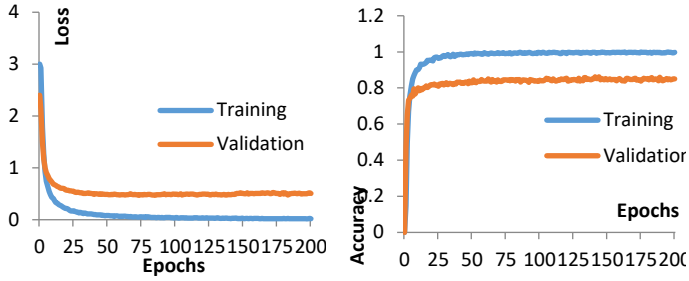


(a) Using the UC Merced land use dataset.

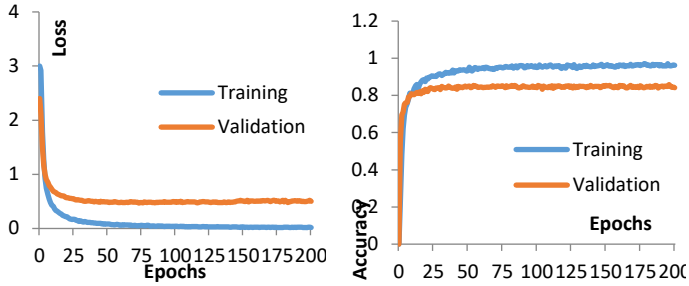


(b) Using the SIRI-WHU dataset.

Figure 11: The loss and the accuracy learning curves for training the DenseNet 169 model.

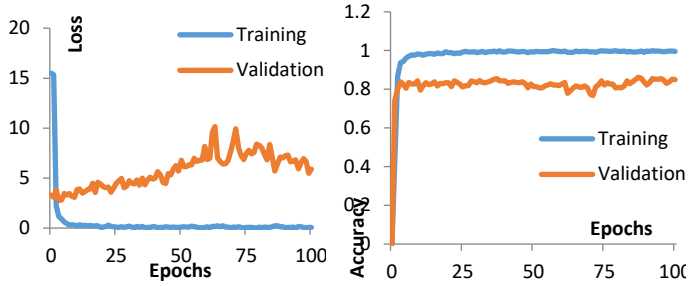


(a) Using the UC Merced land use dataset

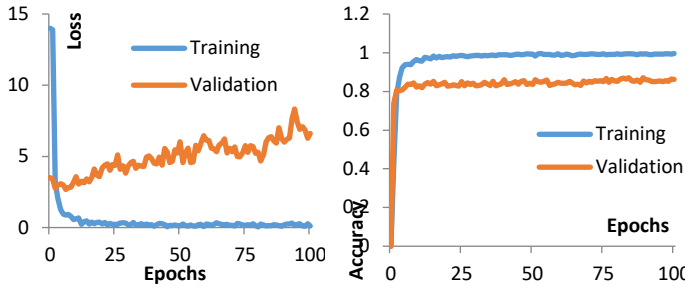


(b) Using the SIRI-WHU dataset

Figure 12: The loss and the accuracy learning curves for training the NASNet Mobile model.

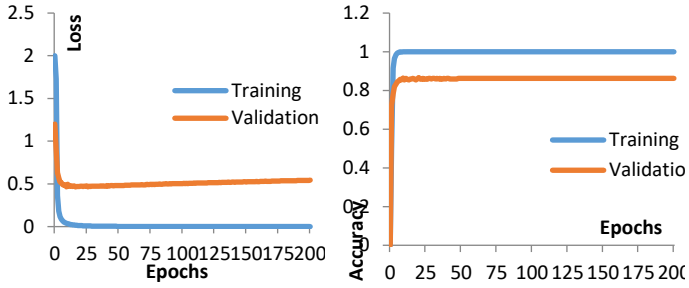


(a) Using the UC Merced land use dataset

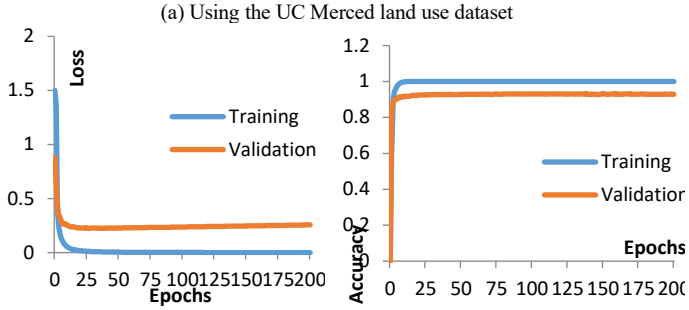


(b) Using the SIRI-WHU dataset

Figure 13: The loss and the accuracy learning curves for training the VGG 16 model.



(a) Using the UC Merced land use dataset



(b) Using the SIRI-WHU dataset

Figure 14: The loss and the accuracy learning curves for training the ResNet 50 model.

From the learning curves it can be determine the number of epochs that achieved the minimum validation loss in each model from the four models that discussed in this study. So, we consider that the training data and the validation data, 80% from dataset, are the new training data. Then, we repeat the same training process for each model with the same hyper-parameters values and the both datasets, and then calculate the OA using the predictions of the test data, 20% from the training set, to assess the performance of each model. Table 4 and figure 15 show the OA for each model using the both datasets.

Table 4: The OA for each model using the both datasets

	The UC Merced land use Dataset	The SIRI-WHU Dataset
The DenseNet 169 model	0.91	0.933
The NASNet Mobile model	0.876	0.896
The VGG 16 model	0.902	0.929
The ResNet 50 model	0.924	0.956

As shown from these results, the ResNet 50 model had the higher OA in this comparative study where the NASNet Mobile model had the lowest OA. In the other hand the OA for the DenseNet 169 model had little higher OA than the VGG 16 model. The use of the SIRI-WHU dataset had higher OA than the use of the UC Merced land use dataset. These results illustrated that the OA had an opposite relation with the dataset image resolution and the dataset number of classes, so the use of the SIRI-WHU dataset which has 12 classes, image resolution 200×200 pixels, and spatial resolution 2 square meters gave higher OA than the use of the UC Merced land use dataset which has 21 classes, image resolution 256×256 pixels, and spatial resolution 0.0929 square meter. The deeper convolution networks give considerable accuracy but the connections between layers may have another influence. The VGG 16 model gave good OA so it had efficient results but its learning curves had some degradation in its validation curves and near to the over-fitting in its training curves. So it may give better results with some additional researches that adjust the optimizations and regularization hyper-parameters. In the other hand the ResNet 50 model, that gave the higher OA in this study, had good learning curves with some little over-fitting. So, with more research and adjusting the regularization hyper-parameters, it is not easy to achieve higher results using this model without any major development. The ResNets are based on the skip layers connections so the layer connections can raise the classification accuracy. The DenseNets may have more connections but still the ResNet 50 model had the higher OA in this comparative study. The NASNets models have layers connections but not more as the DenseNets models, these connections only to determine the previous layer, so its results are low compared with other models in this study. In the other hand the NASNet's model learning curves are good, no degradation and no over-fitting, but with increasing the epochs the validation loss may be raised, so it must have an attention observed for epochs and validation curves through training this model. As a total the deeper convolution networks may give better accuracies but the deeper networks that have layers connections may give the best accuracies.

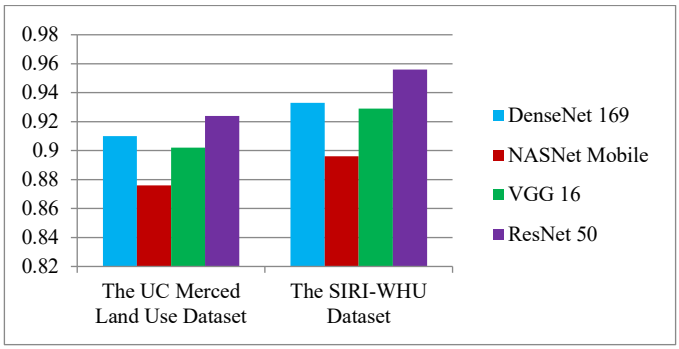


Figure 15: The OA for each model using the both datasets

4. Conclusions

This paper presented a comparative study for the use of the deep convolution models classic networks in classifying the remote sensing images. This comparison illustrated that what the classic network was more accurate for classifying the VHR remote sensing images. The used classic networks in this study were the DenseNet 169, the NASNet Mobile, the VGG 16, and the ResNet 50 models. There were two used datasets in this study; the UC Merced land use dataset and the SIRI-WHU dataset. This comparison was based on the learning curves to check that how much effectiveness of the hyper-parameters values selection and

the overall accuracy to assess the classification model performance. This comparison illustrated that the ResNet 50 model was more accurate than other models that stated in this study, which the overall accuracy of the DenseNet 169 model was little higher than the VGG 16 model. The NASNet Mobile model had the lowest OA in this study. The learning curves elucidated that the adjustment of the hyper-parameters of the VGG 16 model can lead to better overall accuracy where it is not easy to achieve better overall accuracy in the ResNet 50, the DenseNet 169 and the NASNet Mobile models without major developments in these models. The overall accuracy had an opposite relation with the remote sensing images resolution (pixel or spatial) and the number of dataset classes.

In the future, the FC layers can be replaced by other classifiers, and then train these models.

Conflict of Interest

The authors declare no conflict of interest.

References

[1] Michael Bowling, Johannes Furnkranz, Thore Graepel, and Ron Musick, "Machine Learning and Games", Machine Learning, Springer, **63**(3), 211-215, 2006. http://doi.org/10.1007/s10994-006-8919-x

[2] Issam ElNaqa and Martin J. Murphy, "What is Machine Learning", Machine Learning in Radiation Oncology, Cham, Springer, 3-11, 2015. https://doi.org/10.1007/978-3-319-18305-3_1

[3] Tom M. Mitchell, "The Discipline of Machine Learning, Pittsburgh", PA: Carnegie Mellon University, School of Computer Science, Machine Learning Department, **9**, 2006.

[4] Kyung Hwan Kim and Sung June Kim, "Neural Spike Sorting Under Nearly 0-dB Signal-to-Noise Ratio Using Nonlinear Energy Operator and Artificial Neural-Network Classifier", IEEE Transactions on Medical Engineering, **47**(10), 1406-1411, 2000. http://doi.org/10.1109/10.871415

[5] T.Blaschke, "Object Based Image Analysis for Remote Sensing", ISPRS Journal of Photogrammetry and Remote Sensing, Elsevier, **65**(1), pp. 2-16, 2010. https://doi.org/10.1016/j.isprsjprs.2009.06.004

[6] Minu Nair S., and Bindhu J.S., "Supervised Techniques and Approaches for Satellite Image Classification", International Journal of Computer Applications (IJCA), **134**(16), 1-6, 2016. . https://doi.org/10.5120/ijca2016908202

[7] Waseem Rawat, and ZenghuiWang, "Deep Convolutional Neural Networks for Image Classification: A Comprehensive Review", Neural computation, **29**(9), 2352-2449, 2017. http://doi.org/10.1162/NECO_a_00990

[8] Khalid. A. Al-Afandy, Hicham Omara, Mohamed LaZaar, and Mohammed AL ACHHAB, "Artificial Neural Networks Optimization and Convolution Neural Networks to Classifying Images in Remote Sensing: A Review", in The 4th International Conference on Big Data and Internet of Things (BDIoT'19), 23-24 Oct, Rabat, Morocco, 2019. http://doi.org/10.1145/3372938.3372945

[9] Yiting Tao, Miaozhong Xu, Zhongyuan Lu, and Yanfei Zhong, "DenseNet-Based Depth-Width Double Reinforced Deep Learning Neural Network for High-Resolution Remote Sensing Images Per-Pixel Classification", Remote Sensing, **10**(5), 779-805, 2018. http://doi.org/10.3390/rs10050779

[10] Gefei Yang, Utsav B. Gewali, Emmett Ientilucci, Micheal Gartley, and Sildomar T. Monteiro, "Dual-Channel DenseNet for Hyperspectral Image Classification", in IGARSS 2018 - 2018 IEEE International Geoscience and Remote Sensing Symposium, 05 Nov, Valencia, Spain, 2595-2598, 2018. http://doi.org/10.1109/IGARSS.2018.8517520

[11] Jianming Zhang, Chaoquan Lu, Xudong Li, Hye-Jin Kim, and Jin Wang, "A Full Convolutional Network based on DenseNet for Remote Sensing Scene Classification", Mathematical Biosience and Engineering,, **6**(5), 3345-3367, 2019. http://doi.org/10.3934/mbe.2019167

[12] Lingling Li, Tian Tian, and Hang Li, "Classification of Remote Sensing Scenes Based on Neural Architecture Search Network", in 2019 IEEE 4th International Conference on Signal and Image Processing (ICSIP), 19-21 Jul, Wuxi, China, 176-180, 2019. http://doi.org/10.1109/SIPROCESS.2019.8868439

[13] Ali Bahri, Sina Ghofrani Majelan, Sina Mohammadi, Mehrdad Noori, and Karim Mohammadi, "Remote Sensing Image Classification via Improved Cross-Entropy Loss and Transfer Learning Strategy Based on Deep Convolutional Neural Networks", IEEE Geoscience and Remote Sensing Letters, vol. **17**(6), 1087-1091, 2019. http://doi.org/10.1109/LGRS.2019.2937872

[14] Xuan Liu, Mingmin Chi, Yunfeng Zhang, and Yiqing Qin, "Classifying High Resolution Remote Sensing Images by Fine-Tuned VGG Deep Networks", in IGARSS 2018 - 2018 IEEE International Geoscience and Remote Sensing Symposium, 22-27 Jul, Valencia, Spain, 7137-7140, 2018. http://doi.org/10.1109/IGARSS.2018.8518078

[15] Souleyman Chaib, Huan Liu, Yanfeng Gu, and Hongxun Yao, "Deep Feature Fusion for VHR Remote Sensing Scene Classification", IEEE Transactions on Geoscience and Remote Sensing, **55**(8), 4775-4784, 2017. http://doi.org/10.1109/TGRS.2017.2700322

[16] Zhong Chen, Ting Zhang, and Chao Ouyang, "End-to-End Airplane Detection Using Tansfer Learning in Remote Sensing Images", Remote Sensing, **10**(1), 139-153, 2018. http://doi.org/10.3390/rs10010139

[17] Gang Fu, Changjun Liu, Rong Zhou, Tao Sun, and Qijian Zhang, "Classification for High Resolution Remote Sensing Imegery Using a Fully Convolution Network", Remote Sensing, **9**(5), 498-518, 2017. http://doi.org/10.3390/rs9050498

[18] Mingchang Wang, Xinyue Zhang, Xuefeng Niu, Fengyan Wang, and Xuqing Zhang, "Scene Classification of High-Resolution Remotely Sensed Image Based on ResNet", Journal of Geovisualization and Spatial Analysis, Springer, **3**(2), 16-25, 2019. http://doi.org/10.1007/s41651-019-0039-9

[19] Yenan Jiang, Ying Li, and Haokui Zhang, "Hyperspectral image classification based on 3-D separable ResNet and transfer learning", IEEE Geoscience and Remote Sensing Letters, **16**(12), 1949-1953, 2019. http://doi.org/10.1109/LGRS.2019.2913011

[20] S. Natesan, C. Armenakis, and U. Vepakomma, "ResNet-Based Tree Species Classification Using UAV Images", International Archives of the Photogrammetry, Remote Sensing & Spatial Information Sciences, **XLII**, 2019. http://doi.org/10.5194/isprs-archives-XLII-2-W13-475-2019

[21] Jiachen Yang, Yinghao Zhu, Bin Jiang, Lei Gao, Liping Xiao, and Zhihui Zheng, "Aircraft Detection in Remote Sensing Images Based on a Deep Residual Network and Super-Vector Coding", Remote Sensing Letters, Taylor & Francis, **9**(3), 229-237, 2018. http://doi.org/10.1080/2150704X.2017.1415474

[22] Lin Xu and Qiang Chen, "Remote-Sensing Image Usability Assessment Based on ResNet by Combining Edge and Texture Maps", IEEE Journal of Selected Topics in Applied Earth Observations and Remote Sensing, **12**(6), 1825-1834, 2019. http://doi.org/10.1109/JSTARS.2019.2914715

[23] Ahmed Fawzy Gad, "Practical Computer Vision Applications Using Deep Learning with CNNs", Apress, Springer, Berkeley, CA, 2018. https://doi.org/10.1007/978-1-4842-4167-7

[24] Yushi Chen, Hanlu Jiang, Chunyang Li, Xiuping Jia, and Pedram Ghamisi, "Deep Feature Extraction and Classification of Hyperspectral Images Based on Convolutional Neural Networks", IEEE Transactions on Geoscience and Remote Sensing, **54**(10), 6232-6251, 2016. http://doi.org/10.1109/TGRS.2016.2584107

[25] Emmanuel Maggiori, Yuliya Tarabalka, Guillaume Charpiat, and Pierre Alliez, "Convolutional Neural Networks for Large-Scale Remote-Sensing Image Classification", IEEE Transactions on Geoscience and Remote Sensing, **55**(2), 645-657, 2017. http://doi.org/10.1109/TGRS.2016.2612821

[26] Gao Huang, Zhuang Liu, Laurens van der Maaten, and Kilian Q. Weinberger, "Densely Connected Convolutional Networks", in 2017 IEEE Conference on Computer Vision and Pattern Recognition (CVPR), 21-26 Jul, Honolulu, HI, USA, 2261-2269, 2017. http://doi.org/10.1109/CVPR.2017.243

[27] Barret Zoph and Quoc V. Le, "Neural architecture search with reinforcement learning", in International Conference on Learning Representations (ICLR 2017), 24-26 April, Toulon, France, 2017. https://arxiv.org/abs/1611.01578

[28] Karen Simonyan and Andrew Zisserman, "Very deep convolutional networks for large-scale image recognition", in International Conference on Learning Representations (ICLR 2015), 7-9 May, San Diego, USA, 2015. https://arxiv.org/abs/1409.1556

[29] Kaiming He, Xiangyu Zhang, Shaoqing Ren, and Jian Sun, "Deep Residual Learning for Image Recognition", in 2016 IEEE Conference on Computer Vision and Pattern Recognition (CVPR), 27-30 Jun, Las Vegas, NV, USA, 770-778, 2016. http://doi.org/10.1109/CVPR.2016.90

[30] Gebhard Banko, "A Review of Assessing the Accuracy of Classifications of Remotely Sensed Data and of Methods Including Remote Sensing Data in Forest Inventory", in International Institution for Applied Systems Analysis (IIASA), Laxenburg, Austria, IR-98-081, 1998. http://pure.iiasa.ac.at/id/eprint/5570/

[31] Weijia Li, Haohuan Fu, Le Yu, and Arthur Cracknell, "Deep Learning Based Oil Palm Tree Detection and Counting for High-Resolution Remote Sensing Images", Remote Sensing, **9**(1), 22-34, 2017. http://doi.org/10.3390/rs9010022

[32] Jan N. van Rijn, Salisu Mamman Abdulrahman , Pavel Brazdil, and Joaquin Vanschoren, "Fast Algorithm Selection Using Learning Curves", in International symposium on intelligent data analysis, **9385**, Springer, Cham,

22-24 Oct, Saint Etienne, France, 298-309, 2015. http://doi.org/10. 1007/978-3-319-24465-5 26

[33] MartinWistuba and Tejaswini Pedapati, "Learning to Rank Learning Curves", arXiv:2006.03361v1, 2020. https://arxiv.org/abs/2006.03361

[34] Yi Yang and Shawn Newsam, "Bag-Of-Visual-Words and Spatial Extensions for Land-Use Classification", in the 18th ACM SIGSPATIAL international conference on advances in geographic information systems, 2-5 Nov, San Jose California, USA, 270-279, 2010. http://doi.org/10.1145/1869790.1869829

[35] Bei Zhao, Yanfei Zhong, Gui-Song Xia, and Liangpei Zhang, "Dirichlet-Derived Multiple Topic Scene Classification Model for High Spatial Resolution Remote Sensing Imagery", IEEE Transactions on Geoscience and Remote Sensing, **54**(4), 2108-2123, 2016. http://doi.org/10.1109/TGRS.2015.2496185

[36] Ekaba Bisong, "Building Machine Learning and Deep Learning Models on Google Cloud Platform: A Comprehensive Guide for Beginners", Apress, Berkeley, CA, 2019.

[37] Tiago Carneiro, Raul Victor Medeiros Da Nobrega, Thiago Nepomuceno, Gui-Bin Bian, Victor Hugo C. De Albuquerque, and Pedro Pedrosa Reboucas Filho, "Performance Analysis of Google Colaboratory as a Tool for Accelerating Deep Learning Applications", IEEE Access, **6**, 61677-61685, 2018. http://doi.org/10.1109/ACCESS.2018.2874767

[38] Olga Russakovsky and Li Fei-Fei, "Attribute Learning in Large-Scale Datasets", in European Conference on Computer Vision, **6553**, Springer, Berlin, Heidelberg, 10-11 Sep, Heraklion Crete, Greece, 1-14, 2010. http://doi.org/10.1007/978-3-642-35749-7_1

[39] Jia Deng, Alexander C. Berg, Kai Li, and Li Fei-Fei, "What Does Classifying More Than 10,000 Image Categories Tell Us? ", in The 11th European conference on computer vision, **6315**, Springer, Berlin, Heidelberg, 5-11 Sep, Heraklion Crete, Greece, 71-84, 2010. http://doi.org/10.1007/978-3-642-15555-0_6

ASTES

Advances in Science, Technology and Engineering Systems Journal Vol. 5, No. 5, 781-788 (2020)

www.astesj.com

Special Issue on Multidisciplinary Innovation in Engineering Science & Technology

ASTESJ

ISSN: 2415-6698

Development of a Wireless Displacement Estimation System Using IMU-based Device

Tri Nhut Do*, Quang Minh Pham, Hoa Binh Le-Nguyen, Cao Tri Nguyen, Hai Minh Nguyen-Tran

Division of Electronics and Electrical Engineering, Faculty of Engineering, Van Lang University, HCMC 700000, Vietnam

ARTICLE INFO

Article history:
Received: 14 August, 2020
Accepted: 28 September, 2020
Online: 12 October, 2020

Keywords:
Displacement Estimation
Inertial Measurement Unit
Indoor Localization
Wireless Smart Sensor Network
Daily Activities Monitoring System

ABSTRACT

Estimation of displacement is an information required for daily operation monitoring systems to monitor human health or to locate users in buildings, basements, tunnels and similar places which under the same conditions that the global positioning signal (GPS) level is from very weak to completely absent; and is the measurement technique by using multimetric data fusion. Most current displacement estimation methods require a lot of infrastructures and devices such as UWB, wifi access points, cameras. Hence, estimation methods that ultilize inertial measurement unit (IMU) and integrate acceleration to get diplacement are effective alternatives since the three-axis accelerometer embedded in IMU usually low cost, easy to adjust and low noise. The advantage of this approach is that the IMU-based device is compact, easy to install and put on user's body. However, these methods expose some weaknesses when used in large-scale indoor structures such as multi-storey buildings due to the need to compensate azimuth estimation which is drifted overtime and is employed for calculating displacement with refer to earth frame as a base station. This article proposes a low-cost wireless displacement estimation system developed with IMU. The system employs a Kalman-filter type in indirect form for orientation estimates and Median-filter algorithm for classification of motion modes. In order to verify the proposed system in terms of accuracy and feasibility, a device was designed in a wearable form and tetsted on a multi-storey building in university. The wearable device ultilized IMU model MPU9250 and results recored wirelessly via Xbee devices in order to test the system performance in such senarios as climbing/descending staircases only, climbing/descending staircases through one floor combined with walking. Experiments are repeated for root mean square error (RMSE) computation based on the ground-truth. The proposed system performance is evaluated accordingly to RMSE. The experimental results demonstrate RMSE of 3.56%, 1.43%, for climbing/descending staircases only, climbing/descending staircases one floor combined with walking, respectively.

1. Introduction

The wireless displacement estimation system in this article is introduced in order to locate the position of user moving along a path indoor and carrying an wearable device only. Such pre-installed devices as fiducial markers on floor [1], infrared LED landmarks on panel [2], wireless communication devices like radio frequency and wireless local area network [3–5] are not required.

The applications of this system are diverse. High-demand areas of application can be listed including defense applications of tactical planning or strategic coordination for soldiers; social life applications for public safety and elderly care; and firefighter rescue applications when they're stuck and in need of rescue. The common characteristic of the aforementioned applications is the indoor environment with no pre-installed infractructures or devices due to such infractructures as RFID, wireless network, infrared sensor, landmark for vision are unable to installed or have already been destroyed by disaster. Specifically, rescue and security applications often take place in unstable areas that are unsuitable for infrastructure-based systems.

In general, two types of non-infrastructure displacement estimation systems exist and named as the strap-down and the step-and-heading. The strapdown method is integrating the acceleration in order to get displacement. Accumulated errors in the integration process are compensated with reset algorithm in [6]. The step-and-

*Corresponding Author: Tri Nhut Do, Division of Electronics and Electrical Engineering, Van Lang University, 45 Nguyen Khac Nhu Street, District No. 1, Ho Chi Minh City 700000, Vietnam, Cell No. +84938113898, trinhutdo@gmail.com

heading method estimates displacement by combining the step size with the yaw (user heading) which is estimated by quaternion-based filters [7–8].

The infrastructure-free displacement estimation system utilizes sensors such as IMU, force sensor, pressure sensor (barometer), ultra-wide band (UWB), etc. Depending on the specific application needs, the sensors are selected and their positions on user's body can be mentioned as holding in hand [9–10], mounting on foot [11–12], putting at ankle [13], placing at waist [14–16] and attaching at upper torso [17].

All mentioned approaches estimate displacement in two horizontal dimensions. However, Diaz [18] proposed an estimator with IMU put in pocket in order to estimate displacement in the vertical dimension. The inconvenient IMU location for user and the required training are the limitations of Diaz algorithm. Therefore, this article proposes a novel method that doesn't require training but provide a displacement estimation algorithm for indoor three dimensions (3D), which is able to estimate both the horizontal displacement and vertical displacement. The proposed algorithm is based on the double integration of acceleration with reset at step events in order to eliminate accumulate error due to integrating process. The proposed method is tested when a person climbing/descending staircases.

In this article, the IMU is placed at pedestrian's waist as shown in Figure 1 for convenient usage.

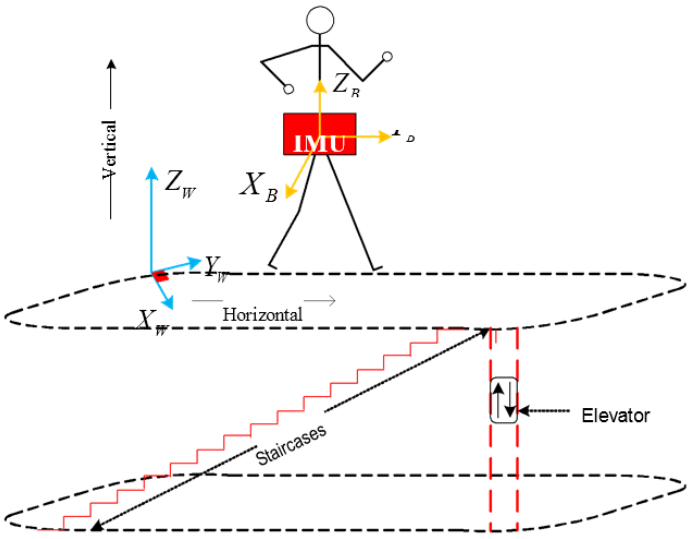


Figure 1: IMU is mounted at pedestrian's waist and used to estimate 3D displacements.

The rest of the article is organized as follows. The proposed system and algorithm to estimate 3D displacements are introduced in section 2. In section 3, the experiment setting is described and the experimental results are shown. Section 4 concludes the article.

2. Proposed Wireless Displacement Estimation System

2.1. System Overview

The proposed wireless displacement system employed the integrating process with novel velocity update algorithm in [6] in order to convert measured acceleration into displacement. Moreover, the system ultilized IMU module MPU9250 for sensing, Xbee devices for wireless communication and Arduino Fio Board for programming the proposed algorithm. The system was implemented within space as in Figure 1 and various experimental scenarios were designed for testing and evaulating as well. People took part in experiments were tasked to wear mobile device at waist, perform multi-activities freely with normal speed. Experiment data was recorded wirelessly in distance of several hundred meters.

2.2. Attitude Estimation System

In order to make the theoretical basis for all math operations in this article, all coordinate systems (or frames) must be assigned and two frames are assigned as illustrated in Figure 1. The subscript notations of W and B indicate for World and Body, respectively. The East-North-Up (ENU) coordinate system is used as the world reference frame ($X_WY_WZ_W$) while the body coordinate system is assumed to rigidly attached to the IMU and the IMU is mounted at the pedestrian's waist.

Let $\hat{\psi}$, $\hat{\theta}$ and $\hat{\varphi}$ be the user heading, IMU pitch and roll angles, respectively. An attitude in three dimensions is estimated based on a quaternion-based Kalman Filter in indirect form by fusing the information from the gyroscope, the accelerometer and the magnetometer.

The employed attitude estimation algorithm has two advantages as follows: 1) reducing computation cost due to dealing with orientation errors instead of dealing direct with orientation which results the state dimension being smaller and its response faster, and 2) two stages update using acceleration and magnetic strength by exploiting two measurements of the difference between accelerometer reading vs the gravity vector and the difference between magnetometer reading vs the magnetic strength vector.

2.3. Classification of Motion Modes

In order to improve displacement estimation accuracy, the motion modes of user carrying IMU must be recognized precisely [19]. Some motion modes including jogging, running, walking with different step sizes have already been done in our previous works [13, 17, 20]. In this article, motion modes of stationary, going up (climbing), going down (descending) staircases and riding a lift are added to update our previous work and enhance our system capabilities. Therefore, the motion modes are organized and indicated by numbers as follows: '0' indicates stationary mode; '1' indicates descending staircases mode; '2' indicates walking on flat surface mode; '3' indicates climbing staircases mode; '4' indicates riding a lift mode; '5' indicates jogging/running mode.

There are many motion modes introduced in [20] and were classified by machine learning based on four decision trees. The device are able to be put in many places including handheld with both portrait and landscape orientations; backpack; purse; belt holder; chest strapped; arm strapped hand still by side; dangling; pocket (consists of pant pocket, shirt pocket, and jacket pocket, in both horizontal and vertical orientations); wrist (ex: smartwatches) and headmount (such as smartglasses).

The algorithm in [20] is a very convenient but it is complicated and time consuming for learning method. Therefore, a simpler method for classification of motion modes is proposed in this article. The entire classification process, as shown Figure 2, consists of: 1) the acceleration in world frame is normalized and compared with a threshold in order to categorize motion modes into stationary, non-stationary and riding a lift modes, and 2) the non-stationary mode is classified into jogging/running, walking, climbing and descending staircases.

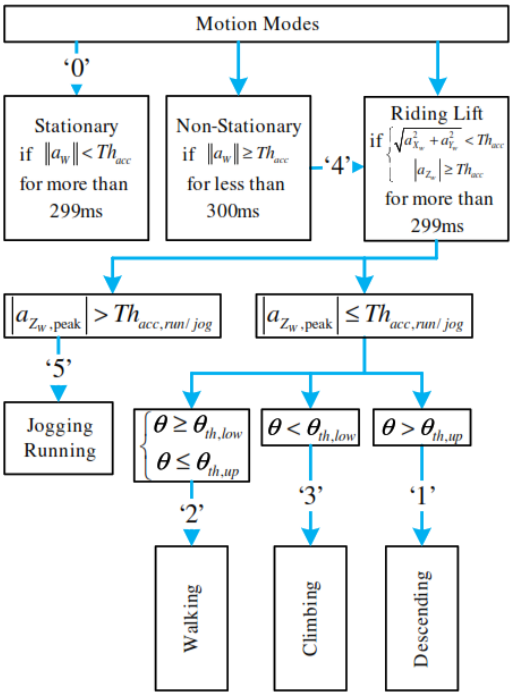


Figure 2: Motion Modes recognized by our work. The notation a_W is the acceleration in world frame and the a_{z_w} is its vertical component. All the Th_{acc}, $Th_{acc,\ run/jog}$, $\theta_{th,\ low}$ and $\theta_{th,\ up}$ are thresholds for motion modes classification.

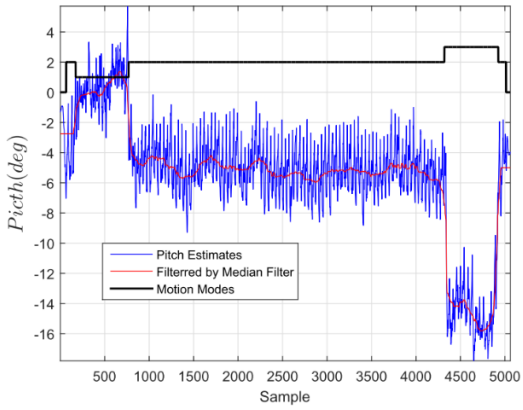


Figure 3: The blue solid line shows pitch angle estimates whereas the red one is the filtered pitch and the black solid line shows the Motion Modes, with values '0', '1', '2', '3' represents modes of stationary, descending staircases, walking and climbing up staircases, respectively.

2.3.1. *Classification for Non-Stationary mode group:*

The mode group of non-stationary consists of walking, jogging/running, climbing/descending staircases. Among them, the climbing/descending staircases motion modes are mentioned in this articles. Basically, classification of climbing/descending staircases is based on the pitch angle thresholds. Firstly, the original pitch estimates (depicted by the blue solid line in Figure 3) are passed through a Median Filter with a 100 samples window before doing a comparison with the pitch angle thresholds. The filtered pitch estimates are depicted by the red solid line in Figure 3. In order to illustrate the feasibility of the classification algorithm, an experiment that a pedestrian performs the following motion modes: stationary, walking, climbing up and descending down staircases with normal step sizes, moving at speed two steps per second, going along with a straight path is conducted and the pitch estimates are shown in Figure 3.

2.3.2. *Classification for Riding Lift mode*

In order to recognize whether a pedestrian riding a lift or not, the surface acceleration and the absolute of vertical acceleration are compared with a threshold. A pedestrian activity is classified into riding a lift mode if the condition shown in Figure 3 is satisfied. A person is tasked to perform a riding lift activity combined with walking then descending staircases in an experiment. Figure 4 proves the feasibility of classification riding a lift mode.

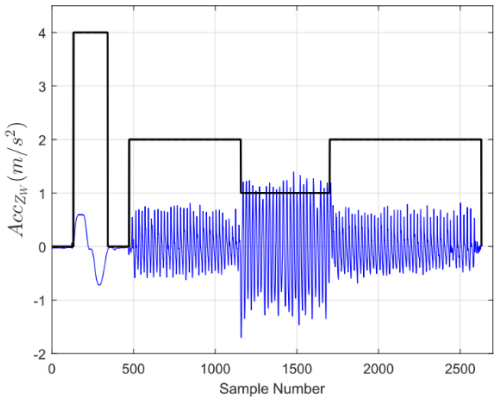


Figure 4: The blue solid line shows vertical acceleration with gravity removal whereas the black solid line shows the Motion Modes, with values '0', '1', '2', and '4' represents modes of stationary, descending staircases, walking and riding a lift, respectively.

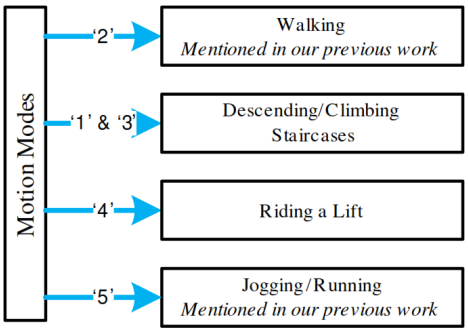


Figure 5: Overview of the proposed in-door localization system. Values '1', '2', '3', '4', '5' represents modes of descending staircases, walking and climbing up staircases, riding a lift and jogging/running, respectively.

2.4. *Displacement Estimation Method*

Authors' previous works [13, 17] described the pedestrian's walking motion and proposed two walking models applied to estimate displacement in two dimensions with the accuracy up to

97%. In order to enhance our displacement estimation system, an estimator applied for displacement estimation in (3D) including vertical and horizontal directions is developed. The details are described in this section.

2.4.1. System Overview

The displacement estimation system in this article consists of different algorithms accordingly to motion modes recognized by above described classification method. Figure 5 shows the block diagram of the proposed system for 3D displacement estimation.

2.4.2. 3D displacement estimation for descending/climbing staircases motion modes

During going up/down, the step events are defined at the extreme peak positions of the vertical acceleration, one component of the global acceleration with gravity removal. The method in [13] is used to detect the peaks.

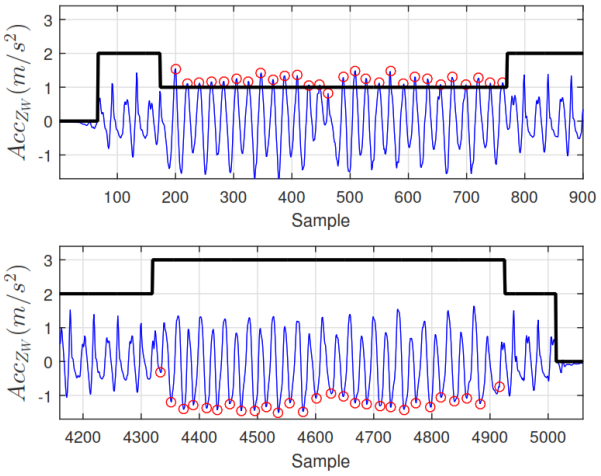


Figure 6: The black solid line shows the Motion Modes, with values '0', '1', '2', '3' represents modes of stationary, descending staircases, walking and climbing up staircases, respectively. The red rings are the extreme peak positions when descending (top) and climbing (bottom).

Figure 6. shows the peaks detected based on the data from the same experiment shown in Figure 3. The blue solid line is the vertical acceleration and the black solid line shows the Motion Modes. The step events are 100% detected.

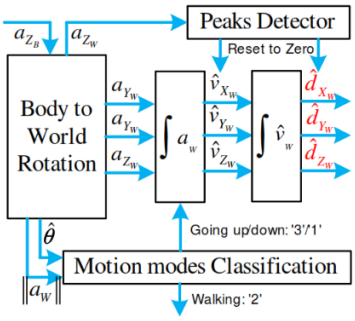


Figure 7: Block Diagram of the estimation algorithm for climbing/descending staircases.

Based on the fact that climbing/descending staircases are the periodic motions and the vertical acceleration is periodic data recored from the IMU mounted on the pedestrian's body, the entire displacement estimation process is able to be considered as the accumulation of segments. Each segment starts from a step event and ended at the next adjacent step event. However, the accumulating error due to integration affects the estimation accuracy as described in [20]. Unlike putting the IMU at the ankle, placing the IMU at pedestrian's waist has no chance of zero velocity interval when the normalized global acceleration is equal to zero. Therefore, the authors propose a method in order to obtain the 3D displacement is that integrating twice from global acceleration with gravity removal and that integrating process is reset to zero for velocity and displacement at the step events. The method is illustrated as in Figure 7. The reseting is called refreshing for segments.

2.4.3. 3D displacement estimation for riding a lift motion mode

The 3D displacement estimation when riding a lift is obtained by double integrating the vertical acceleration with gravity removal in world frame. The method was introduced in our previous work [19]. It is described that the integrated velocity is reset in zero vertical acceleration intervals during riding lift interval. Figure 8 illustrates the integrating process. Firstly, the discrete vertical acceleration with respect to the world frame is in the top plot and is with gravity removal when riding a lift one floor. Secondly, the middle plot is the integrated velocity and the bottom plot is the integrated vertical displacement. The red dot value 'non-zero' in the top plot indicates the zero vertical acceleration intervals where integrated velocity is reset.

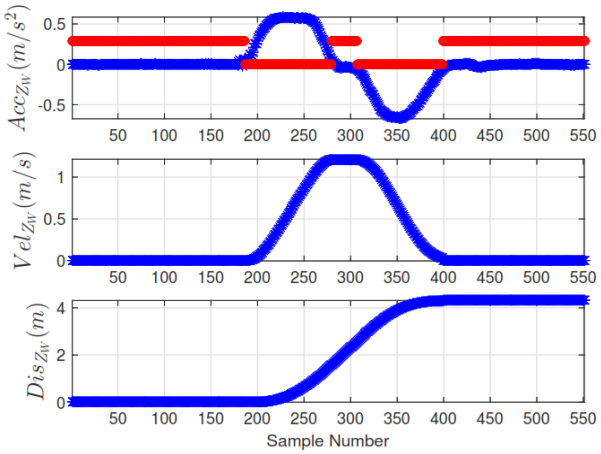


Figure 8: The vertical integration process when riding a lift through one floor.

3. Experiments and Evaluations

The capability of proposed method is tested through experiments conducted by four persons in our research group. In this section, a brief description of the experiment setup is first given, followed by a description of the experimental scenarios and the results obtained.

3.1. Set up

The hardware used to test the proposed method is illustrated in Figure 9, which consists of two parts: 1) the mobile part (attached to the pedestrian) shown in the top portion and 2) the base part shown in the bottom portion. The mobile part consists of an Xbee wireless transmitter, an MPU-9250 IMU sensor board and an Arduino Fio microcontroller Atmega328P board whereas the base part has an Xbee wireless receiver connected to the laptop by

virtual serial port via USB port. The transmitter communicates with Fio board using I^2C communication protocol. The serial baud rate is set at 115200bps.

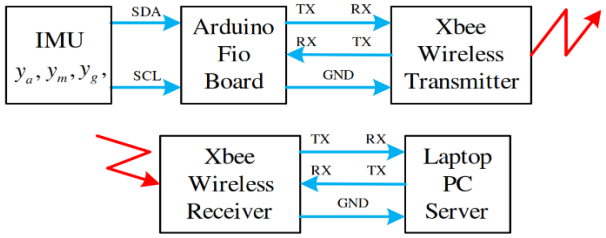


Figure 9: Hardware for experiments, with the mobile part (attached to pedestrian's waist) shown in the top and the base part shown in the bottom.

The proposed algorithm is implemented in the mobile part with the data acquired in every 25 ms and passed through a complimentary filter with 225 ms time constant.

Four experimental scenarios are set and conducted, namely: 1) which is described in section 3.2 is the experiment of going staircases along a straight path with two action modes climbing and descending for 3D displacement accuracy evaluation; 2) which is described in section 3.3 is the experiment of walking along with a triangular path put together with climbing and descending staircases for combination of heading and displacement accuracy evaluation; 3) which is described in section 3.4 is the experiment of riding a lift through floors; and 4) which is described in section 3.5 is the experiment of 3D displacement estimation that consists of many motion modes.

Four people in our research group aging from 25 to 39 with height ranging from 1.6 meters to 1.86 meters are deployed for these experiments, and all the experiments are conducted. Each test is also repeated for four times.

3.2. Results for climbing/descending staircases

For the first experiments scenario, the straight path includes 2m flat path and 15 stairs as shown in Figure 10. Each stair is 15cm in height and 30cm in length. The straight path has 2.25m ground truth in height (vertical direction) and 7.03m ground truth in horizontal direction. It produces 14.06m traveling ground truth in three dimensions.

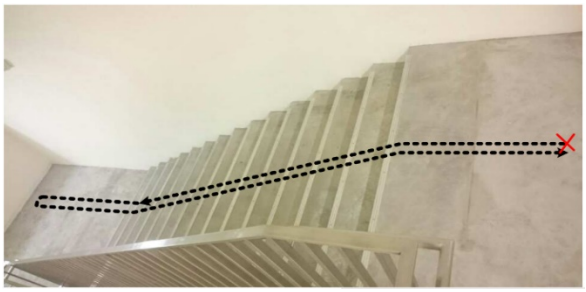


Figure 10: In this figure, the volunteers start from the red mark 'X' and performs motion modes of stationary, descending, climbing along a straight path depicted by the black bold dot line.

On stairs, both horizontal and vertical displacements are obtained by double integration with zero reset at step events. The heading is determined by method in [9]. Figure 11 shows the side view of an experimental result and illustrates the both vertical and horizontal estimates.

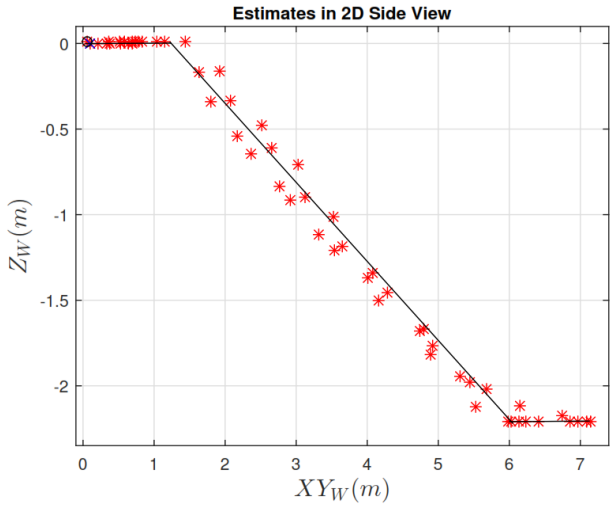


Figure 11: In this figure, both horizontal and vertical estimates are represented by the red asterisk '*' when walking, descending/climbing staircases along with a straight path. (XY_W) is the horizontal direction. The black solid line is the ground truth.

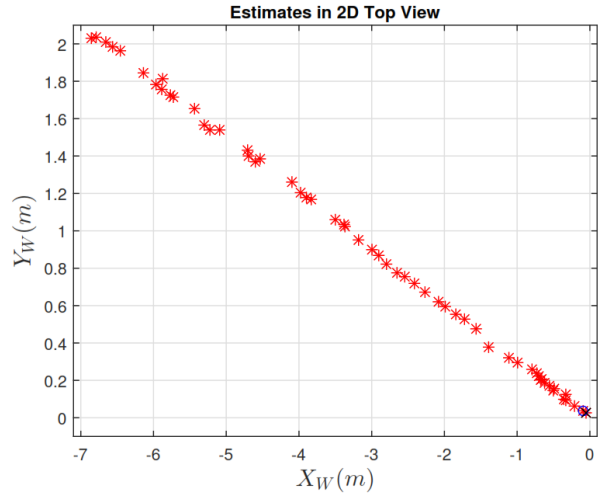


Figure 12: In this figure, the horizontal estimates are represented by the red asterisk '*' when walking, descending/climbing staircases along with a straight path.

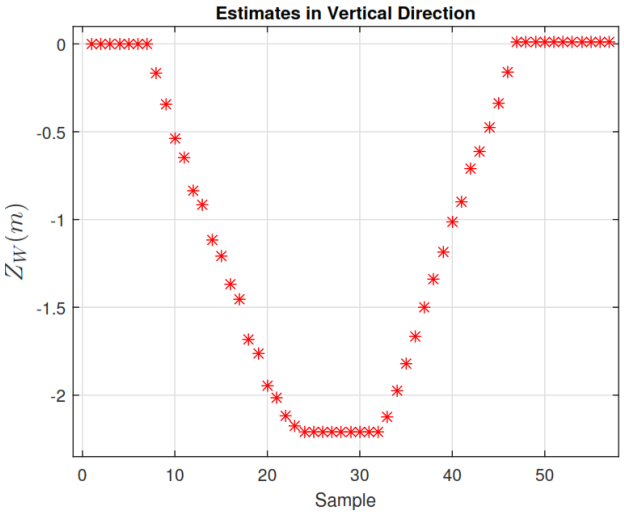


Figure 13: In this figure, the vertical estimates are represented by the red asterisk '*' when walking, descending/climbing staircases along with a straight path.

The vertical estimates are positions of pedestrian in upward direction (Z_W) and the horizontal estimates are computed by taking normalization of pedestrian positions in both north (Y_W) and east (X_W) directions. Let (XY_W) be the representation of horizontal direction.

Next, Figure 12 shows the view from top and illustrates the horizontal estimates only. Finally, Figure 13 illustrates the vertical estimates only.

In the three figures, the red asterisk '*' represents the estimated positions, the blue 'O' represents the starting point and the black 'X' represents the ending point.

3.3. Results for walking and climbing/descending staircases

For the second experimental scenario, a traveling path includes two triangular paths (Figure 14(a)) in two different floors which are connected by 30 stairs of 15cm in height and 30cm in length (Figure 14(c)). The triangle has 3 edges in 11m length and its vertices are circled with 1/3 ring of 1m radius. The pillar in Figure 16(a) is one of triangle vertices. The walking path from a triangle to staircases is 9m for the top level (Figure 14(b)) and 11m for the bottom level (Figure 14(d)). The walking path at middle of staircases is 3m (Figure 14(c)). In order to obtain the highest accuracy in measurement as ground truth for evaluation, the staircase height is measured by Fluke 411D Laser Distance Meter and the number of staircases between two floors are counted. There are 30 staircases with 14.5cm height between two floors at Singapore University of Technology and Design, Building 1. This experimental set produces totally 114.62m traveling ground truth in three dimensions.



(a) Triangular walking path



(b) 9m connecting walking path



(c) 30 Stairs



(d) 11m connecting walking path

Figure 14: The second experimental scenario in the building.

When walking, the walking model and method in [18] is applied for displacement estimation while double intergrating process is employed for displacement estimation when climbing/descending staircases. For illustrating, an experimental result in 3D is shown in Figure 15.

3.4. Evaluation for the first two experimental scenarios

In order to evaluate the method performance, all the Euclidean distances in three dimensions between the starting point and the ending point are computed for both described experimental scenarios. In addition, all the differences between estimated height for each experiment and the staircase height ground truth are also computed for the first experimental scenario. The root means square errors of the Euclidean distances and the height differences are then calculated. The evaluation results are summarized in Table 1.

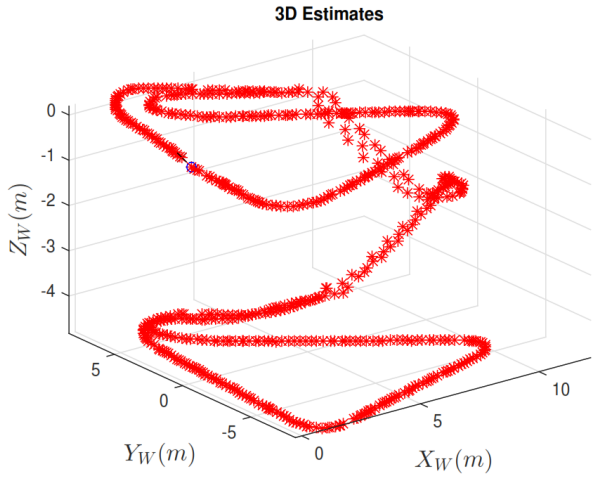


Figure 15: In this figure, the 3D estimates are shown when walking along a triangular path, climbing/descending 30 stairs.

Table 1: Performance of four people conducted experimental scenarios described in Section 3.3

	RMSE [m]	RMSE [%]
3D distance for descending, climbing along with Straight Path	0.5	3.56
Height Differences for descending, climbing along with Straight Path	0.26	11.56
3D distance for travelling on the Triangular Shape Path	1.64	1.43

3.5. Results and evaluations for riding a lift

In this experimental scenario, four members in our research group are tasked to ride a lift upward four times, then downward four times. Three experimental sets are designed such as riding a lift through one floor only as shown in Figure 8, riding lift through multiple floors with one floor stop as shown in Figure 16, riding lift through 40 floors as shown in Figure 17.

Figure 8 shows one of 16 experimental results in total for the first experimental set including 2 upward direction and 2 downward direction rode by 4 persons at Building 1. The experimental results are evaluated by the root mean square error based on the ground-truth of 4.35 meters, which is 0.0334 meters or 0.77%.

Figure 16 shows one of 8 experimental results in total for the second experimental set including 1 upward direction and 1 downward direction rode by 4 persons at Building 1. The experimental results are evaluated by the root mean square error based on the ground-truth of 4.35 meters, which is 0.0384 meters or 0.88%.

Figure 17 shows one of 4 experimental results in total for the third experimental set including 2 upward direction and 2

downward direction rode by 1 person at Block 90. There are 20 staircases with 13.5cm height between two floors of Block 90. The experimental results are evaluated by the root mean square error based on the ground-truth of 2.7 meters, which is 1.7909 meters or 1.66%.

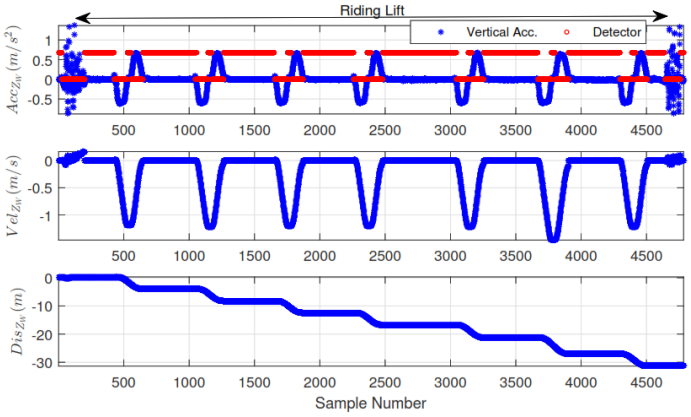


Figure 16: In this figure, the vertical estimates are shown when riding a lift through multiple floors.

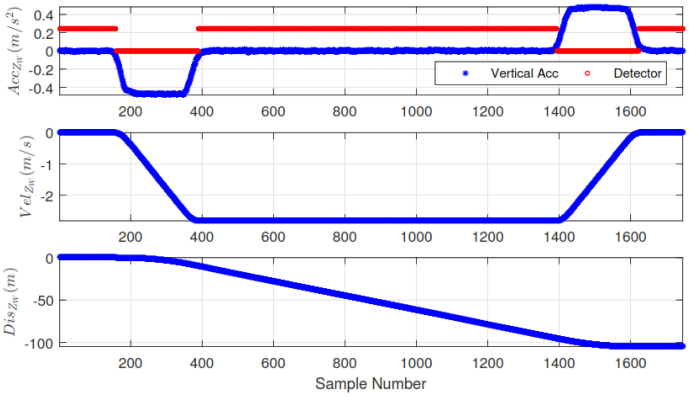


Figure 17: In this figure, the vertical estimates are shown when riding a lift through 40 floors.

3.6. Result and evaluation for 3D displacement estimation

A person is tasked to conduct experiments of walking from starting point, entering a lift, riding a lift upward one floor, followed by a walking out of a lift, descending staircases and walking again to starting point. The experimental result of this scenario is illustrated as in Figure 18.

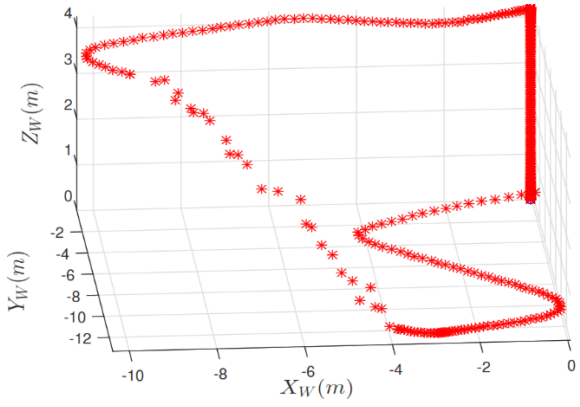


Figure 18: In this figure, the 3D estimates are shown when riding a lift through one floor then walking and descending straircases.

The experiment is repeated 4 times. The Euclidean distances between starting point and ending point are calculated for evaluation, which distance average of four experimental results is 0.71 meters.

4. Conclusion

A simple motion mode classification for climbing/descending staircases comes with an algorithm to estimate both vertical and horizontal displacements by utilizing information from global acceleration with gravity removal have been proposed in this article. The estimation based on integrating process with zero reset at the extreme peaks of the vertical, rather than horizontal, acceleration. Authors have given new method to estimate indoor 3D displacements as a basic for positioning of pedestrian without knowing of stair measurements and provided the most convenient IMU location at waist. In order to verify displacement estimation system's feasibility and evaluate its performance, a range of experiments which are grouped into two sets of experiment including straight path, and triangular shape path are conducted by four subjects. In each set, people who tasked to perform experiments are required to move at normal step size and at speed 2 steps per second. The experimental results have demonstrated the capability of the algorithm via a RMS displacement error of 3.56% for straight path and 1.43% for the triangular shape path.

Finally, the algorithm in this article is only focusing on climbing upstairs and descending downstairs. The displacement estimations when pedestrian acts in other motion modes like standing, walking on escalator and standing in evaluator will be researched in the future work.

Conflict of Interest

The authors declare no conflict of interest.

Acknowledgment

This project is supported by Singapore University of Technology and Design (SUTD) Temasek Lab, Pillar of Engineering Product Development (EPD), Changi 487372, Singapore.

In addition, this project is supported by Van Lang University (VLU) Electronics and Electrical Engineering Division, Ho Chi Minh City 700000, Vietnam.

References

[1] T. N. Do, and Y. S. Suh, "Gait Analysis Using Floor Markers and Inertial Sensors" Sensors, **12**(2), 1594-1611, 2012. https://dx.doi.org/10.3390%2Fs120201594

[2] T. N. Do, and Y. S. Suh, "Gait Analysis System Using Infrared LED Landmarks" Journal of Institute of Control, Robotics and Systems, **17**(7), 641-646, 2011. https://doi.org/10.5302/J.ICROS.2011.17.7.641

[3] H. Liu, H. Darabi, P. Banerjee, and J. Liu, "Survey of wireless indoor positioning techniques and systems" IEEE Transactions on Systems, Man, and Cybernetics, Part C: Applications and Reviews, **37**(6), 1067-1080, 2007. https://doi.org/10.1109/TSMCC.2007.905750

[4] K. El-Kafrawy, M. Youssef, A. El-Keyi, and A. Naguib, "Propagation modeling for accurate indoor wlan rss-based localization" in IEEE 72nd Vehicular Technology Conference Fall, Ottawa, Canada, 2010. https://doi.org/10.1109/VETECF.2010.5594108

[5] L.-H. Chen, E. H.-K. Wu, M.-H. Jin, and G.-H. Chen, "Intelligent fusion of Wi-Fi and inertial sensor-based positioning systems for indoor pedestrian navigation," IEEE Sensors Journal, **40**(11), 4034-4042, 2014. https://doi.org/10.1109/JSEN.2014.2330573

[6] T. N. Do, U-X. Tan, "Novel Velocity Update Applied for IMU-based Wearable Device to Estimate the Vertical Distance" IEEE 1st International Conference on Electrical, Control and Instrumentation Engineering (ICECIE), Kuala Lumpur, Malaysia, 25-25 Nov. 2019. https://doi.org/10.1109/ICECIE47765.2019.8974671

[7] X. Yun, E. R. Bachman, and R. B. McGhee, "A Simplified Quaternion-Based Algorithm for Orientation Estimation from Earth Gravity and Magnetic Field Measurements" IEEE Transactions on Instrumentation and Measurement, **57**(3), 638-650, 2008. https://doi.org/10.1109/TIM.2007.911646

[8] Y. S. Suh, "Orientation estimation using a quaternion-based indirect Kalman filter with adaptive estimation of external acceleration" IEEE Transactions on Instrumentation and Measurement, **59**(12), 3296-3305, 2010. https://doi.org/10.1109/TIM.2010.2047157

[9] V. Renaudin, M. Susi, G. Lachapelle, "Step Length Estimation using Handheld Inertial Sensors" Sensors, **12**(7), 8507-8525, 2012. https://doi.org/10.3390/s120708507

[10] H. Zhang, W. Yuan, Q. Shen, T. Li, and H. Chang, "A Handheld Inertial Pedestrain Navigation System with Accurate Step Modes and Device Poses Recognition" IEEE Sensors Journal, **15**(3), 1421-1429, 2015. https://doi.org/10.1109/JSEN.2014.2363157

[11] H. M. Schepers, E. H. van Asseldonk, C. T. Baten, and P. H. Veltink, "Ambulatory estimation of foot placement during walking using inertial sensors" Journal of Biomechanics, **43**(16), 3138-3143, 2010. https://doi.org/10.1016/j.jbiomech.2010.07.039

[12] E. Bachmann, J. Calusdian, E. Hodgson and X. Yun, "Insitu heading drift correction for human position tracking using foot-mounted inertial/magnetic sensors" IEEE International Conference on Robotics and Automation (ICRA), 5425-5430, Saint Paul, MN, May. 2012. https://doi.org/10.1109/ICRA.2012.6225007

[13] T. N. Do, R. Liu, C. Yuen, and U-X. Tan, "Design of an infrastructureless indoor localization device using an IMU" IEEE International Conference on Robotics and Biomimetics, 2115-2120, China, Dec. 2015. https://doi.org/10.1109/ROBIO.2015.7419086

[14] A. Kose, A. Cereatti, and U. D. Croce, "Estimation of traversed distance in level walking using a single Inertial Measurement Unit attached to the waist" IEEE International Conference in Medicine and Biology Society, 1125-1128, 2011. https://doi.org/10.1109/IEMBS.2011.6090263

[15] J. C. Alvarez, D. Alvarez, A. Lopez, and R. C. Gonzalez, "Pedestrian Navigation Based on a Waist-Worn Inertial Sensor" Sensors, **12**(8), 10536-10549, 2012. https://doi.org/10.1109/I2MTC.2012.6229714

[16] F. Inderst, F. Pascucci, M. Santoni, "3D pedestrian dead reckoning and activity classification using waist-mounted inertial measurement unit" IEEE International Conference on Indoor Positioning and Indoor Navigation (IPIN), 1-9, 2015. https://doi.org/10.1109/IPIN.2015.7346953

[17] T. N. Do, R. Liu, C. Yuen, M. Zhang and U-X. Tan, "Personal Dead Reckoning using IMU mounted on upper Torso and inverted Pendulum Model" IEEE Sensors Journal, 2016. https://doi.org/10.1109/JSEN.2016.2601937

[18] E. M. Diaz, "Inertial Pocket Navigation System: Unaided 3D Positioning" Sensors, **15**(4), 9156-9178, 2015. https://doi.org/10.3390/s150409156

[19] M. Elhoushi, J. Georgy, A. Noureldin, M. J. Korenberg, "Motion Mode Recognition for Indoor Pedestrian Navigation Using Portable Devices" IEEE Transactions on Instrumentation and Measurement, **65**(1), 208-221, 2016. https://doi.org/10.1109/TIM.2015.2477159

[20] T. N. Do, R. Liu, C. Yuen, and U-X. Tan, "Personal Dead Reckoning using IMU device at upper torso for walking to running" IEEE International Conference on Sensors, Orlando, FL, USA, Nov. 2016. https://doi.org/10.1109/ICSENS.2016.7808521

ASTES

Advances in Science, Technology and Engineering Systems Journal Vol. 5, No. 5, 789-798 (2020)

www.astesj.com

Special Issue on Multidisciplinary Innovation in Engineering Science & Technology

ASTESJ

ISSN: 2415-6698

Design and Implementation of Quad-Site Testing on FPGA Platform

Basavaraj Rabakavi[1,*], Saroja V Siddamal[2]

[1]*Department of Electronics and Communication, Government Engineering College, Haveri, 581110, India*

[2]*School of Electronics and Communication, KLE Technological University, Hubli, 580021, India*

ARTICLE INFO

Article history:
Received: 17 August, 2020
Accepted: 21 September, 2020
Online: 12 October, 2020

Keywords:
Multi-Site Testing
Concurrent Testing
Propagation Delay
Quad IC Tester
VLSI
ATE
FPGA
IC Packages

ABSTRACT

As manufacturing efficiency has become a main focus of today's business, it is very critical to surge the throughput by developing different test strategies. With throughput, testing cost also has been recognized as the major challenge in the future of leading semiconductors. Reducing test time is a significant effort to maximize throughput as the complexity increases in future generation outcomes and devices. So, low-cost Automatic Test Equipment (ATE) with parallel test can be promoted as the obvious solution for challenges said above. In parallel testing, multiple devices-under-test (DUT) can be tested at a time that enhances way of testing by increasing product flow, limiting gross test times, and efficient usage of tester. The proposed Integrated Circuit (IC) tester is used to implement multi-site testing (Quad-Site testing) and concurrent testing. It exhibits multi-site efficiency which substantially enhances the throughput by reducing test time. Modular, re-configurable test system provides cost-saving solution. To confirm these effects, authors have presented experimental results for Quad site testing of different ICs namely Decoder, Buffer, Multiplexer and Logic gates. This portable IC Tester handles variety of IC packages like Dual Inline Package (DIP), Small Outline Integrated Circuit (SOIC), Thin Shrink Small Outline Package (TSSOP). With functional test, the proposed tester also verified the AC Parametric tests (i) Propagation Delay is 20ns (ii) Operating frequency with 50MHz for Decoder IC (74HC138). The proposed IC tester consumes 70% less power and throughput enhanced by 11% compared to existing IC testers.

1. Introduction

This paper is an extension of previous work originally presented in the 3rd IEEE International Conference on Electrical, Electronics, Communication, Computers and Optimization Techniques [1]. Integrated Circuits which are more commonly known as ICs, are the central components of every electronic circuits present in modern times. Though it is one of the most important and vital part of the circuit, these ICs are most prone to be the cause of the malfunctioning of the whole design. With the advent of the complex integrated circuits, the problem arises after production of digital circuits to verify its functionality towards the meeting specifications. While delivering a product to market, testing plays an important role in the overall process. It is impossible to dispatch quality chips to the customer without proper testing. However, testing cost is also part of the overall product cost. Since it is very essential to test the IC before actually using them in any applications, an IC tester has been developed in order to eliminate the complex process of circuit troubleshooting [2, 3].

1.1. Types of testing

There are three types of testing: (i) Functional (ii) Parametric (iii) Structural tests. Functional testing is carried out by assigning specific test vectors to device under test, measuring the circuit response and device's functionality. Parametric tests are performed to determine the basic electrical characteristics of the device. DC parametric tests verify threshold levels of voltages and currents, in addition to open/short circuit tests and DC parameters are independent of time. AC characterization tests verify time dependent properties like propagation delays, transition signals (rise and fall) and operating frequency range. In structural testing, test inputs are designed to find out particular faults that might have occurred in circuit due to manufacturing deficiencies. During a structural verification, it is assumed that the circuit design is proper and the intention of the testing is to detect faults because of failures in processing [4].

*Corresponding Author: Basavaraj Rabakavi & Email: bsrabakavi@gmail.com

1.2. Stages of testing

There are four different stages of Very Large-Scale Integration (VLSI) testing; (i) Characterization (ii) Production (iii) Burn-in (iv) Incoming inspection. A characterization test measures the true operating limit values of the product. Before manufacturing, this test is carried out on a current design. Manufacturing test undergoes for smaller duration but checks all relevant parameters of the product. This test covers maximum number of standard faults but all expected functions may not be covered by test inputs. Burn-in makes sure the safety of devices by verifying the devices for longer duration, either continuously or regularly, and causing the wrong products to really fail. System manufacturers carry out incoming inspections on the purchased devices before incorporating them into the system [5].

1.3. Traditional method of testing

Everywhere digital circuits are growing consistently in case of both quantity and complexity. Meantime, automated circuit testing is going tougher, costly and critical. Manufacturing test plays a key role in ensuring the standard of the ICs supplied to the consumer. While ICs consistently integrating greater Built-In Self-Test (BIST) approaches, external testing instrument is still required in case of manufacture testing such as reading of specific configuration data or IC characteristics for assessment of ICs performance. Manufacturing test is carried out by advanced ATE, designed to work consistently with high quality standards. These High performance ATEs (HATEs) are costly and high-power consuming machines [6].

Now a day, there are two major types of ATE instruments exist in market: Highly sophisticated ATE and Low-price ATE. Instruments belongs to highly sophisticated ATEs are Verigy, Advantest, Teradyne etc. and normally used in testing industries and their functioning is closely related to manufacturing stage. Highly sophisticated ATE manufactured by industries such as Advantest are costlier (millions of dollars) and need specialized technical skills to be utilized with precision [7]. Costs can be decreased much further by using Field Programmable Gate Array (FPGA) based hardware and computer software in combination. The advances in FPGA technology supports the development of FPGA based low cost ATE. Low cost FPGA based ATE case study can perform functional tests of digital circuits [8].

1.4. Advanced method of testing

Present product trends need greater parallelism in testing methods and flows of VLSI. The overall price of both wafer and production testing will be increased by high-end ATE. So, the increased price of System on Chip (SoC) testing and the ATE cost are two major worries for the semiconductor companies. Multi-site testing with available low-price ATEs is the only solution to resolve this issue by reducing the cost of test. In both wafer and package stage testing methods, multi-site testing can be utilized [9]. Increasing the degree of parallelism can reduce testing price by decreasing the recognizable test time for every product. Multi-site testing is a classic parallel test method where many devices are tested at the same time. Concurrent method of testing is another parallel technique, in which two or more operational modules related to same product are verified in parallel. If the product and test design engineers are able to make sure that independence in their designs individually, then the testing can be carried out simultaneously [10].

1.5. Necessity

The VLSI circuit manufacturer cannot guarantee the defect free integrated circuits (ICs). It is not feasible for small-scale industries investing huge amounts of money to buy sophisticated IC testers. Similarly, directly replacing ICs mounted on a board may not be desirable solution to repair a malfunction. The limitations of high end ATE machines are high price instrument, imprecision and need large memory. Therefore, all the limitations indicated above lead to the way for designing a new IC tester with low price, high accurate with maximum speed, otherwise advantages of semiconductor technology are purposeless [11].

1.6. Contributions

In previous work [1], Dual IC testing of digital ICs was implemented with feature of functionality test only. In this paper, work is extended to perform propagation delay test, operating frequency test with Quad IC testing simultaneously and also to analyze the power consumption and throughput of the proposed testing system. This paper describes a FPGA based reconfigurable, inexpensive, high speed, indigenous testing platform for standard digital ICs (74/54- types). This IC tester can be implemented with low budget for small or medium-scale industry customers of these ICs & offers fast and detailed check-out functions with minimal operator action.

Rest of the paper is organized as follows. Section 2 describes motivation for designing the multi-site tester. In section 3, concept of multisite testing is discussed. Proposed methodology is described in section 4. Results are discussed in section 5 and followed by the conclusion.

2. History and Motivation

2.1. Manufacturing Process Defects

Various types of defects can occur during the manufacture of any circuit, this leads to errors. There are four categories of defects as age defects, process defects, material defects and package defects. Process defects and material defects arise due to material imperfection during manufacture of the circuit. Age defects arise due to usage of device for longer duration and also with over time. Physical assembling of the circuit can cause package defects and other defects can be caused due to opening or breakage of pins [12]. Addition to mentioned defects, the person working on testing can also cause defects by testing the devices with incorrect test program or sometimes testing procedure itself can cause faulty components. Test instrument without calibration leads to wrong results. The person working on production lab can put good devices in the incorrect bin and also possible that a good device can be stamped with wrong part number [13].

2.2. Need for FPGA

Earlier digital IC testers were implemented using micro-processor or microcontroller family. Test vectors stored in the memory as lookup table are assigned to every IC to be tested. Reconfigurable logic system has programmable interconnections

to allow the user to perform required operation within it and it is known as Programmable Logic Device (PLD) or FPGA. Now a day, PLD's logic density has become more sufficient to implement lot of data processing operations within it. Even though ASICs achievement is more compared to PLD, when same application is realized in both devices, PLD's re-configurability has many advantages. PLD System with applications having high parallelism can be quicker more than hundred times than the microcontroller-based system. FPGA produces the test patterns by using Test Pattern Generator (TPG), rather than storing the test patterns as a lookup table for specific IC [11, 14].

FPGAs provide a greater number of tested devices in the specified period of duration. FPGA supports high standard of parallelism while generating various test vectors that varies in properties, ranging from simple digital circuits to highly complicated digital products [15]. FPGAs have many benefits which consist of more speed, large number of input and outputs, less power consumption, less size, enhanced time-to-market and increased flexibility and re-configurability. The number of I/O pins differs between one device to another device. Additionally, the interconnection between DUT pins and test equipment also varies from device to device. Hence, to perform the tests, the test device must be wise enough to handle pin configurations and input/output allocation of the DUT. For I/O handling issue, FPGA based ATE with reconfiguration property is the solution [16].

2.3. Tester requirement

All devices are not identical even though they pass in production tests. When actually used in the field, some will function for longer time and some will fail early. Out of four testing stages, incoming inspection is one of them. Incoming inspection can be conducted for arbitrary samples depending on the standard device and the system specifications. As the cost of incoming inspection is much less compared to the cost of testing in assembled system, the incoming inspection of components is much necessary in the industry [5]. To carryout incoming inspection, digital IC testers are required in various electronics laboratories and industries during design, after manufacturing stage of different electronics devices [6]. As small-scale industries or assembly housing units cannot offer large amount of investment for high end ATEs, less price ATE or IC testing device is the solution for incoming inspection. The requirement of low-cost tester is not only in industries but also in the academics. The low-cost tester can be achieved by implementing multisite and concurrent testing.

3. Concept of Multi-site Testing

IC testing is an important method to create insulation between good and poor components to make sure the quality of the outgoing goods. Traditionally single site testing method was used for testing. In single site method one DUT was verified at given instance using ATE [17]. Reduction in the testing cost is the repeated challenge of the semiconductor manufacture, and the test time has become important part of the Cost of Test (CoT). Because of high competency, system design companies have low profit margins in market, a continuous check on the low average price and quick time to market is very important [18]. Multi-site parallel testing provides the greatest enhancement to throughput on test, irrespective of the particular task. The multi-site parallel test concept has throughput advantages over traditional parallel test methods. In traditional parallel testing, multiple devices are tested on the same site. Once all testing on one site is completed, the prober indexes to the next site. By contrast, the multi-site parallel testing method is performed on multiple devices on different (multiple) sites at the same time as shown in the Figure.1. This eliminates all dead time between tests, and means there is no waiting for any one test to complete before the prober indexes to the next site. The test program is written so that at a time all similar DUTs are tested.

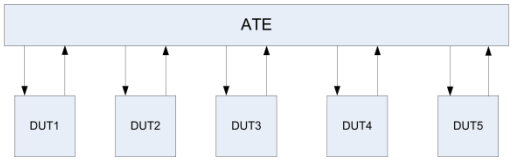


Figure 1: Multi-Site with parallel DUT testing

The total time taken for the group of devices tested at the same time is the addition of the index time t_i and the production test time t_p as shown in the Figure 2. The index time t_i is the time duration to build contact between the bonding pads of the DUTs and the probe interface by making proper positioning. The index time t_i differs on the type of probe station used and it is fixed for each probe station. A normal value of t_i is 0.7sec [19]. The production test t_p is the sum of different tests performed on DUT which may include functionality and characterization test.

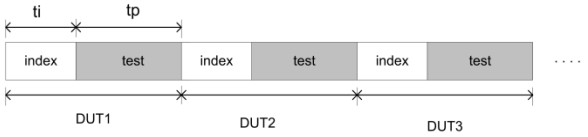


Figure 2: Testing time of DUT consists of index time t_i and test time t_p

If there is no waiting time between replacement of chip being tested is completed with new chip to be tested, then only index time was considered as valid. If immediate replacement of a new chip after the chip being tested is completed, then the indexing time is ignored. If there are no issues like tester downtime and chip contacting problems then test time was considered as valid [20]. The total testing time of a device T_s (Single site test time) can be written as shown in equation (1).

$$T_s = t_i + t_p \quad (1)$$

The Multi-Site-Testing is the test method for simultaneous testing of multiple similar DUTs on single ATE. The test time spent on one device of the Multi-Site-Test is 1/N of the Single-Site-Test. So, Multi-Site-Test testing time is close to time taken by Single-Site-Test. Earlier this test method was utilized for the testing memory devices, but now almost all semiconductor devices are tested with this strategy to decrease the testing cost. The Multi-Site-Test needed N times of the tester resources. Relationship between Multi-Site-Test and Single-Site-Test test timings can be given by Multi Site Efficiency (MSE). MSE is calculated as shown in equation (2).

$$MSE = ((N - T_m/T_s)/(N-1))x100 \quad (2)$$

Where N is the number of devices that can be tested in Multi-Site test, T_m is time consumed for Multi-Site-Test and T_s is time

taken for Single-Site-Test. Generally, Digital circuits MSE is higher than the MSE of analog circuits. i.e. MSE of Digital tests is about 95% and Analog mixed signal MSE is around 60 to 85% [21]. Considering the maximum usage of the ATE, total devices tested per hour i.e. D_{th} for multi-site testing with N number of devices or throughput can be given as in equation (3).

$$D_{th} = (3600 \times N)/T_m \quad (3)$$

4. Proposed Architecture for Quad IC Tester

The proposed architecture of FPGA based Quad IC tester is shown in the Figure 3. It contains FPGA device, devices under test, power supply device and peripheral Interfaces such as switches, LEDs and Displays. In this design, Altera Development board is used for FPGA device (Cyclone II – family) and also for user I/O interfaces. FPGA design consists of various modules as Test Pattern Generation (TPG), Output Response Analyzer (ORA), Input/output compatibility, Frequency Synthesizer and peripheral interface modules.

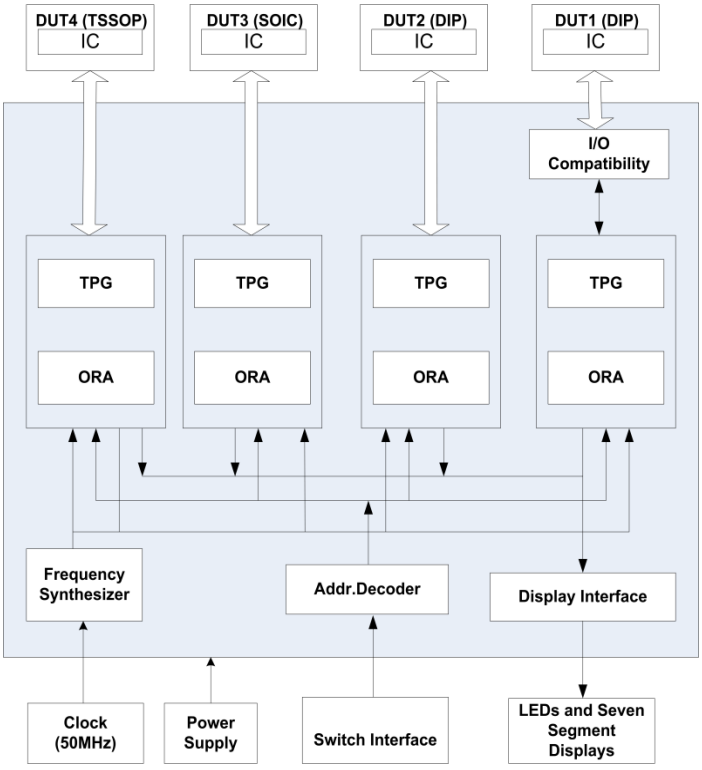


Figure 3: Proposed architecture of Quad IC Tester.

Different test vectors required to test the functionality of the DUT are generated by TPG module. The outputs of the DUT are latched by ORA module to verify with expected ones. If the actual results are similar to the expected results, IC tester displays *P* (PASS), or else *F* (FAIL). Frequency Synthesizer is used to produce various frequencies, which is required for TPG module to generate test vectors and to maintain synchronization among different blocks. As ICs will differ in their Input/Output (I/O) configurations, the I/O compatibility module is required to use single slot for testing different ICs. All the modules are described in the remaining sections.

4.1. Test Pattern Generation

Test Pattern Generation module produces desired test vectors for the device under test. Deterministic, exhaustive, random generations are different ways of producing the test patterns. In present work, exhaustive test patterns are utilized for 100% fault coverage during the testing of IC. In the case of logic gate IC, all quad gates are applied with the same patterns and tested simultaneously. Each different combinational circuit or sequential circuit will have different test patterns generated by Finite State Machine (FSM). Figure 4 shows the FSM for generating test patterns for dual 4:1 multiplexer. This FSM has eight states (S0 to S7) controlled by master clock. FSM is in initial state S0 as long as reset and ebar signals are held high.

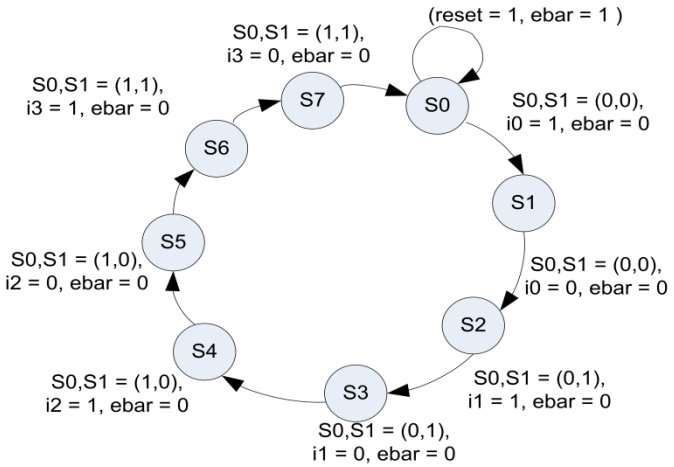


Figure 4: FSM for Generation of Test Patterns for Dual 4:1 MUX

4.2. Output Response Analyzer

The ORA module receives the actual outputs from the DUT and compared with desired values stored in register. Depends on the comparison result, specific bit say R1 will be set as '1' if the result exactly same as desired one, or else it is declared as '0'. In view of complex digital circuits, ORA module is used to verify whole data given in truth table or sequence table of DUT's datasheet with its real outputs, prior to setting of R1 bit. Choice of expected values stored in register is done by setting the switches at the beginning of test, based on the IC inserted in the specific socket. By considering dual 4:1 Multiplexer IC, outputs of multiplexer are captured and stored on every negative edge of input clock into temporarily register i.e. temp [7:0]. This process is continued until input patterns are reached to DUT by FSM in TPG module. Figure 5 shows the FSM for latching the outputs of dual 4:1 MUX.

4.3. Frequency Synthesizer and Input/output Compatibility

The proposed IC tester tests various ICs of different frequencies. Frequency Synthesizer is needed to produce clocks with different frequencies like 2Hz, 0.5MHz, 1.567MHz, 3.125MHz, 6.25MHz, 12.5 MHz, 25MHz. Altera FPGA board consists of 50MHz and 27MHz as master clocks. Binary counters are used to generate various frequencies. Frequency synthesizer module is utilized to calculate propagation delay and operating frequency range of particular IC. Depending upon the modes of

operation like user mode or fast mode, specific frequency is selected for IC testing. IC results are monitored using LEDs with help of 2Hz frequency in user mode. Figure 6 shows frequency generation of 25MHz and 12.5MHz, similarly other frequencies are also generated.

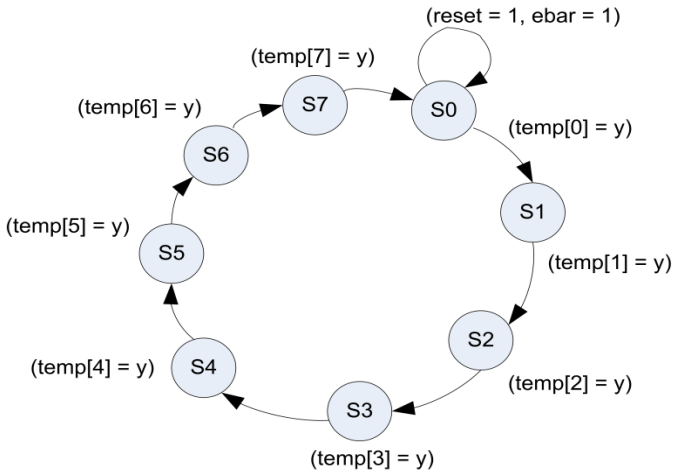


Figure 5: FSM shows output latching of Dual 4:1 MUX

Provision of single slot for testing of various ICs with different I/O connection is the complex problem. If different ICs are to be tested using single socket, then each pin of particular IC need I/O compatibility. This issue is solved by designing I/O compatibility module using multiplexers and tristate buffers. The Figure 7 represents the I/O compatibility logic for single pin. Similarly, all other pins of ICs can be configured as input/output based on the IC selection.

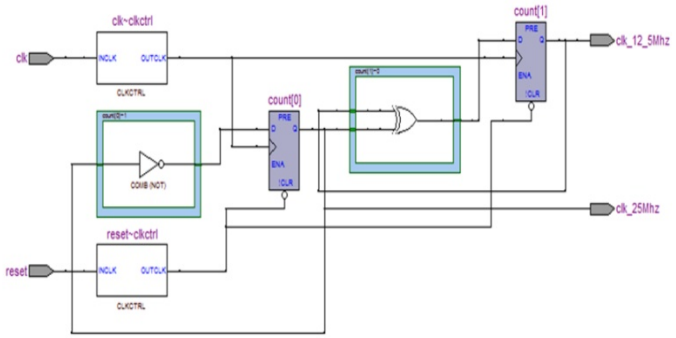


Figure 6: Frequency generation of 12.5MHz and 25MHz

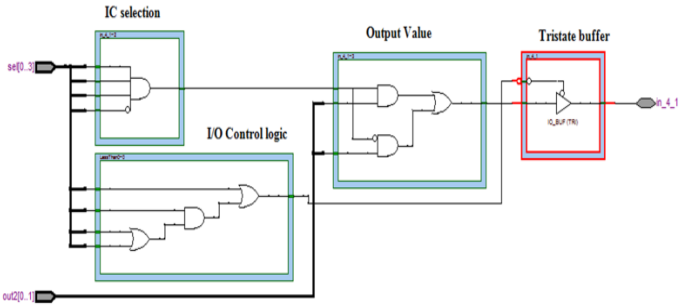


Figure 7: I/O handling logic for single pin of IC

4.4. Propagation delay test and Functional speed test

Propagation delay test is one of the AC Parametric Test of IC. Propagation delay is the addition of switching delay of device and transport delay of interconnects on the track [5]. The process of finding the propagation delay is shown in the Figure 8. Once the test vector of DUT is active i.e. transition from low to high, one pulse is generated. At this time, high frequency counter is started and continues to count till it come across change in output of the device to be tested. The change in output of the device is recognized by pulse generated due to the low to high transition occurs at the device output. Propagation delay is calculated by multiplying the number of counts with time period of master clock used for counter. The equation (4) shows calculation of the propagation delay, where P_d represents propagation delay, C indicates the number of counts from change of input value to the change of output value and T is the time period of the high frequency clock used to run the counter.

$$P_d = C \times T \quad (4)$$

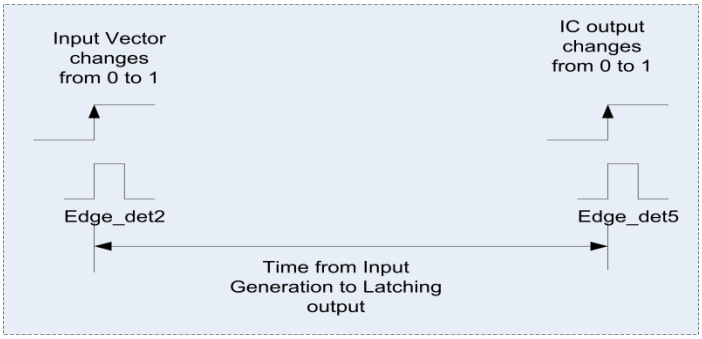


Figure. 8: Process to calculate the propagation delay

Functional Speed Test or Operating Frequency Test of device under test is also one of the AC Parametric tests. Here, the specific test inputs are produced and verified for the performance of the device. The speed at which functionality results of device meet the expected values is called functional speed of the device. The propagation delay test and functionality speed test results are shown in the section 5.

4.5. Quad IC Testing

Most of the existing single IC testers are made up of microprocessor or microcontroller device. The limitations of these testers are sequential execution and a smaller number of input/outputs. In the presented work, the above limitations are overcome by developing test logic with individual FSM for each device. All the FSMs will run in parallel, because of this feature proposed Quad-IC tester can test four different ICs simultaneously.

5. Results and Discussion

The proposed IC tester is designed and developed on target Altera FPGA Development board (Cyclone II – family). The testing logic is developed using Verilog HDL. The design is synthesized using Altera Quartus-II 9.1 tool. Test vectors are produced by TPG modules according to the truth table or sequence table of individual ICs. The functional test of four different ICs, namely Logic gate, Multiplexer, Decoder and

Buffer is performed simultaneously and details of the testing is given in Table 1. Simulation results of TPG and ORA modules are verified for all Digital ICs with respect to its functionality through waveforms. All four ICs are tested in parallel with one-time test and loop test facility by selecting switch as 0/1 respectively. Results are verified through LEDs using IC selection values with fast mode or user mode facility. Status of the result shown in the seven-segment display as IC1P (i.e. First IC is PASS).

Functional test of ICs is carried out with different frequencies by frequency synthesizer to find out the testing speed of IC. Buffer IC is tested with four values namely as 0xff, 0xaa, 0x00, 0x55 in a loop test with 50MHz. Similarly, Decoder IC is tested according to its truth table sequence with 50MHz successfully. Logic gate ICs outputs are verified with 12.5MHz. Multiplexer IC is tested for all combinations of test vectors with 6.25MHz successfully. All the ICs are powered with 5V supply. Table 2 shows the operating frequency and total time required to complete the functionality test of particular IC for all combinations of test vectors.

Propagation Delay test is performed on ten ICs individually and measured values of propagation delays of each IC is given in Table 3. The ICs having 'HC' (High speed CMOS) symbol in their names operate with both voltages '2V' and '5V'. Propagation delay values of ICs differ with respect to supply voltages.

In this work, system clock 50MHz is used to find out the propagation delay. The count value represents the delay between rising edge of test vector to rising edge of gate output. The count value is multiplied with clock period of master clock (i.e. 20ns) which gives the switching delay of the device. In this work, transport delay is considered as negligible (usually in terms of Pico Secs) and it is fixed value. For example, for 74HC86 IC the propagation delay is calculated by using equation (4) i.e. $P_d = C \times T = 2 \times 20ns = 40ns$. In which, C is count value and T is time period of 50MHz clock. Similarly, propagation delay is calculated for all other ICs. Out of ten ICs, eight ICs results are almost similar to the respective datasheet values except two ICs (74HC266 and 74HC153). Reasons may be because of EX-NOR IC has open collector pins, the delay depends on pull up resistor values and MUX IC depends upon its switching activities.

Proposed IC tester also aims to test functionality of ICs with low power consumption. The power consumed by testing logic with respect to each IC is given in the Table 4. Power consumption of developed testing logic is calculated using Powerplay Early Power Estimator Spreadsheet provided by respective FPGA IC vendor (Altera Cyclone II spreadsheet- Now Intel). It will be achieved by filling the utilization of FPGA device i.e. LUTs, FFs, Input/output pins used, clock rate and total fanouts details in the spreadsheet of FPGA family.

The top verilog module or integrated module gives overall power consumption for testing four ICs simultaneously. Power consumption calculated using spreadsheet is static or offline method and for top module it is 169mW. Table 5 shows the power consumed by proposed system in real time during Quad IC testing. The power consumed by FPGA board is calculated by multiplying Icc with Vcc (5V). The current Icc is measured through ammeter placed on power supply path of hardware during Quad IC testing and it is 0.30A. Similarly, board power is calculated before downloading the testing logic onto FPGA device. So, the power consumption of testing logic is calculated by subtracting board power consumption (powered on condition i.e. without code) from power consumed during testing of Quad ICs i.e. 1.5W-1.25W = 0.25W. Total power consumed during testing is 1.5W which is less compared to commercial testers. In the Table 6, the power consumption of the proposed tester is mentioned approximately as 2W by considering enhancement of testing logic to cover variety of ICs.

Table 1: Functional test of Quad ICs

Quad IC Testing (Functionality Test - Simultaneously)								
Sl. No	**Device Name (IC name)**	**Package**	**IC Pins**	**IC Selection**	**Fast mode (1)/User mode (0)**	**Loop test (1)/One time test (0)**	**Expected Result**	**Actual Result**
1	74HC244 (8bit Buffer/Driver)	TSSOP	20	1 (001)	0	0	IC1-PASS	IC1-PASS
2	74HC138D (3:8 Decoder)	SOIC	16	2 (010)	0	1	IC2-PASS	IC2-PASS
3	74HC153N (Dual 4:1 MUX)	DIP	16	3 (011)	1	1	IC3-PASS	IC3-PASS
4	SN74HC86N (Quad XOR Gate)	DIP	14	4 (100)	1	0	IC4-PASS	IC4-PASS

Table 2: Operating Frequency test

Operating Frequency Test			
Sl.No	**Verilog Module name**	**Operating Frequency for Loop Test**	**Time required complete functionality test (Power supply - 5V)**
1	Buffer module	50MHz	80ns (4 values – write and read)

2	Decoder module	50MHz	160ns (8 test vectors)
3	Gate module	12.5MHz	320ns (4 test vectors)
4	MUX module	6.25MHz	1280ns (8 test vectors)

Table 3: Comparison of Real time Propagation Delays with Datasheet values

Propagation Delay Test							
Sl. No	Device (IC)	Values measured using Proposed IC Tester (Actual values)				Values given in Datasheet	
		Power supply (2V)		Power supply (5V)		2V	5V
		Count value	Time taken by devices	Count Value	Time taken by devices	Expected values	
1	74HC86 (EXOR gate)	2	2x20ns = 40ns	1	1x20 = 20ns	40	12
2	74HC138 (Decoder)	2	2x20ns = 40ns	1	1x20 = 20ns	40	15
3	74HC244 (Buffer)	2	2x20ns = 40ns	1	1x20 =20ns	30	11
4	74HC153N (Mux)	4	4x20ns = 80ns	2	2x20 = 40ns	50	17
5	74LS00 (NAND gate)	NA	NA	1	1x20 = 20ns	NA	22
6	74LS02 (NOR)	NA	NA	1	1x20 = 20ns	NA	10
7	74LS08 (AND)	NA	NA	1	1x20 = 20ns	NA	15
8	74LS32 (OR)	NA	NA	1	1x20 = 20ns	NA	15
9	74LS04 (NOT)	NA	NA	1	1x20 = 20ns	NA	10
10	74HC266 (EX-NOR)	18	18x20 = 360ns	18	18x20 = 360ns	150	30

Table 4: Power Consumption of Testing Logic

Power Calculation Through PowerPlay Early Power Estimator Spreadsheet (Offline)						
Individual Modules						
Sl.No	Verilog Modules	Logic		Input/ Output	Clocks	Total (mW)
1	Bufer module	1		36	3	40
2	Decoder module	0		32	3	35
3	MUX module	0		34	3	37
4	Gate module	0		32	3	35
5	Clock module	0		29	3	32
Total = 97 (Pstatic) + 0.179 = 276mW						
Integrated Module						
Sl.No	Module name	P static	Logic	I/O	Clocks	Total (mW)
1	Final module	97	2	63	7	169

5.1 Simulation Results

The Simulation results of TPG and ORA logic modules for each IC under test are verified by using Xilinx ISE 14.3 version through testbench module. Simulation results are described with case study of 74HC138 IC. In TPG module, address and control inputs of decoder are generated at each positive edge of clock. All possible combinations of test vectors are generated as shown in the Figure 9. The outputs from decoder are latched at the falling edge of each clock and stored in register. The 8th output of decoder labeled as y7, latched value shows 0xfe during its active state as shown in the Figure 10.

Similarly, each TPG and ORA module of different ICs are simulated and verified by writing testbench modules. These modules are verified in hardware by implementing on FPGA and tested with physical ICs by sending test vectors to and read the outputs from ICs and compared with expected values.

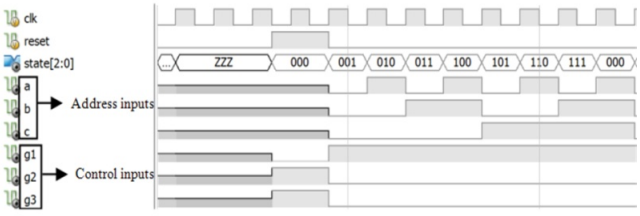


Figure 9: Test Pattern Generation for 3 : 8 Decoder (74HC138 IC)

Table 5: Power consumption in real time testing

Power Values during testing (Real time condition)				
Sl. No	**Module Name**	**Powered on state (No code)**	**Running State (With code)**	**Designed module Power**
1	Final code	0.25Ax5V = 1.25W	0.30Ax5V = 1.50W	(Running code) – (Powered on condition) = 1.50 – 1.25 = 0.25W

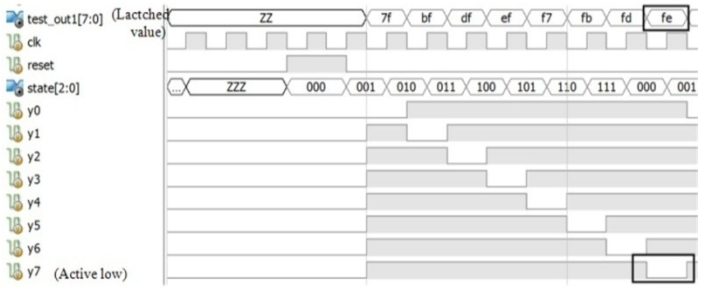


Figure 10: Latching of IC outputs is verified through testbench

Propagation Delay test concept is verified through simulation results as shown in Figure 11. The signal 'edge_det2' shows rising edge of input test vector and signal 'edge_det5' shows rising edge of IC output. The 'count time' register gives the number of counts between the change in the input and output of DUT. The number of clocks marked in the waveform is matched with value stored in the 'count time 'register. This logic is verified through hardware and found the count time value for each IC to be tested. This count time value is multiplied with clock period to get the propagation delay as mentioned in Table 3.

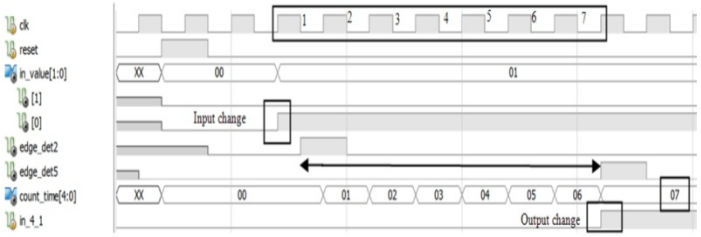


Figure 11. Finding the time between change of input to change of output

5.1. Implementation Results

5.1.1. Dual IC Testing (DIP and SOIC Package)

Dual IC testing presented in paper [1], the Decoder (74138-SOIC) and XOR (7486-DIP) ICs were tested simultaneously. The 7486 – XOR IC was tested by applying all possible test vectors to each gate simultaneously and latched outputs were compared with desired values. 'P' on the seven-segment display represents result status of the individual gate in IC. Figure 12 shows Dual IC testing setup. Results of both ICs were verified through LEDs.

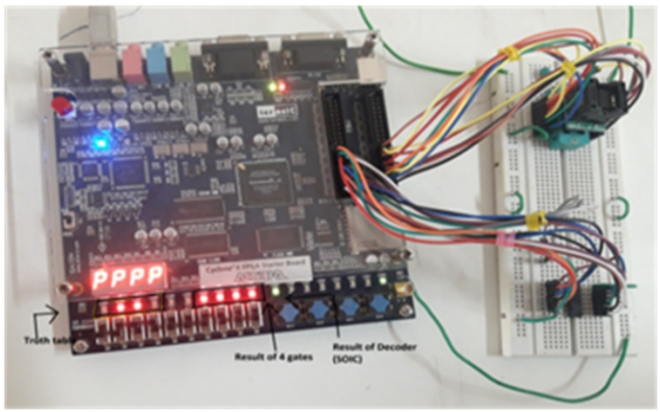


Figure 12: Results of Dual IC tesing (74HC138 and 7486 ICs)

5.1.2. Quad IC testing (TSSOP,SOIC,DIP,DIP- Package)

In Quad IC testing, Buffer - 74HC244 (TSSOP), Decoder - 74HC138 (SOIC), Dual 4:1 MUX - 74HC153 (DIP), XOR Gate - 74HC86 (DIP) ICs with various packages are tested simultaneously. The Figure 13 shows the results of Buffer IC among four ICs. 'IC1P' on the seven segment display represents result status of particular IC as free of error. Buffer IC is tested with fast mode, one time execution method and results shown on LEDs are last combination of test vector i.e. 0x55. IC selection should be set to '001' to monitor Buffer IC result. Similarly, decoder IC also tested in fast and one time execution mode. Both multiplexers in dual 4:1 MUX IC and quad gates in XOR IC are tested at same time. All ICs results are monitored through LEDs by setting switches. Quad IC testing is verified simultaneously without modifying source code.

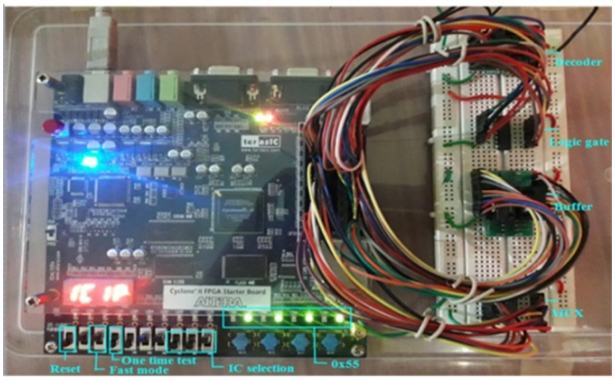


Figure 13: Buffer IC (74HC244) result during Quad IC Testing

The comparison is made between FPGA based Quad-IC tester and available IC testers in market and it is shown in Table 6. The Quad IC tester is having all existing features like multi package support, loop test capability, truth table verification etc. except unknown IC identification. With additional to these features, the Quad IC tester has capability of testing four ICs at a time (parallel execution) with more speed. Throughput calculation is made for single IC and Quad IC testing by using equation (3). The comparison results are demonstrated in the Figure 14 with respect to number of ICs tested per hour. The speed of proposed IC tester is about 0.01sec, which is much lower than speed of existing IC tester i.e. 0.8 sec. Also, Quad IC tester has some more features like

Propagation delay and operating frequency range test. The Altera FPGA Cyclone II EP2C20F484C7 device's (Now its Intel) utilization summary for quad IC testing logic is given in the Figure 15. Implementation of quad IC testing has utilized about 1% of logic and 32% of I/O pins of cyclone II device. So, to provide highly extended support still lot of ICs can be included into tester.

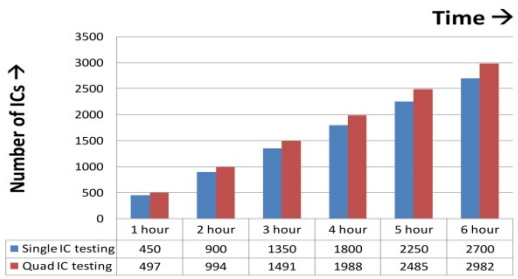


Figure 14: Throughput comparison between Single IC and Quad IC Testing

Quartus II Version	9.1 Build 350 03/24/2010 SP 2 SJ Web Edition
Revision Name	ic_tester_top
Top-level Entity Name	ic_tester_top
Family	Cyclone II
Device	EP2C20F484C7
Timing Models	Final
Met timing requirements	No
Total logic elements	217 / 18,752 (1 %)
Total combinational functions	164 / 18,752 (< 1 %)
Dedicated logic registers	159 / 18,752 (< 1 %)
Total registers	159
Total pins	102 / 315 (32 %)
Total virtual pins	0
Total memory bits	0 / 239,616 (0 %)
Embedded Multiplier 9-bit elements	0 / 52 (0 %)
Total PLLs	0 / 4 (0 %)

Figure 15: Device Utilization summary for Quad IC Testing

6. Conclusion

In this paper, portable Quad-Site Tester for digital ICs is implemented with automatic testing approach on FPGA. Testing has been carried out on Quad ICs simultaneously with features such as Propagation Delay and Operating frequency test along with Functional test. The `concurrent testing with true parallel execution` is the main key of proposed IC tester which greatly reduce the test time and cost compared with traditional testing. The proposed Quad IC tester improves throughput by 11% compared with existing IC testers. In this context, considering index time as 7secs as it is done by manually and testing time is 1sec. If index time becomes less than the execution time, then there will be significant change in throughput. This can be achieved by automatic replacing of ICs using hardware setup.

Also, throughput can be further increased by enhancing the work to Octal-Site testing. The proposed IC tester consumes 70% less power compared to existing IC testers.

In future, proposed work can be enhanced to include analog ICs (ADC, DAC, Opamps, and Analog MUX etc.), peripheral ICs (UART, level translators, drivers etc.) and memories with support of different packages like Thin Small Outline Package (TSOP), Thin Quad Flat Package (TQFP), and Plastic Leaded Chip Carrier (PLCC) etc.

Table 6: Comparison with existing testers

Features	IC Tester (Outside INDIA)	IC Tester (INDIA)	FPGA based Proposed Tester
Quad IC testing (Different type)	No	No	Yes
Package Support	DIP/SOIC	DIP	DIP/SOIC/TSSOP
Parallel Execution	No	No	Yes
Propagation Delay Test	No	No	Yes
Testing Speed	0.8sec	Not shown	0.01sec
Power Consumption	5W	6W	2W
MC/FPGA based	MC based	MC based	FPGA based
Battery operated	Yes	Yes	Can be incorporated in the system
Loop-test capability	Yes	Yes	Yes
Truth table observation	No	Yes	Yes
Counting process observation	No	Yes	Yes
Unknown IC identification	Yes	Yes	Can be enhanced to this feature as proposed IC tester is reconfigurable

Conflict of Interest

The authors declare no conflict of interest.

References

[1] B. Rabakavi, Saroja Siddamal, "Design of High Speed, Reconfigurable Multiple ICs Tester using FPGA Platform", IEEE, ICEECCOT, 909-914, December, 2018. https://doi.org/10.1109/ICEECCOT43722.2018.9001588.

[2] M. S. Zaghloul and M. Saleh, "Implementation of FPGA for decision making in portable automatic testing systems for ICs library & Digital Circuits ," IEEE Applied Imagery Pattern Recongnition Workshop, 2011. https://doi.org/10.1109/AIPR.2011.6176361.

[3] B. Vermeulen, Camelia Hora, Bram Kruseman, Erik Jan Marinissen, Robert van Rijsinge, "Trends in Testing Integrated Circuits", International Test Conference, IEEE, 2004. https://doi.org/ 10.1109/TEST.2004.1387330.
[4] I.A. Grout , Integrated Circuit Test Engineering: Modern Techniques, Springer, 2006.
[5] M.L. Bushnell, Vishwani D. Agrawal, Essentials of Electronic Testing for Digital, Memory and Mixed-Signal VLSI Circuits, Kluwer Academic Publishers, 2002.
[6] S. Fransi, G. L. Farré, L. G. Deiros, and S. B. Manich, "Design and Implementation of Automatic Test Equipment IP Module", ETSYM, 2010. https://doi.org/ 10.1109/ETSYM.2010.5512749.
[7] L. Mostardini, L. Bacciarelli, L. Fanucci, L. Bertini, M. Tonarelli, and M. De Marinis, "FPGA Based Low Cost Automatic Test Equipment for Digital Integrated Circuits", IEEE International Workshop on Intelligent Data Acquisition and Advanced Computing Systems: Technology and Applications, 21-23 September 2009.https://doi.org/ 10.1109/IDAACS.2009.5343031.
[8] A. A. Bayrakci, "ELATE: Embedded low cost automatic test equipment for FPGA based testing of digital circuits", 2017 10th International Conference on Electrical and Electronics Engineering (ELECO), Bursa, 2017, pp. 1281-1285.
[9] H. Kim, Yong Lee, Sungho Kang, "A Novel Massively Parallel Testing Method Using Multi-Root for High Reliability", IEEE Transactions on Reliability, **64**(1), March 2015.https://doi.org/10.1109/TR.2014.2336395.
[10] T. Nakajima, Takeshi Yaguchi, Hajime Sugimura, "An ATE Architecture for Implementing Very High Efficiency Concurrent Testing", International Test Conference, IEEE, 2012. https://doi.org/ 10.1109/TEST.2012.6401551.
[11] Gary L. West, H. Troy Nagle, Jr., Victor P. Nelson, "A Microcomputer-Controlled Testing System for Digital Integrated Circuits", IEEE Transactions on Industrial Electronics and Control Instrumentation, **IECI-27**, No. 4, Nov. 1980.https://doi.org/10.1109/TIECI.1980.351644.
[12] J. Dunbar, "FPGA Based Design for Accelerated Fault-testing of Integrated Circuits" , Master's Theses, Bucknell University, 2010.
[13] A. L. Boudreault, "Automatic Test Equipment in the Production Process", IEEE Transactions on Manufacturing Technology, Volume-4, No.2, December 1975.https://doi.org/10.1109/TMFT.1975.1135861.
[14] Takashi Kitagaki, "Flexible ATE Module with Reconfigurable Circuit and Its Application", International Test Conference, IEEE, 1999.https://doi.org/10.1109/TEST.1999.805826.
[15] J. Romoth, M. Porrmann, and U. Ruckert " Survey of FPGA Applications in the period 2000-2015", Center of Excellence Cognitive Interaction Technology, Bielefeld University, Germany. https://doi.org/10.13140/RG.2.2.16364.56960.
[16] S. S. Tripaliya and P. P. Bansod, "FPGA based IC Tester," IJEEDC, ISSN: 2320-2084 , **3**(5), May-2015.https://doi.org/10.1109/ITC-Asia.2019.00018.
[17] N. Velamati, Robert Daasch, "Analytical Model for Multi-site Efficiency with Parallel to Serial Test Times, Yield and Clustering", 27th IEEE VLSI Test Symposium, 2009.https:doi.org/10.1109/VTS.2009.42.
[18] Y. Lee, Inhyuk Choi, Kang-Hoon Oh, James Jinsoo Ko and Sungho Kang, "Test Item Priority Estimation for High Parallel Test Efficiency under ATE Debug Time Constraints", Teradyne inc. 2017. https://doi.org/10.1109/ITC-ASIA.2017.8097131.
[19] S. Kumar Goel, Erik Jan Marinissen, "On-Chip Test Infrastructure Design for Optimal Multi-Site Testing of System Chips" , Proceedings of the Design, Automation and Test in Europe Conference and Exhibition, 2005. https://doi.org/10.1109/DATE.2005.231.
[20] K. Voon Ching, "A Case Study of Return on Investment for Multi-sites Test Handler in The Semiconductor Industry Through Theory of Industry 4.0 ROI Relativity", International Journal of Recent Contributions from Engineering, Science &IT, **7**(3), 23-40, July 2019. https://doi.org/10.3991/ijes.v7i3.11057.
[21] Y. Takahashi, Akinori Maeda, "Multi Domain Test: Novel Test Strategy to reduce the Cost of Test", 2011 29th IEEE VLSI Test Symposium, 2011. https://doi.org/10.1109/VTS.2011.5783738.

ASTES

Advances in Science, Technology and Engineering Systems Journal Vol. 5, No. 5, 799-807 (2020)

www.astesj.com

Special Issue on Innovative Research in Applied Science, Engineering and Technology

ASTESJ

ISSN: 2415-6698

A Study on Methodology of Improvement the Hydraulic System for Cometto Self-Propelled Trailer System

Hai Minh Nguyen-Tran, Quang Minh Pham, Hoa Binh Le-Nguyen, Cao Tri Nguyen, Tri Nhut Do*

Division of Electronics and Electrical Engineering, Faculty of Engineering, Van Lang University, HCMC, 700000, Vietnam

ARTICLE INFO

Article history:
Received: 19 August, 2020
Accepted: 21 September, 2020
Online: 12 October, 2020

Keywords:
Self-propelled trailers
Hydraulic system
MSPE
Heavy transport

ABSTRACT

In recent years, the transport of large packages with super weight from 100 tons to several thousand tons is no longer a difficult problem due to the continuous development of technology. Experienced transport companies, specializing in transporting heavy goods in Vietnam, have invested in very modern equipment and machinery such as self-propelled trailers of Cometto (Italy) in order to transport safely mentioned parcels of great economic value arrive at the requested location. This trailer can be self-propelled, does not need to use a tractor, and only needs to use a remote-control handheld device. Moreover, the trailer gear shaft can rotate 360 degrees. In particular, the hydraulic system supports trailers operating with high accuracy and absolute safety including functions such as 360-degree rotation, lifting, transmission, braking, etc. In order to improve the performance of trailers when actually used in large projects, an important detail in the trailer's hydraulic system has been inserted a throttle valve with to increase the safety of the hydraulic pump and the entire system as well as the safety of the goods that trailers are transporting. The trailer system has transported the rig with a capacity of up to 3,200 tons in Vietnam, the shipment of 15,000 tons in the world and beyond in the future.

1. Introduction

The operation of moving of oversized and overweight packages onboard is called load-out. The oversized and overweight packages such as: 1) topside, jackets for oil and gas industry; 2) Big equipments for power stations; 3) Super-weighted equipments for oil refineries and thermal power plants.

The load-out task is based on several techniques such as skidding, lifting, float-on, etc and is a high-risk task. In this paper, a self-propelled trailers system is utilized to do load-out task. Adverse events can occur such as trailer overloaded, broken trailer structure, damaged path due to temporary breakdown such as tire explosion, the frequent failure of the Electronic Load Sensing (ELS). Engineers should give priority to solving the problem of damage to the road surface during transportation by many options in many different places [1, 2]. Theoretically, the self-propelled trailer system is navigated by methods such as GPS-based, IMU-based [3], vision-based [4], and combined method of the single mentioned methods [5].

*Corresponding Author: Tri Nhut Do, Division of Electronics and Electrical Engineering, Van Lang University, 45 Nguyen Khac Nhu Street, District No. 1, Ho Chi Minh City 700000, Vietnam, Cell No. +84938113898, trinhutdo@gmail.com

However, this method has many limitations as follows:

- It is difficult to control the synchronous speed of tractors.
- It is difficult to adjust the center to lower the required position because each delegation is a different rotation center.
- It is unable to transport too heavy cargos.

The self-propelled trailers come with many special functions are manufactured by employed the modern technology in order to carry such overlength, overweight and oversized cargos as illustrated in Figure 1. This self-propelled trailer system greatly improves the limitations of the towing method as follows:

- The trailer speed is controlled very synchronously due to the control needs only one person to operate via a remote controller.
- Adjusting the lower center to the expected position is much simpler due to only one driving center is rotated.
- The trailer modules are connected to each others more or less depending on the size and load of packages: Very maneuverable in assembling.
- Distributes loads evenly on the trailer floor via the hydraulic suspension.



Figure 1: A project to load out the gantry using self-propelled trailers

Many leading companies in the world have approached to invest in self-propelled trailer systems. However, several companies in Vietnam also invest but are limited because of the high cost. In particular, Vietranstimex has invested a Cometto self-propelled trailer system that made in Italy [6] and is a Modular Self-Propelled Electric (MSPE) type. During operation, the Cometto system has shown many advanced features such as:

- Flexible assembly: modules are joined together by vertical or horizontal coupling depending on the size and load of packages.
- Mobile steering system: The ability to rotate the package 360 degrees when not moving and many driving modes: wheel steering, parallel steering, single-headed steering.
- The ability to shift the center of steering system in order to adjust the trailer to overcome difficult roads without interfering with the initial programming.

However, the Cometto self-propelled trailer system still presents many problems during operation, including the frequent failure of the ELS valve. Therefore, a new method was proposed in order to handle fastly the ELS valve damage. A throttle valve M is used in series with both tap J and ELS valve. Accordingly, when the ELS valve fails, no matter the status of tap J and without locking tap J, the hydraulic pump is adjusted by turning the throttle valve M only so that the system pressure, which is displayed on the driving pressure gauge, reaches to 200 bar or to 220 bar. The system works stably by those pressures. When more pressure is needed, the throttle valve M continues to be adjusted. After the throttle valve M is installed in the hydraulic system controlling the pump, the self-propelled trailer system works very stably and the proposed self-propelled trailer system has safely transported and launched a lot of oversized and overweight packages.

The remainder of the article is organized as follows: Section II describes in details the origin Cometto self-propelled trailer system and the method to enhance its performance; Section III describes in details the experimental results by applying the proposed method and summarizes the evaluation and Section IV concludes the article.

2. The Cometto self-propelled trailer system and the proposed method

Three problems discussed in this section is organized as follows: Subsection 2.1 introduces the overview of Cometto self-propelled trailer system including Power Pack Unit (PPU) and Modules; Subsection 2.2 specially describes about the main features of PPU hydraulic system; and Subsection 2.3 introduces the proposed method to enhance features of PPU hydraulic system.

2.1. The Cometto self-propelled trailer system

The system consists of main components as follows [7]:

- Power Pack Unit.
- The 4/4/3 electronic-hydraulic module (The module has 4 axes, 4 hydraulic motors, the module width is 3 meters).
- The 6/4/3 electronic-hydraulic module (The module has 6 axes, 4 hydraulic motors, the module width is 3 meters).

The PPU links one or more trailer modules together with either vertical or horizontal configurations as depicted in Figure 2.

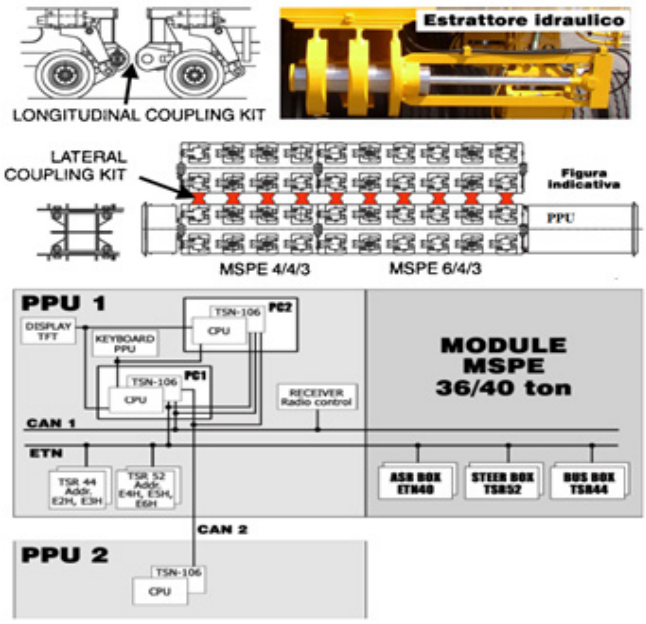


Figure 2: Main components of Cometto system

The number of PPUs and the number of modules is more or less depending on the package weight and package size. However, the system will be only controlled by one remote controller and operated by one person.

The system is operated by a Diesel engine that driving hydraulic pumps, generators and compressors. They provide hydraulic, electrical and steam power for the following main functions:

- Hydraulic drive function.
- Steering control function
- Lifting control function.
- Hydraulic brake function.
- Air brake function when connecting a self-propelled trailer and a non-self-propelled trailer.

2.1.1. The Power Pack Unit

The PPU is considered to be the brain of a self-propelled trailer system. The PPU consists of an electro-electronic control

system [8], a main hydraulic system that determines the functions of the trailer. The PPU can be adjusted in the angle range of 11.8 degrees as depicted in Figure 3.

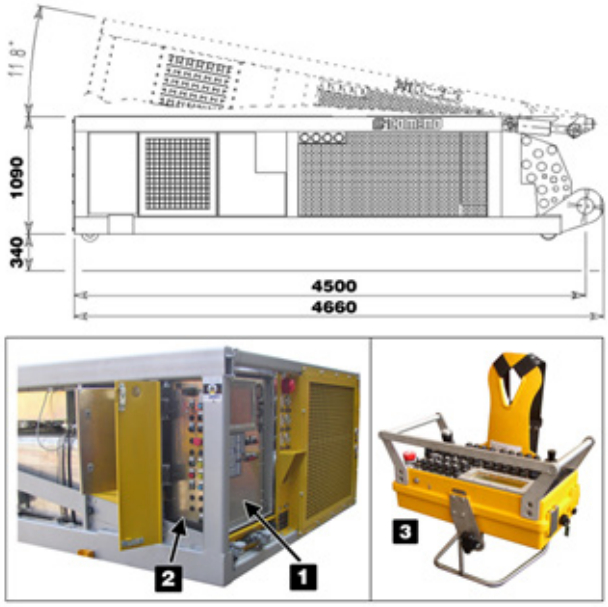


Figure 3: Power Pack and Radio Control

Between two mentioned systems, the hydraulic system, with the parameters listed in Table 1, is improved to make the trailer safer by adding a hydraulic system that controls the pump with a throttle valve. This adding valve replaces the main control valve ELS when this valve is damaged.

Table 1: The PPU hydraulic system parameters

Variable displacement pumps	
Lifting and steering	A11VLO190
Motorization (2 pumps)	A4VG180 + A4VG125
Gear pumps	
Oil cooling pump	SAUER SNP3/90
Pump for hydraulic oil supply to engine coolant radiators fan	SAUER SNP3/44
Pump for overfeeding planetary gearboxes.	SAUER SNP3/44
Pump for hydraulic oil supply to radiator fan	SAUER SNP2-17

Table 2: Module parameters

WEIGHTS	**MSPE 4/4/3 (4 axles)**			**MSPE 6/4/3 (6 axles)**		
Speed (km/h)	0.5	5	10	0.5	5	10
Axle load (2 suspensions), ton	34	34	31	34	34	31
Total gross weight, ton	136	136	124	204	204	186
Dead weight, ton	1.77			26		
Payload, ton	186.3	186.3	106.3	178	178	160
AXLES						
Number of axle lines	4 (8 suspensions)			6 (12 suspensions)		
Number of driven axles	2			4		
Number of braked axles with A.S.R.	2			2		
PLANETARY GEARBOX						
Wheel reducer (code 108.0204)	LOHMANN GFT 17 T3 9357					
Number of wheel reducer	8			8		
Variable displacement motor	A6VE 28HD1/63W					
Input speed	5960 rpm					
Reduction ratio	77.95					
Output speed	76,46 rpm					
Output torque	13881 Nm (10237 ft.lbs)					
Quantity of oil per wheel reducer	2 litres					
Oil type	SPARTAN EP 220~BP Energol GR-XF220					
SLEW GEAR						
Slew gear	IMO WD-HC 0300					
Motor	PARKER VOAC F12-060-MF-INF					

2.1.2. Modules

Modules with parameters such as in Table 2 include 6-axis type (6/4/3) and 4-axis type (4/4/3) with a maximum load for one axle of 3,4 tons. Modules are assembled by 3 types of connection such as mechanical connection, hydraulic connection and electronic connection. The connections are formed by serial configuration (back to back coupling) and parallel configuration (side by side coupling) as depicted in Figure 4.

2.2. The PPU hydraulic system.

The PPU hydraulic system [9] which is depicted in Figure5 consists of 5 pump assemblies as follows:

- One variable delivery pump A11VLO of 190cc (No. 22 in Figure 5) used for the steering and the lifting of the vehicle, and for the lifting cylinders of the Power Pack.
- Two variable delivery pumps: A4VG of 180cc and 125cc (No. **23** and No. **24 in** Figure 5); used for the motorization. Being a closed circuit, each of these two pumps is equipped with an overfeeding pump.
- One fixed delivery pump of 44cc (No. **25 in** Figure 5): this pump is used for overfeeding and piloting of the hydrostatic motors.
- One fixed delivery pump of 17cc (No. **26 in** Figure 5): this pump operates the hydraulic oil radiator fan.
- One further double-body fixed delivery pump of 90cc + 44cc (No.**27** and **27a in** Figure 5)
  - The 90cc pump (No. **27a in** Figure 5) is used for hydraulic oil recirculation in the radiator and in the return filter (No. **11 in** Figure 5).
  - The 44cc pump (No. **27 in** Figure 5) operates the Diesel engine coolant liquid/air radiator fans.

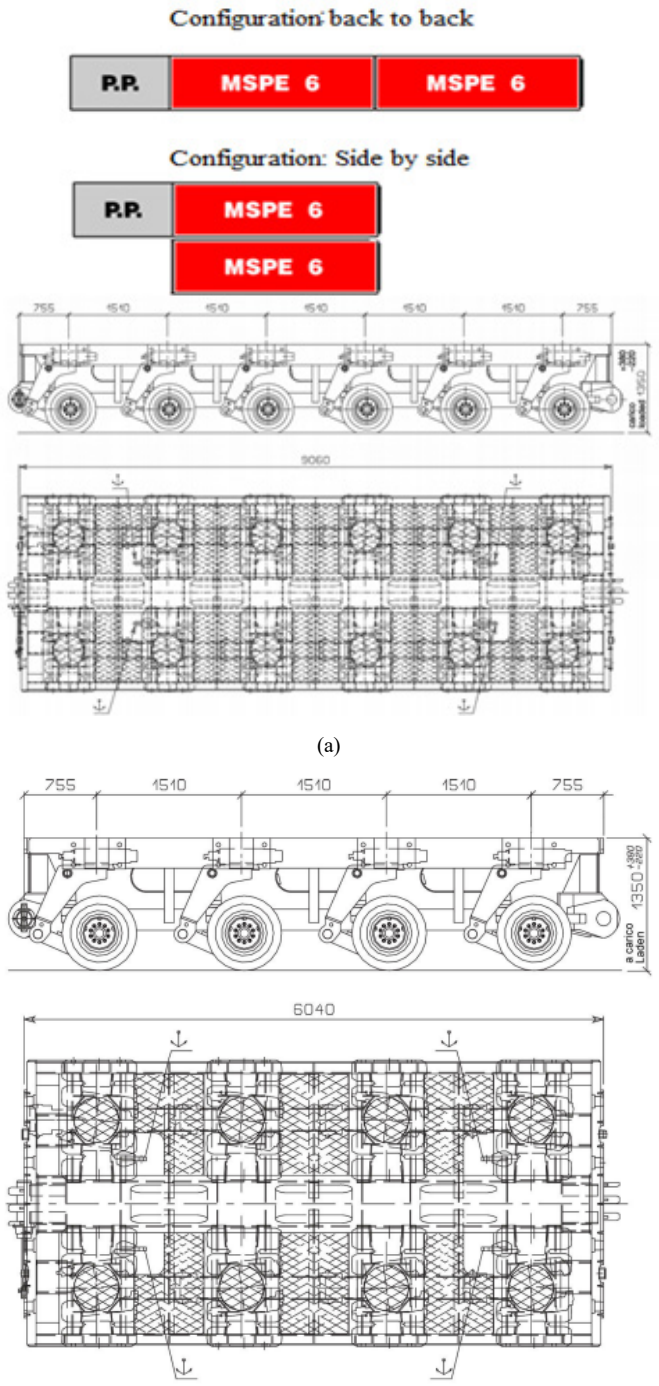


Figure 4: (a) Module Coupling and 6-axis type
(b) 4-axis type

The five pump assemblies are arranged as depicted in Figure 5 and are driven by a MERCEDES 335 KW Diesel engine. The pump assemblies are responsible for ensuring the operation of functions such as transmission, steering, lifting and braking. In particular, the hydraulic control valve ELS determines the operation of the braking, steering and lifting functions by adjusting the supply impeller A11VLO.

The hydraulic braking function: The braking function is to ensure the safety of the entire trailer system and packages. If the valve ELS is broken, the brake pressure cannot reach to 170 bar (as in Figure 6) and therefore the braking function will not work.

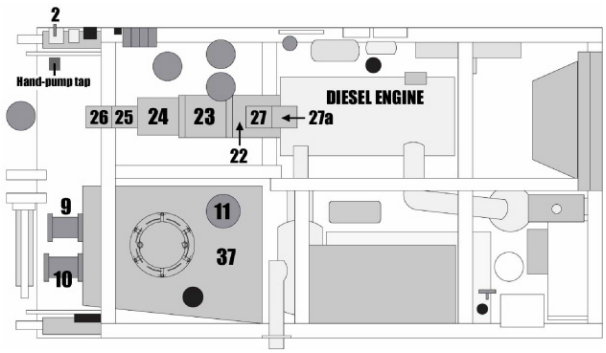


Figure 5: Pump Cluster Positions

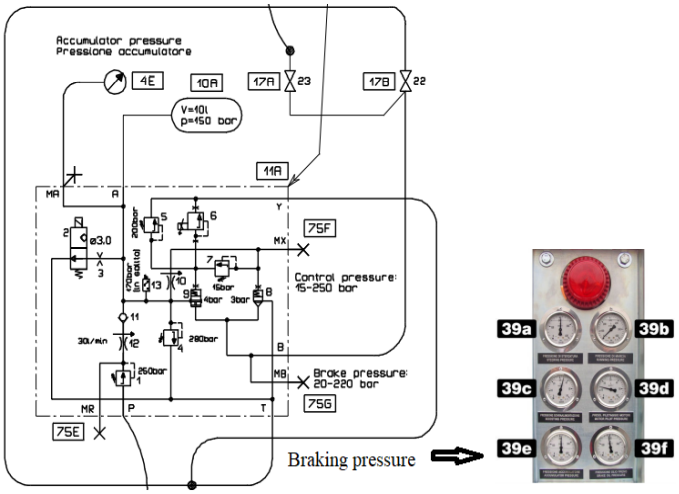
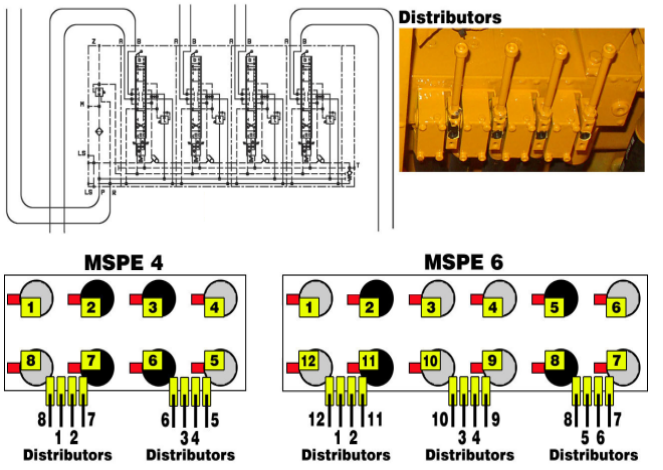
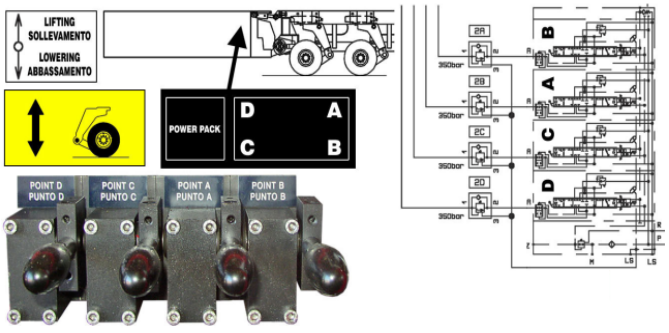


Figure 6: Diagram of the hydraulic braking system



(a)



(b)

Figure 7: (a) The steering; and lifting/lowering function (b)

The hydraulic steering and lifting/lowering function: Diagram of hydraulic steering [9] and lifting/lowering function is shown in Figure 7. In addition, the hydraulic diagram for the pump A11V0 is depicted in Figure 8. The pump A11VO is used to open the steering and lifting/lowering function. This type of pump automatically changes the flow according to the load change. The working pressure of the steering and lifting/lowering function is adjusted by the proportional structure of the pressure reducing valve ELS.

If the load changes, the sensor detects and sends the signal to the central control system, then the controller processes and outputs the appropriate signal controlling the ELS regulating valve (No. **27A in** Figure 8). This valve ELS will regulate the amount of oil that back to the tank in order to control the impeller corresponding to the load.

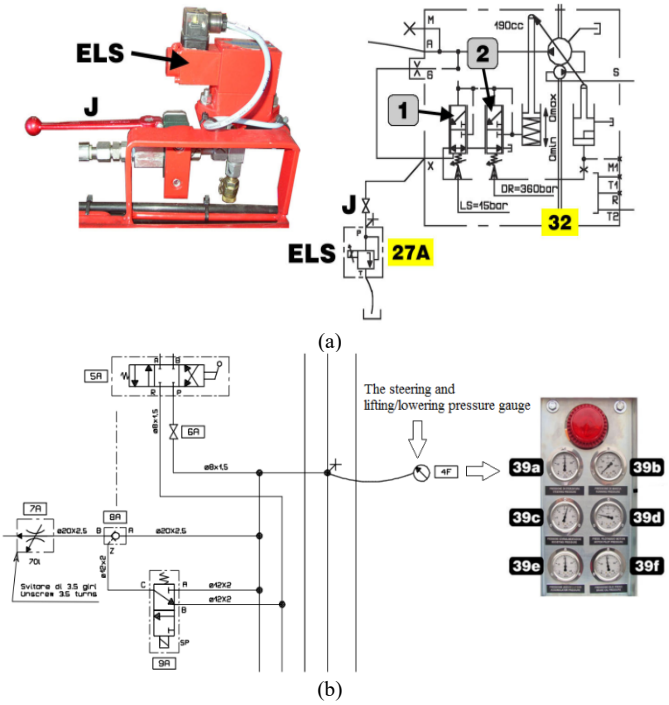


Figure 8: Valse ELS (a) and pressure gauge (b)

2.3. The proposed method

This section deals with the installation of a new throttle valve M [7] which is shown in Figure 9-b that is used to replace the hydraulic control valve ELS if it is unexpectedly damaged or failed.

The valve ELS is controlled by the electronic system with the following description:

- In the case of the diesel engine in starting and stand-by status: the system pressure approximately reaches to 15 bar during engine starting; after 5 seconds, the engine speed reaches to 900 rpm and therefore the system pressure will approximately reach to 220 bar.
- In the case of changing the direction of steering system and aligning it: the initial pressure is approximately 220 bar, the maximum pressure is 300 bar.
- In the case of lifting: The valve pressure is proportional to the load to be lifted. Working pressure is from 220 to 300 bar (approx.). Maximum pump pressure is 300 bar (approx.)
- In the case of lowering: Working pressure is from 220 to 300 bar (approx.)
- Maintain brake pressure from 170 bar to 220 bar.
- Pressure increase

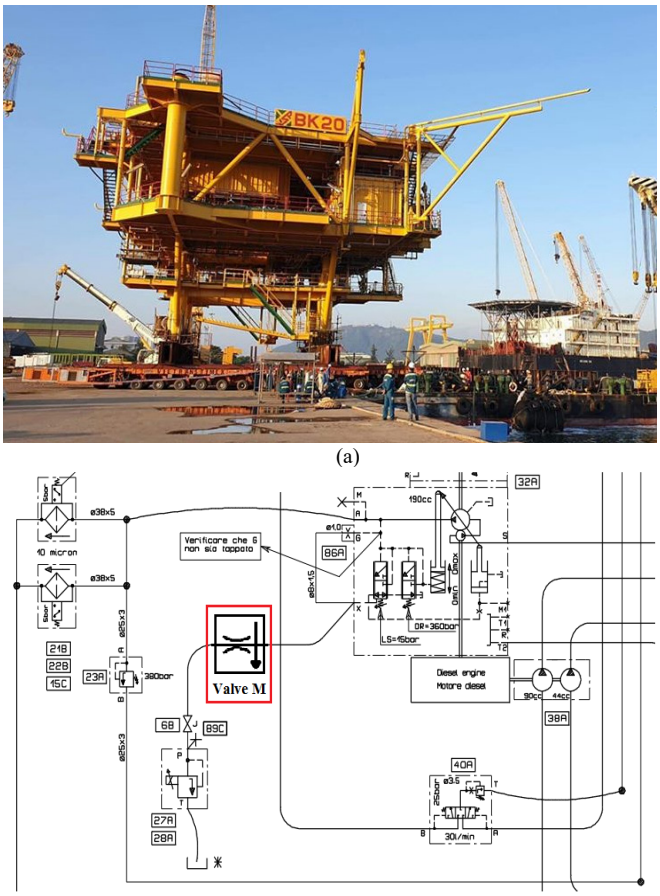


Figure 9: (a) The package is on the bridge leading to the barge (b) Install the throttle valve M into the system

In case of the valve ELS failure (pressure lack in the system), the tap J must be closed. This action allows to increase the pressure in the system to 360 bar again.

Failure of the valve ELS is an important issue because it determines all lifting, lowering, steering and braking functions when the Cometto self-propelled trailer is in operation. Therefore, the failure of this valve is very dangerous for all system because at that time the tap J needs to be closed in order to force the system to operate.

Closing the tap J will cause the pump A11VO to work at full capacity, considered to be high load, the working pressure of the pump and the piping system will be up to 360 bar (as shown in Figure 8, 39a). Diesel engine also works at high power and they often get drowned. Therefore, tap J can only be temporarily locked for a short time but not for long-term use.

Experience is learned during the actual use of self-propelled trailer system, the valve ELS often burns down when in operation because the suction coil of the valve is very hot when working due to the valve ELS is always soaked in electricity and the

environmental temperature in Vietnam is much higher than in Europe (Italy, where the system is made).

In an actual coincidence case, if tap J and valve ELS are damaged at the same time (called valve leakage), all lifting/lowering, steering, braking functions stop operating and cannot be controlled. Packages will overturn if there is a difference in load at any combination in the system that makes it impossible to adjust to the balance point.

Given the nature of transportation of oversized and overweight packages, such damages are very dangerous. Moreover, when the package is lying both on the wharf and on the barge (Figure 9-a) and the tide goes up/down quickly, the incident is absolutely impossible to happen because of much more dangerous. However, if this happens, there must be immediate remedies. And the fastest way to handle when the ELS valve is damaged is an essential issue.

Based on the operating principle of the system, the function of the ELS valve is to regulate the hydraulic oil flow that controls the A11VO impeller. Therefore, the amount of control oil will be at the maximum when this valve is broken. The pump will work as in no-load state, not enough pressure for the modes of steering, lifting/lowering and braking to operate. The proposed method is ultilizing the throttle valve M (as shown in Figure 10), which is located in the main connection between tap J and the ELS valve (as depicted in Figure 9b).



Figure 10: throttle valve M

The proposed method has improved the necessary requirements. Accordingly, when the ELS valve fails, no matter the status of tap J and without locking tap J, the hydraulic pump is adjusted by turning the throttle valve M only so that the system pressure, which is displayed on the steering pressure gauge, reaches to 200 bar or to 220 bar. The system works stably by those pressures. When more pressure is needed, the throttle valve M continues to be adjusted.

The throttle valve M theoretical basis is presented as follows:

2.3.1. Functions

The throttle valve M is responsible for regulating the flow rate in terms of the speed or running time of the actuator. The calculation method is presented in the next section.

2.3.2. Principles

The throttle works on the principle that the flow through the valve depends on the cross section (as shown in Figure 11). The oil flow qv through the gap is calculated using the Torricelli formula in (1) as follows:

$$q_v = \mathrm{C} \cdot A_j \sqrt{\frac{2 \cdot \Delta p}{\rho_j}} \quad (1)$$

where:

$\propto$: Flow coefficient.

A_j: Interstitial area of the gap, $A_j = \frac{\pi d^2}{4}$ [m^2].

$\Delta p = p_1 - p_2$: Pressure at previous and next positions of the gap [N/m^2].

p_j: Density of hydraulic oil [Kg/m^3].

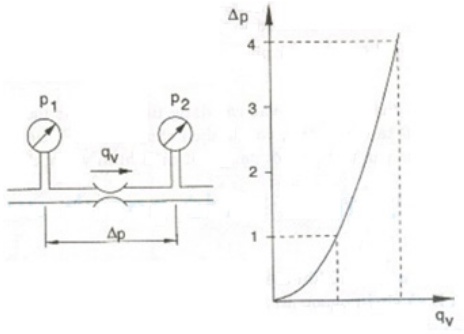
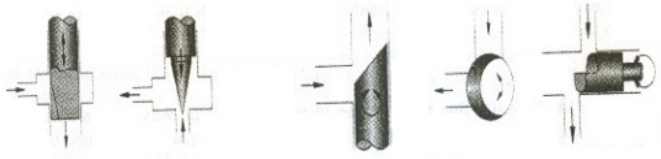


Figure 11: Difference in pressure and flow rate through the gap.

According to the flow control method, throttle can be classified into two main categories: the throttle adjusts axially (as shown in Figure 12-a) and the throttle adjusts around the shaft (as shown in Figure 12-b).



(a) (b)

Figure 12: Classification of throtle vale

Between them, the throttle adjusts axially as shown in Figure 12-a is selected for epxeriment in this article. The specifications requirement for the throttle valve M:

- System maximum working pressure p: 300-440 (Bar).
- Maximum working flow: 30 (l/ph).
- Threaded catch size: 1/2" (PT).
- Working Temperature: -25 ºC ÷ 80ºC.
- Valve Type): APT-04
- Standard size: DIN.

3. The Evaluation of Economic Efficiency

Since installing the throttle valve M into the hydraulic system controlling the pump, the self-propelled trailer system works very stable. The self-propelled trailer system safely and effectively transports a lot of petroleum packages. Some key projects had been applied the proposed method are as follows:

3.1. Hai Su Trang oil rig project in 2013:

Main task: Relocating and launching to barges the 1,700-ton upper block of Hai Su Trang rig at PTSC port, Vung Tau, Vietnam with following details:

- Relocation distance is 500 meters.
- Launching to barges.

While the trailers were moving through the bridge connecting the wharf and the barge, the ELS valve was damaged, the working pressure dropped to nearly 0 bar, the systems stopped working, unable to control the steering, lifting and braking functions. At this time, the technical worker adjusted the valve M so that the steering pressure and lifting/lowering pressure increased to 220 bar. Therfore, the system works again normally with this pressure. All actions only take 1 minute. If the valve M is not utilized, replacing the ELS valve will take 30 minutes or more, this will change the calculation parameters for the pump of bracing barges because the tide changes rapidly.

After the project is completed, our company is highly appreciated by the investors for quick action and mobility.

3.2. Su Tu Nau oil rig project in 2014:

Main task: Relocating and launching to barges the 2,200-ton upper block of Su Tu Nau rig at PTSC port, Vung Tau, Vietnam with following details:

- Relocation distance is 500 meters.
- Launching to barges.

When moving a site (site moving) from the installation location to the wharf, the ELS valve is damaged. At this time, it is very dangerous to stop and replace the ELS valve because the whole trailers and packages is lying in place for more than 30 minutes, that causes very large load impact on the road surface. Therefore, the valve M is adjusted to solve this problem within a minute and to bring the system back to normal operation.

In addition to the two typical projects just mentioned, all projects after Nov, 2014 (as listed in Table 3, 4, 5, 6) with application of the proposed method of improving the hydraulic system for Cometto self-propelled trailers have have made many investors trust our company and give the reputation of Vietranstimex is the leading company in Southeast Asia and the 34th rank in the world in the oversized and overweight transportation.

Table 3: Projects that applied the proposed method (2014-2016)

No.	**Project name; Weight (tons)**	**Port / Place; Time**
1	Load out BK4A Jacket; 1,080	Vietsovpetro Port – Vung Tau; Nov, 2014
2	Site moving DSF - HRD Project; 1,360	PTSC Port – Vung Tau; Nov, 2014
3	Transport gantry crane; 280	Hai Phong to Nha Trang; Mar, 2016
4	Load out Container crane; 560	Phu Huu Port – Ho Chi Minh; Jun, 2016
5	Load out ST-LQ Jacket; 1,279.72	PVC-MS Port – Vung Tau; Aug, 2016
6	Load out ThTC3 Jacket; 992.57	Vietsovpetro Port – Vung Tau; Aug, 2016
7	Load out ST-PIP Module 01 Topside; 1700.29	PTSC Port – Vung Tau; Aug, 2016
8	Load out ST-PIP Module 02 Topside; 2820.57	PTSC Port – Vung Tau; Aug, 2016
9	Load out ST-LQ Topside; 2429.17	PVC-MS Port – Vung Tau; Sep, 2016
10	Load out BKTNG Living Quarters; 823.79	Vietsovpetro Port – Vung Tau; Sep, 2016
11	Site Moving Sumitomo crane; 803	Tan Cang Port – Ho Chi Minh; Sep, 2016
12	Site Moving Container crane; 618.62	Tien Sa Port – Da Nang; Nov, 2016

Table 4: Projects that applied the proposed method (2017)

1	Site Moving Container crane; 560	ITC Phu Huu Port – HCM; Mar, 2017
2	Load out ThTC3 Topside; 1039.94	Vietsovpetro Port – Vung Tau; Mar, 2017
3	Load out DKI 16 Topside; 860	Vietsovpetro Port – Vung Tau; May, 2017
4	Load out DKI 16 Middle; 810	Vietsovpetro Port – Vung Tau; May, 2017
5	Load out DKI 17 Topside; 822.4	Vietsovpetro Port – Vung Tau; May, 2017
6	Load out DKI 17 Middle; 750	Vietsovpetro Port – Vung Tau; May, 2017

7	Load out DKI 18 Topside; 908.48	Vietsovpetro Port – Vung Tau; May, 2017
8	Load out DKI 18 Middle; 750	Vietsovpetro Port – Vung Tau; May, 2017
9	Load out DKI 19 Topside; 863.95	Vietsovpetro Port – Vung Tau; May, 2017
10	Load out DKI 19 Middle; 750	Vietsovpetro Port – Vung Tau; May, 2017
11	Site Moving Container crane; 650	Tan Vu Port – Hai Phong; Aug, 2017
12	Load out C24-P2 Topside; 1660	PTSC Port – Vung Tau; Dec, 2017
13	Load out C24-P2 Jacket; 1750	PTSC Port – Vung Tau; Dec, 2017
14	Load out B12-13 Topside; 1360	PTSC Port – Vung Tau; Dec, 2017
15	Load out B12-13 Jacket; 1679	PTSC Port – Vung Tau; Dec, 2017

Table 5: Projects that applied the proposed method (2018)

1	Load out B12-15 Topside; 1354.32	PTSC Port – Vung Tau; Jan, 2018
2	Load out B12-15 Jacket; 1530	PTSC Port – Vung Tau; Jan, 2018
3	Load out B12-11 Topside; 1781.88	PTSC Port – Vung Tau; Feb, 2018
4	Load out B12-11 Jacket; 1587	PTSC Port – Vung Tau; Feb, 2018
5	Load out B12-17 Topside; 1396	PTSC Port – Vung Tau; Feb, 2018
6	Load out B12-17 Jacket; 1762	PTSC Port – Vung Tau; Feb, 2018
7	Site Moving Container crane; 650	Tan Vu Port – Hai Phong; Mar, 2018
8	Load out CTC1 Jacket; 1025.23	Vietsovpetro Port – Vung Tau; May, 2018
9	Site Moving Container crane; 618.62	Tien Sa Port – Da Nang; Nov, 2018
10	Erection packages at Paper-mill; 150	SePon – Laos; Aug, 2018
11	Erection packages at Paper-mill; 90	SePon – Laos; Aug, 2018
12	Erection packages at Hoang Van Thu Bridge Project (2 packages); 140.3 &83.5	Hai Phong city – Vietnam; Aug, 2018
13	Erection the center arch span bridge from the barge grillage to final elevation by strand jack system; 440.3	Hai Phong city – Vietnam; Aug, 2018
14	Load out CTC1 Topside; 1047.3	Vietsovpetro Port – Vung Tau; Oct, 2018

Table 6: Projects that applied the proposed method (2019-2020)

1	Site moving for H387 & H388 Vessel; 788.5	Dong Xuyen Port – Vung Tau; Fed, 2019
2	Site moving for H765 Vessel; 1057.6	Dong Xuyen Port – Vung Tau; Fed, 2019
3	Load out BK20 Jacket; 721.2	Vietsovpetro Port – Vung Tau; Jul, 2019
4	Load out BK20 Topside; 800	Vietsovpetro Port – Vung Tau; Jul, 2019
5	Load out SVDN Pipes; 3x2000	PV Shipyard Port – Vung Tau; Jul, 2019
6	Site Moving Container crane; 2x700	Bason Port-Phu Mi; September, 2019

7	Site Moving SVDN Jacket; 1200	PTSC Port – Vung Tau; March, 2020
8	Site moving, Loadout,, Launching hight speed ferry	Dong Xuyen Port – Vung Tau; May, 2020

4. Conclusion

The article has proposed a new method of installing the throttle valve M into the hydraulic system for the Cometto self-propelled trailer system. The method has been raised by the practical difficulties arising during the operation of the Cometto self-propelled trailer system for transporting the oversized and overweight packages. The difficulties include suspending the Cometto system, unable to control the steering, lifting and braking functions and that caused by the damage of the hydraulic control valve ELS. The sudden stop of the system makes the packages also being abruptly stopped on the road, which will put high pressure on the road surface, affecting the structure of road and the balance of barges.

With the new installation of a part in the hydraulic system, it has brought a great effect to the business, creating peace of mind for investors, increasing mobility for transport equipment and great reducing troubleshooting time when trailers are under load as well.

However, it is necessary to note that the throttle valve M only replaces the ELS valve in an emergency when the incident occurs because the M valve only works with manual adjustment. This M valve cannot replace the ELS valve completely because the ELS valve opens and closes automatically via electronic card control in the PPU. When the load changes, the ELS valve automatically adjusts accordingly. Therefore, the ELS valve replacement should be performed when the system is maintained after the project.

Moreover, authors would like to introduce in this article a kind of world-specific trailers that have been approached for a long time in the word but it is still very new in Vietnam. Hopefully, much leading transportation companies in Vietnam will equip the system in the future and put them into use more, improve efficiency, increasingly develop oversized/overweight packages transportation industry in order to reach to the world standard. Besides Cometto, there are many companies producing Modular Self-Propelled Electric (MSPE) self-propelled trailer systems such as: Golghofer, Nicolas, Kamag ... Each company has different strengths but all of them enhance advanced operational features for the purpose of absolute safety for goods and people.

Conflict of Interest

The authors declare no conflict of interest.

Acknowledgment

This project is supported by Van Lang University (VLU) Electronics and Electrical Engineering Division, Ho Chi Minh City 700000, Vietnam.

References

[1] L. Černá, V. Zitrický*, and J. Daniš, “The Methodology of Selecting the Transport Mode for Companies on the Slovak Transport Market”, Open Engineering, **7**(1), 2006, doi: 10.1515/eng-2017-0002.

[2] S. Hameed, R. Chandra Prathap, “Study on Impact of Vehicle Overloading on National Highways in Varying Terrains”, International Journal of Engineering Research & Technology (IJERT), **7**(1), 2018, doi: 10.17577/IJERTV7IS010135.

[3] T.N. Do et al., “Personal dead reckoning using IMU mounted on upper torso and inverted pendulum model”, IEEE Sensors Journal, **16**(21), 7600–7608, 2016, doi: 10.1109/JSEN.2016.2601937.

[4] T. Nhut Do, S.Y. Soo, “Foot motion tracking using Vision”, IEEE 54th International Midwest Symposium on Circuits and Systems (MWSCAS), 1–4, 2011, doi: 10.1109/mwscas.2011.6026603.

[5] T.N. Do, S.Y. Soo, “Gait analysis using floor markers and inertial sensors”, International Journal of Sensors, **12**(2), 1594–1611, 2012, doi: 10.3390/s120201594.

[6] Self-Propelled Module Trailer - Use and Maintenance, Cometto, Via Cuneo, 2019.

[7] Self-Propelled Module Trailer - Electronic Manual, Cometto, Via Cuneo, 2019.

[8] Self-Propelled Module Trailer - Electric Electronic Diagrams, Cometto, Via Cuneo, 2019.

[9] Self-Propelled Module Trailer - Hydraulic Diagrams, Cometto, Via Cuneo, 2019.

ASTES

Advances in Science, Technology and Engineering Systems Journal Vol. 5, No. 5, 808-819 (2020)

www.astesj.com

Special Issue on Multidisciplinary Innovation in Engineering Science & Technology

ASTESJ

ISSN: 2415-6698

Innovative Solution for Parking-Sharing of Private Institutions Using Various Occupancy Tracking Methods

Adrian Florea*, Valentin Fleaca, Simona Daniela Marcu

Lucian Blaga University of Sibiu, Department of Computer Science and Electrical Engineering, Sibiu, 550025, Romania

ARTICLE INFO

Article history:
Received: 27 August, 2020
Accepted: 28 September, 2020
Online: 12 October, 2020

Keywords:
parking sharing
embedded system
web application
smart parking
image processing

ABSTRACT

This work presents an innovative solution for parking-sharing of private institutions based on daily occupancy patterns and using different real time tracking methods of vacant parking slots. The research objective consists in finding the most accurate cars detection method, for determining of vacant parking slots and updating them on application web page. Beside the technical innovation represented by image processing algorithms used, this paper promotes the concept of sharing economy with many social benefits like car flow optimization, reducing fuel, pollution, loss of time and creating financial advantages for parking owners. The main software component is a web application which is connected with Raspberry Pi microcontroller, 2 Pi cameras and one fix camera for parking management. It facilitates reserving a place, opening the barrier and allows entering, exiting and revising the number of vacant slots and synchronization with the web application and the supporting database. The web application provides the following facilities: real time parking status view, reservation on a specific time by license plate number, administration module that includes payment system and updates about users and prices, implementation of the gamification concept in the management of parking spaces. The solution was piloted at Lucian Blaga University of Sibiu (LBUS) Romania. The developed solution is flexible, extensible and applicable to crowded university cities, but also to other private organizations that have inefficiently operated parking slots.

1. Introduction

This paper extends the previous work that was presented at the 2018 Thirteenth International Conference on Digital Information Management (ICDIM) [1], by presenting an innovative solution for parking-sharing of private institutions based on daily occupancy patterns and using different real time tracking methods of vacant parking slots.

1.1. The need of innovative smart parking solutions

The general-purpose objective of smart cities is finding smart solutions for increasing the citizens' welfare and comfort by providing high quality services like smart mobility, smart health, and smart environment. Unfortunately, the shortage of parking spaces and, the continuous infrastructure development generates city crowding [2] and traffic congestion. The constant stopping and starting in traffic jams burn the fuel at higher rate in comparison to when someone travels smoothly through the highway. Thus, the congested areas have a higher emission of Carbon Dioxide than other areas [3]. A solution that some countries tried was to put a number of traffic policemen to help manage the traffic in a better way [4]. The problem with this was that a one out of three-traffic policeman suffers from either one or more respiratory morbidities like allergic rhinitis, chest symptoms (cough, wheeze, and breathing difficulty/chest tightness), allergic eye symptoms, sinusitis [5].

Especially in touristic cities, at seaside resorts or others with many visitors yearly, the lack of parking spaces is emphasized by unpopular local authorities' decisions with short or long term effect. For example, in Sibiu, during the theatre festival or international events like auto-moto rallies, the municipality restricts parking places, providing these for guests or organizers. In 2019 there were 700,000 people who visited or participated to shows, more than 4 times the population of Sibiu that produces a further pressure on local drivers. Finding with difficulty a vacant parking place became ordinary activity for most of the drivers.

*Corresponding Author: Adrian Florea, Lucian Blaga University of Sibiu, Department of Computer Science and Electrical Engineering, Sibiu 550025, Romania, Emil Cioran Street, No. 4, Email adrian.florea@ulbsibiu.ro

Studies developed by researchers from Boston University [6] reveals that over 30% of the drivers lost around 8 minutes looking for a free space around the zone where they must stop their car. According to [7], the drivers spend in medium 17 hours yearly looking for vacant places on streets, in lots, or in garages generating tremendous financial losses (tens of billions of dollars) to economy. From our experience in Sibiu, Romania, finding a parking place near the Engineering Faculty takes every morning minimum 10 minutes of searching, beside the fuel costs. Arriving to Faculty earlier with around 20 minutes before starting the classes might solve sometimes this problem. Implementing a smart parking system would shorten the search time for a parking space, reduces CO2 emissions – a key aspect of smart crowded cities, optimizing the car traffic, increasing safety and sometimes even avoid fines caused by illegal parking.

An innovative smart parking system incorporates several important features [8]:

- It helps the business growth and economic development by different solutions like providing incentives for parking or sharing excess spaces of private institutions.
- It helps drivers and municipality to efficiently exploit citywide parking space or providing unexpected (vacant) spaces in real time from private parking which share their spaces.
- It analyses the daily occupancy patterns based on institution / company schedule to understand driver patterns and to predict spaces to be released.

In our smart parking solution, beside innovative technical implementation, the emphasize is on the problem of sharing economy (until the municipalities make new parking lots – a very difficult and time-consuming process, the sharing empty parking places is an acceptable solution with positive economic impact. Especially in big cities finding a parking place represents one of the major challenge of a drivers, and smart parking would represent even urban smart mobility solution for traffic congestion control using parking charges differentiated by time and area. In busy days when most of people are running to work / schools and Saturday afternoon when everybody is engaged in the social and commercial life of the city or during major events when traffic congestion is high, the municipalities' decision factors could coordinate with traffic planners the city mobility to update parking lot status and maximize use of public transit, and alternative transportation options. However, this would be applied by local municipalities. Our proposal is dedicated for private organizations who may share their excess parking places with ordinary traffic drivers without affecting their own employees.

1.2. Scientific motivation based on bibliometric study

As motivation of our research we also present the following bibliometric study, developed by us at the end of June 2020. 812 articles containing the phrase "*smart parking*" in the "Title", "Abstract" or "Keywords" and that appeared at least 25 times in the article's content were selected. The charts were developed using Microsoft Excel and VOSviewer Software (https://www.vosviewer.com/).

Analyzing the period 2011-2020, there is an increasing evolution of the number of articles published in the SCOPUS database, which refers to the phrase "smart parking". The statistics (see Figure 1) were compiled at the end of June 2020 and the number of articles in 2017 has already been reached, despite the reduction in the number of conferences (and implicitly of articles) caused by the COVID-19 pandemic.

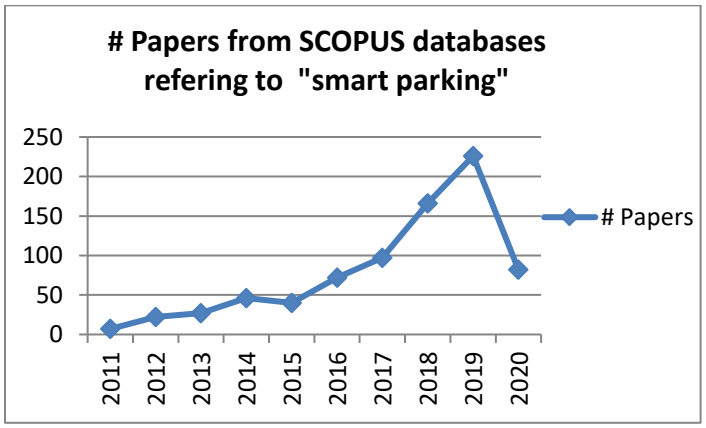


Figure 1. Number of publications indexed in the Scopus databases referring to the concept of smart parking (2011–2020)

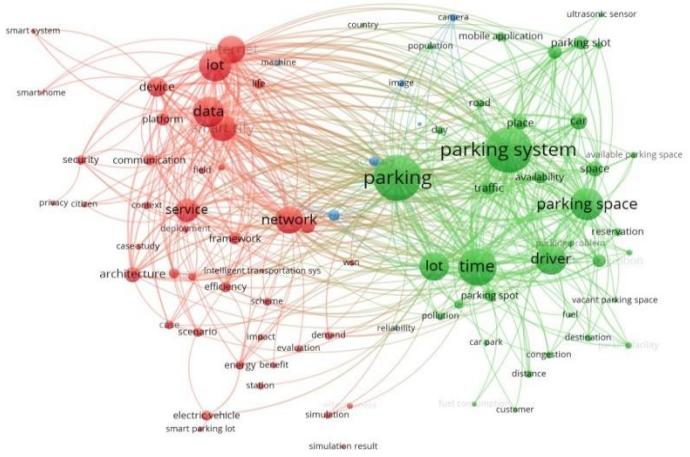


Figure 2. Number of publications indexed in the Scopus databases referring to the concept of smart parking (2011–2020)

By applying clustering algorithms on the selected papers resulted in 87 keywords grouped into three clusters. In Figure 2 is drawn with different colors a map displaying relations between the analyzed keywords. The frequently key terms are presented in the central part of the map. The style information like the size and font of point specific to a certain keyword express its frequency (higher or lower). First, the resulting network is characterized by numerous links and looks rather dense. The first cluster was located around the term "parking" including the most terms defining the problem of smart parking: parking system/lot/space/slot/spot, reservation, road, fuel, congestion, pollution, availability, etc. In the second cluster terms related to solution (most of them technical) can be observed: network, Internet, IoT (of Things), Communication, device, platform, framework, architecture, service, smart system/home/city, etc. The third is the shortest and is strict related to some tools and their performance: image, camera, accuracy, reliability, etc. However, the three clusters do not contain keywords such as "sharing", "economy", and very few or not at all contain "image processing", "machine learning algorithms", "thermo vision camera", etc.

The conclusions of this bibliometric study show us that very few researchers consider the economic view of smart parking and especially the sharing concept in order to create benefits.

Other studies show that there are a lot of startups worldwide that target different aspects of a smart parking: payment, access monitoring or even vacancies but do not analyse the problem from perspective of sharing economy and private parking lots and also does not present technical solutions for detection of free parking spaces [9].

1.3. Premises for success. Brief description of solution proposed

In our previous work [10] we predicted "the occupancy rate of a building" based on embedded system which retrieves data from sensors and, using Multi-Layer Perceptrons we predicted the energy consumption in smart buildings knowing alternative data sources, like the number of cars from parking space. It was computed the correlation between the number of vehicles over time and time-related parameters, like day of week, hour of day, and type of day, for validating the machine learning model of parking lot occupancy. This paper describes in detail the smart parking system implemented at Engineering Faculty of Lucian Blaga University of Sibiu (LBUS), Romania. The occupancy pattern during one year includes around 40 weeks, in rest being holidays. Engineering Faculty contains about 120 parking slots. The institution time scheduler shows that usually after 5 p.m. are much less classes than during the morning. In conclusion, there is a quite high degree of vacancy in the parking which could generate additional income by sharing them.

The proposed solution includes the hardware components (Raspberry Pi Model 3B with a Pi camera) for license plate recognition, the opening / closing the barrier, three led that form the traffic light, and software application for real time detection of each empty parking space based on Motion Detection algorithm; the reserving a parking space for a time interval is done through a web application. Raspberry Pi microcontroller and the WEB application communicate through the Node-RED program that use the MQTT services for transmitting real-time information to the application without the need to refresh the webpage ensuring real time synchronization of web application and database with existing vacant parking spaces.

Our solution provides the next benefits:

- Innovate by relying on the principle of sharing economy / parking sharing of private institutions: analyses the problem from the perspective of creating financial advantages for the owner in conjunction with reducing the disadvantages mentioned above, loss of time, pollution, etc.
- It is based on the profile / schedule of the institution (daily and / or on much longer periods – monthly, annually).
- Innovate by applying image processing methods for monitoring vacancies from parking lot based on daily occupancy patterns and real time tracking of vacant parking slots and updating in real time the web application and the supporting database.
- Provides a multidisciplinary character combining different disciplines of Computer Engineering ranging from Image Processing and classification algorithms specific to Artificial Intelligence, to Embedded Systems and IoT, Web Design, Information Security (payment), targeting social welfare, improving the citizens' life quality.

The rest of the paper is organized into six sections. Section 2 analyses the related works. Section 3 introduces our smart parking solution, its advantages as well as the analysed use-case scenarios. Section 4 presents the application's hardware and software architecture, whilst the Section 5 describes the image processing methods used for finding the vacant slots in the parking space. The Section 6 illustrates some results obtained after software implementation of methods from fifth section. Section 7 emphasizes the paper's conclusions and proposes further work research.

2. Related Work

The reservation-based parking system developed by researchers from Nebraska University, Lincoln, USA [11] focus on parking spaces managing and real-time monitoring. Their solution is based on reservation and the selection of the vacant slot for parking is made based on the walking distance to the destination and the cost. The main drawback of their solution consists in the synchronization problem when more than one motorists apply simultaneously for reservation. A "bottleneck" occur within the system and increases the update time out of the need to serially treat the requests. In our work we solve this problem at the session level of the OSI reference model [12] of communications protocols. Different names for every session are used, and the messages are received and sent only to the specific session.

In [13] the researchers from University of South Florida developed an embedded system for a real-time parking aiming to inform the drivers using a mobile application, about parking spaces availability. Detecting the vacant spaces was done with ultrasonic sensors. When a car is detected in front of the parking lot, the ultrasonic sensor reads and refreshes the number of cars on the entrance display and on the smart phone application. The accuracy suffers in case of golf carts or people because the sensors consider them as cars. Unlike them, our solution of entering and leaving is based on image recognition of license plate number.

The Indian researchers from Pune [14] implemented an intelligent reservation parking system using QR code technology and a camera that reads at parking entrance the QR code and checks its correspondence in database. In our case, the system includes newer and different hardware components than those used in [14] and besides that we implemented image recognition for license plate instead of QR technology, we also use image processing for updating the web application according to cars presence or not from the parking.

Finding vacant parking slot by the drivers becomes an NP-hard problem with various constraints. In [15] a genetic algorithm is used for solving scheduling problems and finding the best parking region into shopping malls and the slot to park the vehicle without affecting medium waiting time. The kernel of their system is a number of autonomous trolleys. These are used to take the vehicles from the entrance to best parking slot identified by the system. The customer can leave their vehicle at the entrance and enjoy the

shopping. The trolley captures the image of the surrounding after the vehicle is successfully parked in the slot. The image and location map is send to the customer mobile application. The main disadvantage is the cost of implementation and the necessity that the customer to have a WiFi connection.

In [16] the author reviews and presents practical examples based on smart technologies for guiding drivers to parking lot in urban areas. There are four categories (from simple to complex) depending on the equipment used and the services provided by parking lot: typical, semi-automatic, automatic and multi-storey. The simplest (typical) involves no equipment and services, the semi-automatic allows payment at the cashier and the operator who operates the barriers, the automatic is fully equipped with an automatic parking equipment and payment on terminals. The disadvantage of first three categories is that these parking systems are not providing information about the occupancy of car parks (free parking spaces) except for the direction and possibly the distance to the destination. The most complex, multi-storey car parks are fully automatic and equipped with smart technologies. Unfortunately, from the administrator's viewpoint their purchasing and correct implementation is costly and from the driver's point of view, the disadvantages are their reliability and detection accuracy (most of the time different of 100%).

Smart parking alternative solutions based on magnetic sensors and IoT systems are revealed by engineering companies. Magnetic sensors, placed on the side of road or parking spot, on the road surface, or in the ground in the form of Inductive-loop detectors, can be used to check the occupancy of the parking lot, determining the number of free spaces left every time a car passes over them and disrupts the magnetic field [17]. The major disadvantages of this solution are the high installation cost and time and require civil engineering.

In [18] are briefly shown examples from Siemens and Huawei IoT-integrated parking management systems. These provide drivers information about the availability of parking lots and connect with municipalities decision factors. The IoT system consists in environmental sensors, a cloud-based web platform enabling also the automated parking payment. Our solution is very close to this system but furthermore promote the idea of parking sharing by private institutions.

In the European project proposal "Unlock the sharing economy for the parking sector" [19] the authors promote the parking sharing concept proposing integration of parking sharing platform into connected and autonomous transportation systems in smart cities. Based on mathematical model and simulation the authors tests how motivated are the drivers to use the platform which includes private parking shared for public. Furthermore they reveal the need for collaboration between academic and industrial partners as co-developers and city councils and local communities as decision makers and private companies as parking sharers.

3. The smart parking solution

This work aims to create an embedded system that solves the parking problem described above. The main software component is a web application which is connected with Raspberry Pi for parking management: reserving a slot and authorizing the entering and exiting and revising the number of vacant slots, real time detection of each empty parking space based on Motion Detection algorithm and synchronization with the web application and the supporting database. Of course the technical implementation is complementary to the sharing economy concept that in order to be efficiently applied requires appropriate understanding the parking occupancy patterns of each private institution. The project development stages are:

- Implementation of hardware-software application for identifying car license plate number and real time detection of each parking space (to determine if they are vacant or not)
- Development of the web application
- Real time synchronization with the web application and database

The web application provides the following facilities:

- Real time parking status view
- Reservation on a specific time by license plate number
- Contact parking management by email
- Administration module that includes updates about users and prices
- Implementation of the gamification concept in the management of parking spaces.

In order to make drivers estimate an exact time at which their car will be parked on that place, is introduced the concept of "Gamification". In this case, this concept aims at reserving parking spaces for as accurate a period of time as possible, in order to better manage vacant spaces and in addition to this, it also has the purpose of reducing fuel, driving time and streamlining traffic at peak hours. This is done using the web application and encourages drivers to make as accurate estimation of time as possible by rewarding them with points that can be used later for parking payment.

Scalability issues and proposal for solving are treated in [1].

3.1. The use case diagrams

In Figure 3 is presented the possible use cases of the application: the involved actors and the actions performed. There are three types of actors: the administrator, a previously enrolled user and the new user. The administrator manages the parking lots and their status; adds new locations and parks; manages new users; allows sign-in of new users; allows and control making the new reservations and set the price for parking. A registered user may see the parking status, may reserve a parking slot into a location, and obviously the sign-in process. The reservation process supposes: choosing the date and time for access, the parking location and slot and providing the license plate. The new user can see the parking status, the contact information and the geographical area of parking location, and he may register.

3.2. Reservation

The smart parking system is reservations-based. Any registered user may reserve a parking slot in case exists at least one vacant. Reservation includes the parking name, parking space (selected by user), hourly rates, the estimated date and time of arrival and

departure. The parking spaces reservation is made from web application. This reservation can only be made if the user already has an account (as new user performed the registration process and then as registered user make the sign-in process).

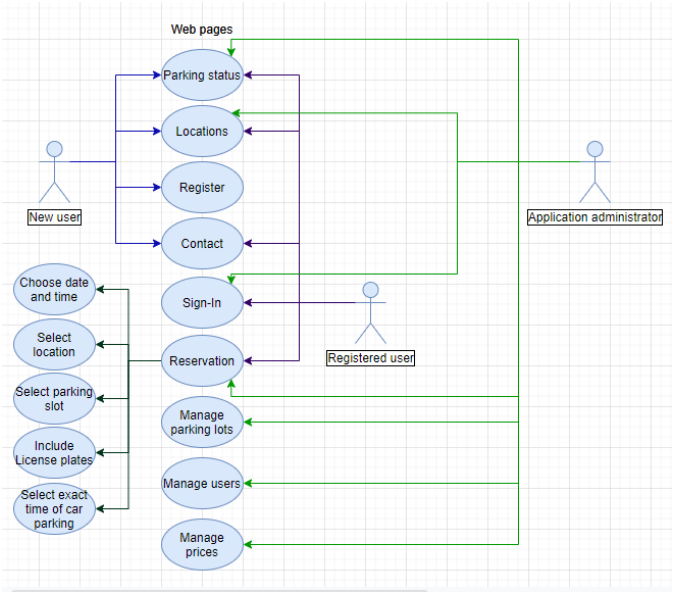


Figure 3. The application use case diagram

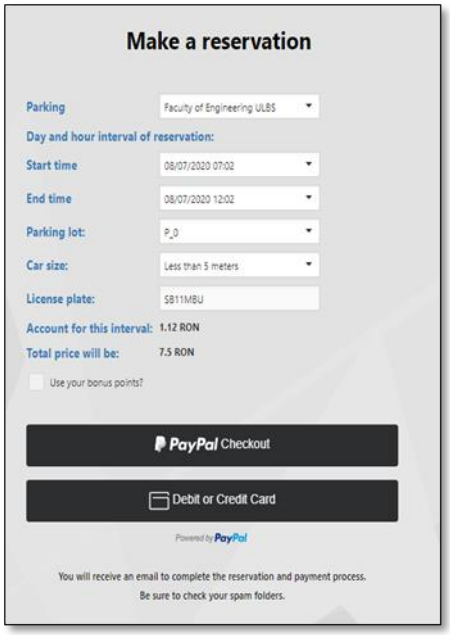


Figure 4. Reservation form

Extending the original work [1], in the Reservation page (see Figure 4) we added hourly payment implementation and the type of parking desired based on car's size (less than 5 meters, between 5-10 meters and higher that 10 meters). This constraint has been implemented to ensure an appropriate number of parking spaces according to the size of the car, otherwise there is a risk that the car is too large compared to the parking space and then two places must be invalidated even if only one car is entered. To change the type of parking is required to access the configuration page, and for each parking space the type is changed by the administrator. Payment implementation buttons have also been added using PayPal technology, which currently perfectly simulates a real payment. This process requires bank protocols which are not finalized yet.

3.3. Real time parking status view

As Figure 5 illustrates, the parking degree of occupancy can view in real time by anyone, and, for the car parked, which are their license plate numbers. The busy spaces are drawn with Red color, and vacant spaces are drawn with Green color. In "Parking status" page can be seen in real time the occupancy of the parking. The parking slots are updated by reloading the page when a message is received from the Node-Red with the parameter "Access". All parking lots are made as dynamic buttons. All parking coordinates together with id and color are taken from database into web application and displayed as buttons of different sizes depending on the parking type. For each set of 4 points that represent a parking space has been made some calculations to determine the parking type. The types of parking can be as follow: normal parking, diagonally parking on the right, diagonally parking on the left and lateral parking (see Figure 5).

In addition to the original work [1], in the Parking Status page all the coordinates corresponding to each parking space are taken and it is determined for each place whether it is straight, lateral or diagonal. These places are displayed on the page according to the coordinates received in the database (x, y) and the corresponding color in real time.

The management of parking in the web application is done in the following way: when a new parking lot is added, the "start" image is taken from the moment the fixed camera is installed in the parking lot, it is sent to Raspberry Pi for processing (is checked if there are parking spaces in the image , how many, and possibly the two-dimensional coordinates x, y for each parking space). This image is added as a background on the real time parking view page and is colored according to coordinates which is occupied in red and the rest in green (similar to Figure 5).

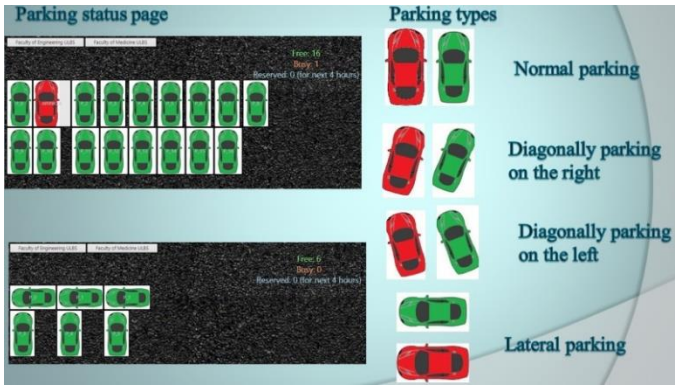


Figure 5. Real time status parking view

3.4. License plate recognition

At the entrance into the parking is checked the car license plate number. When reach in the front of the barrier, the driver push <*I arrive*> button from "Home" page to send instruction to camera for capturing and checking license plate number. If the drivers have a reservation that is +/- 15 minutes around estimated arrived date and time he has access into the parking. Otherwise, it is

checked if exist vacant slots, that are not reserved in the next 4 hours. In the affirmative case the car is authorize to enter in the parking space, otherwise not.

4. The application architecture, tools and programming environment used

This embedded system consists in the following main components:

- Hardware component which contains a Raspberry Pi Model 3B with a two Pi cameras (one for entering and one for exiting from parking lot), a Hikvision camera from the category "Bullet Series Thermal", stepper motor and some LEDs. Raspberry Pi is used together with the library that includes License plate recognition algorithm (OpenALPR algorithm from OpenCV library) that checks the number of license plate with the previously made reservation and opening the gate, parking lot and occupancy detection algorithm, Pi camera used for taking picture of each car arrived on parking entrance to apply license plate recognition algorithm, python script to manage barrier using a stepper motor and providing rotation angles, and another scripts that commands LEDs lighting for semaphore simulation. The Hikvision camera is used for parking monitoring and providing inputs for Motion Detection algorithm.
- ASP .NET web application developed using DevExpress controls. Website structure it consists of several modules who communicate with each other for a better functionality of application. MQTT (Message Queuing Telemetry Transport) and Node-Red are used for communication between web application and Raspberry Pi. The main web components are pre-setting the parking configuration based on the architecture of the location, user registration, parking slot reservation, gamification concept, real time parking visualization with counter for each vacant, occupied and reserved (for next two hours) parking slots, administration module to manage users, parking and prices for each zone.
- MySQL database. The database is essential and structured in such a way as to allow a much better flexibility, efficiency and dynamism so that the web application can be applied much more easily from one parking to another. The MySQL database contains few tables with foreign keys and records in database all reservations, user information, prices, history and the number of free parking spaces.

In Figure 6 is presented the application architecture together with all project stages from online reservation to entering car into a parking space. The first step is Motion Detection algorithm (1) in order to set the parking configurations and saving the coordinates in database (2). When the camera is installed and fixed, the parking spaces in an image captured in real time are delimited with the help of a Python script. The delimited places are saved in the database together with the coordinates and the id corresponding to each place, and the initial colour is green (free places). The Motion Detection algorithm is in real time applied and used for updating the colour corresponding to each place (red - occupied, green - free) in the database and web application. Then, it follows the online reservation (3) and inserting a record in database. When the driver arrives in front of the barrier, he has to push the <I arrive> button from Home page. After all this, the Node-Red is sending using MQTT, messages and instructions from/to application. In step (4), after pushing the *<I arrive>* button the web application through Nod-Red is sending to Raspberry Pi the instruction to take a picture. Then the checking access in parking is start calling OpenALPR algorithm (5) which provide the license plate number (6) to web application. So, if the car that arrives in the front of barrier has a valid reservation (the license plate number is successfully found in database (7) and the result is sent to web application (8)) then the latest grants the permission to enter in the parking space (9) and send this message through Node-Red to Raspberry Pi, the green led is turning on (10), and the barrier opens (11). Otherwise, the red led is turning on. After verification of license plate number, web application sends instructions to turn on / off the lights and open the barrier or not. While all this checks are made, yellow light is on. Finally, if the access is granted, green light is turning on, and the barrier opens. Otherwise, red light is turning on, and the barrier does not open.

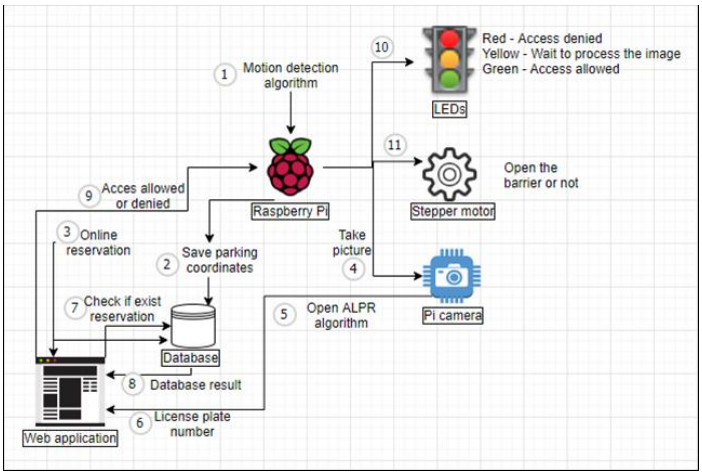


Figure 6. Application hardware-software architecture

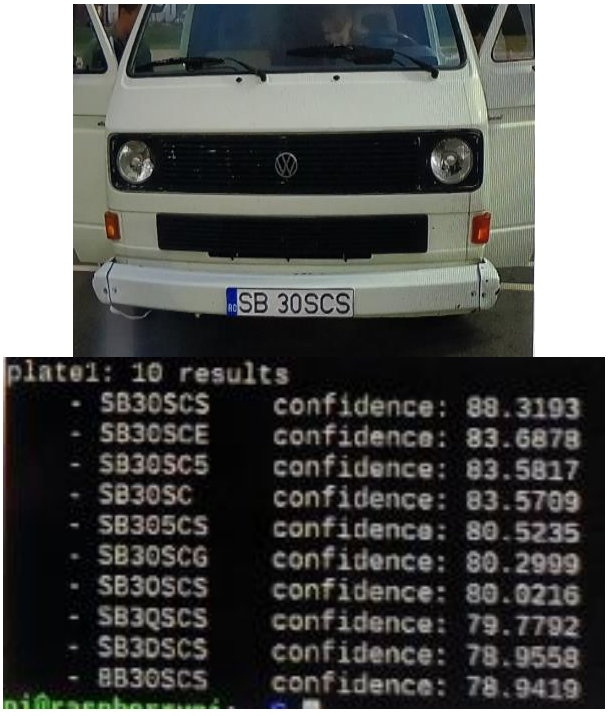


Figure 7. ALPR algorithm (up - image source, down - the result)

For updating the web application and database with the correct number of slots when the car leaves the parking is used the second Pi camera. So, if a car intends to exit from parking the same license plate recognition algorithm is applied. In the web application we check if that license plate number is inside the parking or not. In the affirmative case, is change accordingly the parking slots and opens the barrier and turn on the green led. The contrary case means that the car intends to enter in the parking. Ultrasonic sensors could be alternative solution for detecting the presence or absence of the car. When the car leaves, sensors detect this thing and mark this thing in the database. We opted in this project to use the second Pi camera instead of sensors from simplicity reason.

4.1. Software tools

1) OpenALPR: is an open source library written in C++, Java, Node.js, and Python that analyses video images and streams to identify the license plate numbers [20]. The Computer Vision algorithm is in Python implemented. The output returned is the text represented by the characters of the license plate (see Figure 7).

OpenALPR return license plate number with the higher confidence from ten possible results. The algorithm can be configured to work both with European and American license plate numbers. This library is portable and can be compiled and run on Linux, Mac and Windows. OpenALPR needs the next additional libraries:

- Tesseract OCR: it is one of the most accurate optical character recognition (OCR) engine for various operating systems.
- OpenCV: it is a Computer Vision library enhanced with machine learning algorithms.
- Leptonica: contains software dedicated for image processing and analysis applications. The license plate region detector uses the Local Binary Pattern (LBP) algorithm [21]. LBP is a simple but effective texture operator that labels the pixels of an image by comparing it with neighboring pixels, and considers the result to be a binary number. The advantage of LBP operator consists in its resistance to changes in the level of gray generated mainly by the variation of light.

2) MySQL: is used for database. In Figure 8 can be viewed the database architecture, the structure of the tables, the primary keys of each table and their links to other tables as foreign keys, which allow adjacent selections from several tables (joins), but also allow faster retrieval data in this way.

The Users table contains information about users and their type such as “User”, “Visitor” or “Admin”. The Reservations table contains all reservations made using the online reservation such as parking zone, car size, parking spot where driver should park, time of arrival and departure, license plate number, account that need to be paid before, total price and user id. The History table keeps the temporary information retaining only the vehicles that has entered in the parking and are still there. Here are stored the exactly time of arrival and departure of each car that had access to parking. Price table stores the hourly rate for every parking and ratio for account payment for each parking zone and each parking type. The Parkingzone table stored the name of every parking zone (for the moment “Faculty of Engineering ULBS”, “Faculty of Medicine ULBS”) and in Parking_types table are stored the car size types such as “Less than 5 meters”, “Between 5 and 10 meters” and “Higher than 10 meters”. In table Parking_coordinates are stored information about each parking slot. Every row from this table contains a set of 4 points which determines a parking slot, id from image file and colour in real time (red or green depending if parking slot is vacant or not).

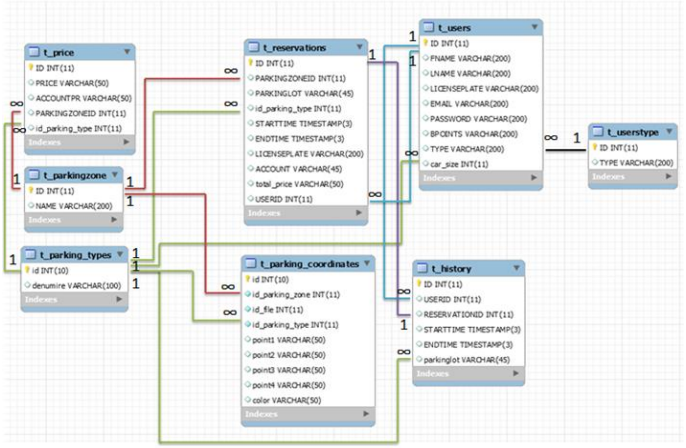


Figure 8. Database architecture

3) Node-Red: represents a programming tool used in general for IoT programming that connects hardware components with API’s and online services in new and interesting ways. To connect the Raspberry Pi, the Pi camera, the LEDs and the stepper motor of the web application is used Node-Red programming tool.

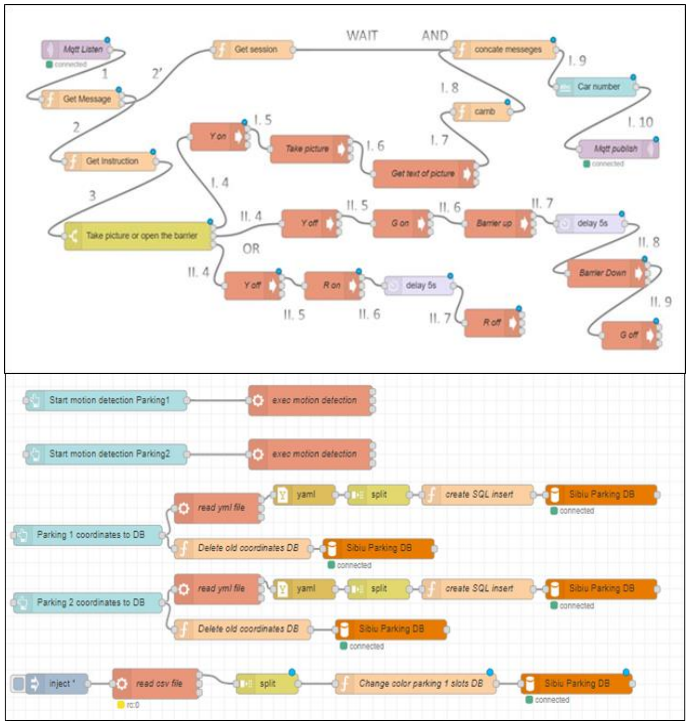


Figure 9. Implementation in Nod-Red of parking access (up) and Motion Detection algorithm (down)

In the upper side of Figure 9 is presented the whole flow of Node-Red. The purple nodes are MQTT nodes. “MQTT in” is waiting for messages from web application while “MQTT out” is sending messages to web application. The nodes with an “f” are functions, the yellow/green node is a switch node, the nodes with

an arrow are execution nodes, delay nodes represent a delay of 5 seconds, and the blue node represents a text output that displays the final message that has to be sent. When a message arrives, using function nodes we get the session and instruction from message. The session is used to know from which web session had been called the instruction, to send back the message only to that session. If instruction is "new Car" we go on the first value of switch. This value generates the execution on commands like turn yellow led on, take a picture, get the license plate number from picture, concatenate with session and send message. The second value of switch determine the fact that the car has access in parking and send the commands to turn off yellow led, turn on the green one, open the barrier, wait 5 seconds, close the barrier and turn off the green led. Last value of switch represents the fact that the car doesn't have access and turns off yellow led, turn on red led, wait 5 second and turn off the red led.

In the down side of Figure 9 are the scripts corresponding to saving coordinates for each parking slot from real time image captured with Hikvision camera when this is installed for the first time; Command to apply Motion Detection algorithm and saving real-time colors to database at each 1 second.

4) DevExpress: provides various controls for ASP .NET web applications. The web application was splited into several modules with different functionalities combined to achieve the goal, and easy understanding from the user perspective. There are implemented the 3 menu types (for Visitor, Users and Administrator) according to the application use case diagram (see Figure 3). The Register form (see Figure 10) is completely made from DevExpress controls. For the web application in order to have similar format for all pages as possible (the only part what differs in pages is the content) a page called "master" is used, in which CSS or JavaScript files can be imported, elements can be added that are desired in the future in all the pages created later, such as menu, footnote, or any other elements whose presence is desired in more than one page. This page is responsible for the layout of the application.

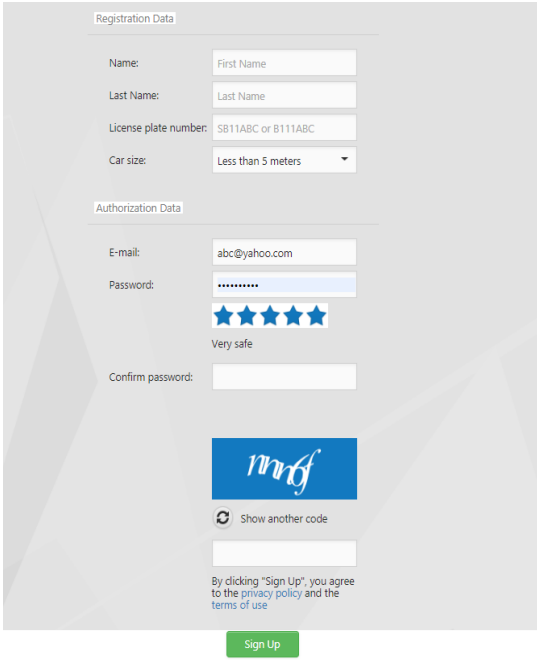


Figure 10. Register form

5) MQTT is a machine-to-machine (M2M) connectivity protocol. The messages are sent and received using an online MQTT broker. The Node-Red receives the message using the MQTT in node. The implementation of MQTT in the web application is done by installing an M2Mqtt service, which uses a PAHO client from Eclipse, the programming being done in JavaScript.

5. Finding the vacant parking slot using Image Processing methods

Finding vacant spaces can be a challenge for large parking lots and especially at rush hours. The technical solution proposed for implementing a smart parking system in this work is based on Image Processing. Different methods was tackled in order to set the best one. The Hikvision camera is positioned on a considerable height (3 meters above the ground), so that it could see the entire parking lot.

In the following are provided brief details about the methods tried and will be discussed in detail the most accurate that is used in the implementation of the smart parking system.

5.1. Using the Hough Transform

First was tried the detection of the parking lot grid using Hough Transform (dedicated to feature extraction and object detection) and Hough Probabilistic for lines [22]. The potential challenge referred to the fact that the parking lot grid is not clear/visible enough from the camera position in case of fog/snow/rain/old paint on pavement/fallen leaves. The approached solutions were:

i) Manual parking lot grid initialization

- Reading the image
- Convert image to grayscale to reduce the info in the photo
- Apply Gaussian Blur to remove even more unnecessary noise
- Detect the edges with Canny detector
- Detect lines with Hough Transform

ii) Machine-Learning algorithm for detecting the grid (fed with multiple photos from different days/weeks/months) which generates as output the parking slots.

On web application, first was tried the rendering of background image every 1 second (and after every 5 seconds) with real time picture from camera. The rendering takes too long. We tried all this on a separated asynchronous thread, but with no success. After that we were thinking about drawing each set of points on a background image from web application. This was a good idea, but wasn't good looking. The main drawback was that other lines appear besides the desired ones and the hard part was that we need to identify the useful lines and remove the rest. We tried to selectively analyze only of the useful part and not of the whole image. Unfortunately the results was not satisfactory. These are presented in the 6.1 section of the paper.

5.2. Car detection via static thermovision camera

The Hikvision camera allows acquiring images both from infrared and visible specter. Thus, the second method aims car detection via static thermovision camera by tracking the engine of the car

(considering that it will dissipate the highest amount of heat). In the database is saved the slot with highest temperature produced by the engine of a new car that is coming from outside the parking. We update as an occupied slot, in the database, and in web application, whenever a new hotspot reaches to a previously vacant slot. A challenge that we faced was finding the correct threshold for the heat level. This is because in the sunny days even the pavement/asphalt can reach the temperature of running engine. To overcome this, we ignore not moving heat spots. This method could be the best for using at night consumes moderate computational power but provides moderate accuracy. The main disadvantage is the cost of camera which is relatively high.

However, were made without success, temperature comparisons relative to the cars that enter the parking lot, against to those that stay and have the engine "cold" or "colder" according to the previous idea that different temperature of the cars represents a concrete indicator regarding a vacant or occupied place (see Figure 13).

5.3. Using Motion Detection algorithm

Detecting a free parking slot based on car motion can be done in multiple ways:

- Car tracking via motion detection – from the moment the barrier is open, is known that only a car would move near the parking entrance and it can be track it up to a point where it parks. The location is saved in the database as occupied. The challenge in this case is that if the driver, on his way to a slot, will stop too much time on the road the tracking will fail (a threshold variable for the motion detection has been reached). Thus, is need variable thresholding time for the tracking (tracking the car until it reaches exactly on a parking spot by calculate the distances towards the nearest available slot's grid lines). It has low computational impact but may not be accurate enough and it does not work well during night
- The second way suppose no car detection or tracking, actually the motion is indirectly determined. It is just detected if a slot is occupied or not by calculating the average of pixels between 4 grid lines. An empty slot has to have a lot of darker pixels (empty slot case) than any other colored pixels (the case when car is parked). The points method (based of pixels between 4 grid lines) provides the best accuracy and is easy integrated in the web application. Basically, in the pre-processing stage (pre-setup), the image is analyzed and is configured the 2D map of the parking lot that is loaded in the web page. Subsequently, the stored information related to the spatial position of the existing parking spaces is kept in database. This motion detector algorithm is based on some coordinates given by user. Thus, user has to give position for each of the parking spots by clicking on the initial image. This process is made only once, when the camera is fixing (pre-setup stage). Each set of 4 points that made up a parking space for all of the spaces in the lot are stored in an *.yml* file. Clicking edges of each parking slot is made using a mouse as a "paintbrush". Then some calculations are made to find out the center of the rectangle (to label each space with a number, used later on web application). After drawing the rectangles, all there was left to do was examine the area of each rectangle to see if there was a car in or not. By taking each rectangle (grayed and blurred), determining the area and doing an average on the pixels, we can tell that there was not a car in the spot if the average was high (more dark pixels) and the rectangle color is changing. One challenge that could arise is if car has a close color to the pavement. In this case, even if a car has the same color as the slot when it is empty, it will still reflect light from the windshields so will result different average color of pixels than an empty slot.

The most benefits of this method are that provide high accuracy and requires moderate to low computational power. By this indirect Motion Detection algorithm is known exactly that a new car which entered in the parking lot cover a previously empty place (however it is not 100% sure that is the reserved place, it would have been useful to combine the algorithm with the above solution that follows the car from the barrier to the parking slot). The introduction of the type of car is necessary and efficient. It allows the display of parking on the web page in a way as close as possible to reality and the parking spaces are updated in real time depending on what colors the Motion Detection algorithm returns for each parking slot (see Figure 14).

Next, we summarize the strengths and the weakness of car detection methods:

Table 1: Algorithms Summary

Algorithm	Advantages	Disadvantages
Hough Transform	• Handle missing data • Express a high level of detail	• Due to the heterogeneity of the objects in the image, the algorithm produces as a result lines that are not part of the parking lot (poles, houses, etc.). • Sensitive to fog / snow / rain / fallen leaves, etc.
via static thermovision camera	• May be successfully used at night • Consumes moderate computational power	• Moderate accuracy • Relative high costs
Motion Detection	• High accuracy • Low computational power	• Limited by the relation between cars color and pavement

6. Comparative results between algorithms

6.1. Results after using Hough Transform for detection of the parking lot grid

In Figure 11 and Figure 12 are presented the original images (two parking lots) and the results respectively after detecting the lines in parking using Hough Transform. OpenCV encapsulates the math of the Hough Transform into HoughLines(). This approach was tested on different videos and real time images but without success.

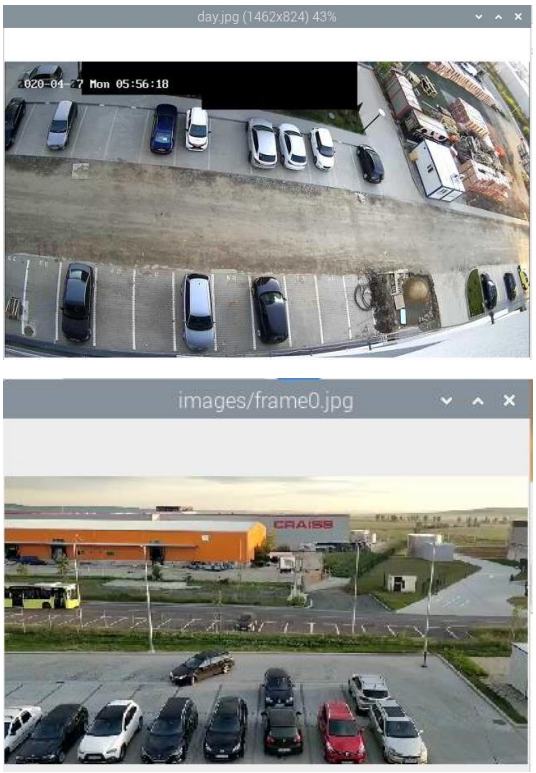


Figure 11. Original images

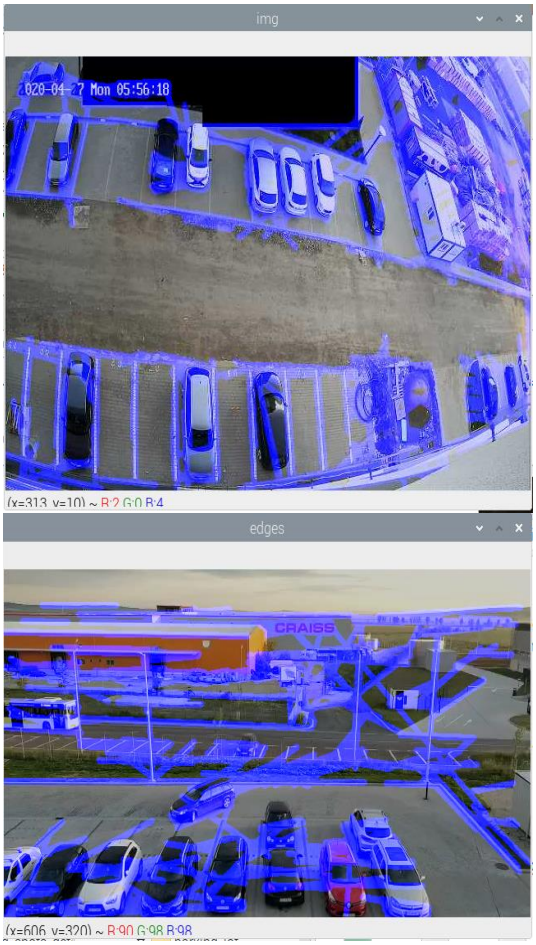


Figure 12. Final result

6.2. Results from thermovision camera

One explanation for the disappointing results may be that the car body insulates the engine from the outside and its high temperature is not captured by the thermovision camera. Also, heated asphalt produces a higher temperature than cars. The Figure 13 illustrates the image of the parking lot captured with the camera both in the infrared and in the visible spectrum. In the Figure 14 it can be seen how the driver getting out of the car has the highest temperature in the image and not the engine. Unfortunately, the method did not help us to accurately identify free parking spaces.

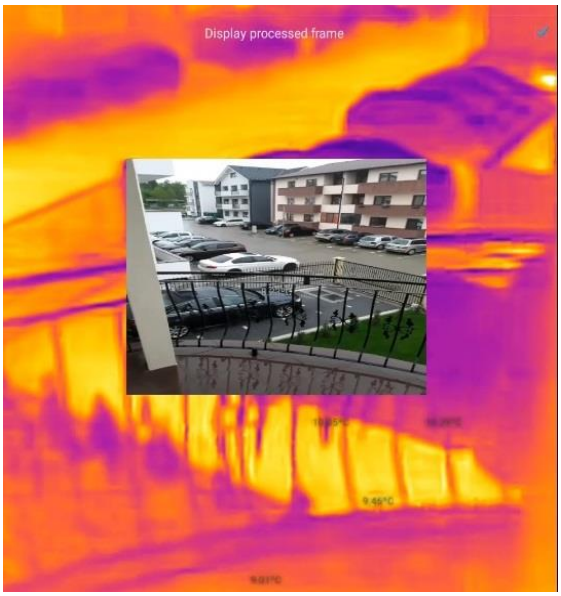


Figure 13. The parking lot seen in both spectrum: infrared and visible

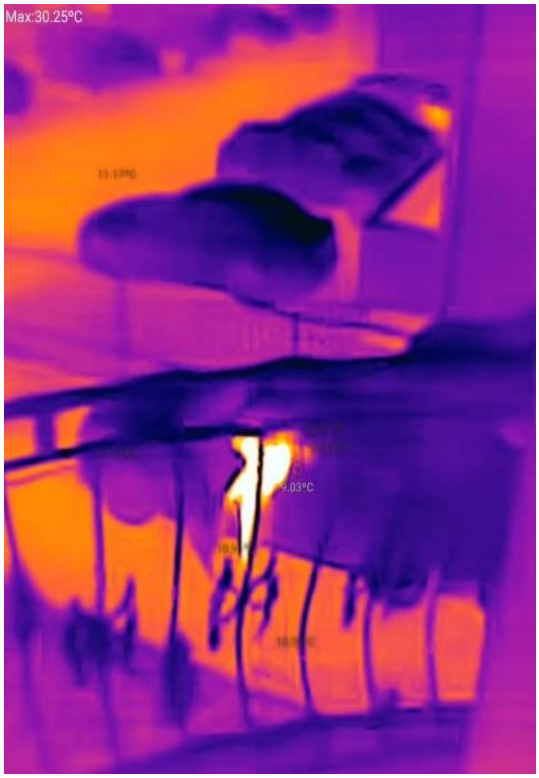


Figure 14. Driver exiting from the car parked seen with thermovision camera

6.3. Results after using Motion Detection algorithm

Looking both to Figure 15 and to Figure 5 it can be seen that the indirect Motion Detection algorithm helps to create a more real 2D structure of the parking lot and using it we can determine the occupancy of the parking space (to know which slots are vacant or not). In the upper side of the Figure 15 is capture the pre-setup stage when are identified the slots (with Blue colour) of the parking, in the middle it can be seen a scenario with two empty spaces and the down side image shows the previous places that are now occupied. It should be mentioned that for a better exemplifying, only the bottom of the test image was treated (since the pre-setup phase) without taking into account the cars and the places from the top of each of the three images. Once the algorithm is implemented, the degree of parking occupancy can be accurately determined at any given time.



Figure 15. Motion Detection algorithm results

7. Conclusions and further work

This paper presents a smart parking embedded system with focus on image processing algorithms as a solution for smart mobility. We implemented and comparatively presented the results of various image processing algorithms like Hough Transform, with thermovision camera and based on motion detection for real time tracking of vacant parking slots or OpenALPR for identifying car license plate number. The accuracy of the identification system of license plate numbers depends on the quality of the camera used. For example, in the first tests we noticed that for the number SB11MBU the number 11 was not read, the result being SBMBU, probably due to the confusion with the letter 'i' or 'I'. Another problem would be the brightness; the 5MP resolution Pi camera is not efficient enough to take clear pictures when the brightness is low. Anyway, with this cost-effective Pi camera we perfectly detected 188 from 204 cars meaning 92.15% accuracy (a reasonable performance).

The main software component of the system is the web application that implements the payment system with different rates depending on the number of hours or days of parking and integrates the gamification concept rewarding the driver with bonuses if he exactly respects the parking period for which he made the reservation. When booking a parking slot, an account is paid to make sure that the slot is available on arrival thus avoiding the queue for payment and the need to change money.

This work brings social, economic and scientific arguments to promote innovation in smart parking and especially promoting the parking sharing concept. Even if we developed a prototype tested at LBUS Sibiu (a town with around two hundred thousand inhabitants) we appreciate that the smart parking system proposed is functional, scalable [1] at least to moderate sized cities and extendable to many private institutions which might share their excessive parking places according to the daily occupancy patterns of their employees. Excess parking spaces of the parking lots of different faculties / universities, but also of private companies can be shared to users in need! If a power outage occurs or the barrier does not work, to avoid creating a long queue at the entrance that could block traffic then the implemented technical solution involves the automatic lifting of the barrier and allowing free entry and exit (without scanning the license plate number) of cars depending on the remaining available space. Even in these conditions, the Motion Detection algorithm and the takeover of the occupied spaces in the web application works, announcing the exact number of free spaces in the parking lot.

There are at least two work directions we will consider in the near future:

- The web application should provide an indication of what would be the best place to park depending on the size of the car based on genetic algorithms.
- With the help of Google Earth or Google Street applications, we will take over the spatial arrangement of the parking lots and we will generate the parking architecture in the web page (see Figure 5), thus offering a greater flexibility for application.

Conflict of Interest

The authors declare no conflict of interest.

Acknowledgment

This work was partially developed under the ERASMUS+ KA2 project "THE FOF-DESIGNER: DIGITAL DESIGN SKILLS FOR FACTORIES OF THE FUTURE", financing contract no.

2018-2553 / 001-001, project number 601089-EPP-1-2018-1-RO-EPPKA2-KA, web: https://www.digifof.eu/

References

[1] S. D. Marcu, A. Florea, "Smart parking system-another way of sharing economy provided by private institutions". In 2018 IEEE Thirteenth International Conference on Digital Information Management (ICDIM), Berlin, Germany, 2018. https://doi.org/10.1109/ICDIM.2018.8846986

[2] E. J. Tomaszewska, A. Florea, "Urban smart mobility in the scientific literature - bibliometric analysis", Engineering Management in Production and Services, **10**(2), 41-55, 2018, https://doi.org/10.2478/emj-2018-0010

[3] A. Florea, L. Berntzen, M. R. Johannessen, D. Stoica, I.S. Naicu, & V. Cazan, "Low Cost Mobile Embedded System for Air Quality Monitoring", In Proceedings of the Sixth International Conference on Smart Cities, Systems, Devices and Technologies (SMART), Venice, Italy (25-29), 2017.

[4] N. Zhao, & Z. Li, "Optimize traffic police arrangement in easy congested area based on improved particle swarm optimization". Procedia-Social and Behavioral Sciences, **138**, 408-417, 2014. https://doi.org/10.1016/j.sbspro.2014.07.219

[5] G. Gowda, & R. Thenambigai, "A Study on Respiratory Morbidities and Pulmonary Functions among Traffic Policemen in Bengaluru City". *Indian journal of community medicine: official publication of Indian Association of Preventive & Social Medicine*, ***45***(1), 23–26, 2020. https://doi.org/10.4103/ijcm.IJCM_102_19

[6] Y. Geng, C. G. Cassandras, "A new smart parking system infrastructure and implementation". Procedia - Social and Behavioral Sciences, **54**, 1278–1287, 2012, https://doi.org/10.1016/j.sbspro.2012.09.842

[7] K. McCoy, "Drivers spend an average of 17 hours a year searching for parking spots", USA TODAY, December 15, 2019, https://eu.usatoday.com/story/money/2017/07/12/parking-pain-causes-financial-and-personal-strain/467637001/, last accessed 25.08.2020.

[8] B. Chan, "Smart parking is innovative, but what it enables is even more innovative", Digital Transformation, Innovation Management, Internet of Things, IoT, Smart City, September 21, 2017, https://strategyofthings.io/smart-parking-innovation, last accessed 25.08.2020.

[9] I.T. Cervera, "Internet of Things & startups: state of the art and emerging trends", Master's thesis, Universitat Politècnica de Catalunya, 2020.

[10] J. A. Oliveira-Lima, R. Morais, J.F. Martins, A. Florea, C. Lima, "Load forecast on intelligent buildings based on temporary occupancy monitoring", Energy and Buildings, **116**, 512-521, 2016, https://doi.org/10.1016/j.enbuild.2016.01.028

[11] H. Wang, "A reservation-based Smart Parking System", Ph.D Thesis, University of Nebraska-Lincoln, 2011.

[12] International Telecommunication Union ITU-T X.200, "Information technology – Open Systems Interconnection – Basic Reference Model: The basic model", July 1994.

[13] O. Dokur, "Embedded System Design of a Real-time Parking Guidance System", MSc Thesis, University of South Florida, October 2015.

[14] F. I. Shaikh, P. N. Jadhav, S. P. Bandarkar, O. P. Kulkarni, N. B. Shardoor, "Smart Parking System Based on Embedded System and Sensor Network", International Journal of Computer Applications in Technology **140**(12):45-51, 2016, https://doi.org/10.5120/ijca2016909532

[15] D. Thomas, B. C. Kovoor, "A genetic algorithm approach to autonomous smart vehicle parking system", Procedia Computer Science, 125, 68-76. 2018, https://doi.org/10.1016/j.procs.2017.12.011

[16] J. Hanzl, "Parking Information Guidance Systems and Smart Technologies Application Used in Urban Areas and Multi-storey Car Parks", Transportation Research Procedia, **44**, 361-368, 2020, https://doi.org/10.1016/j.trpro.2020.02.030

[17] M. Pietruch, "Innovative Technology for Quick and Easy Smart City Parking Solutions", Comarch Telecommunications Blog, May 08 2019, https://www.comarch.com/telecommunications/blog/innovative-technology-for-quick-and-easy-smart-city-parking-solutions/, last accessed 25.08.2020.

[18] Digiteum Team, "Parking IoT Technologies: About Smart Parking Systems", Smart Parking Solutions, November 27, 2019, https://www.digiteum.com/iot-smart-parking-solutions, last accessed 25.08.2020.

[19] W, Liu; H. Haitao, "Unlock the sharing economy for the parking sector", ETH Zurich Research Collection, European Transport Innovation Challenge: Creating Mobility Solutions, 2017, https://doi.org/10.3929/ethz-b-000171167

[20] https://github.com/openalpr/openalpr, Retrieved at 25.08.2020.

[21] D. C. He, L. Wang, "Texture Unit, Texture Spectrum, and Texture Analysis", IEEE Transactions on Geoscience and Remote Sensing, **28**, 509-512, 1990, https://doi.org/10.1109/TGRS.1990.572934

[22] J. Illingworth, J. Kittler, "A survey of the Hough transform", Computer vision, graphics, and image processing, **44**(1), 87-116, 1988, https://doi.org/10.1016/S0734-189X(88)80033-1

ASTES

Advances in Science, Technology and Engineering Systems Journal Vol. 5, No. 5, 820-825 (2020)

www.astesj.com

Special Issue on Multidisciplinary Innovation in Engineering Science & Technology

ASTESJ

ISSN: 2415-6698

Innovative Course Delivery using Analyze – Group – Design – Optimize (AGDO) Methodology: Case Study of Entity-Relationship Model

Aparna Sharma*, Rishabh Singh, Prathamesh Churi, Mahesh Mali

School of Technology Management and Engineering, NMIMS University, Mumbai, 400056, India

ARTICLE INFO

Article history:
Received: 12 August, 2020
Accepted: 25 September, 2020
Online: 12 October, 2020

Keywords:
AGDO
Design
Group
Analyze
ER Diagram

ABSTRACT

*Visualization plays an important role in teaching and learning. The ability of the learner to grasp the visual contents are better than that of textual contents. Traditional teaching methods often revolved around instructions and recitation techniques. However, most of these approaches were dormant and did not call for active learning. The proposed AGDO-Analyze, Group, Design & Optimize methodology was inspired by these obstacles and creates an engaging and wholesome experience for the students. A sample of 47 undergraduate students was used to analyses the feasibility and effectiveness of this teaching mechanism. Students first tackled and **analyzed** the problem statement with their preconceived knowledge. They were then segregated into **groups** wherein they **designed** solutions collectively. Finally, they tried to find an **optimized** solution considering all the suggested designs. Observations were validated based on feedback and how well the students were able to perform. The results revealed that approaches such as AGDO facilitate an immersive learning environment and ensure the quality of teaching. The implications and methodology were further discussed.*

1. Introduction

The current education system in our country has been blamed for all sorts of evil for hundreds of years. Rote learning is still a trouble for our education system, students mug up concepts/theory/methodologies to score marks. The main problem associated with the system is the lack of effective learning pedagogies [1], [2], knowledgeable instructors, and trusted online content. The current assessment process comprises testing the crammed information presented on paper, in such cases the knowledge and skill are given less importance. Teaching pedagogy must emphasize skill-based development which will help students in their professional life [3], [4]

The research work done in [5] reveals the fact that the use of digital video in the classroom increases student engagement. According to the case study in [5]

- It helps to increase the student's motivation to study.
- The learning experience is enhanced.
- Students may get good marks if they are made interested to learn the topic.
- It also increases the team building and communication skills.

Many researchers have observed, learners can gain positive indicators when they watch authentic and real-life clips [6] Information and communications technology is influencing the delivery of education in tertiary institutions. Researchers studied video usage and student beliefs about video instructions for 'beyond classroom' learning and concluded that videos are preferred by students as learning tools compared to other online learning media [7]. In a study conducted, one of the five reasons cited for effective teaching was easy to access to taped teaching sessions, hence rendering the use of video technology in the teaching-learning process as critical [8]. The implementation of this process is not without difficulties. Finding relevant and objective videos that are of optimal length is a challenging and time-consuming task [9]. The proposed AGDO methodology focuses on skill-based learning and makes use of video and audio tools to solve a case study. We agree that it does not apply to all the complex engineering problems.

We conducted a case study on 47 students, in which they had to follow the process of the proposed model. The students were given a problem statement that demanded the development of an entity-relationship model by them. In the initial stage, all students individually analyzed the given problem statement using some

*Corresponding Author: Aparna Sharma, NMIMS University, sharmaaparnasunil@gmail.com

media as a resource for the same. This media including text, images, and videos. After the analysis, the students were grouped and they had discussions about the problem statement and their respective analysis. By listening and understanding the analysis done by every student in the group they moved towards designing the model. The students adapted and improvised on the group's model based on their discussion, the key towards the development of an ideal model lied in the decision making and choices of the groups. After receiving the models from all the groups, their strengths and weaknesses are discussed. The models need to be compared and evaluated to obtain the most suitable model applying to the problem statement through optimization.

Through this research, we are proposing a model that helps the students and teachers to obtain better results by following four basic procedures of A-G-D-O that are- analyze, group, design, and optimize. Apart from the proposed model our results also showed an enhanced understanding level of concepts by the students while using visual data like images and videos rather than the traditional textual way. The study showed a gradual increase in effectiveness with the increase in visuals and animations i.e. from text to images and videos.

2. Motivation

2.1. Skill-based learning

Skill Based Learning (SBL) [10]-[12] is an adaptive method that provides students with external knowledge that is suitable for a particular skill. Psychological research says that by having students learn through the experience of solving problems in place of rote learning, they can learn both contents of study and analyzing strategies [13], [14]

In SBL, student learning focuses on a complex and innovative problem rather than a simple and traditional problem that does not have a single correct answer. Identifying appropriate complex and innovative tasks is the role of an instructor. A complex problem is a problem in which there are multiple ways to solve the problem OR may have to use multiple strategies or algorithms to solve a problem. A complex problem doesn't have a normal and direct answer, it requires thinking and analytical skills which always comes through experience.

According to recent research, Skill Based Learning helps in the following way:

- **Motivating creative skills** – SBL helps to think out of the box and motivates creative skills to solve a particular problem.
- **Develops critical thinking** [15]– SBL helps students to hone analytical and critical thinking skills in all the topics. In this way, rote learning can be avoided, and self-learning can be motivated.
- **Enhances collaborative problem solving** [16] – Constructive criticism is always necessary to solve a problem in the real world. This is only possible if students learn how to work collaboratively in a group in a selfless way. Skill-based learning helps in drawing enhancing strengths and important skills to achieve their goals. While organizing an event or a field-based activity, students work as a team to deliver the desired results.
- **Builds effective written and oral communication** [17] – SBL helps to improvise written and oral communication through reports, presentations, seminars, etc.
- **Hones leadership** – SBL in classrooms also helps to develop leadership skills in students and help them see beyond their self-interests.

However, it is difficult to indulge in the culture of analyzing the things in students by the teacher. A graphical representation/ pictorial view/video can be used to analyze the concepts better [18]. The advantages of Video and Graphics/Image are tabulated in Table 1.

Table 1: Advantages of the use of Text, Images, and Videos in SBL

Parameter	Text	Images /Graphics	Video
Facilitating thinking and problem solving	X	✔	✔
Inspiring and engaging students	X	✔	✔
Easier to be accepted by students	✔	✔	X
More than words can tell	X	✔	✔
Inspired Thinking	X	✔	✔

2.2. Effect of Textual Data, Images, and Videos on Human Brain

Humans are social creatures. They have metamorphosed to communicate in forms of stories, ideas, and visions. Digital storytelling endeavors to stimulate real-life ways of understanding and communication. This allows humans to acknowledge and conceptualize the idea, which is a stark contrast to the notion of the traditional methodology of imparting knowledge through textual scripts [19]. Similarly, a study conducted by Teleiquile also pointed to the fact that people acquire 83% knowledge from vision, 11% from hearing, and 5% from other sources [20]

With the digital boom all over the world, digital technology has become a part and parcel of one's life. These digital reformations have impacted the entire world dynamics, including the field of education [21]. Multimedia such as engaging images and videos arouses interest and enthusiasm. Images and videos accede students in going beyond the four walls of a classroom [22].

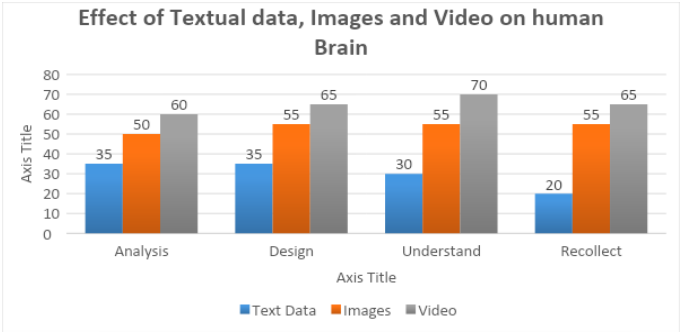


Figure1: Effect of Textual Data, Images, and Video on Human Brain

The problem statement was exercised with a group of 47 students. It was performed and segregated into three levels.

Students were entrusted with a problem definition in different forms and a survey was conducted thereafter, to analyze their understanding for the same. Level One consisted of the problem statement as a two-page textual script. In Level Two, the problem statement was depicted in the forms of images, similar to comics. In Level Three, a five-minute video was outlined in front of the students. All the three stages were recorded and the survey divulged the following results(See figure 1):

3. AGDO Methodology

In the proposed Analyze-Group-Design-Optimize (AGDO) method students work individually as well as in groups to identify basic requirements to solve a real-time complex problem. The AGDO methodology makes use of Graphical con-tents and Skill-Based Learning as described in previous sections. Students get engaged in self-learning and then apply their knowledge to the problem and reflect on what they learned. The instructor acts as a mentor who is passively involved in the learning process rather than actively providing knowledge.

The block diagram of AGDO methodology is drawn in figure 2 below. The diagram depicts the outcomes and strategies of each keyword with the description.

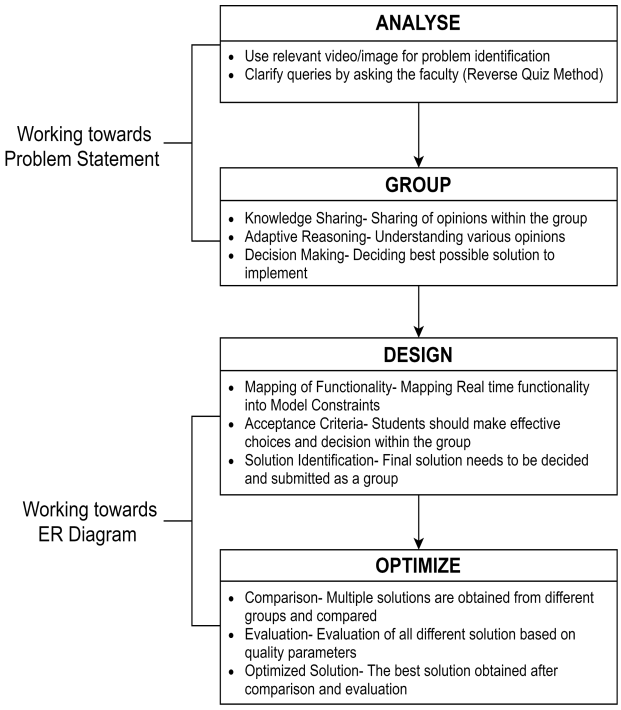


Figure 2: AGDO Methodology Block Diagram

We have experimented with our proposed AGDO methodology for conducting database management lectures to teach data modeling (Entity-Relationship Model). In the proposed AGDO methodology, students will be provided with visual artifacts to **analyze** the real-time problem and model an Entity-Relationship Model. By forming **groups** students will get an opportunity to collaborate and come up with different ideas. By using Adaptive reasoning and Decision-making ability of each group to map functionalities of the system in the **designed** ER diagram. Each group would present their proposed solution, these individual solutions would be evaluated and updated to arrive at an **optimized** solution.

- **Analyze**

  Individual students will analyze the real-time problem using relevant videos/images to felicitate thinking and problem defining abilities. Instructors will continuously monitor progress using the reverse quiz [23] method. The conceptual understanding and progress of the students are confirmed by asking them questions about the same in the reverse quiz method. With a proper understanding of the problems by the students and assurance of the same by the instructors, we move on to the next phase of our model.

- **Group**

  The students are then grouped and asked to have discussions about their analysis by the instructors. Group discussion will ensure active participation and the process of learning by listening to others. Adaptive learning will promote self-determination [24]-[27] among students to provide and accept design decisions proposed by peers. The formation of groups provides several different ideas as well as induction of innovation among peers. Listening skills are a key to this process, better understanding within the group results in better model development. After acceptance of the solution proposed by the peers, groups start with the designing phase of the model.

- **Design**

  After the discussion, adaptation, and improvisation of their respective analysis. Students will come up with mapping real-time functionality into model constraints. Groups will decide the acceptance criteria to make effective choices and decisions within the group. The final solution will be proposed by the project team [23].

- **Optimize**

  All the models developed by every group are collected, discussing the positives and negatives of each. Selecting one model for any problem statement in most cases would not result in the ideal solution. Hence, all proposed solutions are compared and evaluated to obtain the best possible solution using presentation by the groups.

4. Case Study using the AGDO Methodology – Entity-Relationship Model

A case study approach [28] allows us to explore real-life scenarios in a given sample size and identify solutions. Hence, this case study was established to give ideas for designing data models for students. It was effectively conducted with students of Semester III, Computer Engineering who had merely basic knowledge of design process and methodologies. The main objective of this case study was to make students aware of innovative and practical strategies to conceptualize problem statements and eventually, draw ER diagrams for the same. The course name was Relational Database Management System. The total time required for this case study was four hours.

The case study involved following the AGDO methodology and hence conducted in four buckets- Analyze, Group, Design & Optimize. See Figure 3 for the given problem statement.

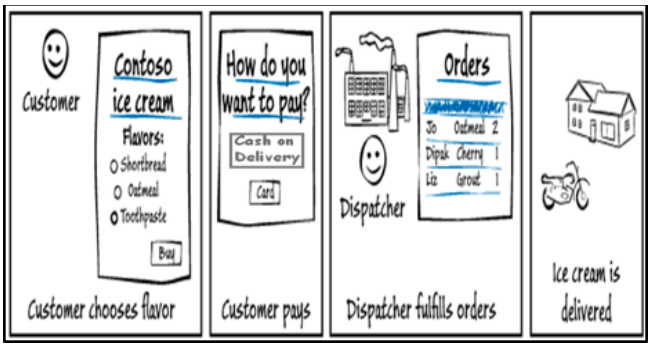


Figure 3: Problem statement

- **Analyze:** A group of 47 students was presented with the above picture. The problem statement involved forming a Relationship Entity Model based on the given picture. The students were expected to analyze the given problem statement, connect it with pre-existing knowledge, and form initial grounds of approaching this problem statement. The system environment consisted of a typical E-Commerce, involving customers (consumers), shopkeepers (vendor), and dispatchers (distributor).

The problem definition of Figure 3 is as follows:

The CoolPoint Ice Cream Delivery System has many flavors of ice cream. The system will allow customers can choose flavors of ice cream from the list, Customer places the order and pays the bill through card or chooses to pay on delivery, Staff gives the order dispatching list to the dispatcher and the dispatcher delivers the ice-cream orders to the respective customers. The system environment is for Customer, Shopkeeper, and Dispatcher.

- **Group:** After analyzing, the students were now grouped into clusters, containing 4 to 5 students. The team goal is to help one another understand the problem statement successfully and to identify the purpose. Each member of the group was accountable individually and collectively. Every member of the group had to work towards a common goal and perform his/her tasks that contribute towards it. In smaller groups, students could now freely discuss and debate their ideas. They also learn by effectively listening [29] to other peers to express their ideas. Grouping calls for an engaging and more confined platform which lets students feel much more confident and accepted within the smaller constraints of a group.

  A sample outcome of this step (Referring figure 3) is given below:

Identify Entities and attributes for each entity.

– To identify entities from the scenario we can use the 'Noun-phases' approach.

– This approach considers all nouns and phases in the problem as entities.

– Then we will take some steps to remove all vague or unnecessary Entities

– If an entity is depending on other entities or entities not having independent existence in the system such entities are enlisted as Weak entities.

– Some problem attributes are given in the problem statement itself. Sometimes attributes are not specified in the problem.

Example Above:

IceCream (Flavor, pricePerScoop)

Customer (Customer_Name, Customer_Mobile, Cust_Address)

Shopkeeper (Customer_Name, Customer_Mobile, Cust_Address)

Dispatcher (Order_Id, Shipping_Address, Ship_Status)

- **Design:** The third step involved them working collaboratively to build on the designing of the ER model. Completion of the ER diagram required each student's work to be combined with that of other students to produce a team effort. They started designing the model by forming and recognizing primitive stages of relations such as (see Figure 4 and 5):



Figure 4: Formation of relationships within entities

Approaches to Identify Relationships

– We can use conjunction used in problem for naming relationship.

– Example, Employee works for a department

– We can also use the name of two entities connected with an underscore as a conjunction for the naming relationship.

– Example, Employee works for a department

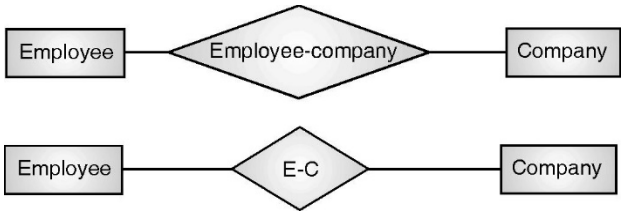


Figure 5: Formation of relationships within entities

- **Optimize:** This problem statement which closely tried to mimic real-world problems, had a wide range of parameters and constraints. The smaller clustered groups presented their contrived designs in front of the entire class. They gave and received feedback on their presented solution. The class then tried to find the optimum solution by comparing all the suggested diagrams by the various groups. The optimized solution was an amalgamation from diagrams received by various groups.

5. Results and Analysis

The usage of AGDO methodology accorded students the skills required to understand real-world problems using visual artifacts such as videos and images. The analyzing stage empowers them to use preconceived knowledge and relate it with the given problem statement. Reverse questioning can lead to a better conceptual

understanding [30] while ensuring continuous assessment by the teacher. Hence, making sure that the results of the analysis obtained are relevant to the topic. The grouping stage allows students to work together and share experiences which leads them to a better understanding of the problem at hand and integrates different perspectives. The designing data model in the group will improve the acceptability of solutions from other peers. Students experience active learning through problem-solving, brain-storming sessions, and group assignments for designing the solutions.

This case study was conducted with the help of student teams in a session regarding RDBMS during a class. After following the proposed AGDO methodology, the student teams came up with multiple solutions, and the one shown in figure 5 was found out to be the optimal one.

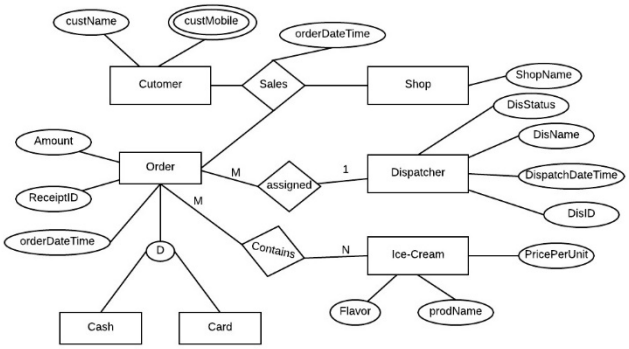


Figure 5: Optimized Solution

This led to the introduction of various metrics such as Problem Statement, Questions, Solutions, and Learning Outcomes that help affluently evaluate the proposed approach. Students were graded according to their performance on these parameters.

The following results can be drawn out of the assessment of the case study post implementing the AGDO methodology: Greater than half the strength of the course, 55.5% (26) of students scored over 90% in successfully understanding and conceptualizing the problem statement. This led us to the direction that students were able to harness the given visual artifacts into meaningful and coherent comprehension. In the category labeled 'Questions', it was observed that 44% of the class could surpass the 80% threshold. This paves the way for the reverse questioning method and group discussions which stimulate and encourage students to probe and ask questions, thereby fueling their curiosity. Similarly, 40.4% (19) scored more than 80% for the solutions that they provided for the given problem statement. 72.3% (34) of students secured over 80% when evaluating the learning outcomes. This, in turn, gave better insights into potential subject outcomes, thus accelerating learning and growth.

In totality, 42.3% (16) of the total students attained above 90% of the maximum marks allocated, while a staggering 93.6% (44) were able to achieve over 80% of the maximum marks. These numbers substantiate the proposed AGDO methodology.

The students gave feedback about the usage of this case study regarding their learning of viewing real-world scenarios for designing IT solutions. Students got the experience of active learning through problem-solving, brainstorming sessions, and group assignments for designing Real-World Systems. Feedbacks provide better insight and help verify the feasibility and efficacy of the proposed method.

Feedback was provided by the 47 participating students on various parameters. They were asked to give the rating on a scale of 0 to 5, zero being the least effective to 5 being most effective. For the first two parameters which were based on the relevancy and ease of understanding of the course, it was observed that images were the most effective medium. While the latter two which were based out of helpfulness and the overall impact indicated the video was the most preferred option. In all four parameters, the textual transmission was rated relatively poorly proving that it was not favored amongst the students. This table reaffirms the advantages of visual artifacts such as videos and images over textual data.

6. Limitations of the AGDO Methodology

AGDO methods motivate skill-based learning and encourage the group working culture among engineers. In industry. Working together in a group is the most important aspect. Engineering leadership is another emerging area of research [31]. The courses like software engineering, Technical Project, Mobile Application Development, Prototype Development, etc. wherein the problem definition and problem formulation is involved, the AGDO methodology is best suited. The theoretical subjects and other self-study-based subjects, the AGDO courses are not appliable.

Another limitation of this paper is the sample size, which is very small for any kind of analysis. Since AGDO methodology was new, we have tested its applicability on a smaller population. In near future, we would like to extend our work to a larger population and we would like to conduct the statistical measures to prove how AGDO methodology helped to build a perfect ER model.

7. Conclusion

There is evidence that suggests that the traditional education reforms, once considered significant, are now struggling to keep up with modernization. Historically, students often resort to ineffective methods such as rote learning or often feel disengaged from the learning process. In the AGDO modus operandi, it tries to eliminate the above by students working collaboratively in groups towards a common goal.

As a denouement of the case study, students were able to discover and learn the subject of the course on their own by questioning, interrogation, and logical ability. Grouping allowed them to weigh, judge, and preview others' ideas with their own. This sanctioned them to construct and assemble ideas which were also accepted by their peers. By using their primary knowledge and associating it with daily life, they were able to optimize the best possible outcome and come up with scalable and practical solutions. AGDO strives to foster an easy understanding of concepts and bring joy to learning. To conclude, this study showed that AGDO is an effective teaching method.

While applying this methodology, it was also observed that in most cases students using visual forms of data like images and videos had better efficiency than that of the students using traditional textual methods. This was a result of the increasing

proficiency of students in technology and a better understanding of concepts through visualization rather than textual descriptions.

References

[1] G. Domik, Fostering collaboration and self-motivated learning: Best practices in a one-semester visualization course, IEEE Computer Graphics and Applications, 2012.

[2] H. J. Holz, A. Applin, D. Joyce, H. Purchase, C. Reed, B. Haberman, Research Methods in Computing : What are they , and how should we teach them ?, Information Systems, 2006.

[3] F. David, R. Abreu, Information technology in education: Recent developments in higher education, in *Iberian Conference on Information Systems and Technologies, CISTI*, 2014, 2014.

[4] W. G. Spady, *Outcome-Based Education: Critical Issues and Answers*, 1994. 1994.

[5] P. Willmot, M. Bramhall, K. Radley, Using digital video reporting to inspire and engage students, The Higher Education Academy, 2012,.

[6] W. A. Almurashi, THE EFFECTIVE USE OF YOUTUBE VIDEOS FOR TEACHING ENGLISH LANGUAGE IN CLASSROOMS AS SUPPLEMENTARY MATERIAL AT TAIBAH UNIVERSITY IN ALULA, 2016.

[7] H. Forbes *et al.*, Use of videos to support teaching and learning of clinical skills in nursing education: A review, *Nurse Education Today*, 2016. 2016.

[8] G. C. Lee, C. C. Wu, Enhancing the teaching experience of pre-service teachers through the use of videos in web-based computer-mediated communication (CMC), *Innovations in Education and Teaching International*, 2006. 2006.

[9] S. Ivanova, Using explainer videos to teach web design concepts, in *The 13th International Scientific Conference eLearning and Software for Education*, 2017, 2017.

[10] K. Kraiger, J. K. Ford, E. Salas, Application of Cognitive, Skill-Based, and Affective Theories of Learning Outcomes to New Methods of Training Evaluation, Journal of Applied Psychology, 1993.

[11] P. Pastor, M. Kalakrishnan, S. Chitta, E. Theodorou, S. Schaal, Skill learning and task outcome prediction for manipulation, in *Proceedings - IEEE International Conference on Robotics and Automation*, 2011, 2011.

[12] C. Gomathi, V. Rajamani, Skill-based education through fuzzy knowledge modeling for e-learning, Computer Applications in Engineering Education, 2018.

[13] A. G. GREENWALD, Cognitive Learning, Cognitive Response to Persuasion, and Attitude Change, in *Psychological Foundations of Attitudes*, 1968, 1968.

[14] R. C. Schank, T. R. Berman, K. A. Macpherson, Learning by doing, in *Instructional-Design Theories and Models: A New Paradigm of Instructional Theory*, 2013, 2013.

[15] M. J. Bezanilla, D. Fernández-Nogueira, M. Poblete, H. Galindo-Domínguez, Methodologies for teaching-learning critical thinking in higher education: The teacher's view, Thinking Skills and Creativity, 2019.

[16] J. Andrews-Todd, C. M. Forsyth, Exploring social and cognitive dimensions of collaborative problem solving in an open online simulation-based task, Computers in Human Behavior, 2020,.

[17] V. Garousi, G. Giray, E. Tuzun, C. Catal, M. Felderer, Closing the Gap between Software Engineering Education and Industrial Needs, IEEE Software, 2020.

[18] L. DE SOUSA, B. RICHTER, C. NEL, The effect of multimedia use on the teaching and learning of Social Sciences at tertiary level: a case study, Yesterday and Today, 2017,.

[19] B. R. Robin, The power of digital storytelling to support teaching and learning, *Digital Education Review*, 2016. 2016.

[20] M. Himanshoo, K. Sharma, Role of ICT in Improving the Excellence of Education, International Journal on Computer Science and Engineering (IJCSE, 2015.

[21] A.-M. Suduc, M. Bîzoi, G. Gorghiu, L.-M. Gorghiu, Digital Images, Video and Web Conferences in Education: A Case Study, Procedia - Social and Behavioral Sciences, 2012.

[22] L. Killian, New Textual Formats: Reading online is re-wiring the human brain and changing how we process information, Dalhousie Journal of Interdisciplinary Management, **5**(1), 2010. https://doi.org/10.5931/djim.v5i1.49

[23] P. Churi, K. Mistry, A. Dhruv, S. Wagh, Alchemizing education system by developing 5 layered outcome based engineering education (OBEE) model, in *Proceedings - 2016 IEEE 4th International Conference on MOOCs, Innovation and Technology in Education, MITE 2016*, 2017, 2017.

[24] J. C. Ortiz-Ordoñez, F. Stoller, B. Remmele, Promoting Self-confidence, Motivation and Sustainable Learning Skills in Basic Education, Procedia - Social and Behavioral Sciences, 2015.

[25] P. Ommundsen, Problem-based learning, in *Inspiring Students: Case Studies on Teaching Required Courses*, 2013, 2013.

[26] D. Boud, G. I. Feletti, *The challenge of problem-based learning*, 2013. 2013.

[27] J. R. Savery, T. M. Duffy, Problem based learning: An instructional model and its constructivist framework, Educational Technology, 1995.

[28] S. Crowe, K. Cresswell, A. Robertson, G. Huby, A. Avery, A. Sheikh, The case study approach, BMC Medical Research Methodology, 2011,.

[29] C. Edwards, Life-long learning, Communications of the ACM, 1993.

[30] J. P. Weaver, R. J. Chastain, D. A. DeCaro, M. S. DeCaro, Reverse the routine: Problem solving before instruction improves conceptual knowledge in undergraduate physics, Contemporary Educational Psychology, 2018.

[31] B. Ahn, M. F. Cox, J. London, O. Cekic, J. Zhu, Creating an instrument to measure leadership, change, and synthesis in engineering undergraduates, Journal of Engineering Education, 2014.

ASTES

Advances in Science, Technology and Engineering Systems Journal
Vol. 5, No. 5, 826-833 (2020)
www.astesj.com
Special Issue on Multidisciplinary Innovation in Engineering Science & Technology

ASTES Journal
ISSN: 2415-6698

Deaf Chat: A Speech-to-Text Communication Aid for Hearing Deficiency

Mandlenkosi Shezi*, Abejide Ade-Ibijola

Formal Structures, Algorithms and Industrial Applications Research Cluster, Department of Applied Information Systems, University of Johannesburg, Bunting Road Campus, Johannesburg, 2006, South Africa

ARTICLE INFO

Article history:
Received:31 July, 2020
Accepted:15 September, 2020
Online:12 October, 2020

Keywords:
Speech-to-Text
Hearing Aids
Communication Aids
Multiple-Speaker Classification
AI for Social Good

ABSTRACT

Hearing impairments have a negative impact in the lives of individuals living with them and those around such individuals. Different applications and technological tools have been developed to help reduce this negative impact. Most mobile applications that have been developed that use Speech-to-Text technology have been inconsistent such that they are not inclusive of all types of hearing impaired individuals, only work under specifically predefined environments and do not support conversations with multiple participants. This makes the present tools less effective and makes hearing impaired participants feel like they are not completely part of the conversation. This paper presents a model that aims to address this by introducing the use of Multiple-Speaker Classification technology in the design of mobile applications for hearing impaired people. Furthermore we present a prototype of a mobile application called `Deaf Chat` *that uses the newly designed model. A survey was conducted in order to evaluate the potential that this application has to address the needs of hearing-impaired people. The results of the evaluation presented a good user acceptance and proved that a platform like* `Deaf Chat` *could be useful for the greater good of those who have hearing impairment.*

1 Introduction

Hearing is a very important ability that many people take for granted until it weakens, or they lose it [1]. Communication impairments have been studied and proven numerous times to have a negative impact on many aspects of an individual's life such that most communication impaired individuals experience mental and emotional challenges [2]–[5].

Hearing disorders have led into negative effects on the social and professional lives of older adults [6, 7]. Hearing impairment has a mass effect on the performance of individuals irrespective of their age group. Children who have any form of hearing impairment have been found to be experiencing continuous behavioral problems and issues with language development [8]. While examining hearing-impaired children, it was found that those who have hearing aids perform far way better compared to those who do not [9]. Using hearing aids reduces listening effort and the possibility of going through mental fatigue as less effort is made for processing speech [10]. This shows the greater potential that technology-based hearing aids could play on the lives of hearing-impaired individuals.

On many instances hearing-impaired individuals must depend on interpreters (mostly family members) to help them communicate with other people [11, 12]. Some also resort to using sign language for communication and others even go to the extent of lip reading [13, 14]. Despite the efforts made, the failure to accommodate the hearing-impaired and the use of insufficient and ineffective communication methods further contributes to depression, loneliness and social anxiety [15]. Alternatively, some people use SMS messaging to communicate with hearing impaired individuals [16], but that is only effective when both parties are at the same geographical location. It is highly imperative to note that SMS is not that much effective when individuals who are engaging in a conversation are not at the same place because one can never know if the other party viewed or received the message or not [17].

The understanding of the problems that hearing-impaired individuals of different ages face gave us motivation to create a platform that can help reduce these problems. With advances in Artificial Intelligence (AI), there has been a movement to create more AI tools for social good. Here, we introduce a model and a tool (named `Deaf Chat` to communicate with hearing impaired individuals based on AI. AI for Social Good can be indelicately described as AI that aims to improve people's lives in more meaningful ways [18]. Hence, creating an AI-powered software tool to support people with hearing impairment is considered as AI for Social Good [19].

*Corresponding Author: Mandlenkosi Shezi, University of Johannesburg, Bunting Road Campus, Johannesburg, South Africa, +27 74 875 1559, mandlashezifbi@gmail.com

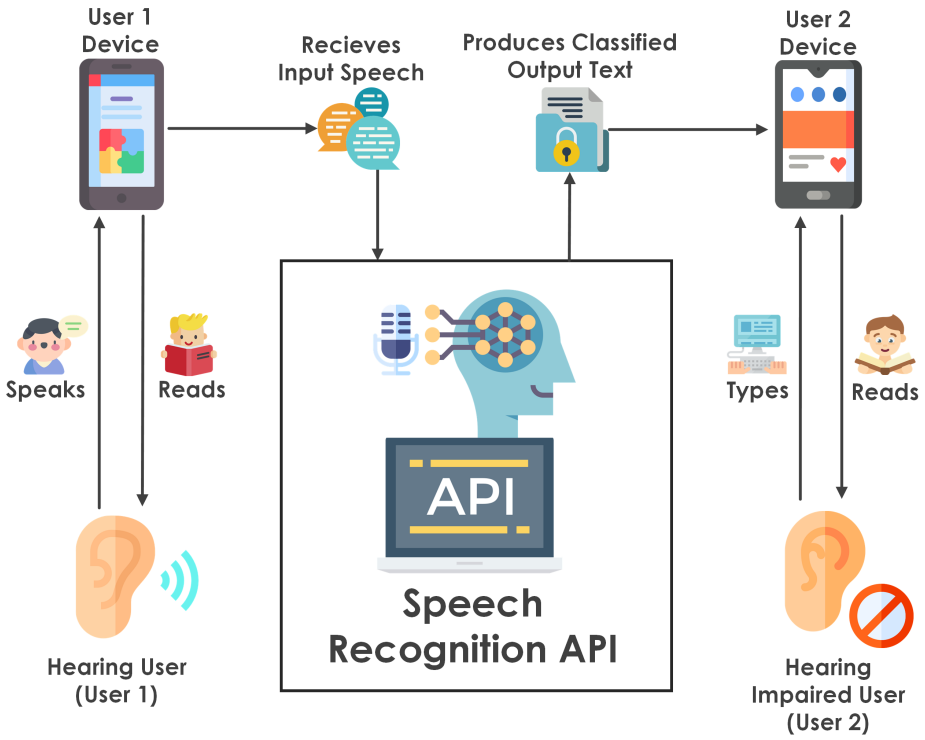


Figure 1: Graphical representation of messaging using the Deaf Chat application

Figure 1 gives a high level overview of how `Deaf Chat` facilitates communication between both hearing and hearing-impaired users. `Deaf Chat` supports both one-to-one chat and group chats, in both modes speech is analysed and classified in the interest of confirming if more than one voice is embedded in a voice note. The process is as follows. A hearing user, pair or group of hearing users will record their speech and the speaker recognition API will process the speech then convert it into classified text. The output text will then be sent to the hearing-impaired user in place of the voice note. Depending on the classification of the hearing-impairment and the preference of the hearing-impaired user, he or she will respond using either speech or text.

The following are the contributions of this paper. We have:

1. conducted an extensive literature review on previous tools used as hearing aids and tools,
2. developed a prototype of a mobile based messaging application called `Deaf Chat` that uses Multiple Speaker Recognition technology to serve as a communication aid for people with hearing deficiency, and
3. evaluated `Deaf Chat` using a survey in order to analyse its potential impact.

This paper is organized as follows. The following section will explore the Background. Section 3 will then follow with Related Work. Section 4 presents the design of the `Deaf Chat` application. Section 5 presents Implementation and Results. Section 6 presents the evaluation. Lastly, Section 7 will conclude the paper by presenting the Conclusion, Recommendations and directions for Future Work.

2 Background

This section provides a detailed view of all the tools that are similar to `Deaf Chat`. The first subsection discusses our problem statement which shows why the development of this solution is necessary.

2.1 Problem Statement

Mobile applications that have been developed to aid hearing-impaired individuals to communicate with each other and with people without disabilities have been focused on creating solutions that are not inclusive of all categories of hearing-impaired individuals, most of them are scenario based and none of them currently support multiple speakers. In order to explore and solve the following problem, the following questions will be addressed:

1. How has technology been used in the design of hearing aids and tools previously?
2. How can Multiple-Speaker Recognition software be incorporated in the design of a new tool to enhance communication with hearing deficient individuals?
3. Can we evaluate this new tool, and show that it can be helpful for hearing impaired individuals?

The following subsection gives a brief background on previously developed tools and how they affect the design of this new tool.

2.2 Classifying Hearing Impaired Individuals

Hearing impairments are one of the most well-known types of impairments around the world. According to the World Health Organization (WHO) [20], there are about 6.1% people who are suffering from hearing loss around the world. It is very important to note that there are different types of hearing impairments, these are distinguished according to the degree of hearing loss one is experiencing [21]. Firstly, some people experience partial hearing loss, an individual living with such a condition is labelled as one who is "hard of hearing" [22]. Secondly, other hearing-impaired individuals cannot hear a thing but can speak, an individual of such a group is called "deaf" [23]. Thirdly, some hearing-impaired individuals can not hear nor speak, and they are called "deaf mute" or "deaf and mute" [24]. Most people use the term "deaf" to describe all three groups but they are not the same.

It is important to understand this as it is a contributing factor that should be considered in the design of mobile applications for the hearing-impaired. The following subsection discusses the two types of hearing aids which are normally the primary aid that hearing-impaired individuals use.

2.3 Types of Hearing Aids

The most common hearing aids that exist are of two types, namely analog and digital hearing aids. Analog hearing aids are less expensive but what makes them unique is that when they amplify sounds, they do not filter noise. Digital hearing aids on the other hand are more advantageous because they can remove unwanted signals of which eliminates noise [25]. Digital hearing aids have been developed spontaneously such that newer versions of them have also gave birth to "smart hearing aid systems" [1]. Smart hearing aid systems consist of digital hearing aids and software for mobile applications that help with providing more flexibility and performance. Smart hearing aid systems enable users to set their environments using the mobile applications of which enables their digital hearing aids to filter noise more suitably [26, 27].

Technology is continuously evolving as time moves. It is important to note that, hearing aids are better suited for people who are living with or rather are experiencing partial hearing loss. This stresses the need for assistive technologies as they are more inclusive. The following section discusses these technologies.

2.4 Assistive Technologies

Assistive technologies can be used to aid people with different special needs and they have created new possibilities for people with living with limiting conditions [27]. These possibilities include help with day-to-day activities, rehabilitative services and others. As a result, these technologies make it possible or rather easier for people with disabilities to complete tasks that were previously difficult, or close to impossible. In the context of hearing-impaired individuals, these are better suited because they cater for all three groups of hearing-impaired individuals.

Some assistive technologies have been developed for educational purposes. GameOhm [28] is a serious game that was developed for electronic engineering students which is based on the Android platform. A serious game is a game which is developed with the purpose of contributing to teaching and learning. Serious games have been applied in numerous fields such as STEM (Science, Technology, Engineering and Medicine), education, business and more. We can easily categorize students as young people as the dominating age group of students is them. On the other hand, it is important to note that assistive technologies are not solely designed for young people.

Elderly people must also be included [26]. Bearing in mind that it is highly possible for elderly people to have more than one disability, the design of assistive mobile application technologies then becomes a major concern. Typically, most elderly people do not easily welcome technology. Making applications that are not user-friendly for them would further contribute negatively. Upon developing mobile applications for the hearing-impaired, developers must go for a user-centered approach and designs must be familiar to that of familiar applications [26, 29]. This enables the user training process to be less complex, which also increases motivation and user acceptance [30].

Upon collecting requirements for assistive technologies, it is important to consider both hardware and software capabilities in accordance to the needs of the targeted disabled users [31]. Different types of software could be used in accordance to the different classifications of hearing-impaired users such as Haptic Feedback software and Speech and Language Processing software. Haptic software technology uses touch to communicate with operators. The most common Haptic software implementations are that of vibration responses made by devices upon different user inputs. The following subsection discusses Speech and Language Processing.

2.5 Overview of Speech and Language Processing

Speech and Language Processing is basically concerned with the conversion of Speech-to-Text and Text-to-Speech. Text-to-Speech software synthesizes written natural language into an audio output, in simple terms it uses Natural Language Processing (NLP) technology to read written text. On the other hand, Speech-to-Text software does the same process but the other way around, it synthesizes spoken language and processes it into written natural language using NLP technology. Such software is often incorporated in the designs of voice assistants, automatic speech recognition (ASR) engines and speech analytic tools [31].

Applications that use Speech and Language Processing technology must be able to convert and transfer messages timely. Time, message transfer and real-time presentation of written text are some of the major challenges of converting speech-to-text in real time [32]. Instant speech-to-text conversion aims to synthesize spoken language into written text nearly concurrently. This is very important as it would enable people living with hearing-impairments to take part in conversations as they would have normally done if they were not experiencing any hearing problems. This would enable their conversations to be more engaging as they do not feel like they slow down participation because of taking too much time to process statements.

It is highly imperative to note that there are some challenges that might arise when converting speech to text in real-time [33]. Challenges are often caused by the nature of how Automatic Speech Recognition (ASR) based tools are built. Automatic speech recogni-

tion software typically needs one to train their speech recognition engine [34, 35]. It is advisable to have a minimum signal-to-noise ratio as noisy environments are inadequately fit. The amount of time spent training the speech recognition engine is directly proportional to the speech recognition engine's performance. However, this condition does not apply in the context of this research. Automatic speech recognition can be used for various purposes ranging from speaker identification [36], speaker classification [37] to speaker verification. This research is mainly concerned with speaker classification.

Speaker classification can separate audio input according to the voices of different speakers. It is not necessary to train a speech recognition engine for speaker classification because speaker classification is aimed at separating speech input from different voices not identifying and verifying predefined speakers. All speakers' voices are treated the same and are not compared against anything as they are viewed as new every time a voice input is synthesized during the use of a newly created speech client. *No literature currently exists on the application of speaker classification techniques for the design of mobile applications for hearing-impaired individuals* but the following subsection discusses some similar work.

3 Related Work

In this section we present an overview of current tools that are similar to `Deaf Chat` and how our tool differs.

3.1 Overview of Current Tools

The most common tools that exist in the market are mobile applications that use Automatic Speech Recognition software to help convert speech to text [17]. The requirements for these tools must be further studied in order to improve usability and usefulness [38]. Assistive technologies for the hearing-impaired must be designed to fit for all and more commercialised as many are only designed for research purposes [39, 27, 40]. Many solutions that are present are flawed as most are one-sided, they either work for a certain group of hearing deficient individuals (deaf, hard of hearing, or mute) or they work only under specifically predefined situations. This is evident in tools like Sign Support [41], which works as an aid in pharmacies only and LifeKey [42], which only works in cases of emergency.

3.2 Examples of Existing Tools

VoIPText is a mobile application that was developed to assist deaf and hard of hearing people. It attempted to apply VoIP (Voice Over IP), speech to text software and instant Automatic Speech Recognition (ASR) functionalities to include hearing deficient individuals in the use of VoIP technology for communication [17]. This tool was based online (dependent on internet connectivity) and its development realized the potential VoIP technology can assist hearing impaired people.

BridgeApp is a mobile application that was designed to assist deaf and mute Filipino Sign Language and American Sign Language speaking people from the Philippines, their user acceptance was positive, and the tool was deemed as useful [31]. This tool makes use of Text-to-Speech, Speech-to-Text, Text-to-Image and Haptic Feedback technology and it only works offline. The tool was only applicable to only predefined scenarios such as being at church, the office and others. Another tool called Ubider was developed for Cypriotic deaf people and it had the ability to convert a natural language into Cypriotic Sign Language [21]. This tool is dependent on the internet. The following subsection shows the gap that exists in current tools.

3.3 The Gap

Many tools have been developed to assist hearing-impaired people and the most common characteristics of these tools are that they are either:

1. online or offline,
2. dedicated only to a specific audience (deaf, mute, hard of hearing or any combination of two of the three categories),
3. they make use of speech to text, text to speech, and automatic speech recognition software.

A model that is inclusive of all three categories of hearing-impaired individuals (deaf, mute or hard of hearing) would make a greater contribution to their lives. This is what we present in this paper — `Deaf Chat`.

4 Design of Deaf Chat

The biggest distinguishing factors that represent how `Deaf Chat` is unique are the algorithm behind it and technologies that it uses. The following subsection gives a brief explanation of the algorithm that represent the app flow in `Deaf Chat`.

4.1 The Deaf Chat Algorithm

`Deaf Chat` has a unique design compared to other messaging applications that exist. It uses speaker diarisation techniques recognize and classify speakers before sending converted speech to text from one user to another. Speaker diarisation refers to the process of separating different voices on a voice input. This term is also spelled as "diarization" and this paper uses both spellings interchangeably. Algorithms 1-3 give a high-level overview of the algorithms behind how `Deaf Chat` was designed and implemented. Algorithm 1 shows how a message is sent from one user to another and how the dialogue process works on a Chat Activity.

```
Data: Text Message
Result: Delivery Notification
initialisation;
message = MakeInput();
SEND message;
if User_2 responds then
    MakeInput();
else
    do nothing;
end
```

Algorithm 1: Chat Activity

Algorithm 2 gives the possibility of two input types which are either text or voice input. This algorithm is a function that takes an argument and results in a text output that is used in Algorithm 1. In the case where a user decides to type text, the input will just be sent as is. In contrast to that, if the user decides to record a voice note the speech will be sent to the Process Speech function.

```
Function MakeInput():
begin
    Data: txt_input or voice_input
    Result: text_message
    if (input==txt_input) then
    begin
        text_message = txt_input;
    end
    else
    begin
        text_message = ProcessSpeech(voice_input)
    end
    end
    return text_message
end
```

Algorithm 2: Make Input Function

As called in Algorithm 2 (`MakeInput` Function), this algorithm shows how `Deaf Chat` interacts with the API which facilitates the classification of speakers. Algorithm 3 takes the voice input from the Make Input function and sends it to the API which then transcribes the speech and returns a string of words. This is continued until the user decides to either stop the recording using the stop button or by just simply sending the currently transcribed text.

```
Function ProcessSpeech():
begin
    Data: voice_input
    Result: text
    text = " ";
    while text = " " do
    begin
        SEND request to API;
        text = RECEIVED response from API;
        return text
    end
    end
end
```

Algorithm 3: Process Speech Function

The following subsection explains the graph structure of `Deaf Chat`.

4.2 Deaf Chat's Operation Flow

Figure 2 shows how users can interact with each other through all the functionalities that `Deaf Chat` has. Users can simply send a text message, media or make use of the diarisation functionality by recording a voice note. In order to save time in development, our prototype showcases the core functionality of our application of which is the separation of speakers from a voice input. The following section will give more thorough insights about the technologies that were used of which is a discussion about what they are and how they were implemented.

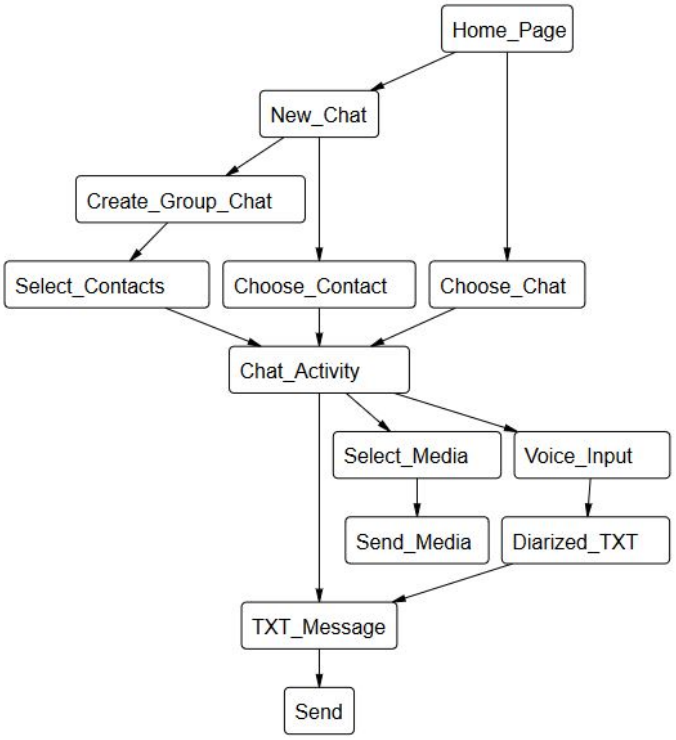


Figure 2: A Graph diagram, showing the operation flow of `Deaf Chat`

5 Implementation and Results

As indelicately mentioned on the previous section, our prototype showcases the core functionality of the `Deaf Chat` tool. By applying the core functionality we improved the quality of the results we were to obtain because incorporating an online chat service would have impacted the response time of the application. The following subsections discuss the two core technologies that we used in the implementation of `Deaf Chat`.

5.1 Android Studio

We used Android Studio IDE to develop our tool. We used the Java programming language to create all our back-end functions and XML (Extensible Markup Language) to create the front end in our activities. Figure 3 shows the chat activity whereby a voice input has been made and processed. The activity has an easy to use interface of which enhances the user experience. In order for a user or a group of users to make an input, one simply has to click the record button and start talking. There is no limit as to how long the user can speak. Furthermore, a user is allowed to edit the output text that has been produced before sending the generated text to the next user.

5.2 IBM Watson API

The IBM Watson API has a number of different features that can be used to build different applications ranging from Chat bots, Text-

to-Speech engines, Speech-to-Text engines and more. In the implementation of our tool, we used the IBM Watson Speech to Text API. It facilitated the conversion of speech from voice notes into classified text.



Figure 3: A Chat Activity showing processed voices of four distinct speakers.

The IBM Watson Speech to Text API manages to do this by applying Deep Neural Network (DNN) models. Within this context, Deep Neural Networks process speech by using powerful algorithms that can identify unique voices and further convert speech into text. The algorithms behind the API also filter noise by excluding unwanted sounds on the transcribed text. The IBM API only supports about 19 language models which include English (USA, Australia and UK), Mandarin, Dutch, French and more. We used the US language model. In order to identify different speakers we enabled diarization on our model and further created some methods that assisted us in formatting our output in a way that is easy to understand for different users.

6 Evaluation

This section presents the results we obtained from numerous individuals who tested the `Deaf Chat` prototype. We uploaded the application's installation file on the internet and then attached a link to an online survey which had 7 questions that respondents had to complete after testing the app. The results can be seen from Figure 4-10. Most of our respondents were between the ages 18-39, and they found the application useful and about 83.7% said that they would recommend it to a hearing impaired person. Only 14% of our respondents found it hard to navigate through the app of which shows that it is user friendly.

According to the results of the survey, `Deaf Chat` can convert Speech to Text and Identify Speakers successfully up to 86% and 88.5%, respectively. We accumulated those results by adding all participants who rated `Deaf Chat` 5 and above. Some respondents who experienced challenges with speech processing outlined that it might be because of their African accents. Some recommendations also included comments that said that `Deaf Chat` would be better if it could support local languages. A small percentage of our respondents outlined that the response rate is slow. Overall, we can conclude that `Deaf Chat` is very useful and performed even better than we had anticipated.

7 Conclusion and Future Work

7.1 Conclusion and Recommendations

In this paper, we have presented a new model and a software prototype for facilitating of communication with hearing-impaired individuals. Our tool can be used to communicate with all three types of hearing-impaired individuals and further makes a contribution into improving the lives of the targeted users. We evaluated our tool using a survey which included participants who are not hearing impaired. Most of our participants found the tool very useful and made recommendations as to how we can improve it so that it is more useful. Some participants had a bad experience because of their accents and we would like to recommend the use of a speech recognition engine that responds faster and supports more accents, and more especially those that are African.

There are many perceptions that the people of South Africa and Africa as a whole have about AI because it has not been used for much social good in South Africa. According to Stats SA [43], about 7.5% people in the population of South Africa are living with a disability. Furthermore, the South African National Deaf Association (SANDA) [44], certifies that it represents about four million deaf and hard of hearing people in South Africa which shows the greater need for more AI tools for Social Good. `Deaf Chat` is one of the first South African AI tools that were developed for Social Good and we perceive that it will open more opportunities for innovative research and development for this particular purpose.

7.2 Future Work

We are going to implement our model and design in an iOS and web based version of `Deaf Chat`. Moreover, we will add additional features such as quick access to emergency services for hearing impaired users.

Acknowledgment The authors would like to give special thanks to Nikita Patel for the rich illustration on this contribution and the whole Formal Structures Lab team for their support during the commencement of this study.

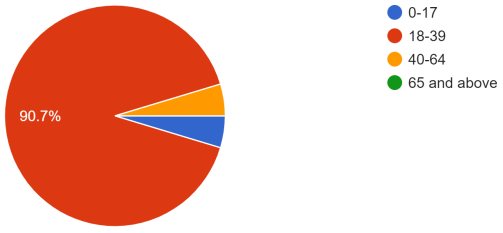


Figure 4: Age group of participants

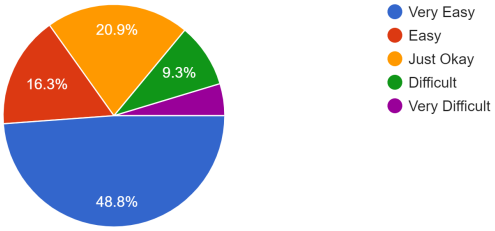


Figure 5: Ease of navigation

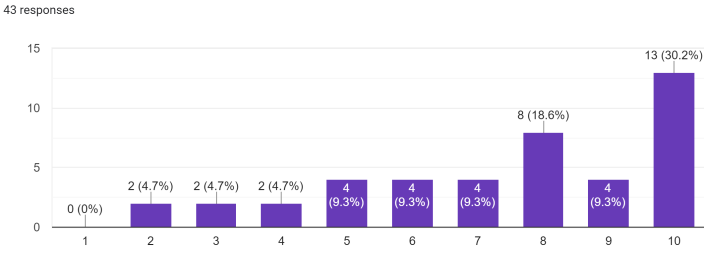


Figure 6: Rating of Speech-to-Text functionality

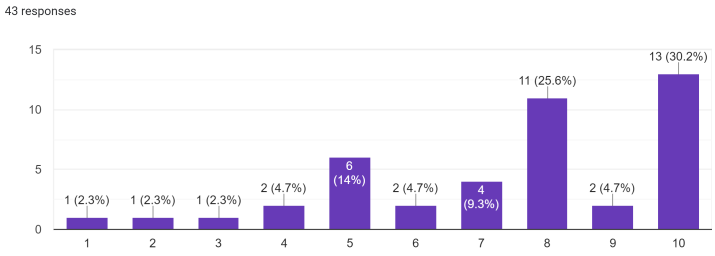


Figure 7: Rating of Speaker Diarization functionality

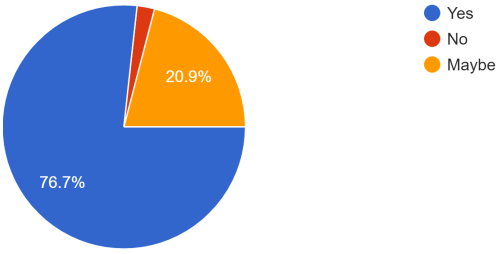


Figure 8: Usefulness of tool to hearing impaired people

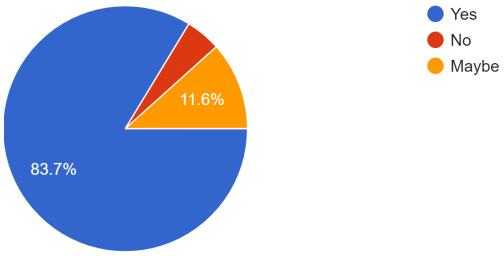


Figure 9: Likeliness to recommend app to hearing impaired person

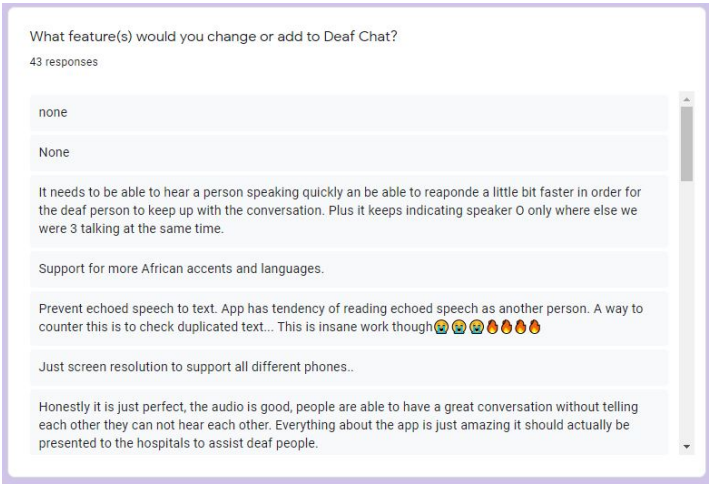


Figure 10: Recommendations

References

[1] W. Shehieb, M. O. Nasri, N. Mohammed, O. Debsi, K. Arshad, "Intelligent Hearing System using Assistive Technology for Hearing-Impaired Patients," in 2018 IEEE 9th Annual Information Technology, Electronics and Mobile Communication Conference, IEMCON 2018, 2018, doi:10.1109/IEMCON.2018.8615021.

[2] D. G. Blazer, D. L. Tucci, "Hearing loss and psychiatric disorders: A review," Psychological Medicine, 2019, doi:10.1017/S0033291718003409.

[3] A. D. Palmer, P. C. Carder, D. L. White, G. Saunders, H. Woo, D. J. Graville, J. T. Newsom, "The impact of communication impairments on the social relationships of older adults: Pathways to psychological well-being," Journal of Speech, Language, and Hearing Research, 2019, doi: 10.1044/2018_JSLHR-S-17-0495.

[4] N. Shoham, G. Lewis, G. Favarato, C. Cooper, "Prevalence of anxiety disorders and symptoms in people with hearing impairment: a systematic review," Social Psychiatry and Psychiatric Epidemiology, 2019, doi: 10.1007/s00127-018-1638-3.

[5] M. I. Wallhagen, W. J. Strawbridge, G. A. Kaplan, "6-year impact of hearing impairment on psychosocial and physiologic functioning." 1996.

[6] A. D. Palmer, J. T. Newsom, K. S. Rook, "How does difficulty communicating affect the social relationships of older adults? An exploration using data from a national survey," Journal of Communication Disorders, 2016, doi:10.1016/j.jcomdis.2016.06.002.

[7] L. C. Gellerstedt, B. Danermark, "Hearing impairment, working life conditions, and gender," Scandinavian Journal of Disability Research, 2004, doi: 10.1080/15017410409512654.

[8] J. Stevenson, D. McCann, P. Watkin, S. Worsfold, C. Kennedy, "The relationship between language development and behaviour problems in children with hearing loss," Journal of Child Psychology and Psychiatry and Allied Disciplines, 2010, doi:10.1111/j.1469-7610.2009.02124.x.

[9] T. Most, "The effects of degree and type of hearing loss on children's performance in class," Deafness and Education International, 2004, doi:10.1179/146431504790560528.

[10] B. W. Hornsby, "The effects of hearing aid use on listening effort and mental fatigue associated with sustained speech processing demands," Ear and Hearing, 2013, doi:10.1097/AUD.0b013e31828003d8.

[11] M. A. HARVEY, "Family Therapy with Deaf Persons: The Systemic Utilization of an Interpreter," Family Process, 1984, doi:10.1111/j.1545-5300.1984.00205.x.

[12] P. Kumar, S. Kaur, "Sign Language Generation System Based on Indian Sign Language Grammar," ACM Transactions on Asian and Low-Resource Language Information Processing (TALLIP), **19**(4), 1–26, 2020.

[13] C. N. Asoegwu, L. U. Ogban, C. C. Nwawolo, "A preliminary report of the audiological profile of hearing impaired pupils in inclusive schools in Lagos state, Nigeria," Disability, CBR and Inclusive Development, 2019, doi:10.5463/dcid.v30i2.821.

[14] R. Conrad, "Lip-reading by deaf and hearing children," British Journal of Educational Psychology, **47**(1), 60–65, 1977.

[15] J. F. Knutson, C. R. Lansing, "The relationship between communication problems and psychological difficulties in persons with profound acquired hearing loss," Journal of Speech and Hearing Disorders, 1990, doi:10.1044/jshd.5504.656.

[16] F. Bakken, "SMS Use Among Deaf Teens and Young Adults in Norway," in The Inside Text, 2005, doi:10.1007/1-4020-3060-6_9.

[17] B. Shirley, J. Thomas, P. Roche, "VoIPText: Voice chat for deaf and hard of hearing people," in IEEE International Conference on Consumer Electronics - Berlin, ICCE-Berlin, 2012, doi:10.1109/ICCE-Berlin.2012.6336486.

[18] Google, "AI for Social Good– Google AI," 2020.

[19] J. Cowls, T. King, M. Taddeo, L. Floridi, "Designing AI for Social Good: Seven Essential Factors," SSRN Electronic Journal, 2019, doi:10.2139/ssrn.3388669.

[20] WHO, "Estimates," 2018.

[21] K. Pieri, S. V. G. Cobb, "Mobile app communication aid for Cypriot deaf people," Journal of Enabling Technologies, 2019, doi:10.1108/JET-12-2018-0058.

[22] A. Stratiy, "The Real Meaning of "Hearing Impaired"," Deaf World: A Historical Reader and Primary Sourcebook, 203, 2001.

[23] T. K. Holcomb, "Deaf epistemology: The Deaf way of knowing," American Annals of the Deaf, 2010, doi:10.1353/aad.0.0116.

[24] A. Ballin, The deaf mute howls, volume 1, Gallaudet University Press, 1998.

[25] P. V. Praveen Sundar, D. Ranjith, T. Karthikeyan, V. Vinoth Kumar, B. Jeyakumar, "Low power area efficient adaptive FIR filter for hearing aids using distributed arithmetic architecture," International Journal of Speech Technology, 2020, doi:10.1007/s10772-020-09686-y.

[26] A. Holzinger, G. Searle, A. N. Witzer, "On some aspects of improving mobile applications for the elderly," in Lecture Notes in Computer Science (including subseries Lecture Notes in Artificial Intelligence and Lecture Notes in Bioinformatics), 2007, doi:10.1007/978-3-540-73279-2_103.

[27] G. Kbar, A. Bhatia, M. H. Abidi, I. Alsharawy, "Assistive technologies for hearing, and speaking impaired people: a survey," 2017, doi:10.3109/17483107.2015.1129456.

[28] A. Jaramillo-Alcazar, C. Guaita, J. L. Rosero, S. Lujan-Mora, "Towards an accessible mobile serious game for electronic engineering students with hearing impairments," in EDUNINE 2018 - 2nd IEEE World Engineering Education Conference: The Role of Professional Associations in Contemporaneous Engineer Careers, Proceedings, 2018, doi:10.1109/EDUNINE.2018.8450948.

[29] C. Siebra, T. B. Gouveia, J. Macedo, F. Q. Da Silva, A. L. Santos, W. Correia, M. Penha, F. Florentin, M. Anjos, "Toward accessibility with usability: Understanding the requirements of impaired uses in the mobile context," in Proceedings of the 11th International Conference on Ubiquitous Information Management and Communication, IMCOM 2017, 2017, doi:10.1145/3022227.3022233.

[30] B. Adipat, D. Zhang, "Interface design for mobile applications," 2005.

[31] M. J. C. Samonte, R. A. Gazmin, J. D. S. Soriano, M. N. O. Valencia, "BridgeApp: An Assistive Mobile Communication Application for the Deaf and Mute," in ICTC 2019 - 10th International Conference on ICT Convergence: ICT Convergence Leading the Autonomous Future, 2019, doi:10.1109/ICTC46691.2019.8939866.

[32] S. Wagner, "Intralingual Speech-to-text conversion in real-time: Challenges and Opportunities," in Challenges of Multidimensional Translation Conference Proceedings, 2005.

[33] S. Rossignol, O. Pietquin, "Single-speaker/multi-speaker co-channel speech classification," in Eleventh Annual Conference of the International Speech Communication Association, 2010.

[34] J. P. Campbell, "Speaker recognition: A tutorial," Proceedings of the IEEE, **85**(9), 1437–1462, 1997.

[35] H. Beigi, "Speaker recognition: Advancements and challenges," New trends and developments in biometrics, 3–29, 2012.

[36] H. E. Secker-Walker, B. Liu, F. V. Weber, "Automatic speaker identification using speech recognition features," 2017, uS Patent 9,558,749.

[37] P. Matejka, O. Glembek, O. Novotny, O. Plchot, F. Grezl, L. Burget, J. H. Cernocky, "Analysis of DNN approaches to speaker identification," in ICASSP, IEEE International Conference on Acoustics, Speech and Signal Processing - Proceedings, 2016, doi:10.1109/ICASSP.2016.7472649.

[38] S. S. Nathan, A. Hussain, N. L. Hashim, "Studies on deaf mobile application: Need for functionalities and requirements," Journal of Telecommunication, Electronic and Computer Engineering, 2016.

[39] S. Hermawati, K. Pieri, "Assistive technologies for severe and profound hearing loss: Beyond hearing aids and implants," Assistive Technology, 2019, doi:10.1080/10400435.2018.1522524.

[40] M. C. Offiah, S. Rosenthal, M. Borschbach, "Assessing the utility of mobile applications with support for or as replacement of hearing aids," in Procedia Computer Science, 2014, doi:10.1016/j.procs.2014.07.079.

[41] M. B. Motlhabi, M. Glaser, M. Parker, W. D. Tucker, "SignSupport: A Limited Communication Domain Mobile Aid for a Deaf patient at the Pharmacy," in Southern African Telecommunication Networks & Applications Conference, 2013.

[42] L. Slyper, M. K. Kim, Y. Ko, I. Sobek, "LifeKey: Emergency communication tool for the deaf," in Conference on Human Factors in Computing Systems - Proceedings, 2016, doi:10.1145/2851581.2890629.

[43] S. SA, "Stats SA profiles persons with disabilities," 2020.

[44] SANDA, "Homepage," 2018.

ASTES

Advances in Science, Technology and Engineering Systems Journal Vol. 5, No. 5, 834-839 (2020)

www.astesj.com

ASTESJ

ISSN: 2415-6698

Providing a Model for Utilizing HRM Tools in Project Management with ISM Technique

Aboozar Zare khafri[*,1], Seyed Mohammad Poorhosseini[2], Amin Zare khafri[3], Seyed Davood Mirtorabi[4]

[1]*Islamic Azad University Najafabad branch, Department of Industrial engineering, Esfahan, Iran*

[2]*Islamic Azad University Tehran Medicine branch, Department of Medical Genetic, Tehran, Iran*

[3]*Researcher of Business Management, Tehran, Iran*

[4]*Legal Medicine Research Center, Tehran, Iran*

ARTICLE INFO

Article history:
Received: 17 March, 2020
Accepted: 28 September, 2020
Online: 12 October, 2020

Keywords:
HRM Tools
ISM

ABSTRACT

An example of the essential factors in ensuring the outcome of project management is the effective use of human resources methods. Researchers' studies have shown that a logical connection exists between "human resource practices" and "project management". The goal of this research was determining a connection between five methods of human resource selection (employee performance appraisal, staff training and development, staff recruitment and selection, employee compensation system and employee welfare) and project management using structural interpretive modeling (ISM) Is. As a result of the present study, it has been observed that hiring and selecting employees and staff welfare are important and influential factors and are at the bottom of the hierarchical structure, these factors are very important for achieving staff training and evolution. Staff capabilities evaluation and their recompense is at a high level of the ISM model, meaning that if shaping methods are performed in project management, it is going to have occurred within the latter a part of the HRM.

1. Introduction

As an idea and content, HRM was suggested in 1980 [1]. The use of resources in any organization is extremely important and effective. Like three constraints (cost, quality, scope), human resources are considered as an example of the essential factors and therefore the most vital factors for any project to be successful. Human resource management includes proper training, hiring experienced workers, acknowledging the importance of the project and using potent methods and strategies to implement the project with the advantage of time and allowance [1]. It is the project manager's duty to successfully and fundamentally do the HRM. Project management involves the utilization of knowledge, expertise, strategies and methods for project activities to satisfy important project needs. This is often done by the utilization and combining the processes of project management to start out, useful preparations, implementation, effective observing, control and closure [2]. Project management and related functions have received more attention in recent years, mainly due to their significance as a reward for administrative actions in contemporary organizations [3]. Because project management is an essential and complicated process that involves the utilization of ideas, the "Project Management Knowledge Set" (PMBOK) is therefore divided to "42 processes" and "5 groups" issued by the Project Management Institute [2]. No wonder that researchers are constantly searching for more links between project management and human resource practices. So far, this research has received the least reward, because, despite extensive research on project success factors [4], the number of successful projects is worryingly inadequate [5]. The main reason for this can be considered the flexibility of the main elements of the success of a project [4]. These factors of project success are often supported the outer or inner situations of related administrations, but a transparent and obvious classification between these factors are often shown in two sorts of project-related success and they are considered as a success both in project and whole HRM project [6] . Project success is

[*]Corresponding author: Aboozar zare khafri, Email: Abozar.zare71@yahoo.com

associated with the effective achievement of the planned goal owing to businesses, so it is associated with the goods or assistance of the organization, while the outcome of the management is associated with the effective achievement of the goals associated with allowance and capital, quality and common processes to control Project [7]. These two important and extensive categorization of project success obviously have one common shared feature, which may be a vital dependence on human resources owing to the previous aspect of success comes from its main power from the latest one [8]. Moreover, because "Employee Recruitment and Selection (ERS), Employee Training and Development (ETD), Employee Performance Assessment (EPA), Employee Compensation System (ECS) [8] and Employee Welfare" are among other important issues. Each of the organization's other employees also communicates with the project manager and the selected team, so the connection between these HR methods and project success (PS) is undeniable. Generally, HRM has an eye-catching effect on project management, managing people and creating value for a project. Today, HRM is part of the company's strategy and considers people as a resource, not a cost. By linking HRM to project management, it can be seen that performance plays a strategically important role. In this article, we discuss the primary significance of HRM in effective project management, so we would like to research how performance and impact of human resource management on project management. By considering this, it is essential to spot ways in which human resource performance can play a strategic role. After identifying these methods, it is necessary to create a model for implementation in any type of project.

2. ISM Process

ISM is an collaborative study method and procedure. During this technique, a group of various elements and factors that are directly and indirectly associated with one another are created in a inclusive and structured efficient model. The model that is formed depicts the form of a drag or complicated problem in an accurate modeled pattern that has diagrams and pictures in addition to words. [9] Interpretive structural modeling (ISM) is a deep-rooted method and approach for recognizing the relationships between particular cases that expresses an issue or a complicated problem. For any complicated problem to be considered, variety of elements could also be associated with an issue or problem. Nevertheless, the direct and indirect relationships between different situational elements are far more accurate than the individual element. ISM begins with identifying factors and variables that are related to the matter or issue, consequently expands to the group analytic method. At that point a textual relationship that is related to the context is defined. After deciding on the set of effective elements and textual relationship, a structural selfinteraction matrix (SSIM) is made supported by the two-by-two analogy of the factors. Next, the SSIM is changed to an accessibility (RM) matrix and its portability is checked. After embedding, a special matrix model is achieved. Then, the elements are split and a new basic model called ISM obtained [9].

3. Steps involved in ISM methodology

Step 1: Structural Self-Interaction Matrix (SSIM)

The ISM process and approach promotes the use of specialist ideas in terms of a variety of effective management methods such as intercommunicating, team design, etc. in building textual relationships between elements. To this end, industry and academics should be conferred to find an essence of an effective textual connection between delegates. The activity and academics should have a deep knowledge of the subject. To analyze the different factors, a "lead" or "impact" textual relationship must be provided. This means that one factor has a significant effect on another. Accordingly, a textual relationships are found between the various identified elements. [9]

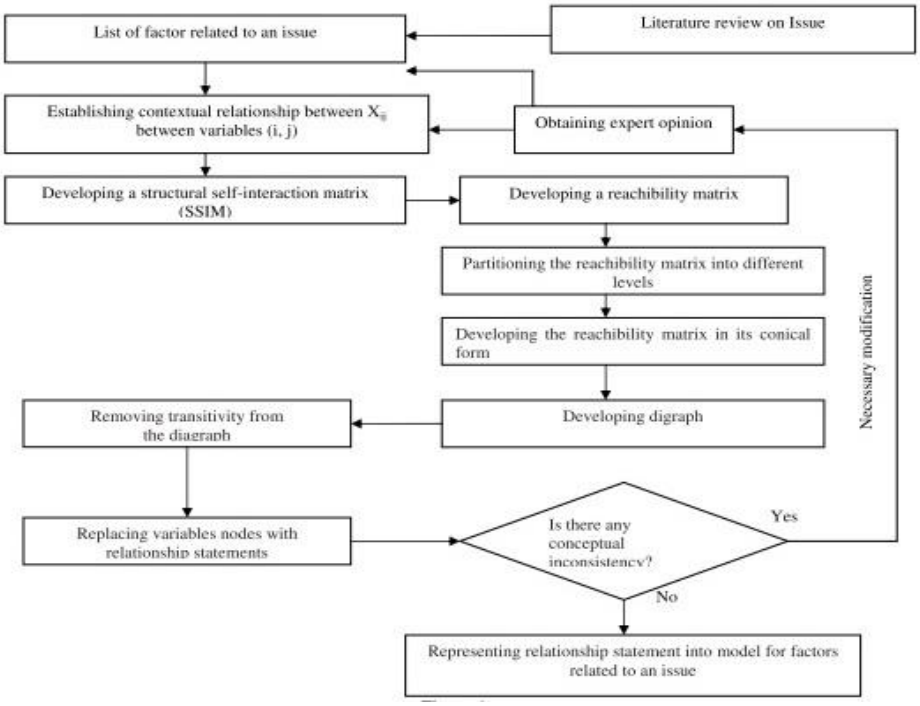


Figure 1: Diagram for developing ISM model [9]

Depending on the proposed textual relationship for each element and the existence of a connection between the two functional elements (i and j), the administration related to the connection goes less than a year. These four distinct symbols are used to indicate the orientation of the connection between two elements (i and j): the connection from element j to element i (ie, element j affects element i) (c) X in both orientations (Elements i and j are independent) (d) O due to the lack of relationship between the elements (i.e. barriers i and j are independent). [9].

Step 2: Discovery of the Matrix

The following important step in the process and method of ISM is to build the first SSIM access matrix. By considering this, SSIM becomes the first access matrix by inserting four different symbols (for example, V, A, X or O) SSIM with 1s or 0s in the first access matrix [9]. The basic practices of this method include: Model 0 input. (B) If the model input (i, j) is in SSIM O, then the input (i, j) in the access matrix is 0 and input (j, i) is 0. (C) If the model input (i, j) is in SSIM A, then the input (i, j) in the access matrix is 0 and input (j, i) is 1. (D) If the model input (i, j) is in SSIM X, the input (i, j) in the access matrix becomes 1 and input (j, i) becomes 1 [9].

Step 3: Level separation

Finally, from the last access matrix, different access sets and priori sets are available for each active item. The access set contains another different agent and element that may have influence on it, while the previous set is another different agent and agent that may have influence on it. After that, the combination of these sets is found in all the elements and factors and the quality of the various elements is checked and investigated. The various elements in which the access set ` level of each element is obtained [9]. This proposed level is very helpful in building the chart and model of ISM.

Step 4: Conical Matrix

In this section, a conical matrix is created by interconnected elements that operate at the same level between different lines and columns of the last access matrix. The driving force of an element obtained through adding its number to the lines and its dependence by adding its number to the columns [9]. Thereafter, the level and level of motivation and confidence is achieved by providing the highest rank in elements with the highest number of rows and columns, respectively.

Step 5: Digraph

At this section, depending on the conical shape of the access matrix, the first diagram containing the transfer links is available. This item is produced with knots and edge lines. Finally, after taking out the indirect links, the final diagram of the model is created. This diagram is used to show the functional elements and their dependence on nodes and edges (this diagram is a perceptible illustration of objects and their interdependence). In this evolution, the top element is at the upper position of the chart and the second element is in the second position, etc. This process continues until the lowest position which is located at the below part of the chart. [9]

4. HRM tools in project management

Employees Recruitment & Selection (ERS)

Experienced and highly capable staff are important resources to promote business increase. On the other hand, low-skilled staff can be very dangerous in business [10]. Reasonable and appropriate selection of employees can guarantee future career success [11]. If the selection process is implemented correctly, the result will be experienced and appropriate employees [12]. The process of staff selection is based on an examination that may determine the quality of the candidate from another is able to anticipate the future effective performance of the candidates. These evaluations are done by observing the values of the inherent characteristics of the candidates and compliance with the criteria set by the company [11].

Employees Training & Development (ETD)

Selected employees are trained to improve the interests of the organization as well as to improve their skills. Whether it is a small-scale firm or an organization or a large-scale firm, they should instruct all their staff to learn new and innovative technologies. Attitudes towards all colleagues change and a very friendly atmosphere is created. If employees are properly trained, their morale will improve compared to their jobs. They will learn new and advanced skills and become more committed to the organization. Investing in this training is appropriate in terms of time as well as additional costs for the firm, but it increases the efficiency of staff, better collaboration among different parts of the firm and thus increases efficiency and overall productivity [13]. This is a good way to transfer information and knowledge to employers. Employers are equipped with the translation of this information and knowledge to increase the efficiency and productivity of the organization and the high quality of management. This should be considered in conjunction with policies and training systems that are critical to human resource development.

Employees Performance Appraisals (EPA)

Employees Performance Appraisals (EPA) is important to organizations towards determining successes or failures as well as boosting employees' performance. This is because enhancing employee performance is the fundamental aim of any appraisal policy in organization. Thus, the EPA as an essential human resource management (HRM) practice in the 21st century is important because will assist organizations in achieving effectiveness and competitiveness. Employee participation may lead EPA.

Employees Compensation System (ECS)

Compensation is the reward received by employees in exchange for their share in the organization.

Effective compensation management is critical to balancing employee and employee relations by providing financial and non-financial compensation to employees. Compensation consists of all payment methods for employees resulting from work. The appropriate compensation strategy motivates employees to put effort in the job and keep on working with greater resolution. It is a supportive factor for organizations to effectively set appropriate, practical and appreciable performance qualities. Compensation strategies must be in line with human resource practices.

Welfare of Staff (SW)

Singh (2009) has shown that the standard of a career life often is conditional on the standard of living of the worker that the manager provides to meet the needs of employees. It is clear that the well-being of workers helps to improve the business environment and encourages employees, which ultimately leads to the superlative performance in corporate output [14]. Appropriate instruction, without-charge medical care, sports sites, public clubs, restaurants, staff management and operations, hospital club recruitment and savings programs, offer individualized matters just like personal counseling and salary adjustments, pension fund and leave employees, loans especially in difficult situations, assistance transferred staff and most importantly help in the field sector that makes employees feel comfortable in the organization [14]. One of the key factors that leads to employee insecurity and hindering the final performance of employees is the delay in payment of workers' salaries. Welfare is defined in different ways and there is no single definition that can be used globally. The Oxford Dictionary defines the term welfare as "the pursuit of a worthwhile life for the worker."

Identify the main sources of risk in the virtual organization (VO)

Many researchers and scholars who have studied in this field have claimed to have identified the places created in the virtual organization. Extensive and comprehensive study of the literature has recognized 13 risk origins and barriers in terms of time of delivery, price and standard and in cases where partnerships are completely eliminated they can be significant and potentially insurmountable causes. This has been a major threat to the visible organization. The level of trust that exists between partners is closely related to the level that partners believe in the honesty, giving, and worthiness of others. Problems arise when there is no trust between the partners of the organization. For example, they have no desire to pass on sensitive information and it is difficult to agree on how they should manage their finances. In short, they are not trying to increase efficiency and improve corporate governance. Trust and commitment are essential to effective co-operation over a period of time and a willingness to share risks. The greater the level of trust among the partners of the organization, the greater the commitment of employees [15]. Without a close and direct relationship between distance and risk, the risk can increase due to the existing environment and some areas create many problems, for example political and legal problems [16].

5. Identification of The Drivers

The key drivers in human resource management are identified through a text review by a team of specialists.

Table 1, presents the integration results of the questionnaires. The maximum and minimum values as a result of the integration were 9 and 4, respectively. In Table 1, level 8 is repeated more than the other levels and indicates the level of confidence. Therefore, in this research, the mentioned value has been selected as a range for the desired position (significance level).

Table 1: Integration Results of the questionnaires

S.No	ERS	ETD	SW	EPA	ECS	VO
ERS		9		8	8	6
ETD	5		6	9	8	7
SW	7	9		8	8	8
EPA	5	9	4		8	6
ECS	8	9	4	5	6	7
VO	4	7	8	5	8	

Table 2, shows the initial accessibility matrix. In this table, based on the significance range (this range is level 8) for the larger values, the number 1 and the smaller values are assigned the number 0. Also, the value of 0 is considered to be equal to 8. One of the advantages of a significant level is the ease of understanding the subject. By studying the results for the initial Reachability, it is observed that as a result of integrating the questionnaires and defining the level of significance, the number of cases marked with 0 is twice as many as the cases marked with 1.

Table 2: Primary Reachability Matrix (SSIM)

S.No	ERS	ETD	SW	EPA	ECS	VO
ERS	1	1	0	0	0	0
ETD	0	1	0	1	0	0
SW	0	1	1	0	0	1
EPA	0	0	0	1	0	0
ECS	0	1	0	0	1	0
VO	0	0	1	0	1	1

By studying the results of this research in Table 3, the last reachability matrix is submitted. This table shows the drawing power values for five selected HR practices. This value is 2 for all selected HR practices. Also, in the dependency row of this table, it is observed that the highest value is related to staff training and development. Other considerations, including employee performance appraisal and employee compensation, fall into the following categories, respectively.

Table 3: The latest reachability matrix

S.No	ERS	ETD	SW	EPA	ECS	VO	Driving power	Row
ERS	1	1	0	0	0	0	2	1
ETD	0	1	0	1	0	0	2	2
SW	0	1	1	0	0	1	2	3
EPA	0	0	0	1	0	0	2	4
ECS	0	1	0	0	1	0	2	5
VO	1	4	1	2	2	1	2	6
Dependence power	1	4	1	2	2	2		

In accordance with the results of previous researchers in this study, reachability set, intersection set and antecedent set values were selected as criteria for evaluating the five methods of human resource selection. Higher values of reachability set indicate the efficiency of the proposed method. According to table 4, it can be seen that Employee Performance Appraisals and Employee Compensation are at a high level of the ISM model. Also, Recruitment & Selection and Staff Welfare are important factors and placed at the bottom of the hierarchical structure.

Table 4: Level Partitions of Drivers Iteration I

HRM Tools	Rechability Set	Antecedent Set	Intersection Set	Level
ERS	1,2	1	1	
VO	3,4	1,2,5	2	
ETD	2,4	1,2,3,5	3	
SW	2,3	3	4	
EPA	4	2,4	5	1
ECS	5	4,5	6	1

In Table 5, in the iteration II, the levels were examined for the desired methods. The results showed that level 2 is assigned by Employees Training & Development. Also, intersection set was obtained for Recruitment & Selection and Employees Training & Development 1 and 2, respectively.

According to Table 5, it is observed that in the iteration III, the Recruitment & Selection and Staff Welfare methods with a level of 3 are important factors and placed at the bottom of the hierarchical structure. Also, the speed antecedent set for Recruitment & Selection and Staff Welfare are obtained as 1 and 2, respectively.

Table 5: Level Partitions of Drivers Iteration II

HRM Tools	Rechability Set	Antecedent Set	Intersection Set	Level
ERS	1,2	1	1	
VO	3	1,2	2	2
ETD	2	1,2,3	3	2
SW	2,3	–	–	

Table 6: Level Partitions of Drivers Iteration III

HRM Tools	Rechability Set	Antecedent Set	Intersection Set	Level
ERS	1	1	1	3
SW	2	2	2	3

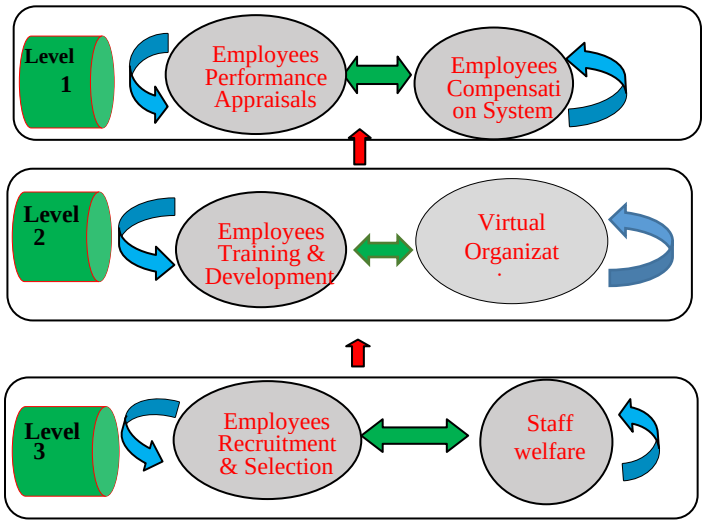


Figure 2: Diagram for developing ISM model

6. Conclusion

This study was conducted to evaluate the significance of selected human resource methods for project success in project-based organizations. The proposed model is very useful and important for understanding the interactions between HRM tools in project

management. In this model, drivers are divided into different levels so that decision makers are aware of the importance of different types of drivers and their implementation methods. A total of 5 types of drivers have been pointed out and an ISM model has been developed.

The model shown in Figure 2 shows that hiring and selection of employees and employee wellbeing are influential factors that are at the bottom of the hierarchical structure and these factors are important for improving staff training and development. The considerations include evaluating employee performance and compensating employees at a high level of the ISM model, meaning that if shaping methods are done in the project, it can happen in the last part of the HRM. In addition, the interaction between management drivers is expected to guide the understanding of the complex situation and create an executive plan.

References

[1] C. Gill, "Dont know, dont care: An exploration of evidence based knowledge and practice in human resource management. Human Resource Management Review, **28**(2), 103– 115, 2018. doi: 10.1016/j.hrmr.2017.06.00

[2] PMI "A Guide to the Project Management Body of Knowledge (PMBOK Guide), (4th Ed.), PMI, Pennsylvania, 2004.

[3] M.A. Kaulio, "Project leadership in multi-project settings: findings from a critical incident study. Int. J. Proj. Manag. **26** (4), 338–347, 2008. https://doi.org/10.1016/j.ijproman.2007.06.005

[4] K. Judgev, "A retrospective look at our evolving understanding of project success. Proj. Manag. J. **36** (4), 19–31, 2005. https://doi.org/10.1177%2F875697280503600403

[5] B. Flyvbjerg, Garbuio, M., Lovallo, D., "Delusion and deception in large infrastructure projects: two models for explaining and preventing executive disaster. Calif. Manag. Rev. **51** (2), 170–193, 2009.

[6] T. Cooke-Davies, "The "real" success factors on projects. Int. J. Proj. Manag. **20** (3), 185–190, 2002.

[7] Müller, R., Turner, R., 2010. Leadership competency profiles of successful project managers. Int. J. Proj. Manag. **28** (5), 437–448.

[8] A.S. Khan, "Human resource management practices and project success, a moderating role of Islamic Work Ethics in Pakistani project-based organizations, International Journal of Project Management, **20** (3), 185–190, 2014.

[9] R. Attri1, N. Dev1 and V. Sharma, "Interpretive Structural Modelling (ISM) approach: An Overview, Research Journal of Management Sciences, ISSN 2319–1171, **8**(5), 2013.

[10] R. M. Guion, S. Highhouse and D. Doverspike, Essentials of Personel Assesment and Selection, New York: Routledge, 3-15, 2016.

[11] C. F. Chien and L. F. Chen, Data mining to improve personnel selection and enhance human capital: A case study in high-technology industry., Expert Systems with Applications, **34**(1), 280-290, 2008. https://doi.org/10.1016/j.eswa.2006.09.003

[12] S. Vasanthi, S. Rabiyathul "Designing Implementing and Evaluating Employee Training Programs, International Journal of Recent Technology and Engineering (IJRTE), **8**(3), 2019

[13] N.M. Musalli et al., "The Relationship Between Staff Development, Organizational Policy, Staff Welfare to Personnel Performance, Mediterranean Journal of Social Sciences, **6**(4), 2015. Doi: http://dx.doi.org/10.5901/mjss.2015.v6n4p288

[14] J.J. Mistry, "Origins of profitability through JIT processes in the supply chain, Industrial Management & Data Systems, **105**(3), 2005.

[15] T. DEWITT, L.C. GIUNIPERO, "Clusters and supply chain management: the Amish experience, International Journal of Physical Distribution & Logistics Management, **36**(5), 2006.

ASTES

Advances in Science, Technology and Engineering Systems Journal Vol. 5, No. 5, 840-846 (2020)

www.astesj.com

ASTESJ

ISSN: 2415-6698

The Curriculum Developer Team Assignment Analysis Using Ones Assignment Method

Elis Ratna Wulan[1,*], Dindin Jamaluddin[2], Iwan Setiawan[3], Chaerul Saleh[4], Dudy Imanuddin Effendi[5]

[1]*Mathematics Department, Science and Technology Faculty, UIN Sunan Gunung Djati Bandung, 40115, Indonesia*

[2]*Islamic Education Department, Tarbiyah and Education Faculty, UIN Sunan Gunung Djati Bandung, 40115, Indonesia*

[3]*Syariah Accounting Department, Islamic Economics and Business Faculty, UIN Sunan Gunung Djati Bandung, 40115, Indonesia*

[4]*Constitutional Law Department, Syariah and Law Faculty, UIN Sunan Gunung Djati Bandung, 40115, Indonesia*

[5]*Islamic Counseling Guidance Department, Da'wah and Communication Faculty, UIN Sunan Gunung Djati Bandung, 40115, Indonesia*

ARTICLE INFO

Article history:
Received: 02 June, 2020
Accepted: 29 September, 2020
Online: 12 October, 2020

Keywords:
Assignment Problem
Curriculum Development
Linear Integer Programming
Ones Assignment Method
Optimal Solution

ABSTRACT

This examination plans to investigate the task issue in the educational program designer group utilizing the Ones Assignment Method. The calculation of this technique as follows. At first characterized the task grid, at that point by utilizing determinant portrayal acquired a diminished framework which has in any event one in each line and segments. At long last, it acquired an ideal answer for task issues by allocating ones to each line and every segment. This strategy depends on making somewhere in the range of ones in the task network and afterward attempt to locate a total task. The huge favorable position of this technique is a methodical system, simple to apply, and can be used for a wide range of task issues with amplify or limit target capacities. The contextual analysis of this exploration is a counseling organization creating science educational program with 5 specialists and 5 phases of educational program arranging and improvement process. The exploration bring about case minimization time of 48 days.

1. Introduction

The significant factor in the investigation of the profitability of a creation framework is the human viewpoint. The practicality of some laborers and their abilities cause the sketchy executing time and cost for the creation attempts [1]. In genuine cases, the effectiveness of the laborers shifts from an assignment to another, with the goal that the best specialist for an undertaking isn't really the best for another errand. Subsequently, appointing the best specialist to each assignment can altogether improve the profitability of the framework [2].

The task issue is the particular type of transportation issue. This is especially significant in the hypothesis of dynamic. The soonest utilization of a direct whole number programming issue is the task issue [1]. Other techniques have been introduced for task issues and different articles have been distributed regarding the matter [3]. See [4], [5], and Taha [6] for the historical backdrop of these strategies [7].

An imperative number of systems has been so far introduced for task issue in which the Hungarian approach is dynamically valuable technique among them [8]. This iterative technique depends on add or take away a steady to each component of a line or section of the cost network, in a minimization demonstrate and make somewhere in the range of zeros in the given cost framework and afterward attempt to locate a total task as far as zeros. By a total task for a cost framework $n \times n$, we mean a task plan containing precisely n doled out autonomous zeros, one in each line and one in every section. The key idea of the task issue is to locate the ideal designation of certain assets to an equivalent number of interest focuses. A task plan is ideal if enhances the absolute expense or expenditure of doing all the occupations [7].

Indeed, [13] demonstrated that the summed up task issue is a NP-complete combinatorial advancement and the current accurate techniques are viable just for specific occurrences where there are no extra limitations. In examination with this exploration, the

*Corresponding Author: Elis Ratna Wulan, elis_ratna_wulan@uinsgd.ac.id

commitment of the introduced research is to propose a strategy for taking care of task issues which is different from the past strategies.

2. Methodology

The task issues are one specific instance of direct programming issues by and large. In business and industry, the board frequently faces issues identified with the ideal task of different profitable sources or diverse proficiency level faculty for various assignments. The Hungarian Method is one of a couple of available dealing with systems for task issues. This strategy was initially developed by an acclaimed mathematician from Hungarian known as D. Konig in 1916 [14].

The utilization of the Hungarian strategy, the quantity of sources allocated must match precisely the quantity of undertakings to be finished. Moreover, every source have to relegated distinctly for one assignment. Along these lines, the task issue will incorporate some *n* sources that have n assignments. There is *n!* potential tasks in an issue because of coordinated blending. This issue can be clarified effectively by the rectangular network structure, in which the lines demonstrate the sources and segments indicating the undertaking or reason [14].

In the transportation model, the creators decide the x_{ij} dissemination which will limit the all-out expense of transport and meet the limit of the source (s_i) just as the goal demand (t_j). The task model might be thought of as an uncommon type of the transportation model. In this model, the *i*th asset or *j*th goal is one by the essential idea, so the ideal estimation of the x_{ij} choice variable must be just zero or one [15].

The overall type of the numerical transportation model condition, as follows:

$$\text{Min}= \sum_{i=1}^{n} \sum_{j=1}^{n} c_{ij}x_{ij} \quad (1)$$

Subject to:

$$\sum_{i=1}^{n} x_{ij} = s_i, \text{ for } i = 1,2, ..., m$$

$$\sum_{j=1}^{n} x_{ij} = t_j, \text{ for } j = 1,2, ..., n$$

where $x_{ij} \geq 0$.

The model is disentangled in the task model with the goal that the s_i value is one so does t_j for the ideal estimation of the x_{ij} choice variable, it must be zero or one. Along these lines, the overall type of the efficient model of task as follows:

$$\text{Min} \sum_{i=1}^{m} \sum_{j=1}^{n} c_{ij}x_{ij} \quad (2)$$

Subject to:

$$\sum_{j=1}^{n} x_{ij} = 1, \text{ for i = 1, 2,.....,m}$$

$$\sum_{j=1}^{m} x_{ij} = 1, \text{ for j = 1, 2,....,n}$$

For details in the assignment matrix displyed in Table 1.

where x_{ij} = 0 or 1, and

x_{ij}= the assignment from *i*th master to *j*th phase

c_{ij}= the cost unit from *i*th master to *j*th phase

Table 1: The Initial Assignment Matrix Form

Master	Phase				Master Capacity per period
	t_1	t_2	⋯	t_n	
s_1	c_{11} x_{11}	c_{12} x_{12}	⋯	c_{1n} x_{1n}	1
s_2	c_{21} x_{21}	c_{22} x_{22}	⋯	c_{2n} x_{2n}	1
⋮	⋮	⋮	⋮	⋮	⋮
s_m	c_{m1} x_{m1}	c_{m2} x_{m2}	⋯	c_{mn} x_{mn}	1
Phase Demand per period	t_1	t_2	⋯	t_{jn}	$\sum s_i$ $\sum t_j$

The educational plan as per Lewis and Miel in [16] is a lot of objectives about individuals' chances to be taught by others and with all the fixings (all transporters of data, procedures, methods, and qualities) in a specific reality setting. Anderson and Bowman, referred to by Akangbou, characterize arranging as a procedure of setting up a lot of choices for future activity. Along these lines, educational plan arranging is worried about setting up a progression of choices about the subject and topic that the educator will show future students [16]. For this situation, the educational program plan must experience certain stages. As per Lewy referred to in [16] is preparation obviously schedule that basically portrays the topic; production of showing materials; and implementation of the educational program in the framework.

There are five phases of activities engaged with the educational program arranging and improvement process, in particular objective setting, specialized activity (Technology), application stage, usage, and assessment [17].

(1) Objective Determination

This capacity includes the assurance of general instructive objectives and particulars of the fundamental goals. The universally useful of instruction is political intrigue. Shared objectives are normally communicated in expansive terms with the goal that the objective gets the accord of most social orders. The broadly useful fills in as a reason for dynamic on school daily ought to be composed and what ought to be educated in school, however in itself it doesn't establish or legitimately decide the useful subtleties of school life [17]. Choices on educational program targets are impacted by three fundamental elements, incorporate students, society, and topic (disciplines) [16,18].

(2) Technology (Selecting and organizing learning experience)

When overall instruction objective has been resolved, proficient organizers start to make an interpretation of it into explicit educational plan exercises. Choices are made on the

targets of explicit subjects, content, instructing learning, educational program groups will build up the primary rendition of learning content that will be utilized in the homeroom. At this stage incorporate composing writings, getting ready practicum materials, understudy courses of action, movement plans, etc [19].

(3) Application

The application stage alludes to preliminaries and modifications in which instructive projects will be tried exactly before they are affirmed for huge scope use. As a rule, little consideration is paid to joining or enhancing proficient intelligence with exact proof. For preliminary work of materials [17]. Numerous educational plans have fizzled in the past because of an absence of educational program testing before usage. A significant number of them are affirmed dependent on emotional decisions of instructive specialists [19].

(4) Implementation

Execution alludes to the open utilization of the educational plan all through the educational system. This will require a few changes in the training framework. A portion of the exercises are the arrangement of instructing and learning and in-administration preparing for school chiefs, instructors, and school administrators [17, 16].

(5) Evaluation

The procedure of assessment as per Tyler, is the way toward deciding the degree to which the reason for instruction is being acknowledged by educational program and instructing programs. At the end of the day, the mission statement isn't just the premise of choice and sorting out the learning experience however the norm on which the program is based. In this way, Tyler expresses that assessment is a procedure where one's desires coordinate the underlying desires as social goals with results. Such educational plan arranging ideas have a characteristic and exceptionally regular intrigue, particularly when advanced with models of modern and framework the executives, apparently a savvy and down to earth approach to survey the achievement of a business as per Tyler in [18].

3. Results and Discussion

The Ones Assignment Method depends on making somewhere in the range of ones in the task network and afterward attempt to locate a total task regarding ones. A task plan containing precisely m appointed free ones, one in each line and one in every segment [7]. The Matrix Ones Assignment decide punishments, partition least or most extreme point in each line and section [8].

This method utilizes one of the determinant properties of $n \times n$ lattice to get the ideal arrangement of the task issue. The ideal arrangement of the task issue in condition (2) doesn't change if the line or section of the cost network is partitioned or increased by a steady. This can be demonstrated as follows:

If every cell form *i*th row and *j*th column divided by p_i and q_j, the new cost element be $c'_{ij} = c_{ij} \times \frac{1}{a_i} \times \frac{1}{b_j}$. Thus, we obtain the new objective function.

$$Z' = \sum_{i=1}^{n}\sum_{j=1}^{n} c'_{ij}x_{ij}$$

$$\sum_{i=1}^{n}\sum_{j=1}^{n}\left(c_{ij} \times \frac{1}{p_i} \times \frac{1}{q_j}\right)x_{ij} \qquad (4)$$

$$Z' = \sum_{i=1}^{n}\sum_{j=1}^{n} c_{ij}x_{ij} \times \frac{1}{p_i q_j}$$

where:

c'_{ij} = the new cost element

x_{ij}= the assignment from *i*th master to *j*th phase

c_{ij}= the cost or time unit from *i*th master to *j*th phase

p_i = *i*th master capacity

q_j = *j*th capacity demand

with $a_i \neq 0 \; \forall_i \; dan \; b_j \neq 0 \; \forall_j$. Thus, obtain

$Z' = Z \times constant.$

This shows the minimization of the target work produces a similar arrangement by limiting Z'. For additional subtleties introduced by the lattice in Table 2 [2].

Table 2: The Cost Matrix Form

Master	**Phase**				
	1	**2**	**3**	⋯	**N**
1	c_{11}	c_{12}	c_{13}	⋯	c_{1n}
2	c_{21}	c_{22}	c_{23}	⋯	c_{2n}
⋮	⋮	⋮	⋱	⋮	⋮
N	c_{n1}	c_{n2}	c_{n3}	⋯	c_{nn}

The algorithm are as follows [7]:

Step 1.

In a minimization (expansion) case, locate the base (greatest) component of each line in the task lattice (state α_i) and compose it on the right-hand side of the network. For additional subtleties, introduced in Table 3.

Table 3: Minimum (Maximum) Cost Of Each Row

Master	**Phase**					***Min***
	1	**2**	**3**	⋯	***N***	
1	c_{11}	c_{12}	c_{13}	⋯	c_{1n}	α_1
2	c_{21}	c_{22}	c_{23}	⋯	c_{2n}	α_2

⋮	⋮	⋮	⋱	⋮	⋮	⋮
N	c_{n1}	c_{n2}	c_{n3}	⋯	c_{nn}	α_n

At that point separate every component of the *i*th line of the network by α_i. These activities make in any event one in each column. For additional subtleties, introduced in Table 4

Table 4: The Divide by Maximum (Minimum) Cell in Row

Master	**Phase**				
	1	**2**	**3**	⋯	***N***
1	c_{11}/α_1	n_{12}/α_1	c_{13}/α_1	⋯	c_{1n}/α_1
2	c_{21}/α_2	n_{22}/α_2	c_{23}/α_2	⋯	c_{2n}/α_2
⋮	⋮	⋮	⋱	⋮	⋮
N	c_{n1}/α_n	n_{n2}/α_n	c_{n3}/α_n	⋯	c_{nn}/α_n
	β_1	β_2	β_3	⋯	β_n

As far as ones for every line and section do task, in any case go to stage 2.

Step 2.

Locate the base (most extreme) component of every section in the task network (say β_j), and compose it underneath *j*th segment. At that point separate every component of *j*th segment of the framework by β_j.

These tasks make at any rate one in every section. Make task as far as ones. On the off chance that no attainable task can be accomplished from step (1) and (2) at that point go to stage 3.

Step 3.

Draw the base number of lines to cover all the value of ones of the grid. On the off chance that the quantity of drawn lines not as much as *n*, at that point the total task is unimaginable, while in the event that the quantity of lines is actually equivalent to *n*, at that point the total task is gotten.

Step 4.

On the off chance that a total task program is unimaginable in sync 3, at that point select the littlest (biggest) component (state *dij*) out of those which don't lie on any of the lines in the above lattice. At that point isolate by *dij* every component of the revealed lines or segments, which *dij* lies on it. This activity makes some new ones to this line or segment.

On the off chance that still a total ideal task isn't accomplished in this new lattice, at that point use stage 4 and 3 iteratively. By rehashing a similar methodology the ideal task will be gotten. At the point when the ideal task has been accomplishing either step (3) or step (4) at that point utilize the need rule, which is to choose the littlest expense in arrangement for the minimization issue and the best benefit for the augmentation issue of all lattice components put away to one side of the network in sync (1), that is α_i.

In this research, the authors explore the new application of the ones assignment algorithm in the field of higher education services, in order to gain optimal time results in solving the curriculum development.

4. Illustrative Example

Think about the accompanying task issue. Allocate the five occupations to the three machines to limit the all out expense. The information is then reproduced for issues in an educational program advancement advisor organization with 5 specialists and 5 phases of educational program arranging and improvement process. More explanation is introduced in Table 5.

Table 5: The Solution Time of Curriculum Planning and Development

Master	**Phase**				
	G	**T**	**A**	**I**	**E**
ERS	24	16	14	30	8
DJ	14	18	2	28	20
IS	18	12	24	12	14
CS	14	12	28	12	20
DIE	18	12	24	20	12

Phase: G (Goal Determination stage), T (Technology stage), A (Application stage), I (Implementation stage), and E (Evaluation stage)

Step 1.

Locate the base component of each column in the task lattice (state α_i) and compose it on the right-hand side of the network, as follows:

Table 6: The Minimum Time on Every Row

Master	**Phase**				
	G	**T**	**A**	**I**	**E**
ERS	24	16	14	30	8
DJ	14	18	2	28	20
IS	18	12	24	12	14
CS	14	12	28	12	20
DIE	18	12	24	20	12

At that point separate every component of the *i*th line of the lattice by α_i. These activities make ones for each column, and the lattice diminishes to the accompanying framework.

Table 7: The Divide by The Minimum Time In Every Row

Master	**Phase**				
	G	**T**	**A**	**I**	**E**

ERS	24/8	16/8	14/8	30/8	8/8
DJ	14/2	18/2	2/2	28/2	20/2
IS	18/12	12/12	24/12	12/12	14/12
CS	14/12	12/12	28/12	12/12	20/12
DIE	18/12	12/12	24/12	20/12	12/12

The operation result displayed in Table 8.

Table 8: The Solution Of Divide By The Minimum Time In Every Row

Master	Phase				
	G	T	A	I	E
ERS	3	2	14/8	30/8	1
DJ	7	9	1	14	10
IS	18/12	1	2	1	14/12
CS	14/12	1	28/12	1	20/12
DIE	18/12	1	2	20/12	1

Step 2.

Presently locate the base component of every section in the task lattice (state β_j), and compose it beneath that segment. The operation result is displayed in Table 9.

Table 9: The Minimum Time in Every Column

Master	Phase				
	G	T	A	I	E
ERS	3	2	14/8	30/8	1
DJ	7	9	1	14	10
IS	18/12	1	2	1	14/12
CS	14/12	1	28/12	1	20/12
DIE	18/12	1	2	20/12	1

At that point partition every component of the *j*th segment of the framework by β_j as follows:

Table 10: The Divide By The Minimum Time In Every Column

Master	Phase				
	G	T	A	I	E
ERS	$\frac{3}{14/12}$	2/1	14/8	$\frac{30/8}{1}$	1/1
DJ	$\frac{7}{14/12}$	9/1	1/1	14/1	10/1
IS	$\frac{18/12}{14/12}$	1/1	2/1	1/1	$\frac{14/12}{1}$
CS	$\frac{14/12}{14/12}$	1/1	$\frac{28/12}{1}$	1/1	$\frac{20/12}{1}$
DIE	$\frac{18/12}{14/12}$	1/1	2	$\frac{20/12}{1}$	1/1

The solution represented in Table 11.

Table 11: The Solution Of Divide By The Minimum Time In Every Column

Master	Phase				
	G	T	A	I	E
ERS	36/14	2	14/18	30/8	1
DJ	6	9	1	14	10
IS	18/14	1	2	1	14/12
CS	1	1	28/12	1	20/12
DIE	18/14	1	2	20/12	1

Thus, we obtain the new objective function as stated in the Equation (4).

Step 3.

Draw a line that passes all the bits 1 to the cross portion. The base number of lines needed to experience all the ones of the network is 5. For more detail presented in Table 12.

Table 12: Lines That Cover All 1 Values in Cell

Master	Phase				
	G	T	A	I	E
ERS	36/14	2	14/18	30/8	1
~~**DJ**~~	~~6~~	~~9~~	~~1~~	~~14~~	~~10~~
IS	18/14	1	2	1	14/12
CS	1	1	28/12	1	20/12
~~**DIE**~~	~~18/14~~	~~1~~	~~2~~	~~20/12~~	~~1~~

The task can be finished in light of the fact that the quantity of lines approaches *n* (request framework). Select the littlest worth speaking to just one line and one segment utilizing the need rules from Table 13.

Table 13: The Minimum Time in Row and Column

Master	Phase				
	G	T	A	I	E
ERS	36/14	2	14/18	30/8	**1**

DJ	6	9	**1**	14	10
IS	18/14	**1**	2	**1**	14/12
CS	**1**	**1**	28/12	**1**	20/12
DIE	18/14	**1**	2	20/12	**1**

Select beginning from the littlest incentive in each line or segment that is Row 2 with esteem 2 in segment 3, line 1 with esteem 8 in section 5, line 3 with esteem 12 in segment 4 (Value 12 on line 3 is double, that is in segment 2 and segment 4, the chose estimation of 12 in segment 4 of the explanation in segment 2 will be spoken to by the worth 12 in line 5), line 5 with esteem 12 in segment 2 (Value 12 in line 5 is double, that is in segment 2 and segment 5, the chose esteem 12 in segment 2 of the explanation in segment 5 has been spoken to by the worth 8 in line 1), and the last line 4 with esteem 14 in segment 1 (The littlest worth in line 4 is the worth 12 in segment 2 and 4. Notwithstanding, segment 2 has been spoken to by an estimation of 12 in line 5 and section 4 has been spoken to by an estimation of 12 in line 3 with the goal that it is chosen to speak to push 4 that is esteem 14 in segment 1). The outcomes are introduced in Table 14.

Table 14: The Final Assignment Result

Master	**Phase**				
	G	**T**	**A**	**I**	**E**
ERS	24	16	14	30	8
DJ	14	18	2	28	20
IS	18	12	24	12	14
CS	14	12	28	12	20
DIE	18	12	24	20	12

: The minimum time for one expert to one operation process

The results in details are as follows:

Table 15: The Time Minimum Result

Master	**Phase**	**Duration (days)**
ERS	Application stage	8
DJ	Evaluation stage	2
IS	Implementation stage	12
CS	The technological stage	14
DIE	The goal-setting stage	12

In this manner, the base chance to embrace educational program arranging and advancement in a science educational plan improvement counseling firm is

$$Z' = \sum_{i=1}^{n}\sum_{j=1}^{n} c'_{ij}x_{ij}$$

$$= \sum_{i=1}^{5}\sum_{j=1}^{5} c'_{ij}x_{ij}$$

$$= c'_{15}x_{15} + c'_{23}x_{23} + c'_{34}x_{34} + c'_{41}x_{41} + c'_{52}x_{52}$$

$$= 8\ (1) + 2\ (1) + 12\ (1) + 14\ (1) + 12\ (1) = 48 \text{ days.}$$

5. Conclusions

In this paper, another and basic technique was presented for taking care of task issues. The new strategy depends on making some ones in the task grid, and discover a task as far as the ones. The need assumes a significant job in this strategy. To improve a task issue, indicate the one in the column that has the biggest component for the amplification issue and the littlest component for the minimization issue on the correct side. After applying this method to the problem of curriculum development, the research results obtained the minimum time to complete curriculum development stages is 48 days. As respects the explaining technique proposed for the task issue in the writing, creating amplify target capacity could be a smart thought for future investigates.

Conflict of Interest

The authors declare no conflict of interest.

Acknowledgment

The authors expressed gratitude to the UIN Sunan Gunung Djati Bandung Rector and his staff for their support to this research.

References

[1] E. R. Wulan et al, "Determine the Optimal Solution for Linear Programming with Interval Coefficients", in 2018 IOP Conf. Ser.: Mater. Sci. Eng. **288** 012061, 2018. https://doi.org/10.1088/1757-899X/288/1/012061

[2] L.E. Idris, and Sukamto, "Modifikasi Metode Hungarian Untuk Menyelesaikan Masalah Penugasan", 2013. available at: http://repository.unri.ac.id [accessed December 5, 2017]

[3] E. R. Wulan, D. Jamaluddin, A. H. Hermawan and T. Ratnasih, "The Application of Assignment Problem Optimal Solution Using Ones Assignment Method in The Curriculum Developer Team," 2019 IEEE 5th International Conference on Wireless and Telematics (ICWT), Yogyakarta, Indonesia, 1-6, 2019. doi: 10.1109/ICWT47785.2019.8978255

[4] M.S. Bazarra, J.J. Jarvis, and Sherali, H.D." Linear programming and network flows", 2005

[5] B.S. Goel, "Operations Research", Fifth Ed., 2405-2416, 1982.

[6] H.A. Taha, "Operations Research, an introduction", 8th Ed, 2007.

[7] H. Basirzadeh, "Ones Assignment Method for Solving Assignment Problems", Applied Mathematical Sciences, **6**(47), 2345 – 2355, 2012.

[8] E.R. Wulan et al, "The comparative analysis of Hungarian assessment, matrix ones assignment and alternate mansi method in solving assignment problem", in J. Phys.: Conf. Ser. **1402** 077090, 2019. https://doi.org/10.1088/1742-6596/1402/7/077090

[9] G.T. Ross, R. M. Soland, "A Branch and Bound Algorithm for the Generalized Assignment Problem." Mathematical programming, **8** (1): 91–103, 1975.

[10] D. Klingman, J. Stutz, "Computational Testing on an Integer Generalized Network Code." 45th Joint National Meeting of the Operations Research Society and the Institute of Management Sciences, Boston, MA, April 1974.

[11] D. Maio, A., and C. Roveda, "An All Zero-one Algorithm for a Certain Class of Transportation Problems." Operations Research, **19** (6): 1406–1418, 1971.

[12] S.E. Moussavi, M. Mahdjoub, O. Grunder, "Productivity improvement through a sequencing generalised assignment in an assembly line system", International Journal of Production Research, **55**(24), 7509-7523, 2017. DOI: 10.1080/00207543.2017.1378828

[13] P.C. Chu, J.E. Beasley, "A Genetic Algorithm for the Generalised Assignment Problem." Computers & Operations Research, **24** (1): 17–23, 1997.

[14] P. Subagyo, “Dasar-dasar Operations Research”. Yogyakarta: BPFE, 1983.
[15] Siswanto, “Operations Research”,Yogyakarta: Erlangga, 2007.
[16] S.D. Akangbou, "Planning the junior secondary school curriculum". In Pai Obanya (edited). Curriculum In Theory and practice. Ibadan: Educational Research and study group, 1984.
[17] R.S. Longe, “Planning for a Responsive curriculum”. In Pai Obanya edited. Curriculum, in theory and in practice Ibadan: Educational Research and study group, 1984.
[18] G.A. Badmus, “Curriculum development and changes in mathematics education in Nigeria”. A paper presented during the mathematics education Summit at National Mathematical Centre, Abuja, February, 2012.
[19] A.B. Festus, K.M. Seraphina, “Curriculum Planning and Development in Mathematics from the Formative Stages”, Journal of Education and Practice, ISSN 2222-1735 (Paper) ISSN 2222-288X (Online), **6**(2), 62 -66., 2015.

ASTES

Advances in Science, Technology and Engineering Systems Journal Vol. 5, No. 5, 847-851 (2020)

www.astesj.com

ASTESJ

ISSN: 2415-6698

The Effect of User Experience from Teksologi

Yanfi Yanfi*, Yogi Udjaja, Adrian Victor Juandi

Computer Science Department, School of Computer Science, Bina Nusantara University, Jakarta, Indonesia 11480

ARTICLE INFO

Article history:
Received: 07 June, 2020
Accepted: 19 September, 2020
Online: 12 October, 2020

Keywords:
Teksologi
User Experience
Gamification
Visually Impaired Children

ABSTRACT

A meaningful User Experience can indicate successful of the application, so it is important to provide positive experience which aims to maximize the usability of an application. The purpose of this current study is to evaluate the user experience of an application called Teksologi: Gamification interactive typing for visually impaired children in Indonesia. User Experience Questionnaire (UEQ) were applied to measure several aspects include attractiveness, dependability, efficiency, perspicuity, novelty, and stimulation. A total of 22 visually impaired participants had been involved for this study. Besides, Alpha Cronbach test and directly check the means of each items inside the scales to draw the conclusions were conducted to examine the consistency of each aspect, then comparison to UEQ benchmark also applied. The result show that all the quality aspect is positive. At the same time, stimulation had the highest value, but perspicuity had the smallest value that enhancement will be needed to make user feel easy to get familiar with the application, easy to learn to use the application.

1. Introduction

Computers nowadays have become a common thing to master. Almost all groups even elementary school children have started to be able to operate computers. Computer lessons are also commonly taught in schools. Unfortunately, some amazingly special schools for the blind (SLB A) have not provided computer lessons in the learning curriculum, especially at the elementary and junior high levels.

The previous work was to create a gamification application for primary school visually impaired in Indonesia by utilizing the Game Development Life Cycle (GDLC). The application included lessons from first to second grade with the competition-based curriculum of 2013. The application has been tested on 11 normal respondents and 5 visually impaired respondents.

This paper extends the gamification interactive typing for Primary School Visually Impaired in Indonesia which fulfills several suggestions [1] with several studies on the context of the effectiveness of learning games for children with visually impaired.

One of the aspects to evaluate the succession of an application is user experience (UX). User inconvenience in using an application or product or service, can indicate failure of an application or product or service, because user satisfaction is one of the key determinants of continuance intention to use application [2].

As mentioned by Farhat, et al. [3] in a paper titled "Usability Evaluation of E-learning Systems in Al-Madinah International University" that there are two types in usability evaluation methods which are inspection methods and testing methods, though the inspection methods based on experts, the testing methods involve end-users and mostly done by filling questionnaires.

There are several UX measurement methods. Some of them are Questionnaire for User Interaction Satisfaction (QUIS), System Usability Scale (SUS), Standardized User Experience Percentile Rank Questionnaire (SUPR-Q), Software Usability Measurement Inventory (SUMI).

Questionnaire for User Interaction Satisfaction (QUIS) [4] is developed to assess user's subjective satisfaction with four aspects such as screen factors, terminology and system feedback, learning factors, and system capabilities. Meanwhile, the System Usability Scale (SUS) is a tool for measuring the usability of a product [5].

Standardized User Experience Percentile Rank Questionnaire (SUPR-Q) that includes four aspects: usability, trust, appearance, and loyalty, is used to measure the quality of the website user experience [6].

Software Usability Measurement Inventory (SUMI) are designed to discover specific usability problems of measuring

*Corresponding Author: Yanfi Yanfi, Bina Nusantara University, Indonesia
Email: eufrasia.yan.fi@binus.ac.id

user' perception of the usability software by either do a product-against-product comparison or compare each product against the standardization database [7].

User Experience Questionnaire (UEQ) was developed by Schrepp. M, et al. [8]. This UEQ model consists of 26 items questionnaire including six aspects: attractiveness, dependability, efficiency, perspicuity, novelty, and stimulation.

Compared to others, UEQ is a measurement that is considered to provide more benefits because it can provide comprehensive measurement results on user experience [9]. UEQ has used to evaluate the user experience of student-centered e-learning management system [10], to evaluate teachers and students' user experience of learning tools for special needs education [11], and to examine user experience for blind and visually impaired in a field setting [12].

This study focuses on renewing the application and evaluate user experience using the User Experience Questionnaire (UEQ). However, in paper [11] it is stated that the UEQ measuring tool which initially evaluates the experience of interactive product users can be applied to assess non-interactive tools used in special needs education, so in this study, the UEQ measuring tool is applied in our interactive application used for children with special needs like visually impaired.

2. Design of Technology

2.1. Current Condition

At present, only a few schools for special needs provide computer lessons, while schools that have provided computer lessons apply 10-finger typing as one of the learning topics for students. Applications that have been made have been able to support students who can type with 10 fingers. Therefore, this study studies the behavior of students who are able and have not been able to type 10 fingers so that it is expected that application improvements can be done to support all students and non-blind students in understanding basic knowledge even though they do not have education in school. The field chosen to conduct this research is a blind school or course located in Jakarta.

2.2. Teksologi

Teksologi is a computer program that helps visually impaired children to learn to type and learn basic knowledge based on a curriculum that has been created using the concept of gamification [1]. Gamification serves to increase the motivation of users so that the application continues used repetitively, so the results obtained are in line with expectations [13][14].

2.3. Interaction

The model of interaction used is to use visuals and sounds, and the controller uses a normal keyboard. The most difficult thing in making this application is to determine the user's user experience, where this requires repeating testing to make improvements so that users feel comfortable when using this application.

2.4. Type of User

There are 2 types of users of Teksologi, namely: those who fully cannot see and are partial. For users who cannot see, they only interact with the sound and the normal keyboard, while those who are partial can interact with the visual, sound, and normal keyboard. What should be noted from partial users is the level of lighting in the application. Moreover, this lighting level must be dark, because if there is a bright color it can dazzle partial users.

2.5. User Experience Questionnaire

User Experience Questionnaire (UEQ) is a tool for evaluating interactive products. In its section, there are several standards needed, i.e. attractiveness, dependability, efficiency, perspicuity, novelty, and stimulation [15]. These things are standards to measure the comfort of users of the application made.

3. Research Method

Previous research explained [1], some improvement and evaluation related user experience were conducted with the hope that this application will be used according to user needs. The improvements produced are as follows:

1. On the home page, here are tutorials and more selection keys like the "space" button, "S", "H", and "Esc" with each function. Besides, the level of this application has reached the sixth level of elementary school.
2. The application also completed with a backspace tone which alerts if the user has deleted the letter.
3. The application provides information about the score, total time, correct inputted number.

To validate the conceptual model of this application, the User Experience Questionnaire (UEQ) is used as the evaluation method to measure several aspects include attractiveness, dependability, efficiency, perspicuity, novelty, and stimulation.

The method to gather the data by applying the interview method to answer the questionnaires, so researchers read and the respondents give the answer for each item in the questionnaire. This data is collected for one week in July 2019 in the school. Nevertheless, students from elementary to senior high school were noticed.

There are 26 questions consists of pairs that meaningfully contradict each other using a Likert scale from 1 (strongly disagree) to 7 (strongly agree) was adopted from the User Experience Questionnaire (UEQ). The distribution aspects of the User Experience Questionnaire are shown in Table 1.

Table 1: User Experience Questionnaires

Aspect	Item
Attractiveness	This application Teksologi is enjoyable
	This application Teksologi is good
	This application Teksologi is pleasing
	This application Teksologi is pleasant
	This application Teksologi is attractive
	This application Teksologi is friendly

Aspect	Item
Dependability	This application Teksologi is predictable
	This application Teksologi is support user in performing the tasks.
	This application Teksologi is secure
	This application Teksologi meets expectations
Efficiency	This application Teksologi is fast
	This application Teksologi is efficient
	This application Teksologi is practical
	The user interface of this application Teksologi looks organized
Perspicuity	This application Teksologi is easy to understand
	This application Teksologi is easy to learn
	This application Teksologi is simple
	This application Teksologi is clear
Novelty	This application Teksologi is creatively design
	This application Teksologi is inventive
	This application Teksologi is leading edge
	This application Teksologi is innovative
Stimulation	This application Teksologi is valuable
	This application Teksologi is exciting
	This application Teksologi is interesting
	This application Teksologi is motivating

Attractiveness represents users' impression of the product while dependability relates to predictable, secure, and meet the expectations. Moreover, efficiency describes users' ability with minimum effort in solving their tasks in the application. Perspicuity relates to how users get familiar with the application includes simple, clear, easy to learn, and easy to understand. In addition, novelty represents innovation and creation of an application while stimulation shows how motivated and excited an application [16].

Several studies [17,18] using Cronbach's Alpha analysis to examine the consistency scale, reliability of the responses. Moreover, in this study with this sample size, Cronbach's Alpha analysis and directly check the means of each item inside the scales to draw the conclusions were also being conducted.

4. Result and Analysis

To evaluate the user experience, the User Experience Questionnaire (UEQ) could have been distributed. The answers from the participants are scaled from -3 to +3. The most negative answer is represented by -3, 0 for neutral, and +3 for the most positive answer.

There are 22 participants for this study. All participants were visually impaired. Table 1 showed that 13 out of 22 (59%) respondents are male and 41% respondents are female with 32% respondents are 10-13 years old, 32% respondents are 14-16 years old, 27% respondents are 17-18 years old, and 9% respondents are more than 20 years old. There are also educational stages as 36% of respondents are Senior High School, 32% of respondents are Junior High School, and 32% of respondents are elementary school.

Table 2: Participants' demographic distribution

Educational Stage:	
Senior High School	36%
Junior High School	32%
Elementary School	32%
Gender:	
Male	59%
Female	41%
Age:	
10-13	32%
14-16	32%
17-18	27%
>20	9%

Figure 1 showed the results of UX measurement in six aspects. Six aspects include attractiveness, dependability, efficiency, perspicuity, novelty, and stimulation. Schrepp, et al. stated that a scale above 0 represent a positive evaluation of this quality aspect while a value below 0 represents a negative evaluation [15]. As a result of all the aspect is higher than 0, so it confirmed that all the quality aspect is positive. At the same time, stimulation had the highest value while perspicuity had the smallest value that enhancement will be needed.

As mentioned in the paper titled "The Evaluation of Academic Website using Eye Tracker and UEQ: a Case Study in Website of XYZ" [19], mean values between -0.8 and 0.8 represent a more or less neutral evaluation of the corresponding scale, while the mean values more than 0.8 represent a positive evaluation. Based on that statement, this evaluation of application Teksologi confirmed positive.

Furthermore, the Cronbach Alpha coefficient [20] was calculated to verify the reliability. The results value of 0.889 is shown in Table 3. As the general rule of thumb is that a Cronbach's alpha of 0.70 and above is good, so all value confirmed reliable and valid.

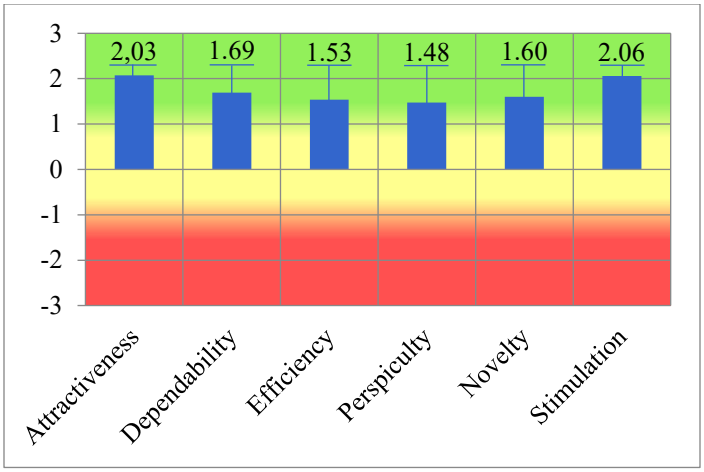


Figure 1: UX measurement scale

Table 3: Reliability Test Results

Cronbach's Alpha	Cronbach's Alpha Based on Standardized Items	N of Items
0.880	0.889	26

To make sure there is nothing potential critical related to the scale consistency, so we examined the means of the single items inside the scales. Figure 2 described that all items are interpreted in the usual way with a highly positive mean, so it confirmed there are no problems with any items in this context.

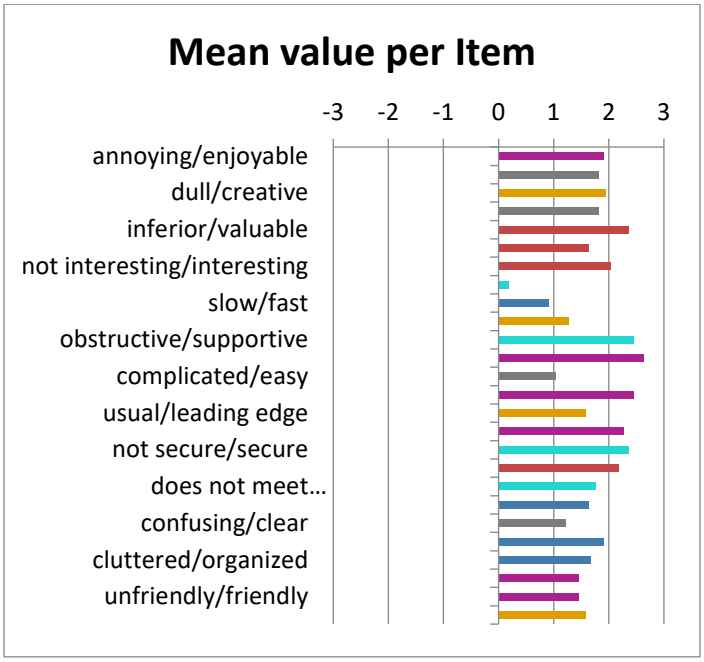


Figure 2: Mean Value per Item

The comparison to benchmark was also conducted (see Figure 3) to decide if this application has sufficient user experience to be successful in the market. However, the common expectation grew over time towards the user experience [16] and a new product established should reach at least the good category in all scales.

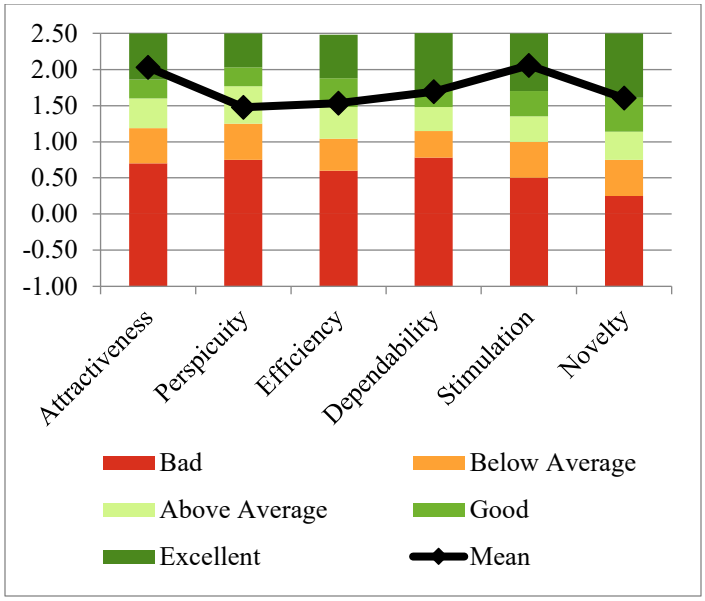


Figure 3: Graph of comparison to benchmark UEQ

As shown in Table 4, Perspicuity is below the good category expectation, so some improvement in this area is needed to be related to make users feel easy to get familiar with the application, easy to learn to use the application.

Table 4: Interpretation results of comparison to Benchmark UEQ

Aspects	Mean	Comparison to Benchmark	Interpretation
Attractiveness	2,03	Excellent	In the range of the 10% best results
Perspicuity	1,48	Above Average	25% of results better, 50% of results worse
Efficiency	1,53	Good	10% of results better, 75% of results worse
Dependability	1,69	Good	In the range of the 10% best results
Stimulation	2,06	Excellent	In the range of the 10% best results
Novelty	1,60	Good	10% of results better, 75% of results worse

5. Conclusion

The study is aimed to examine the user experience of the application called Teksologi: Gamification interactive typing for visually impaired children in Indonesia. The evaluation is conducted with adopted User Experience Questionnaire (UEQ) that assess aspects like efficiency, perspicuity, dependability, attractiveness, stimulation, and novelty.

The evaluation in this current study is conducted to 22 visually impaired participants while the previous study [1], the application is tested by 16 participants (11 normal participants and 5 visually impaired participants).

The study results represented that all the value is confirmed consistently based on the Cronbach alpha test result. In addition, mean value for all aspect more than 0.8 includes attractiveness

(2,03), perspicuity (1,48), efficiency (1,53), dependability (1,69), stimulation (2,06), and novelty (1,60) means positive evaluation.

Compare to the benchmark, attractiveness, and stimulation reach the excellent category, while efficiency, dependability, and novelty in the good category. However, perspicuity is in the above-average category, so some improvements are needed to have sufficient user experience to be successful in the market.

It is recommended that future work apply some aspects' comparison towards the user experience of this application.

Acknowledgement

We truly appreciate all participants' contributions and help especially Sekolah Luar Biasa Tuna Netra (SLB-A) Pembina Tingkat Nasional.

References

[1] Yanfi, Y. Udjaja, A.C. Sari, "A Gamification Interactive Typing for Primary School Visually Impaired Children in Indonesia," in Procedia Computer Science, 2017, doi:10.1016/j.procs.2017.10.032.

[2] W.T. Wang, W.M. Ou, W.Y. Chen, "The impact of inertia and user satisfaction on the continuance intentions to use mobile communication applications: A mobile service quality perspective," International Journal of Information Management, 2019, doi:10.1016/j.ijinfomgt.2018.10.011.

[3] A. Farhat, W.M.S. Yafooz, "Usability Evaluation of E-learning Systems in Al- Madinah International University," **1**(1), 2017.

[4] B.D. Harper, K.L. Norman, "Improving user satisfaction: The questionnaire for user interaction satisfaction version 5.5," Proceedings of Mid Atlantic Human Factors Conference, 1998.

[5] A. Kaya, R. Ozturk, C. Altin Gumussoy, Usability Measurement of Mobile Applications with System Usability Scale (SUS), 2019, doi:10.1007/978-3-030-03317-0_32.

[6] J. Sauro, "SUPR-Q: A Comprehensive Measure of the Quality of the Website User Experience," Journal of Usability Studies, **10**(2), 68–86, 2015.

[7] J. Kirakowski, M. Corbett, "SUMI: the Software Usability Measurement Inventory," British Journal of Educational Technology, 1993, doi:10.1111/j.1467-8535.1993.tb00076.x.

[8] B. Laugwitz, T. Held, M. Schrepp, Construction and Evaluation of a User Experience Questionnaire, 2008, doi:10.1007/978-3-540-89350-9_6.

[9] S. Putro, K. Kusrini, M.P. Kurniawan, "Penerapan Metode UEQ dan Cooperative Evaluation untuk Mengevaluasi User Experience Lapor Bantul," Creative Information Technology Journal, **6**(1), 27, 2020, doi:10.24076/citec.2019v6i1.242.

[10] H.B. Santoso, M. Schrepp, R. Yugo Kartono Isal, A.Y. Utomo, B. Priyogi, "Measuring user experience of the student-centered E-learning environment," Journal of Educators Online, **13**(1), 1–79, 2016.

[11] J. Kadastik, T. Artla, M. Schrepp, "Your Experience is Important! The User Experience Questionnaire (UEQ) - Estonian Version," Rural Environment. Education. Personality. (REEP) : Proceedings of the 11th International Scientific Conference, **11**(May), 281–287, 2018, doi:10.22616/reep.2018.034.

[12] S. Pohjolainen, "Usability and User Experience Evaluation Model for Investigating Coordinated Assistive Technologies with Blind and Visually Impaired," 2020.

[13] Y. Udjaja, V.S. Guizot, N. Chandra, "Gamification for elementary mathematics learning in Indonesia," International Journal of Electrical and Computer Engineering, 2018, doi:10.11591/ijece.v8i5.pp3859-3865.

[14] Y. Udjaja, "Gamification Assisted Language Learning for Japanese Language Using Expert Point Cloud Recognizer," International Journal of Computer Games Technology, 2018, doi:10.1155/2018/9085179.

[15] M. Schrepp, A. Hinderks, J. Thomaschewski, "Construction of a Benchmark for the User Experience Questionnaire (UEQ)," International Journal of Interactive Multimedia and Artificial Intelligence, **4**(4), 40, 2017, doi:10.9781/ijimai.2017.445.

[16] M. Schrepp, A. Hinderks, J. Thomaschewski, "Applying the User Experience Questionnaire (UEQ) in Different Evaluation Scenarios BT - Design, User Experience, and Usability. Theories, Methods, and Tools for Designing the User Experience," 383–392, 2014.

[17] Y. Yanfi, Y. Kurniawan, Y. Arifin, "Factors Affecting the Behavioral Intention of using Sedayuone Mobile Application," ComTech: Computer, Mathematics and Engineering Applications, **8**(3), 137, 2017, doi:10.21512/comtech.v8i3.3722.

[18] F.E. Gunawan, I. Sari, Y. Yanfi, "The consumer intention to use digital membership cards," Journal of Business & Retail Management Research, 2019, doi:10.24052/jbrmr/v13is04/art-10.

[19] A.H. Kusumo, M. Hartono, "The evaluation of academic website using eye tracker and UEQ: A case study in a website of xyz," IOP Conference Series: Materials Science and Engineering, **703**(1), 2019, doi:10.1088/1757-899X/703/1/012049.

[20] L.J. Cronbach, "Coefficient alpha and the internal structure of tests," Psychometrika, 1951, doi:10.1007/BF02310555.

ASTES

Advances in Science, Technology and Engineering Systems Journal Vol. 5, No. 5, 852-863 (2020)

www.astesj.com

ASTESJ

ISSN: 2415-6698

Design of High Output Impedance, Large Voltage Compliance Output Stage of Implantable Hypoglossal Nerve Stimulator (HGNS) for OSA Treatment

Ghada Ben Salah[*,1], Karim Abbes[2], Chokri Abdelmoula[3], Mohamed Masmoudi[1]

[1]*METS Laboratory, Department of Electrical Engineering, National School of Engineers of Sfax (ENIS), University of Sfax, Sfax, 3038, Tunisia*

[2]*METS Laboratory, Department of Physics, Faculty of Sciences of Sfax (FSS), University of Sfax, Sfax, 3038, Tunisia*

[3]*METS Laboratory, Department of Industrial Computing, National School of Electronics and Telecommunications of Sfax (ENET'Com), University of Sfax, Sfax, 3018, Tunisia*

ARTICLE INFO

Article history:
Received: 20 July, 2020
Accepted: 24 September, 2020
Online: 12 October, 2020

Keywords:
Obstructive Sleep Apnea
Electrical stimulation
Output stage
Hypoglossal Nerve Stimulator
Biphasic symmetric current

ABSTRACT

Obstructive Sleep Apnea (OSA) is a potentially common sleep disorder manifested in upper airways' collapse, either partially or completely. If diagnosed late and untreated, it may result in serious complications. The standard golden method, useful for treating OSA, remains the full night Continuous Positive Airway Pressure (CPAP). Yet, due to the ensuing discomfort it incurs on patients, researchers have been motivated to investigate other efficient alternatives, whereby, OSA can be effectively treated. More recently, an increasingly popular OSA treatment solution has been developed that consists in activating the protrusion muscles of the tongue by stimulating the Hypoglossal Nerve (HGN). After discussing the classification topologies of some neural stimulator output design stages, we consider putting forward the design of output stage of Hypoglossal Nerve Stimulator (HGNS), in compliance with the HGN requirements. The proposed HGNS is simulated in cadence software using the 0.35µm CMOS technology and Matlab software. It proved to enable the delivery of a maximum stimulation current of 1mA through 1kΩ resistive load under 3.3V voltage supply. The output stage managed to achieve large voltage compliance of 94% of the voltage supply and high output impedance of 275MΩ at full scale stimulus current. The total power consumption is about 705.87µW.

1. Introduction

Sleep is a complex neurological state, which has a vital role in maintaining sound health conditions and well-being all along the life. The sleep phenomenon associated significance is clearly manifested in the fact that people usually spend about one-third of their life spans asleep. It is worth noting, in this respect, that according to the third edition of the International Classification of Sleep Disorders (ICSD-3) [1], there exist no less than 83 kinds of sleep disorders. Most common among these disorders is the Sleep Apnea-Hypopnea Syndrome (SAHS).

Indeed, according to the ResMed group [2] report released in May 2018, the SAHS is discovered to affect nearly one billion people worldwide (specifically, 936 million people), ten times greater than the previously released 2007 World Health Organization (WHO) published statics (100 million) [3]. Central Sleep Apnea (CSA) and Obstructive Sleep Apnea (OSA) present the two main kinds of the syndrome. Rated as the rarest kind of SAHS, the CSA is considered by researchers to prevail among fewer than 20% of all subjects affected with this pathology. It usually occurs when the brain fails the transmission of nervous messages to the inspiratory muscles to trigger respiration. As for the OSA, it represents the most widely spread type of SAHS, and is recorded to occur among 84% of syndrome administered analyses [4].

Concerning the present work, we are interested in investigating the OSA type, commonly recognized with recurrent episodes of shrinkage and obstruction of the upper respiratory system during sleep (hypopneas and apneas). As the soft back-throat tissue

* Corresponding author: Ghada Ben Salah, ghadabensah92@gmail.com

collapses, the individual struggles harder against the blocked air passage by contracting the tongue and throat muscles allowing oxygen to flow into the lungs. The apnea event lasts for no less than 10 seconds in duration.

Currently, the Continuous Positive Airway Pressure (CPAP) presents the leading OSA therapy mechanism which consists of a mechanical device dubbed that serves to convey a positive flowing of air into the nasal cavities through a facial or nasal mask. The CPAP device has the advantage to maintain, the transmural pressure along the upper airway above P_{crit}, thus, preventing apnea episodes from recurring. It is worthing to note that the wear of this mask is not less than 6 hours to achieve the desired purposes. Despite the recognized therapeutic effectiveness of the CPAP [5], patient non-compliance usually stands as an important issue restricting the usage of such a device. Indeed, an elevated flow is needed to get enough positive airway pressure. Such a flow engenders the deterioration of the mucosal functions as it imposes a difficult burden on the nasal mucosa. Subsequently, several complications could befall, e.g., sneezing attacks, allergic rhinitis, and mucosal blockage. In the long-run, the frequent application of the CPAP might well culminate in other negative impacts linked mainly to epidermis issues, such as eye inflammation, the appearance of blemishes on the subject's face. It is for this reason that 30 to 50% of the CPAP treatment undergoing patients end up with abandoning it throughout the first year of therapy [6,7]. Overall, those with untreated OSA are exposed to significantly severe problems, ranging from hypersomnia to unexpected death [8]. Thus, there is a need for developing a rather effective OSA treatment therapy as an alternative to the CPAP non-compliant patients.

In this respect, pharyngeal dilation via Hypoglossal Nerve (HGN) stimulation has proven to stand as an effective therapeutic approach useful for treating the OSA [9–12]. Accordingly, the motor innervations of the Genioglossus muscle (GG) is the twelfth cranial nerve (XII) which is recognized as the responsible of the tongue protruding and pharynx expansion [13]. The branches associated with the HGN include motor fibers, and an electrical stimulation of those branches helps activate or stir the GG muscle with sensory feedback and then, elevate the tongue to stop the breakdown of the upper airway.

This new therapy is under investigation and in the process of development and completion by multiple groups. In this respect, a comparative study was established among such medical devices as InspireI, InspireII, Apnex, Imthera, and Nyxoah, elaborately treated in [14,15]. The necessity to ensure that the intervention of the HGN stimulator is maintained in such a way as to account exclusively for real apnea events is among the criteria of implant' reliability. In this regard, it is worthing to highlight that it is required to ensure the detection of real apnea events to avoid damage to the other tongue functions.

In this context, a novel OSA detection method is considered that rests on esophageal Pressure (P_{es}) signal detection processing [16]. In the relevant literature, this parameter had not been adopted by investigators in OSA monitoring although it is admitted as the gold standard to detect OSA pathology, according to the recent studies [17]. Therefore, the block diagram illustrated in Figure1 is conceived to stand as a promising prospect for future research dealing with the design of medical implants devoted to the treatment of OSA. The architecture involves an internal implantable device coupled with associated external devices. The external devices wirelessly transmit commands and power to the implantable device.

The duty of delivering electrical pulses to the HGN securely and without causing complications of the nerve cells is eventually attributed to the "output stage" or "driving stage". The HGNS output stage represents a conflict of interest of investigators since it represents functionally the closest part to the biological tissue and any irregularity in HGN stimulation standards may engender tissue damage. The critical aspects, necessary for accomplishing the biomedical and design constraints of the output stage (e.g., large output voltage compliance, high output impedance, low power consumption), usually raise problems as to circuit topology and components. Indeed, Achieving large voltage compliance (ie, very close to the supply voltage), and maintaining high output impedance to keep the desired stimulus current constant disregarding the site and tissue impedances as well as reducing the size and power consumption, have been the major challenges in designing the neural stimulator of output stage circuits to make it more efficient.

In this context, the present work is aimed to put forward a High output impedance, large voltage compliance, and low power consumption output stage for implantable HGNS, specifically conceived to maintain a safe secure treatment of apnea affected subjects and in compliance with the HGN requirements, after discussing the state of the art model topologies relevant to the output stage designs of neural stimulators.

The remainder of this paper is constructed as follows. Section 2 is devoted to depicting the topological classification of neural stimulators, including the related mode, stimulus shape and charge-balanced stimulation techniques. As for Section 3, it involves a thorough description of the proposed HGNS output stage design relevant architecture, with details of the specific blocks they contain. Section 4 is devoted to highlighting the reached simulation results, achieved by means of the cadence virtuoso tool, along with a relevant comparison established with other well recognized output-stage designs. Finally, the major relevant concluding remarks are highlighted in section 5, followed with some propositions for future investigation.

2. Topological classification of neural stimulators

2.1. Stimulus Mode

The output stage of the neural stimulator is responsible for generating electrical stimulation pulses and creating an action potential in the targeted nerve. Generally, the distinct stimulation modes in which the electrical stimulation of nerve cells can be provided are represented in Voltage-Controlled Stimulation (VCS), Charge-Controlled Stimulation (QCS), and Current-Controlled Stimulation (ICS). The entirety of these output stage modes turn out to be bipolar in type so that crosstalk can be reduced, despite the noticeable decrease witnessed in the efficiency parameter. They are usually performed with a Digital-to-Analog Converter (DAC) enclosing binary-weighted transistors or a thermometer code, enabling to control the output signal amplitude and maintain circuit stability.

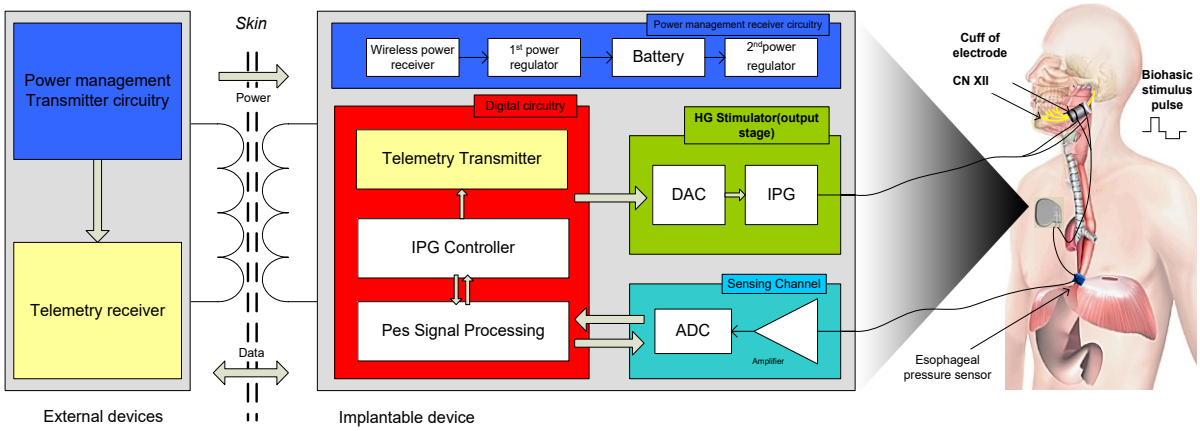


Figure 1: Block diagram of implantable Hypoglossal nerve stimulator.

Concerning the VCS mode, the neural stimulator output is in the form of a voltage, thus, the pulses crossing the tissue demonstrate to depend deeply on the electrode or tissue associated impedance (Ohm's law). Thereby, the exact charge quantity provided to the electrode and tissue turns out to be ineffectively controlled due to impedance variation. However, this approach has the advantage of maintaining rather high power efficiency [18]. As depicted by Figure 2(a), the DAC current source transistors are implemented under the form of a cascode, so as to raise the output impedance and preserve a constant output current, disregarding the fluctuation of the voltage over the load ZL. Still, the static voltage is beneficial for biasing the cascode transistor, as documented by Sivaprakasam et al. [19] as well as Jones et al. [20]. As for [21], the authors considered that the DAC output impedance can also be boosted by the implementation of an active feedback which biased the cascode transistor.

As regards the QCS mode, the charge, directly delivered to the target tissue, is kept under constant control. The major drawback associated with this method lies in the fact that it occupies a large chip area because of the implementation of numerous switched capacitor networks [22].

With respect to the ICS mode, it is widely applied in implantable neural stimulators, whereby, the stimulated current is not concerned by variations of the tissue load. The model ensures direct control to be kept over the tissue delivered charge by means of linear relationship persistent between charge and current. Accordingly, the mode helps ensure the maintaining of a rather effective control and safer stimulation [23,24].

The current mirror constitutes the most obviously clear mode, whereby, the current-mode DAC output current, I_{DAC} can be duplicated or scaled into output current I_{out} by means of load. It is worth noting, in this respect, that the Wide-Swing Cascode (WCS) current mirrors are used to help increase the current source output resistance through a gm factor, whereby, gm stands as the trans-conductance of the cascode transistor (M3), as illustrated through Figure 2(b). Noteworthy, also, is the fact that, contrary to the fully cascode current mirror case, the external voltage V_{bias} is used for biasing the WSC circuit stacking transistors. Accordingly, regulating the biasing voltage V_{bias} contributes to the reduction of the headroom voltage to $2V_{Dsat}$. As regards voltage compliance, it is reduced to V_{DD}-$2V_{Dsat}$.

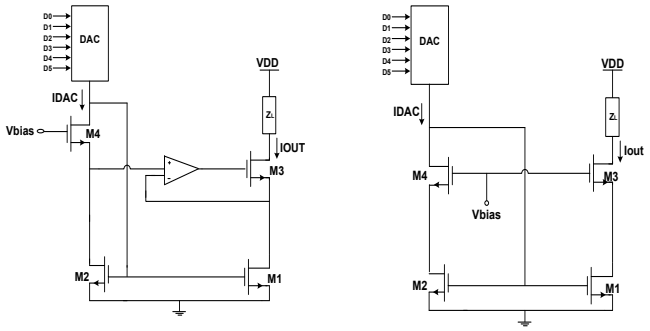


Figure 2: (a) "Folded cascode" FC current mirror with output impedance boosted via active feedback; (b) "Wide-Swing" WS Cascode current mirror, entirely controlled via DAC current mode.

2.2. Stimulus Shape

It is worth highlighting that there exist two commonly recognized stimulus waveforms, widely applied in the field of neural stimulation, namely, the monophasic stimulus form and the biphasic stimulus one.

Regarding the monophasic waveform, it is characterized with a unidirectional pulse, more frequently applied in surface electrode stimulation process, as depicted through Figure 3(a). Noteworthy, however, is that monophasic stimulation culminates in irreversible damage to the biological tissue, because of the charge accumulation on the electrode-tissue interface.

This problem may be prevented by implementation of biphasic stimulation. Indeed, each pulse in the charge-balanced biphasic stimulation process is followed with an inverse polarity pulse, culminating eventually in a succession of a cathodic (negative) phase, succeeded by an anodic (positive) phase, as demonstrated by Figure 3(b). The cathodic phase serves to depolarize nearby axons and triggers the potential action permitting to excite the muscle response. The succeeding anodic phase undertakes to neutralize the primary phase accumulated charge by reversing the damaging electrochemical process, likely to occur at the level of electrode-tissue interface throughout the cathodic phase. The time delay, slightly separating the two stimulation phases, is dubbed interphase gap. Hence, the anodic phase does not impede the action's potential propagation triggered by the cathodic phase. It is for this reason that the biphasic stimulation procedure is considered safer than the monophasic

stimulation procedure, which makes it widely applied and fit for application in neural stimulators to prevent tissue damage [23–25].

Generally, the square pulse (active), supplied by active circuits, turns out to be the stimulus more suitably fit for application in the cathodic phase, while the ensuing anodic phase can be either square or exponentially decaying (active or passive discharging), as illustrated through Figure 3(c), below.

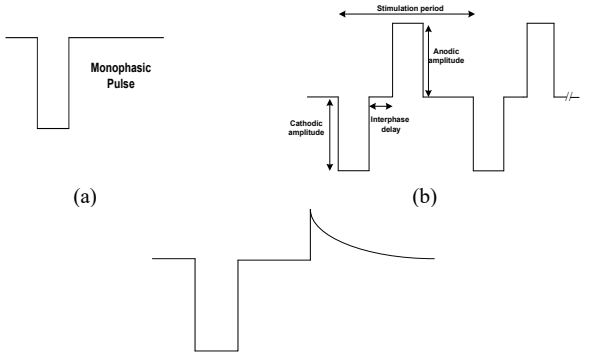


Figure 3: (a) A typical monophasic-stimulus pulses; (b) A symmetric biphasic-stimulus pulse with active-cathodic and passive-anodic phases; (c) A Biphasic stimlus pulse with active-cathodic phase and passive-anodic phases (exponential decay).

2.3. Charge-balanced stimulation

One of the well-established principles of neural stimulation is the achievement of charge balancing among the different stimulus pulses related phases throughout the execution of stimulation process. It is a protecting measure that helps avoid the accumulation of the charge in the biological tissue, likely to result in the rise of electrode potentials to levels inducing water hydrolysis to start. Actually, there exist several reasons for a charge imbalance to take place, mainly, a semiconductor breakdown, current leakages due to cross-talks among neighboring stimulating positions, and wire breakdown. The correction and the generation of the charge imbalance are ensured noticeably by connecting in series the blocking capacitor with each stimulating electrode. Figure 4, below, illustrates three current-mode stimulator configurations deploying a blocking capacitor [26]. The nerve tissue is sited between both of the anodic (A) and the cathodic (C) electrodes, denoting a polarity that indicates the stimulus pulse.

As for the Figure 4(a) depicted circuit [21], the cathodic electrode remains perpetually associated with a reference voltage, usually both of the supply voltages associated midpoint. The cathodic and anodic relevant current supplies are respectively generated by the programmable current sink I_{stimC} and current source I_{stimA}. These current supplies are driven through the load, representing the nerve-electrode impedance, by the control of switches S1 and S2.

Regarding the case in which only a single supply is available, as illustrated through Figure 4(b), both of the anodic and cathodic current supplies turn out to be generated from a single current sink I_{stim}, by inverting the current paths through the S2 switch. Both of the Figure 4(a) and 4(b) displayed configurations indicate charge-imbalance provided solutions. Yet, reaching accurately zero net charges following each stimulation period is not practically feasible owing to the mismatch of timing errors and leakage emanating from nearby stimulating sites. Hence, incorporating the switch S3 seems imposed to help in periodically removing the residual charge by generating an extra passive discharge phase.

As the circuit configurations appearing in Figure 4(a) and 4(b) necessitate the incorporation of the third phase, some investigators consider deploying the passive discharge phase as the principal anodic phase, as clearly described through the Figure 4(c) depicted circuit illustration [27].

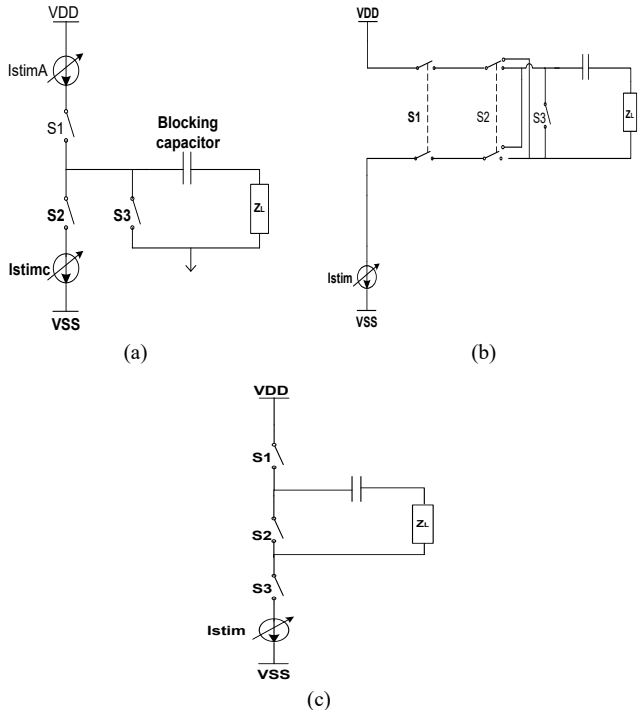


Figure 4: Current-mode stimulator configurations deploying blocking capacitor: (a) dual supplies with active cathodic and active anodic phases; (b) Single supply with active cathodic and active anodic phases; (c) single supplywith active cathodic phase and passive anodic phase.

In general, blocking capacitors stand as critical tools significantly useful for ensuring that DC current cannot, by any means, pass into the electrodes in the event of semiconductor failure resulting from voltage failure or current leakage. More specifically, they are typically considered as off-chip surface-mount components given their highly required value (of a few microfarads in the case of lower-body application stimulators). As for applications in which blocking capacitors are not applicable, due mainly to physical size constraints, other active charge-balancing alternatives turn out to be imposed. In this respect, Sit et al. [28] considered investigating the “Dynamic current balancing” method.

As Figure 5 (a) depicted circuit indicates, the current sink and the PMOS transistor (M1) are respectively responsible for generating both of the cathodic and the anodic phases. Firstly, both of the $S_{cathodic}$ and S_{anodic} switches are on, while the two sampling switches, S_{samp}, are off. When the circuit sets the drain current amplitude of M1 to equate the current sink (as a feedback effect), the resultant bias voltage V_{bias} affect on the M1 gate turns out to be sampled and held. After that, the two S_{samp} switches are on and $S_{cathodic}$ switches off to generate cathodic current. Then, $S_{cathodic}$ switches on and S_{anodic} switches off. As the gate voltage of M1 is

held at V_{bias}, an anodic current, of an amplitude equal to that of the (cathodic) sink, goes through S_{anodic} to the load. According to Ortmanns et al. [29], the "Active charge balancer" method offers the advantadge of providing feedback information about the electrode condition after stimulation.

In the Figure 5 (b) figuring circuit, the extra voltage acquired following a biphasic pulse, is measured and compared to a safe referential benchmark voltage. Should the electrode voltage prove to surpass the safe window, supplementary short stimulation current pulses need be applied to drive the electrode voltage towards a balanced condition. In an attempt to experiment with a rather effective charge-balancing method, Williams et al. conducted a special study [30] relying on the implementation of an "H-Bridge" circuit.

Accordingly, the same current source could be applied to both phases (thus, doing away with the mismatch factor). The current path, as flowing through the electrode, is merely switched/driven, as illustrated through Figure 6. Throughout the cathodic phase, $\varphi 2$ is high with current flowing from electrode B to electrode A. As regards the anodic phase, $\varphi 1$ is high and the current is flowing from electrode A to electrode B. This technique assumes the persistence of an asymmetrical biphasic waveform maintaining a delay between the cathodic and anodic phases.

The architecture has been demonstrated to offer a number of valuable benefits, particularly, decreasing the power consumption range, while initiating action potentials at significantly lower charge thresholds [31], thus, enhancing safety stimulus.

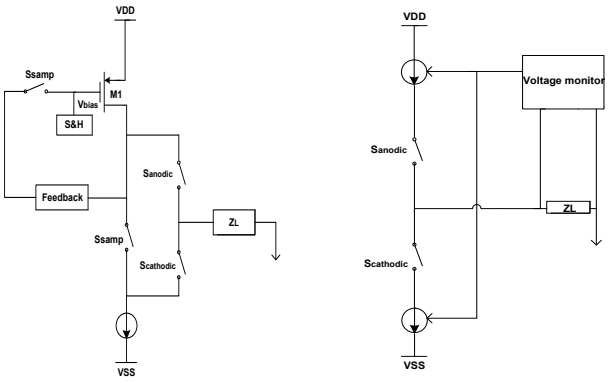


Figure 5: Charge balancing relevant methods: (a) Dynamic current balancing; (b) active charge balancer.

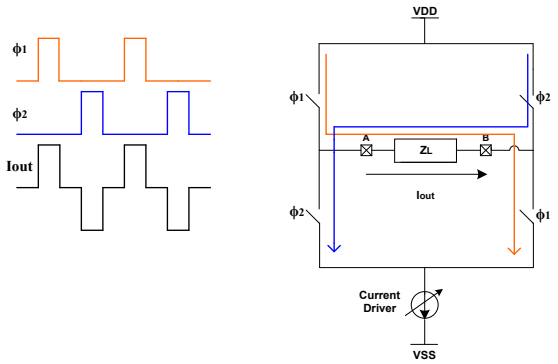


Figure 6: H-bridge architecture highlighting the control of bi-directional current flow insured by Switches, passing through the load ZL.

3. Design of HGNS Output Stage

In this work, the ICS stimulus architecture was opted for as the most optimally fit stimulation pulse generating framework on which the present work is based, rather than the other stimulation modes detailed in the preceding section (i.e., the VCS and QCS).

The conceptual block diagram of the proposed HGNS output stage is described on Figure 7, below. The output stage englobes two main parts. The first current driver part encloses the DAC of type low-voltage, binary-weighted 6-bit current mode and a performing current mirror, while the second part consists in the switch network configuration which provides the generation of biphasic current pulsations by alternating the flow path of the stimulated current, passing within the targeted tissue, as already stated.

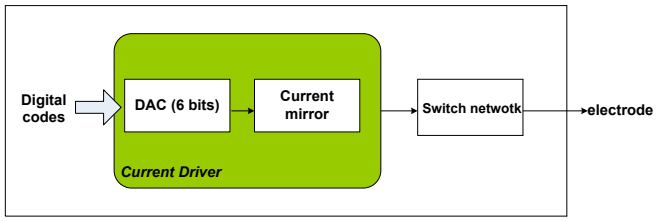


Figure. 7: Conceptual block diagram of the proposed implantable HGNS output stage.

3.1. Current pulse generator design

- *Current* Steering *Digital-to-Analog Converter CS-DAC*

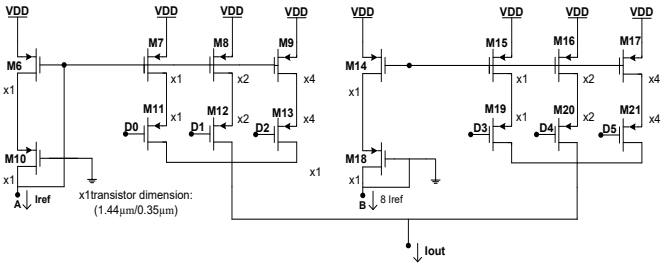
A specific binary-weighted 6-bit Current-Steering Digital to Analog Converter (CS-DAC) is employed in the proposed neural stimulator output stage. Actually, this topology has proved an important capacity to direct conversion without the necessity for a voltage stage. Besides, it guarantees high speed, a small chip-area, and maintains a minimally low power dissipation [32,33].

Figure 8 highlights the advanced CS-DAC circuit, whereby, all the transistors are performing in the saturation region. The circuit of reference current, illustrated on Figure 8(b), provides the reference current types I_{ref1} and I_{ref2} $(8 \times I_{ref1})$, drawn from a reference current I_{ref} of 2.54µA, that are mirrored into transistors M2 and M3. Given the respective sizes of M3 (m=8, W=11,52µm, L=0.35µm) and M2 (m=1, W=1.44µm, L=0.35µm), as figured in the circuit, the drain current of M3 turns out to be 8 times greater than that of M2. In effect, maintaining the same dimensions for M4 and M5 as the transistors M2 and M3, respectively, culminates in having the same drain-source voltages of both transistors M2 and M3. The accuracy of the current copier circuit is proved to be improved by applying this strategy. Figure 8 (a) showed that the currents passing through the drains of the transistors M4 and M5 are mirrored by the transistors M6 and M10 on the left and right sides of the CS-DAC, respectively. The gates of the transistors (M6-M9) and the transistors (M14-M17) are inter-connected to ensure saturation and controlled polarity voltage. This measure is aimed to help in saving and conserving power to the maximum. The PMOS transistors' width range adapts to the copied current in conformity with the size of the reference branch transistors.

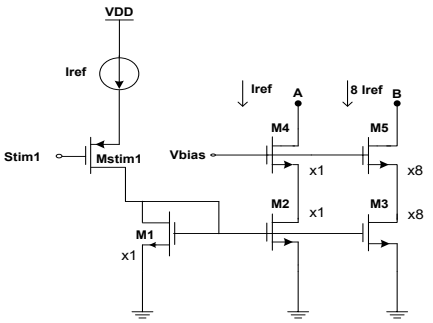
It is also worth mentioning, in this respect, that employing a 6-bit binary-weighted CS-DAC composed of transistors that have the same dimensions in both sides helps remarkably in saving the area of the integrated circuit. Once there is no stimulation current is

produced, the transistor M_{stim1} is implemented to serve in switching off the proposed CS-DAC. Therefore, it plays the role of power conserver when the design is in the mode "stand by". By switching on Mstim1, the input digital codes (D0-D5), which represent the addition to the 6 branches through applying the law of knots, undertake to control CS-DAC total output current. Accordingly, the bits D0 and D5 designate to the Least Significant Bit (LSB) and the Most Significant Bit (MSB), respectively. In the CS type of DAC, PMOS transistors are responsible for monitoring each current source indexed by '*i*'. The current related to this source is $I_i = 2^i.I_{ref}$, where, I_{ref} signifies the current reference by a reference current generator. It also stands for the LSB current $I_{ref} = ILSB$. At a given moment 't_0', if the digital input $\{D_i(t_0)\}$, $0 \le i \le N-1$ is recognized, the total output current of the CS-DAC I_{out} provided to the following module (current mirror) is expressed as follows:

$$I_{out}(t_0) = \sum_{i=0}^{N-1} 2^i I_{ref} \times D_i(t_0) \quad (1)$$



(a)



(b)

Figure 8: The proposed DAC associated (a) schematic circuit; (b) reference current generator.

The static absolute accuracy of the proposed CS-DAC can be described in relation to three fundamental error types, i.e., offset errors, gain errors, and linearity errors. The offset error is defined by a persistent shift in the transmission characteristic of the DAC. Indeed, when the digital input D equal to "000000", the ideal output current must be equal to 0A. If the analog output is unequal to zero, an offset error will be observed. Concerning the gain error, it stands for the difference of the real slope and the perfect slope of the CS-DAC transfer feature. It appears to continue when the slope of the best-fit line by the real transfer characteristic of the DAC is different from the slope of the best-fit line by the ideal one. With respect to the current study case, both of the offset and gain errors are determined by means of the two equations below:

$$Error_{offfset} = \left\{\frac{I_{out}}{I_{LSB}}\right\}_{(000000)} \quad (2)$$

$$Error_{gain} = \left\{\left(\frac{I_{out}}{I_{LSB}}\right)_{(111111)} - \left(\frac{I_{out}}{I_{LSB}}\right)_{(000000)}\right\} - (2^N - 1) \quad (3)$$

Still, we are mainly interested in these two static specifications: Integral Non-Linearity (INL), or relative accuracy as well as Differential Non-Linearity (DNL), which are most highly recognized in the ac performance. The difference calculation of each level from the real and ideal widths presents the Differential nonlinearity. Considering the ideal output value of a certain code D_i is expressed by: $I_{ideal}(D_i) = I_i$, the real value generated by the CS-DAC to the same code is: $I_{real}(D_i) = \tilde{I}_i$. Thus, deviation is directly provided by:

$$d_i = I_{real}(D_i) - I_{ideal}(D_i) = \tilde{I}_i - I_i \quad (4)$$

It is adjusted by accounting for the LSB value:

$$\bar{d}_i = \frac{d_i}{I_{LSB}} = \frac{\tilde{I}_i - I_i}{I_{LSB}} \quad (5)$$

In this context, DNL_i is attributed to the noticeable difference that exists between two variations in a given transitional code, such as:

$$DNL_i = \bar{d}_i - \bar{d}_{i-1} = \frac{\tilde{I}_i - I_i}{I_{LSB}} - \frac{\tilde{I}_{i-1} - I_{i-1}}{I_{LSB}} = \frac{\tilde{I}_i - \tilde{I}_{i-1}}{I_{LSB}} - 1 \quad (6)$$

The positions of the ideal output current are distinct from the positions of the real output current. This difference appearing between both of them defines the INL. It is also characterized with the accumulation of previous DNL errors, as highlighted through the expression below:

$$INL_i = \sum_{K=1}^{i} DNL_K \quad (7)$$

The main drawback of the weighted binary CS-DAC design lies in the persistence of glitches due to the delays caused by the switch of varying currents. These glitches can well engender a reduction in the system's respective dynamic performance [34].

- *Regulated* cascode *current mirror*

The regulated cascode current mirror is responsible for performing an accurate conveyance of stimulus current to the switch network. It is designed for the purpose of effectively satisfying the biomedical micro-stimulations associated key requirements, such as low voltage operation, high output impedance, and large voltage compliance. Long-channel transistors were applied in the cascode topology for increasing the output impedance value. Furthermore, to ensure large voltage compliance, the implemented output transistors should be characterized by high channel widths for limited overdrive voltage. For a voltage compliance benefiting from the maximum amount of voltage supply to take place, a compromise has been introduced in the design of the current mirror. The schematic diagram of the cascode current mirror, figuring in Figure 9 (a), appears to involve a low voltage ($V_b = 0.25V$), which ensures the voltage to drop conveniently to fit for the circuit operation (voltage headroom) and

regulate the power consumption. The bias voltage V_b is determined by the saturation voltage condition (V_{gs} - $V_{th} \leq V_{ds}$), once M22 and M23 are discovered to operate in a saturation region. The four (M22 to M25) transistors bear the same dimensions for a unit gain (25u/1.1u). The concept of this regulated cascade current mirror consists in increasing output impedance of the proposed CS-DAC through assuring the bias of the cascade transistor M24 by active feedback using an Operational Transconductance Amplifier (OTA), as schematically depicted through Figure 9 (b). Applying active feedback serves to ensure that the drain associated with the mirror transistor M25 is held at some constant voltage in a feedback loop to equate the drain voltage associated with M23 (i.e., the OTA should be in the role of voltage follower). The output resistance associated with the regulated cascode current mirror circuit is provided by:

$$R_{out}=A\times r_{025}\times g_{m24}\times r_{024} \quad (8)$$

Where: A denotes the OTA gain; r_{025} designates the output resistance associated with M25 and g_{m24}, and r_{024} stands for the transconductance and output resistance of M24, respectively. The voltage compliance is expressed by:

$$V_c=V_b+V_{gs24}-V_{oD24} \quad (9)$$

Where: V_{gs22} stands for the gate source voltage of M22 and V_{oD24} represents the overdrive voltage of M24. V_{oD} has been defined as the voltage persistent between the transistor gate and source (V_{gs}) in excess of the threshold voltage (V_{th}). It can be determined by the difference outcome perceived between both parameters ($V_{oD} = V_{gs} - V_{th}$). As highlighted by (9), V_b is expected to be elevated to provide large voltage compliance. The transistor M25 may be driven summarily into the triode region due to the boost of V_b, thus, automatically reducing the output impedance. The maximum value for V_b is equal to V_{DD}-V_{gs22}-V_{oD25}, which brings about a voltage compliance of V_{DD}-V_{oD24} -V_{oD25}.

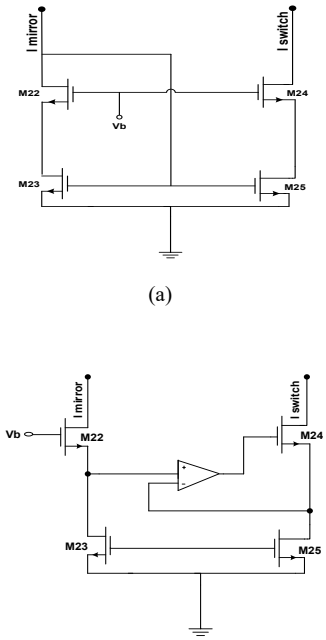


Figure 9: (a) Schematic diagram highlighting the cascode current mirror circuit. (b) The cascode current mirror with active feedback to boost output impedance.

The active feedback insured by the amplifier should allow high input common-mode voltages, and provide sufficient gain useful for reaching a high-level of output impedance. The topology of a single-stage folded-cascode OTA with NMOS input transistors has been designed to fulfill these requirements, as shown through Figure 10. Accordingly, the output impedance is equal to:

$$R_{out}=A\times gm_{27}\times r_{27}\times r_{26} \quad (10)$$

Where: A denotes the OTA provided gain; gm_{27} represents the transconductance of transistor M27; r_{27} designates the output impedance of M27 transistor, and r_{26} refers to the output resistance of M26 transistor.

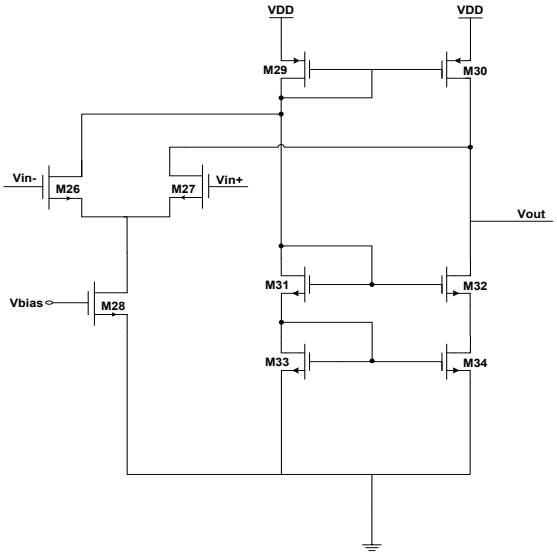


Figure 10: Folded cascode OTA.

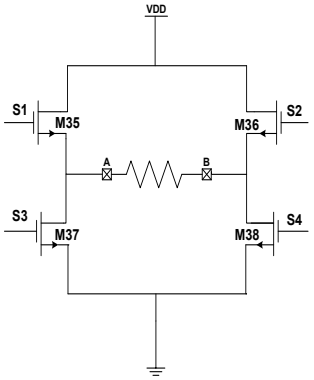
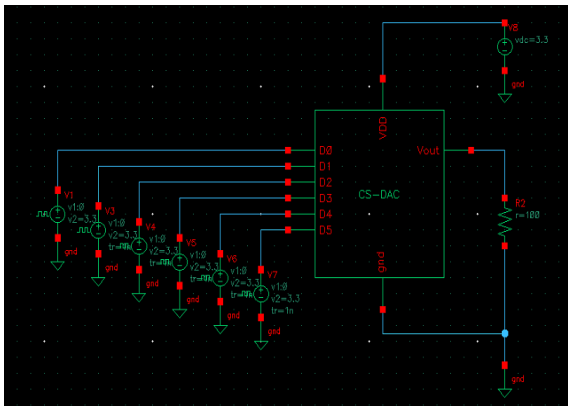


Figure 11: Block diagram of the bi-directional current generation as based on 'H bridge' architecture.

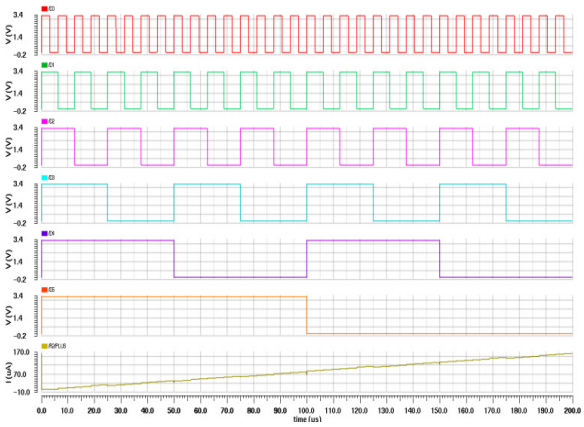
3.2. Switch network configuration

Delivering a bi-directional stimulated current by the output stage of HGNS is preferred than the mono-directional current to the cuff of electrode since it prevents any charge cumul in the biologic tissue. Figure 11 displays the switch network configuration, based on 'H bridge' architecture. This architecture is applied in power-efficient shapes, where a single the full stimulation back-end is functioning under a single-rail supply voltage and only one a current source is disposed. The switches (S1-S4) serve to guide current within the biological tissue in the

requested direction. Activating these switches makes the current circulate in a certain sense whereas turning on the other pair of switchers (S2-S3) orientates the current towards the opposite sense. It follows, therefore, that only a single current source turns out to be needed to make the stimulation current bi-directional. As to the resistance (R) figuring on the schematic diagram, it reflects the similar impedance of the recognized biological tissue between the cuff of electrode. Concerning the switches S5 and S6, they are in charge of grounding the stimulation sites. This mission consists in supplying a special pathway in order to discharge the extra charge caused by the imbalance between the anodic and cathodic periods to prevent any possible tissue damage.



(a)



(b)

Figure 12: (a) Test bench of 6 bits CS-DAC. (b) The CS-DAC related binary input.

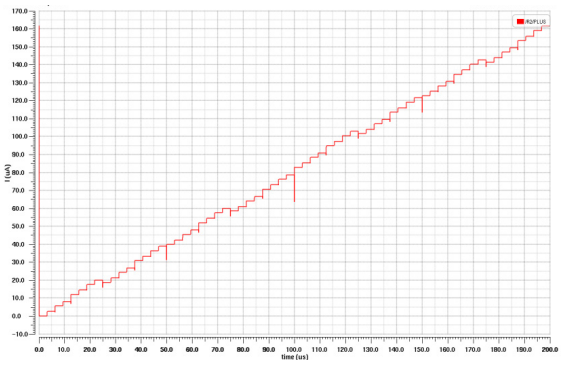


Figure 13: Output Current of the proposed binary weighted CS-DAC.

4. Results and Discussion

4.1. Stimulation results

The performed simulation stage and the relating reached results are achieved by means of Cadence Virtuoso tool for CMOS 0.35µm process technology, under 3.3V supply voltage. Figure 12, below, displays the Test Bench of 6bit CS-DAC along with its input digital codes (D_0, D_1, D_2, D_3, D_4, D_5) ranging from '000000' to '111111'. The resolution of a CS-DAC refers to the number of unique output current levels the converter is able to produce.

In the case of HGNS, a CS-DAC with a resolution of 6 bits is needed, since it enables to produce a range of 64 different current levels at its output. Therefore, operating on a 6-element binary code is sufficient for providing a flexible generation of electrical pulses and helping to save significant chip-area. Indeed, the transient response of simulated output current, associated with the proposed CS-DAC, is discovered to be relatively monotonic, as illustrated through Figure 13, below.

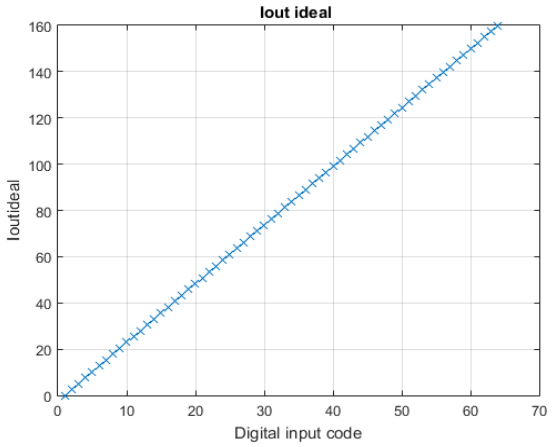


Figure 14: Ideal output current versus DAC input codes.

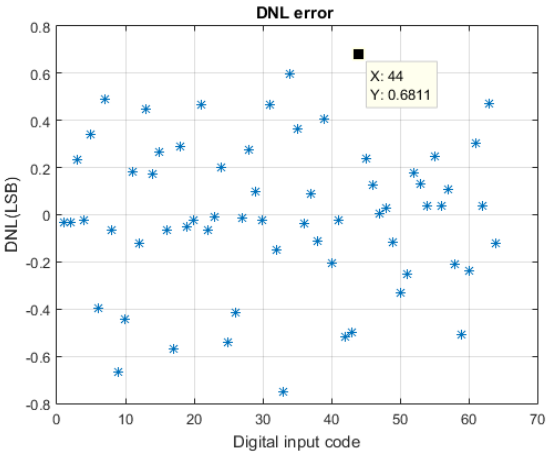


Figure 15: DNL error.

At this level, Matlab software is used for the purpose of determining the proposed CS-DAC associated static performance. The ideal conversion of the digital codes to the current output is depicted on Figure 14. As for the Figure 15 and 16, they respectively indicate the relating DNL and INL performance. The attained results prove to reveal well that the DNL is comprised

between -0.669 and +0.681LSB, and that the INL is within -0.563 to +0.815LSB. The proposed DAC associated specifications are depicted on the Table 1, below:

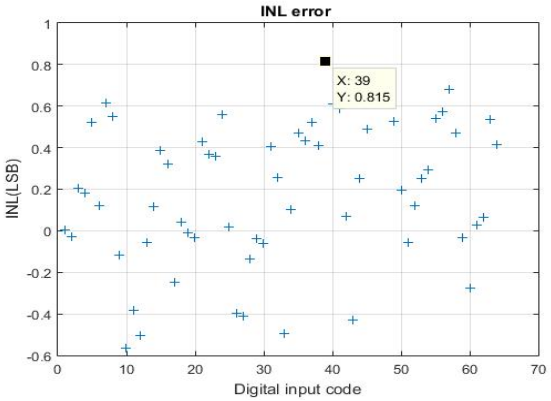


Figure 16: INL error.

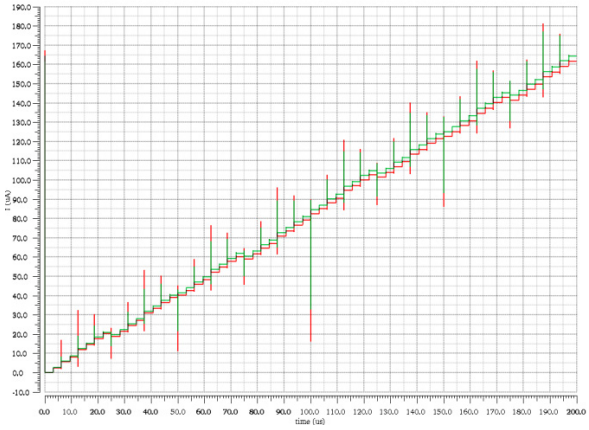


Figure 17: Input and output current concerning the regulated cascode mirror.

Table 1: Performance of the proposed DAC

Parameters	DAC obtained
Supply Voltage (V)	3.3
Approach	Current steering
Resolution (bits)	6
Temperature (°C)	27
Conversion Rate	50
Full Scale Current (µA)	161.05
LSB Size (µA)	2.54
DNL (LSB)	-0.669≤INL≤+0.681
INL (LSB)	-0.563≤INL≤+0.815
Gain error (LSB)	+0.37 LSB
Offset error (LSB)	3.9 10^{-4} LSB
Power dissipation (µW)	89.529

As mentioned in the previous section, the current generator requires a minimum of two steps to convert the input digital bits into the output stimulus current. The digital bits are first converted into an analog current which is applied later to a cascade current mirror. The transient response of the input and output current of the regulated cascode mirror is displayed on Figure 17. Given the imposition of sufficient linearity and adequate transition time of the stimulation current, it is legitimate to ascertain the circuit flexibility. The role allocated to this current mirror lies in raising the DAC output impedance through employing active feedback using an operational trans-conductance amplifier (OTA). As already stated, this OTA bears an NMOS input folded cascode configuration, and helps consume a bias current of 0.88µA. Figure 18 reveals the frequency response relevant to the proposed folded cascade OTA. Based on this figure, the circuit proves to be able to obtain 74dB with a frequency bandwidth of 69 MHz at an input common-mode voltage range of $V_{in} = 250mV$. The performance of the folded cascode OTA is depicted on Table 2, figuring below.

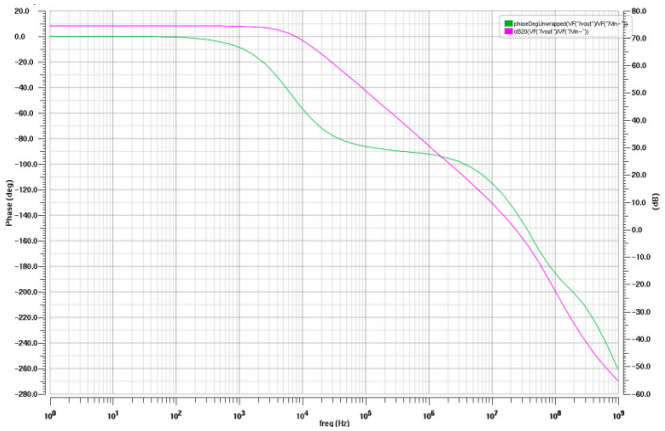


Figure 18: Gain and phase response of AC analysis for the OTA folded cascode.

Table 2: Custom design performance of the proposed OTA

Specifications	Values
Supply Voltage (V)	3.3
DC gain (dB)	>70
GBW(MHz)	69
Phase Margin(degree)	30
Settling Time (µs)	1
Slew Rate (V/µs)	4
ICMR (V)	1.5-2.5
CMRR (dB)	≥60
Output Swing (V)	1-2.8
PSRR (dB)	≥60
Power consumption (µW)	213.9

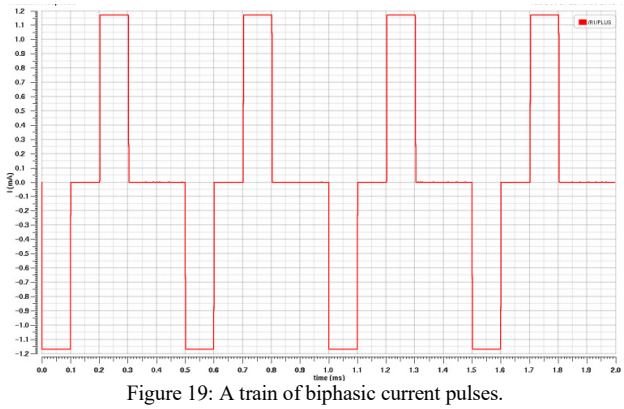


Figure 19: A train of biphasic current pulses.

The operation of generating rectangular biphasic pulses to the load rests heavily on the H-bridge switch network configuration. With respect to the HGNS case, the stimulation charge to the neural tissue of the twelfth cranial nerve needs to be within the range of 0.5mA to 2.5mA, so as not to damage the other tongue-

associated functions. The output stage should be implemented in compliance with a resistive load model, with an impedance rate ranging between 200 and 3KΩ [35]. Figure 19 illustrates the stimulus current pulses under 1k resistive load relevant to four complete stimulation cycles. The stimulation period is set to 500µs with 100µs interphase delay which presents a pause between the cathodic and the anodic phase. The HGNS proves to be capable of providing 1.17ms deliverable stimulus current under 3.3V voltage supply. It exhibits a voltage compliance of 3.1V along with an output resistance of 275 MΩ at full scale stimulus current.

4.2. Comparison with relevant output stage stimulators designs

At this level, a comparison is established with other output stage circuits used in Functional Electrical Stimulation (FES) applications, as figuring on Table 3. Accordingly, a respective summary of the entirety of the relevant aspects is depicted, including the related mode, topology and stimulation parameters. Initially, the aim was to establish a comparison with a number of already advanced OSA disease treating neural-stimulator designs. Nonetheless, neither the related specifications, nor the associated performance of the proposed schemes have been available in the relevant literature. In this respect, Velloso and Souza [36], Chen et al. [37] as well as Cheng et al. [38] designed circuits based on the implementation of a transistor that serves to create a High voltage output in the secondary side of the step-up transformer by switching its primary winding. In turn, the design of the output stage, advanced by Lima and Cordeiro [39], Yochum et al. [40], and Khosravani et al. [41], put forward a common specification, namely, the implementation of a current mirror, whereby, the output current can be regulated. As for Masdar et al. [42], they envisaged the use of LM675 power operational amplifier, operated by a DAC and microcontroller, to produce biphasic impulses with a changeable extent. As for Willand and De Bruin [43], they inserted TIP 50 a high voltage bipolar transistor, activated by means of an operational amplifier, as part of their envisioned output-stage design. With respect to Qu et al. [44], they constructed their proper stimulator output-stage architecture on the basis of an H-bridge switch network, which turns out to involve four controlled switches. Concerning Brunetti et al. [45] elaborated study, a high voltage op-amp (PA78) was adopted, which is considered as a voltage-to-current amplifier, able to generate biphasic current pulses. Regarding Huerta et al. conducted study [46], it rests on the idea of reducing charge accumulation in the biological tissue. To this end, they considered applying special switch-capacitor (SC) converters that produce zero net charge elevated slew-rate impulses, thus, decreasing the feeling of pain. This concise literature review reveals well that, in their greatest parts, the advanced transformers, designed for implementation in voltage-controlled output stages, appear to rest predominantly on the idea of easily increasing voltage levels. They were also liable to provide biphasic stimulus whenever the output stage proves to involve a center tap. Hence, based on this abrupt summary, one could well note that most of the investigators seemed to adopt biphasic current pulses as an effective stimulation topology useful for reducing the undesirable effects of charge accumulation on the biological tissue. In addition, symmetric circuits enclosing an H-bridge configuration proved to exhibit an important safety characteristic, as scientifically demonstrated by relevant research studies. It is in this context that the present research can be set, motivated mainly by the interest to investigate a special design of the output stage construct that rests on a biphasic current stimulation architecture equipped with an H-bridge switch network, relevant to the treatment of OSA disease.

Table 3: Review of the output stage related circuit specifications as figuring in the relevant literature

Research Work	Stimulation Mode	Output Topology	Stimulation Parameters
Velloso and Souza [36]	I	Biphasic	PW: 50 – 500 µs
			f: 20 – 200 Hz
			I: 0 – 100 mA
Chen et al. [37]	V	Monophasic	PW: 20 – 400 µs
			f: 40 Hz
			V: up to 150 V
Cheng et al.[38]	I	Biphasic	f: 200 Hz
			I: 100 mA
Lima and Cordeiro [39]	I	Monophasic	PW: 50 µs – 1ms
			f: 1 – 10 Hz
			I: 0 – 100 mA
Yochum et al.[40]	I	Monophasic/Biphasic	PW:100 – 600 µs
			I: 100mA
Khosravani et al.[41]	I	Monophasic/Biphasic	f: 50 Hz
			I: 0 – 150 mA
Masdar et al.[42]	I	Monophasic/Biphasic	PW: 10 – 500 µs
			I: 10 – 120 mA
Willand and De Bruin[43]	I	Monophasic	PW: 5 ms
			f: 20 Hz
			I: up to 22mA
Qu et al.[44]	I	Monophasic/Biphasic	I: 150 mA
Brunetti et al.[45]	I	Biphasic	PW:10 µs – 5 ms
			f: 0 – 100 Hz
			I: 0 – 120 mA
Huerta et al. [46]	V	Biphasic	PW:10µs –10ms
			f :1 Hz – 15KHz
			V: up to 300 V
The present design	I	Biphasic	PW: 100 µs
			f: 2 KHz
			I: 0 – 1.17 mA

*N.B: the relevant denotations are: f: frequency; I: current; V: voltage; PW: Pulse Width.

Table 4 reports the comparison of Performance summary between the proposed HGNS output stage and other works published in the literature.

Table 4: Performance comparison with previous works

Properties	[24] M.Azin	[47] R.Shulyzki	[48] S.Farahmand	This Work
Technology (µm)	0.35	0.35	0.18	0.35
Output impedance (MΩ)	>45	NA	160	275
Compliance voltage (%)	94	87	94	94
Power consumption (µw)	N/A	750	816	705.87
Stimulation Mode	Current	Current	current	current
Supply voltage (V)	5	3	1.8	3.3
Resolution (bits)	6	N/A	6	6

5. Conclusion

More recently, current OSA pathology treatment concepts turn out to rest on the idea of therapeutic electrical stimulation of the HGN. For this reason, a special architecture of the implantable HGNS was investigated. The stimulator output stage constitutes the most significant part of the implantable stimulator system, given the fact that it is connected directly with the biological tissue, in addition to its responsibility for triggering the stimulated nerve'

potential action. In this regard, an overview of existing topologies relevant to the architecture of neural stimulator output stages was provided, considering the stimulation mode, shape and safety measure characteristics. To this end, an output stage of implantable HGNS has been designed using standard 0.35µm CMOS technology. The goals of such architecture were focused on satisfying low voltage biomedical stimulators constraints fit for HGN stimulation. It proved to achieve an efficient performance comparing to the other output stages of stimulator design. Indeed, the proposed output stage design was able to show large voltage compliance of 3.1V under 3.3V power supply, high output impedance of 275MHz, and consuming an amount of low power consumption of the rate of 705.87µw. It permits the delivery of a maximal stimulation current of 1.17mA to the targeted tissue across a 1KΩ resistive load. As future work, the issue of communication between the pacing module (as a proposed design of output stage HGNS) and sensing module (P_{es} signal processing), which is already treated as part of a previously conducted work is envisaged to investigate. Hence, as the stimulated current pulses' intensity proves to depend highly on the severity of esophageal pressure amplitude decreases, the proposed HGNS architecture, depicted on Figure 1, could well stand as a key design that paves the way for the creation of new generations of HGNS.

Conflict of Interest

The authors declare no conflict of interest.

Acknowledgment

The authors are deeply grateful to Professor: ABDELMOULA Mohamed, Chief of the Maxillo-Facial Surgery Department of the CHU Habib BOURGUIBA University Hospital, Sfax, as well as to Dr. TURKI Mohamed pulmonologist, President of the Tunisian Society of Sleep Medicine (STMS) organization, for their direction, fruitful recommendations, and valuable aid in matters of relating issues.

References

[1] M. J Sateia, "International classification of sleep disorders-third edition highlights and modifications," Chest, **146**(5), 1387–1394, 2014, doi:10.1378/chest.14-0970.

[2] ResMed - Newsroom, The Lancet Publishes: More Than 936 Million Have Obstructive Sleep Apnea Worldwide | Resmed Inc, 2019.

[3] J. Bousquet, N. Khaltaev, eds., Global surveillance, prevention and control of chronic respiratory diseases : a comprehensive approach, WHO Organisation, 2007.

[4] I.T. Morgenthaler, V. Kagramanov, V. Hanak, P. A Decker, "Complex Sleep Apnea Syndrome: Is It a Unique Clinical Syndrome?," Sleep, **29**(9), 1109–110, 2006, doi:https://doi.org/10.1093/sleep/29.9.1109.

[5] J. Guo, Y. Sun, L.-J. Xue, Z.-Y. Huang, Y.-S. Wang, L. Zhang, G.-H. Zhou, L.-X. Yuan, "Effect of CPAP therapy on cardiovascular events and mortality in patients with obstructive sleep apnea: a meta-analysis," Sleep and Breathing, **20**(3), 965–974, 2016.

[6] T. E. Weaver, A. M.Sawyer, "Adherence to Continuous Positive Airway Pressure Treatment for Obstructive Sleep Apnea: Implications for Future Interventions," The Indian Journal of Medical Research, **131**, 245–258, 2010.

[7] I. Smith, V. Nadig, T. J.Lasserson, "Educational, supportive and behavioural interventions to improve usage of continuous positive airway pressure machines in adults with obstructive sleep apnoea," Cochrane Database of Systematic Reviews, **2**, 2009, doi:10.1002/14651858.CD007736.

[8] T. Young, L. Finn, P. E. Peppard, M. Szklo-Coxe, D. Austin, F.J. Nieto, R. Stubbs, K.M. Hla, "Sleep Disordered Breathing and Mortality: Eighteen-Year Follow-up of the Wisconsin Sleep Cohort," Sleep, **31**(8), 1071–1078, 2008, doi:https://doi.org/10.5665/sleep/31.8.1071.

[9] A.R. Schwartz, D.C. Thut, B. Russ, M. Seellagy, X. Yuan, R.G. Brower, S. Permutt, R. A. WISE, P. L.SMITH, "Effect of electrical stimulation of the hypoglossal nerve on airflow mechanics in the isolated upper airway," American Review of Respiratory Disease, **147**(5), 1144–1150, 1993, doi:10.1164/ajrccm/147.5.1144.

[10] D.W. Eisele, A.R. Schwartz, A. Hari, D.C. Thut, P.L. Smith, "The Effects of Selective Nerve Stimulation on Upper Airway Airflow Mechanics," Archives of Otolaryngol Ogy-Head & Neck Surgery, **121**(12), 1361–1364, 1995, doi:10.1001/archotol.1995.01890120021004.

[11] W. Hida, H. Kurosawa, S. Okabe, Y. Kikuchi, J. Midorikawa, Y. Chung, T. Takishima, K. Shirato, "Hypoglossal nerve stimulation affects the pressure-volume behavior of the upper airway.," American Journal of Respiratory and Critical Care Medicine, **151**(2), 455–460, 1995, doi:https://doi.org/10.1164/ajrccm.151.2.7842206.

[12] A. Oliven, R.P. Schnall, G. Pillar, N. Gavriely, N. Odeh, "Sublingual electrical stimulation of the tongue during wakefulness and sleep," Respiration Physiology, **127**(2–3), 217–226, 2001, doi:https://doi.org/10.1016/S0034-5687(01)00254-7.

[13] H. Zhang, J.-Y. Ye, L. Hua, Z.-H. Chen, L. Ling, Q. Zhu, L.-M. Wang, L. Zheng, Y.-H. Zhang, "Inhomogeneous neuromuscular injury of the genioglossus muscle in subjects with obstructive sleep apnea," Sleep and Breathing, **19**(2), 539–545, 2015, doi:https://doi.org/10.1007/s11325-014-1044-3.

[14] G. Ben salah, K. Abbes, C. Abdelmoula, M. Masmoudi, "Hypoglossal nerve stimulation in the treatment of obstructive sleep apnea," in 2017 14th International Multi-Conference on Systems, Signals & Devices (SSD), 429–433, 2017, doi:10.1109/SSD.2017.8166976.

[15] G. Ben salah, K. Abbes, C. Abdelmoula, M. Masmoudi, Obstructive Sleep Apnea treatment Methods: A Comparative Study, 77–96, 2019, doi:10.1515/9783110592566-005.

[16] G. Ben Salah, K. Abbes, Ch. Abdelmoula, M.H. Abdelmoula, M. Turki, M. Masmoudi, "Obstructive Sleep Apnea OSA detection through esophageal Pressure Pes," in 2019 IEEE International Conference on Design & Test of Integrated Micro & Nano-Systems (DTS), 1–4, 2019, doi:10.1109/DTSS.2019.8914748.

[17] V. Skiba, C. Goldstein, H. Schotland, "Night-to-Night Variability in Sleep Disordered Breathing and the Utility of Esophageal Pressure Monitoring in Suspected Obstructive Sleep Apnea," Journal of Clinical Sleep Medicine, **11**(6), 597–602, 2015, doi:https://doi.org/10.5664/jcsm.4764.

[18] D.R. Cantrell, J.B. Troy, "Extracellular stimulation of mouse retinal ganglion cells with non-rectangular voltage-controlled waveforms," in 2009 Annual International Conference of the IEEE Engineering in Medicine and Biology Society, 642–645, 2009, doi:10.1109/IEMBS.2009.5333464.

[19] M. Sivaprakasam, W. Liu, W. Guoxing, J.. Weiland, M.S. Humayun, "Architecture tradeoffs in high-density microstimulators for retinal prosthesis," IEEE Transactions on Circuits and Systems I: Regular Papers, **52**(12), 2629–2641, 2005, doi:10.1109/TCSI.2005.857554.

[20] K.E. Jones, R.A. Normann, "An advanced demultiplexing system for physiological stimulation," IEEE Transactions on Biomedical Engineering, **44**(12), 1210–1220, 1997, doi:10.1109/10.649992.

[21] M. Sivaprakasam, W. Liu, M.S. Humayun, J.D. Weiland, "A variable range bi-phasic current stimulus driver circuitry for an implantable retinal prosthetic device," IEEE Journal of Solid-State Circuits, **40**(3), 763–771, 2005, doi:10.1109/JSSC.2005.843630.

[22] J. Vidal, M. Ghovanloo, "Towards a Switched-Capacitor based Stimulator for efficient deep-brain stimulation," in 2010 Annual International Conference of the IEEE Engineering in Medicine and Biology, 2927–2930, 2010.

[23] J. Lee, H.-G. Rhew, D. R. Kipke, M. P. Flynn, "A 64 Channel Programmable Closed-Loop Neurostimulator With 8 Channel Neural Amplifier and Logarithmic ADC," IEEE JOURNAL OF SOLID-STATE CIRCUITS, **45**(9), 1935–1945, 2010, doi:10.1109/JSSC.2010.2052403.

[24] M. Azin, P. Mohseni, "A high-output-impedance current microstimulator for anatomical rewiring of cortical circuitry," in 2008 IEEE International Symposium on Circuits and Systems, 2502–2505, 2008, doi:10.1109/ISCAS.2008.4541964.

[25] N.S. Davidovics, G.Y. Fridman, B. Chiang, C.C. Della Santina, "Effects of Biphasic Current Pulse Frequency, Amplitude, Duration, and Interphase Gap on Eye Movement Responses to Prosthetic Electrical Stimulation of the Vestibular Nerve," IEEE TRANSACTIONS ON NEURAL SYSTEMS AND REHABILITATION ENGINEERING, **19**(1), 84–94, 2011, doi:10.1109/TNSRE.2010.2065241.

[26] X. Liu, A. Demosthenous, N. Donaldson, "An integrated implantable stimulator that is fail-safe without off-chip blocking-capacitors.," IEEE Transactions on Biomedical Circuits and Systems, **2**(3), 231–244, 2008, doi:10.1109/TBCAS.2008.2003199.

[27] M.B. Bugbee, An implantable stimulator for selective stimulation of nerves.,

University College of London, 2000.
[28] J.-J. Sit, R. Sarpeshkar, "A Low-Power Blocking-Capacitor-Free Charge-Balanced Electrode-Stimulator Chip With Less Than 6 nA DC Error for 1-mA Full-Scale Stimulation," IEEE Transactions on Biomedical Circuits and Systems, **1**(3), 172–183, 2007, doi:10.1109/TBCAS.2007.911631.
[29] M. Ortmanns, A. Rocke, M. Gehrke, H.-Jü. Tiedtke, "A 232-Channel Epiretinal Stimulator ASIC," IEEE Journal of Solid-State Circuits, **42**(12), 2946–2959, 2007, doi:10.1109/JSSC.2007.908693.
[30] I. Williams, G.T. Constandinou, "An Energy-Efficient, Dynamic Voltage Scaling Neural Stimulator for a Proprioceptive Prosthesis," IEEE Transactions on Biomedical Circuits and Systems, **7**(2), 129–139, 2013, doi:10.1109/TBCAS.2013.2256906.
[31] O. Macherey, A. van Wieringen, R.P. Carlyon, J.M. Deeks, J. Wouters, "Asymmetric Pulses in Cochlear Implants: Effects of Pulse Shape, Polarity, and Rate," Journal of the Association for Research in Otolaryngology, **7**(3), 253–266, 2006, doi:10.1007/s10162-006-0040-0.
[32] Z.-Y. Cui, H.-L. Piao, N.-S. Kim, "A 10-bit Current-steering DAC in 0.35-μm CMOS Process," Transactions on Electrical and Electronic Materials, **10**(2), 44–48, 2009, doi:10.4313/TEEM.2009.10.2.044.
[33] H. Aboobacker, A.R. Krishna, R. Jayachandran, "Design, Implementation and Comparison of 8 Bit 100 Mhz Current Steering Dacs," International Journal of Engineering Research and Applications, **3**(4), 881–886, 2013.
[34] A. Van den Bosch, M. Steyaert, W. Sansen, Solving Static and Dynamic Performance Limitations for High Speed D/A Converters, 189–210, 2003, doi:10.1007/0-306-47950-8_10.
[35] M.G. Lima, S.R. Craig Jr, RFID-based apparatus, system, and method for therapeutic treatment of obstructive sleep apnea, 772579525, United States, 2010.
[36] J.B. Velloso, M.N. Souza, "A Programmable System of Functional Electrical Stimulation (FES)," in 2007 29th Annual International Conference of the IEEE Engineering in Medicine and Biology Society, 2234–2237, 2007, doi:10.1109/IEMBS.2007.4352769.
[37] M. Chen, B. Wu, X. Lou, T. Zhao, J. Li, Z. Xu, X. Hu, X. Zheng, "A self-adaptive foot-drop corrector using functional electrical stimulation (FES) modulated by tibialis anterior electromyography (EMG) dataset," Medical Engineering & Physics, **35**(2), 195–204, 2013, doi:10.1016/j.medengphy.2012.04.016.
[38] K.W.E. Cheng, Y. Lu, R.K.-Y. Tong, A.B. Rad, "Development of a Circuit for Functional Electrical Stimulation," IEEE Transactions on Neural Systems and Rehabilitation Engineering, **12**(1), 43–47, 2004, doi:10.1109/TNSRE.2003.819936.
[39] J. De Lima, A.S. Cordeiro, "A low-cost neurostimulator with accurate pulsed-current control," IEEE Transactions on Biomedical Engineering, **49**(5), 497–500, 2002, doi:10.1109/10.995689.
[40] M. Yochum, S. Binczak, T. Bakir, S. Jacquir, R. Lepers, "A mixed FES/EMG system for real time analysis of muscular fatigue," in 2010 Annual International Conference of the IEEE Engineering in Medicine and Biology, 4882–4885, 2010, doi:10.1109/IEMBS.2010.5627264.
[41] S. Khosravani, N. Lahimgarzadeh, A. Maleki, "Developing a stimulator and an interface for FES-cycling rehabilitation system," in 2011 18th Iranian Conference of Biomedical Engineering (ICBME), 175–180, 2011, doi:10.1109/ICBME.2011.6168550.
[42] A. Masdar, B.S.K.K. Ibrahim, M.M.A. Jamil, "Development of wireless-based low-cost current controlled stimulator for patients with spinal cord injuries," in 2012 IEEE-EMBS Conference on Biomedical Engineering and Sciences, 493–498, 2012, doi:10.1109/IECBES.2012.6498175.
[43] M. Willand, H. Debruin, "Design and Testing of an Instrumentation System to Reduce Stimulus Pulse Amplitude Requirements During FES," in 2008 30th Annual International Conference of the IEEE Engineering in Medicine and Biology Society, 2764–2767, 2008, doi:10.1109/IEMBS.2008.4649775.
[44] H. Qu, T. Wang, M. Hao, P. Shi, W. Zhang, G. Wang, N. Lan, "Development of a network FES system for stroke rehabilitation," in 2011 Annual International Conference of the IEEE Engineering in Medicine and Biology Society, 3119–3122, 2011, doi:10.1109/IEMBS.2011.6090851.
[45] F. Brunetti, Á. Garay, J.C. Moreno, J.L. Pons, "Enhancing functional electrical stimulation for emerging rehabilitation robotics in the framework of hyper project," in 2011 IEEE International Conference on Rehabilitation Robotics, 1–6, 2011, doi:10.1109/ICORR.2011.5975370.
[46] S.C.H. Olivares, M. Tarulli, A. Prodic, M.R. Popovic, P.W. Lehn, "A universal functional electrical stimulator based on merged flyback-SC circuit," in 2012 15th International Power Electronics and Motion Control Conference (EPE/PEMC), 3–5, 2012, doi:10.1109/EPEPEMC.2012.6397471.
[47] R. Shulyzki, K. Abdelhalim, R. Genov, "CMOS current-copying neural stimulator with OTA-sharing," in Proceedings of 2010 IEEE International Symposium on Circuits and Systems, 1232–1235, 2010, doi:10.1109/ISCAS.2010.5537284.
[48] S. Farahmand, M.H. Maghami, A.M. Sodagar, "Programmable high-output-impedance, large-voltage compliance, microstimulator for low-voltage biomedical applications," in 2012 Annual International Conference of the IEEE Engineering in Medicine and Biology Society, 863–866, 2012, doi:10.1109/EMBC.2012.6346068.

ASTES

Advances in Science, Technology and Engineering Systems Journal Vol. 5, No. 5, 864-868 (2020)

www.astesj.com

ASTESJ

ISSN: 2415-6698

Primary Healthcare Response to COVID 19 in a District of Callao, Peru

Juan Morales[*, 1], Marlene Raquel Basilio-Rojas[2], Maria Rosa Gonzales-Gonzales[2], Ana Paula Goyzueta[3]

[1]*E-Health Research Center, University of Sciences and Humanities, 15306, Peru*

[2]*Mi Peru Health Center, DIRESA Callao, 07056, Peru*

[3]*Faculty of Health Sciences, University of Sciences and Humanities, 15306, Peru*

ARTICLE INFO

Article history:
Received: 01 August, 2020
Accepted: 19 September, 2020
Online: 12 October, 2020

Keywords:
Primary Health Care
Home Care Services
Coronavirus Infections
Peru

ABSTRACT

Objectives: Describe the clinical characteristics and home care of patients diagnosed with COVID-19 in a Primary Healthcare Facility of the "Mi Peru" district, in the Callao Region, Peru. Materials and methods: Observational and descriptive cross-sectional study. A total of 84 subjects with positive results for Rapid Test IgM / IgG or molecular test (RT-PCR) participated. Results: Of the sample, 59.5% (n=50) were males, 60.7% (n=51) aged 30 to 59 years and 21.4% (n=18) aged 60 to over of age, 67.9% (n=57) were positive on the rapid test and the rest on the molecular test. Diabetes and high blood pressure were the main pathological antecedents. Among the most frequent clinical manifestations were general malaise, fever and cough, with 40.5% (n=34), 36.9% (n=31) and 31% (n=26), respectively. The most frequently prescribed medications were acetaminophen and azithromycin, 25% (n=21), and 21.4% (n=18), respectively. Regarding home monitoring of patients diagnosed with COVID-19, the first week was performed with a higher proportion of those affected, progressively decreasing in the second week. Conclusions: Evidence of an important response to COVID-19 is shown in the scenario of the first level of care. Mild and moderate cases can be treated outpatient and complemented with home monitoring, contributing to the containment of the pandemic.

1. Introduction

COVID-19 is a disease caused by type 2 coronavirus causing severe acute respiratory syndrome (SARS-CoV-2), originated in Wuhan (China) in December 2019, and on 30 January 2020, the World Health Organization (WHO) has declared it as a public health emergency of international importance [1]. Globally, the number of positive cases and the number of deaths from COVID-19 are terrifying, where the region of Americas recorded the highest number of cases in the world, led by the United States of North America and Brazil [2]. In Peru, the first case of COVID-19 was confirmed on 6th of March 2020 [3], since then the number of cases and deaths have had a sustained increase, Lima and Callao manifested the highest percentage [4].

In China, the majority of COVID-19 cases were symptomatic, the proportion of severe cases and the case fatality rate were 25.6% (17.4 to 34.9) and 3.6% (1.1 to 7.2), respectively; older patients and those with comorbidities resulted in more severe symptoms [5]. People with high blood pressure, diabetes, chronic obstructive pulmonary disease, cardiovascular and cerebrovascular disease were associated with serious complications and COVID-19 fatality [6]. Of the patients hospitalized for COVID-19, 20% required the use of Intensive Care Units (ICU) and 13.9% (95% CI 6.2–21.5%) of hospitalized patients had fatal results [7].

COVID-19 pandemic in addition to the enormous consequences for health systems. It also has an impact on the economic plane and on the labor market, both in supply and demand [8]. Social distancing, self-isolation, and travel restrictions forced a decrease in the workforce in all economic sectors and caused the loss of many jobs[9].

For COVID-19, to date, there are no specific medications or vaccines available [10]. So hospital support therapy remains the top priority; however, primary healthcare can play an important role in the COVID-19 response by differentiating patients with respiratory symptoms from those with COVID-19, making an early diagnosis, helping vulnerable people cope with their anxiety

[*] Corresponding author: Juan Morales, E-Health Research Center, University of Sciences and Humanities. Lima, Peru. Email: mdjuanmorales@gmail.com

towards the virus, and reducing the demand for hospital services [11].

In the fight against COVID-19, hospital establishments are the main protagonists; however, the growing demand for services has exceeded the response capacity of hospitals. For this reason, the establishments of the first level of care, which are generally more precarious, assume a more active role and act in two settings, intramural and extramural. The objective of the present study was to describe the clinical characteristics and home care of patients diagnosed with COVID-19 in a Primary Healthcare Facility of the "Mi Peru" district, in the Callao Region, Peru.

2. Materials and Methods

2.1. Design

An observational and descriptive cross-sectional study was held at "Mi Peru" Primary Healthcare Facility, located in the district of the same name, which belongs to the Callao Region. The source of information was the emergency medical records and monitoring records with a positive result for COVID-19. The attentions made by the special team COVID-19, in the period of April and May 2020, were considered.

2.2. Population and sample

Our study population consisted of all patients with a positive test report for COVID-19. All subjects who had a positive result for COVID-19, relevant sociodemographic, and clinical data, as well as information from the home follow-up, were included.

Of a total of 91 cases enrolled in the COVID-19 positive patient registry, seven were excluded because they did not have a record of confirmatory laboratory results. The sample was made up of 84 confirmed cases.

2.3. Study variables and instruments

COVID-19: Disease caused by the SARS-CoV-2 virus (Severe acute respiratory syndrome coronavirus 2), the diagnosis of which was established using the Rapid IgM / IgG Test or molecular test (RT-PCR) for COVID-19, according to the national technical document [12].

Comparison variables: Sex, age, type of test for the diagnosis of COVID-19, the establishment of diagnosis, contacts with people suspected of COVID-19, hospitalization, clinical condition, clinical manifestations, vital functions, body weight, saturation of oxygen, medical prescription, pathological history, and home care services of confirmed cases.

2.4. Statistic analysis

Data were obtained from the emergency medical records and from the home care services registry, then entered into a matrix in the IBM SPSS Statistics 23 program. Qualitative variables were distributed according to frequencies and represented in tables and graphs. For the variables belonging to the vital functions, the means and extreme values were determined.

2.5. Ethical considerations

Access to information sources was made with the authorization of the Chief Medical Officer of the "Mi Peru" Health Center and precautions were taken to safeguard the confidentiality of the data as indicated in the Declaration of Helsinki of the World Medical Association [13]. The Ethics Committee of the University of Sciences and Humanities (CEI Act No. 017-2020) approved the research project.

Table 1: Epidemiological characteristics of people diagnosed with COVID-19, District of "Mi Peru", Callao Region, 2020.

Epidemiological characteristics	n	%
Total	84	100
Sex		
Female	34	40.5
Male	50	59.5
Age (years)		
12-17	2	2.4
18-29	13	15.5
30-59	51	60.7
≥ 60	18	21.4
Type of test		
Molecular	27	32.1
Rapid	57	67.9
Health facility		
Local Health Center	78	92.9
Derivated from a hospital	6	7.1
Contacts		
No apparent contact	65	77.4
Positive contact	2	2.4
Contact with suspect	2	2.4
Sick family member	11	13.1
Deceased relative	3	3.6
Healthcare worker	1	1.2
Hospitalization		
No	81	96.4
Yes	3	3.6
Patient's condition		
Favorable evolution	78	92.9
Died	6	7.1
Referrals to a hospital	2	2.38
Medical history		
Diabetes	3	3.57
High blood pressure	3	3.57
Tuberculosis	1	1.19
Pregnant	2	2.38

3. Results

This study involved 84 patients of both sexes diagnosed with COVID 19, with a mean age of 45.3 years (SD = 16.74; Range: 15 to 98), with an average illness time of 8.65 days (Min. 3, Max. 21).

Of the participants, 59.5% (n=50) were male, 60.7% (n=51) aged 30-59 years and 21.4% (n=18) 60 or over. Of the sample, 67.9% (n=57) were positive to the rapid test and the rest to the molecular test, 92.9% (n=78) were performed at the "Mi Peru" Health Center. Most of the participants had no contact with people suspected of COVID-19; however, 16.7% (n=14) were in contact with a family member who was sick or died of COVID-19, 3.6% (n=3) were hospitalized, and 7.1% (n=6) of the sample died. Diabetes and high blood pressure were the main pathological antecedents among patients diagnosed with COVID-19 (Table 1).

Frequent clinical manifestations among patients diagnosed with COVID-19 were general malaise, fever and cough, with 40.5% (n=34), 36.9% (n=31) and 31% (n=26), respectively. Most frequently prescribed medications were acetaminophen and azithromycin, in 25% (n = 21) and 21.4% (n=18), respectively (Figure 1). During the evaluation, the patients had vital functions outside the normal parameters (Table 2).

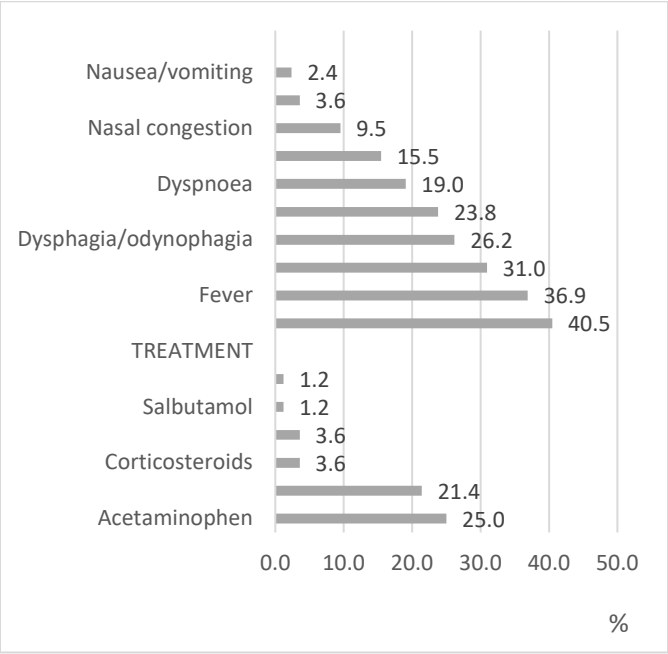


Figure 1: Clinical presentation and treatment in patients diagnosed with COVID-19, "Mi Peru" District, Callao Region, 2020.

Table 2: Vital functions of patients affected by COVID-19, "Mi Peru" district, Callao Region, 2020.

Vital functions	Mean	Min	Max
Systolic blood pressure	110.8	90	140
Diastolic blood pressure	67.2	40	80
Heart rate	91.15	65	116
Breathing rate	22.91	18	26
Temperature	37.15	36	39
Oxygen saturation	94.41	75	100
Body weight	76.77	54	103

Regarding home health monitoring of patients diagnosed with COVID-19, the first week was performed with a higher proportion of those affected, progressively decreasing in the second week (Figure 2).

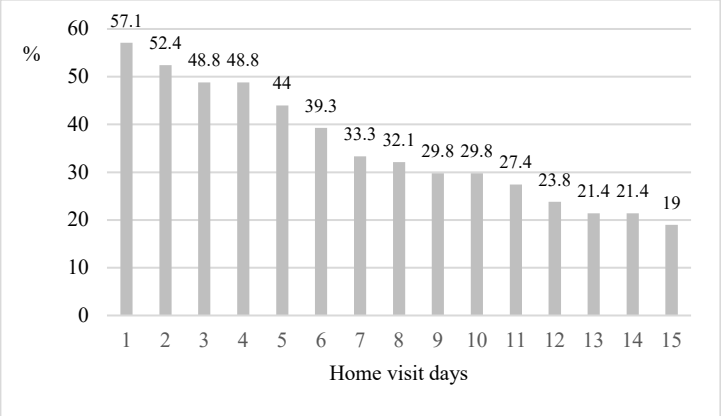


Figure 2: Home monitoring of patients diagnosed with COVID-19, "Mi Peru" district, Callao Region, 2020.

4. Discussion

In the present study, the majority of those affected by COVID-19 were males, mainly adults (30-59 years) and older adults (≥ 60 years). Among the most frequent comorbidities in patients diagnosed with COVID-19 were diabetes mellitus and high blood pressure. Frequent clinical manifestations were general malaise, fever, and cough, with an illness time of approximately one week. Despite having vital functions outside normal parameters, most required only outpatient treatment and home monitoring.

Clinical presentation of COVID-19 is not yet fully clarified, the symptoms vary from mild to severe. To date, the most commonly reported symptoms are fever, cough, myalgia, dyspnea, and less common symptoms include headache, diarrhea, hemoptysis, and a runny nose. Mild symptoms recover after one week, while severe cases experience progressive respiratory distress that can lead to death; the average reported incubation duration was seven days and ranges from two to 14 days [14].

In our research, the most frequent comorbidity in patients diagnosed with COVID-19 was diabetes mellitus and high blood pressure, which are frequent problems in the country and primary healthcare establishments play an important role in control and treatment. These findings are consistent with studies conducted in China, which indicate that the most prevalent comorbidity was high blood pressure and diabetes. Patients with any comorbidity have poorer clinical outcomes, and a higher number of comorbidities is correlated with poorer clinical outcomes [15].

Based on the finding, two pregnant women had positive tests for COVID-19 and only received outpatient treatment. Symptoms of COVID-19 in pregnant women are not different from that of non-pregnant women; vertical transmission has not been reported either. However, they can cause fetal distress, miscarriage, respiratory distress, and premature delivery [16], they can also end in an emergency cesarean section for these complications [17].

Patients with mild symptoms are eligible for isolation, while patients with severe pneumonia require hospitalizations and frequent access to intensive care units [10]. Although to date there

are no specific medications or vaccines available for the treatment of COVID-19, different drug therapies have been tried that have offered a limited level of evidence [10].

Regarding the drugs used in the health response, Azithromycin and Acetaminophen were the most frequently indicated drugs and are among the drugs included in the technical documents of the Ministry of Health (MINSA). According to the Technical Standard of the MINSA, for the management of moderate and severe cases in hospitalized patients, Chloroquine Phosphate or Hydroxychloroquine plus Azithromycin has been considered [12], after, at the proposal of the Peruvian Society of Hematology, Enoxaparin was incorporated in moderate and severe clinical scenarios [18]. In RM N° 270-2020-MINSA, published on 8 May 2020, for mild cases, Hydroxychloroquine plus Ivermectin was considered; while for moderate to severe cases, Hydroxychloroquine, Azithromycin plus Ivermectin [19].

Although vital functions and oxygen saturation were found altered in the initial evaluation, only two patients needed reference for hospital management. In the Health Center of the "Mi Peru" district, the hospitalization service still does not work, so the figure of 3.6% of those hospitalized refers to patients who went alone to some other hospital in the Callao Region and were hospitalized.

Most of the patients were diagnosed at the "Mi Peru" Health Center, with an indication for outpatient treatment and monitored by phone and in person. In-person monitoring was carried out in their homes and consisted of clinical evaluation; verify treatment compliance, providing orientation, and comprehensive sanitary information. Extramural monitoring has been prioritized during the first week of evolution and responds mainly to insufficient human and technological resources. According to the Technical Standard of the MINSA, clinical follow-up must be carried out in all mild cases with or without risk factors during 14 days, the frequency is every 24 hours if it is remote and the face-to-face follow-up every 72 hours or earlier if the evolution Clinic requires it [12]. Most COVID-19 patients can be managed remotely with advice on symptomatic management and self-isolation; consultations can be made by phone, and the video also provides additional visual cues and therapeutic presence [20].

In a scenario where the response capacity of hospital centers has reached its limit, primary healthcare establishments considered as the gateway to the health system and that in Peru they represent 98% of all Establishments [21], which can take a more active role in controlling the pandemic. It is then necessary to strengthen the team that works in these establishments and improve the referral-counter-referral process to optimize limited resources, adding up the effort in the fight against the fearsome pandemic. Strong primary care systems form the basis of any emergency response, trained professionals can provide care across the spectrum of prevention, preparedness, response, and recovery; primary healthcare professionals must also participate in planning and action for risk management of health emergencies [22].

The following limitations should be considered in the study. The sample size has not allowed establishing relationships between the variables; due to the lack of uniformity in the complete filling in of medical records, the frequency of symptoms, treatment, vital functions, and home follow-up has been performed with less than the total number of participants. Despite these limitations, the study shows favorable results and can approximate the scenarios of primary healthcare establishments.

5. Conclusions

Evidence of an important response to COVID-19 is shown in the scenario of the first level of care. Mild to moderate cases can be managed on an outpatient basis and with home follow-up, contributing to the containment of the pandemic. Strengthen the first level of care to continue promoting preventive measures, diagnosis, treatment, and home follow-up, as well as improving the reference system for cases that require management in the hospital setting.

Conflict of Interest

The authors declare no conflict of interest.

Acknowledgment

Special thanks to Dr. Iván Vidal Puma and Glenys Olivos Lecarnaque from the "Mi Peru" Health Center, for the administrative advice.

References

[1] World Health Organization, Rolling updates on coronavirus disease (COVID-19), WHO, (Updated 25 May 2020), 2020.
[2] World Health Organization, Coronavirus Disease (COVID-19), 2020.
[3] Gobierno del Perú, Coronavirus en el Perú: casos confirmados, 2020.
[4] Ministerio de Salud, Sala Situacional COVID-19 Perú, Lima, Perú, 2020.
[5] L. Fu, B. Wang, T. Yuan, X. Chen, Y. Ao, T. Fitzpatrick, P. Li, Y. Zhou, Y. fan Lin, Q. Duan, G. Luo, S. Fan, Y. Lu, A. Feng, Y. Zhan, B. Liang, W. Cai, L. Zhang, X. Du, L. Li, Y. Shu, H. Zou, "Clinical characteristics of coronavirus disease 2019 (COVID-19) in China: A systematic review and meta-analysis," Journal of Infection, **Apr 10**, 2020, doi:10.1016/j.jinf.2020.03.041.
[6] B. Wang, R. Li, Z. Lu, Y. Huang, "Does comorbidity increase the risk of patients with covid-19: Evidence from meta-analysis," Aging, **12**(7), 6049–6057, 2020, doi:10.18632/AGING.103000.
[7] A.J. Rodriguez-Morales, J.A. Cordona-Ospina, E. Gutiérrez-Ocampo, R. Villamizar-Peña, Y. Holguin-Rivera, "Clinical , laboratory and imaging features of COVID-19 : A systematic review and meta-analysis," Travel Medicine and Infectious Disease, **34**(March), 2020, doi:10.1016/j.tmaid.2020.101623.
[8] Organización Internacional del Trabajo, El COVID-19 y el mundo del trabajo: repercusiones y respuestas, 2020.
[9] M. Nicola, Z. Alsafi, C. Sohrabi, A. Kerwan, A. Al-Jabir, C. Iosifidis, M. Agha, R. Agha, "The Socio-Economic Implications of the Coronavirus Pandemic (COVID-19): A Review," International Journal of Surgery, **78**(March), 185–193, 2020, doi:10.1016/j.ijsu.2020.04.018.
[10] C. Scavone, S. Brusco, M. Bertini, L. Sportiello, C. Rafaniello, A. Zoccoli, L. Berrino, G. Racagni, F. Rossi, A. Capuano, "Current pharmacological treatments for COVID-19: what's next?," British Journal of Pharmacology, (April), 1–12, 2020, doi:10.1111/bph.15072.
[11] World Health Organization, Role of primary care in the COVID-19 response, 2020.
[12] Ministerio de Salud del Perú, Documento Técnico. Prevención y atención de personas afectadas por COVID-19 en el Perú, Perú, 2020.
[13] Asociación Médica Mundial, Declaración de Helsinki de la AMM-Principios éticos para las investigaciones médicas en seres humanos.
[14] S.P. Adhikari, S. Meng, Y. Wu, Y. Mao, R. Ye, Q. Wang, C. Sun, S. Sylvia, S. Rozelle, H. Raat, H. Zhou, "Epidemiology, causes, clinical manifestation and diagnosis, prevention and control of coronavirus disease (COVID-19) during the early outbreak period: a scoping review," Infectious Disease Poverty, **9**(29), 1–12, 2020, doi:10.1186/s40249-020-00646-x.
[15] W.J. Guan, W.H. Liang, Y. Zhao, H.R. Liang, Z.S. Chen, Y.M. Li, X.Q. Liu, R.C. Chen, C.L. Tang, T. Wang, C.Q. Ou, L. Li, P.Y. Chen, L. Sang, W. Wang, J.F. Li, C.C. Li, L.M. Ou, B. Cheng, S. Xiong, Z.Y. Ni, J. Xiang, Y. Hu, L. Liu, H. Shan, C.L. Lei, Y.X. Peng, L. Wei, Y. Liu, et al., "Comorbidity and its impact on 1590 patients with COVID-19 in China: a

nationwide analysis," The European Respiratory Journal, **55**(March 2020), 2020, doi:10.1183/13993003.00547-2020.
[16] L. Panahi, M. Amiri, S. Pouy, "Risks of Novel Coronavirus Disease (COVID-19) in Pregnancy; a Narrative Review.," Archives of Academic Emergency Medicine, **8**(1), e34, 2020.
[17] Y. Liu, H. Chen, K. Tang, Y. Guo, "Clinical manifestations and outcome of SARS-CoV-2 infection during pregnancy," Journal of Infection, (January 2020), 2020, doi:10.1016/j.jinf.2020.02.028.
[18] Ministerio de Salud del Perú, Modificación del documento de Prevención Diagnóstico y Tratamiento, RM 240-2020-MINSA, 2020.
[19] Ministerio de Salud del Perú, RM N° 270-2020-MINSA, 2020.
[20] T. Greenhalgh, G.C.H. Koh, J. Car, "Covid-19: A remote assessment in primary care," The BMJ, **368**(March 2020), 1–5, 2020, doi:10.1136/bmj.m1182.
[21] Ministerio de Salud, Plan Nacional de Fortalecimiento del Primer Nivel de Atención 2011 - 2021, Lima-Perú, 2011.
[22] C. Dunlop, A. Howe, D. Li, L.N. Allen, "The coronavirus outbreak: the central role of primary care in emergency preparedness and response," BJGP Open, 2020, doi:10.3399/bjgpopen20x101041.

ASTES

Advances in Science, Technology and Engineering Systems Journal Vol. 5, No. 5, 869-875 (2020)

www.astesj.com

ASTESJ

ISSN: 2415-6698

Path Loss Estimation for Some Korek-Telecom Sites Operating at (1.8) GHz and (2.1) GHz for Urban and Suburban Area in Erbil City

Sattar Othman Hasan*, Sevan Siyyah Abdullah

Salahaddin University-Erbil, Physics Department, College of Education, Erbil, 44001, Iraq

ARTICLE INFO

Article history:
Received: 01 August, 2020
Accepted: 29 September, 2020
Online: 12 October, 2020

Keywords:
Radio wave propagation
Path loss
Derive test
Signal strength

ABSTRACT

This investigation deals with the identification of the suitable empirical models for predicting radio wave propagation path losses in Erbil city of Kurdistan region in Iraq. For this purpose, two sites of Korek Telecom operating at 1800 MHz and 2100 MHz have been selected at urban and sub-urban environments in the city and seven different empirical path loss model named free space model, ECC-33, Stanford Interim University (SUI), Optimized Cost-231, Okumura-Hata, Egli, and Ericson models are tested against experimentally measured path loss values. The path loss was measured experimentally using Sony Ericson handset with complete required equipment and the results are compared to that predicted by each of the mentioned empirical models. The results which have been analyzed through the identification of Root Mean Square Error value achieved by each model revealed that the Optimized Cost-231 and Ericson model provide lowest Root Mean Square Error values. They provide RMSE values of 9.21, 9.38 and 1.58 and 4.12 at operating frequency of 1800 MHz, while at frequency 2100 MHz they gave 7.28, 6.07, 11.86 and 7.54, for sub-urban and urban areas, respectively. Therefore, it was concluded that the Optimized Cost-231 followed by Ericson model would be more reliable and best candidate for use in planning and designing network communication in the urban and suburban areas in the investigated area.

1. Introduction

In Kurdistan region of Iraq, the access to Global System for Mobile Communication (GSM) has become most active industry in 2005 to the present day. The numbers of network service providers continue to increase, but the quality of their services is poor due to several factors. The investigation and identification of the possible factors and proper solutions through scientific findings became necessary towards solving problems faced by the customers [1]. The wireless communication systems are a process by which the electromagnetic waves propagated from one location to another transferring data or information without any wire [2]. With constant increase in the field of GSM for mobile communication, the need for providing high quality data and reliable network services be an urgent issue for user services demands. Generally, development in the wireless communications systems has now become down due to focusing technological advancements. Therefore, in order to obtain reliable and suitable coverage area for wireless communication, high quality with high capacity networks and accurate estimation of signal strength must be taken into consideration [1, 2].

The signal strength of radio wave decreases when propagating between the transmitter and/or receiver due to many factors such as, reflection, diffraction, scattering, path distance, environments (i.e. urban, suburban or rural), height of the transmitter and receiver antennas and absorption by the object of the environment as well as operation frequencies [3]. Such reduction in the power strength of the signal is known as radio wave propagation path loss. Mathematically, it is expressed as the ratio between the transmitted power P_t to received power P_r as given by [4]:

$$\mathrm{PL(dB)} = 10 \log \frac{P_t}{P_r} \quad (1)$$

The models presented in the literature for path loss calculations play an important role in planning and designing of any wireless communication systems. They are based on a series of

* Corresponding Author: Sattar Othman Hasan, sattar.hasan@su.edu.krd

mathematical equations that are used for predicting radio wave propagation signal strength in a definite environment [5]. The proper estimation of radio frequency path losses leads to the development of efficient network planning to operate at high quality with high capacity network.

In recent years, different propagation path loss models were presented to help the wireless systems to provide high quality and service delivery. These models cannot be generalized to all environments, since each of which may applicable for a specific environment and at a certain operational frequency [6]. The main objective of this research is to identify the model environment suitable for predicting radio wave propagation path loss in Erbil city of Kurdistan region in Iraq. The outcome may be assisting the wireless communication companies to plans for the best Global System for Mobile Communication (GSM) networks in the city under consideration.

For this purpose, two of the Korek telecom cellular sites operating at frequencies 1.8 GHz and 2.1 GHz are selected and investigated with the use of seven familiar empirical path loss models. The selected sites are located at Sharawany(sub-urban) and Bakhtiary(urban) which are two districts area in the Erbil city of different location and have different building organization. The procedure of the measured and calculated results is described in the following sections.

2. Empirical models

As previously mentioned, there were different proposed models considered under different circumstances and positions for estimating radio wave path loss. This fact implies that the reliability of any model that predict path loss accurately, based on the terrain in which it is developed.

The most familiar empirical models that are available for estimating radio wave propagation path loss in different environment are, free space, ECC-33, Stanford Interim University (SUI), Optimized Cost-231, Okumura-Hata, Egli and Ericson models. The mathematical equations and their application ranges for each of these models that have been considered in this study are described briefly in the following subsections individually.

2.1. Path loss model for free space

For free-space path loss model, the lost in signal strength is specified only by the frequency operation and separation distance between transmitter and/or receiver without taking into account the signal reflection or absorption by object surrounding the medium. The theoretical derivation of the free space path loss formula is given by [7]:

$$\mathrm{PL_{FSPL}} = 32.45 + 20\log_{10}(d) + 20\log_{10}(f_c) \quad (2)$$

2.2. Okumura –Hata model

The Okumura-Hata model is one of the most familiar models which is very applicable for path loss prediction. Generally, most of path loss empirical models are consolidate form of the Okumura model which can be used at frequencies up to 3 GHz. This model is applicable for a separation ranges of about 100 km between transmitter and receiver and for the receiver height in between 3 m to 10 m. The path loss expression in this model has different form according to the environment of wave propagation and are as follows [8]:

Rural environment (dB)

$$\mathrm{PL(dB)} = 69.55 + 26.16\log_{10}(f_c) - 13.82\log_{10}(h_t) + \left(44.9 - 6.55\log_{10}(h_t)\right)\log_{10}(d) - 4.78\left(\log_{10}(f_c)\right)^2 + 18.33\log_{10}(f_c) + 40.94 \quad (3)$$

Suburban areas path loss (dB)

$$\mathrm{PL(dB)} = 69.55 + 26.16\log_{10}(f_c) - 13.82\log_{10}(h_t) + \left(44.9 - 6.55\log_{10}(h_t)\right)\log_{10}(\mathrm{d}) - 2\left(\log_{10}\frac{f_c}{28}\right)^2 + 10.8 - \mathrm{E} \quad (4)$$

Urban area path loss (dB)

$$\mathrm{PL(dB)} = 69.55 + 26.16\log_{10}(f_c) - 13.82\log_{10}(h_t) + \left(44.9 - 6.55\log_{10}(h_t)\right)\log_{10}(\mathrm{d}) - \mathrm{E} \quad (5)$$

where, $\mathrm{E} = 3.2[\log_{10}(11.75\,h_r)]^2 - 4.97$

In all considered models, the following parameter symbols have the same representation and are as follows [8]-[9]:
h_t: transmitter antenna height in m,
h_r: receiver antenna height in m,
d: distance between base station and mobile receiver in km,
f_c: operating frequency in MHz.

2.3. Optimization Cost-231

The equation of the path loss proposed by this model is an extension of COST-231 by introducing a correction factor through the least square fitting process of the measured data by [8]:

$$\mathrm{PL(dB)} = 41.42 + 33.9\log_{10}(f_c) - 13.82\log_{10}(h_t) - \mathrm{a}(h_r) + [44.9 - 6.55\log_{10}(h_r)]\log_{10}(d) + \mathrm{C_K} \quad (6)$$

The correction factor Ck = 0 dB for suburban and Ck =3 dB for urban environments. the expression for $\mathrm{a}(h_r)$, for sub-urban and rural environments, is:

$$\mathrm{a}(h_r) = (1.11\log(f_c) - 0.7)h_r - (1.56\log(f_c) - 0.8) \quad (7)$$

While $\mathrm{a}(h_r)$ in urban area for $f_c \geq 400$ MHz is:

$$\mathrm{a}(h_r) = (3.20[\log 11.75\,h_r\,]2\,) - 4.97 \quad (8)$$

2.4. Ecc-33 model receiver

The ECC-33 path loss model is proposed by Electronic Communication Committee (ECC) which is considered as an appropriate model for the UHF frequency band. This model derived on the bases of the extrapolation to the measurement path loss data by Okumura model. The general path loss representation formula for this model is [10]:

$$\mathrm{PL(dB)} = \mathrm{A_f} + \mathrm{A_m} - \mathrm{G}_t - \mathrm{G}_r \quad (9)$$

where, G_t and G_r, are transmitter and receiver antenna height gain factor, respectively, while $(\mathrm{A_f})$ represent attenuation due free space [dB] and $(\mathrm{A_m})$ is accounted for median path loss [dB]. They are mathematically defined as given by [11]:

$$\mathrm{A_f} = 92.4 + 20\log_{10}(d) + 20\log_{10}(f_c) \quad (10)$$

$$\mathrm{A_m} = 20.41 + 9.83\log_{10}(d) + 7.894\log_{10}(f_c) + 9.56[\log_{10}(f_c)]^2 \quad (11)$$

$$\mathrm{G}_t = \log_{10}\left(\frac{h_t}{200}\right)\{13.958 + 5.8[\log_{10}(d)]^2\} \quad (12)$$

$$\mathrm{G}_r = [42.57 + 13.7\log_{10}(f_c)][\log_{10}(h_r) - 0.585] \quad (13)$$

for rural and medium city,

$$\mathrm{G}_r = 0.759(h_r) - 1.862 \quad \text{for large city} \quad (14)$$

2.5. Stanford University Interim (SUI) model

The SUI model extended the Hata model by modification of some parameters in order to be applied to a frequency bands up to 3 GHz. In this model, the base station antenna height allows to vary from 10 m to 80 m and the receiver height can take values between 2 m to 20 m. This model proposed different mathematical formula for different types of environment, such as dense urban, hilly regions and rural with moderate vegetation areas. Here, the basic path loss expression for SUI model with its correction factors are presented which given by [12]:

$$\mathrm{PL(dB)} = \alpha + 10\,\beta\log\left(\frac{d}{d_r}\right) + \mathrm{Y}_f + \mathrm{Y}_h + \mathrm{s} \quad \text{for } d > d_r \quad (15)$$

where, (d_r) is the reference distance $(d_r = 100\,m)$, (d) is the separation distance between transmitter and receiver antenna in meters. The parameter (β) is called path loss exponent factor and is determined through the equation below:

$$\beta = \mathrm{a} - \mathrm{b}\,h_t + \frac{c}{h_t} \quad (16)$$

Both (Y_f) *and* (Y_h) are the frequency correction factor and correction factor for receiving antenna height, respectively, and they are given by [13]-[14] as:

$$\mathrm{Y}_f = 6.0\log_{10}\left(\frac{f_c}{2000}\right) \quad (17)$$

For sub-urban and urban city Y_h is expressed as:

$$\mathrm{Y}_h = -10.8\log_{10}\left(\frac{h_r}{2000}\right) \quad (18)$$

While for rural area or small size city is given as:

$$\mathrm{Y}_h = -20.0\log_{10}\left(\frac{h_r}{2000}\right) \quad (19)$$

The shadowing factor is represented by parameter (s) and its values is in between 8.2 dB and 10.6 dB [14]. The value of the constants a , b and c which depend upon the environment types are given in Table 1. Finally, the parameter (α) is known as the intercept factor and is expressed as [10-15]:

$$\alpha = 20\log_{10}\left(\frac{4\pi d_r}{\lambda}\right) \quad (20)$$

where, (λ) is the wavelength in (m),

Table 1: Different terrains and their parameters for SUI model [14-15].

Model Parameter	Urban	Sub-urban	Rural
S	10.6	9.6	8.2
c (m)	12.6	17.1	20.0
b (m^{-1})	0.0075	0.0065	0.0050
a	4.6	4.0	3.6

2.6. Egli model

The Egli model is a reliable model for use in network communication systems for a frequency bands from 3MHz to 3GHz and is usually applicable when a fixed antenna and receiver mobile antenna are line of sight LOS [16]. The Egli path loss model is an empirical model based on real data measurement and it mathematically presented by [16]-[18] as:

$$\mathrm{PL(dB)} = 20\log_{10}(f_c) + \mathrm{P}_l + 76.3 \qquad h_r \leq 10 \quad (21)$$

$$\mathrm{PL(dB)} = 20\log_{10}(f_c) + \mathrm{P}_l + 83.9 \qquad h_r > 10 \quad (22)$$

where,

$$\mathrm{P}_l = 40\log_{10}(d) - 20\log_{10}(h_t) - 10\log_{10}(h_r) \quad (23)$$

2.7. Ericson model

The Ericson company provided a software by their network designing engineers for predicting radio wave path losses so is called Ericson model. This model also stands on the modification of Okumura-Hata model according to the wave propagation environment. The mathematical formula given by this model is expressed as [19].

$$\mathrm{PL(dB)} = \mathrm{a_o} + \mathrm{a_1}\log(d) + \mathrm{a_2}\log(h_t) + \mathrm{a_3}\log(h_t).\log(d) - 3.2\,[\log(11.75\,h_r)^2] + \mathrm{g}(f_c) \quad (24)$$

where:

$$\mathrm{g}(f_c) = 44.49\log(f_c) - 4.78[\log(f_c)]^2 \quad (25)$$

The values of $(\mathrm{a_o}, \mathrm{a_1}, \mathrm{a_2}\ and\ \mathrm{a_3})$ for different environment types are given in Table 2 [11-19].

Table 2: Value of parameters $(\mathrm{a_o}, \mathrm{a_1}, \mathrm{a_2}\ and\ \mathrm{a_3})$ for different environment area [11-19].

Environment	$\mathbf{a_3}$	$\mathbf{a_2}$	$\mathbf{a_1}$	$\mathbf{a_o}$
Rural	0.1	12.0	100.6	45.95
Suburban	0.1	12.0	68.93	43.20
Urban	0.1	12.0	30.20	36.20

3. Materials and method

Erbil town is the capital city of Kurdistan region of Iraq. It is an urban city characterized by sites located near moderate and tall mountains, residential and commercials buildings as well as small size industries and large offices. The GSM service providers in the town are Asia cell, Korek Tel, and Zain operating at 900MHz, 1800 MHz and 2100MHz. For this study, two of Korek Tel towers at two different location Sharawany and Bakhtiari in the city are selected and the methodology for the measurement is employed. Sharawany is regarded as a sub-urban territory due to low population and flat building construction houses which are surrounded by parks and open parking areas. Bakhtiari is considered as an urban region because it consists of many high building towers built of concrete block material and of high dense population markets.

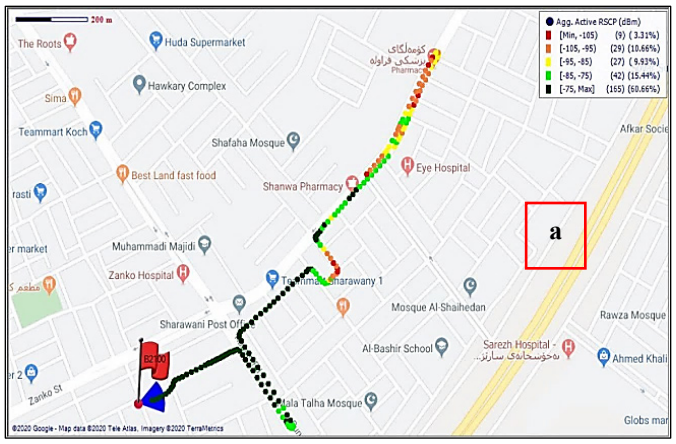
The measurement devices which consists of a laptop with Test Mobile Systems (TEMS) investigator software and all other required accessories installed and arranged inside the deriving car. The received signal strength is measured as the vehicle moves away from the fixed transmitted tower at every 50 m using the Ericsson handset and transferred to the TEMS log file in the laptop. The numbers of data were between 10 to 20 reading for each coverage area. A GPS monitor was attached and used to record coordinates of the sites under investigation and tracking distances covered. The height of the BTS antennas located at Sharawany and Bakhtiari are 20m and 28m, respectively, while the mobile station height is kept at 1.5m. The car which is used for moving away from the base station was driven at a speed of about 30km/hr while the TEMS recorded the received power. Figures 1 show the log files representation of the signal strength level tracking by the GPS indicator during the drive test for suburban and urban areas, respectively.

The frequency was set to 1800MHz for the first test case and then the process is repeated at 2100MHz for the second test case at both mentioned base station towers. The measured received signal power is transferred to the TEMS logs file in the laptop by using Ericsson mobile phones. Measurement were carried out in November 2019 and the field data collection was done with the test drive Korek telecom technique team in the mentioned cells areas. The coordinate of the tower sites with its heights, transmitting power as well as its location and antennas type are presented in Table 3.

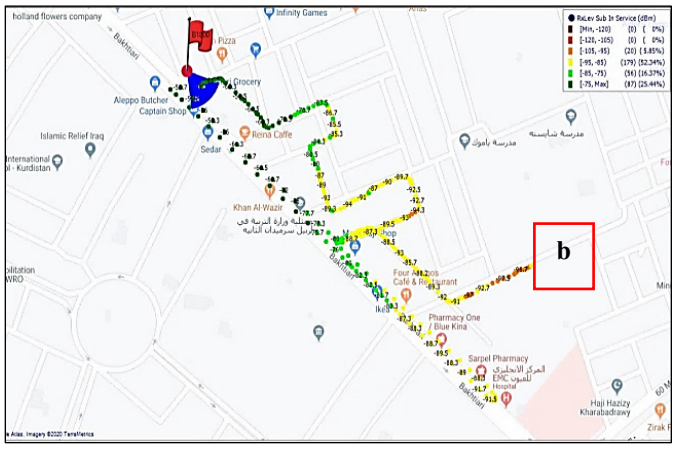
Table 3: Simulation parameters of the selected Korek tower site.

Antenna type	K-80010307	K-800010485
Tower location	Sharawany-A	Bakhteari
Operating frequency (f)	1.8 MHz and 2.1 MHz	
Mobile antenna height (h_r)	1.5 m	
Base station height (h_t)	20 m	28m
Base station power (P_t)	43 dBm	

The measured received signal strength at different distances with the corresponding measured path loss in the mentioned regions and at both operating frequencies are presented in Figures 2 and Figure 3, respectively. These figures indicate that the signal strength power decreases with increasing distance from the towers and also decrease with increasing operation frequencies regarded in this investigation.



(a)



(b)

Figure 1: Log files showing the received signal level distribution for (a) suburban and (b) urban environments.

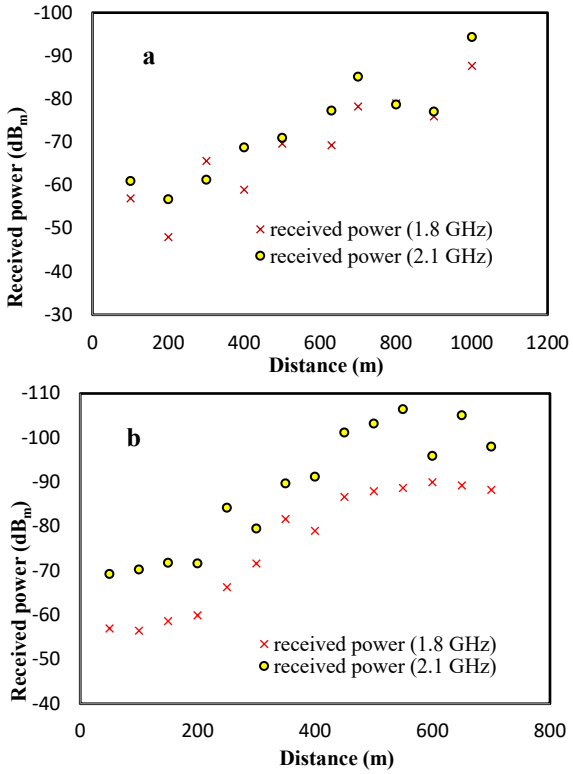


Figure 2: Measured received signal versus distance for (a) suburban & (b) urban environments.

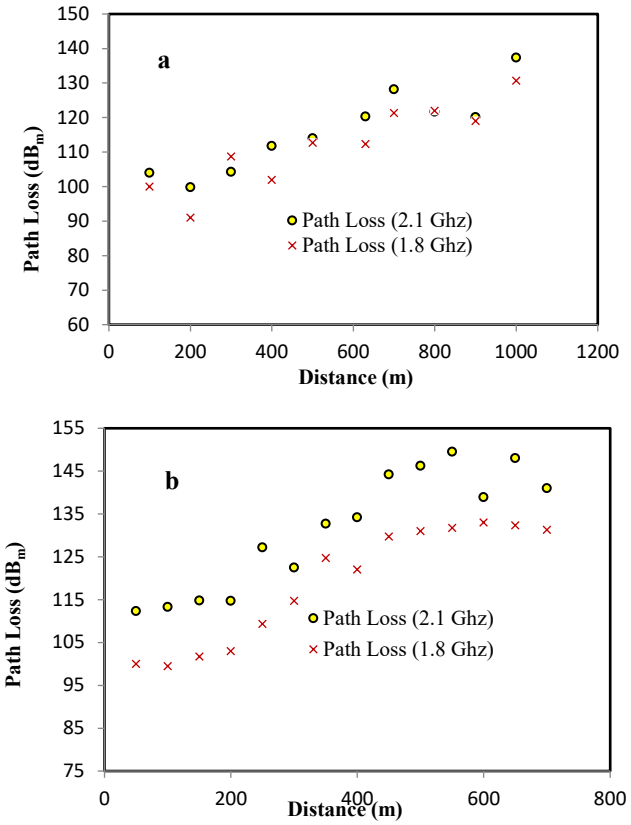


Figure 3: Measured path loss versus distance for (a) suburban & (b) urban environments.

4. Results and discussion

In order to verify which empirical path loss model is reliable and valid for mobile telecommunication systems in Erbil city, the measured path loss data have been compared to the most familiar empirical path loss models. The models that were selected for this study are free space model, ECC-33, SUI, Optimized Cost-231, Okumura-Hata, Egli and Ericson models. The selection of these models is based on the fact that they take various parameters into consideration for the estimation of radio wave propagation path loss, such as separation between antenna base station and mobile receiver, antenna heights and type of environment. Moreover, they are applicable for a frequency ranging from 1800MHz to 2100MHz.

The path loss values for the mentioned prediction models are calculated using equations 2, 4, 5, 6, 9, 15, 21 and 24. The results of the path loss computation with the use of these models and those measured practically are simulated on a MATLAB code developed for this study are shown together on the same path loss distribution graph. The calculated results for suburban are shown in Figures 4 and for urban area are presented in Figure 5 at both operation frequencies of 1800 MHz and 2100MHz, respectively.

Generally, these figures indicate that the path loss increases with distance away from the base station due to many diffractions through obstacle in environment of propagation. The obtained results for sub-urban areas are shown in Figures 4, implies that the Okamura-Hata, ECC-33 and Egli models are overestimated while, SUI with FSPL models provide an underestimated radio wave propagation path loss value.

In addition, the Optimum Cost-231 and Ericson models seem to estimate the radio wave propagation path loss values as close as to that obtained experimentally at both operational frequencies. Moreover, the computed results for urban environment as presented in Figures 5, indicate that the FSPL and SUI models are underestimated while the other models provide values approximately close to that measured experimentally except path loss values predicted by Egli model. Egli model in both environment and at both operational frequencies provide path loss values so far from the measured path loss data.

It can also be observed from these figures that the FSPL model extremely under estimated the path loss in both environments. This may be due to the topography of the sites as the state is hilly in terrain. However, it is also evident from the plots that the optimized Cost-231 model and Ericson model gave a close estimation values for path losses in this environment.

For further confirmation, comparison between measured path loss and the predicted path loss models are also done through the calculation of root mean square value RMSE and mean absolute percentage error MAPE. These two parameters which identify the reliable model accurately for a given environment is obtained by using the following mathematical formula as given by [13] as:

$$RMSE = \frac{1}{n}\sum_{t=1}^{n}\sqrt{(P_{mt} - P_{Rt})^2} \quad (26)$$

$$MAPE = \frac{1}{n}\sum_{t=1}^{n}\left|\frac{(P_{mt}-P_{Rt})}{P_{mt}}\right| \times 100\% \quad (27)$$

where: P_{mt} is the value of measured data, P_{Rt} is the value of predicted path loss values and (n) is the number of data points [20].

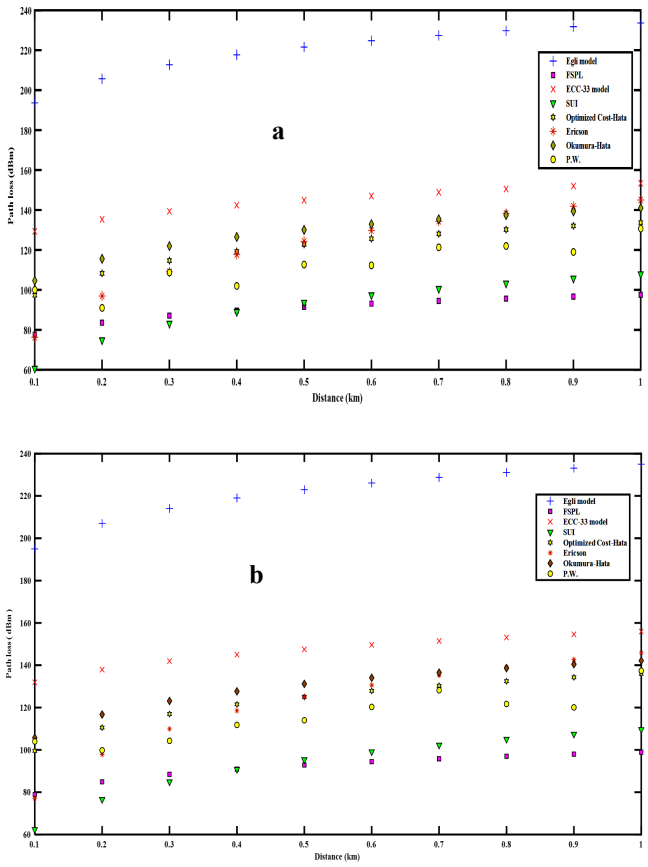


Figure 4: Comparison between measured and different empirical path loss model calculation versus distance from the transmitting tower antenna in suburban area operating at: **(a)**1.8 GHz & **(b)** 2.1 GHz

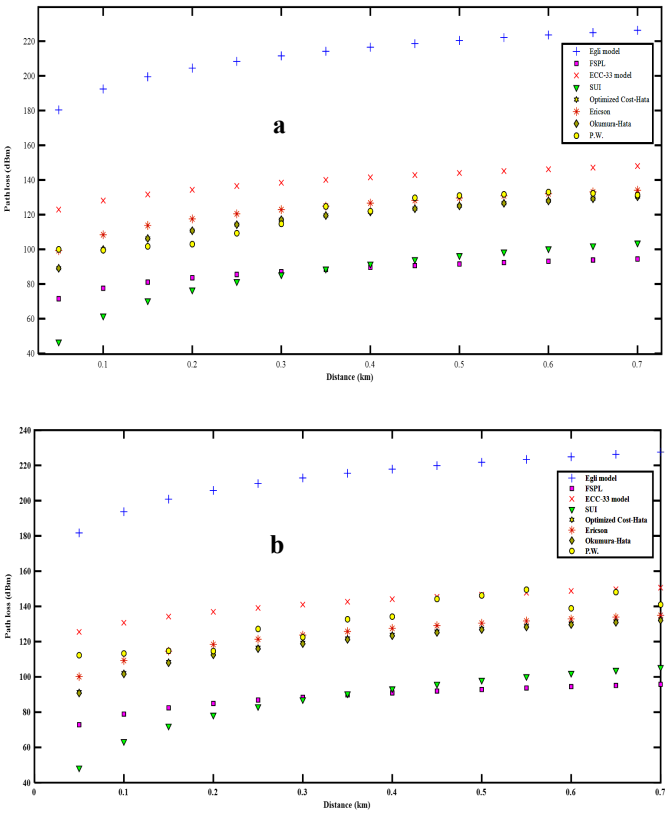


Figure 5: Comparison between measured and different empirical path loss model calculation versus distance from the transmitting tower antenna in urban area operating at: **(a)**1.8 GHz & **(b)** 2.1 GHz

The computed results for each of these two parameters and in both environments with the operation frequencies 1800 MHz and 2100 MHz are presented in Tables 4 and 5, respectively. Generally, the results as depicted in in these two tables reveals that the Optimized Cost-231 followed by Ericson models provide better performance in predicting radio wave path losses compared to the other empirical models considered in this investigation. Since, the Optimized Cost-231 models gives the lowest RMSE 9.21 and 1.58 with MAPE 0.76 and 0.09 at 1800 MHz frequency bands and RMSE 7.28 and 11.86 with MAPE 0.59 and 0.70 at 2100 MHz frequency bands in sub-urban and urban area, respectively.

Table 4: Performance of different path loss models in both environment at frequency of 1.8 GHz.

Model	Sub-Urban		Urban	
	RMSE	MAPE	RMSE	MAPE
FS-Model	38.70	2.55	28.31	1.35
ECC-33	31.38	2.18	16.75	0.87
SUI	20.35	2.09	33.32	2.62
Opt. Cost231	9.21	0.76	1.58	0.09
Okumura-	15.75	1.23	14.73	0.77
Egli	107.89	4.89	92.77	3.12
Ericson	9.387	0.90	4.12	0.22

In addition, it is evident from these tables that the Egli, SUI and FSPL models are not reliable for predicting radio wave path loss in our environment under consideration due to their high RMSE and MAPE values in both environment and at both operation frequencies. Therefore, the Optimized Cost-231 model followed by Ericson model can be used successfully to the network planning and designing problems in the sub-urban and urban areas of the Erbil city.

Table 5: Performance of different Path loss models in both environment at frequency of 2.1 GHz.

Model	Sub-Urban		Urban	
	RMSE	MAPE	RMSE	MAPE
FS-Model	35.85	2.34	17.10	0.80
ECC-33	30.71	2.09	7.72	0.39
SUI	22.80	2.31	44.13	3.43
Opt. Cost231	7.28	0.59	11.86	0.70
Okumura-Hata	12.82	0.99	3.93	0.20
Egli	105.04	4.74	81.56	2.72
Ericson	6.07	0.63	7.54	0.44

5. Conclusions

In this study, the performance of different empirical model has been tested for predicting radio wave propagation path loss for urban and sub-urban areas in Erbil city. It is obviously observed that the Egli and ECC-33 models are overestimated while both FSPL and SUI models are underestimated path loss values in both environment under consideration. In addition, the results also demonstrated that the path loss values evaluated by Optimized Cost-231 and Ericson models are in good agreement with those measured experimentally. Since, the MAPE values provided by Optimized Cost-213 are (0.76, 0.09, 0.59 and 0.70) and that obtained by Ericson are (0.90, 0.22, 0.63 and 0.44) at respective operation frequencies for sub-urban and urban environment, respectively.

Generally, as a results of these calculation one can concluded that the estimation of radio wave propagation path loss value in urban and suburban environment is best estimated by these two models especially Optimized Cost-231 model in the city under consideration as a whole.

Conflict of Interest

The authors declare no conflict of interest.

Acknowledgment

The authors would like to thank the Korek Telecommunication Company for all the cooperation.

References

[1] D. A. Tonga,"Path loss propagation model prediction for GSM mobile networks in nigeria", First International Conference on Information Technology, Communications and Computing (ICITCC 2017), 24-December-2017, doi: 10.5281/zenodo.1130791.

[2] Z. Nadir, "Seasonal pathloss modeling at 900 Mhz for Oman", International Conference on Telecommunication Technology and Applications, **5**, 2011, https://www.researchgate.net/publication/228895216_Seasonal_Pathloss_Modeling_at_900MHz_for_OMAN.

[3] P. K. Sharma , " Comparative study of path loss models depends on various parameters", International Journal of Engineering Science and Technology, **3**(6), 4683-4690, 2011, doi: 10.24018/ejers.2017.2.5.346.

[4] V. Armoogum., K.M.S Soyjaudah., N Mohamudally. and T. Fogarty , " Propagation models and their applications in digital television broadcast network design and implementation", March 2010, doi: 10.5772/8471.

[5] P. Pathania, P. Kumar and B. S. Rana, " Performance evaluation of different path loss models for broadcasting applications", American Journal of Engineering Research (Ajer), **3**(4), 335-342, 2014, https://www.researchgate.net/publication/293326766_Performance_Evaluation_of_different_Path_Loss_Models_for_Broadcasting_applications

[6] K. A. Akpado and A. Adewale," Pathloss prediction for a typical mobile communication system in Nigeria using empirical models", International Jounal of Computer Networks and Wireless Communications (Ijcnwc), **3**(2), 2013, https://www.researchgate.net/publication/241688188_Pathloss_Prediction_for_a_typical_mobile_communication_system_in_Nigeria_using_empirical_models

[7] I. B. Oluwafemi and O. J. Femi-Jemilohun, " Suburban area path loss propagation prediction and optimization at 900 and 1800 MHz", Journal of Engineering and Applied Sciences, **13**(9), 2521-2529, 2018, doi: 10.36478/jeasci.2018.2521.2529.

[8] A. O. Oyubu, " A comparative study of free space and Okumura-Hata models in GSM signal path loss prediction in south-south Nigeria", International Journal of Advencements in Research and Technology, **5**(5), 34-44,2016. https://www.semanticscholar.org/paper/a-comparative-study-of-free-space-and-Okumura-Hata/e1a80e192f191ed861bff040b3e390326db26480.

[9] P. O. Omolaye, G. A. Igwue and G. A. Akpakwu, " Okumura-Hata: a perfect model for driving route UHF investigation", American Journal of Engineering Research, **4**(9), 139-147, 2015. https: //issuu.com/ajer. Research /docs/t04901390147.

[10] K. Ayyappan and P. Dananjayan," Propagation model for highway in mobile communication system", Ubiquitous Computing and Communication Journal, **3**(4), 61-66, 2010, https://citeseerx.ist.psu.edu/viewdoc/download?doi=10.1.1.548.5163&rep=rep1&type=pdf.

[11] J. Chebil, A. K. Lawas and M. D. Rafiqul Islam, " Comparison between measured and predicted path loss for mobile communication in Malasia", World Applied Sciences Journal, **21**, 123-128, 2013, doi: 10.5829 /idosi.wasj.2013.21.mae.99936.

[12] I. Khan and S. A. Kamboh, " Performance analysis of various path loss models for wireless network in different environments", International Journal of Engineering and Advanced Technology, **2**, 161-165, 2012, https: //www.researchgate.net/publication/235459463_Performance_Analysis_of_Various_Path_Loss_Models_for_Wireless_Network_in_Different_Environments.

[13] S. I. Popoola and O. F. Oseni ," Empirical path loss models for GSM network deployment in Makurdi, Nigeria", International Refereed Journal of Engineering and Science, **3**, 85-94, 2014. https://www.researchgate.net/publication/264036911_Empirical_Path_Loss_Models_for_GSM_Network_Deployment_in_Makurdi_Nigeria.

[14] N. Shabbir and M. T. Sadiq," Comparison of radio propagation models for long term evaluation (LTE) network", International Journal of Next Generation Networks (Ijngn), **3**(3), 27-41 2011, doi: 10.5121/ijngn.2011.3303.

[15] N. M. Shebani, A. E. Mohammed , M. A. Mosbah and Y. A. Hassan, "Simulation and analysis of path loss models for WiMax communication system", Research Gate, 692-703, 2013. https://www.researchgate.net/publication/269222079_Simulation_and_Analysis_of_Path_Loss_Models_for_WiMax_Communication_System.

[16] A. O. Akende, F. A. Semire and Z. K. Adeyemo , "Performance analysis and optimization of Cost231-Hata model for mobile communication in Nigeria" International Journal of Computer Applications, , **173**(6), 2017, doi: 10.5120/ijca2017915310.

[17] A. L. Imoize and T. E. Ogunfuwa ,"Propagation measurements of a 4G LTE network in Lagoon Environment", Nigerian Journal of Technological Development, **16**(1), 1-9, 2018, doi: 10.4314/njtd.v16i1.1.

[18] H. Oudira, L. Djouane and M. Garah , "Optimization of suitable propagation model for mobile communication in different area", International Journal of Information Science & Technology, **3**(3), 10-19, 2019. https://www.researchgate.net/publication/332687459_Optimization_of_Suitable_Propagation_Model_for_Mobile_Communication_in_Different_Area

[19] Y. Zakaria, J. Hosek and J. Misurec, "Path loss measurements for wireless communication in urban and rural environments", American Journal of Engineering and Applied Sciences, 94-99, 2015, doi: 10.3844/ajeassp.2015.94.99.

[20] N. Fesseha, Fine-tuning of Cost-231 Hata path loss model for LTE network: the case of 4 Kilo area, M.Sc. Thesis, Addis Ababa University, Ethiopia, 2018.

ASTES

Advances in Science, Technology and Engineering Systems Journal Vol. 5, No. 5, 876-881 (2020)

www.astesj.com

ASTESJ

ISSN: 2415-6698

User's Demographic Characteristic on the Evaluation of Gamification Interactive Typing for Primary School Visually Impaired with System Usability Scale

Yanfi Yanfi*, Yogi Udjaja, Azani Cempaka Sari

Computer Science Department, School of Computer Science, Bina Nusantara University, Jakarta, Indonesia 11480

ARTICLE INFO

Article history:
Received: 13 August, 2020
Accepted: 07 September, 2020
Online: 12 October, 2020

Keywords:
Usability
Gamification
Unity
Visually Impaired
System Usability Scale
Evaluation

ABSTRACT

This paper extends the gamification interactive typing for Primary School Visually Impaired in Indonesia with some development according to previous user's feedback. This study focuses in to renew the application and evaluate the updated application for visually impaired children developed by utility Unity software. Besides, standards of good gamification are worthy of study and can increase the motivation to learn, and it only can happen if it meets the needs of the user. To achieve those goals, it has completed some development on several sections includes the homepage, input text, text size, and scoring. In this paper, System Usability Scale (SUS) is utilized, and some statistical model is conducted such as average, mean, Pearson-Product Moment correlation, T-test, and ANOVA. T-test results show that no difference between the partial and fully visually impaired participant, gender, and participants who used a similar application and not. The grades do not affect the SUS score, so it proved that the collected SUS score as average 75 is an objective result from the users although the average grade is 46. Moreover, both variable usability (0.884) and variable learnability (0.771) are positively correlated toward the System Usability Scale, notwithstanding variable usability and variable learnability is not correlated (0.383). The impact of this research can improve the industries especially the education field in Indonesia and some expectations from that result are included experience, knowledge, and skills of the users that need to be evaluated in further research. Hence, in the future, by using this application, we can increase the standard of living visually impaired people and enhance industry 4.0 in Indonesia.

1. Introduction

The International Organization for Standardization ISO 9241-11 has defined usability as the "Extent to which a product can be used by specified users to achieve specified goals with effectiveness, efficiency, and satisfaction in a specified context of use"[1].

This paper extends the gamification interactive typing for Primary School Visually Impaired in Indonesia to meet some suggestions [2] with some studies on the context of the effectiveness of the games in learning for visually impaired children. According to that paper, several categories include name page, score, subject matter, sound, user experience, and information. This study focuses on updating the application and evaluating the latest application for visually impaired children developed utilizing Unity engine.

There are many models for evaluating the usability of the application or software such as the User Experience Questionnaire (UEQ)[3], Game Experience Questionnaire (GEQ)[4–6], Computer System Usability Questionnaire (CSUQ)[7], Quality Function Deployment (QFD)[8], Questionnaire for User Interface Satisfaction (QUIS), and System Usability Scale (SUS). CSUQ, QUIS, and SUS reach only 30-40% accuracy with a sample size of only 6, while SUS increases about 75% accuracy at a sample size of 8 and reaches 100% at a sample size of 12 as stated by Tullis and Stetson [9]. In this paper, we utilized the System Usability Scale conducted by John Brooke[10]. This system is utilized to access the nutrition application that provides an effective human and virtual coaching approach to raise parent's awareness about children's eating behavior and lifestyle [11]. Moreover, the System Usability Scale (SUS) is also has used to access user satisfaction on interactive maps for the visually impaired [12] and e-learning systems [13]. Furthermore, the questionnaire is modified with

* Corresponding Author: Yanfi Yanfi, Bina Nusantara University, Jakarta-Indonesia, +62 821 2551 9291 & eufrasia.yan.fi@binus.ac.id

GEQ and UEQ so that applications can be tailored to the needs of users.

2. Research Method

Based on the results of research from a previous paper [2], proper gamification standards are feasible to study and can increase learning motivation because user needs are met. After conducting several model evaluations, the applications created ordinarily require the development of user input, so that what is expected is achieved.

This application, which is intended for the blind Primary School in Indonesia, was developed using Unity Engine which has a universal system that can adapt to current technology needs, such as a personal computer, a mobile, head-mounted display, the internet of things, and various platforms (see figure 1).

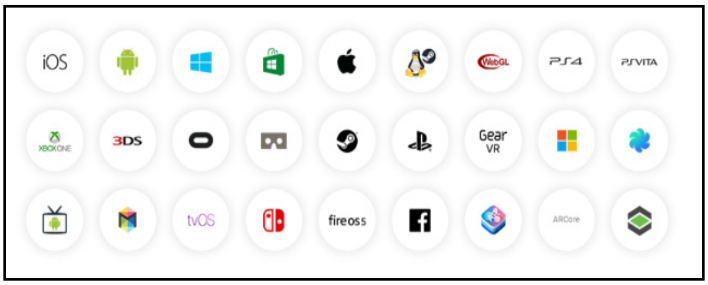


Figure 1: Compatible Platform with Unity Engine [14]

Unity engine also offers all the features needed to create beautiful, engaging, and enhanced content with sustainable engine upgrades with multi-platform support, documentation, forums, and tutorials, and therefore a lot of developers eager to use that engine.

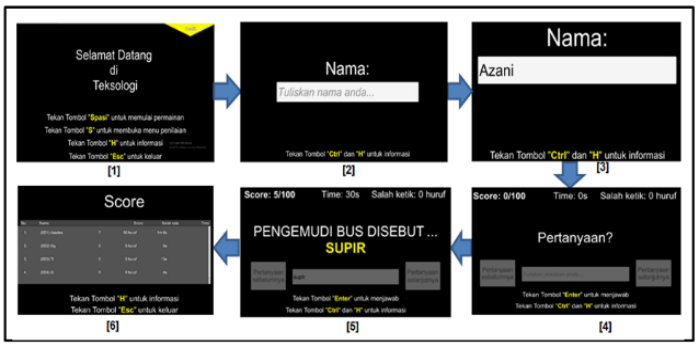


Figure 2: Page Flow of Application

In this paper, we adopted the DECIDE framework to utilize the evaluation. This framework is proposed by Rogers et al. (2011) [15] as a usability evaluation framework. This framework used as a guide for evaluating the usability of the LMS Moodle by Melton [16], Planning Support System (PSS) conducted by Russo et al. (2015) [17], and virtual laboratory of open-source programming in a virtual classroom based on Moodle in 2016 [18]. The phase-in of this framework includes six stages, namely:

1. Determine the Evaluation Goals

In this first phase, we determine the purpose of this evaluation. The purpose is to evaluate the usability of the updated application.

Table 1: Comparison Previous and Current Application

Section	Old Application	New Application
Home Page	The application on the information section is still unclear, some buttons sound ambiguous. More information (tutorial) is required. In addition, the question has not varied and currently available a question of classes 1 and 2 only.	The application is currently equipped with some information (tutorials) and some selection keys: the "space" button to start the game, the "S" button to open the scoring menu, the "H" button for information, and the "Esc" button to exit from game as shown in figure 2 no.1. In addition, the level of this application is more varied, not only for classes 1 and 2 but also for class 3 to class 6 of elementary school that is adapted to the curriculum.
Input text	This application is not equipped with backspace tones, so the user does not know which letters have been deleted. Also, in each question, the user does not get information related to what button information can be used. So that additional information for the user is not clear yet.	Figure 2 no.2 and no.3 show that the application is equipped with backspace tones so that when the user deletes the desired letter, it becomes easier to specify other letters that will be inputted.
Text Size	The text size is small and there is no option to continue to the next question or return to the previous question.	The applications are equipped with larger and clearer text sizes, also, the user can choose to proceed to the next question or return to the previous question. Then on each question page, as shown in figure no.4 and 5, the User knows the position of the letter being typed with information from the application. When the user enters the answer to each question, the application will guide the user to do the next step and some information to go ahead or exit the application.
Scoring	Information obtained by the user including the current generated value, the total time required, number of questions the user has done, and the number of letters incorrectly inputted by the user.	In the current application, as shown in figure no.6, it can display the scores by the user, the total time required, the number of incorrect letters entered by the user, and there are several selection information buttons, namely the "H" button for information and the "Esc" button for exit.

2. Explore the Questions

There are 13 participants included 9 elementary students and 4 teachers with visually impaired. First, the questionnaire included 10 item questions relating to the satisfaction, efficiency, and effectiveness using a Likert scale from 1 (strongly disagree) to 5 (strongly agree) was adopted from System Usability Scale (SUS) to understand usability assessment of user responses to this application.

Table 2: List of Questionnaires

System usability scale	
1.	I think that I would like to use this application frequently.
2.	I found the application unnecessarily complex.
3.	I thought the application was easy to use.
4.	I think that I would need the support of a technical person to be able to use this application.
5.	I found the various functions in this application were well integrated.
6.	I thought there was too much inconsistency in this application.
7.	I would imagine that most people would learn to use this application very quickly.
8.	I found the application very cumbersome to use.
9.	I felt very confident using the application.
10	I needed to learn a lot of things before I could get going with this application.

The SUS questionnaire is shown in Table 2. Positive statements are displayed on odd items as the score is calculated from scale minus 1, while negative statements are displayed on even items as the score is calculated from 5 minus scale. As a result, the SUS score is generated from the total score of all items multiplied 2.5 so it ranges from 0 (completely disable) to 100 (completely usable).

3. Choose the Evaluation and Data Collection Methods

The evaluation is a controlled setting involving users. Before doing testing, the user is given some brief guidance about this application, and then they should fulfill the questionnaire about the application.

4. Identify the Practical Issues

As Russo et al. has stated that some practical issues must be considered when conducting an evaluation [17]. In this issue, the participants have chosen that represent for this application. For that purpose, the teachers, and students from the elementary school with disabilities have asked to participate in evaluating this application. When conducting the evaluation, the participants rely on the voices to fill out the questionnaires, while the questionnaire is given in the written form, so some volunteers read out each question which is then answered orally by the participants and recorded in writing by the volunteer.

5. Decide How to Deal with the Ethical Issues.

The participants have been informed that the collected data during the evaluation and how it is used will be for this research.

6. Evaluate, Analyze, Interpret, and Present the data

In this phase, evaluation has been done and analyzed on the profile of participants such as gender (female or male), age, role (teacher or student with grade), and type of disabilities (fully visual impaired or partial visual impaired). Besides, the experience of using a similar application also asked.

Also, according to Bangor et al. (2008) [19] and Lewis and Sauro [20] in their paper, the SUS questionnaire has two variables are usability (8 items) and learnability (2 items) as implemented in this study. Question numbers 1, 2, 3, 5, 7, and 9 are grouped to the usability variable while question numbers 4 and 10 are grouped to learnability variable. Based on the results of questionnaires, validity is tested by utilizing Pearson-Product Moment correlation while reliability is examined by adopting Cronbach's Alpha method [21].

Subsequently, in the T-test, it can analyze the comparison of SUS score by gender, role, type of disabilities, and their experience of using a similar application. Meanwhile, an analysis of variance (ANOVA) is used to test the hypothesis of a comparison of two or more than two groups. This test has been used in research such as road damage classification [22], factors affecting behavioral intention [23], factors that determine consumer perceptions [24]. In this study, ANOVA is examined to make sure whether the application's score affects the SUS score or not. Therefore, we can make conclusions according to the analysis test that has been carried out.

3. Results and Analysis

According to the data collected with the result in a response rate of 100 percent, as stated in figure 3 and figure 4, they are 7 out of 13 (54%) male participants and the rest (46%) are female participants aged as 69% are 6-11 years old, 8% are 25-34 years old, and 23% are 35-44 years old.

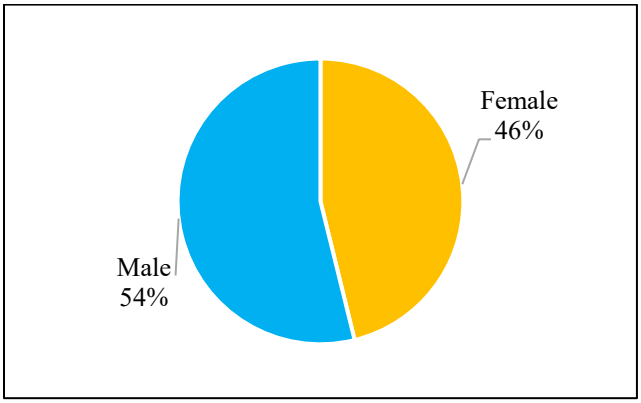


Figure 3: Percentage of Participants by Gender

Based on question 1 to 10, Table 3 shows the results of the SUS calculation. The method to calculate the results can be looked at in session 2. The SUS score has a level acceptable as produced by Bangor et al. (2008) [19]. SUS score below 50 is not acceptable while between 70 and 80 are acceptable although more than 90 are excellent. In this study, the average SUS is 75 of 100 means this system has 75% usable.

Cronbach's Alpha [21] calculation is conducted to examine the reliability and validity of SUS. Hossain reported that reliability is

acceptable when $0.6 \leq \alpha \leq 0.7$ [25]. This finding indicates that this SUS is reliable ($\alpha = 0.601$).

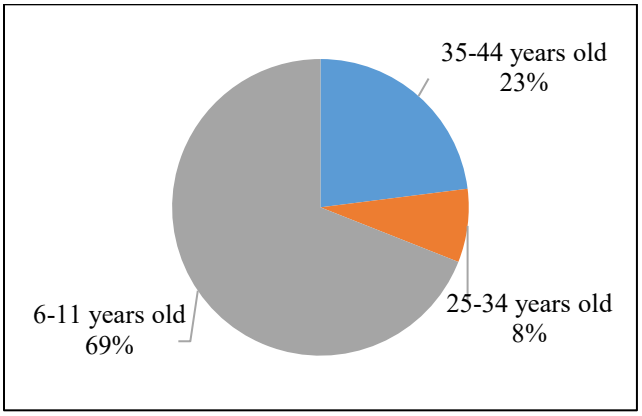


Figure 4: Percentage of Participants by Age

Table 3: SUS Score Results

Participant	Q 1	Q 2	Q 3	Q 4	Q 5	Q 6	Q 7	Q 8	Q 9	Q 10	SUS Score	Grade Score
1	5	3	4	2	5	1	3	1	5	1	85	04
2	5	1	5	2	5	3	4	2	3	2	80	63
3	5	3	5	4	5	5	5	3	4	4	63	37
4	5	3	5	2	4	2	5	2	5	5	75	72
5	5	1	5	5	5	1	5	1	5	5	80	69
6	5	2	4	3	3	2	4	1	4	4	70	60
7	5	3	4	3	5	2	5	2	4	3	75	23
8	5	2	4	3	3	4	5	2	5	3	70	32
9	5	3	4	2	4	3	4	3	4	3	68	46
10	4	3	4	4	4	1	4	2	5	3	70	48
11	5	2	5	3	5	3	5	2	4	4	75	51
12	5	3	4	2	4	2	4	2	5	3	75	73
13	4	1	5	1	4	1	4	1	5	2	90	23

Table 4: Correlation on Usability and Learnability

	ALL	**Usability**
Usability	0.884	1
Learnability	0.771	0.383

Based on the Pearson-Product Moment correlation calculation, both variable usability (0.884) and variable learnability (0.771) are positively correlated toward the System Usability Scale, notwithstanding variable usability and variable learnability are not correlated (0.383) as shown in Table 4.

Moreover, 11 (85%) full visual impaired and 2 (15%) partial visual impaired with the distribution as stated in Figure 5.

According to the results in Table 5, the T-test is conducted to confirm our assumption that the Ha1: SUS score of participants with partial visually impaired differently from the SUS score of participants with totally loss vision, and 5% significant level. Table 4 described that P-Value 0.123 shows statistically that there is no difference between the SUS score of participants with partial visually impaired and the SUS score of participants with fully visually impaired.

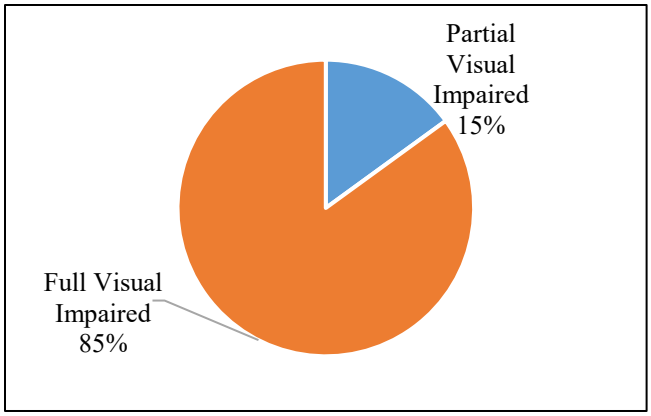


Figure 5: Percentage of Participants by Types of Visually Impaired.

Table 5: T-Test Results on SUS Score of Partial and Full Visual Impaired Participants

	Partial	***Full***
Mean	82.5	73.727
Variance	12.5	50.018
Observations	2	11
Pooled Variance	46.6	
Hypothesized Mean Difference	0	
df	11	
t Stat	1.672	
P(T<=t) one-tail	0.061	
t Critical one-tail	1.796	
P(T<=t) two-tail	0.123	
t Critical two-tail	2.201	

Besides, a T-test was also conducted on gender to compare SUS score between male and female that Ha2: SUS Score of male participants is different from the SUS score of female participants.

Table 6 describes that there is no difference in SUS score by gender.

Table 6: T-Test Results on SUS Score by Gender

	Male	***Female***
Mean	75.429	74.667
Variance	52.952	64.667
Observations	7	6

Pooled Variance	58.277
Hypothesized Mean Difference	0
df	11
t Stat	0.179
P(T<=t) one-tail	0.430
t Critical one-tail	1.796
P(T<=t) two-tail	0.861
t Critical two-tail	2.201

From 13 participants with disabilities, there were 4 (31%) teachers and 9 (69%) students as in Figure 6.

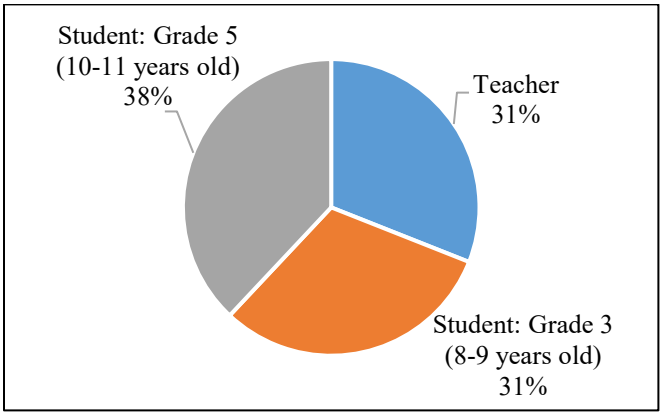


Figure 6: Percentage of Participants by Role

Table 7: T-Test Results on SUS Score by Role

	Student	*Teacher*	*Grade 5*	*Grade 3*
Mean	72.3	81.25	73.6	70.75
Variance	31.75	56.25	52.3	8.917
Observations	9	4	5	4
Pooled Variance	38.432		33.707	
Hypothesized Mean Difference	0		0	
df	11		7	
t Stat	-2.394		0.732	
P(T<=t) one-tail	0.018		0.244	
t Critical one-tail	1.796		1.895	
P(T<=t) two-tail	0.036		0.488	
t Critical two-tail	2.201		2.365	

The T-test also performed comparing the SUS score between students and teachers that Ha3: SUS score of students is different from the SUS score of teachers and Ha4: SUS score on grade 5 is different from the SUS score on grade 3.

The results in table 7 show that there is a difference between the SUS score of students and the SUS score of teachers, but there is no difference between students of grade 3 and grade 5.

Some participants have used a similar application, therefore in this study, a comparison of the SUS score was carried out on participants who had a used similar application and not. The results can be seen in Table 8 that there is no difference in SUS scores between participants who have used a similar application and who have not.

Table 8: T-Test Results on SUS Score from Participants Used Similar Application and Not

	No	*Yes*
Mean	74.8	76
Variance	30.4	183
Observations	10	3
Pooled Variance	58.14545	
Hypothesized Mean Difference	0	
df	11	
t Stat	-0.239	
P(T<=t) one-tail	0.408	
t Critical one-tail	1.796	
P(T<=t) two-tail	0.815	
t Critical two-tail	2.201	

In addition, Moreover, after calculating the SUS Score with some T-test is completed, another hypothesis was developed with the assumption that Ha3: Grades do not affect SUS Score.

P-Value and significance F is more than 5% proved that the user's grade does not significantly affect the SUS score as shown in Table 9.

Table 9: ANOVA and Partial (T) Results

R Square	P-Value	*F*	*Sig. F*
0.061	0.415	0.717	0.415

4. Conclusion

Based on the result, although the average grade is 46, the average SUS score is 75 of 100 shows that this application is 75% fulfill the usability of the application. This SUS is reliable with α = 0.601. Both variable usability (0.884) and variable learnability (0.771) are positively correlated toward the System Usability

Scale, notwithstanding variable usability and variable learnability are not correlated (0.383).

After completed the T-test on the SUS score, it has concluded that no difference between the partial versus fully visually impaired participant, gender differences, and whether participants used similar applications. However, there is the difference between students' SUS score with a mean of 72.3 and teachers' SUS score with a mean of 81.3, even though there is no difference in the SUS score according to student's grade. Also, grades do not affect the SUS score, so it proved that the collected SUS score as average 75 is an objective result from the users although the average grade is 46.

Therefore, some of the expectations from these results including the experience, knowledge, and skills of the users need to be evaluated in future research.

Acknowledgment

We thank Sekolah Luar Biasa Tuna Netra (SLB-A) Pembina Tingkat Nasional, and our participants for their help and contributions.

References

[1] W. ISO, "9241-11. Ergonomic requirements for office work with visual display terminals (VDTs).," The International Organization for Standardization, 1998.

[2] Y. Yanfi, Udjaja, A.C. Sari, "A Gamification Interactive Typing for Primary School Visually Impaired Children in Indonesia," in Procedia Computer Science, 2017, doi:10.1016/j.procs.2017.10.032.

[3] Y. Udjaja, "EKSPANPIXEL BLADSY STRANICA: Performance Efficiency Improvement of Making Front-End Website Using Computer Aided Software Engineering Tool," Procedia Computer Science, **135**, 292–301, 2018, doi:10.1016/j.procs.2018.08.177.

[4] Y. Udjaja, V.S. Guizot, N. Chandra, "Gamification for elementary mathematics learning in Indonesia," International Journal of Electrical and Computer Engineering, **8**(5), 3859–3865, 2018, doi:10.11591/ijece.v8i5.pp3859-3865.

[5] Y. Udjaja, "Gamification Assisted Language Learning for Japanese Language Using Expert Point Cloud Recognizer," International Journal of Computer Games Technology, **2018**, 2018, doi:10.1155/2018/9085179.

[6] D.P. Kristiadi, Y. Udjaja, B. Supangat, R.Y. Prameswara, H.L.H.S. Warnars, Y. Heryadi, W. Kusakunniran, "The effect of UI, UX and GX on video games," in 2017 IEEE International Conference on Cybernetics and Computational Intelligence, CyberneticsCOM 2017 - Proceedings, 2018, doi:10.1109/CYBERNETICSCOM.2017.8311702.

[7] J.R. Lewis, "IBM Computer Usability Satisfaction Questionnaires: Psychometric Evaluation and Instructions for Use," International Journal of Human-Computer Interaction, 1995, doi:10.1080/10447319509526110.

[8] Y. Udjaja, Sasmoko, Y. Indrianti, O.A. Rashwan, S.A. Widhoyoko, "Designing Website E-Learning Based on Integration of Technology Enhance Learning and Human Computer Interaction," in 2018 2nd International Conference on Informatics and Computational Sciences, ICICoS 2018, 2019, doi:10.1109/ICICOS.2018.8621792.

[9] T.S. Tullis, J.N. Stetson, "A Comparison of Questionnaires for Assessing Website Usability ABSTRACT : Introduction," Usability Professional Association Conference, 2004.

[10] J. Brooke, "SUS-A quick and dirty usability scale," Usability Evaluation in Industry, 1996.

[11] S. Gabrielli, M. Dianti, R. Maimone, M. Betta, L. Filippi, M. Ghezzi, S. Forti, "Design of a Mobile App for Nutrition Education (TreC-LifeStyle) and Formative Evaluation With Families of Overweight Children," JMIR MHealth and UHealth, 2017, doi:10.2196/mhealth.7080.

[12] A. Brock, P. Truillet, B. Oriola, D. Picard, C. Jouffrais, "Design and user satisfaction of interactive maps for visually impaired people," in Lecture Notes in Computer Science (including subseries Lecture Notes in Artificial Intelligence and Lecture Notes in Bioinformatics), 2012, doi:10.1007/978-3-642-31534-3_80.

[13] N. Harrati, I. Bouchrika, A. Tari, A. Ladjailia, "Exploring user satisfaction for e-learning systems via usage-based metrics and system usability scale analysis," Computers in Human Behavior, 2016, doi:10.1016/j.chb.2016.03.051.

[14] Unity Technologies, Game engine, tools and multiplatform, Unity Technologies, 2016.

[15] Y.R. Jenny Preece, Helen Sharp, "INTERACTION DESIGN: beyond human-computer interaction, 3rd Edition, Chapter 8: DATA ANALYSIS, INTERPRETATION, AND PRESENTATION. Publisher: John Wiley & Sons," Interactive Computation: The New Paradigm, 2011, doi:10.1007/3-540-34874-3_10.

[16] J. Melton, "The lms moodle: A usability evaluation," Prefectural University of Kumamoto Retrieved …, 2006.

[17] P. Russo, M.F. Costabile, R. Lanzilotti, C.J. Pettit, "Usability of planning support systems: An evaluation framework," in Lecture Notes in Geoinformation and Cartography, 2015, doi:10.1007/978-3-319-18368-8_18.

[18] A. Zakiah, "Evaluation of interaction design of virtual laboratory of open source programming in virtual classroom based on moodle using decide framework case study: C programming," International Journal of Psychosocial Rehabilitation, 2020, doi:10.37200/IJPR/V24I2/PR200708.

[19] A. Bangor, P.T. Kortum, J.T. Miller, "An empirical evaluation of the system usability scale," International Journal of Human-Computer Interaction, 2008, doi:10.1080/10447310802205776.

[20] J.R. Lewis, J. Sauro, "The factor structure of the system usability scale," in Lecture Notes in Computer Science (including subseries Lecture Notes in Artificial Intelligence and Lecture Notes in Bioinformatics), 2009, doi:10.1007/978-3-642-02806-9_12.

[21] L.J. Cronbach, "Coefficient alpha and the internal structure of tests," Psychometrika, 1951, doi:10.1007/BF02310555.

[22] F.E. Gunawan, Yanfi, B. Soewito, "A vibratory-based method for road damage classification," in 2015 International Seminar on Intelligent Technology and Its Applications, ISITIA 2015 - Proceeding, 2015, doi:10.1109/ISITIA.2015.7219943.

[23] Y. Yanfi, Y. Kurniawan, Y. Arifin, "Factors Affecting the Behavioral Intention of using Sedayuone Mobile Application," ComTech: Computer, Mathematics and Engineering Applications, **8**(3), 137, 2017, doi:10.21512/comtech.v8i3.3722.

[24] F.E. Gunawan, I. Sari, Y. Yanfi, "The consumer intention to use digital membership cards," Journal of Business & Retail Management Research, **13**(04), 117–124, 2019, doi:10.24052/jbrmr/v13is04/art-10.

[25] G. Hossain, "Rethinking self-reported measure in subjective evaluation of assistive technology," Human-Centric Computing and Information Sciences, 2017, doi:10.1186/s13673-017-0104-7.

ASTES

Advances in Science, Technology and Engineering Systems Journal Vol. 5, No. 5, 882-892 (2020)

www.astesj.com

ASTESJ

ISSN: 2415-6698

Using the Neural Network to Diagnose the Severity of Heart Disease in Patients Using General Specifications and ECG Signals Received from the Patients

Zahra Jafari[1], Saman Rajebi[2,*], Siyamak Haghipour[1]

[1]*Department of Biomedical Engineering, Tabriz branch, Islamic Azad University, 5157944533, Iran*

[2]*Department of Electrical Engineering, Seraj Higher Education Institute, 5157944533, Iran*

ARTICLE INFO

Article history:
Received: 13 August, 2020
Accepted: 19 September, 2020
Online: 12 October, 2020

Keywords:
Heart disease
Feature combination
Fisher's discriminant ratio
Perceptron neural network
Artificial Intelligence

ABSTRACT

Nowadays, heart diseases cause the maximum death in the world. Also, due to the noticeable increase of heart diseases, studying this field is one of the important matters in medical community. Therefore, this study tries to benefit using information in data base of cardiac arrhythmia and employ arterial intelligent and neural network, in order to improve the speed in getting cardiac signals with minimum errors and maximum certainty.
The dataset for the project is taken from the UCI machine learning repository https://archive.ics.uci.edu/m1/datasets/Arrhythmia. Used data base has 279 characteristics taken from 364 patients that includes general characteristics and ECG signals received from patients. In this study, firstly the primary classification has done with all characteristics, so some parts of information in data base of cardiac arrhythmia with values near zero has omitted. Considering the improvement of accuracy of the classification after omitting the characteristics near to zero, in next level the second series of data in neural networks that has negative effect on classification has omitted. In order to increase the accuracy of neural network and minimize the number of characteristics, the characteristics has classified in multiple classes and the obtained ratio has improved using genetic algorithm. In this level, the best accuracy of the neural classification has obtained but in order to get a network with minimum characteristics possible and preserve the 100% accuracy of the classification, ineffective characteristics has omitted using PCA algorithm.

1. Introduction

Cardiovascular diseases are main reseaon of death in the United States, accounting for a large proportion of deaths around the world [1]. According to the World Health Organization, about 15 million people die annually from cardiovascular disease in the world and this includes 30 percent of all deaths [2].

1.1. Familiarity and Perceptions of heart disease

Heart disease includes conditions such as coronary heart disease, ischemic heart disease, heart attack, cardiac arrhythmia, cerebrovascular disease and other conditions [3]. Cardiac ischemia, heart injury and heart attack are three consecutive stages in which coronary arteries proceed from congestion to full blockage. Ischemia means limited blood supply. In cardiac ischemia, the muscle suffers from a lack of oxygen due to the narrowing of the arteries that supplying blood to the heart and this leads to the reduction in blood flow to the heart. Therefore, there is a mismatch between the blood supply and the blood demand in the heart, and this imbalance can lead to the heart tissue death [4]. Heart injury is a condition in which the blood supply to the heart continues to decline beyond ischemia and tissue damage begins. This condition still can be avoided as no sign of a heart attack has observed [4]. A heart attack or infarction is a condition in which the blood supply to the heart stops and the death of part of the tissue occurs, which is mainly causes by a blockage of the coronary artery following a rupture in the plaque artery wall [5]. An adult's healthy heart during resting usually beats 60 to 100 times a minute. The heart rate below 60 beats per minute at rest is called bradycardia, and a heart rate more than 100 beats per minute at rest is called tachycardia. Sinus bradycardia is a type of slow beating that occurs when the problem starts in the sinoatrial node (SA). The SA node of the heart is the natural pacemaker in the heart. If the electrical impulses in the sinus node are not generated properly, sinus

*Corresponding Author: Saman Rajebi, Department of Electrical Engineering, Seraj Higher Education Institute, Tabriz, Iran, Email: s.rajebi@seraj.ac.ir

bradycardia will occur. In sinus tachycardia, the SA node regularly produces constant beats ranging 160 to 180 beats per minute [6].

Myocardial fibrosis, myocardial infarction, myocardial inflammation, pulmonary embolism, and coronary artery diseases cause the damage to the bundle branch blocks of the heart. Bundle branch blocks are a group of blocks in which the ventricles cannot be depolarized at the same time due to conduction disturbances in the conductive fibers inside the ventricles, and as a result the QRS complex changes in terms of time duration or shape. In the right bundle branch block, there is a conductive disturbance in the right bundle branch of the His, and first the left ventricle is depolarized in normal path, then the right ventricle is depolarized with a delay. Also, in the left bundle branch block, the dysfunction of the left bundle branch of His causes normal depolarization of the right ventricle and delayed depolarization of the left ventricle [7,8].

1.2. Applying pattern recognition methods in identifying heart diseases

Nowadays, in many cases, machines have replaced humans, and most of the physical work that used to be done by humans is now being performed by machines. Although the power of computers in storing, retrieving information and etc. is undeniable, still there are some cases that humans have to do alone. But in general, machine-related cases involve systems in which the human brain is unable to mathematically understand these connections due to the complex connections between components. Over time, the human brain can partially identify the habits of the system by observing the sequence of behaviors of the system and sometimes testing the results obtained by manipulating one of the components of the system. This learning process leads to experience by observing various examples of the system. In such systems, the brain is unable to analyze the system internally and only estimates the system's internal performance and predicts its reactions based on external behaviors. How to manage large amounts of information and use it effectively to improve decision-making is one of the most challenging issues in the modern era. One of the most important research issues in computer science is the implementation of a model similar to the internal system of the human brain for the analysis of various systems based on experience. In this regard, neural networks are one of the most dynamic areas of research in the current era.

The different information received from different channels, along with the general information of individuals, creates a lot of numbers in order to diagnose different heart diseases. This large amount of information makes it difficult to establish pattern recognition structures on one hand, as well as increases detection time on the other hand. In order to use microcontroller systems independent from computers, it is vital to reduce the amount of information received from the person under the study. Also, due to the much lower speed of microcontroller systems compared to computers, this volume reduction will be very significant in the speed of program execution.

Microcontrollers are microprocessors that, in addition to CPU, at least include input and output systems, memory, and memory-connected circuits inside the main chip, and they do not require external intermediary circuits to connect to additional systems. Of course, all microcontrollers are not similar, and some microcontrollers in addition to considerable features include digital to analog and analog to digital converters, or even more facilities. Using advanced architecture and optimal commands, microcontrollers reduce the amount of code generated and increase the speed of program execution. Therefore, a simple microcontroller is used for classification with high accuracy and speed [9].

The present study focuses on the role of each of the features in diagnosis of heart disease, so, we should first mention sampling method and calculating each of the features.

2. Sampling Method

2.1. Obtaining information about heart function

Cardiac signals are received by metal electrodes attached to the limbs and chest and amplify and record by ECG. As shown in figure 1, there are 12 leads in a complete electrocardiography, which include 6 limb leads and 6 chest leads or precordial. Limb leads has two types: standard bipolar leads and amplified unipolar leads. Bipolar leads consist of three leads and are called lead I and II and III or L1 and L2 and L3, and indicate the potential difference between the two points of the body [10].

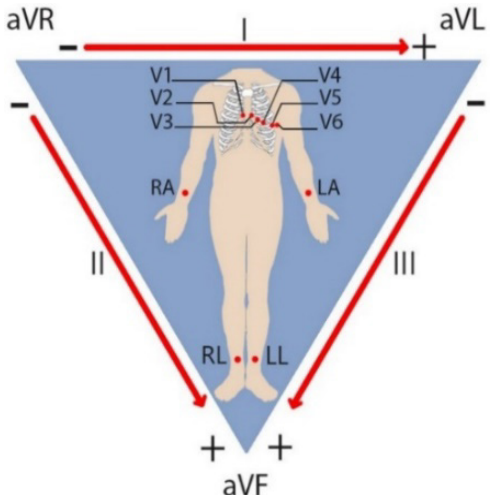


Figure 1: Limb and chest leads [11]

An electrocardiogram (ECG) or ECG is a written record of the potentials generated by the heart that includes specified areas shown in figure 2.

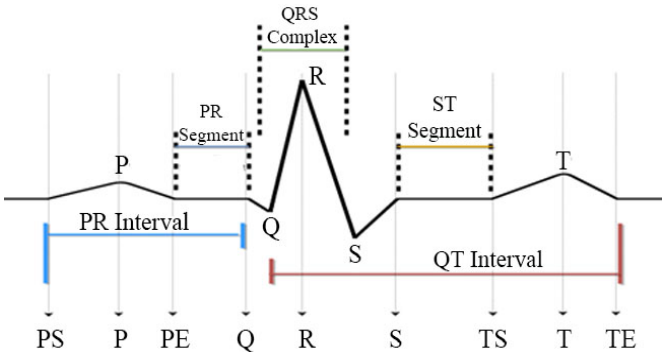


Figure 2: Different areas of an electrocardiogram [12]

In this study, the features of cardiac arrhythmia database were examined. As illustrated in table1, total number of features are 279.

Table 1: All features table

Status	Number of features	Features Name
1	12,14	Vector angles in degrees on front plane of P,J
1	19,31,43,55,67,79, 115,127,139,151	Average width of R' wave of channel DI,DII,DIII, aVR, aVL, aVF,V3,V4,V5, V6
1	20,32,44,56,68,80,92, 104,116,128,140,152	Average width of S' wave of all channels[1]
1	22,34,46,58,70,82,94, 106,118,130,142,154	Existence of ragged R wave of all channels
1	23,35,47,59,71,83,95, 107,119,131,143,155	Existence of diphasic derivation of R wave of all channels
1	24,36,48,60,72,84,96, 108,120,132,144,156	Existence of ragged P wave of all channels
1	25,37,49,61,73,85,97, 109,121,133,145, 157	Existence of diphasic derivation of P wave of all channels
1	26,38,50,62,74,86,98, 110,122,134,146,158	Existence of ragged T wave of all channels
1	27,39,51,63,75,87,99, 111,123,135,147,159	Existence of diphasic derivation of T wave of all channels
1	54	Average width of S wave of channel aVR
1	100,112, 124	Average width of Q wave of channel V2,V3,V4
1	165,175,185,195,205, 215,225,235,245,255, 265,275	Amplitudes of S' wave Of all channels
1	160,162,163	Amplitudes of JJ,R,S waves Of channel DI
1	164,174,194,204,214, 234,244,254, 264,274	Amplitudes of R' wave Of channel DI,DII,aVR,Avl, aVF, V2,V3,V4,V5,V6
1	161,231,241,251	Amplitudes of Q wave Of channel DI,V2,V3,V4
2	10	Vector angles in degrees on front plane of QRS
2	16	Average width of Q wave of channel DI
2	41,101,113	Average width of R wave of channel DIII,V2, V3
2	66, 78	Average width of S wave of channel aVL, aVF,
2	105	Number of intrinsic deflections of channel V2
2	173,176	Amplitudes of S,P waves Of channel DII
2	252,253	Amplitudes of R,S waves Of channel V4
2	261,262,263	Amplitudes of Q,R,S waves Of channel V5
2	272	Amplitudes of R wave Of channel V6
2	187	Amplitudes of T wave Of channel DIII
2	178,208,228	QRSA of channel DII, aVL,V1
2	199,219,269	QRSTA of channel aVR, aVF,V5
2	190,210,220,230,260, 270	Amplitudes of JJ wave Of channel aVR,aVF,V1,V2,V5, V6,
2	192,193	Amplitudes of R,S waves Of channel aVR
2	201	Amplitudes of Q wave Of channel aVL
2	242,243,247	Amplitudes of R,S,T waves Of channel V3
3	5	QRS duration
3	6,7,8,9	P-R,Q-T,T,P intervals
3	11,13	Vector angles in degrees on front plane of T, QRST
3	28,40,52,64,76,88, 136,148	Average width of Q wave of channel DII, DIII, aVR,aVL, aVF,V1,V5,V6
3	17,29,53,65,77, 89, 125,137,149	Average width of R wave of channel DI,DII,aVR, aVL, aVF, V1,V4,V5,V6
3	18,30,42,90,102, 114, 126,138,150	Average width of S wave of channel DI,DII, DIII,V1, V2, V3, V4,V5,V6
3	21,33,45,57,69, 81,93, 117,129, 141,153	Number of intrinsic deflections of channel DI,DII, DIII,aVR,aVL, aVF, V1, V3,V4,V5,V6
3	91,103	Average width of R' wave of channel V1,V2
3	166,186,196,206,216, 226,236,246,256,266, 276	Amplitudes of P wave Of channel DI, DIII, aVR, aVL, aVF,V1,V2, V3,V4, V5,V6
3	167,177,197,207,217, 227,237,257,267,277	Amplitudes of T wave Of channel DI,DII,aVR,aVL, aVF,V1,V2,V4, V5,V6
3	171,181,191,211,221, 271	Amplitudes of Q wave Of channel DII,DIII,aVR,aVF, V1,V6
3	170,180,200,240,250	Amplitudes of JJ wave Of channel DII,DIII,aVL,V3,V4
3	172,182,202,212,222, 232	Amplitudes of R wave Of channel DII,DIII,aVL,aVF, V1,V2
3	183,203,213,223,233, 273	Amplitudes of S wave Of channel DIII,aVL,aVF,V1, V2, V6
3	184,224	Amplitudes of R' wave Of channel DIII,V1
3	168,188,198,218, 238,248,258,268,278	QRSA of channel DI, DIII, aVR,aVF,V2,V3,V4,V5,V6
3	169,179,189,209,229, 239,249,259,279	QRSTA of channel DI,DII, DIII,aVL,V1,V2, V3,V4,V6
4	1	Age
4	2	Sex
4	3	Height
5	4	Weight
5	15	Heart rate

The features include general specifications and ECG signals received from patients. In ECG signals received from the patients, the channels are DI, DII, DIII, aVR, aVL, aVF, V1, V2, V3, V4, V5 and V6, respectively. Features of status 1 have zero or close to zero values, features of status 2 have a negative effect on classification, and features of status 3 are combined features. The main features of 1,2,3, which are defined as status no. 4, and the combined features of 5,14,17 are removed due to their low effect on classification accuracy. Also, features 4 and 15 remained constant from the beginning to the end of the process, which can be observed in table 1 as status number 5.

[1] The ECG signals received from the patient in the channels are DI, DII, DIII , aVR ,aVL, aVF , V1 , V2, V3, V4, V5 and V6, respectively.

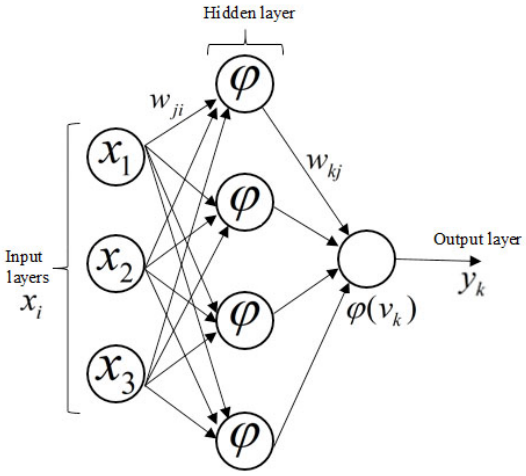
3. Neural Networks

A neural network is one of the most popular classifiers in various researches, especially the classifiers related to heart disease, and etc [13-16].

Among different neural networks, the possibility of implementing perceptron neural networks in microcontrollers is more. The ability to link Arduino microcontrollers to the Simulink environment in Matlab, has made it possible to transfer Perceptron neural networks into Arduino microcontrollers regarding to memory-related items and etc.

3.1. Perceptron Neural Network

One type of neural network is the perceptron neural network which is divided into Single- Layer Perceptron (SLP) and Multi-Layer Perceptron (MLP). Perceptron neural networks are classified as feed forward neural networks. A single layer perceptron can only categorize separate linear problems, and for more complex problems we need to use more layers. Multi-layer feed forward networks consists of one or more middle layers. The multilayer perceptron is a completely interconnected network because each neuron in one layer is connected to all the neurons in the next layer. If some of these connections do not exist, the network is an incomplete connected network [17].



The input-output equations of kth neuron are as follows:

$$Y_k = \varphi(v_k) \tag{1}$$

$$v_k = \sum_{j=1}^{n} W_{jk} x_j \tag{2}$$

where $x_1, x_2, x_3, ..., x_n$ are input signals. u_k is the output of the sum. $W_{k1}, W_{k2}, W_{k3}, ..., W_{kn}$ are the weights of neurons. The final output of the MLP network with a hidden layer is equal to:

$$Y = \sum_{k=1}^{N} W_k Y_k \tag{3}$$

In other words:

$$Y_k = \varphi(\sum_{j=1}^{n} W_{jk} x_j) \tag{4}$$

The active function used in the hidden layer is usually nonlinear. And the transform function in the output layer can be linear or nonlinear.

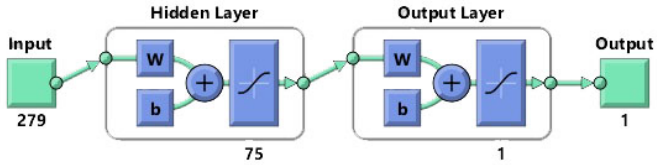
The Perceptron algorithm is a repetitive algorithm, in which the weight and bias vectors are first quantified, and then at each step, the algorithm changes the weight and bias values according to the points that are not accurately categorized to categorize these points correctly. If the given points are not linearly separable, the perceptron algorithm will not end, but if the linear points are separable, the algorithm will end in finite number of steps.

4. Data Analysis

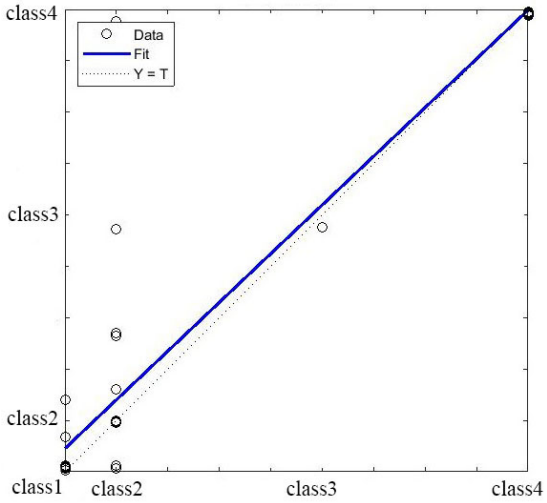
Using all the features, we use a classification to remove and combine low-value features using different methods to improve the accuracy and speed of the neural network.

4.1. Classification with all features

Before analyzing the features, firstly a classification has made in order to evaluate the whole system considering all features. A single layer network is designed as shown in Figure 4.



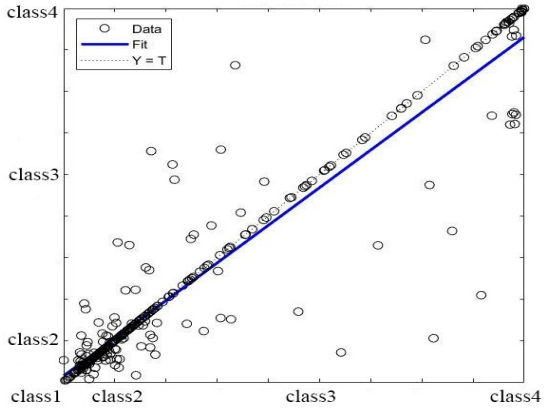
By changing all possible parameters in a Perceptron neural network, including the number of hidden layers, the number of neurons in each layer, and the transform functions of each neuron, the best possible accuracy for the neural network and with the accuracy of 92.324% obtained as shown in figure 5.



The points outside the dash- line indicate an error in classification with the neural network as shown in figure 4.

4.2. Removing features with values close to zero

By studying all the samples, some of the features that had zero value (25 features) or very close to zero (104 features) in all samples were removed from the features. The number of features was reduced from 279 to 150, and the number of features removed at this stage is 129. These features are shown in table 1 as status number 1. By removing the features close to zero, with 150 remaining features, the perceptron neural network has re-formed with a hidden layer as shown in figure 4 with 100 neurons in that layer, and with the optimization of its various parameters, as shown in figure 6 the classification accuracy has increased from 92.324% to 94.579%. The accuracy obtained at this stage indicates the accuracy of our performance in removing the features close to zero.



4.3. Studying the effect of each feature on neural network error rate

To calculate the effect of each feature on the error of neural network, we consider a figure similar to figure 7 as a neural network with one output, which the transform function of each neuron is φ and the number of neurons in the middle layer is m.

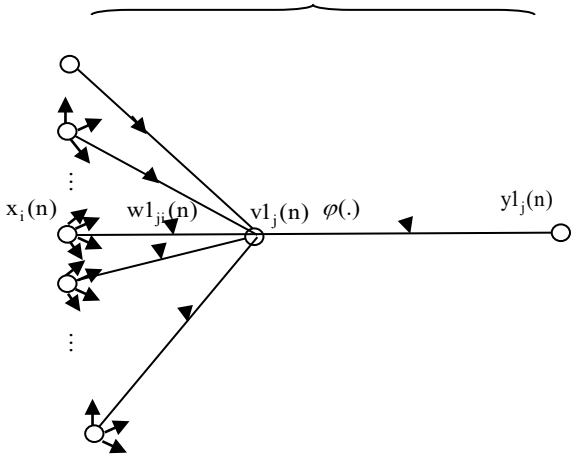


Figure 7: Perceptron neural network output layer with partial specifications

If the optimal output of the network is d and its actual output is y, the network error is defined as follows:

$$e = d - y \tag{5}$$

The total error of a neural network is defined as the sum of the output errors and based on considering an output in the network of figure 7, we have:

$$\xi = \frac{1}{2}\sum (e_k)^2 = \frac{1}{2}e^2 \tag{6}$$

where:

$$y2_k = \varphi(v2_k) \tag{7}$$

On the other hand, according to the weights of the final layer, the input of the last layer neuron is defined as follows

$$v2_k = \sum_{j=1}^{n} y1_j\, w2_{kj} \tag{8}$$

where:

$$y = \varphi v \tag{9}$$

$$v1_j = \sum x_i w1_{ji} \tag{10}$$

To calculate the effect of the weights of the layer shown in figure 7 at the total output of the network , can be written:

$$\frac{\Delta\xi}{\Delta w2_{kj}} = \frac{\partial\xi}{\partial e}\times\frac{\partial e}{\partial y}\times\frac{\partial y}{\partial v}\times\frac{\partial v}{\partial w} \tag{11}$$

where:

$$\frac{\partial\xi}{\partial e} = e_k \;,\; \frac{\partial e}{\partial y} = -1 \;,\; \frac{\partial y}{\partial v} = \varphi'(v2_k) \;,\; \frac{\partial v}{\partial w} = y1_j \tag{12}$$

As a result, Equation 11 can be rewritten as equation 13 using equation 12:

$$\frac{\partial\xi}{\partial w2_{kj}} = e_k \times (-1) \times \varphi'(v2_k) \times y1_j \tag{13}$$

To calculate the effect of pre-final layer weights, consider a figure similar to figure 8.

Considering Equation 13, we can define the effect of the weights of pre-final layer on the total error as follows:

$$\frac{\partial\xi}{\partial w1_{ji}} = (e_k \times (-1) \times \varphi'(v2_k) \times y1_j) w2_{kj} \times \varphi'(v1_j) \times x_i \tag{14}$$

Now it is enough to calculate the effect of each of the features on total error using the following Equation:

$$\frac{\partial\xi}{\partial x_i} = \left[\frac{\partial\xi}{\partial w1_{ji}}\right] \times \frac{\partial w1_{ji}}{\partial x_i}$$

$$= \left[(e_k \times (-1) \times \varphi'(v2_k) \times y1_j) w2_{kj} \times \varphi'(v1_j) \times x_i\right] \times \frac{-v1_j}{(x_i)^2} \tag{15}$$

As all the weights of the last layer affect the total error through each of the features, thus:

$$\frac{\partial \xi}{\partial x_i} = \sum_{j=1}^{m} [e \times (-1) \times \varphi'(v') \times yl_j \times w'_j] \times \varphi'(vl_j) \times \frac{-vl_j}{x_i} \quad (16)$$

At this stage, 6 different neural networks of Perceptron have designed with different parameters and by applying and not applying any of the features in all designed networks, the effect of each feature on the error ratio of classification of the networks has been calculated.

Studying figure 10, 35 features that had caused adverse effects in classification of more than 4 neural networks and were marked red, have identified and removed. These features are shown in Table 1 as status number 2. By removing the specified features, the number of features has reduced from 150 to 115, and again a Perceptron neural network with a hidden layer as shown in figure 4 with 105 neurons in that layer has optimized for classification of different features.

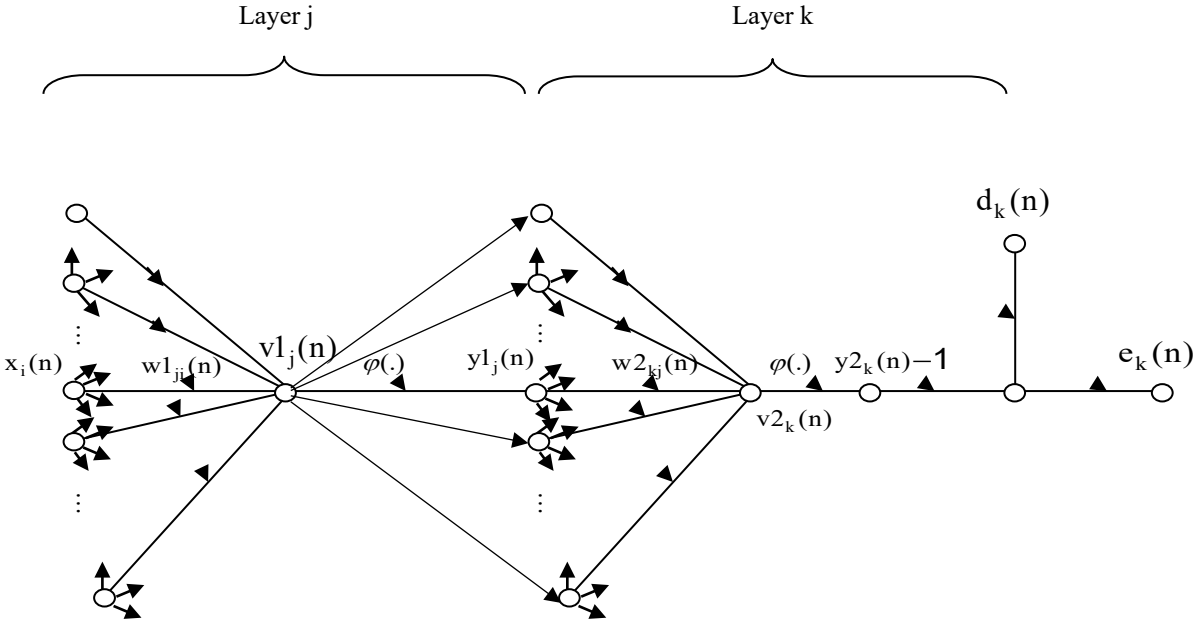


Figure 8: A more detailed view of the output and hidden layers of the Perceptron neural network

The classification accuracy for this neural network, as shown in figure 9, is 97.155%, which has improved compared to the neural network of previous stage with accuracy of 94.579%.

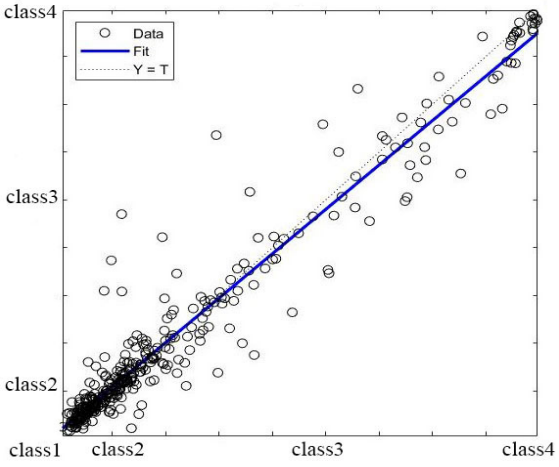


Figure 9: Neural network regression designed with 115 remained features from stages 4-2 and 4-3 with 97.155% accuracy

4.4. Combining features

After removing features with values close to zero as well as features with negative effects on the accuracy of neural network's classification, according to Fisher's discriminant ratio (FDR) and applying optimization on it the remaining 115 features are combined in multiple groups and present the formation of features with suitable performance and more discriminant power among the classes.

To describe the performance of FDR, at first in a two-classes case, it is assumed that the data have Gaussian or quasi-Gaussian distribution. As shown in figure 10, if the average difference between the features of the two classes has increased and their variance have gotten smaller, the discrimination of these two classes will be improved.

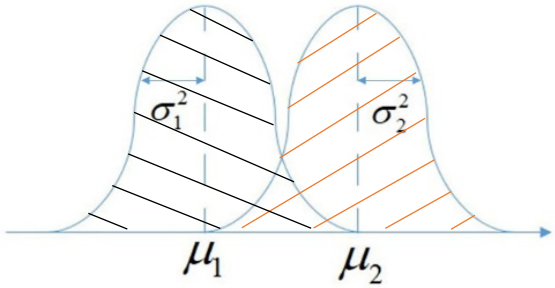


Figure 10: Diagram of detecting the degree of discrimination of two classes [19]

As mentioned, the FDR is defined as follows:

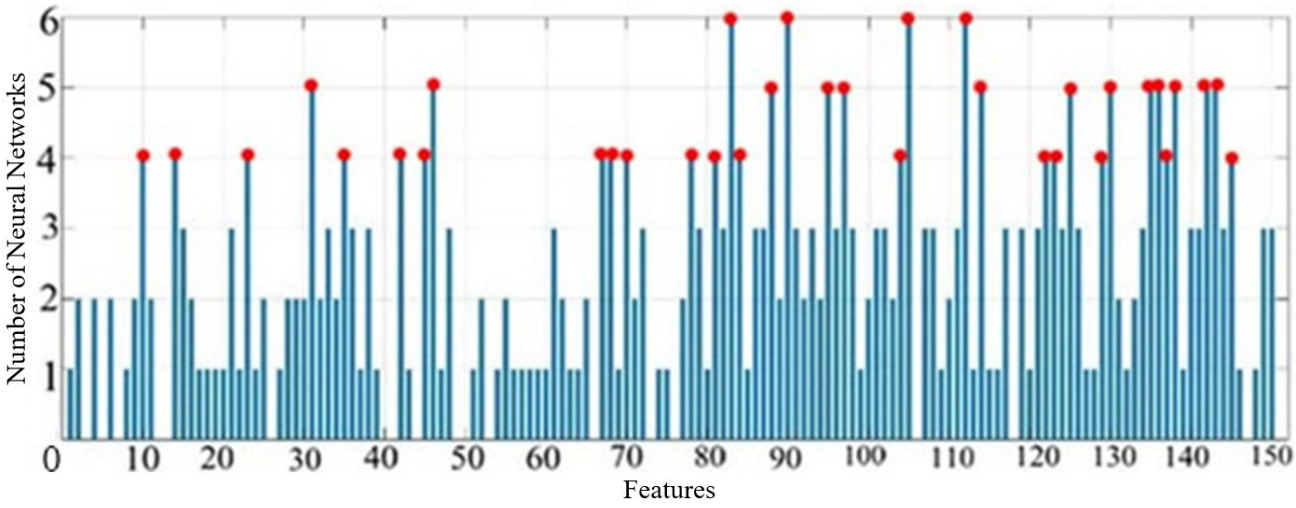


Figure 11: The number of negative effects of each feature on different neural networks tested

$$FDR = \frac{(\mu_1 - \mu_2)^2}{\sigma_1^2 + \sigma_2^2} \tag{17}$$

If the difference between means increases and the variances decreases, the FDR increases. Therefore, increasing FDR means increasing class separation and thus increases the accuracy of classification. Now, if Equation (17) is generalized to a 4 –classes case, we have:

$$FDR = \frac{(\mu_1 - \mu)^2 + (\mu_2 - \mu)^2 + (\mu_3 - \mu)^2 + (\mu_4 - \mu)^2}{\sigma_1^2 + \sigma_2^2 + \sigma_3^2 + \sigma_4^2} \tag{18}$$

where:

$$\mu = (\mu_1 + \mu_2 + \mu_3 + \mu_4)/4 \tag{19}$$

, weights with the form $a = [a_1, a_2, ..., a_n]$ are applied to the given features. Then, using genetic optimization algorithm, the values of these coefficients are determined in such a way that the given FDR is maximized.

The genetic algorithm method is based on minimizing the objective function, but since the goal is to maximize FDR, the fitness function of the genetic algorithm is defined as follows:

$$Fitness.Function = \frac{1}{FDR}$$

$$= \frac{\sigma_1^2 + \sigma_2^2 + \sigma_3^2 + \sigma_4^2}{(\mu_1 - \mu)^2 + (\mu_2 - \mu)^2 + (\mu_3 - \mu)^2 + (\mu_4 - \mu)^2} \tag{20}$$

For example, the features presented in table 2 are combined with the coefficients shown, and after maximizing the FDR with the genetic algorithm, has turned into an optimized feature.

Table 2: Features considered for the combination stated for example

Feature	Coefficient
Amplitude of JJ wave of channel DII	a_1
Amplitude of JJ wave Of channel DIII	a_2
Amplitude of JJ wave Of channel AVL	a_3
Amplitude of JJ wave Of channel V3	a_4
Amplitude of JJ wave Of channel V4	a_5

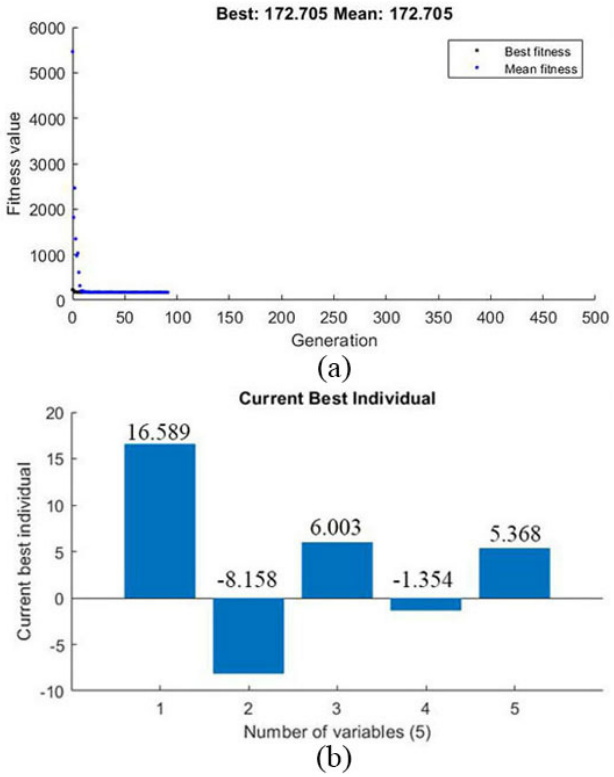


Figure 12: (a) Optimized fitness function for different generations of genetic algorithms (b) Optimized coefficient charts

How to apply the coefficients in Equation (20) is considered as follows:

$$FDR = \frac{a'_{1\times5} \times (\mu_1 - \mu)_{5\times1} (\mu_1 - \mu)'_{1\times5} \times a_{5\times1}}{a' \times \sigma^2_{1_{5\times5}} \times a}$$

$$+\frac{a'_{1\times5}\times(\mu_2-\mu)_{5\times1}(\mu_2-\mu)'_{1\times5}\times a_{5\times1}}{a'\times\sigma^2_{2_{5\times5}}\times a}$$

$$+\frac{a'_{1\times5}\times(\mu_3-\mu)_{5\times1}(\mu_3-\mu)'_{1\times5}\times a_{5\times1}}{a'\times\sigma^2_{3_{5\times5}}\times a}$$

$$+\frac{a'_{1\times5}\times(\mu_4-\mu)_{5\times1}(\mu_4-\mu)'_{1\times5}\times a_{5\times1}}{a'\times\sigma^2_{4_{5\times5}}\times a} \quad (21)$$

After optimization, the optimal value of the fitness function and the values of each of the coefficients are shown in figure 12.

As shown in Figure 12.b, after optimizing a_1=16.589 , a_2=-8.158 , a_3=6.003 , a_4=-1.354 , a_5=5.368 and instead of the features listed in Table 2, the following single features is replaced:

New feature combined

= a_1*Amplitude of JJ wave of channel DII

+ a_2* Amplitude of JJ wave of channel DIII

+ a_3* Amplitude of JJ wave of channel aVL

+ a_4* Amplitude of JJ wave of channel V3

+ a_5* Amplitude of JJ wave of channel V4

Similarly, most other available features are combined in the same way as shown in table 3.

With the processing so far, the number of features has been reduced from 279 to 20. To evaluate the accuracy of the performed processes, again, an optimized Perceptron neural network has designed with a hidden layer as shown in figure 4 with 20 neurons in that layer, and with the remaining 20 features, the accuracy of the classification is 100%, which can be seen in figure 13 of the neural network regression line and in comparison with the regression line of figure 9 with accuracy of 97.155%, the optimal performance of the neural network is observed.

Table 3: Classification of features combined with the values of the coefficients obtained from the genetic algorithm

The number of feature created from the combination	Combined members	Coefficient values
1	28	16.495
	40	5.046
	52	5.027
	64	-5.429
	76	-10.297
	88	4.963
	136	19.642
	148	-19.996
2	17	16.519
	29	5.023
	53	4.99
	65	-5.414
	77	-10.298
	89	4.944
	125	19.612
	137	-19.993
	149	1.465
3	18	19.56
	30	11.841
	42	4.154
	90	-6.005
	102	-14.663
	114	5.76
	126	-9.814
	138	5.654
	150	9.157
4	91	11.651
	103	7.387
5	21	19.717
	33	12.501
	45	11.184
	57	-13.653
	69	6.319
	81	0.819
	93	0.489
	117	-15.581
	129	-2.518
	141	-4.174
	153	-0.581
6	170	19.472
	180	-9.577
	200	7.04
	240	-1.597
	250	6.314
7	171	19.736
	181	-9.717
	191	7.124
	211	-1.611
	221	6.386
	271	16.633
8	172	2.202
	182	2.933
	202	11.031
	212	0.256
	222	-19.972
	232	2.034
The number of features created from the combination	Combined members	Coefficient values
9	183	-2.148
	203	-2.801
	213	-10.351
	223	-0.125
	233	18.791
	273	-1.917
10	184	-10.374
	224	16.532
11	166	-1.103
	186	-3.814
	196	2.629
	206	0.742
	216	-0.72
	226	-6.062
	236	3.689
	246	-2.338
	256	-9.028
	266	-5.158
	276	19.995
12	167	19.997
	177	-2.209
	197	1.261

	207 217 227 237 257 267 277	-5.925 6.124 1.926 -3.214 3.267 1.572 5.651
13	168 188 198 218 238 248 258 268 278	-2.421 14.644 -0.308 -13.025 9.193 -3.083 6.634 -19.895 15.906
14	169 179 189 209 229 239 249 259 279	-2.421 14.644 -0.308 -13.025 9.193 -3.083 6.634 -19.895 15.906
15	11 13	6.067 5.972
16	5 6 7 8 9	-18.087 -17.804 14.276 -9.757 -8.759
17	5 6	-14.284 -5.04

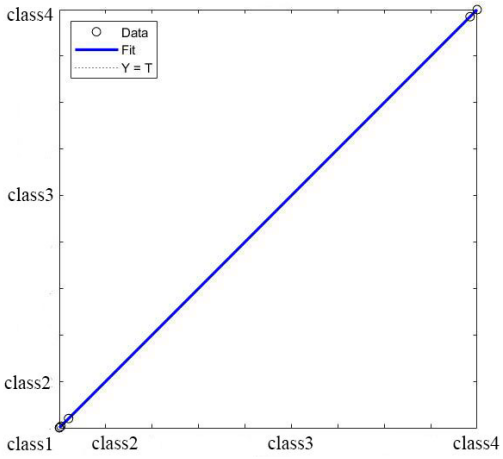


Figure 13: Neural network regression with 20 remaining features after combining features with 100% accuracy

4.5. Selection of final features with Principle Component Analysis (PCA) algorithm

Usually the last step in optimizing and selecting features, is the stage of eliminating no-effect or low-effect features. As the combined features lead to FDR optimization and as a result the classification has reached the most accurate state, it is possible to keep the accuracy of the classification at 100% by eliminating the features that do not have a good effect on classification. To better separation of classes, sometimes you need to make changes to the features. Previously, the application of coefficients to features in order to increase the FDR classification value was investigated. A more general method is now being considered that, in addition to applying coefficients to the feature, also has the ability to make more fundamental changes

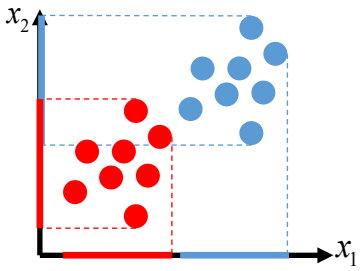


Figure 14: Two-class data arrangement with two features

As shown in figure 14, the two classes with their data are characterized. For these two classes, two features x1 and x2 are considered. Given the degree of separation of class ranges on the axis of each feature, we will notice better discrimination of the x1 feature than the x2.

But if it is possible to make changes to the features of the same problem so that the features have a rotational value of the appropriate amount and shape, then the rotated feature of x1 will have more discrimination ability. How to make these changes to the features so that the maximum discrimination is achieved and also the selection of the top features from the classification point of view, is done using a method called PCA. Mathematically, to make any changes, an interface matrix should be used to make any changes. For example, we will have two features:

$$\begin{bmatrix} x_1 \\ x_2 \end{bmatrix} = \begin{bmatrix} q_{11} & q_{12} \\ q_{21} & q_{22} \end{bmatrix} \times \begin{bmatrix} x_1 \\ x_2 \end{bmatrix} \quad (22)$$

As shown in figure 15 by adjusting the q values correctly, a suitable change can be made to the features so that the data scatter is properly adjusted and thus the classes' discrimination is simplified.

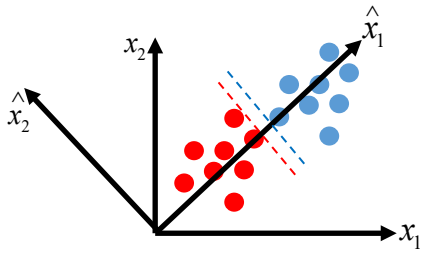


Figure 15: Better class separation after PCA application on features

If the input data is as follows:

$$x = [x_1 \;\; x_2 \;\; \ldots \;\; x_n] \quad (23)$$

And each input data has m attributes, ie:

$$x_i = \begin{bmatrix} x_{i1} \\ x_{i2} \\ \vdots \\ x_{im} \end{bmatrix} \quad (24)$$

The average of all input data in each attribute is assumed to be zero. If this is not the case, the first change in attributes is to subtract each attribute from the average of that attribute in the total data, so that the average of each attribute in all data is zero.

$$E\{x\} = 0 \quad (25)$$

New features will be created according to the following relation:

$$x_i = \begin{bmatrix} q_{11} & q_{12} & & q_{1m} \\ & & & \\ q_{m1} & q_{m2} & & q_{mm} \end{bmatrix} \times x_i \quad (26)$$

The j attribute of the i data changes with the following relation(In this relation, q_j^T represents the j column of the Q matrix.)

$$x_{ij} = q_j^T x_i \quad (27)$$

In general, it can be written like this:

$$x_i = Q^T x_i \quad (28)$$

Considering that the mean of the initial features is considered to be zero and also considering that the members of the Q matrix are fixed numbers, it can be said that the average of the new features that have coefficients of the original features will be equal to zero.

On the other hand, the covariance of the data is described by the following relation:

$$COV(x) = E\{(x-\mu)(x-\mu)^T\} \quad (29)$$

Since the average of the initial data is considered to be zero, as a result, the covariance of the primary data can be shown as follows:

$$COV(x) = E\{x.x^T\} = R \quad (30)$$

According to the above statement, the covariance of the modified data can be shown as follows:

$$COV(\hat{x}) = E\{\hat{x}.\hat{x}^T\} = E\{Q^T x.(Q^T x)^T\} = E\{Q^T x.x^T Q\} = Q^T.R.Q \quad (31)$$

Since the data of all classes are expressed in the form of an x matrix, it can be said that increasing the amount of covariance of the data mean that the data of different classes will be separated from each other. Therefore, the PCA task is defined to increase the covariance value of new data by selecting the appropriate values for the members of the Q matrix.

In the view of the above, the goal is to maximize the covariance of new features.

$$Max Q^T.R.Q \quad (32)$$

To solve the above equation, to find the values of the Q matrix, use no change in the value of the function at the extreme points. So we will have:

$$\Psi(Q) = Q^T R\, Q \quad (33)$$

$$\frac{\partial \Psi(Q)}{\partial Q} = 0 \Rightarrow \Psi(Q+\partial Q) = \Psi(Q)\Big|_{\Psi(Q)_{Max}} \quad (34)$$

$$(Q+\partial Q)^T R\, (Q+\partial Q) = Q^T R\, Q \quad (35)$$

$$Q^T R\, Q + Q^T R\, \partial Q + \partial Q^T R\, Q + \partial Q^T R\, \partial Q = Q^T R\, Q \quad (36)$$

$$\partial Q^T R\, Q = 0 \Rightarrow \partial Q^T Q = 0 \quad (37)$$

$$\partial Q^T R\, Q - \lambda\, \partial Q^T Q = 0 \Rightarrow \partial Q^T (R\, Q - \lambda Q) = 0 \quad (38)$$

$$R\, Q - \lambda Q = 0 \quad (39)$$

$$R\, Q = \lambda Q \quad (40)$$

After solving the above equation by MATLAB software, eigenvalues (and eigenvectors in terms of eigenvalues) are arranged in descending order. New inputs (new features) can be calculated using the initial relation provided.

$$\hat{x}_i = Q^T x_i \quad (41)$$

Instead of selecting all eigenvectors, it is sufficient to obtain a limited number of the best eigenvectors, so that, with minimal data loss, the dimensions of the data can be optimally reduced.

By evaluating the performance of each of the remaining features on the degree of classification, it is possible to eliminate the age features number 1, gender number 2, height number 3, and combination features 5,14,17. The accuracy of the classification maintains on 100%.

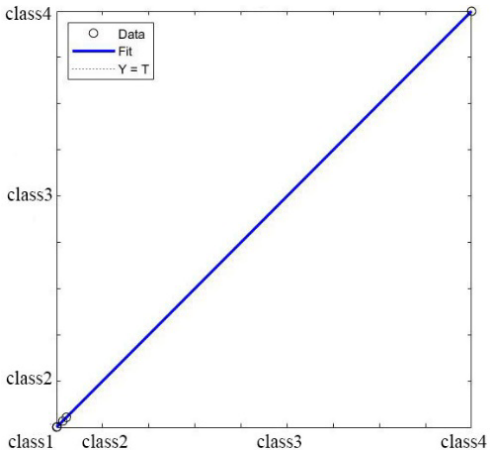


Figure 16: Neural network regression with 14 final features with 100% accuracy

5. Discussion

The accuracy obtained during each of the steps has shown in figure 17.

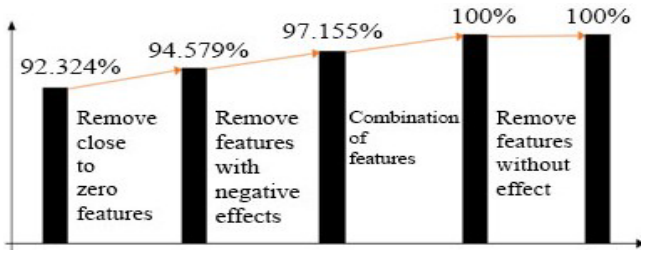


Figure 17: CCR extracted at various stages of feature reduction

In order to use the microcontroller for hardware implementation of the classifier neural network, the problem studied in this paper, in addition to accuracy, the study of occupied memory and performance speed is also of great importance.

Table 4 summarizes the accuracy, speed, and amount of memory occupied by the neural network in a microcontroller in each of the states described.

Table 4: Classification accuracy, execution time and memory occupied with microcontroller with the frequency 16MHz

Occupied memory	Execution time in microcontroller with the frequency 16MHz	Classification accuracy	Number of feature
11602	0.8243125	92.324%	279
6313	0.7830625	94.579%	150
4878	0.7678	97.155%	115
3932	0.714725	100%	20
2948	0.62425	100%	14

6. Conclusion

According to the noticeable increase of heart diseases and importance of the speed of getting the cardiac signals to diagnose and treat the diseases in time, by using artificial intelligent and Perceptron neural network during a multi- stage process by decreasing the number of characteristics, speed of getting the cardiac signals has maximized. During this process firstly the primary classification has done by 279 characteristics and 92.324% accuracy of Perceptron neural network has obtained. In next level, 35 characteristics with values near zero has omitted and second classification has done. The accuracy of the classification has increased from 92.324% to 94.579% and the number of characteristics has decreased from 279 to 150 by omitting the characteristics with values near zero. The effects of each characteristic on the amount of accuracy of neural network has investigated. Characteristics with undesirable effects has identified and the characteristics with undesirable effects on most networks has omitted. Number of characteristics decreased from 150 to 115 and by second classification, 97.155% accuracy obtained. In next level, to increase the accuracy of neural network with multiple classification of the characteristics, the number of characteristics has decreased from 115 to 20 and the accuracy of classification has increased from 97.155% to 100%. In final level, to minimize the number of characteristics and increase the speed of neural network as possible, by omitting ineffective or less effective characteristics in classification and keeping the accuracy on 100%, the number of characteristics has decreased from 20 to 14.

References

[1] P. Christopher, MD. Cannon. "Cardiovascular disease and modifiable cardiometabolic risk factors", Clinical Cornerstone, **8**(3), 11-28, 2007, doi:10.1016/s1098-3597(07)80025-1.

[2] T.A. Gaziano, A. Bitton, Sh. Anand, S. Abrahams-Gessel, A. Murphy, "Growing Epidemic of Coronary Heart Disease in Low- and Middle-Income Countries", Current Problems in Cardiology, **35**(2), 72–115 ,Feb 2010, doi:10.1016/j.cpcardiol.2009.10.002.

[3] M. Naghavi, H. Wang, R. Lozano, A. Davis, X. Liang, M. Zhou, et al, "Global, regional, and national age–sex specific all-cause and cause-specific mortality for 240 causes of death, 1990–2013: a systematic analysis for the Global Burden of Disease Study 2013", Lancet , **385**(9963), 117-171, January 2015, doi:10.1016/S0140-6736(14)61682-2.

[4] C.P. Cannon, "Cardiovascular disease and modifiable cardiometabolic risk factors", Clinical Cornerstone, **8**(3), 11–28, 2007, doi:10.1016/s1098-3597(07)80025-1.

[5] U. Zeymer, K. Schröder, U. Tebbe, et al. "Non-invasive detection of early infarct vessel patency by resolution of ST segment elevation in patients with thrombolysis for acute myocardial infarction. results of the angiographic substudy of the Hirudin for Improvement of Thrombolysis (HIT)-4 trial", Eur Heart J , 22-796, 2001, doi:10.1053/euhj.2000.2290.

[6] S.G. Johnson, M.B. Farrell, A.M. Alessi, M.C. Hyun, "Nuclear Cardiology Technology Study Guide 2nd edition", J. Nucl. Med. Technol. jnmt.116.175018 published ahead of print March 10, United States: SNMMI; 17-19, 2016, doi:10.2967/jnmt.116.175018.

[7] A S. Fauci, E. Braunwald, D L. Kasper, S L. Hauser, D L. Longo, J. Larry Jameson, J. Loscalzo, "Harrison Principles of Internal Medicine", 15th ed. New York: McGraw-Hill; 1386-99, 2001.

[8] G. Hollander, V. Nadiminti, E. Lichstein, A. Greengart, M. Sanders, "Bundle branch block in acute myocardial infarction", American Heart Journal, **105**(5), pp. 738-743, 1983, doi:10.1016/0002-8703(83)90234-x.

[9] J.J. Segura-Juarez, D. Cuesta-Frau, L. Samblas-Pena, M. Aboy, "A microcontroller-based portable electrocardiograph recorder", IEEE Transactions on Biomedical Engineering, **51** (9) , Sep 2004, doi: 10.1109/TBME.2004.827539.

[10] J. Francis, "ECG monitoring leads and special leads", Indian Pacing and Electrophysiology Journal, **16**(3), 92-95, May–June 2016, doi:10.1016/j.ipej.2016.07.003.

[11] P. D. Khandait, N. G. Bawane and S. S. Limaye, "Features extraction of ECG signal for detection of cardiac arrhythmias", Proceedings of the National Conference on Innovative Paradigms in Engineering & Technology (NCIPET'2012), 6-10, 2012, doi:10.1109/MAMI.2015.7456595.

[12] D. Awasthi, S. Madhe, "Analysis of encrypted ECG signal in steganography using wavelet transforms", Electronics and Communication Systems (ICECS), 2nd International Conference on, Coimbatore, 718-723, 2015, doi:10.1109/ECS.2015.7125005.

[13] K. Vanisree, J. Singaraju, "Decision support system for congenital heart disease diagnosis based on signs and symptoms using neural networks", Int. J. Comput. Appl., **19**(6), 6-12, 2011, doi: 10.5120/2368-3115.

[14] A. D. Dolatabadi, S. E. Z. Khadem, B. M. Asl, "Automated diagnosis of coronary artery disease (CAD) patients using optimized SVM", Comput. Methods Programs Biomed, **138**, 117-126, 2017, doi:10.1016/j.cmpb.2016.10.011.

[15] K. Polat, S. shahan, S. Gunesh, "Automatic detection of heart disease using an artificial immune recognition system (AIRS) with fuzzy resource allocation mechanism and k-nn (nearest neighbour) based weighting preprocessing", Expert Syst. Appl., **32**(2), 625-631, 2007, doi:10.1016/j.eswa.2006.01.027.

[16] O. Mokhlessi, H. Masoudi Rad, N. Mehrshad, A. Mokhlessi, "Application of Neural Networks in Diagnosis of Valve Physiological Heart Disease from Heart Sounds", American Journal of Biomedical Engineering, **1**(1),pp. 26-34, 2011, doi:10.5923/j.ajbe.20110101.05.

[17] P.Wallisch, M .Lusignan, M .Benayoun, T I .Baker, A S .Dickey, N G. Hatsopoulos: "MATLAB for Neuroscientists", Second Ed, Academic Press, 501-517, 2014, doi:10.1016/C2009-0-64117-9.

[18] H. Yan, Y. Jiang, J. Zheng, C. Peng, Q. Li, "A multilayer perceptron-based medical decision support system for heart disease diagnosis", Expert Systems with Applications, **30**(2), 272–281, 2005, doi:10.1016/j.eswa.2005.07.022.

[19] L. Sharma, D.K. Yadav, A. Singh, "Fisher's linear discriminant ratio based threshold for moving human detection in thermal video", Infrared Physics & Technology, **78**, 118–128, 2016, doi:10.1016/j.infrared.2016.07.012.

ASTES

Advances in Science, Technology and Engineering Systems Journal Vol. 5, No. 5, 893-901 (2020)

www.astesj.com

ASTESJ

ISSN: 2415-6698

English as a Foreign Language Learning Students' Perceptions of Blended Learning in University Institutions: A Case Study of a University in UAE

Ghadah Al Murshidi*

Department of Curriculum and Instruction College of Education, United Arab Emirates University, 15551, United Arab Emirates

ARTICLE INFO

Article history:
Received: 03 September, 2020
Accepted: 24 September, 2020
Online: 12 October, 2020

Keywords:
Blended Learning
Online teaching TAM
Q- Methodology
EFL Learners

ABSTRACT

This study aims to review English as a foreign language learning students' perception of blended learning on various aspects of learning process. The study seeks to answer the question as to whether there is any correlation among students derived independent variable and their perception with respect to the merits and demerits of online blended learning. The Q-methodology was used whereby the questionnaire method was applied and data collection was supported by the Q-Sort data collection model which involves 251 learners who voluntarily presented themselves for Q-Method procedural participation and learning at third and fourth grade of English Language Teaching at the university identified within United Arab Emirates. The results showed no statistical difference in means for students' perceptions towards blended learning at significant level 0.05. This thus confirms a higher degree of acceptance for blended learning versus old class mode of learning. The study, therefore, concludes that individual student success was highly increased in blended learning encounters as compared to either complete online or wholly face to face learning encounters. Online blended learning has been seen to optimize maximum benefits of old teaching methods and access to online learning materials.

1. Introduction

Times are changing in terms of using modern online technology for delivering instruction to expand distance education to attain maximum learning objectives. Immense advancement in internet services and e-learning technology evolved a blended mode of learning (a combination of traditional face-to-face and modern e-learning) [1]. This mode of blended learning proved to be a strong link among students, faculty members and classrooms with different locations to develop and enhance multiple skills especially learning of different languages. Blended learning is a mode of learning in which use of both ordinary teaching, in accord with advanced modern online teaching, and online learning materials are largely applied in its application [2]. As daily norms and routines are followed, electronic online materials are seemingly acquired to complement learning process [3]. This mode of learning also made use of professional establishment and on job training acquisition sessions [2].

Further, [4], expanded the conceptualization of blended learning as a combination of online and physical individual consociate dissemination in which online platform efficiently replace majority of face-to-face learning time other than serving as a supplement. [5] found out that individual student success was highly revealed in blended learning encounters when related to either complete online or wholly face to face learning encounters. Addition of creativity and innovation to make improvement and ability of teaching has yield new openings in learning field [6]. Blended learning is envisioned to optimize maximum benefit of old teaching techniques and internet material access [7] Despite of the immense benefits, yet, this blended learning mode is not widely adopted in higher education and it has been massively passive all about independent on its cadre, as, many approaches have been laid to keep at bay it's application [8], [6].

Previous reports on the topic have revealed laxity in definitions on its mandate, a disgrace that has resulted into limitation of effective research on its application [4], [9], [10], attributed this to few reasons including lack of teacher's familiarity and adaptability as they perceive it less appropriate in terms of stated that, complications which arise in establishing blended learning module units involve limited support, inadequate period, course structuring resource, technological risk on its accessibility, and requirement to acquire most current learning skill. [11] supported researcher efforts to seek

*Corresponding Author: Ghadah Al murshidi, Email: g_almurshidi@uaeu.ac.ae

investigation of approach to blended learning at curriculum level, expound on the concepts of blended learning from the angle of course instructors. On the other hand, the researches focused to examine the efficient component aspects of blended learning in regard to specific learning lesson, the component aspects demanded for institution level blending, for instance, institution support, were neglected [11]- [13]. To make an illustration, even though Poon (2012) summed up that institution support had a mega significance within his research, this material component has for long time been ignored despite the fact that it was meant for institutional embracing of blended learning. Therefore, this research is particularly conducted to reveal the importance of institution support for blended learning. This paper aims to review students' perceptions of blended learning on various aspects of learning process and will address the following questions,

i. Is there any correlation among students derived independent variable (Abilities to learn online, speed of online information capture, Increased capacity of knowledge acquisition) and their perception with respect to the merits and demerits of Blended Learning? (what is the Perceived Ease of Use of the Blended Learning & Online Learning?)

ii. In which manner does United Arab Emirates university learners perceive effects linked to blended learning regarding how they develop English language learning skills? (How the Perceived usefulness of Blended Learning & Online Learning lead to positive Behavioral Intention to Use?)

iii. How do learners in United Arab Emirates university perceive blending learning model attesting to its merits and demerits? (How the Perceived Ease of Use of Blended Learning & Online Learning lead to Positive Behavioral Intention to Use?)

iv. What do the learners suggest for improvement of disseminating and implementing blended course units within English Department? (How to implement Blended Learning & Online Learning?)

2. Review of Related Literature

2.1. Blended learning

There are many conceptualizations of blended learning available in literature. [14] defines it as "a combination of online and classroom learning activities using resources in an optimal way in order to improve student learning outcomes and to address important institutional issues". The ideological meaning of blended learning is "enhancing integration of online resources and face to face framework for creating a sleek efficient learning encounter" ([15], p. 98). By application of blended learning, instructors have a capacity to make use of online resource materials within daily classwork lesson dissemination to instigate learners, stimulate individual assertive behavior and mold them to become more efficient in their daily learning routine.

According to [16] blended learning is "a flexibility intensified approach with combination of face to face learning activity encompassing online learning capacity which entrusts learners to exchange collectively acquired and individuals' feedback and response within four specified regions, that's, learner feedback, learner strategy, and alternative synchronous or asynchronous assessment ". Meanwhile [17] refer to blended learning as "a concept that includes framing teaching learning process that incorporates both face to face teaching and teaching supported by ICT, i.e., direct instruction, indirect instruction, collaborative teaching, and individualized computer assisted learning". Finally, [18] define blended learning as "a learning program that improves learning effectiveness through extending the access, optimizing the cost of development and time, as well as optimizing learning outcomes.

2.2. Principles of Blended learning

- Blended learning focus on effective achievement of goals.
- Blended learning entails consideration of cumulative learning style frameworks
- Blended learning needs to base on learner's class needs.
- Blended learning availability to learner's knowledge acquisition desire should be present.

It involves 2 modes of interacting: face to face meeting, and website base meeting. Website base interaction may either be synchronously or asynchronously laid [3] The terminology synchronous refers to description of the live on-board training session, online actual time meeting set among course instructors and remotely located learners [19]. Concurrently, asynchronous has a meaning that "instructions stream is just in time, when you require it" [19]. Comparatively face to face learning in conjunction with online learning environment have their merits. However, as [20] points out, "A complexion of learning and teaching techniques all the time will ever be the highest effective criterion for supporting learner's knowledge acquisition as you find out it's the only distinguished mechanism to accept cumulative practices of discussing, interacting, adapting and reflecting on daily learning routines, and essentials of academic knowledge acquisition" [21].

2.3. Importance of blended Learning in Learning English Language

In [6], the author conducted a research study to find out the effectiveness of blended learning on "academic achievements, motivation and learner autonomy" while teaching English language via short stories. A quasi-experimental study was conducted among 116 students by utilizing two different teaching pedagogies i.e. for experimental group a blended learning classroom and at the sometime for a control group a conventional learning classroom was spared. There results depicted more positive effects on students' motivation and learner autonomy variables in case of blended learning in comparison to conventional learning. therefore, it can be concluded that blended learning is effective to be applied in English language classes by having proper technical support and required resources.

Similarly, a study was conducted by [5] to find out the English communication skills need of the undergraduate engineering students at workplace by implying Blended Learning and Project-based Learning Approach. They inferred that Blended Learning Module were supported more for English language leaning particularly, for speaking and listening skills. Thus,

representing the importance of blended learning Module for learning language skills. [18] examined the impact of blended learning on academic achievements of the school students and fond the positive results as compared to the traditional methods of learning. [22] conducted a study to examine the impact of blended learning method on attainment of English language proficiency among the students of 9th grade. They made two groups of female students (50 in each group). One was experimental and other was control. Controlled group was taught English language via traditional method whereas, experimental group was taught by using computerized programs. Results supported the experimental group in terms of more proficiency of learning English language over controlled group representing the importance of blended learning methods in learning English language.

In [23], the auhtor sleeked attention on the outcome of an initially presented model of blended learning and intimately enlisted students' attitude towards English linguistic application while learning medical new words by preparatory medical students at AGU university. He made two assortment of group samples division. One encored a control experimental sample, another one monitored test sample. Outcome implicated none of the samples by statistics significantly illustrated difference amidst the two classified samples regarding individual student achievements in line to attitude towards English. The findings showed also that the control experiment grouped members of the class indicated a reasonable magnitude of contentment pertaining the online learning aspect. [16] conducted a research on the effectivity of making use of blended learning in generating interrogated teacher's training module, and ability to perform. Investigation sample size encompassed 38 English as a foreign language (EFL) voluntary Saudi origin teacher from the school of Arts and Education, Tabuk University. It then followed that the sample to be divided at the two-group differential. From the divisions, group one was instructed to study 4 EFL subjects by means of traditional technique, on the other side group number two was asked to study four correlated subjects making use of blended learning modelled module. Outcomes showed contentiously blended learning module clarified extensively efficient comparison to traditional module while devising voluntary teacher's periodical teaching module. No difference was fond among the two groups depicting the good adaptability level of learners for blended learning method.

In [24], the author investigated elements affecting e-learning student's acceptability for Blackboard in King Khalid University. The study results outlined a demonstration that informant persons made identification of facilitator and inhibitor elements of e-learner's experience initially identified within previous study. They as well indicated that learners are prepared for technology implementation acceptance, ready for shifting towards an e-learning module. Within similar categorized setting, [5] conducted a study on the school officials and learner's perception of electronic learning within English departmental school and made observation response given extensively were motivating and implied that learning became better within electronic learning setting in comparison to traditional classroom criterion. The lynched investigation attempt to find out intensively more detail perception of EFL students in respect to impact blended learning has on their numeral English language learning skill developments, expected merits of the renewed encounter, redundancy of the designed model of learning culminating expected suggestion to enhance quality of website base learning and teaching at the college and universities.

2.4. Perceived Usefulness and Intentions to Use Blended and Online Learning Techniques

According to [25], "perceived usefulness is an individual belief that a technology will make their work better". On the other side, ([26], p. 30) views "perceived usefulness as the degree to which students believe that using technologies will improve their learning performances". Many researchers concede "perceived usefulness" as determinant of the intentions, for using online technologies in learning and teaching activities [27] as, online Learning technologies utilized in teaching facilitate students and teachers with chances to cooperate in creation and sharing of knowledge. "These inform that technologies and tools provide a learning environment in which students can construct their learning experiences and collaborate with others to generate ideas" ([28], p. 18). Therefore, it can be said that students get more benefit out of collaborative learning activities via online system rather than working alone [29]. As stated by [30] that now a day's digital students acquire more knowledge by engaging into relevant and eloquent activities for which online technologies is mandatory.

Additionally, it is imperative to note that online technologies increase blended learning opportunities by creating a learning environment that impart positive effects on students as well as faculty members [5], [31]; [32]. Particularly, language education teachers expressed positive views regarding online learning and specified the pedagogical benefits related to blended learning and online learning technologies [33]. In another study conducted by [34] to examine the adaptability of students towards online learning technologies, they found that according to students few online technologies are very helpful in terms of interaction with fellow beings and teachers and acquisition of more knowledge, and satisfaction with a course etc. [28] expressed that perception of teachers regarding usefulness of online technologies are noteworthy determinants of their intention to use the applications in teaching. Therefore, based on the "Technology Acceptance Model (TAM)", it can be posed that Perceived usefulness of blended and online learning is a significant predictor of intentions to use those technologies in teaching methodologies particularly while teaching and learning English language as foreign language.

H1: The "perceived usefulness" of blended learning & online learning is positively associated with behavioral intention to use blended & online learning technologies.

2.5. Perceived Ease of Use and Intentions to Use Blended and Online Learning Techniques

"Perceived ease of use refers to the degree to which an innovation (technology) is perceived to be easy to understand and use" ([35], p. 33) "Users of a technology can perceive ease of use of technology when they are exposed to or familiar with it" [5] Similarly, stated by [5] learners start using technologies once they perceive it easy to use. On the other hand, ([36], p. 338) declares that "new ideas and innovations that are easier to understand are

adopted more rapidly than those that require adopters to develop considerable new skills and understandings". ([37], p. 320) that "perceived ease of use is the degree that using a specific technology will be free of effort". Additionally, [38] research results revealed that perceived ease of use is a strong predictor of intentions of the students to keep on using the online leaning technologies. Likewise, [5] conducted a cross sectional study among 350 respondents and including teachers and students and fond that perceived ease of use is significant predictor of intentions to use the online technologies and was supported by majority of both students as well as teachers. Therefore, based on the "Technology Acceptance Model (TAM)", it can be posed that Perceived Ease of Use of blended and online learning is a significant predictor of intentions to use those technologies in teaching methodologies particularly while teaching and learning English language as foreign language.

H2: The "perceived ease of use" of blended learning & online learning is positively associated with behavioral intention to use blended & online learning technologies.

2.6. Technology Acceptance Model (TAM), Intentions to Use and Actual System Use

Technology Acceptance Model (TAM) model is applied in this study. The three constructs of the TAM including "perceived usefulness, perceived ease of use, and behavioral intention to use" blended learning and online learning are tested to find out the actual usage of an information system as presented in Figure 1. This implies that teachers and students' readiness to participate in blended and online learning activities are dependent upon their perception about usefulness of these techniques along with ease of sing those. In addition, [27] asserts that there is an affirmative association between intention to use and actual usage of online technology and those intentions are initiated because of Perceived usefulness and Ease of Use of blended and online learning.

Likewise, [39] stated that intentions to use new learning systems results into increased adoption level of the students as well as teachers and ultimately results into more learning capabilities. [40] also concluded that intentions to use technologies leads to actual system usage of those technologies and are aroused on the bases perceived ease of use and perceived usefulness and intentions to use blended and online learning techniques. Therefore, it is posed that in case of high intention to use blended learning and online learning technologies to learn English language, the resultant pledge towards using blended learning and online learning technologies would be high and would be actually predicted by perceived usefulness and perceived ease of use.

H3: There is a positive association between behavioral intention to use blended & online learning technologies and actual system use.

H4: Behavioral intention blended & online learning technologies. mediates the relationship between "perceived usefulness" of blended learning & online learning and actual system use.

H5: Behavioral intention blended & online learning technologies. mediates the relationship between "perceived ease of use" of the blended learning & online learning and actual system use.

2.7. Correlation Hypotheses of the study

H_0; There's correlation between students derived independent variable (Abilities to learn online, speed of online information capture, Increased capacity of knowledge acquisition) and their perception with respect to the merits and demerits of Blended Learning.

$$\mu_1 = \mu_2 = \mu_3 = \mu_4$$

2.8. Theoretical Framework of the Study

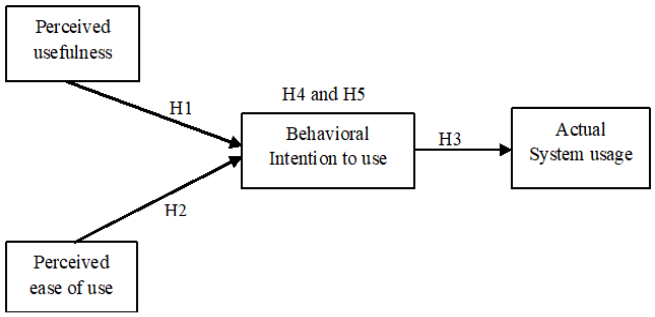


Figure 1: Theractical Framework of the Study

3. Research Methodology

3.1. Research Tools

In this research, the Q method was employed as mixed method research approach. As a part of it, questionnaire method was applied. The criterion for data collection was supported by the Q-Sort data collection model. A model in which differential sample groups were demarcated in individual allotment data collection units. Q methodology application began in 1930 in psychology field. It was later used in institutional research of social sciences. Its main mandate is to unravel objective perspective, perception, attitude and believes from sampled population of learners in their own discourse, [41]; [42]; [43]; [44]. The Q methodology has been visualized as the most merited data collection technique as it reveals where research group data meets on instantaneous commonly standardized ground on specific topic, and in which direction it is deviated, if that's the scenario [42]. It also helps to develop research outcome amongst commonly identified ideas. Within Q research method, we meet a cemented research model known as Q-Sort model. This model provided guidelines for data collection to perform analysis. Individual factors in its structured framework partition an integration of data acquisition and display aspect. The data partition and clarity in depth display made analysis simple. Data collection was streamlined on the hierarchy of statement listings on the Q- Sort scale. The same is guided by individual learner participants' agreement or disagreement choice selections whose items are listed at the brim of heading titles. The Q methodology is a reality-based research methodology preferably noted choice

to measure perceptions aligned to a particular phenomenon, presenting it as a generation of both qualitative and quantitative methods of data collection [45]; [42]; [46]. As we progressed, in this research, the main objective inculcated determination of English as foreign language students' perception on blended learning by participants' inducing a total of 47 judgmental statement clauses involving 36 affirmative and eleven negative expression on the Q-Sort model.

3.2. Data Collection Work Group

The data collection workable group in the research comprised of 251 English language learners who voluntarily presented themselves for Q-Method procedural participation and learning at third and fourth grade of English Language Teaching at the university identified within United Arab Emirates while in their spring semesters of 2018-2019 academic year. The participant respondents initially have had coursework in "Phonetics and Phonology" and "English Literature Responsive Cultural Pedagogy Work" within blended learning designed model. The provisions to have registered and done a blended course unit there before was used as a determination for main criterion in selecting a cumulative total number of 251 learners. It thus followed, the criteria for sampling method in determination of research sample.

Table 1: Description of research sample Size

Independent Variables	**N**	**%**
Student Ability to Learn Online. (Perceived -Usefulness).	9	36%
Speed of online information capture (Perceived Ease of USE)	5	20%
Students' Perceptions about irrelevancy of online blended learning (Behavior Intention)	7	28%
Students' Suggestions on the way forward for Online Blended Learning Implementation, Actual System Use)	4	16%
TOTAL:	25	100%

Note: * Number of Learners in The Sample: 251

3.3. Data collection instrument

Judgmental statement clauses held expression for determination of learners' views at the clinch of 4 headings. A sequential study directive required individual learners to make placement for a total 25 judgmental statement clauses (Nineteen affirmative and six negative) within the Q-Sort model with regard to their individual level of assessment and agreements. This is how the data was collected regardless of the idea that judgmental statement viewpoints within instrument of research was based on the literature.

Q-Sort Model

-1	0	1	2
Disagree	**Neutral**	**Agree**	**Strongly Agree**

4. Results and Analysis

The data of this study was compiled and analyzed by ANOVA (Analysis of Variance), to find out the correlation between students' response statistic with bended learning. The Analysis of Variance (ANOVA) was performed by means of a five-step approach. Let us match one by one systematically to find out what will be the outcome.

- **Step I: Hypotheses review and Level of significance Setup;**

  H0: μ1 = μ2 = μ3 = μ4

  H1: Standard deviated values away from the normal range

  Level of Significance (a) α=0.05

- Step II: **Test statistic identification.**

  We decide to use F statistic as it is the standard ANOVA test statistic. Calculated as follows; F = MSB/MSE.

- **Step III: Decision Rule determined.**

  The degrees of freedom are required to set up a decision rule. In this case we are enabled to get the critical value of F.

  Degrees of freedom calculation.

  Degree of Freedom 1 (df1) = k-1

  Degree of Freedom 2 (df2) = N-k.

  Now in our case, df1=k-1= 4-1=3 for all tables, i.e. Table 1 to Table 4.

  df2 = N - k=100 – 4 = 96 for table 1, 28 – 4 = 24 for table 2, 44 – 4 = 40 for table 3, 16 – 4 = 12 for table 4. From the F table, the F value for test statistic in Table 1 is 2.699, Table 2 is 3.009, Table 3 is 2.839, and Table 4 is 3.490.

  Decision rule is that: Reject H0 in each category if F > 2.699 for table 1, F > 3.009 for table 2, F > 2.839 for table 3, and when F > 3.490 for table 4. Rejection is based on the test statistic in each type of the four categories.

- **Step IV: Computation of the test statistic.**

  In this case we need to complete Analysis of Variance table for ANOVA. We find out sample means, then overall mean after which we will run sum of squares.

$$\mathrm{SSE} = \Sigma\Sigma\left(X - \bar{X}_j\right)^2$$

$$\mathrm{SSB} = \Sigma n_j\left(\bar{X}_j - \bar{X}\right)^2$$

  (Note: Workings in Excel Sheet)

Table 2: Analysis of Variance (ANOVA)

Source of Variation	**Sum of Squares (SS)**	**Degree of freedom (df)**	**Mean Squares (MS)**	**F Value**
Between Treatments 1	-	3	411.828	0.113
Residual Deviation 1	-	96	3639.455	
Between Treatments 2	-	3	739.229	3.000

Residual Deviation 2	-	24	237.188	
Between Treatments 3	-	3	1803.269	0.384
Residual Deviation 3	-	40	4693.318	
Between Treatments 4	-	3	647.064	1.389
Residual Deviation 4	-	12	465.600	

- **Step V: Final Comments**

  We accept H0 hypothesis since 0.113 < 2.699 for table 1, 3.000 < 3.009 for table 2, 0.384 < 2.839 for table 3, and 1.389 < 3.490 for table 4. At significance level of 0.05, there is no statistical difference in means for students' perceptions towards blended learning. This thus confirms a higher degree of acceptance for blended learning versus old class mode of learning.

4.1. Correlation Analysis results:

For analysis purpose Smart PLS 3 was applied. Out of total 251 respondents 55.3 % were male 44.7% were females. The bivariate correlation analysis in table 1 shows that Perceived Usefulness had a significant positive correlation with Behavioral Intention (r=.38, p < .01), Perceived Ease of Use (r=.29, p < .01) and Actual System Usage (r=.37, p < .01). Similarly, Behavioral Intention had a positive correlation with Perceived Ease of Use (r=.66, p < .01) and Actual System Usage (r=.48, p < .01). Likewise, Perceived Ease of Use was found to have a positive correlation with Actual System Usage (r=.55, p < .01). The *** on the path coefficient values show excellent correlation between the variables. The survey questions are able to explain 48.1 % of these relationships.

Table 3: Correlation results

Construct	PU	BI	PEOU	ASU
PU	(0.89)			
BIU	0.38**	(0.87)		
PEOU	0.29**	0.66**	(0.75)	
ASU	0.37**	0.48**	0.55**	(0.79)

Note: Cronbach's alpha(α) are written in parenthesis PU= Perceived Usefulness; BIU= Behavioral Intention to use; Perceived Ease of Use and ASU=Actual System Usage

To establish internal consistency and to ensure reliability of all constructs Cronbach's alpha and construct reliability was checked. Results of Cronbach's alpha in table 3 reveals that it was higher than standard requirement (0.7) for all the study constructs, i.e. Perceived Usefulness (0.89), Behavioral Intention (0.87), Perceived Ease of Use (0.75), Actual System Usage (0.77). One of the major contributions of this research is the provision of new dimension by converging Online Learning technology, blended learning technology Perceived Usefulness, perceived ease of use, the Learner behavioral intention in relation to its impact on online Learning actual Usage. This study further provides clarification and incremental knowledge in context to other researchers.

4.2. Direct and mediation hypothesis.

In table 4 the results depicted that Perceived Usefulness is positively and significantly related to Behavioral Intention of the students (ß = .633***, t=4.160) and Perceived Ease of Use is positively and significantly related to Behavioral Intention of the students (ß = .331***, t=3.552). Therefore, hypothesis1, which projected a positive association between the "Perceived usefulness" of Blended Learning & Online Learning with Behavioral Intention of students to opt for the blended learning and online learning, and hypothesis2, which projected a positive association between "Perceived Ease of Use" of the Blended Learning & Online Learning with Behavioral Intention of students to opt for the blended learning and online learning is fully supported. Similarly, H3, is fully supported by results given in table 4.

Table 4: Hypotheses Testing Results

Hypotheses		Std. Beta	t-Value	p-Values	Findings
H1	PU→ BIU	0.287	2.960	0.000	Supported
H2	PEOU→BIU	0.675	.710	0.010	Supported
H3	BIU→ASU	0.596	5.287	0.000	Supported
H4	PU→BIU→ ASU	0.360	3.618	0.000	Supported
H5	PEU→BIU→ ASU	0.400	4.519	0.000	Supported

Note: PU= Perceived Usefulness; BI= Behavioral Intention to use; Perceived Ease of Use and ASU=Actual System Usage

As depicted in Table 4 the mediation hypotheses ($H_4$and H_5) are supported. An indirect and positive effect of "Perceived usefulness" of Blended Learning & Online Learning was found on Behavioral Intention of students to opt for the blended learning and online learning (B=.360***, t= 3.618, p < 0.001), similarly, an indirect and positive effect of "Perceived Ease of Use" of the Blended Learning & Online Learning was also found on Behavioral Intention of students to opt for the blended learning and online learning (B=.400***, t= 4.519, p < 0.001). The formal two tailed significance test assuming a normal distribution exhibited that for Perceived usefulness the indirect effect was positive and significant. Further, results show the non-zero value for lower limit and upper limit confidence interval which means that results were significant [47].

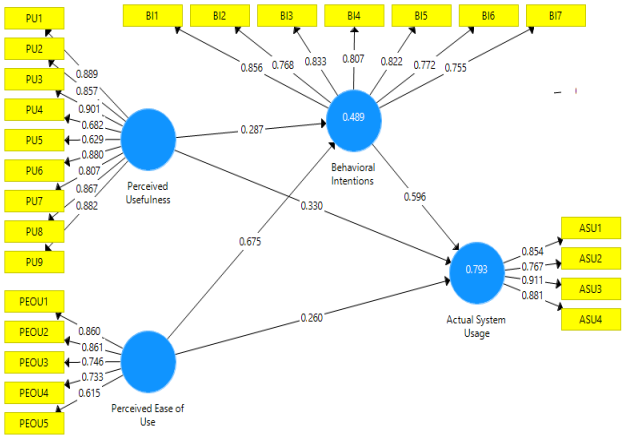


Figure 2: Regression results

5. Discussion

5.1. Students ability to learn online

Current study reveals that Perceived Usefulness and Perceived Ease of Use of Blended Learning & Online Learning directly impact the Behavioral Intention of Students to opt for the blended learning and online learning practices to learn different language (in this study particularly to learn English language) and those behavioral intentions further increase the adoptability level of the students for Actual System Usage. This study disclosed that the blended online learning format in the modules encouraged students to focus their attention on the topics and issues with less distraction. All evidence-based studies made a conclusion that individual student's success was highly revealed in blended learning encounters when related to either complete online or wholly face to face learning encounters. Outcomes showed contentiously blended learning module clarified extensively efficient comparison to traditional module while devising voluntary teacher's periodical teaching module.

In [48], the author indicated intrinsically students whose preference was for enrollment into online course units displayed higher magnitude within individual abilities to entrust online learning also magnificent confidence in relation to online knowledge acquisition compared to the other students using the old learning technique. The study also noted that integration of blended online discussions format in their courses allowed them to construct their own thinking rather than just passively accepting what others thought. This study also noted that blended online learning format encouraged students to be creative i.e. having the ability to think critically of an issue in novel and unusual ways and come up with unique conclusions resulting into enhanced ability to learn English. [49] noted that the magnitude of students' contentment, expectation, opinion, or viewpoints on various unit programs performed a significant role in evaluation of efficiency in learning process and that is a pre-requite for learning a foreign language i.e. English Language.

5.2. Speed of online information

This study also reveals that there was no significance difference (P<0.05) in the speed of online information accessed among the students. The integration of online blended discussion format in their course encouraged in-depth discussion of the ideas and concepts taught in the English language course among students. Also, the online learning discussion format prevented students from wasting time in non-course activities like disturbance, commuting, and unnecessary social interactions. These findings are in line with the study of [50] that mapped Egypt university EFL student's knowledge acquisition skills and contentment linked to website base material components that had individual's contentment with internet illuminated material set. The blended online discussion format encouraged students to spend more time focused on topics and issues at hand very easily. Incorporating learners in an online blended learning session has a huge promising effect on wider knowledge acquisition and at the same time providing response to peer related question sets, live share of borne ideology including acquisition of timely outcomes from their course instructors.

5.3. Students' Perceptions about irrelevancy of Online blended learning capacity of knowledge acquisition

The study noted that Online learning discussion format allowed more students to feel more comfortable asking awkward questions but others thought that lack of social interactions in the online discussions affected their understanding and learning as well as difficulty in participating in the Online discussions since due to the lack of face-to-face interaction aspect during the discussions. However, some students noted that they spent too much time learning to use technology instead of focusing on the discussion part of the module. Others felt that online discussion format in their course made them feel isolated from the instructor. This study found that there is no significant difference in means for students' perceptions towards blended learning.

This concurs with [51] study which confirms a higher degree of acceptance for blended learning versus old class mode of learning and that student's attitude towards blended learning were motivating regarding processes, convenience in usage and satisfaction, putting a contextual comprehension format on course materials. This study has indicated greater motivating perception responses aligned to beneficial aspects of blended online learning, such as the accessibility, convenience, and resource endowment factor. A study by [5] on perception of blended learning within Saudi colleges and university institutions concluded that the merit of this blended online learning model of knowledge acquisition was applauded at the University and College Education Ministry in Saudi since it was found to provide a remedy to the shortcomings emanating within college students learning in response to a highly replicating college learner demography.

In [52] the author noted that e-Learning within Saudi universities and colleges had capabilities and challenges that was envisioned within the e-learning acceptability that was determined by numerous influential factors. One of these factors is the learner's perception towards blended electronic learning. This shows how much the student like online learning and how frequently does the individual student make use of it. This study also noted that student's ability to decide on to blended online learning is significantly influenced by and subject to who surrounds or who is nearby. These are the people they highly value like their tutors, lecturers, or even parents. Furthermore, they perceived notion of whether blended online learning was accessible or not, plays an intensive role on deciding on whether to accept its usability or not. These findings are imperative in the seamless technology use acceptability.

5.4. Students' Suggestions on the way forward for Online Blended Learning

This study has revealed that members of the class indicated a reasonable magnitude of contentment pertaining the online learning aspect. The students' suggestions on the way forward for online blended learning was not statistically difference (P<0.05) indicating that combination of traditional learning process techniques with technological online learning techniques have a positive output to the success of a learner to read and comprehend different languages. These findings are in concurrence with report by [53] who envisaged in a case study

within the Iranian higher education setting that combining traditional learning process instructions with technological reference online material may have an intense output to the success of a learner to read and comprehend. This study also found out that students would recommend the online blended learning courses to their fellow students because of motivation and enjoyable online discussion in the course and appreciated the online discussion of the course with deadline attached to it.

6. Conclusion

As current study examined the factors influencing blended learning adoptions, results revealed that perceived usefulness proved to be the most powerful factor of blended learning along with perceived ease of use that creates intentions to use blended and online learning among teachers and students for learning English Language. The logic can be that blended learning is adopted by academicians in lieu of the fact that they perceive the online technology as useful tool of learning and teaching, therefore, they are interested to focus on the usefulness of the technology as well as its perceived ease of use in adopting it. This study has found out that individual student success was highly revealed in blended learning encounters when related to either complete online or wholly face to face learning encounters. Blended learning has been seen to optimize maximum benefits of old teaching methods and access to online learning materials. This study, therefore, confirms a higher degree of acceptance among students for blended learning versus old class mode of learning technique. We also conclude that there is a significant correlation among students derived independent variable i.e. abilities to learn online, speed of online information capture, Increased capacity of knowledge acquisition, and their perception with respect to the merits and demerits of blended learning.

Conflict of Interest

The authors declare no conflict of interest.

References

[1] X. Li, Y. Yang, S.K.W. Chu, Z. Zainuddin, Y. Zhang, "Applying blended synchronous teaching and learning for flexible learning in higher education: an action research study at a university in Hong Kong," Asia Pacific Journal of Education, 1–17, 2020, doi:10.1080/02188791.2020.1766417.

[2] J.C. Evans, H. Yip, K. Chan, C. Armatas, A. Tse, "Blended learning in higher education: professional development in a Hong Kong university," Higher Education Research and Development, **39**(4), 643–656, 2020, doi:10.1080/07294360.2019.1685943.

[3] P. Bazelais, T. Doleck, "Blended learning and traditional learning: A comparative study of college mechanics courses," Education and Information Technologies, **23**(6), 2889–2900, 2018, doi:10.1007/s10639-018-9748-9.

[4] C.R. Graham, W. Woodfield, J.B. Harrison, "A framework for institutional adoption and implementation of blended learning in higher education," Internet and Higher Education, **18**, 4–14, 2013, doi:10.1016/j.iheduc.2012.09.003.

[5] K.-T. Wong, G.-J. Hwang, P.S. Choo Goh, S.K. Mohd Arrif, N. Wang, J. Chen, M. Tai, J. Zhang, R. Wanchid, N. Van Long, J. Van Exel, G. De Graaf, P.A. Towndrow, C. Cheers, Z. Tatli, H.İ. Akbulut, D. Altinisik, K. Spring, C.R. Graham, D.R. Serrano López, D. Ayuela, M. Auxiliadora, E. González Burgos, A. Serrano Gil, K. Lalatsa, R.D. Rogers, K.R. Seddon, W.S. Robinson, N.A. Rahman, et al., "Cognitive presence in online learning," Education and Information Technologies, **13**(1), 643–656, 2020.

[6] K.T. Wong, G.J. Hwang, P.S.C. Goh, S.K. Mohd Arrif, "Effects of blended learning pedagogical practices on students' motivation and autonomy for the teaching of short stories in upper secondary English," Interactive Learning Environments, **28**(4), 512–525, 2020, doi:10.1080/10494820.2018.1542318.

[7] N.A. Rahman, N. Arifin, M. Manaf, M. Ahmad, N.A. Mohd Zin, M. Jamaludin, "Students' Perception in Blended Learning among Science and Technology Cluster Students," in Journal of Physics: Conference Series, IOP Publishing: 12012, 2020, doi:10.1088/1742-6596/1496/1/012012.

[8] L. Martín-Martínez, V. Sainz, F. Rodríguez-Legendre, "Evaluation of a blended learning model for pre-service teachers," Knowledge Management and E-Learning, **12**(2), 147–164, 2020, doi:10.34105/j.kmel.2020.12.008.

[9] D.J. Lemay, M.M. Morin, P. Bazelais, T. Doleck, "Modeling Students' Perceptions of Simulation-Based Learning Using the Technology Acceptance Model," Clinical Simulation in Nursing, **20**, 28–37, 2018, doi:10.1016/j.ecns.2018.04.004.

[10] C. Porumb, S. Porumb, B. Orza, A. Vlaicu, "Blended Learning Concept and its Applications to Engineering Education," in Advanced Engineering Forum, Trans Tech Publ: 55–64, 2013, doi:10.4028/www.scientific.net/aef.8-9.55.

[11] N. Wang, J. Chen, M. Tai, J. Zhang, "Blended learning for Chinese university EFL learners: learning environment and learner perceptions," Computer Assisted Language Learning, 1–27, 2019, doi:10.1080/09588221.2019.1607881.

[12] T. Doleck, S.P. Lajoie, P. Bazelais, "Social networking and academic performance: A net benefits perspective," Education and Information Technologies, **24**(5), 3053–3073, 2019, doi:10.1007/s10639-019-09913-3.

[13] J. Jia, D. Xiang, Z. Ding, Y. Chen, Y. Wang, Y. Bai, B. Yang, "An effective approach using blended learning to assist the average students to catch up with the talented ones," Knowledge Management and E-Learning, **5**(1), 25–41, 2013, doi:10.34105/j.kmel.2013.05.003.

[14] H. Kanuka, D.R. Garrison, "Cognitive presence in online learning," Journal of Computing in Higher Education, **15**(2), 21–39, 2004, doi:10.1007/BF02940928.

[15] A. Brew, "Disciplinary and interdisciplinary affiliations of experienced researchers," Higher Education, **56**(4), 423–438, 2008, doi:10.1007/s10734-007-9102-4.

[16] M.F. Badawi, "Using Blended Learning for Enhancing EFL Prospective Teachers' Pedagogical Knowledge and Performance.," Online Submission, 2009.

[17] D. Lalima, K.L. Dangwal, "Blended learning: An innovative approach," Universal Journal of Educational Research, **5**(1), 129–136, 2017.

[18] V.K. Ceylan, A. Elitok Kesici, "Effect of blended learning to academic achievement," Journal of Human Sciences, **14**(1), 308, 2017, doi:10.14687/jhs.v14i1.4141.

[19] L. Bielawski, D.S. Metcalf, Blended elearning: Integrating knowledge, performance, support, and online learning, Human Resource Development, 2003.

[20] D. Laurillard, "The educational challaenges for teachers and learners," in Virtual University Conference, 1996.

[21] P.A. Towndrow, C. Cheers, "Learning to communicate effectively in English through blended e-learning," 2003.

[22] D.A. Hijazi, A.S. AlNatour, "The effect of using blended learning method on students' achievement in english and their motivation towards learning it: Blended learning, achievement, and motivation," International Journal of Virtual and Personal Learning Environments, **10**(2), 83–96, 2020, doi:10.4018/IJVPLE.2020070106.

[23] A.A. Alshwiah, "The Effects of a Blended Learning Strategy in Teaching Vocabulary on Premedical Students' Achievement, Satisfaction and Attitude toward English Language.," Online Submission, 2009.

[24] A. AHmad, M. Al-Faqeeh, "Strategic leadership of the heads of academic departments: A field study at the University of Najran," Journal of Education, **1**(146), 571–615, 2011.

[25] R. Echeng, A. Usoro, I. Ewuzie, "Factors to Consider when Enhancing the Use of Web 2.0 Technologies in Higher Education: Students' and Lectures' Views for Quality Use," International Journal for Digital Society, **7**(1), 2016, doi:10.20533/ijds.2040.2570.2016.0138.

[26] K.J. Spring, C.R. Graham, "Thematic patterns in international blended learning literature, research, practices, and terminology," Online Learning Journal, **21**(4), 337–361, 2017, doi:10.24059/olj.v21i4.998.

[27] B.J.J. Muries, "Explaining Electronic Learning Management Systems (ELMS) Continued Usage Intentions among Facilitators in Higher Education Institutions (HEIs) in Tanzania.," International Journal of Education and Development Using Information and Communication Technology, **13**(1), 123–141, 2017.

[28] S.S. Khanal, P.W.C. Prasad, A. Alsadoon, A. Maag, "A systematic review: machine learning based recommendation systems for e-learning," Education and Information Technologies, **25**(4), 2635–2664, 2020, doi:10.1007/s10639-019-10063-9.

[29] F. Ndumbaro, "Exploring students' conceptions of collaborative information use and information use outcomes in credit-based group learning assignments," University of Dar Es Salaam Library Journal, **13**(2), 65–79, 2018.
[30] A. Jimoyiannis, P. Tsiotakis, D. Roussinos, "Social network analysis of students' participation and presence in a community of educational blogging," Interactive Technology and Smart Education, **10**(1), 15–30, 2013, doi:10.1108/17415651311326428.
[31] N. Emelyanova, E. Voronina, "Introducing blended learning in the English language classroom: Students' attitudes and perceptions before and after the course," Knowledge Management and E-Learning, **9**(1), 33–49, 2017, doi:10.34105/j.kmel.2017.09.003.
[32] S. Majid, P. Yang, H. Lei, G. Haoran, "Knowledge sharing by students: Preference for online discussion board vs face-to-face class participation," in Lecture Notes in Computer Science (including subseries Lecture Notes in Artificial Intelligence and Lecture Notes in Bioinformatics), Springer: 149–159, 2014, doi:10.1007/978-3-319-12823-8_16.
[33] W.W.K. Ma, A.H.K. Yuen, "Understanding online knowledge sharing: An interpersonal relationship perspective," Computers and Education, **56**(1), 210–219, 2011, doi:10.1016/j.compedu.2010.08.004.
[34] R. Hartshorne, H. Ajjan, "Examining student decisions to adopt Web 2.0 technologies: Theory and empirical tests," Journal of Computing in Higher Education, **21**(3), 183–198, 2009, doi:10.1007/s12528-009-9023-6.
[35] R.D. Rogers, K.R. Seddon, "Ionic liquids--solvents of the future?," Science, **302**(5646), 792–793, 2003.
[36] W.S. Robinson, "Ecological correlations and the behavior of individuals," International Journal of Epidemiology, **40**(4), 1134, 2011, doi:10.1093/ije/dyr082.
[37] F.D. Davis, "Perceived usefulness, perceived ease of use, and user acceptance of information technology," MIS Quarterly: Management Information Systems, **13**(3), 319–339, 1989, doi:10.2307/249008.
[38] L.W. Leong, O. Ibrahim, M. Dalvi-Esfahani, H. Shahbazi, M. Nilashi, "The moderating effect of experience on the intention to adopt mobile social network sites for pedagogical purposes: An extension of the technology acceptance model," Education and Information Technologies, **23**(6), 2477–2498, 2018, doi:10.1007/s10639-018-9726-2.
[39] S.A. Pradia, "Understanding College Students' Readiness to Use Web 2.0 Technologies in Online Education," ProQuest Dissertations and Theses, 137, 2016.
[40] K. Kazoka, J.E. and Mwantimwa, "Perceived Usefulness and Ease of Use of Web 2.0 tools in University Teaching and Learning in Tanzania," University of Dar Es Salaam Library Journal, **14**(2), 19-37, 2019.
[41] F. Demir, M. Kul, "Modern bir araştırma yöntemi olarak; Q metodu," Ankara: Adalet Yayınları, 2011.
[42] N. Herrington, J. Coogan, "Q methodology: an overview," Research in Teacher Education, **1**(2), 24–28, 2011.
[43] M. Mansoor, T.M. Awan, B. Alobidyeen, "Structure and Measurement of Customer Experience Management," International Journal of Business and Administrative Studies, **6**(4), 171–182, 2020, doi:10.20469/ijbas.6.10001-4.
[44] B.B. Mckeown, D.B. Thomas, In : Q Methodology, Sage publications, 2016.
[45] S.R. Brown, "Q Methodology and Qualitative Research," Qualitative Health Research, **6**(4), 561–567, 1996, doi:10.1177/104973239600600408.
[46] V.E. Job, G. De Graaf, "Q Methodology : A Sneak Preview Q methodology : A sneak preview," (March), 2016.
[47] M. Mansoor, T. Fatima, S. Ahmed, "Signaling Effect of Brand Credibility Between Fairness (Price, Product) and Attitude of Women Buyers," Abasyn Journal of Social Sciences, **13**(1), 263–276, 2020.
[48] A.R. Artino, "Online or face-to-face learning? Exploring the personal factors that predict students' choice of instructional format," Internet and Higher Education, **13**(4), 272–276, 2010, doi:10.1016/j.iheduc.2010.07.005.
[49] B. Akkoyunlu, M.Y. Soylu, "A study of student's perceptions in a blended learning environment based on different learning styles," Educational Technology and Society, **11**(1), 183–193, 2008.
[50] A.M. Aliweh, "The effect of electronic portfolios on promoting Egyptian EFL college students' writing competence and autonomy," Asian EFL Journal, **13**(2), 90–132, 2011.
[51] D. Adas, W.A. Shmais, "Students' Perceptions Towards Blended Learning Environment Using the OCC," An - Najah Univ. J. Res. (Humanities)., **25**(6), 1681–1710, 2011.
[52] K.A.S. Al-Harbi, "e-Learning in the Saudi tertiary education: Potential and challenges," Applied Computing and Informatics, **9**(1), 31–46, 2011, doi:10.1016/j.aci.2010.03.002.
[53] F. Behjat, M. Yamini, M.S. Bagheri, "Blended Learning: A Ubiquitous Learning Environment for Reading Comprehension," International Journal of English Linguistics, **2**(1), 97, 2012, doi:10.5539/ijel.v2n1p97.

ASTES

Advances in Science, Technology and Engineering Systems Journal Vol. 5, No. 5, 902-912 (2020)

www.astesj.com

Special Issue on Multidisciplinary Innovation in Engineering Science & Technology

ASTESJ

ISSN: 2415-6698

Need of E-Recruitment System for Universities: Case of Pulchowk Campus, Nepal

Vijay Yadav*, Ujjwal Gewali, Suman Khatri, Shree Ram Rauniyar, Aman Shakya

Pulchowk Campus, Department of Electronics and Computer Engineering, Lalitpur, 44700, Nepal

ARTICLE INFO

Article history:
Received: 30 August, 2020
Accepted: 28 September, 2020
Online: 12 October, 2020

Keywords:
e-recruitment
job recommendation
candidate filtering
HR management

ABSTRACT

This paper highlights the importance of on-campus online job recruitment system and its role in helping students grab the available job opportunities. It highlights the problems associated with the traditional way of hiring, especially for college students. It also presents some findings and results obtained through various surveys conducted within the campus before and after the deployment of this system. The work presented in this paper is based on an e-recruitment system built for one of the leading engineering institute in Nepal, Pulchowk campus. With some features like job recommendation based on various levels of skill, smart multi-criteria search, graduate tracking, this system proves to be useful for all i.e. companies, students and the campus as well.

1. Introduction

With an increase in production of manpower in various sectors, finding a proper job according to our skill is really a tough task to accomplish. Traditional method of hiring a candidate is proving to be inefficient. It is quite tedious and time consuming. Specially, those candidates who are freshers, don't have any idea regarding the whole process from advertisement to hiring face difficult times in landing to their first job. It's not that they don't have the right skills required for the job, rather most of the time its lack of right information at right time. Some sectors of job are really competitive and is difficult to make through it. But many other sectors have plenty of job opportunities, it's the lack of proper communication channel between employer and job seeker which makes it difficult. The advancement in electronics devices, IT sectors made people realize the need of e-recruitment system. In the beginning phase of development of e-recruitment system it was limited to only few countries and sectors. But today, it has widespread. Even the under developed and developing countries are working to build a proper electronic medium of hiring candidates to manage and mitigate the challenges posed by increasing unemployment in the country, to some extent.

In many developed countries, the universities and campuses have built their own job portal to make it easy for their students to get internships and jobs. This helps students know about the available opportunities at the right time and also establish proper communication channel with the employer. The employer can get their targeted candidate with little effort and less spending. The campuses can also be happy with the improvement in placement rate of their students.

Nepal has a range of web portals that work in the field of hiring of candidates for the jobs that they get through various companies from across the country. JobsNepal, KantipurJob, kumariJob, MeroJob are few of them. Though these commercial jobs are available in large numbers, the concept of job portal for universities and campuses is still a new idea to this country. It's hard to find such a portal in the institute of this country. Through the study and understanding of the importance of dedicated job portal for campuses we came up with the idea to develop an e-recruitment for our own campus. Before developing this system, we conducted surveys among the bachelor's students from the faculties of electronics, computer, electrical and civil engineering. The purpose of these surveys was to know their difficulties faced with traditional system, experiences of using available commercial job portals and perception towards having on-campus job portal.

Here, we are going to present a graphical representation of the process of hiring students that existed before this system and that exists after this system.

*Corresponding Author: Vijay Yadav, vizayyadav123@gmail.com

1.1. Before this system

The Figure 1 below depicts the traditional process of hiring of students that existed in our campus.

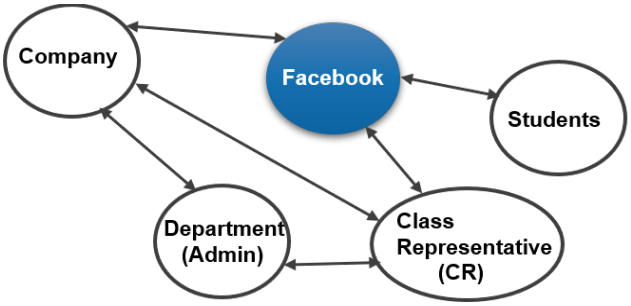


Figure 1: Traditional hiring process

In traditional system, in order to hire students, the company either contacted to various departments of our campus or Class Representative (CR) to circulate the information among students regarding any job vacancies. The department through CR and CR through Facebook page circulated that information. And then when student opened that page, they came to know about any job vacancies. The Facebook page was used for various purposes due to which the job-related information could not be properly communicated.

1.2. After this system

The Figure 2 shows the improvement we brought through the development of this system in the process of hiring students of the campus.



Figure 2: Present day hiring process

As shown in the figure above, a dedicated system is available to manage all the recruitment related activities. Now, company can directly post jobs in the web portal and students can see all the job postings in that portal without anyone's intervention. Companies will contact the department only once in their whole lifetime i.e. at the sign-up process just to verify their identity so that they can start posting jobs and communicate with their potential candidate directly.

1.3. Why this system?

Even though many commercial job portals were available in the market, why we felt the importance of building this system, what edge this system provides over those commercial job portals and how it will benefit the students, we will answer these questions in this section.

Let's have a look at a Figure 3.



Figure 3: Purpose of the system

According to the trend we have seen in last few years, when it comes to hiring a college student for the job, companies prefer students of one institute over others. Also, they post the same vacancies across variety of commercial job portals which is quite costly and time-consuming process. Now, they can simply post their job vacancies in our e-recruitment system which is not only free of cost but also reduces their time in the process of hiring the right candidate. Because it's a simple system with limited user access, the campus also can manage to run this system in free of cost because in the end, it's going to benefit their own students and themselves as they can keep track of the employment situation of their students.

2. Literature review

This paper is an extension of work originally presented in a conference, Artificial Intelligence for Transforming Business and Society (AITB), 2019 [1]. It contains an extensive explanation of the system using various diagrams. Some features which were improved in the system in the last one year have been included in this paper. Those improvements are job recommendation not only based on skills but also on the level of skill like beginner, skilled, advanced and expert, skill verification of students by the department, viewing the location of companies on map, knowing more about the location from where the job has been posted using Foursquare API. It also includes the analysis of data collected before and after the development of this system, through various surveys conducted among the students of the campus. Some data visualization tools have also been used to visualize the skill requirements of the country and places with more job opportunities across the country, using the data collected over the last one year.

Over the last few years technologies have developed a lot. But before that various traditional methods like advertisement through radio, television, newspapers were used to propagate information regarding vacancy opening [2]. Nowadays, people spend more time on internet finding a job rather than reading a newspaper or listening a radio every day. Many breakthroughs are being achieved regarding the speed of the internet which in turn have decreased the price of web surfing. At the same time, we cannot

deny the existence of traditional way of hiring a candidate. Still, the same process of publishing an advertisement on newspaper and hiring a candidate through an interview is considered as the best way to find the right candidate [3]. The major role of online recruitment system is to communicate information regarding the vacancies among the targeted candidates within the right time and in an organized manner in order to fight the increasing unemployment because in some places where even jobs were available, the candidates were unaware of those jobs due to lack of proper communication channel [4]. So, it becomes very important to study the existing situation around the place for which the system is being built. A proper study is needed to know the perception of both employer and job seekers especially the students regarding online recruitment system and traditional system of hiring [5]. Not all the employers looking to find candidate for the job through online process gets satisfactory result after spending considerable amount of money during the process [6]. So, once a system is built it is necessary to analyze the various parameters of the system like cost-effectiveness, security, performance, usability and reliability with the help of group of respondents who are actually going to use the system [7]. Charging a huge amount of money to the employers/ companies is not going to help, especially in the case of on-campus job portal because this will ultimately reduce the number of job postings through this system.

Knowing the purpose of building a job portal is very important because in the past as well many job portals emerged without analyzing the environmental situation required at that point of time and thus, later on were compelled to merge in order to provide better service [8]. Online job recruitment system cannot be useful in every scenario. There are some problems associated with e-recruitment system as well [9]. In some cases, it may prove to be more costly and inefficient. So, while developing a system all factors need to be considered. If done so it can save large amount of money which is spent on advertising and those saved money can be used for training and skill enhancement of the hired candidate [10]. Campuses where mostly non-income generating candidates are available, cost effective system is a must to reduce the economic burden which could come upon the student.

In a fast-paced world of today, it's very difficult to carry on the traditional way of hiring a candidate they are tedious, time consuming and stressful [11]. We live in the world of advertisement. No matter how good the product is, it needs an attractive presentation through advertisement to increase its sale and get desired price for that product. Same thing applies for job. It is directly linked with the life and dreams of an individual. So, he/ she needs to find something inspiring to apply for a job and an e-recruitment provides that platform to the employer to put a proper job posting in order to attract the targeted candidates [12]. Online medium and internet have brought drastic change in the recruitment process impacting both employer and job seeker in a positive way. Internet has become a major tool for both employer and job seeker as it has brought both of them on same platform. It has revolutionized the traditional method of hiring a candidate for the job [13]. It provides an edge to the company to get the best candidate suited for the job. Also, an edge to the job seeker to select from many options available. E-Recruitment system has virtually vanished the boundaries between the countries [14]. It has promoted the concept of globalization. It has reduced the work and time spent by Human Resource Department of companies on hiring process, significantly. It has made the whole process organized and paperless [15].

An individual has to go through various steps and screenings before they finally get a job and for that one should first be able to apply for a job of matched skills [16]. Companies perform those screenings to make sure they have found the right candidate who could sustain in the company for longer period of time because the human resource is what one company can have advantage over others [17]. Skilled and talented human resource makes wise use of resources available within the company and thus makes a company look different in comparison to its competitors. The human resources available within the company should be motivated and possess high morale and companies should help them with these because the conduct, work and efficiency of workforce of companies determine the survival of the company in the business they are involved in [18].

Lots of job are posted on an e-recruitment website on a daily basis. All the job seekers on those platforms don't have same set of skills and it takes lots of time for an individual to find the right job that match up with his/ her skills, if some mechanisms are not employed in the system to recommend jobs to the job seekers based on the skills they possess [19]. So, recommendation system is a must for any e-recruitment system because the main purpose of any e-recruitment system is to reduce the time in the process of hiring.

Nepal is still a developing economy. Many skilled manpower is forced to leave the country in search of job. So, a better and organized system is required to employ those workforces within the country to contribute to its economic development [20]. And, what could be a better than to start identifying the skill of individuals during the college times and helping them find the job that suits their skill. This will not only stop those skilled workforces from going abroad but also help them in contributing to the development of their own country. The college students are more in dilemma when they complete their study and look to find a job for themselves because they don't have any idea regarding where to apply, how the process takes place. They spend much time finding answer to those questions before they land to their first job. So, the e-recruitment system we have built will try to solve these issues. With this system, students will probably be able to get their first job before they complete their studies. Also, they would be familiar with the whole process in advance.

3. System overview

This application is a campus based online recruitment system. The need to build this system was realized when we faced with the traditional method of hiring students by the companies. The

traditional method was time consuming, tedious and unfair to most of the students because the job vacancies came through various individuals in the campus. There was not a dedicated platform for handling only job-related matters due to which the information related to vacancies could not reach to every students of the campus within the time. In fact, we faced this issue multiple times. Until we could get information related to vacancies, some other individuals were already hired. So, we thought of building a system which would treat each student fairly in terms of getting information timely and show casing their skills to the employer. We also defined the role faculty department (Admin) during the hiring process, in this system. There are three actors involved in this system. They are students, companies and faculty departments. Though the role of faculty department during hiring process is minimal, it's vital.

3.1. Basic features of the system

The basic and most important features of an e-recruitment system is shown in Figure 4 The system will help students to build their profile once they are logged in and this profile can be used to generate CV which they can download in the form of PDF. The companies can post job through their own profile. Based on the jobs posted by the companies, the system will recommend the jobs to the students that match with their skills. A secured login is provided to enhance the authenticity of the users.

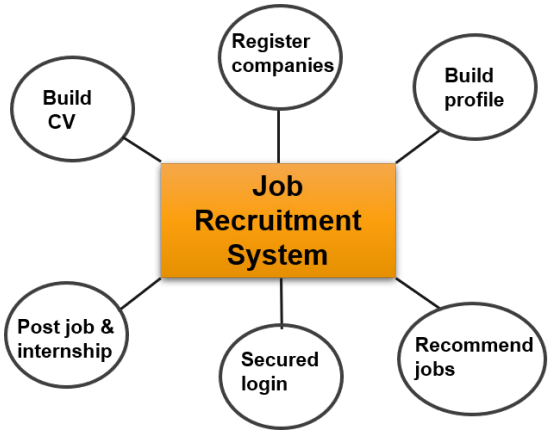


Figure 4: Overview of system

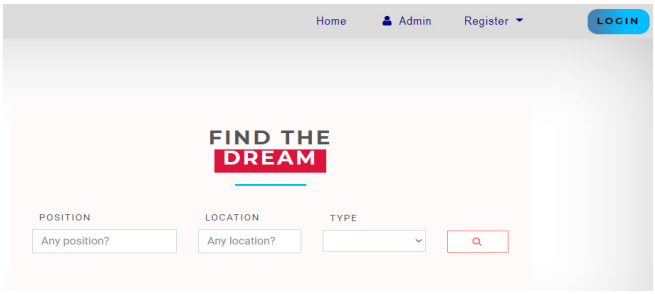


Figure 5: Home page of the system

3.2. Workflow of the system

The state diagram shown in Figure 6 represents various states and the workflow of the system. During the sign-up process, users need to identify themselves as either employer or student. Department does not have to create a separate account as it is already provided with the system. Students having an email account of the campus will only be allowed to create an account. Similarly, the companies can also create an account which they can use to post job vacancies. Students, Companies and Admin are the three actors involved in this system. The whole process of hiring is completed with interactions among these three actors.

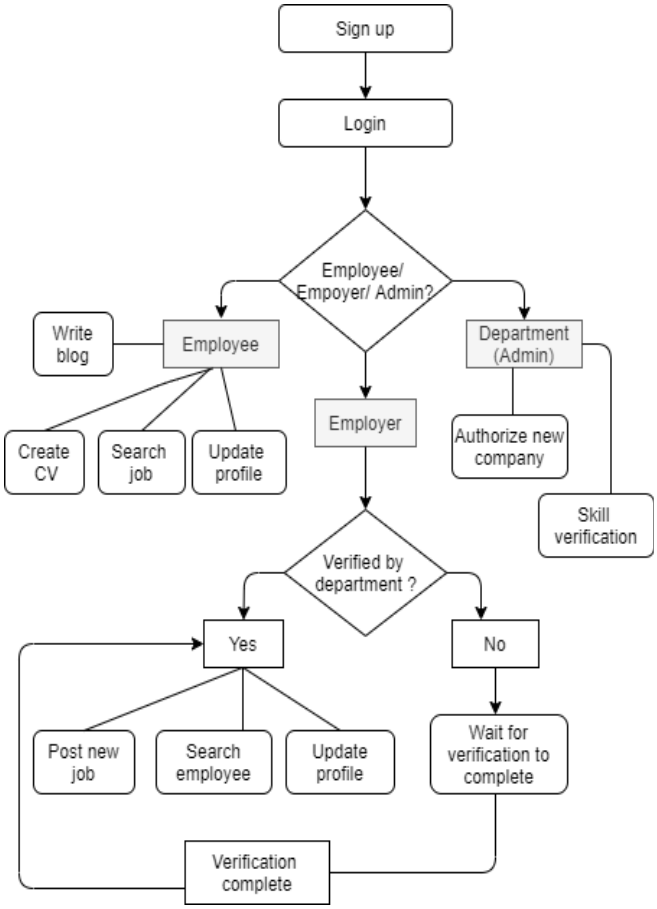


Figure 6: State diagram of the system

The role of all three actors are elaborated below:

Students

Students are the job seekers in this case. All they have to do is to first register themselves into the system. During the registration process, students need to verify their email address. This process does two things, first it verifies whether the email address used is of the campus or not (for e.g.: abcd@pcampus.edu.np), and the next thing is whether the provided email address is associated with particular user or not. The link sent to email for verification will be valid for only few hours. Once the email is verified, users will be asked to update their profile. After updating their profile, they can apply for the job. Also, students will now be visible to the companies in their search results. Students will be notified periodically through email to update their profile to increase the chances to find better job.

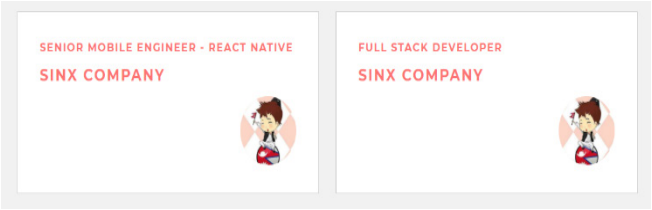


Figure 7: List of jobs the student has applied for

Companies

Companies are the job providers or employers in this case. All they have to do is to create an account to start posting jobs. They have to pass through two verification processes. First, they have to verify their email address and the second is to verify their identity which will be done by the Admin. Once an account is created, a notification will be sent to the Admin to verify whether the company is genuine or not. The admin can match the information provided by the companies during the creation of account or can directly contact with the companies to verify its existence and credibility. As soon as the two-verification processes are completed, companies can start posting jobs. There is no limit on how many jobs a company can post. Also, the posting of jobs will be free of cost to attract sufficient job opportunities towards the campus.

Department (Admin)

It is the center of the system. It controls all the activities of the system. The major task of this actor is to verify the identity of the companies signing up into the system. It can also keep track of the employment condition of the students even after their graduation.

The role of Admin has been extended from the previous version of the system. A separate account will be setup for project supervisors which will have very limited access control over the system. The one who has logged in using this account can only view an interface to verify the skills of the students. Once in a semester the project supervisor can use this account to verify the skill demonstrated by the student during the development of project. Student's profile will have green tick mark displayed along with their skills. This will be an added advantage to the student.

3.3. Software Development model

This application has been developed using prototype model. Since this system was itself a first of its kind in the country, it was very important to incorporate the feedbacks of various parties involved in this system directly of indirectly. Especially, it was very important to get the advices of the users who will actually be using this system. After refining so many prototypes, we finalized a prototype and started building this system. During prototyping, various faults within the design were identified. Also, it became easy for us to train them as most of them were familiar with the design. It also increased the acceptance among the users. The development and testing of the system were carried out simultaneously.

4. System architecture

The various components of this system have been elaborated below:

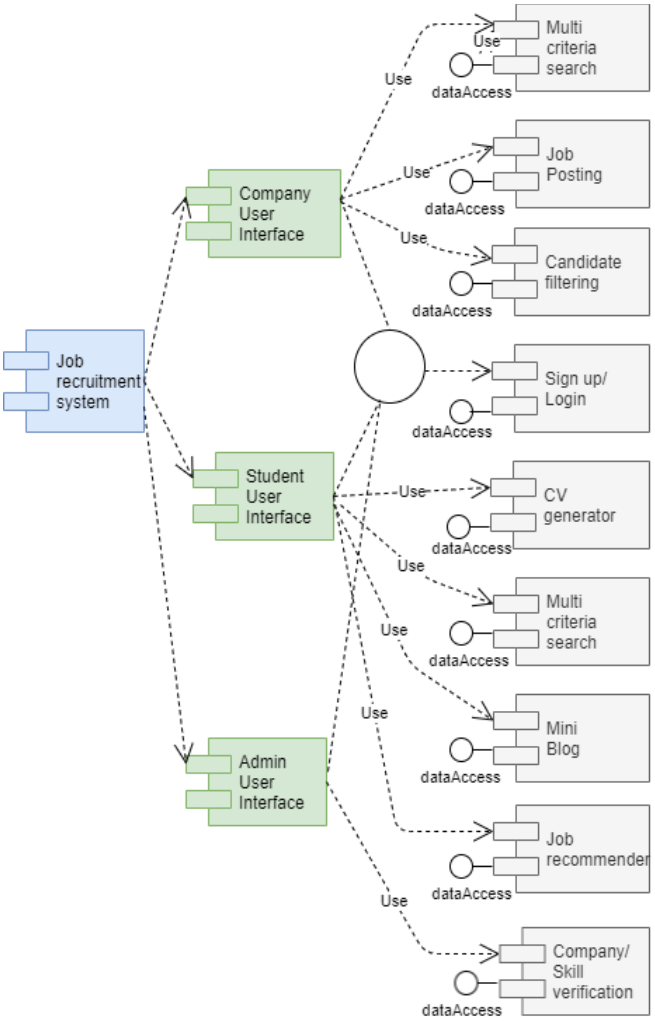


Figure 8: Component diagram of the system

Multi-criteria search

Multiple fields have been provided to both students and companies to make search. Students have been provided with fields like position, location and type to find the jobs more suited to them. Student can search for different positions like programmer, graphics designer, project manager, content writer and so on. Also, they can make search if jobs are available in the location of their choice. Type field represents the type of job like part time, full time, freelance or internship. Students can either use these fields individually or in combinations to make search.

Similarly, companies are provided multiple fields to make search for candidates best suited for the vacancies they have announced. The fields provided in search module of companies are position, qualification, skills, and years of experience. Position has same meaning as that of students. Qualification could be the degree that a particular candidate holds such as Bachelor in Computer Engineering, Masters in Electronics and communication

Engineering and so on. Skills could be technical skills like python, java and non-technical skills like communication, time management and so on. The companies can also use these fields individually or in various combinations.

Not every time the keywords used for searching match exactly to the keywords stored in database. So, Levenshtein distance has been used to approximate the search keyword. It helps to find the result that best represents the keyword entered by users during search process. It calculates the minimum edit required to transform one string to another [21]. The edit mentioned here could be insertion, deletion or substitution.

For example, let us consider someone is trying to make search using skill field and he/she enters PYTON instead of PYTHON.

P	Y	T	H	O	N
P	Y	T	O	N	

The Levenshtein distance between those two words is 3 as three changes are required. Also, we have fixed the maximum permissible to 3. So, in this case the user will successfully get all the results have skill value “PYTHON”.

Job posting

This allows a company to post jobs. There is no limit on how many jobs a single company can post. Also, the posting of job is free of cost. The company needs to add their address very carefully because we have used folium library to point to the address defined by the company, on map of Nepal. This could help student in finding the place easily in case if company calls that individual for the interview. Geopy library has been used to find the latitude and longitude of the place.

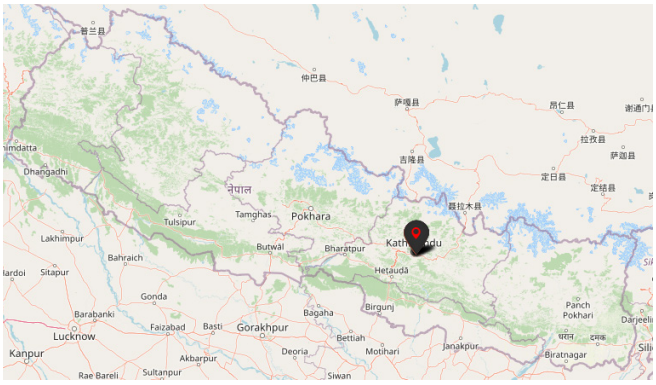


Figure 9: Example of map pointing to the address of company in New Baneshwor, Kathmandu, Nepal

There is also one feature provided called “Explore this place” which will help students get an overview of the place for which the job vacancy has been announced. It uses Foursquare API to find the top ten categories of venues within 500m of that place (if available within its dataset). Since it is still in an initial phase, the free version of Foursquare API has been used. Here also, Geopy library has been used to find the latitude and longitude of the place.

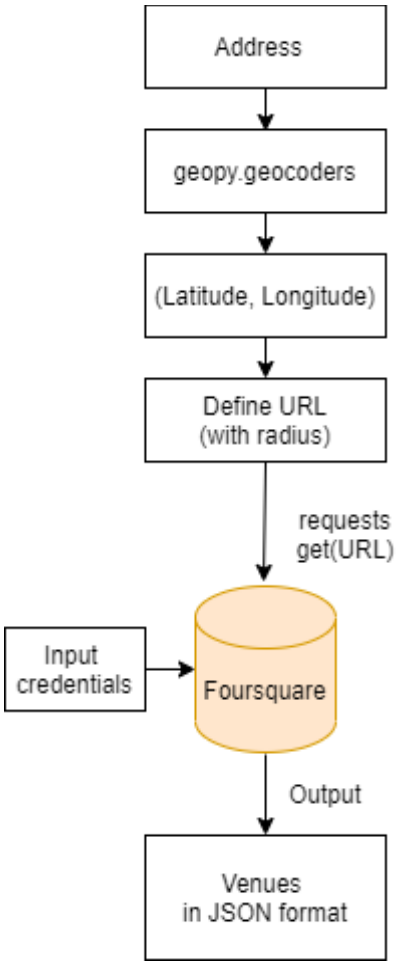


Figure 10: Fetching venues using Foursquare API

The venues fetched in JSON format is properly formatted and displayed in tabular form. Then, according to the availability of each category of venues, they are sorted in descending order to get the list of top ten categories of venues.

	Venues	Total Count
0	Asian Restaurant	5
1	Restaurant	5
2	Café	4
3	Hotel	4
4	Coffee Shop	3
5	Bar	2
6	Food	1
7	Garden	1
8	Himalayan Restaurant	1
9	Hostel	1
10	Bakery	1

Figure 11: Example of top 10 categories of venues within 500m radius of Kathmandu fetched by Foursquare

Candidate filtering

The company after receiving applications from many students regarding any job vacancy can shortlist the students based on their skill, qualification and experience required for the job in order to reduce the time for recruitment. They can also download the CVs of shortlisted students.

Registration/ login

This component is responsible for allowing the users to safely register and log in into the system. During the process of registration or login, it is very important to make sure authentic users are using the system. The number of attempts allowed to make to login into the system have been set to four. Also, for new users the time interval to verify the email has been set to a maximum one hour. Failing to do so will result in suspension of the account in both the cases which could only be activated by the Admin. Also, the password strength is checked during the registration process and during the password change.

CV generator

This component is built for students. It is used to generate CV using the information provided by students during profile creation. Five attractive templates have been provided using which CV can be generated. The generated CV can be downloaded in PDF format as well to use it outside this system. The information displayed on CV would be basic information, education, experience, projects, hobbies, certifications and trainings, skills and languages. Company, if finds the profile of any student interesting can also download his/her CV in PDF format for future reference. This feature saves time and money of students which they spent on various platform for building an attractive CV.



Figure 12: Example of a generated CV

Mini blog

This feature is provided to students which allow them to add short description of what projects or research they are working on. The companies can view these pieces of information when a student apply for the job to their company or when the company search for candidates using search component. Very limited functionalities have been provided with this component to keep it simple and yet useful.

Job recommender

Many jobs are posted in an e-recruitment system on a daily basis by different companies requiring different skills for different jobs. Every student/candidate doesn't possess same set of skills. It would be difficult for them to find the right kind of jobs suited to their skill. So, a recommendation system is a must for any e-recruitment system. Student does not need make search every time they login into the system. In fact, the system itself recommend some jobs to the students based on the skills they have mentioned on their profile. The system first matches the skills of students with the skill required for the job posted and if matched, it will then look for level of skills i.e. beginner, skilled, advanced or expert, required for the job and also possessed by students. The jobs whose both requirements matched with the profile of students will be displayed on top in the recommendation section. The recommendation section is displayed on the home page of students.

Company/ Skill verification

This component is developed for department (Admin). It allows admin to verify the identity of the companies and allow them to post jobs into the system. Also, a separate account is created for project supervisor within admin with limited access control, to verify the skills demonstrated by students during the project or research work. The student having verified skill will have an added advantage. As it is verified by the authorized body, companies can trust that student with those verified skills. It will help companies in taking decision during the process of hiring.

5. Results and discussion

An e-recruitment system we tried to build to solve the existing problems in our own campus, has been implemented successfully. The main motive of building this system was to overcome the shortcomings of traditional method of hiring and provide fair chance to every student to showcase their skills and grab the job opportunities that comes their way. It also helped to bring both the employers and the job seekers on common platform and establish direct communication channel between them.

5.1. Surveys

We will here present some very useful outcomes we got through the various surveys and questionnaires we conducted.

Survey 1

In this survey, we gave two sets of questionnaires were given to the participant. The purpose of this survey was to find the experiences of participants regarding the traditional method of hiring and also commercial job portals. we conducted this survey among 300 students of our campus (mainly comprising the third- and fourth-year students from the faculty of bachelor in computer, electronics and communication, electrical and civil engineering) and here are the results we got.

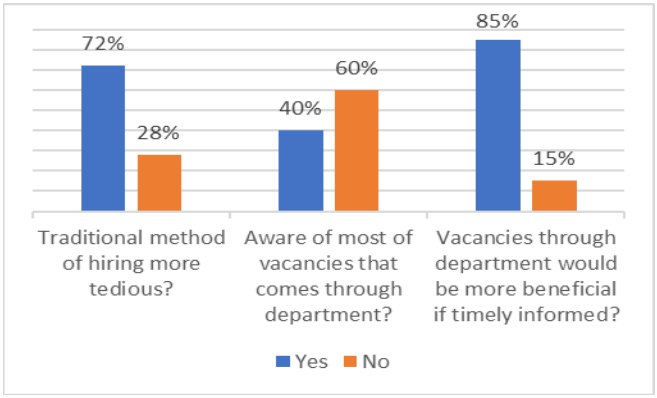


Figure 13: Responses of survey 1.1

The first questionnaire (survey 1.1) comprised 3 questions as shown in Figure 13 We found 72% participants felt traditional method of hiring is more tedious. Only 40% were aware of most of the vacancies that came through department and the other 60% either never came to know about some of the vacancies or knew when they were already expired. Despite that, 85% felt vacancies through the department would be more beneficial if proper communication channel is established between the companies and the students.

The second questionnaire (survey 1.2) comprised 3 questions. The responses are shown in Figure 14.

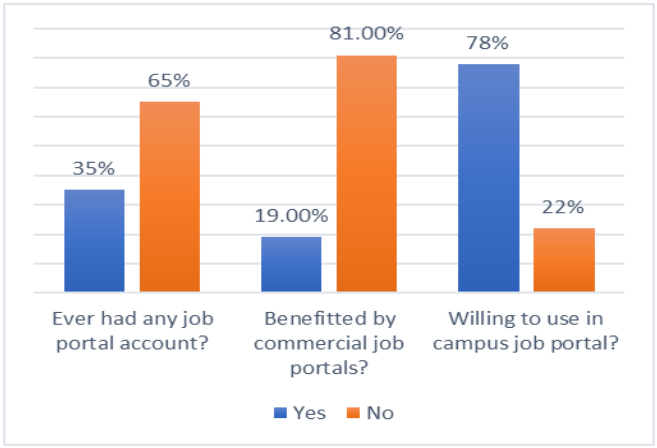


Figure 14: Responses of survey 1.2

In this survey, we found only 35% students had used any job portal website till date. Among them only 19% found worth using it. And 78% were willing to use the job portal site if build only for campus students. They felt it would be more beneficiary for students than those commercial sites that already exists in the market, as this on-campus job portal sites would provide even playing field to all the candidates.

Survey 2

This survey had one questionnaire comprising two questions. The number of participants were 200. Only the fourth-year bachelor's students from the faculty of computer, electronics and communication, electrical and civil engineering were involved.

Result for the question 1: "**What level of job do you look for in the 4th year of your study?**" is shown in Figure 15.

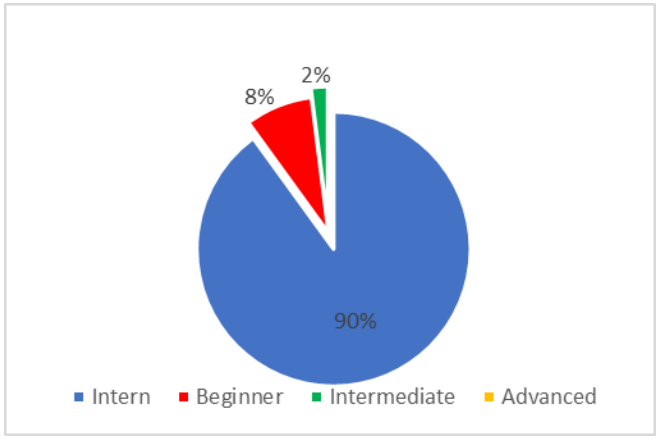


Figure 15: Responses to first question of survey 2

We can see 90% students look for intern position when they are in the fourth year of bachelor's study, as internship is the first step towards the journey of employment. There are some students who start working since the first or second year of bachelor. It is the result of this that in the fourth year, they start looking for beginner or intermediate level of jobs. According to our survey, 8% look for beginner level, 2% for intermediate level and no one for advanced level.

Result for the question 2: "**From which year do you start looking for jobs?**" is shown in Figure 16.

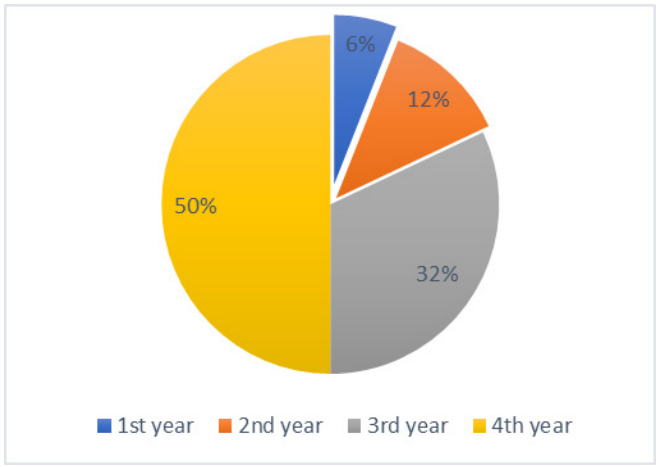


Figure 16: Responses to second question of survey 2

From the Figure 16, we can see 50% of students start looking for jobs from 4th year onwards. Similarly, 32% from 3rd year, 12% from 2nd year and only 6% from 1st year. This result shows as students' progress towards the end of their study, they more actively start looking for jobs. Especially, the numbers increase rapidly towards third and fourth year.

Survey 3

This survey was conducted after the system was brought in use to know if it has served its purpose for which it was developed. 280

students participated in this survey comprising the third- and fourth-year students from the faculty of bachelor in computer, electronics and communication, electrical and civil engineering

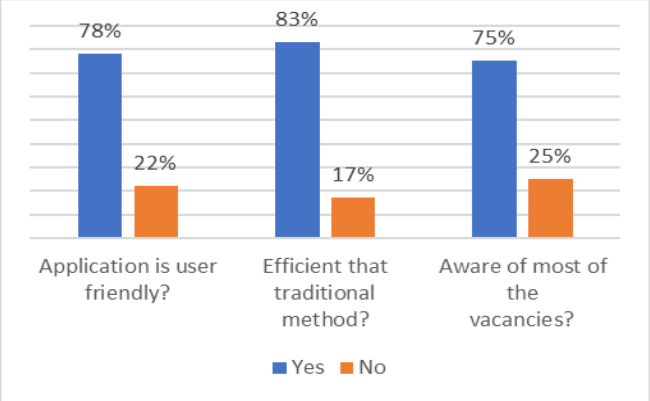


Figure 17: Responses to survey 3

From Figure 17, we can see 78% students found this application user friendly and 83% found it more efficient than the traditional method of hiring. Similarly, 75% who used this system were aware of most of the jobs posted, of their concern. This is actually a good number as it was only 40% in case of traditional method. Looking at these numbers, we feel the system has at least served its purpose to some extent.

Analysis and visualization of number of vacancies received over the period of one-year (i.e. from 2018/08/01 to 2019/07/31) using choropleth map:

5.2. Province wise analysis

From the Table 1 and Figure 18, we can see that Bagmati Province is way ahead in terms of generating employment opportunities. Then comes Province 5, Province 2 and Province 1 respectively. The remaining two provinces i.e. Karnali and Sudurpashchim provinces have not contributed in job openings through this system over the given period of time. This is because many industries and services sectors are situated in the Bagmati province. Also, its contribution to the GDP of the country is much higher than the other provinces.

Table 1: Number of vacancies across provinces of Nepal (Tabular representation)

Province	Number
Bagmati	77
5	15
2	12
1	11
Gandaki	4
Karnali	0
Sudurpashchim	0

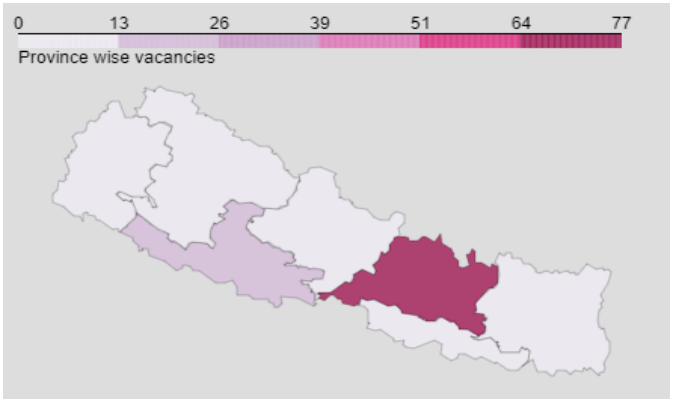


Figure 18: Number of vacancies across provinces of Nepal (Graphical representation)

5.3. District wise analysis

From the Table 2 and Figure 19, we can see Kathmandu district has the highest job openings over the period of one year. Also, we received job vacancies from only 16 out of 77 districts of Nepal. We received zero vacancy from the districts not mentioned in the Table 2. If we exclude Kathmandu and Lalitpur from the list we barely received vacancies from the other districts. This shows the concentration of economy within only few districts of Nepal.

Table 2: Number of vacancies across districts of Nepal (Tabular representation)

District	Number
Kathmandu	42
Lalitpur	24
Rupandehi	8
Morang	7
Dhanusa	5
Chitwan	5
Dang	5
Bhaktapur	4
Kaski	4
Sunsari	3
Parsa	3
Mahottari	2
Bara	2
Makwanpur	2
Kapilvastu	2
Bhojpur	1

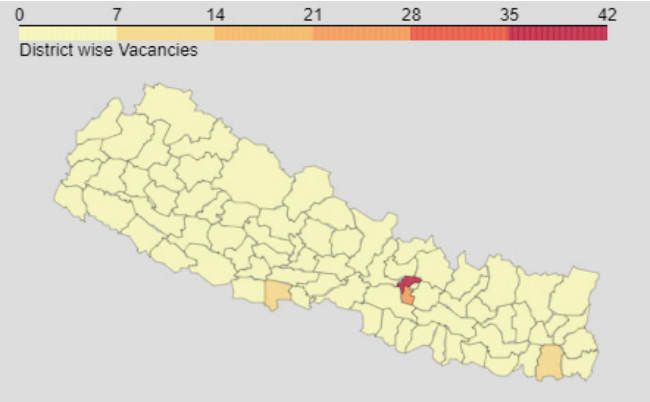


Figure 19: Number of vacancies across districts of Nepal (Graphical representation)

Visualization (using word cloud) of various types of skills that were required for the jobs we received over the period of one year (i.e. from 2018/08/01 to 2019/07/31):



Figure 20: Word cloud of skills that were mentioned for job vacancies

We can visualize in Figure 20 that skills like PHP, SQL, HTML, Python, Web design, Graphics design and so on were more in demand at least over that one-year period.

6. Conclusions and recommendations

We decided to build this e-recruitment system seeing the problems that were faced by the students of our campus. The main idea was to help students overcome the communication gap with the companies and to provide fair chance to every student in the campus to showcase their talent and skills in order to grab any job opportunity that comes their way. And to achieve this, we thought of building a system which could bring both the students and the companies on a single platform so that they can communicate directly and in an organized manner.

This system fulfills many of its purpose. But as it is said nothing is perfect, this system has also some shortcomings which we hope to improve in the upcoming future. We can make a provision to read the information of CV in PDF form, when uploaded to the system instead of enforcing the new users to fill the information manually. We can add blogging feature with advanced functionalities to develop it as a social hub where one can help others in finding a job. We can add online test features to verify the skills mentioned by students in their profile. We can improve the job recommendation using some advanced machine learning algorithms. The notification features informing the students about the job match can be improved. Some inbuilt data analysis tools can be added to provide insights on the current job scenario. Also, feature regarding the sharing of CV on different platforms through this platform can be added.

References

[1] V. Yadav, U. Gewali, S. Khatri, S.R. Rauniyar, A. Shakya, "Smart Job Recruitment Automation: Bridging Industry and University," in International Conference on Artificial Intelligence for Transforming Business and Society, AITB **2019**, 1-6, 2019, doi:10.1109/AITB48515.2019.8947445.

[2] E. Galanaki, "The decision to recruit online: A descriptive study," Career Development International, **07**, 243-251, 2002, doi:10.1108/13620430210431325.

[3] O. Shafique, "Recruitment in the 21 st century," Interdisciplinary Journal of Contemporary Research in Business, **04**(02), 887-901, 2012.

[4] J. Dorn, T. Naz, Integration of Job Portals by Meta-search, 401-412, 2007, doi:10.1007/978-1-84628-858-6_44.

[5] L. Khanam, M.A. Uddin, M.A. Mahfuz, "Students' Behavioral Intention and Acceptance of E-recruitment System: A Bangladesh Perspective," Proceedings of the 12Th International Conference on Innovation and Management, 1297-1303, 2015.

[6] E. Parry, S. Tyson, "An analysis of the use and success of online recruitment methods in the UK," Human Resource Management Journal, **18**(03) 257-274, 2008, doi:10.1111/j.1748-8583.2008.00070.x.

[7] M.G.G. Ventura, R.P. Bringula, "Effectiveness of online job recruitment system : evidence from the university of the east," IJCSI International Journal of Computer Science Issues, **10**(04), 152-159, 2013.

[8] A. Matas, "Internet becomes an on-line opportunity for employers and job hunters," The Washington Post, H2, Nov. 7, 1993.

[9] R. Ramaabaanu, & M. Saranya, "Importance and Problems of E-Recruitment," International Journal of Research (IJR), **01**(09), 2014.

[10] A.J. du Plessis, H. Frederick, "Effectiveness of e-recruiting: empirical evidence from the Rosebank business cluster in Auckland, New Zealand," Science Journal of Business Management, **2012**, 1-19, 2012, doi:10.7237/sisa/126.

[11] S. Mauno, U. Kinnunen, M. Ruokolainen, "Job demands and resources as antecedents of work engagement: A longitudinal study," Journal of Vocational Behavior, **70**(01), 179-171, 2007, doi:10.1016/j.jvb.2006.09.002.

[12] M.O. Fred, U.M. Kinange, "Effectiveness of E-Recruitment in Organization Development," Management and Economic Journal, **02**(04) 2018, 294-301.

[13] B. Raghavendra, C. Priyanka, G. Chaithanya, "A study on E recruitment,"

International Journal of Advance Research in Science and Engineering, **07**(03), 2018.
[14] R. Rani, "E-Recruitment and its impact upon job seekers: A contemporary approach," International Journal of Advanced Research and Innovative Ideas in Education, **02**(04), 2016.
[15] Y. Gupta, "Literature review on E-Recruitment: A step towards paperless HR," International Journal of Advance Research in Computer Science and Management Studies, **04**(01), 2016.
[16] F. Ramadhani, M. Zarlis, "Analysis of e-Recruitment System Design," International Journal of E-Education, e-Business, e-Management and e-Learning, **09**, 38–45.
[17] M.R. Karim, M.S. Miah, A. Khatun, "E-Recruitment in Practice: A Study on Jobseekers' Perception in Bangladesh," Global Disclosure of Economics and Business, **04,** 2015, doi:10.18034/gdeb.v4i1.150.
[18] R. et al Patel, "E-Recruitment Challenges and Methods used in Modern Organization," International Journal of Advance Research in Computer Science and Management Studies, **04**(12), 2016.
[19] P. Manjare, R. Munde, "An Effective Job Recruitment System Using Content-based Filtering," International Research Journal of Engineering and Technology(IRJET), **04**(03) 2017.
[20] B.R. Poudel, "Online Recruitment: A Cognitive Perspective of Job Seekers in Nepal," Journal of Business and Social Sciences, **02**(01) 2018, doi:10.3126/jbss.v2i1.22823.
[21] K. Kukich, "Techniques for Automatically Correcting Words in Text," ACM Computing Surveys (CSUR), 1992, doi:10.1145/146370.146380.

ASTES

Advances in Science, Technology and Engineering Systems Journal Vol. 5, No. 5, 913-919 (2020)

www.astesj.com

Special Issue on Multidisciplinary Innovation in Engineering Science & Technology

ASTESJ

ISSN: 2415-6698

Effect of Cover Number on Distilled Water Production of Distillers with a Novel Water Feeding

Mirmanto Mirmanto*, Made Wirawan, I Made Adi Sayoga, Abdullah Abdullah, Muhamad Faisal

Jurusan Teknik Mesin, Universitas Mataram, Mataram, 83125, Indonesia

ARTICLE INFO

Article history:
Received: 03 September, 2020
Accepted: 29 September, 2020
Online: 12 October, 2020

Keywords:
Distiller
Glass cover
Seawater
Distilled water

ABSTRACT

An experimental study on the effect of a cover number of solar distillers with a continuous seawater feeding system was conducted. The seawater feeding in this study was a continuous feeding, which was not utilized yet in the previous studies. Three identical distillers i.e. single caver distiller, double cover distiller, and triple cover distiller were designed and examined. The material tested in this study was seawater taken from Tanjungkarang beach, Mataram, NTB, Indonesia, and converted into distilled water through distillation processes. The overall size of the distillers used was 1136 mm x 936 mm x 574 mm (outer dimension), while the absorber plat size was 0.8 m x 1 m. The experiment was performed in July 2019 from 09.00 to 16.00 local time. The results showed that increasing the number of glass cover decreased the amount of distilled water. The single cover distiller resulted in 949 ml a day, while the double and triple cover distillers resulted in 260 ml and 88 ml a day. The distiller with 3 glass covers was hotter than others so that the seawater vapour could not condense on the glass cover. Therefore, the distiller with a single glass cover was recommended.

1. Introduction

Many regions in Indonesia always have freshwater shortages in the dry season; e.g. Gunung Kidul, East Jawa, Central and East Lombok, and East Nusa Tenggara. Meanwhile, freshwater is essential substantive for a human being. The human being cannot live without fresh water. Therefore, efforts to fulfil the demands freshwater are crucial. However, to have freshwater requires much cost. Is there a cheap device to produce freshwater?

Indeed, devices to make freshwater have been available and they are quite sophisticated. One of the devices is reverse osmosis (RO). Researches on RO have been rigorously conducted by many previous researchers, e.g. [1-2]. Nevertheless, the price of the RO is still expensive and its operational cost is high enough. Also, it needs electrical energy. Then, RO is suitable for the production of large quantities of water and applicable electrical energy. However, for the community who have no electrical power and they are in low economic class, RO may not be a choice. Is there a cheaper way of producing freshwater?.

Yes, there is a cheaper way for this; that is a distilling system. The distilling system can be performed for several cases; e.g. distilling dirty water, distilling seawater, distilling rainwater. However, the energy used for distilling is high and expensive. When the distilling system is run using liquid fuel or wood or gases, then this method is quite expensive. Consequently, this method is not suitable for people with low economic levels. The heat used for the distilling system can be from many sources such as solar energy (solar thermal distilling), mechanic energy, electrical energy, chemical energy and so on. Meanwhile, the process of distilling is also various; e.g. evaporation-condensation, filtration, and crystallization as reported by in [3].

Some distilling techniques that are being developed are solar chimneys, greenhouses, natural vacuum, adsorption desalination, membrane distillation (MD), membrane bioreactors (MBR), forward osmosis (FO), and ion exchange resins (IXR). RO followed by multistage flashing (MSF) and multi-effect distillation (MED) systems are the most widely applied desalination. According to the 2015 International Desalination Association (IDA), more than 300 million people depend on water produced by 18426 destinations in 150 countries, which provide more than 86.8 million cubic meters per day as explained in [4].

Western countries and developed countries prefer RO systems because of efficient power consumption, while Middle Eastern and Gulf countries prefer MSF and MED systems because oil sources are abundant. The largest desalination plant which started operating at the end of 2014 was Ras Al-Khair in Saudi Arabia. The plant produces around 728,000 cubic meters of desalination

* Corresponding Author: M. Mirmanto, Jl. Majapahit no. 62, Mataram, NTB, 83125, Indonesia, +6282111738971, m.mirmanto@unram.ac.id

water per day by implementing MSF and RO technology as revealed in [5]. In [6], it was stated that the second-largest desalination plant was Carlsbad in California. United States produces around 190,000 cubic meters of desalination water per day by applying RO technology, opened in December 2015. Nevertheless, that's not the case for low-income communities.

The simplest desalination technology is the solar still distillation (SD) system, which is suitable for remote areas with low water demand because this system has low productivity, [7-9]. However, the problem for this distiller model is that its water production capacity is very low because the productivity depends on the device areas and environmental conditions.

In reference [9], the supply of freshwater is only 0.5 litres per day, and a pyramid-shaped distiller with a size of 1 m x 1 m and a total height of about 50 cm was used. In [8], the yield of freshwater obtained was only 15 ml/hour, with a tool area of 1 m². For this reason, some studies modify solar still distillation with various absorber models and multilevel models. Multilevel models have been studied in [6], nevertheless, the effect of the cover number on freshwater production was not yet investigated.

Recently, research on solar distillation using three different forms of the absorber was conducted in [10]. The form of absorber used was a flat plate, stringy absorber, and finned absorber. He explained that the fin absorber produced larger freshest water. Unfortunately, he did not examine the cover number in his study. Meanwhile, increasing the cover number raises the water temperature in the basin of the distiller. The more amount of glass is expected to be able to evaporate more seawater so that the distilled water becomes more numerous. Besides that, this distillation tool uses a continuous system, unlike distillers that have been studied by previous researchers. The continuous feed water creates the seawater level inside the basin constant. Consequently, the effect of water thickness in the basin can be eliminated and the water production continuously occurs. To analyze experimental data, equations about heat transfer, evaporation and condensation are taken from [7-9]. The equations determine the heat input, heat use and heat loss to the environment. The long term aim of this study is obtaining the cheapest, simplest, easy to operate, distiller, but the distiller has high water productivity.

2. Research Method

The research apparatus comprised of three identical distillers. One distiller had one cover, another distiller contained 2 covers and the rest included 3 covers. The absorbers of the three distillers were made of a galvalume flat plate. The apparatus is indicated in Figure 1. The distiller with a single cover is case A, the distiller with double covers is case B, and the distiller with triple covers is case C. The dimension of the distillers was 1136 mm x 936 mm x 574 mm, while the areas of absorbers were 1 m x 0.8 m.

The seawater was poured down in the top reservoir, and then it flowed forward the distiller chamber. After the level of the seawater inside the distiller reached a certain height, the valve with a floating ball closed by its self. However, when the vaporization took place so that the seawater level decreased, the valve opened automatically and the new seawater came into the distiller basin and so on until the complete experiments were done for one day. Using this method, the seawater level remained constant. This was called a novel feeding seawater or a continuous seawater feeding. This system, however, was not utilized yet in the previous studies. The seawater level in the basin was kept at approximately 4 cm. The temperatures in this current study were verified by K type thermocouples that were calibrated with an accuracy of ± 0.5°C. The solar power was measured using a pyranometer Lutron SPM-1116SD with accuracy was employed to record the solar power with an accuracy of ± 5% reading (stated in the device specification). Meanwhile, the wind velocity around the distillers was predicted using an anemometer Benetech GM8901 with an accuracy of ± 3% reading as stated in the specification brochure. The experiments were conducted at the Universitas Mataram at positions of 08° 33' - 08° 38' South Latitude and 116° 04' - 116° 10' East Longitude. The freshwater obtained was weighed at every hour using a digital scale. The density of the seawater was measured by weighing it on the scale and putting it in the glass volume. It was of approximately 1111 kg/m³.

Parameters tested in this study were temperatures, solar power, wind velocity, and distilled water. The solar power, temperatures, and distilled water were measured directly, while other parameters such as useful heat, the heat lost and efficiency were calculated. Some equations employed to analyze the parameter data were taken from [7-9].

Heat input is heat from the sun (solar power) multiplied by aperture area and glass cover transmissivity. The heat passes through the glass cover can be estimated using Eq. (1) that was taken from [11].

$$Q_{in} = \tau I A \tag{1}$$

Q_{in} is the heat input (W) absorbed by the absorber plate in the distiller basin; τ is the transmissivity of the glass cover 0.88 as reported in [12-13]. For the double cover distiller, the transitivity was obtained to be 0.8^2, and for the triple cover distiller, the emissivity was determined as 0.8^3. Meanwhile, the heat that is used for heating the seawater from the initial temperature to the final temperature is expressed in Eq. (2). Equation (2) can be obtained in [14].

$$Q_s = mc_p(T_f - T_i)/t \tag{2}$$

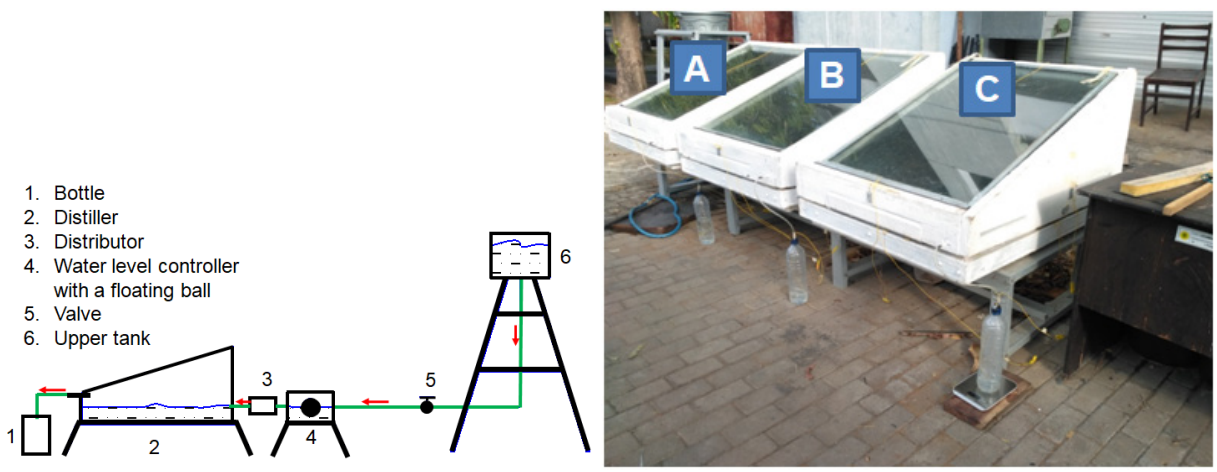
Q_s is the sensible heat (W), m indicates the seawater mass in the basin (kg), c_p represents the specific heat (J/kg°C), T_f and T_i are the final and initial temperatures (°C), while t is the time (s). Besides sensible heat, as expressed in Eq. (2), there is latent heat. The latent heat is the heat that is used for evaporating the seawater inside the distiller and written in Eq. (3) that can be found in [14].

$$Q_l = m_l h_{fg}/t \tag{3}$$

Q_l is the latent heat (W), m_l is the mass of the distilled water (kg), h_{fg} is energy for evaporation (J/kg). For that, according to [14], the total heat can be written as:

$$Q = Q_s + Q_l \tag{4}$$

Efficiency parameter is a parameter that shows the distiller performance. The efficiency can be expressed as Eq. (5) that can be attained in [14].



(a) (b)

Figure 1: Schematic diagram of the apparatus; (a) process line schematic, (b) photograph, Faisal [10].

$$\eta = \frac{Q}{Q_{in}} \quad (5)$$

3. Results and discussion

Figure 2 shows the solar power that was recorded during experiments for case A, case B, and case C at three days in June 2019 at Jurusan Teknik Mesin, Universitas Mataram, Indonesia. The solar power recorded was not influenced by the cases because all the distillers were close together; therefore, the solar power for the three distillers was the same. In figure 2, the solar power increases with the observation time and then it reaches a peak at about 13.00 (local time). After 13.00, it decreases continuously. However, the trends were also found in the previous studies conducted by Faisal [10], and Mirmanto et al. [15]. Nevertheless, on the third day, at around 10.00 (local time), solar power decreased. That was caused by the temporary cloud covering the sun. The solar power was recorded at every hour for figure 2, therefore, the effect of the cloud can be seen clearly. Then, the solar power was averaged and the results of recording solar power were 414.5 W/m² (day 1), 530.4 W/m² (day 2), and 537.2 W/m² (day 3). Of course, the results of recording solar power from day to day were different, they depended on the brightness of the sun. However, in general, solar power has a maximum value at around 13.00 (local time), because at 13.00 the sun shines brightly and also has maximum heat radiation. After 13.00 the solar power decreases further till at 16.00 (local time). Based on solar power, the heat input can be estimated using Eq. (1) and the calculation result is presented in figure 3.

Meanwhile, the heat input is different for each distiller because of the number of the glass cover. For the single cover, the transmissivity is approximate 0.88, while for the double and triple covers; the transmissivities are 0.7744 and 0.681 respectively. Hence, increasing the number of covers decreases transmissivity.

Figure 3 shows the trend of solar power, in general, increases with the time until it reaches a peak value at about o'clock local time. After that, the solar power decreases continuously until the experiment is complete. This phenomenon was due to the sun cycles. The sun rises, afternoon, and then sunset.

The experimental heat input is shown in figure 3. The heat input was calculated using Eq. (1) on the experimental data basis. The trend of this parameter is almost the same as that of solar power trends. However, the magnitudes for the three cases are different. This was due to the different number of the cover. The higher the number of covers, the lower the transmissivity.

Recorded absorber temperatures are presented in figure 4. The trends of the temperature are different from that of solar power. The temperatures increase with the observation time, then after at around 13.00 o'clock, they are flat until the experiment is finished at about 16.00 o'clock. For the single cover, the absorber temperature at after 13.00 o'clock is constant, while that of double and triple covers still increases fairly. This trend indicates that adding the number of covers elevates the absorber temperature. This could happen because the heat inside the distiller was difficult to be emitted back to the ambient. It was trapped by the number of glass covers and the gaps between the cover. Nevertheless, distillers with multiple covers had higher heat losses than that with a single cover. The heat loss occurred due to the high different temperatures between the absorber and the ambient. Mostly the heat loss happened through the conduction mode. The heat flowed through the distiller walls and bottom.

To know further the effect of cover numbers, let's see Figure 5. Figure 5 shows the recorded seawater temperatures. Figure 5 indicates that trends of the seawater temperatures are almost the same as the trends of the absorber temperatures. The seawater temperatures increase with time and then get constant. Moreover, the magnitudes of the temperatures are nearly the same. This was caused by the direct contacts of absorber and seawater. Previous studies also showed similar findings, e.g. in [8, 10, 15].

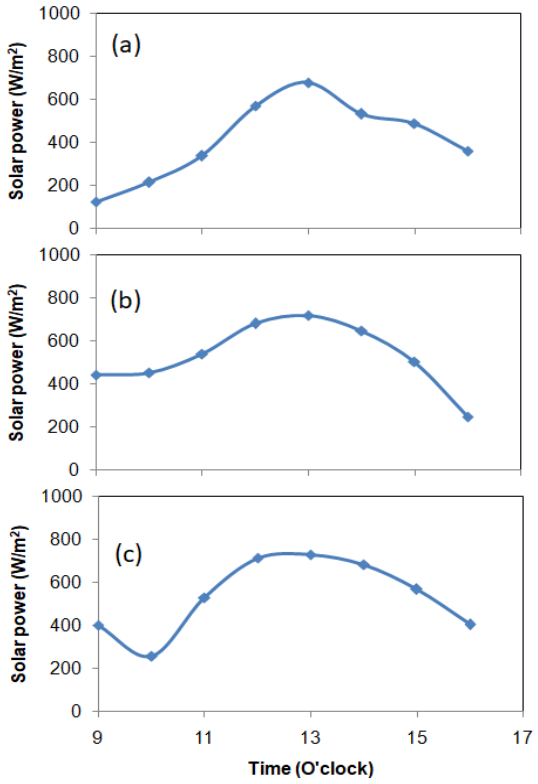


Figure 2: Recorded solar power: (a) day 1, (b) day 2, and (c) day 3

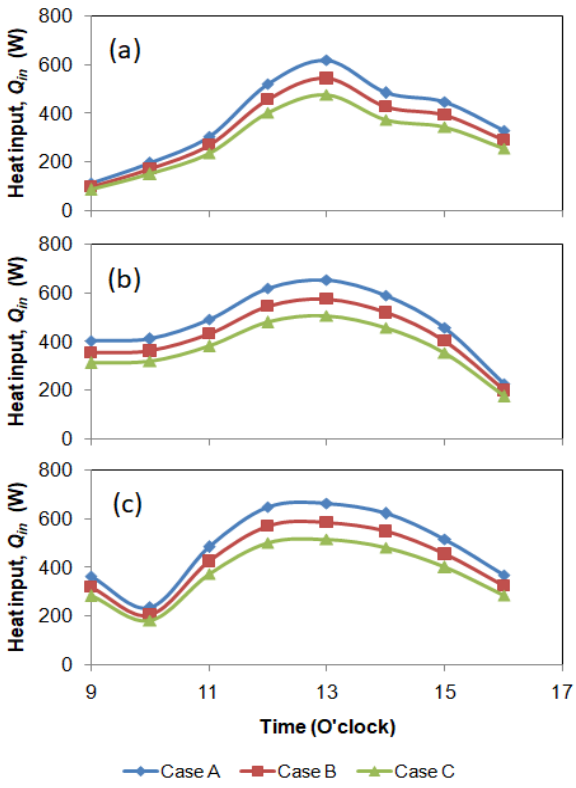


Figure 3: Calculated heat input (Q_{in}) for the three cases: (a) day 1, (b) day 2, and (c) day 3.

Another parameter recorded in this study was the amount of distilled water. Distilled water production per hour is presented in Figure 6, and the accumulated distilled water production is given in Figure 7, while the distilled water daily production is shown in Figure 8. The distilled water density was measured to be of approximately 995.2 kg/m³ at 30°C. The hourly distilled water production seems irregular, sometimes it is much and other times it is less. This was due to the sky and environmental conditions. At the time where the sky was clear, the distilled water production was high and vice versa. This phenomenon was also found in [10, 16]. The distilled water production obtained in [10] was greater than that of [16]. This was due to the different day.

Figures 6 and 7 show that the distiller with a single cover produces larger hourly distilled water. This phenomenon was due to the cover temperatures. The cover of the distiller that contacts directly to the vapour for the single cover distiller was lower than that of double and triple covers. Therefore, when the vapour came up to the cover, it could be easily condensed. However, for the double and triple cover distillers, the lower glass cover that touched the vapour had a higher temperature, as a result, the vapour could not condense. When the glass covers were removed from the distillers at the end of the experiment, the vapour coming out from the distillers with double and triple covers was much larger than that from the single cover distiller. Moreover, the absorber and seawater temperatures for the distiller with double and triple covers were higher than that of the distiller with a single cover. Hence, why did the distillers with double and triple covers result in less distilled water? This was due to the less condensed vapour on the glass cover. Furthermore, the results of this study were less than that of [17, 18]. This was due to the simple shape of the distillers utilized in this current study.

Different from hourly distilled water production, accumulated distilled water production increased with time, see figure 7. This finding was also found by previous researchers; e.g. [15, 17]. In [16], the total distilled water production was almost 1500 ml a day. They started their experiment at 9.00 local time and finished at 16.00 local time. Meanwhile, this study produced maximum distilled water of 949 ml.

Heat transfer calculation results are presented in figure 8. The heat transfer here is called useful heat; Q. Q can be computed using Eq. (4) that comprises sensible heat and latent heat. The useful heat increased drastically at the beginning of the experiments. After at 10.00 am, the useful heat decreased continuously till the experiments were finished. The trend of the useful heat was due to heat absorption. At the beginning of the experiment, much heat could be absorbed because the seawater temperature was still low. At this level, the heat transfer occurring was sensible heat. The heat was used for heating the seawater inside the distiller. As the seawater temperature increased, the heat absorbed decreased, and the heat transfer mode changed to a combined heat transfer; e.g. sensible and evaporation heat transfer. The evaporation heat transfer is called latent heat transfer. For this case, the seawater changed to vapour.

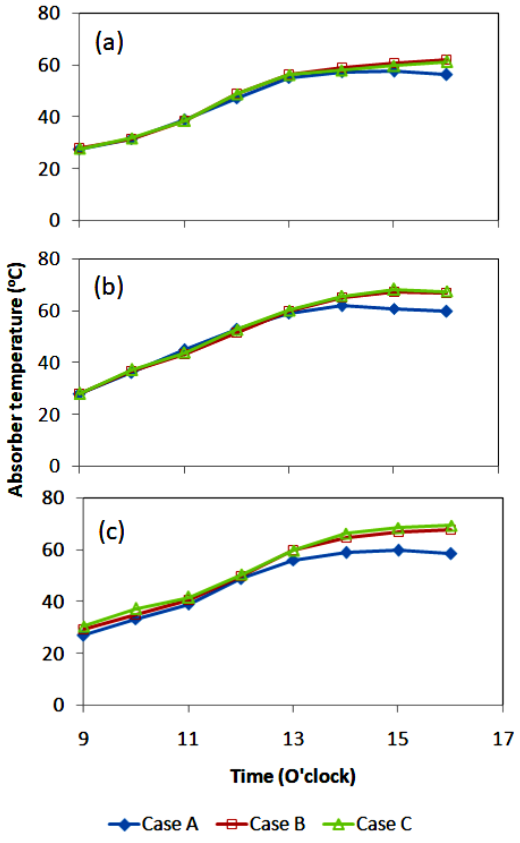


Figure 4: Trends of the absorber temperatures for three cases: (a) day 1, (b) day 2, and (c) day 3.

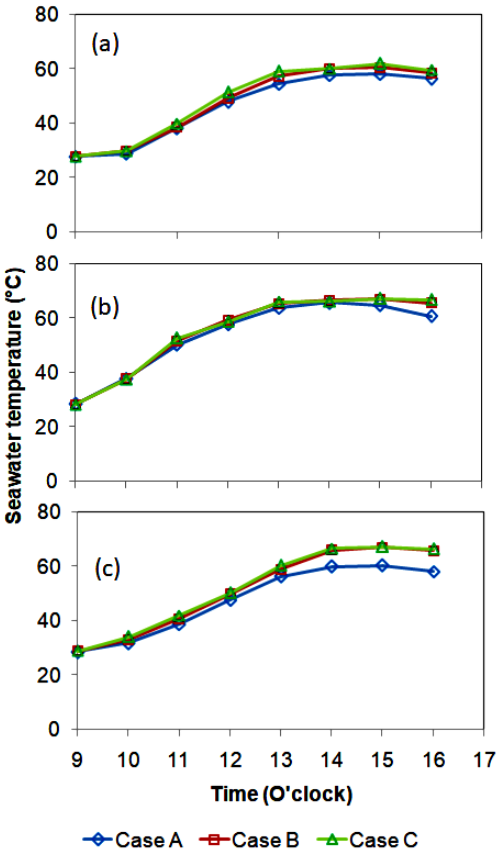


Figure 5: Seawater temperature for the three distillers; (a) day 1, (b) day 2, and (c) day 3.

In figure 8, the useful heat contained sensible and latent heat. The useful heat was predicted using equations (2) and (3). The mass of the vapour condensed was used to estimate the latent heat. For case A, the distilled water production was larger than for cases B and C, as a result, the useful heat obtained for case A also was higher than for the other two cases. This was due to the larger condensation for case A.

Another variable that indicates the performance of the distiller is efficiency. Efficiency is a comparison of useful energy to heat input. The useful heat is Q and the heat input is Q_{in}. Q_{in} is estimated using Eq. (1). Therefore, efficiency can be predicted using Eq. (5) and the calculated efficiency is presented in figure 9.

Figure 9 indicates that the trend of efficiency is almost the same as the trend of the useful heat. At the beginning of experiments, the efficiency increased sharply, and it reached that peak value. After the peak value was achieved, the efficiency decreased continuously until the experiments finished. However, for case A, the efficiency trend was a little bit different. At around 15.00 o'clock, it increased again. This occurred because the production of distilled water was still ongoing, but the heat input was down. For cases B and C the distiller still generated much vapour, but the lower layer of the glass cover was still hot, then the vapour could not condense, as a result, the useful heat (latent heat) was low. Consequently, the efficiency for case B and C was lower than that for case A.

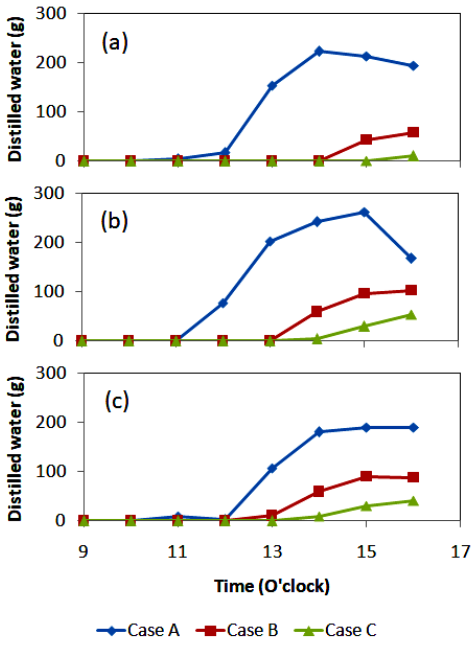


Figure 6: Hourly distilled water production obtained for three days. (a) day 1, (b) day 2, and (c) day 3.

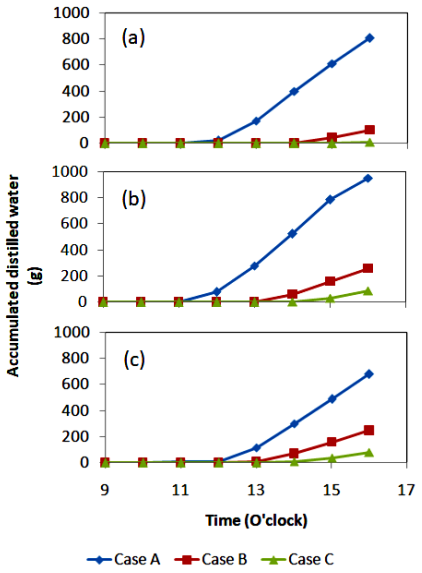


Figure 7: Accumulated distilled water production; (a) day 1, (b) day 2, and (c) day 3.

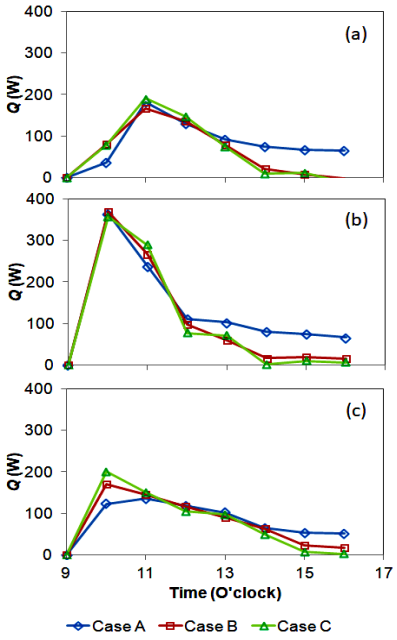


Figure 8: Useful heat transfer in the distillers for the three cases and three days.

4. Conclusions

The study to know the effect of glass cover number on the distilled water production was conducted with several tested parameters and continuous feeding seawater. Some findings that can be stated are: the solar power in Indonesia has a large potential; the hourly distilled water productions are scatter depending on sky conditions. The major remark in this study is that much-distilled water production can be achieved just using single cover; less vapour can be condensed in the double and triple cover distillers; the largest efficiency is obtained for the single cover distiller. A single cover distiller is recommended to be utilized for producing freshwater.

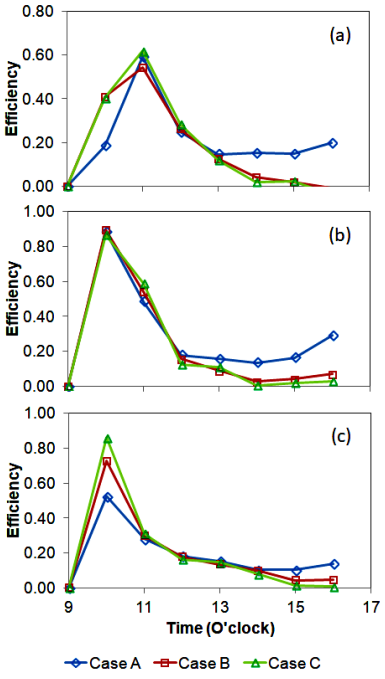


Figure 9: Distiller efficiency for the three cases and three days.

Acknowledgement

The author would like to thank the DRPM for the funding and Jurusan Teknik Mesin, Universitas Mataram for the facility.

Nomenclature

A	=	Aperture area (m²).
c_p	=	Specific heat (J/kg K).
I	=	Solar power (W/m²).
m	=	Seawater mass (kg)
Q	=	Useful heat (W).
Q_{in}	=	Heat input (W).
Q_l	=	Latent heat (W).
Q_s	=	Sensible heat (W).
t	=	Time (s).
T_i	=	Initial seawater temperature (°C).
T_f	=	Final seawater temperature (°C).
η	=	Efficiency

References

[1] A.H. Slocum, M.N. Haji, A.Z. Trimble, M. Ferrara, S.J. Ghaemsaidi, "Integrated pump hydro reverse osmosis system", Sustainable Energy Technologies and Assessments, **18**, 80-89, 2016. doi:10.1016/j.seta.2016.09.003

[2] N.K. Khanzada, S.J. Khan, P.A. Davies, "Performance evaluation of reverse osmosis (RO) pre-treatment technologies for in-land brackish water treatment", Desalination, **406**, 44-50, 2017. doi:10.1016/j.desal.2016.06.030

[3] A. Alkaisi, R. Mossad, A. Sharifian-Barforoush, "A review of the water desalination systems integrated with renewable energy", Energy Procedia, **110**, 268 – 274, 2017. doi:10.1016/j.egypro.2017.03.138.

[4] M. Baawain, B.S. Choudri, M. Ahmed, M., A. Purnama, "An Overview: desalination, environmental and marine outfall systems", Recent Progress in Desalination, Environmental and Marine Outfall Systems, **1**, 3-10, 2015. doi:10.1016/j.egypro.2017.03.138.

[5] S.M. Cheong, G.W. Choi, H.S. Lee, "Barriers and solutions to smart water grid development", Environmental Management, **57(3)**, 509-615, 2016. doi:10.1007/s00267-015-0637-3

[6] N. Heck, A. Paytan, D.C. Potts, B. Haddad, "Coastal residents' literacy about seawater desalination and its impacts on marine ecosystems in California", Marine Policy, **68**, 178-86, 2016. doi:10.1016/j.marpol.2016.03.004

[7] Water and waste water tratement spesialist yang dipercaya dalam proses pengolahan air, tirtamandiri.com.

[8] A. Mukadim, M. Wirawan, I.B. Alit, "Analisa pengaruh variasi bentuk absorber pada alat destilasi air laut terhadap kenaikan suhu air dalam ruang pemanas dan jumlah penguapan air yang dihasilkan", Dinamika Teknik Mesin, **3(2)**, 127-135, 2013.

[9] Mirmanto, Destilasi surya pengubah air laut menjadi air tawar. Laporan Penelitian DPP/SPP, Universitas Mataram, 2003.

[10] M. Faisal, Pengaruh variasi absorber alat distilasi air laut tenaga surya terhadap produksi air tawar, Skripsi, Jurusan Teknik Mesin, Universitas Mataram, 2019.

[11] J.A. Duffie, W.A. Beckman, "Solar Engineering of Thermal Processes", 4th Edition y John Wiley & Sons, Inc., Hoboken, New Jersey, 2013.

[12] B.Y. Idi, D.K. De, "Transmissivity of the glazing surface of a solar flat plate collector based on the metrological parameters of Yola, Nigeria", Journal of American Science, **7(1)**, 639-643, 2011.

[13] M. Syahri, "Rancang bangun sistem desalinasi energi surya menggunakan absorber bentuk separo elip melintang", Prosiding Seminar Nasional Teknik Kimia "Kejuangan", Pengembangan Teknologi Kimia untuk Pengolahan Sumber Daya Alam Indonesia, Yogyakarta, 22 Februari, 2011.

[14] J.P. Holman, "Heat Transfer", 8th Edition. McGraw-Hill Inc., USA, 1997.

[15] M. Mirmanto, M. Wirawan, I.M.A. Sayoga, S. Syahrul, M. Faisal, A. Abdullah, "Effect of absorber types of conventional distillers on the amount of distilled water production", Frontiers in Heat and Mass Transfer, **13**, 1-7, 2019. doi:10.5098/hmt.13.10.

[16] Abdullah, "Pengaruh jumlah *cover* alat distilasi air laut tenaga surya terhadap poduksi air tawar", Skripsi, Jurusan Teknik Mesin, Universitas Mataram, 2019.

[17] A.A. Kabeel, "Performance of solar still with a concave wick evaporation surface", Energy, **34**, 1504–1509, 2009. doi:10.1016/j.energy.2009.06.050.

[18] Mulyanef, Marsal, R. Arman, K. Sopian, K., "Sistem distilasi airlaut tenaga surya menggunakan kolektor plat datar dengan tipe kaca penutup miring", Teknik Mesin, Universitas Bung Hatta, Padang, Indonesia, 2014.

ASTES

Advances in Science, Technology and Engineering Systems Journal
Vol. 5, No. 5, 920-926 (2020)
www.astesj.com
Special Issue on Multidisciplinary Sciences and Engineering

ASTES Journal
ISSN: 2415-6698

Using Big Data Analytics to Predict Learner Attrition based on First Year Marks at a South African University

Gcobisile Matafeni[*,1], Ritesh Ajoodha[1]

[1]*School of Computer Science and Applied Mathematics. The University of the Witwatersrand, Johannesburg. 2050. South Africa.*

ARTICLE INFO

Article history:
Received: 17 August, 2020
Accepted: 21 September, 2020
Online: 12 October, 2020

Keywords:
Expert system
predicting student success
statistical models
learner attrition

ABSTRACT

Due to high failure rates many students end up spending unnecessary years struggling to qualify and subsequently accumulate unnecessary debt. In this paper, our principal contribution is to provide an expert system that statistically predicts the success of a first year student in an undergraduate Science programme given only academic merit in their subject matter. Over the past decades, much work has been done in the field of predicting student success in first year computer science and in other first year courses. Historically, other authors focused on using linear statistical models to predict student success. These models had limitations as the prediction was designed for inference as compared to machine learning techniques. This paper presents an approach of using the naïve Bayes classifier, support vector machines and decision trees as models that can be used to predict the completion of an undergraduate science degree. This was done by firstly training the classifiers and then testing them. The support vector machine achieved the best accuracy (87%) in predicting the completion of a science degree based only on first year marks, this was followed by the naïve Bayes model (86.36%) and the decision tree (65.62%) came last.

1 Introduction

The prevalence of high failure rates in South African universities results in students spending unnecessary years struggling to qualify and subsequently accumulate unnecessary debt. A view that is generally agreed upon is that acceptance into a university programme often proves to be life changing. The prospect of obtaining a degree is sometimes a promise of higher income and improves ones standard of living [1]. The idea of students having the ability to know after their first year of study which courses to take in order to maximize their chances of succeeding is helpful. Historically, institutions of higher learning have been struggling to improve their throughput rates over the years. Since the dawn of the democratic dispensation, enrolment rates in higher education institutions have sky rocketed while the dropout rates have increased significantly [2]. To mitigate drop-out rates and improve success, this paper will attempt to build a model for calculating the probability of a student completing an undergraduate degree at Wits University in order to promote early interventions focused on student success.

Some useful features to recognize the success of a student in first year computer science include using the Scholastic Aptitude Test (SAT) and the American College Testing (ACT) scores across different subjects [3, 4]. The approach in this paper will have the ability to calculate the alternative streamlines that might align a student with better options, so that they can reconsider their academic standing. In [3], the authors used statistical analysis in order to build a linear model that described the correlations using all linear combinations of the dependent variables. [5] made use of a step-wise discriminant analysis to identify all significant factors in a study group of 87 freshman computer science majors. The above papers demonstrate the methodologies that rely on using statistical models to perform the classification task. The purpose of this study is to explore the correlation between first year academic results and the probability of completing a Science degree at a South African university.

In this paper we trained the following three machine learning classification models: naïve Bayes classifiers, support vector machines, and decision trees to predict student attrition given their first year marks. The support vector machine achieved the best accuracy (87%) in predicting the completion of a science degree based only on first year marks, this was followed by the naïve Bayes model (86.36%) and the decision tree (65.62%) came last.

Our principal contribution from this paper, to stand along other contributions of this kind [6]–[8], is to provide a predictive model that statistically predicts the success of a first year student to complete their undergraduate Science degree given their first year marks. This will enable and promote early interventions to encourage stu-

[*]Corresponding Author: Gcobisile Matafeni, The University of the Witwatersrand, Johannesburg, +27 65 9940 231 & matafenigcobisile@gmail.com

dent success.

This paper is structured as follows: section II reviews the related work; section III discusses the research methodology that was used to conduct the relevant experiments; section IV presents the qualitative results of the experiments and a discussion. Lastly, section v provides a summary of this paper, it also suggests some future work that can be explored.

2 Related Work

In [9], the authors attempt to deduce student attrition at a South African higher-education institution with the aim of identifying students who are likely to be in need of academic support so that a focus could be provided on improving their academic performance. The techniques used in the above paper are; Decision Trees, K-Star, naïve Bayes, Support Vector Machines, Random Forests, and Linear Logistic Regression. In [10], the authors attempt to provide a data-driven solution to the data-congested environment of attributes related to student success and contribute towards preventing the increased dropout rates at South African higher education institutions. The techniques used in the above paper are; Decision Trees, K-Star, naïve Bayes, Support Vector Machines, feed-forward neural networks, and linear regression models. In this research we are concerned with predicting the completion of an undergraduate science degree based only on first year marks. This research will be adapted from the work in the literature survey which focused on predicting student success in first year computer science by using marks from high school. This section provides the necessary background and related work that was used during the research project.

2.1 Predicting success at first year computer science

In this section, we look at different approaches that were used to predict the performance of first year students who majored in computer science. We first evaluate how multiple factors were used for this purpose, we then move into how mathematics as a single subject was used for prediction purposes. Lastly, we look at how English as another single subject was used for prediction purposes.

2.1.1 Predicting success using multiple factors

There are many approaches that can be used to look at what affects student performance in first year courses. One approach is to use multiple variables to compute the probability of succeeding in a freshmen major. In [3], 13 variables were used and these were independent to each other, these included the American College Testing (ACT) scores for mathematics, the American College Testing (ACT) scores for English, the American College Testing (ACT) scores for natural science and the student's class rank to name a few. The American College Testing (ACT) are assessments that are used to measure the college readiness of high school students in America. The authors focused their study on a sample size of 269 students. For every variable; the mean, standard deviation, minimum and the maximum were calculated. Utilizing the correlations that were developed, a linear model was used to fit the data and the results indicated that it was possible to calculate the probability of a pass or a fail in an introductory computer science course. In [4], the authors used multiple factors to predict the performance in a computer science major and some of their work which focused on ACT English and other scores was extended in [3]. In [4], the authors consider the SAT scores, the sex of the student and their high school grades. By combining all of these, they developed a linear discriminant as a function to perform classification. In a data sample of 256 students, they were able to successfully classify 175 students which is 68.4% of the data into the correct group.

In [5], the author studied 10 factors and used these to find their relationship to student success in a first year computer science major. The ACT scores were used similarly to what [3] used in their variables. According to [5], the placement factors that reduced the failure rate in first year were the ACT English scores and the UTM mathematics placement scores, with the former scores being the best predictor. To identify the factors that contribute to the forecasting of success, a discriminate function was used. In [5], the author found that the other factors were not significant to be used as predictors. [4] found SAT mathematics and verbal scores as best predictors but did not indicate which one was the best predictor. In [11], the author builds a model that forecasts the success in a programming course, with the hope of counseling students to make informed decisions. On top of using past academic achievement as used in [3]–[5], the author includes certain cognitive skills and personality traits. The study focused on a sample size of 120 students that was randomly selected from a population of 600 students. The variables that were used in this paper are both independent and dependent, and they are 21 in total. This is significantly more variables in comparison to the number of variables that were used in other papers; [3]–[5]. The multiple regression equation that was developed was able to classify 61 students out of 79 (77.2%). The approach of using multiple factors to build a model for predicting the success of students worked in the papers mentioned above but there are other approaches.

2.1.2 Predicting success using Mathematics

In [12], the author uses the IBM Aptitude Test for Programmer Personnel (ATTP) scores to classify the students who are doing different computing courses, one based on COBOL and the other based on FORTRAN. The study focused on 46 students who had written the ATTPs. A positive correlation between the FORTRAN course and the arithmetical component of the ATTP was found, another correlation was found between the letter series and the COBOL course. The only factor that was used for forecasting the performance in an introductory computer course were the ATTP scores which is a different approach from using a combination of variables. In a paper that focuses on a commerce degree, the author [13] argues for the use of mathematics as a single variable rather than the matric aggregate to predict the performance in first year. The study focused on results that spanned a period of 4 years. The approach used was to take the individual mathematics scores and compare them to pass rates in first year. According to [13], a good mark in matric mathematics is the best predictor of first year success compared to the matric aggregate scores.

2.1.3 Predicting success using English

Similar to the approaches used in [12] and [13], in [14] the authors use a single factor to predict the success in first year computer sci-

ence. The paper studies the correlation between success in English and the actual performance in first year. Analysis took place by use of qualitative data from a survey and an in-depth quantitative look at matric results. Results show that language scores from matric results are better predictors of success. In contrast, a recent publication by [13] argues about an important relationship between mathematics results in matric and the performance in a commerce degree. The argument is of great importance as it bases its findings on the same matric results as in [14]. Also, in [13] the author did not consider language in their study and according to [14] there is a possibility that it might have been a factor. As alluded to earlier, [4] states that it is inappropriate to only use a single matric subject as a predictor of success for a first year computer science major. A holistic approach is to use the matric aggregate as a predictor. It is worthy revisiting the findings of [5], the research found that amongst the several variables that were used in the study, the best single predictor for success were the ACT English scores. The overall best predictor for success in computer science was the combination of UTM mathematics and ACT English placement scores. The predictor that was developed in [5] was able to to successfully reduce the failure rate in computer science the following year from 28% to 18% as stated in [14].

3 Research Methodology

Predicting the success of a first year computer science student is affected by many variables as demonstrated in [3]. The background to the problem has been presented in the previous section and it also lays out the different approaches that have been used by other authors who focused on first year performance by using previous student grades. It must be noted that the previous authors who are surveyed in the literature had their focus on predicting success in first year computer science and other first year courses. This research will be taking this work further by trying to predict the completion of a science degree based only on first year marks. The naïve Bayes classifier, support vector machines and decision trees can be used to build classification models for this particular problem area as presented in section II. These classification models will use the first year marks as training data.

3.1 Data and Preprocessing

The study participants were learners who studied at a South African higher-education institution. The study ethics application has been approved by the Human Research Ethics Committee of the University (Non-Medical). The ethics application addresses key ethical issues of protecting the identity of the learners involved in the study and ensuring the security of data. The clearance certificate protocol number is H19/03/02. The dataset had a total of 216 features with 8557 observations. The features were selected according to their relevance in order to serve our aims and objectives. The data was received in a spreadsheet format and this had to be converted into a format that Weka can work with. Weka can work with comma separated values (csv) or attribute-relation format files (arff), the spreadsheet was converted into a csv file. The spreadsheet was read into an iPython notebook which uses Python and a package called pandas to work with stored data, this platform makes it easy to perform exploratory data analysis. The student numbers were anonymized in order to protect the students identity. The dataset contained students who did their year of study 1,year of study 2 and year of study 3 and in our case since we were working with year of study 1 so we dropped the other records (YOS2 and YOS3). After dropping the unnecessary rows, the rows that were left contained the subject and its mark for each student, say student x, the first 6 rows would be student x with the 6 subjects they did in first year with the corresponding marks and Progression Outcome Type. Since each student had more than one row identifying them we performed a transpose on the given table so that each record is one unique student with the columns having the subject matters and marks. The last column was the class label which was either a Yes or a No for the Progression Outcome Type. There was 216 features in total after the data was prepared correctly. The data was then saved onto a Weka readable format in order to run the supervised learning algorithms.

3.2 Classification Models

After the implementation of the classifiers the focus shifted to evolving the models in order to improve their accuracy. This was done by performing feature extraction and selection techniques. A 10-fold cross validation scheme was used.

3.2.1 Naïve Bayes

The naïve Bayes pre-defines a finite set of mutually exclusive classes and assumes that all of the features are conditionally independent given the class label of each instance [15], [16]

3.2.2 Support Vector Machine

SVMs are a type of supervised learning algorithm that can be applied to both regression and classification problems. In SVMs, the required hyperplanes and weights are learned during training, these have the required optimal plane and correctly chosen support vectors. The default kernel used by Weka is the RBF with gamma equal 1/k. [17], [18]

3.2.3 Decision Tree

The decision tree is based on the J48 algorithm that is also known as Iterative Dichotomiser 3, in this research this will construct a tree from top down using the ID3 algorithm. [19]

After performing the feature extraction techniques we chose one supervised learning algorithm in order to see if the accuracies were comparable to the generalized models. Training was done on the Correlation, Information Gain and Wrapper Evaluation attributes. The tailored degrees have their specified subjects so for each category the training was performed as well. After learning the parameters of the classifiers, these will be used to either confirm or reject the hypothesis through testing.

4 Experimental Results

In the previous section we discussed how the hypothesis of the research project would be tested and in this section we look at the performance of the machine learning techniques that were mentioned in section III. Firstly, we do simple plots of the data distribution in order to have a better picture of our data and then we evaluate the performance of the 3 main techniques. This evaluation occurs on the full dataset that has 216 features and the results will be subsequently recorded. We then perform feature extraction using the techniques that were also mentioned in section III, we use one of them (of the three algorithms) in order to observe if there's any improvement on the model after feature extraction. The last batch of experiments involve training models for tailored degrees in the Faculty of Science, this is done due to the fact that in the initial models we generalized students in the Faculty. The tailored degrees fall under four categories which are; Physical Sciences, Mathematical Sciences, Biological and Life Sciences and the last one is Earth Sciences. The algorithms were ran on Weka (Waikato Environment for Knowledge Analysis) which is tool developed at the University of Waikato, New Zealand [20].

4.1 Graphs

The stacked plot in Figure 1 represents the distribution of the Progression Outcome Type, and this is referred to as the class label. The color blue represents students that have successfully completed their degrees in record time (3 years) and red represents the class of students that have not completed their degrees. The total number of unique students is 8557 for a period of 7 years.

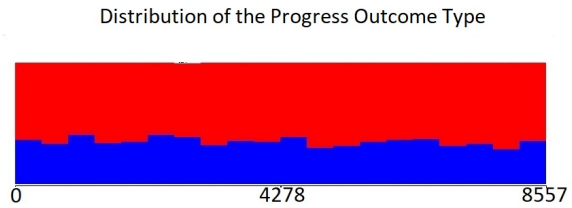


Figure 1: Stacked plot of the distribution of Progress Outcome Type

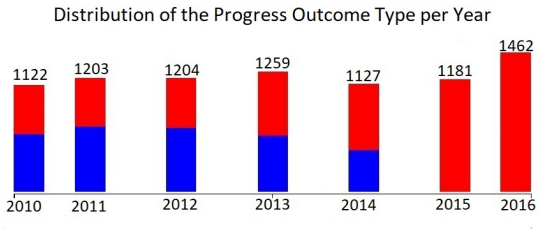


Figure 2: Stacked bar plot of the Progress Outcome Type per year

Figure 2 represents a stacked bar plot that compares the Progress Outcome Type for each year from 2010 until 2016. Blue represents students that have completed their degrees in record time and the color red represents students that have not completed their degrees. The last two years, 2015 and 2016 have students that have not completed their degrees which is a strange phenomenon because we would expect that in every 3 year cycle there would be students that complete their degrees. Students that enrolled in 2014 should have completed their degrees in 2016, and the same applies to students that enrolled in 2013, these students should have completed their degrees in 2015. This strange observation in Figure 2 can be accounted to the second phase of the research methodology, we might have dropped students who completed their degrees in 2015 and 2016 by mistake. This might have been caused by the format in which we received the dataset.

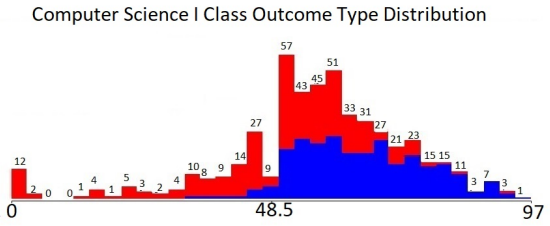


Figure 3: A plot that represents the distribution of Computer Science I marks

Figure 3, we have a stacked plot of the distribution of marks in Computer Science I. The plot resembles a normal distribution (Gaussian) which is what we expected for a set of marks for any given course. There are outliers in the Computer Science I marks and these are located at the far left in the plot.

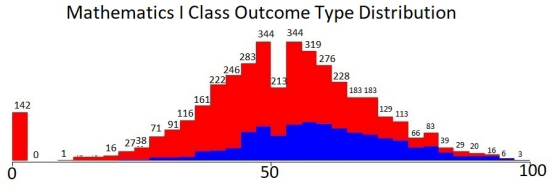


Figure 4: A plot that represents the distribution of Mathematics I marks

Figure 4 illustrates a stacked plot of the distribution of marks in Mathematics I major. The plot resembles a normal distribution (Gaussian) more than the Figure 3, this is because we have more data points than before. There are also outliers to the far left of the stacked plot. Given that there is 216 possible courses that are features of the data, the same phenomenon of normally distributed marks can be generalized to these but we plot only 2 diagrams for the purpose of illustration.

Figure 5a represents the results of the 3 different machine learning algorithms that were used to test the hypothesis. The support vector machine outperformed the naïve Bayes and the decision tree. The results of the decision tree are the worst from the first two algorithms as an accuracy of 65.62% cannot be deemed as reasonable given that the support vector machine achieved an accuracy of 87%.

Figure 5b, Figure 5c and Figure 5d represent the Confusion Matrices for the respective algorithms that are in Figure 5a. These tables describe the performance of each algorithm and this is another way of representing the accuracy of each algorithm.

Algorithm	Correctly Classified	Incorrectly Class.
naïve Bayes	7391 [**86.3636**%]	1167 [**13.6364**%]
Support Vector Machine	7446 [**87.0063**%]	1112 [**12.9937**%]
Decision Tree	5616 [**65.9663**%]	2942 [**34.3772**%]

(a) A table that compares the accuracies of the algorithms

P	F	
2622	363	P = Pass
804	4769	F = Fail

(b) Confusion Matrix of the naïve Bayes

P	F	
2380	605	P = Pass
507	5066	F = Fail

(c) Confusion Matrix of the support vector machine

P	F	
2979	6	P = Pass
2936	2637	F = Fail

(d) Confusion Matrix of the decision trees

Figure 5: Tabulated results of the different algorithms

Extraction Technique	Correctly Classified	Incorrectly Class.
Correlation	7393 [**86.387**%]	1166 [**13.613**%]
Information Gain	7387 [**86.3169**%]	1171 [**13.6831**%]
Wrapper Evaluation	6968 [**81.4209**%]	1590 [**18.5791**%]

(a) A table that compares the accuracies of the algorithms

P	F	
2696	289	P = Pass
876	4697	F = Fail

(b) Confusion Matrix of the naïvee Bayes (Correlation)

P	F	
2640	345	P = Pass
826	4747	F = Fail

(c) Confusion Matrix of the naïve Bayes (Information Gain)

P	F	
2437	548	P = Pass
1042	4531	F = Fail

(d) Confusion Matrix of the naïve Bayes (Wrapper Evaluator)

Figure 6: Tabulated results of the feature extraction techniques

Degree	Correctly Classified	Incorrectly Class.
Physical Sciences	7392 [**86.3753**%]	1166 [**13.6247**%]
Mathematical Sciences	7198 [**86.3169**%]	1360 [**15.8916**%]
Biological and Life Sciences	7357 [**81.4209**%]	1201 [**14.0337**%]
Earth Sciences	7396 [**81.4209**%]	1162 [**13.5779**%]

(a) A table that compares the accuracies for the different degree fields

P	F	
2753	232	P = Pass
934	4639	F = Fail

(b) Confusion Matrix of the naïve Bayes (Physical Sciences)

P	F	
2771	214	P = Pass
1146	4427	F = Fail

(c) Confusion Matrix of the naïve Bayes (Mathematical Sciences)

P	F	
2784	201	P = Pass
1000	4573	F = Fail

(d) Confusion Matrix of the naïve Bayes (Earth Sciences)

P	F	
2746	239	P = Pass
923	4650	F = Fail

(e) Confusion Matrix of the naïve Bayes (Wrapper Evaluator)

Figure 7: Tabulated results of the different degree fields

In Figure 8 we have a bar plot that compares the accuracy of the three algorithms. The legend of the plot indicates that the red color represents the category of the correctly classified instances and the cyan represents the incorrectly classified instances.

4.2 Results with Feature Extraction using Naïve Bayes

Figure 6a represents the results of the naïve Bayes classifier that was used on the 3 feature extraction techniques namely, correlation, information gain, and wrapper evaluation.

The Figure6b, 6c and 6d represent the Confusion Matrices for the respective algorithms that are in Table 6a.

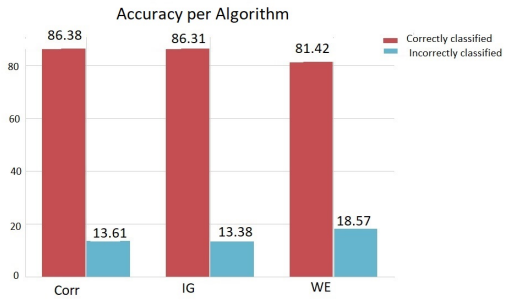


Figure 8: Bar plot

In Figure 8 we have a bar plot that compares the accuracy of the three feature extraction techniques.

4.3 Predicting the completion of a field specific Bachelor of Science degree based on first year marks

Figure 7a represents the results of the field specific degrees in the Faculty of Science. The naïve Bayes classifier was used for each of the 4 fields. The correctly classified instances for each of the fields have comparable accuracies and these are also comparable to the generalized case which uses the 216 features. Given that some students when they start their first year's of study they pursue field specific degrees, the model was also tested for field specific degrees in order to see whether we could test our hypothesis for these cases.

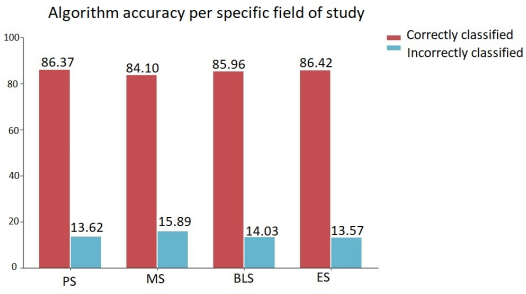


Figure 9: Bar Plot

In Figure 9 we have a bar plot that compares the accuracy of the the naïve Bayes when used on each of the four field specific degrees in the Faculty of Science. The graphical representation gives a better picture than Figure 7a and the Confusion Matrix tables. Here we are able to visually analyze the accuracy of each field specific degree when the naïve Bayes classifier is applied.

5 Conclusion

Our primary objective of this research was to build a model that can successfully predict the completion of a student's Science degree based only on their first year marks. To achieve this, we first conducted research on different machine learning techniques, analyzed their advantages and limitations of each. According to the literature survey, we selected the naïve Bayes classifier, support vector machine and the decision tree. These have reasonable performances in theory that is why they were selected to be used in this research. Data preprocessing was used in order to package the data into the correct format and the feature extraction techniques were used in order to minimize the effect of over-fitting. Following a certain methodology, we conducted experiments on the selected models and on their variations. The methodology we performed can be easily extended to build other models that can be used for prediction purposes.

To evaluate the predictive performance of the models, this research applied a combination of features to the given models and their accuracies were determined. The computation time of each model is comparable except to the support vector machine that took some time do build. The experiment results show that our hypothesis is true and the support vector machine is considered as the most efficient model that produces results of reasonable accuracy. This was followed by the naïve Bayes and the decision tree had the worst performance. The naïve Bayes classifier was chosen purely on discretion when it was used for the feature extraction techniques and the field specific degrees. The support vector machine could have been chosen as well for this purpose as it had a comparable accuracy. The results of the feature extraction techniques and the field specific degrees were comparable to the general case.

A lot of factors were not taken into account when building the necessary models, i.e. the social circumstances of a particular student, whether a student is on financial aid, personal preferences and this affects the future work of the research. It can also be argued that the gender of the student might also affect the performance of a particular student, so this can improve future models.

It would be interesting to apply these models on a dataset with more variables that describe the learners academic trajectory. It would also be interesting to compare the predictive across models trained from various South African institutions in order to discover if the same features drive success and failure at difference institutions. Further work could explore optimising the hyper-parameters used in this study to optimise on accuracy. Deep neural networks or other probabilistic graphical models, such as Bayesian networks, could be used to provide better explanatory power of the influence that these features play in determining student success. These models do not make a lot of assumptions about our data and they can also be used to achieve the research objectives.

Conflict of Interest The authors declare no conflict of interest.

Acknowledgement This work is based on the research supported in part by the National Research Foundation of South Africa (Grant number: 121835).

References

[1] L. Thurow, "Education and economic equality," in In The Public Interest, 66, 1972.

[2] I. Scott, "A proposal for undergraduate curriculum reform in South Africa: The case for a flexible curriculum structure," in In Council on Higher Education, 2013.

[3] D. Butcher, W. Muth, "Predicting success in an introductory computer science course," in Communications of the ACM, 263–268, ACM, 1985.

[4] P. Campbell, G. G. McCabe, "Predicting the success of freshmen in a computer science major," in Oxford: Clarendon, 1102–1113, 1984.

[5] E. Gathers, "Screening freshmen computer science majors," in ACM SIGCSE Bulletin, 44–48, ACM, 1986.

[6] N. Ndou, R. Ajoodha, A. Jadhav, "A Case Study: Educational Data-mining to Determine Student Success at Higher Education Institutions," in The International Multidisciplinary Information Technology and Engineering Conference, 2020.

[7] N. Mngadi, R. Ajoodha, A. Jadhav, "A Conceptual Model to Identify Vulnerable Undergraduate Learners at Higher-Education Institutions," in The International Multidisciplinary Information Technology and Engineering Conference, 2020.

[8] N. Philippou, R. Ajoodha, A. Jadhav, "Using Machine Learning Techniques and Matric Grades to Predict the Success of First Year University Students," in The International Multidisciplinary Information Technology and Engineering Conference, 2020.

[9] R. Ajoodha, A. Jadhav, S. Dukhan, "Forecasting Learner Attrition for Student Success at a South African University," in In Conference of the South African Institute of Computer Scientists and Information Technologists 2020 (SAICSIT '20), September 14-16, 2020, Cape Town, South Africa. ACM, New York, NY, USA, 10 pages., ACM, 2020, doi:https://doi.org/10.1145/3410886.3410973.

[10] R. Ajoodha, S. Dukhan, A. Jadhav, "Data-driven Student Support for Academic Success by Developing Student Skill Profiles," in International Multidisciplinary Information Technology and Engineering Conference. ISBN: 978-1-7281-9519-9., IEEE, 2020.

[11] T. Hostetler, "Predicting student success in an introductory programming course," in ACM SIGCSE Bulletin, 40–43, 1983.

[12] C. Capstick, J. Gordon, A. Salvadori, "Predicting performance by university students in introductory computing courses," in ACM SIGCSE Bulletin, 21–29, 1975.

[13] D. Tewari, "Is matric math a good predictor of student's performance in the first year of university degree? A case study of faculty of management studies, University of Kwazulu-Natal, South Africa," in In International Journal of Science Education, 233–237, 2014.

[14] S. Rauchus, B. Rosman, G. Konidaris, I. Sanders, "Language performance at high school and success in first year computer science," in ACM SIGCSE Bulletin, 2927–2948, 2006.

[15] Z. Ghahrami, "An Introduction to Hidden Markov Models and Bayesian Networks," in Journal of Pattern Recognition and Artificial Intelligence, 9–15, 2001.

[16] D. Pham, G. Ruz, "Unsupervised training of bayesian networks for data clustering," in In Proceedings of the Royal Society of London A: Mathematical, Physical and Engineering Sciences, 2927–2948, 2009.

[17] D. Isa, L. Lee, V. Kallimani, R. Rajkumar, "Text document preprocessing with the bayes formula for classification using the support vector machine," in IEEE Transactions on Knowledge and Data engineering, 1265–1272, 2008.

[18] D. Boswell, "Introduction to Support Vector Machines," Carlifonia Institute of Technology, 2002, doi:http://www.work.caltech.edu/~boswell/IntroToSVM.pdf.

[19] D. Isa, L. Lee, V. Kallimani, R. R. Rajkumar, "Decision Tree Learning," in In Machine Learning, 52–57, 1997.

[20] R. Remco, E. Bouckaert, M. Frank, "Weka Manual," in In Weka Manual for version 3.6.9, University of Waikato, New Zealand, 2008.

ASTES

Advances in Science, Technology and Engineering Systems Journal
Vol. 5, No. 5, 927-933 (2020)
www.astesj.com

ASTES Journal
ISSN: 2415-6698

Performance Analysis of Selective Repeat ARQ Protocol Used in Digital Data Transmission Over Unreliable Channels

Fayza A. Nada*

Department of Information Technology, Faculty of Computers and Information, Suez University, Egypt

ARTICLE INFO

Article history:
Received: 21 June, 2020
Accepted: 28 September, 2020
Online: 12 October, 2020

Keywords:
ARQ Protocols
Sliding Window
Selective Repeat ARQ
Service Time
Error control
Queuing Systems
Performance Analysis

ABSTRACT

Stop and Wait (SW) ARQ, Go Back N (GBN) ARQ, and Selective Repeat (SR) ARQ are the main ARQ (Automatic-Repeat-reQuest) protocols used to ensure reliable delivery of digital data at correct sequence. These protocols are implemented at the DLC (Data Link Control) sub layer of Data Link Layer (DLL) of OSI (Open System Interconnection) network model. The main task of such protocols is controlling errors and providing smooth and reliable transmission between communicating nodes. This is mostly done by using acknowledgements and timeouts to satisfy reliable data transmission over unreliable channels. This paper completes measuring the performance of SR ARQ protocol. We study and analyze the service time distribution of SR ARQ protocol used in digital data transmission over unreliable channels. Stochastic Process and Markov Chains have been used to study the proposed network model. Closed and analytic expressions of the Probability Generating Function (PGF) of service time are calculated considering two different situations (short and long messages). Moreover, expressions for first and second moments of the service time are derived. ARQ protocols are basically applied on shortwave radio to provide reliable delivery of signals and in peer-to-peer protocols that provide reliable data transmission. The obtained results can be applied in simulations of similar communication systems and may be adopted in approximating some relevant systems.

1 Introduction

Reliable data transmission requires applying some error control mechanisms. ARQ (Automatic Repeat reQuest) protocols are error control protocols implemented at layer 2 (Data Link Layer) and Layer 4 (Transport layer) to provide reliable transmission of digital data over unreliable communication links, with correct order . To do so, ARQ protocols depend on ACKnowledgements (ACK) (or Negative AcKnowledgements (NAK)) and timeouts. Most likely, the receiver implements some error detection technique (ex. Cyclic Redundancy Check (CRC)) to check if the received packet is error free or not. Then, the receiver sends either an ACK or NAK to the sender to tell whether the packet is correctly received or not. On the other hand, the sender sets some timeout interval after sending each packet. If no ACK is received before the timeout, the sender usually re-transmits the packet. This process is repeated until either an ACK is received or number of re-transmissions attempts is exceeded. There are three basic types of ARQ protocols: Stop and Wait (SW) ARQ, Go Back N (GBN) ARQ, and Selective Repeat (SR) ARQ. All will be explained in the next section.

In [1], "The SW ARQ protocol adopted the idea of SR ARQ protocol considering different packet size depending on the link state. The proposed SW ARQ scheme proved better performance compared to traditional SW ARQ protocol considering either the simulation results or the obtained analytical results". However, in [2], "SR ARQ protocol is applied within Adaptive Modulation System (AMS). It studied the throughput of SW ARQ protocol using different fading links. Moreover, It considered the link estimated transmission errors in the analysis of the throughput and conducted a type of comparison with the link throughput assuming perfect transmission link".In [3], "a Reliable SR ARQ (RB-SR ARQ) protocol is suggested with parity check codes of low density. This spoils the reliability of the estimated bits at the decoder side to re-transmit these unreliable bits". But in [4], "the link Round Trip Time (RTT), which specifies the receiving instant of the receiver feedback, is considered to be a fixed amount. It has been shown that, the changing of RTT has limited effect on delay analysis". While [5] "modelled and analyzed the delay resulted from the packet resequencing of time division duplexing that applies SR ARQ error control scheme. Keeping in mind that link transmission errors may initiate and motivate the packet resequencing procedure at the receiver side, Markov Chains assumptions have been applied to give prediction for the effect of resequencing delay on the Quality of Service (QoS)". Also, "discussion of SR ARQ strategy for underwater acoustic networks

*Corresponding Author: Fayza A. Nada, Department of Information Technology, Faculty of Computers and Information, Suez University, Egypt, f.nada@suezuni.edu.eg

has been presented in [6]. It has been shown that, performance of a given size multiuser networks can be optimized through adjusting the point-to-point communication time".

As ARQ protocols provide reliable data transmission over unreliable transmission links, they have wide range of applications. ARQ protocols are basically applied on shortwave radio to ensure reliable delivery of signals. Add to this, there are different applications for the same function of ARQ protocols such as Transmission Control Protocol (TCP), High-Level Data Link Control (HDLC) protocol, and Xmodem. The service time analysis of GBN ARQ protocol was presented in [8]. However, In [9], we started service time analysis of SR ARQ protocol for transmission of short messages over noisy channels and obtained the service time distribution for this special case. Moreover, the first and second moments of service time distribution were also calculated. The future research plan includes doing validation and simulations for all results obtained in [8, 9] accompanied by a wide comparison between all discussed ARQ protocols.

Obviously, the service time analysis of SR ARQ protocol has not been considered properly before. Service time can be considered as a type of QoS measurement and evaluation metric. No doubt, analyzing and studying the service time of ARQ protocols is essential because it sheds the light on factors affecting the service time. If such factors are handled properly, service time may be reduced. The main contribution of this article is studying and analyzing the service time of SR ARQ protocol based on a new mathematical model. This study depends on applying stochastic processes and Markov Chains in view of probability and statistics theories to obtain an analytical formula of Probability Generating Function (PGF) of service time distribution of SR ARQ protocol. Also, closed form expressions of first and second moments of obtained PGF are also derived. The rest of this article proceeds as follows: Next section demonstrates the basic ARQ protocol types showing the basic strategy of each and differences between them. Section 3 explains the used mathematical model assumptions. Then, the PGF of service time distribution is discussed and derived in section 4 for two different cases (short and long messages). Moreover, the first and second moments of service time distribution are calculated in each case. Conclusion is the last section.

2 Basic ARQ Protocols

In data transmission, reliable data transfer is an important issue. TCP protocol is responsible of this service. The major ARQ flow control schemes are: SW ARQ, GBN ARQ, and SR ARQ. Each ARQ protocol has specific strategy for controlling transmission errors. Some ARQ protocols use the concept of sliding window, where the transmitter can send many packets before receiving any ACKs. Both GBN ARQ and SR ARQ protocols are sliding window protocols. The sliding window (also known as windowing) is an imaginary box to hold packets. In such protocols, both the sender and the receiver have buffers called the sending window and the receiving window respectively (Figure 1).

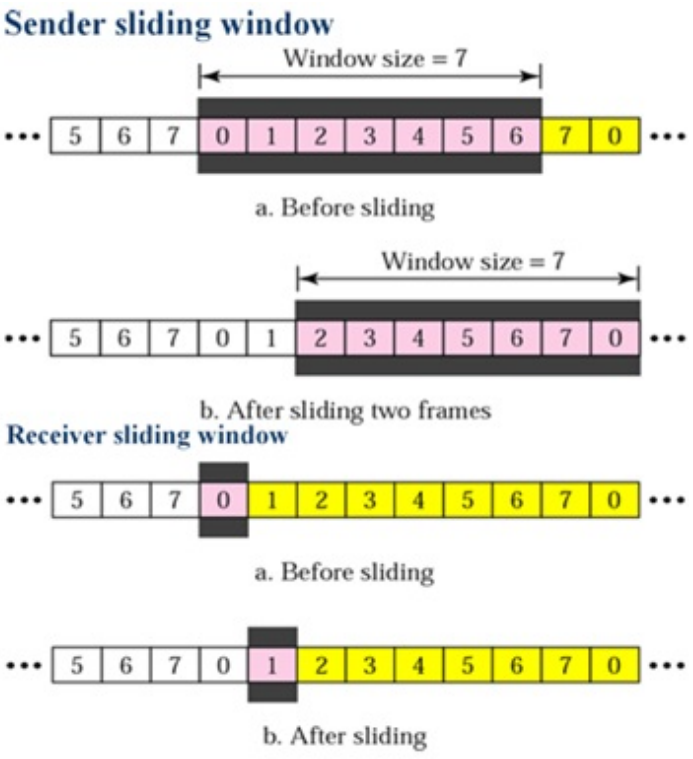


Figure 1: Sender Sliding Window

Actually, The sending window size is somehow dependent on the sequence number field of the packet header. If the size of the sequence number field of the packet header is n bits, then the sequence numbers of packets will range from 0 to $2^n - 1$. Consequently, the sending window size can not exceed $2^n - 1$ packets too. Thus, in order to accommodate a sending window size of 7 packets, the length of sequence number field should be 3 bits.

2.1 Stop and Wait (SW) ARQ Protocol

SW ARQ protocol is an error and flow control strategy used for unidirectional data traffics over unreliable communication links. It applies the ACKs and timeouts modules. The sender saves a copy of each sent packet. Then, it waits for a predefined time period (timeout) to receive an ACK from the receiver. If an ACK is received, the sender sends the next packet. On the other hand, The receiver checks each received packet and apply an error detection scheme (ex. CRC). After that, either ACK or NAK is sent to the sender. The packet is re-transmitted if the timer expired or a NAK is received. However, if the ACK is lost, and the packet is re-transmitted again, the receiver discards the duplicated frame (Figure 2).

2.2 Go Back N (GBN) ARQ Protocol

According to GBN ARQ protocol, the sender is able to send a block of packets (that depends on the size of the sending window) before receiving the ACK of any sent packets. After sending all packets of the sending window ($2^n - 1$ packet, where n is the size of the sequence number field of the packet header), the sender stops and checks the received ACKs (if any). Receiving ACKs indicates that the window will slide down and more packets can be sent. However,

in GBN ARQ protocol, the receiver is adjusted to receive ordered packets only. Which means, receiver will discard out-of-order packets (even if they are correct) and does not send ACKs for them. If a packet is lost (or damaged), the receiver sends a NAK. In such case, the sender re-transmits again all packets in the sending window (Figure 3).

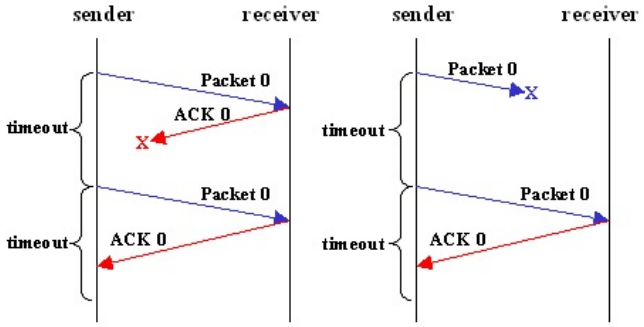


Figure 2: Stop and Wait ARQ Protocol

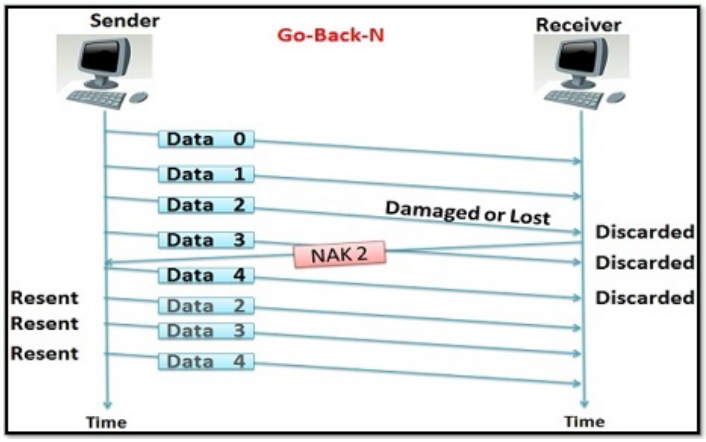


Figure 3: Go Back N ARQ Protocol

2.3 *Selective Repeat (SR) ARQ Protocol*

Implementation of SR ARQ protocol is much similar to GBN ARQ protocol. The sender sends a block of packets (that depends on the size of the sending window) without waiting for receiving the ACK of any sent packets. After that, the sender stops and checks the received ACKs (if any). By receiving ACKs, sending window slides down and more packets can be sent. However, in SR ARQ protocol, the receiver is programmed to hold and buffer the out of order packets (if correct). Actually, the receiver sends ACKs for all correctly received packets whether they are ordered or not. Typically, The receiver is able to put the received packets in correct order before sending to the upper layers. If a packet is lost (or damaged), the receiver sends a NAK for this packet. In such case, the sender re-transmits only the packet indicated by the NAK. Although both GBN ARQ and SR ARQ protocols are sliding window protocols, it can be noted that, SR ARQ protocol is more complex than GBN ARQ protocol as it requires application of extra logic, sorting and storage modules at both sender and receiver (Figure 4).

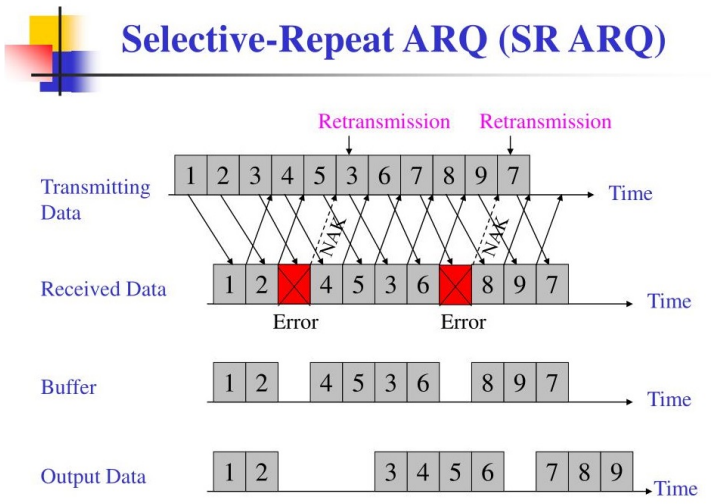


Figure 4: Selective Repeat ARQ Protocolh

3 Model Assumptions

Since this work is an extension to our work done in [9], similar mathematical model assumptions are adopted here:

- The model includes a transmitter, a receiver, and a slotted communication link.
- Data is divided to packets of fixed size.
- At messages level, SW ARQ protocol is applied while SR ARQ protocol is applied at packets level.
- Service time interval is specified by the time between starting and completing transmission of each message.
- Time is considered to be of equal time slots.
- Service discipline is assumed to be FCFS.
- The RV A represents the number of messages arriving in each slot, with PGF denoted by $A(z)$

$$a_n = \Pr[A = n], \quad A(z) = \sum_{n=0}^{\infty} a_n z^n. \tag{1}$$

- The buffer of the transmitter is considered to be of infinite capacity.
- Messages are divided to packets where each packet fits one slot.
- The RV B represents the number of packets in each message (message size), with PGF denoted by $B(z)$

$$b_n = \Pr[B = n], \quad B(z) = \sum_{n=1}^{\infty} b_n z^n. \tag{2}$$

- Transmission errors occur randomly and follow a Bernoulli process. That is, if p is the probability of damage in the transmitted packet, $1-p$ is the probability of successful packet transmission, and ε represents the link bit error rate, then p can be written as

$$p = 1 - (1-\varepsilon)^N, \tag{3}$$

  where N specifies the size of the transmitted packet in bits.

- The receiver uses a return communication link to send feedback regarding the received packet (ACK or NAK, depending on the status of the received packet).
- The RV R represents the number of packets transmitted during the RTT (duration, measured in milliseconds, from sending a packet till receiving a response from a receiver).
- No errors are assumed while sending on the return communication link.

4 PGF of Service Time In SR ARQ Protocol

In this section, the PGF $S(z)$ of the service time distribution of a message in SR ARQ protocol is discussed and derived. We consider a message consisting of i packets and deal with two different cases.

4.1 Case 1 (Short messages): $i \leq R+1$

We have analyzed and presented this case in detail in [9] and these are the main results obtained from that analysis

$$\begin{aligned} S_i(z) &= \sum_{l=0}^{\infty}\sum_{k=1}^{i}(1-p^{l+1})^{k-1}p^l(1-p)(1-p^l)^{i-k} \\ &\times z^{k-1+(l+1)(R+1)} \\ &= (1-p)\sum_{l=0}^{\infty}\sum_{k=1}^{i}(1-p^{l+1})^{k-1}p^l(1-p^l)^{i-k} \\ &\times z^{k-1}(z^{(l+1)})^{(R+1)}. \end{aligned} \tag{4}$$

But we have

$$(1-p^{l+1})^{k-1} = \sum_{m=0}^{k-1}(-1)^m \binom{k-1}{m}(p^{l+1})^m \tag{5}$$

$$(1-p^l)^{i-k} = \sum_{n=0}^{i-k}(-1)^n \binom{i-k}{n}(p^l)^n. \tag{6}$$

Substituting from (5) and (6) in (4), we get

$$\begin{aligned} S_i(z) &= (1-p)z^R \\ &\times \sum_{l=0}^{\infty}\sum_{k=1}^{i}\sum_{m=0}^{k-1}\sum_{n=0}^{i-k}(-1)^{m+n}\binom{k-1}{m}\binom{i-k}{n} \\ &\times (p^l)^{m+n+1}p^m z^k (z^l)^{R+1}. \end{aligned} \tag{7}$$

But

$$\begin{aligned} &\sum_{l=0}^{\infty}\sum_{k=1}^{i}\sum_{m=0}^{k-1}\sum_{n=0}^{i-k}(p^l)^{m+n+1}(z^l)^{R+1} \\ &= \sum_{k=1}^{i}\sum_{m=0}^{k-1}\sum_{n=0}^{i-k}\frac{1}{1-z^{R+1}p^{m+n+1}}. \end{aligned} \tag{8}$$

Substituting from (8) in (7), then

$$\begin{aligned} S_i(z) &= (1-p)z^R\sum_{k=1}^{i}\sum_{m=0}^{k-1}\sum_{n=0}^{i-k}\binom{k-1}{m}\binom{i-k}{n} \\ &\times \frac{(-1)^{m+n}p^m z^k}{1-z^{R+1}p^{m+n+1}}. \end{aligned} \tag{9}$$

Moreover, the first moment (mean) and the second moment of the service time were obtained, in the form

$$\begin{aligned} E[S_i] &= (1-p) \\ &\times \sum_{k=1}^{i}\sum_{m=0}^{k-1}\sum_{n=0}^{i-k}\binom{k-1}{m}\binom{i-k}{n}(-1)^{m+n}p^m \\ &\times \frac{\begin{array}{c}R+k-Rp^{m+n+1}-kp^{m+n+1} \\ +Rp^{m+n+1}+p^{m+n+1}\end{array}}{(1-p^{m+n+1})^2} \\ &= (1-p) \\ &\times \sum_{k=1}^{i}\sum_{m=0}^{k-1}\sum_{n=0}^{i-k}\binom{k-1}{m}\binom{i-k}{n}(-1)^{m+n}p^m \\ &\times \frac{(R+1)+(k-1)(1-p^{m+n+1})}{(1-p^{m+n+1})^2}. \end{aligned} \tag{10}$$

$$\begin{aligned} E[S_i^2] &= (1-p) \\ &\times \sum_{k=1}^{i}\sum_{m=0}^{k-1}\sum_{n=0}^{i-k}\binom{k-1}{m}\binom{i-k}{n}\frac{(-1)^{m+n}p^m}{(1-p^{m+n+1})^3} \\ &\times \Big(\Big[(K+R)^2-(R+1)\Big](1-p^{m+n+1})^2 \\ &+ [3R(R+1)+2k(R+1)]\,p^{m+n+1}(1-p^{m+n+1}) \\ &+ (R+1)(1-p^{m+n+1})+2(R+1)^2p^{2(m+n+1)}\Big). \end{aligned} \tag{11}$$

4.2 Case 2 (Long messages): $i > R+1$

Consider a message consisting of i packets such that $i > R+1$. Let us define the *continuous transfer phase* to be the period between the beginning of transmission of first packet to the end of the first trial of the $(R+1)^{th}$ packet. After the end of the continuous transfer phase, the $i-(R+1)$ packet are transmitted and also NAKed packets are retransmitted. Let us define the point of the beginning of slot $R+1$ before ending the continuous transfer phase to be a *critical point*. Note that the $i-(R+1)^{st}$ ACKs are received before the end of the continuous transfer phase (at the last but one). Therefore, the $i-(R+1)^{st}$ transmission takes place at the last slot before the critical point. Let $S1_i$ slots include transmission of $i-(R+1)$ packets. {explanation : The packets of the message are transmitted continuously as in the previous case (continuous transfer phase)

until the slot number $R+1$. This slot starts the reply for the previously transmitted message (ACK or NAK). So, this slot represents the beginning of the transmission of both new and NAKed packets. That is why we call it a critical point. After all the new packets have been transmitted, the retransmission tail, which includes the transmission of the NAKed packets only, starts. So S_i here is

$$S_i = S1_i + S2_i, \tag{12}$$

where the message consists of i packets, and

$S1_i$: RV that represents the service time of the packets transmitted before the critical point.

$S2_i$: RV that represents the service time of the packets transmitted after the critical point. $S1_i$ can be defined as

$$\begin{aligned} S1_i &= \sum_{k=1}^{i-(R+1)} S1_{i_k} \\ &= S1_{i_1} + S1_{i_2} + \cdots + S1_{i_{i-(R+1)1}}, \end{aligned} \tag{13}$$

where the message consists of i packets, and

$S1_{i_1}$:Service time of the 1^{st} packet of the message.

$S1_{i_2}$:Service time of the 2^{nd} packet of the message.

$S1_{i_{i-(R+1)}}$:Service time of the $i-(R+1)^{th}$ packet of the message.

Let $S1_i(z)$ be the PGF of $S1_i$, then

$$\begin{aligned} S1_i(z) &= E[z^{S1_i}] \\ &= E\left[z^{\sum_{k=1}^{i-(R+1)} S1_{i_k}}\right] \\ &= E\left[z^{S1_{i_1}}.z^{S1_{i_2}}\cdots z^{S1_{i_{i-(R+1)}}}\right] \\ &= [S1_{i_k}(z)]^{i-(R+1)}, \end{aligned} \tag{14}$$

where $S1_{i_k}(z)$ denotes the PGF of the RV representing the service time of the $i-(R+1)^{st}$ packets of the message. Suppose that any of the $i-(R+1)^{st}$ is unsuccessfully transmitted for l times. So

$$S1_{i_k}(z) = \sum_{l=0}^{\infty} p^l(1-p)z^{l+1}. \tag{15}$$

Substituting for $S1_{i_k}(z)$ from (15) in (14), then

$$S1_i(z) = \left(\sum_{l=0}^{\infty} p^l(1-p)z^{l+1}\right)^{i-(R+1)} \tag{16}$$

$$= \left(\frac{(1-p)z}{1-pz}\right)^{i-(R+1)}. \tag{17}$$

Now, we proceed to find the distribution of $S2_i$, which represents the service time of the packets transmitted after the critical point. Actually, the rest of the message can be considered as a new message consisting of $R+1$ packets. Then, its transmission will be exactly as in *case 1*. Thus, the distribution of $S2_i$ will be the same as that of S_{R+1} considered in *case 1*, with PGF $S_{R+1}(z)$. However, since both the RVs $S1_i$ and $S2_i$ are mutually independent, then, the PGF of S_i is given by

$$S_i(z) = S1_i(z)S_{R+1}(z). \tag{18}$$

Now we are ready to get PGF $S(z)$ of the service time of SR ARQ protocol from what we obtained in *case 1* and *case 2*.

$$\begin{aligned} S(z) &= \sum_{i=1}^{\infty} b_i S_i(z) \\ &= \sum_{i=1}^{R} b_i S_i(z) + \sum_{i=R+1}^{\infty} b_i \left(\frac{(1-p)z}{1-pz}\right)^{i-(R+1)} \\ &\times S_{R+1}(z) \\ &= \sum_{i=1}^{R} b_i S_i(z) + S_{R+1}\left(\frac{1-pz}{(1-p)z}\right)^{(R+1)} \\ &\times \left[B\left(\frac{(1-p)z}{1-pz}\right) - \sum_{i=1}^{R} b_i \left(\frac{(1-p)z}{1-pz}\right)^{i}\right]. \end{aligned} \tag{19}$$

From which we can find the first moment ($E[S]$) and the second moment ($E[S^2]$), as follows

$$\begin{aligned} E[S] &= \frac{d}{dz}S(z)\Big|_{z=1} \\ \frac{d}{dz}S(z) &= \sum_{i=1}^{R} b_i S_i'(z) + S_{R+1}(z).(R+1) \\ &\times \left(\frac{1-pz}{(1-p)z}\right)^{R}\left(-\frac{p}{(1-p)z} - \frac{1-pz}{(1-p)z^2}\right) \\ &\times \left(B\left(\frac{(1-p)z}{1-pz}\right) - \sum_{i=1}^{R} b_i \left(\frac{(1-p)z}{1-pz}\right)^{i}\right) \\ &+ S_{R+1}(z)\left(\frac{1-pz}{(1-p)z}\right)^{(R+1)} \\ &\times \left(\begin{array}{c} B'\left(\frac{(1-p)z}{1-pz}\right)\left(\frac{(1-p)pz}{(1-pz)^2} + \frac{(1-p)}{(1-pz)}\right) \\ -\sum_{i=1}^{R} i b_i \left(\frac{(1-p)z}{1-pz}\right)^{i-1} \\ \times\left(\frac{(1-p)pz}{(1-pz)^2} + \frac{(1-p)}{(1-pz)}\right)\end{array}\right) \\ &+ S_{R+1}'\left(\frac{1-pz}{(1-p)z}\right)^{(R+1)}\left[B\left(\frac{(1-p)z}{1-pz}\right)\right. \\ &\left. - \sum_{i=1}^{R} b_i \left(\frac{(1-p)z}{1-pz}\right)^{i}\right]. \end{aligned} \tag{20}$$

Substituting for $z=1$ in (20), thus

$$\begin{aligned} E[S] &= \frac{d}{dz}S(z)\Big|_{Z=1} \\ &= \sum_{i=1}^{R} b_i E[S_i] + (R+1) \\ &\times \left(-\frac{p}{(1-p)} - 1\right)\left(1 - \sum_{i=1}^{R} b_i\right) \\ &+ B'(1)\left(\frac{p}{(1-p)} + 1\right) - \sum_{i=1}^{R} i b_i \left(\frac{p}{(1-p)} + 1\right) \\ &+ S_{R+1}'(1)\left(B(1) - \sum_{i=1}^{R} b_i\right) \end{aligned}$$

$$= \sum_{i=1}^{R} b_i E[S_i] + \left(1 - \sum_{i=1}^{R} b_i\right) E[S_{R+1}] \tag{21}$$
$$+ \frac{E[B] + \sum_{i=1}^{R}(R+1-i)b_i - (R+1)}{(1-p)}.$$

Now we have

$$E[S^2] = \left.\frac{d}{dz}S(z)\right|_{z=1} + \left.\frac{d^2}{dz^2}S(z)\right|_{z=1}. \tag{22}$$

Finding $\frac{d^2}{dz^2}S(z)$, substituting for $z = 1$, and after some manipulation, we get

$$\begin{aligned}
\left.\frac{d^2}{dz^2}S(z)\right|_{z=1} &= \sum_{i=1}^{R} b_i S_i^{''}(1) + (R+1) \\
&\times \left(\frac{2p}{(1-p)} + 2\right)\left(1 - \sum_{i=1}^{R} b_i\right) \\
&+ R(R+1)\left(-\frac{p}{(1-p)} - 1\right)^2 \\
&\times \left(1 - \sum_{i=1}^{R} b_i\right) \\
&+ 2(R+1)\left(-\frac{p}{(1-p)} - 1\right) \\
&\times \left(-\sum_{i=1}^{R} i b_i \left(\frac{p}{(1-p)} + 1\right)\right. \\
&\left. + \left(\frac{p}{(1-p)} + 1\right) B^{'}(1)\right) \\
&+ 2S_{R+1}^{'}(1)(R+1) \\
&\times \left(-\frac{p}{(1-p)} - 1\right)\left(1 - \sum_{i=1}^{R} b_i\right) \\
&+ 2S_{R+1}^{'}(1)\left(-\sum_{i=1}^{R} i b_i \left(\frac{p}{(1-p)} + 1\right)\right. \\
&\left. + \left(\frac{p}{(1-p)} + 1\right) B^{'}(1)\right) \\
&+ \left(\begin{array}{l} -\sum_{i=1}^{R} i b_i \left(\frac{2p^2}{(1-p)^2} + \frac{2p}{(1-p)}\right) \\ \quad -\sum_{i=1}^{R} i(i-1)b_i \end{array} \right) \\
&\times \left(\frac{p}{(1-p)} + 1\right)^2 \\
&+ \left(\frac{2p^2}{(1-p)^2} + \frac{2p}{(1-p)}\right) \\
&\times B^{'}(1) + \left(\frac{p}{(1-p)} + 1\right)^2 B^{''}(1)\Big) \\
&+ S_{R+1}^{''}(1)\left(1 - \sum_{i=1}^{R} b_i\right).
\end{aligned} \tag{23}$$

Hence

$$\begin{aligned}
\left.\frac{d^2}{dz^2}S(z)\right|_{z=1} &= \sum_{i=1}^{R} b_i S_i^{''}(1) + (R+1) \\
&\times \left(\frac{2}{(1-p)}\right)\left(1 - \sum_{i=1}^{R} b_i\right) \\
&+ R(R+1)\frac{1}{(1-p)^2}\left(1 - \sum_{i=1}^{R} b_i\right) \\
&- 2(R+1)\frac{1}{(1-p)^2}E[B] \\
&+ 2(R+1)\sum_{i=1}^{R} i b_i \frac{1}{(1-p)^2} \\
&- 2E[S_{R+1}](R+1) \\
&\times \left(\frac{1}{(1-p)}\right)\left(1 - \sum_{i=1}^{R} b_i\right) \\
&-2E[S_{R+1}]\sum_{i=1}^{R} i b_i \left(\frac{1}{(1-p)}\right) \\
&+ 2E[S_{R+1}]\left(\frac{1}{(1-p)}\right)E[B] \\
&- \sum_{i=1}^{R} i b_i \left(\frac{2p}{(1-p)^2}\right) \\
&- \sum_{i=1}^{R} i^2 b_i \frac{1}{(1-p)^2} + \sum_{i=1}^{R} i b_i \frac{1}{(1-p)^2} \\
&+ \left(\frac{2p}{(1-p)^2}\right)E[B] + \frac{1}{(1-p)^2}B^{''}(1) \\
&+ S_{R+1}^{''}(1)\left(1 - \sum_{i=1}^{R} b_i\right).
\end{aligned} \tag{24}$$

Now, substituting for $\left.\frac{d}{dz}S(z)\right|_{z=1}$ and $\left.\frac{d^2}{dz^2}S(z)\right|_{z=1}$ from (21) and (24) in (22) and after simplification, we get

$$\begin{aligned}
E[S^2] &= \sum_{i=1}^{R} b_i E[S_i^2] + \left(1 - \sum_{i=1}^{R} b_i\right) E[S_{R+1}^2] \\
&+ \frac{2(R+1)\left(1 - \sum_{i=1}^{R} b_i\right) - (R+1)\left(1 - \sum_{i=1}^{R} b_i\right)}{(1-p)} \\
&+ \left(1 - \sum_{i=1}^{R} b_i\right)\left(\frac{(R+1)}{(1-p)}\left[\frac{R}{1-p} - 2E[S_{R+1}]\right]\right) \\
&+ \frac{E[B]}{(1-p)} \times \left(2E[S_{R+1}] - \frac{2(R+1)}{(1-p)} + \frac{p}{1-p}\right) \\
&+ \frac{E[B^2]}{(1-p)^2} + 2(R+1)\sum_{i=1}^{R} i b_i \frac{1}{(1-p)^2} - \\
&- \sum_{i=1}^{R} i^2 b_i \frac{1}{(1-p)^2}
\end{aligned}$$

$$+\frac{\begin{array}{c}\sum_{i=1}^{R} ib_i - 2p\sum_{i=1}^{R} ib_i - \sum_{i=1}^{R} ib_i \\ +p\sum_{i=1}^{R} ib_i - 2(1-p)E[S_{R+1}]\sum_{i=1}^{R} ib_i\end{array}}{(1-p)^2}$$

$$= \sum_{i=1}^{R} b_i E[S_i^2] + \left(1 - \sum_{i=1}^{R} b_i\right) E[S_{R+1}^2]$$

$$+ \frac{E[B^2]}{(1-p)^2} + \frac{E[B]}{(1-p)}$$

$$\times \left(2E[S_{R+1}] - \frac{2(R+1)}{(1-p)} + \frac{p}{1-p}\right)$$

$$+ \left(1 - \sum_{i=1}^{R} b_i\right)\left(\frac{(R+1)}{(1-p)}\begin{bmatrix} 1+\frac{R}{1-p} \\ -2E[S_{R+1}] \end{bmatrix}\right)$$

$$- \sum_{i=1}^{R} \frac{b_i}{(1-p)^2}\begin{bmatrix} i^2 + [p + 2(1-p)E[S_{R+1}] \\ -2(R+1)]i \end{bmatrix},$$

which can be written in the final form

$$E[S^2] = \sum_{i=1}^{R} b_i E[S_i^2] + \frac{E[B^2]}{(1-p)^2} + \frac{E[B]}{(1-p)}$$

$$\times \left(2E[S_{R+1}] - \frac{2(R+1)}{(1-p)} + \frac{p}{1-p}\right)$$

$$+ \left(1 - \sum_{i=1}^{R} b_i\right)\begin{pmatrix} E[S_{R+1}^2] + \frac{(R+1)}{(1-p)} \\ \times\left[1 + \frac{R}{1-p} - 2E[S_{R+1}]\right] \end{pmatrix}$$

$$- - \sum_{i=1}^{R} \frac{b_i}{(1-p)^2}\begin{bmatrix} i^2 + [p + 2(1-p) \\ \times E[S_{R+1}] - 2(R+1)]i \end{bmatrix}. \quad (25)$$

5 Conclusion

ARQ protocols are applied at DLL and Transport Layer of OSI network model to control transmission errors at these layers. SW ARQ, GBN ARQ, and SR ARQ are the main ARQ protocol types. They use ACKs, timeouts, and the concept of sliding window to satisfy reliable data transmission over noisy channels. This paper studies and analyzes the service time distribution of SR ARQ protocol. The model is discussed with aid of stochastic processes and Markov Chains. The PGF of the service time distribution is calculated considering transmission of short and long messages. The First and second moments of service time distribution are derived as well. Results of the analysis can be used either in simulation or approximations of relevant communication models.

References

[1] C. Jin, W. Jinlong, "A novel selective repeat stop-wait ARQ for half-duplex channels,"in 2002 IEEE Region 10 Conference on Computers, Communications, Control and Power Engineering. TENCOM '02. Proceedings. 28-31 Oct. 2002, Beijing, China, DOI: 10.1109/TENCON.2002.1180350.

[2] J. Yun, W. Jeong, M. Kavehrad, "Throughput analysis of selective repeat ARQ combined with adaptive modulation for fading channels,"in MILCOM 2002. Proceedings. 7-10 Oct. 2002, Anaheim, CA, USA, DOI: 10.1109/MILCOM.2002.1180532.

[3] F. Huang, X. Yi, T. Wang, "Reliability-Based Selective Repeat Hybrid ARQ Protocol on Low Density Parity,"in 16^{th} International Conference on Artificial Reality and Telexistence–Workshops (ICAT'06). 29 Nov.-1 Dec. 2006, Hangzhou, China, DOI: 10.1109/ICAT.2006.104.

[4] L. Badia, "A Markov Analysis of Selective Repeat ARQ with Variable Round Trip Time,"IEEE Communications Letters, **17**(11) , 2184 - 2187, 2013, DoI: 10.1109/CEIT.2016.7929028.

[5] F. Chiti, R. Fantacci, A. Tassi, "Evaluation of the Resequencing Delay for Selective Repeat ARQ in TDD-Based Wireless Communication Systems,"IEEE Transactions on Vehicular Technology, **63**(5), 2450 - 2455, 2014, DOI: 10.1109/TVT.2013.2291432.

[6] S. Azad, P. Casari, M. Zorzi, "The Underwater Selective Repeat Error Control Protocol for Multiuser Acoustic Networks: Design and Parameter Optimization,"IEEE Transactions on Wireless Communications, **12**(10), 4866 - 4877, 2013, DOI: 10.1109/TWC.2013.090413.121306.

[7] F. Nada, "Service Time Analysis of Go Back N ARQ Protocol,"in 7th International Conference on Advanced Machine Learning and Technologies and Applications (AMLTA2021), March 20-22, 2021, To appear.

[8] F. Nada, "Service Time Distribution of Selective Repeat ARQ Protocol Used In Transmitting Short Messages Over Noisy Channels,"in 12th International Conference on Electrical Engineering (ICEENG), 7-9 July 2020, Cairo, Egypt, DOI: 10.1109/ICEENG45378.2020.9171772.

ASTES

Advances in Science, Technology and Engineering Systems Journal
Vol. 5, No. 5, 934-943 (2020)
www.astesj.com

ASTES Journal
ISSN: 2415-6698

Classification of Handwritten Names of Cities and Handwritten Text Recognition using Various Deep Learning Models

Daniyar Nurseitov[1,2], Kairat Bostanbekov[1,2], Maksat Kanatov[1,2], Anel Alimova [1,2], Abdelrahman Abdallah[*2,3], Galymzhan Abdimanap [2,3]

[1]*Satbayev University, Almaty, 050010, Kazakhstan*

[2]*National Open Research Laboratory for Information and Space Technologies, Almaty, 050010, Kazakhstan*

[3]*MSc Machine Learning & Data Science , Satbayev University, Almaty, 050010, Kazakhstan*

ARTICLE INFO

Article history:
Received: 18 July, 2020
Accepted: 30 September, 2020
Online: 12 October, 2020

Keywords:
Deep Learning
Convolutional neural networks
Recurrent neural networks
Russian handwriting recognition
Connectionist Temporal Classification

ABSTRACT

This article discusses the problem of handwriting recognition in Kazakh and Russian languages. This area is poorly studied since in the literature there are almost no works in this direction. We have tried to describe various approaches and achievements of recent years in the development of handwritten recognition models in relation to Cyrillic graphics. The first model uses deep convolutional neural networks (CNNs) for feature extraction and a fully connected multilayer perceptron neural network (MLP) for word classification. The second model, called SimpleHTR, uses CNN and recurrent neural network (RNN) layers to extract information from images. We also proposed the Bluechet and Puchserver models to compare the results. Due to the lack of available open datasets in Russian and Kazakh languages, we carried out work to collect data that included handwritten names of countries and cities from 42 different Cyrillic words, written more than 500 times in different handwriting. We also used a handwritten database of Kazakh and Russian languages (HKR). This is a new database of Cyrillic words (not only countries and cities) for the Russian and Kazakh languages, created by the authors of this work.

1 Introduction

This paper is an extension of work originally presented at International Conference on Electronics, Computer and Computation (ICECCO) [1]

Handwriting text recognition (HTR) is the process of changing handwritten characters or phrases into a format that the computer understands. It has an active network of educational researchers studying it for the past few years as advances in this subject help to automate different types of habitual tactics and office work. An example could be a painstaking seek of a scientific document inside heaps of handwritten ancient manuscripts by a historian, which is requires a huge amount of time.

Converting these manuscripts right into a virtual layout using HTR algorithms could permit the historian to find the data within a few seconds. Other examples of ordinary work that need automation will be the tasks associated with signature verification, author recognition, and others. The digitized handwriting text could make contributions to the automation of many corporations' business approaches, simplifying human work. Our nation postal carrier, as an instance, does not have an automated mail processing gadget that recognizes handwritten addresses on an envelope. The operator has to work manually with the data of any incoming correspondence. Automation of this commercial cycle of mail registration might dramatically decrease postal carrier fees on mail shipping.

The key advances in HTR in mail communication are primarily aimed at finding solutions to the problems of recognition of the region of interest in the images, text segmentation, elimination of interference when working with text background noises, such as missing or ambiguous bits, spots on paper, detection of skew.

The whole cycle of recognizing handwritten addresses of a written correspondence using machine learning from start to end will consist of the following steps:

- Letters are put face-up on a conveyor in motion.
- A snapshot is taken at a certain place of the conveyor.
- The machine handles the snapshot and issues addresses to

[*]Corresponding Author: Abdelrahman Abdallh, Satbayev University, Almaty, Kazakhstan & abdoelsayed2016@gmail.com

both the sender and the receiver.

- The address is passed to the sorting and tracking system.

Any supervised machine learning problem requires labeled input data on which to train the model. In our case, it is necessary to train at least two models: one to determine the areas of the image where the text is located, and the other to recognize words. Forms for collecting handwriting samples by keywords were designed and launched. A set of data was formed from scanned images of the front sides of envelopes with handwritten text for training in determining the areas of interest in the image. A model was trained to detect an area of handwritten text on the face of an envelope. The algorithm for segmentation of the detected text block by lines and words was implemented using the construction of histograms.

Offline handwritten address recognition is a special case of Offline Cursive Word Recognition (CWR). The main difference is that the set of words for recognition is limited to words that can occur in addresses. To solve the problem of handwriting recognition, machine learning methods are used, namely, RNN and CNN in HTR (Bluche [2],Puigcerver [3]).

Russian and Kazakh languages are very difficult and challenging when it comes in recognizing text language, where writers can write the character contact together like in Figure 1, so the segmentation of characters can be impossible.

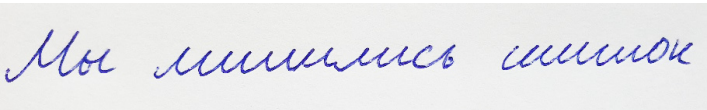


Figure 1: An example of Russian text which difficult to recognize "Мы лишились шишок" ("My lishilis shishok")

This project aims at further study of the challenge of classifying Russian handwritten text and translating handwritten text into digital format. Handwritten text is a very broad concept, and for our purposes we decided to restrict the reach of the project by specifying the meaning of handwritten text. In this project we took on the task of classification of the handwritten word, which could be like a sequence writing. This research will be combined with algorithms segmenting the word images into a given line image, which in turn can be combined with algorithms segmenting line images into a given image of an entire handwritten page. Our research will take the form of the end-to-end user program and will be a fully functional model that serves the user to solve the problem of transformation of a handwritten text to the digital format. The aim of the work is to implement such a recognition handwritten system that will be able to recognize Russian and Kazakh handwriting words written by different writers. We use the HKR database [4] as training, validation and test set. The main contributions covering several key techniques proposed in our system can be highlighted as follows.

1. Pre-processing of the snapshot input (noise elimination, horizontal alignment). An unprocessed snapshot is forwarded as input data at this step. Here the noise is reduced, and the object's angle of rotation is measured along the axis perpendicular to the plane.
2. Segmentation of areas by word within the text. Handwritten words are described at this stage of service, and they are cut into rectangular areas within the text for further recognition.
3. Recognition of Words. After the snapshot segmentation into separate areas of words has been effective, direct word recognition will begin.

In this article we evaluated models using two methods: in the first method the standard performance measures are used for all results presented: the character error rate (CER) and word error rate (WER) [5]. The CER is determined as the deviation from Levenshtein, which is the sum of the character substitution (S), insertion (I) and deletions (D) required to turn one string into the other, divided by the total number of characters in the ground truth word (N). Similarly, the WER is calculated as the sum of the number of term substitutions (Sw), insertion (Iw) and deletions (Dw), which are necessary for transformation of one string into the other, divided by the total number of ground-truth terms (Nw). The second method is calculation of the character accuracy rate(CAR) and word accuracy rate(WAR).

This article considers four main models based on artificial neural networks (ANN). Russian and Kazakh handwriting recognition is implemented using Deep CNN [6], SimpleHTR model [7], Bluche [2], and Puigcerver [3].

The paper is structured as follows: Section 2 describes the related work, Section 3 presents the description of models proposed in the work. Comprehensive results are presented in Section 4, and conclusions in Section 5.

2 Related Work

In offline HTR, the input features are extracted and selected from images, then ANN or HMM are used to predict the probabilities and decode them for the final text. The main disadvantage of HMMs is that they cannot predict long sequences of data. HMMs have been commonly used for offline HTR because they have achieved good results in automatic speech recognition [8, 9]. The basic idea is that handwriting can be perceived as a series of ink signals from left to right that is similar to the sequence of acoustic signals in voice. The inspiration for the hybrid HMM research models came from:

1. offline HTR [10, 11],
2. offline HTR using conventional HMMs [12],
3. automatic speech recognition using hybrid HMM/ANN models [13, 14],
4. and online HTR [15].

On the other hand, RNNs such as gated recurrent unit (GRU) [16] and long short term memory (LSTM) [17] can solve this problem. RNN models have shown remarkable abilities in sequence-to-sequence learning tasks such as speech recognition [18], machine tranlation [19], video summarization [20], automated question answer [21] and others.

To transform a two-dimensional image for offline HTR it is necessary to take the image as a vector and forward it to an encoder and decoder. The task is solved by HTR, GRU and LSTM, which

take information and feature from many directions. These handwriting sequences are fed into RNN networks. Due to the use of Connectionist Temporal Classification (CTC) [22] models, the input feature requires no segmentation. One of the key benefits of the CTC algorithm is that it does not need any segmented labeled data. The CTC algorithm allows us to use data alignment with the output.

A new system called Multilingual Text Recognition Networks (MuLTReNets) was proposed by Zhuo [23]. In particular, the main modules in the MuLTReNets are: the function extractor, script identifier and handwriting recognition. In order to convert the text images into features shared by the document marker and recognizer, the Extractor function method combines spatial and temporal information. The handwriting recognizer adopts LSTM and CTC to perform sequence decoding. The accuracy of script recognition achieves 99.9%.

A new attention-based fully gated convolutional RNN was proposed by Abdallah [24], this model was trained and tested on the HKR dataset [4]. This work shows the effect of the attention mechanism and the gated layer on selecting relative features. Attention is one of the most influential ideas in the Deep Learning community. It can be used in image caption [25], automated question answer [21], and other problems in deep learning achieving good results. Attention mechanism was first used in the context of Neural Machine Translation using Seq2Seq Models. It also achieved the state-of-the-art for offline Kazakh and Russian handwriting dataset [4]. Atten-CNN-BGRU architecture achieves 4.5% CER in the first dataset and 19.2% WER in HKR dataset and 6.4% CER and 24.0% WER in the second test dataset.

A multi-task learning scheme in Tassopoulou [26] research, teaches the model to perform decompositions of the target sequence with target units of varying granularity, from fine to coarse. They consider this approach as a way of using n-gram knowledge in the training cycle, indirectly, while the final recognition is made using only the output of the unigram. Unigram decoding of such a multi-task method demonstrates the capacity of the trained internal representations, placed on the training phase by various n-grams. In this research, pick n-grams as target units and play with granularities of the subword level from unigrams till fourgrams. The proposed model, even evaluated only on the unigram task, outperforms its counterpart single-task by absolute 2.52% WER and 1.02% CER, in a greedy decoding, without any overhead computing during inference, indicating that an implicit language model is successfully implemented.

The Weldegebriel [27] for classification proposes a hybrid model of two super classifiers: the CNN and the Extreme Gradient Boosting (XGBoost). CNN serves as an automatic training feature extractor for raw images for this integrated model, and XGBoost uses the extracted features as an input for recognition and classification. The hybrid model and CNN output error rates are compared to the fully connected layer. In the classification of handwritten test dataset images, 46.30% and 16.12% error rates were achieved, respectively. As a classifier, the XGBoost gave better results than the conventional fully connected layer.

A fully convolutional handwriting model suggested by Petroski [28] utilizes an unknown length handwriting sample and generates an arbitrary symbol stream. Both local and global contexts are used by the dual-stream architecture and need strong pre-processing steps such as symbol alignment correction as well as complex post-processing steps such as link-time classification, dictionary matching, or language models. The model is agnostic to Latin-related languages using over 100 unique symbols and is shown to be very competitive with state-of-the-art dictionary methods based on standard datasets from IAM [29] and RIMES [30]. On IAM, the fine-tuned model achieves 8.71% WER and 4.43% CER and hits 2.22% CER and 5.68% WER on RIMES.

Also, a fully convoluted network architecture proposed by Ptucha [31] that outputs random length symbol streams from the handwritten text. The stage of pre-processing normalizes the input blocks to a canonical representation that negates the need of expensive recurrent symbol alignment. To correct the oblique word fragments a lexicon is developed and a probabilistic character error rate is added. On both lexicon-based and arbitrary handwriting recognition benchmarks, their multi-state convolutional approach is the first to show state-of-the-art performance. The final convolutional method achieves 8.22% WER and 4.70% CER.

Arabic handwritten character recognition based on deep neural network uses CNN models with regularization parameters such as batch normalization to prevent overfitting proposed by Younis [32]. Deep CNN was applied for the AIA9k [33] and AHCD [34] databases, and the accuracy of classification for the two datasets was 94.8% and 97.6%, respectively.

3 Proposed work

In this section four architectures for Handwriting recognition are discussed:

1. Deep CNN models[6].
2. SimpleHTR model[7].
3. Bluche[2].
4. Puigcerver[3].

3.1 Data

In this section, we will describe two types of datasets:

The first dataset contains handwritten cites in Cyrillic words. It contains 21,000 images from various handwriting samples(names of countries and cities). We increased this dataset for training by collecting 207,438 images from available forms or samples.

The second HKR for Handwritten Kazakh & Russian Database [4] consisted of distinct words (or short phrases) written in Russian and Kazakh languages (about 95% of Russian and 5% of Kazakh words/sentences, respectively). Note that both languages are Cyrillic written and share the same 33 characters. Besides these characters, there are 9 additional specific characters in the Kazakh alphabet. Some examples of HKR dataset are shown in Figure 2.

This final dataset was then divided into Training (70%), Validation (15%), and Test (15%) datasets. The test dataset itself was split into two sub-datasets (7.5% each): the first dataset was named

TEST1 and it consisted of words that were not included in the Training and Validation datasets; the other sub-dataset was named TEST2 and consisted of words that were included in the Training dataset but had completely different handwriting styles. The main purpose of splitting the Test dataset into TEST1 and TEST2 datasets was to check the difference in accuracy between recognition of unseen words and words seen in the training stage but with unseen handwriting styles.

3.2 Deep CNN Models

In this experiment, the old approach for classifying images using various deep CNN models was used. To obtain right distribution of records, pre-processing image strategies and data enlargement methods have been used. Three types of models were considered in the experiment: The experiment consists of three options:

1. Simple model of the CNN [35],
2. MobileNet [36],
3. MobileNet with small settings.

Experiment 1 In this experiment, CNN model was used to train and evaluate the dataset, this model includes 2 conventional layers and a softmax layerr [37], which produces probabilities for classification. This model is usually used in character classification like MNIST handwritten digit database [38]. The image data feedforward to the model were (512x61x1). 10% of the dataset was used for evaluate the model.

Experiment 2 and 3 In this section we will describe the MobileNet architecture, which consists of 30 layers. The MobileNet model is shown in Figure 3. For more information, see [36]. This architecture contains 1x1 convolution layer, Batch Normalization, ReLU activation function, average pooling layer and softmax layer, which is used for classification. In Experiment 2 we trained the model for 150 iterations, with Adadelta optimization method [39] where the initial learning step with learning rate (LR) = 1.0 was used.



Figure 2: Some Sample of Dataset

3.3 SimpleHTR model

This experiment in our studies used the SimpleHTR system developed by Harald [7]. The proposed system makes use of an ANN, wherein numerous layers of the CNN are used to extract features from the input photo. Then the output of these layers is feed to RNN. RNN disseminates information through a sequence. The RNN output contains probabilities for each symbol in the sequence. To predict the final text, the decoding algorithms are implemented into the RNN output. CTC functions (Figure 4) are responsible for decoding probabilities into the final text. To improve recognition accuracy, decoding can also use a language model [22].

The CTC is used to gain knowledge; the RNN output is a matrix containing the symbol probabilities for each time step. The CTC decoding algorithm converts those symbolic probabilities into the final text. Then, to improve the accuracy, an algorithm is used that proceeds a word search in the dictionary. However, the time it takes to look for phrases depends on the dimensions of the dictionary, and it cannot decode arbitrary character strings, including numbers.

Type / Stride	Filter Shape	Input Size
Conv / s2	$3 \times 3 \times 3 \times 32$	$224 \times 224 \times 3$
Conv dw / s1	$3 \times 3 \times 32$ dw	$112 \times 112 \times 32$
Conv / s1	$1 \times 1 \times 32 \times 64$	$112 \times 112 \times 32$
Conv dw / s2	$3 \times 3 \times 64$ dw	$112 \times 112 \times 64$
Conv / s1	$1 \times 1 \times 64 \times 128$	$56 \times 56 \times 64$
Conv dw / s1	$3 \times 3 \times 128$ dw	$56 \times 56 \times 128$
Conv / s1	$1 \times 1 \times 128 \times 128$	$56 \times 56 \times 128$
Conv dw / s2	$3 \times 3 \times 128$ dw	$56 \times 56 \times 128$
Conv / s1	$1 \times 1 \times 128 \times 256$	$28 \times 28 \times 128$
Conv dw / s1	$3 \times 3 \times 256$ dw	$28 \times 28 \times 256$
Conv / s1	$1 \times 1 \times 256 \times 256$	$28 \times 28 \times 256$
Conv dw / s2	$3 \times 3 \times 256$ dw	$28 \times 28 \times 256$
Conv / s1	$1 \times 1 \times 256 \times 512$	$14 \times 14 \times 256$
$5\times$ Conv dw / s1	$3 \times 3 \times 512$ dw	$14 \times 14 \times 512$
$5\times$ Conv / s1	$1 \times 1 \times 512 \times 512$	$14 \times 14 \times 512$
Conv dw / s2	$3 \times 3 \times 512$ dw	$14 \times 14 \times 512$
Conv / s1	$1 \times 1 \times 512 \times 1024$	$7 \times 7 \times 512$
Conv dw / s2	$3 \times 3 \times 1024$ dw	$7 \times 7 \times 1024$
Conv / s1	$1 \times 1 \times 1024 \times 1024$	$7 \times 7 \times 1024$
Avg Pool / s1	Pool 7×7	$7 \times 7 \times 1024$
FC / s1	1024×1000	$1 \times 1 \times 1024$
Softmax / s1	Classifier	$1 \times 1 \times 1000$

Figure 3: The MobileNet architecture

Operations CNN: the input images are fed to the CNN layers. These layers are responsible for extracting features. There are 5x5 filters in the first and second layers and 3x3 filters in the last three layers. They also contain non-linear RELU function and max pooling layer that summarizes images and makes them smaller than the input. Although the height of the image is reduced 2-fold in each layer, the feature maps (channels) are added so as to get the output feature map (or sequence) 32 to 256 in size.

RNN: the feature sequence contains 256 signs or symptoms per time step. The relevant information is disseminated by RNN via these series. LSTM is one of the famous RNN algorithms that carries information at long distances and offers more efficient training functionality than typical RNNs. The output RNN sequence is

mapped to a 32x80 matrix.

CTC: receives the output RNN matrix and the predicted text during the neural network learning process, and determines the loss value. CTC receives only the matrix after processing and decodes it into the final text. There should be no more than 32 characters for the length of the main text and the known text.

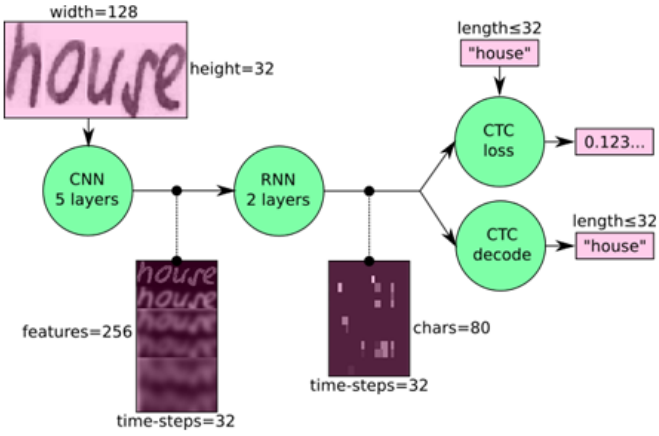


Figure 4: SimpleHTR model, where green icons are operations and pink icons are data streams

Data Input: This is a size 128 to 32 gray file. Images in the dataset usually do not exactly have this size, so their original dimension is changed (without distortion) until they are 128 in width and 32 in height. The image is then copied to a target image of 128 to 32 in white. Then the gray values are standardized, which simplifies the neural network process.

3.4 Bluche model

Bluche model [2] proposes a new neural network structure for modern handwriting recognition as an opportunity to RNNs in multi-dimensional LSTM. The model is totally based on a deep convolutional input image encoder and a bi-directional LSTM decoder predicting sequences of characters. Its goal is to generate standard, multi-lingual and reusable tasks in this paradigm using the convolutional encoder to leverage more records for transfer learning.

The encoder in the Bluche model contains 3x3 Conv layer with 8 features, 2x4 Conv layer with 16 features, a 3x3 gated Conv layer, 3x3 Conv layer with 32 features, 3x3 gated Conv layer, 2x4 Conv layer with 64 features and 3x3 Conv layer with 128 features. The decoder contains 2 bidirectional LSTM layers of 128 units and 128 dense layer between the LSTM layers. Figure 5 shows the Bluche architecture.

3.5 Puigcerver model

Modern approaches of Puigcerver model [3] to offline HTR dramatically depend on multidimensional LSTM networks. Puigcerver model has a high level of recognition rate and a large number of parameters (around 9.6 million). This implies that multidimensional LSTM dependencies, theoretically modelled by multidimensional recurrent layers, might not be sufficient, at least in the lower layers of the system, to achieve high recognition accuracy.

The Puigcerver model has three important parts :

- Convolutional blocks: they include 2-D Conv layer with 3x3 kernal size and 1 horizontal and vertical stride. number of filters is equal to 16n at the n-th layer of Conv.
- Recurrent blocks: Bidirectional 1D-LSTM layers form recurrent blocks, that transfer the input image column-wise from left to right and from right to left. The output of the two directions is concatenated depth-wise.
- Linear layer: the output of recurrent 1D-LSTM blocks are fed to linear layer to predict the output label. Dropout is implemented before the Linear layer to prevent overfitting (also with probability 0.5).

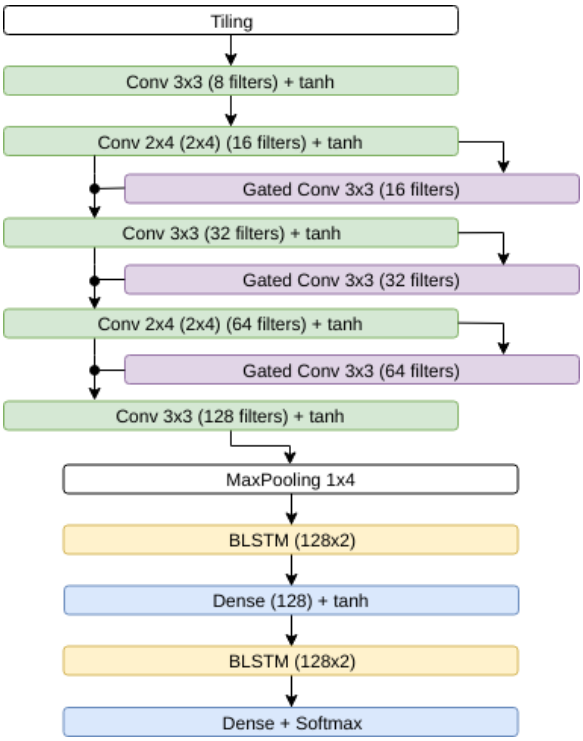


Figure 5: Bluche HTR model

In the new Puigcerver version multidimensional LSTM is used. The difference between regular LSTM networks and multidimensional LSTM is that the former introduce a recurrence alongside the axis of 1-dimensional sequences (as an instance, speaking time-axis or picture writing-direction). In comparison, the latter has a recurrence alongside two axes (generally the x-axis and y-axis in pics). This allows us to use in the latter model unconstrained, two-dimensional information, doubtlessly capturing long-time term dependencies throughout each axis. Figure 6 shows the Puigcerver architecture.

3.6 Experiment Materials

All models have been implemented using the Python and deep learning library called Tensorflow [40]. Tensorflow allows for transparent

use of highly optimized mathematical operations on GPUs through Python. A computational graph is defined in the Python script to define all operations that are necessary for the specific computations.

The plots for the report were generated using the matplotlib library for Python, and the illustrations have been created using Inkscape, which is a vector graphics software similar to Adobe Photoshop. The experiments were run on a machine with 2x "Intel(R) Xeon(R) E-5-2680" CPUs, 4x "NVIDIA Tesla k20x" and 100 GB RAM. The use of a GPU reduced the training time of the models by approximately a factor of 3, however, this speed-up was not closely monitored throughout the project, hence it could have varied.

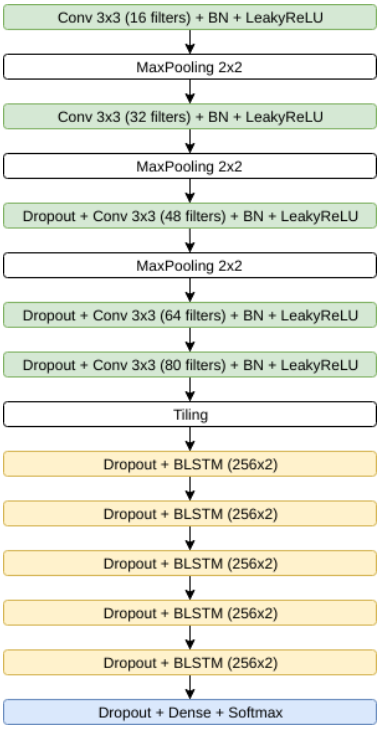


Figure 6: Puigcerver HTR model

4 Results

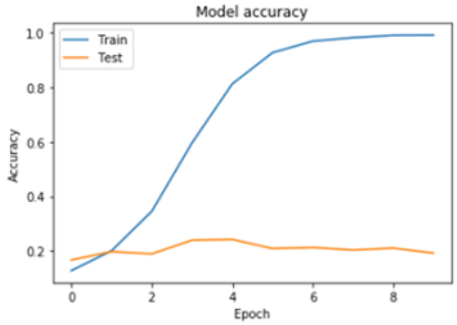
This section will discuss the results of the four models on two different datasets. Deep CNN models were trained and evaluated on the first dataset, SimpleHTR model was trained and evaluated on the two datasets and finally Bluche and Puigcerver were trained and evaluated on the second dataset.

4.1 Deep CNN Result

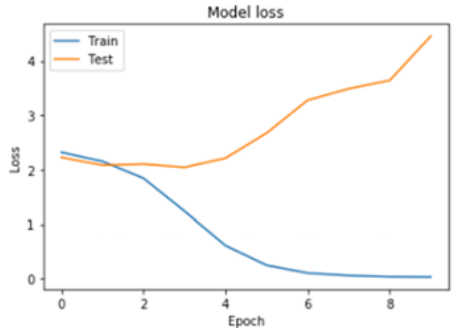
For the current experiments, only ten classes from the first dataset were selected: Kazakhstan, Belarus, Kyrgyzstan, Tajikistan, Uzbekistan, Nur-Sultan, Almaty, Aktau, Aktobe, and Atyrau.

Experiment 1 The simple CNN model result is presented. There were 150 iterations in the learning process, and we showed the effects of 10 iterations in the following (Figure 7): In Figure 7, the model goes into a re-learning state after the first iteration, where the results on the training data improve rapidly and the results on the test data, on the contrary, degrade. This means that the model achieves overfitting on this dataset. For this experiment the minibatch of 32 size and the value of the learning rate (lr = 0.01) was used.

Experiment 2 and 3 Figure 8 shows the results after the 10th iteration of learning, and as we can see, the model only learns correctly after the 3rd iteration.



(a)



(b)

Figure 7: First experiment results: (a) Model accuracy, (b) Model error

The Adadelta optimization method is used and we track the learning behavior, we found that the initial value (lr=1.0) is very large and is not suitable and is to be reduced. Therefore, Experiment 3 was carried out exactly as Experiment 2, the difference is lr=0.01 with minibatch of size 32.The results of Experiment 3 are shown in Figure 9.

The Adadelta optimization method is used and we track the learning behavior, we found the initial value (lr=1.0) is very large and is not suitable and need to reduce it.Therefore, Experiment 3 was carried out exactly as Experiment 2, the difference is lr=0.01 with minibatch of size 32.The results of Experiment 3 are shown in Figure 9. From Figure 9,we can see that the initial iterations have become more correct. However, in the 6th iteration, the model shows a large resonance relative to the entire graph. The reasons for this behavior are still being studied; one of the probable reasons could be small amount of data

The results of the experiments show that the MobileNet Model is better than the simple CNN network because MobileNet is trained on a large dataset for feature extract. This means that the CNN model did not have enough data for training for the feature extract. In order to test this hypothesis, the methods of affinity transformation such as stretching image and other distortions were designed to further increase the data and repeat experiments. After 10 epochs,

the training method had the early stop because of overfitting of the models due to the lack of the dataset used in these experiments.

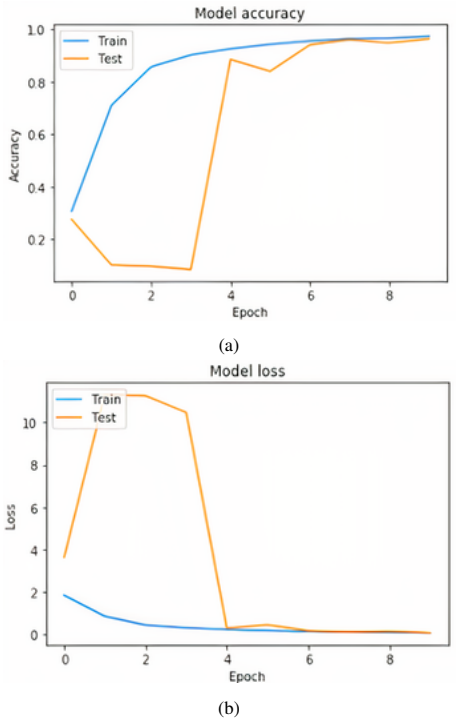


Figure 8: Second experiment results using MobileNet (lr = 1.0): (a) Model accuracy, (b) Model error

4.2 SimpleHTR model

SimpleHTR model is training, validation, and test on two different datasets. In order to launch the model learning process on our own data, the following steps were taken:

- Words dictionary of annotation files has been created
- DataLoader file for reading and pre-possessing the image dataset and reading the annotation file belongs to the images
- The dataset was divided into two subsets: 90% for training and 10% for validation of the trained model.

To improve the accuracy and decrease the error rate we suggest the following steps: firstly, increase the dataset by using data augmentation; secondly, add more CNN layers and increase the input size; thirdly, remove the noise in the image and cursive writing style; fourthly, replace LSTM by bidirectional GRU and finally, use decoder token passing or word beam search decoding to constrain the output to dictionary words.

First Dataset For learning on the collected data, the SimpleHTR model was processed, in which there are 42 names of countries and cities with different handwriting patterns. Such data has been increased by 10 times. Two tests were performed: with cursive word alignment and without alignment. After learning the values on data validation presented in Table 1 were obtained.

This table shows SimpleHTR recognition accuracy for different Decoding Methods (bestpath,beamsearch,wordbeamsearch) The best path decoding only uses the NN output and calculates an estimate by taking the most probable character at each position. The beam search only uses the NN output as well, but it uses more data from it and hence provides a more detailed result. The beam search with character-LM also scores character-sequences that further boost the outcome.

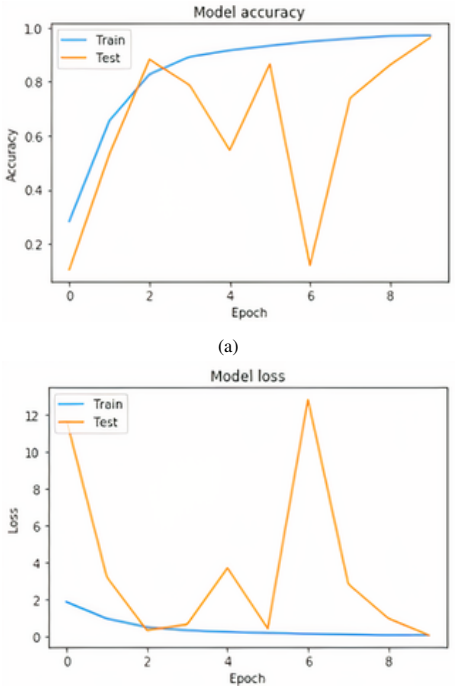


Figure 9: Third experiment results using MobileNet (lr = 0.01): (a) Model accuracy, (b)Model error

Table 1: RECOGNITION ACCURACY OF HANDWRITTEN CITY NAMES WITH VARIOUS DECODING METHODS

Algorithm	alignment of cursive		no alignment	
	CER	WAR	CER	WAR
bestpath	19.13	52.55	17.97	57.11
beamsearch	18.99	53.33	17.73	58.33
wordbeamsearch	16.38	73.55	15.78	75.11

Figure 10 shows an image with the name of the region that was submitted to the entrance, and in Figure 11 we can see the recognized word “South Kazakhstan” (“Yuzhno-Kazakhstanskaya” in Russian) with a probability of 86 percent.

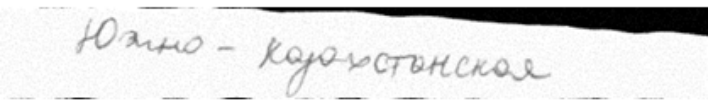


Figure 10: Example of image with phrase ”South-Kazakhstan” in Russian

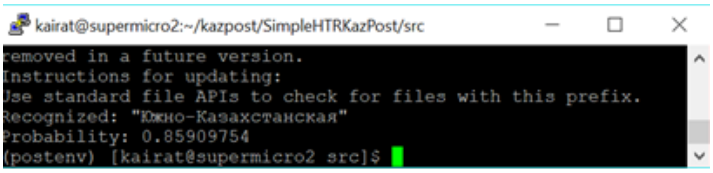


Figure 11: Result of recognition

Second Dataset (HKR Dataset) The SimpleHTR model showed in the first test of the dataset 20.13% Character error rate (CER) and second dataset 1.55% CER. We also evaluated the SimpleHTR model by each Character accuracy rate (Figure 12). Word error rate (WER) was 58.97% for TEST1and 11.09% for TEST2. The result for TEST2 shows that the model can recognize words that exist in the Training dataset but have completely different handwriting styles. The TEST1 dataset shows that the result is not good when the model recognizes the words that do not exist in Training and Validation datasets.

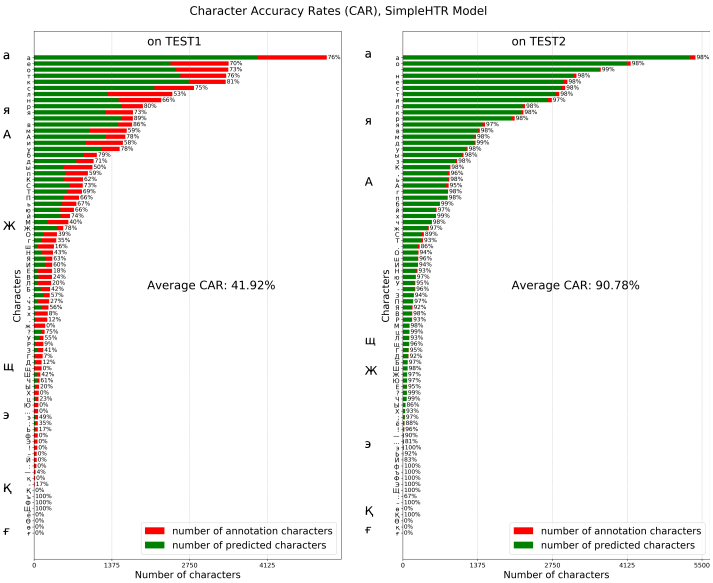


Figure 12: Character Accuracy Rate for SimpleHTR model

4.3 *Bluche and Puigcerver models*

After training, validation, and test datasets were prepared, and models were trained, comparative evaluation experiments were conducted. The Bluche and Puigcerver model were trained on the second dataset (HKR dataset). We evaluated these models by the standard performance measures used for all results presented: CER and WER. For all models the minibatch of 32 size and Early Stopping after 20 epochs without improvement in validation loss value and lr=0.001 were set. For the best use of each model, within the 20 tolerance epochs, ReduceLROnPlateau schedule [41] with a decay factor of 0.2 after 10 epochs without improvement in validation loss value was also used.

Table 2 shows the result of comparison between the two models. We can observe that the Puigcerver has a higher error rate compared with the Bluche because the Puigcerver model has many parameters (9.6M) and overfitting on the dataset.

Table 2: CER, WER for Bluche and Puigcerver

Algorithm	TEST1		TEST2	
	CER	WER	CER	WER
Bluche	16.15%	59.64%	10.15%	37.49%
Puigcerver	73.43%	96.89%	54.75%	82.91%

Figure 13 and 14 present the character accuracy rate which shows how the model detects each character.

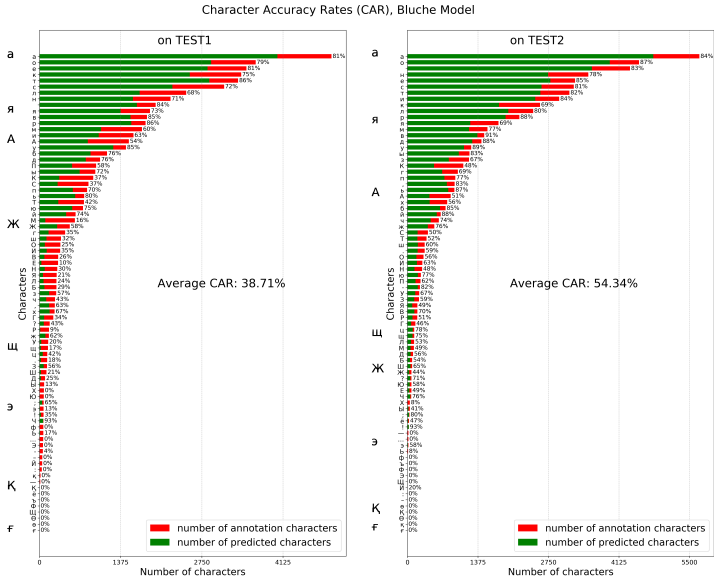


Figure 13: Bluche HTR model performance on TEST1 and TEST2 dataset

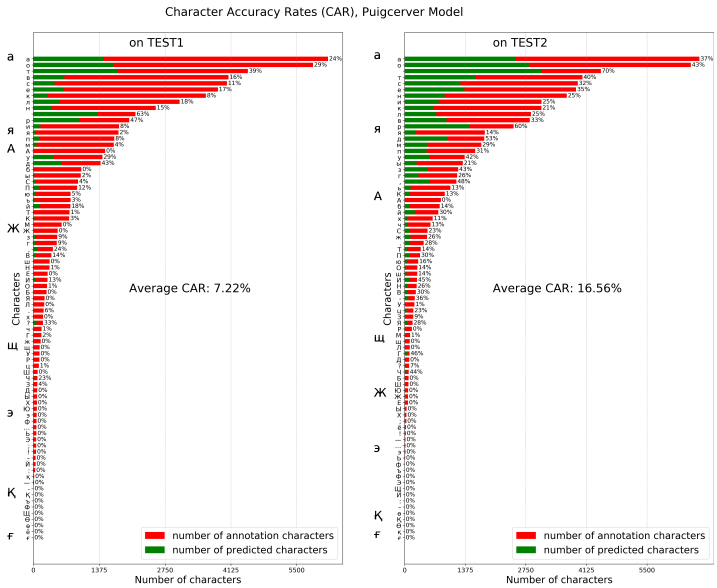


Figure 14: Puigcerver HTR model performance on TEST1 and TEST2 dataset

5 Conclusion

Two interrelated problems are considered in the paper: classification of handwritten names of cities and HTR using various deep learning

models. The first model is used for classification of handwritten cities based on deep CNN and the other three models (SimpleHTR, Bluche, Puigcerver) are used for HTR which contains CNN layers, RNN layers, and the CTC decoding algorithm.

Experiments on classification of handwritten names of cities were conducted using various machine learning methods and the following results for recognition accuracy were obtained on the test data: 1) 55.3% for CNN; 2) 57.1% for SimpleHTR recurrent CNN using best-path decoding algorithms, 58.3% for Beamsearch and 75.1% wordbeamsearch is The best result was shown by for Wordbeamsearch, which uses a dictionary for the final correction of the text under recognition.

Experiments on HTR were also conducted with various deep learning methods and the following results for recognition accuracy were obtained for the two test datasets: 1) Bluche model achieved 16.15% CER and 59.64% WER in the first test dataset and 10.15% CER and 37.49% WER in the second dataset; 2)The Puigcerver HTR model showed 73.43% CER and 96.89% WER in the first test dataset and 54.75% CER and 82.91% WER in the second dataset; 3)The SimpleHTR model showed 20.13% CER and 58.97% WER in the first test dataset and 1.55% CER and 11.09% WER in the second dataset.

Acknowledgment The work was carried out within the framework of the grant project No. AR05135175 with the support of the Ministry of Education and Science of the Republic of Kazakhstan.

References

[1] N. Daniyar, B. Kairat, K. Maksat, A. Anel, "Classification of handwritten names of cities using various deep learning models," in 2019 15th International Conference on Electronics, Computer and Computation (ICECCO), 1–4, IEEE, 2019, doi:10.1109/ICECCO48375.2019.9043266.

[2] T. Bluche, R. Messina, "Gated convolutional recurrent neural networks for multilingual handwriting recognition," in 2017 14th IAPR International Conference on Document Analysis and Recognition (ICDAR), volume 1, 646–651, IEEE, 2017, doi:10.1109/ICDAR.2017.111.

[3] J. Puigcerver, "Are multidimensional recurrent layers really necessary for handwritten text recognition?" in 2017 14th IAPR International Conference on Document Analysis and Recognition (ICDAR), volume 1, 67–72, IEEE, 2017, doi:10.1109/ICDAR.2017.20.

[4] D. Nurseitov, K. Bostanbekov, D. Kurmankhojayev, A. Alimova, A. Abdallah, "HKR For Handwritten Kazakh & Russian Database," arXiv preprint arXiv:2007.03579, 2020.

[5] V. Frinken, H. Bunke, Continuous Handwritten Script Recognition, 391–425, Springer London, London, 2014, doi:10.1007/978-0-85729-859-1_12.

[6] S. Albawi, T. A. Mohammed, S. Al-Zawi, "Understanding of a convolutional neural network," in 2017 International Conference on Engineering and Technology (ICET), 1–6, IEEE, 2017, doi:10.1109/ICEngTechnol.2017.8308186.

[7] H. Scheidl, Handwritten text recognition in historical documents, Master's thesis, Technische Universität Wien, Vienna, 2018, diplom-Ingenieur in Visual Computing.

[8] A. El-Yacoubi, M. Gilloux, R. Sabourin, C. Y. Suen, "An HMM-based approach for off-line unconstrained handwritten word modeling and recognition," IEEE Transactions on Pattern Analysis and Machine Intelligence, **21**(8), 752–760, 1999, doi:10.1109/34.784288.

[9] R. Plamondon, S. N. Srihari, "Online and off-line handwriting recognition: a comprehensive survey," IEEE Transactions on pattern analysis and machine intelligence, **22**(1), 63–84, 2000, doi:10.1109/34.824821.

[10] H. Bunke, "Recognition of cursive Roman handwriting: past, present and future," in Seventh International Conference on Document Analysis and Recognition, 2003. Proceedings., 448–459, IEEE, 2003, doi:10.1109/ICDAR.2003.1227707.

[11] H. Bunke, S. Bengio, A. Vinciarelli, "Offline recognition of unconstrained handwritten texts using HMMs and statistical language models," IEEE transactions on Pattern analysis and Machine intelligence, **26**(6), 709–720, 2004, doi:10.1109/TPAMI.2004.14.

[12] J. Gorbe-Moya, S. E. Boquera, F. Zamora-Martínez, M. J. C. Bleda, "Handwritten Text Normalization by using Local Extrema Classification." PRIS, **8**, 164–172, 2008, doi:10.5220/0001742801640172.

[13] Y. Bengio, "A connectionist approach to speech recognition," in Advances in Pattern Recognition Systems Using Neural Network Technologies, 3–23, World Scientific, 1993, doi:10.1142/9789812797926_0002.

[14] R. Gemello, F. Mana, D. Albesano, "Hybrid HMM/Neural Network basedSpeech Recognition in Loquendo ASR," URL http://www. loquendo. com/en/.[Online], 2010, doi:10.1.1.93.2006.

[15] A. Graves, M. Liwicki, H. Bunke, J. Schmidhuber, S. Fernández, "Unconstrained on-line handwriting recognition with recurrent neural networks," in Advances in neural information processing systems, 577–584, 2008.

[16] J. Chung, Ç. Gülçehre, K. Cho, Y. Bengio, "Empirical Evaluation of Gated Recurrent Neural Networks on Sequence Modeling," CoRR, **abs/1412.3555**, 2014.

[17] S. Hochreiter, J. Schmidhuber, "Long Short-Term Memory," Neural Computation, **9**(8), 1735–1780, 1997, doi:10.1162/neco.1997.9.8.1735.

[18] A. Y. Hannun, C. Case, J. Casper, B. Catanzaro, G. Diamos, E. Elsen, R. Prenger, S. Satheesh, S. Sengupta, A. Coates, A. Y. Ng, "Deep Speech: Scaling up end-to-end speech recognition," CoRR, **abs/1412.5567**, 2014.

[19] I. Sutskever, O. Vinyals, Q. V. Le, "Sequence to Sequence Learning with Neural Networks," CoRR, **abs/1409.3215**, 2014.

[20] N. Srivastava, E. Mansimov, R. Salakhudinov, "Unsupervised learning of video representations using lstms," in International conference on machine learning, 843–852, 2015, doi:10.5555/3045118.3045209.

[21] A. Abdallah, M. Kasem, M. Hamada, S. Sdeek, "Automated Question-Answer Medical Model based on Deep Learning Technology," Proceedings of the 6th International Conference on Engineering & MIS 2020, 2020, doi:10.1145/3410352.3410744.

[22] A. Graves, S. Fernández, F. Gomez, J. Schmidhuber, "Connectionist temporal classification: labelling unsegmented sequence data with recurrent neural networks," in Proceedings of the 23rd international conference on Machine learning, 369–376, 2006, doi:10.1145/1143844.1143891.

[23] Z. Chen, F. Yin, X.-Y. Zhang, Q. Yang, C.-L. Liu, "MuLTReNets: Multilingual Text Recognition Networks for Simultaneous Script Identification and Handwriting Recognition," Pattern Recognition, 107555, 2020, doi:10.1016/j.patcog.2020.107555.

[24] A. Abdallah, M. Hamada, D. Nurseitov, "Attention-based Fully Gated CNN-BGRU for Russian Handwritten Text," arXiv preprint arXiv:2008.05373, 2020.

[25] L. Huang, W. Wang, J. Chen, X.-Y. Wei, "Attention on attention for image captioning," in Proceedings of the IEEE International Conference on Computer Vision, 4634–4643, 2019, doi:10.1109/ICCV.2019.00473.

[26] V. Tassopoulou, G. Retsinas, P. Maragos, "Enhancing Handwritten Text Recognition with N-gram sequence decomposition and Multitask Learning," 2020, doi:10.13140/RG.2.2.29336.83200.

[27] H. T. Weldegebriel, H. Liu, A. U. Haq, E. Bugingo, D. Zhang, "A New Hybrid Convolutional Neural Network and eXtreme Gradient Boosting Classifier for Recognizing Handwritten Ethiopian Characters," IEEE Access, **8**, 17804–17818, 2019, doi:10.1109/ICFHR-2018.2018.00024.

[28] F. P. Such, D. Peri, F. Brockler, H. Paul, R. Ptucha, "Fully convolutional networks for handwriting recognition," in 2018 16th International Conference on Frontiers in Handwriting Recognition (ICFHR), 86–91, IEEE, 2018.

[29] U.-V. Marti, H. Bunke, "The IAM-database: an English sentence database for offline handwriting recognition," International Journal on Document Analysis and Recognition, **5**(1), 39–46, 2002, doi:10.1007/s100320200071.

[30] E. Grosicki, M. Carré, E. Augustin, F. Prêteux, "La campagne d'évaluation RIMES pour la reconnaissance de courriers manuscrits," in Colloque International Francophone sur l'Ecrit et le Document, 2006, doi:10.1016/S0031-3203(97)00137-4.

[31] R. Ptucha, F. P. Such, S. Pillai, F. Brockler, V. Singh, P. Hutkowski, "Intelligent character recognition using fully convolutional neural networks," Pattern recognition, **88**, 604–613, 2019, doi:10.1016/j.patcog.2018.12.017.

[32] K. S. Younis, "Arabic handwritten character recognition based on deep convolutional neural networks," Jordanian Journal of Computers and Information Technology (JJCIT), **3**(3), 186–200, 2017, doi:10.5455/jjcit.71-1498142206.

[33] M. Torki, M. E. Hussein, A. Elsallamy, M. Fayyaz, S. Yaser, "Window-Based Descriptors for Arabic Handwritten Alphabet Recognition: A Comparative Study on a Novel Dataset," CoRR, **abs/1411.3519**, 2014.

[34] A. El-Sawy, M. Loey, H. El-Bakry, "Arabic handwritten characters recognition using convolutional neural network," WSEAS Transactions on Computer Research, **5**, 11–19, 2017, doi:10.1109/IACS.2019.8809122.

[35] Y. Kim, "Convolutional Neural Networks for Sentence Classification," CoRR, **abs/1408.5882**, 2014.

[36] A. G. Howard, M. Zhu, B. Chen, D. Kalenichenko, W. Wang, T. Weyand, M. Andreetto, H. Adam, "MobileNets: Efficient Convolutional Neural Networks for Mobile Vision Applications," CoRR, **abs/1704.04861**, 2017.

[37] R. Memisevic, C. Zach, M. Pollefeys, G. E. Hinton, "Gated Softmax Classification," in J. D. Lafferty, C. K. I. Williams, J. Shawe-Taylor, R. S. Zemel, A. Culotta, editors, Advances in Neural Information Processing Systems 23, 1603–1611, Curran Associates, Inc., 2010.

[38] Y. LeCun, C. Cortes, "MNIST handwritten digit database," 2010.

[39] M. D. Zeiler, "ADADELTA: An Adaptive Learning Rate Method," CoRR, **abs/1212.5701**, 2012.

[40] M. Abadi, A. Agarwal, P. Barham, E. Brevdo, Z. Chen, C. Citro, G. S. Corrado, A. Davis, J. Dean, M. Devin, S. Ghemawat, I. J. Goodfellow, A. Harp, G. Irving, M. Isard, Y. Jia, R. Józefowicz, L. Kaiser, M. Kudlur, J. Levenberg, D. Mané, R. Monga, S. Moore, D. G. Murray, C. Olah, M. Schuster, J. Shlens, B. Steiner, I. Sutskever, K. Talwar, P. A. Tucker, V. Vanhoucke, V. Vasudevan, F. B. Viégas, O. Vinyals, P. Warden, M. Wattenberg, M. Wicke, Y. Yu, X. Zheng, "TensorFlow: Large-Scale Machine Learning on Heterogeneous Distributed Systems," CoRR, **abs/1603.04467**, 2016.

[41] A. Vinciarelli, J. Luettin, "A new normalization technique for cursive handwritten words," Pattern recognition letters, **22**(9), 1043–1050, 2001, doi: 10.1016/S0167-8655(01)00042-3.

ASTES

Advances in Science, Technology and Engineering Systems Journal Vol. 5, No. 5, 944-954 (2020)

www.astesj.com

Special Issue on Multidisciplinary Innovation in Engineering Science & Technology

ASTESJ

ISSN: 2415-6698

Dense SIFT–Flow based Architecture for Recognizing Hand Gestures

Suni S S[*,1] K Gopakumar[2]

[1]*LBS Centre for Science & Technology, University of Kerala, Kerala, 695033, India*

[2]*TKM College of Engineering, Kollam, Kerala, 691005, India*

ARTICLE INFO

Article history:
Received: 04 July, 2020
Accepted: 29 September, 2020
Online: 20 October, 2020

Keywords:
Human-computer interaction
Hand segmentation
Scale Invariant Feature Transform
Support Vector Machine
K-Nearest Neighbour
Hand gesture recognition

ABSTRACT

Several challenges like changes in brightness, dynamic background, occlusion and inconsistency of camera position make the recognition of hand gestures difficult in any vision-based method. Diversity in finger shape, size, distribution and motion dynamics is also a big constraint. This leads to the motivation in developing a dense Scale Invariant Feature Transform (SIFT) flow based architecture for recognizing dynamic hand gestures. Initially, a combination of three frames differencing and skin filtering technique is used for hand detection to reduce the computational complexity followed by a SIFT flow technique to extract the features from the detected hand region. SIFT flow vectors obtained from every pixel can lead to overfilling, data redundancy and dimension disaster. A dual layer belief propagation algorithm is utilized to optimize the feature vectors to resolve the dimensionality problem. Support Vector Machine (SVM) and K-Nearest Neighbors (KNN) classifiers are used to evaluate the performance of the developed framework. Experiments were conducted on hand gesture database for HCI, Sebastien Marcel Dynamic Hand Posture Database and RWTH German finger spelling database. The simulation results demonstrate that the developed architecture has excellent performance on the uneven background and varying camera position and it is robust against image noise. A comparative analysis with the state of the art methods illustrates the effectiveness of the architecture.

1. Introduction

Man's innate, innovative and intentional desire to grab and cope up with the smart devices and interactive systems in the modern era is fathomless. Recent studies show that 80% of the population uses smart decision making systems in one or another way [1]. For example, a person who is doing multiple tasks can change display of computer using a hand movement or gesture, while reading newspaper. Artificial intelligence leaps to the zenith that it becomes an art in presenting artistic perfection and accuracy increasing the percentage of digitalized people resulting restless efforts to propose new algorithms for interacting with machines. Numerous approaches are there to tap and convert gesture movement captured using vision sensors to decision support systems [2,3]. The work of Liu and Zhang was a human computer conversation based on hand gestures from the video streams using Hu invariant moments and support vector machine [2]. A system to recognize the basketball referee signals from videos using image segmentation and support vector machine classifier was build [3].

In human computer interaction systems, the present and widely used trend is dynamic texture based techniques [4,5] and multimodal feature based frameworks [6,7] because of its powerful representation. One of the most broadly used features is local binary pattern (LBP) introduced by Ojala [8] for texture classification, that proved to be useful in computer vision applications. The authors of [4] was developed a dynamic texture based technique for human-computer interaction using volumetric spatiograms of local binary patterns. The approach is congenial to detect static and dynamic gestures with the expense of high dimensional feature vectors. A spatio temporal descriptor called directional local ternary pattern from three orthogonal planes was introduced by the authors of [5] to classify the dynamic scenes and utilized convolutional neural network for detection. However, performance of these systems are found to be affected by external environment such as complex background and image noise and most of the systems perform well only for specific dataset. Human

[*] Corresponding Author: Suni S S, suni.ss@gmail.com

gestures are unique in velocity and motion scale. Another work was to build a multimodal feature based framework that fuses shape and movement information for recognizing facial expressions. The design uses histogram of gradients and optical flow features to obtain the video descriptor [6]. The authors of [7] developed a framework that uses combination of moments and directional wavelet local binary pattern for recognizing human actions. These methods give higher recognition rate at the cost of high dimensionality of feature vectors. The present attempt is to reduce the changes between distinct people performing the same gesture and to exaggerate the coherence of the gestures. Some of the constraints observed in the above mentioned literature are summarized as follows:

- Most feature vectors are calculated on limited number of pixels in an image. So it will not take the micro scale variations of movements (eg: finger movements). This will affect the overall accuracy of the system.
- Suggested methods are not strong enough to avoid image noise.
- High dimensionality of feature vectors leads to increase in computational time.
- Most of the systems perform well only for specific dataset. Robustness is needed.

To solve the above-mentioned drawbacks, a newly refined descriptor, dense SIFT flow that preserves the local appearance features of the image and the temporal variations (movement) of the video can be utilized. Dense SIFT flow algorithm calculates the flow vectors of the SIFT image. The proposed architecture is invariant to rotation, scale, illumination, view point and noise.

The main contributions of this work are,

- An architecture that accounts the spatial and temporal consistency, and can be manage to adapt itself to diverse lighting environments. Moreover, it can improve the system accuracy when connected with gesture identification methods.
- In the pre-processing stage to reduce the computational complexity and dimensionality of feature vector a hand segmentation method is applied.
- A sift flow algorithm that captures features from video frames in terms of spatial coherence and motion. It improves the discriminative power and effectiveness of the feature vector.
- System is tested for three different databases with varying background and viewpoints. The results obtained indicates the robustness of the system.

The rest of the article is framed as follows: Related works in the field of gesture recognition are detailed in Section 2. Theoretical framework of the proposed approach is given in section 3. The classifiers and its detection process is explained in section 4. Simulations, performance evaluations, comparative study of proposed algorithm with other existing methods are illustrated in section 5 followed by conclusion in section 6.

2. Related works

Attention has been focused in describing hand gesture using different feature based approaches, i.e., local and global feature based approaches. Recognition of hand gestures involves segmentation, preprocessing, feature extraction, gesture description and representation & classification.

Mostly, the state of movement of objects in the whole frame is represent as optical flow at a given time. Optical flow enables the foreground object motion study under static background. The methods based on the optical flow [9-11] are mostly used one to find the displacement of an entity in a image sequence. Estimation of optical flow captures local dynamics in the temporal domain and is computatinally efficient. The authors of [9] improved the classical optical flow algorithm by adding median filtering during optimization, that help to preserve better motion details. Dense optical flow algorithm is applied to label data for convolutional neural networks for motion detection in one work [10]. Another work [11] which utilized optical flow to detect moving objects and to estimate depth using triangulation. Optical flow algorithm with Kalman filter is successfully used for tracking multiple objects [12]. The authors of [13] proposed a solution with very low time complexity and accuracy for the estimation of dense optical flow. To detect obstacles at the time of landing of a moving air vehicles, a self-supervised learning (SSL) technique based on optical flow cues was developed [14]. All these approaches, however, do not take into account the characteristic temporal dynamics of all micro variations in movements and are limited to preserve local appearance representations.

A new system is introduced by authors of [15] based on a Single-Shot Multibox Detector (SSD) deep learning algorithm for hand gesture recognition. The system identifies the hand gestures in complex scenes with limited test cases. The authors of [16] build a framework that uses knowledge from multiple modalities by utilizing separate 3D convolutional neural networks (3D-CNNs) for recognizing dynamic hand gestures. The authors of [17] integrated density clustering and image entropy to obtain the key frames to enhance the performance of fast and robust gesture recognition and feature combination technique is also introduced. They also created two datasets named Action3D and Hand Gesture datasets. A dynamic hand gesture recognition system using skeletal representation of hand introduced in [18]. The system used a hand topology technique called later hand skeletal data to capture kinematic descriptors from the gesture frames and were encoded in using a multi-level temporal pyramid and a Fisher kernel. Mahayuddin and Saif [19] has described a method to improve learning process of mathematics using modified extrusion method for recognizing hand gestures which converts 2D shape to 3D shape. The method achieved good accuracy, but robustness of the system has to tested. Handling the large dataset is also a big concern.

The idea of using local appearance based feature like SIFT was introduced by Lowe [20]. SIFT algorithm converts an image into a set of local feature vectors. Each of these feature vectors is is distinctive and invariant to any image translation, rotation or scaling. After introduction of this feature, it has been applied in the different areas of video processing problems like gesture recognition, image registration and image retrieval. Hossein-Nejad and Nasri utilized SIFT features and RANdom SAmple Consensus (RANSAC) transform in image registration for extracting and matching features [21]. SIFT features are applied in gender and gaze recognition problem and produced good results in [22]. One

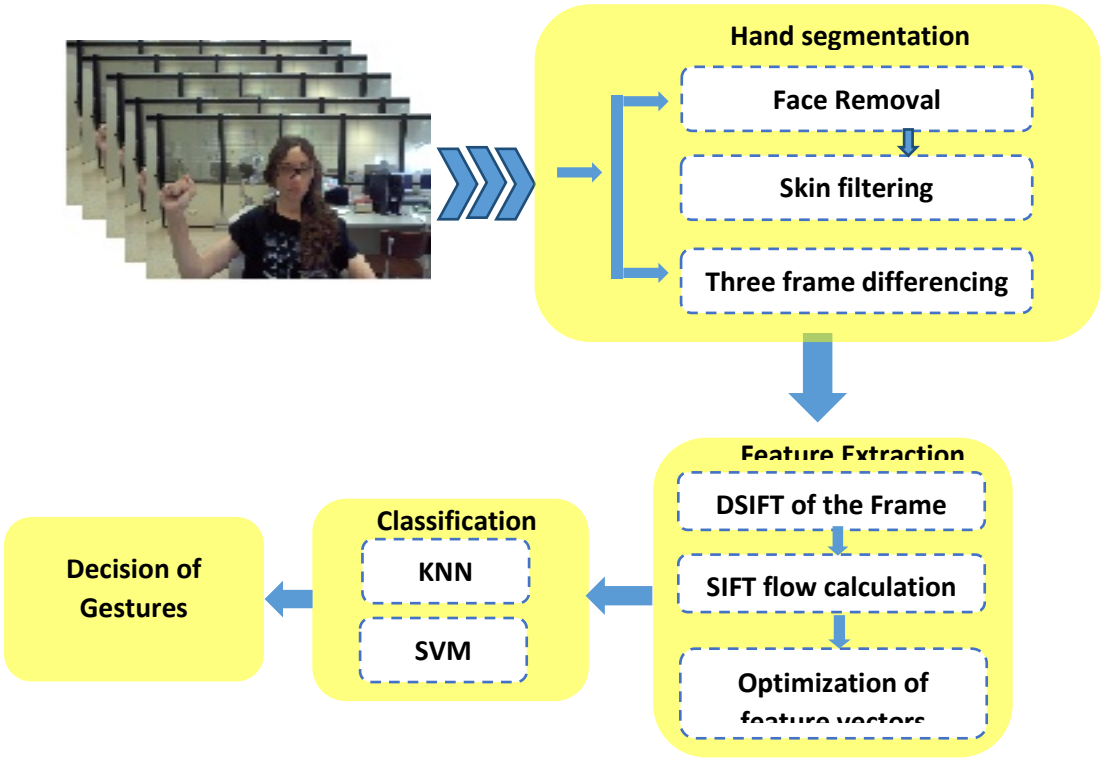


Figure 1: Proposed architecture of hand gesture recognition

disadvantage of using this feature matching method is that they become computationally expensive. Furuya and Ohbuchi [23] introduced the dense sampling of SIFT and a fast encoding algorithm for the application of 3D model retrieval. The dense SIFT algorithm takes the local gradient information of all pixels in an image and has the limitation for capturing motion dynamics of the video. This leads to the motivation in developing a SIFT flow based framework that captures spatial and motion features for detection.

SIFT flow vectors generated are high dimension. Optimization is necessary to reduce the dimensionality of feature vectors. Numerous methods are used for optimizing the SIFT descriptors. Daixian adopt key point location optimization using Chamfer distance [24]. The technique is proved to be reduce computation time and achieves good accuracy. Here the optimization was done before descriptor generation. VSA(Vector Symbolic Architecture) is an encoding technique which converts the high dimensional vectors into the sparse discrete representation [25]. The mapping is one of the key constraints when working on real time data. The double layer belief propagation was proved to be a good optimization technique for SIFT flow vectors [26].

A framework is developed for dynamic hand gesture recognition, wherein multimodal behavior of the image sequences in terms of spatial coherence and motion is extracted. In this application, a descriptor called dense sift flow is utilized which takes flow vectors of the local gradients. Dense SIFT flow refers to taking dense sampling in space of all image sequences. An algorithm is applied that performs gesture analysis to recognize and take decisions to interact with machines. It yields dense sift flow fields that are robust to image noise. Thus, the final video descriptor achieves highly discriminative hand gesture representation. The method is invariant to scale, rotation, illumination, view point and noise. It is observed that the developed architecture gives a better recognition rate.

3. Our Architecture

The prime motivation of the proposed work is to build an efficient framework which can capture shape and motion features from image frames for recognizing hand gestures. There are four phases in the present approach: pre-processing, feature extraction, optimization and detection. In the first stage, the hand is segmented by using three frame differencing and skin filtering [24]. The feature vectors are evaluated using dense SIFT flow algorithm and create a descriptor representation that can express the particular gesture. Classifiers are trained with feature vectors and then assign the new descriptors into various categories of gestures. The proposed architecture of a hand gesture recognition system is shown in Figure 1. The subsections will describe the SIFT flow algorithm and its optimization.

3.1. Hand Segmentation

Hand segmentation is the first step in any hand gesture recognition process. The work flow of hand segmentation process is shown in Figure 2. There are three main processes that combined together to achieve the segmented image. They are hand region tracking, skin filtering, and three frame differencing of both color and grayscale image frames [27].

Initially, the face of the person performing gesture is identified and eliminated from the second image of the video using the Viola–Jones algorithm [28, 29]. Skin filtering operation [30] is performed after removing the face to retrieve only the skin

coloured objects from the image frames. In the meantime, three-frame differencing is carried out with the first three frames of both coloured and grayscale sequences. Morphological operations (AND/OR) are done as shown in Figure 2 to attain the expected results. The desired hand is obtained from the combined results of the three-frame differencing and skin filtering. But, it has been notifying that some small skin coloured objects are also present with the desired hand. Thus, the largest binary linked object is selected and is treated to be the required hand in the scene.

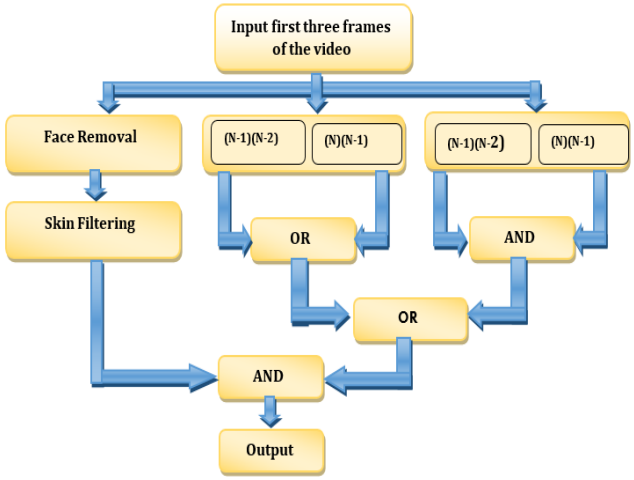


Figure 2: Work flow of Hand segmentation process

Algorithm for Hand Segmentation

Input :*Colour image frame from the video*
Output: *Segmented Hand Image*

1. For n =1 to 3 do
2. I(n) = input colour image frame
3.%%%Colour to gray scale conversion of image
4. I1(n) = rgb I(n) to the grayscale image conversion
5. if n =2 then
6.%%%Face detection of image
7.J = face detection using Viola – Jones algorithm
8.%% Removing face
9.J1 = Remove face J from frame I(n)
10.J2 = Skin filtering of J1 image
11. end if
12. if n =3 then
13.K1 = Skin filtering of (I(n-2) – I(n-1))
14. K2 = Skin filtering of (I(n-1)-I(n))
15.L = OR (K1, K2)
16.M1 = Grey to binary (I(n-2) – I(n-1))
17.M2 = Grey to binary (I(n-1)-I(n))
18.P = AND(M1,M2)
19.Q = OR(P,L)
20.R = AND (Q,J2)
21. %% Biggest binary linked object is selected
22.Seg_image = BBLOB(R)
23.end if
24.end for



Figure 3: Result of hand segmentation algorithm

Figure 3 shows the result of hand segmentation algorithm. The yellow box is the segmented hand region.

3.2. SIFT flow algorithm

3.2.1. Dense SIFT

Object tracking problems are usually solved using visual extraction algorithms. Dense SIFT (Dense scale invariant feature transform) is an innovative step in this field conducive even there is change in the background and appearance of the tracked object during tracking [31]. The process of extraction of dense SIFT is done by taking SIFT histogram for all pixels at a single scale having overlapping patches. A dense sampling assures a good characterization of foreground gestures as well as the consistency of features in the adjacent image frames. The following steps have been used to obtain dense SIFT descriptor. For each pixel of a segmented grey scale image the derivative value ρ and the derivative direction θ can be represented as

$$\rho(x,y) = \sqrt{dx^2 + dy^2}$$
$$\theta(x,y) = \tan^{-1}\frac{x}{y} \quad (1)$$

SIFT descriptor indicates the neighbourhood gradient information. As such, every pixel in an image, select 16 x16 neighbourhood, into 4 x4 cell array. The histogram of derivative direction comprising each block of size 4x4 is obtained and quantizing the orientation into 8 bins. Thus obtaining 4 x4 x 8 = 128 dimensional SIFT description for a pixel. Figure 4 shows the principle of SIFT local feature generation.

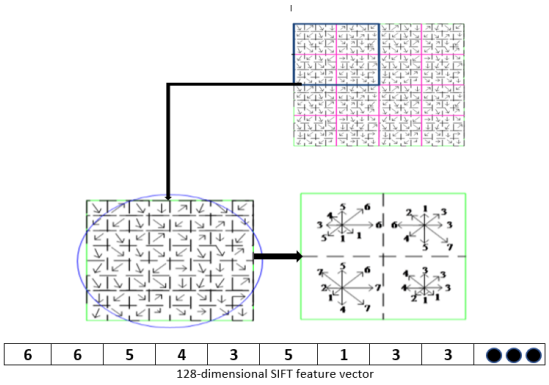


Figure 4: Principle of SIFT feature generation

3.2.2. SIFT flow algorithm

The Dense optical flow [32] opened the avenue of tracking the flow fields very densely from two consecutive SIFT images. SIFT flow is the latest innovative step by authors of [26] and is formulated to adjust an image frame to its nearest neighbor for huge image changes in scale. SIFT flow vector is obtained as follows. Assume $p = (x, y)$ be the grid coordinates of the image frames and $\omega(p) = (v(p), u(p))$ be the flow vector at Where $v(p)$ and $u(p)$ are integers with L possible states. s_1 and s_2 be the two SIFT images and ϵ contains all spatial neighborhoods (4 neighbourhood). The objective energy function of SIFT flow is designed as,

$$E(\omega) = \sum_p \min(\|s_1(p) - s_2(p + \omega(p))\|_1, t) \quad + \tag{3}$$

$$\sum_p \eta(|v(p) + u(p)|) \quad + \tag{4}$$

$$\sum_{(p,q)\in\varepsilon} \min(\alpha|v(p) - v(q)|, d) \quad + \quad \min(\alpha|u(p) - u(q)|, d) \tag{5}$$

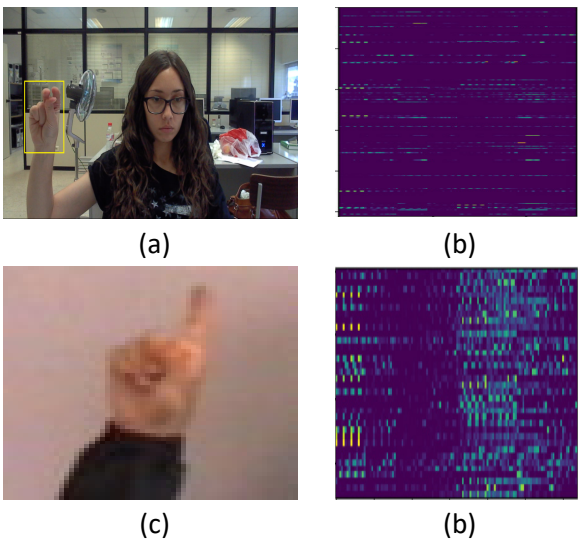


Figure 5: Sample image and its dense SIFT image (a) shows the sample image from hand gesture database for HCI. (b) shows its dense SIFT image. (c) shows sample image from Sebastien Marcel Dynamic Hand Posture Database (d) its dense SIFT image

The data term in (3) is a SIFT descriptor match constraint to be matched via the flow vector $\omega(p)$. The small displacement constraint in (4) allows the flow vector to be as small as possible when no other information is available. The smoothness term inhibits (5) the neighboring pixels to have similar displacement. In this objective energy function, truncated L1 norm is used as a matching threshold in both the smoothness and data term with $d$and t respectively (d=0.1, t=0.01). Figure 5 shows the sample image and its dense SIFT image.

3.2.3. Optimization of feature vector

A dual layer loopy belief propagation method is utilized for optimizing the objective energy function (5) [31]. Figure 6 shows the components in horizontal and vertical direction using dual layer loopy belief propagation. The direct application of SIFT flow vectors to the high dimensional image will result in poor performance. Hence, a coarse to fine SIFT flow matching method is used to formulate the correspondence between two consecutive frames, to accelerate the speed and matching performance.

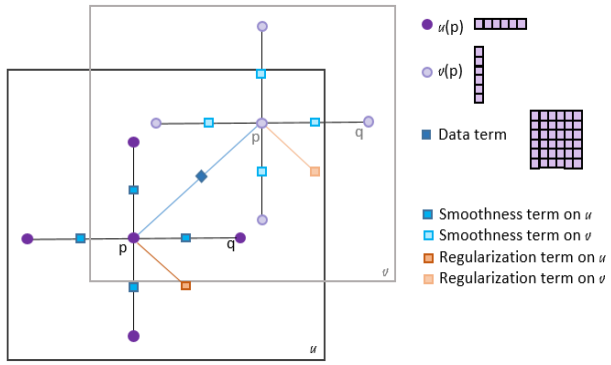


Figure 6: Illustration of Dual-layer belief Propagation [32]. Vertical and horizontal components of objective function

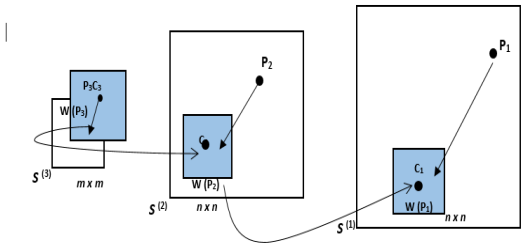


Figure 7: Coarse-to-fine SIFT flow matching process on a pyramid. Blue Square shows the searching window for P_k at pyramid level k.

The foremost aim is to calculate the flow at the coarse level of image patch, constantly resulting and the flow is refined from coarse to fine level [26]. The process is demonstrated in Figure 7. The SIFT images s_1 and s_2 are represented as 's'. A sift pyramid $\{s(k)\}$ is created where $s(1) = s$ and $s(k+1)$ is smoothed and down sampled from $s(k)$. The pyramid level at K, Pk is the coordinate of the pixel to match. Ck is the centroid or offset of the searching window and the right match is $\omega(Pk)$. At the loop pyramid levels $s(2), P3$ is the centroid of the searching window with size mxm. Then the belief propagation converges, at this

level. The system transfers the optimized flow vector $\omega(P3)$ to the next finer level $C2$, where searching window of $P2$ is centered. The process continues from $s(3)$ to $s(1)$ till the flow vector $\omega(P1)$ is obtained. The computational complexity is reduced to a factor of $O(h2logh)$. Thus, the algorithm become very energy efficient by doubling η and retain α and d. Figure 7 shows the process of matching method from coarse to fine SIFT flow.

4. Recognition of hand gestures

4.1. KNN classifier

The SIFT flow vectors generated in the feature extraction stage is used to train the classifiers to assess the performance of the designed system. KNN classifier is selected here, because of its capability of handling large training data. Training was done in the system for two values of k such as 3 and 5. The draw votes in recognition process can be eliminated by selecting odd values of k. 'Leave one group out cross validation' strategy is utilized for testing.

4.2. Support Vector Machine Classifier

The aim of the detector stage is to create a SVM classifier with all data samples of extracted feature vectors. This supervised learning classifier splits the data samples of various categories by calculating a maximum-margin boundary between them. The system is trained using feature vectors of videos from selected database with quadratic, radial, linear and polynomial kernel based SVM classifiers. The classifier was selected because it has been tested successfully in various image classification and object detection tasks. SVM with four kernels is trained with different training videos in hand gesture database. It is seen that radial function based SVM performs better than others. Hence SVM with RBF kernel is used for testing. 'Leave one group out cross-validation' technique is used for testing.

5. Results and Discussion

All test procedures are conducted using Matlab 2014a on a i5 2.7GHz computer with 8.00GB RAM. To analyze the proposed algorithm, we performed the set of experiments with three databases such as hand gesture database for HCI [4,33], Sebastien Marcel Dynamic Hand Posture Database [34] and RMTH German finger spelling database [35]. The performance parameters of the system are analyzed on the basis of certain metrics such as sensitivity, specificity and accuracy [36,37]. The parameters are defined as follows.

$$\text{Sensitivity} = TP/(TP+FN) \quad (6)$$

$$\text{Specificity} = TN/(TN+FP) \quad (7)$$

$$\text{Accuracy} = (TP+TN)/(TP+TN+FP+FN) \quad (8)$$

$$\text{F1 Score} = 2TP/(2TP+FP+FN) \quad (9)$$

$$\text{Negative predictive value} = TN/(TN+FN) \quad (10)$$

where TN, TP, FN, and FP are true negatives, true positives, false negatives and false positives respectively. A comparative analysis has been done with different state of art methods.

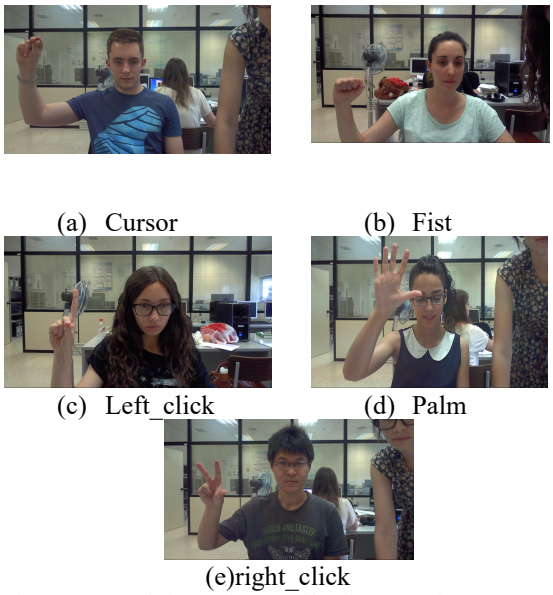
5.1. Performance Analysis

5.1.1. Performance Analysis with Hand gesture Database for HCI

The database contains a group of $1280\,x\,720$ pixel resolution color image frames that are generated for human computer interaction applications using Senz3D sensor [4]. This was generated for testing the mouse functionalities such as left and right click, curser, fist and palm. The samples were captured in realistic way with uneven environment. It composed of two sets of image frames. Five various gestures performed by distinct people are contained in Set 1 and Set 2. For testing, individual videos were created. Samples of hand gesture image frames are shown in Figure 8.

In the first stage, process of hand detection is done and the resolution (width is reduced by a factor of 5 and height is reduced by a factor of 3) of the image frames is reduced. Thus the process will lessen the computational complexity and dimension of the feature vectors and saves the computational time. The feature vectors are generated with the Dense SIFT flow algorithm and are tested with KNN and SVM classifiers.

Evaluation is done using KNN classifier with two values of K=3, K=5. The performance analysis based on recognition rate is provided in the Fig .9. It shows that the highest recognition rate of 87.8% with K = 5 is obtained for the testing video of seq 5 and the average recognition rate is 85.9%.



(a) Cursor (b) Fist

(c) Left_click (d) Palm

(e)right_click

Figure 8: Sample image frames of hand gestures for HCI

The system is tested for using KNN classifier with K =3 and K =5. The performance analysis is provided in Table. 1. The highest training and testing accuracy were achieved for k = 5.

The system is validated using SVM classifier with various kernel functions such as polynomial, linear, radial basis and quadratic in hand gesture database and the performance analysis is shown in Figure 10. The performance level shows SVM classifier with radial basis kernel produces better results than the other kernels and it gives 97.6%.

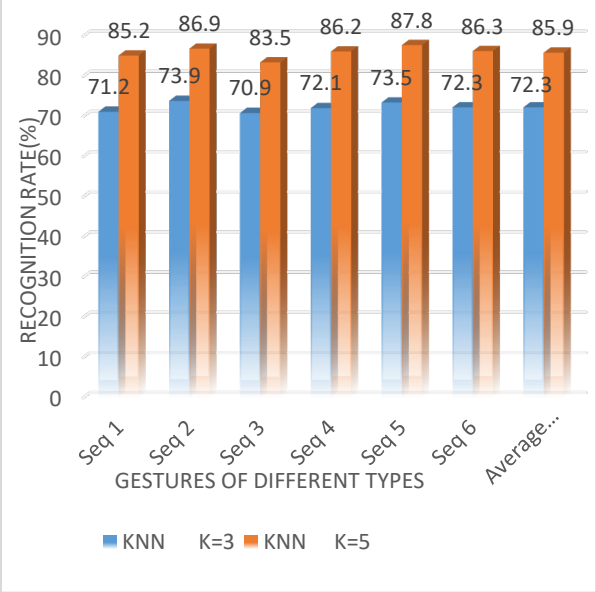


Figure 9: Performance of the system for various hand gestures on hand gesture database using KNN with K=3 and K=5

Table 1: Accuracy of algorithm on hand gesture database using KNN classifier

Expt	K = 3		K = 5	
	Training accuracy	Testing accuracy	Training Accuracy	Testing Accuracy
Subject 1	0.768	0.712	0.873	0.852
Subject 2	0.769	0.739	0.891	0.869
Subject 3	0.748	0.709	0.852	0.835
Subject 4	0.751	0.721	0.878	0.862
Subject 5	0.772	0.735	0.902	0.878
Subject 6	0.758	0.723	0.889	0.863
Mean Accuracy	**0.761**	**0.723**	**0.881**	**0.859**

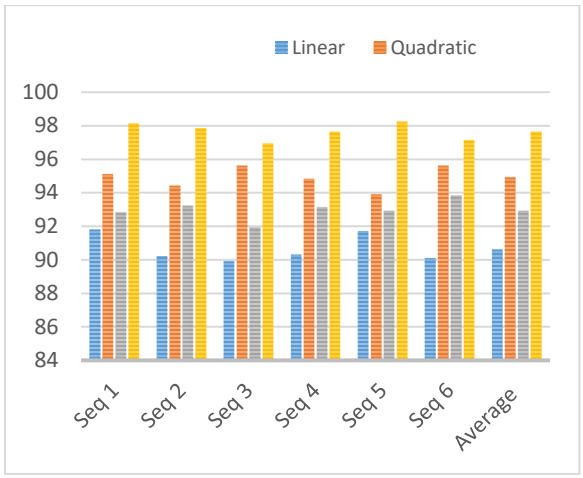


Figure 10: Performance of the system using SVM classifier with different kernels

Group of experiments were done using the multiclass SVM classifier with rbf kernel. Table. 2 shows the evaluation based on accuracy in both training and testing phase. The mean accuracy is obtained as 0.976 which is better as compared with the existing methods.

Table 2: Accuracy of algorithm on hand gesture database using SVM classifier

Gestures	Training accuracy	Testing accuracy
Subject 1	0.998	0.981
Subject 2	0.982	0.978
Subject 3	0.978	0.969
Subject 4	0.989	0.976
Subject 5	0.991	0.982
Subject 6	0.986	0.971
Mean Accuracy	**0.987**	**0.976**

5.1.2. Performance analysis with Sebastien Marcel Dynamic Hand Posture Database

The dynamic hand posture database [34] consists of image frames for four hand gestures such as Rotate, Click, No, and Stop-Grasp-Ok from 10 different persons with various resolution ranges from 50 x 50 pixels to 80 x 80 pixels. Figure 11 shows the Sample image frames.



(a)Clic (b)StopGraspOk (c)No (d)Rotate

Figure 11: Sample frames from Sebastien Marcel Dynamic Hand Posture Database

Table 3 and Table 4 show confusion matrix obtained for the four dynamic hand gestures using KNN classifier with K =3 and K = 5. We observed that the size of hand gestures ranges from 50 × 50 pixels to 80 × 80 pixels, didn't affect the efficiency of the framework in terms of recognition rate and computational time. Some of the frames 'clic' and 'no' hand gestures seem to be same that is why the recognition rate is less for these gestures while using KNN classifier.

Table. 3: Confusion matrix for hand gesture database using KNN with K=3

Gesture	Clic	No	Rotate	StopGraspOk	Recognition Rate(%)
Clic	11	3	0	1	73.3
No	3	10	1	0	71.4
Rotate	1	1	9	2	69.2
StopGraspOk	1	0	3	11	73.3

Table. 4. Confusion matrix for hand gesture database using KNN with K=5

Gesture	Clic	No	Rotate	StopGraspOk	Recognition Rate(%)
Clic	12	3	0	0	80.3
No	2	12	0	0	85.7
Rotate	1	0	11	1	84.6
StopGraspOk	1	0	2	12	80.0

For efficient classification, multi SVM classifier is used and got the recognition rate of 100%. Table. 5 shows performance matrix.

Table. 5: Confusion matrix for hand gesture database using SVM with rbf kernel

Gesture	Clic	No	Rotate	StopGraspOk	Recognition Rate(%)
Clic	15	0	0	0	100
No	0	14	0	0	100
Rotate	0	0	13	0	100
StopGraspOk	0	0	0	15	100

Figure 12 shows the system performance analysis for different types of classifiers based on true positive rate and false positive rate. From the observation, we can say that the SVM classifier with radial basis kernel gives better results. The experiments reveals that the developed framework gives good results for dynamic gestures with different illuminations and resolution levels.

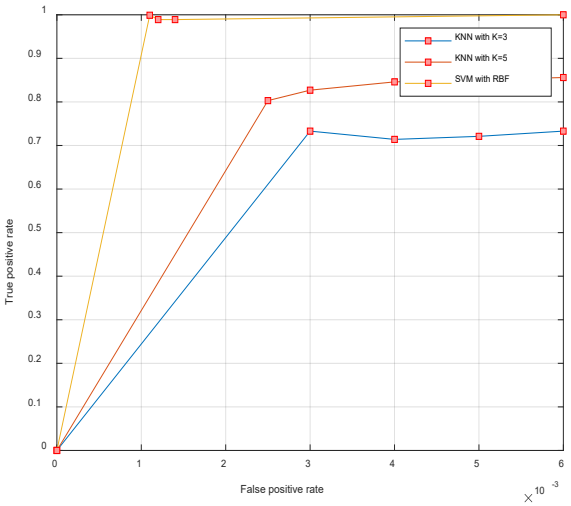


Figure 12: System performance with classifiers

5.1.3. Performance Analysis with RMTH German finger spelling Database

The database [35] consists of gestures of 35 types denoting 1 to 5 numbers, the symbols A to Z, 'SCH and the German umlauts Ä, Ö, Ü. It contains five dynamic gestures captured in uneven environment with varying camera positions. Among 1400 image sequences in the dataset, 700 videos are used for testing. The videos are captured at the rate of 25 frames per second with 320*240 pixels of resolution. The sample image sequences are shown in Figure 13.



Figure 12: Sample frames from RWTH German finger spelling database

The testing and evaluations are performed on five dynamic gestures of RWTH gesture database and confusion matrix obtained is shown in Table 6. The recognition rate achieved is 93% with SVM classifier (rbf kernel). The performance analysis in Figure 13 reveals that the dense SIFT flow-based framework provides better results for gestures from uneven background.

Table 6: Confusion matrix attained for five gestures in RMTH gesture Database

Gesture types	J	Z	Ä	Ö	Ü	Recognition Rate in %
J	18	0	0	2	0	90
Z	0	18	0	0	2	90
Ä	0	1	19	0	0	95
Ö	0	0	1	19	0	95
Ü	0	0	1	0	19	95

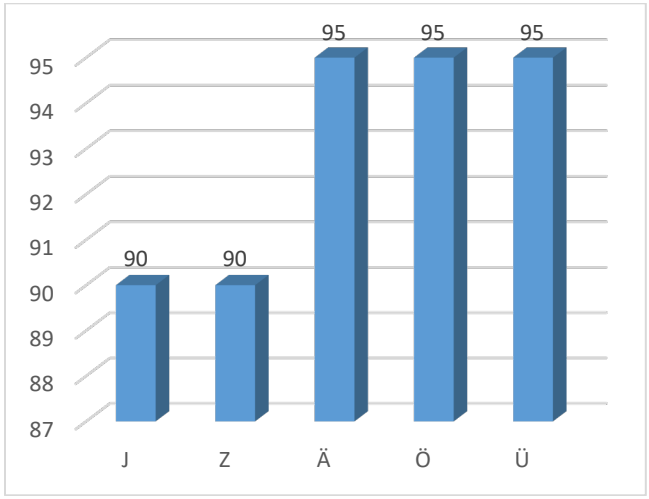


Figure 13: Performance of the system using SVM classifier with rbf kernel

Table 7: Performance Metrics of SVM (rbf) classifier on three different databases

Metric	Hand gesture Database for HCI	Sebastien Marcel Dynamic Hand Posture Database	RMTH German finger spelling Database
Accuracy(%)	97.6	100	93
Sensitivity(%)	97.6	100	93.1
Specificity(%)	98.8	100	94.7
Negative Predictive Value(%)	99.1	100	95.8
F1 Score(%)	97.8	100	92.9
Response time(Sec)	34	28	37

Table 7: Performance comparison of the proposed architecture with the state of the art methods on Hand gesture database

Method	Subject1	Subject2	Subject3	Subject4	Subject5	Subject6	Mean Accuracy
VS-LBP[4]	0.951	0.962	0.939	0.931	0.801	0.959	0.927
LBP+ Moments [7]	0.942	0.918	0.937	0.923	0.851	0.923	0.915
TPM-SLB$_s$P$_{8,1,10,8,1}$ [33]	0.974	0.961	0.976	0.960	0.926	0.975	0.965
TPM-SLBP$_{8,1,10,8,3}$ [33]	0.980	0.957	0.981	0.972	0.924	0.974	0.962
PHOG_TOP+ Optical flow based framework [39]	0.967	0.971	0.942	0.939	0.892	0.962	0.946
Dense SIFT flow based framework	**0.981**	**0.978**	**0.969**	**0.976**	**0.982**	**0.971**	**0.976**

Table 8: Comparative analysis of the proposed method with existing techniques on RMTH German Finger spelling database

Study	Technique	Error rate
Reference [35]	Thresholding with skin color probability+ camshift tracking	35.7%
Reference [38]	features from hand movements and contour shape	27.6%
Reference [39]	PHOG_TOP+ Optical flow based framework	11%
Proposed architecture	Dense SIFT flow	**7%**

From Table. 7, the accuracy of the proposed architecture on the selected datasets come out to be well (97.6% for hand gesture database for HCI, 100% for Sebastien Marcel dynamic hand posture database and 93% for RMTH German finger spelling database). The negative predictive value and specificity records higher values. Higher sensitivity is recorded. Response time of the proposed architecture is very good (< 37). So, the system can work well in real time applications.

5.2. Comparative Analysis

The developed Dense SIFT flow-based framework for hand gesture recognition differs from other methods, in terms of various preprocessing and filtering techniques. Therefore, it is hard to make a quantitative analysis with the state of the art methods. However, we have analyzed performance based on accuracy with existing approaches on the hand gesture database and tabulated on Table 7. **T**he global and local spatial information with temporal data utilizes in volumetric spatiograms of local binary pattern (VS-LBP), achieves the accuracy of 0.927 [4]. The authors of [7] developed an algorithm that fuses directional wavelet Local Binary Pattern (LBP) and moments and obtained the accuracy of 0.914. But it is sensitive to dynamic backgrounds. The Temporal Pyramid Matching of Local Binary Pattern (TPM-LBP) algorithm created by authors of [33] achieved good recognition rate with the expense of computational complexity. In one of recent work [39], hand gesture recognition based on pyramid histogram of gradients (PHOG) and optical flow achieves a recognition rate of 94.6% with the expense of high dimensional feature vectors. From this analysis, we can found that proposed architecture shows considerable improvement in recognition rate and work well in non-uniform background and varying viewpoints.

Table. 8 illustrates the comparative analysis of the proposed architecture with existing techniques on RMTH German finger spelling database based on error rate. The authors of [35] generated a hidden Markov model emission probabilities based on the appearance features to detect the hand gestures and was achieved an error rate of 35.7%. The features from contour shape (orientation, seven hu moments area and perimeter) and motion of hand (angle and velocity of movement) are used to detect hand gestures and achieved a better error rate 27.6% [38]. Another work [39] obtained 11% of error rate by using a multiple feature based framework. The proposed SIFT flow based architecture attained an error rate of 7%. The outcome of the framework is promising in the light of the fact that some of the symbols are very identical in database, for example the gestures for M, N and A.

6. Conclusions

In this paper, we have proposed a novel architecture for hand gesture recognition based on dense SIFT flow. A hand segmentation method is introduced in the pre-processing stage, which utilizes the three frame differencing and skin filtering to reduce the dimensionality of feature vectors. SIFT flow algorithm calculates the displacement between SIFT features of all pixels in

two consecutive sequences in a video. The flow vectors generated are invariant to image rotation and scale, image noise, illumination and camera view point. The KNN classifier and Support vector machine classifier is used for testing effectiveness of features. The present design can further benefit from improvements in SIFT flow estimation and hand segmentation technique. This approach considers the spatial and temporal consistency, and it is capable of accommodating itself to various illuminations. The evaluation results showed that the presented architecture can achieve high accuracies even for non-even background and image noise. As a result of comparison, we determined that our architecture has better recognition accuracy (0.976 for hand gesture database for HCI) than the state of the art methods.

However, a few aspects remain untapped, which may lead to further investigation. Even though our framework provides good results in various levels, it is computationally a little bit expensive. Hence developing faster and more accurate framework will certainly receive more attention in the future. In hand segmentation stage, adding a good key frame extraction technique may well significantly improve both speed and accuracy. And this problem is definitely worth further enhancement.

Conflict of Interest

The authors declare that there are no conflicts of interest regarding the publication of this paper.

References

[1] T.H. Davenport, "From analytics to artificial intelligence", Journal of Business Analytics, **1**(2), 73 -80, 2018. https://doi.org/10.1080/2573234X.2018.1543535

[2] Y. Liu, P. Zhang, "Vision-Based Human-Computer System Using Hand Gestures", Proceedings of International Conference on Computational Intelligence and Security, Beijing, China, 2009.

[3] J. Zemgulys, V. Raudonis, Rytis Maskeliūnas and Robertas Damaševičius, "Recognition of basketball referee signals from videos using Histogram of Oriented Gradients (HOG) and Support Vector Machine (SVM)" Procedia Computer Science **130**, 953–960, 2018.

[4] I. Ana, R Carlos "Human-computer interaction based on visual hand- gesture recognition using volumetric spatiograms of local binary patterns", Computer Vision and Image Understanding, Special Issue on Posture & Gesture, **141**, 126-137, 2015.

[5] M. Azher Uddin, Mostafijur Rahman Akhond and Young-Koo Lee, "Dynamic Scene Recognition Using Spatiotemporal Based DLTP on Spark", IEEE Access, 6, 66123 – 66133, 2018.

[6] X. Fan and T. Tjahjadi, "A spatial – temporal framework based on histogram of gradients and optical flow for facial expression recognition in video sequences", Pattern Recognition, **48**(11), 3405-3416, 2015. https://doi.org/10.1016/j.patcog.2015.04.025

[7] M.N. AI-Berry, A.M. Mohammed "Fusing directional wavelet local binary pattern and moments for human action recognition", IET ComputerVision, **10**(2), 1-10, 2015.

[8] T. Ojala, M. Pietikainen and Topi Maenpaa, "Multiresolution Gray Scale and Rotation Invariant Texture Classification with Local Binary Patterns", IEEE Transactions on Pattern Analysis & Machine Intelligence, **24**(7), 971-987, 2002.

[9] D. Sun, Roth, S. and Black, M.J., "A quantitative analysis of current practices in optical flow estimation and the principles behind them", International Journal of Computer Vision, **106**(2), 115–137, 2014.

[10] J. Walker, "Dense optical flow prediction from a static image", Proceedings of IEEE International Conference on Computer Vision (ICCV), 2443–2451, 2015.

[11] S.-Lara, L., Sun, D., Jampani, V. and Black, M.J., "Optical flow with semantic segmentation and localized layers", Proceedings of IEEE Conference on Computer Vision and Pattern Recognition (CVPR), 3889–3898, 2016.

[12] S. Shantaiya, "Multiple object tracking using Kalman filter and optical flow", European Journal of Advances in Engineering and Technology, **2**(2), 34–39, 2015.

[13] T. Kroeger et al., "Fast optical flow using dense inverse search", Proceedings of European Conference on Computer Vision, 471–488, 2016.

[14] H.W. Ho et al., "Optical-flow based self-supervised learning of obstacle appearance applied to MAV landing", Robotics and Autonomous Systems, **100**, 78–94, 2018.

[15] P. Liu, Xiangxiang Li, Haiting Cui, Shanshan Li and Yafei Yuan, "Hand Gesture Recognition Based on Single-Shot Multibox Detector Deep Learning", Mobile Information Systems, Article ID 3410348, 2019.

[16] M. Abavisani, Hamid Reza Vaezi Joze and Vishal M. Patel, "Improving the Performance of Unimodal Dynamic Hand-Gesture Recognition with Multimodal Training", Proceedings of the IEEE/CVF Conference on Computer Vision and Pattern Recognition (CVPR), 1165-1174,2019.

[17] H. Tang et al., "Fast and Robust Dynamic Hand Gesture Recognition via Key Frames Extraction and Feature Fusion", Neurocomputing, **331**, 424-433, 2019.

[18] Q.D. Smedta et al., "Heterogeneous hand gesture recognition using 3D dynamic skeletal data", Computer Vision and Image Understanding, **181**, 60-72, 2019.

[19] Z. Rasyid et al., "Efficient Hand Gesture Recognition Using Modified Extrusion Method based on Augmented Reality", Test Engineering and Management **83**(5-6), 4020-4027, 2020.

[20] D. G. Lowe, "Distinctive image feautres from scale-invariant keypoints," Int. J. Comput. Vis., **60**(2), 91–110, 2004.

[21] Z. Hossein-Nejad and Mehdi Nasri, "An adaptive image registration method based on SIFT features and RANSAC transform", Computers & Electrical Engineering, **62**(C), 524-537, 2017. https://doi.org/10.1016/j.compeleceng.2016.11.034

[22] W. Zhang et al., "Gender and gaze gesture recognition for human-computer interaction", Computer Vision and Image Understanding, **149**(C), 32-50, 2016. https://doi.org/10.1016/j.cviu.2016.03.014

[23] T. Furuya and R. Ohbuchi, "Dense sampling and fast encoding for 3D model retrieval using bag-of-visual features", Proceedings of the ACM International Conference on Image and Video Retrieval, Article 26., 2009.

[24] Z. Daixian, "SIFT algorithm analysis and optimization," 2010 International Conference on Image Analysis and Signal Processing, Zhejiang, 2010, 415-419, doi: 10.1109/IAS2010.5476084.

[25] D. Simon, " A New Building Material for Artificial General Intelligence", Proceedings of the 2008 conference on Artificial General Intelligence , 414–418, 2008.

[26] C. Liu et al., " SIFT Flow: Dense Correspondence across Scenes and Its Applications", IEEE Transactions on Pattern Analysis and Machine Intelligence, **33**(5), 978 – 994, 2011. DOI: 10.1109/TPAMI.2010.147

[27] J. Singha, Amarjit Roy and Rabul Hussain Laskar, "Dynamic hand gesture recognition using vision-based approach for human–computer interaction", Neural Comput & Applic, **29**, 1129–1141 ,2018.

[28] P. Viola, "Rapid object detection using a boosted cascade of simple features", Proceedings of the IEEE conference on computer vision and pattern recognition, **1**, 511–518, 2001.

[29] P. Viola "Robust real-time face detection", International Journal of Computer Vision, **57**(2), 137 -154, 2004.

[30] D. Chai "Face segmentation using skin-color map in videophone applications", IEEE Trans Circuits and Systems for Video Technology, **9**(2), 551–564, 1999. DOI: 10.1109/76.767122

[31] Y. Liu, "Multi-focus image fusion with dense SIFT", Information Fusion, **23**, 139 -155, 2015.

[32] H. Wang, "Dense Trajectories and Motion Boundary Descriptors for Action Recognition", International Journal of Computer Vision, **103**(1), 60–79, 2013.

[33] I. Ana et al., "Temporal Pyramid Matching of Local Binary Subpatterns for Hand-Gesture Recognition", IEEE Signal Processing Letters, .**23**(8), 1037 -1041, 2016. DOI: 10.1109/LSP.2016.2579664

[34] S. Marcel, O. Bernier, J-E. Viallet and D.Collobert, "Hand gesture recognition using Input/Output Hidden Markov Models", Proceedings of 4th International Conference on Automatic Face and Gesture Recognition (AFGR), 2000.

[35] A. Ahmed et al., "Modeling and Simulation of Office Desk Illumination Using ZEMAX," in 2019 International Conference on Electrical, Communication, and Computer Engineering (ICECCE), 1–6, 2019. DOI: 10.1109/ICECCE47252.2019.8940756

[36] P. Baldi et al., "Assessing the accuracy of prediction algorithms for classification: an overview", Bioinformatics Review, **5**(5), 412-424,2000.
[37] T. Raghuveera, R Deepthi, R Mangalashri and R Akshaya. A depth-based Indian Sign Language recognition using Microsoft Kinect. Sadhana; 2020:45:34.
[38] M.S. Abdalla, "Dynamic Hand Gesture Recognition of Arabic Sign Language using Hand Motion Trajectory Features", Global Journals Inc. (USA), 13, 2013.
[39] S. S. Suni and K. Gopakumar, "Fusing Multimodal features for Recognizing Hand Gestures," 2019 Second International Conference on Advanced Computational and Communication Paradigms (ICACCP), 1-6, 2019. doi: 10.1109/ICACC2019.8882910.

ASTES

Advances in Science, Technology and Engineering Systems Journal Vol. 5, No. 5, 955-959 (2020)

www.astesj.com

Special Issue on Multidisciplinary Innovation in Engineering Science & Technology

ASTESJ

ISSN: 2415-6698

Scattering of H-Wave by a Moving Dispersive Conducting Complex Object

Esmail Mohamed Abuhdima*, Gurcan Comert, Ahmed El Qaouaq, Ashleigh Nicole Reeves

Computer Science, Physics and Engineering, Benedict College, Columbia, SC 29204, USA

ARTICLE INFO

Article history:
Received: 04 July, 2020
Accepted: 29 September, 2020
Online: 20 October, 2020

Keywords:
Moving conducting cylinder
Scattered phase and magnitude
Dispersive conducting cylinder

ABSTRACT

The effect of the moving dispersive conducting complex scatterer on the scattering of incident H-wave is investigated herein. In this research, a simulation shows how the scattered phase and magnitude of a moving (rotating and translating) circular cylinder with higher conductivity, made of dispersive material, is affected in the case of incident H-wave (TE-mode) polarization. The Franklin transformation is applied to study the scattering of incident wave by a rotating dispersive higher conductivity cylinder, and then the effect of translating dispersive higher conductivity cylinder is investigated by applying the Lorentz transformation. This effect is studied at different speed of rotation. Also, this work shows that the pattern of scattered phase and magnitude are changed in terms of incident frequency. Moreover, a created model is used to demonstrate the impact of moving dispersive higher conductivity cylinder using backscattered static data which is generated using a comprehensive computational electromagnetics software (FEKO). The comparison between patterns of scattering of incident H-wave by a moving dispersive and non-dispersive higher conductivity cylinder is considered to show clear behavior of scattering patterns, in terms of the material of scatterer.

1. Introduction

The research is an expansion of the previous study published in 2019 IEEE International Conference on Wireless for Space and Extreme Environments (WiSEE) [1]. In previous work, the scattering of incident E-wave and H-wave by a rotating dispersive higher conductivity cylinder was investigated. The simulation result of this previous work shows a periodic pulse during rotation of dispersive conducting cylinder. It is found that the duration of these pulses is directly proportional to the speed of rotating dispersive higher conductivity cylinder, but inversely proportional to radius of dispersive higher conductivity cylinder. The difference between backscattered field of stationary case and backscattered field of rotating case is clear explicit in the incident H-wave polarization. For this reason, the incident H-wave is considered herein to study the effect of moving (rotating and translating) higher conductivity cylinder on the characteristic of the backscattered field. First of all, the Lorentz conversion is applied to figure out the effect of dispersive translating dispersive higher conductivity cylinder on the characteristics of the backscattered field. Secondly, Franklin conversion and Lorentz conversion are applied to study the characteristics of the backscattered phase and magnitude of moving dispersive conducting cylinder. Moreover, a created model is used to demonstrate the movement (rotation and translation) of dispersive higher conductivity cylinder using backscattered static data that is generated using FEKO. This data inserts into proposed model to demonstrate rotation and translation.

2. Scattered phase and magnitude

The effect of translation and rotation of a dispersive higher conductivity cylinder on scattered field (phase and magnitude) is investigated. The mathematical expression of scattered phase and magnitude is found by applying Lorentz and Franklin conversion [2]. Figure 1 shows the block diagram of the research problem.

It is assumed that a rotating dispersive higher conductivity cylinder is translated in the x-direction. Also, the incident wave propagates in the x-direction. Since, the magnetic field is in z-direction, so the electric filed is in y-direction by applying Maxwell's equations. Also, the direction of rotation is in the φ direction.

*Corresponding Author: Esmail Mohamed Abuhdima, Faculty of Computer Science, Physics and Engineering, Benedict College, Columbia, SC, USA. Email: esmail.abuhdima@benedict.edu

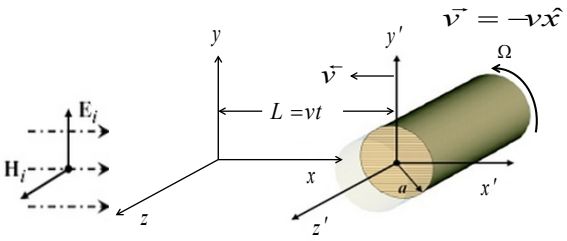


Figure 1: H-wave of moving dispersive conducting cylinder inrotatranslation

2.1. The effect of translating dispersive conducting cylinder

In this part, Lorentz conversion is applied to discuss the scattering of incident H-wave by a translating dispersive higher conductivity cylinder. The incident H-wave is defined as [3]

$$H_z^i = e^{j(\omega t - kx)} \tag{1}$$

where ω is the angular frequency and k called wavenumber. The electrical field is computed by

$$\bar{E}^i = \frac{1}{j\omega\varepsilon_o}\nabla\times\bar{H}^i = \hat{y}\frac{jk}{j\omega\varepsilon_o}\left[e^{j(\omega t-kx)}\right] = \hat{y}z_c e^{j(\omega t-kx)}, \tag{2}$$

where $z_c = \sqrt{\frac{\mu_o}{\varepsilon_o}}$ .These fields, which are defined by (1) and (2), are in laboratory frame. The Lorentz conversion is applied to compute fields in the co-moving frame using [4]

$$\bar{H}'_{\perp} = \gamma\left(\bar{H}_{\perp} - \bar{v}\times\bar{D}\right), \tag{3}$$

Where $\gamma = \left[1-\left(\frac{v}{c}\right)^2\right]^{-1/2}$, D is an electrical flux density, and v is a speed of translation.

The expression of scattered magnetic field in co-moving frame can write as [5]

$$\bar{H}_z^{sc\prime} = e^{j\omega' t'}\sum_{-\infty}^{+\infty} C_n H_n^{(2)}\left(k'r'\right)e^{jn\phi'} \tag{4}$$

where C_n is the unknown scattered coefficient. The unknown amplitude coefficient can be found by applying the boundary condition as $C_n = -\gamma\left[1+\frac{v}{c}\right]j^{-n}\frac{J'_n(k'a)}{H'^{(2)}_n(k'a)}$ [5].

The expression of magnetic field in the laboratory frame is computed using [6]

$$\bar{H}^{sc} = \gamma\left(\bar{H}_{\perp} + \bar{v}\times\bar{D}\right) \tag{5}$$

The backscattered magnetic field is given by

$$\bar{H}_z^{sc} = -\frac{e^{-jkr\left(1+2\frac{v}{c}\right)}}{\sqrt{r}}\sqrt{\frac{2j}{\pi k'}}\left(1+2\frac{v}{c}\right)e^{j\omega t\left(1+2\frac{v}{c}\right)}\sum_{-\infty}^{+\infty}\frac{J'_n\left(ka\left(1+2\frac{v}{c}\right)\right)}{H'^{(2)}_n\left(ka\left(1+2\frac{v}{c}\right)\right)}e^{jn\pi} \tag{6}$$

Equation (6) defined the backscattered magnetic field by translating very good dispersive conducting circular cylinder. It is seen that when $v = 0$ (stationary case), (6) leads to (11-115) that generated by Balanis [7], in the case of scattering of incident H-wave by a stationary perfect conducting cylinder.

2.2. Effect of movement

The scattering of incident H-wave by a rotating dispersive higher conductivity cylinder is investigated by taking the Franklin conversion. The expression of the magnetic field is written as [3]

$$H_z^i = e^{-jkx} = \sum_{-\infty}^{+\infty} j^{-n}J_n(kr)e^{jn\varphi}. \tag{7}$$

Fields inside the dispersive conducting cylinder is computed using Maxwell's equations as following [9],

$$H_Z = \sum_{-\infty}^{+\infty} A_{hn}J_n\left(\gamma_n r\right)e^{jn\varphi}, \tag{8}$$

where A_{hn} is the unknown transmission coefficient. The expression of scattered magnetic field can define as [9]

$$H_z^{sc} = \sum_{-\infty}^{+\infty} B_{hn}H_n^{(2)}\left(kr\right)e^{jn\varphi}, \tag{9}$$

where B_{hn} is the unknown scattering constant. This unknown scattering coefficient is found using the boundary conditions on the surface of the dispersive conducting cylinder [10] and [11]. These coefficients are defined by

$$B_{hn} = \frac{j^{-n}\left[kJ'_n(ka)J_n(\gamma_n a)\left(\alpha^2\dot{o}_r(\omega)+n\frac{\Omega\dot{o}_r(\omega)}{\omega}\right)-c\gamma_n J_n(ka)J'_n(\gamma_n a)\left(1+n\frac{\Omega}{\omega c\dot{o}_o}\right)\right]}{c\gamma_n J'_n(\gamma_n a)H_n^{(2)}(Ka)\left(1+n\frac{\Omega}{\omega c\dot{o}_o}\right)-kJ_n(\gamma_n a)H'^{(2)}_n(ka)\left(\alpha^2\dot{o}_r(\omega)+n\frac{\Omega\dot{o}_r(\omega)}{\omega}\right)} \tag{10}$$

$$A_{hn} = \frac{j^{-n}\left[J_n(ka)H'^{(2)}_n(ka)\left(\left(1+n\frac{\Omega}{\omega c\dot{o}_o}\right)\right)-J'_n(ka)H_n^{(2)}(Ka)\left(1+n\frac{\Omega}{\omega c\dot{o}_o}\right)\right]}{H'^{(2)}_n(ka)-J'_n(\gamma_n a)H_n^{(2)}(Ka)\left(1+n\frac{\Omega}{\omega c\dot{o}_o}\right)\left(\frac{c\gamma_n}{k\alpha^2\dot{o}_r(\omega)}\right)} \tag{11}$$

where $\gamma'^2_n = k'^2N^2\left(1-jq\right)+\frac{n\omega'\Omega}{2c^2}\left(N^2-1-j\frac{N^2q}{2}\right)$. The scattering of incident H-wave by a rotating dispersive higher conductivity cylinder is computed using (9). An approximation to Lorentz transformation $\omega' = \omega\left(\frac{c+v}{c-v}\right)\square\ \omega\left(1+2\frac{v}{c}\right)$ and $k' = k\left(\frac{c+v}{c-v}\right)\square\ k\left(1+2\frac{v}{c}\right)$ is substituted into (9) to find the

mathematical model of the effect of movement of dispersive higher conductivity cylinder on the backscattered field. The formula of a backscattered field is given by

$$H_z^{sc} = \sum_{-\infty}^{+\infty} B_{mn} H_n^{(2)}(kr) e^{jn\varphi}, \qquad (12)$$

where B_{mn} is the unknown moving scattering constant. It is written as

$$B_{mn} = \frac{j^{-n}\left[kJ_n'(k'a)J_n(\gamma_n'a)\left(\alpha^2\dot{o}_r'(\omega')+n\frac{\Omega\dot{o}_r'(\omega')}{\omega}\right)-c\gamma_n'J_n(k'a)J_n'(\gamma_n'a)\left(1+n'\frac{\Omega}{\omega' c\dot{o}_o}\right)\right]}{c\gamma_n'J_n'(\gamma_n'a)H_n^{(2)}(K'a)\left(1+n'\frac{\Omega}{\omega' c\dot{o}_o}\right)-k'J_n(\gamma_n'a)H_n^{(2)}(k'a)\left(\alpha^2\dot{o}_r'(\omega')+n'\frac{\Omega\dot{o}_r'(\omega')}{\omega'}\right)},$$

where $\varepsilon_r'(\omega') = 1-\frac{\omega' p^2}{\omega'^2 + j\omega'\Gamma}$, $n'(\omega')^2 = 1+j\frac{\sigma(\omega')}{\omega'\varepsilon_o}$, $\sigma'(\omega') = \varepsilon_o \frac{\omega' p^2}{-j\omega'+\Gamma}$, $\omega p^2 = \frac{nq^2}{m_e\varepsilon_o}$, q is the electron charge, m_e called mass of charge, Γ called damping coefficient, and ε_o is vacuum electric permittivity [1]. The backscattered field (far field), can be defined as

$$\mathrm{H}_m^{\mathrm{sc}} = -\hat{z}\sqrt{\frac{2j}{\pi k'}}\sum_{-\infty}^{+\infty} B'_{mn} e^{jn\pi}. \qquad (13)$$

The new proposed model is shown in Figure 2. The characteristic of this model is computed as $\mathrm{H}_m^{\mathrm{sc}} = \mathrm{H}_s^{\mathrm{sc}} \times A(s)$, so

$$A(s) = \frac{\mathrm{H}_m^{\mathrm{sc}}}{\mathrm{H}_s^{\mathrm{sc}}} = \frac{-\sqrt{\frac{2j}{\pi k'}}\sum_{-\infty}^{+\infty} B'_{mn} e^{jn\pi}}{\frac{1}{\sqrt{\pi k}}\sum_{-\infty}^{+\infty}\frac{J_n'(ka)}{H_n^{(2)\prime}(Ka)} e^{jn\pi}}, \qquad (14)$$

where $\mathrm{H}_s^{\mathrm{sc}}$ is scattered magnetic field of stationary perfect conducting cylinder [7].

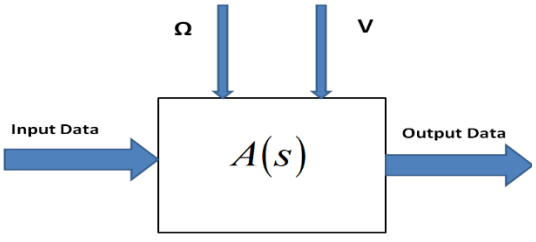


Figure 2: Proposed model

3. Numerical result

Equation (13) defines the far field (backscattered phase and magnitude) of moving dispersive higher conductivity cylinder. It is considered that the dispersive higher conductivity cylinder has a radius equal to $0.03m$ and the incident frequency changes from 2GHz to 20GHz. In this simulation, the conductivity of cylinder's martial is $\sigma = 5.76\times10^7\ s/m$ (Copper). This simulation is taken place using a specific values of $\beta_a = \Omega a/c = 0.009$ and $v/c = 0.02$.

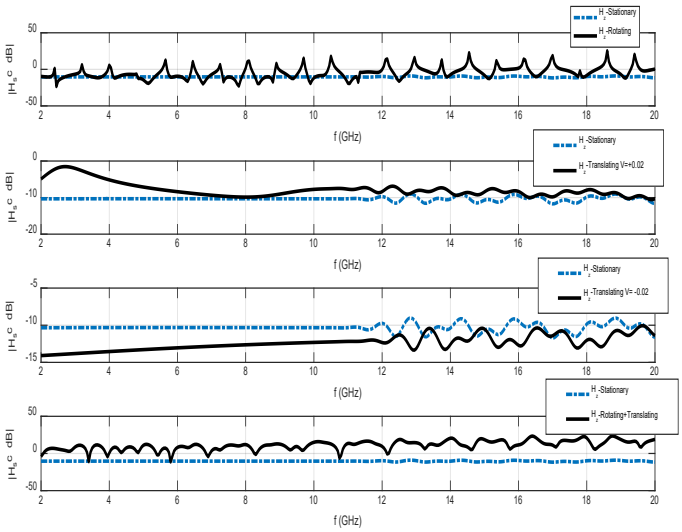


Figure 3: Magnitude of backscattered H-wave

It is shown the backscattered field (phase and magnitude) of the rotating, translating and moving dispersive higher conductivity cylinder cases in comparison with stationary case are shown in Figure 3. The graphs' y-axis and the x-axis represent the magnitude the operating frequency of backscattered magnetic field respectively. The first graph is a comparison of the backscattered magnitude of a stationary and a rotating dispersive higher conductivity cylinder. The blue line represents the stationary case, and the rotating case is represented by black line. Visibly it is observed that the black line (rotating case) shows pulses as frequencies increases and the blue line (stationary case) shows tiny ripples in higher frequencies, as shown in the first graph.

The second and the third graph show the comparison of the backscattered magnitude of a stationary and translating very good dispersive conducting cylinder, that is heading in a positive direction (away from the source) and the negative direction (towards the source). When the dispersive higher conductivity cylinder is heading in a positive direction, the backscattered magnitude is shifted in the higher frequencies in comparison with the stationary case. On the contrary, the backscattered magnitude is shifted in the lower frequencies when the dispersive higher conductivity cylinder is heading in the negative direction. The effect of a moving dispersive higher conductivity cylinder on the backscattered magnitude is shown in the fourth graph. The backscattered magnitude shows a pulses and negative slop in the moving case.

Figure 4 shows the backscattered phase of rotating, translating and moving cases. The first graph shows the difference between the backscattered phases of stationary and rotating. This difference shows up as a periodic pulse. In the translating case, the difference between the backscattered phase of stationary and translating cases is shown in the second and third graphs. When the dispersive higher conductivity cylinder is heading in a positive direction, the phase difference appears as a series of pulses. The widths of these

pulses increase as the dispersive higher conductivity cylinder heads in a positive direction. Also, slope of the pulses in the case of a positive translation is negative. On the contrary, the width of the pulses decreases when the dispersive higher conductivity cylinder heads in the negative direction. In this case, the slope of the pulses is positive. In comparison to the past work, the backscattered phase and amplitude of the moving non-dispersive conducting cylinder with high conductivity showed up a sinusoidal behavior, especially in higher frequencies [12]. The effect of movement of dispersive higher conductivity cylinder is shown in graph four.

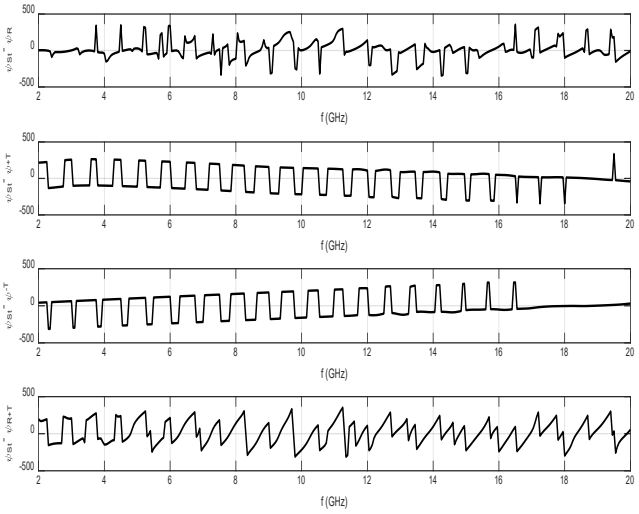


Figure 4: Phase of backscattered H-wave

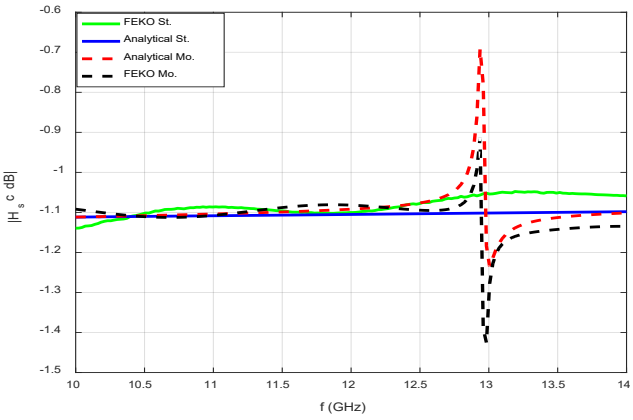


Figure 5: Magnitude of backscattered H-wave

The dispersive higher conductivity cylinder that is displayed in Figure 1 constructed by using a comprehensive computational electromagnetics software (FEKO). To construct the geometry of problem (Figure 1), It is assumed the radius, the height and the conductivity of cylinder are $a = 0.025\,m$, $h = 0.1\,m$ and $\sigma = 5.76\times10^{7}\ s/m$ respectively. Also, the range of simulation frequency is from 10 GHz to 14GHz.

In this part, the generated stationary static data is inserted into proposed model that is sown in Figure 2. Figure 5 and Figure 6 show that the analytical and simulation results of the backscattered phase and magnitude show a similar behavior in the stationary (St) and moving (Mo) cases.

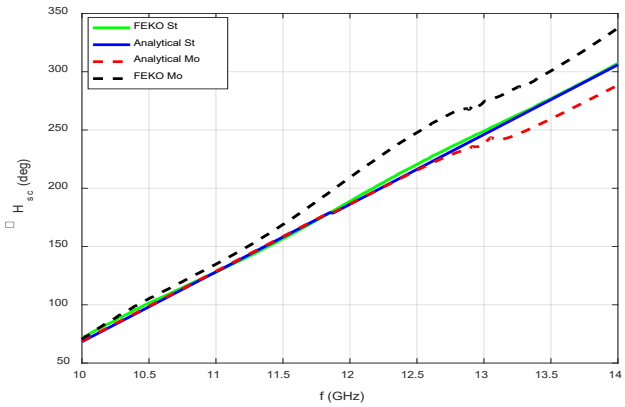


Figure 6: Phase of backscattered H-wave

4. Conclusion

In this research, the backscattered phase and magnitude of movement dispersive conducting cylinder is studied in the case of incident TE mode. The effect of the movement of the dispersive higher conductivity cylinder on the scattering of incident H-wave is studied. In this research, a mathematical model that represents the moving backscattered field (magnitude and phase) is created using Franklin and Lorentz conversion. It is found that the effect of the rotation shows as a periodic pulse on the patterns of backscattered phase and magnitude. Also, simulation result shows that the duration of pulses is affected when a speed and radius of dispersive higher conductivity cylinder are changed. In the translating case, the backscattered magnitude of an incident H-wave is shifted in the direction of higher frequencies when the dispersive higher conductivity cylinder moves away from the source of incident wave. Conversely, the backscattered magnitude of the incident H-wave is shifted in the lower frequencies when dispersive higher conductivity cylinder moves towards the source of incident wave. The phase difference of a backscattered field appears as series pulses in the translating mode. The slop of pulses is negative and the width of pulses increases when the dispersive higher conductivity cylinder moves away from the source of incident wave. When the dispersive higher conductivity cylinder moves towards the source of incident wave, the slop of pulses is positive and the width of pulses decreases. The demonstration results of the proposed model and an analytical results gives a similar backscattered phase and magnitude patterns. In comparison to the past work, the pattern of backscattered phase and amplitude of dispersive higher conductivity cylinder showed a periodic pulse. However, the pattern of backscattered phase and amplitude of non-dispersive higher conductivity cylinder showed a sinusoidal behavior, especially in higher frequencies. These phenomena display the impact of the electrical properties of material of scatterer on the scattering pattern of an incident H-wave.

Acknowledgment

The research is supported by the Center for Connected Multimodal Mobility (C2M2). Authors would also like to acknowledge U.S. Department of Homeland Security (DHS) Summer Research Team Program Follow-On, FY19 US

Department of Education MSEIP Grant Award P120A190061, and National Science Foundation (NSF, No. 1719501, 1436222, and 1400991) grants. Any ideas, results, epilogue or commendation that are expressed in this study are for those author(s), and do not necessarily reverberate the opinions of (C2M2), USDOT, DHS, U.S. Department of Education, or NSF. The U.S. Government suppose no liability for contents or utilize therefrom.

References

[1] E. Abuhdima, Gurcan Comert, Ahmed Elqaouaq, Ashleigh Reeves and Williams Kellen, "Scattering of EM waves from a Rotating Dispersive Very Good Conducting Cylinder," in 2019 IEEE International conference on wireless for space and extreme environments, October, 2019.

[2] Philip Franklin, "The meaning of rotation in the special theory of relativity," Proc. Nat. Acad. Sci., **8**(9), 1922.

[3] Harrington, Time Harmonic Elecromagnetic Fields, McGraw-Hill, 234, 1961.

[4] E. Abuhdima and R. Penno, "A New Model for Simulation of Scattered EM Fields from a conducting Cylinder in Rotation and Translation using Static Data," in IEEE NAECON-OIS, 2017.

[5] Abuhdima, Esmail, "Simulation of the Scattered EM Field of a Moving Dynamic Object Using Static Data," Ph. D Thesis, University of Dayton, 2017.

[6] H. Gholizade, "Radar Cross Section of Moving Objects," The European physical journal, 2013.

[7] C. A. Balanis, Advanced Engineering Electromagnetics, John Wiley &Sons, Inc, 1989.

[8] E. Abuhdima and R. Penno, "Simulation of the scattered EM fields from a rotating conducting cylinder," in IEEE International Radar, 2015.

[9] P. Hillion, "Scattering by a rotating circular conducting cylinder I," Mathematical physics, **41**, 1998.

[10] P. Hillion, "Scattering by a rotating circular conducting cylinder II," Mathematical physics, **41**, 1998.

[11] D. De Zutter, "Scattering by a rotating circular cylinder with finite conductivity, " IEEE Transactions on Antenna and Propagation , **AP-31**(1), 166-169, 1983.

[12] E. Abuhdima and R. Penno,"The Effect of Rotation and Translation upon the Scattered EM Fields of a Conducting Cylinder," in NAECON-OIS, 2016.

ASTES

Advances in Science, Technology and Engineering Systems Journal Vol. 5, No. 5, 960-965 (2020)

www.astesj.com

Special Issue on Multidisciplinary Sciences and Engineering

ASTESJ

ISSN: 2415-6698

Total Family Risk in Families who go to Popular Dining Rooms in a Vulnerable Area of Collique, Comas

Hernan Matta-Solis[1,*], Rosa Perez-Siguas[1], Eduardo Matta-Solis[1], Melissa Yauri-Machaca[2]

[1]*Research and Intellectual Creativity Direction, Universidad María Auxiliadora, 15408, Lima-Perú*

[2]*Research and Technology Direction, Business on Making Technologies, 15307, Lima-Perú*

ARTICLE INFO

Article history:
Received: 04 August, 2020
Accepted: 28 September, 2020
Online: 20 October, 2020

Keywords:
Family
Family relationships and risk
Popular dining rooms
Threatened family

ABSTRACT

The family can be referred to as a basic nucleus of society, where it must be fully formed as a group and guarantee the safety and development of its members. Increasing social inequality affects society and also the families that comprise it. It is a study with a quantitative approach, with a non-experimental, descriptive and cross-sectional design. The population consisted of 240 heads of families who go to 12 Popular Dining Rooms of a Vulnerable Area of Collique. The data collection technique was the survey-interview and the instrument used was the RFT 5-33 questionnaire of 5 dimensions and 33 items. The total family risk in families who go to Popular Dining Rooms of a Vulnerable Area of Collique in Comas, it is presented as follows, 172 participants representing 72% are threatened families; 41 participants representing 17% are families with low risk and 27 participants representing 11% are families with high risk. Regarding dimensions, threatened families predominated in all, in psycho-affective conditions with 94%, in health services and practices with 91%, in housing and neighborhood conditions with 62%, in socioeconomic situation with 85% and in child management with 85%. The total family risk that predominated is threatened families, followed by families with high risk and families with low risk. Regarding the dimensions of the main variable, threatened families predominate in all of them. The dimension with the highest high-risk value is housing and neighborhood conditions.

1. Introduction

The family, as the basic nucleus of society, must develop plenty as a group and guarantee the safety and development of its members. Growing social inequality affects society and the families that make it up, this problem affects and destabilizes family dynamics, exposing and making it vulnerable to existing social problems [1].

Similarly, it not only makes families vulnerable to social problems but also to psycho-affective emotional and motivational problems where these aspects compromise the development of self-esteem, self-confidence and the fulfillment as a person of each family member, altering the development of values and optimal functionality that benefits the family [2].

In the family, there is a diversity of problems that are accentuated more frequently, and there are no ways to solve them, couples who are at the head of the family nucleus choose divorce or separation as a solution, a situation that affects the Family structure and functioning [3], also, family ruptures bring relevant psychosocial consequences for their members, many times these affect the personality of their children [4].

According to the National Program Against Family and Sexual Violence of the Ministerio de la Mujer y Poblaciones Vulnerables, it indicates the frequency of cases of different types of violence, where the main type of violence is psychological, followed by physical, sexual and economic. In relation to the age groups with the types of violence given in women, cases of violence were attended in the first semester of 2018, where it was found that 72% of young and adult women said they had suffered some type of violence, followed 22% to girls and adolescents and 5% to older women [2].

In the same way, the Instituto Nacional de Estadística e Informática mentions the complaints registered by the National Police on family violence due to marital and family problems, according to department, during 2016, they show that Lima has

*Corresponding Author: Hernan Matta-Solis, Email: hernan.matta@uma.edu.pe

the highest number of complaints with 28 699 reports, followed by Arequipa with 9,748 reports [5].

In the research study carried out in Colombia, it shows the results obtained in families of schoolchildren where the level of total family risk shows that 55% of families are at a threat risk level, 37% at a low risk level and 8% at high risk level; when evaluating the individual risk categories of the five factors studied according to RFT 5-33, all the factors are classified as threatened and the factor related to housing and neighborhood is located in its highest frequency at 21% [6].

In the research study carried out in Colombia, the results of the characterization of the total family risk show that in the group of adolescents, 57% of the total are threatened families and 8% are families with high risk. From the measurement of adolescents, 57% are threatened families and 8% are families with high risk, from it is measured by caregivers, 66% are threatened families and 15% are families with low risk [7].

In the research study carried out in Peru, they mention the results of the total family risk, they found 35 families that represent 31% of the total are family with high risk, 58 families that represent 51% of the total are threatened and 20 families that represent 18% of the total have low risk. Regarding the dimensions of the total family risk, those that present a high risk are the housing and neighborhood conditions, they have 46 families that represent 41%, and in health services and practices they have 41 families that represent 36% [8].

The objective of the research work is to determine the total family risk in families who go to Popular Dining Rooms of a Vulnerable Area of Collique in Comas, which it will allow to observe what the family risk is in families. This study is important since it will provide with relevant and real data about the vulnerability of families exposed to risky conditions that can compromise all family members.

In the present research work, the Total Family Risk questionnaire also known as RFT Questionnaire 5-33 will be used as a collection instrument.

The data collection was processed through the survey of families who go to Popular Dining Rooms of a Vulnerable Area of Collique in Comas, the data to be entered was carried out in a data matrix that will be designed in the statistical program IBM SPSS Statistics Base 25.0, it proceeded to its corresponding analysis, which will allow to make statistical tables so that they can be described and interpreted in results and discussions, respectively.

The following research work is structured as follows: In section II, the development of the data collection process of the families who go to a popular dining room of Collique in Comas will be presented and also the guidelines to consider. In section III, the results will show the total family risk in families who go to Popular Dining Rooms of a Vulnerable Area of Collique in Comas according to the measures based on the variable. In section IV, it presents the discussions of the research work and in section V, the conclusions.

2. Methods

In this part, the type and design of the research will be developed, also the population and the sample that will be carried out in the research work, the inclusion and exclusion criteria in detail and finally the technique and the instrument for collecting data.

2.1. Research type and design

The present study has the characteristics of the quantitative approach. Regarding the research design, this study is non-experimental, descriptive and cross-sectional [9].

2.2. Population

This study was carried out in the total population. This is made up of 240 family managers who go to a popular dining room of Collique in Comas. The family heads identified in their entirety is women.

Inclusion criteria

- Family managers who live in the area at least 1 year old
- Family managers who consume food in a popular dining room of Collique in Comas.
- Family managers who are physically and/or mentally able to answer an interview.
- Family managers who wish to participate and sign the informed consent for participation in the study.

Exclusion criteria

- Family managers who do not live in the study jurisdiction.
- Family managers who do not consume food in the Popular Dining Room linked in the study.
- Family managers who are not physically and/or mentally capable of answering an interview.
- Family managers who do not wish to participate and do not sign the informed consent to participate in the study.

2.3. Technique and instrument

The data collection technique to be used in this study will be the survey, since a structured instrument is used to capture a good amount of information from the participants in the data collection process [10].

In the present research work, the Total Family Risk questionnaire also known as RFT Questionnaire 5-33 will be used as a data collection instrument, which is made up of 5 factors or dimensions, in which 33 main items are distributed.

The 5 factors or dimensions are: psycho-affective conditions, health practices and services, housing and neighborhood, socioeconomic situation and child management. The answers are all dichotomous for each of the items, if it is at risk, it is given a value of 1 and if there is an absence of it, it is valued at 0. Between 5 to 12 risks of 33 possible, it has families threatened, between 13 and 33 risks of 33 possible, it is families with high risk, and 0 to 4 risks of 33 possible, it has families with low risk. The final value

of the variable Total family risk has three values: families with high risk, threatened families and families with low risk [11].

The values as families with high risk, is based as a situation where the family is exposed to dangers in which it can compromise all the members; threatened families is the situation where the family is vulnerable to dangerous situations where one or all the members of the family would be compromised and families with low risk, refers to the situation that the family is at some type of risk but that can be controlled by the family members.

2.4. Place and Application of the Instrument

The survey to measure total family risk was carried out in families who go to a popular dining room of Collique in Comas.

In order to start data collection, administrative procedures were previously carried out at the university in order to obtain the cover letter stating the title of the study. With this document, steps were taken regarding authorizations to access the popular dining room of Collique in Comas. In a first contact, the people in charge of the Popular Dining Room were happy to support the development of the study.

By identifying the number of families who go to Popular Dining Rooms, it coordinated with the representatives of the popular dining room to date the most appropriate time to collect the data.

The data collection was carried out in the second quarter of the year (April to June of the year), this was carried out mainly during the hours in which family managers went to the popular dining rooms to coordinate the purchase of their food. In some cases, the family heads suggested that the interview be conducted at their home. An average time of approximately 15 to 25 minutes was taken with each family head.

It is important to mention the nursing staff present at the research site since they carry out their controls in popular dining room, weight and height screening is done in families, especially in children and adolescents since they are in a growth stage and development which is very important in their diet, so that they are not prone to get diseases.

3. Results

Below, there are graphs of the surveys carried out following the guidelines corresponding to the research work:

In Figure 1, it has the data of the study participants, where it can observe regarding to the family risk in families who go to popular dining room, 172 participants that represent 71.7% of the total are threatened families, 41 participants that represent the 17.1% of the total are families with low risk and 27 representing 11.3% are families with high risk.

In the Figure 2, it can see regarding to the Total Family Risk in its psycho-affective conditions dimension, in families who go to Popular Dining Rooms, that 226, which represents 94%, are threatened families and 14, which represents 6%, represents Families with high risk. In its dimension, health services and practices, in families who go to Popular Dining Rooms, 219, representing 91% are threatened families and 21, representing 9%, are families with high risk, in its dimension, housing and neighborhood conditions, in families that go to Popular Dining Rooms, that 149 participants representing 62% are threatened families and 91 participants that represent 38% are families with high risk, in their socioeconomic situation dimension, in families that go to Popular Dining Rooms, that 203 participants that represent 85% are threatened families and 37 participants that represent 15% are families with high risk and in their dimension child management, in families who go to Popular Dining Rooms, that 204 participants representing 85% are threatened families and 36 participants representing 15% are families with high risk.

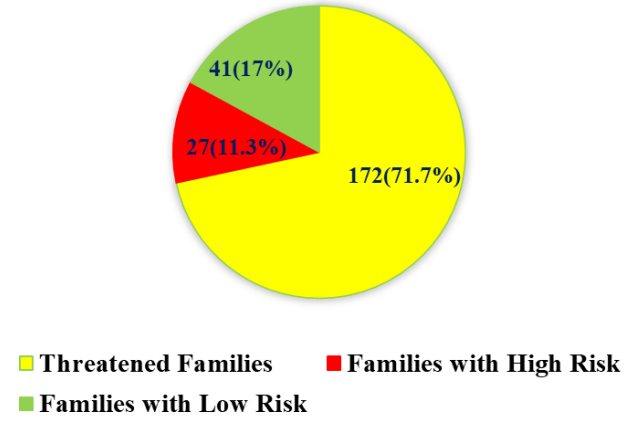


Figure 1: Total Family Risk in Families who go to Popular Dining Rooms in a Vulnerable Area of Collique, Comas – 2018

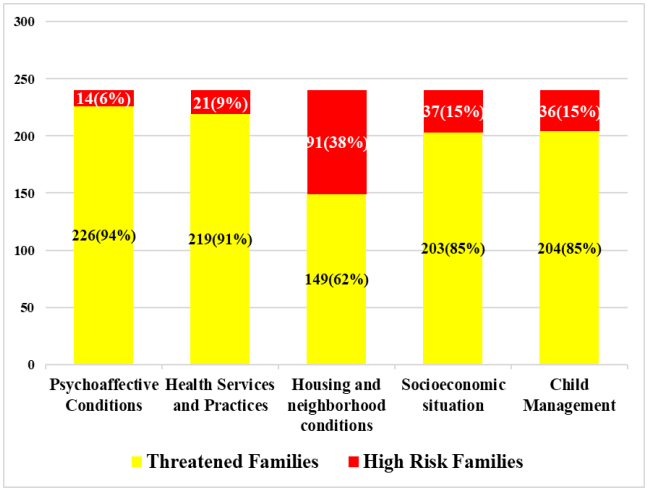


Figure 2: Total family risk according to its dimensions in families who go to Popular Dining Rooms in a Vulnerable Area of II of Collique, Comas - 2018

In Table 1, it has the study participants from popular dining rooms in a vulnerable area of Collique, Comas, where it can see that, in the "Los Diamantes" popular dining room 100% represent the threatened families, in the " Nuestra Señora de Luz" popular dining room 94.1% represents threatened families, 5.9% represents families with high risk, in the "Cruz de Motupe" popular dining room 92% represents threatened families, 8% represents families with low risk, in the "El Buen Pastór" popular

Table 1: Total Family Risk in Families who go to Popular Dining Rooms in a Vulnerable Area of Collique, Comas.

			TOTAL FAMILY RISK - Risk level			
			Threatened Families	Families with High Risk	Families with Low Risk	Total
Popular Dining Rooms	Virgen de Fatima	Count	13	0	3	16
		% in the dining room	81,2%	0,0%	18,8%	100,0%
	Micaela Bastidas	Count	13	2	1	16
		% in the dining room	81,2%	12,5%	6,3%	100,0%
	Corazón de Jesus	Count	18	9	4	31
		% in the dining room	58,1%	29,0%	12,9%	100,0%
	Iglesia Evangelica	Count	13	4	0	17
		% in the dining room	76,5%	23,5%	0,0%	100,0%
	Nuestra Sra. de la Luz	Count	16	1	0	17
		% in the dining room	94,1%	5,9%	0,0%	100,0%
	Victor Raul Haya de la Torre	Count	10	1	13	24
		% in the dining room	41,6%	4,2%	54,2%	100,0%
	Corazon de Jesus ll	Count	17	4	1	22
		% in the dining room	77,3%	18,2%	4,5%	100,0%
	Cruz de Motupe	Count	23	0	2	25
		% in the dining room	92,0%	0,0%	8,0%	100,0%
	Los Diamantes	Count	11	0	0	11
		% in the dining room	100,0%	0,0%	0,0%	100,0%
	Milagros de Jesus	Count	14	1	13	28
		% in the dining room	50,0%	3,6%	46,4%	100,0%
	El buen Pastor	Count	19	2	0	21
		% in the dining room	90,5%	9,5%	0,0%	100,0%
	Los Diamantes ll	Count	5	3	4	12
		% in the dining room	41,7%	25,0%	33,3%	100,0%
Total		Count	172	27	41	240
		% in the dining room	71,7%	11,3%	17%	100,0%

dining room 90.5% represent threatened families, 9.5% represent families with high risk, in “Micaela Bastidas” popular dining room 81.2% represent to threatened families, 12.5% represent families with high risk and 6.3% represent families with low risk, in the "Virgen de Fátima" popular dining room 81.2% represent threatened families, 18.8% represent families with low risk in the “Corazón de Jesús II” popular dining room 77.3% represent threatened families, 18.2% represent families with high risk and 4.5% represent families with low risk, in the "Iglesia Evangélica" popular dining room 76.5% represents threatened families, 23.5% represents families with high risk, in the “Corazón de Jesús” popular dining room 58.1% represents threatened families, 29% represents families with high risk and 12.9% represent families with low risk, in the “Milagros de Jesús” popular dining room 50% represent threatened families, 3.6% represent families with high risk and 46.4 % represents families with low risk, in the "Los Diamantes II" popular dining room 41.7% represents threatened families, 25% represents families with high risk and 33.3% represents families with low risk and in the “Victor Raúl Haya de la Torre” popular dining room 41.6% represents threatened families, 4.2% represents families with high risk and 54.2% represent families with low risk.

The results of this study can be interpreted that the total family risk of families who go to popular dining room is linked to the promotion of family health, since it is very important to know the consequences that exist in families, whether due to disorganization within the family, family dysfunction, or diseases, that allow us to act on it and have the ability to make changes in families that present some type of difficulties.

4. Discussion

The total family risk assessment allows guiding family health care, ensuring the health of each member of the family group and the context in which they take place [12]. For this reason, the importance of putting into practice the proposal of Pilar Amaya, who involves a series of factors and dimensions that allow to see the family's problems in an integral way [11].

The findings proposed by Pilar Amaya, who emphasizes in her instructions that threatened families present between 5 and 12 risks in relation to the 33 items that are part of the risk assessment; these families are characterized by the presence of emotional and affective alterations that result in an adverse environment for the optimal development of the family members. These family groups have difficulties in accessing public health services, in addition to their precarious situation being this situation a threat to the members of the family group. Total family risk is a dynamic concept, that is, it is changing and can be altered over time [11,13]. We agree with what was pointed out by Barboza E. and collaborators, who in their respective studies indicate that this group of threatened families must be given due attention, since they can become families with high risk, which would worsen their situation [14].

In relation to its psycho-affective conditions dimension, threatened families predominated, followed by families with high risk. A threatened family must be monitored to see its evolution over time, in order to prevent the family from becoming involved in more risks, this dimension is closely linked to the mental and emotional health of families, in which it is altered in the interpersonal relationships between family members. Becerra et al. point out in their results in relation to psycho-affective conditions that affective needs are important to satisfy and preserve the mental health of families, therefore, at an emotional level, it will depend on how the family can face situations where the role and the dynamics in the family are not altered [8].

In terms of health services and practices, threatened families predominated, followed by families with high risk. In the study, the basic needs of health benefits are increasingly difficult because most families do not predispose with time because they are mainly engaged in activities that generate income to cover their basic needs, where the health is prioritized in the background, because many of them, due to their educational level, do not value health care, also, they do not know about the care provided by health facilities in their jurisdiction. We agree with what was stated by Giraldo M., who in his study that the distance and lack of involvement of the health establishment with its population has led to the underutilization of the health services available there, where families do not perceive the related risks with their health, also their members, this often causes health problems that evolve over time and can generate unfavorable sequelae in the family [7].

In terms of housing and neighborhood conditions, threatened families predominated, followed by families with high risk; Compared to the other dimensions, this presents a higher risk in families. Health or illness is the result of a dynamic interrelation between families and the environment that surrounds them, although it is true that the environment has a direct link with being healthy in different ways, which is why it improves living conditions and improves the health levels of family members. However, the study showed environmental sanitation problems, where the lack of support from the municipality, the lack of organization and participation of families in caring for their environment has been very high, but that there is no culture in themselves that allow them to prioritize that aspect. In the study by Soto A. and collaborators, findings were evidenced in relation to deficiencies in this aspect and that attributes the socioeconomic conditions and the lack of support from the authorities to improve the environment and adapt the place to live [12]. In the same way, Millan M. and collaborators also point it out in their study associate the socioeconomic situation with the development and adequacy of homes and their sanitation, where unsanitary conditions constitute a risk for all family members [15].

In its socioeconomic situation dimension, threatened families predominated, followed by families with high risk, on the analysis of this dimension conditions the development of a family, because it explains the shortcomings and constraints that families go through in their daily lives, where the Precarious work and education are points that compromise the family and its members. In the same way, Pérez R. and collaborators highlight that education and job insecurity make it difficult for family members to know and access their social rights as citizens, therefore social assistance is important since it allows them to fulfill a palliative function given the needs of families, and that it is important that government institutions and the state promote decent and sustained employment for the population [16].

Finally, in its dimension child management, threatened families predominated followed by families with high risk, in the study the results were alarming, because the health of the child in this community is prioritized as second plane. The risk that minors are exposed to where the conditions of housing, neighborhood and

the economic situation of the family are determinants that sustain the well-being of the child, coincides with the study by Cabello E. et al. [17].

5. Conclusions

It is concluded that the total family risk in families who go to popular dining room of Collique in Comas, where threatened families predominated, followed by families with low risk and families with high risk, is suggested to the health establishment of the jurisdiction, implement as part of its extramural activities, a program of visits to families with high risk, so that it can specifically identify their problems and be able to address them comprehensively.

It is concluded that more variables should be introduced in future studies, in order to establish new possibilities of relating the main variable total family risk with other variables that allow a better understanding of family health and the risks of families in all their dimensions.

It is concluded that studies with qualitative and mixed approaches should be developed that allow a deeper understanding of the problem that these families are going through, this will give a better picture when analyzing family health and the care that is oriented to improve it.

It is suggested that the nursing professional continuously monitor the area through a program of home visits directed from the results of this study, focusing on the growth and development of children and adolescents, their diet, care, and the family relationship.

Conflicts of Interest

The authors declare that they have no conflict of interest.

References

[1] M.E. Benítez-Pérez, "La familia: Desde lo tradicional a lo discutible," Revista Novedades En Población, **13**(26), 58–68, 2017.

[2] Ministerio de la Mujer y poblaciones Vulnerables, Observatorio Nacional de las Familias, MIMP, 1–12, 2018.

[3] Superintendencia Nacional de Registros Públicos, Crece inscripción de divorcios a nivel nacional, Lima - Perú, 2017.

[4] M. Jiménez Arrieta, M. Amarís Macías, M. Valle Amarís, "Afrontamiento en crisis familiares: El caso del divorcio cuando se tienen hijos adolescentes," **28**(1), 99–112, 2012.

[5] Instituto Nacional de Estadística e Informática, Denuncias registradas por la Policía Nacional sobre violencia familiar, según departamento, Lima - Perú, 2017.

[6] S. Diaz Cardenas, K. Ramos Martinez, K.M. Arrieta Vergara, "Asociacion del nivel de riesgo familiar total y caries dental en escolares de La Boquilla, Cartagena," Avances En Enfermería, **31**(2), 43–52, 2013.

[7] D.M. Giraldo Ocampo, Caracterización de riesgo familiar total en familias con adolescentes escolarizados, Universidad nacional de Colombia, Bogota - Colombia, 2014.

[8] W.I. Becerra Cubas, J.S. Diaz Pareja, J.P. Rocha Durand, Riesgo familiar total en familias del sector 1 del Asentamiento Humano Juan Pablo II Los Olivos - 2013, Universidad de Ciencias y Humanidades, Lima-Perú, 2015.

[9] R. Hernández Sampieri, C. Fernández Collado, P. Baptista Lucio, Metodología de la Investigación, 6a Edición, McGraw-Hill Education, México, 2014.

[10] F. Alvira-Martín, La encuesta: una perspectiva general metodológica, 2a edición, Centro de Investigaciones Sociológicas, Madrid-España, 2011.

[11] P. Amaya, Instrumento de riesgo familiar total RFT : 5-33 : manual aspectos teoricos, psicometricos de estandarización y de aplicación del instrumento., 1st ed., Universidad Nacional de Colombia, Bogotá, 2004.

[12] A.M. Soto González, V.F. Velásquez G., "Riesgo Familiar Total de Familias desplazadas residentesen el Municipio de Bugalagrandade (Valle de Cauca, Colombia)," Hacia La Promoción de La Salud, **20**(1), 126–139, 2015, doi:10.17151/hpsal.2015.20.1.9.

[13] N.C. Charrys Bravo, "Riesgo familiar total en familias con mujeres diagnosticadas con neoplasia de mama - Dialnet," Revista Ciencia y Cuidado, **14**(2), 8–21, 2017.

[14] E.L. Barboza Delgado, L.I. Prado Pérez, P. Vega Tarazona, Riesgo familiar total en familias de niños menores de 5 años del Asentamiento Humano 19 de Mayo, Los Olivos - 2018, Universidad de Ciencias y Humanidades, Lima-Perú, 2018, doi:10.22258/uch.thesis/217.

[15] M.E. Millan Ambrocio, Riesgo Familiar Total y tipo de familia en el Asentamiento Humano Santa Rosa Alta sector VII del distrito del Rímac, Lima 2017, Universidad Norbert Wiener, 2018.

[16] R.E. Pérez Siguas, H.H. Matta Solís, T.M. Espinoza Moreno, C.R. Paredes Tafur, "Caracterización del riesgo familiar total y tipo de familia en pobladores de un asentamiento humano de un distrito de Lima Norte | Pérez Siguas | Peruvian Journal of Health Care and Global Health," Peruvian Journal of Care and Global Health, **1**(1), 2017.

[17] E.Y. Cabello Huerta, J.B. Francisco Yauri, S.J. Mayta Guanilo, Riesgo familiar total de las familias con niños preescolares de la institución educativa inicial Semillitas de Amor I Puente Piedra – 2015, Universidad de Ciencias y Humanidades, Lima - Perú, 2017.

ASTES

Advances in Science, Technology and Engineering Systems Journal Vol. 5, No. 5, 966-972 (2020)

www.astesj.com

Special Issue on Multidisciplinary Sciences and Engineering

ASTESJ

ISSN: 2415-6698

Health-Related Quality of life in Students of an Education Institution of Ventanilla

Lucia Silva-Bueno[1], Brian Meneses-Claudio[2], Hernan Matta-Solis[1,*], Lourdes Matta-Zamudio[1]

[1]*Faculty of Health Sciences, Universidad de Ciencias y Humanidades, 15314, Lima-Perú*

[2]*Image Processing Research Laboratory (INTI-Lab), Universidad de Ciencias y Humanidades, 15314, Lima-Perú*

ARTICLE INFO

Article history:
Received: 03 August, 2020
Accepted: 28 September, 2020
Online: 20 October, 2020

Keywords:
Adolescents
Quality of life
Students
Health
Adolescent psychology

ABSTRACT

The Health-related quality of life corresponds to the perception that people have of their level of well-being, considering aspects of their lives and their impact on their state of health. The studies were initially carried out in a population that presented both acute and chronic pathologies and covered practically all areas of medical specialties; subsequently, the interest focused on studying health-related quality of life in the general population and then in the population of children and adolescents. That is why, in this research work, the evaluation of the adolescent to prevent future problems was raised; to carry out the evaluation, the questionnaire called KIDSCREEN 52 was used, which consists of 52 closed questions divided into 10 dimensions, providing an idea of how the adolescent feels. The following results were obtained: The Health-related quality of life in adolescents of an Educational Institution of Ventanilla, where 430 students representing 59.1% have high quality of life and 298 students representing 40.9% have medium quality of life; according to its dimensions, adolescents from the Educational Institution of Ventanilla, its most affected dimension was economic resources, with 64 students representing 8.8% having a low level. In the relationship with parents' dimension, it appreciates that 3.4% of students do not have a good family atmosphere since they do not live with their parents, but with uncles and/or grandparents.

1. Introduction

Health-related quality of life (HRQL) defined as "individual and group perceived physical and mental health". It has been used to evaluate medical care from the patient's point of view and as a subjective indicator of social well-being [1]. It corresponds to the perception that people have of their level of subjective well-being, considering various aspects of their lives and their impact on their state of health. Studies in HRQL were initially carried out in a population that presented both acute and chronic pathologies and covered practically all areas of medical specialties; subsequently, the interest was concentrated in studying HRQL in the general population and then in the population of children and adolescents. Currently, studies in school children and adolescents have increased [2]. HRQL in childhood and adolescence is useful for describing the health of a population and establishing comparisons between subgroups with certain characteristics (for example, sociodemographic, regional, etc.). In pediatric clinical practice, the study of HRQL can facilitate knowledge of health status, study the effect of different treatments, identify levels of morbidity and facilitate clinical decisions [3]. Adolescents are considered as individuals in constant development, that is why they need to grow in a balanced and healthy way within a safe and structured environment, in order to develop positively on a physical, educational, emotional and social level [4].

In the research work [5] in 2017, it was indicated that a total of 550 adolescents aged 16 ± 1 years completed the questionnaires. 39% consumed alcohol in the last month, 31% smoked, 33% used marijuana, and 33% admitted using multiple drugs. High-risk alcohol consumption was associated with a lower perception of psychological well-being, self-perception, and the school environment. This last dimension was affected in those who admitted the use of marijuana during the last month. Multiple drug use (three substances) was associated with a lower perception of physical and psychological well-being, self-perception, relationship with parents, family life and the school environment; in conclusion, high-risk alcohol consumption and multiple drug use (three substances) have a negative impact on the HRQL of school-age adolescents.

*Corresponding Author: Hernan Matta-Solis, Mr., +51 1 999751065 & hmatta@uch.edu.pe

In [6] in 2019, the authors explain that of the 723 adolescents, 13% reported having been bullied; there were no gender differences within this finding. However, more boys than girls reported that they had bullied others. Both bullying and intimidation of others were associated with a lower HRQL; however, being bullied was associated with lower scores. Greater self-efficacy was associated with better HRQL. Self-efficacy contributed significantly to predicting variation in HRQL. In conclusion, being involved in bullying, as a victim or bully, is associated with a lower HRQL. The association between general self-efficacy and HRQL indicates that self-efficacy could be a resource to increase HRQL in adolescents. Their findings highlight the importance of focusing on self-efficacy beliefs as an intervention strategy to improve self-efficacy and HRQL in adolescents involved in bullying.

In [7] in 2018, the authors presented that girls and adolescents aged 17-18 years presented significantly higher psychosomatic symptoms, both groups also scored worse in all dimensions of HRQL, although only the dimensions related to physical well-being, mental well-being and mood and stress reached significance. All psychosomatic symptoms were inversely associated with the 10 dimensions of the KIDSCREEN-52. The regression models performed showed that sadness, difficulty concentrating and difficulty sleeping were the predictors of the worst HRQL in both sexes and age groups, and these variables explained between 30% and 41% of the variance in the HRQL of adolescents. In conclusion, psychosomatic symptoms are more frequent in girls and older adolescents, and predictors of worse HRQL. It is important to differentiate them from medical conditions to avoid unnecessary interventions. As expressions of emotional distress, they must be evaluated and treated comprehensively because they interfere with daily life and increase the vulnerability of adolescence.

The general objective of the study is to determine the health-related quality of life in students of an educational institution. To do this, reviewing various studies verifies that there is no research on this area, neither from this population that currently has problems most of them in the psychological field. In the review of national and international scientific literature, it is evident that there are few scientific researches that use the KIDSCREEN 52 in their work on health-related quality of life, and it is evident that most of the researchers are international. In Callao, and specifically in the place where the research work is carried out, there is no evidence of other research on this topic, which is why this research wants to fill the knowledge gap.

The technique used is the survey. The data collection instrument was the KIDSCREEN 52, which consists of 52 items distributed in its ten dimensions (physical well-being, psychological well-being, mood, self-perception, autonomy, relationship with parents, financial resources, friends and social support, social environment and social acceptance). After completing the field work, the data was entered into a matrix in Microsoft Excel 2016, and then exported to the IBM SPSS Statistics Base 23.0 statistical package, in which the mainly descriptive analysis was performed.

2. Methodology

2.1. Population and sample

In the present study, it worked with the total population (N=728), which is made up of adolescents between 12 and 18 years old of the 2019 school year from a public school in the Ventanilla district, the 21 classrooms have around 700 students, each participant was selected according to the inclusion and exclusion criteria of the study; in addition, each participant was informed about the objectives and scope of the study, and then invited to bring the corresponding informed consent and assent signed.

Table 1: Distribution of classrooms at the secondary level of the Jorge Portocarrero Rebaza educational institution

Grade	Shifts	Classrooms	Total students
First	Afternoon	5	164
Second	Afternoon	5	177
Third	Morning	4	162
Fourth	Morning	4	119
Fifth	Morning	3	106
Total		21	728

2.2. Inclusion and Exclusion Criteria

Inclusion criteria:

- All students who present the consent of their parents and informed assent by them.
- Students between 8 and 18 years old.
- Students who have attended the day of the survey.

Exclusion criteria:

- Students over 18 years old.
- Students who do not wish to take the survey.

2.3. Analysis of the variable

The present study presents Health-related quality of life as the main variable, according to its nature, it is a qualitative variable and its measurement scale is ordinal.

The health-related quality of life (HRQL) corresponds to the perception that people have of their level of subjective well-being, considering various aspects of their lives and their impact on their state of health [2]. It is the perception that high school adolescents of II.EE Jorge Portocarrero Rebaza has about their position in life, in the cultural context and value systems in which they operate and in relation to their objectives, expectations, standards and concerns also, it is expressed by physical well-being, psychological well-being, mood, self-perception, autonomy, relationship with parents, financial resources, friends and social support, social environment and social acceptance, which will be measured with the KIDCREEN 52 questionnaire.

The technique used in the study for the data collection process was the survey, this technique contemplates a set of standardized procedures that wants to obtain a significant amount of data quickly and efficiently.

Regarding the data collection instrument that allowed to measure the main variable Health-related quality of life, the KIDSCREEN 52 questionnaire was used. It is financed by the European Commission within the "Quality of life and management of living resources" Fifth Framework Programmed (QLC-CT-2000-00751) and was held for 3 years; they are a group of instruments developed and standardized for the topography of Health-related quality of life (HRQL - Health related to quality of life), in children and adolescents aged 8 to 18 years [8].

The KIDSCREEN-52 tool was developed jointly by 13 European countries, including Spain, following a simultaneous intercultural protocol. This ensures that future comparisons can be made between different countries. Later it has been adapted to different countries in Latin America, such as Venezuela and Argentina. The instrument was constructed using psychometric studies based on classical test theory and more advanced models, such as Item Response Theory (IRT). Based on the KIDSCREEN implementations, a computer-adaptive trial version was also developed using an IRT-based methodology. The original Spanish version of the KIDSCREEN-52 (KIDSCREEN-52-ES) was culturally adapted according to the International Test Commission (ITC) guidelines. We carry out the adaptation following the instructions of the KIDSCREEN Group. There were two stages: First, an adjusted linguistic validation of the instrument was performed. This consisted in the forward and backward translation of the instrument and harmonization until obtaining a semantic and conceptually equivalent version to the original. To maintain the validity of the content of the instrument, the items had to be formulated and expressed in an acceptable and culturally relevant way for Colombian children and adolescents. Subsequently, a pilot study was conducted to examine the validity of the instrument and correct any content or format errors [9].

This instrument is made up of 52 main items which are distributed in 10 dimensions, being these:

Physical well-being: This dimension measures the physical activity of the person, the sensation of energy and everything about the physical part of the person.

- High: Indicates that the participant performs well in physical activities and maintains an adequate physical level.
- Medium: Indicates that the participant alternately performs physical activities but also maintains a good level of physical well-being.
- Low: Indicates that the participant performs minimal physical activities.

Psychological well-being: In this dimension, the person's emotions and satisfaction with life are measured.

- High: Indicates that the participant has their emotions in constant control.
- Medium: Indicates that the person may at times be unable to control their emotions.
- Low: Indicates that the person cannot control their emotions when faced with any situation.

Mood: The level of stress that the person presents and if it presents depressive states are measured.

- High: The person can control and maintain a balance regarding stress.
- Medium: The person may at times not be able to control stress adequately.
- Low: The person may present depressive states due to not being able to adequately control stress.

Self-perception: The perception of its physical appearance and body image and if it feels satisfied with it.

- High: The person appreciates and values their body appearance and feels satisfied.
- Medium: The participant may sometimes not appreciate their body appearance.
- Low: The participant is not satisfied with their image and physical appearance.

Autonomy: Opportunities for activities in their free time are perceived.

- High: The participant has opportunities to do activities in their free time.
- Medium: The participant has some opportunities for activities in their free time.
- Low: The participant has few opportunities to do activities in their free time.

Relationship with parents: The family atmosphere is perceived.

- High: The participant has a very good family relationship.
- Medium: Presents a medium family atmosphere, there may be some problems between family members.
- Low: It presents a bad family atmosphere.

Economic resources: The perception of the family's financial capacity is measured.

- High: Presents adequate family financial capacity to meet the family's needs.
- Medium: Presents an adjusted family financial capacity but still satisfies the basic expenses of the family.
- Low: Presents an adjusted financial capacity.

Friends and social support: The relationship with classmates and/or friends is measured.

- High: Good relationship with classmates.
- Medium: Good relationship with some classmates.
- Low: Bad relationship with classmates.

Social environment: The perception of the ability to concentrate and cognition is measured, in addition to feelings about school.

- High: The participant presents a good concentration and cognition within the school.
- Medium: Presents a regular cognition within the school.

- Low: The participant does not show adequate concentration and cognition in school.

Social acceptance: Measures the feeling of rejection from friend or people around.

- High: The participant does not present any rejection from its colleagues.
- Medium: Presents some rejection of its colleagues.
- Low: Presents rejection by their peers, the participant suffers from bulling by their peers.

Reliability of the KIDSCREEN 52 data collection instrument

The reliability of the instrument was determined based on the Cronbach's alpha statistic, which presents an internal consistency index of 0.885 (α> 0.6). Therefore, a high level of general reliability of the instrument is identified.

Reliability	Cronbach's alpha	0,885
	No. of elements	52

Validity of the data collection instrument Health-related quality of life KIDSCREEN 52

To determine the validity of the instrument, the Kaiser-Meyer-Olkin (KMO) sample adequacy index and the Barttlet sphericity test were used. After the analysis, a sample adequacy coefficient of 0.928 and a significance value of 0.000 (x2 = 20481.828; g.l. = 1326; p <0.05) were obtained in the Barttlet sphericity test. Given the above data, an acceptable validity of the instrument can be identified.

	Measure of sampling adequacy of Kaiser-Meyer-Olkin		0,928
Validity	Bartlett's test of sphericity	X^2 approximate	2048
		gl	1,828
		Sig.	1326
			0,000

2.4. Data Collection

Authorization and prior coordination for data collection

In order to start the data collection process, steps were taken to access the institution where the field work will be carried out.

At first during the month of September of the year 2019, a request letter of introduction to the Professional School of Nursing of the Universidad de Ciencias y Humanidades to formally manage the permit and be able to carry out the surveys at the Jorge Portocarrero Rebaza educational institution.

In a second moment, it coordinated with the director of the Jorge Portocarrero Rebaza educational institution, Mr. Rafael Salvador Mimbela, and the importance of the research was explained to him, authorization was requested for the development of the work, to which he agreed.

Application of data collection instrument

On October 4th, 2019, the survey was carried out in the students who attended the educational institution, they were 11 classrooms in the morning shift and 10 classrooms in the afternoon shift with 40 students for each classroom. The time used in each classroom was approximately 25 minutes. In each classroom, an authorization document was requested from the parent or guardian of the adolescent, since the informed consent had to be signed. At the time of the delivery of the questionnaire, each classroom was informed how it should be filled out correctly since they were closed-response questions based on marking with an "X" in each question, the students were clarified in their doubts having more doubts the students from first years of secondary study. At the conclusion of the data collection procedure, the correct filling and coding of each of the sheets with the instrument was verified. It is important that a professional carry out this type of research, in this case I as a nursing professional went to explain the correct filling of the questionnaire since nursing is prepared in all areas of health such as the psychological area among others and therefore prepared for any doubt of the group of questions presented by each dimension of the instrument. As the reader can see in the Figure 1, it shows the application of the survey in the Education Institution.



Figure 1: Application of the surveys in the Educational Institution

2.5. Statistical analysis methods

At the end of the data collection process, a matrix prepared in the Microsoft Excel spreadsheet will be entered, then these will be exported to the statistical program IBM SPSS Statistics Base 23.0, it will proceed to its corresponding analysis. As it is a descriptive design research, the methods of descriptive statistics will be used for data analysis; where the tables of absolute and relative frequencies will be used, the measures of central tendency, among other tests for the analysis of the sociodemographic information, also corresponding to the variables and dimensions involved. Finally, tables and graphs will be obtained according to the sociodemographic data, general and specific objectives of the study; for later description and discussion.

3. Results

Below are three summary tables; the first will show the demographic data of the students who participated in the study, the second table shows the result of the variable Quality of life related to health, and the third table shows the results of each dimension.

Table 2: Sociodemographic data in students of an Educational Institution of Ventanilla (N = 728)

Age	**Minimum – Maximum**	**Media (D.T.)**
	12 – 18	14.06 (± 1.505)
Sex	**Frequency (f)**	**Percentage (%)**
Female	357	49.0
Male	371	51.0
Degree of the interviewee	**Frequency (f)**	**Percentage (%)**
First high school	164	22.5
Second high school	177	24.3
Third high school	162	22.3
Fourth high school	119	16.3
Fifth high school	106	14.6
Study shift	**Frequency (f)**	**Percentage (%)**
Morning	389	53.4
Afternoon	339	46.6
Type of Family	**Frequency (f)**	**Percentage (%)**
Nuclear	424	58.2
Single parent	176	24.2
Extended	33	4.5
Expanded	58	8.0
Reconstituted	26	3.6
Family equivalent	6	.8
Single person	5	.7
Disability, illness or medical problem	**Frequency (f)**	**Percentage (%)**
No	622	85.4
Yes	106	14.6

In Table 2, it has the sociodemographic data of the study participants, a total of 728 students. Regarding the age of the study participants, it was determined that they fluctuate in a range from 12 to 18 years old, with an average of 14.06 (+ 1.505) years old. Regarding sex, it was found that 51.0% are male. Fourth and fifth year of secondary school have the lowest percentages of students with 16.3% and 14.6% respectively. The majority of respondents, equivalent to 53.4%, study in the morning shift. 58.2% of the sample claims to be part of a nuclear family. Only 14.6% claim to have a disability, difficulty or some medical problem.

Table 3: Health-related Quality of life in adolescents of an Educational Institution of Ventanilla (N = 728)

		N	**%**
Health-related quality of life	**Low**	0	0.0
	Medium	298	40.9
	High	430	59.1
Total		728	100

In Table 3, it can see the health-related quality of life in adolescents of an Educational Institution of Ventanilla, where 430 students representing 59.1% have high quality of life and 298 students representing 40.9% have medium quality of life.

Table 4: Health-related Quality of life according to its dimensions, in adolescents of an Educational Institution of Ventanilla (N = 728)

		N	**%**
Physical well-being	**Low**	23	3.2
	Medium	360	49.5
	High	345	47.4
Psychological well-being	**Low**	6	0.8
	Medium	239	32.8
	High	483	66.3
Mood	**Low**	25	3.4
	Medium	219	30.1
	High	484	66.5
Self-perception	**Low**	7	1.0
	Medium	260	35.7
	High	461	63.3
Autonomy	**Low**	27	3.7
	Medium	333	45.7
	High	368	50.5
Relationship with parents	**Low**	25	3.4
	Medium	267	36.7
	High	436	59.9
Economic resources	**Low**	64	8.8
	Medium	400	54.9
	High	264	36.3
Friends and social support	**Low**	14	1.9
	Medium	254	34.9
	High	460	63.2
Social environment	**Low**	18	2.5
	Medium	321	44.1
	High	389	53.4
Social acceptance	**Low**	18	2.5
	Medium	166	22.8
	High	544	74.7

In Table 4, it can see the Health-related quality of life according to its dimensions in adolescents of an Educational Institution of Ventanilla, where the most affected dimension was that of economic resources with 64 students representing 8.8% having a level low. In the physical well-being dimension, it is noted that it presents a medium quality of life with a percentage

of 49.5%, giving an idea that adolescents from that educational center practice physical activity both inside and outside the educational institution. In the psychological well-being dimension, it is noted that they present a high quality of life of 66.3%, revealing that adolescents from the educational institution present emotions where they prioritize the positive ones and satisfaction with life. In the mood dimension, it is noted that it presents a high level with a total of 66.5%, thus expressing that the students present a balanced level of stress. In the self-perception dimension, it can observe that it presents a result of 63.3%; which corresponds to a high level, demonstrating that students have a good perception of their body image and physical appearance. In the autonomy dimension, it is noted that it presents a high level with a percentage of 50.5% showing that the educational institution does allow them to have time for their activities in their free time. In the relationship with parents' dimension, it appreciates that 3.4% of students do not have a good family atmosphere since they do not live with their parents, but with uncles and/or grandparents. In the economic resources dimension, it is noted that they present a medium level with a percentage of 54.9%, reflecting that the financial capacity of the parents is not low but that it does not cover the maximum with respect to the expenses of the students, since it was observed that most students have one or more siblings studying in lower grades. Regarding the friends and social support dimension, it presents a high level with a total of 63.2%, reflecting that the students have good communication with their classmates or friends who do not study with them. In the social environment dimension, it reflects a high level with a total of 53.4%, which shows a good feeling about school, also a good ability to concentrate and a positive feeling about school. Finally, in the social acceptance dimension, it is observed that a total of 2.5% presents a low level, reflecting that in the educational institution there are some students who express rejection of their peers.

4. Discussion

In the following study, the issue of health-related quality of life is raised from the point of view of promoting adolescent health, which wants to contribute to educational institutions which are part of adolescent educational training, which must include programs that allow adolescents to enhance their ability to interrelate and adequately shape their personality.

The participants in this study were high school students from a public school in the province of Callao, who had an average age of 14 years, from a lower-middle socioeconomic level in the district where the school is located, who mostly belonged to a nuclear family. Most of the students in this study did not have any significant physical disabilities, illnesses, or medical problems.

At a general level, it was found that the students who participated in this study had high levels of HRQL, this because they were very clear about their personal goals and objectives, optimistically seeing their future, as in other studies on the same subject, such as the study of Hidalgo et al [1], in this study it is evident that the present one focuses on school adolescents, which results in a low level HRQL since the students affirmed that they presented bullying among their classmates, thus demonstrating a Health-related quality of life from medium to low, therefore it is asked to delve into the dimensions that present difficulties.

Compared to other studies, this research only worked with the variable Health-related quality of life since the instrument used focuses directly on that variable and the type of population, therefore the KIDSCREEN 52 compared to its two existing types, holistically assesses the age group of people who carried out the research work.

The research work wants to demonstrate the related quality of life in adolescents since in these times, that group of people present problems most of them in the psychological part. In the following research work, it wants to demonstrate that the adolescent is a holistic person and therefore it must be studied in all its dimensions; In this study group, it verified that the educational institution presents few problems due to the result found that was between a medium and high level with respect to the variable Health-related quality of life.

5. Conclusions

It is concluded that the Health-related quality of life is the set of manifestations that a person presents most of them in the subjective part (emotions, sensations, among others); this is influenced by the state of health that is presented at the time; this already gives an idea of how the adolescent feels at the school stage. In this case, what we are looking for with this study is to give us an idea of how the adolescent feels at that moment.

It is concluded that the educational institution, the director provided the support for the realization of the survey and later the processing of the information given by the study population. The study was also successfully carried out thanks to the teachers of the institution since they offered class time and especially to the students who were the study population, since they were predisposed to collaborate with the study.

As a future research work, other health professionals are expected to carry out research work in localities where populations are vulnerable, such as the case of Pachacutec-Ventanilla; since other research could be carried out with other groups of people and thus obtain relevant results to complement the improvement of the Peruvian population.

Conflicts of Interest

The authors declare no conflict of interest.

References

[1] C. Hidalgo, T. Molina, R. Molina, R. Sepúlveda, V. Martínez, Montaño, Bullying y calidad de vida relacionada con la salud en adolescentes escolares Chilenos. Rev Med Chil. 2015; **143**(6):716–23. http://dx.doi.org/10.4067/S0034-98872015000600004

[2] E. González et al., "Diferencias de género en la calidad de vida relacionada con la salud en adolescentes escolarizados chilenos Gender differences in health-related quality of life of Chilean adolescent students. Rev Med Chil. 2016; **144**(3):298–306. http://dx.doi.org/10.4067/S0034-98872016000300004

[3] L. Rajmil, "Advances and challenges in the measurement of health related quality of life in the child and adolescent population. An Pediatr [Internet]. 2019; **90**(5) :261–2.: https://doi.org/10.1016/j.anpedi.2019.01.011

[4] I. Bica , J. Costa, "Original Article Sociodemographic infl uence in health-related quality of life in adolescents. Acta Paul Enferm. 2020;**33**:1–7. https://doi.org/10.37689/acta-ape/2020ao0054

[5] F. Vilugrón, C.A. Hidalgo et al., "Uso de sustancias psicoactivas y calidad de vida relacionada con la salud en adolescentes escolarizados. Rev Med Chil. 2017; **145**(12):1525–34. http://dx.doi.org/10.4067/s0034-98872017001201525

[6] K. Haraldstad et al., "Associations between self-efficacy, bullying and

health-related quality of life in a school sample of adolescents: a cross-sectional study. BMC Public Health. 2019; **19**(1):1–9. https://doi.org/10.1186/s12889-019-7115-4

[7] R.M. Fuentes-Chacón et al., "Psychosomatic symptoms as an expression of the deterioration of the health-related quality of life in adolescents. Aten Primaria. 2018; **50**(8):493–9. doi: 10.1016/j.aprim.2017.06.009

[8] KIDSCREEN-52 - kidscreen.org [Internet]. Available from: https://www.kidscreen.org/español/cuestionario-kidscreen/kidscreen-52/

[9] J. Valencia, P. Galvañ, C. Martínez, C. García, R. Martínez. Adjusted linguistic validation and psychometric properties of the Colombian version of KIDSCREEN-52. J Child Heal Care. 2019; **23**(1):20–34. https://doi.org/10.1177/1367493518777291

ASTES

Advances in Science, Technology and Engineering Systems Journal Vol. 5, No. 5, 973-983 (2020)

www.astesj.com

Special Issue on Economic Impact of COVID-19 on Companies & Consumers

ASTESJ

ISSN: 2415-6698

Covid-19 Pandemic Lockdown: The Consequences Towards Project Success in Malaysian Construction Industry

Muneera Binti Esa, Farah Salwati Binti Ibrahim*, Ernawati Binti Mustafa Kamal

Construction Management Department, School of Housing, Building and Planning, Universiti Sains Malaysia, Gelugor, Penang, 11800, Malaysia

ARTICLE INFO

Article history:
Received: 11 August, 2020
Accepted: 06 September, 2020
Online: 20 October, 2020

Keywords:
Covid-19
Lockdown
Movement Control Order (MCO)
Malaysia Construction Industry
Project Success

ABSTRACT

The Covid-19 is a pandemic issue that is causing widespread global disruption forcing lockdowns in many countries including Malaysia as an effort in disconnecting the virus from spreading. As an initiative, the Malaysia government has call for the Movement Control Order (MCO) as one of the lockdown alternatives starting on 18th March 2020. Due to that, the MCO has given a huge impact on Malaysia's industries including the construction industry. Hence, to successfully deliver projects, time and cost become the essential component which in this current scenario, most of the on-going projects declined to deliver the project according to the time and cost as planned. Thus, this paper intends to explore the consequences of the Movement Control Order (MCO) towards project success. In getting an authentic data and fast feedback from the respondents during this current scenario, uses alternate methods as face to face interview is not encouraged. The interview sessions were held thru telephone conversation with 8 contractors in Klang Valley and Penang which randomly selected based on contractor listing in Malaysian Construction Industry Development Board (CIDB) website and content analysis are used to figure out the main consequences using Nvivo software. Results from the interviews found that the MCO has resulted in 6 main impacts consists of (1) regulation compliance; (2) safety; (3) additional time for project delivery; (4) increase in development cost; (5) limited human resources supplies; and (6) limited resource availability on-site. These shows the MCO has given the negative impact to the project success. This result is important for the government to ensure their awareness on the consequences of the MCO towards construction industry and facilitate the construction players to overcome the six factors mentioned in this paper.

1. Introduction

The 2019 Novel Coronavirus or Covid-19 is currently a pandemic issue that is spreading globally [1] which have affected 9.54 million people and 485,000 recorded in 215 countries up to 25th June 2020 [2]. This pandemic was first identified in Wuhan City, located in Hubei Province in China [1,3,4]. Due to that, on January 11, 2020, the Covid-19 was recognised as a global pandemic by the World Health Organization. Then, on 30th January 2020, the Emergency Committee of the World Health Organization (WHO) has declared the on-going Covid-19 outbreak to be a global Public Health Emergency of International Concern (PHEIC) which the PHEIC defined as an *"extraordinary event" that "constitute a public health risk to other States through the international spread of disease" and "potentially require a coordinated international response",* this definition implies the situation faced is a serious, sudden, unusual or unexpected situation that can give a huge insinuation to the public health beyond the State's national border and it may require immediate internal action [5]. In the situation of Covid-19, the PHEIC is significant to prevent the outbreak from affecting other countries with weak health system.

Due to rapid spreading of Covid-19 among the people, a lockdown has been implemented in several countries affected by the virus to disconnect the virus from spreading. The lockdown is divided into two categories which are the nationwide traffic restriction and stay at home movement [6]. Hence, many sectors were advised to stop their operations and services during the lockdown including the construction sector [7]. In Malaysia's situation, the Covid-19 is not as worse as in United State of

*Corresponding Author: Farah Salwati Binti Ibrahim, Construction Management Department, School of Housing, Building and Planning, Universiti Sains Malaysia, 11800 Gelugor, Penang, Malaysia, farahsalwati@gmail.com

America (USA), Russia, United Kingdom, Brazil, Spain, Italy and China. However, tight measures have been implemented by the Malaysia government to prevent this pandemic from wide spreading. Like other countries, Malaysia has also implemented nationwide traffic restriction and stay at home order since 18th March 2020 until this date (RMCO). The government has imposed restriction in term of movement control order (MCO) with a special standard operation procedure (SOP) and not a tight lockdown as China's.

Furthermore, Covid-19 pandemic is not just affecting human health but also bringing the economy to the worst level where all the industry was severely hit. Therefore, construction activities were also facing project suspension and cancellation due to shortage of materials, equipment and parts because of the lockdown. Hence, most of the supplier had to close their businesses and they cannot deliver the requested materials during that time. Moreover, there are several consequences of lockdown to the construction industry as recorded in United State of America (USA) in term of time, cost, resource availability and construction worker layoff [8]. As for Malaysia, the government has also halted all construction progress within MCO phase 1 to phase 3.

In line with the issue, this paper intends to explore the consequences of the Movement Control Order (MCO) towards the project success in Malaysia's context. Hence, this paper will be explaining the theoretical background about the movement control order (MCO) and the related project success factors. Then, methodology used for this study will also be enlighten, followed by the findings, discussions and the conclusion for this study. It is important to acknowledge the consequences of the MCO towards project success because the result from this study will assist the government and industry to plan a post-Covid-19 roadmap to enhance the construction industry in the future specifically to overcome the issues of the consequences among affected construction players like contractor.

2. Theoretical Background

This section provides a theoretical background for the paper. The first part discusses the Movement Control Order in Malaysia's context, followed by the literature of project success and the current state of the Malaysian construction industry.

2.1. *Lockdown Alternative in Malaysia: Movement Control Order (MCO)*

Movement Control Order (MCO) known as *cordon sanitaire* refers to the restriction on the people movement from one place to another either locally or internationally which can cause spreading of unexpected disease or viruses. This movement control has been used as a preventive measure to stop the spreading of unwanted diseases or viruses. Moreover, the MCO in Malaysia was enforced under the Control and Prevention of Infectious Diseases Act 1988 and the Police Act 1967 [9]. In Malaysia, the government has implemented four (4) types of MCO as this date according to the situation needed with differing Standard of Operation (SOP) which are;

2.1.1. Movement Control Order (MCO)

MCO applied nationwide in Malaysia where most of the main sectors are not allowed to operate during this time and most of the workers are encouraged to work from home or stay at home to minimize the virus transmission started from 18th March until 28th April 2020 in three phases with every phase allocating 14 days of quarantine time [10]. To ensure the MCO successfully breaks the chain of Covid-19, there are six (6) restrictions or orders imposed during the MCOs period which are [9];

- Complete restriction of movement and gatherings nationwide, including religious activities, sports, social and cultural events. To enforce this restriction, all houses of worship and business premises are to be closed, except supermarkets, public markets, sundry shops and convenience stores selling essential goods.
- Complete travel restriction for all Malaysians going overseas and mandatory to undergo health checks and voluntary self-quarantine for 14 days.
- Complete restriction to foreign visitors and tourists into Malaysia.
- Closing of all kindergartens, public and private schools including day schools and residential schools, international schools, Tahfiz centres and all other institutions of learning in primary, secondary and pre-university levels
- Closing of all public and private institutions of higher learning nationwide including skills training institutes.
- Closing of all government and private premises except those involved in essential services such as water, electricity, energy, telecommunications, post, transportation, irrigation, oil, gas fuel, lubricants, broadcasting, finance, banking, health, pharmacy, fire prevention, prisons, ports, airports, security, defence, cleaning, food supply & retail.

2.1.2. Enhanced MCO (EMCO)

This EMCO phase started from 27th March and it only applied within certain areas with high cases of Covid-19 such as in Simpang Renggam, Johor; Sungai Lui, Selangor; City One, Kuala Lumpur; Selangor Mansion and Malayan Mansion, Kuala Lumpur; Jalan Masjid India, Kuala Lumpur and Wholesale Market in Selayang. In this EMCO, the government has announced this control to curb the spreading of the Covid-19 as well as to make it easier for the authorities to trace the cases unit by unit throughout the EMCO period. Therefore, the government has categorised the affected area in three colour zoning (red zone, yellow zone and green zone) as a differentiation to show the level of the affected area according to the numbers of Covid-19 active cases recorded. The red zone represents the area with more than 41 cases recorded and will be designated as EMCO area for fourteen (14) days or until the cases reduced to satisfied level. Meanwhile, for the yellow zone, it represents areas that recorded cases within 1-40 cases and for the green zone, represent "zero" cases area. There are a few accomplishments in the EMCO which are;

- All residents are prohibited from exiting the EMCO area throughout the EMCO.
- All non-residents and visitors are prohibited from entering the area throughout the EMCO
- All business activities are to be closed, except for the shops selling daily essential items in buildings
- Residents are allowed to use food delivery services
- A medical base will set up in the EMCO area.
- All in and out points of the EMCO will be sealed.

- The Royal Malaysian Police (PDRM), Malaysian Armed Forces (ATM), Angkatan Pertahanan Awam (APM) and Jabatan Sukarelawan Malaysia (RELA) will act as administers in the EMCO area.

2.1.3. Conditional MCO (CMCO)

Then, after the number of new Covid-19 cases have dropped to below 100 cases per day, the government has announced Conditional MCO (CMCO) as Phase 4 MCO starting on 4th May 2020 until 9th June 2020 [11], seeing a more relaxed implementation of CMCO regulation compared to the previous MCO regulations where certain sectors are allowed to reopen their business. The main purpose of this CMCO is to help the government regenerate and regain the momentum of Malaysia's economy, a step up from essential sectors only previously. Thus, starting 4th May 2020, the sectors that have obtained the permission to reopen their business from MITI (Ministry of International Trade and Industry) are allowed to operate but with a tight SOP (Standard Operational Procedures) determined by the government. There are few conditions and requirements that need to be fulfilled by the employers and employees in preventing the virus from spreading in their workplace including the construction sectors. According to the Prime Minister, within the MCO phase 1 to phase 3 period, the government has lost around RM 2.4 billion per day, meaning the total losses is around RM63 billion until 1st May 2020 and if the MCO continues for one more month, the overall total losses will reach RM98 billion [11]. Related to that, the construction sector also estimated about RM 11.6 billion per day in losses as stated by Minister of Work Department, Dato' Sri Hj Fadillah in *Bernama TV* interview session on 5th May 2020. Therefore, the implementation of CMCO is important for the government and industry to generate income but the prevention of the Covid-19 from spreading is still highly prioritised.

2.1.4. Recovery MCO (RMCO)

Starting on 10th June until 31st August 2020, the RMCO will take over as an exit strategy for the MCO and CMCO, where in this phase more economic sectors are allowed to be operated, sport and recreational as well as domestic travelling also are allowed but with a tight SOP. Moreover, education sectors are starting to gradually reopen in phases as in 24th June, only form 5 and 6 starts their school session while kindergarten will reopen on July, 1st. In the construction industry, the RMCO facilitated the industry to increase their productivity to produce sufficient construction materials to be supplied, as more skilled workers and working time returns back to normal.

Somehow, the MCOs, as well as the CMCO and RMCO with tight SOP, hugely impacted the construction industry either the established companies or small and medium companies. The consequences are not only related to the financial aspects but also impacting the project success as well as the project performance. Due to that, the productivity of the project performance has dropped and to deliver a project is seen to be hard during this time.

2.2. *Project Success*

In defining the project success, it is vital to clearly understand the terms of project success to avoid misleading information to this study. The definition of a project success is broad, ambiguous and subjective [12–14] as well as multidimensional in concepts [14–16] based on the process and the nature of the project [17]. Project success is frequently defined by the previous authors as the achievement of the project's objective, which in construction development, the project can be classified as project success when it efficiently achieved the iron triangle of time, cost, and scope or quality of the project outcome [18–20]. Moreover, [21] has defined "success" as the accomplishment of an aim in which the outcome is favourable.

Meanwhile, [22] expressed that project success is an accumulation of factors such as timely completion, within the budget, according to the specification and customer satisfaction. Then, [23] have defined the project success according to the project level where the project duration, monetary cost (budgeting) and project performance are highlighted as the key project success in their perspective. Additionally, there are a variety of factors that contribute to the project success other than factors mentioned above which the factors are according to the specific objectives for each of the projects such as safety, leadership, communication, teamwork, cognitive skill and so on [24]. Overall, project success is not just about completion of a project within the defined scope, time, and cost, nonetheless it is also about gaining the customer acceptance, stakeholder satisfaction, commercialization, and future project opportunity [25, 26]. Otherwise, for current construction industry, defining and measuring success lead to discussions on efficiency and effectiveness of the organizational, team and individual performance in managing the project lifecycle [18]. Despite that, there are different parties involved in a project such as the client, architect, contractor, and various surveyors and engineers which each of them will have his or her view of success according to their job scope [27]. Therefore, there is no common set of project success definition agreed yet due to the nature of the projects which are unique and differs widely in the practice.

According to the [25] there are two types of project success that needs to be precisely understood the differences between it; which are the project success "factors" and the project success "criteria". The *Project success factors* are related to the elements of a project that when it is influenced, it will increase the likelihood of success and act as the independent variables that make success more likely. Moreover, it is also referred to 'how to achieve' the project success [28]. Meanwhile, the *Project success criteria* is a measurement that used to judge on the success or failure of a project; these are the dependent variables that measures the success by focusing on "what to achieve" in the project. Besides, the success factors presence the inputs to the management system that directly or indirectly contribute to the success of a project, while success criteria are measures by which success of a project is judged [22]. Numerous previous studies on project success concentrated on identifying the success factors rather than success criteria as their subject because it is important to identify the success factors for a project before establishing which criteria should be used to judge or determine the project success [29]. Due to this explanation, this study indicates that the project success factors are the relevant type to be studied in this research because at the end of this research, the outcome will contribute to the body of knowledge for the industry and the government on what factors are affected due to the MCO in delivering a successful project; beneficial for them to overcome the issue based on the factors produced by this study.

Besides the listed project success factors as discussed above, the safety and health condition either the workers or the environment of construction sites and regulatory compliance should be one of the factors in successfully deliver the project

according to the current situation faced. It is because to ensure the project can be operated as usual without distressed project progress, the construction players need to play important roles in closely implementing the SOP announced by the government.

2.3. *Current Situation in Malaysia Construction Industry*

On 13th of April 2020, the Prime Minister has announced that the main services including construction sector is allowed to operate during the CMCO but with a strict SOP [11]. Later on 30th May, there are 28 of workers affected by Covid-19 in a construction site located in Jalan Ampang [30]. Hence, to overcome the spreading of Covid-19 in construction site while still be in full operation, the government has declared a specific SOP for construction sectors on 1st May 2020 stated under Act 520. This SOP also applicable for all construction sector related professional services (Quantity surveyor, engineers, architect firm etc.). Moreover, in the SOP, the developers and contractors are fully responsible to ensure their site workers and staffs follows all the terms and conditions particularly to keep the workers' health and hygiene as a priority. Besides, any violation of the SOP will cause the construction site to be closed.

As at 15th May 2020, CIDB has declared that within 20th April to 18th May 2020, there are 515 or 11% of the construction site in the whole Malaysia successfully complied to the SOP, meanwhile, 167 (4%) are non-compliance (warning notice) and seven (7) are ordered to be closed. Besides, there are 3,870 (85%) construction sites still not resuming their project at that time. Furthermore, as recorded on 22nd June 2020 through CIDB Telegram Channel, the operating construction site increased to 2245 (84%). Meanwhile, 437 (16%) construction site were issued warning notice and 19 (1%) of the construction site are ordered to be closed because of SOP non-compliance such as not implementing Covid-19 screening tests for the workers, not registered with CIDB, does not provide Covid-19 health supervisor and 90% not practising the SOP properly in the construction site. From the increment of the project which is successfully compliance to SOP, it was proven that the construction players have a good awareness and understanding regarding to SOP imposed by the government.

There are 15 actions highlighted by the government in the SOP for construction industry including the (1) Preparation of information and Documentation for the project (2) Workers management (3) Workers transportation vehicle (4) Workers movement (in-out construction site) (5) transportation of construction materials and supplies (6) Information blasting and awareness regarding the SOP in construction site (7) Emergency management and response (8) contact tracing (9) the entrance of the construction site/premise (10) Compliance that need to be implement while carrying out construction work (11) Toilet management (12) Time-break management (13) Procedure for returning from work (14) Accommodation at construction site/premises and (15) Record all the related data in for SOP compliance as required by the government [31].

Starting from the first phase until the third phase of MCO most of the construction site is directed to be closed by the government for approximately 6 weeks except for critical development categories. Due to this, most of the project schedule is interrupted and causes delay in delivering the project. The delay is not only related to the project progress on site; it also affected the suppliers who deliver the materials due to the restricted movement from one place to another place. The machinery availability is also limited and this caused hectic to the construction players. To overcome the lagging progress, extra work from all parties, additional time and cost should be prepared by the developers and contractors. Additionally, the limited number of workers are allowed to work on-site in conjunction with the social distancing hugely impacted the project's progress as well as productivity. In getting more precise information regarding the current scenario of the construction industry in Malaysia and the consequences that the construction players are facing now, this research is essential to be explored.

3. Methodology

In producing accurate and apparent data, a qualitative method of research was used for this study. A qualitative method chosen for this study is due to the appropriate method in collecting the data where the respondents experience the issue or problem under the study and the data was produced subjectively from their minds [32]. A stratified random sampling technique was used in this study in which simple random subsample was taken from different strata in the same or equal characteristic [33]. This technique is less in error and enhanced the precision of the sample selection. In this case, the population of this study is Malaysian construction players and the strata consists of contractors. Then, for subsample selection, a simple random sampling is used for each of the strata group. This study was conducted in Klang Valley and Penang where both of these areas are currently active in developing new construction project.

Table 1: Respondents Profile

Respondents	R1	R2	R3	R4	R5	R6	R7	R8
Designation	Contractor	Contractor	Contractor	Contractor	Contractor	Contractor	Contractor	Contractor
Years of Experience	5	10	20	10	15	1	7	10
Current Project	Housing	Housing	Housing	Housing	Housing	Housing	Housing	Housing
Expected Completion Time **Before** MCO	3 y	3 y	4y	8m	3.5y	3.2y	4y	4y
Expected Cost **Before** MCO (RM'000)	50	900	1.5 mil	470	1.5 mil	130 mil	NA	42 mil
Expected Completion Time **After** MCO	TBA	3.2y	4.6y	11m	4y	3.5y	4.7m	4.4y
Expected Cost **After** MCO (RM'000)	70	900	1.51 mil	611	1.8 mil	132 mil	Increase 20% from previous	42 mil

Due to the MCO, most of the construction company halted the construction activities and the employees are encouraged to work from home. Hence, the telephone conversation is selected as the medium for interviewing them. Before conducting the interview, the researchers have set the eligibility criteria of the respondent for this study such as respondents is a contractor, have an active project, involved in the construction project in Klang Valley and Penang, and registered with CIDB. Firstly, the researchers had selected a few companies through CIDB website, then the researchers browsed the selected company's website to identify their on-going project. After being satisfied with the criteria, the invitation email was sent to the respondents using their registered email in CIDB website. From 20 emails sent out, only 8 contractors gave feedback and willing to be part of this study. According to [34], the amount of the useable data obtained from each respondent is more important than the number of the participants in which the greater the amount of useable, the fewer the number of participants is needed. It also supported by [35] where the number of interviews between five and twenty-five interviews is enough to understand about their experience in that situation. Hence, eight respondents are adequate in getting feedback related to this study. Table 1 shows the respondents' profile.

An exploratory study has been conducted in this study by using semi-structured interview with the contractors based on their experience during the MCO. There are 17 questions were developed by the researchers which were designed to allow respondents to express their opinion and experience freely during the interview session. The interview was divided into 3 sections involving the social demographic which includes working experience in the construction field, current project, expected completion date & total development cost before MCO and expected completion date & total development cost after MCO. The next section is to measure their understanding and awareness on the SOP for the construction industry during the MCO and RMCO. Then, the last section is about the consequences of the MCO towards project success. The duration for each of the interview session was about 30 to 40 minutes. The questions for the interview were developed based on the previous literature and focused on factors generated by the previous project success factors namely; time, cost, human resource, resource availability, safety prevention and regulatory compliance.

Then, the data obtained from the interview were analysed using content analysis which according to the [36] the data for qualitative mainly consist of words, which can have several meanings and could lead into wrong interpretation, therefore the content analysis is used because it can identifying the quote, coding the quotes and categorising the codes and also mapping approach being used to find the relationship between the different categories. Thus, content analysis was being used in this study to analyse the data gathered from the interview by using Nvivo Software. Nvivo Software can quickly run the frequent word in the script to find the same theme, provides word cloud and the connection between the theme can easily be identified. During the telephone conversation, the researchers had recorded the interview session and the data was transcribed manually by the researchers. Then, the transcribed script was analysed using Nvivo which then the results are based on the highest theme that shows in the shape of boxes. The bigger box shows the high consequences event and vice versa. From the content analysis, this study found that there are 6 themes listed as the main consequences' factors of the MCO towards the project success.

4. Finding and Discussion

From the consequences of the MCO towards project success, this paper has classified the consequences into two which are in the perspective of *negative* where the factors turns the project to not achieving the success and *positive* views for the factors that help the project successful delivered because it is important to address both of these views to help the government, industry and construction players understand the current scenario as well as to guide them for planning post-Covid-19 for the industry.

4.1. *General Consequences of MCO*

From the content analysis, 6 themes were emerged from this study. These themes were further grouped into two general themes which are negative consequences and positive consequences of MCO towards the project success. The following findings and discussions are structured around themes that were mentioned by respondents as shown in Table 2. Meanwhile, the subthemes were considered as the factors influencing the theme in achieving the project success was shown in Figure 1 as the conceptual framework for this study. The first theme that was identified was time, which consists of delay on hand overring the project due to delay in material supplying, changing in work breakdown as well as rescheduling the project timeline because of time-lapsed during the MCO period. Cost emerged as the second theme, comprised of cost in providing hygiene kits (face mask, hand sanitizer, soap), Covid-19 tests for workers, cost in appointing Covid-19 Health Supervisor to oversee Covid-19 prevention on-site and cost in providing transportation for the workers to promote social distancing among the workers. Then, the safety aspect becomes the third theme with several subthemes which are significant in preventing the workers from the pandemic cluster like compulsory recording the daily temperature, social distancing, Covid-19 test for all foreign workers, workers management (movement, arrangement, job scope), workers hygiene, contact tracing, break time management, worker's residential management and regularly educate the workers about the pandemic. The fourth theme is related to the regulatory compliance which is the most significant in ensuring the project can be operated and the authority reserves the right to authorize or terminate the site due to noncompliance of SOP. The human resource theme consisted of the level of workers expertise (skilled, semi-skilled and unskilled), limited of workers at any one time at the same space, low productivity due to limited workers and working time as well as the termination of workers to reduce the project cost. The final and the sixth theme that was observed was the resource availability in the market and site which are limited including the material, equipment as well as skilled workers.

Table 2: The Results of the Consequences of MCO towards Project Success

Respondent	TIME				COST				SAFETY									REGULATION COMPLIANCE		HUMAN RESOURCES				RESOURCE AVAILABILITY	
	DP	RE	DM	BR	HK	COV	HS	TR	DT	SD	COV2	WM	WH	CT	TBM	WRM	EDU	FULL	VIS	WE	LW	LP	WL	LME	LSW
R1	/	/	/		/	/	/		/	/	/	/	/		/	/	/	/	/	/	/			/	/
R2	/	/			/	/			/	/	/	/	/	/	/			/	/		/	/			/
R3	/	/	/		/	/			/	/			/					/	/		/	/		/	
R4	/	/	/		/	/	/		/	/	/				/	/		/	/	/	/	/		/	
R5	/	/	/		/	/		/	/	/	/	/						/	/	/	/	/		/	
R6	/			/	/	/	/		/	/		/	/	/			/	/	/	/		/	/	/	/
R7	/	/		/	/	/	/	/	/	/	/			/				/	/	/	/	/		/	/
R8	/	/		/	/	/			/		/	/		/	/	/		/	/	/	/		/	/	/
TOTAL	8	7	4	3	8	8	4	2	8	7	6	5	4	4	4	3	2	8	8	6	7	6	2	7	5

Subthemes	Abb.
Delay on hand overring the project	DP
Rescheduling the project	RE
Delay on material supply	DM
Change the work breakdown	BR
Cost for providing hygiene kit (face mask, hand sanitizer, soap)	HK
Covid-19 test	COV
Cost appointing the Covid-19 Health Supervisor	HS
Providing worker's transportation	TR
Daily Temperature	DT
Social distancing	SD
Covid-19 test for all foreign workers	COV2
Workers management (movement, arrangement, job scope)	WM
Workers hygiene	WH

Subthemes	Abb.
Contact tracing	CT
Time break management	TBM
Worker's residential management	WRM
Educate the workers about the pandemic	EDU
Fully compliance the SOP regulation	FULL
An unexpected visit from the authority	VIS
Workers expertise	WE
Limited workers	LW
Low productivity	LP
Workers layoff/termination	WL
Limited material & equipment in the market and on-site	LME
Limited Skill workers	LSW

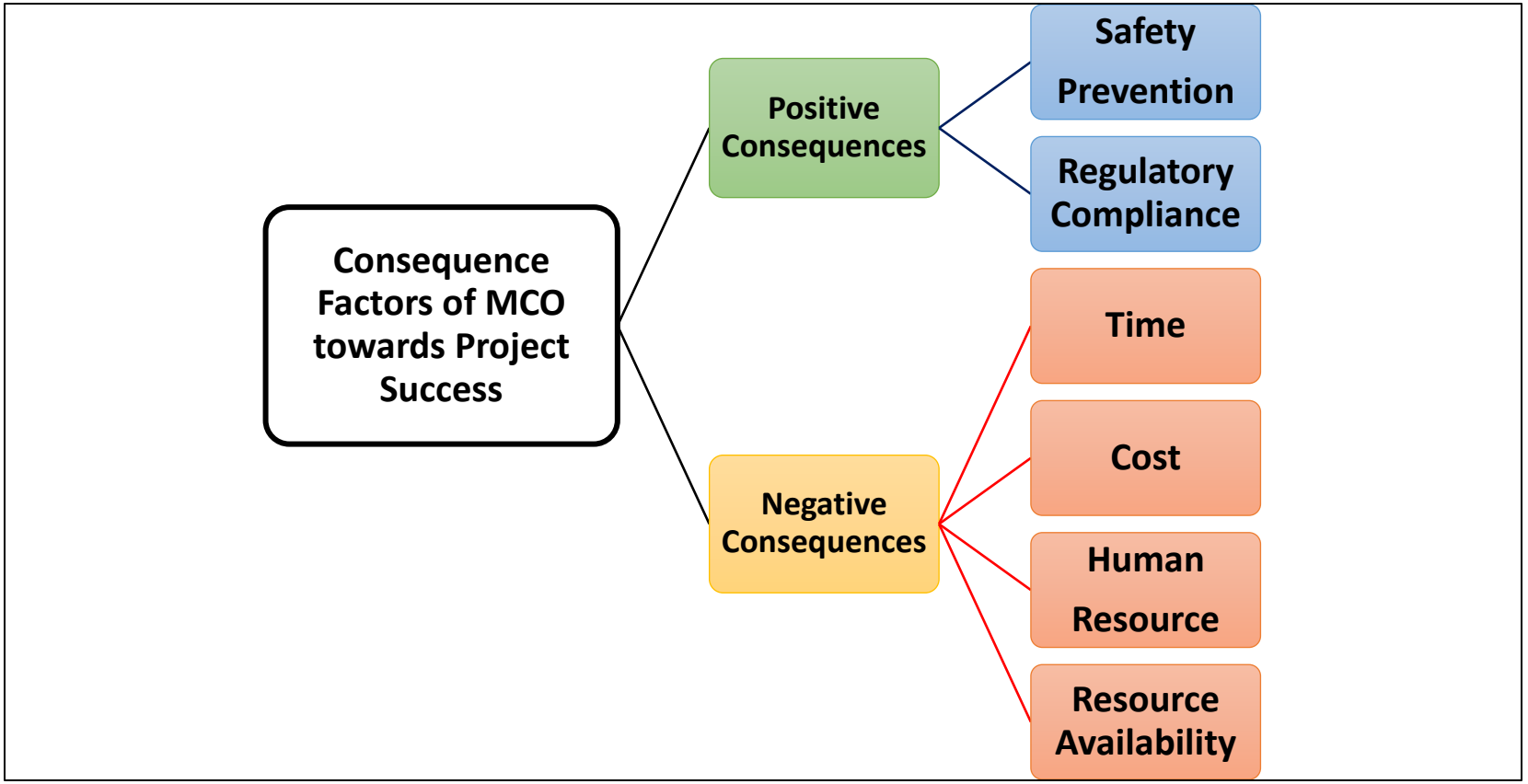


Figure 1: The Conceptual Framework of Consequences of MCO towards Project Success

4.2. *Negative Consequences*

The consequences of the MCO towards the project success gave negative impact mainly to (i) time, (ii) cost, (iii) human resources and (iv) resource availability in the market as well as on-site. Therefore, the construction players and government need to give more attention to these negative consequences factors in order to overcome the project delay, project losses and to optimize the project timeline and the project performance.

4.2.1. Time

Time is considered as one of the main factors that gave high impact to the project success, the project is considered successful when it can be delivered on time to the client within the budget and good in quality [37,38]. In the event of any delay, it will cause an extension of time and rise in cost, in which the project failed to achieve the success [25]. In regard to time, it has found that the MCO has delayed the handing over of the project to the client and this were affected by several issues like delayed material supply due to the manufacturers halting their business, as well as the supplier, cannot across the state or region during the MCO period. Due to that, the contractors need to reschedule the project timeline and change the work breakdown which invited stress among the contractors to fulfil the client requirement with tight budgeting in limited working time. Somehow, there are respondents mentioning that they are facing the extended time in their project of 2 to 7 months to complete the project development. As quoted by most of the respondents regarding the consequences of time during the MCO in Malaysia such as;

Respondent's Feedback on Consequences of Time – Delay & Extended of time
"delay on hand over the project, delay on material supply most of the work breakdown need to change and rearrange the time schedule"
"it's important to cover all the previous delay work"
"difficulties to hand over the project which delayed 2 months from the actual delivery time"
"our project delay for 2 months from the previous completion time"
"project timeline due to the limited time in term of working hours, material delivery and number of workers allowed in any one time. So, the project will be delayed for about 7 months from the actual timeline"

4.2.2. Cost

In term of cost, the respondents have mentioned that they are facing cost increment between RM 100,000 to RM 300,000 for their housing project of which 2 respondents facing a huge cost increment due to their big project involving the development of public project housing under Armed Forces. Meanwhile, another 4 respondents are involved in affordable housing project. Moreover, there are 2 respondents remaining at the same cost as the previous costing before the MCO because their project is already at the final stage therefore not much work to revise. Based on the respondent's feedback, the increment of the project costing because of two additional requirements highlighted in the SOP, the first cause is providing all the workers with face mask, hand sanitizer, keeping the site in good hygiene also cost of regularly sanitize the areas frequently used by the workers. Then, the second cause is related to Covid-19 tests that is compulsory to the workers especially the foreign workers before resuming their work on-site. Furthermore, 4 of respondents mentioned that appointing a Covid-19 team or health supervisor in the construction site will also increase the cost of their project. Below is the respondent's explanation regarding the consequences of MCO towards the costing aspect in construction project;

Respondent's Feedback on Consequences of Cost – Provide the workers with safety kits
"We also need to provide face mask, hand sanitizer and hand soap to promote hygiene among the workers, but the cost of providing the face mask is high due to daily usage"
"increased total development cost from the original because according to the SOP we need to provide face mask, hand sanitizer"
Respondent's Feedback on Consequences of Cost – Provide the workers with Covid-19 Test
"The most influential cost aspect is COVID-19 tests for the workers especially the foreign worker, you already know that the price for 1 test per person is between RM 150 to RM 300, so if we have about 20 persons foreign workers, so it will cost us a lot"
"running Covid-19 test to all workers especially the foreign workers before we resume work on site. The covid-19 test is expensive and you can calculate by yourself how many should we spend on that test if we have more than 10 workers, it will cost thousands of Ringgit Malaysia, huge cost"
Respondent's Feedback on Consequences of Cost – Providing Health Supervisor/Covid-19 Team at site
"we also need to appoint a health-supervisor as representative to manage and monitor the safety on-site including to monitor our compliance with all the SOP. This will also be an additional cost that we need to bear"
"we also need to appoint a health supervisor on-site to monitor the regulation compliance among the staffs and labourers on-site who can update us on the daily SOP compliance on-site"

4.2.3 Human Resources

The third negative consequences of MCO towards project success is focused on human resource which included the limited numbers of workers and skilled workers allowed to work in one time in the same area or space in practicing social distancing among the workers. Due to that, it will give a negative impact to the project productivity, previously the workers managed to complete 30% to 50% of work in one area or space with a few workers in one day but for this current situation, the productivity slid down between 10% to 30% according to the project. Other than that, the MCO also causes some of the unskilled workers layoff due to limited budget to hire them without any relevant skills. The skilled and semi-skilled workers are seen to be significant in this constricted project timeline [37].

Respondent's Feedback on Consequences of Human Resource – Limited number of workers & Skilled workers
"limited number of workers allowed to work in one time to ensure the social distancing are implemented, this will affect the productivity of work per day and the daily percentage of project completion"
"the limited numbers of workers allowed to work in one time also get us headache because some work need lots of people in one time so we need to arrange it by minimizing the workers and job scope"

"to maintain our project financial, some of unskilled workers are laid off because we need a skilled worker to work faster and reduce the error risk"

4.2.4. Resource Availability

Finally, limited resource availability on-site and in the market such as manpower, materials and machinery are also a challenging situation during the MCO period and causes time as well as cost overrun. According to [37], the construction delays causing risks on time and cost are including the materials, manpower, plants and equipment, changes, scheduling and control as well as government relation which all of these are related to the MCO situation.

Respondent's Feedback on Consequences of Resource Availability
"Resource are very limited in current situation due to the manufacturer are closed for a few weeks, so the supplier cannot get their sources and the limited resource in market has cause the price to go up. Other than that, the supplier also cannot deliver the exact amount that we need in one time because they need to get permission from the police before they can travel and deliver the material to us. So, we need to hold some of the work because of inadequate material"
"limitation on resource availability either in term of human, materials and machineries. All are interconnected by each other"

4.3. *Positive Consequences*

Besides the negative consequences of MCO, there are also positive consequences that give good impact to the construction industry. According to the respondents, all of them agreed that the MCO is a good initiative to disconnect the Covid-19 from spreading especially in the construction site where most of the time the social distancing and cleanliness are hard to practice. But, through this study, it can be seen that with the new SOP imposed by the government, changed the construction site into a better site and human resource management. The improvement of the safety practice aspect and the regulatory compliance by the construction players are the positive consequences that has been practised in the construction industry since the Covid-19 pandemic.

4.3.1. Safety Prevention

The safety in construction site is significant to ensure the site is free from hazards and to minimize the accidents in construction site [39]. At the same time, to increase the probability of project success, attention to construction safety need to be heightened in preventing the workers and other related parties from illness and accidents thus avoiding unnecessary cost and delays [40]. In the pandemic situation, every worker, supplier, staffs or any person who visited the construction site must be thermally scanned before entering the site. Moreover, the workers especially the foreign workers are compulsory to get Covid-19 test before they are allowed to work in construction site. Other than that, the contractor, as well as the construction workers, are responsible for managing the social distancing and hygiene in their construction site. In conjunction with that, the contractors practicing a proper workers' residential, time-break schedule (to make sure the canteen is not crowded in one time), worker's transportation for purpose of social distancing and control the worker's movement to minimize the spreading of the Covid-19.

Respondent's Feedback on Consequences of Safety Prevention
"daily temperature must be recorded for all workers before entering the site"
"compulsory for covid-19 test for all workers before our project resume back as usual to prevent the pandemic"
"For daily check, the body temperature is recorded for all of the person working or entering the site including the worker, supplier, site clerk, engineer and other related parties"
"All foreign and local workers are compulsory to be tested for covid-19 before they are allowed to work"
"make a marked area for practicing social distancing in worker's residential, café area, prayer room. We also record all the workers details and movements for contact tracing as well as the project detail"
"managing the workers on-site include managing their residential, time break scheduling, record all the movements and also provide transportation for our workers and we are strictly concerned regarding the hygiene"

4.3.2. Regulatory Compliance

In construction industry, the regulatory compliance is essential because failure to meet the regulation requirement means the project failed to meet the core requirement that has been decided [41]. In this research, it was found that this theme is significant in determining whether the construction site is allowed to operate or not because the authorities will randomly conduct an unexpected checking to the construction site and if the site is not properly implementing the SOP, their project will get warning notice or ordered to be closed. This tight regulation is good to practice in the construction industry to make sure all the construction workers and staffs are in a safe condition. The respondents also aware about the important to comply the SOP on the site.

Respondent's Feedback on Consequences of Regulation Compliance
"This part is hard to comment because it was related to the government order, so like it or not we need to comply to the SOP for construction because once we agree with that SOP, we need to adhere to it. The authorities will visit our project in unexpected time so we need to always be ready in term of project details, project documentation, workers detail and move in and out parties in the site for contact tracing"
"if you comply to all the SOP so you will be safe even if the authorities make unexpected spot check to your site. Then, we need to prepare a proper documentation management to record the project detail and the workers. Actually, it is difficult to manage all this, but if you want to save your project like it or not you need to do it"

4.4. *Discussion*

Based on the 6 consequence factors that have been decided in this study, the regulatory compliance became the main factor to determine if the project either is allowed to continue to work or closed during this pandemic issue. Once the project is directed to be closed because of non-compliance of the SOP, the project will be facing delay, losses and the cost will keep increasing day by day and in the end the project will be stuck and abandoned. Hence, the regulatory compliance is essential in this pandemic situation.

Then, followed the safety prevention factors, in which the safety precaution is important to prevent the workers and the construction site from being a new cluster for spreading the virus. There are several preventive actions that has been introduced by the Ministry of Health in the SOP and this safety prevention is connected to the regulatory compliance. The awareness and understanding regarding these two issues are seen to be positive due to the number of projects allowed to operate is getting higher.

Another 4 factors such as time, cost, human resource and resource availability is turned to negative aspect during this pandemic issue due to the movement control order for 6 weeks. The project timeline and costing need to rescheduled and recalculated which caused extended time and increasing costs. However, the project will still need to be done even if it will stress the contractors and workers to deliver the project within the new adjusted time and cost. In conjunction with that, the low production by manufacturers for suppling the materials will cause an extension of time because there is higher demand but low in supply. It also happened to the supply of machinery and limited skilled workers in this hectic situation. Furthermore, the contractors need to be more particular with all the issues in the construction site to minimize the error in the project progress and at the same time comply to the SOP especially in practising social distancing, hygiene and worker's health. From the discussion above, the MCO has gave high impact to the 6 consequence factors mentioned above and the government should give due concern to all the factors to facilitate the construction players especially those categorized as small and medium construction companies because most of them are affected during this MCO.

Due to these 6 factors, there are still have a few factors that attached with these factors, but in this current situation only these 6 factors are mainly have given high influenced to the project either it can be successfully delivered or not. Thus, the limited information from the respondents also being the limitation in this research due to the telephone conversation which sometimes having distressing because of the noise, unfocused of respondents while answered the questions and no face reaction can be detected.

5. Conclusion and Future Work

Based on the negative and positive consequences recorded through the interview session, the MCO has given lots of hindrances to the construction players compared to the positive consequences on the project success. The extension of time in delivering the project, the increased project costing and limited resource have hastened the project to achieve the project success. Currently, to facilitate the construction industry survival in this critical situation especially for the small and medium contractors' companies, CIDB has announced "CIDB Prihatin Initiative" with nine (9) schemes such as deferment on the levy payment, deferment of construction personnel skill training and fee payment for skill competency assessment. Also, the compulsory requirement for Covid-19 test is a burden to the contractors because of its cost, however, on 23rd June 2020, the government facilitate by CIDB and SOCSO (Social Security Organization) has launched a new initiative to help the construction players on this issue by providing them with a free Covid-19 test for the foreign workers especially for the small and medium construction company.

Through all the discussion in this paper, it can be concluded that MCO has given a lot of negative impacts towards the project success whereby the contributing factors to project success such as time, cost and resource availability are affected by the MCO. With limited additional time and tight budget has caused stress among the contractors especially for the project that needs more than RM 100,000 additional cost to complete their project (Refer Table 1). In another view, MCO has taught people about the self-care in preventing the Covid-19 especially in term of regularly practising good hygiene and social distancing. At the same time, it was observed that the SOP compliance level amongst construction players is seen to be better and this new norm should be maintained in the construction industry to avoid the second wave of Covid-19 in Malaysia. For further works, this research will continue to be conducted on other construction players including the AEC (Architecture, Engineering and Construction) company in Malaysia to investigate the impact of MCO to their organization.

Conflict of Interest

The authors declare no conflict of interest.

Acknowledgment

This research was supported by the Fundamental Research Grant Scheme (FRGS), Ministry of Higher Education [Grant No: FRGS/1/2019/TSSI11/USM/02/1]; Academic Research Grant School of Housing, Building and Planning, Universiti Sains Malaysia (1001.PPBGN.808005) and USM Fellowship Scheme

References

[1] X. Gao, J. Yu, "Public governance mechanism in the prevention and control of the COVID-19 : information , decision-making and execution," Journal of Chinese Governance, **0**(0), 1–20, 2020, doi:10.1080/23812346.2020.1744922.
[2] WHO, Coronavirus Disease (COVID-19) Outbreak Situation, World Health Organization, 2020.
[3] L. Wang, Y. Wang, D. Ye, Q. Liu, "A review of the 2019 Novel Coronavirus (COVID-19) based on current evidence," International Journal of Antimicrobial Agents, 105948, 2020, doi:10.1016/j.ijantimicag.2020.105948.
[4] T. Singhal, "A Review of Coronavirus Disease-2019 (COVID-19)," The Indian Journal of Pediatrics, 2020, doi:10.1007/s12098-020-03263-6.
[5] World Health Organization, WHO Emergencies Coronavirus Emergency Committee Second Meeting, 2020.
[6] Z. Yuan, Y. Xiao, Z. Dai, J. Huang, Y. Chen, "A Simple Model to Assess Wuhan Lock-down Effect and Region Efforts during COVID-19 Epidemic in China Mainland," Bulletin of the World Health Organization, 2020.
[7] S. Brown, L. Claeys, "Six Steps Construction Companies Can Take to Ride Out the Coronavirus Shock," Associated General Contractors of America, 2020.
[8] AGC, "Construction Layoffs Spread Rapidly as Coronavirus Shuts Down Projects, In Contrast to Job Gains Through February in Most Metroos," The Associated General Contractor of America, 2020.
[9] PMO, Speech By Prime Minister of Malaysia on 16 March 2020, 1–4, 2020.
[10] PMO, Perutusan Perdana Menteri Malaysia 18 Mac 2020, 1–6, 2020.
[11] PMO, Teks Perutusan Khas Perdana Menteri Malaysia Sempena Hari Buruh 1 Mei 2020, 1–17, 2020.

[12] D. Chan, "Cognitive Misfit of Problem-Solving Style at Work : A Facet of Person – Organization Fit," Organizational Behavior and Human Decision Process, **68**(3), 194–207, 1996.
[13] S.M. Sabry Elattar, "Towards Developing an Improved Methodology for Evaluating Performance and Achieving Success in Construction Projects," Scientific Research and Essay, **4**(6), 549–554, 2009.
[14] S.M.H.M. Al-tmeemy, H. Abdul-Rahman, Z. Harun, "Future Criteria for Success of Building Projects in Malaysia," International Journal of Project Management, **29**, 337–348, 2011, doi:10.1016/j.ijproman.2010.03.003.
[15] R. Atkinson, "Project Management : Cost , Time and Quality , Two Best Guesses and A Phenomenon , Its Time to Accept Other Success Criteria," International Journal of P, **17**(6), 337–342, 1999.
[16] A.J. Shenhar, J.J. Renierg, "Improving PM : Linking Success Criteria to Project Type," in Southern Alberta Chapter, Project Management Institute, Symposium "Creating Canadian Advantage through Project Management", Calgary, May 1996., 12, 1996.
[17] L.A. Ika, "Project Success as a Topic in Project Management Journals," Project Management Journal, **40**(4), 6–19, 2009, doi:10.1002/pmj.
[18] R. Müller, K. Jugdev, "Critical success factors in projects: Pinto, Slevin, and Prescott – the elucidation of project success," International Journal of Managing Projects in Business, **5**(4), 757–775, 2012, doi:10.1108/17538371211269040.
[19] R. Joslin, R. Müller, "The impact of project methodologies on project success in different project environments," 2015, doi:10.1108/IJMPB-03-2015-0025.
[20] M.M. Raziq, F.M. Borini, O.F. Malik, M. Ahmad, M. Shabaz, "Leadership styles, goal clarity, and project success: Evidence from project-based organizations in Pakistan," Leadership and Organization Development Journal, **39**(2), 309–323, 2018, doi:10.1108/LODJ-07-2017-0212.
[21] Oxford Dictionary, Oxford Dictionry, 2019.
[22] L.D. Nguyen, S.O. Ogunlana, D.T. Xuan Lan, "A Study on Project Success Factors in Large Construction Projects in Vietnam," Engineering, Construction and Architectural Management, **11**(6), 404–413, 2004, doi:10.1108/09699980410570166.
[23] M. Albert, P. Balve, K. Spang, "Evaluation of project success : a structured literature review," International Journal of Managing Projects in Business, **10**(4), 2017, doi:10.1108/IJMPB-01-2017-0004.
[24] J. Zuo, X. Zhao, Q.B.M. Nguyen, T. Ma, S. Gao, "Soft skills of construction project management professionals and project success factors: A structural equation model," Engineering, Construction and Architectural Management, **25**(3), 425–442, 2018, doi:10.1108/ECAM-01-2016-0016.
[25] T. Cooke-Davies, "The '" Real "' Success Factors on Projects," International Journal of Project Management, **20**, 185–190, 2002.
[26] P. Serrador, R. Turner, "The Relationship Between Project Success and Project Efficiency," Project Management Journal, **46**(1), 30–39, 2015, doi:10.1002/pmj.
[27] V. Sanvido, F. Grobler, K. Parfitt, M. Guvenis, M. Coyle, "Critical Success Factors for Construction Projects," Journal of Construction Engineering and Management, **118**(1), 94–111, 1992.
[28] W.M. Wan Abdullah, Critical Factors in Project Success: A Study of Public Sector Construction Projects in Malaysia., Universiti Malaysa, Malaysia, 2010.
[29] M. Podgórska, M. Pichlak, "Analysis of project managers' leadership competencies: Project success relation: what are the competencies of polish project leaders?," International Journal of Managing Projects in Business, 2019, doi:10.1108/IJMPB-08-2018-0149.
[30] M. Bavani, Developers, Contractors in KL Construction Sites to get Workers tested for Covid-19., The Star, 2020.
[31] N. National Security Council, Standard of Procedure for Construction Sector, 2020.
[32] J.. Creswell, J.. Creswell, Research Design Qualitative, Quantitative and Mixed Method Approaches, Fifth Edit, SAGE Publication, London, United Kingdom, 2018.
[33] Z. Mahmud, Hanbook of Research Methodology, A Simplified Version., Fourth Edi, UiTM Press, Kuala Lumpur, Malaysia, 2015.
[34] J.M. Morse, "Determining Sample Size," Qualitative Health Research, **10**(1), 3–5, 2000.
[35] J.. Creswell, Research Design Qualitative, Quantitative and Mixed Method Approaches, 4th Editio, 2014, doi:10.1192/bjp.112.483.211-a.
[36] Z. Zakaria, N. Mohamed Ali, A.T. Haron, A. Marshall-Ponting, Z. Abd Hamid, "Exploring the Adoption of Building Information Modelling (BIM) in the Malaysian construction industry: A Qualitative approach.," International Journal of Research in Engineering and Technology, **2**(8), 384–395, 2013, doi:10.1017/CBO9781107415324.004.
[37] C. Ramanathan, S.P. Narayanan, A.B. Idrus, "Construction Delays Causing Risks on Time and Cost - a Critical Review," Australasian Journal of Construction Economics and Building, **12**(1), 37–57, 2012.
[38] S.G. Tadewos, D. Patel, "Factors influencing Time and Cost Overruns in Road Construction Projects : Addis Ababa , Ethiopian Scenario : Review paper," International Research Journal of Engineering and Technology (IRJET), **5**(1), 177–180, 2018.
[39] S. Kanchana, P. Sivaprakash, S. Joseph, "Studies on Labour Safety in Construction Sites," The Scientific World Journal, 1–6, 2015.
[40] V.K. Bansal, "Application of geographic information systems in construction safety planning," International Journal of Project Management, **29**(1), 66–77, 2011, doi:10.1016/j.ijproman.2010.01.007.
[41] J.D. Schwierking, V.S. Anantatmula, "The Effective Practitioner Project Management and Regulatory Compliance: The Missing Ingredient?," Baltzer Science Publishers, (May), 48–61, 2015.

ASTES

Advances in Science, Technology and Engineering Systems Journal Vol. 5, No. 5, 984-990 (2020)

www.astesj.com

Special Issue on Multidisciplinary Innovation in Engineering Science & Technology

ASTESJ

ISSN: 2415-6698

The Impact of Innovation on the Performance of Manufacturing Enterprises in Vietnam

Thi Anh Van Nguyen*, Khac Hieu Nguyen

Department of Industrial Management, HCMC University of Technology and Education, Ho Chi Minh City, 700000, Vietnam

ARTICLE INFO

Article history:
Received: 23 August, 2020
Accepted: 29 September, 2020
Online: 20 October, 2020

Keywords:
Product Innovation
Technology Innovation
Organization Innovation
Firm Performance
Manufacturing Enterprises

ABSTRACT

This paper examines the impact of innovation on the performance of manufacturing enterprises in Vietnam. Innovation is measured by product innovation (3 observed variables), technology innovation (8 observed variables), and organization innovation (6 observed variables) while firm performance is measured by revenue and profit. The OLS regression model was used with data collected from 806 enterprises in four industrial sectors. The results show that innovation has a positive effect on firm performance. From the results, some implications are proposed to improve the performance of manufacturing enterprises in Vietnam.

1. Introduction

Nowadays, with the changing business environment, innovation is the key to decide the success or failure of many businesses. In the world, innovation takes place quickly and strongly. Many studies show that innovation (technological innovation, product innovation, organizational innovation) has a positive effect on the performance of enterprises. However, most of the studies in Vietnam focusing on small and medium-sized enterprises and these studies mostly ignored the impact of the innovation factor on the performance of enterprises. Ho Chi Minh City is the largest economic center in Vietnam, and a place to welcome investment waves as well as technological innovations. In recent years, the city has had a policy of investing in the development of four key industries: the Food processing industry; Pharmaceutical-rubber industry; Mechanical industry and Electronics & Information technology. However, measuring the impact of policies as well as the innovation on performance is an issue of little concern. This is a research gap for the authors to implement the study **"The impact of innovation on the performance of manufacturing enterprises in Vietnam".** This paper examines the relationship between innovation (including technological innovation, product innovation, organizational innovation) and business performance (including revenue and profits). From the results, the paper proposes some recommendations to improve the performance of enterprises in four key industries in Ho Chi Minh City.

In this article, innovation includes technological innovation, product innovation, and organizational innovation. Business performance is analyzed and measured based on revenue and profit.

2. Literature review and research model

This section presents related concepts such as innovation, product innovation, technological innovation, organizational innovation, and the four key industries. Studies of the impact of innovation on the performance will be reviewed in the following part. Finally, a research model will be proposed based on the previous researches.

2.1. Related concepts

2.1.1 Innovation:

Innovation has become the main driving force of economic strength and national competitiveness. Most people think that innovation only brings technological aspects to create outstanding new products, such as Apple's iPad, Sony's PlayStation, or applying artificial intelligence to business, etc. Others argue that innovation is only associated with research and development (R&D) activities conducted at national universities and laboratories. This concept is too limited because innovation has a much broader meaning [1].

Innovation nowadays is understood as "a new idea, creative thought, or new imagination in the form of equipment or methods". Innovation is often seen as the application of better solutions to meet new requirements and existing market needs. The innovation takes place through the provision of new products, new processes, new services, new technologies or new efficient business models

*Corresponding Author: Thi Anh Van Nguyen, Email: anhvan@hcmute.edu.vn

[2]. Innovation is related invention, but not like it, because innovation is most likely related to the actual implementation of an invention (i.e. new/improved ability) to create a meaningful impact in the market or society, and not all innovations require an invention [3], [4].

A fairly complete definition of the Organization for Economic Co-operation and Development (OECD)'s innovation is "implementing a new product or a significant improvement (for a particular product or service), a new process, marketing method, or a new organizational method in business practices, workplace organization, or external relations " [5]. From here, we can see the concept of innovation including technology and non-technology. In this study, the concept of innovation used includes product/service innovation; technological innovation and organizational innovation.

2.1.2. Product innovation

Product innovation refers to the creation and introduction of new products and services, whereby the direction of innovation is associated with the speed of innovation (necessary time to develop new products), the ability to replace regular products with improved versions and the ability to launch new products to new markets [5] [6].

2.1.3. Technology innovation

Technology innovation is the replacement of a major part or the whole of an existing technology with more advanced and more efficient technology. Technology innovation aims to increase the productivity, quality and efficiency of the production process or create a new product or service to serve the market.

Technological innovation includes new products and processes and significant technological changes of products and processes [7]. An innovation has been made if it is launched in the market. Technological innovation is inevitable for companies that want to develop and remain competitive or achieve the goal of entering new markets [8]. There are many variables that represent technological innovation such as: technology infrastructure (computers, internet, R&D costs, etc.); government support for technology; enterprise competencies (enterprise training, technology strategic plan, ...) and corporate culture (human resource level, management support, ...).

2.1.4. Organization innovation

Organization innovation involves upgrading management processes through new business approaches. Organization innovation can improve business performance by supporting necessary changes, reducing transaction and administrative costs, improving workplace satisfaction, reducing input costs [9]. Organization innovation includes training programs, product design programs, and management group creativity in problem-solving [10]. In 2006, authors proposed that organizational innovation involves management efforts to refresh organizational habits, procedures, mechanisms or systems to create ultimate ecological innovation.

2.1.5. Four key industries

According to the Ho Chi Minh City General Statistics Office [11], the codes for the four key industries are shown in Table 1 as follows:

Table 1: Industries belong to 4 key industries groups

Key industries group	Industry code	Industry name
Foods (1)	11	Beverage manufacturing
Pharmaceutical chemicals - Rubber (2)	20	Chemicals and chemical products manufacturing
	21	Medicine, pharmaceutical chemicals and pharmacognosy manufacturing
	22	Rubber and plastic products manufacturing
Mechanical (3)	24	Metal production
	25	Manufacturing products from prefabricated metal (except machinery and equipment)
	28	Producing machines and equipment not classified in any category
	29	Motor vehicles manufacturing
	30	Other means of transportation manufacturing
	27	Electrical equipment manufacturing
Electronics and information technology (4)	26	Manufacturing electronic products, computers and optical products

2.2. Study overview

2.2.1. Overview of related research works in the world

Currently, the issue of innovation is being strongly concerned in the world, especially with the strong development of the industrial revolution 4.0. Therefore, there are a lot of researches related to this field. In the context of the topic, the author reviews a number of studies related to the question of how innovation affects the company's operating results such as revenue, profits, and costs.

In 2008, the researcher collected data from 7302 companies in Europe to test the relationship of using technology via the internet, different types of innovation and the performance of enterprises. Research results indicated that all types of product and process innovation (including products related to e-commerce and traditional products) have positive effects on revenue and labor force growth [12]. Another research studied small and medium-sized companies in Portugal on the relationship between Total Quality Management (TQM), customer orientation, innovation and the operation of businesses [13]. The author concluded that most of the components of TQM affect customer orientation and business performance. Meanwhile TQM does not affect innovation. However, innovation affects business performance [13].

In 2010, the research on 600 small and medium-sized companies in Australia was done and proposed that the enterprise formal structure and innovation strategy are the main keys affecting enterprises' operations [14].

In 2014, the relationship between innovation (process innovation, product innovation, organizational innovation) to the performance of enterprises in 121 enterprises in Taiwan were investigated in some other papers. They suggested that

organizational innovation has the most positive impact on the performance of businesses. Meanwhile, process innovation and product innovation affect organizational innovation, and organizational innovation affects the performance of businesses [15].

In 2017, Rangus and Slavec examined the relationship between organizational characteristics, firm's innovation and firm performance. After studying 421 manufacturing and service companies in Slovenian, they proposed that innovation has a positive impact on the performance of businesses [16].

Recently, a study used the Ordinary Least Squares (OLS) and simultaneous equation models to analyze large data which included 63303 firms from 13 different European Union countries. The results showed that both human capital and the number of adopted eco-innovation strategies influenced positively firm performance [17]. Another study analyzed the impact of innovation on firm performance in developing economies. The study used data from 8,551 enterprises which were surveyed between 2014 and 2016 covering 19 Sub Saharan African countries. The CDM model and ordinary least squares method were adopted to analyze the effect of domestic R&D on innovation output, and the contribution of innovation to firm performance in the sub region. The result showed that both product and process innovations had a positive and significant effect on firm performance [18].

In general, although studies are conducted at different times in many countries, the results are quite similar in testing the relationship between innovation and business performance.

In the industrial revolution 4.0 and the current globalization, innovation is really an urgent issue for businesses in Vietnam in general and Ho Chi Minh City in particular. However, according to experts, the rate of innovation in Vietnamese enterprises is very low. There are nearly 600,000 businesses in the country, most of them are using technology lagging behind the average level of the world from two to three generations.

Ho Chi Minh City is an important economic, cultural and educational center of Vietnam. The industrial production value of Ho Chi Minh City accounts for about 45% of industrial output value in the southern key economic region and contributes about 26% of the national industrial production scale [19]. The investment policy of Ho Chi Minh City is to focus on investing in four key industries: mechanical engineering, electronics, chemicals - rubber - plastic and food processing. However, studies on innovation issues in these enterprises and the impact of innovation on business performance are limited.

Most of the research on innovation and business performance in Vietnam is about small and medium enterprises (SMEs). In 2008, some researchers examined the relationship between innovation and export at Vietnamese SMEs and concluded that innovation has an impact on export [20]. For instance, some authors surveyed 389 SMEs in Can Tho City in 2011. The results showed that factors such as the level of access to government support policies, the education level of the business owner, the size of the business, the social relationship of the enterprise and the revenue growth rate affect the efficiency of business operation of SMEs in the Can Tho city [21].

One of the few studies on innovation to business results of Vietnamese enterprises was conducted by Quan Minh Nhut in 2018 [22]. The author surveyed primary information from 55 randomly selected agricultural enterprises representing the agricultural enterprises in Ben Tre province. After studying the effect of the scientific and technological investment on enterprises' business results, discriminatory analysis results showed that there are 4 statistically significant factors affecting the difference of enterprises' profit: total revenue, investment capital for application of science and technology, type of enterprises and market expansion [22].

Finally, in 2019, some authors did research on the drivers of firm productivity, focusing on the role of international management standards certification in Vietnam. They concluded that the possession of an internationally recognized standard certificate leads to significant productivity. They also proposed that the effect of certification on productivity is particularly strong for firms with technological innovation [23].

2.3. Research model

From the above results, most of the researches concluded that innovation has a positive impact on the performance of enterprises. Therefore, the author proposes a research model with the dependent variable as the business performance of the enterprise, measured by revenue and profit. Independent variables are product innovation, technological innovation and organizational innovation.

After reviewing the above studies, the author proposes the following model:

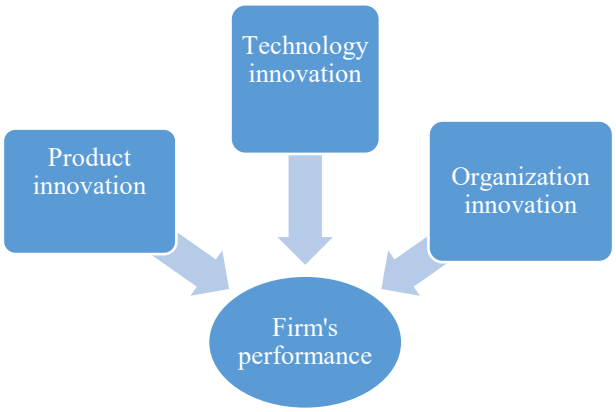


Figure 1: Proposed Research model

3. Research methodology and data

In order to test the proposed research model (Figure 1), the author uses Ordinary Least Squares (OLS) regression. There are many studies which did research about firm performance by OLS method and the results are consistent and reliable [17], [18], [24]-[26]. In this study, the authors suggest dependent variable denoted by Yi, independent variable denoted by Xi and error denoted as u_i, a constant β1 and a vector of regression coefficients β2. The regression equation is expressed as follows:

In which, Yi is a vector of dependent variables including: Revenue, Profit, Xi is an independent variable vector. Details of variable encoding and definitions are shown in the following table.

$$Y_i = \beta_1 + \beta_2 X_i + u_i$$

Table 2: Variables names and definitions

Variable name	Definition
Revenue	Log10 revenue of the enterprise in 2018 (Unit: Million VND)
Profit	Log10 profit of the enterprise in 2018 (Unit: Million VND)
Product Innovation	
New products/services	Binary variable, equal to 1 if the enterprise develops new products/services or innovates the existing products/services.
Quantity of new product types	Quantity of new products/services launched to the market in 2018
Cost for testing new products/services	Cost for testing new products/services in 2018. (Unit: Million VND)
Technology Innovation	
New technology investment	Binary variable, equal to 1 if there is any technology innovation or improvement of the current technology.
Cost of hiring machines and technology	Expenses for hiring/buying specialized machines, equipment, software and new technologies in 2018. (Unit: Million VND)
Cost of improving machines and technology	Expenses for the improvement of machines, equipment, specialized software and technologies in 2018. (Unit: Million VND)
Cost of technology project research	Expenses for technology project research in 2018. (Unit: Million VND)
Level of computer equipment	Level of computer equipment is calculated by the quantity of current equipment dividing by the actual quantity of the equipment needed for work.
Using internet/computer network	Binary variable, equal to 1 if the enterprise use internet or computer network
Private information website	Binary variable, equal to 1 if the enterprise has its own portal/website.
Cloud computing model	Binary variable, equal to 1 if the enterprise uses cloud computing model for work.
Organization Innovation	
New marketing method	Binary variable, equal to 1 if the enterprise has a new marketing method, new experience for customers.
New management method	Binary variable, equal to 1 if the enterprise has implemented a new management and organization method.
Research & Development (R&D)	Binary variable, equal to 1 if the enterprise has R&D department.
Science and Technology Development Fund	Binary variable, equal to 1 if the enterprise has established Science and Technology Development Fund.
Training cost	Labor/human resource training costs in technology hiring/innovation/research activities in 2018 (Unit: Million VND).
Government's support	Binary variable, equal to 1 if the government assists in innovation.

The data was from the surveys conducted in enterprises in four key industries including: Food processing industry; Pharmaceutical-rubber industry; Mechanical industry and Electronics & Information technology. The results obtained 806 qualified answers.

4. Research results and discussion

4.1. Descriptive statistics

Survey results collected 806 qualified samples, of which enterprises in the field of mechanical manufacturing - automation accounted for 47.8%; plastic - rubber sector (29.5%); food processing (16%); and the lowest is information technology - electronics and telecommunications (6.7%).

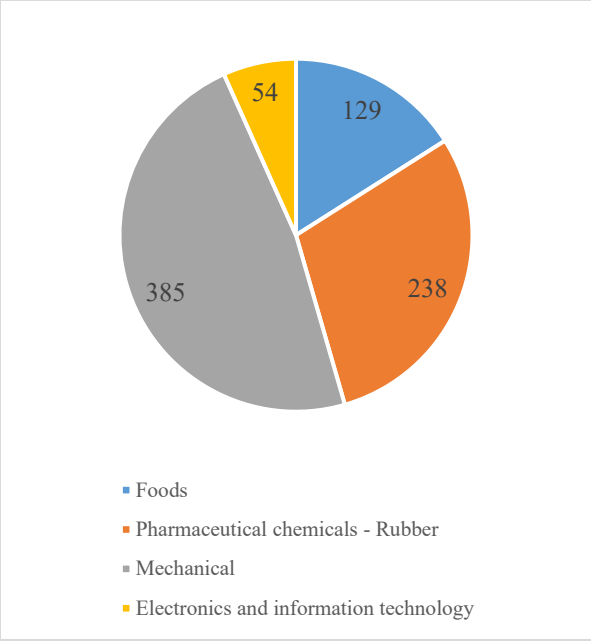


Figure 2: Number of surveyed companies in four sectors

4.2. Regression results with the dependent variable REVENUE and PROFIT.

To see the impact of innovation on the performance of enterprises, the authors analyze data by the OLS regression method. Details of regression analysis results are presented in Table 3 and Table 4. In order to ensure that the regression model is not faulty, the authors tested multi-collinearity and heteroscedasticity error of the model. The results of the multi-collinearity test show that all the magnification coefficients are less than two, hence, we can conclude that the regression equation does not occur the multi-collinearity phenomenon. The heteroscedasticity error is checked by the White test. The results show that there is no heteroscedasticity error because of the significance of Prob (F)> 10%.

Table 4: Regression results with the dependent variable is REVENUE

Observed variables	Coef	P-Value	VIF
Intercept	3.866	0.000	
Cost of hiring machines and technology	0.000001**	0.028	1.10
Expenses for improving machines and technology	0.000111***	0.000	1.07
Cost of technology project research	-0.000004	0.834	1.19

Cost for testing new service/products	0.000027***	0.004	1.06
Training cost	0.000324*	0.078	1.24
Quantity of new product types	0.00408	0.254	1.15
Level of computer equipment	0.000384	0.579	1.04
Using internet/computer network	0.367**	0.045	1.07
Private information website	0.2581***	0.000	1.18
Cloud computing model	-0.0519	0.529	1.15
Government's support	0.1935**	0.005	1.12
R&D	-0.0357	0.680	1.31
Science and Technology Development Fund	0.212	0.239	1.16
New products/services	0.0349	0.701	1.67
Investment in new technologies	0.2904***	0.000	1.61
New marketing method	-0.2525***	0.009	1.49
New management method	0.5946***	0.000	1.23
R-squared	0.302649		
F-statistic	20.06607***		
Prob(F-statistic)	0.000000		

Note: *, ** and *** represent for the level of significance 10%, 5% and 1%, respectively.

The results of the regression analysis show that the factors affecting revenue are Expenses for hiring machines and technology; Expenses for improving machines and technology; Cost for testing new service/products; Training costs; Using internet/computer network; Private information website; Government's support; Investment in new technologies; New marketing methods; New management method.

Table 5: Regression results with the dependent variable is PROFIT

Variable	Coef	P-Value	VIF
Intercept	5.1103	0.000	
Cost of hiring machines and technology	0.000001***	0.000	1.10
Expenses for improving machines and technology	0.000023***	0.000	1.07
Cost of technology project research	-0.000004	0.126	1.19
Cost for testing new service/products	0.000008***	0.000	1.06
Training cost	0.000082***	0.004	1.24
Quantity of new product types	0.001156**	0.037	1.15
Level of computer equipment	0.000172*	0.108	1.03
Using internet/computer network	0.0101	0.722	1.07
Private information website	-0.00092	0.915	1.18
Cloud computing model	-0.0051	0.691	1.15
Government's support	0.0027	0.800	1.12
R&D	0.0305**	0.023	1.31
Science and Technology Development Fund	0.1019***	0.000	1.16
New products/services	0.0143	0.309	1.67
Investment in new technologies	-0.0018	0.879	1.61
New marketing method	0.0006	0.967	1.49
New management method	0.02431***	0.007	1.23
R-squared	0.261308		
F-statistic	16.37629***		
Prob(F-statistic)	0.000000		

Note: *, ** and *** represent for the level of significance 10%, 5% and 1%, respectively.

The results of the regression analysis show that the factors affecting profit are: Expenses for hiring machines and technology; Expenses for improving machines and technology; Cost for testing new services/products; Training costs; Quantity of new product types; Level of computer equipment; R&D; Science and Technology Development Fund; New management method.

4.3. Research results discussion

Factors positively affecting both revenue and profit: Cost of hiring machines and technology; Expenses for improving machines and technology; Cost for testing new services/products; Training cost; New management method. Specifically, the greater the cost of hiring/buying specialized machines, equipment, software and new technologies in 2018, the greater the revenue and profit. The results for the cost of improvements to machines, equipment, specialized software, technology in 2018, costs for testing new products/services and training costs in 2018 are similar. These results appear to be new contributions for firm performance studies.

Normally, we assume that cost will decrease revenue and profit. However, the results in this case show that the following costs will help revenue and profit increase: expenses for hiring/buying machinery and equipment, specialized software, new technology; cost of improvements to machines, equipment, specialized software, technology; costs for testing new products/services; costs for training labors/human resources in hiring/innovating/technology research activities in 2018.
In [27], the author presented these costs to be called prevention costs or quality costs in the company. These costs are not only to ensure the creation of a product/service that meets market needs, but also to prevent customers from being dissatisfied with the product/service, thereby reducing the failure costs of the company. Therefore, these costs bring many benefits such as increasing customer satisfaction, increasing sales and profits.

In addition, the observed variable "new management method" has a positive impact on revenue and profit of businesses with a significant level of p = 1%. In an organization, management greatly affects the performance of the company. With the business environment constantly changing, it is required that the management method must be improved and refreshed to suit the general context. That is the reason why implementing a new management and organization method in businesses positively affects revenue and profit.

Factors that only affect revenue: Using internet/computer networks; Private information website; Government's support; Investment in new technologies; New marketing method. Specifically, the revenue of businesses will be higher if businesses use internet or computer network, has private information website, get support from the government, invest in new technology or innovate the existing technology. The results are same as the results of some previous studies. However, if the enterprises apply new marketing methods, new experiences for customers, the revenue will decrease. The use of supporting tools such as computers, internet, websites will help businesses operate more effectively, leading to better sales. Businesses that have support in innovation will also have a better competitive advantage, hence, the revenue is also better. However, according to the analysis results, the revenue of the businesses that have new marketing methods and new experiences for customer's decreases; This may be due to the high cost of these marketing methods or the inappropriate marketing methods, resulting in low efficiency.

Factors that only affect profit: Quantity of new product types; Level of computer equipment; R&D; Science and Technology Development Fund. The study results show that the more the new types of services/products are launched to the market in 2018, the higher profit the businesses get. Furthermore, the higher level of

computer equipment, the greater the profit. Also, if the businesses have R&D department or have Science and Technology Development Fund, the profit will increase. The results are equivalent to the results of some previous studies.

5. Conclusions and policy implications

The analysis results show that the factors of technology innovation, product innovation and organizational innovation all have observable variables affecting the revenue and profit of enterprises in four key industries in Ho Chi Minh City. The authors propose a few recommendations to improve business performance for these businesses as follows:

First, businesses should invest in prevention costs such as: innovation costs, costs of testing new products/services; training costs. These costs are essential for the sustainable development of businesses, improving operational efficiency as well as business performance[27].

Second, enterprises need to improve and innovate management methods in the organization to suit the business environment. The research results show that the "new management method" has the greatest positive impact on both revenue and profit. This reaffirms the role of management in the organization. Nowadays, there are many management methods in the world that Vietnamese enterprises can apply such as: ISO 9001, ISO 14001, ISO 22000, ISO 27000, etc. Businesses choose for themselves the most appropriate management model depending on the different industries and fields of operations. And it is greatly important to constantly improve and innovate to keep up with the changes in the business environment and organizational context.

Third, businesses should equip themselves with supporting tools such as computers, internet, private websites, etc. With the development of information technology nowadays, the above tools do not only help businesses increase revenue (according to analysis results), but also help businesses improve working efficiency, enhance brands, reach customers more easily, thereby improving the competitive advantage of businesses.

Fourth, the government needs to promote the support of innovation for businesses. The support here is not only financial but also support for skills training, management method updates to raise awareness as well as skills for workers; create a transparent startup ecosystem, a fair playing field for businesses. *Finally,* enterprises should have a research and development department or set up a science and technology (S&T) development fund. According to the analysis results in 4 key industries in Ho Chi Minh City, enterprises that have either of these two sections will have higher profits. As experts have said, the philosophy in any management system is "do it right from the beginning". R&D departments or S&T development funds are the original incubators for ideas. If this nursery produces good seeds, of course the results will be good.

Limitation of the study: Although the paper has achieved some results, the research still has some limitations. The study only analyzes data in a specific period of time, has not yet analyzed data to see the fluctuation of the dependent variable over time. The thesis has just verified the results by logit regression model but has not compared the results with other models. The study was conducted only in Ho Chi Minh City but not in other localities in Vietnam. The authors hope to carry out further studies to improve the above limitations.

References

[1] National Department of Science and Technology Information, "Report "Global innovation policy"," 2012. [Online]. Available: http://www.vista.gov.vn/.

[2] S. Maranville, "Entrepreneurship in the Business Curriculum," J. Educ. Bus., **68**(1), 27–31, Oct. 1992.

[3] P. Frankelius, "Questioning two myths in innovation literature," J. High Technol. Manag. Res., **20**(1), 40–51, 2009. https://doi.org/10.1016/j.hitech.2009.02.002

[4] K. Bhasin, "This Is The Difference Between 'Invention' And 'Innovation,'" 2012. [Online]. Available: https://www.businessinsider.com/this-is-the-difference-between-invention-and-innovation-2012-4.

[5] OECD, "Measuring Innovation: A New Perspective," 2010. [Online]. Available: http://www.oecd.org/.

[6] D. I. Prajogo and A. S. Sohal, "The integration of TQM and technology/R&D management in determining quality and innovation performance," Omega, **34**(3), 296–312, Jun. 2006.

[7] E. OECD, Presentación Oslo Manual 2018(October. 2018.

[8] V. Souitaris, "Technological trajectories as moderators of firm-level determinants of innovation," Res. Policy, **31**(6), 877–898, Aug. 2002. https://doi.org/10.1016/S0048-7333(01)00154-8

[9] M. Shafiq et al., "Towards successful global software development." In Proceedings of the Evaluation and Assessment in Software Engineering, 445-450. 2020. DOI: https://doi.org/10.1145/3383219.3383283

[10] P. Kemp, R., Pearson, "Final Report MEI Project about Measuring Ecoinnovation: Deliverable 15 of MEI Project," 2008.

[11] Ho Chi Minh City General Statistics Office, "Statistical Yearbook," 2018. [Online]. Available: http://www.pso.hochiminhcity.gov.vn/.

[12] P. Koellinger, "The relationship between technology, innovation, and firm performance-Empirical evidence from e-business in Europe," Research Policy, **37**(8), 1317–1328, 2008. https://doi.org/10.1016/j.respol.2008.04.024

[13] J. Carlos Pinho, "TQM and performance in small medium enterprises," Int. J. Qual. Reliab. Manag., **25**(3), 256–275, Mar. 2008. https://doi.org/10.1108/02656710810854278

[14] M. Terziovski, "Innovation practice and its performance implications in small and medium enterprises (SMEs) in the manufacturing sector: a resource-based view," Strateg. Manag. J., p. n/a-n/a, 2010.

[15] C. C. J. Cheng, C. Yang, and C. Sheu, "The link between eco-innovation and business performance: a Taiwanese industry context," J. Clean. Prod., **64**, 81–90, Feb. 2014.

[16] K. Rangus and A. Slavec, "The interplay of decentralization, employee involvement and absorptive capacity on firms' innovation and business performance," Technol. Forecast. Soc. Change, **120**, 195–203, 2017.

[17] M. Madaleno, M. Robaina, M. Ferreira Dias, and M. Meireles, "Dimension effects in the relationship between eco-innovation and firm performance: A European comparison," Energy Reports, **6**, 631–637, Feb. 2020.

[18] B. A. Asunka, Z. Ma, M. Li, and O. A. Anaba, "Linking Innovation to Firm Performance in Developing Countries: the Role of Trade Liberalization," Eur. J. Bus. Manag. Res., **5**(3), 2020.

[19] N. Thao, "Ho Chi Minh City focuses on developing 4 key industries," 2017. [Online]. Available: http://www.ipcs.vn/vn/tp-ho-chi-minh-tap-trung-phat-trien-4-nganh-cong-nghiep-trong-yeu-W1422.htm.

[20] A. N. Nguyen, N. Q. Pham, C. D. Nguyen, and N. D. Nguyen, "Innovation and exports in Vietnam's SME sector," Eur. J. Dev. Res., **20**(2), 262–280, Jun. 2008.

[21] Q. N. Nguyen and V. N. Mai, "Factors affecting business performance of small and medium-sized enterprises in Can Tho City," Sci. J. Can Tho Univ.**19b**, 122–129, 2011.

[22] Q. M. Nhựt, "The effects of science and technology investment on business performance of agricultural enterprises in Ben Tre province," Can Tho Univ. J. Sci., **54**(1), p. 187, 2018.

[23] E. Calza, M. Goedhuys, and N. Trifković, "Drivers of productivity in Vietnamese SMEs: the role of management standards and innovation," Economics of Innovation and New Technology, **28**(1), 23–44, 2019.

[24] M. L. Yeh, H. P. Chu, P. J. Sher, and Y. C. Chiu, "R&D intensity, firm performance and the identification of the threshold: Fresh evidence from the panel threshold regression model," Appl. Econ., **42**(3), 389–401, 2010.

[25] N. Kraiczy and N. Kraiczy, Innovation and firm performance, July. 2013.

[26] Vu, Nguyen, Ho, and Vuong, "Determinants of Vietnamese Listed Firm Performance: Competition, Wage, CEO, Firm Size, Age, and International Trade," J. Risk Financ. Manag., **12**(2), 62, Apr. 2019.

[27] J. S. Oakland, Total quality management and operational excellence: Text with cases. 2014.

ASTES

Advances in Science, Technology and Engineering Systems Journal Vol. 5, No. 5, 991-996 (2020)

www.astesj.com

Special Issue on Multidisciplinary Innovation in Engineering Science & Technology

ASTESJ

ISSN: 2415-6698

Matrix-based Minimal Cut Method and Applications to System Reliability

Emad Kareem Mutar*

Department of Mathematics, Directorate of Education Babylon, Babylon, 51005, Iraq

ARTICLE INFO

Article history:
Received: 23 August, 2020
Accepted: 29 September, 2020
Online: 20 October, 2020

Keywords:
Reliability
Network model
Graph theory
Reliability method
Complex system
Optimal design

ABSTRACT

In this paper, we present a new method to deduce minimal cut sets depending on the minimal path sets of the complex systems (networks) to generate the Incidence Matrix, and then compared it with the truth table of the system. This comparison, based on some algebraic properties, gives minimal-cut sets of the complex network with an algorithm in Mathematica software. In addition, the minimal cut sets completely characterize the operating state of the system and equal to the complex system structural function information. So, the distinguish of the operational states of the system give us information about the binary operational states for some components. The system failure time is also given immediately if the failure times of the component parts are known.

1. Introduction

The main objective of a system reliability evaluation is to provide a certain probabilistic information on potential system component failures since a real design project needs to be evaluated in terms of reliability. A system can be defined as a stochastic graph G = (V, E) which contains the vertices set (nodes) and the edges set (links) of the system [1], [2]. The edges and vertices are usually prone to failures. In our system discussions, we claim that the edges go drop by design while the vertices function perfectly. The edge failures should be probabilistic [3]. A system can be described as working if a source vertex communicates with the vertex in the sink. In this case, it called reliability of two-terminal systems [4].

A cut set is a collection of components whose failure removes all the connections between the sources and the sinks of the system and thus leads to system failure, but a minimal cut set is a cut set that cannot be delivered in working condition without creating a path from the source to the sink, i.e., each minimal cut set causes system failure [5]. Conversely, the failure rate is not immediate or obvious [6].

In graph theory and computer science, a square matrix representing a finite graph is an adjacency matrix. The matrix elements indicate whether or not the vertical pairs are adjacent to the graph. The adjacent matrix for a finite simple graph is a (0,1) matrix with zeros at its diagonal [7]. The adjacent matrix is symmetrical if the graph is undirected (i.e. all its edges are bi-directional). The adjacent graph matrix should be separated from its incidence matrix [8]. We construct a set of minimal path set based on the matrix properties of the graph and then use the algebraic properties and multiplication to find the system's minimal cut set. Song and Kang [9], [10] presented a matrix-based system reliability approach which can be tested with simple matrix calculations for evaluating the reliability of complex system stats. Hassan and Mutar [11] have recently researched the architecture of electrical device reliability models (geometry point of view) used within spacecraft, which is considered a spacecraft's high-pressure oxygen supply system (HPOSS) [12]. With exception of current system reliability approaches, the complexity depends heavily on the details. The complexity of the formulas is not affected as the efficiency of the method is calculated with simple matrix calculations.

A connection matrix is a matrix with rows as minimal path sets and columns representing system components, then compared it to the system truth matrix. Based on some algebraic properties, this relation results in minimal cutting sets of the system. So the Matrix-based minimal cut structure of the system can be accomplished through algebraic manipulation of *the transpose of a* incidence matrix with the truth matrix . From that, we form a matrix in which the rows represent the minimal cut, and columns represent the components of the system then, we find the reliability of the system or obtain information about the system failure. Generally, this method is used to find the reliability of systems by using the *Mathematica* software.

*Corresponding Author: Emad Kareem Mutar, Email: emad77math@gmail.com

This paper presents a minimal cut method based on matrix and applies it to a simple system and engineering structures (looking at as networks), as seen in Figure 1. The units may be linked as a complex configuration. In a spacecraft, that reflects a HPOSS, i.e. the HPOSS in the cabin by the array of controls and valves from a high-pressure oxygen tank. This system consists of several components connected in a complex form for quantifying. The Matrix-based minimal cut analysis uses the representation of the incidence matrix whose elements indicate whether vertex–edge pairs are important in evaluating the minimal path sets of the systems. Then the matrix of **minimal cut** formulation of a system can be obtained depending on the minimal path sets of the systems. Generally, for solving complex models, we give an algorithm for calculating all minimal cuts, we use the Mathematica program to implement. We also gives powerful ideas to understand the MTTF of complex systems [13].

2. Models of network reliability

A reliability block diagram of a system is a graph whose edges are the system components, while there exists a pair of nodes called terminal nodes, in the backup power supply diagram. This describes the functional relationship between the components, and indicates if there exists a path between the terminal nodes which contains only edges with functional components (making, consequently, the entire system functional; in the contrary case, this is non-functional). It shows the functional relationship between the components, and indicates there is a path between the terminal nodes that contains only edges with functional parts. Otherwise it is not functional. The graphical model represents the reliability structure of the system like series , parallel and complex structures.

The system S consists of n components $X_1, X_2, X_3, \dots, X_n$ which can only work or fail in one of two states. Then we can define the boolean (binary) indicator variables for each component or S system for these states. The system design and connection paths reflect the reliability structure of the system which might or might not be the system's functional block diagram. As a practical illustration of engineering systems, modules can then be attached to a complicated configuration as illustrated in Figure 1. is a spacecraft's high-pressure oxygen supply system (HPOSS) [11] [12].

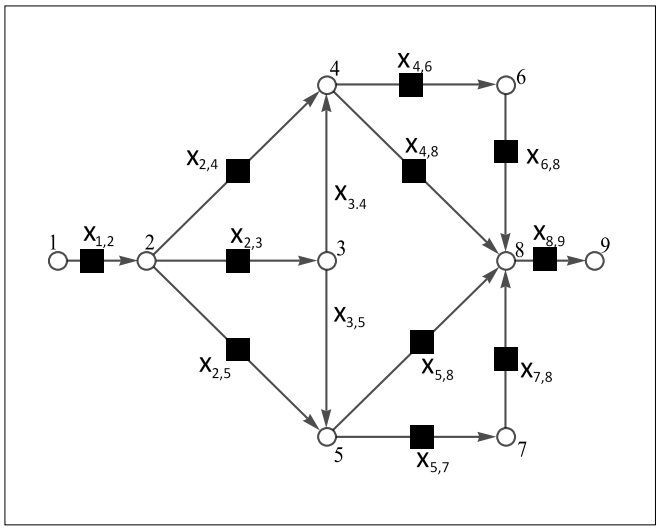


Figure 1: Reliability block diagram of system S.

As an illustration, we will study a simple model is a basic reliability block diagram with 3 subsystems as Figure 2, then we formulate a general Algorithm for complex models.

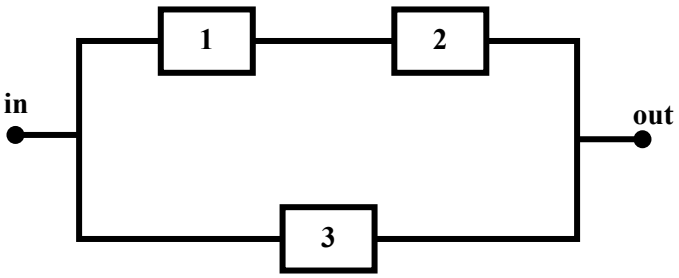


Figure 2: Reliability block diagram of system S.

3. Matrix-based minimal path deduction

The graph G = (V, E) represents the components' logical relations inside a piece of equipment. It is not necessarily the graphical representation of the system, but the system's functional components. In the graph theory, the minimal path is the problem of selecting a path from which no component can be removed without disconnecting the connections between the scour and sink node in a graph such that the sum of its constituent edges is minimized.

Consider a system that has different $\boldsymbol{X_i}$ states with its ith component, $i = 1, \dots, n$. The connection matrix (CN) is constructed in order to create the minimal paths by adding a (n × n) adjacent matrix of a simple graph with the identity matrix (unit matrix) in size n, to obtain 1's in the main diagonal, that is

$$\begin{bmatrix} 0 & a_{12} & \cdots & a_{1n} \\ a_{21} & 0 & \cdots & a_{2n} \\ \vdots & \vdots & \ddots & \vdots \\ a_{n1} & a_{n2} & \cdots & 0 \end{bmatrix} + \begin{bmatrix} 1 & 0 & \cdots & 0 \\ 0 & 1 & \cdots & 0 \\ \vdots & \vdots & \ddots & \vdots \\ 0 & 0 & \cdots & 1 \end{bmatrix}$$

Then we get the following matrix of connection

$$CN = \begin{bmatrix} 1 & a_{12} & \cdots & a_{1n} \\ a_{21} & 1 & \cdots & a_{2n} \\ \vdots & \vdots & \ddots & \vdots \\ a_{n1} & a_{n2} & \cdots & 1 \end{bmatrix} \quad (1)$$

where $\{1,2, \dots, n\}$ is the set of vertices, and $a_{ij} = (i, j)$ is the edge between vertex i and vertex j, if there is a connection between vertex i and vertex j then $a_{ij} = X_j$, otherwise $a_{ij} = 0$ .For example , in Figure 1, the simple model has the following connection matrix

$$CN = \begin{bmatrix} 1 & x_2 & x_3 \\ 0 & 1 & x_3 \\ 0 & 0 & 1 \end{bmatrix}$$

Therefore, we finding the minimal path between a two-terminal system as a special case of the paths problem, the minimal path vector for a system can be constructed by removes vertices which are either source or sink in the (CN) matrix, one at a time, until only the source vertex and sink vertex are present in the matrix [13]. When a vertex is deleted, the connection matrix inputs

are modified using the following equation for the remaining vertices:

$$a_{ij}^{1} = a_{ij} + a_{il}a_{lj}, \tag{2}$$

if vertex 1 is removed, where $i \neq j, i \neq l, j \neq l$ and $1 \leq i \leq n, 1 < j \leq n$ for $i = 1, 2, \dots, n$. Otherwise $a_{ij}^{1} = 1$ iff $i = j$.

The system shown in Figure 2 can be formulated as graph with directed edge (component) x_j of simple model is a basic RBD with 3 subsystems for i *and* j= 1,2,3. So the all minimal paths of the system are $\{X_2, X_3\}, \{X_3\}$.

Generally, for finding all minimal paths of series, parallel and complex system. A minimal path deduction algorithm to calculate all the minimal paths [14]. Based on the communication matrix and equation (1) by using the *Mathematica* software.

Algorithm 1: Minimal path deduction

```
mtrix = AdjacencyMatrix[
    G = Graph[Table[i, {i, 1, 9}], {1 ↔ 2, 2 ↔ 3, 1 ↔ 3}]];
n = VertexCount[G];
CN =
  MapIndexed[If[Equal @@ #2, 1, # Subscript[x, ## & @@ #2]] &,
     #, {2}] &@matr;
ClearAll[a]
a[m_, r_] := Module[{inds = DeleteCases[Range@Length@m, r]},
  Table[m[[i, j]] + If[i ≠ j, 1, 0] m[[i, r]] m[[r, j]],
   {i, inds}, {j, inds}]]
a[CN, 2];
ai = Nest[a[#, 2] &, CN, n - 2];
Mipaths = Expand[Part[ai, 1, 2]];
baseSet[Mipaths_] :=
 DeleteDuplicates[SortBy[MonomialList[Mipaths],
   {Head, Length}], Denominator[#2 / #1] == 1 &]
baseSet[Mipaths]
```

Applying the algorithm (1) to the complex model in Figure 1, all the minimal path sets can be obtained

$\{X_{1,2}\, X_{2,4}\, X_{4,8}\, X_{8,9}\}$, $\{X_{1,2}\, X_{2,5}\, X_{5,8}\, X_{8,9}\}$,

$\{X_{1,2}\, X_{2,4}\, X_{4,6}\, X_{6,8}\, X_{8,9}\}$, $\{X_{1,2}\, X_{2,3}\, X_{3,4}\, X_{4,8}\, X_{8,9}\}$,

The use of this approach is good practice by marking the source vertex as the first vertex and the sink vertex as the last vertex. Each intermediate node is deleted one by one until a 2×2 matrix is left with a_{12} represent summation of all minimal paths. Therefore, removing node i implies removing row i and column i from the original connection matrix where $2 < i < n - 1$ for a network with perfect n nodes [2].

4. Matrix-based minimal cut deduction

This method is based on minimal path mainly. The incidence matrix of minimal paths can be obtained from all minimal paths by use of a set of all minimal paths [3]. Assume that n minimal paths are defined by $P_1, P_2, \dots, P_n$. These paths will create a matrix while the paths represent the rows and the components represent the columns of the matrix. we determine the incidence matrix (IM) of all the minimal paths, of the form:

$$IM = \begin{array}{c} \\ P_1 \\ P_2 \\ \vdots \\ P_m \end{array} \begin{array}{c} \begin{array}{cccc} x_1 & x_2 & \cdots & x_n \end{array} \\ \begin{bmatrix} a_{11} & a_{12} & \cdots & a_{1n} \\ a_{21} & a_{22} & \cdots & a_{2n} \\ \vdots & \vdots & \ddots & \vdots \\ a_{m1} & a_{m2} & \cdots & a_{mn} \end{bmatrix} \end{array} \tag{3}$$

where $a_{ij} \in \{0,1\}$ with $i = 1, 2, \dots, m$, $j = 1; 2, \dots, n$ and $a_{ij} = 1$ iff $X_j \in P_i$, otherwise $a_{ij} = 0$. Appling to the system illustrated in Figuer 2, we obtain incidence matrix as follows.

$$IM = \begin{bmatrix} 1 & 1 & 0 \\ 0 & 0 & 1 \end{bmatrix}$$

Based on the algebraic properties, we can form the truth matri x (TM) depending on the listing of a limited number of system s ates, which is the most common approach. The true matrix of the graph is an n-dimensional vector consisting of 1s and 0s in raws and the components represent the columns of the matrix. If the ith of a state is 1, component i shall be in that state; otherwise it shall be down, illustrates the system model in Figure 2 its sample space divided into $m = 2^3 = 8$. The TM matrix of the three component sates is

$$TM = \begin{bmatrix} 0 & 0 & 0 \\ 0 & 0 & 1 \\ 0 & 1 & 0 \\ 0 & 1 & 1 \\ 1 & 0 & 0 \\ 1 & 0 & 1 \\ 1 & 1 & 0 \\ 1 & 1 & 1 \end{bmatrix}$$

Then, we perform the multiplication process between *the transpose of a* incidence matrix (IM) and the truth matrix (TM) such that incidence matrix is $n \times m$ matrix and the truth matrix is $p \times m$ matrix, then A is an $p \times n$ matrix with entries, so the comparison matrix is formed as in the equation

$$A = TM.(IM)^T \tag{4}$$

The calculation in equation (4) can be done simply by matrix-based multiplication with improved efficiency. This is illustrated by an example in Figure 1 .

.

$$A = \begin{bmatrix} 0 & 0 \\ 0 & 1 \\ 1 & 0 \\ 1 & 1 \\ 1 & 0 \\ 1 & 1 \\ 2 & 0 \\ 2 & 1 \end{bmatrix}$$

The process of this multiplication produces a new matrix that represents a fracture that helps to find parts and malfunctions in the system and the components that stop that we use the least property of Boolean algebra between the elements of the matrix rows according to the formula:

$$\boldsymbol{V} = \boldsymbol{min}\{\boldsymbol{a_{ij}} \,|\boldsymbol{j} \in \{\boldsymbol{1,2,3,\dots,n}\}\} \quad (5)$$

So for above example $v = (0,1,0,1,0,0,1)$ Whereas, this object represents the diameter elements in a matrix that create with, then we Then we make $V.I_n = diag(P_1, P_2, P_3, \dots, P_n)$ and remove the zero rows of the previous result. This is a job for logical indexing. Then we take

$$\boldsymbol{N(v)} = \begin{bmatrix} p_1 & 0 & \cdots & 0 \\ 0 & p_2 & \cdots & 0 \\ \vdots & \vdots & \ddots & \vdots \\ 0 & 0 & \cdots & p_n \end{bmatrix} \quad (6)$$

The matrix above represents the process of intersecting minimal paths to find the cut sets , so we use the equation

$$CSM = N(v).IM \quad (7)$$

The CSM matrix include all cuts in rows and the components are arranged according to the columns in sequence , then the conditions of component failures are given by a single matrix.

$$CSM = \begin{matrix} \\ C_1 \\ C_2 \\ \vdots \\ C_m \end{matrix} \begin{matrix} \begin{matrix} x_1 & x_2 & \cdots & x_n \end{matrix} \\ \begin{bmatrix} a_{11} & a_{12} & \cdots & a_{1n} \\ a_{21} & a_{22} & \cdots & a_{2n} \\ \vdots & \vdots & \ddots & \vdots \\ a_{m1} & a_{m2} & \cdots & a_{mn} \end{bmatrix} \end{matrix} \quad (8)$$

Then remove any cuts that include other cuts to generate minimal cuts as following

$$MCS = min\{C_i \,|i \in \{1,2,3,\dots,m\}, \forall C_i \in CSM\} \quad (9)$$

The CSM matrix of the three component in above example in Fig. (2) is

$$CSM = \begin{bmatrix} 0 & 1 & 1 \\ 1 & 0 & 1 \\ 1 & 1 & 1 \end{bmatrix}$$

For the edge x_j, the minimal cut is $\{x_1x_3, x_2x_3\}$.

Generally, for finding all minimal cuts of series, parallel and complex system. A minimal cut deduction algorithm to calculate all the minimal cuts [14]. Based on the CSM matrix and equation (9) by using the *Mathematica* software.

Algorithm 2: minimal cut deduction

```
M = rep@baseSet[Mipaths];
var = Variables[M];
M1 =
  var # & /@ CoefficientRules[M][[All, 1, 1]] /.
   x_i_,j_ → 1;
mat = M1;
sets = Tuples[{0, 1}, n1];
sets.Transpose[mat];
r = Pick[sets,
   Unitize[Min /@ (sets.Transpose[mat])], 1];
Sort[r.Array[Subscript[x, #] &, n1] /.
   Plus → Times];
b = DeleteDuplicates[r, #1 #2 == #1 &];
Micuts =
  Sort[b.Array[Subscript[x, #] &, n1] /.
    Plus → Times];
```

Applying the algorithm to the complex model in Figure 1, all minimal cuts can be obtained

$\{X_{1,2}\, X_{2,4}\, X_{4,8}\, X_{8,9}\}$, $\{X_{1,2}\, X_{2,5}\, X_{5,8}\, X_{8,9}\}$,
$\{X_{1,2}\, X_{2,4}\, X_{4,6}\, X_{6,8}\, X_{8,9}\}$, $\{X_{1,2}\, X_{2,3}\, X_{3,4}\, X_{4,8}\, X_{8,9}\}$,
$\{X_{1,2}\, X_{2,3}\, X_{3,5}\, X_{5,8}\, X_{8,9}\}$, $\{X_{1,2}\, X_{2,5}\, X_{5,7}\, X_{7,8}\, X_{8,9}\}$,
$\{X_{1,2}\, X_{2,3}\, X_{3,4}\, X_{4,6}\, X_{6,8}\, X_{8,9}\}$, $\{X_{1,2}\, X_{2,3}\, X_{3,5}\, X_{5,7}\, X_{7,8}\, X_{8,9}\}$

5. Minimal cat system reliability method

This method determines the reliability of a systems by using the minimal cut set and the inclusion-exclusion rule [15]. A cut Set is a set of components that fail to interrupt all the connections between source and sink, which causes device failure [16]. Then the system reliability can be written as

$$R_{System} = Pr\left(\prod_{i=1}^{n}(1 - C_i)\right) \quad (10)$$

where $C_i, i = 1,2,\dots,n$ represent all the minimal cuts, and $Pr(C_i) = Q_i$ where $Q_i = 1 - R_i$. Therefore, the probability of system failure is determined by a simple vector calculation

$$C_i = [X_1 \quad X_2 \quad \dots \quad X_n]$$

For example , in Figure 2, the system model has the following minimal cut vectors

$$C_1 = [0 \quad 1 \quad 1]$$
$$C_2 = [1 \quad 0 \quad 1]$$

So the minimal cut are $\{X_1X_3, X_2X_3\}$. These Reliability System can be generated easily by using the *Mathematica* software. Using equation (10) subsequently, the Reliability System is obtained as

$$\begin{aligned} R_{System} &= Pr(1 - C_1) \times Pr(1 - C_2) \\ &= (1 - Q_1Q_3)(1 - Q_2Q_3) \\ &= (1 - (1 - R_1)(1 - R_3))(1 - (1 - R_2)(1 - R_3)) \\ &= R_3 + R_1R_2 - R_1R_2R_3 \end{aligned}$$

So, we get

$$R_{System} = R_3 + R_1R_2 - R_1R_2R_3 \quad (11)$$

In general, the Reliability System for the union of minimal cuts is obtained using Mathematica processes

Algorithm 3: Minimal cat system reliability method

```
Micuts = Sort[b.Array[Subscript[x, #] &, n1] /. Plus → Times];
Qs = 1 - Expand[Product[1 - i, {i, Micuts}]] /. x_i_^n → x_i;
Rs = Expand[1 - Qs /. x_i_ → 1 - x_i]
Rsystem = Rs /. x_i_ → R_i
```

The minimal cut method based on the matrix has Firstly, as a result of calculating the connection matrix independently from a system definition, the reliability of a system event is calculated, the complexity of system reliability evaluations is not related to the concept of system states. Secondly, the matrix-based method helps one to understand easily and solve the failure rate of the system. Third, if component failure probabilities or statistical dependency are incomplete, the matrix-based method helps one to achieve the

shortest possible limit for all general system states. Fourth, recent developments in matrix-based computer languages and software, including Mathematica software, have made it easier and more efficient to implement matrix calculations. Finally, in this paper, the examples deal with two-state systems. The proposed approach is applicable to general multi-state component systems.

6. The Mean Time to Failure (MTTF)

The transformations we use are called linearizing transformations, which researchers have used in the past to evaluate the values of constants to best match a collection of data. The exponential function is of the form $R(t) = \lambda e^{-\mu t}$, and the ln-transformation of R(t) matches it with $lnR(t) = \mu t + ln\,\lambda$, mapping an exponential to a linear expression [17]. In particular, this approach refers to circumstances where the rate of the quantity change is directly commensurate with the radioactive decay (see [18], p.483] for further details). The exponential function also represents a curve whose form mainly depends on the exponent 's constant.

- If a > 0, then R(t) increases as t increases,
- If a < 0, then R(t) decreases as t increases.

Because of the interpretation of the Mean Time to Failure, we obtain

$$R(t) = \lambda e^{-\mu t} \tag{12}$$

where $\mu \geq 0$ and $\lambda \geq 1 > 0$: The function (15) is decreasing and satisfies the Reliability conditions. Let us also consider the polynomial of reliability (11). We assume that exponential functions correspond to $R_1, R_2 R_3$, where $\mu_i \geq 0$ and $\lambda_i \geq 1 > 0$, for $i = 1,2,3$. Then we obtain

$$R(t) = \lambda_3 e^{-\mu_3 t} + \lambda_1\lambda_2 e^{-(\mu_1+\mu_2)t} - \lambda_1\lambda_2\lambda_3 e^{-(\mu_1+\mu_2+\mu_3)t} \tag{13}$$

By using the above equation and mimicking the MTTF definition, we get

$$\begin{aligned}\text{MTTF} = \int_0^{\infty} & \boldsymbol{\lambda_3 e^{-\mu_3 t} + \lambda_1\lambda_2 e^{-(\mu_1+\mu_2)t}} \\ & \boldsymbol{- \lambda_1\lambda_2\lambda_3 e^{-(\mu_1+\mu_2+\mu_3)t}}\, dt \\ = \boldsymbol{\lambda_3} & \boldsymbol{\lim_{n\to\infty}} \int_0^n \boldsymbol{e^{-\mu_3 t}\, dt} + \boldsymbol{\lambda_1\lambda_2} \boldsymbol{\lim_{n\to\infty}} \int_0^n \boldsymbol{e^{-(\mu_1+\mu_2)t} dt} \\ & \boldsymbol{- \lambda_1\lambda_2\lambda_3} \boldsymbol{\lim_{n\to\infty}} \int_0^n \boldsymbol{e^{-(\mu_1+\mu_2+\mu_3)t} dt}\end{aligned}$$

Therefore, the integration leads to

$$MTTF = \frac{\lambda_3}{\mu_3} + \frac{\lambda_1\lambda_2}{\mu_1\mu_2} - \frac{\lambda_1\lambda_2\lambda_3}{\mu_1\mu_2\mu_3}$$

The above relationship through which it is possible to deduce the time for the failure of the system and then relay the components to give the longest time as a system.

7. The failure rate of the system reliability

In order to evaluate the system failure rates for the reliability system (11) used as a simple example with constant failure rate components. Consider the equation (12) of one component; the reliability of the component selected is given

$$R_c(t) = \lambda e^{-\mu t}$$

The failure rate is defined as the relationship between the density of probability and the reliability function

$$h(t) = \frac{f(t)}{R(t)} = \frac{-\frac{dR(t)}{dt}}{R(t)} \tag{14}$$

Then, by equation (14), we get

$$R_c(t) = \frac{\mu\lambda e^{-\mu t}}{\lambda e^{-\mu t}} = \mu$$

where a is constant. We note the failure rate of the component is constant. Generally speaking, we get the equation (13) from the equation (14), we obtain

$$h(t) = \frac{\boldsymbol{\lambda_3\mu_3 e^{-\mu_3 t} + \lambda_1\lambda_2(\mu_1+\mu_2)e^{-(\mu_1+\mu_2)t} - \lambda_1\lambda_2\lambda_3(\mu_1+\mu_2+\mu_3)e^{-(\mu_1+\mu_2+\mu_3)t}}}{\boldsymbol{\lambda_3 e^{-\mu_3 t} + \lambda_1\lambda_2 e^{-(\mu_1+\mu_2)t} - \lambda_1\lambda_2\lambda_3 e^{-(\mu_1+\mu_2+\mu_3)t}}}$$

The failure rate of the system for the failure rate of components in the complex system as constants is therefore time-related [19]. We find that if the component failure rate is constant, the system failure rate is also constant. In other words, the system's failure rate is always equal to the stable state failure rate [20].This is thus an correct representation of the state of polynomial multivariate reliability based on the values of the constants .

A practical example of engineering systems has been used with the proposed algorithm, components can be connected in a complex system, as shown in Figure 1. Including 9 nodes and 9 edges. The patterns representing system states and component problems can be defined effectively using matrix-based programming languages and applications. In addition, we obtain the failure rate equation, which results in an incremental failure of one variable being reduce by improving the pairing component, and which, obviously, provides a mathematical basis for the failure rate. This result demonstrates that our approach increases accuracy without increasing the assessment time.

8. Conclusions

This paper clearly defines a new method of deducing minimal cuts according to minimal path sets of complex systems, using the minimal cuts approach in a simplified form. The Matrix-based minimal cat approach can calculate the Reliability of complex system states by simply calculating matrix. Using matrix-based programming languages and applications, the matrices representing the system states and the component problems can be effectively defined. The components (the system) also proven to be exponentially time dependent; furthermore, we achieve a failure rate equation indicating that a gradual failure of a component can be balanced by the improvement of the pairing

component, and naturally gives a mathematical foundation for the failure rate. When the states of component failure are dependent largely. In some instances, we find a state failure rate and display certain components to be the efficient elements responsible for the device failure.

References

[1] Y.H. Kim, K.E. Case, P.M. Ghare, "A method for computing complex system reliability," IEEE Transactions on Reliability, **21**(4), 215–219, 1972, doi:10.1109/TR.1972.5215997.

[2] W. Kuo, M.J. Zuo, Optimal reliability modeling: principles and applications, John Wiley & Sons, 2003.

[3] J.-L. Marichal, "Structure functions and minimal path sets," IEEE Transactions on Reliability, **65**(2), 763–768, 2016, doi:10.1109/TR. 2015.2513017.

[4] S. Kharbash, W. Wang, "Computing two-terminal reliability in mobile ad hoc networks," in 2007 IEEE wireless communications and networking conference, IEEE: 2831–2836, 2007, doi:10.1109/WCNC. 2007.525.

[5] R.N. Allan, Reliability evaluation of power systems, Springer Science & Business Media, 2013.

[6] S.M. Alghamdi, D.F. Percy, "Reliability equivalence factors for a series–parallel system of components with exponentiated Weibull lifetimes," IMA Journal of Management Mathematics, **28**(3), 339–358, 2017, doi:10.1093/imaman/dpv001.

[7] G.T. Gilbert, "Positive definite matrices and Sylvester's criterion," The American Mathematical Monthly, **98**(1), 44–46, 1991, doi:10.1080/000 29890.1991.11995702.

[8] M.B. Javanbarg, C. Scawthorn, J. Kiyono, Y. Ono, Minimal path sets seismic reliability evaluation of lifeline networks with link and node failures, 1–12, 2009, doi:10.1061/41050%28357%29105.

[9] W.-H. Kang, J. Song, P. Gardoni, "Matrix-based system reliability method and applications to bridge networks," Reliability Engineering & System Safety, **93**(11), 1584–1593, 2008, doi:10.1016/j.ress.2008. 02.011.

[10] W.-H. Kang, Y.-J. Lee, J. Song, B. Gencturk, "Further development of matrix-based system reliability method and applications to structural systems," Structure and Infrastructure Engineering, **8**(5), 441–457, 2012, doi:10.1080/15732479.2010.539060.

[11] Z.A.H. Hassan, E.K. Muter, "Geometry of reliability models of electrical system used inside spacecraft," in 2017 Second Al-Sadiq International Conference on Multidisciplinary in IT and Communication Science and Applications (AIC-MITCSA), IEEE: 301–306, 2017, doi:10.1109/AIC-MITCSA.2017.8722980.

[12] K.K. Aggarwal, Reliability engineering, Springer Science & Business Media, 2012.

[13] Y. Kobayashi, M. Hayashi, "A new approximation method to evaluate system reliability," in 2017 IEEE International Symposium on Local and Metropolitan Area Networks (LANMAN), IEEE: 1–2, 2017, doi:10. 1109/LANMAN.2017.7972141.

[14] S.S. Skiena, The algorithm design manual: Text, Springer Science & Business Media, 1998.

[15] K. Dohmen, "Inclusion-exclusion and network reliability," The Electronic Journal of Combinatorics, R36–R36, 1998, doi:10.37236/ 1374.

[16] J.E. Biegel, "Determination of tie sets and cut sets for a system without feedback," IEEE Transactions on Reliability, **26**(1), 39–42, 1977, doi:10.1109/TR.1977.5215071.

[17] Z.A.H. Hassan, C. Udrişte, "Equivalent reliability polynomials modeling EAS and their geometries," Annals of West University of Timisoara-Mathematics and Computer Science, **53**(1), 177–195, 2015, doi:10.1515/awutm-2015-0010.

[18] T. Pyzdek, P.A. Keller, Quality engineering handbook, CRC Press, 2003.

[19] L. Xu, Y. Chen, F. Briand, F. Zhou, M. Givanni, "Reliability measurement for multistate manufacturing systems with failure interaction," Procedia CIRP, **63**, 242–247, 2017, doi:10.1016/j.procir. 2017.03.124.

[20] H. Pham, "Commentary: Steady-state series-system availability," IEEE Transactions on Reliability, **52**(2), 146–147, 2003, doi:10.1109/TR. 2003.811164.

ASTES

Advances in Science, Technology and Engineering Systems Journal Vol. 5, No. 5, 997-1006 (2020)

www.astesj.com

Special Issue on Multidisciplinary Innovation in Engineering Science & Technology

ASTESJ

ISSN: 2415-6698

Renewable Electric Power from the Equine Treadmill: An Evaluation of the Potential

Faizan Dastgeer*, Hasan Erteza Gelani

Department of Electrical Engineering, University of Engineering and Technology, Lahore, FSD Campus, Faisalabad, 38000, Pakistan

ARTICLE INFO

Article history:
Received: 23 August, 2020
Accepted: 29 September, 2020
Online: 20 October, 2020

Keywords:
Aerobic Power
Anaerobic Power
Distributed Generation
Efficiency
Equine Exercise
Horse

ABSTRACT

Horse power – the prime mover that has been there with humans for ages; chiefly used for transportation in the early days, and later, also used as an energy source leading to the conception of the term – horse power (hp). The current paper presents an interdisciplinary effort that brings forward an approach for evaluation of the potential of renewable power extractable from this prime mover once again. Specifically, the focus is towards extracting power from the equine treadmills (dry-type) whereby the incline of the machine is replaced by an equivalent (or pseudo-equivalent) energy generation mechanism leading to the coupling of renewable power with an equine workout. This approach comprises aerobic power (evaluated from oxygen uptake data) as well as anaerobic power (evaluated from plasma lactate data) – each of which is estimated from the difference values between equine running on a flat treadmill and when the mill is inclined. Furthermore, a literature review mentioning different inventions as well as some research efforts directed towards tapping somatic energy of animals is included in the manuscript. Also, a section dedicated towards assumptions/weak points helps judge the applicability of the presented work.

1. Introduction

For centuries, humans have benefitted from animals in one way or the other. Animals such as camels, cows and goats have provided us with milk as well as meat, hides (leather) have been used for a variety of purposes, and in the transportation department – they have been there, whether it was a draft work such as moving heavy loads by oxen carts or it was a high speed transit benefitting from the pace of Equus Caballus i.e. the horse. Despite living in close proximity for ages, the dawn of modern lifestyle has parted animals from their human beneficiaries, especially for the city dwellers who can obtain milk and meat from the market; besides getting access to a variety of honey, eggs and even leather and wool products in a superstore. As regards the transport, it has been taken up largely by fossil-fuel based automobiles. So, has this separation been for the good, or have we lost something that we shouldn't have – this may be deemed a debatable issue. Reference [1] mentions in its abstract that the positive effects of human-animal interaction have been researched by various studies and it has been shown that animal-assisted activities can be used to improve the physical and mental health of humans. The authors of [1] present a study concerning effect of equine-assisted activities (EAA) on prosocial behavior of adolescents and conclude that '… in this sense EAA has a protective effect on the behavior of adolescents'. Reference [2] identifies equine grazing, domestic biodiversity, land use, tourism and equine work as five 'green assets' of equines and mentions a case (with its certain conditions) which showed that for the same amount of carbon emissions, a donkey could prepare larger agricultural land area than a machine. The authors of [3] present a study of effects of horse riding upon children and deduce that riding a half-breed horse or a pony had a positive effect on causing the go- and no-go (self-control) reaction on children and it even improved solving of arithmetic problems.

Orienting towards the topic of the current paper, the horse in particular, has been serving humankind for ages. It offers the highest sprint speed (surpassing other rideable animals such as camels and steers) coupled with human-friendliness as well as ease of keeping. However, as the 20th century witnessed the spread of automotive industry, the horse can now be found in equestrian sports and leisure riding (exceptions may include draft work). One of the equipment used for equine exercise as well as research is the treadmill. Furthermore, some of the treadmills can have an incline function where the mill is tilted (w.r.t. ground) to increase the intensity of equine workout without reaching maximal speeds. The current paper makes the argument: why not keep the mill flat while extracting an equivalent amount of energy electrically, thus maintaining the exercise while generating clean renewable energy. To this end, the paper provides an approach for evaluating the amount of power that can be generated by an average horse.

The idea of energy generation from the horse via an equivalent (-to-incline) treadmill is unorthodox as well as interdisciplinary – involving Electrical Engineering (Power Engineering and Power

*Corresponding Author: Faizan Dastgeer, Email: faizandastgeer@uet.edu.pk

Electronics) as well as Equine Science (may include bio-mechanics as well as Equitation Science). The subsequent literature review mentions various inventions and research papers directed towards generation of energy from animate prime-movers.

2. Literature Review

This literature review is neither intended to define the scope of various inventions/research efforts nor may it be considered as a compact summary encompassing all the inner details of the inventions/research efforts.

Energy capture via treadmills is a fascinating concept with a fair number of research efforts. A US patent is presented in [4] which mentions that the invention provides a system and method for electricity generation via using animals like horses. The invention is different from treadmills; over here, the animal moves on trolleys which in turn move on a track. An elaborate system of gears, springs and levers converts the biological energy into rotational energy for an electric generator. The inventor says that this device is superior to a treadmill which only uses a half of the force of movement. He further goes on to say that it is envisioned that a treadmill like free running environment may be developed without departing from the invention. Also, it has been mentioned that the specific intention for the device is for rural areas with limited or non-existent electricity generation.

An exercise machine is presented in the patent [5], for large animals such as dairy cows. The invention is a treadmill type device and includes hoof abrasion system as well as a treadmill cleaning or flushing system. The inventor argues that as exercise gives a lot of benefit to humans, in a similar way it can be beneficial to dairy cows. A frame supports an endless track, upon which the animal will walk. One embodiment of the device includes a power generation system, wherein the walking energy of cow powers an electric generator. Energy may be stored or fed to the grid.

Continuing the treadmills, the patent [6] presents a treadmill for humans which can generate electric power. According to the inventor, a manually operated treadmill that can generate power for itself or for other electrical equipment may be beneficial for various environmental and practical reasons. In an exemplary embodiment the kinetic energy (KE) of the treadmill which the user imparted to the running belt is converted to electrical power via the power generation system.

Furthermore, the patents [7–10] also mention inventions using animate prime movers for electricity generation. The patent [7] mentions a mechanical platform comprising five stages used to convert energy from animals such as camels and horses into electrical energy. The multiple stages include a rotating base, air compression mechanism, a steam device and a dynamo for electricity generation.

Movement of livestock for energy production has been used by [8]. The patent presents equiangular radial levers which will generate moment of force when driven by livestock. Eventually, KE will be converted to electrical energy. The patent [9] uses a treadmill for harnessing animal power while the animal is walking on the belt and its head is in the feed end. It also gives the idea of getting more work from a powerful animal and vice versa; via a computer system developed for this. The patent [10] harnesses equine power where horses move in a circular path driving a central shaft via gears which drives a synchronous generator.

Looking at research publications, Fuller and Aye [11] are of the view that human and animal somatic energy is a forgotten source of renewable power. The paper mentions that on a global scale, the energy (authors are not exactly focusing on electrical energy) contributed by humans and animals is estimated to be twice that of the wind power. In the authors' words, "the paper makes the case that human and animal power be seen as renewable sources of energy"; the authors further say that the techniques for using these energy sources should be deemed "as part of the 'renewables' family." Posing the question why human and animal powers are not included in well-known renewable energy forms, the authors answer that several explanations are possible; these include human/animal powered technologies not being very fashionable and lack of support from big companies. Despite the paper not being targeted towards generation of electrical energy and being largely discussing rural habitat – it has been mentioned that the relevance of such technologies for developed countries should not be overlooked.

The authors of reference [12] give the idea of using animal draft power as well as biogas for electricity generation for rural areas. Animals are attached to rods connected to a circular plate which is connected to a chain sprocket system which transmits power to an electrical generator via a gear box. Estimated energy output (without including electrical component losses) is 18kWh/day from twelve oxen.

Energy generation via human treadmills is presented in [13–15]. Both electrical energy (generated via permanent magnet DC machine) and mechanical energy (used by a special washing machine) have been exploited in [13]. The system is not grid connected and detailed measures for maintaining (nearly constant) treadmill speed have not been mentioned. An elaborate work presenting hardware setup for a grid connected treadmill is mentioned in [14], where an infra-red sensor senses user position on the treadmill; consequently a three-phase permanent magnet synchronous machine connected to the belt is operated as either a motor (if the user leads reference) or as a generator. The synchronous machine receives/supplies power from/to a DC bus via a three phase AC/DC converter which operates the machine via field-oriented control. The DC bus is connected to the grid via a single phase bi-directional converter operated via single phased d-q frame. In [15], the authors present another human treadmill where the generated energy may be used for charging a battery or for a low voltage CFL.

In short, this section has mentioned efforts of various authors and inventors who have worked towards the idea of harnessing the energy of animate prime movers. However, the specific idea of generating electric energy from flattening the inclined dry-type treadmill for an exercising horse is rather unorthodox and thus could not be covered in literature review – although, instances of treadmills where horses walk to generate mechanical power (e.g. for wood splitting) may be found from sources other than published research literature.

3. Work, Metabolic Cost & Horse Power

3.1. Work

Encyclopedia Britannica defines work, in physics, as "measure of energy transfer that occurs when an object is moved over a distance by an external force at least part of which is applied in the direction of the displacement." Work is the product of force and the displacement: hence, if the displacement is opposite to force,

the work is negative. For example, in humans, if the triceps brachii is used for a fast accelerated extension of the fore-arm along the horizontal plane i.e. parallel to the ground surface – the muscle performs positive work, however, before reaching the straightening of the arm (i.e. the max extended position), the biceps brachii naturally exerts a decelerating force and slows down the arm – thus performing negative work. Another way to look at this is that the triceps accelerated the forearm, thus imparting KE; while the biceps decelerated the forearm thus extracting that kinetic energy. Consequently, the net work, performed by the body upon the forearm limb is zero (another way to comprehend net zero work is that the limb returns to same energy state KE = 0, Potential Energy (PE) = as before). However, internally both the muscles consumed metabolic energy (explained subsequently) of the body while applying their respective contractive forces.

3.2. Internal Work

Work performed upon the limbs w.r.t. the Center of Mass (COM) of the body may be regarded as internal work e.g. the protraction phase of an equine forelimb during a gallop, when the limb is moving forward (being protruded) may easily be comprehended as a case of internal work.

3.3. External Work

This is the work performed by the limbs to move (upward and/or forward) the COM of the body e.g. in the stance phase (hoof touching the ground) of an equine gallop, the propulsive part which accelerates the body, is performing external work.

As a summary, the stance phase includes external works – negative and then positive, when the COM is braking and then accelerating respectively, while the swing phase (hoof not touching ground) includes internal work. On a level locomotory activity such as walking, at a constant speed, for horses or humans, the *net* external work performed by the body is zero (energy expended against aerodynamic drag is not included in this). Alternative argument for the zero work concept is that the body is undergoing no *net* change in its KE or PE per stride. Reference [16] mentions this, that in level walking or running, the net work per stride is zero.

However, the body is still expending metabolic energy (discussed subsequently) which is being used up in

i. Internal work
ii. Within stride External work – this includes the decelerating and accelerating work per stride. Reference [17] gives graphs of within-stride KE variation for equine walk, trot and gallop.

3.4. Metabolic Cost

Metabolic cost for a physical activity refers to the energy expended by metabolic reactions within the body for performing that activity. For locomotion, the metabolic cost becomes Joules expended per meter of covered distance i.e. J/m; on per kg of body mass it is augmented to Jkg-1m-1. The portion of released energy which is converted to mechanical work decides the efficiency of the muscles; [18] quotes this efficiency to be in the range of 25 – 30% and mentions it to be a product of two efficiencies

- Phosphorylative coupling efficiency (around 60%)
- Efficiency of contractive coupling (around 49%)

For equine performance, [19] mentions that the energetic cost (expressed as kJ/min) is essentially linear with speed, with the condition that the animal can change gait freely. A relationship on per kg basis is provided as well, this relationship may be given as

$$Energy\ (kcal/min) = 0.0289 + 0.00074 * speed(m/min) \quad (1)$$

The author of [19] further mentions that Adenosine Triphosphate (ATP), the immediate source of energy in muscles, is quite limited (6mmol/kg of muscle mass) – it has to be replenished for muscular contractions lasting more than a second or two. The aerobic and anaerobic processes (utilizing and not utilizing oxygen respectively) are the pathways for the release of energy in the body leading to the replenishment of ATP for muscular contractions. The intensity of both the pathways can respectively be judged via

- Oxygen uptake - VO_2 (also symbolized as $\dot{V}O_2$), which is the volume of oxygen consumed given as ml.kg-1.min-1.
- Blood lactacte concentration mmol/L

3.5. Horse Power

How much power can a horse generate? 1horse-power i.e. 746 Watts? Actually, the authors of [20] say that one horse (600kg mass and assumption of 100 W/kg of muscle mass) could in theory give 24hp; it has been further mentioned that realistic estimate of peak performance is around 12 – 14.9hp. The term horse power was coined by James Watt when he was commercializing his steam engine. Watt observed that during a day's work, a horse would expend a power of 33,000 ft-lbf/min [20], equivalent to 745.7Nm/s. This unit came to be known as horse power. As this power value was intended to show a replacement potential of horses by steam engines, hence it is not an indicator of peak equine potential; rather a through-out-the-day power which a horse could deliver.

4. Treadmills

The first equine treadmill dates back to 1960 as mentioned in [21] and the initial studies were focused on metabolic variables. Treadmills were subsequently adopted in kinematic studies as well as for equine exercising. The incline function of the treadmills can increase the exercise intensity, consequently a maximal workout may be achieved at sub-maximal speeds. More recently, water treadmills have been introduced which can increase exercise intensity due to drag of water.

4.1. Scope of the current paper

The scope of the current paper is towards evaluating the potential of renewable electrical power generate-able via the equine dry type treadmill. If the treadmill is kept flat, and an adaptive/controllable energy generation unit is coupled with it that may be grid-tied or connected to a battery bank – the exercise/study intensity may be adjusted equivalent to the value that the inclined mill offered, thus producing clean renewable energy at the same time. The scope of the current paper is different from many citations quoted in literature review; over here, rather than being the primary objective, energy production may be regarded as a secondary objective, wherein the chief purpose may be the exercising of the horse.

4.2. Direct and Indirect Assessment Methods – why mgv_v is not used.

Reference [22] examines speed of racehorses on different gradients on an undulating racecourse. The authors say that the

race horses reduce speeds on inclines and the speed detriment corresponds to trade-off between metabolic costs of height gain and horizontal galloping. The paper mentions that the power required to move up an incline may be expressed as

$$power = mgv_v \; where \; v_v = v_h.s \qquad (2)$$

m and g are the body mass and gravity, v_v and v_h are the vertical and horizontal components of velocity and s is the slope of the gradient. The paper calculates that moving up a 10% incline at 8m/s i.e. at v_v = 0.8m/s equates to 8W/kg.

In the current effort, an indirect assessment of the power generatable via equine treadmill is presented. This indirect approach uses ΔVO_2 and Δlactate values (between flat and incline) for the power assessment – details of the methodology are presented in the sections 5 and 6. A direct assessment of the power actually being expended on the vertical mill, via the use of (2) has not been performed (although there are research efforts which use this approach for the treadmills). We refrain from using it because we are of the view that this approach is not exactly applicable to treadmills where the center of mass (COM) may not move absolutely the same as its movement on an actual uphill incline. A subsequent kinematic study or a prototype demonstration may be able to verify or disprove the results of this paper – in light of such results, the currently presented approach may be reworked to look for a discrepancy and readjusted as per need.

For use of ΔVO_2, we present the case of [23] where an uphill/downhill (incline of ±8%) treadmill work (for humans) was simulated on a flat treadmill, via the use of a horizontal force applied to the waist of the runner (speed 2.5m/s). For the uphill case, despite the Pearson correlation coefficient given to be 0.42 and the authors regarding the VO2 correlation between the two methods (uphill simulation on flat treadmill and actual inclined treadmill) to be not significant; still, the mean VO_2-net (ml.kg-1.min-1) values for simulated incline and actual treadmill incline running were fairly close. These values were reported to be (Mean±SD) equal to 38.6±2.19 and 37.2±4.25 for simulated and actual treadmill incline respectively. An observation of the graphical results presented in the paper shows that, out of the eleven humans tested, three gave VO_2 results for the simulated method to be very close to the actual inclined treadmill, and the remaining eight were distributed so that six gave higher VO_2 for the simulated method while two gave otherwise. For the current paper, the fair proximity in the average VO_2-net values for simulated and actual treadmill incline as mentioned earlier, may be regarded as a basis for the provided approach of evaluating the equine renewable power potential from an average horse.

Moreover, it is worth mentioning that an alteration in the ground reaction forces (GRFs) is also expected as the treadmill is changed from inclined to horizontal while maintaining exercise intensity. We deem such an alteration to GRFs beyond the scope of the current paper. However, we do like to mention that the GRFs on an inclined treadmill are already not the same as those on a flat track apparently; the change from inclined to horizontal, might just be in-favor-of, or benign-to, the exercising equine.

5. Evaluation of The Potential: The Aerobic Contribution

5.1. Evaluating the generatable renewable power

We present an indirect metabolic approach for evaluation of the power expended on inclined treadmills at different slopes. The authors of [24] have examined effect of treadmill incline on VO_2 and other parameters for five horses. The VO_2 has been plotted against treadmill speed for different inclines (reproduced here in Figure 1). Attempting to describe their data mathematically, the authors say that for 2.5% and 0% (i.e. flat), the VO_2 vs. speed relationship could be best defined by second order polynomials while for 5%, 7.5% and 10%, the relationship was described via linear regression. Table 1 gives various coefficient values for their relationships.

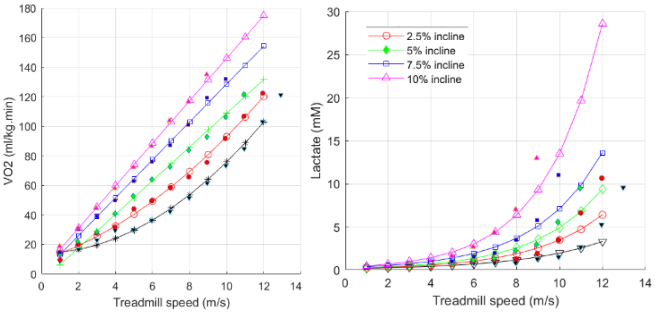
Table 1: Speed and incline relationship coefficients of [24]

Coefficients / Incline	x^2	x^1	x^0
0%	0.61	0.10	13.89
2.5%	0.43	4.08	9.29
5%	-	11.40	-5.11
7.5%	-	12.82	0.43
10%	-	14.38	2.30

'x' represents the horizontal axis quantity of speed in m/s. The y-axis quantity is VO_2 in $m,kg^{-1}min^{-1}$. Linear regression coefficient values are means only - non-inclusive of ± SE

Fig 1. plots the VO_2 and lactate concentrations (after taking antilog of $\log_{10}$ values) obtained from provided relationships as well as those obtained from the provided graphs (from [24], Figure 1A for VO_2 and Figure 4A for lactate conc. – mean values acquired via) using a MATLAB based graph digitizer program [25]. Some of the points for lactate concentration (e.g. lactate mM at 9m/s for 10% incline) with large variation between graph based and regression equation based values have been approximated to their graph digitized values. The current work takes the data of [24] and calculates the differences of oxygen uptake ΔVO_2 between each incline and the flat e.g. for the 2.5% incline $\Delta VO_{2\text{-}2.5\%}$ may be obtained as

$$\Delta VO_{2-2.5\%} = VO_{2-2.5\%} - VO_{2-0\%} \qquad (3)$$



(a) (b)

Figure 1: (a) VO_2 and (b) Plasma lactate concentrations vs treadmill speed – empty symbols are for values obtained from relationships, filled symbols are for values acquired from graph

Subsequently, the joule equivalent of oxygen ($O_{2\text{-}J\text{-}eqv}$) is taken to be 21.1 J/ml O_2 [26]. The extra power expended (not exactly expended – rather, this is the power extractable at 0% incline to produce a similar/same energetic response) for vertical motion at 2.5% incline denoted by $p_{mech\text{-}aer\text{-}2.5\%}$ may be expressed as

$$p_{mech-aer-2.5\%} = CRS_{CF} * \Delta VO_{2-2.5\%} * O_{2-J-eqv} * m_{equ} * \eta_{mscl} * (1/60) \qquad (4)$$

where η_{mscl} represents locomotor muscle efficiency, m_{equ} represents the equine mass, 1/60 converts from minutes to seconds and CRS_{CF} is the correction factor for Cardio-Respiratory system oxygen

demand explained subsequently. Furthermore, (5) provides a look at (4) in terms of dimensions (units)

$$Watts\ (J.s^{-1}) = ml.kg^{-1}.min^{-1} * J.ml^{-1} * kg * min.s^{-1} \quad (5)$$

Next we assume a value of 30% for η_{mscl} [17] and a 492 kg equine body mass (as in [24]). The factor CRS_{CF} is a rather crude approximation of the VO_2 used up by the heart and lungs. The web article [27] (although not exactly for the equine heart) provides values for the myocardial oxygen consumption (MVO_2) to be 8ml O_2 per minute per 100g, for the cardiac state of 'resting heart rate' while for the state of 'heavy exercise', the value is raised to 70ml O_2 per min. per 100g. Next we assume the lowest activity state of locomotion at 1m/s on the treadmill of 0% incline (i.e. flat mill) to be equivalent to the resting state for MVO_2. The corresponding VO_2 for this state equals to 8.8ml/kg.min (obtained via graph digitization). Furthermore, [28] presents mean heart weight of racing type (Thoroughbreds and Standardbreds) horses to be about 0.86% of bodyweight – hence, for the ongoing study mean heart mass is taken to be 0.86% of m_{equ} which equals about 4.2 kg. Consequently,

$$total\ MVO_2 = 4.2kg * 80ml.kg^{-1}.min^{-1} = 336\ ml.min^{-1} \quad (6)$$

and the MVO_2 as a percentage of total VO_2 roughly equals

$$\frac{total\ MVO_2}{total\ VO_2} = \frac{336\ ml.min^{-1}}{8.8 * 492\ ml.min^{-1}} \approx 0.078 \rightarrow 7.8\% \quad (7)$$

Performing similar calculations for the highest speed point (10m/s) for 7.5% treadmill slope (as it corresponds to the highest heart rate provided by [24]) and using the 'heavy exercise' cardiac state, total MVO_2 equals

$$total\ MVO_2 = 4.2kg * 700ml.kg^{-1}.min^{-1} = 2940\ ml.min^{-1} \quad (8)$$

and

$$\frac{total\ MVO_2}{total\ VO_2} = \frac{2940\ ml.min^{-1}}{132.2 * 492\ ml.min^{-1}} \approx 0.045 \rightarrow 4.5\% \quad (9)$$

subsequently, we approximate the total MVO_2 to be equal to 5% of the total MVO_2 being taken up for any given speed and slope. This is obviously a crude approximation, and a more detailed approach can involve use of multiple values for the *total MVO_2/total VO_2* ratio which can yield multiple values of CRS_{CF}.

Continuing towards the lungs, [29] mentions that the lung consumes 5% of whole body oxygen uptake – using this value as it is (although [29] is neither for equines nor for exercise) and combining it with the estimated 5% value of the total MVO_2, means that about 10% VO_2 is being consumed by the cardio-respiratory system for its own functionality – hence, 90% VO_2 is the value available to the rest of the body. The CRS_{CF} is then taken to be 90% (i.e. 0.9) thus showing that (only) 90% of the $\Delta VO_{2\text{-}2.5\%}$ in (4) is available for the evaluation of $p_{mech\text{-}aer\text{-}2.5\%}$.

Figure 2 shows plots of $p_{mech\text{-}aer\text{-}2.5\%}$ and the mechanical power values for other inclines. Also shown are the metabolic power values generated at different speeds and inclines. A relatively light exercise of 2.5% incline at 5m/s (3 – 6m/s has been regarded as most energy efficient speeds regardless of incline by [24]) is generating around 500 Watts of clean power – assuming a 30 minute exercise and an 80% efficiency of the power extraction and conversion system, 400W may be supplied to the grid for half an hour.

5.2. Sketching the metabolic power lines

Figure 2 also shows metabolic power $p_{met\text{-}aer}$ lines. These are sketched by looking for speed points of the same (chosen value of) metabolic power on curves of different inclines – this is achieved via a spline interpolation of speed vs. metabolic power (at different inclines) data - the metabolic power e.g $p_{met\text{-}aer\text{-}2.5\%}$ has been evaluated as

$$p_{met-aer-2.5\%} = VO_{2-2.5\%} * O_{2-J-eqv} * m_{equ} * (1/60) \quad (10)$$

Subsequently, corresponding to the speed point acquired and the $p_{met\text{-}aer}$ value in consideration, $p_{mech\text{-}aer}$ points are obtained for each incline. Connecting these points constitutes the linear joints of the $p_{met\text{-}aer}$ lines. Lastly, for the selected metabolic powers a spline extrapolation is performed using the speed points and corresponding $p_{mech\text{-}aer}$ points towards the upper end of the figure.

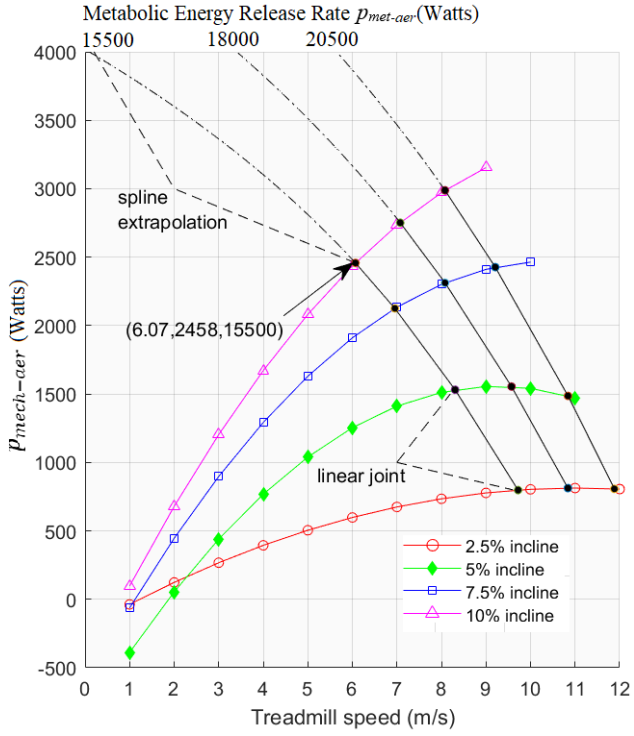


Figure 2: Power generation potential for various inclines. In general, the $p_{mech\text{-}aer}$ values beyond 3m/s may be deemed practical, while errors in speed points of 1 & 2m/s may be attributed to corresponding cluttered VO_2 data of Figure 1(a). The top horizontal axis shows metabolic power lines for different speeds and inclines. A single point (x_{bottom}, y, x_{top}) e.g. (6.07m/s, 2458W,15500W) is to be interpreted as release of 15500W metabolic energy where the horse is moving at 6.07m/s (on the incline of 10%) wherein the aerobic mechanical power generatable via flattening the mill is 2458W.

5.3. Power and Energy

For a discussion about energy, three points α, β and γ are taken from Figure 2; the coordinates are taken as (x_{bottom}, y, x_{top}) i.e. (speed, $p_{mech\text{-}aer}$, $p_{met\text{-}aer}$). These points are (approximately):

$\alpha \rightarrow$ (6.07m/s, 2458W,15500W) - 10 %incline
$\beta \rightarrow$ (8.08m/s, 2312W, 18000W) - 7.5%incline
$\gamma \rightarrow$ (8.08m/s, 2988W, 20500W) - 10 %incline

It may be seen that, while the operating point α can deliver mechanical power value of 2.46kW; the point β is delivering slightly lesser power of 2.31kW, while depleting metabolic energy at a higher rate of 18kW. Consequently, the potential of energy generation at α is higher than that of β. Furthermore, γ is showing even higher potential of delivering about 3 kW but the depletion rate of metabolic energy is also huge - a 20.5kW, hence a probable reduced time duration for maintaining a healthy workout at the point γ, may reduce its energy potential. A detailed analyses of

energy generation potentials for different equine breeds, exercise schedules for various gaits, treadmill slopes and speeds incorporating the data of on-set of fatigue/maximum exhaustion (e.g. [30] mentions Times to Fatigue of 45 and 20.2 minutes for an Arab and a Thoroughbred horse exercised at 4.5m/s, 6% incline) is deemed beyond the scope of the current which is aimed at presenting methodology for the evaluation of power that may be generated.

5.4. Point of optimum (aerobic) mechanical power generation

Looking for the point of optimum power generation potential, Figure 3 plots treadmill speed (including and beyond 3m/s) versus treadmill slope (the four inclines) versus $p_{mech\text{-}aer} : p_{met\text{-}aer}$ ratio at the different points.

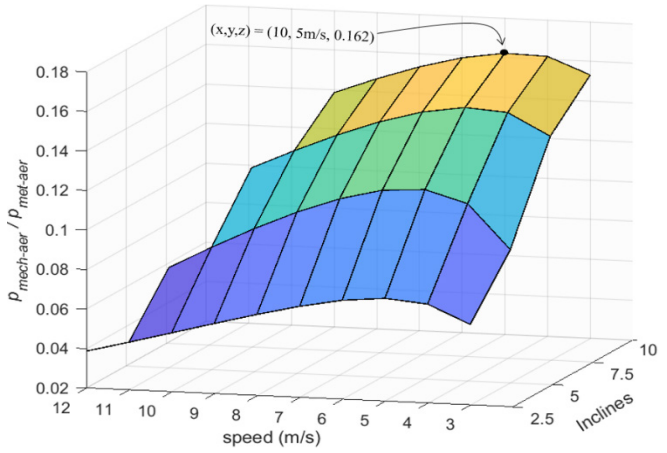


Figure 3: Treadmill speed vs. Treadmill Slope vs. $p_{mech\text{-}aer} : p_{met\text{-}aer}$ ratio. Speed points 1 and 2 m/s are ignored for reason mentioned in Figure2 caption.

The highest value of 0.162 for the $p_{mech\text{-}aer} : p_{met\text{-}aer}$ ratio was found to occur at the speed of 5m/s for the treadmill slope of 10%. With respect to the treadmill slope, Figure 3 shows a trend of increase in $p_{mech\text{-}aer} : p_{met\text{-}aer}$ ratio and w.r.t the speed, highest $p_{mech\text{-}aer} : p_{met\text{-}aer}$ ratio values are achieved around 5m/s. It may be noted that this is in line with the top values of economy of locomotion ($ml.kg^{-1}.m^{-1}$) occurring in range of 3 – 6 m/s as evaluated for the initial data (of the current study) by [24] - which further mentions high speed locomotion to be less efficient (for flat and 2.5% incline).

Lastly, towards the end of this section, it is worth mentioning that the methodology described here may be considered to be only an approach towards the evaluation of the potential. The values are not definitive – with variations arising from different factors such as equine body mass and precision in value of energy released per ml of O_2 etc. Reference [24] has itself mentioned that the regression coefficients for the speed and VO_2 relationship have range from 11.1 to 19.61 in different studies. It has been further mentioned that the variations in studies may be due to differences in methodology including different factors such as horse breed, bodyweight as well as treadmill acclimation.

6. The Anaerobic Contribution

This section provides an approach to assess the anaerobic (lactic) contribution to energy and power for equine exercise on inclined treadmill. Once again, the data of [24] has been used which has provided plasma lactate concentration graphs as well as linear regression log10 lactate concentration versus speed relationships. Mean values have been used excluding the standard deviations – the same was the case for aerobic approach. The difference in plasma lactate concentration between each incline and the flat treadmill have been evaluated. These differential lactate values represent the additional exertion expended due to the incline of the treadmill and are converted to corresponding delta (Δ i.e. difference) metabolic energetic approximations as expressed in (11) for the 2.5% incline. Differing from the approach of aerobic contribution where a portion of the VO2 was given to the cardiorespiratory system, over here, lactate value are assumed to be a result of the activity of exercising muscles only.

$$e_{met-\Delta-2.5\%} = \Delta_{lact-2.5\%} * lact_{p\rightarrow b} * lact_{O2-eqv} * O_{2-J-eqv} * m_{equ} \quad (11)$$

where,

- $e_{met\text{-}\Delta\text{-}2.5\%}$ is the Δ metabolic energy for the anaerobic pathway for the 2.5% incline
- $\Delta_{lact\text{-}2.5\%}$ is the difference in lactate concentrations between the 2.5% incline and flat treadmill – units of Δ_{lact} are milli moles per litre (the units may be symbolized as mM)
- $lact_{p\rightarrow b} = 1.5^{-1}$ is a factor to represent a 1.5 times reduced concentration of blood lactate as compared to plasma lactate as mentioned by [31]
- $lact_{O2\text{-}eqv}$ is $3ml O_2$/mmol lactate (per litre blood) – it is the oxygen equivalent of blood lactate as described in [26]
- $O_{2\text{-}J\text{-}eqv}$ is the Joule equivalent of O_2 equal to 21.1 J/ml O_2 as used by [26]; a slight variation of 20.92 J/ml O_2 has been used by [32]
- m_{equ} is the mean equine mass of 492 kg as in [24]

Subsequently, (12) shows calculation of the corresponding mechanical power generation $p_{mech\text{-}anaer}$ which is evaluated by taking difference of two consecutive energy points $\Delta e_{met\text{-}\Delta}$ and dividing this by the two minutes of interval length for lactate measurement as mentioned by [24] (which mentions blood sample collection during last 15s of each interval) – also, as for the case of aerobic power, the metabolic to mechanical conversion is achieved assuming η_{mscl} i.e. muscular mechanical efficiency of 30% as in case of aerobic power. Figure 4 presents the results of $p_{mech\text{-}anaer}$ for the different inclines and speed points.

$$p_{mec-anaer-2.5\%} = \Delta e_{met-\Delta} J/120s * \eta_{mscl} \quad (12)$$

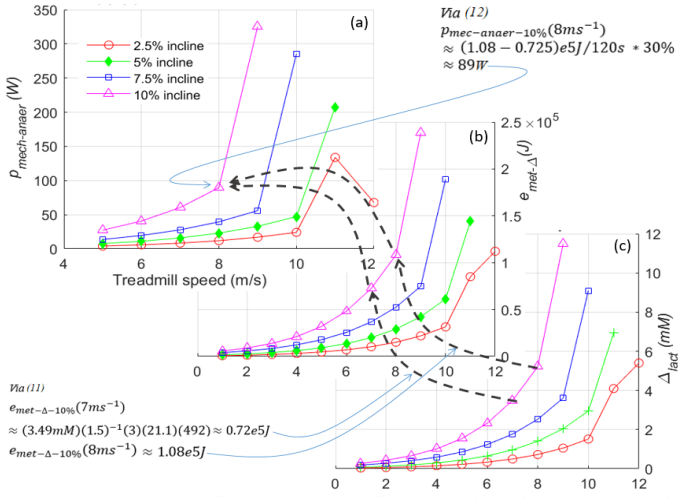


Figure 4: Anaerobic contribution composite figure. (a), (b) and (c) show anaerobic mechanical power, metabolic energy (y-axis in 10e5 Joule) and the differential lactate concentration values respectively. The horizontal axis shows treadmill speed for each subfigure. A single point of (a) e.g. (8m/s, 89W) for the 10% incline

indicates that, 89W of power generation potential is available corresponding to this point and metabolically, this power will be generated via anaerobic pathway.

Interestingly, Figure4 shows that for 12m/s at 2.5% slope, the power potential is actually reduced and this may be attributable to the fact that at this speed, the lactate threshold for the flat mill has also been crossed (as may be seen from Figure 1b) – consequently, the differential anaerobic energy is reduced and hence the power graph shows a dip. Furthermore, anaerobic alactic contributions could not be evaluated in this study because of in-availability of corresponding data in [24], however, these may be deemed minor - [32] mentions the alactic energy contributions to be around 0.1% for supramaximal exercises in their study.

7. Including the Drag

Aerodynamic drag becomes considerable as speed increases. [33] calculates this drag via $½C_D\rho Av^2/body\text{-}mass$ (with $C_D = 0.9$, $\rho = 1.29$ kg/m^3, $A = 1$m^2, $v = 12$m/s and $mass = 550$kg) to be equal to 0.15 Jkg^{-1}m^{-1}. Converting this to power translates into 990 J/s i.e. about 1kW. It has been mentioned by [33] that, while the drag is often considered negligible, it is actually a larger proportion of the external mechanical work compared to what was considered before. So, a horse galloping on the track at 12m/s is expending about 1kW of external mechanical work for countering the aerodynamic drag forces. Consequently, as the same horse is exercising at 12m/s on a high speed treadmill, extracting 1kW of power can make the equine work-out closer (in terms of power consumed) to the over track exercise. Figure 5 plots variations in the mechanical power $p_{mech\text{-}drag}$, calculated as in (13), expended (in over-ground running) for overcoming the drag

$$p_{mech-drag} = \frac{1}{2}C_D\rho Av^3 \qquad (13)$$

at various speeds while including the effect of variation in air density ρ as it varies from 1.2 kg/m3 to 1.29 kg/m3.

The two data points selected in the figure show a pmech-drag difference of about 230Watts between the extremes of ρ for the speed of 18m/s. From the figure, around 3.4kW of power generation potential is available as the same workout of 18m/s in an atmosphere of ρ = 1.29 kg/m3 is being carried out on a high speed equine treadmill.

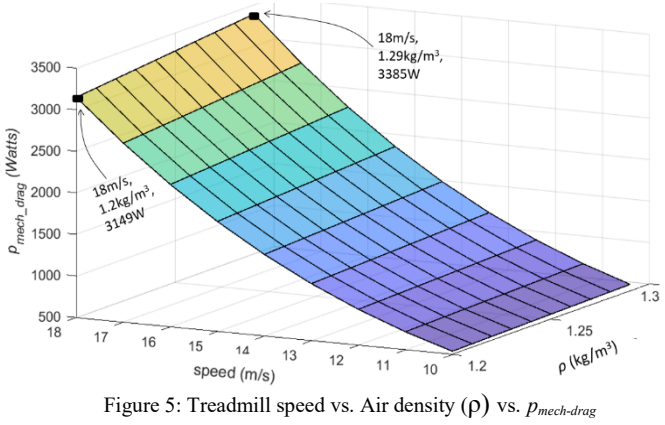


Figure 5: Treadmill speed vs. Air density (ρ) vs. $p_{mech\text{-}drag}$

Furthermore, [34] mentions a case where the exercise on flat treadmill provided a lower cardiac and blood lactate response as compared to exercise on ground at the same speeds. A treadmill incline of 3.5% was found to give heart rate closer to that of the track exercise (especially in the range of 9.1 – 10m/s). Again, if appropriate energy is being extracted from a treadmill, this might give a better replication of the over track exercise while generating renewable power at the same time.

8. Total Mechanical Power: Combining Aerobic and Anaerobic Portions

8.1. Total Generatable Power

Figure 6 presents a wholesome picture – curves for total generatable mechanical power $p_{mech\text{-}total}$ via combining the contribution from the aerobic and anaerobic mechanical powers have been sketched. Except for the last (or second last for 2.5% incline) speed points, the $p_{mech\text{-}total}$ lines are generally quite close to the pmech-aer lines, hence the anaerobic contribution is clearly far less than that of the aerobic part. Furthermore, the rise in $p_{mech\text{-}total}$ lines towards the last speed points may also be explained from Figure 4, which shows a significant rise in $p_{mech\text{-}anaer}$ for the last speed points (except for 2.5%). The dip in $p_{mech\text{-}anaer}$ for 2.5% incline is briefly explained in section 6.

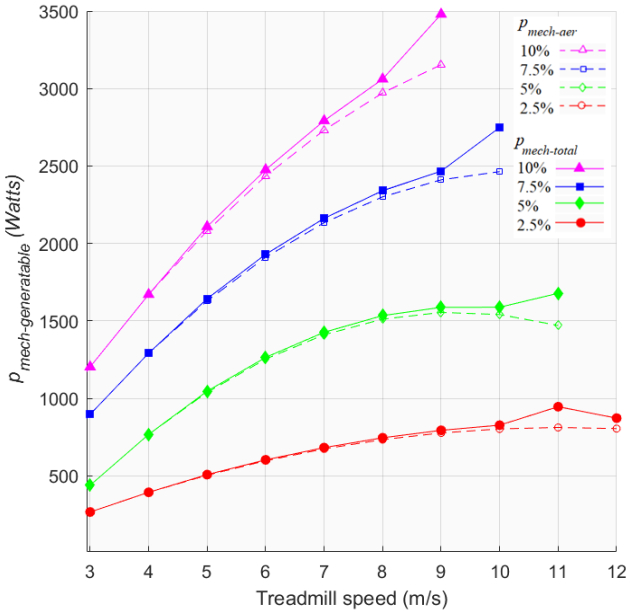


Figure 6: Total generatable power evaluated via combining aerobic and anaerobic portions. The speed points 1 and 2 m/s are ignored for reason mentioned in Figure2 caption.

8.2. Total Expended Power – Revisiting mgv_v concept

Reference [35] summarizes various studies mentioning efficiency for vertical mechanical work for different species – in case of horses the efficiency falls in range of 35 – 40%. If this is true and if a 35% value may be taken for the η_{mscl} variable ([22] mentions use of 35% for vertical efficiency for horses), then the $p_{mech\text{-}total}$ curves, now renamed as $p'_{mech\text{-}total}$, are re-plotted in Figure 7 using the altered value for η_{mscl} (for both the aerobic and anaerobic contributions). Also, plotted are the mgv_v lines for different slopes.

The results of Figure 7 showed an interesting behavior – except for the 7.5% incline (which presents an over-estimation scenario), the mgv_v lines are generally close to the evaluated $p'_{mech\text{-}total}$ curves around the range of 4 - 6m/s (the region is shaded and may be named '*High Proximity Region' (HPR)*). Now if η_{mscl} is truly equal to 35%, the results may be interpreted as suggesting that in a certain speed range, the equine locomotion is involving movement of the whole body, quite the same as it would do on an actual

incline – while at other speeds, the COM is moving lesser vertically compared to how it would have to move on an actual uphill incline.

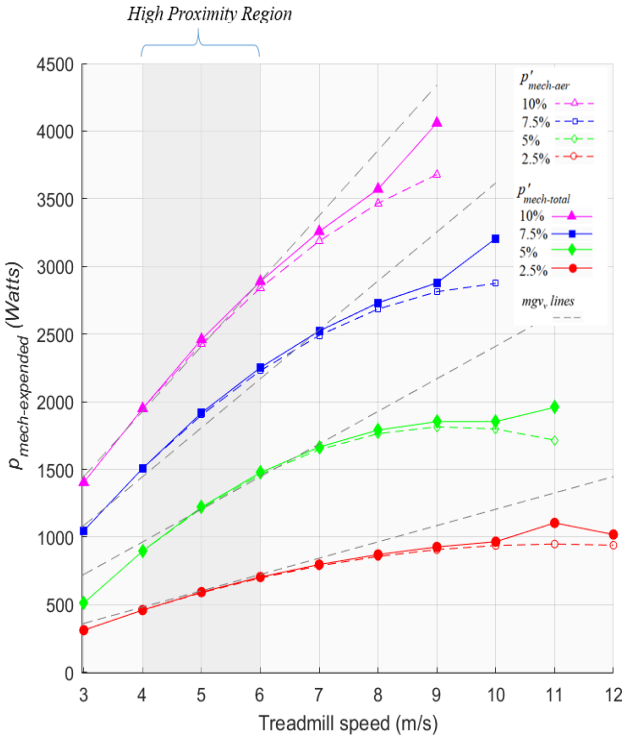


Figure 7: Total expended power evaluated via using 35% muscle efficiency. The speed points 1 and 2 m/s are ignored for reason mentioned in Figure2 caption.

9. The Electrical Power Generatable

The generatable mechanical power $p_{mech\text{-}total}$ is finally converted to electrical power which may be supplied to the grid. Different conversion schemes may be employed, however, for the sake of providing an approach for the evaluation of the potential, the current effort assumes a simple scheme. A DC generator is assumed to be coupled with the treadmill belt, thus converting $p_{mech\text{-}total}$ to p_{dc}. A fixed efficiency of 80% is taken for this conversion.

Next, a grid-tied DC/AC inverter is assumed to convert p_{dc} to AC power $p_{elect\text{-}ac}$ supply-able to distribution electrical power system. For this DC/AC conversion, the Fronius IG Plus 12 curve is selected from [36] ('Figure 4. Typical per unit efficiency curves for grid-connected solar inverters'), graph points are obtained via digitization (using 'grabit' [25]) and curve fitting is used which expresses the efficiency characteristic via (14)

$$Inverter\ Efficiency\ = ax^b + c \qquad (14)$$

where a = - 0.6217, b = -1.183, c = 96.98 and x represents the x-axis point of p_{dc} pu (the p_{dc} per unit is obtained via dividing any actual p_{dc} by 3000Watts which is taken as the rating of the inverter). Subsequently, p_{dc} is converted to $p_{elect\text{-}ac}$ according to the (14). Figure 8 presents the inverter efficiency characteristics (digitized points and the curve fitting approximation) as well as the $p_{elect\text{-}ac}$ lines.

10. Assumptions and Weak Points

The purpose of this section is to summarize some of the weak points/assumptions of the presented effort – this may lead to future improvements as well as better evaluation of the quality of results.

1. Use of ΔVO_2 and Δlactate values (section 4.2)

A justification is provided in the section. Furthermore, due to this assumption, the work may not be applicable to every single

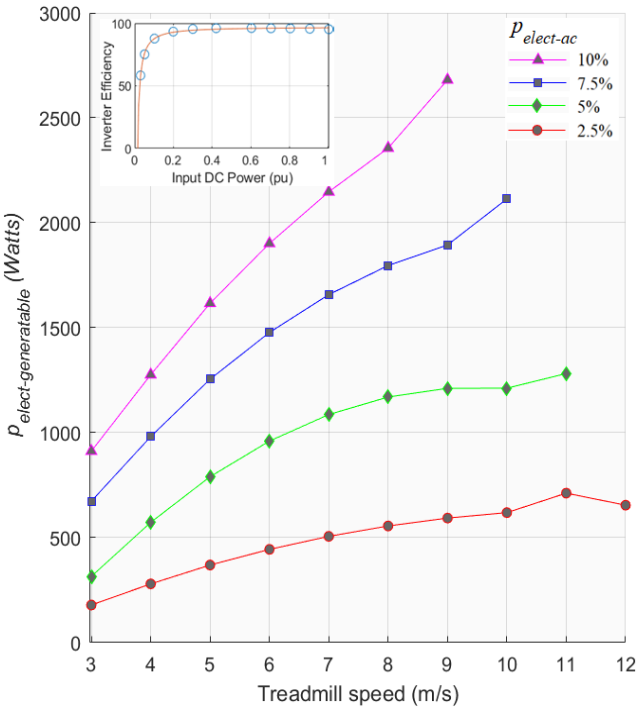


Figure 8: Total generatable (and grid deliverable) ac electrical power from the renewable exercising equine animate prime mover. Inset sub-figure presents inverter efficiency curve – circles show digitized graph points while the curve shows plot of the equation obtained via curve fitting.

individual horse, rather, it would be applicable to an average horse – in other words, if the approach of [23] (which is for humans and for ΔVO_2 only, and not for Δlactate) can be extended to this work (including Δlactate) , then the results should be applicable on the average to different equines with plus minus deviations individually.

2. Variation in $O_{2\text{-}J\text{-}eqv}$ (sections 5.1 & 6)

Depending upon respiratory exchange ratio, O2-J-eqv can vary from 19.61 to 21.1 [26]. The current study does not take any such variation into account - $O_{2\text{-}J\text{-}eqv}$ = 21.1 J/ml O_2.

3. *CRS_{CF} (section 5.1)*

The cardio-respiratory system correction factor is a crude approximation with various assumptions – derivational details are mentioned in the appropriate section.

4. *η_{mscl} (sections 5.1 & 6)*

The mechanical efficiency of muscles (for horizontal locomotion) is taken equal to 30%, also, any variation in this value has not been accounted.

5. *Using mean values only*

From the basic reference [24], which is the source of the treadmill VO_2 and lactacte data – only the mean values are taken and standard deviations have not been included.

6. *$lact_{O2\text{-}eqv}$ (section 6)*

As per our understanding, the current work is not explicitly involving any lactate clearance alongside lactate generation.

7. *Vertical η_{mscl} (section 8.2)*

A fixed value of 35% has been used.

8. *Efficiency of DC generator (section 9)*

A fixed value of 80% has been used. This is a far from true assumption, as the actual efficiency will vary with operating point. However, it may be said that the purpose of section 10 is mainly to convey the idea of $p_{mech\text{-}total}$ to $p_{elect\text{-}ac}$ conversion, so, for the DC/AC inverter, the efficiency variation with changing operating point has been used and then, to keep things simple, this variation was not used for the DC generator.

11. Contributions to Body of Knowledge

As per the understanding of the authors, the following points may be regarded as the contributions of the manuscript

- Bringing forward a novel concept of harvesting energy from an equine exercise treadmill – thus presenting a case of renewable energy generation from animate prime-movers, without compromising the original purpose i.e. exercise of the treadmill machine.
- Presenting an approach to quantify the generatable power from an exercising equine.

12. Conclusion

The paper has presented the idea of tapping renewable energy from the inclined treadmill for equine exercise. The somatic energy of the horse has long been used by humans – the current paper uses it for electricity generation, albeit maintaining exercise as the primary function of the treadmill workout. For determining the amount of the generatable power, a detailed approach has been presented which includes power of aerobic and anaerobic metabolism as well as the conversion into electrical power.

The paper does rely upon assumptions, but an effort has been made to clearly mention them. The (deemed) contributions to the body of knowledge have been mentioned as well. On the whole, the paper is an interdisciplinary effort presenting a novel concept as well as a subsequent quantitative methodology for estimation of the potential.

Acknowledgments

The paper humbly and gratefully acknowledges the contribution of Dr. Shahid in guiding towards the topic, and the contribution of Dr. Zaheer in support with biological topics.

References

[1] I.Z. Pelyva, R. Kresák, E. Szovák, Á.L. Tóth, "How Equine-Assisted Activities Affect the Prosocial Behavior of Adolescents," International Journal of Environmental Research and Public Health, **17**(8), 2020, doi:10.3390/ijerph17082967.

[2] A. Rzekęć, C. Vial, G. Bigot, "Green Assets of Equines in the European Context of the Ecological Transition of Agriculture," Animals, **10**(1), 2020, doi:10.3390/ani10010106.

[3] N. Ohtani, K. Kitagawa, K. Mikami, K. Kitawaki, J. Akiyama, M. Fuchikami, H. Uchiyama, M. Ohta, "Horseback Riding Improves the Ability to Cause the Appropriate Action (Go Reaction) and the Appropriate Self-control (No-Go Reaction) in Children," Frontiers in Public Health, **5**, 8, 2017, doi:10.3389/fpubh.2017.00008.

[4] Gomez-Nacer, "Animal Powered Electricity Generator," Patent US20050161289A1, 2005.

[5] A.R. Smith, "Bovine Treadmill," Patent US7654229B2, 2010.

[6] D.G. Bayerlein, V.E. Emons, N. Oblamski, "Power generating manually operated treadmill," Patent US9956450B2, 2018.

[7] S. Al-Zamil, "Mechanical platform for producing clean energy by means of animals منصة ميكانيكية لانتاج طاقة نظيفة تعمل بواسطة الحيوانات," Patent WO2017061906A1, 2017.

[8] T.-C. Chang, "Livestock power generation system," Patent US20160344260A1, 2016.

[9] W. Taylor, "Animal power generator," Patent US20110266091A1, 2011.

[10] A.K. Bayen, "A system for generating electricity using nonconventional source," Patent WO2019186582A1, 2019.

[11] R.J. Fuller, L. Aye, "Human and animal power – The forgotten renewables," Renewable Energy, **48**, 326–332, 2012, doi:10.1016/j.renene.2012.04.054.

[12] H.M.D.P. Wijethunge, T.G.P. Priyadarshana, "Micro hybrid power plant design with animal draft power and biogas for a rural village," in 2013 IEEE Global Humanitarian Technology Conference: South Asia Satellite (GHTC-SAS), 213–217, 2013, doi:10.1109/GHTC-SAS.2013.6629918.

[13] Sahil, P.K. Sharma, N. Hari, N. Kumar, D. Shahi, "An innovative technique of electricity generation and washing machine application using treadmill," in 2016 IEEE 1st International Conference on Power Electronics, Intelligent Control and Energy Systems (ICPEICES), 1–5, 2016, doi:10.1109/ICPEICES.2016.7853524.

[14] H.T. Yang, T.H. Tseng, T.H. Ai, Y.H. Wu, S.H. Yeh, "A grid-connected energy conversion system for a treadmill with auto-transferring modes between a motor and a generator," in IECON 2015 - 41st Annual Conference of the IEEE Industrial Electronics Society, 316–321, 2015, doi:10.1109/IECON.2015.7392118.

[15] S. Ali, S. Murtaza, A. Katiyar, "Design of manual treadmill with electricity generator for energy saving," International Journal of Research in Engineering and Applied Sciences, **5**, 12–15, 2016.

[16] D.F. Preedy, G.R. Colborne, "A method to determine mechanical energy conservation and efficiency in equine gait: a preliminary study," Equine Veterinary Journal, **33**(S33), 94–98, 2001, doi:10.1111/j.2042-3306.2001.tb05368.x.

[17] A.E. Minetti, L.P. Ardigò, E. Reinach, F. Saibene, "The relationship between mechanical work and energy expenditure of locomotion in horses," Journal of Experimental Biology, **202**(17), 2329–2338, 1999.

[18] L.A. Peyré-Tartaruga, M. Coertjens, "Locomotion as a Powerful Model to Study Integrative Physiology: Efficiency, Economy, and Power Relationship," Frontiers in Physiology, **9**, 1789, 2018, doi:10.3389/fphys.2018.01789.

[19] D.F. McMIKEN, "An energetic basis of equine performance," Equine Veterinary Journal, **15**(2), 123–133, 1983, doi:10.1111/j.2042-3306.1983.tb01734.x.

[20] R. Stevenson, R. Wassersug, "Horsepower from a horse," Nature, **364**, 195, 1993, doi:10.1038/364195a0.

[21] M.M.S. Van Oldruitenborgh-Oosterbaan, H.M. Clayton, "Advantages and disadvantages of track vs. treadmill tests," Equine Veterinary Journal, **31**(S30), 645–647, 1999, doi:10.1111/j.2042-3306.1999.tb05305.x.

[22] Z.T. Self, A.J. Spence, A.M. Wilson, "Speed and incline during Thoroughbred horse racing: racehorse speed supports a metabolic power constraint to incline running but not to decline running," Journal of Applied Physiology, **113**(4), 602–607, 2012, doi:10.1152/japplphysiol.00560.2011.

[23] P. Gimenez, P.J. Arnal, P. Samozino, G.Y. Millet, J.-B. Morin, "Simulation of uphill/downhill running on a level treadmill using additional horizontal force," Journal of Biomechanics, **47**(10), 2517–2521, 2014, doi:https://doi.org/10.1016/j.jbiomech.2014.04.012.

[24] M.D. Eaton, D.L. Evans, D.R. Hodgson, R.J. Rose, "Effect of treadmill incline and speed on metabolic rate during exercise in thoroughbred horses," Journal of Applied Physiology, **79**(3), 951–957, 1995, doi:10.1152/jappl.1995.79.3.951.

[25] GRABIT - Extract (pick out) data points off image files, May 2020.

[26] C.B. Scott, A primer for the exercise and nutrition sciences: thermodynamics, bioenergetics, metabolism, Humana Press/Springer Science, 2008.

[27] R.E. Klabunde, Myocardial Oxygen Demand, Aug. 2020.

[28] H. Kline, J.H. Foreman, "Heart and Spleen Weights as a Function of Breed and Somatotype," in 3rd International Conference on Equine Exercise Physiology (ICEEP), 17–21, 1991.

[29] M.D. Loer Stephan A., M.D. Scheeren Thomas W. L., M.D.F. Tarnow Jorg, "How Much Oxygen Does the Human Lung Consume?," Anesthesiology: The Journal of the American Society of Anesthesiologists, **86**(3), 532–537, 1997.

[30] S.J. Wickler, H.M. Greene, K. Egan, A. Astudillo, D.J. Dutto, D.F. Hoyt, "Stride parameters and hindlimb length in horses fatigued on a treadmill and at an endurance ride," Equine Veterinary Journal, **38**(S36), 60–64, 2006, doi:10.1111/j.2042-3306.2006.tb05514.x.

[31] S. Franklin, K. Allen, 2 - Laboratory exercise testing, W.B. Saunders: 11–24, 2014, doi:https://doi.org/10.1016/B978-0-7020-4771-8.00002-8.

[32] S.L. Bond, P. Greco-Otto, R. Sides, G.P.S. Kwong, R. Léguillette, W.M. Bayly, "Assessment of two methods to determine the relative contributions

of the aerobic and anaerobic energy systems in racehorses," Journal of Applied Physiology, **126**(5), 1390–1398, 2019, doi:10.1152/japplphysiol.00983.2018.

[33] Z.T.S. Davies, A.J. Spence, A.M. Wilson, "External mechanical work in the galloping racehorse," Biology Letters, 2019, doi:10.1098/rsbl.2018.0709.

[34] E. Barrey, 10 - Biomechanics of locomotion in the athletic horse, W.B. Saunders: 189–211, 2014, doi:https://doi.org/10.1016/B978-0-7020-4771-8.00010-7.

[35] G.K. Snyder, C.A. Carello, "Body mass and the energy efficiency of locomotion: Lessons from incline running," Comparative Biochemistry and Physiology Part A: Molecular & Integrative Physiology, **150**(2), 144–150, 2008, doi:https://doi.org/10.1016/j.cbpa.2006.09.026.

[36] R.S. Faranda, H. Hafezi, S. Leva, M. Mussetta, E. Ogliari, "The Optimum PV Plant for a Given Solar DC/AC Converter," Energies, **8**(6), 4853–4870, 2015, doi:10.3390/en8064853.

ASTES

Advances in Science, Technology and Engineering Systems Journal Vol. 5, No. 5, 1007-1012 (2020)

www.astesj.com

Special Issue on Multidisciplinary Innovation in Engineering Science & Technology

ASTESJ

ISSN: 2415-6698

Control of Soft Robotic Artificial Muscle with Hand Gesture Using Leap Motion Sensor

Victoria Oguntosin*, Akindele Ayoola E

Department of Electrical & Information Engineering, Covenant University, Ota, Ogun State, 112233, Nigeria

ARTICLE INFO

Article history:
Received: 01 June, 2020
Accepted: 18 July, 2020
Online: 20 October, 2020

Keywords:
Artificial Muscles
Pneumatic Actuator
Soft robot
Gesture-based control
Leap motion sensor

ABSTRACT

We describe the control design strategy used to control a soft robotic artificial muscle composed of silicone rubber using hand gesture signals. This artificial muscle is actuated with pneumatics, and therefore, the control strategy employed is through the regulation of air pressure within the inner chambers. Using the hand gestures of bringing the hands apart and together, the artificial muscle can be made to expand and contract with the gesture interface from the leap motion sensor. The advantage of the employed hand gesture control compared to switch control is that it provides a more natural interface for the regulation of air pressure within the artificial muscle through the use of electronic and automatic control. Possible areas of application include the use of the soft muscles for rehabilitation purposes and the combined system for developing a physiotherapy gaming device to exercise the hands and fingers of individuals that need to strengthen the muscles of the hands and fingers.

1. Introduction

Soft robots are specialized sets of actuators that possess infinite degrees of freedom and, therefore, able to perform complex motions and manipulations, which would be difficult for rigid manipulators to perform. The control of such infinite degrees of freedom is, therefore, an integral part of the study and design of soft actuators. This paper aims to control a soft robotic artificial muscle using gesture-based control. This paper is an addition to the study initially presented in International Conference on Soft Computing & Machine Intelligence (ISCMI) [1], which employs hand gestures to control a soft rotary actuator. In this work, the same principle is employed to contract and expand a Soft Robotic Muscle using gesture signals.

The pneumatic air within pneumatically powered soft actuators can be controlled using manual or electronics control. Manual control involves the operation of the control hardware such as piston and cylinder via manual operation [2] while electronics operation makes use of electronic devices such as air pump and ON/OFF solenoid valves for the control hardware interfaces [3][4]. While electronics control has the superior advantage of automatic control compared with manual operation of pistons and cylinders, an electronics-free control system is sought after. This is because soft robots are inherently compliant, and as such, can be used in environments where Electromagnetic Interferences (EMI) needs to be minimized. An electronics-free control system is required because the air pump and solenoid valves used for electronics control generate EMI waves and, as such will limit the use of soft robots in such controlled environments. Electronics-free control makes use of fluidic valves, logic circuits, and fluidic processors. The switching valves and pumps are composed entirely of silicone rubber [5].

Soft robot control can be over a long-distance communication channel [6]. The transfer of control commands from the master device to a slave device via a remote communication channel results in delays. For instance, a teleoperated soft actuator controlled on the master side using hand gestures has been studied for the measured delays. With the Message Queuing Telemetry Transport (MQTT) server utilized to convey packets of data over the internet to the soft actuator, delays, which include communication delays, elastic saturation delays occurring as a result of non-linear effects of pneumatic action, delays due to noise and hardware imperfections were observable. A Kalman filter [7] has been used to effectively minimize the delay due to elastic saturation.

Unlike silicone-based soft roots that move via material stretching, fabric-based eversion robots are made from non-extensible nylon fabric. Therefore, more complex control such as

*Victoria Oguntosin, Department of Electrical & Information Engineering, Covenant University, KM 10, Idiroko Road, Ota, Ogun State, Zip Code: 112233, Nigeria, Contact No: +2349018107052
Email: victoria.oguntosin@covenantuniversity.edu.ng

extension, steering, tip position, and orientation, and variable stiffness control is possible using air pressure control [8].

As a result of the multiple degrees of freedom exhibited by soft robots, it implies that multiple sensors are required to measure these degrees of freedom for feedback control. Embedding a large number of sensors within a soft robot is impractical because embedded sensors can limit movement [9] and can give rise to increased material and computational cost. Therefore, an observer or estimator is necessary to estimate the states of the soft robot based on the available measurements from the sensors available. Before observer design can be done, a model of the soft robot is first required. A soft robot has been modeled using a network of wavelet and a Kalman filter used to predict output measurements [10].

In this paper, a soft robotic muscle described in [11] is controlled for contraction and expansion using a gesture device. The choice of an artificial muscle based soft device compared to other forms of the soft actuator is due to its ability to contract and expand in such a manner that can follow natural motions of the hands. Soft robotic muscles made of silicone have the advantage of high contractibility [12] and high force compared to conventional McKibben muscles [13]. Soft robotic muscle actuators make use of vacuum pressure to contract via buckling of air channels [14] and make use of air pressure to expand via the opening of air channels [11]. This is In contrast to McKibben's artificial type muscles that shorten when pressurized air enters into the inner air cavities [15]. The novelty of the proposed solution is the control of artificial muscles for expansion and contraction purposes via hand gestures. Possible areas of application include the use of the soft muscles for rehabilitation purposes and the combined system for game purposes – a physiotherapy gaming device can be developed to exercise the hands and fingers of individuals that need to strengthen the muscles of the hands and fingers.

Hand gesture recognition refers to the combination of specialized sensors with mathematical algorithms to recognize the movement of the hands with the intention of controlling devices without touch. The applications of hand-gesture systems are in the areas of robotics, home automation, automatic sign language recognition, phone, and computer security and gaming devices. The sensors used for gesture recognition include magnetic sensors, inertial measurement units, single cameras, depth cameras, stereo cameras, and gesture-based gaming controllers. Hand gesture sensors can make use of 3D model-based algorithms, Skeletal-based algorithms (such as the Kinect and Leap Motion sensors), Appearance-based models (such as cameras) or Electromyography-based models (such as EMG electrodes) to track hand movements and recognize the gestures.

An accelerometer system for drawing English letters and Arabic numerals as well as recognizing directional movement for gaming, was implemented [16] as a hand recognition device for recognizing the handwritten gestures. Hand movement is captured with the use of an accelerometer while the DTW algorithm processes it and sent to a mobile device using the BlueTooth interface. The gesture recognition and motion detection algorithm were validated by collecting hand gesture and directional motion trace for three participants. Being an accelerometer based system, the device performed best with directional movement detection compared to shape and digits recognition.

In order to miniaturize hand gesture devices, a microsystem consisting of ultrasonic traducers was proposed [17]. The hand gestures implemented include hand tap, hand click, hand rotate, hand press, and hand rub, which are precisely the way people use the fingers in actual scenarios. Ultrasonic sensors were used to distinguish the movement of the hands, and RF signal processing algorithms were used to excerpt features for the machine learning classifiers. Accuracies of conventional classification methods with Radio Frequency (RF) and end-to-end architecture for 9 subjects were analyzed with accuracy greater than 80% for all the classifiers.

A segmentation method that uses both depth and RGB color data from a scene using a Kinect sensor to obtain the hand position and convex hull detection algorithm for identification of the fingertips position was presented [18]. The hand gesture image is first extracted, after which contour information is removed to give a sketch of the hand with palm and finger location highlighted. From the presented results, the proposed method was found to accurately determine hand gestures in realtime with distances of 0.6m, 1.0m, 1.5m, and 2.0m from the sensor. The gesture recognition rate was between 96.67% - 98.88% for the six gestures.

A multimodal hand gesture recognition system comprising of the combined use of a single Inertial Measurement Unit (IMU) and pressure-based transducers placed on the wrist has been evaluated [19]. The multimodal approach eliminates the problem of using a single IMU as a hand gesture detection system due to arm movements. The system comprised of an IMU unit (3-axis accelerometer, and 3-axis gyroscope) and acoustic signals (10 microphones) placed on the wrists of 10 subjects in order to detect and track thirteen common gestures for hand signaling.

A method for detecting gestures of the hand [20] using soft skin tactile sensors to measure wrist movements instead of using the more conventional methods involving IMUs, EMG, and FSR has been implemented. Eight specific gestures comprising the movement of the wrist could be distinguishable using the novel sensor. Filtering techniques were used to filter out pulse rate noise, which could be misinterpreted as a movement of the wrist. The verification of the performance of the proposed sensor involved comparison tests between the sensor with an EMG and FSR sensor was conducted. 97–99% accuracy of the stain sensor was obtained compared to the EMG and FSR sensors suggesting the superiority of the novel gesture recognition method with the tested conventional methods. Other conventional methods that have been used to control soft actuators other than hand gestures [21] include eye movement and tracking [22].

This section provided an introduction with background material on soft robotics control. It also describes hand gesture sensors and systems. Section two provides a description of the hand gesture control strategy employed to control the contraction and expansion of the soft robotic artificial muscle. Results and discussion are offered in Section three. The last section, Section four, provides a conclusion for the work.

2. Hand Gesture Control Design of Soft Robotic Muscle

In this work, a hand gesture system that controls a soft robotic muscle for contraction and expansion actuation is implemented.

The system design comprises of the hardware and software design. The hardware system consists of a leap motion sensor to detect the hands and the soft robotic muscle. The software system is made up of the control algorithms that detect the gestures responsible for contracting and expanding the soft muscles.

2.1. Leap Motion Sensor Interface

The Leap Motion device continually detects hand, finger, or tool-like objects inside its field of view when powered ON via connection to a computer. Three infrared LEDs and two infrared cameras within the device facilitate hand motion tracking. The device is able to track any object located with its 150^0 viewing area with a distance of 0.50m from it in the upward direction and 0.25m from it in other directions [23]. Hand and fingers can be detected by the Leap using the Software Development Kit (SDK) libraries. The leap sensor is displayed in Figure 1.

The leap motion sensor tracks the movement of the hands within its FOV by measuring distances in three directions, called the X, Y, and Z directions. The X distance is changed when a positioned hand moves left or right, the Y distance changes with a hand moving up and down from the sensor, while the Z distance changes with a positioned hand moving forward or backward.

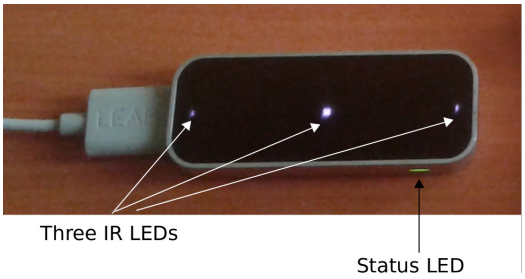


Figure 1: The Leap Motion sensor powered via USB connection to a computer; the green status LED is ON and the three infrared LEDs come ON as shown.

2.2. Soft Robotic Muscle Interface

The Soft Robotic Muscle (SRM) used is the same described in [24]. The detailed fabrication process, together with mathematical equations describing its model, is presented in [11]. The SRM muscle is comprised of soft modular units arranged in series to improve the rate of shortening. The SRM muscle contracts upon the application of vacuum pressure and expands to its original length when positive pressure is applied to its inner chambers. The muscle is also able to bend bi-directionally by controlled variation of air and vacuum pressure within its inner walls. The SRM muscle is shown in Figure 2. The parameters of muscle include the wedge angle, $\theta = 60^0$, wedge length, l_l=20mm, number of modular units, n=9, air channel height, h_c=40mm, wall thickness, t=2.5mm, and muscle length, l=160mm. The soft robotic muscle can contract and expand partially. The zero position of the SRM is at its normal length of 160mm; its contacted length is 104mm while its expanded length is 170mm.

2.3. Integrated Hand Gesture and Soft Robotic Interface

The software aspect of the system involves designing the hand gesture system responsible for contracting and expanding the SRM muscle. This process first begins with detecting the two hands and then implementing the software that measures the distance between both hands. Two gestures which we term the "contracting" and "expanding" gestures are implemented. The two gestures are described as follows:

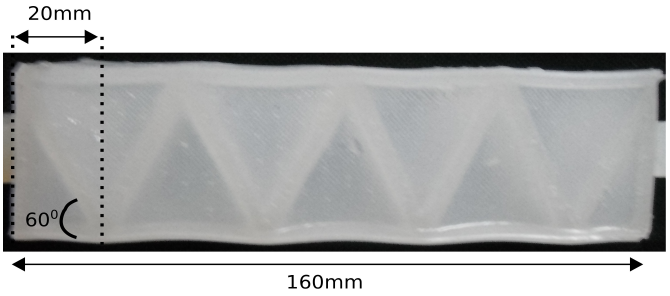


Figure 2: SRM Muscle having a total length of 160mm and defining angle of wedge as 60^0, wedge length is 20mm, number of wedges is 9, the height of air channel equals 40mm and wall thickness is 2.5mm

- **Contraction gesture**: This gesture is represented by bringing both hands together, i.e., decreasing the distance between the left and right hands.
- **Expansion gesture**: This gesture is represented by bringing both hands farther apart, i.e., increasing the distance between the left and right hands.

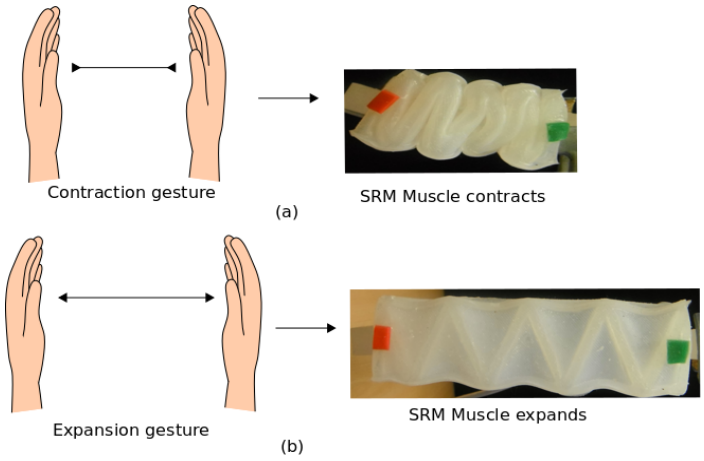


Figure 3: From (a), when the contraction gesture is executed, the SRM muscle contracts; From (b), when the expansion gesture is executed, the SRM muscle expands to its original length.

The two gestures were developed because they follow the natural motions of how a human will contract and expand the muscle as if holding it physically without an actuating source. Therefore, when the contraction gesture is executed, control commands are sent to the SRM muscle to contract it. Conversely, when the expansion gesture is performed, a control command from the leap sensor interface is sent to the electronics hardware [4] to cause the expansion of the soft robotic muscle. The rationale behind using a leap sensor is so that expansion and contraction control of the SRM muscle can be implemented over a remote distance. This gesture interface allows for a master-slave control where the master is the movement of the two hands, and the slave is the soft robotic muscle that follows the motions of the master. The pictorial representation of the system design is seen in Figure 3.

The software flowchart for implementing the integrated system comprising hand gesture detection and soft robotic muscle control is shown in Figure 4. As seen from the Figure, the distance between

the two hands is measured; if this distance is decreasing, i.e., its value is reducing, that means that a contraction gesture is being executed and a command is sent to the SRM muscle to contract it. If the measured distance is increasing, i.e., its value is getting larger from the previous timestamp, which means that an expansion gesture is being executed, and a command is sent to the SRM muscle to expand it to its normal resting length. If there is no change in the distance measured between the consecutive timestamps, then no gesture is being executed, and the SRM muscle does not change in length.

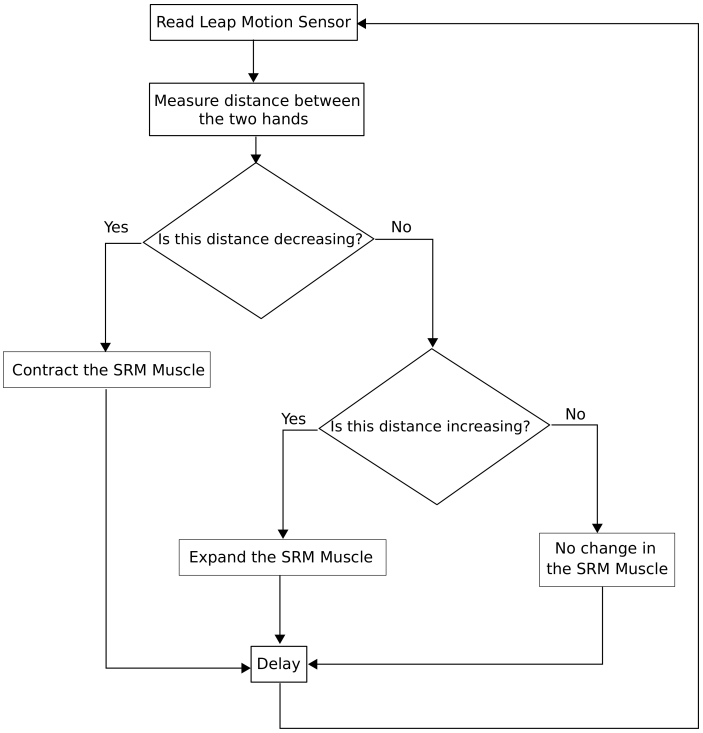


Figure 4: Flow chart for the control of soft robotic artificial muscle with hand gesture signals using the leap motion sensor

3. Results and Discussion

The controller hardware setup consisting of the electronic circuit, leap motion sensor, SRM Muscle, supply pumps for negative and positive pressurized air is shown in Figure 5. The detailed explanation of the experiment and description of the used circuit board and controller can be found in [3][4]. Through the USB connection of the Leap device to a computer, interpreted gestures commands are sent to the controller hardware with the microcontroller and leap connected to the same computer interface for the transfer control commands.

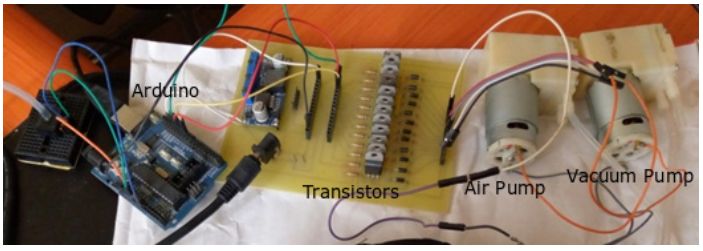


Figure 5: The hardware controller for the hand gesture system consisting of the controller circuitry, vacuum pump for contracting the muscle and air pump for expanding the SRM Muscle

Figure 6 shows absolute vacuum pressure and contraction ratio as a function of during contraction. A maximum absolute vacuum pressure of -20kPa is observed for a maximum contraction ratio of 0.35. The measured contraction time is 4 seconds

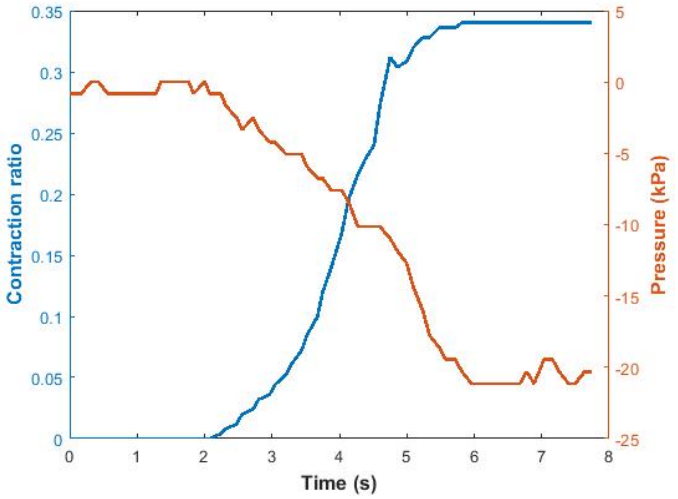


Figure 6: Contraction of the SRM Muscle, the contraction ratio moves from 0 to 0.35 of the muscle length in 4s, the vacuum pressure is shown to move from 0kPa to -20kPa during contraction

When the SRM Muscle is undergoing contraction, contraction ratio, and absolute vacuum pressure move from zero to the contraction ratio of 0.35 and vacuum pressure of -20kPa, respectively. Figure 7 shows absolute vacuum pressure and contraction ratio as a function of during expansion. The contraction ratio moves from 0.35, which is the contracted ratio to 0, which is the original muscle resting position in 6 seconds. The vacuum pressure is shown to move from -20kPa to -0kPa during expansion.

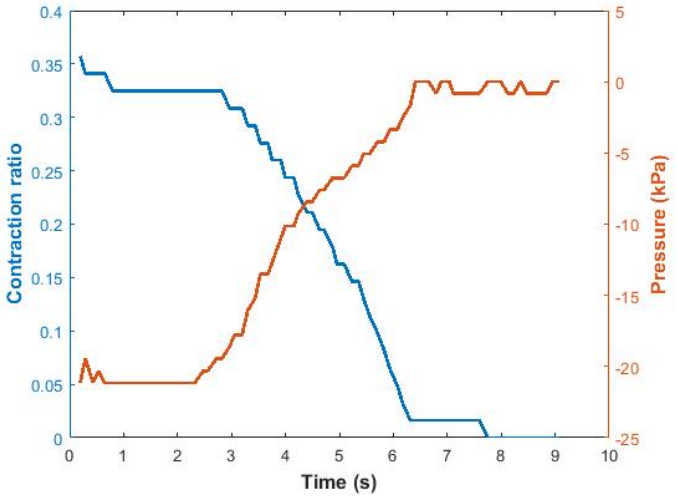


Figure 7: Expansion of the SRM Muscle, the contraction ratio moves from 0.35 which is the contracted form to 0 which is the original muscle resting position in 6s, the vacuum pressure is shown to move from -20kPa to -0kPa during expansion

When the SRM Muscle is undergoing expansion, contraction ratio, and absolute vacuum pressure move a contraction ratio of 0.35 and vacuum pressure of -20kPa to zero as shown. Through the use of the leap sensor to control the soft muscle, closed-loop

control operation of the SRM muscle opens the possibility to obtain a specified muscle contraction. To achieve the desired operation, visual information from the users' eyes measures the appropriate contraction or expansion length while control signals are sent to contract and expand the SRM muscle.

The novelty of the proposed solution is the control of artificial muscles for expansion and contraction purposes via hand gestures. Possible areas of application include the use of the soft muscles for rehabilitation purposes and the combined system for game purposes – a physiotherapy gaming device can be developed to exercise the hands and fingers of individuals that need to strengthen the muscles of the hands and fingers.

The demonstration of the control of the Soft Robotic Artificial Muscle with a hand gesture using the leap motion sensor is shown in Figure 8. A user performs the contraction and expansion gesture using the Leap motion sensor as a hand gesture interface to create contraction and contraction movements of the Soft Robotic Muscle. As shown, both hands must be within the 150^0 field of view of the leap sensor in order that the accurate distance between the hands is measured. Also, both hands should be within 0.50m from the sensor in the upward direction and 0.25m from the sensor in the x and y direction.



Figure 8: A user performs the contraction and expansion gestures using the Leap motion sensor as hand gesture interface to create contraction and contraction movements of the Soft Robotic Muscle

4. Conclusions

A control design strategy for the control of artificial muscles using hand gesture signals have been proposed and implemented through the regulation of air pressure within the inner chambers. The artificial muscle can be made to expand and contract as a result of interpreted gesture commands from the leap motion device. The advantage of the employed hand gesture control compared is that it provides a more natural interface for the regulation of air pressure within the artificial muscle through the use of electronic and automatic control. Applications of this work include teleoperated control of a soft robotic muscle using the natural motions of how the muscle will be contracted and expanded if it is physically held.

Conflict of Interest

The authors declare no conflict of interest.

Acknowledgment

The authors acknowledge the management of Covenant University, Ota, Nigeria, for the publication support fund.

References

[1] V. Oguntosin, A. Akindele and E. Oladimeji, "Gesture-Based Control of Rotary Pneumatic Soft Robot Using Leap Motion Controller" in 6th International Conference on Soft Computing & Machine Intelligence(ISCMI), 2019, 169-174, 2019, DOI: 10.1109/ISCMI47871.2019.9004295

[2] F. Ilievski, A.D. Mazzeo, R.F. Shepherd, X. Chen and G.M. Whitesides, "Soft Robotics for Chemists" Angewandte Chemie,, **123**(8): 1930-1935. 2011, DOI: 10.1002/anie.201006464

[3] V. Oguntosin, S. Nasuto, and Y. Hayashi, "Embedded Fuzzy Logic Controller for Positive and Negative Pressure Control in Pneumatic Soft Robots" in UKSim-AMSS 19th International Conference on Computer Modelling & Simulation, 2017, 63–68. 2017, DOI: 10.1109/UKSim.2017.41

[4] V. Oguntosin, S. J. Nasuto and Y. Hayashi, "A Compact Low-Cost Electronic Hardware Design for Actuating Soft Robots", International Journal of Simulation Systems, Science & Technology (IJSSST), **16**(3), 1–11, 2016, DOI: 10.5013/IJSSST.a.16.03.06

[5] S. T. Mahon, A. Buchoux, M. E. Sayed, L. Teng and A. A. Stokes, "Soft Robots for Extreme Environments: Removing Electronic Control", IEEE International Conference on Soft Robotics, 782-787, 2019. DOI: 10.1109/ROBOSOFT.2019.8722755

[6] P..D..S..H. Gunawardane, R..E..A. Pallewela and Nimali T. Medagedara, "Tele-Operable Controlling System for Hand Gesture Controlled Soft Robot Actuator" in 2nd IEEE International Conference on Soft Robotics (RoboSoft), 2019, DOI: 10.1109/ROBOSOFT.2019.8722756

[7] P.D.S.H. Gunawardane, R.E.A Pallewela, A.P.T.D. Pathirana and N. T. Medagedara, "Kalman Filter Based Approach to Overcome Elastic Saturation and Pneumatic Disturbances in Tele-Operated Soft Actuators" in Advances in Manufacturing Technology XXXIII, 2019, DOI:10.3233/ATDE190023

[8] A. Ataka, T. Abrar, F. Putzu, H. Godaba, and K. Althoefer, "Model-based Pose Control of Inflatable Eversion Robot with Variable Stiffness", IEEE Robotics and Automation Letters, 2020, DOI: 10.1109/LRA.2020.2976326

[9] V. Oguntosin, A. Akindele, O. Alashiri,. "Vision Algorithms for Sensing Soft Robots", Journal of Physics: Conference Series, **1378**(3), 2019, DOI: 10.1088/1742-6596/1378/3/032102

[10] J. Y. Loo, K. C. Kong, C. P. Tan1 and S. G. Nurzaman "Non-linear System Identification and State Estimation in a Pneumatic Based Soft Continuum Robot", IEEE Conference on Control Technology Applications, 2019, DOI: 10.1109/CCTA.2019.8920693

[11] V. Oguntosin, A. Akindele, "Design and Characterization of Artificial Muscles from Wedge-Like Pneumatic Soft Modules." Sensors and Actuators A: Physical, 2019, DOI: 10.1016/j.sna.2019.07.047

[12] K. Han, N. Kim, and D. Shin, "A Novel Soft Pneumatic Artificial Muscle with High-Contraction Ratio", Soft Robotics, **00** (00), 2018, DOI: 10.1089/soro.2017.0114

[13] S. M. Mirvakili and I. W. Hunter, "Artificial Muscles: Mechanisms, Applications, and Challenges" Advanced Materials, 1704407, 1-28, 2017, DOI: 10.1002/adma.201704407

[14] D. Yang, M. S. Verma, J. So, B. Mosadegh, C. Keplinger, B. Lee, F. Khashai, E. Lossner, Z. Suo, and G. M. Whitesides, "Buckling Pneumatic Linear Actuators Inspired by Muscle", Advanced Materials Technologies, 1600055, 1-6, 2016, DOI: 10.1002/admt.201600055

[15] T. Abrar, F. Putzu, J. Konstantinova and K. Althoefer, "EPAM: Eversive Pneumatic Artificial Muscle" in 2nd IEEE International Conference on Soft Robotics (RoboSoft), 2019, DOI: 10.1109/ROBOSOFT.2019.8722787

[16] A. Ahmed et al., "Modeling and Simulation of Office Desk Illumination Using ZEMAX," in 2019 International Conference on Electrical, Communication, and Computer Engineering (ICECCE), 1–6, 2019. DOI: 10.1109/ICECCE47252.2019.8940756

[17] Y. Sang, L. Shi, and Y. Liu, "Micro Hand Gesture Recognition System Using Ultrasonic Active Sensing", IEEE Access, **6**, 49339-49347, 2018, DOI: 10.1109/ACCESS.2018.2868268

[18] X. Ma and J. Peng, "Kinect Sensor-Based Long-Distance Hand Gesture Recognition and Fingertip Detection with Depth Information", Hindawi Journal of Sensors, 5809769, 1-9, 2017. DOI: 10.1155/2018/5809769

[19] N. Siddiqui, R. H. M. Chan, "Multimodal hand gesture recognition using single IMU and acoustic measurements at wrist" PLoS ONE **15**(1): e0227039. 2020, 1-12. DOI: 10.1371/journal.pone.0227039

[20] B. Sung-Woo and L. Seok-Pil, "Implementation of Hand Gesture Recognition Device Applicable to Smart Watch Based on Flexible Epidermal Tactile Sensor Array", MDPI micromachines, **10**, 692, 1-15, 2019. DOI:10.3390/mi10100692

[21] V. Oguntosin and A. Abdulkareem, "Design of a pneumatic soft actuator controlled via eye tracking and detection", Heliyon. **6**(7):e04388, 2020, DOI: 10.1016/j.heliyon.2020.e04388
[22] V. Oguntosin and A. Abdulkareem, "Hand gesture control and design of a rotary pneumatic soft actuator using leap motion sensor". Int J Intell Robot Appl, 2020, DOI: 10.1007/s41315-020-00140-5
[23] B. Sanders, Mastering Leap Motion. Packt Publishing, 2014
[24] V. Oguntosin, "Development of Soft Modular Robotics," Ph.D Thesis, University of Reading, 2017. ISNI: 0000 0004 6499 6177

ASTES

Advances in Science, Technology and Engineering Systems Journal Vol. 5, No. 5, 1013-1019 (2020)

www.astesj.com

Special Issue on Innovative Research in Applied Science, Engineering and Technology

ASTESJ

ISSN: 2415-6698

Fabrication and Properties of Hybrid Membranes Based on Poly (Vinyl Alcohol), Sulfosuccinic Acid and Salts of Heteropolyacid with or without Silica for Fuel Cells Applications

Said Maarouf [1,*], Zouhair Alouane[1,2], Bouchra Tazi[2], Farhate Guenoun[1], Khalil Fouad[3]

[1]*Laboratoire de Chimie Biologie Appliquée à l'Environnement, Faculté des Sciences, Université Moulay. Ismail, Zitoune Meknès, B.P. 11201, Maroc*

[2]*Laboratoire de Chimie, DSB, Ecole Nationale d'Agriculture. km. 10, Route Haj Kaddour,.B.P. S/40, Meknès, 50001, Maroc*

[3]*Laboratoire de Chimie Appliquée (LCA). Faculté des Sciences et Technique,– Route d'Imouzzer Fès, B.P. 2202, Maroc*

ARTICLE INFO

Article history:
Received: 24 June, 2020
Accepted: 21 September, 2020
Online: 20 October, 2020

Keywords:
Fuel cells
Polymer electrolyte membranes
Poly (vinylalcohol)
Silicotungstic acid
Sulfosuccinic acid

ABSTRACT

Novel ionic polymers were synthesized by crosslinking of poly (vinylalcohol) (PVA) with sulfosuccinic acid (SSA) and silicotungstic acid (SiWA) with or without silica. The polymer electrolyte membrane fuel cell (PEMFC) was developed using solution casting method. Infrared (IR) spectra revealed that the Keggin structure was insered in the PVA films. The thermal decomposition of the PVA/SSA/SiWA/SiO_2 membranes showed good thermal stability up to 200°C. Water uptake ranged between 31% and 88%. The maximum conductivity has been found to be 6,72.10^{-3} S.cm^{-1} at room temperature for PVA/SSA/SiWA containing 10% of silica weight. The ion exchange capacity of this membrane was 1,75 mmol.g^{-1}. The results showed that these membranes presented very promising performances for use in Proton Exchange Membrane Fuel Cells.

1. Introduction

Exhaustion of non-renewable fossil fuel invokes the development of environmentally friendly alternative energy sources. Fuel cells are being considered as interesting alternatives power sources for a wide range of applications, ranging from portable devices to electric vehicles [1, 2]. Fuel cells are of great interest in the recent research due to their attractive properties. They offer many advantages, such as environmentally benign, high energy efficiency and lower emission of pollutants [3, 4]. The principal component in PEMFCs is the proton exchange membrane (PEM) which is used as proton (or charge carriers) provider from anode to cathode. The membrane must be proton conductor with mechanical strength and chemical stability. The perfluorosulfonated membrane, Nafion produced by Dupont is the most used as a polymer in PEMFCs because of its combined chemical, electrochemical, and mechanical stabilities with high proton conductivity (~0.1 S.cm^{-1}) at ambient temperature [5].
However, it possesses some drawbacks, and especially its high cost; presents a high water swelling characteristic which reduces the lifespan of the membrane and decrease in conductivity at elevated temperature [6]. So, the utilization of Nafion membrane in fuel cell is limited. Therefore, "Hydrocarbon" proton conducting membranes have been designed as an alternative to perfluorinated membranes [7,8]. High performance polyarylenes are resistant to oxidation, thermo-stable and are mechanically strong with a relatively high glass transition temperature (Tg), sulfonated poly (ether ether) ketone [9], sulfonated polyimide [10], polybenzimidazole [11], sulfonated polyposphazene [12] and sulfonated poly(vinylalcohol) (PVA) [1,13], have been synthesized.
However, to enhance the proton conductivity of the polymers, a high acid content is needed. Unfortunately, this can decrease the mechanical strength of the composite membranes, or, even worse, degrade it, especially at higher temperatures [14].
Among the materials investigated, Poly (vinylalcohol) (PVA) has attracted great attention due to its good mechanical properties, chemical stability, low cost, film forming ability, and high hydrophilic behavior [15,16]. The PVA membranes are poor proton conductors and dissolve in water. Hence, to impart protonic conductivity as well as mechanical stability to PVA membranes, a crosslinking agent containing sulfonic acid group

*Corresponding Author: Said Maarouf, Email: saidmaarouf576@gmail.com

can be used, such as concentrated sulfuric acid, sulfosuccinic acid (SSA), acid sulfophthalic [13,17].

Many researchers have studied the properties of cross-linked PVA/SSA membranes as a function of SSA content. Recently, C.González, and A. Greus studied the proton-conducting membrane based on PVA/SSA/GO. Their experimental results showed the proton conductivity of the order of $2{,}06.10^{-3}$ S.cm^{-1} for the PVA/SSA humidified membrane [18]. Furthermore, Kim and al. demonstrated that the PVA/SSA/silica hybrid membranes prepared via a sol-gel process presents excellent proton conductivity [1].

In general, heteropolyacids (HPAs), and SiO_2 have served as an essential inorganic proton conductor for organic-inorganic hybrid membranes [19–22]. HPAs, a class of superionic conductor in their fully hydrated condition and thus it provides high proton conducting pathway [23,24]. For example, hydrated silicotungstic acid (H4 SiW12 O40 •28H2 O) has an ionic conductivity of 2.10^{-2} S.cm^{-1} at room temperature [25–27]. However, HPAs are generally water-soluble. Consequently, a major research objective is to fix the HPAs in stable structure by forming composites which can maintain or increase the proton conductivities of the membranes [22,28,29].

In our previous studies [30,31], we have synthesized the HPA and SiO_2 based hybrid membranes (PVA/PVP/SSA/HPAs/SiO_2). These membranes showed that proton conductivity increase significantly with the HPAs content. Silica was also added in the membranes preparation solution in order to improve thermal and mechanical stabilities of the PVA/PWA membranes.

The aim of this study was to prepare membranes for possible PEMFC. To do this, PVA/SiWA/SiO_2 hybrid membranes containing sulfonic acid groups were synthesized using solution casting method. Sulfonic acid groups were introduced into the PVA matrix by modifications of the chemical structure of the PVA through esterification with sulfosuccinic acid (SSA), which has sulfonic acid groups. In addition heteropolyacid and silica particles in the polymer matrix at varying concentrations, which were expected to achieve high proton conductivity, thermal stability and high water uptake. The effect of membrane thicknesses has also been studied. Ion exchange capacities have been studied for PVA/SSA/10wt.%SiWA/SiO_2 membranes. The prepared composite polymer electrolyte membranes have been characterized by various techniques TGA, and FTIR.

2. Experimental

2.1. Materials

Poly(vinylalcohol) with a molecular weight of 70.000 g.mol^{-1} was received from Sigma Aldrich. Sulfosuccinic acid 70wt.% from sigma Aldrich, Silicotungstic acid from Panreac, Silica 60A°,from sigma Aldrich.

2.2. Membrane preparation

10 wt% PVA solution was prepared by dissolving the pre-weighed amount of PVA in deionized water at 80°C for at least 4 h. The solution of PVA was mixed with SSA in mass ratio of 0,10g at 80°C for 3 hours. Then, Silicotungtic acid (0% - 40%) was added to the above solution and stirred for 2 hours at 80°C to produce PVA/SSA/SiWA membrane. Silica (1% - 15%) was subsequently added to the above solution and stirred at 70°C for about 4 hours to produce PVA/SSA/SiWA/SiO_2 membrane. The solvent was removed by evaporation at room temperature for 16 h, then the cast membranes were allowed to dry at 60°C for 24 h. and then in the oven at 140°C for 1 hour. Membranes thicknesses in the dray state are about 50 to 650 µm.

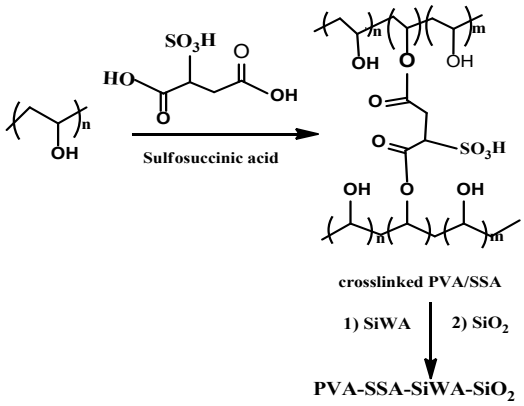


Figure 1: Molecular structure of PVA/SSA polymer matrix and silicotungstic acid with silica.



Figure 2: Homogeneous, transparent thin film of PVA-SSA-SiWA-SiO_2

2.3. Water Uptake

Membrane samples were dried at 60 °C for 24 h and weighed after (Wdry). Then immersed in boiling water during 24 h. The membranes were then removed, and the samples were finally weighed (Wwet). The water uptake of the membrane is deduced using the following equation:

$$WU = \frac{Wwet - Wdry}{Wdry} * 100 \quad (1)$$

2.4. Proton conductivity

Resistances were measured using a cell coupled with potentiostat-galvanostat–Amel instrument (70-50), the measurement cell is show in Figure 3 and has been described elsewhere (Table.1). It composed of two identical compartments linked with two platinum electrodes with the same surface as the membrane. In addition, in each compartment, Luggin capillaries are connected to two saturated calomel electrodes. The membrane is placed between the two compartments during measurements. The ionic conductivity of the membranes was determined by polarization. In 1M NaCl solution, the potential drop between the two references electrodes was measured, following application of a constant direct current (0.5 - 5 mA). The proton conductivity (σ) was obtained using the following equation:

$$\sigma = \frac{e}{RS} \quad (2)$$

where σ is the ionic conductivity in S.cm^{-1}, R is the Resistance of the membrane in Ω, e is the thickness of the membrane in cm, and S is the membrane surface in cm^2.

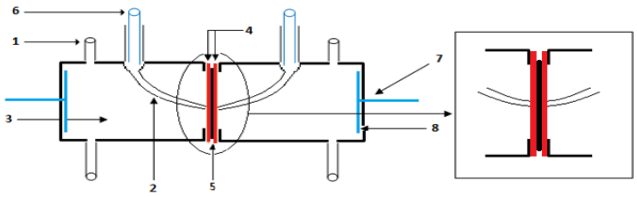


Figure 3: measurement cell of proton conductivity.

Table 1: Description of measurement cell of proton conductivity

1: Capillary (allow entry and exit of the solutions). 2: Capillary Luggin. 3: Electrolyte. 4: Teflon gaskets.	5: Membrane. 6: Reference electrodes. 7: Stem platinum. 8: Platinum electrodes.

2.5. FTIR spectroscopy

The spectrum of the membranes was recorded with a MVP 2 STAR ART DIAMANT (600-4000 cm^{-1}, resolution $4cm^{-1}$).

2.6. Thermal gravimetric analysis (TGA)

TGA was accomplished by thermogravimetric analyzer, TA 60 SHIMADZU TG-DTA. The samples were then heated from 25 °C to 600 °C at a heating rate of 20 °C.min^{-1}.

2.7. Ion exchange capacity (IEC) and fixed ion concentration

IEC has been determined by titration method. A sample membrane (0,375g to 0,765g) was immersed in a 250 ml of 1M HCl solution and stirring for 1h to change them into the H^+ form. The samples were then washed with deionized water to remove excess HCl, and then equilibrated with 230 ml of NaCl (0.1M) + 20 ml of NaOH (0.1M) solution for 24h at room temperature to permit the exchange between protons and sodium ions. Thereafter, 25 ml of the solution was titrated with HCl (0.1M) to evaluate the amount of H^+ generated from the exchange process. From the titration, the ion exchange capacity was determined from the following relation:

$$IEC = \frac{n(H^+)}{(W_{dry})} \quad (3)$$

where $n(H^+)$ is the number of moles of proton sites present in the membrane and Wdry is the weight of the dry membrane. Fixed ion concentration (FIC) can be determined from the following equation:

$$FIC = \frac{IEC}{WU} \quad (4)$$

where (WU) is the water uptake of the membrane sample.

3. Results & Discussions

3.1. Thermal gravimetric analysis (TGA)

The thermal degradation behavior of PVA/SSA, PVA/SSA/SiWA, and PVA/SSA/SiWA/SiO_2 composites membranes was illustrated in figure 4. Three major stages of the thermal decomposition can be considered. The first stage of the decomposition, which occurs between 25 and 200 °C, is the loss of absorbed water molecules formed after the esterification reaction of the membranes. Most of the absorbed water molecules in the membranes are supposed to exist in a bound state rather than in free molecules state. The water molecules seem to have been bound directly to the polymer chains and / or the $–SO_3H$ groups via hydrogen bonds [1]. The second decomposition stage between 200 and 400°C, is the degradation of the sulfonic acid groups ($–SO_3H$). The final major decomposition step comes about between 400 and 500 °C, which is ascribed to decomposition of salt of silicotungstic acid combined with silica. It is seen from TGA curves, that the thermal stability of the hybrid membranes is improved probably due to the additive effect of SiWA and SiO_2 fillers and the chemical cross-linked reaction between the PVA and SSA.

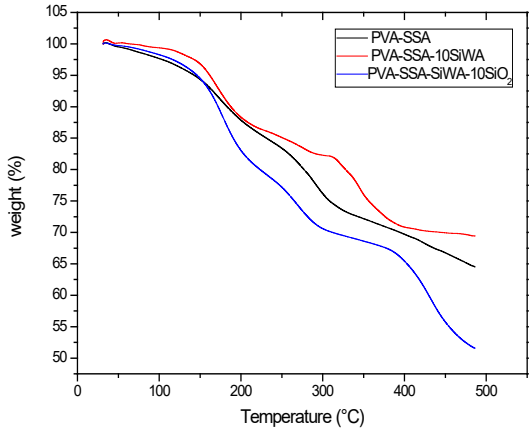


Figure 4: TGA curves for PVA/SSA, PVA/SSA/SiWA, and PVA/SSA/SiWA/SiO_2.

3.2. Fourier transform infrared spectroscopy

Figure 5 represents the F.T.I.R spectrum of the PVA/SSA, PVA/SSA/SiWA and PVA/SSA/SiWA/SiO_2 composite membranes. In the PVA/SSA/SiWA blend membranes, the characteristic ester absorption band (–COO) appeared around $1710cm^{-1}$ [32], and the band at $1030cm^{-1}$ is attributed to ($-SO_3H$) group [32]. These spectral data confirm the esterification between –OH in PVA and –COOH in SSA [1]. The peaks at $3300cm^{-1}$ (OH stretching), $2921cm^{-1}$ (symmetric CH_2–), and the band at $1420cm^{-1}$ is for (-CH3) bending which are characteristic of PVA. The peaks at 969.03; 914.16; 789.04 and $1141.89cm^{-1}$ which are respectively attributed to the W=Od, W-Ob-W and W-Oc-W and O-Si-O. The presence of these peaks in the spectra F.T.I.R confirms that silicotungstic acid is inserted into the blend membranes PVA/SSA/SiWA, the characteristic bands (Si-O-Si) appeared around 1082.14 and $1219.31cm^{-1}$ were observed in the spectra of the PVA/SSA/SiWA/SiO_2 hybrid membrane. This demonstrates that the esterification reaction was complete between the Poly (vinylalcohol) chains and the sulfosuccinic acid.

3.3. Water uptake and proton conductivity of the membrane PVA/SSA/SiWA

Figure 6 shows the water uptake and proton conductivity of the membranes PVA/SSA/xwt.%SiWA as function of the silicotungtic acid content. The water uptake varies from 47% to

60%. As shown in Figure 6, The water uptake increases with the increase of silicotungstic acid, and the maximum is obtained for 10wt.% of SiWA. After that, the addition of silicotungstic acid leads to a decrease in water uptake of the membrane. Invese behavior can be explained by the chemical structure of the PVA/SSA network. An increase in water uptake at low SiWA content maybe is due the restricted degree of their swelling as also of the hydrophilicity of silicotungstic acid to due presence of keggin cage in PVA/SSA/HPA bridged-matrix [33,34].

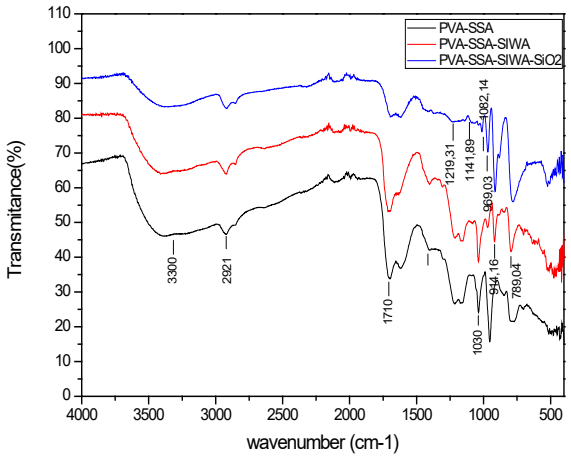


Figure 5: F.T.I.R spectra of PVA/SSA, PVA/SSA/SiWA, and PVA/SSA/SiWA/SiO_2 hybrid membranes.

The proton conductivity has been determined, as shown in this figure; the ionic conductivity of PVA/SSA/xwt.%SiWA membranes varies from 1,100.10^{-3} S.cm^{-1} to 3,015.10^{-3} S.cm^{-1}. The higher value is obtained for the composition PVA/SSA/10wt.%SiWA, which is much higher than that of the pure PVA films and pure 12-tungstogermanic heteropolyacid [35]. The results indicated that PVA film, composited with sulfosuccinic acid and silicoptungstic acid is a new kind of excellent high proton conductor.

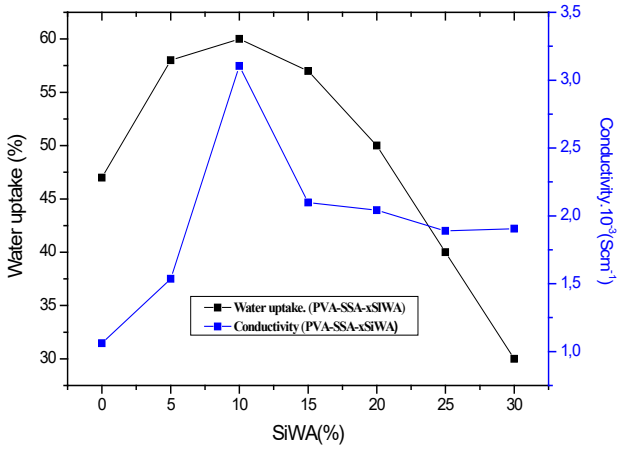


Figure 6: water uptake and proton conductivity of the hybrid membranes PVA/SSA/xwt.%SiWA with different amounts of SiWA.

Figure 7 shows a plot of water uptake of the membranes PVA/SSA/10wt.%SiWA as a function of the membrane thickness. The water absorption increases with the thickness of the membrane in the range 100 - 600 µm. It therefore goes from 28% for the PVA/SSA/10wt.%SiWA membrane of 110 µm thickness to 64% for the PVA/SSA/10wt.%SiWA membrane of 550 µm thickness.

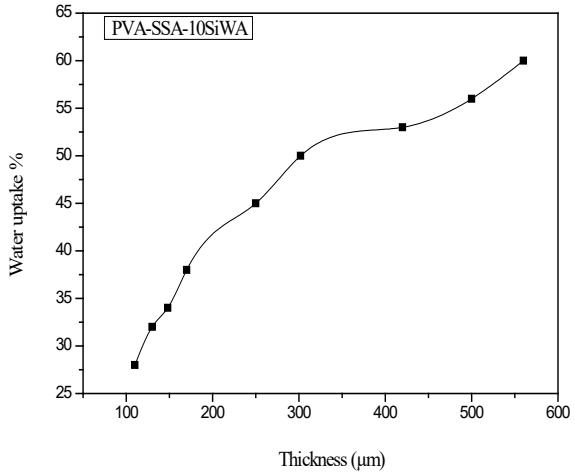


Figure 7: Water uptake of PVA/SSA/10wt.%SiWA membrane with thicknesses.

Figure 8 represents the ionic conductivity of the membrane PVA/SSA/10wt.%SiWA at saline media (NaCl 1M) as a function of the membranes thickness at room temperature. Ionic conductivity values increase from 0,567.10^{-3} to 3,668.10^{-3} S.cm^{-1} In line with thickness values from 100 to 650µm thick. This agrees well with the published results of B. Tazi and al. [22].

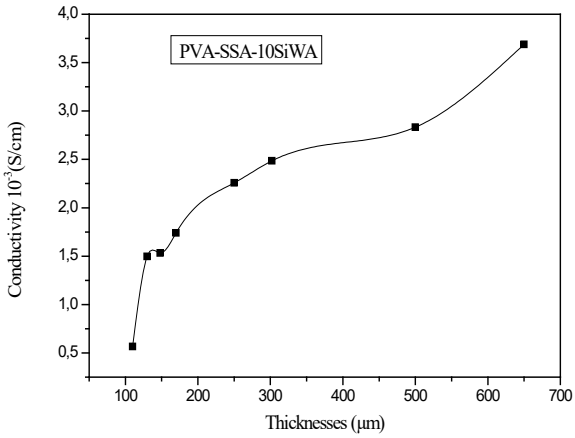


Figure 8: Proton Conductivity of PVA/SSA/10wt.%SiWA membrane with thicknesses.

3.4. Water uptake and proton conductivity of the membrane PVA/SSA/10wt.%SiWA/SiO_2

The water uptake of the membranes PVA/SSA/SiWA/ywt.%SiO_2 as function of SiO_2 content (0wt.%≤ y ≤16wt.%) varies from 60% to 88%. As shown in figure 9. We notice that the water uptake varies with the silica percentage. Hence, the maximum which is equal to 88% was obtained for the

membrane PVA/SSA/SiWA/10wt.%SiO_2. Thus, over 10 wt.% of silica, the water uptake of this membrane starts decreasing.

This figure shows that the ionic conductivities of PVA/SSA/SiWA/ywt.%SiO_2 membranes increase with the increase weight of SiO_2 percentage. The ionic conductivities go from 3,105.10^{-3} S.cm^{-1} for the membrane without SiO_2 to 6,720.10^{-3} S.cm^{-1} for the membrane containing SiO_2 (Table 2). The proton conductivity of the membrane based on PVA/SSA/SiWA/10wt.%SiO_2 reaches a maximum of 6,72.10^{-3} S.cm^{-1}, and decreases when the SiO_2 content exceeds 10 wt.%. The obtained value is higher than that of the Nafion®112 membrane (5,9.10^{-3} S.cm^{-1}) [36]. This is in agreement with the results which show that the latter membrane also has the best hydration rate. These membranes then experience a decrease in proton conductivity when the SiO_2 content exceeds 10 %. The inverse behaviors of the water uptake and ion exchange capacity (IEC) explain this behavior. As figure 12 shows. These results indicate that an inverse in water content can lead to higher proton conductivity at a low SiO_2 content. However, large adsorption of water in membranes does not simply improve proton conductivity, but also dilutes the charges carries [5], which causes a decrease in proton conductivity at high SiO_2 content in the membranes.

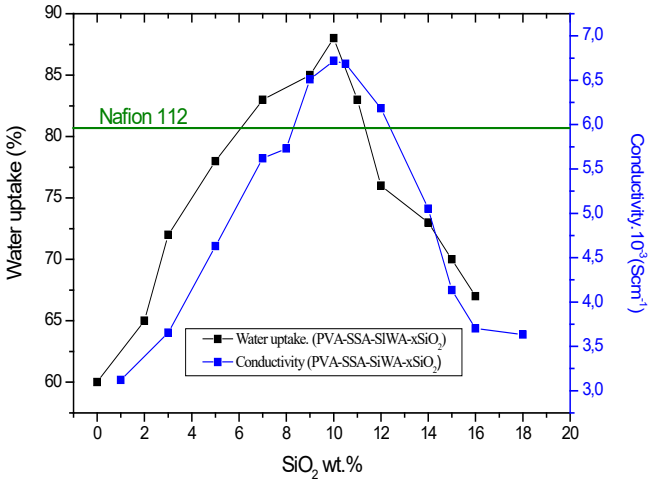


Figure 9: water uptake and proton conductivity of the membranes PVA/SSA/SiWA/ywt.%SiO_2 with different amounts of SiO_2

Table 2: Ionic conductivities (S.cm^{-1}) for Nafion®112, PVA-SSA-10wt.%SiWA and PVA-SSA-SiWA-10wt.%SiO_2 membranes

Membranes	Nafion®112	PVA/SSA/10wt. %SiWA	PVA/SSA/SiWA /10wt.%SiO_2
Ionic conductivity 10^{-3}S.cm^{-1}	5,900	3,105	6,720

Figure 10 shows the ionic conductivity of PVA/SSA/SiWA/10wt.%SiO_2 composite membrane as function thicknesses. The ionic conductivity of the composite membranes are in the order of 10^{-3} S.cm^{-1}. This figure shows that the ionic conductivity of the membrane increases when the membrane thickness increases. It goes from 0,672.10^{-3} S.cm^{-1} for the PVA/SSA/SiWA/10wt.%SiO_2 membrane 110 µm thick to 6,72.10^{-3} S.cm^{-1} for PVA/SSA/SiWA/10wt.%SiO_2 membrane 450 µm thick, for thicknesses greater than 450 µm the ionic conductivity remains close to 6,72.10^{-3} S.cm^{-1}.

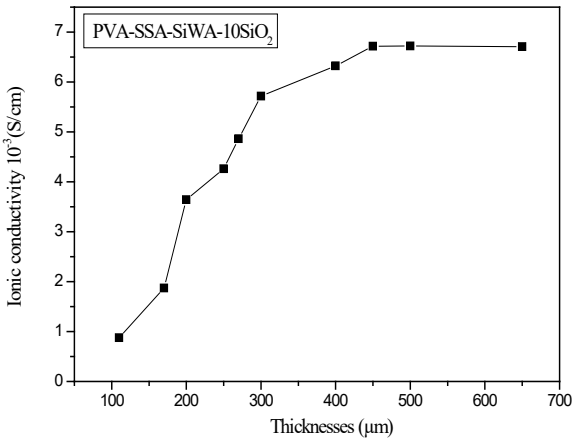


Figure 10: Proton Conductivity of PVA/SSA/SiWA/10wt.%SiO_2 membrane with thicknesses

3.5. Ion exchange capacity and fixed ion concentration

Figure 11(a,b) shows a plot of the ion exchange capacity (IEC) and fixed ion concentration as function of SiWA content. As shown in figure 11(a), the IEC of PVA/SSA/SiWA hybrid membrane varies from 0,90 to 2,20 mmol.g^{-1}, and increases with SiWA content up to a maximum value of 2,20 mmol.g^{-1} obtained with PVA/SSA/35wt.%SiWA hybrid membrane, the value obtained is higher than Nafion 115 (0,90 mmol.g^{-1}) [36]. This result indicates that an increase in silicotungstic acid content can lead to higher ion exchange capacity. At low HPA concentrations, the looser interaction between PVA and SiWA would provide less compact space for protons to be transported rather easily, resulting in higher ion exchange capacity. However, as the HPA concentration increased further, the interaction between PVA and SiWA would became stronger. The stronger interactions between not only PVA and SiWA but also PVA and SSA seem to inhibit the proton transport through the composite membranes, leading to lower ion exchange capacity.

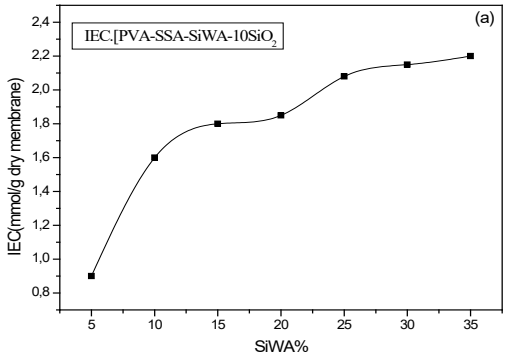


Figure 11(a): Effect of SiWA content on ion exchange capacity of PVA/SSA/SiWA membranes.

As shown in figure 11(b), the fixed ion concentration (FIC) of the PVA/SSA/SiWA hybrid membrane. The (FIC) values were observed to increase greatly from 5 to 35wt.% SiWA. The ion concentration sites increased with increasing the weight percent of silicotungstic acid. The ion concentration sites increased with the add of silicotungstic acid.

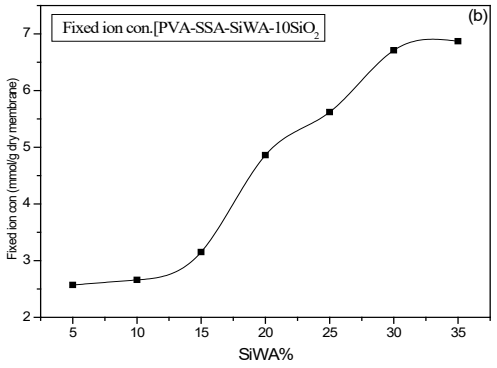


Figure 11(b): Effect of SiWA content on fixed ion concentration of PVA/SSA/SiWA membranes.

Figure 12 shows the IEC and water uptake of the membranes PVA/SSA/SiWA/ywt.%SiO_2 as function of SiO_2 content. As shown in this plot, the measured IEC value of the PVA/SSA/SiWA/ywt.%SiO_2 hybrid membranes decreases as the silica content increases from 2 to 10%.

in the other side, the water uptake of the PVA/SSA/SiWA/ywt.%SiO_2 membranes increases with the increase of SiO_2 content and reaches a maximum value of 88% for 10%.wt SiO_2 content membrane.

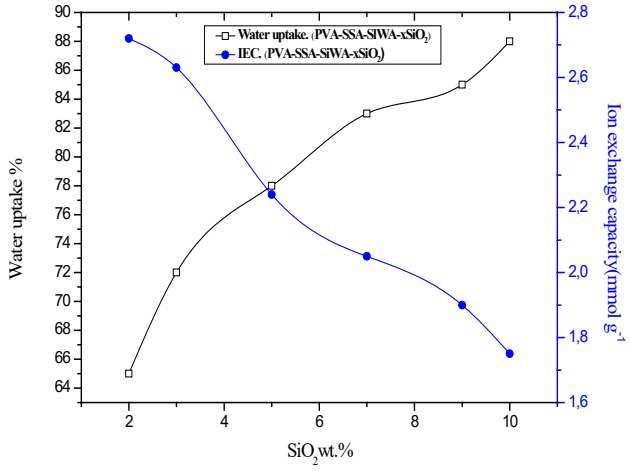


Figure 12: Water uptake and ion exchange capacity of the membranes based on PVA/SSA/10wt.%SiWA/ywt.%SiO_2

4. Conclusion

In the present work, we synthesized a new proton-conducting polymer membrane based on PVA/SSA/SiWA/SiO_2. The composite membranes were characterized by various techniques. The crosslinked networks and the formation of the intermolecular interactions between the hydroxyl groups on PVA and sulfosuccinic acid in membranes were proved with FTIR study. TGA showed that the membranes are thermally stable up to 200 °C. Moreover, high proton conductivity was obtained at room temperature for the membranes PVA/SSA/10wt.%SiWA and PVA/SSA/SiWA/10wt.%SiO_2, are about $3,105.10^{-3}$ and $6,72.10^{-3}$ $S.cm^{-1}$ respectively. The obtained ion exchange capacities values decreases as the SiO_2 content increases and reaches a maximum value of 1,75 $mmol.g^{-1}$ for the membrane PVA/SSA/SiWA/10wt.%SiO_2. This value is higher than that of the standard values of Nafion®112 and Nafion® 115 commercial membranes (use as reference membranes), which do not exceed 1 $mmol.g^{-1}$. Therefore, it can be concluded that the new composite polymer electrolyte membrane PVA/SSA/SiWA/10wt.%SiO_2 shows potential applications in PEMFC.

References

[1] D.S. Kim, H.B. Park, J.W. Rhim, Y.M. Lee, "Preparation and characterization of crosslinked PVA/SiO2 hybrid membranes containing sulfonic acid groups for direct methanol fuel cell applications," Journal of Membrane Science, **240**(1–2), 37–48, 2004. https://doi.org/10.1016/j.memsci.2004.04.010

[2] J. Qiao, T. Okada, H. Ono, "High molecular weight PVA-modified PVA/PAMPS proton-conducting membranes with increased stability and their application in DMFCs," Solid State Ionics, **180**(23–25), 1318–1323, 2009. https://doi.org/10.1016/j.ssi.2009.08.010

[3] M.M. Hasani-Sadrabadi, E. Dashtimoghadam, S.R. Ghaffarian, M.H.H. Sadrabadi, M. Heidari, H. Moaddel, "Novel high-performance nanocomposite proton exchange membranes based on poly (ether sulfone)," Renewable Energy, **35**(1), 226–231, 2010. https://doi.org/10.1016/j.renene.2009.05.026

[4] C.-C. Yang, "Synthesis and characterization of the cross-linked PVA/TiO2 composite polymer membrane for alkaline DMFC," Journal of Membrane Science, **288**(1–2), 51–60, 2007. https://doi.org/10.1016/j.memsci.2006.10.048

[5] J. Qiao, T. Hamaya, T. Okada, "New highly proton-conducting membrane poly (vinylpyrrolidone)(PVP) modified poly (vinyl alcohol)/2-acrylamido-2-methyl-1-propanesulfonic acid (PVA–PAMPS) for low temperature direct methanol fuel cells (DMFCs)," Polymer, **46**(24), 10809–10816, 2005. https://doi.org/10.1016/j.polymer.2005.09.007

[6] M.-C. Clochard, T. Berthelot, C. Baudin, N. Betz, E. Balanzat, G. Gébel, A. Morin, "Ion track grafting: A way of producing low-cost and highly proton conductive membranes for fuel cell applications," Journal of Power Sources, **195**(1), 223–231, 2010. https://doi.org/10.1016/j.jpowsour.2009.07.016

[7] C.H. Park, C.H. Lee, M.D. Guiver, Y.M. Lee, "Sulfonated hydrocarbon membranes for medium-temperature and low-humidity proton exchange membrane fuel cells (PEMFCs)," Progress in Polymer Science, **36**(11), 1443–1498, 2011. https://doi.org/10.1016/j.progpolymsci.2011.06.001

[8] W. Vielstich, A. Lamm, H.A. Gasteiger, Handbook of fuel cells: fundamentals technology and applications, Wiley New York, 2003.

[9] L. Li, J. Zhang, Y. Wang, "Sulfonated poly (ether ether ketone) membranes for direct methanol fuel cell," Journal of Membrane Science, **226**(1–2), 159–167, 2003. https://doi.org/10.1016/j.memsci.2003.08.018

[10] J. Fang, X. Guo, S. Harada, T. Watari, K. Tanaka, H. Kita, K. Okamoto, "Novel sulfonated polyimides as polyelectrolytes for fuel cell application. 1. Synthesis, proton conductivity, and water stability of polyimides from 4, 4 '-diaminodiphenyl ether-2, 2 '-disulfonic acid," Macromolecules, **35**(24), 9022–9028, 2002. https://doi.org/10.1021/ma020005b

[11] J. Lobato, P. Canizares, M.A. Rodrigo, J.J. Linares, "PBI-based polymer electrolyte membranes fuel cells: temperature effects on cell performance and catalyst stability," Electrochimica Acta, **52**(12), 3910–3920, 2007. https://doi.org/10.1016/j.electacta.2006.11.014

[12] Q. Guo, P.N. Pintauro, H. Tang, S. O'Connor, "Sulfonated and crosslinked polyphosphazene-based proton-exchange membranes," Journal of Membrane Science, **154**(2), 175–181, 1999. https://doi.org/10.1016/S0376-7388(98)00282-8

[13] J.-W. Rhim, H.B. Park, C.-S. Lee, J.-H. Jun, D.S. Kim, Y.M. Lee, "Crosslinked poly (vinyl alcohol) membranes containing sulfonic acid group: proton and methanol transport through membranes," Journal of Membrane Science, **238**(1–2), 143–151, 2004. https://doi.org/10.1016/j.memsci.2004.03.030

[14] H. Chen, S. Wang, F. Liu, D. Wang, J. Li, T. Mao, G. Liu, X. Wang, J. Xu, Z. Wang, "Base-acid doped polybenzimidazole with high phosphoric acid retention for HT-PEMFC applications," Journal of Membrane Science, **596**, 117722, 2020. https://doi.org/10.1016/j.memsci.2019.117722

[15] L. Lebrun, E. Da Silva, M. Metayer, "Elaboration of ion-exchange membranes with semi-interpenetrating polymer networks containing poly (vinyl alcohol) as polymer matrix," Journal of Applied Polymer Science, **84**(8), 1572–1580, 2002. https://doi.org/10.1002/app.10420

[16] G. Hirankumar, S. Selvasekarapandian, M.S. Bhuvaneswari, R. Baskaran, M. Vijayakumar, "AC impedance studies on proton conducting polymer electrolyte complexes (PVA+ CH 3 COONH 4)," Ionics, **10**(1–2), 135–138, 2004. DOI: 10.1007/BF02410322

[17] C. Chanthad, J. Wootthikanokkhan, "Effects of crosslinking time and amount of sulfophthalic acid on properties of the sulfonated poly (vinyl alcohol) membrane," Journal of Applied Polymer Science, **101**(3), 1931–1936, 2006. https://doi.org/10.1002/app.23660

[18] C. González-Guisasola, A. Ribes-Greus, "Dielectric relaxations and conductivity of cross-linked PVA/SSA/GO composite membranes for fuel cells," Polymer Testing, **67**, 55–67, 2018. https://doi.org/10.1016/j.polymertesting.2018.01.024

[19] P. Staiti, A.S. Arico, V. Baglio, F. Lufrano, E. Passalacqua, V. Antonucci, "Hybrid Nafion–silica membranes doped with heteropolyacids for application in direct methanol fuel cells," Solid State Ionics, **145**(1–4), 101–107, 2001. https://doi.org/10.1016/S0167-2738(01)00919-5

[20] S.P. Nunes, B. Ruffmann, E. Rikowski, S. Vetter, K. Richau, "Inorganic modification of proton conductive polymer membranes for direct methanol fuel cells," Journal of Membrane Science, **203**(1–2), 215–225, 2002. https://doi.org/10.1016/S0376-7388(02)00009-1

[21] B. Ruffmann, H. Silva, B. Schulte, S.P. Nunes, "Organic/inorganic composite membranes for application in DMFC," Solid State Ionics, 162, 269–275, 2003. https://doi.org/10.1016/S0167-2738(03)00240-6

[22] B. Tazi, O. Savadogo, "Effect of Various Heteropolyacids (HPAs) on the Characteristics of Nafion®-HPAS Membranes and their H~ 2/O~ 2 Polymer Electrolyte Fuel Cell Parameters," Journal of New Materials for Electrochemical Systems, **4**(3), 187–196, 2001.

[23] I. V Kozhevnikov, "Catalysis by heteropoly acids and multicomponent polyoxometalates in liquid-phase reactions," Chemical Reviews, **98**(1), 171–198, 1998. https://doi.org/10.1021/cr960400y

[24] M. Misono, "Heterogeneous catalysis by heteropoly compounds of molybdenum and tungsten," Catalysis Reviews Science and Engineering, **29**(2–3), 269–321, 1987. https://doi.org/10.1080/01614948708078072

[25] O. Nakamura, I. Ogino, T. Kodama, "Temperature and humidity ranges of some hydrates of high-proton-conductive dodecamolybdophosphoric acid and dodecatungstophosphoric acid crystals under an atmosphere of hydrogen or either oxygen or air," Solid State Ionics, **3**, 347–351, 1981. https://doi.org/10.1016/0167-2738(81)90111-9

[26] P. Staiti, "Proton conductive membranes constituted of silicotungstic acid anchored to silica-polybenzimidazole matrices," Journal of New Materials for Electrochemical Systems, 4(3), 181–186, 2001.

[27] O. Nakamura, T. Kodama, I. Ogino, Y. Miyake, "High-conductivity solid proton conductors: Dodecamolybdophosphoric acid and dodecatungstophosphoric acid crystals," Chemistry Letters, **8**(1), 17–18, 1979. https://doi.org/10.1246/cl.1979.17

[28] C.W. Lin, Y.F. Huang, A.M. Kannan, "Cross-linked poly (vinyl alcohol) and poly (styrene sulfonic acid-co-maleic anhydride)-based semi-interpenetrating network as proton-conducting membranes for direct methanol fuel cells," Journal of Power Sources, **171**(2), 340–347, 2007. https://doi.org/10.1016/j.jpowsour.2006.10.081

[29] S.M.J. Zaidi, S.D. Mikhailenko, G.P. Robertson, M.D. Guiver, S. Kaliaguine, "Proton conducting composite membranes from polyether ether ketone and heteropolyacids for fuel cell applications," Journal of Membrane Science, **173**(1), 17–34, 2000. https://doi.org/10.1016/S0376-7388(00)00345-8

[30] S. Maarouf, B. Tazi, F. Guenoun, "Synthesis and characterization of new composite membranes based on polyvinylpyrrolidone, polyvinyl alcohol, sulfosuccinic acid, phosphomolybdic acid and silica," J Chem Pharmaceut Res, **8**, 387–395, 2016.

[31] S. Maarouf, B. Tazi, F. Guenoun, "Preparation and Characterization of New Composite Membranes containing Polyvinylpyrrolidone, Polyvinyl alcohol, Sulfosuccinic acid, Silicotungstic acid and Silica for Direct Methanol Fuel Cell applications."," J. Mater. Environ. Sci., **8**, 2870–2876, 2017.

[32] J.E. Castanheiro, A.M. Ramos, I.M. Fonseca, J. Vital, "Esterification of acetic acid by isoamylic alcohol over catalytic membranes of poly (vinyl alcohol) containing sulfonic acid groups," Applied Catalysis A: General, **311**, 17–23, 2006. https://doi.org/10.1016/j.apcata.2006.05.039

[33] F. Lufrano, G. Squadrito, A. Patti, E. Passalacqua, "Sulfonated polysulfone as promising membranes for polymer electrolyte fuel cells," Journal of Applied Polymer Science, **77**(6), 1250–1256, 2000. https://doi.org/10.1002/1097-4628(20000808)77:6<1250::AID-APP9>3.0.CO;2-R

[34] S. Hietala, M. Koel, E. Skou, M. Elomaa, F. Sundholm, "Thermal stability of styrene grafted and sulfonated proton conducting membranes based on poly (vinylidene fluoride)," Journal of Materials Chemistry, **8**(5), 1127–1132, 1998. DOI: 10.1039/A708288F

[35] Q. Wu, S. Tao, H. Lin, G. Meng, "Preparation, characterization and proton-conductivity of silica gel containing 71 wt.% 12-tungstogermanic heteropoly acid," Materials Chemistry and Physics, **64**(1), 25–28, 2000. https://doi.org/10.1016/S0254-0584(99)00244-8

[36] S. Anisa, A. Utami, "Preparation of Sulfonated PVA-TMSP Membranes for Direct Methanol Fuel Cell," Makara Journal of Science, 95–100, 2013. https://doi/org/10.7454/mss.v16i2.1403

ASTES

Advances in Science, Technology and Engineering Systems Journal Vol. 5, No. 5, 1020-1027 (2020)

www.astesj.com

Special Issue on Multidisciplinary Innovation in Engineering Science & Technology

ASTESJ

ISSN: 2415-6698

Dissection of Quantitative Trait Loci (QTL), annotation of Single Nucleotide Polymorphism (SNP), and Identification of Candidate Genes for Grain Yield in *Triticum turgidum* L. var durum

Issame Farouk[*,1], Ahmad Alsaleh[2], Jihan Motowaj[3], Fatima Gaboun[4], Bouchra Belkadi[1], Abdelkarim Filali Maltouf[1], Zakaria Kehel[3], Ismahane Elouafi[5], Nasserelhaq Nsarellah[4], Dimah Habash[6], M. Miloudi Nachit[3]

[1]*Laboratory of Microbiology and Molecular Biology, Department of Biology, Faculty of Sciences, Med V University, Rabat, 10000, Morocco*

[2]*Dept. Science and Technology Bozok University, Yozgat, 66100, Turkey*

[3]*ICARDA. Av. Med Belarbi Alaoui, BP6299, Al Irfane, Rabat, 10000, Morocco*

[4]*INRA. Institut National de Recherche Agronomique Av. Med Belarbi Alaoui, Al Irfane, Rabat, 10000, Morocco*

[5]*ICBA. Dubai, 14660, United Arab Emirates*

[6]*Securewheat, AL3, St. Albans, UK*

ARTICLE INFO

Article history:
Received: 29 June, 2020
Accepted: 04 October, 2020
Online: 20 October, 2020

Keywords:
Durum wheat
SNP
Candidate genes
Grain yield
QTL
Linkage map

ABSTRACT

Durum wheat (Triticum turgidum L. var durum) is among the most important crops in the world. High and stable grain yield in diverse environments is the major objective in durum breeding programs. This trait is linked to the quantitative trait loci (QTL). For the detection of QTL linked to the grain yield, it is necessary to construct a high-density genetic linkage map. The aims of this study were to detect the candidate genes comprised in the QTLs on 2A chromosome linked to grain yield and annotate the single nucleotide polymorphisms (SNPs). The linkage map of Lahn/Cham1 population was used to identify QTLs. In multi-environmental analysis and employing bioinformatic approaches, 583 sequences corresponding to the SNPs markers selected from the detected QTL regions were analyzed, 122 SNP sequences were annotated of which 53% of the candidate genes were involved in stresses tolerance, 29.5% in plant development and growth, and 3.3% in cell transport. Moreover, 1.6% of candidate genes were retrotransposon and transposon 2.4% with unknown function. Further 9.8% were related in other cellular processes. The results also showed that 66.7% of the candidate genes harbored on 4B chromosome, were involved in stresses tolerance and 33.3% in plant development and growth. Additionally, in the specific and stressed environments analysis, the DNA sequences of the four QTL detected on 2A chromosome were used for homology search, 546 candidate genes were identified of which some were present in several QTL (F-box gene family, hydroxyproline-rich glycoprotein-like), retrotransposons and transposons and others. This study provided information on employing SNPs markers to detect candidate genes linked with grain yield trait in durum wheat in contrasting environments (dry, cold, hot).

1. Introduction

Durum wheat (*Triticum turgidum* L. var durum) is a tetraploid wheat, its genome is constituted by seven homoeologous groups of chromosomes A and B. Its grain use is reported in [1, 2]. The nutritional values for durum grain were published in earlier research works [1-3]. Grain yield is related to the QTL additive effects and to their interactions with the environment. Several wheat genetic linkage maps were constructed with various molecular markers, such as Restriction Fragment Length Polymorphism (RFLP), Amplified Fragment Length

[*]Corresponding Author: Issame Farouk, Email: issame.farouk@gmail.com

Polymorphism (AFLP), Simple Sequence Repeats (SSR) and other markers [4-13]. The construction of saturated maps with large number of molecular markers of Single Nucleotide Polymorphism (SNP) [14-16] and Diversity Array Technology (DArT) [10, 17-23] are fundamental to detect candidate genes for desirable traits in crops, such as durum wheat. Both markers (SNP and DArT) are small sequence of DNA. These sequences can be compared with the public databases [URGI (Unité de Recherche Génomique Info) Blast of the Institut National de la Recherche Agronomique (INRA, France) and NCBI (National Center for Biotechnology Information, the USA)] to identify the candidate genes involved in a QTL controlling a specific trait. Recently the markers (SNP and DArT) were used for QTLs regions detection and for the identification of the candidate genes involved in these QTLs of wheat [24-29]. The high and stable grain yield across diverse environments constitutes the principal aim for durum breeding programs.

The aims of this work were to: 1) identify the SNPs mapped into QTL regions; 2) extend the SNPs sequence analysis in terms of functional and comparative analysis; and 3) identify the candidate genes constituting the QTLs harbored by 2A chromosome and linked to grain yield.

2. Materials and methods

2.1. *Plant materials*

The genetic population used in this study (Lahn/Cham1) was published in [8, 30] and presented in the conference [31]. The population was phenotyped for grain yield in 11 contrasting environments (cold / drought / heat). The characteristics of the parents: Lahn and Cham1 were described in earlier paper [8, 30].

The Lahn/Cham1 genetic map that consisted of 1425 SNPs, 216 SSR and 31 other molecular markers was constructed using IciMapping program v 4.1.0.0 was presented in [31].

The QTLs linked to grain yield detected using this map were used for candidate genes identification and SNPs annotation.

2.2. *SNPs annotation and candidate genes identification*

The methodology used for the SNPs annotation and the candidate genes identification is as flowing:

For the QTLs detection in specific and stressed environments, 9 QTLs were detected, 4 of which were localized on 2A, due to its strong contribution to grain yield [32, 33], the full DNA sequence of 2A chromosome were downloaded from URGI and the 4 DNA sequences corresponding to the 4 QTL were isolated based on markers flanking of these QTL regions [24, 25, 29] using the GeneStudio software. More informations about the environments, DNA sequences size, environmental conditions, QTL intervals and flanking markers are summarized in Table 1. Thereafter, the sequences isolated were served as queries for Blast search in NCBI against Rice and *Brachypodium* genomes to identify the candidate genes composing these QTLs detected in the four environments (EP, INC, RF, and RQ), see Figure 1

In multi- environmental analysis, the 583 SNPs selected from the QTLs regions and harbored by durum chromosomes [31] were analyzed through Blast (Basic Local Alignment Search Tool) search homology using the URGI Blast of (INRA), France (https://urgi.versailles.inra.fr/blast/blast.php) with the aim to expand the SNP sequences in terms of length [34] (Figure 2).

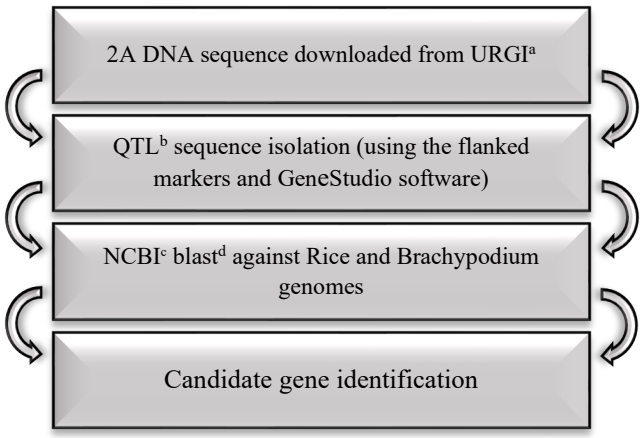


Figure 1: Candidate genes identification in specific and stressed environments

Subsequently, the derived genomic sequences (280bp) were served as query to identify the candidate genes using Blast search homology in NCBI (National Center for Biotechnology Information, the USA), see Figure 2. The Venn diagram was used to present the results.

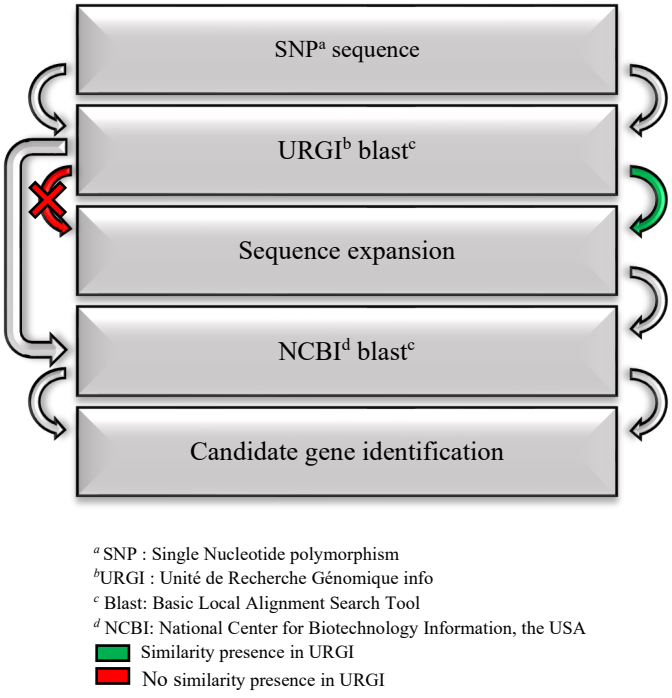


Figure 2: Candidate genes identification in multi-environmental analysis

More details about the candidate genes identified in combined and in specific environments QTLs analysis are shown in supplementary materials S1 and S2, respectively.

Table 1: QTL detected on 2A chromosome with the environmental conditions, QTL peak positions in cM, QTL regions interval size in centimorgan (cM) and in Mega bases (Mb) and with QTLs region flanking markers.

Environment	Environmental Conditions	Peak position (cM)	QTL[a] interval size		Flanking markers	
			cM	Mb	Left marker	Right marker
EP[b]	Cold	142	5.02	1.33	wsnp[f]_2280363	wmc[g]177bp190
INC[c]	Drought (vetch incorporation)	046	5.90	2.64	wsnp[f]_998898	cnl[h]127bp435
RF[d]	Drought	270	3.59	4.57	wsnp[f]_1000185	gwm[i]312bp189
RQ[e]	Heat	063	6.49	0.10	wsnp[f]_2276833	gwm[i]636bp111

[a]QTL: Quantitative Trait Loci

[b]EP: Early planting at Tel Hadya / Syria (ICARDA main station), 36°0.1'N 36°56'E, 284m, the sowing is in mid-October, 330mm of rainfall and 70mm of irrigation at sowing, the temperatures were 2 °C at Tillering and 20 °C at flowering

[c]INC: Incorporated in field (vetch biomass incorporation in soil) at same station, the sowing date in Mid-November with 330mm as rainfall, the temperatures were 8 °C at tillering and 24 °C at flowering

dRF: Rainfed (vetch above biomass harvested, no incorporation in soil) at the same station, sowing in Mid-November, the rainfall temperatures are also the same

eRQ: Raqqa station (35°57' N 39°0'E, 295m) with chickpea rotation, sowing in Mid-November, the rainfall was 150mm and 450 mm of irrigation, were 10 °C at tillering and 30 °C at flowering

[f]SNP: Single Nucleotide Polymorphism

[g]wmc: Wheat Microsatellite Consortium (SSR)

[h]cnl: Cornell University (EST-SSR)

[i]gwm: Gatersleben Wheat Microsatellite (SSR)

3. Results

3.1. *Candidate genes detection in specific and stressed environments*

The search for candidate genes in the QTLs corresponding to the environments (dry / cold / heat) show the presence of 407 candidate genes in Rice as in *Brachypodium* databases. Moreover, in the Rice database 139 genes identified were retrotransposons and transposons that have showed no correspondence in *Brachypodium* database.

3.1.1. Dry environment

As for the dry environments (RF and INC), the QTLs detected in these environments (Table 2) spanned on 4.57 Mb for RF and 2.64 Mb for INC. In RF (dryland) were identified 147 candidate genes and in INC (dryland with incorporation of vetch crop) 376 candidate genes, including genes involved in stress tolerance (biotic and abiotic stress) and in other cellular processes, the retrotransposons and transposons were also present in the two QTLs with a high frequency especially in the RF environment (Supplementary: Table S1). Also, it was noticed that the incorporation of legume vetch in the soil increased the expression of candidate genes. This expression is higher in dryland with vetch incorporation in soil (INC) than in dryland without vetch incorporation in the soil (RF). This may be due to increased availability of nitrogen and water through the organic matter incorporation in the soil.

3.1.2. Cold environments

In the cold environment (EP) characterized by low temperature during the tillering developmental stage (Table 2), the QTL detected was spanned on 1.33 Mb, it contained 17 candidate genes among those involved in plant development and abiotic/biotic stress tolerance: as Germin-like protein 8-14, protein far1-related sequence 5, putative FBD-associated F-box protein, Photosystem II 44 kDa protein and others. The retrotransposons and transposons are also present in this QTL (Supplementary: Table S1).

Table 2: The environmental conditions, the number of candidate genes identified for the four QTL linked to grain yield of the four stressed environments (EP, INC, RF and RQ) with the QTL interval size, and the number of candidate genes identified for Rice and *Brachypodium*

Environment	**Environmental Conditions**	**QTL[a] Interval size (Mb)**	**Candidates genes number**	
			Rice	***Brachypodium***
EP[b]	Cold	1.33	017	012
INC[c]	Drought (vetch incorporation)	2.64	147	113
RF[d]	Drought	4.57	376	277
RQ[e]	Heat	0.10	006	005

[a]QTL: Quantitative Trait Loci

[b]EP: Early planting at Tel Hadya / Syria (ICARDA main station), 36°0.1'N 36°56'E, 284m, the sowing is in mid-October, 330mm of rainfall and 70mm of irrigation at sowing, the temperatures were 2 °C at Tillering and 20 °C at flowering

[c]INC: Incorporated in field (vetch biomass incorporation in soil) at same station, the sowing date in Mid-November with 330mm as rainfall, the temperatures were 8 °C at tillering and 24 °C at flowering

[d]RF: Rainfed (vetch above biomass harvested, no incorporation in soil) at the same station, sowing in Mid-November, the rainfall temperatures are also the same

[e]RQ: Raqqa station (35°57' N 39°0'E, 295m) with chickpea rotation, sowing in Mid-November, the rainfall was 150mm and 450 mm of irrigation, were 10 °C at tillering and 30 °C at flowering

Table 3: SNPs annotated and not annotated in A and B genomes

Genome	SNPs			
	Annotated	Not annotated	Total	Percentage of SNPs annotated (%)
1A	15	24	39	38.46
2A	17	63	80	21.25
3A	6	33	39	15.38
4A	8	31	39	20.51
5A	1	11	12	08.33
6A	5	14	19	26.31
7A	7	46	53	13.20
A genome	**59**	**222**	**281**	**20.99**
1B	17	35	52	32.69
2B	16	63	79	20.25
3B	2	10	12	16.66
4B	9	64	73	12.32
5B	5	28	33	15.15
6B	13	29	42	30.95
7B	1	10	11	09.10
B genome	**63**	**239**	**302**	**20.86**

3.1.3. Hot environments

Further, the QTL detected in the hot environment (RQ) which is characterized by high temperatures during the anthesis developmental stage compared with the other environments (Table 2), the QTL region was spanned on a small interval of 0.1Mb that contained 6 genes, the first one is an LRR receptor-like serine/threonine-protein kinase gene involved in plant resistance to pathogens and the others are a retrotransposons and transposons (Supplementary: Table S1).

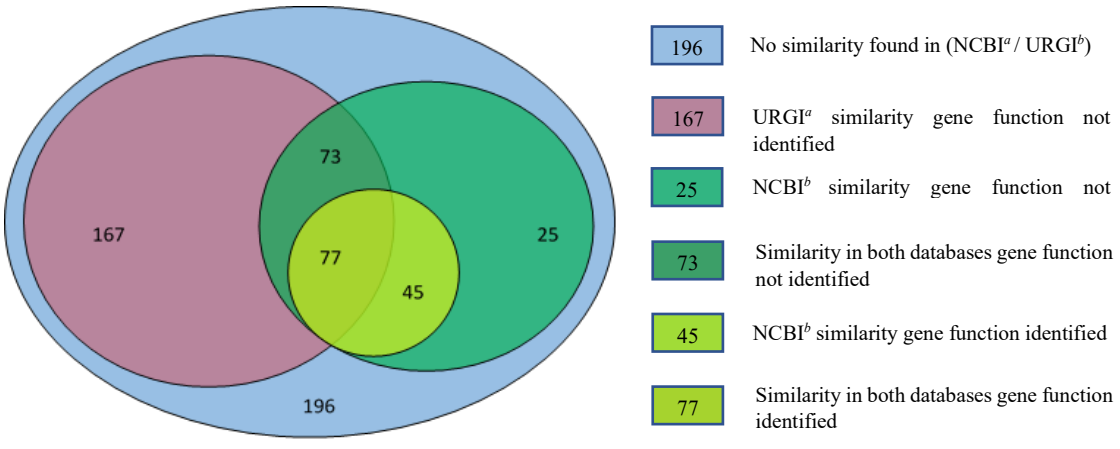
3.2. *Mapping of SNPs to identify candidate genes*

Of the mapped SNPs, 80 were mapped on 2A. Additional information for other chromosomes is shown in Table 3.

As for the candidate genes number, the 2A along 1B harbored the highest number (17), while in terms of annotation percentage for other chromosomes see Table 3.

The SNPs sequences availability provides the possibility of identifying gene loci contributing to grain yield.

Among the 583 SNP sequences selected, 122 sequences were annotated. the candidate genes involved in various growth, development processes, and stress tolerances have been identified, of which 77 sequences were enlarged with URGI database and annotated with NCBI. Whereas the remaining 45 SNPs sequences were annotated directly with NCBI, as no-similarity presence was available to enlarge in URGI database (Figure 3). Several sequences did not show any similarity in URGI and NCBI databases



[a]URGI : Unité de Recherche Génomique info
[c]NCBI: National Center for Biotechnology Information. The USA

Figure 3: Annotation and similarity study on Venn diagram of SNP.

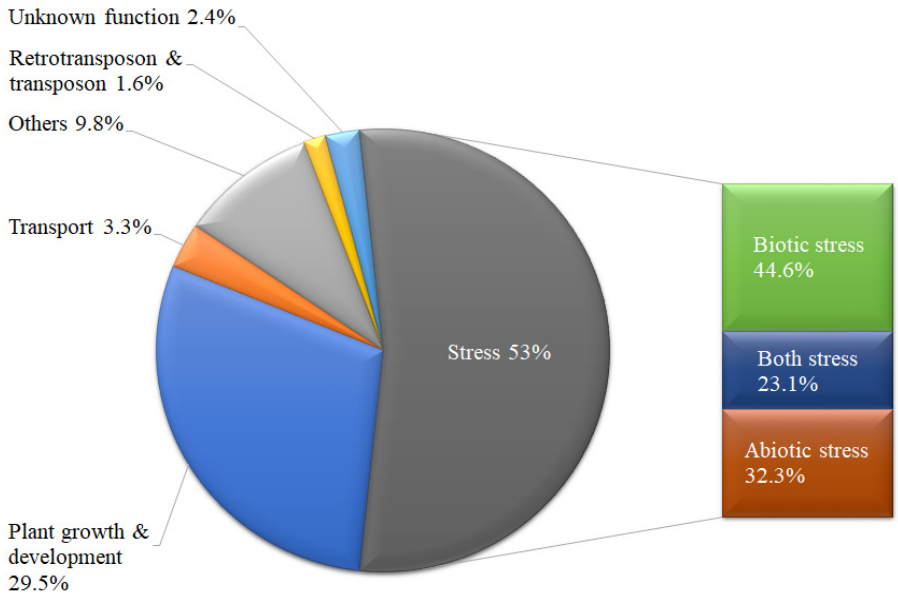


Figure 4: Functional classification of candidate genes co-located with QTLs linked to grain yield.

The 583 SNPs marked on Venn diagram (Figure 3) showed that 77 sequences were annotated (candidate genes identified) with similarity presence with both databases; while 45 sequences were annotated with similarity presence only in NCBI. Further, 73 were not annotated but had similarity in both databases. Also 167 SNP had similarity only in URGI and 25 only in NCBI, consequently both sets of SNPs were not annotated). The remaining196 sequences were not annotated, showing no similarity in the two databases.

The analysis with bioinformatic tools showed that 53% of candidate genes found were related to stresses tolerance, with 44.6% of them to biotic stress [powdery mildew, stem rust (sr32), leaf rust (lr10, lr34)], 32.3% to abiotic stress (cold heat, drought, salinity) and 23.1% to both stresses; 29.5% to plant development and growth; 3.3% to cell transport, and 1.6% to retrotransposon and transposon; and only 2.4% were with unknown function.

Further, 9.8% were involved in other cellular processes (secondary metabolism, pigments, herbicide detoxification, wall formation, etc.), see Figure 4. More informations about the SNPs annotation and candidate gene functions were shown in the supplementary table (S2).

Some candidate genes are involved in several processes, such as the basic helix-loop-helix (bHLH) proteins pertaining to the superfamily of transcription factors (TFs) and linked with wsnp_3026224. These proteins have been linked with the regulation of diverse biological processes as growth, development, and response to diverse stresses.

Moreover, in the 4BS, 57.1% of candidate genes found, were linked to stresses tolerance and 42.9% in plant development and growth.

4. Discussion

4.1. *Candidate genes detection in specific and stressed environments*

We found among 9 QTLs related to grain yield, four were located on 2A chromosome, these QTLs were detected in diverse stressed environments: EP characterized by cold, INC and RF by drought, and RQ by heat. These results are in accordance with several studies on grain yield QTLs located on 2A chromosome [24, 32, 33].

4.1.1. Dry environment

In the dry environment (INC), among the candidate genes were serpin-Z5, Probable glucuronosyltransferase Os04g0103100, Chalcone synthase 1, Fatty acid amide hydrolase isoform X1, Amino acid permease 3 (Supplementary: Table S1). This is in the agreement with the study of [30] where the transcriptomic pattern under progressive water stress of the two parents: Lahn and Cham1 (parents of the current studied population) and one recombined inbred line where the candidate genes cited above showed an overexpression. Such as the candidate gene coding for the mitochondrial metalloendopeptidase OMA1 identified in the QTL of the dry environment RF (Supplementary: Table S1). This was also confirmed by [30]. Similarly, the F-box and associated protein family were overexpressed in the dry environments RF and INC (Supplementary Table S1), but under cold stress was downexpressed [35]. Some genes of this large family under abiotic stress may be over or underexpressed depending on the stress [36]. As for the candidate gene coding for the Hydroxyproline-rich glycoprotein-like identified in the QTLs detected in the dry and cold environments: RF, INC, and EP (Supplementary: Table S1), this gene was associated with drought

tolerance in barley [37] and with the resistance to bacterial pathogen in rice [38].

Further, other candidate genes identified in the dry environment (RF): GDSL esterase/lipase EXL3; the cold environment (EP): UDP-glycosyltransferase 79-like isoform, and the glutathione S-transferase identified in both environments (Supplementary: Table S1). These genes play role in plant development and growth through the action on ABA homeostasis [39]; germination and growth [40]; detoxification and plant pathogen resistance [41].

4.1.2. Cold environment

In the cold environment (EP), among the candidate genes composing the QTL detected: 5'-3' exoribonuclease 3 isoform X1, NADH dehydrogenase; as for the QTL of dry environment (RF), it contains the genes: starch synthase3, chloroplastic/amyloplastic and a photosystem I P700 chlorophyll an apoprotein A1 candidate gene. While the gene coding for the Photosystem II 44 kDa protein were identified in the QTLs for the cold (EP) and dry (RF) environment, as for the ankyrin repeat family protein-like it was found in the INC environment (Supplementary Table S1). All these candidate genes expression was altered under water stress [30]. Some candidate genes identified in QTLs for INC and RF environments like zinc finger family genes play an important role in physiological traits of yield potential under heat stress [27]. Moreover, in the QTL for the RF environment, the gene coding for BTB/POZ and MATH domain-containing protein 2 was highly repeated in this QTL, this gene is involved in heat tolerance and in plant growth and development [42].

4.1.3. Hot environment

In the hot environment RQ, six candidate genes were identified, one coding for LRR receptor-like serine/threonine-protein kinase RCH1 involved in resistance to pathogens [43, 44]. The remaining candidate genes were belonging to the family of retrotransposon/transposase. This gene family was also present in the other QTLs especially in RF (dry environment) with a high frequency. The abundance of this gene family presence can be explained by their involvement in stress conditions, [30] reported that the activity of these genes was altered under water stress and by the fact that the retrotransposon/transposon may represents 80 to 90% of wheat genome [45].

4.2. *Detection of candidate genes in other chromosomes*

Additionally, the presence of the wsnp_993293 SNP marker in the chromosome 1A and its linkage with the candidate gene implicated in powdery mildew resistance, confirms earlier mention on one parent of the population (Lahn) that carries moderate resistance to powdery mildew. Additionally, the wsnp_2265986, located in the 1B chromosome and linked to 3-ketoacyl-CoA synthase 6-like, this candidate gene plays also a role in abiotic (drought, heat and cold) and in biotic stress resistance. This reflects the genes carried by the second parent Cham1 for good drought and heat tolerance, osmotic adjustment, and proline content.

The candidate genes covered the entire genome and were linked to different biotic (powdery mildew, rust, etc.) and abiotic (drought, cold, heat, etc.) stress resistance / tolerance (Fig 4).

In the current work, a large part of candidate genes harbored by the 2A, in addition to 4B chromosome, were related to stress tolerance. They were also involved in plant growth and development. The 4BS results corroborate earlier studies [25, 46-50] on the importance of the 4BS and its contribution to grain yield in stressed environments.

5. Conclusion

The candidate genes found were linked to yield performance under drought and temperature extreme conditions. Also, this study showed the importance of 2A chromosomes for contrasting environments (drought, cold, and heat).

In this study specific and general candidate genes were detected. For the specific environments, the candidate genes in cold environment (EP) involved the genes of 5'-3'exoribonuclease 3 isoform X1 and NADH dehydrogenase. As for the dry environment (RF) the genes included were starch synthase3, chloroplastic/amyloplastic, and a photosystem I P700 chlorophyll. Further, in the dry environment (RF), the gene coding for BTB/POZ and MATH domain-containing protein2 was highly repeated in this environment. This gene is also effectuates heat tolerance, plant development and growth. Similarly, the ankyrin repeat family protein-like was found in the dry environment (INC), it contains the genes synthase3, chloroplastic/amyloplastic and photosystem I P700 chlorophyll. For the general candidate genes involved in diverse stressed environments, the following genes were identified: The Photosystem II 44 kDa protein were identified in the cold (EP) and the dry (RF) environments. Also, some of the candidate genes are operating in all 3 stresses, such as the zinc finger family genes. This gene also plays a significant role in physiology of yield potential under heat stress frequently.

5.1.1. Conflict of Interest

The authors declare no conflict of interest.

5.1.2. Acknowledgement

We would like to thank the International Center for Agricultural Research in Dry Area (ICARDA) for the financial support of this study and the support staff of the CIMMYT/ICARDA durum-breeding program.

5.1.3. References

[1] I. Elouafi, MM. Nachit, "A genetic linkage map of the Durum x *Triticum dicoccoides* backcross population based on SSRs and AFLP markers, and QTL analysis for milling traits" Theor Appl Genet, **108**(3), 401-413, 2004. https://doi.org/10.1007/s00122-003-1440-8

[2] MM. Nachit, "Durum wheat breeding for Mediterranean drylands of North Africa and West Asia. In: Rajram S, Saari EE, Hetel GP (eds) Durum Wheats" Challenges and Opportunities. CIMMYT, Ciudad Obregon, Mexico, **14**, 14–27, 1992.

[3] El Yadini, I. Kahama, M. Labhilili, A. El Yadini, M. Azeqour, "La technique TILLING comme nouvelle biotechnologie pour la protection et l'amélioration du blé dur (TILLING : A new biotechnological method for protection and improvement of durum wheat)" J Mater Env Sci, **4**, 931-934, 2013.

[4] M. Maccaferri, M. Sanguineti, S. Corneti, J. Ortega, M. Salem, J. Bort, E. DeAmbrogio, L. del Moral, A. Demontis, A. El-Ahmed, "Quantitative trait loci for grain yield and adaptation of durum wheat (*Triticum durum* Desf.) across a wide range of water availability" Genetics, **178**(1), 489-511, 2008. https://doi.org/10.1534/genetics.107.077297

[5] B. Heidari, BE. Sayed-Tabatabaei, G. Saeidi, M. Kearsey, K. Suenaga, P. Gulick, "Mapping QTL for grain yield, yield components, and spike features in a doubled haploid population of bread wheat" Genome, **54**(6), 517-527, 2011. https://doi.org/10.1139/g11-017

[6] A. Blanco, M. Bellomo, A. Cenci, C. De Giovanni, R. D'ovidio, E. Iacono, B. Laddomada, M. Pagnotta, E. Porceddu, A. Sciancalepore, "A genetic linkage map of durum wheat" Theor App Genet **97**(5-6), 721-728, 1998. https://doi.org/10.1007/s001220050948

[7] SA. Dura, MA. Duwayri, MM. Nachit, "Detection of molecular markers associated with yield and yield components in durum wheat (*Triticum turgidum* L. var. *durum* Desf.) under drought conditions" Afr J Agr, **8**(19), 2118-2128, 2013. https://doi.org/10.5897/AJAR11.2031

[8] MM. Nachit, I. Elouafi, A. Pagnotta. A. El saleh, E. acono, M. Labhilili, A. Asbati, M. Azrak, H. azzam, D. Benscher, M. Khairallah, JM. Ribaut, OA. Tanzarella, E. Porceddu, ME. Sorrells, "Molecular linkage map for an intraspecific recombinant inbred population of durum wheat (*Triticum turgidum* L. var. *durum*)". Theor App Genet, **102**, 177-186, 2001. https://doi.org/10.1007/s001220051633

[9] A. Alsaleh, FS. Baloch, M. Derya, M. Azrak, B. Kilian, H Özkan, MM. Nachit, "Genetic Linkage Map of Anatolian Durum Wheat Derived from a Cross of Kunduru-1149× Cham1". Plant Mol Biol Rep, **33**, 209-220, 2014. https://doi.org/10.1007/s11105-014-0749-6

[10] Mantovani, M. Maccaferri, MC. Sanguineti, R. Tuberosa, I. Catizone, P. Wenzl, B. Thomson, J. Carling, E. Huttner, E. DeAmbrogio, "An integrated DArT-SSR linkage map of durum wheat" Mol Breed, **22**(4), 629-648, 2008. https://doi.org/10.1007/s11032-008-9205-3

[11] M. Nagel, S. Navakode, V. Scheibal, M. Baum, MM. Nachit, M. Röder, A. Börner, "The genetic basis of durum wheat germination and seedling growth under osmotic stress" Biol Plantarum, **58**, 681–688, 2014. https://doi.org/10.1007/s10535-014-0436-3

[12] KJ. Haile, MM. Nachit, H. Karl, B. Ayele, SM. Röder, "QTL mapping of resistance to race Ug99 of Puccinia graminis f. sp. tritici in durum wheat (*Triticum durum* Desf.)" Mol Breed, **30**, 1479–1493, 2012. https://doi.org/10.1007/s11032-012-9734-7

[13] S. Dura, M. Duwayri, MM. Nachit, F. Al Sheyab, "Detection of molecular markers associated with yield and yield components in durum wheat (*Triticum turgidum* L. var. *durum*) under saline conditions" Crop Past Sci, 64(10), 957-964, 2013. https://doi.org/10.5897/AJAR11.2031

[14] RM. Poecke, M. Maccaferri, J. Tang, HT. Truong, A. Janssen, NJ. Orsouw, S. Salvi, MC. Sanguineti, R. Tuberosa, EA Vossen, "Sequence based SNP genotyping in durum wheat" Plant Biotech J, **11**(7), 809-817, 2013. https://doi.org/10.1111/pbi.12072

[15] D. Trebbi, M. Maccaferri, P. de Heer, A. Sørensen, S. Giuliani, S. Salvi, M. Sanguineti, A. Massi, E. van der Vossen, R. Tuberosa, "High-throughput SNP discovery and genotyping in durum wheat (*Triticum durum* Desf.)" Theor App Genet, **123**(4), 555-569, 2011. https://doi.org/10.1007/s00122-011-1607-7

[16] W. Zhang, S. Chao, F. Manthey, O. Chicaiza, JC. Brevis, V. Echenique, J. Dubcovsky, "QTL analysis of pasta quality using a composite microsatellite and SNP map of durum wheat" Theor App Genet, **117**(8) 1361-1377, 2008. https://doi.org/10.1007/s00122-008-0869-1

[17] A. Blanco, P. Colasuonno, A. Gadaleta, G. Mangini, A. Schiavulli, R. Simeone, AM. Digesù, P. De Vita, AM. Mastrangelo, L. Cattivelli, "Quantitative trait loci for yellow pigment concentration and individual carotenoid compounds in durum wheat" J Cereal Sci, **54**(2), 255-264, 2011. https://doi.org/10.1016/j.jcs.2011.07.002

[18] A. Blanco, G. Mangini, A. Giancaspro, S. Giove, P. Colasuonno, R. Simeone, A. Signorile, P. Vita, AM. Mastrangelo, L Cattivelli, "Relationships between grain protein content and grain yield components through quantitative trait locus analyses in a recombinant inbred line population derived from two elite durum wheat cultivars" Mol Breed, **30**(1), 79-92, 2011. https://doi.org/10.1007/s11032-011-9600-z

[19] A. Gadaleta, A. Giancaspro, S. Giove, S. Zacheo, G. Mangini, R. Simeone, A. Signorile, A. Blanco, "Genetic and physical mapping of new EST-derived SSRs on the A and B genome chromosomes of wheat" Theor App Genet, **118**(5), 1015-1025, 2009. https://doi.org/10.1007/s00122-008-0958-1

[20] D. Marone, G. Laidò, A. Gadaleta, P. Colasuonno, D. Ficco, A. Giancaspro, S. Giove, G. Panio, M. Russo, P. De Vita, L. Cattivelli, R. Papa, A. Blanco, "A high-density consensus map of A and B wheat genomes" Theor App Genet, **125**(8), 1619-1638, 2012. https://doi.org/10.1007/s00122-012-1939-y

[21] MA. Russo, DBM. Ficco, D. Marone, P. De Vita, V. Vallega, C. Rubies-Autonell, C. Ratti, P. Ferragonio, V. Giovanniello, N. Pecchioni, "A major QTL for resistance to soil-borne cereal mosaic virus derived from an old Italian durum wheat cultivar" J Plant Interact, **7**(4), 290-300, 2012. https://doi.org/10.1080/17429145.2011.640437

[22] J. Ahmad et al., "Study of Physio-chemical Properties of POSS/Mineral Oil based Nanofluids," in 2018 International Conference on Power Generation Systems and Renewable Energy Technologies (PGSRET), 1–5, 2018. DOI: 10.1109/PGSRET.2018.8685972

[23] Z. Peleg, Y. Saranga, T. Suprunova, Y. Ronin, MS. Röder, A. Kilian, AB. Korol, T. Fahima, "High-density genetic map of durum wheat x wild emmer wheat based on SSR and DArT markers" Theor App Genet, **117**, 103–115, 2008. https://doi.org/10.1007/s00122-008-0756-9

[24] H. Tura, J. Edwards, V, Gahlaut, M. Garcia, Sznajder, U. Baumann, F. Shahinnia, M. Reynolds, P. Langridge, HS. Balyan, "QTL analysis and fine mapping of a QTL for yield-related traits in wheat grown in dry and hot environments" Theor App Genet, 1-19, 2019. https://doi.org/10.1007/s00122-019-03454-6

[25] D. Xu, W. Wen, L. Fu, F. Li, J. Li, L. Xie, X. Xia, Z. Ni, Z. He, S. Cao, "Genetic dissection of a major QTL for kernel weight spanning the Rht-B1 locus in bread wheat" Theor App Genet, **132**(11), 3191-3200, 2019. https://doi.org/10.1007/s00122-019-03418-w

[26] R. Mérida-García, G. Liu, S. He, V. Gonzalez-Dugo, G. Dorado, S. Gálvez, I. Solís, P. Zarco-Tejada, J. Reif, P. Hernandez P, "Genetic dissection of agronomic and quality traits based on association mapping and genomic selection approaches in durum wheat grown in Southern Spain" PloS one **14**(2), e0211718, 1-24, 2019. https://doi.org/10.1371/journal.pone.0211718

[27] S. Pradhan, MA. Babar, G. Bai, J. Khan, D. Shahi, M. Avci, J. Guo, J. McBreen, S. Asseng, S. Gezan, et al, "Genetic dissection of heat-responsive physiological traits to improve adaptation and increase yield potential in soft winter wheat" BMC Genomics **21**, 315, 1-15, 2020. https://doi.org/10.1186/s12864-020-6717-7

[28] M.S. Rahman, K.J. Linsell, J.D. Taylor, M.J. Hayden, N.C. Collins, K.H. Oldach, "Fine mapping of root lesion nematode (*Pratylenchus thornei*) resistance loci on chromosomes 6D and 2B of wheat" Theor App Genet **133**, 635-652. 2020. https://doi.org/10.1007/s00122-019-03495-x

[29] J. Yu, Y. Miao, S. Yang, Z. Shi, N. Miao, M. Ding, H. Zhang, Y. Jiang, J. Rong, "Identification and mapping of a photoperiod response gene (QPpd.zafu-4A) on wild emmer wheat (*Triticum turgidum* L.) chromosome 4AL" Euphytica **215**, 146, 1-12, 2019. https://doi.org/10.1007/s10681-019-2469-3

[30] D. Habash, M. Baudo, M. Hindle, S. Powers, M. Defoin-Platel, R. Mitchell, M. Saqi, C. Rawlings, K. Latiri, J. Araus, et al, "Systems responses to progressive water stress in durum wheat" PloS one, **9**, e108431, 1-21, 2014. https://doi.org/10.1371/journal.pone.0108431

[31] I. Farouk, F. Gaboun, Z. Kehel, A. Alsaleh, B. Belkadi, I. Elouafi, J. Motowaj, A. Filali maltouf, MM. Nachit, "Dissection of QTL linked to grain yield and identification of candidate genes involved in grain yield formation using comparative SNP sequences analysis," in 2020 IEEE the first International Conference on Innovative Research in Applied Science, Engineering and Technology (IRASET), Meknes, Morocco, pp. 1-6, 2020. https://doi.org/10.1109/IRASET48871.2020.9091989

[32] S. Li, J. Jia, X. Wei, X. Zhang, L. Li, H. Chen, Y. Fan, H. Sun, X. Zhao, T. Lei, et al, "A intervarietal genetic map and QTL analysis for yield traits in wheat" Mol Breeding **20**, 167-178, 2007. https://doi.org/10.1186/s12870-018-1308-3

[33] S. Sukumaran, M.P. Reynolds, C. Sansaloni, "Genome-Wide Association Analyses Identify QTL Hotspots for Yield and Component Traits in Durum Wheat Grown under Yield Potential, Drought, and Heat Stress Environments". Front Plant Sci **9**, 81, 1-16, 2018. https://doi.org/10.3389/fpls.2018.00081

[34] P. Colasuonno, MA. Maria, A. Blanco, Gadaleta, "Description of durum wheat linkage map and comparative sequence analysis of wheat mapped DArT markers with rice and *Brachypodium* genomes" BMC Genet, **14**, number (114), 1-9, 2013. https://doi.org/10.1186/1471-2156-14-114

[35] C. Xin, R. Hou, F. Wu, Y. Zhao, H. Xiao, W. Si, ME. Ali, L. Cai, J. Guo, "Analysis of cytosine methylation status in potato by methylation-sensitive amplified polymorphisms under low-temperature stress" J Plant Biol, **58**, 383-390, 2015. https://doi.org/10.1007/s12374-015-0316-1

[36] M. Jain, A. Nijhawan, R.Arora, P. Agarwal, S. Ray, P. Sharma, S. Kapoor, AK. Tyagi, JP. Khurana, "F-Box Proteins in Rice. Genome-Wide Analysis, Classification, Temporal and Spatial Gene Expression during Panicle and Seed Development, and Regulation by Light and Abiotic Stress" Plant Physiol, **143**, 1467-1483, 2007. https://doi.org/10.1104/pp.106.091900

[37] SF. Abou-Elwafa, "Identification of genes associated with drought tolerance in barley" Biol Plantarum **62**, 299-306. 2018. https://doi.org/10.1007/s10535-017-0765-0

[38] IS. Kumar, N. Zaharin, K. Nadarajah, "In silico identification of resistance and defense related genes for bacterial leaf blight (BLB) in rice" J Pure Appl Microbiol, **12**, 1867-1877, 2018. https://dx.doi.org/10.22207/JPAM.12.4.22

[39] Z. Liu, J-P. Yan, D-K. Li, Q. Luo, Q. Yan, Z-B. Liu, L-M. Ye, J-M. Wang, X-F. Li, Y. Yang, "UDP-Glucosyltransferase71C5, a Major Glucosyltransferase, Mediates Abscisic Acid Homeostasis in Arabidopsis" Plant Physiol, **167**, 1659-1670, 2015. https://doi.org/10.1104/pp.15.00053

[40] C-P. Lai, L-M. Huang, L-FQ. Chen, M-T. Chan, J-F. Shaw, "Genome-wide analysis of GDSL-type esterases/lipases in Arabidopsis" Plant Mol Biol, **95**, 181-197, 2017. https://doi.org/10.1007/s11103-017-0648-y

[41] G. Gullner, T. Komives, L. Király L, P. Schröder, "Glutathione S-Transferase Enzymes in Plant-Pathogen Interactions" Front Plant Sci **9**, 1836, 1-19, 2018. https://doi.org/10.3389/fpls.2018.01836

[42] K. Morimoto, N. Ohama, S. Kidokoro, J. Mizoi, F. Takahashi, D. Todaka, J. Mogami, H. Sato, F. Qin, J-S. Kim, et al, "BPM-CUL3 E3 ligase modulates thermotolerance by facilitating negative regulatory domain-mediated degradation of DREB2A in *Arabidopsis*" Proceedings of the National Academy of Sciences **114**(40), E8528-E8536, 2017. https://doi.org/10.1073/pnas.1704189114

[43] S. Padmarasu, DJ. Sargent, A. Patocchi, M. Troggio, P. Baldi, G. Linsmith, L. Poles, M. Jänsch, M. Kellerhals, S. Tartarini, R. Velasco, "Identification of a leucine-rich repeat receptor-like serine/threonine-protein kinase as a candidate gene for Rvi12 (Vb)-based apple scab resistance" Mol Breeding, **38** ,73, 1-14, 2018. https://doi.org/10.1007/s11032-018-0825-y

[44] D. Pradhan, D. Mathew, SK. Mathew, PA. Nazeem, "Identifying the markers and tagging a leucine-rich repeat receptor-like kinase gene for resistance to anthracnose disease in vegetable cowpea [*Vigna unguiculata* (L.) *Walp*.]" J Hortic Sci Biotech, **93**, 225-231, 2018. https://doi.org/10.1080/14620316.2017.1362962

[45] V. Jamilloux, J. Daron, F. Choulet, H. Quesneville, "De novo annotation of transposable elements: tackling the fat genome issue" Proceedings of the IEEE, **105**, 474-481, 2016. https://10.1109/JPROC.2016.2590833

[46] A.A. Diab, R. Kantety, N. Ozturk, D. Benscher, MM. Nachit, M. Sorrells, "Drought-inducible genes and differentially expressed sequence tags associated with components of drought tolerance in durum wheat" Sci Res Essay, **3**, 009-026, 2008.

[47] D. Habash, Z. Kehel, M. Nachit, "Genomic approaches for designing durum wheat ready for climate change with a focus on drought" J Exp Bot, **60**(10), 2805-2815, 2009. https://doi.org/10.1093/jxb/erp211

[48] MM. Nachit, "Association of grain yield in dryland and carbon isotope discrimination with molecular markers in durum (*Triticum turgidum* L. var. *durum*)" In Proceedings of 9th International Wheat Genetics Symposium, Saskatoon, ed. A.E. Slinkard, Canada, 218–223, 1998.

[49] M.M. Nachit, I.Elouafi, "Durum wheat adaptation in the Mediterranean dryland: Breeding, stress physiology, and molecular markers" In Challenges and strategies for dry-land agriculture, eds. S.C. Rao and J. Ryan, CSSA. Madison, WI: Crop Science of America and American Society of Agronomy, **32**, 203–218, 2004. https://doi.org/10.2135/cssaspecpub32.c13

[50] J. Li, S. Wen, C. Fan, M. Zhang, S. Tian, W. Kang, W. Zhao, C. Bi, Q. Wang, S. Lu, et al, "Characterization of a major quantitative trait locus on the short arm of chromosome 4B for spike number per unit area in common wheat (*Triticum aestivum* L.)" Theor Appl Genet, **133**, 2259–2269, 2020. https://doi.org/10.1007/s00122-020-03595-z

ASTES

Advances in Science, Technology and Engineering Systems Journal Vol. 5, No. 5, 1028-1035 (2020)

www.astesj.com

Special Issue on Multidisciplinary Innovation in Engineering Science & Technology

ASTESJ

ISSN: 2415-6698

Understanding Risk Assessment in the Context of Fractional Ownership using Ethereum Smart Contract

Mohamed Laarabi*, Abdelilah Maach

Mohammadia school of Engineers, Mohammed V University, Rabat, 10090, Morocco

ARTICLE INFO

Article history:
Received: 31 July, 2020
Accepted: 27 September, 2020
Online: 20 October, 2020

Keywords:
Smart contracts
Block chain
Non-fungible assets
Risk Assessment

ABSTRACT

Ethereum smart contract system has seen a steady adoption as it continues to support tens of thousands of contracts. This feature has evolved to give a practical shape to the ideas leading up to fractional ownership transfer, using advanced smart contracts such as ERC-981. However, alongside its numerous benefits, various risks arise with the actual implementation of the ERC-981. This paper documents high-level processes and risk factors involved in the transfer-system, building a theoretical risk model based on Electre Tri-framework belonging to MCDA classification/sorting models. This model deals with detecting problems that are pre-defined on a central reference. The approach is illustrated through several stages: following comparison between the methods of risk analysis towards a risk assessment model, proposing recommendations and solutions. The framework was able to detect 18 major risks and bugs assigned to 6 categories.

1. Introduction

In the past, the value of fractional ownership of assets (such as the right of publicity, trade secrets, copyrights, software, and real estates) have had little to no understanding as an asset, leading in some cases to a determination of having no value as assets. [1]. Fractional ownership of assets has been classified as "intangible" on corporate balance sheets regarding intellectual rights, such as products and technologies based in large portions upon such intellectual property [2]. They have also frequently been assigned little or no concrete value.

In large measures, placing a value on a co-ownership of the property has been difficult [1], and has led to some confusion over the valuation of the property at the time of selling, leading to the conventional diminution of value placed on the property.

Fractional ownership transfer is one of the most complex-prone operations. Many attempts have been made to develop dependable and accurate selling methods and evaluation for co-ownership of property assets, most unsuccessful because of the long process and the huge risk associated with the transaction.

However, selling a property for co-ownership is becoming a main target for the new era of decentralized ledger technologies using blockchain plate forms and as a base for developing larger multi-unit projects such as (tokenization, colored coins) [3]. Addressing multiple complications in the design of the contract, aiming to reduce unnecessary costs and time expenditure while enhancing transparency, by using this technology it becomes possible to tokenize existing financial assets - equities, debt instruments, the share of investment funds, or real estate by representing them in the form of tokens.

The decentralized ledger is a design pattern that underpins the Bitcoin cryptocurrency it can be described as a ledger of any transactions or contracts maintained in decentralized form across different levels [3]. However, its capacity to validate interaction amongst participant nodes is a vital key enabler for participants that require mutually distrusting peers to conduct their affairs. One such use is the smart contract, designed to encode rules to reflect any kind of multi-party interaction [4]. With the huge amount of investment in the decentralized ledger technologies, especially blockchain, and its rapid evolution as a trend towards being accepted as a new solution to record, share and synchronize transactions in their respective electronic ledgers [5]. Ethereum smart contracts are becoming the preferred mechanism to implement a wide range of applications, including financial instruments (e.g., Ether, mining, and saving wallets.).

A smart contract is a program that runs on the block chain and has its correct execution enforced by the consensus protocol. A contract can encode any set of rules represented in its programming language, offering new solutions such as [6]:

- ERC20: for fungible assets,
- ERC721: for non-fungible tokens, used for collectibles and games,

*Corresponding Author: Mohamed Laarabi, Mohammadia school of Engineers, Mohammed V University, Rabat, 10090, Morocco, Cell No. 00 212 6 61 95 42 22, laar.mohamedd@gmail.com

- ERC777: for fungible tokens, provide a new use and building on past learnings that match with ERC20,
- ERC1155: allowing for a single smart contract to represent multiple fungible and non-fungible tokens.

However, despite the expressiveness of the smart contracts, the present form of these technologies lacks transactional privacy. There are numerous risks that need to be identified and documented when going through the process of tokenizing an asset and selling it. The entire sequence of actions taken in a smart contract is propagated across the network and/or recorded on the blockchain and therefore are publicly visible [7]. Even though parties can create new pseudonymous public keys to increase their anonymity, the values of all transactions and balances for each (pseudonymous) public key are publicly visible [8].

The main purpose of this study is to document several new zones and factors of risks and bugs on the Ethereum's smart contracts as well as the whole tokenization process.

We formalize a theoretical decision framework alongside with a risk assessment model, proposing recommendations and solutions for the documented risks. We provide a new approach of handling co ownership of property, a frame work able to detect major risks and bugs.

The rest of the article is organized as follows: Section 2 provides a review of risks and deferent methods of risk assessment alongside with MCDA classification/ sorting techniques to handle fractional rights. Section 3 the contextual setting and the main risk factors. Section 4 presents applications of these techniques in a framework that can be used in a risk assessment model for real cases, as well as listing some multi-criteria decision that supports the transfer of fractional rights using smart contract which can be developed for classification and sorting model development in general. In Section 5, we will be discussing the results and provide a summary. Finally, section 6 concludes the paper and discusses some interesting future research extensions and directions.

2. Related work and Open Challenges

The concept of tokenization is not recent. In monetics, tokenization is the process of substituting bank data (card number) with disposable data called "tokens". This solution helps to reassure the wearer especially in payment on the Internet or in NFC. For the trader, this is a way to reduce the perimeter of PCI-DSS since no sensitive items will be stored in his information system. For the bearer's bank (issuer), it is simply a way to reduce fraud [3].

the author mainly explains that the process of tokenization is highly promising for illiquid assets: their valuation is now sanctioned by low rate of liquidity in important proportions (which he calculate at "25% to 35 %"). Tokenization will increase market depth by opening markets to more participants, resulting in more exchanges. Traditional assets will be tokenized because they will lose the liquidity premium if they do not (such as real estate, residential assets, or artistic works), therefore, individuals could collectively acquire a valuable painting for a local museum through a sale of tokens, even if none of them can afford to buy the painting individually [9].

Following the literature review, two major types of assets are more easily "tokenizable" than others: -Intangible assets (patents, carbon credits, copyrights.) because of their lack of physical existence, these assets can lend themselves more easily than others to this tokenization process, even though some laws barriers can make the transfer process more expensive and complex, these assets are easier to tokenize, they can often be divided into multiple units (such as bitcoins) and all tokens can be associated with a general set of interchangeable asset components (example: 10kg gold), conversely, non-fungible active ingredients are less suitable for tokenization. For example, when securitized, mortgages are often grouped with other loans with similar but not identical characteristics.

In this paper, we will only be focusing on the risks occurring the tokenization of non-fungible assets using smart contract that's runs on Ethereum's platform, as we assume that the risks presented are much more complex and require more documentation.

Many papers presented methods for risk measurement based on different criteria, from classification models to multi-criteria methods [8, 9]. In recent years, formal methods have been largely used to analyze tokenization using smart contracts with the aim of verifying the security protocols of potential risks with untrusted codes. One of the most cited problems has been the infamous DAO attack, taken millions of dollars during a crowdfunding service and caused a huge bug in the Ethereum's blockchain. Among methods of classification and sorting, the MCDA method is used to assign selected areas to one of the four collapse risk classes previously defined by a committee of experts. By convention, Class 1 is the class corresponding to the highest risk, and Class 4 is the least significant risk [10].

The classification or risk has been the subject of extensive archiving work leading to the development of a geographic information system (GIS) [11]. The choice of areas to be classified according to risk was the subject of a pre-assigned selection procedure presented in table 1. The data available for each area is either quantitative (probability rate, depth, tokens) or qualitative (presence of a fault, nature of the fraud). These data are used, first, to identify the so-called homogeneous areas (with constant characteristics in their perimeter) [9], and on the other hand, to select the so-called (at-risk areas), presenting a predisposition to the occurrence of a collapse off chain or smart contract infrastructure in other words (operational, strategic). We first present the procedure for selecting the areas studied and the criteria chosen for the prioritization of these areas, then we explain the principle of prioritization based on the Electre- tri method [9]. Finally, we illustrate the course of the method.

3. Contextual Setting and Methods

On the block chain, risks are a major concern. In addition to their ability to cause losses of money and time, they can also degrade the performance of these systems and render them incapable of achieving their objectives [11]. However, in order to consider tokenizing non-fungible assets using smart contracts, it is crucial to assess the feasibility of it. In this section, we are interested in presenting the main methods used to manage risks and their influencing factors.

Many works characterize risk using two distinct components of "probability" and "severity". The probability represents an average value of its eventuality over a period of time. As for severity, it is defined as the amount of damage [12], following the occurrence of a dreaded event. In a two-dimensional space, a risk can be presented by a point admitting an 'S' severity component

and a probability component 'P' (see figure 1). It is important to note that there are different types of risks that can reach a system. According to the author these "risks" can be internal (industrial, bugs, errors), external (legal framework, economical), or chronic [11]. In this work, we are interested in documenting all of those risks, specifically risks that can damage the platform of a transaction, degradation of the production tool as well as human errors, [13]. We will limit ourselves, in terms of causes of damage, to technical failures, human errors and organizational problems.

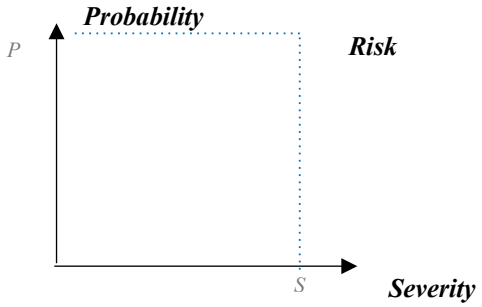


Figure 1: Representation of risk in a two-dimensional space, axis (Y) represent probability while axis (X) represent severity

The previous section illustrated the philosophy of conventional methods for risk analysis. These methods are based mainly on an iterative approach that allows, depending on the method, to identify and analyze a particular type of danger (dangerous phenomena, failures) [14]. The methods are based on the representation of results in different forms (such as diagrams, tables), however, and despite their proliferation, the methods that are dedicated to risk assessment, have certain limitations that can compromise the quality of their results, some of these methods present their results in different forms that can limit the risk detection in the system. In terms of quantifying the impact of risks, conventional methods are generally based on a qualitative risk assessment. For example, in the APR and AMDEC methods, a criticality index is given to each risk, this index is unreliable as it is calculated from qualitative indices of probability and severity. As for the fault tree method, it provides a quantification reliable probability of an adverse event, however, the assessment of the severity of the event remains unreliable [15]. Given the limitations of conventional risk analysis methods, other risk analysis methods have emerged. One of those methods is MCDA methods of classification and sorting, simply defined as an algorithm, which from the elements of a comparison matrix, can document the most likely risks [9]. During our analysis of the existing risk factors, we found various work aimed at integrating risk factors in different zones. Among them, some work has tried to identify only internal risks [5], others focused on integrating the inclusion of certain risk effects in the external environment [9] (see figure 2). In addition, another category of contribution was interested in the automatic conversion of multiple risk factors to one model [16]. We present in the following sections the frame work used in order to document all the risk factors [17].

4. Risk Assessment

Similar to the above definitions of risk, there are several definitions of risk management. Among these definitions, we will settle for the one given by NASA [18], which defines risk management as a process in which the program/project team is responsible for identifying, analyzing, planning, tracking, monitoring, and communicating risks effectively [19]. According to this definition, risk management is a practice of character methodical and ordered as an iterative process (see figure 3). It aims to reduce the impact of hazards to a level described as acceptable, given the efforts spent on its implementation [20].

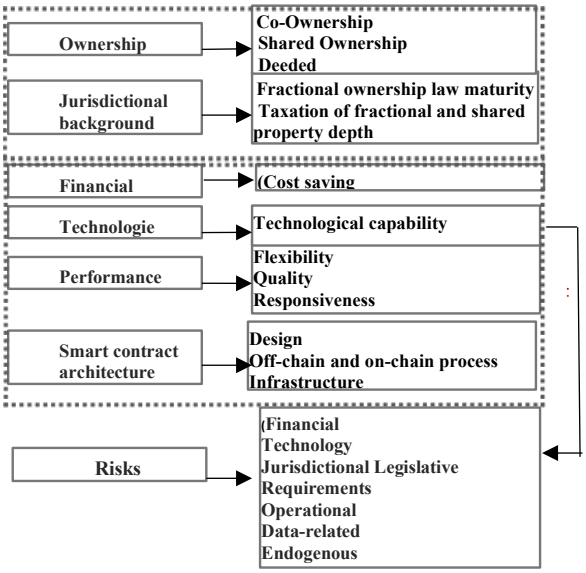


Figure 2: Factors influencing fractional ownership transfer

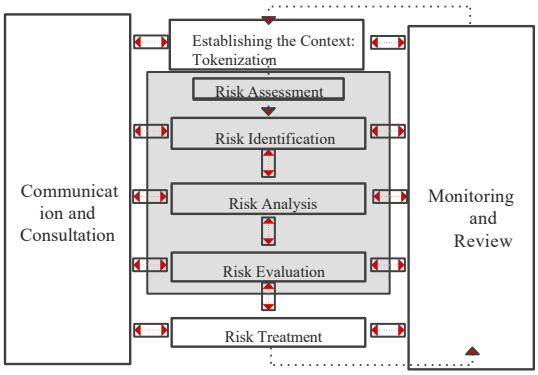


Figure 3: Risk assessment Process

4.1. Risk identification: Identifying risks that need to be assessed

It is important to note that, like any production system, tokenizing assets using Ethereum smart contract is subject to a multitude of risks [6], however, given the mission of tokenizing non-fungible assets, some risks can have a huge impact, as they affect in some cases the life savings of the users, causing in the process some dramatic damages [17]. Identifying risks aims to represent and describe the dysfunctions that can occur in a system (see table 1) [9]. A malfunction is characterized by an alteration that reaches the behavior of elements of a system already identified, in general, a function fails if it does not achieve the objective to which it is intended, with the desired quality [11].
These malfunctions represent events with different natures. Based on literature and available data, we are able to identify 6 major categories:

Table 1: Categories of risks in non-fungible tokenization

Category	Risk
Operational	R1- Lack of a standardized mode of operation, function and security deficiencies R2- Server/Infrastructure Breach R3- Poor service performance: failure in attaining an acceptable degree of responsiveness and flexibility R4- On and off chain information's disorder R5- lack of privacy
Financial	The transaction costs of the public block chain are high. R7- Lack of recipients and users
Technology	R8-Poor implementation of the smart contract to failure in the execution phase
Data Related	R9- Private keys information's leakage R10-Latent information asymmetry between sellers and buyers. (Wang and Regan 2002)
Legal Framework	R11-Insufficient basis for cooperation and information exchange R12- Absence of legal framework R13- Legal taxes basis inadequate or overly rigid
Endogenous	R14- Prior supervisory approval not required R15- No definition of significant ownership, nor qualitative criteria to determine ownership R16- Unrealistic or high expectations regarding the service provide performance R17- Inadequate response to week audits and control R18- Loss of control over the service provider

4.2. Risk Analysis

Risk analysis is the systematic use of information to identify risk factors and target entities and estimate risk [9]. The risk factor is a parameter that is thought to play a role in the accidental sequence without being proven to be a direct or indirect cause. Estimating risk is defined as a "process used to assign values to the probability and consequences of a risk" [8]. As for risk estimation, the stakeholder may consider cost, benefits, concerns, and other variables required for risk assessment.

Two major risk analysis approaches are used in risk analyses: "Deterministic approach" that consists of identifying events that could lead to an accident by looking for the worst possible case (the worst-case scenario) and assigning extreme gravity to its potential consequences [9], and the "probabilistic approach" that involves calculating probabilities for the occurrence of events that are part of the process of materializing a given accident-scenario [18].

Table 2: Deterministic risk assessments

Deterministic risk assessments	Description
Single scenario	Risks are defined and handled as static entities and outputs have fixed values [4]
Maximum-credible scenario'	The scenario selected may be a 'worst-case scenario' or 'most likely scenario' (i.e. based on a historical event) [8]
Stochastic Dominance	A partial order between random variables [11]
Consequence/probability matrix	Matrix with different layers of severity at the top and the levels of probability [12]

4.3. Deterministic Risk Analysis

In this paper, we will use the deterministic approach that has been generally adopted in high-risk areas such as nuclear, military, guided transport, where the slightest significant risk is tracked down and reduced at source [9]. It consists of identifying events that could lead to an accident scenario by looking for the worst possible case and assigning extreme gravity to its potential consequences, this means that deterministic risk analysis only has a single and specific outcome based on the scenario being assessed [18]. Using a scenario-based approach can be extremely useful for communicating risk assessment results to non-experts.

4.4. Risk evaluation

Evaluating a risk is a process used to assign values to the probability and consequences of a risk. It's a fundamental requirement for risk evaluation to identifier risk functions. As we are using Elctre-tri method, we categorize the parameters that we have mentioned earlier (such as fragility, vulnerability, likelihood and occurrence), into categories with the same nature in order to have a significant results. The natures of some parameters can vary significantly from one function to another [18, 19]. Using the MSDC tri method oblige us to choose categories with the same nature. Selecting appropriate functions is an essential aspect of risk evaluation as a mediocre selection can cause unsound decision making and unintentionally increase risk [9]. There is a significant challenge and a huge barrier to both the selection criteria and development of effective risk frame work as the parameters used are strongly limited by the availability of data:

- Financial impact
- Ethuriem Infrastructure impact
- Security impact
- Regulation impact
- Technological impact
- Likelihood of occurrence
- Risk mitigation effort

Once the severity, frequency of occurrence is estimated, the risk is assessed from a risk graph, of which here is a prototype (see figure 4).

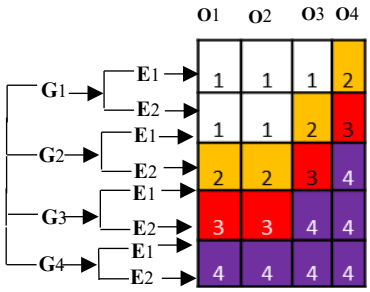


Figure 4: Prototype of a risk graph

As we pointed out in section 3, it is worth remembering that our ontological commitment is minimal, therefore, the user can either accept our risk graph (see figure 4), or define its own levels of severity [12], as well as the frequency of occurrence and/or exposure, they may also consider gravity if they chose to use the hazard analysis approach such as ODA (preliminary hazard analysis) [19]. In fact, many papers tried to provide a risk model based on ODA such as model-checking of smart contracts that contain three layers capturing respectively the behavior of Ethereum blockchain, the smart contracts themselves and the execution framework [20]. However, they don't consider external factors outside the platform as relevant, unlike our framework that work as a formal verification technique based on a description of

the variables. This technique consists in performing an efficient systematic inspection of all possible risk factors described by the risk assessment model in order to satisfy the conditions in our first step of building a risk model [21].

Table 3: Risk acceptability criteria

Area of criticality	Risk acceptability	
Negligible	Acceptable	Risks that do not require the approval of the guardianship authority.
Acceptable		Risks requiring proper control and agreement from the supervisory authority.
Undesirable		Risks that cannot be reduced or insufficient and require agreement from the guardianship authority.
Unacceptable		Risks to be reduced.

5. Method Proposed

By identifying 18 risks (see table 1), by applying the Electre-tri method, we were able to classify those risks into four zones (see table 2). The Four proposed zones are built-in after assigning each risk to a specific area. The outranking concept by building binary relationships among each alternative and the profiles that bound each category. This method proposes both procedures for assigning to the collapsing risk classes under the two scenarios pessimist and optimistic procedure [19]. The pseudo-disjunctive procedure of the Electre-tri method corresponds to the procedure optimized with the outranking relation [16].

5.1. Implementation of the ELECTRE-TRI method and Results

Each of the 18 risks must be assigned to qualified zones to take on the implementation of the risk management. Nevertheless, Ethereum platform face an organizational challenges in controlling risk [20], due to the clutter of the continuum of risk reduction measures. We will devote this part to build a theoretical model formulation using Electre-tri.

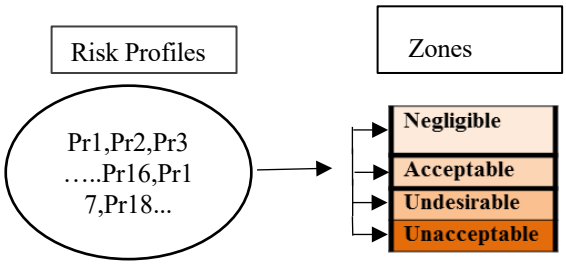


Figure 5: Risk level assignment

Zones are necessarily exclusive and orderly (with the Electre-tri method), zone 1 being the riskiest, the Pr_1 profile, is presented on each criterion, a risk at least as high as Pr_2, Pr_2, also presents, on each criterion, a risk at least as high as Pr_3, (see figure 7). The set of comparisons, on each criterion 9, between the evaluation of a Z_1 zone, and each Pr_n profile provides a partial response to the entry of an area into a risk class h (figure 6 and 7)

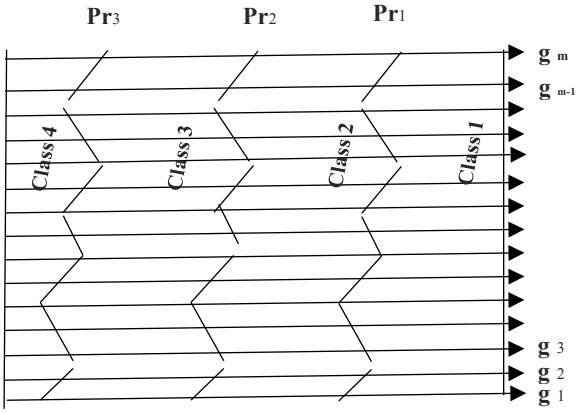


Figure 6: Position of principle of Pr_h class profiles on each criterion g_j.

The data available are tainted with uncertainties, Electre-tri allows it to be taken into account through the introduction of two thresholds [8, 9]. The threshold of indifference q_j and the threshold of preference P_j, they represent, respectively, the minimum and maximum margin of uncertainty related to the nature of the data and the calculations to be made and are defined as follows (see figure 7)

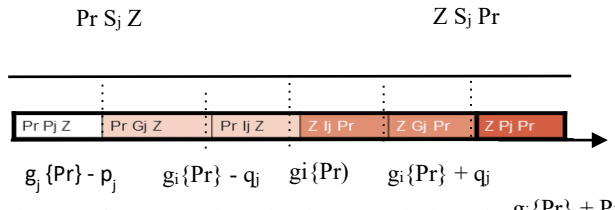


Figure 7: Three Comparison Situations, on Criterion J, between a Z zone and an Pr (S) profile at least as risky as, (I) indifference, (Q) low riskier and (P) strictly riskier.

- If $lg_j,(Z,) – g_j (Pr_j)l$ is less than q_j, it is considered that this difference is not significant and that $g_j(Z_j)$ and $g_j (Pr_h))$ are practically equivalent; it will be said then that zone Z, and the low profile of the h class, Pr_h, are indifferent (l_j) from the point of view of the g_j ($Z_j I_j Pr_h$) criterion;

- If $lg_j(Z_j) – g_j (Pr_h)l$ is greater than p_j, this difference is considered significant; in the event that $g_j (Z_j)$ is greater than $g_j (Pr_h)$, it will be said that zone Z, is strictly riskier than the low profile of the h class, Prh, for the gj criteria, (ZjPj Prh); Prh is strictly riskier (Pj) and that Z, in reverse (Prh PjZj)

-If the threshold of preference p_j is not equal to the threshold of indifference q_j, the interval between these two values represents a range of ambiguity in which the risk is presumed to be higher without the difference $lg_j(Z_j) - g_i (Pr_n)l$ can be considered truly significant. It will be said that zone Z, is weakly riskier (Q_i) than Pr_h, for the criterion g_j (Z Q, Pr_h); Pr_h is weakly p_j us risky than Z, in reverse (Pr_h Q, Z,)'. By convention, if an area is indifferent to a low profile of a class, the area is then assigned to that class: we can say that the risk class is closed from below [9]. Therefore, if a Z, presents a risk assessment on each criterion, between the risk assessment made for Pr_n and Pr_h, then Z_j is assigned to class h, however, this case is rarely encountered.

Two extreme logics of sorting to risk classes are then possible: either Z, is assigned in the class the lowest encounter on a criterion, Z, is assigned to the highest class met on a criterion. These two logics imply a principle of caution which is, in the first case, minimum and, in the second case, maximum. To mitigate these two logics, Electre- tri proposes two assignment procedures: a pseudo-conjunctive procedure and a pseudo-disjunctive procedure [9]. To achieve this, a credibility index σ is introduced. This index, which takes a value between 0 and 1, aggregates, taking into account importance of risk, partial comparisons, criterion by criterion, and expresses the credibility with which one can consider overall that a Z, is more risky than a Pr_h profile [22].

In this case, it will be said that the area outperforms (S) the profile. When this index is worth 1, it means that the assertion (Z, is riskier than Pr_h) is completely credible (100% credibility resulting from the adherence of all criteria to this assertion).When it is worth 0, it means that this assertion is not at all credible (credibility of 0% resulting from the rejection of the assertion by all the criteria or by one of the criteria that imposes its veto).When it takes a value between 0 and 1, it means that the (opinions - are divided (some criteria validate the assertion while others oppose it)[9]. The credibility index then expresses the force with which the favorable criteria are expressed, corrected by the opposite force of the adverse criteria. When it's above 0.5, this means that an absolute majority of criteria is in favor of the assertion. The credibility index that makes it possible to judge this upgrade relationship is rated o(Z,Pr_h).In Electre- tri, one must also calculate the credibility index of the inverse relationship, noted o (Pr_h, Z), because the calculation of this index is not commutative. [23]

To judge whether or not a Z zone enters a class h, f credibility index o(Z,Pr_h) is compared to a parameter λ (including enter 0,5 and 1) that expresses the desired level of requirement to validate that entry. For example, an λ=0,6 means that it is hoped that at least 60% of the criteria (including risk importance) will be favorable to entry into the class. Three situations are possible and only possible if:

-If the Z is indifferent to Pr_h when: $\sigma(Z, Pr_h) \geq \lambda$ and $\sigma(Pr_h, Z_j) \geq \lambda$ => Z_j I Pr_h ;
-If the Z is preferred to Pr_h when: $\sigma(Z, Pr_h) \geq \lambda$ and $\sigma(Pr_h, Z_j) < \lambda$=> Z_j I Pr_h ;

-Pr_h is preferred to the Z when: $\sigma(Z, Pr_h) < \lambda$ and $\sigma(bh, Z_j) \geq \lambda$=> Z_j I Pr_h ;

-Is incomparable to Pr_h when: $\sigma(Z, Pr_h) < \lambda$ and $\sigma(Pr_h, Z_j) < \lambda$=> Z_j I Pr_h ;
Out of the two sorting procedures offered by the Electre- tri method, pseudo-disjunctive is the most prudent. This procedure involves assigning a Z-zone, to an h-class, if:

- Z, has a strictly higher level of risk than the low profile Prn (Z,P Pr_h), Z_j and low profile Pr_n present the same level of risk (Z,I Pr_n), or Z_j and the low profile Pr_h presents incomplete levels of risk (Z_j ,R Pr_h);

- And if none of the previous situations is valid when comparing Z, and the Pr_h .profile, (low profile of class h-1).

From the moment the first condition is checked by a Pr_h profile, it is also verified by all the lower n profiles
($Pr_{k>h}$).

The assignment h class can therefore be characterized by the highest h value such as Prn_, violates the first condition. This corresponds to the lowest profile such as Pr_{hj1} presents a strictly higher risk level than Z.

It is important to note the λ parameter [21], which adjusts the allocations of areas to risk classes, is chosen by the user and raises the question of the degree of severity (or requirement) with which the allocations from the zones to the classes are to be dealt with [8], it must be greater than 0.5 to mean that, in order to validate an assignment from an area to a class, it is necessary that more than half of the criteria validate the assertion based on their respective weight or importance. Since importance of risks are different, it is important not to leave the decision to a single criterion, even if it is the most important [15].

Table 4: Comparative analysis between multi-criteria methods

Multi-criteria methods	Criteria	Benefits	Disadvantages
Weighted sum = WSM	Quantitative	Simple, known, no change to the underlying problem [28].	Drafting criteria, need for homogeneity of units and scales of criteria [28].
Goal-Programming GP	Quantitative	Suitable for initial internships in the decision-making process [29].	No qualitative criteria [29].
MAUT = Multiple Attribute Utility Theory	Quantitative and qualitative	Accommodates scales of units of different criteria.Mathematically represents the decision-making process [30].	Little intervention from the decision maker. Difficulty establishing utility functions [30].
AHP = Analytic Hierarchy Process	Quantitative and qualitative	Great flexibility, varied range of unstructured problems [31].	Decision-makers' comparisons of potentially tricky criteria and alternatives [31].
ELECTRE 1 = Elimination And Choices Translating Reality	Quantitative and qualitative	First method of upgrade. Suitable for the problems of choice between alternatives [23].	Effects of significant thresholds. (too) simple modeling of the decision-making process.Real criteria only [23].
ELECTRE 2 - Elimination And Choices Translating Reality	Quantitative and qualitative	Represents the decision-maker's preference, indifference and veto in front of two alternatives by fixed values [23].	Real criteria only [23].
ELECTRE 3 = Elimination And Choices Translating Reality	Quantitative and qualitative	Represents the decision-maker's preference, indifference and veto in front of two alternatives by an index between 0 and 1 (introduction of quasi-criterion and blur).Stable results [23].	Implementation of the full potential of this delicate method. No physical interpretation of certain parameters (discordance thresholds).Results can be difficult to interpret [23].
ELECTRE 4 - Elimination And Choices Translating Reality	Pseudo-criteria (fuzzy logic)	No weighting of the criteria but no criteria can be preponderant or negligible in relation to the others.Use fuzzy logic [32] .	Little flexibility in calculations [32].

The advantage of our model in the light of literature as we have said, is that the semantics of our model is given by a system of functions what can be more or less complex. Thus, the main challenge in our framework is the combinatory explosion of the framework. Nevertheless, this technique combined with Electre-tri has a huge potential to check most of risks in the design process

of the smart contract [24]. The Electre- tri method always come up with a solution, however, the downside is that the proposed solution may be far from returning to the original classification if there are inconsistencies in the decision making process. In addition, the complexity of the calculations means that the theoretical model only works in cases where neither the criteria nor the alternatives are too numerous. [25] The algorithms used often rely on linear programming algorithms, whose computational time increases rapidly with the number of input variables (criteria and/or instances). [26, 27]

For example, Kappalab's capacity calculation is limited to less than 10 criteria, which is more than enough in our case (it is common to consider that a problem with more than 6 or 7 criteria is a poorly defined problem) but not necessarily in machine learning .Taking into account the particular structure of machine learning problems may reduce computational time, particularly for "utility" or " Electre- tri" method, this is an important step in the decision-making process, to inform on the options for this choice, a summary of the main characteristics of the methods described in the papers presented in table 4. Implementation of these tools may require the expertise of someone who will serve decision-makers and stakeholders. [26] These tools must be implemented in a decision-making process that can, depending on the case, be relatively complex and time-consuming and involve experts and members of civil society. The use of a facilitator who is familiar with the tools and conditions of their implementation can then be useful, especially for knowledge and preference management aspects. This theoretical framework is improved if it has a structured approach, it is with this in mind, that the decision-making tools described in this paper were designed, helping stakeholders and top management to reach consensus [27].

6. Conclusion

In this paper, we have introduced a unified theoretical framework for handling fractional rights using Ethereum smart contracts, which runs on the blockchain. This study links jurisdictional studies to computer science which deserves further investigations. While this direction of research has been already pointed out in other contributions, our results are meant to serve as a model for top management in order to handle a situation where they are too many criteria that are not connected. As we pointed out in our paper, this is achieved by expressing the decision-making process as a formula and solving arithmetic constraints.
Risk analysis on the Ethereum requires effective methods and tools to respond to the urgency with which risk sometimes needs to be managed. This method makes it possible to formalize expert knowledge through criteria that all contribute to the explanation of risk even when the knowledge of the phenomena involved is partial or imprecise.

The conclusions provided by Electre- tri serve as consultation between experts and decision-makers, their robustness depends on several aspects, including the reliability of data. To this end, Electre- tri imposes sensitivity analyses on the various parameters. It exploits such as weights, thresholds, and the λ fuzzy index before providing robust conclusions.

We believe that there is still much work to be done. As regards our results, several questions must be considered. First of all, we will be working on providing a new template for smart contracts to handle fractional rights, also we will be providing a real case study using our new template studying the response behavior of these templates regarding their abilities to handle different variables and information's.

In conclusion, it is necessary to clarify that the method used does not intend to provide a forecast, but rather, a risk assessment, taking into account the availability of data, we will continue in our research aiming to provide a safer template to transfer non fungible assets using smart contracts.

Conflict of Interest

The authors declare no conflict of interest.

References

[1] M.D. Jones, system of fractional ownership of ntellectual.patent no.: us 7,720,740 b2.date of patent: may 18, 2010

[2] M. Zeilinger, "Digital Art as 'Monetised Graphics': Enforcing Intellectual Property on the Blockchain," Philosophy & Technology, **31**(1), 15–41, 2018, doi:10.1007/s13347-016-0243-1.

[3] M. Mohammadi, A. Al-Fuqaha, M. Guizani, J.-S. Oh, "Semisupervised Deep Reinforcement Learning in Support of IoT and Smart City Services," IEEE Internet of Things Journal, **5**(2), 624–635, 2018, doi:10.1109/JIOT.2017.2712560.

[4] Kalra, S. Goel, M. Dhawan, S. Sharma, "ZEUS: Analyzing Safety of Smart Contracts," in Proceedings 2018 Network and Distributed System Security Symposium, Internet Society, Reston, VA, 2018, doi:10.14722/ndss.2018.23082.

[5] R. Shinde, O. Nilakhe, P. Pondkule, D. Karche, P. Shendage, "Enhanced Road Construction Process with Machine Learning and Blockchain Technology," in 2020 International Conference on Industry 4.0 Technology (I4Tech), IEEE: 207–210, 2020, doi:10.1109/I4Tech48345.2020.9102669.

[6] M. Alharby, A. van Moorsel, "Blockchain Based Smart Contracts : A Systematic Mapping Study," Computer Science & Information Technology (CS & IT), 125–140, 2017, doi:10.5121/csit.2017.71011.

[7] BEN-ARI, Adi,A System and method for blockchain smart contract data privacyinternational search report (art. **21**(3)),62/259,090 24 november, 2015

[8] A. Kosba, A. Miller, E. Shi, Z. Wen, C. Papamanthou, "Hawk: The Blockchain Model of Cryptography and Privacy-Preserving Smart Contracts," in 2016 IEEE Symposium on Security and Privacy (SP), IEEE: 839–858, 2016, doi:10.1109/SP.2016.55.

[9] L. Luu, D.-H. Chu, H. Olickel, P. Saxena, A. Hobor, "Making Smart Contracts Smarter," in Proceedings of the 2016 ACM SIGSAC Conference on Computer and Communications Security, ACM, New York, NY, USA: 254–269, 2016, doi:10.1145/2976749.2978309.

[10] G.W. Peters, E. Panayi, Understanding Modern Banking Ledgers Through Blockchain Technologies: Future of Transaction Processing and Smart Contracts on the Internet of Money, 239–278, 2016, doi:10.1007/978-3-319-42448-4_13.

[11] N. Atzei, M. Bartoletti, T. Cimoli, A Survey of Attacks on Ethereum Smart Contracts (SoK), 164–186, 2017, doi:10.1007/978-3-662-54455-6_8.

[12] C.F. Torres, J. Schütte, R. State, "Osiris," in Proceedings of the 34th Annual Computer Security Applications Conference, ACM, New York, NY, USA: 664–676, 2018, doi:10.1145/3274694.3274737.

[13] B. Roy, D. Bouyssou, Comparison of a Multi-Attribute Utility and an Outranking Model Applied to a Nuclear Power Plant Siting Example, 482–494, 1985, doi:10.1007/978-3-642-46536-9_35.

[14] J. Figueira, B. Roy, "Determining the weights of criteria in the ELECTRE type methods with a revised Simos' procedure," European Journal of Operational Research, **139**(2), 317–326, 2002, doi:10.1016/S0377-2217(01)00370-8..

[15] C. Liu, H. Liu, Z. Cao, Z. Chen, B. Chen, B. Roscoe, "Finding Reentrancy Bugs in Smart Contracts," in 2018 IEEE/ACM 40th International Conference on Software Engineering: Companion (ICSE-Companion), IEEE, Gothenburg: 65–68, 2018..

[16] O. Deck, M. Al Heib, F. Homand, "Taking the soil–structure interaction into account in assessing the loading of a structure in a mining subsidence area," Engineering Structures, **25**(4), 435–448, 2003, doi:10.1016/S0141-0296(02)00184-0.

[17] J.R. Figueira, S. Greco, B. Roy, R. Słowiński, "An Overview of ELECTRE Methods and their Recent Extensions," Journal of Multi-Criteria Decision

Analysis, **20**(1–2), 61–85, 2013, doi:10.1002/mcda.1482.
[18] C. Harland, R. Brenchley, H. Walker, "Risk in supply networks," Journal of Purchasing and Supply Management, **9**(2), 51–62, 2003, doi:10.1016/S1478-4092(03)00004-9.
[19] S. Scheuer, D. Haase, V. Meyer, "Towards a flood risk assessment ontology – Knowledge integration into a multi-criteria risk assessment approach," Computers, Environment and Urban Systems, **37**, 82–94, 2013, doi:10.1016/j.compenvurbsys.2012.07.007.
[20] Z. Nehai, P.-Y. Piriou, F. Daumas, "Model-Checking of Smart Contracts," in 2018 IEEE International Conference on Internet of Things (iThings) and IEEE Green Computing and Communications (GreenCom) and IEEE Cyber, Physical and Social Computing (CPSCom) and IEEE Smart Data (SmartData), IEEE: 980–987, 2018, doi:10.1109/Cybermatics_2018.2018.00185.
[21] K. Govindan, M.B. Jepsen, "Supplier risk assessment based on trapezoidal intuitionistic fuzzy numbers and ELECTRE TRI-C: a case illustration involving service suppliers," Journal of the Operational Research Society, **67**(2), 339–376, 2016, doi:10.1057/jors.2015.51.
[22] A. Ahmed et al., "Modeling and Simulation of Office Desk Illumination Using ZEMAX," in 2019 International Conference on Electrical, Communication, and Computer Engineering (ICECCE), 1–6, 2019. DOI: 10.1109/ICECCE47252.2019.8940756
[23] U. Okoro, A. Kolios, L. Cui, "Multi-criteria risk assessment approach for components risk ranking – The case study of an offshore wave energy converter," International Journal of Marine Energy, **17**, 21–39, 2017, doi:10.1016/j.ijome.2016.12.001.
[24] E. Mengelkamp, J. Gärttner, K. Rock, S. Kessler, L. Orsini, C. Weinhardt, "Designing microgrid energy markets," Applied Energy, **210**, 870–880, 2018, doi:10.1016/j.apenergy.2017.06.054.
[25] N. Xiao, H.Z. Huang, Y. Li, L. He, T. Jin, "Multiple failure modes analysis and weighted risk priority number evaluation in FMEA," Engineering Failure Analysis, **18**(4), 1162–1170, 2011, doi: 10.1016/j.engfailanal.2011.02.004.
[26] S. Sterlacchini, S. Frigerio, P. Giacomelli, M. Brambilla, "Landslide risk analysis: a multi-disciplinary methodological approach," Natural Hazards and Earth System Sciences, **7**(6), 657–675, 2007, doi:10.5194/nhess-7-657-2007.
[27] K. Bhargavan, N. Swamy, S. Zanella-Béguelin, A. Delignat-Lavaud, C. Fournet, A. Gollamudi, G. Gonthier, N. Kobeissi, N. Kulatova, A. Rastogi, T. Sibut-Pinote, "Formal Verification of Smart Contracts," in Proceedings of the 2016 ACM Workshop on Programming Languages and Analysis for Security - PLAS'16, ACM Press, New York, New York, USA: 91–96, 2016, doi:10.1145/2993600.2993611.
[28] S. Kaddani, D. Vanderpooten, J.-M. Vanpeperstraete, H. Aissi, "Weighted sum model with partial preference information: Application to multi-objective optimization," European Journal of Operational Research, **260**(2), 665–679, 2017, doi:10.1016/j.ejor.2017.01.003.
[29] B. Bankian-Tabrizi, K. Shahanaghi, M. Saeed Jabalameli, "Fuzzy multi-choice goal programming," Applied Mathematical Modelling, **36**(4), 1415–1420, 2012, doi:10.1016/j.apm.2011.08.040.
[30] D. Von Winterfeldt, G.W. Fischer, Multi-Attribute Utility Theory: Models and Assessment Procedures, Springer Netherlands, Dordrecht: 47–85, 1975, doi:10.1007/978-94-010-1834-0_3.
[31] M. Younas, S.H.I. Jaffery, M. Khan, M.A. Khan, R. Ahmad, A. Mubashar, L. Ali, "Multi-objective optimization for sustainable turning Ti6Al4V alloy using grey relational analysis (GRA) based on analytic hierarchy process (AHP)," The International Journal of Advanced Manufacturing Technology, **105**(1–4), 1175–1188, 2019, doi:10.1007/s00170-019-04299-5.
[32] M.A. Alghamdi, N.O. Alshehri, M. Akram, "Multi-Criteria Decision-Making Methods in Bipolar Fuzzy Environment," International Journal of Fuzzy Systems, **20**(6), 2057–2064, 2018, doi:10.1007/s40815-018-0499-y.

ASTES

Advances in Science, Technology and Engineering Systems Journal Vol. 5, No. 5, 1036-1041 (2020)

www.astesj.com

Special Issue on Multidisciplinary Sciences and Engineering

ASTESJ

ISSN: 2415-6698

Social skills and Resilience in Adolescent of Secondary Level of a public Educational Institution in Puente Piedra Lima - 2020

Niurka Jacome-Olacua[1], Joselyne Rodríguez-Paucar[1], Prhitty Marin-Garcia[1], Brian Meneses-Claudio[2,*], Hernan Solis-Matta[1], Eduardo Matta-Solis[3]

[1]*Faculty of Health Sciences, Universidad de Ciencias y Humanidades, 15314, Lima-Perú*

[2]*Image Processing Research Laboratory (INTI-Lab), Universidad de Ciencias y Humanidades, 15314, Lima-Perú*

[3]*Health Sciences, Instituto Peruano de Salud Familiar, 15304, Lima-Perú*

ARTICLE INFO

Article history:
Received: 03 August, 2020
Accepted: 28 September, 2020
Online: 20 October, 2020

Keywords:
Social skills
Resilience
Teenagers
Relationship with the opposite sex
Spirituality

ABSTRACT

Social skills and resilience are very important aspects for mental health; therefore, it is necessary to take into account the positive contribution in the development of adolescents, they are in a vulnerable stage, adapting to physical, mental, emotional, etc. changes. Adolescents, not knowing how to handle the difficulties that may arise, if they do not have the ability to face it and show their positive qualities, can easily fall into depression, student desertion, early pregnancy, addictions to toxic substances (alcohol, tobacco and drugs). That is why in this study to measure social skills, the Elena Gismero Scale of Social Skills questionnaire data collection instrument was used, it has 33 items, 28 refer to the lack of assertion or social skills deficit, 5 of them refers to a positive sense. For resilience, the Connor-Davidson Resilience Scale will be used, it has 25 items. The results obtained with respect to social skills show that in the dimension positive interactions with the opposite sex shows the low level 14.3%, which is equivalent to 45 students, they are presenting difficulties in relating to the opposite sex, regarding resilience in the dimension of spirituality, the low level of 21.7%, indicates that 65 students do not have positive attitudes to fulfill their purposes. The minimum age was 11 years, the maximum age was 17 years, the mean being 13.39 in terms of sex, males predominate with a number of 154 students and 146 females.

1. Introduction

According to the World Health Organization and the Pan American Health Organization, they consider that in recent years adolescents from 13 to 16 years old have suffered from some mental health problem such as stress, depression or apprehension, the use of technology, cyberbullying as well as the condition that adolescents live, whether in areas where violence is used [1].

In Peru, it is estimated that there are 295 thousand people who have limitations to relate either by conduct or their way of thinking, feeling and managing their emotions, showing that 67.8% of them, which is equivalent to 200 thousand people, have moderate and severe limitations [2].

A study carried out on the main problem adolescents face reveals that pregnancy is one of the consequences of not using contraceptive methods, due to lack of information or the myths they believe, followed by that is the state of how they live and the economic income that each family has, the physical abuse that the adolescent faces, these problems leads to the adolescent tending to suffer mental health problems such as stress, depression or apprehension, the use of technology, cyberbullying.

On the other hand, a study on depression in Peruvian adolescents was carried out in a report prepared by the Instituto Nacional de Salud Mental del Perú (INSM) with the result that 7% of the constitutional province of Callao Lima - Peru, suffers from depression disorder, being the most frequent. In the Peruvian Amazon jungle, they reported a prevalence of 1.9%, most relevant in women with 2.2% being adolescents from Lima [3].

*Corresponding Author: Brian Meneses-Claudio, Mr., +51 1 950159924 & bmeneses@uch.edu.pe

A study of 352 adolescents on alcohol consumption in the city of Cajamarca revealed that 5.5% of adolescents have alcohol problems. In addition, a comparison was made in which men have a high risk of alcohol consumption with 9.5%, while women have a 3.8% high risk of alcohol consumption [5].

A study was carried out to determine the consumption of toxic and alcohol in adolescents in which 55% of its population were women between 13 and 14 years of age, 70.9% of adolescents consume alcohol. On the other hand, it was evident that 26.4% use tobacco and 14.2% cannabis. However, people who did not consume both products presented better mood and a good family relationship, therefore a good school environment [5].

However, a study was conducted to determine the relationship between resilience and self-concept with social support in a group of adolescents, resulting in a positive correlation of 26.6% in family support and support from friends, women showed a high level of self-concept with 25.4%, as opposed to men who obtained 21.1% [6].

This study will show the most relevant signs that the adolescent presents in order to intervene and therefore avoid future consequences such as stress, depression, alcoholism and drug addiction. In addition, it has been identified through a bibliographic review of the National and International scientific articles that there is a lack of research in mental health in adolescents [6]. The objective of this study is to determine the relationship of social skills and resilience in adolescents of secondary level in a Public Educational Institution of Puente Piedra.

The Elena Gismero Scale of Social Skills questionnaire will be used to measure social skills, it has 33 items. The answers consist of 4 alternatives that are “I do not identify myself at all; most of the time I do not act or I would not "as well as" I very much agree and I would feel or act like this in most cases" [7]. On the other hand, the Connor-Davidson resilience instrument will be used to propose 25 items, which are distributed in 5 dimensions that are personal competence, confidence in one's own instincts, tolerance of adversity, positive acceptance of change, control and spiritual influence¨ [8]. The data from this research will be entered into the statistical software SPSS 24.0, since it is a correlational design study, the Pearson's Chi-square correlation test will be used for data analysis to evaluate the general objective of the study and a descriptive analysis to see the behavior of the main variables of the study.

The following research work is structured as follows: In section II, the methodology that was carried out to apply the survey collection technique will be presented. Section III will deal with the results showing the sociodemographic data of Social Skills and Resilience in adolescents, indicating the high, medium and low level according to its dimensions. In section IV, it will present the discussions of the research work. Finally, in section V, the conclusions of the research work.

2. Methodology

In this section, the steps for completing the questionnaire will be explained, in addition to showing the sociodemographic data.

2.1. Research Focus and Design

The present research is of quantitative approach, as for the methodological design, it is a cross-sectional correlational research.

2.2. Population and Sample

The population is made up of 300 students from the María de Los Ángeles 3070 Educational Institution which involved 154 men and 146 women, the mean age being 13.39.

2.3. Inclusion Criteria

- Students who are in the first to fifth year of high school in the Puente Piedra district.
- Students whose Parents have signed the informed consent to participate in the study.
- Students who agree to participate in the research study.

2.4. Study Variable

The present study presents two main variables that are social skills, these are a group of strategic behaviors that help developing a capacity for adolescents to contribute to solving a social situation in a way that is acceptable to both the person and the environment social, resilience is the ability that it develops people or group, to deal with difficult adversity such as trauma or a situation. Social skills and resilience in adolescents at the secondary level of a public educational institution.

2.5. Data Collection Technique

The technique to be used in this research work will be a questionnaire. As they are 2 variables, it presents Elena Gismero's Social Skills questionnaire consisting of 33 items, divided into 6 dimensions in which self-expression in social situations, the defense of its own rights as a consumer, the expression of anger or disagreement, being able to say no and cut interactions, make a request, and initiate positive interactions with the opposite sex. 28 of the items refer to the lack of assertion or deficit in social skills, and the remaining 5 refer to the positive sense. The responses are dichotomous for each of them, consisting of 4 response options, “I do not identify myself in absolute; most of the time it does not happen to me or it would not "as well as the positive responses" I would feel or act like this in most cases; strongly agree". In the sum of the results, it obtains high global scores, the adolescent would be expressing its social abilities and in different contexts its desertion capacity [7]. Regarding resilience, the Connor-Davidson Resilience Scale was used, it has 24 items divided into 5 dimensions that will assess personal competence, confidence in one's instincts, tolerance of adversity, positive acceptance of change and control, and spiritual influence [8].

2.6. Procedure for Data Collection

Arrangements will be made to the authorities to access the educational institution. First, it processed the letter of presentation of the university, the team went to the educational institution and presented ourselves to the director of the current campus. The team initiates activities such as classroom accounting. Regarding the student census, the assistant principal provided with an updated list, which allowed to identify the number of students available between 1st and 5th grade of secondary school. When identifying the number of students, coordinated with the assistant principal to carry out the surveys in an average time of one month, The time it took to do the surveys was approximately 15 to 20

minutes per classroom, the team surveyed 4 classrooms per day, two days a week, at the time of conducting the surveys, it was quiet since the teachers collaborated so that everything is carried out correctly, as future health personnel, by applying the surveys the team has been allowed to see more closely the means of how they socialize, to know the capacities that some develop in their environment, among the needs, etc. The team also make sure that the filling and process is correct and detect in a timely manner some erroneous process that may have been presented.



Figure 1: Carrying out the Survey on adolescents in secondary education at the María de los Ángeles Educational Institution N° 3070, in the Puente Piedra district - Lima, 2019.

3. Results

The tables are showing the research results and the relationship between social skills and resilience.

Table 1: Sociodemographic Data on Social Kkills and Resilience in adolescents of Secondary Education of the María de Los Angeles N° 3070 Educational Institution, District of Puent Piedra - Lima, 2020 (n = 300)

Participant Information	**Total**	
	N	**%**
Total	300	100
Gender		
Female	146	48,7
Male	154	51,3
Who do adolescents live with?		
Parents	191	63,7
Other relatives	108	36,0
Alone	1	0,3
Types of Family		
Nuclear	184	61,3
Extended	115	38,3
Aggrandized	1	0,3
Study Grade		
First	72	24,0
Second	87	29,0
Third	40	13,3
Fourth	70	23,3
Fifth	31	10,3

In Table 1, it has the sociodemographic data of the study participants, there were 300 adolescents from secondary education. The minimum age is 11 years old; the maximum age is 17 years old; the average is 13.39 years old.

Regarding gender, the male sex predominated with 154 students representing 51.3%, followed by the female with 146 students representing 48.7%.

Regarding the dimension; Who do students live with? the highest percentage was that they live with their parents with a population of 191, which is equivalent to 63.7%, followed by other relatives, 108 (36.0) and only 1 (0.3).

The type of family nuclear families predominates with 184 (61.3%) cases, extended family with 115 (38.3%) cases and aggrandized with 1 (0.3%) cases. Regarding the study grade, the distribution is heterogeneous, the students of the First grade 72 (24.0%), the second grade 87 (29.0%) and the fourth grade 70 (23.3%) exceed in proportion to those of third grade 40 (13.3%) and fifth grade 31 (10.3%) of high school.

Table 2: Social Skills and Resilience in adolescents of Secondary Education of the María de Los Angeles N ° 3070 Educational Institution, of the Puente Piedra District - Lima, 2019 (N = 300)

Resilience			
Spearman's Rho	**Social skills**	**Correlation coefficient**	0,086
		Sig. (Unilateral)	0,068
		N	300

Test correlation coefficient is + 0.086 ($p<0.05$). Regarding the previous results, there is no statistical evidence to confirm that there is a relationship between the variables Social Skills and Resilience.

Table 3: Social Skills in Adolescents of Secondary Education of The María De Los Angeles N ° 3070 Educational Institution, of the Puente Piedra District - Lima, 2019 (N = 300)

		N	**%**
Social Skills	**Low Level**	0	0,0
	Medium Level	292	97,3
	High Level	8	2,7
Total		300	100,0

In Table 3, it can see the social skills of secondary school adolescents from the María de los Ángeles No. 3070 Educational Institution, in the Puente Piedra District - Lima where a population of 300 adolescents, 292 Students representing the 97.3 have medium level when making requests, 8 adolescents representing 2.7% have a high level when saying no and cutting

off interactions and 0.0% do not present a low level when initiating positive interactions with the opposite sex.

Table 4: Resilience, in adolescents of Secondary Education of the María de Los Angeles N ° 3070 Educational Institution, of the Puente Piedra District - Lima, 2019 (N = 300)

		N	%
Resilience	**Low Level**	1	0,3
	Medium Level	174	58,0
	High Level	125	41,7
Total		300	100,0

In Table 4, the resilience in adolescents of secondary education of the María de los Ángeles N ° 3070 Educational Institution of the Puente Piedra district - Lima 2019, where 174 adolescents representing 58% have a medium level of adaptation and capacity to recover, 125 adolescents representing 41.7% have a high level of control and purpose and finally 1 adolescent representing 0.3% has a low level of spirituality.

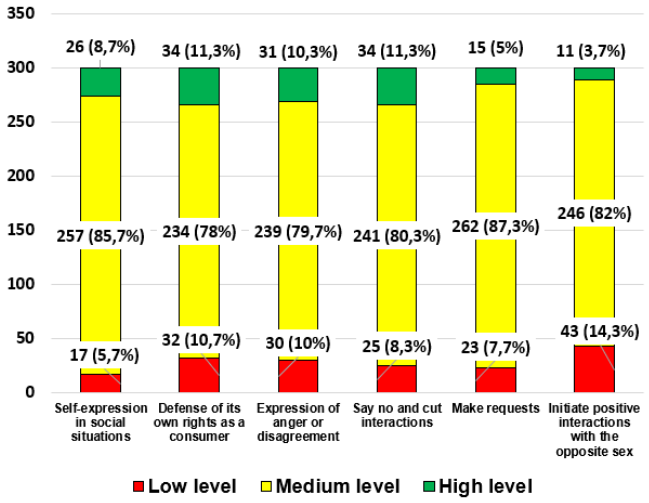


Figure 2: Social skills according to their dimensions in adolescents of Secondary Education of the María de Los Angeles N ° 3070 Educational Institution, of the Puente Piedra District - Lima, 2019 (N = 300)

In Figure 2, it can observe social skills according to their 6 dimensions, where the most affected dimension with low level was to initiate positive interactions with the opposite sex with 43 representing 14.3% adolescents followed by the defense dimension of the its own rights as a consumer 32 that represents 10.7% of the population, the dimension of expression of anger or disagreement with 30 that represents 10%, the dimension of saying no and cutting interactions with 25 which is 8.3%, the dimension of making requests with 23 representing 7.7%, the self-expression dimension with 17 which is 5.7%. The medium level dimension is to make requests with 262 adolescents, which is equivalent to a percentage of 87.3%, the self-expression dimension with 257 represents 85.7% of the population, the dimension of initiating positive interactions with the opposite sex 246 students represent 82%, the dimension saying no and cutting interactions with 241 represents 80.3%, expression of anger or disagreement 239 which represents a percentage of 79.7%, the dimension of defense of its own rights as a consumer with 234 which represents 78%, the dimension of high level that is say no and cut interactions with 34 which represents 11.3%.

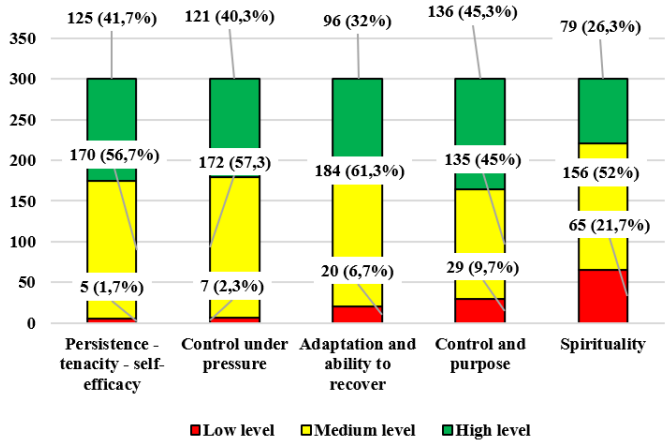


Figure 3: Resilience according to its dimensions in adolescents of Secondary Education of the María de Los Angeles N ° 3070 Educational Institution, of the Puente Piedra District - Lima, 2019 (N = 300)

In Figure 3, it can see resilience according to its dimensions, where the most affected dimension was spirituality with 65 which represents 21.7% of adolescents, the control and purpose dimension with 29 which represents 9.7% of the population, the adaptation dimension and ability to recover with 20 which represents a percentage of 6.7%, followed by the control dimension under pressure with 7 which represents a percentage of 2.3% of adolescents, the persistence-tenacity-self-efficacy dimension with 5 represents a 1.7%. The medium level dimension is adaptation and ability to recover with 184 which represents 61.3%, followed by the control dimension under pressure with 172 which represents 53.3% of adolescents, the persistence-tenacity-self-efficacy dimension with 170 represents 56.7%, spirituality with 156 which represents a percentage of 52%, control and purpose with 135 represents 45%. The high level dimension is control and purpose with 136 which represents a percentage of 45.3% of adolescents.

The importance of knowing the data from this study will contribute to the school authorities are going to detect any problem that may be harmful to students, such as student desertion, dependence on toxic substances such as alcohol, tobacco, drugs, depression, among others. It will also contribute to the health level in which it allows to directly identify the needs and deficits that adolescents may present, this stage is important since they can develop mentally as appropriate as possible and thus be able to focus with more attention to health Mental that is at the limit of risk in what is social skills and resilience.

4. Discussion

In the present research work, it shows that 58.0% of the students are at a medium level with respect to resilience, presenting higher percentages in the dimensions of spirituality, a percentage of 52.0% and in control under pressure shows the 61.3%. Corroborating data on resilience in adolescence is that in the first grades there is a significant decrease in resilience, but it also shows that in intermediate grades, such as 3rd grade, it is still low, but partially recovering in later grades. as 4th and 5th grades [9].

A study was carried out in which the effects of behavior in a social skills program in young people between 14 and 18 years of age in vulnerable situations were identified, for which two interventions were carried out, which they called pre-test and post-test, giving as result in the first one an average of 28.40% and in the post, result 86.64%. This research work also obtain similar results which reinforces the risk that adolescents are in [10].

A research work was carried out in an Educational Institution regarding the well-being in adolescence in which they looked for the relationship between resilience and subjective well-being in adolescents between 12 and 15 years old, resulting in the relation between the subjective well-being and resilience in which have an average of 74.80% in their total sample, making women the most affected [11].

On the other hand, a research on the resilience implied regarding sex and educational level was carried out, it is observed that the students who participated in the research, have a high level of resilience in what is behavioral involvement, 20.29%, which is important that make more emphasis on the emotions of adolescents in schools [12].

Compared with the reviewed studies, we reinforce that the results obtained in this study show that adolescents are at a risk level. Regarding resilience, which is worrisome since if this is not treated in time, adolescents can present difficulties to develop and easily fall into consequences such as depression, student desertion, etc. It was also evidenced that students with fewer grades represent a lower level of resilience, but that would recover progressively since in the higher grades they represent a higher level. In the following study of resilience, it indicates that women would be the most affected regarding to well-being in adolescence and resilience, even though our predominant population are men with a percentage of 51.3%, it is vitally important to be aware of warning signs. Regarding to social skills, in the analyzed study, we have obtained similar results, which reinforces the importance of this study since it is necessary for the authorities to pay attention to the possible problems that the students may have, and to act as soon as possible with the support of mental health professionals and thus the quality of development of these adolescents can be improved, reinforcing their self-esteem, ability to face adversities and improve their social skills, being able to be an important contribution to society. What we want is demonstrate that at this stage of life, it is necessary to be aware because it is very easy for social problems to appear and it is also a stage where if the qualities and mental health are reinforced, these adolescents can be positively motivated resulting in good citizens.

5. Conclusion

Regarding Social Skills and Resilience in adolescents at the secondary level of a Public Educational Institution in Puente Piedra District, it was found that there is no significant relationship between these 2 variables.

Regarding social skills in its self-expression dimension in social situation, the medium level predominated with 85.5%, followed by the high level 8.7%, low level 5.7%, the defense of its own rights as a consumer dimension, the medium level predominated 78%, followed by the high level 11.3%, low level 10.7%, in its dimension expression of anger or disagreement, the medium level predominated 79.7% followed by the high level 10.3%, low level 10%, in its dimension saying no and cutting interactions predominated the medium level with 80.3%, followed by the high level 11.3%, low level 8.3%, in its dimension making requests predominated the medium level with 87.3%, followed by low level 7.7% the high level with 5%, in its dimension to initiate positive interactions with the opposite sex, the medium level predominated with 82%, followed by the low level with 14.3%, high level 3.7%.

It can conclude that the social skills in this study indicate that 6 dimensions that the measurement scale has, 5 of them are at a medium level, followed by high level and low level. The 6th dimension must be taken into consideration, initiate positive interactions with the opposite sex, which has an medium level of 82%, but followed by this is the Low level with 14.3% and the high level obtains 3.7 %; this would represent that students are at risk, the 6th dimension is the most worrisome since adolescents could have difficulties in relating with the opposite sex, although it is true that it considers that they are in a stage of attraction and infatuation typical of age, for this reason, it is worrying that this dimension may decrease, the authorities of this institution should have professional advice such as psychologists who can detect the reason why this interaction is decreasing, which may be an alarm sign such as low self-esteem, upbringing, family history (such as dysfunctional families, among others), leading to difficulties in developing this stage normally. Using this study, we demonstrate and emphasize that it is necessary to take mental health into account at this stage of life, since these adolescents will be the future of the country and society. Take into account how necessary is to carry out a timely control, schools or colleges and especially families add mental health as one of their priorities.

Regarding resilience in its persistence-tenacity-self-efficacy dimension, the medium level predominates with 56.7%, followed by the high level with 41.7%, low level 1.7%; in its control dimension under pressure, the medium level predominates with 57.3%, followed by the high level 40.3%, low level 2.3%; in its adaptation and ability to recover dimension, the medium level predominated with 184 which represents 61.3%, followed by the high level 32%, low level 6.7%; in its control and purpose dimension, a high level predominated with 45.3%, followed by a medium level 45%, low level 9.7%; in its spirituality dimension, a medium level predominated with 52%, followed by a high level 26, 3%, low level 21.7%.

It can conclude that the Resilience in the present study showed that, in the 5 dimensions of the measurement scale, they are all at a medium level, followed by the high level and finally the low level. But in the spirituality dimension, at the low level it is 21.7% which is equivalent to 65 students, this amount is very high, comparing it with the results obtained in the low levels of the other dimensions, this is worrying since that dimension refers to the conformist attitude indicator, this means that 65 students do not have positive attitudes to be able to set a goal and finish it, which is very likely that they do not want to improve their quality of life, this could be considered an alarm sign and is necessary to seek the intervention of medic professionals, psychologists among others, in order to detect the reason for this attitude, they will be able to make a more complete observation. The authorities of the institution must act as

soon as possible so that this is improved and good mental health can be guaranteed in these adolescents, and in this way enhance their capacities to face the difficulties that arise.

Conflicts of Interest

The authors declare no conflict of interest**.**

References

[1]. W.H.O. Pan American Health Organization, Los jóvenes y la salud mental en un mundo en transformación, PAHO, 2018.

[2]. Ministerio de Salud, Prioridades de Investigación en Salud, Instituto Nacional de Salud, 2016.

[3]. L. Donatus, D.J. Sama, J.M. Tsoka-Gwegweni, S.N. Cumber, "Factors associated with adolescent school girl's pregnancy in kumbo east health district north west region Cameroon," Pan African Medical Journal, **31**(3), 1–11, 2018, doi:10.11604/pamj.2018.31.138.16888.

[4]. J.S. Navarro-Loli, M. Moscoso, G. Calderón-De La Cruz, "Research on depression in adolescents in Peru: a systematic review," Liberabit: Peruvian Psychology Journal, **23**(1), 57–74, 2017, doi:10.24265/liberabit.2017.v23n1.04.

[5]. R. Leal, L. Vásquez, "INFLUENCIA DE LOS ESTILOS DE CRIANZA Y LA RESISTENCIA A LA PRESIÓN DE GRUPO SOBRE EL CONSUMO DE ALCOHOL EN ADOLESCENTES DE LA CIUDAD DE CAJAMARCA," Perspective Journal, **17**(1), 33–45, 2016.

[6]. A. Rodríguez-Fernández, E. Ramos-Díaz, I. Ros, A. Fernández-Zabala, "Relaciones de la resiliencia con el autoconcepto y el Apoyo Social Percibido en una muestra de adolescentes," Psychology Action, **12**(2), 1, 2015, doi:10.5944/ap.12.2.14903.

[7]. E. Gismero, EHS. Escala de Habilidades Sociales, 3rd ed., TEA Ediciones, Madrid-España, 2010, doi:10.5901/ajis.2016.v5n3s1p36.

[8]. M.I. Soler Sánchez, M. Meseguer de Pedro, M. García Izquierdo, "Propiedades psicométricas de la versión española de la escala de resiliencia de 10 ítems de Connor-Davidson (CD-RISC 10) en una muestra multiocupacional," Latin American Journal of Psychology, **48**(3), 159–166, 2015, doi:10.1016/j.rlp.2015.09.002.

[9]. I. Axpe, I. Ros, E. Ramos, "Resiliencia y bienestar subjetivo en estudiantes de secundaria en funcion de variables sociopersonales," Proceedings of 3rd International Congress of Educational Sciences and Development, **26**(4), 15–19, 2018.

[10]. J. Redondo-Pachecho, J.S. Parra-Moreno, M. Luzardo-Briceño, "Efectos comportamentales de un programa de habilidades sociales en jóvenes de 14 a 18 años en situación de vulnerabilidad," Pensando Psicología, **11**(18), 45–58, 2015, doi:10.16925/pe.v11i18.1003.

[11]. A. Rodríguez-Fernández, E. Ramos-Díaz, I. Ros, A. Fernández-Zabala, L. Revuelta, "Bienestar subjetivo en la adolescencia: El papel de la resiliencia, El autoconcepto y el apoyo social percibido," Psychology Sum, **23**(1), 60–69, 2016, doi:10.1016/j.sumpsi.2016.02.002.

[12]. A. Rodríguez-Fernández, E. Ramos-Díaz, I. Ros, A. Fernández-Zabala, L. Revuelta, "Resiliencia e implicación escolar en función del sexo y del nivel educativo en educación secundaria," Open School, **44**(2), 1–6, 2015, doi:10.1016/j.aula.2015.09.001.

ASTES

Advances in Science, Technology and Engineering Systems Journal Vol. 5, No. 5, 1042-1049 (2020)

www.astesj.com

Special Issue on Multidisciplinary Sciences and Engineering

ASTESJ

ISSN: 2415-6698

A Cavity Structure based Flexible Piezoelectric for Low-Frequency Vibration Energy Harvesting

Khairul Azman Ahmad[*,1], Siti Noraini Sulaiman[1], Noramalina Abdullah[2], Muhammad Khusairi Osman[1]

[1]*Faculty of Electrical Engineering, Universiti Teknologi MARA, Cawangan Pulau Pinang, Permatang Pauh, Pulau Pinang, 13500, Malaysia*

[2]*School Of Electrical & Electronic Engineering, Universiti Sains Malaysia, Engineering Campus, Seberang Perai Selatan, Nibong Tebal Pulau Pinang, 14300, Malaysia*

ARTICLE INFO

Article history:
Received: 03 August, 2020
Accepted: 28 September, 2020
Online: 20 October, 2020

Keywords:
Flexible piezoelectric energy harvester
Low-frequency vibration energy
Interdigitated electrode circuit

ABSTRACT

Piezoelectric energy harvesters (PEH) can be used in many areas of application, including human walking, railways, pavements and bridges. Piezoelectric energy harvesters are currently based on two types of external forces, namely pressure load and mechanical oscillation or vibration. A vibration energy harvesting (VEH) is a mechanical oscillation in a piezoelectric energy harvester that harvested electric energy. In the market, there is available energy harvesting device in good electric energy harvesting and very sensitivity. However, the price is too high and the fabrication process is too complex. Furthermore, one of the aimed of the research is to install the energy harvesting device at rotary compressor machine which has noise vibration frequency at 1 kHz to 10 kHz. This paper presented a cavity structure-based flexible piezoelectric vibration energy harvester (FPVEH) based on an IDE circuit for low-frequency vibration applications. A cavity structure (IDE circuity) combine with the flexible circuit (polyimide) and flexible membrane (polyvinylidene fluoride, PVDF) will increase the electric energy harvesting and sensitivity of the device. Therefore, the four designs (Design A to D) are used to investigate the effect of the electrode finger width and the gap between the electrode fingers (to investigate the cavity structure applying in the design). All designs have been characterized by FEA simulation using COMSOL Multiphysics 5.0 and experimental work using a sieve shaker vibration machine. A sieve shaker machine is worked as vibration frequency calibrator. However, the sieve machine can operate at 5 kHz and 7 kHz. Since these two vibration frequencies are in targeted vibration frequency. It is used as vibration frequency calibrator in this experimental work. The results from the FEA simulation and experimental work show the Design D has the highest electric energy harvesting compare to other designs. It has electric energy harvesting at 27.3 V for 1 minutes period. Design D has a wide electrode finger width and the wide gap between electrodes compare to other designs. The vibration frequency was also given the impact to energy harvesting whereby the vibration frequency at 5 kHz has the highest electric energy harvesting compare to vibration frequency at 7 kHz.

1. Introduction

Previously, the research [1] has been looked up into a vibration effect towards PMUT design and then, it has been energised and stored in a capacitor. This paper is an extension of work originally presented in 9th International Conference on Control System, Computing and Engineering (ICCSCE2019) [1]. The paper will look into the flexible membrane (PVDF) and cavity design (the gap between electrodes) in PMUT for energy improvement.

Recently, numerous studies have been investigated the use of piezoelectric energy harvesters (PEH) in various fields of application, such as human walking [2], railways [3], pavements [4–6], and bridges [7]. Several applications have emerged based on frequency and vibration studies [8]-[10], while others have been

*Corresponding Author: Khairul Azman Ahmad, azman062@uitm.edu.my

based on load or pressure acting on an energy harvesting device [4] and [11].

Flexible piezoelectric energy harvesting (FPEH) systems use elastomer pillars based on a piezoelectric polymer, whereby the stored energy has been converted into electrical energy in the clamped boundary on the piezoelectric layer [12]. Double-sided tribological layers, including polydimethylsiloxane (PDMS) and PDMS/multiwall carbon nanotubes with flexible polyvinylidene fluoride (PVDF), have been used as a triboelectric mechanism to enhance the performance of electric harvesters at various frequencies [13]. A flexible piezoelectric energy harvester with a sandwich structure using PIN-PMN-PT/epoxy has also been designed for wearable applications. The sandwich structure and the interdigitated electrode (IDE) film increase the flexural modulus of the membrane, resulting in a high electrical output [11]. The flexible piezoelectric energy harvester has been further developed using lead-free (Na0.5Bi0.5) TiO3-BaTiO3 piezoelectric nanofibers, which exhibit a high peak voltage output with a high load resistance [14]. Polymer piezoelectric materials, in collaboration with a beating mechanism, have been shown to generate a large force during low-frequency vibration and thus generate large output [15]. In one study, a piezoelectric PZT film was clamped to one end of a fixed wall and a load was mounted onto its other end [3]. This is called a cantilever piezoelectric beam model, and it has since been used in many vibration-type piezoelectric energy harvesters [3], [9], [16], [17].

Many researchers are examining the relationship between vibration and a resonance frequency that is capable of increasing the output power [8]. A vibration energy harvester with multiple nonlinear techniques can broaden the bandwidth of energy harvesting systems; however, there is a need to tune the resonance frequency [18], [19]. This design uses a parallel-plate structure consisting of a suspended spring-plate, which is a very complicated design and extra work is needed to tune the frequency [18]. A resonant vibration energy harvester was developed based on the cantilever model that can achieve a high strain and thus maximize the output power [20]. Another study on broadening the bandwidth in piezoelectric energy harvesters used a bi-stable composite laminate. This bi-stable piezoelectric energy harvester has a high geometrical nonlinear response that can broaden the frequency bandwidth during vibration [21]. Besides, a bimorph piezoelectric vibration energy harvester with flexible piezoelectric material was designed to improve the output power while lowering the resonance frequency. The bimorph-type piezoelectric increases the deflection, and this increases the strain inside the piezoelectric material and thereby improves the output power [9].

This paper presents a flexible piezoelectric vibration energy harvester (FPVEH) for use in low-frequency vibration energy harvesting applications. The energy harvesting device that available in the market can produce low energy harvester. There is an available energy harvesting device that can produce high electric energy harvester and sensitive to vibration frequency in the market. However, the price is a too high and complicated fabrication. The aimed of this research is to design and characterize a cavity structure-based flexible piezoelectric energy harvesting for low-frequency vibration applications. Beside of that, this design is to improve the quality of electric energy harvester and sensitive to vibration frequency. The target vibration frequencies are in the range 1 kHz to 10 kHz because the device will be installed at the rotary compressor that has noise vibration frequency from 1 kHz to 10 kHz. However, the available vibration frequency calibrator that is sieve shaker machine only can support 5 kHz and 7 kHz frequency. Since these two frequencies are in the range of target vibration frequencies, this sieve shaker has been used as vibration frequency calibrator in the experiment.

The four designs of FPVEH involving different in the gap between electrodes and different in the width of electrode fingers have been simulated and tested and demonstrated a significant performance in the result. All of these will be explained in the next section. The contribution of this research is a cavity design which is the gap between electrode fingers and a flexible circuit that has significant performance in electric energy harvesting. The investigation of different electrode fingers gap will be shown the significant of cavity design in FPVEH. The next section presents the design and methodology for the piezoelectric vibration energy harvester, while the finite element analysis (FEA) simulation method and experimental method are also described. The FEA simulation results and experimental results are discussed in the results and discussion section, and the last section presents the conclusion.

2. Design and Method

The PMUT design and method are presented in this section. A cavity-based flexible piezoelectric energy harvesting has been elaborated in terms of structure and mechanical properties that related to energy harvesting. Furthermore, a procedure and method are presented in this section.

2.1. IDE Circuits Structure

Four different IDE circuits have been designed to examine the effect of the different gap between electrodes of FPVEH and the electrode finger width of the FPVEH that harvested the electrical energy. Hereby, the electrode finger width and electrode finger gap were the two parameters that were investigated in low-frequency vibration. The design parameters are shown in Table 1. The schematic diagram of the IDE circuit is shown in Figure 1 and is referred to as Design A.

Table 1: IDE circuit design parameters

Parameter	Design A(mm)	Design B(mm)	Design C(mm)	Design D(mm)
IDE width	0.5	0.5	1.0	1.0
IDE gap	0.5	1.0	0.5	1.0
IDE length	20.5	26.0	25.0	29.0

As presented for Design A in Figure 1, the electrode finger gap between the positive and negative electrodes was 0.5 mm, the electrode finger width was 0.5 mm, and the IDE circuit length was 20.5 mm.

Polyvinylidene fluoride (PVDF) was attached to the top of the IDE circuit. The IDE circuit was made of polyimide (PI) as a dielectric and flexible membrane, and copper (Cu) was used for the finger electrode of the IDE circuit. The 3M tape was attached

on top of PVDF and IDE circuit and then worked together as a new structure flexible membrane in harvesting electric potential difference of low-frequency vibration. The schematic diagram of the flexible piezoelectric vibration energy harvester (FPVEH) designed in this study is shown in Figure 2.

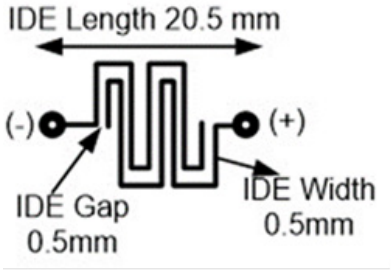
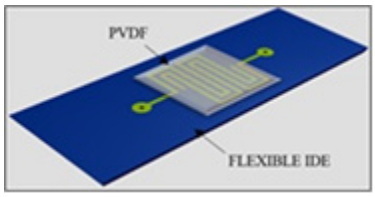
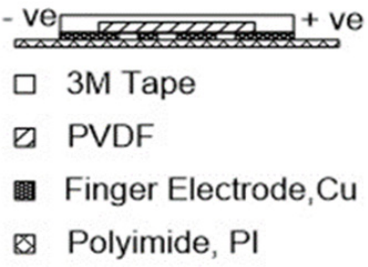


Figure 1: Schematic diagram of IDE circuit Design A.



(a)



(b)

Figure 2: Schematic diagram of the flexible piezoelectric vibration energy harvester; (a) top view and (b) side view.

The thicknesses of the 3M tape, PVDF, Cu and PI are shown in Table 2. The contribution in this design of FPVEH is a cavity added between PVDF and PI and clamped by electrode fingers at both ends left and right. It gives more flexure to the membrane and oscillates smoothly if there an external force acting on both top and bottom membrane. The four IDE circuit designs were created using Proteus 8 software; these are illustrated in Figure 3. The fabricated IDE circuit is depicted in Figure 4, whereby the yellow material is a coverlay made from PI and the shiny circuit is made from Cu. The completed fabrication of the FPVEH is shown in Figure 5.

Table 2: The thickness of material in flexible piezoelectric vibration energy harvester design.

Material name	Thickness (mm)
3M tape	0.88
PVDF	0.11
Finger electrode, Cu	0.035
Polyimide, PI	0.025

The readout circuitry for the energy harvester system is presented in Figure 6, and it is also called a full-bridge rectifier circuit, consisting of four diodes, a capacitor and a resistor. This full-bridge rectifier circuit converted the AC electric potential difference from the FPVEH into DC voltage and stored it in a capacitor. The value of the capacitor was 47 μF and it was used as a filter to reduce the ripple voltage while also acting temporary storage. The resistor had a value of 1 kΩ and was used as a load. A 1N4007 diode was considered suitable for use in low-power consumption because its peak-to-peak voltage was around 70 V.

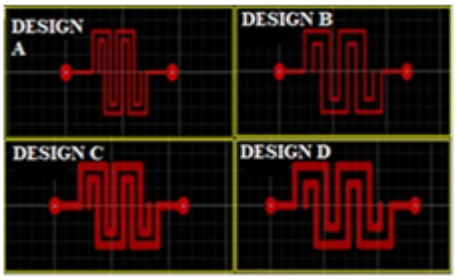


Figure 3: The four IDE circuit design in Proteus software.



Figure 4: A fabricated IDE circuit.

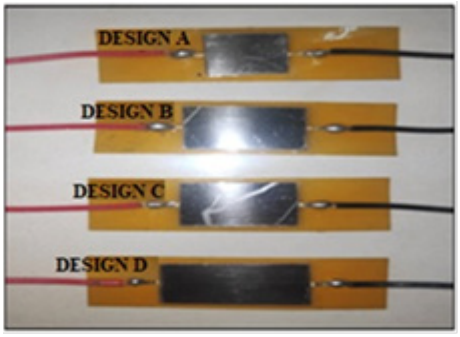


Figure 5: The completed fabrication of the FPVEH.

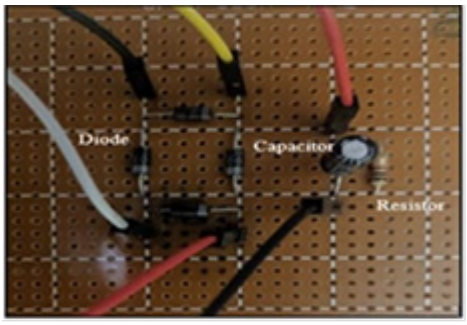


Figure 6: A full-bridge rectifier circuit.

2.2. Simulation Method

In the FEA simulation method, COMSOL Multiphysics 5.0 presented the direct piezoelectric effect on the piezoelectric material and elastic material. Firstly, defined the gravitational acceleration as amount 9.764 ms^{-2} in parameter definitions. A mass is represented of a pressure or a load per unit area with 0.5 MPa also has been defined in parameter definitions.

Then, set up the geometry in the geometry column. The flexible circuit consists of polyimide and copper, Cu is shown in Figure 7. Then, the geometric has been set up until the geometric structure shown in Figure 8. It consisted of 3M tape at the top layer followed by PVDF, copper and polyimide.

Then, set the material properties in the material properties column. The material properties of all materials are shown in table 3.

Table 3: Mechanical properties of all material

Material name	Mechanical properties		
	Young's modulus (GPa)	Poisson ratio (na)	Density (kg/m^3)
PVDF	8.3	0.18	1780
Copper, Cu	128	0.36	8920
Polyimide	7.5	0.35	1420
3M Tape	0.0045	0.499	980

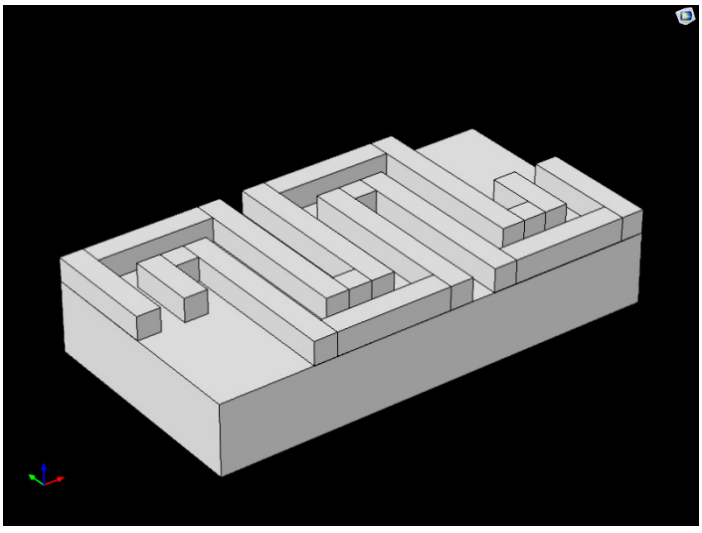


Figure 7:. Top view of set up flexible circuit in the geometric column in COMSOL Multiphysics

Next, select the suitable physics studies such as solid mechanics, electrostatics and Multiphysics. Selected the proper domain and put in physics studies column. For example, all materials are solid, then all domain belongs to solid mechanics. In solid mechanics, both ends at the left and right of the FPVEH are clamped. These clamped made the FPVEH oscillated freely when there was an external force acted on the surface of the membrane from the top or bottom. Then, select PVDF as an electrostatic domain. PVDF is a material that can convert mechanical property to electrical property and put the domain it into electrostatics study.

Then, select the suitable mesh, for instance, used size normal in the range 0.342 mm to 1.9 mm, used swept and the distribution, and select all domain put into distribution column. The mesh of geometry is shown in Figure 9.

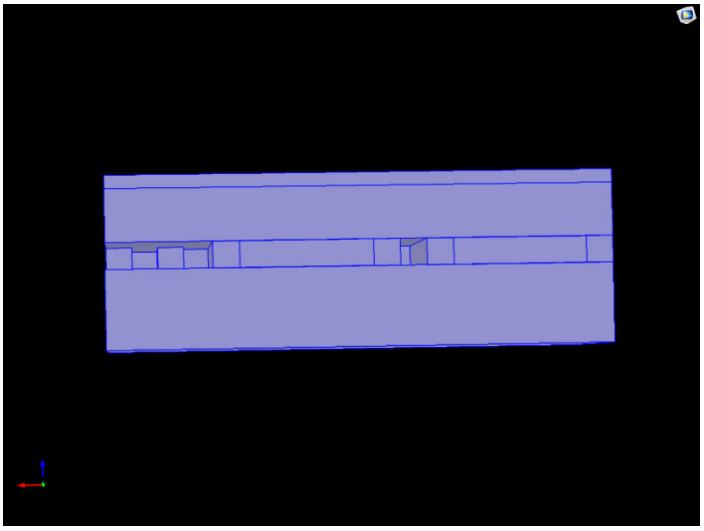


Figure 8: Side view of completed geometric setup in COMSOL Multiphysics

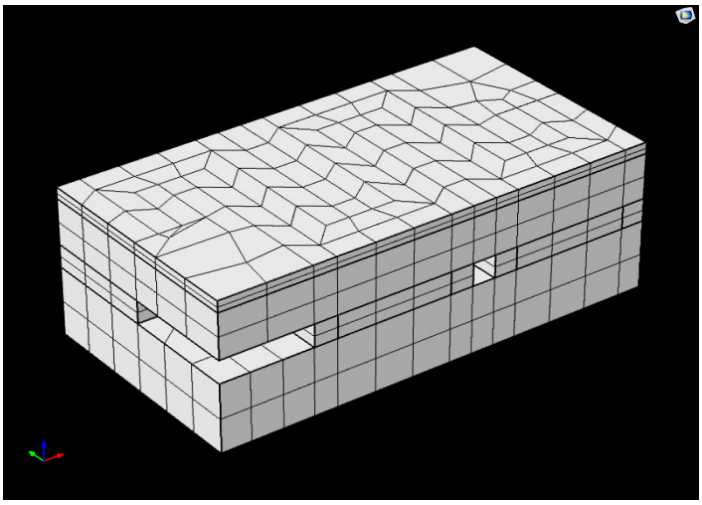


Figure 9: Mesh of geometry

Then, select the frequency domain as the study method. Furthermore, selected frequency range from 0 to 10 kHz with step 0.5 kHz as frequency input and put into the frequency domain. Lastly, in the result, the electric potential and electrical displacement were selected for plotted the graph. In electric potential result, the graph total voltage against frequency input has been plotted whereby in electrical displacement, the graph membrane displacement against frequency input has been plotted.

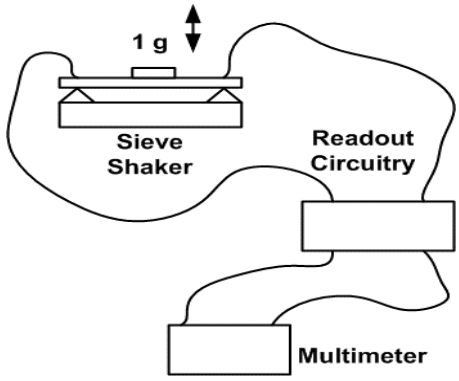
2.3. Experimental method

In this experimental, two parameters have been studied such as the effects of different electrode finger width of FPVEH and the effect of the different gap between electrodes of FPVEH during vibration. The electrical output voltage has been used as a benchmark of different studies to indicate the performance of the energy harvesting device. The four designs of FPVEH with different electrode finger and the different gap between electrodes have been tested using a sieve shaker to characterize their performances.

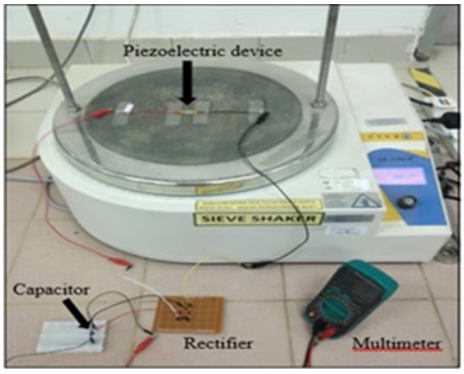
In experimental, a sieve shaker machine has been used to apply a vibration effect to the FPVEH. The FPVEH was placed on top of sieve shaker with both ends clamped using foam tape. Foam tape was worked as clamped at both ends as shown as a triangle in Figure 10 (a). The gravitational acceleration as amount 9.764 ms^{-2} has been set up to the sieve shaker machine with 0.5 MPa mass load. As one of the aimed of this research is to obtain electric harvesting energy from the rotary compressor within the range of frequency noise 1 to 10 kHz. In the laboratory, there is no calibrator machine can support 1 kHz to 10 kHz vibration. However, this sieve shaker machine can be operated at 5 kHz and 7 kHz only. Since the operation frequency, 5 kHz and 7 kHz are still in the range of rotary compressor frequency noise (1 kHz to 10 kHz), this sieve shaker machine has been used as a calibrator vibration machine.

The sieve shaker has a function to set time duration. The time duration can be used for investigating the energy stored in the period of time. The sieve shaker can support the period of 1 minute, 5 minutes, 10 minutes, 15 minutes and 20 minutes.

The output measurements comprised the electric field charge collected in the capacitor. Each of four designs (Design A to D) energy harvesting device was placed on top of the sieve shaker machine, and its electrodes were connected to the readout circuitry. The output of readout circuitry was measured by multimeter, and then it was observed and recorded the measurements. The experiment utilized the sieve shaker vibration machine to characterize the performance of four designs of different electrode finger width of FPVEH and different of the gap between electrodes of FPVEH that caused by vibration were shown in Figure 10.



(a)



(b)

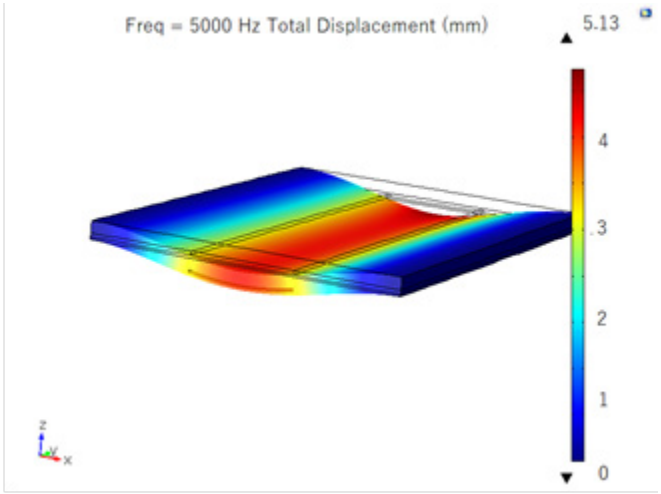
Figure 10: The experimental method to characterize the four designs with a different electrode finger width of FPVEH and the different gap between electrodes of FPVEH caused by vibration, (a) the schematic diagram, and (b) test field.

3. Results and Discussion

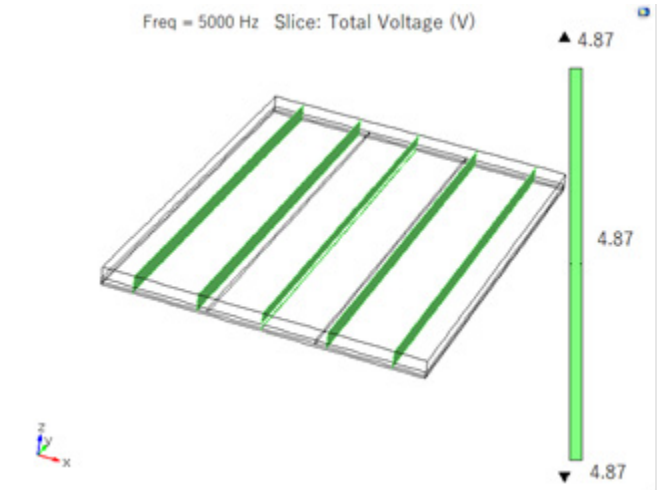
This section is divided into two parts that, respectively, present the simulation results and the experimental results. In the simulation results, two investigations were conducted to examine the effect of different IDE electrode finger widths and different IDE electrode gaps on the displacement of the membrane and the subsequently harvested an electric field accordingly to frequency input given. In the experimental result, the investigations were done on four designs with different electrode fingers width and different electrode gap (Design A to D) that have been affected on potential different, V by the energy harvesting device.

3.1. Simulation Results

FEA simulation is performed to characterize the total displacement of the membrane and the total electric potential difference harvested caused by the different of IDE electrode finger width and IDE electrode accordingly to the frequency input given. Figure 11 presents the simulation results for an IDE electrode finger width and gap of 1.0 mm and 1.0 mm, respectively for input frequency, 5000 Hz.



(a)



(b)

Figure 11: Simulation results for an IDE electrode finger width of 1.0 mm and an IDE electrode finger gap of 1.0 mm according to 5000 Hz; (a) displacement of the membrane (mm), (b) and total electric potential difference (V).

Figure 11(a) shows that the centre of the FPVEH membrane between the electrodes gap has been displaced by about 5.13 mm towards the negative z-axis at a frequency of 5000 Hz. The gap between the electrode fingers created a cavity between the PVDF and the polyimide. Therefore, the displacement of the flexure membrane increased when pressure was exerted on the surface of the FPVEH. Figure 11(b) shows that the FPVEH has a total electric potential difference of 4.87 volts for a frequency of 5000 Hz. Hence, Figure 11 was demonstrated the flexural membrane that has relation with total electric potential difference harvested by the FPVEH.

The simulation results for the four different electrode finger widths and gaps (Design A to D) are shown in Figure 12. The results show Design D with electrode finger width 1.0 mm and the gap between electrodes 1.0 mm has the highest electrical energy harvesting value compare to all design. Furthermore, Design D and Design C that has the same electrode finger width are the higher electric energy harvester compare to design B and Design A which are the smaller size of electrodes fingers width.

Next, Design D has higher electric energy harvesting compare to Design C whereby the Design D has a higher gap between electrodes compare to Design C. The Design A and Design B which are smaller in electrode fingers width and the gap between electrodes has lower electric energy harvesting. Subsequently, the vibration frequency has given the impact on harvested electric energy at low-frequency vibration applications whereby in the results shown the total voltage is highest at 5 kHz vibration frequency. It can show that the resonance frequency of Design D is at 5 kHz.

3.2. Experimental Results

In this section, the experiment results have been demonstrated. The investigation on the different electrode finger width of FPVEH and the different gap between electrodes of FPVEH were demonstrated. As explained in methodology, all four FPVEH designs (Design A to D) with different electrode finger and the different gap between electrodes were measured using a multimeter and sieve shaker as a vibrator calibrator. Table 4 is tabulated the experimental results of Design A, Design B, Design C and Design D for the different lengths of the periods.

The tabulated results are plotted in Figure 13. Figure 13 shows that the electric potential difference harvested by all four designs (Design A to D) increase relative to the increase in the length of time. Design D has an electrode finger width of 1.0 mm and a gap between the electrode fingers of 1.0 mm, and it has the highest electric potential difference value compared to the others. In addition to that, Design D and Design C with an electrode finger width of 1.0 mm have higher electric potential difference value compare to Design A and Design B that have lower an electrode finger width at 0.5 mm. Therefore, the wide electrode finger width has affected the electric potential difference value to increase.

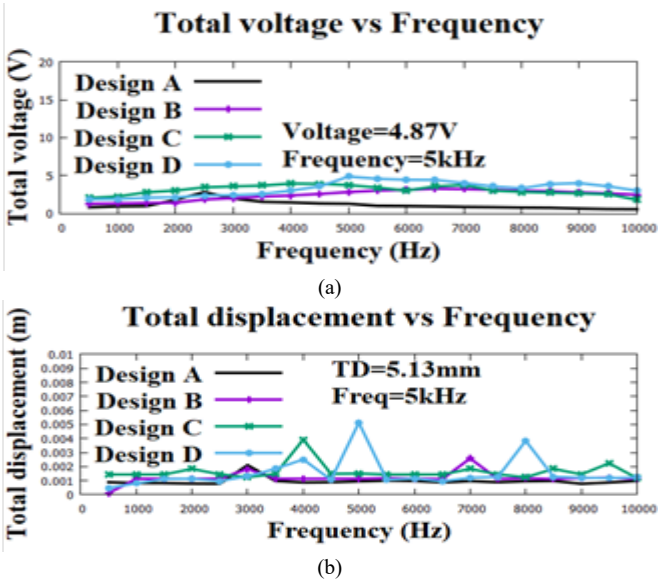


Figure 12: Simulation results for the four different electrode finger widths and gaps based on different frequency input; (a) total voltage (V) vs frequency (Hz), and (b) total displacement (mm) vs frequency (Hz).

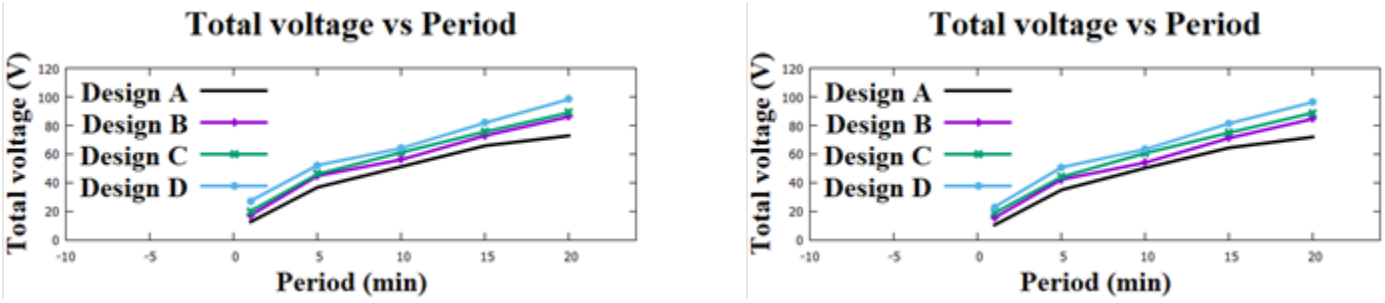
Furthermore, Design D has higher electric potential difference value compare to Design C which indicates the gap between electrode fingers also affected an increase of electric potential difference value. Therefore, the increase of the electrode fingers gap has higher electric potential difference value.

Next, it can be seen that the electric potential difference harvesting in Figure 13(a) has a higher value compared to the value in Figure 13(b). The electric potential difference harvested in the experiment using the sieve shaker machine at 5 kHz was higher than at 7 kHz. Hence, the frequency vibration will affect electric energy harvesting by FPVEH.

In Figure 13 (a), Design D with an electrode finger width of 1.0 mm and electrode finger gap of 1.0 mm has the highest electric potential difference harvesting at 98.4 volts. The frequency of the sieve shaker machine is 5 kHz.

Table 4: Tabulated data for Design A, Design B, Design C, and Design C

Period (min)	Total Voltage stored (V)							
	Design A		Design B		Design C		Design D	
	Amplitude 5 kHz	Amplitude 7 kHz	Amplitude 5 kHz	Amplitude 7 kHz	Amplitude 5 kHz	Amplitude 7 kHz	Amplitude 5 kHz	Amplitude 7 kHz
1	12.6	10.4	17.1	15.5	20.1	18.9	27.3	23.0
5	36.8	35.0	44.8	42.2	46.0	44.0	52.2	50.8
10	51.3	50.3	56.2	54.1	61.2	60.7	64.1	63.4
15	65.9	64.5	73.0	71.3	75.7	75.0	82.0	81.5
20	72.9	72.0	86.2	84.7	89.0	88.9	98.4	96.4



(a) (b)

Figure 13: Total electric potential difference by experimental vibration results for the different designs and different lengths of time; (a) 5 kHz vibration and (b) 7 kHz vibration.

Table 5 shows the summary of the previous study that designed the vibration piezoelectric energy harvesting and their performances. The highest voltage has been harvested by [21] at 12 V with a resonance frequency of 19.1 Hz. The design can energise high voltage however, it needs to tune their frequencies until it reached the high electrical potential differences. The previous design was used PCB as substrate and it was hard to bend, thus the flexible circuit has been used to replace PCB as a substrate that can bend together with PVDF substrate. Therefore, more electrical energy has been produced. In this work has shown the significant performance in increasing the electric energy harvesting.

Table 5: Summary of previous study and their achievement.

Author	Method	Achievement
[22]	Design PEH using clamped-clamped beam with proof mass.	Voltage: 4.5V at 1 g Resonance Frequency: 42.8 Hz Displacement of plate: 1.56 mm Stress: 8Mpa
[23]	Design multi-layer piezoelectric energy harvester (MPEH).	Voltage: 3.79V at 1 g Resonance frequency: 91 Hz
[24]	Design PEH based macro-fibre composite	Voltage: 2.8 V in 2.12 s Resonance frequency: 8 Hz
[25]	Design metamaterial beam with double-layer resonators.	Voltage: 0.48 V Resonance frequency: 348 Hz
[21]	Design PEH based cantilever tunable beam.	Voltage: 12 V at 0.7 g Resonance frequency: 120 rad/s = 19.1 Hz
[1]	Previous work, design interdigitated electrodes on the PCB board with PVDF membrane and 1.0 mm finger width.	Voltage = 322 mV at 1 ($9.764\ m^{-2}$) g and 1 minutes, Voltage = 0.005 V at 1 s. Frequency = 50 Hz
This work.	Design flexible piezoelectric based on PVDF and polyimide substrate.	Voltage = 27.3 V at 1 g ($9.764\ m^{-2}$) and 1 minutes, Voltage = 0.455 V at 1s. Frequency = 5 kHz.

4. Conclusion

This paper presented an investigation into the effect of electrode finger width as well as the gap between the electrode fingers and vibration frequency on the potential difference harvested by an FPVEH. The novel of FPVEH presented here was successfully designed and fabricated using IDEs, a flexible printed circuit, PVDF and 3M tape. The new structure flexible membrane and novel cavity design in FPVEH were successfully presented in this paper.

The experiment showed that the electrode finger gap had a greater effect on the electric potential difference harvesting by the FPVEH than the width between the electrode fingers. In this experiment with different setting frequencies at vibration machine was shown that the electric potential difference harvesting by all four designs using vibration machine at 5 kHz have higher than the electric potential difference harvesting by all four designs using vibration machine at 7 kHz. This indicates the vibration frequency has affected the electric potential difference has been harvested. Design D is the best design that harvesting the highest electric potential difference of 98.4 volts with a frequency input of 5 kHz. These concluded that the increases of electrode finger gap of FPVEH, and the wide of electrode finger width of FPVEH can increase the potential difference that harvesting by FPVEH. Moreover, the vibration frequency was also gave affected to energy harvesting when the results show that the vibration of 5 kHz has higher electric potential difference compare to vibration of 7 kHz that been harvested by FPVH.

Furthermore, a cavity that is a gap between electrodes has caused the increases of electrical energy harvesting by FPVEH. As a recommendation for future research, we propose the use of a power bank as a form of storage that can keep the electrical energy harvesting.

Conflict of Interest

The authors would like to declare that it is no conflict of interest in this paper publication.

Acknowledgement

The authors would like to acknowledge and express their highest appreciation to Research Management Unit (RMU), Universiti Teknologi MARA, Cawangan Pulau Pinang, Kampus Permatang Pauh for funding this fee of the paper. The authors also would like to express appreciation to Adavances Control System and Computing Research Group (ACSCRG), Universiti Teknologi MARA, Cawangan Pulau Pinang, Kampus Permatang Pauh for their contributions to this research.

References

[1] K.A. Ahmad, M.F. Abdullah, N. Abdullah, "Design and Characterization of an Interdigitated Electrode PVDF based Energy Harvesting Device," in 2019 9th IEEE International Conference on Control System, Computing and Engineering (ICCSCE), 172–177, 2019, doi:10.1109/ICCSCE47578.2019.9068549.

[2] A.C. Turkmen, C. Celik, "Energy harvesting with the piezoelectric material integrated shoe," Energy, **150**, 556–564, 2018, doi:10.1016/j.energy.2017.12.159.

[3] M.Y. Gao, P. Wang, Y. Cao, R. Chen, C. Liu, A rail-borne piezoelectric transducer for energy harvesting of railway vibration, Journal of Vibroengineering, **18**(7), 4647–4663, 2016, doi:10.21595/jve.2016.16938.

[4] C. Wang, S. Wang, Z. Gao, X. Wang, "Applicability evaluation of embedded piezoelectric energy harvester applied in pavement structures," Applied Energy, **251**, 113383, 2019, doi:10.1016/j.apenergy.2019.113383.

[5] X. Xu, D. Cao, H. Yang, M. He, "Application of piezoelectric transducer in energy harvesting in pavement," International Journal of Pavement Research and Technology, **11**(4), 388–395, 2018, doi:10.1016/j.ijprt.2017.09.011.

[6] X. Zhao, H. Xiang, Z. Shi, "Piezoelectric energy harvesting from vehicles induced bending deformation in pavements considering the arrangement of harvesters," Applied Mathematical Modelling, **77**, 327–340, 2020, doi:10.1016/j.apm.2019.07.048.

[7] G. Yesner, A. Jasim, H. Wang, B. Basily, A. Maher, A. Safari, "Energy harvesting and evaluation of a novel piezoelectric bridge transducer," Sensors and Actuators A: Physical, **285**, 348–354, 2019, doi:10.1016/j.sna.2018.11.013.

[8] L. Lamprecht, R. Ehrenpfordt, C.K. Lim, A. Zimmermann, "A 500 Hz-wide kinetic energy harvester: Outperforming macroscopic electrodynamic arrays with piezoelectric arrays," Mechanical Systems and Signal Processing, **119**, 222–243, 2019, doi:10.1016/j.ymssp.2018.09.025.

[9] T. Tsukamoto, Y. Umino, S. Shiomi, K. Yamada, T. Suzuki, "Bimorph piezoelectric vibration energy harvester with flexible 3D meshed-core structure for low frequency vibration," Science and Technology of Advanced Materials, **19**(1), 660–668, 2018, doi:10.1080/14686996.2018.1508985.

[10] X. Wang, H. Xiao, "Dimensionless Analysis and Optimization of Piezoelectric Vibration Energy Harvester," International Review of Mechanical Engineering (IREME), **7**(4), 607-624–624, 2013, doi:10.15866/ireme.v7i4.3812.

[11] Z. Zeng, L. Gai, A. Petitpas, Y. Li, H. Luo, D. Wang, X. Zhao, "A flexible, sandwich structure piezoelectric energy harvester using PIN-PMN-PT/epoxy 2-2 composite flake for wearable application," Sensors and Actuators A: Physical, **265**, 62–69, 2017, doi:10.1016/j.sna.2017.07.059.

[12] H.G. Çetin, B. Sümer, "A Flexible Piezoelectric Energy Harvesting System for Broadband and Low-frequency Vibrations," Procedia Engineering, **120**, 345–348, 2015, doi:10.1016/j.proeng.2015.08.631.

[13] Y. Zhu, B. Yang, J. Liu, X. Wang, X. Chen, C. Yang, "An Integrated Flexible Harvester Coupled Triboelectric and Piezoelectric Mechanisms Using PDMS/MWCNT and PVDF," Journal of Microelectromechanical Systems, **24**(3), 513–515, 2015, doi:10.1109/JMEMS.2015.2404037.

[14] B. Liu, B. Lu, X. Chen, X. Wu, S. Shi, L. Xu, Y. Liu, F. Wang, X. Zhao, W. Shi, "A high-performance flexible piezoelectric energy harvester based on lead-free (Na0.5Bi0.5)TiO3–BaTiO3 piezoelectric nanofibers," Journal of Materials Chemistry A, **5**(45), 23634–23640, 2017, doi:10.1039/C7TA07570G.

[15] H.-H. Huang, K.-S. Chen, "Design, analysis, and experimental studies of a novel PVDF-based piezoelectric energy harvester with beating mechanisms," Sensors and Actuators A: Physical, **238**, 317–328, 2016, doi:10.1016/j.sna.2015.11.036.

[16] Y. Kuang, M. Zhu, "Design study of a mechanically plucked piezoelectric energy harvester using validated finite element modelling," Sensors and Actuators A: Physical, **263**, 510–520, 2017, doi:10.1016/j.sna.2017.07.009.

[17] J. Fu, Y. Hou, M. Zheng, M. Zhu, "Flexible Piezoelectric Energy Harvester with Extremely High Power Generation Capability by Sandwich Structure Design Strategy," ACS Applied Materials & Interfaces, **12**(8), 9766–9774, 2020, doi:10.1021/acsami.9b21201.

[18] X. Wang, C. Chen, N. Wang, H. San, Y. Yu, E. Halvorsen, X. Chen, "A frequency and bandwidth tunable piezoelectric vibration energy harvester using multiple nonlinear techniques," Applied Energy, **190**, 368–375, 2017, doi:10.1016/j.apenergy.2016.12.168.

[19] M. Yuan, Z. Cao, J. Luo, J. Zhang, C. Chang, "An efficient low-frequency acoustic energy harvester," Sensors and Actuators A: Physical, **264**, 84–89, 2017, doi:10.1016/j.sna.2017.07.051.

[20] S. Du, Y. Jia, S.-T. Chen, C. Zhao, B. Sun, E. Arroyo, A.A. Seshia, "A new electrode design method in piezoelectric vibration energy harvesters to maximize output power," Sensors and Actuators A: Physical, **263**, 693–701, 2017, doi:10.1016/j.sna.2017.06.026.

[21] C. Lihua, X. Jiangtao, P. Shiqing, C. Liqi, "Study on cantilever piezoelectric energy harvester with tunable function," Smart Materials and Structures, **29**(7), 075001, 2020, doi:10.1088/1361-665X/ab859f.

[22] A. Damya, E. Abbaspour Sani, G. Rezazadeh, An innovative piezoelectric energy harvester using clamped–clamped beam with proof mass for WSN applications, Microsystem Technologies, 9, 2018, doi:10.1007/s00542-018-3890-6.

[23] Q. Lu, L. Liu, F. Scarpa, J. Leng, Y. Liu, "A novel composite multi-layer piezoelectric energy harvester," Composite Structures, **201**, 121–130, 2018, doi:10.1016/j.compstruct.2018.06.024.

[24] S. Balguvhar, S. Bhalla, "Evaluation of power extraction circuits on piezo-transducers operating under low-frequency vibration-induced strains in bridges," Strain, **55**(3), 2019, doi:10.1111/str.12303.

[25] J.S. Chen, W.J. Su, Y. Cheng, W.-C. Li, C.-Y. Lin, "A metamaterial structure capable of wave attenuation and concurrent energy harvesting," Journal of Intelligent Material Systems and Structures, **30**(20), 2973–2981, 2019, doi:10.1177/1045389X19880023.

Advances in Science, Technology and Engineering Systems Journal Vol. 5, No. 5, 1050-1055 (2020)

www.astesj.com

Special Issue on Multidisciplinary Innovation in Engineering Science & Technology

ASTESJ

ISSN: 2415-6698

VLSI Architecture for OMP to Reconstruct Compressive Sensing Image

Santosh Bujari[1,*], Saroja V Siddamal[2]

[1]Department of Electronics and Communication, SKSVMACET, Laxmeshwar, 5812116, India

[2]School of Electronics and Communication, KLE Technological University, Hubli, 580021, India

ARTICLE INFO

Article history:
Received: 03 August, 2020
Accepted: 28 September, 2020
Online: 20 October, 2020

Keywords:
Nyquist Criteria
Matching Pursuit
Sparsity
Threshold
FHT

ABSTRACT

A real-time embedded system requires plenty of measurements to fallow the Nyquist criteria. The hardware built for such a large number of measurements, is facing the challenges like storage and transmission rate. Practically it is very much complex to build such costly hardware. Compressive Sensing (CS) will be a future alternate technique for the Nyquist rate, specific to some applications where sparsity property plays a major role. Software implementation of Compressive Sensing takes more time to reconstruct a signal from CS measurements using the Matching Pursuit (MP) algorithm because of fetching, decoding, and execution policy. It is necessary to build hardware in CS. The author proposes one such VLSI Architecture (Hardware) for $256\ X\ 256$ *and* $512\ X\ 512$ *image. Various random matrices like Bernoulli, Partial Hadmard, Uniform Spherical, and Random Matrix are used to build hardware. FHT (Foreward Transform) with* $\pm 2\ to\ 6$ *threshold is applied to get CS measurements. The reconstruction time, Signal to Noise ratio (SNR), and Mean Square Error (MSE) are measured. Multiple time experiments are carried out and results show that for an image of size* $256\ x\ 256$*, SNR is* $25\ dB$ *and MSE is 166. For the image of size* $512\ x\ 512$*, the values are* $27dB$ *and 182. However, both the input images are resized to* $256\ X\ 256$ *so the reconstruction time is* $2.62\mu sec$ *which is less is compared to software implementation.*

1. Introduction

The digital sensing and processing based on the Nyquist criteria made a tremendous impact on real-time applications. The scale of data accumulated by digital conversion has increased from a few to exponential growth. In many emerging applications it will be very complex to store and transmit over the communication channel. Therefore, it is very much essential to find out an alternative for the Nyquist criteria which can reconstruct the signals with few numbers of samples than the Nyquist criteria. The Compressive Sensing theory (CS) [1-7], which is an asymmetric concept [8] with the simple decoder and dumb encoder, can reconstruct the sparse signals when the samples are acquired other than the Nyquist criteria.

$$Z = \Psi A \tag{1}$$

The signal acquisition in CS theory is the product of random measurement matrix (Ψ) and analog signal (A) leads to CS measurements (Z) [9, 10] defined by equation (1).

Z Ψ = I. N X N Identity matrix A

$$\text{N X 1}\begin{bmatrix} Z1 \\ Z2 \\ Z3 \\ Z4 \\ \vdots \\ \vdots \\ ZN \end{bmatrix} = \begin{bmatrix} 1 & 0 & 0 & 0 & \cdots & \cdots & 0 \\ 0 & 1 & 0 & 0 & \cdots & \cdots & 0 \\ 0 & 0 & 1 & 0 & \cdots & \cdots & 0 \\ 0 & 0 & 0 & 1 & \cdots & \cdots & 0 \\ \vdots & \vdots & \vdots & \vdots & \ddots & \cdots & \vdots \\ \vdots & \vdots & \vdots & \vdots & \vdots & \ddots & \vdots \\ 0 & 0 & 0 & 0 & \cdots & \cdots & 1 \end{bmatrix} * \begin{bmatrix} A1 \\ A2 \\ A3 \\ A4 \\ \vdots \\ \vdots \\ AN \end{bmatrix} \text{N X 1}$$

(2)

The Nyquist criterion as shown in equation (2), is extended to illustrate compressive theory, where A is an analog signal, Ψ is unity (identity) matrix of size N X N and Z is the Nyquist samples. In CS unity matrix is replaced with a random matrix such as Bernoulli Matrix [11], Uniform Spherical, Partial Hadmard, etc. Samples that are obtained by multiplying the analog signal with the random matrix are called CS measurements (Z) as shown in equation (3).

Z Ψ $m\ X\ N$ *matrix* A

*Corresponding Author: Santosh Bujari, santoshbujari@gmail.com

$$\begin{bmatrix} Z1 \\ Z2 \\ \vdots \\ Zm \end{bmatrix} = \begin{bmatrix} \Psi_{11} & \Psi_{12} & \Psi_{13} & \Psi_{14} & \cdots & \cdots & \Psi_{1N} \\ \Psi_{21} & \Psi_{22} & \Psi_{23} & \Psi_{24} & \cdots & \cdots & \Psi_{2N} \\ \vdots & \vdots & \vdots & \vdots & \vdots & \vdots & \vdots \\ \Psi_{m1} & \Psi_{m2} & \Psi_{m3} & \Psi_{m4} & \cdots & \cdots & \Psi_{mN} \end{bmatrix} \begin{bmatrix} A1 \\ A2 \\ A3 \\ A4 \\ \vdots \\ \vdots \\ AN \end{bmatrix} \quad (3)$$

These CS measurements are related to only sparse (big amplitude) signal, that's why m is less than N. Random matrix is modified as shown in equation (4) by including only those columns related to sparsity. Remaining signals (N − K) are not processed which may be located anywhere in the signal. Therefore, CS is an asymmetric theory.

$$Z \qquad \Psi \quad m\,X\,K \;\; matrix \qquad A$$

$$\begin{bmatrix} Z1 \\ Z2 \\ \vdots \\ Zm \end{bmatrix} = \begin{bmatrix} \Psi_{11} & \Psi_{12} & \Psi_{13} & \Psi_{14} & \cdots & \cdots & \Psi_{1K} \\ \Psi_{21} & \Psi_{22} & \Psi_{23} & \Psi_{24} & \cdots & \cdots & \Psi_{2K} \\ \vdots & \vdots & \vdots & \vdots & \vdots & \vdots & \vdots \\ \Psi_{m1} & \Psi_{m2} & \Psi_{m3} & \Psi_{m4} & \cdots & \cdots & \Psi_{mK} \end{bmatrix} \begin{bmatrix} A1 \\ A2 \\ \vdots \\ AK \end{bmatrix} \quad (4)$$

Various Matching Pursuit algorithms [12] are used to solve the linear equation (4). Orthogonal Matching Pursuit (OMP) is compatible for sparse recovery [13-15]. This OMP will search the sparse related columns iteratively which appears in the random matrix. These are the best approximate-correlated columns that correspond to the sparse signal. One best-correlated column is searched in the iterations and removed from the random matrix. Like this finally updated matrix (C) of dimension K x K is obtained. The sparse reconstructed signal is obtained by solving the Least Square Problem (LSP). The complete OMP procedure is bellowed:

1. **Declaration:** Declare residual Resi = Y, matrices $Q = zeros\,(m,K)$, $R = zeros\,(K,K)$, $R_{inv} = zeros\,(K,K)$ and the index set $C = zeros(m,k)$. Initialize iteration i to 1.
2. **Search Index:** Search the most correlated index by solving the optimization problems and generate Q and R matrices.

$$\mathrm{KK_i} = \arg\max_{j=1..N} \left| < \mathrm{Resi_{i-1}}, \Psi_j \right|$$

$$\Psi_j = Q_j R_j$$

3. **Residual Status Update:** Revise the index set c and estimate the residual.

$$C_i = \mathrm{C_{i-1}} \cup \{\mathrm{KK_i}\}$$

$$\mathrm{R_{inv}} = [\mathrm{R_{inv}}\ \Psi_{\mathrm{c_i}}]$$

$$Resi_i = Resi_{\mathrm{i-1}} - (Q_{\mathrm{i-1}} * \mathrm{Q_{i-1}}')Resi_{\mathrm{i-1}}$$

4. **Iterations:** $\boldsymbol{i = i + 1}$ and go back to search index step suppose $i < K$.
5. **LSP: Least Square problem,** Find the inverse corresponding $\boldsymbol{c}$ to get reconstructed sparse signal

$$A_R = (\mathrm{R_{inv_j}} * \mathrm{Q_j}' * \mathrm{Z_j})_{\mathrm{j=1.....K}}$$

Further write up of the paper is as follows. 2 briefs design methodology. In 3 VLSI architecture is proposed. The results of the work are shown in 4. Finally, work is concluded with future work in 5.

2. Design Methodology

2.1. OMP (Reconstruction Algorithm) Blocks

OMP is a sequential algorithm (as shown in Figure1) where the Optimization block is formed by combining the Search Index and Residual update. CS measurements (Z) which are in HEX format (256 X 256), Random Matrix (Ψ) of dimensions 128 x 256 and sparsity count (K = 64) are applied as inputs. Correlated columns (Ψ = 64 X 64) related sparse signals are identified. From these correlated columns, reconstructed signal ($\mathrm{C_K}$) is calculated by taking the inverse of the matrix as shown in equation (5) and (6) in LSP.

$$\mathbf{Z_K = C_K \Psi_K} \quad (5)$$

$$\mathbf{C_K = \Psi_K^{-1} Z_K} \quad (6)$$

$$\mathbf{A_R = IFHT\,(C_K)} \quad (7)$$

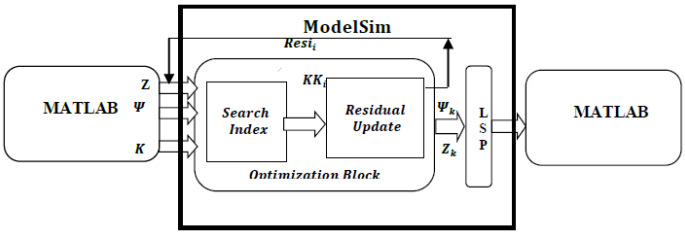


Figure 1: OMP Blocks

2.2. Input for OMP Architecture

MATLAB tool is used to generate input for OMP Architecture. The unsigned gray image of any dimensions is resized into to 256 X 256. Double Precision format for processing purposes and integer format for display purpose is followed. Since the image does not exhibit sparsity property in the normal domain so it is converted into FHT (Foreward Hadmard Domain). Less magnitude coefficient values are treated as zero by selecting a proper threshold value. This is asymmetric contrast to the Nyquist criteria. These zero value signals may be located anywhere in the image. These are converted to in HEX number and stored as a text file which is used as input for OMP VLSI Architecture. The complete procedure of creating a text file is shown in Figure2.

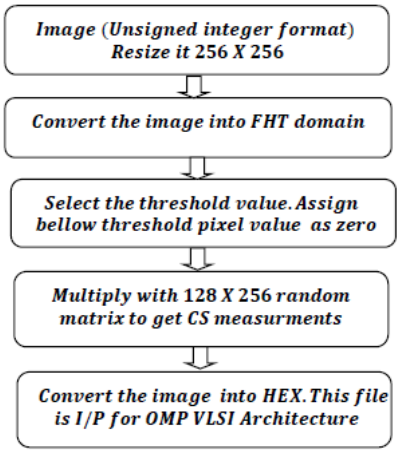


Figure 2: Text File Creation Flow

3. Proposed VLSI Architecture

The text file which is obtained from the previous step and the random matrix are stored in different RAM in the proposed OMP architecture as shown in Figure3. The tree structure (Wallace tree) as shown in Figure4 is used to obtain the inner product vector. The CS measurements in the form of 3 x 3 dimensions are applied to the Wallace tree along with random variables.

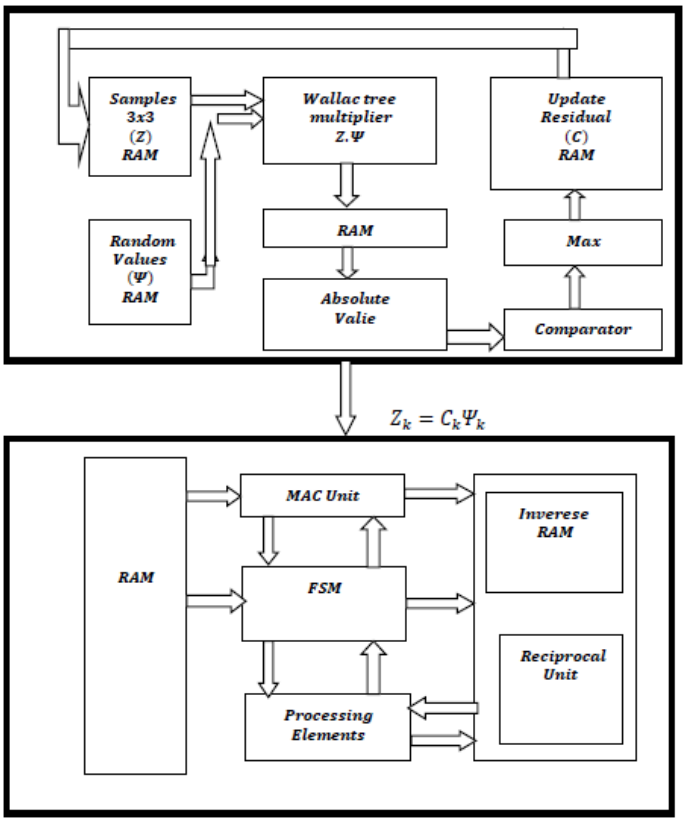


Figure 3: Proposed OMP Architecture

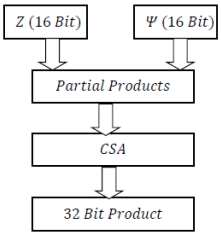


Figure 4: Multiplier (Wallace Tree)

In this proposed architecture, a carry-save adder (CSA) as shown in Figure5 is used to perform the fast addition of partial products. At the beginning of the calculations, the accumulator register is reset to zero. Then, the first partial product, P, is selected by the multiplexer and applied to the 16-bit adder. The other input of the adder comes from the 16-bit register. Hence, at this stage, the output of the 16-bit adder will be Acc=P + 0=P. With the upcoming clock tick, this will be stored in the accumulator register. Next, the second partial product, Q, will be chosen by the multiplexer. This will be added to the current value of the 16-bit register which gives Acc = P + Q. This procedure will be repeated for the remaining partial products. With each clock tick, a new partial product will be added and the result will be stored in the 16-bit register. The control unit is used to generate an appropriate signal for the select input of the multiplexer. Speed up of the 16-bit adder is achieved by implanting a carry-lookahead structure for a 16-bit adder.

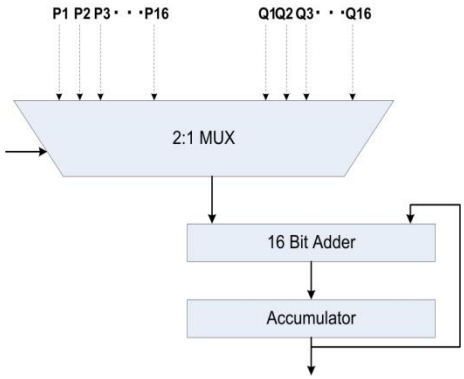


Figure 5: Carry save Adder

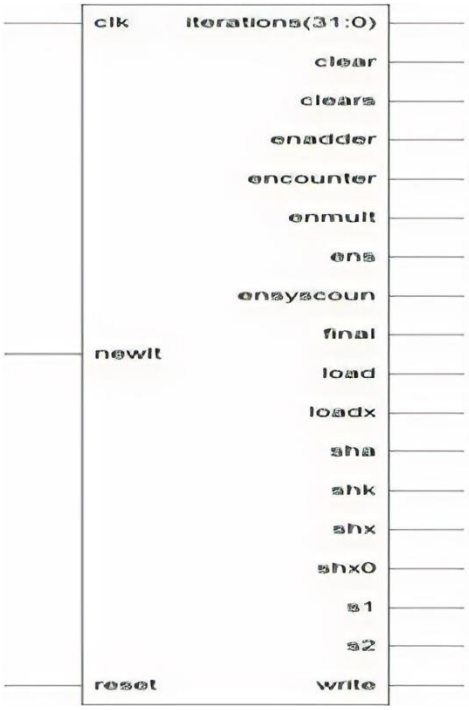


Figure 6: Control Path Block

In a single clock cycle, it cannot be completed since the carry bit has to propagate. CSA is required in different stages of the OMP algorithm. This adder architecture is critical as it is used for many numbers of operations. The complexity of the adder depends on the operation like subtraction, multiplication, and division. In general carry-save adders connected in a tree-like structure can reduce the number of operations from m to $m-1$ compare to parallel adders. This in turn contributes to reconstruction time. Within the tree structure, an adder is designed using $2:1$ multiplexers which can reduce the delay of higher multiplexers and it address reconstruction time. Once the product vector is obtained from the tree structure, the maximum value, and its corresponding column numbers are calculated using a comparator, and values are

stored in RAM represented as update residual in architecture. Later these values are removed from text files and like this for every 3x3 sample process repeats iteratively. This process repeats until K(Sparsity Count) values are searched. Finally, $Z_k = C_k \Psi_k$ values are obtained from the optimization block and later applied to the LSP block. As the matrix size increases, the number of computations like multiplication, addition/subtraction, and division is increasing. That's why the image is divided into a 3x3 matrix. All submatrix are processed iteratively which contributes towards reconstruction time. From the Optimization block, all the sparse signal information is obtained and it is stored in RAM of LSP architecture. The arithmetic right shifts are used in LSP to perform division and reciprocal operations. Shifting one bit right is dividing by 2 in binary. Compared to a division operator, a shift operator will execute in less number of cycles in all most all processor. This contributes to the reduction of reconstruction time. Moreover, it can be reused for shift operations wherever it is necessary. The entire LSP operation is controlled by the control path block as shown in Figure6, which is implemented in the form of a state diagram as shown in Figure7.

Depending upon the state diagram and data the control signals are generated, and the data out (reconstruction signal) will be calculated. Finally, these reconstructed signals are stored in the output text file.

3.1. State diagram

- Reset S_0: At the beginning, LSP architecture is initialized by storing all the signals (Z_k) obtained from the Optimization block. This state is considered a reset state. If control signal reset $= 0$, LSP remains in the same state otherwise new state will be initialized.
- New System S_1: Since LSP iterative in nature, the iteration counter is initialized to zero based on a clear signal in this state.
- New Iteration S_2: Values (Z_K, Ψ_k) is loaded in this state based on Load and loadx signal. When clears signal is in high, loaded values will be sent to the calculation state.
- Calcs S_3: Architecture in this state will start calculation (division) using processing elements and shift operator if sha and Shax signal is high. At the same time counter is incremented. It will be in the same state if the number of calculations is not equal to the number of elements considered. When the calculations become equal to number with counter then it will go to the next state called wait state.
- Wait S_4: Results of division obtained from the previous state are collected in this state.
- Calculation Reciprocal state S_5: (CalcR) In this state reciprocals are calculated iteratively on the outcomes obtained from the previous state. Encounter signals trigger the counter to keep track of the number of iterations. When the counter becomes equal to the number of iterations, state transition will occur based on shx.
- Calcx S_6: When the number of calculations is not equal to the number of reciprocal elements then S1 and S2 signals will be high which keeps reciprocal calculation in progress. If the number of calculations (iterations) is equal to K and then state changes to countsys state. If iteration is not equal to K then state transition switches to S_2 and the process repeats until all K blocks are completed.

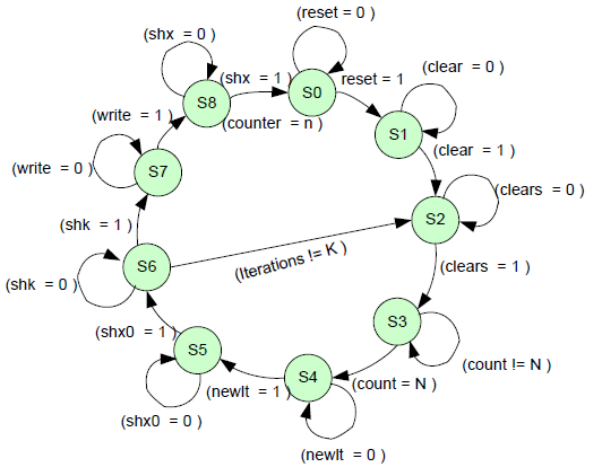


Figure 7: LSP State Diagram

- Countsys S_7: Once all K blocks are processed, memory is initialized in this state to store the results. State transition occurs when Write becomes high.
- Savex S_8: In this state, results are updated on the output text file.

All the control signals generated by the state diagram will be reflected in the LSP data path which is as shown in Figure 8.

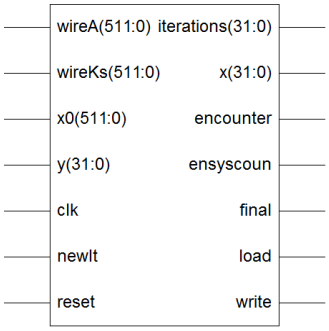


Figure 8: LSP Data Path

4. Results

On Intel Core with 1.2GH$_z$ processor and 3GB memory, several time experiments are carried out. Obtained results are tabulated to analyze the performance of our proposed architecture. Bellow steps are followed to get the results.

- Select any Image of dimensions more than or equal to 256 X 256.
- Create a text file in HEX.
- Use text file in Test-bench and reconstruct signal which will be stored in the output text file.
- Read the output text file and display it after processing

Steps 1, 2, and 4 are carried out in MATLAB 2014A. For the third step, the ModelSim PE Student Edition is used. Standard Lena image of dimension 256 x 256 and 512 X 512 with different image formats are used as input to the proposed architecture. Several times process is repeated and only the average value of selected parameters [16] is analyzed.

- MSE: Difference between original and reconstructed signal which is estimated using MSE defined by equation (8).

$$\text{MSE} = \sum_n \frac{(\text{A}-\text{Arec})^2}{\text{n}} \quad (8)$$

- Reconstruction time: Time taken by OMP VLSI architecture to generate output file which is measured in second.
- SNR: The amount of noise present in the signal reconstructed using OMP VLSI architecture which is defined by equation (9).

$$\text{SNR} = 10\log_{10}\left(\frac{\sum_n \text{A}^n}{\sum_n(\text{A}-\text{Arec})^2}\right) \quad (9)$$

4.1. Analysis of Image Reconstruction Quality

- Standard Lena Image ($\text{N} = 256$ and 512).
- Measurement Matrix: $(128 \text{ X } 256)$
- Number of CS measurements = 128X 1.
- FHT transform coder.
- Threshold value ($\pm T_r$)= 3



Figure 9: Reconstructed 256 *X* 256 and 512 *X* 512 Image

Figure 9 is the reconstructed image using OMP VLSI Architecture indicates that the quality of the image degraded which will be one of the future challenges of OMP VLSI architecture. Simulation results of this work compared with MATLAB implementation [17] and Virtex 5 implantations [18, 19] as shown in Table I. Compared with other simulation work, the proposed design takes less reconstruction time. The reduction in reconstruction time is mainly due to less processing elements as input 3x 3 is fed into the system iteratively. To process 256x256 at a time require more hardware and more time to reconstruct

Table 1: Comparison of Proposed Design with Other Similar Work

Platform	**[17]**		**[18]**	**[19]**	**Proposed**
Tools Used	***MATLAB***		***Xilinx***		***Xilinx***
Target Device	***NA***		***Virtex − 5***		***Virtex − 4***
Signal Size (N)	256	512	256	256	256
Measurements (m)	128	128	64	64	128
Sparsity Count (K)	64	64	8	8	64
Reconstruction Time	***9sec***	***15sec***	***17μS***	***22μS***	***2.62μS***
MSE	550	580	-	-	166.60
SNR (dB)	23	26	-	-	25.91

4.2. Varying T_r with FHT Domain

Normally large amplitude signals hold most of the important information about the input. Even by neglecting lesser value amplitude signals, information can be extracted. To remove small amplitude signal threshold value from ± 2 to $\pm 6$is used in the FHT domain. To minimize the number of measurements larger threshold value should be selected. However, it affects the quality of the reconstructed signal. Therefore trade-off between the quality of the reconstructed signal and reconstruction time will be the parameter for selecting proper threshold value. Experiment analysis shows that for $\text{N} = 256$ or 512, the FHT threshold value should not be more than ± 7. SNR for different threshold is almost the same as shown in table 2.

Table 2: Threshold and SNR Analysis

Image Size	**Threshold ($\pm T_r$)**	**SNR (dB)**
256 X256	**2**	**25**
	4	**25**
	6	**25**

4.3. Device Utilities

Table 3 shows the device utilization report using the Xilinx ISE 8.1i version tool. Verilog code implemented on target device namely xc4vlx15-12sf363 (Vertex 4 FPGA). However, our work [1] and [17] are continued in this paper and the main objective of reduction of reconstruction time is achieved. The analysis and optimization of area, power consumption, and other VLSI parameters are considered as future work for this paper.

Table 3: Device Utilization Summary

Logic Utilization	**Used**	**Availability**	**Utilization**
Slices	2116	6144	34%
Slice F/F	2257	12288	18%
4 Input LUTs	3523	12288	28%
Bonded IOBs	212	240	88%
GCLKs	1	32	3%

5. Conclusion and Future Work

This paper presents semi-VLSI architecture which contributes to developing hardware, especially for the Compressive Sensing image. The implemented architecture has equal reconstruction for both 256x256 and 512x512 image i.e 2.62μS since it is resized to256x256. This is far better than software implementation and some hardware implementation. For FHT (Foreward Transform) ± 2 to 6 (less than 7) is to be used as a threshold for proper reconstruction. 25db and 27dB are the SNR for an image of size 256 x 256 and 512x512 respectively. Mean Square Error (MSE) is 166 which is less as observed in software. Finally, our work concludes that one of the objectives (reconstruction time) is achieved. Analysis and optimization of some objectives like area, power consumption, and other VLSI parameters are considered as future work of this paper

Conflict of Interest

The authors declare no conflict of interest.

References

[1] S. Santosh, V. Siddamal, "A Survey and Theoretical View on Compressive Sensing and Reconstruction", I.J.Image, Graphics and Signal Processing, 2016, DOI: 10.5815/ijigsp.2016.04.01 MECS Journal

[2] D. L. Donoho, "Compressed sensing," in IEEE Transactions on Information Theory, **52**(4), 1289-1306, April 2006. DOI: 10.1109/MSP.2007.914728

[3] E. J. Candes and M. B. Wakin, "An Introduction To Compressive Sampling," in IEEE Signal Processing Magazine, **25**(2), 21-30, March 2008. DOI: 10.1109/MSP.2007.914731

[4] Shreyas Joshi, Saroja V. Siddamal "Performance Analysis of Compressive Sensing Reconstruction" IEEE sponsored 2nd International Conference on Electronics and Communication Systems (ICECS 2015), pp-724-729, 26th to 27th February KNU Coimbatore 2015, 978-1-4788-7225-8/15/$31.00 ©2015 IEEE.

[5] J. Romberg, "Imaging via Compressive Sampling," in IEEE Signal Processing Magazine, **25**(2), 14-20, March 2008. DOI: 10.1109/MSP.2007.914729

[6] K. V. Siddamal, Shobha P Bhat, Saroja V. S "A survey on compressive sensing" IEEE sponsored 2nd International Conference on Electronics and Communication Systems (ICECS 2015), 639-643, 26th to 27th February KNU Combaiture 2015, 978-1-4788-7225-8/15/$31.00 ©2015 IEEE.

[7] R. Baraniuk, M. Davenport, R. DeVore, and M. Wakin. "A simple proof of the restricted isometric property for random matrices". Const. Approx., **28**(3):2538211; 263, 2008.

[8] M. Davenport, J. Laska, P. Boufouons, and R. Baraniuk. "A simple proof that random matrices are democratic". Technical report TREE 0906, Rice Univ., ECE Dept., Nov. 2009.

[9] M. Davenport, P. Boufounos, M. Wakin, and R. Baraniuk. "Signal processing with compressive measurements". IEEE J. Select. Top. Signal Processing, **4**(2):4458211; 460, 2010.

[10] M. Davenport, J. Laska, P. Boufouons, and R. Baraniuk. "A simple proof that random matrices are democratic". Technical report TREE 0906, Rice Univ., ECE Dept., Nov. 2009.

[11] U. Dias and M. E. Rane, "Comparative analysis of sensing matrices for compressed sensed thermal images," 2013 International Mutli-Conference on Automation, Computing, Communication, Control and Compressed Sensing (iMac4s), Kottayam, 2013, 265-270.

[12] Meenakshi and Sumit Budhiraja, "A survey of Compressive Sensing Based Greedy Pursuit Reconstruction Algorithms", IJIGSP, **7**(10), 1-10, Pub. Date: 2015-9-8

[13] J. A. Tropp and A. C. Gilbert, "Signal Recovery From Random Measurements Via Orthogonal Matching Pursuit," in IEEE Transactions on Information Theory, **53**(12), 4655-4666, Dec. 2007.

[14] Lin Bai, Patrick Maechler, Michel and Hubert Kaeslin, "High Speed Compressed Sensing Reconstruction on FPGA using OMP and AMP", IEEE 2012.

[15] Pierre B, Hasan R and Abbes A, "High Level Prototyping and FPGA Implementation of The OMP Algorithm", in Information Sciences, Signal Processing and their Application Conference, 11th IEEE International Symposium on, 2012.

[16] A. Ahmed et al., "Modeling and Simulation of Office Desk Illumination Using ZEMAX," in 2019 International Conference on Electrical, Communication, and Computer Engineering (ICECCE), 1–6, 2019. DOI: 10.1109/ICECCE47252.2019.8940756

[17] S. S. Bujari and S. V. Siddamal, "Image Reconstruction Using Compressive Sensing Technique for Hardware Implementation," 2018 International Conference on Electrical, Electronics, Communication, Computer, and Optimization Techniques (ICEECCOT), Msyuru, India, 1042-1046, 2018. doi: 10.1109/ICEECCOT43722.2018.9001308.

[18] J. L. V. M. Stanislaus and T. Mohsenin, "Low-complexity FPGA implementation of compressive sensing reconstruction," in Proc. Int. Conf. Comput. Netw. Commun. (ICNC), 671–675, 2013.

[19] J. L. V. M. Stanislaus and T. Mohsenin, "High performance compressive sensing reconstruction hardware with QRD process," in Proc. IEEE Int. Symp. Circuits Syst. (ISCAS), May, 29–32, 2012.

ASTES

Advances in Science, Technology and Engineering Systems Journal Vol. 5, No. 5, 1056-1063 (2020)

www.astesj.com

Special Issue on Multidisciplinary Innovation in Engineering Science & Technology

ASTESJ

ISSN: 2415-6698

Essential Features/Issues of a Multi-Phase Switching Synchronous Buck Regulator

Hani Ahmad-Assi*, Nour Sultan Gammoh, Mariana Awni Al Bader

Electrical Engineering Department, King Abdullah II School of Engineering, Princess Sumaya University for Technology, Amman, 11941, Jordan

ARTICLE INFO

Article history:
Received: 30 August, 2020
Accepted: 28 September, 2020
Online: 20 October, 2020

Keywords:
Multi-phase buck converter
Phase shedding
Fast-transient
Current sensing

ABSTRACT

This paper addresses essential features/issues and proposes solutions that would improve the overall performance of a multi-phase buck converter. Low efficiency at light load is addressed with phase shedding, load fast transient and regulated output voltage spiking/dipping is addressed with novel helper technique at the point of load (output node). An Integrated current sensing is utilized to implement over-current-protection (OCP), in addition to its inherent function in current mode control. The phase shedding developed technique was used to enhance the efficiency of the converter. The number of phases rather increases or decreases, depending on the desired load. The proposed fast transient helper circuit is tested by inserting a 500mA transient current step in 100µs. Worst case spike of a 79.1mV was achieved at the output node; which is a reduction of 49.4% of the original response (160mV without the helper circuit). Worst case of a 35mV of output voltage dip was achieved; which is a reduced by 45.4% compared to the original response (77.1mV without the helper circuit). An integrated current sensing technique using current mirroring to equalize the drain voltages of main and replica (sense) PMOS devices was utilized. With this technique, the current in the replica (sense) PMOS device is a scaled down version of the current in the main PMOS device. The sensed currents from all three phases are added up and converted to a voltage. This voltage is compared to a reference voltage that represents the limit for over-current. This reference voltage is set to be 20% higher than the average total currents in the three phases combined.

1. Background

This paper is an extension of work originally presented in Power Electronics and Drive Systems (2019 IEEE 13th International Conference on PEDS). Unlike single phase converters, multiphase buck converters are considered one of the state-of-art regulator topologies that provide high current capability (example, some CPUs requires 10A-15A or even more at their peak performances). Compared to a single-phase converter, multi-phase converters were proven to have many benefits, such as higher efficiency, lower component sizes, and reduced output current and voltage ripple [1].

Different features and techniques are addressed in this paper to study the behaviour of the multiphase buck converter. In [2], phase shedding (PS) is defined as a technique used to improve the converter efficiency by disconnecting some phases at light load. When the load decreases, there is no need for using all the phases in the circuit, however, it is possible to reduce the number of phases as the output current is being distributed between those reduced phases. In [3], fast transient is presented as a technique that will guarantee a low transient spike/dip and preserve a stable supply voltage. The two main objectives for using the fast transient are having the shortest recovery time and having the smallest output voltage spike/dip. In [4], integrated current sensing was presented as a technique to implement over-current protection (OCP), and current-mode feedback control. Many different schemes have been executed to utilize the inductor current sensing techniques. Most of these current sensing schemes have limiting constraints such as high-power dissipation, difficult implementation and control, and process-dependence..

2. Features/Issues

In [1], the single-phase buck converter was used as a first step to develop a functional multi-phase buck converter. In this paper, it was also used to test the features added to the final multi-phase design (consists of power and control stages). The buck converter

*Hani Ahmad, Princess Sumaya University for Technology, Al-Jubaiha, Amman, Jordan;ZIP code 11941; PO BOX 1438, 00962795930140, h.ahmad@psut.edu.jo

(the power stage) was designed by sweeping the width of both NMOS and PMOS transistors so that it would handle the current passing through them. The width of the NMOS was chosen to be 23m and the width of the PMOS which is usually 2-3 times larger than the width of the NMOS, was chosen to be 53.2m. These sizes were selected based on RdSon which is designed to be within the typical industrial standard range of (50-100) mΩ.

This paper discusses three features/issues that will be added to the power stage of the design, starting from single phase to the three-phase final design. This is done to observe the impact of the features on each phase. The three features/issues are Phase Shedding, Fast Transient, and Integrated current sensing which will be discussed in the sub-sections A, B, and C.

The schematic design and simulation results of the proposed circuits were done in LTspice using 180nm standard CMOS technology [5].

2.1. Phase Shedding

Phase Shedding technique is defined as the disconnection of phases in multi-phase buck converters when using different loads. This technique is a requirement to achieve the highest efficiency possible. To implement this feature, an NMOS transistor is utilized to realize an ON/OFF switch function as shown in

Figure 1. This NMOS is added to the single-phase buck converter and placed at the output node as shown in Figure 2. An NMOS was chosen due to its smaller size and faster response when it is compared to a PMOS device. To make an NMOS transistor turns on, a voltage source (Vsource) is connected to its gate and to make it turns off, its gate is grounded.

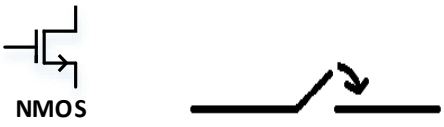


Figure 1: NMOS is used to implement an ON/OFF switch

Vsawtooth in the control stage is adjusted depending on the number of phases in the circuit. In multiphase converter, phase difference is applied to specify the angle that will be used depending on the number of phases in the circuit. Equation 1 was used to define the angle for each implementation. For single phase, the angle is at 0°. For two-phases, the angles are at 0° and 180°. For three-phases, the angles are at 0°, 120°, and 240°. As the number of phases increases, the ripple at the output is reduced.

$$360°/n \text{ ; where n is the number of phases} \qquad 1$$

Single-phase buck converter is utilized to test this phase shedding technique as shown in Figure 2. In this case, Vsawtooth was considered to be at 0°. The parameters used in the single-phase design are listed in Table *1*: Parameters for the single-phase buck converterTable 1 with Vin = 3.3V, Vref = 1.2V, and Vsupply = 2.19V.

Table 1: Parameters for the single-phase buck converter

Power stage	Control stage
Inductor (L1) = 2.17µH	Resistor (R2) = 13.3kΩ
Capacitor (C1) = 15µF	Resistor (R3) = 12.2kΩ
Resistor (R1) = 2.5Ω	Resistor (R4) = 53.7kΩ
	Capacitor (C2) = 86.07µF
	Resistor (R5) = 100kΩ
	Capacitor (C3) = 0.318nF

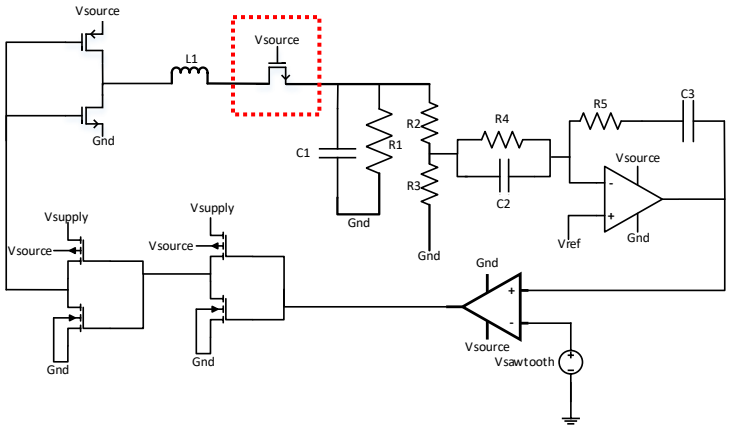


Figure 2: Single-phase Buck converter with NMOS switch used for Phase Shedding

When the NMOS is ON, the output voltage is 2.5V and the output current is 1A as seen in Figure 3.

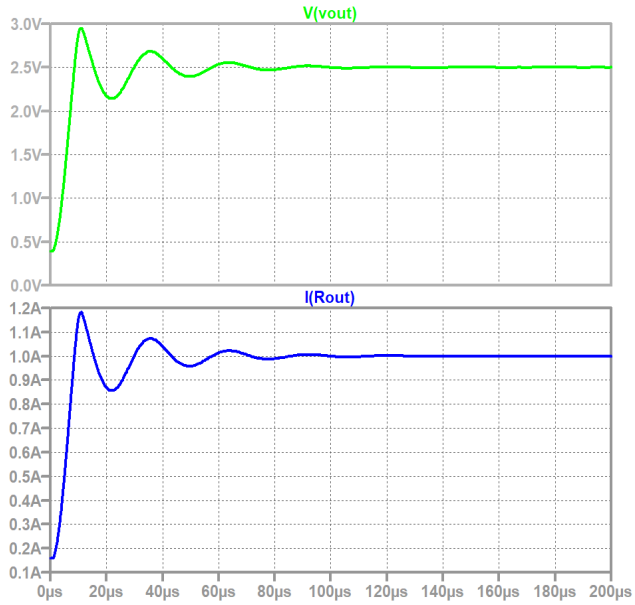


Figure 3: Output voltage and load current when switch is ON

Since the single-phase converter has the minimum number of phases, there is no need to turn off the NMOS switch. Therefore, a two-phase converter was used next to implement the effect of phase shedding as seen in Figure 4. The resistor R1 is a simple representation of the load impedance. Based on Ohm's law, $R = V/I$ and since the voltage is fixed (regulated), the current is changing (due to adding a phase). Since the current is changing, R1 is changed to fit the number of active phases (each phase adds same amount of current in this scenario). For two phase case, R1

is 1.25Ω and Vsawtooth was considered to be the summation of two signals at 0° and 180°.

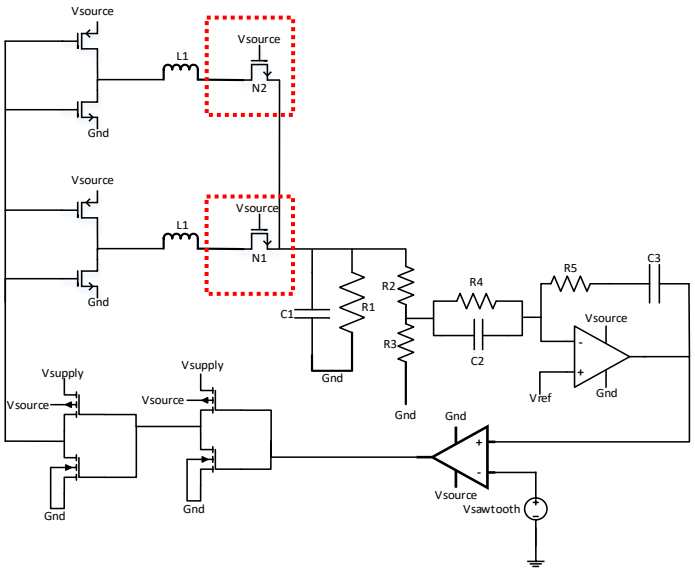


Figure 4: Two-phase Buck converter with NMOS switches used for Phase Shedding

When both N1 and N2 are ON, this means that both phases are being active. In this case, the output voltage is 2.5V and the output current is 2A, having 1A distributed in each phase as demonstrated in Figure 5. When N1 is ON and N2 is OFF, or vice versa, R1 is changed to 2.5Ω due to the number of active phases being decreased. This is donebased on equation 1 above and it consequently maintains output voltage at 2.5V. The output current is now 1A as observed in Figure 6. The results are summarized in Table 2.

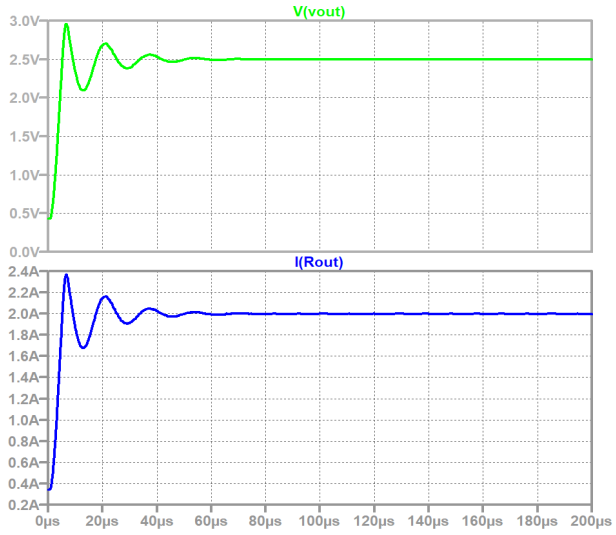


Figure 5: Output voltage and load current when both switches are ON

Table 2: Phase shedding results for two switches

N1	N2	Voltage / V	Current / A
ON	ON	2.5	2
ON	OFF	2.5	1

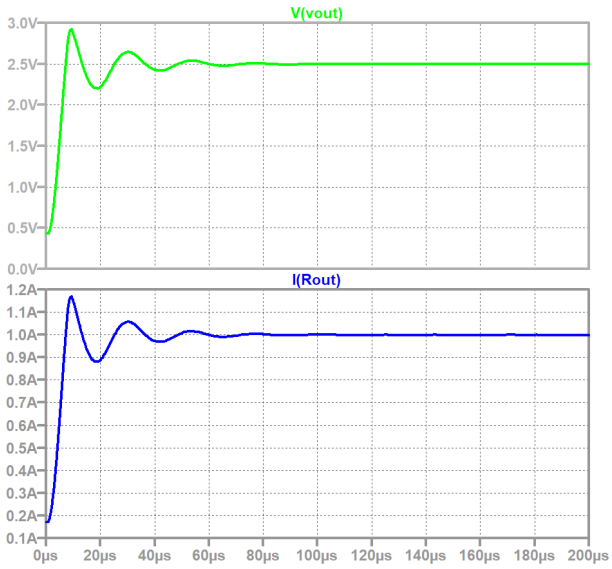


Figure 6: Output voltage and load current when one of the switches is ON

Applying this technique to the three-phase buck converter means having different load and different Vsawtooth. In three-phase scenario, R1 is decreased to 0.833333Ω and the summation of three sawtooth signals is used at 0°, 120°, and 240°. Figure 7 depicts this implementation.

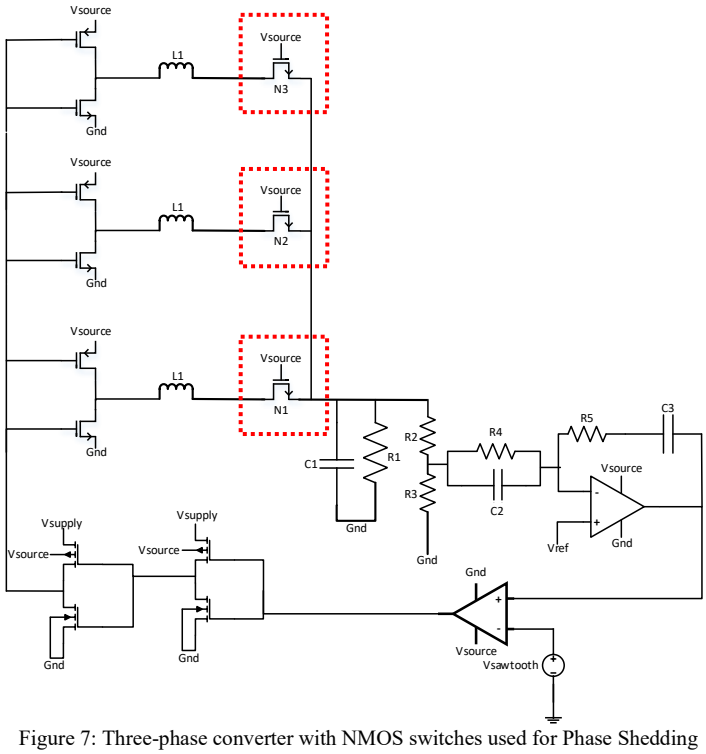


Figure 7: Three-phase converter with NMOS switches used for Phase Shedding

When N1, N2, and N3 are all ON, all phases are used, resulting in having an output voltage of 2.5V and an output current of 3A, having 1A distributed in each phase as shown in Figure 8. When N1 and N2 are ON and N3 is OFF (one phase is OFF), the used R1 is 1.25Ω as it is similar to the two-phase buck converter. The output voltage remains 2.5V and the output current is 2A (1A in each phase) as observed in Figure 9. When N1 is ON and N2

and N3 are OFF (one phase is ON), the simulation results are similar to the single-phase buck converter having 2.5V as an output voltage and 1A as an output current as depicted in Figure 10. The results are summarized in Table 3.

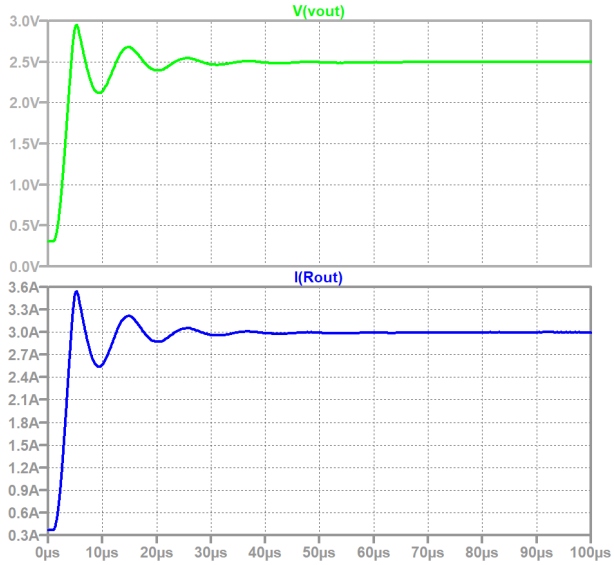


Figure 8: Output voltage and load current when all switches are ON

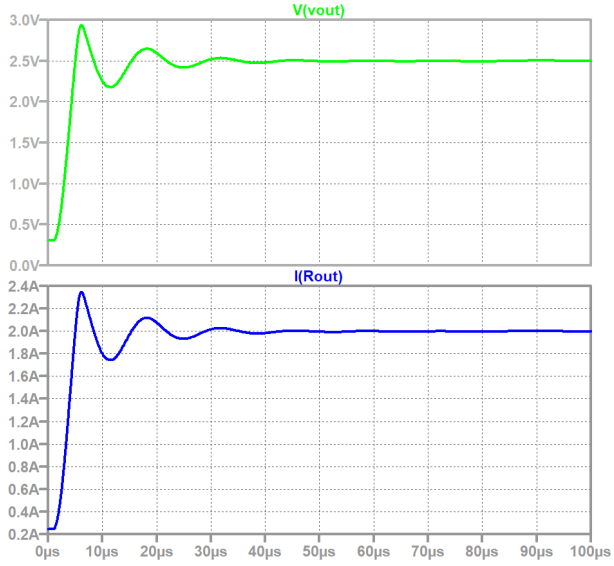


Figure 9: Output voltage and load current when one of the switches is OFF

Table 3. Phase shedding results for three switches

N1	N2	N3	Voltage / V	Current / A
ON	ON	ON	2.5	3
ON	ON	OFF	2.5	2
ON	OFF	OFF	2.5	1

2.2. Fast-Transient

As previously discussed, a current source can be used to force a step in the load current which would cause a spike or a dip in the output voltage [1]. The importance of the fast-transient feature is that the current profile of modern high-performance devices (such as a microprocessor) is very dynamic in nature which means a change from few microamps to full peak value within very small interval of time (say microseconds or even less) is expected. This definitely causes a spike/dip in the regulated output voltage. The dip below 10% of the regulated voltage may cause malfunctioning of the devices in the circuit. A spike above 10% of the regulated output voltage may cause damage to some devices (exceeds breakdown voltage).

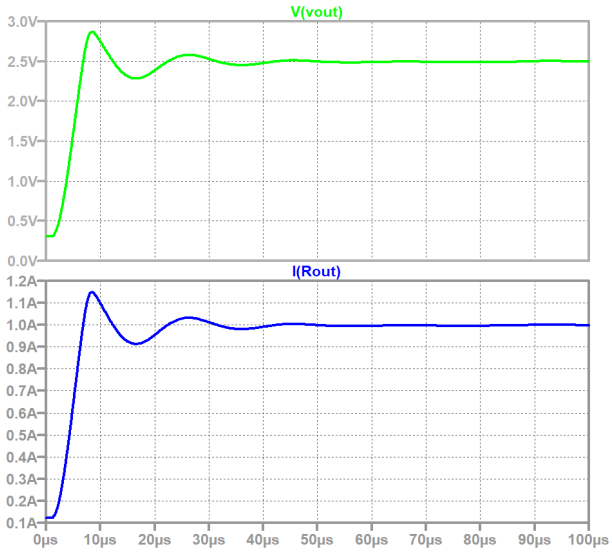


Figure 10: Output voltage and load current when one of the switches is ON

A transient current was inserted to test the response time that would take the controller to pull back the output to its regulated state and to measure the amount of worst spike/dip of the output voltage. In this paper, the current source with pulse signal of 500mA step (in both directions) was added parallel to the load to force the output voltage spike or dip. To mitigate/prevent this kind of problem, a proposed two-part circuitry was developed to assist in minimizing the voltage spike and dip to stay within the tolerable range. The developed solution is shown in Figure 11. The main job of the resistor voltage divider in helper circuit is to put the initial value for the gate voltage such that the transistor is off in the normal operating conditions (no load transient).

When spike occurs at the Vout node, the capacitor (C1) acts as a short circuit (due to high frequency signal of the fast-current step) which causes the gate voltage to increase. Therefore, NMOS transistor immediately starts to turn on. To overcome the spike, NMOS transistor starts pulling current from Vout node and this brings the spike back toward the regulated value. Results are shown in Figure 12 to Figure 15.

Table 4: Parameters of the helper circuits

Spike	Dip
Resistor (R1) = 30kΩ	Resistor (R3) = 32kΩ
Resistor (R2) = 1kΩ	Resistor (R4) = 1kΩ
Capacitor (C1) = 10µF	Capacitor (C2) = 1µF
NMOS size= 70mm	PMOS size= 200mm

When dip occurs at the Vout node, the capacitor (C2) acts as a short circuit which causes the gate voltage to decrease. Hence, PMOS transistor immediately starts to turn on. To overcome the dip, PMOS transistor starts pushing current to Vout node and this

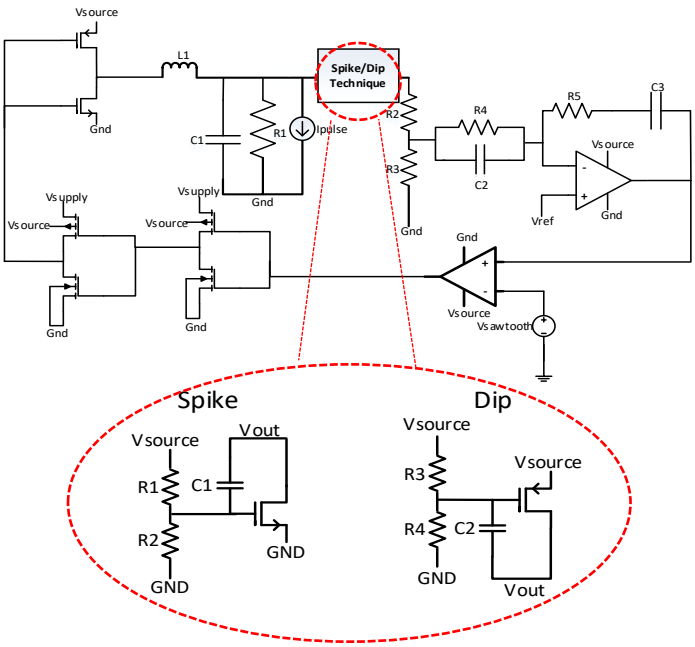


Figure 11: The helper circuits at the point of load



Figure 12: Output voltage spike without the helper circuit

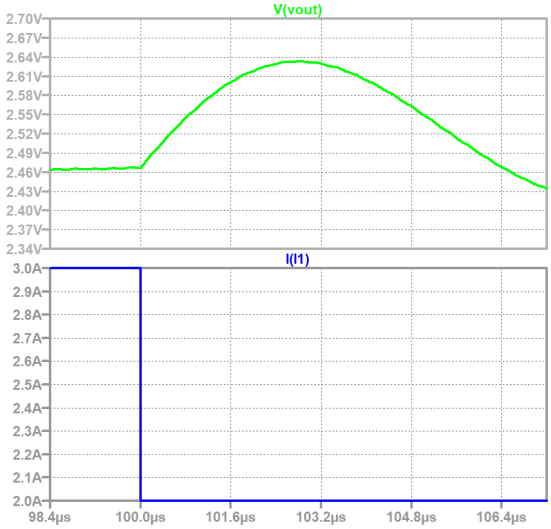


Figure 13: Zoomed-in graph when spike occurs without helper circuit

brings the output voltage back towards its regulated value. Results are shown in Figure 16 to Figure 19. The values of the helper circuits are shown in Table 4.

This fast-transient technique is introduced to the three-phase buck converter. One of the benefits is that the voltage ripple decreases as the number of phases in the circuit increases [1].

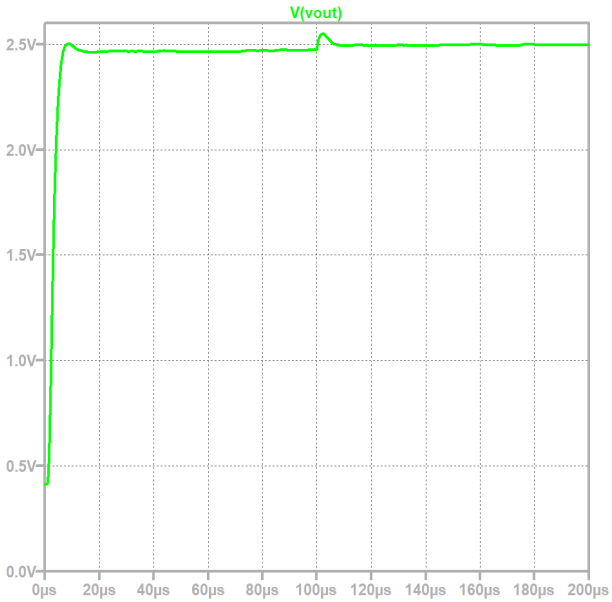


Figure 14: Output voltage spike with the helper circuit

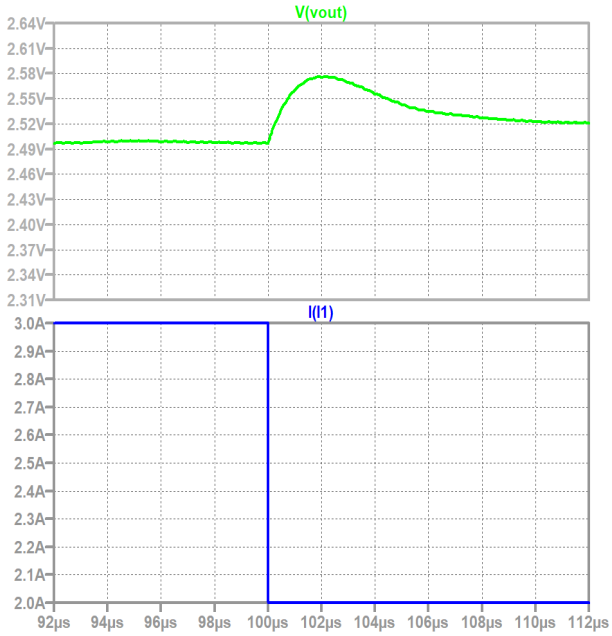


Figure 15: Zoomed-in graph when spike occurs with helper circuit

Table 5: Fast Transient results

Fast transient	Before the helper circuit	After the helper circuit
Spike	160mV	79.1mV
Dip	77.1mV	35mV

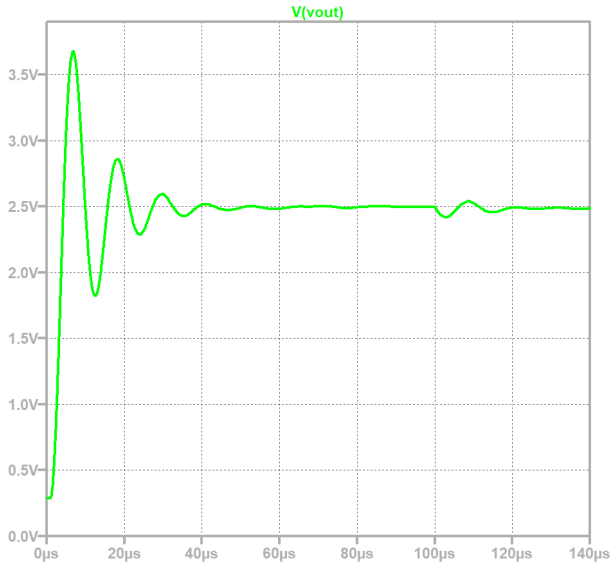


Figure 16: Output Voltage Dip without the helper circuit

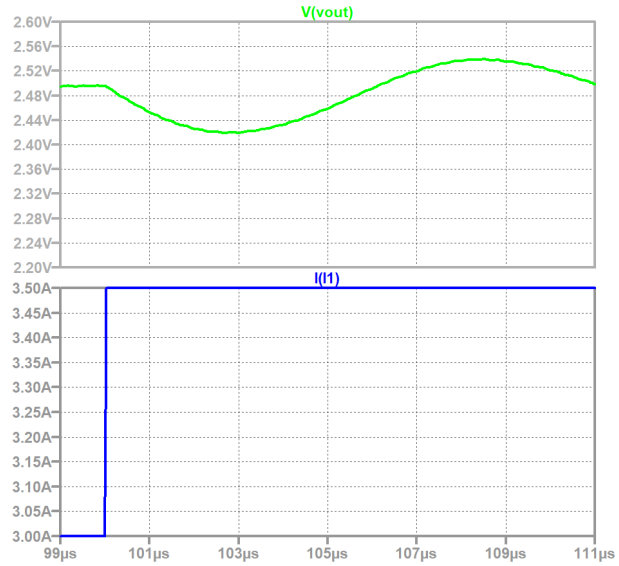


Figure 17: Zoomed-in graph when dip occurs without helper circuit

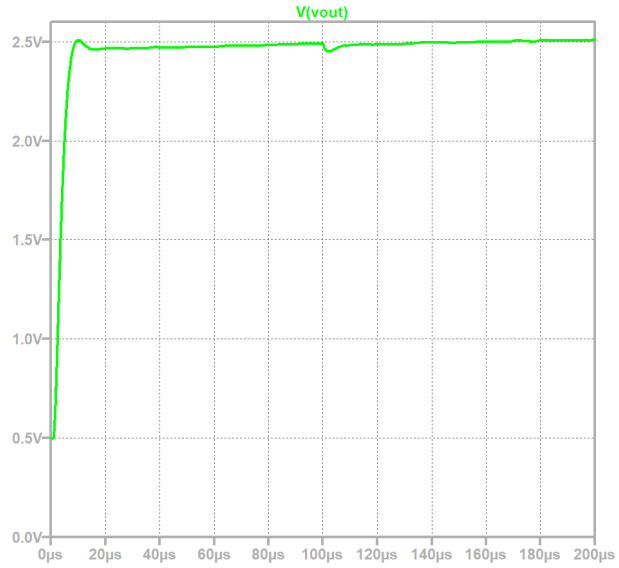


Figure 18: Output voltage Dip with the helper circuit

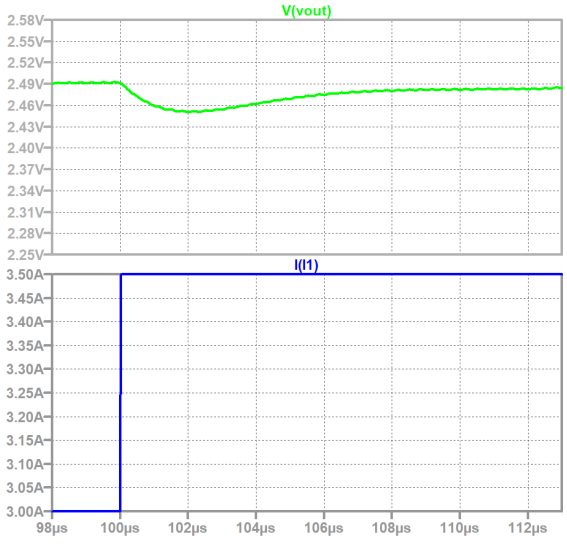


Figure 19: Zoomed-in graph when dip occurs with helper circuit

2.3. Integrated Current Sensing using Current Mirroring

Current sensing can be achieved using many conventional techniques such as Series-Sense Resistor [6]. This a simple technique that uses a resistor in series with an inductor is depicted in Figure 20. When knowing the value of the resistor, the voltage sensed across it will determine the current flowing through the inductor. This method allows higher power loss therefore, it has negative impact on the efficiency of the converter. The series resistor method can also be used by placing the sense resistor in series with the PMOS or NMOS.

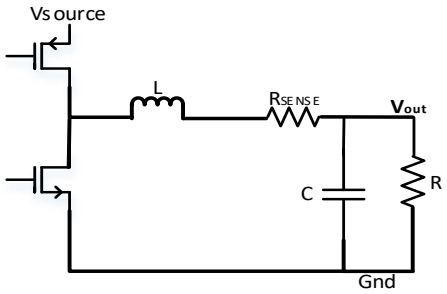


Figure 20: An example of series resistor used in current sensing

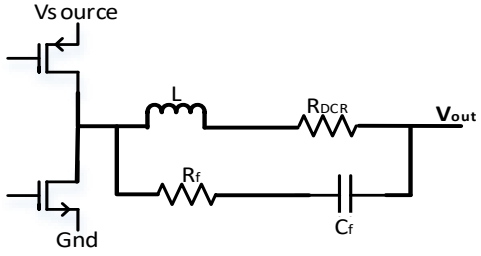


Figure 21: Integrated current sensing by adding a parallel capacitor Cf to the convertor's inductor L

DC resistance (DCR) of switching inductors with a low-pass RC circuit connected in parallel with the inductor is considered to be another method to sense the current as presented in Figure 21 [4]. The disadvantage of using this method is that the RC circuit

has to be chosen based on the inductor and resistor values which is not an easy task as some components are integrated, and others are not.

An Op-Amp can also be used as an additional method for a current sensing technique as shown in Figure 22 [6]. The Op-Amp is used to force the drain voltages of the transistors (power and sense) in the DC-DC converters to be equal. However, if the power and sense transistors width ratio increase (for efficiency reasons), the accuracy of the circuit degrades. The Op-Amp needs to have a high bandwidth and a high gain to have a very accurate current sensing method. Practically, there is not an Op-Amp that complies perfectly to the previous requirements.

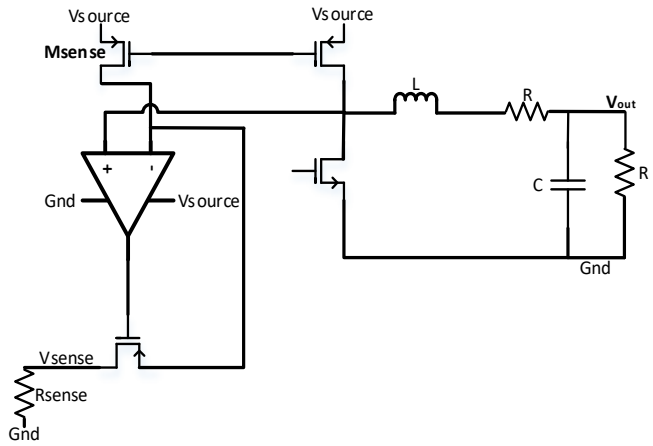


Figure 22: Integrated current sensing using op-amp and sense FET

The selected method for current sensing is the current mirroring circuit [7]. This method is selected due to the higher accuracy in addition to higher efficiency it provides compared to the previous mentioned methods. As shown in Figure 23, MP2 was connected to be a replica (sense) device for MP1. The two sources and gates are physically connected. The drains of these two devices are forced to be equal via the current mirror. Of course, each terminal of the main device and the corresponding sense device need to be equal in value since the both main and sense devices act as switches. The relationship between MP1 and MP2 sizes is presented as a ratio of 1: K. The drain currents flowing through MP1 and MP2 then will have a value of Ip1 and Ip2 which equals to Ip1/K.

In this current-sensing circuit, to have accurate current sensing, the voltages at NB and NC need to be almost equal (drain voltages for main and sense devices). As MP1 and MP2 are turned on, then MN1 is turned off, therefore the voltage at NB and NC is high because of currents Ip2 and Isense are equal and vice versa. This method can force the voltages at nodes NB and NC to be equal as noticed in Figure 24. The width of the transistor MP1 was chosen to have a value of W1 and transistor MP2 was chosen to have a width of W2 which equals to W1/K.

For the current mirror transistors, size sweeping/optimization was conducted to equalize both nodes NB and NC.

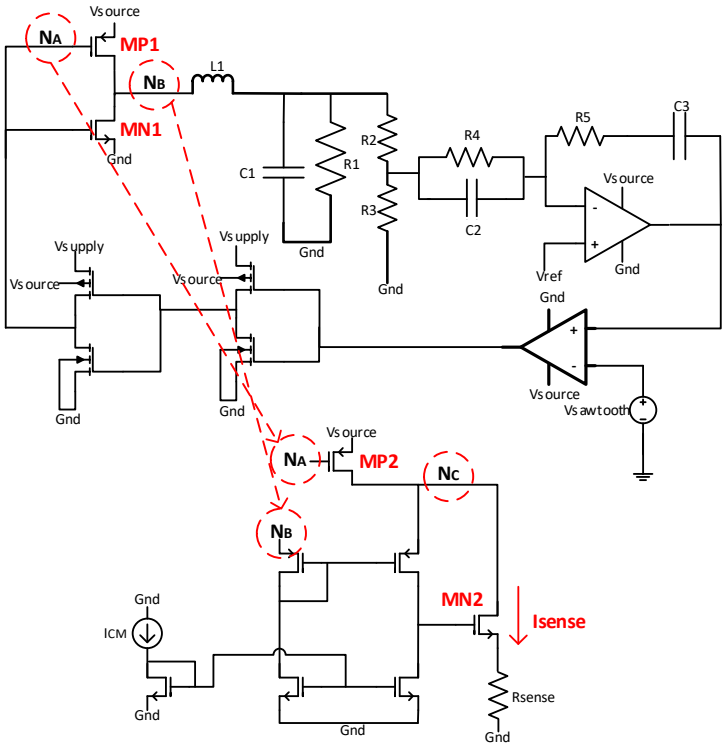


Figure 23: Integrated current sensing based on current mirror

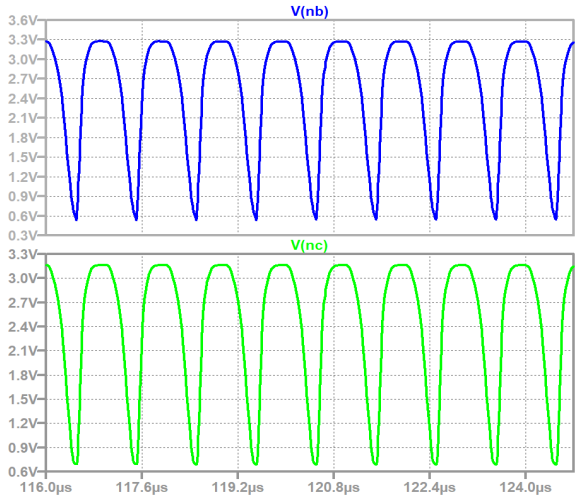


Figure 24: Voltages at Nodes NB and NC

Figure 25 shows the currents Ip1 and Ip2. It can be observed that Ip1 is identical to Ip2 except for the scaling factor of 1: K (Ip2=Ip1/K).

The sensed voltage across Rsense represents the output current of the converter. The output current can be sensed using two different options. The first option is by assuming that all phases are balanced and carry the same current which is 1A per phase. In this case, a single-phase converter can be used to represent whether an over-current condition has occurred or not. Therefore, a single-phase is enough to represent the total current of multi-phase converter. If Isense for the single phase is exceeded by 20% of a reference value, an over-current has occurred and switching will be halted.

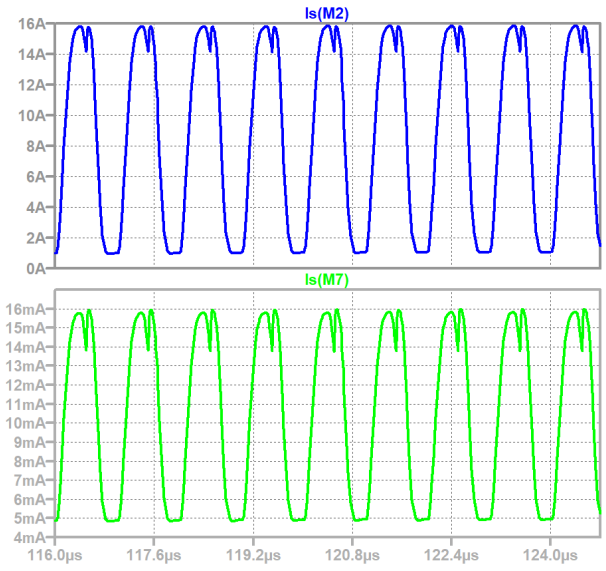


Figure 25: Ip1 and Ip2 of main and sense PMOSs

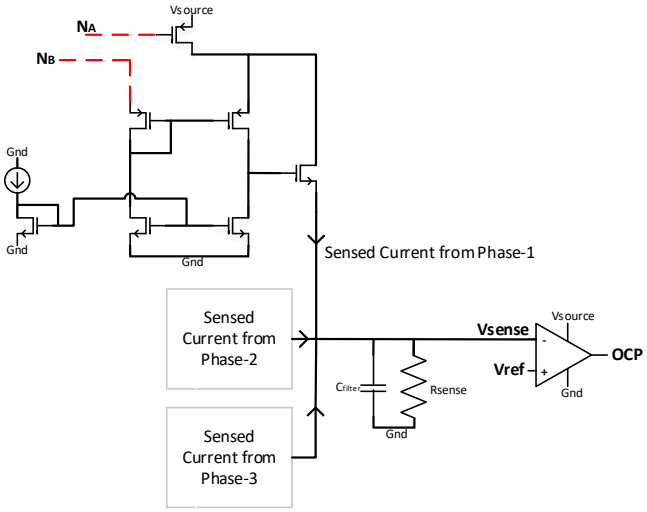


Figure 26: Option two combined sensed current for Three-Phase

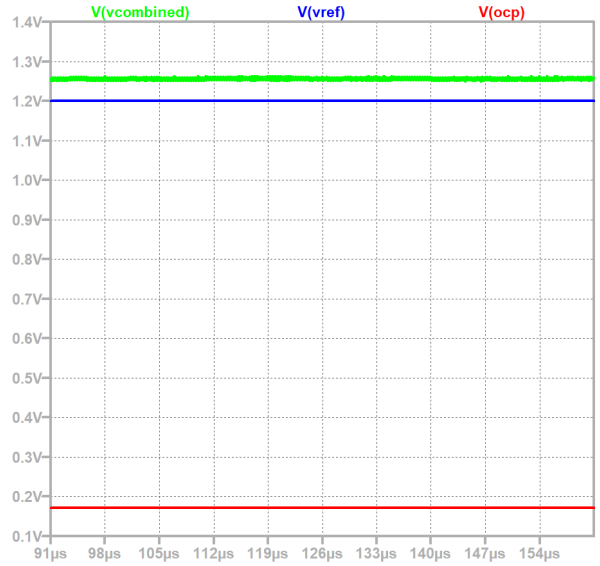


Figure 27: Three-Phase OCP indicator

Another option is possible by combining sensed currents of all phases together regardless of having the current being balanced between phases or not. In this case, the combined current, which is the total current of the converter, is 3A. A reference voltage with a value of 1.2V is presented to assist in detecting an over-current. The sensed voltage is compared to the reference voltage, therefore, if the sensed voltage value is higher than the reference voltage, then no over-current has occurred and vice versa. Of course, this 1.2V is a reference voltage that represent 20% higher than typical 3A. When over-current has occurred then the switching must be halted to protect the circuit. The second option was selected in this paper due to its higher practical value with the assumption of no current balancing. As a result, no over-current was detected in the final design as seen in Figure 26 and Figure 27.

3. Conclusion

It is well known that a multi-phase buck converter has higher capabilities, and efficiency compared to the single-phase buck converter. The phase shedding technique was implemented in the three-phase buck converter utilizing NMOS switches as they are used to disconnect some phases at light load. When the load decreases, there is no need for using all the phases in the circuit. It was concluded that by increasing the number of phases, the efficiency would be improved.

The proposed fast transient helper circuit is tested by inserting a 500mA transient current step in 100µs. Worst case spike of 79.1mV was achieved; which is a reduction of 49.4% of the original response (160mV) without the helper circuit. Worst case of 35mV of a voltage dip was achieved; which is a reduced by 45.4% compared to the original response (77.1mV) without the helper circuit. Moreover, the integrated current-sensing technique using current mirroring was used in the three-phase buck converter to detect the occurrence of an over-current, in order to protect the components in the circuit. A reference voltage with 20% higher than typical value is used to indicate an occurrence of an over current.

References

[1] N. S. Gammoh, M. A. Al-Bader and H. Ahmed-Assi, "Design and Simulation of a Three-Phase Switching Synchronous Buck Regulator," 2019.
[2] A. Costabeber, P. Mattavelli and S. Saggini, "Digital Time-Optimal Phase Shedding in Multiphase Buck Converters," 2010.
[3] Y. Zeng and H.-z. Tan, "Fast-transient DC-DC converter using an amplitude-limited error amplifier with a rapid error-signal control," 2019.
[4] Y.-S. Roh, Y.-J. Moon, J. Park, M.-G. Jeong and C. Yoo, "A Multiphase Synchronous Buck Converter With a Fully Integrated Current Balancing Scheme," 2015.
[5] 6 January 2012. [Online]. Available: http://ptm.asu.edu/modelcard/180nm_bulk.txt.
[6] H. P. Forghani-zadeh and G. A. Rincon-Mora, "Current-Sensing Techniques for DC-DC Converters," 2002.
[7] C.-H. Chang and R. C. Chang, "A Novel Current Sensing Circuit for a Current-Mode Control CMOS DC-DC Buck Converter," 2005.

ASTES

Advances in Science, Technology and Engineering Systems Journal Vol. 5, No. 5, 1064-1074 (2020)

www.astesj.com

Special Issue on Innovative Research in Applied Science, Engineering and Technology

ASTESJ

ISSN: 2415-6698

Comparison by Correlation Metric the TOPSIS and ELECTRE II Multi-Criteria Decision Aid Methods: Application to the Environmental Preservation in the European Union Countries

Mohammed Chaouki Abounaima*, Loubna Lamrini, Noureddine EL Makhfi, Mohamed Ouzarf

Laboratory of Intelligent Systems and Applications, Faculty of Sciences and Technologies, Sidi Mohammed Ben Abdellah University, Fez 35000, Morocco

ARTICLE INFO

Article history:
Received: 02 September, 2020
Accepted: 23 September, 2020
Online: 20 October, 2020

Keywords:
Multi-Criteria Decision Aid
Metric correlation
Ranking Quality
TOPSIS
ELECTRE
The Europe 2020 indicators
Environmental Preservation

ABSTRACT

This article is part of the field of Multi-Criteria Decision Aid (MCDA), where several criteria must be considered in decision making. All criteria are generally as varied as possible and express different dimensions, and aspects of the decision problem posed. For more than four decades, several MCDA methods have emerged and have been applied perfectly to solve a large number of multi-criteria decision problems. Several studies have tried to compare these methods directly with one another. Since each method has its disadvantages and advantages, a direct comparison between the two methods is normally far from common sense and becomes subjective. In this article, we propose a rational and objective approach that will be used to compare the methods between them. This approach consists of using the famous correlation measure to evaluate the quality of the results obtained by different MCDA approaches. To prove the effectiveness of the proposed approach, experimental examples, as well as a study of real cases, will be studied. Indeed, a set of indicators, known as The Europe 2020 indicators, are defined by the European Commission (EC) to control the smart, sustainable and inclusive growth performance of the European Union countries (EU). In this proposed real study, a subset of indicators is used to compare the performance of environmental preservation and protection of the EU states. For this, the two-renowned methods MCDA ELECTRE II and TOPSIS are used to classify from the best to the worst CE countries with regard to environmental preservation. The results of the experiment that the proposed ranking quality measure is significant. For the case study shows that the ELECTRE II method results in a better ranking than that obtained by the TOPSIS method.

1. Introduction

This present article is an extension of the paper published at the international conference IRASET'20 [1]. In this article, we have shown the importance of the correlation metric to evaluate the quality of the ranking results of the MCDA methods. In this paper, we will suggest an extension of the measurement of quality, this time considering the relative importance of the criteria selected. Indeed, in numerous multi-criteria decision problems, the decision-makers (DMs) do not have the same vision and the same levels of importance of the criteria, which is naturally given the priorities of the choices are not always equal and even sometimes conflicting.

For taking into consideration the criteria importance, the MCDA methods use a weighting system, represented by a set W, in which the highest weight is assigned to the most important criterion, and the lowest weight is assigned to the least important criterion. The difference between the MCDA methods lies in the approach used to aggregate the criteria with their weights to select the best choice with regard to the criteria considered.

Nowadays, the field of MCDA has known a remarkable abundance of methods which have emerged and applied to several areas [2], [3] such as Human Resources, Health, Industry and Logistic Management, Economy Management, Energy Management, Water Resources Management, the Environment Management, and recently some methods are used in applications on the fight against Covid19 [4]. Generally, an MCDA problem is defined by considering a finite set A of n alternatives, where each alternative is described by a family F of m criteria. In MCDA

*Corresponding Author: Mohammed Chaouki ABOUNAIMA, Laboratory of Intelligent Systems and Applications, Faculty of Sciences and Technologies, Sidi Mohammed Ben Abdellah University, Fez 35000, Morocco. medchaouki.abounaima@usmba.ac.ma

discipline, three obvious problematics are possible. The first allows ranking the set *A* from the best to the bad alternative, known as Ranking Problematic. The second consists in classifying the set *A* into predefined classes, called Sorting Problematic. Finally, in the third decision problem, we find to select the best alternative, known as Choice Problematic. In this article, we discuss the ranking problematic. Prospects are possible to apply the results of this paper to the other two problematics.

For the same ranking problematic, there are many MCDA methods are proposed in multi-criteria analysis literature, each with its resolution process as well as its advantages and disadvantages [5]. Thus, for a given multi-criteria ranking problem, the DM obtains several proposals for ranking solutions, and it becomes not obvious to opt objectively for a single solution.

The approach proposed in this work allows us to remedy this inconvenience of the choice embarrassment of ranking solutions. Indeed, a metric will be defined to evaluate the quality of each ranking solution obtained. The ranking which gives a better quality will, therefore, be retained. In the first version of the proposed metric [1] no reference was made to the importance of the criteria. It was supposed that all the criteria are treated with the same importance, i.e. each criterion is not considered more interesting than others. In this paper, we extend this metric for measuring the quality of a ranking to the general case where all the criteria do not necessarily have the same importance.

The proposed correlation metric not only can be used to distinguish the best ranking among several results of the MCDA methods, but it can also be used to guide and help the DM to perform the robustness analysis. The latter is a primordial activity and highly recommended in the multi-criteria analysis [6]. Indeed, the primary motivation for this activity is since the data provided by the DMs are often subject to uncertainty and imprecision, in particular at the level of the choice of the parameters required by specific MCDA methods is not sometimes obvious for DMs, as in the case of criteria weights [7]. The uncertain and imprecise choices of parameters will undoubtedly have repercussions on the quality of the final result. The robustness analysis then consists in verifying the stability of the results by testing a set of slightly different values of parameters. The metric thus proposed could help to compare objectively all the results obtained by the robustness analysis.

Intending to prove and illustrate the significance and importance of the ranking quality measure, we propose a real case study that aims to rank the European Union countries according to the level of preservation environmental. In fact, a set of indicators are defined and monitored by the European Commission, known as Europe 2020 indicators, to compare and control the smart sustainable and inclusive growth performance of all the EU countries (http://epp.eurostat.ec.europa.eu/portal/page/portal/europe_2020_indicators/headline_indicators). In the proposed case study, a subset of indicators is selected as criteria, and all relate to environmental performance. As for the example of these indicators: “Waste generated except main mineral waste”, “Recycling rate of e-waste”, “Exposure to PM10 pollution”, “Exposure of the urban population to air pollution by fine particles”, “Final energy consumption”, “Greenhouse gas emissions”, “Share of renewable energies”, and etc. A total of 11 indicators are selected. In first exploitation, these indicators are used by the two-popular methods MCDA ELECTRE II and TOPSIS to rank and evaluate the environmental performance of the EU countries. All results obtained are compared based on quality measurement.

The case study remains valid and open to all other MCDA ranking methods. The choice of methods used in this paper is only illustrative.

The rest of the article is structured as follows. In the second section, a brief reminder will be given on MCMA methods. In section III, a reminder of the ELECTRE II and TOPSIS methods will be presented. Section IV presents the case study to rank the EU countries according to the environmental preservation performance. In section V, we will present the extension of the ranking quality measurement approach. In section VI, all the numerical experiments for the test example and the case study will be detailed. Lastly, the paper will be concluded with new and possible research axes.

2. Overview of MCDA methods

2.1. *Background*

Certainly, the decision-making is often multi-criteria, where several criteria are considered to find a solution, such as a better choice, a ranking or a sorting, according to the problematics mentioned above. The criteria adopted are often contradictory insofar as a better choice in relation to one criterion is not necessarily so for another criterion, as price and quality are two contradictory criteria. In addition, the criteria are not always expressed on the same measurement scale and can represent from different points of view [8]: such as political, military, economic, comfort, social, education, investment cost, environmental impact, etc.

In some MCDA methods, such as the Weighted Sum method [9] and TOPSIS method [3] all criteria are normalized and aggregated into a single criterion, called synthesis criterion, on the basis of which the final decision will be made. Note that any transformation of the criteria by normalization will not be innocent and will have an influence on the final solution. Indeed, the final solution may depend on the normalization operation used, so these methods are to be used with recklessness [10].

Nowadays, the MCDA field has experienced great progress both in theory and in application [11]. Many methods have emerged, each has its own approach to aggregate criteria, and each has its advantages and disadvantages. There are currently two main resolution processes [12].

The first process is known as the Synthesis Criteria Approach. The principle of the methods of this approach is to transform the multi-criteria problem into a simple mono-criterion problem, by the first normalization of all the criteria, and then an aggregation of all the normalized criteria into a single decision criterion. As an example of these methods, we find the method of the weighted sum (WSM) [7], [9], the method of programming by objective [13], TOPSIS method [3] and many other methods. In this paper, the TOPSIS method will be used. The second resolution process takes the name of outranking approach. Whose main idea is to develop a relationship, by comparing the alternatives two by two, named

outranking relation and denoted by S. This relation S will be used in a second step of the process to find the compromise solution according to the problem to be solved: problematic choice, classification or sorting. There are numerous methods which are based on the principle of this approach, of which we cite the two popular methods: the methods family PROMETHEE (Preference Ranking Organization METHod for Enrichment of Evaluations) [14], and the methods family ELECTRE (Elimination And Choice Translating Reality) [15], [16]. In this paper, the ELECTRE method will be used and compared to the method TOPSIS.

The principal objective of the presented paper is to propose a rational tool to compare MCDA methods objectively. Several authors have tackled this question, but for the majority of them, they have tried to compare the methods directly according to their resolution processes. For example, we cite the works [17], [18]. The direct comparison between methods, for example, based on their own characteristics and the approach to which they belong, will undoubtedly be a devoid comparison of objectivity, as each method has its limitations and advantages. We propose to use the correlation metric as a tool to compare the results obtained by the ranking methods instead of a direct comparison.

2.2. *The data necessary for an MCDA method*

The data hypotheses of an MCDA problem are at least the set of n alternatives *A*, which contains all the possible solutions, and a set of m criteria *F*, which are the dimensions along which the alternatives will be evaluated.

The following Table 1, called the performance matrix *M* [16], summarizes all the data which we need in a decision problem.

Table 1: Sample Table

Criteria						
Weights		*g1*	...	*gj*	...	*gm*
		w1	...	*wj*	...	*wm*
		Min/Max	...	*Min/Max*	...	*Min/Max*
Alternatives	*X1*	*g1(X1)*	...	*gj(X1)*	...	*gm(X1)*
	...	...	...	...	...	...
	Xi	*g1(Xi)*	...	*gj(Xi)*	...	*gm(Xi)*
	...	...	...	...	...	...
	Xn	*g1(Xn)*	...	*gj(Xn)*	...	*gm(Xn)*

In this paper, the following notations will be deployed:

- $A = \{X_1, ..., X_i, ..., X_n\}$ are the n alternatives.
- $F = \{g_1, ..., g_j, ..., g_m\}$ are the m criteria, $m \geq 2$.
- Min means that the criterion to be minimized
- Max means that the criterion to be maximized
- $W = \{w_1, ..., w_j, ..., w_m\}$ are the weights of criteria.
- $g_j(X_i)$ is the evaluation of the alternative Xi on the criterion g_j.

3. The remainder of the MCDA ELECTRE II and TOPSIS methods

The ELECTRE II and TOPSIS methods are considered among the most widely used methods in the MCDA field. Several research works and real applications have successfully deployed these two methods [8], [19]. However, the two methods proceed differently. The ELECTRE II method is a method which is the basis of the outranking approach, while the TOPSIS method is a method which is part of the approach of the unique synthesis criterion. The common point between the two methods is that both are able to rank the alternatives of set A from the best alternative(s) to the bad alternative(s); moreover, they take as starting data the decision matrix M and a set W of criteria weights.

In this section, we present the algorithms of the two methods, which we will need for the case study.

3.1. *The TOPSIS method*

The TOPSIS method (Technique for Order Preference by Similarity to Ideal Solution) [3] is developed to rank all the alternatives of the set A from the best alternative(s) to the bad alternative(s). As shown in Figure 1, the TOPSIS method starts with a normalization of the decision matrix M, then it calculates a Euclidean distance between all the alternatives and two reference solutions Ab, and Aw, respectively called Ideal Solution and Anti-Ideal Solution. Then the similarity Swi, called the relative closeness, is calculated between each alternative Xi and the tow solutions Ab and Aw. Lastly, the alternatives are ranked according to the similarities Sw, thus calculated.

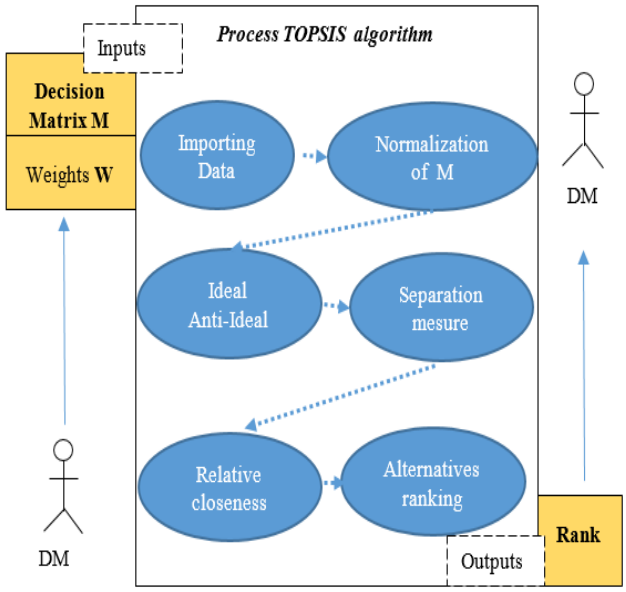


Figure 1: Process TOPSIS algorithm

TOPSIS algorithm proceeds in the following seven steps:

- Step 1: Establishment of the performance matrix

In the first step, we build the decision matrix *M* which is composed of *m* criteria and *n* alternatives, as shown in Table 1.

- Step 2: Normalization of the performance matrix

To compare the performances of the alternatives by the Euclidean distance, one of the conditions imposed by the TOPSIS method is that all the performances must be expressed on the same measurement scale. In this step, a normalization is then calculated. This normalization consists of replacing each performance *gj(Xi)* by an equivalent normalized performance calculated by the following equation 1.

$$r_{ij} = \frac{g_j(X_i)}{\sqrt{\sum_{k=1}^{n} g_j(X_k)}} \quad (1)$$

For the rest of the decision process, the decision matrix M is therefore replaced by the new normalized matrix $R = (r_{ij})_{n\times m}$.

- Step 3: Construction of weighted normalized decision matrix T.

For taking into account the importance wj of criteria in the decision-making process, the matrix R is again replaced by a new matrix $T = (t_{ij})_{n\times m}$ which is obtained by the following equation 2:

$$t_{ij} = \frac{w_j \times r_{ij}}{\sum_{j=1}^{m} w_j} \quad (2)$$

In equation 2, the performance of alternative Xi on criterion gj is reinforced by the weight of criterion gj. The performance will, therefore, be multiple depending on the importance of the criterion.

- Step 4: Calculation of the Ideal solution Ab and the anti-ideal solution Aw

In step 4, we determinate the worst solution Aw and the best solution Ab. For each criterion gj, we calculate the performances Abj and Awj by the following equations 3 and 4.

$$A_{bj} = \begin{cases} \max\limits_{i=1\ to\ n} t_{ij} \ \ if\ g_j\ is\ a\ criterion\ to\ be\ maximized \\ \min\limits_{i=1\ to\ n} t_{ij}\ if\ g_j\ is\ a\ criterion\ to\ be\ minimized \end{cases} \quad (3)$$

The worst solution Aw is calculated in an opposite way to the best solution Ab, it is obtained by the following formula 4.

$$A_{wj} = \begin{cases} \min\limits_{i=1\ to\ n} t_{ij} \quad if\ g_j\ is\ a\ criterion\ to\ be\ maximized \\ \max\limits_{i=1\ to\ n} t_{ij} \quad if\ g_j\ is\ a\ criterion\ to\ be\ minimized \end{cases} \quad (4)$$

- Step 5: Calculation of the Euclidian distance between each action Xi and the Ab and Aw

We calculate by equations (5) and (6) the Euclidean distance between all the alternatives Xi and the solutions Aw and Ab.

$$d_i^+ = \sqrt{\sum_{j=1}^{m} (t_{ij} - A_{wj})^2} \quad (5)$$

And

$$d_i^- = \sqrt{\sum_{j=1}^{m} (t_{ij} - A_{bj})^2} \quad (6)$$

- Step 6: Calculation the similitude coefficient Sw to Aw and Ab

For each action Xi, the similarity S_{wi}, called the relative closeness, is calculated, by equation 7, between each action Xi and the Ideal Ab solution and the Anti-Ideal solution Aw. This similarity is the Euclidean distance between the action Xi and the Anti-Ideal Aw attenuated by the sum of the two distances from Xi to the solutions Aw and Ab. An alternative obtains so the best ranking when its similarity is better.

$$s_{wi} = \frac{d_i^-}{d_i^+ + d_i^-} \quad (7)$$

- Step 7: Rank the actions in descending order by similitude coefficient

Lastly, the actions are ranked from the best action to the bad action according to similarities s_{wi} $(i=1, \ldots, n)$ calculated.

In summary, the main idea of the TOPSIS method is an alternative will be better when it is closer to the Ideal Ab solution and further from the Anti-Ideal Aw solution.

2.3. *ELECTRE II method*

The ELECTRE family of methods currently has 6 different methods ELECTRE I, IS, II, III, VI, and ELECTRE TRI [8][10]. The six versions have the same principle of constructing an outranking relation in the first step of the method, and then its exploitation in the second step. However, the six ELECTRE methods are distinguished by the problem posed (choice, sorting or ranking), and whether the DM hesitates to prefer an alternative x to another alternative y, in the case where the alternatives have very similar performances.

In this article, we will compare the ELECTRE II method and the TOPSIS method on the basis of the real case study on environment preservation and the quality measurement of ranking.

The ELECTRE II method [10][12], like all the other versions, proceeds in two phases. In the first phase, two outranking relations S^1 and S^2 are developed. In the second phase, the relations S^1 and S^2 are exploited to rank the alternatives.

In the approach to developing the outranking relation, pairwise comparisons between pairs of alternatives (x, y) are performed. For all ELECTRE versions, the outranking relation S is developed as follows:

xSy, if two conditions are satisfied:

• x is better than y for most criteria (majority principle)

• without there being a criterion for which y has a preference much greater than that of x (principle of minority).

The two conditions of majority and minority are known as the concordance condition and the non-discordance condition.

- Step 1: Construction of relations S^1 and S^2

In ELECTRE II method, we construct two relations S^1 and S^2, such that S^1 is included in S^2, i.e.: if xS^1y then xS^2y. To do this we require two thresholds of concordance c1 and c2, and two thresholds of discordance, which all verify: c1>c2 and d1<d2.

The relation S^1 is, therefore, more stringent than the relation S^2, because the majority of criteria required to satisfy the condition of concordance in relation S^1 is much larger than that required for the relation S^2: c1>c2. In addition, the maximum acceptable difference to reject the discordance effect is too small in S^1 and larger in S^2: d1<d2.

The S^1 and S^2 outranking relations are called respectively the "strong outranking" relation and the “weak outranking" relation: $x\ S^1y \Longrightarrow x\ S^2y$.

The concordance threshold defines the minimum majority required of the criteria that match the assertion of the outranking relation. As an example, a concordance threshold of 0.6 requires a

majority of more than 60% of criteria to accept the concordance test.

However, the discordance threshold defines the maximum difference supported between the performance of two alternatives on a given criterion to accept the second discordance test.

The construction of the two outranking relations S^1 and S^2 is formulated by the following equation 8.

$$xS^i y \Leftrightarrow \begin{cases} \text{Concordance condition :} \\ c(x,y) = \dfrac{\sum wj}{\sum wj} \geq ci \\ 1 \leq j \leq m \\ \text{Non - discordance condition :} \\ \forall\, gj \in F / gj(x) > gj(y) : \; gj(x)\text{-}gj(y) \leq dji \end{cases} \quad (8)$$

For $i \in \{1,2\}$

- Step 2: Exploitation of relations S^1 and S^2

After the construction in the first step of the two relations S^1 and S^2, we calculate two reverse pre-orders, the first, named *P1*, is obtained by exploring the graph, corresponding to the relation S^1, from the root to the leaves. A second pre-order, named *P2*, is obtained by exploring the graph in the reverse direction, this time starting from the leaves towards the root. Then the two pre-orders *P1* and *P2* are combined to give a final median pre-order *P* of the form $P = \frac{P1+P2}{2}$.

Lastly, the alternatives having obtained the same rank in the ranking median *P*, will be separated according to the second relation S^2.

4. A real case application

The Europe 2020 indicators (http://epp.eurostat.ec.europa.eu/portal/page/portal/europe_2020_indicators/headline_indicators) are set up and deployed by the European Commission (EC) in order to control the objectives of the strategy set out for smart, sustainable and inclusive growth in the member states of the European Union (EU). The objectives of sustainable growth aim for a more resource-efficient, greener, and more competitive economy. It is decided to achieve a 20% reduction in greenhouse gas emissions from 1990 levels, in addition, an increase in the share of renewable energy sources in energy consumption. All of the above objectives must be measurable and comparable. This is why the main indicators have been defined by the EC to facilitate the monitoring of the progress of the indicators in each member state, of which we cite:

- Greenhouse gas emissions;
- Share of renewable energies in gross final energy consumption;
- Contributions to eco-innovation;
- Waste management and recycling;
- Water management and production;
- Energy intensity of the economy;
- Employment rate by sex;
- Early leavers from education and training;
- The population at risk of poverty or exclusion;
- Integration rate of emigrants;
- Etc.

The different indicators can reflect the diversity of performance in each country. Also, they measure the level of progress of the goals over time and can, therefore, be used for comparison purposes at the European and international level.

In the case study presented in this paper, the study focuses on the level of ecological conservation performance and environmental preservation in the EU. For this, a subset of the Europe 2020 indicators is used. More precisely, all the indicators having a direct and indirect relationship with the environmental dimension are retained. The list of indicators selected is not exhaustive and remains the first exploitation of the institutional database developed and put online by Eurostat (https://ec.europa.eu/eurostat/).

The annual values recorded on the indicators cover several years from the years 1990 to the year 2018. For the indicators selected for the evaluation of environmental performance, we have deployed the latest data available on each indicator and each country. Some countries are excluded from the study because they lack information on certain indicators, such as Switzerland.

As shown below, there are a multitude and varied of conflicting indicators and not necessarily reducible into a single indicator. The multi-criteria approach is, therefore, essential to compare and classify European countries according to the different indicators. The European countries represent the set *A* of the alternatives, and the indicators constitute the set *F* of the criteria. The proposed problematic consists of ranking the EU member states, according to environmental performance. The decision matrix *M* is shown in Table 2, and a brief description of the criteria is given below.

Table 2: Performance matrix for selected indicators

Country	Indicators	Criterion g1	Criterion g2	Criterion g3	Criterion g4	Criterion g5	Criterion g6	Criterion g7	Criterion g8	Criterion g9	Criterion g10	Criterion g11
		MIN	MAX	MIN	MIN	MAX	MIN	MIN	MIN	MIN	MAX	MAX
	Weights	1	1	1	1	1	1	1	1	1	1	1
X1	Germany	1897	38.7	0.06	12.7	7.34	215.37	291.75	441.22	70.44	16.481	137
X2	Austria	1886	50.1	3.77	13.8	24.08	27.91	31.8	50.65	102.66	33.426	119
X3	Belgium	3383	38.6	0	12.9	6.56	36.33	46.84	71.37	82.67	9.423	83
X4	Bulgaria	2527	68.8	77.59	23.8	2.56	9.91	18.36	26.76	57.16	20.528	50
X5	Croatia	828	81.3	99.08	19	6.94	6.85	8.18	17.21	75.23	28.024	88
X6	Denmark	1657	38.5	0	9.2	9.75	14.96	17.96	32.44	70.69	35.708	115
X7	Spain	1480	41	1.32	12.1	9.28	86.84	124.63	202.66	119.74	17.453	105

Country	Indicators	Criterion g1	Criterion g2	Criterion g3	Criterion g4	Criterion g5	Criterion g6	Criterion g7	Criterion g8	Criterion g9	Criterion g10	Criterion g11
		MIN	MAX	MIN	MIN	MAX	MIN	MIN	MIN	MIN	MAX	MAX
	Weights	1	1	1	1	1	1	1	1	1	1	1
X8	Estonia	8965	69.8	0	5.3	20.57	2.96	6.17	6.34	49.98	29.996	81
X9	Finland	2595	48.2	0	4.9	13.09	25.84	32.99	30.04	81.41	41.162	121
X10	France	1455	36.6	0.39	12	7.01	146.61	238.91	343.07	83.1	16.593	112
X11	Greece	1328	32.9	28.64	14.7	9.32	15.95	22.42	44.88	90.84	18.002	83
X12	Hungary	1119	51.1	58.88	20.9	3.92	18.54	24.49	43.33	67.82	12.489	73
X13	Ireland	1765	47.7	0	7.7	2.63	12.27	14.54	45.37	113.6	11.061	94
X14	Italy	1799	32.1	49.28	19.4	15.17	116.47	147.24	274.75	84.41	17.775	112
X15	Latvia	1065	40.6	3.78	13.6	14.47	4.18	4.69	9.18	45.95	40.292	82
X16	Luxembourg	2697	45.5	0	11.2	4.39	4.35	4.46	9.09	94.16	9.059	138
X17	Netherlands	2539	42.1	0	11.3	3.18	50.27	64.71	101.8	88.58	7.385	92
X18	Poland	2090	36.1	70.09	23.8	3.33	71.93	101.06	217.98	87.42	11.284	59
X19	Portugal	1148	43.5	0.89	12	5.93	16.91	22.64	40.75	118.9	30.322	101
X20	Romania	1084	25	21.55	20.4	2.43	23.53	32.48	74.27	46.84	23.875	66
X21	United-Kingdom	1813	42.2	0	10	2.64	134.67	176.27	329.4	61.59	11.017	110
X22	Slovakia	1459	46.5	40.2	17.5	9.85	11.11	15.79	21.92	59.16	11.896	68
X23	Slovenia	1457	33.4	4.81	19.7	10.01	4.98	6.67	10.98	94.35	21.149	107
X24	Sweden	2136	47	0.16	5.4	20.29	32	46.78	32.69	75.28	54.645	132
X25	Czechia	1214	46.5	31.12	18.4	14.76	25.32	40.39	64.11	64.82	15.15	100

* Source: The institutional sources of data are European Commission - Directorate-General for Environment (DG ENV)- Eco-innovation Observatory.

In this first analysis of the indicators, we consider that no criterion is privileged over the others. In other words, all the criteria have a weight equal to 1.

- Criterion 1: Waste generated except main mineral waste

This indicator is defined as all hazardous and non-hazardous waste produced in a country per year and per capita. The total annual number of kilograms of waste produced per person measures the indicator.

- Criterion 2: Recycling of electronic waste (e-waste)

This criterion e-waste is a rate which is estimated by multiplying the “collection rate” by the “reuse and recycling rate”.

The indicator is expressed as a percentage (%).

- Criterion 3: Exposure to PM10 pollution

This criterion expresses the percentage of citizens living in urban areas exposed to concentrations of particles <10 µm (PM10) exceeding the daily limit value (50 µg / m3).

The European Environment Agency collects air quality data on an annual basis.

- Criterion 4: Exposure of urban citizens to atmospheric pollution by fine particles

This criterion expresses the concentration of suspended particles PM10 and PM2.5 weighted according to the urban population potentially exposed to air pollution.

The particles PM10 and PM2.5 are harmful, and they can cause serious lung inflammation.

- Criterion 5: Agricultural area covered by organic farming

The criterion is expressed in terms of the share of the agricultural area using only organic farming. It is a criterion that we choose to maximize in the ranking.

- Criterion 6: Final energy consumption

By "final energy consumption" we mean the sum of the energy consumption of the transport industry in the residential sector, services, and agriculture. This quantity is relevant for measuring energy consumption in the last resort of energy use and for comparing it with the objectives of the Europe 2020 strategy. More information can be found on the statistics of energy savings on Statistics Explained.

This indicator is measured in millions of tons of oil equivalent (TOE)

- Criterion 7: Primary energy consumption

By "primary energy consumption" is meant gross domestic consumption with the exception of any non-energy use of energy products (e.g. natural gas used not for combustion but for the production of chemicals). This quantity is relevant for measuring actual energy consumption and for comparing it with the Europe 2020 targets.

This indicator is measured in millions of tons of oil equivalent (TOE)

- Criterion 8: Greenhouse gas emissions in the sectors included in the effort distribution decision

The calculation of the indicator is based on the emissions covered by the decision on shared effort 406/2009 / EC. The decision on the shared effort provides for annual quantified commitments for emissions not covered by the emissions trading system (ETS). The emissions governed by the decision are calculated by deducting the verified emissions relating to the ETS from the CO2 emissions associated with domestic flights and the NH3 emissions from the total national emissions.

- Criterion 9: Greenhouse gas emissions to the base year 1990

This indicator shows trends in total anthropogenic greenhouse gas emissions contained in the “Kyoto basket”. It

presents the total annual emissions compared to 1990 emissions. The "Kyoto basket" includes the following greenhouse gases: carbon dioxide (CO2), methane (CH4), nitrous oxide (N2O), and so-called fluorinated gases (hydrofluorocarbons, per-fluorinated hydrocarbons, nitrogen trifluoride (NF3) and sulfur hexafluoride - SF6). These gases are grouped into a single unit according to specific factors corresponding to their global warming potential (GWP). Aggregate greenhouse gas emissions are expressed in CO2 equivalent units.

The EU as a whole is committed to reducing its greenhouse gas emissions by at least 20% by 2020 compared to 1990.

- Criterion 10: Use of renewable energies

This criterion expresses the level of use of renewable energies.

This indicator is then to be maximized in the ranking.

- Criterion 11: The eco-innovation index

The criterion is calculated on the basis of 16 sub-indicators from 8 data sources in 5 thematic areas: contributions to eco-innovation, eco-innovation activities, consequences of eco-innovation, results in terms of 'efficient use of resources and socio-economic results.

The overall index of an EU country is evaluated by the average of these 16 sub-indicators. It shows how each country practices eco-innovation compared to the EU average.

This indicator is then to be maximized in the ranking.

5. The proposed approach to measure the quality of rankings

5.1. Process of the extension approach

For the extension of the quality measure of any ranking P, we propose to compare this ranking P to all the rankings induced by the criteria. Indeed, it is so easy to rank the alternatives on each criterion gk, and we baptize this rank by P^k. The quality measurement then makes it possible to measure the correlations between the P ranking and the various P^k rankings.

In practice, the rankings P^k and P are replaced by the comparison matrices R^k and R given by the equations 9 and 10. In order to consider the differences between the importance of the criteria, the final result of the comparisons is aggregated by a weighted average of the correlations between the R and R^k.

The approach proceeds in three steps: In the first step, the comparison matrices R^k induced by the different criteria gk are evaluated. In the second step, the comparison matrix R induced by the ranking P result of the MCDA method is evaluated. In the last step, all the matrices R^k are compared to the matrix R. The results of the comparison are then aggregated with the weighted average. The approach is presented as follows.

- Step 1: Compute the comparisons matrix R^k induced by the criterion gk

Let $(R_{ij}^K)_{i.j\in\{1.....n\}}$ be the comparison matrix R^k induced by the criterion gk. This matrix is calculated by the formula 9.

$$R_{ij}^k = \begin{cases} 1 \; if \; gk(i) > gk(j) \\ 0 \qquad otherwise \end{cases} \tag{9}$$

The matrix R^K contains only the numbers 0 and 1. The value 1 means that the alternative i is preferred to the alternative j according to the criterion gk.

- Step 2: Compute the comparisons matrix R induced to the ranking P

The matrix R is calculated by formula 10.

$$R_{ij} = \begin{cases} 1 \; if \; "i" \; is \; better \; ranked \; than \; j \; in \; the \; ranking \;\; P \\ 0 \qquad\qquad\qquad\qquad\qquad\qquad\qquad\qquad otherwise \end{cases} \tag{10}$$

The value 1 indicates that the action i is ranked before the action j for the MCDA method used.

- Step 3: Evaluate the quality for the ranking P

As the example E1 of the experiment section proves, a P ranking will be better if it follows the same direction of all the P^k rankings of the gk criteria. This amounts to measuring the dependence between the matrix R and each matrix R^k. The dependence between the matrices is measured mathematically by the correlation coefficient [1]. To take into account all the correlations calculated as well as the relative importance of the criteria W, the quality measure $Q(P)$ is then calculated by a weighted average, which is given by the following formula (11).

$$Q(P) = \frac{\sum_{k=1}^{m} w_k \times \text{correlation}(R^k, R)}{\sum_{k=1}^{m} w_k} \tag{11}$$

With:

$$\text{correlation}(X,Y) = \frac{\sum_{i=1}^{n}\sum_{i,\,j=1}^{n}(X_{ij}-\bar{X})\times(Y_{ij}-\bar{Y})}{\sqrt{\sum_{i=1}^{n}\sum_{i,\,j=1}^{n}(X_{ij}-\bar{X})^2} \times \sqrt{\sum_{i=1}^{n}\sum_{i,\,j=1}^{n}(Y_{ij}-\bar{Y})^2}} \tag{12}$$

- X and Y are two square matrices of order n.

$$\bar{X} = \frac{1}{n(n-1)} \times \sum_{\substack{i,\,j=1 \\ i\neq j}}^{n} X_{ij}$$

- is the empirical average a square matrix X of order n.

5.2. Propriety: Equivalence between P and R

Let P be a ranking and R the comparison matrix deduced from P. The matrix is given by the equations (1) or (2) and let Xi be any alternative of A.

The rank of Xi in P can be deduced from the matrix R and conversely. In other words, the vector P and the matrix R are equivalent. Indeed, by definition, from ranking P we can build the

matrix R. Now, we suppose that we only have the matrix *R*. If for the alternative *Xi* we calculate the sum of all the values 1 on its line of the matrix *R*. Let *L* be this value, so we have $L(Xi)=\sum_{j=1}^{n} R_{ij}$.

The value *L(Xi)* gives the number of alternatives that are classified behind *Xi*. The ranking *P* is obtained by sorting the alternatives *Xi* in decreasing order of the values *L(Xi)*.

As an essential result of this propriety, it is that the comparison between two any comparison matrices *R1* and *R2* gives the same result as the direct comparison of the rankings *P1* and *P2* associated because as we have just demonstrated, the comparison matrices of and rankings are equivalent.

We will show in the discussion paragraph this equivalence at the base of the numerical results obtained by the case study.

6. Numerical experimentation and discussion

6.1. Numerical results of the experimentation example

To show that the metric of correlation proposed gives a significant result for the measurement of the quality of the rankings, we propose a sample of 15 varied rankings. In this example, we consider an MCDA problem of 3 criteria: *F={g1, g2, g3}*, and a set of four alternatives *A={A1, A2, A3, A4}*. For the simplification of the example, we propose that the three criteria give the same ranking: *A1> A2> A3> A4*, as shown in Table 2 below. This ranking expresses that the alternatives *A1*, *A2*, *A3* and *A4* are respectively in rank 1, 2, 3 and 4.

Moreover, we choose the three criteria with the same weighting *w1=w2=w3=1*.

Table 3: The criteria rankings *P1*, *P2*, and *P3*

Alternatives/Rankings	P1(g1)	P2(g2)	P3(g3)
X1	1	1	1
X2	2	2	2
X3	3	3	3
X4	4	4	4

The matrices R^1, R^2 and R^3 induced by the three criteria *g1*, *g2* and *g3* are given by Table 4.

Table 4: Matrices induced by the criteria R^1, R^2, and R^3

	X1	X2	X3	X4
X1	0	1	1	1
X2	0	0	1	1
X3	0	0	0	1
X4	0	0	0	0

The 15 rankings are chosen as an experiment to determine the significance of the proposed correlation metric. We have carefully chosen these rankings in order to cover almost all possible cases. Moreover, to show how the quality can vary according to these classifications choices. Table 4 gives all the rankings selected for the test.

In total, we propose two borderline cases of rankings with other intermediate cases. The first limit ranking is the ranking E1: X1>X2>X3>X4 which is the same as all the rankings given by the criteria g1, g2 and g3. The second limit ranking is the E15 ranking: X4> X3> X2> X1, which is the opposite of the three classifications given by the three criteria. The 13 other cases are the rankings intermediate where the alternatives permute their ranks between cases E1 and E15.

In this experiment, we also consider the case where the rankings can contain alternatives obtained from the same ranks. It is the case of the rankings E11, E12, E13 and E14.

Table 5 summarizes the calculated quality results for the 15 selected rankings. An interpretation of the results will be given in the following discussion section.

Table 5: Quality measurement for the 15 rankings

Example number	Ranking *P*	*Q(P)*
E1	X1>X2>X3>X4	1.0000
E2	X1>X3>X4>X2	0.4667
E3	X2>X1>X3>X4	0.7333
E4	X2>X3>X1>X4	0.4667
E5	X2>X3>X4>X1	0.2000
E6	X3>X1>X2>X4	0.4667
E7	X3>X2>X4>X1	-0.0667
E8	X3>X4>X2>X1	-0.3333
E9	X4>X1>X3>X2	-0.0667
E10	X4>X2>X1>X3	-0.0667
E11	X1>X2>X3=X4	0.8704
E12	X1>X2=X3=X4	0.6202
E13	X1=X2>X3>X4	0.8704
E14	X1=X2>X3=X4	0.7454
E15	X4>X3>X2>X1	-0.6000

The graph illustrated by Figure 2 below represents the variation in the quality *Q(P)* of the 15 selected test rankings.

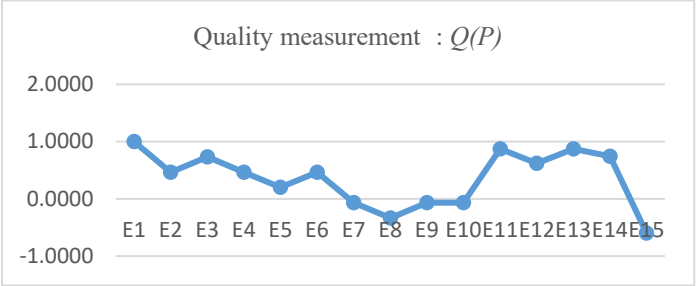


Figure 2: Graphical representation of variations of the quality measurement of rankings

The graph undoubtedly proves that the quality measure *Q(P)* is significant. Indeed, for the ideal-ranking, *E1: X1>X2>X3>X4*, which coincides with the three rankings induced by the three supposed criteria *g1*, *g2* and *g3*, gives a maximum quality, which is worth *Q(E1)=1*. From more, the ranking *E15: X4>X3>X2>X1*, which is opposed to the three rankings induced by the three criteria *g1*, *g2* and *g3*, gives the most inferior quality which is worth *Q(E15)=-0.63*. For all other cases of rankings, even for rankings with equal rank, the quality varies between 1 and -0.63. In addition, that depends on the ranks of the alternatives.

In summary, the quality remains close to the maximum value when the alternatives keep almost the same ranks of the rankings induced by the criteria. And, the quality becomes poorer when the alternatives score far from the ranks of the rankings induced by the criteria.

6.2. Numerical results of the study case

For the comparison and ranking of European countries according to performance and environmental preservation, we use the two methods TOPSIS and ELECTRE II at the base of the decision matrix *M* illustrated by Table 2. The rankings obtained by the two methods are given in Table 8.

Ranking of countries by the TOPSIS method

We calculate the *swi* similarities, given by equation 7, for each country. Then we rank the countries in descending order according to the *swi* scores thus calculated. The result of the ranking obtained by the TOPSIS method is given in Table 8.

Ranking of countries by the ELECTRE II method

The first step of the ELECTRE II method consists of calculating the matrix of concordance indices *C(Xi, Xk),* given by equation 8, for all pairs *(Xi, Xk)* of countries. Then, in the second step of the method, we build the two outranking relations *S1* and *S2*, as indicated previously in the method remainder paragraph. For the concordance thresholds to be provided, we choose c1=0.8 and c2= 0.6. These values are the standard choices of several MCDA software. Moreover, for the discordance thresholds, we choose d1=60% of the extent of each criterion. Furthermore, d2=80% of the extent for each criterion, see Table 6.

The extent of a criterion *gj* is given by *extent(gj)=Max(gj(a))-Min (gj (a)))* for any *a* of *A*.

In MCDA, for the case of the ELECTRE method, it is strongly recommended to make a robustness analysis [6], which shows the stability of results. This analysis involves testing multiple values for the parameters required by the method, such as concordance and discordance thresholds, and seeing how the results obtained by the method may change depending on the parameter values used. For this reason, we choose the second test of discordance values. However, we keep the same concordance thresholds, because we obtained almost the same rankings for different values of concordance thresholds. The values used are the best thresholds which disperses the ranking of countries as much as possible.

Table 7 below summarizes all the parameters used for the ELECTRE II method. Furthermore, it gives two versions of results according to the parameters provided: ELECTRE II V1 and ELECTRE II V2.

Table 6: The discordance thresholds for d_2 =80% for extent and d_1 = 60% for extent

	Criterion 1	Criterion 2	Criterion 3	Criterion 4	Criterion 5	Criterion 6	Criterion 7	Criterion 8	Criterion 9	Criterion 10	Criterion 11
Extent	8137.000	56.300	99.080	18.900	21.650	212.410	287.290	434.880	73.790	47.260	88.000
d1	4882.20	33.78	59.45	11.34	12.99	127.45	172.37	260.93	44.27	28.36	52.80
d2	6509.60	45.04	79.26	15.12	17.32	169.93	229.83	347.90	59.03	37.81	70.40

Table 7: Discordance and concordance thresholds

Thresholds	ELECTRE II V1	ELECTRE II V2
d1	80%	90%
d2	60%	80%
c1	0.60	0.60
c2	0.80	0.80

Table 8: Rankings obtained by the ELECTRE II and TOPSIS methods

Code	County	Rank TOPSIS	Rank ELECTRE II V1	Rank ELECTRE II V2
X24	Sweden	1	2	4
X15	Latvia	2	1	2
X2	Austria	3	6	6
X9	Finland	4	2	3
X6	Denmark	5	3	5
X23	Slovenia	6	5	7
X19	Portugal	7	5	5
X16	Luxembourg	8	3	5
X13	Ireland	9	8	9

Code	County	Rank TOPSIS	Rank ELECTRE II V1	Rank ELECTRE II V2
X25	Czechia	10	8	13
X11	Greece	11	7	12
X22	Slovakia	12	7	10
X20	Romania	13	13	17
X3	Belgium	14	12	15
X8	Estonia	15	4	1
X17	Netherlands	16	13	16
X12	Hungary	17	9	14
X7	Spain	18	13	18
X4	Bulgaria	19	10	11
X5	Croatia	20	3	8
X21	United-Kingdom	21	11	17
X18	Poland	22	16	22
X14	Italy	23	14	19
X10	France	24	14	21
X1	Germany	25	15	20

Table 9: Comparison of ELECTRE II method to TOPSIS method

	Correlation between R and R^K											
	R1	*R2*	*R3*	*R4*	*R5*	*R6*	*R7*	*R8*	*R9*	*R10*	*R11*	*Q(P)*
ELECTRE II V1	0.10	0.35	0.18	0.33	0.32	0.54	0.57	0.68	0.10	0.48	0.17	0.35
ELECTRE II V2	-0.03	0.39	0.23	0.34	0.35	0.60	0.62	0.72	0.09	0.46	0.13	0.36
TOPSIS	0.04	0.14	0.22	0.28	0.32	0.37	0.43	0.48	-0.04	0.38	0.21	0.26

Comparison of ELECTRE II method to TOPSIS method

All this work aims to show how quality measurement can be used as a rational tool to compare the results obtained by several methods objectively. This same tool can be used to compare the results of the robustness analysis, as is the case of the ELECTRE II V1 and ELECTRE II V2 versions. To choose the best ranking, we use the quality measure of rankings *Q(P)* given by equation 11. Table 9 gives the results of the comparison between the ELECTRE methods, for versions V1 and V2, and the TOPSIS method.

Where R is the comparison matrix of the ranking P result of the method. R^k is the comparison matrix induced by the criterion gk, with $1 \leq k \leq 11$.

According to this Table 9, we can confirm that the ranking obtained by the ELECTRE II V2 method is the best ranking to be prescribed and recommended to the decision-maker.

According to the rankings results of the three methods ELECTRE II V1, ELECTRE II V2 and TOPSIS, almost all the most industrialized countries, such as Germany, France, and Italy, are placed at the end of the rankings, but more or less not with the same ranks in the three rankings. This result is well justified by the fact that most industrial and developed countries consume much energy and have high rates of carbon dioxide emissions CO2. Except for Sweden, Denmark and Austria, which are industrial countries, but according to the three rankings, they are considered among the top five most environmentally conservative countries in Europe.

According to the numerical results, the robustness analysis is very useful in the MCDA context, where the parameters are sometimes very vague and uncertain concerning the decision-maker. For example, the countries having obtained equal ranks, in the ELECTRE II V1 version, were separated into countries with different ranks in the ELECTRE II version, which gave the best ranking in terms of the measurement of quality *Q(P)*.

7. Conclusions

In summary, this article has addressed the following contributions.

On the one hand, a quality measure at the base of the correlation metric of the matrices, which takes into account the relative importance is proposed. This proposed quality measurement is a rational tool for the decision-maker to compare the rankings results of several MCDA methods adopted for its decision problem to be solved.

On the other hand, in order to prove the significance of the proposed quality measure, an experimental test was tested. This example clearly showed the relevance of the proposed measure. In addition, a real application on the preservation of the environment in the countries of the European community was studied. This case study has been proposed to practically illustrate the meaning and

relevance of quality measurement to compare MCDA methods. Two popular methods ELECTRE II and TOPSIS were used and compared on the basis of quality measurement. It turns out that the ELECTRE II method gives a better ranking.

Besides, it was shown that the quality measurement *Q(P)* could be very useful to support the decision-maker in the operation of the robustness analysis. An illustrated example of the robustness analysis has been done on the ELECTRE II method.

The results obtained in this article apply to the case of ranking methods. In our future works, we intend to use the metric for evaluating the quality of the rankings for the case of sorting and choosing problematics.

References

[1] M.C. Abounaima, F.Z. El Mazouri, L. Lamrini, N. Nfissi, N. El Makhfi, M. Ouzarf, "The Pearson Correlation Coefficient Applied to Compare Multi-Criteria Methods: Case the Ranking Problematic," in 2020 1st International Conference on Innovative Research in Applied Science, Engineering and Technology, IRASET 2020, 2020, doi:10.1109/IRASET48871.2020.9092242.

[2] M. Aruldoss, "A Survey on Multi Criteria Decision Making Methods and Its Applications," American Journal of Information Systems, **1**(1), 31–43, 2013, doi:10.12691/ajis-1-1-5.

[3] M. Behzadian, S. Khanmohammadi Otaghsara, M. Yazdani, J. Ignatius, "A state-of the-art survey of TOPSIS applications," Expert Systems with Applications, **39**(17), 13051–13069, 2012, doi:10.1016/j.eswa.2012.05.056.

[4] O.S. Albahri, J.R. Al-Obaidi, A.A. Zaidan, A.S. Albahri, B.B. Zaidan, M.M. Salih, A. Qays, K.A. Dawood, R.T. Mohammed, K.H. Abdulkareem, A.M. Aleesa, A.H. Alamoodi, M.A. Chyad, C.Z. Zulkifli, "Helping doctors hasten COVID-19 treatment: Towards a rescue framework for the transfusion of best convalescent plasma to the most critical patients based on biological requirements via ml and novel MCDM methods," Computer Methods and Programs in Biomedicine, **196**, 105617, 2020, doi:10.1016/j.cmpb.2020.105617.

[5] S. Greco, M. Ehrgott, J.R. Figueira, Multiple Criteria Decision Analysis: State of the Art Surveys, Springer, 2016.

[6] H. Aissi, B. Roy, "Robustness in Multi-criteria Decision Aiding," Trends in Multiple Criteria Decision Analysis, 87–121, 2010, doi:10.1007/978-1-4419-5904-1_4.

[7] G. Kumar, N. Parimala, "A Sensitivity Analysis on Weight Sum Method MCDM Approach for Product Recommendation," in Distributed Computing and Internet Technology, Springer, Cham: 185–193, 2019, doi:10.1007/978-3-030-05366-6_15.

[8] K. Govindan, M.B. Jepsen, "ELECTRE: A comprehensive literature review on methodologies and applications," European Journal of Operational Research, **250**(1), 1–29, 2016, doi:10.1016/j.ejor.2015.07.019.

[9] J.R.S.C. Mateo, "Weighted Sum Method and Weighted Product Method," Multi Criteria Analysis in the Renewable Energy Industry, 19–22, 2012, doi:10.1007/978-1-4471-2346-0_4.

[10] Bernard Roy, Denis Bouyssou, Aide multicritère méthodes et cas, Economica, Paris, 1993.

[11] E.K. Zavadskas, Z. Turskis, S. Kildienė, "State of art surveys of overviews on MCDM/MADM methods," Technological and Economic Development of Economy, **20**(1), 165–179, 2014, doi:10.3846/20294913.2014.892037.

[12] F.Z. El Mazouri, M.C. Abounaima, K. Zenkouar, "Data mining combined to the multicriteria decision analysis for the improvement of road safety: case of France," Journal of Big Data, **6**(1), 2019, doi:10.1186/s40537-018-0165-0.

[13] N. Vivekanandan, K. Viswanathan, S. Gupta, "Errata to: Optimization of cropping pattern using goal programming approach," OPSEARCH, **47**(1), 104, 2010, doi:10.1007/s12597-010-0007-0.

[14] M. Behzadian, R.B. Kazemzadeh, A. Albadvi, M. Aghdasi, "PROMETHEE: A comprehensive literature review on methodologies and applications," European Journal of Operational Research, **200**(1), 198–215, 2010, doi:10.1016/j.ejor.2009.01.021.

[15] I. Emovon, O.S. Oghenenyerovwho, "Application of MCDM method in material selection for optimal design: A review," Results in Materials, **7**, 100115, 2020, doi:10.1016/j.rinma.2020.100115.

[16] F.Z. El Mazouri, M.C. Abounaima, K. Zenkouar, A.E.H. Alaoui, "Application of the ELECTRE III Method at the Moroccan Rural Electrification Program," International Journal of Electrical and Computer Engineering (IJECE), **8**(5), 3285–3295, 2018, doi:10.11591/ijece.v8i5.pp3285-3295.

[17] M. Wang, S.-J. Lin, Y.-C. Lo, "The comparison between MAUT and PROMETHEE," in 2010 IEEE International Conference on Industrial Engineering and Engineering Management, 753–757, 2010, doi:10.1109/IEEM.2010.5675608.

[18] J.M. Sánchez-Lozano, M.S. García-Cascales, M.T. Lamata, "Comparative TOPSIS-ELECTRE TRI methods for optimal sites for photovoltaic solar farms. Case study in Spain," Journal of Cleaner Production, **127**, 387–398, 2016, doi:10.1016/j.jclepro.2016.04.005.

[19] Y. Çelikbilek, F. Tüysüz, "An in-depth review of theory of the TOPSIS method: An experimental analysis," Journal of Management Analytics, **7**(2), 281–300, 2020, doi:10.1080/23270012.2020.1748528.

Advances in Science, Technology and Engineering Systems Journal Vol. 5, No. 5, 1075-1092 (2020)

www.astesj.com

Special Issue on Multidisciplinary Innovation in Engineering Science & Technology

ASTESJ

ISSN: 2415-6698

Nature Inspired and Transform Based Image Encryption Techniques: A Comparative Study

Bhagyashri Pandurangi R[*,1], Chaitra Bhat[2], Meenakshi R. Patil[3]

[1]Department of Electronics and Communication Engineering, KLS Gogte Institute of Technology, Belagavi, 590008, India

[2]Robert Bosch Engineering and Business Solutions, EEA, Bengaluru, 560 103, India

[3]Electronics and Communication Engineering, Jain AGM Institute of Technology, Jamakhandi, 587301, India

ARTICLE INFO

Article history:
Received: 01 September, 2020
Accepted: 29 September, 2020
Online: 20 October, 2020

Keywords:
Bio inspired techniques
Chaotic maps
Fractional transforms
Radial Hilbert transforms
Transform domain encryption

ABSTRACT

In this paper, performances of two variations of chaos based algorithms are compared. First algorithm is a self-adaptive color image encryption algorithm is proposed based on Radial Hilbert Transform and chaos. This technique uses chaotic random phase masks operated on the transformed pixels to increase the randomness in confusion and diffusion operations. Also, a random jumbling process is used at the final stage to increase the randomness in the cipher image. Part of the plain image is used to generate the keys for encrypting another part. Second algorithm is inspired by the bio operations resembling confusion and diffusion. Use of a scrambler improves the performance of this algorithm. Proposed work elaborates the results of the suitability analysis conducted on various kinds of input images, namely, satellite images, face images and handwritten signature images. Performance parameters considered for the analysis include horizontal correlation, vertical correlation, diagonal correlation, and net changing pixel rate, unified average change in intensity, entropy and encryption time taken by the encryption techniques.

1. Introduction

With the increase in multidimensional applications of internet based multimedia content, secure transmission of multimedia data including images has become the need of the day. Biometric image based security is deployed in all the electronic gadgets. Electronic transactions are involved in day today life. Various multimedia applications include transmission variety of images though the computer networks. Image encryption algorithms vary in the way they are developed, the domain in which they encrypt and the inputs they accept. Since the algorithms need to satisfy a variety of constraints imposed by different applications, there is a need for adaptivity. Adaptive encryption algorithms meet the security standards without compromising the quality of the transmission. Self-adaptive encryption techniques improve the security of the encryption. Bringing adaptivity at various stages of encryption algorithm is a promising field of current era.

As image security is an elementary requirement in variety of applications ranging from IoT to aerospace communication, variety of constraints are imposed on the encryption methods.

Researchers have developed various algorithms to meet the specifications of the application intended. Based on implementation, image encryption techniques can be classified into cover a wide range of classes including:

- Nature Inspired Encryption
- Parallel Encryption
- Transform Domain Encryption
- Partial / Selective Encryption
- Self-Adaptive Encryption, etc

Many hybrid algorithms are developed recently with a proper blend of these classes, considering the relative advantages of various classes. For the comparative study proposed, two different algorithms are considered. First one is based on nature inspired encryption and the second is a blend of transform domain and self-adaptive encryption.

Majority of the nature inspired encryption algorithms are based on genetic algorithms (GA). Efficient image encryption algorithms exploit the basic techniques of the GAs which simulate processes in natural systems necessary for evolution.

2. Literature Survey

Genetic algorithms initialize a random population and define fitness of population (p). These algorithms randomly choose

*Corresponding Author: Bhagyashri Pandurangi R, brpandurangi@git.edu

parents from p. Crossover operation is carried out on these parents, resulting in the creation of new population (p+1). The new population is mutated and the fitness of population (p+1) is determined. The entire process is repeated until best individual is good enough. This concept can be effectively used in the accomplishment of confusion and diffusion of pixels required for encryption. Genetic Algorithms possess the following limitations:

- requires a greater number of iterations for optimum solution
- convergence is spread across many parameters [1].

To overcome these limitations, it is essential to find and to improve GA and to increase the speed of convergence. Various methods have been proposed to improvise the efficiency of GA [2-7]. In [8], a Chaos Genetic Algorithm (CGA) is proposed that employs logistic map to create the initial population. Limitation of this technique is that it still cannot generate diverse content in mutation for some complex circumstances. Work taken up in [9] is a feature selection method based on chaos GA using two different chaotic maps to keep up and improve the capability in global searching.

Various approaches to achieve confusion and diffusion based on genetic operations are presented in [10-14]. They utilize the fitness function for key generation and generation of cipher image. The pixels are permuted with DNA (Deoxyribo nucleic acid) based combinations to improve the encryption quality. A scheme for the security of medical images based on the features of genetic algorithms is discussed in [15]. Limitations of these algorithms are that few of the parameters are not tested for the cipher images. The algorithms are efficient but complex in nature. Work in [16] cryptanalyzes a DNA based color encryption technique. Also, there is a different approach using predicted key pair values to breach the security of these algorithms as demonstrated in [17].

Since the DNA based techniques do not change the pixel values non-linearly, they are prone to known plaintext attack. If one plain image is compromised, the enciphered image can be easily reconstructed without the help of keys. Optical encryption techniques target parallel processing of the image with multiple degree of freedom.

The image pixels are multiplied with random phase masks in the process of Double Random Phase Encryption (DRPE) in spatial and frequency domain. Optical encryption is performed with the keys generated in the transform domain. Work presented in [18-25] describe encryption techniques based on various transforms including fractional Fourier transform (FrFT), Radial Hilbert transform (RHT), Discrete Cosine Transform (DCT) and Hartley transform (HT). Optical encryption exploits several image parameters, including color, amplitude, phase, spatial frequency, polarization, etc., to arrive at a robust and secure encryption. Also, the complications can be regulated by proper selection of the number of rounds and the fractional order.

Fractional transforms play a vital role in image encryption. They exhibit many beneficial assets of general transforms, and have an additional independent component, its fraction. If this fraction equals to zero, the output image is a modulated version of the input image. When the fraction equals to one, fractional transform is equivalent to the original regular transform. With the fraction varying from zero to unity, different versions of the signals interpolating between modulated form and the regular transformed version can be generated. Thus, the free component serves as a key for encipherment.

The fractal compression technique is another promising method for image encryption. It is a lossy compression technique that suits for the images having high similarity at different parts. Natural and texture images are the best examples for this kind of images. A compression-encryption algorithm based on the fractal coding is discussed in [26]. Even though the compression ratio is high, the algorithm suffers at the quality of encryption. Balancing the compression ratio and the encryption quality is an interesting topic for current research.

Fractional Fourier transform has found effective in image encryption and noise removal. A multiple parameter FrFT based scheme is discussed in [27], in which, the order is considered as a vector. This scheme provides flexibility for the dimension of transform order and improvises the strength of encrypted image while retaining low computational complexity and hardware cost. Fractional Fourier transform with vector power multi-parameters is another general form of the FrFT which has great significance in information processing security. Performance of various transform based techniques is compared in [28]. Even though it claims that chaos based encryption with discrete wavelet transform gives better performance, the NPCR (number of changing pixel rate) and UACI values need to be improved. A properly designed scrambler can improve these parameters.

Remote sensing (RS) is a booming technology that provides the dynamic information of the earth surface remotely and without contact. Remote sensing technology has been developed with an exponential rate due the improved research on the computers and graphic and playing a vital role in the national, economic, construction and defense related issues [29].

Latest studies of primary focus are on the protection of digital contents communicated using RS technology. Satellite remote sensing utilizes image distribution and characteristics with various structures of remote sensing image [30]. Recently purposeful hack assaults have demonstrated that interruption into satellite information is not an unimaginable assignment. A group at the Embry Riddle Aeronautical University figured out how to get National Oceanic and Atmospheric Administration (NOAA) satellite symbolism with fundamental contraption worked as a component of an exploratory venture and by utilizing open sources accessible from the Internet [31].

Cryptanayzers have been successful in breaking few of these algorithms with known/chosen plaintext cryptanalysis. The reason is that the same set of encryption keys are used to encipher different input plain images. Unfortunately, all these cryptosystems use the same key for quite a long period. The key set can be easily compromised by encrypting some distinct images like a completely white image or completely black image, and then associating the result with the equivalent enciphered output. In order to make the algorithms robust against the kind of attacks, a plaintext-related diffusion and confusion needs to be incorporated. The key stream rudiments can be selected under the control of plain pixel. Secret keys must be associated not only to the control parameters but also to the parameters related to plain

image, in order to make the known/chosen plaintext attack harder to succeed.

Self-adaptive encryption is considered as a method that has the encryption considering input image details. The dependency on the plain image content is strongly desirable characteristics of a good encryption algorithm since two images differing with few pixels will get encrypted into totally dissimilar patterns. The proposed technique generates the encryption keys dependent on the plain image features. Also, the technique arrives at a second level of self adaptivity since one part of the image gets encrypted by the influence of the other part.

Optical systems deploy transform based algorithms, which include, Fourier transform (FT), the fractional Fourier transform (FrFT), radial Hilbert transform (RHT). To add to these, there are also discrete fractional Fourier transform (DfrFT), discrete fractional cosine transform (DFrCT), and discrete fractional Sine transform (DFrST). Haar wavelet transform de-correlates the image pixels by decomposing into averaging and differencing components [32].The Hilbert transform exhibits edge enhancing properties and hence finds its use in processing of images and phase observation [33]. Radial Hilbert transform can increases the strength with expanded key space [34].

Satellite images are widely used in various applications including remote sensing, weather forecasting and vegetation based analysis, mineral/rock differentiation, plant species identification, forest classification, coastal water analysis, soil/vegetation differentiation, etc. [35]. Satellite images can be classified as infrared images, water vapor and visible images. Some features of the satellite images are high correlation among the pixels, bulkiness and large size. Since most of them are confidential, the traditional encryption methods lack in efficiency for bulky images and have a poor speed. To encrypt bulky images, a secure and high speed encryption algorithm is necessary.

The paper compares the performance of chaos based bio-inspired image encryption [36] and chaos based self-adaptive encryption using radial Hilbert transform [37]. The test is performed with three sets of images, namely, satellite images, face images and signature images as input data. Self-adaptive technique divides the plain image into sub-images and adds chaos. The encrypted image after jumbling yields an unsystematic, disordered image [38]. In the second method, image encryption is accomplished using multi-point crossover and mutation serving as bio-operational tools for confusion and diffusion.

3. Description of proposed techniques

3.1. Chaos Based Self Adaptive Encryption Using Radial Hilbert Transform (Technique 1)

Proposed technique employs Radial Hilbert transform. Hilbert Transform in fractional domain has been explored by Lohmann et al. [39]. Hilbert Transform has a special feature that it selectively emphasizes the features of the given input image during the spatial filtering process. Generally Hilbert Transform applied to an image builds its edge-enhanced version. In support to this, the fractional HT modifies the nature of the edge enhancement. A Hilbert filter yields an edge-enhanced image in a single dimension. 2D edge enhancement for the image can be accomplished by merging the response of two Hilbert filters orthogonal to each other. Still, these transformed images preserve the basic symmetry in rows and columns. A uniformly edge-enhanced image is the result of its radial version of the Hilbert transform. Since the Hilbert transform is helpful in enhancing the edges of one the input image, it is commonly used in image processing and phase observation. Three dimensional radially symmetrical Hilbert transform is mathematically represented as

$$H(a, b, 3) = \exp(i * x * \theta(a, b, 3)) \quad (1)$$

where x is a user defined parameter.

Self-adaptive encryption employs the keys generated form one part of the image to encrypt the other part. Proposed algorithm has the following components.

3.1.1. Image Encryption

Flow diagram of algorithm is as shown in Fig.1.Plane images are initially re-sized to MxN and divided into 4 sub-images with size (M/2, N/2). It is divided into four sub-images (I_1, I_2, I_3 and I_4). First sub-image I_1 is encrypted using three input parameters: radial Hilbert transform, random chaos mask and a key x selected by the user. The Second sub-image I_2 is encrypted with a key calculated as the fraction of mean to standard deviation the previous sub-image I_1. This value also functions as an input to the radial Hilbert transform. Remaining sub-images are encrypted similarly. The encrypted sub-images are joined together and pixel positions are jumbled using a randomly generated matrix to get the final encrypted image. For decipherment, conjugate of the radial Hilbert transform and two random chaos masks are considered.

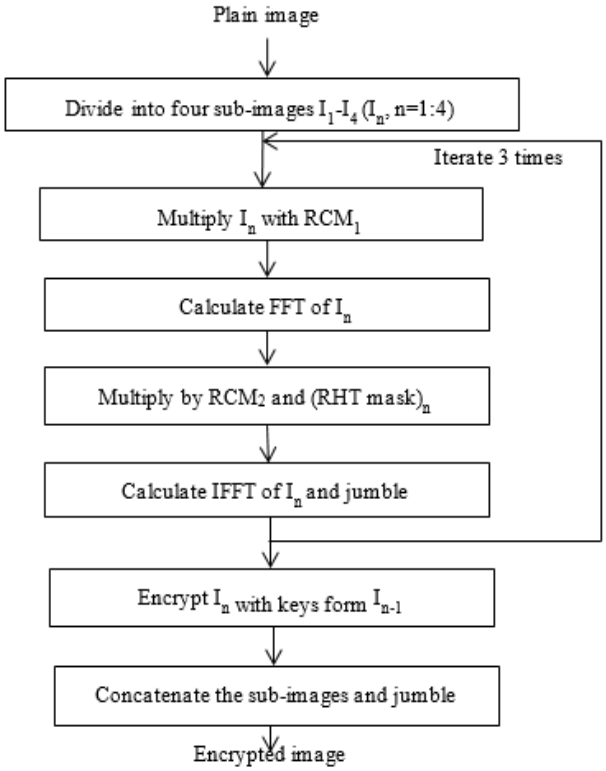


Figure 1: Radial Hilbert transform based image encryption process

3.1.2 Creation of Random Chaos Mask (RCM)

Two random three dimensional matrices having dimensions equal to that of the plain image 'i' are considered. These are considered as A_1 and A_2. Two random matrices are generated as

$$Ø_1(a, b, 3) = \exp(i * \theta_1(a, b, 3)) \quad (2)$$

$$Ø_2(a, b, 3) = \exp(i * \theta_2(a, b, 3)) \quad (3)$$

where $Ø(x, y, 3)$ is the random chaos mask generated, $\theta(x, y, 3)$ is the Fourier transform of randomly generated matrix. These values are utilized in the generation of chaotic images A1 and A2 using logistic map which serve as a random chaos masks. The process is depicted in Figure 2.

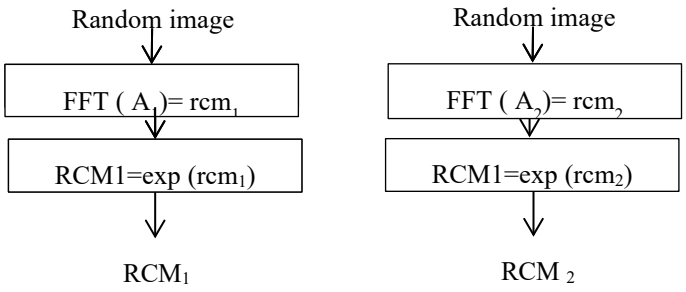


Figure 2: Generation of random phase mask (RCM)

3.1.3 Transformation with Radial Hilbert Transform

Each of sub-images undergoes a transformation as per equation (4), where x is a user defined value for sub- image I_1. For I_2-I_4, x is fraction of mean and standard deviation of previous sub-images. $\theta(a,b,3)$ is the imaginary part of the Fourier transform for the sub- image I_n and H(a,b,3) is the Hilbert transform for sub-image I_n. By introducing radially symmetrical Hilbert transform, we can use it in three dimensions. The equation for radial Hilbert transform is given by

$$H(m, n, 3) = \exp(i * x * \theta(m, n, 3)) \quad (4)$$

The conjugate of radial Hilbert transform parameter is expressed as

$$H_1(a, b, 3) = \exp(-i * x * \theta(a, b, 3)) \quad (5)$$

3.1.4 Results

The algorithm is applied on color images downloaded from Bhuvan, a Geo-portal of ISRO [40]. The images published on Bhuvan in 2D/3D domain are captured using many sensors and inform about the water, soil and land.

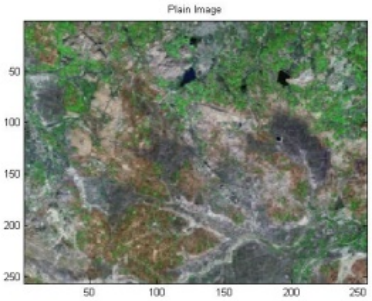


Figure 3: Input image for encryption

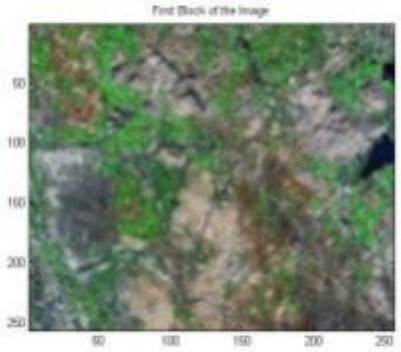


Figure 4: Sub-image I_1

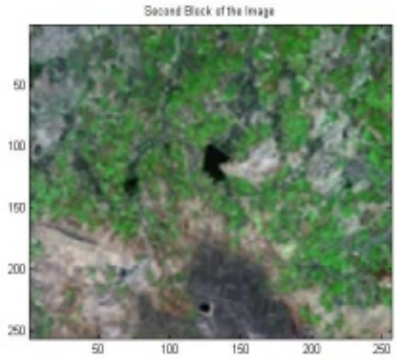


Figure 5: Sub-image I_2

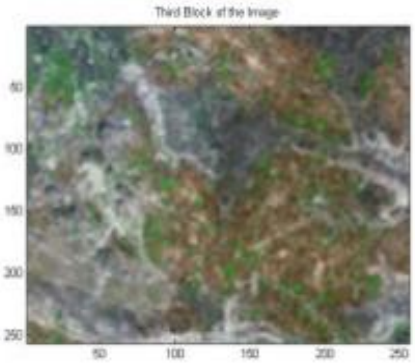


Figure 6: Sub-image I_3,

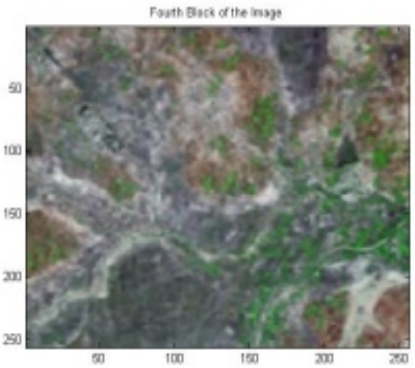


Figure 7: Sub-image I_4

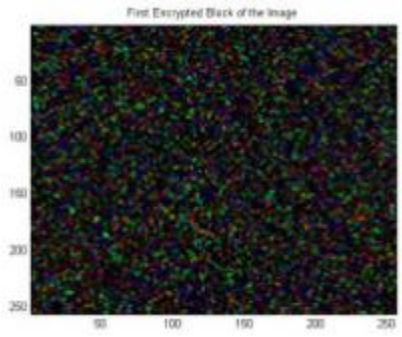


Figure 8: First encrypted block

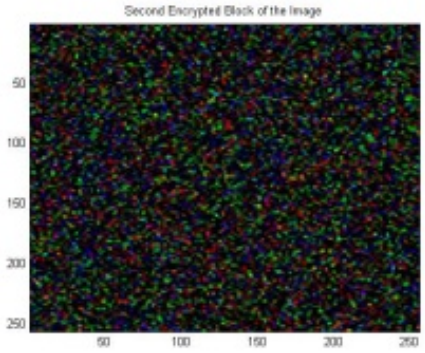


Figure 9: Second encrypted sub-block

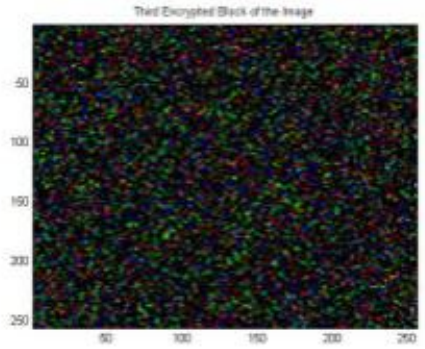


Figure 10: Third encrypted sub-block

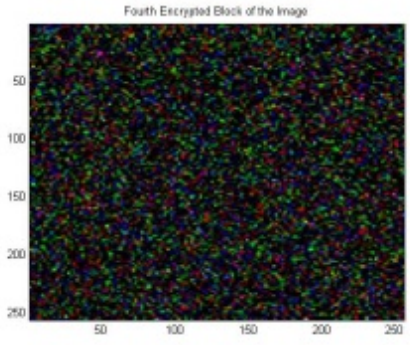


Figure 11: Fourth encrypted sub-block

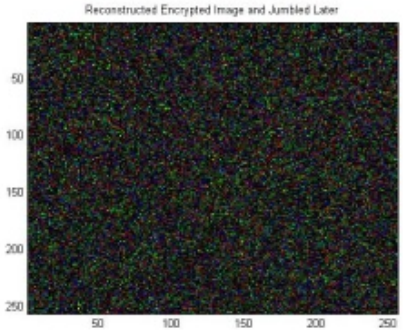


Figure 12: Complete encrypted image

Input satellite image shown in Figure 3 is divided into four smaller sub-images as displayed in Figure 4 -7. Each block is encrypted by the keys generated using the previous sub-image. The process is iterated three times for the entire image. Encrypted sub-images are displayed in Figure 8-11. Complete encrypted image is presented in Figure 12.

3.1.4.1 Histogram Analysis

Histogram analysis provides an overview of strength of confusion and diffusion for an image encryption algorithm, in presence of statistical attack. Histogram of plain image is obtained as shown in figure 13 (a) – (c). Histogram of encrypted image is shown by figure 14 (a) – (c). Histogram of the encrypted image gets exponentially distributed due to radial Hilbert transform.

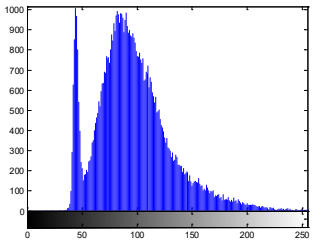


Figure 13(a): Histogram of plain image red channel

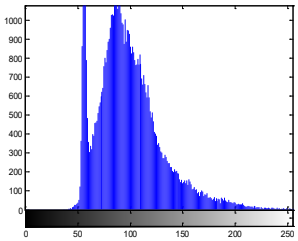


Figure 13(b): Histogram of plain image green channel

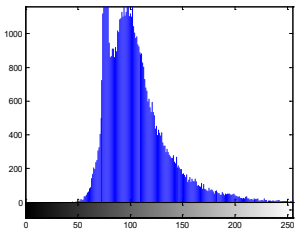


Figure 13(c): Histogram of plain image blue Channel

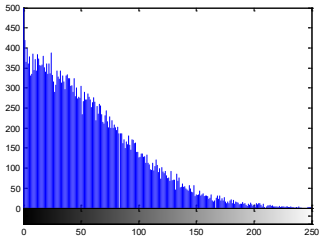


Figure 14(a): Histogram of encrypted image red channel

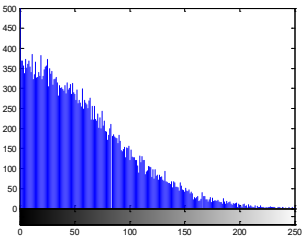


Figure 14 (b) Histogram of encrypted image green channel

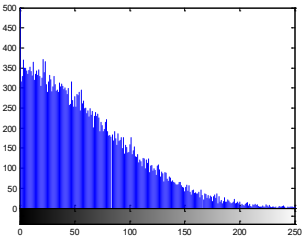


Figure 14(c): Histogram of encrypted image blue channel

3.1.4.2 Correlation of Two adjacent pixels

Correlation coefficients r(x,y) in horizontal, vertical and diagonal directions are calculated with the equation 6.

$$r(x,y) = \frac{COV(x,y)}{\sqrt{D(x)}\sqrt{D(y)}} \quad (6)$$

where x and y are values of two neighboring pixels in the image, D(x) equals to the variance of x and COV(x, y) indicates the covariance of x and y.

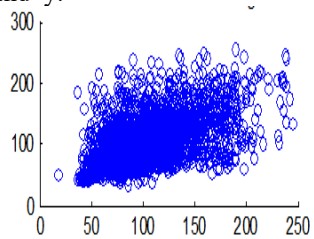


Figure 15(a): Horizontal pixel distribution of plain image for red plane

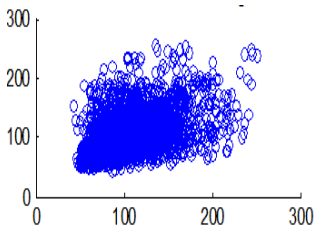


Figure 15(b): Horizontal pixel distribution of plain image for green plane

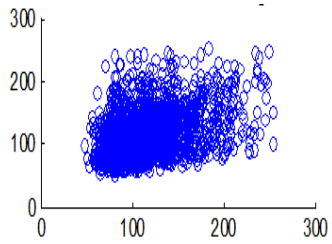


Figure 15(c): Horizontal pixel distribution of plain image for blue plane

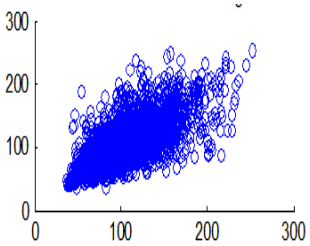


Figure 16(a): Vertical pixel distribution of plain image for red plane

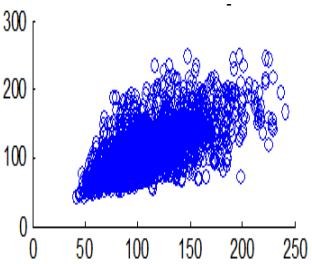


Figure 16(b): Vertical pixel distribution of plain image for green plane

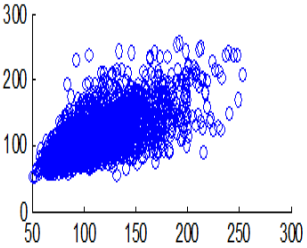


Figure 16(c): Vertical pixel distribution of plain image for blue pixel

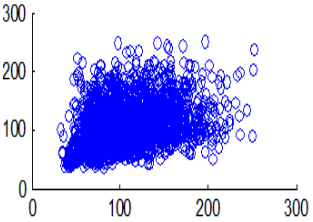


Figure 16(a): Diagonal pixel distribution of plain image for red plane

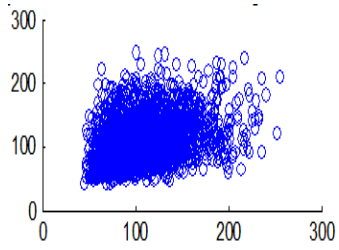


Figure 16(b): Diagonal pixel distribution of plain image for green plane

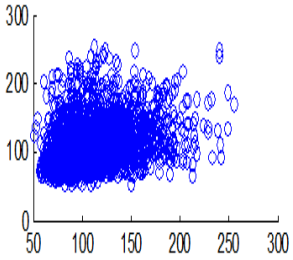


Figure 16(c): Diagonal pixel distribution of plain image for blue pixel

The experiment was conducted with 4096 pairs of neighboring pixels selected arbitrarily from the plain image and the enciphered image. Pixel distribution in Horizontal, Vertical and Diagonal directions corresponding to plain satellite image and encrypted image are plotted in figures 14 (a) –(c), 15 (a) – (c), 16 (a) –(c) and 17 (a) – (c), 18 (a) – (c), 19 (a) – (c) respectively. Encrypted image exhibits a uniform pixel distribution, which is a desirable property of a good encrypting algorithm to resist the statistical attacks. Correlation coefficients are given in table 1.

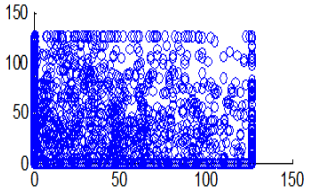


Figure 17(a): Horizontal pixel distribution of encrypted image for red plane

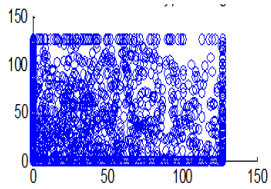


Figure 17(b): Horizontal pixel distribution of encrypted image for green plane

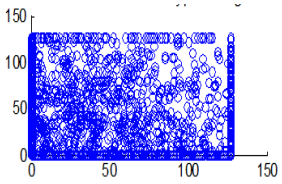


Figure 17(c): Horizontal pixel distribution of encrypted image for blue plane

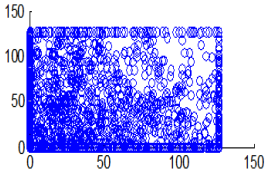


Figure 18(a): Vertical pixel distribution of encrypted image for red plane

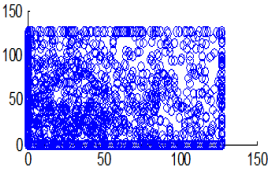


Figure 18(b): Vertical pixel distribution of encrypted image for green plane

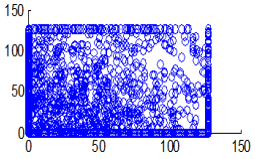


Figure 18(c): Vertical pixel distribution of encrypted image for blue plane

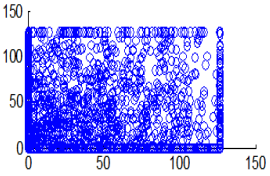


Figure 19(a): Diagonal pixel distribution of encrypted image for red plane

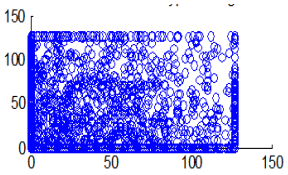


Figure 19(b): Diagonal pixel distribution of encrypted image for green plane

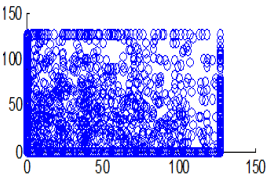


Figure 19(c): Diagonal pixel distribution of encrypted image for blue plane

Table 1: Correlation coefficients of two adjacent pixels in plain and encoded image

	Plain Image			Cipher Image		
Color	*R*	*G*	*B*	*R*	*G*	*B*
HC	0.6316	0.5629	0.5239	0.0057	-0.0013	0.0027
VC	0.7814	0.7525	0.7312	-0.0072	0.0393	-0.0021
DC	0.5247	0.5058	0.4179	-0.0056	-0.0189	-0.0170

3.1.4.3 Sensitivity Analysis

Since this algorithm encrypts one sub-image 3 times it is less prone to differential attacks. The initial key is obtained from the user and a special operation on the initially encrypted image acts as the input for the next part of the original image using radial Hilbert transform. This makes the algorithm more powerful as the complete image cannot be decrypted at once with a single key.

Four unique keys are required to decrypt the complete image. Input to radial Hilbert transform is image dependent. If the input given to radial Hilbert transform while decrypting is changed slightly, it leads to error propagation to the complete sub-image. The whole encrypted image changes as the sub images are interdependent. Thus the sensitivity is four times more than the algorithm with single key for the whole image. Figure 20 shows the deciphered image with a wrong key.

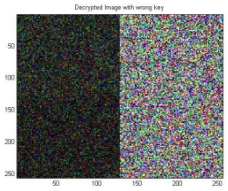


Figure 20: Deciphered image with a wrong key

To resist brute force attack, the algorithm must possess a very large key space. The technique proposed exhibits key sensitivity up-to 24 bits after the decimal point (10^{24}) and before the decimal point. There can be a range of 10^{2128} combinations of keys.

3.1.4.4 Differential analysis

3.1.4.5 Entropy Analysis

Information entropy of an image is a basic parameter to measure the randomness of pixels. A value of entropy near to 8 implies a random distribution.

Table 2: NPCR, UACI and entropy results

	Encrypted Image		
Color	*R*	*G*	*B*
NPCR (%)	99.6368	99.6017	99.6201
UACI (%)	33.5262	33.6828	33.5840
Entropy (bits)	7. 7499	7. 4897	7.3896

3.2. Nature Inspired Technique (Technique 2)

The general block diagram of the proposed encryption algorithm is shown in figure 21. The process includes a quantification unit, a logistic map generator, a mutation block, a crossover block and a scrambler. Chaotic sequence generator generates four chaotic sequences. The quantifier transforms these chaotic sequences into four streams of keys applied to crossover and mutation operations. Crossover unit alters the order of the image pixels along the horizontal and vertical direction (confusion). The mutation unit disguises the encryption image with a random mask image (diffusion). The scrambler alters the position of the image pixels using a random sequence. Functionality of the various units is described as follows:

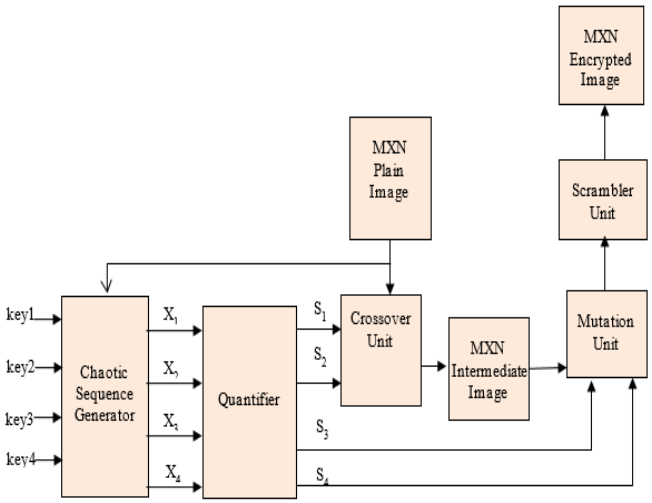


Figure 21: Architecture of the nature inspired image encryption algorithm

3.2.1 Chaotic Sequence Generator

Chaotic generator unit produces four random sequences with logistic map depending on the control parameters (μ1, μ2, μ3, μ4) and initial seed values (X_{10}, X_{20}, X_{30}, X_{40}). These keys form the set of shared secret values used in the cryptosystem. All the plain image pixels are added up and divided by (MxNx255). This fractional value is scaled down to 10% and added with the initial parameters. Thus the chaotic sequences generated are dependent on initial keys as well as the plain image. This makes the encryption algorithm stronger as the values X_1, X_2, X_3 and X_4 are not same with any two different images. Logistic map is used for the generation of chaotic sequences.

3.2.2 Quantifier

The quantifier receives four chaotic arrays X_1- X_4 produced by the chaotic map and reforms them to four sequences S_1- S_4. The length of the 1st and 3rd key streams is chosen equal to M, and the length of the 2nd and 4th key streams is made equal to N, where M × N is the dimension of the plain image.

3.2.3 Crossover Unit

Let K_i and K_i+1 denote two sequential elements present in the key stream. Rows/columns numbered Ki and K_i+1 are undergo crossover process. Cut points occupy the positions in accordance with the following equation:

$$r_1 = \max\{1, |K_i - K_{j_} + 1|\text{modL}\} \quad (7)$$

$$r_2 = \max\{1, r_1 + |K_i - K_{j_} + 1|\text{modL}\} \quad (8)$$

$$r_k = \max\{1, r_{k-1} + |K_M - K_N + 1|\text{modL}\} \quad (9)$$

where k refers to the number of cut points, L = M or N = the length of the row/column, and (r_1, r_2, …, r_K) are the localities of

cut points. Crossover operation at multiple points is executed by exchanging the even or odd numbered sectors of i and j.

3.2.4 Mutation Unit

Mutation unit disguises the transitional values rearranged after crossover by XORing with a random image. The random mask image is generated before the encryption process starts and shared between the two end users. Mutation unit changes each and every pixel in the intermediary image by XORing with an arbitrary pixel selected by the values of the S_3 and S_4 from the secrete mask image. Any $(i, j)^{th}$ pixel in the enciphered image is attained by XORing the corresponding pixel in the transitional image and $(p_i, q_j)^{th}$ pixel of the enciphered image, where $p_i \epsilon S_3$ and $q_i \epsilon S_4$.

3.2.5 Scrambler Unit

The scrambling is incorporated by altering the positions of the mutated image pixel values as per the elements in a random sequence generated by a random seed. The process for a sample sequence {2, 3, 1… N} is tabulated in table 3.

Table. 3: Scrambler unit design

	Random Sequence					
Random Sequence		2	3	1	…	N
	2	(2,2)	(2,3)	(2,1)	…	(2,N)
	3	.	.	.	.	.
	.	.	.	.	.	.
	..	.	.	.	.	.
	N	(N,2)	(N,3)	(N,1)	..	(N, N)

3.2.6 Experimental results

A sample satellite image shown in Figure 22 is enciphered using the proposed method. Key used is {3.7158, 0.11, 3.89858, 0.25, 3.76158, 0.35, 3.8458, 0.6520}. Figure 23 shows the encrypted image.



Figure 22: Original image,



Figure 23: Encrypted Image

3.2.6.1 Histogram Analysis

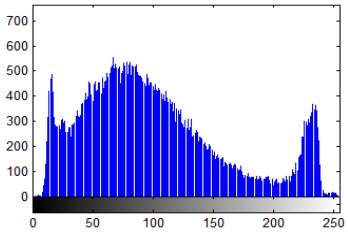


Figure 24(a): Histogram of plain image for red plane

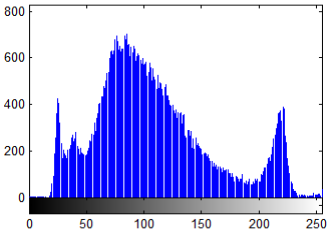


Figure 24(b): Histogram of plain image for green plane

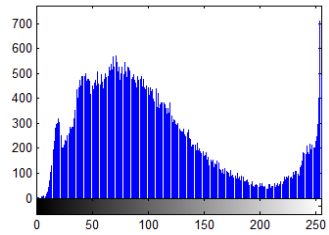


Figure 24(c): Histogram of plain image for blue plane

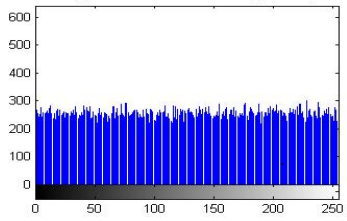


Figure 25(a): Histogram of cipher image for red plane

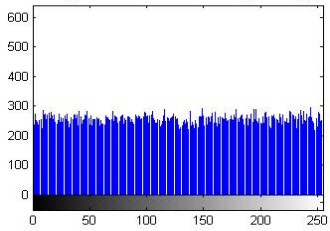


Figure 25(b): Histogram of cipher image for green plane

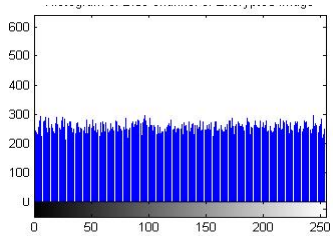


Figure 25 (c): Histogram of cipher image for blue plane

The histograms of plain image are presented in figure 24 (a)-(c). From figure 25(a)-(c), it is witnessed that the histogram of the encrypted image differs completely from the histogram of the plain image and has a uniform distribution, which is the desired property to make the algorithm hard for cryptanalysis.

3.2.6.2 Correlation Analysis

Correlation between two contiguous pixels corresponding to the plain image and cipher image is tested in this experiment. Horizontal, Vertical and Diagonal pixel distribution of plain image and cipher image for red, green and blue planes is shown in figures 26 (a) –(c), 27(a) –(c), 28(a)-(c) and 39(a)-(c), 40(a) –(c), 41(a)-(c) respectively. It is observed that the distribution is almost same and uniformly distributed for all the three-color planes in the cipher image.

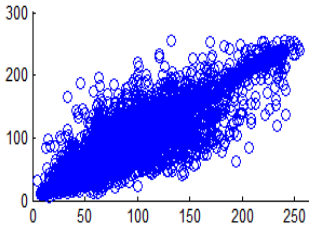


Figure 26(a): Horizontal pixel distribution of plain image for red plane

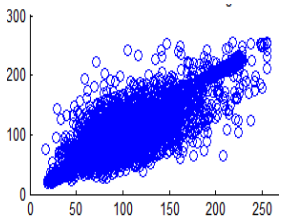


Figure 26(b): Horizontal pixel distribution of plain image for green plane

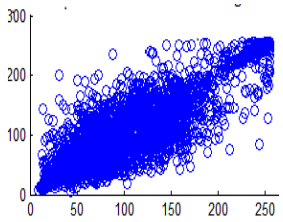


Figure 26(c): Horizontal pixel distribution of plain image for blue plane

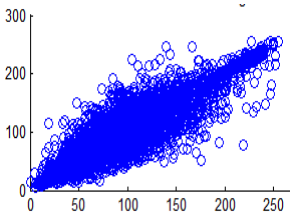


Figure 27(a): Vertical pixel distribution of plain image for red plane

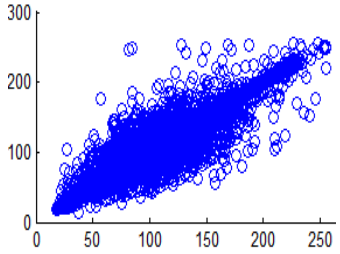


Figure 27(b): Vertical pixel distribution of plain image for green plane

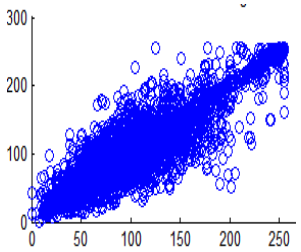


Figure 28(c): Vertical pixel distribution of plain image for blue plane

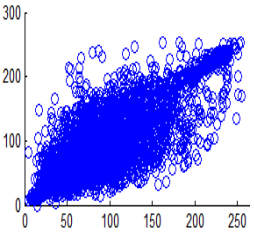


Figure 29(a): Diagonal pixel distribution of plain image for red plane

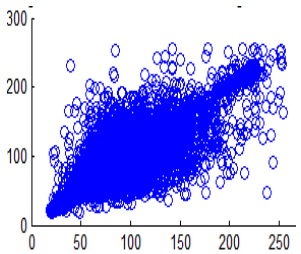


Figure 29(b): Diagonal pixel distribution of plain image for green plane

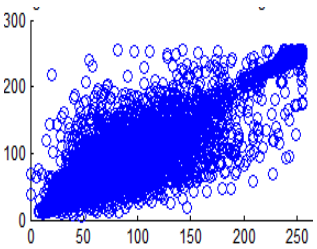


Figure 29(c): Diagonal pixel distribution of plain image for blue plane

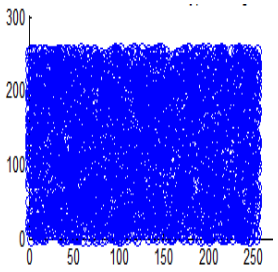


Figure 30(a): Horizontal pixel distribution of cipher image for red plane

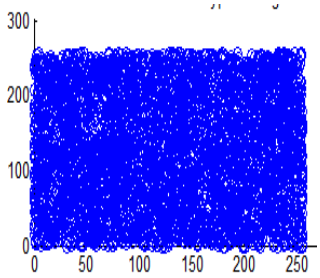


Figure 30(b): Horizontal pixel distribution of cipher image for green plane

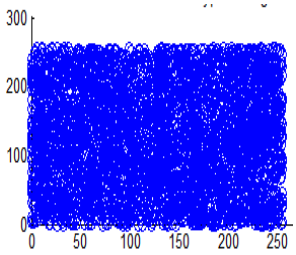


Figure 30(c): Horizontal pixel distribution of cipher image for blue plane

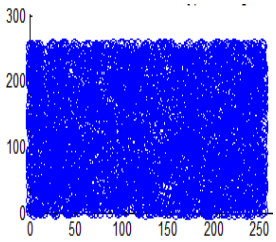


Figure 31(a): Vertical pixel distribution of cipher image for red plane

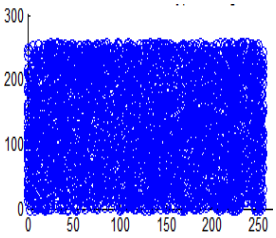


Figure 31(b): Vertical pixel distribution of cipher image for green plane

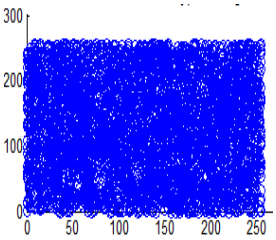


Figure 31(c): Vertical pixel distribution of cipher image for blue plane

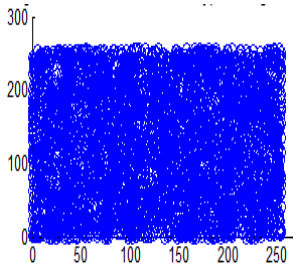


Figure 32(a): Diagonal pixel distribution of cipher image for red plane

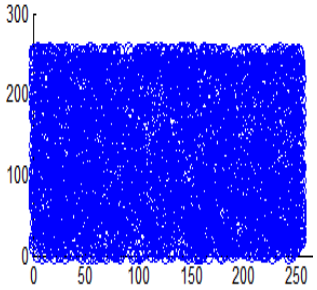


Figure 32(b) Diagonal pixel distribution of cipher image for green plane

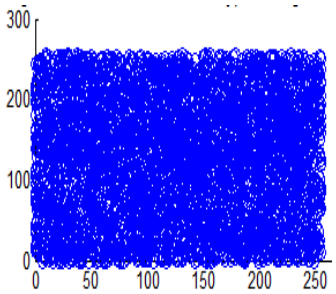


Figure 32(c): Diagonal pixel distribution of cipher image for blue plane

The following equations are used to obtain the correlation coefficients r(x,y) in horizontal (HC), vertical (VC) and diagonal (DC) directions:

$$r(x,y) = \frac{COV(p,q)}{\sqrt{D(p)}\sqrt{D(q)}} \quad (10)$$

where p and q represent gray scale values of two neighboring pixels in the image, D(p) denotes the variance of p and COV (p, q) indicates the covariance of p and q.

The experiment was executed by selecting 4096 random adjacent pixel sets from the plain image and the ciphered image. Correlation coefficients are calculated using equation 3.3 and documented in table 4. It can be observed that the cipher image correlation coefficients are uniformly distributed in the range of 0-255 for all the three planes. This shows the strength of the algorithm towards statistical attacks.

Table 4: Correlation coefficients of two neighboring pixels in input and enciphered image

	Plain Image			Cipher Image		
Color	*R*	*G*	*B*	*R*	*G*	*B*
HC	0.9545	0.9491	0.9223	-0.0005	-0.0008	0.0185
VC	0.9680	0.9558	0.9542	-0.0006	-0.0266	0.0052
DC	0.9269	0.9034	0.8875	-0.0242	-0.0109	-0.0051

3.2.6.3 Differential Analysis

The number of changing pixel rate and the unified averaged changed intensity are effective parameters used in the assessment of the robustness of an image encryption algorithm against differential attacks. Parameter NPCR implies the number of pixels

changed over the encrypted image with only one single pixel in the plain image being varied. The UACI index represents difference in the intensity between plain and encrypted images on an average. The equations 1.9 and 1.10 are used in the calculation of NPCR and UACI respectively. The results for input satellite image shown in figure 3.5(a) are given in table 5 that shows the resistance at differential attacks

Table 5: NPCR, UACI and entropy results

	Encrypted Image		
Color	*R*	*G*	*B*
NPCR (%)	99.6368	99.6017	99.6201
UACI (%)	33.5262	33.6828	33.5840
Entropy (bits)	7.9974	7.9974	7.9973

4. Comparative Study

A huge variety of chaos based image encryption algorithms have been modeled and developed in the past few years. Usually these algorithms are tested on a single image and the conclusion is drawn based on the performance parameters obtained. There arises a need to test the algorithms for a set of images with identical features and decide about the suitability of the algorithms for the input dataset. Proposed work attempts to analyze the results obtained with the algorithms tested using three datasets, namely, satellite images, face images and handwritten signature images. Sample images from each of these datasets are shown in Figure 33, 34 and 35.



Figure 33: Satellite image



Figure 34: Face image



Figure 35: Signature Image

The three datasets have a vast variation in their features. Satellite images have many small segments which show a high level of pixel variations. Also, the content is massive. Face images have few different segments with identical colors. Content is almost uniform in a segment. Signature images have only two colors, blue and white. Pixels are almost identical except the blue colored area. Fifty images belonging to each class are considered in the comparative study.

4.1. Statistical features

Statistical parameters for the three sample images are provided in table 2. Satellite images have almost equal variation in the three planes, with an average centered at the middle value in the range of 0-255. Face images have a bit higher deviation in the three planes and the average is smaller as compared to satellite images. Signature images are centered at near white pixel because of the large white background. Variation is quite different for the three planes. However, all the three sets follow an identical pattern with respect to the correlation coefficients.

Table 5: Statistical parameters for the three datasets

Parameter	Satellite image	Face image	Signature image
mean	102.0983	85.4429	212.9507
standard deviation (R plane)	45.7829	53.3737	91.6546
standard deviation (G plane)	40.5145	44.4940	95.4395
standard deviation (B plane)	50.0683	52.0977	10.6353
correlation coefficient (R plane)	1	1	1
correlation coefficient (G plane)	0.8618	0.9209	0.9999
correlation coefficient (B plane)	0.9715	0.9480	0.3898
Entropy	7.303112	7.307502	2.740406

Results obtained with fifty images from each dataset are compared in the following section to decide about the suitability of the algorithm for the particular dataset. Performance parameters considered for the analysis include horizontal correlation, vertical correlation, diagonal correlation, net changing pixel rate, unified average change in intensity, entropy and encryption time taken by the encryption technique.

4.2. Results for Satellite Images

Fifty satellite images are considered for testing. They are RGB images with sizes varying from 128x128 to 1024x1024 pixels. The images are resized to 256x256 to bring the uniformity in the result. Performance parameters included in the analysis are correlation coefficient, NPCR, UACI, entropy and time required for encryption. Figure 36 (a) to (f) shows the plot of the pixel correlations for fifty encrypted satellite images.

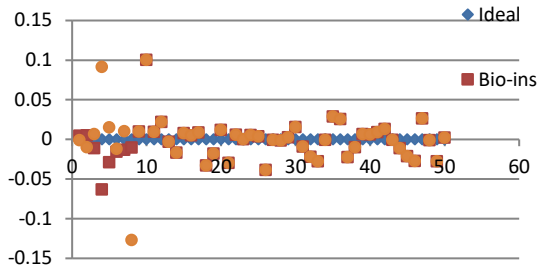


Figure 36(a): Horizontal correlation for 50 images

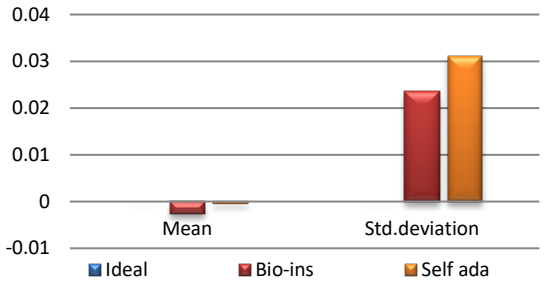


Figure 36(b): Mean Horizontal Correlation

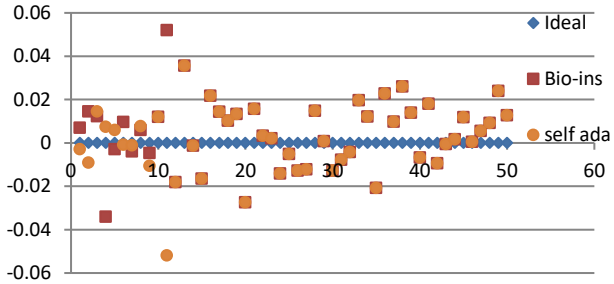


Figure 36 (c): Vertical Correlation for fifty images

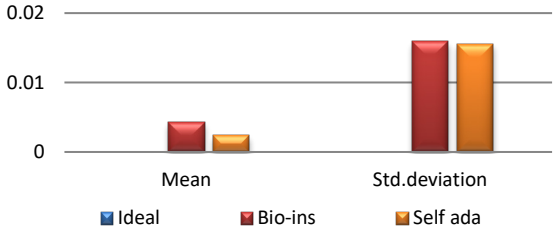


Figure 36 (d): Mean vertical correlation

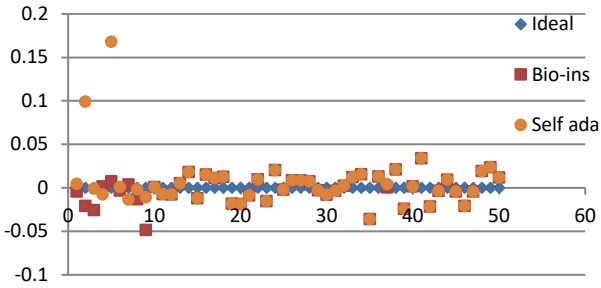


Figure 36(e): Diagonal Correlation for fifty images

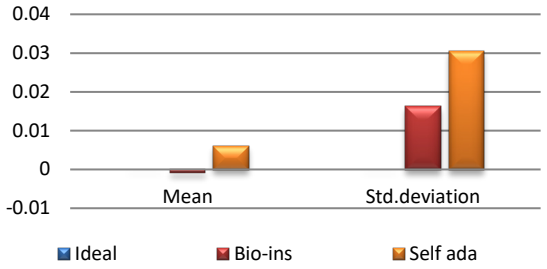


Figure 36(f): Mean Diagonal Correlation

Results of performance comparison for satellite images are displayed in Figure 37.

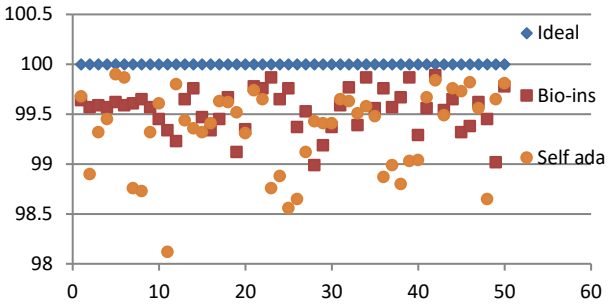


Figure 37(a): NPCR for fifty images

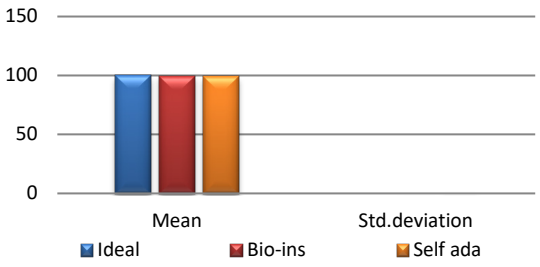


Figure 37 (b): Mean NPCR

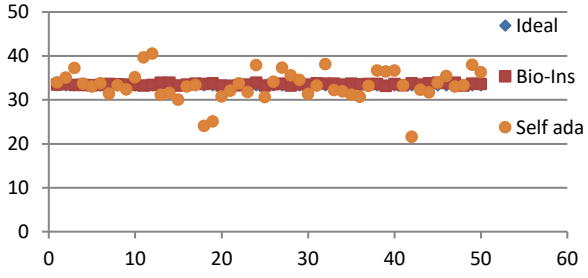


Figure 37(c): UACI for fifty images

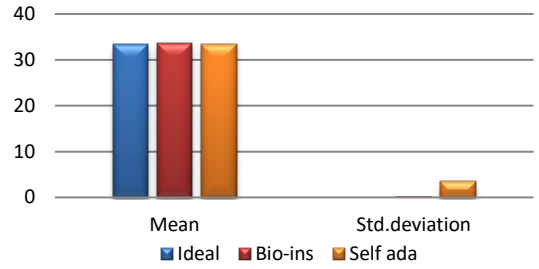


Figure 37(d): Mean UACI

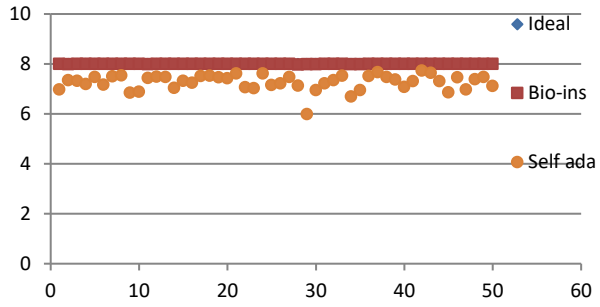


Figure 37(e): Entropy for fifty images

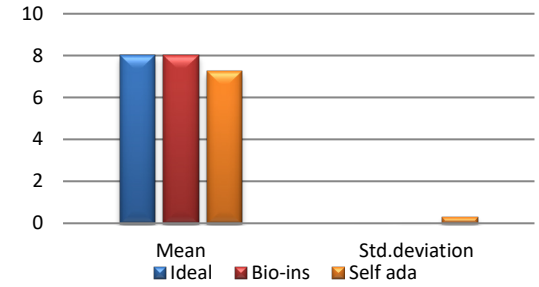


Figure 37(f): Mean Entropy

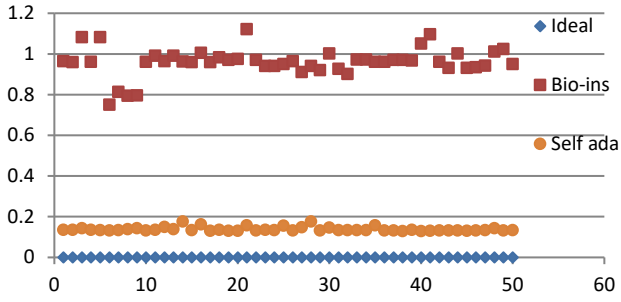


Figure 37(g): Encryption time for fifty images

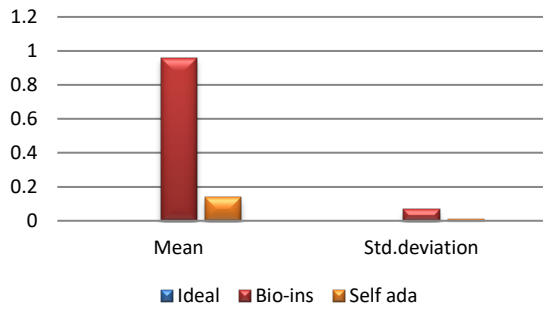


Figure 37(h): Mean encryption time

Referring to these results, Bio-inspired technique performs well with respect correlation coefficients, but requires more time for encryption. Self-adaptive method works well except entropy. Since the satellite images are generally bulky in size and sometimes need to be transmitted in real time, encryption time is also an important parameter to decide the capability of an algorithm. Self-adaptive encryption technique seems to be more time-efficient for the encryption of the satellite images.

4.3. Results for Face Images

Fifty RGB color images containing human face are provided as the inputs for testing. These images are obtained from an open source database [41] and have size of 180x200 pixels. Figure 38(a) to (f) displays the correlation parameters obtained for the fifty encrypted face images.

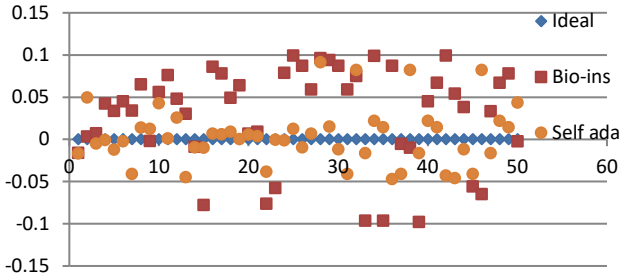


Figure 38(a): Horizontal Correlation for fifty images

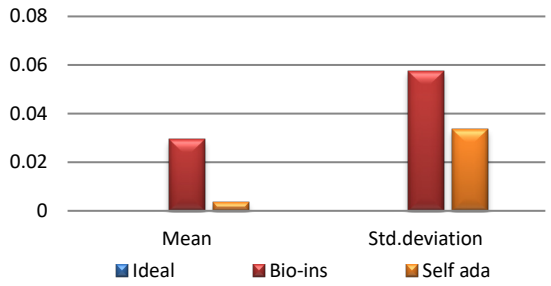


Figure 38(b): Mean Horizontal Correlation

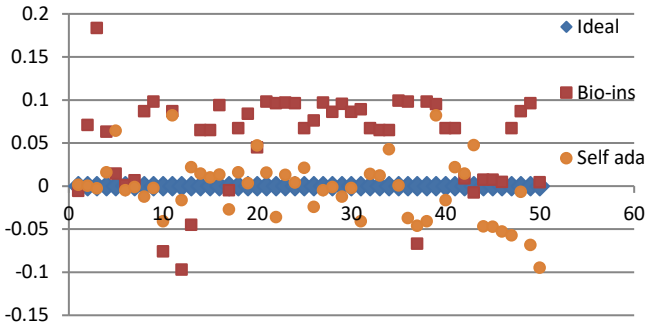


Figure 38(c): Vertical Correlation for fifty images

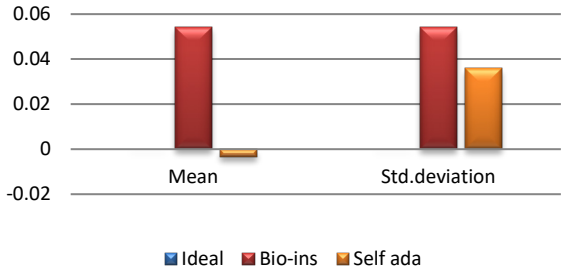


Figure 38(d): Mean Vertical correlation

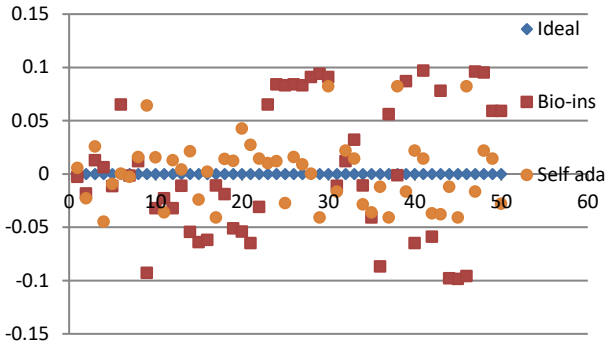


Figure 38(e): Diagonal correlation for fifty images

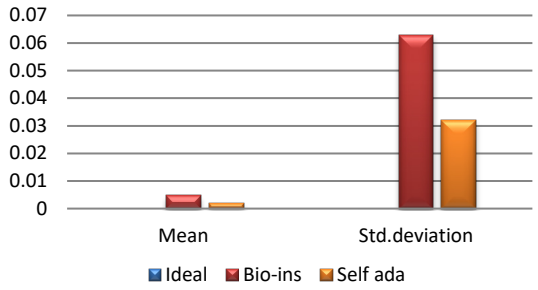


Figure 38(f): Mean Diagonal Correlation

Performance comparison for face images is visualized in Figure 39.

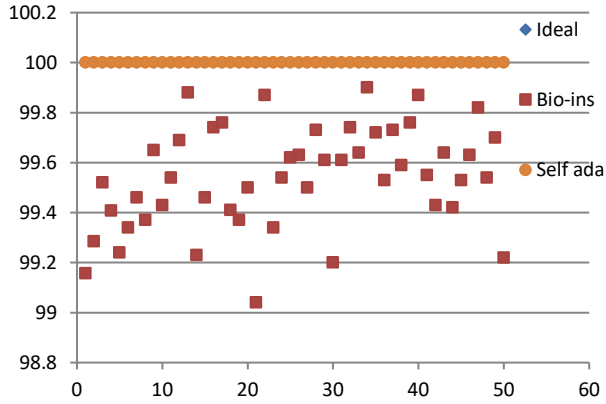


Figure 39 (a): NPCR for fifty images

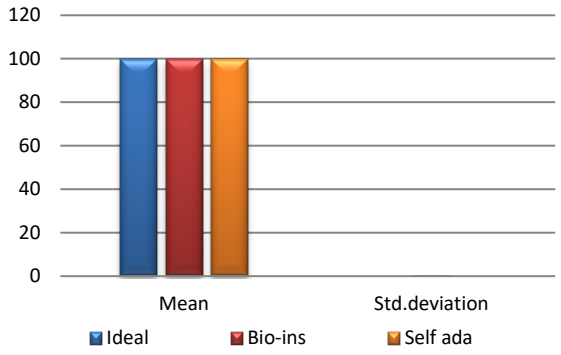


Figure 39(b): Mean NPCR

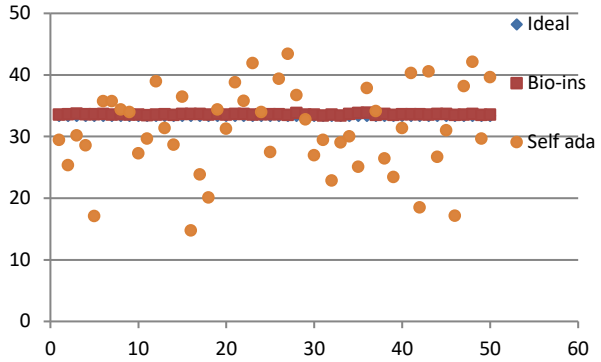


Figure 39(c): UACI for fifty images

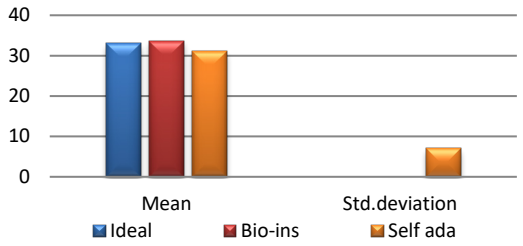


Figure 39(d): Mean UACI

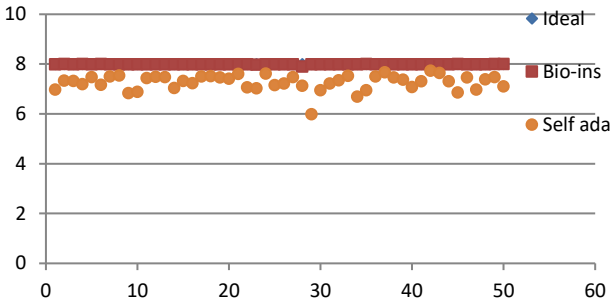


Figure 39(e): Entropy for fifty images

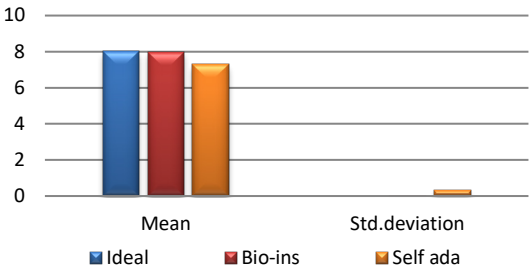


Figure 39(f): Mean Entropy

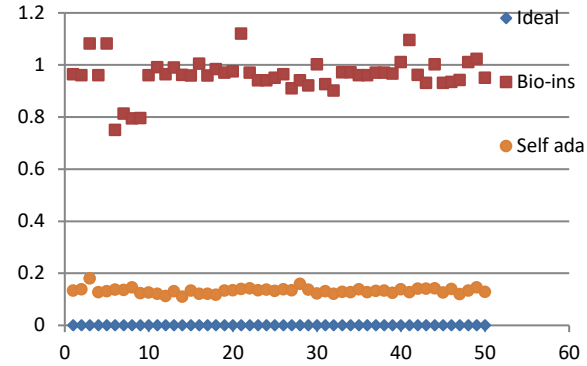


Figure 39(g): Encryption time for fifty images

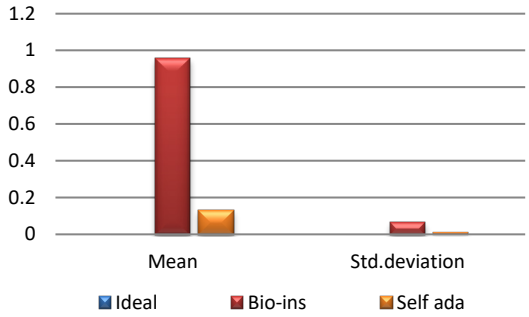


Figure 39(h): Mean Encryption time

Results show that bio-inspired algorithm performs low with correlation test and takes more time for encryption. Self-adaptive algorithm is the fastest but lacks in performance with respect to UACI and entropy values. Face has an important significance in biometric based identification and authentication applications. However, the size of the images does not vary much and the need for real time transmission has limited scope. Hence, any of these algorithms can be chosen for encryption of this kind of images.

4.4. Results for Signature images

Fifty sample signatures are collected from fifty different people with a mobile app. Signatures are RGB images with size varying from 320x320 pixels to 675x675 pixels with white background. Performance parameters obtained for the fifty signature images are documented in Figures. 40 (a) to (f) and 41(a) to (h)

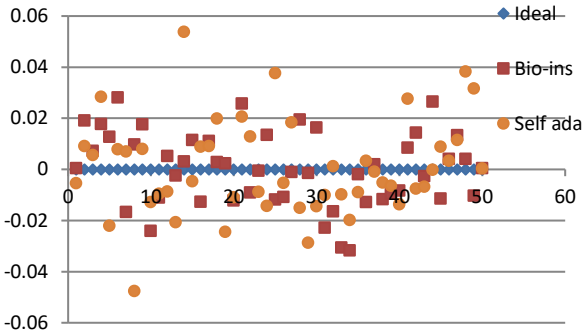


Figure 40(a): Horizontal correlation of fifty images

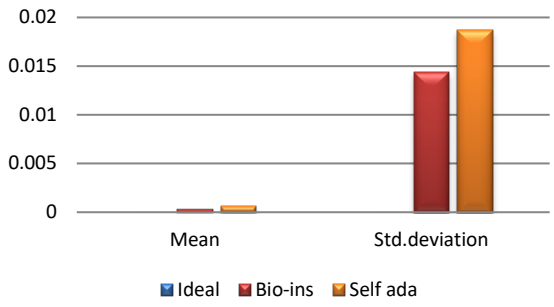


Figure 40(b): Mean Horizontal correlation

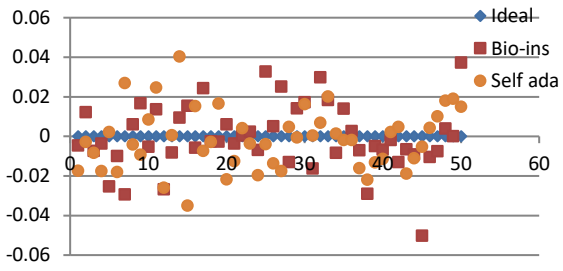


Figure 40(c): Vertical correlation for fifty images

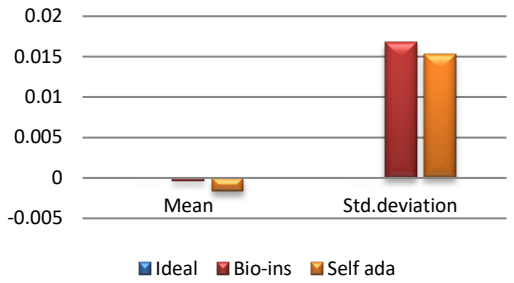


Figure 40(d): Mean vertical correlation

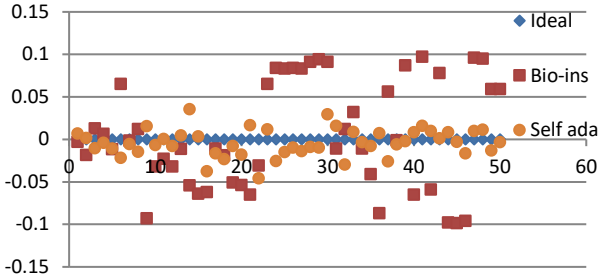


Figure 40(e): Diagonal correlation for fifty images

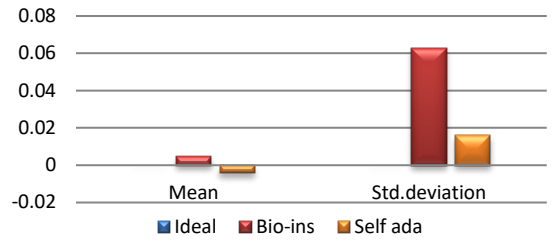


Figure 40(f): Mean Diagonal correlation

Below images Performance comparison for signature images from figure 41 (a) – (g)

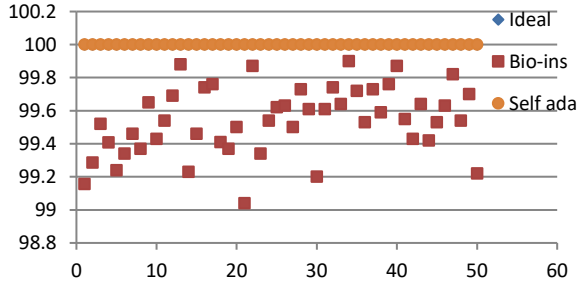


Figure 41(a): NPCR for fifty images

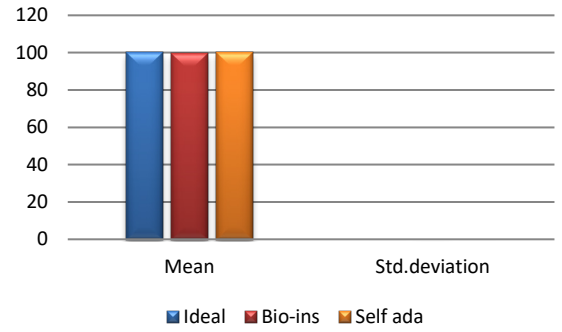


Figure 41(b): Mean NPCR

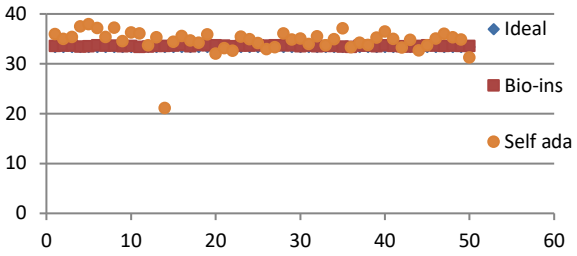


Figure 41(c): UACI for fifty images

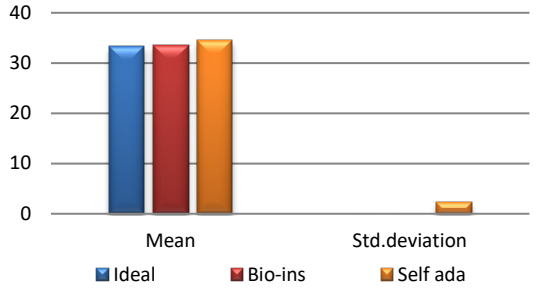


Figure 41(d): Mean UACI

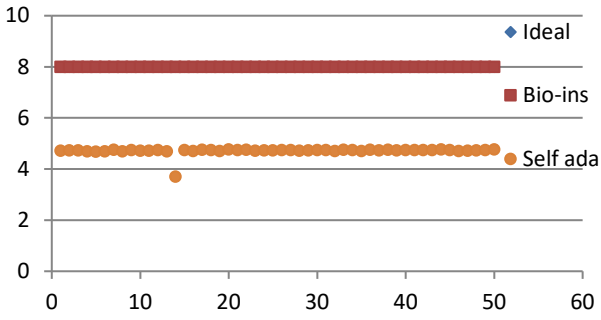


Figure 41(e): Entropy for fifty images

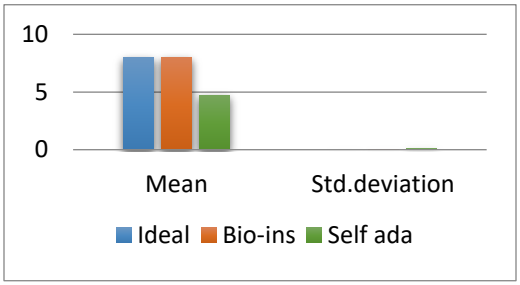


Figure 41(f): Mean Entropy

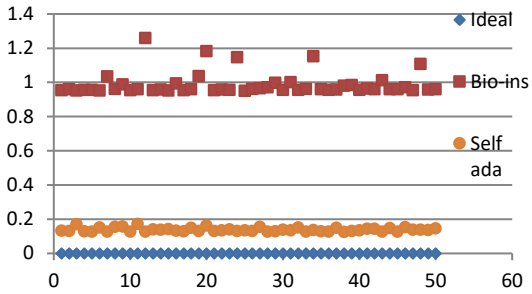


Figure 41(g): Encryption time for fifty images

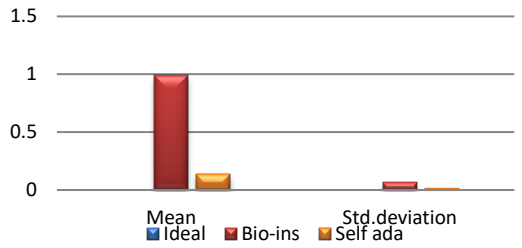


Figure 41(h): Mean encryption time

It can be observed that nature inspired encryption technique performs high for correlation, NPCR, entropy and UACI. Self-adaptive technique has high performance for correlation, NPCR and time, with entropy and UACI values deviating from the ideal values.

Signature images are mainly involved in online shopping and banking applications. Security of them is the primary factor rather than the time taken. Real time processing of these images has limited scope. Also, size of the signature images is not bulky and does not vary much. Therefore, nature inspired technique suits better for the signature image encryption in comparison with the self-adaptive technique.

5. Conclusion and future scope

Suitability analysis is performed on three datasets with different statistical features. Results obtained reveal that the bio-inspired technique provides better performance with respect to NPCR, UACI and entropy, but takes more time to encrypt. Self-adaptive encryption performs well in consideration with correlation and NPCR. Limitation of this method is its low performance in the UACI and entropy tests. Suitability analysis finds out that satellite images can be encrypted more efficiently using self-adaptive method. Performance is almost equal for face images. Signature image encryption can achieve better quality by using bio-inspired method and fast partial method.

References

[1] M. Javidi and R. Hosseinpourfard, "Chaos Genetic Algorithm Instead Genetic Algorithm", The International Arab Journal of Information Technology, . **12**(2), 163-168, March 2015. https://doi.org/10.1007/s11633-017-1107-6

[2] D. Haufu, L. Xiao-lu., L. Xue, "An Improved Genetic Algorithm for Combinatorial Optimization," in Proceedings of the IEEE International Conference on Computer Science and Automation Engineering, Shanghai) 58-61, 2011. https://doi.org/10.1109/CEC.2014.6900496

[3] K. Tang, "An Improved Genetic Algorithm based on A Novel Strategy for Nonlinear Programming Problems," Computers and Chemical Journal, **35**(3), 615-621, 2011. https://doi.org/10.1016/j.compchemeng.2010.06.014

[4] F. Ye F., Y. Haiyang, and J. Xueshou, "An Improved Constrained Optimization Genetic Algorithm," in Proceedings of IEEE International Conference on ICIS, Xiamen, China) 435-439, 2010. https://doi.org/10.1109/ICICISYS.2010.5658317

[5] K. Shankar, P Eswaran, "An Efficient Image Encryption Technique Based on Optimized Key Generation in ECC Using Genetic Algorithm", Artificial Intelligence and Evolutionary Computations in Engineering Systems, , **394**, 705-714. https://doi.org/10.1007/978-81-322-2656-7_64.

[6] H. Nematzadeh, RasulEnayatifar, bHomayunMotameni, Frederico GadelhaGuimarães, Vitor NazárioCoelho, "Medical image encryption using a hybrid model of modified genetic algorithm and coupled map lattices", **110**, 24-32, 2018. https://doi.org/10.1016/j.optlaseng.2018.05.009.

[7] X. Wang, Hui li Zhang, "A novel image encryption algorithm based on genetic recombination and hyper-chaotic systems", Nonlinear Dynamics, **83**, 333-346, 2016. https://doi.org/10.1007/s11071-015-2330-8.

[8] Cheng T., Wang C., Xu M., and Chau W., "Optimizing Hydropower Reservoir Operation using Hybrid Genetic Algorithm and Chaos," Water Resources Management, **22**(7), 895-909, 2008. https://doi.org/10.1007/s11269-007-9200-1

[9] Chao-Lin Kuo, et.al, "Image Encryption Based on Fuzzy Synchronization of Chaos Systems", IEEE 37th Annual Computer Software and Applications Conference)45 3-461, 2013. https://doi.org/10.1109/COMPSAC.2013.23

[10] Abdul Hanan Abdullaha, Rasul Enayatifara,, Malrey Lee, "A hybrid genetic algorithm and chaotic function model for image encryption", International Journal on Electronics and Communication (AEÜ), **66**, 806– 816,2012. https://doi.org/10.1016/j.aeue.2012.01.015

[11] A. Ahmed et al., "Modeling and Simulation of Office Desk Illumination Using ZEMAX," in 2019 International Conference on Electrical, Communication, and Computer Engineering (ICECCE), 1–6, 2019. doi: 10.1109/ICECCE47252.2019.8940756.

[12] V. Srikanth, et.al, "Bit-Level Encryption of Images using Genetic Algorithm", TECHNIA, International Journal of Computing Science and Communication Technologies, **3**(1), 2010. https://doi.org/10.1007/978-3-642-30111-7_75

[13] K.A Al-Utaibi., El-Alfy, "A bio-inspired image encryption algorithm based on chaotic maps", IEEE Congress on Evolutionary Computation (CEC)) 87-92, 2010. https://doi.org/10.1109/CEC.2010.5586463

[14] Hassan Al-Mahdi , Yaser Fouad, "Design and analysis of DNA Binary Cryptography Algorithm for Plaintext", International Journal of Engineering and Technology (IJET), 10(3) 699-706, 2018. https://doi.org/10.21817/ijet/2018/v10i3/181003055

[15] Narendra K. Pareek, Vinod Patidar, "Medical image protection using genetic algorithm operations", Soft Computing, **20**(2), 763–772, 2016. https://doi.org/10.1007/s00500-014-1539-7

[16] Yuansheng Liu,et.al, "Cryptanalyzing a RGB image encryption algorithm based on DNA encoding and chaos map", Optics & Laser Technology, 60(6)111–115, 2014. https://doi.org/10.1016/j.optlastec.2014.01.015

[17] H. Wen et.al, "Breaking an Image Encryption Algorithm Based on DNA Encoding and Spatiotemporal Chaos', Entropy, **21**(7), 246-263, 2019. https://doi.org/10.3390/e21030246

[18] Areeba Fatima, Isha Mehra and Naveen K Nischal , "Optical image encryption using equal modulus decomposition and multiple diffractive imaging", Journal of optics, **18**, 2016, 10.1088/2040-8978/18/8/085701.

[19] R. Kumar, Basanta Bhaduri, "Optical image encryption using Kronecker product and hybrid phase masks", Optics & Laser Technology, **95**, 51-55, 2017. https://doi.org/10.1016/j.optlastec.2017.03.041

[20] Ravi Kumar, Basanta Bhaduri, "Optical image encryption in Fresnel domain using spiral phase transform", Journal of optics, **19**, 2017. 10.1088/2040-8986/aa7cb1

[21] M. Joshi, Chandra Shakher, Kehar Singh, "Image encryption and decryption using fractional Fourier transform and radial Hilbert transform', Optics and Lasers in Engineering, **46**(1), 522– 526, 2008. https://doi.org/10.1016/j.optlaseng.2008.03.001

[22] S. Liu, "A review of optical image encryption techniques", Optics & Laser Technology, **57**(1), 327–342, 2014. https://doi.org/10.1016/j.optlastec.2013.05.023

[23] Z. Liu, et.al, "Color image encryption by using the rotation of color vector in Hartley transform domains", Optics and Lasers in Engineering, **48**, 800–805, 2010. https://doi.org/10.1016/j.optlaseng.2010.02.005

[24] N. Singh, A. Sinha, "Optical image encryption using fractional Fourier transform and chaos", Optics and Lasers in Engineering, **46**(2) 117–123, 2008. https://doi.org/10.1016/j.optlaseng.2007.09.001

[25] Y. Liang & G. Liu "Color image encryption combining a reality-preserving fractional DCT with chaotic mapping in HIS space". Multimedia Tools and Applications, **75**(11), 6605-6620, 2016. https://doi.org/10.1007/s11042-015-2592-7

[26] Dr. Emad S. Othman, Dr. Mohammed M. Sakre, "Compression and Encryption Algorithms for Image Satellite Communication", International Journal of Scientific & Engineering Research, **3**(9), 1-4, 2012.

[27] Qiwen Ran, et.al, "Vector power multiple-parameter fractional Fourier transform of image encryption algorithm", Optics and Lasers in Engineering, **62**, 80–86, 2014. https://doi.org/10.1016/j.optlaseng.2014.05.008

[28] Ensherah A. Naeem, et.al, "Efficient implementation of chaotic image encryption in transform domains", The Journal of Systems and Software, **97**(3), 118–127, 2014. https://doi.org/10.1016/j.jss.2014.07.026

[29] R. A. Schowengerdt, "Remote sensing, third edition: models and methods for image processing", Academic Press, 2006.

[30] Anil K. Jain, et.al, "Statistical Pattern Recognition: A Review", IEEE Transactions on Pattern Analysis and Machine Intelligence, 2000. https://doi.org/10.1109/34.824819

[31] Panigrahi, Sushant, and Toran Verma, "Texture image classification using neuro fuzzy approach." International Journal of Engineering and Computer Science, **2**(1), 2309-2313, 2013.

[32] Sura F. Yousif, ""Grayscale Image Confusion and Diffusion Based on Multiple Chaotic Maps", 1st International Scientific Conference of Engineering Sciences - 3rd Scientific Conference of Engineering Science (ISCES), 2018. https://doi.org/10.1109/ISCES.2018.8340538

[33] Jianhua Wu, Mengxia Zhang and Nanrun Zhou,"Image encryption scheme based on random fractional discrete cosine transform and dependent scrambling and diffusion", Journal of Modern optics, 2016. https://doi.org/10.1080/09500340.2016.1236990

[34] P. Maan, Hukum Singh, "Non-linear Cryptosystem for Image Encryption Using Radial Hilbert Mask in Fractional Fourier Transform Domain", 3D Research, **9**(53), 112-119, 2018. https://doi.org/10.1007/s13319-018-0205-8

[35] V. Srikanth, et.al, "Bit-Level Encryption of Images using Genetic Algorithm", TECHNIA, International Journal of Computing Science and Communication Technologies, 3, issue1, 2010.

[36] R. Bhagyashri. Pandurangi, Meenakshi R. Patil, "A Nature Inspired Color Image Encryption Technique to Protect the Satellite Images", International Journal of Current Engineering and Technology, **9**(3), May 2019. https://doi.org/10.14741/ijcet/v.9.3.4

[37] R. Bhagyashri. Pandurangi, Meenakshi R. Patil, Chaitra Bhat, "Comparison of Bio-inspired and Transform based Encryption Algorithms for Satellite Images", Third IEEE International Conference on Electrical, Electronics, Communication, Computer Technologies and Optimization Techniques (ICEECCOT), Mysore, India, December 2018. https://doi.org/10.1109/ICEECCOT43722.2018.9001344

[38] H. Gao, et.al, "A new chaotic algorithm for image encryption", Chaos, Solitons& Fractals, **2**(29), 393-399, July 2006. https://doi.org/10.1016/j.chaos.2005.08.110

[39] Adolf W. Lohmann, David Mendlovic, and Zeev Zalevsky, "Fractional Hilbert transform," Optics Letters, **21**(4), 281-283, 1996. https://doi.org/10.1364/OL.21.000281

[40] https://bhuvan-app1.nrsc.gov.in/imagegallery/bhuvan.html

[41] http://cmp.felk.cvut.cz/~spacelib/faces/faces94.html

ASTES

Advances in Science, Technology and Engineering Systems Journal Vol. 5, No. 5, 1093-1098 (2020)

www.astesj.com

Special Issue on Multidisciplinary Sciences and Engineering

ASTESJ

ISSN: 2415-6698

Posture Recognition Method for Caregivers during Postural Change of a Patient on a Bed using Wearable Sensors

Kodai Kitagawa[1,*], Koji Matsumoto[1], Kensuke Iwanaga[1], Siti Anom Ahmad[2], Takayuki Nagasaki[3], Sota Nakano[4], Mitsumasa Hida[1,5], Shogo Okamatsu[1,6], Chikamune Wada[1]

[1]*Graduate School of Life Science and System Engineering, Kyushu Institute of Technology, Kitakyushu, 8080196, Japan*

[2]*Malaysian Research Institute of Ageing (MyAgeing™), Universiti Putra Malaysia, Serdang, Selangor, 43400, Malaysia*

[3]*Department of Rehabilitation, Tohoku Bunka Gakuen University, Sendai, 9818550, Japan*

[4]*Department of Rehabilitation, Kyushu University of Nursing and Social Welfare, Tamana, 8650062, Japan*

[5]*Department of Physical Therapy, Osaka Kawasaki Rehabilitation University, Kaizuka, 5970104, Japan*

[6]*Department of Physical Therapy, Kitakyushu Rehabilitation College, Kanda, 8000343, Japan*

ARTICLE INFO

Article history:
Received: 09 September, 2020
Accepted: 10 October, 2020
Online: 20 October, 2020

Keywords:
Posture recognition
Caregiver
Patient handling
Lower back pain
Wearable sensor
Machine learning

ABSTRACT

Caregivers experience lower back pain due to their awkward postures while handling patients. Therefore, a monitoring system to supervise caregivers' postures using wearable sensors is being developed. This study proposed a postural recognition method for caregivers during postural change while handling a patient on a bed. The proposed method recognizes foot positions and arm movements by a machine learning algorithm using inertial data on the trunk and foot pressure data obtained from wearable sensors. An experiment was conducted to evaluate whether the proposed method could recognize three foot positions and three arm movements. Participants provided postural change for a simulated patient on a bed (patient: supine to lateral recumbent) under nine conditions, including different combinations of the three foot positions and three arm movements; the experiment was repeated ten times for each condition. Experimental results showed that the proposed method using an artificial neural network with all features obtained from an inertial measurement unit and insole pressure sensors could recognize arm movements and foot positions with an accuracy of approximately 0.75 and 0.97, respectively. These results suggest that the proposed method can be used in a monitoring system tracking a caregiver's posture.

1. Introduction

Recently, many caregivers have experienced lower back pain owing to frequent patient handling [1–2]. Previous studies have suggested that caregivers should maintain an appropriate posture based on body mechanics during patient handling [3–4]. Accordingly, previous studies have developed monitoring systems to supervise the postures of caregivers to prevent lower back pain [5–8].

Lin et al. developed a robot patient comprising an inertial measurement unit (IMU), angular position sensors, and servo motor encoders and found that the robot could classify correct and incorrect transfer methods [5]. Huang et al. developed an automatic evaluation method for patient transfer skills using two Kinect RGB-D sensors [6, 7]. Their study showed that this method could improve the patient transfer skill of students [7]. Itami et al. developed a monitoring system using electromyography, goniometer, and inclination sensor [8]. This system could monitor skills and lumbar loads of patient handling [8]. These systems are useful for monitoring caregivers' postures; however, these systems have limitations in terms of workspace and usability because they

*Corresponding Author: Kodai Kitagawa, Kyushu Institute of Technology, Japan, kitagawakitagawa156@gmail.com

require vision-based devices, multiple specialized sensors, or robots. Previous study reported that assistive devices for caregivers should be time-efficient, cost-effective, and suitable for various workspaces [9]. Hence, there is a need to develop wearables and simple monitoring systems for caregivers' postures.

PostureCoach is a wearable and simple system for preventing lower back pain among caregivers [10]. This system can provide real-time biofeedback using the trunk angle obtained from only two IMUs [10]. Previous investigations have shown that PostureCoach can reduce the lumbar spine flexion in a beginner who handles patients [10]. However, this system cannot suggest caregiver ways to adjust to an appropriate posture because the system measures only the trunk angle. Several factors, such as the foot position and arm movement, are useful to achieve suitable postures to prevent lower back pain during patient handling [11–13]. Therefore, a simple and wearable system that monitors the trunk angle, foot position, and arm movement is being develop [14].

Figure 1 shows the flow of the proposed monitoring system for caregivers' postures. The proposed system monitors a caregiver's posture using wearable sensors mounted on the caregiver's trunk and shoes (Step 1). The proposed method evaluates several factors such as trunk angle, foot positions, and arm movements using sensor data obtained from the wearable sensors (Step 2). If the evaluated factors are unsuitable, the proposed system informs the caregiver to adjust their posture (Step 3).

Our previous study proposed a postural recognition method during sit-to-stand assistive motions but could not consider other patient-handling aspects and various foot positions and arm movements [14]. Several patient-handling aspects, such as providing postural change to turn a patient on a bed, cause lumber load among caregivers [12, 15]. Such a type of patient handling causes lower back pain among caregivers as a patient is frequently repositioned on a bed [15]. As explained above, arm movements and foot positions are important factors for patient handling [11-13]. Thus, this study proposes the recognition method for various foot positions and arm movements of caregivers using a postural recognition method during postural change for a patient on a bed.

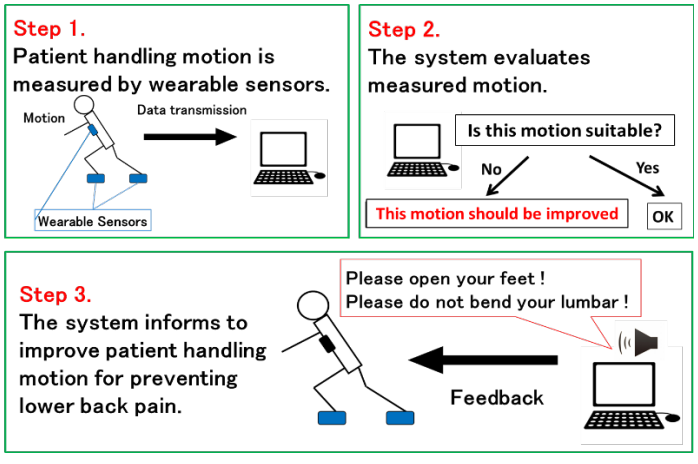


Figure 1: Monitoring system for patient-handling motion.

This section discusses the background, previous studies of this paper. The remainder of this paper is organized as follows. Section 2 mentions the objective and contribution of this paper. Section 3 explains the proposed method for postural recognition during postural change while handling a patient on a bed. Section 4 describes the experiments conducted to evaluate whether the proposed method can recognize a caregiver's posture during patient handling. Section 5 presents experimental results and discussions. Finally, section 6 presents conclusions.

2. Objective and Contribution

The objective of this study is proposal of a novel posture recognition method for wearable monitoring system to prevent lower back pain among caregivers. Furthermore, this study explores appropriate combination of wearable sensors and machine learning algorithms for the proposed method.

The contribution of this study is as follows. The proposed method will be applied to suggest an appropriate posture for caregivers because this method recognizes both arm movements and foot positions. This study presents the novel posture recognition method using sensor fusion consisted of IMU and insole pressure sensor. As a scientific contribution, this method using sensor fusion of wearable sensor has a potential to be applied to posture recognition related to occupational health. In addition, the appropriate combination of wearable sensors and machine learning algorithms shown in this study will be useful in the research area of computer science and wearable systems.

3. Proposed Method

3.1. Overview

Figure 2 shows a block diagram of the proposed postural recognition method. The proposed method measured postural information by wearable sensors. Machine learning algorithm using features obtained from wearable sensors generated function for postural recognition. Caregiver's posture such as arm movement and foot position were recognized by generated function. The details of each component are described below.

3.2. Input (wearable sensors)

The IMU attached on the trunk and insole pressure sensors measured postural information during patient handling. The IMU (Logical Product Co., Japan) measures the three-axis acceleration and angular velocity of the trunk for features of the machine learning algorithm. Insole pressure sensors are fabricated by arranging eight FlexiForce sensors (Tekscan, USA) on each foot. Because the FlexiForce sensors are thin and flexible, they are suitable for measuring forces between various surfaces, such as an insole [16]. Furthermore, the FlexiForce sensors can be used in real time applications owing to the lack of linearity, non-repeatability, and hysteresis [17]. Front and rear forces on each foot are measured using insole pressure sensors as features for the machine learning algorithm. These sensor data were measured at a 1-kHz sampling rate.

3.3. Machine learning-based recognition

Seven features (mean, maximum, minimum, standard deviation, root mean square, kurtosis and skewness) were extracted for machine learning algorithm. These features were extracted from each sensor data using a sliding window technique with a 1.0-s window size and 50% overlap. These features, window

size, and overlap were selected based on the previous researches about posture recognition using wearable sensors [18–19].

The machine learning algorithm recognized three arm movements and three foot positions during postural change while handling a patient on a bed. In this study, artificial neural network, decision tree, and support vector machine were selected as machine learning algorithm for the proposed method because these three algorithms were used for wearable sensor-based posture recognition [19-20]. Details of the recognition models were described below.

Artificial neural network is applied to complex relationship between input and output by nonlinear and flexible decision boundary [19-21]. The artificial neural network-based model consists of input layer, hidden layer and output layer [19-20]. In our proposed method, the features obtained from the wearable sensors were inputted to the input layer, and the recognized posture was outputted from the output layer. Hidden layer was set function for learning the relationship between features obtained wearable sensor and postures. The specifications and parameters in artificial neural network of proposed method is shown in Table 1.

Decision tree provides if-then rules which have free of ambiguity [22-24]. If-then rules generated by decision tree consist of root, internal and leaf nodes [22]. The root and internal nodes have threshold of features for recognition. Position and features of these nodes are determined based on comparison of entropy for all features [23]. Leaf nodes are defined as recognition output via root and internal nodes. When these nodes are too many and complex, recognition model has problem such as over fitting [24]. Thus, decision tree has several parameters to adjust number of nodes [24]. The specifications and parameters of decision tree in our proposed method is shown in Table 2.

Support vector machine is applied to nonlinear data without over fitting by large margin separation and kernel function [25]. Kernel function provides efficient calculation in nonlinear feature spaces [25]. Large margin separation is required for generalization performance of support vector machine [25]. The specifications and parameters of support vector machine in our proposed method is shown in Table 3.

Comparison of these machine learning algorithms was necessary in order to determine the appropriate algorithm depends on the target postures [19–20]. In this study, the proposed method was compared to investigate which algorithm could recognize patient handling motion using these wearable sensors.

Table 1: Specifications and parameters for artificial neural network of the proposed method.

Specification / Parameter	Status / Value	
Number of Node / Neuron	Input Layer	70 (based on features)
	Hidden Layer	70
	Output Layer	3 (based on postures)
Activation Function	Hidden Layer	Sigmoid
	Output Layer	Linear
Learning Rate	0.3	
Momentum	0.2	
Training	Back Propagation	

3.4. Output (recognized posture)

In the proposed method, arm movements and foot positions were recognized as postural factors. The monitoring system shown in previous section will provide caregiver the appropriate posture based on recognition results.

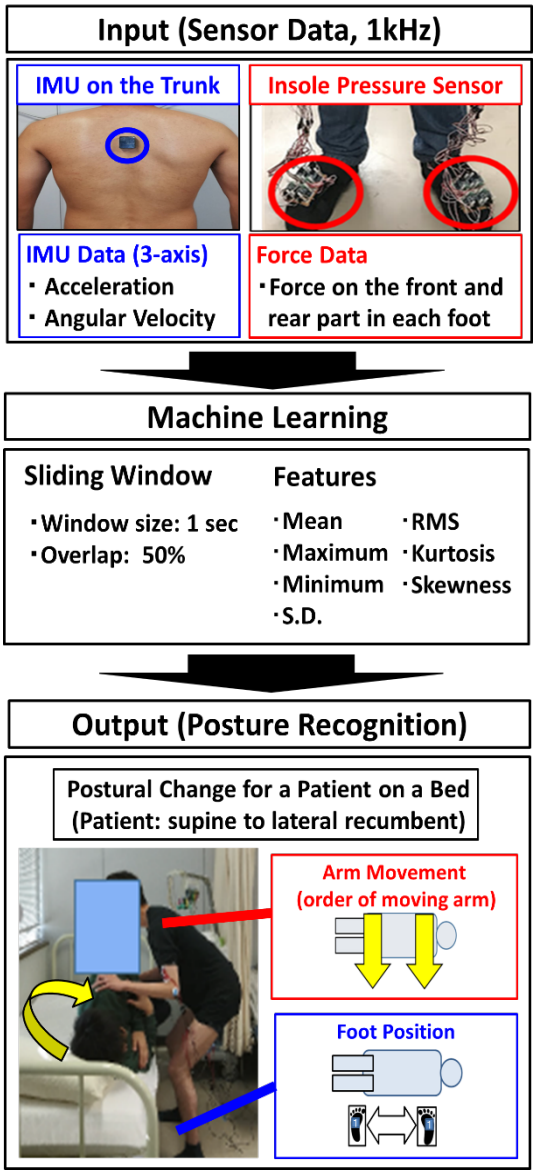


Figure 2: Proposed postural recognition method.

Table 2: Specifications and parameters for decision tree of the proposed method.

Specification / Parameter	Status / Value
Algorithm	J48 (entropy-based)
Confidence Factor for Pruning	0.25
Minimum Number of Samples per Leaf Node	2
Number of Folds for Data Segmentation	3

Table 3: Specifications and parameters for support vector machine of the proposed method.

Specification / Parameter	Status / Value
Training	Sequential Minimal Optimization
Kernel	Polynomial Kernel
c (weight for slack variable)	1.0

4. Experiment

Four young healthy males (24.75 ± 0.83 years, 1.72 ± 0.05 m, 67.00 ± 10.79 kg) were participants as caregivers. One young healthy male (25.00 years, 1.69 m, 70.00 kg) participated as a simulated patient. All participants provided their verbal informed consent to the experiment.

The four participants (caregivers) were asked to perform a postural change for the simulated patient on a bed under nine postural conditions. The nine conditions were a combination of the three arm movements and three foot positions shown in Figure 3. Each participant (caregiver) repeated this motion ten times for each condition. Data for the proposed method were measured by wearable sensors (IMU and insole pressure sensors) at 1-kHz sampling frequency for each trial.

The proposed method recognized the three arm movements and three foot positions by processing data obtained from the sensors using the machine learning algorithm. This experiment compared the recognition performance of three machine learning algorithms to determine the appropriate algorithm for the proposed method. Furthermore, the recognition performances of three feature patterns ("IMU," "Insole Sensor," and "All") were compared to verify the effectiveness of the sensors and features.

The metrics of accuracy and F-measure were used to evaluate the recognition performance of the algorithms. These evaluation metrics were calculated according to

$$\text{Accuracy} = \frac{TP + TN}{TP + TN + FP + FN} \quad (1)$$

$$\text{Precision} = \frac{TP}{TP + FP} \quad (2)$$

$$\text{Recall} = \frac{TP}{TP + FN} \quad (3)$$

$$\text{F-measure} = \frac{2 \times Precision \times Recall}{Precision + Recall} \quad (4)$$

where TP denotes true positive and represents the number of correct recognition for positive samples, TN denotes true negative and represents the number of correct recognition for negative samples, FP denotes false positive represents the number of samples incorrectly recognized as positive in actual negative samples, and FN denotes false negative and represents the number of samples incorrectly recognized as negative in actual positive samples. The accuracy of the proposed method was evaluated based on the recognition performance of each algorithm using the feature patterns. The F-measure of each arm movement and foot position was calculated using the harmonic mean of precision and recall as the overall performance. These metrics were calculated by ten-fold cross validation using data obtained from all trials and participants.

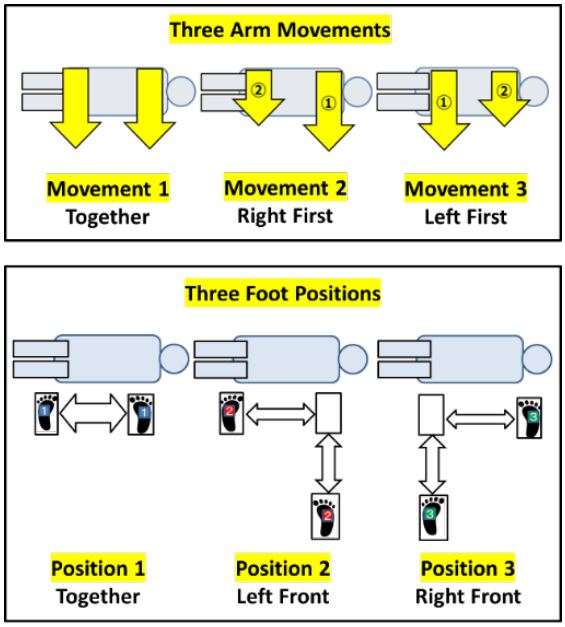


Figure 3: Postural conditions in the experiment.

5. Results and Discussion

Tables 4 and 5 show the accuracy and F-measure of the proposed method. The results show that the combination of artificial neural network and all features obtained from both IMU and insole pressure sensors achieved the best performance for postural recognition. In this combination, the proposed method could recognize arm movements and foot positions with an accuracy of approximately 0.75 and 0.97, respectively. These results suggest the possibility of using the proposed recognition method in monitoring systems to prevent lower back pain.

A comparison between the machine leaning algorithms showed that the artificial neural network exhibited the best performance for both accuracy and F-measure. Therefore, the artificial neural network was deemed the most suitable machine learning algorithm for the proposed method. The artificial neural network's best performance was attributed to its nonlinear and flexible decision boundary, which was effective for wearable sensor data [19-21].

A comparison between feature patterns showed that the proposed method yielded the best performance for accuracy and F-measure when all features obtained from both IMU and insole pressure sensors were used. These results indicated that both IMU and insole pressure sensors were effective and necessary for the proposed method. Moreover, in foot position recognition, the proposed method using only insole pressure sensors achieved a great performance. These findings indicate that the insole pressure sensors could detect the force distribution depending on the foot positions. However, the proposed method could not recognize arm movements using only the insole pressure sensors. Thus, IMU was also considered necessary for the proposed method. Table 6 shows the confusion matrices of the proposed method using the artificial neural network and all features for postural recognition. These results showed that the proposed method achieved good performance for foot position recognition. The reason for this

performance, as explained earlier, was that insole pressure sensors in the shoes could detect relevant features related to foot positions. However, the proposed method incorrectly recognized arm movement between movements 1 and 3 because there was no sensor on the upper limbs. Placing additional sensors on the upper limbs could obstruct care activities. Thus, the optimal position to place an IMU on the trunk to detect arm movement without additional sensors should be explored.

The limitation of this study is that the proposed method was not evaluated in an actual workspace and under various aspects of patient handling, such as assisting transfer. Moreover, the proposed method should be tested for female participants, patients of different ages, and caregivers. Furthermore, other feature selection patterns and algorithms should be examined to improve the performance of the proposed postural recognition method. Following further tests and improvements on the proposed method, the postural monitoring system to prevent lower back pain will be implemented based on the proposed postural recognition method.

Table 4: Accuracy of the proposed method.

Algorithm	Feature Pattern	Accuracy	
		Arm Movement	Foot Position
Artificial Neural Network	IMU	0.691	0.693
	Insole Sensor	0.508	0.971
	All	**0.755**	**0.979**
Decision Tree	IMU	0.616	0.635
	Insole Sensor	0.634	0.938
	All	0.645	0.930
Support Vector Machine	IMU	0.586	0.591
	Insole Sensor	0.364	0.958
	All	0.599	0.972

Table 5: F-measure of the proposed method.

Algorithm	Feature Pattern	F-measure					
		Arm Movement			Foot Position		
		1	2	3	1	2	3
Artificial Neural Network	IMU	0.637	0.760	0.674	0.675	0.629	0.776
	Insole Sensor	0.486	0.539	0.497	0.959	0.976	0.980
	All	**0.707**	**0.813**	**0.742**	**0.974**	**0.978**	**0.985**
Decision Tree	IMU	0.575	0.695	0.571	0.627	0.587	0.694
	Insole Sensor	0.595	0.681	0.622	0.915	0.954	0.945
	All	0.632	0.682	0.619	0.902	0.951	0.938
Support Vector Machine	IMU	0.593	0.646	0.510	0.617	0.438	0.700
	Insole Sensor	0.325	0.429	0.309	0.942	0.970	0.964
	All	0.591	0.653	0.552	0.962	0.975	0.980

In future work, the optimal placement of sensors will be explored to improve the accuracy of postural recognition in the proposed method. Moreover, other machine learning algorithms will be tested to determine a more suitable algorithm for the proposed method. Furthermore, a modified version of the proposed recognition method should be evaluated under various conditions. Finally, a monitoring system will be implemented based on the modified postural recognition method to prevent lower back pain due to patient handling.

Table 6: Confusion matrices of posture recognition (using an artificial neural network with all features).

(A) Arm Movement

		Recognized		
		Movement 1	Movement 2	Movement 3
Actual	Movement 1	259	42	72
	Movement 2	40	326	26
	Movement 3	63	35	277

(B) Foot Position

		Recognized		
		Position 1	Position 2	Position 3
Actual	Position 1	387	6	3
	Position 2	7	364	1
	Position 3	5	2	365

6. Conclusion

In this study, the posture recognition method for caregivers during postural change for a patient on a bed was proposed. The experimental results showed that the proposed method could recognize a caregiver's posture. The proposed method using novel sensor fusion with machine learning will also be useful for posture recognition in other various application.

Conflict of Interest

The authors declare no conflict of interest.

Acknowledgment

The first author is grateful for a scholarship from the Nakatani Foundation for Advancement of Measuring Technologies in Biomedical Engineering.

References

[1] S. Kai, "Consideration of low back pain in health and welfare workers," Journal of Physical Therapy Science, **13**(2), 149–152, 2001, doi:10.1589/jpts.13.149.

[2] A. Holtermann, T. Clausen, M.B. Jørgensen, A. Burdorf, L.L. Andersen, "Patient handling and risk for developing persistent low-back pain among female healthcare workers," Scandinavian Journal of Work, Environment & Health, **39**(2), 164–169, 2013, doi:10.5271/sjweh.3329.

[3] R. Ibrahim, O.E.A.E. Elsaay, "The effect of body mechanics training program for intensive care nurses in reducing low back pain," IOSR Journal of Nursing and Health Science, **4**(5), 81–96, 2015, doi:10.9790/1959-04548196.

[4] A. Karahan, N. Bayraktar, "Determination of the usage of body mechanics in clinical settings and the occurrence of low back pain in nurses," International Journal of Nursing Studies, **41**(1), 67–75, 2004,

doi:10.1016/s0020-7489(03)00083-x.
[5] C. Lin, T. Ogata, Z. Zhong, M. Kanai-Pak, J. Maeda, Y. Kitajima, M. Nakamura, N. Kuwahara, J. Ota, "Development and Validation of Robot Patient Equipped with an Inertial Measurement Unit and Angular Position Sensors to Evaluate Transfer Skills of Nurses," International Journal of Social Robotics, 1–19, 2020, doi:10.1007/s12369-020-00673-6.
[6] Z. Huang, A. Nagata, M. Kanai-Pak, J. Maeda, Y. Kitajima, M. Nakamura, K. Aida, N. Kuwahara, T. Ogata, J. Otha, "Automatic evaluation of trainee nurses' patient transfer skills using multiple kinect sensors," IEICE TRANSACTIONS on Information and Systems, **97**(1), 107–118, 2014, doi:10.1587/transinf.E97.D.107.
[7] Z. Huang, A. Nagata, M. Kanai-Pak, J. Maeda, Y. Kitajima, M. Nakamura, K. Aida, N. Kuwahara, T. Ogata, J. Otha, "Self-help training system for nursing students to learn patient transfer skills," IEEE Transactions on Learning Technologies, **7**(4), 319–332, 2014, doi: 10.1109/TLT.2014.2331252.
[8] K. Itami, T. Yasuda, Y. Otsuki, M. Ishibashi, T. Maesako, "Development of a checking system for body mechanics focusing on the angle of forward leaning during bed making," Educational Technology Research, **33**(1–2), 63–71, 2010, doi: 10.15077/etr.KJ00006713267.
[9] S. Sivakanthan, E. Blaauw, M. Greenhalgh, A.M. Koontz, R. Vegter, R.A. Cooper, "Person transfer assist systems: a literature review. Disability and Rehabilitation," Assistive Technology, 1–10, 2019, doi: 10.1080/17483107.2019.1673833.
[10] M. Owlia, M. Kamachi, T. Dutta, "Reducing lumbar spine flexion using real-time biofeedback during patient handling tasks," Work, **66**(1), 41–51, 2020, doi: 10.3233/WOR-203149.
[11] K. Kitagawa, T. Nagasaki, S. Nakano, M. Hida, S. Okamatsu, C. Wada, "Optimal foot-position of caregiver based on muscle activity of lower back and lower limb while providing sit-to-stand support," Journal of Physical Therapy Science, **32**(8), 534–540, 2020, doi:10.1589/jpts.32.534.
[12] B. Schibye, A.F. Hansen, C.T. Hye-Knudsen, M. Essendrop, M. Böcher, J. Skotte, "Biomechanical analysis of the effect of changing patient-handling technique," Applied Ergonomics, **34**(2), 115–123, 2003, doi: 10.1016/S0003-6870(03)00003-6.
[13] Q. An, J. Nakagawa, J. Yasuda, W. Wen, H. Yamakawa, A. Yamashita, H. Asama, "Skill Extraction from Nursing Care Service Using Sliding Sheet," International Journal of Automation Technology, **12**(4), 533–541, 2018, doi:10.20965/ijat.2018.p0533.
[14] K. Kitagawa, T. Uezono, T. Nagasaki, S. Nakano, C. Wada, "Classification Method of Assistance Motions for Standing-up with Different Foot Anteroposterior Positions using Wearable Sensors," in 2018 International Conference on Information and Communication Technology Robotics (ICT-ROBOT2018), 1–3, 2018, doi:10.1109/ICT-ROBOT.2018.8549912.
[15] H. Wardell, "Reduction of injuries associated with patient handling," Aaohn Journal, **55**(10), 407–412, 2007, doi:10.1177/216507990705501003.
[16] A.M. Almassri, W.Z. Wan Hasan, S.A. Ahmad, A.J. Ishak, A.M. Ghazali, D.N. Talib, C. Wada, "Pressure sensor: state of the art, design, and application for robotic hand," Journal of Sensors, **2015**, 846487, 2015, doi:10.1155/2015/846487.
[17] A.M. Almassri, W.Z. Wan Hasan, C. Wada, "Evaluation of a Commercial Force Sensor for Real Time Applications," ICIC Express Letters, Part B: Applications, **11**(5), 421–426, 2020, doi:10.24507/icicelb.11.05.421.
[18] S. Pirttikangas, K. Fujinami, T. Nakajima, "Feature selection and activity recognition from wearable sensors," in 2006 International Symposium on Ubiquitous Computing Systems (UCS2006), 516–527, doi:10.1007/11890348_39.
[19] M.F. Antwi-Afari, H. Li, Y. Yu, L. Kong, "Wearable insole pressure system for automated detection and classification of awkward working postures in construction workers," Automation in Construction, **96**, 433–441, 2018, doi:10.1016/j.autcon.2018.10.004.
[20] M.F. Antwi-Afari, H. Li, J. Seo, A.Y.L. Wong, "Automated detection and classification of construction workers' loss of balance events using wearable insole pressure sensors," Automation in Construction, **96**, 189–199, 2018, doi:10.1016/j.autcon.2018.09.010.
[21] S. Dreiseitl, L. Ohno-Machado, "Logistic regression and artificial neural network classification models: a methodology review," Journal of Biomedical Informatics, **35**(5–6), 352–359, 2002, doi:10.1016/S1532-0464(03)00034-0.
[22] Y.Y. Song, L.U. Ying, "Decision tree methods: applications for classification and prediction," Shanghai archives of psychiatry, **27**(2):130-135, 2015, doi:10.11919/j.issn.1002-0829.215044.
[23] Y. Zhang, S. Lu, X. Zhou, M. Yang, L. Wu, B. Liu, P. Phillips, D. Wang, "Comparison of machine learning methods for stationary wavelet entropy-based multiple sclerosis detection: decision tree, k-nearest neighbors, and support vector machine," Simulation, **92**(9), 861-871, 2016, doi:10.1177/0037549716666962.
[24] T. Wang, Z. Qin, Z. Jin, S. Zhang, "Handling over-fitting in test cost-sensitive decision tree learning by feature selection, smoothing, and pruning," Journal of Systems and Software. **83**(7), 1137-1147, 2010, doi: 10.1016/j.jss.2010.01.002.
[25] A. Ben-Hur, C.S. Ong, S. Sonnenburg, B. Schölkopf, G. Rätsch, "Support vector machines and kernels for computational biology," PLoS Comput Biol, **4**(10), p.e1000173, 2008, doi: 10.1371/journal.pcbi.1000173.

Advances in Science, Technology and Engineering Systems Journal Vol. 5, No. 5, 1099-1110 (2020)

www.astesj.com

ASTESJ

ISSN: 2415-6698

Load Evaluation with Fast Decoupled-Newton Raphson Algorithms: Evidence from Port Harcourt Electricity

Ogbuefi Uche Chinweoke[1,2], Ibeni Christopher[*,3]

[1]*Department of Electrical Engineering, University of Nigeria, Nsukka, Enugu State, 410001, Nigeria*

[2]*Africa Centre of Excellence (ACE-SPED), University of Nigeria, Nsukka, Enugu State, 410001, Nigeria*

[3]*Rivers State University, Nkpolu- Oroworukwo, Port Harcourt, Rivers State, 500001, Nigeria*

ARTICLE INFO

Article history:
Received: 06 June, 2020
Accepted: 11 September, 2020
Online: 20 October, 2020

Keywords:
Load Flow Evaluation
Distribution System
MATLAB
Fast Decoupled
Capacitor Bank
Injection Substation

ABSTRACT

The undulated power supply has dropped to its worst reliability index in most parts of the city despite the installations of distribution transformers to improve the power. In this work, examination of Port Harcourt Town Zone 4 (Z4), Rivers State power distribution system forcing on its operation, planning for future expansion of the system, and sharing of power between utilities was done. The objective was to unravel the problematic recurrent blackouts as a result high power loss, that is (I^2R) in the line; low voltage profile, poor cos Ø at the load end, excessive loading of feeder transformers, and conductors rating inadequacy at the receiving end of the 33KV Distribution part of the substation. A comprehensive study was carried out on the system with the formation of node admittance matrix. Programmable codes were written using MATLAB script to resolve the static power flow equations defined applying Fast decoupled-Newton Raphson calculation procedure centered on the advantages of time and PC memory space (PC-MS). Thus, the node voltage and the other variables like branch flows and phase angles were gotten, and network losses were reduced. However, the results obtained were compared with that gotten from Electrical Transient Analyzer Program (ETAP) application software. It was seen that the two results got were related. The general net power gotten was (129.741 MW, 83.818 MVAr) applying the Fast Decoupled-Newton-Raphson load flow technique in MATLAB programming environment after the addition of receptive power through the means of the capacitor bank to the affected nodes. The total net power that is real and reactive got employing ETAP programming were (125.765 MW, 92.782 MVAr).

The overall line losses were enhanced by 0.246 reductions. That is from (4.75MW, 10.05MVAr) to (3.58MW, 7.57MVAr) of the entire real power losses.

1. Introduction

Generally, electrical power is transmitted from the sending end side to the receiving end substations. At the receiving side, the voltage is stepped down to a lesser value of the sending end value, most times accompanied by some technical and economic challenges. As a result of these challenges, electrical energy being the hub of modern technologies as well as the foundation of industrialization, has driven every nation to improve electrical power generation as well as enhancing the power transmission and distribution systems in order to make it efficient and meet-up with the growing power demand of the respective nations, thus massive upgrading. Despite the perceived upgrade to enhance the power wheeling capacity of the transmission line and its ancillary parts, low voltages are still felt in some areas and this has prompted the installation of distribution generators without adequate arrangement, accordingly causing the over-loading of the different feeders and some other issues. Thus, a few zones are under-used whereas certain transformers are over stacked. In this study, the combined Fast Decoupled - Newton Raphson method was utilized to study the Port Harcourt Zone 4 power network. The Port Harcourt Z4 substation includes 4-distribution transformers using a complete installed capacity/limit of approximately 164.9MVA with nine (9) serving feeders. However, the authority of the substation has attributed blame on poor power situation on

*Corresponding Author *IBENI, Christopher., Rivers State University, Nkpolu-Oroworukwo, Port Harcourt, Rivers State, 500001, Nigeria. cibeni@yahoo.com, uche.ogbuefi@unn.edu.ng,

insufficient megawatts, adding that there had been a reduction in the megawatts allotted to the substation from 693.9MW to between 149.7MW/159.5MW. This shortage of megawatts forced the company to embark on recurrent load shedding to ensure the limited-megawatts available go round consumers. These are the key problems to be looked upon in the distribution network for proper utilization of the available power. Hence, the objective of this paper is to formulate a load flow program based on the combined Fast Decoupled - Newton- Raphson load flow method. Analyze, and take care of the issue of successive blackouts brought about by heavy power (I^2R) losses in the line, low voltage experienced, poor cosØ at the load end, over-loading of feeders, and transformers in the 33kV distribution network.

2. Related Work

Availability of adequate electrical energy supply is an indispensable enabler for the social-economic advance of any nation [1, 2]. Several numeral of resourceful and dependable power flow solution techniques, like, Gauss-Seidel (GS), Newton-Raphson (NR), Fast Decoupled Load Flow (FDLF), and so on were reviewed as in [3, 4]. In an earlier era and now, they were widely and excellently used for network analysis, operation, control, and planning. However, in the investigation of distribution networks with high resistance to reactance proportions (Resistance/Reactance) an exceptional network becomes relevant. Power flow study is an indispensable requirement for power system planning, expansion, and assessment, etc. Many scholars have carried out great research for the improvement of computer programs (CP) to enhance large power system power flow investigation [5, 6]. Though, these comprehensively useful programs may experience convergence complexities with radial distribution networks when many nodes are to be resolved [5-7] and, thus, development of a special program (SP) becomes crucial for distribution study. The result formulation and procedure may be accurate or estimated, with balanced values anticipated for either on-line or detached on line use, and intended to be applied for either single-case several-case assessments [3, 8]. The load flow methodology is a key device in application programming for the network distribution management. These approaches can be classified as node-based or branch-based procedure. The node-based class utilizes node voltages and or currents infusion as state variables to address the load flow issue. Here, the most prominent techniques incorporate system equivalence approach strategy, Z-node approach, Fast Decoupled calculation, and Newton-Raphson's approach. The branch-based procedure uses either branch currents, and or branch flows as main variables for the solution of the load flow issue. Regressive and forward range based procedures, as well as ring impedance calculation algorithms, can be arranged in group ass in [7]. The power losses in electricity are most cases higher at the distribution lines compared to that of the transmission systems. This is usually due to the higher R/X ratio at the distribution lines [2, 6, 9].

2.1. Load Flow Solution methodology for Radial Distribution network

According to [6, 10] power flow procedure is planned for transmission networks rather than distribution systems. Much of the algorithm has been modified in literature. The necessity for dependability, exactness, storage ability, and quick calculation assumes a significant function in any latest power flow proposed distribution analysis. In this study, it was stated that a new distribution power flow methodology must consider complex network so order that the storing capacity can be reduced to achieve the result fast, and in fewer iteration for both online and offline applications [8, 10].

2.2. The Theory of Diakoptic Built On Fast Decoupled Power Flow Algorithm

The hypothesis is reasonable for dispersed processing of load flow problem. The studies can be performed in a very shorter period if calculations for various subsystems of an incorporated network are done simultaneously utilizing a few workstations. However, when distributed processing preparation is carried out continuously in actual time, information should be gathered from nearby points and only a generally little information base is to be updated locally at normal interims. The Reduction of transmission line information over long significant distances to the central workstation can be achieved [8, 10].

2.3. Load Flow Analysis using ETAP Software Simulation

This product is a computer-based model that simulates a continuous real-time stable state power system process. It facilitates the calculation of system line losses, reactive and real power flow, and node voltage profiles [9-11]. ETAP software is used for designing and coordinating of relays in the distribution network [10, 12]. To carry out a power flow study to analyze the performance of the electrical system during abnormal and normal working conditions, and giving the proof expected to upgrade or optimize circuit uses, create functional voltage profiles; identifies transformer tap settings, minimize MVAr, and MV losses. Besides, to help in developing equipment specification guidelines.

2.4. Analysis of the Load Flow Problem in Power System Planning Studies

According to [7, 11, 13], load flow or power flow is the movement of active and reactive power from generators to different load points of the system. This examination is an exceptionally basic instrument utilized by power system engineers for planning and deciding the steady-state activity of a power network. In [10, 12, 14] power system is presented as an electric circuit that comprises of generators, transformers, circuit breakers, lines, etc. to decide the different hub voltages, phase angles, dynamic and responsive power flows through the system [15]. The analysts or researchers in [14, 16, 17] said that the primary proof acquired from the load/power flow consists of voltage and phase angles at a given node number. The load flow problem equations are nonlinear and this requires an iterative technique to solve it.

2.5. Power Perturbation Technique for Study of Power Network Load Flow

Perturbation technique theory is a new power flow technique which goal is to try to improve the convergence rate by linearizing the load flow equation where more attention is given to the voltage values (V) and the phase angle (δ) in every recalculation step. This

procedure is quicker, and it gives more precise results than the regular or normal Gauss-Seidal power flow computation method, having been tested on the IEEE 118-node, 30-node, 14-node, and 5-node systems [2, 18, 19]. Reduction of the computational challenges by decreasing the total equations, approximating the Jacobian matrix structure, and other different factors are the opinions of most developed existing algorithms.

3. Methodology of the Research

Among various power flow solution algorithms, power flow models depend more on the Newton-Raphson (NR) based algorithm. Various decoupled polar alternatives of the NR methodology have been tried for minimizing the storage capacity limit and calculation period associated with the load flow remedy. In this study, the tools needed for the study are line parameters, node information, MATLAB applications programming, a PC; MATLAB programming codes utilizing a Fast-decoupled load flow calculations approach. ETAP programming will be additionally utilized for examination, comparism, and result justification. The FDLF technique was utilized for the study being considered. The system was modeled and demonstrated using the Electrical Transient Analyzer Program (ETAP programming) for simulation purposes employing fast decoupled. The universal purpose NR method of power flow studies was used for solving initial values.

3.1. Power Flow Equations

Sample of Node of a Power System network is as shown in Figure 1(a & b) for illustration purposes.

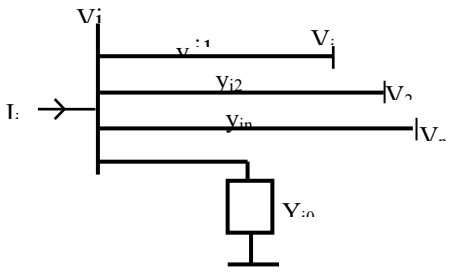


Figure. 1(a): Sample of a Power System Model Bus for the Network

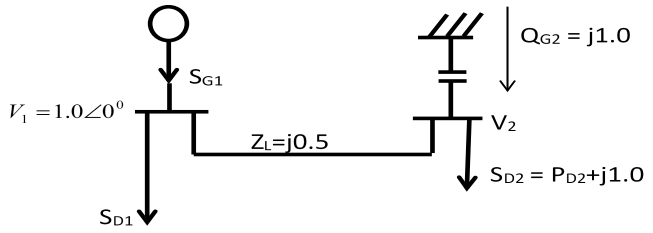


Figure 1(b): Two Bus System Network

The capacitor, in this case, injects a specified power in the system, while the voltage is controlled.

$$S_2 = S_{G2} - S_{D2} = -\mathrm{P}_{D2} \quad . \tag{1}$$

Using Kirchhoff current law (kcl) from Figure 1(b) we obtain

$$\mathrm{Ii} = (y_{i0} + y_{i1} + y_{i2} + \ldots \mathrm{yin})\,\mathrm{Vi} - y_{i1}\,V_1 - y_{i2}\,V_2 - \ldots - y_{in}\mathrm{Vn}. \tag{2}$$

$$I_i = V_i \sum_{j=0}^{n} Y_{ij} - \sum_{j=0}^{n} Y_{ij} V_j \quad where\ j \neq i \tag{3}$$

$$P_i + jQ_i = V_i I_i^* \quad .$$

Substituting Ii from the above equation into 3

$$\left(P_i - jQ_i\right)/V_i^* = V_i \sum_{j=0}^{n} Y_{ij} - \sum_{j=0}^{n} Y_{ij} V_j \quad where\ j \neq i \tag{4}$$

Equation 3 can be written as in Equation 5

$$I_i = \sum Y_{ij}\ V_i \quad . \tag{5}$$

And the polar representation

$$I_i = \sum \left|Y_{ij}\right|\left|V_j\right| \angle \theta_{ij} + \delta_{ij}, \tag{6}$$

The complex power at node I is given as

$$P_i - jQ_i = \left|V_i\right| \angle -\delta_i \sum \left|Y_{ij}\right| \angle \theta_{ij} + \delta_{ij} \quad .$$

Separating real and imaginary parts

$$P_i = \sum_{j=1}^{n} \left|V_i\right|\left|V_j\right|\left|Y_{ij}\right| \cos\left(\theta_{ij} - \delta_i + \delta_j\right), \tag{7}$$

$$Q_t = -\sum_{j=1}^{m} \left|V_i\right|\left|V_j\right|\left|Y_{ij}\right| \sin\left(\theta_{ij} - \delta_i + \delta_j\right) \quad . \tag{8}$$

Equations 7 and 8 constitute a set of non- linear algebraic equations in terms of independent variables, voltage values in per unit, and phase angle in radians. Using the Taylor series approach in expanding Equations 7 and 8 with the initial estimate and neglecting all higher-order terms results in a set of equations as shown below:

$$\begin{bmatrix} \Delta P \\ \Delta Q \end{bmatrix} = \begin{bmatrix} J_1 & J_2 \\ J_3 & J_4 \end{bmatrix} \begin{bmatrix} \delta\Delta \\ \Delta|V| \end{bmatrix} \tag{9}$$

The diagonal and off-diagonal elements of J1 are

$$\frac{\partial Pi}{\partial \delta i} = \sum_{j \neq j}^{n} \left|V_i\right|\left|V_j\right|\left|Y_{ij}\right| \sin\left(\theta_{ij} - \delta_i + \delta_j\right), \tag{10}$$

$$\frac{\partial Pi}{\partial \delta i} = -\left|V_i\right|\left|V_j\right|\left|Y_{ij}\right| \sin\left(\theta_{ij} - \delta_i + \delta_j\right) \quad j \neq i \quad . \tag{11}$$

The diagonal and off-diagonal of J4 are;

$$\frac{\delta Qi}{\delta |V_i|} = -2\left|V_i\right| \left| Y_{ii} \sin\theta_{ii} - \sum_{i \neq j} \left| V_i \right| \left| Y_{ij} \right| \sin\left(\theta_{ij} - \delta_i + \delta_j\right) \right| \tag{12}$$

$$\frac{\partial Qi}{\partial |V_i|} = -|V_i||Y_{ii}|\sin\left(\theta_{ij} - \delta_i + \delta_j\right) \quad (13)$$

Table: 1: 33KV Feeders and Injection Substations at port Harcourt Town Zone 4

Port Harcourt Town 33KV Feeder (Amadi Junction-Nzimiro Road)			33/11KV Injection Substations	
Fdr S/N	Feeder Name	Installed Transformer Capacity (MVA)	Feeder Name	Transformer Installed Capacity (MVA)
1	UST feeder	30	RSUST Agip NAOC	2x15 1x7.5 2x3
2	Secretariat Feeder	45	Secretariat Marine Base Juanuta	2x7.5 2x15 1x2.5
3	Borokiri Feeder	60	Borokiri Eastern Bypass	1x15 1x15
4	Silver Bird Feeder		Silver Bird Kidney Island	1x15 1x1.5
5	UTC Feeder		UTC Water Works	1x15 1x15
6	Rumuolumeni Feeder		UOE School of Nursing Naval Base Master Energy	1x7.5 1x15 2x2.5 1x1.5
7	Nzimiro Feeder, etc.	30	Nzimiro-Old Diobu, Owerri Road, etc	3x15

The terms $\Delta Pi^{(k)}$ and $\Delta Qi^{(k)}$ in Equations 9 are the differences between the computed and scheduled quantities, called power mismatch or residual, expressed as in Equations 14 and 15.

$$\Delta P_i^{(k)} = P_i^{(sch)} - P_i^{(k)} \quad (14)$$

$$\Delta Q_i^{(k)} = Q_i^{(sch)} - Q_i^{(k)} \quad (15)$$

The new estimates for node voltage are

$$\delta_i^{(k-1)} = \delta_i^{(k)} - \Delta P_i^{(k)}. \quad (16)$$

$$\left|Vi^{(k+1)}\right| = \left|Vi^{(k)}\right| + \Delta\left|Vi^{(k)}\right|. \quad (17)$$

3.2. Formulation of Power Flow Equations

A complex unified system with several nodes interconnected through transmission lines can be described as a power system. The load flow issue includes the calculation of voltage values and phase angle at every node, real and reactive power flow in all subsystems in the network under predictable or consistent state condition. Formulation and calculation of node admittance matrix is the starting point in the solution of power flow which is formed from transmission line parameters. In this manner, a contextual analysis is taking from Port Harcourt Town (zone 4) on the 33KV Distribution System of active feeders with 165MVA as a complete installed limit of the Transformers. The breakdown of the distribution transformers added to the incoming substation is as shown in Table 1 while Figure 2 depicts the 33KV Distribution System of the substations used as the case study.

3.3. Line Parameters for Port Harcourt Town, 33KV Distribution Network

Consider the line Parameters of the 33KV Distribution System, the conductors are evenly sorted and are overhead lines. The spacing between FACT as in the case of the Nigerian 33KV distribution system is 88cm. (that is, D = 0.88m) and. Figure 3 is the phi representation of per phase Line.

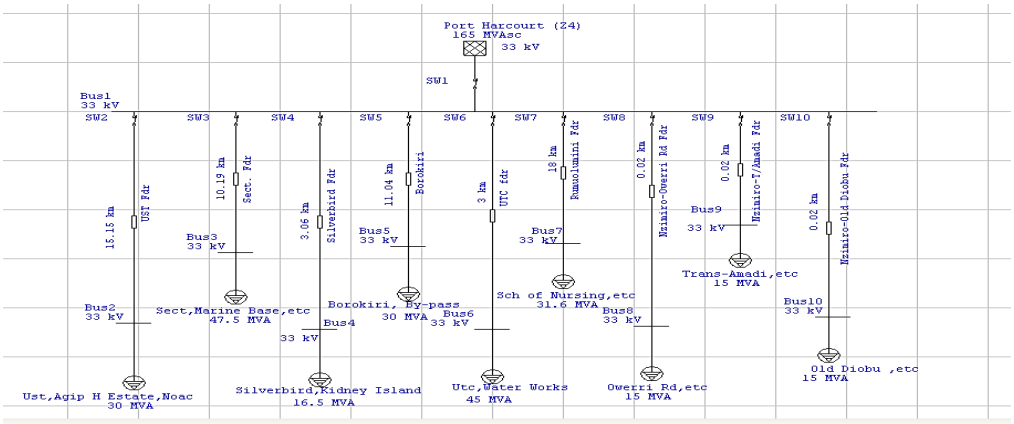
For the UST Feeder (33KV) on Node 2 at 15.15km to Incoming Substation; with Conductor Cross-Sectional Area, A = 182mm2ACSR/GZ. (Aluminum conductor steel fortified with electrifies).

$$\text{Radius of conductor, } R = \sqrt{\frac{A}{\pi}} \quad \text{m.} \quad (18)$$

$$R = \sqrt{\frac{182x10^{-6}}{\pi}} = 0.00761 \text{ m.}$$

$$GMD = \sqrt{D_{RY}\, x\, D_{YB}\, x\, D_{RB}} = 1.26D. \quad (19)$$

$$DGMD = 1.26D. \quad (20)$$



DGMD = 1.26 x 0.88 = 1.1088m or 1.109m.

Resistivity of Aluminum, $\rho = 2.826\ x\ 10^{-8}\Omega.m\ at\ 20^0C$

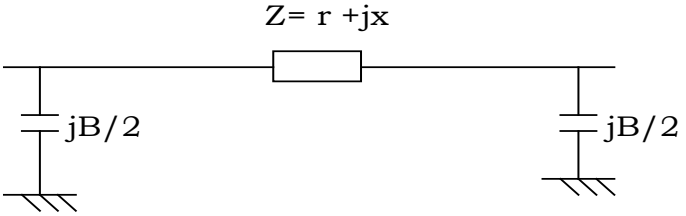


Figure 3: Π Representation of a Line (Per Phase)

$$R_0 = \frac{1000\,\rho}{A(m^2)} \quad \Omega/_{Km.} \tag{21}$$

$R_{(UST)}$ = 0.1552$\Omega/_{km}$ x 15.15km = 2.352 Ω.

Per-Kilometer Reactance, (X_0)

$$X_0 = 0.1445\ log_{10}\left(\frac{DGmD}{R}\right) + 0.0157 \quad \Omega/_{Km.} \tag{22}$$

$X_{(UST)}$ = 4.970 Ω.

$Z_{(UST)} = 2.352 + j4.970\ \Omega.$

Per – Kilometer Capacitive Susceptance**, (b_o),**

$$\boldsymbol{bo = \frac{7.58}{log_{10}\left(\frac{DGmD}{R}\right)}\ x\ 10^{-6}\ 1/_{\Omega.km}} \tag{23}$$

$b_{(UST)}$ = 3.504 x 10^{-6} x 15.15km = 53.1 x 10^{-6} $1/_{\Omega}$ or siemens

Shunt admittance (susceptance) value for **Node 1-2** for UST Feeder Network.

Given $b_{(UST)}$ = 53.1 x 10^{-6} $1/_{\Omega}$,

Qc (UST) = 0.5 x 33^2 x 53.1 x 10^{-6} = 0.0289 MVAr.

Per-Unit Values of the Line Parameters for Port Harcourt Town, 33KV Distribution Network

Assume: 100MVA as Base MVA, (S Base)

33KV as Base Voltage

$$\text{Base impedance, } \boldsymbol{Z_b = \frac{(kV^2_{base})}{MVA_{base}}} \tag{24}$$

Base impedance, $Z_b = \frac{33^2}{100} = 10.89\Omega.$

Per Unit impedance of the UST feeder,

$$Z_{(UST)pu} = 0.216 + j0.456\ pu.$$

Per unit capacitive susceptance value for UST feeder, $Bpu_{(UST)}$

$$\text{Bpu} = \frac{(\boldsymbol{Bshunt*MVAr})}{\boldsymbol{SBase}}\ \text{pu.} \tag{25}$$

Bpu(UST) = $\frac{(BshuntMVAr)}{SBase} = j0.000289$ pu.

We compute the complex power demanded at the load side bearing in mind the percentage loading. Note that, the loading capacity is due to available power

Per Unit Load Parameter at Each Feeder for Port Harcourt Town, 33KV Distribution Network

UST Feeder (Node 1-2) for Port Harcourt Town, 33KV Distribution Network

SD = 30MVA, Percentage loading =60%, Pf= cosφ= 0.8, Rf = sinφ = 0.6.

SD(1-2) = 30x0.6=18MVA, PD(UST)=18x0.8 =14.4MW, QD(UST)=18x0.6 =10.8MVAr

On 100 MVA base, the per unit values of the complex power demand, we have

$P_{D(UST)} = \frac{14.4MW}{100MVA} = 0.144\ pu$, $Q_{D(UST)} = \frac{10.8MVAr}{100MVA} = j0.108\ pu$

$$S_{D(pu)} = (\ P_{D(UST)} + jQ_{D(UST)}) = (\boldsymbol{0.144 + j0.108})p$$

Nzimiro-Trans-Amadi Feeder (Node 1-9) for Port Harcourt Town, 33KV Distribution Network

SD = 15MVA, Percentage loading = 80%, Pf = cosφ = 0.8, Rf = sinφ = 0.6

SD (1-9) = 15x0.8 = 12MVA, PD (NZ-A.) = 12x0.8 = 9.6MW, QD (NZ-A.) = 12x0.6 = 7.2MVAr

On 100 MVA base, the per unit values of the complex power demand, we have

$P_{D(NZ-A.)} = \frac{9.6MW}{100MVA} = 0.096\ pu$, $Q_{D(NZ-A.)} = \frac{7.2MVAr}{100MVA} = j0.072\ pu.$

$$S_{D(pu)} = (\ P_{D(NZ-A)} + jQ_{D(NZ-A)}) = (\boldsymbol{0.096 + j0.072})pu.$$

Nzimiro-Old-Diobu Feeder (Node 1-10) for Port Harcourt Town, 33KV Distribution Network.

SD = 15MVA, Percentage loading = 80%, Pf = cosφ = 0.8, Rf = sinφ = 0.6.

SD (1-10) = 15x0.8 = 12MVA, PD (NZ-OD.) = 12x0.8 = 9.6MW, QD (NZ-OD.) = 12x0.6 = 7.2MVAr

On 100 MVA base, the per unit values of the complex power demand, we have

$P_{D(NZ-OD.)} = \frac{9.6MW}{100MVA} = 0.096\ pu$, $Q_{D(NZ-OD.)} = \frac{7.2MVar}{100MVA} = j0.072\ pu.$

$$S_{D(pu)} = (\ P_{D(NZ-OD)} + jQ_{D(NZ-OD)}) = (\boldsymbol{0.096 + j0.072})pu.$$

The complex power received from the grid network to the 33KV node is 165MVA at a power factor of 0.8, we have Srec =

(130+j100.8) MVA. Where 130MW is the real power and 100.8MVar is the reactive power demanded on the 33kV node.

The summary of the 33kV Distribution node network data under consideration are shown in Tables 2 and 3. It is much better

to compute all other parameters using the per unit values. To realize its real values we multiply the per unit values by the base values assumed at the beginning.

3.4. Mathematical Model of Fast Decoupled Power Flow Method

In a power network, the net infused active and receptive power at an ith node are mathematically represented by:

$$P_i = \sum_{j=1}^{nb} |V_i||V_j|\left(G_{ij}\cos\theta_{ij} + B_{ij}\sin\theta_{ij}\right) \quad . \qquad (26)$$

$$Q_i = \sum_{j=1}^{nb} |V_i||V_j|\left(G_{ij}\sin\theta_{ij} - B_{ij}\cos\theta_{ij}\right) \quad . \qquad (27)$$

where Vi and Vj, represent voltage levels at the ith and jth nodes separately; Gij+ jBij is the ijth component of the Y-node; and "n" the entire number of nodes. The linearized power flow Eqns. (26) and (27) are stated or given in reduced forms:

$$\begin{bmatrix} \Delta P \\ \Delta Q \end{bmatrix} = \begin{bmatrix} J1 & J2 \\ J3 & J4 \end{bmatrix} \begin{bmatrix} \Delta\theta \\ \Delta V \end{bmatrix} \qquad (28)$$

We compute the complex power demanded at the load side bearing in mind the percentage loading.
Note that, the loading capacity depends on the available power.

Table 2: Line Data for Port Harcourt Town, 33KV Distribution Network

S/No	Feeders	Impedance code	Impedance, Z_{series} (pu)	Admittance, Y (pu)	Susceptance B/2 (pu)
1.	(Node 1-2) UST	$Y_{1,2}$	0.2159 + j0.4567	0.8460-j1.7897	j0.0002890
2.	(Node 1-3) Secretariat	$Y_{1,3}$	0.1452 + j0.3072	1.2576-j2.6607	j0.0001940
3.	(Node 1-4) Silver bird	$Y_{1,4}$	0.0436 + j0.0922	4.1916-j8.8638	j0.0000584
4.	(Node 1-5) Borokiri	$Y_{1,5}$	0.1573 + j0.3328	1.1608-j2.4561	j0.0002110
5.	(Node 1-6) UTC	$Y_{1,6}$	0.0427 + j0.0904	4.2719-j9.0441	j0.0000572
6.	(Node 1-7) Rumuolemeni	$Y_{1,7}$	0.2565 + j0.5426	0.7120-j1.5064	j0.0003430
7.	(Node 1-8) Owerri Road	$Y_{1,8}$	0.0003 + j0.0006	666.67-j1333.3	j0.00000038
8.	(Node 1-9) Nzimiro Trans- Amadi	$Y_{1,9}$	0.0003 + j0.0006	666.67-j1333.3	j0.00000038
9.	(Node 1-10) Old Diobu	$Y_{1,10}$	0.0003 + j0.0006	666.67-j1333.3	j0.00000038

Table 3: Node Data for Port Harcourt Town (Zone 4), 33KV Distribution Network (Initials Input)

Node	Type	Vsp (pu)	P_D (pu)	Q_D (pu)
1	slack	1.00	0	0
2	PQ	1.00	0.144	0.108
3	PQ	1.00	0.228	0.171
4	PQ	1.00	0.079	0.059
5	PQ	1.00	0.144	0.108
6	PQ	1.00	0.234	0.176
7	PQ	1.00	0.187	0.142
8	PQ	1.00	0.096	0.072
9	PQ	1.00	0.096	0.072
10	PQ	1.00	0.096	0.072

Table 4: Results for the Solutions after Injection of Reactive Power into the Under-Voltage Feeders (ETAP)

Feeders	Results before Injection of Reactive Power				Results after Injection of Reactive Power				
	Initial Load (Power) Received		Bus Volts (KV)	% Drop in Volt	Reactive Power Injected	New Bus Volts (KV)	New Net power Received		% Drop in Volt
	MW	MVar	KV	%	MVar	KV	MW	MVar	%
2	12.8	9.6	29.83	9.61	21.7	32.799	13.6	10.2	0.6
3	20.1	15.1	29.37	11.0	33.8	32.333	23.4	17.6	2.0
5	14.4	10.8	30.60	8.3	19.1	32.261	15.5	11.6	2.2
7	13.9	10.4	28.46	13.9	23.9	32.274	16.2	12.2	2.2

The sub-networks J1 and J4 in Eqn. 28, have a similar order because of the absence of the Q-V equations at PV nodes. A few presumptions are made as in previous studies in the formation of the FDPF model from Eqn. (28) the sub-matrices J2 and J3 are disregarded. Subsequent to joining the assumptions, the subsequent FDPF conditions become:

$$\left[\frac{\Delta P'}{V}\right]=[B'][\Delta\theta] \quad . \tag{29}$$

$$\left[\frac{\Delta Q'}{V}\right]=[B'']][\Delta V] \quad . \tag{30}$$

where

$$\Delta P'_i = P_{scheduled,t} - P_{calculated,1} - P_{shunts,1}$$

$$\Delta Q'_i = Q_{Scheduled,f} - Q_{calculated,t} - Q_{Shunts,i} \tag{31}$$

The suffix "i" represents the ith node, Q-shunts,i; and P-shunts,i are the reactive and real powers, because of lumped shunts at the ith node. It ought to be noticed that the order for the Jacobians $[B']$ are (nb-1) by (nb – 1) in Eqns. (29) while that of $[B'']$ in Eqn. (30) is (nb –mb -1) by (nb – mb – 1) where mb is the total number of voltage-controlled nodes. At the point when both $[B']$ and $[B'']$ are of the similar order of (nb -1), the matrices are real, sparse, and just contain system parameters. These matrices are only factorized once, stored, and are held and fixed all through the iteration. The result of Eqns. (29) and (30) are given by Eqn. (32) and (33):

$$[\Delta\theta] = [B']^{-1}\left[\frac{\Delta P'}{V}\right]. \tag{32}$$

$$[\Delta V] = [B'']^{-1}\left[\frac{\Delta Q''}{V}\right]. \tag{33}$$

Thus, by utilizing an abridged fast decoupled load flow technique, the voltage values and change in phase angle can be determined.

3.5. Fast Decoupled Power Flow for Radial Distribution System

In the Radial Distribution network, the massive R-X ratio constitutes problems in the convergence of the normal ordinary load flow calculation. Hence, for excellent convergence, some modifications in the load flow methods are applied. The model can be represented by a radial interconnection of networks of the fundamental structure depicted in Figure 4. The dotted lines from the co-generator, shunt capacitor, and load to the ground are to demonstrate that these components might be interconnected in floated delta-design since a given branch might be two-phase or single-phase as situation demands.

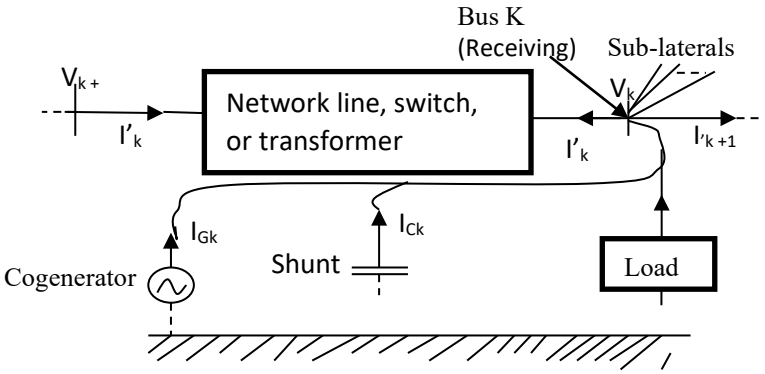


Figure 4: The Building Block diagram of a Radial Distribution System

One of the key ideas driving our techniques is that the current and voltage at one node can be expressed as an element of the current and voltage on the other node. If we let the equation be:

$$W_k = \begin{bmatrix} V_k \\ \\ I_{k+1} \end{bmatrix} \tag{34}$$

The branch update function [I] is given beneath as:

$$W_{k-1} = gk(W_k) \tag{35}$$

Where Wk is a vector containing the real and imaginary parts of the voltages and current flows at node k. The factor gk is controlled by the sub-laterals joined at node k like as the models for distribution lines, switches, loads, transformers, co-generators, and shunt capacitors. From Vk we can calculate the flows as a result of the loads, co-generators shunt and, capacitors, given Ik + 1 and the currents Ij taken into sub-laterals branching out from node k, applying KCL at node k to the calculate current [I] given by Eq. 36:

$$I'_k = I_{GK} + I_{CK} + I_{LK} _ I_{k_1} - \sum_{J \in AK} Ij \tag{36}$$

Where Ak is the set of nodes adjacent to node k on sub-laterals.

From Eqn. (36), we calculate the voltage and current at the main side given the voltage and current at the auxiliary or secondary "I" as in Eq. 37:

$$\begin{bmatrix} I_K \\ I_{K'} \end{bmatrix} = \begin{bmatrix} Y_k^{pp} & Y_k^{ss} \\ Y_k^{sp} & Y_k^{sp} \end{bmatrix} \begin{bmatrix} V_{k-1} \\ V_k \end{bmatrix} \tag{37}$$

Therefore by solving equation (37), we get;

$$V_{k-1} = \left(Y_k^{sp}\right)^{-1} \left(I_{k'} - Y_k^{ss} V_k\right). \tag{38}$$

$$I_k = \left(Y_k^{pp}\right)^{-1} \left(I_{k'-1} + Y_k^{ss} V_k\right). \tag{39}$$

So that by applying this formulation or definition we get the converged values easily and faster than the other normal techniques.

a. Formulation for Fast Decoupled Power Flow Method

The stepwise calculation procedure to solve the power flow issue by applying the Fast Decoupled Power Flow Method is as given in [3] and as summarized thus: Creation of the node admittance Y as indicated by the lines given by the IEEE standard node test system, identification of all kinds of nodes according to the IEEE standard and setting all node initial value of $1\angle 0 p.u$, Creation of the matrices B1 and B11 Where B1 and B11 are the imaginary part of the node admittance matrix of Y_{node}, Calculating the value ΔP and ΔQ mismatches, Check the convergence status, Calculation of real and reactive power at every node, and checking if MVAr of generator nodes are within the cutoff points, Update of the voltage magnitude V and the voltage angle δ at every node. The current can then be determined from the calculated Y node using Eqn. (36)

$$\begin{bmatrix} I_k \\ I_{k'} \end{bmatrix} = \begin{bmatrix} Y_k^{pp} & Y_k^{ps} \\ Y_k^{sp} & Y_k^{ss} \end{bmatrix} \begin{bmatrix} V_{k-1} \\ V_k \end{bmatrix} \tag{40}$$

If convergence is attained Display the load flow result, calculation, and show the line flows, current, and losses.

$$\text{Percentage Voltage Drop ; } V_d = \frac{V_S - V_R}{V_S} \times 100\% \tag{41}$$

b. Capacitor Bank

Line compensators are introduced in the network because of line losses and other line limitations to reduce losses. In the system under study, shunt capacitors are applied over an inductive load to give part of the reactive VARs required by the load to keep the voltage within the anticipated range. They can also be applied through capacitive loads and in light load situations to consume some amount of the main (leading) VARs for accomplishing voltage regulation. Capacitors are connected either directly to a node or through the tertiary winding of the primary transformer and are installed along the line as to limit mishaps in form of losses, voltage drop, also improves loading power factor. The shunt capacitor banks introduce reactive power into the system and compensate for line losses. To avoid much harmonic in line FACTS devices suffice.

Implementation of the Fast-Decoupled Load Flow in MATLAB. The program is implemented in the MATLAB programming language and is run in MATLAB Software development environment. The software modules files (M-files) results are as presented in appendices A1 to A3:

3 Results and Analysis

The results obtained are shown in Figs 5, 6, A1 to A3, and Tables 4 to 9 using the Fast decoupled-N-R procedures inserted in ETAP programming. The outcomes of the studied power flow and its parameters determined utilizing MATLAB program are represented in Figs. 5, 6, and Tables 4 and 5. The power flow study of the 33KV Distribution system making use of Port Harcourt Town, Zone 4, are presented in appendix A1 to A3 for different results sections from the utilization of the methods and simulation of the system as follows:

Injection of Reactive Power into the Feeder (via Capacitor Bank) using ETAP

Feeder 2 (Node 1-2): The initial net load (Power) received was 9.59 MVAr and 12.76 MW with a voltage drop of 0. 961. But after injection of 21.67 MVAr of reactive power through a capacitor bank, (Cap 1- rated 22MVAr), the voltage drop reduces to 0.0059 while the new net load (power) became 10.18 MVAr and 13.57MW, new node voltage becomes 0.994 with an angle of -5.48 degree as in Table 4.

Feeder 3 (Node 1-3): The initial net load (Power) received was 15.09 MVAr and 20.14 MW with a voltage drop of 0.11. But, after the injection of 33.79 MVAr of reactive power, - 0.49MW through

a capacitor bank, (Cap 2- rated 35MVAr), and the voltage drop reduces to 0.02 while the new net load (power) became 17.58 MVAr and 23.46MW. The new node voltage becomes 0.9798 with an angle of -6.08 degree. Table 4 shows the summary of reactive power injected into the feeders to improve the voltage profile and the net power received, using ETAP.

Injection of Reactive Power into the Feeder (via Capacitor Bank) using MATLAB

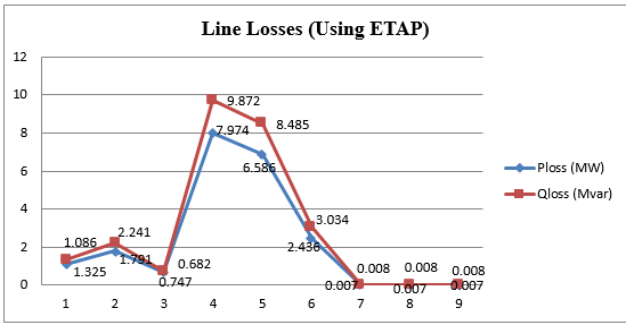


Figure 5: Feeder Power Losses before Injecting Reactive Power (ETAP)

In the new input node data, we have injected reactive power via the capacitor bank. The results are as in Table 5. The values of the reactive power injected were as follows: Node-2 @ 20 MVar, Node-3 @ 30MVar, Node-5 @ 20MVar and Node-7 @ 22MVar. (Check along QGi)

Table 5: New Input Bus Data Injecting Reactive Power (MATLAB)
New Bus Data Input with Capacitor Bank

Bus	Type	V_{sp}	Theta	P_{Gi}	Q_{Gi}	P_{Li}	Q_{Li}	Q_{min}	Q_{max}
1	SL	1.00	0.00	0.00	0.00	0.00	0.00	0.00	0.00
2	PQ	1.00	0.00	0.00	**20.00**	14.40	10.80	-5.00	5.00
3	PQ	1.00	0.00	0.00	**30.00**	22.80	17.10	-3.00	5.00
4	PQ	1.00	0.00	0.00	0.00	7.90	5.90	0.00	0.00
5	PQ	1.00	0.00	0.00	**20.00**	14.40	10.80	-5.00	10.00
6	PQ	1.00	0.00	0.00	0.00	23.40	17.60	0.00	0.00
7	PQ	1.00	0.00	0.00	**22.00**	18.70	14.20	-6.00	15.00
8	PQ	1.00	0.00	0.00	0.00	9.60	7.20	0.00	0.00
9	PQ	1.00	0.00	0.00	0.00	9.60	7.20	0.00	0.00
10	PQ	1.00	0.00	0.00	0.00	9.60	7.20	0.00	0.00

From the voltage profile, the network required more power injection and some tap setting. In Table 7, **M** means the bus voltage is marginal while C mean critical.

Table 6: Results for 10 Bus/9 Feeder System Load Flow Solutions before Injection of Reactive Power (ETAP)

Bus	Type	V KV	Angle	P. Received $P_{S(rec)}$	$Q_{S(rec)}$	P. Dispatched P_{disp} MW	Q_{disp} MVar	Demand $-P_{net}$ MW	$-Q_{net}$ MVar
1	slack	33.00	0.0	130.001	100.846	-	-	-	-
2	PQ	**29.82**	-1.5	0	0	13.905	10.940	12.819	9.614
3	PQ	**29.65**	-1.5	0	0	21.742	17.203	19.949	14.962
4	PQ	32.64	-0.2	0	0	7.886	5.938	7.818	5.863
5	PQ	**30.68**	-1.1	0	0	14.026	10.894	13.229	9.922
6	PQ	31.89	-0.5	0	0	24.789	18.928	24.122	18.092
7	PQ	**27.81**	-2.4	0	0	18.851	15.344	16.415	12.311
8	PQ	32.99	0.0	0	0	9.601	7.200	9.600	7.199
9	PQ	32.99	0.0	0	0	9.601	7.200	9.600	7.199
10	PQ	32.99	0.0	0	0	9.601	7.200	9.600	7.199

Table 7: Line Losses and Voltage Drop before Injection of Reactive Power (using ETAP)

Bus	Power Losses P_{Line} (MW)	Q_{Line} (MVar)	Vd % Drop in $V_{mag.}$	conditions	Remarks
1-2	1.086	1.325	**9.7**	9.7% >5%	Under Voltage (C)
1-3	1.791	2.241	**11.0**	11.0% > 5%	Under Voltage (C)
1-4	0.682	0.747	1.08	1.08% < 5%	Acceptable
1-5	7.974	9.721	**8.3**	8.3% > 5%	Under Voltage (M)
1-6	6.860	8.485	3.35	3.35% < 5%	Acceptable
1-7	2.436	3.034	**13.9**	13.9% > 5%	Under Voltage (C)
1-8	0.007	0.008	0.01	0.01%<< 5%	Acceptable
1-9	0.007	0.008	0.01	0.01% << 5%	Acceptable
1-10	0.007	0.008	0.01	0.01% << 5%	Acceptable
Total	**6.8502**	**8.485**			

Table 8: Summary of the Bus Voltages before and after Injection of Reactive Power (with MATLAB)

Bus Voltage before Injecting Reactive Power				**Bus Voltage after Injecting Reactive Power**		
B/ No	Bus Volt (KV)	Angle (degree)	% Vd	Bus Volt (KV)	Angle (degree)	% Vd
1	**33.000**	0.000	0.000	**33.000**	0.000	0.000
2	**30.525**	-0.043	7.490	**33.244**	-0.085	0.740

3	**31.307**	-0.045	5.130	**33.085**	-0.088	0.260
4	**32.716**	-0.004	0.860	**32.703**	-0.005	0.910
5	**31.574**	-0.030	4.320	**33.201**	-0.062	0.609
6	**32.155**	-0.012	2.560	**32.119**	-0.014	2.670
7	**29.651**	-0.069	10.15	**32.567**	-0.123	1.310
8	**32.997**	-0.000	0.000	**32.997**	-0.000	0.010
9	**32.997**	-0.000	0.000	**32.997**	-0.000	0.010
10	**32.997**	-0.000	0.000	**32.997**	-0.000	0.010

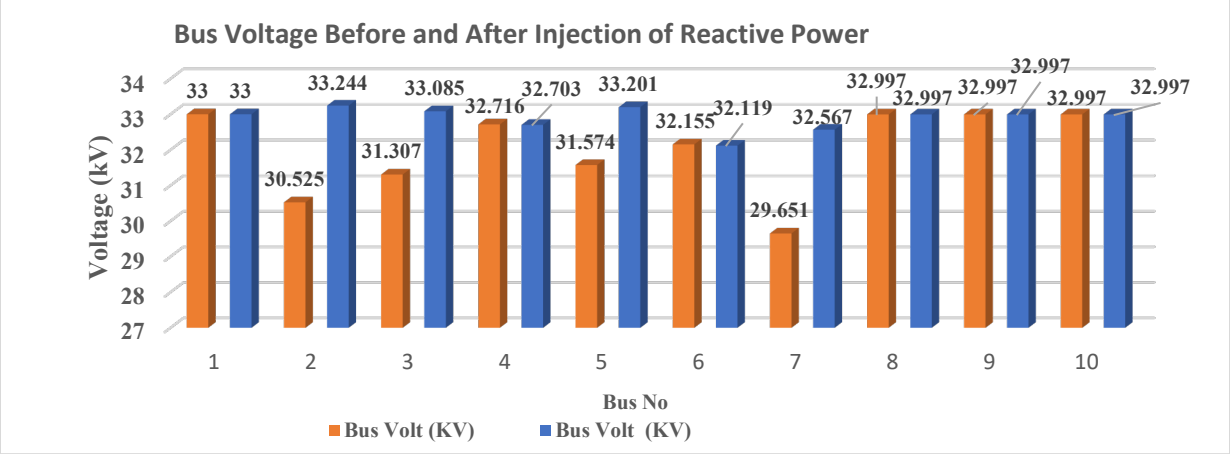


Figure 6: Bus Voltage before and after Injection of Reactive Power

Table 9: Summary of the Net-load/Power and line Losses before and after Injection of Reactive power into Z4 station

Bus Net Load (Power) Received before Injecting Reactive Power					Bus Net Load (Power) Received after Injecting Reactive Power			
B/No	P_{Net} (MW)	Q_{Net} (MVa)	Line Loss (MW)	(MVar)	P_{Net} (MW)	Q_{Net} (MVar)	Line Loss (MW)	(MVar)
2	14.400	10.774	0.7657	1.6197	14.400	9.229	0.62241	1.31659
3	22.800	17.083	1.3094	2.7704	22.800	12.920	0.99193	2.09863
4	7.900	5.894	0.0398	0.0842	7.900	5.894	0.04313	0.09120
5	14.400	10.780	0.5302	1.1217	14.400	9.221	0.45441	0.96139
6	23.400	17.594	0.3557	0.7530	23.400	17.595	0.38635	0.81795
7	18.700	14.172	1.7492	3.7003	18.700	7.833	1.08263	2.29020
8	9.602	7.201	0.0004	0.0008	9.604	7.196	0.00042	0.00086
9	9.602	7.201	0.0004	0.0008	9.604	7.196	0.00042	0.00086
10	9.602	7.201	0.0004	0.0008	9.604	7.196	0.00042	0.00086
Total	**130.406**	**97.9**	**4.7512**	**10.0517**	**130.412**	**84.28**	**3.58212**	**7.57854**

4. Discussion

Power flow is a significant and fundamental device for the study of any power system and also applied in the operation, arranging for future development/upgrade of power systems. It will help in deciding the best mode of operation of the existing networks.

The results of the voltage values in nodes, 2, 3, 5, and 7 were not within the acceptable range because its node voltage was critical while node 6 is marginal and is within the required range. The steady-state MW and MVAr delivered to the slack node is not equal to the sum of the load (Power) demanded at each node. The transmitted/injected power and the power expected/net power at the load point were not equal, due to power losses on each feeder. The total disposable power received was *129.741 MW and 83.818 MVAr* with Fast Decoupled Newton-Raphson technique in MATLAB Environment after incorporation of Capacitor bank to the nodes that were influenced by unsatisfactory voltage drop, while the entire net load got using ETAP programming was 92.782 MVAr and 125.765 MW.

The Voltage drop at Node 6, 8, 9, and 10 are within the acceptable range. These nodes Voltage drops are less than or equal to the acceptable 0.05 of the nominal voltage drop. Figure 6 above, shows the Node Voltage profile before and after the injection of Reactive Power.

The total power (line) losses on the feeders have been reduced from 10.05MVAr and 4.75MW to 7.57MVAr and 3.58MW. This gives 0.246 reductions of the entire real power loss after the addition of reactive power into the black nodes.

5. Conclusion

The analysis of this work has revealed the areas of consideration and urgent attention. The use of Fast Decoupled Load Flow study with MATLAB and the use of ETAP programming helps the examination precisely and proactive with less need for memory space. The load dispatched from the grid system to the transmission substation was not satisfactory thus every receiving substation has a fraction of sharing the available power or load.

The simulated results show that more power is required from the grid network to the receiving substations through the Port Harcourt Town (Z4) control transmission center. In this way, without a satisfactory power source from the grid system, alternative energy supply or distributed generation suffices or, calls for load shading as the only way out.

The entire power losses adding up to 10.05MVAr and 4.75MW on the 33KV distribution system require the update of the system by distributing or adding more load from the grid to these essential distribution centers, or alternative power generation should be sourced to beef up else load shedding becomes the only option. However, the recommendation and installation of the line compensator as "ccapacitor bank" at the affected nodes improved the voltage profile. Giving a 0.246 decrease in real power loss when capacitor banks were introduced on problem nodes for better enhancement.

5.1. Recommendations

1. We recommend that the 33KV distribution system be made more reliable by increasing the number of protective elements, capacitors banks, and transformers as realized from the results obtained. Also, intermittent power flow analysis and maintenance should be carried out.
2. The reactive power required locally at the nodes can be utilized to limit or minimize the losses on the line related with the system.
3. The substations for the network in this study should be made to perform at least 20 to 25 percent below the supply power to the secondary distribution system.

Conflict of Interest

The authors declare no conflict of interest.

Acknowledgment

My warm appreciation & respect to all the staff of the Port Harcourt Electricity Distribution Company of Nigeria (PHEDC), Moscow Road, Port Harcourt; all staff of Transmission Company of Nigeria, Port Harcourt Zone, for making this research work a worthwhile success. My sincere appreciation also goes to all the members of N.S.E and staff of the Rivers State University, Port Harcourt. My inmost sincere thanks to the African Centre of Excellence for Sustainable Power & Energy Development (**ACE-SPED**) University of Nigeria, Nsukka, Enugu State, Nigeria.

References

[1] I.A. Adejumobi, G. A. Adepoju, and K.A. Hamzat, " Iterative techniques for load Flow Study: A Comparative Study for Nigeria 330KV Grid System as a Case Study" International Journal of Engineering and Advanced Technology (IJEAT) ISSN: 2249-8958, **3**(1), October 2013

[2] C.S Indulkar and K. Ramalingam "Load flow Analysis with voltage-sensitive loads" Joint International Conference on Power System Technology and IEEE Power India Conference 2008. DOI: 10.1109/ICPST.2008.4745151

[3] H. K. Okyere, H. Nouri, H. Maradi and Li Zhenbiao " Statcom and load tap changing transformer (LTC) in Newton Raphson Power Flow: Bus voltage constraint and losses" 42nd International Universities Power Engineering Conference 2007

[4] M. Sailaja Kumari and M. Sydulu " A fast and reliable quadratic approach for Q-adjustments in Fast M Applied to power systems, 2006

[5] J. Nanda, V. Bapi Raju, P.R. Bijwe, M. L. Kothari and M. Joma "New findings of convergence properties of fast decoupled load flow algorithms", IEE Proceedings C- Generation, transmission and Distribution, 1991

[6] T. Ochi, D. Yamashita, K. Koyanagi, & R. Yokoyama, "The Development and Application of Fast Decoupled Load Flow Method for Distribution Systems with High R/X Ratios Lines", In 2013 IEE PES Innovative Smart Grid Technologies Conference, Washington DC, USA. Retrieved from https://waseda.pure.elsevier.com. 25th, July 2016.

[7] F.S. Abu-Mouti, & M.E. El-Hawary, A New and Fast Power Flow Solution Algorithm for Radial Distribution Feeders including Distributed Generations", Institute of Electrical & Electronics Engineering Transactions on Power Systems, 2668 – 2672, 2007.

[8] B. Stott and O. Alsace " Fast Decoupled Loaf Flow" IEEE Transaction on Power Apparatus and Systems, PAS-93, 1974

[9] G. B Jasmon and L.H.C. C Lee, " Stability of Load flow techniques for distribution system voltage stability analysis", IEE Proceedings C- generation transmission and Distribution, **138**(6), 479-484, Nov 1991

[10] A. Sharma, Deep Kiran and Bijaya K Panigrahi, " Planning the coordination of overcurrent relays for distribution systems considering network reconfiguration and load restoration", IET Generation, Transmission and Distribution, 2018

[11] P. S. Bhowmik, S. P. Bose, D. V. Rajan, and S. Deb, "Power flow analysis of power system using power Perturbation method" IEEE Power Engineering and Automation Conference, 2011

[12] H. M. Gibson Sianipar, Giri Angga Setia and M. Fatahillah Santosa, "Implementation of Axis Rotation fast Decoupled Load Flow on distribution systems" 3rd conference on power Engineering and Renewable Energy (ICPERE), 2016

[13] R. Mageshvaran, R.I. Jacob, V. Yuvaraj, P.Rizwankhan, T. Vijayakumar, & V. Sudheera, , "Implementation of Non-Traditional Optimization Techniques (PSO, CPSO, HDE) for the Optimal Load Flow Solution", TENCON 2008 - 2008 IEEE Region 10 Conference, 19-21.doi:10.1109/tencon.2008.4766839, 2008.

[14] S. Vasanthara, "Electric power systems" Electric renewable Energy Systems, 2016

[15] W. Xi-Fan, Song, Yonghua and Irving Malcolm "Modern Power System Analysis", (3rd ed*.),* New York: Mc-Graw-Hill, 2008.

[16] H. A. Raza et al., "Analysis the effect of 500kv High-Voltage Power Transmission Line on the Output Efficiency of Solar-Panels," in 2019 International Conference on Electrical, Communication, and Computer Engineering, 1–6, 2019. doi: 10.1109/ICECCE47252.2019.8940803

[17] H. D. Chiang, "A decoupled load flow method for distribution power network algorithms analysis and convergence study", Electric Power Energy System, **3**(3), 9-13,1991. https://doi.org/10.1016/0142-0615(91)90001-C

[18] M.S. Srinivas, "Distribution load flows: A Brief Review", IEEE Power Engineering Society Winter meeting 2000, **2**, 942-945,2000

[19] S. M. Lutful Kabir, A Hasib Chowdhury, Mosaddequr Rahman and J. Alam "Inclusion of slack bus in Newton-Raphson load flow study" 8th International Conference on Electrical and Computer Engineering 2014

APPENDIX A: Some Simulated Results

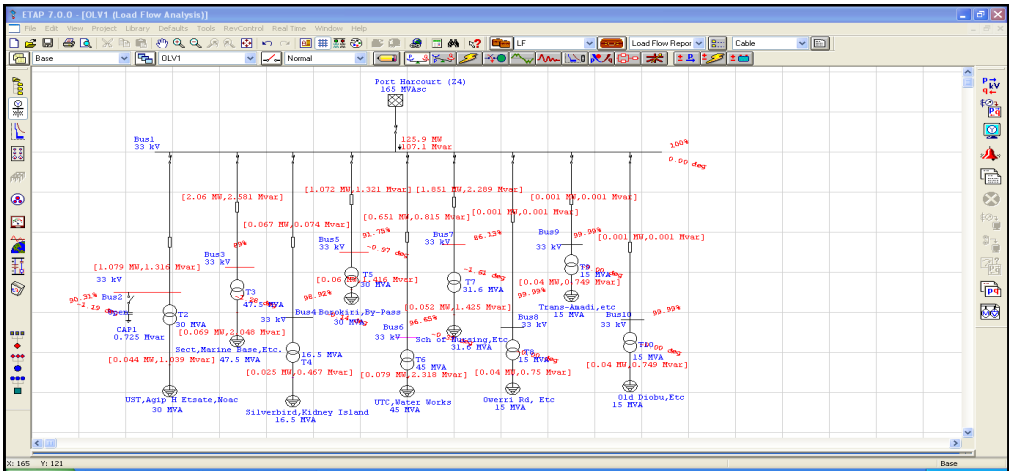


Figure A1: The Simulated 33KV Distribution Network (with Power Losses indicated) before addition of Capacitors Bank

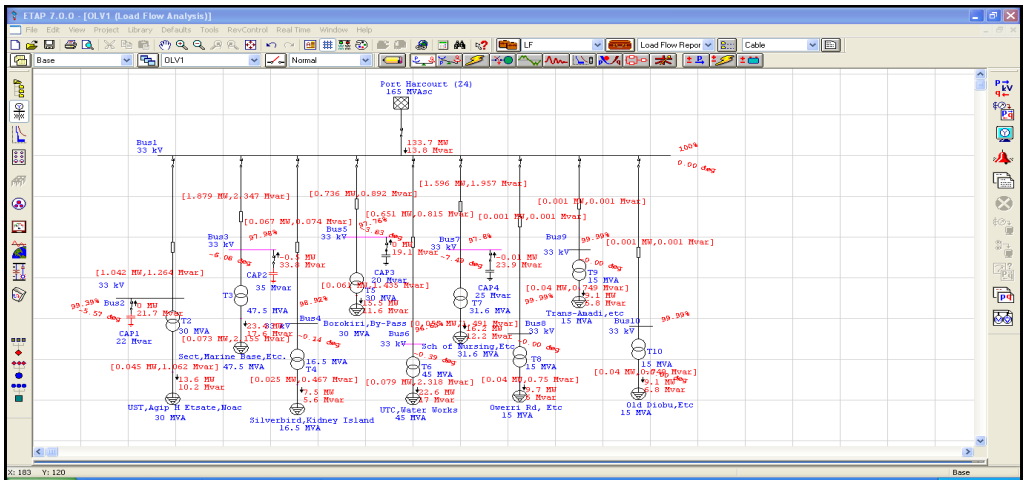


Figure A2: Simulated Result for 33KV Distribution Network (with Power Losses indicated) after the addition of Capacitors Bank

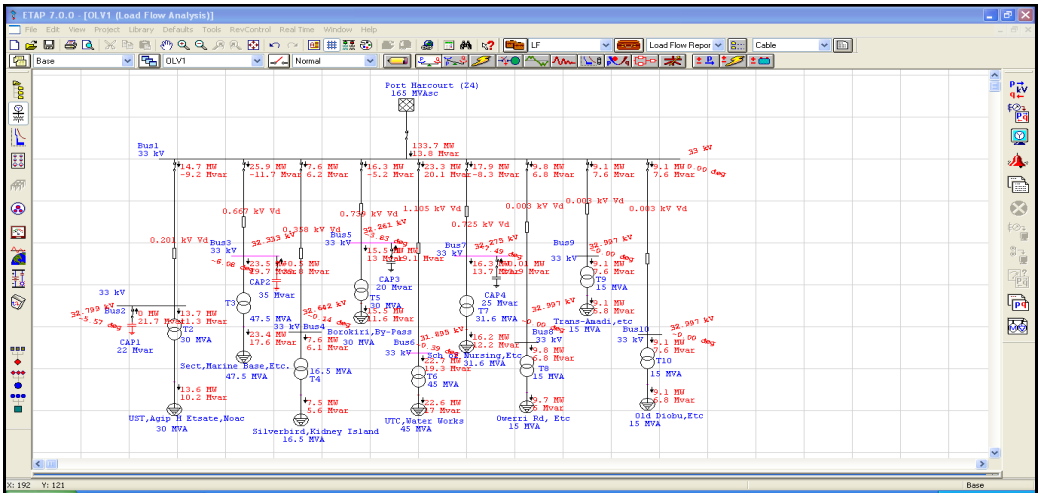


Figure A3 4.10: Result of the Simulated 33KV Distribution Network (with % Voltage Drop indicated) after addition of Capacitors Bank

ASTES

Advances in Science, Technology and Engineering Systems Journal Vol. 5, No. 5, 1111-1117 (2020)

www.astesj.com

ASTESJ

ISSN: 2415-6698

Design and Implementation of Aerial Vehicle Remote Sensing and Surveillance System, Dehazing Technique Using Modified Dark Channel Prior

Hasn Mahmood Khudair[1], Taif Alawsi[2,*], Anwaar A. Aldergazly[1], A. H. Majeed[1]

[1]*Al Nahrain University, Department of Laser and Optoelectronics Engineering, Baghdad, 10001, Iraq*

[2]*Sapienza University of Rome, Department of Information Engineering, Electronics and Telecommunication, Rome, 00100, Italy*

ARTICLE INFO

Article history:
Received: 13 June, 2020
Accepted: 18 September, 2020
Online: 20 October, 2020

Keywords:
Unmanned Aerial Vehicle (UAV)
Remote Sensing
Dehazing
Dark Channel Prior (DCP)

ABSTRACT

After studying the aviation problems in Iraq, on one hand, and because Iraq has various weather characteristics due to its different terrains (i.e. mountains, plain fields, and deserts). We discussed these problems with pilots and aviation specialists, and came to the conclusion that the main offset faced is vision deficiency is foggy and dusty weather. Thus, the Iraqi aviation reconnaissance system was developed to overcome this hurdle by implementing instant image rendering by developing this technology to remove fog and such hazy particles utilizing dark channel prior (DCP) image processing algorithm since this method is highly capable of resolving the fog/haze weather condition problems. The DCP algorithm suggested showed a reasonable enhancement of the images with foggy, hazy, and dusty conditions when the Unmanned Aerial Vehicle (UAV) was used to capture images at various altitudes correspondent to the same height most helicopters and reconnaissance UAVs fly at. Our main contribution is based on the evaluation of optimal values of DCP parameters/metrics to the hazy images and performs UAV image dehazing and enhancement.

1. Introduction

The presence of haze reduces the perception of the Aerial imagery observed by the captured image in the UAV. Such deterioration affects computer vision systems' efficiency in aerial vehicle applications, including video monitoring, automatic vehicle navigating, and remote sensing. Light dispersion is caused by suspended objects, just like droplets of water or smog that can reduce the visibility in hazy environments. The degree of visibility losses depends upon the intensity and range among view objects and the observational location of the suspended particles in that environment. During the past years, studies have concentrated on creating effective computational methods to eliminate the effects of haze in aerial photogrammetry of the exterior surroundings. For example, the processing of many views captured during various hazy circumstances is an algorithm on which the research is based [1]. The algorithm we modified and implemented in this research is based on the DCP algorithm which is commonly utilized in the defogging algorithm. The processing of the DCP algorithm based on the scattering process resulting from fog and weather circumstances, photographs from low altitudes can be decayed. Such unfavorable environmental conditions reduce the color and contrast of the views and thus its radiometric performance. The article provides a way of image restoration collected from aerial vehicle (AV) sites. Across the course of the study, an algorithm for low-altitude imaging has been developed and environmental adjustment algorithms based on a model for atmospheric dispersion were being shown. Performance testing of the system of dehazing suggested had been performed by only using subjective metrics like the SSIM, PSNR, RMS, normalized cross-correlation, Universal Image Quality Index, the root mean square error (RMSE). Investigations showed that utilizing the dehazing algorithm, could minimize the adverse effects of haze and enhance the quality of aerial imagery dependent on the PSNR scale [2-5].

2. Literature Review

The dark channel prior (DCP) algorithm is considered to be widely used in fog reduction and image enhancement, which was suggested primarily [1]. Such an algorithm separates the scene across hazy and foggy zones. In [6], the author utilized bilateral and denoise processing to obtain that graph of the transmission [7]. In [8], the author was using the edge smoothing filter of the DCP and conducted multiscale acoustic manipulation. In [9], the author suggested a way of utilizing contrast hazy dependence, i.e. fog-free scenes are better over hazy photographs. Due to weather effects,

*Corresponding Author: Taif Alawsi, Iraq, Baghdad, +9647714202625 & taif.alawsi@uniroma1.it

lighting, shadows, and occlusion, roads in imagery show its complex characteristics, which make road mining difficult. In [10], the author proposed an automatic method of aerial extraction for a vague Retinex based aerial images and an improved Canny Operator with the shape criteria. The monitoring and line detection method has been researched for invariant illumination images. In [11], the author studied the bioinspired classificatory for remote sensing imaging surveillance mining, which takes into account the dynamic conditions of weather such as hazy and foggy weather.

3. Theoretical Background

3.1. Hazy Environment

A captured scene in the existence of fog as shown in Figure 1 which can be seen in a uniform medium using an algorithm to atmospheric optics as follows:

$$I(x)=J(x)t(x)+A(1-t(x)) \quad (1)$$

The formula of transmission function in the medium can be described as follow:

$$t(x)=exp(-Bd(x)) \quad (2)$$

A definition for all the variables/constants in the equations above can be seen in Table 1. Overall, the problem is the restoration of the reflectance function J(x), t(x), and also B for the foggy view I(x). This must be mentioned whether model dehazing is an unrecognized concern since the only single hazy image can approximate the J(x) functions and also the variables b and A.

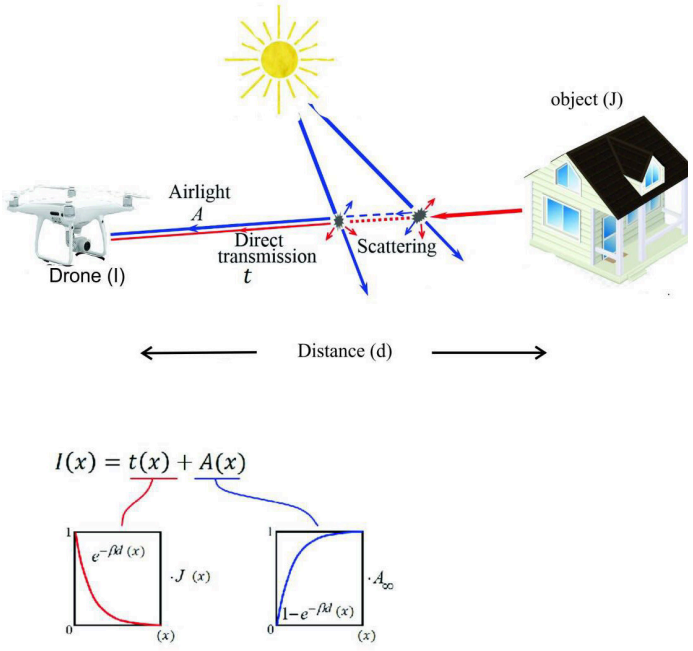


Figure 1: The main scheme of the hazy environment can be affected by the surveillance system

3.2. Dark Channel Prior (DCP) Algorithm

The DCP is shown in three RGB color filters via calculating the minimum spatial illumination values for the bright object, accordingly [9]:

$$DC(x) = \min_{c\in\{r,g,b\}}\left\{\min_{x\in\Omega_{sq}}\left\{\frac{I^c(x)}{\hat{A}^c}\right\}\right\} \quad (3)$$

The DCP algorithm considered the most widely used method of dehazing algorithms which can be illustrated as following [12]

1) A simplistic, rational, clear, and true inference is derived from an outdoor natural picture of statistical characteristics.
2) No modification to dehazing is made before the collection of the initial meaning variables are calculated.

Table 1: Mapping the definition of each symbol in the equations

Symbol	Quantity
I(x)	Single hazy image
A	Scalar constant (airlight)
t(x)	Medium transmission function
J(x)	Reflectance function of the scene (haze-free image)
d(x)	Scene depth from the camera viewpoint
β	Attenuation coefficient determined by the weather condition
Ω	A subset of pixel coordinates defining a square structure around the central coordinates x.
MSE	Mean Square Error
RMSE	Root Mean Square Error
PSNR	Peak Signal to Noise Ratio

3.3. Suggested Dark Channel Prior Algorithm

A modified DCP algorithm was suggested in this article for the surveillance system in foggy/hazy/dusty weather conditions, which is illustrated in Figure 2.A. The input image has the desired criteria to be enhanced using the DCP algorithms, these criteria were a foggy indoor image, foggy outdoor image, and dusty outdoor image. After capturing the images in the UAV with the desired conditions, these images were processed by MATLAB® to calculate the image quality parameters/metrics. Then applying the DCP algorithms to dehaze/defog the images and then again calculate the parameter/metrics for the dehazed image. The final step will be the optimization of the parameters/metrics and then getting the final output of the dehazed images, as shown in Figure 2.B. The procedure described above was repeated for three different algorithms based on the DCP. The snapshots of the MATLAB® programming for image dehazing is shown in Figure 3.

Mainly based on five steps described in the experimental implementation section in this article. We modified the DCP algorithm by calculating the attenuation coefficient of different images under different hazy conditions then varying the attenuation coefficient (α) until the images were dehazed and enhanced the resolutions by varying and modifying the DCP algorithm to obtain modified DCP used in different hazy conditions in different heights.

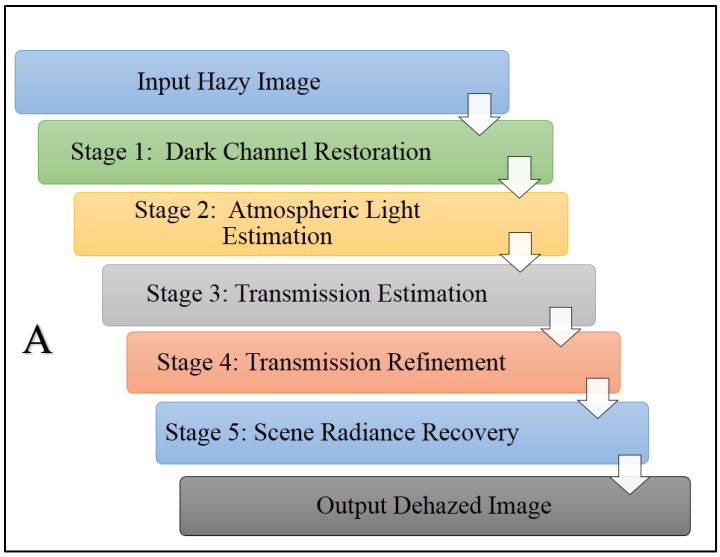


Figure 2: Schematic illustration for the DCP algorithm (a) Steps for the DCP algorithm (b) Dehazing workflow for our suggested DCP algorithm

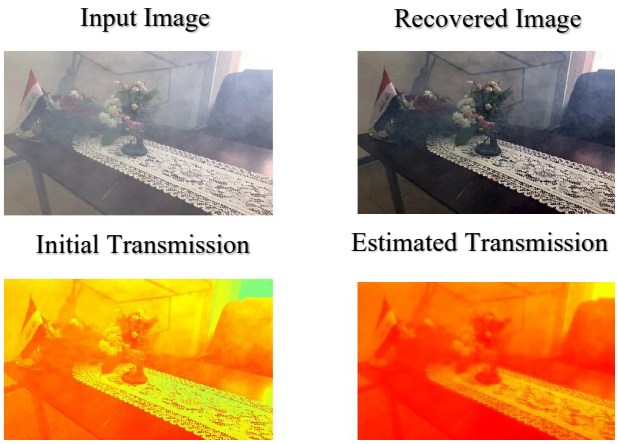


Figure 3: The DCP approach on an experimental image captured in our lab

Utilizing the atmospheric scattering model, the system reconstructs an image from a hazy scene. A general dehazing parameter is used by the process to modify the degree of haze removal so that the image does not look over defogging. An effective methodology to dehaze an image using modified DCP as shown in Figure 2.

4. Dark channel restoration

It is presumed that one channel (red, green, or blue) is usually very dark, except for the sky, with a given pixel in a color image of a natural scene. Which allows for accurate measurement of the dark channel. The dark channel $J^{dark}(x)$ is for a hazy image J(x) in the following equation:

$$J^{dark}(x) = \min_{c\in\{r,g,b\}} \left\{ \min_{y\in\Omega(x)} \{J^c(y)\} \right\} \quad (4)$$

where: J^c is a color channel of J and y is a local patch centered at x.

1. Atmospheric light estimation

When the atmosphere is gloomy and the sunlight (S) is overlooked and even the ambient light (A_∞) is considered the brightest pixel in an eyelid is considered to be the strongest eyelid. Thus, the brightest pixel can be brighter than the atmospheric light by utilizing the following equation:

$$J(x) = R(x)(S + A_\infty) \quad (5)$$

$$I(x) = R(x)St(x) + R(x)A_\infty t(x) + (1 - t(x))A_\infty \geq A_\infty$$

Where: A_∞ is the brightest pixels in an eyelid image intensity without haze is ranging between 0 ⩽R ⩽1.

2. Transmission estimation

Transmission is estimated as follows after estimating the atmospheric light

$$t(x) = 1 - \omega \min_{y\in\Omega(x)} \left\{ \min_c \left\{ \frac{I^c(y)}{A_\infty^c} \right\} \right\} \quad (6)$$

Where: ω is the haze kept in the photo to prevent unnatural scenes (ω= 0.95).

3. Transmission Refinement

Soft matting Laplacian [11] is applied to smooth objects along the edges to refine the transmission map. It dramatically increases the computing time.

4. Scene Radiance Recovery

Which may deduce that we apply to the Equation:

$$J(x) = \left(\frac{I(x) - A_\infty}{\max(t(x), t_0)} \right) + A_\infty \quad (7)$$

We set t_0 = 0.1 so that the dimly enhanced image will be avoided.

The optimization of our modified DCP technique was obtained by testing the quality of captured images to get the attenuation

coefficient (α) which referred to the haze in the scene. Then the image is processed and by varying the attenuation coefficient (α) values we aim to get better results in dehazing. The values of α that have been taken in our algorithm are three values (α =0.5, 0.7, 0.9) and we compared our results with previous DCP algorithms.

5. Experimental Work

5.1. Images Capturing Setup

The experimental setup used for capturing the desired foggy/hazy/dusty scene in this research employed the following tools:

UAV: The UAV used was the Phantom 4 Pro model, produced by Dji co.® (China), with high specifications and camera quality. The UAV is equipped with a 20 Mpix camera as well as an AV navigation system in addition to a variety of other features relevant to the research at hand, such as snapshots, good battery life, GPS, and easy-to-control joysticks, as shown in Fig 4.A. The purpose of using the UAV in this research is primarily to scan the designated terrain, capture photographs in foggy, hazy, and dusty conditions to be used for image analysis and processing by the dark channel prior algorithm.

Fogger: Is utilized for generating foggy-like environmental circumstances. By adding the fogging liquid that consists of a chemical material which turns into a white water vapor due to heating initiated by the fogger. The reason for using the fogger is to generate the fog required to obtain a foggy condition essential for the reconnaissance, which can be very useful in indoor conditions, as shown in Figure 4.B.

The room (Lab): We used two different rooms with a 5x6 m^2 area and 5x4 m^2, where the heights are equal for both rooms (3 m) suitable for photography and reconnaissance as shown in Figure 4.A, and Figure 5.

The software used in our research are as follows:

- MATLAB® software was utilized for aerial photogrammetry processing with DCP algorithm implementation.
- UAV Deploy® and DJI Go® applications are utilized as a UAV pilot to control and capture the scene, as shown in Figure 4.C.

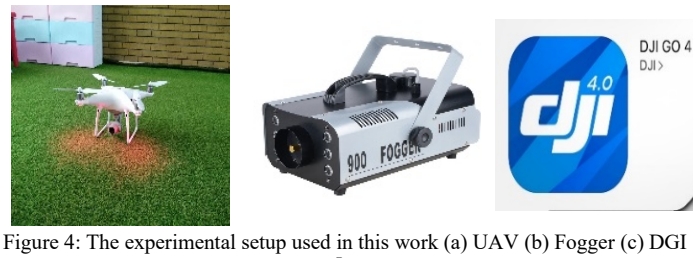


Figure 4: The experimental setup used in this work (a) UAV (b) Fogger (c) DGI GO® App

Our suggested algorithm is obtained by using the UAV (Phantom 4 Pro V_2) that has the modern specifications to uptake the surveillance. This is done by gathering the information by capturing images in different foggy/hazy/dusty conditions. The images were then processed in MATLAB® 2019 with different DCP algorithms and were processed. We have selected the value of attenuation coefficients that give the clearest scenes for images haze removal and then enhance the dehazing image.

5.2. Experimental Implementation

The equipment used in this research was installed as was described in the previous section. After that the fogger was switched on after the addition of the fogging substance, the UAV was launched at the given designated route for reconnaissance and the UAV was programmed to take one photograph per second. We programmed the UAV to take photographs at various heights (3 m, 25 m, and 10 m for the foggy indoor, dusty outdoor, foggy outdoor images, respectively) with the presence of fog in the research environment. After conducting the reconnaissance and collecting the photographs, we have transferred the photos from the UAV's memory card to the PC for photo rendering to be enhanced and conduct our calculation (Image quality metrics, normalized cross-correlation, and (PSNR/RMSE)). We processed the images using MATLAB® software by inserting the suggested algorithm that we have developed to enhance the image and remove the fog. The images were enhanced and the fog was removed by inserting two previous algorithms to compare the result as well as developing future researches to address some of the weak points of such studies. Two previous articles were chosen to compare their results after applying the captured images in the previously chosen algorithms. The calculation for Image Quality parameters/metrics; normalized cross-correlation, (PSNR), Average Difference, Structure Content, Max Difference, Normalized Absolute Error then the results of our calculations were compared and contrasted with QFP of our algorithm and the chosen scene as is shown in Figure 5.

6. Results

The output dehazed images obtained from the suggested algorithm on the selected images are shown below with a comparison of two other DCP algorithms [13]. The images were selected in various weather conditions as shown in Figure 6 under DCP, we also calculated the image quality parameters/metrics and compared them with our modified algorithm. The algorithms used in the comparison are He, et al [14] algorithm and Fattal's [15] algorithm. The selected circumstances that we have been testing our modified DCP are foggy indoor image, as shown in Figure 6.A, dusty outdoor image, as presented in Figure 6.B, and dusty outdoor image, as depicted in Figure 6.C, respectively. The altitude of the images A, B, and C are 3, 25, and 10 m, respectively. Images in Figure 6 were processed by three different DCP algorithms, the input images have different conditions of haze/fog and therefore different results are shown for each image. Our method gives more enhancement and clearer output in comparison with the other DCP algorithms.



Figure 5: Experimental implementation setup of our study for the hazy environment using UAV in indoor conditions

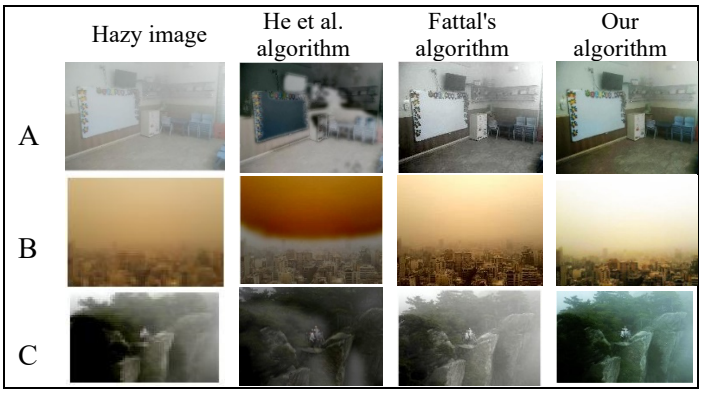


Figure 6: Dark Channel Prior algorithms used for dehazing in various algorithms in three different hazy circumstances (images from the experimental setup) (a) Indoor foggy image (b) Outdoor dusty image (c) Outdoor foggy image

Table 2 below provides the comparative calculations of image quality parameters/metrics and the comparison between these values which are discussed in the discussion section. The image quality parameters/metrics were calculated using MATLAB® software.

Other comparative results for the DCP algorithms were used for images obtained from Google® with foggy and dusty environmental conditions, the altitude of the images A, B, and C are 80, 125, 50 m, respectively, as shown in Figure 7. The image quality metrics/parameters for these sets of images are presented in Table 3.

Table 2: The Q indices for the images A, B, and C, respectively

Image Q indices	He et al algorithm	Fattal's algorithm	Our algorithm
Image (A) (Foggy Indoor) (Altitude 3 m)			
MSE	8.43e+03	3.07e+03	2.69e+03
PSNR	8.87	13.25	13.84
Normalized Cross-Correlation	0.58	0.82	0.86
Average Difference	68.53	37.15	35.85
Structure Content	2.28	1.36	1.27
Max Difference	236	255	146
Normalized Absolute Error	0.41	0.25	0.18
Image (B) (Dusty Outdoor) (Altitude 25 m)			
MSE	5.25e+03	1.14e+03	1.89e+03
PSNR	10.93	17.58	15.36
Normalized Cross-Correlation	0.57	0.78	0.86
Average Difference	55.65	-11.84	-22.56
Structure Content	2.69	0.76	0.78
Max Difference	115	117	64
Normalized Absolute Error	0.42	0.21	0.18
Image (C) (Foggy Outdoor) (Altitude 10 m)			
MSE	2.23e+03	1.84e+03	1.64e+03
PSNR	14.64	15.49	15.98
Normalized Cross-Correlation	0.53	0.82	0.87
Average Difference	38.2	-32.19	-32.34
Structure Content	3.01	0.54	0.51
Max Difference	162	118	111
Normalized Absolute Error	0.47	0.38	0.38

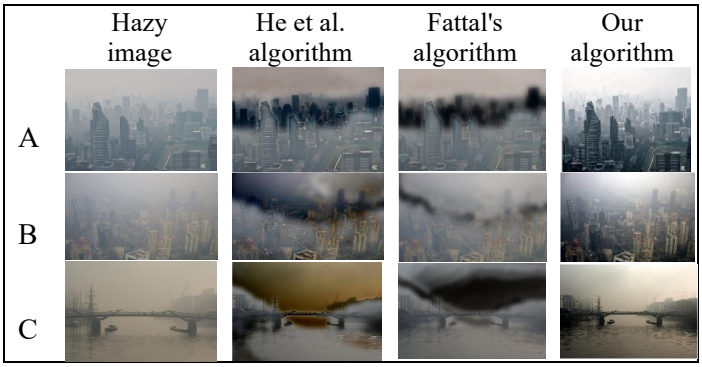


Figure 7: Dark Channel Prior algorithms used for dehazing in various algorithms in three different hazy circumstances with different altitudes (images from Google®) (a) 80 m (b) 125 m (c) 50 m

Figure 8 shows a selective comparison for the metrics of the three processed images of Fig, 6.A, 6.B, and 6.C, respectively, the comparison was done with our method and two previous methods for (a) PSNR (b) Normalized Absolute Error.

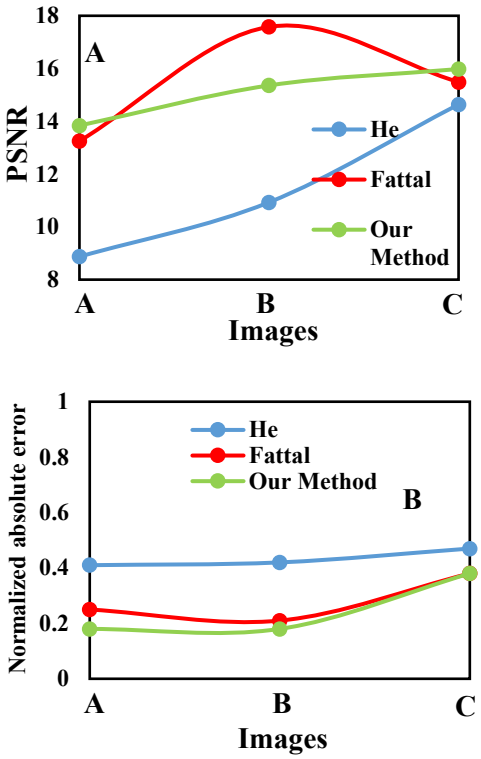


Figure 8: Comparison of the DCP methods (a) PSNR (b) Normalized absolute error

Table 3: The Q indices for the images A, B, and C, respectively

Image Q indices	He et al algorithm	Fattal's algorithm	Our algorithm
Image (A) (Altitude 80 m)			
MSE	3.32e+03	3.25e+03	2.94e+03
PSNR	12.92	13.01	13.44
Normalized Cross-Correlation	0.72	0.75	0.87
Average Difference	37.5	35.95	35.1
Structure Content	1.67	1.62	0.9
Max Difference	174	180	254
Normalized Absolute Error	0.28	0.28	0.26
Image (B) (Altitude 125 m)			
MSE	4.61e+03	5.11e+03	2.3e+03
PSNR	11.5	11	14.5
Normalized Cross-Correlation	0.63	0.62	0.94
Average Difference	54.54	50.18	13.64
Structure Content	2.37	2.05	1.03
Max Difference	164	167	255
Normalized Absolute Error	0.39	0.41	0.19
Image (C) (Altitude 50 m)			
MSE	3.86e+03	2.13e+03	2.61e+03
PSNR	12.26	12.52	13.95
Normalized Cross-Correlation	0.62	0.72	0.84
Average Difference	50.18	54.18	1.83
Structure Content	2.2	2	0.9
Max Difference	148	187	255
Normalized Absolute Error	0.37	0.49	0.22

7. Discussion

From the previous experimental work and their implementation, the output dehazed images obtaining from the DCP algorithm on the selected images as shown in Figure 6 and Figure 7 using the image capturing setup and images in Google® which includes three DCP algorithms. These results illustrate the differences between using the DCP algorithms that have been developed over the years. Our modified DCP algorithm that has been developed gave high image quality in outer photogrammetry that used in monitoring systems in hazy weather such as foggy and dusty environments. In calculations obtained using our algorithm, noticing that the values in indoor hazy aerial photogrammetry (Table 2, Figure 6.A), the MSE, average difference, structure content, max difference, and normalized absolute error values reduced respectively while the PSNR and the normalized cross-correlation values raised to give good quality and eliminate the haze effect on the imagery. In the dusty weather test (Table 2, Figure 6.B), the MSE, average difference, max difference, normalized cross-correlation, and the normalized absolute error values were reduced by using our modified DCP algorithm while PSNR and structure content better in Fattal's algorithm. For outdoor hazy aerial image (Table 2, Figure 6.C), the MSE, average difference, structure content, and max difference values respectively reduced. While there are comparatively increasing in the other parameters. Even if the images were taken apart from the setup as shown in Figure 7, the suggested algorithm is enhancing the image and removing the fog and dust in the surrounding environment and producing a clear view of the scene (Table 3, Figure 7.A, Figure 7.B, Figure 7.C).

The restriction and other related algorithms based upon statistics of the proposed method in which image values with particular images, e.g., obtained in very different examples cannot be used (harsh weather conditions). If only part of the object in the picture is obscured by heavy fog, using the algorithm would distort the image's color reproduction and degrade as a result affects the spectral image quality which utilized radiometric correction with low impact. The atmosphere is important for the accuracy of subsequent remote sensing analyses in low altitudes; therefore, calibration panels with a proven reflection coefficient should be used to check device calibration in the processed image and estimate radiometric error. Also, geophysical limitations are not included in the proposed method, for example, variables like humidity.

8. Conclusions

This paper demonstrates the results of research into low altitude dehazing picture methods. The DCP algorithm has been used to eliminate the haze induced by the negative effect of the low atmosphere on UAV images. The variables of our algorithm were empirically determined. We have a strategy dedicated to low altitude photos, in particular for the most commonly used altitudes (in the range below 30 meters) for remote sensing with the UAV. The efficiency of the system proposed was assessed and many qualitative metrics that were used to establish the effectiveness of our suggested algorithm. In comparison with other common methods used for dehazing images, the results of our experiments showed the effectiveness of our process. Moreover, the image data collection in various heights and atmospheric conditions is obtained by careful assessment of weather conditions using the UAV. We have shown that our approach is of significant value in terms of improving the image quality in different weather conditions.

Conflict of Interest

The authors declare no conflict of interest

Acknowledgment

We would like to acknowledge the department of laser and optoelectronics engineering at Al Nahrain University.

References

[1] K. He, J. Sun, X. Tang, "Single image haze removal using dark channel prior," IEEE Transactions on Pattern Analysis and Machine Intelligence, **33**(12), 2341–2353, 2011, doi:10.1109/TPAMI.2010.168..

[2] A. Mazur, M. Kacprzak, K. Kubiak, J. Kotlarz, K. Skocki, "The influence of atmospheric light scattering on reflectance measurements during photogrammetric survey flights at low altitudes over forest areas," Forest Research Papers, **79**(1), 59–68, 2019, doi:10.2478/frp-2018-0007.

[3] S. Zhang, and J. Yao, Single image dehazing using fixed points and nearest-neighbor regularization, Computer Vision – ACCV 2016 Workshops Springer, 2016.

[4] K. He, J. Sun, and X. Tang, "Single image haze removal using dark channel prior," in IEEE transactions on pattern analysis and machine intelligence

33.12: 2341-2353, 2011.doi:10.1109/TPAMI.2010.168.
[5] Y. Xu, J. Wen, L. Fei, Z. Zhang, "Review of Video and Image Defogging Algorithms and Related Studies on Image Restoration and Enhancement," IEEE Access, **4**(c), 165–188, 2016, doi:10.1109/ACCESS.2015.2511558.
[6] S. Lee, S. Yun, J.H. Nam, C.S. Won, S.W. Jung, "A review on dark channel prior based image dehazing algorithms," Eurasip Journal on Image and Video Processing, **2016**(1), 1–23, 2016, doi:10.1186/s13640-016-0104-y.
[7] Y. Huang, W. Ding, H. Li, "Haze removal for UAV reconnaissance images using layered scattering model," Chinese Journal of Aeronautics, **29**(2), 502–511, 2016, doi:10.1016/j.cja.2016.01.012.
[8] C. Pat S. Jr., Atmospheric, solar, and M.T.F. corrections for ERTS digital imagery, S.l. : s.n., 1975.
[9] R. Richter, "Atmospheric correction of DAIS hyperspectral image data," Computers and Geosciences, **22**(7), 785–793, 1996, doi:10.1016/0098-3004(96)00016-7.
[10] D. Chowdhury, M. Sarkar, M. Z. Haider, S. A. Fattah, and C. Shahnaz, "Design and implementation of a cyber-vigilance system for anti-terrorist drives based on an unmanned aerial vehicular networking signal jammer for specific territorial security," in IEEE Region 10 Humanitarian Technology Conference (R10-HTC), 2017. doi:10.1109/R10-HTC.2017.8288995.
[11] S.A. Fattah, M.Z. Haider, D. Chowdhury, M. Sarkar, R.I. Chowdhury, M.S. Islam, R. Karim, A. Rahi, C. Shahnaz, "An aerial landmine detection system with dynamic path and explosion mode identification features," in GHTC 2016 - IEEE Global Humanitarian Technology Conference: Technology for the Benefit of Humanity, Conference Proceedings, 745–752, 2016, doi:10.1109/GHTC.2016.7857361.
[12] H. Liu, J. Yang, Z. Wu, Q. Zhang, "Fast single image dehazing based on image fusion," Journal of Electronic Imaging, **24**(1), 013020, 2015, doi:10.1117/1.jei.24.1.013020.
[13] E. Woloszyn, An Overview of Meteorology and Climatology, Ph.D. Thesis Gdansk University of Technology, Poland, 2009.
[14] K. He, J. Sun, X. Tang, "Guided image filtering," IEEE Transactions on Pattern Analysis and Machine Intelligence, **35**(6), 1397–1409, 2013, doi:10.1109/TPAMI.2012.213.
[15] R. Fattal, "Single image dehazing," ACM Transactions on Graphics, **27**(3), 2008, doi:10.1145/1360612.1360671.

ASTES

Advances in Science, Technology and Engineering Systems Journal Vol. 5, No. 5, 1118-1125 (2020)

www.astesj.com

ASTESJ

ISSN: 2415-6698

Design and Implementation a Novel System for Estimation Precise Transfer Function of DC Motor

Falih Salih Alkhafaji[*,1], Wan Zuha Wan Hasan[2], Nasri Sulaiman[3], Maryam bt. Mohd. Isa[3]

[1]*Ministry of Industry, State Company for Electrical and Electronic Industries,10052, Baghdad, 10001, Iraq*

[2]*Institute of Advanced Technology (ITMA), University Putra Malaysia, 43400, Serdang, Selangor, 45500, Malaysia*

[3]*Department of Electrical and Electronic Engineering, Faculty of Engineering, UPM, 43400, Serdang, Selangor, 45500, Malaysia*

ARTICLE INFO

Article history:
Received: 30 June, 2020
Accepted: 04 October, 2020
Online: 20 October, 2020

Keywords:
HSMDAQS
TF
PI controller
DC motor
Estimation

ABSTRACT

A precise modelling plant system is substantial to improve the design of the DC motor controller, where a low accurate model may cause an unacceptable controller system. This study presents a hardware-in-the-loop (HIL) system for design a high speed motor data acquisition system (HSMDAQS) and injected collected data (ICD) Simulink model to estimate accurately the transfer function (TF) of a DC motor, without needing motor's specification, providing high accuracy estimation tool that can be used to develop the design of a DC motor controller. The proposed system generates synching data to be imported into system identification (Sys Ident) application through a serial port. To show the performance design, a comparative study has been conducted between the experimental realization and simulation results in terms of dead time(td), rise time(tr), and settling time(ts), using a scope simulator. It was used three different DC motors to demonstrate the effectiveness of our approach in terms of average error step responses (AE-SR). The estimation results show that the best FIT between the response of the estimated TF and the collected data augmented by 95.03 % and stabilized despite using different motor's speed. A comparison step response between experimental and simulation shows a very low deviation and minimized AE-SR below 10% for all tested motors. The developed system could be applied in a wide range of industrial applications, offering faster with accurately capturing data, high precision stabilized platform, a simpler implementation for dynamic systems, lower computational cost design, and flexibility.

1. Introduction

This paper is an extension of work originally presented in the Prime Asia 2019 conference [1]. DC motors are being used in robotic systems, home appliance and an electric vehicle and many other applications in case of simple structure, high performance, low-cost installation, and easy control speed. However, DC motor systems still have nonlinear parameters, variation in load dynamics, unpredictable inputs and disturbances, that affect their quality. Therefore, these motors should be controlled and analyzed to improve their performance [2-5].The concept of a real-time processing must be considered when an engineer designs develops and deploys a new automation and control system[6].The improvement of DC motors' control arrangement to enhance their response characteristics is one way of reducing the amount of consumed energy and enhance the efficiency of the machines. Control systems engineering requires a knowledge of at least two basic components: (1)the plant model which describes the mathematically modeled behavior of the system;(2)the desired output [7]. For those systems are known their specifications, The DC motor can be mathematically modelled by using the dynamic equivalent circuit of DC motors based on the second order system as given in equation 1 [8, 9] .

$$P(s) = \frac{\dot{\theta}}{V(s)} = \frac{K}{(Js+b)(Ls+R)+K^2} \quad \frac{[rad/sec]}{V} \tag{1}$$

For DC motor with zero load, the TF from can be simplified as a first order system as given in equation 2.

$$P(s) = \frac{\frac{1}{Ke}}{\frac{Jm\,R}{Kt\,Ke}S+1} = \frac{a}{TS+1} \quad \frac{[rad/sec]}{V} \tag{2}$$

[*]Corresponding Author: Falih Salih Alkhafaji, falih_alkafaji1@yahoo.com

where J is the moment of inertia of the rotor,b is motor viscous friction constant, θ is the speed of the shaft, L is the electric inductance is the resistance of the coil, Kt is the motor torque and Ke is the back emf

By contrast, modelling TF not so straightforward in case of not all manufactured motors are provided their specifications, which was considered the first problem in the field of controller system [10] .One of the most interesting criteria to improve the controller schemes is the optimized TF model. Therefore , it is necessary to base the control system design on a process model [11]. Consequently, the structure of a TF model should be accurately realized that is without following a suitable estimation process , the classical approaches for compensator design and stability analysis are rendered ineffectual [12-17], especially for controller based PID and PI algorithm, that were extensively applied to enhance the speed performance in terms of step response characteristics td, tr, ts and overshoot [18, 19].However, the common problem in dynamic systems, that is impossible to describe the real plant system exactly in case of unbalancing behavior between controller and plant system. As some techniques are better than others for any given application, each method has its advantages and disadvantages [20].To estimate an approximate model for an unknown system's specification, it is desired to load a certain input signal and to collect the output with thanks to Sys Ident, providing simplified models for complex systems from time-series data [21 , 22]. However, the errorless of parameter estimation depends on the preciseness of data information and sampling time.Therefore, the precision of acquiring data determined the accurate level of estimation models [23]. There are numerous studies focusing on estimation TF model of plant systems, several using costly data acquisition (DAQ)system based Sys Ident application for loading and collecting input /output data [24, 25], others using digital oscilloscope based Sys Ident [26, 27].By contrast, improve the accuracy of DAQ system could be considered the best solution to boost the precise estimation, and if the modeling of TF can be acquired precisely, the control system could be greatly improved performance [28].

The objective of this study is to obtain high accuracy mathematical model for DC motors without need their specifications, providing low cost design, besides investigating the simulation and experimental realization in terms of step response characteristics to show the efficiency of the proposed system. This paper proposed a novel HSMDAQS coupled with ICD Simulink model to improve the accuracy of collecting data to be used with Sys Ident application to formulate the mathematical models. The novel system has several advantages such faster and accurately capturing data, high precision stabilized platform, a simpler implementation for dynamic systems, flexibility and reducing the total parts cost design less than 20 US dollars. It is well known that the Sys Ident application is very limited, but the proposed methodology assists the novel system to minimize significantly the error capturing data (injected signal and θ) leads to increase the accuracy of TF form. The contributions of this study are: (1) Design a novel HSMDAQS to guarantee capturing data with very low error; (2) high precision stabilized system (3) improve the estimation of TF model for unknown system's specification; (4) highly sensitives tool for measuring the deviation between experimental results and simulation. In order to verify the estimated TF models, a comparison between the simulation and the actual motor performed in terms of step response characteristics.

This article is organized as follows: Section 2 presents the proposed system design to estimate TF and provides a brief description of the hardware design and Simulink model. Section 3 presents the results of the estimation TF models, besides simulation and experimental results are carried, highlighting the step response characteristics, further discussing the comparison between them. Finally, the conclusion and recommendation are presented in section 4.

2. System design

This section presents the multi-steps of design methodologies to estimate accurately the mathematical model of a DC motor, giving a brief detail about the injected signals and the collected data in a time domain specification. The proposed method relies on four parts:(1) design HSMDAQS;(2) implement ICD Simulink model;(3) software and hardware setup;(4) using Sys Ident to estimate TF form. The proposed HSMDAQS has been employed to inject a different signal, and to acquire θ data, to be imported into Sys Ident application. It is chosen three diverse DC motors (M1, M2, M3) to investigate the effectiveness of the proposed HSMDAQS in terms of AE-SR. The speed motors M1,M2,M3 are 56,400,107 RPM respectively. The M1 and M3 are gearbox type with a reduction ratio equal to 1/10 for both, where M2 is a speed type. These motors are unknown dynamic parameters. Physically, to acquire data in data output, the tested motors were connected with HSMDAQS via a driver amplifier, where the collected output data imported from the dual hall encoder sensor (DHES) through collecting data port. By using a model-based design technique, it is designed ICD Simulink model to be implemented on HSMDAQS to inject step pulse and to collect data out. It is essential to calibrate the θ by measuring the RPM on a tachometer and scope simulator then adjusting the potentiometer of HSMDAQS to ensure that the recording data from the scope simulator is corresponding with the tachometer reading. This step is very important to minimize the divergence between experimental and simulation results. The communication between HSMDAQS and DHES is designed to inject signal to drive a motor and to acquire data out from DHES.

Figure 1 shows the proposed methodology to estimate precise TF model, it can be summarized into seven steps to meet the objective as follows:(1)connect HSMDAQS with PC through port6;(2)calibrate HSMDAQS by measuring θ in scope simulator and tachometer then proceed the adjustment between them to meet maximum similarity between experimental and simulation results;(3)using switching mode to inject one of the five different signals (square and triangle) wave by setting values as shown in Table 1;(4)acquiring data in data out and convert them into the time domain using iddata command to create a data object of (y, u, Ts);(5)import created data object into Sys Ident application to proceed the estimation process;(6) repeat again the same procedure with other injected signals until reached to signal 5;(7) from data model info, select the maximum percentage of best FIT that achieve high accurate TF model . The steps began with the measurement of data in data out of the tested motors M1, M2, M3 under different signals and voltages for a different speed with sampling time (Ts) equal to 0.02s to be imported into Sys Ident toolbox to evaluate a TF model of the tested motors. In this stage, the tested DC motor will begin to spin proportionally with the amplitude of the injected signal for the 30sec. The generated pulses are counted through the ICD model via Arduino analog inputs analog outputs. At this moment, the data in data out is ready to be imported accurately into the Sys Ident application.

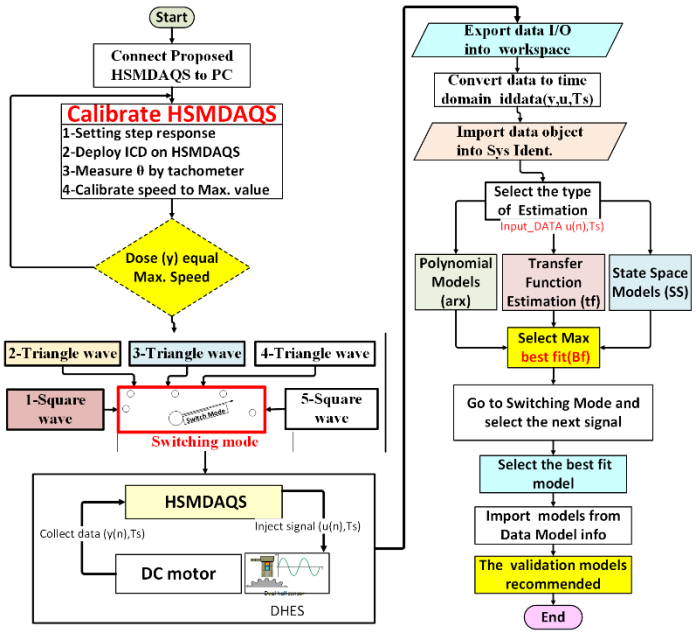


Figure 1: Methodology to estimate precise TF model

Table 1: Setting injected step signals

shape	No	Amplitude (V)	Period (s)	Pulse Width(s)	Pulse Delay (ms)
Square	Sig1	12	10/Ts	5/Ts	100
	Sig5	6	8/Ts	4/Ts	50
		Vector Amplitude(V)		Vector Time(ms)	
Triangle	Sig2	[0 ,6, 0 ,6 ,0]		[750 ,1500, 2250, 3000]	
	Sig3	[0 ,2.4, 4.8 ,2.4 ,0]		[132.5 ,2653, 3975, 5.300]	
	Sig4	[0 ,1.8, 3.6 ,1.8 ,0]		[0 ,1250, 2500, 3755,5000]	

2.1. Hardware design

As shown in Figure 2, the proposed HSMDAQS platform-constructed to be used as a high-speed capturing data. The platform constructed based on Arduino Uno with several electrical devices, HIL technique to communicate with the ICD Simulink model. It is used RF520 MOSFET to derive the tested motors, and designed a collecting data port to acquire data in data out, besides using a potentiometer to improve the accuracy of the collected data by calibrating the injected signal regarding maximum speed for each tested motors.

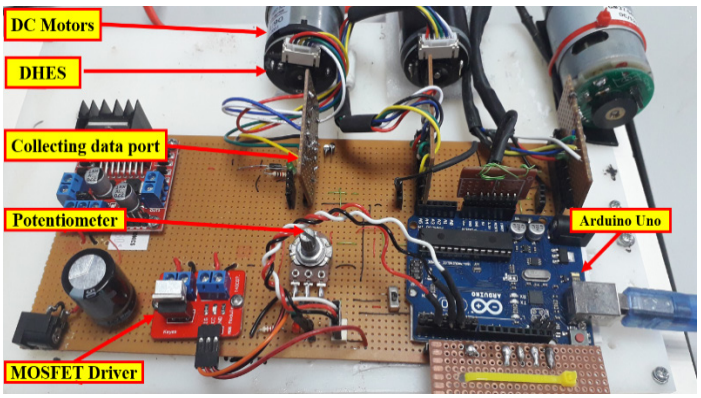


Figure 2: Proposed HSMDAQS

2.2. Proposed ICD simulink model

As shown in Figure 3, the ICD model is constructed based on Simulink block sets to run the HSMDAQS on external mode. It is designed several subsystem blocks such as a signal generator, count mode (CM), and selective switching mode (SSM). Figure 4 shows the SSM subsystem which contains five block set switches (SW) connected serially, to generate multiple signals. It is designed to choose one signal between five generated signals depending on setting the truth table, as illustrated in Table 2.

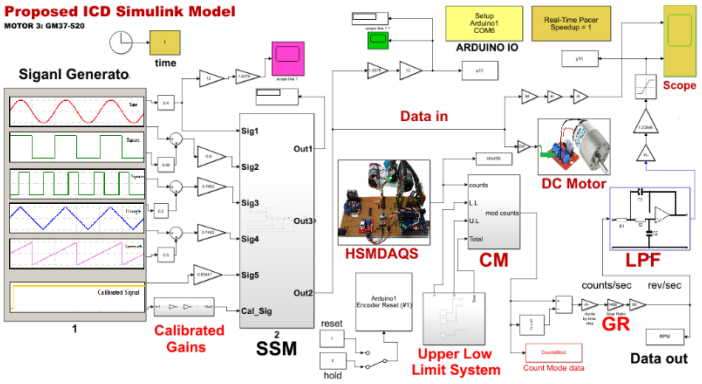


Figure 3: Proposed ICD simulink model

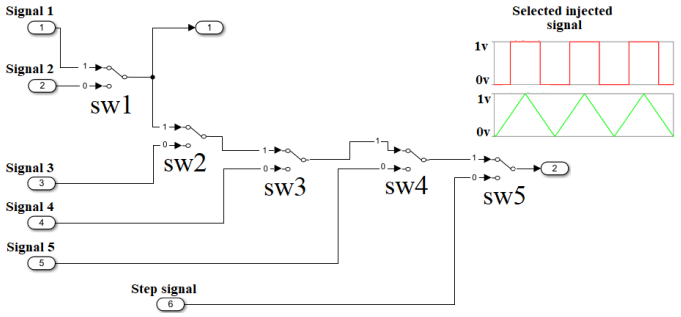


Figure 4: The SSM subsystem

Table 2: Suggested setting logic switching.

Signal No.	Shape	Sw1	Sw2	Sw3	Sw4	Sw5
Signal1	Sequare	1	1	1	1	1
Signal2	Triangle	0	1	1	1	1
Signal3	Triangle	x	0	1	1	1
Signal4	Triangle	x	x	x	0	1
Signal5	Sequare	x	x	x	x	0

Figure 5 shows the shape of generated signals (square and triangle) to inject into the tested DC motors. Based on selective switching mode, it can be chosen the shape of the signal depending on setting truth table, by setting sw1,2,3,4,5 on appropriate logic level to get the desired signal, for example, to generate triangle wave (signal 2), it should be setting sw1 on logic 0 and others switches on logic 1, and to generate square wave (signal 5), the sw4 should setting on logic 0 and sw5 on logic 1. Finally, to calibrate the generating voltage on 12V, it is suggested to inject the step response signal to drive the motor by setting sw5 on logic 0.

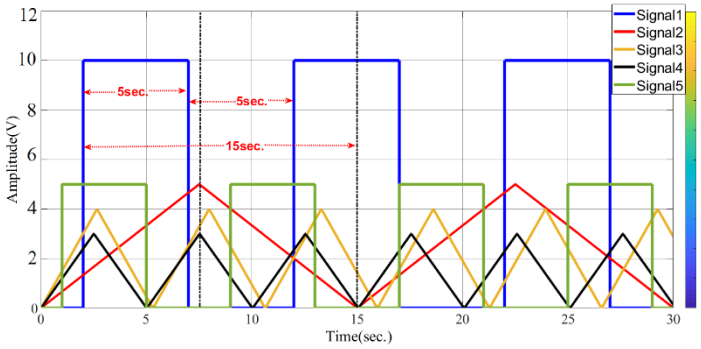


Figure 5: Five different injected signals into DC motors

The C.M subsystem designed to evaluate the motor's speed based on count pulses, and to make a comparison between the present counts to the previous one from the last sample, and to specify whether a rollover has occurred between (-32768 to 32767), then to adjusts the cumulative number of counts and to remove the overflow counting. Examine the DHSE, it is observed some a certain error between the injected signals (u)and the angular speed signal (y), also when increasing the RPM speed, the capturing θ will become not smooth with augmented error as shown in Figure 6.

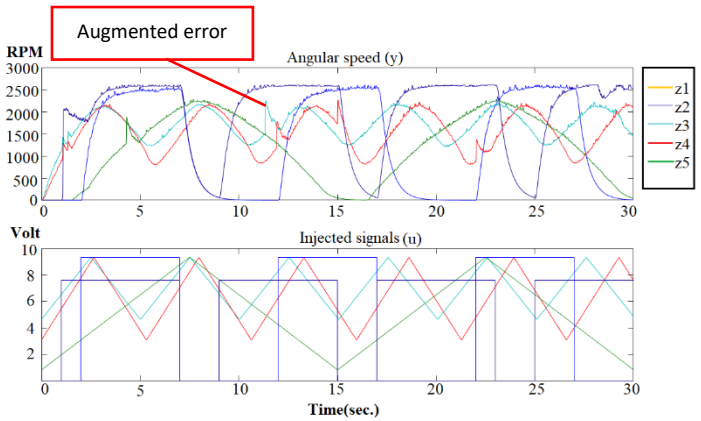


Figure 6: Five different injected signals and θ

To reduce the effect of noise ,it is suggested to design a low pass filter (LPF) to be implemented on the ICD model, by measuring the cut off frequency(Fo) at maximum speed for tested motor as given in equation 3 , to find a filter constant (Fil_c) as represented in equation 4.Based on scope simulator recording, the measuring cutting frequencies for the tested motors M1,M2,M3 are 73HZ,187HZ,95HZ respectively. To cut unwanted these frequencies, it should be evaluated the TF of the LPF motor as given in equation 5.

$$Fo = \frac{1}{2\pi .Fil_c} \tag{3}$$

$$Fil_c = \frac{1}{2\pi.Fo} \tag{4}$$

$$LPF(TF) = \frac{Vout}{Vin} = \frac{1}{Fil_c\ S + 1} \tag{5}$$

The resulted TF form of the LPF of each DHSE of the M1, M2, M3 are shown in equations 6, 7 ,8 respectively.

$$LPF(M1) = \frac{1}{2.1\,x10^{-3}\ S\ +1} \tag{6}$$

$$LPF(M2) = \frac{1}{0.85x10^{-3}\ S + 1} \tag{7}$$

$$LPF(M3) = \frac{1}{1.67x10^{-3}\ S\ +1} \tag{8}$$

2.3. Software setup

By using a model-based design technique to construct the proposed ICD model and to do the communication with HSMDAQS, it is followed two steps. Firstly, by installing the ARDUINO I/O block set on MATLAB respiratory using the IDE ARDUINO program to scratch the application on the Arduino board. This program acts as a server for passing information between the hardware and the Simulink model. Together, these elements allow us to access Arduino digital inputs/outputs, analog inputs and read encoders through the Simulink model. Secondly, run MATLAB as an administrator to run the ICD model based on ARDUINO I/O block set that has been appeared in the respiratory library. Once the ARDUINO I/O Simulink block set installed, the Arduino IO block set (Digital Write block, the Encoder Read block, the Arduino IO Setup block, and the Real-Time Pacer block) are ready to be used for hardware communication. The sketch IDE program runs continuously and receives the commands from the ICD model via the serial port to executes the commands and returns a result. The final Arduino communication setting located on the workspace detecting that the port connection with the Arduino Uno board is connected through com6. For further information about Simulink block sets for communicating with an Arduino Uno board, programming code refers to [30].

Afterward, set the current MATLAB directory to the location of the file install_ arduino.m (in the Arduino IO/ folder), this will be allowed the update path to be saved continuously. Finally, importing ARDUINO I/O Simulink block set into the respiratory library by typing (install Arduino) at the MATLAB command line to run the IDE script through Simulink. The script simply adds the relevant Arduino IO folders to the MATLAB path and saves the path. After completing these steps, the proposed HSMDAQS is ready to communicate with the ICD model to inject a signal and to collect data out from DHES.

2.4. Hardware setup

Figure 7 shows the hardware setup for acquiring data to be used with the Sys Ident toolbox. In this process for the data acquisition, the tested motors connected with HSMDAQS via collecting data port. To run the hardware-based Simulink model, it should keep communication between PC and HSMDAQS through collecting data port, using serial data port com6. This process provides additional advantages, for instance, more synching data, measured real-time via scope simulator further rejecting noisy data by proceeding further modifications through running hardware.

The communication between HSMDAQS and DHES through the ICD model will be beginning by sending the injected signal via pin A0 (Analog write) to drive the motor, then acquiring data in data out from DHES via (Digital read pins) D2 and D3, which already connected with Phases A and B of a DHES. Hence, sending a voltage through pin A0 input signal (data-u) and the encoder block set receives a couple of data through Digital read pins to generate single output speed data(y).

To run the proposed HSMDAQS in real-time, it should be configured Arduino board on Simulink using configuration parameter setting, by selecting Tools > Run on Target Hardware > Run. Afterward, the ICD model activated to acquire data in data

out in time domain specification, which will be run internally on the host computer.

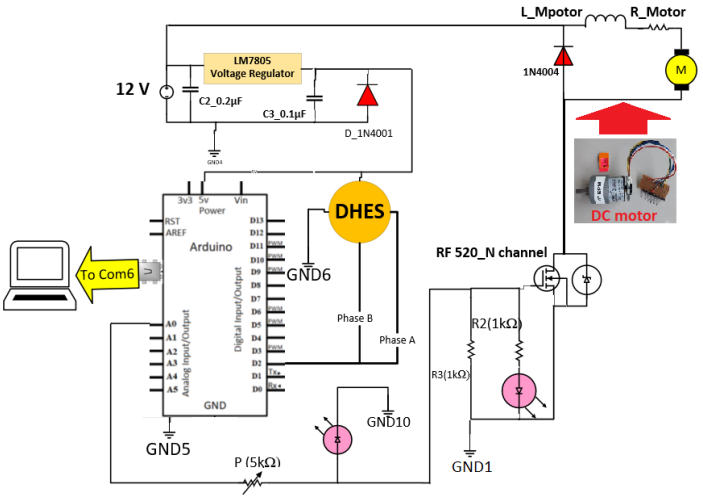


Figure 7: Hardware setup

2.5. Analysis based System Identification

This stage demonstrates how to estimate the TF model of M1, M2, M3 by acquiring data out θ based proposed HSMDAQS hardware to be imported into the Sys Ident toolbox. Mainly, this is done by modifying parameters within a given model until its output synchronizes as well as possible with the measured output. To check the validation of the proposed TF, it is taken a close look at the model's output compared to the measured one on a data by finding the best FIT using the Model output box. By contrast, the accuracy of collecting data specifies the level of the best FIT estimation. Therefore, the HSMDAQS hardware should be designed to acquire synching data with lower noise.

Based on Sys Ident, it is used various estimated models, such as TF, state-space (SS), and polynomial (arx)models to choose a better estimation. It is essential to prepare the HSMDAQS for acquiring data. Firstly, connected M1, M2, M3 with the HSMDAQS system through data collecting port. Secondly, it is injected five various signals (triangle, square) waves to excite the system and to record the θ data. The reason behind using different injected signals is to provide sufficient data for model validation as PRBS signals, besides increasing the capability for finding a better accurate TF form. Figure 8 shows the several steps need to be followed to inject different signals and to collect the set of θ data from DHES using ICD Simulink model-based HSMDAQS as following:(1) run proposed HSMDAQS platform based proposed ICD Simulink model ;(2) using suggested SSM to inject five different signals with a frequency between 0.5 to 5 HZ;(3) the signal logging feature in Simulink will create a data set object in a workspace containing all the logged signals as time-series objects;(4) export five sets of data in data out (u, y) into the workspace, where (u) represents to an input signal and (y) to θ;(5) prepared the acquired data for estimation and validation, by converting the exported data into the time domain denoted data object using iddata command, to be imported into a workspace with Ts equal to 0.02s;(6) import created data objects (z1, z2, z3, z4, z5) into Sys Ident.

Figure 9 shows the estimation process to obtain a TF form. Firstly, it is selected the θ data object (z1, z2, z3, z4, z5) imported from the workspace/MATLAB into Sys Ident application, then using three different estimation types; Polynomial model(arx), State Space model (SS)and TF model. Afterward, specify the number of poles and zeros for different cases. Next, the estimation for each data object is figured as an impulse response time characteristic. Ultimately, it can be imported the TF model (TF1, TF2, TF3, TF4, TF5) and best FIT estimation for each impulse response by clicking the estimation box as shown in Figure 9.

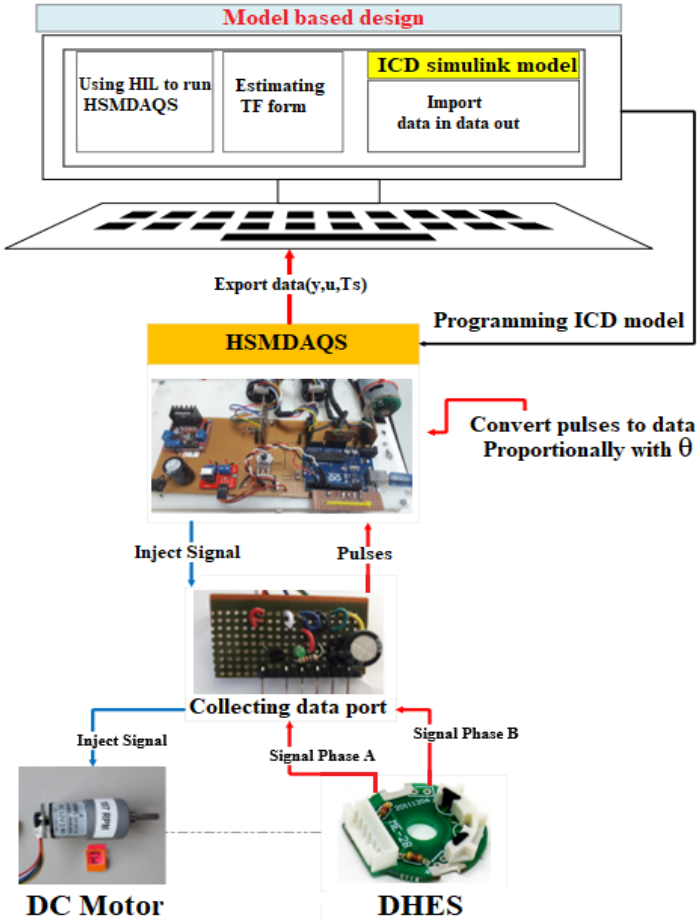


Figure 8: Acquiring data based HSMDAQS

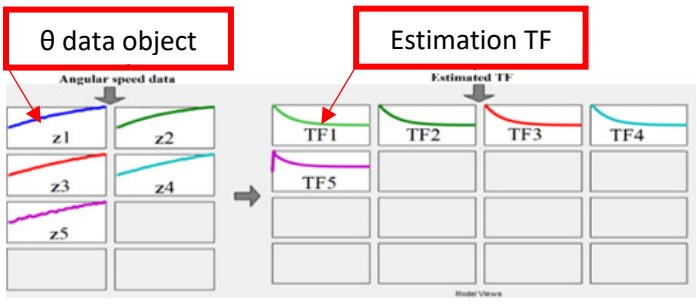


Figure 9:Importing data object into Sys Ident application

3. Results and Discussion

This section presents the estimation TF models based HSMDAQS, besides measuring the simulation and experimental step response parameters in terms of td, tr, ts, and SST, where the AE-SR is the performance indices used for the comparison of the results.

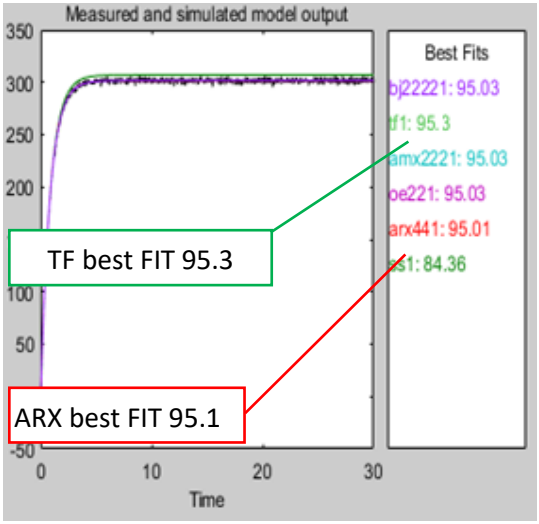


Figure 10: Model Output box for selection the estimation models

```
From input "u1" to output "y1":
  6.419
  ----------
  s + 0.7606
Name: tf_1st_order
Continuous-time identified transfer function.
```

```
From input "u1" to output "y1":
  6.399
  ---------
  s + 1.188
Name: tf7
Continuous-time identified transfer function.
```

```
From input "u1" to output "y1":
  436.5
  ---------
  s + 1.582
Name: tf7
Continuous-time identified transfer function.
```

Figure 11: Estimated TFs form (a), for M1,(B)for M2,(c)for M3

3.1. Estimation TF model

It is used the Model Output box to show the best FIT of estimation. It is observed, when increasing the order of the estimation system, the best FIT will remain at the same value, therefore it is selected the first order system for the estimation because of the availability of a simple formula for designing a PID controller [31]. The estimated models are compared and selected regarding to the highest best FIT percentage. As shown in Figure 10, it is displayed that the best FIT of the estimated models are enhanced in TF form by 95.3 % and ARX by 95.01%, that means the novel HSMDAQS has rejected the noise significantly. The justification behind using three different types of DC motors is to verify the best FIT estimation in different conditions. It is observed that even though using different RPM speeds, the best FIT results are still the same value. That is mean the proposed HSMDAQS has excellent stability despite using different motor's speed. Consequently, it is possible to use the proposal for any other types of DC motor even in industrial applications to estimate TF.

From Figure 11, it is important to highlight that the estimated TFs for M1, M2, M3, shown an absolute structure models due to low error capturing data.

3.2. Simulation results

In order to evaluate the proposed TFs models of each DC motor, there are several experiments are performed to obtain step response characteristics. Hence, the simulation scenarios are carried out with 3 estimated TFs models for the tested motors M1, M2, M3. The step response results were investigated by using a scope simulator as shown in Figure 12. It is observed that the tr and ts measured in the second unit for all tested motors.

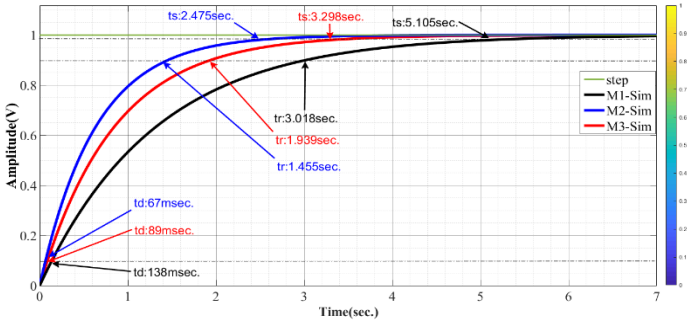


Figure 12: Simulation step response characteristics of M1,M2,M3

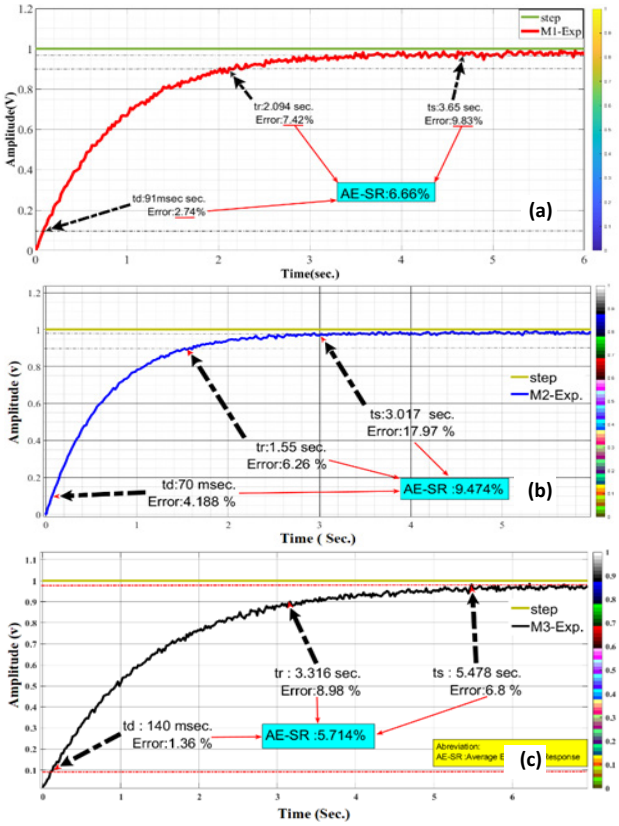


Figure 13: Actual step response of the tested motors,(a)M1 ,(b)M2,(c)M3

3.3. Experimental results

Figure 13 shows the plotted experimental results of the step response characteristics for M1, M2, M3. The experimental tests have shown that the step response characteristics are very convergence to simulation results.

To show the efficiency of the proposed HSMDAQS, the comparison between experimental and simulation results is performed. The deviation time (Δt) of the step response between experimental and simulation for each response parameter is represented in equation 9. The percentage error of the step response (PE-SR) and AE-SR can be calculated as represented in equations 10 ,11 respectively.

$$\Delta t = t(experimental) - t(simulation) \quad (9)$$

$$\text{PE-SR\%} = \left(\frac{\Delta t}{t\ (experimental)}\right) x100 \quad (10)$$

$$\text{AE-SR\%} = \frac{PE-SR(td)+PE-SR(tr)+PE-SR(ts)}{3} \quad (11)$$

Table 3 highlights the comparison parameters between (simulation based models) and (experimental based HSMDAQS) in terms of td, tr, ts. It appears that the curves based on the proposed TF models are closer to the experimental results and the maximum AE-SR is less than 10%. Confidently, the HSMDAQS provides an acceptable △t [32, 33], shows the magnificent performance design to be utilized as the best solution for estimating high-quality TF form that can be utilized in a wide range of industrial applications.

Table 3: Simulation and experimental results comparison

Parameters	M1	M2	M3
△td(ms)	2.49	2.93	1.88
△tr(ms)	155.64	97.25	298.03
△ts(ms)	359.9	542.32	372.89
PE-SR (td) %	2.74	4.18	1.36
PE-SR (tr) %	7.42	6.26	8.98
PE-SR (ts) %	9.83	17.97	6.8
AE-SR %	6.66	9.47	5.71

4. Conclusion

In this study, we have proposed a modern methodology and designed HSMDAQS to estimate the high accuracy TF model for unknown DC motor's specifications. It was observed from the quantification of the results, despite there are three different tested DC motors was used in this approach, but the best FIT resolution of estimation stabilized and enhanced by 95.3 %, besides reducing AE-SR below 10%. Graphically, when experimental realization and simulation results are compared, basic similarities between them were observed. The developed system could be used to improve many design sectors, offering faster with accurately capturing data, high precision stabilized platform, simpler implementation for dynamic systems, lower computational cost design and flexibility.

Ultimately, it is recommended to use the proposed system to enhance the speed performance of a PI controller-based DC motor for the CNC machine. In the future, we will intend to implement the proposed HSMDAS on a Field Programmable Gate Array (FPGA), by taking in consideration variable reference speed, variable load and current limiting protection.

Conflict of Interest

The authors declare no conflict of interest.

Acknowledgment

The authors would like to thanks to UPM and MOE (MOE-FRGS scheme (03-01-17-1893FR).) for supporting and funding this research.

References

[1] F.S.M. ALKhafaji, W.Z.W. Hasan, M. Isa, N. Sulaiman, "A HSMDAQ System for Estimating Transfer Function of a DC motor," Proceedings Prime Asia 2019 ,25–28, 2019.

[2] A. Jaya, E. Purwanto, M.B. Fauziah, F.D. Murdianto, G. Prabowo, M.R. Rusli, "Design of PID-fuzzy for speed Control of Brushless DC Motor in Dynamic Electric Vehicle to Improve Steady-State Performance," Proceedings IES-ETA 2017 - International Electronics Symposium on Engineering Technology and Applications, 2017-Decem, 179–184, 2017, doi:10.1109/ELECSYM.2017.8240399.

[3] E. Gelik, H. Gor, "Enhanced Speed Control of a DC Servo System Using PI+DF controller tuned by stochastic fractal search technique," Journal of the Franklin Institute, 1–28, 2019, doi:10.1016/j.jfranklin.2018.11.020.

[4] Y. Naung, A. Schagin, H.L. Oo, K.Z. Ye, Z.M. Khaing, "Implementation of Data Driven Control System of DC Motor by Using System Identification Process," Proceedings of the 2018 IEEE Conference of Russian Young Researchers in Electrical and Electronic Engineering, ElConRus, 1801–1804, 2018, doi:10.1109/EIConRus.2018.8317455.

[5] W.G. Soliman, D. V. Rama Koti Reddy, D.A. Reddy, "Microprocessor-Based Performance Indices Analysis of Individual Systems Distributed Motion Control Strategies," A Springer Nature Journal, **2**(1), 1–11, 2020, doi:10.1007/s42452-019-1832-2.

[6] M. Torre, Halliburton, Designing real-time process controllers, Control Engineering, 2014. [Online].Available: https://www.controleng.com/articles/designing-real-time-process-controllers.

[7] A.Y. Al-Maliki, K. Iqbal, "PID-Type FLC Controller Design and Tuning for Sensorless Speed Control of DC Motor," Advances in Science, Technology and Engineering Systems Journal, **3**(6), 515–522, 2018, doi:10.25046/aj030660.

[8] A. Martinez, An Introduction to Control Systems: Designing a PID Controller Using MATLAB's SISO Tool, ALL ABOUT CIRCUITS, 2015.[Online].Available: https://www.allaboutcircuits.com/technical-articles/an-introduction-to-control-systems-designing-a-pid-controller-using-matlabs.

[9] E.S. Addasi, "Modelling and Simulation of DC-Motor Electric Drive Control System with Variable Moment of Inertia," ACEEE Int ernational Journal on Electrical and Power Engineering, Identification and Control, **4**(1), 52–57, 2013, doi: 01.IJEPE.4.1.

[10] F.S.M. Alkhafaji, W.Z.W. Hasan, M.M. Isa, N. Sulaiman, "Proposed a Novel Method for Optimization DC Motor Controller," Procceding of the 5th IEEE International Conference on Smart Instrumentation, Measurement and Applications (ICSIMA) , 2018.

[11] W. Wu, "DC Motor Identification Using Speed Step Responses," Proceedings of the 2010 American Control Conference, 1937–1941, 2010, doi:10.1109/ACC.2010.5531349.

[12] S. Arun Jayakar, G.M. Tamilselvan, "Mathematical modelling and Robust PID controller Design for Compressed Air Pressure Control Process," An International Journal of Applied Mathematics and Information Sciences, **13**(4), 561–567, 2019, doi:10.18576/amis/130407.

[13] V.D. Yurkevich, N.A. Stepanov, "PWM Speed Control of DC Motor based on Singular Perturbation Technique," International Congress on Ultra Modern Telecommunications and Control Systems and Workshops, 434–440 , 2014, doi:10.1109/ICUMT.2014.7002140.

[14] N. Tripathi, R. Singh, E. Engineering, N. Gwalior, M. Pradesh, "Analysis of Speed Control of DC Motor – A Review Study," International Research Journal of Engineering and Technology (IRJET) e-ISSN:2395-0056, **02**(08), 1616–1621, 2015.

[15] W. Wu, "DC Motor Parameter Identification Using Speed Step Responses," Hindawi Publishing Corporation journal of Modelling and Simulation in Engineering, **2012** ,1–5, , doi:10.1155/2012/189757.

[16] D.X. Liu, "Design and Development of DC Motor Speed Control System based on ARM," Advanced Materials Research, **926**(930),1239–1242, 2014, doi:10.4028/www.scientific.net/amr.926-930.1239.

[17] T.A. Tutunji, "DC Motor Identification Using Impulse Response Data," EUROCON 2005- The International Conference onComputer as a tool, 1734–1736, 2006, doi:10.1109/eurcon.2005.1630309.

[18] J.M. Esposito, M.G. Feemster, J.M. Watkins, "Role of a MATLAB Real-Time Hardware Interface within a Systems Modeling Course," Proceedings of the 2004 American Society for Engineering Education Annual Conference and Exposition, **16**(1), 41–50, 2006.

[19] F.S.M. Alkhafaji, W.Z.W. Hasan, M.M. Isa, N. Sulaiman, "Robotic Controller : ASIC versus FPGA — A Review," Journal of Computational and Theoretical Nanoscience, **15**(1), 1–25, 2018, doi:10.1166/jctn.2018.7119.

[20] Y. Naung, S. Anatolii, Y. Htet Lin, "Speed Control of DC Motor by Using Neural Network Parameter Tuner for PI-controller," Proceedings of the 2019 IEEE Conference of Russian Young Researchers in Electrical and Electronic Engineering, ElConRus2019, 2152–2156, 2019, doi:10.1109/EIConRus.2019.8656911.

[21] F.S.M. Alkhafaji, W.Z.W. Hasan, M.M. Isa, N. Sulaiman, "A Novel Method for Tuning PID Controller," "Journal of Telecommunication, Electronic and Computer Engineering," **10**(1-12), 33–38, 2018.

[22] S. Khan, A. Paul, T. Sil, A. Basu, R. Tiwari, S. Mukherjee, U. Mondal, A. Sengupta, "Position Control of a DC Motor System for Tracking Periodic Reference Inputs in a Data Driven Paradigm," 2016 International Conference on Intelligent Control, Power and Instrumentation, ICICPI 2016, 17–21, 2017, doi:10.1109/ICICPI.2016.7859665.

[23] S. Adewusi, "Modeling and Parameter Identification of a DC Motor Using Constraint Optimization Technique," IOSR Journal of Mechanical and Civil Engineering (IOSR-JMCE) ,**13**(6), 46–56, 2016, doi:10.9790/1684-1306024656.

[24] B. Nayak, S. Sahu, "Parameter Estimation of DC Motor Through Whale Optimization Algorithm," International Journal of Power Electronics and Drive Systems(IJPEDS), **10**(1), 83–92, 2019, doi:10.11591/ijpeds.

[25] T.A. Tutunji, A. Saleem, "A Methodology for Identification and Control of Electro-Mechanical Actuators," MethodsX 2, 219–231, 2015, doi:10.1016/j.mex.2015.04.001.

[26] D. Ramasubramanian, Identification and Control of DC Motors,MS.c Thesis, Escola Tècnica Superior d'Enginyeria Industrial de Barcelona, 2016.

[27] M. Fruk, G. Vujisić, T. Špoljarić, "Parameter Identification of Transfer Functions Using MATLAB," Procceding International Convention on Information and Communication Technology, Electronics and Microelectronics (MIPRO) , 697–702, 2013, doi:10.1002/cpe.3949.

[28] M. Idrees et al., "Fuzzy Logic Based Calculation and Analysis of Health Index for Power Transformer Installed in Grid Stations," in 2019 International Symposium on Recent Advances in Electrical Engineering (RAEE), 4, 1–6, 2019. doi: 10.1109/RAEE.2019.8887016.

[29] G.Y. Chen, J.W. Perng, "PI Speed Controller Design based on GA with Time Delay for BLDC Motor Using DSP," Procceding of 2017 IEEE International Conference on Mechatronics and Automation, ICMA 2017, 1174–1179, 2017, doi:10.1109/ICMA.2017.8015983.

[30] C.Giampiero, Legacy MATLAB and Simulink Support for Arduino - File Exchange-MATLAB Central, 2016. [Online]. Available: https://www.mathworks.com/matlabcentral/fileexchange/32374-legacy-matlab-and-simulink-support-for-arduino

[31] D. Xue, Y.Q. Chen, D.P. Atheron,"PID controller Design," in Linear Feedback Control: Analysis and Design with MATLAB,183–235, 2007.doi.org/10.1137/1.9780898718621

[32] W.L. Oberkampf, M.F. Barone, "Measures of Agreement Between Computation and Experiment: Validation Metrics," Journal of Computational Physics, **217**(2006), 5–36, 2006, doi:10.1016/j.jcp.2006.03.037.

[33] T. Magraner, A. Montero, S. Quilis, J.F. Urchueguía, "Comparison Between Simulation and Experimental Results for The Energy Performance of Geocool Geothermal Experimental Plant," Proceedings of the 11th International Conference on Thermal Energy Storage, (June), 2009.

ASTES

Advances in Science, Technology and Engineering Systems Journal Vol. 5, No. 5, 1126-1136 (2020)

www.astesj.com

Special Issue on Multidisciplinary Innovation in Engineering Science & Technology

ASTESJ

ISSN: 2415-6698

Tolerance of Characteristics and Attributes in Developing Student's Academic Achievements

Wongpanya Nuankaew[1], Pratya Nuankaew[2,*]

[1]*Faculty of Information Technology, Rajabhat Mahasarakham University, Maha Sarakham, 44000, Thailand*

[2]*School of Information and Communication Technology, University of Phayao, Phayao, 56000, Thailand*

ARTICLE INFO

Article history:
Received: 03 July, 2020
Accepted: 15 October, 2020
Online: 22 October, 2020

Keywords:
Academic Achievement Attributes
Educational Data Mining
Lifelong Learning
Learning Strategies
Learning Analytics

ABSTRACT

The purpose of this research is to study the relevance of factors for the analysis of the effectiveness of suitable educational institutions that illustrate the significance of the characteristics and attributes of the student's academic achievements and to identify the acceptance and tolerance of each attribute, which supports lifelong learning. The data used in this research is 1109 students who used and tested the institution recommender system based on student context and educational institution application. The research methodology focuses on the study of user involvement and application analysis. There are six significant phases of the research: business understanding, data understanding, data preparation, modeling, evaluation, and deployment. The machine learning tools and data mining techniques are k-means, k-medoids, decision trees, cross-validation methods, and confusion matrix. From the data analysis, it can be concluded that the overall level of satisfaction with the application is accepted (average = 3.70, S.D. = 0.84). In addition, the prototype model has been developed for predicting and recommending appropriate institutions for the learner has moderate accuracy levels (92.25%), and the results of the self-test data model are very accurate at the highest level, which is equal to 93.78%. Finally, this research demonstrates the relevance and success of education engineering projects. It demonstrates a worthy accomplishment. For future research, the researchers aim to construct and develop applications that promote and support the findings of this research.

1. Introduction

Education and learner sustainability are the main goals of Thailand's government and the United Nations (UN) as defined in the Sustainable Development Goals (SDGs) [1,2], which are aimed and set as the world target success in 2030 [1]. The results are from an extensive research related to the development in quality of education. Numerous research studies showed a variety of educational outcomes [3–5], such as the development of learners' theories, learning styles, educational models, and educational technology.

Most of the research results is abstract and difficult to develop into a model or method that can be effectively implemented. In addition, there are many ways to take the next step towards student achievement, as shown in Figure 1. The question asked is "what is truly reasonable in theoretical practice for student characteristics?"

While there are many theories for the development of learning, there seems to be no technology and method to present reasonable and appropriate models, tools and strategies for learners. The combination of the two academic domains between engineering and education that had occurred is called Education Engineering (EE). In addition, it has completely changed the current radical educational system to be known as "Disruptive Technology" [6,7]. However, the researchers tried to study and carry out the research by applying the two knowledge together [8–14]. The discovery was that there were too many research areas that have yet to be explored. Figure 2 shows the studies and research related to the research results of the past researchers.

From Figure 2, the researchers gathered the hot issues, critical problems, data set, student information, research models, and research results in many perspective [2,8]. Preliminary studies have driven the researchers to conduct research studies to develop learners' potential and significantly increase the learners' academic achievement. Therefore, this research has important objectives and goals for studying the relevance and success of

*Corresponding Author: Pratya Nuankaew, School of Information and Communication Technology, University of Phayao, Phayao, 56000, Thailand, +66 89 961 4832 & pratya.nu@up.ac.th

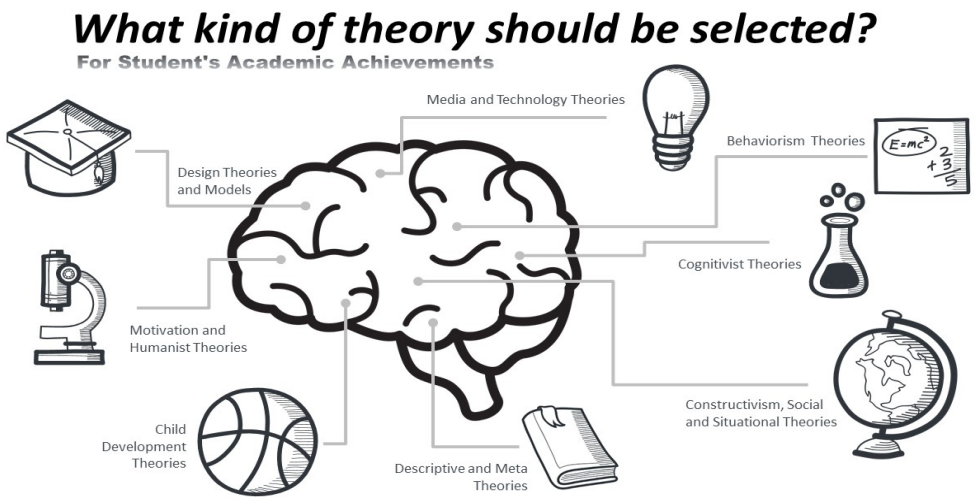


Figure 1: World of Learning Theory



Figure 2: Areas of research being offered

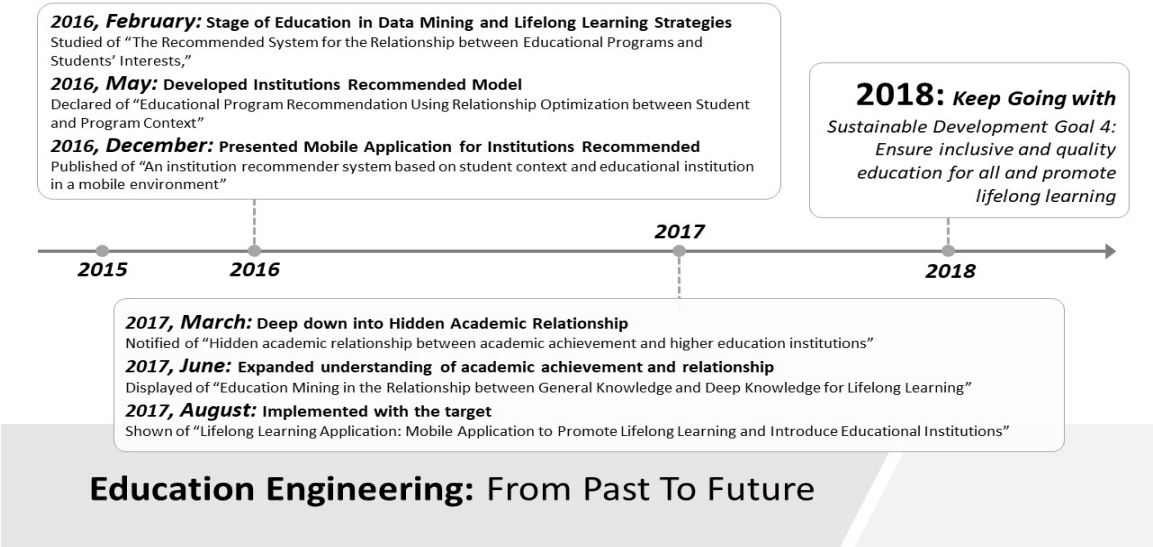


Figure 3: Research Progress

research that demonstrate the significant attributes of the student's academic achievements, and to identify the acceptance and tolerance of each attribute.

The important process of this research is therefore aimed at the model chosen from the previous research to improve the application that had been developed [10,15]. After that, the data collected from 1109 actual users were analyzed and searched for factors that supported and encouraged learners to meet the needs and suitability between the learners and the educational institutions. This is the main objective of the research.

The outline of this research is divided into four sections. Section 1 leads the reader to understand the problem. Section 2 is the presentation of literature, related work and research methods. Section 3 is a summary of the research results and discussions. Finally, the last section is the summarized conclusion.

2. Literature Reviews and Related Works

This section summarizes the overview of research related to the moment of research in engineering education. Areas of education engineering in the paper are scoped into five stages: traditional problems, students' academic achievement, engineering education, technology of education engineering, and how can education engineering work.

2.1. Thailand's educational policy and problems

Since 1999, education in Thailand has been improved and educational opportunities have presented for the public. The system provides the learning process for personal and social development with factors available conducive to continuous lifelong learning [5]. Everything seems beautiful for Thai students [6]. While twenty years have passed, Thailand's education system is still hopeful that there is light at the end of the tunnel. The failure of a test to measure students' achievement is a good example [16]. However, when considering the factors, learners are most important for developing because no matter how the system has changed, the end result should be the learner's achievement. Finding the identity of the learner to present what is worthy for her/him is the first priority [10].

2.2. Student's Academic Achievements

Certifications and degrees are not a measure of a person's achievements, but it is a tool that helps everyone find what they want and expect in life. Academic results are an opportunity for learners to find what they are. At the same time, grading the exam and testing can be used to determine the advancement and recognition of students' knowledge, however there is a need on considering what determines to be for success as the process may require more testing.

Student's academic achievements can be judged from many perspectives, such as the dimension of learning styles, student's emotions, academic motivation, and hidden academic relationship [2,9,17]. Considering the reasonableness of the individual is more important than anything.

2.3. Education Engineering

Education and Engineering has changed over time, where the desire to achieve "the best practices" requires a clear framework. For the best, finding the answer requires research, which also requires a method, technology, theoretical, and application that depends on the researcher's needs [17,18].

It is only a minority researcher that mentions engineering education [3,19]. To combine the education and engineering requires a step by step framework for developing the best practice models. In addition, in-depth research using modern technology also supports learning theory by finding and developing models that are sensible to learners. No matter how smart and important the technology is, the emphasis of educational development is to develop the learning processes, analytical thinking, and ability to apply their knowledge to solve problems and increase knowledge [10].

2.4. Education Engineering Technology

Educational engineering technology is the use of technology for effective education for learners. It resulted from a change known as disruptive technology [7, 8]. There are many programs and applications that support Thailand's education, which bring in novel and advanced technology for managing in order to achieve better student performance [4,20,21]. The results show different aspects of the development in the education process.

2.5. Implemented Education Technology

A good example is on how the application of engineering knowledge is integrated into the educational process [5]. It provides and explains the advanced technology application, which consists of five steps: requirement definition, system and software design, implementation and unit testing, integration and system testing, and operation and maintenance. All steps are the key principles in the development of knowledge, research, and discoveries to be practically usable [5, 11, 16].

2.6. Thailand's educational policy and problems

This research was conducted and studied logically, as illustrated in the study period in Figure 3. Their research has started to focus on education engineering since the year 2016 and has proposed concepts of applied engineering and education for the education models in Thailand. At this stage, it presented their research from the past to the future, which consists of six main steps. The first step is defining the research problems. The second step is finding the significant and appropriate attributes. The third step is development of the model. The fourth step is building the application. The fifth step is testing and deploying the application. Finally, the sixth step is applying the application to the targets

2.6.1. Defining the Research Problems

It started in early 2016, which presented the idea of matching students to universities [5]. The research problem is "how to introduce and match diverse students to different contexts of educational institutions" as shown in Figure 4.

The results of their research found that Thailand's education system and interest to study are important factors in choosing universities and influencing the decision of studying at a higher education level [16]. The data used in their research was 256 students from two universities: (1) the Rajabhat Mahasarakham University, Maha Sarakham, Thailand and (2) the University of Phayao, Phayao, Thailand.

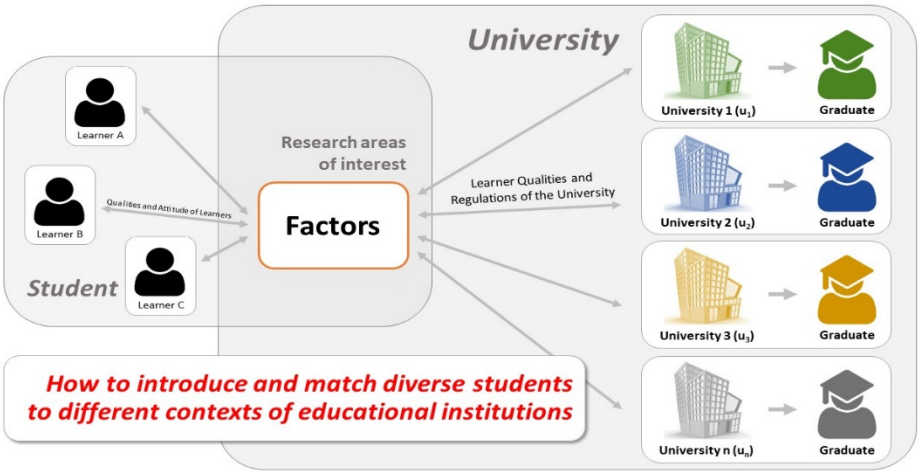


Figure 4: Matching Students to Universities

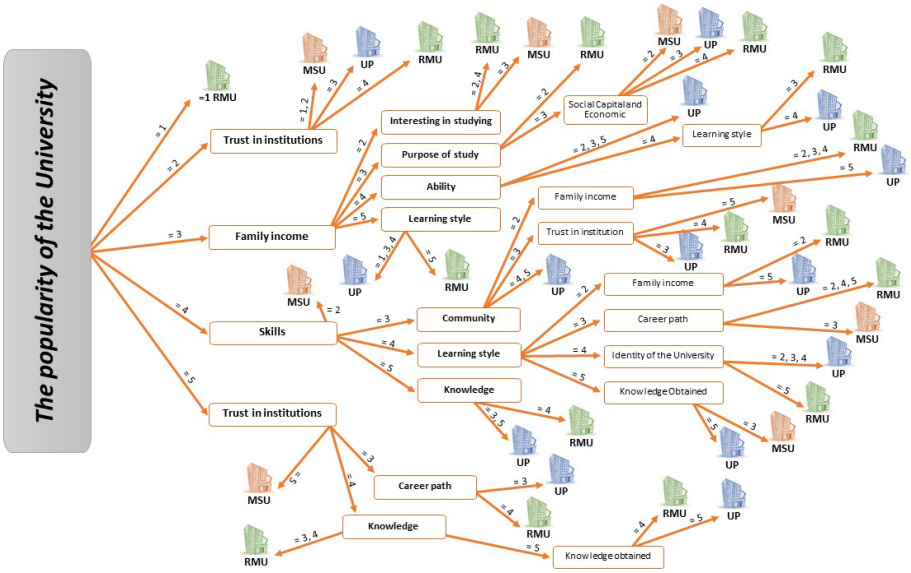


Figure 5: Appropriate Model with Decision Tree [23]

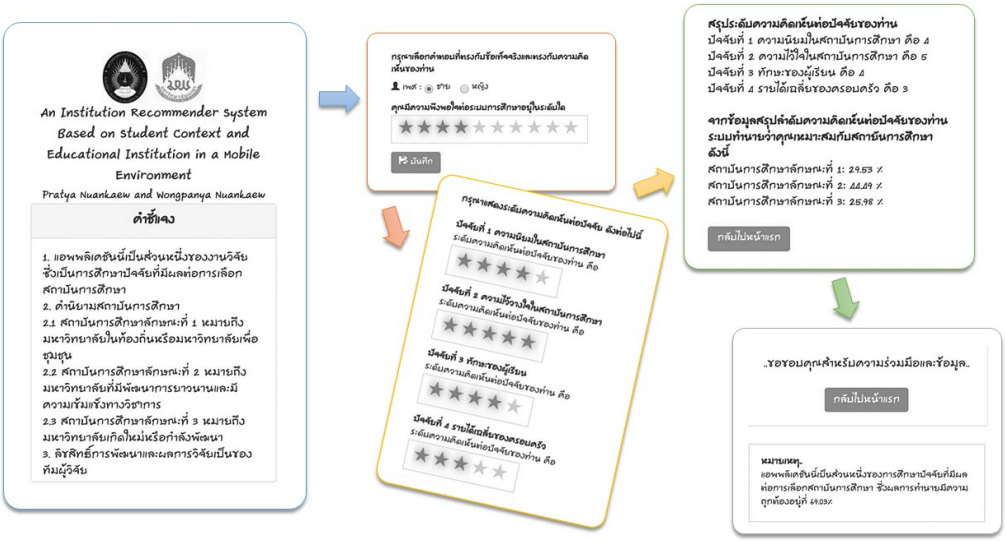


Figure 6: Institution Recommender Mobile Application

2.6.2. Finding Significant and Appropriate Attributes

After the success of the study in the problems of the decision to study at a higher level, the researchers conducted the study to find factors that are important matching components between the learners and the educational institutions [22]. The data used in the research was 885 students from three universities: (1) the Rajabhat Mahasarakham University, Maha Sarakham, Thailand, (2) the Maha Sarakham University, Maha Sarakham, Thailand, and (3) the University of Phayao, Phayao, Thailand.

The result is the acceptance of the factors studied. It was found that the factors associated with their research consisted of 19 significant factors including 15 factors of student's context and 4 factors of program's context, as shown in Table 1.

Table 1: Significant and Appropriate Attributes [23]

Perception and Perspective	Statement and Details
Student's Context	*Student's Interests*
	Stage 1.1 Interest in studying Stage 1.2 Career path Stage 1.3 Identity of the University Stage 1.4 Knowledge obtained Stage 1.5 Education system
	Student's Characteristics
	Stage 2.1 Student Abilities Stage 2.2 Student Skills Stage 2.3 Student Knowledge Stage 2.4 Learning Styles of Student
	Student's Environment
	Stage 3.1 Social capital and Economic Stage 3.2 Trust in institutions Stage 3.3 Personal decision Stage 3.4 Family income Stage 3.5 Community Stage 3.6 Purpose of study
Program's Context	*Program's Context*
	Stage 4.1 The popularity of the University Stage 4.2 Curriculum Stage 4.3 Education standard Stage 4.4 Quality assurance

2.6.3. Model Development

After studying and analyzing perceptions of factors that are important to the choice of continuing education between students and institutions [23], the data collected the satisfaction level with factors having been analyzed and developed by data mining techniques and machine learning tools. The result is a decision tree model that is shown in Figure 5. Figure 5 illustrates the decision tree obtained from the appropriate model.

All among 19 factors, 15 factors can determine whether the students are suitable to learn at that particular university.

2.6.4. The Application Development

After modeling success, the mobile applications have been developed [5]. Their application consists of three important steps: (1) introduction of the application, (2) prediction of interest at a higher education level, and (3) recommendation of an appropriate institution for the user. The structure and working process of the application is shown in Figure 6.

2.6.5. Testing and Deployment

The application in the previous section was searched for performance, which used a satisfaction questionnaire from 431 samples [5]. It consisted of 186 high school students, 191 university students, 12 staffs and 42 lectures in the universities. The testing process consisted of four main stages: functional requirement testing, functional testing, usability testing, and security testing. According to their results, it indicated that the total satisfaction toward the application are highest, which is equal to 4.32, and the groups with the highest levels of satisfaction are university students, which is equal to 4.43. It can be concluded that the application is appropriate and reasonable for students who wish to study at a higher education level [5].

2.6.6. Applied Application to the Targets

After the prototype application was created [5], it was applied to 1,109 students from the three universities; Rajabhat Mahasarakham University, Mahasarakham University, and University of Phayao to test the application [11]. Based on the data collected, they found that the relationships were more expected and exceeded that was supported by Thailand's educational system. It is defined as a "Nest Relationship" or "Hidden Relationship". The results of their research demonstrate the different levels of relationships that are influenced by the Grade Point Average (GPA), school size, community environment, and school friends. It is consistent with the hypothesis that was predicted as shown in Figure 7.

From the findings and additional information collected, the research studied on matching the right students with the most appropriate institutions. The research aimed on developing the knowledge and seeking the best tools for the learner, which have research related to the development tools in education engineering, machine learning, active learning theory, and data mining in education [2, 5, 9, 12].

3. Research Methodology

The purpose of this research is to study the relevance of factors for the analysis of the effectiveness of suitable educational institutions that illustrate the significant of the characteristics and attributes of the student's academic achievements, and to identify the acceptance and tolerance of each attribute, which supports lifelong learning. The data collection used in this research is 1109 students who used and tested the institution recommender system based on student context and educational institution application [11]. The research methodology focused on the study of user involvement and application analysis. It consisted of six main steps in data analysis for data mining management [23,24]: business understanding, data understanding, data preparation, modeling, evaluation, and deployment.

3.1. Business Understanding

The business understanding presents the viewpoint of research problems [24]. Understanding the overview of the problem will enable the research goals to be defined clearly. Thus, the research problem of this research is to screen the groups of testers who tested the applications [11], and to use the data collected to study the group's behavior.

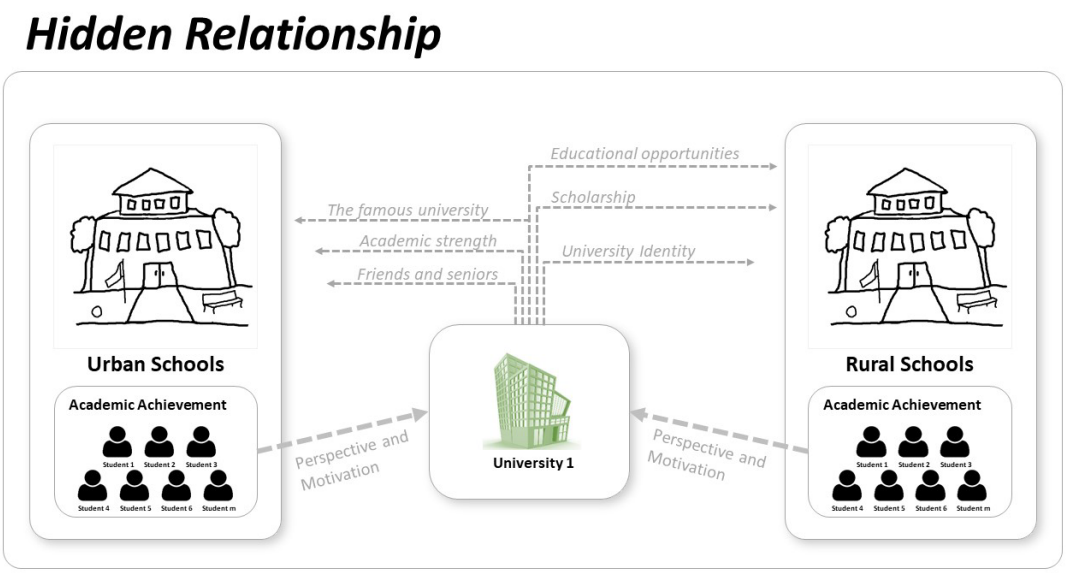


Figure 7: Thinking cycle of students toward the institution

3.2. Data Understanding

Data understanding is closely linked to the business understanding of activities which are aimed at identifying data quality problems, discovering the insight into the data, and examining the attractiveness of problems from hidden data [24]. Therefore, the research designed the data collection to be consistent with the research objectives. The characteristics of the data consisted of specifying the educational institution of the data providers and showing the level of attitude towards the factors that the researcher is studying.

3.3. Data Preparation

Data preparation is a process of data management for use in the development of prototype models. In addition, it prepares data in formats such as tables and records, including feature selection, feature management, data cleaning, construction of the new attributes, and so on [24]. In this research, it was compiled and prepared as summarized in Table 2 to Table 3.

Table 2: Data Collection

Institutions	Data Collection	
	Providers	*Percentage*
MSU: Maha Sarakham University	345	31.11%
RMU: Rajabhat Mahasarakham University	478	43.10%
UP: University of Phayao	286	25.79%
Total:	**1109**	**100%**

From Table 2, it shows that the largest number of tester who provided the data was Rajabhat Mahasarakham University, which had 478 tester or equal to 43.10 percent of all data providers. In addition, the summary of general statistics from data collection is shown in Table 3, referring to the accepted factors from Table 1.

From Table 3, it can be concluded that the overall perception and perspective on the overall factors averages at 3.70 (S.D. = 0.84), which is the most accepted point of view is program's context. It has an average of 4.00 (S.D. = 0.89). Therefore, it can be concluded that the providers accept all factors as a whole, with particular emphasis on the program's context.

Table 3: Data Analysis

Perception and Perspective	Data Collection (n = 1109)		
	Stages	*Means*	*S.D.*
Student's Context	*Student's Interests*		
	Stage 1.1	3.80	0.81
	Stage 1.2	3.74	0.85
	Stage 1.3	3.85	0.79
	Stage 1.4	3.82	0.74
	Stage 1.5	3.63	0.87
	Average	*3.77*	*0.82*
	Student's Characteristics		
	Stage 2.1	3.75	0.81
	Stage 2.2	3.63	0.74
	Stage 2.3	3.71	0.69
	Stage 2.4	3.40	0.78
	Average	*3.63*	*0.77*
	Student's Environment		
	Stage 3.1	3.61	0.81
	Stage 3.2	4.03	0.72
	Stage 3.3	3.27	0.90
	Stage 3.4	3.49	0.89
	Stage 3.5	3.20	0.84
	Stage 3.6	3.41	0.93
	Average	*3.50*	*0.89*
Program's Context	*Program's Context*		
	Stage 4.1	4.08	0.83
	Stage 4.2	4.12	0.74
	Stage 4.3	4.00	0.67
	Stage 4.4	3.79	0.70
	Average	*4.00*	*0.75*
	Total Average	*3.70*	*0.84*

3.4. Modeling

The modeling phase is the selection of tools suitable for the data collected to meet the research questions and goals [24]. Therefore, the researchers selected the machine learning tools and data mining techniques, which consisted of two types of tools: clustering tools consisting of k-means [25] and k-medoids [26], and classification tools consisting of decision tree [5, 11, 12].

The k-means is the most common algorithm used in an iterative refinement technique. It is also called Lloyd's algorithm [26], especially in the computer science community. The k-mean algorithm is performed by switching between two steps: (1) the assignment step, which assigns each observation to the cluster with the closest mean. (2) updates the procedure which is calculated a new means to be a centroid of observations in a cluster.

The k-medoids algorithm is a clustering algorithm that is associated with the k-means and the medoid shift algorithm. Both the k-means and k-medoids algorithms have some characteristics which divide the data set into groups. K-means is an attempt to reduce the total squared error, while the k-medoids reduce the sum of the dissimilarities between the points labeled in the cluster and the point that determines the center of that cluster [27].

The decision tree is one of the learning methods used in statistics, machine learning, and data mining. It works by determining data from observations and separating data for use in data consideration and finding predictive results. The benefit is getting important factors, which are caused by the nodes or the decision-making part of the model [5, 11, 12].

3.5. Evaluation

The goal of the evaluation is to assess the results and review the process [14,23]. The tools that are used in the research include cross-validation methods as shown in Figure 8, and confusion matrix as mentioned in Figure 9. Figure 8 displays the separation of data for evaluating the model. The cross-validation method divides the data into two parts. The first part is used for modeling and the remainder to test the model. In addition, model evaluation requires a tool called a confusion matrix [12, 14, 15, 24] to test the model's performance, with the principles shown in Figure 9.

Figure 9 presents the composition of the confusion matrix performance, which is composed of the actual class and the predicted class. An important benefit of the performance of the confusion matrix is the ability to determine the model's ability to predict results, such as the predictive ability or accuracy, model precision, model sensitivity, and model specificity (recall measurement). These values are used to determine the actual performance model. Moreover, Figure 9 also demonstrates the formulas and methods for calculating the various performance parameters in detail.

3.6. Deployment

The implementation is intended to be used in further applications [24]. The researcher aims to improve and use it in the next academic year (academic year 2021). It has been described in applying an activity recommendation as the following:

3.6.1. Testing Model Results

As mentioned above, the tools used to evaluate the model consist of two parts: cross-validation method, and confusion matrix. This section describes the implementation of assessment tools in the research.

The testing process divides the data into two parts according to the cross-validation method principles, but the division is divided into three types. The first type is 5-Fold cross-validation, which used 4-Fold (80%) for modeling and 1-Fold (20%) for testing. The second type is 10-Fold cross-validation, which used 9-Fold (90%) for modeling and 1-Fold (10%) for testing. The last type is leave-one-out cross-validation, which used 99% of data for modeling and 1% of data for testing. However, each time the cross-validation test is reported, the model results are also tested using the confusion matrix too.

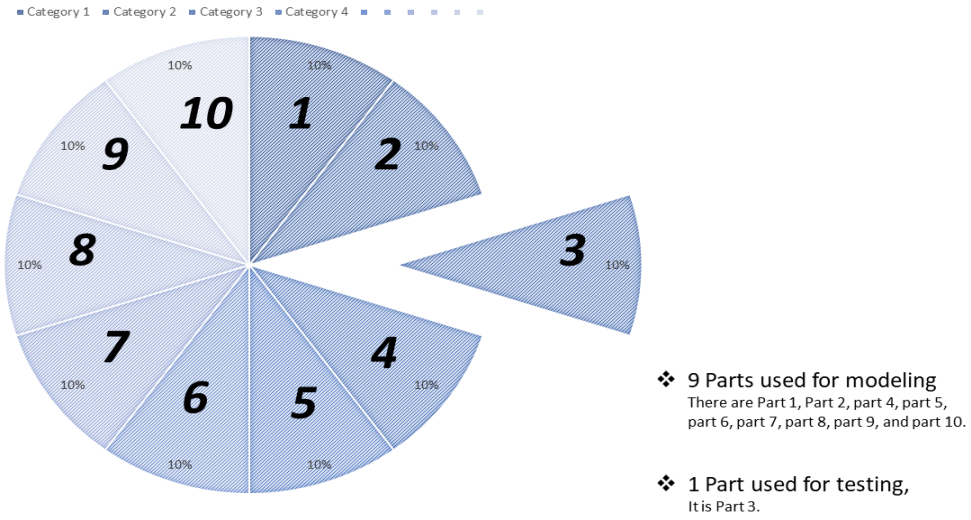


Figure 8: Cross-Validation Method

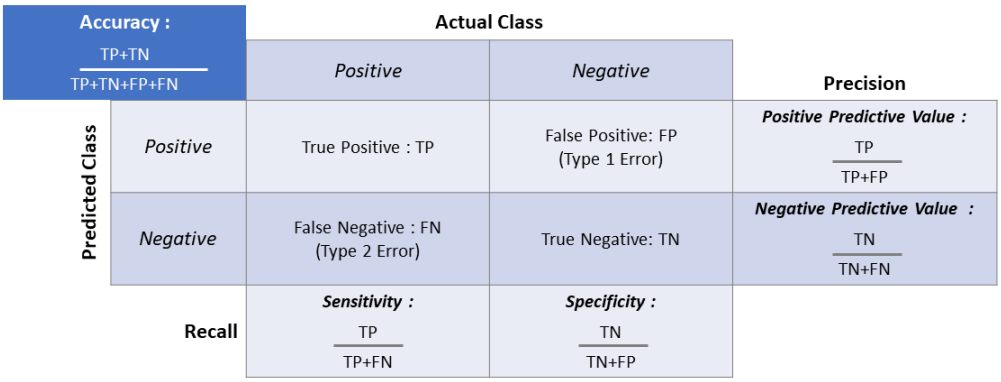


Figure 9: Confusion Matrix Performance

3.6.2. *Applying Model Results*

The applying model results are in three parts: generate a decision tree model for decision-making, test the decision tree model with data collection, and conclude the centroid of k-means. All details are presented on the section of research results and discussion.

4. Research Results and Discussion

In the research results, the researchers classified the research report into three parts which are modeling results, model testing results, and model applying results.

4.1. Modeling Results

Modeling results are the various models on different criteria, such as defining the unequal depth of the decision tree, and determining the different types of cross-validation method tests, which have the results shown in Table 4 and Table 5.

Table 4: Modelling Results from k-Means Clustering

Cluster Number	Decision Tree Depth	Cross-Validation Method Types		
		5-Fold	*10-Fold*	*Leave-one-out*
3 Clusters	Level 3	88.10%	88.46%	88.64%
	Level 4	88.73%	88.55%	89.00%
	Level 5	89.27%	89.18%	88.91%
	Level 6	89.63%	89.90%	89.90%
	Level 7*	91.07%	91.16%	92.25%*
	Level 8	91.52%	92.24%	92.25%
	Level 9	91.61%	92.24%	91.88%
4 Clusters	Level 3	47.61%	47.43%	47.07%
	Level 4	47.97%	47.88%	47.79%
	Level 5	58.97%	59.24%	59.24%
	Level 6	60.32%	61.59%	60.50%
	Level 7	65.10%	63.30%	63.39%
	Level 8	80.61%	79.44%	78.72%
	Level 9*	88.28%*	87.65%	87.65%
5 Clusters	Level 3	54.82%	54.73%	54.64%
	Level 4	55.46%	55.82%	55.91%
	Level 5	60.50%	59.87%	60.23%
	Level 6	63.12%	62.13%	60.50%
	Level 7	68.98%	66.72%	65.46%
	Level 8*	83.94%*	74.56%	66.28%
	Level 9	87.91%	85.12%	83.95%

From Table 4, it shows that the k-means model with the highest accuracy is the decision tree model that is classified into 3 clusters by dividing the model testing into the leave-one-out cross-validation method with a depth of 7 levels of the decision tree model and has an accuracy of 92.25%.

However, the test results classified by other clusters yielded a lower accuracy. For example, the 4 clusters with the highest results are 88.28% and the 5 clusters have the highest results of 83.94%.

Table 5: Modelling Results from k-Medoids Clustering

Cluster Number	Decision Tree Depth	Cross-Validation Method Types		
		5-Fold	*10-Fold*	*Leave-one-out*
3 Clusters	Level 3	78.00%	77.37%	76.01%
	Level 4	80.25%	81.24%	81.61%
	Level 5	84.67%	83.50%	77.37%
	Level 6	88.10%	86.83%	91.52%
	Level 7	90.62%	89.72%	90.35%
	Level 8	91.25%	91.25%	91.07%
	Level 9*	91.62%	91.97%*	91.61%
4 Clusters	Level 3	77.37%	76.38%	75.74%
	Level 4	78.08%	80.08%	81.33%
	Level 5	81.96%	83.32%	81.70%
	Level 6	84.49%	86.30%	86.93%
	Level 7	88.19%	89.18%	90.08%
	Level 8	90.26%	90.72%	91.52%
	Level 9	91.61%	91.62%*	90.62%
5 Clusters	Level 3	78.99%	78.54%	77.01%
	Level 4	82.23%	82.42%	81.15%
	Level 5	84.76%	85.39%	85.57%
	Level 6	86.65%	86.66%	86.38%
	Level 7	88.73%	88.73%	88.73%

Cluster Number	Decision Tree Depth	Cross-Validation Method Types		
		5-Fold	*10-Fold*	*Leave-one-out*
	Level 8	90.53%	89.36%	88.64%
	Level 9	91.96%*	90.81%	90.98%

From Table 5, it shows that the k-medoids model with the highest accuracy is the decision tree model that is classified into 3 clusters by dividing the model testing into the 10-fold cross-validation method with a depth of 9 levels of the decision tree model and has an accuracy of 91.97%.

However, the test results classified by other clusters yielded a lower accuracy. For example, the 4 clusters with the highest results are 91.62% and the 5 clusters have the highest results of 91.96%.

Table 6: Model Testing Results

Accuracy: 92.25%		Actual Class			*Precision Class*
		True Cluster_0	*True Cluster_1*	*True Cluster_2*	
Predicted Class	*Pred. Cluster_0*	185	*4*	*7*	94.39%
	Pred. Cluster_1	7	*423*	*31*	91.76%
	Pred. Cluster_2	21	*16*	*415*	91.81%
Recall Class		86.85%	95.49%	91.61%	

Table 7: Decision Tree Model

```
Stage 4.1 > 3.5
|  Stage 3.6 > 3.5
|  |  Stage 3.1 > 2.5
|  |  |  Stage 3.5 > 3.5: cluster_2 {cluster_2=268}
|  |  |  Stage 3.5 ≤ 3.5
|  |  |  |  Stage 3.3 > 3.5: cluster_2 {cluster_0=1, cluster_2=56, cluster_1=3}
|  |  |  |  Stage 3.3 ≤ 3.5
|  |  |  |  |  Stage 3.1 > 3.5: cluster_2 {cluster_2=11, cluster_1=3}
|  |  |  |  |  Stage 3.1 ≤ 3.5: cluster_1 {cluster_1=3}
|  |  Stage 3.1 ≤ 2.5: cluster_2 {cluster_0=1, cluster_2=3}
|  Stage 3.6 ≤ 3.5
|  |  Stage 1.4 > 2.5
|  |  |  Stage 1.3 > 2.5
|  |  |  |  Stage 3.2 > 2.5
|  |  |  |  |  Stage 3.5 > 3.5: cluster_2 {cluster_0=1, cluster_2=25, cluster_1=5}
|  |  |  |  |  Stage 3.5 ≤ 3.5: cluster_1 {cluster_0=6, cluster_2=30, cluster_1=423}
|  |  |  |  Stage 3.2 ≤ 2.5: cluster_0 {cluster_0=3}
|  |  |  Stage 1.3 ≤ 2.5
|  |  |  |  Stage 1.4 > 4: cluster_2 {cluster_2=2}
|  |  |  |  Stage 1.4 ≤ 4: cluster_0 {cluster_0=8}
|  |  Stage 1.4 ≤ 2.5: cluster_0 {cluster_0=4}
Stage 4.1 ≤ 3.5
|  Stage 4.4 > 4.5: cluster_2 {cluster_0=1, cluster_2=29, cluster_1=1}
|  Stage 4.4 ≤ 4.5
|  |  Stage 1.4 > 4.5
|  |  |  Stage 3.2 > 3.5: cluster_2 {cluster_2=9}
|  |  |  Stage 3.2 ≤ 3.5: cluster_0 {cluster_0=2,}
|  |  Stage 1.4 ≤ 4.5
|  |  |  Stage 2.3 > 4.5: cluster_2 {cluster_0=1, cluster_2=3}
|  |  |  Stage 2.3 ≤ 4.5
|  |  |  |  Stage 1.2 > 3.5
|  |  |  |  |  Stage 3.1 > 3.5: cluster_2 {cluster_0=10, cluster_2=16, cluster_1=1}
|  |  |  |  |  Stage 3.1 ≤ 3.5: cluster_0 {cluster_0=18, cluster_1=1}
|  |  |  |  Stage 1.2 ≤ 3.5: cluster_0 {cluster_0=157, cluster_2=1, cluster_1=3}
```

4.2. Model Testing Results

From the results of the prototype model development, it can be concluded that the model with the highest accuracy is the development of the model from k-means clustering, with the appropriate number of 3 clusters and the leave-one-out cross-validation result with an accuracy of 92.25%. Details of the testing developed model are shown in Table 6.

4.3. Model Applying Results

From the model that has been selected and demonstrated the performance of the model, this section shows the decision tree model in Table 7; the decision tree rules for self-testing is shown in Table 8, and the centroid of each cluster is shown in Table 9. In addition, a summary of the members from the collected datasets described by source classified by cluster. It is shown in Table 10.

Table 7 shows the decision tree models, which are the selected models from the tests in Table 8 and Table 9.

Table 8: Model Applying Results

Rule	Condition (If)	Prediction (Then)
1	If Stage 4.1 > 3.5 and Stage 3.6 > 3.5 and Stage 3.1 > 2.5 and Stage 3.5 > 3.5	Then, suitable for cluster_2 = 100%
2	If Stage 4.1 > 3.5 and Stage 3.6 > 3.5 and Stage 3.1 > 2.5 and Stage 3.5 ≤ 3.5 and Stage 3.3 > 3.5	Then, suitable for cluster_0 = 1.67%, suitable for cluster_1 = 5.00%, and suitable for cluster_2 = 93.33%.
3	If Stage 4.1 > 3.5 and Stage 3.6 > 3.5 and Stage 3.1 > 2.5 and Stage 3.5 ≤ 3.5 and Stage 3.3 ≤ 3.5 and Stage 3.1 > 3.5	Then, suitable for cluster_1 = 21.43%, and suitable for cluster_2 = 78.57%.
4	If Stage 4.1 > 3.5 and Stage 3.6 > 3.5 and Stage 3.1 > 2.5 and Stage 3.5 ≤ 3.5 and Stage 3.3 ≤ 3.5 and Stage 3.1 ≤ 3.5	Then, suitable for cluster_1 = 100%
5	If Stage 4.1 > 3.5 and Stage 3.6 > 3.5 and Stage 3.1 ≤ 2.5	Then, suitable for cluster_0 = 25.00%, and suitable for cluster_2 = 75.00%.
6	If Stage 4.1 > 3.5 and Stage 3.6 ≤ 3.5 and Stage 1.4 > 2.5 and Stage 1.3 > 2.5 and Stage 3.2 > 2.5 and Stage 3.5 > 3.5	Then, suitable for cluster_0 = 3.23%, suitable for cluster_1 = 16.13%, and suitable for cluster_2 = 80.65%.
7	If Stage 4.1 > 3.5 and Stage 3.6 ≤ 3.5 and Stage 1.4 > 2.5 and Stage 1.3 > 2.5 and Stage 3.2 > 2.5 and Stage 3.5 ≤ 3.5	Then, suitable for cluster_0 = 1.31%, suitable for cluster_1 = 92.16%, and suitable for cluster_2 = 6.54%.
8	If Stage 4.1 > 3.5 and Stage 3.6 ≤ 3.5 and Stage 1.4 > 2.5 and Stage 1.3 > 2.5 and Stage 3.2 ≤ 2.5	Then, suitable for cluster_0 = 100%
9	If Stage 4.1 > 3.5 and Stage 3.6 ≤ 3.5 and Stage 1.4 > 2.5 and Stage 1.3 ≤ 2.5 and Stage 1.4 > 4.0	Then, suitable for cluster_2 = 100%
10	If Stage 4.1 > 3.5 and Stage 3.6 ≤ 3.5 and Stage 1.4 > 2.5 and Stage 1.3 ≤ 2.5 and Stage 1.4 ≤ 4.0	Then, suitable for cluster_0 = 100%
11	If Stage 4.1 > 3.5 and Stage 3.6 ≤ 3.5 and Stage 1.4 ≤ 2.5	Then, suitable for cluster_0 = 100%
12	If Stage 4.1 ≤ 3.5 and Stage 4.4 > 4.5	Then, suitable for cluster_0 = 3.23%, suitable for cluster_1 = 3.23%, and suitable for cluster_2 = 93.55%.
13	If Stage 4.1 ≤ 3.5 and Stage 4.4 ≤ 4.5 and Stage 1.4 > 4.5 and Stage 3.2 > 3.5	Then, suitable for cluster_2 = 100%

Rule	Condition (If)	Prediction (Then)
14	If Stage 4.1 ≤ 3.5 and Stage 4.4 ≤ 4.5 and Stage 1.4 > 4.5 and Stage 3.2 ≤ 3.5	Then, suitable for cluster_0 = 100%
15	If Stage 4.1 ≤ 3.5 and Stage 4.4 ≤ 4.5 and Stage 1.4 ≤ 4.5 and Stage 2.3 > 4.5	Then, suitable for cluster_0 = 25.00%, and suitable for cluster_2 = 75.00%.
16	If Stage 4.1 ≤ 3.5 and Stage 4.4 ≤ 4.5 and Stage 1.4 ≤ 4.5 and Stage 2.3 ≤ 4.5 and Stage 1.2 > 3.5 and Stage 3.1 > 3.5	Then, suitable for cluster_0 = 37.04%, suitable for cluster_1 = 3.70%, and suitable for cluster_2 = 59.26%.
17	If Stage 4.1 ≤ 3.5 and Stage 4.4 ≤ 4.5 and Stage 1.4 ≤ 4.5 and Stage 2.3 ≤ 4.5 and Stage 1.2 > 3.5 and Stage 3.1 ≤ 3.5	Then, suitable for cluster_0 = 94.74%, and suitable for cluster_1 = 5.26%.
18	If Stage 4.1 ≤ 3.5 and Stage 4.4 ≤ 4.5 and Stage 1.4 ≤ 4.5 and Stage 2.3 ≤ 4.5 and Stage 1.2 ≤ 3.5	Then, suitable for cluster_0 = 97.52%, suitable for cluster_1 = 1.86%, and suitable for cluster_2 = 0.62%.

Correct: 1040 out of 1109 training examples (93.78%).

Table 8 shows the model test results using the collected data. It shows the validity and suitability of the model at 93.78%, which concludes nicely that the selected model is reasonable.

Table 9: Average within Centroid for each cluster

	Stage and Cluster			
	Stages	*Cluster_0*	*Cluster_1*	*Cluster_2*
Student's Context	*Student's Interests*			
	Stage 1.1	3.19	3.72	4.15
	Stage 1.2	2.94	3.62	4.23
	Stage 1.3	3.03	4.24	3.85
	Stage 1.4	3.11	3.81	4.16
	Stage 1.5	3.15	3.60	3.88
	Student's Characteristics			
	Stage 2.1	3.20	3.72	4.04
	Stage 2.2	3.15	3.52	3.98
	Stage 2.3	3.30	3.58	4.04
	Stage 2.4	2.81	3.06	4.03
	Student's Environment			
	Stage 3.1	2.87	3.48	4.09
	Stage 3.2	3.14	4.33	4.15
	Stage 3.3	2.94	2.88	3.81
	Stage 3.4	3.07	3.04	4.13
	Stage 3.5	3.00	2.67	3.83
	Stage 3.6	3.11	2.72	4.23
Program's Context	*Program's Context*			
	Stage 4.1	3.01	4.36	4.29
	Stage 4.2	3.54	4.18	4.33
	Stage 4.3	3.37	4.08	4.22
	Stage 4.4	3.23	3.67	4.17
Total Number of Items: 1109		*213 Items*	*443 Items*	*453 Items*

Table 9 shows the average within centroid for each cluster. The benefit of this study and Table 9 is that it can be used to recommend suitable educational institutions according to the learner interest clusters. In addition, a classification of interest clusters by educational institutions is presented in Table 10.

Table 10 shows the details of the data collected by classification for the groups analyzed in the study. It was discovered that clusters of members from the collected datasets were unclearly distributed. Therefore, in future research, the researcher should suggest research tools to improve the more balanced distribution of datasets.

Table 10: Details of Each Cluster from Data Collection

Institutions	Data Collection		
	Cluster_0	*Cluster_1*	*Cluster_2*
MSU: Maha Sarakham University	72 Items	171 Items	103 Items
RMU: Rajabhat Mahasarakham University	58 Items	223 Items	197 Items
UP: University of Phayao	83 Items	49 Items	153 Items
Total Number of Items: 1109	*213 Items*	*443 items*	*453 items*

However, the data collection were 1109 people who provided attitudes and satisfaction to the research. It can be concluded that the overall level of satisfaction with the study is accepted (average = 3.70, S.D. = 0.84), as shown in Table 3.

In addition, the prototype model has been developed for predicting and recommending the appropriate institutions for the learner, which has moderate accuracy levels (92.25%) shown in Table 4 and Table 6. Moreover, the results of the self-test data model are very accurate at the highest level, which is equal to 93.78% (Correct: 1040 out of 1109 training examples) as shown in Table 7. Therefore, it can be concluded that this study was successful. It can develop highly accurate models and also have high performance model testers.

5. Conclusions

From this research, the researcher can summarize according to the research objectives as follows: (1) to study the relevance of factors for the analysis of the effectiveness of suitable educational institutions, and (2) to identify the acceptance and tolerance of each attribute, which supports lifelong learning.

The conclusion was obtained from the study of the relevance of factors by using machine learning tools and data mining techniques in the development of prototype models. It was discovered that the developed model is highly effective, with the ability to summarize 11 predictive factors: stage 1.2, stage 1.3, stage 1.4, stage 2.3, stage 3.1, stage 3.2, stage 3.3, stage 3.5, stage 3.6, stage 4.1, and stage 4.4 as shown in Table 7. While studying factors acceptance, it was found that the overall level of acceptance was at a medium level (average = 3.70, S.D. = 0.84). When the researcher has considered all dimensions, it was found that all factors had been accepted, as shown in Table 3. With the research study by collecting a total data of 1109 people from three universities (Rajabhat Mahasarakham University, the Maha Sarakham University, and the University of Phayao), the researcher concluded that this research achieved its objectives with five machine learning tools and data mining techniques: k-means, k-medoids, decision tree, cross-validation methods, and confusion matrix.

For future research, the researchers aim to construct and develop applications that promote and support the findings of this research.

Conflict of Interest

The authors declare no conflict of interest.

Acknowledgment

This research is supported by the two organizations: (1) The Faculty of Information Technology, Rajabhat Mahasarakham University, Maha Sarakham, Thailand. (2) The School of Information and Communication Technology, University of Phayao, Phayao, Thailand. The researchers would like to thank the advisor, lecturers, students, technicians, and all respondents for their entire support.

References

[1] U.N. Desa, "Transforming our world: The 2030 agenda for sustainable development," 2016.

[2] W. Nuankaew, P. Nuankaew, S. Bussaman, P. Tanasirathum, "Hidden academic relationship between academic achievement and higher education institutions," in 2017 International Conference on Digital Arts, Media and Technology (ICDAMT), 308–313, 2017, doi:10.1109/ICDAMT.2017.7904982.

[3] F. Bellotti, R. Berta, A. De Gloria, E. Lavagnino, A. Antonaci, F. Dagnino, M. Ott, M. Romero, M. Usart, I.S. Mayer, "Serious games and the development of an entrepreneurial mindset in higher education engineering students," Entertainment Computing, **5**(4), 357–366, 2014.

[4] S. Fungchomchoei, U. -mapor. Kardkarnklai, "Exploring the intercultural competence of Thai secondary education teachers and its implications in English language teaching," Procedia-Social and Behavioral Sciences, **236**, 240–247, 2016.

[5] A. Navy, "Higher Education Reform In Thailand: Toward Quality Improvement And University Autonomy," KATHA-The Official Journal of the Centre for Civilisational Dialogue, **9**(1), 1–16, 2013.

[6] M. Flavin, "Disruptive technologies in higher education," Research in Learning Technology, **20**, 2012, doi:10.3402/rlt.v20i0.19184.

[7] S. Gallagher, G. Garrett, "Disruptive education: Technology-enabled universities," The United States Studies Centre at the University of Sydney, 2013.

[8] P. Nuankaew, P. Temdee, "Online Mentoring Model by Using Compatible Different Attributes," Wireless Personal Communications, **85**(2), 565–584, 2015, doi:10.1007/s11277-015-2755-x.

[9] P. Nuankaew, P. Temdee, "Determining of compatible different attributes for online mentoring model," in 2014 4th International Conference on Wireless Communications, Vehicular Technology, Information Theory and Aerospace Electronic Systems (VITAE), 1–5, 2014, doi:10.1109/VITAE.2014.6934434.

[10] K. Pupara, W. Nuankaew, P. Nuankaew, "An institution recommender system based on student context and educational institution in a mobile environment," in 2016 International Computer Science and Engineering Conference (ICSEC), 1–6, 2016, doi:10.1109/ICSEC.2016.7859877.

[11] P. Nuankaew, "Dropout Situation of Business Computer Students, University of Phayao," International Journal of Emerging Technologies in Learning (IJET), **14**(19), 115–131, 2019.

[12] P. Nuankaew, W. Nuankaew, K. Phanniphong, S. Imwut, S. Bussaman, "Students Model in Different Learning Styles of Academic Achievement at the University of Phayao, Thailand," International Journal of Emerging Technologies in Learning (IJET), **14**(12), 133–157, 2019.

[13] W.S. Nuankaew, P. Nuankaew, D. Teeraputon, K. Phanniphong, S. Bussaman, "Perception and Attitude Toward Self-Regulated Learning of Thailand's Students in Educational Data Mining Perspective," International Journal of Emerging Technologies in Learning (IJET), **14**(09), 34–49, 2019.

[14] P. Nuankaew, W. Nuankaew, K. Phanniphong, R. Fooprateepsiri, S. Bussaman, "Analysis Dropout Situation of Business Computer Students at University of Phayao," in: Auer, M. E., Hortsch, H., and Sethakul, P., eds., in The Impact of the 4th Industrial Revolution on Engineering Education, Springer International Publishing, Cham: 419–432, 2020, doi:10.1007/978-3-030-40274-7_42.

[15] P. Nuankaew, W. Nuankaew, T. Thamma, "The Recommended System for the Relationship between Educational Programs and Stu-dents' Interests," in International Conference on Digital Arts, Media and Technology, 2–3A–4: 34, 2016.

[16] J. Witte, "Education in Thailand after the crisis: A balancing act between globalization and national self-contemplation," International Journal of Educational Development, **20**(3), 223–245, 2000.

[17] N. Omar, M.M. Mohamad, A.N. Paimin, "Dimension of learning styles and students' academic achievement," Procedia-Social and Behavioral Sciences, **204**, 172–182, 2015.

[18] P.R. Medwell, P.N. Grimshaw, W.S. Robertson, R.M. Kelso, "Developing sports engineering education in Australia," Procedia Engineering, **34**, 260–265, 2012.

[19] A. Rezvanfar, M. Ghorbanian, F. Shafiee, "An investigation of the behaviour of agricultural extension and education engineering students in Tehran University towards employability," Procedia-Social and Behavioral Sciences, **152**, 65–69, 2014.

[20] S. Rongraung, S. Kanokorn, "Soft skills for private Ba," Procedia-Social and Behavioral Sciences, **112**, 956–961, 2014.

[21] W. Techataweewan, U. Prasertsin, "Development of digital literacy indicators for Thai undergraduate students using mixed method research," Kasetsart Journal of Social Sciences, **39**(2), 215–221, 2018.

[22] P. Nuankaew, W. Nuankaew, P. Temdee, "Institution recommendation using relationship optimisation between program and student context," International Journal of Higher Education and Sustainability, **2**(4), 279–302, 2019.

[23] R. Wirth, J. Hipp, "CRISP-DM: Towards a standard process model for data mining," in Proceedings of the 4th international conference on the practical applications of knowledge discovery and data mining, Citeseer: 29–39, 2000.

[24] P. Chapman, J. Clinton, R. Kerber, T. Khabaza, T. Reinartz, C. Shearer, R. Wirth, "CRISP-DM 1.0: Step-by-step data mining guide," SPSS Inc, **9**, 13, 2000.

[25] G. Hamerly, J. Drake, Accelerating Lloyd's algorithm for k-means clustering, Springer: 41–78, 2015.

[26] H.-S. Park, C.-H. Jun, "A simple and fast algorithm for K-medoids clustering," Expert Systems with Applications, **36**(2), 3336–3341, 2009.

[27] Silhouettes: A graphical aid to the interpretation and validation of cluster analysis, Journal of Computational and Applied Mathematics, **20**, 53–65, 1987, doi:10.1016/0377-0427(87)90125-7.

ASTES

Advances in Science, Technology and Engineering Systems Journal Vol. 5, No. 5, 1137-1146 (2020)

www.astesj.com

Special Issue on Multidisciplinary Innovation in Engineering Science & Technology

ASTESJ

ISSN: 2415-6698

Feature Extractors Evaluation Based V-SLAM for Autonomous Vehicles

Mounir Amraoui[*,1], Rachid Latif[1], Abdelhafid El Ouardi[2], Abdelouahed Tajer[3]

[1]*LISTI, ENSA Ibn Zohr University, Agadir, 80000, Morocco*

[2]*SATIE Paris-Saclay University, Orsay, 91405, France*

[3]*LISA, ENSA Cadi Ayyad University, Marrakech, 40140, Morocco*

A R T I C L E I N F O

Article history:
Received: 07 August, 2020
Accepted: 08 October, 2020
Online: 22 October, 2020

Keywords:
V-SLAM
Feature Extraction
Detectors
Descriptors
Bio-inspired algorithms
Front-end processing

A B S T R A C T

Visual Simultaneous Localization and Mapping known as V-SLAM, is an essential task for autonomous vehicles. It can be carried out using several sensors, in particular with on board cameras. To locate a vehicle, SLAM algorithms are based on two main tasks. The first task (front-end kernel) is intended to process images in order to provide features (called also landmarks or primitives) of the perceived environment. The second task (back-end kernel) is intended for localization and environment reconstruction.
This work focuses on the front-end task which uses extractors (detectors and descriptors) in a stereo-vision system. Several feature detectors and descriptors exist in the state of the art. The aim of this paper is to evaluate the possible combinations of detectors and descriptors to achieve a precise localization while considering the processing times. The study is extended to bio-inspired extractors. The evaluation is achieved with SLAM algorithms over well-known indoor and outdoor datasets. Experimental results highlight the performance of bio-inspired extractors and their potential integration in designing vision systems for real-time SLAM applications.

1. Introduction

Simultaneous localization and mapping (SLAM) [1] are a complex task aiming to reconstruct a map during a vehicle motion in parallel while localizing its position. This problem can be solved by using complicated algorithms, where many threads should be executed simultaneously, since the need is to recognize at the same time the vehicle pose and process previously detected landmarks for pose estimation and mapping. It is known that in ordinary circumstances a map cannot be achieved without knowing the precise position, while to know it, a map with landmarks is needed. The pose recognition is done by using feature extractors, that are a combination between feature detectors and descriptors. A SLAM algorithm can use input data issued from one or many sensors, to estimate the robot position. However, for a higher accuracy, a fusion of different sensors data is required.
Vision SLAM systems use a camera to detect a maximum of key Points (KP). Some software approaches are then developed to improve the quality of detected features, by enhancing description and detection algorithms. Both these tasks are the main ingredient for back-end kernels (localization, mapping and building environment) of any real-time vision SLAM application.

Despite some weakness like sensitivity to light, vision SLAM systems need a powerful architecture for image processing. This could be improved based on a hardware software co-design.

Back-end and front-end algorithms, both dependent as shown in figure 1, are continuously object of improvement and will keep being, as well as all other researches related to the embeddability on heterogeneous architectures and parallel implementation. The works in [2, 3] are among many similar studies, an example where the SMG-SLAM and EKF-SLAM, were accelerated on a field-programmable gate array (FPGA).

Most of feature extractors are mainly based on existing algorithm but are solving their drawbacks or improving their weaknesses, to be more robust against environment changes.

There are many ways to determine a key-point, also called a landmark in image processing depending on its type, since it could be a corner, a blob, an edge or a ridge. However, a recent survey [4] related to advances on feature extraction and description algorithms, show that the most used method is the corner detection, due to its algorithmic moderated complexity and the improved calculation adopted formulas, which has an impact on the number of memory access and CPU usage. Corners, called interest points, can be obtained by intersection of at least two edges.

[*]Corresponding Author: Mounir Amraoui, LISTI, ENSA Ibn Zohr University, E-mail: mounir.amraoui@edu.uiz.ac.ma

The corner detector is based on the edge detector. It is represented by a set of pixels that have rapid change in direction. Each of these pixels have at least two dominants and various directions of the corresponding point in a local area.

The quality of a corner detector can be evaluated by applying above criterions on the same corner, for multiple images and under different environment effects such as light changes, rotation, translation, and image resolution.

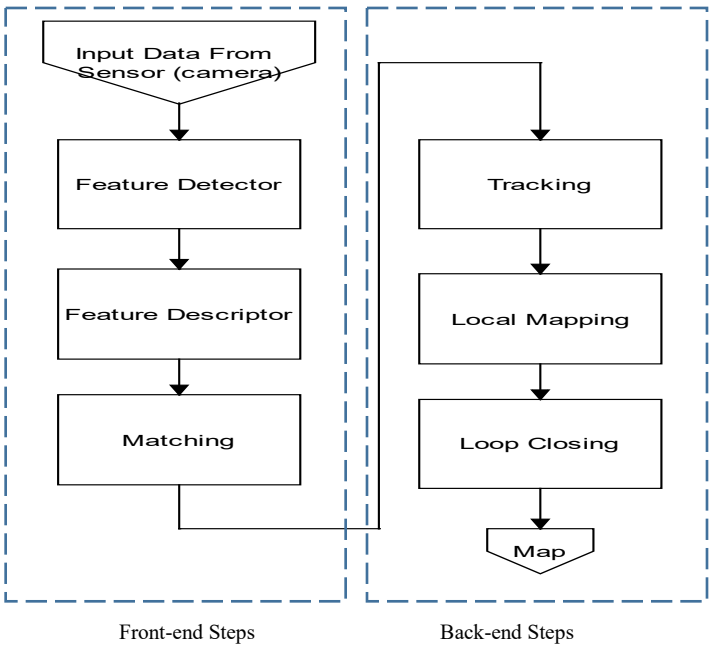


Figure 1: Front-End / Back-end main sequence for V-SLAM

As per [5] Harris represented by equation (1), was evaluated as the most stable, with the lower computational complexity compared to other corner detectors, such as Shi-Tomasi [6] and Forsner [7].

$$f(\Delta x, \Delta y) \approx (\Delta x, \Delta y)\, M \begin{pmatrix} \Delta x \\ \Delta y \end{pmatrix} \quad (1)$$

Where, in a given 2-dimensional grayscale image I, $(x, y)\epsilon\, w$ (window) are the image patch, $(\Delta x, \Delta y)$ is the shift and M is a Matrix structure tensor represented by:

$$M = \sum_{(x,y)\epsilon w} \begin{bmatrix} IxIx & IxIy \\ IxIy & IyIy \end{bmatrix}$$

$$= \begin{bmatrix} \sum_{(x,y)\epsilon w} IxIx & \sum_{(x,y)\epsilon w} IxIy \\ \sum_{(x,y)\epsilon w} IxIy & \sum_{(x,y)\epsilon w} IyIy \end{bmatrix} \quad (2)$$

Hence based on [5], for lower threshold values Harris detects many features together with noisy data from the image, which is considered as a weakness. Since Harris cannot set multiple threshold values for each image feature detection, it needs to be enhanced.

To solve such issue an accelerated segment test model, mathematically simple, was developed and proved with better performance, since it can determine if the interest point is a corner or not, only by evaluating the point neighborhood. Based on this concept some very known detector was developed, such as Feature Accelerated Segment Test (FAST) [8], which is also considered as an enhancement of SUSAN [9] and Harris corner detectors.

There are other different approaches for corner detection, that can detect interest points using a genetic programming for automatic image operator synthesis, like the one developed by Trujillo and Olague [10] in 2011. This method can be competitive, but it is more used for object recognition and need to be trained based on a bag of features.

To perform the desired task in an optimal way, the representation of the complete initial image data must be reduced by eliminating redundant features. So, a descriptor is applied once the feature detection is done, to provide complementary attributes such as gradient, magnitude and orientation.

Several descriptors like SIFT, SURF, BRIEF, ORB or BRISK has been successfully applied for tracking and object detection tasks, but most of pervious evaluation works were related to the computational complexity of algorithms.

In this work, our contribution is a study of detectors and descriptors to select the suitable extractor combination dedicated to the V-SLAM. The study considers constraints of processing times and precision for autonomous vehicles. It is extended to bio-inspired extractors and their integration into a back-end V-SLAM system.

The following section is related to the state-of-the-art and the essential concepts, to highlight and explain the reasons behind each selection and present also advantages and drawbacks of the chosen feature descriptors and detectors. Then, the evaluation methodology will be presented in section 3. Section 4 shows the results related to the processing times and precision of the evaluated extractors. It presents also front-end experimental tests which lead us to select an extractor for a full SLAM evaluation (back-end evaluation). The last section gives a general holistic view point and a conclusion.

2. Related Work

2.1. Feature detectors

FAST: based on AST (Accelerated Segment Test) and stands for Feature Accelerated Segment Test, is a corner detector that exceeds the other detectors in both computational performance and repeatability as per [11]. This method consists on the examination of the intensity for a given central pixel p in a radius r circle following a mathematical representation, where the intensity value Ip of the corresponding pixel p and a threshold t are used in three intervals:

$$S_{p\to x} = \begin{cases} d, & I_{p\to x} \le I_{p-t} & (darker) \\ s, & I_{p-t} < I_{p\to x} < I_{p+t} & (similar) \\ b, & I_{p+t} \le I_{p\to x} & (brighter) \end{cases} \quad (3)$$

where, $S_{p\to x}$ is the state, $I_{p\to x}$ is the intensity of the pixel x and t is a threshold.

There is a way to make this process faster by evaluating *n* successive pixels from the circle. Based on the brightness and darkness of these pixels, the evaluated pixel can be identified as a feature or not.

Authors in [11] has optimized the algorithm to achieve higher computational efficiency with improved processing speed, by defining the order in which the test is done and applying a non-maximum suppression (NMS), to pixels that have successfully verified the segment test. The idea is mathematically represented by:

$$V = max \begin{cases} \Sigma(pixel\ values - p)\ if\ (value - p) > t \\ \Sigma(p - pixel\ values)\ if\ (p - value) > t \end{cases} \quad (4)$$

In this equation, *p* refers the central pixel, *t* is a threshold and "*pixel values*" correspond to the *N* contiguous pixels in the corresponding circle.

The AST processing speed depends mainly on the pixel from which the evaluation is starting first. Therefore, the decision tree can be computed based on the distribution of the learnt set of the corner configuration for a given environment.

AGAST: Adaptive and Generic Accelerated Segment Test, is a corner detector developed by Elmar Mair et al. [12] where a binary decision tree is computed. This method is common and does not require any adaptation to new environments. However, it is more memory consuming due to the number of memory access to weight the various pixels. The decision tree is optimal for a given probability of similar pixels in the AST mask.

Also, the corner detector is automatically adapted to the environment by combining two trees, to make, with only one-pixel delay, the optimal decision tree for the image region. Hence, it results in a corner detector that does not need a training task, while maintaining the same corner repeatability and response as FAST.

By varying the nucleus (*Ps)*, the decision tree can be balanced. The system is then represented as follow:

$$S_{n\to x} = \begin{cases} d, & I_{n\to x} < I_{n-t} & (darker) \\ \bar{d}, & I_{n\to x} \not< I_{n-t} \wedge S'_{n\to x} = u & (notdarker) \\ s, & I_{n\to x} \not< I_{n-t} \wedge S'_{n\to x} = \bar{b} & (simillar) \\ \bar{s}, & I_{n\to x} \not> I_{n+t} \wedge S'_{n\to x} = \bar{d} & (simillar) \\ \bar{b}, & I_{n\to x} \not> I_{n+t} \wedge S'_{n\to x} = \bar{b} & (notbrighter) \\ b, & I_{n\to x} > I_{n+t} & (brighter) \end{cases} \quad (5)$$

where, $S'_{n\to x}$ is the previous state, *I* is the pixel brightness and *u* refers to an unknown state.

Therefore, when the environment switches at consecutive pixels from homogenous to structured, AGAST can be less efficient than FAST. However, it is not possible practically due to the mirroring effect of dissimilar pixels, also because a random brightness distribution does not exist on a natural image.

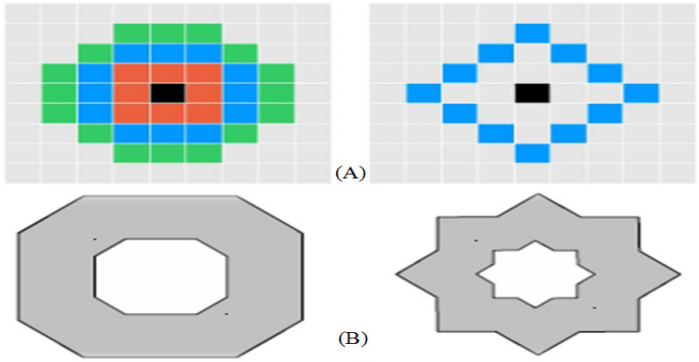
SURF: Stands for Speed Up robust Feature, it is inspired and developed based on SIFT [13]. The main motivation of this feature detector and descriptor is to overcome SIFT's low processing time and computational complexity. SURF [14] has been reported to be up to a few times faster than SIFT without compromising the performance.

For a given pixel, SURF calculate first the Haar-wavelet responses in x and y-direction, around the key-point in a circular neighborhood of radius 6. Integral images are also used on big scales wavelets for fast filtering. The second step in the process is to calculate the main orientation of the feature descriptor, by making the sum of vertical and horizontal wavelet responses in a scanning area, then changing the scanning orientation by adding π/3, and re-calculating until to find the largest sum value.

STAR: It is distinguished from SIFT and SURF which find extrema at sub-sampled pixels that consequently reduces accuracy of feature localization at larger scales. This feature detector is a derivative from CenSurE (Center Surround Extrema) feature detector [15]. It was integrated to the well-known Open source Computer Vision library.

Aiming to create a multiscale detector with full spatial resolution, this detector uses a bi-level approximation of the Laplacian of Gaussians (LoG) filter. So instead of the simple circular shape, the mask is represented by a circle with 2 overlapping squares: 1 upright and 1 45-degree rotated, resulting in a polygon with thick borders, to be invariant to rotations and to enable the use of integral images for efficient computation (see figure 2). This configuration is computationally better compared to the other scale-space detectors and presents real-time implementation possibilities.

The masks shape used in feature detection for each method is given by Figure 2.



ORB: Stands for Oriented FAST and Rotated BRIEF (Binary Robust Binary Robust Independent Elementary Features) [16]. The ORB detector is developed based on FAST to find key-point then applies Harris corner detector measuring method to give the top N points among them. But since FAST does not compute the orientation, the authors in [16] came up with enhancing modifications.

The ORB detector creates a multiscale image pyramid, with versions of image at different resolutions, where each level in the pyramid contains a subsampled version than the previous level. Once this process is finished, FAST detector is used to detect key-points at each level, and therefore ORB is partial scale invariant.

2.2. Features descriptors

BRIEF: Stands for Binary Robust Independent Elementary Features. This feature descriptor as per [17] uses a binary subsequent matching, with Hamming distance method to compute the descriptors similarities. This algorithm is much faster and computationally efficient.

Due to the high sensitivity to noise, BRIEF performs a smoothing to the image before applying the actual descriptor, using a simple averaging filter.

The value of each contributing bit to the descriptor, is given by the comparison of intensity values of two points inside an image segment centered on the currently described feature. The value of this bit is equal to 1 if the first point intensity of this pair is higher than the second point intensity value, otherwise it is equal to 0.

A few sampling strategies were tested by the authors to select the point pairs, show that sampling according to the Gaussian distribution centered on the described feature point, results in best performances.

For BRIEF, the initial smoothing is done with a 9x9 pixels rectangular averaging filter, the image patch is a 48x48, and the proposed descriptor is 512-bit long. The size of the window can be modified to be fitted to the application.

ORB: The Oriented FAST and Rotated BRIEF descriptor, uses a modified version of BRIEF (Binary Robust Binary Robust Independent Elementary Features).

Since Standard BRIEF descriptor performs weakly on rotation, ORB drives BRIEF depending on the orientation of key-points (KP's). The algorithm constructs a lookup table of pre-computed BRIEF patterns, to get a rotated version S_θ, where the angle is discretized by an incrementation of 12° degrees. then use the correct set of points S_θ to compute its descriptor.

BRISK: The Binary Robust Invariant Scalable Key-point (BRISK) [18], is a key point detector and descriptor inspired by AGAST [12] and BRIEF [17]. It uses AGAST for detection, which is an upgrading of FAST in term of processing time while preserving the similar detection performance.

To achieve scale invariance, the key-point is detected using a non-maxima suppression and interpolation across all scales space pyramid. To describe the features, authors have used symmetric patterns instead of using learned or random patterns.

For long-distance and to determine orientation, several sample point comparisons were used. The relative difference in intensity of the displacement vector is weighted and stored. These vectors are weighted. The computed average is used to find the major gradient direction of the patch.

FREAK: Fast Retina Key point [19], inspired from the biological human retina. The detection concept is based on summing the estimated local gradients over selected point pairs to provid the feature orientation.

To allow applying coarser discretization of rotation, a specific biologically inspired point sampling pattern is used which also results on saving memory space.

To reject false matches and accelerate the computation time, the feature description used is BREIF-based binary string. This allows a sampling pattern approach by comparing the most distinctive characteristics feature neighborhood to the point pairs carrying the information.

HOOFR: Hessian ORB-Overlapped FREAK [20] is a FREAK descriptor-based method combined with the ORB detector, with enhancements on the detection algorithm to speed up the process, improve memory allocation and reliability, the matching process timing is then reduced because the descriptor size is 256 instead of 512 compared to FREAK. HOOFR has three steps:

1- The first step consists on extracting key points from training data and building the description: a matrix M is created using all possible pairs where each key-point has its own descriptor. The number of key-points is equivalent to rows and the size of descriptor is equivalent to the number of columns.

2- The second step aims to define the variance value of the binary distribution, by computing the average for each column limited between 0 and 1. A mean value of 0.5 indicates the maximum variance desired to have a discriminant feature.

3- Finally, the third step consist on processing all columns to maintain only 256 columns that have the greatest variances.

ZEON: Defined by H. Angrish [21] as a new technique combining features of, SURF [14], BRISK [17] and FREAK [19], to overcome each method drawback. The main purpose of this improvement is to increase the extraction robustness and accuracy. This new proposed technique is intended to use features of SURF and BRISK as well as the detection capabilities of FREAK as a first step. This will provide a certain edge and will not add massive time strains to the new method timing.

3. Evaluation Methodology

First, we will develop and set many combinations of different feature detectors and descriptors. All extractors will be evaluated in terms of processing time and accuracy for different set of images of well-known outdoor dataset, using different lighting condition and at different camera rates. Results from the first step will be analyzed to select only the best candidate that could be used in a real time SLAM system for automotive application. For this reason, we will consider the first three high score combinations taking into consideration the compromise between processing time and accuracy. At the end, we will make a full implementation of the selected extractors with a V-SLAM algorithm, to be able to evaluate the behavior of each extractor and define the most robust solution versus back-end constraints related to rotation, filtering, type of landmarks, lighting, sensor noise or ground truth. The evaluation methodology will also take indoor scenes.

4. Experimental Results

4.1. Front-End Evaluation

The adopted method for front-end process evaluation, is using a calibrated monocular camera to get image input, focusing on the number of detected features, the processing time of each extractor combination and the matching time.

To make an objective comparison, the same image is used where the calibration settings described in Table 1 are similar for each set of images given by KITTI benchmark [22].

The hardware configuration shown in Table 1.

Table 1: Hardware and software configuration

CPU: Intel i5 core ™ @ 2.60 GHZ GPU : NVIDIA GeForce GTX 1060 Max-Q 6GiB RAM: 12 GB	
Scale factor	1.6
Initial threshold	20
Scale level	8
Min threshold	7
Max Feature	1000

The number of features is set to a fix value number to limit the image maximum interest points that can be found by using a descriptor, 1000 is the highest number found during experiment, so it is set to be a reference value to make the comparison and to calculate the detector accuracy. All values are given after calculating the means. Figure 3 gives examples of proceeded images with their respective resolutions.



(A) Street: Image resolution: 1392 x 512 pixels. Labels: 1 Cars, 0 Vans, 0 Trucks, 0 Pedestrians, 0 Sitters, 0 Cyclists, 0 Trams, 0 Misc.



(B) Cars: Image resolution: 1392 x 512 pixels. Labels: 5 Cars, 2 Vans, 1 Trucks, 0 Pedestrians, 0 Sitters, 0 Cyclists, 0 Trams, 0 Misc.

Figure 3: Outdoor images of KITTI dataset [22] used for evaluation.

Some extractors can be used, in the same time, as detectors and descriptors like ORB and SURF. Therefore, the description task is done in parallel with the detection task. From the other hand and since it is expected that the extractors will not have the same number of detected features, the processing time will be higher for the ones with high number of detections. So, the given value will consider the total processing time divided by the number of detected features as presented in Table 2 and Table 3.

Table 2: Processing time evaluation for different combinations of detectors-descriptors vs number of detected features using the image from figure 3 (A).

	Image (A): Street		
Descriptor	Detector	Number of detected features	Total detection and description processing time per feature (ms)
FREAK	FAST	956	0.046
	STAR	643	0.12
	ORB	213	0.291
	SURF	684	0.409
	AGAST	950	1.065
ORB	FAST	946	0.037
	STAR	660	0.106
	SURF	967	0.278
	ORB	500	0.036
	AGAST	939	1.399
BRISK	FAST	988	0.041
	STAR	660	0.126
	ORB	402	0.239
	SURF	896	0.355
	AGAST	980	1.357
BRIEF	FAST	951	0.035
	STAR	660	0.12
	ORB	500	0.144
	SURF	973	0.197
	AGAST	944	1.292
ZEON	FAST	3353	0.018
	STAR	654	0.124
	ORB	371	0.396
	SURF	971	0.346
	AGAST	3382	0.374
SURF	FAST	8115	0.049
	STAR	660	0.127
	ORB	500	0.57
	SURF	1334	0.31
	AGAST	8217	0.177

Table 3: Processing time evaluation for different combinations of detectors-descriptors vs number of detected features using the image from figure 3 (B)

	Image (B): Cars		
Descriptor	Detector	Number of detected features	Total detection and description processing time per feature (ms)
FREAK	FAST	960	0.05
	STAR	741	0.09
	ORB	206	0.30
	SURF	691	0.47
	AGAST	957	1.39
ORB	FAST	953	0.05
	STAR	760	0.10
	SURF	969	0.25
	ORB	500	0.19
	AGAST	947	1.45
BRISK	FAST	988	0.07
	STAR	760	0.11
	ORB	414	0.21
	SURF	897	0.28
	AGAST	984	1.49
BRIEF	FAST	956	0.04
	STAR	760	0.09
	ORB	500	0.15
	SURF	973	0.25
	AGAST	952	1.57

ZEON	FAST	982	0.06
	STAR	753	0.11
	ORB	373	0.37
	SURF	862	0.38
	AGAST	980	1.37
SURF	FAST	1000	0.06
	STAR	760	0.13
	ORB	500	0.55
	AGAST	1000	0.40

As shown in the above tables, it is clear that FAST as feature detector, is the most improved among all evaluated detectors because it provides the lower processing time with the maximum points of interest. Nonetheless, the total time is evaluated as the mean of the sum of all processing times needed for a feature detection and description for several iterations. Having a high number of detected features necessarily leads to a higher processing time needed for matching process. To evaluate this effect, the matching time and accuracy are then calculated according to the following formula:

$$\%Accuracy = \frac{\Sigma(True\ Positives + True\ negatives)}{\Sigma(\ Total\ cases)} * 100 \quad (6)$$

Table 4 gives the time spent per feature to have the corresponding match, based on image (B) from figure 3.

Table 4: Matching time using Brut force for SURF, and Hamming distance for the remaining descriptors

Descriptor	Detector	Number of matched Features	Matching time (ms)	% Acc
FREAK	FAST	869	0.139	90.52%
	STAR	683	0.035	92.17%
	ORB	193	0.049	93.69%
	SURF	638	0.055	92.33%
	AGAST	875	0.079	91.43%
ORB	FAST	891	0.061	93.49%
	STAR	720	0.064	94.74%
	SURF	885	0.040	91.33%
	ORB	471	0.038	94.20%
	AGAST	885	0.046	93.45%
BRISK	FAST	896	0.138	90.69%
	STAR	702	0.103	92.37%
	ORB	388	0.048	93.72%
	SURF	852	0.068	94.98%
	AGAST	897	0.113	91.16%
BRIEF	FAST	896	0.056	93.72%
	STAR	722	0.049	95.00%
	ORB	482	0.038	96.40%
	SURF	938	0.040	96.40%
	AGAST	894	0.065	93.91%
ZEON	FAST	870	0.155	88.59%
	STAR	681	0.086	90.44%
	ORB	348	0.054	93.30%
	SURF	632	0.101	73.32%
	AGAST	590	0.063	60.20%
SURF	FAST	845	0.187	84.50%
	STAR	658	0.120	86.58%
	ORB	463	0.062	92.60%
	AGAST	408	0.162	40.80%

Based on above result, a complete evaluation is conducted for front-end vision SLAM system where, we can conclude that if we seek for speed and low processing time, BRIEF-FAST is the best descriptor-detector combination to be selected. However, if the priority is given to higher accuracy, the BRIEF-ORB, and BRIEF-SURF is those that must be chosen. Also, as it is seen, the FAST algorithm is better in terms of processing time and number of detected features than all actual known detectors. Therefore, any evaluation will depend strongly on the associated descriptor and matching process. However, from another side, ORB descriptor, is the best descriptor in term of accuracy.

Additionally, the evaluation of the bio-inspired FREAK descriptor has proven that it has the lowest matching time performance, beside good results on both accuracy and processing time.

To narrow down and make the choice of the most adapted combination for automotive application, we must look for a combination that fulfil both the minimum processing time and the highest accuracy, which will leave us with 3 extractor combinations as shown below in Table 5. The remaining combination will be ignored, because they do not fulfill requirement and could lead to incorrect final mapping results.

This choice can be justified by the fact that any automotive vision SLAM application must be real time. Therefore, a low processing time has the advantage, but it does not mean that the precision can be high. The best combinations are the ones shown in the Table 5.

Table 5: High score combination leading to a compromise between the maximum accuracy percentage and the minimum processing time

Extractor	Total detection and description processing time per feature (ms)	Matching time (ms)	Total Processing time (ms)	% Acc
BRIEF-FAST	0.04	0.056	0.096	93.72%
ORB-FAST	0.05	0.061	0.111	93.49%
FREAK-STAR	0.09	0.035	0.125	92.17%

In a similar way to BRISK and BRIEF, FREAK uses also a binary string, but it has an optimized false matching algorithm which reduces the processing time during matching process, giving the advantage to be used for real time V-SLAM applications.

The second evaluation step is to apply the selected extractors to a full V-SLAM algorithm to evaluate the behavior considering back-end constraints (localization and mapping kernel).

4.2. Back-End Evaluation

For an objective evaluation, we implemented an algorithm based on ORB-SLAM2 and modify it to incorporate additional detectors and descriptors functional blocks. We used the already prepared class from OpenCV.

The matching method is based on the Brut force matcher which uses Hamming method to calculate distance. The intended stereo-vision system has three main parallel threads with an additional loop executed also in a separate thread.

The used datasets are an indoor sequence from Tum, fr2/desk [23] running at 10 FPS, and an outdoor sequence from the well-known KITTI dataset [24] running at 30 FPS. The reason behind this choice is because these datasets has a denser co-visibility graph and therefore the local map contains more key frames and points to evaluate object reconstruction and SLAM/odometry methods under different texture, illumination and structure conditions. The sequence is schematized in Figure 4. The obtained results are given by Figure 5.

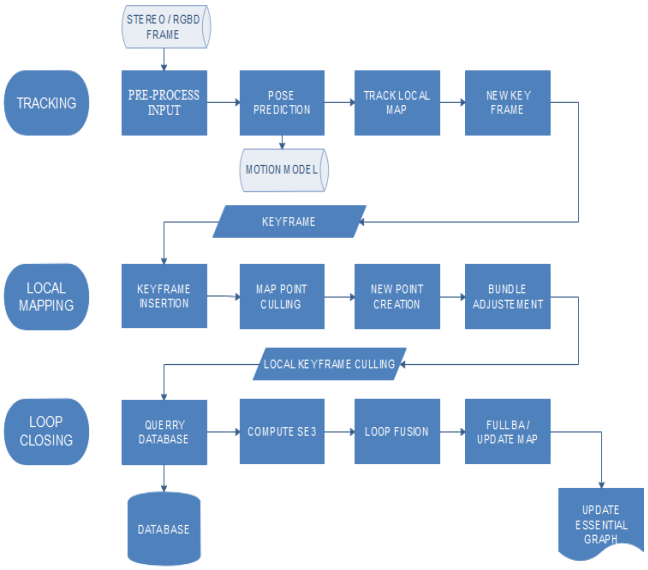


Figure 4: V-SLAM threads executed in parallel

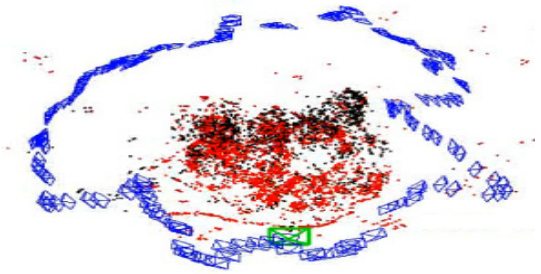
where:

- **Tracking:** a separate thread where every frame is localized by extracting feature and matching it to the local map. A local Mapping loop is then applied.
- **Local Mapping**: minimize the reprojection error, optimize and manage the local map, by performing a bundle adjustment (BA) loop.
- **Loop Closing**: it enhances the pose-graph by correcting the accumulated drift, within large loops.

To allow the system to continue loop detection and creating the map, a fourth thread of Full bundle adjustment, also called Full BA [25] is launched when the optimization process is aborted, and loop closing is finished.

Once the full BA finishes, the updated subset of key frames and points are merge and optimized, with the non-updated key frames and points that where inserted while the optimization was running. This is done by propagating the correction of updated key frames.

Indoor mapping results are shown in Figure 6 with the resulting path compared to the ground truth, that is provided initially with the dataset. Camera calibration data are also provided by [23].



(a)

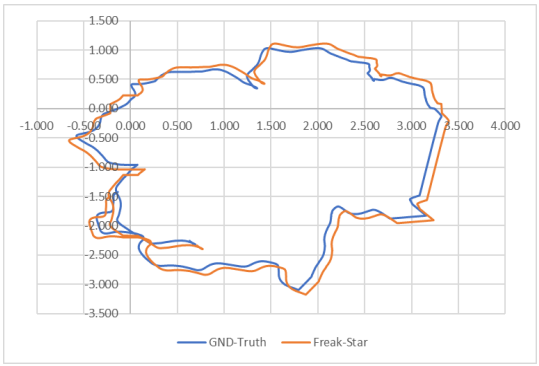


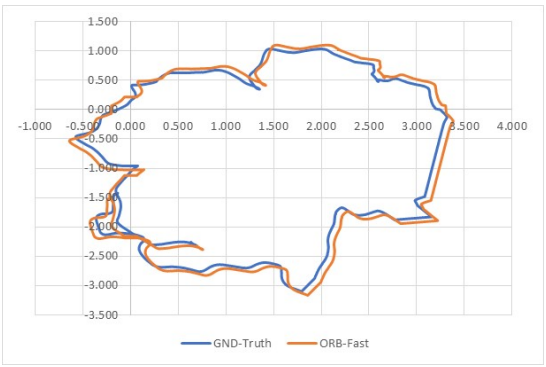
(b)



(c)

Figure 5: Dense point reconstruction from estimated keyframe poses: (a), sensor (camera) pose, (b) maps in TUM, fr2/desk. (c), KITTI_00 dataset tracked by the visual odometry system indicated in blue.





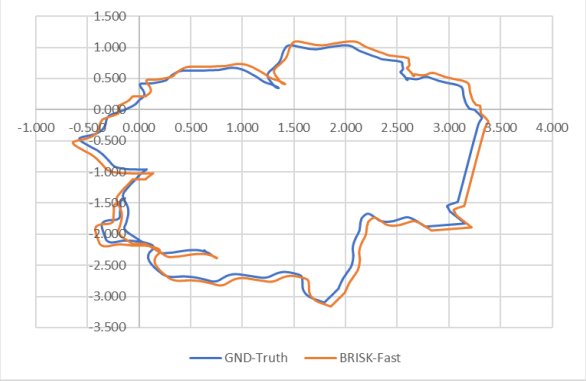


Figure 6: Pose-graph corresponding to indoor dataset, from up to down, for BRIEF-FAST, ORB-FAST, and FRAEK-STAR with comparison to ground-truth for TUM, fr2/desk

Bellow, the Figure 7 shows the evaluation using the outdoor dataset where the resulting path is compared to the ground truth given by [24].

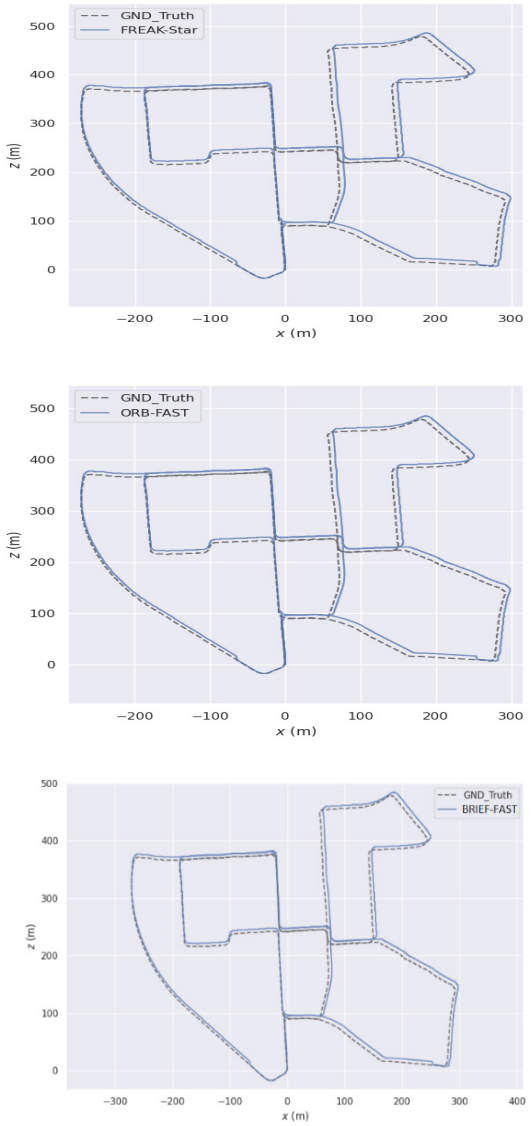


Figure 7: Pose-graph corresponding to outdoor dataset for BRIEF-FAST, ORB-FAST and FRAEK-STAR from up to down with comparison to ground-truth for KITTI dataset 00.

To compare both reconstructions, we used both metrics: the absolute trajectory error (ATE) and relative pose error (RPE) since they directly measure the difference between the ground-truth and the generated trajectory when using visual SLAM algorithms.

The estimated poses are associated to ground truth poses using the timestamps, then aligned using singular value decomposition. Finally, the difference between each pair of poses is computed. The output value is the mean, median, and the standard deviation of these differences, the RPE calculate the rotational errors. Results are given in Table 5 and Table 6 bellow.

Table 6: Translational and rotational errors calculated based on relative pose error (RPE) and absolute trajectory error ATE for 10000 pose pairs for TUM, fr2/desk indoor dataset.

FPS = 10		FREAK-STAR	ORB-FAST	BRISK-FAST
Translational Error (m)	RMSE	0.050	0.044	0.429
	Mean	0.045	0.028	0.027
	Median	0.047	0.017	0.017
	STD	0.021	0.034	0.033
	Min	0	0	0
	Max	0.103	0.148	0.143
Rotational Error (deg)	RMSE	9.85	3.73	3.618
	Mean	3.52	1.5	1.51
	Median	0.014	0.011	0.010
	STD	9.206	3.394	3.285
	Min	0	0	0
	Max	35.629	18.801	18.223

Table 7: Translational and rotational errors calculated based on relative pose error (RPE) and absolute trajectory error ATE for KITTI-00 outdoor dataset.

FPS = 30		FREAK-STAR	ORB-FAST	BRISK-FAST
Translational Error (m)	RMSE	8.623	7.914	6.707
	Mean	8.364	7.680	6.510
	Median	7.223	6.633	5.633
	STD	2.096	1.908	1.616
	Min	0.000	0.000	0.000
	Max	10.212	9.377	7.963
Rotational Error (deg)	RMSE	0.538	0.505	0.429
	Mean	0.294	0.278	0.250
	Median	0.264	0.250	0.227
	STD	0.451	0.422	0.349
	Min	0	0	0
	Max	14.079	12.562	10.161

Indoor dataset is considered as an environment with low lighting variations, where a robot is moving in a low speed. Additionally, the camera is held by a human, so the rotational effects are also much more important and unexpected. While the outdoor dataset is an environment that presents better other constraints like high speed, lighting changes and lower camera rotation, because it is fixed in the same position during the vehicle motion.

Considering above results, it is crystal clear that BRISK-FAST introduces the minimum rotational and translational error. Hence it has a better performance in term of trajectory precision in both shorter and longer distances.

From the other hand, FREAK-STAR extractor performance is acceptable for short distances and in environment with low variations, since it has the minimum standard deviation with

lowest maximum translational error, but the rotation can be considered as a weakness compared to the ORB-FAST and BRISK-FAST extractors.

To summarize, even if all above three methods results are very close to each other, related to timing performance, a bio-inspired extractor based on FREAK has a low complexity since it uses a binary string like BRISK and BRIEF. It has an optimized matching algorithm reducing processing time. It is suitable to be implemented on a GPU or FPGA due to the number of threads that could be executed in parallel. For these reasons a parallel implementation will give the advantage to the bio-inspired algorithm and make it the more suitable for a real time Visual SLAM application.

5. Discussion and Conclusion

FAST is still till today the most adjusted feature detector despite of its known drawbacks. The reason behind this statement is that, as per above results, the other descriptors were outperformed in terms of processing time and the number of detected features. Hence, due to this fact any selection of a descriptor merged with FAST will lead to the minimum detection time. However, this descriptor used in a SLAM application must run together with a descriptor and a matching process, which is affecting the global timing performance, as also demonstrated in this paper.

The matching process is a task that must be considered when selecting the combination of detector/descriptor, since the algorithm could lose more time during this step especially when the dataset has much more Key-points that need to be matched. This is clearly shown during experiments done in the current work, where pros and cons of every detector/descriptor combination are analyzed.

Additionally, a proof of consistency, accuracy and speed is made in this study with regards to the bio-inspired extractors, that still need to be improved to have lower rotational and translational error and the processing time. A new descriptor called HOOFR [20] try to improve theses weaknesses and an evaluation of this descriptor combined with different detectors in a full SLAM system could be achieved as a perspective with a parallel implementation on a heterogeneous architecture. This could be a solution leading to promising results.

Conflict of Interest

The authors declare no conflict of interest.

Acknowledgment

This research is supported by Information Systems and Technologies Engineering Laboratory, LISTI. *ENSA Ibn Zohr University, Agadir, Morocco* and *SATIE Paris-Saclay University, Orsay, France*.

References

[1] H. Durrant-Whyte, T. Bailey, "Simultaneous localization and mapping: part I", IEEE Robotics & Automation Magazine. **13** (2), 99-110, 2006. doi:10.1109/mra.2006.1638022. ISSN 1070-9932

[2] D. T. Tertei, J. Piat and M. Devy, "FPGA design and implementation of a matrix multiplier-based accelerator for 3D EKF SLAM," 2014 International Conference on ReConFigurable Computing and FPGAs (ReConFig14), Cancun, 2014, pp. 1-6, doi: 10.1109/ReConFig.2014.7032523

[3] G. Mingas, E. Tsardoulias, L. Petrou "An FPGA implementation of the SMG-SLAM algorithm" Microprocessors and MicrosystemsVolume 36, Issue 3, May 2012, 190-204.

[4] E. Salahat, "Recent Advances in Features Extraction and Description Algorithms: A Comprehensive Survey" arXiv:1703.06376v1 [cs.CV] 19 Mar 2017.

[5] J. Sánchez, N. Monzón and A. Salgado "An Analysis and Implementation of the Harris Corner Detector". Image Processing on Line. 8: 305–328, 2018. doi:10.5201/ipol.2018.229

[6] H. Kadhim, Araheemah, W. "A Comparative Between Corner-Detectors (Harris, Shi-Tomasi&FAST) in Images Noisy Using Non-Local Means Filter". Journal of Al-Qadisiyah for Computer Science and Mathematics, 11(3), Comp Page 86-93, 2019.

[7] A.S. Eltanany et al., "Key Point Detection Techniques". In: Hassanien A., Shaalan K., Tolba M. (eds) Proceedings of the International Conference on Advanced Intelligent Systems and Informatics 2019. AISI 2019. Advances in Intelligent Systems and Computing, **1058**. Springer, Cham, 2020.

[8] E. Rosten "Machine learning for high-speed corner detection », in 9th European Conference on Computer Vision, Graz, Autriche, **7**(13), 430-443, 2006.

[9] X. Chen, et al. Corner detection and matching for infrared image based on double ring mask and adaptive SUSAN algorithm. Opt Quant Electron **50**, 194, 2018.

[10] L. Trujillo and G. Olague, "Automated design of image operators that detect interest points". Evolutionary Computation. **16** (4): Archived from the original on 2011-07-17, 2008.

[11] R. Edward; R. Porter; T. Drummond "FASTER and better: A machine learning approach to corner detection". IEEE Transactions on Pattern Analysis and Machine Intelligence. **32** (1): 105–119. arXiv:0810.2434, 2010. doi:10.1109/TPAMI.2008.275. PMID 19926902..

[12] E. Mair, G. D. Hager, D. Burschka, M. Suppa, and G. Hirzinger, "Adaptive and generic corner detection based on the accelerated segment test," in Proceedings of the 11th European Conference on Computer Vision: Part II, Heraklio, 183–96, 2010.

[13] M. Safdari, P. Moallem and M. Satari, "SIFT Detector Boosted by Adaptive Contrast Threshold to Improve Matching Robustness of Remote Sensing Panchromatic Images," in IEEE Journal of Selected Topics in Applied Earth Observations and Remote Sensing, **12**(2), 675-684, Feb. 2019, doi: 10.1109/JSTARS.2019.2892360.

[14] X. Qu, "Evaluation Of Sift And Surf For Vision Based Localization "International Archives of the Photogrammetry, Remote Sensing & Spatial InformationSciences . **41**(B3), 685-692, 2016.

[15] M. Agrawal, K. Konolige, M.R. Blas, "CenSurE: Center Surround Extremas for Realtime Feature Detection and Matching. In: Forsyth D., Torr P., Zisserman A. (eds) Computer Vision – ECCV 2008. ECCV 2008. Lecture Notes in Computer Science, **5305**. Springer, Berlin, Heidelberg, 2008.

[16] E. Rublee, V. Rabaud, K. Konolige and G. Bradski, "ORB: An efficient alternative to SIFT or SURF," 2011 International Conference on Computer Vision, Barcelona, 2011, 2564-2571, doi: 10.1109/ICCV.2011.6126544.

[17] M. Calonder, Lepetit, V., Strecha, C., Fua, P.: BRIEF: binary robust independent elementary features. ECCV'10 Proceedings of the 11th European Conference Computer Vision: Part IV, 2010.

[18] S. Leutenegger, M. Chli and R. Y. Siegwart, "BRISK: Binary Robust invariant scalable keypoints," 2011 International Conference on Computer Vision, Barcelona, 2011, 2548-2555, doi: 10.1109/ICCV.2011.6126542.

[19] A. Ahmed et al., "Modeling and Simulation of Office Desk Illumination Using ZEMAX," in 2019 International Conference on Electrical, Communication, and Computer Engineering (ICECCE), 1–6, 2019. doi: 10.1109/ICECCE47252.2019.8940756.

[20] D. Nguyen, A. El Ouardi, E. Aldea and S. Bouaziz, "HOOFR: An enhanced bio-inspired feature extractor," 2016 23rd International Conference on Pattern Recognition (ICPR), Cancun, 2977-2982, 2016.

[21] H. Angrish. Navjot Kaur. Raman Chadha." A Novel Technique to Detect Local Features in Digital Images" IJSTE - International Journal of Science Technology & Engineering **2**(3), September 2015.

[22] A. Geiger and Philip Lenz and Christoph Stiller and Raquel Urtasun," Vision meets Robotics: The KITTI Dataset", International Journal of Robotics Research (IJRR), 2013, Geiger2013IJRR.

[23] F. Steinbruecker, J. Sturm and D. Cremers, In Workshop on Live Dense Reconstruction with Moving Cameras at the Intl. Conf. on Computer Vision (ICCV), 2011.

[24] A. Geiger and Philip Lenz and Raquel Urtasun "Are we ready for Autonomous Driving? The KITTI Vision Benchmark Suite", Conference on Computer Vision and Pattern Recognition (CVPR), 2012.

[25] D. P. Frost, O. Kähler and D. W. Murray, "Object-aware bundle adjustment for correcting monocular scale drift," 2016 IEEE International Conference on Robotics and Automation (ICRA), Stockholm, 2016, 4770-4776, doi: 10.1109/ICRA.2016.7487680.

ASTES

Advances in Science, Technology and Engineering Systems Journal Vol. 5, No. 5, 1147-1153 (2020)

www.astesj.com

Special Issue on Multidisciplinary Innovation in Engineering Science & Technology

ASTESJ

ISSN: 2415-6698

Effects of Resting Actions Using Smart Toys During Break Times on Concentration in E-learning

Takashi Ito[1], Kenichi Takahashi[*,2], Tomoko Kajiyama[2]

[1]*Aoyama Gakuin University, Department, Institute of Industrial and Systems Engineering, Kanagawa, 252-5258, Japan*

[2]*Hiroshima City University, Department of Intelligent Systems, Hiroshima, 731-3194, Japan*

ARTICLE INFO

Article history:
Received: 24 August, 2020
Accepted: 15 October, 2020
Online: 22 October, 2020

Keywords:
Refresh
Resting action
Smart toys
Effect
Break times

ABSTRACT

This study conducted experiments to investigate the effects of resting actions of e-learners during break times on keeping and improving the concentrations of learners in e-learning. Two smart toys (a dog-type robot "aibo" and a toy drone) were used for the resting actions. Two types of experiments were conducted to examine the effects: one is a work type experiment (simple mathematical calculation) and the other is a memorizing type experiment (learning of English words). In those experiments, the learners played with one of the smart toys during the resting times between the learning sessions and performed certain actions accordingly. The experimental results were combined with the previous study using a humanoid robot "RoBoHoN." A questionnaire was also employed to investigate the feeling of the learners. The experiments showed that the "playing with aibo" action refreshed the learners effectively in the mathematical experiment, while the "playing with RoBoHoN" action was effective in the learning experiment.

1. Introduction

In recent years, e-learning has been actively used with the development of ICT [1]. E-learning is the education and learning way that combines the Internet with PCs and mobile terminals. With e-learning, learners can deeply understand the content by learning iteratively and utilizing videos and voices. Also, learners can take advantage of good features of e-learning, such as learning at any time and place and furnishing functions for learners to select learning contents suitable to their knowledge level and to repeat lessons, as well as the variety of devices used for e-learning, such as tablets and smartphones. As a result, learning effect by e-learning is expected to be higher than the conventional learning using paper media. Additionally, with e-learning systems, the management and utilization of learning data become easy.

On the other hand, since e-learning is mainly used for individual learning, there is no instructor present and there is no opportunity that learners communicate with instructors and other students. The stimulation from instructors and friends is small, which can decrease their willingness to learn gradually. Thus, it is not easy for learners to keep motivation and concentration high, and learners can easily get bored to abandon learning, which is one of the important problems to be solved for e-learning [2].

In order to challenge the problem, various systems have been proposed, e.g., a system with a function to praise and scold students with images according to their learning performance, a system that measures student concentration and learning states during learning using Kinect, a system introducing game-based learning, intelligent collaborative e-learning systems, an e-learning platform, and portfolio assessment in elearning environment [3-6].

Another important factor is to provide appropriate break times in order to maintain motivation and concentration of learners. A study investigated the effect on student learning performance by introducing a break during a 90-minute lecture at a university [7]. It showed that taking a short break of about 8-10 minutes improved the learning performance: After the break, drowsiness of students decreased and their concentration increased. In addition, for VDT (visual display terminal) work, a study examined the lengths of an appropriate work time and the break time in order to reduce the burden on the mind and body and to improve work performance [8]. They suggested that one session of continuously working on a VDT is less than one hour and a 10–15 minute break between working sessions is desirable. Also, work on the way how office workers using VDTs spent their break times influenced their working efficiency was published [9], and Japan's Ministry of Health, Labor and Welfare recommends occupational health management guidelines regarding the use of

[*] Corresponding Author: Kenichi Takahashi, Hiroshima City University, +81-82-848-2872, 6961643@hiroshima-cu.ac.jp

VDTs [10]. Further, apps for supporting learners in the break time has been proposed [11]. The authors consider that it is important to introduce appropriate resting actions during break times for efficient and effective learning in e-learning that usually uses the VDT equipment.

In our research, a web-based e-learning system equipped with functions to improve or maintain learning motivation and concentration has been developed, such as a ranking function, a function that praises or scolds students appropriately with images and a sound, and a function for learners to present problems to one another [3]. In addition, a learning system equipped with games to investigate the effect of fun and relaxation of the games has been developed [12]. The games are one that refreshes learners by quick physical motion (shooting flies on a screen) and one that relaxes learners by taking care of a dog without heavy physical movement. These studies showed that refreshing by playing games during the break times between learning sessions is effective on improving learners' will to learn and maintaining the degree of concentration during e-learning. Furthermore, to examine what kinds of resting actions during break times keep or increase the concentration, we have conducted mathematical calculation experiments and English word memorizing experiments previously [13], [14]. The resting actions(behaviors) during the break times are: "playing the beat-fly game," "playing the dog-care game," "reading a book," "listening to music," and "doing nothing." We have showed that the type of these resting actions influences the degree of concentration.

Additionally, there was a study that introduced new resting actions and investigated the influence of the learner's motivation for learning and concentration. In this study, we performed the same experiments using two types of works as in our previous study: "simple work" (the learners solve continuously simple numeric calculation with four arithmetic operations for 15 minutes per work session) and "learning work" (they memorize English words for 30 minutes per learning session). In the study, we introduced the interaction with communication robots, "RoBoHoN" and "aibo", as new resting actions [15]. The study confirmed that the break time using "playing with aibo" had a good relaxing effect, and had a positive effect on simple learning such as numeric calculation with arithmetic operations. However, it is not appropriate for memorization learning such as English word learning, while a break time using "playing with RoBoHoN" gave better results.

In this study, we employ resting actions using a "toy drone" and aibo, and investigate how they affect the learning motivation, concentration, and learning results. The resting action using aibo in this study was the same as that in the previous study [15]. We also conducted two types of experiments for e-learning: simple work in which students try to calculate the numeric questions of four arithmetic operations continuously for 15 minutes and memorizing in which students try to remember new English words for 30 minutes. After the experiments, the learners were asked to answer a questionnaire and respond to statements, in order to examine how they felt the effect the resting actions had on their concentration in the experiments. We discuss the effect of the resting actions after combining these experimental results with the results in our previous study [15].

2. Smart Toys

Recently with the development of artificial intelligence technology, various robots become popular. For example, a robot can make dialogue and conversation with humans. We call those robots smart toys. As these smart toys become popular, they are used for children's learning, while the privacy and security problems occurs [16-18].

This study employed smart toys in order to refresh the feeling of the learners by the resting actions. In the experiments, the learners perform different types of resting actions during break times: "playing with a toy drone" (in which the learners manipulate a toy drone to finish a toy course), "playing with RoBoHoN" (in which the learners play five kinds of games with a humanoid robot), and "playing with aibo" (in which the learners play with a dog-shaped robot by talking and touching).

2.1. RoBoHoN

"RoBoHoN" is a fourth-generation mobile communication robot developed by Sharp Corporation [19]. RoBoHoN works as a smartphone and has functions to talk with users and to make actions through the original apps. In our experiments, using software called "Scratch Pack for RoBoHoN," four actions were programmed so that the learners can play with RoBoHoN during break times. We refer to these actions together as "playing with RoBoHoN."

The four actions used for RoBoHoN are as follows.

1) Raise a flag: RoBoHoN speaks a command such as "raise a red (or white) flag", and the learner tries to obey the command correctly.

2) Answer a riddle: RoBoHoN speaks randomly one of five programmed riddles, and the leaner tries to answer it.

3) Guess who-I-am: RoBoHoN pretends to be a thing, a person, or an animal, and gives hints, such as "I am a humanoid". The learner guesses what or who RoBoHoN is from those hints spoken by RoBoHoN. The game continues giving other hints until the learner hits the correct answer or the number of hints becomes a certain number.

4) Dance: RoBoHoN can dance randomly one of more than 20 dances with music.

2.2. aibo

A pet robot "aibo" is developed by Sony Corporation [20]. It can walk on four legs and behaves like a puppy. It can recognize persons and changes its behavior gradually as the person interacts it frequently. The latest version of "aibo" employs artificial intelligence techniques and network functions such as expressing emotions and online backup of data. The first "aibo" was developed in 1999, and now new "aibo" developed in 2017 was on sale. With the introduction of artificial intelligence, the technology has improved the robot to show more puppy-like gestures and reactions.

In our previous research, we conducted experiments based on the idea that it will be effective to interact with "aibo", a robot that imitates a puppy, as well as to interact with actual small animals, since a certain improvement effect on e-learning was obtained [21]. In this study, we also adopted "aibo" for one of the resting actions from the same viewpoint. We asked the learners to interact with "aibo" during the break times between sessions. "aibo" performs various actions (behaviors) in response to human words. Specific keywords cause "aibo" to behave as if a dog behaves such

as "hands" and "sitting", and unique behaviors such as "dance" and "high touch". In addition, there are a special ball and a bone toy that can be used for play. "aibo" can learn tricks gradually by being praised with the words "good" or "good dog" and by being stroked in the part of the head, chin, and the back of its body.

2.3. Toy Drone

A drone refers to a remote-controlled or autonomous unmanned aerial vehicle. In the present, it is actively utilized for industrial use in various scenes.

Toy drones are inexpensive to buy, often have a small and lightweight body, and are simple to operate. With these features, even a beginner can easily operate the drone. The toy drone "Tello" developed by Ryze Technology Co. was used in this research [22]. We can use a smartphone as a controller to operate it by connecting the dedicated app to the drone. It can also be operated by connecting the app to a dedicated controller via Bluetooth. A small camera mounted on the front of the drone constantly captures the scenes in front of the drone, which are displayed in real time on the screen of the smartphone. The flight mode can be selected by the app. Acrobatic flight and various aerial photography functions can be easily executed.

In this study, we adopted a resting action called "playing with a toy drone" for comparison with the resting actions of different types of smart toys: "aibo" and "RoBoHoN." They were used for resting to refresh the mood by communicating with the robot. On the other hand, the "playing with a toy drone" action presents "fun" by performing precise operations of the drone, which requires concentration.

We asked the learners to operate the toy drone during the break times between work or learning sessions. A dedicated controller linked to the app is used to operate the drone. We can operate the drone more easily by linking the app with the controller. In order to enable the learners to operate the drone in the 3-minute break time, we completed various connections between the app and the controller in advance. In addition, before the experiments, we distributed the document summarizing how to operate the drone to the learners. Since the experiments were conducted indoors, flight mode functions were limited by eliminating dangerous acrobatic flights.

We constructed a drone course to have the learners perform precise operations. A gimmick of arches, a tunnel, and a slalom were placed for the drone to finish the course in about 1 to 2 minutes per lap. As for the arches, we prepared two patterns: one with multiple arches placed in curve side by side, and the other with multiple arches placed in different altitudes on the floor and a chair. The tunnel was made with multiple arches placed at narrow intervals in the same altitude. The slalom was made of rods of different lengths so that the drone goes forward in zigzags avoiding rods. Figure 1 shows the course used for the experiment. The course shown in Figure 1 is a basic form. We changed the difficulty of the course by changing the layout if the learner desired.

3. Experiments Incorporating Resting Actions

In this Section, we describe the results of the mathematical experiment and the English-word learning experiment, and discuss how the different types of resting actions affect learning motivation and maintenance of concentration. We estimate the effects of the resting actions on simple work (mathematical calculation) and learning work (memorizing English words) through the experiments. In the experiments, ten male students majoring computer science and belonging to our laboratory in our university served as participants and were divided into 2 groups of 5 students. The each group performed one of the resting actions during break times, but it did the same resting action in the mathematical experiment and the learning experiment to examine the effect of the same resting action on different types of work. In addition, we compared and discussed the learning results of this research with the results of the previous study using "aibo" and "RoBoHoN." We employed the correct-answer rate and the average number of answers as metrics for the mathematical experiment, and test score improvement as the metric for the learning experiment. We divided the learners to one of the groups through preliminary experiments so that the ability of each group is roughly equal.

3.1. Mathematical Experiment

The mathematical experiment is composed of three work sessions and two breaks between the work sessions. Figure 2 shows the flow of the experiment. The work session is 15 minutes long, and the resting time is 3 minutes. Figure 3 shows an example of mathematical calculation. The learner continuously calculates similar problems for 15 minutes in a work session. The mathematical experiment provides simple work in which learners tackle continuously to calculate simple numeric equations for 15 minutes. The numeric questions to be solved were produced by the automatic formula generation program of the system.

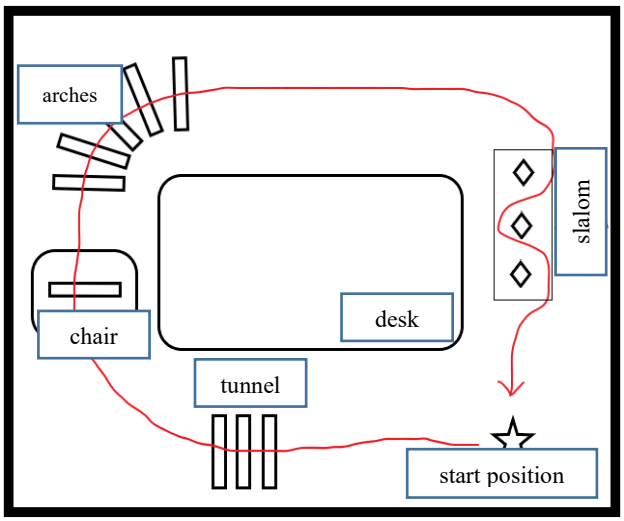


Figure 1: The basic course used for the toy drone

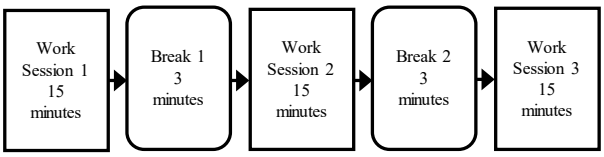


Figure 2: The flow of the mathematical experiment

Figure 4 illustrates the average correct-answer rates for the three actions. As for the aibo group, the result of the previous work [17] was incorporated with the result of the experiment in this study. From Figure 4, it can be seen that all groups tend to increase

the correct-answer rate from the first to second work sessions and to decrease the correct-answer rate from the second to third work sessions. Among them, the drone group shows that the degree of the tendency is large, whereas that of the RoBoHoN group is small. The correct-answer rate of the aibo group behaves between the RoBoHoN group and the drone group. Considering the decrease of concentration due to fatigue in the latter half of the work sessions, the average correct-answer rate of the drone group is significantly decreased in the second to third work sessions because the resting action using the drone operations heavily needs the concentration, while the average correct-answer rate of the RoBoHoN group is gently decreased. Also, the increase of the correct-answer rate of the RoBoHoN group from the first to second work sessions is small. Regarding the aibo group, the overall average correct-answer rate is low, while the tendency is between the RoBoHoN group and the drone group. Thus, we can say that the relaxing/refreshing effect of the resting action using the drone that influences learning motivation is low, because it needs the tense concentration.

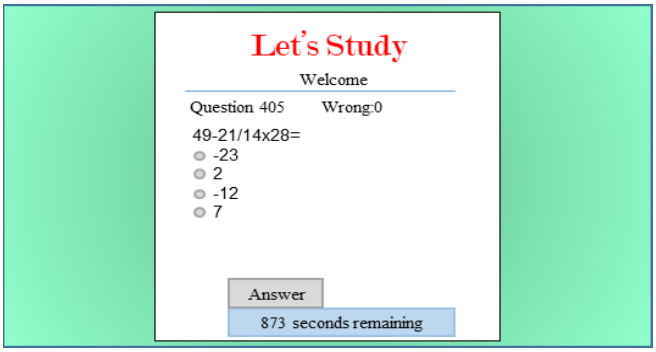


Figure 3: An example of mathematical calculation

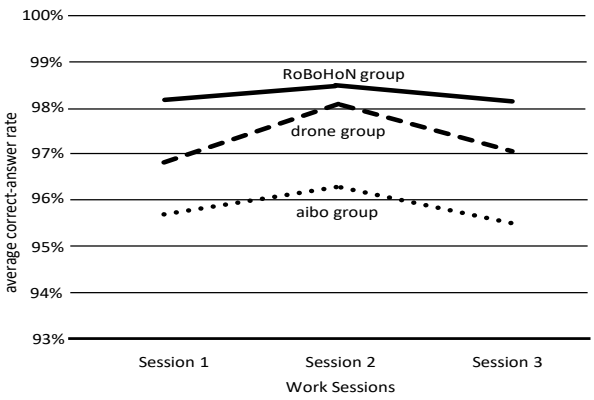


Figure 4: Correct-answer rates for RoBoHoN, aibo, and drone groups in the mathematical experiment

Figure 5 shows a graph summarizing the number of correct answers and the number of incorrect answers. Comparing the average number of answers shows that for all groups the number of answers in the second session is larger than that in the first one. Note that the increase of the number of answers by the drone group was large. However as the session proceeded, the learners became tired, and the number of answers decreased from the second to third sessions. Comparing the number of incorrect answers indicates that the numbers of the answers for all groups decreased except for the second to third sessions of the aibo group as the experiment proceeded, which suggests that the effect of the resting actions on learning was positive. Looking at Figure 5, it can be said that difference of the number of answers among the sessions is smallest for the aibo group.

In the mathematical experiment, the correct-answer rate for "playing with RoBoHoN" was a little higher than that for "playing with aibo," while the number of answers for "playing with aibo" was larger, indicating that "playing with aibo" was more effective to keep improve concentration. The authors believe that the resting behavior using aibo could provide a high refreshing/relaxing effect, and it can be considered as effective in improving learning motivation while maintaining moderate concentration.

3.2. Learning Experiment

In the English-word learning experiment, the learners were requested to memorize 200 English words for 30 minutes. In the experiment, two 30-minute learning sessions were held, and a 3-minute break was placed between the learning sessions, as shown in Figure 6. In the experiment, we asked the learners to learn 200 English words provided by the e-learning system. A post-learning test was administered to check to see whether they memorized English words or not, immediately after the second session. An example of a question for English word learning is shown in Figure 7. Note that the group of the resting action was the same group as the mathematical experiment in order to verify the effectiveness of the resting action.

Both the pre-learning test and the post-learning test consist of 50 words. The pre-learning test was performed about a week before the experiment to prevent the learners from memorizing the English words in the test. The score of the pre-learning test was used as a baseline for comparison.

We employed the score increase rate to evaluate the learning effect of the resting actions. The increase rate was calculated as follows, where IR is the score increase rate, P1 is the score on the pre-learning test, and P2 is the score on the post-learning test. The full score of each test was 50.

$$\mathrm{IR} = \frac{P2-P1}{50-P1} \times 100(\%) \qquad (1)$$

Figure 8 shows a graph summarizing the average increase rate of each group. We can see from Figure 8 that the RoBoHoN group had the highest average increase rate. In the memorization problem, it is necessary to remember the contents memorized in the learning sessions before the break time, and thus the resting action with high relaxation and refreshing effect is not appropriate, since the learners tend to forget the content. The authors considered that resting actions with a moderate refreshing effect is suitable. Also the positive effect was obtained for the aibo group in this experiment because the average increase rate was positive. On the other hand, the drone group has the lowest average increase rate. The resting action using the drone needs tense concentration for operating the drone, and had the high refresh effect, indicating that the resting action using the drone is not suitable.

Therefore, we can conclude that RoBoHoN-based resting action is suitable and effective for memorization learning such as English-word learning, because the score increase rate for the "playing with RoBoHoN" group was higher.

3.3. Questionnaire and Summary

At the time the learners finished each of the mathematical experiment and the learning experiment, we conducted a questionnaire. The questionnaire includes descriptive questions

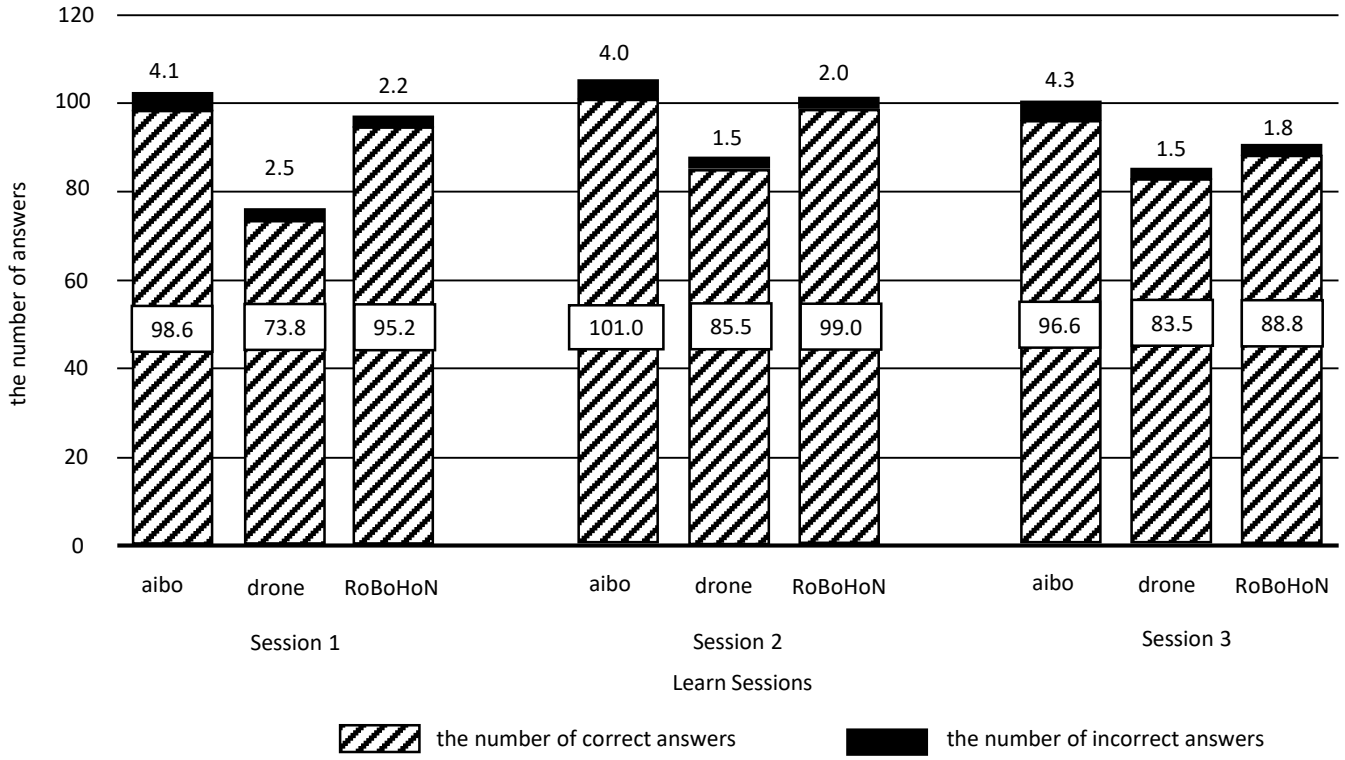


Table 1: Average Scores on Survey

Statement	RoBoHoN group		aibo group		drone group	
	Math	Eng	Math	Eng	Math	Eng
The game-playing with the smart toy during breaks were effective.	3.8	3.4	4.1	4.3	3.2	2.8
I felt refreshed after taking a break.	4.0	3.0	4.1	4.1	3.8	3.4
Playing with the smart toy improved my concentration.	3.6	3.0	3.7	3.8	3.4	2.8

and three selective questions. In the selective questions, the learners select a score on a five-point scale (5: strongly agree --- 1: strongly disagree). The questionnaire was conducted to investigate how the learners felt the effect of the resting actions.

Table 1 summarizes the evaluation results of the questionnaire obtained from aibo, drone, and RoBoHoN groups in the mathematical and the learning experiments. We can see from Table 1 that the aibo group gave the highest evaluation score for each question in both the mathematical experiment and the learning experiment, which shows higher refreshing and concentration effect than other groups did. The evaluation for the learning experiment was higher than the mathematical experiment, indicating that the resting action by aibo gave more refreshment in the learning experiment than in the mathematical experiment. We can see in Figure 5 that the number of answers was larger than those of the other groups, while in Figure 4 the correct-answer rate is the lowest, but the difference was less than 3%. Many learners said that they regarded aibo as a robot rather than as an animal. In the limited resting time, aibo didn't behave as ordered by the learners, and that may be stressful to them. We also see in Figure 8 that the score increase rate was positive, and the resting action worked well.

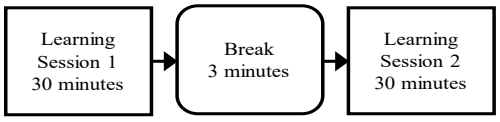


Figure 6: The flow of English-word learning experiment

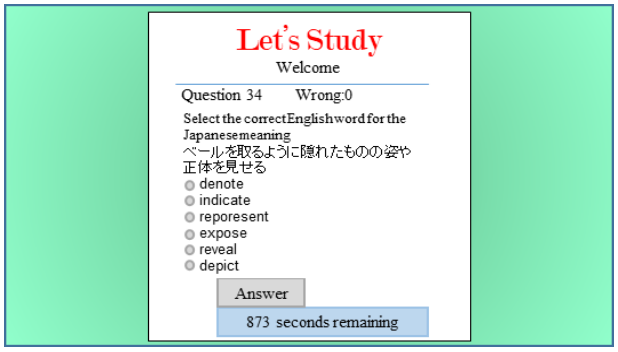


Figure 7: An example of an English-word question

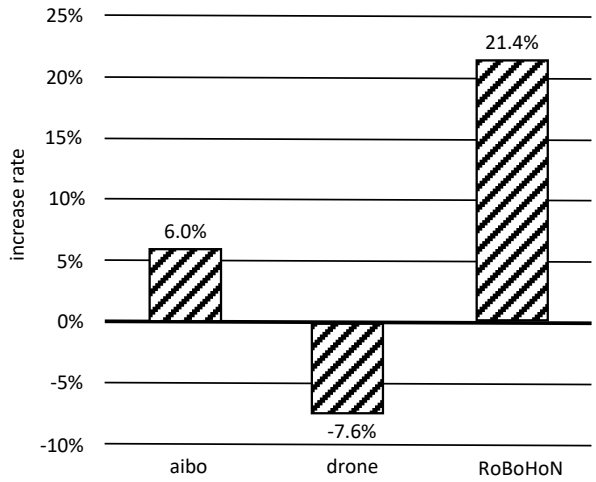


Figure 8: The average increase rates for RoBoHoN, aibo, and drone groups

The RoBoHoN group has the second highest rating scores. In this group, the evaluation of the mathematical experiment is also higher than that of the English experiments. We see in Figure 5 that the number of answers in the mathematical experiment was the second highest, while the increase rate in Figure 8 was highest in the English learning experiment, which shows that the resting action was effective in the learning experiment. The drone group has the lowest evaluation scores. They were refreshed in the mathematical experiment, while they gave evaluation score 2.8 and didn't concentrate in the learning experiment. The "playing with the drone" action needs concentration for precise operations, and that makes the learners feel stress. Thus, the authors considered that "playing with the drone" was not appropriate for the English word problem.

3.4. Summary

The "playing with aibo" action showed the best results as the resting action for the simple work regarding keeping and improving concentration, while the "playing with RoBoHoN" action shows the highly rated results in the English learning experiment.

The authors considered that the reason why the "playing with aibo" action was effective for the mathematical experiment was the high refreshment effect of the dog-shaped robot. The learners had to continue calculating simple mathematical problems for 15 minutes in the mathematical experiment and the "playing with aibo" highly refreshed the learners. On the other hand, in the English learning experiment, the "playing with RoBoHoN" action gained the highest score increase rate, although the evaluation scores of the "playing with aibo" group on the questionnaire were higher than those of the "playing with RoBoHoN" group. Thus, the feeling of refreshment by the learners themselves during the learning was different from the experimental results. Additionally, the "playing with RoBoHoN" action using language communication that has the moderate refreshing effect seems more suitable than the "playing with aibo" action that completely refreshed one's feeling. The "playing with a drone" behavior needs tense concentration on operation of the drone, and it was not appropriate for e-learning.

Future task includes further experiments with more participants of variety types and investigation from psychological point of view to evaluate the effect of the resting actions accurately, and the improvement of the learning system. It also includes experiments with other methods for relaxation than smart toys and discussion about the effect of those methods comprehensively in association with the type of learning.

4. Conclusion

In this study, we investigated the improvement of learner's concentration to learn and the learning will by using smart toys (either aibo or a toy drone) for e-learning, and discussed the effect by integrating the previous study using RoBoHoN . We compared the effect of the resting actions using aibo, RoBoHoN, and a toy drone among smart toys, since they have different features. We chose the functions that are considered to be effective for learning as the resting behavior and explained them so that the learners who touch the toys for the first time can operate the toys as they want. We found that that the "playing with aibo" action was effective for simple work like mathematical calculation, because the action had a well-balanced effect of improving concentration and learning motivation. Also we found that the "playing with RoBoHoN" action provides a moderate relaxing effect and was effective for English word memorizing. The "playing with a toy drone" action was not appropriate as a resting action, since some participants felt frustration to operate the drone.

Conflict of Interest

The authors declare no conflict of interest.

Acknowledgment

The authors would like to thank Mr. Masaki Ueta for collaboration on this work. This research was supported by a Grant-in-Aid for Scientific Research JP16K00485.

References

[1] Proseeds Inc., Merits and demerits of introducing e-learning, http://www.pro-seeds.com/trend/meritdemerit.html, Accessed in Aug. 2019 .

[2] A. Tominaga, C. Kogo, "Development and issues in Practical studies of e-learning", The Annual Report of Educational Psychology in Japan, **53**, 156–165, 2014 .

[3] M. Takeue, K. Shimada, K. Takahashi, M. Inaba, "Experiments of displaying images to keep the motivation in e-learning," Conference Proceedings - IEEE International Conference on Systems, Man and Cybernetics, 120–125, 2012, doi:10.1109/ICSMC.2012.6377687.

[4] T. Ito, S. Kotake, K. Takahashi, I. Inaba, M. Inaba, "Detecting Concentration of Students Using Kinect in E-learning," 450–456, 2017, doi:10.12792/icisip2017.082.

[5] T. Ito, K. Kamiya, K. Takahashi, M. Inaba, "A method for identification of students' states using kinect," Advances in Intelligent Systems and Computing, **935**, 341–350, 2019, doi:10.1007/978-3-030-19063-7_28.

[6] R. Takaoka, M. Shimokawa, T. Okamoto, "Special Section on Knowledge-Based Software Engineering A Development of Game-Based Learning Environment to Activate," **4**, 911–920, 2012.

[7] A.Yamazaki, "Effect of introducing small breaks during class hours on health promotion and learning performance," Journal of humanities and sciences, Nihon University, **24**(1-3), 33-58, 2019 .

[8] Y.Horie, "A study on optimum term of work hour with rest pause for VDT workers," Journal of Japan human factors and ergonomics society, Japan, **23**(6), 373-383, 1987 .

[9] T. Miki, T. Terada, et al., "Research of the effects of the break time on work performance," IPSJ SIG Technical Report, **2018-UBI-57**(3), 1–8, 2018 .

[10] Ministry of Health, Labour and Welfare, "Guidelines for occupational health management in VDT work," http://www.mhlw.go.jp/file/06-Seisakujouhou-11200000-Roudoukijunkyoku/0000184703.pdf, Accessed in Aug. 2019 .

[11] D. Hirama, A. Minaduki, "A development of an interval-supported application for VDT-work," Conference of Information processing sciety of Japan, 4-125 – 4.126,2014.

[12] M. Takeue, K. Takahashi, and M. Inaba, "Fundamental Experiments on Effects of Games in Rest Time between Learning," IPSJ SIG Technical Report, **2014-CE-124**(17) , 1–8, 2014 .
[13] K. Yamasaki, K. Takahashi, and M. Inaba, "Effect of the way of spending the rest time on learning," Conference of Japan Society for Fuzzy Theory and Intelligent Informatics, Kyushu Chapter, C-203, 83–86, 2015 .
[14] J. Kawaguchi, T. Ito, K. Takahashi, and M. Inaba, "Influence of How to Spend Recess in E-learning," Conference of IEICE Engineering Sciences Society, A-11-4, 151, Sapporo, Japan, 2016 .
[15] Y. Yasumura, T. Ito, K. Takahashi, T. Kajiyama, "Effects on Concentration of Different E-Learner Resting Behaviors in Reponse to Communication Robot Actions during Break Times," Proceedings of the 2020 14th International Conference on Ubiquitous Information Management and Communication, IMCOM 2020, 0–4, 2020, doi:10.1109/IMCOM48794.2020.9001742.
[16] L. Plowman, R. Luckin, "Interactivity, Interfaces, and Smart Toys," Computer, **37**(2), 98–100, 2004, doi:10.1109/MC.2004.1266302.
[17] F.D. Faraci, M. Papandrea, A. Puiatti, S. Agustoni, S. Giulivi, V. Drapuzzo, S. Giordano, F. Righi, O. Barberis, E. Thommen, E. Rossini, "AutoPlay: A smart toys-kit for an objective analysis of children ludic behavior and development," MeMeA 2018 - 2018 IEEE International Symposium on Medical Measurements and Applications, Proceedings, 2018, doi:10.1109/MeMeA.2018.8438636.
[18] S. Shasha, M. Mahmoud, M. Mannan, A. Youssef, "Playing with danger: A taxonomy and evaluation of threats to smart toys," IEEE Internet of Things Journal, **6**(2), 2986–3002, 2019, doi:10.1109/JIOT.2018.2877749.
[19] Sharp Corporation, "RoBoHoN," http://global.sharp/corporate/news/160414.html, Accessed in Aug. 2019.
[20] Sony corporation, "aibo," https://us.aibo.com/, Accessed in Aug. 2019.
[21] Mail Online, "The power of cute: How looking at pictures of baby animals can help improve your concentration levels," https://www.dailymail.co.uk/news/article-2210614/The-power-cute-How-looking-pictures-baby-animals-help-improve-concentration-levels.html, Accessed in Aug. 2019.
[22] Ryze Technology Co.,Ltd, "Tello," https://www.ryzerobotics.com/jp/tello/, Accessed in Aug. 2020.

ASTES

Advances in Science, Technology and Engineering Systems Journal Vol. 5, No. 5, 1154-1161 (2020)

www.astesj.com

Special Issue on Multidisciplinary Innovation in Engineering Science & Technology

ASTESJ

ISSN:2415-6698

A Proactive Mobile Edge Cache Policy Based on the Prediction by Partial Matching

Lincan Li[1], Chiew Foong Kwong[1,*], Qianyu Liu[2]

[1]*Department of Electrical and Electronic Engineering, University of Nottingham Ningbo China, Ningbo, 315100, China*

[2]*International Doctoral Innovation Centre, University of Nottingham Ningbo China, Ningbo, 315100, China*

ARTICLE INFO

Article history:
Received: 28 August, 2020
Accepted: 15 October, 2020
Online: 22 October, 2020

Keywords:
Cache
Latency
Cache Hit Rate
Content Prediction
Location Prediction

ABSTRACT

The proactive caching has been an emerging approach to cost-effectively boost the network capacity and reduce access latency. While the performance of which extremely relies on the content prediction. Therefore, in this paper, a proactive cache policy is proposed in a distributed manner considering the prediction of the content popularity and user location to minimise the latency and maximise the cache hit rate. Here, a backpropagation neural network is applied to predict the content popularity, and prediction by partial matching is chosen to predict the user location. The simulation results reveal our proposed cache policy is around 27%-60% improved in the cache hit ratio and 14%-60% reduced in the average latency, compared with the two conventional reactive policies, i.e., LFU and LRU policies.

1. Introduction

This article is an extended version of a conference paper presented in 2018 at the Biomedical Engineering, Healthcare, Robotics, and Artificial Intelligence 2018 [1].

With the ubiquitous emergence of the smart mobile devices, e.g., the mobile phones, as well as the trend towards high data rate applications, exponential mobile data have been generated in the wireless network while the current network cannot support the fast growth of the mobile data traffic [2], [3]. As a result, the storage capacity of the wireless network needs to be expanded and the conventional way is the dense-deployment of the base stations (BSs). However, it costs a lot for the mobile operator to upgrade this infrastructure [4]. Therefore, a more cost-effective approach is needed and the caching technique is regarded as an ideal approach [5].

By deploying the cache devices at the edge of the wireless network in proximity to the users, e.g., BSs and user terminals (UTs), and storing the popular contents at the cache devices [6], [7], users can directly retrieve the contents from the edge nodes rather than the remote core network via the backhaul links [8]. Hence, the content access latency can be decreased due to the reduced content transmission distance [9]. In parallel, duplicated requests for the same contents from the core network to the edge of the network can be avoided, which reduces the potential data congestion of the network [10]. Furthermore, due to the increasingly decreased prices of the cache devices, the storage capacity of the wireless network can be more cost-effectively boosted compared to the conventional way [4].

Due to the limited storage capacity of the cache devices, only a part of the contents can be stored in the edge cache devices. Hence, multiple works are focusing on how to design an efficient cache content placement policy. The most common approaches are least frequently used (LFU) and least recently used (LRU), which are referred to as reactive cache policies that determine whether to cache a specific content after it has been requested [11], [12]. In detail, LRU always caches the most recently requested contents while LFU caches the most frequently requested contents [13]. While the reactive cache policy is not efficient during peak hours. Hence, the proactive caching strategy is introduced, by which the content can be cached before the request, and hence the users can access the preferred content immediately when they arrive in new areas.[14], [15].

There are many proactive schemes have been investigated. In [16], a threshold-based proactive cache scheme based on reinforcement is presented, aiming at minimising the average energy cost. In this case, the time variation of the content is considered, which means the content popularity is changed over time rather than static. In practice, only the content whose lifetime is not expired has the potential to be cached. In [17], a caching scheme is presented to improve the cache hit rate and reduce

*Corresponding Author: Chiew Foong Kwong, c.f.kwong@nottingham.edu.cn

energy consumption by predicting the content popularity distribution. In [18], a proactive cache based on the estimation of the content popularity is presented, targeting at increasing the cache hit rate and decreasing the content transmission expenditure. Motivated by deep learning which can improve the accuracy of the content prediction, many works utilise deep learning for proactive caching. In [19], deep learning is utilised to predict the future probability of the content and the predicted content with a high probability will be cached. In [20], a proactive cache policy is proposed based on a deep recurrent neural network model which can predict the future content requests.

Table 1: Summary of existing cache policies.

Policy	Contribution
[11] [12]	LFU and LRU are explained to manage the cache content updating.
[16]	A reinforcement learning-based proactive cache policy is proposed to minimise energy consumption. Here, content popularity is a time-varying variable and only the contents whose lifetime are not expired can be considered to be cached or not.
[17]	An accurate content popularity prediction is adopted to improve the cache hit rate and reduce energy consumption.
[18]	A proactive cache policy is proposed to increase the cache hit rate and decrease the content transmission cost. Here, transfer learning is applied to evaluate the content popularity, and a greedy algorithm is adopted to deal with the cache problem.
[19]	A deep learning algorithm is applied to predict the future probability of the content, and the content with a high predicted probability will be pre-cached.
[20]	A proactive cache policy is proposed to alleviate the data congestion and reduce the average latency, in which a deep recurrent neural network algorithm is adopted to predict future content requests.
[21]	A long-short term memory (LSTM) network is utilised to predict the direction of the moving vehicles, and the proactive cache problem is modeled as MDP and solved by a heuristic ε_n-greedy algorithm.
[22]	A two-layer cache network consisting of several MSBs and SBSs is proposed to improve the cache hit ratio and reduce the average latency. Here, the adjacent SBSs can communicate with each other. Besides, the users with different moving speeds are clustered into different layers, i.e. the MBS or the SBS.
[23]	A cooperative cache framework is proposed to increase the cache hit ratio and reduce access latency. Here, a PPM algorithm is adopted to predict vehicles' probability of arriving in the hot areas.

Besides, in [21], a proactive cache policy for the vehicular network is proposed, where the roadside units (RSUs) are equipped with the cache capability under high mobility of the moving vehicles. There, a long-short term memory (LSTM) network is utilised to predict the direction of the moving vehicles. Then the proactive cache problem is modeled as a Markov decision process (MDP) problem and solved by a heuristic ε_n-greedy algorithm. In [22], Gao *et al*. design a proactive cache scheme for the hierarchical network where each small base station (SBS) can perceive the user mobility of its adjacent small base stations (SBSs), aiming at maximising the cache hit rate and minimising the transmission latency. In specific, the users with different moving speeds are clustered into different layers and the cached content deployment problem is solved by a genetic algorithm. In [23], a cooperative cache framework is introduced to increase the cache hit rate and minimise the access latency, in which the prediction by partial matching (PPM) is utilised to predict the vehicles' probability of arriving at the hot areas. The vehicles with long sojourn time in a hot spot are equipped with cache capability and are regarded as cache nodes. A summary of the aforementioned works is shown in Table 1.

Different from the aforementioned works singly considering the prediction of the content popularity or the users' location, this extended paper designs a proactive cache policy jointly considering the prediction of the user preference and the user location to minimise the average latency and maximise the cache hit rate, which to the best of our knowledge has not been considered in the prior research works. In detail, a practical scenario is considered, in which the BSs are distributed and the users are mobile. A backpropagation (BP) neural network, one of the deep learning methods, is applied to predict the user preference based on the historical content requests. Furthermore, the user's future location is predicted via PPM which has been introduced in our previous work [1], and the user's preferred content is pre-cached at the location in which the user will highly arrive. The main contributions of this paper are as follows:

- This paper focuses on minimising the average latency and maximising the cache hit rate by jointly considering the content popularity prediction and user location prediction.
- The BP neural network is applied to predict the content popularity, and PPM is chosen to predict the user location.
- The effect of the several parameters on the cache performance is investigated, i.e., the Zipf parameter, the content size, the transmission rate, the distance of the backhaul link, and the distance between the user and the BS.

The remainder of this paper is organised as follows. The system model and the problem formulation are shown in section 2. Section 3 introduces the proactive cache policy. We show the simulation results in section 4 and conclude in section 5.

2. System model and problem formulation

In this section, we describe the system model, state the assumption, and formulate the problem.

2.1. System model

For each time slot t whose period is one hour, the proposed proactive cache policy adopts the PPM algorithm to obtain the probability of the user arriving at different locations. The location with the highest value is regarded as the future location. In parallel, the prediction of the user preference is trained via the BP neural network. Once the predicted user preference and the future location are obtained, the popular contents in the user preference are pre-cached at the future location. Consequently, once the user arrives in this location in the next time slot (t+1), the user can immediately obtain the requested content. However, if the prediction is not accurate, the BS needs to retrieve the requested content from the core network and then send it to the users, which imposes a more latency consumption issue.

As shown in Figure 1, the distributed cache architecture consists of the following network equipment (NE): a core network, $\mathcal{M}$ cache-enabled BSs, and $\mathcal{N}$ mobile users. The $\mathfrak{m}^{th}$ BS is denoted by BS_m for $1 < \mathfrak{m} < \mathcal{M}$, the n^{th} user is denoted by U_n for $1 < n < \mathcal{N}$, the circular coverage area of BS_m is denoted as A_m, and the set of the users served by BS_m is denoted as U_m. Let $\mathcal{F}_n=\{\mathfrak{f}_{n1}, \mathfrak{f}_{n2},\ldots, \mathfrak{f}_{n\mathfrak{k}}\}$ denotes the set of $\mathfrak{k}$ contents requested by U_n. The content popularity distribution of a user, *i.e.* user preference, follows Zipf distribution law [24]. The popularity of the $\mathfrak{R}^{th}$ content requested by U_n is characterized as:

$$\mathfrak{p}_n(\mathfrak{R}, \mathfrak{M}, \mathfrak{U}) = \frac{\frac{1}{\mathfrak{R}^{\mathfrak{M}}}}{\sum_1^{\mathfrak{U}} \frac{1}{\mathfrak{U}^{\mathfrak{M}}}}, \quad (1)$$

where $\mathfrak{R}$ is the rank of the content in $\mathcal{F}_n$, $\mathfrak{M}$ is the Zipf parameter for $0< \mathfrak{M}<1$, and $\mathfrak{U}$ is the total number of contents in $\mathcal{F}_n$.

Let $\mathcal{F}_{U_m}$ represents the set of the contents requested at BS_m, $\mathfrak{p}_{U_\mathfrak{m}}$ represents the content popularity at BS_m and $\mathcal{C}=\{1,2,\ldots, \mathcal{H}\}$ represents the library of all the contents requested by $\mathcal{N}$ mobile users served by $\mathcal{M}$ BSs. Assume each BS can store $\mathfrak{k}$ contents at most for $\mathfrak{k}< \mathcal{H}$, and each content has the same size $\mathcal{B}$. Besides, one user only requests one content at most for each time slot *t*.

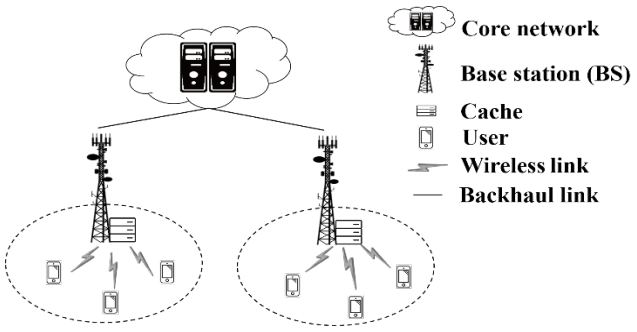


Figure 1: The cache-enabled network.

2.2. Problem formulation

Based on the mention before, our target is to minimise the access latency $\mathfrak{T}$, which is comprised of the transmission latency and propagation latency [25]. The transmission latency is caused by transmitting the content from EN_i to EN_j [26], in which EN_i and EN_j are any two network equipment. According to [27], the transmission rate $\mathbb{R}_{(i,j)}$ is calculated as:

$$\mathbb{R}_{(i,j)}= \mathrm{B}\log_2(1+\frac{\rho\mu}{\sigma^2}), \quad (2)$$

where B (Hz) is the available spectrum bandwidth, ρ is the transmitted power, σ^2 is the noise power and μ is the channel gain between EN_i and EN_j.

Therefore, the transmission latency $\mathfrak{T}_{t_{(i,j)}}^{c}$ based on the size of the requested content c and the transmission rate is derived as:

$$\mathfrak{T}_{t_{(i,j)}}^{c}=\frac{\mathcal{S}}{\mathbb{R}_{(i,j)}}, \quad (3)$$

where $\mathcal{S}$ is the size of requested content c.

The propagation latency $\mathfrak{T}_{p_{(i,j)}}^{c}$ is defined as the time of propagating the requested content c from EN_i to EN_j. Affected by the propagation speed of the electromagnetic wave and the distance between the EN_i and EN_j, the propagation latency $\mathfrak{T}_{p_{(i,j)}}^{c}$ is expressed as:

$$\mathfrak{T}_{p_{(i,j)}}^{c}=\frac{\mathcal{J}_{(i,j)}}{v}, \quad (4)$$

where v is the propagation speed of the electromagnetic wave in the corresponding channel, $\mathcal{J}_{(i,j)}$ is the distance between EN_i and EN_j.

Therefore, the access latency is expressed as:

$$\mathfrak{T} = \mathfrak{T}_{t_{(i,j)}}^{c} + \mathfrak{T}_{p_{(i,j)}}^{c} \quad (5)$$

$$= \frac{\mathcal{S}}{\mathbb{R}_{(i,j))}} + \frac{\mathcal{J}_{(i,j)}}{v}. \quad (6)$$

In detail, the content can be directly retrieved from BS if it is hit at the BS, i.e., the content is cached at the BS. Hence the latency $\mathfrak{T}_{hit}$ of cached content is shown as:

$$\mathfrak{T}_{hit}= \frac{\mathcal{S}}{\mathbb{R}_{(u,b)}} + \frac{\mathcal{J}_{(u,b)}}{v_{hit}}, \quad (7)$$

where $\mathbb{R}_{(u,b)}$ is the transmission rate between a user and a BS, $\mathcal{J}_{(u,b)}$ is the distance between a user and a BS, and v_{hit} is the propagation speed of the electromagnetic wave in the air.

Otherwise, the content needs to be retrieved from the core network via the backhaul links if the content is missed at the BS, i.e., the content is not cached at the BS. According to [28], the transmission rate $\mathbb{R}_{(u,core)}$ from the core network to the BS is shown as

$$\mathbb{R}_{(b,core)}= \mathrm{R}^*, \quad (8)$$

where R^* is the maximal transmission rate of the network.

Therefore, the latency of a missed content $\mathfrak{T}_{missed}$ consisting of the transmission latency $\mathfrak{T}_{t_{(u,core)}}^{c}$ and the propagation latency of a missed content is expressed as:

$$\mathfrak{T}_{t_{(u,core)}}^{c} = \frac{\mathcal{S}}{\mathrm{R}*}+\frac{\mathcal{S}}{\mathbb{R}_{(u,b)}}, \quad (9)$$

$$\mathfrak{T}_{p_{(u,core)}}^{c} = \frac{\mathcal{J}_{(u,b)}}{v_{hit}} + \frac{\mathcal{J}_{(b,core)}}{v_b}, \quad (10)$$

$$\mathfrak{T}_{missed} =\frac{\mathcal{S}}{\mathbb{R}_{(u,b)}} + \frac{\mathcal{S}}{\mathrm{R}*} +\frac{\mathcal{J}_{(u,b)}}{v_{hit}} + \frac{\mathcal{J}_{(b,core)}}{v_b}, \quad (11)$$

where $\mathcal{J}_{(u,b)}$ is the distance between the user and the BS, $\mathcal{J}_{(b,core)}$ is the distance between the BS and the core network, and v_b is the propagation speed of the electromagnetic wave in the backhaul link.

Therefore, the average system latency $\overline{\mathfrak{T}}$ is calculated as:

$$\overline{\mathfrak{T}}=\frac{\sum_1^N[\left(\frac{\mathcal{S}}{\mathbb{R}_{(u,b)}}+\frac{\mathcal{J}_{(u,b)}}{v_{hit}}\right)+(1-\mathcal{Z})(\frac{\mathcal{S}}{\mathrm{R}*}+\frac{\mathcal{J}_{(b,core)}}{v_{bk}})]}{N}, \quad (12)$$

where $\mathcal{Z}$ is the cache hit rate and is calculated as follows:

$$\mathcal{Z} = \frac{\sum_{n=1}^{\mathcal{N}} \sum_{1}^{\mathcal{G}} F(R_{i_{U_n}})}{\sum_{n=1}^{\mathcal{N}} \mathcal{G}}, \quad (13)$$

where $R_{i_{U_n}}$ is the content requests of U_n, $\mathcal{G}$ is the number of request times of $R_{i_{U_n}}$. The $F(R_{i_{U_n}})$ is calculated as

$$F(R_{i_{U_n}}) = \begin{cases} 1, & R_{i_{U_n}} \text{ is cached} \\ 0, & R_{i_{U_n}} \text{ is not ccahed} \end{cases} \quad (14)$$

The problem of minimising the average system latency is modeled as follows

$$\mathbf{P_1}: \min \overline{\mathfrak{T}} \quad (15)$$

$$\text{s.t. } 0 < v_{bk} < v_{hit} \leq 3 \times 10^8 m/s \quad (16)$$

$$0 \leq \mathcal{Z} \leq 1 \quad (17)$$

3. The proactive cache based on the content popularity prediction and future location prediction

In this section, a proactive cache policy is proposed to address **P_1**. Firstly, the user preference is predicted according to the backpropagation (BP) neural network. Besides, we introduce the future location prediction based on the prediction by partial matching (PPM) algorithm. The proposed cache policy minimises the average system latency by pre-caching the predicted popular content at the correspondingly predicted location.

3.1. The content popularity prediction based on backpropagation neural network

User preference is the content probability distribution of individual user and content popularity is the content probability distribution of a cluster of users. Due to the characteristic of the user preference that a small number of contents account for most of the data traffic, the cache policy considers caching the popular content to reduce the complexity of the computation. Hence, the set of the popular contents of U_n is denoted as $\mathbb{P}_{U_n} = \{y_{U_n}^1, y_{U_n}^2, \ldots, y_{U_n}^k\}$, which contains k samples by choosing the top k contents with the highest probability from the user preference. Therefore, the set of the popular contents at BS$_m$ is denoted as $\mathbb{P}_{BSm} = \{\mathbb{P}_1, \mathbb{P}_2, \ldots \mathbb{P}_{U_n} \ldots, \mathbb{P}_{U_m}\}$.

After obtaining the popular content database of BS$_m$, the BP neural network, as shown in Figure 2, is applied to predict the content popularity. The proposed neural network is comprised of three layers, namely the input layer, hidden layer, and output layer. The number of the neuron cells in the input layer and the output layer is equal to the cache storage k. The content requests of U_n are collected each hour and denoted as a training data set. Besides, two continuous training data sets are chosen to optimise the parameter of the neural network. The value y_{in} for the input layer is the request times of the top k popular contents in the former training data set. The value y_{real} is the request times of the top k popular contents in the latter training data set. Furthermore, mean squared error (MSE) is utilised as the loss function in the content prediction. The *MSE* is formulated as

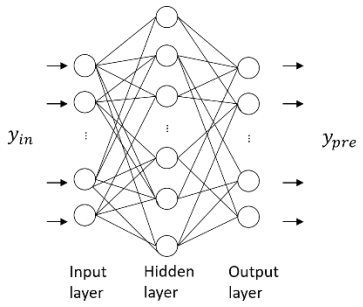
$$\text{MSE} = \frac{\sum_{1}^{k} (y_{real} - y_{pre})^2}{k}, \quad (18)$$

where y_{pre} is the value of the output layer.

Besides, the Relu function is chosen as the activation function, which is expressed as

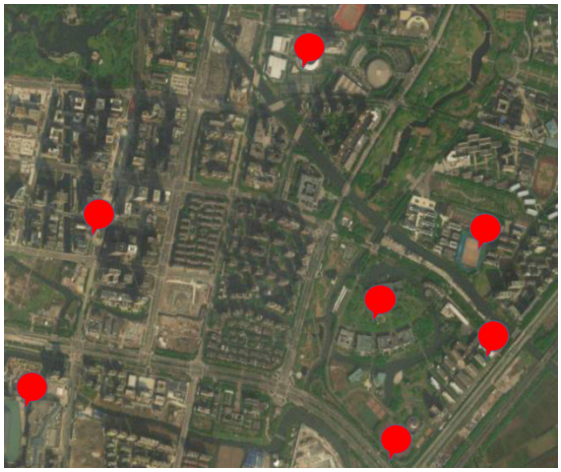
$$Relu(y_{in}) = \begin{cases} 0, & y_{in} < 0 \\ y_{in}, & y_{in} \geq 0 \end{cases}. \quad (19)$$

With the help of stochastic gradient descent (SGD), the proposed neural network can optimally predict the content popularity after enough training.



3.2. The future location prediction based on a prediction by partial matching

Before the location prediction, the historical location information is collected from a real environment model as shown in Figure 3. The areas labeled by red symbols are regarded as the hot spots with long sojourn time. The historical location information sequence is denoted as $\mathcal{L}$ which is related to the hot spots.



After obtaining the historical location information $\mathcal{L}$, PPM is applied to predict the user's future location. PPM is a data compression method based on the finite context and it has been proven effective for the location prediction [23]. The probability of the future location y appearing after the given context *Con* is model as *P(ycon),* where *Con* is the sequence of the location and the length of the sequence is called order [29]. Furthermore, PPM proposes an escape mechanism to deal with the zero-frequency problem [30]. When escape occurs, *i.e. y* is missed after *Con*. Then the PPM outputs an escape probability defined as

Pesc(esc|Con). The computation of PPM is shown in Algorithm 1. Firstly, PPM checks whether *y* appears after *Con*. If *y* appears, PPM records the number of appearing times and outputs the probability $P(y|Con)$, otherwise, PPM outputs the escape probability *Pesc(esc|Con)*. Under the escape situation, PPM restarts to check whether *y* appears after the new *Con* (the order of which is the original order minus 1). The process is finished until *y* appears after *Con* or the order is -1. The predictive probability of the future location is the multiple of the sub-probabilities and the calculation is shown as:

$$P = \prod_1^{step} P_i, \tag{20}$$

$$P_i = \begin{cases} P(y|Con) = \frac{N_y}{N_{esc}+N_{Con}}, \ y\ appears\ after\ Con \\ Pesc(esc|Con) = \frac{N_{esc}}{N_{esc}+N_{Con}}, \ y\ escapes\ after\ Con \end{cases}, \tag{21}$$

where P_i is the probability of step *i*, N_y represents the number of the times of *y* appearing after *Con*, N_{esc} represents the number of the characters appearing after *Con*, and N_{Con} represents the number of the times of all the characters appearing after *Con*.

Once the probabilities of the possible locations are obtained via PPM, these obtained probabilities are ranked in descending order. The location with the highest probability is regarded as the future location.

Algorithm 1 PPM algorithm

Input: historical data $\mathcal{L}$

Output: the probability *P* of the future location *y*

```
Initialize P=0
order = h, j =1
if y appears after Con
    P_j=P(y|Con)
    Process finished
else
    P_j=P(esc|Con)
    h - =1, j + =1
    Restart the step 3-7
The process is finished until y appears after Con or h =-1.
Output j, and P=∏_1^j P_j
```

Here is an example to help understand PPM computation by giving a user path $\{L_1, L_3\}$ and the future location L_4 in the historical data sequence $\mathcal{L}$ ={$L_1, L_2, L_3, L_4, L_5, L_1, L_3, L_1, L_4, L_1, L_2, L_4, L_3, L_4, L_1$}. First, since the sequence{ L_1, L_3, L_4 } cannot be found from the historical data sequence, the escape probability P(esc| L_1, L_3) is outputted based on *Pesc(esc|Con)* in Eq. (21), as shown in Eq. (22). Then the new order is 1 and consequently, the new context is { L_3 }. The new sequence { L_3, L_4 } can be found from the historical date sequence, and therefore the probability P(L_4| L_3) is obtained based the $P(y|Con)$ in Eq. (21), as shown in Eq. (23). Finally, the probability P(L_4| L_1, L_3) is obtained based on Eq. (20), as shown in Eq. (24).

$$\mathrm{P}(\mathrm{esc}|\ L_1, L_3) = \frac{N_{(\mathrm{esc}|\ L1,L3)}}{N_{(\mathrm{esc}|\ L1,L3)}+N_{(L1|\ L1,L3)}} = \frac{1}{1+1} = \frac{1}{2}, \tag{22}$$

where $N_{(\mathrm{esc}|\ L1,L3)}$ is the number of the characters appearing after $\{L_1, L_3\}$, and $N_{(L1|\ L1,L3)}$ is the number of the times of all the characters appearing after $\{L_1, L_3\}$ since only L_1 appears after $\{L_1, L_3\}$.

$$\mathrm{P}(L_4|\ L_3) = \frac{N_{(L4|\ L3)}}{N_{(\mathrm{esc}|\ L3)}+N_{(L4|\ L3)}+N_{(L1|\ L3)}} = \frac{2}{2+2+1} = \frac{2}{5}, \tag{23}$$

where $N_{(L4|\ L3)}$ is the number of L_4 appearing after L_3, $N_{(\mathrm{esc}|\ L3)}$ is the number of the characters appearing after L_3 and $N_{(L1|\ L3)}$ is the number of L_1 appearing after L_3. The sum of $N_{(L4|\ L3)}$ and $N_{(L1|\ L3)}$ is called the number of the times of all the characters appearing after L_3.

$$P(L4|L1, L3) = P(esc|L1,L3) \times P(L4|L3) = \frac{1}{2} \times \frac{2}{5} = \frac{1}{5}, \tag{24}$$

3.3. The pre-deployment of the popular content at the future location

In each time slot *t*, the users' future locations in which users will highly arrive at the next time slot *t+1* are predicted via PPM. In parallel, the user preference at *t+1* is predicted via BP neural network. The top *w* contents with the highest number of request times are regarded as the popular contents in the future. After that, these popular contents are pre-deployed at the corresponding future location. Hence, in the next time slot *t+1*, if the prediction is correct, users can immediately obtain their preferred contents, which extremely reduces the average system latency.

4. Simulation results and analyzation

In this section, we consider a distributed BS caching network which consists of 10 BS, 30 users, and 6 locations. The number of content requests of each user is 3000. The comprehensive simulation shows the performance of our proposed policy, LFU, and LRU in terms of the average latency and cache hit rate. The specific parameter settings are shown in Table 2. The program is modeled via PyTorch language in Pycharm software.To further show the improvement of our proposed policy in terms of the cache hit rate and the reduction of our proposed policy in terms of the cache hit rate compared with LFU and LRU policies, we propose the growth ratio $\mathcal{P}_G$ and the reduction ratio $\mathcal{P}_R$, which are expressed as:

$$\mathcal{P}_G = \frac{\mathcal{C}_{our} - \mathcal{C}_{existing}}{\mathcal{C}_{existing}}, \tag{25}$$

$$\mathcal{P}_R = \frac{\overline{\mathfrak{T}}_{existing} - \overline{\mathfrak{T}}_{our}}{\overline{\mathfrak{T}}_{existing}}, \tag{26}$$

where $\mathcal{C}_{our}$ and $\mathcal{C}_{existing}$ is the cache hit rate of our proposed policy and any one of the LFU and LRU policies, respectively. $\overline{\mathfrak{T}}_{our}$ and $\overline{\mathfrak{T}}_{existing}$ is the average latency of our proposed policy and any one of the LFU and LRU policies, respectively.

Table 2: The simulation parameter settings

symbol	value

v_{bk}	1×10^7 m/s
v_{hit}	3×10^8 m/s
$\mathbb{R}_{(i,j)}$	10~50 Mbps
σ^2	1W
ρ	3W
$\mathcal{J}_{(u,b)}$	10~50km
$\mathcal{J}_{(bs,core)}$	100km
$\mathcal{B}$	30Kb~450Kb
$\mathfrak{M}$	1.1~1.8
$\mathcal{Q}$	1%~10%
δ	2%~10%

Figure 4 reveals the cache hit rate (represented in percentage) of our proactive policy and the conventional reactive policies, *i.e.,* LFU and LRU. The number of the total content requests is 6000, the Zipf parameter of each user varies between 1.7 and 1.8. Besides, to demonstrate the effect of the cache capacity on the cache performance, we introduce the cache capacity ratio $\delta = \frac{\mathcal{h}}{\mathcal{H}}$. And in this simulation, we assume δ= 2%, 4%, 6%, 8% and 10%. Horizontally, the cache hit rates of LFU, LRU, and our proposed policy increase with the larger cache capacity ratio. The tendency demonstrates that increasing the cache capacity can improve the cache hit rate since more popular contents can be cached. We also notice that our proactive policy has the highest cache hit rate, which is around 10-25% higher than that of LFU and LRU policies, no matter how the Zipf parameter varies. Therefore, our proposed policy outperforms the other two policies.

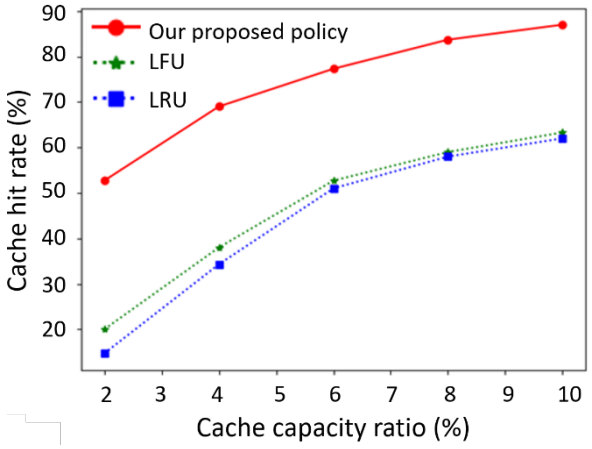


Figure 4: The cache hit rate vs. cache capacity ratio $\delta = \frac{\mathcal{Q}}{\mathcal{H}}$.

Figure 5 investigates the effect of the Zipf parameter $\mathfrak{M}$ on the cache hit rate of our proposed policy with the other two policies as mentioned before. We assume δ is 10%, and the Zipf parameter of each user varies in the range [1.1, 1.2], [1.2, 1.3], [1.3, 1.4], [1.4, 1.5], [1.5, 1.6], [1.6, 1.7] and [1.7, 1.8]. As the Zipf parameter grows, the cache hit rates of all the cache policies increase. The reason is that fewer contents are taking up more content requests as the Zipf parameter grows, and hence the popular content becomes more popular. Considering the fixed number of the total content request, the number of content reduces. With the same capacity, the cache has a higher chance to store more contents and the cached contents are more popular, which contributes to a higher cache hit rate. Furthermore, the slopes of the three curves are gradually reduced. The reason is with the larger Zipf parameter, the newly cached popular contents have fewer content requests compared with the initially cached contents. We also notice that the two reactive policies have a relatively close cache hit rate, and the cache hit rate of our proposed policy is around 24%-38% higher than that of the two reactive policies.

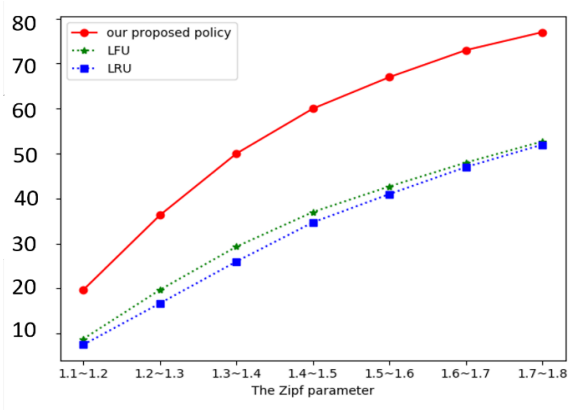


Figure 5: The cache hit rate vs. the Zipf parameter.

The relation between the average latency and the size of the content is displayed in Figure 6. Here, the size of the content is 30Kb, 200Kb, 200Kb, 250Kb, 300Kb, 350Kb, and 450Kb, respectively. Besides, we set the cache capacity ratio δ is 10% and the fluctuation of the Zipf parameter is between 1.7 and 1.8, the distance between the user and the BS is 10km and the distance of the backhaul link is 100km. As the size of the content grows, the average latencies of all the policies increase. The reason is the transmitter consumes more time to send the content into the channel as the size of the content grows. Vertically, the average latency obtained by our proposed policy is around 60% reduced compared with LFU and LRU regardless of the size of the content, which implies our proposed policy outperforms the two reactive policies.

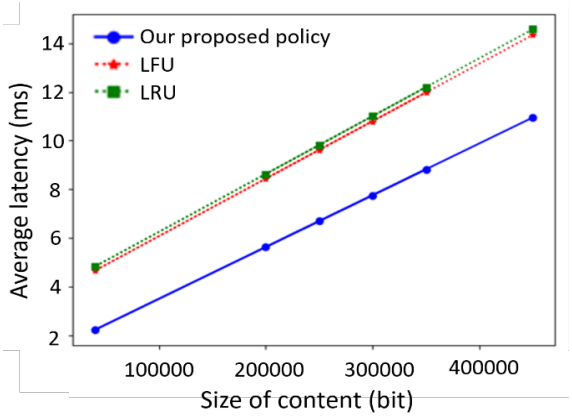


Figure 6: The average latency vs. the size of the content.

Figure 7 shows the relationship between the average latency and the transmission rate between the user and BS. Here, the content size is 400Kb, the storage capacity ratio is 10%, the distance between the user and the BS is 10km and the distance of the backhaul link is 100km. The transmission rate between user and BS is 10Mbps, 20Mbps, 30Mbps, 40Mbps, and 50Mbps, respectively. As the transmission rate between user and BS grows,

the average latencies of all the policies reduce. The reason is that, with the larger transmission rate, the latency between the user and the BS is reduced. Also, the average latency of our proposed policy is 31%-64% reduced compared with the other two policies.

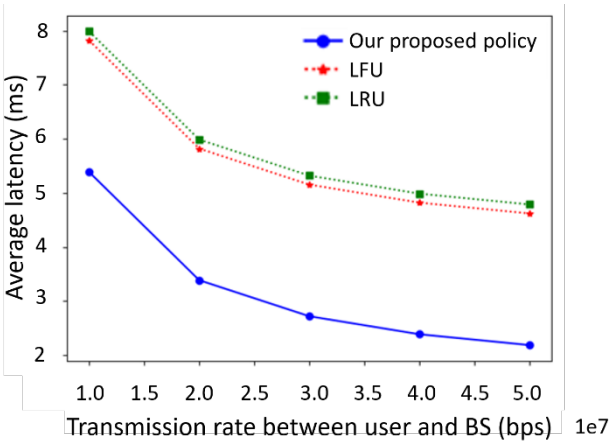


Figure 7: The average latency vs. transmission rate between the user and the BS.

As shown in Figure 8, the average latency is plotted as a function of the Zipf parameter. Here, the Zipf parameter of each user varies in the range [1.1, 1.2], [1.2, 1.3], [1.3, 1.4], [1.4, 1.5], [1.5, 1.6], [1.6, 1.7] and [1.7, 1.8], respectively. Besides, the transmission rate between the user and the BS is 50Mbps, the content size is 400Kb, the storage capacity ratio δ is 10%, the distance between the user and the BS is 10km and the distance of the backhaul link is 100km. As the Zipf parameter increase, the average latencies of three policies are reduced. The reason is that, with the increase of the Zipf parameter, more contents are cached locally, and hence fewer contents need to be retrieved from the remote core network. And the latency from the BS is lower than from the core network. Also, as the Zipf parameter grows, the slopes of the three curves gradually decrease. The tendency is caused since the newly cached contents are less popular than the initially cached contents. Furthermore, our proposed policy is around 14%-53% reduced in terms of the average latency compared with the two reactive policies.

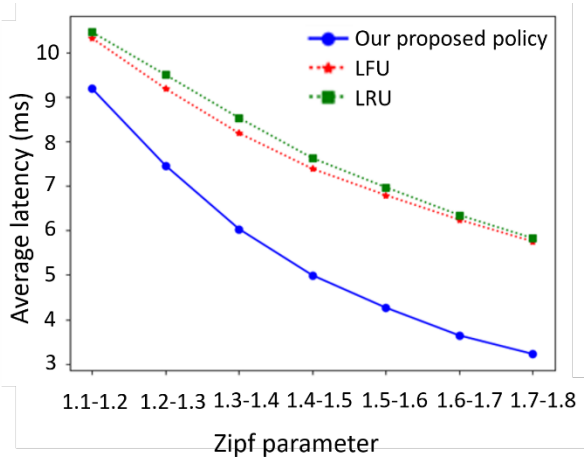


Figure 8: The average latency vs. Zipf parameter.

The effect of the cache capacity ratio δ on the average latency is shown in Figure 9. In this simulation, we assume δ= 2%, 4%, 6%, 8% and 10%. Besides, the content size is 400Kb, the transmission rate is 50Mbps, the distance between the user and the BS is 10km and the distance of the backhaul link is 100km. The cache capacity ratio δ is varied from 2% to 10%. It can be noticed that the average latencies of three policies decrease with the increment of the cache capacity ratio. The fact is that a larger cache capacity means more contents can be cached. As a result, more long-distance propagation time consumption from the core network to the BS can be avoided. Also, the average latency of our proposed policy is around 35%-55% reduced compared with the LFU and LRU.

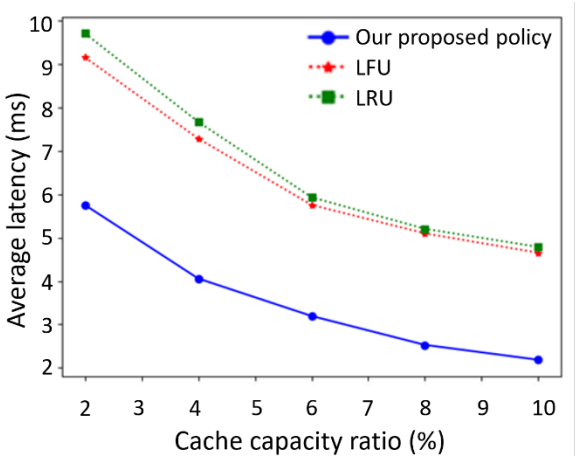


Figure 9: The average latency vs. cache capacity ratio.

5. Conclusion

In this paper, a proactive cache policy is proposed in a distributed manner to minimise the average latency, as well as maximising the cache hit rate. An accurate prediction is achieved to make sure the proactive cache policy can have a high cache performance. In specific, a BP neural network is applied to predict the content popularity, and a PPM algorithm is applied to predict the user location. The simulation results (Fig.4 and Fig.5 simulations) reveal our proposed cache policy is around 10%-38% improved in terms of the cache hit rate no matter how the cache capacity and Zipf parameter vary, compared with LFU and LRU policies. As for the average latency, our proposed policy has at least 14% decrease no matter how parameters change, i.e., the variation of the content size (Fig.6 simulation), the transmission rate between the user and BS (Fig.7 simulation), the Zipf parameter (Fig.8 simulation) and the cache capacity (Fig.9 simulation). Consequently, our proposed policy outperforms LFU and LRU policies.

References

[1] L. Li, C.F. Kwong, F. Chen, Q. Liu, J. Wang, 'Predicting future location in mobile cache based on variable order of prediction-by-partial-matching algorithm', in IET Conference Publications, 4–4, 2018, doi:10.1049/cp.2018.1729.

[2] E. Bastug, M. Bennis, E. Zeydan, M.A. Kader, I.A. Karatepe, A.S. Er, M. Debbah, 'Big data meets telcos: A proactive caching perspective', Journal of Communications and Networks, **17**(6), 549–557, 2015, doi:10.1109/JCN.2015.000102.

[3] Cisco, 'Cisco Annual Internet Report (2018–2023)', Cisco, 1–41, 2020.

[4] R. Wang, X. Peng, J. Zhang, K.B. Letaief, 'Mobility-aware caching for content-centric wireless networks: Modeling and methodology', IEEE Communications Magazine, **54**(8), 77–83, 2016, doi:10.1109/MCOM.2016.7537180.

[5] Y. Mao, C. You, J. Zhang, K. Huang, K.B. Letaief, 'A Survey on Mobile Edge Computing: The Communication Perspective', IEEE Communications Surveys and Tutorials, **19**(4), 2322–2358, 2017, doi:10.1109/COMST.2017.2745201.

[6] F.M. Modesto, A. Boukerche, 'An analysis of caching in information-centric vehicular networks', IEEE International Conference on Communications, 2017, doi:10.1109/ICC.2017.7997019.

[7] Y. Li, C. Zhong, M.C. Gursoy, S. Velipasalar, 'Learning-based delay-aware caching in wireless D2D caching networks', IEEE Access, **6**, 77250–77264, 2018, doi:10.1109/ACCESS.2018.2881038.

[8] S. Zhang, N. Zhang, P. Yang, X. Shen, 'Cost-Effective Cache Deployment in Mobile Heterogeneous Networks', IEEE Transactions on Vehicular Technology, **66**(12), 12264–12276, 2017, doi:10.1109/TVT2017.2724547.

[9] Z. Luo, M. LiWang, Z. Lin, L. Huang, X. Du, M. Guizani, 'Energy-Efficient Caching for Mobile Edge Computing in 5G Networks', Applied Sciences, **7**(6), 557, 2017, doi:10.3390/app7060557.

[10] S. Wang, X. Zhang, Y. Zhang, L. Wang, J. Yang, W. Wang, 'A Survey on Mobile Edge Networks: Convergence of Computing, Caching and Communications', IEEE Access, **5**, 6757–6779, 2017, doi:10.1109/ACCESS.2017.2685434.

[11] H. Ahlehagh, S. Dey, 'Video-aware scheduling and caching in the radio access network', IEEE/ACM Transactions on Networking, **22**(5), 1444–1462, 2014, doi:10.1109/TNET.2013.2294111.

[12] S. Shukla, O. Bhardwaj, A.A. Abouzeid, T. Salonidis, T. He, 'Proactive Retention-Aware Caching with Multi-Path Routing for Wireless Edge Networks', IEEE Journal on Selected Areas in Communications, **36**(6), 1286–1299, 2018, doi:10.1109/JSAC.2018.2844999.

[13] Y. Jiang, M. Ma, M. Bennis, F.C. Zheng, X. You, 'User preference learning-based edge caching for fog radio access network', IEEE Transactions on Communications, **67**(2), 1268–1283, 2019, doi:10.1109/TCOMM.2018.2880482.

[14] N. Golrezaei, A. Molisch, A.G. Dimakis, G. Caire, 'Femtocaching and device-to-device collaboration: A new architecture for wireless video distribution', IEEE Communications Magazine, **51**(4), 142–149, 2013, doi:10.1109/MCOM.2013.6495773.

[15] E. Bastug, M. Bennis, M. Debbah, 'Living on the edge: The role of proactive caching in 5G wireless networks', IEEE Communications Magazine, **52**(8), 82–89, 2014, doi:10.1109/MCOM.2014.6871674.

[16] S.O. Somuyiwa, A. Gyorgy, D. Gunduz, 'A Reinforcement-Learning Approach to Proactive Caching in Wireless Networks', IEEE Journal on Selected Areas in Communications, **36**(6), 1331–1344, 2018, doi:10.1109/JSAC.2018.2844985.

[17] M. Yan, C.A. Chan, W. Li, L. Lei, Q. Shuai, A.F. Gygax, I. Chih-Lin, 'Assessing the energy consumption of 5G wireless edge caching', 2019 IEEE International Conference on Communications Workshops, ICC Workshops 2019 - Proceedings, **7**, 2019, doi:10.1109/ICCW.2019.8756642.

[18] T. Hou, G. Feng, S. Qin, W. Jiang, 'Proactive Content Caching by Exploiting Transfer Learning for Mobile Edge Computing', GLOBECOM 2017 - 2017 IEEE Global Communications Conference, 1–6, 2017, doi:10.1109/GLOCOM.2017.8254636.

[19] K. Thar, N.H. Tran, T.Z. Oo, C.S. Hong, 'DeepMEC: Mobile edge caching using deep learning', IEEE Access, **6**, 78260–78275, 2018, doi:10.1109/ACCESS.2018.2884913.

[20] L. Ale, N. Zhang, H. Wu, D. Chen, T. Han, 'Online proactive caching in mobile edge computing using bidirectional deep recurrent neural network', IEEE Internet of Things Journal, **6**(3), 5520–5530, 2019, doi:10.1109/JIOT.2019.2903245.

[21] L. Hou, L. Lei, K. Zheng, X. Wang, 'A Q -Learning-Based Proactive Caching Strategy for Non-Safety Related Services in Vehicular Networks', IEEE Internet of Things Journal, **6**(3), 4512–4520, 2019, doi:10.1109/JIOT.2018.2883762.

[22] N. Gao, X. Xu, Y. Hou, L. Gao, 'A Mobility-aware Proactive Caching Strategy in Heterogeneous Ultra-Dense Networks', IEEE International Symposium on Personal, Indoor and Mobile Radio Communications, PIMRC, **2019**–**Septe**, 2019, doi:10.1109/PIMRC.2019.8904364.

[23] L. Yao, A. Chen, J. Deng, J. Wang, G. Wu, 'A Cooperative Caching Scheme Based on Mobility Prediction in Vehicular Content Centric Networks', IEEE Transactions on Vehicular Technology, **9545**(c), 1–10, 2017, doi:10.1109/TVT.2017.2784562.

[24] D. Liu, C. Yang, 'Caching at Base Stations with Heterogeneous User Demands and Spatial Locality', IEEE Transactions on Communications, **67**(2), 1554–1569, 2019, doi:10.1109/TCOMM.2018.2876424.

[25] F. Jiang, Z. Yuan, C. Sun, J. Wang, 'Deep Q-Learning-Based Content Caching With Update Strategy for Fog Radio Access Networks', IEEE Access, **7,** 97505–97514, 2019, doi:10.1109/access.2019.2927836.

[26] Y. Li, M.C. Gursoy, S. Velipasalar, 'A delay-aware caching algorithm for wireless D2D caching networks', 2017 IEEE Conference on Computer Communications Workshops, INFOCOM WKSHPS 2017, 456–461, 2017, doi:10.1109/INFCOMW.2017.8116419.

[27] H. Wu, J. Zhang, Z. Cai, F. Liu, Y. Li, A. Liu, 'Towards Energy-Aware Caching for Intelligent Connected Vehicles', IEEE Internet of Things Journal, **4662**(c), 1–1, 2020, doi:10.1109/jiot.2020.2980954.

[28] J. Zhang, X. Hu, Z. Ning, E.C.H. Ngai, L. Zhou, J. Wei, J. Cheng, B. Hu, V.C.M. Leung, Joint resource allocation for latency−sensitive services over mobile edge computing networks with caching, **6**(3), 4283−4294, doi:10.1109/JIOT.2018.2875917.

[29] I. Burbey, T.L. Martin, 'Predicting future locations using prediction-by-partial-match', Proceedings of the First ACM International Workshop on Mobile Entity Localization and Tracking in GPS-Less Environments - MELT '08, 1, 2008, doi:10.1145/1410012.1410014.

[30] S.K. Pulliyakode, S. Kalyani, 'A Modified PPM Algorithm for Online Sequence Prediction Using Short Data Records', IEEE Communications Letters, **19**(3), 423–426, 2015, doi:10.1109/LCOMM.2014.2385088.

ASTES

Advances in Science, Technology and Engineering Systems Journal
Vol. 5, No. 5, 1162-1171 (2020)
www.astesj.com
Special Issue on Multidisciplinary Innovation in Engineering Science & Technology

ASTES Journal
ISSN: 2415-6698

Improvised E-Rickshaws for Indian Roads by Effective Battery-Ultracapacitor Hybridization

Shimin Vayal Veetil[*,1], Varsha Shah[1], Makarand Lokhande[2]

[1]*Department of Electrical Engineering, Sardar Vallabhbhai National Institute of Technology, Surat, 395007, India*

[2]*Department of Electrical Engineering, Visvesvaraya National Institute of Technology, Nagpur, 440010, India*

ARTICLE INFO

Article history:
Received: 23 July, 2020
Accepted: 28 September, 2020
Online: 22 October, 2020

Keywords:
Battery-Ultracapacitor
Electric Vehicles
Energy Management
Fuzzy Logic
Regenerative Braking

ABSTRACT

The revolution in the electrification of conventional vehicles due to increased petroleum prices and environmental concerns has had its impact on three-wheeler vehicles as well. Motorized three-wheeled vehicles, known as Auto-rickshaws, are a standard mode of transportation in India. Existing battery operated electric rickshaws (known as E-rickshaws) available in major cities of India faces challenges like insufficient charging facility, low driving range, high battery cost, battery replacement/disposal, etc. A battery-ultracapacitor (UC) hybrid energy source is proposed in this paper to overcome these issues. Two energy sources of complementary characteristics, when operated in tandem, can enhance the overall performance of a vehicle in terms of weight, volume, and efficiency. An Erickshaw with battery-UC hybrid energy sources is modeled in Matlab-Simulink in this paper. The vehicle dynamics are calculated real-time based using a GPS based PerformanceBox tool of VBOX motorsport for Surat city. A fuzzy logic-based approach was employed for efficient energy management between these two sources with efficient utilization of regenerative power generated while braking. The system was later tested on Real-Time Hardware-in-Loop (HIL) environment to validate the simulation results. It was observed that the addition of an additional source with complementary characteristics had enhanced the performance of vehicle operation.

1 Introduction

India, holding the second largest population in the world [1], is also home to some of the most polluted cities across the globe [2]. Fourteen of the twenty most polluted cities in the world are in India according to a recent study based on $PM_{2.5}$ particulate matter [3]. A major contributor towards pollution in these cities are emissions from motorized vehicles [4]. The rise in air pollution has escalated the research towards improving air quality across the country. Also incompetent petroleum resources which kept the growth of economy in check for the past few decades have raised the necessity to identify alternate fuel propelled vehicles for transportation. Transportation electrification was hence identified as a potential breakthrough to answer all these concerns faced by the country in the present decade and for future.

Three wheeled motorized vehicles called as Auto-rickshaws, capable of carrying three to four passengers plays a vital role in public transportation in India along with trains and buses. Unlike the other two, auto-rickshaws are preferred for shorter traveling distances (preferably inside cities) due to its compact size. A Tier-I city (with more than 4 million population) accommodates more than 50,000 auto-rickshaws [5] in India. That can account to 4-5% or sometimes even high as 10% of total vehicle population of a city. These vehicles can be a considerable source of air pollutants and is also a major customer of petroleum resources [6]. Electrification of auto-rickshaws can thereby lead to a better and cleaner mode of urban public transportation and can also urge the public to opt for them due to the improvisations in comfort, safety and cost to travel [7].

Battery operated electric vehicles are gaining public and industry interest in the past couple of decades [8]. A battery operated auto-rickshaw (termed as E-rickshaw) was first introduced in the streets of New Delhi in 2010. Many researches on implementation of E-rickshaws/vehicles in different states and cities across the country and their economical and environmental impacts are available in literature. The technical and commercial issues hindering the

[*]Corresponding Author: Shimin Vayal Veetil, Department of Electrical Engineering, S. V. National Institute of Technology, Surat, 395007, India, +91 83477 68150 & ds14el004@eed.svnit.ac.in

popularity of electric vehicles in Pune was discussed in [9]. The merits, demerits and the challenges faced by adopting E-rickshaw as a possible mode for public transportation in the roads of West Bengal was discussed in [10]. A 24% fuel economy with hybridization and optimization was observed by [11] in their study on parallel electric hybrid E-rickshaws. A compact, robust and affordable hybrid system was developed and tested on a Bajaj RE auto-rickshaw by [12] and identified that the fuel consumption and CO_2 emissions was significantly reduced by 21%.

There are many techno-commercial areas for improvisation in the design and development of E-rickshaws in India. Driving range is a major issue faced by e-rickshaws [13] along with waste management of used battery [14]. Another concern is method of power generation for charging batteries employed in E-rickshaws. One major aspect is the use of renewable energy for charging of the vehicle batteries which will lead to complete zero emissions [15]. Using conventional energy sources for electricity generation may result in zero tail-pipe emissions but will have less to no impact in global control of air pollution. Many literature is available on bonding renewable sources with electric vehicles. Incorporating solar energy as one of the energy source for electric vehicles and their economic impacts were studied in [16] and [17]. A correlative analysis study of a solar assisted three-wheeled rickshaw with various drive trains of hybrid configurations was carried out in [18]. A fuel cell based E-rickshaw which employs a fuzzy logic controller was proposed in [19]. In [20], a control scheme for solar rickshaw with maximum power point tracking algorithm (MPPT) was designed.

A rigorous review on various electrical energy storage technologies compatible for vehicular applications was carried out in [21] and [22]. The battery technologies available for electric vehicles including Li-ion batteries, lead acid batteries, Ni-MH batteries and ultracapacitors are discussed in [14]of which lithium-ion battery yields the lowest operating costs and GHG emissions (compared to lead-acid batteries). The research on lead-acid batteries, Li-ion batteries and ultracapacitor are gaining considerable significance in India as well [23]. Applications of different energy sources in Indian context was studied in [24]. Hybridization of energy sources with complementary characteristics to improve performance of electric vehicles [25] is attracting considerable interest these days. Hybridization of energy sources to achieve improved performance is been practiced in various applications [26, 27]. Hybridization enhances the performance of each sources involved, but with introducing complexity in its control. A study on possible methods for coupling a battery with an ultracapacitor for enhanced performance in electric vehicles was carried out in [28]. A study on different energy sources available for electric vehicles, their hybridization and energy management strategies was carried out in [29]. Performance improvement of a mild hybrid vehicle by hybridization of battery with ultracapacitor was suggested in [30].

Energy management between the hybrid sources employed in an electric vehicle calls for special care for ensuring optimum performance of both. The different control strategies viz. Rule based control strategy, Fuzzy rule based control strategy, Linear programming, Dynamic programming, Stochastic control strategy, Genetic algorithm, Particle swarm optimisation etc., for power split in a hybrid electric vehicle was discussed in [31]. A model predictive control strategy for sharing of power between a battery and ultracapacitor for a plug-in hybrid electric vehicle (PHEV) was proposed in [32] and has achieved significant improvement in performance. A data fusion approach for energy management in a fuel cell hybrid electric vehicle was proposed in [33]. The energy management strategy for a Fuel cell/Battery/Ultracapacitor hybrid electric vehicle is achieved by implementing an intelligent control technique constructed based on Fuzzy Logic Control (FLC) in [27]. A Fuzzy logic based energy management for a parallel hybrid electric vehicle was proposed by [34] considering torque demand and battery SOC as its inputs.

Presently, there is little to no work carried out in hybridization of energy sources in E-rickshaws in India which is the motivation for this work. In this paper the vehicle dynamics of an E-rickshaw is modeled in Matlab-Simulink for a standard Indian City Driving Cycle (IDC) which was calculated using a GPS based PerformanceBox tool of VBOX motorsport for Surat city. The system was later tested on a Real-time simulation environment to validate the results. The paper is divided into following sections. In section 2, the vehicle dynamics of an E-rickshaw is modeled to calculate the total tractive force. System architecture of an E-rickshaw is carried out in section 3 for a standard Indian City Driving Cycle (IDC). In section 4, the energy management between battery and ultracapacitor using a fuzzy logic based approach was discussed and the vehicle was tested for different driving conditions. The Matlab-Simulink simulation results are discussed in section 5 followed by a brief discussion on validation of the system implementation in Real-time environment in section 6. The paper concludes with discussions and conclusion in section 7.

2 Vehicle Dynamics of an E-rickshaw

The structure of a conventional auto-rickshaw is shown in Figure 2. The specifications of the auto-rickshaw is shown in Table 1 [12] whose parameters are taken as reference to design the E-rickshaw power-train.

Table 1: Specifications of Conventional Auto-rickshaw (Model: Bajaj RE 2S Petrol

Specifications	Values
Gross vehicle weight, M	610 Kg
Kerb weight	272 Kg
Tyres, r_w	4.00-8, 4PR
Roll resistance, C_r	0.015
Air drag coefficient, C_d	0.44
Frontal surface area, A_f	2.0 m^2

Load power requirement is calculated based on the drive cycle and vehicle dynamics. Energy source sizing is carried out based on this power requirement.

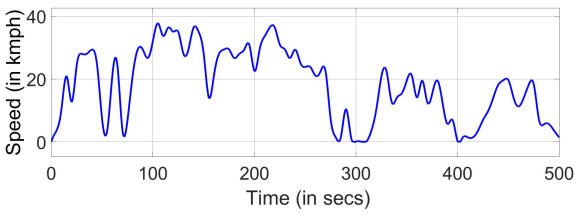


Figure 1: Indian City Drive Cycle (IDC) for Surat City

The drive cycle was calculated using a GPS based Performance-Box tool of VBOX motorsport for Surat city and is chosen because the E-rickshaw is desired to be operated in cities. The load power requirement was calculated for the calculated standard Indian city driving cycle shown in Figure 1. Battery and ultracapacitor was sized based on this power requirements. Modeling of vehicle dynamics is explained in detail in the following sections.

2.1 Total Tractive force

The forces acting on a vehicle needs to be understood for an effective modeling of vehicle dynamics. The forces acting on an auto-rickshaw while hill climbing is shown in Figure 2. The tractive force generated by the electric motor of the vehicle has to experience and overcome these forces namely (a) Rolling resistance force (b) Aerodynamic drag (c) Grade resistance force and (d) Acceleration force [35].

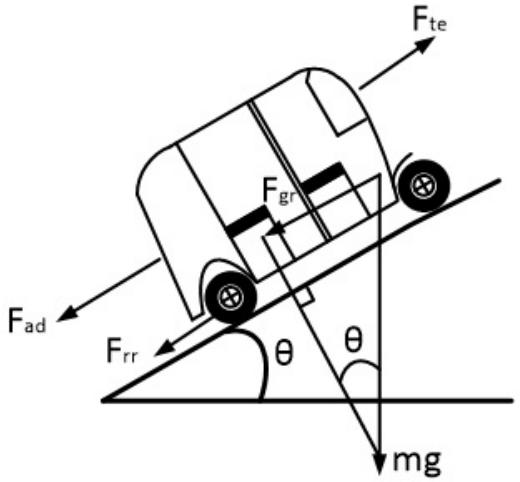


Figure 2: Forces acting on an auto-rickshaw moving along a slope

The major forces acting on an E-rickshaw and their expressions are shown in Table 2. Here, M is the mass of the vehicle in kg, g is the gravitational constant, i.e., 9.81 m/s^2, C_r is the coefficient of rolling resistance, ρ is the air density in kg/m^3, A is the frontal area of vehicle in m^2, C_d is the drag coefficient, v is the velocity of the vehicle in m/s, θ is the clockwise angle made by the slope of the road with the horizontal plain and a is the acceleration of the vehicle in m/s^2.

The total tractive force is the force required to propel the vehicle forward by overcoming all the above mentioned forces acting on the vehicle. Neglecting all other forces acting directly or indirectly on the vehicle, the total tractive force can be obtained from the Eq 1

$$F_{te} = F_{rr} + F_{ad} + F_{gr} + F_{af} \quad (1)$$

3 E-rickshaw System Architecture

The sizing of every components like energy source,electric motor, power electronic converters etc., of an E-rickshaw depends on the vehicle parameters and driving patterns. The total tractive force required by the vehicle for propulsion was calculated using Eq 1. System parameters like mass of the vehicle, frontal area etc., is available from Table 1. Vehicle velocity and acceleration is obtained from drive cycle data. Required load power is calculated as the product of total tractive force and velocity. The energy flow in a conventional electric-rickshaw is as shown in Figure 3. The vehicle dynamics of an auto-rickshaw is modeled in Matlab-Simulink environment.

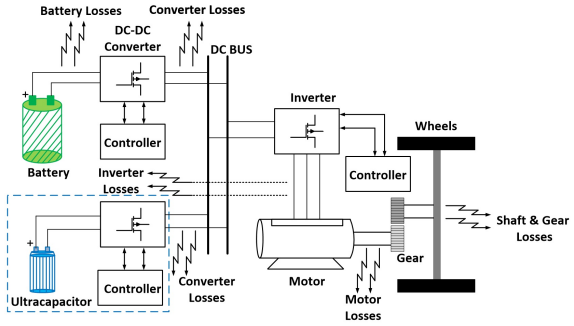


Figure 3: Energy flow diagram of an E-rickshaw with losses

The E-rickshaw is designed for the Indian City Drive Cycle (IDC) as shown in Figure 1 measured for a total time of 500 secs. The vehicle, being operated in the cities are desired to be run at a speed not more than 40 kmph due to the frequent starts and stops in traffic. The peak velocity is observed to be nearer at 38 kmph.

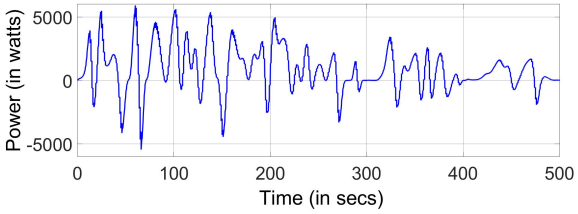


Figure 4: Load Power Requirement for Indian Drive Cycle (IDC)

The load power requirement for Indian City Drive Cycle (IDC) is shown in Figure 4. The peak power requirement was found to be approximately 5.0 kW. Considering the losses at each stages of transmission of power (source, converter and inverter), the required power to be provided by the E-rickshaw energy source was calculated. Assuming a constant source voltage of 48V (most of the E-rickshaws in India are operated with 48V Lead acid battery), the source current is calculated and is shown in Figure 5.

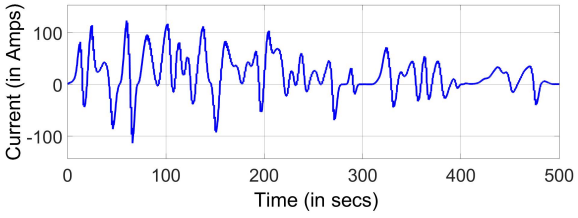


Figure 5: Source current for IDC

The proposed E-rickshaw is expected to have a driving range of 75 kms and the total distance travelled a day is expected to be 150 kms, there by calling for twice charging a day. The normal charging period is 2.5-3 hours. Figure 6 (a) shows the average speed at which E-rickshaw commutes inside a city. The vehicle covers a total distance of 2.548 kms at the end of 500 secs (Figure 6 (b)) at an average speed of 18.3 kmph.

Table 2: Forces Acting on an E-rickshaw

Force	Definition	Expression
Rolling Resistance force, F_{rr}	The force experienced by the vehicle due to friction between the tyres and the running surface.	C_r.M.g
Aerodynamic drag, F_{ad}	The force experienced by the vehicle due to friction with the surrounding air.	$\frac{1}{2}.\rho.\text{A}.C_d.V^2$
Grade Resistance force, F_{gr}	The force required to drive the vehicle upward on a slope.	M.g.Sinθ
Acceleration force, F_{af}	The force which is needed to accelerate the vehicle for different running velocities.	M.a

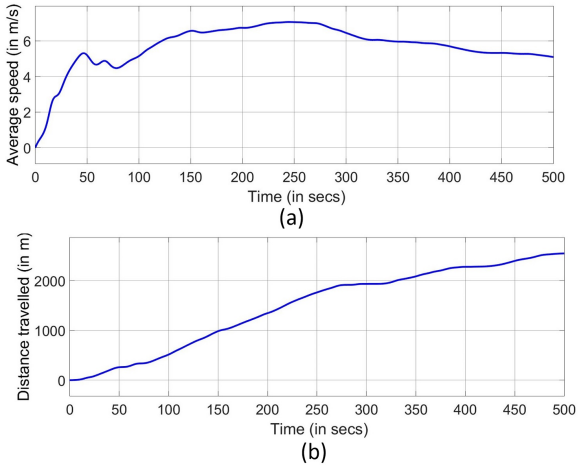


Figure 6: (a) Average Speed of an E-rickshaw (b) Total Distance travelled at the end of 500 secs

4 Fuzzy Logic based Energy Management

A fuzzy logic based approach for energy management was adopted in this paper due to its adaptive nature to the non-linear environment of electric vehicles. The source current shown in Figure 5, the battery and ultracapacitor state of charge (SOC) are taken as reference to split the energy requirement between battery and ultracapacitor for propelling the E-rickshaw as shown in Figure 7.

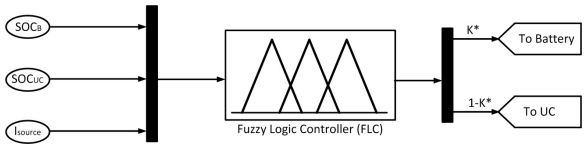


Figure 7: Fuzzy Logic controller

The three fundamental rules adopted for ensuring an optimum energy management was;

- Battery will be providing the average power requirements (cruising).
- Ultracapacitor will be providing the peak power requirements (accelerating).
- Ultracapacitor will be absorbing the generated braking power which shall be followed by battery, if necessary (regenerative braking).

Battery, being a high energy density device is designed to provide the average power requirement and ultracapacitor is designed to provide the peak power requirement as it is a high power density device and can charge/discharge at a higher rate. The battery is designed not to discharge at more than 2C rate where C-rate is the rate at which a battery is discharged with respect to its maximum capacity. Based on the power requirements, the battery and ultracapacitor ratings are chosen as shown in Table 3

Table 3: Ratings of Battery and Ultracapacitor

Function	Battery	UC
Type	Li-ion	Maxwell
Rating	48V, 20 AH	48V, 165F
Cell Specification	3.7 V	2.7 V
Cell Combination	13-series	18-series
Stored Energy	960 Wh	53 Wh
Absolute Maximum Current	60 A	1900 A
Weight	8 KG	14.2 KG
Charge temperature	-40 to 65°C	0 to 45°C
Discharge temperature	-40 to 65°C	-20 to 60°C

4.1 Cruising mode of operation

When an E-rickshaw is running at a constant speed thereby consuming a non-varying power, the vehicle can be said to be in cruising or coasting mode of operation. The source current requirement will be average in this case whereby enabling the battery to supply the total power required (case-I; see Table 4). Depending on the state of charge (SOC) of battery and ultracapacitor, either of them is chosen for acting as the propelling power source of the vehicle (case-II). A threshold SOC of 20% is chosen for both battery and ultracapacitor for the state of health (SOH) concerns of both. Falling of SOC below the threshold value will alert the driver for an immediate stop of the vehicle and signals external plug-in charging of the battery (case-III). An average current of 17.6A was found to be drawn from the source during cruising mode of operation. Hence an upper threshold of 40A (considering 2C-rate of discharge) was set as the maximum possible current to be drawn from the battery.

4.2 Accelerating mode of operation

During acceleration the power requirement of the e-rickshaw will reach its peak thereby making the battery unable to supply the same.

Table 4: Fuzzy rules for Optimum Energy Management between Battery and Ultracapacitor

Mode	Case	(if) Source current	(and) Battery SOC	(and) UC SOC	Battery	UC
Cruising	I	$0 < i \leq 40$	$20\% \leq SOC \leq 100\%$	XX	1	0
	II	$0 < i \leq 40$	$0\% \leq SOC < 20\%$	$20\% \leq SOC \leq 100\%$	0	1
	III	$0 < i \leq 40$	$0\% \leq SOC < 20\%$	$0\% \leq SOC < 20\%$	0	0
Accelerating	IV	$40 < i \leq I_{MAX}$	XX	$20\% \leq SOC \leq 100\%$	0	1
	V	$40 < i \leq I_{MAX}$	XX	$0\% \leq SOC < 20\%$	0	0
Braking	VI	i < 0	XX	$0\% \leq SOC < 100\%$	0	1
	VII	i < 0	$0\% \leq SOC < 100\%$	= 100%	1	0
	VIII	< 0	= 100%	= 100%	0	0

Ultracapacitor (UC) hence will take care of the peak power requirements of the vehicle being a high power density device (case IV). The UC is designed based on the maximum current the device has to support (here approximately 120A) for a short duration of time. The capacitance of UC is calculated using Eq 2.

$$dV = \frac{i}{C}.dt + iR \tag{2}$$

where, dV is the change in voltage in volts
i is the current in Amperes
dt is the total discharge time in seconds and,
R is the equivalent series resistance in ohms
The change in voltage is the desired maximum voltage drop of an ultracapacitor. Since 75% of energy in a UC gets consumed within 50% of terminal voltage drop, the change in voltage is kept as 24V (i.e., 50% of 48V). The total discharge time is kept equal to the vehicle test time i.e., 500 secs. Assuming the time constant RC=0.7, substituting for R in Eq 2 yields,

$$C = \frac{i}{dV}.dt + i.\frac{0.7}{dV} \tag{3}$$

For an optimum calculation of capacitance of the ultracapacitor, the regenerative power gained during deceleration/braking is also considered. Hence the capacitance is calculated considering the average time and peak power requirement during the stages (acceleration/regenerative braking) it is needed by the vehicle. If the UC can no longer meet the power requirements of the vehicle (case-V), an external/internal charging of the same has to be done for efficient performance of the vehicle.

4.3 Regenerative Braking mode of operation

E-rickshaw, while decelerating/braking will be having a considerable amount of energy stored in it in the form of kinetic energy. In conventional vehicles this energy is wasted as heat energy in brake drums through mechanical braking as there is no provision to store it. In an E-rickshaw this energy can be stored in both battery and ultracapacitor with ultracapacitor being a more suitable choice due to its higher charge/discharge rate (case-VI). Battery cannot be exposed to higher currents for long time as it effects its state of health which makes it a lesser preferable choice for absorbing the regenerative braking power. Depending on the state of charge (SOC) of both battery and ultracapacitor, this recovered energy can be stored in either of them. If the UC is completely charged then the remaining regenerative power will be absorbed by battery depending on its SOC (case-VII). If both energy sources are fully charged and still there is a flow of regenerative power then it will be dissipated across the available mechanical brakes (case-VIII).

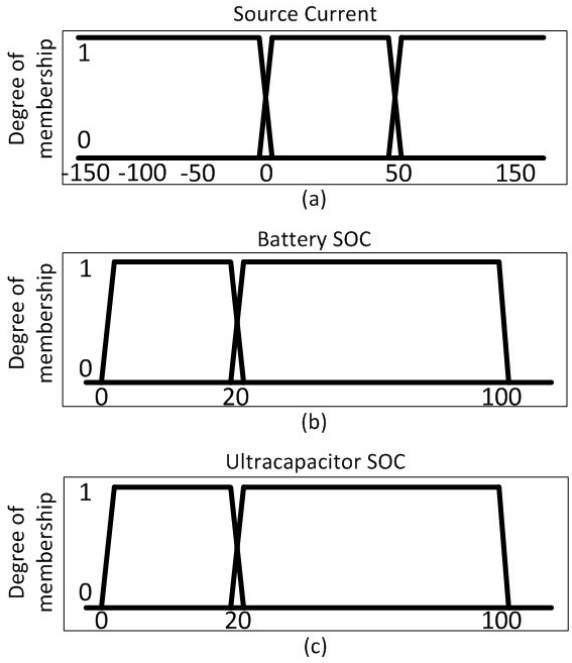


Figure 8: Membership functions for (a) Source current (b) Battery SOC and (c) Ultracapacitor SOC

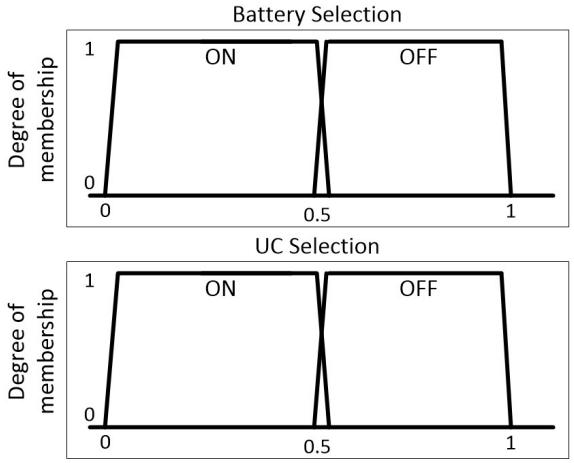


Figure 9: Membership functions for (a) Battery Selection and (b) Ultracapacitor Selection

The fuzzy rules set for an optimum energy management considering the efficient absorption of regenerative power is discussed in Table 4. The input membership functions of the fuzzy logic controller namely source current, battery SOC and ultracapacitor SOC are shown in Figure 8. The output membership functions for selection of energy sources are shown in Figure 9.

5 Simulation Results

Th vehicle has been tested in Matlab-Simulink environment for different conditions of battery and ultracapacitor. The results are discussed in detail below.

5.1 Case-I: Both Battery and UC fully charged (Batt-SOC=100% & UC-SOC=100%)

Both battery and ultracapacitor is assumed to be fully charged at start (i.e., Initial SOC = 100%). Depending on the power requirement, battery SOC and ultracapacitor SOC, the load power is shared between battery and ultracapacitor as shown in Figure 10.

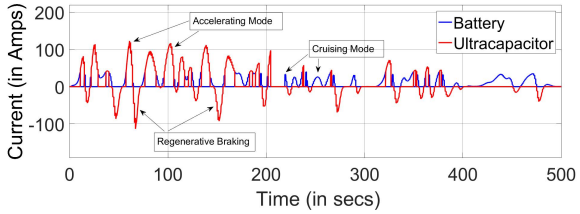


Figure 10: Case-I: Power split between Battery and UC

It is evident that during the cruising mode of operation battery is supplying the required power and during peak power requirement (accelerating mode) and while regenerative braking ultracapacitor supplies/absorbs power respectively.
The state of charge (SOC) of the battery and ultracapacitor is shown in Figure 11.

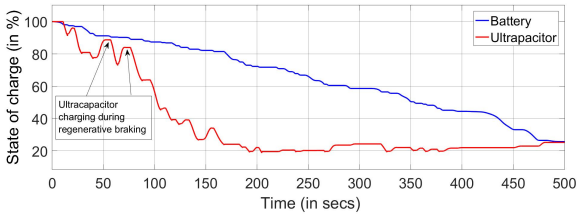


Figure 11: Case-I: Battery and UC SOC comparison

The terminal voltage characteristics (V_T) of the battery and ultracapacitor when operated at Indian drive cycle is shown in Figure 12.

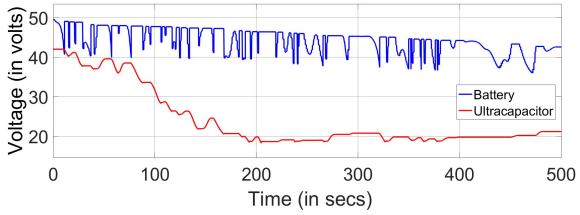


Figure 12: Case-I: Battery and UC Voltage (V_T) comparison

The vehicle is able to operate during all three modes of driving i.e., cruising, accelerating and regenerative braking. During regenerative braking the ultracapacitor is being charged as shown in Figure 11. Battery is able to supply the required power for a longer duration when hybridized with an ultracapacitor when compared to operated alone thereby improving its state of health. Ultracapacitor has successfully absorbed the generated power during braking thereby improving vehicle performance and energy efficiency.

5.2 Case-II: Battery fully charged but UC less charged (Batt-SOC=100% & UC-SOC=25%)

Battery is assumed to be fully charged at start (i.e., Initial SOC = 100%) and ultracapacitor is assumed to be 75% discharged.

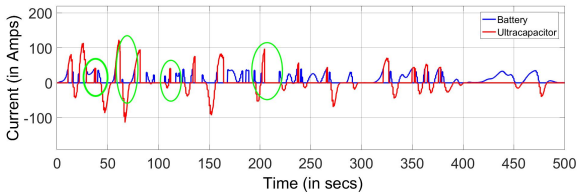


Figure 13: Case-II: Power split between Battery and UC

Depending on the power requirement, battery SOC and ultracapacitor SOC, the load power is shared between battery and ultracapacitor as shown in Figure 13 for a standard Indian drive cycle (IDC).
During the cruising mode of operation battery is supplying the required power but during peak power requirement (accelerating mode) the ultracapacitor is unavailable to meet the system requirements once its SOC level reaches below 20% (see the highlighted areas in Figure 13). While regenerative braking, ultracapacitor absorbs power which is later used to meet the vehicle requirements while accelerating mode of operation. The state of charge (SOC) of the battery and ultracapacitor is shown in Figure 14.

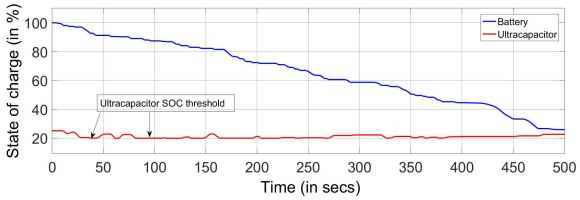


Figure 14: Case-II: Battery and UC SOC comparison

The terminal voltage characteristics (V_T) of the battery and ultracapacitor is shown in Figure 15.Since the ultracapacitor is discharged already by 75%, its terminal voltage will be 24V, as the depth of discharge will be 75% in an ultracapacitor by the time its terminal voltage falls by half.

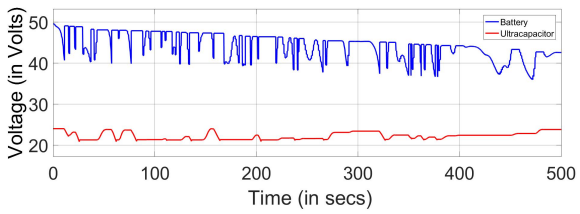


Figure 15: Case-II: Battery and UC Voltage (V_T) comparison

The vehicle is able to operate only during cruising mode of driving. While accelerating the ultracapacitor is only able to meet the demands of the vehicle till its SOC reaches the bottom threshold of 20%. Once the SOC of the ultracapacitor falls below its lower threshold, the vehicle may no longer be able to accelerate thereby hindering its performance hugely. The driver may have to charge the ultracapacitor externally (Plug-In) or internally (through battery) to ensure smooth operation of the vehicle. Interestingly, during regenerative braking the ultracapacitor can still be charged as shown in Figure 14. Once the SOC level reaches above the lower threshold of 20% it can resume it duties and can contribute to the vehicle operation as before.

5.3 *Case-III: UC fully charged but Battery less charged (Batt-SOC=25% & UC-SOC=100%)*

Battery is assumed to be initially charged at 25% (i.e., Initial SOC = 25%) and ultracapacitor is assumed to be fully charged.

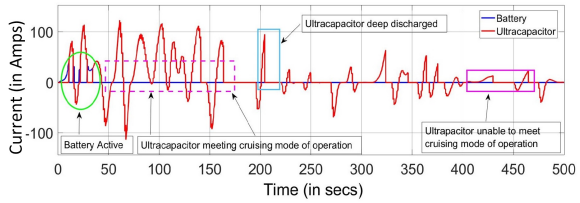


Figure 16: Case-III: Power split between Battery and UC

Depending on the power requirement, battery SOC and ultracapacitor SOC, the load power is shared between battery and ultracapacitor as shown in Figure 16.

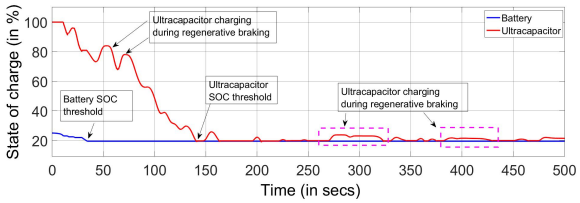


Figure 17: Case-III: Battery and UC SOC comparison

Since battery is very low charged, it cannot meet the vehicles' demands after its SOC falls below the threshold value of 20%. Once the battery SOC is below 20% the ultracapacitor may continue to meet the vehicle average and peak demands till its SOC reaches 20% (see the highlighted areas in Figure 16). While regenerative braking, ultracapacitor absorbs power which is later used to meet the vehicle requirements during accelerating mode of operation. The state of charge (SOC) of the battery and ultracapacitor is shown in Figure 17.

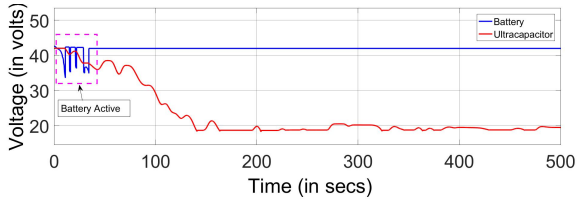


Figure 18: Case-III: Battery and UC Voltage (V_T) comparison

The terminal voltage characteristics (V_T) of the battery and ultracapacitor when operated at Indian drive cycle is shown in Figure 18. Since the battery is discharged already by 75%, its terminal voltage will be non-linearly reduced initially. The battery is active till its SOC reaches the lower threshold value. Once both the energy sources are below its lower threshold value of SOC, the driver has to perform an external charging of battery accompanied by an external (Plug-In) or internal (through battery) charging of ultracapacitor to ensure smooth operation of the vehicle. While regenerative braking, ultracapacitor absorbs power which is later used to meet the vehicle requirements during accelerating mode of operation.

6 Implementation Results

The proposed fuzzy logic based power-split between battery and ultracapacitor was experimentally tested in laboratory environment using the Xilinx made Spartan3 FPGA board (XC3S5000). A two-channel Agilent make DSO-X2002A is used to record the performance in real-time. The Indian city drive cycle generated from actual measured data is recreated in lab and is shown in Figure 19.

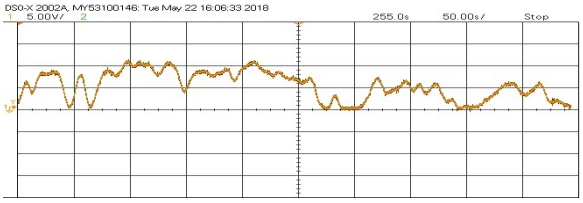


Figure 19: Real-time Indian City Drive Cycle at laboratory environment

The current to be drawn from the energy source(s) to meet the vehicle demands are shown in Figure 20.

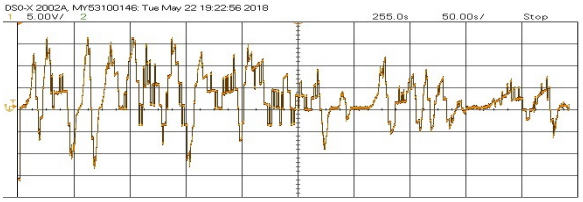


Figure 20: Source current requirement of E-rickshaw

The vehicle simulated in Matlab-Simulink was successfully recreated in a Real-time environment. The current drawn from the energy source for various modes of vehicle operation was observed to be closely matched with simulation results.
Al the three cases of vehicle operation based on battery and ultracapacitor state of charge (SOC) tested earlier with Matlab-Simulink was tested in laboratory environment. The results were found to be matching and is discussed briefly below.

6.1 *Case-I: Both Battery and UC fully charged (Batt-SOC=100% & UC-SOC=100%)*

Both battery and ultracapacitor is fully charged. As seen earlier, the vehicle is able to operate during all three modes of driving i.e., cruising, accelerating and regenerative braking. Ultracapacitor is being charged during regenerative braking as shown in Figure 21.

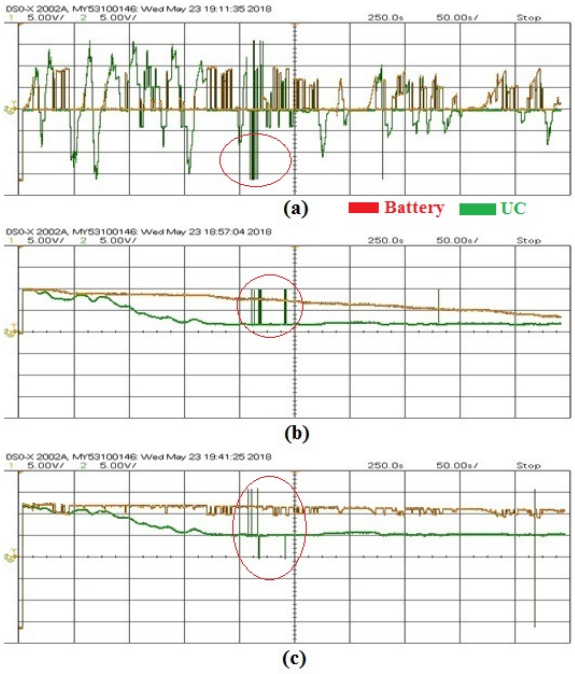


Figure 21: Case-I: Battery and UC (a) Current (b) SOC and (c) Voltage (V_T) comparison in Real-time laboratory environment

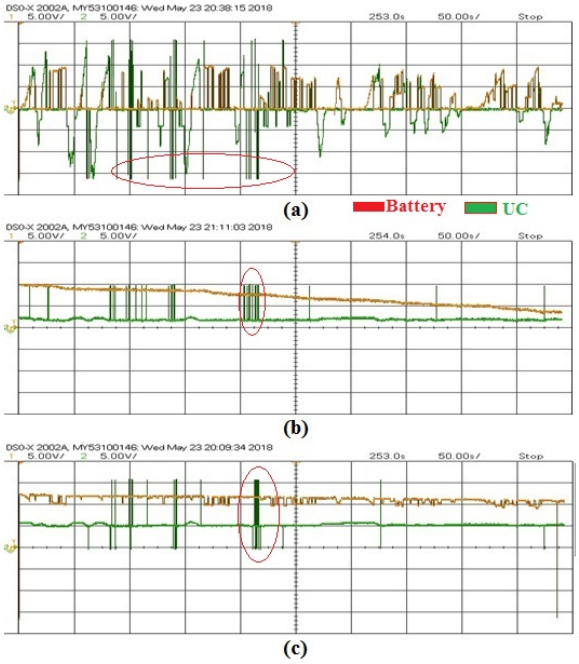


Figure 22: Case-II: Battery and UC (a) Current (b) SOC and (c) Voltage (V_T) comparison in Real-time laboratory environment

As the system is run for 500 seconds, few noises are present in the results which are highlighted in the results plotted. For average power requirements battery is acting as the energy source and for peak power requirements ultracapacitor is the source. Vehicle performance and energy efficiency is improved as ultracapacitor has successfully absorbed the generated power during braking.

6.2 *Case-II: Battery fully charged but UC less charged (Batt-SOC=100% & UC-SOC=25%)*

Battery is full charged but ultracapacitor is charged at 25% SOC. It can be seen that during the cruising mode of operation battery is supplying the average power required but during accelerating mode the ultracapacitor is unavailable to meet the system peak power requirements once its SOC level reaches below 20% as shown in Figure 22. Ultracapacitor absorbs the regenerative braking power. Ultracapacitor is only able to meet the demands of the vehicle till its SOC reaches the bottom threshold of 20%. Once the SOC falls below its lower threshold, the vehicle may no longer be able to accelerate thereby hindering its performance hugely calling for an external/internal charging based on system architecture.

6.3 *Case-III: UC fully charged but Battery less charged (Batt-SOC=25% & UC-SOC=100%)*

Battery is charged at 25% whereas ultracapacitor is fully charged. Since battery is very low charged, it cannot meet the vehicles' demands after its SOC falls below the threshold value of 20%. Ultracapacitor may continue to meet the vehicle average and peak demands till its SOC reaches 20% once the battery SOC is below 20% as shown in Figure 23. Ultracapacitor absorbs power while regenerative braking.

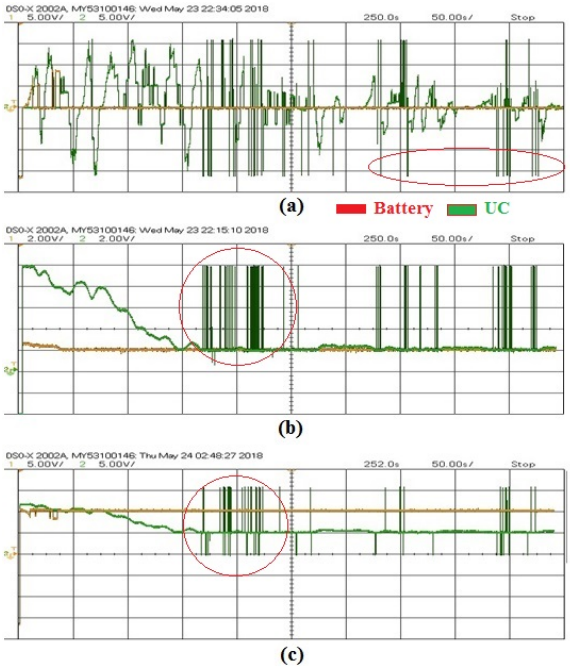


Figure 23: Case-III: Battery and UC (a) Current (b) SOC and (c) Voltage (V_T) comparison in Real-time laboratory environment

The battery is active energy source till its SOC reaches the lower threshold value of 20%. Once both the energy sources are below its lower threshold value of SOC, the driver has to perform an external charging of battery accompanied by an external (Plug-In) or internal (through battery) charging of ultracapacitor ensure smooth operation of the vehicle.

7 Discussion and conclusion

Rickshaws, even-though being a common mode of transportation is subjected to very less research to improve its performance. Conventional E-rickshaws which employ a single energy source, has a lot of limitation in terms of driving range. In Indian scenario, E-rickshaws‘ success will be always measured by its driving range and cost. It is identified that combining a high power density device (UC) for sharing peak power demand with the traditional high energy density device (battery) will improvise the vehicle performance which was not earlier attempted in E-rickshaws. An improved SOC and terminal voltage characteristics can increase the driving range of the E-rickshaw. Also since the UC is able to meet the peak power demands, battery can be sized for a much lesser average current demand. This will considerably reduce the size and cost of the vehicle. Since the battery in a traditional e-rickshaw occupies almost 15-20% of its kerb weight, any minute reduction in weight and size of the battery will always result in better performance. Also UC possess faster charge/discharge characteristics than battery which can be utilized in absorbing regenerative power during deceleration and braking in a better way.
This paper have attempted for the hybridization of energy sources for an E-rickshaw system architecture in Indian scenario. The performance improvement was justified using simulation and implementation in real-time results in this paper. Successful implementation of a fuzzy logic based energy management algorithm has enhanced the performance of E-rickshaw. The vehicle dynamics was calculated real-time based on an Indian city drive cycle calculated using a GPS based PerformanceBox tool of VBOX motorsport. The vehicle was tested for three different driving modes of operation and three different battery and ultracapacitor state of charge conditions. It was found that the algorithm was working perfectly with less computation time and complexity. Implementation of a hybrid energy source for an E-rickshaw can extend its driving range. Also successful absorption of the generated regenerative power can further enhance the vehicle performance.

References

[1] J. Bremner, A. Frost, C. Haub, M. Mather, K. Ringheim, E. Zuehlke, et al., “World population highlights: Key findings from PRB’s 2010 world population data sheet,” Population Bulletin, **65**(2), 1–12, 2010.

[2] S. K. Guttikunda, R. Goel, P. Pant, “Nature of air pollution, emission sources, and management in the Indian cities,” Atmospheric environment, **95**, 501–510, 2014, doi:https://doi.org/10.1016/j.atmosenv.2014.07.006.

[3] BBC, “Indian cities dominate world air pollution list,” 2018.

[4] H. Mayer, “Air pollution in cities,” Atmospheric environment, **33**(24-25), 4029–4037, 1999, doi:https://doi.org/10.1016/S1352-2310(99)00144-2.

[5] A. Mani, M. Pai, R. Aggarwal, “Sustainable urban transport in India: role of the auto-rickshaw sector,” 2012.

[6] J. Shah, N. Iyer, “Module 4c: two-and three-wheelers,” Sustainable transport: a sourcebook for policy-makers in developing cities. GTZ, Eschborn, 2004.

[7] J. Pucher, N. Korattyswaroopam, N. Ittyerah, “The crisis of public transport in India: overwhelming needs but limited resources,” Journal of public transportation, **7**(3), 5, 2004, doi:http://doi.org/10.5038/2375-0901.7.4.1.

[8] M. S. Kumar, S. T. Revankar, “Development scheme and key technology of an electric vehicle: An overview,” Renewable and Sustainable Energy Reviews, **70**, 1266–1285, 2017.

[9] V. Gulhane, M. Tarambale, Y. Nerkar, “A scope for the research and development activities on Electric Vehicle technology in Pune city,” in Electric and Hybrid Vehicles, 2006. ICEHV’06. IEEE Conference on, 1–8, IEEE, 2006.

[10] D. Majumdar, T. Jash, “Merits and Challenges of E-Rickshaw as An Alternative form of Public Road Transport System: A Case Study in the State of West Bengal in India,” Energy Procedia, **79**, 307–314, 2015, doi: https://doi.org/10.1016/j.egypro.2015.11.492.

[11] S. Tatipamula, “Study of a Parallel Electric Hybrid Three-Wheeled Motor Taxi,” IJCA Proceedings on International coriference on Green Computing and Techn% gy ICGCT, **1**, 38–41, 2013.

[12] T. Hofman, S. Van Der Tas, W. Ooms, E. Van Meijl, B. Laugeman, “Development of a micro-hybrid system for a three-wheeled motor taxi,” World Electric Vehicle Journal, **3**(3), 1, 2009.

[13] M. Mruzek, I. Gajdáč, L. Kučera, T. Gajdošík, “The possibilities of increasing the electric vehicle range,” Procedia engineering, **192**, 621–625, 2017.

[14] S. Manzetti, F. Mariasiu, “Electric vehicle battery technologies: From present state to future systems,” Renewable and Sustainable Energy Reviews, **51**, 1004–1012, 2015.

[15] A. Poullikkas, “Sustainable options for electric vehicle technologies,” Renewable and Sustainable Energy Reviews, **41**, 1277–1287, 2015.

[16] R. Kumar, “Evolution of solar rickshaw technology vis-à-vis economic feasibility,” in Advances in Electrical, Electronic and Systems Engineering (ICAEES), International Conference on, 646–651, IEEE, 2016.

[17] M. Sameeullah, S. Chandel, “Design and analysis of solar electric rickshaw: A green transport model,” in Energy Efficient Technologies for Sustainability (ICEETS), 2016 International Conference on, 206–211, IEEE, 2016.

[18] P. Mulhall, S. M. Lukic, S. G. Wirasingha, Y.-J. Lee, A. Emadi, “Solar-assisted electric auto rickshaw three-wheeler,” IEEE transactions on vehicular technology, **59**(5), 2298–2307, 2010.

[19] M. A. Mallouh, L. McInnes, B. Surgenor, B. Peppley, “Intelligent Control for optimal performance of a fuel cell Hybrid Auto Rickshaw,” Energy Procedia, **29**, 367–376, 2012.

[20] B. Masood, R. A. Naqvi, R. M. Asif, “Designing of a control scheme for the solar rickshaw in comparative study with conventional auto rickshaw,” in Engineering Technology and Technopreneuship (ICE2T), 2014 4th International Conference on, 324–329, IEEE, 2014.

[21] M. Hannan, M. Hoque, A. Mohamed, A. Ayob, “Review of energy storage systems for electric vehicle applications: Issues and challenges,” Renewable and Sustainable Energy Reviews, **69**, 771–789, 2017.

[22] G. Ren, G. Ma, N. Cong, “Review of electrical energy storage system for vehicular applications,” Renewable and Sustainable Energy Reviews, **41**, 225–236, 2015.

[23] A. K. Rohit, K. P. Devi, S. Rangnekar, “An overview of energy storage and its importance in Indian renewable energy sector: Part I–Technologies and Comparison,” Journal of Energy Storage, **13**, 10–23, 2017.

[24] A. Singh, P. Karandikar, N. Kulkarni, “Feasibility of energy storage systems in different applications for sustainable energy,” in Emerging Technological Trends (ICETT), International Conference on, 1–6, IEEE, 2016.

[25] A. F. Burke, “Batteries and ultracapacitors for electric, hybrid, and fuel cell vehicles,” Proceedings of the IEEE, **95**(4), 806–820, 2007.

[26] H. Fathabadi, “Fuel cell hybrid electric vehicle (FCHEV): Novel fuel cell/SC hybrid power generation system,” Energy Conversion and Management, **156**, 192–201, 2018.

[27] S. Ahmadi, S. Bathaee, A. H. Hosseinpour, “Improving fuel economy and performance of a fuel-cell hybrid electric vehicle (fuel-cell, battery, and ultracapacitor) using optimized energy management strategy,” Energy Conversion and Management, **160**, 74–84, 2018.

[28] L. Kouchachvili, W. Yaïci, E. Entchev, “Hybrid battery/supercapacitor energy storage system for the electric vehicles,” Journal of Power Sources, **374**, 237–248, 2018.

[29] N. Sulaiman, M. Hannan, A. Mohamed, E. Majlan, W. W. Daud, “A review on energy management system for fuel cell hybrid electric vehicle: Issues and challenges,” Renewable and Sustainable Energy Reviews, **52**, 802–814, 2015.

[30] S. S. Kulkarni, N. Gandhi, N. Chaithanya, S. Govindarajan, “Ultra-Capacitor based Hybrid Energy Storage and Energy Management for Mild Hybrid Vehicles,” Technical report, SAE Technical Paper, 2014.

[31] W. Enang, C. Bannister, “Modelling and control of hybrid electric vehicles (A comprehensive review),” Renewable and Sustainable Energy Reviews, **74**, 1210–1239, 2017.

[32] S. Zhang, R. Xiong, F. Sun, "Model predictive control for power management in a plug-in hybrid electric vehicle with a hybrid energy storage system," Applied Energy, **185**, 1654–1662, 2017.

[33] D. Zhou, A. Al-Durra, F. Gao, A. Ravey, I. Matraji, M. G. Simões, "Online energy management strategy of fuel cell hybrid electric vehicles based on data fusion approach," Journal of Power Sources, **366**, 278–291, 2017.

[34] M. Dawei, Z. Yu, Z. Meilan, N. Risha, "Intelligent fuzzy energy management research for a uniaxial parallel hybrid electric vehicle," Computers & Electrical Engineering, **58**, 447–464, 2017.

[35] J. Larminie, J. Lowry, Electric vehicle technology explained, John Wiley & Sons, 2012.

ASTES

Advances in Science, Technology and Engineering Systems Journal Vol. 5, No. 5, 1172-1183 (2020)

www.astesj.com

Special Issue on Multidisciplinary Innovation in Engineering Science & Technology

ASTESJ

ISSN: 2415-6698

Advanced Control Strategies on Nonlinear Testbench Dynamometer System for Simulating the Fuel Consumption

Marika Fanesi, David Scaradozzi*

Dipartimento di Ingegneria dell'Informazione (DII), Università Politecnica delle Marche, Ancona, 60121, Italy

ARTICLE INFO

Article history:
Received: 26 June, 2020
Accepted: 28 September, 2020
Online: 22 October, 2020

Keywords:
Engine-in-the-loop
Nonlinear dynamometer system
Testbench
Electric motor
Automotive

ABSTRACT

The adoption of Engine-in-the-loop technology shows real behaviour. This study presents a test runs simulation platform with real engine data. In addition, a test bench model is a demand approach that offers a significant potential to provide an excellent reproducibility of test runs. The platform includes the data integration to upgrade tests run and a comparison with previous results using the advancing control techniques designed. The dynamometer system presents significantly non-linearity. The adaptive control approach, integrated into the Model Predictive Control on the vehicle, allows increasing the tests run performance. The results show how the real data can improve performance and the validation of the system integrating the updated driving cycle and maintaining EiL approach. The conclusion showed the significant benefits regarding the control methods used.

Abbreviation

AMPC	Adaptive Model Predictive Controller
CO2	Carbon dioxide
DSM	dynamometer system motor
DUT	Device Under Test
EiL	Engine-in-the-Loop
EM	Electric Motors
EUDC	Extra-Urban Driving Cycle
FTP	Federal Test Procedure
ICE	Internal Combustion Engines
IM	Induction Motor
KF	Kalman Filter
LS	Least Square Algorithm
MHEV	Mild Hybrid Electric Vehicles
MIMO	Multiple Input Multiple Output
NEDC	New European Driving Cycle
PID	Proportional Integral Controller
UDC	Urban Driving Cycles
XiL	X-in-the-Loop
WLTP	World Light-duty vehicles Test Procedure

1. Introduction

Nowadays, in automotive industries, analysis and testing of Electric Motors (EMs) and Internal Combustion Engines (ICEs) are the key elements. Accuracy and efficiency are further improved and allows to evaluate the vehicles' production. However, to achieve these, the test benches are fundamentals. A novel data approach for advanced control strategies applied on a modelled test benches was introduced in a paper originally presented at the 23rd International Conference on System Theory, Control and Computing (ICSTCC) in 2019 [1], for which this work is an extension.

The tests are not limited to the EMs or ICEs in that the integration and combination of components are relevant. In the vehicles, brakes [2-4], energy management [5, 6], power devices [7, 8], sensors [9, 10], batteries [11-13], front steering [14, 15], are strongly analysed to increase vehicles' performances. Every component needs to be tested determining robustness, reliability, fault-tolerant [16-21] and, in case of traditional and Mild Hybrid Electric Vehicles (MHEVs), the engine has to respect the limits and the restriction regarding fuel consumption and, consequently, emissions [22-25]. To reduce costs, the virtualisation and the introduction of simulation's platform are included in the industry process [26, 27]. Considering the relevance of real data, in the last decade is introduced a new approach that includes the use of real components in the virtual tests. These techniques are called X-in-the-Loop (XiL) and include Engine-in-the-Loop, Hardware-in-the-Loop, Software-in-the-Loop, Model-in-the-Loop and Human-in-the-loop [28-32]. The XiL is used in different fields, as marine systems [33, 34], power units [36], home automation and robots [37], educational science [38].

*Corresponding Author: David Scaradozzi, Università Politecnica delle Marche, Email: d.scaradozzi@univpm.it

Engine-in-the-Loop (EiL) techniques allow testing of the electric motors and internal combustion engines. EiL is widely used to ensure precision on testbench. This type of simulations allows to reduce simulation timing and to simulate testing scenarios leading to higher efficiency. Another significant benefit is the reduction of costs that this technology enables. The strengths of this approach include the adaptability of the system with different hardware and the reliability of the measured data deriving from the real engine. The EMs and the ICEs tested, most of the time, are prototypes [39, 40] and this excludes the possibility to have a reliable model of the EM or the ICE to be included in the simulation. The Eil technique allows the integration of EMs or ICEs, and it is significant in that the modelling of these demonstrates a different behaviour from the real. The solution is identified in the EiL approach [41, 42]. Based on that, the simulation and control of the Induction Motor (IM) on the testbench become essential, and to efficiency, the parametric model of IM must be identified. The overall model is affected by accuracy and nonlinear behaviour [43-45]. The partial linearization of the motor helps to define the real-non-linear behaviour. A first step of calibration is needed to assure proper performance. The introduction of control techniques in these systems increase precision and real-behaviour and point to manage tests easily. To guarantee reliability and security, final design and implementation of the control strategies are required. Generally, this phenomenon is described and controlled utilising methods to achieve more accurate results. An adaptive control leads to higher efficiency and performance compared to conventional control [46-49].

With the paper, the authors describe a possible solution to design an EiL architecture and an improvement of the control quality in a real environment. This paper aims to compare the results obtained, adding real-driving conditions and upgrading the driving cycles presented. The work is organised as follow: in the next paragraph (Background and review) is shown the background related to two critical elements that influence the automotive industry, the market and the legislation concerning driving cycles and the Engine-in-the-loop state of the art; in the third paragraph (Nonlinear system) the models of the testbench and others components are presented including a section with the calibration test; then the adaptive control strategies are introduced and integrate to the system to increase the robustness and dynamics (Control strategy). The results are presented in the Simulation and discussion paragraph that shows an adaptive control used in the simulation of the overall system in a real environment applied to the new driving cycles.

2. Background and review

In this section, the authors present a review about the background, including the market reasons that guided the choice of development and implemented a specific configuration model. In this section is introduced also the driving cycles used in the simulation for the validation of the system and includes an Engine-in-the-loop methods review.

2.1. Automotive Market

In the automotive market, electric motors have been introduced recently. In the industries, the most critical challenge is the reduction of carbon dioxide (CO_2). The combination of engine and the electric motor in the vehicles guarantees excellent performance and the car's production has adapted to the growing market. These represent a radical innovation in the industries and allowed an expansion of the market. The key challenges are:

- Complexity and reduction of costs
- Different market
- Virtualisation process
- Industries landscape

Based on these four points, it is clear that in the future, the changes are fast and in different directions [50, 51].

Nowadays, vehicles include a lot of components, and the complexity is growing. Nevertheless, the market requests the reduction of costs and lower price. For this reason, a solution developed with the introduction of new technologies and features is to enter in the electrification process. Thus, a conventional vehicle with ICE become a hybrid vehicle [52]. At the same time, are developing new systems and safety, and performances are increased. This electrification process is essential to the point of becoming an evaluation factor. However, the main challenge remains the costs reduction. The governments help to achieve this target with new stricter limits and regulations regarding the emissions and pollutants, and these restrictions reflect in differentiation of the markets [53]. The differentiation of the markets has developed the adaptability of the automotive industries that need to supply vehicles based on sales. To be competitive, the approach uses the virtualisation process [54, 55]. This process combines the connectivity with accessibility and increases the use of digital resources. The virtualisation is a potential technique and represents an opportunity applies to the driving experience. Another added value in the car is the communication and interaction. Besides, the development of new powertrain technologies and innovative solutions for active safety and infotainment change and it is based on the industry landscape. Europe needs to be reconstructed and adapt the capacity of industries; East Asia is a competitive emerging market. Each challenge is dependent and interconnected from the others and to capture future growth strategic choice, appropriate investments and resources are essential [56-58].

2.2. Driving Cycles development

The driving cycles are evolved and upgraded based on government and legislation of every countries and are founded on the market's choices. The studied methodologies are not limited to the choice of driving cycles capable of making consumption real but include also to monitor energy consumption. An important aspect is the central role of driving cycles in emission measurement [59]. The pollutants, carbon dioxide, volatile organic compounds, nitrogen oxides and particulate are the results of the combustion of fuel and are regulated by countries directives. Emissions depend on different parameters and for this reason is classified based on vehicles types: cars, vans, buses, trucks and motorcycles.

In this paper, the authors illustrate driving cycles which had considered explicitly for the presented testbench. The driving cycles are described throughout some features shown in Table 1.

Table 1: Driving Cycles features

Feature	Detail
Distance	Total distance
Time	Total time Driving Time Acceleration Time Braking Time
Speed	Average Driving Speed Minimum Speed Maximum Speed
Acceleration	Average Driving Acceleration Minimum Acceleration Maximum Acceleration
Stops	Number of Stops Average Stop duration

The tests most used in the last ten years are:

- UDC or ECE-15: The Urban Driving Cycles represent a typical driving condition in Europe in a busy city with traffic and with a maximum speed of 50 km/h;
- EUDC: The Extra-Urban Driving Cycle is the high-speed road in the European cities with a maximum speed of 120 km/h;
- NEDC: The New European Driving Cycle is a combination of the UDC and EUDC, with four repetitions of UDC and once of EUDC;
- FTP-72 is the Federal Test Procedure used in US to simulate an urban road with multiple stops;
- FTP-75: Federal Test Procedure derived from FTP-72 is a city driving cycle with are a series of tests defined by the US Environmental Protection Agency (EPA),
- ARTEMIS Urban: is chassis dynamometer system procedure used in Europe with driving patterns derived from the analysis of a database containing real data and it is considered the urban track.
- ARTEMIS Rural: is chassis dynamometer system procedure as ARTEMIS Urban with the different that it is considered the rural road;
- ARTEMIS Motorway: as ARTEMIS Urban is chassis dynamometer system procedure and it is considered the motorway track.

These driving cycles are significant for new cars in that allow to test and know emission and pollutants. Lastly, as presented in the introduction, the validation tests assure that the results reflect real-world emission. This driving cycle is integrated into the system proposed in the following section to enhance the results on [1].

2.3. The engine in the loop

Engine-in-the-loop is a recent technique that makes possible to run a modelled testbench with an ICE reproducing the same conditions as when the engine is mounted in the real vehicle. Eil is a vehicle simulation linked and, in this technique, physical hardware called control unit, and an engine are integrated in a model of a testbench or a vehicle and driver model. The virtual testbench environment includes:

- High power
- Low inertia in the DSM

These perform a reasonable powertrain control and permit a detail emission evaluation.

The simulation of other components brings many benefits as repeatability and flexibility and can brush up the whole system. For this reason, the Eil approach results in an ideal choice for testbenches in that the accuracy, time-to-run and performance are highly improved [60, 61]. At the other hand, the request of this technique is the projecting of the entire system and for the high-speed real-time controller to have an adequate manage of the models implemented [62-66]. The fast response of the dynamometer loads the connected engine and the virtual vehicle follow the specific driving cycle target track as in the real world. Another influencer of the acceleration and speed is the vehicle pedal effect by the driver. In detail, the system includes an input-output behaviour deriving from the physical engine system and requests reasonable accuracy and response [67, 68]. The dynamics of the engine subsystem, along with the main subsystem testbench model and variables influence, is analysed to prevent fault. In automotive, the control strategy needs to be integrated into the control unit parameterising the whole virtual vehicle modelled and driveline configurations. The effects on the engine and performance are easily analysed as fuel consumption. In this use case, the relevant step is the calibration of the system in the virtualisation process and to reach a well-configurated testbench [69-71]. In automotive, the Eil is used during the development of new engine in that the testing of prototypes reduces the bugs and fastly improve the overall number. The development uses advanced simulation and modelling tools to realise a system with precise modelled functions that work together with physical hardware and processes. The virtualisation allows testing and validation of parameters and function guarantying highly quality [72-74]. However, several factors, as real-time computational complexity and calibration efforts, might lead to select faster and less-expensive techniques. The various combination and choice of vehicle calibration can limit in terms of management and testing functionalities, and the calibration steps must fit the engine behaviour. For these reasons and due to the architectural complexity of the Mild Hybrid Electric Vehicles, designing models for specific EM and ICE an adapt the entire system including interactions to the model is extremely difficult if even possible [75-77]. The major challenge is the satisfaction of the requirements during the Eil simulation.

3. Nonlinear system

The testbench detailed schema used in the present paper is shown in Figure 1. This collects some components: an inverter, the dynamometer motor (DSM) and the Device Under Test (DUT). On the EiL approach, the DUT could be an ICE (Internal Combustion Engine) or an EM (Electric Motor).

3.1. The Dynamometer System model

A general detailed model of the Dynamometer System is often too costly due to the induction machine typical non-linearity. Moreover, the parametrisation of the IM non-linearity is highly demanding for a standard automotive testbench commissioning process. Furthermore, the inverter includes a static controller with an unknown structure. The DSM is designed as a low-pass filter with fast dynamics with a simplified nonlinear mathematical model of DUT. The plant considered includes the inertia and the two parts of the testbench is treated as two mass oscillators. The model can be expressed as:

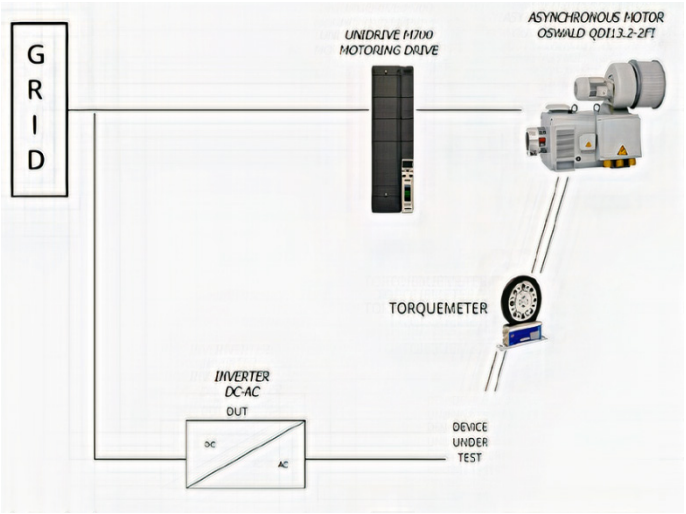


Figure 1: Dynamometer System

$$\Delta\dot{\varphi} = \omega_{EM} - \omega_D \tag{1}$$

$$\theta_{EM}\dot{\omega}_{EM} = T_{EM} - c\Delta\varphi - d(\omega_{EM} - \omega_D) \tag{2}$$

$$\theta_D\dot{\omega}_D = c\Delta\varphi + d(\omega_{EM} - \omega_D) - T_D \tag{3}$$

where:

$_{EM}$ is referred to DUT and can be consider as Engine or E-Motor,

$_D$ is applied to the dynamometer,

ω_x is the speed,

θ_x the inertia,

Δ_φ the torsion of the shaft,

T_x the estimated or measured torque,

c is the stiff constant

d is the damping.

For run the testbench model, the first tread is the calibration of the system as explained in the next paragraph.

3.2. Calibration Process

The calibration plays a crucial role in a testbench. The parameters setting is often a necessary step which influences the tests. The calibration process is a signal that allows assessing the exact initial configuration. The computation is real-time for the DSM. Parameters in the first step are set with an offline estimation. Then, the torque signal starts with a fixed amplitude and increasing frequency, and it is evaluated the response. The previous calibration phase is repeated increasing magnitude and testing the new value of amplitude for every frequency. The online calculation provides time constant for the system. This dynamic calibration has been achieved considering the transfer function between reference torque and IM air gap torque and shaft speed. In a MIMO (Multiple Input Multiple Output) systems, a controller with low overshoot is significant for improving dynamics compensation and consider the different steady-state. Considering that the reference for the inverter is a torque signal, the test is run in the torque mode. This calibration process is essential for estimate the parameters, evaluate the results obtained, select the model parameters and helps to interpret the well-fit model flexibility. To assure a good fit the evaluation of the model is essential and there are many concepts to guarantee the single-best fit [78]. However, the authors choose to focus this paper on the Engine-in the loop approach and on the advanced control strategies applied.

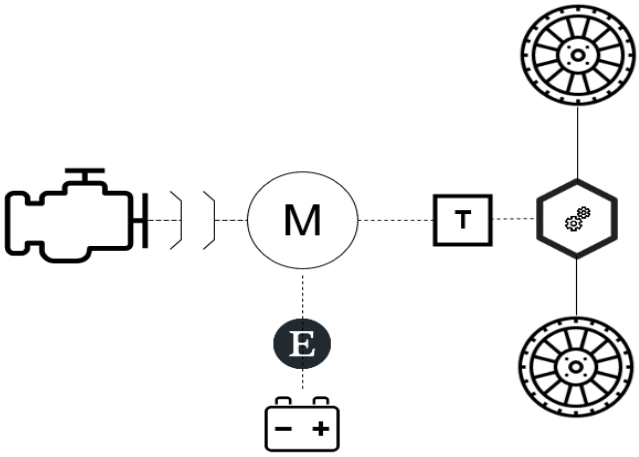


Figure 2: P2 Configuration: in order ICE, clutch, EM with Electronics and Battery pack, Transmission, Differential and Wheel.

3.3. P2 configuration

A testbench can simulate different types of ICE and EM; furthermore, the configuration of the vehicles can be changed, and this requires a different set of parameters and connected device. The structure considered is the parallel hybrid P2 of a Mild Hybrid Electric Vehicle. The P2 configuration is shown in figure 2. The EM (M) is placed in front of the transmission (T) and provide torque to compensate torque for dragging the ICE. The output torque derives from both ICE and EM. The vehicle can operate in pure electric mode, charge-battery mode, engine mode and parallel mode. Based on the way, the behaviours and the performances are

different. In the designed testbench it is possible to test every way during a driving cycle. The virtual model of the vehicle implemented with the integration of the Eil techniques is shown in the next section.

3.4. Vehicle Model

Based on the virtual vehicle developed presented in [1], lateral and vertical dynamics are included. The analysis of the static and dynamic behaviour is necessary to have a stable model of the vehicle. A multitude of parameters influences the stability and a representation of the main components is required to have a reliable system. For define the static behaviour, the steady-state cornering equations are introduced. The yaw velocity defines the steady steady-state $\dot{\Psi}$ and the sideslip angle β that are constant.

For the steady-state case, the torque balance influenced by the front and the rear wheel is:

$$F_{sf} \cdot I = -m \cdot a_y \cdot I_r \tag{4}$$

$$F_{sr} \cdot I = -m \cdot a_y \cdot I_f \tag{5}$$

with the tyre side forces:

$$F_{sf} = c_{sf} \cdot \alpha_f \tag{6}$$

$$F_{sr} = c_{sr} \cdot \alpha_r \tag{7}$$

where for small slip angles α results:

$$\alpha_f = \delta + \beta - \frac{I_f \cdot \dot{\Psi}}{v} \tag{8}$$

$$\alpha_r = \delta + \beta - \frac{I_r \cdot \dot{\Psi}}{v} \tag{9}$$

The equations become:

$$c_{sf} \cdot \left(\delta + \beta - \frac{I_f \cdot \dot{\Psi}}{v}\right) = \frac{I_r}{I} \cdot m \cdot a_y \tag{10}$$

$$c_{sr} \cdot \left(\beta + \frac{I_r \cdot \dot{\Psi}}{v}\right) = \frac{I_f}{I} \cdot m \cdot a_y \tag{11}$$

In the case of steady-state cornering, (10) and (11) are equal and the sideslip angle β are constant, so $\dot{\beta}$=0. The prediction of driving behaviour results:

$$\delta = \frac{I}{r} + \frac{m}{I} \cdot \left(\frac{I_r}{c_{sf}} - \frac{I_f}{c_{s_r}}\right) \cdot a_y \tag{12}$$

And based on (12), considering that $\frac{1}{r} = \frac{\dot{\psi}}{v}$ and $a_y = v \cdot \dot{\Psi}$, the stationary yaw amplification factor can be written as:

$$\frac{\dot{\psi}}{\delta} = \frac{v}{I + \frac{m}{I} \cdot \left(\frac{I_r}{c_{sf}} - \frac{I_f}{c_{sr}}\right) \cdot v^2} \tag{13}$$

$$\frac{\dot{\psi}}{\delta} = \frac{v}{I + \frac{d\delta}{da_y} \cdot v^2} \tag{14}$$

where:

F is the force
F_{sf} is side front
F_{sr} is side rear
I is the inertia
m is the mass of the vehicle
a_y is the acceleration
$\dot{\Psi}$ is the yaw velocity
β is the sideslip angle
v is the driving speed
c is the stiffness of tyre slip
α is the slip angle front or rear
δ is the wheel steering angle
r is the instantaneous curve radius.

The static behaviour shows the output variable $\dot{\Psi}$ divide for input variable δ that represent the stationary yaw amplification factor (13) that is related to the driving speed v. These equations are significant to define the vehicle's model and its behaviour. An essential prediction about the driving behaviour of a car while cornering results from these equations. The necessary steering angle input while navigating around a corner is composed of two parts: one part depends on geometric data, and the second part describes the influence of lateral acceleration. Driving at higher speeds in addition to low rates necessary input steering angle includes the steering angles at higher speeds which can increase or reduce the steering angle. This is very important for the interactions between the driver inputs and vehicle handling in the driver and vehicle control loop. While cornering, the driver must input a steering angle, which depends on the curve radius, and the present lateral acceleration. The reason that the steering angles depend on the lateral acceleration is that at the vehicle wheels while experiencing lateral force, a slip angle results, which usually differ for the front and rear wheel.

3.5. Electric Motor and Battery

In a Mild Hybrid Electric Vehicle, the electric motor can work as motor or generator based on the situation. The model of an EM is composed by an electronics unit setting on torque control mode, the EM and a battery pack. However, there are some constraints in terms of nominal value and maximum value of speed and torque. The operating range of motors in the electric vehicles is directly linked to the battery capacity. The battery has an enhanced capacity, compared with conventional cars, and this increases the operating range and decreases the emissions.

4. Control strategy

To face the non-linearities of the system, the feedback is supervised by an Adaptive Model Predictive Controller (AMPC). Its aim is performing robustness and reliability. The thought control pattern permits to improve the performance of the vehicle under study and the testbench behaviour concerning dead time compensation typical of such complex system. The controller presented strategy is necessary to guarantee disturbances rejection modified by the nonlinear behaviour of the vehicle. The schema in fig. 3 represents the action of the AMPC controller. The torque reference is the input of the dynamometer system placed as input of the inertia model. The control loop process handles the action

of driver and the vehicle reaction. Therefore, the steering behaviour in the single-track road is included in the response of the control vehicle as to the static behaviour.

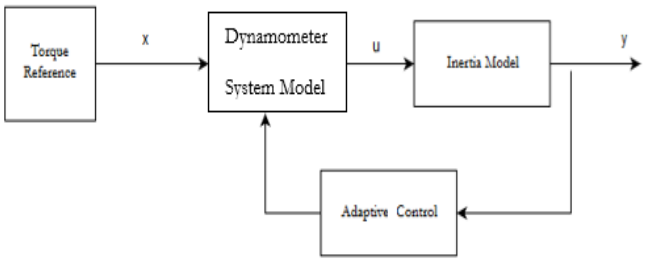


Figure 3: Control schema

The implemented control follows the same strategy explained in [1]. The Kalman filter inside is implemented as:

$$x_{k+1} = Ax_k + Bu_k + w_k \quad (15)$$

where x_{k+1} and x_k are the discrete-time instant system state variables at k+1 and k respectively. u_k is the control vector and A,B are the matrices that link the state variables at time k to k+1 and w is the weight at time k.

The equations for the online state estimation on MATLAB/Simulink are as follow. The state prediction uses the matrices that represent an optional extension for the system, which are linearised in a non-stationary operating point.

State prediction:

$$X(.|k) = \Psi \cdot x(k) + Y \cdot u(k-1) + \theta \cdot \delta u(.|k) + Xi$$

Output prediction:

$$Y(.|k) = \gamma \cdot X(.|k) \quad (16)$$

Free response:

$$f(.|k) = \gamma \cdot \Psi \cdot x(k) + Y \cdot u(k-1) \quad (17)$$

Free control error:

$$e(.|k) = r(.|k) - f(.|k) \quad (18)$$

This implemented function generates the matrices used for the prediction. The adaptive controller executes in parallel an online Kalman Filter (KF) state estimator combined with a Least Square Algorithm (LS) for parameters estimation.

$$Min\ J(x) = \big(Z - h(x)\big)^T W \big(Z - h(x)\big) \quad (19)$$

Based on the nonlinear state estimation model. The objective function is the minimisation of the weighted square of error.

$$J(x) = \sum \frac{(z_i - h_i(x))^2}{\sigma_i^2} \quad (20)$$

The process includes:

- State update
- Update variance of the state error
- Gain matrix of the Kalman Filter
- Update estimation state, the variance disturb on state and loop.

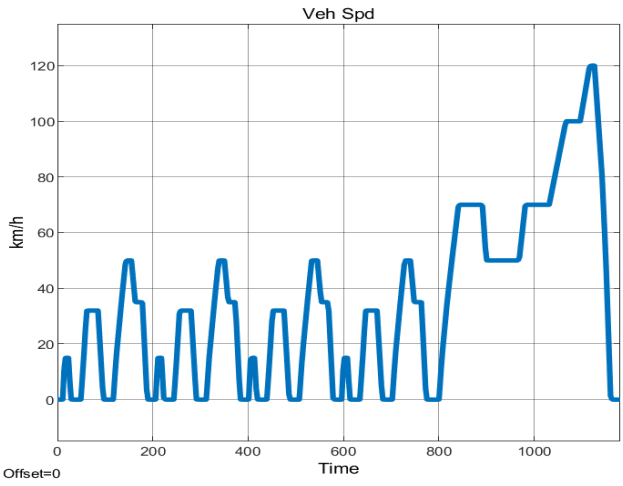
In detail, the evaluated estimation of the target is adjusted for each time, and the parameters are evaluated until the fulfilled qualities are gained. The KF is utilised for the dead-time compensation of DSM. In the KF and the A(k) and B(k) lattice are updated each progression in the calculation by the LS. The controller is additionally adjusted by the online estimation of the parameter by the LS. The evaluation of disturbance with the dead-time compensation is critical to address the distortion and the non-linearity in the general model. The undesirable deformation and significant suppression of oscillations is accomplished utilising this methodology.

5. Simulations and discussions

To verify the proposed method, the DSM model and the controller is developed using the MathWorks Matlab/Simulink software. The preliminary outcomes obtained simulating the vehicle on the testbench is shown in [1]. Based on these previous results, the simulations are enhanced, adding the updated driving cycles presented in section 2.

Table 2: Use Case table

Driving Cycle	Description			
	Time (s)	Distance (m)	Average Speed (km/h)	Fuel Consumption (gr CO_2/km)
NEDC	1180	11023	33.6	47,49
WLTP	1477	23262	44.5	50,95
FTP-72	1369	12070	31.5	52,81
FTP-75	2474	17770	34.12	49,14
ARTEMIS Urban	993	4870	17.6	102,45
ARTEMIS Rural	1082	17272	57.5	32,48
ARTEMIS Motorway	1068	28735	96.9	16,74



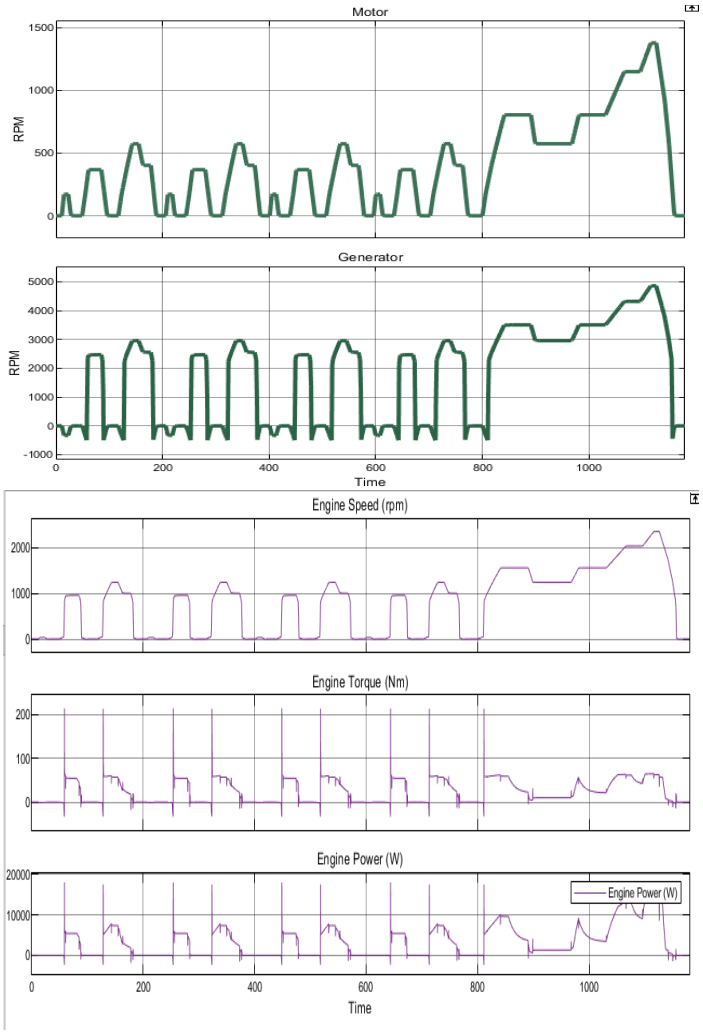
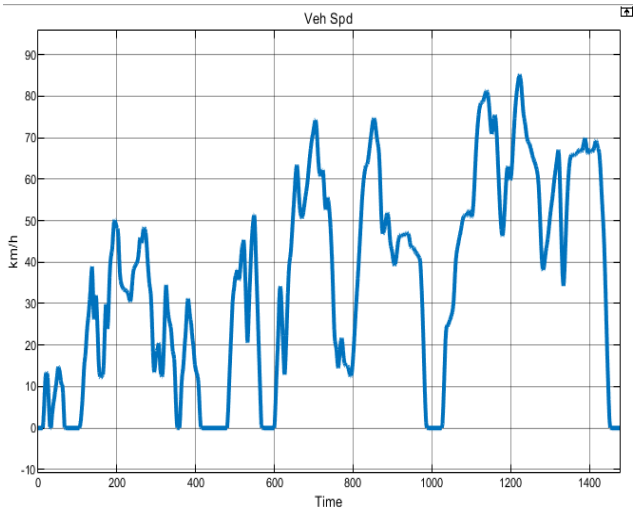


Figure 4: NEDC Cycle

Indeed, the AMPC performances exceed those of the conventional PID controller. Including the real-world disturbances on the vehicle, the PID controller no guarantees a fast, accurate response. For this reason, the authors test the considered driving cycles with AMPC controller by adding noise derived from the road.



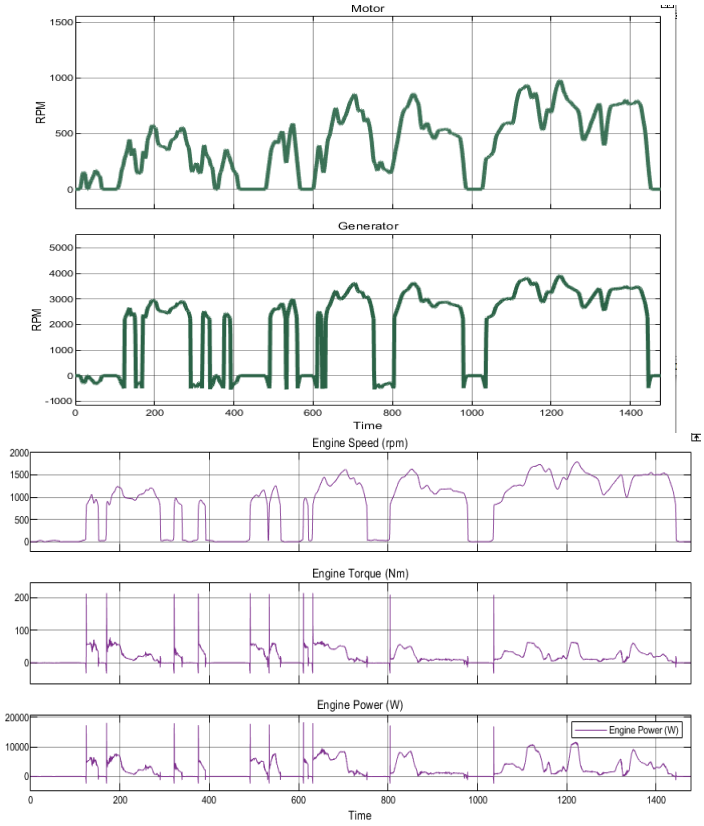


Figure 5: WLTP cycle

The torque request is based on the gas pedal value. The driving profiles are employed to examine the EiL test and to characterise the control system. Non-quantifiable amounts are assessed by filtering or with validated models. The AMPC controller results progressively strong, and the error is contained within 1.7 rpm to 2.8 rpm that is in the requirement of 3 rpm. This requirement derives from the possibility to measure not less than 3 rpm that results in the sensibility of the inverter. The error range is not changed, and this confirms and validates the control strategy. Every test procedure provides information about the behaviour of the control vehicle. Using Eil approach is important to maintain a defined speed minimum quantifiable with the physical process. The AMPC controls the reference quickly to the single setpoints while fulfilling the limitations. In the MHEVs this configuration is strongly used and the AMPC supply the ideal torque requested by the motor speed controller with more precision and control the values and references. The accuracy demonstrates through using AMPC improve the vehicle system and the reliable. The driving cycles are presented as a plot of the vehicle's speed: NEDC (Fig. 4), WLTP (Fig. 5), FTP-72 (Fig. 6), ARTEMIS Urban (Fig.7), Rural (Fig.8), Motorway (Fig.9). Furthermore, are shown the behaviour of electric motor modelled as motor or generator and the response of the engine, including the speed, the torque and the power. The description of every driving test cycle is in Table 2. The results are not only limited to the validation of the AMPC analysing the behaviour and the satisfaction of the requirements in that the emission for each test cycle is calculated. Table 2 shows the emission value for the driving cycles. The tests were chosen to cover a broad working range to investigate performance, and the controller results precise and accurate.

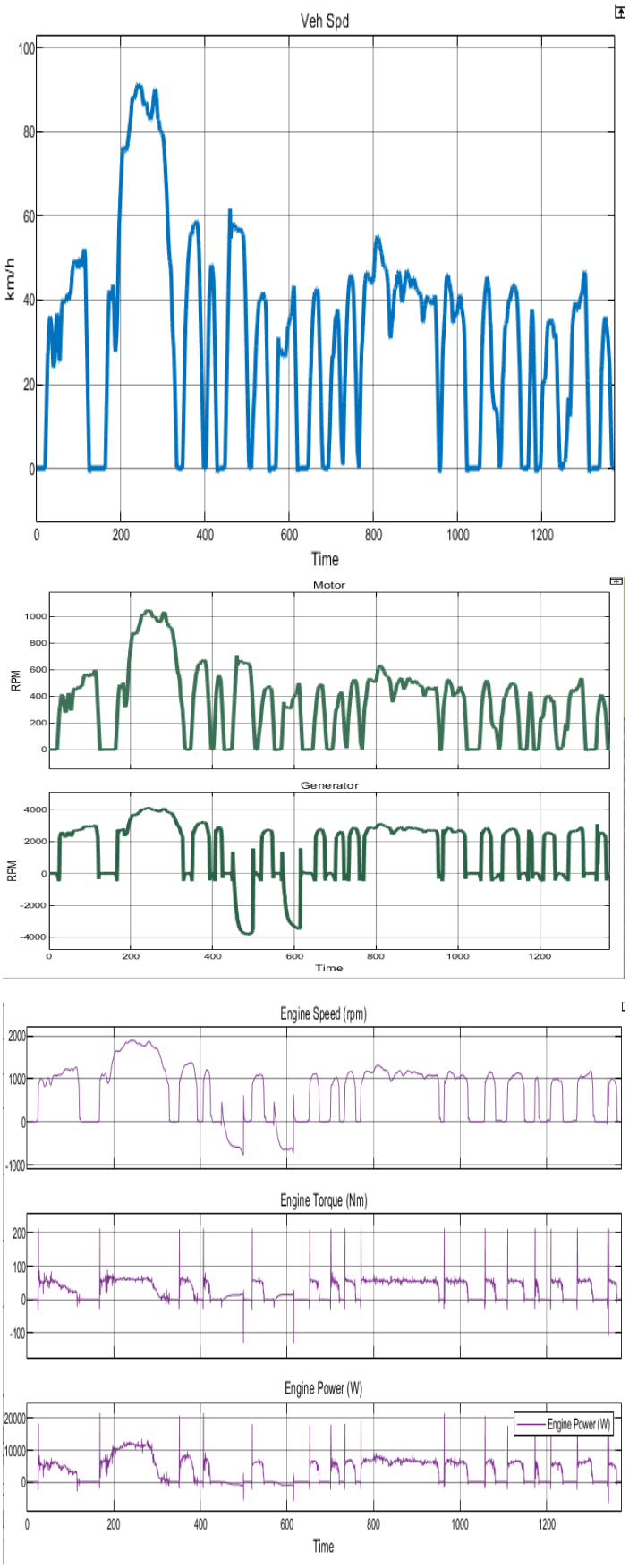


Figure 6: FTP-72 cycle

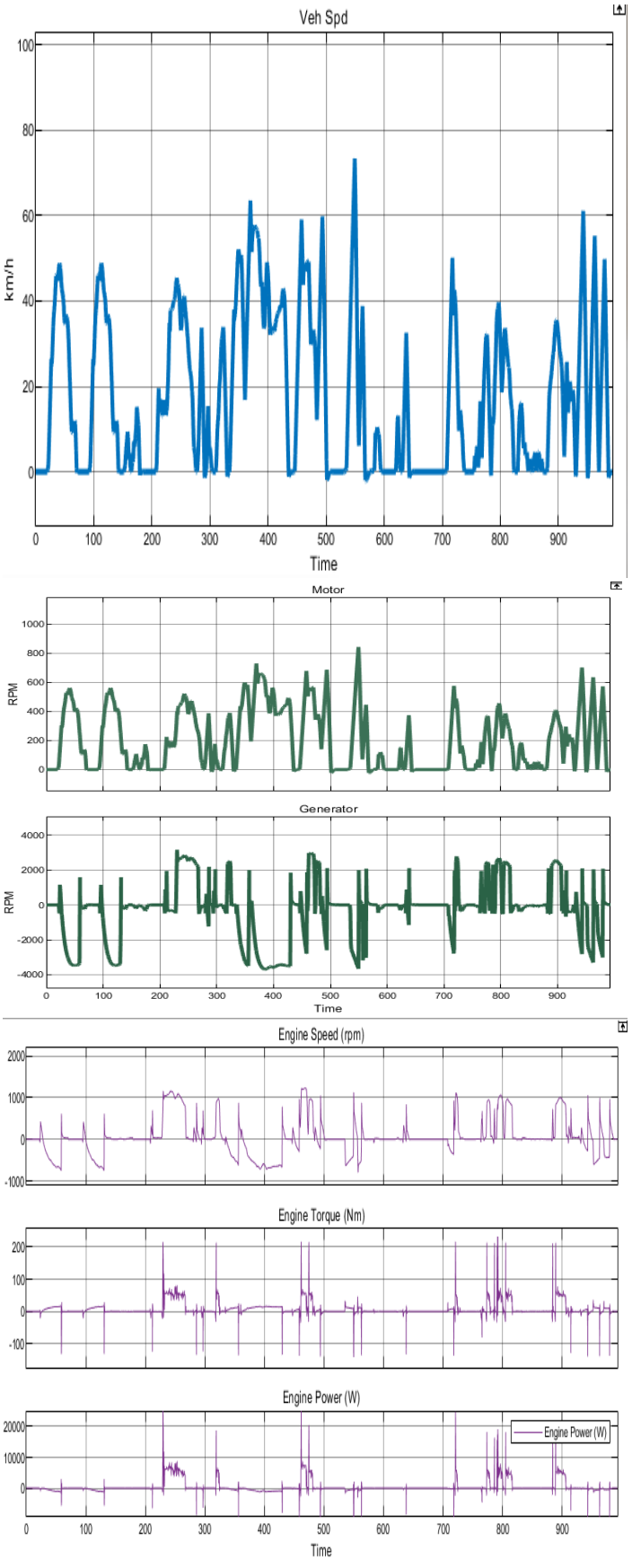


Figure 7: ARTEMIS Urban

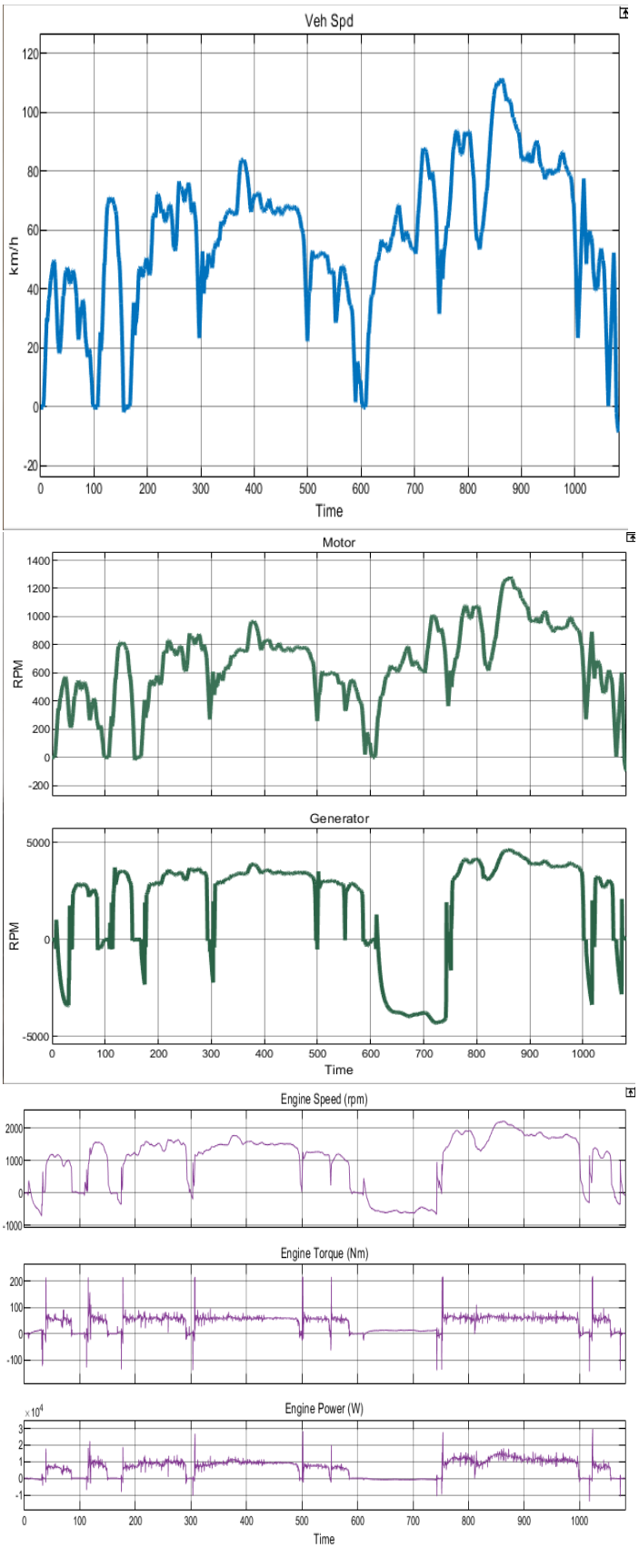


Figure 8: ARTEMIS Rural

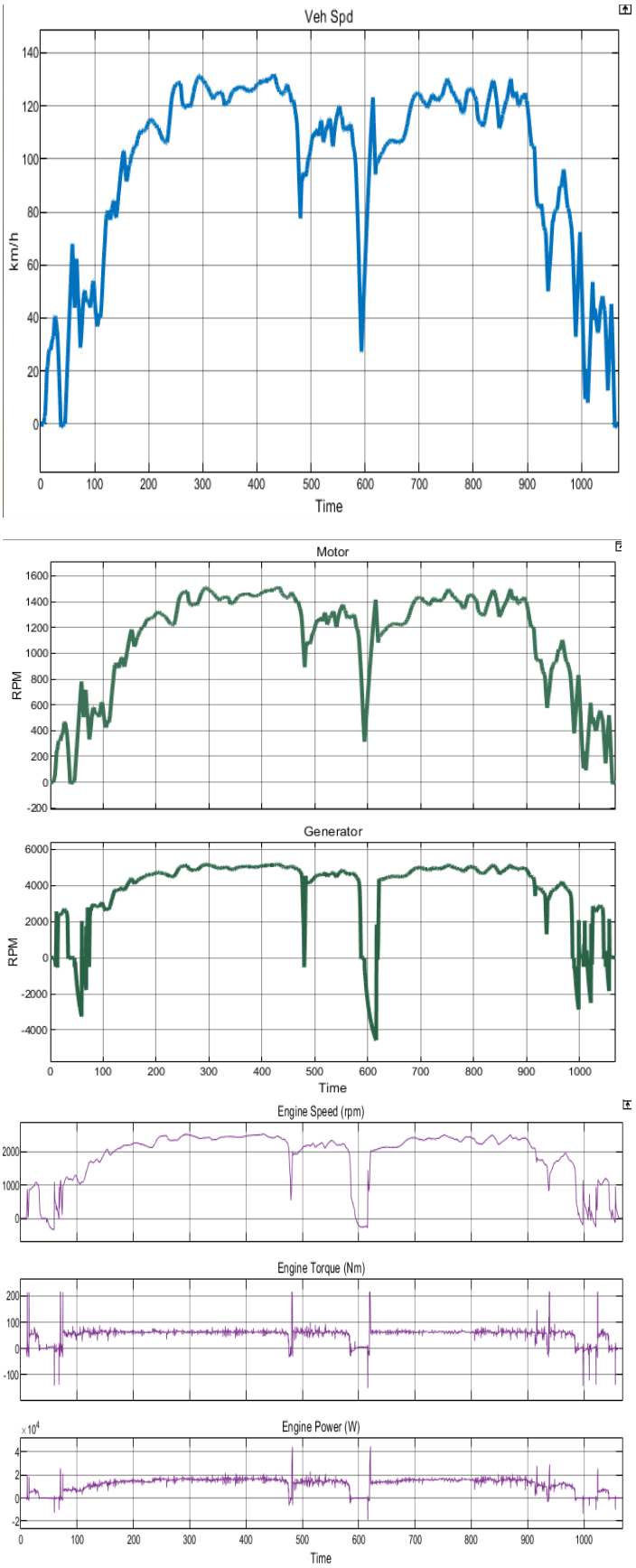


Figure 9: ARTEMIS Motorway

6. Conclusions and outlook

The results confirm the notable performances of the control strategy that allow characterising, with real feedback, the vehicles feature adding the disturbance to the road, a conventional control does not guarantee an accurate and fast response. Nevertheless, the AMPC disturbance rejection is strong, and the outcomes on the real system show excellent efficiency. This output is enhanced by measuring fuel consumption, and the results strongly validate the potential of this control strategy. Furthermore, the extension of driving cycles of the different country shows the R&R of the system. Overall, the research findings show that the nonlinear control strategies demonstrate outstanding disturbance rejection qualities. The flexibility of the testbench model can be investigated to find the single-best fit as the methods for assessing it. Moreover, these results can be extended to different vehicle's configuration as P3 and P4 and full electric vehicles in order to improve systems efficiency.

References

[1] M. Fanesi, D. Scaradozzi, "Adaptive control for non-linear test bench dynamometer systems," in 2019 23rd International Conference on System Theory, Control and Computing, ICSTCC 2019 - Proceedings, Institute of Electrical and Electronics Engineers Inc.: 768–773, 2019, doi:10.1109/ICSTCC.2019.8885558.

[2] J. Ko, S. Ko, H. Son, B. Yoo, J. Cheon, H. Kim, "Development of Brake System and Regenerative Braking Cooperative Control Algorithm for Automatic-Transmission-Based Hybrid Electric Vehicles," IEEE Transactions on Vehicular Technology, **64**(2), 431–440, 2015.

[3] F. Naseri, E. Farjah, T. Ghanbari, "An Efficient Regenerative Braking System Based on Battery/Supercapacitor for Electric, Hybrid, and Plug-In Hybrid Electric Vehicles With BLDC Motor," IEEE Transactions on Vehicular Technology, **66**(5), 3724–3738, 2017.

[4] S. Khastgir, "The simulation of a novel regenerative braking strategy on front axle for an unaltered mechanical braking system of a conventional vehicle converted into a hybrid vehicle," in 2013 Eighth International Conference and Exhibition on Ecological Vehicles and Renewable Energies (EVER), 1–6, 2013.

[5] H. Wang, Y. Huang, A. Khajepour, "Cyber-Physical Control for Energy Management of Off-Road Vehicles With Hybrid Energy Storage Systems," IEEE/ASME Transactions on Mechatronics, **23**(6), 2609–2618, 2018.

[6] H. Fathabadi, "Plug-In Hybrid Electric Vehicles: Replacing Internal Combustion Engine With Clean and Renewable Energy Based Auxiliary Power Sources," IEEE Transactions on Power Electronics, **33**(11), 9611–9618, 2018, doi:10.1109/TPEL.2018.2797250.

[7] C. Sun, S.J. Moura, X. Hu, J.K. Hedrick, F. Sun, "Dynamic Traffic Feedback Data Enabled Energy Management in Plug-in Hybrid Electric Vehicles," IEEE Transactions on Control Systems Technology, **23**(3), 1075–1086, 2015, doi:10.1109/TCST.2014.2361294.

[8] Z. Amjadi, S.S. Williamson, "Power-Electronics-Based Solutions for Plug-in Hybrid Electric Vehicle Energy Storage and Management Systems," IEEE Transactions on Industrial Electronics, **57**(2), 608–616, 2010, doi:10.1109/TIE.2009.2032195.

[9] X. Li, Q. Xu, "A Reliable Fusion Positioning Strategy for Land Vehicles in GPS-Denied Environments Based on Low-Cost Sensors," IEEE Transactions on Industrial Electronics, **64**(4), 3205–3215, 2017, doi:10.1109/TIE.2016.2637306.

[10] S. Saponara, P. Tisserand, P. Chassard, D. Ton, "Design and Measurement of Integrated Converters for Belt-Driven Starter-Generator in 48 V Micro/Mild Hybrid Vehicles," IEEE Transactions on Industry Applications, **53**(4), 3936–3949, 2017, doi:10.1109/TIA.2017.2687406.

[11] R. Romagnoli, L.D. Couto, M.M. Nicotra, M. Kinnaert, E. Garone, "Computationally-efficient constrained control of the state-of-charge of a Li-ion battery cell," in 2017 IEEE 56th Annual Conference on Decision and Control (CDC), 1433–1439, 2017, doi:10.1109/CDC.2017.8263855.

[12] J. Shen, A. Khaligh, "A Supervisory Energy Management Control Strategy in a Battery/Ultracapacitor Hybrid Energy Storage System," IEEE Transactions on Transportation Electrification, **1**(3), 223–231, 2015, doi:10.1109/TTE.2015.2464690.

[13] E. Kamal, L. Adouane, "Hierarchical Energy Optimization Strategy and Its Integrated Reliable Battery Fault Management for Hybrid Hydraulic-Electric Vehicle," IEEE Transactions on Vehicular Technology, **67**(5), 3740–3754, 2018, doi:10.1109/TVT.2018.2805353.

[14] S. Yim, J. Choi, K. Yi, "Coordinated Control of Hybrid 4WD Vehicles for Enhanced Maneuverability and Lateral Stability," IEEE Transactions on Vehicular Technology, **61**(4), 1946–1950, 2012, doi:10.1109/TVT.2012.2188921.

[15] S. Di Cairano, H.E. Tseng, D. Bernardini, A. Bemporad, "Vehicle Yaw Stability Control by Coordinated Active Front Steering and Differential Braking in the Tire Sideslip Angles Domain," IEEE Transactions on Control Systems Technology, **21**(4), 1236–1248, 2013, doi:10.1109/TCST.2012.2198886.

[16] A.H. Hajimiragha, C.A. Canizares, M.W. Fowler, S. Moazeni, A. Elkamel, "A Robust Optimization Approach for Planning the Transition to Plug-in Hybrid Electric Vehicles," IEEE Transactions on Power Systems, **26**(4), 2264–2274, 2011, doi:10.1109/TPWRS.2011.2108322.

[17] C. Quinn, D. Zimmerle, T.H. Bradley, "An Evaluation of State-of-Charge Limitations and Actuation Signal Energy Content on Plug-in Hybrid Electric Vehicle, Vehicle-to-Grid Reliability, and Economics," IEEE Transactions on Smart Grid, 3(1), 483–491, 2012, doi:10.1109/TSG.2011.2168429.

[18] H. Yu, Z. Liu, "Fault Analysis and Fault-Tolerant Control of Electric Motor Drive System in HEV," in 2012 Fifth International Conference on Intelligent Computation Technology and Automation, 177–180, 2012, doi:10.1109/ICICTA.2012.51.

[19] L. Zhang, Y. Fan, C. Li, C. Liu, "Design and Analysis of a New Six-Phase Fault-Tolerant Hybrid-Excitation Motor for Electric Vehicles," IEEE Transactions on Magnetics, **51**(11), 1–4, 2015, doi:10.1109/TMAG.2015.2447276.

[20] A. Berthon, F. Gustin, M. Bendjedia, J.M. Morelle, G. Coquery, "Inverter components reliability tests for hybrid electrical vehicles," in 2009 IEEE 6th International Power Electronics and Motion Control Conference, 763–768, 2009, doi:10.1109/IPEMC.2009.5157487.

[21] A. Drosu, G. Suciu, A. Scheianu, I. Petre, "An Analysis of Hybrid/Electric Vehicle Monitoring Systems and Parameters," in 2019 Electric Vehicles International Conference (EV), 1–5, 2019, doi:10.1109/EV.2019.8892923.

[22] Y. Cheng, C. Lai, J. Teh, "Application of Particle Swarm Optimization to Design Control Strategy Parameters of Parallel Hybrid Electric Vehicle with Fuel Economy and Low Emission," in 2018 International Symposium on Computer, Consumer and Control (IS3C), 342–345, 2018, doi:10.1109/IS3C.2018.00093.

[23] S.A. Zulkifli, S. Mohd, N. Saad, A.R.A. Aziz, "Influence of motor size and efficiency on acceleration, fuel economy and emissions of split-parallel hybrid electric vehicle," in 2013 IEEE Symposium on Industrial Electronics Applications, 126–131, 2013, doi:10.1109/ISIEA.2013.6738981.

[24] S.A. Rahman, Nong Zhang, Jianguo Zhu, "A comparison on fuel economy and emissions for conventional hybrid electric vehicles and the UTS plug-in hybrid electric vehicle," in 2010 The 2nd International Conference on Computer and Automation Engineering (ICCAE), 20–25, 2010, doi:10.1109/ICCAE.2010.5451533.

[25] A.Y. Saber, G.K. Venayagamoorthy, "Plug-in Vehicles and Renewable Energy Sources for Cost and Emission Reductions," IEEE Transactions on Industrial Electronics, **58**(4), 1229–1238, 2011, doi:10.1109/TIE.2010.2047828.

[26] C.M. Martinez, X. Hu, D. Cao, E. Velenis, B. Gao, M. Wellers, "Energy Management in Plug-in Hybrid Electric Vehicles: Recent Progress and a Connected Vehicles Perspective," IEEE Transactions on Vehicular Technology, **66**(6), 4534–4549, 2017, doi:10.1109/TVT.2016.2582721.

[27] V. Delafosse, S. Stanton, T. Sekisue, Junsik Yun, "A methodology to use simulation at every stage of a hybrid vehicle design," in 2012 IEEE Vehicle Power and Propulsion Conference, 1134–1138, 2012, doi:10.1109/VPPC.2012.6422618.

[28] H. Zhang, Y. Zhang, C. Yin, "Hardware-in-the-Loop Simulation of Robust Mode Transition Control for a Series–Parallel Hybrid Electric Vehicle," IEEE Transactions on Vehicular Technology, **65**(3), 1059–1069, 2016, doi:10.1109/TVT.2015.2486558.

[29] Zheng Li, Zetao Ma, Shumei Cui, "Design and research on engine emulation system of HEV power train hardware-in-the-loop simulation platform," in 2014 IEEE Conference and Expo Transportation Electrification Asia-Pacific (ITEC Asia-Pacific), 1–6, 2014, doi:10.1109/ITEC-AP.2014.6941031.

[30] N. Shidore, A. Ickes, T. Wallner, A. Rousseau, M. Ehsani, "Evaluation of ethanol blends for PHEVs using engine-in-the-loop," in 2011 IEEE Vehicle Power and Propulsion Conference, 1–8, 2011, doi:10.1109/VPPC.2011.6043041.

[31] Wang Lei, Yang Yalian, Peng Zhiyuan, Yang Guo, Hu Xiaosong, "Research on hybrid electrical vehicle based on human-in-the-loop simulation," in 2014 IEEE Conference and Expo Transportation Electrification Asia-Pacific (ITEC Asia-Pacific), 1–5, 2014, doi:10.1109/ITEC-AP.2014.6940738.

[32] Wu Kai, Zhang Tong, Zhu Maotao, Zhou Jianhao, "Hardware-in-the-loop simulation for multi-energy management controller of Hybrid Electric Vehicle in a virtual car environment," in 2011 International Conference on Electric Information and Control Engineering, 5061–5064, 2011, doi:10.1109/ICEICE.2011.5776933.

[33] J. Zhou, G. Ouyang, M. Wang, "Hardware-in-the-Loop Testing of Electronically-Controlled Common-Rail Systems for Marine Diesel Engine," in 2010 International Conference on Intelligent Computation Technology and Automation, 421–424, 2010, doi:10.1109/ICICTA.2010.40.

[34] Y. Liu, M. Steurer, P. Ribeiro, "A novel approach to power quality assessment: real time hardware-in-the-loop test bed," IEEE Transactions on Power Delivery, **20**(2), 1200–1201, 2005, doi:10.1109/TPWRD.2005.844251.

[35] J. Wang, H. Lee, J. Wang, C. Lin, "Robust Environmental Sound Recognition for Home Automation," IEEE Transactions on Automation Science and Engineering, **5**(1), 25–31, 2008, doi:10.1109/TASE.2007.911680.

[36] A.M. Pavan, S. Castellan, G. Sulligoi, "An innovative photovoltaic field simulator for hardware-in-the-loop test of power conditioning units," in 2009 International Conference on Clean Electrical Power, 41–45, 2009, doi:10.1109/ICCEP.2009.5212086.

[37] J. Domaszewicz, S. Lalis, A. Pruszkowski, M. Koutsoubelias, T. Tajmajer, N. Grigoropoulos, M. Nati, A. Gluhak, "Soft Actuation: Smart Home and Office with Human-in-the-Loop," IEEE Pervasive Computing, **15**(1), 48–56, 2016, doi:10.1109/MPRV.2016.5.

[38] M. Karakose, "Hardware, software, and human in the loop education supported with social network analysis and mining," in 2016 15th International Conference on Information Technology Based Higher Education and Training (ITHET), 1–5, 2016, doi:10.1109/ITHET.2016.7760721.

[39] M. Hafner, T. Finken, M. Felden, K. Hameyer, "Automated Virtual Prototyping of Permanent Magnet Synchronous Machines for HEVs," IEEE Transactions on Magnetics, **47**(5), 1018–1021, 2011, doi:10.1109/TMAG.2010.2091675.

[40] X. Zeng, S. Zheng, D. Song, "Modeling and dynamic simulation of a virtual prototype for applying automobile differential into hybrid electric vehicle as power-slit device," in 2010 International Conference on Computer Application and System Modeling (ICCASM 2010), V3-82-V3-87, 2010, doi:10.1109/ICCASM.2010.5620147.

[41] R.S. Vadamalu, C. Beidl, "Explicit MPC PHEV energy management using Markov chain based predictor: Development and validation at Engine-In-The-Loop testbed," in 2016 European Control Conference (ECC), 453–458, 2016, doi:10.1109/ECC.2016.7810326.

[42] Y. Kim, A. Salvi, A.G. Stefanopoulou, T. Ersal, "Reducing Soot Emissions in a Diesel Series Hybrid Electric Vehicle Using a Power Rate Constraint Map," IEEE Transactions on Vehicular Technology, **64**(1), 2–12, 2015, doi:10.1109/TVT.2014.2321346.

[43] Liyong Yang, Xiaolin Peng, Zhengxi Li, "Induction motor electrical parameters identification using RLS estimation," in 2010 International Conference on Mechanic Automation and Control Engineering, 3294–3297, 2010, doi:10.1109/MACE.2010.5535653.

[44] J. Xiaochun, Y. Geng, W. yunfei, "A Parameter Identification Method for General Inverter-fed Induction Motor Drive," in 2006 CES/IEEE 5th International Power Electronics and Motion Control Conference, 1–5, 2006, doi:10.1109/IPEMC.2006.4778331.

[45] B. Zhu, K. Rajashekara, H. Kubo, "Comparison between current-based and flux/torque-based model predictive control methods for open-end winding induction motor drives," IET Electric Power Applications, **11**(8), 1397–1406, 2017, doi:10.1049/iet-epa.2016.0517.

[46] M. Pakmehr, T. Yucelen, "Adaptive control of uncertain systems with gain scheduled reference models and constrained control inputs," in 2014 American Control Conference, 691–696, 2014, doi:10.1109/ACC.2014.6859326.

[47] D. Bourlis, J.A.M. Bleijs, "Gain scheduled controller with wind speed estimation via Kalman filtering for a stall regulated variable speed wind turbine," in 2009 44th International Universities Power Engineering Conference (UPEC), 1–5, 2009.

[48] T. Ertuğrul, M.A. Adli, M.U. Salamci, "Model reference adaptive control design for helicopters using gain scheduled reference models," in 2016 17th International Carpathian Control Conference (ICCC), 182–187, 2016, doi:10.1109/CarpathianCC.2016.7501090.

[49] E. Gruenbacher, L. del Re, "Robust inverse control for combustion engine test benches," in 2008 American Control Conference, 2852–2857, 2008, doi:10.1109/ACC.2008.4586926.

[50] C. Yang, M. Zha, W. Wang, K. Liu, C. Xiang, "Efficient energy management strategy for hybrid electric vehicles/plug-in hybrid electric vehicles: review and recent advances under intelligent transportation system," IET Intelligent Transport Systems, **14**(7), 702–711, 2020, doi:10.1049/iet-its.2019.0606.

[51] J.E. Siegel, D.C. Erb, S.E. Sarma, "A Survey of the Connected Vehicle Landscape—Architectures, Enabling Technologies, Applications, and Development Areas," IEEE Transactions on Intelligent Transportation Systems, **19**(8), 2391–2406, 2018, doi:10.1109/TITS.2017.2749459.

[52] M. Traub, A. Maier, K.L. Barbehön, "Future Automotive Architecture and the Impact of IT Trends," IEEE Software, **34**(3), 27–32, 2017, doi:10.1109/MS.2017.69.

[53] T. Sivakumaran, F. Köhne, M. Toth, "Identification of critical success factors for emerging market entry planning processes in the automotive industry," in 2015 IEEE International Conference on Industrial Engineering and Engineering Management (IEEM), 1694–1698, 2015, doi:10.1109/IEEM.2015.7385936.

[54] L. Hanwu et al., "Regularity of Current Dispersal in Different Kinds of Grounding Electrode," in 2018 IEEE International Conference on High Voltage Engineering and Application (ICHVE), 1–4, 2018. doi: 10.1109/ICHVE.2018.8642240

[55] A. Balluchi, L. Benvenuti, M.D. di Benedetto, C. Pinello, A.L. Sangiovanni-Vincentelli, "Automotive engine control and hybrid systems: challenges and opportunities," Proceedings of the IEEE, **88**(7), 888–912, 2000, doi:10.1109/5.871300.

[56] H. A. Raza et al., "Analysis the effect of 500kv High-Voltage Power Transmission Line on the Output Efficiency of Solar-Panels," in 2019 International Conference on Electrical, Communication, and Computer Engineering, 1–6, 2019. doi: 10.1109/ICECCE47252.2019.8940803

[57] A.R. Mahayadin, I. Ibrahim, I. Zunaidi, A.B. Shahriman, M.K. Faizi, M. Sahari, M.S.M. Hashim, M.A.M. Saad, M.S. Sarip, Z.M. Razlan, M.F.H. Rani, Z.M. Isa, N.S. Kamarrudin, A. Harun, Y. Nagaya, "Development of Driving Cycle Construction Methodology in Malaysia's Urban Road System," in 2018 International Conference on Computational Approach in Smart Systems Design and Applications (ICASSDA), 1–5, 2018, doi:10.1109/ICASSDA.2018.8477619.

[58] A. Charadsuksawat, Y. Laoonual, N. Chollacoop, "Comparative Study of Hybrid Electric Vehicle and Conventional Vehicle Under New European Driving Cycle and Bangkok Driving Cycle," in 2018 IEEE Transportation Electrification Conference and Expo, Asia-Pacific (ITEC Asia-Pacific), 1–6, 2018, doi:10.1109/ITEC-AP.2018.8432599.

[59] A.R. Salisa, N. Zhang, J.G. Zhu, "A Comparative Analysis of Fuel Economy and Emissions Between a Conventional HEV and the UTS PHEV," IEEE Transactions on Vehicular Technology, **60**(1), 44–54, 2011, doi:10.1109/TVT.2010.2091156.

[60] J. Liu, L. Zhang, Q. Chen, S. Quan, R. Long, "Hardware-in-the-loop test bench for vehicle ACC system," in 2017 Chinese Automation Congress (CAC), 1006–1011, 2017, doi:10.1109/CAC.2017.8242913.

[61] M.H. Salah, T.H. Mitchell, J.R. Wagner, D.M. Dawson, "A Smart Multiple-Loop Automotive Cooling System—Model, Control, and Experimental Study," IEEE/ASME Transactions on Mechatronics, **15**(1), 117–124, 2010, doi:10.1109/TMECH.2009.2019723.

[62] J. Zhao, J. Wang, "Adaptive Observer for Joint Estimation of Oxygen Fractions and Blend Level in Biodiesel Fueled Engines," IEEE Transactions on Control Systems Technology, **23**(1), 80–90, 2015, doi:10.1109/TCST.2014.2313003.

[63] A. Pratt, M. Ruth, D. Krishnamurthy, B. Sparn, M. Lunacek, W. Jones, S. Mittal, H. Wu, J. Marks, "Hardware-in-the-loop simulation of a distribution system with air conditioners under model predictive control," in 2017 IEEE Power Energy Society General Meeting, 1–5, 2017, doi:10.1109/PESGM.2017.8273757.

[64] D. Michalek, C. Gehsat, R. Trapp, T. Bertram, "Hardware-in-the-loop-simulation of a vehicle climate controller with a combined HVAC and passenger compartment model," in Proceedings, 2005 IEEE/ASME International Conference on Advanced Intelligent Mechatronics., 1065–1070, 2005, doi:10.1109/AIM.2005.1511151.

[65] S. Jiang, M. Smith, J. Kitchen, A. Ogawa, "Development of an Engine-in-the-loop Vehicle Simulation System in Engine Dynamometer Test Cell," in SAE Technical Papers, 2009, doi:10.4271/2009-01-1039.

[66] T. Jung, M. Kötter, J. Schaub, C. Quérel, S. Thewes, H. Hadj-amor, M. Picard, S.-Y. Lee, Engine-in-the-Loop: A Method for Efficient Calibration and Virtual Testing of Advanced Diesel Powertrains: Antriebsentwicklung im digitalen Zeitalter 20. MTZ-Fachtagung, 209–224, 2019,

doi:10.1007/978-3-658-25294-6_12.
[67] F.C. Nemtanu, I.M. Costea, D. Buretea, L.G. Obreja, "Hardware in the loop simulation platform for intelligent transport systems," in 2017 IEEE 23rd International Symposium for Design and Technology in Electronic Packaging (SIITME), 247–250, 2017, doi:10.1109/SIITME.2017.8259901.
[68] R. Isermann, J. Schaffnit, S. Sinsel, "Hardware-in-the-Loop Simulation for the Design and Testing of Engine-Control Systems," IFAC Proceedings Volumes, **31**(4), 1–10, 1998, doi:https://doi.org/10.1016/S1474-6670(17)42125-2.
[69] M. Nasri, M. Kargahi, M. Mohaqeqi, "Scheduling of Accuracy-Constrained Real-Time Systems in Dynamic Environments," IEEE Embedded Systems Letters, **4**(3), 61–64, 2012, doi:10.1109/LES.2012.2195294.
[70] B.J. Bunker, M.A. Franchek, B.E. Thomason, "Robust multivariable control of an engine-dynamometer system," IEEE Transactions on Control Systems Technology, **5**(2), 189–199, 1997, doi:10.1109/87.556024.
[71] A. Ahmed et al., "Modeling and Simulation of Office Desk Illumination Using ZEMAX," in 2019 International Conference on Electrical, Communication, and Computer Engineering (ICECCE), 1–6, 2019. DOI: 10.1109/ICECCE47252.2019.8940756
[72] R. Jayaraman, A. Joshi, V. To, G. Kaid, "Fidelity Enhancement of Power-Split Hybrid Vehicle HIL (Hardware-in-the-Loop) Simulation by Integration with High Voltage Traction Battery Subsystem," 2018, doi:10.4271/2018-01-0008.
[73] H. Holzmann, K. Hahn, J. Webb, O. Mies, "Simulation-Based ESC Homologation for Passenger Cars," ATZ Worldwide, **114**, 40–43, 2012, doi:10.1007/s38311-012-0218-5.
[74] U. Baake, K. Wüst, M. Maurer, A. Lutz, "Testing and simulation-based validation of ESP systems for vans," ATZ Worldwide, **116**, 30–35, 2014, doi:10.1007/s38311-014-0021-6.
[75] G. Siva Sankar, R. Shekhar, C. Manzie, T. Sano, H. Nakada, "Fast Calibration of a Robust Model Predictive Controller for Diesel Engine Airpath," 2018.
[76] A. White, G. Zhu, J. Choi, "Hardware-in-the-Loop Simulation of Robust Gain-Scheduling Control of Port-Fuel-Injection Processes," IEEE Transactions on Control Systems Technology, **19**(6), 1433–1443, 2011, doi:10.1109/TCST.2010.2095420.
[77] H. Schuette, M. Ploeger, "Hardware-in-the-Loop Testing of Engine Control Units - A Technical Survey," SAE Transactions, **116**, 86–107, 2007.
[78] V.D. Veksler, C.W. Myers, K. Gluck, "Model flexibility analysis.," Psychological Review, 122 4, 755–769, 2015.

ASTES

Advances in Science, Technology and Engineering Systems Journal Vol. 5, No. 5, 1184-1188 (2020)

www.astesj.com

ASTESJ

ISSN: 2415-6698

Development of the Surface Roughness Model in the Grinding Processes

Nhu-Tung Nguyen, Dung Hoang Tien, Do Duc Trung *

Faculty of Mechanical Engineering, Hanoi University of Industry, Hanoi, 100000, Vietnam

ARTICLE INFO

Article history:
Received: 08 August, 2020
Accepted: 17 October, 2020
Online: 22 October, 2020

Keywords:
Surface Roughness Model
Grinding Grain
Undeform Chip Thickness

ABSTRACT

This paper presents a research about the modelling of surface roughness in the grinding process. Based on the analyzed results about the surface roughness models from the previous studies, this study was performed to develop a surface roughness model in the grinding process. The surface roughness model is proposed with two hypotheses about the shape and ratio of the number of scratches of the grinding grains leaving on the workpiece surface. The first hypothesis is that the shapes of scratches of the grinding grains leave on the workpiece surface with five types including the triangle, the curved arc, the parabolic, the semi-circular, and the curved arc of a quarter circle. The second hypothesis is that the ratios of the number of the scratches with different shapes of the grinding grains leaving on the workpiece surface are the same (all are equal to 20%). This research paper discusses about the modelling of surface roughness when considering many shapes of scratches of the grinding grains left on the machining surface. This proposed model can be used to calculate the surface roughness in grinding processes of the different pairs of grinding wheels and workpieces. The developed surface roughness model has been applied to calculate the surface roughness during the grinding of SUJ2 steel using an aluminum oxide grinding wheel. Calculated surface roughness using proposed model were quite close to the experimental results. The average difference between calculated and the experimental results was about 14.84%. This study offers a promising ability to calculate the machining surface roughness in the grinding processes.

Nomenclature

a - Cutting depth.

a_d - Grinding wheel dressing depth.

b_s - Grinding wheel width.

C - Grinding grain concentration (for diamond and CBN grinding wheels).

d_e - Equivalent diameter of grinding wheel.

d_g - Diameter of the grinding grain.

d_s - Grinding wheel diameter.

d_w - Workpiece diameter.

$E(h)$ - Expectation of the undeformed chip thickness.

$E(R_a)$ - Expectation of the surface roughness.

h - Undeformed chip thickness in grinding processes.

f - Ratio of the part volume of particle (participated in the cutting processes) and the volume of particle.

L - Contact length between the grinding wheel and the machining surface.

M - Graininess of the grinding wheel (The number of sieve holes per square inch of the sieve).

N - Number of dynamic cutting grinding particles per unit area of grinding wheel surface.

r - Ratio between the length and the height of the chip.

S - Structure number of the grinding wheel (for normal grinding wheel).

s_d - Grinding wheel dressing feed rate.

s_t - Plunge feed rate.

V_g - Volume ratio of the grinding particles in the grinding wheel.

v_s - Grinding wheel velocity.

v_w - Workpiece velocity.

*Corresponding Author: Do Duc Trung, Faculty of Mechanical Engineering, Hanoi University of Industry, Vietnam, doductrung@haui.edu.vn

1. Introduction

Grinding method is one of the most common machining methods in the metal cutting processes. This method is often chosen as a finishing machining process to machine the surfaces with requirement of high dimension precision and high surface quality [1, 2].

Surface roughness has much influence on the working ability and the life of the mechanical products. So, the surface roughness is often selected as one of the most important factors to evaluate the efficiency of a grinding process. However, in the investigation of grinding surface roughness, the experimental method costs much time and money usually. Besides, this method is only applied to a few specific cases, the application ability of experimental results is the limitation [3] and [4].

The grinding surface roughness was modeled by different methods. In this study, the surface roughness models in the previous studies were analyzed, and then a new surface roughness model was developed to calculate the surface roughness in the grinding processes. The accuracy of the development surface roughness model has been validated through the experiments of grinding processes.

2. A brief review of some surface roughness models in the grinding processes

To overcome the limitations of the experimental methods, many studies were performed to model the grinding surface roughness by different methods. The surface roughness models were built depending on the parameters of the grinding processes as presented in the Table 1.

From the Table 1, it seems that the surface model was modeled by only considering the relationship between surface roughness and the workpiece velocity, grinding wheel velocity, the grinding wheel diameter, and the contact length between the grinding wheel and the machining surface [3]. In this model, the effect of characteristic parameters of grinding wheel such as the graininess of the grinding wheel, the structure number of the grinding wheel, etc. on the surface roughness has not mentioned. So, it is difficult to apply this model in different cases when using different grinding wheels.

In the model 2, the surface roughness was built depending on the velocity of workpiece and velocity of grinding wheel [5], [6]. In these studies, the effect of other parameters on the surface roughness was evaluated through the adjustment coefficients R_1 and the exponential number x_1. So, to apply this model in the calculation of surface roughness, the experiments must be conducted to determine the values of the coefficients R_1 and x_1. Similarly, to apply the model (3), the experiments must be performed to determine to coefficients R_2 and x_2 [7].

In the Table 2, some surface roughness models were presented based on the specific machining conditions. These models can be directly used to calculate the surface roughness. However, these models were only applied to calculate the surface roughness for the case the workpiece material, the grinding wheel types to be the same that one in the proposed research models.

Table 1: Surface roughness models – Type 1

Source	Model	Note	No.
[3]	$R_a = \frac{1}{9\sqrt{3}}\left(\frac{v_w L}{v_s d_s^{1/2}}\right)^2$	The surface roughness was built for surface grinding processes.	(1)
[5] and [6]	$R_a = R_1\left(\frac{v_w a}{v_s}\right)^{x_1}$	R_1 and x_1 are the constants that depend on the machining conditions and can be determined by experimental method.	(2)
[7]	$R_a = R_2 s_d^{0.5}\, a_d^{0.25}\left(\frac{v_w a}{v_s}\right)^{x_2}$	R_2 and x_2 are the constants that depend on the machining conditions and can be determined by experimental method.	(3)

Table 2: Surface roughness model - Type 2

Source	Model	Grinding wheel	Workpiece	No.
[8]	$R_a = 12.9 s_d^{0.54} a_d^{0.34}\left(\frac{v_w}{v_s}\right)^{0.38}\left(\frac{s_t}{b_s}\right)^{0.43}$	38A60K5VBE	4140 steel	(4)
[9]	$R_a = 0.92 * 0.3574^{0.094} * h$	HY-180x13x31.75-	C45 steel	(5)
[10] and [11]	$R_a = 0.487\, T_{av}^{0.3} \quad for \quad 0 < T_{av} < 0.254$ $R_a = 0.7866\, T_{av}^{0.72} \quad for \quad 0.254 < T_{av} < 2.54$ Where: $T_{av} = 12.5 \times 10^3 \frac{d_g^{16/27} a_p^{19/27}\left(1 + \frac{a_d}{d^e}\right)}{s_d^{16/27}\left(\frac{v_w}{v_s}\right)}$	2A80K4VFMB	AISI 52100 steel	(6)

In the Table 3, the surface roughness models were built depending on the undeformed chip thickness and the adjustment coefficient (R). These models were built based on the theory of cutting processes in which these models did not depend on the specific machining conditions (grinding wheel types, workpiece materials, and so on). So, these models can be applied in a wider range than the above models. Besides, the undeformed chip thickness that has the relationship to the many parameters of the grinding processes including the cutting parameters, the grinding wheel geometry, etc. This relationship would be presented in the detail in the next sections.

Table 3: Surface roughness model - Type 3

Models	Note	No.
$E(R_a) = 0.37\,E(h)$, [4]	Hypothesis was that shapes of scratches of the grinding particles leaving on the workpiece surface was the triangle.	(7)
$E(R_a) = 0.423\,E(h)$, [12]	Hypothesis was that shapes of the scratches of the grinding particles leaving on the workpiece surface was the curved arc.	(8)
$E(R_a) = 0.396\,E(h)$, [13]	Hypothesis was that shapes of scratches of the grinding particles leaving on the workpiece surface was the parabolic.	(9)
$E(R_a) = 0.471\,E(h)$, [14]	Hypothesis was that shapes of scratches of the grinding particles leaving on the workpiece surface was the semi-circular.	(10)
$E(R_a) = 0.92\,E(h)$, [15]	Hypothesis was that shapes of scratches of the grinding particles leaving on the workpiece surface was the curved arc of a quarter circle.	(11)

The above cited surface roughness models showed that depending on the different hypotheses about the shapes of the scratches of the grinding grains left on the workpiece surface. Few literatures were performed to confirm the exact shape of each of the scratches of the grinding grains left on the workpiece surface. It can be inferred that during the grinding processes, the geometry of the grinding grains is always changing (texture, form, self-dressing, and so on). These features on each cut of grinding grains left on the workpiece surface will always change. The shapes of scratches of the grinding grains left on the workpiece surface did not retain the shapes like that one in the hypotheses of the previous literatures. Hence, it is necessary to develop a surface roughness model considering the different shapes of scratches of the grinding grains left on the workpiece surface.

3. Developing a surface roughness model in grinding process

In this study, the surface roughness modelling was performed for grinding processes. The surface roughness model was built with two hypotheses as following:

The first hypothesis is that the shapes of the scratches of the grinding grain left on the workpiece surface are of five types such as triangle, curved arc, parabolic, semi-circular, and curved arc of a quarter circle.

The second hypothesis is that the ratios of the number of the scratches with different shapes of the grinding grains leaving on the workpiece surface are the same (all are equal to 20%).

Basing on above two hypotheses and the analyzed results from Table 3, the surface model that was proposed in this study as presented by (12).

$$E(R_a) = 0.516\,E(h) \tag{12}$$

Where $E(R_a)$ - The expectation of the surface roughness.

$E(h)$ - The expectation of thickness of undeformed chip.

The undeformed chip thickness (h) has been mentioned in many studies. However, to present of this study in detail and clearly, the undeformed chip thickness was determined as following: According to reference [16], the undeformed chip thickness (h) that was calculated by (13) and (14).

$$h = 2\sqrt{\frac{1}{N.r}\frac{v_w}{v_S}\sqrt{\frac{a}{d_e}}} \tag{13}$$

$$d_e = \frac{d_S.d_W}{d_S \pm d_W} \tag{14}$$

According to reference [17], it was difficult to determine the value of "r", that was selected in the range from 10 to 20. In this study, the value of "r" was chosen by 20 (selecting according to previous studies [18] and [19]).

According to reference [19], the value of "N" that was determined by (15).

$$N = 4f\frac{1}{d_g^2}\frac{1}{\sqrt[3]{\left(\frac{4\pi}{3\,V_g}\right)^2}} \tag{15}$$

According to reference [18], it was also difficult to determine the value of "f". In almost case, it can be assumed that half of a grinding grain that participated in cutting process. It means that $f = 0.5$.

d_g is diameter of grinding grain that was determined from (16) to (18).

$$d_g = 15.2/M \tag{16}$$

The value of V_g was selected depending on the grinding wheel structure number (S). With common grinding wheel, the structure number is from 0 to 16, the value of V_g is determined by (17) which means if the structure number increases one time, the volume of the grinding particles in the grinding wheel decreases 2%. According to reference [3] the maximum value of V_g does not exceed 60%.

$$V_g\,(\%) = 2(32 - S) \tag{17}$$

$$V_g\ (\%) = 0.25 * C \quad (18)$$

For the cases of the diamond and CBN grinding wheels, V_g is determined according to the sign of the grinding particle concentration as listed in Table 4, [20]. From this table, for the diamond and CBN grinding wheels, the grinding particle concentration was determined by (18).

Table 4: The V_g of several diamond and CBN grinding wheel [20]

Concentration sign, C	25	50	75	100	125	150	175	200
V_g (%)	6.25	12.50	18.75	25.00	31.25	37.50	43.75	50.00

From the (12) to (18), the surface roughness can be calculated by the block diagram with the parameters of the grinding process (r , f, v_w, v_s, a, d_s, M, S, C và d_W) as shown in the Figure 1.

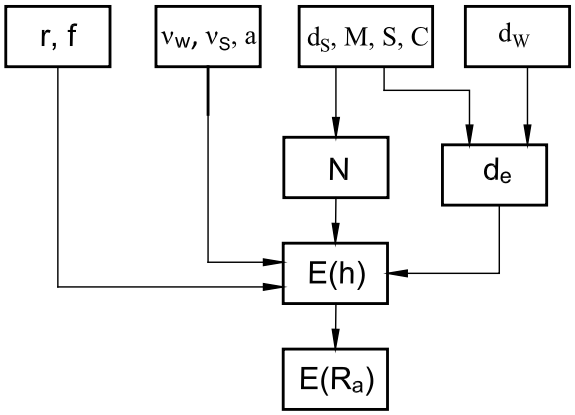


Figure 1: Block diagram of surface roughness calculation

4. Validation of the developed surface roughness model

The SG-5010AHR surface grinding machine was used to perform the experiments (Figure 2). The experimental workpiece was steel SUJ2 with the dimensions: length of 80 mm, width 40 mm, and height of 10 mm (Figure 3). This steel is often chosen for the fabrication of parts with high precision and surface gloss such as bearings, mold guide shafts, gears, etc. This study used an aluminum oxide grinding wheel with the symbol Cn100GV1x250x30x75x35m/s. This grinding wheel was produced by Hai Duong Grinding Stone Company (Viet Nam).



Figure 2: Experimental machine



Figure 3: Experimental workpieces (SUJ2 steel)

In experimental method, 6 experiments were performed with the change of depth of cut, and 6 experiments were performed with the change of the workpiece velocity. Before each experiment, grinding wheel was dressed with a dressing depth of 0.01 mm and the dressing feed rate of 150 mm/min, respectively. Surface roughness SJ-210 tester was used to measure surface roughness (Ra) of the product. The basic parameters of this measuring equipment are shown in Table 5. And then, the measured results were used to compare to the calculated results by using proposed model of surface roughness. The compared results were described in Figure 4 and Figure 5. Figure 4 showed the surface roughness when calculating and measuring with varying depth of cut. For example: with point 6 in Figure 4: when the depth of cut is 10 (µm), the surface roughness when measuring and calculating are 1.92 (µm) and 1.57 (µm), respectively. Figure 5 showed the calculated surface roughness and the measured surface roughness when changing the workpiece velocity. For example: with point 11 in Figure 5: when the workpiece velocity is 11 (m/min), the surface roughness in the measurement and calculation are 1.42 (µm) and 1.72 (µm), respectively.

Table 5: Parameter of SJ301 surface tester (Mitutoyo – Japan)

Model	SJ-301
Trademark	Mitutoyo
Display	Touch screen and integration printer
Monitor	14.5cm (5.7 inch)
Cable length	1 m
Measurement method	Induction method
Sliding radius	40 mm
Measurement force	0.75 mN
Interface port	RS-232 C
Resistance wear standard	EN ISO, VDA, ANSI, JIS
Digital filter	2RC -75%, 2RC -75%
Auto rest	after 5 minutes

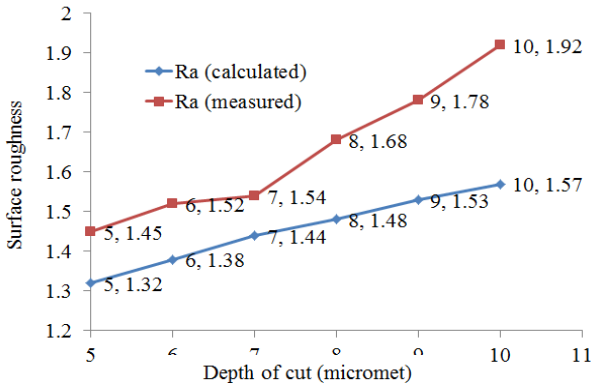


Figure 4: Measured and calculated surface roughness with the change of the cutting depth

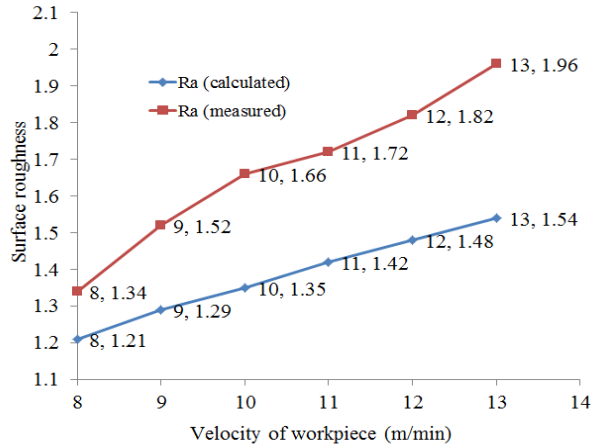


Figure 5: Measured and calculated surface roughness with the change of the workpiece velocity

The results of Figures 4 and Figures 5 illustrates that by using proposed model, the calculated and experimental results were quite close to each other. The average difference between the calculated and experimental results was 11.51% considering the depth of cut and 18.18 % for change in the velocity. The average difference between the calculated and experimental results was 14.84% for all cases.

5. Conclusion

The conclusion of this paper was drawn based on the investigation:

- A new model of surface roughness has been proposed considering different shapes of abrasive cuts left on the surface of the workpiece.

- The evaluation of the proposed surface roughness model in this study was carried out when grinding the SUJ2 steel using the aluminum oxide grinding wheel. The results inferred that the calculated surface roughness was quite close to the experimental.

In addition, the parameters of grinding wheel dressing mode, cooling lubrication parameters, and others also considered in the surface roughness model will be implemented in the further research.

Acknowledgment

The authors thank for support from Hanoi University of Industry (https://www.haui.edu.vn) in the experimental research.

References

[1] O. Kazuhito, T. Kazuya, A. Tomoya, T. Shinya, "Quick On-Machine Measurement of Ground Surface Finish Avaiable for Mass Production Cylindrical Grinding Process," International Journal of Automation Technology, **9**(2), 176-183, 2015, doi:https://doi.org/10.20965/ijat.2015.p0176

[2] L. Tao, D. Zhaohui, L. Lishu, S. Shuailong, L. Wei, L. Chengyao, "Experimental Analysis of Process Parameter Effects on Vibrations in the High-Speed Grinding of a Camshaft," Strojniški vestnik - Journal of Mechanical Engineering, **66**(3), 175-183, 2020.

[3] M. Stephen, G. Changsheng, Grinding technology theory and applications of machining with abrasives, Insustrial press, New York. 2008.

[4] L.R. Hecker, Y.L. Steven, "Predictive modeling of surface roughness in grinding," International Journal of Machine Tools and Manufacture, **43**, 755-761, 2003, doi:https://doi.org/10.1016/S0890-6955(03)00055-5

[5] R. Snoeys, J. Peters, and A. Decneut, "The Significance of Chip Thickness in Grinding," Annals of the CIRP, **23**, 227-237, 1974.

[6] S.M. Kedrov, "Investigation of Surface Finish in Cylindrical Grinding Operations," Machines and Tooling, **51**(1), 40-45, 1980.

[7] S. Akram, B. Robert, W. Andrew, "Investigation of single-point dressing overlap ratio and diamond-roll dressing interference angle on surface roughness in grinding," Transactions of the Canadian Society for Mechanical Engineering, **34**(2), 295-308, 2010.

[8] C.W. Lee, T. Choi, and Y.C. Shin, "Intelligent Model-based optimisation of the surface grinding process for heat treated 4140 steel alloys with Aluminium oxide grinding wheels," Journal of Manu-facturing an Engineering, **125**, 65-76, 2003, doi:10.1115/1.1537738

[9] V.T. Nguyen, D.T. Do, H.K. Le, H.A. Le, "Prediction of Surface Roughness When Surface Prediction of Surface Roughness When Surface," Universal Journal of Mechanical Engineering, **8**(2), 92-96, 2020, doi:10.13189/ujme.2020.080203

[10] R.P. Lindsay, R.P., and S. Hahn. "On the surface finish-metal removal relationship in precision grinding," Annals of the CIRP, 95(3), 815–820, 1973, https://doi.org/10.1115/1.3438231

[11] X.M. Wen, A. A. O Tay, A. Y. C Nee, "Micro-Computer-based optimization of the surface grind-ing process," Journal of Material Processing Technology, **29**,75-90, 1992, doi:https://doi.org/10.1016/0924-0136(92)90426-S.

[12] A. Sanjay, P.V. Rao, "A probabilistic approach to predict surface roughness in ceramic grinding," International Journal of Machine Tools & Manufacture, **45**(6), 609–616, 2005, doi:https://doi.org/10.1016/j.ijmachtools.2004.10.005.

[13] A. Sanjay, P.V. Rao, "Surface roughness prediction model for ceramic grinding," International Mechanical Engineering Congress and Exposition, **79180**, 2005, doi:10.1115/IMECE2005-79180.

[14] K.K. Sanchit, A. Sanjay, "Predictive modeling of surface roughness in grinding," CIRP Conference on Modelling of Machining Operations, **31**, 375 - 380, 2015, doi:https://doi.org/10.1016/j.procir.2015.04.092.

[15] K.S. Krishna, A. Sanjay, D. Raj, "Surface Roughness Prediction in Grinding: A Probabilistic Approach," MATEC Web of Conferences, **82**(01019), 2016, doi:10.1051/matecconf/20168201019

[16] V.G. Anne, P.V. Rao, "A new chip-thickness model for performance assessment of silicon carbide grinding," Int J Adv Manuf Technol, **24**, 816–820, 2004, doi:https://doi.org/10.1007/s00170-003-1788-6.

[17] B.F. Nabil, S. Habib, B. Chedly, "Ground surface improvement of the austenitic stainless steel AISI304 using cryogenic cooling," Surface & Coatings Technology, **200**(16), 4846-4860, 2006, doi:https://doi.org/10.1016/j.surfcoat.2005.04.050

[18] J.E. Mayer. G.P. Fang, "Effect of grit depth of cut on strength of ground ceramics," Annals CIRP, **43**(1), 309-312, 1994, doi:https://doi.org/10.1016/S0007-8506(07)62220-3

[19] X. Hockin, S. Jahanmir, L.K. Ives, "Effect of grinding on strength of tetragonal zirconia and zirconia-toughned alumina," Journal of Machining Science Technology, **1**, 49-66, 1997, doi:https://doi.org/10.1080/10940349708945637

[20] https://www.noritake.co.jp/eng/catalog_type/download/8aa6080c86465c93cfebd53c07689c7f.pdf

ASTES

Advances in Science, Technology and Engineering Systems Journal
Vol. 5, No. 5, 1189-1195 (2020)
www.astesj.com
Special Issue on Multidisciplinary Innovation in Engineering Science & Technology

ASTES Journal
ISSN: 2415-6698

Synthesis of SQL Queries from South African Local Language Narrations

George Obaido[*,1,2], Abejide Ade-Ibijola[2], Hima Vadapalli[1]

[1]*School of Computer Science and Applied Mathematics, University of the Witwatersrand, Johannesburg, 2001, South Africa.*

[2]*School of Consumer Intelligence and Information Systems, University of Johannesburg, Johannesburg, 2001, South Africa.*

ARTICLE INFO

Article history:
Received: 25 August 2020
Accepted: 18 October 2020
Online: 24 October 2020

Keywords:
Language translation
Synthesis of things
JFA applications
SQL queries

ABSTRACT

English remains the language of choice for database courses and widely used for instruction in nearly all South African universities, and also in many other countries. Novice programmers of native origins are mostly taught Structured Query Language (SQL) through English as the medium of instruction. Consequently, this creates a myriad of problems in understanding the syntax of SQL as most native learners are not too proficient in English. This could affect a learner's ability in comprehending SQL syntaxes. To resolve this problem, this work proposes a tool called local language narrations to SQL (`Local-Nar-SQL`) that uses a type of Finite Machine, such as a Jumping Finite Automaton to translate local language narratives into SQL queries. Further, the generated query extracts information from a sample database and presents an output to the learner. This paper is an extension of work originally presented in a previous study in this field. A survey involving 145 participants concluded that the majority found `Local-Nar-SQL` to be helpful in understanding SQL queries from local languages. If the proposed tool is used as a learning aid, native learners will find it easier to work with SQL, which will eliminate many of the barriers faced with English proficiencies in programming pedagogies.

1 Introduction

According to Linguists, English has much of its vocabulary borrowed from French and Latin, but it remains a Germanic language in terms of structure and sounds [1]–[2]. English is the predominant language of instruction used at most universities and remains the *de facto* language of communication for many industry sectors [3, 4]. It is interesting to note that many of the world's population do not speak English as their first language, but it is vastly used for communication and dissemination of knowledge [5, 6]. Most programming and scripting languages, such as C, Java, Python and Structured Query Language (SQL) have keywords, declarations and documentations based in English [6]–[7]. Even online resources, such as forums, blogs and developers communities that aid the learning of programming are primarily in English [8, 9]. For example, Stack Overflow, which is one of the largest online communities for developers, enforces that all questions and answers are posted in English. Hence, for a novice programmer to be proficient in programming, English is a necessity [10].

SQL is the most popular query declarative language used for performing operations on relational databases [11, 12]. As a standardised language, many of its syntaxes and statements are English-like, and SQL has found numerous applications in both industry and academia [13, 14]. Listing 1 shows examples of the SQL SELECT query statements that depict English-like formation. These set of queries would retrieve one or more records from a targeted database's table.

Listing 1: SQL SELECT statement query

```
SELECT * FROM myrecordinfo;

SELECT DISTINCT firstname, lastname
FROM myrecordinfo;

SELECT * FROM myrecordinfo
WHERE firstname='karabo' AND lastname='hlophe';

SELECT * FROM Customers
WHERE country='South Africa'
OR city = 'Pietermaritzburg';
```

[*]Corresponding Author: George Obaido, University of the Witwatersrand, School of Computer Science and Applied Mathematics, Johannesburg, 2001, South Africa. Email: rabeshi.george@gmail.com & Contact: +27832227427

South Africa is a multilingual country with eleven official languages [15]–[16]. Most South African learners prefer to communicate in their local dialects, rather than English [17, 16]. Educational instruction for learning programming requires a good proficiency in English, which creates numerous challenges for a local student whose native language is not English [6, 18, 19]. Just like any other programming language, anecdotal evidence has shown that SQL is hard for students [11]–[13], [20]. Even the straightforward, English-like syntax of SQL is misleading [21, 22]. Other studies have identified that the burden of remembering SQL keywords and database schemas are often challenging [20, 23]. These challenges have made it crucial for researchers and developers to create *culturally-agnostic* aids that would assist learners to improve their understanding of SQL. Such systems could be developed to enable learners express their requests in *free-forms* using local language narrations. To our knowledge, this is the first study that attempts to translate South African local language narrations into SQL queries.

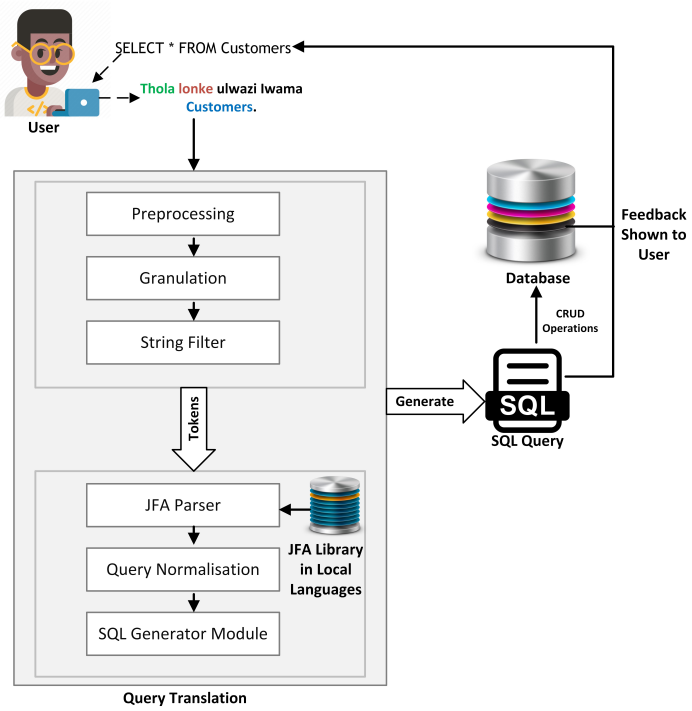


Figure 1: The translation process (adapted from [11])

This paper is an extension of work originally presented in [11], where natural language specifications were translated into SQL queries. We extended the use of a Jumping Finite Automaton, a type of Finite Machine for the translation of local language specifications into SQL queries. This idea was further implemented into a desktop-based application called `Local-Nar-SQL`. The process of translating the local language specifications into SQL queries is presented in Figure 1. Here, a user provides narrations in a local language, that is then processed by `Local-Nar-SQL`. The system preprocesses and passes the provided narrations to the JFA parser for matches. Further, the tokens are matched and a query is generated, which is made available to the user. In this paper, the following contributions were made. This study has:

1. developed a method for the recognition of local language specifications using a JFA,
2. extended this approach into a tool, called `Local-Nar-SQL`, for the translation of local language specifications into SQL queries, and
3. evaluated this approach using human subjects and presented initial results.

The rest of this paper is organised as follows: Section 2 highlights the background and related works, Section 3 presents the methodology used for this study, Section 4 shows the implementation and results details, the evaluation information is provided in Section 5 and Section 6 concludes the paper and highlights discussions for future studies.

2 Background

This section presents the problems as research questions, highlights the motivation behind this work and discusses related work.

2.1 Research Questions

This study attempts to solve the following problems:

1. how can we successfully translate local language narrations into SQL queries?
2. can we describe a JFA and implement this into a tool that addresses the above problem?
3. what are human perceptions of the developed tool?

These problems were addressed in Section 3, 4 and 5.

2.2 Motivation

English proficiency is a problem in South Africa English proficiency remains a major concern for local students learning programming [10]. Many programming language constructs, keywords, API methods and libraries are mostly written in English, which pose a great deal of difficulty for a local learner [6, 18, 19].

Decolonisation of science Issues regarding the decolonisation of the science curriculum is currently being debated in South Africa and the rest of the world [24]. Many local learners agree that the legacies of apartheid (entrenched colonialism) are still evident in education sectors, built by western perspectives, which might impinge access to learning [25, 26].

Comprehension problems in SQL Generally, the English-like syntax of SQL is misleading for learners [12, 14]. Similarly, most query interfaces are built to report errors in English, which might be confusing for learners to decipher [27, 28].

Abstract nature of programming From a novice learners' perspective, the process of learning a new programming language remains a daunting task [29, 30]. Even so, the abstract nature of programming has resulted in high failure rates for Computer Science (CS) disciplines [31, 32].

2.3 Why Local Language Narrations

In Section 2.2, it was seen that English language poses numerous difficulties for local language learners. An ideal approach would be to enable such learners to express their intention, free from natural language ambiguities – *in narrations*. Narrations have been shown to provide textual explanations for programming and scripting language paradigms [11, 13, 32]. This practice allows learners to express their requests in *free-forms*, ignoring programming language syntax. Such *free-forms* allow learners to express their requests in their local language, free from English language ambiguities. For programming languages, especially in low-resource settings, such an approach has been tried in [7, 33, 34].

2.4 Related Work and Terms

This section presents similar work in the area of language translations and the applications of JFA.

Language Translation An evolutionary method for translating Portuguese language into SQL query [35], a pattern matching approach for translating Hindi language into SQL query [36], Telugu language translation into SQL query [37], translating Italian language to SQL query [38], translating Chinese language into SQL query [39] and Arabic translation into SQL queries [40]–[41].

JFA Applications Abstraction of frequently asked questions (FAQs) for comprehension purposes [42], synthesising SQL queries from narratives [11] and the automatic comprehension of tweets [43].

SQL Comprehension Generating narratives of SQL queries [12], generating narratives of nested SQL queries [14], generating SQL queries from visual specifications [13] and synthesising SQL queries from verbal specifications [44].

The method used in this paper is a JFA, and definitions of this term are as follows.

Definition 1 (A Jumping Finite Automaton (JFA) [45]) *A JFA is a five-tuple, M = (Q, Σ, R, s, F) where:*

1. *Q is a bounded set of states,*
2. *Σ is an input alphabet,*
3. *R is the bounded set of rules, where py → q (p,q ∈ Q, y∈Σ),*
4. *s∈Q is the start state, and*
5. *F⊆Q is the final state.*

3 Methodology

This section presents the methodology for this study. To begin, local languages were abstracted into a JFA, then queries were normalised, where irrelevant details were removed. Next, a query was generated.

3.1 Abstracting Local Languages to SQL

For local language abstraction into a JFA, entities were identified with colours, such as query types ($\sum_{QT} = a_x$) in green, attributes ($\sum_{CT} = b_y$) in red and relations ($\sum_{ET} = c_z$) in blue. This information is presented in Table 1. The Chinook DB [46] was selected for our use-case with a corpus containing a total of 120 different local languages conversions. This database contains a typical digital music store, consisting of eleven tables and multiple records. Some examples of the JFA abstractions are presented.

Table 1: JFA symbols 1 - 30

a_x	b_y	c_z
a_0 Khombisa	b_0 EmployeeID	c_0 Employee
a_1 Ungitholele	b_1 LastName	c_1 Genre
a_2 Ngitholela	b_2 FirstName	c_2 Customer
a_3 Ukuthola	b_3 Title	c_3 Mediatype
a_4 Usika	b_4 ReportTo	c_4 Track
a_5 Fumana	b_5 Address	c_5 Invoice_item
a_6 Khetha	b_6 State	c_6 Invoice
a_7 Enta	b_7 City	c_7 Phone
a_8 Faka	b_8 PostalCode	c_8 Playlist_track
a_9 Susa	b_9 Fax	c_9 Album
a_{10} Funda	b_{10} Country	c_{10} Artist
a_{11} Wys	b_{11} Email	–
a_{12} Vind	b_{12} CustomerID	–
a_{13} Lys	b_{13} SupportRepID	–
a_{14} Kry	b_{14} TrackID	–
a_{15} Plaas	b_{15} ArtistID	–
a_{16} Opdateer	b_{16} InvoiceID	–
a_{17} Verwyder	b_{17} MediaTypeID	–
a_{18} Skep	b_{18} InvoiceLineID	–
a_{19} Lees	b_{19} Name	–
a_{20} Nghenisa	b_{20} UnitPrice	–
a_{21} Sula	b_{21} Composer	–
a_{22} Susa	b_{22} Company	–
a_{23} Engetela	b_{23} Al | Alle | Alles	–
a_{24} Tumbuluxa	b_{24} Konke | Yonke	–
a_{25} Tlakusisa	b_{25} Yothe | Vhothe	–
a_{26} Ulonga	b_{26} –	–
a_{27} Ubvisa	b_{27} –	–
a_{28} Udadzisa	b_{28} –	–
a_{29} Utomola	b_{29} –	–
a_{30} Usika	b_{30} –	–

- Ek will al die customer besonderhede vind

Example 1 above shows a query request sentence in Afrikaans. The English translation for this sentence is: "I want to find all the customer's details". The equivalent JFA shows:

$$\mathbf{M} = (\{I, J, K, L\}, \{b_{23}, c_2, a_{12}\}, R, I; \{L\})$$

where $\{I, J, K, L\}$ are the states,
$\{b_{23}, c_2, a_{12}\}$, are the input alphabets,
R is the set of rules,
I is a start state, and
$\{L\}$ is a final state.

with

$$\mathbf{R} = \{Ib_{23} \rightarrow J, Jc_2 \rightarrow K, Ka_{12} \rightarrow L\}$$

accepts

$$\text{L(M)} = \{w \in \{b_{23}, c_2, a_{12}\}^*: |b_{23}| = |c_2| = |a_{23}|\}$$
$$\text{i.e. } b_{23} = al; c_2 = customers; a_{12} = vind$$

$$\begin{aligned} b_{23}c_2a_{12}a_{12}c_2\underline{I}b_{23} &\curvearrowright b_{23}c_2a_{12}\underline{J}a_{12}c_2 && [Ib_{23} \rightarrow J] \\ &\curvearrowright b_{23}c_2a_{12}\underline{K}a_{12} && [Jc_2 \rightarrow K] \\ &\curvearrowright \underline{L}b_{23}c_2a_{12} && [Ka_{12} \rightarrow L] \end{aligned}$$

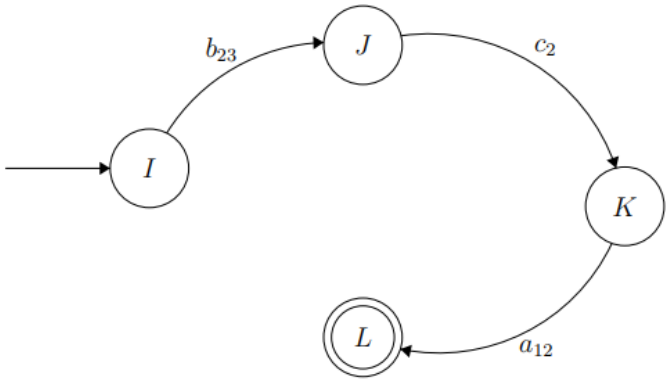


Figure 2: An example of a sample JFA

Figure 2 shows an example of a sample JFA with three transitions. The diagram consists of four states, labelled as $\{I, J, K, L\}$, where the start state is I and accepting state is L. Ib_{21} begins the movement with the *al* keyword, then Jc_2 shows the movement with the *customer* keyword, and the transition, Ka_{12} ends with the *vind* keyword. Since local languages are rich in vocabulary, the input alphabet may differ in another language, which might result in a change in the states and transitions.

- Ngifuna ukuthola yonke imininingwane ya ma customer

The above sentence is the Zulu translation of: "I want to find all the customer's details". The equivalent JFA shows:

$$\mathbf{M} = (\{I, J, K, L\}, \{a_3, b_{24}, c_2\}, R, I; \{L\})$$

where $\{I, J, K, L\}$ are the states,
$\{a_3, b_{24}, c_2\}$, are the input alphabets,
R is the set of rules,
I is a start state, and
$\{L\}$ is a final state.

with

$$\mathbf{R} = \{Ia_3 \rightarrow J, Jb_{24} \rightarrow K, Kc_2 \rightarrow L\}$$

accepts

$$\text{L(M)} = \{w \in \{a_3, b_{24}, c_2\}^*: |a_3| = |b_{24}| = |c_2|\}$$
$$\text{i.e. } a_3 = ukuthola; b_{24} = yonke; c_2 = customers$$

$$\begin{aligned} b_{24}a_3c_2b_{24}c_2\underline{I}a_3 &\curvearrowright b_{24}a_3c_2\underline{J}b_{24}c_2 && [Ia_3 \rightarrow J] \\ &\curvearrowright b_{24}a_3c_2\underline{K}c_2 && [Jb_{24} \rightarrow K] \\ &\curvearrowright \underline{K}b_{24}a_3c_2 && [Kc_2 \rightarrow L] \end{aligned}$$

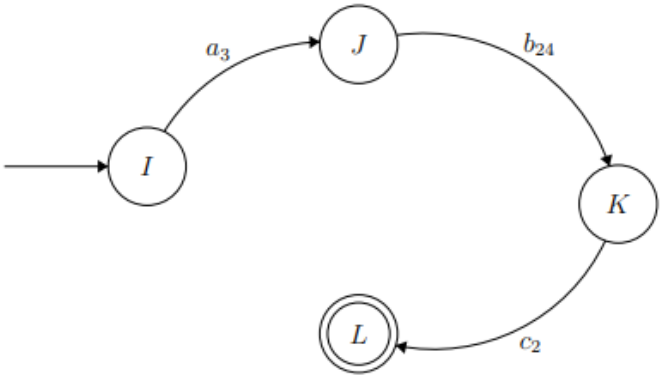


Figure 3: An example of a sample JFA

Figure 3 shows an example of a JFA with three transitions. The four states as shown in the diagram are $\{I, J, K, L\}$, with I representing the start state and L denoting the accepting state. Ia_3 begins the movement with the *ukuthola* keyword, then Jb_{24} shows the next input label with the *yonke* keyword, Kc_2 ends with the *customer* keyword. It is interesting to note that these examples only cater for a single relation. We may have situations of many states and transitions, taking into account the input statement provided by the learner.

3.2 *Normalising Queries*

At the normalisation phase, irrelevant details were removed and keywords that appears in our JFA design were used to semantically form a query. The normalisation process is passed to the SQL query generator, which is then used to create and retrieve records from the Chinook DB. As illustrated in Table 2, each local language word is mapped to a query operation. This stage is useful for the SQL generation phase.

Table 2: Mapping Local Language Keywords

Keywords	Query Operation
Ukuthola, Thola, Ngtholele, Fumana, Ngitholela, Vind, Kies	SELECT
Al, Alle, Alles, Konke, Yonke, Yothe, Vhothe	ALL
Skep, Usika, Dala	CREATE
Faka, Plaas, Ulonga	INSERT
Susa, Lees, Verywyder, Utomola, Ubvisa Vhothe	DELETE

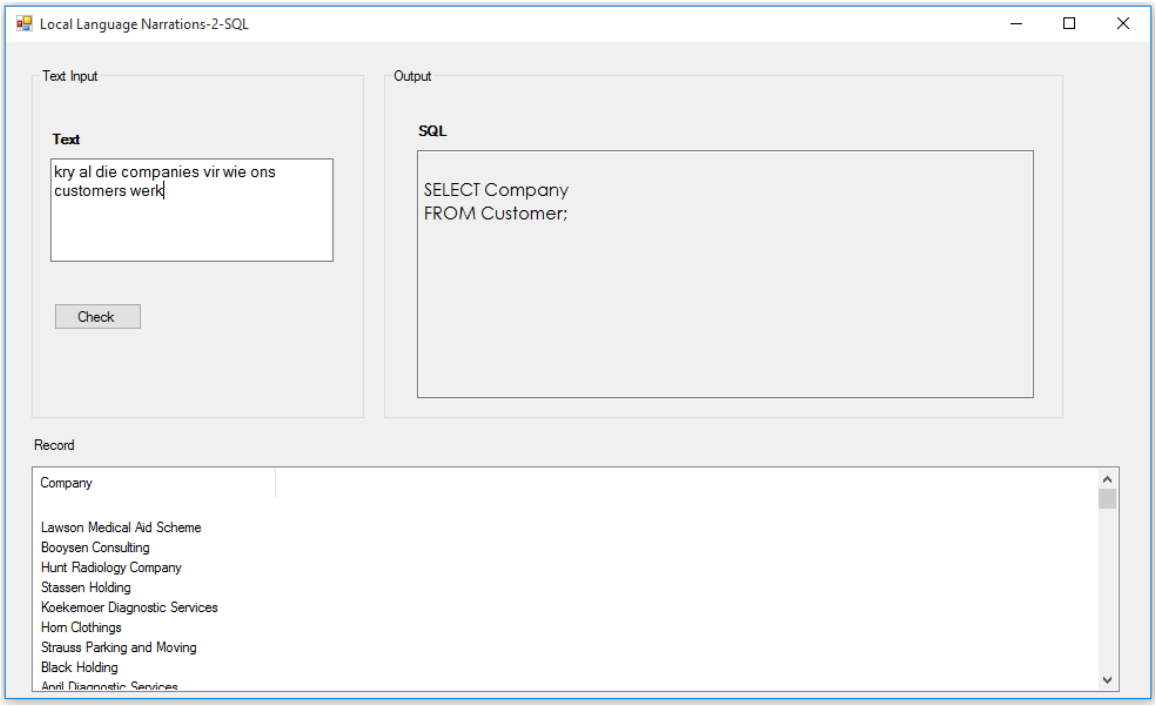


Figure 4: A sample output of `Local-Nar-SQL`

3.3 Generating SQL Queries

This phase takes information from the normalisation phase to semantically generate a query. The generated query is used against the Chinook DB, which then produces an output. Since this task is limited to a single relation, the JFA algorithm was useful for this purpose. Similarly, the task was quite straightforward.

4 Implementation and Results

In Section 3, JFA technique was described which showed how a query is generated. Here, the implementation and results of the local language narration process are presented. The JFA approach was implemented using the Microsoft C# .NET framework[1], which was developed into a software tool, called `Local-Nar-SQL`.

`Local-Nar-SQL` was created to allow a native learner to specify a query request in any of the eleven local languages spoken in SA. The software tool uses the learner's input to generate a query and retrieve records from the sample database. Further, the result is made available to the learner. The sample database used for our use-case was the ChinookDB[2], which contains multiple records. A sample output of this request is provided in Figure 4.

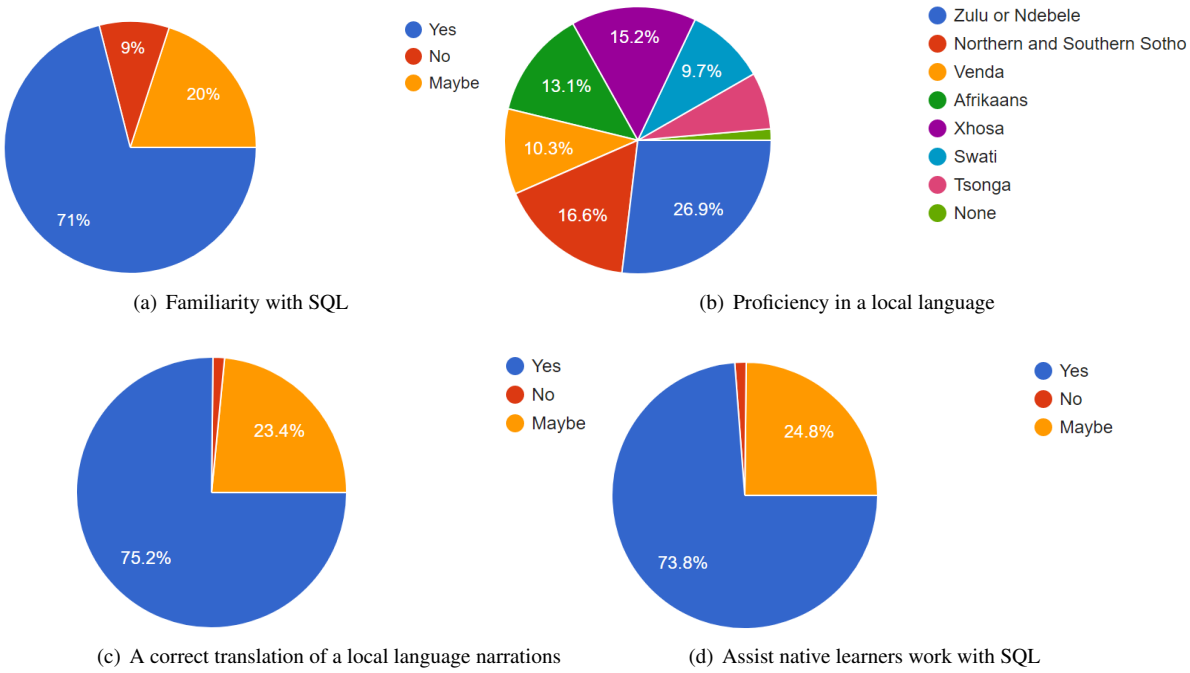
5 Evaluation

A total of 145 participants participated in a survey that was conducted online. The majority of the participants are native language learners who are familiar with programming and have taken numerous computer science courses. The questions for the survey is available via `https://forms.gle/uSXn8TZpBEWmnGk66`. The results are presented in Figure 5.

Of the responses received, 71% indicated familiarity with SQL, whilst 9% of respondents claimed no familiarity with SQL and 20% were unsure of their answers (Figure 5(a)). The participants were asked about their native language proficiencies. Approximately 29% of learners were proficient in Zulu, 16.6% were proficient in Northern and Southern Sotho, 15.2% claimed to be proficient in Xhosa and 13.1% admitted to being proficient in Afrikaans. The remaining respondents were proficient in Venda (10.3%), Swati (9.7%) or Tsonga (6.9%), and 1.4% of the participants did not list any of these native languages (Figure 5(b)). Furthermore, the participants were asked if the `Local-Nar-SQL` tool provided a correct translation of local language narrative to SQL: 75.2% affirmed that the tool was accurate, 23.4% were unsure and 1.4% indicated no (Figure 5(c)). When the participants were asked if they think that the tool will assist native learners work with SQL, about 73.8% affirmed that the tool would assist learners, 24.8% were unsure and 1.4% indicated no (Figure 5(d)).

The survey showed that the majority of the learners found the `Local-Nar-SQL` tool to be useful and helpful towards their interest of learning SQL. If our proposed tool is used as a learning aid, native learners will find it easier to work with SQL, which will eliminate many of the barriers faced with English proficiencies in programming pedagogies.

[1] https://docs.microsoft.com/en-us/dotnet/framework/
[2] https://github.com/lerocha/chinook-database



(a) Familiarity with SQL

(b) Proficiency in a local language

(c) A correct translation of a local language narrations

(d) Assist native learners work with SQL

Figure 5: The survey results

6 Conclusion and Future Work

This paper presented an extended version of a JFA for the automatic synthesis of SQL queries from local language narrations. This automata-based algorithm was further implemented into a software tool called `Local-Nar-SQL`, designed for native learners to specify query request in any of the eleven official South African languages of their choice. `Local-Nar-SQL` takes these requests, generates a query and produces an output that is presented to the learner. If implemented on a large scale, this tool will serve as:

1. a comprehension aid: With `Local-Nar-SQL`'s textual and translation approaches, it can improve the cognitive workload of a native learner towards understanding the SQL concept.
2. a learning aid: The *free-form* approach offered by the tool will enable native learners improve and enhance their SQL query skills.
3. a solution to English language barriers: Native learners are not required to attain a high English proficiency to use `Local-Nar-SQL`. Since local languages are widely spoken in South Africa, it is seen that this tool will stimulate a native learner's interests in becoming proficient in SQL.

To this end, our evaluation results showed that the majority of learners agreed that this tool will be helpful to native learners yearning to be proficient in SQL. Our evaluation results are consistent with the works of [38] where majority of the native participants agreed that the developed tool helped serve their information needs . In the future, we aim to improve this study to accommodate nested SQL query and other query operation tasks. Also, it would be interesting to conduct a performance evaluation on our proposed tool. Such information would provide us with the accuracy of `Local-Nar-SQL`.

Conflict of Interest The authors declare no conflict of interest.

Acknowledgment This work is based on research supported by the National Research Foundation (NRF) of South Africa (Grant Number: 119041). Any opinion, findings and conclusions or recommendations expressed in this material are those of the authors and therefore the NRF does not accept liability in regard thereto.

References

[1] R. D. Fulk, "English as a Germanic language," Companion to the history of the English language, 1–8, 2008.

[2] D. Borodenko, "Formation of the English Language," Science progress in European countries: New concepts and modern solutions, 304 – 427, 2019.

[3] F. Ndhlovu, L. Siziba, "English in Southern Africa," in The Social and Political History of Southern Africa's Languages, 65–92, Springer, 2018.

[4] S. Passera, A. Kankaanranta, L. Louhiala-Salminen, "Diagrams in contracts: Fostering understanding in global business communication," IEEE Transactions on Professional Communication, **60**(2), 118–146, 2017, doi: DOI:10.1109/TPC.2017.2656678.

[5] O. Inbar-Lourie, "English only? The linguistic choices of teachers of young EFL learners," International Journal of Bilingualism, **14**(3), 351–367, 2010, doi:https://doi.org/10.1177%2F1367006910367849.

[6] P. J. Guo, "Non-native English speakers learning computer programming: Barriers, desires, and design opportunities," in Proceedings of the 2018 CHI conference on human factors in computing systems, 1–14, 2018.

[7] A. G. Soosai Raj, E. Zhang, S. Mukherjee, J. Williams, R. Halverson, J. M. Patel, "Effect of Native Language on Student Learning and Classroom Interaction in an Operating Systems Course," in Proceedings of the 2019 ACM Conference on Innovation and Technology in Computer Science Education, 499–505, 2019.

[8] A. Nguyen, P. Rigby, T. Nguyen, D. Palani, M. Karanfil, T. Nguyen, "Statistical translation of English texts to API code templates," in 2018 IEEE International Conference on Software Maintenance and Evolution (ICSME), 194–205, IEEE, 2018.

[9] A. Barua, S. W. Thomas, A. E. Hassan, "What are developers talking about? an analysis of topics and trends in Stack Overflow," Empirical Software Engineering, **19**(3), 619–654, 2014.

[10] K. Reestman, B. Dorn, "Native Language's Effect on Java Compiler Errors," in Proceedings of the 2019 ACM conference on international computing education research, 249–257, 2019.

[11] G. Obaido, A. Ade-Ibijola, H. Vadapalli, "Synthesis of SQL Queries from Narrations," in 6th International Conference on Soft Computing & Machine Intelligence (ISCMI), 195–201, IEEE, 2019.

[12] A. Ade-Ibijola, G. Obaido, "S-NAR: generating narrations of SQL queries using regular expressions," in Proceedings of the South African Institute of Computer Scientists and Information Technologists, 1–8, 2017.

[13] G. Obaido, A. Ade-Ibijola, H. Vadapalli, "Generating SQL queries from Visual Specifications," in Annual Conference of the Southern African Computer Lecturers' Association, 315–330, Springer, 2018.

[14] G. Obaido, A. Ade-Ibijola and H. Vadapalli, "Generating narrations of nested SQL queries using context-free grammars," in 2019 Conference on Information Communications Technology and Society (ICTAS), 1–6, IEEE, 2019.

[15] H. Brookes, "Youth Language in South Africa: The Role of English in South African Tsotsitaals," English in multilingual South Africa: The linguistics of contact and change, 176–195, 2020.

[16] F. Banda, "The dilemma of the mother tongue: Prospects for bilingual education in South Africa," Language culture and curriculum, **13**(1), 51–66, 2000, doi:https://doi.org/10.1080/07908310008666589.

[17] S. Coetzee-Van Rooy, "Being English in multilingual South Africa," World Englishes, 2020.

[18] Y. Pal, S. Iyer, "Classroom versus screencast for native language learners: Effect of medium of instruction on knowledge of programming," in Proceedings of the 2015 ACM conference on innovation and technology in Computer Science Education, 290–295, 2015.

[19] A. K. Veerasamy, A. Shillabeer, "Teaching English based programming courses to English language learners/non-native speakers of English," International Proceedings of Economics Development and Research, **70**, 1–6, 2014.

[20] A. Migler, A. Dekhtyar, "Mapping the SQL Learning Process in Introductory Database Courses," in Proceedings of the 51st ACM Technical Symposium on Computer Science Education, 619–625, 2020.

[21] S. Prabhu, S. Jaidka, "SQL and PL-SQL: Analysing teaching methods," in The Proceedings of the Computing and Information Technology Research and Education New Zealand (CITRENZ), 105–109, 2019.

[22] S. Ardeleanu, "SQL: Beauty and the Beast," in Relational Database Programming, 17–30, Springer, 2016.

[23] J. Heller, "Use SQL More Often with Basic Dynamic SQL," in Pro Oracle SQL Development, 339–353, Springer, 2019.

[24] J. de Beer, N. Petersen, "Decolonisation of the science curriculum: a different perspective (# cookbook-labs-must-fall)," 2016.

[25] V. Mudaly, "Decolonising the mind: Mathematics teachers explore possibilities for indigenising the school curriculum," Journal of Education (University of KwaZulu-Natal), **74**, 67–84, 2018, doi:http://dx.doi.org/10.17159/2520-9868/i74a05.

[26] L. Le Grange, "Decolonising the university curriculum: Leading article," South African Journal of Higher Education, **30**(2), 1–12, 2016.

[27] M. Llopis, A. Ferrández, "How to make a natural language interface to query databases accessible to everyone: An example," Computer Standards & Interfaces, **35**(5), 470–481, 2013.

[28] J. Barzdins, M. Grasmanis, E. Rencis, A. Sostaks, A. Steinsbekk, "Towards a More Effective Hospital: Helping Health Professionals to Learn from their Own Practice by Developing an Easy to use Clinical Processes Querying Language," Procedia Computer Science, **100**, 498–506, 2016.

[29] A. Ade-Ibijola, S. Ewert, I. Sanders, "Introducing Code Adviser: A DFA-driven electronic programming tutor," in International Conference on Implementation and Application of Automata, 307–312, Springer, 2015.

[30] A. O. Ade-Ibijola, Automatic novice program comprehension for semantic bug detection, Ph.D. thesis, 2016.

[31] M. Konecki, "Problems in programming education and means of their improvement," DAAAM international scientific book, **2014**, 459–470, 2014.

[32] A. Ade-Ibijola, S. Ewert, I. Sanders, "Abstracting and narrating novice programs using regular expressions," in Proceedings of the Southern African Institute for Computer Scientist and Information Technologists Annual Conference 2014 on SAICSIT 2014 Empowered by Technology, 19–28, 2014.

[33] A. G. Soosai Raj, K. Ketsuriyonk, J. M. Patel, R. Halverson, "Does Native Language Play a Role in Learning a Programming Language?" in Proceedings of the 49th ACM technical symposium on computer science education, 417–422, 2018.

[34] K. Varadarajan, M. L. Chu, "Declarative programming model with a native programming language," 2020, US Patent 10,585,653.

[35] A. Afonso, L. Brito, O. Vale, "An evolutionary method for natural language to SQL translation," in Asia-Pacific Conference on Simulated Evolution and Learning, 432–441, Springer, 2008.

[36] R. Kumar, M. Dua, "Translating controlled natural language query into SQL query using pattern matching technique," in International Conference for Convergence for Technology, 1–5, IEEE, 2014.

[37] R. Reddy, N. Reddy, S. Bandyopadhyay, "Dialogue based question answering system in Telugu," in Proceedings of the Workshop on Multilingual Question Answering-MLQA, 1–8, 2006.

[38] L. Siciliani, P. Basile, G. Semeraro, M. Mennitti, "An Italian Question Answering System for Structured Data based on Controlled Natural Languages." in CLiC-it, 1–6, 2019.

[39] X. Meng, S. Wang, "Nchiql: The chinese natural language interface to databases," in International Conference on Database and Expert Systems Applications, 145–154, Springer, 2001.

[40] B. Al-Johar, A portable natural language interface from Arabic to SQL, Ph.D. thesis, University of Sheffield, 1999.

[41] H. Bais, M. Machkour, L. Koutti, "An independent-domain natural language interface for relational database: Case Arabic language," in 2016 IEEE/ACS 13th International Conference of Computer Systems and Applications (AICCSA), 1–7, IEEE, 2016.

[42] N. E. Okwunma, "Automatic comprehension of customer queries for feedback generation," 2018, MSc thesis.

[43] S. Obare, A. Ade-Ibijola, G. Okeyo, "Jumping Finite Automata for Tweet Comprehension," in 2019 International Multidisciplinary Information Technology and Engineering Conference (IMITEC), 1–7, IEEE, 2019.

[44] G. Obaido, A. Ade-Ibijola, H. Vadapalli, "TalkSQL: A Tool for the synthesis of SQL Queries from Verbal Specifications," in International Multidisciplinary Information Technology and Engineering Conference (IMITEC) Vanderbijlpark, South Africa, 1–9, 2019.

[45] A. Meduna, P. Zemek, "Jumping finite automata," International Journal of Foundations of Computer Science, **23**(07), 1555–1578, 2012.

[46] B. Schultheiss, A. Vollebregt, C. Hummelink, "Storing heterogeneous helicopter signal data: Advantages of using an XML database," in 2007 IEEE Autotestcon, 469–475, IEEE, 2007.

ASTES

Advances in Science, Technology and Engineering Systems Journal
Vol. 5, No. 5, 1196-1203 (2020)
www.astesj.com

ASTES Journal
ISSN: 2415-6698

A Proposal of Exercise and Performance Learning Assistant System for Self-Practice at Home

Irin Tri Anggraini[1], Achmad Basuki[1], Nobuo Funabiki [*,2], Xiqin Lu[2], Chih-Peng Fan[3], Yu-Chung Hsu[3], Cheng-Hsien Lin[3]

[1]*Departement of Multimedia Creative, Politeknik Elektronika Negeri Surabaya, Surabaya,60111,Indonesia*

[2]*Department of Electrical and Communication Engineering, Okayama University, Okayama,700-8530, Japan*

[3]*Department of Electrical Engineering, National Chung Hsing University, Taichung,40227, Taiwan*

A R T I C L E I N F O

Article history:
Received: 11 June, 2020
Accepted: 15 October, 2020
Online: 24 October, 2020

Keywords:
EPLAS
exercise
performance
indoor
Yoga
practice
OpenPose

A B S T R A C T

Due to pandemic spreads of COVID-19 *and increasing populations of seniors, exercises or performance practices at home have become important to maintain healthy lives around the world.* World Health Organization (WHO) *has announced the physical health determines the* Quality of Life (QoL) *of a human. Unfortunately, a lot of people have no exercise and may be in unhealthy conditions. In this paper, we propose an* Exercise and Performance Learning Assistant System (EPLAS) *to assist people practicing exercises or learning performances by themselves at home. EPLAS adopts inexpensive devices and free software for low-cost implementation. It offers a video content of model actions by an instructor to be followed by the user, where the reaction is rated by comparing the feature points of the human bodies extracted by an open-source software* OpenPose. *For evaluations, we conduct experiments of applying EPLAS with five* Yoga *poses to* 41 *persons in Indonesia, Japan, and Taiwan, and confirm the effectiveness of the proposal.*

1 Introduction

Nowadays, the population of old people has rapidly increased around the world. The rapid increase of seniors may cause large negative impacts to the societies in many countries, if they have unhealthy lives. *World Health Organization (WHO)* has announced that the physical health determines the *Quality of Life (QoL)* of a human [2]. To achieve the stability and prosperity of the country, it is one of the most important policies for many countries to advance the QoL and health of the people including seniors.

However, a lot of seniors are in unhealthy conditions, may stay at home all the time, and do never have exercises. Before this study, we had interviews 20 seniors in Indonesia, and found that about 50% of them are suffering from pains in the bodies. More specifically, five seniors feel pains on their legs, three seniors on the backs, and two seniors on the shoulders. Nevertheless, our survey found that in one week on average, three seniors have exercises at more than three times, one has three times, two have two times, and six have one time. The remaining seniors have no exercise at all. Only 15% of them have regular exercises outside their homes more than three times a week to alleviate pains.

Besides, pandemic spreads of *COVID-19* force people to stay at home in order to avoid infections among them [3]. Then, many people have lost opportunities of having regular exercises in daily lives, such as walking to offices, schools, or shopping centers, and enjoying sports or trainings in outdoors, fields, or gyms. The similar situations to seniors may also cause health problems to a lot of people around the world.

In this paper, we propose an *Exercise and Performance Learning Assistant System (EPLAS)* to assist people practicing exercises or learning performances by themselves at home. EPLAS offers a video content showing the model movement of an instructor for some exercise or performance such as *Yoga*, *Tai Chi*, or dance. The user should follow the actions suggested by the instructor as similarly as possible. In EPLAS, the *rating function* is implemented to rate the user reaction to each action of the instructor. It calculates the difference between the coordinates of the feature points in the image of the instructor and in that of the user. If the difference is small, the function gives the higher rate, since both actions are similar.

The feature points are actually extracted by applying *OpenPose* [4] to the corresponding images of the instructor

*Corresponding Author: Nobuo Funabiki, Dep. of Electrical and Communication Engineering, Okayama University, Okayama, Japan, Email: funabiki@okayama-u.ac.jp. This paper is an extension of the work originally presented in 2019 International Electronics Symposium (IES) [1].

and the user to each action. *OpenPose* is a popular open-source program for real-time human pose estimation, and has been developed by researchers at Carnegie Mellon University. It can estimate the poses of multiple persons in one image at the same time. First, *OpenPose* detects the *feature points* called *keypoints* of every person in the image. Then, it allocates them to distinct individuals in the image. The source codes and documents can be accessed at *GitHub*.

For evaluations of the proposal, we prepared videos of five simple *Yoga* poses, and asked 41 persons in Indonesia, Japan, and Taiwan to practice the Yoga poses using EPLAS. Then, we asked 20 persons including the Yoga instructor to evaluate each pose of every participant subjectively. The results show the strong correlation exists between the subjective evaluation results and the rating function outputs in EPLAS. The rating function also points out the feature points to be improved in each pose. Thus, the effectiveness of the proposal is confirmed.

The rest of this paper is organized as follows: Section 2 explores relevant studies in literature. Section 3 presents the overview of EPLAS Section 4 presents the rating function in EPLAS. Section 5 shows evaluation results of EPLAS. Finally, Section 6 concludes this paper with future works.

2 Related Works in Literature

In this section, we discuss related works to this paper in literature. Some of the papers focus on evaluating physical exercises for seniors using *robot interactions* or *electrical muscles*, and on helping seniors to record the personal health with the physical health record such as *Fuzzy System*, *Exergames*.

In [5], the author proposed a unique fuzzy system design for adjusting the cycle ergometer workload to the physical work capacity of the individual, and observed the physical work capacity by measuring the heart rate and the muscular-fatigue-related index. A set of fuzzy membership functions were adopted for three different phases during a trial exercise with a progressively increasing workload.

In [6], the author presented the design, implementation, and user study evaluation of a *socially assistive robot (SAR)* system, which has been designed to engage elderly users in physical exercises aimed at achieving health benefits and improving the quality of life (QoL).

In [7], the author showed a moderate therapeutic effect associated with the self-application of the neuromuscular electrical stimulation (NMES) application protocol that targets improvements in the muscle strength and the cardiovascular exercise capacity of an elderly person. This work is the promising first step towards the development of an NMES application protocol that could eventually be widely used by seniors to counteract the detrimental effects of aging.

In [8], the author proposed a study for understanding why seniors still perceive the usability of *Personal Health Records* as low in spite of the publicly available guidelines. *Personal Health Records* focuses on user generated contents where health websites provide information for users to consume.

In [9], the author proposed the design, implementation, wide deployment, and evaluation of the low-cost physical exercise and gaming (exergaming) *FitForAll (FFA)* platform. The system usability, the user adherence to exercise, and the efficacy are explored. The design of FFA is tailored to elderly people, distilling literature guidelines and recommendations. The FFA architecture introduces standard physical exercise protocols in exergaming software engineering, as well as, standard physical assessment tests for the augmented adaptability through the adjustable exercise intensity.

In [10], the author developed an exercise-management platform with an end-user application software and a connective sport device to collect and store the elderly individual's exercise data as a reference for diagnosis and treatments. Compared to traditional methods for encouraging sports, this platform uses *Near Field Communication (NFC)* for automatically collecting data.

In [11], the author studied the correlation between the sense of presence and the attitude towards physical exercises in an active game-based exercise training program for older adults. The hypothesis in this study is that the more positive attitude towards physical exercises would lead to a higher sense of presence. There is the significant positive correlation between them in this program.

In [12], the author supported the positive effects of exergaming playing on the elderly's attitude towards exergames, psychosocial well-being (sociability and loneliness), and inter-generational perceptions. Exergames could be used as a good intervention to improve social interactions among the elderly and promote the healthy and active ageing. *Senior Activity Centres (SAC)* may introduce exergames and organize it as a weekly activity. Policymakers can use exergames to create an environment for elderly to take physical exercises, maintain social relationships, and in turn, improve the elderly's psychosocial well-being.

In [13], the author developed a sensor resistance-band for objective exercise measurements and preliminary trials of activities' classifications by using the artificial intelligence. The preliminary experiments show that the sensor resistance-band can be used as the replacement equipment of the traditional resistance-band in handling for data collections. A future study will be based on the sensed resistance-band to quantify the exercises objectively in elderly people.

In [14], the author presented a design of *Embedded based Assistive System for Yoga (EASY)* and its implementation for Yoga postures analysis, using *Kinect* and *LabVIEW*. The authors claimed that the novelty of the proposal is the integration of the skeleton method and the golden template techniques to identify the amount of deviation while performing the asana postures. However, there is no detail on how to extract the skeletons accurately, and also no detail on what is the golden template method.

In [15], the author presented a Yoga pose evaluation method using *OpenPose*. This method calculates the angle of the human pose at the important feature point, including the elbow and the knee, using the to-and-fro feature points together, and compares the angle of the instructor pose and that of the user pose.

3 Proposal of EPLAS

In this section, we propose the *Exercise and Performance Learning Assistant System (EPLAS)* to help people to practice exercises and learn performances by themselves at home.

3.1 Required Devices

In EPLAS, a personal computer (PC) displays a video on the monitor and rates the user reaction. The PC camera should be installed to capture the motion of the user. For more realistic instructions, a flat wall in the room can be used as the monitor by adopting a projector. The wireless mouse will be used to control the PC by the user, because the user needs to stay at a distance place from the PC so that the PC camera can detect the whole body of the user. Depending on the exercise, the user may sit on a chair during the exercise.

Table shows the specifications of the adopted PC. A high-performance computer that has a lot of GPUs will be necessary to evaluate dynamic movements of poses using *OpenPose*, which will be in future studies.

Table 1: Specifications of PC.

item	specification
manufacturer	Dell Inc.
model	Inspiron 24-5459
processor	Intel(R) Core(TM) i5-6400T
memory	8GB RAM
OS	Microsoft Windows 10

To reduce the cost, an inexpensive computing device such as *Raspberry Pi* [16] can be used instead of the PC. In this case, a webcam, a monitor, and a keyboard are additionally required because *Raspberry Pi* does not contain them.

3.2 Implemented Functions

For efficient self-practices by users, EPLAS provides the following functions:

1. Content selection function
   A user can select and start the video of the exercise or performance to be practiced.

2. Mirror function
   A user can view the movement or reaction of himself/herself on the monitor to each action of the instructor during the practice.

3. Rating function
   A user can know the accuracy of his/her reaction to each action of the instructor.

3.3 Utilization Procedure

The user can use EPLAS for the self-practice by the following procedure:

1. Set up the necessary devices for EPLAS at home properly. Put it in front of the user. Here, it is necessary to make sure that the whole body of the user is detected by the camera.

2. Start running the EPLAS software.

3. Sit on a chair if necessary.

4. Select and run one video content at EPLAS.

5. Practice the exercise or performance by following the movements of the instructor in the video.

6. Reflect the practice by the result of the rating function.

3.4 EPLAS User Interface

For the trial use of EPLAS, we implemented simple user interface functions that run only on *Chrome* [17] browser. *Chrome* offers rich functions and is now very popular around the world. When the interface is opened, the EPLAS menu in Figure 1 appears. It displays the five yoga poses that are available currently. There are Mountain Pose, Side Bend Pose, Warrior Pose, Seated 1 Pose and Seated 2 Pose. Then, the user chooses one of them and start the exercise.



Figure 1: Menu interface.

When one of the yoga pose is chosen, the corresponding exercise interface in Figure 2 appears. This interface has three views.

The *left top view* displays the current movement or reaction of the user for the *mirror function*. This camera display function is realized using the built-in camera function in *Chrome*. Thus, the request for the camera access permission pops up automatically. By permitting it, the moving image of the camera appears there. The moving image can be recorded on the browser, if necessary.

The *right top view* displays the video of the exercise or performance by an instructor. By imitating the movements of the instructor in this view, the user can practice or enjoy the exercise or performance learning.

The *left bottom view* displays the recorded moving image of the user. By clicking the button, the user can see his/her movement or reaction for the instructor video. The recorded moving image will be used in the *rating function* in the next section.

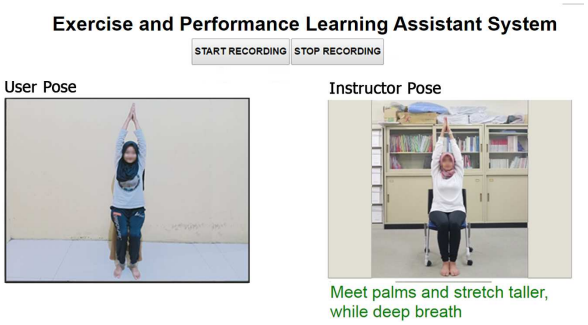


Figure 2: Exercise interface.

4 Rating Function

In this section, we present the *rating function* using *OpenPose* to give a numerical feedback on the quality of movements or poses of the user in an exercise or a performance.

4.1 Idea in Rating Function

From a photo or a video frame containing a human body, *OpenPose* can extract the *coordinates* of the 18 feature points of the body on the coordinate system of the photo/frame, called *keypoints*. Figure 3 illustrates the feature points for determining a human pose. Here, we note that *OpenPose* can handle multiple human bodies in the same photo/frame at the same time. Then, we consider that the difference of the coordinates between the instructor pose and the user pose for the same action is a proper index to evaluate the accuracy of the user reaction.

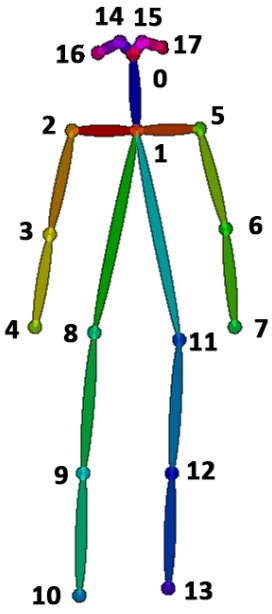


Figure 3: 18 feature points by *OpenPose*.

4.2 Coordinate System Adjustment

However, the coordinate systems of two photos/frames can be different by the camera architecture or the distance between the subject and the camera. Since the instructor photo/video should be taken beforehand at a different place using a different camera, the coordinate system for the user pose must be adjusted to be coincident with that for the instructor pose as much as possible.

In this paper, we adjust the x-coordinate and the y-coordinate of the feature points through the *liner functions*, $x' = a_x x + b_x$, $y' = a_y y + b_y$, independently. The values of the coefficients, a_x, b_x, a_y, and b_y, are obtained by applying the *least-squares method* to the x-coordinates or the y-coordinates of the 18 feature points to minimize the difference between the instructor pose and the user pose, respectively.

4.3 Feature Point Pickup for Improvements

On a feature point of the user pose, if the corresponding coordinate is much different from that of the instructor pose, the user should care the point intensively to improve the whole pose or reaction. In this paper, we calculate the *Euclid distance* between the user/instructor coordinates for every feature point, and take the average and the standard deviation of the Euclid distances for all the points. Then, we choose the summation of the average and the standard deviation for the *threshold*, and pick up the feature points whose Euclid distance is larger than this threshold. In other words, we regard the 16% of the instances as abnormal, assuming they follow the normal distribution.

4.4 Procedure

Now, we present the procedure of the rating function for one pose. When multiple poses are rated, this procedure should be repeated for them.

1. Select the photo or capture the video frame that contains the pose to be rated. Here, the final pose to be rated is often longer that the other transition poses.
2. Run *OpenPose* and extract the coordinates of the 18 feature points.
3. Repeat these steps for both the instructor photo/video and the user photo/video.
4. Apply the *least squares method* to the x-coordinates and the y-coordinates of the feature points to minimize the difference between the instructor photo/frame and the user one.
5. Adjust the x- and y-coordinates of the feature points for the user pose by using the linear functions.
6. Calculate the Euclid distance between the two coordinates corresponding to each feature point after the adjustments.
7. Calculate the average and the standard deviation of the Euclid distances to the 18 feature points.
8. Take the summation of the average and the standard deviation as the threshold.
9. Pick up any feature point of the user pose if the Euclid distance is larger than both this threshold and the minimum threshold, and notice it to the user to be improved. Here, the minimum threshold should be selected properly.

To avoid pointing too many feature points to be improved, we select the points whose Euclid distance is larger than both the calculated threshold and the minimum threshold. If no feature point is selected for a pose, we select the point whose Euclid distance is the largest among the points in the pose, so that the user can know which part should be improved. For the minimum threshold, we choose the average threshold among the 41 persons in this paper. In future studies, the minimum threshold will be tuned into the proper value. In both figures, we mark the selected feature points.

4.5 Advantages of Proposal

The rating function of the proposal is applied to the important static postures of each Yoga pose where the user keeps the same body state for a while. The Euclid distances of the coordinates of the *feature points* found by *OpenPose* between the instructor and the user are calculated. Then, the correctness of the Yoga pose is evaluated at every feature point by comparing the distance with the threshold that is given by the summation of the average Euclid distance among all the feature points and its standard deviation. If the distance is larger than the threshold, the function feedbacks that the corresponding point should be improved. Thus, the proposal points out the individual feature points to be improved for the user.

Besides, the proposal gives the overall evaluation of the whole posture of the user. The larger threshold suggests the worse pose, since it becomes larger when the difference between the user's pose and the instructor's pose is large. By comparing the thresholds between the users, the best/worst users and their Yoga poses can be known. Furthermore, by reviewing the past thresholds, the user can know his/her improvements, which will be in future works.

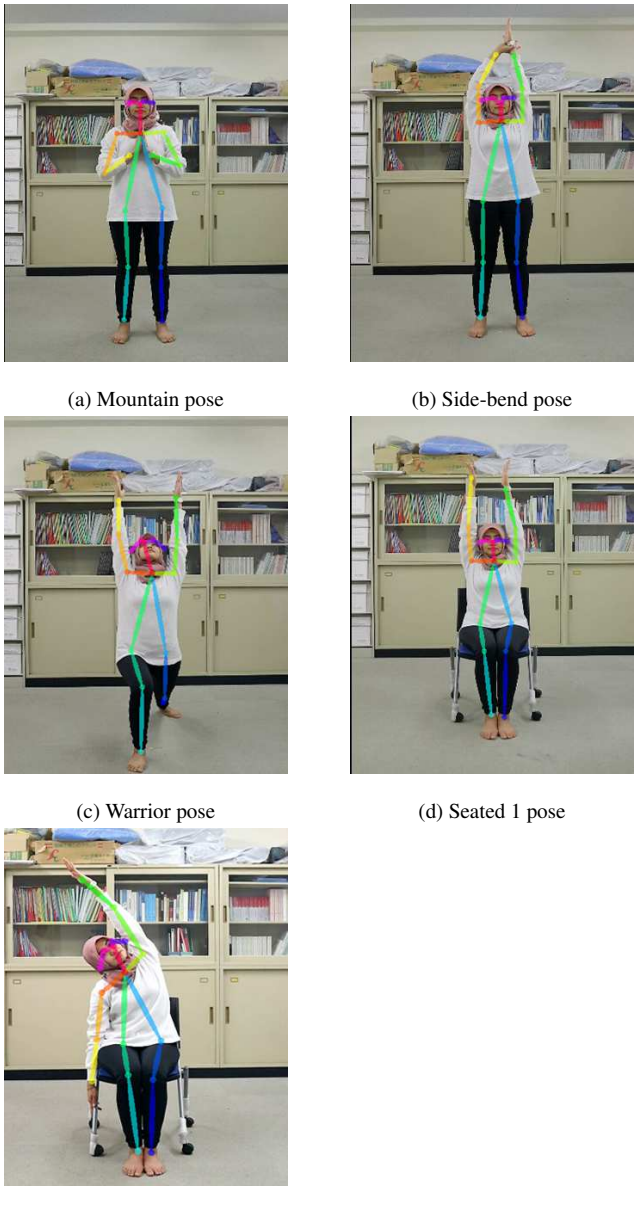
5 Evaluations

In this section, we evaluate the proposed EPLAS using five *Yoga* poses and the rating function through application to 41 persons in Indonesia, Japan, Myanmar, and Taiwan. We evaluate the user pose by objective evaluation using *OpenPose* by comparing the result of keypoint and JSON fie between the instructor Pose and the User Pose. Then we made a form subjective evalulation by scoring the instructor and 19 corespondence.

5.1 Evaluation Setup

For evaluations, we adopted the conventional personal computer (PC) in Table , because only the static postures are evaluated in the current system. It is noted that high-performance computer that has a lot of GPUs will be necessary to evaluate dynamic movements of poses using *OpenPose*, which will be in future studies.

Then, we prepared the videos for five *Yoga* poses in Figure 4, and asked 41 persons in Indonesia, Japan, Myanmar and Taiwan with various ages, to practice them by following the movements of the instructor as the EPLAS users. Then, we manually selected the frames for the final poses by the instructor and the users from the recorded videos, where the final pose stopped for several seconds. By following the procedure in Section 4, we calculated the threshold for each *Yoga* pose of every user. The correctness of the static posture of the Yoga pose is evaluated at every feature point in our proposal. For the static posture, we calculate the threshold by taking the summation of the average Euclid distance among all the feature points between the instructor and the user and its standard deviation, and compare the Euclid distance at every feature point with this threshold. If the distance is larger than the threshold, our system feedbacks to the user that the corresponding feature point should especially be improved for the better static posture, among the feature points. The larger threshold suggests the worse pose, since the threshold becomes larger when the difference between the user's pose and the instructor's pose is large. By comparing the thresholds between users, a user can know who shows the good performance and who does the bad one. Also, by reviewing the recorded thresholds, the user can know the improvements of the performance



(a) Mountain pose

(b) Side-bend pose

(c) Warrior pose

(d) Seated 1 pose

(e) Seated 2 pose

Figure 4: Five *Yoga* poses by instructor.

Then, for the subjective evaluation, we requested the Yoga instructor in the videos and 19 users among the 41 users, to rate each pose of every user in the experiments with three points by showing the instructor's photo and the user's photo. The goodness of a Yoga pose can be subjective. In this rating, we asked them to rate 1 if they feel the pose in the photo is good, 2 if they feel it is neutral, and 3 if they feel it is bad. Then, we calculated the subjective results and comparing the subjective result with our system results.

5.2 Results for Individual Users

First, we discuss the evaluation results for individual users. Table 2 shows the rating results by the proposal and the subjective evaluation results for individual users. For each one of the 41 users in the experiments, this table presents the gender, the age, the average of the average Euclid distances among the 18 feature points for the five *Yoga* poses, the average of the standard deviations (SD) of the Euclid distances for the five poses, the average of the thresholds (TH), and the average of the total subjective rating results for the five poses among 41 users.

Then, to confirm the validity of the proposed rating function, we calculated the correlation coefficient between the average thresholds and the average rating results among the 41 users. The value is 0.746, which suggests the strong correlation exists between them. Actually, the two graphs in Figure 5 suggest the similarity between the average thresholds and the subjective rating results of the 41 users.

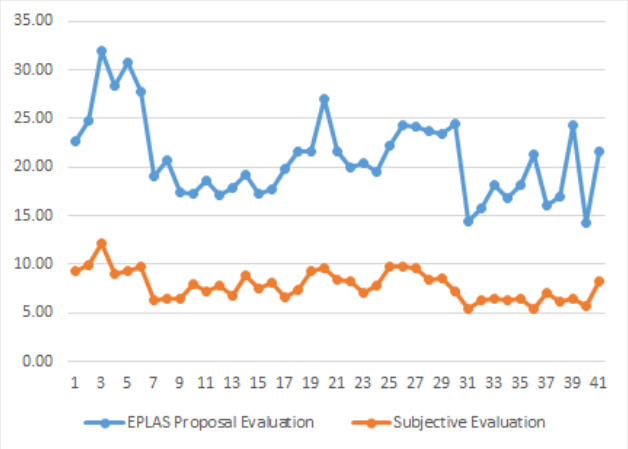


Figure 5: Average thresholds and rating results of 41 users.

When the average thresholds are compared among the users, younger users have smaller thresholds than older users, in general. As mentioned before, the threshold is given by the summation of the average and the standard deviation of the Euclid distances. The correlation coefficient between the age and the average threshold is 0.660, and that between the age and the average rating result is 0.628. Both suggest the moderate correlations.

Table 2: Application results of 41 users.

ID	gender	age	distance	SD	TH	rating
1	male	78	14.62	8.04	22.66	9.35
2	male	70	15.80	8.99	24.79	9.95
3	female	68	20.03	12.01	32.04	12.2
4	female	67	17.61	10.79	28.40	9.05
5	male	65	18.89	11.89	30.77	9.25
6	male	72	18.42	9.39	27.81	9.75
7	female	46	12.21	6.82	19.03	6.3
8	female	18	14.04	6.62	20.66	6.4
9	female	26	10.88	6.59	17.46	6.5
10	female	25	10.94	6.30	17.24	7.9
11	male	16	11.39	7.24	18.63	7.25
12	male	21	10.65	6.48	17.14	7.8
13	female	30	11.06	6.88	17.94	6.8
14	female	66	11.48	7.78	19.26	8.85
15	male	25	10.89	6.37	17.25	7.55
16	male	26	10.50	7.18	17.68	8.1
17	female	56	12.16	7.64	19.80	6.6
18	female	32	13.82	7.83	21.64	7.3
19	female	19	12.93	8.64	21.57	9.25
20	female	68	16.97	10.00	26.97	9.55
21	female	52	12.91	8.77	21.68	8.4
22	female	53	13.67	6.34	20.01	8.2
23	male	13	11.94	8.40	20.35	7
24	male	16	11.96	7.59	19.55	7.85
25	male	54	13.68	8.56	22.23	9.75
26	male	56	14.19	10.18	24.37	9.8
27	male	68	14.83	9.40	24.23	9.65
28	female	50	14.53	9.22	23.75	8.4
29	female	48	14.77	8.71	23.48	8.5
30	female	58	13.89	10.60	24.49	7.15
31	male	58	9.45	5.04	14.49	5.35
32	male	26	10.05	5.76	15.81	6.3
33	female	25	11.41	6.77	18.18	6.45
34	male	26	10.70	6.11	16.81	6.3
35	male	30	10.93	7.17	18.10	6.4
36	female	27	13.16	8.16	21.32	5.35
37	male	30	10.22	5.88	16.10	7
38	female	25	11.22	5.81	17.02	6.1
39	male	32	14.55	9.70	24.25	6.4
40	female	26	8.90	5.34	14.23	5.75
41	male	23	12.23	7.52	19.74	7.75
max		78	20.03	12.01	32.04	12.20
min		13	8.90	5.04	14.23	5.35
ave		41.22	13.04	7.91	20.95	7.79

5.3 Results for Five Poses

Next, we discuss the evaluation results for individual poses. Table 3 compares the average thresholds between the five poses. It indicates that *Seated 2* exhibits the largest threshold (31.85), while *Side-bend* does the smallest threshold (12.41). As illustrated in Figure 4 (e), to stretch the left arm and bend it deeply at *Seated 2* may be difficult for seniors, which makes the threshold large.

Table 3: Comparisons of average thresholds among five poses.

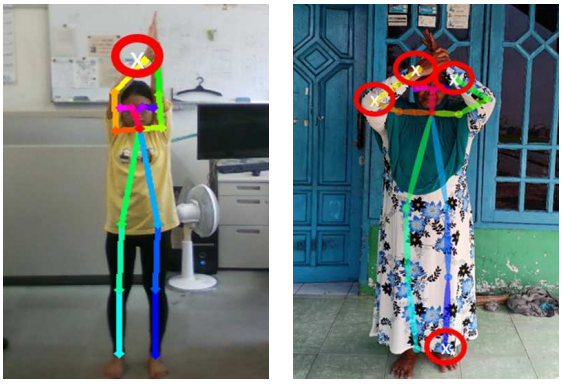
pose	max	min	ave
Mountain	60.65	11.50	25.64
Side-bend	27.18	6.54	12.41
Warrior	38.42	9.40	18.96
Seated 1	45.24	9.00	15.90
Seated 2	51.70	11.61	31.85

5.4 *Discussions of User Poses with Smallest and Largest Thresholds*

Among the 41 users, the 26-year lady at ID-40 exhibits the smallest average threshold (14.23 = 8.9 + 5.04) and the 68-year lady at ID-3 does the largest average threshold (32.04 = 20.03 + 12.01). Figures 6 and 7 show their poses for *Side-bend* and *Seated 2*. Clearly, the difference of the performance quality can be noticed between their poses.

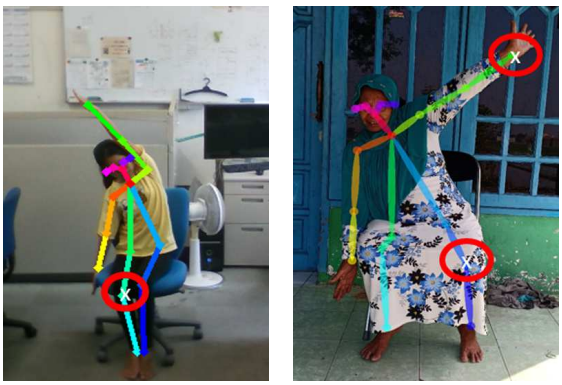
In these figures, the feature points that should be improved are pointed out by the marked crosses for further improvements of the poses. They are extracted in the rating function, where the Euclid distances are larger than the thresholds. Here, the average threshold value among the 41 users in Table 3 is used for the minimum threshold.

In Figure 6 (a), the right hand is pointed, because it is not stretched sufficiently, if compared with the instructor in Figure 4 (b). In Figure 6 (b), the three points in the both hands are pointed out, where the both arms should be stretched. It is noted that due to the pain, this lady cannot stretch the arms. Besides, the left leg is also pointed out, because the both legs are not parallel. In Figure 7 (a), the right leg is pointed, because the both legs are not parallel. In Figure 7 (b), the left hand is pointed out, where the left arm should be stretched and bended to the right side. Besides, the left leg is pointed out, because the both legs are not parallel. It is expected that the users will improve their poses by caring these feature points.



(a) smallest threshold user (b) largest threshold user

Figure 6: Comparison of *Side-bend* poses.



(a) smallest threshold user (b) largest threshold user

Figure 7: Comparison of *Seated 2* poses.

6 Conclusion

This paper proposed the *Exercise and Performance Learning Assistant System (EPLAS)* to assist people practicing exercises or learning performances by themselves at home. Using an open-source software *OpenPose*, the *rating function* was implemented to evaluate the user pose and point out the *feature points* to be improved. For evaluations, the instructor videos of five *Yoga* poses were prepared, and EPLAS was applied to 41 persons with various ages and genders in Indonesia, Japan, and Taiwan. The quality of the poses was also subjectively evaluated by 20 persons, where the strong correlation was observed between the subjective results and the rating function outputs. Besides, EPLAS pointed out the feature points to be improved in each pose. Thus, the effectiveness of the proposal was confirmed. In future works, we will improve user interfaces for easy operations by seniors, collect a variety of exercise/performance video contents, evolve the rating function for evaluating dynamic motions, and apply EPLAS to more various people for evaluations.

References

[1] I. T. Anggraini, A. Basuki, and N. Funabiki, "A proposal of entertainment and performance learning assistant system for seniors," in Proc. Int. Elec. Symp. (IES), 14-18, 2019.

[2] `https://www.who.int/mental_health/publications/whoqol/en/`.

[3] `https://www.who.int/health-topics/coronavirus#tab=tab_1`.

[4] `https://github.com/CMU-Perceptual-Computing-Lab/openpose`.

[5] T. Kiryu, I. Sasaki, K. Shibai and K. Tanaka, "Providing appropriate exercise levels for the elderly," IEEE Eng. Med. Biol. Mag., **20**(6), 116-124, 2001.

[6] J. Fasola and M.J Mataric "Using socially assistive human–robot interaction to motivate physical exercise for older adults," Proc. IEEE, **100**(8), 2512-2526, 2012. DOI: 10.1109/JPROC.2012.2200539

[7] B. Caulfield, A. Prendergast, G. Rainsford, and C. Minogue, "Self directed home based electrical muscle stimulation training improves exercise tolerance and strength in healthy elderly," in Proc. IEEE Eng. Med. Biol. Soc. (EMBS), 7036-7039. 2013.

[8] S. Ogunseye, S. X.Y. Komiak, and P. Komiak, "The impact of senior-friendliness guidelines on seniors' use of personal health records," in Proc. Int. Conf. Health. Inform. (ICHI), 597-602, 2015.

[9] E. I. Konstantinidis, A. S. Billis, C. A. Mouzakidis, V. I. Zilidou, P. E. Antoniou, and P. D. Bamidis, "Design, implementation and wide pilot deployment of FitForAll: an easy to use exergaming platform improving physical fitness and life quality of senior citizens," IEEE J. Bio. Health Inform., **20**(1), 189-200, 2016. DOI: 10.1109/JBHI.2014.2378814

[10] H. Wu, K.-Y. Lin, P. Liu, T. Hung, Z. Xiao, J. Chen, R. Lai, W. Wang, Y. Wang, and Z. Ye, "Development of an exercise management platform for the elderly," in Proc. IEEE Int. Conf. Cons. Elect. - Taiwan (ICCE-TW), 399-400, 2017.

[11] A. M. Campelo and L. Katz, "Physical literacy promotion in older adults using active video gaming: a sense of presence and attitudes towards exercise," in Proc. IEEE Game., Enter., Media Conf. (GEM), 163-166, 2018.

[12] C. Li, J. Li, T. P. Pham, and Y. Theng, "Promoting healthy and active ageing through exergames: effects of exergames on senior adults' psychosocial well-being," in Proc. Int. Conf. Cyberworld., 288-291, 2018.

[13] J. Ma, E. Hogervorst, D. Magistro, V. Chouliaras, and M. Zecca "Development of sensorised resistance band for objective exercise measurement: activities classification trial," in Proc. Int. Conf. IEEE Eng. Med. Biol. Soc. (EMBS), 3942-3945, July 2018.

[14] M. C. Chinnaiah, T. P. Kausalya Nandan, P. Haritha, S. Dubey, and I. A. Pasha, "A new deliberation of embedded based assistive system for Yoga," in Proc. Int. Symp. Embed. Comput. Syst. Design (ISED), 42-47, 2018.

[15] M. C. Thar, K. Win, and N. Funabiki "A proposal of Yoga pose assessment method using pose detection for self-learning," in Proc. Int. Conf. Adv. Inform. Tech. (ICAIT), 137-142, 2019.

[16] `https://www.raspberrypi.org/`.

[17] Chrome Browser, `https://www.chrome.com/`.

ASTES

Advances in Science, Technology and Engineering Systems Journal Vol. 5, No. 5, 1204-1213 (2020)

www.astesj.com

Special Issue on Multidisciplinary Innovation in Engineering Science & Technology

ASTESJ

ISSN: 2415-6698

Examination of a Skill Sampling Method of an Athlete Using the Athlete's Movement and Eye Movement for the Development of an AI Coach

Takuya Sarugaku[*,1], Jun Lee[2], Yasuaki Matsumoto[2], Mitsuho Yamada[1]

[1]*Graduate School of Information and Telecommunication Engineering, Tokai University, 108-0074, Japan*

[2]*Takei Scientific Instruments Co., Ltd., 956-0113, Japan*

ARTICLE INFO

Article history:
Received: 27 August, 2020
Accepted: 17 September, 2020
Online: 24 October, 2020

Keywords:
Sports
AI
4K
Gaze movement
Wireless eye movement measurement device

ABSTRACT

From amateur players who enjoy sports throughout their lives to top athletes who participate in international competitions, interest in improving sports skills is growing. Coaches and their coaching are indispensable for improving sports skills, but it is difficult for many athletes, especially amateur athletes, to secure coaching. However, we thought that anyone could easily receive coaching through the use of an artificial intelligence (AI) coach. In order to bring about AI coaching, learning is important. The set of learning data must include data such as players' skills as they correspond to their gaze and performance. In particular, it is thought that analyzing gaze movement during sports may provide insight into exceptional athletic skills. In this study, we propose a skill sampling method of collecting learning data for the specific purpose of creating an AI coach, using a wireless eye movement measurement device and 4K imaging.

1. Introduction

There is growing interest in sports, including the promotion of lifelong sports with an eye on the aging population, as well as the improvement of the skills of athletes aiming to participate in the Olympic Games and other international competitions. Many people from professionals to amateurs wish to improve their athletic ability and enjoy sports as a regular activity. Having a good coach is essential to improve sports skills, however, not everyone has access to a superior coach. We believe that by extracting the skills of both athletes and coaches, and applying learning data, it is possible to develop an AI robot that can coach anytime and anywhere.

An important task in realizing such AI is to include skill learning. It is necessary to collect learning data as a set of both players' and coaches' performances, gazes, and ideal skills. However, to the best of our knowledge, no such sets of learning data yet exist. In the present paper, we examine a skill sampling method of collecting learning data based on the performance and gaze of an athlete.

We focused on eye movement because we believe that it is essential for players during sports to watch the ball, to watch the opponent, and to observe the situation of the game. In fact, in an experiment that analyzed the eye movements of athletes performing on a gymnastics pommel horse, it was confirmed that posture fluctuations can be predicted from the stability of eye movements [1]. In martial arts such as kendo and fencing, it is said that it is important to maintaim a wide field of view by concentrating on a single point without moving one's eyes (as the Japanese proverb says, *enzan no metsuke*: "eyes on the far mountain" in a rough English translation)[2]. In a study by Natsuhara et al. [3], experts and semi-experts in football clarify whether there is a difference in eye movements during play depending on skill.

It is thought that an examination of eye movements during competition in various sports can reveal the points of attention and important gaze points for each sport.[4-8] For example, in relation to eye movements, experiments that block vision while a subject shoots a basketball have demonstrated that visual information at the final stage of the shot is important [9].

However, simply measuring eye movements without further context leaves it unclear what game situation brought about those eye movements. Therefore, combining athlete images taken from different directions with eye movement data can help match the movement of the athlete at any given point to the specific playing situation and eye movement. By connecting an actual athlete's action output with data obtained in this way, a set of learning data can be obtained. The required learning data vary by sport. In table

[*]Corresponding Author: Takuya Sarugaku, Email: tky.j10@fuji.tokai-u.jp

tennis, for example, useful data include the players' gaze, posture and movements, how to hit the ball, the score rate, etc. In dance, on the other hand, in addition to data on the dancer's gaze, posture and movements, it is also useful to know his or her velocity of rotation, etc. It is necessary to construct a database that associates the characteristic play of skilled athletes with results such as score rate and rotation speed.

In this paper, we examine a skill sampling method based on an athlete's performance and gaze in order to acquire a data set to be used in creating an AI coach. First, we consider the configuration and accuracy evaluation of a wireless eye movement measurement device developed to easily measure the eye movements of athletes who exercise intensely. Next, we present the results of experiments conducted during table tennis and dance rotation as examples of data acquisition.

2. Configuration of a wireless eye movement measurement device

Many sports science experiments using eye movements have been conducted [10]. In the work [11], experiments have been conducted with the aim of elucidating the role of head, eye and arm movements during table tennis competitions, using eye movement measuring devices and other equipment. However, the eye movement measurement device used in this experiment requires a wired connection to an interface PC and control unit etc, which is difficult to measure in competitions with a lot of distance to travel or competitions involving rotation. In addition, the study [12] describes the eye movements and shooting strategy in soccer penalty kicks. The eye movement measurement device used in this study was linked to a PC via a 10m fire wire cable from a recording device in a pouch wrapped around the waist, so it was not possible to measure in a completely free state. One study by [4] measured the eye movements of athletes watching competition videos. As in these examples, few studies have measured eye movements in a state where athletes are free to compete.

There are several reasons why it is difficult to measure the eye movements of athletes during competition. First, wired devices can hinder the athlete's performance. Also, calibrated sensors may be displaced by the intense movement of the athlete and, when a sensor shifts, the experimenter may not notice the shift unless measurement status can be confirmed in real time. We solved these problems using wireless measurement devices and by enabling real-time monitoring and recalibration of the measurement situation. Figure 1 shows the configuration of the developed eye movement measurement device, and a person wearing the device is shown in Figure 2. A video transmitter and external control system with a mouse were added to a TalkEye Lite system (Takei Science Instruments Co., Ltd., Niigata, Japan), which uses a corneal reflection method. The experimenter can control recording start/stop, offset of the line of sight, etc. with a Bluetooth mouse by watching a display transmitted wirelessly. Two devices can be used at the same time. Because experimental data is recorded in the TalkEye Lite, there are no direct effects of the wireless delay. The device can be fixed to the head with a hook and loop fastener so that the eye movement sensors do not slip off during exercise.

Figure 3 shows the operation screens shown on the external display: (a) is the eye movement calibration screen, (b) is an offset button for correcting the displacement of gaze movement when the subject gazes at the center of the field of view before the experiment, and (c) is the experimental screen. Basic operation is possible wirelessly when the athlete carries the eye movement measuring equipment in a backpack. It is possible to measure the gaze movement of two athletes simultaneously by radio.

We evaluated the accuracy of this eye movement recording system using a dancer who agreed to serve as a subject for the experiments discussed in Section 4. We had the dancer perform two high-speed turns and compared eye movement accuracy before and after the turns. Five-point calibration was applied, as shown in Figure 4. The distributions of the gaze points when the subject gazed at the calibration points before and after two high-speed turns are shown in Figure 5. The subject's accuracy before turning was x: -0.82±0.64 deg., y:-0.72±0.69 deg., and that after turning was x: 0.92±0.87 deg., y:-1.71±1.75 deg. Considering that the diameter of the fovea, which has the highest resolution on the retina, is about 1 degree, it was confirmed that eye movement accuracy barely changes at all with high-speed turns. However, it was confirmed that the dancer's gaze shifted upward when viewing the lower index point after rotation.

The maximum transmission distance of video in the room is 19.7m, and the maximum distance at which the TalkEye Lite can be controlled is 43m. The device weighs 1.3 kg. The size of the goggles with the eye movement sensors and a field of view camera is 19 cm in length, 21 cm in width, and 9 cm in height.

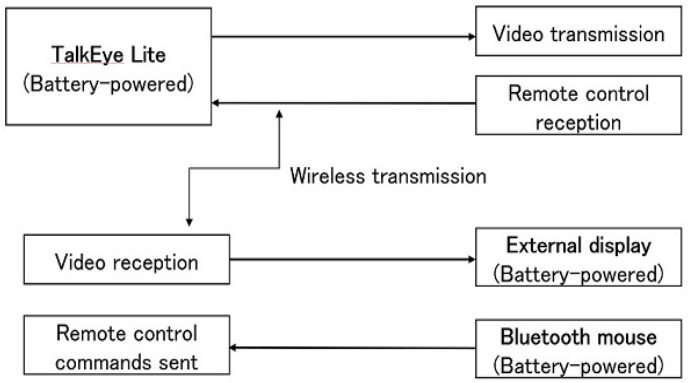


Figure 1: Configuration of the developed device



Figure 2: A person wearing the device (the eye movement measurement device is in the backpack)

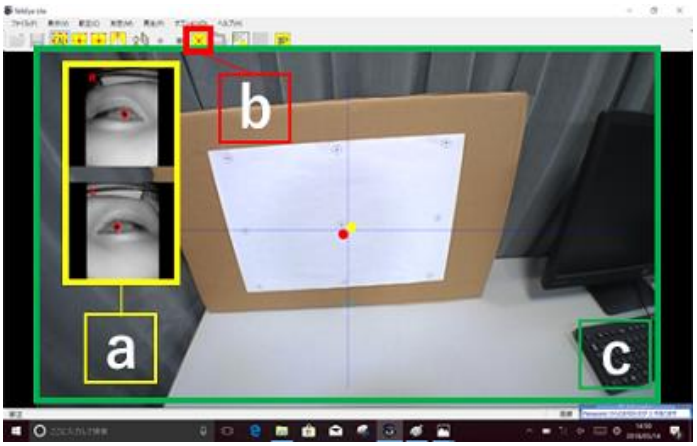


Figure 3: The operation screens shown on the external display

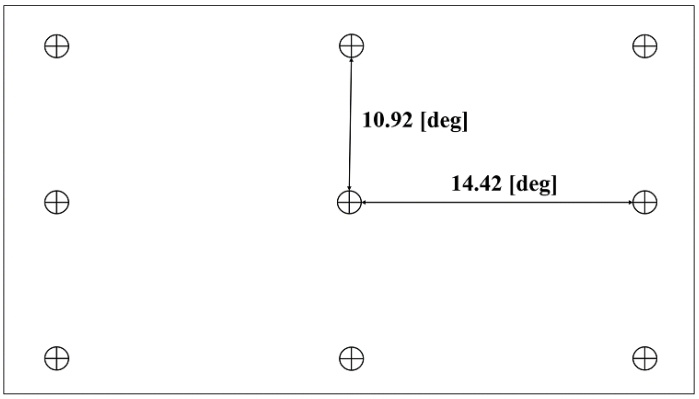


Figure 4: Fixation points for five-point calibration

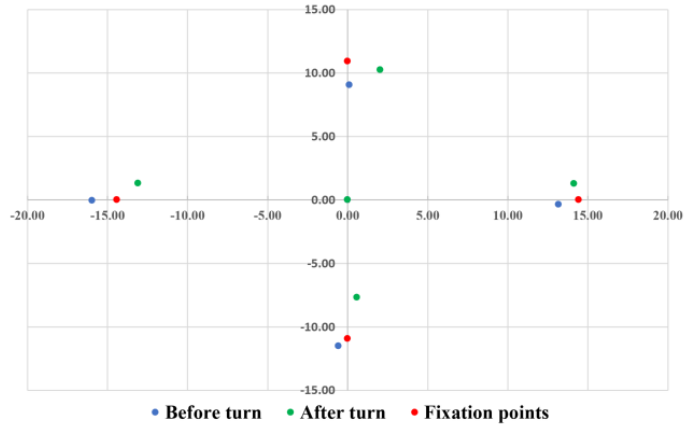


Figure 5: Distributions of the gaze points when the subjects gazed at the calibration points before and after two high-speed turns

3. Measurement of gaze movement during table tennis play

We first conducted experiments on table tennis as an example to demonstrate the wireless function of our device. Our subjects were two players on the table tennis team at Tokai University Takanawadai Junior & Senior High School. A table tennis table was brought to our 4K studio, each athlete wore a backpack device, and the eye movement of each was acquired. In order to record the actions of the athletes, video was taken with a 4K camera from the front and the side of the table tennis table and were recorded synchronously with recording by the eye movement measurement device. Figure 6 shows the layout of the equipment during the experiment, and Figure 7 shows an image taken during play.

An example of an image edited after measurement is shown in Fig8. "Cam 1" in Figure 8 shows the performance of Player A, "Cam 2" shows the movement of the ball during the game, and "Cam 3" shows the performance of Player B. The images marked "Player A" and "Player B" in the figure show their respective lines of sight. In addition to the images of the two athletes' gaze movement superimposed on the image from each camera, the expression and movement of the athletes during the game are displayed. Our 4K system makes it possible for individual images to maintain a resolution quality nearly as good as that of high-definition television even when we divided an image, as in this figure; high-precision analysis was thus possible.

The purpose of this experiment was to sample the athlete's characteristic eye movements and performance during table tennis by using the above analysis method. The specific data to be collected include information on the athlete's gaze and performance during rallies, for example. These data will be useful in the creation of an AI coach. An example of analysis using this apparatus is shown in Figure 9, which shows the gaze movement of both players at the moment Player A hits the ball. The left and right lines of sight are indicated by the yellow and green numbers, respectively, where their number indicates their order.

Furthermore, we propose a method to compare the body and eye movements of Players A and B in the time series shown in Figure 10. Figure 10 compares the actions and lines of sight of Players A and B. Here, for greater clarity, the ball is circled in white and the line of sight is circled with yellow dots. The area over which the gazing points were distributed is expressed by the size of the circle.

In this sequence, Player B hits the ball at Time (a) [Column a, Row 3], and Player A hits the ball at Time (f) [Column f, Row 1]. Let us first focus on Player A. Looking at Player A's line of sight [Row 2] at Time (a) [Column a], Player A looks at Player B's racket at the moment Player B hits the ball. At Times (b-f) [Columns b-f, Row 2], it can be confirmed that Player A continues watching the flying ball. Player A's movement at Time (d) [Column d, Row 1] confirms that he starts to drop his waist to return the ball. Comparing Times (e), (f) and (g) [Columns e-g, Row 1], we see that Player A's waist has dropped most at Time (g) [Column g, Row 1], after he has finished hitting the ball. In addition, we can confirm that he follows the ball and gazes at his partner's racket at Times (f-h) [Columns f-h, Row 2].

Next, when we examine Player B's line of sight where he follows the trajectory of the flying ball at Time (a) [Column a, Row 4], and after hitting the ball toward Player A at Time (b) [Column b, Row 4], it can be seen that his eye follows the trajectory of the ball as it flies to Player A. Also, Player B's movement at Time (a) [Column a, Row 3] confirms that he is leaning forward to hit the ball. The sequence at Times (f-h) shows that Player A hit the ball higher than at Times (a-c), and this is confirmed by comparing Player B's movement [Column b, Row 3] and [Column g, Row 3] and continuing into Time (h) as he follows the downward motion of the ball [Column h, Row 4].

Judging from the relative sizes of the circles of yellow dots, Player B's eye movement area is larger than Player A's. Head movement was judged from images of the table tennis table taken by each player's field-of-view camera. Images from Player A's

field-of-view camera [Row 2] moved largely along the vertical direction, and changes in the image of the table are therefore large. In contrast, the images from Player B's field-of-view camera [Row 4] show little change, suggesting that his head moved only a little. These results indicate that Player A's head movement supplemented his eye movement since his eye movement area was small, while Player B did not need to supplement his eye movement with head movement. In this regard, the coach of the high school table tennis team pointed out that small head movement during a game, like Player B's, is better.

Time (g) in Figure 10 also shows another characteristic result. When the ball hit by Player A reaches the top of its trajectory after bouncing off the table, Player B looks at the highest point of the ball. It is known that the rotation direction of the ball is easy to see when the vertical velocity of the ball is nearly at the top of its trajectory. In other words, we were able to capture the moment when Player B looked at the top of the trajectory to determine the rotation direction of the ball.

Two important features of our system are that two wireless eye movement analysis devices can be employed simultaneously and that it uses high-definition 4K imaging, making it possible to extract such moments from rallies between two players. By using two devices, it is possible to know the athletes' tactics using gaze. We believe that this can be useful as a sports video analysis method or as a new training method. By using this method, the athlete's body movement, situation, and eye movement can be obtained simultaneously at any point during competition. At present, coaching emphasizes movement but, by using gaze data, it is possible to provide coaching based on the information skilled athletes obtain from their own gaze and from their own plays as well as those of their opponents. Furthermore, a database can be created in which these measured data are combined with the score rate, smash success rate, etc. By then using this information as learning data, an AI coach that can teach expert skills can be created.

4. Measurement of gaze movement during dance

Next, let us consider an experimental example of dance. Considerable research on figure skating is currently being conducted. Resistance to vestibular system input is typically weak in novices who have just started figure skating, and it has been noted that they are remarkably susceptible to physiological and mental disorders. Rotation experiments using a Barany chair have shown heartbeat irregularities and malfunction of the coordination of movements of the hands and feet [13].

It is difficult to measure eye movements while a subject is rotating during competition. Therefore, experiments have been conducted in which circulation vection is generated using virtual reality in order to examine eye movements closely related to the vestibulo-ocular reflex (VOR). In a comparison of professional skaters and beginners in which the angle of the view to be displayed was changed, significant differences were observed all components of eye movement (decrease in fixation time, decrease in saccade amplitude, increase in blinking, etc.) in results corresponding to a visual angle exceeding 180°[14].

These studies show that training of the vestibulo is an important aspect of figure skating training, and eye movement is useful for evaluation. From the point of view of training athletes for sports that require high speed rotation, such as figure skating and dancing, the athlete should set the gaze position at the time of rotation at a single point and suppress the VOR, which is the function of the semicircular canal at the back of the ear. This is said to prevent eye movement in the direction opposite to the rotation of the head, which occurs to compensate for head movement during head rotation [15-17].

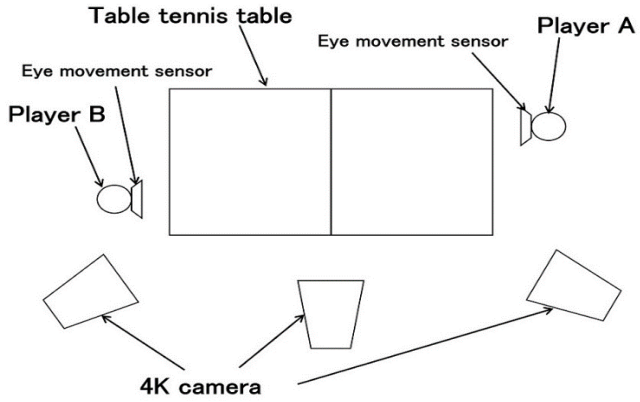


Figure 6: Arrangement of the developed equipment



Figure 7: Photo taken during measurement



Figure 8: Edited image

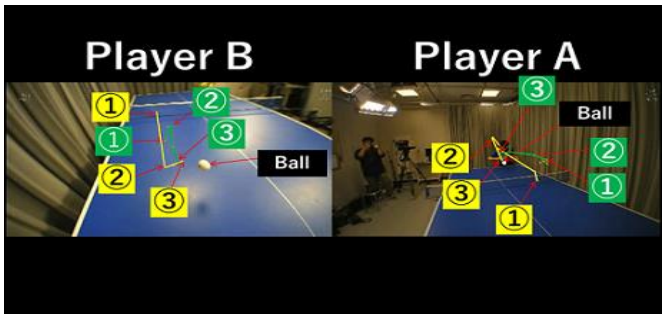


Figure 9: Analysis example

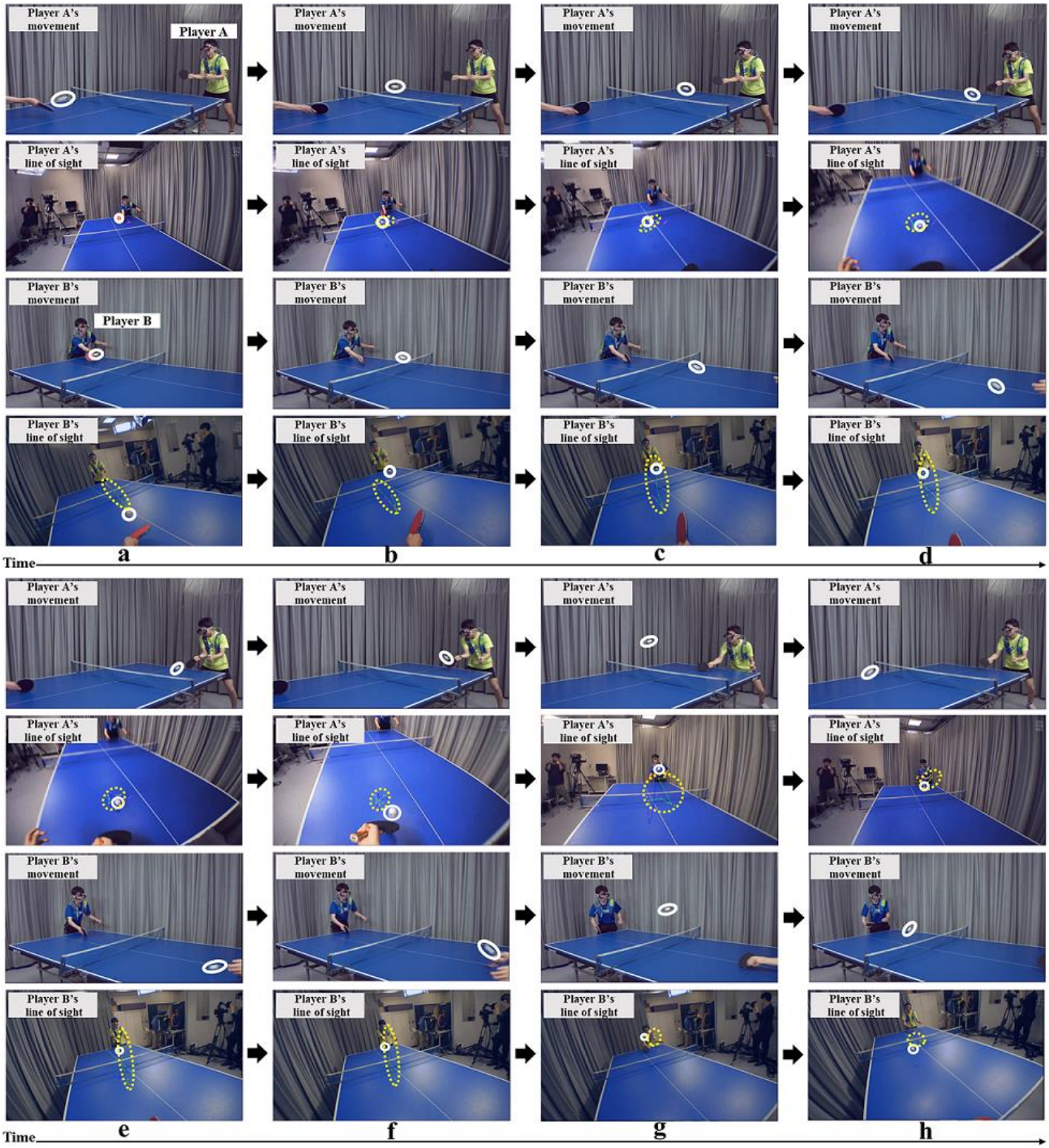


Figure 10: Body and eye movements of Players A and B in a time series

Previous studies have used rotating chairs and images such as VR environments but to the best of our knowledge, none have actually measured eye movements during performance. Since the athlete rotates, a wired system is impossible and a wireless system is indispensable. Furthermore, since the system undergoes heavy centrifugal force during rotation, it is necessary to ensure that the goggles for eye movement measurement do not shift, and robustness is also required for the eye movement measurement device itself. Additionally, due to the intense motion during performance, it is possible that the calibration of the eye movement device may shift. Thus, it is necessary for the experimenter to be able to recalibrate the eye movement measuring apparatus during performance of subject.

We believe that the device introduced in the present study meets the requirements for eye movement measurement during dance. In the present dance experiment, a dance expert with a dance history of 17 years beginning at the age of 4 wore a wireless eye movement measurement device and rotated in place. To the best of our knowledge, there have been no reported examples of eye movement measurement during dance using a wireless-type eye movement measurement device. All experiments were conducted at the 4K studio of our university, and videos were taken with GoPro from the top, and with a 4K camera from the front, right and left; all videos were recorded synchronously with the wireless eye movement measurement device. The sampling rate was 120 Hz for the GoPro device, 60 Hz for the 4K camera, and 30 Hz for the wireless eye movement measurement device. The experimental set-up is shown in Figure 11 and 12.

After the experiment, we edited the video from the three recording devices, and found the rotation angles of the head and body. An example of the edited video is shown in Figure 13. Images of the dancer's eye movement and of the dancer from various directions were recorded in high definition using a 4K production system. The purpose of this experiment was to sample a dancer's characteristic eye movements and body posture and movement during a dance competition. As mentioned above, to the best of our knowledge, there has been no actual measurement of gaze during a dance turn. Our proposed skill sampling method can clarify not only the gaze of the spinning dancer, but also his or her movement. A sequence of images from a dance turn is shown in Figs.14-17. Figure 14 shows the series of images taken from overhead, and the same sequence is then shown from the front (Figure 15), from the right (Figure 16), and from the left (Figure 17). A picture was taken every 45°, and the numbers correspond across the different views. The present method makes it possible to acquire the relationships among the body, head, and eye movements of a dancer during a dance.

Figs.18 and 19 are graphs of the subject's lines of sight at the time of rotation. The solid line shows the rotation angle of the head, the broken line shows that of the body, and the dotted line shows that of the right eye (gaze). Where there is no dotted line, the subject blinked and eye movement could not be acquired. The color of each line corresponds to the number of the trial. The left vertical axis in Figure 18 shows the angle between the head and the body, the right vertical axis shows the angle of the line of sight, and the horizontal axis shows the corresponding numbers of the frames on the wireless eye movement measuring device. In Figure 19, the vertical axis shows the velocity of the corresponding rotation angle, and the horizontal axis shows the numbers of the frames on the wireless eye movement measuring device. First, let us focus on head movement. The head does not move significantly until Frames 7-10 in Figure 18. This is because the athlete is trying to look at his chosen front fixation point. After that, the head rotates rapidly from Frame 8 onward, overtaking the body, which rotated previously. The velocity of the head rotation angle reaches its maximum in Frames 10-14 in Figure 19, and the average of the velocity of the head rotation angle of 11 trials is 1712±112 deg/sec. Next, let us examine the motion of the body. The velocity of the body rotation angle (Figure 19) reached its maximum with the same timing as the head, at Frames 8-12. However, it can be seen that there is no large change in speed compared to the head; the body rotates at an approximately constant speed. The dancer's eye moves to the left until Frame 11, at which point the body and the head are both rotating to the right, indicating that the dancer is gazing at his chosen front fixation point on the left. Some data were lost due to blinking but, after 18 frames, the body and head passed right behind and turned to the right, and the dancer was gazing at his chosen front fixation point on the right. Eventually, the body and head rotate 360 degrees and again face the front and the eye movement is also 0 degrees, but before that time, a number of sawtooth-like eye movements like OKN (optokinetic nystagmus) that pass through the predetermined frontal fixation point and back again have occurred.

Next, Figs. 20 and 21 show the rotation angle and rotation angle velocity of a typical trial. The axes in Figs. 20 and 21 are the same as those in Figs. 18 and 19. The forms at the bottom of Figs.20 and 21 show the direction of the body, head, and eyes (arrow) at points corresponding to the images in Figs.15-17. These figures are intended to make it easier to match the athlete's body movements with other data obtained at the same point. From ⑤ to ⑥ , the subject blinked and we were unable to acquire eye movement data. Figure 20 shows that the body rotates first, followed by the head, which turns rapidly around a body rotation angle of about 90° (③ in Figs. 14-17, 20 and 21) until the body rotation angle reaches about 140 deg (④ in Figure 14-17, 20 and 21), when the head begins to lead. Figure 21 confirms that the maximum velocity reached 1920 deg/sec when the head was sharply turned. The velocity of the body rotation angle did not change as rapidly as that of the head.

Generally, the eye rotates in the direction opposite to that of the rotation of the head due to the VOR, but when the head is rotating at a high speed, the VOR is prevented, and we confirmed that the eye did not move in Figure 21 (④ and ⑤). Furthermore, the video from the field-of-view camera of the wireless eye movement measuring device confirmed that the subject continued to gaze at the front camera between 0° and 90° (① - ③ in Figure 14-17, 20 and 21) and between 270° and 360° (⑦ - ⑨ in Figure 14-17, 20 and 21). From Figure 20, it was confirmed that the eye rotated to the left from the front as it rotated (① - ④), and from the right to the front after turning (⑦ - ⑨), in order for the dancer to gaze at a point that he had chosen in advance (the front camera, in this example) even as the body rotated. After that, eye movement showed a large reverse in direction at ⑦. Regarding gaze position, it was confirmed that the dancer gazed at a point that he had chosen in advance by asking "Where do you look when you are turning?" after the experiment.

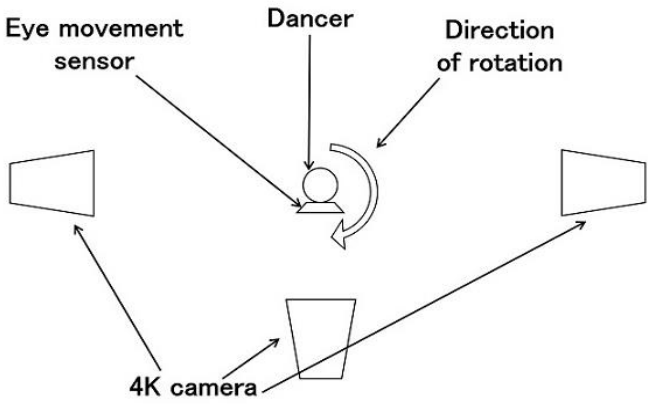


Figure 11: Experimental set-up from the top

Generally speaking, when one sits on a rotating chair and rotates, the VOR causes dizziness. However, a dancer keeps his or her posture steady without dizziness by watching a certain point while rotating [11-13]. To the best of our knowledge, the present study is the first time that this could be confirmed through the use of an eye movement measuring device. The present method makes it possible to acquire the relationships among the body, head, and eye movements of a dancer while dancing. By using this skill sampling method to create a database of the head, body, and eye movement data obtained from many skilled athletes, an AI coach that can teach beginners the optimal rotation method can be created.

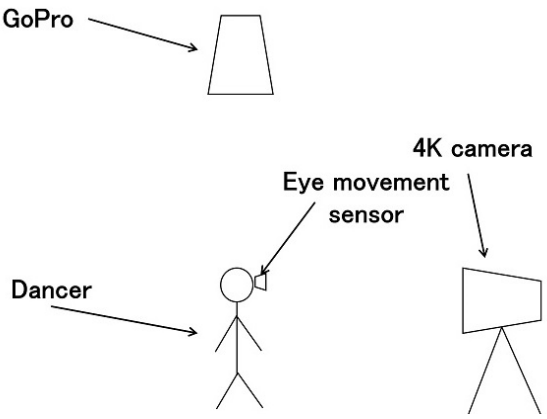


Figure 12: Experimental set-up from the side

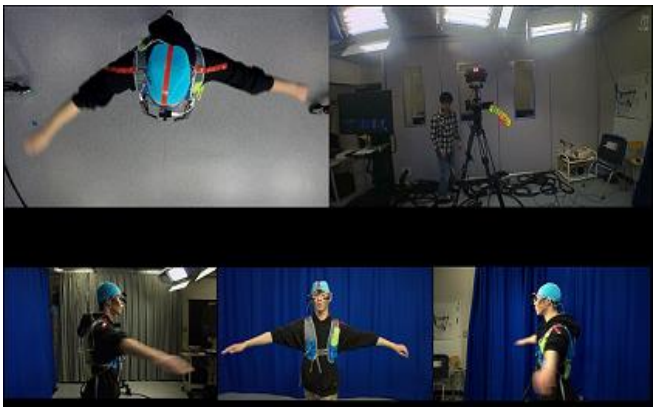


Figure 13: Video output after editing

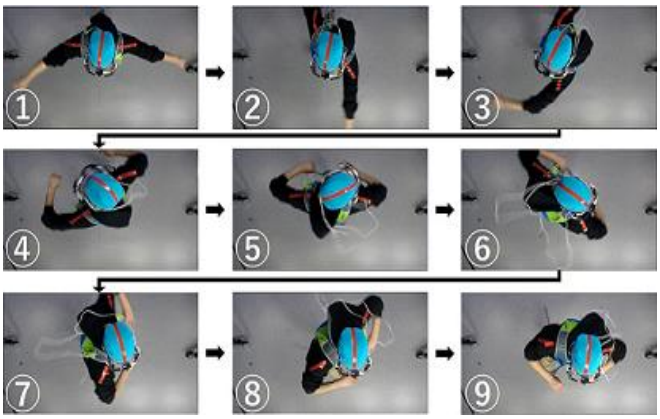


Figure 14: View from the top

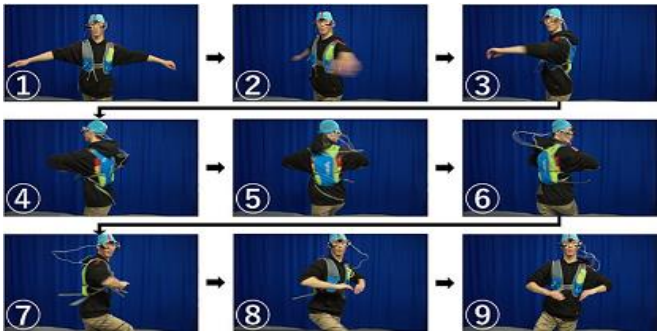


Figure 15: View from the front

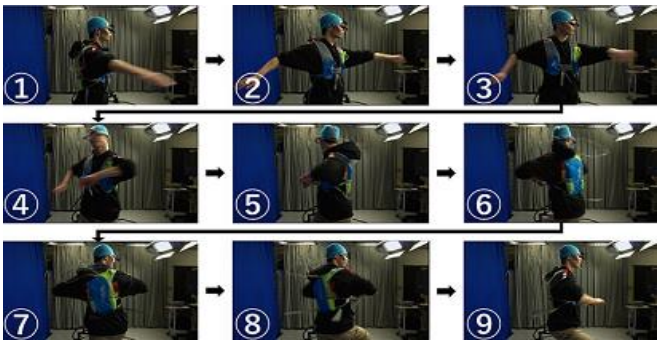


Figure 16: View from the right side

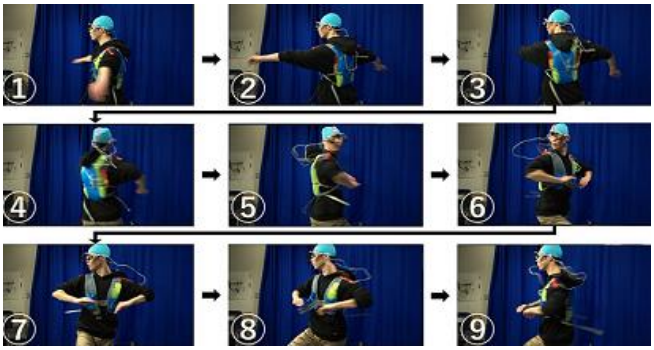


Figure 17: View from the left side

5. Conclusion

There is a big difference in the level of sports ability to aim for, from the promotion of lifelong sports aimed at healthy longevity to the training of athletes who are able to compete in the Olympic Games and other international competitions. For this reason, coaches for many different levels of athletes are required. However, it cannot be said that there are enough coaches, except for athletes who are aiming for professional sports and the Olympics. If an individual learns tips for improving and enjoying various sports, he or she will be able to start sports at an early age and continue throughout life; such tips may also help the handicapped and the elderly. Therefore, if we can develop an AI coach that can teach these tips, we believe that the shortage of coaches can be solved at once.

However, learning data are required in order to develop AI robots. For example, if the goal is a successful shot in soccer, the performance of the athlete up to that point and during the immediate situation becomes learning data. The situation during a game changes every second, and the exact same game situation is rarely, if ever, reproduced. Additionally, the athlete does not experience all possible game situations and does not calculate the

next play based on all past experiences during games. It is possible to develop an AI coach that can make judgments similar to those of the skilled athlete by applying as much learning data and as many outcomes as possible. To the best of our knowledge, no analysis of the behavior of athletes during a match or performance has yet been carried out for this purpose. Therefore, given the fact that the eye movements of advanced and beginner athletes differ significantly in various skills, and taking advantage of the superb resolution of 4K imaging, which allows images taken during play to be synthesized with high resolution, we worked on building databases that make it possible to learn from the eye movements and performance of athletes during a game or performance. In this paper, we present measurement examples of athletes both playing table tennis and performing dance rotation, and analysis examples using 4K video; these data can be used to create a database.

In table tennis, the analysis included data collected when two players were competing, specifically, data regarding eye movement, the position of the racket, and the position of the ball. In the case of dance rotation, eye movement, head movement, and body movement during rotation were examined. The data introduced here are those of non-professional athletes and are not necessarily sufficient as input for learning data. However, by applying our skill sampling method with cooperation from top athletes, it will be possible to collect the necessary data. Using our method, we would like to develop AI coaching through the use of learning data that match eye movements, body movements, game situations and outcomes during play.

Acknowledgment

This work was supported in part by the Hoso Bunka Foundation (2018/2019 Grant Cycle). We would like to express our sincere gratitude to the table tennis team at Tokai University Takanawadai Junior & Senior High School for kindly allowing us to take movies of them playing. We also thank Mr. Hiroki Kudo in our laboratory who danced for our dance experiment.

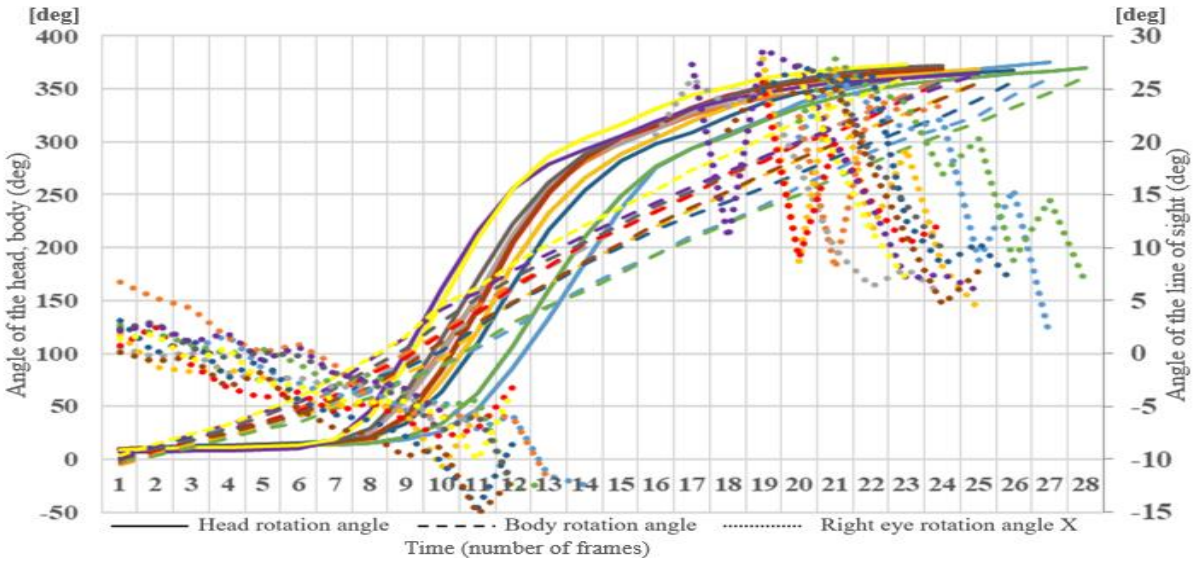


Figure 18 : Angle of gaze, head, body (11 trials)

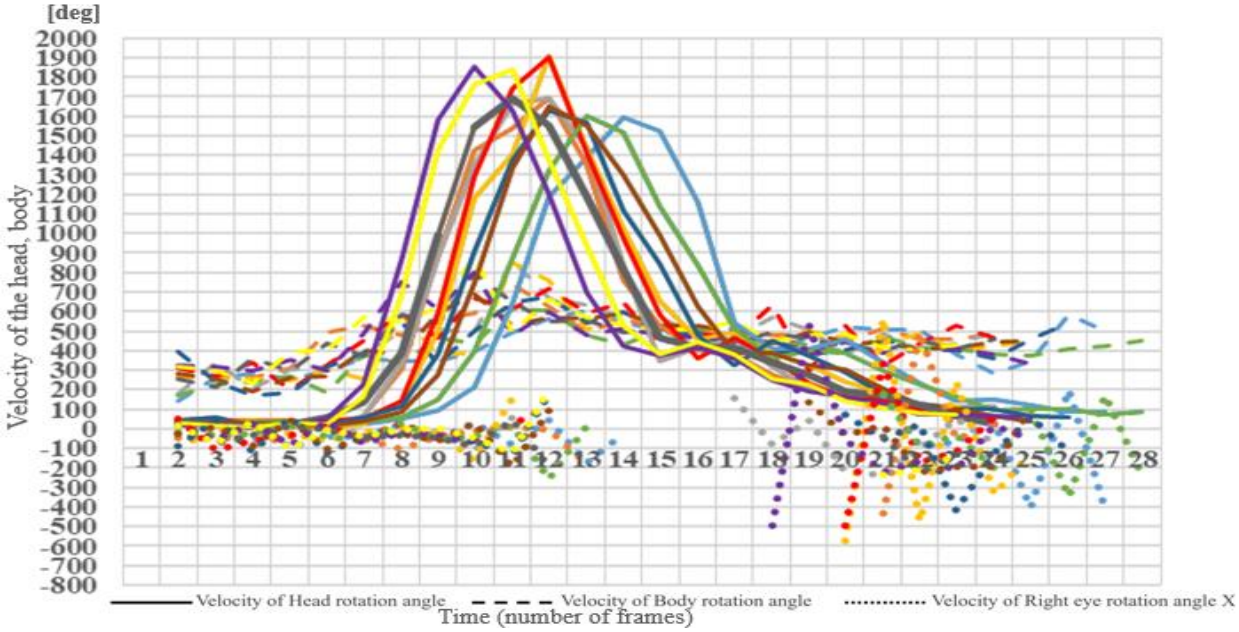


Figure 19 : Velocity of gaze, head, and body rotation angle (11 trials)

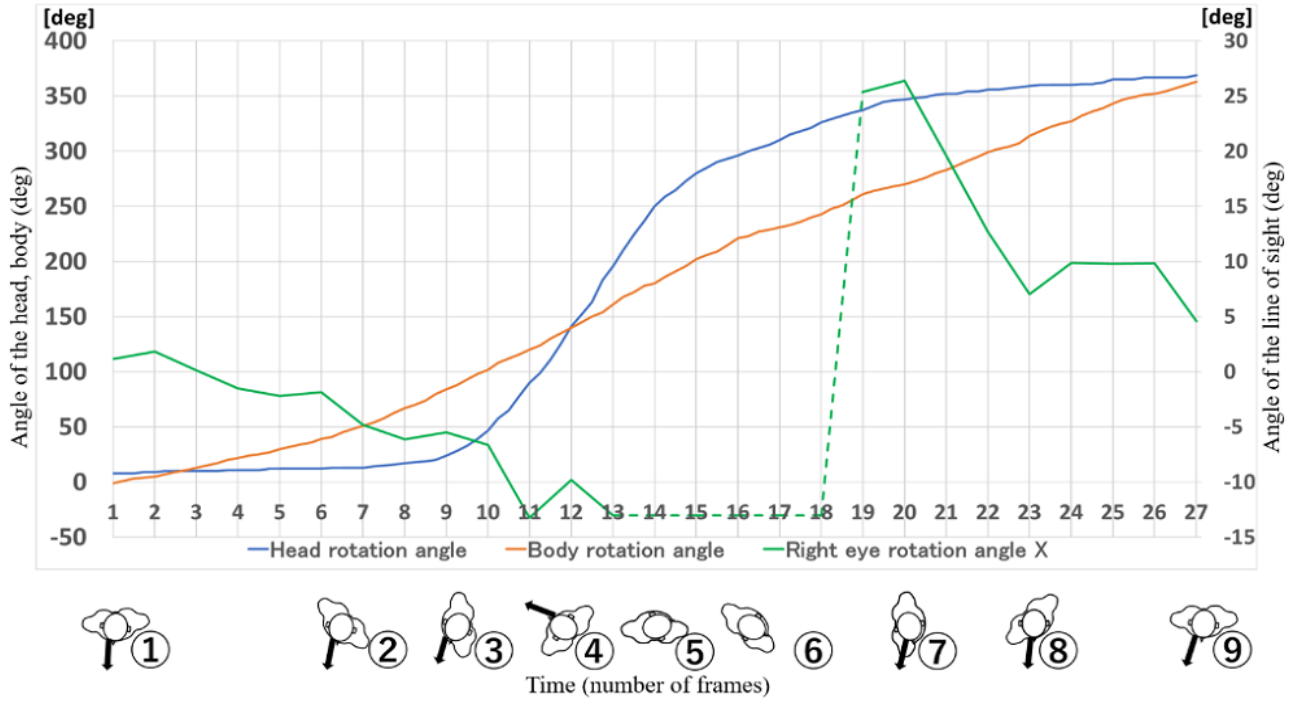


Figure 20 : Angle of gaze, head, body

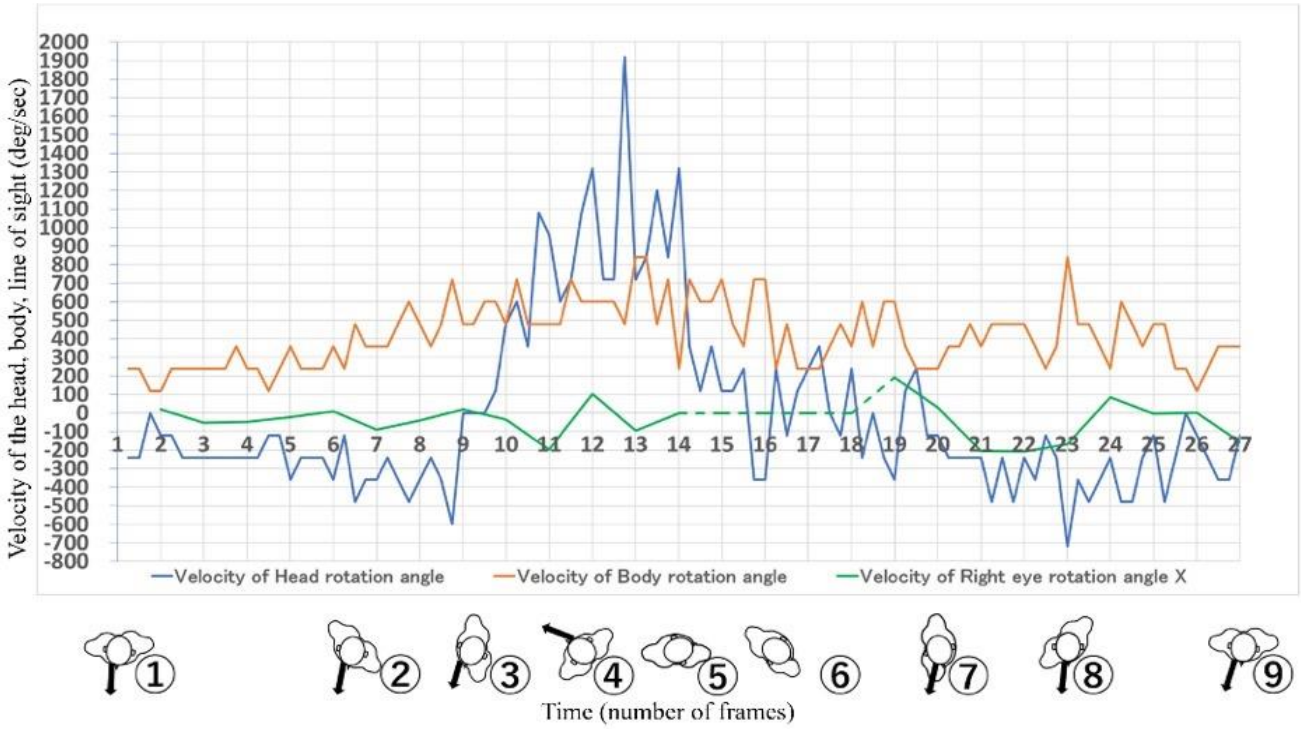


Figure 21 : Velocity of gaze, head, and body rotation angle

References

[1] Y. Sato, "Gaze Behavior during Circles on Pommel Horse", Bulletin of College of Commerce (comprehensive cultural studies), Nihon University, **24**(1,2,3), 221-236, 2019.

[2] K. Hasegawa et al., "Study on the Point of Observation the Moment of Stroke : With Special Reference to the Point of Observation," Metsuke", in Kendo", The bulletin of School of Physical Education, Tokai University, **16**, 55-60, 1987.

[3] T. Natsuhara et al., "Soccer ni okeru senjyutsuteki handan wo tomonau pasu no suikou wo sasaeru ninchi purosesu (Cognitive process that supports the execution of a path with tactical judgment in football)", Japan J. Phys. Educ. Hlth. Sport Sci., **60**(1), 71-85, 2015, doi:10.5432/jjpehss.14001.

[4] E. Hiroshi Edagawa, Monthly Book OCULISTA, No.58, 1, 2018.

[5] Z. Jian, W. Kazuhiko, M. Mai, " A study on anticipatory accuracy and visual search strategy of skilled and novice soccer players:Compared between 1 vs. 1 and 3 vs. 3 situations", Jpn J. Phys. Educ. Health Sport Sci., **53**(1), 29-37, 2008, doi: 10.5432/jjpehss.0478.

[6] Y. Mizusaki, H. Nakamoto, S. Mori, " The Effect of Visual Occlusion during Quiet Eye Training on Free-Throw Accuracy in Novice Basketball Player", Annals of Fitness and Sports Science, National Institute of Fitness and Sports in Kanoya, **47**, 21-28, November, 2013.
[7] M. Takahashi et al., " Visual Behavior of Expert Baton Twirlers during Catching Tasks", The Japanese journal of ergonomics, **46**(1), 31-36, February, 2010, doi: 10.5100/jje.46.31
[8] T. Kato, T. Fukuda, " Visual Search Strategies of baseball batters during the preparatory phase of batting", The Japanese journal of ergonomics, 38(6), 333-340, December, 2002, doi: 10.5100/jje.38.333.
[9] R. Oudejans, van de Langenberg RW, Hutter RI, "Aiming at a far target under different viewing conditions: visual control in basketball jump shooting.", Hum Mov Sci, **21**, 457-480, 2002, doi:10.1016/s0167-9457(02)00116-1.
[10] S. Hüttermann, B. Noël, D. Memmert, "Eye tracking in high-performance sports: Evaluation of its application in expert athletes", IJCSS – **17**(2), 2018, doi:10.2478/ijcss-2018-0011.
[11] S.T. Rodrigues, Joan N Vickers, Andrew Mark Williams, "Head, eye and arm coordination in table tennis", Journal of Sports Sciences, **20**,187-200, April, 2002, doi: 10.1080/026404102317284754.
[12] G. Wood, Mark R Wilson, "Gaze behaviour and shooting strategies in football penalty kicks: Implications of a 'keeper-dependent approach", International journal of sport psychology **41**(3), pp.293-312, November, 2010.
[13] J. Wetzig, M.Reiser, E.Martin, N.Bregenzer, R.J.von Baumgarten, "Unilateral centrifugation of the otoliths as a new method to determine bilateral asymmetries of the otolith apparatus in man", Acta Astronautica, **21**, 519-525, 1990, doi:10.1016/0094-5765(90)90070-2.
[14] G.Y. Menshikova, Aterm I. Kovalev, Oxana A. Klimova, Alexander M. Chernorizod, "Eye movements as indicated of vestibular dysfunction", Perception, **44**, 8-9: 1103-1109, First Published August 14, 2015, doi:10.1177/0301006615594916.
[15] R. Letzter, "The brutal neuroscience of figure skating: How spinning athletes overcome dizziness", https://www.livescience.com/61795-ice-skating-brain-spin-dizzy.html, February 16, 2018.
[16] A. Kheradmand, "Why don't figure skaters get dizzy when they spin", https://www.scientificamerican.com/article/why-don-t-figure-skaters-get-dizzy-when-they-spin/, July 24, 2013.
[17] C. Dehesdin, "Spin, Dance, Jump, Repeat!, Why don't figure skaters get dizzy?", http://www.slate.com/articles/news_and_politics/explainer/2010/02/spin_dance_jump_repeat.html, February 10 2014.

ASTES

Advances in Science, Technology and Engineering Systems Journal Vol. 5, No. 5, 1214-1224 (2020)

www.astesj.com

Special Issue on Economic Impact of COVID-19 on Companies & Consumers

ASTESJ

ISSN: 2415-6698

Strategic Model to Assess the Sustainability and Competitiveness of Focal Agri-Food Smes and their Supply Chains: A Vision Beyond COVID 19

Yonatan López-Santos[*,1], Diana Sánchez-Partida[2], Patricia Cano-Olivos [2]

[1]*Instituto Tecnológico Superior de Tepexi de Rodríguez, Tecnológico Nacional de México, Tepexi de Rodríguez, 74690, México*

[2]*Department of Logistics and Supply Chain Management, Universidad Popular Autónoma del Estado de Puebla, Puebla 72410, Mexico*

ARTICLE INFO

Article history:
Received: 01 September, 2020
Accepted: 28 September, 2020
Online: 24 October, 2020

Keywords:
Sustainable Supply Chain Management (SSCM)
Analytic Hierarchy Process (AHP)
Small and Medium-sized Enterprises (SMEs)
Agri-food sector
Strategic planning
COVID-19

ABSTRACT

There have been disruptions in local and global food supply chains around the world due to the COVID-19 pandemic. It has led to rethink various aspects and to consider various trends in the food sector, encourage a more rapid transition and evolution to the Sustainable Supply Chain Management (SSCM), to counteract current problems and to help towards a more sustainable and competitive vision. However, there is a strategic disconnection in SSCM between sustainability and strategies related to competitive advantage. Therefore, the objective of this research is to propose a decision-making model to assess the sustainability and competitiveness strategically of a Mexican agri-food focal SME (Small and Medium-sized Enterprise) that leads its supply chain. It is validated with comparative analysis in the productive taro activity through the Analytic Hierarchy Process (AHP) that contributes to prevent or to face problems such as the COVID-19 pandemic and climate change. This research is based on a case study methodology divided into four stages. Three presented alternatives are assessed and compared by thirty-five criteria: a) A current situation without sustainability, b) Cost leadership strategy considering sustainability, and c) Differentiation strategy considering sustainability. The conclusions indicate more feasibility and compatibility to achieve sustainability with a differentiation strategy than with a cost leadership strategy. The current crisis should lead us to think beyond COVID-19, as we have more challenges ahead, such as climate change, environmental impacts, poverty, among other aspects that could cause instability around the world. Therefore, the current situation should be an impetus to further progress towards the 17 Sustainable Development Goals, in this case, through the theory of SSCM. That is why this model contributes strategically to the SSCM, to develop greater long-term resilience in the Mexican agri-food focal SMEs and their supply chains.

1. Introduction

Currently, there are disruptions in both local and global food supply chains around the world due to the pandemic [1]-[3] caused by the new coronavirus [4], better known as COVID 19. It has led to thinking in various scientific fields and everyday life, as in the present manuscript, which contemplates the acceleration of various changes to move towards Sustainable Supply Chain Management (SSCM) and competitiveness, especially in the food sector. Some adversities that have placed Mexico as one of the countries at the most significant risk to COVID-19 are obesity and overweight [5], mainly caused by poor nutrition from ultra-processed foods [6].

Also, this pandemic has exposed social deficiencies in textile supply chains by the ease of firing employees who have been subcontracted, violating their labor rights [7]. Therefore, after COVID-19, there will be challenges, opportunities, and potential solutions in agri-food supply chains considering some sustainable aspects, among which climate change stands out [8]. A climate shock would place food supply chains in vulnerable circumstances,

[*]Corresponding Author: Yonatan López Santos, Instituto Tecnológico Superior de Tepexi de Rodríguez, Puebla, Mex., yls_27@hotmail.com, https://orcid.org/0000-0001-8249-3256

exacerbating poverty, food insecurity, and the impact on the environment [9] aspects considered by the SSCM.

However, there are few studies on SSCM, especially on its environmental and social aspects [10], [11]. There is little implementation of the SSCM theory in emerging economies [12], [13], as in Mexico [14]. The SSCM theory also has several theoretical gaps derived from the disconnection between sustainability and strategies related to competitive advantage, known as this combination as Sustainable Competitive Advantage (SCA). SCA is challenging to evaluate and measure since there is no factual theoretical basis [15]. The poor results of the implementation of sustainable strategies to improve competitiveness [16] make it difficult to introduce them into regular SSCM practice [17].

In emerging countries, the SSCM practices adoption does not necessarily imply improved cost performance or short-term profitability [18]. Likewise, a case was found where clients do not necessarily accept higher prices for acquiring sustainable products [17]. Therefore, the SSCM theory seems to be incompatible in some cases between the economic part and the social and environmental parts [17]. That is, if sustainability is considered together with Porter's cost leadership strategy [19], there may not be compatible. Hence, this discordance is reflected in the supply chains of both large, and Small and Medium Enterprises (SMEs), with an even greater emphasis on emerging countries such as Mexico. As a result, decision making becomes a challenge at the strategic level in SSCM, since there are no well-established metrics, as pointed out in the literature review [20]. Therefore, the objective of the research is to propose a decision-making model to assess the sustainability and competitiveness strategically of a Mexican agri-food focal SME that leads its supply chain, validated with comparative analysis in the productive taro activity through the Analytic Hierarchy Process (AHP) that contributes to prevent or face problems such as the COVID-19 pandemic and climate change. It is expected that the results of the strategic model contribute with knowledge at a strategic level to the SSCM, in order to understand the generic strategies and their relationship with sustainability, demonstrating their possible compatibilities.

2. Literature review

2.1. Sustainable Supply Chain Management

Sustainability is a term derived from Sustainable Development, being an increasingly important instrument for economic growth. Sustainable Development is defined as [21]:

"A development that meets the needs of the present without compromising the ability of future generations to meet their own needs " [21].

Sustainability must be taken into account in the design of supply chains [22]. Certain aspects of Supply Chain Management (SCM) are related to the environmental, social, and economic aspects of Sustainable Development, conceptualizing SSCM as [10]:

"The strategic, transparent integration and achievement of an organization's social, environmental, and economic goals in the systemic coordination of key interorganizational business processes for improving the long-term economic performance of the individual company and its supply chains" [10].

That is why SSCM is based on long-term partnerships [23], even if these are difficult to achieve [24] and also costly [17]. Likewise, the level of interest in SSCM practices by companies or organizations is different and depends on what they are producing [25]. To replace SCM with SSCM, companies or organizations need both conventional performance criteria and sustainability requirements [11]. Besides, as it is known, both SCM and SSCM have three levels of planning; strategic planning, tactical planning, and operational planning [26], so when sustainability is integrated into SCM, it causes changes at each level, making strategic planning more relevant.

2.2. Sustainable Supply Chain Management and Competitiveness

On the one hand, there are no signs where competitiveness is strategically considered within the central SSCM literature reviews [20], [23]. On the other hand, the theory of Creating Shared Value (CSV) [27] from the theory of Competitive Advantage [19] does not consider sustainability in-depth, nor does it consider external pressures. However, it has happened that legal norms and sanctions applied (external pressures) to companies become the primary motivations for companies to implement SSCM initiatives [28], which contradicts the internal motivation of the companies [27]. Furthermore, CSV, a relatively new theory, focuses more on large companies, even multinationals, leaving considerable research opportunities in SMEs.

Hence, this research proposes a model for Mexican agri-food focal SMEs that integrates sustainable and competitive strategies within the SSCM theory. These strategies will be based on Porter's two generic strategies [19]: 1) Cost leadership; consists of low costs and economies of scale, and 2) Differentiation; consists of being unique in some value need for clients. It is essential to clarify that it is challenging to achieve a low-cost and differentiation strategy simultaneously, although this does not mean that it is impossible [19].

2.3. Analytic Hierarchy Process and Supply Chains

The AHP is a general theory of measurement developed by Saaty in 1971-1975; this method is used to make a consistent measurement of physical and psychological events, giving them equal importance without sacrificing anything [29]. Therefore, the AHP is a technique for decision making where certain situations with ideas, feelings, and emotions are quantified, which affect the decision-making process, thus obtaining a numerical scale to prioritize the decision alternatives [30].

This tool has also been applied in various areas such as assessment of risk factors in agriculture [31]; natural resources management [32]; location of an SME [33]; benchmarking [34]; among others. According to the literature review [35], there are no applications of AHP for strategic decision-making in sustainable agri-food supply chain models.

2.4. The Sustainable Supply Chain and Mexican Agri-food SMEs

The percentage of SMEs in Mexico is 99.8%, contributing 34.7% to the Gross Domestic Product (GDP) and creating 73.8%

of jobs [36], [37]. The productivity of SMEs is at a lower level than expected, so their entry into the international market and their permanence in the local or national market is difficult [37] due to changes in globalization. Therefore, in order to improve the SMEs, it is necessary to provide strategies that contribute to the current economic panorama, since there are companies where a conservative attitude persists, waiting to introduce structural changes [38].

The performance of focal companies in encouraging sustainable supply chains is vital because they drive and govern the supply chain [23]. There are few studies of Mexican agri-food focus companies that lead a sustainable supply chain [14]. It is normal since, SSCM theory is in an early stage of research [11]. However, some research has been found in the Mexican agri-food sector that includes only aspects of sustainability without considering supply chains, where they show how to develop sustainable enterprises through local networks of eco-farmers [39]. Likewise, the implications of fair trade and inclusion of local people in cooperatives or farmers' associations, trying to connect producers directly with clients [40]. Other studies have a more theoretical scope, a model [41] and a methodological proposal [42], focusing on sustainable agri-food SMEs without considering supply chains. In other words, agribusinesses still individualize their efforts without realizing that they are part of a supply chain.

In Mexico, there are studies on Clean Production and SMEs that contribute to the theory of SSCM. These point out that SMEs mostly play the role of suppliers for large companies; that is, they are not leaders in supply chains, so they are not focal companies [43]- [46]. However, there are projects that try to include the local population in competitive businesses with environmental and social aspects [47], [48]. Nevertheless, according to a literature review in [14], all these attempts are still far from achieving sustainability [14].

2.5. The malanga (Colocasia esculenta) production

The malanga, taro or Colocasia esculenta, is a plant that is cultivated for its corms, which are used in human and animal food and has various industrial uses [49], [50].

There are several ways to transform malanga into food; regional nutritionists have even recommended it as a valuable food; however, more in-depth research is required [51]. One of the most remarkable ways to consume it is in the meal. The nutritional value that taro provides through a meal is highlighted in a study [52], where it is obtained that according to fiber fractions, the meal is an alternative for the elaboration of balanced foods.

The volume of national production in 2015 was 16,552,000 kilograms, equivalent to $66,364,000 national current pesos, and the price was 15,800 Mexican pesos per thousand kilograms [53]. The leading producers are in the states of Oaxaca, Tabasco, and Veracruz [54]. Mexican malanga production is used for self-consumption and is sold to the domestic market [54] and the United States and Canada [54], [55].

3. Methodology

Several research methods are used in SSCM theory, as SSCM is at an early stage, these methods are seen as a complement to others to gain diverse theoretical perspectives [11]. This study is mainly based on the case study methodology [56], to research a phenomenon in its context. It allows selecting and studying an economically successful Mexican agri-food focal SME within its productive activity to relate its situation to the theoretical gaps and thus propose a strategic decision-making model.

Three experts participate in the development of this methodology and model. They propose the following four methodological stages through Figure 1.

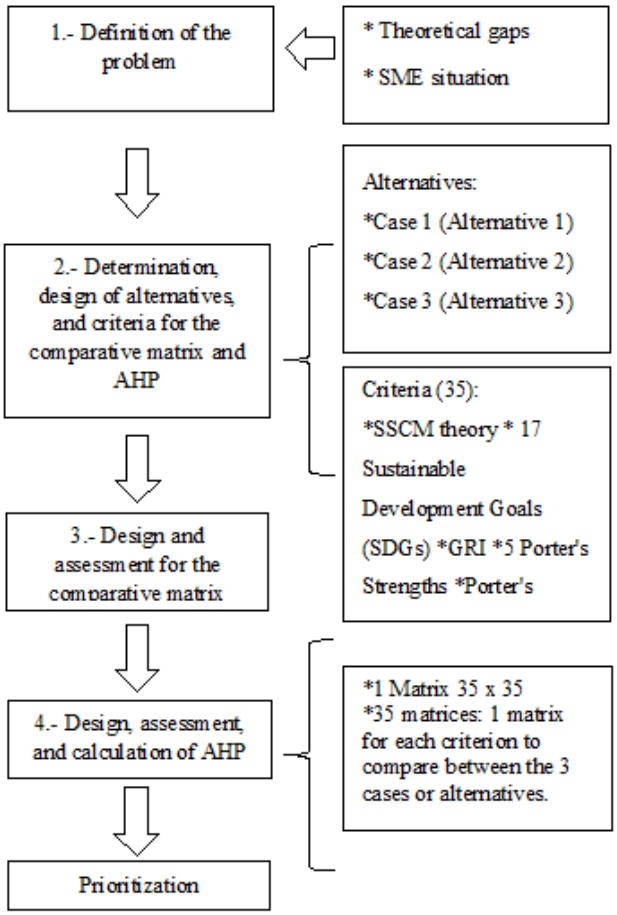


Figure 1: Methodological scheme.

Stage 1. Definition of the problem: It consists of creating a team of experts to know the essential characteristics of the company and to define the problem theoretically.

This research was carried out in a Mexican agri-food focal SME that leads its supply chain in the productive taro activity. This Veracruz-based company, the most economically successful one, is classified in Mexico as a medium-sized company by its number of employees [57], so it is also classified as an SME.

According to the information collected, this SME has been developed without any planning of strategies without considering competitive and sustainable strategies. The collaboration between the members of its supply chain is not ideal, so it is far from being a sustainable supply chain. This SME does not have a generic strategy, according to Porter's positioning matrix [19]. However, this company involuntarily competes with low prices to perform its exports; it is based on a cost leadership strategy. Its competitive situation is threatened when other competitors replace taro with

lower prices in the foreign market. For this reason, a model is designed to integrate strategies of competitiveness and sustainability, and then be assessed with the AHP.

Stage 2. Determination, design of alternatives, and criteria for the comparative matrix and AHP: It consists of identifying the alternatives and criteria used in the AHP methodology. In this stage, the participation of experts is essential to provide feedback and consensus on the alternatives and criteria used in strategic, competitive, sustainable, and SSCM issues.

Stage 3. Design and assessment for the comparative matrix: It is a based analysis process on the logic of the experts, to compare two or more cases, to assimilate their reciprocal differences so that the attributes or criteria for comparing the case studies are established in [58], [59]. In this research, the case studies are considered as alternatives. Each attribute or criterion is assigned a weight or percentage value and then a value from 1 to 5 (1. Very low, 2. Low, 3. Medium, 4. High, 5. Very high) between each case and each criterion.

Stage 4. Design, assessment, and calculation of AHP: The matrix is designed to develop the calculations of AHP [60], the determined criteria are compared A1...An with their respective weights w1,...,wn, this allows to formalize a square matrix, as shown in Figure 2:

$$A = \begin{array}{c|cccc} & A_1 & A_2 & \dots & A_n \\ \hline A_1 & w_1/w_1 & w_1/w_2 & \dots & w_1/w_n \\ A_2 & w_2/w_1 & w_2/w_2 & & w_2/w_n \\ \vdots & \vdots & \vdots & & \vdots \\ A_n & w_n/w_1 & w_n/w_2 & & w_n/w_n \end{array}$$

Figure 2: Square matrix. Source: Saaty [60].

The Saaty scale is used to assign the weights for each criterion [61, 62], shown in Table 1.

Table 1: AHP Fundamental Scale. Source: Saaty [61], [62].

Intensity of importance	*Definition*	*Explanation*
1	Equally important.	Both elements contribute equally to ownership or judgment.
3	Moderately more important one element than the other.	Judgment and prior experience favor one element over the other.
5	Strongly more important one element than the other.	Judgment and prior experience favor one element over the other strongly.
7	Much more vital importance of one element over the other.	One element dominates strongly. Its dominance is proven in practice.
9	The extreme importance of one element over the other.	One element dominates the other with the most significant possible order of magnitude.

The values 2, 4, 6 and 8 are used when the degree of importance is intermediate between two odd numbers in the scale; and when the definition and explanation, is inverted, the reciprocal values of the scale are used (1/2, 1/3, 1/4, 1/5...1/9) [61], [62].

Then, Equation 1, because it is a reciprocal matrix, has positive inputs, that is, $aji = 1/aij$. So, if this matrix is multiplied by the transposition of the vector $wT = (w_1, \dots., w_n)$, the vector nw is obtained. In this way, Equation 1 is obtained:

$$Aw = nw \quad (1)$$

However, with the Saaty technique, it is only possible to work with a limited number of "n" criteria [61], [62]; for that reason, the Alonso and Lamata's technique [63], [64] is used since it allows to work with a matrix that has a more significant number of "n" criteria, allowing different degrees "α," to fulfill the requirement of consistency of the AHP technique.

3.1. Proposed model

Figure 3 shows the sequence of the proposed model, designed for SMEs through the productive taro activity, applied in a medium-sized company. This model, through the AHP technique, assesses the sustainability and competitiveness strategically of a Mexican agri-food focal SME that is the leader of its supply chain in the productive taro activity.

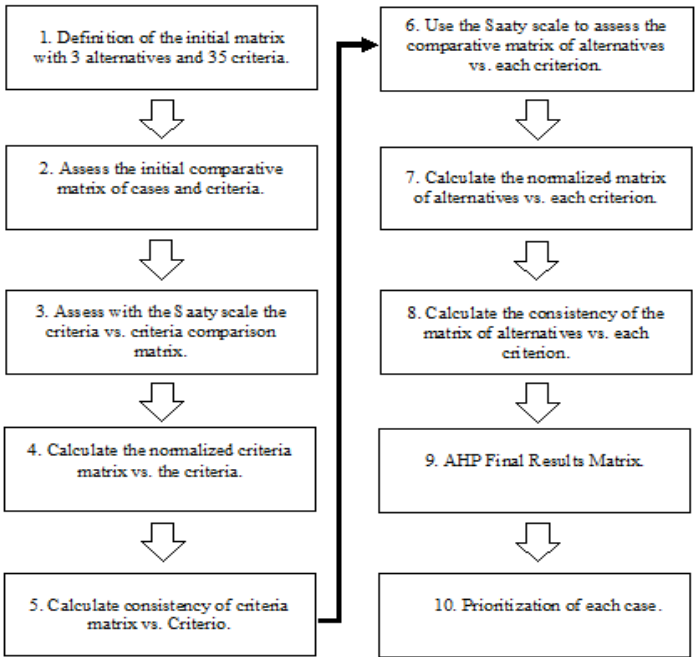


Table 2: Model alternatives or cases.

Alternatives (Cases)		
Alternative 1	Alternative 2	Alternative 3
a) The current state without sustainability (Case 1)	b) Cost leadership strategy with the possibility of sustainability (Case 2)	c) Differentiation strategy with the possibility of sustainability (Case 3)

Step 1. Definition of the initial matrix with three alternatives and 35 criteria.

Table 2 presents the three proposed alternatives, which represent three cases: a) case 1; it is the current state of the SME and its supply chain without considering sustainability, b) case 2; it is the strategy of cost leadership with the possibility of involving

sustainability and c) case 3; it is the strategy of differentiation with the possibility of involving sustainability. These last two alternatives are taken from Porter's two main generic strategies [19].

Table 3 shows the 35 criteria related to economic, competitive, environmental, social, and sustainable aspects from a strategic perspective. These criteria were determined and designed based on the five competitive forces [65], the Porter diamond [66], the SSCM theory [20], [23], the 17 Sustainable Development Goals [67] and the Sustainability Reporting Guidelines [68]. The authors selected these 35 criteria through an exhaustive analysis, representing the most updated and essential aspects of each theory. The theories reflected in these 35 criteria are SSCM, Competitive Advantage, and Sustainable Development.

Table 3: Classification of criteria.

Aspects	***Criteria***	
Economic and competitive	C_1	Scale Economies
	C_2	Product differentiation
	C_3	Brand positioning
	C_4	Input differentiation
	C_5	Impact of inputs on cost or differentiation
	C_6	The relative price performance of substitutes
	C_7	The propensity of buyers to substitute
	C_8	High negotiating power of the buyer
	C_9	Industry Rivalry (High, considering that the competition is international)
	C_{10}	Low labor cost
	C_{11}	Horizontal and vertical cooperation
	C_{12}	Technology and Innovation
	C_{13}	Administrative and production knowledge
	C_{14}	Government policy (No intervention)
	C_{15}	Consumer's level of acquisition
Environmental	C_{16}	Materials
	C_{17}	Energy
	C_{18}	Water
	C_{19}	Biodiversity
	C_{20}	Emissions
	C_{21}	Regulatory compliance and environmental standards
	C_{22}	Supplier selection based on environmental performance
Social	C_{23}	Labor Practices, Decent Work, Health and Safety at Work
	C_{24}	Investment in training and education based on labor practices, human rights, and social impact
	C_{25}	Diversity and equality of opportunity and redistribution
	C_{26}	Supplier selection based on labor practices, human rights, and social impact
	C_{27}	Child and forced labor
	C_{28}	Rights of the indigenous population
	C_{29}	Local communities
	C_{30}	Fight against corruption
	C_{31}	Regulatory compliance and social standards
	C_{32}	Product Responsibility
	C_{33}	Consumer Awareness of Sustainability
	C_{34}	Food security, improved nutrition, and promotion of sustainable agriculture
Sustainable	C_{35}	Partnerships to Achieve the Goals: Strengthening the Means of Implementation and Revitalizing the Global Partnership for Sustainable Development

Table 4 shows the initial matrix, which contains the three alternatives or cases, and the thirty-five criteria.

Table 4: Initial matrix.

Criteria	***Alternatives (Cases)***		
	a) Alternative 1 (Case 1)	b) Alternative 2 (Case 2)	c) Alternative 3 (Case 3)
	a) The current state without sustainability	b) Cost leadership strategy with the possibility of sustainability	(Case 2) c) Differentiation strategy with the possibility of sustainability
C_1	Assessment 1/a	Assessment 1/b	Assessment 1/c
C_2	Assessment 2/a	Assessment 2/b	Assessment 2/c
…	…	…	…
…	…	…	…
C_{35}	Assessment 35/a	Assessment 35/b	Assessment 35/c

Step 2. Assess the initial comparative matrix of cases and criteria

In Table 5, the importance of each criterion is assessed according to a scale of 1 to 100 points, then the weight (percentage) of each criterion is calculated, and finally, the assessment is made between each case and each criterion, assigning values of 1, 2, 3, 4, and 5 (where 1 equals very low, 2 = low, 3 = medium, 4 = high, and 5 = very high).

Table 5: Initial assessment of cases and criteria.

Criteria	Alternatives (Cases)			Points for each criterion (From 1 to 100)	Weight (Percentage)
	a) Alternative 1 (Case 1)	b) Alternative 2 (Case 2)	c) Alternative 3 (Case 3)		
C_1	Assessment 1/a	Assessment 1/b	Assessment 1/c		
C_2	Assessment 2/a	Assessment 2/b	Assessment 2/c		
⋮	…	…	…		
⋮	…	…	…		
C_{35}	Assessment 35/a	Assessment 35/b	Assessment 35/c		
				$\sum_{i=1}^{35} C_i$	$\sum_{i=1}^{35} C_i$

Step 3. Assess with the Saaty scale the criteria vs. criteria comparison matrix.

In Table 6, the criteria versus criteria assessment are made according to the Saaty scale [61], [62], taking as reference the weight (percentage) of Table 5.

Table 6: Assessment with Saaty scale [61], [62].

Criteria	***Criteria***			
	C_1	C_2	….	C_{35}
C_1	Saaty assessment w_1/w_1	Saaty assessment w_1/w_2	….	Saaty assessment w_1/w_{35}
C_2	Saaty assessment w_2/w_1	Saaty assessment w_2/w_2	….	Saaty assessment w_2/w_{35}
⋮	⋮	⋮	….	⋮
⋮	⋮	⋮	….	⋮
C_{35}	Saaty assessment w_{35}/w_1	Saaty assessment w_{35}/w_2	….	Saaty assessment w_{35}/w_{35}
	$\sum_{i=1}^{n} C_1$	$\sum_{i=1}^{n} C_2$	….	$\sum_{i=1}^{n} C_{35}$

Step 4. Calculate the normalized criteria matrix vs. the criteria.

Performing the normalization of Table 6, each assessment is divided by the total sum of each criterion. Once the normalization is done, the next step is to calculate the weighting of each criterion, which is obtained by averaging each criterion, see Table 7.

Table 7: Normalized matrix.

Criteria	***Criteria***				***Weighting***
	C_1	C_2	…	C_{35}	
C_1	(Saaty assessment w_1/w_1)/ $(\sum_{i=1}^{n} C_1)$	(Saaty assessment w_1/w_2)/ $(\sum_{i=1}^{n} C_2)$	…	(Saaty assessment w_1/w_{35})/ $(\sum_{i=1}^{n} C_{35})$	**Row average C_1**
C_2	(Saaty assessment w_2/w_1)/ $(\sum_{i=1}^{n} C_1)$	(Saaty assessment w_2/w_2)/ $(\sum_{i=1}^{n} C_2)$	…	(Saaty assessment w_2/w_{35})/ $(\sum_{i=1}^{n} C_{35})$	**Row average C_2**
⋮	⋮	⋮		⋮	⋮
⋮	⋮	⋮		⋮	⋮
C_{35}	(Saaty assessment w_{35}/w_1)/ $(\sum_{i=1}^{n} C_1)$	(Saaty assessment w_{35}/w_2)/ $(\sum_{i=1}^{n} C_2)$		(Saaty assessment w_{35}/w_{35})/ $(\sum_{i=1}^{n} C_{35})$	**Row average C_{35}**

Step 5. Calculate consistency of criteria matrix vs. criteria

Multiply the evaluated matrix (Table 6) by the weighting vector in Table 7, then add the products to obtain the λmax "o" nmax, which indicates if there is consistency in the matrix, according to α [63], [64].

Step 6. Use the Saaty scale to assess the comparative matrix of alternatives vs. each criterion.

In Table 8, each alternative is evaluated and compared with the alternative of each criterion. In this case, 35 matrices will be obtained, representing each criterion; each matrix is 3x3.

Table 8: Assessment with Saaty scale [61], [62].

Criterion C_1			
Alternatives vs. alternatives comparison matrix (3x3)			
Alternatives	a) Alternative 1 (Case 1)	b) Alternative 2 (Case 2)	c) Alternative 3 (Case 3)
Alternative 1 (Case 1)	Saaty assessment w_1/w_1	Saaty assessment w_1/w_2	Saaty assessment w_1/w_3
Alternative 2 (Case 2)	Saaty assessment w_2/w_1	Saaty assessment w_2/w_2	Saaty assessment w_2/w_3
Alternative 3 (Case 3)	Saaty assessment w_3/w_1	Saaty assessment w_3/w_2	Saaty assessment w_3/w_3
Total (Sum)	$\sum_{i=1}^{n} C_1$	$\sum_{i=1}^{n} C_2$	$\sum_{i=1}^{n} C_3$

Step 7. Calculate the normalized matrix of alternatives vs. each criterion.

This normalization consists of dividing each assessment by the sums in Table 8, then averaging the normalization of each alternative, to obtain the weighting, as shown in Table 9.

Table 9: Normalized matrix.

Criterion C1				
Normalized matrix (3x3)				
Alternatives	Alternative 1 (Case 1)	Alternative 2 (Case 2)	Alternative 3 (Case 3)	**Average Vector C_1/A_n**
Alternative 1 (Case 1)	(Saaty assessment w_1/w_1)/ $(\sum_{i=1}^{n} C_1)$	(Saaty assessment w_1/w_2)/ $(\sum_{i=1}^{n} C_2)$	(Saaty assessment w_1/w_3)/ $(\sum_{i=1}^{n} C_3)$	**Row average Alternative 1 (C_1/A_1)**
Alternative 2 (Case 2)	(Saaty assessment w_2/w_1)/ $(\sum_{i=1}^{n} C_1)$	(Saaty assessment w_2/w_2)/ $(\sum_{i=1}^{n} C_2)$	(Saaty assessment w_2/w_3)/ $(\sum_{i=1}^{n} C_3)$	**Row average Alternative 2 (C_1/A_2)**
Alternative 3 (Case 3)	(Saaty assessment w_3/w_1)/ $(\sum_{i=1}^{n} C_1)$	(Saaty assessment w_3/w_2)/ $(\sum_{i=1}^{n} C_2)$	(Saaty assessment w_3/w_3)/ $(\sum_{i=1}^{n} C_3)$	**Row average Alternative 3 (C_1/A_3)**

Step 8. Calculate the consistency of the matrix of alternatives vs. each criterion

This calculation is done in the same way as in step 5. The matrix in Table 8 is taken by the average vector in Table 9. This procedure is done for all 35 criteria.

Step 9. AHP Final Results Matrix.

Making this matrix, only the average vectors of the 35 matrices calculated in step 7 are taken, and finally, the weights of step 4 are taken from Table 10.

Step 10. Prioritization of each case.

It is the last step in our proposed model to obtain the prioritization of each case or alternative. First, each of the average vectors of each alternative is multiplied by the weighting with the same criterion, resulting in 35 products. Then, the resulting products are added up to obtain the prioritization of each alternative (Table 10).

Table 10: Normalized matrix (3x3).

Criteria/Cases (Alternatives)	*Alternative 1 (Case 1)*	*Alternative 2 (Case 2)*	*Alternative 3 (Case 3)*	*Weighting*
C_1	Average Vector C_1/A_1	Average Vector C_1/A_2	Average Vector C_1/A_3	Weighting C_1
C_2	⋮	⋮	⋮	Weighting C_2
⋮	⋮	⋮	⋮	⋮
⋮	⋮	⋮	⋮	⋮

C_{35}	Average Vector C_{35}/A_1	Average Vector C_{35}/A_2	Average Vector C_{35}/A_3	Weighting C_{35}
Prioritization	Prioritization 1	Prioritization 2	Prioritization 3	

4. Results

Table 11 shows the comparative matrix of the three alternatives against the thirty-five criteria. This table is the beginning of the application of the AHP technique.

Table 11: Initial comparative matrix of cases and criteria.

Criteria		*Alternatives (Cases)*			*Points for each criterion (From 1 to 100)*	*Weight (Percentage)*
		a) The current state without sustainability (Case 1)	b) Cost leadership strategy with the possibility of sustainability (Case 2)	c) Differentiation strategy with the possibility of sustainability (Case 3)		
C_1	Scale Economies	3	3	1	66	2.84%
C_2	Product differentiation	1	1	5	66	2.84%
C_3	Brand positioning	1	3	5	60	2.58%
C_4	Input differentiation	1	3	5	40	1.72%
C_5	Impact of inputs on cost or differentiation	1	4	4	40	1.72%
C_6	The relative price performance of substitutes	1	3	3	62	2.67%
C_7	The propensity of buyers to substitute	1	1	5	75	3.23%
C_8	High negotiating power of the buyer	1	1	5	80	3.44%
C_9	Industry Rivalry (High, considering that the competition is international)	1	1	5	80	3.44%
C_{10}	Low labor cost	2	3	3	38	1.64%
C_{11}	Horizontal and vertical cooperation	1	2	5	90	3.87%
C_{12}	Technology and Innovation	2	3	5	72	3.10%
C_{13}	Administrative and production knowledge	2	3	5	73	3.14%
C_{14}	Government policy (No intervention)	3	2	5	79	3.40%
C_{15}	Consumer's level of acquisition	1	2	5	81	3.49%
C_{16}	Materials	1	2	5	45	1.94%
C_{17}	Energy	1	2	5	68	2.93%
C_{18}	Water	1	2	5	67	2.88%
C_{19}	Biodiversity	2	2	5	56	2.41%
C_{20}	Emissions	2	2	5	57	2.45%
C_{21}	Regulatory compliance and environmental standards	2	3	5	89	3.83%
C_{22}	Supplier selection based on environmental performance	1	2	5	90	3.87%
C_{23}	Labor Practices, Decent Work, Health and Safety at Work	2	3	5	40	1.72%
C_{24}	Investment in training and education based on labor practices, human rights, and social impact	1	3	5	39	1.68%
C_{25}	Diversity and equality of opportunity and redistribution	1	3	5	41	1.76%
C_{26}	Supplier selection based on labor practices, human rights, and social impact	1	3	5	90	3.87%
C_{27}	Child and forced labor	4	4	5	57	2.45%
C_{28}	Rights of the indigenous population	3	3	5	56	2.41%
C_{29}	Local communities	3	3	5	53	2.28%
C_{30}	Fight against corruption	2	3	5	67	2.88%
C_{31}	Regulatory compliance and social standards	2	3	5	89	3.83%
C_{32}	Product Responsibility	3	3	5	68	2.93%
C_{33}	Consumer Awareness of Sustainability	1	2	5	85	3.66%
C_{34}	Food security, improved nutrition, and promotion of sustainable agriculture	3	3	4	67	2.88%
C_{35}	Partnerships to Achieve the Goals: Strengthening the Means of Implementation and Revitalizing the Global Partnership for Sustainable Development	1	2	4	97	4.18%
					2323	**100%**

Continuing with the AHP technique, it is essential to know the consistency of the matrix. Since it is too large (35 x 35), it requires using the Alonso and Lamata's consistency criteria [63], [64], where λmax is considered to accept or reject the consistency. According to calculations made with an α of 0.1, λmax has a value of 38,845, which indicates that this matrix has an adequate consistency, allowing the continuation of the AHP technique.

In Table 12, the comparison between the alternatives is made according to criterion 1 (C1), then it is normalized (average vector); this procedure is performed for the 35 criteria.

Table 12: Comparative matrix of cases for each criterion.

Criterion C1: Scale Economies				***Normalized matrix***			
Alternatives	Case 1 (Alternative 1)	Case 2 (Alternative 2)	Case 3 (Alternative 3)	Case 1	Case 2	Case 3	Average Vector
Case 1 (Alternative 1)	1	1	5	4/9	4/9	4/9	0.45
Case 2 (Alternative 2)	1	1	5	4/9	4/9	4/9	0.45
Case 3 (Alternative 3)	1/5	1/5	1	0.09	0.09	0.09	0.09
Total ($\sum_{i=1}^{n} C_i$)	2.20	2.20	11.00				

In Table 13, the final result of AHP can be seen, where the weights of the 35 x 35 matrix and the average vectors of the 35 comparative matrices of the three cases by criterion are shown. The final result is the prioritization of each case. This prioritization can be interpreted as the final assessment or evaluation that each case has according to the 35 criteria.

Case 1 (alternative 1) has a low value (9.49%) because its current situation is casual, here there are no defined strategies, the collaboration of the supply chain is not ideal, sustainability is not contemplated, among other aspects defined in stage 1.

While case 2 (alternative 2), with the strategy of cost leadership with the possibility of sustainability, shows a percentage of 17.30%. Based on the current situation, this percentage indicates that the combination of this strategy with sustainability would be more challenging to carry out compared to case 3. It does not mean that it is impossible, but it would be more challenging to shift to sustainability. It is difficult for organizations to compete with unsustainable low-cost products in the foreign market in the current situation, making it somewhat unfeasible to have this strategy along with sustainability. It could increase their costs and lead to unequal competition.

Finally, case 3 (alternative 3), referring to the strategy of differentiation with the possibility of sustainability, has the highest value (73.21%). It indicates better compatibility and strategic feasibility between competitiveness and sustainability. It is because sustainability could be more easily aligned while providing a competitive advantage. However, a more significant challenge to achieving full sustainability can be seen in the supply chain of this SME because it is in the agri-food sector. If it goes more in-depth at the farmer level, it is difficult to achieve 100 % sustainability because it would need to reach a natural ecosystem to do so [69].

Table 13: AHP final results.

Criteria / Cases (Alternatives)	***Case 1 (Alternative 1)***	***Case 2 (Alternative 2)***	***Case 3 (Alternative 3)***	***Weighting***
C_1	0.4545	0.4545	0.0909	0.0178
C_2	0.0909	0.0909	0.8182	0.0178
C_3	0.0612	0.2157	0.7231	0.0106
C_4	0.0612	0.2157	0.7231	0.0050
C_5	0.0667	0.4667	0.4667	0.0050
C_6	0.0909	0.4545	0.4545	0.0110
C_7	0.0909	0.0909	0.8182	0.0362
C_8	0.0909	0.0909	0.8182	0.0391
C_9	0.0909	0.0909	0.8182	0.0391
C_{10}	0.1429	0.4286	0.4286	0.0044
C_{11}	0.0685	0.1549	0.7766	0.0737
C_{12}	0.0833	0.1932	0.7235	0.0339
C_{13}	0.0833	0.1932	0.7235	0.0350
C_{14}	0.1932	0.0833	0.7235	0.0374
C_{15}	0.0685	0.1549	0.7766	0.0414
C_{16}	0.0685	0.1549	0.7766	0.0058
C_{17}	0.0685	0.1549	0.7766	0.0209
C_{18}	0.0685	0.1549	0.7766	0.0192
C_{19}	0.1111	0.1111	0.7778	0.0095
C_{20}	0.1111	0.1111	0.7778	0.0097
C_{21}	0.0833	0.1932	0.7235	0.0665
C_{22}	0.0685	0.1549	0.7766	0.0737
C_{23}	0.0833	0.1932	0.7235	0.0050
C_{24}	0.0612	0.2157	0.7231	0.0046
C_{25}	0.0612	0.2157	0.7231	0.0056
C_{26}	0.0612	0.2157	0.7231	0.0737
C_{27}	0.2000	0.2000	0.6000	0.0097
C_{28}	0.1429	0.1429	0.7143	0.0091
C_{29}	0.1429	0.1429	0.7143	0.0087
C_{30}	0.0833	0.1932	0.7235	0.0192
C_{31}	0.0833	0.1932	0.7235	0.0665
C_{32}	0.1429	0.1429	0.7143	0.0209
C_{33}	0.0685	0.1549	0.7766	0.0632
C_{34}	0.2000	0.2000	0.6000	0.0192
C_{35}	0.0833	0.1932	0.7235	0.0823
Prioritization	**0.0949**	**0.1730**	**0.7321**	**1**

5. Discussion

This study shows that there are more compatibility and feasibility between the differentiation strategy and sustainability, causing at the same time a competitive advantage. While some strategic incompatibilities can be observed with the cost leadership strategy and sustainability, the effects are presented in the costs and, consequently, the competitiveness. It coincides that SSCM practices do not necessarily reduce costs related to sustainability [17], [18].

The proposed model shows a high degree of difficulty in assessing sustainability and competitiveness strategically. It was validated through a Mexican agri-food focal SME. The model demonstrates that it is possible a large number of criteria for decision-making, considering Alonso and Lamata's terms [63], [64]. To carry out this assessment, it is necessary to have an in-depth and particular knowledge of the company's situation, its environment, and its supply chain. It agrees that particular circumstances of each supply chain must be assessed, considering all factors, both internal and external, which may vary over time [20].

Everything indicates that the effects of the COVID-19 pandemic will drive and accelerate a change in people's eating habits [70], prioritizing consumption in local food supply chains [71]. All of the above, together with climate change and its effects [8], [9], as well as changes in the governmental agendas of various countries due to the COVID-19 pandemic [1], such as Mexico, would lead to an increase of SSCM practices in local, national and international food sector.

The COVID-19 pandemic can be taken as a reference for issues such as food insecurity and ultra-processed food products that affect the health and welfare of people. The crisis that has brought this pandemic should lead us to think further, as we have more challenges ahead, such as climate change, environmental impacts, poverty, among other aspects that could cause instability around the world. Thus, the current situation should be a lesson on what is wrong, and an impetus to further progress towards the 17 Sustainable Development Goals, in this case, through the SSCM theory. The SSCM must continue to evolve in order to improve food supply chains, so this model contributes to the strategic planning of the SSCM in order to develop greater long-term resilience in Mexican agri-food SMEs.

6. Conclusions

This study finds more feasibility and compatibility to achieve sustainability with a differentiation strategy than with a cost leadership strategy. As could be seen, strategies have an essential role in promoting sustainability and competitiveness. Therefore, they must be considered in SSCM's strategic planning and tactical and operational planning, aligning them and fitting them to the core business of the focal companies and the supply chain members. It is also found that the proposed strategic initiatives in SSCM would lead to a competitive advantage due to the difficulty of replicating them.

The proposed model provides support to assess and develop the sustainable and competitive part of the strategic planning in SSCM, without running the economic risks that an implementation represents. It highlights how complex it may be to assess an SME and its supply chain strategically due to the high number of criteria used, but at the same time, these criteria provide important aspects for decision making.

This strategic model contributes to prevent or face problems such as the COVID-19 pandemic and climate change, providing knowledge to the SSCM. It is designed to apply to both small and medium-sized focal companies that lead their supply chain in the food sector, considering sustainability and competitiveness strategically through specific metrics.

In future research, it is intended to apply the model to more small and medium Mexican agri-food companies that lead their supply chains to carry out comparative case studies to contribute knowledge to the SSCM theory and, at the same time to continue executing and improving the proposed model.

Conflict of Interest

The authors declare no conflict of interest.

Acknowledgment

The authors are thankful to the Instituto Tecnológico Superior de Tepexi de Rodríguez, and to the UPAEP (Universidad Popular Autónoma del Estado de Puebla) for the support and collaboration of this research. Likewise, Dr. Yonatan thanks CONACYT (Consejo Nacional de Ciencia y Tecnología) from Mexico for the support during his doctoral studies.

References

[1] Economic Commission for Latin America and the Caribbean & Food and Agriculture Organization of the United Nations, COVID-19 Report ECLAC-FAO. Preventing the COVID-19 crisis from becoming a food crisis. United Nations, 2020. https://www.cepal.org/en/publications/45726-preventing-covid-19-crisis-becoming-food-crisis-urgent-measures-against-hunger

[2] S. Singh, R. Kumar, R. Panchal, M.K. Tiwari, "Impact of COVID-19 on logistics systems and disruptions in food supply chain," International Journal of Production Research, 1–16, 2020, doi:10.1080/00207543.2020.1792000.

[3] P. Udmale, I. Pal, S. Szabo, M. Pramanik, A. Large, "Global food security in the context of COVID-19: A scenario-based exploratory analysis," Progress in Disaster Science, 7, 100120, 2020, doi:10.1016/j.pdisas.2020.100120.

[4] F. Wu, S. Zhao, B. Yu, Y.-M. Chen, W. Wang, Z.-G. Song, Y. Hu, Z.-W. Tao, J.-H. Tian, Y.-Y. Pei, M.-L. Yuan, Y.-L. Zhang, F.-H. Dai, Y. Liu, Q.-M. Wang, J.-J. Zheng, L. Xu, E.C. Holmes, Y.-Z. Zhang, "A new coronavirus associated with human respiratory disease in China," Nature, **579**(7798), 265–269, 2020, doi:10.1038/s41586-020-2008-3.

[5] L.M. Castillo, C. O., Castillo, M.P., Limón, J.L., Tamayo, La colisión de dos pandemias: COVID-19 y obesidad, 2020. http://www.doctorcarbajo.com/doc/OBESIDAD_Y_COVID-19.pdf

[6] J. Eaton, Pillars of the Nutrition Transition: The Global Impacts of Ultra-Processed Foods and Beverages on Overweight and Obesity and National Nutrient Supplies, 2020. https://openscholarship.wustl.edu/art_sci_etds/2180

[7] A. Majumdar, M. Shaw, S.K. Sinha, "COVID-19 debunks the myth of socially sustainable supply chain: A case of the clothing industry in South Asian countries," Sustainable Production and Consumption, **24**, 150–155, 2020, doi:10.1016/j.spc.2020.07.001.

[8] N.J. Rowan, C.M. Galanakis, "Unlocking challenges and opportunities presented by COVID-19 pandemic for cross-cutting disruption in agri-food and green deal innovations: Quo Vadis?," Science of The Total Environment, 748, 141362, 2020, doi:10.1016/j.scitotenv.2020.141362.

[9] J. Sarkis, P. Dewick, J.S. Hofstetter, P. Schröder, "Overcoming the Arrogance of Ignorance: Supply-Chain Lessons from COVID-19 for Climate Shocks," One Earth, **3**(1), 9–12, 2020, doi:10.1016/j.oneear.2020.06.017.

[10] C.R. Carter, D.S. Rogers, "A framework of sustainable supply chain management: moving toward new theory," International Journal of Physical

Distribution & Logistics Management, **38**(5), 360–387, 2008, doi:10.1108/09600030810882816.
[11] S. Seuring, "Supply chain management for sustainable products - insights from research applying mixed methodologies," Business Strategy and the Environment, **20**(7), 471–484, 2011, doi:10.1002/bse.702.
[12] Q. Zhu, J. Sarkis, K. Lai, Y. Geng, "The role of organizational size in the adoption of green supply chain management practices in China," Corporate Social Responsibility and Environmental Management, **15**(6), 322–337, 2008, doi:10.1002/csr.173.
[13] M. Ehrgott, F. Reimann, L. Kaufmann, C.R. Carter, "Social Sustainability in Selecting Emerging Economy Suppliers," Journal of Business Ethics, **98**(1), 99–119, 2011, doi:10.1007/s10551-010-0537-7.
[14] Y. López Santos, "La administración de la cadena de suministro sustentable y las pequeñas y medianas empresas de economías emergentes: caso México / The Sustainable Supply Chain Management and the Small and medium-sized enterprises of emerging economies: The case of Mexico," RICEA Revista Iberoamericana de Contaduría, Economía Y Administración, **8**(15), 54–81, 2019, doi:10.23913/ricea.v8i15.124.
[15] G. Vinayan, S. Jayashree, G. Marthandan, "Critical Success Factors of Sustainable Competitive Advantage: A Study in Malaysian Manufacturing Industries," International Journal of Business and Management, **7**(22), 2012, doi:10.5539/ijbm.v7n22p29.
[16] R.C. Walke, V. Topkar, S. Kabiraj, "Managing Risk for Green Supply Chain Management : Competitive Strategies for Manufacturing Companies," Skyline Business Journal, **6**(1), 1–10, 2010. https://www.skylineuniversity.ac.ae/pdf/sbj/SBJ2010.pdf#page=7
[17] J. Wolf, "Sustainable Supply Chain Management Integration: A Qualitative Analysis of the German Manufacturing Industry," Journal of Business Ethics, **102**(2), 221–235, 2011, doi:10.1007/s10551-011-0806-0.
[18] A. Esfahbodi, Y. Zhang, G. Watson, "Sustainable supply chain management in emerging economies: Trade-offs between environmental and cost performance," International Journal of Production Economics, **181**, 350–366, 2016, doi:10.1016/j.ijpe.2016.02.013.
[19] M. Porter, Ventaja Competitiva. Creación y sostenimiento de un desempeño superior, (Segunda Edición Reformada),Grupo Editorial Patria, México, 2015.
[20] P. Ahi, C. Searcy, "An analysis of metrics used to measure performance in green and sustainable supply chains," Journal of Cleaner Production, **86**, 360–377, 2015, doi:10.1016/j.jclepro.2014.08.005.
[21] World Commission on Environment and Development, Our Common Future, Oxford University Press, Oxford, 1987.
[22] P. Chopra, S., Meindl, Administración de la Cadena de Suministro. Estrategia, planeación y operación, Pearson, México, 2013.
[23] S. Seuring, M. Müller, "From a literature review to a conceptual framework for sustainable supply chain management," Journal of Cleaner Production, **16**(15), 1699–1710, 2008, doi:10.1016/j.jclepro.2008.04.020.
[24] O. Chkanikova, "Sustainable supply chain management: Theoretical literature overview," International Institute for Industrial Environmental Economics, Lund University., 2012.
[25] L.B. da C. Dalé, L.B. Roldan, P.B. Hansen, "Analysis of Sustainability Incorporation by Industrial Supply Chain in Rio Grande do Sul State (Brazil)," Journal of Operations and Supply Chain Management, **4**(1), 25, 2011, doi:10.12660/joscmv4n1p25-36.
[26] A. Rushton, P. Croucher, P. Baker, The handbook of logistics & distribution management, Kogan Page Limited, Great Britain , 2010.
[27] M.E. Porter, M.R. Kramer, "Creating Shared Value," Harvard Business Review, **89**(1/2), 62–77, 2011.
[28] J. Koplin, "Integrating Sustainability into Supply Management - Cooperation with Suppliers for Managing Environmental and Social Guidelines and Standards," 1–17, 2003.
[29] R.W. Saaty, "The analytic hierarchy process—what it is and how it is used," Mathematical Modelling, **9**(3–5), 161–176, 1987, doi:10.1016/0270-0255(87)90473-8.
[30] H. A. Taha, Investigación de operaciones, Pearson Educación, México, 2012.
[31] R. Toledo, A. Engler, V. Ahumada, "Evaluation of Risk Factors in Agriculture: An Application of the Analytical Hierarchical Process (AHP) Methodology," Chilean Journal of Agricultural Research, **71**(1), 114–121, 2011, doi:10.4067/S0718-58392011000100014.
[32] I. Sánchez Cohen, G. Díaz Padilla, H. Macías Rodríguez, J. Estrada Ávalos, "Proceso jerárquico analítico para la toma de decisiones en el manejo de los recursos naturales," Revista Mexicana de Ciencias Agrícolas, **1**(3), 306–316, 2010. http://www.scielo.org.mx/scielo.php?script=sci_arttext&pid=S2007-09342010000300003
[33] E. Martínez Rodríguez, "Aplicación del proceso jerárquico de análisis en la selección de la lozalización de una PYME," Anuario Jurídico Y Económico Escurialense, **40**, 523–542, 2007.
[34] P.K. Dey, "Benchmarking project management practices of Caribbean organizations using analytic hierarchy process," Benchmarking: An International Journal, **9**(4), 326–356, 2002, doi:10.1108/14635770210442680.
[35] O. Ahumada, J.R. Villalobos, "Application of planning models in the agri-food supply chain: A review," European Journal of Operational Research, **196**(1), 1–20, 2009, doi:10.1016/j.ejor.2008.02.014.
[36] Secretaría de Economía, Segundo informe de labores 2013-2014, 2014. https://www.profeco.gob.mx/transparencia/informe_labores_SE_2013-2014.pdf
[37] Diario oficial de la federación, Programa de Desarrollo Innovador 2013 – 2018, 2013. http://www.dof.gob.mx/nota_detalle_popup.php?codigo=5326479
[38] M. Ramírez, J. Delgado, "Modelo de alianza estratégica con base en la empresa integradora para PYMES con tecnología tradicional," in 14 Convención Científica de Ingeniería y Arquitectura, La Habana, Cuba, 2008. https://www.researchgate.net/profile/Mercedes_Delgado_Fernandez/publication/314142824_Modelo_de_alianza_estrategica_con_base_en_la_empresa_integradora_para_PYMES_con_tecnologia_tradicional/links/58b6f9f292851c471d47a0c2/Modelo-de-alianza-estrategica-con-base-en-la-empresa-integradora-para-PYMES-con-tecnologia-tradicional.pdf
[39] M.T. Magallón Diez, M.T. Montoya Flores, "Sustentabilidad y Organizaciones. Reflexiones a partir del análisis de la 'Red de Ecoproductores y Consumidores Origen Volcanes.'. (Spanish)," Administracion Y Organizaciones, **14**(27), 123–148, 2011.
[40] N. Mun, J. Seo, "Fair trade for coffee producing small-scale farmers in Mexico.," Portes: Revista Mexicana de Estudios Sobre La Cuenca Del Pacifico, **6**(11), 27–49, 2012.
[41] E. Michelena Fernández, F. Espinosa Mejía, "Modelo de administración para la operación sustentable y gestión de la calidad en las agroindustrias de café: Estudio de caso," Ingeniería Industrial, **28**(3), 4, 2007. https://www.redalyc.org/pdf/3604/360433564004.pdf
[42] E. Kú, V., Pool, L., Mendoza, J. Aguirre, "Propuesta metodológica para evaluar proyectos productivos con criterios locales de sustentabilidad en Calakmul, México," Avances En Investigación Agropecuaria, **17**(1), 9–34, 2012.
[43] B. van Hoof, T.P. Lyon, "Cleaner production in small firms taking part in Mexico's Sustainable Supplier Program," Journal of Cleaner Production, **41**, 270–282, 2013, doi:10.1016/j.jclepro.2012.09.023.
[44] B. van Hoof, M. Thiell, "Collaboration capacity for sustainable supply chain management: small and medium-sized enterprises in Mexico," Journal of Cleaner Production, 67, 239–248, 2014, doi:10.1016/j.jclepro.2013.12.030.
[45] B. van Hoof, "Organizational learning in cleaner production among Mexican supply networks," Journal of Cleaner Production, **64**, 115–124, 2014, doi:10.1016/j.jclepro.2013.07.041.
[46] B. van Hoof, M. Thiell, "Anchor company contribution to cleaner production dissemination: experience from a Mexican sustainable supply programme," Journal of Cleaner Production, **86**, 245–255, 2015, doi:10.1016/j.jclepro.2014.08.021.
[47] M. Rosas-Baños, R. Lara-Rodríguez, "Desarrollo endógeno local sustentable y propiedad común: San pedro el alto, México," Cuadernos de Desarrollo Rural, **10**(71), 59–80, 2013. https://revistas.javeriana.edu.co/index.php/desarrolloRural/article/view/6268
[48] V. M. Toledo, B. Ortiz-Espejel, Regiones que caminan hacia la sustentabilidad. Una geopolítica de las resistencias bioculturales, Universidad Iberoamericana Puebla. 1-139, México, 2014.
[49] C. Martínez, M. Muñozcano, J. Santoyo, Paquete tecnológico para el establecimiento de malanga, Colección RP, México.
[50] C. Olguín, Manual para el cultivo de Malanga, 1997.
[51] M.D.C. Olguín-Palacios, C., Álvarez-Ávila, "La malanga (Colocasia esculenta (L.) Schott) bajo un enfoque de investigacion-desarrollo," AGROProductividad, **4**(4), 2011. https://go.gale.com/ps/anonymous?id=GALE%7CA382656502&sid=googleScholar&v=2.1&it=r&linkaccess=fulltext&issn=&p=IFME&sw=w
[52] L. Madrigal-Ambriz, J. Hernández-Madrigal, M. Carranco-Jáuregui, M. Calvo-Carrillo, R. Casas-Rosado, "Caracterización física y nutricional de harina del tubérculo de 'Malanga' (Colocasia esculenta L. Schott) de Actopan, Veracruz, México.," Archivos Latinoamericanos de Nutrición, **68**(2), 175–183, 2018. https://search.proquest.com/openview/cf1f760852cdc0cab6bc4ffe9df9370d/1?pq-origsite=gscholar&cbl=2032499
[53] Servicio de Información Agroalimentaria y Pesquera, Datos abiertos. Estadística de Producción Agrícola, 2017. http://infosiap.siap.gob.mx/gobmx/datosAbiertos.php.
[54] V. Asiain, A., Arvizu, E., Gallardo, F., Chalate, H., Acosta, J. Moreno,

Tipología y caracterización de los sistemas de producción de malanga en los estados de Oaxaca, Tabasco y Veracruz, México, 2017.
[55] Y. López Santos, E. Arvizu Barrón, A. Asiain Hoyos, Y. Mayett Moreno, J.L. Martínez Flores, "Análisis competitivo de la actividad productiva de la malanga: un enfoque basado en la teoría de Michael Porter / Competitive analysis of the taro productive activity: an approach based on the Michael Porter´s theory," RIDE Revista Iberoamericana Para La Investigación Y El Desarrollo Educativo, 8(16), 729–763, 2018, doi:10.23913/ride.v8i16.366.
[56] R. Yin, "Case Study Research. Design and Methods", Sage. Publications, London, 1994.
[57] Diario Oficial de la Federación, Acuerdo por el que se establece la estratificación de las micro, pequeñas y medianas empresas, 2009. http://dof.gob.mx/nota_detalle.php?codigo=5096849&fecha=30/06/2009
[58] G. Sartori, L. Morlino, La Comparación en las Ciencias Sociales.Alianza Editorial, Madrid, 1994
[59] A. Pérez-Liñán, El Método Comparativo: Fundamentos y Desarrollos Recientes, Universidad de Pittsburgh, Pittsburgh, 2007.
[60] T.L. Saaty, "A scaling method for priorities in hierarchical structures," Journal of Mathematical Psychology, **15**(3), 234–281, 1977, doi:10.1016/0022-2496(77)90033-5.
[61] T.L.Saaty, The Analytic Hierarchy Process. McGraw-Hill, New York, 1980.
[62] T.L. Saaty, "How to Make a Decision: The Analytic Hierarchy Process," Interfaces, **24**(6), 19–43, 1994, doi:10.1287/inte.24.6.19.
[63] J.A. Alonso, M.T. Lamata, A Statistical Criterion of Consistency in the Analytic Hierarchy Process, 67–76, 2005, doi:10.1007/11526018_8.
[64] J.A. Alonso, M.T. Lamata, "Consistency in the analytic hierarchy process: a new approach," International Journal of Uncertainty, Fuzziness and Knowledge-Based Systems, **14**(4), 445–459, 2006, doi:10.1142/S0218488506004114.
[65] M. Porter, "The five competitive forces that shape strategy," Harvard Business Review, 86(1), 2008.
[66] M. Porter, "The Competitive Advantage of Nations," Harvard Business Review, **68**(2), 73–91, 1990.
[67] United Nations, La Asamblea General adopta la Agenda 2030 para el Desarrollo Sostenible, 2015. http://www.un.org/sustainabledevelopment/es/2015/09/la-asamblea-general-adopta-la-agenda-2030-para-el-desarrollo-sostenible/
[68] Global Reporting Initiative, G4 Sustainability Reporting Guidelines. Reporting principles and standard disclosures, Global Reporting Initiative, Amsterdam, Netherlands, 2013.
[69] S.R. Gliessman, Agroecology, CRC Press, 2006, doi:10.1201/b17420.
[70] M. del R. Vergara-Castañeda, A., Lobato-Lastiri, M., Díaz-Gay, M., Ayala-Moreno, "Cambios en el comportamiento alimentario en la era del COVID-19," Revista Latinoamericana De Investigación Social, **3**(1), 27–30, 2020. https://repositorio.lasalle.mx/handle/lasalle/1767
[71] J.E. Hobbs, "Food supply chains during the COVID-19 pandemic," Canadian Journal of Agricultural Economics/Revue Canadienne D'agroeconomie, 68(2), 171–176, 2020, doi:10.1111/cjag.12237.

ASTES

Advances in Science, Technology and Engineering Systems Journal Vol. 5, No. 5, 1225-1232 (2020)

www.astesj.com

ASTESJ

ISSN: 2415-6698

Interactive Virtual Rehabilitation for Aphasic Arabic-Speaking Patients

Sherif H. ElGohary*, Aya Lithy, Shefaa Khamis, Aya Ali, Aya Alaa el-din, Hager Abd El-Azim

Biomedical Engineering and Systems Department, Faculty of Engineering, Cairo University, Giza, 12613, Egypt

ARTICLE INFO

Article history:
Received: 04 August, 2020
Accepted: 19 September, 2020
Online: 24 October, 2020

Keywords:
Aphasia
Arabic
Convolutional neural networks
Rehabilitation
Signal processing
Speech and language disorders

ABSTRACT

Objective: Individuals with aphasia often experience significant problems in their daily lives and social participation. Technologies that address speech and language disorders deficit in merging between therapist's major role and reinforcing the training between sessions at home. It also lacks the Arabic language attention; however, current systems are typically expensive and lack amusement. Moreover, cumulative feedback for both patient and therapist incapacitates the whole home rehabilitation process. This project sought to address these issues by developing an interactive rehabilitation-based system for people with aphasia. Methods: A virtual reality (VR) environment is created providing real-life situations with task specific training of comprehension in addition to a virtual speech-language pathologist (SLP) representing lip motions for correct pronunciation of target words. A speech recognition convolutional neural networks (CNN) algorithm based on signal processing is created and trained on ten isolated Arabic words. We tempted log-spectrograms and Mel-frequency cepstral coefficients (MFCC) as feature extractors for the CNN model which is then integrated for accurate evaluation of input speech from the aphasic patient providing a real-time feedback resulting in measuring speech improvement and sends it to the SLP through the network via a website platform. Results: Our speech recognition assessment algorithm results in a recognition accuracy of 95.2 % using Log-Spectrograms feature extraction method and 92.6 % using MFCC. Significance & Conclusion: We hypothesize that this interactive VR therapy combined with speech function training will result in faster word retrieval and improve language ability of patients with aphasia and that our outcomes contribute to the development of a home-based language and speech therapy.

1. Introduction

Aphasia is the most common language disorder caused by traumatic brain injury or most commonly a stroke. Stroke is the 3rd leading cause of long-term disabilities in the world [1]. According to the world stroke organization, there are over 13 million emerging strokes each year [2] and to the stroke association in the United Kingdom, around a third of stroke survivors experience some level of aphasia [3]. Aphasia is a disorder that results from damage to portions of the brain that are responsible for language production and comprehension which impairs the expression and understanding of language and speech as well as reading and writing [4].

The most common two types of aphasia are Broca's and Wernicke's. Broca's aphasia is associated with the damage to the frontal lobe of the brain in which patients can understand speech and know what they want to say but they cannot express it and is also referred to as non-fluent aphasia because of the halting and effortful speech quality [5]. On the contrary, people with Wernicke's aphasia suffer from damage in the temporal lobe of the brain and have difficulties in language comprehension while producing speech itself is not much affected, therefore, it is referred to as fluent aphasia [5]. Patients mostly suffer from significant problems in their daily lives and social participation which leads to depression, isolation, embarrassment and preventing the expression of everyday needs [6], and therefore, greatly reduce quality of life.

Usually, traditional rehabilitation therapy aims at restoring or improving the impaired functions. It helps patients retrieve their

*Corresponding Author: Sherif H. ElGohary, Biomedical Engineering and Systems Department, Faculty of Engineering, Cairo University, Giza, 12613, Egypt, (+20)1020031012 & Email: sh.elgohary@eng1.cu.edu.eg

ability to speak and express as the speech-language pathologists (SLPs) focus on motor production of speech sounds. It depends on the SLP showing the patient some cards or photos of an object while pronouncing its name with a very accurate and relatively slow lip motion so that the patient could mimic it and train several times. But, most often, patients feel embarrassed from their pathologists in addition to that the treatment progress is relatively slow [7].

A range of mobile phone applications have widely spread out for people with stroke, aphasia, brain injury, or dementia. Some of them focus on language and conversation training in a very primitive way and most of the rest are used as communication tools to help patients communicate with other people in form of icons being pressed to say what they need in the time; however, there is still a huge lack in technological solutions that focus on the rehabilitation process itself especially that dealing with Arabic language.

Arabic language is the 6th most used language based on the number of native speakers. Nearly 250 million people use Arabic as their first language and it is the second language for around four times that number [8]. There are three types of the Arabic language: Classical Arabic which is the most formal type, Modern Standard Arabic with some simplifications on the classical and is used in writings and formal speeches, and Colloquial (dialectal) Arabic. Each country or region within a country has its own dialect. Colloquial Arabic is considered the most important for a language rehabilitation process as it is the language used in daily conversations and informal writings.

For the available rehabilitation digital solutions, we found a focus on virtual therapists to validate the tele-rehabilitation delivery by using pre-recorded voices or scripts like in Web-ORLA developed by Cherney et al. [9] and Aphasia Scripts developed by Van et al. [10] which are more reading treatment for people with aphasia so, they are too complicated for people with severe comprehension or reading impairment. Another solution called EVA project developed at City University of London [11] is a multi-user online virtual world headed towards speech training through navigating different environments and conversation; however, it is represented in a fantasy and non-immersive world.

Moreover, virtual reality (VR) has been explored and proved to be an effective rehabilitation method in many physical disabilities' rehabilitations [12], [13] and in other communication disorders such as autism [14], [15] and stuttering [16]. Although this potential has not yet been fully directed to aphasia disorder, there has been some work that investigated the effectiveness of VR in aphasia rehabilitation [17], [18] and proved it to be effective as patients were more attracted and concentrated.

In this paper, we propose a new VR-based rehabilitation approach for Arabic-speaking aphasic patients, which provides them the flexibility and convenience of getting therapy at their homes, with an access to real-life simulation, speech, comprehension, and categorization training in addition to a virtual SLP representing lip motions for correct articulation of words. The boost of an Artificial Intelligence (AI) speech recognition algorithm based on isolated words independent of speakers is integrated for accurate evaluation of input speech from the aphasic patient providing a real-time feedback resulting in measuring speech and comprehension improvement. And taking the Internet of Things (IOT) advantages into account for automatic data transfer over the network to send feedback to the therapist via a website platform for remote following up.

2. System Description

The flow block diagram of the proposed system is depicted in Figure 1. We have created a game-like virtual rehabilitation environment in which we simulate the traditional therapy approach. Therefore, the environment is divided into two significant parts, which can be customized separately depending on the patient's case. The first one is the virtual SLP clinic representing the vocalization learning part based on the very accurate lip movement with several repetitions. Secondly, is the training part which focuses on comprehension problems in which we provide real-life situations with interactive and categorization tasks.

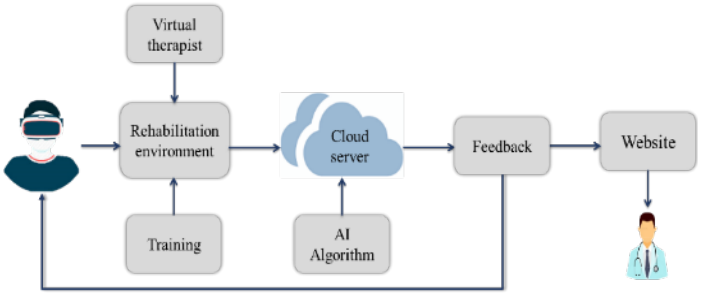


Figure 1: System flow block diagram.

All the manipulations within the game that are in the form of input voice from the patient are continuously recorded and inputted to an algorithm for measuring and calculating speech production and comprehension improvement. A feedback report is sent to the real therapist via a website platform for following up and also an on-screen feedback will be appearing in the game for encouraging the patient. A cloud server connects the whole cycle of sending and receiving data.

3. Methodology

3.1. Rehabilitation Environment

We designed the virtual environment simulating the real rehabilitation pattern but in the form of a game-like scenario to be more interactive and fun. Unity3D (version 2019.3.13f1) game engine was used as the main development platform with C# scripting language to control the various assets. The game activities were divided into two main parts; the virtual therapist or SLP clinic and the training part.

3.1.1. Virtual Therapist

Based on our interviews with different SLPs and their instructions, lip motions are considered the most important part in speech rehabilitation generally and in aphasic cases specially, including synchronization of articulators' movement [19] and also according to a pilot study about the effects of silent visuomotor cueing on verbal execution [20]. Thus, we started by designing a realistic room in unity (shown in Figure 2), representing the clinic's room.



Figure 2: Virtual therapy room.

We created a virtual SLP represented as a humanoid avatar character created using Daz3D studio using Genesis2 characters for rendering the very accurate lip motions of correct pronunciation of words. The character is then exported from Daz3D studio as an FBX object format with its animation and imported into the clinic's scene in Unity as shown in Figure 3. This part is responsible for encouraging the patient to learn words and practice pronunciation regularly.

Patients interact using a screen UI button to make the avatar start saying the targeted word and after listening and observing target speech patterns for reference, another button is used for patient voice input via the device's microphone. Then, a useful screen feedback appears to correct speech deficits and encourage improvement in speech legibility.



Figure 3: Avatar character's lip motions after importing in Unity and the UI screen buttons.

3.1.2. Training Part

For the training part, we designed a city-like environment containing a variety of locations of daily living situations, for example: street, living room and kitchen; sample scenes are shown in Figure 4. Designing real-life scenes was considered so that the patient feels as if he/she is in the real world with free movement and scene navigation. This part focuses mainly on comprehension measurement and how to deal with things in real life with its denotations through carrying out some assigned tasks either categorization and matching or voice input ones.

a) Navigation Exercises

In all scenes in this part, the player can navigate freely in the area and if he/she selects an object that belongs to the specific category of training in the time, the name of this object is pronounced so he can train by listening and learning vocabulary of objects while wandering in the place.

b) Comprehension Tasks

In order to work on patient's ability to comprehend objects' meanings in an interactive manner, one of the categorization-based tasks that is assigned to him while moving is that a food bar is placed in the screen corner (see Figure 5), decreased over time and at a moment, an icon appears that guides the patient to click by mouse on any food around and so, the bar gets refilled and he can keep proceeding.



Figure 4: Sample scenes from the training environment.



Figure 5: Interactive task based on words categories.

3.2. Algorithm Generation

For the AI algorithm used in voice data processing, we created a convolutional neural network (CNN) model using TensorFlow module with python programming language to train the data of targeted words in Arabic language and then testing the patient's speech of those words to assess the patient's improvement. The following parts illustrate the steps followed in order to build the algorithm.

3.2.1. Data Acquisition

The undergoing dataset consists of collected audio data of frequent speech of some targeted words in colloquial Egyptian Arabic language. The words were selected based on different major categories used in speech therapy.

We collected the dataset consisting of 12,804 utterances of 10 short words; each word repeated 5 times by the same person; by participants of both genders; about 199 females and 58 males with ages greater than 18. The mother tongue of all participants is Egyptian Arabic.

3.2.2. Pre-processing

Data preprocessing is a data mining technique that is used to transform the raw data into a useful and efficient format. For the purpose of data preparation for the system, we applied several preprocessing steps as shown in Figure 6.

a) Noise Removal

The Noise reduction effect dramatically reduces background and broadband noise with a minimal reduction in the signal quality.

We used fre:ac – a free audio converter desktop application for background noise reduction which implicitly uses recurrent neural networks models for noise reduction (RNNoise).

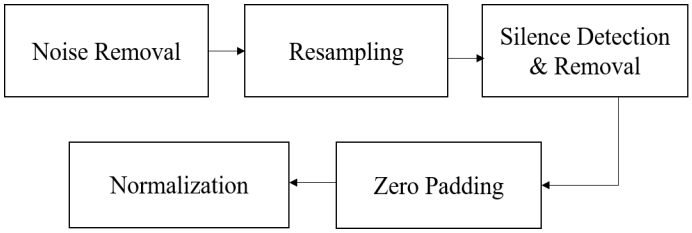


Figure 6: The pipeline of preprocessing steps.

b) Resampling

Resampling is usually done to interface two systems which have different sampling rates. The sampling rates of our collected data were different. So, we resampled all audio signals to 16000 Hz.

c) Silence Detection and Removal

Silence detection and removal help to maintain an acceptable end-to-end delay for the audio signal. We applied silence detection algorithm by segmenting the audio file into chunks of constant size equals to 0.01 s and comparing each chunk's amplitude in decibels with the silence threshold which equals to – 45 dB

d) Zero Padding

Because of the different lengths of the collected audio files, we unified the length of all signals to be one second for each command in the dataset. We applied zero padding at the end of each record that was less than one second.

e) Normalization

In order to overcome the problem that the speech is loud in some portions and quiet in others. Having this variance in volume can hinder transcription, so we had to normalize the audios.

The method that was followed, is used for standard amplitude normalization by scaling the whole audio to the maximum amplitude.

3.2.3. Data Augmentation

We performed this step to generate more data from the available dataset and increase the diversity of it to make our model invariant to perturbations and enhance its ability to generalize. We augmented the dataset randomly by several techniques such as adding a random factor of white noise between 0.004 to 0.009, shifting the starting point of the audio, and then padded it to its original length, increasing signal's amplitude (loudness) by a gain of 5-10 dB and applying random cropping by a mask of random silence of the time that is chosen to be saved and the remaining parts of the audio will reset to zero. After applying data augmentation, the dataset size became 77,040 utterances.

3.2.4. Features Extraction

The most common two approaches in speech recognition are to convert raw audio signals to spectrograms or to extract features using Mel-frequency Cepstral Coefficients (MFCC) [21-23].

As proven that convolutional neural networks work well with image recognition tasks [24], in this paper we followed the two approaches and compared results to choose the best approach that fits our system.

a) Spectrogram Generation

First, we converted the prepared uniform raw data to its log-spectrograms; which are two-dimensional matrices, as a representation of the audio signal in frequency domain and used it as an input to the CNN. The audio signal is used in time domain and broken up into chunks, each chunk is a small frame size of the speech signal data. It is between 0.02-0.04 s and is assumed to be a stationary signal. If the chunk size is more than 0.04 s, the signal will act as a non-stationary signal and if the chunk size is less than 0.02 s, it won't have enough samples to extract features from it. Then Fast Fourier Transform (FFT) is applied for each chunk to calculate the magnitude of the frequency spectrum. Then the spectrum is rotated by 90 degrees to make the frequency in the vertical axis and the amplitude is represented by mapping it to color. These spectrums have some imaginary values, so, a log for the spectrum is applied to visualize it, then these spectrums are added side by side to form the spectrogram. Some spectrograms are visualized in Figure 7.

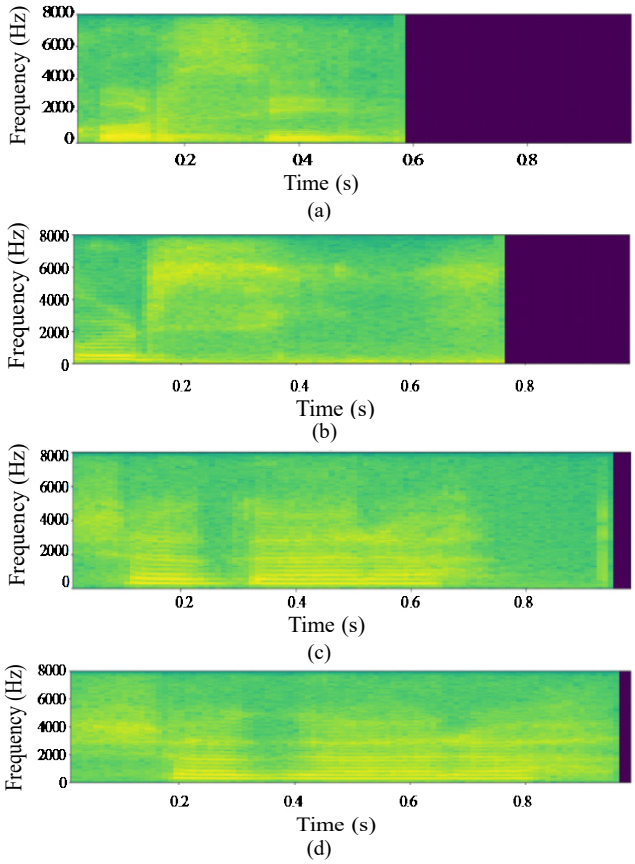


Figure 7: Spectrogram representation of two words in Arabic, each recorded from two different persons: (a), (b) for "chair" and (c), (d) for "tree". Sample rate = 16000 Hz, then frequencies in the range [0-8000] according to Nyquist theory.

b) MFCCs Generation

The MFCCs help to understand the speech and try to determine how sound comes out. To create the MFCC, we used the audio signal in the time domain and frame blocking into frames. Then

the Hamming windowing Framing process produces discontinuity frames. Fast Fourier transform (FFT) is applied for each frame to calculate the magnitude of the frequency spectrum. The magnitude spectrum is warped according to Mel scale. Then the magnitude spectrum is segmented into a number of critical bands by means of a Mel filter bank. Then the logs of the powers at each of the Mel frequencies were taken.

The logarithm of the filter bank outputs are called the Mel spectrum. After that, we applied the discrete cosine transform (DCT) of the list of the Mel spectrum to convert it into the time domain. The MFCCs are the amplitudes of the resulting list of the Mel spectrum as shown in Figure 8.

3.2.5 Classification

After extracting the features from the audios, the input became images. These images were used as input to the CNN model. We built our model to classify between 10 words in Arabic language. Thus, we knew if the target word is said or not, and improvement measurements are to be followed.

a) Model Architecture

Our model represents the CNN architecture with three convolutional and pooling layers and one dense layer. Additionally, we add batch normalization to increase stability and dropout to avoid overfitting.

For the hyperparameters of each convolutional layer, we used 32 filters each with a window size of 3×3 with 1 stride. We used max-pooling layers each of 2×2 window cell size with 2 strides after each convolutional layer for down sampling the input by halve. For the dropout hyperparameter, the probability of training a given node in a layer is 0.2.

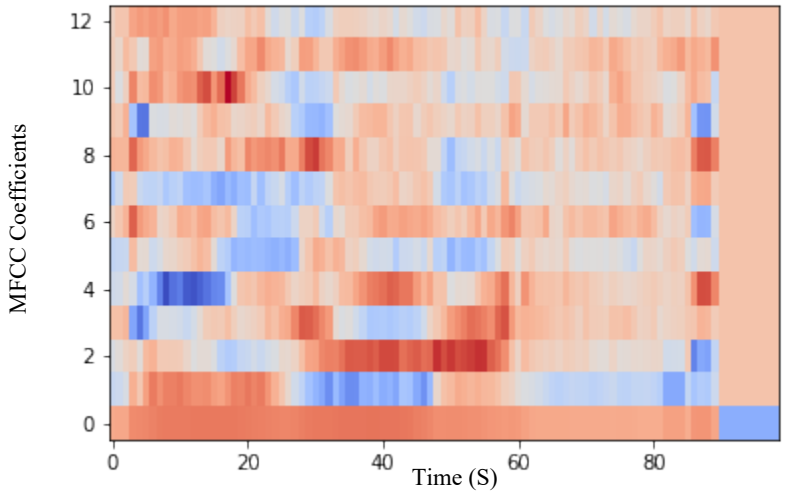
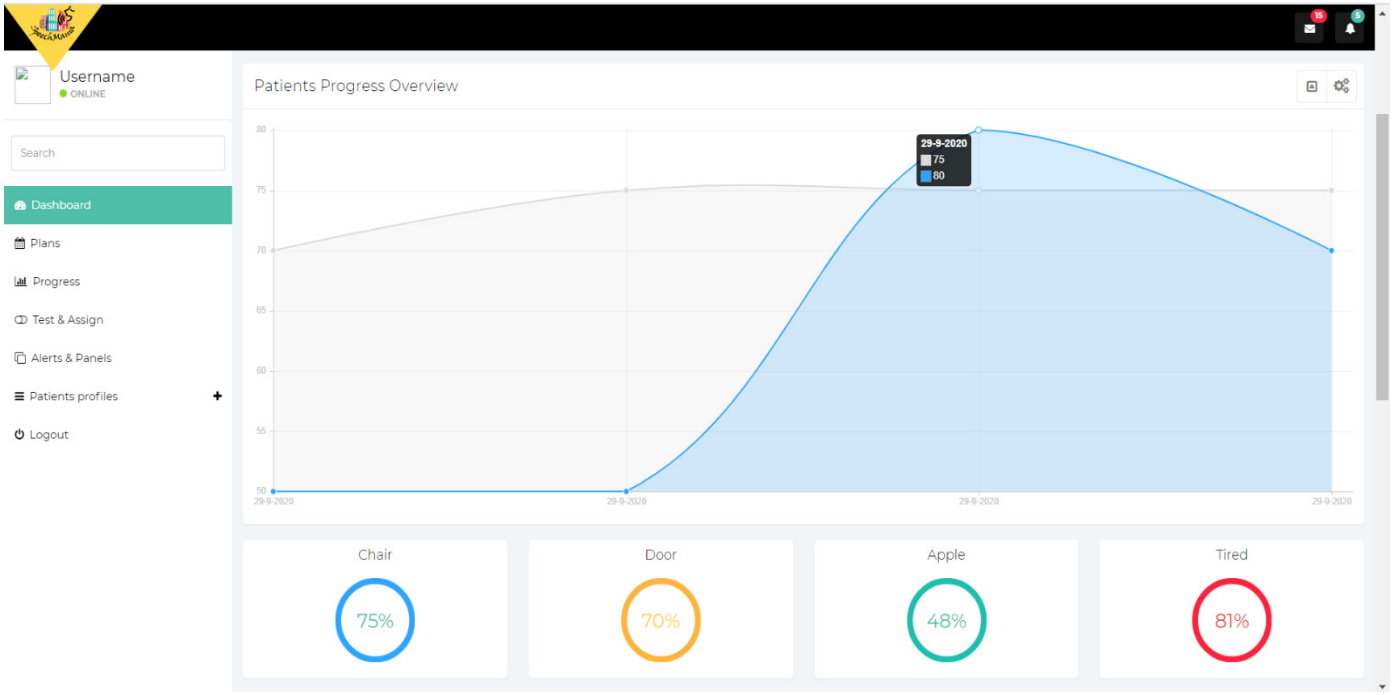


Figure 8: The MFCCs representation of a speech audio signal for “chair”.



Firstly, we organized the dataset and divided it into train and validation sets with a validation ratio of 0.25. Next, we implemented CNN model considering a loss function to be local minimum so, we used standard Adam optimizer minimizing categorical cross-entropy and monitor accuracy in the course of training.

With regard to the training parameters, we used a number of epochs = 15 and batch size = 64. Moreover, early stopping has been added in order to stop the training once validation loss function starts to increase.

3.3. Feedback System

During the game, the voice of the patients is continuously taken to a cloud server using Artificial Intelligence of Things (AIOT) providing real-time feedback to their speech improvement. The feedback is divided into two parts, the first one is an on-screen feedback to guide the patients and encourage improvement in speech and comprehension.

The second one is to be shared via a website with the actual therapist for remote follow-up and to see the progress report of his patients using the AIOT system and assign needed tasks and effective rehabilitation plan.

3.3.1. Website Architecture

The website was created using HTML, CSS, JavaScript and Bootstrap. It consists of three main parts; the home page, therapist authentication page and the most important part is the therapist's dashboard shown in Figure 9. It enables therapists to follow up their patients' progress through the rehabilitation timeline and assign needed tasks.

The feedback is visualized by a curve for each task along the rehabilitation timeline and accumulation of the improvement percentages for learning words, considering the good experience and emphasizing the functionality.

3.3.2. Cloud Server

After evaluating different cloud service providers, we chose Google Firebase mainly because of the ease of use. It offers the needed storage and real-time database for our system so we can store and retrieve data in a game made with Unity3D and share resources between the AI model, the rehabilitation environment, and the website.

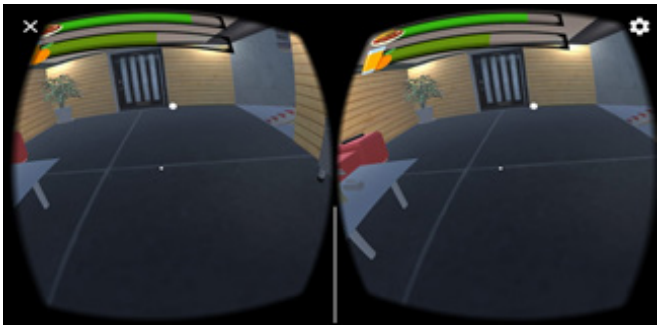


Figure 10: Final VR application on android operating system.

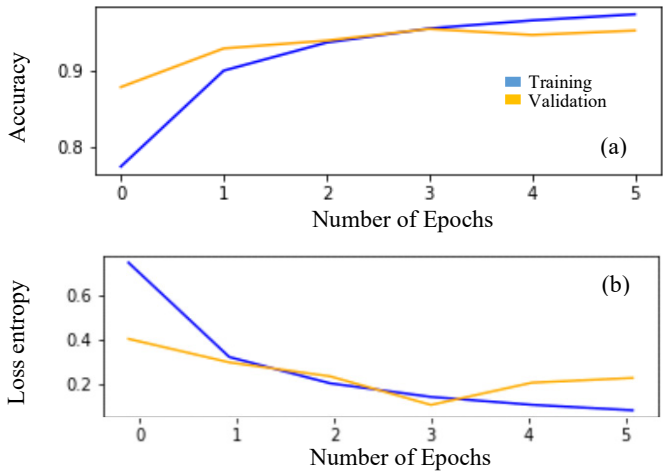


Figure 11: Results of the model on the spectrograms dataset after applying augmentation. (a) Classification Accuracy and (b) Cross Loss Entropy.

4. Results

4.1. VR environment build

Finally, the whole integrated system is built as an interactive computer-aided system on regular PCs and as VR mobile phone application consolidating immersivity concept. Figure 10 shows a final look of the system built on an android device.

Table 1: Comparison of the model accuracy using the two techniques used in feature extraction applied on both datasets.

Feature extraction method	**Dataset**	
	Without augmentation	Augmented data
Log Spectrograms	92.17 %	95.2 %
MFCC	90.7 %	92.6 %

4.2. Speech recognition model results

We tested the CNN model using the two approaches of feature extraction. First, we started with the spectrograms' dataset calculating the accuracy over validation set to obtain the validation accuracy. The final accuracy and loss on the validation set of spectrograms were obtained at the 3rd epoch where the accuracy was 92.17 % and the validation loss was 0.33. Then, we tested the model on the dataset after extracting MFCCs from it and also got the accuracy and loss on the validation set. The final accuracy and loss on the validation set were obtained at the 5th epoch where the accuracy was 90.7 % and 0.39 validation loss.

After applying the augmentation techniques to the original data, we extracted spectrogram and MFCC features and again tested the model on them. The final accuracy and loss on the validation set of spectrograms are shown in Figure 11 where an accuracy of 95.2 % and a validation loss of 0.22 were obtained at the 5rd epoch. Extracting the MFCC features results in an accuracy of 92.6 % and the validation loss was 0.39.

Results of recognition accuracy of both techniques applied on the dataset before and after augmentation are summarized and compared in Table 1.

Table 2: Precision, recall and f1-score calculated for the testing set of the 10 words (classes) on each one of the four models used.

	Log-Spectrogram						MFCC					
	Before Augmentation			**After Augmentation**			**Before Augmentation**			**After Augmentation**		
Classes	**Precision**	**Recall**	**f1-score**	**Precision**	**Recall**	**f1-score**	**Precision**	**Recall**	**f1-score**	**Precision**	**Recall**	**f1-score**
تفاح /Apples	0.500	0.40	0.44	1.00	1.00	1.00	0.40	0.40	0.40	0.57	0.80	0.67
كرسي / Chair	0.00	0.00	0.00	0.43	0.75	0.55	0.17	0.25	0.20	0.33	0.25	0.29
باب / Door	1.00	0.50	0.67	0.57	1.00	0.73	0.67	0.50	0.57	0.50	0.50	0.57
آكل / Eat	0.00	0.00	0.00	1.00	0.75	0.86	0.00	0.00	0.00	0.50	0.25	0.33
عصير /Juice	0.08	0.25	0.13	1.00	0.75	0.86	0.50	0.25	0.33	1.00	0.25	0.40
جنيه / Pound	0.50	0.25	0.33	1.00	0.50	0.67	0.33	0.50	0.40	0.60	0.75	0.67
تاكسي /Taxi	0.00	0.00	0.00	0.33	1.00	0.50	0.00	0.00	0.00	0.00	0.00	0.00
تعبان /Tired	0.36	0.80	0.500	1.00	0.60	0.75	0.38	0.60	0.46	0.60	0.60	0.60
شجرة / Tree	0.50	0.25	0.33	1.00	0.50	0.67	1.00	0.25	0.40	0.50	0.25	0.33
مايه / Water	0.00	0.00	0.00	1.00	1.00	1.00	1.00	0.60	0.75	0.67	0.80	0.73

The testing process is done with 15 speakers with the same ratio of males and females in the training set. We obtained about 2 or 3 records of mimicked sounds of multiple cases of patients from each speaker; thus, a total of 40 data points is used to evaluate the performance of the model. Then, we applied all the preprocessing steps on each audio in the test set. Table 2 shows the precision, recall, and f1-score in the classification report of the test data when applying the four trained models.

5. Conclusion

This paper addresses the problems of language and speech dysfunction after stroke or traumatic brain injury. We proposed a computer aided Arabic-based rehabilitation system for people with aphasia as a regular PC interactive game and a VR-based mobile application. Language comprehension and speech production are assessed and measured using a CNN algorithm to provide feedback for both patients and the SLPs via a website for remote follow-up. In the purpose of speech assessment, we build four speech recognition models. Experimenting two feature extraction methods and apply them on the collected audio dataset and one more time after augmenting these data.

The test results showed that the best model was obtained when applying data augmentation techniques on the spectrogram dataset with a training accuracy of 95.2 %.

In future work, more testing and enhancing of the model will be applied, adding more categories of words and more tasks for training and a clinical study will be done to validate our system performance and patient's acceptance of this new rehabilitation method.

Conflict of Interest

The authors declare no conflict of interest.

Acknowledgment

We would like to thank Dr. Nahla Rifaie, Professor and head of phoniatrics unit at faculty of medicine, Ain Shams University for contributing with all needed information about the medical condition and the idea of accurate lip syncing, in addition to arranging periodic consultations for validation. We also grateful for each participant who devoted his/her time to help us in collecting the dataset and for Cairo University, the Academy of Scientific Research & Technology, and ITIDA as well for providing us the needed fund to proceed with the project.

References

[1] W. Johnson, O. Onuma, M. Owolabi, S. Sachdey, "Stroke: a global response is needed," Bulletin of the World Health Organization, **94**(9), 634-634A, 2016, doi: 10.2471/BLT.16.181636.

[2] M. Lindsay, B. Norrving, R. L. Sacco, M. Brainin, W. Hacke, S. Martins, J. Pandian, V. Feigin, "World stroke organization (WSO): global stroke fact sheet 2019" International Journal of Stroke, **14**(8), 806–817, 2019. doi: 10.1177/1747493019881353.

[3] United Kingdom, State of the nation: stroke statistics, JN 1718.250, 2018.

[4] National Institute on Deafness and Other Communication Disorders, NIDCD fact sheet | voice, speech and language: Aphasia, NIH Pub. No. 97-4257, 2015.

[5] National Aphasia Association, aphasia definitions fact sheet.

[6] K. Hilari, S. Byng, "Health-related quality of life in people with severe aphasia," International Journal of Language and Communications Disorders, **44**(2), 193–205, 2009, doi: 10.1080/13682820802008820.

[7] O. L. Backus, L. D. Henrry, J. L. Clancy, H. M. Dunn, Aphasia in Adults: The Rehabilitation of Persons with Loss or Disturbance of the Faculty of Speech Resulting from Brain Injury, University of Michigan Official Publication, 1945.

[8] I. K. Hamed, M. Elmahdy, S. Abdennadher, "Collection and Analysis of Code-switch Egyptian Arabic-English Speech Corpus," in the 11th International Conference on Language Resources and Evaluation, 2018.

[9] L. R. Cherney, S. V. Vuuren, "Telerehabilitation, virtual therapists, and acquired neurologic speech and language disorders," Seminars in Speech and Language, **33**(3), 243-57, 2012, doi: 10.1055/s-0032-1320044.

[10] S. V. Vuuren, L. R. Cherney, "A virtual therapist for speech and language therapy," In: Bickmore T., Marsella S., Sidner C. (eds) Intelligent Virtual Agents. Lecture Notes in Computer Science, **8637**, Springer, Cham, 2014, doi: 10.1007/978-3-319-09767-1_55.

[11] J. R. Galliers, S. Wilson, J. Marshall, R. Talbot, N. Devane, T. Booth, C. Woolf, H. Greenwood, "Experiencing eva park, a multi-user virtual world for people with aphasia," ACM Transactions on Accessible Computing, **10**(4), 15, 2017, doi: 10.1145/3134227.

[12] H. S. Lee, Y. J. Park, S. W. Park, "The effects of virtual reality training on function in chronic stroke patients: A systematic review and meta-analysis," Biomed Research International, 2019, doi: 10.1155/2019/7595639.

[13] J. Thomas, C. France, S. Leitkam, M. Applegate, P. Pidcoe, S. Walkowski, "Effects of real-world versus virtual environments on joint excursions in full-body reaching tasks," IEEE Journal of Translational Engineering in Health and Medicine, **4**, 1-8, 2016, doi: 10.1109/JTEHM.2016.2623787.

[14] S. Parsons, S. Cobb., "State-of-the-art of Virtual Reality technologies for children on the autism spectrum," European Journal of Special Needs Education , **26**(3), 355-366, 2011, doi: 10.1080/08856257.2011.593831.

[15] N. S. Rosenfield, K. Lamkin, J. Re, K. Day, L. Boyd, E. Linstead, "A virtual reality system for practicing conversation skills for children with autism," Multimodal Technologies and Interaction, **3**(2), 28, 2019, doi: 10.3390/mti3020028.

[16] B. Brundage, A. B. Hancock, "Real enough: using virtual public speaking environments to evoke feelings and behaviors targeted in stuttering assessment and treatment," American Journal of Speech-Language Pathology, **24**(2), 139-149, 2015, doi: 10.1044/2014_AJSLP-14-0087.

[17] Y. Zhang, P. Chen, X. Li, G. Wan, C. Xie, X. Yu, "Clinical research on therapeutic effect of virtual reality technology on broca aphasia patients," in IEEE International Conference on Information Technology, 2, 2017, doi: 10.1109/INCIT.2017.8257880.

[18] M. Horváth, C. Dániel, J. Stark, C. Sik Lanyi, "Virtual reality house for rehabilitation of aphasic clients," Transactions on Edutainment III, **5940**, 231–239, 2009, doi: 10.1007/978-3-642-11245-4_20.

[19] N. Sebkhi, D. Desai, M. Islam, J. Lu, K. Wilson, M. Ghovanloo, "Multimodal speech capture system for speech rehabilitation and earning," IEEE Transactions on Biomedical Engineering, **64**(11), 2639-2649, 2017, doi: 10.1109/TBME.2017.2654361.

[20] K. Grechuta, B. Rubio Bellaster, R. Esp´ın Munn´e, T. Usabiaga Bernal, B. Molina Herv´as, R. San Segundo, P. F.M.J. Verschure, "The effects of silent visuomotor cueing on word retrieval in broca's aphasics: a pilot study," in IEEE International Conference on Rehabilitation Robotics, 2017, doi: 10.1109/ICORR.2017.8009245.

[21] J. Gibson, M. Van Segbroeck, S. Narayanan, "Comparing Time-Frequency Representations for Directional Derivative Features," in Interspeech, 612–615, 2014.

[22] M. Alsulaiman, G. Muhammad, Z. Ali, "Comparison of Voice Features for Arabic Speech Recognition," in IEEE 6th International Conference on Digital Information Management, **6**, 2011, doi: 10.1109/ICDIM.2011.6093369.

[23] S. Prasomphan, "Improvement of speech emotion recognition with neural network classifier by using speech spectrogram," in International Conference on Systems, Signals and Image Processing ,2015, doi: 10.1109/IWSSIP.2015.7314180.

[24] N. Jmour, S. Zayen, A. Abdelkrim, "Convolutional neural networks for image classification" in IEEE International Conference on Advanced Systems and Electric Technologies, 2018, doi: 10.1109/ASET.2018.8379889.

ASTES

Advances in Science, Technology and Engineering Systems Journal Vol. 5, No. 5, 1233-1246 (2020)

www.astesj.com

Special Issue on Multidisciplinary Innovation in Engineering Science & Technology

ASTESJ

ISSN: 2415-6698

Design and Development of Electronic Sensor and Monitoring System of Smart Low-cost Phototherapy Light System for Non-Invasive Monitoring and Treatment of Neonatal Jaundice

Paul Cabacungan[1,*], Carlos Oppus[1,2], Gregory Tangonan[1], Nerissa Cabacungan[3], John Paul Mamaradlo[1], Neil Angelo Mercado[1]

[1]*Ateneo Innovation Center, Ateneo de Manila University, Quezon City, 1108, Philippines*

[2]*Electronics, Computer, and Communications Engineering Department, Ateneo de Manila University, Quezon City, 1108, Philippines*

[3]*Ateneo Grade School, Ateneo de Manila University, Quezon City, 1108, Philippines*

ARTICLE INFO

Article history:
Received: 31 August, 2020
Accepted: 28 September, 2020
Online: 24 October, 2020

Keywords:
Phototherapy
Neonatal Jaundice
Yellow Detection
Irradiance
Sensor and Monitoring System

ABSTRACT

This paper showcases our previous and continuously improving development at Ateneo Innovation Center (AIC) and partners in designing and further enhancing the existing Low-cost Phototherapy Light System (LPLS) and Improved Low-cost Phototherapy Light System (ILPLS) to the new Smart Low-cost Phototherapy Light System (Smart LPLS) with non-invasive jaundice monitoring for newborns with Neonatal Jaundice (NNJ). Developing this tool will help determine the intensity of yellowish color in infants and can monitor NNJ in a non-invasive way. The system is envisioned to be integrated with Mobile or Near Cloud as part of Smart Nursing Station together with other hospital equipment for monitoring, collection, and management of medical records and services. Its solar-power features for off-grid and remote deployments were also explored. This contribution is an extension of the Intelligent Sensors and Monitoring System for Low-cost Phototherapy Light for Jaundice Treatment that was presented in the International Symposium on Multimedia and Communication Technology (ISMAC) in 2019.

1. Introduction

This contribution is an extension of the previous development [1-3] of the Ateneo Innovation Center (AIC) in the development of a phototherapy system for the treatment of infants with jaundice. The system has been proven to be reliable and effective, with over 30 patients treated [2, 3] during clinical investigation. Our previous efforts described that this unit has been developed at far less cost and may achieve similar results like the commercially available units.

Neonatal jaundice (NNJ) occurs in 25% to 60% of full-term newborns and 80% of preterm newborns in the first two weeks of life, as studied by Cecelia Henny-Harry and her research partner [4]. It is a benign transient physiological event in the majority of newborns but can cause irreversible brain damage and kernicterus in some infants if the serum bilirubin levels are high. Various mechanisms involved in producing this 'physiological' increase in total serum bilirubin include increased production of bilirubin due to lysis of red blood cells, decreased ability of liver cells to clear bilirubin and increased enterohepatic circulation. Any condition that further increases bilirubin production or alters the transport or metabolism of bilirubin increases the severity of physiological jaundice [5].

The main indicator of NNJ is the presence of high levels of bilirubin. Among the effects of high levels of bilirubin caused by rapid RBC metabolism is the increased levels of carbon monoxide in the body, which sometimes causes neurologic dysfunction [6]. Adults may also contract jaundice by having elevated serum bilirubin levels. Jaundice in adults is often an indicator of underlying condition, such as hepatitis or liver disease, and injury [7]. The recurrence of jaundice or its persistence can have astounding and long-standing effects on the health and overall welfare of the patient.

Some factors that increase the likelihood of contracting jaundice are genetics, hospital setting, and social-economic status. In addition, persons of African, Mediterranean, Middle Eastern, or Southeast Asian descent are more likely to contract jaundice [8]. With this in mind, we can infer that Filipinos belonging to lower-income households will be more susceptible to this disease, and so

*Corresponding Author: Paul Cabacungan, pcabacungan@ateneo.edu

are communities with little to no access to sufficient medical services.

Phototherapy is the most frequently used treatment when serum bilirubin levels exceed physiological limits. To initiate phototherapy without delay is the most important intervention for infants with severe hyperbilirubinemia. Phototherapy uses blue light to convert bilirubin into water-soluble photo-products that can bypass the hepatic conjugating system and be excreted without further metabolism. The clinical response to phototherapy depends on the efficacy of the phototherapy device, as well as the infant's rates of bilirubin production and elimination [9]. Phototherapy, despite being the recommended standard treatment for hyperbilirubinemia in newborns, may not be accessible to many people most especially in developing countries. This is due to its high procurement and maintenance cost ranging from PHP 150,000 to PHP 350,000 (USD 3,100 to USD 7,000) [10]. In the Philippines, for rural clinics and maternity hospitals to be accredited by Philippine Health Insurance Corporation (PhilHealth), a tax-exempt Government Corporation attached to the Department of Health that administer the National Health Insurance Program [11], they must possess an operating phototherapy system for jaundiced infants.

For more efficient operations, clinics and hospitals need a detailed digital record of consultation or confinement such as demographic data of the patient, identity of attending medical staff, medical and laboratory procedures and results, among others. In the case of NNJ, rural hospitals will need chemical reagents and a hematology analyzer to administer actual bilirubin counting of blood samples. Access to comprehensive patient digital records and to needed reagents and medical devices is usually problematic, especially in remote areas. When an infant is suspected to be suffering from NNJ, the doctors resort to physical inspection to assess the existence or degree of jaundice.

In 2016, Ateneo Innovation Center together with its partner pediatricians conducted a two-year pilot study and clinical investigation to evaluate the capability of the LPLS in lowering bilirubin levels among healthy term infants diagnosed with indirect hyperbilirubinemia admitted at the nursery, OB ward, and pediatric ward of a tertiary hospital in Metro Manila. [2,3]. Figure 1 shows the LPLS administered by a pediatrician during the clinical investigation, after passing through all the necessary protocols required by the ethics committee.



Figure 1: Infant diagnosed with indirect hyperbilirubinemia underwent phototherapy using the LPLS prototype in a tertiary hospital in Metro Manila, Philippines

The clinical investigation revealed that 16% of the total number of patients completed treatment after 24 hours of phototherapy under the LPLS and were classified to be in the low risk zone while 36% completed treatment after 48 hours. The total bilirubin significantly decreased by 16.5% ($p = 0.0001$) from baseline bilirubin levels after 24 hours. There was a significant 29.9% mean percentage of reduction in bilirubin level after 48 hours. The proportion of subjects in the high-risk zone during baseline to 24th hour went down significantly from 80% to 28% ($p = 0.0003$). In the same manner, comparing baseline to 48th hour, the percentage of subjects in the high-risk zone went down from 80% to 9.5% ($p = 0.0001$). Figure 2 shows the graphical representation of the results.

After the clinical investigation, there were no reported occurrences of rebound hyperbilirubinemia. No patient experienced any complication while on treatment. This makes the system safe and effective in lowering total serum bilirubin among healthy term infants with indirect hyperbilirubinemia [3].

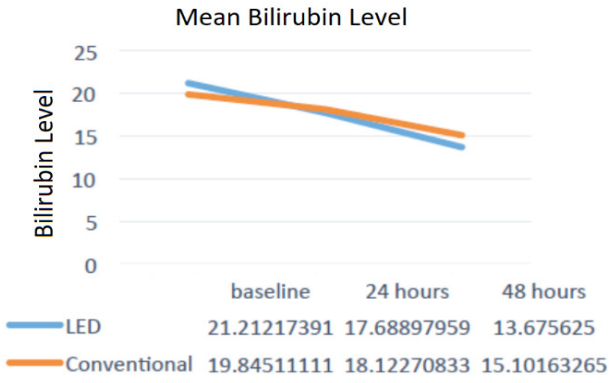


Figure 2: Mean TSB levels in both groups at different period [3]

Ateneo Innovation Center developed further the Low-cost Phototherapy Light System (LPLS), shown in Figure 3, with the integration of sensors making it an Improved Low-cost Phototherapy Light System (ILPLS) as seen in Figure 4. ILPLS was designed to have the same functions, to provide the same treatment, and to keep its low cost, as the original prototype.

The main components of the ILPLS were the eight pieces of 7-watt LED blue spotlight, which were more robust and had the same cost as the 3-watt bulbs of the LPLS. The wavelength was within the 400 - 500 nanometers (peak at 460nm) which are specifically used for administering phototherapy [12]. The measured irradiance was three times stronger than that of the 3-watt bulb and its unit exceeded the total irradiance of the previous unit. The bulbs were positioned alongside each other at 13 centimeters apart (from center to center). This engineering design made the light beams overlap by 43% resulting in a more intensified lighting. There is an 11% intersection of light beams coming from the bulbs positioned across each other, which are 22 centimeters apart. The 22-centimeter distance was an engineering trade-off to give way to the fans that provide fail-safe mechanisms. During the 120-hour operation, the ILPLS bulbs performed in an acceptable temperature range of 35.8 to 39.0 °C, with ambient average temperature of 32.5 degree Celsius. No issues were encountered at all. An additional 10-watt computer fan was also installed.



Figure 3: Low-cost Phototherapy Light System (LPLS)



Figure 4: Improved Low-cost Phototherapy Light System (ILPLS)

The sensor and monitoring system were also introduced and successfully integrated into the ILPLS without affecting the unit's optimal functioning. The camera system is intended to provide digital records of the patient's ID, time stamp, unit tag and audio tags by medical personnel. The smart camera was able to transmit images and sounds within the 10-meter radius in a laboratory setting, despite the presence of walls, demonstrating that data collection at nearby stations is possible. The location of the phototherapy unit is crucial to readily interface with nursing stations and hospital medical records. This approach is scalable and useful to situations where multiple phototherapy units are operated at the same time. It can easily record the data of the ongoing phototherapy and supplement the nurses' records. Four light dependent resistors (LDRs) were installed to ensure emission of appropriate light intensity. The two-in-one sensor was also able to measure temperature and humidity inside the light box. Alarms would signal readings beyond threshold, adding safety features to the system.

Ateneo Innovation Center acknowledges the long-standing problem of the people in remote and off grid communities who have little or no access to this device. Through the efforts of this organization, professors, students, and different organizations continue to collaborate and work together in developing innovative designs and ideas that provide solutions with impact on the betterment of society. This paper presents another Ateneo Innovation Center's development that aims to address a need in remote settings - the Smart Low-cost Phototherapy Light System (SLPLS) with non-invasive jaundice monitoring for neonatal jaundice.

Shown in this paper is how we are developing new sensor and monitoring systems that enhance the performance of our low-cost phototherapy light systems and facilitate data collection and sharing with patients' families and the stakeholders. Having a digital record to determine the progress and success of treatment, doctors can monitor and assess the progress of the treatment in a more scientific way. We are developing yellow jaundice sensors that can monitor the treatment of the patient and can provide a possible basis for detection. We explore different color sensor experiments, using accessible devices and open source applications that can be integrated into our latest prototype. We also demonstrate optical techniques for color measurement that can be a tool for obtaining a digital record of the degree of jaundice. Lastly, we deal with an important aspect of the development - solar powering of the phototherapy system for 24/7 performance in case of power outage or blackouts and remote deployment. To further prove that this system is effective enough to be used as an alternative than that of a commercial unit, we have yet to conduct further tests with actual human subjects that will be supervised by medical personnel.

2. System Overview

This paper describes the most recent Smart LPLS prototype with further improvements to its electronic sensor and monitoring system. We also present non-invasive methods that will help determine the intensity of yellowness in infants as a way of detecting NNJ. The Smart LPLS is composed of eight 7-Watt LED bulbs at the top and the additional ten 10-watt LED tube light pieces at the bottom, as seen in Figure 5. This makes the system more robust compared to the 3-watt and 7-watt LED bulbs used in previous prototypes presented earlier. These additional T5 LED tube lights are 90% more efficient than traditional light bulbs, 60% compact than fluorescent bulbs, and have a lifespan of 30,000 hours.

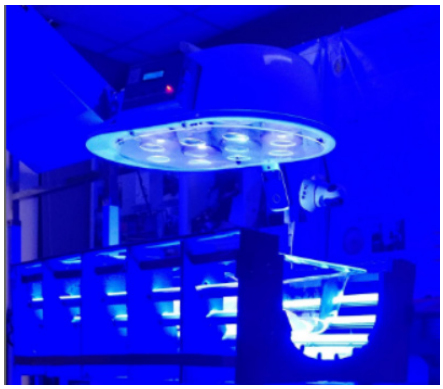


Figure 5: New Smart Low-cost Phototherapy Light System

To easily monitor the system's performance, an automated system that stores data about the device's light intensity and bulb temperature and records ambient humidity was installed. An alarm system that activates the warning lights if sensor readings are in critical level and if the bulbs need to be replaced are built into the system. A time setting feature is also included to manually set the time of operation and automatically turn-off the device. The system diagram for the smart sensor and monitoring system can be seen in Figure 6.

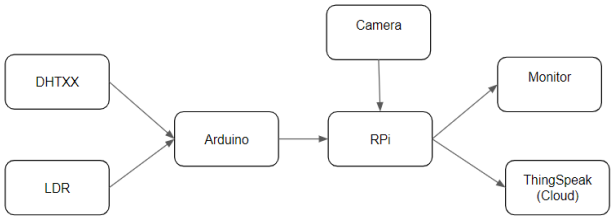


Figure 6: System diagram for the smart sensor and monitoring system

The DHT22 sensor, which can measure both humidity and temperature, is placed inside the system. Meanwhile, the photoresistors or the light dependent resistors (LDRs) are placed near the phototherapy light to monitor the light intensity. Both are connected to the Arduino which will send data to the Raspberry Pi later. While the Arduino is feeding sensor data to the Raspberry Pi, a camera may also be connected to it. The Processing IDE will process the data and display everything in one window through the monitor where people can see if everything is as expected. Measured data like temperature, humidity, light intensity, and images are sent to ThingSpeak IoT platform, which can be used to send data to the cloud from any Internet-enabled device. Users can configure actions and alerts based on real-time data and unlock the value of data through visual tools.

The non-invasive jaundice treatment monitoring feature of the Smart LPLS aims to provide an alternative platform for physicians to conduct a non-invasive method to check how severe the jaundice of an infant is while on treatment. Blood analysis is currently used to determine bilirubin level in the blood. This process is invasive, and the results may take some time. Physical inspection may also be done but the accuracy of results depends heavily on the skill of the medical practitioner performing the inspection. In our experience, provincial hospitals often lack the necessary reagents to carry out these tests, necessitating an alternate measurement. Developing a tool that will determine the intensity of yellowish color in infants can give immediate and accurate detection of NNJ in a non-invasive way. Also, commercial phototherapy systems and bilirubinometers are expensive and rural hospitals might not have the financial resources to afford these. The sensor will be helpful in gauging and monitoring if the phototherapy treatment is sufficient and successful in treating the jaundice in infants. If phototherapy was not enough, blood transfusion might be needed. The system may store collection of readings and activate a warning light indicator if sensor readings that are related to bilirubin level go beyond the set ceiling, indicating that the condition cannot be managed through phototherapy light and a more aggressive treatment approach such as blood transfusion is needed. The same automation system can also activate a different warning light if sensor readings go below a set floor, indicating the full treatment of NNJ. This means that the infant can be removed from phototherapy light exposure.

In *Table 1*, we compared the prototypes with a commercially available unit. What sets the Smart LPLS apart from the previous prototypes are the top and bottom irradiation. This results in a 360° light exposure, without the need to tilt the baby every two hours. Moreover, the irradiance of top-mounted lights is three times stronger than the minimum required irradiance of 30 µW/cm²/nm for NNJ treatment. In addition, the bottom-mounted lights provide an irradiance of 34 µW/cm²/nm, leading to an expectation for faster treatment. Despite the installation of more lights, the Smart LPLS has two fans with air vents to provide safety mechanisms.

The Smart LPLS for off-grid deployment with a total unit cost of PHP 38,000.00 or around USD 780.00 uses energy efficient LED bulbs and tubes having a full width half maximum wavelength range of 439.66 nm to 467.64 nm that is within the curing wavelength of 400-500 nm, irradiance of 34µW/cm²/nm, with top & bottom lights still within the minimum wavelength, additional air vents, sensors and monitoring system, and with integrated non-invasive yellow detection feature. We have listed our estimates of the baseline system costs, however, due to time constraints and the current setup of the research laboratory, the systematic optimization in relation with its cost discussing the reliability, longevity, and efficiency is of pending approval by medical authorities will be discussed in future publications.

Table 1: Comparison of Smart LPLS with its Predecessors and Commercial Unit

Parameters	**LPLS**	**ILPLS**	**Smart LPLS**	**Commercial Unit**
Light Bulb	Twenty 3watt LED bulbs	Eight 7-watt LED spotlights	Eight 7-watt LED and Ten 10-watt LED tubes	Five 20-watt Fluorescent
Wavelength	462.1 nm to 476.4 nm	437.8 nm to 458.48 nm	437.8 nm to 458.48 nm; and 439.66 nm to 467.64 nm	(5 white and 2 blue)
Irradiance at 30 cm. average distance	84 µW/cm² /nm	90 µW/cm² /nm	90 and 34 µW/cm² /nm	70 µW/cm² /nm
Total Power	75 watts	90 watts	240 watts	400 watts
Ventilation	one fan	two fans	two fans with air vents	air-cooled
Sensor and Monitoring System	none	present	present	none
Integrated Non-invasive yellow monitoring	none	none	present	none
Unit Cost	Php20k	Php35k	Php38k	Php150k

Since 2015, the Ateneo Innovation Center has been studying and exploring the Near Cloud or Mobile Cloud, recognizing its powerful computing and caching capabilities in the context of disaster resilience, education, and healthcare. The concept of caching is powerful especially in a telecom infrastructure-less environment. This technology uses a combination of a plug computer, preloaded content, and key web applications on terabyte drives at fiber-like speeds. It addresses limited bandwidth and connectivity by providing valuable preloaded content and acting as a gateway to the Internet [13-15].

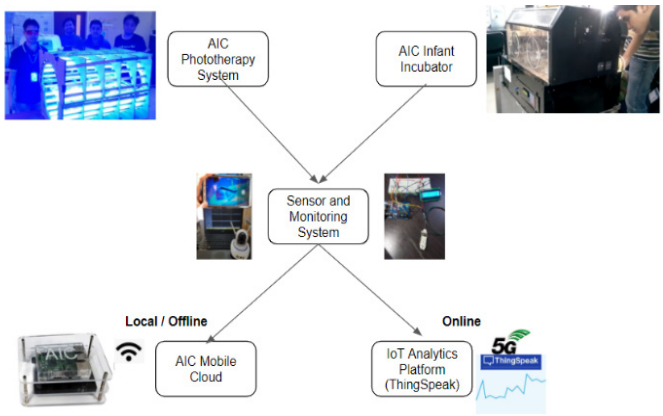


Figure 7: Smart LPLS as part of the envisioned Smart Nursing Station

We foresee this system to be part of a Smart Nursing Station, which diagram is in Figure 7, wherein a visual and auditory monitoring system is implemented to remotely oversee infants from the nurse station. The cameras will capture image and recordings of the infant that will serve as logs and be written in baby's medical records. It also sends alerts and data to the medical doctor or staff if there are any updates. Medical records and images of patients can be easily archived and retrieved if stored locally in the Near Cloud. Having the patient's data in the cloud also promotes interoperability and seamless transfer of data among the various stakeholders and speeds up healthcare delivery. This therefore closes the Medical Data Loop and promotes 5G and mobile cloud architectures in academic and business settings as well as for applications in sustainable and resilient communities [16].

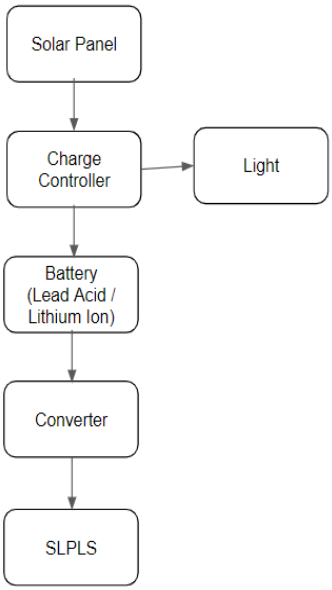


Figure 8: Off grid setup for Smart LPLS

In our previous study, we were able to run the system for 10 hours powered by two 50-ampere-hour commercial lead acid car batteries that were pre-charged by two 50-watt solar panels [1]. In this study, we continue to explore ways to make the system energy-efficient to be easily supported by solar powering. Ultimately, we hope to deploy the Smart LPLS in remote areas using the set-up shown in Figure 8.

3. Review of Related Literature

Total body phototherapy exposure (TBPE) is a new and effective technique to avoid the risks of invasive exchange blood transfusion (EBT) in neonates with jaundice. TBPE consists of top- and bottom-mounted lights to provide whole body phototherapy light exposure. Ogah Emeka Onwe and his research team in 2019 used an imported phototherapy light unit that has an average spectral irradiance of 34 µW / cm^2 / nm and 50 µW/cm^2/nm in the top and bottom lights, respectively, and a peak wavelength of 455 - 470 nm. It was reported that out of 82 severely jaundiced cases, all TBPE cases were successfully discharged except for two mortalities due to related exchange blood transfusion complications [17].

In general, the same authors found that TBPE is an efficient and a good non-invasive alternative to EBT intervention [17]. It is also affordable for resource-constrained settings. But some limitations were encountered during the study. The frequent occurrences of unannounced power failures at the hospital facility might have adversely affected the overall treatment time. Also, the identification of qualified subjects for inclusion in the study was limited due to poor record keeping.

In determining jaundice condition in infants, the practice of visual assessment is quite subjective and needs a lot of experience from the medical practitioner to determine severity of jaundice condition, as stated in The Journal of Pediatrics by Arieh Riskin and his co-researchers [18]. Thus, medical practitioners can use devices which can measure the levels of jaundice in infants without blood analysis. Infants under treatment can still have increased bilirubin levels which is very dangerous when not recognized immediately. On the other hand, infants with decreased bilirubin levels can only be verified upon examining the blood. In the absence of total bilirubin serum (TBS) test and hematology analyzer, a database of infant's yellowish skin color across varied skin tones may be helpful in the visual assessment of the patients' condition.

Methods of digitally sensing color pigment from reflected light may offer a simple and objective way of determining the existence or severity of jaundice condition during visual inspection. Current procedure of detecting jaundice in infants, such as newborn screening (NBS) test, is done by physicians through visual inspection and blood analysis to measure the bilirubin level. The study of Hafizon Baharuddin and his group in 2010 presented an infrared sensor that detects bile pigments, but blood extraction is still needed to assess the bilirubin level [19].

A method for measuring jaundice using non-contact optical devices at the conjunctiva of human subjects was described by Nabarun Polley and his colleagues in 2015 [20]. The light from the source is transmitted through the six excitation fibers of the excitation arm and incident on the subject (conjunctiva). The diffused light is collected by the detection fiber and transmitted through the detection arm to the spectrograph. The spectral response corresponding to the conjunctiva is processed and generated in the laptop computer as shown in Figure 9 below.

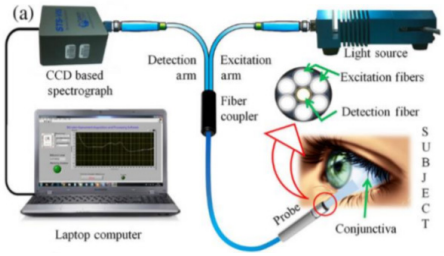


Figure 9: Use of non-contact optical devices at the conjunctiva of human subject

In the figure below, the comparative spectral response of a normal volunteer and a jaundice patient using the wavelength calibration of their setup has been established with a He-Ne laser (632.8 nm), fluorescent lamp, and emission/absorption of a number of dyes including aqueous bilirubin solution are shown. A distinct difference in the spectral appearance is visible; the contribution of yellow pigment deposited in the conjunctiva of the jaundice patients is higher compared to the normal volunteer. An absorption spectrum of aqueous bilirubin solution is also included in Figure 10 as reference.

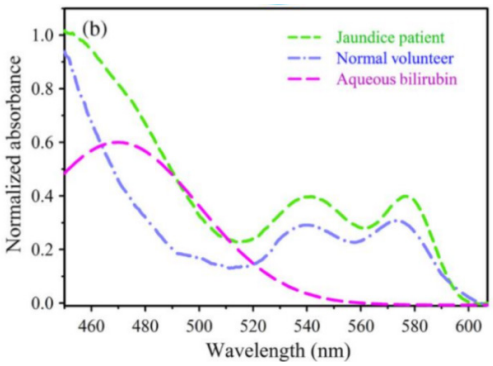


Figure 10: The comparative spectral response of conjunctiva of a normal volunteer and jaundice patient

They have also developed a non-invasive and practical device for measurement of bilirubin levels. While serum bilirubin measurements are still required for precise diagnosis, the proposed device shows the potential that reduce frequent blood sampling. This procedure may be difficult to use knowing that newborns sleep most of the time and their eyes are small and sensitive.

4. Results and Discussion

This is a design and engineering study with no infants or humans involved, with no cross-reference with real jaundice patients and no photos during treatment and corresponding bilirubin measurements were taken due to ethics concerns and time constraints. This study was partially funded by Ateneo de Manila University, where the authors are affiliated with, so there is no conflict of interest to be declared.

4.1. Increased Surface Exposure

The main component of the phototherapy treatment is the blue light which is provided by the blue LEDs. Using LEDs also reduces the risks of complications such as progressive skin damage brought about by conventional ultraviolet light used by standard phototherapy light treatments. To ensure the efficiency and effectiveness of the device, light intensity, the distance from the subject of phototherapy, the area of exposure, the duration of the treatment and the amount of bilirubin present in the body of the subject must be taken into consideration.

The blue light source in the Smart LPLS is coming from the top-mounted spotlights and bottom-mounted tube-type LEDs. The Smart LPLS has a wavelength that peaks at 253.99 nm and has a full width at half maximum (FWHM) range of 439.66 nm to 467.64 nm. Its irradiance was measured from an oval grid with a length of 60 cm and width of 40 cm from 35 different data points. The average distance of the measuring device (RS Pro) from the phototherapy light mimics the distance of the infant patient from the phototherapy light which is about 30 cm. The measured irradiance is 34 $\mu w/cm^2/nm$, which is also above the minimum required irradiance of 30 $\mu w/cm^2/nm$.

The additional set of phototherapy lights installed under the transparent bassinet also acts as the frame and stand of the whole system. The existence of bottom-mounted lights provides additional irradiation that may shorten treatment time.

4.2. Monitoring of Neonatal Jaundice Patient

One of the significant features of the Smart LPLS is the color sensor to monitor the treatment progress of the infant with jaundice based on the intensity of skin yellowness.

We are convinced in the importance of having a patient monitoring process when the phototherapy light system is deployed in remote areas without reagents and hematology analyzer. The cost of transcutaneous bilirubinometer (TcB) is similarly prohibitive making it difficult to find in remote areas.

This paper presents the use of inexpensive electronic sensors and devices that can detect even small color changes in the infant's skin by image processing. A low-cost method of skin tone simulation that is digitally generated and classified to detect change in yellow pigments can also address the restrictive financial resources in the rural areas. The sample size is limited only to the number of images we have conducted in our initial tests. Though the tests exhibit promising results, the data gathered are patient specific since we covered only three colors of skin.

4.2.1. Profiling the Sensors

For the non-invasive jaundice monitoring feature of the Smart LPLS, we utilized HD web camera and Raspberry Pi, Arduino, and color sensors, and RGB phone app to monitor patients non-invasively. We implemented the yellow detection feature by quantifying the reading of different sensors based on their profile.

4.2.2. Creation of Yellow Swatches

Due to time and ethical constraints, especially during this COVID-19 pandemic, yellow level detection tests using different sensors were done using printed yellow swatches, not using human subjects. We created a standard swatch of yellow that varies from 0% to 100% with increments of 10%. We also tested the swatches with plastic film to compare it with different opacities. We are envisioning that doctors can use this plastic film or transparency swatches by putting it on a non-jaundice skin (with similar tone as the infant's skin) and comparing it with the

level of yellowing in a jaundiced infant's skin. The jaundiced infant's condition can be initially verified through blood test and correlate with the increments of yellowness represented in the swatches. The image or data can then be evaluated by the supervising doctor remotely or check the history of treatment of the baby.

RGB color picker was used to make yellow swatches that will be detected by the sensor and the camera. It is based on the color theory that all visible colors can be made using the additive primary colors of red, green, and blue. Hue (H), saturation (S), and value (V) are the main color properties that allow us to distinguish between different colors.

Hue is described by the dominant wavelength and is the first item we refer to when adding in the three components of a color and it refers to a color having full saturation. value refers to the lightness or darkness of a color. Value on the other hand indicates the quantity of light reflected. Saturation lastly defines the brilliance and intensity of a color [21]. In color theory, a tint is a mixture of a color with white, which reduces darkness, while a shade is a mixture with black, which increases darkness. Both processes affect the resulting color mixture's relative lightness [22].

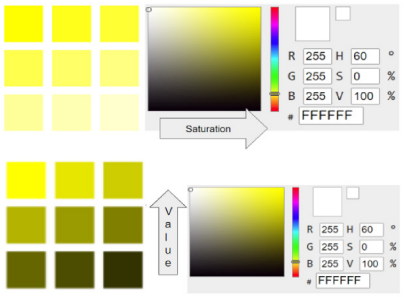


Figure 11: Different levels of Saturation (S) and Value (V) to obtain yellow swatches

Changing the S while maintaining H and V in constant values will give us different saturation levels of yellow. Also, shades of yellow in RGB have R and G values at 255. As the transparency decreases, B value increases from 0 to 255. At 100% transparency, B is at its maximum value at 255, while 0% transparency is at minimum value at 0.

4.2.3. TCS3200/TCS230 RGB Color Sensor

In building the intelligent system, codes were developed to be used for the microcontrollers, sensors, and actuators. Calibration and testing of the system were also conducted to ensure the efficiency of the system. To jumpstart the tests using a detector to gauge the yellowness level of the skin, we used the TCS3200 / TCS230 RGB color sensor that has an array of photodiodes with 4 different filters and is mostly used for color recognition projects and can detect a wide variety of colors based on wavelength [23]. By selectively choosing the photodiode filter's readings, we were able to detect the intensity of the yellow and other different colors. This sensor has a current-to-frequency converter which converts its readings into a square wave with frequency that is proportional to the light intensity of the chosen color [23].

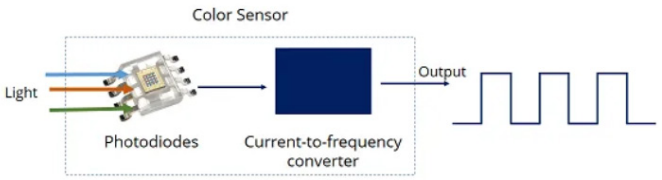


Figure 12: TCS3200 / TCS230 color sensor [23]

The sensor was connected to the Arduino and was able to receive serial data RGB values ranging from 0 - 255. This sensor can accurately reproduce colors which were monitored by getting output from the Arduino. Processing3 IDE was used to verify by sight the similarity of the actual color and sensed color by taking in the serial data from the sensors, and visualize the color seen by the device by using the RGB value attained, and displaying it on a computer screen.

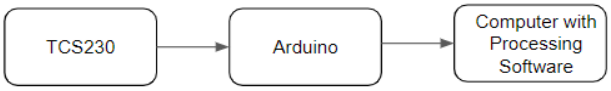


Figure 13: Block diagram for basic TCS3200 / TCS230 sensor test

Initially, we used a clear filter and set the control pins S2 and S3 to HIGH and LOW, respectively. We calibrated and enclosed the color sensor in a box to prevent ambient light from contaminating the sensor and concentrate the light reflected to the sensor.

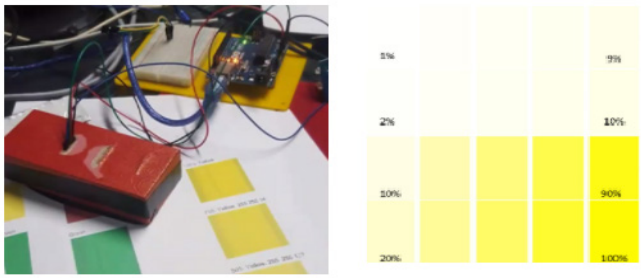


Figure 14: Enclosed TCS3200 / TCS230 and color swatches

Running the serial monitor will provide values that are dependent on the selected frequency-scaling and the condition of ambient light. The R, G, and B values differ due to the different sensitivity of each photodiode type, as seen in *Figure 15*. To represent the detected colors with the RGB Model with values from 0 to 255, we will use the *map()* function to map or convert the readings to values from 0 to 255.

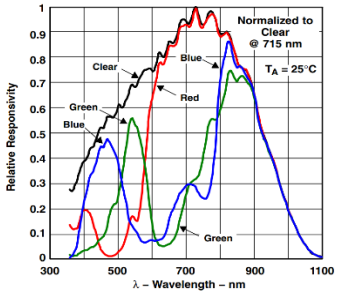


Figure 15: TCS3200 / TCS230 spectral responsivity diagram

We profiled and checked the sensor to set baseline data. The graph in Figure 16 shows that the sensor can detect colors normalized to different values. The sensor is more responsive to more colors.

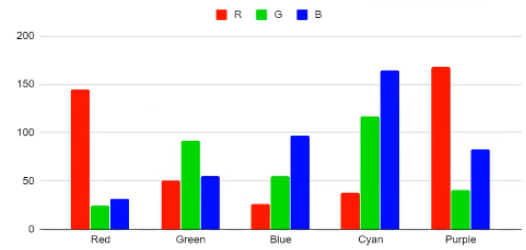


Figure 16: TCS3200 / TCS230 color profiling

We interpreted the theoretical RGB values for different shades of yellow as seen in Figure 17. Both R and G values are at 255 while B is at 255 if the color is at 0% opacity or 100% transparency. Meanwhile, B is at 0 when the yellow swatch is at 0% transparency. Once transparency increases, B increases as well, at a linear rate. Using this information, we compared the graph obtained by the blue values of the sensor, to the true-blue values of yellow swatches.

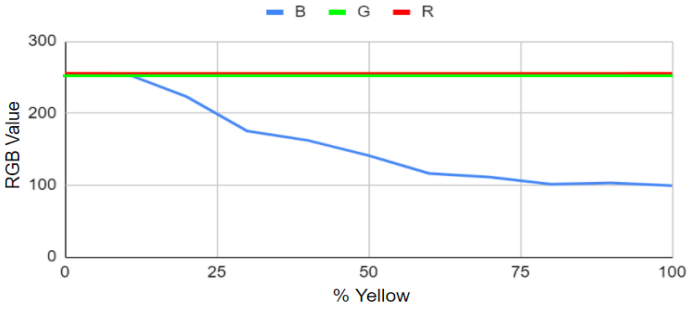


Figure 17: Theoretical and expected RGB values with different yellow values

As expected, a downward curve is shown in Figure 18 with 0% to 60% yellow of sensor values in line with the theoretical values, but it started to deviate from the theoretical value at around 60% yellow. We found that the sensor was able to accurately determine the B values of the swatches ranging from 40% to 100% transparency. The yellow pigment absorbs blue light and it allows red and green light to pass through or reflect from its surface.

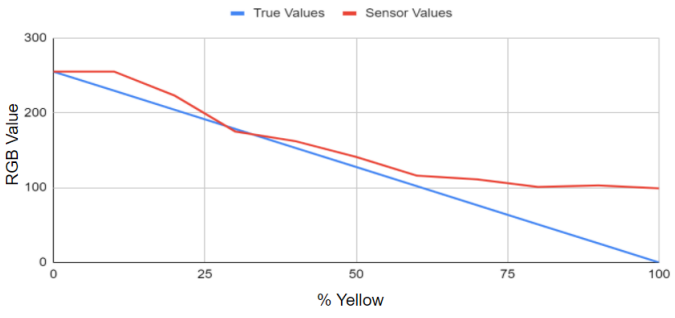


Figure 18: Theoretical vs sensor values of B values using without color filter

We also applied various color filters to the TCS3200 sensor and saw any changes or improvements in performance. In Figure 19, the experimental setup using the color filter of the sensor was shown. The built in LED of the sensor as the light source will shine light in the yellow swatches. Light will be bounced off the color filter that will be detected by the TCS3200 / TCS230 sensor which will generate a pulse width modulation data will proceed to the Arduino and be sent in the serial monitor.

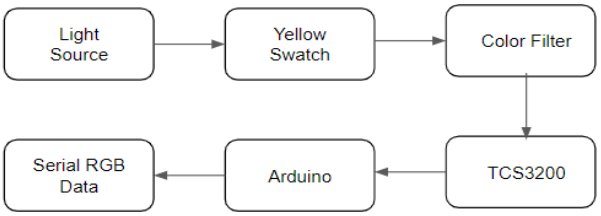


Figure 19: Experimental setup using TCS3200 / TCS230 sensor with filter

In Figure 20, a blue filter was placed in between the swatches and the sensor. For the blue level to be detected by the photodiode, we set the control pins S2 and S3 to LOW and HIGH, respectively. Green and red are not in constant 255 because of the filter and blue, as expected, the graph also shows a downward curve. It can be observed that blue dips in accuracy past 30% and none of the values follow the ideal relationship between blue values and yellow percentage.

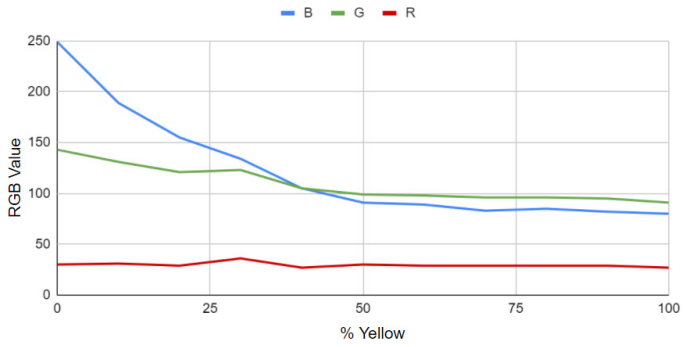


Figure 20: TCS3200 / TCS230 sensor using blue filter

None of the values are constant, but blue seems to be decreasing in a similar curve as it did with the other test. Looking at the results from the blue filter and no filter tests, blue values from the sensor seem close to the true values from 0% - 60%.

4.2.4. ISL29125 RGB Color Sensor with IR Filter

We also conducted tests and determined the performance of the ISL29125 sensor without filters and compared it to the true RGB values and each other. ISL29125 is a low power, high sensitivity, RGB color light sensor with an I2C interface and operates at 3.3V TTL and 56 uA typical supply. Its state-of-the-art photodiode array provides an accurate RGB spectral response and excellent light source to light source variation. It has integrated IR filter and compensation and outputs the actual light intensity with analog-to-digital converter and is designed to reject IR in light sources that allows the device to operate from well-lit to dark rooms. All the features of the device are controlled by the registers. The device is designed for operation under dark glass cover which significantly attenuates visible light and passes the infrared light without much attenuation. The device has an on-chip passive optical filter designed to block or reject most of the

incident infrared. This sensor is often used in ambient light color detection and / or correction [24].

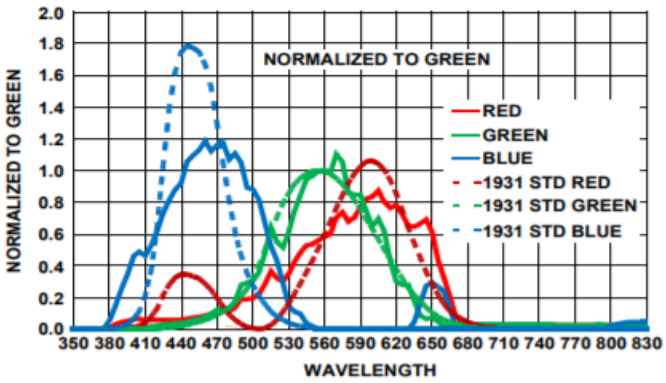


Figure 21: ISL29125 responsivity [24]

Housing for the sensor was created to keep out any ambient light from interfering with the received data. Using the ISL29125 with I2C interface can be both an advantage and disadvantage as it operates at 3.3V TTL and a logic converter is needed if Arduino is used since the datasheet specifies 4V as absolute max voltage while using less pins. An LED in series with a 510 Ohm resistor was used because there is no built-in light for the sensor.

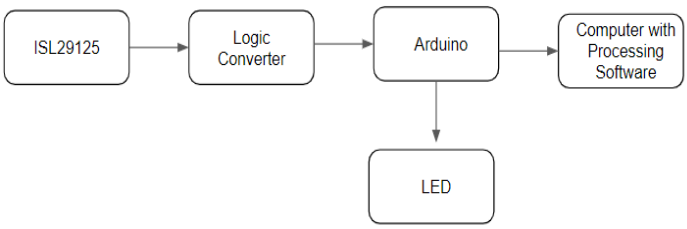


Figure 22: Block diagram for ISL29125 color sensor test

The sensor has three configurable settings. At CONFIG1, mode can be picked that determines what colors does the sensor samples, light intensity range from 375 lux to 10,000 lux depending on lighting condition, choose between 12 or 16 bit ADC precision depending on speed and precision, and sets the behavior of the interrupt pin if to be used as an input that triggers sensor sampling. CONFIG2, on the other hand, provides the option to set the level and range of active infrared compensation and lastly CONFIG3 that sends an interrupt to the Arduino once RGB values reach a certain threshold. In this test, we used the default configuration by enabling all the RGB, set the light intensity range to 10,000 lux, 16-bit ADC, high IR compensation on the lower range, and no interrupts.

We also profiled and checked the sensor to set baseline data. The graph in *Figure 23* shows that the ISL29125 sensor can detect colors normalized to different values. The sensor has slower deviation to colors as compared to the TCS3200.

The ISL29125 was used in determining the RGB values in different yellow swatches and it shows in Figure 24 that Red is constant at 255. Green, on the other hand, showed a downward trend from 232 at 25% yellow to 184 at 100% yellow. Blue, as expected, followed a downward trend as well from 161 at 25% to 63 at 100% yellow.

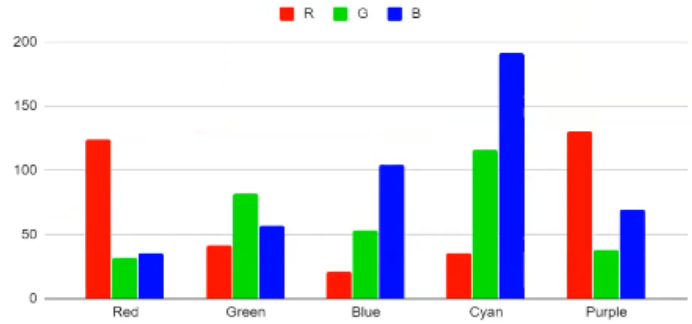


Figure 23: ISL29125 color profiling

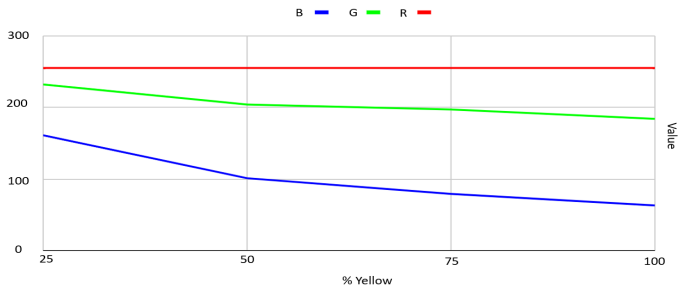


Figure 24: Test using ISL29125 sensor

Instead of using a white LED to illuminate the subject or surface, we used a red LED to test the reflectance of the surface for a specific color. In theory, red should reflect some, if not all, the red LED's light and sensor readings should be relatively higher compared to those that absorb instead of reflecting. This was seen in the data where the sensor read Red from colors where the red values were maxed out.

As seen in Tables 2 and 3, white, red, yellow, and purple swatches reflected red as expected. Values correspond to their measured RGB values and by looking at their full measured Red data of the swatches with red illuminant, white has the highest red value measured tied with yellow, then followed by purple, and lastly red. This order is also seen when measuring the colors using a white illuminant where White has the highest red value with red reading the lowest. Whether a white or red illuminant is used, the measured values are proportional in that their order from 'most red' to 'least red' is the same regardless of the illuminant.

Table 2: ISL29125 with red LED illuminant

Swatch Color	Red Value
White (#FFFFFF)	68
Red (#FF0000)	44
Yellow (#FFFF00)	66
Purple (#FF00FF)	58
Black (#000000)	0
Cyan (#00FFFF)	0
Green (#00FF00)	0
Blue (#0000FF)	0

Table 3: ISL29125 with white LED illuminant

Swatch Color	Red Value
White (#FFFFFF)	255
Red (#FF0000)	124
Yellow (#FFFF00)	255
Purple(#FF00FF)	130

The other colors had 0 color red reflected as detected by the sensor because by theory, they did not reflect red. This was done only with one red LED and compared to the white LED used in the earlier tests. Since the highest measured value is only 68 for red illuminant as to 255 of the white illuminants, the red LED might be too dim compared to the white illuminant. For further tests, it is recommended to install more LEDs for illumination since its dimness may not reflect the whole swatch or sample picture. It may be possible that the other colors do not reflect red but realistically they still could reflect a little red due to the color accuracy of the printers. Other colors may also be tried as well such as the suggested pulsing of Red and Green for Yellow. Proper calibration is also needed as the sensor's datasheet specifies very specific methods and processes to calibrate.

We also conducted an IR compensation test using the ISL29125 sensor which provides a programmable active IR compensation which allows fine tuning of residual infrared components from the output, which allows optimizing the measurement variation between differing IR-content light sources. There are two ranges set by B7:0 in the compensation register. In the library they are labeled as Offset and No Offset. B5:0 configures the specific value within the ranges. The preset values are HIGH, MED, LOW, but any 6-bit value can be set as the compensation. This combined with the offset gives 128 possible values for the active IR compensation. *Figure 25* shows a typical system measure for both IR Comp Adjust and IR Comp Offset.

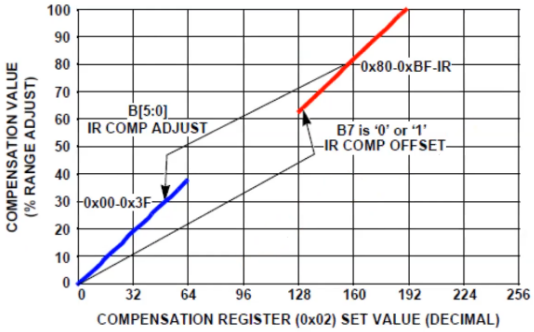


Figure 25: IR compensation set [24]

Using yellow swatch in this IR compensation test, Red and Blue have constant values as seen in Figure 26. When testing on colors, only the green color varied. With the highest IR compensation, the value of green is at its lowest. On the other hand, if there is no IR compensation set, green is at its highest.

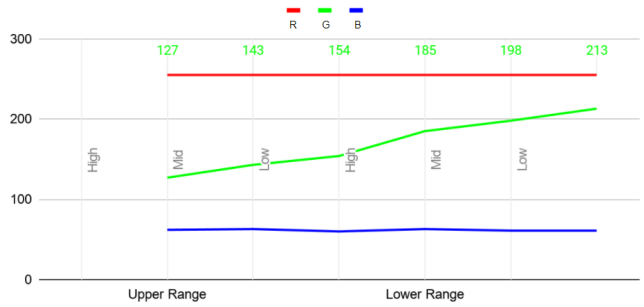


Figure 26: IR compensation using ISL29125 sensor

To test the difference on how the IR compensation works, the sensor was used on the same swatch while changing the IR modes between measurements. The measured values are seen in Figure 27. Since this printed color swatch was used, the most accurate value is the one with no offset / IR compensation.



Figure 27: IR compensation using ISL29125 sensor

In these series of tests using sensors, both TCS3200 and ISL29125 perform similarly and the deciding factor would be whether configuring the sensor is needed. The power draw of the ISL29125 may be considered as it can be set to standby / power down mode to consume much less power. Another consideration is the footprint of the two sensors, the TCS230 is bigger and has 4 LEDs mounted. From the documentation, the ISL29125 is designed for operation under dark glass cover which could be an option and the purpose of the IR configuration.

4.2.5. Web Camera

For yellow color detection using a camera, we obtained image samples for different yellow levels using enclosed camera set-up and gathered its RGB values and used the weighted sum to quantify color level. Using off-the-shelf web camera is a low-cost platform in detecting the yellow levels of NNJ among infants.

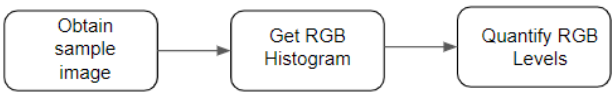


Figure 28: Flowchart for yellow color detection using camera

For this test, we used A4Tech PKS 730G (480p) Web Camera with 16MP camera sensor which supports up to 480p and with built-in LED. The camera was enclosed in a cup to prevent stray light from being detected by the camera. The camera could be connected to a laptop or low-cost Raspberry Pi computer via USB. The captured photo was then loaded to Processing software to

obtain the histogram of the image, generate a CSV file and quantify the R,G and B values using weighted average technique.



Figure 29: Test setup for yellow color detection using camera

Sample images from different levels of yellow opacity (0% most transparent; 100% most opaque) were obtained using the camera and the RGB values, using weighted average of the RGB histogram, were recorded as shown in *Figure 30*.

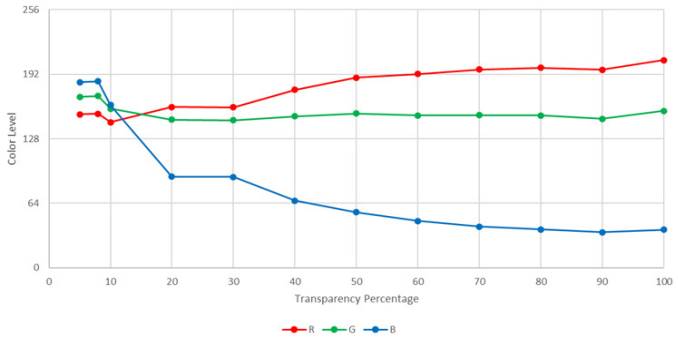
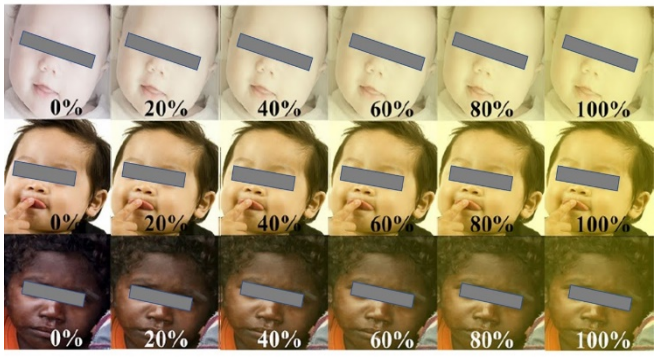


Figure 30: Different yellow levels for A4Tech PKS 730G

Theoretically, the red and green levels must remain constant and the blue level decreases as the yellow opacity level increases. From Figure 30, it could be observed that the red and green values started to stabilize at 50% yellow while values of blue followed a downward curve.

We expect fewer blue values as the blue color is absorbed by yellow, like how the phototherapy treatment works. To simulate the condition of a patient with NNJ, pictures of children with white, brown, and black skin tones were taken. The image used for the white skin tone swatch was from *pexels.com*, a free stock photo sharing website [25] while for the brown and black skin tone photo was from the photo collection of the author.



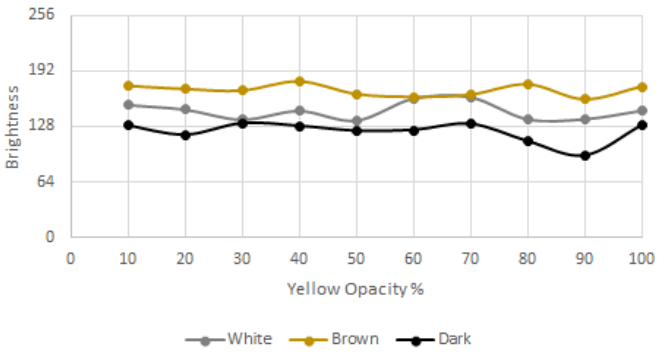


Figure 32: Red level for different baby skin types with yellow overlay

The yellow level corresponded to the opacity level of the yellow color. The swatches were built using Adobe Photoshop and were printed on a transparency sheet. The forehead area was chosen because face pictures were more available, and the said area had a strong correlation with serum bilirubin, as stated by Gwendoline Chimhini and her research collaborators [26].

In Figure 32, the brown skin type had a higher red level detected by the camera due to the brown color having red as the dominant color (brown RGB = 150, 75, 0). This test did not consider the reddening of the baby, particularly the white baby, due to blood or other sickness.

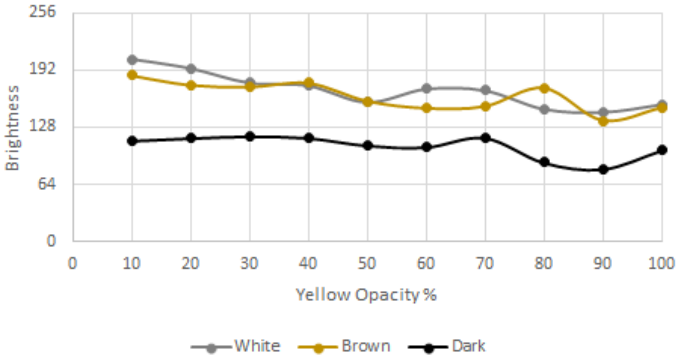


Figure 33: Blue level for different baby skin types with yellow overlay

In Figure 33, the blue levels detected for white and brown babies with yellow transparency overlaid were increasing as the yellowing of the baby decreased. This was due to the yellow color absorbing the blue. The decrease in yellow increased reflection of the blue level. However, for the black baby, no significant change in blue level was observed.

The improved electronic sensor and monitoring system complements the ability of doctors in observing and managing the condition of infants with NNJ and assists the doctors and patients in having a digital copy of medical records. In the future, we will explore and record various skin tones and nail colors of Filipino infants in photos as reference. The detection of the intensity of yellowness will be tested by placing different shades of yellow pigment over varied skin tones or nail colors.

4.2.6. Smartphone RGB Color Application

We also explored the use of Color Meter app, a simple color meter free mobile application that allows users to pick live colors and displays RGB color on the screen and the hexadecimal

(HTML) color code that is used in graphics and web applications that can detect changes in RGB values. We used a Samsung S9+ smartphone with $f/1.5$ and $f/2.4$ (Dual Aperture) 12-megapixel camera and to explore the RGB values at zero and 100% yellowness.

The changes in RGB values are detected upon overlay of different levels of yellowness (0% to 100% yellow) on varied skin tones represented by white-, brown- and dark-skinned photos of infants, as seen in *Figure 34*. The graph shows the different amount of reflectance of RGB colors upon overlay of zero percent yellow transparency and one hundred percent yellow transparency on three skin tones.

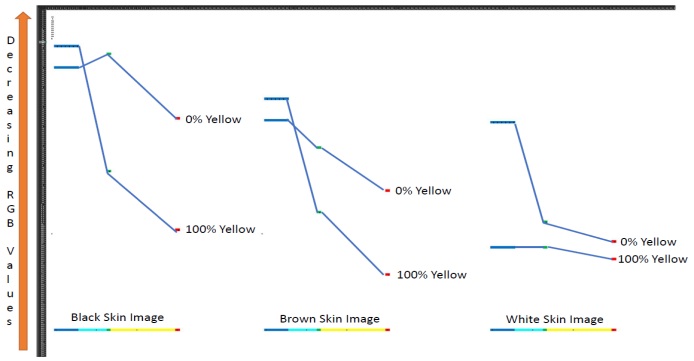


Figure 34: RGB values that correspond with zero percent and one hundred percent yellowness in three skin tones

Note that we flipped the graph by showing the lower values as you go up. In doing so, the behavior of the lines mimics the graph presented by Nabarun Polley and his team in 2015 on the absorption rate of colors in conjunctiva of infants with and without jaundice.

In summary, the color experimentation revealed the following results in Table 4 below.

Table 4: Changes of RGB values from zero to 100% yellow

Skin Tone	Blue Color Values	Red/Green Color Values
White	Decreased	Decreased
Brown	Decreased	Increased
Dark	Decreased	Increased

Zero and 100% yellowness show differences in scores of RGB. With white skin tones, all RGB scores went down in 100% yellowness indicating greater reflectance of light in jaundiced skin. In both brown and dark skin tones, Red and Green values increased while Blue score decreased when yellowness moved from zero to 100%. Thus, jaundiced babies with brown- and dark-skin tone tend to reflect Red and Green colors more than the non-jaundiced infants.

Varied percentages of yellowness in between zero and 100% bring about changes in the RGB scoring. Detection of smaller increments of yellowness will be further explored. We are also looking for a spectroscopic approach related to the study of Nabarun Polley and his team which will be reported soon.

4.3. Mobile or Near Cloud for Smart Nursing Station

The smart sensor and monitoring system of the Smart LPLS can be integrated with the Mobile or Near Cloud as part of the Smart Nursing Station for medical use cases. The main component of this Near Cloud System is the Raspberry Pi, a low-cost, credit card sized microcomputer that offers various interfaces. Raspbian, a Debian-based operating system, is burned to the micro SD card for the Raspberry Pi to function. For easy deployment, the system should be portable and have the necessary processing power for its essential functions.

Since content are cached in the Near Cloud node, the medical doctors and nurses as Mobile or Near Cloud clients can upload, download, or stream prepositioned health and medical data remotely in their own most convenient time using their Wi-Fi enabled devices. To observe security measures, administrators can identify users and set restrictions. Server-side encryption feature encrypts files stored on the server and files on remote storage. When encryption is enabled, all files are encrypted and decrypted by the software application and saved on the remote storage. Also, Wi-Fi Protected Access version 2 or WPA2, a method of securing your network with the use of the optional Pre-Shared Key authentication, is offered by the node. Time-based one-time passwords was also enabled for the system to add another layer of access security to the system.

This technology complements the off-grid setup of the Smart LPLS as it is readily deployable, works with or without internet connection, and can be powered by using a mobile power bank or DC adapter. It is of great value in remote health facilities for patient monitoring of select few doctors who work in barrios lacking in medical equipment and supplies, as featured by Juan Alfonso Leonardia and his co-proponents [27]. Its architecture features load-sharing and can be interconnected with other Near Cloud nodes via an inner wireless mesh network using B.A.T.M.A.N-adv routing protocol.

4.4. Improving Power Storage for Off-grid Deployment

Phototherapy treatment usually requires exposure of the infant patient for an extended period. However, deployment of a phototherapy unit in remote areas can present issues on power supply which is either intermittent or totally off grid. To address this problem, we designed the smart LPLS to be more energy-efficient, which makes provision of solar powering less costly and more feasible. We tested and compared the performance of lithium ion, motorcycle, and car batteries. The use of car and motorcycle batteries in powering a system in off grid deployment had been studied in a recent publication by Paul Cabacungan and his co-researchers [28].

In this paper, an experimentation on the discharging rate of the 12-volt lead-acid battery and 120 lithium-ion batteries (all of them with a lifespan of 3-5 years) was conducted using a seven-watt LED bulb. The lead-acid battery was connected to a 7-watt LED

bulb while the lithium-ion battery that was uniformly configured (Li-ion UC), i.e. with uniform number of battery cells in parallel, was attached to the same bulb with converter. A lithium-ion battery that was reconfigured (Li-ion RC), i.e., 45-30-45 batteries in parallel, used a charge controller instead of a converter. Results are shown in Table 5 below.

Table 5: Comparison of lead acid and lithium-ion batteries

	Ampacity	**Volume (sq.cm.)**	**Weight (kg.)**	**Duration of Discharging**
Lead Acid	50 AH	8840	15	26 hours
Li-ion UC	40 AH	3500	3	5 hours
Li-ion RC	40 AH	3500	3	17.75 hours

Results showed that lead-acid batteries took longer to discharge compared to lithium-ion. However, lithium-ion has its advantages in remote deployment - being twice smaller and 5 times lighter. Moreover, when batteries are discharged below their manufacturer-stated end-of-life discharge voltage, cells are permanently damaged, preventing it from ever being recharged. Lithium-ion batteries require low maintenance because each cell, once damaged, can be individually replaced without having to replace all the batteries in the system.

We have also done initial power calculations for a set of 10 conventional 60 cm LED strips with 36 LEDs each. 3 LEDs draw 20 milliamperes at 12 V to consume a total of 28.8 watts, about 70% less power consumption than the T5 LED. In using LED strips, an overall power consumption is estimated to decrease from 240 watts (SPLS) to 90 watts (SPLS off-grid), which already includes power usage of the charge controller, sensor, and monitoring system.

For future innovations, another prototype with top and bottom-mounted phototherapy lights that will operate on DC can be explored to eliminate the power consumed by the DC to AC converter and the T5 LED tubes' internal AC to DC converters. This prototype can use LED strips with transparent outer cover, which is expected to provide greater irradiance compared to T5 LED with translucent cover that limits light intensity.

5. Conclusion and Future Works

We presented an improved architecture and design for the current system, making the Smart LPLS a viable option for rural and underserved areas with limited resources to treat newborn patients with jaundice. The integration of skin color monitoring aids medical doctors by providing a non-invasive method of possible detection and monitoring of jaundice condition. Several approaches are being taken as we describe how we are developing a complementary system of transparencies that doctors can use in the field with photos to determine the severity of the yellowing and will aid in monitoring the progress of the treatment. We acknowledge the limitation of the current results on skin color monitoring, having tried the transparencies only on images with three specific kinds of skin color. We cannot claim a generalized conclusion yet, thus, we recommend that for future development, we can increase the sample size and cover a wider variety of skin colors. Also, aside from the usual placing of sensors on the forehead and chest, we explore putting it on other parts of the body such as nails, palm or sole.

The robust LED spotlights mounted on top and the additional T5 LED tube lights at the bottom offer more powerful and faster jaundice treatment due to greater irradiance. Its low power consumption and solar powering provision make it easily deployable even in remote off grid health systems. The Mobile Cloud System provides easy access to data which can supplement the patient's existing records.

The initial tests conducted in several patients exhibit results that are promising with treatment outcome and safety features comparable to commercial units available in the market today. However, we have yet to conduct further tests with actual human subjects, under the supervision of medical personnel to generalize results. To sum up, the Smart Low-cost Phototherapy Light System integrated with additional functions can still be made more energy-efficient, appropriately deployable in off-grid locations and yet maintain its affordable cost.

Acknowledgment

The prototypes built by Ateneo Innovation Center went under extensive research acceptance tests in public hospitals in Metro Manila by our collaborators – Dr. Vanessa Marie Calabia, Dr. Viel Bagunu, Dr. Ma. Lucila Perez, and Dr. Jeremie De Guzman. We thank them for their efforts and valuable feedback. We are grateful to our researchers, Mr. Alfonso Agustin, Mr. Alfonso Cuezon, Mr. Reymond Cao, Mr. Kerwin Caballas, Mr. Lawrence Ibarrientos, Mr. Lemuel Emman Tan and the interns and OJTs who worked in th research center for the past five years. In their capacities, they gave their valuable assistance in the different stages of fabricating the prototypes. We are indebted to the University Research Council (URC) of the Ateneo de Manila University for granting financial support to come up with this paper and to explore further developments of the Smart LPLS. Our gratitude goes to the Ateneo Innovation Center for serving as a hub for the phototherapy light system developments since its initial conceptualization.

References

[1]. P. Cabacungan, C. Oppus, J. De Guzman, G. Tangonan, I. Culaba and N. Cabacungan, "Intelligent Sensors and Monitoring System for Low-cost Phototherapy Light for Jaundice Treatment," 2019 International Symposium on Multimedia and Communication Technology (ISMAC), Quezon City, Philippines, 1-6, August 2019, doi:10.1109/ISMAC.2019.8836133.

[2]. V. Calabia, M. Perez, G. Tangonan, P. Cabacungan, I. Culaba, and J. De Guzman. "Bilirubin lowering effect and safety of a prototype low cost blue light emitting diode (LED) phototherapy device in the treatment of indirect hyperbilirubinemia among healthy term infants in a tertiary government hospital: a pilot study," arXiv preprint arXiv:2008.08875, August 2020.

[3]. V. Bagunu and M. Perez, "Comparative study of Prototype Low-Cost Light Emitting Diode Phototherapy Device versus Conventional Fluorescent Phototherapy in the Treatment of Indirect Hyperbilirubinemia among Term Infants in a Tertiary Government Hospital," Unpublished, August 2018.

[4]. C. Henny-Harry and H. Trotman, "Epidemiology of neonatal jaundice at the University Hospital of the West Indies," The West Indian Medical Journal,

61(1), 37-42, January 2012.
[5]. P. Kumar, D. Chawla, and A. Deorari, "Light-emitting diode phototherapy for unconjugated hyperbilirubinemia in neonates," Cochrane Database of Systematic Reviews, **12**(7969), December 2011, doi:0.1002/14651858.CD007969.pub2.
[6]. S. Moerschel, L. Cianciaruso, and L. Tracy, "A practical approach to neonatal jaundice," American Family Physician, **77**(9), 1255-1262, May 2008.
[7]. M. Fargo, S. Grogan, and A. Saguil, "Evaluation of Jaundice in Adults," American Family Physician, **95**(3), February 2017.
[8]. E. Gurley, A. Halder, P. Streatfield, H. Sazzad, T. Nurul Huda, M. Jahangir Hossain, and S. Luby, "Estimating the burden of maternal and neonatal deaths associated with jaundice in Bangladesh: possible role of hepatitis E infection," American Journal of Public Health, **102**(12), 2248-2254, December 2012, doi:10.2105/AJPH.2012.300749.
[9]. Iowa Department of Public Health, "Managing Newborn Hyperbilirubinemia and Preventing Kernicterus Progeny,"http://www.idph.state.ia.us/hpcdp/common/pdf/perinatal_newsletters/progeny_june2013.pdf. Accessed: August 2020
[10]. World Health Organization International, "Bilirubinometer - Core medical equipment - Information," https://www.who.int/medical_devices/innovation/bilirubinometer.pdf. Accessed: August 2020.
[11]. PhilHealth, "Agency's Mandate And Functions," https://www.philhealth.gov.ph/about_us/mandate.html#gsc.tab=0. Accessed: August 2020.
[12]. H. Vreman, R. Wong, and D. Stevenson, "Phototherapy: current methods and future directions," Seminars Perinat, **28**, 26-33, October 2004, doi: 10.1053/j.semperi.2004.09.003.
[13]. J. dela Cruz, N. Libatique and G. Tangonan, "Design of a Disaster Information System using Mobile Cloud Wireless Mesh with Delay Tolerant Network," 2019 IEEE Global Humanitarian Technology Conference (GHTC), Seattle, WA, USA, 1-8, October 2019, doi: 10.1109/GHTC46095.2019.9033450.
[14]. N. Mercado, Design and Demonstration of Near Cloud System for Digital Education and Disaster Resiliency, MS ECE thesis, Electronics, Computer and Communications Engineering, Ateneo de Manila University, Quezon City, Philippines, May 2020.
[15]. J. Mamaradlo, Design and Demonstration of a Mobile Cloud System for Smart Transportation System Use Case, MS ECE thesis, Electronics, Computer and Communications Engineering, Ateneo de Manila University, Quezon City, Philippines, May 2020.
[16]. J. Mamaradlo, N. Mercado, N. Libatique, G. Tangonan, R. Solis, V. Rodriguez, B. Dingel, C. Pineda, and C. Lopez, "University campus 5G testbed and use case deployments in the Philippines," SPIE Proceedings, Broadband Access Communication Technologies XIV, **11307**, January 2020, doi:3. 10.1117/12.2549903 2020.
[17]. O. Onwe, O. Ezeanosike, C. Obu, O. Daniyan, and H. Amadi, "Economic cost savings with the use of total body phototherapy for the treatment of severe neonatal jaundice in Nigeria," Journal of Pediatrics and Neonatal Care, **9**(6), December 2019, doi: 10.15406/jpnc.2019.09.00401.
[18]. A. Riskin, A. Tamir, A. Kugelman, M. Hemo, and D. Bader, "Is Visual Assessment of Jaundice Reliable as a Screening Tool to Detect Significant Neonatal Hyperbilirubinemia?," The Journal of Pediatrics, January 2008, doi: 10.1016/j.jpeds.2007.11.003
[19]. H. Baharuddin, M. Sulong, A. Joret, T. Rahman, and N. Ismail, "Bile Pigments Detection via IR Sensor," Proceedings of EnCon2010 3rd Engineering Conference on Advancement in Mechanical and Manufacturing for Sustainable Environment, Kuching, Sarawak, Malaysia, April 2010.
[20]. N. Polley, S. Saha, S. Singh, A. Adhikari, S. Das, B. Choudhury, and S. Pal, "Development and optimization of a noncontact optical device for online monitoring of jaundice in human subjects," Journal of Biomedical Optics, **20**(6), June 2015, doi: 067001
[21]. Learn Leight Cotnoir, "Hue, Value, Saturation," http://learn.leighcotnoir.com/artspeak/elements-color/hue-value-saturation/. Accessed: August 2020
[22]. P. Mollica, Color Theory: An essential guide to color-from basic principles to practical applications (Artist's Library), Walter Foster Publishing, 17, January 2013.
[23]. Random Nerd Tutorials, "Guide for TCS230/TCS3200 Color Sensor with Arduino," https://randomnerdtutorials.com/arduino-color-sensor-tcs230-tcs3200/. Accessed: August 2020.
[24]. Renesas Electronics, "ISL29125 | Light-to-Digital Sensors," https://www.renesas.com/us/en/products/sensors/ambient-light-sensors/light-to-digital-sensors/device/ISL29125.html. Accessed: August 2020.
[25]. Pexels.com, "Photo of Couple with Baby Sitting," https://www.pexels.com/photo/photo-of-couple-with-a-baby-sitting-3995914/. Accessed: August 2020.
[26]. G. Chimhini, S. Chimhuya, and V. Chikwasha, "Evaluation of transcutaneous bilirubinometer (DRAEGER JM 103) use in Zimbabwean newborn babies," Maternal Health, Neonatology and Perinatology, **4**(1), April 2018.
[27]. J. Leonardia, H. Prytherch, K. Ronquillo, R. Nodora and A. Ruppel, "Assessment of factors influencing retention in the Philippine National Rural Physician Deployment Program," BMC Health Services Research, **12**(411), November 2012.
[28]. P. Cabacungan, G. Tangonan, and N. Cabacungan, "Water - Electricity - Light System (WELS): Technology Innovations," 2020 International Journal of Recent Technology and Engineering (IJRTE), **8**(6), 3061-3068, March 2020, doi: 10.35940/ijrte.F8103.038620

ASTES

Advances in Science, Technology and Engineering Systems Journal Vol. 5, No. 5, 1247-1260 (2020)

www.astesj.com

Special Issue on Economic Impact of COVID-19 on Companies & Consumers

ASTESJ

ISSN: 2415-6698

Resilience Assessment of System Process Through Fuzzy Logic: Case of COVID-19 Context

Saloua Said[*,1], Hafida Bouloiz[1], Maryam Gallab[2]

[1]*National School of Applied Sciences (ENSA), Systems Engineering and Decision Support Laboratory (LISAD), IBN ZOHR University, Avenue Tamesoult, Agadir, BP 80000, Morocco*

[2]*Engineers' Mohammadia School (EMI), LERMA, Mohammed V University, Avenue Ibn Sina, Agdal, Rabat, BP 765, Morocco*

ARTICLE INFO

Article history:
Received: 08 September, 2020
Accepted: 05 October, 2020
Online: 24 October, 2020

Keywords:
Resilience assessment
Process
Fuzzy logic
3R process
COVID-19

ABSTRACT

The present work is undertaken as part of research studies aiming to provide sociotechnical systems with a decision-making tool that supports them in assessing the resilience of their processes. The ultimate objective is to fix the identified imperfections in order to steadily gain strength and effectiveness to cope with new and existing threats and challenges. In that respect, this paper presents a framework called 3R process whose goal is to calculate the resilience score for a process based on several parameters and grade it on the resilience scale. In order to achieve this, a fuzzy model has been put in place and graphic user interfaces have been designed so that the 3R process becomes an integral part of daily working practices. Finally, a real case company example in the context of COVID-19 is exposed towards putting into practice the proposed model.

1. Introduction

In an increasingly uncertain and volatile world, sociotechnical systems, which are complex systems incorporating technical (machines and technology that provide an authentic link between the user input and the system's output) and social (people and society) systems that both have interactions between them, and those interactions are a key factor in the success or failure of system performance [1], are bending over backwards to become more resilient in order to be able to react to change as quickly as possible and to treat challenges and mistakes as a learning opportunity. An obvious case in point is the Nokia organization. This company, at one point, had 32% of the global market share in smartphones and mobile phones [2]. However, as it is well known, Nokia fell from grace with respect to the mobile phones market. They misread the North American market and they did not respond correctly when Apple and Samsung introduced new products and it took them too long to catch up. Eventually, they had to sell their mobile phone business to Microsoft, and effectively had to exit the mobile phone market, which they dominated only a few years earlier. Nevertheless, what makes Nokia such an interesting case of resilient organization is that despite the fact that Nokia made a mistake, it has been putting back together an organization. They refocused on their core transmission on business, they have been thinking how to position their navigational services and connecting with other organizations to produce new software, new kinds of handsets. The organization did not fall apart and was able to remake itself. In fact, their stock price, from the time they sold the business to Microsoft to recently, doubled. Indeed, what is important for every system is to develop resilience capabilities such as the ability to sense what is happening out in its environment and to compare that with what is done inside the organization, and, as necessary make the changes [3]. The question now being asked is how a system can assess its own resilience level so it can take stock of its strengths and weaknesses, threats and opportunities in terms of dealing with disturbances and returning to normal function.

In fact, several attempts have been made to find new approaches and frameworks that help in the resilience assessment. Amongst these, there are methods established to evaluate resilience of critical infrastructures, such as defining a generalized index that serves for quantifying the resilience under various scenarios [4], or designing a quantitative method to assess distinct elements in a critical infrastructure system [5].

Furthermore, different frameworks were proposed for the assessment of supply chain resilience, for example, elaborating an assessment model in order to measure organizational, business and labor resilience performance of supply chain [6], or developing a

[*]Corresponding Author: Saloua SAID, National School of Applied Sciences, IBN ZOHR University, Avenue Tamesoult, BP 80000, Agadir, Morocco, +212 623407567, saloua.said.5@gmail.com

framework that integrates the concepts of resilience with risk management techniques in order to understand how a supply chain reacts to disruptions as a function of time [7].

Idem for urban communities as establishing a methodology for evaluating the earthquake resilience [8], or putting into place a workbook that helps urban areas incorporate resilience thinking into their planning practice [9], and so forth.

Moreover, measuring and quantifying resilience has proved challenging and research works in this field are not so numerous. However, some researchers have sought to contribute to fill this gap by developing methods aimed at calculating resilience. For example, we can find quantitative models explaining how to compute resilience of manufacturing [10] or nuclear power [11] plants, physical networks [12], mass railway transportation [13], and the list goes on.

In this same perspective, the 3R process dedicated to assigning a resilience level to sociotechnical system processes is described in this paper. This framework is based on the resilience scale [14], a scoring system, which is composed of five echelons: 0.Unconscious (Processes belonging to this category have no resilience processes associated with them), 1.Informed (These processes are warned of resilience without any elaborated resilience processes), 2.Aspiring (These processes are beginners and try to set up resilience processes), 3.Progressing (These processes overcome less serious disruptions within a reasonable time. However, the consequences can be more devastating in serious situations), 4.Expert (For this kind of processes, the anticipated situations are perfectly manageable. As per the unforeseen situations, they try to adapt to changes), and which aims to assess the level of resilience of a given process. The present work will go beyond this qualitative description to find out how this scale can be used by a sociotechnical system in order to assess the resilience of its own processes by attributing a resilience score to each process.

For this purpose, the first section will be devoted to the selection of needed indicators. This step is of such importance since the indicators provide the necessary information for decision-making and constitute a basis for our calculation model. However, in order to be able to accomplish these missions, the indicators should be relevant. This means that they should be specific so that the results can be clearly identified, measurable and quantified, practical and useable, available (it should be possible to collect the data), be transparent in methodology and selection and well-grounded in scientifically [15]. After this, the "3R" process will be defined in the second section. This method relies mainly on three concepts, which are (1) resources that can be considered, among others (time, budget, regulations…) as a constraint that may limit the achievement of the process objective [16], (2) risks, which are undesirable events that may happen several times can have a negative impact on the process [17], (3) Resilience, which is the ability of a system to manage disturbances and to adapt to changes without ceasing the activity[18]. In this section, a model explaining extensively the 3R process that is divided into two steps (Definition of parameters and resilience assessment) will be derived, the way of calculating the resilience score using fuzzy logic, a procedure that has already proved its effectiveness in many fields, will be explicitly shown, and graphic user interfaces will be developed. Then, a real case company example in the context of COVID-19 is presented in the penultimate section. The purpose is to check the reliability of the proposed method through assessing the resilience of a process of a huge company in face of this exceptional crisis. At the end of this paper, conclusions and opportunities for further work will be exposed.

2. Selection of indicators

The role of resilience processes is to ensure the continued availability of resources, in case of disruptions, in order to avoid failures. This objective can be achieved through resistance, recovery, and anticipation [19]. Thus, the selection of indicators will be in relation with these three missions.

As per resistance, a variety of metrics can be considered [20]:

- The meantime between failures (MTBF), which indicates the expected time between consecutive failures.
- The operational availability that expresses the percentage of time a process is available to users.
- The operational reliability, which is defined as the ability of a process to operate at the normal service level for a specified period of time.
- The Maximum Tolerable Period of Disruption (MTPD) that measures the time for which a process can be available before entirely stopping the system activity. It depends on the system business objectives and thus determined by the organization. The importance of this indicator lies in the fact that it has an impact on the recovery metrics [21]. Furthermore, the MTPD is identified as one of the inputs used to prepare the response plans [22].

In the light of the foregoing, the MTPD is picked up and the criticality of processes will be defined according to the value of MTPD.

Table 1: The selected indicators

Resilience process mission	Indicator	Description
Resistance	MTPD	Time after which operations of the site are critically impacted, in case of a full process unavailability.
Recovery	RT	Time required for the system to resume normal operation after a disruption.
Anticipation	WIT	The time needed to implement an anticipated workaround for a disturbance.
Anticipation	WMTTL	The period during which a workaround perform normally.

Regarding recovery, the following metrics can be listed [23]:

- Recovery Point Objective (RPO) describes the period of time in which data must be restored after a disruption.
- Recovery Time Objective (RTO) is the period during which the system must recover.

- Mean Down Time (MDT) is the mean time that a system is not operational.
- Recovery time, which is the time it takes for a process to return to normal operation after a failure is occurred. It is shown in a research work about the relationship between recovery and resilience that the recovery time depends on, among others, the resilience of the system and the scale of the perturbation [24]. It is considered also as the period within which it takes a system to return to a stable state [25]. This metric is chosen as one of the parameters used to define the process criticality.

As for anticipation, the notion of "workaround" is addressed. It may be defined, according to the Cambridge Dictionary, as "a way of dealing with a problem or making something work despite the problem, without completely solving it". In other words, it is an alternative solution, which allows continuing the operation in short term. For instance, we can define, as workaround, for raw material shortage, borrowing from the stock of another plant. In terms of indicators, Workaround Implementation Time (WIT) and Workaround Maximum Tolerable Time Length (WMTTL) are selected. WIT is the amount of time it takes to implement an anticipated workaround for the present situation, and WMTTL is the absolute maximum length of time for which an implemented workaround can be maintained.

The featured indicators are presented in the table 1.

3. 3R process

The 3R process is a novel method and an instrument for decision-making aimed at assessing the resilience of sociotechnical systems processes. This process is built on three essential concepts: Resource, Risk, and Resilience, and is conducted in two stages, which are the definition of parameters and the resilience assessment. A model of the 3R process is proposed in figure 1.

This begins with the selection of a sociotechnical system process for which resilience will be assessed. Thereafter, the concerned resource is identified. This latter may fall under one of the following categories: (1) Infrastructures (Buildings, Racks, Dock lanes, Doors…), (2) Devices/Equipment (Pick-to-light, Conveyer Belt, Tape machine, Forklift…), (3) People (Management, Certified staff, External Human Resources…), (4) IT/Hardware (Computer, Printer, Server, Network…), (5) IT/Software (ERP, Local applications…), (6) Consumables (Box, Plastic film, Labels, Pallet…), (7) Utilities (Electricity, Water, Stream, Gas…). Then, a potential risk that threaten the selected resource is chosen. In general, there are six types of risks: (1) General resources (All risks directly impacting facilities and services (Supplier Bankrupt, Power outage…), (2) Internal staff (All events impacting human resources (Loss of key personnel, Strike, Epidemic…)), (3) IT (All incidents concerning data and IT resources availability (Virus, Hacking…)), (4) Natural disaster (All incidents with natural causes (Earthquake, flood, hurricane…)), (5) Regulation (All incidents impacting the authorization to make business (Lawsuit, Customs issue…), (6) Social (External) (All personal incidents external to the system (Riots, Terrorism, Bomb Threat)).

When this is done, the next step is to define parameters. The aim is to attribute values to the four indicators detailed in the previous section. For each one, time ranges should be defined and the process criticality level should be identified based on these intervals. As regards WIT and WMTTL, before proceeding with this exercise, the existence of workarounds should be checked, and if not found, workarounds must be put in place.

The criticality level helps determine the priority ranking of processes as per their potential risk of failures. In the present work, five process criticality levels are considered: (1) Very low, (2) Low, (3) Medium, (4) High, (5) Very high. An example of intervals for the selected indicators (MTPD, RT, WIT, and WMTTL) is given in the tables below.

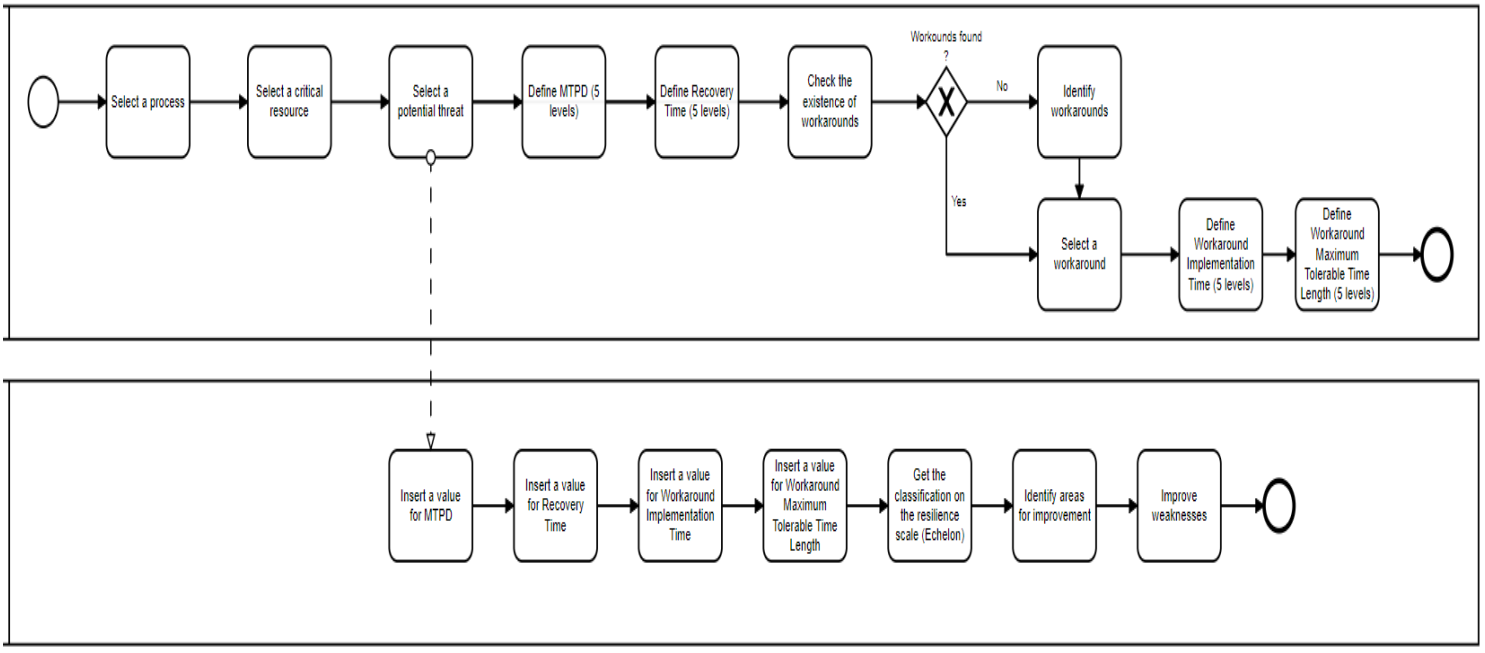


Figure 1: 3R process model

Table 2: The process criticality levels for MTPD

Level	Process criticality	Description	Comment
5	Very high	MTPD < 4h	The risk of failure is very high since the process can carry on functioning only 4 hours during the disturbance before completely ceasing its activity.
4	High	4h ≤ MTPD < 1 day	The risk of failure is high since the process can carry on functioning between 4 hours and 1 day during the disturbance before completely ceasing its activity.
3	Medium	1 day ≤ MTPD < 3 days	The risk of failure is medium since the process can carry on functioning between 1 day and 3 days during the disturbance before completely ceasing its activity.
2	Low	3 days ≤ MTPD < 5 days	The risk of failure is low since the process can carry on functioning between 3 and 5 days during the disturbance before completely ceasing its activity.
1	Very low	5 days ≤ MTPD < 1 week	The risk of failure is very low since the process can carry on functioning between 5 days and 1 week during the disturbance before completely ceasing its activity. This is a sufficient time for the process to recover.

Table 3: The process criticality levels for RT

Level	Process criticality	Description	Comment
1	Very low	RT < 1 day	The risk brought about by the disruption is very low since the process can recover in less than 1 day.
2	Low	1 day ≤ RT < 3 days	The risk brought about by the disruption is low since the process can recover in a period of time between 1 day and 3 days.
3	Medium	3 days ≤ RT < 5 days	The risk brought about by the disruption is medium since the process can only recover in a period of time between 3 and 5 days.
4	High	5 days ≤ RT < 1 week	The risk brought about by the disruption is high since the process can only recover in a period of time between 5 and 7 days.
5	Very high	1 week ≤ RT	The risk brought about by the disruption is very high since the process can only recover in more than 1 week.

Table 4: The process criticality levels for WIT

Level	Process criticality	Description	Comment
1	Very low	WIT < 1 day	The risk of failure is very low since the anticipated workaround can be implemented in less than 1 day.
2	Low	1 day ≤ WIT < 3 days	The risk of failure is low since the anticipated workaround can be implemented in a period of time between 1 day and 3 days.
3	Medium	3 days ≤ WIT < 5 days	The risk of failure is medium since the anticipated workaround can be implemented only in a period of time between 3 and 5 days.
4	High	5 days ≤ WIT < 1 week	The risk of failure is high since the anticipated workaround can be implemented only in a period of time between 5 and 7 days.
5	Very high	1 week ≤ WIT	The risk of failure is very high since the anticipated workaround can be implemented only in more than 1 week.

Table 5: The process criticality levels for WMTTL

Level	Process criticality	Description	Comment
5	Very high	WMTTL < 1 day	The risk of failure is very high since the anticipated workaround can be maintained only for less than 1 day.
4	High	1 day ≤ WMTTL < 3 days	The risk of failure is high since the anticipated workaround can be maintained only for a period of time between 1 day and 3 days.
3	Medium	3 days ≤ WMTTL < 5 days	The risk of failure is medium since the anticipated workaround can be maintained only for a period of time between 3and 5 days.
2	Low	5 days ≤ WMTTL < 1 week	The risk of failure is low since the anticipated workaround can be maintained for a period of time between 5 and 7 days.
1	Very low	1 week ≤ WMTTL	The risk of failure is very low since the anticipated workaround can be maintained for more than 1 week.

Table 6: The process criticality levels for the selected indicators

Criticality level					
Indicator	Very low	Low	Medium	High	Very high
MTPD (days)	[5 , 7[	[3 , 5[	[1 , 3[	[1/6 , 1[	[0 , 1/6[
RT (days)	[0 , 1[	[1 , 3[	[3 , 5[	[5 , 7[	[7 , +∞[
WIT (days)	[0 , 1[	[1 , 3[	[3 , 5[	[5 , 7[	[7 , +∞[
WMTTL (days)	[7 , +∞[	[5 , 7[	[3 , 5[	[1 , 3[	[0 , 1[

Table 7: Definition of parameters: Example of application

Action	Description
Select a process	Quality Control. It includes : - Raw material control - Finished goods and components control - Microbiology control
Select a resource	The critical resources for this process are: - Infrastructure: Light, air conditioning, fume hood, microlab, raw material sampling booth… - Equipment: Component control equipment, finished goods and packaging control equipment, raw material and assay control equipment, micro control equipment… - People: raw material and assay control: Basic chemical knowledge, micro control: micro knowledge.
Select a threat	The potential threats for this process are: Lab unavailable, reagent supply shortage, scanners or printers unavailable, more than half of the team missing, equipment unavailable…
Define MTPD (Five levels)	Cf. Table 6
Define recovery time (Five levels)	Cf. Table 6
Check the existence of workarounds	If No →Identify workarounds If Yes →Select a workaround
Identify workarounds	-**Lab unavailable**→Externalization of quality control to another plant. **- More than half of the team missing**→Borrow people from production department. **- Reagent supply shortage** →Borrow from another plant. **- Equipment unavailable**→Delegate part of the activity to another plant.
Select a workaround	Select one of the workarounds already identified
Define WIT (Five levels)	Cf. Table 6
Define WMTTL (Five levels)	Cf. Table 6

The process criticality levels for the four selected metrics are gathered in table 6 (1/6 day stands for 4 hours)

An example of application of the first part of the 3R process model is given in the process analysis template hereafter (table 7).

The second and most important step of the 3R process model is “resilience assessment”. Its aim is to explain how to rate sociotechnical system processes on the resilience scale. In figure 1, it can be noticed that this part consists in determining inputs in order to obtain the echelon at the output. This will help the process identify the areas for improvement and afterwards overcome weaknesses.

In order to design the 3R process model, fuzzy logic will be used. This is an approach of data mining, which enables the modelling of a decision process in a situation of uncertain reasoning or incomplete information [26]. A fuzzy inference system (FIS) is defined as a system that uses fuzzy membership functions to make a decision [27]. In our case, Mamdani approach is adopted. This is a nonlinear mapping process on the base of fuzzy logic, which involves three components: fuzzification, inference rules, and defuzzification. The proposed fuzzy model is implemented using the programming language python, which is versatile and easy to use with a large and rich library.

The first step in the fuzzy model is to import scikit-fuzzy, which is a fuzzy logic Python package, using the following code block:

```
import numpy as np
import skfuzzy as fuzz
from skfuzzy import control as ctrl
```

Afterwards, the inputs (MTPD, Recovery time (RT), Workaround implementation time (WIT), Workaround maximum tolerable time length (WMTTL)) and the output (Echelon) should be defined. Values included between 0 and 8 for the inputs according to Table 6, and 0 and 5 for the output according to the resilience scale (5 echelons (0, 1, 2, 3 and 4)). The code portion is inserted hereunder:

```
MTPD = ctrl.Antecedent (np.arange (8), 'MTPD')
WIT = ctrl.Antecedent (np.arange (8), 'WIT')
WMTTL = ctrl.Antecedent (np.arange (8), 'WMTTL')
RT = ctrl.Antecedent (np.arange (8), 'RT')
Echelon = ctrl.Consequent (np.arange (0, 5, 1), 'echelon')
```

Next, auto-membership function should be populated (Five intervals). Membership functions are used in fuzzy systems to represent input values. The code snippet is added below:

```
MTPD.automf (5)
WIT.automf (5)
WMTTL.automf (5)
RT.automf (5)
```

Then, membership functions are built based on resilience scale and table 6. Our choice was to go with the triangular membership functions (trimf) that are frequently used in many applications of fuzzy sets owing to their simplicity and which are suitable in this case (because they are defined by a lower limit a, an upper limit b, and a value m, where a < m < b) [28], [29]. The functions are shown hereafter

```
Echelon['Unconscious'] = fuzz.trimf(Echelon.universe, [0, 0, 1])
Echelon['Informed'] = fuzz.trimf(Echelon.universe, [1, 1, 2])
Echelon['Aspiring'] = fuzz.trimf(Echelon.universe, [2, 2, 3])
Echelon['Progressing'] = fuzz.trimf(Echelon.universe, [3, 3, 4])
Echelon['Expert'] = fuzz.trimf(Echelon.universe, [4, 4, 5])
MTPD['Very high'] = fuzz.trimf(MTPD.universe, [0, 0, 0.16])
MTPD['High'] = fuzz.trimf(MTPD.universe, [0.16, 0.16, 1])
MTPD['Medium'] = fuzz.trimf(MTPD.universe, [1, 3, 3])
MTPD['Low'] = fuzz.trimf(MTPD.universe, [3, 5, 5])
MTPD['Very low'] = fuzz.trimf(MTPD.universe, [5, 7, 7])
WIT['Very low'] = fuzz.trimf(WIT.universe, [0, 0, 1])
WIT['Low'] = fuzz.trimf(WIT.universe, [1, 1, 3])
WIT['Medium'] = fuzz.trimf(WIT.universe, [3, 3, 5])
WIT['High'] = fuzz.trimf(WIT.universe, [5, 5, 7])
WIT['Very high'] = fuzz.trimf(WIT.universe, [7, 7, 8])
WMTTL['Very high'] = fuzz.trimf(WMTTL.universe, [0, 0, 1])
WMTTL['High'] = fuzz.trimf(WMTTL.universe, [1, 1, 3])
WMTTL['Medium'] = fuzz.trimf(WMTTL.universe, [3, 3, 5])
WMTTL['Low'] = fuzz.trimf(WMTTL.universe, [5, 5, 7])
WMTTL['Very low'] = fuzz.trimf(WMTTL.universe, [7, 7, 8])
RT['Very low'] = fuzz.trimf(RT.universe, [0, 0, 1])
RT['Low'] = fuzz.trimf(RT.universe, [1, 1, 3])
RT['Medium'] = fuzz.trimf(RT.universe, [3, 3, 5])
RT['High'] = fuzz.trimf(RT.universe, [5, 5, 7])
RT['Very high'] = fuzz.trimf(RT.universe, [7, 7, 8])
```

Thereafter, fuzzy rules are defined in order to express pieces of knowledge. Given the large number of identified rules, a few examples are provided in the table hereunder:

Table 8: Examples of Fuzzy rules

Example 1						
MTPD = Very low & RT = Very low						
Echelon		WIT				
		Very low	Low	Medium	High	Very high
WMTTL	Very low	Expert	Expert	Expert	Progressing	Progressing
	Low	Expert	Expert	Expert	Progressing	Progressing
	Medium	Expert	Expert	Progressing	Progressing	Progressing
	High	Progressing	Progressing	Progressing	Progressing	Progressing
	Very high	Progressing	Progressing	Progressing	Progressing	Progressing
Example 2						
MTPD = Very low & RT = High						
Echelon		WIT				
		Very low	Low	Medium	High	Very high
WMTTL	Very low	Progressing	Aspiring	Aspiring	Aspiring	Aspiring

	Low	Aspiring	Aspiring	Aspiring	Aspiring	Aspiring
	Medium	Aspiring	Aspiring	Aspiring	Aspiring	Aspiring
	High	Aspiring	Aspiring	Aspiring	Aspiring	Aspiring
	Very high	Aspiring	Aspiring	Aspiring	Aspiring	Aspiring
Example 3						
MTPD = High & RT = High						
Echelon		WIT				
		Very low	Low	Medium	High	Very high
WMTTL	Very low	Informed	Informed	Informed	Informed	Informed
	Low	Informed	Informed	Informed	Informed	Informed
	Medium	Informed	Informed	Informed	Informed	Informed
	High	Informed	Informed	Informed	Unconscious	Unconscious
	Very high	Informed	Informed	Informed	Unconscious	Unconscious

Table 9: Values of inputs

Indicator	Value	Level	Interpretation
MTPD	3	Medium	The process can resist for 3 days before failing to function. Then, its criticality is medium.
WIT	5	High	It takes 5 days to implement the anticipated workaround. This is a long response time to the perturbation.
WMTTL	1	High	The implemented workaround can remain operational for one day, which is not sufficient.
RT	7	Very high	The process can reach its normal functioning within 7 days. This means that the duration of the disturbance lasts for a long time.

In example 1, MTPD and RT are very low, which means that the two first missions of resilience process (resistance and recovery) are perfectly fulfilled. It remains to be seen if the last mission (anticipation) is also fully accomplished or not. Accordingly, the output (Echelon) will oscillate between progressing and expert.

In example 2, the RT decreases, which conveys a much-needed effort to enhance recovery, and thus the process climbs down in the resilience scale from progressing to aspiring. It cannot be informed or unconscious because the resilience process is already set up with at least one mission that really holds water (resistance).

Regarding the last example, MTPD and RT are high, which is to say that resistance and recovery of the process are weak. Therefore, depending on the performance of anticipation, the echelon varies between informed and unconscious.

Subsequently, a control system (a nonlinear Single Input-Single Output (SISO) discrete-time process based on a set of rules [30]) is created using the code block hereunder

```
resiliencescale_ctrl = ctrl.ControlSystem ([rule1, rule2,…, rule n])
```

Later, this control system is simulated through specifying the inputs. The table hereafter gathers the values attributed to the four indicators in the present example.

```
resiliencescale.input ['MTPD'] = 3
resiliencescale.input ['WIT'] = 5
resiliencescale.input ['WMTTL'] = 1
resiliencescale.input ['RT'] = 7
resiliencescale.compute ()
```

Finally, simulation results is visualized (cf. Code blow& figure 2)

```
print (resiliencescale.output['echelon'])
Echelon.view(sim=resiliencescale)
```

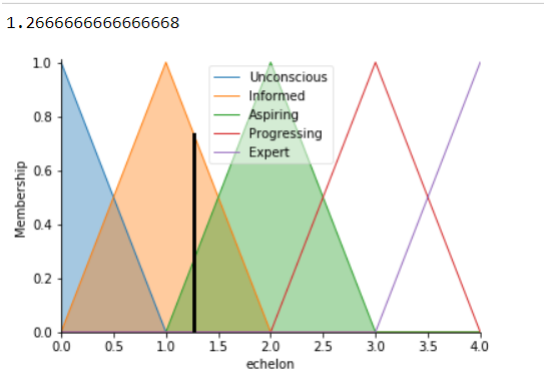


Figure 2: Simulation results

According to the plot above, the resilience echelon is about 1.27. That is to say, by referring to the resilience scale, the process

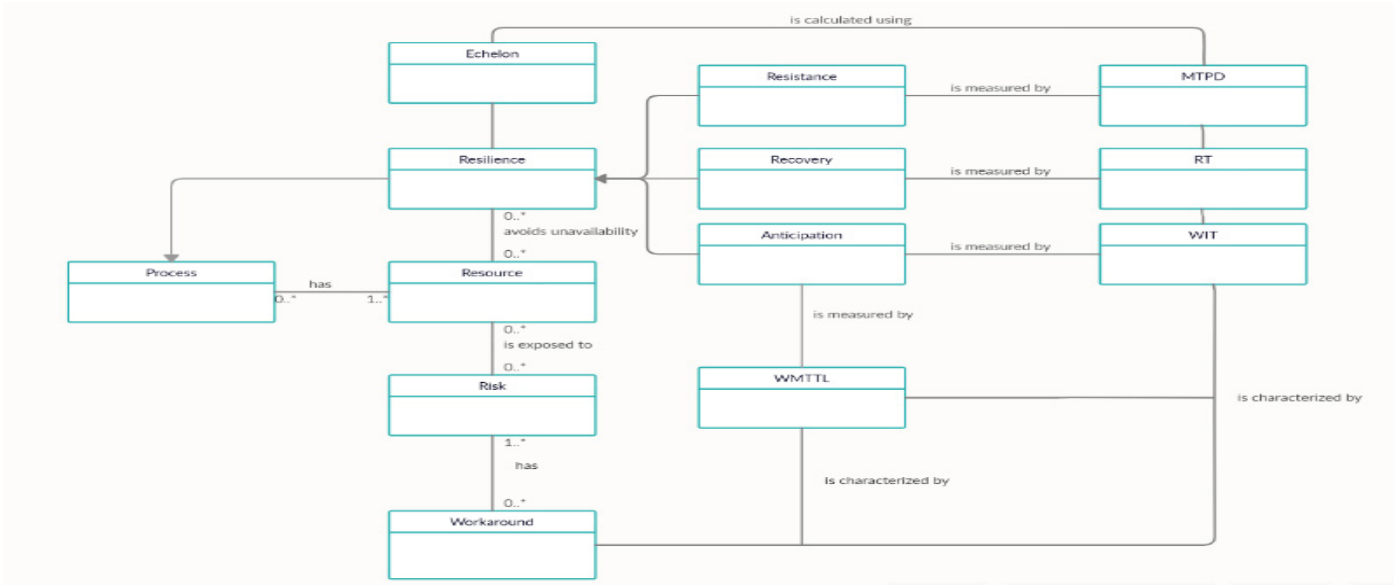


Figure 3: A conceptual metamodel representing the 3R process

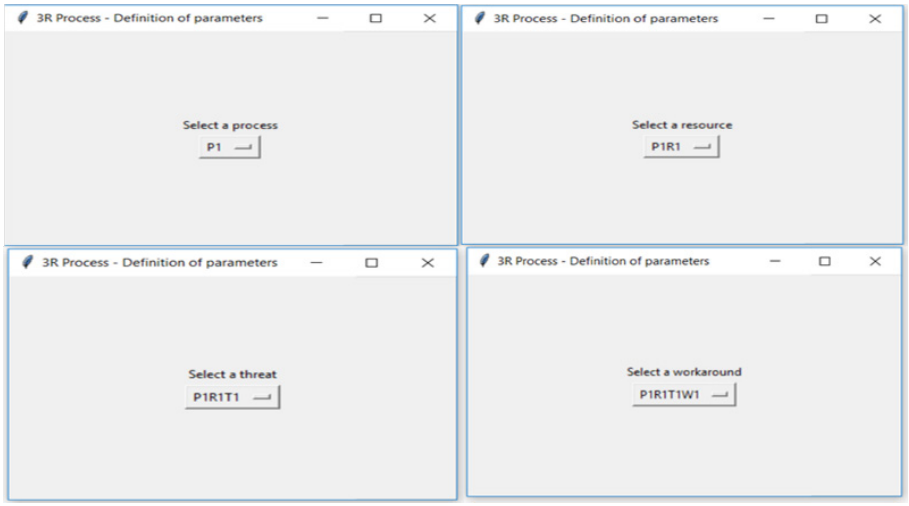


Figure 4: Definition of parameters – User interfaces

under study is informed. It is poorly developed with regard to resilience. An associated resilience process must be set up in order to enhance its resilience. The aim is to improve:

- the resistance of the process and its resource to the disruption through increasing the MTPD
- the recovery through the reduction of the recovery time (RT)
- the anticipation through putting in place well elaborate workarounds, reducing WIT and increasing WMTTL for each workaround.

In order to make this model usable for sociotechnical systems and a core part of their processes, a user interface should be designed. For this purpose, a model is elaborated using UML language (Cf. figure 3).

As can be seen, the metamodel illustrated by figure 3 formulates the following points:

- A process has one or more resources.
- A resource is exposed to one or more risks.
- A risk can have one or several identified workarounds. It may also have no created workarounds.
- There are processes called resilience processes.
- The existence of resilience processes in the sociotechnical systems help avoiding unavailability of resources.
- An echelon (Resilience score) is attributed to each process of the sociotechnical system based on the existence of associated resilience processes.
- The missions of resilience processes are resistance, recovery and anticipation.
- Resistance is measured using MTPD.
- Recovery is measured using RT.
- Anticipation is measured using WIT and WMTTL. These two indicators characterize workarounds.
- The echelon is calculated through MTPD, RT, WIT and WMTTL.

Firstly, the database should be populated with the list of all the processes in a sociotechnical system. Then, for each process, the critical resources should be identified. After this, the potential threats should be presented for each resource. Next, the verification should be carried out, for each risk, to ensure that anticipated workarounds are available. If this is not the case, workarounds should be developed to compensate for the lack. Thereafter, criticality levels (Very high, high, Medium, Low, Very low) should be determined for MTPD, RT, WIT and WMTTL.

In the second place, the parameters can be defined via the user interfaces dedicated for this purpose and which are developed using the framework Tkinter of Python (cf. figure 4)

Then, based on the chosen criteria, the resilience of the selected process can be assessed. Figure 5 illustrates that values of the indicators MTPD, RT, WIT and WMTTL should be inserted to get the resilience score of the process.

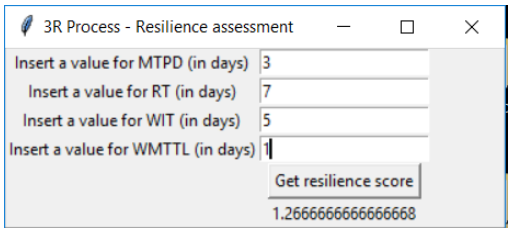


Figure 5. User interface corresponding to resilience assessment

It is clear that for the selected combination ((Process(P1), Resource(P1R1), Threat (P1R1T1), Workaround (P1R1T1W1)), the resilience score is 1.27. That is to say, according to the resilience scale, the process P1 is informed and there is no elaborated resilience process associated with it. The first thing to be done is to try to enhance the resistance of the process/resource to the risk P1R1T1 through increasing the MTPD in order to avoid the activity interruption and at the same time attempt to recover more quickly. Furthermore, the workaround implementation time should be sharply reduced and the functioning of the workaround P1R1T1W1 should last longer at least until recovery.

On the basis of the given example, the 3R process can be considered as a decision-making tool that helps sociotechnical systems assess their processes as per resilience and hence identify improvement opportunities with the aim of building a system capable of weathering the continuing uncertainty surrounding business environment nowadays.

4. A real case company example – COVID-19 context

COVID-19 is having an unprecedented impact on sociotechnical systems (societies, companies…) and people's livesand will continue to do so into the foreseeable future. Since the first day, the selected company, which is one of the largest and best-known enterprises operating in the cosmetics sector, has been working on the COVID-19 outbreak in order to ensure its employees' safety. Country by country as well as globally, the evolution of the situation has been carefully monitored and decisive measures to limit everyone's risk to exposure have been taken. In order to evaluate the resilience of the company processes against this worldwide crisis, the 3R process method will be applied.

First, the physical distribution process (PDP) is chosen as an example. It is a part of the supply chain organization. Its aim is to ensure that the service to the consumer required by the business is met at the best possible costs by optimizing the inbound (reception and returns), internal (putaway and replenishment) and outbound (order preparation and shipping) physical flows whilst guaranteeing quality and safety in a sustainable environment. The table below summarizes all the crisis phases that the PDP has passed through.

Table 10: PDP behavior during pandemic phases

Crisis step	Events / Country decisions	Supply Chain Impact	PDP Impact	Risk	Workaround
Before outbreak	Pre epidemic decisions	Localize Goods close to the market	Increase pallets to Customer & International Affiliates	Storage saturation	Increase storage capacity (internal or external)
Before outbreak	Pre epidemic decisions	Business Continuity Plans (BCP) & Secondary backup Distribution Center (DC)	Secondary DC carry additional stock	Storage Saturations/Unable to move product systematically	Work with IT to prioritize Storage location creation needed and Catalog extension; Identify key 3PLs that can support pop-up DCs where needed
Before outbreak & Outbreak phase	Epidemic decisions	Lead-time increase	Transport capacity	Lack of carriers and freight-forwarders capacity	Give to suppliers mid-term visibility in order to book slots and capacity + alert Transportation Team if no positive answer from freight-forwarders
Before outbreak &	Epidemic decisions	Costs increase	Transportation costs increase	Spot extra charges for airfreight but also risk on road and sea freight	Inform Transportation Team about requests from freight-forwarders especially for intercontinental flows (sea freight, rail freight & airfreight)

Outbreak phase					
Outbreak phase	Shops closing by authorities without proper anticipation / Population confined at home	Order delivery not possible as shops are closed	Unusual amount of parcels returns to DCs: Cancellation of orders that could've begun picking	Return area capacity saturation unable to manage the flow	Define in advance how to manage this unusual return flow: resize return area / outsource?
Outbreak phase	Shops closing by authorities without proper anticipation / Population confined at home	Customer orders in portfolio not relevant.	Unusual amount of parcels returns to DCs	Useless workload in picking Return area capacity saturation	Verify if customer can still receive goods / reprocessing order portfolio (cancel useless orders)
Outbreak phase	Shops closing by authorities without proper anticipation / Population confined at home	Massive slowdown of order and still inbound flows to come	Increase of pallets to store	storage saturation/"lack of work" for labor on-site	Increase storage capacity (internal or external) Release time while communicating retention bonus plan for future Reduce shift hours throughout day
Outbreak phase	Shops closing by authorities without proper anticipation / Population confined at home	Online orders booming	Increase of e-commerce orders	Capacity (preparation and delivery)	Labor share where sites are in close proximity Work through weekends
Outbreak phase	School closing	Part of employee obliged to stay at home to baby-sit the children	Part of employee in home office / not working (if home office not feasible)	Capability reduction	Identify what are the key processes, the key customers that have to be prioritized: Set-up daycare alternative & reimbursement : alternate shift schedules
Outbreak phase	Health and Safety instructions		Temperature measurement before entering for all employees => delays in workers' access to the DC	Capability reduction	Several simultaneous controls or with thermal camera Verify temperature measurement system data privacy compliancy
Outbreak phase	Health and Safety instructions		Disable fingerprint access control	Less access control	Replaced by personal cards
Outbreak phase	Health and Safety instructions		Flexibility or workforce reduction to	Capability reduction	Extra hours/ Extra shifts

			lower people concentration. Keep a minimum distance of 1 m from other operators. Canteen flow regulation.		
Outbreak phase	Health and Safety instructions		A Covid-19 case confirmed for a DC employee	Capability reduction	Identify what are the key processes, the key customers that have to be prioritized; Shutdown area for 3 hours, neighborhood survey & sanitize area; If site is shutdown, go to secondary DC; Have approved sanitation suppliers confirmed for cleaning support
Outbreak phase	3PL crisis management	Ensure 3PLs follow Health and Safety instructions and have a strong crisis management internally		capability reduction / lock down due to inappropriate actions	Ask 3PL to present measures activated and BCP action plan
Outbreak phase	Stop of none essential activity / epidemic situation in the DC	DC Lock down	Stock not available and shipping stopped		Define heroes products Map heroes products stocks positions worldwide Map twins heroes products worldwide Prepare process to use these twins products
Outbreak phase	DC closed due to government regulation	DC Lock down	Stock not available and shipping stopped	Unable to load products	Prepare list of key SKUs; Preload trailers where items have sufficient coverage based on risk of local government shutdown
Restart period	confine constraints removal	Orders pic	Huge activity at restart	Unable to meet demand	Prepare additional locations for preparation; Offer retention bonus for temporary employees based on seniority

As mentioned previously, the first step of the 3R process method is the definition of parameters. For such needs, the human factor is picked up as a resource. Then, the threat chosen, based on the table above, is capability reduction due to school closing. Finally, the workaround selected is alternating shift schedules. As per the four indicators, they are determined as follows (table 11)

Table 11: The four indicators time ranges for PDP

MTPD			
Level	Process criticality	Description	Comment
5	Very high	MTPD < 1 month	The risk of failure is very high since the PDP can handle the capability reduction only for less than 1 month before completely ceasing its activity.
4	High	1 month ≤ MTPD < 3 months	The risk of failure is high since the PDP can handle the capability reduction only for a period of time between 1 month and 3 months before completely ceasing its activity.
3	Medium	3 months ≤ MTPD < 5 months	The risk of failure is medium since the PDP can handle the capability reduction only for a period of time between 3 and 5 months before completely ceasing its activity.
2	Low	5 months ≤ MTPD < 9 months	The risk of failure is low since the PDP can handle the capability reduction for a period of time between 5 and 9 months before completely ceasing its activity.

1	Very low	MTPD ≥ 9 months	The risk of failure is very low since the PDP can handle the capability reduction for more than 9 months before completely ceasing its activity. This is a sufficient time for the process to recover.
RT			
Level	Process criticality	Description	Comment
1	Very low	RT < 1 month	The risk brought about by the disruption is very low since the process can recover in less than 1 month.
2	Low	1 month ⩽ RT < 3 months	The risk brought about by the disruption is low since the process can recover in a period of time between 1 month and 3 months.
3	Medium	3 months ⩽ RT < 5 months	The risk brought about by the disruption is medium since the process can only recover in a period of time between 3 and 5 months.
4	High	5 months ⩽ RT < 12 months	The risk brought about by the disruption is high since the process can only recover in a period of time between 5 and 12 months.
5	Very high	1 year ⩽ RT	The risk brought about by the disruption is very high since the process can only recover in more than 1 year.
WIT			
Level	Process criticality	Description	Comment
1	Very low	WIT < 1 month	The risk of failure is very low since the anticipated workaround can be implemented in less than 1 month.
2	Low	1 month ⩽ WIT < 3 months	The risk of failure is low since the anticipated workaround can be implemented in a period of time between 1 month and 3 months.
3	Medium	3 months ⩽ WIT < 5 months	The risk of failure is medium since the anticipated workaround can be implemented only in a period of time between 3 and 5 months.
4	High	5 days ⩽ WIT < 9 months	The risk of failure is high since the anticipated workaround can be implemented only in a period of time between 5 and 9 months.
5	Very high	9 months ⩽ WIT	The risk of failure is very high since the anticipated workaround can be implemented only in more than 9 months.
WMTTL			
Level	Process criticality	Description	Comment
5	Very high	WMTTL < 1 month	The risk of failure is very high since the anticipated workaround can be maintained only for less than 1 month.
4	High	1 month ⩽ WMTTL < 3 months	The risk of failure is high since the anticipated workaround can be maintained only for a period of time between 1 month and 3 months.
3	Medium	3 months ⩽ WMTTL < 5 months	The risk of failure is medium since the anticipated workaround can be maintained only for a period of time between 3 and 5 months.
2	Low	5 months ⩽ WMTTL < 9 months	The risk of failure is low since the anticipated workaround can be maintained for a period of time between 5 and 9 months.
1	Very low	9 months ⩽ WMTTL	The risk of failure is very low since the anticipated workaround can be maintained for more than 9 months.

Afterwards, the second step, which is the resilience assessment, should be initiated. Therefore, the inputs are specified in the table below.

Table 12: Specification of inputs

Input	Value (in months)	PDP criticality level
MTPD	12	Very low
RT	Uncertain (Given the fact that there is no visibility concerning the termination of the crisis). For calculation purposes, 12 is taken as value.	Very high
WIT	4	Medium
WMTTL	8	Low

By using the 3R process tool, the plot below (figure 6) is obtained.

By inference, the physical distribution process is aspiring. In fact, the Novel Coronavirus outbreak has some particularities that differentiate it from other disruptions. As a result, the

corresponding resilience process is not yet completely set up. The resistance mission is functioning very well and the anticipation mission is under development. However, the recovery mission is still very ambiguous.

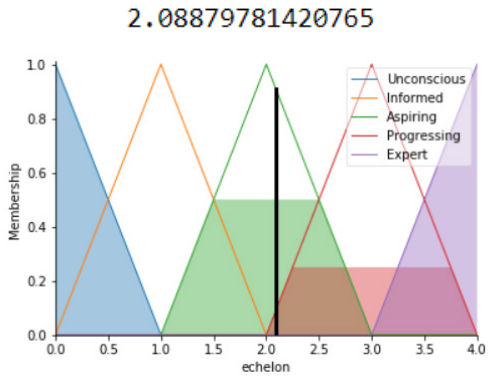


Figure 6: Simulation results for PDP

5. Conclusion

The presented work pointed out a method that can be used by sociotechnical systems to evaluate the resilience of their processes. First and foremost, the resilience scale with its five echelons (0. Unconscious, 1. Informed, 2. Aspired, 3. Progressing, 4. Expert) and three missions (resistance, recovery and anticipation) was introduced. Then, indicators related to these missions have been outlined (MTPD for resistance, RT for recovery, WIT and WMTTL for anticipation). Afterwards, the 3R process was detailed. The 3Rs stand for Resource, Risk and Resilience. This framework is divided into two parts, the first one is the definition of parameters, which consists in determining process criticality levels according on the four selected indicators. Time ranges are defined for the metrics and for each process, critical resources, potential risks and anticipated workarounds are selected and resilience is evaluated for all possible combinations. As for the second part, it is about the resilience assessment. In order to calculate the resilience score (echelon) and rank the process on the resilience scale, fuzzy logic has been used. A fuzzy model has been elaborated and user interfaces have been developed in order to enable decision makers to evaluate their systems and build their resilience. In short, the major advantages of this process are summarized as follows. First, this is a generic method that can apply to any system and help it to define the key indicators, related to resistance (MTPD), recovery (RT) and anticipation (WIT and WMTTL): the three functions of a resilience process, and identify plausible workarounds. Second, it provides a resilience score and a rating as per the resilience scale, which can be useful for detecting and improving weaknesses and also increasing strength and effectiveness to deal with adverse events. Finally, by applying fuzzy logic in the 3R process, the vagueness and uncertainty faced can be overcome. In the last section, a study has been conducted to look at the impact of the COVID19 sanitary crisis on a real case company example and how resilience plays a crucial role in preventing the worst from happening and resuming gradually the normal course of events. In fact, the exposed real case study shows that the pandemic situation has negatively affected the functioning of the studied process. In the aftermath, the process works on improving its resilience, especially, the recovery mission. In the future work, attempts will be made to establish new methods serving to evaluate the resilience of sociotechnical system processes and enhance it.

Conflict of Interest

The authors declare no conflict of interest.

References

[1] G. Fischer, T. Herrmann, "Socio-Technical Systems", International Journal of Sociotechnology and Knowledge Development, **3**(1), 1-33, 2011, doi:10.4018/jskd.2011010101

[2] Nokia reports fourth-quarter 2004 net sales of EUR 9.1 billion, EPS EUR 0.23. (2005, January 27). Retrieved from https://www.nokia.com/system/files/files/q4-2004-earnings-release-pdf.pdf

[3] C. G. Worley, E. E. Lawler, T. Williams, "The agility factor: Building adaptable organizations for superior performance", San Francisco, CA: Jossey-Bass, 2014.

[4] S. A. Argyroudis, S. A. Mitoulis, L. Hofer, M. A. Zanini, E. Tubaldi, D. M. Frangopol, "Resilience assessment framework for critical infrastructure in a multi-hazard environment: Case study on transport assets", Science of The Total Environment, **714**, 2020, 136854, doi:10.1016/j.scitotenv.2020.136854

[5] D. Rehak, P. Senovsky, M. Hromada, T. Lovecek, "Complex approach to assessing resilience of critical infrastructure elements", International Journal of Critical Infrastructure Protection, **25**, 125–138, 2019, doi: 10.1016/j.ijcip.2019.03.003

[6] J. Vargas, D. González, "Model to assess supply chain resilience", International Journal of Safety and Security Engineering, **6**(2), 282–292, 2016, doi: 10.2495/safe-v6-n2-282-292

[7] A. K. Ravulakollu, L. Urciuoli, B. Rukanova, Y.-H. Tan, R. A. Hakvoort, "Risk based framework for assessing resilience in a complex multi-actor supply chain domain", Supply Chain Forum: An International Journal, **19**(4), 266–281, 2018, doi: 10.1080/16258312.2018.1540913

[8] O. Kammouh, A. Z. Noori, G. P. Cimellaro, S. A. Mahin, "Resilience Assessment of Urban Communities", ASCE-ASME Journal of Risk and Uncertainty in Engineering Systems, Part A: Civil Engineering, **5**(1), 2019, 04019002, doi: 10.1061/ajrua6.0001004

[9] M. M. Sellberg, C. Wilkinson, G. D. Peterson, "Resilience assessment: a useful approach to navigate urban sustainability challenges", Ecology and Society, **20**(1), 2015, doi: 10.5751/es-07258-200143

[10] A. C. Caputo, P. M. Pelagagge, P. Salini, "A methodology to estimate resilience of manufacturing plants", IFAC-PapersOnLine, **52**(13), 808–813, 2019, doi: 10.1016/j.ifacol.2019.11.229

[11] J. T. Kim, J. Park, J. Kim, P. H. Seong, "Development of a quantitative resilience model for nuclear power plants", Annals of Nuclear Energy, **122**, 175–184, 2018, doi: 10.1016/j.anucene.2018.08.042

[12] N. Ahmadian, G. J. Lim, J. Cho, S. Bora, "A Quantitative Approach for Assessment and Improvement of Network Resilience", Reliability Engineering & System Safety, **200**, 106977, 2020, doi: 10.1016/j.ress.2020.106977

[13] K. Adjetey-Bahun, B. Birregah, E. Châtelet, J.-L. Planchet, "A model to quantify the resilience of mass railway transportation systems", Reliability Engineering & System Safety, **153**, 1–14, 2016, doi: 10.1016/j.ress.2016.03.015

[14] S. Said, H. Bouloiz, M. Gallab, "A new structure of sociotechnical system processes using resilience engineering", International Journal of Engineering Business Management, **11**, 2019, 184797901982715, doi: 10.1177/1847979019827151

[15] V. Cornescu, R. Adam, "Considerations Regarding the Role of Indicators Used in the Analysis and Assessment of Sustainable Development in the E.U", Procedia Economics and Finance, **8**, 10–16, 2014, doi: 10.1016/s2212-5671(14)00056-2

[16] V. Llamas, T. Coudert, L. Geneste, J. Romero-Bejarano, A. de Valroger, "Proposition of an agile knowledge-based process model", IFAC-PapersOnLine, **49**(12),1092-1097, 2016.

[17] D. Ristic, "A TOOL FOR RISK ASSESSMENT", Safety Engineering, **3**(3), 2013.

[18] O. Gluchshenko, "Definitions of Disturbance, Resilience and Robustness in ATM Context" DLR Report IB 112-2012/28, DLR,Institute of Flight Guidance, Germany, 2012.

[19] S. Said, H. Bouloiz, M. Gallab, "Resilience Engineering: A Restructuring Of Processes Toward The Building Of Resilient Sociotechnical Systems" in 2019 4th World Conference on Complex Systems (WCCS), doi:

10.1109/icocs.2019.8930797
[20] ENISA, "Measurement Frameworks and Metrics for Resilient Networks and Services: Technical report", 2011. Retrieved from https://www.enisa.europa.eu/publications/metrics-tech-report/at_download/fullReport
[21] E. Zambon, D. Bolzoni, S. Etalle, M. Salvato, "A Model Supporting Business Continuity Auditing and Planning in Information Systems" in Second International Conference on Internet Monitoring and Protection (ICIMP 2007), doi:10.1109/icimp.2007.4
[22] S. A. Torabi, R. Giahi, N. Sahebjamnia, "An enhanced risk assessment framework for business continuity management systems", Safety Science, **89**, 201-218, 2016, doi:10.1016/j.ssci.2016.06.015
[23] M. Wiboonrat, K. Kosavisutte, "Optimization strategy for disaster recovery" in 4th IEEE International Conference on Management of Innovation and Technology, 2008, doi:10.1109/icmit.2008.4654446
[24] I. A. Leemput, V. Dakos, M. Scheffer, E. H. Nes, "Slow Recovery from Local Disturbances as an Indicator for Loss of Ecosystem Resilience", Ecosystems, **21**(1), 141-152, 2017, doi:10.1007/s10021-017-0154-8
[25] Z. Fu, D. Li, O. Hararuk, C. Schwalm, Y. Luo, L. Yan, S. Niu, "Recovery time and state change of terrestrial carbon cycle after disturbance", Environmental Research Letters, **12**(10), 2017, 104004, doi:10.1088/1748-9326/aa8a5c
[26] N. H. Chan, H. Y. Wong, "Data mining of resilience indicators", IIE Transactions, **39**(6), 617–627, 2007, doi: 10.1080/07408170600899565
[27] A. Hossain, A. Rahman, "Sensor-Controlled Intelligent Vehicle Systems: Demand and Needs for a Global Automotive Landscape", Comprehensive Materials Processing, 473–497, 2014, doi:10.1016/b978-0-08-096532-1.01321-2.
[28] J. Zhao, B. Bose, "Evaluation of membership functions for fuzzy logic controlled induction motor drive" in IEEE 2002 28th Annual Conference of the Industrial Electronics Society, IECON 02, 2002, doi:10.1109/iecon.2002.1187512
[29] B. M. Moreno-Cabezali, J. M. Fernandez-Crehuet, "Application of a fuzzy-logic based model for risk assessment in additive manufacturing R&D projects", Computers & Industrial Engineering, **145**, 106529, 2020, doi:10.1016/j.cie.2020.106529
[30] R.-E. Precup, M.-L. Tomescu, S. Preitl, E. M. Petriu, C.-A. Dragoş, "Stability Analysis of Fuzzy Logic Control Systems for a Class of Nonlinear SISO Discrete-Time Systems", IFAC Proceedings, **44**(1), 2011, 13612–13617, doi: 10.3182/20110828-6-it-1002.00937

ASTES

Advances in Science, Technology and Engineering Systems Journal Vol. 5, No. 5, 1261-1265 (2020)

www.astesj.com

ASTESJ

ISSN: 2415-6698

An Empirical Study on Factors Influencing the Intention to use Mobile Learning

Malik Khlaif Gharaibeh[1,*], Natheer Khlaif Gharaibeh[2]

[1]*School of Business, Jadara University, Irbid, 21110, Jordan*

[2]*College of Computer Science and Engineering, Taibah University, Yanbu, 41911, Saudi Arabia*

ARTICLE INFO

Article history:
Received: 26 July, 2020
Accepted: 18 October, 2020
Online: 24 October, 2020

Keywords:
Mobile learning
ISSM
Trust

ABSTRACT

Lately, the use of mobile learning has increased in higher education at a global level. Especially after the new Coronavirus (Covid-19). Therefore, trust issues towards the benefits of mobile learning are still important matters just as important as quality dimensions (e.g. service quality, information quality and system quality) for both technology and its content. These three factors are existing in the Information System Success Model (ISSM), but the trust is not clearly present. Hence, this study is attempting to explain the impact of trust in addition to the three quality dimensions of the ISSM on the usage intention of mobile learning among students in two Jordanian universities. The data were gathered by a self-administered questionnaire and SPSS version 23 is used by performing linear regression analysis to analyze it. The findings showed that trust, service quality, system quality, and information quality positively and significantly affect the intention to use mobile learning. This study will help researchers, decision-makers and system designers by gaining valuable implications in developing proper strategies and creating effective and practical approaches through learning via mobile devices.

1. Introduction

Because of rapid development and increasing capabilities of technology and the progress of 4th industrial revolution in the last two decades, many business transformations have emerged, mobile applications are considered one of the most important transformations, as a result, many applications have been developed in the field of education. For that reason, the academic sector is making great efforts to activate and introduce this new method of smart learning in its environment [1-3]. Such service encourages researches to study this type of technology in terms of its effect on students [4], whether it is university or school Mobile learning occupied important role in the educational process [5]. The goal of this research is to make effective use of mobile applications in the educational sector especially after the global emergence of Coronavirus, which caused difficulties and frustrations for both teachers and students.

Mobile learning can be defined as "learning across multiple contexts, through social and content interactions, using personal electronic devices" [6]. The article [7] claimed that mobile learning is an extension of electronic learning in which a smartphone is used. In more detail, Mobile learning technology changed the way students and learners manage learning activities with one another, and also facilitated knowledge sharing between them [8-10]. Also, The paper [11] indicated that mobile learning is not only limited to a mobile device but also includes learning via any portable phone e.g. PDA and tablet. In short, it is a technology that allows students to carry out their daily educational work with higher quality, in addition to its advantage that it is portable and it can be used regardless of location and time [5, 12].

There are many features and functions that mobile learning offers to students, such as downloading books and study materials, making phone calls, responding to e-mail quickly, capturing pictures, and interacting easily with lecturers and colleagues outside the campus [13, 14]. Mobile learning also provides benefits to universities in that it provides multiple educational services for students at a relatively low cost [15, 16]. Mobile learning is a very important step for any educational institution because that gives it a competitive advantage and in the near future the use of these services in educational institutions will be inevitable, especially in universities [17].

At present, it seems that the application of the mobile learning service faces technical and un-technical restrictions (such as any

[*]Corresponding Author: Malik Khlaif Gharaibeh, Address: Jadara University, Contact No: 00962779919484 & Email: malik.gh@jadara.edu.jo

new technology in developing countries), thus the rate of adoption of this service is less than expected [18-20]. The paper [21] pointed out that students need a deeper and broader understanding of how to use these applications. Form a theoretical perspective, a few studies have been measured on the adoption of university students for mobile learning in Jordan. Hence, it is a good idea to study this spreading technology. Given that Jordan has a good wireless network infrastructure and penetration rate of mobile phones is high [22]. Statistics revealed that 90 percent of Jordanian families have a smartphone, around also 89 percent have an Internet subscription [23-25]. More specifically, Jordan has enhanced its 4G coverage and its improvement is directed towards mobile terminals. It also has got high in both mobile broadband and smartphone penetration rate [26-29].

This study attempts to explain the determinants affecting the adoption intention to use mobile learning among university students'. The current study adds to the prior work on mobile learning in two points. First, previous researches shed light on TAM, IDT, and UTAUT in studying mobile learning acceptance/adoption/intention to use e.g. [30-32]. Despite the important role of trust in technology, the relationship between students' trust and adoption intention in the context of mobile learning has rarely been examined [32]. This study interested in investigating the relationship between trust and intention to use mobile learning. Second, whereas previous research was more concerned with the influence of the innovation characteristics and new technology, which already exists in TAM, UTAUT, and IDT. This study takes another direction by incorporating quality dimensions with trust to explore the factors of intention to use mobile learning among students'.

2. Theoretical Foundation and Hypothesis Development

ISSM is extensively adapted among researchers to investigate the acceptance/adoption of many information systems [33-35] (see Figure 1). The article [36] Stated that ISSM is a robust model because it has a solid theoretical basis for many successful empirical types of research. This model consists of three independent variables that affect positively the intention of use and acceptance. "System quality is defined as the degree to which the system users believe that a system is easy to use, user-friendly, easy to learn, easy to connect to, and enjoyable to use" [37]. "information quality is defined as the degree to which system users think that online learning information is up-to-date, accurate, relevant, comprehensive, and organized" [38]. "Service quality is referred to through these attributes: tangible, reliability, responsiveness, assurance, functionality, interactivity, and empathy" [39].

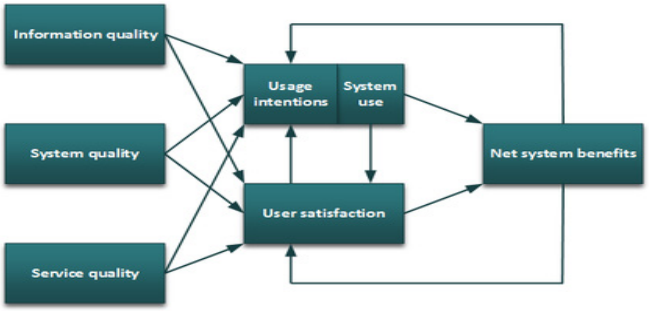


Figure 1: Information System Success Model (ISSM)

Previous studies used this model in the context of electronic learning. For example, the article [40] added transformational leadership in ISSM to study the adoption of online learning. They found that overall quality positively affects the adoption of online learning. Another study conducted by the article [36], results showed that quality dimensions which include; system quality, service quality, and information quality significantly affect user satisfaction of electronic learning.

In this regard, sseveral previous studies also used ISSM in different information systems contexts. The paper [41] investigated factors affecting the success of banking systems. The results showed that system quality, service quality, and information quality positively affect intention and acceptance of banking systems. The article [42] concluded that these 3 quality dimensions are core determinants in affecting users' trust and satisfaction of phone-call-related applications. The article [43] also found that these quality dimensions have a positive and direct impact in Accounting Information Systems (AIS) success at the organizational level. Table 1 summarizes the most important studies that have been conducted in adopting mobile learning. Through the table, it has been observed that most of these studies used two models, namely TAM and UTAUT2, while this study used ISS Model to increase and deepen the understanding regarding mobile learning as this model contains variables that have not been measured Sufficient in the previous studies.

Table 1: Previous studies in acceptance/adoption of mobile learning area

Author/s	Focus	Model	Results
Shin and Kang, 2015.	Using Mobile Learning Management System at an Online University and Its Effect on Learning Satisfaction.	expanded TAM model	The results revealed that self-efficacy, personal innovativeness, and system accessibility have a significant influence on perceived ease of use. Subjective norm and relative advantage did not influence perceived ease of use. Subjective norm and relative advantage exhibited a positive influence on perceived usefulness. Perceived usefulness is the most influential factor affecting students' intention to use mobile learning.
Laura Briz-Ponce et al, 2017	Learning with mobile technologies - Students' behavior.	TAM and UTAUT	Social Influence raised to be an important factor towards the Attitude and Intention of using Mobile Learning. Ease of perception seems to be the main factor affecting the Social Influence and the reliability for recommending this technology for learning was the main factor that affected the Intention. Overall, findings provide support for Technology Acceptance Model.
Jose Carlos et al 2016.	Mobile Learning and pre-service teachers: An assessment of the intention .	expanded TAM model	The analysis supported all the hypotheses proposed, that the stronger relationships were those established between perceived usefulness and behavioral intention, perceived ease of use and perceived usefulness, and self-efficacy and perceived ease of use.
Hamidi and Chavoshi, 2018	Adoption of mobile learning in higher education.	expanded TAM model	Character and personal attributes, perceived usefulness and perceived ease of use did not influence the intention. Context has a direct and positive effect on both usefulness and ease of use. Ease of use has a positive effect on usefulness. Trust and the culture of using the application truly impacts the behavioral intention. Personal features and characters have a significant positive effect on the culture of using.
Al-Adwan et al 2018.	Solving the mystery of mobile learning adoption in higher education.	expanded UTAUT model	The results reveal that effort expectancy, performance expectancy, trust expectancy, self-management of learning, system functionality and social influence are significant determinants of m-learning adoption.

Based on positive recommendations and results of previous studies [44]. We extended ISSM by adding trust to develop an inclusive model for evaluating the intention to use mobile learning. These intentions will be increased when learners/students believe that mobile learning application is beneficial in their learning process. This study proposed four hypotheses as following:

H1: System quality positively affects intention to use mobile learning.

H2: Service quality positively affects intention to use mobile learning.

H3: |Information quality positively affects intention to use mobile learning.

H4: Trust positively affects intention to use mobile learning.

The present study depends on previous studies in developing the proposed research model and associated hypotheses. This study aims to discover the possible impact of trust and quality dimensions, which are information quality, service quality, and system quality on the intention to use mobile learning as see Figure 2.

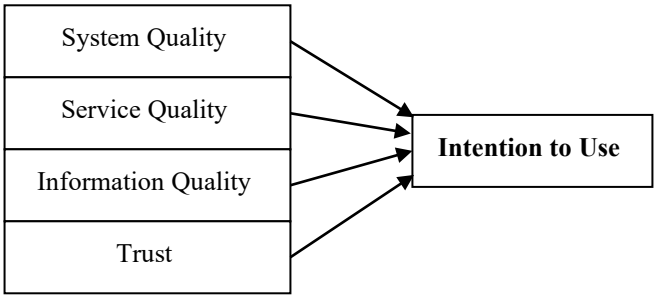


Figure 2: Proposed Research Framework

3. Methodology

The sample in this study was represented by university students enrolled in two Jordanian universities namely: The University of Jordan and Yarmouk University. A quantitative method (questionnaire) was used to collect the necessary data in this study, including two sections, the first section containing personal information of participants (gender, income, and internet frequency usage). In the second section covering 20 items to evaluate the four variables, a five Likert scale for all items was used with values from 1 "strongly disagree" to 5 "strongly agree". These items were carefully selected from related literature and different areas of IS/IT research. 480 answers were received. Out of these, 30 participants were not users of mobile learning, hence, these surveys were not included in this study. Besides that, 20 were incomplete and 12 answers were removed due to non-seriously in filling out (e.g. identical responses for each question). So 418 surveys were considered in this study for statistical analysis. The data collection period lasted twenty-five days between February 2 and February 27, 2020. Finally, SPSS version 23 was used to analyze data.

4. Results and Discussion

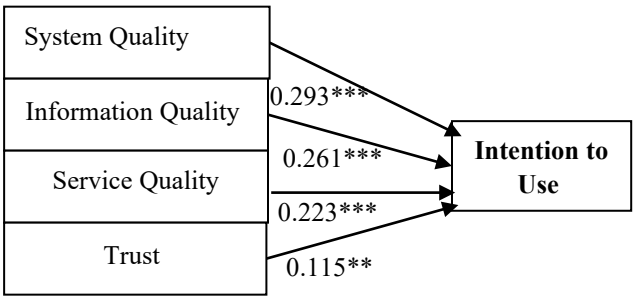
The results of the item-total correlation for each item exceeded the minimum acceptable value which is 0.5 as suggested by the article [45]. Cronbach's alphas also were measured for each construct. The result showed that all items were more than 0.70 therefore all items were kept for more statistical analysis. Besides, items of this study were loaded on the component matrix. It was be found that all coefficients were greater than the lowest acceptable level of 0.70 [46]. For hypotheses testing, all hypotheses in this study were accepted. Regarding H1, system quality (most significant factor) has been found positively affect intention to use mobile learning applications in Jordan ($\beta = 0.293$, $p < 0.001$). This result provides support for the articles [33, 34] findings based on ISSM. The results of prior studies also found system quality as a vital variable in using on-line learning, e.g., the study by the article [36] found that service quality is a vital variable in the adoption of online learning.

For H2, service quality has been found positively affect intention to use mobile learning ($\beta = 0.261$, $p < 0.001$) which supports the result of the articles [33, 34] based on ISSM. The results of prior studies also found the service quality as a vital variable in using online learning, e.g., the study by the article [40] /found that the service quality is a vital variable in the adoption of online learning. For H3, information quality has been found positively affect intention to use mobile learning ($\beta = 0.223$, $p < 0.001$) which supports the result of the articles [33, 34] based on ISSM. The results of prior studies also found information quality as a vital variable in using on-line learning [35, 40]. For H4, this study reveals the important role of trust in intention to use process ($\beta = 0.115$, $p < 0.01$). This role has been found in other studies in the context of mobile learning by the paper [47] which they discovered that trust dimensions play a major role in influencing users to use mobile learning. The results of hypotheses testing are summarized in Figure 3.

The results offer valuable information for both top management and system designers regarding the enhancement of students' desire for the use of mobile learning. The current paper concluded that the presence of effective leadership and management support in universities leads to raising motivation of students to use mobile learning. According to survey results, the respondents have a good level of readiness to use such an application. This means that the level of conviction in the use of mobile learning among students depends greatly on the quality of the service provided to them, so the higher the quality of information, the quality of the system, and the quality of the service, this leads to a greater conviction for the use of this application. In addition, those responsible for these applications must provide updated, easy-to-understand, and complete information. In this way, the students' motivation will increase to use this service, since they will notice the many benefits as a result of using it. The justification for this positive path between the dimensions of quality and intention to use is that the Jordanian government has strengthened the communications infrastructure, and therefore the service provided is considered to be cheap and of high quality. This study found that the trust factor is very important in adopting mobile learning. This importance stems from that it motivates the student to use this application, as well as the student influences the decision of his/her colleagues to adopt such applications and thus the level of confidence affects the adoption of the service, in other words, the more confidence in the service increases, the greater the percentage Use it among students and vice versa.

During the last decade, and through an integrated plan by the government, Jordan has achieved tremendous development in terms of infrastructure in the field of communications. This strategic plan for the educational sector in moving towards mobile learning is in line with Queen Rania's vision, who believes that the general trend in the future in universities and schools will be in e-learning. She always urges researchers to conduct more studies in order to motivate students to use this technology in education [18]. This trend in Jordanian universities towards e-learning would give these universities a competitive ability at the global level, which in

turn raises the ranking of universities on approved standards such as THE and QS rankings. This important issue has increased the desire to realize the determinants that affect the students' intention to use mobile learning in higher education.



**p<0.01, ***p<0.001

Figure 3: Findings of path analysis

5. Conclusion

Technology is changing constantly, and the demand for smartphones is increasing. The many features of the smartphone have attracted many users around the globe. This leads to a higher demand for mobile learning and thus a change in the university education system. From a theoretical perspective, quality dimensions are a vital facet in electronic learning as well it has a high impact on the level of understanding. Besides that, the current study showed that trust in mobile learning applications has a positive effect, as well as high trust motivates the intention to use. However, this study can be improved by conducting a study include the public and private universities, in this way, a comprehensive model in the context of mobile learning can be constructed that extends quality dimensions and trust for local context applications.

6. Limitations and Future Research

This study contains several limitations, which are useful for future research. Firstly, the sample of this study was confined to academic institutions in Jordan, and therefore the difficulty of generalizing the results to other countries. Besides that, a sample of this study included only respondents using mobile learning, and those who do not use this service were excluded, so future studies can include users who are not satisfied with this service and study the reasons for refusing to use this service. Third, the moderate effect of demographic factors e.g. gender, income, and familiarity with mobile applications have not been taken into consideration, and it is expected that these factors will affect students' intention to use mobile learning. Finally, given that mobile learning is still in an early stage at the application level in educational and academic institutions in Jordan, therefore we recommend future studies to use the innovation diffusion theory [48] as it is very appropriate in the early stages before the diffusion of new technology.

Conflict of Interest

The authors declare no conflict of interest.

References

[1] Y.M. Huang, and P.S. Chiu, The effectiveness of a meaningful learning-based evaluation model for context-aware mobile learning. British Journal of Educational Technology, **46**(2): 437-447, 2015. doi:10.1111/bjet.12147.

[2] G. Fulantelli, D. Taibi, and M. Arrigo, A framework to support educational decision making in mobile learning. Computers in human behavior, **47**, 50-59, 2015. doi.org/10.1016/j.chb.2014.05.045.

[3] M. Al-Okaily et al., Dataset on the Acceptance of e-learning System among Universities Students' under the COVID-19 Pandemic Conditions. Data in Brief, 2020. 32: 106176, doi.org/10.1016/j.dib.2020.106176.

[4] I. Han, and W.S. Shin, The use of a mobile learning management system and academic achievement of online students. Computers & Education, 2016. 102:.79-89, doi.org/10.1016/j.compedu.2016.07.003.

[5] M. Al-Emran, H.M. Elsherif, and K. Shaalan, Investigating attitudes towards the use of mobile learning in higher education. Computers in Human behavior, **56**: 93-102, 2016. doi.org/10.1016/j.chb.2015.11.033.

[6] H. Crompton, A historical overview of mobile learning: Toward learner-centered education. Handbook of mobile learning, 3-14, 2013.

[7] N.S. Alzaza, N.S. and A.R. Yaakub, Students' awareness and requirements of mobile learning services in the higher education environment. American Journal of Economics and Business Administration, **3**(1): 95-100, 2011.

[8] S. Homan, and K. Wood, Taming the Mega-Lecture: Wireless Quizzing. Syllabus Magazine, October 7-8. 2003.

[9] M.A. Emran, and K. Shaalan. E-podium Technology: A medium of managing Knowledge at Al Buraimi University College via Mlearning. in Proceedings of the 2nd BCS International IT Conference 2014, doi.org/10.14236/ewic/bcsme2014.

[10] A. Abu-Al-Aish, and S. Love, Factors influencing students' acceptance of m-learning: An investigation in higher education. The International Review of Research in Open and Distributed Learning, **14**(5): 82-107, 2013. doi.org/10.19173/irrodl.v14i5.1631.

[11] A. Matias, and D.F. Wolf, Engaging students in online courses through the use of mobile technology. Cutting-edge Technologies in Higher Education, 6 part (D): Emerald Group Publishing Limited, Bingley, 115-142, 2013. doi.org/10.1108/S2044-9968(2013)000006D007.

[12] A.I. Saroia, and S. Gao, Investigating university students' intention to use mobile learning management systems in Sweden. Innovations in Education and Teaching International, **56**(5): 569-580, 2019. doi.org/10.1080/14703297.2018.1557068.

[13] B. Handal, J. MacNish, and P. Petocz, Adopting mobile learning in tertiary environments: Instructional, curricular and organizational matters. Education Sciences, **3**(4): 359-374, 2013. doi:10.3390/educsci3040359

[14] F. Mubuke, et al., The Predictability of Perceived enjoyment and Its Impact on the intention to use Mobile learning systems. Asian Journal of Computer Science And Information Technology, **1**(1): 1-5, 2017. doi.org/10.15520/ajcsit.v6i851.

[15] M.A. Almaiah, M.M. Alamri, and W.M. Al-Rahmi, Analysis the effect of different factors on the development of Mobile learning applications at different stages of usage. IEEE Access, **8**: 16139-16154, 2019. 10.1109/ACCESS.2019.2963333.

[16] B. Pynoo, et al., Predicting secondary school teachers' acceptance and use of a digital learning environment: A cross-sectional study. Computers in Human behavior, **27**(1): 568-575, 2011. DOI: 10.1016/j.chb.2010.10.0

[17] S. Criollo, S. Luján, and A. Jaramillo. Advantages and disadvantages of M-learning in current education. in World Engineering Education Conference (EDUNINE). IEEE, 2018. DOI: 10.1109/EDUNINE.2018.8450979.

[18] M.A. Almaiah, M.A. Jalil, and M. Man, Extending the TAM to examine the effects of quality features on mobile learning acceptance. Journal of Computers in Education, **3**(4): 453-485, 2016. doi.org/10.1007/s40692-016-0074-1.

[19] A. Chavoshi, A. and H. Hamidi, Social, individual, technological and pedagogical factors influencing mobile learning acceptance in higher education: A case from Iran. Telematics and Informatics, **38**: 133-165, 2019. doi.org/10.1016/j.tele.2018.09.007.

[20] 20. Almaiah, M.A. and O.A. Alismaiel, Examination of factors influencing the use of mobile learning system: An empirical study. Education and Information Technologies, 2019. 24(1): 885-909, doi.org/10.1007/s10639-018-9810-7

[21] L. Briz-Ponce, and J.A. Juanes-Méndez, Mobile devices and apps, characteristics and current potential on learning. Journal of Information Technology Research (JITR), **8**(4): 26-37, 2015. 10.4018/JITR.2015100102.

[22] M.K. Gharaibeh, and M.R.M. Arshad, Determinants of intention to use mobile banking in the North of Jordan: extending UTAUT2 with mass media and trust. Journal of Engineering and Applied Sciences, **13**(8): 2023-2033, 2018. dx.doi.org/10.36478/jeasci.2018.2023.2033.

[23] The Jordan Times, ICT, Internet usage among Jordanian households increases — ministry. 2018.

[24] M.K. Gharaibeh, and M.R.M. Arshad, The Impact of Demographic Factors and Visual Aesthetics of Mobile Application Interface on Intention to Use

Mobile Banking in Jordan. Journal of Theoretical & Applied Information Technology, **96**(4): 937-945, 2018.
[25] Gharaibeh, M.K., N.K. Gharaibeh, and M.V. De Villiers, A Qualitative Method to Explain Acceptance of Mobile Health Application: Using Innovation Diffusion Theory. International Journal of Advanced Science and Technology, 2020. 29(4): 3426-3432.
[26] GCI, Jordan GCI 2018. 2018.
[27] M. Gharaibeh, and M.R.M. Arshad, Current status of mobile banking services in Jordan. World Applied Sciences Journal, **34**(7): 931-935, 2016. 10.5829/idosi.wasj.2016.34.7.153.
[28] M. Gharaibeh, M.R. Arshad, and N.K. Gharaibeh, Using the UTAUT2 model to determine factors affecting adoption of mobile banking services: A qualitative approach. International Journal of Interactive Mobile Technologies (iJIM), **12**(4): 123-134, 2018.doi.org/10.3991/ijim.v12i4.8525.
[29] N. Gharaibeh, et al., Exploring Intention to use Mobile Commerrce: Integrating UTAUT2 with Social Media. International Journal of Scientific and Technology Research, **9**(3): 3826-3833, 2020.
[30] L. Briz-Ponce, et al., Learning with mobile technologies–Students' behavior. Computers in Human Behavior, **72**: 612-620, 2017. doi.org/10.1016/j.chb.2016.05.027.
[31] P. Sánchez, M.S. Olmos, and P.F.J. García, MLearning and pre-service teachers: An assessment of the behavioral intention using an expanded TAM model. Computers in Human Behavior, **72**: 644-654, 2017. doi.org/10.1016/j.chb.2016.09.061.
[32] H. Hamidi, and A. Chavoshi, Analysis of the essential factors for the adoption of mobile learning in higher education: A case study of students of the University of Technology. Telematics and Informatics, **35**(4): 1053-1070, 2018. doi.org/10.1016/j.tele.2017.09.016.
[33] W.H. Delone, and E.R. McLean, The DeLone and McLean model of information systems success: a ten-year update. Journal of management information systems, **19**(4): 9-30, 2003. doi.org/10.1080/07421222.2003.11045748.
[34] W.H. DeLone, and E.R. McLean, Information systems success: The quest for the dependent variable. Information systems research, **3**(1): 60-95, 1992. doi.org/10.1287/isre.3.1.60.
[35] A.H. Aldholay, et al., The role of compatibility as a moderating variable in the information system success model: The context of online learning usage. International Journal Of Management And Human Science, **2**(1): 9-15, 2018.
[36] R. Freeze, et al., IS success model in e-learning context based on students' perceptions. Journal of Information systems education, **21**(2): 173-184, 2019.
[37] S. Petter, and E.R. McLean, A meta-analytic assessment of the DeLone and McLean IS success model: An examination of IS success at the individual level. Information & Management, **46**(3): 159-166, 2009. doi.org/10.1016/j.im.2008.12.006.
[38] T. Acton, et al., DeLone & McLean success model as a descriptive tool in evaluating the use of a virtual learning environment, in International Conference on Organizational Learning, Knowledge and Capabilities. 2009.
[39] F. Lin, S.S. Fofanah, and D. Liang, Assessing citizen adoption of e-Government initiatives in Gambia: A validation of the technology acceptance model in information systems success. Government Information Quarterly, **28**(2): 271-279, 2011. doi.org/10.1016/j.giq.2010.09.004.
[40] A.H. Aldholay, et al., The role of transformational leadership as a mediating variable in DeLone and McLean information system success model: The context of online learning usage in Yemen. Telematics and Informatics, **35**(5): 1421-1437, 2018. doi.org/10.1016/j.tele.2018.03.012.
[41] A. Jaafreh, Evaluation information system success: Applied delone and McLean information system success model in context banking system in KSA. International Review of Management and Business Research, **6**(2): 829-845, 2017.
[42] C. Lin, and Y.-J. Chang. The Application of IS Success Model on Continuous Intention and Information Sharing for Caller ID Apps Usage. in International Conference on HCI in Business, Government, and Organizations, Springer, 2018.
[43] A. Al-Okaily, et al., Measuring Success of Accounting Information System: Applying the DeLone and McLean Model at the Organizational Level. Journal of Theoretical and Applied Information Technology, **98**(14): 2697-2706, 2020.
[44] A. Al-Okaily, et al., Accounting information system effectiveness from an organizational perspective. Management Science Letters, **10**(16): 3991-4000, 2020. 10.5267/j.msl.2020.7.010.
[45] J. Hair, et al., Multivariate data analysis: A global perspective. **7,** Pearson Upper Saddle River, NJ, 2010:
[46] A. Field, Discovering Statistics Using SPSS (2nd ed). London: Sage Publications, 2005.
[47] E. Ibrahim, and N. Walid, Trust contributing factors in m-learning technology. Procedia-Social and Behavioral Sciences, **129**: 554-561, 2014. 10.1016/j.sbspro.2014.03.713.
[48] E.M. Rogers, Diffusion of innovations.Simon and Schuster, 2010.

ASTES

Advances in Science, Technology and Engineering Systems Journal Vol. 5, No. 5, 1266-1272 (2020)

www.astesj.com

Special Issue on Multidisciplinary Innovation in Engineering Science & Technology

ASTESJ

ISSN: 2415-6698

Agricultural Data Fusion for SmartAgro Telemetry System

Ioana Marcu[1,*], Ana-Maria Drăgulinescu[1], Carmen Florea[1], Cristina Bălăceanu[2], Marius Alexandru Dobrea[2], George Suciu[2]

[1]*Telecommunication Department, University Politehnica of Bucharest, 010082, Romania*

[2]*R&D Department, Beia Consult International, Bucharest, 010082, Romania*

ARTICLE INFO

Article history:
Received: 16 July, 2020
Accepted: 15 October, 2020
Online: 24 October, 2020

Keywords:
Precision Agriculture
Data Fusion
Reliability
Sensors

ABSTRACT

Smart agriculture concept uses innovative solutions including IoT and Cloud storage features, dedicated sensors for monitoring basic agricultural parameters, new communications protocols, etc. SmartAgro architecture comprises a telemetry system for Key Performance Indicators (KPIs) such as air & soil temperature, air & soil relative humidity, leaf wetness, etc. The current paper outlines the reliability of the implemented system by comparing and analyzing data collected in spring 2019 and spring 2020. The relevance of this season consists in great air variations due to the transition from winter to summer. Being monitored in a vine area near Bucharest, these data may be useful for different statistics related to grapes culture in this season and can be used by interested parties for future predictions related to vine crops. Moreover, in this paper, data fusion will allow advanced data management and coherence achievement among collected data.

1. Introduction

This paper is an extension of work originally presented in SIITME'19 conference [1]. In [1] the authors presented the telemetry system with its main advantages consisting in solar panel supply and data reliability. The current work extends the demonstration of the system's reliability by processing data from Spring 2019 and Spring 2020. In addition to the previous work, data fusion will be used to fill the gaps between the recorded data and to ensure a proper system's management.

Considering all climate changes, the evolution of the agriculture plays an important role in the lives and well-being of people, since it represents a source of food for population and, respectively for domestic animals. Climate change influences agriculture in different ways. Changes in temperature and precipitation are already affecting crop yields [2]. Consequently, people must adapt to and implicitly adjust the solutions used to ensure food or water quality, for irrigation and daily use [3]. The health of soils and crop, also, is very important, as it affects the quality and quantity of agricultural crops [4, 5].

When required to evaluate successful analysed crops, the key performance indicators (KPIs) must be considered since they are quantitative, practical, directional, and actionable. Depending on the analysed corps, KPIs differ. For example, based on KPIs crop usage can be tracked to evaluate the production and to monitor the overall costs. The most significant impacts of KPIs on agriculture are increased productivity, profit and time save [6].

An important role in the precision agriculture is played by IoT platforms. Using them, the quality of the crops can be enhanced by real time data acquisition, processing and decision making. These data are converted, thus, in useful information for farmers, and, also, in a facile understandable manner [7]. Capturing, transmitting, storing and processing the volume of information collected by sensors connected on the IoT platform, show a number of challenges, in particular, regarding integration technologies, communications, databases and computing. A middleware platform which alleviates these issues is FIWARE. FIWARE is a technology supported by the European Commission to make possible the IoT in the context of the Future Internet [8].

SmartFarmNet is an IoT platform that automatically collects data from soil, as fertilization and irrigation. The data is then automatically correlated, and the invalid data is filtered-out from the perspective of assessing crop performance. Also, with the help of the platform the crop forecasts can be computed, and the farmers receive personalized crop recommendations for any farm [9].

There are also platforms which are specialised on only one aspect such as SWAMP. Within SWAMP project there was developed and assessed an IoT-based smart water management platform for precision irrigation in agriculture. The platform was

*Corresponding Author: Ioana Marcu, Email: ioana.marcu@upb.ro

built in such manner that it can be configured and deployed in different ways. Thus, the platform can deal with the requirements and limitations of different countries, climate, soils, and crops, which require flexibility to adapt to a range of deployment configurations involving mixed technologies [10].

Data fusion techniques applied on data collected by different sensors used in agricultural area allow a better understanding of parameters' evolution and advanced data management, especially in cases where the data volume is huge [11], [12]. Yet, the applicability domain is not limited only to agriculture, but it can comprise different applications that are sensor-based and that imply multiple data sources.

The current paper aims to emphasize the role of the implemented SmartAgro telemetry system in ensuring reliable data for further use in statistics and specialized predictions. Data fusion methods will allow additional processing that will offer a global perspective of the monitored parameters. The paper is organized as follows: Section 2 presents the related work on data fusion solution for key parameters monitored in precision agriculture; Section 3 contains the description of SmartAgro telemetry system and in Section 4 system's setup and relevant monitoring results are presented. Data fusion implications are outlined in Section 5 and Section 6 comprises Conclusions.

2. Data Fusion for Agricultural Area

According to [13], when acquirred data present high and diverse information, data fusion considers the juxtaposition of large set of data to ensure reliable, homogeneously and fair overview of the collected information. The advantage of data fusion of data received from multiple different sensors relies in "an improved estimate of physical phenomenon via redundant observations" [14]. The efficiency of data fusion was previously demonstrated in precision agriculture domain [15-18]. In [15], authors present the benefits on crop monitoring of 2D and 3D data fusion for a vineyard monitoring and use the results in order to classify vines in serveral classes by processing data from multiple sources (different sensors, Unmanned Aerial Vehicle (UAVs), etc). In 2012, in [16] different data fusion methods were used (e.g. multiple linear regression (SMLR), partial least squares regression (PLSR) and principal components analysis combined with stepwise multiple linear regression (PCA+SMLR) techniques) to predict multiple soil properties. Authors' conclusions indicate that data fusion techniques are more relevant in clayey field and worse in sandy field and, in addition, these methods can improve the quality of soil sensing in precision agriculture if appropriate sensors are selected. Later, in 2017, sensor data fusion for soil health assessment was applied in [17] and, as a result, faster determination of soil health was achieved by merging data gathered from all sensors. In a more advanced manner, in [18] sensing data fusion methods are involved in crop detection. Authors use an efficient method of fusing multi-source remote sensing images with a convolution neural networks (CNN) for semantic segmentation to identify crops (93% succesful rate) in detecting and identifying crops.

In this paper we use data fusion technique on agricultural KPIs to fill the gaps and to create a complete picture of their variation even in the absence of their recording by the telemetry system.

3. ADCON-based Architecture of Telemetry System

Monitoring of KPIs (such as air and soil temperature, crop state, air and soil relative humidity) for a vine located in a residential area close to Bucharest was performed using an ADCON-based telemetry system (called SmartAgro). The selected season was spring since it is a season in which high variations may be observed because of the transition from winter to summer (two seasons with extreme temperatures). Figure 1 illustrates the new concept of SmartAgro telemetry system in which different dedicated agricultural sensors are interconnected for main parameter's monitoring.

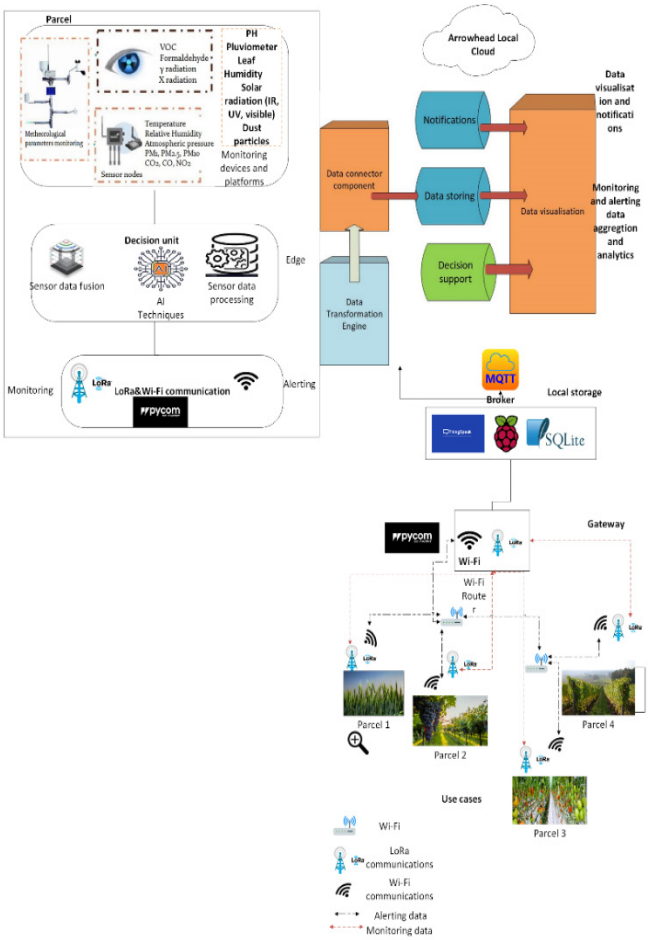


Figure 1: SmartAgro innovative architecture [19]

The data acquired from the agricultural sensors were centralized into a database and were used to highlight the impact of measured parameters on crops [19]. The architecture differs from the traditional ones by introducing two new levels consisting in: *The Edge level*: at this level telemetry data are passed through a decision-making system based on artificial intelligence techniques for data analysis and detection of abnormal values. Also, at this level, the data are classified as belonging to alert scenarios or simple monitoring. This determines the optimization of communication, in terms of traffic and energy consumption. LoRa technology is proposed for monitoring data, a technology known for extremely low energy consumption and for the field very extensive coverage. For scenarios involving alerts and critical change of parameters, Wi-Fi (short range) or 4G technology can

still be used for a large coverage area. Further, *the Local Storage level* has a role in storing relevant, processed, analysed, and labelled data to reduce latencies in alert scenarios and for applications. on-field, off-line. Additional functionalities of the proposed telemetry system are given in [19].

4. Extended monitoring results

To demonstrate the reliability of the system, extended monitoring results are presented. The measurements were performed in 2019 and 2020 and the data were acquired each 6 hours per day, starting with 8 a.m.

4.1. Air temperature monitoring

Figure 2 illustrates the variation of air temperature during Spring of 2019 and 2020.

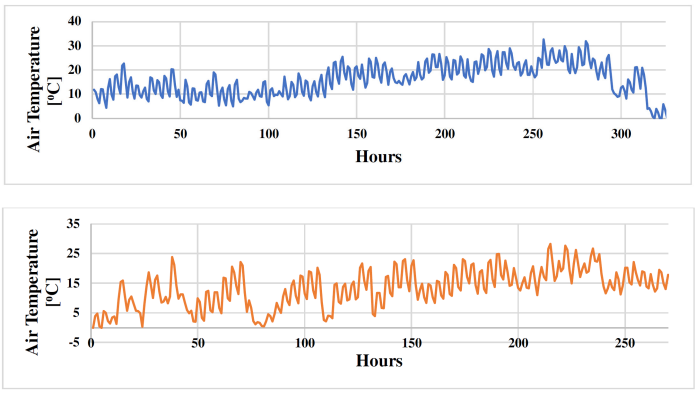


Figure 2: Air temperature variation in Spring 2019 (up), Spring 2020 (down)

Based on results in Figure 2, it can be seen the patterns of the day-night air temperature variation, also called Day/Night Differential (DIF). Higher temperature peaks can be observed in Figure 3. DIF value has multiple significances: firstly, DIF values were related to plant growth. Moreover, values of DIF around 8°C were proved to provide the best plant growth, whereas DIF values between 12°C and 22°C showed a low correlation to the predicted results in [20] for Chrysanthemum.

From the air temperature data provided by SmartAgro platform in the two seasons (Spring 2019 and Spring 2020), we can state that in Spring 2019 the plant growing should have been more pronounced, as the DIF was lower than 12°C.

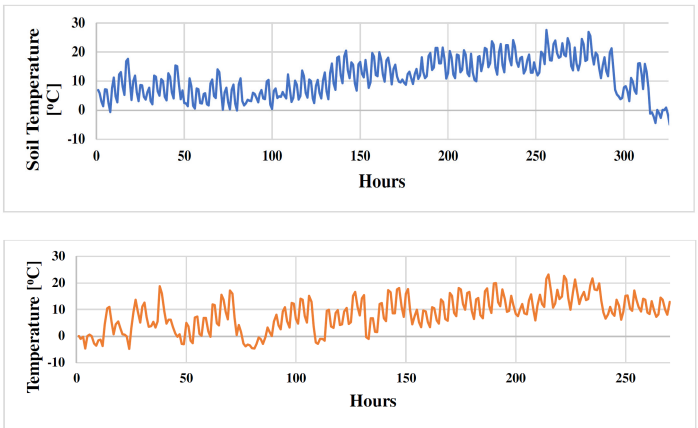


Figure 3: Soil temperature variation in Spring 2019 (up), Spring 2020 (down)

4.2. Soil temperature monitoring

From Figure 3, which outline the variation of soil temperature for Spring 2019 and Spring 2020, there can be observed that the patterns are identical with their correspondent air temperature data in Spring 2019 and, respectively, in Spring 2020, with the exception of a temperature offset of -5°C for both Spring 2019 and for Spring 2020.

4.3. Relative air humidity monitoring

From Figure 4, which depicts the variation of relative air humidity for Spring 2019 and Spring 2020, it can be observed that the supersaturation phenomenon was similarly frequent in both years. This is related to the prediction of the rainfall and appears when the air humidity reaches 100%.

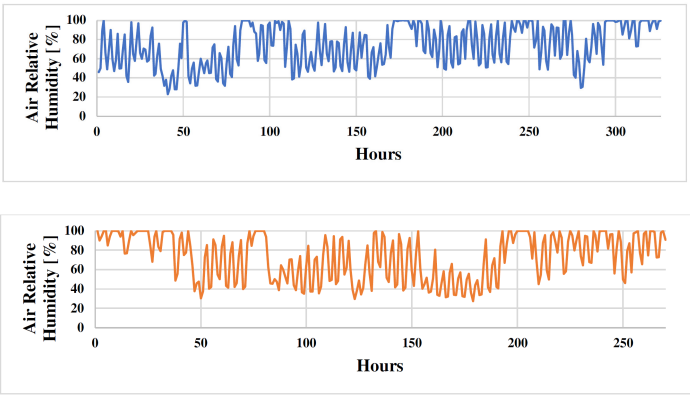


Figure 4: Relative air humidity variation in Spring 2019 (up), Spring 2020 (down)

4.4. Relative soil humidity monitoring

Figure 5 emphasizes the variation of relative soil humidity for Spring 2019 and 2020.

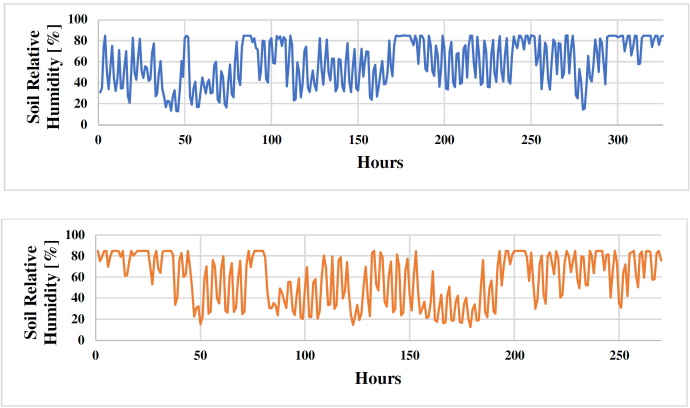


Figure 5: Relative soil humidity variation in Spring 2019 (up), Spring 2020 (down)

From Figure 5, it can be noticed that, similar to the soil and ambient temperature, the soil and ambient humidity follows the same pattern, with an offset of -15% both in Spring 2019 and in Spring 2020.

4.5. Leaf wetness monitoring

Figure 6 presents the leaf wetness variation for Spring 2019 and 2020. It can be observed that several peaks occur especially

after 21:00 p.m. From the analysed data, there is no evidence of correlation between the air humidity and the leaf wetness, nor between air temperature and leaf wetness.

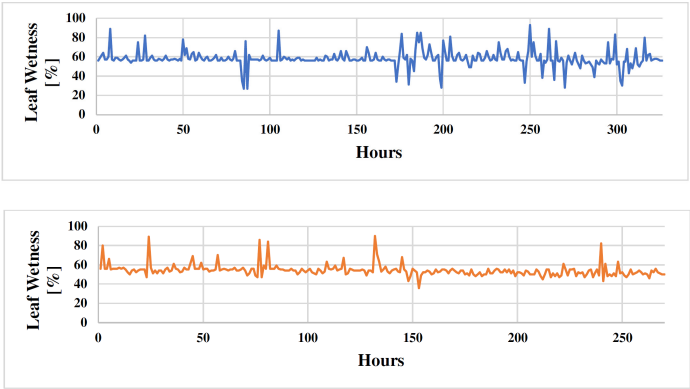


Figure 6: Leaf wetness variation in Spring 2019 (up), Spring 2020 (down)

5. Agricultural Data Analysis

The previous graphical representations did not reveal the absence of some data or the heterogeneity of the data. For example, from the previous graphs there cannot be noticed the absence of the samples for certain moments of the day or even the fact that the samples were not acquired at the same moment every day. Moreover, the data were not acquired each day.

The time intervals for data collection are March 4th, 2019 and May 31st, 2019 (Spring 2019) and March 1st, 2020 and May 28th, 2020 (Spring 2020), respectively. Analysing data of a real acquisition, it can be remarked that the samples were collected at the time moments given in Table 1.

Table 1: Classification of the samples based on the moment of acquisition

Hours (0-24)	No. of Days (ND)	ND (2019)	ND (2020)	Total Samples
3, 9, 15, 21	98	57	41	392
2, 8, 14, 20	48	23	25	192
3, 9	1	0	1	2
9, 15, 21	3	2	1	9
2	1	0	1	1
	Total			**596**

Unfortunately, missing data determine different issues concerning the predictions and forecasts or the decisions taken by the support decision systems integrated in the overall architecture. Nevertheless, sensor data fusion techniques can bring many benefits such that the faults triggered by the data gaps can be mitigated. For exemplification, two variables are considered: air temperature and soil temperature. They were chosen after the analysis of the samples acquired because the vectors storing their values comprise NaN values, that is, there are missing samples in air temperature and soil temperature data because of system failures.

In Figure 7, it is illustrated the graphical representation of the air temperature variation at 3 a.m. and 2 a.m. for each of the days in which the data were collected, more precisely, in the intervals March 4th, 2019 and May 31st, 2019 (88 days) and March 1st, 2020 and May 28th, 2020 (88 days). Figure 7 highlights small, but important, data gaps.

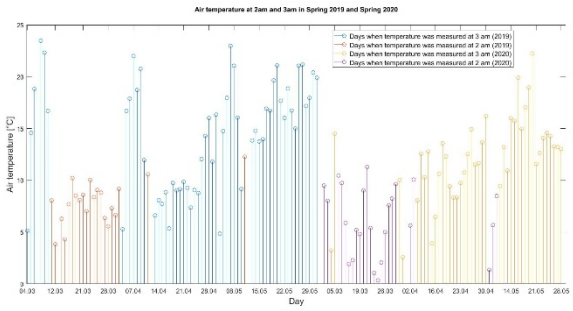


Figure 7: Air temperature measured at 2am and 3am in Spring 2019 and Spring 2020

In Figure 8, it is highlighted the soil temperature variation during the same seasons, and it can be noticed that also soil temperature data is missing. In addition, as previously mentioned, the soil temperature follows the same variation pattern as in the case of air temperature and, by computing the difference between air and soil temperature, a constant value of 5°C is determined. Therefore, finding a method to determine an approximate value for air temperature will also succeed in determining the approximate value for soil temperature, too, and vice versa.

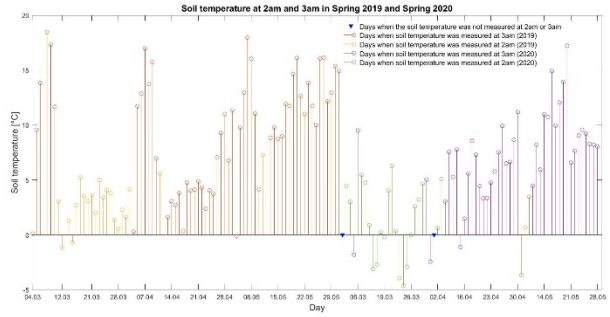


Figure 8: Soil temperature measured at 2am and 3am in Spring 2019 and Spring 2020

Further, the choice of soil temperature and air temperature variables will be justified with respect to the variation of the other parameters. Analyzing the graphical representation of air relative humidity (Figure 9), soil humidity (Figure 10) and leaf wetness (Figure 11) variations, missing data can be also observed (samples missing before and after March 13, 2019), but the data gaps are affecting all variables. The only variables that experience isolated data gaps when all the other parameters are represented are soil temperature and air temperature.

In Figure 9, air relative humidity variation for the same moment of day for Spring 2019 and Spring 2020 is represented. It can be observed that the minimum air relative humidity recorded in Spring 2019, at 2 a.m., is 37.78 % and it was recorded on March 24th, 2019, while the maximum value of 100% was reached 7 times (March 11-12, 2019; March 15, 2019; April 11th-12,2019; May 11th-12,2019).

Regarding the air relative humidity measured at 3 a.m., in Spring 2019, the minimum value was 55.74% on March 9th, 2019,

while the maximum value (100%) was reached 10 times (10% in March, 40% in April, 50% in May).

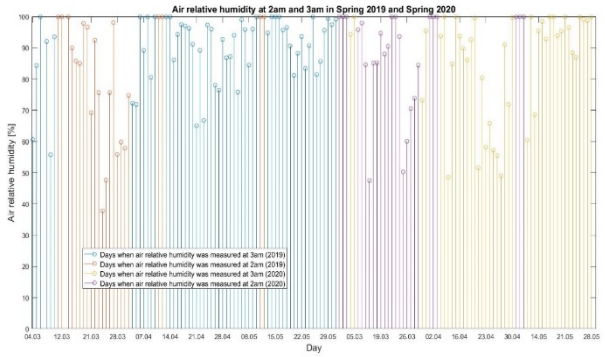


Figure 9: Air relative humidity measured at 2am and 3am in Spring 2019 and Spring 2020

In Spring 2020, the minimum value of the air relative humidity measured at 2 am was 47.45% on March 16, 2020, whereas the maximum value (100%) recorded at 2 a.m. was reached 10 times (40% in March, 30% in April and 30% in May).

Concerning the samples acquired at 3 a.m. in Spring 2020, the minimum value of air relative humidity was recorded on 13.04.2020 (48.57%), whereas the maximum value of 100% was reached 9 times (22.2 % in March, 11.1% in April and 66.7% in May).

Computing the difference between soil humidity and air humidity, a constant difference of 15% is achieved and it can be seen that the variations patterns are identical (Figure 10). This can be proven also by computing the standard deviation (SD) for each season for the two possible time moments of acquisition (2 a.m. and 3 a.m.) for both variables. For both soil and air humidity variables, the values of the standard deviation coincide and are given in Table 2.

Table 2: Standard deviation of soil and air humidity for Spring 2019 and Spring 2020 (at 2am and 3 am)

Season	SD (2am)	SD (3am)
Spring 2019	19.49	10.92
Spring 2020	15.76	16.85

Therefore, by finding the approximate value of the air relative humidity, the approximate value of the soil humidity can also be determined.

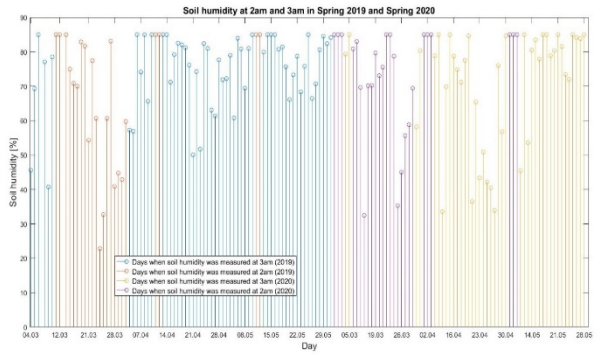


Figure 10: Soil humidity measured at 2am and 3am in Spring 2019 and Spring 2020

Finally, in Figure 11, the variation of the leaf wetness is depicted. The standard deviation (STD) of the leaf wetness parameter was computed.

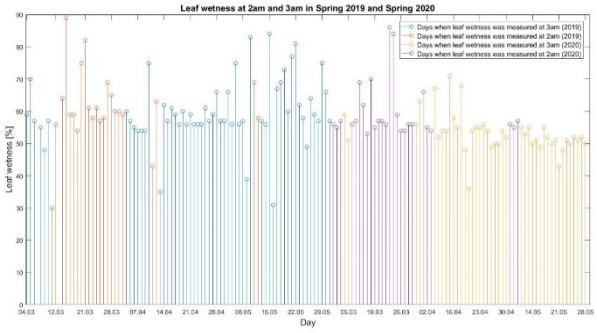


Figure 11: Leaf wetness measured at 2am and 3am in Spring 2019 and Spring 2020

The lowest values of SD were obtained for Spring 2020 3 a.m. (a small value with respect to Spring 2019 was also obtained for 2 a.m.), while the highest one is obtained for Spring 2019 (2 a.m.). The small variation of leaf wetness values in Spring 2020 is highlighted in the graphical representation, too. All values of the standard deviation are given in Table .

Table 3: Standard deviation of leaf wetness for Spring 2019 and Spring 2020 (at 2am and 3 am)

Season	SD (2am)	SD (3am)
Spring 2019	11.66	10.00
Spring 2020	8.64	6.04

6. Proposed data fusion algorithm

Next, based on the data analysis performed in Section 5, we proposed a data fusion algorithm based on a hybrid decision tree. Here, the hybrid attribute is given due to the fact that, with respect to the traditional binary tree approach, in the proposed algorithm three cases may arise: the value of the parameter is in range (1), the value of the parameter is out of range (2), the value of the parameter is not available (3). When a sample of a parameter is not available at the querying moment (case 3), the algorithm commands the estimation block that computes an estimated value of the parameter based on current samples of the other parameters and based on previous samples of the required parameter. In Figure 12, the proposed algorithm was depicted. In Table 4, the parameters acronyms and their meanings are given.

Table 4: Parameters acronyms and significance

Acronym	Significance
t_air	Normal air temperature range
t_soil	Normal soil temperature range
rh_air	Normal air relative humidity range
rh_soil	Normal soil relative humidity range
leaf_wet	Normal leaf wetness range
T_air	Current air temperature sample
T_soil	Current soil temperature sample
RH_air	Current air relative humidity sample
RH_soil	Current soil relative humidity sample
Leaf_w	Current leaf wetness sample

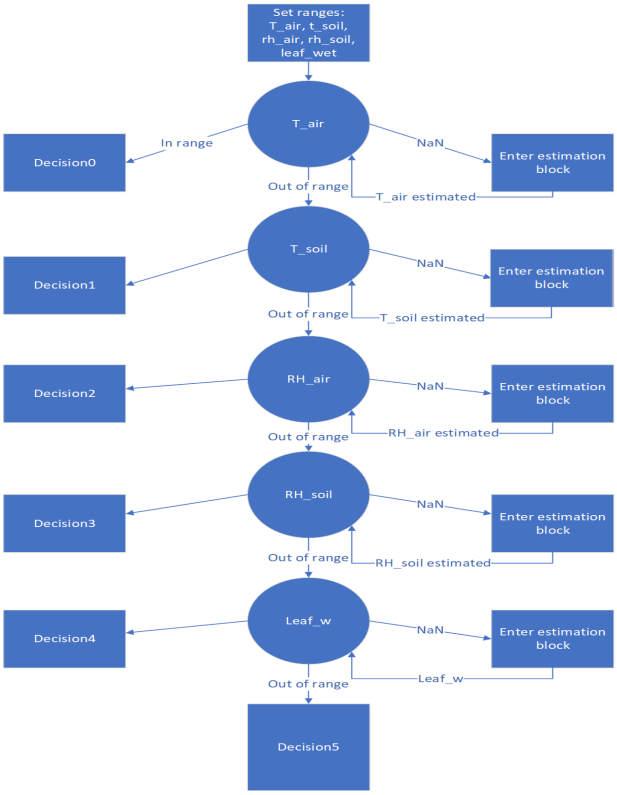


Figure 12: Hybrid decision tree for data fusion-based decision making

The correlation between the parameters is depicted in Figure 13-18.

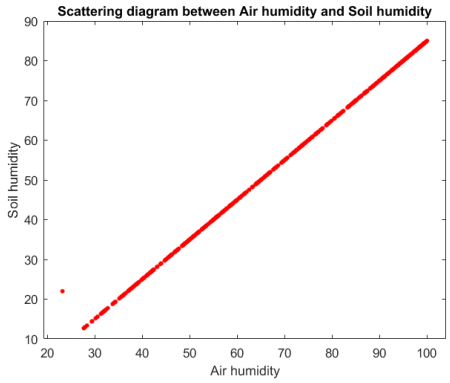


Figure 13: Scattering diagram of air humidity and soil humidity

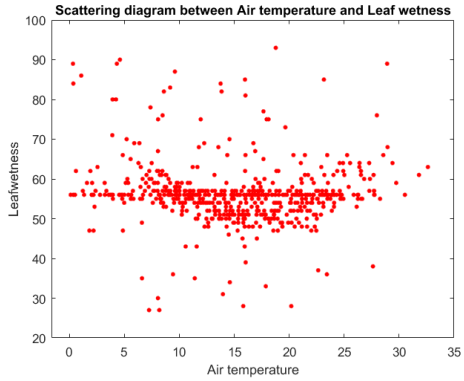


Figure 14: Scattering diagram of air temperature and leaf wetness

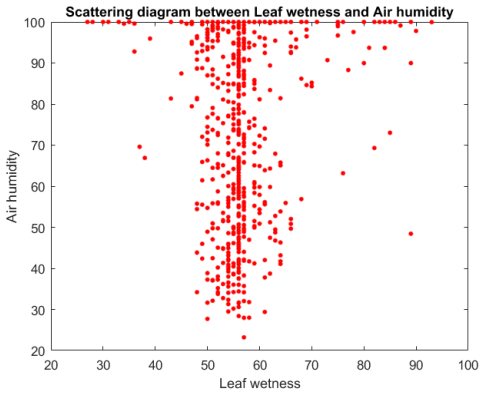


Figure 15: Scattering diagram of leaf wetness and air humidity

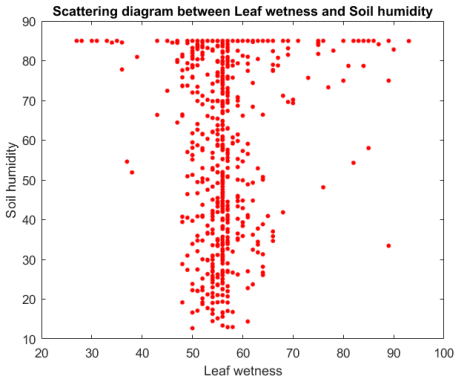


Figure 16: Scattering diagram of leaf wetness and soil humidity

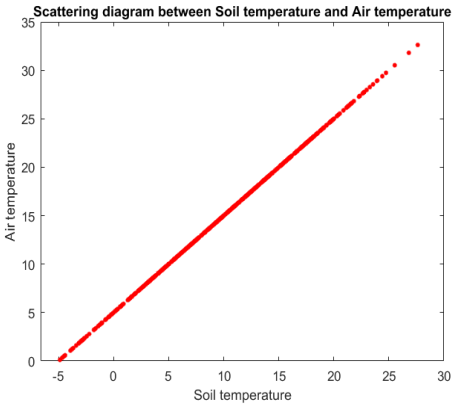


Figure 17: Scattering diagram of soil temperature and air temperature

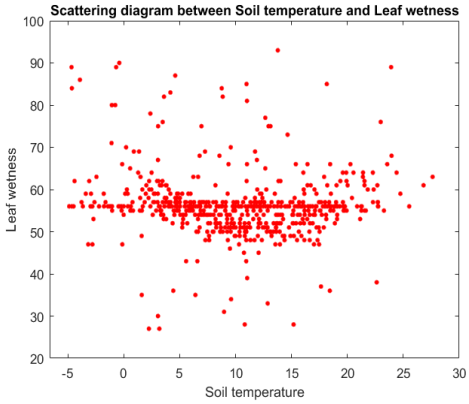


Figure 18: Scattering diagram of soil temperature and leaf wetness

7. Conclusions

Agriculture is an on-going evolving domain since worldwide survival depends in on it a great manner. Telemetry systems developed for crop and field monitoring (such as SmartAgro) play important roles in providing crucial KPIs related to air & soil temperature and/or air & soil humidity, as well as crop diseases detection. The architecture of the implemented SmartAgro system is highlighted by two relevant levels: The Edge level and the Local Storage level. They enable data classification and use parameters improvement in various cases such as alert scenarios and for applications. on-field, off-line.

Being equipped with multiple different, SmartAgro provides massive quantity of data for the monitored parameters. In this paper, the reliability of the recorded data provided by the telemetry system is outlined by performing measurements in 2 consecutive years (2019 and 2020) with a frequency of 6h/ day.

Based on the collected data related to the air temperature in Spring 2019 and Spring 2020, it can be noticed that Spring 2019 was a more favourable season for plant growing since the DIF was lower than 12°C. The variation of soil temperature led to the observation that the patterns are identical with their correspondent air temperature data in both seasons (Spring 2019 and Spring 2020). Further, by recording data on relative soil humidity and leaf wetness there was observed that there is no evidence of correlation between the monitored parameters. Yet, the similarities in variations during Spring 2019 and Spring 2020 demonstrates the reliability of the data recorded using SmartAgro telemetry system.

Since it was noticed that the monitored parameters have not been collected at the same moment in time with regularity, data fusion technique was used to fill the gaps and to provide a global overview on the behaviour of the system. Two KPIs have been considered: air temperature and soil temperature. Using data fusion, it was proven that:

- By finding a method to determine an approximate value for air temperature will also succeed in determining the approximate value for soil temperature, too, and vice versa.
- By finding the approximate value of the air relative humidity, the approximate value of the soil humidity can also be determined.

As conclusion, the goals of data fusion referring to advanced data management and coherence achievement among collected data were achieved within this research.

Conflict of Interest

The authors declare no conflict of interest.

Acknowledgment

The work presented in this paper was funded by SmartAgro project subsidiary contract no. 8592/08.05.2018, from the NETIO project ID: P_40_270, MySmis Code: 105976 and DISAVIT project, code EUROSTARS-2019-E!113655-DISAVIT/2020 and Operational Programme Human Capital of the Ministry of European Funds through Financial Agreement 51675/09.07.2019, SMIS Code 125125.

References

[1] I. Marcu, G. Suciu, C. Balaceanu, A.-M. Dragulinescu, M. A. Dobrea, "IoT Solution for Plant Monitoring in Smart Agriculture", 2019 IEEE 25th International Symposium for Design and Technology in Electronic Packaging (SIITME), Cluj-Napoca, Romania, Romania, Oct. 2019, DOI: 10.1109/ECAI46879.2019.9041952

[2] European Environment Agency, Climate change adaptation in the agriculture sector in Europe, EEA Report No 04/2019 (ISBN 978-92-9480-072-5)

[3] M. Uzunoglu, M. S. Alam, "Dynamic modeling, design, and simulation of a combined PEM fuel cell and ultracapacitor system for stand-alone residential applications" in IEEE Trans. Ener. Conv., **21**(3), 767–775, 2006. https://doi.org/10.1109/TEC.2006.875468

[4] I. Hadade, T. M. Jones, F. Wang, L. di Mare, "Software Prefetching for Unstructured Mesh Applications" in 2018 IEEE/ACM 8th Workshop on Irregular Applications: Architectures and Algorithms (IA3), Dallas, TX, USA, 2018. https://doi.org/10.1109/IA3.2018.00009

[5] H. Lihua, "Analysis of Fuel Cell Generation System Application," Ph.D Thesis, Chongqing University, 2005.

[6] https://blog.agrivi.com/post/measuring-kpis-for-increasing-productivity

[7] M. H. Nehrir, C. Wang, Modeling and Control of Fuel Cells: Distributed Generation Applications, Wiley-IEEE Press, 2009.

[8] R. Martínez, JA Pastor, B. Álvarez, A. Iborra, "A Testbed to Evaluate the FIWARE-Based IoT Platform in the Domain of Precision Agriculture" Sensors (Basel). 2016; **16**(11):1979, 2016. doi:10.3390/s16111979

[9] F.J. Ferrández-Pastor, J.M. García-Chamizo, M. Nieto-Hidalgo, J. Mora-Martínez, "Precision Agriculture Design Method Using a Distributed Computing Architecture on Internet of Things Context" Sensors (Basel). **18**(6):1731, 2018. doi:10.3390/s18061731

[10] C. Kamienski, J.P. Soininen, M. Taumberger, et al. "Smart Water Management Platform: IoT-Based Precision Irrigation for Agriculture" Sensors (Basel). 2019; **19**(2), 276. Published 2019. doi:10.3390/s19020276

[11] E-agriculture in Action: Big Data for Agriculture. Bangkok, FAO and ITU. 2019. Available online: http://www.fao.org/3/ca5427en/ca5427en.pdf

[12] X. Shi, X. An, Q. Zhao, H. Liu, L. Xia, X. Sun, Y. Guo, "State-of-the-Art Internet of Things in Protected Agriculture", Sensors (Basel). 2019 Apr; **19**(8): 1833, 2019

[13] A. de Juan, R. Tauler, Data Fusion Methodology and Applications, Elsevier, 2019

[14] P. Rashinkar, V. S. Krushnasamy, "An overview of data fusion techniques" in 2017 International Conference on Innovative Mechanisms for Industry Applications (ICIMIA), Bangalore, India, 2017, DOI: 10.1109/ICIMIA.2017.7975553

[15] L. Comba, A. Biglia, D. Ricauda Aimonino, P. Barge, C. Tortia, P. Gay, "2D and 3D data fusion for crop monitoring in precision agriculture" in 2019 IEEE International Workshop on Metrology for Agriculture and Forestry (MetroAgriFor), Portici, Italy, 2019, DOI: 10.1109/MetroAgriFor.2019.8909219

[16] H. S. Mahmood, W. B. Hoogmoed, E. J. van Henten, "Sensor data fusion to predict multiple soil properties", Precision Agric **13**, 628–645, 2012. DOI 10.1007/s11119-012-9280-7

[17] K. S. Veuma, K. A. Suddutha, R. J. Kremerb, N. R. Kitchena "Sensor data fusion for soil health assessment" Geoderma **305,** 53–61, 2017.

[18] J. Pena, Y. Tan, W. Boonpook, "Semantic segmentation based remote sensing data fusion on crops detection", Journal of Computer and Communications, **7**(7), 53-64., 2019 DOI: 10.4236/jcc.2019.77006

[19] I. Marcu, G. Suciu, C. Bălăceanu, A. Vulpe, and A.-M. Drăgulinescu, "Arrowhead Technology for Digitalization and Automation Solution: Smart Cities and Smart Agriculture" Sensors, **20**(5), 1464, Mar. 2020.

[20] SM Carvalho, E Heuvelink, R Cascais, O. van Kooten. Effect of day and night temperature on internode and stem length in chrysanthemum: is everything explained by DIF?. Ann Bot. **90**(1):111-118, 2002. doi:10.1093/aob/mcf154

ASTES

Advances in Science, Technology and Engineering Systems Journal Vol. 5, No. 5, 1273-1281 (2020)

www.astesj.com

Special Issue on Multidisciplinary Innovation in Engineering Science & Technology

ASTESJ

ISSN: 2415-6698

Laser Deprocessing Technique and its Application to Physical Failure Analysis

Yanlin Pan*, Jia Rui Thong, Pik Kee Tan, Siong Luong Ting, Chang Qing Chen

GLOBALFOUNDRIES Singapore Pte. Ltd., QRA-EFA, Singapore, 738406, Singapore

ARTICLE INFO

Article history:
Received: 26 August, 2020
Accepted: 18 October, 2020
Online: 24 October, 2020

Keywords:
Laser deprocessing
PFA
Bit-counting
TEM

ABSTRACT

This paper is an extension of work originally presented in IPFA 2019. In the original work, a new memory bit-counting method in physical failure analysis (PFA) using laser deprocessing technique (LDT) is introduced. In the present paper, LDT will be further exploited and the methodology applied to PFA will be fully discussed. Compared to the conventional methods that involve high-cost equipment such as focused ion beam (FIB) and reactive ion etcher (RIE), the novel LDT method using a laser system instead lowers the cost by more than 5 times and shortens the failure analysis (FA) cycle time by up to 45%. The new improved methodology can significantly increase PFA throughput especially in semiconductor foundries, and facilitate more applications in other types of FA labs.

1. Introduction

In modern electronic industry, the development of the integrated circuit (IC) design and technology node of semiconductor devices poses increasing challenges to PFA techniques due to the higher density of transistors and metal layers in a chip [1]. As one of the failure analysis (FA) branches for defect identification and yield improvement, PFA acts an important role in analyzing memory failure devices, where bit-counting and marking on the failed bits are necessary for the final physical imaging of the defect in transmission electron microscopy (TEM).



Figure 1: Illustration of typical PFA workflow for memory failure devices.

A typical PFA workflow for memory failure devices is illustrated in Figure 1. The workflow starts from RIE removing the inter-metal dielectric to expose the metal of each layer. Then it is followed by mechanical polishing using polisher with polishing slurry on the rotating cloth platen. During the polishing, optical microscope (OM) and scanning electron microscope (SEM) inspection are engaged to monitor and inspect the sample surface. When the sample reaches certain layers, bit-counting in the memory blocks of the device will be attempted to locate and mark the failed bits for TEM analysis.

In static random access memory (SRAM) devices, bit-counting in the memory blocks can be done as the sample reaches Metal2 (M2) or lower metal layer in which both bit lines (BLs) and word lines (WLs) are identifiable and countable. However, in the cases that request for critical dimension (CD) measurements on Via2 (V2) layer or cases where V2 deformation/void defect is highly suspected, traditional method of mechanically delayering away M3 that will damage part of V2 is no longer suitable. In non-volatile memory (NVM) devices, the memory bit-counting is even more challenging, since the metal layer (here it is M5) blocking the WLs directly lands on the memory cells (Figure 2a, b). There have been numerous FA studies on SRAM/NVM devices, from hard short/open failure [2-4] to subtle defect induced marginal failure [5-7]. After the electrical fault isolation (EFI) or bit-map analysis, memory bit-counting is the key step for TEM analysis or transistor-level probing to locate the defect. Prior to the laser deprocessing technique (LDT) assisted method was developed, there were two conventional methods of bit-counting used in SRAM/NVM device.

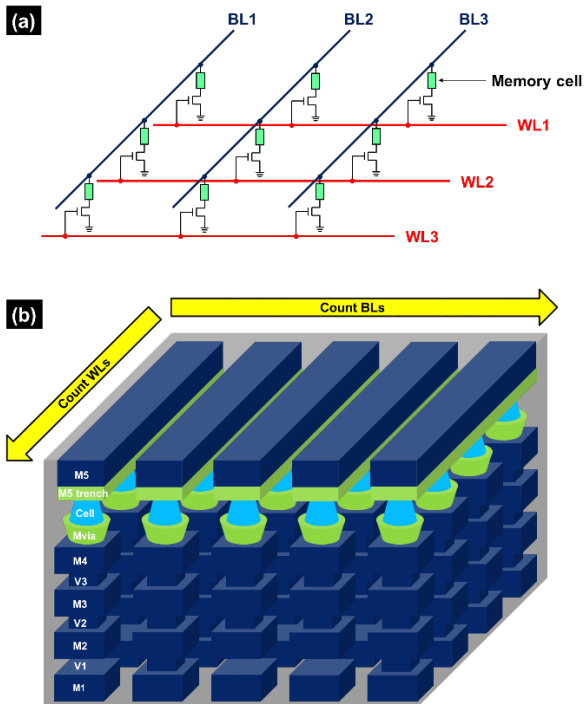


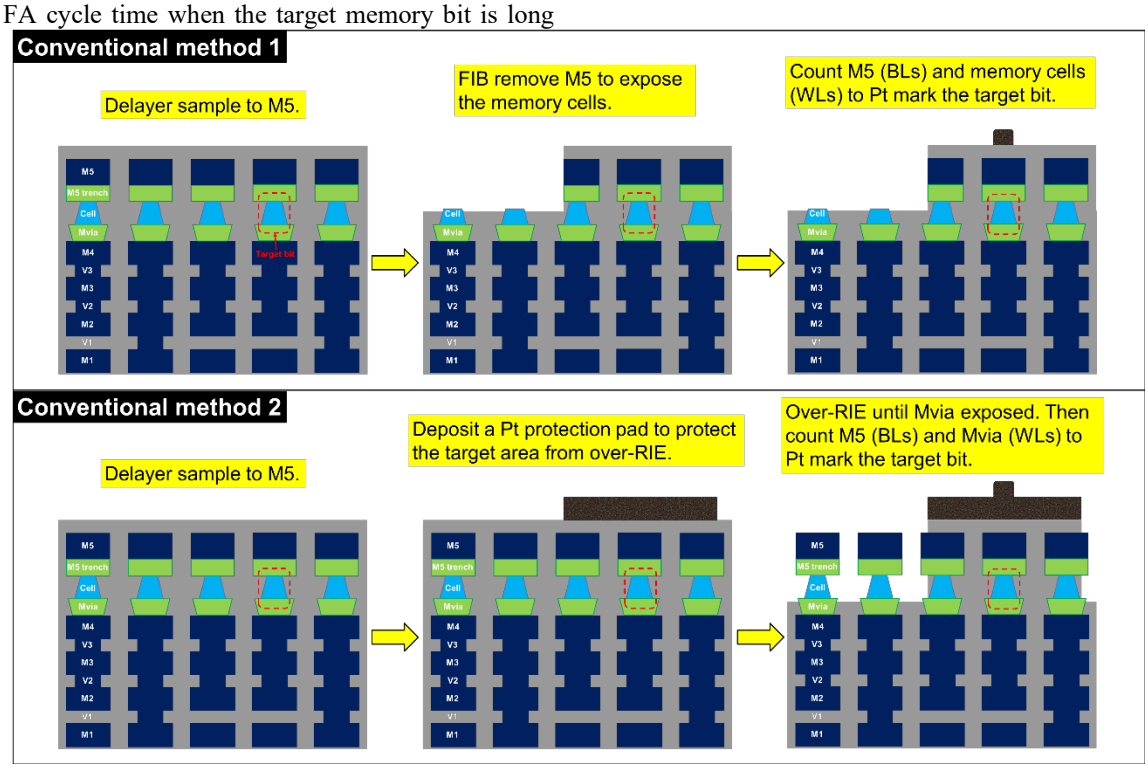
Figure 2: Typical circuit diagram (a) and bit-counting (b) of memory arrays in NVM devices.

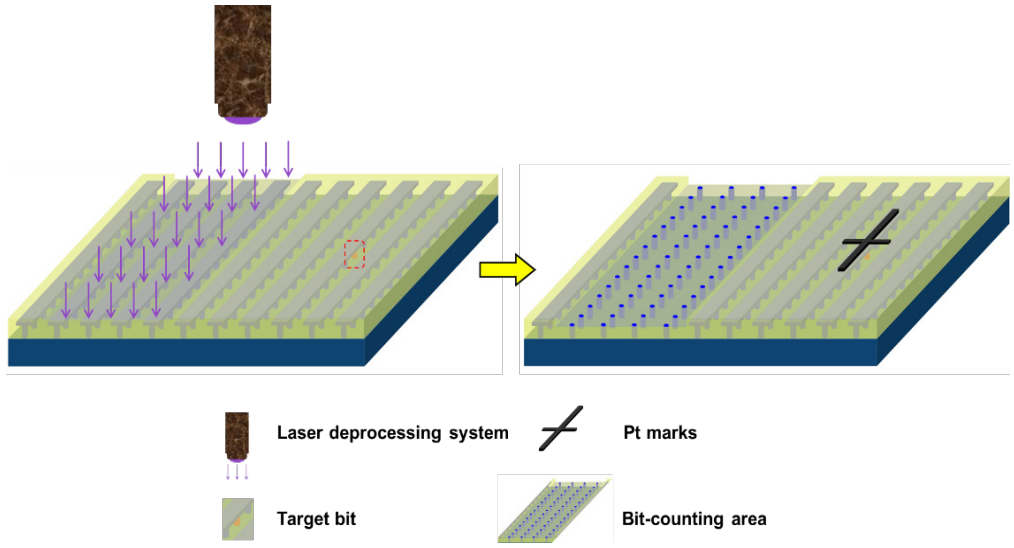
One method is using focused ion beam (FIB) to remove M5 near the target BL to count the exposed cells as counting WLs. The other method is over-RIE the sample surface to expose and count the Memory Via (Mvia) as WLs (Figure 3). The first method has the advantages of real-time monitoring and localized milling, however it requires a FIB-SEM dual-beam system of which the cost is much higher than that of a SEM single-beam system, and much longer FA cycle time when the target memory bit is long distance from the memory block edge. The second method needs only a SEM single-beam system, but it comes with possible sample damage from the Pt protective pad missing the target memory bit. Besides this, for advanced technology node such as 28nm or below, the Mvia size deceases smaller than that of M5, which makes the method by over-RIE not workable. Therefore, new methods with fast cycle time and low cost for the bit-counting in memory devices are highly desired.

In this paper, we will introduce an innovative LDT assisted memory bit-counting method that is applicable to both SRAM and NVM devices. LDT is fast, simple, and has been used to secure an uneven sample surface and remove unwanted layers [1, 8]. LDT employs pulse laser with high peak power to irradiate the sample and physically remove material from the surface, which is economical, efficient, and user-friendly. Moreover, through a systematical parametric study, LDT is able to create uniform deprocessed surface in a large area on various types of materials.

2. Experiments

The experiments were conducted on a 40 nm SRAM device and a 28 nm NVM device. A mechanical polisher (ALLIED HighTech TwinPrep 5) with polishing cloth (Spec-Cloth), and polishing slurry (0.05 µm or 3 µm diamond suspension) was used for mechanical polishing. A SEM single-beam system (FEI Magellan^{TM} 400L) equipped with a gas injection system was used for sample inspection and Pt marking. An optical microscope (ZEISS Axiotron) was used for optical inspection on the sample surface. For LDT, a laser system (New Wave Research Ezlaze3) was used for the sample deprocessing. The laser source emits a pulse laser (wavelength: 532 nm, energy range: 0 to 0.6 mJ, pulse width: ~5 ns) which was integrated into a probe station (Cascade Microtech PM5).





Parameters including laser output power, number of laser shots, and magnification of optical lens were studied on the dummy area of the NVM sample at M5 level. For different devices and materials, the same workflow can be followed to obtain the optimal parametric condition for laser deprocessing in each case. The window size of the laser is adjustable without power shift. Maximum size for 20× lens magnification was 150 µm × 150 µm. TEM sample preparation was performed using a FIB-SEM dual-beam system (FEI Helios NanoLab 450S). TEM analysis and energy dispersive X-ray (EDX) mapping were performed using a 200 kV Field Emission TEM (JEOL JEM-2100F) equipped with a SDD-EDX detector (Oxford X-MaxN 100TLE).

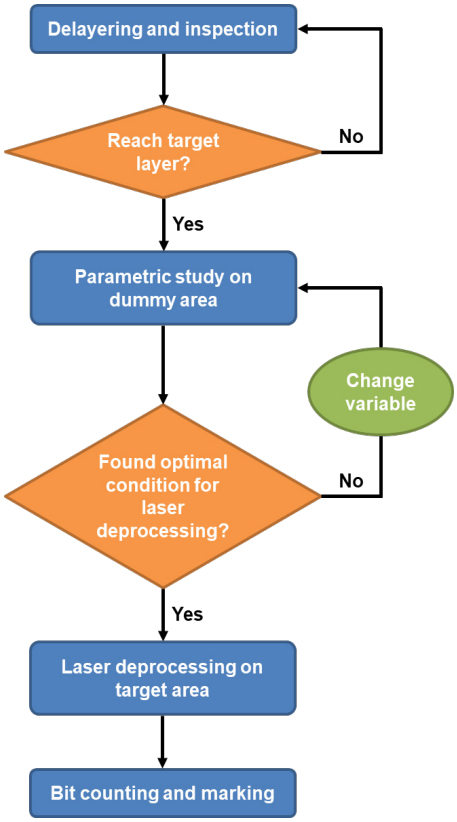


Figure 5: LDT assisted PFA workflow for memory failure devices.

A schematic illustration of LDT in NVM devices is shown in Figure 4. Before the laser deprocessing on the target location, a series of parametric experiments were carried out on the dummy area. Figure 5 shows the LDT assisted PFA workflow for memory failure devices. Here the parametric variables include the work mode of laser energy, attenuation level, lens magnification, and the number of laser shots. For the selection of each parameter, we used parametric arrays to determine the optimal condition in terms of the surface uniformity of the deprocessed sample. A uniform sample surface is critical to the bit-counting accuracy. Any false counting could result in missing the defect.

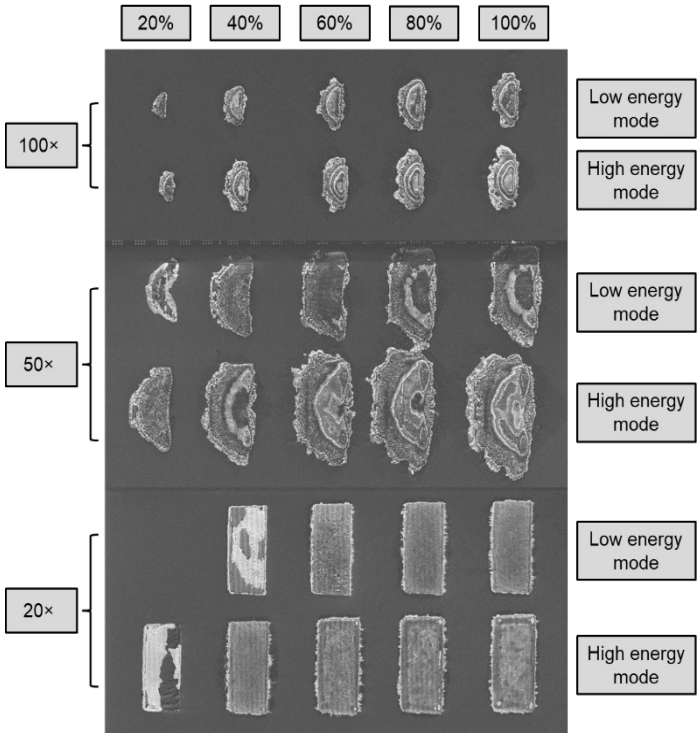


Figure 6: SEM images of the laser deprocessed surfaces of the NVM devices under different energy mode, attenuation level (%), and lens magnification.

2.2. Selection of laser power and lens magnification

Figure 6 shows the SEM images of the laser deprocessed surfaces of the NVM devices under different laser power and lens magnification. From the results, we can see that 100× and 50× lens created a very uneven and deformed surface with multiple layers exposed, regardless of energy mode and attenuation level. So we narrowed down the selection to 20× lens arrays. In low energy mode, 80% attenuation level delivered the most uniform deprocessed surface at the NVM cell level. In high energy mode, the best results were delivered by 40% attenuation level.

The surface uniformity of low energy mode at 80% attenuation level and high energy mode at 40% attenuation mode are comparable for the bit-counting, as shown in Figure 7. However, in low energy mode, the 100% attenuation level makes use of 0.2 mJ of energy while in high energy mode, at 100% attenuation level, the machine makes use of 0.6 mJ of energy. Therefore, output energy of 80% attenuation level in low energy mode is 0.8 × 0.2 mJ = 0.16 mJ, which is lower than 0.4 × 0.6 mJ = 0.24 mJ for 40% attenuation level in high energy mode. Considering the fact that lower laser energy is safer for the sample, low energy mode and 80% attenuation level were selected for the laser deprocessing for memory bit-counting.

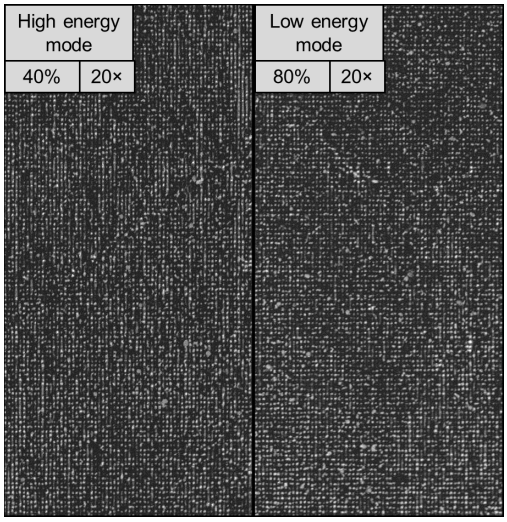


Figure 7: High magnification SEM images of the laser deprocessed surfaces of the NVM devices under 40% attenuation level in high energy mode and 80% attenuation level in low energy mode.

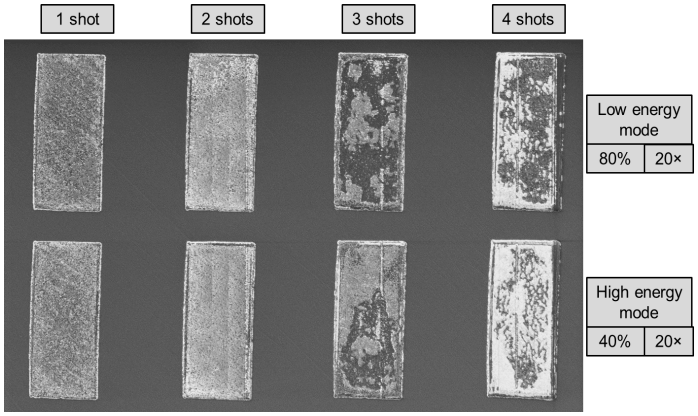


Figure 8: SEM images of the laser deprocessed surfaces of the NVM devices under different number of laser shots.

The experiments above were all from a single laser shot. In this section, using the lens and the attenuation level selected for each energy mode, a boundary test was performed on the maximum number of laser shots on the same surface before the surface becomes uneven again. In some cases, the layer on top of the bit-counting layer might be too thick and need more than one shot of laser to remove. Figure 8 shows the SEM images of the laser deprocessed surfaces of the NVM sample under different numbers of shots. It can be seen that the surfaces for each shot started to become uneven after the second shot was made on the same surface. This could be due to that the third shot was shone on the critical interface between the non low-k dielectric layer (memory cells and Mvia) and the ultra low-k dielectric layer (M4 and below). The unevenness was greatly increased during the third shot because of the big difference in the mechanical removal rate (up to 10 times) between the non low-k and the ultra low-k materials [9]. The experimental results would differ from case to case. For this NVM device, one shot of laser which created uniform bit-counting area (Figure 7) was selected.

2.4. Boundary limitations of laser shots

To understand the damage induced by laser shots to the memory bits, TEM analysis was done on the boundary of the laser deprocessed area. The results (Figure 9) show that four bits (Bit 1, 2, 3, 4) adjacent to the deprocessing area were damaged by the laser shot due to the thermal effect. Similar to other parameters, boundary limitations are dependent on the sample materials and surface conditions, and should be studied on the dummy area first to avoid damaging to the target bits.

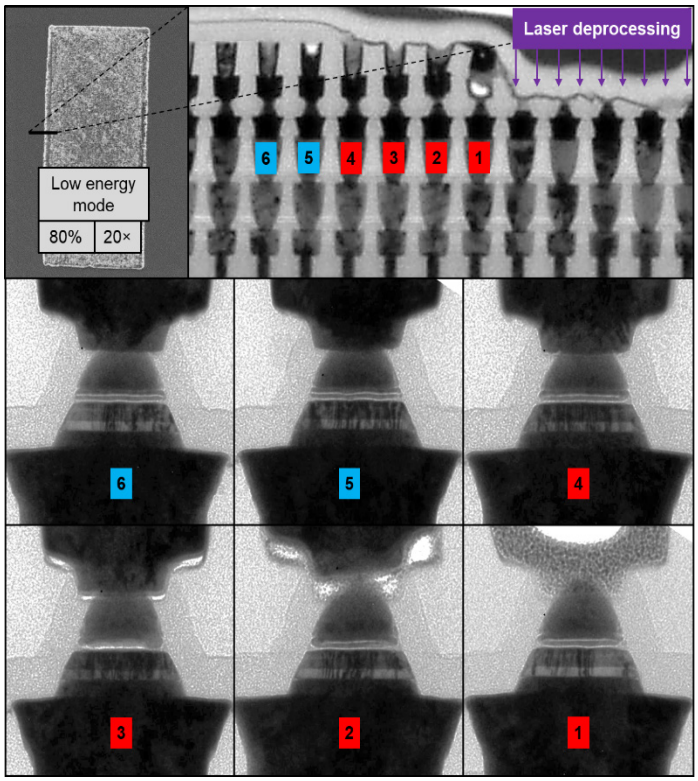


Figure 9: SEM images of the laser deprocessed surfaces of the NVM devices under different energy mode, attenuation level (%), and lens magnification.

2.5. Operation procedure of LDT assisted memory bit-counting

The procedure steps below describe how to utilize LDT to perform the memory bit-counting in SRAM/NVM devices.

1) Delayer the sample and stop at one layer before the bit-counting layer (M5 for NVM, M3 for SRAM) by mechanical polishing and inspection.
2) Make a SEM Pt mark at the target BL as a "sight" for the laser deprocessing process in OM (this step can be skipped for SRAM devices with small memory blocks).
3) Remove M5 (NVM) or M3 (SRAM) layer at certain distance (referring to the boundary limitations of laser shots) from the target BL to expose the memory cells by laser deprocessing (Figure 4). For SRAM devices, an extra deprocessed area for counting WLs is needed.
4) Water-polish the sample to clean the laser burst debris off the deprocessed area.
5) In the deprocessed area, count the exposed memory cells as WLs and M5 lines as BLs to locate the target bit from the NVM memory block (Figure 4). For SRAM devices, both WLs and BLs will also be identifiable and countable from M2 or below.
6) Make SEM Pt marks on the located target bit accordingly for TEM analysis (Figure 4).

Table 1: Operation time usage (in hours) of the conventional methods and the new LDT method for NVM devices.

	Pt mark target BL	Deposit Pt protection layer	Over RIE	FIB milling	Laser deprocessing	Counts WLs	Total
Conventional method 1	N/A	~0.6	~0.2	N/A	N/A	~0.7	~1.5
Conventional method 2	~0.3	N/A	N/A	~0.8	N/A	~0.5	~1.5
New method	~0.3	N/A	N/A	N/A	~0.1	~0.5	~0.9

In Table 1, the operation time usage of the conventional methods and the new LDT method for NVM devices are compared, which is evaluated under the same experimental conditions. The time usage of each operation step may vary with different devices, requirements of the cases and experiences of the operators. It can been seen that the LDT method can shorten the time usage by up to 45%.

Table 2: Summary of the advantages and disadvantages of the conventional methods and the new LDT method.

	Advantages	Disadvantages
Conventional method 1	Localized milling, real-time monitoring	High cost, Long FA cycle time
Conventional method 2	Low cost	Long FA cycle time, High risk of sample damaging, Not suitable for advanced technology node
New method	Low cost, Short FA cycle time	Sample dependent setting of laser parameters

Table 2 shows the advantages and disadvantages of the conventional methods and the new LDT method. Although the new method needs parametric study on the sample, the one-time effort eventually significantly saves FA time and FA cost.

3. Results and Discussion

3.1. Case study on NVM device

In this case, a 28 nm NVM device was performed with PFA using LDT. Figure 10 is the M5 graphic data system (GDS) layout of the device. After wafer sort, the bitmap information was provided in the data log. According to the e-test results, the NVM chip suffered from single-bit short failure (Figure 10).

The sample was polished to M5 layer, and then continued with LDT for bit-counting (Figure 11). First, a 45° angled e-beam Pt line mark was deposited in SEM as the reference for the laser deprocessing below the target BL (located by M5 GDS layout), and was deposited long and thick (SEM: 10 kV at 0.8 nA; Rate of deposition: 10 μm [length] × 2 μm [thickness] in 5 mins) to be clearly visible in OM. Second, at around 20 BLs to the right of the target bit, LDT was used to create a laser exposed area at the level of memory cells, in which the WLs were counted and marked according to the WL address. Finally, Pt marks were deposited on the located target bit for the following TEM analysis.

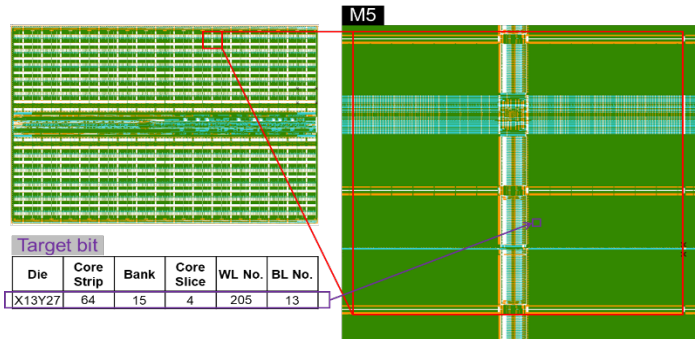


Figure 10: M5 GDS layout of 28 nm NVM device.

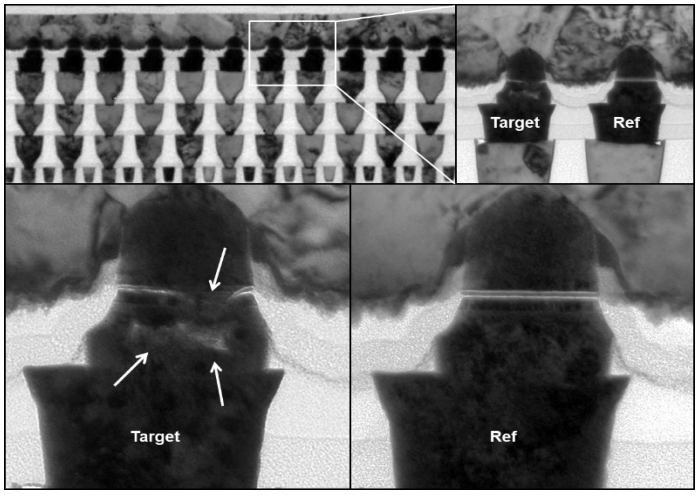


Figure 12: TEM images (Y direction along M5 as shown in Figure 11) of the failed bit and the reference bit.

TEM results of the sample are shown in Figure 12. From the TEM images, metal void and collapsed insulator layer were found at the failed bit. The metal void in the lower cell electrode should form in the first place, and then induce the uneven deposition of the insulation layer and the breakdown of the memory cell.

Figure 13 shows the scanning transmission electron microscope (STEM) images of another case where the TEM sample was cut across M5 to compare between different BLs from

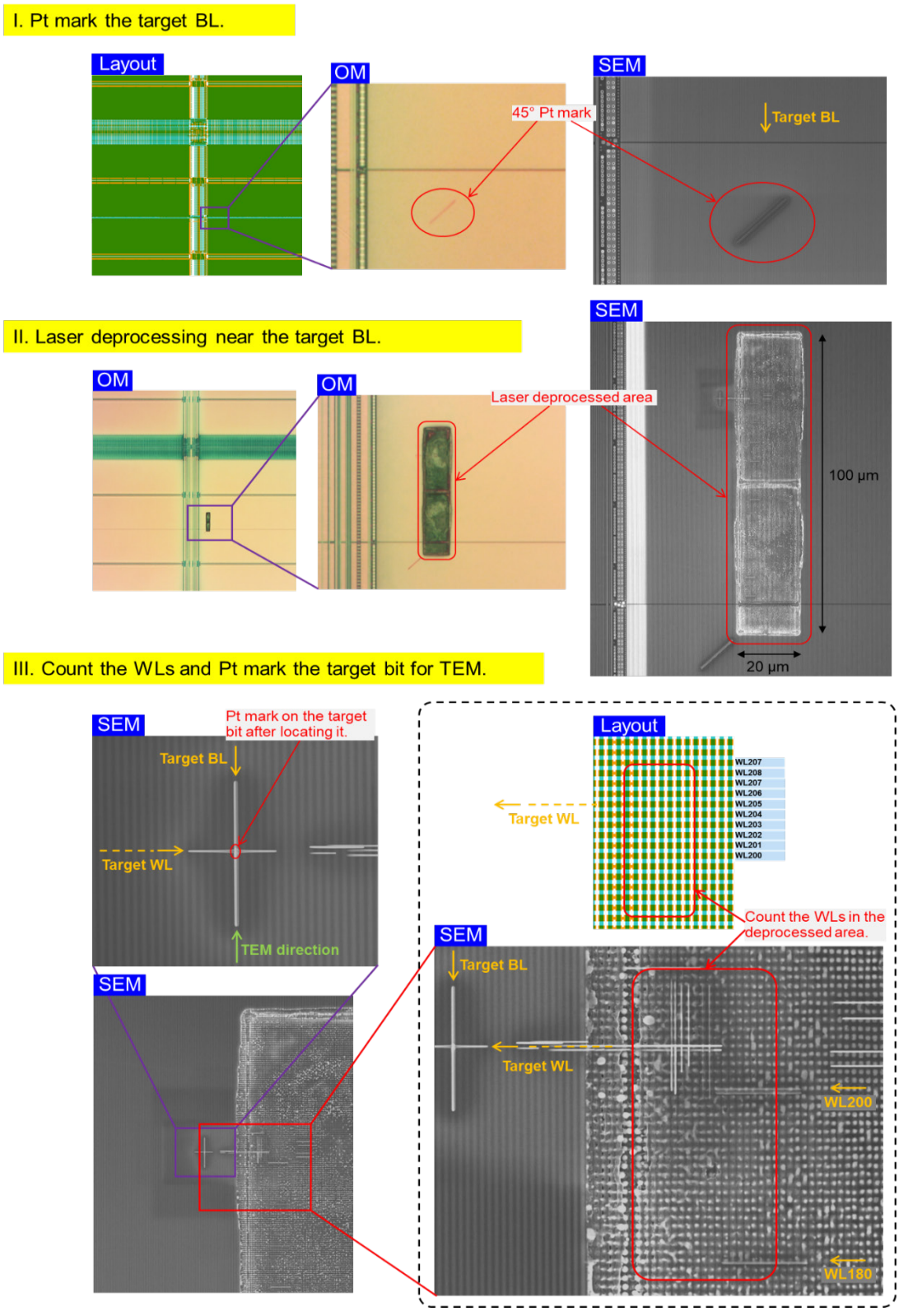


Figure 11: Schematic illustration of LDT assisted bit-counting at M5 in NVM devices.

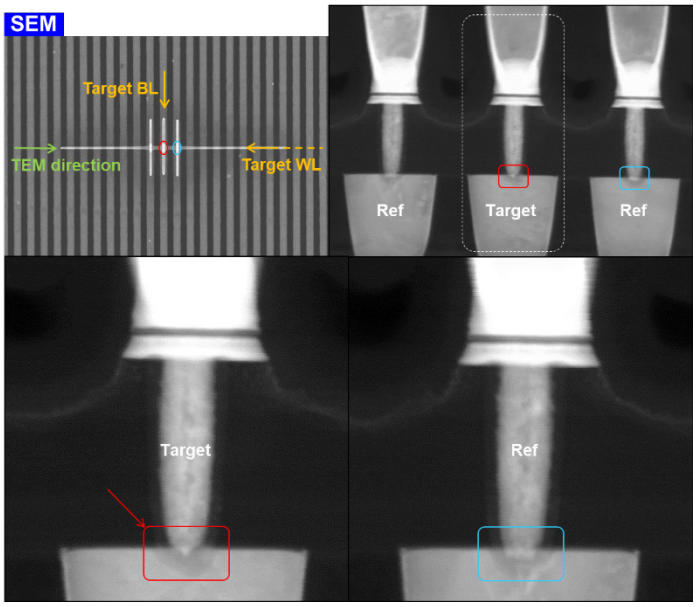


Figure 13: STEM images (X direction across M5) of the failed bit and the reference bit.

the same WL. From the results, abnormal profile at the bottom of the Mvia was found at the failed bit, which caused high landing resistance of the bit. It is worth to mention that, cutting along Y direction, even when the conventional methods aim at wrong WL by a few bits, the real target bit is usually still covered in the TEM sample so it can be corrected in the TEM analysis. However, in the X direction cut, wrong counting due to the insufficient exposing of the memory bits using conventional methods will result in missing the defect. Therefore, the LDT method offers the advantage of efficiently creating a bit-counting area and locating the target WLs in a high success rate.

3.2. Case study on SRAM device

In the SRAM case, a 40nm device with SRAM blocks was found to suffer from a 3-bits cluster failure. Through a series of analysis, Cu void defect in V1/V2 is suspected to result in the random wafer pattern, so the delayering must stop at M3 level to measure the V2 CD. However, without a reference, bit-counting at M3 is not practical, as seen from the GDS layout of SRAM devices (Figure 14). At M3, BLs and WLs are all not able to be properly identified. If we all the way polish to V2, the top portion of V2 will be damaged and the CD measurements will become impossible.

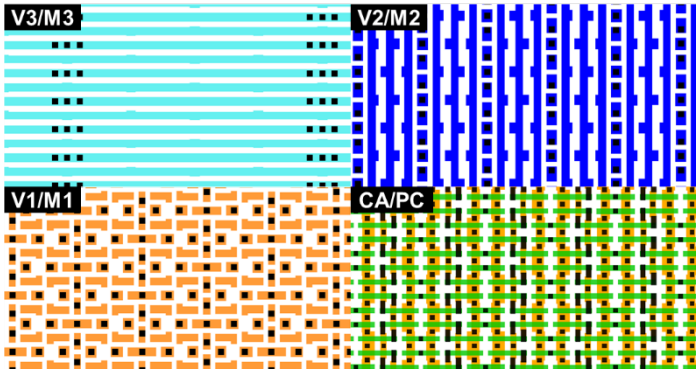


Figure 14: Typical GDS layout of SRAM devices.

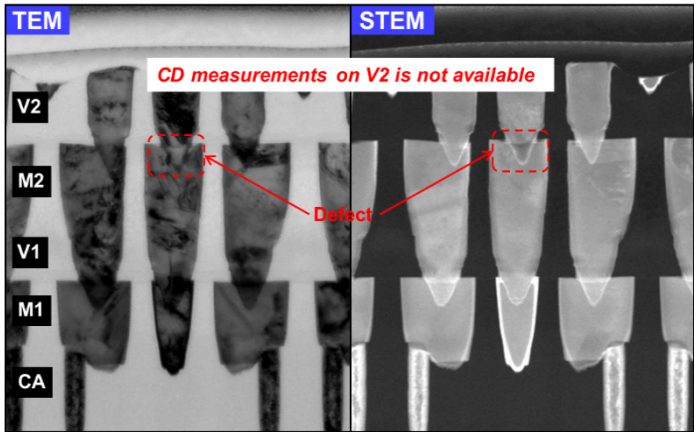


Figure 15: TEM/STEM images of a failed SRAM sample preparation. Top portion of V2 has been damaged.

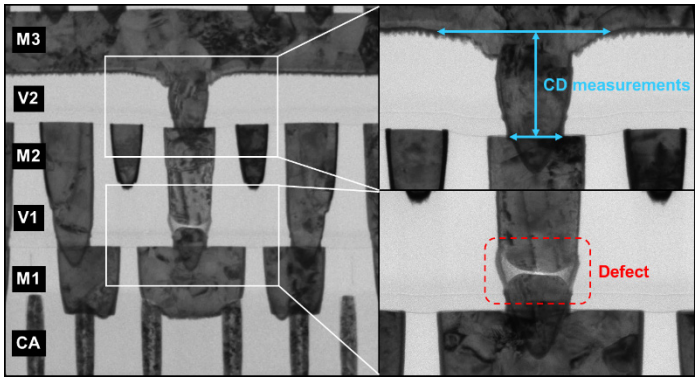


Figure 16: High/low magnification TEM imaging on the failed bits.

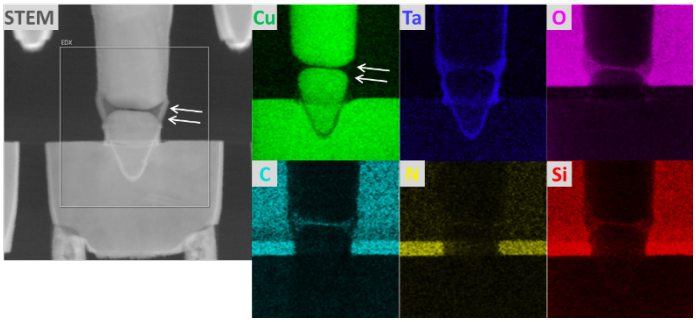


Figure 17: EDX mapping analysis on the failed bit. Defect of Cu void is observed, as arrowed in the Cu quant map.

Figure 15 shows a failed SRAM sample preparation. To solve the problem, we used LDT to create two reference areas (one for counting BLs and the other one for counting WLs) near the failed bit (Figure 18). In the reference areas, bits at V1/M1 level are clearly visible for the counting of WLs and BLs, while the target area is still at M3.

By counting and marking the WLs/BLs in the reference area, the failed bit was located and marked. TEM sample preparation was then performed on the marked bit. The TEM results are shown in Figure 16. From the high/low magnification TEM images, metal void was found at the bottom of V1. CD measurement on V2 was also taken. EDX analysis was then performed on the void area (Figure 17), in order to study the mechanism of the void formation. The EDX quant maps showed that Cu diffusion/migration occurred at the arrowed void area. Therefore, oxidation/corrosion

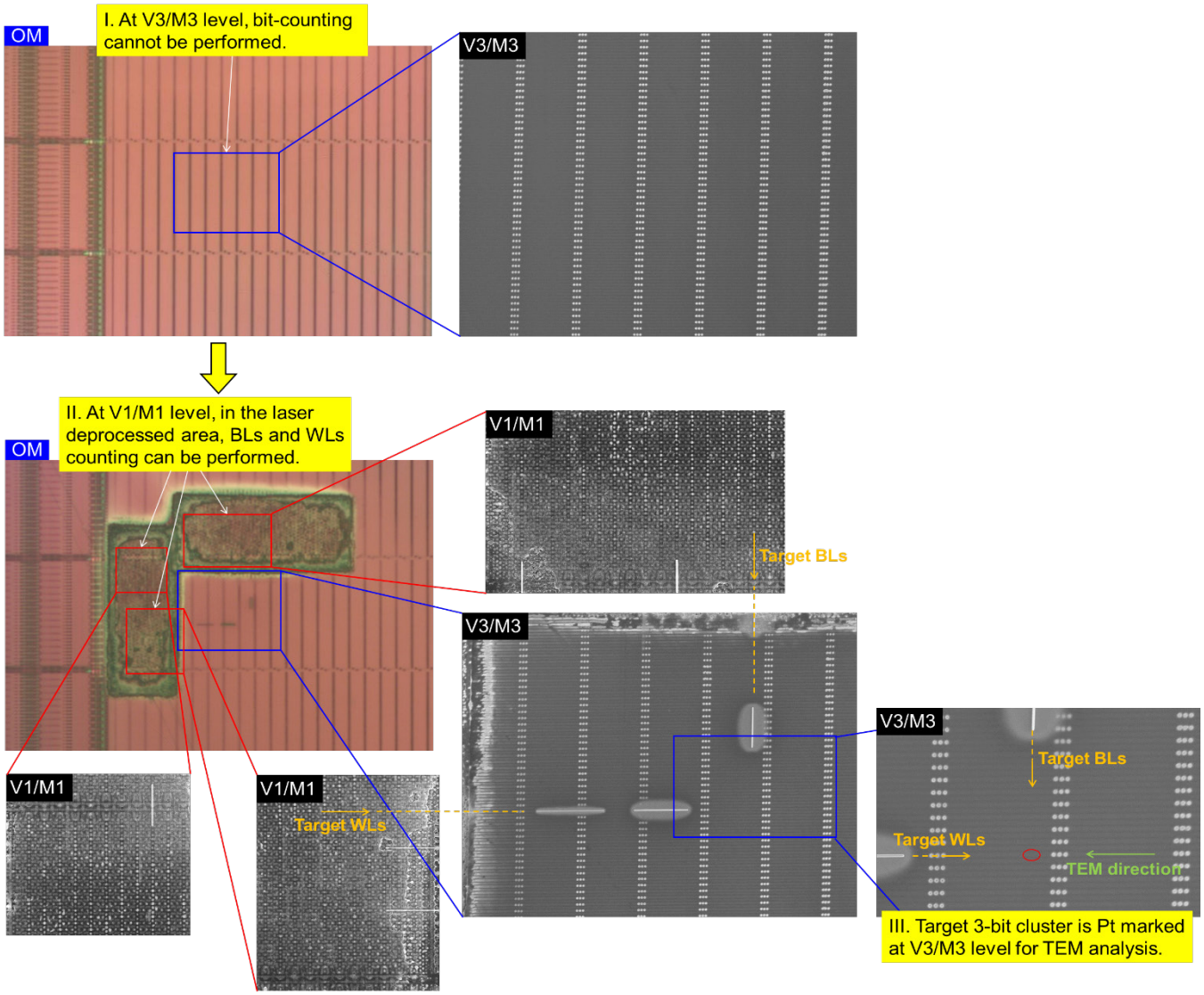


Figure 18: Schematic illustration of LDT assisted bit-counting at M3 in SRAM devices.

of the seed Cu layers could be the root cause of the failure. The high aspect ratio of the metal trench in the dual damascene process could introduce thinner seed Cu layer at the trench bottom. In the subsequent bulk Cu plating, the H+ ions in the electrolyte may attack the Cu seed layer as an acid etchant, since the electrons in the current flowing through the thinning portion were not enough to neutralize the excess H+ ions. This would finally induce the formation of the void at the bottom of either V1 or V2.

4. Conclusion

In this paper, an innovative LDT assisted PFA technique is fully exploited and discussed. Compared to the conventional methods that involve high-cost equipment, this new method employing a pulse laser system instead significantly lowers the FA cost (by more than 5 times) and shortens the FA cycle time (by up to 45%), and facilitates potential applications in other FA areas such as pre-EFI sample preparation, large size cross-sectional analysis, etc. Moreover, only basic FA skills such as using OM and SEM are required to manipulate this new method which is suitable for FA engineers from all different levels.

Conflict of Interest

The authors declare no conflict of interest.

Abbreviations

BL	Bit-Line
CD	Critical Dimension
EDX	Energy Dispersive X-ray
EFI	Electrical Fault Isolation
FA	Failure Analysis
FIB	Focused Ion Beam
GDS	Graphic Data System
IC	Integrated Circuit
LDT	Laser Deprocessing Technique
Mvia	Memory Via
NVM	Non-Volatile Memory
OM	Optical Microscope
PFA	Physical Failure Analysis

RIE Reactive Ion Etching
SEM Scanning Electron Microscope
SRAM Static Random Access Memory
STEM Scanning Transmission Electron Microscope
TEM Transmission Electron Microscope
V*x* Via*x*, *x* is layer number

References

[1] H. H. Yap, P. K. Tan, L. Zhu, H. Feng, Y. Z. Zhao, R. He, H. Tan, B. H. Liu, Y. M. Huang, D. D. Wang, J. Lam, Z. H. Mai, "Application of Laser Deprocessing Technique in PFA on Chemical Over-etched on Bond-pad Issue," Microelectronics Reliability, **64**, 357-361, 2016, doi:10.1016/j.microrel.2016.07.057.

[2] S. Ikeda, Y. Yoshida, K. Ishibashi, Y. mitsui, "Failure Analysis of 6T SRAM on Low-voltage and High-frequency Operation," in 2003 IEEE Transactions on Electron Devices, 1270-1276, 2019, doi:10.1109/TED.2003.813474.

[3] Z. G. Song, "SRAM Failure Analysis Evolution Driven by Technology Scaling," in 2014 IEEE International Symposium on Physical and Failure Analysis of Integrated Circuits (IPFA), 2014, doi:10.1109/IPFA.2014.6898207.

[4] P. Egger, C. Burmer, "SRAM Failure Analysis Strategy," in 2003 International Symposium for Testing and Failure Analysis (ISTFA), 177-183, 2003.

[5] C. Q. Chen, P. T. Ng, S. P. Neo, P. K. Tan, A. C. T. Quah, J. Zhu, "Application of Nanoprobing on Subtle Defects in the Embedded Non-volatile Memory Device," in 2019 International Symposium for Testing and Failure Analysis (ISTFA), 2019.

[6] W. T. Chang, T. E. Hsieh, "Advance Static Random Access Memory Soft Fail Analysis Using Nanoprobing and Junction Delineation Transmission Electron Microscopy," Journal of Vacuum Science & Technology B: Microelectronics and Nanometer Structures Processing, Measurement, and Phenomena, **25**, 202, 2007.

[7] T. Mizutani, T. Saraya, K. Takeuchi, M. Kobayashi, T. Hiramoto, "Transistor-level Characterization of Static Random Access Memory Bit Failures Induced by Random Telegraph Noise," Japanese Journal of Applied Physics, **55**, 04ED05, 2016, doi:10.7567/JJAP.55.04ED05.

[8] Y. Z. Zhao, Q. J. Wang, P. K. Tan, H. H. Yap, B. H. Liu, H. Feng, H. Tan, R. He, Y. M. Huang, D. D. Wang, L. Zhu, C. Q. Chen, F. Rivai, J. Lam, Z. H. Mai, "Application of Fast Laser Deprocessing Techniques on Large Cross-section View Area Sample with FIB-SEM dual beam system," Microelectronics Reliability, **64**, 362-366, 2016.

[9] Y. L. Pan, P. K. Tan, S. L. Ting, C. Q. Chen, "Advanced Sample Preparation Techniques for Rescuing Damaged Samples with Cracks, Scratches, or Unevenness in Delayering," in 2020 IEEE International Symposium on Physical and Failure Analysis of Integrated Circuits (IPFA), 2020.

ASTES

Advances in Science, Technology and Engineering Systems Journal Vol. 5, No. 5, 1282-1287 (2020)

www.astesj.com

Special Issue on Multidisciplinary Innovation in Engineering Science & Technology

ASTESJ

ISSN: 2415-6698

An Overview on CryptDb and Word2vec Approaches

Hana Yousuf[1], Asma Qassem Al-Hamad[2], Said Salloum[1,3,*]

[1]*Faculty of Engineering & IT, The British University in Dubai, 345015, UAE*

[2]*Librarian and information department, Imam Abdulrahman Bin Faisal University, 1982, KSA*

[3]*Research Institute of Sciences & Engineering, University of Sharjah, 27272, UAE*

ARTICLE INFO

Article history:
Received: 24 June, 2020
Accepted: 07 October, 2020
Online: 24 October, 2020

Keywords:
Big data
CryptDB
SQL databases
Word2Vec
Secure vectorization

ABSTRACT

Big data is a vast data set that was used in many areas. Online applications are subject to theft of confidential information because opponents can exploit software errors to access private data, and because curious or malicious officials can capture and lose data. CryptDB is a functional system that provides security and confidentiality through a set of operations. The obvious confidentiality of these attacks is for applications supported by SQL databases. It works by executing SQL queries on encrypted data using robust coding systems that support SQL. Word2Vec outputs word vectors that can be displayed as a large piece of text, or even we first train data. Word2Vec forms and word similarity assessment. Without a doubt, this article calls for proper research that sheds light on the security features using CryptDB to prevent data theft and privacy breaches in the server. The motivation of this research is to have an overview of CryptDB and Word2Vec implementation on the existing research approaches.

1. Introduction

The theft of private data is a big issue [1–3], especially for online applications [4–11]. The SQL databases may be attacked and vulnerable to sensitive information or theft since they can exploit the bugs to gain access to private information. Also, the attackers can capture and leak the data to those who require them. Hence, the dataset must be safeguarded. CryptDB provides confidentiality against the attackers through SQL databases [10]. The processes are encrypted in SQL by collecting effective SQL aware encryption schemes. The process can also be used to encrypt the credential keys so that an item can be decrypted with simply a password. Since the processes and data are encrypted, the database administrator will not view the data. Even if there is an attack on the server, the attacker will not access the decrypted data. CryptDB can handle multiple queries simultaneously and has less overhead.

Word2vec is one type of word embedding technique used to represents a string in a set of real numbers. This is a technique used in Natural Language Processing (NLP) through deep learning to extract data from the requested document. Word2Vec represents the input text as a statistical or vector form using a two-layer neural net that process text using. Word2vec's applications extend on the far side than analyzing sentences; it can be used in an application that has a well-defined pattern

The motivation to carry out this research is to have an overview of Word2Vec and CryptDB approaches and identify the challenges in the current process in both techniques.

1.1. CryptDb

One of the most widely known machines is employed in various shifts in classification tasks. Two threats are tackled by CryptDB [12]. The first of these is a curious database administrator (DBA) that attempts to learn private data (such as financial statements, health records, personal information, etc.) by sneaking into the DBMS server; however, CryptDB does not allow the DBA to access the private data. The other threat is an adversary that acquires full control of the application and DBMS services. Here, no guarantees can be offered by CryptDB for users logged in the application when an attack occurs; however, it can make sure that the data of the users who are not logged in is protected from threats. A simple solution is to create a different database encryption key

*Corresponding Author: Said Salloum, University of Sharjah, UAE. Tel: +971507679647 Email: ssalloum@sharjah.ac.ae

for every user not applicable for their data in applications, including shared data, such as conference review sites and bulletin boards [13].

The CryptDB's function is to perform queries on encrypted information. The main reason for this practice is that SQL uses a specific set of factors; each can effectively support encrypted data [13]. CryptDB combats with these challenges using three core ideas:

- The first one is to run SQL questions on encrypted information. CryptDB applies this concept by employing an encryption methodology that supports SQL and takes advantage of the truth that all SQL inquiries comprise a well-defined set of primitive factors, like Equality Confirmation, framework comparisons, total (amounts), and links. By adjusting known encryption systems (for correspondence, increments, and work confirmation) and employing a new encryption strategy to ensure the protection of joins, CryptDB encrypts each data component so that DBMS can execute the converted information [14]. CryptDB is practical security since it uses essentially symmetric-key encryption in order to prevent completely identical encryption, and runs an unmodified DBMS program (utilizing custom capacities).
- The second strategy is flexible encryption based on the query. A few encryption systems pass more data to the DBMS server than others but should undergo some queries. To avoid leaking all information encryption to the database management system, CryptDB carefully alters the SQL encryption framework for any specific data element, based on queries. To execute these modifications effectively, CryptDB utilizes 'onions of encryption'. Onions are a new approach to store numerous encryption texts within the database and maintain a distance from exorbitant re-encryption [13].
- The third concept is to link encryption keys to users' passwords so that every information within the database can be decrypted by employing a keychain established within the client's password who can approach that data. If the client does not log on to the app and the rival does not know the password, the adversary will not decode the user's information even if the DBMS and the application server are completely under threat [13]. To form a critical chain that captures the app's protection and sharing arrangement, CryptDB permits the developers to give policy comments through the SQL app chart and identifying clients who have access to each part of the information.

1.2. Word2Vec

Google developed Word2vec in 2013 [12], which is a neural network through which text data is processed. Word2vec is not a single algorithm, it is made up of two learning models, which are the Common Bag of Word bag (CBOW) and Skip grams. The word is predicted by CBOW based on its context, while in Skip-Gramm, context determines a word. Word2Vec ultimately developed in a model word vector by feeding the text. Word2Vec first generates a vocabulary from group training text and learning vector representations for every word [12]. The architecture of the word2vec algorithm is given in Figure 1.

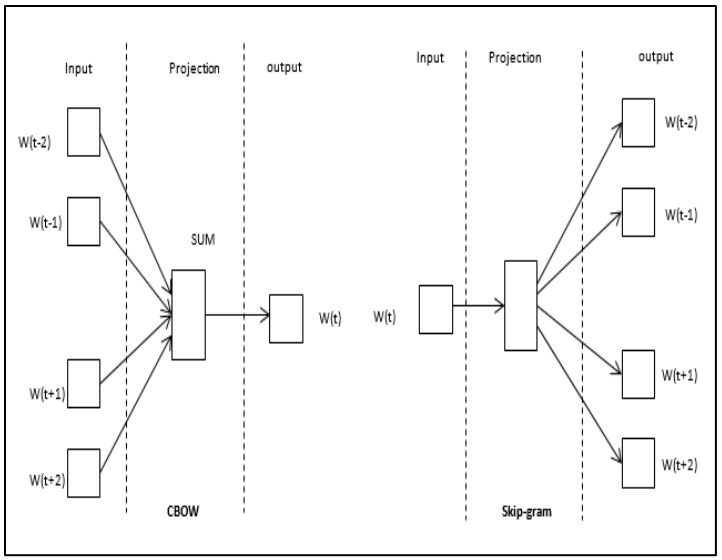


Figure 1: Word2Vec Architecture

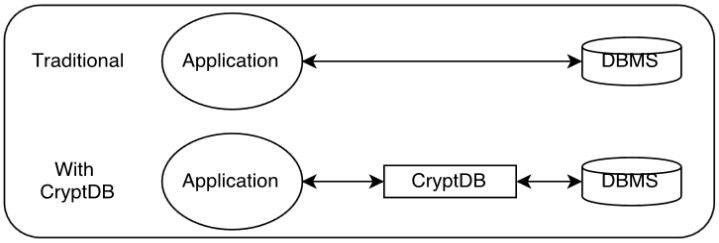


Figure 2: CryptDB along with traditional DB [12].

The purpose of using Word2vec is to cluster the vectors of similar words along in vector-space, then detect the similarity by measuring cosine similarity; it creates vectors that are distributed numerical representations of the word. Word2vec will build extremely accurate guesses of a word's definition based on previous presences. The guesses are used to construct a word that associate with the other word in the sentence.

2. Literature Review

A study by [15] has used effective Galois Field mathematical environments for encrypting algorithms effectively. The increase in network sensor systems and network databases has led to more interest in using cryptology in sensors algorithms and databases. Vectorized Advanced Encrypted Standard (AES) has been implemented for the database systems. Due to vectorization, the implementation is very small and requires 100 times smaller code than ordinary AES implementation. It is also fast and has an effective design. The implementation achieves higher speed which is comparable to real-time prototyping with OpenSSL with good database analytics and processing.

Researchers of [16] have introduced a ciphertext policy with constant sizes known as Cipher-text Policy Hidden Vector Encryption (CP-HVE). An HVE is a unique type of anonymous IBE, which uses identity as the main parameters where the attributes linked with the ciphertext or secret keys contain wild-cards. Two different schemes have been used, one with a composite ordered bi-linear group and a prime ordered bilinear group. Both of these schemes have high security by differentiating

the ciphertext from plaintext. This vectorized encryption has the ability to have a regular size than the other HVE methods.

HVE was also implemented by [17], a type of predictive encryption technique that supports conjunctive equality and ranges on the encrypted data. A novel HVE scheme has been built that is fully secure under standard assumptions. The proposed scheme is based on bilinear maps that are more advantageous for the private keys and pairing computations for decryptions. Tag-based dual system encryption has been developed to hide the vector components and compress the tag's values into one. It is challenging to extend the HVE along with IBE for supporting a higher hierarchical mechanism. Hence, it is still challenging to construct HVE for providing encryption-based security. The number of pairings in the computations is high, which must be reduced in the future to increase the speed of the processes.

In [18], author has described the types of CryptDB. Random (RND) is a type of CryptDB that relatively provides the most security that is selected under a probabilistic adaptive plain text attack. Here, two equal halves of data are mapped into different ciphertexts. RND ensures that computations are performed on ciphertexts directly. RND uses encryptions like AES and Blowfish simultaneously with a random initialization vector. AES is used more than Blowfish for 64-bit block sizes since AES has 128-bit blocks that cause the ciphertexts to be very long. For high security, it is assumed that the server does not change results.

3. CryptDB is a solution for facing the threats

CryptDB works by intercepting all SQL queries in that database proxy and rewrites queries to perform for encrypted data. All inquiries pass through the agent. The agent encrypts and decrypts all data, and some parameters change while maintaining the query's semantics. The DBMS server never receives decryption. A clear text key so that confidential data is not displayed to ensure that strange DBA cannot access private information (Threat 1).

To protect themselves from compromises in applications, proxy servers, and DBMS servers (Threat 2), developers comment on the specific SQL schema different principles; its keys to decode different parts database. They are also making a slight change to their apps, providing encryption keys to the proxy. The agent specifies which parts of the database are to encrypt under any key. The result is that CryptDB guarantees the confidentiality of data owned by users who are not logged in within one. The compromise that just logs in the admin recognizes and corrects the settlement. CryptDB protects data confidentiality, but it does not guarantee its safety, freshness, or completeness of the results returned to implementation. The opponent who threatens the application, the agent, or a malicious DBMS or DBA server that can delete one or all data stored in the database. Attacks on users' computers, Cross-site scripting outside of CryptDB. The security guarantees are provided for in these threat models [19].

3.1. Threat 1: DBMS Server compromise

CryptDB provides security against a curious DBA or another external attacker in this threat while offering complete access to the DBMS server's data. It focuses on confidentiality (data privacy) rather than availability or integrity. It is presumed that the attacker is passive, wanting to get access to confidential data without modifying queries presented by the application, query results, or the data within DBMS. This threat comprises DBMS software being compromised, gaining root access to DBMS, and access to the RAM of physical machines. There is now a greater degree of database consolidation in enterprise data centers, databases are being outsourced to public cloud computing infrastructures, and third party-DBAs are being used, which is why it is becoming very important to deal with this threat [19–21].

The goal of CryptDB is to ensure that the data remains secure from this threat by carrying out SQL queries over the encrypted data DBMS server. The agent uses secret keys for encrypting the entire data; it includes or incorporates them in the outgoing DBMS queries [22]. This tries to make it possible to use the DBMS server to process queries for encrypted data, similar to an unencrypted database. This is done by activating the particular functions for data elements required for encrypted data. The DBMS should have the ability to identify the factors it consists of. There is the same column; however, the actual content items are different. Hence, the DBMS server should be activated by the proxy to identify the relationships among the data required for query processing. SQL-enabled encryption should be used as it is capable of adapting vigorously. CryptDB, when issuing requests, manages the relationships it reveals between lines to the server. The order of the items in the column is not known, which is not even required to learn more about the rest of the columns. When DBMS is needed, CryptDB will identify it by carrying out an ORDER command or determine MAX or MIN items within this column, and not by any other method [22].

3.2. Threat 2: Arbitrary threats

It is possible that the proxy and DBMS server infrastructure experience arbitrary security breaches. Due to the opponent, the method used in Threat 1 is not adequate. It is now possible to access the keys used to encrypt the complete database. To deal with this, different data elements (for example, data for various users) should be encoded using different keys. The application database schema should be suspended to present further privacy guidelines to choose the key developers who would be using each data item. It is still impossible for strange DBA to obtain private data on a DBMS server (Threat 1). The application server or proxy can become decrypted—data from only the presently registered (stored in the proxy). Data from the users who are not active will not be encrypted with the keys available to the attacker and will stay confidential. CryptDB provides substantial guarantees in this configuration in dealing with the arbitrary server-side breaches, including the ones that obtain root access to the proxy or application. CryptDB leaks the majority of the data users that have been active for some time. Concerning an SQL attack, the compromise duration comprises of the SQL queries of the attacker. The system is considered vulnerable until the attacker's email address stays within the database [22], [23].

4. CryptDB Implementation

SQL queries are carried out by CryptDB using encrypted data. There is a lack of trust in the DBMS machines and administrators; however, the application and the proxy can be trusted. CryptDB allows the DBMS server to perform SQL queries on encrypted data, just like how it would be carrying out the same queries on

plaintext data. No modifications in the existing applications are required. Usually, the DBMS query plan for an encrypted query is similar to the actual query, except that the operators forming the query, like projections, selections, aggregates, joins, and orderings, are done on cipher tests. In a few scenarios, modified operators are used. A secret master key MK is stored by CryptDB's proxy, in addition to the database scheme and the existing encryption layers of each column [24]. An anonymized schema is observed by the DBMS server (where the names of tables and columns are substituted with opaque identifiers), encrypted user data, and certain auxiliary tables utilized CryptDB. CryptDB-specific user-defined functions (UDFs) are also provided by CryptDB to the server, using which the server can use ciphertexts for specific functions [24]. Four steps are followed when processing a query in CryptDB.

- A query is presented by an application, which is intercepted and rewritten by the proxy: each table and column name is anonymized. With the master key MK's help, each constant is encrypted in the query using an encryption scheme that is most appropriate for the required operation.
- It is determined by the proxy whether the DBMS server should be provided keys to modify the encryption layers before issuing the query. If this is the case, then an UPDATE query is issued at the DBMS server that brings about a UDF to modify the relevant columns' encryption layer.
- The encrypted query is forwarded by the proxy to the DBMS server, which performs it using standard SQL (often bringing about UDFs for performing aggregation or keyword search).
- The encrypted query result s returned by the DBMS server that is decrypted by the proxy and sent back to the application.

5. Word2Vec Implementation

We prepare our data to be trained using the Word2Vec model. We are taking the below sentence as an example:

We must love life

Step-1: Consider the word 'we' as input and 'must listen' is the output word as follows:

Input	Output
We	must
We	love

Step-2: Now consider 'must' as input word; the output will be the close words as follows

Input	Output
We	must
We	love
Must	we
Must	love
Must	life

Step-3: The same will be done for the rest of the sentence as follows:

Input	Output
We	must
We	love
Must	we
Must	love
Must	life
Love	we
Love	must
Love	life
Love	must
Love	live

At the end of creating a training sample for the sentence, we gotten samples. After that, we will obtain Word2Vec embedding by having a data set consists of 4000 unique words and word vectors size 80 each.

- Vocabulary Size = 4000
- Word vector size =80

The input will be our input vector, and the output will be the probability of nearby vectors. The learned weight matrix can be extracted after the model finishes the training process, and the word vector can be extracted, as shown in Figure 2 and Figure 3.

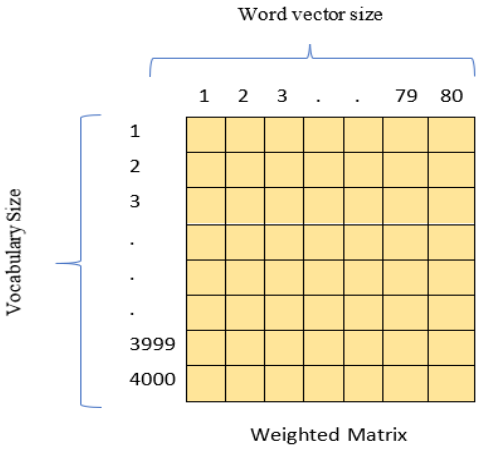


Figure 2: The weight matrix has a size of 4000 x 80.

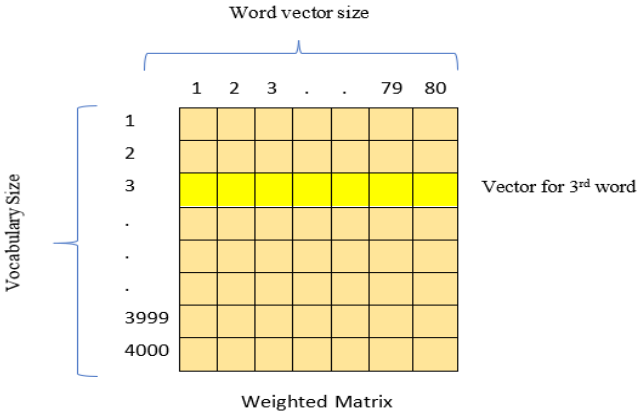


Figure 3: Vector representation for the 3rd word

The above shows how to have a word embedding using Word2Vec. Similar words in the vocabulary set will have similar vectors pointing toward the same direction for example, life and living will have the same direction as shown in Figure 4.

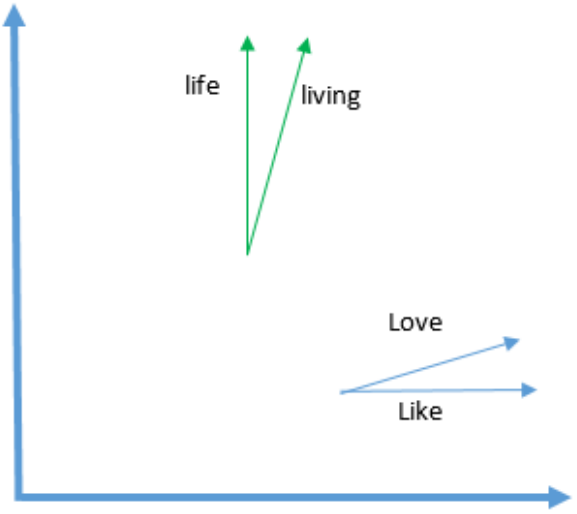


Figure 4: The vector direction for similar words

6. Conclusions and Future Work

CryptDB is a system that offers a logical and powerful level of confidentiality against two considerable threats that attack database-backed applications, i.e., curious DBAs and arbitrary compromises of the application server and the DBMS. Three steps are followed by CryptDB to achieve its objectives: efficiently performing queries over encrypted data through a novel SQL-aware encryption strategy, dynamically modifying the encryption level using onions of encryption to decrease the information given to the untrusted DBMS server, and linking encryption keys to under passwords such that only authorized users can get access to encrypted data. Word2Vec method is an effective data processing technique. It takes into account the significant data dimension issue when handling large-scale training data to offer a means of grouping similar data. This method may be employed to decrease the data dimension.

The CryptDB and Word2Vec approaches will be used together to provide a secure word embedding.

Acknowledgment

This is a part of project done in British University in Dubai.

References

[1] M. Alshurideh, B. Al Kurdi, S.A. Salloum, I. Arpaci, M. Al-Emran, "Predicting the actual use of m-learning systems: a comparative approach using PLS-SEM and machine learning algorithms," Interactive Learning Environments, 1–15, 2020.
[2] M. AlShamsi, S.A. Salloum, M. Alshurideh, S. Abdallah, Artificial Intelligence and Blockchain for Transparency in Governance, Springer: 219–230.
[3] J. Almaazmi, M. Alshurideh, B. Al Kurdi, S.A. Salloum, "The Effect of Digital Transformation on Product Innovation: A Critical Review," in International Conference on Advanced Intelligent Systems and Informatics, Springer: 731–741, 2020.
[4] A.Y. Zainal, H. Yousuf, S.A. Salloum, "Dimensions of Agility Capabilities Organizational Competitiveness in Sustaining," in Joint European-US Workshop on Applications of Invariance in Computer Vision, Springer: 762–772, 2020.
[5] H. Yousuf, S. Salloum, "Survey Analysis: Enhancing the Security of Vectorization by Using word2vec and CryptDB."
[6] S.K. Yousuf H., Lahzi M., Salloum S.A., "Systematic Review on Fully Homomorphic Encryption Scheme and Its Application.," In: Al-Emran M., Shaalan K., Hassanien A. (Eds) Recent Advances in Intelligent Systems and Smart Applications. Studies in Systems, Decision and Control, Vol 295. Springer, Cham, 2021.
[7] S.A. Salloum, R. Khan, K. Shaalan, "A Survey of Semantic Analysis Approaches," in Joint European-US Workshop on Applications of Invariance in Computer Vision, Springer: 61–70, 2020.
[8] S.A. Salloum, M. Alshurideh, A. Elnagar, K. Shaalan, "Machine Learning and Deep Learning Techniques for Cybersecurity: A Review," in Joint European-US Workshop on Applications of Invariance in Computer Vision, Springer: 50–57, 2020.
[9] S.A. Salloum, M. Alshurideh, A. Elnagar, K. Shaalan, "Mining in Educational Data: Review and Future Directions," in Joint European-US Workshop on Applications of Invariance in Computer Vision, Springer: 92–102, 2020.
[10] S.A. Salloum, A.Q. AlHamad, M. Al-Emran, K. Shaalan, A survey of Arabic text mining, 2018, doi:10.1007/978-3-319-67056-0_20.
[11] S.A. Salloum, M. Al-Emran, A.A. Monem, K. Shaalan, Using text mining techniques for extracting information from research articles, 2018, doi:10.1007/978-3-319-67056-0_18.
[12] Y.-C. Chang, M. Mitzenmacher, "Privacy preserving keyword searches on remote encrypted data," in International Conference on Applied Cryptography and Network Security, Springer: 442–455, 2005.
[13] K.C. M. Viktor, "Big data: A revolution that will transform how we live, work, and think," Houghton Mifflin Harcourt, 2013.
[14] N. Aburawi, CryptDB mechanism on graph databases, 2020.
[15] J. Kepner, V. Gadepally, B. Hancock, P. Michaleas, E. Michel, M. Varia, "Parallel vectorized algebraic AES in Matlab for rapid prototyping of encrypted sensor processing algorithms and database analytics," in 2015 IEEE High Performance Extreme Computing Conference (HPEC), IEEE: 1–8, 2015.
[16] T.V.X. Phuong, G. Yang, W. Susilo, "Efficient hidden vector encryption with constant-size ciphertext," in European Symposium on Research in Computer Security, Springer: 472–487, 2014.
[17] J.H. Park, K. Lee, W. Susilo, D.H. Lee, "Fully secure hidden vector encryption under standard assumptions," Information Sciences, **232**, 188–207, 2013.
[18] R.A. Popa, C.M.S. Redfield, N. Zeldovich, H. Balakrishnan, "CryptDB: protecting confidentiality with encrypted query processing," in Proceedings of the Twenty-Third ACM Symposium on Operating Systems Principles, 85–100, 2011.
[19] K. Lang, "Newsgroups Data Set," Available at: Qwone. Com/~ Jason/20Newsgroups/.[Accessed 30-Sep-2015], 20AD.

[20] H.H.O. Nasereddin, A.J. Darwesh, "An Object Oriented Programming on Encrypted Database System (CryptDB)," Journal of Talent Development and Excellence, **12**(1), 5140–5146, 2020.
[21] X. Jiang, X. Kong, Z. Xu, "Research on order-preserving encryption scheme based on CryptDB," in Journal of Physics: Conference Series, IOP Publishing: 32106, 2020.
[22] S.S.M. Chow, J.-H. Lee, L. Subramanian, "Two-Party Computation Model for Privacy-Preserving Queries over Distributed Databases.," in NDSS, Citeseer, 2009.
[23] H. Yousuf, A.Y. Zainal, M. Alshurideh, S.A. Salloum, Artificial Intelligence Models in Power System Analysis, Springer: 231–242.
[24] S. Rizvi, A. Mendelzon, S. Sudarshan, P. Roy, "Extending query rewriting techniques for fine-grained access control," in Proceedings of the 2004 ACM SIGMOD international conference on Management of data, 551–562, 2004.

ASTES

Advances in Science, Technology and Engineering Systems Journal
Vol. 5, No. 5, 1288-1298 (2020)
www.astesj.com
Special Issue on Multidisciplinary Sciences and Engineering

ASTES Journal
ISSN: 2415-6698

A Circular Invariant Convolution Model-Based Mapping for Multimodal Change Detection

Redha Touati[*,1,2], Max Mignotte[1], Mohamed Dahmane[2]

[1]*Vision lab, Département d'Informatique et de Recherche Opérationnelle (DIRO), Université de Montréal, QC, H3T 1J4, Canada*

[2]*R & D vision Département, Centre de Recherche Informatique de Montréal (CRIM), Montréal, QC, H3T 1J4, Canada*

ARTICLE INFO

Article history:
Received: 02 September, 2020
Accepted: 18 October, 2020
Online: 26 October, 2020

Keywords:
Multisource
Multisensor
Mutilooking
Unbalanced satellite images
Circular invariant convolution model
Line minimization process
Change detection
Mapping or projection model

ABSTRACT

The large and ever-increasing variety of remote sensing sensors used in satellite imagery today explains why detecting changes between identical locations in images that are captured, at two separate times, from heterogeneous capturing systems is a major and challenging recent research problem in the field of satellite imaging for fast and accurate determination of temporal changes. This work presents an original concentric circular invariant convolution model that aims at projecting the first satellite image into the imaging modality of the second image. This allows the two images to have identical statistics so that one can then effectively use a classical monomodal change detection method. The invariant circular convolution kernel parameters are estimated in the least squares sense using a conjugate gradient routine whose optimal direction is determined by a quadratic line search algorithm. After the projection of the before image into the imaging modality domain associated with the after image is achieved, a basic pixel-by-pixel difference permits the estimation of a relevant soft difference map which is segmented into two classes by a multilevel Markovian technique. A series of experiments conducted on several pair of satellite images acquired under different imaging modalities, resolution scales, noise characteristics, change types and events, validates the effectiveness of this strategy. The experimentation shows that the proposed model can process different image pairs with less re-striction about the source images and natural event, coming from different sensors or from the same sensor, for detecting natural changes.

1 Introduction

The ever-increasing number of Earth observation satellites, which use today new high-tech sensors, are often technologically quite different from those that have provided the satellite images so far archived. This heterogeneity of satellite image data has thus lately contributed to the advent and development of a novel and rapidly growing research interest in remote sensing and geoscience imaging commonly known as multi-modal (or heterogeneous) change detection (MCD). The purpose of the multimodal CD (MCD) [1, 2] is to detect and precisely locate any change in land cover between at least two satellite images taken in the same place, at different times and under different acquisition conditions. It usually concerns CD models that process heterogeneous satellite images, *i.e.* provided by different satellite sensor types which may combine active and passive sensors such as SAR/optical or by one sensor type, with two heterogeneous SAR, optical or others or finally by different satellites using the same satellite sensor but under different specifications, looks, wavelengths, or calibrations [3].

Recently, MCD has aroused a lot of attention and interest in satellite imagery thanks to its consistency and coherence with our environment favouring the emergence of increasingly heterogeneous images. Nevertheless, it is a difficult procedure because MCD has to be flexible enough to treat a multi-modal image pair, for solving the problems usually considered by the traditional single-modality CD methods [4, 5] including damage, land, environmental monitoring or city planning.

In the literature, the proposed MCD approaches can be classified under four classes. The first class includes the simplest methods which use local descriptors [6] or similarity measures [6]–[9], using invariance properties relative to the imaging modality processed. The second category gathers the methods that do not have assumptions about the data distributions and are thus non-parametric. This includes algorithms using machine learning techniques that learn from the training samples [10]–[19] or from unsupervised parameter,

[*]Corresponding Author: Redha Touati, Email: touatire@iro.umontreal.ca

without requiring any training phase, for example the least squares (LSQ) Multidimensional scaling (MDS) and energy-based model, integrating data-driven pixel pairwise constraints, introduced in [20]. The third group relies on parametric methods trying to model common statistical features or relationship between the different imaging modalities or between the different multisource data *via* a set of multivariate distributions [21]–[27] or through a pixel pairwise modeling integrated in a Markov Random Field (MRF) model [28]. Finally, the last category regroups algorithmic procedures essentially relying on a projective transformation of the heterogeneous images to a common intermediate feature space, where the projected satellite images would ultimately share the same statistical characteristics and on which any conventional homogeneous CD models could be subsequently used [29]–[38]. This category can encompass also the procedures projecting the first image in the imaging modality of the second image or inversely [39]. The method presented in this work fits fully into this sub-category.

More precisely, this work presents a concentric circular invariant convolution mapping which aims at projecting the *before* image onto the imaging modality of the *after* image. In this way, we ensure that the statistics of the pre and after-event satellite images are nearly identical and that a classical monomodal CD procedure can then be efficiently used, as easily as if the two images came from the same imaging modality or sensor with the same settings (specifications/calibrations/wavelength).

To this end, we will show that, once the mapping is done by the proposed convolutive model, the pixel-wise difference image estimated from the image pair shows good likelihood distributions properties corresponding to the "change" and "no change" label classes; that is to say, presenting a mixture of distributions not too far from normal distributions and also not too flat (*i.e.* large or non-informative) so that a binary segmentation with an unsupervised Markovian model to be efficient, despite the big difference between the imaging modalities that could be confronted in multi-modal satellite imagery and which will be evaluated in this paper.
As an amelioration of our convolution model-based mapping [1], in the present research we propose a circular invariant model. Furthermore, a three dimensional (3D) convolution based mapping strategy was adopted in the specific case of MCD using two color images (or multispectral). A battery of tests was conducted to quantify the benefits of such improvements.

It is worth mentioning that convolution model estimation has also been widely experienced and analyzed in different image processing problems as image restoration [40] or 2D or 3D deconvolution issues [41]–[44].

The reminder of this paper is structured as follows: Section 2 describes the proposed projection model based on a concentric circular invariant convolution representation and the unsupervised Markovian approach. Section 3 presents the results and an experimental comparison with state of the art multimodal CD methods. Section 4 concludes the paper.

2 Proposed MCD Model

Let I_b and I_a, be the bi-temporal remote sensing image pair of N pixels, captured in the same area, at two consecutive times (*i.e*, before and after a given event), and coming from different imaging systems or sensors. Let $I_b^\sharp$ and $I_a^\sharp$ also be the informational part of the image or the semantic information of the scene concretely representing the set of real objects and materials imaged in I_b and I_a. The acquisition system, related to respectively the pre-event and post-event image can be modeled by the following linear models: $I_b = I_b^\sharp * u_b$ and $I_a = I_a^\sharp * u_a$ where "$*$" is the convolution operator and u_b and u_a mathematically model the underlying structure of the Point Spread Function (PSF) of the pre-event and post-event data acquisition system [45].

This modeling framework defines a reliable and efficient way for projecting the before-change image to the domain or imaging system of the after-change image image. It consists to apply the following operation to the pre-event image: $(I_b * u_b^{*-1}) * u_a = I_b^\sharp * u_a$ where "u_b^{*-1}" represents the inverse convolution operator of u_b (giving $u_b^{*-1} * u_b = \delta$, such as δ is the Dirac impulse function) or by commutativity and associativity of the convolution product, applying the convolution operator $u_{b\mapsto a} = (u_b^{*-1} * u_a) = (u_a * u_b^{*-1})$ to I_b. This operation allows us to convert the original MCD issue into a conventional monomodal CD method which is used in the case of a pair of images having the same acquisition mode and therefore having the same statistics.

In order to reliably find $u_{b\mapsto a}$, the simplest strategy is to search for the convolution filter parameters that will minimize in the LSQ context, the energy function given by equation 1:

$$\hat{u}_{b\mapsto a} = \arg\min_{u} \overbrace{\sum_{(x,y)\in S_{nc}} \Big([I_b(x,y) * u_{b\mapsto a}(x,y)] - I_a(x,y)\Big)^2}^{E(u_{b\mapsto a})} \tag{1}$$

where S_{nc} is the set of pixels that do not belong to the class label "change" and which must be evaluated in the final change detection map. As first approximation for $\hat{u}_{b\mapsto a}$, we can take for S_{nc}, the set of all pixels in the image. This can be justified because the area of change is usually quite small in proportion to the image which, also, can be considered (in a very first approximation) as noisy observations or outliers in the image data with which it is shown that the LSQ estimator performs well (especially thanks to the fact that the function $E(u_{b\mapsto a})$ to be minimized is convex with regard to the parameter vector of the convolution filter $u_{b\mapsto a}$). As a result, different efficient minimization procedures can be adopted [47].

In this work, we use a combination of conjugate gradient and a line minimization search routine guaranteeing a considerably increased convergence speed compared to other minimization methods. Another advantage of such a minimization technique consists on its ability to integrate some hard constraints on $u_{b\mapsto a}$. In our case, since the two imaging modalities are circular invariant, we constraint $u_{b\mapsto a}$ to be also circular invariant. To this end, at each iteration k of the conjugate gradient descent (CGD), we simply average each of the $(sz \times sz)$ parameter values of $u_{b\mapsto a}^{[k]}$ that are equidistant (in the L_1 distance sense) from the center of the convolution filter

Table 1: Heterogeneous datasets description

No	Dates	Area	Image size	Event	Satellite
1	Sept. 1995 - Jul. 1996	Sardinia, It	412×300	Lake overflow (30 m.)	Landsat-5 (NIR band) / Optical
2	Nov. 1999 - Oct. 2000	Gloucester, Uk	330×590	Flooding (≈ 40 m.)	SAR-ERS / Spot
3	July 2006 - July 2007	Gloucester, Uk	2325×4135	Flooding (0.65 m.)	TerraSAR-X / QuickBird 2
4	Feb. 2009 - July 2013	Toulouse, Fr	4404×2604	Construction (2 m.)	TerraSAR-X / Pleiades
5	May 2012 - July 2013	Toulouse, Fr	2000×2000	Construction (0.52 m.)	Pleiades / WorldView 2
6	2001 - Jan. 2002	Congo, Af.	400×800	Nyiragongo volcano eruption (10 m.)	Radarsat (3 / 5-looks)
7	June 2008 - June 2013	Island town, Chn.	415×403	Urbanization (8 m.)	Radarsat-2 / Google Earth
8	June 2008 - Sept. 2012	Shuguang village, Chn	419×342	Building construction (8 m.)	Radarsat-2 / Google Earth
9	June 2008 - June 2009	Yellow river, Chn.	409×367	River's drying up (8 m.)	Radarsat-2 (1 / 4-looks)
10	Aug. 2013 - Aug. 2015	Wehe river, Xi'an city, Chn.	392×303	flooding (2 m.)	GF-1 (≠ bands) [46]
11	1999 - 2000	Gloucester, Uk	990×554	flooding (≈ 25 m.)	SPOT/NDVI [17]
12	May 2002 - July 2009	Hubei Campus, Chn	240×240	Building construction (2.44 m.)	QuickBird / IKONOS
13	April 2005 - July 2009	Wuhan University, Chn.	400×400	Building construction (3.28 m.)	QuickBird / IKONOS

(see Algorithm 1). This allows us to integrate this constraint with a linear complexity with respect to the $(sz \times sz)$ parameters of the convolution filter. This overall minimization routine is presented in our basic model [1].

Algorithm 1 Concentric Circular Constraint

$u(x, y)$ Convolution filter of dim. $(sz \times sz)$ **[input]**
$u^{\circ}(x, y)$ Circular invariant filter **[output]**
TAB$[x][y]$ 2D table (length,width)= $(2sz,2)$ of floats

- Fill the table TAB$[i][j]$ with zeros

for *each cell of* $u(i, j)$ *with coordinates* (i, j) **do**

- $d \leftarrow L_1$distance from (i, j) to the center of u
- TAB$[d][0] \leftarrow$ TAB$[d][0] + u(i, j)$
- TAB$[d][1] \leftarrow$ TAB$[d][1] + 1$

for *each cell of* $u^{\circ}(i, j)$ *with coordinates* (i, j) **do**

- $d \leftarrow L_1$distance from (i, j) to the center of u°
- $u^{\circ}(i, j) \leftarrow$ TAB$[d][0]$/TAB$[d][1]$

In order to improve this approximation of $\hat{u}_{b\mapsto a}$, we can formulate the LSQ estimation problem of the convolution filter parameters as a fixed point problem involving a contraction mapping. Technically speaking, the first estimation of $\hat{u}_{b\mapsto a}$ allows us to obtain $I_{b\mapsto a}(x, y) = I_b(x, y) * u_{b\mapsto a}(x, y)$, corresponding to the image pre-event image projected on the modality of the post-event image. A simple pixel-by-pixel difference between $I_{b\mapsto a}(x, y)$ and $I_a(x, y)$ enables us then to produce an output image of absolute difference that is subsequently binarized to the "change" and the "non-change" class label. To this end, a Gaussian kernel is used to model the distribution of each class and the Expectation Maximization (EM) [48] algorithm is used both to estimate the parameters of this weighted distribution mixture but also to give an approximate estimate of S_{nc} (*i.e.*, the pixels that does not belong to the class label "change") with a binarization scheme in the Maximum Likelihood (ML) sense. This process allows us to finally better estimate $\hat{u}_{b\mapsto a}$ (see Eq. 1). This process is repeated until the stability of the algorithmic steady state fixed point thus defined is reached. This fixed point-based strategy yields to the following iterative procedure:

$$\hat{u}_{b\mapsto a}^{[k+1]} = \arg\min_{u} \sum_{(x,y)\in S_{nc}^{[k]}} \Big([I_b(x, y) * u_{b\mapsto a}(x, y)] - I_a(x, y) \Big)^2 \quad (2)$$

$$\Phi_D^{[k+1]} = \mathrm{EM}\Big\{ \big| \overbrace{[I_b(x, y) * u_{b\mapsto a}^{[k+1]}(x, y)]}^{I_{b\mapsto a}^{[k+1]}(x,y)} - I_a(x, y) \big| \Big\}_{D^{[k+1]}(x,y)} \quad (3)$$

$$S_{nc}^{[k+1]} = \mathrm{ML}_{\text{binarization}}\{\Phi_D^{[k+1]}, D^{[k+1]}(x, y)\} \quad (4)$$

where $S_{nc}^{[0]}$ stands for the whole image pixels and $\Phi_D^{[k+1]}$ is the parameter vector of the two weighted normal kernels evaluated by the EM procedure (at iteration $k + 1$) on the difference image $D(x, y)$. $\mathrm{ML}_{\text{binarization}}\{\Phi_D^{[k+1]}, .\}$ represents the binarization algorithm, based on $\Phi_D^{[k+1]}$, in the Maximum Likelihood sense.

A second enhancement can be incorporated in this iterative procedure by simply inverting the direction of temporality of the two (before and after) satellite images in the algorithm introduced in our basic model [1]. Concretely, the estimation of $\hat{u}_{a\mapsto b}$ can be done by $I_{a\mapsto b}(x, y) = I_a(x, y) * u_{a\mapsto b}(x, y)$. This allows us to obtain another difference map between $I_{a\mapsto b}(x, y)$ and $I_b(x, y)$. The reverse estimate can be used along with the original one to obtain an average estimate ensuring an improved (less noisy) difference image $D(x, y)$ (see Algorithm 2).

In the case where the image before or after is a single-band image and the second image (possibly a multi-band) is then converted into gray levels and this pair of greyscale images are used as explained in Algorithm 3. A third improvement is proposed in the particular case where we have at our disposal two images before and after in colors (or with $b > 1$ color bands). In this case, the mapping and a difference map $D(b, x, y)$ is estimated for each of the b images individually and sequentially. A difference map is defined finally as

the L_∞ distance, for each pixel (x, y), between the b-components of each pixel ($D(x, y) \leftarrow \max_b D(b, x, y)$) as illustrated in Algorithm 2.

After the fixed point becomes stable (concretely when $S_{nc}^{[k]} \approx S_{nc}^{[k+1]}$, or after $L_{\max}^{P}$, a maximal number of iterations is reached), the parameter vector of the Gaussian kernel mixture Φ_D (given by the EM procedure) is used to classify the difference map into two classes, once again, in the Sequential Maximum *A Posteriori* (SMAP) sense by using the multiscale, fine-to-coarse and coarse-to-fine segmentation procedure [49].

This overall minimization routine is summarized in Algorithm 2 and in Algorithm 3 for a N-band image pair.

Algorithm 2 Convolution-Based Multimodal Change Detection

$S(x, y)$	Binary change detection map [**output**]
$I_b(x, y)$	The before image [**input**]
$I_a(x, y)$	The after image [**input**]
$D(x, y)$	Difference map
Φ_D	Vector parameters
$L_{\max}^{EM}$	Maximal number of iterations for EM
$L_{\max}^{P}$	Maximal number of fixed-point iterations

1. Initialization

• Set $S(x, y)$ with labels "no change" for each pixel

2. Fixed Point Estimation Step

Repeat

• Estimate $u_{b\mapsto a}$ and $u_{a\mapsto b}$ (see [1])

• Circular constraint on $u_{b\mapsto a}$ and $u_{a\mapsto b}$

• $D(x, y) = |[I_b(x, y) * u_{b\mapsto a}(x, y)] - I_a(x, y)|$
. $+ |[I_a(x, y) * u_{a\mapsto b}(x, y)] - I_b(x, y)|$

• $\Phi_D \leftarrow$ EM estimation ($L_{\max}^{EM}$ iter.) on $D(x, y)$

• $S^{[l]} \leftarrow$ ML binarization of $D(x, y)$ based on Φ_D

• $k++$

Until $k < L_{max}^{P}$ (**or** $S(x, y)^{[l]} \neq S(x, y)^{[l-1]}$);

3. Segmentation Step

• $S(x, y) \leftarrow$ SMAP on $D(x, y)$ based on Φ_D

3 Experimental Results

3.1 Heterogeneous Dataset Description

Our strategy is validated by conducting a set of evaluation scenarios on thirteen dissimilar heterogeneous datasets exhibiting different multi modality imaging data such as cross-sensor or multisensor (#1,#5,#12,#13), multisource (#2,#3,#4,#7,#8), multi-looking (#6,#9,#11) or multispectral images (#10)) with different resolution levels and image sizes and imaging a wide variety of changed events which are degraded by a wide variety of both noise type and levels as depicted in Table 1.

In all the experimental results, we recall that if one of the two images is in grayscale, we must convert the other image (colors or with b (> 1) bands) into grayscale to apply algorithm 2. Otherwise, if the two images contain the same number of bands (b), we rely on algorithm 3.

In addition, for computational reasons, we have reduced the image size so that the widest edge of it is at most equal to 500 pixels. For the estimation stage, the size sz of the convolutional (square) filter was set to 9, with a maximal iteration number $L_{\max}^{G}$ set to 200 and a fixed-point iteration number $L_{\max}^{P}$ equal to 2. The iteration number $L_{\max}^{EM}$ used in the EM algorithm is 12 iterations (see our basic model [1]). For the segmentation stage, the depth of the SMAP was set to $d = 9$ [49]. The regularization parameter θ was fixed to 0.9 (a value commonly used for this SMAP fine-to-coarse, coarse-to-fine segmentation algorithm [49, 54]).

Algorithm 3 CBMCD For N-Band Image pair

$S(x, y)$	Binary change detection map [**output**]
$I_b(b, x, y)$	The before image with $b < N$ bands [**input**]
$I_a(b, x, y)$	The after image with $b < N$ bands [**input**]
$D(x, y)$	Difference map
Φ_D	Vector parameters
$D(b, x, y)$	Temporary map with $b < N$ bands
$L_{\max}^{EM}$	Maximal number of iterations for EM
$L_{\max}^{P}$	Maximal number of fixed-point iterations

1. Initialization

• Set $S(x, y)$ with labels "no change" for each pixel and fill $D(k, x, y)$ with zeros

2. Fixed Point Estimation Step

Repeat

for *each band b of* $[I_b(b, x, y), I_a(b, x, y)]$ **do**

• Estimate $u_{b\mapsto a}$ and $u_{a\mapsto b}$

• Circular constraint on $u_{b\mapsto a}$ and $u_{a\mapsto b}$

• $D(b, x, y) = |[I_b(b, x, y) * u_{b\mapsto a}] - I_a(b, x, y)|$
. $+ |[I_a(b, x, y) * u_{a\mapsto b}] - I_b(b, x, y)|$

• $\Phi_D \leftarrow$ EM ($L_{\max}^{EM}$ iterations) on $D(b, x, y)$

• $D(x, y) \leftarrow \max_b D(b, x, y)$

• $S \leftarrow$ ML binarization of $D(x, y)$ based on Φ_D

• $k \leftarrow k + 1$

Until $k < L_{max}^{P}$ (**or** $S(x, y)^{[l]} \neq S(x, y)^{[l-1]}$);

• $\Phi_D \leftarrow$ EM ($L_{\max}^{EM}$ iterations) on $D(x, y)$

3. Segmentation Step

• $S(x, y) \leftarrow$ SMAP on $D(x, y)$ based on Φ_D

3.2 Convolution Filter Estimation Step Result

For all the test scenarios, the maximum iteration number used in the conjugate gradient descent combined with the minimization line

process, is sufficient to ensure the convergence of the minimization procedure. As example, we show, in Figure 1, how evolves the error rate along the minimization process. In addition, for all the scenarios, we estimate for $u_{b\mapsto a}$ or $u_{a\mapsto b}$ a convolution filter (that can be likened to a point spread function (PSF)) which is quite different from one dataset to another since the frequency response (or modulation transfer function) of the imaging modality is also quite different for each pair of imaging multi-modalities. Besides, the convolution filter size sz is also justified, enough because small values of parameters are estimated at the edges of the rectangular filter in all the tested cases (see Figure 2) for an example of convolution filter estimate).

3.3 Results & Evaluation

We evaluate and compare the obtained results using the classification rate accuracy that measures the correct changed and unchanged pixels percentages: ACC and the F-measure Fm which can be defined in the equations 5 and 6.

$$ACC = \frac{TP + TN}{TP + TN + FN + FP} \tag{5}$$

$$Fm = \frac{2TP}{2TP + TN + FN + FP} \tag{6}$$

where TP and TN are the true positives and negatives. FN and FP designate the false negatives and positives.

Table 2 shows a comparison between our segmentation results and the different supervised and unsupervised state-of-the-art methods [9, 12, 16, 17, 20, 23]–[27, 32, 38, 51]–[53].

Figures 3, 4 and 5 compare qualitatively the obtained results. The average accuracy rate of our proposed model is higher than the supervised and unsupervised state-of-the-art methods, obtained by our proposed MCD model on the thirteen heterogeneous dataset is 87.78% with a F-measure equals to 0.444. Compared to these results, our preliminary model (non-circular invariant) [1] gave essentially the same result in terms of rate accuracy but with a much lower F-measure which did not exceed 0.389.

Globally, we notice that our approach works efficiently when a) the considered MCD problem tends towards the simple monomodal CD problem; in other words, in the case of a simple imaging modality which is not too different between the pre-event and post-event image (*e.g.*, when there are similar sensors involving slightly different noise laws between the before and after images), or b) in the case of a couple of images with high resolution, or c) in the case of

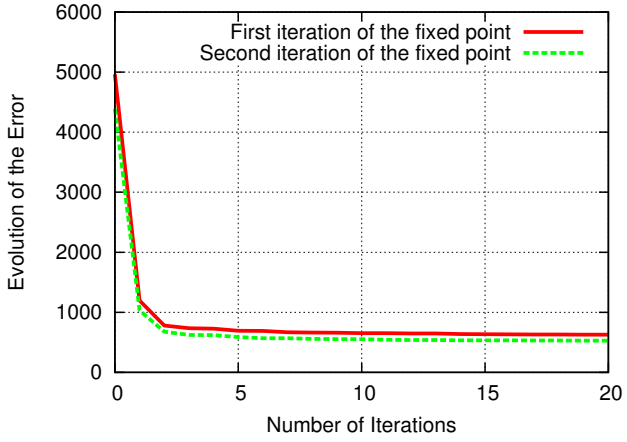


Figure 1: Cost function evolution (see Eq. (1) for the estimation of $u_{b\mapsto a}$ associated to dataset #1

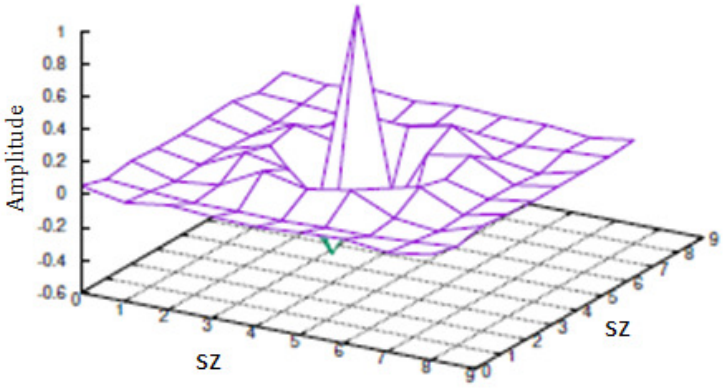


Figure 2: 9×9 Convolution filter estimate $u_{b\mapsto a}$ associated to dataset #1

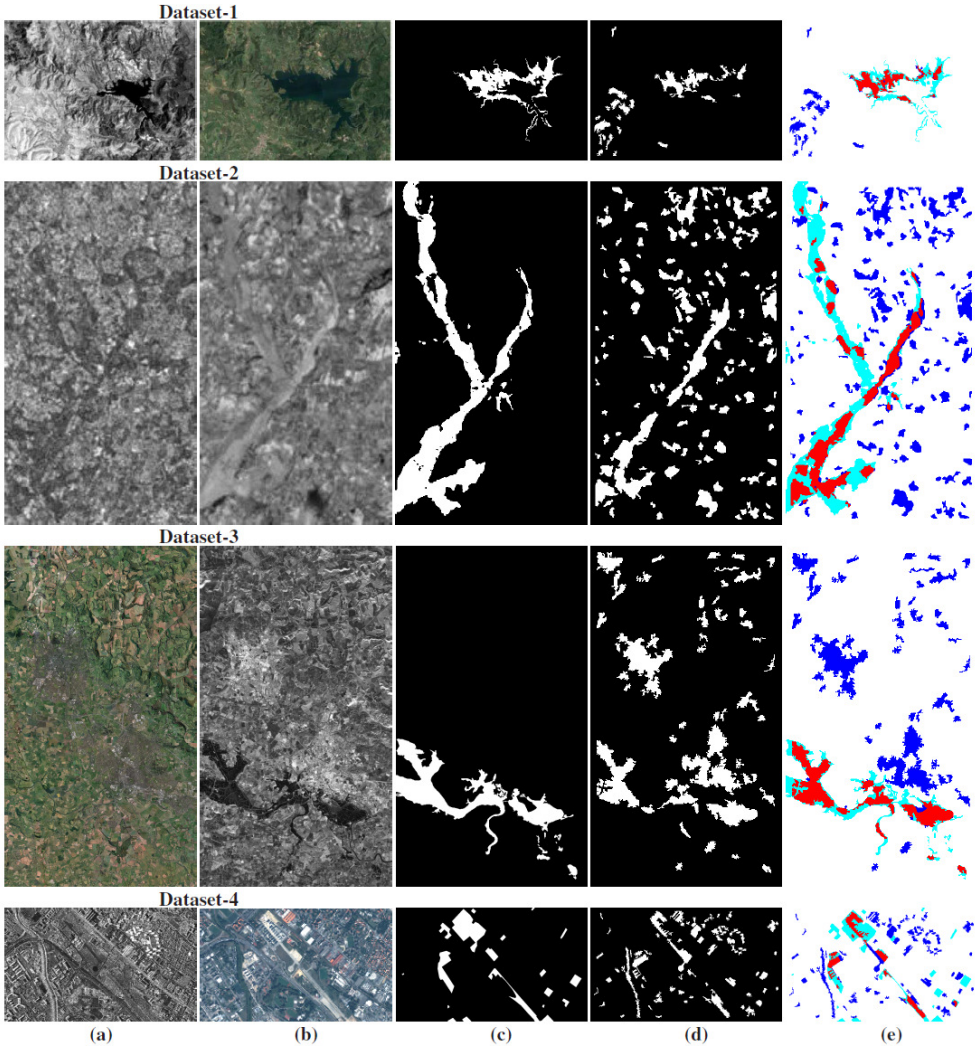


Figure 3: Multimodal datasets. (a) image t_1, (b) image t_2, (c) the ground truth; (d) binary map segmentation, (e) confusion map estimated by our model with white (TN), red (TP), blue (FP), cyan (FN) colors

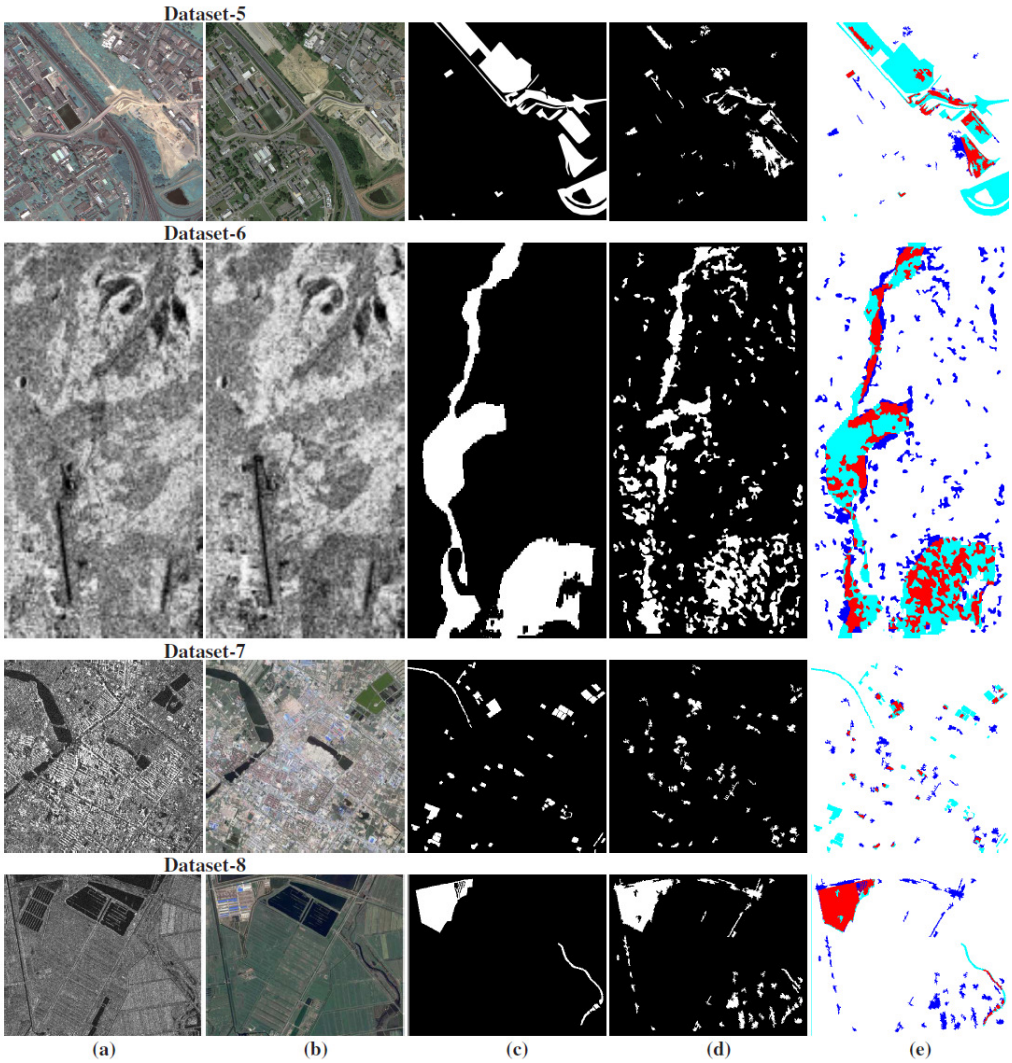


Figure 4: Multimodal datasets. (a) image t_1, (b) image t_2, (c) the ground truth; (d) binary map segmentation, (e) confusion map estimated by our model with white (TN), red (TP), blue (FP), cyan (FN) colors

simple changed events images with a simple uniform texture; as example, a city is flooding by a river (inducing an uniform texture for a new zone or also in building construction or structure with a uniform texture very different from the rest of the image). Conversely, our approach is a little less suitable when it comes to processing a bi-temporal images in which the variability between the before and after images is more important. Otherwise said, in the case of an imaging modality resulting from the combination of active and passive sensors, thus inducing a combination of multiplicative and additive noises in the before and after images with a dissimilar noise law. Also for images pairs with a low spatial resolution and showing complex changed events; as example, urban site construction (replacing a complex texture zone by the new complex texture area).

It requires about 54 seconds to the MCD to process an image. The processing time depends on the estimation problem complexity, the size of image, and the mono or multichanel based estimation (or 660 seconds for the set of 13 image pairs considered in this validation study) using a code with non-optimized C++ version running on $i7-930$ Intel CPU with 2.8 GHz Linux machine.

4 Conclusion

We have presented in this work an efficient mapping model for the change detection problem in multimodal imagery relying on the parametric estimation of an invariant circular convolution CD model. Optimization of the model was performed on a convex quadratic error function using a conjugate gradient routine, whose optimal direction is determined by a quadratic line minimization algorithm, and formulated as a fixed point problem involving a contraction mapping. This allows us to project the before image in the imaging modality space of the second image and inversely so that a difference change map is then computed pixel by pixel and efficiently binarized with a multiscale Markov model. Our proposed strategy seems well suited for the multimodal change detection issue and robust enough against images provided under different resolution levels, type or level of noise and exhibiting a variety of natural event.

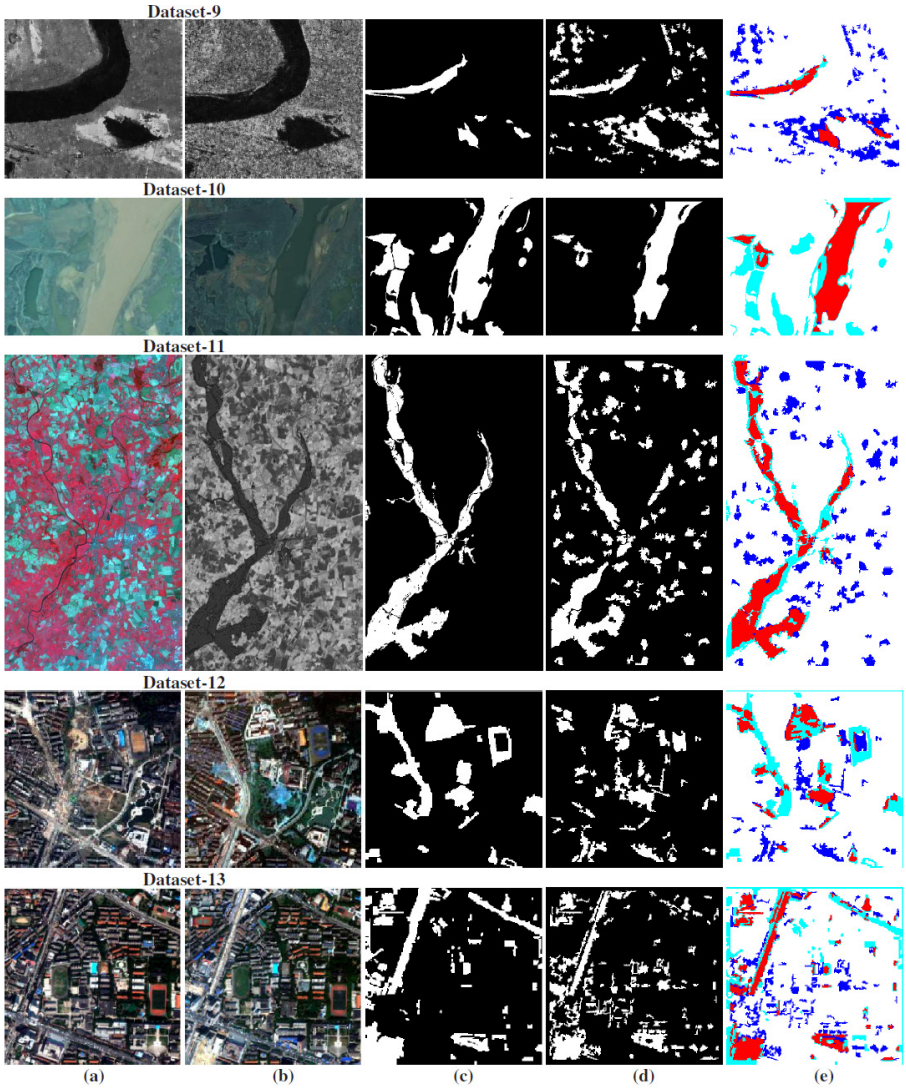


Figure 5: Multimodal datasets. (a) image t_1, (b) image t_2, (c) the ground truth; (d) binary map segmentation, (e) confusion map estimated by our model with white (TN), red (TP), blue (FP), cyan (FN) colors

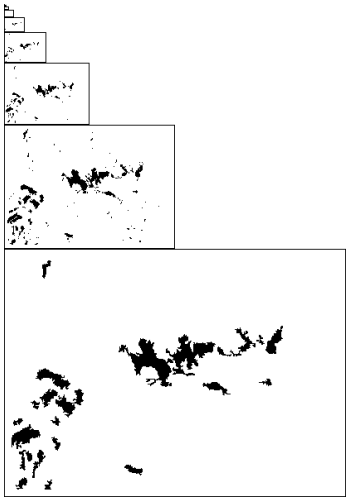


Figure 6: SMAP-based segmentation obtained for the dataset #1

Table 2: Results comparison.

Dataset [#1]	Accuracy rate
Proposed model	**0.942**
Touati et al. [38]	0.942
Zhang et al. [12]	0.975
PCC [12]	0.882

Dataset [#2]	Accuracy rate
Proposed model	**0.835**
Liu et al. [32]	0.818
Liu et al. [32]	0.655

Dataset [#3]	Accuracy rate
Proposed model	**0.896**
Touati et al. [20]	0.949
Touati et al. [9]	0.932
Touati et al. [38]	0.943
Prendes et al. [26]	0.844
Correlation [26]	0.670
Mutual Information [26]	0.580

Dataset [#4]	Accuracy rate
Proposed model	**0.882**
Touati et al. [20]	0.867
Touati et al. [38]	0.878
Touati et al. [38]	0.881
Prendes et al. [50, 27]	0.918
Prendes et al. [25]	0.854
Copulas [23, 25]	0.760
Correlation [23, 25]	0.688
Mutual Information [23, 25]	0.768
Difference [51, 25]	0.782
Ratio [51, 25]	0.813

Dataset [#5]	Accuracy rate
Proposed model	**0.866**
Touati et al. [20]	0.853
Touati et al. [9]	0.870
Touati et al. [38]	0.877
Prendes et al. [26, 27]	0.844
Correlation [26, 27]	0.679
Mutual Information [26, 27]	0.759
Difference. [51, 27]	0.708
Ratio [51, 27]	0.661

Dataset [#6]	Accuracy rate
Proposed model	**0.818**
Chatelain et al. [24]	0.749
Correlation [24]	0.713
Ratio edge [24]	0.737

Dataset [#7]	Accuracy rate
Proposed method	**0.946**
zhan et al. [52]	0.979

Dataset [#8]	Accuracy rate
Proposed model	**0.949**
Touati et al. [38]	0.967
Liu et al. [16]	0.976
PCC [16]	0.821

Dataset [#9]	Accuracy rate
Proposed model	**0.882**
zhan et al. [52]	0.991

Dataset [#10]	Accuracy rate
Proposed model	**0.862**
zhan et al. [52]	0.937

Dataset [#11]	Accuracy rate
Proposed model	**0.882**
HPT [17]	0.826

Dataset [#12]	Accuracy rate
Proposed model	**0.835**
Tang et al. [53]	0.986
Multiscale [53]	0.991

Optical/Optical [#13]	Accuracy rate
Proposed model	**0.815**
Tang et al. [53]	0.959
Multiscale [53]	0.966

Acknowledgement

The authors thank the researchers whose shared the *multi-modal* dataset.

References

[1] R. Touati, M. Mignotte, M. Dahmane, "Multimodal change detection using a convolution model-based mapping," in eighth International Conference on Image Processing Theory, Tools and Applications, IPTA 2019, Istanbul, Turkey, November 2019, 2019, doi:10.1109/IPTA.2019.8936127.

[2] N. Longbotham, F. Pacifici, T. Glenn, A. Zare, M. Volpi, D. Tuia, E. Christophe, J. Michel, J. Inglada, J. Chanussot, Q. Du, "Multi-Modal Change Detection, Application to the Detection of Flooded Areas: Outcome of the 2009-2010 Data Fusion Contest," IEEE J. Sel. Topics Appl. Earth Observ., **5**(1), 331–342, 2012, doi:10.1109/JSTARS.2011.2179638.

[3] L. Su, M. Gong, P. Zhang, M. Zhang, J. Liu, H. Yang, "Deep Learning and Mapping Based Ternary Change Detection for Information Unbalanced Images," Pattern Recognition, **66**(C), 213–228, 2017, doi:10.1016/j.patcog.2017.01.002.

[4] R. Hedjam, M. Kalacska, M. Mignotte, H. Z. Nafchi, M. Cheriet, "Iterative Classifiers Combination Model for Change Detection in Remote Sensing Imagery," IEEE Transactions on Geoscience and Remote Sensing, **54**(12), 6997–7008, 2016, doi:10.1109/TGRS.2016.2593982.

[5] R. Touati, M. Mignotte, "A multidimensional scaling optimization and fusion approach for the unsupervised change detection problem in remote sensing images," in sixth IEEE International Conference on Image Processing Theory, Tools and Applications, IPTA'16, Oulu, Finland, December 2016, 1–6, 2016, doi:10.1109/IPTA.2016.7821021.

[6] G. Liu, J. Delon, Y. Gousseau, F. Tupin, "Unsupervised change detection between multi-sensor high resolution satellite images," in 24th European Signal Processing Conference, EUSIPCO 2016, Budapest, Hungary, August 29 - September 2, 2016, 2435–2439, 2016, doi:10.1109/EUSIPCO.2016.7760686.

[7] V. Alberga, "Similarity Measures of Remotely Sensed Multi-Sensor Images for Change Detection Applications," Remote Sensing, **1**(3), 122–143, 2009, doi:10.3390/rs1030122.

[8] D. Brunner, G. Lemoine, L. Bruzzone, "Earthquake Damage Assessment of Buildings Using VHR Optical and SAR Imagery," IEEE Transactions on Geoscience and Remote Sensing, **48**(5), 2403–2420, 2010, doi:10.1109/TGRS.2009.2038274.

[9] R. Touati, M. Mignotte, M. Dahmane, "A new change detector in heterogeneous remote sensing imagery," in 7th IEEE International Conference on Image Processing Theory, Tools and Applications (IPTA 2017), Montreal, Canada, Qc, 2017, doi:10.1109/IPTA.2017.8310138.

[10] G. Camps-Valls, L. Gómez-Chova, J. Muñoz-Marí, J. L. Rojo-Álvarez, M. Martínez-Ramón, "Kernel-Based Framework for Multitemporal and Multisource Remote Sensing Data Classification and Change Detection," IEEE Trans. Geoscience and Remote Sensing, **46**(6), 1822–1835, 2008, doi:10.1109/TGRS.2008.916201.

[11] P. Du, S. Liu, J. Xia, Y. Zhao, "Information Fusion Techniques for Change Detection from Multi-temporal Remote Sensing Images," Inf. Fusion, **14**(1), 19–27, 2013, doi:10.1016/j.inffus.2012.05.003.

[12] P. Zhang, M. Gong, L. Su, J. Liu, Z. Li, "Change detection based on deep feature representation and mapping transformation for multi-spatial-resolution remote sensing images," ISPRS Journal of Photogrammetry and Remote Sensing, **116**, 24–41, 2016, doi:10.1016/j.isprsjprs.2016.02.013.

[13] M. Gong, P. Zhang, L. Su, J. Liu, "Coupled Dictionary Learning for Change Detection From Multisource Data," IEEE Trans. Geoscience and Remote Sensing, **54**(12), 7077–7091, 2016, doi:10.1109/TGRS.2016.2594952.

[14] W. Zhao, Z. Wang, M. Gong, J. Liu, "Discriminative Feature Learning for Unsupervised Change Detection in Heterogeneous Images Based on a Coupled Neural Network," IEEE Trans. Geoscience and Remote Sensing, **55**(12), 7066–7080, 2017, doi:10.1109/TGRS.2017.2739800.

[15] N. Merkle, P. F. S. Auer, R. Muller, "On the Possibility of Conditional Adversarial Networks for Multi-Sensor Image Matching," in Proceedings of IGARSS 2017, IGARSS 2017, 1–4, Fort Worth, Texas, USA, 2017, doi:10.1109/IGARSS.2017.8127535.

[16] J. Liu, M. Gong, K. Qin, P. Zhang, "A Deep Convolutional Coupling Network for Change Detection Based on Heterogeneous Optical and Radar Images." IEEE Transactions Neural Netw. Learn. Syst., 2018, doi:10.1109/TNNLS.2016.2636227.

[17] Z. Liu, G. Li, G. Mercier, Y. He, Q. Pan, "Change Detection in Heterogenous Remote Sensing Images via Homogeneous Pixel Transformation," IEEE Transactions on Image Processing, **27**(4), 1822–1834, 2018, doi:10.1109/TIP.2017.2784560.

[18] R. Touati, M. Mignotte, M. Dahmane, "Anomaly feature learning for unsupervised change detection in heterogeneous images: A deep sparse residual model," IEEE Journal of Selected Topics in Applied Earth Observations and Remote Sensing, **13**(1), 588–600, 2020, doi:10.1109/JSTARS.2020.2964409.

[19] R. Touati, M. Mignotte, M. Dahmane, "Partly uncoupled siamese model for change detection from heterogeneous remote sensing imagery," Journal of Remote sensing and GIS, **9**(1), 2020, doi:10.35248/2469-4134.20.9.272.

[20] R. Touati, M. Mignotte, "An energy-based model encoding non-local pairwise pixel interactions for multi-sensor change detection," IEEE Transactions on Geoscience and Remote Sensing, **56**(1), 2018, doi:10.1109/TGRS.2017.2758359.

[21] B. Storvik, G. Storvik, R. Fjørtoft, "On the Combination of Multisensor Data Using Meta-Gaussian Distributions," IEEE Trans. Geoscience and Remote Sensing, **47**(7-2), 2372–2379, 2009, doi:10.1109/TGRS.2009.2012699.

[22] G. Mercier, G. Moser, S. Serpico, "Conditional copula for change detection on heterogeneous SAR data," in 2007 IEEE International Geoscience and Remote Sensing Symposium, 2394–2397, 2007, doi:10.1109/IGARSS.2007.4423324.

[23] G. Mercier, G. Moser, S. Serpico, "Conditional copulas for change detection in heterogeneous remote sensing images," IEEE Transactions on Geoscience and Remote Sensing, **46**(5), 1428–1441, 2008, doi:10.1109/TGRS.2008.916476.

[24] F. Chatelain, J. Y. Tourneret, J. Inglada, "Change Detection in Multisensor SAR Images Using Bivariate Gamma Distributions," IEEE Transactions on Image Processing, **17**(3), 249–258, 2008, doi:10.1109/TIP.2008.916047.

[25] J. Prendes, M. Chabert, F. Pascal, A. Giros, J. Tourneret, "A New Multivariate Statistical Model for Change Detection in Images Acquired by Homogeneous and Heterogeneous Sensors," IEEE Transactions on Image Processing, **24**(3), 799–812, 2015, doi:10.1109/TIP.2014.2387013.

[26] J. Prendes, M. Chabert, F. Pascal, A. Giros, J. Tourneret, "Performance assessment of a recent change detection method for homogeneous and heterogeneous images," Revue Française de Photogrammétrie et de Télédétection, **209**, 23–29, 2015.

[27] J. Prendes, New statistical modeling of multi-sensor images with application to change detection, Ph.D. thesis, Toulouse, 2015.

[28] R. Touati, M. Mignotte, M. Dahmane, "Multimodal change detection in remote sensing images using an unsupervised pixel pairwise-based Markov Random Field model," IEEE Trans. on Image Processing, **29**(1), 757–767, 2020, doi:10.1109/TIP.2019.2933747.

[29] M. Xu, C. Cao, H. Zhang, Y. Xue, Y. Li, J. Guo, C. Chang, Q. He, M. Gao, X. Li, "Change detection of the Tangjiashan barrier lake based on multi-source remote sensing data," in 2009 IEEE International Geoscience and Remote Sensing Symposium, volume 4, IV–303–IV–306, 2009, doi:10.1109/IGARSS.2009.5417373.

[30] M. Volpi, F. de Morsier, G. Camps-Valls, M. Kanevski, D. Tuia, "Multi-sensor change detection based on nonlinear canonical correlations," in 2013 IEEE International Geoscience and Remote Sensing Symposium - IGARSS, 1944–1947, 2013, doi:10.1109/IGARSS.2013.6723187.

[31] C. Wu, B. Du, L. Zhang, "Slow Feature Analysis for Change Detection in Multispectral Imagery," IEEE Transactions on Geoscience and Remote Sensing, **52**(5), 2858–2874, 2014, doi:10.1109/TGRS.2013.2266673.

[32] Z. G. Liu, G. Mercier, J. Dezert, Q. Pan, "Change Detection in Heterogeneous Remote Sensing Images Based on Multidimensional Evidential Reasoning," IEEE Geoscience and Remote Sensing Letters, **11**(1), 168–172, 2014, doi: 10.1109/LGRS.2013.2250908.

[33] M. Volpi, G. Camps-Valls, D. Tuia, "Spectral alignment of multi-temporal cross-sensor images with automated kernel canonical correlation analysis," ISPRS Journal of Photogrammetry and Remote Sensing, **107**, 50–63, 2015, doi:10.1016/j.isprsjprs.2015.02.005.

[34] X. Chen, J. Li, Y. Zhang, L. Tao, "Change Detection with Multi-Source Defective Remote Sensing Images Based on Evidential Fusion," ISPRS Annals of Photogrammetry, Remote Sensing and Spatial Information Sciences, 125–132, 2016, doi:10.5194/isprsannals-III-7-125-2016.

[35] D. Tuia, D. Marcos, G. Camps-Valls, "Multi-temporal and Multi-source Remote Sensing Image Classification by Nonlinear Relative Normalization," ISPRS Journal of Photogrammetry and Remote Sensing, 2016, doi: 10.1016/j.isprsjprs.2016.07.004.

[36] Z. Liu, L. Zhang, G. Li, Y. He, "Change detection in heterogeneous remote sensing images based on the fusion of pixel transformation," in 20th International Conference on Information Fusion, FUSION 2017, Xi'an, China, July 10-13, 2017, 1–6, 2017, doi:10.23919/ICIF.2017.8009656.

[37] L. T. Luppino, S. N. Anfinsen, G. Moser, R. Jenssen, F. M. Bianchi, S. B. Serpico, G. Mercier, "A Clustering Approach to Heterogeneous Change Detection," in Image Analysis - 20th Scandinavian Conference, SCIA 2017, Tromsø, Norway, June 12-14, 2017, Proceedings, Part II, 181–192, 2017, doi:10.1007/978-3-319-59129-2_16.

[38] R. Touati, M. Mignotte, M. Dahmane, "Change detection in heterogeneous remote sensing images based on an imaging modality-invariant MDS representation," in 25th IEEE International Conference on Image Processing (ICIP'18), Athens, Greece, 2018, doi:10.1109/ICIP.2018.8451184.

[39] L. T. Luppino, F. M. Bianchi, G. Moser, S. N. Anfinsen, "Remote sensing image regression for heterogeneous change detection," CoRR, **abs/1807.11766**, 2018, doi:10.1109/MLSP.2018.8517033.

[40] S. Benameur, M. Mignotte, J.-P. Soucy, J. Meunier, "Image restoration using functional and anatomical information fusion with application to SPECT-MRI images," International Journal of Biomedical Imaging, **2009**, 12 pages, 2009, doi:10.1155/2009/843160.

[41] D. Kundur, D. Hatzinakos, "Blind image restoration via recursive filtering using deterministic constraints," in Proc. International Conference on Acoustics, Speech, and Signal Processing, volume 4, 547–549, 1996, doi: 10.1109/ICASSP.1996.547737.

[42] M. Mignotte, J. Meunier, "Unsupervised restoration of brain SPECT volumes," in Vision Interfaces, VI'00, 55–60, Montréal, Québec, Canada, 2000.

[43] M. Mignotte, J. Meunier, "Blind deconvolution of SPECT images using a noise model estimation," in SPIE Conference on Medical Imaging, volume 3979, 1370–1377, San Diego, CA, USA, 2000, doi:10.1117/12.387647.

[44] M. Mignotte, J. Meunier, "Three-dimensional blind deconvolution of SPECT images," IEEE trans. on Biomedical Engineering, **47**(2), 274–281, 2000, doi: 10.1109/10.821781.

[45] N. B. Smith, A. Webb, Introduction to Medical Imaging: Physics, Engineering and Clinical Applications, Cambridge Texts in Biomedical Engineering, Cambridge University Press, 2010, doi:10.1017/CBO9780511760976.

[46] T. Zhan, M. Gong, J. Liu, P. Zhang, "Iterative feature mapping network for detecting multiple changes in multi-source remote sensing images," ISPRS Journal of Photogrammetry and Remote Sensing, **146**, 38 – 51, 2018, doi: 10.1016/j.isprsjprs.2018.09.002.

[47] W. H. Press, S. A. Teukolsky, W. T. Vetterling, B. P. Flannery, Numerical Recipes in C, Cambridge University Press, Cambridge, USA, 2nd edition, 1992.

[48] A. Dempster, N. Laird, D. Rubin, "Maximum likelihood from incomplete data via the EM algorithm," Royal Statistical Society, 1–38, 1976, doi: 10.1111/j.2517-6161.1977.tb01600.x.

[49] C. Bouman, M. Shapiro, "A Multiscale Random Field Model for Bayesian Image Segmentation," IEEE Trans. on Image Processing, **3**(2), 162–177, 1994, doi:10.1109/83.277898.

[50] J. Prendes, M. Chabert, F. Pascal, A. Giros, J.-Y. Tourneret, "Change detection for optical and radar images using a Bayesian nonparametric model coupled with a Markov random field," in Proc. IEEE International Conference on Acoustic, Speech, and Signal Processing, ICASSP'15, Brisbane, Australia, 2015, doi:10.1109/ICASSP.2015.7178223.

[51] O. D. Team, "The ORFEO Toolbox Software Guide," 2014, available at http://orfeo-toolbox.org/.

[52] T. Zhan, M. Gong, J. Liu, P. Zhang, "Iterative feature mapping network for detecting multiple changes in multi-source remote sensing images," ISPRS Journal of Photogrammetry and Remote Sensing, **146**, 38–51, 2018, doi: 10.1016/j.isprsjprs.2018.09.002.

[53] Y. Tang, L. Zhang, "Urban Change Analysis with Multi-Sensor Multispectral Imagery," Remote Sensing, **9**(3), 2017, doi:10.3390/rs9030252.

[54] M. Mignotte, C. Collet, P. Pérez, P. Bouthemy, "Sonar image segmentation using an unsupervised hierarchical MRF model," IEEE Trans. on Image Processing, **9**(7), 1216–1231, 2000, doi:10.1109/83.847834.

ASTES

Advances in Science, Technology and Engineering Systems Journal Vol. 5, No. 5, 1299-1307 (2020)

www.astesj.com

Special Issue on Multidisciplinary Innovation in Engineering Science & Technology

ASTESJ

ISSN: 2415-6698

C-Band FMCW Radar Design and Implementation for Breathing Rate Estimation

Mohammad Mohammad Abdul-Atty[1], Ahmed Sayed Ismail Amar[1,*], Mohamed Mabrouk[2]

[1]*Department of Electronics and Communications Engineering, Ain Shams University, Cairo, 18655, Egypt*

[2]*Electrical Engineering Department, Alexandria University, Alexandria, 22301, Egypt*

ARTICLE INFO

Article history:
Received: 31 July, 2020
Accepted: 28 September, 2020
Online: 26 October, 2020

Keywords:
FMCW
Radar
Human
Breathing
Detection

ABSTRACT

In this paper, a portable Frequency Modulated Continuous Wave (FMCW) radar system was designed and implemented for human movements and breathing detection. The radar operates with a frequency band ranges from 4.7 to 4.9GHz. The radar sub-systems were designed and simulated using up to date computer-aided-design tools before implementation. The Voltage Controlled Oscillators (VCO), high gain antenna, low loss power divider/combiner, and a high selectivity bandpass filter were implemented, and their parameters were measured using a microwave analyzer. The simulated results and the measured results show a significant correlation. The new RF front end module components enhanced the radar signal-noise-ratio (SNR), and the breathing rate detection. The Digital Signal Processing (DSP) is implemented on the Field Programmable Gate Array (FPGA) board for movement and breathing signals detection processing in real-time. Highly sensitive detection, configurability, low cost, low power consumption, and portability were considered in the designed system. We believe that the enhanced reconfigurable radar system will be helpful in several biomedical monitoring applications.

1. Introduction

Human breathing estimation is very important in security, medical, and homecare applications [1]. In security applications, special military troops use the human breathing detection devices to detect human behind walls in case of building enforcement operations. In medical applications, vital signs monitoring was proposed in US patent in 1990 [2]. After that, human breathing and heartbeat estimation instruments for medical application were introduced since 1993 [3]. Hospitals use human breathing radars to estimate the breathing especially for burned skin or COVID-19 patients where it is preferred not to contact the medical crew. In homecare applications, the population of Americans edged more than 65 years will grow to 90 million people in 2050 [4]. These old peoples who lives alone need to be monitored using breathing and heartbeat detection radars to detect sudden medical problems and report them to an emergency medical center.

Radar systems may be designed to be pulsed or continuous wave transmitters depending on the required application. Frequency modulated continuous wave (FMCW) radars outperforms the pulsed radars in transmitting higher average power with its capability of measuring the target range, especially for small cross section area targets. Because of that, FMCW radars were used in human breathing and heartbeat estimation and human movements detection applications [5]. In [6], a 24.15 GHz FMCW radar with a scanning bandwidth of 72 MHz was used to extract the human heartbeat rate signal. In [7], a 24 GHz FMCW radar was used for heartbeat rate estimation. The clutter noise was canceled but the effect of human limbs motion decreased the human breathing estimation rate accuracy. According to the selection of the operating frequency band, the human chest cross section area has its highest value in the frequency band 3-4 GHz and the received signal-to-noise ratio is high in the frequency band 4-6 GHz [8], [9] .However, many FMCW radars for human breathing rate estimation were designed and implemented in other frequency bands such as 2.4 GHz, 9.6GHz, 24GHz, and 77GHz [7], [10]-[13]. The harmonics of the human breathing frequency may interfere with the heartbeat rate that result in heartrate estimation failure [10]. One of the most effective methods is to use comb filters to remove these harmonics [14]. For C-band biomedical radars, the state-of-the-art presented the radar systems without considering configurability, cost, and design reliability which is covered in this paper.

*Corresponding Author: Ahmed Sayed Ismail Amar, 434 king Faisal street, Cell No. +0201065664849 & ahmed.s.i.amar@ieee.org

Most uses of radar can be classified as detection, tracking, or imaging. In this research, the scope is on radar detection. The most fundamental problem in radar is detection of an object or physical phenomenon. This requires determining whether the receiver frontend output at a given time represents the echo from a reflecting object or only noise. Detection process starts with using the techniques of signal acquisition and interference reduction necessary to perform these tasks. These techniques were discussed briefly in [15] and the signal is then processed for a decision. Detection decisions are usually made by comparing the amplitude of the signal to a threshold which may be set a priori in the radar design, which is not preferred because noise changes over time, or may be computed adaptively from the radar data.

Digital signal processing on the radar returns can be implemented using main task functions such as: Moving Target Indicators (MTI), Constant False Alarm Rate (CFAR), digital integrators, and target information packet extractors [16]. These main functions can be set to be configurable. For example, CFAR techniques have been developed in the last few decades such as order statistics CFAR (OS-CFAR) [17], cell average CFAR (CA-CFAR) [18], greatest of CFAR (GO-CFAR) [19], and smallest of CFAR (SO-CFAR) [20]. Each one of these techniques is suitable for specific environmental conditions. The DSP can be design to select the desirable technique by the user.

In this paper, a configurable C-band FMCW radar is designed and implement for human breathing detection. Section 2 presents the principal of operation. Section 3 present the Radio Frequency (RF) components design and implementation. Section 4 is the measurements results, section 5 presents the conclusion, and section 6 discusses the future work .

2. Principles of Operation

The FMCW radar range resolution depends on the transmitted signal bandwidth while the maximum range can be calculated from the chirp time interval. (Figure 1.a) shows the linear variation of the transmitted frequency from f_start to f_stop where the bandwidth is equal to $f_{stop} - f_{start}$. The chirp time is T_chirp, that the maximum range is equal to $C \times T_{chirp}/2$, where C is the light propagation velocity. The transmitted signal $x_t(t)$ can be presented by:

$$x_t(t) = A_T \cos(2\pi f_{start}.t + \pi \frac{BW}{T_{chirp}} t^2 + \varphi(t)) \quad (1)$$

where, A_T is the amplitude of the transmitted signal, BW is the bandwidth, and $\varphi(t)$ is the transmitter phase noise. When a transmitted signal hit a target, it reflects with attenuated amplitude and time shift related to the target range. The received signal $x_t(t)$ can be presented by:

$$x_r = A_R \cos(2\pi f_{start}(t - \tau_d) + \pi \frac{BW}{T_{chirp}}(t - \tau_d)^2 + \varphi(t - \tau_d)) \quad (2)$$

where, A_R is the attenuated received signal amplitude, and τ_d is the round-trip delay from the radar antenna to the target and back again to the radar, and is given by:

$$\tau_d = \frac{2R}{c} \quad (3)$$

where, R is the target range. When the received signal is mixed with the transmitted one, the output can be presented by:

$$y(t) = \frac{1}{2} * A_T * A_R \cos[(2\pi f_{start} t + \pi \frac{BW}{T_{chirp}} t^2 + \varphi(t) - 2\pi f_{start}(t - \tau_d) - \pi \frac{BW}{T_{chirp}}(t - \tau_d)^2 - \varphi(t - \tau_d))] \quad (4)$$

$$y(t) = A \cos(2\pi f_{start}\tau_d + 2\pi \left(\frac{BW}{T_{chirp}}\tau_d\right) t - \pi \frac{BW}{T_c}\tau_d^2 + \Delta\varphi(t)) \quad (5)$$

After simplifying $y(t)$, it can be expressed as,

$$y(t) = A \cos[(2\pi f_b t + \varphi_b(t) + \Delta\varphi(t))] \quad (6)$$

where, A it the amplitude of the received signal (t) , f_b is the beat frequency and it is equal to $\frac{BW}{T_{chirp}}\tau_d$, $\varphi_b(t)$ is the received signal phase and it equals to $2\pi f_c \tau_d - \pi \frac{BW}{T_c}\tau_d^2$, $\Delta\varphi(t)$ is the phase noise and it equals to $\varphi(t) - \varphi(t - \tau_d)$. When the target is moving with a specific speed, Doppler frequency adds to the beat frequency and becomes $f_b + f_D$, where f_D is the Doppler frequency. (Figure 1.b), shows the phase difference between the two mixed signals ($f_b + f_D$).

The phase noise is not considered in this research. The term $\pi\,(BW/T_{chirp})\,\tau_d^2$ is very small compared to f_b and can be neglected. Then, the beat signal which is equal to $2\pi f_{start}\tau_d + \frac{BW}{T_{chirp}}\tau_d$, is processed to extract the target parameters.

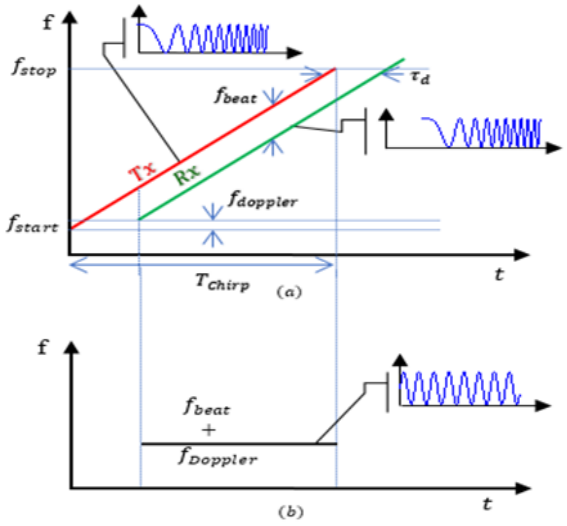


Figure 1: Sawtooth based FMCW radar basic concept: (a) Transmitted and received signal in the frequency-time domain, and (b) single target beat signal

3. System Design

In this section, the design of a C-band FMCW radar for human breathing rate estimation is presented. The system is implemented using RF components and configurable digital signal processing subsystem.

3.1. General Overview of the Proposed Radar

(Figure 2) shows the block diagram of the proposed radar. A single channel architecture is utilized in this design, in order to reduce hardware and memory resources, computation complexity, hence; a cost effective design can be achieved

A function generator board is used to control the Voltage Controlled Oscillator (VCO) to generate a chirp signal with a frequency ranged from 4.7-4.9 GHz. The VCO output is divided into two different ports using 3dB equally power divider. The output of the first port of the divider is connected to a bandpass filter (BPF) from 4 GHz to 5 GHz. The filter output then is sent to the power amplifier with a 20dB gain, and transmitted through a horn antenna with 16.5dB gain. The receive antenna which has the same gain of the transmitter antenna, receives the signal, then a 24dB Low Noise Amplifier (LNA) is used to amplify this signal, then the signal is sent to a BPF operates from 4 GHz to 5 GHz, then this signal is mixed with a replica of the transmitted signal coming from the second port of the power divider, to perform the frequency down conversion. A Low Pass Filter (LPF) then is used to filter the mixer output signal from the unwanted signals. An 8-bit Analog-to-Digital Converter (ADC) is used to digitize the analog signal, then the digital data is passed to the FPGA for signal processing. A PC is connected to the FPGA output for further processing, and a screen is connected directly to the FPGA to show the targets and the target history.

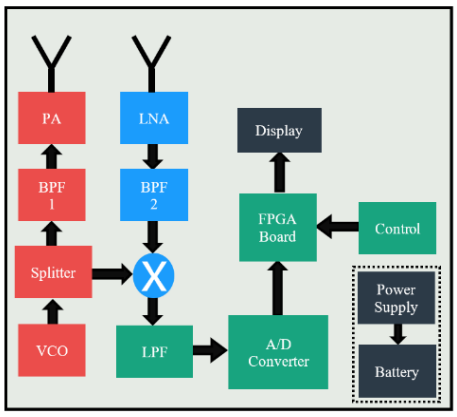


Figure 2: Proposed Radar general block diagram.



Figure 3: Fabricated radar system.

3.2. Radar System Parameters

A 75 cm range resolution is achieved by using 200 MHz sweep bandwidth from the VCO.

The following equation is used to determine the range resolution.

$$R_{res} = \frac{c}{2*BW} \quad (7)$$

where C is the light speed, and BW is the proposed bandwidth. (Figure 3) shows the fabricated radar system, which considers the radar components fixation.

In this design, a chirp duration T_c of 1 ms is chosen. Table 1 shows a listed ssystem parameters. A sampling rate of 2.048 MHz is used for sampling the signal with a band of frequencies that includes the targeted f_b. The beat frequeny can be calculated using equation (6), by measuring the delay time between the transmitted signal and the received signal, the mixer can do this job by mixing these two signals, then the range can be measured. (Figure 4) shows the collected radar data: the x-axis is the fast time direction, each column represents one range cell, while y-axis is the slow time direction, each row represents one complete received chirp or one Coherent Processing Interval (CPI). To get the target's range, then Fast Fourier Transform (FFT) can be performed in the fast time direction, while performing FFT in the slow time direction gets the target's doppler information. (Figure 4) shows the target's movement in many range cells, while another stationary target exists in the same range cell across the slow time direction.

Table 1: Radar system parameters

Parameter	Value
Output Power	16 dBm
Center Frequency (f_c)	4.8 GHz
Sweep Bandwidth (BW)	200 MHz
Sampling Rate (f_s)	2.048 MSPS
FFT Points	2048 point
Chirp Duration T_c	1 ms
Frequency resolution	1 KHz
Range resolution	0.75 m
Maximum Number of Available Range Cells	1024 Range Cell
Range of Interest	15 m
Battery Used	11.1v/5A
Power Consumption	19.98 W
Radar operation time for a single charge	2.5 Hours
Device Cost	800 $

3.3. Radar RF Front End Module

In our previous work, the (VCO), bandpass filter, power divide/combiner, and the antenna were designed and fabricated for a human breathing radar system [21]. In this work, a step forward in the design and fabrication was accomplished by introducing

more analysis and design tuning. The radar Radio Frequency-Front End Module (RF-FEM) circuits are enhanced to improve the (SNR) of the received signal, and therefore improving the breathing rate detection. The new (RF-FEM) circuits are improved to be low cost, compact, high selectivity, low insertion loss in the passband, high isolation in the stopband, excellent return loss, equal phase, and equal amplitude. The (RF-FEM) architecture consists of a single transmitter and a single receiver as presented in (Figure 2). In the transmitter subsystem, a monolithic (VCO) chip TGV2562-SM is utilized to generate frequencies from 4.7 to 4.9 GHz In order to generate a chirp waveform with a preselected bandwidth, a sawtooth signal is used. The VCO printed circuit board is designed, fabricated on Rogers RO4003 substrate material with dielectric material $\varepsilon_r = 3.38$, thickness (h) of 0.203 mm, and loss tangent ($tan\delta = 0.0022$) as shown in (Figure 5). The VCO circuit is measured using N9918A spectrum analyzer, and the VCO output sweeps over the range from 4.7 to 4.9GHz.

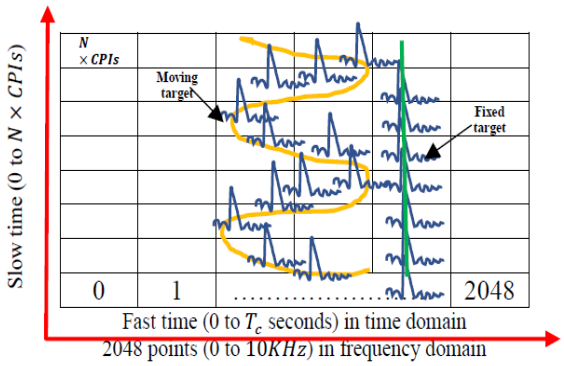


Figure 4: Radar data collection.

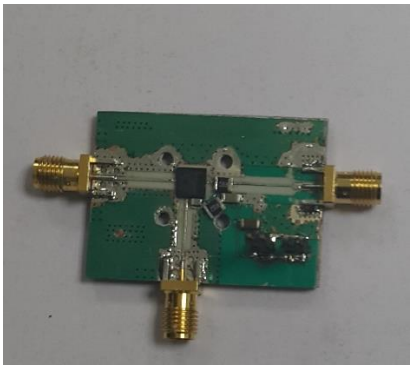


Figure 5: Fabricated printed circuit board of the VCO

equations (Figure 2) shows that the VCO output is connected to a 2-way power splitter. the output signal divides into two paths, a BPF in the transmitter subsystem, and a mixer in the receiver subsystem. (Figure 6) shows the design of a compact microstrip two-way equal Wilkinson RF power divider resonates at 4.8 GHz using CST software. the simulation results within the passband have good matching, isolation, and less than 0.15dB losses as shown in (Figure 6). The proposed power splitter is fabricated on Rogers RT6006 substrate with dielectric constant $\varepsilon_r = 6.15$, thickness (h) of 0.64 mm, and loss tangent (tanδ= 0.0023) and tested using N9918A Vector Network Analyzer (VNA). The measured results show minimum insertion loss 0.2dB, Return Loss, isolation below -23dB in the operating frequency band as shown in (Figure 7).

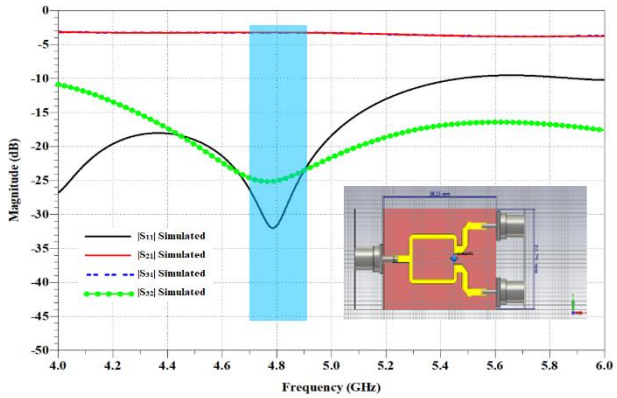


Figure 6: Power divider simulation results and the design structure

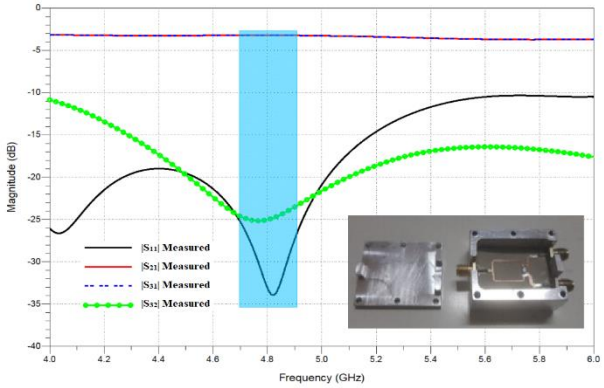
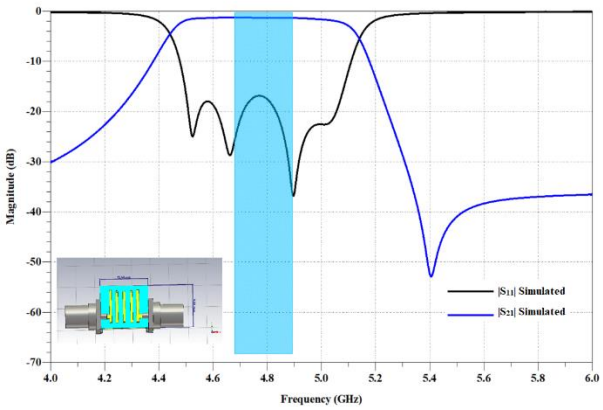


Figure 7: Measured S-parameters results of the fabricated power divider.

A high selectivity BPF is used to select the proposed RF signal on the transmitter subsystem and the receiver subsystem. The design of the presented BPF is based on a microstrip interdigital filter using CST software as shown in (Figure 8). The order of the interdigital filter is five. the simulation results of the proposed wideband BPF is illustrated in (Figure 8). The filter is fabricated on the epoxy Rogers 6006 substrate. Both measured and simulated results of the proposed wideband BPF have low insertion loss -1.1 dB, and good return loss. A good match is found between them the simulated and measured results. The simulated S-parameters are centered at 4.8 GHz while the measured results are shifted slightly and centered at 4.75 GHz as shown in (Figure 9). Any small difference between simulated and measured results from maybe a result of the standard manufacture defects and the copper surface roughness [22].

The BPF output on the transmitter subsystem is amplified via the use of a ZRON-8G+ Mini-Circuits power amplifier. The output of the amplifier is attached to a high gain transmitter antenna. The transmitter antenna is a pyramid horn antenna operating at C-band. (Figure 10) shows the design model and the simulated return loss of the horn antenna using CST software. The simulated results of 3-D radiation patterns of the antenna are given in (Figure 11). The antenna gain is more than 16.5 dB over the operating bandwidth. The horn antenna is fabricated from an aluminum sheet with 3mm thickness as shown in (Figure 12). The simulated results using the CST simulator are compared with the measured one and it achieves

good agreements. The antenna return loss was measured using N9928A Field Fox handheld microwave VNA. As illustrated in (Figure 12), the simulated and measured return loss results of the antenna are less than -10 dB in the operating bandwidth.



Figurer 8: CST structure of the interdigital filter and the simulation results.

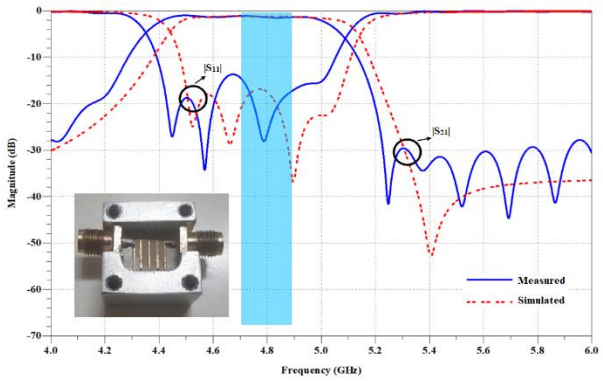


Figure 9: Measured and simulated results of the proposed BPF.

Next, the RF echo signals are received in the receiver subsystem via the receiving antenna, which is a composition of clutter and targets. The receiving antenna is the same as the transmitter antenna. The antenna output is amplified using ZX60-542LN+ Mini-Circuits (LNA). A BPF filter follows the LNA to select the proposed bandwidth. The filtered signal in the receiver subsystem and the output signal from the power splitter in the transmitter subsystem is mixed, using a wideband frequency mixer ZX05-14-S+ to convert the signal to baseband down.

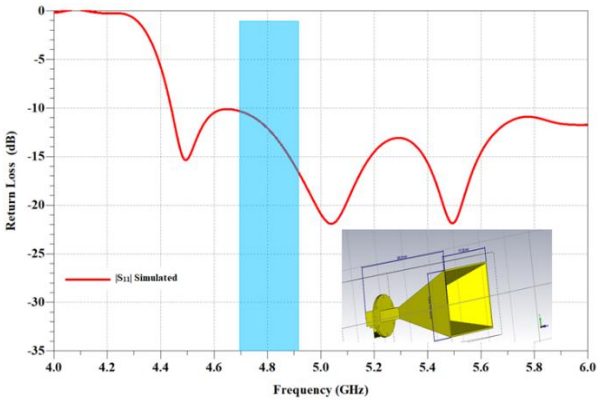


Figure 10: Simulated return loss and the 3D view of the proposed antenna.

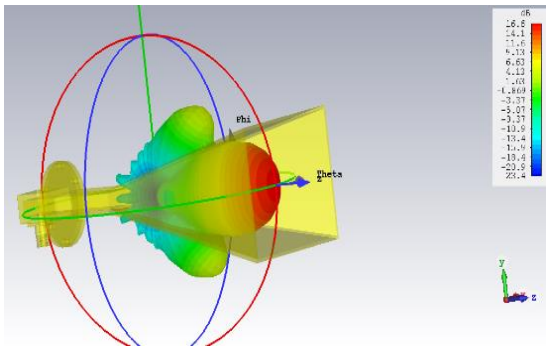


Figure 11: 3D view of the Radiation pattern.

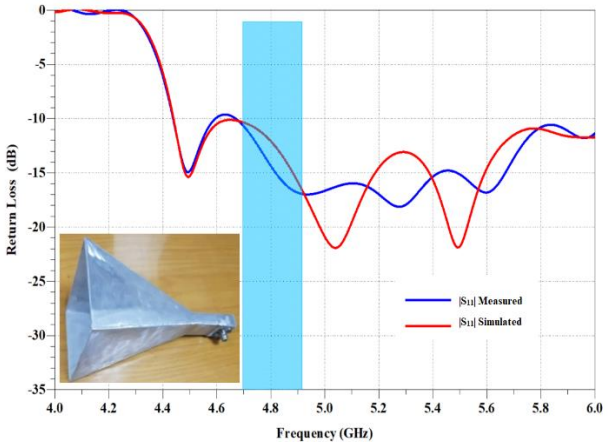


Figure 12: Measured and simulated return loss results.

3.4. Signal Processing

The output of the mixer contains two major frequency components, Sum and difference of the received signal and the reference signal. The signal of interest is the low frequency which contains the target information, Range and Doppler. A LPF is designed and implemented with a cutoff frequency of 1 MHz to filter the mixer output signal from the high frequency components, (Figure 13) shows the filter response. The filtered signal then passes through a 8-bit ADC at 2.048 MSPS sampling rate. The FPGA receives the signal for signal processing.

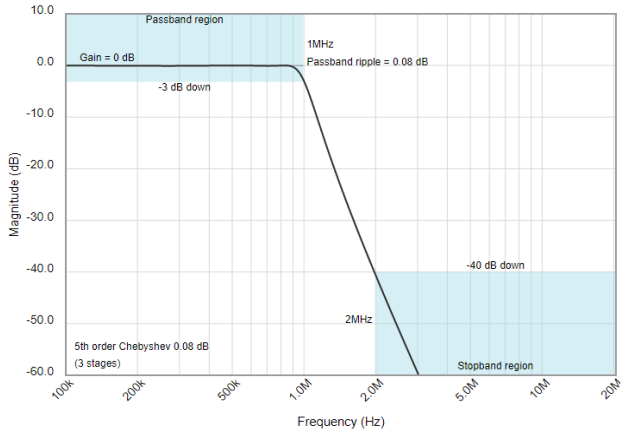


Figure 13: Frequency response of the baseband LPF.

An FPGA board of type XILINX Nexys4, Artix-7 XC7A100T FPGA board, is used for the implementation of the signal processor. A pipelined (FFT) at 2048 point is applied to the ADC

output in the fast time direction as shown in (Figure 14) to extract the frequency component corresponding to the actual range.

Figure 14.a shows that the chirp signal is received continuously through the receiver antenna and the LNA for a single moving target. Figure 14.b shows the resultant signal form the mixer output, which contains the target's information, the range and the Doppler. The amplitude of the signal increases and decreases depending on whether the target is approaching or drifting away from the radar. Figure 14.c shows the spectrum of the received signal after performing FFT, a target's frequency appears with the largest amplitude which changes with the change of the received target signal. The spectrum for each chirp then is stored in a memory Figure 14.d, so that a second FFT can be performed in the slow time for Doppler estimation as shown in Figure 14.e.

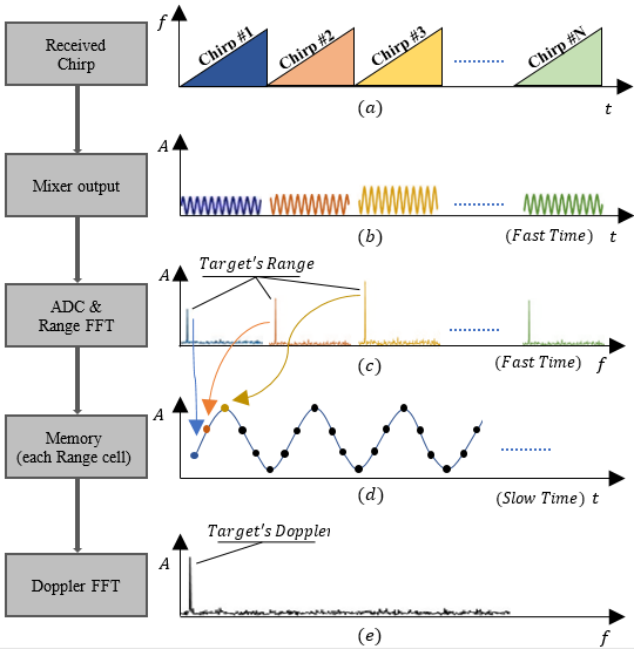


Figure 14: (a) Received chirps, and (b) Mixer output, and (c) Beat frequency in frequency domain, or spectrum of each chirp and (d) Storing target's data into memory for second FFT (slow time), and (e) Slow time FFT for Doppler estimation.

(Figure 15) shows the general block diagram of the digital signal processor. After, the Moving Target Indicator (MTI) is applied to the first FFT output, to remove the stationary targets. MTI can be enabled/disabled, it depends on the target parameters and the environmental conditions, and either one pulse or two pulse cancellers can be selected depending on the targeted speed measurement of the moving target. Then, an adaptive Constant False Alarm Rate (CFAR) is applied, and either Smallest-of-CFAR (GOCFAR) or Greatest-of-CFAR (SOCFAR) can be selected, both having the widow size adjustable (16 or 32).

A decision based on an adjustable number of successive target hits is made using a binary integrator; it can be manually turned on or off during the device run-time operation, and the required number of successive hits can be adjusted during the run-time operation as well, without affecting the radar operation.

All the parameters that can be configured, are perfectly synchronized by the synchronizer to avoid any errors due to removing/adding signal processing blocks or changing numbers within each block in real time, during run time operation. The output block can be separately sent directly to a host PC using serial communication protocol during run-time to monitor and track the received signal in each block, as well as for further analysis, testing and processing.

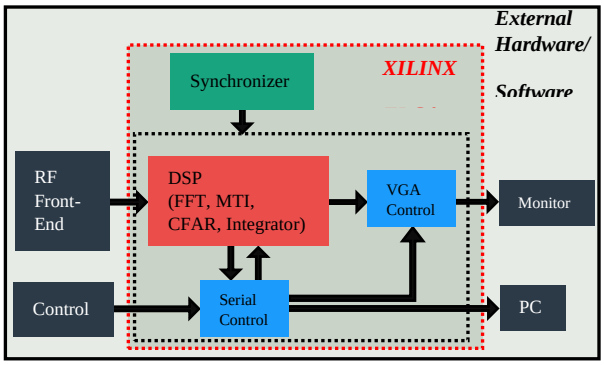


Figure 15: Developed Digital Signal Processing block diagram using XILINX FPGA.

3.5. Simulation Results

The simulation process is based on a simulated target from the MATLAB software, the simulated target then is processed in MATLAB software, the same MATLAB generated target is then processed in ModelSim software (FPGA simulator) , then the signal processing is applied, The outputs of FFT from both MATLAB and ModelSim are compared with each other, the same is applied to the MTI and CFAR. The results show that the outputs of the MATLAB and FPGA are identical. (Figure 16) shows the simulation criteria.

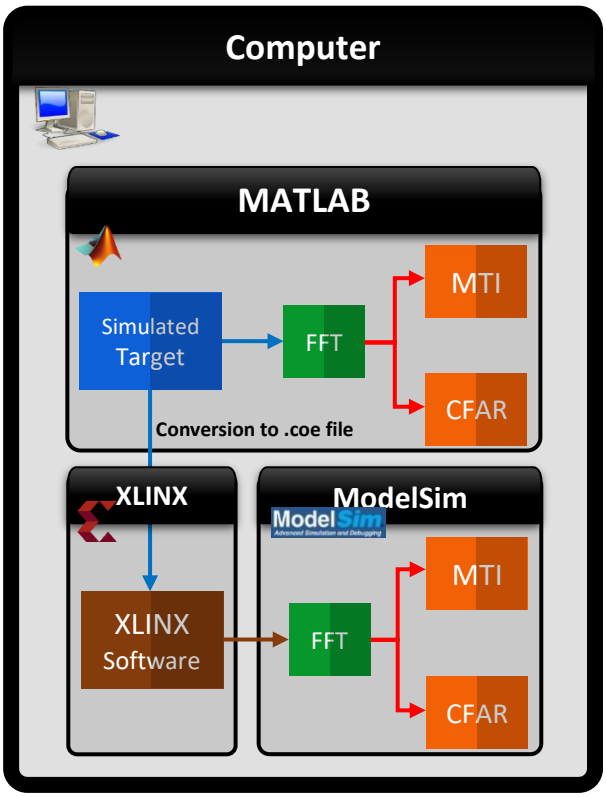


Figure 16: Developed Digital Signal Processing block diagram using XILINX FPGA.

4. Experimental Results

In this section, two experiments are presented, in the first experiment, a breathing signal is estimated from a human sitting in front of the radar device. In the second experiment, an FFT process is applied to a received signal from a human target moving back and forth within certain range from the radar, the FFT-processed data then is sent to the PC.

4.1. Breathing Detection

In this experiment (the first experiment), three measurements were taken from a human in three scenarios:

A human is sitting at a distance of 2.25m, 6m and a measurement without any target in front of the radar for results comparison.

(Figure 17) shows the breathing signal at the 3rd range cell (2.25 m) in time domain, after applying first FFT, the received breathing signal is caused by the human chest movement. After performing the 2nd FFT, a peak appears in the frequency domain which represents the breathing frequency, as shown in (Figure 18)

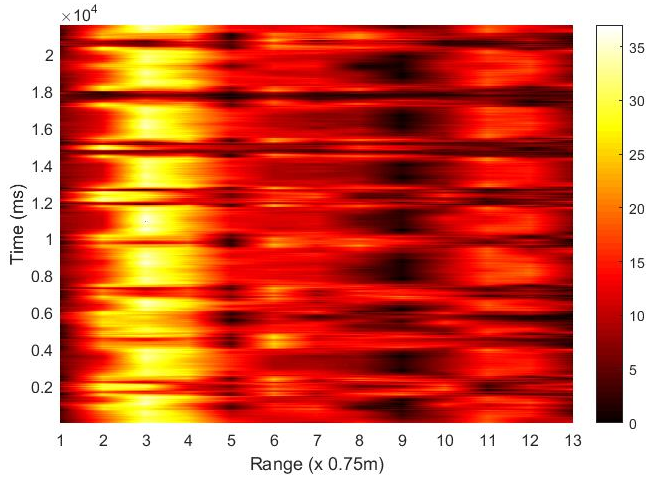


Figure 17: Time domain breathing signal at the 3rd range cell.

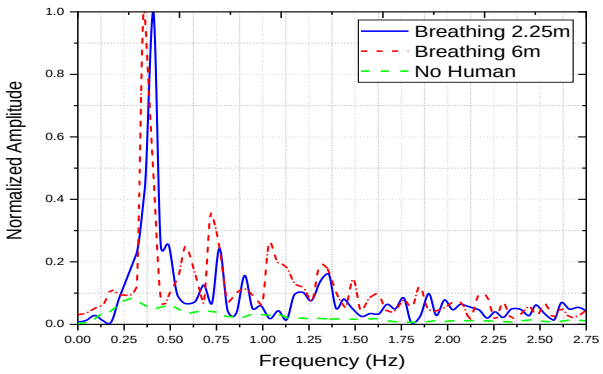


Figure 18: Breathing signal detection results of two ranges.

(Figure 18) shows that a breathing signal has been successfully extracted. Two peaks are detected at 0.4Hz and 0.37Hz detected at a distance 2.25m and 6m, respectively, which represent the breathing signal. To assure that the output peaks represent the breathing signal, not noise signal from the surrounding area or the thermal noise, a measurement was taken without a human in front of the radar, the result as in (Figure 17) green dashed line shows that the breathing frequency disappeared.

4.2. Movement Detection

In the second experiment, The radar device was placed in the free space, and there was two tanks in the left of the radar as shown in (Figure 19). The first data collected without a moving target shows a weak signal at 15 meters as the two tanks was placed on the left of the radar as shown in (Figure 20), a human is moving within 15m back and forth as shown in collected data in (Figure 21), the figure shows that the target appears distinguishable from the noise, as a result of the new RF components presented in this paper.



Figure 19: Measurement setup.

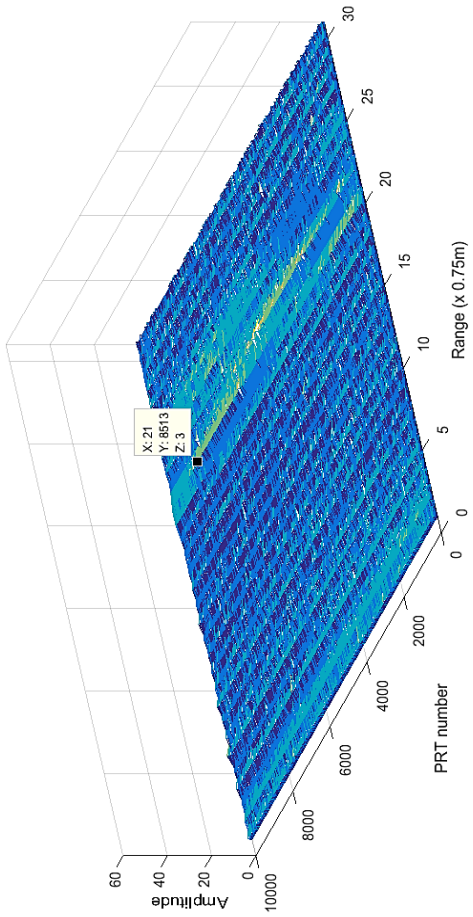


Figure 20: Data collected without moving target.

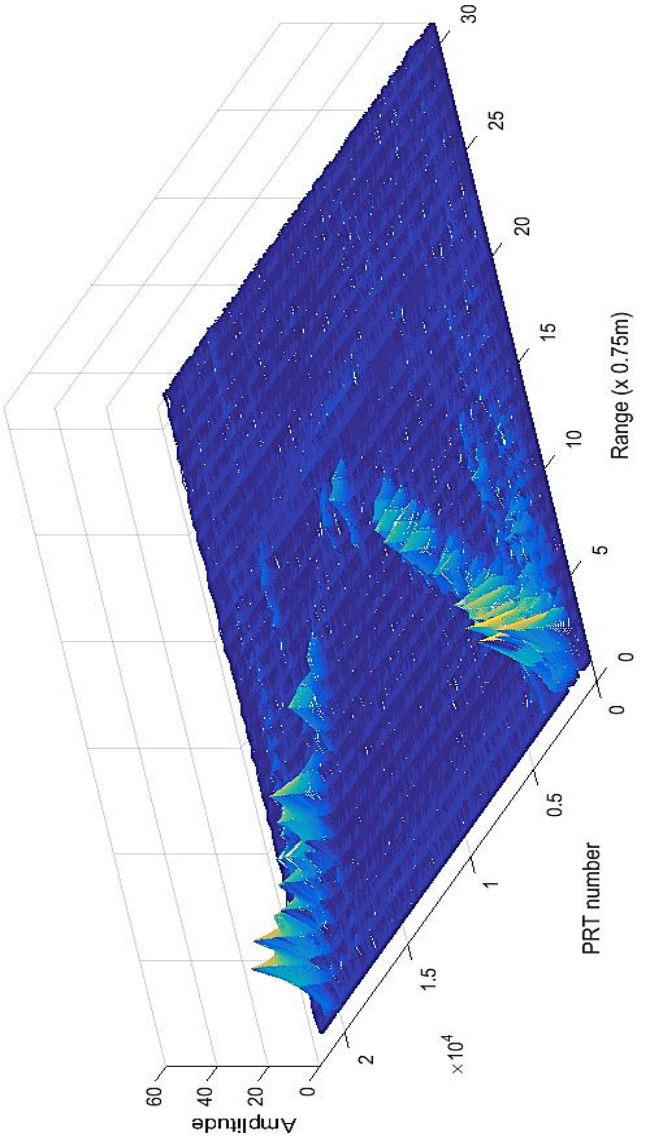


Figure 21: Data collected with the moving target.

4.3. System complexity:

In this paper, the proposed radar system contains IF components and RF components, The RF components comprises new simple RF designs yet with the best performance, while the readymade components are available in the market for commercial use.

The IF section contains the custom locally manufactured boards for this specific radar system, like ADC, LPF, Function Generator (FG) and power supply with attached battery, all were made by locally available components which made the IF section the cheapest part in the system. The FPGA is chosen carefully by calculating the needed resources for the DSP algorithm, that assures the best choice of the FPGA to avoid the high cost FPGAs.

The whole system was intended to be designed as simple as possible, to assure the availability of the required components, the reliability of usage, simplicity in maintenance, with the best performance as shown in previous sections.

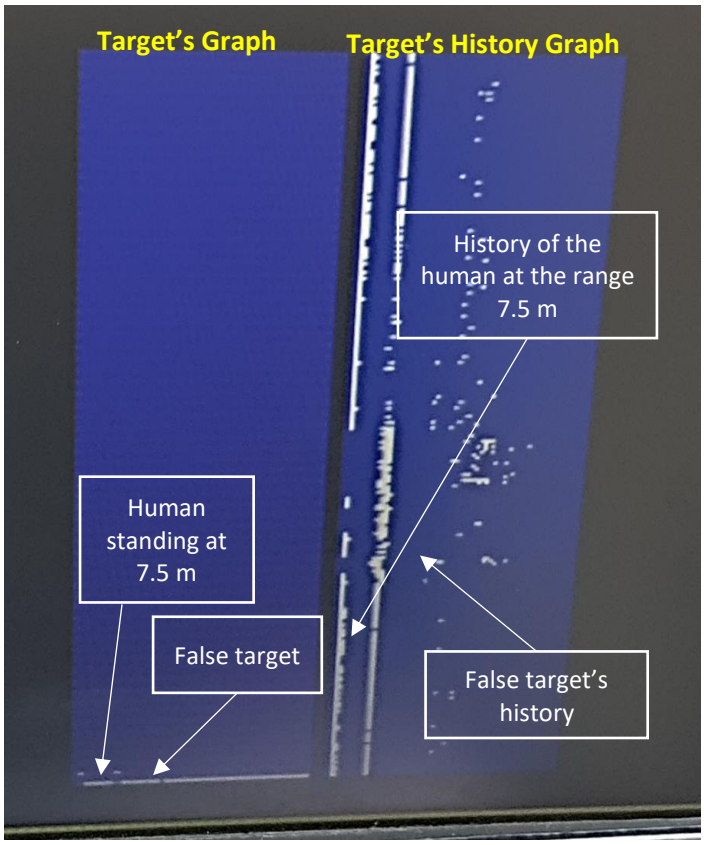


Figure 22: Real target detected on the monitor from the FPGA directly.

Table 2: Previous Work Comparison

Parameter	This Work	[23]	[24]
Start frequency	4.7 GHz	2.1 GHz	8 GHz
Bandwidth	200 MHz	12.5 MHz	4 GHz
ADC sampling rate	2.048 MSPS	25 MSPS	1 MHz
Sweep period	1 ms	1 ms	100 ms
Power Output	16 dBm	33 dBm	2 dBm
Configurability	Yes	No	No
FMCW software	No software required (Windows and Ubuntu are optional)	GNU Radio (Ubuntu)	GNU Radio (Windows)
Cost	Low	High	High

The monitoring system is a key component in this system, the system does not require a software at all, however, an optional software is designed for target monitoring. A Video Graphics Array (VGA) algorithm is implemented on FPGA, taking the advantage of the remaining FPGA resources to show the signal processing results on the VGA screen directly as shown in (Figure 22) and assures the real time detection of the targets and breathing signal. The monitor screen can show the received signal in time domain/frequency domain, breathing signal in time domain/frequency domain, CFAR target output with 5 seconds target history. Switching between all the outputs on the screen can be controlled using the configuration control screen. One

advantage of the VGA controller is that the system takes only 10 seconds to boot.

The monitoring system is a key component in this system, the system does not require a software at all, however, an optional software is designed for target monitoring. A Video Graphics Array (VGA) algorithm is implemented on FPGA, taking the advantage of the remaining FPGA resources to show the signal processing results on the VGA screen directly as shown in (Figure 22) and assures the real time detection of the targets and breathing signal. The monitor screen can show the received signal in time domain/frequency domain, breathing signal in time domain/frequency domain, CFAR target output with 5 seconds target history. Switching between all the outputs on the screen can be controlled using the configuration control screen. One advantage of the VGA controller is that the system takes only 10 seconds to boot.

4.4. Previous Work Comparison

Table 2 Shows a comparison between the proposed radar system and some other developed radar devices. The comparison shows that the proposed radar system is gaining the advantage of the configurability function, with relatively better price, in addition to that, our system does not require any software or operating system for the operation.

5. Conclusion and Future Work

In this paper, a reconfigurable radar system is proposed. The radar device is designed for human movement as well as for breathing detection. The proposed radar system is implemented using a new low-cost RF front end component and a reconfigurable radar signal processor. The radar device is aimed to operate in different situations and multiple environmental conditions. Depending on the required situations, MTI, CFAR and binary integrator can be configured for better performance. The system parameters can be reconfigured during the run time; without affecting the working efficiency. The Proposed radar system is compact and low cost compared to other radar systems with some similar parameters and operates in outdoor and indoor scenarios.

This research work will be extended by using software-defined radio (SDR), to generate the LFMCW waveform and to implement the digital receiver and DSP subsystem. SDR will help in generating different transmitted waveform configurations, decreasing the main to side-lobe level of the transmitted waveform, decreasing the overall size of the radar system, and reducing the cost. After that, many adjustments to the system can help in increasing the operating range and the breathing rate estimation accuracy. Additionally, some functions will be added to the VGA screen for ease to use, like adding grids, numbers and letters.

References

[1] M. Mabrouk, S. Rajan, M. Bolic, I. Batkin, H.R. Dajani, V.Z. Groza, "Model of human breathing reflected signal received by PN-UWB radar," 2014 36th Annual International Conference of the IEEE Engineering in Medicine and Biology Society, EMBC **2014**, 4559–4562, 2014, doi: 10.1109/EMBC.2014.6944638.

[2] S. Sharpe, Seals, J.; MacDonald, A.H.; Crowgey, S.R. Non-Contact Vital Signs Monitor. U.S. Patent **4**,958,638, 25 September 1990.

[3] J. Pan, "Medical Applications of Ultra-Wideband (UWB)," Hadley, 2007.

[4] T. R. Frieden, "The State of Aging and Health in America," Atlanta, 2013.

[5] F. Quaiyum, L. Ren, S. Nahar, F. Foroughian, A.E. Fathy, "Development of a reconfigurable low cost multi-mode radar system for contactless vital signs detection," IEEE MTT-S International Microwave Symposium Digest, **6**, 1245–1247, 2017, doi: 10.1109/MWSYM.2017.80 58832.

[6] D. Zhang, M. Kurata, T. Inaba, "FMCW radar for small displacement detection of vital signal using projection matrix method," International Journal of Antennas and Propagation, **2013**(1), 1–6, 2013, doi: 10.1155/2013/57198 6.

[7] H. Lee, B.H. Kim, J.K. Park, J.G. Yook, "A novel vital-sign sensing algorithm for multiple subjects based on 24-GHz FMCW Doppler radar," Remote Sensing, **11**(10), 2019, doi: 10.3390/rs11101237.

[8] N. Maaref, P. Millot, C. Pichot, O. Picon, "A study of UWB FM-CW radar for the detection of human beings in motion inside a building," IEEE Transactions on Geoscience and RemoteSensing, **47**(5), 1297–1300, 2009, doi: 10.1109/TG RS.2008.2010709.

[9] [9] A. Nezirovic, A.G. Yarovoy, L.P. Ligthart, "Experimental Verification of Human Being Detection Dependency on Operational UWB Frequency Band." IEEE International Conference on Ultra-Wideband, Singapore, 305-310, 2007, doi: 10.1109/ICUWB.2007.4380960.

[10] L. Anitori, A. De Jong, F. Nennie, "FMCW radar for life-sign detection," 2009 IEEE Radar Conference, 1-6, 2009, doi: 10.1109/RADAR .2009.4976934.

[11] C. Gu, G. Wang, T. Inoue, C. Li, "Doppler radar vital sign detection with random body movement cancellation based on adaptive phase compensation," 2013 IEEE MTT-S International Microwave Symposium Digest, 1-3, 2013, doi: 10.1109/MWSYM.2013.6697618.

[12] A. Ahmad, J.C. Roh, D. Wang, A. Dubey, "Vital signs monitoring of multiple people using a FMCW millimeter-wave sensor," 2018 IEEE Radar Conference (RadarConf18), **4**, 1450–1455, 2018, doi:10.1109 /RADA R.2018.8 37 8778.

[13] M. Alizadeh, G. Shaker, J.C.M. De Almeida, P.P. Morita, S. Safavi-Naeini, "Remote monitoring of human vital signs using mm-Wave FMCW Radar," IEEE Access, **7**(4), 54958–54968, 2019, doi: 10.1109/ACCESS. 2019.2912956.

[14] M. Mabrouk, S. Rajan, M. Bolic, M. Forouzanfar, H.R. Dajani, I. Batkin, "Human Breathing Rate Estimation from Radar Returns Using Harmonically Related Filters," Journal of Sensors, 2016, doi: 10.1155/2016/9891852.

[15] M. I. Skolnik, Radar Systems, New York: McGraw-Hill, 2001.

[16] M. Mabrouk, W. Mohamed, S. Aly, H.M. Hassan, "MTD Design and Implementation Using Short Coherent Processing Interval Phase Trace," Proceedings of 172nd ISERD International Conference, Cairo, Egypt ,40-44, 2019.

[17] R. Sor, J.S. Sathone, S.U. Deoghare, M.S. Sutaone, "OS-CFAR Based on Thresholding Approaches for Target Detection," Proceedings - 2018 4th International Conference on Computing, Communication Control and Automation, ICCUBEA **2018**, 1–6, 2018, doi: 10.1109/ICCUBEA.2018.8697389.

[18] C. Xu, Y. Li, C. Ji, Y. Huang, H. Wang, Y. Xia, "An improved CFAR algorithm for target detection," International Symposium on Intelligent Signal Processing and Communication Systems, ISPACS 2017 -Proceedings, 883–888, 2017, doi: 10.1109/ISPACS .2017.8266600.

[19] X. Meng, Y. He, N. Aeronautical, E. Academy, "Two Generalized Greatest of Selection CFAR Algorithms," CIE International Conference on Radar Proceedings (Cat No.01TH8559), Beijing, China, 359–362, 2001, 359-362, doi: 10.1109/ICR.2001.984700.

[20] Meng Xiangwei, Guan Jian, He You, "A generalized smallest of selection CFAR algorithm [radar signal processing]," 130–132, 2004, doi: 10.1109/radar.2003. 1278724.

[21] M.M. Abdul-atty, M. Mabrouk, S. Elramly, "Design and Implementation of a Low Cost FMCW Radar with Configurable Signal Processor for Human Movement and Breathing Detection," International Journal of Electrical, Electronics and Data Communication, **7**(9), 36–41, 2019, doi: RW.18042019.12277.

[22] X. Chen, "EM modeling of microstrip conductor losses including surface roughness effect," IEEE Microwave and Wireless Components Letters, **17** (2), 94–96, 2007, doi: 10.1109/LMWC.2006.890326.

[23] JIAXI ZHU, "LOW-COST, SOFTWARE DEFINED FMCW RADAR FOR OBSERVATIONS OF DRONES". M.Sc. thesis, Oklahoma univ., Norman, Oklahoma, 2017.

[24] A. Anghel, G. Vasile, R. Cacoveanu, C. Ioana, S. Ciochina, "Short-Range wideband FMCW radar for millimetric displacement measurements," IEEE Transactions on Geoscience and Remote Sensing, **52** (9), 5633–5642, 2014, doi: 10.1109/TGRS.2013.2291573.

ASTES

Advances in Science, Technology and Engineering Systems Journal Vol. 5, No. 5, 1308-1314 (2020)

www.astesj.com

Special Issue on Economic Impact of COVID-19 on Companies & Consumers

ASTESJ

ISSN: 2415-6698

Approach to a Logistic Model to Reduce Costs for Delivery at Home of a Seller of Supplies in Times of Coronavirus

Hernán Washington Samaniego Guevara*

Logistics and Supply Chain, Popular Autonomous University of the state of Puebla (UPAEP) and Business Administration, Salesian Polytechnic University, Quito, Av. October 12th 23-52, Ecuador

ARTICLE INFO

Article history:
Received: 19 August, 2020
Accepted: 13 October, 2020
Online: 26 October, 2020

Keywords:
Logistic
Savings method
Cost
Interactions
Routes

ABSTRACT

Logistics is a science and art that has been widely used by large commercial chains, whose main objectives focus on the distribution of products or services. This understanding has generated various logistics studies directed towards those businesses, without considering that science can also be applied to small or medium enterprises.
The present study initially executes a bibliographic review of multiple works done by several authors that confirm that studies related to the field of logistics can be aimed at any organization. The theoretical investigation of this study is therefore widely supported.
This work is focused on helping a small enterprise continue offering its services during the pandemic caused by the worldwide presence of COVID-19. Hence, the purpose of this research is to present a logistics model that will allow a small supermarket to continue its commercial activities in Quito, Ecuador, in compliance with diverse regulations issued by the Ecuadorian Government. The logistical model uses the methodology called savings method developed by Clarke and Wright.
The designed model produces as a main outcome the establishment of short-distance home delivery routes of provision to customers by the supermarket, thereby achieving significant savings in time and money. Additionally, the design and implementation of the model can serve as an example to be replicated in similar businesses.

1. Introduction

The logistics service well thought out is vital for the survival of a small, medium, or large enterprise. On many occasions, logistics has been visualized as the last link of the delivery of any product or service. Generally, it is the client who must go to a store to use a particular service or purchase a good [1].

However, this thought necessarily had to be reconsidered due to a worldwide health problem, which required looking at businesses from another perspective, forcing companies to modify their ways of doing businesses. Otherwise, they ran the risk of being pushed out of the market from not adapting to the policies issued by the local and national governments which affect the inhabitants of the city of Quito, Ecuador.

For this reason, a small supply chain has had to adapt to the policies and conditions issued by these organizations, which state that the enterprise could work only by home delivery while the government prohibits on-site service at their facilities. Therefore, in accordance with mandated policies, a logistics model was designed for home delivery by looking for a way to reach customers at minimal cost and adapting the enterprise's activities to an integration process necessary for its commercial survival [2].

With these considerations, the supermarket object of study could choose to halt its activities and possibly resume them when the health situation caused by the pandemic has finished, or continue working while adapting them to the state's policies [3]. These realities demonstrated the need to find a solution by characterizing and identifying the logistical management of the provision of the supermarket services in its work context in Quito, Ecuador. The study, carried out with the support of the business owner, has the following objectives: highlighting the logistical routes applicable for this business-type, based primarily on innovation; and the work-family subsistence of those who are involved directly in these activities [4].

*Corresponding Author: Hernán Washington Samaniego Guevara, Email: hernanwashington.samaniego@upaep.edu.mx

This study is organized into several sections that present the bibliographic review, the methodology applied, the results achieved, and finally, the conclusions based on the total research carried out.

2. Literature review

Logistics in business is a novelty derived from the concept that it adds value to essential products or services for customer satisfaction and sales [5]. Conversely, for other authors, by citing the American Production and Inventory Control Society (APICS), the term logistics is considered the art and science of obtaining, manufacturing and distributing material and products at a place and in adequate quantities [6]. Therefore, logistics can be considered a science that combines the art of satisfying clients at the moment and placetheydesire.

Logistics is big business in the United States of America. In that country, it represents 8 to 9 % of the Gross Domestic Product (GDP), and this percentage is growing [6]. In Europe, the logistics sector in 2018 represented 8% GDP in most of the countries from the European Union [7].

The use of logistics in any production or service chain is always going to be related to its costs. For example, in the United States, Japan, and Europe, the logistics costs represent under 10% GDP, while in Mexico it represents 13.5% GDP. In India and China it represents 17% and 22% GDP, respectively [8]. In general, in the first world countries, it is noticed in efficient use of their transport systems, including maritime systems, while in the third world countries, it is more common to see a high degree of bureaucracy, as well as inefficiency [8].

According to the Inter-American Development Bank (DIB), in Latin America, the inefficiency of supply chains, and logistics performance in particular hinders competitiveness. Currently, logistics costs represent between 18% and 35% of final product value, which exceeds the percentage registered by the member countries of the Organization for Economic Cooperation and Development (OECD), which is 8% [9]. Additionally, the logistics costs in Latin America and the Caribbean are between 50% and 100% of those of the countries from the OECD [9].

In Ecuador, specifically in Quito, according to a study done by the Municipality of the Metropolitan District of the city, the costs associated with logistics represent between 50% and 60% of the costs incurred by enterprises in production or generation of services [10]. This represents a reasonable limit that halts home delivery in general. Only an approximate percentage of 5% of organizations provide this kind of service [11]. Under this perspective, it is feasible to establish a logistics model that fits the required conditions, which can be used and applied by the supermarket without generating high costs that would increase substantial economic losses for the business.

The logistics model has been studied based on many aspects, for example, the study made in 2014 [9], in which it is established an analysis of the provision of home health services in the Cauca valley in Colombia [4]. In this research, the authors are focused on showing a diagnosis for the institutions authorized by the Ministry of Health of that country, which objective is to characterize how the home health care providers (HHC) make logistical decisions associated with the service delivery process and identify opportunities for improvement and research. The diagnosis of that model is based on the application of a semi-structured survey, which evaluated six work axis and the maturity degree of the service processes, by showing in its results that it is required more integral management with the logistics decisions and supported on the knowledge of the epidemiologic and demographic profile of the population served [4].

In 2018, in Mexico, the logistics related to the means of transportation and local development of an exporting organization of table grape was studied; this study is characterized by determining the critical processes in the enterprise operation by looking for ways to develop management efficiency mechanisms to meet market demands in product delivery times to customers with minimal operation costs, but without establishing a specific model to comply with [12].

In a study, a logistic model is proposed to reduce the costs of the furniture painting sub-process, whose central objective is to minimize reprocessing and reduce its costs. This is achieved by identifying the behavior of the costs incurred in production through the use of tools and techniques that add value to the products and by increasing the profit margin as those tools are used [2].

In 2017, a compilation of logistic models is presented to solve problems related to integration, coordination, sustainability, and mobility that arise in the urban distribution of goods; specifically focused on an update of scientific literature with a subsequent categorization of the models and techniques used so that in the future the solutions presented would be implemented [13]. Another study called personalization degree of logistic services: service and performance priorities is presented. The authors focus their research efforts on analyzing the relationship between the types of logistic services required and the supply chain priorities, generating two hypotheses related to this study, which result in a significant association between the variables studied [14].

Another author conducted a logistics study in small and medium-sized companies in the state of Jalisco-Mexico [15], whose focus is on determining knowledge of the logistical state in the business sector of the area of study, which describes the main problems that affect logistics performance and, therefore, the export efficiency of the state. The obtained results indicate that there is an association between logistics and export business efficiency in the state previously mentioned [15]. Additionally, the executed work describes the logistical problem is in its primary nodes, customs, carriers, and customs agents. Identifying the primary type of problem defined in this study has a cultural nature because work is not done as an integrated system; each node is seen as unique and essential throughout the value chain,

without understanding that it generates a high cost in the export efficiency of the state [15].

One of the few studies made for small and medium-sized companies (SMEs) in Mexico seeks to strengthen the importance of their competitive position through a conceptual model of logistical management via control of the variables involved [16]. It achieves a conceptual reference for SMEs so that they can reach logistical performance according to their needs by integrating resources, skills, and systems and allowing them to accomplish a competitive advantage regarding other companies [16].

In studies carried out in 2019, other authors analyzed the evaluation of the supply chain by considering the direct relationship between a logistical field and the supply chain, and presenting an evaluation model related to companies of the metalworking sector. The model elaborated comprises five aspects: supply, storage, inventory management, distribution, transportation and/or reverse logistics [17]. These factors include a set of variables that evaluate the planning, execution, measurement, and control of the supply chain management. The conclusion was that in the metalworking sector, due to its sustained growth over time, it is necessary to continuously optimize and improve its processes through permanent monitoring, which facilitates the operational processes that actively contribute to an even more significant growth of this type of organization [17].

The lines above have presented various studies carried out by authors who have executed research work in Latin American countries, who present various scientific analyses related to the logistics field. Logistics, in being a science, can be used anywhere in the world and in any labor field [13]. Ecuador is not exempt from such analyses. The research executed by different authors is mainly focused on theoretical works. Some of them study reverse logistics as a differentiation strategy for dynamic markets, highlighting a qualitative-theoretical, historical-logical, analytical-synthetic, and inductive-deductive approach; they seek in this way to highlight that companies that have applied reverse logistics have improved their competitiveness by reducing costs [18].

Their credibility is reflected in the market due to their efforts to minimize the environmental footprint; concluding that the application of the practices covered by reverse logistics increases the possibilities of differentiation from the competition, since it generates trust and security in consumers [18]. Additionally, other authors present a logistics study in a textile company, analyzing the processes that show the most significant difficulties, in which they focus on the processes of production, logistics, and sales, via the use of documentary tools that identify elements that will allow them to recognize logistical processes for companies in the textile sector that contribute to improving the competitiveness of the sector in general, and present as a result a documentary study that facilitates the improvement of processes through strategic decision making [19].

A similar study to those previously mentioned deals with the evolution of digital information in commercial and integral logistics. The research objective of this work was to review the best catalog for searches, trends, and behavior of scientific production over the years by using web tools such as the Scielo catalog, Scopus, and Redalyc; and by specifying trends through Google Trends and Publish or Perish software, presenting a compendium of relevant logistical studies [20].

A document called Research in Logistics and Transport was elaborated, which was based on comparing Ecuador with other countries from the Andean region (Bolivia, Colombia, and Peru) with regards to studies carried out that concern this topic. The comparison looks at competitive aspects of the countries, and relates each one of the points found as relevant factors to identify which country within the Andean region has the most significant development and research concerning logistics and transport [21].

Logistics can be applied to any labor or scientific field. Thus many people consider it a factor that generates competitive advantage [21]. Under this premise, a study focused on the cosmetics and personal care products industry is analyzed. In that study, the authors present a methodological proposal where they analyze factors and variables that characterize this commercial sector and allow the use of the logistics processes and resources in this type of enterprise by practically and directly explaining how these factors should be used along with their variables [22]. In a different approach, the existing relationship between logistics and the environment was studied through content analysis published with relation to logistical studies and supply chain done between 2005 and 2015, while concluding that it is necessary to design support tools for the inclusion of new processes in logistical issues [23].

The research results of a study that relates supplier management to supply chain management show the proposed model that address an existing relationship between an adequate search of suppliers and a strict control of the supply compliance, by providing vital input to generate efficient strategies in this field, and by collaborating on agreements with the suppliers [24].

Finally, it is useful to address a study that performs a competitive diagnostic of the logistical point of view in the central geographical zone of Ecuador. The authors consider the implementation of integral logistics as a competitive advantage in the current global environment. Moreover, they establish that the management of retail stores contributes to cost-reduction if operations are simplified and information flow is improved [25].

When analyzing each of the works presented by the diverse research to which we refer, a high percentage of conceptual studies based on theories applicable to the logistics field are evidenced. However, they do not specify the concrete application of any methodology that allows companies to make practical decisions in the field. This does not mean there is an inability to apply those studies, rather that they leave open the real possibility of using them in different organizations that require it. Based on

what was analyzed, the study presented below describes how a small supermarket can avoid stopping the sale of its products to customers that request home delivery, by finding efficient routes through the interpretation of a methodology that allows savings in time and cost.

It is important to note that the model designed was structured for a small supply delivery business which lacks the logistical infrastructure owned by medium and giant supermarket chains. The study generates practical-scientific knowledge that can be replicated by other similar organizational structures.

3. Methodology

From the regulations issued by control entities in Ecuador due to the type-2 coronavirus that causes severe acute respiratory syndrome SARS-CoV-2-COVID-19 [26], the sales percentages, in most business, have decreased significantly. Given this situation, among the decrees issued by the Ecuadorian state, the possibility of executing door-to-door sale of food and supplies made by small supermarkets and/or grocery stores was defined by decree number 1052, issued by the Presidency of the Republic of Ecuador [3]. Hence, the study carried out is focused on establishing a logistical model that prioritizes the delivery of supplies or provisions to residential complexes located in the sector known as La Vicentina, in order for the SME to cover the largest number of clients in unique places.

Faced with the present situation, a model of logistical transportation was designed, by using the savings method authored by Clarke and Wright which has persisted for many years [27].

Clarke and Wright's model has been one of the most implemented algorithms to solve the vehicle route problem method (VRP), and it consists in doing a limited exploration of the search space and giving an acceptable quality solution in a moderate time. The algorithm is developed starting from a solution with two routes (0,.., i,…,0) y (0,…, j,…,0), which can be combined by generating a single route (0,…, i, j,…,0) [28].

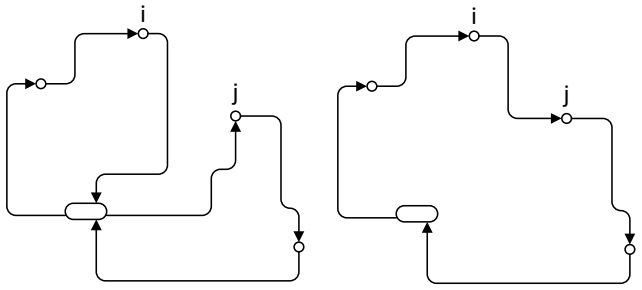


Figure 1: Clarke and Wright's algorithm

Clarke and Wright's method details a very flexible procedure that allows the management of a wide range of practical constraints, and whose resolution on a computer is relatively fast [28]. This method applies to the designed model because the comparisons of the optimal results in small problems, such as in this study case, have shown that the effectiveness of its application generates solutions at 2% of the optimum on average [5].

The objective of using the savings method is to minimize the total distance covered by the vehicles and indirectly minimize the number of vehicles required to make local stops [5]. The logic of the applied model is mainly based on the fact the small supermarket has only one available vehicle. Therefore, by using Clarke and Wright's algorithm, the mathematical model only considers the existence of a central warehouse as the starting point for all deliveries. The objective function of the proposed model is determined by:

Minimize:

$$\sum_{i\epsilon V} \sum_{j\epsilon V} CijXij$$

The constraints applicable to the proposed model are specified by:

$$\sum_{i\epsilon V} Xij = 1, \qquad \forall j \in V \therefore \{0\}$$

$$\sum_{j\epsilon V} Xij = 1, \qquad \forall i \ \in V \ \therefore \{0\}$$

$$\sum_{i\epsilon V} Xio = k$$

$$\sum_{j\epsilon V} Xio = k$$

$$\sum_{i \nexists S} \sum_{j\epsilon S} Xij \ \geq r(s), \forall S \subset V \therefore \{0\}, S \neq \emptyset$$

$$Xij \ \in \{0,1\}, \forall i,j \ \in V$$

Constraint number 5 impedes the presence of subtours, where r(S) is the number of vehicles required to meet the demand in S.

Constraints numbers 5 and 6 have cardinalities that grow exponentially with n, thus, they are replaced with a family of constraints with polynomial cardinality [28]. For the study case, they were set according to the following:

$$ui - uj + Qij <= Q - dj$$

Considering that $di + dj <= Q$

Therefore: $di <= ui <= Q$

where:

V: node set V= {V*0*, V*1*, V*2*,…..V*n*}, V*o* is the warehouse

A: edge set A= {(i, j): i, j ϵV, i≠j}

d*i*: node demand i

k: number of available vehicles

Q: vehicle capacity

By mathematically setting the model design, it is possible to verify that its theoretical characteristics are necessary and ideal to establishing a pattern on which the vehicle belonging to the business returns to its facilities only when it has made all the deliveries. The designed model establishes that this delivery is adapted to the needs of the businesses that are the objects of study, and it can be used for a long time [27]. Considering the opinion of an epidemiological expert whose statements say that the SARS-Cov2 virus will remain for an indefinite time, forcing businesses and people to adapt to living with it, if desired the world economy and its activities to be regularized [29]. In such circumstances, the savings method for the programming and route design is adjusted to the supermarket's needs, by seeking the maximum savings in cost and distances to cover.

Subsequently, and with the theoretical support provided below, with the help of Google Maps, it is possible to visualize the specific places where supplies and provisions are to be delivered, which are identified numerically with small blue circles, as shown in Figure 2.

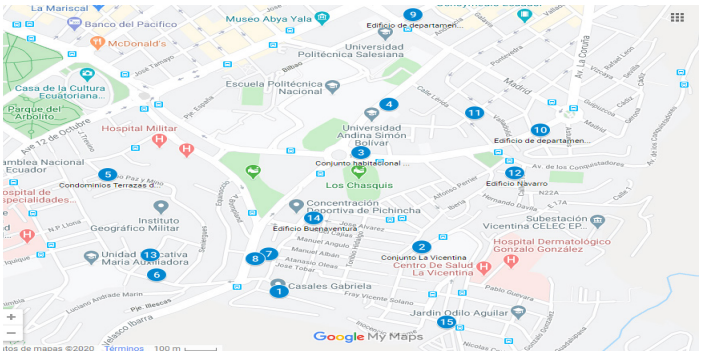
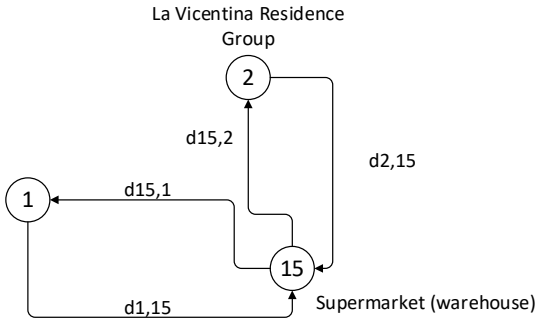


Figure 2: locations of delivery sites

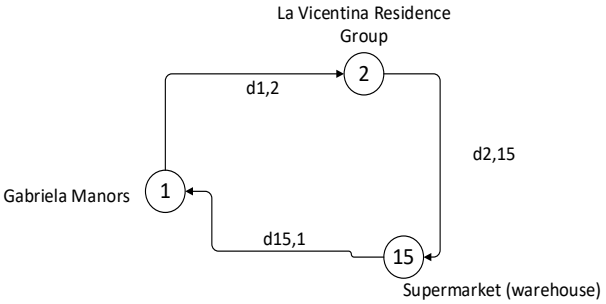


Initial route: route distance= d15,1 + d1,15 + d15,2 + d2,15

Figure 3: the maximum distance route

Initially, with the help of a single vehicle, by simulating covering each stop and immediately returning to the supermarket, identified as number 15, the route to be covered would result in the maximum distance experienced for the delivery of supplies, as is represented in Figure 3.

Nevertheless, when considering the saving of minimizing the distance that must be covered, the vehicle can combine a route or many routes, which would be found by algebraically subtracting the initial distance with the proposal represented in Figure 4:



Combination of two stops=d15,1 + d1,2 + d2,15

By carrying out the algebraic operation of the operations previously defined in Figures 2 and 3, a savings value of Z = d15.1 + d2.15 - d1.2 would be obtained. This calculation is performed for all pairs of stops. The pair of stops with the highest savings value is selected for the respective combination.

This process is a continuous combination because, to combine single stops as in the previous case, the process can add another stop on a route that already contains multiple stops. For example, if point 7 were inserted between stops 1 and 2 where those points are on the same route, the value to be saved would be expressed as follows: Z = d15.7 + d7.15 + d1.2 - d1.7 - d2.7. On the other hand, if stop seven were inserted after the last stop, point 2, the value of the route savings would be: Z = d2, 15 - d2, 7 + d15, 7. By contrast, if stop 7 were inserted before stop 1, the value of the savings would be: Z = d7, 15 - d7, 1 + d1, 15. These savings calculations are repeated as progress is made in solving the problem. With this procedure, the highest savings value identifies the stop that should be considered for inclusion in a route.

If a particular stop, due to some circumstance or constraint, cannot be included, such as the route being excessively long or the capacity of the sole vehicle being exceeded, the stop with the next highest savings value is considered for inclusion; in the same way, this process would be repeated until all points or stops have been considered. This argument is supported due the strength of the method is the ability to simultaneously assign a stop to a specific route and place it in an area in the sequence of the route. In such circumstances, before accepting a stop on a route, the route must be provided with the new stop [5].

Therefore, the use of the only available vehicle by the supermarket must be programmed to send all orders for the week according to the schedule issued by government-controlled entities (06h00-13h00). Such orders can only be complied with by having only one departure in the morning and returning after all deliveries have been made. It is important to note that the dispatchers will be fed before and/or after the delivery of all the provision requests, considering that there is no constraint on this

issue. The average driving speed is 50 km/h, in compliance with the maximum speed limit allowed within the city of Quito. Additionally, the calculation of the costs related to the dispatches – based on the salaries or wages of the staff that make the deliveries, the budget for the purchase of supplies and provisions to be delivered, fuel consumption, and car maintenance costs – equates to an economic value of USD 5.50 per kilometer driven.

The model is posed in the software Logware Version 5.0 for Windows, which is formed by a collection of useful programs to analyze a wide variety of issues related to the management of logistic supply chains. The software has a module named "Route" that allows the user to determine the shortest route in a route network and to input multiple constraints based on the designed model.

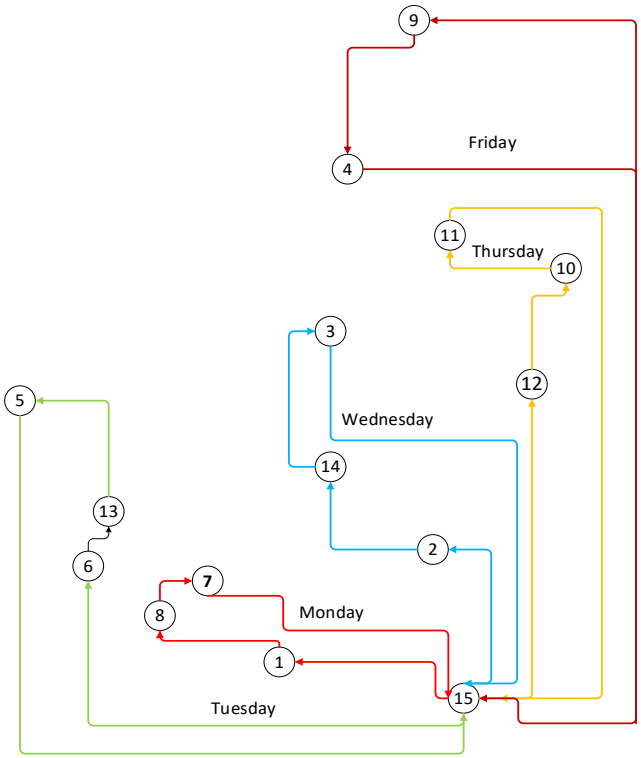


Figure 5: delivery provision routes

When these data were input into this software, and after several ride simulations, the feasible sequences to be implemented were found according to the details in Table 1.

When carrying out the respective work in Logware through the use of the "Route" software which allows the user to consider several additional constraints within savings assessment, enter the respective data, and execute route simulations the feasible sequences to be implemented were found, and are detailed in Table 1.

According to the data found and the determined economic value based on kilometers driven, the weekly cost for home delivery of provisions is USD 206.30. The graphical representation of the routes is illustrated in Figure 5.

Table 1: Optimal Routes to deliver provisions

Route	Sequence	Start Time	End Time	Route Distance (km.)	Route Time (hours)	Delivery Weight (pounds)	Truck size (pounds)
Monday	15,1,8,7,15	08:00	11:00	6.32	3:00	750	1000
Tuesday	15,6,13,5,15	08:00	11:30	7.55	3:30	775	1000
Wednesday	15,2,14,3,15	08:00	11:30	6.83	3:30	790	1000
Thursday	15,12,10,11,15	08:00	12:30	8.05	4:30	900	1000
Friday	15,9,4,15	08:00	12:00	8.76	4:00	810	1000
TOTAL				37.51	17.9	4,025	

Source: Logware for Windows

4. Conclusion

The result achieved with this study provides an opportunity for a small supermarket to be able to continue with its work by delivering provisions at home in its direct area of influence while covering the largest number of customers through direct delivery in residential complexes. The model reflects the optimal weekly routes that the supermarket under study must use in order to comply with its customer's orders and thereby achieve significant savings in time and related costs.

This model was developed using the "savings method" logistics methodology through the Route module of the software program Logware, which facilitated running various simulations of routes that could potentially be applied. This software allows the user to find the shortest driven route in a route network, while making it possible to cover those distances at lower costs than empirical methods. The ideal route found shows that the transport of provisions can be performed weekly by covering a total distance of 37.51 kilometers at a cost of USD 206.30.

The results achieved enabled the supermarket to continue working in compliance with the requirements of the state control authorities of Ecuador, while also allowing a certain number of collaborators to keep their jobs and continue working during a difficult time for labor and economy. The formulation of the logistics model designed by using the savings method made it possible to form a model that has a sequential distribution of daily routes, thus facilitating the identification of additional constraints that could be used in the future to determine certain possible events that may be studied. It is important to mention that the model proposed for the supply business can be replicated by similar businesses, or by commercial establishments that want to make home deliveries while optimizing time and money.

The future work to perform is the determination and allocation of routes to new customers, considering especially that the global health problem will not be easily solvable in the short term, and that this model will allow the supermarket to increase its number of customers.

References

[1] O. Hernández, A. Jarrinson, F. Jiménez, T. Aguilar, "Suppliers and management models in the supply chain: Manufacturing SMEs of Aguascalientes", Acounting and administrative sciences, **7**(1), 21-28, 2017.
[2] S. Rave, D. Arias, J. Garcia, " Proposal of a logistic model to reduce costs of

the painting sub-process in furniture Bovel Ltda", Scientia Et Technica, **20**(3), 240-246, 2015.
[3] Presidency of the Republic of Ecuador, "Decree Number 1052", 5 May 2020.Available:https://www.telecomunicaciones.gob.ec/wpcontent/uploads/2020/07/Decreto_Ejecutivo_No._1052_20200415200635.pdf
[4] E, Valentina, O. Galvis, D. López, J. Mock-Kow, I. Zapata, C. Vidal, "Logistics management in the provision of home care services in Valle del Cauca: characterization and diagnosis", Management studies, **30**(133), 441-450, 2014, doi:org/10.1016/j.estger.2014.06.004
[5] R. Ballou, Logistics. Supply chain management. Pearson, 2004.
[6] R. Jacobs, R. Chase, Operation Administration. Production and supply chain. Mc Graw Hill Education, 2019.
[7] Group Ibertransit Excellence Moves the World, "The logistics sector already represents 8% of the GDP sector", 15 September, 2019. Available: https://www.ibertransit.com/sector-logistico-8-pib
[8] Milenio 2020, "Logistics costs in Mexico", 2 September 2019. Available: https://www.milenio.com/opinion/varios-autores/emprendiendo-con-sentido-humano/costos-de-la-logistica-en-mexico.
[9] Inter-American Development Bank, "Regional Logistics Observatory. Logistics Costs", 20 July 2016. Available: http://logisticsportal.iadb.org/
[10] Municipality of the Metropolitan District of Quito, "Economic and productive situation of the DMQ". 6 November 2017. Available: http://gobiernoabierto.quito.gob.ec/wpcontent/uploads/documentos/pdf/diagnosticoeconomico.pdf.
[11] Development Bank of Latin America, "Logistics roadmap in Ecuador will improve national competitiveness". 15 November 2019. Available: https://www.caf.com/es/actualidad/noticias/2019/11/hoja-de-ruta-logistica-en-ecuador-permitira-mejorar-la-competitividad-nacional/
[12] B, Hurtado, J. Robles, J. Preciado, N. Banuelos, "Transportation logistics and local development in Sonoran table grape export organizations", Social studies, **28**(51), 2-25, 2018, doi:org/10.24836/es.v28i51.563
[13] M. Arango, C. Gómez, C. Serna, "Logistic models applied in the urban distribution of goods". EIA Magazine, **14**(28),. 57-76, 2017, doi:org/10.24050/reia.v14i28.1055
[14] F. Duhamel, J. Duran, "Degrees of customization of logistics services: service priorities and performance". Nova Scientia, **7**(13), 286-313, 2014.
[15] O. Gil, "Logistics: key to the global competitiveness of small and medium-sized companies in the state of Jalisco in Mexico". Paakat: Magazine of Technology and Society, **6**(11), 22-44, 2016.
[16] P. Cano, F. Orue, J. Martinez, J. Mayett, G. López, "Logistics management model for small and medium-sized companies in Mexico", Acounting and administration, **60**(1), 181-203, 2015.
[17] K. Salas-Navarro, J. Meza, T. Obredor, N. Mercado, "Evaluation of the supply chain to improve competitiveness and productivity in the metalworking sector in Barranquilla, Colombia", Technological information, **30**(2), 25-32, 2019, doi:org/10.4067/S0718-07642019000200025
[18] J. Ruiz, M. González, L. Carménate, "Reverse logistics as a differentiation strategy for dynamic markets. Machala-Ecuador". Innova Research Journal **5**(2), 140-156, 2020, doi:org/10.33890/innova.v5.n2.2020.1291
[19] F. Jaramillo, G. Granja, V. Del Pozo, "The logistics processes of textile and clothing companies: case of the textile company hilandería unida s.a .Guayaquil-Ecuador". In 2018 ECOTEC Society remainds and perspectives congress (ECOTEC), 55-62, 2018.
[20] J. Guamanquispe, M. Mancheno, D. Altamirano, S. Chaluisa, "A growing approach to the development of integral logistics. Ambato-Ecuador", Constructivism Web, **4**(1), 116-134, 2019, doi:org/10.23857/pc.v4i1.876.
[21] J. Chicaiza, F. Sandaya, "Research in logistics and transportation: comparison between the countries of the Andean region; challenges and opportunities for its development in Ecuador", in 2015 ESPE Science and technology congress (ESPE), 275-280, 2015, doi.org/10.24133/cctespe.v10i1.60
[22] J. Orjuela, O. Diaz, A. González, "Characterization of logistics in the supply chain for cosmetics and personal care products", Scientific Magazine, **1**(28), 81-96, 2017, doi: 10.14483/udistrital.jour.RC.2016.28.a7
[23] J. Silva, "Supply chain management: a review from logistics and the environment". Sciencie and engineering, **11**(22), 51-59, 2017.
[24] D. Calero, J. Gamboa, M. Mancheno, "Logistics organization, competitive diagnosis in commercial warehouses in zone 3 of Ecuador", POCAIP, **5**(17), 158-181, 2020, doi:org/10.23857/fipcaec.v5i5.190.
[25] World Health Organization (WHO), "Naming the coronavirus disease (COVID-19) and the virus that causes it". 5 May 2020. Available: https://www.who.int/emergencies/diseases/novel-coronavirus 2019/technical-guidance/naming-the-coronavirus-disease-(covid-2019)-and-the-virus-that-causes-it
[26] J. Ascencio, R. Bustos, J. Jiménez, J. Balbuena, A. Zamora, "Automatic Wizard for design of distribution routes", Technical Publication, **14**(1), 2-25, 2018.
[27] R. Álvarez, Proposal for resolution of the vehicle routing problem in the logistics operator Operar S.A., for transport and distribution of dry food products of the group Nutresa S.A", **12**(2), 6-41, 2017.
[28] P. Cano, "Vehicle Routing Problem VRP", in 2020 UPAEP. Operations Research (UPAEP), 1-7, 2020.
[29] R. Rodríguez, "Interview with Tom Frieden", 7 May 2020. Available: https://www.elconfidencial.com/tecnologia/ciencia/2020-0507/coronavirus-diez-verdades-tom-frieden-experto-epidemiologico-eeuu_2583939/

ASTES

Advances in Science, Technology and Engineering Systems Journal
Vol. 5, No. 5, 1315-1328 (2020)
www.astesj.com
Special Issue on Multidisciplinary Innovation in Engineering Science & Technology

ASTES Journal
ISSN: 2415-6698

Evaluating the Impact of Semantic Gaps on Estimating the Similarity Using Arabic Wordnet

Mamoun Abu Helou *

Management Information System Department, Al-Istiqlal University, Jericho, 11590, Palestine

ARTICLE INFO

Article history:
Received: 30 August, 2020
Accepted: 21 October, 2020
Online: 26 October, 2020

Keywords:
Lexical ontologies
Arabic wordnet
Semantic gaps
Semantic structure
Semantic similarity measure

ABSTRACT

Knowledge-based approach is wield used in various NLP applications. For example, to evaluate the semantic similarity between words, the semantic evidence in lexical ontologies (wordnets) is commonly used. The success of the English WordNet (EnWN) in this domain has inspired the creation of several wordnets in different languages, including the Arabic WordNet (ArWN). The English synsets have been extended to Arabic synsets through translation, which have introduced semantic gaps in ArWN structure. Therefore, compared to EnWN, ArWN has limited coverage in terms of lexical and semantic knowledge. This paper explores to what degree the richness of the wordnets' semantic structure influences the semantic evidence that can be used in wordnet-based applications, in particular the effect of filling the semantic gaps in ArWN. The paper studies the performance of applying English-based and Arabic-based similarity measures over ArWN. A set of experiments was performed by applying six path-based semantic similarity measures over Arabic benchmark dataset to investigate the usability and efficacy of the enriched structure of ArWN. The Performance measures, Person Correlation and Mean Square Error, are computed against and compared to human judgment benchmark. The obtained results demonstrate that the semantic similarity between words can be significantly improved when filling the semantic gaps. In addition, the experiment findings show that Arabic-based measures competitively perform well compared to the English-based measures. Further, ArWN enhanced structure is also available for public.

1 Introduction

In Natural Language Processing applications, a common task is to estimate the semantic similarity among words [1]. Lexical resources, such as, bilingual and multilingual dictionaries, thesauruses, lexical ontologies (wordnets), machine translation services among others, are widely used to estimate the similarity [2]. For instance, various tasks of natural language processing, knowledge engineering, and computational linguists have exploited the lexical and semantic knowledge encoded in the English WordNet (EnWN) [3, 4]; including sense disambiguation, information retrieval, text summarization, and question answering [5]–[6].

EnWN has been expanded to provide multilingual knowledge in many wordnet projects [7]–[8]. The Arabic WordNet (ArWN) [9] has extended EnWN by translating English synsets. However, English synsets that do not have translation in Arabic introduce *semantic gaps* in ArWN's semantic structure. For instance, synsets containing a single and polysemous word are difficult to determine their meaning by means of direct translation; in fact, more evidence is required to disambiguate their meaning [10]–[11]. Thus, similarity measures designed for English (i.e., English-based similarity measures) may not be effective in the same way when applied over resources in other languages; in this work we consider Arabic language.

Experiment findings in [12] showed that ArWN has limited coverage of lexical and semantic knowledge compared to EnWN. Further attempts have been made to improve the content of ArWN [9], [13]–[14]. However, resolving the semantic gaps was not considered. In [15, 16] they studied the performance of different similarity measures over ArWN. However, no explicit configuration was stated when calculating the similarity scores. Further, no explanation was given on how some semantic similarity scores were reported.

In [17], a preliminary study was conducted to examine the impact of the semantic gaps on estimating the semantic similarity scores using ArWN. They examined the impact of improving the semantic structure of ArWN on estimating the similarity between Ara-

*Corresponding Author: Mamoun Abu Helou, MIS Dept., Al-Istiqlal University, mabuhelou@pass.ps.

bic synsets. The semantic gaps were analyzed and identified. Then new synsets in Arabic were added to ArWN and mapped to their corresponding synsets in English, using interactive cross-lingual mapping approach [18]. The impact of the enriched ArWN was studied in semantic similarity experiment using only one English-based semantic similarity measure.

In this paper we extend previous work presented in [17]; a large scale experiment is conducted to further examine the degree to which wordnet-based applications can be influenced by improving their semantic structure, mainly considering ArWN. In particular, the main contributions of this work can be summarized as follow.

(i) Four settings are defined and applied over two variants of ArWN structure. In the experiment six path-based similarity measures are applied over ArWN and EnWN; including, four English-based similarity measures (Path [19], Li [2], WuP [20], and Lch [21]), and two Arabic-based similarity measures (AWSS [22], and Aldirey [16]).

(ii) Study to which extent the semantic similarity measures that are developed for Arabic-based applications can perform efficiently well compared to English-based similarity measures. A comprehensive comparison between the similarity measures over the different configurations is provided, for both EnWN and ArWN.

The similarity scores obtained from the different measures, in the different settings, are compared to a standard benchmark for Arabic word pairs obtained from the AWSS dataset [23]. Two measures, the Person Correlation and the Mean Square Error measures, are used to quantify the performance of the similarity measures. Reported values indicate the importance of the semantic evidence obtained from the enrichment process, and its significant effect on estimating the semantic similarity between words. In addition, the results show that Arabic-based measures performs competitively good compared to English-based measures.

The rest of this paper is organized as follows. Section 2 overviews related works on building wordnets, and the development of wordnet-based semantic similarity measures. Section 3 and describes the approach used to evaluate the impact of Semantic Gaps on estimating the Similarity over ArWN. Section 4 discusses experiments conducted: the benchmark dataset, the performance measures, and the obtained results. Finally Section 5 draws some conclusions and outlines future work.

2 Related works

This section provides an overview of the construction of wordnets and the ArWN contents; presents wordnet-based semantic similarity measures, which will be used in the experiment.

2.1 Wordnets overview

Wordnets, also known as lexical ontologies [24], are considered to be a resource of lexical and semantic knowledge, which organize natural language words (lexicons) into synsets. A synset is a collection of synonym words that express one meaning in a specific context (i.e., concept) [3, 25].

In wordnets, words are arranged in a lexical database. Words can have several senses, such that each sense of a given word is identified by a number and its part of speech type. For instance, the sense *village#n#2* indicates the second (#2) nominal (#*n*) sense of the word "*village*". Words are linked through lexical relations, for example, *antonym* and *synonymy* relations. When a word can have more than one meaning, it is called *polysemous word*, which can be member of several synsets. Otherwise, it is called *monosemous word*, which is a member of a single synset. For example, the word "*village*" has three noun senses as defined in EnWN; which are indicated in the following set of synsets:{{village#n#1, smalltown#n#1, settlement#n#2}, {village#n#2, hamle#n#3}, {Greenwichvillage#n#1, village#n#3}}.

Synsets are related by semantic relations. The *Hypernymy* and *Hyponymy* relations are considered to be the key semantic relations that form the semantic structure in wordnets. Hypernymy is described as the inverse of Hyponymy. For instance, in Figure 1 the synset {village#n#2, hamle#n#3} is hypernymy of the synset {settlemt#n#6}, while the synset {settlemt#n#6} is hyponymy of the synset {village#n#2, hamle#n#3}. Further, definitions (glosses) are also attached to synsets to convey their meaning. For example, the word sense *village#n#2* defined as "a settlement smaller than a town" [1].

The $HyperTree$ of a given synset (i.e, word sense) is defined as the sequence of synsets that are linked with hypernymy relations, which connect a synset with its ancestor synsets up to the root node. The function $HyperTrees(word)$ produces the set of HyperTrees which a given word belongs. Figure 1 shows an excerpt of nominal HyperTrees in English and their correspondence in Arabic [2].

EnWN has been manually produced at Princeton University over the past three decades [3, 4]. EnWN 's success in many computational language domains has inspired the development of similarly structured lexicons, for both individual and multiple languages [26], such as EuroWordNet [7], BalkaNet [27], Polylingual WordNet [8], universal wordnet [28],MultiWordNet [29], WikiNet [30],and Arabic WordNet [9].

Computational linguistics has defined the Inter-Lingual Index [7], to establish links between different wordnets which is considered to be independent of language. For instance, near-equivalence and equivalence semantic relations are used to link synsets from the individual wordnets to the Inter-Lingual Index. Wordnets for several languages have been developed under the guidance of the Global WordNet Association [3], which seeks to organize the creation and linking of wordnets. Further, the Open Multilingual WordNet project [31] offers access to open wordnets in a number of languages, which are all connected to the latest version of EnWN (v3.0) [4].

[1] Definitions can be accessed at http://wordnetweb.princeton.edu/perl/webwn.
[2] In the following, for both Arabic and English senses, the *pos* (*n*) identification is removed for readability, as they all nominal senses.
[3] http://globalwordnet.org/
[4] http://compling.hss.ntu.edu.sg/omw/.

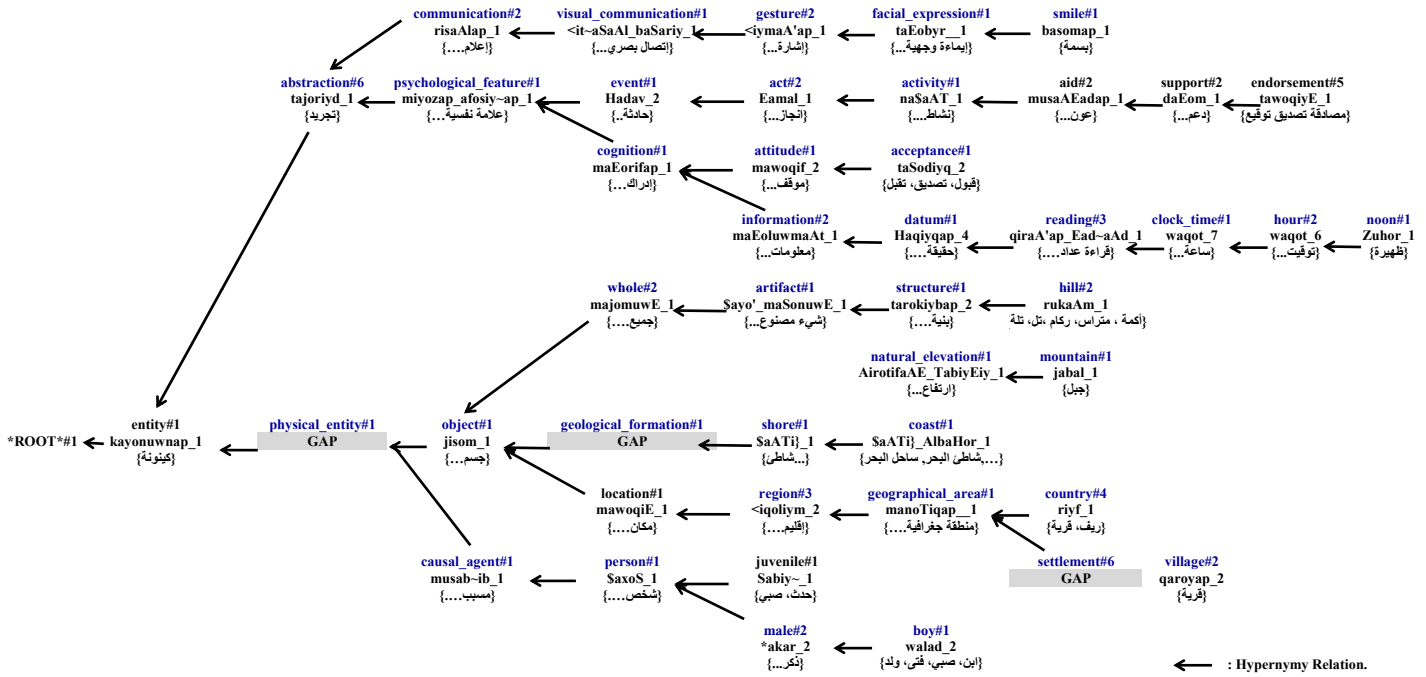


Figure 1: An excerpt of nominal HyperTrees from EnWN and its correspondences in ArWN.

2.2 *Arabic wordnet contents*

In the construction of ArWN [9], the extend method has been adopted. English Synsets have been translated into Arabic; and the structure of the EnWN (v2.0) has been inherited by ArWN . In the release of ArWN (v2.0) [5], 23,841 Arabic words, such as broken plurals, Named Entities, and roots have formed 11,296 synsets. Twenty-two types of semantic relationships have been used to connect synsets that formed 161,705 semantic links. Consequently, and in comparison with EnWN, which contains 147,306 words (117,659 synsets) [6]; one can observe that ArWN has a limited coverage in terms of semantic relations and lexicons [12].

To this end, many attempts have been made to enhance the quality of ArWN by expanding its lexical coverage [13, 9] or semantic relationships [32, 14] by different approaches. In [32] they released their work under the Lexical Markup Framework. However, the public release of ArWN ignores the synsets that are not linked to EnWN [31]. Nevertheless, synsets (semantic gaps) which are resolved in this work will be made for public [7] . In future work we plan to compile an *xml* format of ArWN enhanced structure, to enable researcher to utilize the ArWN in different applications.

2.3 *Wordnet-based similarity measures*

In linguistics, philosophy and information theory, estimating the semantic similarity between concepts is extensively studied [2, 15], which is a common and crucial task in many NLP applications, text summarization, word sense disambiguation, entailment, machine translation, among many others [33]–[6], [34, 35].

Estimating the semantic similarity between words is calculated by measuring the similarity between concepts (synsets) associated with the words [2]. Given two words, one can calculate the semantic similarity by exploiting wordnet (i.e, a lexical knowledge base). The lexical and semantic knowledge in wordnet have been used in many semantic similarity measures, which are originally designed and evaluated over EnWN (English-based measures) [36, 2].

In [15] they defined four broad categories of the similarity measures; Path-based similarity measures [2, 16, 19, 20, 21, 22]; information content similarity measures [37, 38]; feature-based similarity measures [39]; and hybrid similarity measures [40, 41]. There have been few works concerned with the similarity of Arabic; AWSS measure [22] and Aldiery measure [16]. These have mainly adapted measures from those constructed for English. In particular, Li measure [2] was adapted, which is a path-based measure that consider the depth of concepts in the HyperTrees; the distance between two compared concepts; and the depth of the least common concept (*lsc*) that subsumed two compared concepts. Noting that, these measures needs to tune weighting parameters to find the optimal values [22, 16]. In this regards, several preliminary experiments are necessary to find the best weights that provide the optimal values.

An attempt to investigate the performance of the similarity measures over ArWN was conducted in [15]. They studied the performance of seven measures; including AWSS measure [22]. All measures were applied over 40 word pairs that are selected from AWSS dataset [23], which are also considered as the benchmark dataset in this work. The experiments findings [15] showed that

[5] ArWN obtained from the AWN browser available at: AWNBrowser; or as XML file available at: Open Multilingual Wordnet
[6] EnWN-3.0 available at: https://wordnet.princeton.edu/download
[7] Full list of the Semantic Gaps available at:https://fas.alistiqlal.edu.ps/cv-2-ar.html

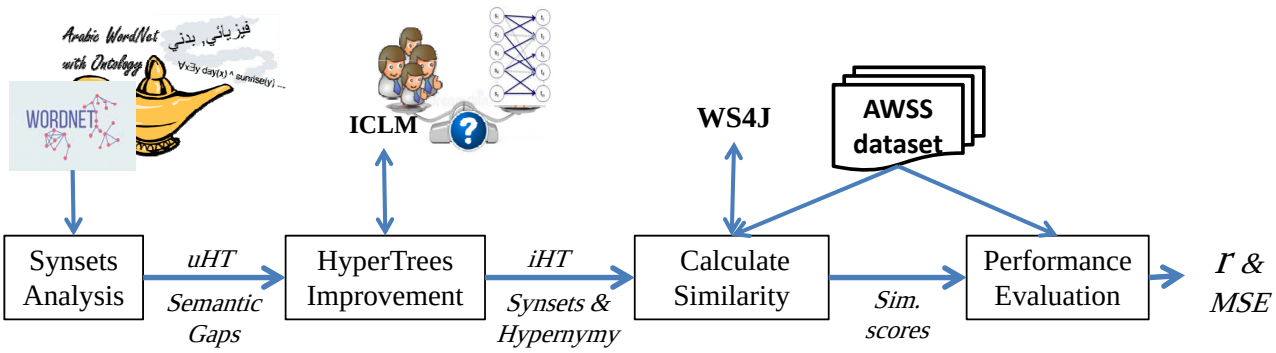


Figure 2: The adopted approach overview

WuP measure [20] has the best performance in estimating the semantic similarity between Arabic word pairs. The experiments in [16] also introduced a competitive Arabic-based similarity measures (Aldiery measure) in comparison to WuP measure.

In [17] they further studied the impact of enhancing the HyperTree over the Wup measure. This work adopted and extend their experimental configurations and examine further the impact of the enhanced semantic structure of ArWN over Six measures including English and Arabic path-based measure, further details are provided in Section 4.

Recall that, for a given concepts c_i and c_j, the function $Sim_m(c_i, c_j)$ calculates the semantic similarity between c_i and c_j, where m indicates the name of the measure. Next the description of the measures used in the experiment is given.

1. *Path* measure [19] finds the shortest path between the two concepts, by counting the number of edge (hypernymy relation) between the concepts, in order to compute the semantic similarity. Path measure which is considered as the pioneer similarity measure is defined in equation (1).

$$sim_{path}(c_i, c_j) = \frac{1}{len(c_i, c_j)} \tag{1}$$

Where the length function, $len(c_i, c_j)$, returns the length of the shortest path between c_i and c_j in the wordnet semantic hierarchy. For example, in Figure 1, $len(hill\#2, mountain\#1) = 3$, and $Sim_{path}(hill\#2, mountain\#1) = 0.333$.

2. *Wup* measure [20] calculates the similarity by computing the distance between the two concepts and the maximum depth of the least common concept (lsc) that subsumed the two concepts under evaluation. WuP measure is defined in equation (2).

$$sim_{WuP}(c_i, c_j) = \frac{2 * d(lcs(c_i, c_j))}{d(c_i) + d(c_j)} \tag{2}$$

Where $d(c_i)$ is the depth of the concept c_i using edge counting in the semantic hierarchy, $lcs(c_i, c_j)$ is the least common subsumer of c_i and cj, $d(lcs(c_i, c_j))$ is the maximum length between lcs of c_i and c_j and the *root* of the hierarchy, where $d(entity) = 1$. For example in Figure 1, $d(hill\#2) = 7$, $d(mountain\#1) = 7$, $d(lcs(hill\#2, mountain\#1) = 6$, and $Sim_{Wup}(hill\#2, mountain\#1) = 0.857$.

3. *Lch* measure [21] uses the length of the shortest path between the two concepts, and also the maximum depth of the semantic hierarchy of a given part of speech type. Lch measure is defined in equation (3).

$$sim_{Lch}(c_i, c_j) = -\log \frac{len(c_i, c_j)}{2 * maxDepth_{pos}} \tag{3}$$

Where, $maxDepth_{pos}$ is the maximum depth of the hypernymy structure for a given part of speech. For instance, $maxDepth_n$ is 20 and 15 in EnWN and ArWN, respectively. For example in Figure 1, $Sim_{Lch}(hill\#2, mountain\#1) = -log(3/2 * 20) = 2.590$.

Noting that the Lch scores reported in Section 4 are normalized into the range 0 to 1 by dividing Lch scors over 3,688, Hence, $Sim_{Lch}(hill\#2, mountain\#1) = 0.702$.

4. *Li* measure [2] computes the similarity using non-linear function, which consumes the shortest length between concepts and the minimum depth of the concepts in the semantic hierarchy. Li measure is defined in equation (4).

$$sim_{Li}(c_i, c_j) = e^{\alpha * len(c_i, c_j)} \frac{e^{\beta * d(lcs(c_i, c_j))} - e^{-\beta * d(lcs(c_i, c_j))}}{e^{\beta * d(lcs(c_i, c_j))} + e^{-\beta * d(lcs(c_i, c_j))}} \tag{4}$$

Noting that the parameters α and β need to be calculated manually for good performance. The optimal parameters are $\alpha = 0.2$ and $\beta = 0.6$ as reported in [2]. For example, $Sim_{Li}(hill\#2, mountain\#1) = 0.548$.

5. *AWSS* measure [22] is an Arabic-based measure that adapted Li measure to compute semantic similarity with modification on the depth and length computation to be proper for ArWN [23]. AWSS measure is defined in equation (5).

$$sim_{AWSS}(c_i, c_j) = e^{-\alpha * d(lcs(c_i, c_j))} * \tanh(\beta * len(c_i, c_j)) \tag{5}$$

Where the parameters α and β are the length and depth factors respectively. The optimal performance was obtained at $\alpha = 0.162$ and $\beta = 0.234$ as reported in [22]. For example in Figure 1, $len(rukaAm_1, Jabal_1) = 4$ and $d(lcs(rukaAm_1, Jabal_1)) = 8$, then $Sim_{AWSS}(rukaAm_1, Jabal_1) = 0.201$.

Table 1: Semantic gaps frequency distribution in ArWN for nominal synsets

Semantic Gaps	1	1	1	1	1	1	1	2	3	1	1	2	1	6	3	3	2	11	1	7	12	11	15	**88**
Freq	4525	187	100	50	48	46	36	30	24	17	15	14	12	10	9	8	7	6	5	4	3	2	1	**5493**

6. *Aldiery* measure [16] is an Arabic-based measure also adapted Li measure to compute semantic similarity with modification on the depth and length computation to be proper for ArWN. Aldiery measure is defined in equation (6).

$$sim_{Aldiery}(c_i, c_j) = \tanh(\frac{2 * d(lcs(c_i, c_j))}{d(c_i) + d(c_j)} + W(\frac{1}{len(c_i, c_j)} + \frac{\log(len(c_i, c_j))}{\log(maxDepth_{pos})})) \quad (6)$$

Where [16] defines $W = 0.5$. For example in Figure 1, $d(rukaAm_1) = 8$, $d(Jabal_1) = 7$, $len(rukaAm_1, Jabal_1) = 4$, and $d(lsc(rukaAm_1, Jabal_1)) = 8$, and $maxDepth_n = 15$, then $Sim_{Aldiery}(rukaAm_1, Jabal_1) = 0.692$.

Noting that, the similarity functions defined above consume either words, or word senses as parameters. In the first case, the similarity function returns the highest similarity score for all the possible combination of word senses for the two given words. In the second case, it returns the similarity score between the two defined senses.

In addition, the six measures defined in the equations (1,2,3,4,5, and 6) are path-based measures, this study focus on the impact of the structure without interference of other semantic evidence such as features extracted from corpuses, which depend on the quality of the used cuprous, as well as the availability of resources in Arabic.

On the other hand, Path, WuP, and Lch measures are considered as linear path-based measures, while Li measure is a non-linear path based measure. AWSS and Aldiery are also non-linear path based measures, which are derived from Li and purposely developed for Arabic.

Observe that, for the Path, Wup, and Lch measures no weights are required to be tuned. While the other measures need to find optimal value of the defined weights. The four English-based measures, as well as the two Arabic-based measures are selected because they achieved good performance against other measures [22, 16], and to compare the performance between the measures using Arabic benchmark dataset.

3 Evaluating the impact of semantic gaps on estimating the similarity

This section presents the approach that is used to evaluate the impact of enhancing the structure of ArWN on estimating the semantic similarity. Figure 2 illustrates the main phases of the approach, which are explained as follow.

1. **Synset Analysis**. In this phase the semantic gaps are identified through a comparison between the structures of ArWN (v2.0) and EnWN (v3.0). In particular, for each nominal synset in ArWN, Hypernymy relations are compared with their EnWN correspondences. The HyperTrees for each synset in ArWN is compared with its correspondence HyperTrees in EnWN. For example, Figure 1 indicates two semantic gaps in the ArWN $HyperTree(\$aATi\}_AlbaHor_1, ساحل)$ ={*ROOT*#1 , kayonuwnap_1, *GAP*, jisom_1, *GAP*, $aATi}_1, $aATi}_AlbaHor_1} [8], where the correspondence HyperTree in EnWN is, HyperTree(coast#1) = {*ROOT*#1, entity#1, physical entity#1, object#1, geological formation#1, shore#1, coast#1}.

   In total, [17] reported that 5,493 (69%) of the 7,960 nominal synsets in ArWN have at least one semantic gap. In particular, compared to the structure of EnWN, the semantic gaps have been resulted from the missing of 88 synsets in ArWN.

   The distribution frequency of the semantic gaps in ArWN is reported in Table 1, "Semantic Gaps" refers to the number of synsets that have the reported freq, and "Freq" indicates the number of HyperTrees that have at least one semantic gap. For instance, the first column reports an English synset ({"physical-entity#1"}) that has no correspondence in Arabic, introduces 4,525 semantic gaps in ArWN. While the 8^{th} column indicates two synsets ({"armed-service#1",...}, and {"health-care-provider#1",...}), each introduces 30 semantic gaps in ArWN. Last column reports the totals.

2. **HyperTrees Improvement**. In this phase ICLM Web application [18] is used to fill the identified semantic gaps. ICLM is a semi-automatic matching approach that supports feedback provided by multiple users. In ICLM the number of users that are asked to perform each mapping task is estimated based on the lexical characterization of concepts under evaluation, i.e., on the estimation of the ambiguity conveyed by the concepts involved in mappings [42], with the assumption that as the selection tasks difficulties increase, more users agreement is required.

   The candidate matching of the source concepts in Arabic are automatically computed to the English target concepts using a lexical based disambiguation algorithm [43]. The study [42] recommended that combining lexical resources improves the quality of translations and provide a valuable support for candidate match retrieval in cross-lingual ontology matching problems. Accordingly, translations of the missing synsets are collected by combining lexical knowledge from different external resources. English synset translation was

[8] Represents the HyperTree of the first nominal sense for the word ساحل.

[9] https://translate.google.com/

[10] https://babelnet.org/

[11] https://www.almaany.com/ar/dict/ar-en/

Table 2: Top ten Frequent Semantic Gaps in ArWN with EnWN correspondence sysnets

	EnWN synset	Freq	Semantic gaps in ArWN
1	{physical entity}	4,525	{كيان مادي}
2	{substance}	187	{جوهر، مادة}
3	{defender, guardian, protector, shielder}	100	{مدافع ، وصي، حارس، حامي، مدافع، ولي}
4	{variety, assortment, miscellanea,...}	50	{تشكيلة،تنوع، مجموعة منوعة منوعات}
5	{aristocrat,blue blood, patrician}	48	{رفيع الجناب، نبالة، نسب أصيل، النبيل، الأرستوقراطي}
6	{formataion, geological formation}	46	{تشكيل ، التكوين الجيولوجي ، التشكلات الجيولوجية}
7	{deceiver, beguiler, cheat, cheater, ...}	36	{مخادع، مضل ، غشاش ، محتال ، دجال}
8	{armed service, service, military service}	30	{القوة المسلحة ، الخدمة العسكرية}
9	{health care provider, health professional,...}	30	{مقدم عناية صحية ، مزود الرعاية الصحية الأولية، الصحة المهنية}
10	{wrongdoer, offender}	24	{مذنب، مجرم ، ظالم ، معتد، آثم}

collected from; Google Translate[9], BabelNet[10], and Almaany dictionary[11].

The difficulties of the mapping selection tasks, that is determining the number of user which are asked to perform the task, are estimated using lexical characteristics of concepts under evaluation: Ambiguity of lexicalization, Synonym-richness, and Uncertainty in the selection Step. The mapping tasks are validated by some users based on a CAUTIOUS strategy. The task difficulty level is estimated as Low, Mid, and High level. One, three, or five users are asked to perform the Low, Mid, or High tasks, respectively.

In [17] ten users (bilingual speakers) are asked to validate the mapping tasks, that is, to fill a semantic gap in ArWN, and accordingly define new link with EnWN, hence, import the semantic relations among the concepts. The top ten frequent semantic gap are listed in Table 2. As a result 94% of the identified gaps are resolved, that is more than 98% of HyperTrees are filled in.

Observe that, some concepts are hard to resolve, and more evidences are needed. For Example, {mechanism#3}, {attache#1}, and {climber#1} synsets, which contain a single and polysemous word, are hard to determine their meaning with direct translation and no context [42], for this reason in the validation task users did not reach an agreement. Noting that, the semantic gaps for every word sense in the benchmark dataset used in the experiment are resolved.

3. **Calculate Similarity**. In this phase similarity measures defined in Section 2.3 are applied over the ArWN and EnWN using Arabic benchmark dataset (AWSS dataset [23]). Different configuration explained in Section 4.4 are applied to calculate the semantic similarity using the WS4J online application (see Section 4.1). Similarity scores are reported and passed to the next phase.

4. **Performance Evaluation**. In this phase the obtained similarity scores are compared with Human Rating benchmark [23] using two performance measures; The Person Correlation measure (r) and the Mean Squared Error (MSE). Further details are provided in the experiment Section 4.3

4 Experiment

The conducted experiment aims at studying the efficacy of the semantic evidence in ArWN. In particular, the experiment focuses on the improvement of hypernymy relations in the semantic structure of ArWN. The experiment studies the extent to which the semantic structure of ArWN affects measuring the semantic similarity between concepts. This section reports and discusses the results obtained from running a set of configurations for measuring the semantic similarity scores over ArWN and EnWN.

Next sections present the tool which is used to calculate the semantic similarity scores, the benchmark dataset, the measures used to evaluate the performance of the structure improvement, and discuss obtained results.

4.1 Similarity Measure Tools

Significant efforts are being made in developing similarity measures to consume ArWN content. For example, the Java ArWN API [12]. The application consumes Arabic words with diacritics (vocalized), whereas the benchmark dataset in this experiment contains unvocalized (without diacritics) word pairs. If Arabic words are vocalized, similar to the work done in [16, 15], then their senses will be defined in advance. The experiment's configuration *DS* (see Section 4.4) studies the performance of determining the word senses on the similarity scores.

To avoid predefined senses, in this experiment the similarity scores are obtained using the $WS4J$ online application [13]. In computing the scores, $WS4J$ uses EnWN's semantic structure (v3.0), which is used to measure the similarity scores between Arabic words. Noting that, in this experiment Arabic senses under evaluation have the same structure of their correspondence senses in English, as the semantic gaps in ArWN has been improved and linked to EnWN(v3.0). The similarity scores between the Arabic concepts are then measured using their correspondence concepts in EnWN. In addition, $WS4J$ provides the description of all HyperTree of words under evaluation. The HyperTrees which returned for EnWN are validated to obtain Arabic words' HyperTrees with semantic gaps as depicted in Figure 1. For instance, this information is necessary to measure the similarity scores in *uHT* configuration,

[12] https://sourceforge.net/projects/javasourcecodeapiarabicwordnet
[13] http://ws4jdemo.appspot.com/

details are provided in Section 4.4.

4.2 Benchmark dataset

Similar to the work performed in [15, 16], the AWSS benchmark [22] will be used in this experiment. The obtained similarity scores will be compared with Human Judgments obtained from the dataset of AWSS [23]. The AWSS dataset contains 70 nominal word pairs of Arabic, divided into three similarity levels, Low, Medium, and High; 40 word pairs are selected and used in this experiment, listed in Table 3,which are also used in [15, 16].

Table 3: Arabic word pairs benchmark dataset

NO.	Sim. level	En Word Pairs		Ar Word Pairs	HR
1	Low	Coast	Endorsement	ساحل تصديق	0.01
2	low	Noon	String	ظهر خيط	0.01
3	low	Stove	Walk	موقد مشي	0.01
4	low	Cord	midday	حبل ظهيرة	0.02
5	low	Signature	String	توقيع خيط	0.02
6	low	Boy	Endorsement	صبي تصديق	0.03
7	low	Boy	Midday	صبي ظهيرة	0.04
8	low	Smile	Village	ابتسامة قرية	0.05
9	low	Noon	Fasting	ظهر صيام	0.07
10	low	Glass	Diamond	كاس الماس	0.09
11	low	Sepulcher	Sheikh	ضريح شيخ	0.22
12	low	Countryside	Vegetable	خضار ريف	0.31
13	mid	Tumbler	Tool	قدح اداة	0.33
14	mid	Laugh	Feast	عيد ضحك	0.34
15	mid	Girl	Odalisque	فتاة جارية	0.49
16	mid	Feast	Fasting	عيد صيام	0.49
17	mid	Coach	Means	حافلة وسيلة	0.52
18	mid	Sage	Sheikh	حكيم شيخ	0.56
19	mid	Girl	Sister	فتاة اخت	0.6
20	mid	Hen	Pigeon	دجاجة حمامة	0.65
21	mid	Hill	Mountain	تل جبل	0.65
22	mid	Master	Sheikh	سيد شيخ	0.67
23	mid	Food	Vegetable	طعام خضار	0.69
24	mid	Slave	Odalisque	عبد جارية	0.71
25	mid	Run	Walk	جري مشي	0.75
26	high	Cord	String	حبل خيط	0.77
27	high	Forest	Woodland	غابة احراش	0.79
28	high	Sage	Thinker	حكيم مفكر	0.82
29	high	Journey	Travel	رحلة سفر	0.84
30	high	Gem	Diamond	جوهرة الماس	0.84
31	high	Countryside	Village	ريف قرية	0.85
32	high	Cushion	Pillow	مسند مخدة	0.85
33	high	Smile	Laugh	ابتسامة ضحك	0.87
34	high	Signature	Endorsement	توقيع تصديق	0.89
35	high	Tools	Means	اداة وسيلة	0.92
36	high	Sepulcher	Grave	ضريح قبر	0.93
37	high	Boy	Lad	صبي فتى	0.93
38	high	Wizard	Magician	ساحر مشعوذ	0.94
39	high	Coach	Bus	حافلة باص	0.95
40	high	Glass	Tumbler	كاس قدح	0.95

Noting that, some words in the dataset benchmark are not covered in ArWN. For instance, the words " موقد" stove, " ساحر" wizard, and " مشعوذ" magician are not covered in ArWN, hence, the 3^{rd} and 38^{th} word pairs are not covered in the experiment. While, the words "ابتسامة" smile and "جوهرة" Gem, which are also not covered in ArWN, instead the words "بسمة" and "جوهر" are used to measure the similarity scores, respectively.

4.3 Performance Measures

The obtained similarity scores are evaluated against human ratings benchmark (*HR*), which is a human judgment similarity scores of Arabic nominal word pairs obtained from the dataset of AWSS.

Two measures are used to quantify the performance of the obtained similarity scores. The Person Correlation measure (r) defines the strength of the linear relationship between the obtained similarity scores and *HR*; the Mean Squared Error (MSE) calculates the average squared difference between the similarity scores and *HR*. The best performance is indicated by a similarity measure with the smallest MSE value and r value is close to 1. While the negative r value means that the obtained scores are increase as the *HR* ratings decrease. In addition, the similarity scores are compared to the performance results reported in [15, 16], which are listed in Table 4.

Table 4: Performance measures reported in [16, 15]

#	**Measure**	r	MSE
1	WuP	0.94	0.01648
2	LCH	0.89	0.03708
3	Path	0.75	0.16038
4	LI	0.85	0.10205
5	AWSS	0.88	0.04424
6	Aldiery	0.96	0.01893

4.4 Experimental settings

Six path-based semantic similarity measures, which are defined in equations (1,2,3,4,5, and 6), will be applied over the Arabic word pairs benchmark dataset, which is described in Section 4.2. Using the following configurations, the similarity measures are applied over ArWN and EnWN to quantify the efficiency of ArWN structure enrichment:

1. *UnDefined Senses* (uDS): calculates the semantic similarity between given words without determining their senses. In this setting, which is considered as the default setting of the similarity measures, the similarity measure returns the maximum score obtained from the all possible combination of the senses of the given words.

2. *Defined Senses* (DS): calculates the semantic similarity between given words senses (i.e, sense are determined in advance). By extending the work in [17], the sense of each word pairs under evaluation is determined based on a majority vote (consensus) approach. Similar to the tasks of filling the semantic gaps [17, 18] (see Section 3), the CAUTIOUS strategy is adopted, where users are avoided to decide among word pairs that share the same words.

3. *wordnets Translation* ($wnTrans$): calculates the semantic similarity over ArWN by selecting the senses that match the

Table 5: uDs configuration over ArWN

					iHT						uHT					
NO.	Ar Word Pairs Senses		En Word Pairs Senses		WuP	LCH	Path	LI	AWSS	Aldiery	WuP	LCH	Path	LI	AWSS	Aldiery
1	$aATi}_1	taSodiyq_2	shore#1	acceptance#1	0.308	0.298	0.100	0.113	0.086	0.451	0.364	0.358	0.125	0.168	0.119	0.504
2	mu&ax~irap_1	xayoT_1	back#2	cord#4	0.706	0.436	0.167	0.301	0.335	0.808	0.667	0.436	0.167	0.300	0.312	0.781
3																
4	Hamol_1	Zuhor_1	gestation#2	midday#1	0.316	0.207	0.071	0.058	0.063	0.504	0.316	0.207	0.071	0.058	0.063	0.504
5	tawoqiyE_1	daliyl_2	endorsement#5	lead#3	0.444	0.272	0.091	0.109	0.123	0.633	0.444	0.272	0.091	0.109	0.123	0.633
6	Sabiy~_1	taSodiyq_2	juvenile#1	acceptance#1	0.308	0.298	0.100	0.113	0.086	0.451	0.333	0.326	0.111	0.138	0.102	0.475
7	Sabiy~_1	Zuhor_1	juvenile#1	midday#1	0.235	0.207	0.071	0.051	0.045	0.379	0.250	0.227	0.077	0.062	0.053	0.394
8	basomap_1	qaroyap_1	smile#1	village#1	0.375	0.272	0.091	0.105	0.102	0.553	0.375	0.272	0.091	0.105	0.102	0.553
9	Zuhor_1	Sawom_1	noon#1	fasting#1	0.364	0.188	0.067	0.049	0.065	0.574	0.364	0.188	0.067	0.049	0.065	0.574
10	kuwb_1	AlomAs_1	glass#2	diamond#2	0.353	0.248	0.083	0.086	0.087	0.535	0.267	0.248	0.083	0.076	0.062	0.411
11	maqaAm_1	ra}iyos_1	shrine#1	head#4	0.500	0.272	0.091	0.110	0.139	0.687	0.556	0.326	0.111	0.164	0.192	0.720
12	riyf_1	xuDaAr_1	country#4	vegetable#1	0.375	0.272	0.091	0.105	0.102	0.553	0.286	0.272	0.091	0.092	0.073	0.429
13	sahom_3	adaAp_2	arrow#2	instrument#1	0.857	0.922	1.000	0.819	0.826	0.943	0.842	0.546	0.250	0.449	0.499	0.874
14	<iHotifaAl_1	DaHik_2	laughter#2	celebration#2	0.824	0.546	0.250	0.449	0.485	0.864	0.824	0.546	0.250	0.449	0.485	0.864
15	fataAp_1	xaAdim_1	girl#1	retainer#2	0.762	0.436	0.167	0.301	0.361	0.842	0.737	0.436	0.167	0.301	0.351	0.827
16	Eiyod_1	Sawom_1	celebration#2	fasting#1	0.700	0.395	0.143	0.246	0.298	0.811	0.700	0.395	0.143	0.246	0.298	0.811
17	HaAfilap_1	wasiylap_1	coach#5	means#2	0.778	0.486	0.200	0.368	0.412	0.845	0.750	0.486	0.200	0.367	0.394	0.828
18	fayolasuwf_1	ra}iyos_1	philosopher#1	head#4	0.762	0.436	0.167	0.301	0.361	0.842	0.737	0.436	0.167	0.301	0.351	0.827
19	fataAp_1	>xot_1	girl#1	sister#1	0.696	0.358	0.125	0.202	0.261	0.815	0.667	0.358	0.125	0.202	0.254	0.796
20	dajaAjap_1	HamaAm_1	hen#1	pigeon#1	0.828	0.436	0.167	0.301	0.376	0.879	0.815	0.436	0.167	0.301	0.374	0.872
21	rukaAm_1	jabal_1	hill#2	mountain#1	0.533	0.358	0.125	0.199	0.201	0.692	0.500	0.395	0.143	0.233	0.195	0.649
22	say~id_1	ra}iyos_1	sir#1	head#4	0.762	0.436	0.167	0.301	0.361	0.842	0.737	0.436	0.167	0.301	0.351	0.827
23	TaEaAm_3	xuDaAr_1	food#2	vegetable#1	0.857	0.624	0.333	0.548	0.545	0.875	0.833	0.624	0.333	0.546	0.507	0.861
24	xaAdim_1	xaAdim_1	retainer#2	retainer#2	1.000	0.922	1.000	0.819	0.835	0.958	1.000	0.922	1.000	0.819	0.826	0.957
25	jaroy_1	ma$oy_1	run#7	walk#1	0.909	0.624	0.333	0.549	0.604	0.905	0.909	0.624	0.333	0.549	0.604	0.905
26	Habol_1	gazol_1	cord#1	thread#1	0.941	0.734	0.500	0.670	0.690	0.918	0.933	0.734	0.500	0.670	0.671	0.913
27	dagol_1	dagol_1	jungle#1	jungle#1	1.000	0.922	1.000	0.818	0.754	0.950	1.000	0.922	1.000	0.815	0.701	0.947
28	fayolasuwf_1	mufak~ir_1	philosopher#1	intellect#3	0.900	0.624	0.333	0.549	0.597	0.900	0.889	0.624	0.333	0.549	0.587	0.894
29	riHolap_1	safar_1	journey#1	travel#1	0.952	0.734	0.500	0.670	0.710	0.926	0.952	0.734	0.500	0.670	0.710	0.926
30	HajarN_kariym_1	AlomAs_1	gem#2	diamond#2	0.875	0.624	0.333	0.549	0.570	0.886	0.857	0.624	0.333	0.548	0.545	0.875
31	riyf_1	riyf_1	country#4	country#4	1.000	0.922	1.000	0.819	0.811	0.955	1.000	0.922	1.000	0.818	0.789	0.953
32	wisaAdap_1	wisaAdap_1	cushion#3	cushion#3	1.000	0.922	1.000	0.819	0.811	0.955	1.000	0.922	1.000	0.818	0.789	0.953
33	basomap_1	DaHik_2	smile#1	laugh#1	0.533	0.358	0.125	0.199	0.201	0.692	0.533	0.358	0.125	0.199	0.201	0.692
34	tawoqiyE_1	tawoqiyE_1	endorsement#5	endorsement#5	1.000	0.922	1.000	0.819	0.835	0.958	1.000	0.922	1.000	0.819	0.826	0.957
35	>adaAp_1	wasiyolap_1	tool#2	means#1	0.941	0.734	0.500	0.670	0.690	0.918	0.941	0.734	0.500	0.670	0.690	0.918
36	qabor_1	qabor_1	grave#2	grave#2	1.000	0.922	1.000	0.819	0.826	0.957	1.000	0.922	1.000	0.819	0.811	0.955
37	Sabiy~_2	Sabiy~_2	spring chicken#1	spring chicken#1	1.000	0.922	1.000	0.819	0.835	0.958	1.000	0.922	1.000	0.819	0.826	0.957
38																
39	HaAfilap_1	HaAfilap_1	coach#5	coach#5	1.000	0.922	1.000	0.819	0.835	0.958	1.000	0.922	1.000	0.819	0.826	0.957
40	kuwb_1	kuwb_1	glass#2	glass#2	1.000	0.922	1.000	0.819	0.826	0.957	1.000	0.922	1.000	0.819	0.811	0.955

	Performance Measures											
Sim. level	Correlation r						Correlation r					
all	0.858	0.774	0.658	0.787	0.806	0.831	0.850	0.814	0.712	0.825	0.840	0.826
low	0.060	-0.115	-0.162	-0.131	-0.074	0.155	-0.075	-0.088	-0.139	-0.135	-0.090	-0.089
mid	0.122	-0.095	-0.127	-0.077	-0.075	-0.052	0.103	0.269	0.324	0.239	0.188	0.050
high	0.152	0.314	0.393	0.265	0.300	0.177	0.171	0.314	0.393	0.267	0.345	0.197
Sim. level	MSE						MSE					
all	0.066	0.045	0.104	0.055	0.047	0.109	0.064	0.038	0.092	0.048	0.044	0.104
low	0.118	0.050	0.010	0.015	0.016	0.247	0.118	0.057	0.010	0.017	0.016	0.240
mid	0.072	0.056	0.178	0.087	0.071	0.101	0.067	0.031	0.142	0.067	0.057	0.091
high	0.020	0.030	0.109	0.056	0.050	0.009	0.020	0.030	0.109	0.056	0.053	0.008

translations defined in the benchmark dataset. In *wnTrans* the maximum similarity score is selected, such that the ArWN and the EnWN cover the Arabic word and its translation in English, respectively. Otherwise, the default setting *uDS* is applied.

4. *Upper Bound* (*UB*): calculates the semantic similarity between given words senses, such that, *UB* selects the sense pair that maximize correlation *r* values and minimize *MSE* values w.r.t the *HR* ratings (benchmark dataset). *UB* indicates the optimal scores for the considered experiment settings.

5. *Unimproved HyperTrees* (*uHT*): calculates the semantic similarity using ArWN while ignoring the structure enhancement. That is, the semantic gaps are considered in calculating the similarly scores.

6. *Improved HyperTrees* (*iHT*): calculates the semantic similarity using the enhanced structure of ArWN.

4.5 Results & Discussion

Tables 5, 6, 7, and 8 report the semantic similarity scores using six similarity measures, which resulted from applying *uDS*, *DS*, *wnTrans* and *UB* configurations over ArWN; respectively. Such that two variants, *uHT* and *iHT*, are considered. The tables also list the Arabic senses and their correspondences senses in English, which are used to provide the obtained similarity scores. Table 9 reports the semantic similarity scores that are obtained from applying *uDs*, *DS*, and *UB* configurations over EnWN. English-based

Table 6: DS configuration over ArWN

					iHT						uHT					
NO.	Ar Word Pairs Senses		En Word Pairs Senses		WuP	LCH	Path	LI	AWSS	Aldiery	WuP	LCH	Path	LI	AWSS	Aldiery
1	$aATi}_AlbaHor_1	tawoqiyE_1	coast#1	endorsement#5	0.235	0.207	0.071	0.051	0.045	0.379	0.267	0.248	0.083	0.076	0.062	0.411
2	Zuhor_1	gazol_1	noon#1	thread#1	0.200	0.154	0.059	0.028	0.028	0.343	0.211	0.170	0.063	0.034	0.033	0.354
3																
4	Habol_1	Zuhor_1	cord#1	midday#1	0.211	0.170	0.063	0.034	0.033	0.354	0.222	0.188	0.067	0.042	0.038	0.366
5	tawoqiyE_1	gazol_1	endorsement#5	thread#1	0.211	0.170	0.063	0.034	0.033	0.354	0.222	0.188	0.067	0.042	0.038	0.366
6	walad_1	tawoqiyE_1	boy#1	endorsement#5	0.235	0.207	0.071	0.051	0.045	0.379	0.250	0.227	0.077	0.062	0.053	0.394
7	walad_1	Zuhor_1	boy#1	midday#1	0.222	0.188	0.067	0.042	0.038	0.366	0.235	0.207	0.071	0.051	0.045	0.379
8	basomap_1	qaroyap_2	smile#1	village#2	0.235	0.207	0.071	0.051	0.045	0.379	0.267	0.248	0.083	0.076	0.062	0.411
9	Zuhor_1	Sawom_1	noon#1	fasting#1	0.364	0.188	0.067	0.049	0.065	0.574	0.364	0.188	0.067	0.049	0.065	0.574
10	kuwb_1	AlomAs_1	glass#2	diamond#2	0.353	0.248	0.083	0.086	0.087	0.535	0.267	0.248	0.083	0.076	0.062	0.411
11	qabor_1	ra}iyos_1	grave#2	head#4	0.444	0.272	0.091	0.109	0.123	0.633	0.375	0.272	0.091	0.105	0.102	0.553
12	riyf_1	xuDaAr_1	country#4	vegetable#1	0.375	0.272	0.091	0.105	0.102	0.553	0.286	0.272	0.091	0.092	0.073	0.429
13	kuwb_1	>adaAp_1	glass#2	tool#2	0.222	0.922	1.000	0.683	0.371	0.691	0.235	0.207	0.071	0.051	0.045	0.379
14	DaHik_2	<iHotifAl_1	laugh#1	celebration#1	0.400	0.298	0.100	0.128	0.120	0.574	0.400	0.298	0.100	0.128	0.120	0.574
15	fataAp_1	xaAdim_1	girl#1	retainer#2	0.762	0.436	0.167	0.301	0.361	0.842	0.737	0.436	0.167	0.301	0.351	0.827
16	<iHotifAl_1	Sawom_1	celebration#1	fasting#1	0.526	0.298	0.100	0.135	0.163	0.703	0.526	0.298	0.100	0.135	0.163	0.703
17	HaAfilap_1	wasiylap_1	coach#5	means#2	0.778	0.486	0.200	0.368	0.412	0.845	0.750	0.486	0.200	0.367	0.394	0.828
18	fayolasuwf_1	ra}iyos_1	philosopher#1	head#4	0.762	0.436	0.167	0.301	0.361	0.842	0.737	0.436	0.167	0.301	0.351	0.827
19	fataAp_1	>xot_1	girl#1	sister#1	0.696	0.358	0.125	0.202	0.261	0.815	0.667	0.358	0.125	0.202	0.254	0.796
20	dajaAjap_1	HamaAm_1	hen#1	pigeon#1	0.828	0.436	0.167	0.301	0.376	0.879	0.815	0.436	0.167	0.301	0.374	0.872
21	rukaAm_1	jabal_1	hill#2	mountain#1	0.533	0.358	0.125	0.199	0.201	0.692	0.500	0.395	0.143	0.233	0.195	0.649
22	say~id_1	ra}iyos_1	sir#1	head#4	0.762	0.436	0.167	0.301	0.361	0.842	0.737	0.436	0.167	0.301	0.351	0.827
23	TaEaAm_1	xuDaAr_1	food#1	vegetable#1	0.571	0.395	0.143	0.243	0.236	0.716	0.500	0.395	0.143	0.233	0.195	0.649
24	Eabod_1	xaAdim_1	slave#1	retainer#2	0.842	0.546	0.250	0.449	0.499	0.874	0.824	0.546	0.250	0.449	0.485	0.864
25	jaroy_1	ma$oy_1	run#7	walk#1	0.909	0.624	0.333	0.549	0.604	0.905	0.909	0.624	0.333	0.549	0.604	0.905
26	Habol_1	gazol_1	cord#1	thread#1	0.941	0.734	0.500	0.670	0.690	0.918	0.933	0.734	0.500	0.670	0.671	0.913
27	dagol_1	dagol_1	jungle#1	jungle#1	1.000	0.922	1.000	0.818	0.754	0.950	1.000	0.922	1.000	0.815	0.701	0.947
28	fayolasuwf_1	mufak~ir_1	philosopher#1	intellect#3	0.900	0.624	0.333	0.549	0.597	0.900	0.889	0.624	0.333	0.549	0.587	0.894
29	riHolap_1	safar_1	journey#1	travel#1	0.952	0.734	0.500	0.670	0.710	0.926	0.952	0.734	0.500	0.670	0.710	0.926
30	HajarN_kariym_1	AlomAs_1	gem#2	diamond#2	0.875	0.624	0.333	0.549	0.570	0.886	0.857	0.624	0.333	0.548	0.545	0.875
31	riyf_1	qaroyap_2	country#4	village#2	0.824	0.546	0.250	0.449	0.485	0.864	0.857	0.624	0.333	0.548	0.545	0.875
32	wisaAdap_1	wisaAdap_1	cushion#3	cushion#3	1.000	0.922	1.000	0.819	0.811	0.955	1.000	0.922	1.000	0.818	0.789	0.953
33	basomap_1	DaHik_2	smile#1	laugh#1	0.533	0.358	0.125	0.199	0.201	0.692	0.533	0.358	0.125	0.199	0.201	0.692
34	tawoqiyE_1	tawoqiyE_1	Endorsement#5	Endorsement#5	1.000	0.922	1.000	0.819	0.835	0.958	1.000	0.922	1.000	0.819	0.826	0.957
35	>adaAp_1	wasiyolap_1	tool#2	means#1	0.941	0.734	0.500	0.670	0.690	0.918	0.941	0.734	0.500	0.670	0.690	0.918
36	qabor_1	qabor_1	grave#2	grave#2	1.000	0.922	1.000	0.819	0.826	0.957	1.000	0.922	1.000	0.819	0.811	0.955
37	muraAhiq_1	Tifol_1	adolescent#1	child#1	0.900	0.624	0.333	0.549	0.597	0.900	0.889	0.624	0.333	0.549	0.587	0.894
38																
39	HaAfilap_1	HaAfilap_1	coach#5	bus#1	1.000	0.922	1.000	0.819	0.835	0.958	1.000	0.922	1.000	0.819	0.826	0.957
40	kuwb_1	kuwb_1	glass#2	glass#2	1.000	0.922	1.000	0.819	0.826	0.957	1.000	0.922	1.000	0.819	0.811	0.955

	Performance Measures											
Sim. level	Correlation r						Correlation r					
all	0.925	0.799	0.607	0.824	0.877	0.933	0.920	0.859	0.688	0.864	0.878	0.925
low	0.810	0.853	0.875	0.901	0.882	0.776	0.564	0.687	0.712	0.756	0.738	0.478
mid	0.736	-0.156	-0.389	0.018	0.463	0.636	0.698	0.770	0.702	0.739	0.695	0.686
high	0.130	0.234	0.290	0.199	0.242	0.150	0.136	0.229	0.288	0.193	0.279	0.161
Sim. level	MSE						MSE					
all	0.028	0.042	0.131	0.065	0.052	0.061	0.026	0.034	0.118	0.062	0.057	0.053
low	0.044	0.020	0.007	0.005	0.005	0.135	0.042	0.026	0.007	0.006	0.007	0.125
mid	0.024	0.060	0.207	0.104	0.076	0.055	0.022	0.033	0.176	0.099	0.088	0.042
high	0.018	0.043	0.158	0.076	0.067	0.008	0.018	0.040	0.152	0.071	0.067	0.008

similarity (Path, lch, WuP, and Li measures) scores are reported for each configuration. English senses that are used to compute the scores are also reported.

Observe that the word senses are defined differently based on the applied configuration. For example, the word boy "صبي" is selected differently w.r.t the applied configuration; in Table 5, in the *uDS* setting the selected sense is (Sabiy _1, juvenile#1) [14], in *DS* (Table 6) and *wnTrans* (Table 7) settings the selected sense is (walad_1, boy#1), and in *UB* (Table 8) setting the sense is (walad_2, boy#2). Moreover, considering *wnTrans* setting, the translation which are defined in the AWSS benchmark for 13 Arabic words that exist in 17 word pairs, does not exist in the mapping between ArWN and EnWN; the words and their translation are {signature: توقيع ; sepulcher: ضريح; sheikh: شيخ; countryside: ريف; tumbler: قدح; feast: عيد; odalisque: جارية; sage: حكيم; thinker: مفكر; pillow: مخدة; signature: توقيع; lad: فتى}. For example, the word "توقيع" has one sense in ArWN "*tawoqiyE_1*", which is mapped into the "*endorsement*#5" in EnWN, while none of the five senses for the word "*signature*" in EnWN is mapped into ArWN. Noting that 28 word pairs out of the 40 word pairs has at least one missing correspondence sense in EnWN when considering *uHT* setting, For example; similarity scores of the 21st word pairs (Hill "تل"; mountain "جبل"); which is also illustrated in

[14] Represents Arabic sense in ArWN and its correspondence in EnWN

Table 7: wnTrans configuration over ArWN

NO.	Ar Word Pairs Senses		En Word Pairs Senses		iHT						uHT					
					WuP	LCH	Path	LI	AWSS	Aldiery	WuP	LCH	Path	LI	AWSS	Aldiery
1	$aATi}_AlbaHor_1	tawoqiyE_1	coast#1	endorsement#5	0.235	0.207	0.071	0.051	0.045	0.379	0.267	0.248	0.083	0.076	0.062	0.411
2	Zuhor_1	xayoT_2	noon#1	string#9	0.353	0.248	0.083	0.086	0.087	0.535	0.353	0.248	0.083	0.086	0.087	0.535
3																
4	Habol_1	Zuhor_1	cord#1	midday#1	0.211	0.170	0.063	0.034	0.033	0.354	0.222	0.188	0.067	0.042	0.038	0.366
5	tawoqiyE_1	xayoT_2	endorsement#5	string#9	0.375	0.272	0.091	0.105	0.102	0.553	0.375	0.272	0.091	0.105	0.102	0.553
6	walad_1	tawoqiyE_1	boy#1	endorsement#5	0.235	0.207	0.071	0.051	0.045	0.379	0.250	0.227	0.077	0.062	0.053	0.394
7	walad_1	Zuhor_1	boy#1	midday#1	0.222	0.188	0.067	0.042	0.038	0.366	0.235	0.207	0.071	0.051	0.045	0.379
8	basomap_1	qaroyap_1	smile#1	village#2	0.235	0.207	0.071	0.051	0.045	0.379	0.267	0.248	0.083	0.076	0.062	0.411
9	Zuhor_1	Sawom_1	noon#1	fasting#1	0.364	0.188	0.067	0.049	0.065	0.574	0.364	0.188	0.067	0.049	0.065	0.574
10	kuwb_1	AlomAs_1	glass#2	diamond#2	0.353	0.248	0.083	0.086	0.087	0.535	0.267	0.248	0.083	0.076	0.062	0.411
11	maqaAm_1	ra}iyos_1	shrine#1	head#4	0.500	0.272	0.091	0.110	0.139	0.687	0.556	0.326	0.111	0.164	0.192	0.720
12	riyf_1	xuDaAr_1	country#4	vegetable#1	0.375	0.272	0.091	0.105	0.102	0.553	0.286	0.272	0.091	0.092	0.073	0.429
13	kuwb_1	>aadaAp_1	tool#1	glass#2	0.778	0.922	1.000	0.818	0.789	0.927	0.750	0.486	0.200	0.367	0.394	0.828
14	DaHik_2	<iHotifaAl_1	laugh#1	celebration#2	0.375	0.272	0.091	0.105	0.102	0.553	0.375	0.272	0.091	0.105	0.102	0.553
15	fataAp_1	xaAdim_1	girl#1	retainer#2	0.762	0.436	0.167	0.301	0.361	0.842	0.737	0.436	0.167	0.301	0.351	0.827
16	Eiyod_1	Sawom_1	day#3	fasting#1	0.316	0.207	0.071	0.058	0.063	0.504	0.316	0.207	0.071	0.058	0.063	0.504
17	HaAfilap_1	wasiylap_1	coach#5	means#2	0.778	0.486	0.200	0.368	0.412	0.845	0.750	0.486	0.200	0.367	0.394	0.828
18	fayolasuwf_1	ra}iyos_1	philosopher#1	head#4	0.762	0.436	0.167	0.301	0.361	0.842	0.737	0.436	0.167	0.301	0.351	0.827
19	fataAp_1	>xot_1	girl#1	sister#1	0.696	0.358	0.125	0.202	0.261	0.815	0.667	0.358	0.125	0.202	0.254	0.796
20	dajaAjap_1	HamaAm_1	hen#1	pigeon#1	0.828	0.436	0.167	0.301	0.376	0.879	0.815	0.436	0.167	0.301	0.374	0.872
21	rukaAm_1	jabal_1	hill#2	mountain#1	0.533	0.358	0.125	0.199	0.201	0.692	0.500	0.395	0.143	0.233	0.195	0.649
22	say~id_1	ra}iyos_1	sir#1	head#4	0.762	0.436	0.167	0.301	0.361	0.842	0.737	0.436	0.167	0.301	0.351	0.827
23	TaEaAm_1	xuDaAr_1	food#1	vegetable#1	0.571	0.395	0.143	0.243	0.236	0.716	0.500	0.395	0.143	0.233	0.195	0.649
24	xaAdim_1	xaAdim_1	retainer#2	retainer#2	1.000	0.922	1.000	0.819	0.835	0.958	1.000	0.922	1.000	0.819	0.826	0.957
25	jaroy_1	ma$oy_1	run#7	walk#1	0.909	0.624	0.333	0.549	0.604	0.905	0.909	0.624	0.333	0.549	0.604	0.905
26	Habol_1	xayoT_2	cord#1	string#9	0.286	0.272	0.091	0.092	0.073	0.429	0.308	0.298	0.100	0.113	0.086	0.451
27	gaAbap_1	dagol_1	forest#1	jungle#1	0.308	0.298	0.100	0.113	0.086	0.451	0.333	0.326	0.111	0.138	0.102	0.475
28	fayolasuwf_1	mufak~ir_1	philosopher#1	intellect#3	0.900	0.624	0.333	0.549	0.597	0.900	0.889	0.624	0.333	0.549	0.587	0.894
29	riHolap_1	safar_1	journey#1	travel#1	0.952	0.734	0.500	0.670	0.710	0.926	0.952	0.734	0.500	0.670	0.710	0.926
30	HajarN_kariym_1	AlomAs_1	gem#2	diamond#2	0.875	0.624	0.333	0.549	0.570	0.886	0.857	0.624	0.333	0.548	0.545	0.875
31	riyf_1	qaroyap_2	country#4	village#2	0.824	0.546	0.250	0.449	0.485	0.864	0.857	0.624	0.333	0.548	0.545	0.875
32	wisaAdap_1	wisaAdap_1	cushion#3	cushion#3	1.000	0.922	1.000	0.819	0.811	0.955	1.000	0.922	1.000	0.818	0.789	0.953
33	basomap_1	DaHik_2	smile#1	laugh#1	0.533	0.358	0.125	0.199	0.201	0.692	0.533	0.358	0.125	0.199	0.201	0.692
34	tawoqiyE_1	tawoqiyE_1	Endorsement#5	Endorsement#5	1.000	0.922	1.000	0.819	0.835	0.958	1.000	0.922	1.000	0.819	0.826	0.957
35	>adaAp_1	wasiyolap_1	tool#2	means#1	0.941	0.734	0.500	0.670	0.690	0.918	0.941	0.734	0.500	0.670	0.690	0.918
36	qabor_1	qabor_1	grave#2	grave#2	1.000	0.922	1.000	0.819	0.826	0.957	1.000	0.922	1.000	0.819	0.811	0.955
37	walad_1	Sabiy~_2	boy#1	spring chicken#1	0.800	0.486	0.200	0.368	0.424	0.858	0.778	0.486	0.200	0.368	0.412	0.845
38																
39	HaAfilap_1	HaAfilap_1	coach#5	bus#1	1.000	0.922	1.000	0.819	0.835	0.958	1.000	0.922	1.000	0.819	0.826	0.957
40	kuwb_1	kuwb_1	glass#2	glass#2	1.000	0.922	1.000	0.819	0.826	0.957	1.000	0.922	1.000	0.819	0.811	0.955

	Performance Measures											
Sim. level	Correlation r						Correlation r					
all	0.787	0.703	0.540	0.703	0.719	0.757	0.787	0.763	0.616	0.763	0.762	0.774
low	0.615	0.569	0.583	0.610	0.645	0.586	0.391	0.555	0.576	0.538	0.470	0.318
mid	0.453	0.067	-0.082	0.088	0.152	0.345	0.434	0.473	0.397	0.466	0.452	0.407
high	0.672	0.656	0.627	0.647	0.658	0.693	0.665	0.643	0.624	0.635	0.653	0.689
Sim. level	MSE						MSE					
all	0.051	0.061	0.155	0.097	0.089	0.082	0.050	0.051	0.140	0.087	0.084	0.076
low	0.062	0.027	0.008	0.006	0.006	0.170	0.065	0.033	0.007	0.006	0.007	0.167
mid	0.046	0.065	0.199	0.114	0.096	0.071	0.043	0.039	0.165	0.094	0.085	0.059
high	0.047	0.084	0.230	0.153	0.147	0.021	0.044	0.078	0.221	0.144	0.144	0.019

Figure 1, before the enhancement of the ArWN structure, the $HyperTree$ has two semantic gaps {*geological formation*#1} and {*physical entity*#1}; while The $HyperTree$(جبل) has one semantic gap, which is {*physical entity*#1}.

The performance measures r and MSE are reported for every configuration in the bottom ofTables 6, 5, 7, and 8; including the performance for each similarity level. Observe that, r values show that iHT achieves better performance compared to uHT. While; MSE values indicate that uHT has less difference in similarity scores than iHT, compared to HR rates. In fact, the values of MSE are strongly influenced by uHT, the semantic gaps. Noting that when $HyperTrees$ of two senses have the same semantic gaps; the lcs is reduced which decreases the similarity scores. This gives less difference in similarity scores compared to HR rates. In particular, this happens for MSE values at mid similarity level. For examples, in row 10, the $HyperTrees$ of the word pairs (Glass; Diamond) has the {*physical entity*#1} as a semantic gap. That is, $d(glass\#2) = 9$; $d(diamond\#2) = 8$ and $d(lcs(glass\#2, diamond\#2)) = 3$; while $d(kuwb_1) = 8$; $d(AlomAs_1) = 7$; $d(lcs(kuwb_1, AlomAs_1)) = 2$.

Furthermore, $wnTrans$ configuration scored the worst performance; this is due to the low Arabic word coverage. A significant finding is that, the richness of ArWN content has a high effect on the evaluation the semantic similarity between the concepts, in terms of the coverage of lexical and semantic relations.

Performance measures in [15, 16]; presented in Table 4; showed that WuP measure scored the best MSE value 0.0165 with 0.94 for r; and comparatively $Aldiery$ measure has obtained the values 0.96

Table 8: UB configuration over ArWN

					iHT						uHT					
NO.	Ar Word Pairs Senses		En Word Pairs Senses		WuP	LCH	Path	LI	AWSS	Aldiery	WuP	LCH	Path	LI	AWSS	Aldiery
1	$aATi}_AlbaHor_1	tawoqiyE_1	coast#1	endorsement#5	0.235	0.207	0.071	0.051	0.045	0.379	0.267	0.248	0.083	0.076	0.062	0.411
2	Zuhor_1	gazol_1	noon#1	thread#1	0.200	0.154	0.059	0.028	0.028	0.343	0.211	0.170	0.063	0.034	0.033	0.354
3																
4	Habol_1	Zuhor_1	cord#1	midday#1	0.211	0.170	0.063	0.034	0.033	0.354	0.222	0.188	0.067	0.042	0.038	0.366
5	tawoqiyE_1	gazol_1	endorsement#5	thread#1	0.211	0.170	0.063	0.034	0.033	0.354	0.222	0.188	0.067	0.042	0.038	0.366
6	walad_2	tawoqiyE_1	boy#2	endorsement#5	0.222	0.188	0.067	0.042	0.038	0.366	0.235	0.207	0.071	0.051	0.045	0.379
7	walad_2	Zuhor_1	boy#2	midday#1	0.211	0.170	0.063	0.034	0.033	0.354	0.222	0.188	0.067	0.042	0.038	0.366
8	basomap_1	qaroyap_2	smile#1	village#2	0.235	0.207	0.071	0.051	0.045	0.379	0.267	0.248	0.083	0.076	0.062	0.411
9	mu&ax~irap_1	Sawom_1	back#2	fasting#1	0.200	0.154	0.059	0.028	0.028	0.343	0.211	0.170	0.063	0.034	0.033	0.354
10	kuwb_1	AlomAs_1	glass#2	diamond#2	0.353	0.248	0.083	0.086	0.087	0.535	0.267	0.248	0.083	0.076	0.062	0.411
11	qabor_1	$ayox_2	grave#2	senator#1	0.400	0.227	0.077	0.073	0.089	0.601	0.333	0.227	0.077	0.070	0.074	0.519
12	riyf_1	xuDar_1	country#4	green#7	0.353	0.248	0.083	0.086	0.087	0.535	0.267	0.248	0.083	0.076	0.062	0.411
13	kuwb_1	>adaAp_1	glass#2	tool#2	0.222	0.922	1.000	0.683	0.371	0.691	0.235	0.207	0.071	0.051	0.045	0.379
14	DaHik_1	Eiyod_1	laughter#2	day#3	0.375	0.272	0.091	0.105	0.102	0.553	0.375	0.272	0.091	0.105	0.102	0.553
15	fataAp_1	xaAdim_1	girl#1	retainer#2	0.762	0.436	0.167	0.301	0.361	0.842	0.737	0.436	0.167	0.301	0.351	0.827
16	<iHotifAl_1	Sawom_1	celebration#1	fasting#1	0.526	0.298	0.100	0.135	0.163	0.703	0.526	0.298	0.100	0.135	0.163	0.703
17	HaAfilap_1	wasiylap_1	coach#5	means#2	0.778	0.486	0.200	0.368	0.412	0.845	0.750	0.486	0.200	0.367	0.394	0.828
18	fayolasuwf_1	$ayox_2	philosopher#1	senator#1	0.696	0.358	0.125	0.202	0.261	0.815	0.667	0.358	0.125	0.202	0.254	0.796
19	fataAp_1	>xot_1	girl#1	sister#1	0.696	0.358	0.125	0.202	0.261	0.815	0.667	0.358	0.125	0.202	0.254	0.796
20	dajaAjap_1	HamaAm_1	hen#1	pigeon#1	0.828	0.436	0.167	0.301	0.376	0.879	0.815	0.436	0.167	0.301	0.374	0.872
21	rukaAm_1	jabal_1	hill#2	mountain#1	0.533	0.358	0.125	0.199	0.201	0.692	0.500	0.395	0.143	0.233	0.195	0.649
22	say~id_1	$ayox_1	lord#3	graybeard#1	0.696	0.358	0.125	0.202	0.261	0.815	0.667	0.358	0.125	0.202	0.254	0.796
23	TaEaAm_3	xuDar_1	food#2	green#7	0.800	0.546	0.250	0.449	0.464	0.850	0.769	0.546	0.250	0.447	0.431	0.831
24	Eabod_1	xaAdim_1	slave#1	retainer#2	0.842	0.546	0.250	0.449	0.499	0.874	0.824	0.546	0.250	0.449	0.485	0.864
25	jaroy_1	ma$oy_1	run#7	walk#1	0.909	0.624	0.333	0.549	0.604	0.905	0.909	0.624	0.333	0.549	0.604	0.905
26	Habol_1	xayoT_1	cord#1	cord#4	0.750	0.486	0.200	0.367	0.394	0.828	0.714	0.486	0.200	0.366	0.367	0.805
27	dagol_1	dagol_1	jungle#1	jungle#1	1.000	0.922	1.000	0.818	0.754	0.950	1.000	0.922	1.000	0.815	0.701	0.947
28	fayolasuwf_1	mufak~ir_1	philosopher#1	intellect#3	0.900	0.624	0.333	0.549	0.597	0.900	0.889	0.624	0.333	0.549	0.587	0.894
29	riHolap_1	safar_1	journey#1	travel#3	0.857	0.546	0.250	0.449	0.508	0.883	0.857	0.546	0.250	0.449	0.508	0.883
30	HajarN_kariym_1	AlomAs_1	gem#2	diamond#2	0.875	0.624	0.333	0.549	0.570	0.886	0.857	0.624	0.333	0.548	0.545	0.875
31	riyf_1	qaroyap_2	country#4	village#2	0.824	0.546	0.250	0.449	0.485	0.864	0.857	0.624	0.333	0.548	0.545	0.875
32	wisaAdap_1	wisaAdap_1	cushion#3	cushion#3	1.000	0.922	1.000	0.819	0.811	0.955	1.000	0.922	1.000	0.818	0.789	0.953
33	basomap_1	DaHik_2	smile#1	laugh#1	0.533	0.358	0.125	0.199	0.201	0.692	0.533	0.358	0.125	0.199	0.201	0.692
34	tawoqiyE_1	tawoqiyE_1	endorsement#5	endorsement#5	1.000	0.922	1.000	0.819	0.835	0.958	1.000	0.922	1.000	0.819	0.826	0.957
35	>adaAp_1	wasiyolap_1	tool#2	means#1	0.941	0.734	0.500	0.670	0.690	0.918	0.941	0.734	0.500	0.670	0.690	0.918
36	qabor_1	qabor_1	grave#2	grave#2	1.000	0.922	1.000	0.819	0.826	0.957	1.000	0.922	1.000	0.819	0.811	0.955
37	muraAhiq_1	Tifol_1	adolescent#1	child#1	0.900	0.624	0.333	0.549	0.597	0.900	0.889	0.624	0.333	0.549	0.587	0.894
38																
39	HaAfilap_1	HaAfilap_1	coach#5	bus#1	1.000	0.922	1.000	0.819	0.835	0.958	1.000	0.922	1.000	0.819	0.826	0.957
40	kuwb_1	kuwb_1	glass#2	glass#2	1.000	0.922	1.000	0.819	0.826	0.957	1.000	0.922	1.000	0.819	0.811	0.955

	Performance Measures											
Sim. level	Correlation r						Correlation r					
all	0.935	0.787	0.580	0.813	0.874	0.945	0.934	0.849	0.662	0.856	0.879	0.943
low	0.825	0.696	0.710	0.765	0.815	0.828	0.621	0.458	0.456	0.509	0.591	0.613
mid	0.815	-0.087	-0.358	0.093	0.537	0.739	0.806	0.792	0.734	0.766	0.773	0.788
high	0.345	0.415	0.402	0.419	0.465	0.333	0.372	0.413	0.401	0.417	0.509	0.369
Sim. level	MSE						MSE					
all	0.023	0.046	0.144	0.073	0.058	0.054	0.022	0.037	0.131	0.070	0.062	0.047
low	0.035	0.019	0.008	0.007	0.006	0.114	0.034	0.025	0.008	0.008	0.008	0.105
mid	0.022	0.060	0.205	0.105	0.074	0.055	0.018	0.033	0.175	0.099	0.084	0.041
high	0.015	0.054	0.193	0.096	0.083	0.006	0.015	0.051	0.186	0.091	0.085	0.006

and 0.0189 for r and MSE; respectively. Nevertheless, [15, 16] did not explicitly state which configuration was considered in calculating the similarity scores. For instance. in Table 8; where the UB scores indicate the best value for r is 0.945 (with 0.542 for MSE); which is obtained by *Aldiery* measure; and the best MSE value is 0.0203 (with 0.935 for r); which is obtained by WuP measure. Further, in [15, 16] semantic similarity scores were reported to be equal to zero for the word pairs in rows $1-9$, which are at the low similarity level, and the word pair in row 21 was considered as not covered ArWN, hence, this increased the r values and reduced MSE values. However, no explanation is provided.

Overall, the reported performance values show that the enhancement of the semantic structure has a strong effect on estimating the semantic similarity between the concepts. Observe that, word pairs at low and mid similarity levels gives better r values than high similarity level. While words pairs in high similarity level gives better MSE values. in other words, similarity measures obtained best coloration values when the concepts are not similar. Both ArWN and EnWN, r and MSE measures indicate that best performance is achieved when word senses are determined in advance, i.e., DS configuration. However, it is important to distinguish the approach which is used to define the sense, in this work consensus based approach is used.

In other hand; the user feedback based approach, ICLM application that adopted to fill the semantic gaps, shows its effectiveness in selecting the senses, such that scores obtained in DS are close to optimal scores achieved with upper bound setting UB. Further, Arabic-based measure *Aldiery* performs better than $AWSS$, also

Table 9: uDS, DS, and UB configuration over EnWN

	uDS						DS						UB					
NO.	En Word Pairs senses		WuP	LCH	Path	LI	En Word Pairs senses		WuP	LCH	Path	LI	En Word Pairs senses		WuP	LCH	Path	LI
1	coast#4	endorsement#2	0.632	0.436	0.125	0.202	coast#1	endorsement#1	0.286	0.350	0.091	0.092	coast#1	endorsement#5	0.235	0.285	0.071	0.051
2	noon#1	string#9	0.353	0.326	0.083	0.086	noon#1	string#9	0.353	0.326	0.083	0.086	noon#1	string#2	0.182	0.202	0.053	0.019
3	stove#2	walk#5	0.632	0.436	0.125	0.202	stove#1	walk#1	0.167	0.175	0.048	0.013	stove#1	walk#6	0.160	0.162	0.045	0.010
4	cord#2	midday#1	0.316	0.285	0.071	0.058	cord#1	midday#1	0.211	0.248	0.063	0.034	cord#3	midday#1	0.190	0.216	0.056	0.023
5	signature#5	string#7	0.737	0.514	0.167	0.301	signature#1	string#1	0.235	0.285	0.071	0.051	signature#4	string#2	0.200	0.232	0.059	0.028
6	boy#1	endorsement#1	0.286	0.350	0.091	0.092	boy#1	endorsement#5	0.235	0.285	0.071	0.051	boy#2	endorsement#5	0.222	0.266	0.067	0.042
7	boy#1	midday#1	0.222	0.266	0.067	0.042	boy#1	midday#1	0.222	0.266	0.067	0.042	boy#2	midday#1	0.211	0.248	0.063	0.034
8	smile#1	village#1	0.375	0.350	0.091	0.105	smile#1	village#1	0.375	0.350	0.091	0.105	smile#1	village#2	0.235	0.285	0.071	0.051
9	noon#1	fasting#1	0.364	0.266	0.067	0.049	noon#1	fasting#1	0.364	0.266	0.067	0.049	noon#1	fasting#1	0.364	0.266	0.067	0.049
10	glass#1	diamond#2	0.667	0.514	0.167	0.300	glass#1	diamond#1	0.353	0.326	0.083	0.086	glass#4	diamond#3	0.148	0.138	0.042	0.007
11	sepulcher#1	sheikh#1	0.476	0.326	0.083	0.090	sepulcher#1	sheikh#1	0.476	0.326	0.083	0.090	sepulcher#1	sheikh#1	0.476	0.326	0.083	0.090
12	countryside#1	vegetable#2	0.400	0.305	0.077	0.073	countryside#1	vegetable#2	0.400	0.305	0.077	0.073	countryside#1	vegetable#1	0.353	0.326	0.083	0.086
13	tumbler#2	tool#1	0.737	0.514	0.167	0.301	tumbler#2	tool#1	0.737	1.000	1.000	0.818	tumbler#1	tool#4	0.316	1.000	1.000	0.775
14	laugh#1	feast#2	0.400	0.376	0.100	0.128	laugh#1	feast#2	0.400	0.376	0.100	0.128	laugh#2	feast#1	0.333	0.305	0.077	0.070
15	girl#1	odalisque#1	0.833	0.564	0.200	0.368	girl#1	odalisque#1	0.833	0.564	0.200	0.368	girl#3	odalisque#1	0.750	0.472	0.143	0.247
16	feast#2	fasting#1	0.526	0.376	0.100	0.135	feast#2	fasting#1	0.526	0.376	0.100	0.135	feast#4	fasting#1	0.500	0.350	0.091	0.110
17	coach#5	means#2	0.778	0.564	0.200	0.368	coach#5	means#2	0.778	0.564	0.200	0.368	coach#1	means#2	0.526	0.376	0.100	0.135
18	Sage#1	Sheikh#1	0.762	0.514	0.167	0.301	Sage#1	Sheikh#1	0.762	0.514	0.167	0.301	Sage#3	Sheikh#1	0.636	0.404	0.111	0.165
19	girl#1	sister#4	0.957	0.812	0.500	0.670	girl#1	sister#1	0.696	0.436	0.125	0.202	girl#1	sister#1	0.696	0.436	0.125	0.202
20	Hen#2	pigeon#1	0.846	0.564	0.200	0.368	hen#2	pigeon#1	0.846	0.564	0.200	0.368	hen#4	pigeon#1	0.828	0.514	0.167	0.301
21	hill#1	mountain#1	0.857	0.702	0.333	0.548	hill#1	mountain#1	0.857	0.702	0.333	0.548	hill#2	mountain#1	0.667	0.404	0.111	0.165
22	master#2	Sheikh#1	0.900	0.702	0.333	0.549	master#2	Sheikh#1	0.900	0.702	0.333	0.549	master#7	Sheikh#1	0.667	0.404	0.111	0.165
23	food#2	vegetable#1	0.857	0.702	0.333	0.548	food#2	vegetable#1	0.857	0.702	0.333	0.548	food#1	vegetable#1	0.571	0.472	0.143	0.243
24	slave#1	odalisque#1	0.727	0.472	0.143	0.247	slave#1	odalisque#1	0.727	0.472	0.143	0.247	slave#2	odalisque#1	0.696	0.436	0.125	0.202
25	run#7	walk#1	0.909	0.702	0.333	0.549	run#7	walk#1	0.909	0.702	0.333	0.549	run#6	walk#1	0.750	0.472	0.143	0.247
26	cord#1	string#1	0.941	0.812	0.500	0.670	cord#1	string#1	0.941	0.812	0.500	0.670	cord#3	string#2	0.762	0.514	0.167	0.301
27	forest#2	woodland#1	1.000	1.000	1.000	0.818	forest#2	woodland#1	1.000	1.000	1.000	0.818	forest#2	woodland#1	1.000	1.000	1.000	0.818
28	Sage#1	thinker#1	0.857	0.624	0.250	0.449	Sage#1	thinker#1	0.857	0.624	0.250	0.449	Sage#1	thinker#1	0.857	0.624	0.250	0.449
29	journey#1	travel#1	0.952	0.812	0.500	0.670	journey#1	travel#1	0.952	0.812	0.500	0.670	journey#1	travel#3	0.857	0.624	0.250	0.449
30	Gem#5	diamond#1	0.952	0.812	0.500	0.670	Gem#5	diamond#1	0.952	0.812	0.500	0.670	gem#2	diamond#2	0.875	0.702	0.333	0.549
31	countryside#1	village#2	0.778	0.564	0.200	0.368	countryside#1	village#2	0.778	0.564	0.200	0.368	countryside#1	village#2	0.778	0.564	0.200	0.368
32	cushion#3	pillow#1	0.941	0.812	0.500	0.670	cushion#3	pillow#1	0.941	0.812	0.500	0.670	cushion#3	pillow#1	0.941	0.812	0.500	0.670
33	smile#1	laugh#2	0.875	0.702	0.333	0.549	smile#1	laugh#2	0.875	0.702	0.333	0.549	smile#1	laugh#2	0.875	0.702	0.333	0.549
34	signature#1	endorsement#4	0.941	0.812	0.500	0.670	signature#1	endorsement#4	0.941	0.812	0.500	0.670	signature#1	endorsement#4	0.941	0.812	0.500	0.670
35	tool#2	means#1	0.941	0.812	0.500	0.670	tool#1	means#2	0.824	0.624	0.250	0.449	tool#2	means#1	0.941	0.812	0.500	0.670
36	sepulcher#1	grave#2	0.941	0.812	0.500	0.670	sepulcher#1	grave#2	0.941	0.812	0.500	0.670	sepulcher#1	grave#2	0.941	0.812	0.500	0.670
37	boy#1	lad#2	0.952	0.812	0.500	0.670	boy#1	lad#2	0.952	0.812	0.500	0.670	boy#1	lad#2	0.952	0.812	0.500	0.670
38	wizard#2	magician#2	1.000	1.000	1.000	0.819	wizard#2	magician#2	1.000	1.000	1.000	0.819	wizard#2	magician#2	1.000	1.000	1.000	0.819
39	coach#5	bus#1	1.000	1.000	1.000	0.819	coach#5	bus#1	1.000	1.000	1.000	0.819	coach#5	bus#1	1.000	1.000	1.000	0.819
40	glass#2	tumbler#2	0.947	0.812	0.500	0.670	glass#2	tumbler#2	0.947	0.812	0.500	0.670	glass#2	tumbler#2	0.947	0.812	0.500	0.670

Performance Measures												
sim. level	correlation r				correlation r				correlation r			
all	0.856	0.851	0.726	0.865	0.949	0.832	0.623	0.845	0.965	0.801	0.565	0.796
low	-0.071	-0.247	-0.241	-0.231	0.697	0.246	0.223	0.310	0.731	0.570	0.645	0.776
mid	0.666	0.604	0.542	0.612	0.675	0.010	-0.289	0.093	0.791	-0.319	-0.488	-0.309
high	0.261	0.268	0.234	0.279	0.139	0.174	0.173	0.170	0.611	0.550	0.422	0.601
sim. level	MSE				MSE				MSE			
all	0.066	0.038	0.104	0.046	0.036	0.040	0.126	0.056	0.016	0.043	0.160	0.091
low	0.150	0.089	0.011	0.021	0.059	0.056	0.008	0.008	0.035	0.035	0.007	0.006
mid	0.055	0.013	0.125	0.051	0.046	0.044	0.174	0.081	0.010	0.068	0.250	0.174
high	0.008	0.018	0.161	0.062	0.009	0.023	0.179	0.073	0.005	0.026	0.205	0.088

Aldiery measure provided a competitive performance in comparison to WuP measures.

5 Conclusion & Future Work

Six path-based similarity measures including English and Arabic based measures are applied over ArWN and EnWN to examine the effect of the improvement of the lexical and semantic coverage on wordnet-based semantic similarity measures. wo variants uHT and iHT of ArWN structure are considered in the experiment to evaluate the impact of filling the semantic gaps on estimating the semantic similarity. The efficacy of the improved structure is examined by experiments in the context of semantic similarity. The semantic similarity scores for a benchmark dataset, human rating for 40 Arabic nominal word pairs, are calculated over ArWN and EnWN in different configurations (uDs, DS, $wnTrans$, and UB). The obtained performance values indicate the importance of the semantic evidence gained with the enrichment process; and its signification effect on estimating the semantic similarity between concepts. Moreover, when considering Arabic-based measures the experiment results showed that *Aldiery* measure performs better than $AWSS$ measure. Beside that, *Aldiery* measure has provided a competitive performance in comparison to the English-based WuP measures. Finally, the resolved semantic gaps of the new structure are made for public.

As a future direction, we plan to compile *xml* format of the new structure, and to integrate it with available ArWN resources (i,e., ArWN release available at Open Multilingual WordNet [31]). It is also interesting is to study the effect of the semantic gaps over NLP applications; for instances Question Answering similar to the work presented in [44], and word sense disambiguation [33, 35] in the context of Arabic.

References

[1] D. Jurafsky, J. H. Martin, Speech and Language Processing (2Nd Edition), Prentice-Hall, Inc., Upper Saddle River, NJ, USA, 2009.

[2] Y. Li, Z. A. Bandar, D. Mclean, "An Approach for Measuring Semantic Similarity between Words Using Multiple Information Sources," IEEE Trans. on Knowl. and Data Eng., **15**(4), 871–882, 2003, doi:10.1109/TKDE.2003.1209005.

[3] G. A. Miller, "WordNet: A Lexical Database for English," Commun. ACM, **38**(11), 39–41, 1995, doi:10.1145/219717.219748.

[4] C. Fellbaum, editor, WordNet An Electronic Lexical Database, The MIT Press, Cambridge, MA ; London, 1998.

[5] F. Christiane, H. Amanda, "When WordNet Met Ontology," in Ontology Makes Sense - Essays in honor of Nicola Guarino, 136–151, 2019, doi: 10.3233/978-1-61499-955-3-136.

[6] N. Bouhriz, F. Benabbou, E. H. B. Lahmar, "Word Sense Disambiguation Approach for Arabic Text," (IJACSA) International Journal of Advanced Computer Science and Applications, **7**(4), 2016, doi:10.14569/IJACSA.2016.070451.

[7] P. Vossen, "Eurowordnet: A Multilingual Database Of Autonomous And Language-Specific Wordnets Connected Via An Inter-Lingualindex," International Journal of Lexicography, **17**(2), 161–173, 2004, doi:10.1093/ijl/17.2.161.

[8] M. Arcan, J. P. McCrae, P. Buitelaar, "Polylingual Wordnet," CoRR, **abs/1903.01411**, 2019.

[9] H. Rodríguez, D. Farwell, J. Farreres, M. Bertran, M. A. Martí, W. Black, S. Elkateb, J. Kirk, P. Vossen, C. Fellbaum, "Arabic WordNet: Current State and Future Extensions," in Proceedings of the Forth International Conference on Global WordNet, 2008.

[10] G. A. Miller, W. G. Charles, "Contextual correlates of semantic similarity," Language & Cognitive Processes, **6**(1), 1–28, 1991.

[11] F. Bond, L. Morgado da Costa, M. W. Goodman, J. P. McCrae, A. Lohk, "Some Issues with Building a Multilingual Wordnet," in Proceedings of the 12th Language Resources and Evaluation Conference, 3189–3197, European Language Resources Association, Marseille, France, 2020.

[12] L. Abouenour, K. Bouzoubaa, P. Rosso, "On the evaluation and improvement of Arabic WordNet coverage and usability," Language Resources and Evaluation, **47**, 2013, doi:10.1007/s10579-013-9254-z.

[13] H. Rodríguez, D. Farwell, J. Ferreres, M. Bertran, M. Alkhalifa, A. Martí, "Arabic WordNet: Semi-automatic Extensions using Bayesian Inference," 2008.

[14] M. A. Batita, M. Zrigui, "The Enrichment of Arabic WordNet Antonym Relations," in A. Gelbukh, editor, Computational Linguistics and Intelligent Text Processing, 342–353, Springer International Publishing, Cham, 2018, doi:10.1007/978-3-319-77113-7_27.

[15] N. Mohammed, D. Mohammed, "Experimental Study of Semantic Similarity Measures on Arabic WordNet," International Journal of Computer Science and Network Security, **17**(2), 2017.

[16] M. G. Aldayri, The semantic similarity measures using Arabic ontology, (Master's theses Theses and Dissertations Master). Middle East University, Jordan, 2017.

[17] M. A. Helou, "Effects of Semantic Gaps on Arabic WordNet-Based Similarity Measures," in 2019 International Conference on Innovative Computing (ICIC), 1–10, 2019, doi:10.1109/ICIC48496.2019.8966672.

[18] M. A. Helou, M. Palmonari, "Multi-user Feedback for Large-scale Cross-lingual Ontology Matching," in Proceedings of the 9th International Joint Conference on Knowledge Discovery, Knowledge Engineering and Knowledge Management, Funchal, Madeira, Portugal, November 1-3, 57–66, 2017, doi:10.5220/0006503200570066.

[19] R. Rada, H. Mili, E. Bicknell, M. Blettner, "Development and application of a metric on semantic nets," in IEEE Transactions on Systems, Man and Cybernetics, 17–30, 1989, doi:10.1109/21.24528.

[20] Z. Wu, M. Palmer, "Verbs semantics and lexical selection," in Proceedings of the 32nd annual meeting on Association for Computational Linguistics, 133–138, Association for Computational Linguistics, Morristown, NJ, USA, 1994.

[21] C. Leacock, M. Chodorow, "Combining local context and WordNet similarity for word sense identification," WordNet: An electronic lexical database, **49**(2), 265–283, 1998.

[22] F. A. Almarsoomi, J. D. OShea, Z. Bandar, K. Crockett, "AWSS: An Algorithm for Measuring Arabic Word Semantic Similarity," in 2013 IEEE International Conference on Systems, Man, and Cybernetics, 504–509, 2013, doi:10.1109/SMC.2013.92.

[23] F. A, Almarsoomi, J. D, O'Shea, Z. A, Bandar, K. A, Crockett, "Arabic Word Semantic Similarity," International Journal of Cognitive and Language Sciences, **6**(10), 2497 – 2505, 2012, doi:10.5281/zenodo.1080052.

[24] G. Hirst, "Ontology and the Lexicon," in eds. S. Staab, R. Studer, editors, Handbook on Ontologies and Information Systems, Heidelberg, Springer, 2004, doi:https://doi.org/10.1007/978-3-540-24750-0_11.

[25] G. A. Miller, C. Leacock, R. Tengi, R. T. Bunker, "A semantic concordance," in Proceedings of the workshop on Human Language Technology, HLT '93, 303–308, Association for Computational Linguistics, Stroudsburg, PA, USA, 1993.

[26] H. Graeme, "Overcoming Linguistic Barriers to the Multilingual Semantic Web," in P. Buitelaar, P. Cimiano, editors, Towards the Multilingual Semantic Web, 3–14, Springer Berlin Heidelberg, 2014, doi:10.1007/978-3-662-43585-4.

[27] D. Tufis, D. Cristea, S. Stamou, "BalkaNet: Aims, Methods, Results and Perspectives. A General Overview," In: D. Tufiş (ed): Special Issue on BalkaNet. Romanian JSTI, 2004.

[28] G. de Melo, G. Weikum, "Towards a universal wordnet by learning from combined evidence," in D. W.-L. Cheung, I.-Y. Song, W. W. Chu, X. Hu, J. J. Lin, editors, CIKM, 513–522, ACM, 2009, doi:10.1145/1645953.1646020.

[29] E. Pianta, L. Bentivogli, C. Girardi, "MultiWordNet: developing an aligned multilingual database," in Proceedings of the 1st Inter. Global Wordnet Conference, 2002.

[30] V. Nastase, M. Strube, B. Boerschinger, C. Zirn, A. Elghafari, "WikiNet: A Very Large Scale Multi-Lingual Concept Network," in N. Calzolari, K. Choukri, B. Maegaard, J. Mariani, J. Odijk, S. Piperidis, M. Rosner, D. Tapias, editors, LREC, European Language Resources Association, 2010.

[31] F. Bond, R. Foster, "Linking and Extending an Open Multilingual Wordnet," in ACL (1), 1352–1362, The Association for Computer Linguistics, 2013.

[32] M. M. Boudabous, N. Chaâben Kammoun, N. Khedher, L. H. Belguith, F. Sadat, "Arabic WordNet semantic relations enrichment through morpho-lexical patterns," in 2013 1st International Conference on Communications, Signal Processing, and their Applications (ICCSPA), 1–6, 2013.

[33] E. Bilel, "Arabic word sense disambiguation: a review," Artif. Intell. Rev., **52**(4), 2475–2532, 2019, doi:10.1007/s10462-018-9622-6.

[34] A. Budanitsky, G. Hirst, "Evaluating WordNet-based Measures of Lexical Semantic Relatedness," Comput. Linguist., **32**(1), 13–47, 2006, doi: 10.1162/coli.2006.32.1.13.

[35] N. Bouhriz, F. Benabbou, E. H. Benlahmar, Y. Zidoun, "Arabic Word Semantic similarity: a survey," in 1st International Conference On Research In Applied Mathematics And Computer, Casablanca, Morroco, 2019.

[36] H. Rubenstein, J. B. Goodenough, "Contextual correlates of synonymy," Commun. ACM, **8**(10), 627–633, 1965, doi:10.1145/365628.365657.

[37] P. Resnik, "Using information content to evaluate semantic similarity in a taxonomy," in IJCAI'95: Proceedings of the 14th international joint conference on Artificial intelligence, 448–453, Morgan Kaufmann Publishers Inc., San Francisco, CA, USA, 1995.

[38] D. Lin, "An Information-Theoretic Definition of Similarity," in J. W. Shavlik, J. W. Shavlik, editors, ICML, 296–304, Morgan Kaufmann, 1998.

[39] M. Lesk, "Automatic sense disambiguation using machine readable dictionaries: how to tell a pine cone from an ice cream cone," in SIGDOC '86: Proceedings of the 5th annual international conference on Systems documentation, 24–26, ACM, New York, NY, USA, 1986, doi:https://doi.org/10.1145/318723.318728.

[40] Z. Zhou, Y. Wang, J. Gu, "New model of semantic similarity measuring in wordnet," in 3rd International Conference on Intelligent System and Knowledge Engineering, volume 1, 256–261, 2008, doi:10.1109/ISKE.2008.4730937.

[41] M. A. Helou, A. Abid, "Semantic Measures based on Wordnet using Multiple Information Sources," in KDIR 2010 - Proceedings of the International Conference on Knowledge Discovery and Information Retrieval, Valencia, Spain, October 25-28, 2010, 500–503, 2010.

[42] M. A. Helou, M. Palmonari, M. Jarrar, "Effectiveness of Automatic Translations for Cross-Lingual Ontology Mapping," J. Artif. Intell. Res., **55**, 165–208, 2016, doi:10.1613/jair.4789.

[43] M. A. Helou, M. Palmonari, "Cross-lingual lexical matching with word translation and local similarity optimization," in Proceedings of the 11th International Conference on Semantic Systems, SEMANTICS 2015, Vienna, Austria, September 15-17, 97–104, 2015, doi:10.1145/2814864.2814888.

[44] Y. Regragui, L. Abouenour, F. Krieche, K. Bouzoubaa, P. Rosso, "Arabic WordNet: New Content and New Applications," in In Proceeding of the 8th Global Wordnet Conference (GWN 2016), 2016.